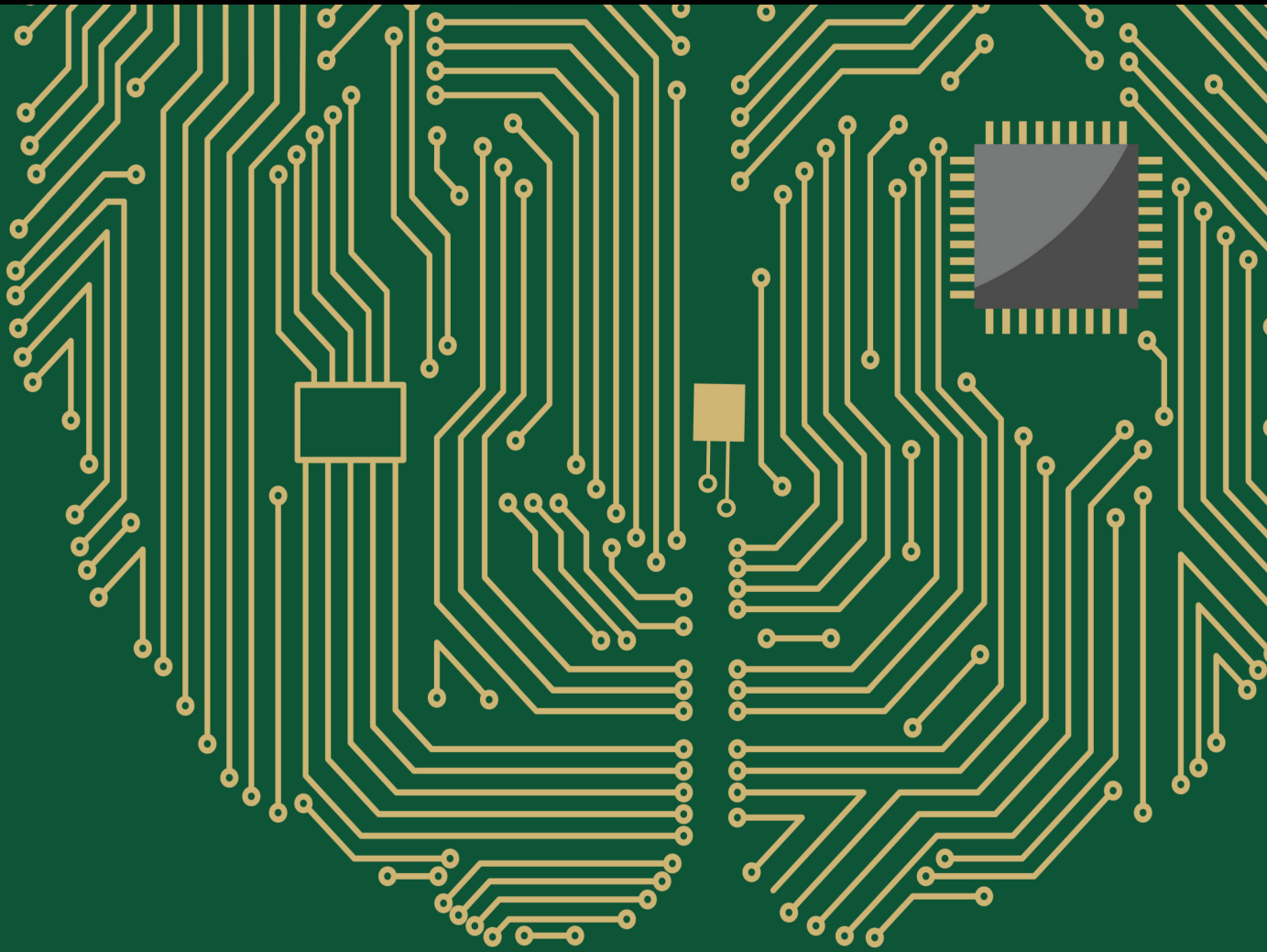


Lightweight Computational Intelligence for Sequential Data Analysis in Edge Computing

Lead Guest Editor: Le Sun

Guest Editors: Sudha Subramani, Subramanian Venkatesan, and Siuly Siuly





Lightweight Computational Intelligence for Sequential Data Analysis in Edge Computing

Computational Intelligence and Neuroscience

Lightweight Computational Intelligence for Sequential Data Analysis in Edge Computing

Lead Guest Editor: Le Sun

Guest Editors: Sudha Subramani, Subramanian
Venkatesan, and Siuly Siuly



Copyright © 2023 Hindawi Limited. All rights reserved.

This is a special issue published in "Computational Intelligence and Neuroscience." All articles are open access articles distributed under the Creative Commons Attribution License, which permits unrestricted use, distribution, and reproduction in any medium, provided the original work is properly cited.

Chief Editor

Andrzej Cichocki, Poland

Associate Editors

Arnaud Delorme, France
Cheng-Jian Lin , Taiwan
Saeid Sanei, United Kingdom

Academic Editors

Mohamed Abd Elaziz , Egypt
Tariq Ahanger , Saudi Arabia
Muhammad Ahmad, Pakistan
Ricardo Aler , Spain
Nouman Ali, Pakistan
Pietro Aricò , Italy
Lerina Aversano , Italy
Ümit Ağbulut , Turkey
Najib Ben Aoun , Saudi Arabia
Surbhi Bhatia , Saudi Arabia
Daniele Bibbo , Italy
Vince D. Calhoun , USA
Francesco Camastra, Italy
Zhicheng Cao, China
Hubert Cecotti , USA
Jyotir Moy Chatterjee , Nepal
Rupesh Chikara, USA
Marta Cimitile, Italy
Silvia Conforto , Italy
Paolo Crippa , Italy
Christian W. Dawson, United Kingdom
Carmen De Maio , Italy
Thomas DeMarse , USA
Maria Jose Del Jesus, Spain
Arnaud Delorme , France
Anastasios D. Doulamis, Greece
António Dourado , Portugal
Sheng Du , China
Said El Kafhali , Morocco
Mohammad Reza Feizi Derakhshi , Iran
Quanxi Feng, China
Zhong-kai Feng, China
Steven L. Fernandes, USA
Agostino Forestiero , Italy
Piotr Franaszczuk , USA
Thippa Reddy Gadekallu , India
Paolo Gastaldo , Italy
Samanwoy Ghosh-Dastidar, USA

Manuel Graña , Spain
Alberto Guillén , Spain
Gaurav Gupta, India
Rodolfo E. Haber , Spain
Usman Habib , Pakistan
Anandakumar Haldorai , India
José Alfredo Hernández-Pérez , Mexico
Luis Javier Herrera , Spain
Alexander Hošovský , Slovakia
Etienne Hugues, USA
Nadeem Iqbal , Pakistan
Sajad Jafari, Iran
Abdul Rehman Javed , Pakistan
Jing Jin , China
Li Jin, United Kingdom
Kanak Kalita, India
Ryotaro Kamimura , Japan
Pasi A. Karjalainen , Finland
Anitha Karthikeyan, Saint Vincent and the
Grenadines
Elpida Keravnou , Cyprus
Asif Irshad Khan , Saudi Arabia
Muhammad Adnan Khan , Republic of
Korea
Abbas Khosravi, Australia
Tai-hoon Kim, Republic of Korea
Li-Wei Ko , Taiwan
Raşit Köker , Turkey
Deepika Koundal , India
Sunil Kumar , India
Fabio La Foresta, Italy
Kuruva Lakshmana , India
Maciej Lawrynczuk , Poland
Jianli Liu , China
Giosuè Lo Bosco , Italy
Andrea Loddo , Italy
Kezhi Mao, Singapore
Paolo Massobrio , Italy
Gerard McKee, Nigeria
Mohit Mittal , France
Paulo Moura Oliveira , Portugal
Debajyoti Mukhopadhyay , India
Xin Ning , China
Nasimul Noman , Australia
Fivos Panetsos , Spain

Evgeniya Pankratova , Russia
Rocío Pérez de Prado , Spain
Francesco Pistolesi , Italy
Alessandro Sebastian Podda , Italy
David M Powers, Australia
Radu-Emil Precup, Romania
Lorenzo Putzu, Italy
S P Raja, India
Dr.Anand Singh Rajawat , India
Simone Ranaldi , Italy
Upaka Rathnayake, Sri Lanka
Navid Razmjooy, Iran
Carlo Ricciardi, Italy
Jatinderkumar R. Saini , India
Sandhya Samarasinghe , New Zealand
Friedhelm Schwenker, Germany
Mijanur Rahaman Seikh, India
Tapan Senapati , China
Mohammed Shuaib , Malaysia
Kamran Siddique , USA
Gaurav Singal, India
Akansha Singh , India
Chiranjibi Sitaula , Australia
Neelakandan Subramani, India
Le Sun, China
Rawia Tahrir , Iraq
Binhua Tang , China
Carlos M. Travieso-González , Spain
Vinh Truong Hoang , Vietnam
Fath U Min Ullah , Republic of Korea
Pablo Varona , Spain
Roberto A. Vazquez , Mexico
Mario Versaci, Italy
Gennaro Vessio , Italy
Ivan Volosyak , Germany
Leyi Wei , China
Jianghui Wen, China
Lingwei Xu , China
Cornelio Yáñez-Márquez, Mexico
Zaher Mundher Yaseen, Iraq
Yugen Yi , China
Qiangqiang Yuan , China
Miaolei Zhou , China
Michal Zochowski, USA
Rodolfo Zunino, Italy

Contents

Retracted: Analysis of Psychological Changes and Intervention Mechanism of Elderly Groups Based on Deep Learning Analysis Technology

Computational Intelligence and Neuroscience

Retraction (1 page), Article ID 9861698, Volume 2023 (2023)

Retracted: A Study on the Impact of Digital Finance on Regional Productivity Growth Based on Artificial Neural Networks

Computational Intelligence and Neuroscience

Retraction (1 page), Article ID 9847181, Volume 2023 (2023)

Retracted: Railway Traffic Emergency Management Relying on Image Recognition Technology in the Context of Big Data

Computational Intelligence and Neuroscience

Retraction (1 page), Article ID 9835971, Volume 2023 (2023)

Retracted: Analysis and Prediction of Corporate Finance and Exchange Rate Correlation Based on Machine Learning Algorithms

Computational Intelligence and Neuroscience

Retraction (1 page), Article ID 9828963, Volume 2023 (2023)

Retracted: Artificial Intelligence-Based Recommendation and Application of Public Services in Smart Cities

Computational Intelligence and Neuroscience

Retraction (1 page), Article ID 9792364, Volume 2023 (2023)

Retracted: Development Strategy of Intelligent Digital Library without Human Service in the Era of "Internet +"

Computational Intelligence and Neuroscience

Retraction (1 page), Article ID 9757085, Volume 2023 (2023)

Retracted: Fuzzy Logic-Based Machine Learning Algorithm for Cultural and Creative Product Design

Computational Intelligence and Neuroscience

Retraction (1 page), Article ID 9827480, Volume 2023 (2023)

Retracted: Design and Implementation of Dance Online Teaching System Based on Optimized Load Balancing Algorithm

Computational Intelligence and Neuroscience

Retraction (1 page), Article ID 9830149, Volume 2023 (2023)

Retracted: Design of a Multimedia-Assisted Distance English Teaching System for College Students

Computational Intelligence and Neuroscience

Retraction (1 page), Article ID 9815654, Volume 2023 (2023)

Retracted: Feasibility Analysis and Discrete Dynamic Modeling of Physical Education Teaching Strategy Based on Intelligent Computing

Computational Intelligence and Neuroscience

Retraction (1 page), Article ID 9813451, Volume 2023 (2023)

Retracted: Construction and Analysis of Indicators of the Labor Education System Based on the Gray Correlation Degree Model

Computational Intelligence and Neuroscience
Retraction (1 page), Article ID 9781506, Volume 2023 (2023)

Retracted: Design and Optimization of Aesthetic Education Teaching Information Platform Based on Big Data Analysis

Computational Intelligence and Neuroscience
Retraction (1 page), Article ID 9761050, Volume 2023 (2023)

Retracted: Data Sharing Method of College Dance Teaching Resource Database Based on PSO Algorithm

Computational Intelligence and Neuroscience
Retraction (1 page), Article ID 9895407, Volume 2023 (2023)

Retracted: Research on Virtual Interactive Animation Design System Based on Deep Learning

Computational Intelligence and Neuroscience
Retraction (1 page), Article ID 9875219, Volume 2023 (2023)

Retracted: A Deep Learning-Based Piano Music Notation Recognition Method

Computational Intelligence and Neuroscience
Retraction (1 page), Article ID 9864216, Volume 2023 (2023)


Retracted: Application of Intelligent Image Matching and Visual Communication in Brand Design

Computational Intelligence and Neuroscience
Retraction (1 page), Article ID 9854212, Volume 2023 (2023)

Retracted: Construction and Analysis of Performance Evaluation Index System for Chinese Small and Medium-Sized Enterprises Based on Fuzzy Hierarchical Analysis Model

Computational Intelligence and Neuroscience
Retraction (1 page), Article ID 9849832, Volume 2023 (2023)

A Factorization Deep Product Neural Network for Student Physical Performance Prediction

Xiaoxia Jiao 
Research Article (8 pages), Article ID 4221254, Volume 2022 (2022)

[Retracted] Design and Implementation of Dance Online Teaching System Based on Optimized Load Balancing Algorithm


Qirong Yang 
Research Article (10 pages), Article ID 3829118, Volume 2022 (2022)

[Retracted] Development Strategy of Intelligent Digital Library without Human Service in the Era of "Internet +"

Hongmei Wang and Jian Ding 
Research Article (11 pages), Article ID 7892738, Volume 2022 (2022)




Contents

Impact Analysis of Basketball Exercise Strength Based on Machine Learning in the Mental Health of College Students

Ran Zhang 


Research Article (9 pages), Article ID 9628446, Volume 2022 (2022)

Review on Security Issues and Applications of Trust Mechanism in Wireless Sensor Networks

Zhengxin Xia , Zhe Wei , and Huan Zhang 



Review Article (9 pages), Article ID 3449428, Volume 2022 (2022)

Design of Cross-Platform Information Retrieval System of Library Based on Digital Twins

Shanshan Shang , Zikai Yu, Kun Jiao, Yingshi Huang, Hua Guo, and Guozhong Wang



Research Article (10 pages), Article ID 7999091, Volume 2022 (2022)

Modeling and Robust Tracking Decoupling Control of a Coaxial Unmanned Helicopter Based on the Improved Alternating Direction Method of Multipliers

Anan Xu , Fang Wang , and Ming Chen



Research Article (12 pages), Article ID 3647784, Volume 2022 (2022)

Intelligent Identification of Coal Crack in CT Images Based on Deep Learning

Jinxia Yu, Chengyi Wu , Yingying Li , and Yimin Zhang

Research Article (10 pages), Article ID 7092436, Volume 2022 (2022)

Study on Personalized Recommendation Algorithm of Online Educational Resources Based on Knowledge Association

Ziqian Xu  and Sheng Jiang 

Research Article (9 pages), Article ID 2192459, Volume 2022 (2022)

Style Transfer of Chinese Art Works Based on Dual Channel Deep Learning Model

Yan Tang 






Research Article (11 pages), Article ID 4376006, Volume 2022 (2022)

Research on Movement Analysis and Guidance in Dance Learning Based on Data Mining

Guangle Yin  and Jing Liu



Research Article (9 pages), Article ID 9327442, Volume 2022 (2022)

Efficient Lattice-Based Ring Signature Scheme without Trapdoors for Machine Learning

Qing Ye , Yongkang Lang , Zongqu Zhao , Qingqing Chen , and Yongli Tang 


Research Article (13 pages), Article ID 6547464, Volume 2022 (2022)

Construction and Application of the Talent Training System in Colleges and Universities Based on the Fuzzy Analytic Hierarchy Process

Yan Yu  and Jun Qiu 




Research Article (10 pages), Article ID 7295875, Volume 2022 (2022)

Research on Monitoring of Gymnastics Facilities and Intelligent Optimal Distribution of Gymnastics Venues Based on Internet of Things

Hongbo Liu and Yuzhen Wang 


Research Article (9 pages), Article ID 6164448, Volume 2022 (2022)

SchizoGoogLeNet: The GoogLeNet-Based Deep Feature Extraction Design for Automatic Detection of Schizophrenia

Siuly Siuly , Yan Li , Peng Wen , and Omer Faruk Alcin


Research Article (13 pages), Article ID 1992596, Volume 2022 (2022)

Interactive Design of Business English Learning Resources Based on EDIPT Multimodal Model

Xiaomei Yang and Shi Qi 


Research Article (9 pages), Article ID 1264847, Volume 2022 (2022)

Personalized Information Service System of Smart Library Based on Multimedia Network Technology

Juan Wang 


Research Article (10 pages), Article ID 2856574, Volume 2022 (2022)

Using Pitch Feature Matching to Design a Music Tutoring System Based on Deep Learning

Jing Jiang 




Research Article (7 pages), Article ID 4520953, Volume 2022 (2022)

Evaluation of Enterprise Accounting Data Management Based on Maturity Model

Jun Xiang 


Research Article (9 pages), Article ID 3891475, Volume 2022 (2022)

A Fast Data Transmission Method of Vehicle-Road Cooperative Communication Based on the Clustering Algorithm

Weifeng Wang , Zijian Wang, Yang Xu , Xinpeng Yao, and Yulin Ma 



Research Article (8 pages), Article ID 9162360, Volume 2022 (2022)

Construction and Application of Farmers' Practical Teaching System in Vocational Education Based on Big Data Mining Technology

Wei Peng and Zhibin Tang 

Research Article (9 pages), Article ID 6075719, Volume 2022 (2022)

An English Flipped Classroom Teaching Model Based on Big Data Analysis

Wang Sa , Li Dan, Du Juan, Yu Fei, and Wang Wei 

Research Article (11 pages), Article ID 7391258, Volume 2022 (2022)

Detection and Analysis of Human Cells Based on Artificial Neural Network

Jun Yao and Hongji Yuan 

Research Article (10 pages), Article ID 4600840, Volume 2022 (2022)


Contents

Task Offloading and Resource Allocation Strategy Based on Deep Learning for Mobile Edge Computing

Zijia Yu , Xu Xu , and Wei Zhou 


Research Article (11 pages), Article ID 1427219, Volume 2022 (2022)

Text Analysis and Policy Guidance of Emotional Intonation of Enterprise Management Based on Deep Learning

Ni Yang and Jing Qiu 


Research Article (8 pages), Article ID 3428078, Volume 2022 (2022)

[Retracted] Artificial Intelligence-Based Recommendation and Application of Public Services in Smart Cities

Jin Zhou 


Research Article (10 pages), Article ID 8958865, Volume 2022 (2022)

Prediction and Evaluation Method of e-Commerce Service Satisfaction Based on Intelligent Computing Method

Fang Tu and Bo Tu 


Research Article (9 pages), Article ID 2730660, Volume 2022 (2022)

Application of Convolutional Neural Network in Motor Bearing Fault Diagnosis

Shuiqin Zhou, Lepeng Lin, Chu Chen, Wenbin Pan, and Xiaochun Lou 

Research Article (11 pages), Article ID 9231305, Volume 2022 (2022)

Intelligent Optimization Method of Resource Recommendation Service of Mobile Library Based on Digital Twin Technology

Shanshan Shang , Zikai Yu, Aili Geng, Xiuxiu Xu, Huizhen Ma, and Guozhong Wang


Research Article (10 pages), Article ID 3582719, Volume 2022 (2022)

Trusted Data Analysis and Consensus Mechanism of Product Traceability Based on Blockchain

Yang Kang, Qiang Li , and Yuanyong Liu


Research Article (10 pages), Article ID 3035231, Volume 2022 (2022)

Web Log Analysis and Security Assessment Method Based on Data Mining

Jingquan Jin and Xin Lin 


Research Article (9 pages), Article ID 8485014, Volume 2022 (2022)

Deep Learning-Based Correlation Analysis between the Evaluation Score of English Teaching Quality and the Knowledge Points

Yuanyuan Li 

Research Article (10 pages), Article ID 4102959, Volume 2022 (2022)

Deep Learning Algorithm for Online College Physical Education Teaching with Flipping Classroom

Zhengqiang Chen 

Research Article (12 pages), Article ID 8742661, Volume 2022 (2022)

Time Series Data Prediction and Feature Analysis of Sports Dance Movements Based on Machine Learning

DongXia Zheng  and Yi Yuan 


Research Article (12 pages), Article ID 5611829, Volume 2022 (2022)

Efficiency Evaluation and Influencing Factors Analysis of Logistics Industry based on Multiobjective Intelligent Computing

Tingyan Zhou  and Wenxing Li


Research Article (10 pages), Article ID 3098160, Volume 2022 (2022)

Lightweight Deep Learning Model for Marketing Strategy Optimization and Characteristic Analysis

Yang Su , Chonghong Wang, and Xuejiao Sun


Research Article (9 pages), Article ID 2429748, Volume 2022 (2022)

The Intervention of Data Mining in the Allocation Efficiency of Multiple Intelligent Devices in Intelligent Pharmacy

Xiaohua Li, Benren Tan , Jinkun Zheng, Xiaomei Xu, Jian Xiao, and Yanlin Liu



Research Article (12 pages), Article ID 5371575, Volume 2022 (2022)

Analysis of Teaching Tactics Characteristics of Track and Field Sports Training in Colleges and Universities Based on Deep Neural Network

Wei Wang 

Research Article (11 pages), Article ID 1932596, Volume 2022 (2022)

Intelligent Evaluation of Public Sports Service Based on Intuitionistic Fuzzy Set Theory

Yu Shao  and Rong Bo 


Research Article (8 pages), Article ID 4748730, Volume 2022 (2022)

Nonlinear Dynamic Response Analysis of a Three-Stage Gear Train Based on Lightweight Calculation for Edge Equipment

Dongdong Ren, Yangwu Yao , Huiyuan Wang , Huixian Qu, and Guoqiang Wang

Research Article (8 pages), Article ID 4724504, Volume 2022 (2022)

Prediction and Estimation of River Velocity Based on GAN and Multifeature Fusion

Yan Wang, Weiwei Chen , and Yulan Wang





Research Article (10 pages), Article ID 7316133, Volume 2022 (2022)

Optimized Deep Neural Network and Its Application in Fine Sowing of Crops

Bing Li  and Jiyun Li

Research Article (10 pages), Article ID 3650702, Volume 2022 (2022)


Video Image Moving Target Recognition Method Based on Generated Countermeasure Network

Zilong Li , DaiHong Jiang , Hongdong Wang , and Dan Li 

Research Article (8 pages), Article ID 7972845, Volume 2022 (2022)


Contents

Gear Fault Diagnosis and Life Prediction of Petroleum Drilling Equipment Based on SOM Neural Network

Linzhu Lu, Jie Liu , Xin Huang, and Yongcai Fan


Research Article (7 pages), Article ID 9841443, Volume 2022 (2022)

Identification of Sports Athletes Psychological Stress Based on K-Means Optimized Hierarchical Clustering

Jun Huang 

Research Article (7 pages), Article ID 6555797, Volume 2022 (2022)

[Retracted] Data Sharing Method of College Dance Teaching Resource Database Based on PSO Algorithm

Xulong ZhuGe and Haibin Cao 


Research Article (9 pages), Article ID 2162981, Volume 2022 (2022)

[Retracted] Construction and Analysis of Indicators of the Labor Education System Based on the Gray Correlation Degree Model

Ling Huang 


Research Article (8 pages), Article ID 2281469, Volume 2022 (2022)

[Retracted] Design and Optimization of Aesthetic Education Teaching Information Platform Based on Big Data Analysis

Xingxing Wu and Hai Gu 



Research Article (9 pages), Article ID 5109638, Volume 2022 (2022)

Personalized Recommendation Algorithm for Movie Data Combining Rating Matrix and User Subjective Preference

Chang Liu 


Research Article (11 pages), Article ID 2970514, Volume 2022 (2022)

Antiocclusion Visual Tracking Algorithm Combining Fully Convolutional Siamese Network and Correlation Filtering

Xiaomiao Tao , Kaijun Wu , Yongshun Wang, Panfeng Li, Tao Huang, and Chenshuai Bai

Research Article (9 pages), Article ID 8051876, Volume 2022 (2022)

[Retracted] Application of Intelligent Image Matching and Visual Communication in Brand Design

Ming Liu  and Wenyan Zhong



Research Article (9 pages), Article ID 5964851, Volume 2022 (2022)

An Improved Logistic Regression Method for Assessing the Performance of Track and Field Sports

Songling Zheng  and Xi Man


Research Article (10 pages), Article ID 6341495, Volume 2022 (2022)

Traffic Flow Prediction and Analysis in Smart Cities Based on the WND-LSTM Model

SuYuan Ma  and MingYe Zhao 


Research Article (9 pages), Article ID 7079045, Volume 2022 (2022)

A Lightweight CNN Model Based on GhostNet

Zhong Wang and Tong Li 


Research Article (12 pages), Article ID 8396550, Volume 2022 (2022)

Optimization and Analysis of Intelligent Accounting Information System Based on Deep Learning Model

Suzhen Feng and Ran Zhong 


Research Article (9 pages), Article ID 1284289, Volume 2022 (2022)

Research on the Evaluation of Moral Education Effectiveness and Student Behavior in Universities under the Environment of Big Data

Rui Zhu 


Research Article (9 pages), Article ID 2832661, Volume 2022 (2022)

Analysis of Strategies and Skills of English Translation Based on Coverage Mechanism

Bin Liu  and Jing Wang



Research Article (7 pages), Article ID 7767045, Volume 2022 (2022)

[Retracted] Construction and Analysis of Performance Evaluation Index System for Chinese Small and Medium-Sized Enterprises Based on Fuzzy Hierarchical Analysis Model

Mengning He  and Raquel Pérez Estebanez





Research Article (8 pages), Article ID 1230786, Volume 2022 (2022)

Research on Perceptual Integrity of Distributed Digital Media Based on AWTC-TT Algorithm Optimization

Xiaobo Zhang  and Rongrong Shen 


Research Article (9 pages), Article ID 9675529, Volume 2022 (2022)

Construction and Analysis of Discrete System Dynamic Modeling of Physical Education Teaching Mode Based on Decision Tree Algorithm

Caixia Wang , Xiaoyun Wei , Aiqian Yang , and Haiyan Zhang 

Research Article (11 pages), Article ID 2745146, Volume 2022 (2022)

Research on Architectural Planning and Landscape Design of Smart City Based on Computational Intelligence

Nan Shao 


Research Article (9 pages), Article ID 1745593, Volume 2022 (2022)

GMAIR: Unsupervised Object Detection Based on Spatial Attention and Gaussian Mixture Model

Weijin Zhu , Yao Shen , Mingqian Liu , and Lizeth Patricia Aguirre Sanchez 

Research Article (13 pages), Article ID 7254462, Volume 2022 (2022)


Secure Clustering Strategy Based on Improved Particle Swarm Optimization Algorithm in Internet of Things

Zhanbiao Bao 

Research Article (9 pages), Article ID 7380849, Volume 2022 (2022)


Contents

Design and Implementation of Trace Inspection System Based upon Hyperspectral Imaging Technology

Yuchen Wang and Zhongyuan Ji 


Research Article (13 pages), Article ID 9524190, Volume 2022 (2022)

Short-Term Demand Forecast of E-Commerce Platform Based on ConvLSTM Network

Zan Li  and Nairen Zhang

Research Article (10 pages), Article ID 5227829, Volume 2022 (2022)

Design of Intelligent Evaluation System for College Students' Mental Health Based on Big Data

Tao Hu, Xiaojun Zhang , and Na Li



Research Article (10 pages), Article ID 7119994, Volume 2022 (2022)

Innovation and Integration Development of the Cultural Industry Based on Mapping Knowledge Domains

Jiangong Lian  and Dan Liang


Research Article (8 pages), Article ID 4725196, Volume 2022 (2022)

Research on the Application of Artificial Neural Network-Based Virtual Image Technology in College Tennis Teaching

Ruizhe Hu  and Xiaocan Cui 

Research Article (12 pages), Article ID 4935121, Volume 2022 (2022)

MRI Radiogenomics in Precision Oncology: New Diagnosis and Treatment Method

Xiao-Xia Yin , Mingyong Gao, Wei Wang, and Yanchun Zhang


Review Article (13 pages), Article ID 2703350, Volume 2022 (2022)

Analysis of Diversified Radio and Television Data Based on Adaptive Least Squares Support Vector Machine

Jing Liu and Minnan Cang 


Research Article (14 pages), Article ID 4235088, Volume 2022 (2022)

[Retracted] Railway Traffic Emergency Management Relying on Image Recognition Technology in the Context of Big Data

Fei Dong and Yuanyuan Ma 

Research Article (12 pages), Article ID 1920196, Volume 2022 (2022)

Application of Human Posture Recognition Based on the Convolutional Neural Network in Physical Training Guidance

Qingyu Wang 


Research Article (11 pages), Article ID 5277157, Volume 2022 (2022)

Deep Learning-Based Optimization Algorithm for Enterprise Personnel Identity Authentication

Tiejun Chen 


Research Article (9 pages), Article ID 9662817, Volume 2022 (2022)

Research on Image Recognition of Gymnastics Sports Injuries Based on Deep Learning

Peng Jia  and Yixiong Xu


Research Article (12 pages), Article ID 8987006, Volume 2022 (2022)

Financial Data Analysis and Application Based on Big Data Mining Technology

Jinfeng Cheng 

Research Article (8 pages), Article ID 6711470, Volume 2022 (2022)

[Retracted] Research on Virtual Interactive Animation Design System Based on Deep Learning

Bing Liu 


Research Article (10 pages), Article ID 5035369, Volume 2022 (2022)

[Retracted] Analysis and Prediction of Corporate Finance and Exchange Rate Correlation Based on Machine Learning Algorithms

Ke Zhang, Xiaofei Wang , Junjie Wang, Sinan Wang, and Feng Hui


Research Article (9 pages), Article ID 2850604, Volume 2022 (2022)

Design and Optimisation of an Enterprise Digital Management System Based on IoT Monitoring

Shengwen Wang 


Research Article (7 pages), Article ID 3264485, Volume 2022 (2022)

High-Performance Computing Analysis and Location Selection of Logistics Distribution Center Space Based on Whale Optimization Algorithm

Lijuan Yang  and Xiedong Song


Research Article (9 pages), Article ID 2055241, Volume 2022 (2022)

[Retracted] Design of a Multimedia-Assisted Distance English Teaching System for College Students

Haili Feng 


Research Article (8 pages), Article ID 2184600, Volume 2022 (2022)

Design of Optimum Portfolio Scheme Based on Improved NSGA-II Algorithm

Yiqian Zhou, Weinan Chen, and Deqin Lin 


Research Article (9 pages), Article ID 7419500, Volume 2022 (2022)

Design of Cloud Storage-Oriented Sports Physical Fitness Monitoring System

Zhou Zheng and Yang Liu 



Research Article (10 pages), Article ID 1889381, Volume 2022 (2022)

The Empirical Analysis of Bitcoin Price Prediction Based on Deep Learning Integration Method

Shengao Zhang, Mengze Li, and Chunxiao Yan 

Research Article (9 pages), Article ID 1265837, Volume 2022 (2022)


Research on Discrete Dynamic Modeling of Learner Behavior Analysis in English Teaching

Junru Fu  and Lingmei Cao 

Research Article (9 pages), Article ID 1914996, Volume 2022 (2022)


Contents

[Retracted] Fuzzy Logic-Based Machine Learning Algorithm for Cultural and Creative Product Design

Taihua Lan 


Research Article (7 pages), Article ID 7747192, Volume 2022 (2022)

Research and Application of Clustering Algorithm for Text Big Data

Zi Li Chen 


Research Article (8 pages), Article ID 7042778, Volume 2022 (2022)

High Performance Computing Simulation of Intelligent Logistics Management Based on Shortest Path Algorithm

Zongchao Wei 


Research Article (10 pages), Article ID 7930553, Volume 2022 (2022)

Prediction and Planning of Sports Competition Based on Deep Neural Network

Jin Xu 


Research Article (9 pages), Article ID 1906580, Volume 2022 (2022)

[Retracted] Feasibility Analysis and Discrete Dynamic Modeling of Physical Education Teaching Strategy Based on Intelligent Computing

Ge Wang 


Research Article (8 pages), Article ID 4093924, Volume 2022 (2022)

Research on Cross-Contrast Neural Network Based Intelligent Painting: Taking Oil Painting Language Classification as an Example

Xi Zeng 

Research Article (10 pages), Article ID 7827587, Volume 2022 (2022)

Prediction of Labor Unemployment Based on Time Series Model and Neural Network Model

Xitao Liu and Lihui Li 


Research Article (8 pages), Article ID 7019078, Volume 2022 (2022)

[Retracted] A Deep Learning-Based Piano Music Notation Recognition Method

Chan Li 


Research Article (9 pages), Article ID 2278683, Volume 2022 (2022)

Analysis of Sentiment and Personalised Recommendation in Musical Performance

Dan Wang 


Research Article (6 pages), Article ID 2778181, Volume 2022 (2022)

Evaluation of Financial Subsidy for Agriculture Based on Combined Algorithm

Kexin Chen and Zhenyu Wang 


Research Article (8 pages), Article ID 6587460, Volume 2022 (2022)

[Retracted] A Study on the Impact of Digital Finance on Regional Productivity Growth Based on Artificial Neural Networks

Jia Li, Fangcheng Sun, and Meng Li 







Research Article (7 pages), Article ID 7665954, Volume 2022 (2022)

Intelligent Control Method for Loss Distribution Balance of High-Power Photovoltaic Grid-Connected Inverters

Yi Xu , ErYong Zou, and FengPing Tang


Research Article (10 pages), Article ID 7240834, Volume 2022 (2022)

Correlation-Based Anomaly Detection Method for Multi-sensor System

Han Li , Xinyu Wang , Zhongguo Yang , Sikandar Ali , Ning Tong , and Samad Baseer 



Research Article (13 pages), Article ID 4756480, Volume 2022 (2022)

Short Sequence Chinese-English Machine Translation Based on Generative Adversarial Networks of Emotion

Hua Wang 



Research Article (10 pages), Article ID 3385477, Volume 2022 (2022)

An Efficient Resource Management Optimization Scheme for Internet of Vehicles in Edge Computing Environment

Anqing Zhu  and Youyun Wen 

Research Article (8 pages), Article ID 3207456, Volume 2022 (2022)

Intrusion Detection Model for Industrial Internet of Things Based on Improved Autoencoder

Wumei Zhang  and Yongzhen Zhang 



Research Article (8 pages), Article ID 1406214, Volume 2022 (2022)

Research on Brand Image Evaluation Method Based on Consumer Sentiment Analysis

ZhengMin Li 





Research Article (8 pages), Article ID 2647515, Volume 2022 (2022)

Research on Audio Recognition Based on the Deep Neural Network in Music Teaching

Yun Cui  and Fu Wang 


Research Article (8 pages), Article ID 7055624, Volume 2022 (2022)

Efficient Linkable Ring Signature Scheme over NTRU Lattice with Unconditional Anonymity

Qing Ye , Mengyao Wang , Hui Meng , Feifei Xia , and Xixi Yan 

Research Article (14 pages), Article ID 8431874, Volume 2022 (2022)

[Retracted] Analysis of Psychological Changes and Intervention Mechanism of Elderly Groups Based on Deep Learning Analysis Technology

Yue Gao and Qi Fan 

Research Article (8 pages), Article ID 1686219, Volume 2022 (2022)


Contents

Redactable Blockchain Trust Scheme Based on Reputation Consensus for MEC

YongLi Tang , Shuai Wu , and XiaoJun Wang 


Research Article (14 pages), Article ID 3269445, Volume 2022 (2022)

Research on Video Captioning Based on Multifeature Fusion

Hong Zhao, Lan Guo , ZhiWen Chen, and HouZe Zheng

Research Article (14 pages), Article ID 1204909, Volume 2022 (2022)

Intelligent Tourism Information Service Model considering Tourist Experience in the Environment of Internet of Things

Han Liu 

Research Article (10 pages), Article ID 5252218, Volume 2022 (2022)

Design of Multimedia English Online Teaching Platform under Wireless Network Communication Technology

He Dan 

Research Article (10 pages), Article ID 1894067, Volume 2022 (2022)

Retraction

Retracted: Analysis of Psychological Changes and Intervention Mechanism of Elderly Groups Based on Deep Learning Analysis Technology

Computational Intelligence and Neuroscience

Received 3 October 2023; Accepted 3 October 2023; Published 4 October 2023

Copyright © 2023 Computational Intelligence and Neuroscience. This is an open access article distributed under the Creative Commons Attribution License, which permits unrestricted use, distribution, and reproduction in any medium, provided the original work is properly cited.

This article has been retracted by Hindawi following an investigation undertaken by the publisher [1]. This investigation has uncovered evidence of one or more of the following indicators of systematic manipulation of the publication process:

- (1) Discrepancies in scope
- (2) Discrepancies in the description of the research reported
- (3) Discrepancies between the availability of data and the research described
- (4) Inappropriate citations
- (5) Incoherent, meaningless and/or irrelevant content included in the article
- (6) Peer-review manipulation

The presence of these indicators undermines our confidence in the integrity of the article's content and we cannot, therefore, vouch for its reliability. Please note that this notice is intended solely to alert readers that the content of this article is unreliable. We have not investigated whether authors were aware of or involved in the systematic manipulation of the publication process.

In addition, our investigation has also shown that one or more of the following human-subject reporting requirements has not been met in this article: ethical approval by an Institutional Review Board (IRB) committee or equivalent, patient/participant consent to participate, and/or agreement to publish patient/participant details (where relevant).

Wiley and Hindawi regrets that the usual quality checks did not identify these issues before publication and have since put additional measures in place to safeguard research integrity.

We wish to credit our own Research Integrity and Research Publishing teams and anonymous and named external researchers and research integrity experts for contributing to this investigation.

The corresponding author, as the representative of all authors, has been given the opportunity to register their agreement or disagreement to this retraction. We have kept a record of any response received.

References

- [1] Y. Gao and Q. Fan, "Analysis of Psychological Changes and Intervention Mechanism of Elderly Groups Based on Deep Learning Analysis Technology," *Computational Intelligence and Neuroscience*, vol. 2022, Article ID 1686219, 8 pages, 2022.

Retraction

Retracted: A Study on the Impact of Digital Finance on Regional Productivity Growth Based on Artificial Neural Networks

Computational Intelligence and Neuroscience

Received 3 October 2023; Accepted 3 October 2023; Published 4 October 2023

Copyright © 2023 Computational Intelligence and Neuroscience. This is an open access article distributed under the Creative Commons Attribution License, which permits unrestricted use, distribution, and reproduction in any medium, provided the original work is properly cited.

This article has been retracted by Hindawi following an investigation undertaken by the publisher [1]. This investigation has uncovered evidence of one or more of the following indicators of systematic manipulation of the publication process:

- (1) Discrepancies in scope
- (2) Discrepancies in the description of the research reported
- (3) Discrepancies between the availability of data and the research described
- (4) Inappropriate citations
- (5) Incoherent, meaningless and/or irrelevant content included in the article
- (6) Peer-review manipulation

The presence of these indicators undermines our confidence in the integrity of the article's content and we cannot, therefore, vouch for its reliability. Please note that this notice is intended solely to alert readers that the content of this article is unreliable. We have not investigated whether authors were aware of or involved in the systematic manipulation of the publication process.

Wiley and Hindawi regrets that the usual quality checks did not identify these issues before publication and have since put additional measures in place to safeguard research integrity.

We wish to credit our own Research Integrity and Research Publishing teams and anonymous and named external researchers and research integrity experts for contributing to this investigation.

The corresponding author, as the representative of all authors, has been given the opportunity to register their agreement or disagreement to this retraction. We have kept a record of any response received.

References

- [1] J. Li, F. Sun, and M. Li, "A Study on the Impact of Digital Finance on Regional Productivity Growth Based on Artificial Neural Networks," *Computational Intelligence and Neuroscience*, vol. 2022, Article ID 7665954, 7 pages, 2022.

Retraction

Retracted: Railway Traffic Emergency Management Relying on Image Recognition Technology in the Context of Big Data

Computational Intelligence and Neuroscience

Received 3 October 2023; Accepted 3 October 2023; Published 4 October 2023

Copyright © 2023 Computational Intelligence and Neuroscience. This is an open access article distributed under the Creative Commons Attribution License, which permits unrestricted use, distribution, and reproduction in any medium, provided the original work is properly cited.

This article has been retracted by Hindawi following an investigation undertaken by the publisher [1]. This investigation has uncovered evidence of one or more of the following indicators of systematic manipulation of the publication process:

- (1) Discrepancies in scope
- (2) Discrepancies in the description of the research reported
- (3) Discrepancies between the availability of data and the research described
- (4) Inappropriate citations
- (5) Incoherent, meaningless and/or irrelevant content included in the article
- (6) Peer-review manipulation

The presence of these indicators undermines our confidence in the integrity of the article's content and we cannot, therefore, vouch for its reliability. Please note that this notice is intended solely to alert readers that the content of this article is unreliable. We have not investigated whether authors were aware of or involved in the systematic manipulation of the publication process.

Wiley and Hindawi regrets that the usual quality checks did not identify these issues before publication and have since put additional measures in place to safeguard research integrity.

We wish to credit our own Research Integrity and Research Publishing teams and anonymous and named external researchers and research integrity experts for contributing to this investigation.

The corresponding author, as the representative of all authors, has been given the opportunity to register their agreement or disagreement to this retraction. We have kept a record of any response received.

References

- [1] F. Dong and Y. Ma, "Railway Traffic Emergency Management Relying on Image Recognition Technology in the Context of Big Data," *Computational Intelligence and Neuroscience*, vol. 2022, Article ID 1920196, 12 pages, 2022.

Retraction

Retracted: Analysis and Prediction of Corporate Finance and Exchange Rate Correlation Based on Machine Learning Algorithms

Computational Intelligence and Neuroscience

Received 3 October 2023; Accepted 3 October 2023; Published 4 October 2023

Copyright © 2023 Computational Intelligence and Neuroscience. This is an open access article distributed under the Creative Commons Attribution License, which permits unrestricted use, distribution, and reproduction in any medium, provided the original work is properly cited.

This article has been retracted by Hindawi following an investigation undertaken by the publisher [1]. This investigation has uncovered evidence of one or more of the following indicators of systematic manipulation of the publication process:

- (1) Discrepancies in scope
- (2) Discrepancies in the description of the research reported
- (3) Discrepancies between the availability of data and the research described
- (4) Inappropriate citations
- (5) Incoherent, meaningless and/or irrelevant content included in the article
- (6) Peer-review manipulation

The presence of these indicators undermines our confidence in the integrity of the article's content and we cannot, therefore, vouch for its reliability. Please note that this notice is intended solely to alert readers that the content of this article is unreliable. We have not investigated whether authors were aware of or involved in the systematic manipulation of the publication process.

Wiley and Hindawi regrets that the usual quality checks did not identify these issues before publication and have since put additional measures in place to safeguard research integrity.

We wish to credit our own Research Integrity and Research Publishing teams and anonymous and named external researchers and research integrity experts for contributing to this investigation.

The corresponding author, as the representative of all authors, has been given the opportunity to register their agreement or disagreement to this retraction. We have kept a record of any response received.

References

- [1] K. Zhang, X. Wang, J. Wang, S. Wang, and F. Hui, "Analysis and Prediction of Corporate Finance and Exchange Rate Correlation Based on Machine Learning Algorithms," *Computational Intelligence and Neuroscience*, vol. 2022, Article ID 2850604, 9 pages, 2022.

Retraction

Retracted: Artificial Intelligence-Based Recommendation and Application of Public Services in Smart Cities

Computational Intelligence and Neuroscience

Received 3 October 2023; Accepted 3 October 2023; Published 4 October 2023

Copyright © 2023 Computational Intelligence and Neuroscience. This is an open access article distributed under the Creative Commons Attribution License, which permits unrestricted use, distribution, and reproduction in any medium, provided the original work is properly cited.

This article has been retracted by Hindawi following an investigation undertaken by the publisher [1]. This investigation has uncovered evidence of one or more of the following indicators of systematic manipulation of the publication process:

- (1) Discrepancies in scope
- (2) Discrepancies in the description of the research reported
- (3) Discrepancies between the availability of data and the research described
- (4) Inappropriate citations
- (5) Incoherent, meaningless and/or irrelevant content included in the article
- (6) Peer-review manipulation

The presence of these indicators undermines our confidence in the integrity of the article's content and we cannot, therefore, vouch for its reliability. Please note that this notice is intended solely to alert readers that the content of this article is unreliable. We have not investigated whether authors were aware of or involved in the systematic manipulation of the publication process.

Wiley and Hindawi regrets that the usual quality checks did not identify these issues before publication and have since put additional measures in place to safeguard research integrity.

We wish to credit our own Research Integrity and Research Publishing teams and anonymous and named external researchers and research integrity experts for contributing to this investigation.

The corresponding author, as the representative of all authors, has been given the opportunity to register their agreement or disagreement to this retraction. We have kept a record of any response received.

References

- [1] J. Zhou, "Artificial Intelligence-Based Recommendation and Application of Public Services in Smart Cities," *Computational Intelligence and Neuroscience*, vol. 2022, Article ID 8958865, 10 pages, 2022.

Retraction

Retracted: Development Strategy of Intelligent Digital Library without Human Service in the Era of “Internet +”

Computational Intelligence and Neuroscience

Received 3 October 2023; Accepted 3 October 2023; Published 4 October 2023

Copyright © 2023 Computational Intelligence and Neuroscience. This is an open access article distributed under the Creative Commons Attribution License, which permits unrestricted use, distribution, and reproduction in any medium, provided the original work is properly cited.

This article has been retracted by Hindawi following an investigation undertaken by the publisher [1]. This investigation has uncovered evidence of one or more of the following indicators of systematic manipulation of the publication process:

- (1) Discrepancies in scope
- (2) Discrepancies in the description of the research reported
- (3) Discrepancies between the availability of data and the research described
- (4) Inappropriate citations
- (5) Incoherent, meaningless and/or irrelevant content included in the article
- (6) Peer-review manipulation

The presence of these indicators undermines our confidence in the integrity of the article’s content and we cannot, therefore, vouch for its reliability. Please note that this notice is intended solely to alert readers that the content of this article is unreliable. We have not investigated whether authors were aware of or involved in the systematic manipulation of the publication process.

Wiley and Hindawi regrets that the usual quality checks did not identify these issues before publication and have since put additional measures in place to safeguard research integrity.

We wish to credit our own Research Integrity and Research Publishing teams and anonymous and named external researchers and research integrity experts for contributing to this investigation.

The corresponding author, as the representative of all authors, has been given the opportunity to register their agreement or disagreement to this retraction. We have kept a record of any response received.

References

- [1] H. Wang and J. Ding, “Development Strategy of Intelligent Digital Library without Human Service in the Era of “Internet +”,” *Computational Intelligence and Neuroscience*, vol. 2022, Article ID 7892738, 11 pages, 2022.

Retraction

Retracted: Fuzzy Logic-Based Machine Learning Algorithm for Cultural and Creative Product Design

Computational Intelligence and Neuroscience

Received 13 September 2023; Accepted 13 September 2023; Published 14 September 2023

Copyright © 2023 Computational Intelligence and Neuroscience. This is an open access article distributed under the Creative Commons Attribution License, which permits unrestricted use, distribution, and reproduction in any medium, provided the original work is properly cited.

This article has been retracted by Hindawi following an investigation undertaken by the publisher [1]. This investigation has uncovered evidence of one or more of the following indicators of systematic manipulation of the publication process:

- (1) Discrepancies in scope
- (2) Discrepancies in the description of the research reported
- (3) Discrepancies between the availability of data and the research described
- (4) Inappropriate citations
- (5) Incoherent, meaningless and/or irrelevant content included in the article
- (6) Peer-review manipulation

The presence of these indicators undermines our confidence in the integrity of the article's content and we cannot, therefore, vouch for its reliability. Please note that this notice is intended solely to alert readers that the content of this article is unreliable. We have not investigated whether authors were aware of or involved in the systematic manipulation of the publication process.

Wiley and Hindawi regrets that the usual quality checks did not identify these issues before publication and have since put additional measures in place to safeguard research integrity.

We wish to credit our own Research Integrity and Research Publishing teams and anonymous and named external researchers and research integrity experts for contributing to this investigation.

The corresponding author, as the representative of all authors, has been given the opportunity to register their agreement or disagreement to this retraction. We have kept a record of any response received.

References

- [1] T. Lan, "Fuzzy Logic-Based Machine Learning Algorithm for Cultural and Creative Product Design," *Computational Intelligence and Neuroscience*, vol. 2022, Article ID 7747192, 7 pages, 2022.

Retraction

Retracted: Design and Implementation of Dance Online Teaching System Based on Optimized Load Balancing Algorithm

Computational Intelligence and Neuroscience

Received 25 July 2023; Accepted 25 July 2023; Published 26 July 2023

Copyright © 2023 Computational Intelligence and Neuroscience. This is an open access article distributed under the Creative Commons Attribution License, which permits unrestricted use, distribution, and reproduction in any medium, provided the original work is properly cited.

This article has been retracted by Hindawi following an investigation undertaken by the publisher [1]. This investigation has uncovered evidence of one or more of the following indicators of systematic manipulation of the publication process:

- (1) Discrepancies in scope
- (2) Discrepancies in the description of the research reported
- (3) Discrepancies between the availability of data and the research described
- (4) Inappropriate citations
- (5) Incoherent, meaningless and/or irrelevant content included in the article
- (6) Peer-review manipulation

The presence of these indicators undermines our confidence in the integrity of the article's content and we cannot, therefore, vouch for its reliability. Please note that this notice is intended solely to alert readers that the content of this article is unreliable. We have not investigated whether authors were aware of or involved in the systematic manipulation of the publication process.

Wiley and Hindawi regrets that the usual quality checks did not identify these issues before publication and have since put additional measures in place to safeguard research integrity.

We wish to credit our own Research Integrity and Research Publishing teams and anonymous and named external researchers and research integrity experts for contributing to this investigation.

The corresponding author, as the representative of all authors, has been given the opportunity to register their agreement or disagreement to this retraction. We have kept a record of any response received.

References

- [1] Q. Yang, "Design and Implementation of Dance Online Teaching System Based on Optimized Load Balancing Algorithm," *Computational Intelligence and Neuroscience*, vol. 2022, Article ID 3829118, 10 pages, 2022.

Retraction

Retracted: Design of a Multimedia-Assisted Distance English Teaching System for College Students

Computational Intelligence and Neuroscience

Received 25 July 2023; Accepted 25 July 2023; Published 26 July 2023

Copyright © 2023 Computational Intelligence and Neuroscience. This is an open access article distributed under the Creative Commons Attribution License, which permits unrestricted use, distribution, and reproduction in any medium, provided the original work is properly cited.

This article has been retracted by Hindawi following an investigation undertaken by the publisher [1]. This investigation has uncovered evidence of one or more of the following indicators of systematic manipulation of the publication process:

- (1) Discrepancies in scope
- (2) Discrepancies in the description of the research reported
- (3) Discrepancies between the availability of data and the research described
- (4) Inappropriate citations
- (5) Incoherent, meaningless and/or irrelevant content included in the article
- (6) Peer-review manipulation

The presence of these indicators undermines our confidence in the integrity of the article's content and we cannot, therefore, vouch for its reliability. Please note that this notice is intended solely to alert readers that the content of this article is unreliable. We have not investigated whether authors were aware of or involved in the systematic manipulation of the publication process.

Wiley and Hindawi regrets that the usual quality checks did not identify these issues before publication and have since put additional measures in place to safeguard research integrity.

We wish to credit our own Research Integrity and Research Publishing teams and anonymous and named external researchers and research integrity experts for contributing to this investigation.

The corresponding author, as the representative of all authors, has been given the opportunity to register their agreement or disagreement to this retraction. We have kept a record of any response received.

References

- [1] H. Feng, "Design of a Multimedia-Assisted Distance English Teaching System for College Students," *Computational Intelligence and Neuroscience*, vol. 2022, Article ID 2184600, 8 pages, 2022.

Retraction

Retracted: Feasibility Analysis and Discrete Dynamic Modeling of Physical Education Teaching Strategy Based on Intelligent Computing

Computational Intelligence and Neuroscience

Received 25 July 2023; Accepted 25 July 2023; Published 26 July 2023

Copyright © 2023 Computational Intelligence and Neuroscience. This is an open access article distributed under the Creative Commons Attribution License, which permits unrestricted use, distribution, and reproduction in any medium, provided the original work is properly cited.

This article has been retracted by Hindawi following an investigation undertaken by the publisher [1]. This investigation has uncovered evidence of one or more of the following indicators of systematic manipulation of the publication process:

- (1) Discrepancies in scope
- (2) Discrepancies in the description of the research reported
- (3) Discrepancies between the availability of data and the research described
- (4) Inappropriate citations
- (5) Incoherent, meaningless and/or irrelevant content included in the article
- (6) Peer-review manipulation

The presence of these indicators undermines our confidence in the integrity of the article's content and we cannot, therefore, vouch for its reliability. Please note that this notice is intended solely to alert readers that the content of this article is unreliable. We have not investigated whether authors were aware of or involved in the systematic manipulation of the publication process.

Wiley and Hindawi regrets that the usual quality checks did not identify these issues before publication and have since put additional measures in place to safeguard research integrity.

We wish to credit our own Research Integrity and Research Publishing teams and anonymous and named external researchers and research integrity experts for contributing to this investigation.

The corresponding author, as the representative of all authors, has been given the opportunity to register their agreement or disagreement to this retraction. We have kept a record of any response received.

References

- [1] G. Wang, "Feasibility Analysis and Discrete Dynamic Modeling of Physical Education Teaching Strategy Based on Intelligent Computing," *Computational Intelligence and Neuroscience*, vol. 2022, Article ID 4093924, 8 pages, 2022.

Retraction

Retracted: Construction and Analysis of Indicators of the Labor Education System Based on the Gray Correlation Degree Model

Computational Intelligence and Neuroscience

Received 25 July 2023; Accepted 25 July 2023; Published 26 July 2023

Copyright © 2023 Computational Intelligence and Neuroscience. This is an open access article distributed under the Creative Commons Attribution License, which permits unrestricted use, distribution, and reproduction in any medium, provided the original work is properly cited.

This article has been retracted by Hindawi following an investigation undertaken by the publisher [1]. This investigation has uncovered evidence of one or more of the following indicators of systematic manipulation of the publication process:

- (1) Discrepancies in scope
- (2) Discrepancies in the description of the research reported
- (3) Discrepancies between the availability of data and the research described
- (4) Inappropriate citations
- (5) Incoherent, meaningless and/or irrelevant content included in the article
- (6) Peer-review manipulation

The presence of these indicators undermines our confidence in the integrity of the article's content and we cannot, therefore, vouch for its reliability. Please note that this notice is intended solely to alert readers that the content of this article is unreliable. We have not investigated whether authors were aware of or involved in the systematic manipulation of the publication process.

Wiley and Hindawi regrets that the usual quality checks did not identify these issues before publication and have since put additional measures in place to safeguard research integrity.

We wish to credit our own Research Integrity and Research Publishing teams and anonymous and named external researchers and research integrity experts for contributing to this investigation.

The corresponding author, as the representative of all authors, has been given the opportunity to register their agreement or disagreement to this retraction. We have kept a record of any response received.

References

- [1] L. Huang, "Construction and Analysis of Indicators of the Labor Education System Based on the Gray Correlation Degree Model," *Computational Intelligence and Neuroscience*, vol. 2022, Article ID 2281469, 8 pages, 2022.

Retraction

Retracted: Design and Optimization of Aesthetic Education Teaching Information Platform Based on Big Data Analysis

Computational Intelligence and Neuroscience

Received 25 July 2023; Accepted 25 July 2023; Published 26 July 2023

Copyright © 2023 Computational Intelligence and Neuroscience. This is an open access article distributed under the Creative Commons Attribution License, which permits unrestricted use, distribution, and reproduction in any medium, provided the original work is properly cited.

This article has been retracted by Hindawi following an investigation undertaken by the publisher [1]. This investigation has uncovered evidence of one or more of the following indicators of systematic manipulation of the publication process:

- (1) Discrepancies in scope
- (2) Discrepancies in the description of the research reported
- (3) Discrepancies between the availability of data and the research described
- (4) Inappropriate citations
- (5) Incoherent, meaningless and/or irrelevant content included in the article
- (6) Peer-review manipulation

The presence of these indicators undermines our confidence in the integrity of the article's content and we cannot, therefore, vouch for its reliability. Please note that this notice is intended solely to alert readers that the content of this article is unreliable. We have not investigated whether authors were aware of or involved in the systematic manipulation of the publication process.

Wiley and Hindawi regrets that the usual quality checks did not identify these issues before publication and have since put additional measures in place to safeguard research integrity.

We wish to credit our own Research Integrity and Research Publishing teams and anonymous and named external researchers and research integrity experts for contributing to this investigation.

The corresponding author, as the representative of all authors, has been given the opportunity to register their agreement or disagreement to this retraction. We have kept a record of any response received.

References

- [1] X. Wu and H. Gu, "Design and Optimization of Aesthetic Education Teaching Information Platform Based on Big Data Analysis," *Computational Intelligence and Neuroscience*, vol. 2022, Article ID 5109638, 9 pages, 2022.

Retraction

Retracted: Data Sharing Method of College Dance Teaching Resource Database Based on PSO Algorithm

Computational Intelligence and Neuroscience

Received 25 July 2023; Accepted 25 July 2023; Published 26 July 2023

Copyright © 2023 Computational Intelligence and Neuroscience. This is an open access article distributed under the Creative Commons Attribution License, which permits unrestricted use, distribution, and reproduction in any medium, provided the original work is properly cited.

This article has been retracted by Hindawi following an investigation undertaken by the publisher [1]. This investigation has uncovered evidence of one or more of the following indicators of systematic manipulation of the publication process:

- (1) Discrepancies in scope
- (2) Discrepancies in the description of the research reported
- (3) Discrepancies between the availability of data and the research described
- (4) Inappropriate citations
- (5) Incoherent, meaningless and/or irrelevant content included in the article
- (6) Peer-review manipulation

The presence of these indicators undermines our confidence in the integrity of the article's content and we cannot, therefore, vouch for its reliability. Please note that this notice is intended solely to alert readers that the content of this article is unreliable. We have not investigated whether authors were aware of or involved in the systematic manipulation of the publication process.

Wiley and Hindawi regrets that the usual quality checks did not identify these issues before publication and have since put additional measures in place to safeguard research integrity.

We wish to credit our own Research Integrity and Research Publishing teams and anonymous and named external researchers and research integrity experts for contributing to this investigation.

The corresponding author, as the representative of all authors, has been given the opportunity to register their agreement or disagreement to this retraction. We have kept a record of any response received.

References

- [1] X. ZhuGe and H. Cao, "Data Sharing Method of College Dance Teaching Resource Database Based on PSO Algorithm," *Computational Intelligence and Neuroscience*, vol. 2022, Article ID 2162981, 9 pages, 2022.

Retraction

Retracted: Research on Virtual Interactive Animation Design System Based on Deep Learning

Computational Intelligence and Neuroscience

Received 25 July 2023; Accepted 25 July 2023; Published 26 July 2023

Copyright © 2023 Computational Intelligence and Neuroscience. This is an open access article distributed under the Creative Commons Attribution License, which permits unrestricted use, distribution, and reproduction in any medium, provided the original work is properly cited.

This article has been retracted by Hindawi following an investigation undertaken by the publisher [1]. This investigation has uncovered evidence of one or more of the following indicators of systematic manipulation of the publication process:

- (1) Discrepancies in scope
- (2) Discrepancies in the description of the research reported
- (3) Discrepancies between the availability of data and the research described
- (4) Inappropriate citations
- (5) Incoherent, meaningless and/or irrelevant content included in the article
- (6) Peer-review manipulation

The presence of these indicators undermines our confidence in the integrity of the article's content and we cannot, therefore, vouch for its reliability. Please note that this notice is intended solely to alert readers that the content of this article is unreliable. We have not investigated whether authors were aware of or involved in the systematic manipulation of the publication process.

Wiley and Hindawi regrets that the usual quality checks did not identify these issues before publication and have since put additional measures in place to safeguard research integrity.

We wish to credit our own Research Integrity and Research Publishing teams and anonymous and named external researchers and research integrity experts for contributing to this investigation.

The corresponding author, as the representative of all authors, has been given the opportunity to register their agreement or disagreement to this retraction. We have kept a record of any response received.

References

- [1] B. Liu, "Research on Virtual Interactive Animation Design System Based on Deep Learning," *Computational Intelligence and Neuroscience*, vol. 2022, Article ID 5035369, 10 pages, 2022.

Retraction

Retracted: A Deep Learning-Based Piano Music Notation Recognition Method

Computational Intelligence and Neuroscience

Received 25 July 2023; Accepted 25 July 2023; Published 26 July 2023

Copyright © 2023 Computational Intelligence and Neuroscience. This is an open access article distributed under the Creative Commons Attribution License, which permits unrestricted use, distribution, and reproduction in any medium, provided the original work is properly cited.

This article has been retracted by Hindawi following an investigation undertaken by the publisher [1]. This investigation has uncovered evidence of one or more of the following indicators of systematic manipulation of the publication process:

- (1) Discrepancies in scope
- (2) Discrepancies in the description of the research reported
- (3) Discrepancies between the availability of data and the research described
- (4) Inappropriate citations
- (5) Incoherent, meaningless and/or irrelevant content included in the article
- (6) Peer-review manipulation

The presence of these indicators undermines our confidence in the integrity of the article's content and we cannot, therefore, vouch for its reliability. Please note that this notice is intended solely to alert readers that the content of this article is unreliable. We have not investigated whether authors were aware of or involved in the systematic manipulation of the publication process.

Wiley and Hindawi regrets that the usual quality checks did not identify these issues before publication and have since put additional measures in place to safeguard research integrity.

We wish to credit our own Research Integrity and Research Publishing teams and anonymous and named external researchers and research integrity experts for contributing to this investigation.

The corresponding author, as the representative of all authors, has been given the opportunity to register their agreement or disagreement to this retraction. We have kept a record of any response received.

References

- [1] C. Li, "A Deep Learning-Based Piano Music Notation Recognition Method," *Computational Intelligence and Neuroscience*, vol. 2022, Article ID 2278683, 9 pages, 2022.

Retraction

Retracted: Application of Intelligent Image Matching and Visual Communication in Brand Design

Computational Intelligence and Neuroscience

Received 25 July 2023; Accepted 25 July 2023; Published 26 July 2023

Copyright © 2023 Computational Intelligence and Neuroscience. This is an open access article distributed under the Creative Commons Attribution License, which permits unrestricted use, distribution, and reproduction in any medium, provided the original work is properly cited.

This article has been retracted by Hindawi following an investigation undertaken by the publisher [1]. This investigation has uncovered evidence of one or more of the following indicators of systematic manipulation of the publication process:

- (1) Discrepancies in scope
- (2) Discrepancies in the description of the research reported
- (3) Discrepancies between the availability of data and the research described
- (4) Inappropriate citations
- (5) Incoherent, meaningless and/or irrelevant content included in the article
- (6) Peer-review manipulation

The presence of these indicators undermines our confidence in the integrity of the article's content and we cannot, therefore, vouch for its reliability. Please note that this notice is intended solely to alert readers that the content of this article is unreliable. We have not investigated whether authors were aware of or involved in the systematic manipulation of the publication process.

Wiley and Hindawi regrets that the usual quality checks did not identify these issues before publication and have since put additional measures in place to safeguard research integrity.

We wish to credit our own Research Integrity and Research Publishing teams and anonymous and named external researchers and research integrity experts for contributing to this investigation.

The corresponding author, as the representative of all authors, has been given the opportunity to register their agreement or disagreement to this retraction. We have kept a record of any response received.

References

- [1] M. Liu and W. Zhong, "Application of Intelligent Image Matching and Visual Communication in Brand Design," *Computational Intelligence and Neuroscience*, vol. 2022, Article ID 5964851, 9 pages, 2022.

Retraction

Retracted: Construction and Analysis of Performance Evaluation Index System for Chinese Small and Medium-Sized Enterprises Based on Fuzzy Hierarchical Analysis Model

Computational Intelligence and Neuroscience

Received 25 July 2023; Accepted 25 July 2023; Published 26 July 2023

Copyright © 2023 Computational Intelligence and Neuroscience. This is an open access article distributed under the Creative Commons Attribution License, which permits unrestricted use, distribution, and reproduction in any medium, provided the original work is properly cited.

This article has been retracted by Hindawi following an investigation undertaken by the publisher [1]. This investigation has uncovered evidence of one or more of the following indicators of systematic manipulation of the publication process:

- (1) Discrepancies in scope
- (2) Discrepancies in the description of the research reported
- (3) Discrepancies between the availability of data and the research described
- (4) Inappropriate citations
- (5) Incoherent, meaningless and/or irrelevant content included in the article
- (6) Peer-review manipulation

The presence of these indicators undermines our confidence in the integrity of the article's content and we cannot, therefore, vouch for its reliability. Please note that this notice is intended solely to alert readers that the content of this article is unreliable. We have not investigated whether authors were aware of or involved in the systematic manipulation of the publication process.

Wiley and Hindawi regrets that the usual quality checks did not identify these issues before publication and have since put additional measures in place to safeguard research integrity.

We wish to credit our own Research Integrity and Research Publishing teams and anonymous and named external researchers and research integrity experts for contributing to this investigation.

The corresponding author, as the representative of all authors, has been given the opportunity to register their agreement or disagreement to this retraction. We have kept a record of any response received.

References

- [1] M. He and R. P. Estebanez, "Construction and Analysis of Performance Evaluation Index System for Chinese Small and Medium-Sized Enterprises Based on Fuzzy Hierarchical Analysis Model," *Computational Intelligence and Neuroscience*, vol. 2022, Article ID 1230786, 8 pages, 2022.

Research Article

A Factorization Deep Product Neural Network for Student Physical Performance Prediction

Xiaoxia Jiao 

Department of Physical Education Bengbu University, Bengbu 233030, China

Correspondence should be addressed to Xiaoxia Jiao; jxx@bbc.edu.cn

Received 30 March 2022; Revised 18 June 2022; Accepted 13 August 2022; Published 19 November 2022

Academic Editor: Le Sun

Copyright © 2022 Xiaoxia Jiao. This is an open access article distributed under the Creative Commons Attribution License, which permits unrestricted use, distribution, and reproduction in any medium, provided the original work is properly cited.

As we all know, sports have great benefits for students. However, with more and more learning pressure, students' physical education has not been paid attention to by teachers and parents, so the analysis and prediction of physical education performance have become significant work. This paper proposes a new method (factorization deep product neural network) for PE course score prediction. The experimental results show that, compared with the existing performance prediction methods (LR, SVM, FM, and the DNN), the proposed method achieves the best prediction effect on the sports education dataset. Compared with the traditional optimal methods, the accuracy and AUC of DNN are both improved by 2%. In addition, there is also a significant improvement in accuracy, recall, and F1. In addition, this study found that considering two or more features at the same time has a certain influence on the prediction results of students' grades. The proposed feature combination method can learn feature combinations automatically, consider the influence of first-order features, second-order features, and high-order features in the meantime, and acquire the relationship information between each feature and performance. Compared with single-feature learning, the proposed method in this paper can enhance prediction accuracy significantly. Moreover, several dimensionality reduction methods are used in this paper, and we found that the PCA model for data processing outperformed all the benchmark models.

1. Background

In the information age, a large amount of data has been accumulated in all walks of life, under which there is often some useful knowledge and valuable information. At present, technologies related to machine learning and data mining are widely used in business, finance, medicine, and other fields.

With the fast development of the Internet, universities have increasingly perfected their digital campuses, and all kinds of educational data have been accumulated. However, there is often some potential knowledge and information in the massive educational data that can promote the development of education. ML data mining and other related technologies are used to provide valuable information for teachers, students, and educational researchers, so as to

scientifically improve teaching methods and make comprehensive management decisions. Therefore, it is worth studying the way how better teaching efficiency and educational output are obtained from the big data of education. From the 1990s to the beginning of this century, with the fast development of the Internet, the education informatization has gradually entered the network era, and distance education and online education have attracted more and more educators' attention. The current mainstream education environment can be roughly divided into traditional classroom education and new online education, such as MOOC. Educational data mining deals with various problems in teaching, practice, and educational research through theories and technologies in multiple disciplines including pedagogy, computer science, statistics, and psychology. Currently, EDM application scenarios can be mainly divided

into four categories: student performance prediction, student modeling, a recommendation system, and visualization.

2. Related Works

At present, education quality has become the top priority in education. Improving the quality of education is one of the unyielding determinations of educators. Now many scholars have conducted research on the prediction of students' academic performance. Early research mainly focused on collecting student learning data (such as traditional classroom teaching test scores) from the educational administration system. Students' consumption behavior data are collected from students' campus cards to predict scores. Burman used the records collected by questionnaires to classify learners into high, average, and low levels according to their academic performance based on students' psychological parameters, including personality, motivation, psychosocial background, learning strategies, learning methods, and socioeconomic status, by using a multiclassifier support vector machine [1]. A team including Sweeney used SVD, SVD-KNN, factorizers, and other recommendation system methods to predict the grades of the next semester and made a comprehensive analysis of the predicted results [2]. Sweeney proposed a method of mixed decomposer and random forest to predict students' scores by taking advantage of the course scores learned by students [3]. A team including Polyzou proposed a sparse linear and low-rank matrix decomposition model to predict future course scores based on students' historical course scores [4]. Yi et al. predicted students' scores through a multikernel support vector machine combined with an optimization algorithm, and then successfully evaluated the teaching quality [5]. AI-based methods play an increasingly important role in teaching quality evaluation [6, 7] and student performance prediction [8, 9].

Recently, with the development of the Internet and the continuous improvement of online learning platforms, the data related to MOOC students' learning has attracted more and more attention from relevant researchers. A team including Jiang used the interaction records of learners' first week on the platform and the performance data of homework to predict whether learners would eventually obtain certificates based on the logistic regression model [10]. Brinton and MChiang developed an algorithmic model relying on the decomposing machine and K-nearest neighbors (KNN) to predict whether a student answers a question correctly for the first time in a MOOC [11]. Lorenzo and Gomez-Sanchez adopted logistic regression, stochastic gradient descent, stochastic forest, and support vector machine models to predict whether the indicator, compared with the previous indicator at the end of the chapter, the three participation indicators (video, exercise, and assignment), would decline [12]. Hlosta builds a student performance prediction model based on machine learning methods (logistic regression, support vector machine,

random forest, naive Bayes, and integrated learning XGBoost) in accordance with the data generated in the current course to evaluate whether students have the risk of dropping out [13]. A team including Aljohani deployed a deep long and short-term memory model based on student interaction records on online platforms (such as clickstream data) to explore student performance prediction, and the results showed that the model could predict pass/fail courses in the first 10 weeks of student interaction in a virtual learning environment with an accuracy of about 90% [14].

Compared with the application of the classical ML-based model to education such as LR [15], SVM [16], Decision Tree [17], GBDT [11], and BNs [18], the DL-based model such as RNN [19] and CNN [20] can also be used to enhance the results in the field of education.

To sum up, some achievements have been made in the study of performance prediction, but there are still some problems and shortcomings.

First, in the traditional classroom grade prediction problem, the main data information comes from some data generated during the course, such as the in-class assignment grades and unit test grades. The characteristics of the course grade prediction can be achieved until the end of the course, which leads to the late predicted results, so the method has a certain lag and the data are sparse and single, so that it cannot provide effective technical support for the teaching and management work in the early stage of the course.

Second, with a lack of other relevant course grade information, the existing online platform course grade prediction research mainly focuses on the log data of learners on the learning platform, such as the learning time on the online learning platform and the number of clicks on the learning video. In addition, in existing research, manual feature engineering is commonly used, which is highly dependent on the professional knowledge and experience of engineers, which affects the prediction accuracy of the method to a certain extent.

Third, most of the data used in the existing research on performance prediction come from the dataset constructed by researchers themselves, and the data are generally not enough. For mainstream research methods such as machine learning algorithms, there are certain requirements on the amount of data. If the data are insufficient, it is difficult to train a better model, which leads to low accuracy of prediction to a certain extent. In view of the above problems, in this paper, two kinds of different data are used to put forward different performance prediction models, so as to improve the accuracy of performance prediction.

To sum up, under the background of educational data mining, this paper carries out in-depth and systematic research on student performance prediction from the perspectives of traditional classroom teaching scenarios and MOOC online platform courses. The research focus is mainly on improving the predictability and accuracy of the method. In the following sections, the main research content of this paper is briefly introduced.

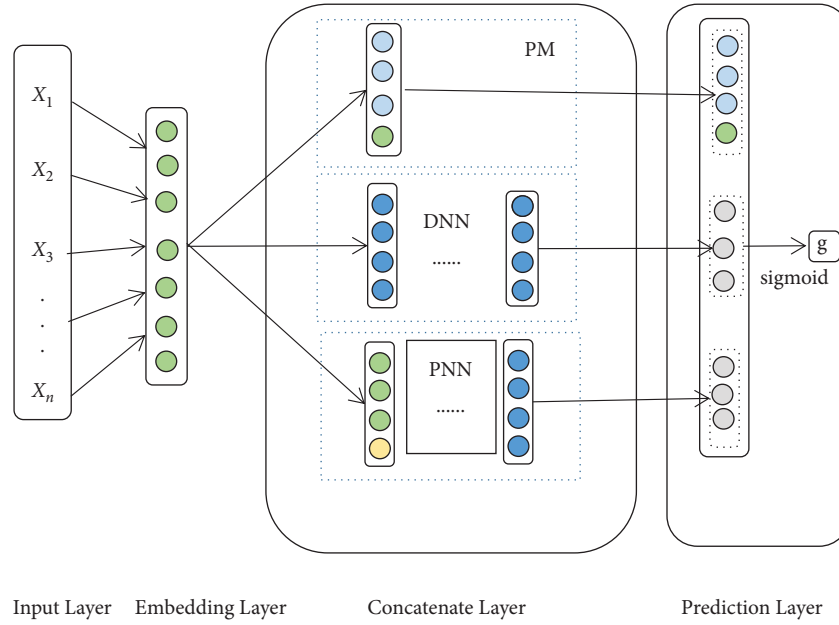


FIGURE 1: FDPN model framework.

3. Sports Course Score Prediction Model Based on Feature Combination

3.1. Problem Definition. Given a student feature set F determined by the student attribution features expressed as $student_attr = \{s_1, s_2, \dots, s_m\}$, course attribution features expressed as $course_attr = \{c_1, c_2, \dots, c_n\}$, and the student learning behavior feature expressed as $behavior = \{b_1, b_2, \dots, b_k\}$. Namely, $F = \{student_attr, course_attr, behavior\}$, where m , n , and k are the number of features, respectively. For the student, his final course score was y_i . $y = \{0, 1\}$ is a class set divided by grades, where 0 indicates a student grade failure and 1 indicates a student grade pass. Student grade prediction aims to predict the grade category y_i according to the student feature F .

3.2. Model Framework. This chapter aims at mining and analyzing the data related to students' learning based on deep learning technology to realize the accurate prediction of students' academic performance. By so doing, timely help and guidance can be provided to students at risk of failing exams. Therefore, this chapter proposes a performance prediction model (factorization deep product neural network, FDPN) based on feature combination, course attributes, and students' learning behavior features. The model framework is shown in Figure 1. The FDPN contains 3 layers:

- (1) Embedding layer: narrow the dimension of the original high-dimensional features and map them to the low-dimensional feature vector.
- (2) Concatenate layer: this layer is composed of three parts: factorization machine, DNN, and product neural network (PNN). FM is used to express

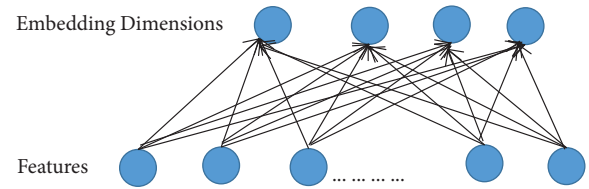


FIGURE 2: Structure of the embedding layer.

first-order and second-order features, and DNN and PNN are used to represent higher-level features.

- (3) Prediction layer: through splicing, the low-level and high-level features are combined to get the final features with richer information, so as to better predict students' performance.

3.2.1. Embedding Layer. Because the raw data are relatively sparse, a dimensional reduction is made to obtain a low-level representation of the features. Changing the initial feature to a lower-dimensional vector representation can make the data relatively dense and reduce computational effort. Figure 2 shows the structure of the embedding layer. Mapping the output of the embedding layer could be introduced as follows:

$$a = [e_1, e_2, \dots, e_p]. \quad (1)$$

Where a represents the embedding feature, e_i represents number i embedding feature, p refers to the number of embedding features, and $p \leq (m + n + k)$.

3.2.2. Concatenate Layer

(1) *Factorization machine.* The FM, as proposed by Rendle [21], is for learning feature interactions. As shown in the formula:

$$y_{fm} = w_0 + \sum_{i=2}^p w_i e_i + \sum_{i=1}^p \sum_{j=i+1}^p w_{ij} e_i e_j, \quad (2)$$

where w_0 , w_i , and w_{ij} are the weights of each feature. The factorization machine is represented by a first-order feature of logistic regression learning, and the second-order features of learning information are accumulated by the dots of vector. The last output value y_{fm} in the FM layer is transferred as input to the part of the input in the prediction layer.

DNN [22] is more capable of learning. The output of the embedding layer is the input of the first hidden layer of the DNN, and the calculation formula of the first hidden layer is shown in the following formula:

$$h_1 = f(w_o e_p + b_o). \quad (3)$$

Assuming that there are l hidden layers, which directly output y_{dm} to the input part of the prediction layer, the final output value of DNN is shown in the following formula:

$$y_{dm} = f(w_{l-1} h_{l-1} + b_{l-1}), \quad (4)$$

where $f(\cdot)$ is the activation function of the hidden layer, whose activation function is the ReLU [23].

(ii) *Product neural network.* The product neural network (PNN) is a feed-forward deep neural network [24] containing the product layer. In the PNN, the input information not only contains first-order feature-related information but also second-order features. Therefore, the product layer enriches the information of the input deep neural network. Its second-order features are calculated in (5), where p represents the inner product of the embedding layer vectors e_i and e_j .

$$p = \langle e_i \cdot e_j \rangle = \begin{bmatrix} e_j^1 \\ e_j^2 \\ \vdots \\ e_j^p \end{bmatrix} = \sum_{i=1}^p \sum_{j=i+1}^p w_{ij} e_i e_j. \quad (5)$$

The input vector of the PNN is composed of the first-order feature vector output by the embedding layer and the second-order feature vector generated by the interaction of the embedding layer. The calculation is shown as follows:

$$x_{pnn} = [a; p]. \quad (6)$$

The final output value y_{pnn} of the PNN is calculated, as in formula (4), which distinguishes itself from the DNN by varying the input feature vector from the embedded layer to the first hidden layer. The output values of the last hidden layer node of the PNN will be transmitted directly as input to the part node of the prediction layer input.

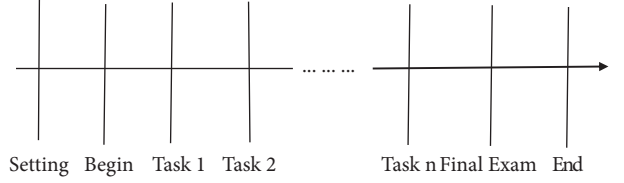


FIGURE 3: Learning process.

3.2.3. *Prediction Layer.* The prediction layer's primary task is to combine the low- and higher-order feature representations of FM, DNN, and PNN output in the network layer and predict the grade categories of the target students. More comprehensive and accurate students' performance can be predicted by integrating the features.

In this paper, features including y_{fm} , y_{dm} , and y_{pnn} are integrated through concatenation [25]. This process can be formalized as follows:

$$f = [y_{fm}; y_{dm}; y_{pnn}], \quad (7)$$

where f is the final feature after integrating of y_{fm} , y_{dm} and y_{pnn} . Finally, the feature f is input into the perceptron of the Sigmoid [26, 27] activation function to obtain the probability of the student course grade category.

From the above, FDPN includes three parts: FM, DNN, and PNN, and the final result is obtained from the following formula:

$$g = \text{Sigmoid}(f). \quad (8)$$

3.3. *Loss Function.* This paper employs the cross-entropy loss function and employs the L2 regularization parameter [27]. The loss function of the model is as follows:

$$\text{loss} = -\frac{1}{n} \sum_{i=1}^n y_i \log g + \lambda \|\theta\|^2, \quad (9)$$

where n is the total number of training data, y_i is the grade category of the data, g is the predicted probability of the number i grade category of the data, and $\lambda \|\theta\|^2$ is the L_2 regular term, θ is the set of all parameters of the model.

4. Experiments

4.1. *Data Set.* In this study, part of the data comes from the Open University Learning Analysis Data set (OULAD), which contains basic information, registration, and learner learning activity records from seven sport online courses from 2013 to 2014. Figure 3 shows the learning process of using the Open University platform. First of all, the Open University opens up a course for students to apply for the course registration, and then students begin their learning. The courses of the Open University usually last for nine months, and learners are required to complete corresponding learning tasks during the learning process. Finally, learners take the final examination, and the course ends.

TABLE 1: Data description.

Number	Features	Descriptions
1	Highest degree	The highest degree of students when enrolled in the course
2	Environmental index	The environment of the area during the course
3	Age group	Students age group
4	Times of attempts	The number of times a student tried a particular module
...
52	Shared information	Times of clicking on the course and faculties' shared information before class
53	Sources	Times of clicking on the PDF resources, such as books
54	Related information	Times of clicking on the information on the website and activities related to that information

TABLE 2: Confusion matrix.

Actual situation	Predicted results	
	Positive	Negative
Positive	TP (true and positive)	FN (false and negative)
Negative	FP (false and positive)	TN (true and negative)

The description of the data set is introduced in Table 1. Numbers 1 to 54 refer to the highest degree of students who register for the course, the environment index in school learning, age, times of trying a specific module, credits of students who are currently learning, . . . , and times of clicking additional information before the course, such as video, tape, website, environment index of learning the module, times of clicking shared information between staff before the course, times of click PDF resources like books before the course and clicking information on the website and related activities.

According to the above descriptions, 22347×33 valid data are preprocessed.

4.2. Evaluation Indicators. The evaluation indexes in this paper include accuracy, precision, recall, F1, and AUC (area under the curve), which measure the model classification prediction performance.

$$\begin{aligned}
 \text{Accuracy} &= \frac{TP + TN}{TP + TN + FP + FN}, \\
 \text{Precision} &= \frac{TP}{TP + FP}, \\
 \text{F1} &= \frac{2 * \text{Precision} * \text{Recall}}{\text{Precision} + \text{Recall}}.
 \end{aligned} \tag{10}$$

The meanings of TP, FP, FN, and TN are shown in Table 2:

5. Analysis

5.1. Influence of Different Parameters on FDPN Model Performance

5.1.1. Number of Neurons in the Hidden Layer. This model contains two deep neural networks. When a network contains multiple hidden layers and the number of neurons in each hidden layer is not the same, a lot of experimentation is

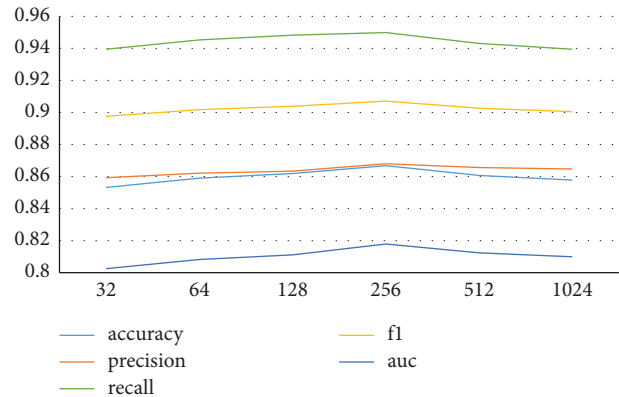


FIGURE 4: The comparison result of neural units in the hidden layer.

TABLE 3: The comparison result of neural units in the hidden layer.

Number	Accuracy	Precision	Recall	F1	AUC
32	0.8532	0.8593	0.9395	0.8976	0.8025
64	0.8590	0.8621	0.9453	0.9018	0.8082
128	0.8619	0.8634	0.9483	0.9039	0.8111
256	0.8668	0.8680	0.9499	0.9071	0.8179
512	0.8607	0.8656	0.9431	0.9027	0.8124
1024	0.8578	0.8647	0.9395	0.9005	0.8099

required. In this paper, the same number of neurons is set in the hidden layer of the two neural networks to simplify the experiment. The experimental results are shown in Figure 4 and Table 3. Six experiments are conducted in turn to change the number of neurons. From the experimental results, it can be seen that when the number of neurons is 256, the recall rate is about 95%, the AUC is about 82%, the accuracy is about 86.6%, and the precision rate is 86.8%. The model performance is optimal because, with the increase in the number of neurons, the model can learn more feature information. However, when the neurons increase to a certain number, no more effective information can be learned by the model, and even the noise that degrades the prediction performance of the model may be generated. Therefore, in deep neural network training, too many neurons should be moderated. Model training and learning comparison are needed to select the optimal number of neurons.

5.1.2. Different Activation Functions. The activation function of hidden layer neurons is related to the prediction

effect about DAF. Due to the binary classification model used in this paper, the model finally predicts the output unit with the Sigmoid function, and the settings of the remaining activation functions are the same. Among ReLU, Tanh, and Sigmoid, ReLU and Tanh are better used in deep learning models, so this experiment only compares the ReLU activation function and the Tanh activation function of the hidden neuron activation function. Table 4 introduces the experimental results. We can find that, when the activation function is ReLU, the prediction accuracy, recall rate, F1, and AUC of the FDPN model are increased by about 2%, and the prediction effect of the hidden layer neuron activation function with ReLU is better than that of the Tanh function. In particular, this chapter makes use of two feed-forward neural networks, in which the ReLU activation function performs better than the Tanh function and will be used in the last part of our study.

5.1.3. The Number of Layers in the Hidden Layer. The model presented in this paper contains two feed-forward neural networks, DNN and PNN, with different numbers of hidden layers and different predictive power of the models. To simplify the experiment, the number of hidden layers in two neural networks is the same; that is, the number of hidden layers is increased from 1 to 3 layers. The experimental results are shown in Table 5. From the experimental results, it can be seen that when the hidden layer is 1 and 2, the model has a good performance, and when the hidden layer is 3, the model prediction effect is significantly reduced. As the number of layers increases, the evaluation index drops, mainly because the more layers, the more complex the structure, and the larger the calculation amount, the more likely the problem of over-fitting the model will appear. Therefore, the number of layers of the hidden layer is still set to be 1 layer in the subsequent experiments of this paper.

5.2. Effect of the Model Structure on the Performance. The influencing factors mainly include first-order representations and second-order representations of FM learning features and different higher-order representations of DNN and PNN learning features. In this paper, the three structures are combined for learning to predict performance. In the experiments of this section, the different feature combination structures are compared to observe the effect of the structure on the model's performance. The experimental results are shown in Table 6.

Experimental results showed that the single-structure FM, DNN, and PNN slightly performed worse, and the Deep FM, DNN + PNN, and FM + PNN of both structures that have combined feature learning are slightly better than the single structure. The FDPN model is the optimal one because it considers both first, second, and two different higher-order feature representations, during which more potentially effective information is used in performance prediction. In conclusion, the FDPN performance prediction model has a significant prediction effect and can improve prediction performance.

TABLE 4: The comparison result of the activation functions.

Activation functions	Accuracy	Precision	Recall	F1	AUC
<i>Tanh</i>	0.8440	0.8610	0.9209	0.8899	0.7988
<i>ReLU</i>	0.8668	0.8680	0.9499	0.9071	0.8179

TABLE 5: The comparison result of the layers of the hidden layers.

Numbers of layers	Accuracy	Precision	Recall	F1	AUC
1	0.8668	0.8680	0.9499	0.9071	0.8179
2	0.8503	0.8639	0.9275	0.8946	0.8050
3	0.7823	0.8814	0.7882	0.8322	0.7788

TABLE 6: The result of the deep learning benchmark models.

Different structures	Accuracy	Precision	Recall	F1	AUC
FM	0.8431	0.8552	0.9281	0.8902	0.7933
DNN	0.8440	0.8554	0.9294	0.8908	0.7939
DeepFM	0.8485	0.8603	0.9297	0.8937	0.8008
PNN	0.8576	0.8646	0.9392	0.9004	0.8098
DNN + PNN	0.8614	0.8660	0.9437	0.9032	0.8131
FM + PNN	0.8625	0.8670	0.9440	0.9039	0.8147
FDPN	0.8668	0.8680	0.9499	0.9071	0.8179

TABLE 7: The result of the benchmark models.

Models	Accuracy	Precision	Recall	F1	AUC
LR	0.7990	0.8400	0.8728	0.8561	0.7557
SVM	0.8324	0.8464	0.9229	0.8830	0.7793
FM	0.8431	0.8552	0.9281	0.8902	0.7933
DNN	0.8440	0.8554	0.9294	0.8908	0.7939
DeepFM	0.8485	0.8603	0.9297	0.8937	0.8008
PNN	0.8576	0.8646	0.9392	0.9004	0.8098
FDPN	0.8668	0.8680	0.9499	0.9071	0.8179

5.3. Experiment Comparison. In this paper, LR, SVM, FM, DNN, DeepFM, PNN, and other deep learning models are used as comparative models. By performing comparative experiments on the sports dataset, the results are shown in Table 7 to verify that the proposed FDPN model has the best prediction performance.

The experimental results in Table 7 show that, compared with the existing performance prediction methods (LR, SVM, FM, and the DNN), this paper achieves the best prediction effect on the sports education dataset. Compared with the optimal traditional methods, DNN accuracy and AUC are both improved by 2%. In addition, there are also significant improvements in accuracy, recall, and F1. The method based on feature combination is better than the four traditional performance prediction methods. This is mainly because the traditional performance prediction method adopts features directly as a classification feature input for model learning training and only the low or high features are taken into consideration, with the exception of the different effects of low and high feature combinations on the final

TABLE 8: The result of the benchmark dimensionality reduction models.

Models	Accuracy	Precision	Recall	F1	AUC
LDA-FDPN	0.8616	0.8628	0.9442	0.9017	0.8130
LPP-FDPN	0.8710	0.8723	0.9545	0.9115	0.8219
PCA-FDPN	0.8789	0.8802	0.9632	0.9198	0.8294
FDPN	0.8668	0.8680	0.9499	0.9071	0.8179

performance. For the other two feature combination methods (DeepFM and PNN), this paper extracts the feature information, including first and second-order features and two different higher-order features, and thus the prediction ability of the model can be greatly improved to achieve a good prediction effect. Through the experiment, the effectiveness of the model was also confirmed. We use LDA (Latent Dirichlet Allocation) and LPP (Locality Preserving Projects) methods for combination comparison. LDA is a generation model for document topics. Make a guess about the topic distribution of the document. This model can represent all topics in the document set in the form of a probability distribution and realize topic clustering and text classification through the probability distribution of each topic. LPP is a linear manifold learning algorithm, which can preserve the local manifold structure of the original dataset and keep it in low-dimensional space. LPP is completely unsupervised; the eigenvectors of LPP are statistically correlated and not orthogonal. This means that LPP does not introduce category tags in the process of feature extraction, and category tags are of great significance for guiding feature extraction for classification problems.

Table 8 shows different performances under different dimensionality reduction methods. It can be found that the FDPN model after PCA dimensionality reduction achieves the best experimental results. In addition, we can also find that compared with the FDPN model alone, the use of the LDA method does not improve the final classification results; compared with the FDPN model alone, the LPP method improves the final classification result but is not as good as the PCA method.

6. Conclusion

This paper presents a new feature combination and structure model for the shortcomings of existing sports course performance prediction methods. We proposed a new method (factorization deep product neural network) for PE course score prediction. The experimental results show that, compared with the existing performance prediction methods (LR, SVM, FM, and the DNN), this paper achieves the best prediction effect on the sports education dataset. Compared with the optimal traditional methods, the DNN accuracy and AUC are both improved by 2%. In addition, there are also significant improvements in accuracy, recall, and F1. The model proposed by us provides an effective method for predicting students' performance in physical education courses.

Data Availability

The experimental data used to support the findings of this study are available from the corresponding author upon request.

Conflicts of Interest

The author declares that there are no conflicts of interest.

Acknowledgments

This work was sponsored in part by the Humanities and Social Sciences Project of Bengbu College (2021sk05zd).

References

- [1] I. Burman and S. Som, "Predicting students academic performance using support vector machine," in *Proceedings of the 2019 Amity International Conference on Artificial Intelligence (AICAI)*, pp. 756–759, Dubai, United Arab Emirates, 2019.
- [2] M. Sweeney, J. Lester, and H. Rangwala, "Next-term student grade prediction[C]," in *Proceedings of the 2015 IEEE International Conference on Big Data (Big Data)*, pp. 970–975, Santa Clara, CA, 2015.
- [3] M. Sweeney, H. Rangwala, and J. Lester, "Next-term student performance prediction: a recommender systems approach," arXiv preprint arXiv: 1604.01840, 2016.
- [4] A. Polyzou and G. Karypis, "Grade prediction with models specific to students and courses," *International Journal of Data Science and Analytics*, vol. 2, no. 3-4, pp. 159–171, 2016.
- [5] Y. Yi, H. Zhang, H. Karamti et al., "The use of genetic algorithm, multikernel learning, and least-squares support vector machine for evaluating quality of teaching," *Scientific Programming*, vol. 2022, Article ID 4588643, 11 pages, 2022.
- [6] A. Abdelhadi and M. Nurunnabi, "Engineering student evaluation of teaching quality in Saudi arabia," *International Journal of Engineering Education*, vol. 35, no. 1A, pp. 262–272, 2019.
- [7] B. Li, Y. Fei, and H. Liu, "An artificial intelligence based model for evaluation of college students' ability and characteristics through teaching evaluation," *Journal of Intelligent and Fuzzy Systems*, vol. 40, no. 1, pp. 1–11, 2020.
- [8] K. C. Jaiswal, P. D. Pathak, V. J. Pawar, and K. D. Kharat, "Prediction of degree student achievement analysis," *IOP Conference Series: Materials Science and Engineering*, vol. 1070, no. 1, Article ID 012057, 2021.
- [9] Y. Su, S. Wang, and Y. Li, "Research on the improvement effect of machine learning and neural network algorithms on the prediction of learning achievement," *Neural Computing & Applications*, vol. 34, no. 12, pp. 9369–9383, 2021.
- [10] S. Jiang, M. Warschauer, and A. Williams, "Predicting MOOC performance with week 1 behavior," in *Proceedings of the 7th International Conference on Educational Data Mining*, pp. 273–275, Worcester: Worcester Polytechnic Institute, London, UK, 2014.
- [11] C. G. Brinton and M. Chiang, "MOOC performance prediction via clickstream data and social learning networks," in *Proceedings of the 2015 IEEE conference on computer communications (INFOCOM)*, pp. 2299–2307, Kowloon, Hong Kong, 2015.
- [12] M. L. Bote-Lorenzo and E. Gómez -Sánchez, "Predicting the decrease of engagement indicators in a MOOC," in

- Proceedings of the Seventh International Learning Analytics & Knowledge Conference*, pp. 143–147, Vancouver, BC, 2017.
- [13] M. Hlosta, Z. Zdrahal, and J. Zendulka, “Ouroboros: early identification of at-risk students without models based on legacy data,” in *Proceedings of the Seventh International Learning Analytics & Knowledge Conference*, pp. 6–15, ACM, Vancouver, BC, 2017.
- [14] N. R. Aljohani, A. Fayoumi, and S. U. Hassan, “Predicting at-risk students using clickstream data in the virtual learning environment,” *Sustainability*, vol. 11, no. 24, p. 7238, 2019.
- [15] S. Jiang, A. Williams, and K. Schenke, “Predicting MOOC performance with week 1 behavior,” 2014.
- [16] B. Amnueypornsakul, S. Bhat, and P. Chinprutthiwong, “Predicting attrition along the way: the UIUC model,” in *Proceedings of the EMNLP 2014 Workshop on Analysis of Large Scale Social Interaction in MOOCs*, 2014.
- [17] C. Taylor, K. Veeramachaneni, and U. M. O’Reilly, “Likely to stop? Predicting stopout in massive open online courses,” *Computer Science*, 2014.
- [18] J. Liang, Y. Jian, and Y. Wu, “Big data application in education: dropout prediction in edx MOOCs,” in *Proceedings of the IEEE Second International Conference on Multimedia Big Data*, IEEE, Taipei, Taiwan, April 2016.
- [19] L. Carmen, A. I. Molina, and A. Cruz-Lemus José, “Learning Analytics to identify dropout factors of Computer Science studies through Bayesian networks,” *Behaviour & Information Technology*, vol. 37, no. 11, pp. 1–15, 2018.
- [20] M. Fei and D. Y. Yeung, “Temporal models for predicting student dropout in massive open online courses,” in *Proceedings of the IEEE International Conference on Data Mining Workshop*, IEEE, Melbourne, Fla, USA, November 2015.
- [21] W. Wei, Y. Han, and C. Miao, “Deep model for dropout prediction in MOOCs,” in *Proceedings of the 2nd International Conference*, Belgium, March 2017.
- [22] S. Rendle, “Factorization machines with libFM,” *ACM Transactions on Intelligent Systems and Technology (TIIST)*, vol. 3, no. 3, pp. 1–22, 2012.
- [23] P. Covington, J. Adams, and E. Sargin, “Deep neural networks for youtube recommendations,” in *Proceedings of the 10th ACM conference on recommender systems*, pp. 191–198, Boston, MA, 2016.
- [24] V. Nair and G. E. Hinton, “Rectified linear units improve restricted Boltzmann machines,” in *Proceedings of the Icml*, pp. 807–814, Haifa, Israel, 2010.
- [25] Y. Qu, H. Cai, and K. Ren, “Product-based neural networks for user response prediction,” in *Proceedings of the 2016 IEEE 16th International Conference on Data Mining (ICDM)*, pp. 1149–1154, Barcelona, Spain, 2016.
- [26] A. V. Nefian, L. Liang, and X. Pi, “Dynamic Bayesian networks for audio-visual speech recognition,” *EURASIP Journal on Applied Signal Processing*, vol. 2002, no. 11, p. 15, 2002.
- [27] A. C. Marreiros, J. Daunizeau, S. J. Kiebel, and K. J. Friston, “Population dynamics: v,” *NeuroImage*, vol. 42, no. 1, pp. 147–157, 2008.

Retraction

Retracted: Design and Implementation of Dance Online Teaching System Based on Optimized Load Balancing Algorithm

Computational Intelligence and Neuroscience

Received 25 July 2023; Accepted 25 July 2023; Published 26 July 2023

Copyright © 2023 Computational Intelligence and Neuroscience. This is an open access article distributed under the Creative Commons Attribution License, which permits unrestricted use, distribution, and reproduction in any medium, provided the original work is properly cited.

This article has been retracted by Hindawi following an investigation undertaken by the publisher [1]. This investigation has uncovered evidence of one or more of the following indicators of systematic manipulation of the publication process:

- (1) Discrepancies in scope
- (2) Discrepancies in the description of the research reported
- (3) Discrepancies between the availability of data and the research described
- (4) Inappropriate citations
- (5) Incoherent, meaningless and/or irrelevant content included in the article
- (6) Peer-review manipulation

The presence of these indicators undermines our confidence in the integrity of the article's content and we cannot, therefore, vouch for its reliability. Please note that this notice is intended solely to alert readers that the content of this article is unreliable. We have not investigated whether authors were aware of or involved in the systematic manipulation of the publication process.

Wiley and Hindawi regrets that the usual quality checks did not identify these issues before publication and have since put additional measures in place to safeguard research integrity.

We wish to credit our own Research Integrity and Research Publishing teams and anonymous and named external researchers and research integrity experts for contributing to this investigation.

The corresponding author, as the representative of all authors, has been given the opportunity to register their agreement or disagreement to this retraction. We have kept a record of any response received.

References

- [1] Q. Yang, "Design and Implementation of Dance Online Teaching System Based on Optimized Load Balancing Algorithm," *Computational Intelligence and Neuroscience*, vol. 2022, Article ID 3829118, 10 pages, 2022.

Research Article

Design and Implementation of Dance Online Teaching System Based on Optimized Load Balancing Algorithm

Qirong Yang 

Music College of Qilu Normal University, Jinan 250000, Shandong, China

Correspondence should be addressed to Qirong Yang; yqr1234562022@163.com

Received 13 June 2022; Revised 2 August 2022; Accepted 10 August 2022; Published 10 October 2022

Academic Editor: Le Sun

Copyright © 2022 Qirong Yang. This is an open access article distributed under the Creative Commons Attribution License, which permits unrestricted use, distribution, and reproduction in any medium, provided the original work is properly cited.

With the continuous improvement of the network hardware environment, people turn the demand target to the network application environment and the construction of information resources. How to build a network teaching platform for general undergraduate teaching to ensure the stability of the system and high-quality services during operation especially large-scale concurrent access will inevitably lead to the increase in the business volume of each core part of the network, the number of visits, and data traffic. With the growth of the network, the corresponding processing power and computing intensity also increase rapidly, which causes problems such as overloading of core network equipment, network bottlenecks, and network congestion. Simply pursuing high-performance hardware to solve problems will undoubtedly result in high cost investment; moreover, equipment with excellent performance cannot meet the needs of the current rapidly growing business volume. According to the design goal of the dance online teaching platform, to meet the online teaching load requirements of many people at the same time, the pressure of the web server cluster must be great. Because many people in online at the same time put too much pressure on the web server, this part of the network cannot be processed in time, which leads to the phenomenon that the performance of this part and even the whole network is degraded. In severe cases, it will even cause network communication services to come to a standstill, that is, the so-called deadlock phenomenon. If the protocol software cannot detect congestion and reduce the packet sending rate, the network will be paralyzed due to congestion. This situation will cause the problem of movement delay for online dance teaching, which will seriously affect the quality of teaching. Therefore, the dance online course system should be continuously improved, the quality of online courses should be continuously improved, and the study of the practical application of load balancing technology in the network teaching environment has become an important means to solve the relationship between supply and demand of network teaching. According to the experimental analysis, when the number of Worker' actuators is fixed, the execution time span of MakeSpan increases with the increase of tasks, while the time required by the optimized load balancing algorithm proposed in this paper increases by 1.32 s on average with the increase of tasks, and the time required by heuristic algorithm and bee colony algorithm increases by 3.68 s and 3.45 s on average with the increase of tasks. On the whole, the optimized load balancing algorithm proposed in this paper has obvious advantages.

1. Introduction

The online dance teaching platform is a digital virtual environment for teachers and students to implement teaching activities. On it, teachers can easily design courses, prepare courses, make teaching courseware and guidance, guide students to study, check students' learning situation, and make scientific and nonquantitative evaluations of students' learning in a timely manner; students can easily obtain all kinds of required learning resources and various course

learning-related materials deposited on the network and conduct real-time or non-real-time two-way interaction with teachers, while managers use the dance online teaching platform to organize teachers and students of the whole school to effectively carry out teaching activities and understand and evaluate teaching activities such as teachers and students who choose courses at any time [1–3]. According to the goal of online dance teaching, to meet the load requirements of many people learning at the same time, the pressure on the server cluster is very great. If the server

processing is not timely to form a network jam, then the action will be delayed in teaching, which will seriously affect the teaching quality.

To deal with the increasingly prominent network bottleneck problem, the traditional solution is often to improve the performance of a single machine to achieve the optimal configuration, which has played a role in certain programs, but the problem of insufficient load is still prominent or multiple servers are used to share different tasks; that is to say, each server plays a different role; for example, one server provides static pages, another server provides dynamic pages, and so on. The structure of this server is asymmetric. The way of distribution, management, and maintenance is very inconvenient [4]. This paper highlights load balancing techniques based on this problem. Its basic design method is to dynamically distribute and allocate customer requests and make the servers in a symmetrical distribution structure; that is to say, each server can respond to the outside world and provide services independently, and each server is in the same position; through the software, the external requests are distributed reasonably and evenly to each server in the symmetrical structure, and the external response is completed independently, and the high load of the website is truly realized.

The focus of this paper is to study and improve a dynamic load balancing algorithm, so that tasks can be efficiently executed in parallel, and the load balance of each machine can improve the parallel resource utilization and overall performance of the task scheduling system. The basic idea is due to the different processing capabilities of each computing node in a task scheduling system, the speed of processing tasks will also be different [5]; lightly loaded nodes can be selected as Thief according to a certain strategy and then go to heavy-loaded nodes. It steals task execution and shares tasks with overloaded nodes, shortens the time span of the system MakeSpan, and improves the overall efficiency of the system [6]. Multitask scheduling in parallel computing is regarded as a classic problem in scheduling system research, and its computational complexity is also recognized as a strong NP problem. So far, the research has not found a most efficient scheduling algorithm. One of the advantages of cloud computing is that it can use a large number of heterogeneous and low-configured resources to realize collaborative computing, thereby reducing the total computing cost [7]. In the cloud computing environment, due to the diversity of computing nodes, geographical dispersion, and various types of resources, multiple tasks also have different characteristics. Businesses need to consider the service quality and cost of cloud computing data centers. The experimental heuristic algorithm and bee colony algorithm are compared with the optimized load balancing algorithm proposed in this paper to verify the performance and load balancing rate of the improved algorithm. During the experiment, the final completion time of the task is used, and compared with other algorithms, the overall performance is improved.

Chapter arrangement of this paper: the first chapter introduces the related research on dance online teaching by relevant scholars; the second chapter introduces the

optimized load balancing algorithm proposed in this paper; the third chapter introduces the dance online teaching based on the optimized load balancing algorithm. The problems existing in the platform are optimized; the fourth chapter is the summary of the full text.

The innovation of this paper: although online dance teaching has been developed for a period of time, a scientific and complete online course system has not yet been formed. The pressure on the server cluster must be great. Since many people online at the same time put too much pressure on the web server, this part of the network cannot be processed in time, which leads to the phenomenon that the performance of this part and even the whole network is degraded. This situation will cause the problem of movement delay for online dance teaching, which has a serious impact. Based on this problem, this paper proposes an optimized load balancing algorithm and studies how to distribute a large number of tasks equally to the appropriate computer nodes in the system for computing and executing tasks, so that the total task execution time MakeSpan is the shortest, and the load balance of each node in the system is achieved and can make full use of computer resources.

2. Related Work

The traditional teaching mode is limited to face-to-face teaching by deeds and deeds. Although this method allows students to see every dance posture and detail taught by the teacher, the students cannot quickly recall the details of the class over time, and the teacher's attitude towards each student is very difficult. Dance demonstrations are not replayable, which greatly limits their application. For the massive amount of information available on the Internet, in the same way that the majority of students often go online, they will browse the corresponding websites to obtain educational resources and access relevant question banks to obtain teaching materials and so on. All these provide huge resources for the development of distance education [8].

Wu design connects motion capture with contemporary sports, fully analyzes the role of motion capture in contemporary physical education teaching, and proposes motion parameters obtained by motion capture technology to monitor motion characteristics in real time and timely monitor motion technology. Diagnosis and analysis assist the coach to judge the standard degree of the athlete's movement in time, analyze the movement of the athlete, and give real-time correction and guidance to the standardization of the athlete's movement [9]. Jiang and Wang proposed to use motion capture to diagnose and analyze the situation in sports training in a timely manner. The coach can improve the training content purposefully based on the real-time activity data captured, thereby improving the effect of physical education and making physical education more effective [10]. Wu uses motion capture technology to assist golf teaching. Wallace uses the motion analysis system to analyze the professional technical movements of golfers, explores the golf players' postures of lifting and hitting the ball, and analyzes the players' movements through real-time captured motion data. It provides the theoretical basis for

the development of the field [11]. Raheb et al. combined motion capture technology with volleyball training, analyzed the volleyball players' movement postures such as serving and catching, and established a set of movement posture database. Through experimental data analysis, volleyball teaching was improved. The quality of education and the technical level of students have brought volleyball teaching into the digital age. Real-time acquisition allows for timely diagnosis and analysis of the situation during motion and reflects the quantitative parameters of the video and images [12]. Maggio et al. introduced the centerless load balancing algorithm and application in grid computing. However, the research on distributed load balancing algorithms is still in its infancy, lacking mature and reliable practical verification methods, and the existence of multiple coordinating nodes can easily cause system network congestion [13]. Han et al. proposed a walking mapping algorithm based on the premise of motion capture and applied it to a humanoid biped robot. Through the effective experimental verification of two robots with different sizes, weights, walking rules, and step lengths, the robot is similar to humans and effectively solves a series of problems caused by the sliding of feet and the ground. Using the Kalman filtering algorithm to predict motion states for unlabeled monocular video sequences of human gait, a quantitative method is proposed to automatically identify and track human motion poses and point out wrong poses [14]. Yan uses motion capture to create animation, optimizes the production process, and studies animation synthesis and elimination of slippage, pointing out that motion capture will become the development trend of animation creation in the future [15]. Aiming at the shortcomings of the current dance online teaching system, Xie proposed and developed a new dance online teaching system based on the B/S model from the perspective of the scale and regularization of online dance teaching [16]. Y. Zhang and M. N. Zhang analyzed the importance of online distance education in the new educational environment, combined with the reality of online teaching with multimedia technology, and expounded the specific design plan for the main functional modules of the system front desk [17]. Cheng et al. introduced the manifestations of online dance teaching resources, online learning methods, online dance teaching platforms, online teaching forms, and online dance teaching evaluation. The concept of education technology, including its specific connotation and theoretical basis, has been designed and developed in an all-round way, including the editing and directing process and online teaching process of online courses, which has broadened the vision of educational technology research and formed the theoretical prototype of the concept of curriculum editing and direction [18]. Wang and Zheng believed that the online teaching platform provides users with a wealth of online learning methods and resources. On the basis of introducing E-Learning, CC-MS, and OSCMS, combined with the online and offline teaching mode, an INM-based teaching method is proposed. The article uses the information network model to model the entity relationship, the entity complex information modeling, and the dynamic modeling for the online teaching system. Finally, the key technologies of the system

are given, including load balancing, database access, cascade query, schema-less data addition, and so on, to support the specific implementation of the system [19].

Classroom teaching based on the network environment provides objective conditions for practical research for the implementation of the learning theory of dance courses. At the same time, dance courses can better guide online interactive classroom teaching and promote the development of two-way activities between teaching and learning. Based on the research of the above related literature, the research on network congestion and online dance teaching is blank. Based on this problem, this paper proposes an online dance teaching model based on the optimized load balancing algorithm.

3. Optimize the Load Balancing Algorithm

In the current teaching reform with a high degree of integration of information technology and education and teaching, a series of education and teaching modes such as blended teaching mode, project-based teaching mode, and inquiry-based teaching mode have emerged, which will inevitably speed up the construction of data resource bases based on various disciplines. The construction of dance teaching resources is complex and diverse. In addition to the integration of online dance resources, data collection of students' learning evaluation, learning habits, and learning methods plays an important role in the generation of benign teaching [20]. The intelligent action analysis software scoring system provides the data generated by students' learning for the resource construction of dance discipline. Through the feedback information of students' learning effect and the evaluation data information of learning process, it is more convenient for teachers to formulate and adjust teaching strategies reasonably, summarize students' learning, provide high-quality and effective online resources for online teaching mode of dance, and give full play to the advantages of the network.

Load balancing is a cheap, effective, and transparent method based on the existing network structure, which aims at expanding the bandwidth of the original network equipment and servers, increasing the network throughput, strengthening the data processing capability and improving the flexibility and availability of the network, and solving the contradiction between the network supply and the business demand. Usually, load balancing is used for two purposes. One is to share a large amount of concurrent access or data traffic on multiple node devices for separate processing, so as to reduce the time for users to wait for a response; the other is to share a single heavy-load operation to multiple nodes. Parallel processing is performed on the node devices. After the processing of each node device is completed, the results are summarized and returned to the user, which greatly improves the processing capacity of the system. Therefore, in order to build an efficient and stable dance online teaching environment, it is necessary to consider how to construct the system hardware and design the software system to avoid the possible risks of network bottlenecks, network congestion, and even application service crashes. A software load

balancing solution refers to the installation of one or more additional software on the operating system of one or more servers to achieve load balancing. It is based on a specific environment, has the characteristics of simple configuration, flexible use, and low cost, and can meet general load balancing requirements. Its technical structure is shown in Figure 1.

Routing is a parameter that reflects the basic performance of a network. It can be used as a constraint condition for path selection and an important criterion for measuring the quality of a path. The measurement parameters often used in the network include bandwidth, delay, delay jitter, cost, packet loss rate, and so on. Based on the different properties of various metric parameters, these metric parameters have various synthetic forms, namely, additive metric, multiplicative metric, and concave metric. The additive metric is determined jointly by the characteristics of all links on the path, such as delay, delay jitter, cost, hop count, and so on, all belong to additive metrics. Its synthesis rule is the metric parameter value of the entire transmission path, that is, the sum of the metric parameter values of each component link, and the cumulative sum of the metric parameter values of the transmission path is shown in the following formula:

$$s(p) = \sum_{i=1}^n s(x_i). \quad (1)$$

The multiplicative metric is the product of all link metrics on the path, and the law is the product of each link metric parameter value, as shown in the following formula:

$$s(p) = \prod_{i=1}^n s(x_i). \quad (2)$$

Available bandwidth, remaining capacity of router buffer, and so on are commonly used concave metrics. The synthesis rule is that the metric parameter value of the path is the smallest among the metric parameter values of each link, and the concave metric is determined by the bottleneck link on the path, such as shown in the following:

$$s(p) = \min [s(x_i)]. \quad (3)$$

In order to reduce the complexity of routing calculation, the usual practice is to select a metric from the additive or multiplicative measures, such as delay or number of nodes, and combine the nonadditive and multiplicative measures such as bandwidth and resource type as constraints. A path selection is made. In addition, the establishment of the above theorem has a prerequisite; that is, the various additive or multiplicative measures should be independent and uncorrelated with each other.

The basic idea of load balancing technology is that multiple servers in a cluster system are symmetrical, and each server has the same status and can respond to service requests independently without the assistance of other servers. By using some load sharing technology, the task request submitted by the client is evenly distributed to a

server in the system, and the server that receives the task request can respond to the client independently. Consistency of server content often relies on shared storage, synchronized updates, or databases. This paper analyzes the number of three kinds of task stealing and gives its core implementation function code. For more clarity, comparison is shown in Table 1.

Since the work-stealing algorithm needs to migrate related tasks when stealing tasks, there will be some communication and delay overhead. When considering reducing the overhead caused by these problems, this paper improves on Thief task stealing timing. The two stealing timings are stealing tasks when the node is idle and stealing tasks when the node is about to be idle.

Task reorganization is to estimate the node performance and regroup the tasks according to the estimated results. Research shows that the node performance mainly depends on RAM and CPU and is closely related to the number of completed tasks. Therefore, when the number of assigned tasks changes, the formula for calculating the number of tasks is shown as follows:

$$N = (1 - C)\alpha + (1 - M)\beta. \quad (4)$$

The memory size of a computer node is an important factor affecting computer performance. It is generally determined by the storage size of the memory card in the node, and usually the node is not simply performing a task; it is always in parallel. Multiple tasks are performed. Therefore, before it executes a task, it also needs to determine how much memory space there is in the node, which can be provided to the task to be executed to determine whether the memory requirement of the task can be met. The memory space calculation of the execution node is shown in the following formula:

$$\text{Ram } S = \text{Ram } R - \text{Ram } U. \quad (5)$$

When the ready task queue on a Worker is empty, that is, the Worker is currently in an idle state and needs dance teaching tasks, it will become thick and send a task dance teaching request to the central task scheduling server Scheduler. The central task scheduler Scheduler finds out the Worker with the largest load according to the stored load information of each Worker and sends the relevant information of the Worker to Thief; Thief can access the relevant Worker after receiving the relevant information sent by the Scheduler and perform dance teaching operations. Different next nodes can be selected in different areas, that is, in a load network environment, facing many choices, how to make the best choice will be a concentrated expression of the advantages and disadvantages of the algorithm. The first is the parameter value to measure the performance of a certain feature of the node, and its formula is shown as follows:

$$T_i = T(v_1, v_2, \dots, v_m). \quad (6)$$

The eigenvalue of a certain characteristic of a node is jointly determined by multiple vectors, and the eigenvalues of different load points are determined under the influence

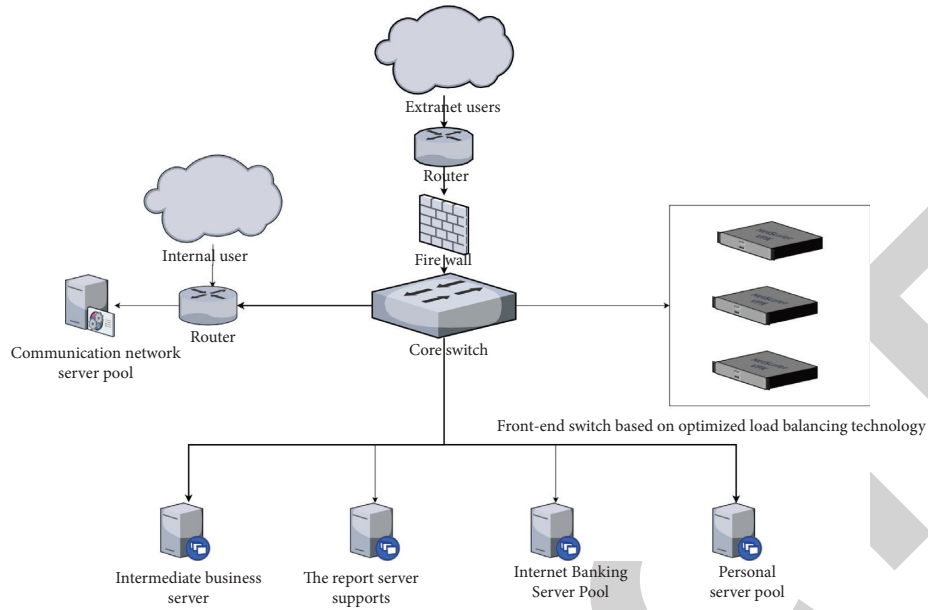


FIGURE 1: Optimized load balancing technology model.

TABLE 1: Comparison of the number of stealing tasks in different tasks.

	Additive series	Multiplication series	Dichotomy
Initial value	Stealinitial	Stealinitial	None
Number of steals for the n th time	$N * stealinitial$	Stealinitial	Half the number of victim tasks
Functional interface	Intsetstealnum (worker victim)	Intsetstealnum (worker victim)	Intsetstealnum (worker victim)

of multiple vectors. The selection formula is shown as follows:

$$T(t + 2) = f(T(t), \kappa). \tag{7}$$

In the case of a large number of users accessing the web server concurrently, how to apply some software mechanism for load balancing in a cluster of web servers to ensure better quality of access for users. Ultimately, the purpose of building a complete, unified, technologically advanced, efficient, stable, safe, and reliable management information system is achieved.

4. Design of Dance Online Teaching System

4.1. Analysis of Correlation Causes of Network Congestion and Action Delay. At present, a series of education and teaching modes such as the high integration of information technology and education and teaching, blended teaching mode, project-based teaching mode, and inquiry-based teaching mode have emerged, which will inevitably speed up the construction of data resource bases based on various disciplines. The construction of online dance resources is complex and diverse. In addition to the integration of online dance resources, the data collection of students' learning evaluation, study habits, and learning methods plays an important role in the generation of benign teaching. The

platform server structure of dance online teaching is shown in Figure 2.

Because servlet runs on the server side, it can generate web pages dynamically and can share data among various programs, so it is easy to realize database connection pool.

Resin is a container for parsing JSPs and servlet, and it supports load balancing to improve reliability. Resin comes with its own Http server and also serves as an srun server. In addition, Resin supports the database buffer pool very well, and the DBPool it provides encapsulates the buffer pool, so long as it is configured in Resin.conf and then referenced in the compiled jsp or servlet. The dance online course system must be continuously improved, and the quality of online courses must be continuously improved. Although online dance teaching has developed over a period of time, a scientific and complete online course system has not yet been formed. Online courses are random, and many of them are not of high quality in terms of teaching content and recording, which affects the teaching effect. According to the design goal of the dance online teaching platform, to meet the online teaching load requirements of many people at the same time, the pressure of the web server cluster must be great. Because many people in online at the same time put too much pressure on the web server, this part of the network cannot be processed in time, which leads to the phenomenon that the performance of this part and even the whole network is degraded. In severe cases, network

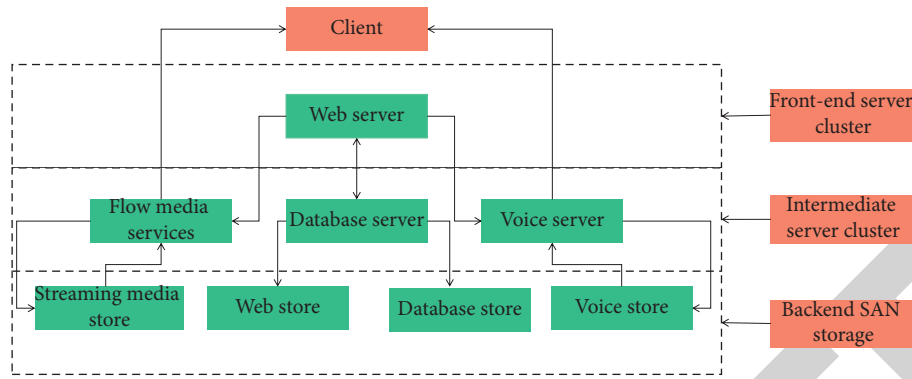


FIGURE 2: The logical structure of the server cluster of the dance online teaching platform.

communication services may even come to a standstill, that is, a so-called deadlock phenomenon occurs, causing data packets sent through the network to experience extremely long delays due to the network being crowded with data packets. If the protocol software fails to detect congestion and reduce the rate at which packets are sent, the network will be paralyzed by congestion. This situation will cause the problem of movement delay for online dance teaching, which will seriously affect the quality of teaching.

The action intelligence analysis software scoring system provides the data information generated by students' learning for the resource construction of dance disciplines. Through the feedback information of students' learning effects and the evaluation data information of the learning process, it is more convenient for teachers to formulate and adjust teaching strategies rationally. Summarize students' learning, provide high-quality and effective online resources for the dance blended teaching model, and give full play to the advantages of the network.

4.2. Dance Online Teaching Platform Based on Optimized Load Balancing. The reason for studying the load balancing technology in the dance online teaching system is that the dance online teaching platform is built for a large-scale user group, providing HTTP, FTP, RTSP, MMS, PNA, and other online or offline methods. It is a kind of network application, which has high requirements on the real-time performance, stability, and data consistency and integrity of the system, and integrates a variety of services.

Load balancing is based on the existing network structure, aiming to expand the bandwidth of the original network equipment and servers, increase the network throughput, strengthen the data processing capability, improve the flexibility and availability of the network, and solve the problem between the network supply and the business demand. Usually, load balancing is used for two purposes. One is to share a large amount of concurrent access or data traffic on multiple node devices for processing, so as to reduce the time for users to wait for a response; the other is to share a single heavy-load operation to multiple nodes. Parallel processing is performed on the node devices. After the processing of each node device is completed, the results are summarized and returned to the user, which greatly

improves the processing capacity of the system. Finally, the purpose of building a complete, unified, technologically advanced, efficient, stable, safe and reliable management information system is achieved.

According to the above analysis of the application characteristics and service types of the dance online teaching platform, this paper adopts a combination of hardware and software to balance the system load. That is, the server cluster technology is selected on the system hardware architecture, and the software load balancing solution is adopted at the same time. A software load balancing solution refers to the installation of one or more additional software on the operating system of one or more servers to achieve load balancing. It is based on a specific environment, has the characteristics of simple configuration, flexible use, and low cost, and can meet general load balancing needs. Cluster technology refers to the technical method of dividing the existing servers into several groups by analyzing the service types accessed by customers, so that multiple servers in the same group can handle certain or similar service requests, so that a large number of concurrent accesses can be shared to the corresponding servers or server groups for processing according to their types. By configuring Resin.conf, enable Resin's own load balancing engine. Resin's load balancing engine can actually start multiple Java response processes and perform load balancing through internal mechanisms. Assuming $n = 3$ here, this paper adopts the configuration scheme of multiple IP addresses and one port.

The test of the system is mainly aimed at concurrent access to examine the responsiveness of the system. The specific method is to use the concurrent access test tool to directly access the database query page in the platform. The test tool adopts the ab test tool that comes with Apache. The test process is divided into a single server running test and two servers running the test at the same time. In these two environments, the number of requests the system responds to per second and the processing time of each request are tested, respectively. The test results are shown in Figures 3 and 4.

It can be seen from the figure that the number of responses per second of the dual-server service is much higher than that of the single-server service when there is a small number of concurrency. With the continuous increase of the number of concurrency, the single and dual-machine

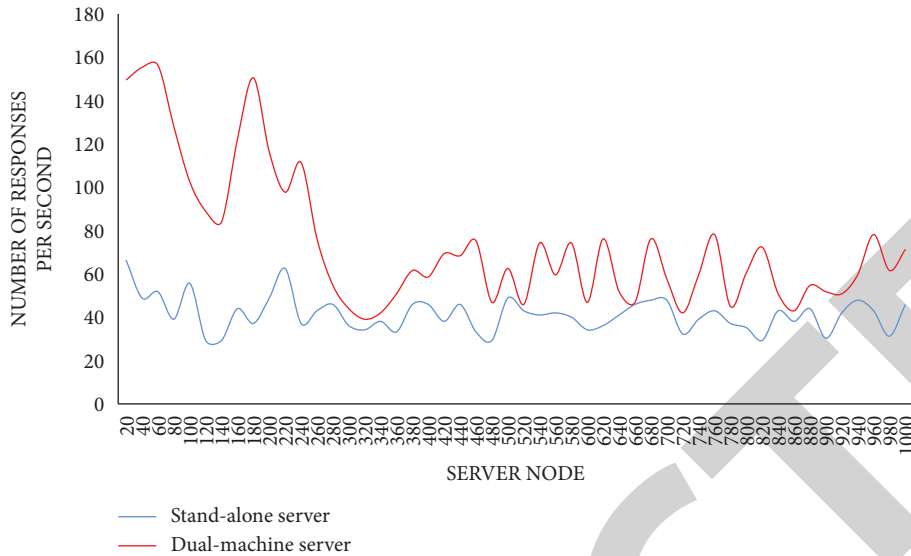


FIGURE 3: Number of responses per second in single-server and dual-server service environments.

services will reach a certain dynamic balance, but the dual-machine service waveform is higher than the single-machine service waveform. This is because Resin parsing and NFS services are required internally during dual-server services, which will temporarily affect the number of responses. However, as the number of concurrency continues to increase, the number of responses for dual-server services will increase; according to the number of user visits, the growth of the amount of stored data can flexibly increase the number of servers and the capacity of network storage to effectively control the service quality of the entire system.

4.3. Experiment on Scheduling Optimization of Dance Online Teaching Server. The web server cluster is the unified portal for the external services of the dance online teaching system, and the user generates a service request relationship with the web server cluster through the browser. On the corresponding servers in the web server cluster, each server responds separately. In the intermediate server cluster, the database server is used to store various dynamic information, courseware resources, and user data; the streaming media server mainly provides streaming media-based courseware on-demand and video services, and the voice server provides real-time online voice interaction services. And all the intermediate server clusters have their own network storage.

The modular combination of various functions of the system should be carried out in accordance with the principles of low coupling and high aggregation. The level of coupling itself represents the strength of the interdependence and connection between programs among the various modules of the system while the level of aggregation represents the intrinsic relationship between the functional programs of each module itself. Here, the module differentiation is carried out in the form of low coupling, which is to reduce the dependencies between modules as much as possible, so that their respective program codes are

independent of each other, so that it is not easy to be confused in development, and it is also conducive to the testing and maintenance of project code. The problem will not have too much impact on other modules; the purpose of using the high-aggregation form is to make the implementation codes within the module itself closely interconnected, so that the function of the module can be used more smoothly and closely. The ultimate goal of this design method is to improve the maintainability of the system design and its later scalability. This paper conducts experiments on the Cloud Sim platform and gives some experimental results for further verification. In order to make the experimental results of this paper more accurate, the number of virtual machines in the experiment is 50 and 100. Every time a group of data is tested, 20 task requests are input, and all the obtained values are recorded as the experimental data of this paper. The experimental results are shown in Figure 5.

The experimental results are stable in a certain range, which proves that the load balancing algorithm is stable in the process of executing cloud task allocation, which shows that the algorithm can ensure that the task allocation can be completed in a limited time when applied to the actual cloud platform. Due to the initial random selection of samples and assignment of tasks to select the first virtual machine, coupled with the uncertainty of the selection results in the iterative formula, the algorithm results will be unstable. Stability means that the experimental results will be stable in a certain range of values, and the curve of the optimal results will tend to be stable. This is because there will always be the best possible results in the system. Then, as the number of experiments increases, the optimal results of the system will tend to a stable value, while the worst results have no rules to follow, and the curve fluctuates greatly. In theory, concentrating all tasks on one virtual machine will produce the worst result, but in fact the algorithm selection strategy guarantees that this situation is impossible, and tasks will be allocated to different virtual

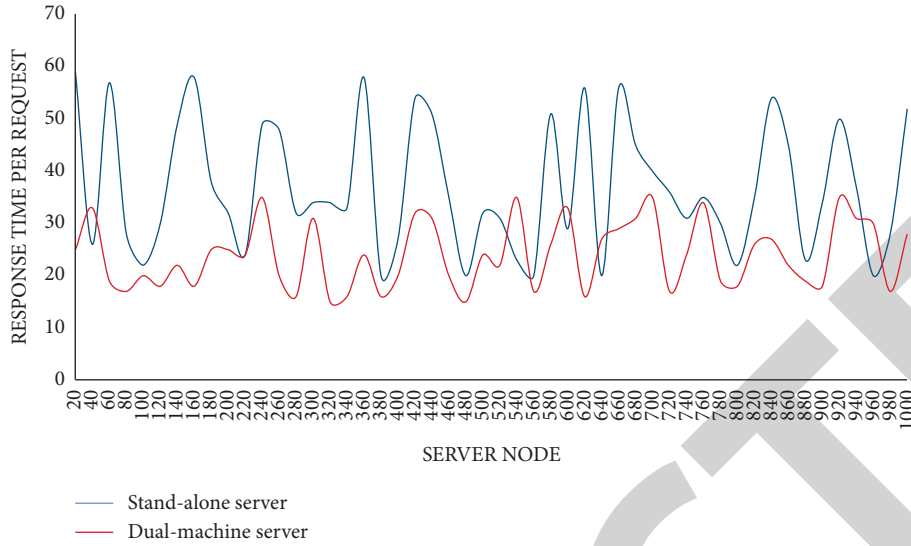


FIGURE 4: Corresponding time of each request in single-machine and dual-machine service environment.

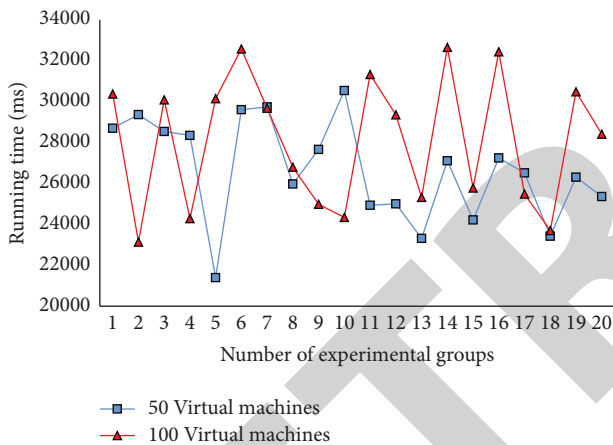


FIGURE 5: 20 experimental results of cloud tasks under different virtual machines.

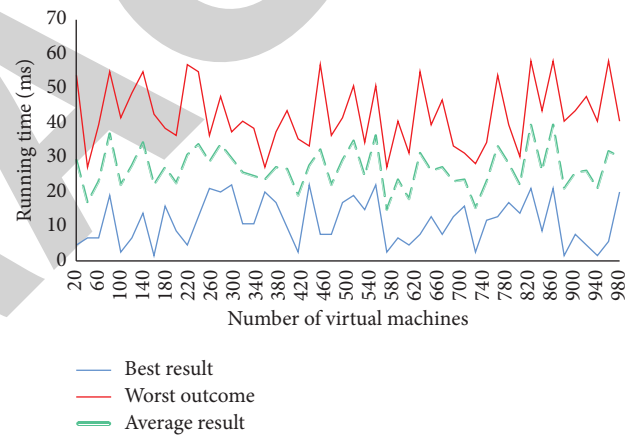


FIGURE 6: The results of different virtual machines changing the experiment.

machines for execution, so the most bad results do not appear stable. In this paper, the optimal result of the experiment is calculated by adjusting the number of virtual machines. The worst result and the average result are used to simulate the number of network task nodes in the simulation dance online teaching. The experimental results are shown in Figure 6.

In all graphs, the best, worst, and average curves grow roughly linearly. This is because when the virtual machine is fixed, as the number of cloud tasks grows, the system consumes more time complexity. Moreover, the linear growth of the average result in the figure can indicate that the load balancing algorithm does not depend on the change of the virtual machine, and the algorithm is stable and independent. The average curve in the graph measures the average efficiency of the algorithm. In the first half of the curve, the curve shows steady growth, which shows the stability of the algorithm. In the range that the virtual machine can bear, the algorithm has stable efficiency.

4.4. Comparison of Optimized Load Balancing Algorithms. In order to verify the validity of the experiment, the optimized load balancing algorithm proposed in this paper is compared with the heuristic algorithm and the bee colony algorithm, and three Work task executors are set to execute the task. The index test results are shown in Figure 7.

It can be seen from the figure that when the number of Worker executors is certain, as the number of tasks increases, the execution time span MakeSpan increases, and the time required for the optimized load balancing algorithm proposed in this paper to complete the task increases on average with the increase in the amount of tasks (1.32 s). As a comparison, the time required for the heuristic algorithm and the bee colony algorithm task increases on average by 3.68 s and 3.45 s with the increase of the task volume. Overall, the optimized load balancing algorithm proposed in this paper has obvious advantages. It is not difficult to find from the test results that the number of servers and the capacity of network storage can be flexibly increased to

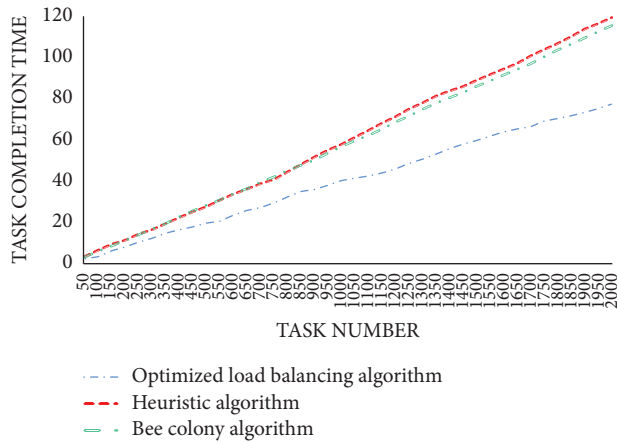


FIGURE 7: Comparing the completion time of different algorithms under worker.

effectively control the service quality of the entire system according to the growth of the number of users accessing the platform and the amount of stored data.

5. Conclusions

Load balancing is an important aspect that affects the performance of the scheduling system. At present, with the reduction of computer hardware cost and the popularity of high-speed networks, network-based parallel computing and distributed computing are also popular. In the dance online teaching platform, by increasing the number of web servers and application servers, server clusters are realized, and at the same time, Resin analysis is used between the web server clusters to achieve load balancing, which effectively improves the system service performance and increases the number of users supported by the system. Quantity makes the system highly scalable and flexible. Practice has proved that with a certain number of Worker executors, with the increase of tasks, the execution time span of MakeSpan increases, and the time required for the optimized load balancing algorithm proposed in this paper to complete the task increases on average by 1.32 s; as a comparison, the time required for the heuristic algorithm and the bee colony algorithm task increases on average by 3.68 s and 3.45 s with the increase of the task volume. Overall, the optimized load balancing algorithm proposed in this paper has obvious advantages. Applying load balancing technology in the establishment of an online dance teaching platform for large-scale user groups is an inexpensive and effective method to expand server bandwidth and increase throughput. It can not only increase network data processing capacity but also improve network performance. This case has great reference significance for building similar large-scale network applications.

When studying the work of dynamic load balancing algorithm, the factors of resources, tasks, and other indicators are considered less, which is far behind the factors affecting scheduling in the actual scene. In the future research and design of dynamic load balancing algorithm, we

should try our best to make the defined indexes closer to the actual application scenarios.

Data Availability

The labeled dataset used to support the findings of this study is available from the corresponding author upon request.

Conflicts of Interest

The author declares that there are no conflicts of interest.

References

- [1] C. H. Wei and M. Jixin, "Design and implementation of a TCP long connection load balancing algorithm based on negative feedback mechanism," *Journal of Physics: Conference Series*, vol. 2, no. 2, pp. 74–84, 2020.
- [2] N. Yao, "Design and implementation of English teaching management system based on web," *International English Education Research: English Edition*, vol. 2, no. 1, pp. 34–42, 2018.
- [3] P. Zhang and H. B. Yang, "Design and implementation of teaching process control system based on activiti," *Software Guide*, vol. 5, no. 13, pp. 74–83, 2018.
- [4] L. Zhu, J. Sun, and M. Zhou, "Design and implementation of dance video teaching system based on Spring MVC architecture," *Modern Electronics Technique*, vol. 5, no. 10, pp. 288–293, 2019.
- [5] G. H. LuJingrong, "Online teaching wireless video stream resource dynamic allocation method considering node ability," *Scientific Programming*, vol. 7, no. 10, pp. 64–71, 2022.
- [6] E. Zhang and Y. Yang, "Music dance distance teaching system based on Ologit model and machine learning," *Journal of Ambient Intelligence and Humanized Computing*, vol. 7, no. 33, pp. 1–17, 2021.
- [7] L. I. Shu-Hong, S. O. Music, and S. University, "A probe into the construction of practical teaching system of dance in colleges and universities," *Journal of Shaoguan University*, vol. 7, no. 2, pp. 144–150, 2017.
- [8] M. Shang, "Thoughts on the reform of higher vocational dance teaching based on big data," *Journal of Physics: Conference Series*, vol. 1852, no. 2, Article ID 022084, 2021.
- [9] H. Wu, "Design of embedded dance teaching control system based on FPGA and motion recognition processing," *Microprocessors and Microsystems*, vol. 83, no. 3, Article ID 103990, 2021.
- [10] C. Jiang and R. Wang, "Design and implementation of the dance teaching live broadcasting system based on the distance education platform," *International English Education Research: English Edition*, vol. 8, no. 2, p. 3, 2019.
- [11] F. Wu, "On the frustration among college English teachers in video-based online teaching in China west ethnic area," *Overseas English*, vol. 3, no. 19, p. 2, 2021.
- [12] K. E. Raheb, M. Stergiou, A. Katifori, and Y. Ioannidis, "Dance interactive learning systems: a study on interaction workflow and teaching approaches," *ACM Computing Surveys*, vol. 52, no. 3, pp. 1–37, 2020.
- [13] L. A. Maggio, B. J. Daley, and D. D. Pratt, "Honoring thy self in the transition to online teaching," *Academic Medicine*, vol. 1, no. 5, pp. 78–83, 2018.
- [14] L. Han, S. O. Music, and A. N. University, "Thinking on highlighting the local characteristics of anhui in the dance

Retraction

Retracted: Development Strategy of Intelligent Digital Library without Human Service in the Era of “Internet +”

Computational Intelligence and Neuroscience

Received 3 October 2023; Accepted 3 October 2023; Published 4 October 2023

Copyright © 2023 Computational Intelligence and Neuroscience. This is an open access article distributed under the Creative Commons Attribution License, which permits unrestricted use, distribution, and reproduction in any medium, provided the original work is properly cited.

This article has been retracted by Hindawi following an investigation undertaken by the publisher [1]. This investigation has uncovered evidence of one or more of the following indicators of systematic manipulation of the publication process:

- (1) Discrepancies in scope
- (2) Discrepancies in the description of the research reported
- (3) Discrepancies between the availability of data and the research described
- (4) Inappropriate citations
- (5) Incoherent, meaningless and/or irrelevant content included in the article
- (6) Peer-review manipulation

The presence of these indicators undermines our confidence in the integrity of the article’s content and we cannot, therefore, vouch for its reliability. Please note that this notice is intended solely to alert readers that the content of this article is unreliable. We have not investigated whether authors were aware of or involved in the systematic manipulation of the publication process.

Wiley and Hindawi regrets that the usual quality checks did not identify these issues before publication and have since put additional measures in place to safeguard research integrity.

We wish to credit our own Research Integrity and Research Publishing teams and anonymous and named external researchers and research integrity experts for contributing to this investigation.


The corresponding author, as the representative of all authors, has been given the opportunity to register their agreement or disagreement to this retraction. We have kept a record of any response received.

References

- [1] H. Wang and J. Ding, “Development Strategy of Intelligent Digital Library without Human Service in the Era of “Internet +”,” *Computational Intelligence and Neuroscience*, vol. 2022, Article ID 7892738, 11 pages, 2022.

Research Article

Development Strategy of Intelligent Digital Library without Human Service in the Era of “Internet +”

Hongmei Wang¹ and Jian Ding^{2,3} 

¹Northeast Forestry University, Library, Harbin 150040, China

²Harbin Conservatory of Music, Harbin 150028, China

³Postdoctoral Program of Heilongjiang Hengxun Technology Co., Ltd., Harbin 150090, China

Correspondence should be addressed to Jian Ding; dingjian@hrbcm.edu.cn

Received 10 June 2022; Revised 18 July 2022; Accepted 20 August 2022; Published 10 October 2022

Academic Editor: Le Sun

Copyright © 2022 Hongmei Wang and Jian Ding. This is an open access article distributed under the Creative Commons Attribution License, which permits unrestricted use, distribution, and reproduction in any medium, provided the original work is properly cited.

Internet technology has a great impact on the application and development of libraries. In order to provide users with more convenient and efficient services, this paper puts forward the development strategy of unmanned intelligent digital libraries in the era of “Internet +.” Design by IntelliSense module, network transmission module, data storage and analysis module, and intelligent service module of no wisdom digital library service mode, IntelliSense module using RFID technology, close range wireless communication technology, and other Internet technologies to collect the wisdom of unmanned services of all kinds of information in the digital library; use network transmission module of the wireless LAN network, Internet technology such as RFID network to transmit information collected to store in a data storage and analysis module; and at the same time using k -means clustering algorithm in data mining techniques such as analysis of collected data, based on the analysis results provide users with intelligence services such as search, wisdom is recommended. The experimental results show that the developed strategy meets the expected functional requirements, can accurately perceive the location of data, and effectively realize the intelligent service function.

1. Introduction

Under the background of the Internet era, compared with previous libraries, the system service of smart digital libraries is becoming more and more perfect, and the information behavior of users presents the characteristics of the Internet [1]. Users’ access to information has taken on a new form and is constantly developing in the direction of intelligence, informatization, digitization, and modernization [2], and information behavior is becoming more and more convenient. In the “Internet +” era, information resources are more abundant and platform systems are more integrated. However, at present, there are some problems in the service of a smart digital library, which need to be handled in time, establish and improve the mechanism, and improve the service quality of the smart digital library. “Internet +”

brings a new development opportunity for the construction of a smart digital library. Combined with the construction of a smart digital library, it can use “Internet +” to fuse different information [3], cross-border integrate information, and achieve the goal of information service. “Internet +” is the product of social development and the crystallization of science, technology, and economic development [4]. The construction of the smart digital library is affected by the Internet. It combines other industries with library information so that library information can be combined with all industries and fields that can be connected and contact institutions in different places.

The concept of a smart digital library was first put forward by foreign library circles [5]. Whether it is theoretical research or practical research, its starting point and purpose are to realize the universality and intelligence of a

smart digital library, so as to provide users with intelligent and personalized services. Around 2003, the library of University of Oulu in Finland launched a service called “smart library” [6]. Smart library is a space-free and perceptible mobile library service that can be used anywhere there is Internet. As for the definition of a smart digital library, different scholars in China have given different expressions from different angles. From the perspective of sensor computing, Yan Dong proposed that smart digital library = library + Internet of Things + cloud computing + intelligent equipment [7]; from the perspective of big data and ubiquitous learning, Wang Weiqiu proposed that smart digital library was the integration of digital library, intelligent perception equipment, big data analysis, and ubiquitous learning space [8]; from the perspective of humanized service and management, Pingping proposed that the smart digital library had changed the interaction mode between users and library facilities, systems and information resources through modern information technology, so as to make the service and management of the library more intelligent [9]. Based on the views of the abovementioned scholars, it can be considered that the smart digital library should be a new generation library that takes the digitization of resources as the premise and is based on the Internet of Things technology, Internet technology, and mobile terminals, guided by the needs of readers, is not limited by space, can be perceived, and continuously improves the reader experience, which is the future development direction of the library.

In recent years, with the continuous development of ubiquitous Internet technology based on mobile Internet and Internet of Things and the continuous expansion of mobile terminal functions, the information service mode based on situational perception, ubiquitous computing, intelligent judgment, and multidimensional interaction will be the main direction of the development of smart library in the future. At present, some scholars have done relevant research on the development strategy of a smart digital library. Wu introduced the intelligent library personalized recommendation service system based on intelligent technology [10]; combined with the characteristics of a ubiquitous and intelligent smart library, Bi et al. constructed a hierarchical model of a ubiquitous smart library from the bottom-up from the perspective of user service [11]; and Cui and Wu introduced the intelligent service system of Library of Nanjing University, including the construction and transformation of physical venues, the construction of information service platform and the construction of intelligent services, and introduced the construction and implementation of its intelligent library in detail [12, 13].

In order to predict the future development of the unmanned service command digital library, this paper studies the development strategy of the unmanned service smart digital library in the era of “Internet +,” and provides users with smart search, smart recommendation, and other smart services, hoping that the research content can improve the service quality of the smart digital library.

2. Materials and Methods

“Internet +” refers to a new form of business developed by the Internet under the impetus of innovation 2.0, and a new form of economic and social development evolved and spawned by the Internet under the impetus of knowledge society innovation 2.0. “Internet +” is a further practical achievement of Internet thinking. It represents an advanced productive force, promotes the continuous evolution of economic forms, drives the vitality of social and economic entities, and provides a broad network platform for the reform, innovation, and development of unmanned smart digital libraries.

2.1. Resource Feature Extraction of Unmanned Intelligent Digital Library. The intelligent service mode of an unmanned intelligent digital library is composed of four main parts: intelligent sensing module, network transmission module, data storage and analysis module, and intelligent service module, as shown in Figure 1.

Intelligent sensing module refers to the use of a variety of Internet technologies to connect users, information resources, unmanned intelligent digital libraries, and so on so that they become an organic whole, so as to achieve the interconnection of information among the three.

When extracting the resource features of the unmanned service intelligent digital library, it is regarded as the combination of the user’s interests and the resource characteristics, that is, the matching of the student’s personalized portrait and the resource features of the unmanned service intelligent digital library. Therefore, after completing the construction of the personalized portrait of students, the resource features of the unmanned intelligent digital library are extracted [8]. Then the matching calculation is carried out for the attribute characteristics of the resources of the unmanned intelligent digital library, and the conditions are provided for the subsequent resource recommendation and detailed display. In the specific operation, it is necessary to determine the distribution of resource data of the unmanned intelligent digital library. In the heterogeneous data storage environment of the unmanned intelligent digital library, the decision-making feature preference of resource data is introduced, and the integration of student personalized portrait and resource feature data is realized. In this process, the following formula can be used:

$$W_{abc} = \frac{A_a}{\sum_{i=1} (B_i - C_i)}. \quad (1)$$

In Equation (1), W_{abc} represents the resource characteristic data of the unmanned intelligent digital library obtained through the abovementioned operation; A_a represents a user personalized portrait tag corresponding to the feature data; B_i represents the characteristic value of all unmanned smart digital library resources; C_i represents the personalized portrait label of the student corresponding to a specific unmanned intelligent digital library resource. According to the abovementioned equation, complete the

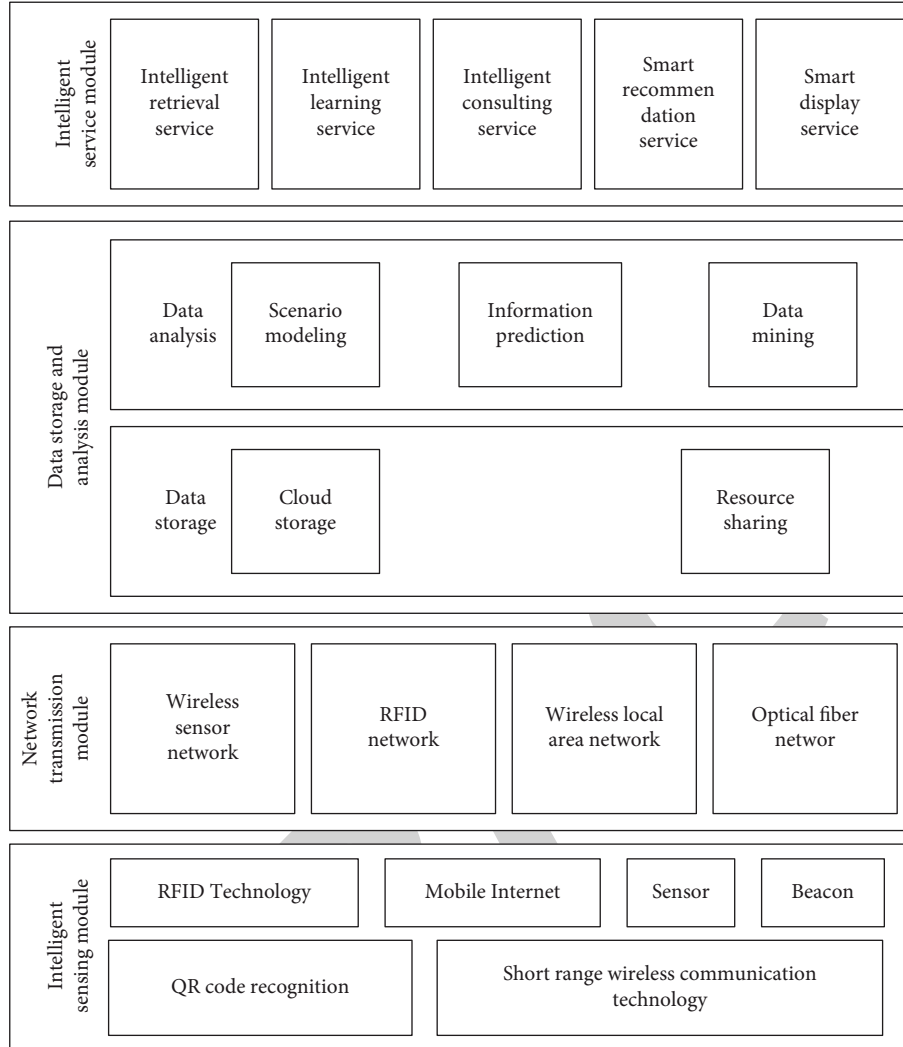


FIGURE 1: Intelligent service mode of unmanned digital library.

fusion of student personalized portrait and resource feature data, and then need to fuse all resource feature data. The specific equation is given as follows:

$$G_H = K_L \times K_J \times W_{abc}. \quad (2)$$

In Equation (2), G_H represents the objective function of resource feature extraction of unmanned intelligent digital library; K_J represents the weight coefficient during feature extraction under a certain recommended delay J condition; and K_L represents the feature extraction weight when the consumption is L in the feature extraction of the resources of an unmanned intelligent digital library. According to the abovementioned operations, the integration of various resources in the unmanned intelligent digital library is realized. After the integration, the feature data needs to be reconstructed in multidimensions. The fusion matching method can be introduced to reconstruct the data, and the reconstructed data can be imported into the recommendation database of the unmanned intelligent digital library according to the abovementioned operation, so as to complete the resource feature extraction task of the entire digital unmanned intelligent digital library.

2.2. RFID-Based Book Location Sensing Algorithm. FRID technology is used to collect book locations in an intelligent digital library without human service. According to the workflow of FRID technology, the sensing method based on frequency domain phase difference is used to sense the distance between tag reader and tag in the two-dimensional space of an intelligent digital library without human service; based on the two-dimensional spatial distance sensing results of the intelligent digital library without human service, the trilateral measurement method is selected to sense the three-dimensional coordinate position data of the book tag to be perceived in the intelligent digital library without human service.

2.2.1. Two-Dimensional Distance Perception. According to the working process of FRID technology, the reader transmits carrier signals with different frequencies [14–16]. After a certain distance, the signal is received and reflected by the book tag. The reader obtains the reflected signal and determines the distance between the book target (the tag to be perceived) and the tag reader (the location coordinates

are known) based on the signal phase difference. The specific process is given as follows.

Ignoring the time required for the process from book tag receiving to transmitting carrier signal, Δs and a are respectively used to represent the time required for the process from reader transmitting carrier signal to receiving reflected signal and the propagation speed of RF signal in the air, so as to obtain the expression of speed distance d :

$$d = a\Delta s, \quad (3)$$

where β and p are respectively represented the phase and carrier frequency experienced by the reader carrier signal from the transmission to reception.

2.2.2. 3D Position Perception. After determining the distance between the book tag to be perceived and the tag reader in the two-dimensional space of the intelligent digital library without human service, it can select the trilateral measurement method to perceive the three-dimensional coordinate position data of the book tag to be perceived in the intelligent digital library without human service [17].

d_i ($i = 1, 2, 3$) represents the distance between the three readers and the tag, and the coordinate (x_i, y_i) ($i = 1, 2, 3$) of each reader is known, so as to obtain

$$d_i = \sqrt{[(x_i - x_0) + (y_i - y_0)]^2}. \quad (4)$$

On this basis, the position coordinate (x_0, y_0) of the book tag to be perceived in the intelligent digital library without human service can be determined by constructing the equation.

The distance relationship between the reader i and the book tag to be perceived in the three-dimensional space of the intelligent digital library without human service can be described by the following equation:

$$d_i^2 = [(x - x_i) + (y - y_i) + (z - z_i)]^2. \quad (5)$$

Equation (5) is defined as a spherical equation. Since the tag is a common point, according to the geometric relationship, the position data of the book tag to be perceived in the intelligent digital library without human service determined by four readers [18] can be obtained, so as to obtain the distance equation group between the book tag and the reader.

From the abovementioned description, it can be seen that accurately obtaining the distance between the book tag to be perceived and the tag reader in the two-dimensional space of the intelligent digital library without human service is the basis for obtaining the high-precision three-dimensional position coordinate data of the books in the intelligent digital library without human service.

If the distance between each tag reader and the book tag has high accuracy, and the tag reader is set in different corners of the intelligent digital library without human service, which can avoid multiple tag readers from being in the same straight line with the book tag, then Equation (5) must have a unique solution. However, in the process of actually perceiving the book located in the intelligent digital

library without human service, the calculation result of the distance between the tag reader and the book tag has a certain error [19], resulting in no solution in Equation (5). In order to solve this problem, it is necessary to use the selected gradient descent method to calculate the solution that makes Equation (5) approximate.

A coordinate position of the book tag to be perceived in the environment of the intelligent digital library without human service is selected, and Equation (6) is used to determine the distance between each reader and the coordinate point of the book to be perceived as follows:

$$d_{0i} = \sqrt{[(x_0 - x_i) + (y_0 - y_i) + (z_0 - z_i)]^2}. \quad (6)$$

The actual distances d_i and d_{0i} between the book tag and the i th reader are subtracted to obtain the error w_{0i} .

After perceiving the relevant information of the intelligent digital library without human service, it can use the network transmission module to transmit the perceived data to the data storage and analysis module and store it. Data mining technology is used to analyze the perceived data, and realize different smart services according to the analysis results.

2.3. Data Storage Analysis of Intelligent Digital Library without Human Service Based on Data Mining. Based on the perceived data information of the intelligent digital library without human service, a personalized service-oriented big data mining process of the intelligent digital library without human service is designed, as shown in Figure 2.

According to Figure 2, data mining, also known as knowledge discovery in the database, is a hot topic in the field of artificial intelligence and database research. It helps decision-makers adjust market strategies, reduce risks and make correct decisions. In the big data mining implementation scheme shown in Figure 2, the main modules are divided into data collection, role modeling, algorithm implementation and result storage, and front-end application. Role modeling, algorithm implementation, and result storage belong to the offline part, and the online part involves data collection and front-end application [20].

2.3.1. K-Means Clustering Algorithm. The clustering algorithms in the process of data analysis stored in the intelligent digital library without human service mainly include hierarchy-based, partition-based, and density-based algorithms [21], among which the most commonly used and effective is the partition-based K-means clustering algorithm. Its specific implementation process is given as follows:

- (1) Firstly, randomly select k vectors as the center of each class.
- (2) Let E be a two-dimensional membership matrix of $c \times n$. If the j -th vector x_j belongs to class i , the element e_{ij} in matrix E is 1, otherwise, it is 0. That is, for each $k \neq j$ and when $\|X_j - C_i\| \leq \|X_j - C_k\|$, e_{ij} value is 1, otherwise the value of e_{ij} is 0.

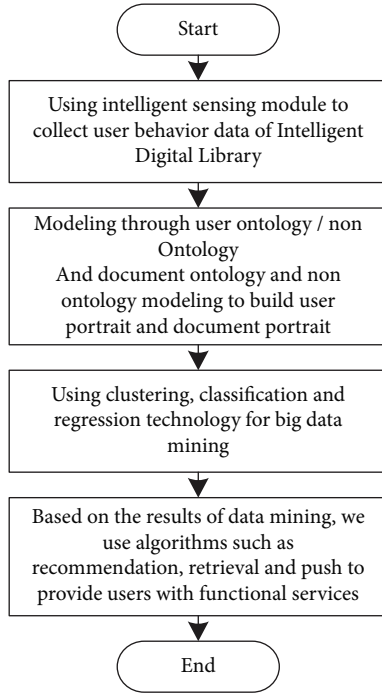


FIGURE 2: Implementation process of data mining.

- (3) Calculate the value of objective function J according to e_{ij} , and stop if it is less than a threshold or the difference between two consecutive times is less than a threshold.
- (4) Calculate the center C_i of each cluster G_i according to e_{ij} : $C_i = \sum_{i \in G_j} X_i / |G_i|$, and G_i is the number of elements in the cluster. Then go back to step (2).

Although K-means algorithm has attracted much attention due to its advantages such as simplicity and efficiency, it still has some limitations, mainly as follows:

- (1) Clustering results are excessively dependent on the selection of initial values [22], and the accuracy and stability of clustering results are poor
- (2) The algorithm is very sensitive to outliers [23], and there are large errors in the clustering results

2.3.2. Improved K-Means Algorithm. To solve the above-mentioned problems, an improved K-means algorithm based on the principle of natural nearest neighbor density and maximum-minimum distance is proposed to optimize the selection of initial clustering centers. Starting from the internal distribution characteristics of the stored data in the intelligent digital library without human service [24], the algorithm can adaptively determine the data density, avoid the problem of artificial parameter setting, and objectively and truly reflect the distribution characteristics of the stored data in the intelligent digital library without human service, so as to find a high-quality initial center to solve the disadvantage that the initial center point randomly selected by the traditional K-means algorithm is not representative. At the same time, it can eliminate the influence of outliers on

the clustering results, so as to improve the accuracy and effectiveness of the final analysis results when clustering the relevant data of the intelligent digital library without human service. The improved algorithm flow is given as follows.

Step 1. For the relevant data set of the intelligent digital library without human service, find out the natural nearest neighbor of the relevant data sample point x_i of each intelligent digital library without human service according to the natural nearest neighbor search algorithm, and determine the density function of the relevant data points of each intelligent digital library without human service. The equation is given as follows:

$$d_e(x_i) = \frac{1}{\sum_{x_j \in NN_{nb(i)}(i)} k_i(x_i, x_j)} \times n_b(i). \quad (7)$$

In Equation (7), $n_b(i)$ represents the number of times that the relevant data sample points of the intelligent digital library without human service appear in the r neighborhood of the relevant data sample objects of the other unserviceable smart digital libraries, that is, the number of natural nearest neighbors of sample i , $NN_{nb(i)}(i)$ represents the natural nearest neighbor set of the relevant data points of each intelligent digital library without human service, and $k_i(x_i, x_j)$ is the European distance between the relevant data points x_i and x_j of the intelligent digital library without human service.

Step 2. Delete the relevant data sample points of sparse intelligent digital library without human service satisfying condition to obtain the relevant data intensive sample point set X' of an intelligent digital library without human service.

Step 3. Select the highest density in X' , i.e., x of $dens_{\max}(x)$, as the first initial clustering center c_1 ; the longest distance mentioned above is the standard [25], to look for the second center point c_2 ; and so on until we get k initial clustering centers $C = \{c_1, c_2, \dots, c_k\}$.

Step 4. Calculate the attribute weight of the dataset.

Step 5. Calculate the weighted Euclidean distance between all the relevant data sample points of the intelligent digital library without human service and the k initial cluster centers obtained in step 3, where $x \in X$ and $c \in C$. Assign each relevant data point of the intelligent digital library without human service to the nearest center [26], forming k clusters, and each cluster is represented by its cluster center.

Step 6. Recalculate the cluster center according to the clustering results of step 5.

Step 7. Repeat step 5 with the results in step 6 as input until the cluster center does not change or the cluster reaches the maximum number of iterations.

Step 8. Output k class clusters.

It can be achieved through the abovementioned process.

3. Experimental Results

This paper studies the development strategy of the intelligent digital library without human service in the “Internet +” era. Taking the University Library as the research object, this paper adopts the development strategy to build an intelligent digital library without human service and verifies the actual performance of the development strategy studied in this paper through experiments. The results are given as follows.

3.1. Functional Test. The main content of the functional test is to test the performance of book borrowing and automatic return under the development strategy studied in this paper. In order to ensure the robustness of book borrowing and automatic book return to the input content, the black box test method is adopted based on the functional requirements of different module designs.

3.1.1. Performance Test of Book Borrowing. The black box test method is used to test the book borrowing function under the development strategy of this paper. The test cases, expected outputs, and actual outputs are shown in Table 1.

According to the analysis of Table 1, under the development strategy of this paper, book borrowing first needs to scan the user’s library card to determine the user’s identity. After determining the identity of the book borrower, it needs to scan the books to bind the relevant information of the book borrower (library card number) and book information (ISBN number), and then click the OK button to complete the book borrowing. According to the analysis of Table 1, the book borrowing function under the development strategy of this paper can identify whether the user’s relevant information (library card number) is registered or not, judge the upper limit of books that can be borrowed according to the user’s relevant information (library card number), and prompt “user does not exist” for unregistered users.

The actual output of the relevant test cases in Table 1 is completely consistent with the expected output, which shows that the book borrowing function under the development strategy of this paper meets the expected requirements.

3.1.2. Performance Test of the Automatic Book Return Module. The black box test method is used to test the automatic book return function of the research object under the development strategy of this paper. The test cases, expected outputs, and actual outputs are shown in Table 2.

Analysis of Table 2 shows that the automatic book return function under the development strategy of this paper can identify whether the books exist, whether they are borrowed, whether they are returned, and the location of the returned books. The actual output of the relevant test cases in Table 2 is completely consistent with the expected output, which shows that the design of the automatic book return function under the development strategy of this paper meets the expected requirements.

3.2. Position Perception Error Analysis. Select different types of books (poetry books, astronomy books, and medical books) and analyze the perception results of book sample location data under the development strategy of this paper. The results are shown in Figures 3–5.

From Figure 3 to Figure 5, under the development strategy of this paper, the position perception error of different types of book samples in different directions is controlled within 4.5 cm, which is significantly lower than the standard position perception error threshold of 10 cm generally recognized in relevant fields. The reason is that this method designs a personalized service-oriented big data mining process for unattended smart digital libraries based on the perceived data information of unattended smart digital libraries, which is conducive to controlling errors to a certain extent. This shows that under the development strategy of this paper, the position perception accuracy of different types of book samples is higher.

3.3. Data Mining Performance Analysis. Taking the user information in the research object as an example, according to the cluster center obtained from the clustering results, the medical book users are divided into five interest groups, and the clustering accuracy under different K values is analyzed. The results are shown in Figure 6, the specific situation of clustering division is shown in Figure 7, and the book recommendation is realized according to the user clustering results, and results are shown in Figure 8.

According to the analysis of Figure 6, under the conditions of different K values, the clustering accuracy of the method in this paper shows a trend of gradually increasing at first and then significantly decreasing. When the K value is increased from 3 to 8, the clustering accuracy of this method is improved from 93.5% to 98.5%; with the continuous improvement of K value, the clustering accuracy of this method gradually decreases. When the K value reaches 12, the clustering accuracy of this method will be less than 90%. This shows that the optimal clustering accuracy can be obtained when the K value in this method is 8.

After the user’s interest group division results shown in Figure 7 are obtained, the borrowing record data of “Tonghao” users in the interest group can be analyzed as part of the reference basis for recommendation in the next step. For example, for target user 07, who likes traditional Chinese medicine, find out the most similar users in the interest group (user 33 and user 48), And recommend the relevant borrowing of these users to the user (see Figure 8). According to the analysis of Figure 8, most of the data borrowed by users 33 and 48 are borrowed by user 07, which shows that this method can effectively realize the intelligent recommendation function.

4. Recommendations

In view of the current development status of China’s intelligent digital library without human service, this paper puts forward the following suggestions for the development of intelligent digital libraries without human service.

TABLE 1: Test cases and output of book borrowing function.

Test case ID	Expected output	Actual output
1	Please scan books	Please scan books
2	Please scan the library card	Please scan the library card
3	Wrong library card number input	Wrong library card number input
4	Exceeding the maximum borrowing amount	Exceeding the maximum borrowing amount
5	Borrowing succeeded	Borrowing succeeded

TABLE 2: Test cases and output of automatic book return module.

Test case ID	Expected output	Actual output
1	Return the book successfully	Return the book successfully
2	The ISBN number of this book does not exist	The ISBN number of this book does not exist
3	Please scan books	Please scan books
4	The book has been returned	The book has been returned
5	This book is placed in column X of XX cabinet in XX district	This book is placed in column X of XX cabinet in XX district

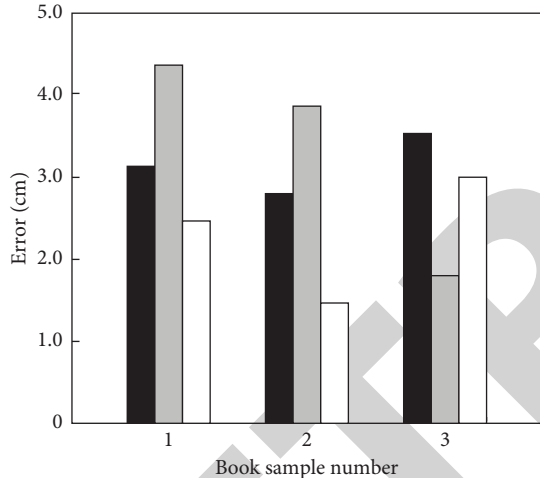


FIGURE 3: Poetry books.

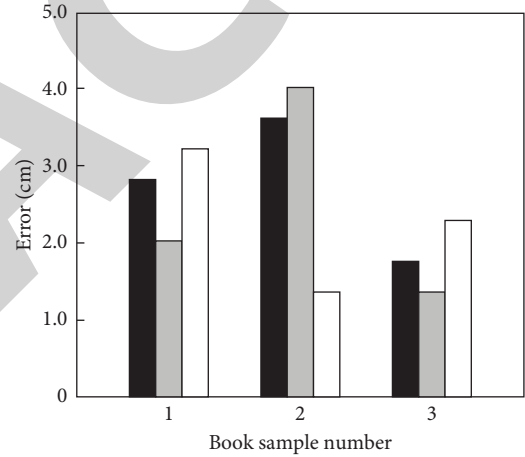


FIGURE 5: Medical books.

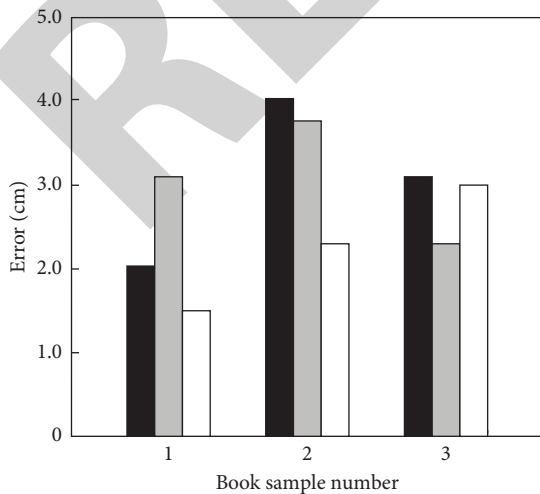


FIGURE 4: Astronomical books.

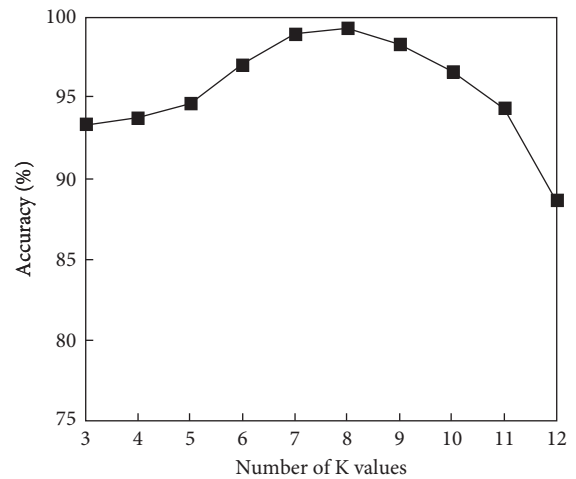


FIGURE 6: Clustering accuracy under different K values.

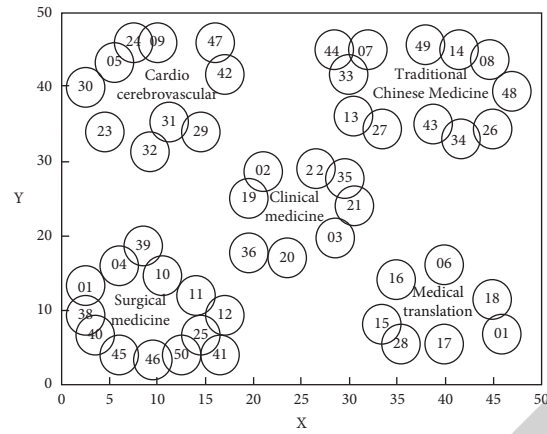


FIGURE 7: Clustering results.

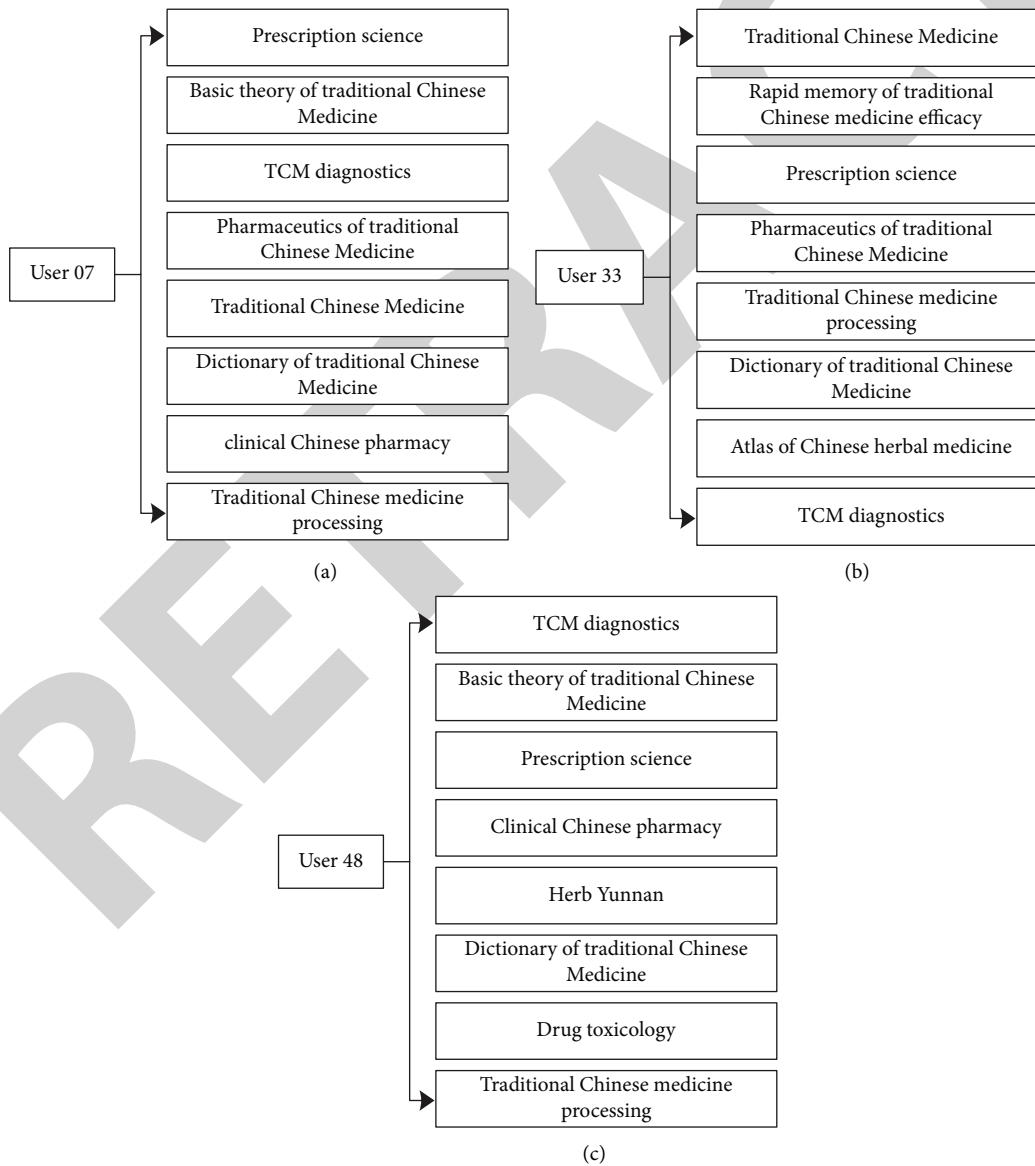


FIGURE 8: Recommended results (a) User 07. (b) User 33. (c) User 48.

4.1. Strengthening Top-Level Design and Formulating the Action Plan of "Internet + Library". "Internet +" has become a new engine to promote social, economic, and cultural development. The state council, provinces and cities, and industries have successively formulated "Internet +" action plans. "Internet +" also has a profound impact on libraries and promotes the transformation and development of libraries. Libraries should seize the opportunity, strengthen top-level design, scientifically formulate the "Internet + library" action plan, clarify the objectives, paths, and key measures of library transformation under the "Internet +" background, explore the implementation scheme of the "Internet + library" action plan and accelerate the deep integration of the Internet and libraries; it should strive to explore the impact of "Internet +" on library service concept, service mode, resources, organization, management, etc., have the courage to break down various obstacles incompatible with the development of "Internet +," speed up the reform process, stimulate innovation vitality, and improve service efficiency and efficiency. In this regard, Zhejiang Provincial Public Library is at the forefront of national libraries. In July 2015, Zhejiang Library, together with 11 municipal public libraries in the province, jointly released the "Internet +" action plan of Zhejiang Public Libraries, proposing to make library services more accessible through cross-border integration, make resources easier to find, enrich resource supply, and enable the public to enjoy more fair, efficient, high-quality and convenient public cultural services.

4.2. Establishing and Improving the System and Articles of Association to Ensure the Storage Security of Digital Information Resources. In order to improve the service quality of digital library and ensure the effectiveness of information resources, colleges and universities need to constantly update the mechanism and concept, do a good job in the resource management and development of digital libraries, give full play to the role and value of digital library, and realize the goal of scientific management of digital library. In order to improve the service quality and order of digital library, during the construction of the university library, it is necessary to build an information resource service system, based on the interaction of administration, economy and law, give full play to the advantages of administrative and economic means, and give full play to the role of the legal system, so as to fully implement administrative, economic and legal standards, establish and improve systems and mechanisms, and form a service system for rational use and efficient management of information resources.

At the same time, it is necessary to do a good job in the management of professional equipment and computer equipment. In order to maintain and test the security of digital library in time and ensure the security and efficiency of electronic resources and network information, we should give full play to our own advantages, strengthen the management of electronic equipment and computer equipment, build and optimize the rules and regulations system so that it can have a legal basis. In the library service of colleges and

universities, only by doing a good job in the management planning of digital literature and information resources can the computer application level be improved, the digital and information resources can be stored safely for a long time, the utilization and development of information resources can be done well, and the scientific and technological achievements can be fully combined with social development so that the library service of colleges and universities can develop toward the direction of digital society and actively adapt to the digital era.

4.3. Making a Good Job in the Construction of Service Content. The digital library of colleges and universities has the characteristics of ubiquity and digitization. College teachers and students can obtain information for the first time in different environments and at different times. In order to ensure the scientificity and rationality of information construction, it is necessary to do a good job in the construction of information resource service content.

4.3.1. Providing Information Independently. This is an intelligent service mode. The service effect of information resources is good, and college teachers and students are in a passive receiving state. To predict the information of college teachers and students, it can analyze the topics of interest, analyze the information needs of college teachers and students and the contact and rules of information resources, and push the content of interest for college teachers and students, so as to provide information independently, mainly in the form of information push and data mining.

4.3.2. Transmitting Information Automatically. This information resource transmission mode focuses on the system construction mode. In the system construction, the intelligent construction function is added to achieve the goal of personalized service. After university teachers and students give keywords, intellectualization can respond in time, and provide a large amount of information resources and effective product information for university teachers and students after inquiry, sorting, collection, and arrangement. Information transmission is the main form of information automation. It increases the timeliness of information interaction and reflects the advantages of digital technology and information technology.

4.4. Increase Expenditure and Make a Good Job in Team Building.

- (1) Colleges and universities should do a good job in software and hardware construction, improve the expenditure on software and hardware, adjust and optimize the collection structure of the digital library, and reasonably divide the comparison between e-books and paper books. It also needs to reduce paper financial expenditure, give full play to the advantages of network resources, and increase the storage of e-book resources. During the construction of the digital library, it is gradually

transitioning from traditional library construction to digital library construction, to formulate a reasonable system and planning scheme, and constantly adjust the collection policy, information purchase, literature planning, and other work. In the document collection scheme and planning, we should improve the collection of electronic information text and increase the financial expenditure on electronic document information, so that the electronic document information resources occupy a large proportion in the library, which is conducive to the development of comprehensive digital library services.

- (2) Do a good job in team building. Paying more attention to the construction of a talented team is conducive to the realization of personalized and professional services of University Digital Library. It should introduce professional and technical personnel and management talents, realize technical and orderly management and improve the professionalism and gradient of talent structure. As for the digital library, it is different from the previous libraries. It does not need a large area of space, does not need to build a large number of reading rooms, changes the previous paper reading form, and realizes the goal of electronic reading. Therefore, colleges and universities can transfer the network resource information and digital information collected by the library itself, or act as the supporter and guides of the network resources of the digital library, and use guidance and training to make readers increase their ability to obtain network resources and improve the ability to obtain digital information resources. In detail, colleges and universities need to enrich the level of talents, educate and train librarians in network technology and digital technology, enhance the quality of librarians, establish a reward and punishment system, employ advanced technicians, and give full play to the maximum service goal of a digital library.

5. Conclusion

This paper studies the development strategy of unmanned intelligent digital libraries in the era of "Internet +" and draws the following conclusions:

- (1) The book borrowing function under the development strategy of this paper can identify whether the relevant information of users has been registered.
- (2) The actual output under the development strategy in this paper is completely consistent with the expected output, indicating that the automatic return function design under the development strategy in this paper meets the expected requirements.
- (3) The position sensing errors of different types of book samples in different directions are controlled within 4.5 cm, and the accuracy of position sensing is high.
- (4) The proposed method can obtain the optimal clustering accuracy and effectively realize the intelligent recommendation function, with strong practical application performance and more convenient and efficient service for users.

Data Availability

The raw data supporting the conclusions of this article will be made available by the authors, without undue reservation.

Conflicts of Interest

The authors declare that they have no conflicts of interest regarding this work.

Acknowledgments

This work was sponsored in part by the project of Heilongjiang Library and Information Work Committee (2021-082-A and 2021-076-B).

References

- [1] B. H. Li, Z. N. Chen, X. D. Chai et al., "Overall development of the Internet plus initiative against the backdrop of intelligence plus," *Chinese Journal of Engineering Science*, vol. 22, no. 4, pp. 1-9, 2020.
- [2] P. Zhao, H. Zhou, C. Zhao et al., "Purification, characterization and immunomodulatory activity of fructans from *Polygonatum odoratum* and *P. cyrtoneuma*," *Carbohydrate Polymers*, vol. 214, no. 5, pp. 44-52, 2019.
- [3] D. M. Wang and G. M. Weng, "Thoughts on the development of intelligent elderly care in rural areas under the background of "Internet +,"" *Jiangsu Agricultural Sciences*, vol. 47, no. 15, pp. 76-80, 2019.
- [4] J. L. Chu, J. H. Ren, and Y. H. Wang, "From digital libraries to smart libraries," *Journal of Academic Libraries*, vol. 40, no. 02, pp. 52-58, 2022.
- [5] X. X. Yao and B. J. Gao, "Exploration and vision of digital transformation of academic Li-braries," *Journal of Library Science in China*, vol. 48, no. 02, pp. 13-24, 2022.
- [6] V. Prokop and J. Stejskal, "Cross-generation analysis of e-book consumers preferences—a prerequisite for effective management of public library," *Information*, vol. 11, no. 2, pp. 72-81, 2020.
- [7] Y. Liang and B. Lou, "Design of an information management system for the case library of business management courses," *International Journal of Emerging Technologies in Learning (iJET)*, vol. 16, no. 07, pp. 203-210, 2021.
- [8] M. Rahimi, M. Rosman, M. N. Ismail, and M. N. Masrek, "Investigating the determinant and impact of digital library engagement: a conceptual framework," *Journal of Digital Information Management*, vol. 17, no. 4, pp. 214-222, 2019.
- [9] R. Pingping, "Application situation model and ecological system construction of digital twin library from the perspective of "cloud intelligence" fusion," *Information Studies: Theory & Application*, vol. 44, no. 12, pp. 41-47+9, 2021.
- [10] J. Z. Wu, "Building an intelligent library:opportunities, challenges and innovations," *Library Journal*, vol. 40, no. 12, pp. 4-11, 2021.

Research Article

Impact Analysis of Basketball Exercise Strength Based on Machine Learning in the Mental Health of College Students

Ran Zhang 

Hubei University of Automotive Technology, Shiyan 442002, Hubei, China

Correspondence should be addressed to Ran Zhang; 20150020@huat.edu.cn

Received 17 April 2022; Revised 3 June 2022; Accepted 27 June 2022; Published 27 September 2022

Academic Editor: Le Sun

Copyright © 2022 Ran Zhang. This is an open access article distributed under the Creative Commons Attribution License, which permits unrestricted use, distribution, and reproduction in any medium, provided the original work is properly cited.

In the current environment of globalization, the communication between people is gradually getting closer, and the society is becoming more and more complex. With the continuous development and progress of science and technology, people are more skilled in applying science and technology to their own concerns. College students are about to enter the society, will feel multiple pressure from family, school, and society, study and life problems will gradually convert into mental health problems, and we need to use machine learning basketball exercise to positively affect the mental health quality of college students. The improvement of living conditions makes people pay more attention to their physical and mental health, and learn to use machine learning sports reasonably, not only basketball exercise, to improve mental health diseases. However, we need to use machine learning to identify the different effects of different basketball exercise intensity on mental health, in order to ensure that the most appropriate basketball exercise intensity brings good aspects to the mental health of college students. Through the investigation and data sampling, it can be concluded that the machine learning-based basketball exercise intensity has a positive impact on the mental health of college students.

1. Introduction

With the continuous development and progress of society, people pay more attention to their physical and mental health, not only due to physical health but also pay more attention to mental health. In the social environment with the rapid development of computer networks, the use of machine learning for emotion recognition has attracted wide attention. People care about the body of their family and friends. Emotional recognition has very broad application prospects in many fields of medical care, online education, and other fields. The designed emotion recognition algorithm is essentially a multi-classifier integration algorithm to achieve better results by integrating classical machine learning classifiers. After the data information collected by the sensor is processed centrally, it is inserted into the algorithm of emotion recognition for calculation. The calculated results are analyzed and the results are displayed, and the long and short results are summarized to provide guidance for the subsequent research path and direction [1].

This article introduces the data types and sources of machine learning for us, introduces a variety of machine learning algorithms, combined with the actual situation in the field of mental health, improve different machine learning algorithms, recognize its advantages and disadvantages, combined with the advantages of traditional psychological tools and machine learning to machine learning in the field of mental health. Finally, it is summarized to play a positive role in effectively solving the prevention of psychological problems [2].

Basketball as a kind of aerobic exercise is an important way to improve mental health problems and maintain mental health problems. After years of research, many research results have shown that basketball can improve psychological problems. This article is to study whether the intensity of basketball exercise has an impact on the mental health of college students. The machine learning method and statistical research results show that the different intensities of basketball exercise will indeed have different positive effects on the mental health of college students. But we need

more experiments to support this result [3]. In the moderate exercise intensity group and no exercise group, they had interpersonal social interaction, anxiety sensitivity, more than depression paranoia, and psychosis, which was in line with the comparable conditions in statistics. Through the experiment, small-intensity basketball has improved interpersonal social fear and other symptoms to a certain extent [4]. It discusses the influence of basketball exercise intensity on the mental health of college students, provides guidance methods and related research materials for college physical education activities, and concludes that basketball sports of different intensity can improve the mental health of college students [5].

Sports and mental health are interrelated. They restrain and influence each other. Strengthening sports basketball can enhance students' interest and learning motivation, and improve the mental health environment of college students. Effective exercise can make college students effectively control their psychological emotions and pressure, and also improve their interpersonal relationships and adaptability to the environment. Therefore, sports have a certain impact on the mental health of college students [6]. The article thinks that sports have a positive guide to college students' psychological problems. This phenomenon will produce different reactions because of the different intensity, frequency, and even time of exercise. Later, the calculation method of machine learning should be used to study the influence mechanism of physical activities on college students [7].

This study discusses the influence of low- and medium-intensity basketball on self-esteem and mental health and provides the basis for physical education and mental health education. There was no difference in self-esteem before and after intervention in the control group. Low-intensity basketball activities have an impact on the mental health of students in the experimental group. After the intervention, students in the moderate intensity group scored lower in obsessive-compulsive disorder, interpersonal sensitivity, depression, phobia and anxiety, mental quality, and general scores. In conclusion, middle- and low-intensity basketball is beneficial to boys' self-esteem and mental health, and the middle-intensity group is better than the low-intensity group [8].

After years of intensive study, the most pressing problem that college students must face is employment. With the sustained development of China's economy and the accelerated pace of social progress, the society's demand for talents comprehensiveness and adaptability is increasing. However, under the influence of long-term exam-oriented education, college students are only satisfied with the required courses at present, resulting in a lack of professional knowledge and the ability to solve practical problems, narrow-mindedness, poor flexibility, creativity, and operational ability. With the significant difference between campus and society, most college students will feel pressure from all aspects when they first enter the society. For example, they lack effective learning methods, have strong social responsibility and self-study ability, have poor understanding and mastery of professional knowledge, poor sense of unity, poor social practice and operation ability, and

poor cognitive ability. Moreover, they often have great communication barriers and cannot correctly evaluate themselves and others [9].

Strengthening sports can improve students' physical quality. Physical and mental exercise is to achieve physical health and mental happiness through physical activities. Academics have long studied the relationship between physical exercise and mental health and reached a consensus that physical exercise has a positive promoting effect. College students are the future talents of this country. Under the national policy of attaching importance to talent building, more and more attention is paid to students' mental health [3]. This study compares the students who use mastery learning methods with those who use nonmastery learning methods [10].

This study aimed to explore the influence of different sports events, intensity, and time on college students' anxiety and depression. College students' sports participation, perceived motor score, and self-rating anxiety scale were discussed in depth. The relationship between the intensity and frequency of basketball exercise and mental health anxiety and depression was studied. Anxiety and depression exist among most ordinary students. College students can take different sports to improve their mental health [11]. Basketball can effectively improve the emotional state and physical level of college students and promote the mental health of male college students [12]. College students' mental health education is playing an increasingly important role in higher education. How to cultivate good mental health through physical education is a difficult problem faced by all educators in China. Let students know more about basketball, and by participating in the basketball team experience, they can improve their social skills, so that college students can better deal with all kinds of social relationships in campus life and study, and build a good mental health quality [13]. Traditional exercise prescription is for physical health, but many current college students need mental health. We should pay attention to how to improve the traditional sports prescription and strengthen their mental health adaptability. Take basketball as an exercise form of mental health prescription [14].

2. Machine Learning Algorithm

2.1. KNN Algorithm. KNN algorithm is one of the classical algorithms in machine learning [15]. Its core idea is that if the K most adjacent samples in the feature space belong to a certain type, the sample also belongs to the current type and has the characteristics of that type. The formula for calculating the distance between the two samples is

$$L_p(x_i, x_j) = \left(\sum_{l=1}^n |x_i^{(l)} - x_j^{(l)}|^p \right)^{1/p}, \quad (1)$$

where P is the variable parameter, when $P=1$, the formula represents the Manhattan distance; when $P=2$, the formula represents the European distance; when $P \rightarrow \infty$ the formula represents the Chebyshev distance.

2.2. Random Forest Algorithm. Random forest algorithm cannot be separated from the decision tree. Random forest algorithm consists of multiple decision trees, and there is no connection between different decision trees. The prediction results of the random forest algorithm are the results of the classification displayed by most decision trees. The random forest algorithm is more accurate and stable compared to the results predicted by a single decision tree.

2.2.1. Detection Process of a Random Forest. The detection of random forest is using a single decision tree to detect characteristic samples step by step, and then uses the minority-obeying majority voting mechanism to judge the final boundary result. The binary segmentation function is defined as follows:

$$h(x, \theta_j) = \begin{cases} 0, & \text{left,} \\ 1, & \text{right,} \end{cases}$$

$$\theta = (k, \tau), h_1(x, \theta) = [x(k) < \tau],$$

$$\theta = (k_1, k_2, \tau),$$

$$h_2(x, \theta) = [x(k_1) - x(k_2) < \tau].$$
(2)

In the formula $h(x, \theta_j)$ —The binary segmentation function at the current node;

θ_j —Characteristic properties and the corresponding threshold of the sample x stored at the node j ;

τ —Threshold value of property k for sample x at node j .

2.2.2. Training Process in the Random Forest. Each decision tree was trained independently. The training sample set of the decision tree includes feature samples and the corresponding artificial labeled samples. Use the Gini exponentially split feature attributes to generate decision trees. The samples are processed as follows:

$$\text{Gini}_j = (S_j^L, S_j^R),$$

$$S_j^L = \{(x, y) \in S_j | h(x, \theta_j) = 0\},$$

$$S_j^R = \frac{S_j}{S_j^L}.$$
(3)

In the formula S_j —The training sample $S_j \in X \times Y$, X at the node j represents the feature sample, and Y represents the marker sample;

Gini_j —The Gini index at the node j ;

S_j^L —A nonboundary sample at the current node j ;

S_j^R —Samples belonging to the motion target boundary;

Redefining the Gini exponential splitting function for the dichotomy case:

$$H(S_j) = \sum_y p_y (1 - p_y),$$

$$\text{Split} = \sum_{k \in \{L, R\}} \frac{|S_j^k|}{|S_j|} H(S_j^k), \text{Gini}_j = H(S_j) - \text{Split}.$$
(4)

In the formula $H(S_j)$ —Split indicators at the nodes j calculated using the Gini index;

y —is a certain structured label, which has a variety of structures;

p_y —Probabilities corresponding to the structured label l ;

Split—Formula representation of the second half of the information gain standard function.

2.3. ID3 Algorithm. The ID3 algorithm is the earliest decision tree algorithm. The information gain is calculated by the following formula:

$$\text{info}(X) = - \sum_{i=1}^n p_i \log_2 p_i,$$

$$\text{info}_A(X) = - \sum_{j=1}^m p_j \text{info}(j),$$

$$\text{Gain}(A) = \text{info}(X) - \text{info}_A(X),$$
(5)

where X is the set of all training samples located at the current node, n is the n species of classification corresponding to the sample set, p_i is the i corresponding probability, m is the m value cases for the attribute A , and p_j is probability that the attribute A is worth j .

2.4. C4.5 Algorithm. ID3 algorithms are prone to fitting with few training samples and more algorithm parameters. In view of this deficiency, Quinlan has improved the ID3 algorithm, and the improved algorithm is called the C4.5 algorithm.

The C4.5 algorithm can disperse the continuous attributes based on the ID3 algorithm and can handle the training data with missing attribute values. C4.5. Definition of the algorithm:

$$\text{Split Info}_A(X) = - \sum_{j=1}^m p_j \log_2 p_j,$$

$$\text{Gain Ratio}(A) = \frac{\text{Gain}(A)}{\text{Split Info}_A(X)},$$
(6)

where m is the m values of the attribute A , $\text{Split Info}_A(X)$ is the amount of information that A contains in the current sample X , and $\text{Gain Ratio}(A)$ is information gain ratio corresponding to attribute A .

2.5. CART Algorithm. The CART algorithm adopts the Gini exponential splitting properties, and the splitting criteria are as follows:

$$\text{Gini}(X) = 1 - \sum_{i=1}^n p_i^2, \text{Gini}_A(X) = \sum_{k=1}^m \frac{N_k}{N} \text{Gini}(K).$$
(7)

In the formula $\text{Gini}(X)$ —The Gini index value of the current sample set X ;

p_i —The probability corresponding to the sample set category i ;

m —Attribute A has m values. The current sample can be divided into m subsets;

N_k —Total number of samples corresponding to the k th subset;

Gini $_A(X)$ —Gini split values for split by attribute A .

2.6. Expectation-Maximization Algorithm. The EM algorithm is an effective method to find maximum likelihood estimation or maximum posterior estimation with hidden variable models [16]. It is widely used in natural language processing, psychology, quantitative genetics, and other problems. The EM algorithm was proposed in 1977 by Arthur Dempster, Nan Laird, and Donald Rubin. The method is simple and effective in operation [17].

Log-likelihood function for a given Gaussian mixture distribution is as follows:

$$\ln p(X|\pi, \mu, \Sigma) = \sum_{n=1}^N \ln \sum_{k=1}^K \pi_k N\left(x_n | \mu_k, \Sigma_k\right). \quad (8)$$

Seek the maximum likelihood estimate of the parameter θ , namely:

$$\theta_{ML} = \arg \max_{\theta} \ln p(X|\theta). \quad (9)$$

Using the EM algorithm to estimate the parameters simplifies the problem.

First, finding the partial guide for the mean μ_k of each component of $\ln p(X|\pi, \mu, \Sigma)$ relative to the mixed Gaussian distribution can obtain:

$$0 = - \sum_{n=1}^N \frac{\pi_k N(x_n | \mu_k, \Sigma_k)}{\sum_{j=1}^K \pi_j N(x_n | \mu_j, \Sigma_j)} \gamma(z_{nk}). \quad (10)$$

Multiplies the above equation by \sum_k^{-1} and rearranges it to obtain

$$\mu_k = \frac{1}{N_k} \sum_{n=1}^N \gamma(z_{nk}) x_n, \quad (11)$$

where N is defined as

$$N_k = \sum_{n=1}^N \gamma(z_{nk}). \quad (12)$$

Through the calculation of the above formula, the mean μ_k of the Gaussian component is the case of the Gaussian mixture distribution. Then, following the same method, $\ln p(X|\pi, \mu, \Sigma)$ for each μ_k , you can obtain

$$\sum_k = \frac{1}{N_k} \sum_{n=1}^N \gamma(z_{nk}) (x_n - \mu_k)(x_n - \mu_k)^T. \quad (13)$$

Observing the equation above shows that the form of the solution of the parameter μ_k in a mixed Gaussian distribution is similar to the solution of the covariance in a single Gaussian distribution.

Finally, the corresponding per-mixing coefficient π_k is obtained by maximizing $\ln p(X|\pi, \mu, \Sigma)$. Specifically, the constraint of π_k can be incorporated into the objective function by introducing the Lagrangian coefficient, subsequently maximizing the new objective function:

$$\ln p(X|\pi, \mu, \Sigma) + \left(\sum_{k=1}^K \pi_k - 1 \right). \quad (14)$$

Similarly, it can be obtained by finding the partial guidance for π_k :

$$0 = \sum_{n=1}^N \frac{\pi_k N(x_n | \mu_k, \Sigma_k)}{\sum_{j=1}^K \pi_j N(x_n | \mu_j, \Sigma_j)} + \lambda. \quad (15)$$

Subsequently, using the characteristic of $\sum_{k=1}^K \pi_k = 1$ to sum the probability π_k of each component, you can simplify the following results: $\lambda = -N$. Bring $\lambda = -N$ into the original to eliminate, and rearrange, and finally obtain

$$\pi_k = \frac{N_k}{N}, \quad (16)$$

where π_k is the mixing coefficient for the k th component in the mixed Gaussian distribution.

3. Status Quo of Basketball Sports in China

As is known to all, basketball has become a well-known popular sport in China. People from primary school students to middle-aged and elderly people participate in basketball. This sport spans all ages and gender races, and everyone gets together to play basketball.

With the development of artificial intelligence and the progress of machine learning methods, in recent years, domestic basketball research has gradually developed in the direction of combining theory and practice. Compared with foreign anaerobic basketball training, aerobic training is more inclined in China. In recent years, with the help of machine learning science concepts and equipment, China has enriched basketball training methods. However, the index system for assessing the level of basketball mainly lies in special speed, strength, and endurance. The research on basketball training in China mainly focuses on physical quality, thus ignoring the mental health state, but the real basketball sport should lie in the comprehensive combination of form, function, and quality, and then the physical fitness level combined with people's health. The difference in basketball exercise intensity not only brings us physical changes but also is a process of physical and mental pleasure, which can shed negative energy and negative emotions.

In the physical education activities of colleges and universities, basketball has always been a hot course, which shows the love of college students for basketball, and observing every college basketball court, is always people, full of, filled with the power of youth. Under the multiple pressure of contemporary college students, basketball is no good way to relieve pressure and relax, so basketball exercise under machine learning can really improve the mental health quality of college students.

Guo Haoran put forward the research [18] on the teaching and education of basketball courses in colleges and universities in the Experimental Research of Introducing Physical Fitness Education on Improving the Teaching Effect of Basketball Public Courses in Colleges and Universities. It means hoping to combine basketball with physical education practice, Add basketball education to physical education, While improving the quality of physical education in colleges and universities while promoting the benefits of basketball exercise, Has the following benefits: (1) is a major breakthrough to improve the traditional sports teaching, Better improve the traditional basketball teaching; (2) Improving the focus of traditional physical education teaching, Pay more attention to the physical and mental health of college students; (3) Better popularization of basketball exercise brings not only the physical benefits, It can also promote the development of mental health.

4. Mental Health Analysis

4.1. Implications of Health and Mental Health. The United Nations Health Organization defines health as: "Health is not only without physical defects, but also with a complete physical, psychological state and social adaptability." Thus, a healthy person is not only a healthy body but also needs a healthy mind. Although there are many controversies in society, even if each person's ideas are different, but mental health is a part of human health.

So what to measure the mental health of college students. Combined with the relevant research at home and abroad, and starting from the actual conditions of the psychological development and mental health of Chinese college students, it should be reflected from the following aspects: (1) healthy and stable mood; (2) strong and brave quality; (3) positive social adaptability; and (4) personality integrity and behavior coordination [19].

4.2. Physical Education Teaching and the Mental Health of College Students. Sports teaching relationship with college students' mental health [20], the characteristics of college students' psychological development, state, motivation development level and master sports knowledge, sports skills, and the main basis of design, arrangement of physical education teaching, reasonable arrangement, and scientific organization sports teaching can make some possibility of psychological development become reality to promote the healthy development of students' psychology. With the progress of sports psychology and the popularization of mental health knowledge, people also gradually realize that physical exercise can not only strengthen physical fitness but also promote mental health.

Physical education teaching is to consciously adjust students' emotions in the process of participation, enhance the communication between students, enhance students' confidence, cultivate the courage to struggle, cultivate a strong will quality, as well as physical education teaching to make students get healthy ideas, and establish healthy behavior. Its main aspects are to promote the development of

students' cognition, promote the development of students' emotions, promote the development of students' will and quality, promote the development of students' personality, slow down stress and improve mental health [21].

4.3. Current Quo of Mental Health of College Students. In the current rapidly developing information age, college students have to bear the triple pressure from their families, schools, and society. According to relevant statistics, about 20% of college students have different degrees of mental health problems, which we should take corresponding positive measures so that college education can cultivate high-quality talents to meet the social development and needs.

However, because of people's high expectations and requirements for college students, their self-concern and life goals, the mental health problems of college students are significantly higher than other groups of the same age, so they must be paid great attention to Colleges and universities are related to the mental health problems of college students. Schools should proceed from reality, carry out a large-scale psychological investigation and in-depth and meticulous research and analysis, use scientific sampling and standards to judge the mental health status of college students, and provide accurate and effective teaching methods for the development of mental health education [22].

4.4. Impact and Effect of Sports on the Mental Health of College Students. As we all know, physical exercise can effectively improve the sensitivity and coordination of the human body. But in fact, this is only one aspect of physical exercise in colleges and universities. In physical exercise, students get exercise not only physical exercise but also mental health exercise, like physical exercise, which is a process of self-improvement in continuous understanding and self-improvement. College students can improve their thoughts, morality, will, emotion, and other aspects through physical exercise. Basketball is an important branch in physical sports [23].

5. Example Analysis

5.1. Experiment Preparation. The 40 students from Chongqing University were selected. Among them, 20 basketball (10 male and female) and 20 ordinary college students (10 male and female) were selected for physical testing and psychological testing.

First, understand the acceptance intensity of basketball at each level and then make basketball prescription for ordinary college students; the basketball teacher is responsible for the guidance, three times a week, 1.5 hours, for 8 consecutive weeks according to the set intensity of fitness activities.

The following data were obtained from the identification survey of the value of physical exercise among 200 random students (Table 1) and the degree of daily physical and mental feelings of college students (Table 2).

It can be seen from Table 1 that most college students have a positive attitude towards physical exercise, and the positive influence of college students on physical activities is relatively

TABLE 1: College students' identification of the value of sports (unit: %).

Content	In full agreement	Largely agree	Disagree	Pussyfoot	Total
Sports can promote physical and mental health	76.8	22.8	0.4	0	100
Sports can enrich your spare time life	65.0	33.3	1.2	0.4	100
Sports can develop good living habits	46.3	46.7	3.7	3.3	100
Sports can relax	44.7	54.9	0.4	0	100
Sports can cause fatigue and affect learning	2.4	8.5	80.9	8.1	100

TABLE 2: Daily physical and mental feeling degree of college students (unit: %).

	Insentience	Sometimes feel	Often feel	Total
Physical fatigue	8.5	81.7	9.3	100
Mental fatigue	10.6	73.2	16.3	100
Feel underexercised	20.3	68.3	11.4	100
Feel that obesity is happening	44.7	37.4	17.9	100

high, indicating that college students have a relative sense of identity for the improvement of physical and mental health of physical exercise, including basketball exercise.

It can be seen from Table 2 that college students usually feel physical fatigue and mental fatigue in daily life. In addition, most students think that physical exercise can bring changes, which proves that contemporary college students have independent personality and positive attitude towards life.

5.2. Basketball Quality Test for Students. As for the statistics of the basketball level of the selected students (Figure 1), it can be seen that very few college students participate in the basketball level and obtain the basketball level certificate.

Considering the difference between basketball special students and ordinary college students at the speed of 5 km/h, Figure 2 shows the right step length of basketball special students is not significantly different from that of ordinary college students, but the left step length of ordinary college students is slightly larger than that of special basketball students. It can be seen that basketball exercise for step length and step width change is not big.

Figure 3 is a comparison of the gait cycle of basketball students and ordinary college students at 5 km/h. The gait cycle of basketball students is less than that of ordinary college students. After a long time of basketball training, basketball exercise has a certain effect on the gait cycle.

Figure 4 shows the statistics of step frequency speed change for special basketball special students and ordinary college students. Step frequency refers to the number of steps per unit time, expressed as in (times/per minute). At 9–13 km/h, with the increasing speed of basketball special students and ordinary college students, the pace frequency also showed an increasing trend. However, the pace frequency of basketball special students is more stable, which shows that basketball exercise has improved the stability of human sports.

5.3. The Impact of Basketball on College Students' Body

5.3.1. Effect of Basketball on Heart and Lung Function. Table 3 is an 8-week basketball training for ordinary college students. Through basketball training, the function

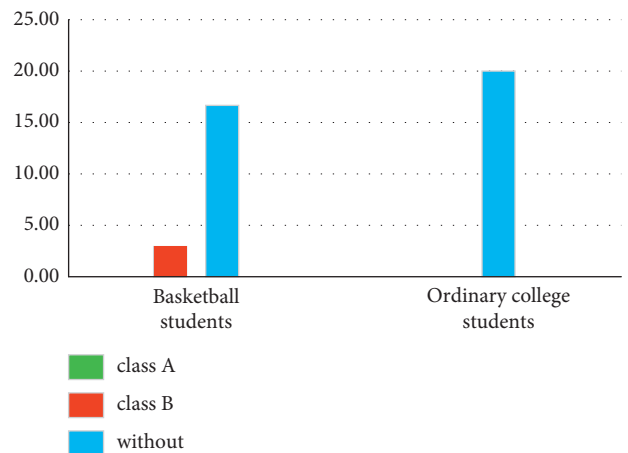


FIGURE 1: Basketball level.

of the body has a significant impact. Before and after 8 weeks of basketball training, the indicators of cardio-pulmonary function of college students after exercise are significantly improved compared with those before exercise. Basketball has a positive impact on improving the body's heart function and promoting the improvement of vascular function.

5.3.2. Influence of Basketball Exercise on the Physical Quality of College Students. As can be seen from Table 4, all the quality tests after exercise are higher than those before exercise. After exercise, the speed of running and 50 meters is significantly higher than before exercise, but the speed of 1000 meters is not much different, indicating that the sensitivity and speed of college students need to be improved, but the endurance is difficult to change. The improvement of pull-up quality shows that the upper limb strength quality of college students needs to be improved. Eight weeks of basketball exercise has a certain impact on the speed, endurance, sensitivity, and the explosive power of the upper and lower limbs of college students. The basic physical quality is improved greatly, and the effect is remarkable.

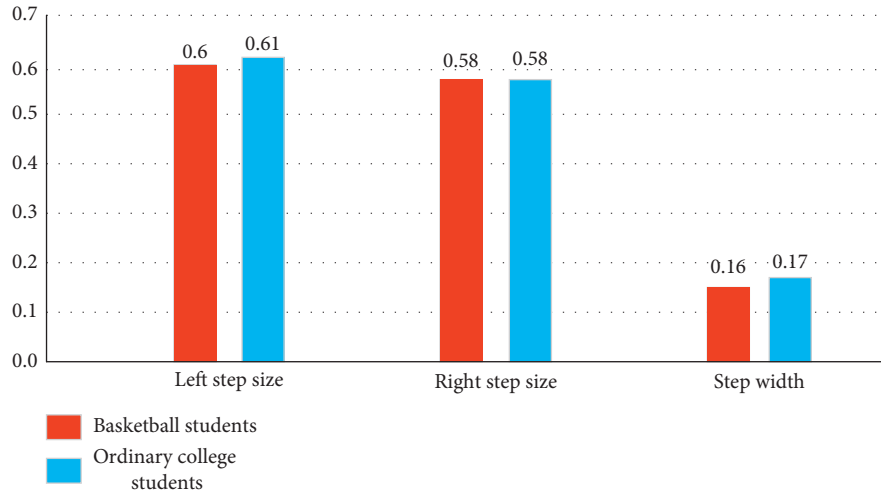


FIGURE 2: Step length and width of each group at 5 km/h (m).

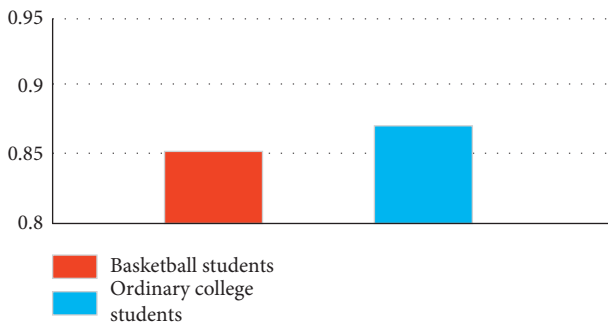


FIGURE 3: Gait cycle of each group at 5 km/h (seconds).

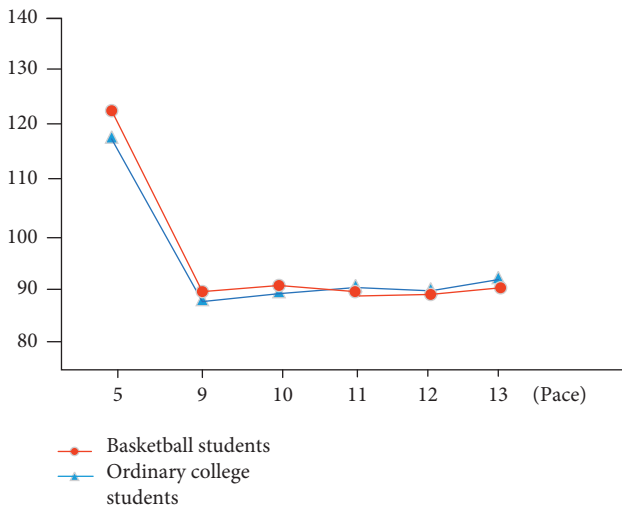


FIGURE 4: Changes in step frequency with speed in each group (times/minute).

5.3.3. *Impact of Basketball Exercise on the Physical Shape of College Students.* As can be seen from Table 5, before and after the basketball exercise, the muscle and bone weight of college students increased, the muscle volume increased, and the bone density and bone mass increased. Body mass index BMI: $18.5 < BMI < 23$ was within the normal range.

TABLE 3: Comparison of heart and lung function before and after basketball exercise (20 people).

Index	Front	Behind	P
Pulse (b/min)	80.84 ± 2.72	73.94 ± 2.10	<0.05
Diastolic pressure (kPa)	73.74 ± 2.29	67.05 ± 1.65	<0.05
Systolic pressure (kPa)	121.53 ± 2.68	116.89 ± 1.89	<0.05
Step index	57.17 ± 1.44	59.30 ± 1.37	<0.05
Vital capacity (ml)	4480.79 ± 134.65	4565.78 ± 127.96	<0.05
Spiro-index (ml/kg)	68.15 ± 2.48	69.40 ± 2.32	<0.05

TABLE 4: Comparison of various qualities before and after basketball exercise (20 people).

Index	Front	Behind	P
Shuttle run (s)	11.11 ± 0.16	10.54 ± 0.11	<0.05
Push-up (individual)	27.74 ± 2.60	30.21 ± 2.24	>0.05
Pull-up (individual)	3.74 ± 0.61	6.68 ± 1.34	<0.05
Grip (N)	50.39 ± 1.22	54.85 ± 1.29	<0.05
Bending (cm)	10.14 ± 1.07	10.21 ± 1.70	>0.05
Vertical jump (cm)	50.37 ± 1.98	56.10 ± 1.57	<0.05
Long jump (cm)	2.51 ± 0.04	2.61 ± 0.04	<0.05
50 meters (s)	7.50 ± 0.11	7.30 ± 0.11	<0.05
1000 meters (s)	3.97 ± 0.18	3.73 ± 0.17	>0.05

5.4. *The Influence of Basketball Exercise on Psychological Problems.* The results of Table 6 were obtained through the investigation:

Through the analysis of the results in Table 6 and Figure 5 above, we can see that the basketball exercise in machine learning has a positive impact on the mental health problems of college students, especially the differences in interpersonal relationships. It shows that the exercise of different intensities of basketball has a significant effect on improving the mental health level of college students. Through the basketball exercise activities, the physical quality and the mental health of college students have been

TABLE 5: Comparison of each circumference, skinfold thickness, and derived index before and after basketball exercise (20 people).

Index	Front	Behind	<i>P</i>
Stature (cm)	174.46 ± 1.37	175.26 ± 1.34	<0.05
Weight (kg)	67.13 ± 3.09	66.91 ± 2.90	>0.05
Bust (cm)	91.52 ± 1.85	89.84 ± 1.75	<0.05
Upper-arm circumference (cm)	30.60 ± 2.55	27.43 ± 0.64	>0.05
Waistline (cm)	76.94 ± 2.59	74.78 ± 2.10	<0.05
Hipline (cm)	93.49 ± 1.55	92.96 ± 1.46	>0.05
Thigh circumference (cm)	53.57 ± 1.35	53.48 ± 1.33	>0.05
Three humerus head (cm)	10.15 ± 1.34	9.27 ± 1.14	<0.05
Loin (cm)	13.30 ± 2.01	12.24 ± 1.88	<0.05
Belly (cm)	10.58 ± 1.40	9.66 ± 1.26	<0.05
BMI (kg/m ²)	21.97 ± 0.84	21.71 ± 0.79	<0.05
WHR	0.82 ± 0.016	0.80 ± 0.012	<0.05

TABLE 6: Comparison of student SCL-90 test results before and after basketball exercise.

	Before the experiment	After the experiment	<i>P</i>
Somatization	1.517 ± 0.407	1.489 ± 0.334	>0.05
Forced symptoms	1.719 ± 0.452	1.576 ± 0.487	<0.05
Interpersonal relation	1.699 ± 0.324	1.424 ± 0.289	<0.05
Depressed	1.531 ± 0.419	1.389 ± 0.392	<0.05
Anxious	1.395 ± 0.281	1.282 ± 0.269	<0.05
Hostile	1.282 ± 0.195	1.165 ± 0.264	<0.05
Terrifying	1.484 ± 0.262	1.416 ± 0.261	>0.05
Bigoted	1.197 ± 0.287	1.101 ± 0.236	<0.05
Psychiatric sex Add	1.208 ± 0.218	1.132 ± 0.212	<0.05
	1.412 ± 0.365	1.394 ± 0.313	>0.05

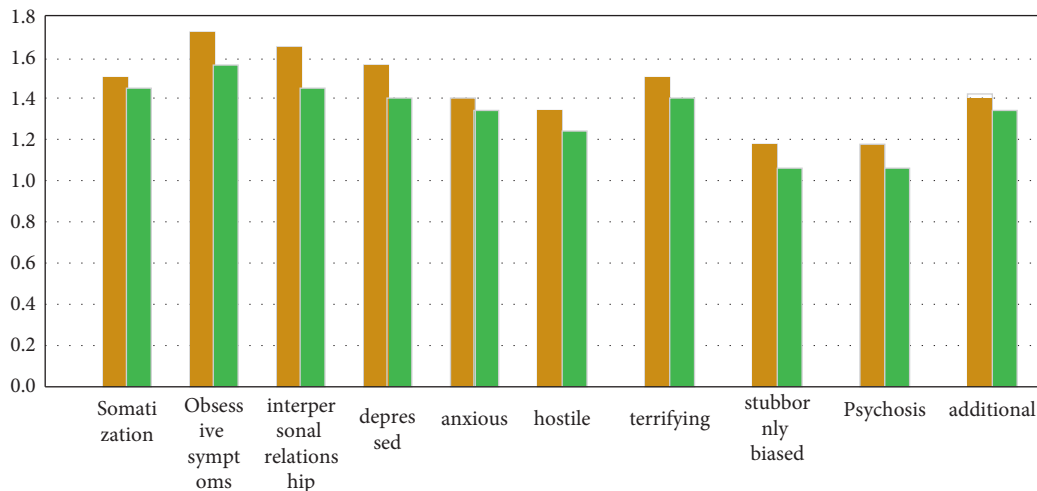


FIGURE 5: Comparison of SCL-90 test results of students before and after exercise.

improved. Using machine learning methods to achieve different degrees of basketball training intensity can indeed improve the mental health quality of college students [24].

6. Conclusion

In view of the impact of basketball exercise on the mental health of college students, the introduction of machine learning is preliminarily studied, but further research is still

needed. The application of machine learning technology methods, especially decision tree methods, has just started in the field of mental health research and faces many uncertainties and challenges, but it has broad application prospects.

- (1) Aiming at the forefront of machine learning development, we constantly introduce the latest machine learning technology methods. Taking the field of mental health research as the focus of research, we

can compare and analyze the characteristics of different basketball exercise intensity through simulation experiments, so as to further improve the ability of machine learning to judge and simulate the strength of basketball exercise.

- (2) In the face of the doubts in the field of traditional basketball education, to study the interpretability of deep learning. Based on domain knowledge, interpretable machine learning models should be established to promote the development of interdisciplinary research in the field of basketball sports education and mental health research.
- (3) For the basketball exercise fully reasonable use of machine learning technology and algorithm and exercise intensity of test and experiment, for the changes in mental health analysis, take the optimal scheme, not only can improve the students' sports and learning enthusiasm, but can also bring positive influence for college students' mental health.

Data Availability

The experimental data used to support the findings of this study are available from the author upon request.

Conflicts of Interest

The author declares that there are no conflicts of interest regarding this work.

References

- [1] S. He, *The Design and Implementation of the Mobile Emotion Analysis System Based on Machine Learning*, pp. 20–26, Xidian University, Xi'an, China, 2020.
- [2] Q. Hu, "Evaluation of different intensity physical exercise on improving the mental health and mental resilience of college students," *School Health in China*, vol. 40, no. 1, p. 3, 2019.
- [3] J. Insler, "The effects of recreational basketball on mood," *Dissertations & Theses - Gradworks*, vol. 13, no. 1, p. 2, 2013.
- [4] F. Zhu and J. Yan, "The impact of small and medium-sized intensity basketball exercise on the mental health of male college students," *China Organization Engineering Research*, vol. 10, no. 20, pp. 35–37, 2006.
- [5] X. Jia, T. Jin, and Q. Wang, "Machine learning and its application in the mental health field," *Journal of Ningbo University: Education Science Edition*, vol. 43, no. 4, p. 6, 2021.
- [6] K. Zheng, "On the influence of physical exercise on students' mental health and its mechanism," *China-ASEAN Expo*, vol. 280, no. 4, 2013.
- [7] C. Qi and Xu Pei, "Effects of physical exercise on students' mental health and its mechanism," *Journal of Wuhan University of Physical Education*, vol. 37, no. 5, p. 3, 2003.
- [8] F. S. Zhu and J. Yan, "Effects of basketball activity on self-esteem and mental health among male college students," *Chinese Journal of School Health*, pp. 30–42, 2006.
- [9] D. Wang, "The effects of basketball on students' social adaptation ability and mental health," *International Journal of Technology Management*, vol. 20, no. 2, p. 5, 2013.
- [10] Y. Ming, "Research on promotion of mental health of college students based on auxiliary idea of physical exercise," *Chinese Journal of School Health*, vol. 10, no. 3, p. 4, 2013.
- [11] C. L. Blakemore, H. G. Hilton, J. M. Harrison, T. L. Pellett, and J. Gresh, "Comparison of students taught basketball skills using mastery and nonmastery learning methods," *Journal of Teaching in Physical Education*, vol. 11, no. 3, pp. 235–247, 1992.
- [12] X. Z. Li, "Influence of different physical exercise item, intensity and time on anxiety, depression and self-concept of college students," *Chinese Journal of Clinical Rehabilitation*, vol. 10, no. 2, pp. 112–134, 2005.
- [13] C. Y. Chen, "An experimental study of influence of basketball exercise on mental health of male collegians," *Journal of Guangzhou Sport University*, vol. 2, no. 3, pp. 23–28, 2009.
- [14] L. I. Da-Peng, "The influence of physical exercise on the mental health of college students," *Bulletin of Sport Science & Technology*, vol. 4, no. 2, pp. 64–73, 2012.
- [15] L. I. Ke-Ke, "Discussion about mental health prescription of basketball activities for college students," *Journal of PLA Institute of Physical Education*, vol. 1, no. 2, pp. 7–12, 2003.
- [16] E. F. Che ha, T. P. Andriacchi, and J. Favre, "Speed, age, sex, and body mass index provide a rigorous basis for comparing the kinematic and kinetic profiles of the lower extremity during walking," *Journal of Biomechanics*, vol. 58, pp. 1–20, 2017.
- [17] A. Guzik, M. Druzicki, G. Przysada, M. Szczepanik, K. Bazarnik-Mucha, and A. Kwolek, "The use of the Gait Variability Index for the evaluation of individuals after a stroke," *Acta of Bioengineering and Biomechanics*, vol. 20, no. 2, pp. 171–177, 2018.
- [18] B. L. Arnold and R. J. Schmitz, "Examination of balance measures produced by the biodex stability system," *Athletic Training*, vol. 33, no. 4, pp. 23–327, 1998.
- [19] T. L. Heiden and D. G. Lloyd, "Timothy R. Ackland. Knee joint kinematics, kinetics and muscle co-contraction in knee osteoarthritis patient gait," *Clinical Biomechanics*, vol. 24, no. 10, pp. 143–151, 2009.
- [20] R. Ferber, L. R. Osternig, M. H. Woollacott, N. J. Wasielewski, and J.-H. Lee, "Gait mechanics in chronic ACL deficiency and subsequent repair," *Clinical Biomechanics*, vol. 17, no. 4, pp. 274–285, 2002.
- [21] M. Berchuck, T. P. Andriacchi, B. R. Bach, and B. Reider, "Gait adaptations by patients who have a deficient anterior cruciate ligament," *The Journal of Bone and Joint Surgery*, vol. 72, no. 6, pp. 871–877, 1990.
- [22] G. Wexler, D. E. Hurwitz, C. A. Bush-Joseph, T. P. Andriacchi, and B. R. Bach, "Functional gait adaptations in patients with anterior cruciate ligament deficiency over time," *Clinical Orthopaedics and Related Research*, vol. 348, pp. 166–175, 1998.
- [23] J. S. Day, D. J. Murdoch, and G. A. Dumas, "Calibration of position and angular data from a magnetic tracking device," *Journal of Biomechanics*, vol. 33, no. 8, pp. 1039–1045, 2000.
- [24] S. J. Preece, L. P. Kenney, M. J. Major, T. Dias, E. Lay, and B. T. Fernandes, "Automatic identification of gait events using an instrumented sock," *Journal of NeuroEngineering and Rehabilitation*, vol. 8, no. 1, p. 32, 2011.

Review Article

Review on Security Issues and Applications of Trust Mechanism in Wireless Sensor Networks

Zhengxin Xia ^{1,2}, Zhe Wei ³, and Huan Zhang ³

¹College of Continuing Education, Nanjing University of Posts and Telecommunications, Nanjing 210042, China

²Engineering Research Center of Medicine Information, Nanjing University of Posts and Telecommunications, Nanjing 210042, China

³School of Computer Science, Civil Aviation Flight University of China, Guanghan 618307, China

Correspondence should be addressed to Zhe Wei; findwei@foxmail.com

Received 13 July 2022; Revised 28 August 2022; Accepted 7 September 2022; Published 27 September 2022

Academic Editor: Le Sun

Copyright © 2022 Zhengxin Xia et al. This is an open access article distributed under the Creative Commons Attribution License, which permits unrestricted use, distribution, and reproduction in any medium, provided the original work is properly cited.

The scale of wireless sensor networks changes depending on specific application tasks. How to design a relatively simple security mechanism that can extend with the expansion of network scale is an arduous task. As the wireless sensor network mostly adopts the decentralized organization form, once the network nodes are distributed adequately, it is difficult to find out the failure of any node. In addition, the node has weak resistance to physical damage, so any node in the network may potentially become a cause of security vulnerability. In this study, firstly, the security standards that wireless sensor networks should have and the current security challenges faced by the network are discussed in detail, and the importance of security issues in wireless sensor networks is pointed out. Secondly, this paper studies and analyzes the current situation of wireless sensor network security problems including the internal and external attacks and the active and passive attacks. Thirdly, this paper also discusses the significance, concept, and characteristics of reputation and trust, the division and composition of reputation and trust system, and the common applications of the reputation and trust mechanism in wireless sensor networks.

1. Introduction

The objects processed by computer systems are mainly abstract things, and these systems do not have insight into the real physical world. Sensors are able to measure the physical quantities such as temperature, pressure, light wave, velocity, electromagnetic wave, and so on and convert the measurement results into electronic signals. Therefore, for computer systems or computable devices, sensors build a bridge from the abstract world to the real world so that the former can obtain almost all kinds of physical information in the real world. However, different from the traditional wired networks, wireless sensor networks, or WSNs, we usually do not need centralized management or fixed infrastructure such as base station and access point. Sensor nodes form the network automatically, and the network cost is relatively low. Therefore, WSNs can be used in situations where there

is no infrastructure, or for security reasons, the existing infrastructure does not meet certain conditions. Although WSNs are widely used, security and reliability should be the prerequisite for these applications.

In this study, firstly, the security standards that wireless sensor networks should have and the current security challenges are discussed in detail, and the importance of security issues in wireless sensor networks is pointed out. Besides, it is of vital importance to develop new security technologies or modify existing security technologies for wireless sensor networks because some traditional security technologies cannot run directly on the network nodes due to their relatively complex algorithms. Secondly, this paper studies and analyzes the current situation of wireless sensor network security problems including the internal and external attacks and the active and passive attacks. Thirdly, this paper also discusses the significance, concept, and

characteristics of reputation and trust, the division and composition of reputation and trust system, and the common applications of the reputation and trust mechanism in wireless sensor networks.

2. Security Standards and Challenges

In any computer-related environment, security is considered as a nonfunctional requirement, which is not only used to maintain the availability and reliability of the whole system but also related to the protection of information and system. However, in wireless sensor networks, security issues are particularly important because on the one hand, the hardware functions of network nodes are seriously limited, and it is necessary to provide sufficient protection to protect them from malicious attacks; on the other hand, the deployment environment of wireless sensor networks makes it easy for the enemy to obtain sensor nodes illegally and destroy them [1–4]. Any destruction and interference to nodes will have a certain impact on the information obtained in the real world. It is due to the above reasons that WSNs security objectives should have the following standards [5–8], which is shown in Figure 1.

Confidentiality. Confidentiality generally refers to that unauthorized users cannot obtain confidential or sensitive information, such as network routing information, topology information, and node geographic location information. In wireless sensor networks, confidentiality provides a basic security service for the important data transmitted between network nodes. Confidentiality also ensures that the nodes cannot be eavesdropped or tampered by the third party during data transmission. In the specific implementation process, confidentiality is generally achieved by the secret key mechanism; that is, data packets are encrypted at the sender and decrypted at the receiver. Without the relevant secret key, it is difficult for attackers to access the encrypted information. In addition, it should be pointed out that the data transmitted between nodes does not need to be encrypted. For example, only the data part in the packet is encrypted during data transmission, while in other applications, only the header of the packet is encrypted to protect the identity information of nodes.

Availability. Availability ensures that network services exist for authorized users; that is, when authorized users need to use some network services, these services exist and are available. In wireless sensor networks, on the one hand, data availability ensures that all nodes submit data to the base station on time, and whenever necessary, the whole network can provide relevant services. In addition, the availability also ensures that nodes are safe and available in the presence of certain attacks.

Integrity. Integrity makes the data in the whole path between the sender and the receiver without being

changed by the enemy [9]. In wireless sensor networks, the integrity of data is particularly important because the nodes are often exposed and unattended, and the communication channel between nodes is also open. Therefore, the transmitted data are easy to be interfered by the enemy channel making the integrity of the data changed.

Authentication. Authentication enables one party to ensure the legal identity of the other party with whom to communicate, that is, to ensure that the other party is not illegal or fake. In wireless sensor networks, authentication makes the sensing data obtained by the network to come from reliable information sources, and authentication also ensures the reliable identity of communication nodes in the network. In the actual operation of the network, each node should check whether the data it receives come from the real sender.

Data Freshness. Data freshness ensures that the sensing data sent by nodes in wireless sensor networks is up to date rather than out of date. Data freshness also ensures that the data sent by nodes to base stations can reflect the current situation. At the same time, data freshness can also be used to prevent malicious nodes from sending outdated and invalid information [10].

Forward and Backward Secrecy. Because nodes in the wireless sensor network have certain constraints on energy supply, some nodes will quit the network due to energy exhaustion after working for a certain period of time. At the same time, according to different application scenarios, there might be new nodes in the network. Therefore, it is necessary to prevent the exiting nodes from breaking the confidentiality of the network, and similarly, it is also necessary to prevent nodes that have just joined the network from cracking any previously used confidential information [11].

Access Control and Nonrepudiation. Only authorized users can access and use the resources and services provided by the network. Generally, the network should specify the member's permission or the permission group to which the member belongs in advance. Nonrepudiation means that the receiving node cannot deny the data packets it has received, and the sending node cannot deny the data packets it has sent.

The scale of wireless sensor networks will change depending on specific application tasks. How to design a relatively simple security mechanism that can extend with the expansion of network scale is an arduous task. In most cases, it is necessary to find a compromise between the network performance and the of security mechanism. As the wireless sensor network mostly adopts the decentralized organization form, once the network nodes are distributed adequately, it is difficult to monitor the actual working state of each node, and it is difficult to find out the failure of any node. In addition, the node has weak resistance to physical damage, so any node in the network may potentially become a cause of security vulnerability.

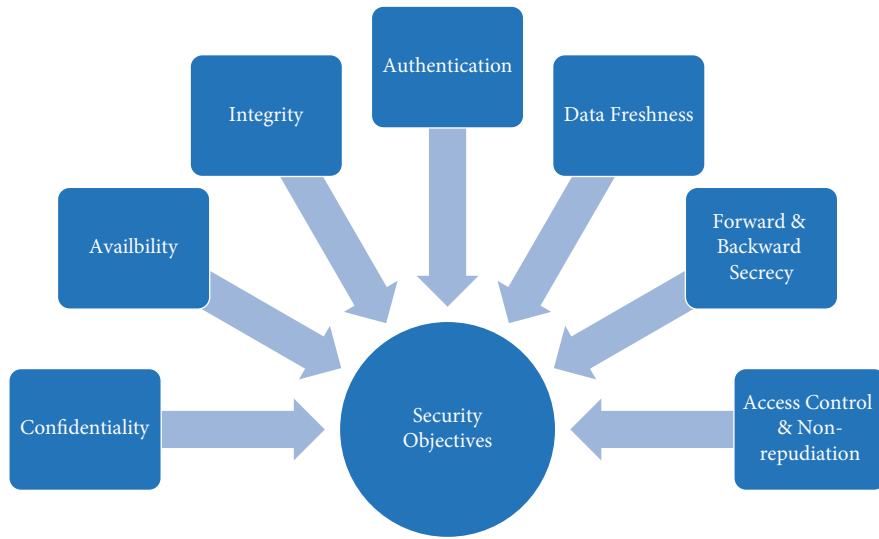


FIGURE 1: Security objectives of WSNs.

3. Internal/External and Passive/Active Attacks

In wireless sensor networks, due to the deployment environment and the limited hardware structure, sensor nodes are more vulnerable to the attacks. Wireless sensor network attacks can be divided into external attacks and internal attacks, and internal attacks are the main security risks of the network. This is because the malicious behavior of nodes in the network or network attacks launched by malicious nodes often disturbs and destroys the normal working nodes in the network. If these attacks are not prevented and handled, they will bring great harm to the whole network. In addition, network attacks can be further divided into active attacks and passive attacks, and active attacks are more harmful in ad hoc wireless sensor networks [12]. WSN attacks are shown in Figure 2.

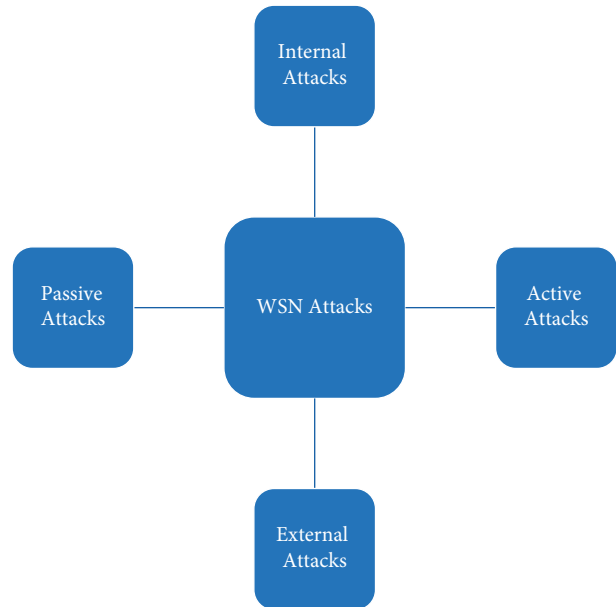


FIGURE 2: WSN attacks.

3.1. Internal Attacks and External Attacks. In wireless sensor networks, all nodes are cooperative entities. External attackers are isolated from the network and have no access to the network. Generally, the impact of attacks launched by external attackers on the network is limited, but once the attacker captures the internal nodes of the network and destroys them, such as programming the captured nodes again to execute malicious programs or using nodes with more computing and storage capabilities to replace the captured nodes, the attacks become internal attacks. In contrast, the internal attack is more destructive to the network because the internal nodes are often regarded as legitimate nodes. Internal attacks are more difficult to detect and prevent; for example, the captured nodes can steal confidential information from encrypted data, transfer false information, and modify routing data.

3.2. Passive Attacks and Active Attacks. In passive attacks, the attacker’s purpose is to eavesdrop on the flowing information in the network without being detected by the system. Through

passive participation in network internal activities, attackers can also obtain a large number of data and conduct data analysis to extract key information. However, due to the lack of clues left by passive attackers, it is difficult to be found.

In active attacks, the attacker can make use of the security loopholes in the network protocol to launch a variety of attacks, such as modifying and deleting the data packets in the routing to make the routing protocol unreliable; for example, in the replay attack, the attacker will maliciously resend the valid routing data packets sent before. The direct result is that the data packets are sent to the wrong destination or make invalid loops in the network, which will eventually lead to network congestion.

Further, a successful active attack by an attacker will seriously damage the function of the network and cause the system to make a wrong judgment and decision. In addition,

the more serious threat comes from the physical accessibility of nodes in ad wireless sensor networks. After the attacker locates the sensor node through the communication information, it captures the node and then obtains the key information and other encrypted contents of the captured node through a certain way. Once the attacker succeeds, the attacker can use the encrypted information to monitor the network or inject illegal information into the network. In addition, malicious nodes will also take the way of impersonating legitimate nodes for active attacks. However, different from passive attacks, since the attacker actively participates in the internal activities of the network, there will be signs of malicious attacks in the network.

Stealthy attack is the most common active attack in the data fusion of wireless sensor networks. Its purpose is to inject false data into the data fusion process and ultimately change the decision of base station nodes. In ad hoc wireless sensor networks, decision-making is usually based on all the data collected by nodes, so once there is false data injection, the whole decision-making result may be changed [13]. In response to stealthy attack, Ref. [14] uses eyewitness nodes to ensure that all fusion data are valid, while in Ref. [15], statistical methods are used to test the effectiveness of the fusion data.

4. Trust Mechanism

4.1. Concept and Definition. In social science, trust can be understood as follows [16–19]: in social networks, trust refers to the behavior that one party voluntarily relies on the other party in a special environment; trust can also be understood as an intention, i.e., one party intentionally relies on the other party.

In the field of computer science, for example, in a routing information request task, the former is the trustor and the latter is the trusted party. When the routing information is successfully transmitted, it is considered to be a node with good behavior, and then its trust value will be increased; on the contrary, when providing wrong routing information, a node is considered as a malicious node, and the corresponding reduced reputation value is applied as a punishment method. In this mechanism, trust is undoubtedly a double-edged sword. On the one hand, it will consume some resources of the system, and on the other hand, it will greatly improve the security of the system.

4.2. Division and Composition of Trust. According to the storage and access of reputation information, the reputation and trust system can be divided into centralized system and decentralized/distributed system. Large e-commerce websites such as Amazon mostly adopt the centralized reputation system and store reputation data in the database associated with websites [20]. For wireless sensor networks, although the centralized reputation system has certain advantages, due to the special structure of network and network nodes, the network system often adopts the decentralized reputation system. In wireless sensor networks, the reputation and trust mechanism has the following characteristics:

- (1) The mechanism of reputation and trust provides incentives for the benign development of node behavior; that is, it makes nodes more responsible for their own behavior
- (2) The reputation and trust mechanism provides the prediction of the future behavior of nodes, which can assist in decision-making;
- (3) The reputation and trust mechanism makes the nodes with good behavior avoid cooperating with the nodes that lack trust. The malicious behavior of nodes leads to the low reputation of nodes themselves, which also makes such nodes have no more opportunities to participate in network cooperation;
- (4) The reputation and trust mechanism is also conducive to the detection of selfish nodes in the network and timely isolation of malicious nodes in the network.

5. Common Applications of Trust

Reputation and trust mechanisms have been widely studied and applied in distributed systems such as ad hoc networks, P2P networks, grid computing, pervasive computing, and e-commerce. In wireless sensor networks, the reputation and trust mechanism can be combined with other network function algorithms to provide better guarantee and service for the network. Specifically, the reputation and trust mechanism can be applied to the following aspects of wireless sensor networks:

5.1. Trusted Data Fusion. In order to ensure the reliability and credibility of data fusion in wireless sensor networks, studies in Refs. [21–33] introduced the reputation mechanism into the network data fusion scheme. In order to deal with the potential malicious nodes in the process of data fusion, combined with reputation management and encryption technology, Ref. [21] proposed a trust-based security data fusion method named blind observation. By adapting the order preserved encryption technology and the sigmoid trust model, the blind observation method can distinguish malicious nodes without decrypting the data sent to the base station and checking the data inside. The security and reliability of data fusion can be ensured by this method. However, in ad hoc wireless sensor networks, the captured or attacked nodes still hold network encrypted information, which is not discussed in Ref. [21].

In order to improve the security of data fusion, Ref. [23] proposed a trust-based intranetwork data fusion method. This method uses the tree data fusion structure and a reputation model based on binomial distribution to detect malicious behavior of nodes. In Ref. [23], the reputation measurement of a node is evaluated by the data it sends, its routing behavior, and its availability. In order to achieve the purpose of reliable data fusion, network nodes only send data to the data fusion nodes whose credibility is higher than the specified threshold value for fusion operation. Although this method may provide security for data fusion, it does not discuss whether the qualified data fusion nodes can rotate to

balance the energy distribution of nodes. In addition to using the tree data fusion structure, Refs. [24, 25] also use the cluster structure. In Ref. [25], the data from the node are weighted according to the reputation of the corresponding node, and the common node selects the fusion point according to the reputation of the data fusion node.

To obtain high quality sensory data, Ref. [28] proposed an energy efficient data fusion method ETA based on the binomial reputation model. ETA adopts the cluster node topology structure and uses the reputation mechanism to select the nodes that meet the requirements as data fusion nodes. In addition, in order to find the best path from ordinary nodes to data fusion nodes, ETA also takes into account the residual energy of nodes on the path and the availability of links. In this method, each node maintains two reputation tables: the reputation table about the link availability of the neighbor node and the reputation table about the data fusion ability of the neighbor node. ETA assumes that the location of each node and base station are known in advance and that there is no malicious node injecting false data in the network. But ETA also has the following problems: each node in the cluster must send its data to the upstream node designated by the base station node, which will increase the complexity of the network; to determine the availability of the link between nodes, each node must send data to its neighbor nodes, which will bring extra cost to the network.

RDAs [22] improve the robustness of data fusion by using the reputation mechanism to identify and isolate malicious nodes in the wireless sensor network data fusion algorithm. The nodes in RDAs adopt the cluster structure and distributed-reputation mechanism. Each node keeps the reputation information of other nodes in the cluster locally and shares the reputation information with other nodes in the cluster. RDAs use LEACH as the underlying data fusion protocol and use the reputation model based on binomial distribution as the node reputation evaluation method.

To ensure the reliability and credibility of data transmitted in WSNs, Ref. [29] proposes a trust evaluation model and data fusion mechanism, which is composed of behavioral trust, data trust, and historical trust. The data trust can be obtained by processing the sensor data, and according to the sensing and forwarding behavior of nodes, the behavior trust is computed. Reference [30] proposes a data fusion and transfer learning empowered granular trust mechanism to handle the data reliability. In order to prevent privacy disclosure and task destruction, a dynamic reward and punishment mechanism is designed to encourage honest users and accurately assess user trust. Reference [31] introduces a data fusion trust model based on rational attributes. It relies on different time attributes to identify the trust of available services, and deep machine learning is used to recursively analyze the attributes and uncertainty characteristics of service providers in continuous shared instances to fuse data with less uncertainty. Reference [32] proposes a trust fusion method consistent with the consortium chain to reach consensus and complete self-organized trust decentralized collaborative learning. In this method, consensus candidates will check others' trust level

to ensure that they tend to integrate consensus with users with high trust. Reference [33] proposes a lightweight privacy protection trust evaluation scheme, which can fully balance trust evaluation and privacy protection under low cost so as to facilitate distributed data fusion.

5.2. Trusted Routing. In wireless sensor networks, all nodes are not only the sender of data sets but also the routing and transmission of data from third-party nodes. Therefore, how to route data to the destination through the reliable transmission path becomes one of the key problems in the design and operation of wireless sensor networks when some nodes in the network behave abnormally and violate the specified standards.

Most routing protocols in wireless sensor networks only consider how to maintain the path connectivity between the source node and the destination node and use methods such as the shortest path or minimum spanning tree to construct the data path. However, the above methods rarely consider whether the intermediate nodes involved in the path will cooperate with other nodes to complete the routing and transmission of data packets. Therefore, it is reasonable to think that some intermediate nodes for their own interests (such as legitimate nodes do not respond to the route to save their energy and illegal nodes tamper with data or selectively discard packets) do not complete the routing or packet delivery task according to the protocol. If the routing protocol in wireless sensor network does not have a method to identify selfish behavior or malicious behavior of nodes, the established path may contain the above two kinds of nodes. Therefore, the path may be unstable, the reliability and integrity of data transmission cannot be guaranteed, and the efficiency of the whole network is also low [34].

In order to improve the reliability and security of routing protocols in wireless sensor networks and protect the network from the influence of abnormal behaviors of nodes, the reputation system is combined with the routing protocols of wireless sensor networks in Ref. [34], and the abnormal behaviors of nodes are divided into two categories: selfish behaviors and malicious behaviors. Different processing methods are adopted according to different abnormal behaviors of nodes, the reputation mechanism based on Bayesian theory is combined into the network routing protocol, and the reliability of each node is evaluated according to the data packet delivery. Finally, the reliable data routing path is established according to the reliability of the node.

According to the observation results of data transmission behavior of nodes, Ref. [34] divides sensor nodes into three categories: friendly, selfish, and malicious. The friendly node will submit the received data packets as they are to ensure the integrity of the submitted data; selfish nodes will randomly discard all or part of the data packets due to their own physical conditions, such as lack of power supply energy, overload, and other reasons, so as to maintain their own physical conditions, and selfish nodes will undoubtedly reduce the reliability of the network; the security and integrity of the network system are often reduced by malicious

nodes modifying the contents of the received data packets or deliberately routing the data packets to the wrong receivers.

Reference [35] proposes a trust model based on node behavior to deal with malicious nodes in opportunistic routing and forwarding candidate set. By using pruning and filtering mechanisms, it deletes malicious suggestions and uses dynamic weight calculation method to combine direct trust and indirect trust to get the comprehensive trust. In order to resist attacks such as black hole and selective forwarding, Ref. [36] proposes a trust aware secure routing protocol to resist these attacks, in which each node calculates the comprehensive trust value of its neighbors based on the direct trust, the indirect trust, the volatility factor, and the residual energy. Reference [37] proposes an atomic search sunflower optimization method to provide trust based routing. The method is designed by combining sunflower optimization with atomic search optimization and uses multiple trust factors to identify and isolate attacks and optimize network performance. By using the Markov chain prediction model, Ref. [38] proposes a reliability trust evaluation model for secure routing based on the combination of internal states of nodes and external interaction between nodes. By selecting security nodes based on tolerance constants and selecting opportunity nodes from security nodes for routing, Ref. [39] proposes a routing algorithm based on energy aware trust and opportunity, which uses multipath routing technology with the multihop communication mechanism within and between clusters.

5.3. Malicious Node Detection. The security threats of wireless sensor networks come not only from external attacks but also from internal attacks of internal nodes. Although traditional security mechanisms such as the encryption mechanism and the authentication mechanism can prevent some external attacks, these security mechanisms are not so effective for attacks launched by internal nodes with abnormal behavior. Reference [40] proposed a malicious node detection mechanism based on the reputation mechanism. This method adopts the reputation model of Bayesian statistical inference and adds the indirect reputation recommendation from the third party. In Ref. [41], the behavior of malicious nodes modifying data packets was identified by every node monitoring each other. By analyzing the signal strength of data readings received by the physical layer of wireless sensor network nodes, Ref. [42] identifies and prevents malicious nodes that send noise to the network and cause channel conflict. Based on the binomial reputation model, Ref. [43] proposed a location aware method for malicious node isolation and deletion in wireless sensor networks.

In addition, in order to effectively isolate malicious nodes, Ref. [44] introduces the reputation system into the routing protocol. Its basic principle is that any node in the network uses a certain mechanism to monitor its neighbors and evaluates its trust value according to the behavior of the monitored node; when the reputation value of a neighbor node is less than the defined threshold value, the neighbor node will be considered as a suspicious node. In this

algorithm, the change of trust value of neighbor nodes only depends on the observer node. Each observer node shares its suspicious node information, so the noncooperative node will be punished soon. However, this method cannot identify the cheating behavior of malicious nodes. It is only a theoretical framework, and no specific and effective reputation evaluation method is given.

To avoid being judged as a malicious node by the reputation system when the reputation value is lower than the predefined reputation threshold value, and finally isolated by the system, some malicious nodes will attack intermittently and maintain good behavior in the period of not launching the attack so as to obtain a good reputation so that their reputation is generally higher than the reputation threshold. In order to solve the above problems, Ref. [45] proposed a malicious node identification method based on node reputation and time series analysis. In this method, malicious suspected nodes with the above characteristics are defined as subaggressiveness nodes. However, this method does not mention which specific reputation model to select nor does it discuss how to combine with the specific reputation model and gives the corresponding test results. It also does not present the specific method of selecting standard time series parameters.

Reference [46] proposes a malicious node detection method based on online learning algorithm. This method first calculates the credibility of each path in the network according to the collected data packets, then models the path reputation obtained through online learning algorithm, and calculates the trust of each node, and detects malicious nodes through the clustering algorithm. The collaboration-based malicious detection mechanism proposed by Ref. [47] includes a data trust module and a reputation calculation module, which ensures honest data communication and reduces the false positive rate of malicious nodes. Reference [48] proposes an effective malicious node detection scheme based on weighted trust, which can detect malicious nodes in clustered wireless sensor networks. By considering the false positive and false negative examples, the node behavior can be truly handled. Reference [49] proposes a method called perceptron based detection, which uses perceptron and K-means method to calculate the trust value of nodes and detect malicious nodes accordingly, and by optimizing the network routing, the detection accuracy is further improved. Reference [50] proposes a blockchain trust model for malicious node detection in wireless sensor networks. It uses the blockchain smart contract, the quadrilateral measurement and the positioning method of wireless sensor network to realize the detection of malicious nodes in the three-dimensional space.

Some common applications of trust are shown in Table 1.

As the sociologist Niklas Luhmann said, "Trust and integrity are necessary in our life, it makes the various components of society integrate into one." Reputation and trust are playing an increasingly important role in human society. In addition, in multiagent systems, due to the uncertainty of agent behavior and in order to protect well-behaved entities from malicious entities, reputation and

TABLE 1: Common applications of trust.

Representative references	Trust data fusion	Trusted routing	Malicious node detection
[21]	×		
[22]	×		
[23]	×		
[24]	×		
[25]	×		
[26]	×		
[27]	×		
[28]	×		
[29]	×		
[30]	×		
[31]	×		
[32]	×		
[33]	×		
[34]		×	
[35]		×	
[36]		×	
[37]		×	
[38]		×	
[39]		×	
[40]			×
[41]			×
[42]			×
[43]			×
[44]			×
[45]			×
[46]			×
[47]			×
[48]			×
[49]			×
[50]			×

trust mechanism have been widely adopted and used as a social method [51]. However, the reputation and trust mechanism cannot be simply attributed to security issues. Security is used to prevent an entity from foreign invasion, ensure that another entity is designated with the entity, ensure that the sender and receiver of the message are designated entities, and prevent information from being illegally obtained by other entities. In contrast, reputation and trust are complex and diversified issues. Reputation and trust not only play a role in decision-making but also provide powerful tools for the establishment of relationships among entities in the insecure real world [43]. The reputation and trust mechanism has become an important supplementary tool for many types of network security solutions.

6. Conclusions

Due to the lack of infrastructure, wireless sensor networks are vulnerable to a variety of attacks. Without adequate security and physical protection, the number and types of applications of wireless sensor networks will be greatly reduced. Therefore, the security problems of wireless sensor networks need to be solved. As an effective supplement to the traditional security mechanism, the reputation and trust mechanism has attracted the attention of scholars and gradually introduced into ad hoc wireless sensor networks. Nowadays, it has obtained extensive theoretical research and application research, such as the selection of trusted routing

path, malicious node identification, and so on. The reputation and trust mechanism can effectively encourage nodes to cooperate and take certain measures to punish malicious behavior of nodes, which not only improves the performance of the network but also enhances the security of the network. In this paper, the security standards and security challenges in wireless sensor networks are discussed in detail. In addition, this paper also discusses the background, significance, concept, and characteristics of reputation and trust, the division and composition of reputation system, and the common applications of reputation and trust mechanism in wireless sensor networks.

Data Availability

The data used to support the findings of this study are available from the corresponding author upon request.

Conflicts of Interest

The authors declare that there are no conflicts of interest regarding the publication of this paper.

Acknowledgments

The authors would like to express their gratitude to the support and help from the Civil Aviation Information Technology Research Center of CAFUC. This work was partially supported by the Scientific Project of CAFUC

under grant nos. JG2022-06 and J2022-042, Civil Aviation Professional Project under grant nos. 0252109 and MHJY2022038, Sichuan Education Reform Project under grant no. JG2021-521, Central University Education Reform Project under grant no. E2022078, and Sichuan Science and Technology Program under grant nos. 2022YFG0190 and 2022JDR0116.

References

- [1] J. Lopez, R. Roman, and C. Alcaraz, "Analysis of security threats, requirement, technologies and standards in wireless sensor networks," in *Foundation of Security Analysis and Design V*, pp. 289–228, Springer, Berlin, Germany, 2009.
- [2] J. Li, L. Yu, J. Zhao, C. Luo, and J. Zheng, "TSTE: a time-variant stochastic trust evaluation model in social networks," *KSII Transactions on Internet and Information Systems*, vol. 11, no. 6, pp. 3273–3308, 2017.
- [3] N. Battat, A. Makhoul, H. Kheddouci, S. Medjahed, and N. Aitouazzoug, "Trust based monitoring approach for mobile ad hoc networks," in *Ad-Hoc, Mobile, and Wireless Networks*, pp. 55–62, Springer, Cham, Switzerland, 2017.
- [4] X. Wu, "A robust and adaptive trust management system for guaranteeing the availability in the internet of things environments," *KSII Transactions on Internet and Information Systems*, vol. 12, no. 5, pp. 2396–2413, 2018.
- [5] J. Peng, H. Zhou, Q. Meng, and J. Yang, "Big data security access control algorithm based on memory index acceleration in WSNs," *Journal on Wireless Communications and Networking*, vol. 2020, no. 1, 2020.
- [6] J. Y. Yu, E. Lee, S. R. Oh, Y. D. Seo, and Y. G. Kim, "A survey on security requirements for WSNs: focusing on the characteristics related to security," *IEEE Access*, vol. 8, pp. 45304–45324, 2020.
- [7] C. Huang, M. Ma, X. Liu, A. Liu, and Z. Zuo, "Unequal probability marking approach to enhance security of trace-back scheme in tree-based WSNs," *Sensors*, vol. 17, no. 6, p. 1418, 2017.
- [8] M. S. Abdalzaher and O. Muta, "Employing game theory and TDMA protocol to enhance security and manage power consumption in WSNs-based cognitive radio," *IEEE Access*, vol. 7, pp. 132923–132936, 2019.
- [9] A. D. Wood and J. A. Stankovic, "Denial of service in sensor networks," *Computer*, vol. 35, no. 10, pp. 54–62, 2002.
- [10] A. A. Pirzada and C. McDonald, "Establishing trust in pure ad-hoc networks," in *Proceedings of the 27th Australasian Conference on Computer Science*, vol. 26, pp. 47–54, Dunedin, New Zealand, January, 2004.
- [11] E. C. H. Ngai and M. R. Lyu, "Trust and clustering based authentication services in mobile ad hoc networks," in *Proceedings of the 24th International Conference on Distributed Computing Systems Workshops*, pp. 582–587, Tokyo, Japan, March, 2004.
- [12] Y. Zhou, Y. Fang, and Y. Zhang, "Securing wireless sensor networks: a survey," *IEEE Communications Surveys & Tutorials*, vol. 10, no. 3, pp. 6–28, 2008.
- [13] Z. Wei, S. Yu, and W. Ma, "Defending against internal attacks in healthcare-based WSNs," *Journal of Healthcare Engineering*, vol. 202110 pages, Article ID 2081246, 2021.
- [14] Y. Yang, X. Wang, S. Zhu, and G. Cao, "SDAP: a secure hop-by-hop data aggregation protocol for sensor networks," *ACM Transactions on Information and System Security*, vol. 11, no. 4, pp. 1–43, 2008.
- [15] H. Chan, A. Perrig, B. Przydatek, and D. Song, "SIA: secure information aggregation in sensor networks," *Journal of Computer Security*, vol. 15, no. 1, pp. 69–102, 2007.
- [16] J. Cheng, J. Li, N. Xiong, M. Chen, H. Guo, and X. Yao, "Lightweight mobile clients privacy protection using trusted execution environments for blockchain," *Computers, Materials & Continua*, vol. 65, no. 3, pp. 2247–2262, 2020.
- [17] S. Kaur and V. K. Joshi, "Hybrid soft computing technique based trust evaluation protocol for wireless sensor networks," *Intelligent Automation & Soft Computing*, vol. 26, no. 2, pp. 217–226, 2020.
- [18] L. Sun, Q. Yu, D. Peng, S. Subramani, and X. Wang, "Fogmed: a fog-based framework for disease prognosis based medical sensor data streams," *Computers, Materials & Continua*, vol. 66, no. 1, pp. 603–619, 2020.
- [19] Y. L. Sun, Z. Han, W. Yu, and K. J. R. Liu, "A trust evaluation framework in distributed networks: vulnerability analysis and defense against attacks," in *Proceedings of the 25TH IEEE International Conference on Computer Communications*, pp. 1–13, Rennes, France, April, 2006.
- [20] C. Jia, L. Xie, X. Gan, W. Liu, and Z. Han, "A trust and reputation model considering overall peer consulting distribution," *IEEE Transactions on Systems, Man, and Cybernetics - Part A: Systems and Humans*, vol. 42, no. 1, pp. 164–177, 2012.
- [21] N. Poolsappasit, M. Busby, and S. K. Madria, "Trust management of encrypted data aggregation in a sensor network environment," in *Proceedings of the IEEE 13th International Conference on Mobile Data Management*, pp. 157–166, Bengaluru, India, November, 2012.
- [22] C. R. Perez-Toro, R. K. Panta, and S. Bagchi, "RDAS: reputation-based resilient data aggregation in sensor network," in *Proceedings of the 7th Annual IEEE Communications Society Conference on Sensor, Mesh and Ad Hoc Communications and Networks*, pp. 1–9, Boston, MA, USA, July, 2010.
- [23] H. Feng, G. Li, W. Lu, and L. Huang, "Trust based secure in-network data processing schema in wireless sensor networks," *Journal of Networks*, vol. 6, no. 2, pp. 295–302, 2011.
- [24] Y. Ni, L. Tian, and X. Shen, "The research of dynamic data fusion based-on node behavior trust for WSNs," in *Proceedings of the International Conference on Computer Design and Applications*, pp. 534–538, Qinhuangdao, China, June, 2010.
- [25] G. P. Gupta, M. Misra, and K. Garg, "Energy and trust aware mobile agent migration protocol for data aggregation in wireless sensor networks," *Journal of Network and Computer Applications*, vol. 41, pp. 300–311, 2014.
- [26] H. Alzaid, E. Foo, and J. G. Nieto, "RSDA: reputation-based secure data aggregation in wireless sensor networks," in *Proceedings of the 9th International Conference on Parallel and Distributed Computing, Applications and Technologies*, pp. 419–424, Dunedin, New Zealand, December 2008.
- [27] C. Liu, Y. Liu, and Z. Zhang, "Improved reliable trust-based and energy-efficient data fusion for wireless sensor networks," *International Journal of Distributed Sensor Networks*, vol. 9, no. 5, pp. 1–11, 2013.
- [28] Z. Taghikhaki, N. Meratnia, and P. J. M. Havinga, "Energy-efficient Trust-based aggregation in wireless sensor networks," in *Proceedings of the IEEE Conference on Computer Communications Workshops*, pp. 584–589, Shanghai, China, April 2011.
- [29] Z. Chen, L. Tian, and C. Lin, "Trust model of wireless sensor networks and its application in data fusion," *Sensors*, vol. 17, no. 4, p. 703, 2017.

- [30] H. Lin, S. Garg, J. Hu, X. Wang, M. J. Piran, and M. S. Hossain, "Data fusion and transfer learning empowered granular trust evaluation for Internet of Things," *Information Fusion*, vol. 78, pp. 149–157, 2022.
- [31] S. Baskar, R. Selvaraj, V. M. Kuthadi, and P. M. Shakeel, "Attribute-based data fusion for designing a rational trust model for improving the service reliability of internet of things assisted applications in smart cities," *Soft Computing*, vol. 25, no. 18, pp. 12275–12289, 2021.
- [32] K. Wang, C. M. Chen, Z. Liang et al., "A trusted consensus fusion scheme for decentralized collaborated learning in massive IoT domain," *Information Fusion*, vol. 72, pp. 100–109, 2021.
- [33] Z. Liu, J. Ma, J. Weng et al., "LPTE: a lightweight privacy-preserving trust evaluation scheme for facilitating distributed data fusion in cooperative vehicular safety applications," *Information Fusion*, vol. 73, pp. 144–156, 2021.
- [34] L. Yang, J. M. Kizza, A. Cemerlic, and F. Liu, "Fine-grained reputation-based routing in wireless ad hoc networks," in *Proceedings of the IEEE Intelligence and Security Informatics*, pp. 75–78, New Brunswick, NJ, USA, May, 2007.
- [35] B. Su, C. Du, and J. Huan, "Trusted opportunistic routing based on node trust model," *IEEE Access*, vol. 8, pp. 163077–163090, 2020.
- [36] H. Hu, Y. Han, H. Wang, M. Yao, and C. Wang, "Trust-aware secure routing protocol for wireless sensor networks," *ETRI Journal*, vol. 43, no. 4, pp. 674–683, 2021.
- [37] P. P. Jadhav and S. D. Joshi, "Atom search sunflower optimization for trust-based routing in internet of things," *Int J Numer Model*, vol. 34, no. 3, Article ID e2845, 2021.
- [38] L. Gong, C. Wang, H. Yang, Z. Li, and Z. Zhao, "Fine-grained trust-based routing algorithm for wireless sensor networks," *Mobile Networks and Applications*, vol. 26, no. 6, pp. 2515–2524, 2021.
- [39] M. Hajiee, M. Fartash, and N. Osati Eraghi, "An energy-aware trust and opportunity based routing algorithm in wireless sensor networks using multipath routes technique," *Neural Processing Letters*, vol. 53, no. 4, pp. 2829–2852, 2021.
- [40] G. Yin, G. Yang, Y. Wu, X. Yu, and D. Zuo, "A novel reputation model for malicious node detection in wireless sensor network," in *Proceedings of the 4th International Conference on Wireless Communications, Networking and Mobile Computing*, pp. 1–4, Dalian, China, October 2008.
- [41] K. F. Ssu, C. H. Chou, and L. W. Cheng, "Using overhearing technique to detect malicious packet modifying attacks in wireless sensor networks," *Computer Communications*, vol. 30, no. 11–12, pp. 2342–2352, 2007.
- [42] P. Reindl, K. Nygard, and X. Du, "Defending malicious collision attacks in wireless sensor networks," in *Proceedings of the IEEE/IFIP International Conference on Embedded and Ubiquitous Computing*, pp. 771–776, Washington, DC, December, 2010.
- [43] G. V. Crosby, L. Hester, and N. Pissinou, "Location-aware, trust-based detection and isolation of compromised nodes in wireless sensor networks," *International Journal on Network Security*, vol. 12, no. 2, pp. 107–117, 2009.
- [44] S. Buchegger and J. Boudec, "Performance analysis of the CONFIDANT protocol," in *Proceedings of the 3rd ACM International Symposium on Mobile Ad Hoc Networking & Computing*, pp. 226–236, Lausanne, Switzerland, June, 2002.
- [45] i, L. Dan, Z. Jianyi, L. Hongwei, Z. Hongliang, and X. Yang, "Malicious node detection in wireless sensor networks using time series analysis on node reputation," *Journal of Convergence Information Technology*, vol. 7, no. 15, pp. 8–16, 2012.
- [46] B. Li, R. Ye, G. Gu, R. Liang, W. Liu, and K. Cai, "A detection mechanism on malicious nodes in IoT," *Computer Communications*, vol. 151, pp. 51–59, 2020.
- [47] S. Sultan, Q. Javaid, A. J. Malik, F. Al-Turjman, and M. Attique, "Collaborative-trust approach toward malicious node detection in vehicular ad hoc networks," *Environment, Development and Sustainability*, vol. 24, no. 6, pp. 7532–7550, 2022.
- [48] F. Zawaideh and M. Salamah, "An efficient weighted trust-based malicious node detection scheme for wireless sensor networks," *International Journal of Communication Systems*, vol. 32, no. 3, Article ID e3878, 2019.
- [49] L. Liu, Z. Ma, and W. Meng, "Detection of multiple-mix-attack malicious nodes using perceptron-based trust in IoT networks," *Future Generation Computer Systems*, vol. 101, pp. 865–879, 2019.
- [50] W. She, Q. Liu, Z. Tian, J. S. Chen, B. Wang, and W. Liu, "Blockchain trust model for malicious node detection in wireless sensor networks," *IEEE Access*, vol. 7, pp. 38947–38956, 2019.
- [51] I. Pinyol and J. Sabater-Mir, "Computational trust and reputation models for open multi-agent systems: a review," *Artificial Intelligence Review*, vol. 40, pp. 1–25, 2013.

Research Article

Design of Cross-Platform Information Retrieval System of Library Based on Digital Twins

Shanshan Shang ¹, Zikai Yu,² Kun Jiao,¹ Yingshi Huang,¹ Hua Guo,¹ and Guozhong Wang³

¹Library, Shanghai University of Engineering Science, Shanghai 201620, China

²Assembly Department, Shanghai Aerospace Equipments Manufacturer, Co., Ltd., Shanghai 200245, China

³Institute of Artificial Intelligence Industry, Shanghai University of Engineering Science, Shanghai 201620, China

Correspondence should be addressed to Shanshan Shang; 91130001@sues.edu.cn

Received 14 July 2022; Revised 8 August 2022; Accepted 13 August 2022; Published 27 September 2022

Academic Editor: Le Sun

Copyright © 2022 Shanshan Shang et al. This is an open access article distributed under the Creative Commons Attribution License, which permits unrestricted use, distribution, and reproduction in any medium, provided the original work is properly cited.

In order to improve the library's ability of cross-platform information retrieval and data scheduling and distribution, a library cross-platform information retrieval system based on digital twin technology is designed. Using data warehouse decision support and data source structured query methods, the spectral characteristics of Library cross-platform information resources are extracted. Using the method of Hadoop data parallel loading, the library cross-platform operation data is divided into decision-making data, computing resource pool data, and Hadoop parallel loading data. A library cross-platform information digital twin parallel retrieval and information fusion feature matching model is established, and the retrieval channels are allocated through multiple complex and balanced task scheduling sequences. According to the queue configuration model of Library cross-platform information retrieval, the optimization design of Library cross-platform information retrieval system is realized. The simulation test results show that the designed system has good recall ability of cross-platform information retrieval data, and improves the utilization rate of cross-platform resources and the dynamic scheduling ability of online resources.

1. Introduction

The design of Library cross-platform information retrieval system is based on the analysis of cloud data quality of service (QoS) [1], combined with the load parameter analysis of mesos slave node. The method of dynamic scheduling of cloud resources is used to extract the characteristics of cross-platform virtual resource allocation of the library [2]. Using virtual machine matching and dynamic node adaptive allocation methods, the design of Library cross-platform information retrieval system is realized.

The design of library cross-platform information retrieval system is based on the analysis of the Quality of Service (QoS) of cloud data [3], combined with the load parameter analysis of Mesos-Slave nodes, using the method of dynamic scheduling of cloud resources, extracting the characteristics of library cross-platform virtual resource allocation, and using the methods of virtual machine

matching and dynamic node adaptive allocation to realize the design of library cross-platform information retrieval system [4]. The design methods of library cross-platform information retrieval system mainly include QoS dynamic resource node scheduling method, CaaS (Container-as-a-Service) scheduling method, and particle swarm optimization scheduling method. In 2011, the National Institute of Standards and Technology, NIST) proposes to use Tanimoto coefficient as the characteristic quantity of stable matching between container and virtual machine to carry out cross-platform information retrieval and resource scheduling in libraries, but the adaptability level of this method for cross-platform scheduling in libraries is not high. Reference [5] designed a library information retrieval system based on big data analysis technology. Firstly, the functions of library information retrieval system are described, and the overall framework of library information retrieval system is established; then the hardware subsystem and software

subsystem of library information retrieval are designed in detail, and the library information retrieval algorithm is described in detail. However, this method has a large computational cost, and the reliability allocation ability of physical machine selection is poor [6, 7].

In view of the above problems, this paper proposes a library cross-platform information retrieval system based on digital twin technology. According to the extracted spectrum features of Library cross-platform information resources, a digital twin parallel retrieval and information fusion feature matching model is established. Through the dynamic allocation of multiple complex and balanced task scheduling sequences, the optimization design of Library cross-platform information retrieval model is realized. The experimental results show that this method has better advantages in improving the cross-platform information retrieval ability of the library.

2. Overall Structure Design and Functional Components of the System

2.1. Overall Structure Design of the Cross-Platform Information Retrieval System of the Library. In order to realize the design of cross-platform information retrieval system of library based on digital twin technology, combining with the middleware design scheme, the API Server is established, the Kubernetes node model is stored, combining with the analysis of Web API (API server is an important management API layer of k8s). It is responsible for providing restful API access endpoints and persisting data to etcd server. In the kubernetes cluster, the API server acts as the location of the interaction portal. API server is not only responsible for interacting with etcd (other components will not directly operate etcd, only API server does so) but also provides a unified API call entry. All interactions are centered on API server. Storage kubernetes node model (kubernetes, or k8s for short) is an abbreviation that replaces the eight characters “ubernet” in the middle of the name with eight. It is an open source application used to manage containerized applications on multiple hosts in the cloud platform. Kubernetes’ goal is to make the deployment of containerized applications simple and efficient. Kubernetes provides a mechanism for application deployment, planning, updating, and maintenance. The traditional application deployment method is to install applications through plug-ins or scripts. The disadvantage of this is that the operation, configuration, management, and all life cycles of the application will be bound to the current operating system. This is not conducive to the upgrade, update/rollback of the application. Of course, some functions can be realized by creating virtual machines. However, virtual machines are very heavy and not conducive to portability. The new method is implemented by deploying containers. Each container is isolated from each other. Each container has its own file system. Processes between containers will not affect each other, and computing resources can be distinguished. Compared with virtual machines, containers can be deployed quickly. Because containers are decoupled from underlying facilities and machine file systems, they can be migrated between different clouds and

different versions of operating systems. Containers occupy less resources and deploy faster. Each application can be packaged into a container image. The one-to-one relationship between each application and the container also gives the container greater advantages. Containers can be used to create container images for applications at the build or release stage, because each application does not need to be combined with other application stacks, nor does it depend on the production environment infrastructure, which enables a consistent environment from R & D to testing and production. Similarly, containers are lighter and more “transparent” than virtual machines, which are easier to monitor and manage, and Web API (Message services are conceptually similar to traditional middleware). Due to the technical and commercial complexity, they have not been developed on a large scale. The web-based communication service visible in the short term is Amazon Simple Queue Service. This service facilitates secure and scalable queue based communication between any application. There is no general web computing service black box that can be accessed through API, but there are many technologies pointing in this direction. The first is ALEXA vertical search platform, which will be mentioned more in the search service section below. The second is grid computing, such as sun grid, datasynapse’s gridserver, or platform’s symphony. Encapsulating arbitrary computing tasks in the API is a very challenging task, and it may take many years for this service to become widely popular. Information services provide a large amount of specific information, including geographic data like Google Maps API, product data like Amazon e-commerce, Amazon historical pricing services. and the latest Yahoo! Answer’s API, etc. What these services have in common is that they all provide simple APIs to access massive amounts of data, which may lead to unpredictable cross applications between isolated information. Because of the foundation and dominance of search in the web domain, search services constitute a key part of the new web infrastructure. Google Search API is an earlier and now a typical search abstraction mechanism. Another example is the Alexa search platform, whose design has led to a series of vertical search engines that challenge Google’s position. It is quite interesting that technically, the Alexa search platform is more like a computing service, but it is limited to the search field. This means the possibility of other services, such as sorting services or data transformation services. The last category I broadly call Web2.0 services. The name is not necessarily relevant, but it includes services such as del.icio.us, flickr, basecamp. John Musser compiled some very influential APIs in programmable web. These specific services will become the users of other services mentioned above in the future, but their value is more reflected in the fact that they provide clear, specific, and simple APIs to view and change the information we have. Although they look more like molecules than atoms, they are such basic services in today’s web domain that it makes sense to treat them as components. New web platforms are changing the rules of the game. With the leverage of these infrastructures, it is possible to launch complex and intelligent applications in a very compact time slice. The mere fact that developers do not

have to worry about scaling the problem is encouraging. In other words, Amazon's ten-year experience in large-scale distributed computing was immediately presented to everyone at a very feasible price. It is possible to build intelligent web applications or desktop applications that make full use of the power of these web services because these applications do not have to worry about infrastructure, but focus more on availability, ease of use, context and semantics! Storage API. In order to unify and standardize the operation APIs of these clients, the storage API is introduced. Through the storage API, we can view the available storage space and the used space, and even control whether the user needs to be reminded when the user data are cleared. Harbo functional components. In the early versions, the functions of harbor mainly focused on the management of docker images. Harbor developers hope that users can push and pull images simultaneously through a unified address, and use the graphical interface to browse and manage images. As for the push and pull functions, docker's open source distribution project is widely used. It can support different types of storage, and is relatively mature and stable. Therefore, harbor chooses distribution to handle the push and pull requests for client images, and provides management functions by adding other components around distribution. On the one hand, this method reduces the development workload; on the other hand, since distribution is basically the de facto standard of the image warehouse, it ensures the stability of the image push and pull functions. Later, with the iteration of the version, harbor gradually reduced its dependence on distribution. However, in terms of image read-write, access, and other functions, distribution is still a bridge between harbor and user storage. The random link node forwarding control is adopted to realize the design of ES log service, monitoring service, alarm service, and other functional modules of library cross-platform information retrieval system [8–12]. The specific process is shown in Figure 1.

Data sharing is the key technology of library cross-platform information retrieval, which means that users in different places, using different computers and different software, can read the data stored in other systems, and can perform various operations, calculations, and analyses on library cross-platform information. If you want to share cross-platform information in libraries, you should first integrate cross-platform information and data in libraries. You need to analyze the characteristics of heterogeneous data sources, formulate a series of standards and specifications to realize the standardized design of cross-platform information retrieval system in libraries, and process data to achieve the purpose of integration. On this basis, you should provide access interfaces to users. Users do not need to care about the specific sources of data but only need to get the data they want through the provided data access interface for cross-platform information retrieval in libraries [13]. The data integration system model of library cross-platform information retrieval system is shown in Figure 2.

Library cross-platform information metadata is descriptive information of data and information resources, that is, data describing data. The metadata of HDFS is composed

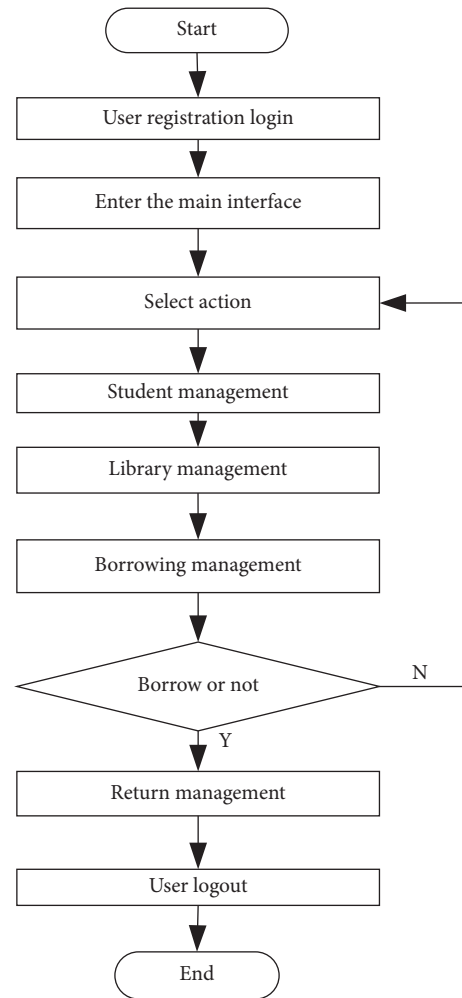


FIGURE 1: Library cross-platform information retrieval flow chart.

of the attributes, affiliation, and distribution location of Block. In HDFS, the management and maintenance of library cross-platform information metadata is completed by NameNode, which is the single failure point of the whole file system [14]. To ensure the reliability of cross-platform information metadata in libraries, HDFS uses two persistent ways, editlog and fsimage, to store metadata in disk. Among them, editlog records the historical information of cross-platform information metadata operation in the library in the form of operation log, and saves it after the record is completed; the fsimage is a kind of stored image file, which is mainly aimed at the checkpoint of regular backup of library cross-platform information metadata in HDFS steps and are expressed as follows: In the application resource pool, on the basis of the resource pool conversion of Slave node, a new log file is generated by the notification of Secondary NameNode, which is deployed in the access and retrieval node, and the data are fed into MySQL. The system logic framework of cross-platform information retrieval in the library is shown in Figure 3.

According to the system logic framework of library cross-platform information retrieval shown in Figure 2, based on image service, authentication service, and ES log

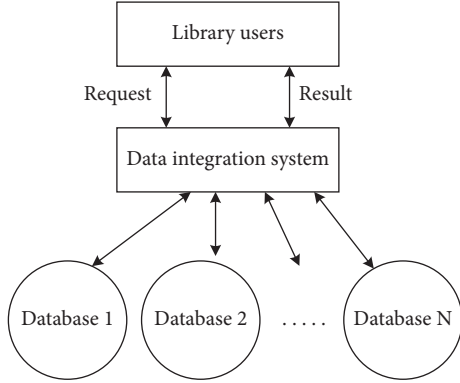


FIGURE 2: Data integration system model of cross-platform information retrieval system in library.

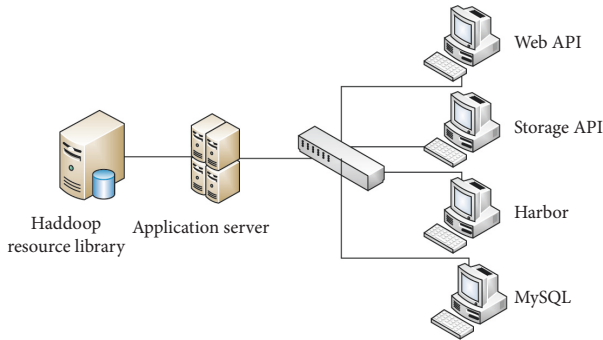


FIGURE 3: System logic framework of cross-platform information retrieval in libraries.

service control methods, the node automatic deployment system model of library cross-platform information retrieval is established [15]. The mirror image of compilation environment is pulled from Harbor warehouse, and Jenkins Master static scanning method is adopted to establish the distribution model of library cross-platform information retrieval system assembly line and core integrated deployment module [16]. The data extraction and program compilation of library cross-platform information retrieval are realized in MySQL underlying cloud database, and the dynamic monitoring model of library cross-platform information retrieval is established from the perspectives of source code construction, code compilation, and image construction, and the architecture diagram of library cross-platform information retrieval system is obtained, as shown in Figure 4.

According to the library cross-platform information retrieval system shown in Figure 3, the data warehouse decision support and data source structured query method are adopted to extract the spectrum characteristic quantity of library cross-platform information resources, and Dockerfile is used to generate the mirror image. The cross-platform information data packet of application library is deployed to Kubernetes cluster, and the functions of creating, configuring, executing, and deleting the cross-platform of library are realized through the module management of application package [17].

2.2. Library Cross-Platform Information Retrieval Module Function Component Analysis. The functional modules of the library cross-platform information retrieval system are divided into mirror compilation sub-module, application deployment sub-module, user interaction module, application package management module, dependency management module, and mirror management module. The specific process is shown in the Figure 5.

Among them, the mirror compilation sub-module is controlled by code version management and generates the mirror image through Dockerfile, which is also within the management scope of Kubernetes cluster. The network design of library cross-platform information retrieval platform is carried out by ZigBee and GPRS networking technologies [18]. The ZigBee data acquisition node of library cross-platform information retrieval is designed as the bottom node of library cross-platform information retrieval system, and the data of library cross-platform information retrieval is uploaded to the central server through GRPS. The original data collection, local information processing, and information fusion of library cross-platform information retrieval are realized at the sensor node [19–21]. The Kubernetes structure diagram of library cross-platform information retrieval system is shown in Figure 6.

In Figure 6, TCP/IP and X.25 protocols are adopted to realize the physical layer access and RF interface output control of the library cross-platform information retrieval system, and the distributed networking scheme is adopted to realize the online scheduling and resource virtualization configuration of the library cross-platform resources under MVB bus control protocol [22].

3. Mathematical Modeling of Cross-Platform Information Retrieval Model in Library

3.1. Feature Extraction of Retrieval Information. Based on the balanced allocation method of library cross-platform information retrieval physical space resources, the balanced allocation of library cross-platform resources is carried out [23], as shown in the Figure 7.

In the cross-platform data computing center of the library, a dynamic allocation model of resources between physical machines and virtual machines is established, and the physical machine set of the cross-platform data center of the library is $G(O) = (V, E, L, \mu, \eta)$, $\eta: E \rightarrow L_E$, and V, E, L, μ, η are the data set of CPU, memory, bandwidth, and hard disk resources in virtual machines, which, respectively, represent the corresponding CPU, memory, bandwidth, and hard disk resource data parameters [24]. Data set $G_1 = (M_1^\alpha, M_1^\beta, Y_1)$, a_{m_i} ($i = 1, 2, \dots, m$) are introduced into different library cross-platform information retrieval container numbers, and the number of hard disk resources as the library cross-platform information center constitutes a feature set. At the information sampling time t and $t + \tau$, the clustering center is initialized to satisfy t_i , so that

$$\begin{aligned} \dot{m}_i(t) &= -a_i m_i(t) + b_i (p_i(t - \sigma), p_2(t - \sigma), \dots, p_n(t - \sigma)), \\ \dot{p}_i(t) &= -c_i p_i(t) + d_i m_i(t - \tau), \end{aligned}$$

(1)

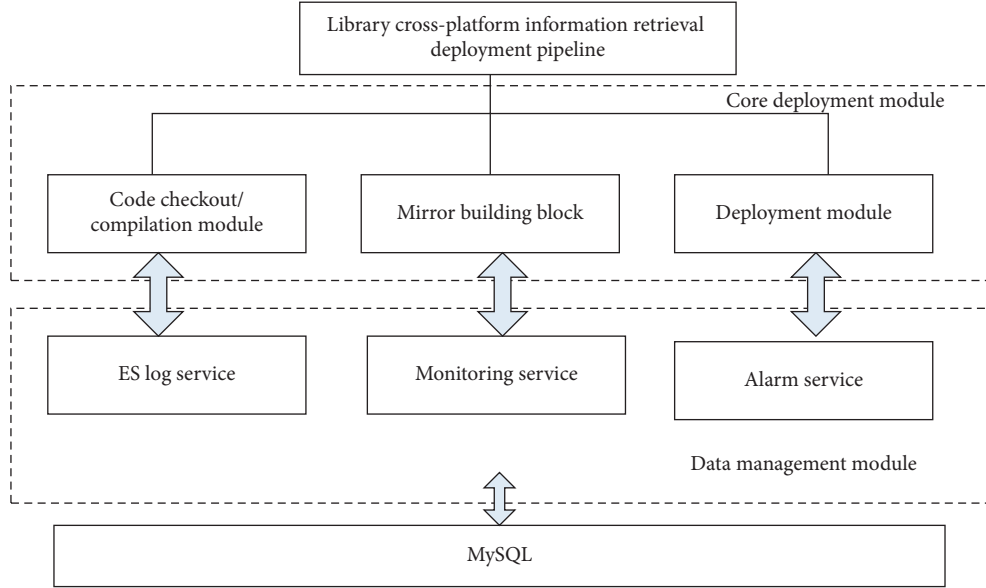


FIGURE 4: Architecture diagram of cross-platform information retrieval system in library.

is the fuzzy clustering center of user behavior attribute data feature vector in library cross-platform information retrieval. The attribute set of library cross-platform storage distribution space is obtained by using the feature sequence training reconstruction method of user behavior attribute data. $B = \{b_1, b_2, \dots, b_m\}$ is the attribute category set of the cross platform information retrieval user behavior attribute data of the library to be mined. Calculate the utilization rate of the physical machine at the time of initialization or migration, and obtain that the central link distribution of the cross platform switch of the library is a_i . The deployment attribute value of the library cross platform information retrieval on the virtual machine M is $\{c_1, c_2, \dots, c_k\}$. According to the deployment of library cross-platform information retrieval nodes on virtual machine M , the information entropy is obtained. By using the methods of information entropy feature extraction and dissimilarity measurement, the resource scheduling fuzzy set $(u, u_t) \in C_t(K, H_x^s \times H_x^{s-1})$ is obtained, the workload sum is obtained, and the CPU utilization rate of the moment is analyzed to obtain the control constraint parameters of library cross-platform information retrieval. The cross-platform running data of the library is divided into decision-making data, computing resource pool data, and Hadoop parallel loading data. By adopting digital twin technology and data clustering method, the digital twin parallel retrieval and information fusion feature matching model of the cross-platform information retrieval system of the library is established, and the information entropy analysis model of the cross-platform resource scheduling of the library is obtained, and the optimized analytical feature components of the cross-platform resource control of the library satisfy:

$$(u_k, \Sigma_k) \sim NiW(v_k, V_k), \quad (2)$$

where in

$$\begin{cases} u_k | \Sigma_k \sim N(\hat{u}_k, \hat{\Sigma}_k), \\ \Sigma_k \sim iW(v_k - d - 1, \Lambda_k), \end{cases} \quad (3)$$

where in $iW(\cdot)$ represents the conduction information function of library cross-platform resource scheduling, parameters v_k and V_k represent the association rule set of library cross-platform resource allocation, d is the information entropy dimension, \hat{u}_k is the load of library cross-platform physical machines, and $\hat{\Sigma}_k$ is the dynamic load balancing parameter of library cross-platform resources. Aiming at the checkpoint of regular backup of metadata in HDFS, the library cross-platform information output rule set of each physical machine is obtained as follows:

$$\begin{aligned} p(x_k | X_{k-1}, Y_{k-1}) &= p(x_k | x_{k-1}, y_{k-1}), \\ p(y_k | X_k, Y_{k-1}) &= p(y_k | x_k), \end{aligned} \quad (4)$$

where in x_k is the sum of the cross-platform information loads of T library, y_{k-1} is the utilization rate of all containers collected by the cross-platform information scheduling server of the library, and X_{k-1} and Y_{k-1} are the simulated minimum physical machine loads and energy consumption, respectively. The cross-platform running data of the library is divided into decision-making data, computing resource pool data, and Hadoop parallel loading data, and the model parameters of cross-platform information retrieval of the library are constructed based on digital twin technology estimation by adopting energy consumption simulation and sorting methods [25].

3.2. Cross-Platform Information Retrieval System of Library. The digital twin parallel retrieval and information fusion feature matching model of the cross-platform information

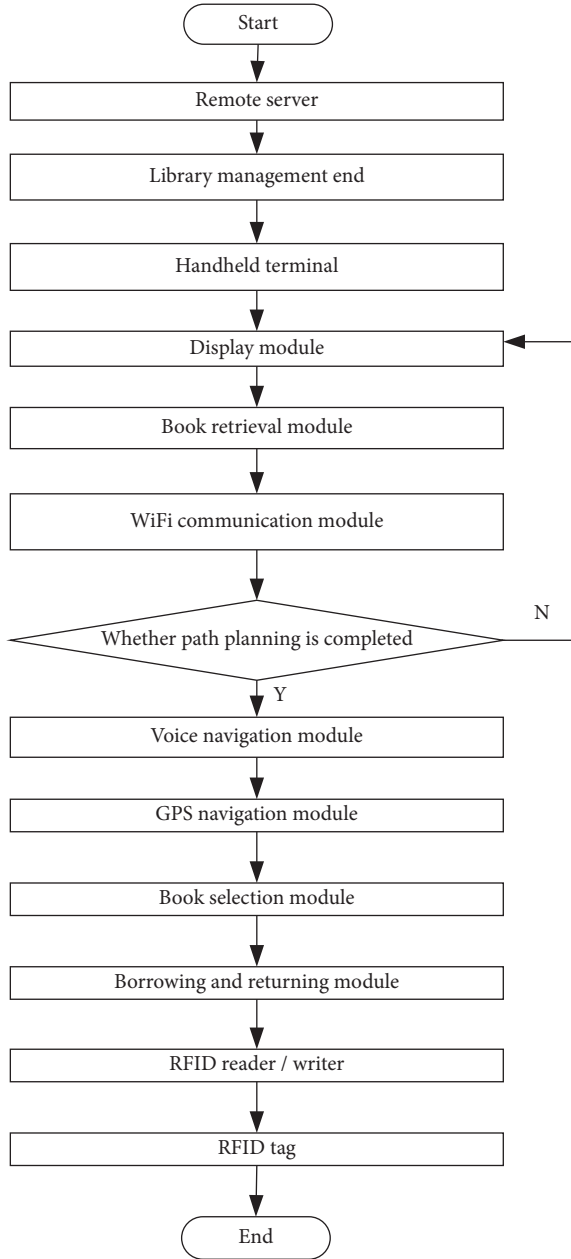


FIGURE 5: Functional component analysis flow chart of library cross-platform information retrieval module.

retrieval system of the library is established, and the four-dimensional parameters of the cross-platform information entropy distribution of the library by the dynamic allocation of multiple complex and balanced task scheduling sequences is given, which are described as follows:

- (1) Random: the random migration target under the guarantee of task service quality.
- (2) FirstFit: the optimization fitness value of library cross-platform scheduling according to the physical machine of the data center.
- (3) MostFull: Calculate the initial target probability density parameters of all available physical machines,

indicating the maximum information entropy under the polling scheduling mechanism.

- (4) LeastFull: Calculate the information entropy and waiting time of all available library cross-platform information.

Based on the construction of 4-dimensional parameters, under multiple Load Balance Service (LBS) mechanisms, the container complex balanced scheduling is carried out. Based on the digital twin technology estimation, the algorithm implementation steps of the library cross-platform information retrieval system are described as follows:

Step 1. Put the idle and closed physical machines into the resource scheduler at the cross-platform resource control end of the library, and get the load parameter X .

Step 2. The task quality mechanism is sorted by the maximum load to obtain the library cross-platform resource feature distribution set E , and the CPU utilization rate of each physical machine in the container E is estimated based on digital twin technology.

Step 3. Move the feature quantity of library cross-platform information retrieval resources in E into X .

Step 4. Set a proprietary conversion engine between the data source and the target data warehouse, and use the round-robin mechanism to calculate the energy consumption of the cross-platform resource retrieval of the library in E , so as to obtain the maximum complex resource ranking.

Step 5. NameNode receives the notification from Secondary NameNode to generate a new log file. Select the physical machine with the smallest simulation value in E .

According to the above algorithm design, the library cross-platform information retrieval channel is dynamically allocated through multiple complex and balanced task scheduling sequences, and the library cross-platform information retrieval queue configuration model [26] is adopted to realize the optimal design of the library cross-platform information retrieval system.

4. Simulation and Result Analysis

In order to verify the application performance of this method in realizing library cross-platform resource scheduling and monitoring, the following experiments are carried out with reference [4] and reference [5] as comparative methods.

4.1. *Establishment of Experimental Platform.* First, the HBase high availability cluster is built. The regionserver of HBase is deployed on the three dat nodes of the Hadoop cluster. Each node backs up each other to ensure high availability of data. HBase's HMaster service is deployed on two NameNode nodes of HDFS, and deploying two HMaster can ensure the high availability of the cluster and prevent single-point failure. Here, an independent ZooKeeper cluster is used, but the ZooKeeper that comes with

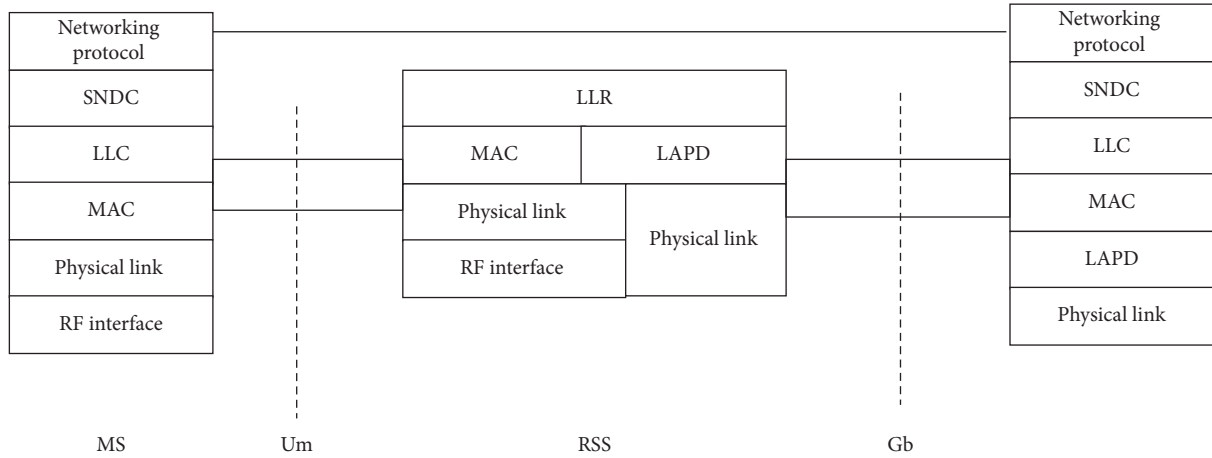


FIGURE 6: Kubernetes structure diagram of library cross-platform information retrieval system.

HBase is not used. When creating an HBase table, if the node failure, thus affecting the whole storage operation.

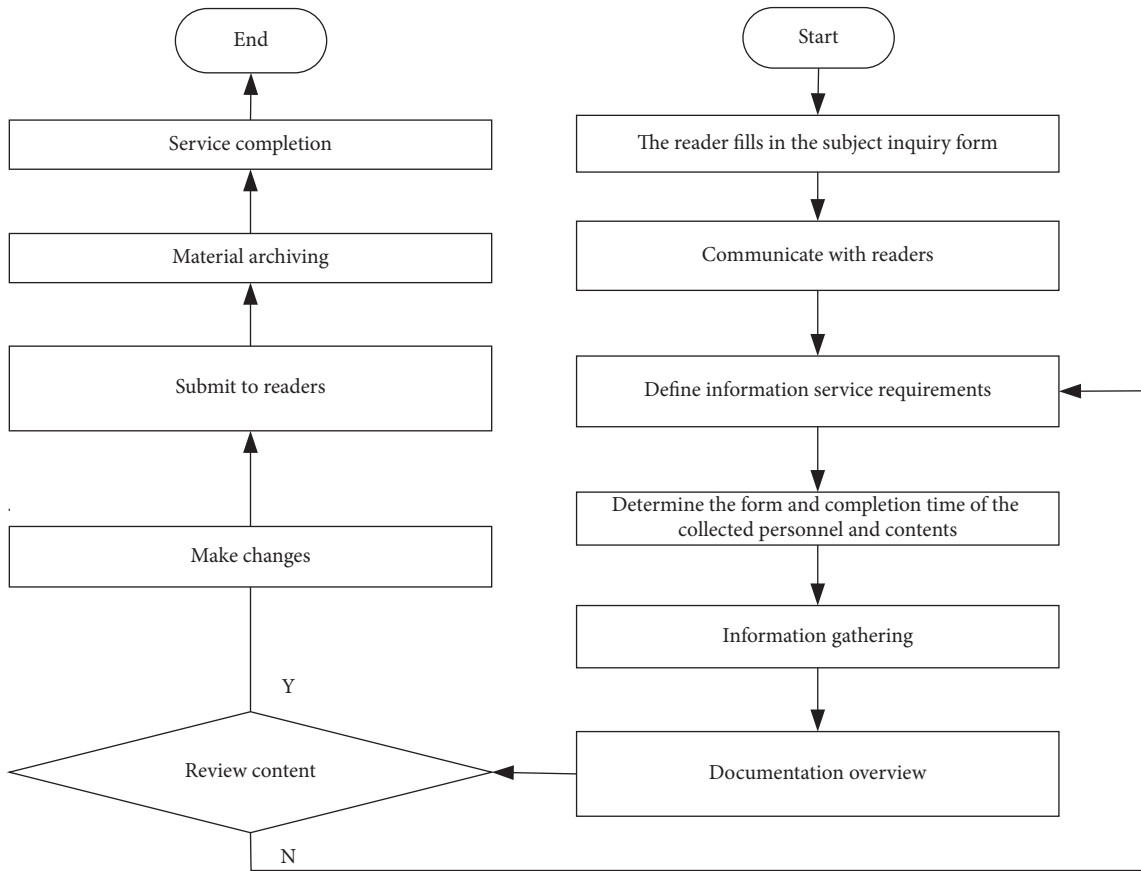


FIGURE 7: Flow chart of feature extraction for cross-platform information retrieval in library.

preallocated Region is not specified, a Region will be created by default. When massive data are written concurrently, all the data will be written into the default Region. Only when it is known that it cannot be loaded will the Split operation be performed, and it will be divided into two regions. In this process, there will be two problems: the data are all stored in one Region, which is prone to single

The underlying disk Split operation will consume a lot of cluster IO resources. Based on this problem, this paper integrates the RowKey characteristics of the cross-platform resource table of the library, designs a reasonable pre-partition scheme, solves the hot issues by creating multiple empty Region in advance, and adjusts the load balance of the cluster. Reasonable design of RowKey can make the

TABLE 1: Task allocation parameters of library cross-platform resource scheduling.

Platform	Memory buffer capacity/mb	Retrieve task queue length/kbps
Platform1	16.840	799.891
Platform2	868.511	472.017
Platform3	556.266	461.907
Platform4	495.678	277.859
Platform5	717.503	169.823
Platform6	99.289	65.178
Platform7	804.483	87.130
Platform8	959.692	803.154
Platform9	984.799	898.029
Platform10	801.790	151.836

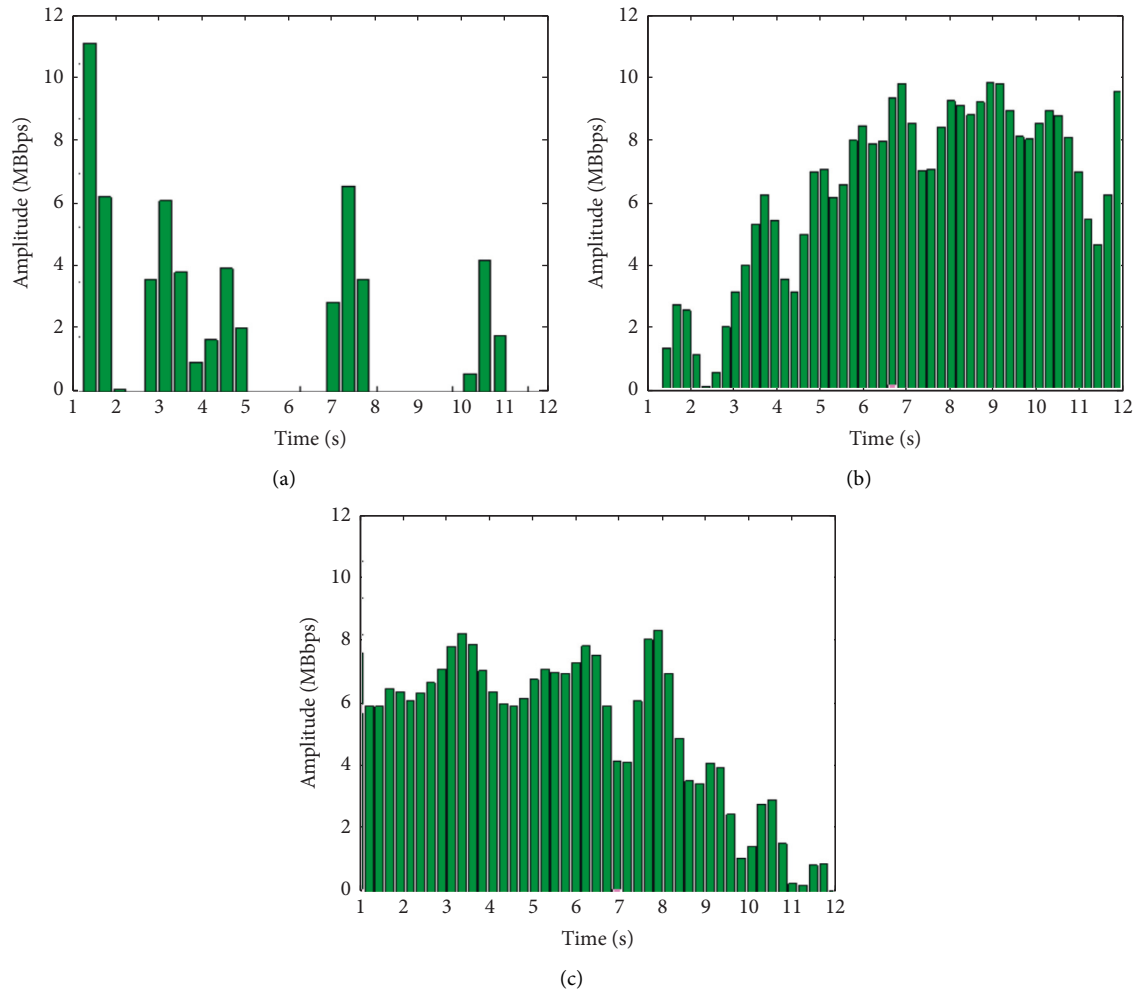


FIGURE 8: Histogram sequence of cross-platform resource allocation in library. (a) Platform1. (b) Platform2. (c) Platform3.

concurrent requests in each Region evenly distributed (tend to be even), so that the IO efficiency can reach the highest. Matlab is used for simulation test. The number of cross-platform nodes in the library is 1200, the length of cross-platform information resource distribution sampling in the library is 1024, the number of training samples is 200, the data size is 800 Mbyte, and the maximum memory buffer capacity of each library is 5600. See Table 1 for the task allocation parameters of cross-platform resource scheduling in the library.

4.2. Cross-Platform Resource Allocation Histogram of Library. According to the parameter configuration in Table 1, the library cross-platform resources are monitored, and the histogram sequence of library cross-platform resources configuration is shown in Figure 8.

4.3. Experimental Results and Analysis. According to the library cross-platform resource allocation in Figure 8, the library cross-platform information retrieval queue

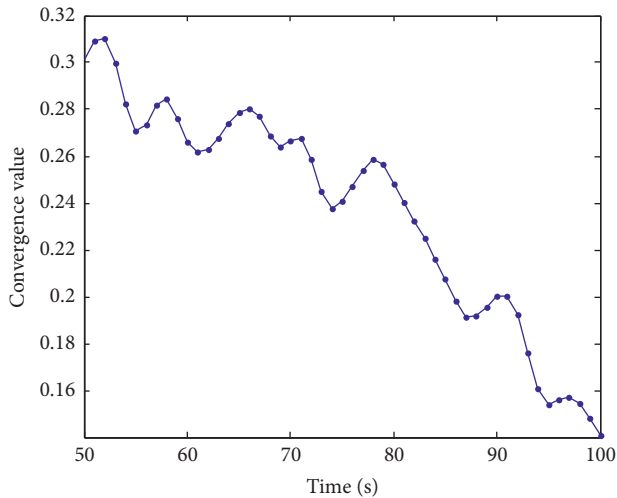


FIGURE 9: Convergence curve of resource allocation.

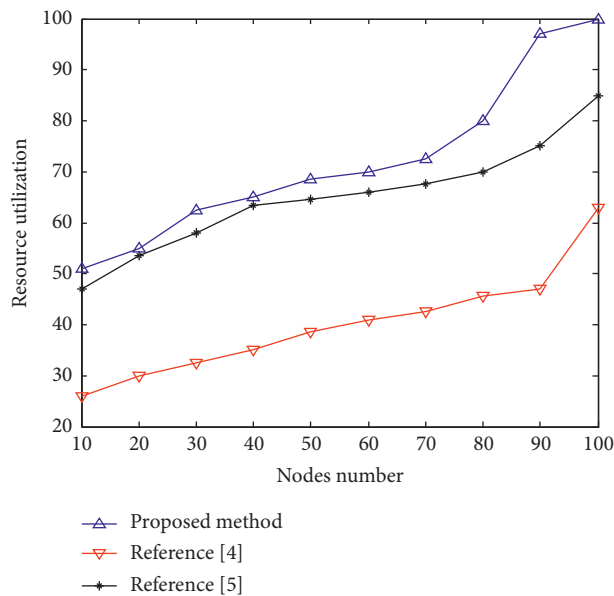


FIGURE 10: Comparative test of resource utilization rate.

configuration model is adopted to realize the optimal configuration of the library cross-platform information retrieval system. Taking the convergence value as the index, the resource allocation of this method is tested after 100 s. The faster the convergence speed is, the better the resource allocation performance of this method is. The convergence curve of resource allocation is shown in Figure 9.

By analyzing Figure 9, it can be concluded that the cross-platform information retrieval of the library by this method has good convergence for resource allocation.

After the application of this method [4] and [5], the library information retrieval resource utilization rate of 100 nodes is tested. The higher the value, the higher the resource utilization rate of the corresponding method and the better the retrieval performance. The comparison results are shown in Figure 10.

Analysis of the simulation results in Figure 10 shows that this method has better data recall ability for library cross-platform information retrieval, which improves the resource utilization rate by 32.3% compared with the traditional method.

5. Conclusions

In order to improve the performance of cross-platform library information retrieval, this paper designs a library cross-platform information retrieval system based on digital twins. The following conclusions can be drawn from the above research:

- (1) This paper constructs an optimized library cross-platform information retrieval and queue scheduling model, and controls and stores the library cross-platform information resource allocation through network server transmission.
- (2) The test shows that the resource utilization rate of information retrieval is higher and the convergence of resource allocation is better in 10 library cross platforms.
- (3) The next step is to refine the library information to further improve the retrieval performance of the design system.

Data Availability

The raw data supporting the conclusions of this article can be obtained from the corresponding author without undue reservation.

Conflicts of Interest

The authors declared that they have no conflicts of interest regarding this work.

References

- [1] B. Lei, J. Wang, and Q. Zhao, "Novel network virtualization architecture based on the convergence of computing, storage and transport resources[J]," *Telecommunications Science*, vol. 36, no. 7, pp. 42–54, 2020.
- [2] C. Xu, D. Yang, and L. He, "Research on cloud computing resource pool load balancing scheduling strategy[J]," *Science and Technology Innovation Herald*, vol. 17, no. 20, pp. 106–111, 2020.
- [3] M. He, "Design of library mass information classification and retrieval system based on data mining[J]," *China Computer & Communication*, vol. 32, no. 11, pp. 153–154, 2020.
- [4] L. Li, J.-F. Wang, and H. Liu, "Hardware supported methods of multi-VM switching and dynamic bandwidth allocation [J]," *Microelectronics & Computer*, vol. 37, no. 1, pp. 93–98, 2020.
- [5] Y. Wu, "Design and research of library information retrieval system based on big data analysis technology[J]," *Modern Electronics Technique*, vol. 43, no. 19, pp. 167–170, 2020.
- [6] Q. Ye and Z. Fang, "Simulation of quantum learning algorithm on virtual resources allocation optimization[J]," *Computer Simulation*, vol. 37, no. 6, pp. 288–292, 2020.

- [7] L. Fei and Y. Guo, "Design of book information retrieval system based on cloud computing and artificial intelligence technology[J]," *Electronic Design Engineering*, vol. 28, no. 18, pp. 60–64, 2020.
- [8] C. Liang, J. Cui, and B. Yin, "Quality detection algorithms for multi-node communication links in wireless sensor networks [J]," *Science Technology and Engineering*, vol. 21, no. 29, pp. 12649–12654, 2021.
- [9] Y. Li, Z. He, and K. Wang, "Link prediction method based on topological tightness of resource transmission nodes[J]," *Computer Engineering*, vol. 47, no. 1, pp. 50–57, 2021.
- [10] Y. Wang, "A design of network information resource retrieval system of digital libraries based on a meta-search engine[J]," *Journal of Nanjing Institute of Technology*, vol. 19, no. 2, pp. 36–39, 2021.
- [11] C. Zhao and L. Wang, "Design of intelligent library cloud retrieval system based on data mining technology[J]," *Modern Electronics Technique*, vol. 43, no. 2, pp. 60–63, 2020.
- [12] X. Zhang, "Design of cross-language information retrieval system based on bidirectional clustering of user logs[J]," *Modern Electronics Technique*, vol. 44, no. 24, pp. 158–162, 2021.
- [13] J. Niu, Y. Zhang, and J. Zheng, "Data logic analysis and retrieval based on graph database[J]," *Electronic Design Engineering*, vol. 30, no. 2, pp. 180–183, 2022.
- [14] L. Xu, "A brief history of library systems and their metadata management," *Library Tribune*, vol. 41, no. 10, pp. 118–126, 2021.
- [15] J. Wang, "Design of digital library information retrieval model based on big data analysis technology[J]," *Modern Electronics Technique*, vol. 43, no. 17, pp. 155–157, 2020.
- [16] J. Zhao, "Design of information retrieval system for hidden information feedback of network users based on big data[J]," *China Computer & Communication*, vol. 33, no. 6, pp. 125–127, 2021.
- [17] W. Xiong, "Analysis and application research of efficient data packet capture technology based on DPDK technology[J]," *Telecom Power Technologies*, vol. 37, no. 21, pp. 181–183, 2020.
- [18] D. Wang, C. Duan, and G. Ma, "Design of wireless energy data acquisition system based on ZigBee and GPRS[J]," *Metrology & Measurement Technique*, vol. 49, no. 2, pp. 23–25, 2022.
- [19] J. Liu, "Distributed multi-sensor information fusion based on weighted number of sensors[J]," *Information & Technology*, vol. 44, no. 2, pp. 22–27, 2020.
- [20] Z. Xiao, "Research on educational information fusion method based on intelligent data collection and processing," *Modern Electronics Technique*, vol. 43, no. 24, pp. 140–143, 2020.
- [21] W. Zhong, "Library integrated information retrieval method based on random forest[J]," *Journal of Anhui Vocational College of Electronics and Information Technology*, vol. 20, no. 4, pp. 1–5, 2021.
- [22] X. Chen and Y. Hu, "Distributed network storage and coding scheme based on balanced data placement strategy[J]," *Application Research of Computers*, vol. 37, no. 4, pp. 1194–1199, 2020.
- [23] L. I. U. Wen, "Big data information resource allocation method based on nash equilibrium solution[J]," *China Computer & Communication*, vol. 33, no. 11, pp. 180–182, 2021.
- [24] Y. Xu and J. Li, "AN efficient allocation mechanism for cloud resource-dynamic virtual machine instance[J]," *Computer Applications and Software*, vol. 38, no. 8, pp. 92–98, 2021.
- [25] X. Ren, "Creation and simulation of large-scale communication optimization model based on 5G technology[J]," *Adhesion*, vol. 49, no. 5, pp. 162–165, 2022.
- [26] Z. Han, Y. Gu, and R. Zhai, "Review of researches on users' knowledge change during online information search processes abroad[J]," *Information Studies: Theory & Application*, vol. 45, no. 2, pp. 204–212, 2022.

Research Article

Modeling and Robust Tracking Decoupling Control of a Coaxial Unmanned Helicopter Based on the Improved Alternating Direction Method of Multipliers

Anan Xu ¹, Fang Wang ², and Ming Chen²

¹School of Aeronautic Science and Engineering, Beihang University, Beijing 100191, China

²Institute of Unmanned System, Beihang University, Beijing 100191, China

Correspondence should be addressed to Anan Xu; xuanan2017@buaa.edu.cn

Received 10 June 2022; Revised 18 July 2022; Accepted 13 August 2022; Published 26 September 2022

Academic Editor: Le Sun

Copyright © 2022 Anan Xu et al. This is an open access article distributed under the Creative Commons Attribution License, which permits unrestricted use, distribution, and reproduction in any medium, provided the original work is properly cited.

In this paper, a robust tracking control strategy based on the dynamic feedback linearization method is proposed for the nonlinear and highly coupled dynamic characteristics of coaxial unmanned helicopter. The mathematical model of the coaxial unmanned helicopter is determined by fault analysis. Then the high-order state system is dynamically feedback linearized by extending the state variables, and the dynamic characteristics of the zeros are analyzed according to the expected tracking characteristics of the inner loop. The pole placement of the subsystem realizes robust monitoring of height and position commands by designing robust compensators. On this basis, an outer loop proportional derivative controller is designed for the horizontal positioning subsystem to realize position tracking. Loop tracking simulation ensures the good separation characteristics of feedback linearization method, and trajectory tracking simulation under fault conditions ensures the control ability and durability of the designed controller.

1. Introduction

Under the background of decentralized consensus optimization, composite proxy networks work together on a common decision variable to minimize the sum of their local target activities and limit the information exchange between neighbors. To do this, check the problem first, and then apply Alternating Direction Method of Multipliers (ADMM). In this method, individuals are iteratively calculated and data are exchanged among neighbors. It is found that this method converges rapidly and is considered to be sustainable [1]. For convex optimization problems, we propose an extended Lagrangian method, in which the cost function is the sum of two terms, one of which can be separated into variable blocks and the other lies between continuous variable blocks [2]. Loop is an effective algorithm for solving complex monotone inclusion and convex optimization problems, which consists of many simple blocks. Promoting PRS and ADMM can automatically adapt to the regularity of the problem and provide an

improved worst case without convergence regularity. All results are obtained through simple techniques [3]. ADMM is widely used to solve structural cone optimization problems. This paper proves that ADMM is a widely used method for solving large-scale multiblock optimization models, and it can also achieve good convergence [4]. ADMM odds are one of the most effective and successful methods to solve different combinations. Multiblock ADMM is a natural extension of ADMM and a general pattern that is very useful for solving various nonconvex optimization problems. Finally, we propose simulation studies and practical applications to support the correctness of the theoretical statements [5]. In this paper, a sPADMM method is proposed to solve the minimization problem of three-block separable cones, where the second block is the constraint of strong convex functions and connected linear equations (6). In this paper, the control problem of a new rotor/duct fan helicopter is studied. By observing the response of a helicopter to steering input, it is found that the coaxial duct fan has the general hinge characteristics different

from traditional helicopters, that is, the strong coupling between ascending and tilting, vertical and rotating motions. The simulation results ensure the correctness of the analysis and control scheme [7]. The design process of strong control of a coaxial micro helicopter is introduced. The process begins with the establishment of a nonlinear dynamic model reflecting all the key elements of a helicopter. Then, the position and climb control controllers are designed using the identified and verified models, and successful flight tests are carried out on the actual system [8]. In this paper, two different methods are used to model a new type of small assembled coaxial helicopter. The system is simulated in two ways and controlled by a PID controller. Simulation results show that the method is effective and can be used to design robust controllers [9]. In this paper, two different methods are used to model a new type of small assembled coaxial helicopter. The system is simulated in two ways and controlled by a PID controller. Simulation results show that the method is effective and can be used to design robust controllers [10]. The initial boundary of closed-loop control of the ideal model of a model autonomous helicopter on the arbitrary flight path is considered. In this paper, a theorem is proved, which sets the limits of the initial fault and trajectory parameters in advance to ensure the acceptable tracking performance of the system. The analysis is expected to be used to validate the work design process [11]. Aiming at the serious nonlinear coupling problem of hydraulic flight simulator, a dynamic robust disconnection compensation method is proposed. This method can disconnect without disconnecting the network. Simulation results show the efficiency of disconnecting the controller. The nonlinear coupling problem in the simulator system is repaired [12]. A robust adaptive fuzzy relative-derived inverse dynamic disengagement control based on the fuzzy linear extended state is proposed and applied to trajectory tracking of the two-degree-of-freedom spherical motion mechanism. The simulation and experimental results ensure the high performance of the controller [13]. Based on the high-dimensional nonlinear system model of the gyro-stabilized platform, a robust control design method for multiple input-output objects is proposed based on eigen structure assignment and quantitative feedback theory. Simulation results show that the EA/QFT method enables designers to understand the design process more intuitively and improves the flexibility between system performance and controller complexity. The results show that even if the spacecraft moves violently, the target tracking system still has good resolution and high-tracking accuracy [14]. The purpose of this paper is to monitor the position and trajectory of a three-stage pneumatic muscle-guided parallel robot without the pressure sensor. An adaptive and durable controller based on the pressure sensor is proposed. The experimental results show that the system not only has good steering accuracy and motion stability but also has strong anti-interference ability [15].

2. Unmanned Helicopter Classification

2.1. Unmanned Helicopter with the Rotor Tail Rotor. The rotor-tail rotor in unmanned helicopter is “rotor + tail rotor,” which is the most common unmanned helicopter type,

so it is also called the conventional unmanned helicopter. In the unmanned helicopter with this configuration, a pair of main rotors is used as lifting components on the fuselage, and the rotor traction is adjusted by controlling the common lifting of the main rotors. By adjusting the pitch angle of the main rotor regularly, the inclination angle of the front and rear wings is adjusted, thus controlling the flight of the helicopter. At the same time, a pair of stern rotors is designed in the vertical plane of the tail of the fuselage to balance the reaction torque generated when the rotors turn to the fuselage and realize stability and heading control. The rotor-tail rotor-unmanned helicopter has been proposed, and the related dynamic analysis and flight technology are mature, and the research results are abundant. As shown in Figures 1 and 2, the unmanned Hummingbird A160 T helicopter designed and manufactured by Boeing Company of the United States and the unmanned AV500 W designed and manufactured by China Aviation Industry Corporation both use this assembly design.

2.2. Variable Structure Unmanned Helicopter. When an unmanned helicopter flies forward at high speed, the supersonic speed of the front tip produces shock wave effect, which greatly increases the aerodynamic drag of the rotor and limits the forward speed of the helicopter. Variable lift unmanned helicopter adopts variable lift axis technology, flies at low speed in helicopter mode, and relies on rotor as lift and steering device to realize short-distance or vertical take-off. By changing the direction of rotor rotation axis to fixed-wing flight mode, the flight speed is gradually increased, which avoids the problems of supersonic overspeed and rotor vibration, and thus improves the forward flight speed. Improved from unmanned helicopters. However, this kind of unmanned helicopter has both aerodynamic characteristics of helicopter and fixed-wing aircraft, and its flight mode is complex. The aerodynamic characteristics of each mode are quite different, and its stability is poor, which increases the design difficulty. Flight control system and flight stability. As shown in Figure 3, only the V-22 Osprey tilt-rotor aircraft and V-22 unmanned V-247 tilt-rotor aircraft of Bell Helicopter Company of America were introduced. At present, China has also done a lot of research on tilt-rotor UAV. Figure 4 shows the first self-developed tilt-rotor UAV “Rainbow”-10 displayed in Zhuhai Flight Exhibition 2018.

2.3. Coaxial Unmanned Helicopter. A coaxial unmanned helicopter has two upper and lower rotors rotating in opposite directions, and the direction is controlled by manipulating the torque difference between the upper and lower rotors. The coaxial unmanned helicopter cancels the design and transmission structure of the stern machine, eliminates stern machine failure caused by the stern swing, reduces the weight of unmanned helicopter, and improves the conversion efficiency between the engine and the rotor elevator. At the same time, the fuselage volume of unmanned helicopter is reduced, the structural load is concentrated on the center of gravity, the moment of inertia of helicopter’s



FIGURE 1: "Hummingbird" A160T unmanned helicopter.



FIGURE 4: "Rainbow"-10 unmanned tilt-rotor aircraft.



FIGURE 2: AV500W unmanned helicopter.



FIGURE 5: Ka-52 armed helicopter.



FIGURE 3: V-247 unmanned tilt-rotor aircraft.



FIGURE 6: TD450 coaxial unmanned helicopter.

rising and tilting is reduced, the steering torque of unmanned helicopter is improved, and the maneuverability of unmanned helicopter is improved. Figure 5 shows the Russian armed Ka-52 helicopter installed in the Russian Air Force for high-altitude reconnaissance and low-altitude operations. Figure 6 shows the TD450 coaxial unmanned helicopter developed in China, which is applied in the field of agricultural plant protection.

2.4. Unmanned Helicopter with Circular Duct. In the annular passage, the unmanned helicopter connects the fuselage with the passage and installs lifting components in the annular passage to reduce the aerodynamic drag of airflow to the rotor during flight. Unmanned helicopters usually use coaxial reversing rotors to balance reverse torque in annular pipes. It is characterized by small overall size and high aerodynamic efficiency at low speed. It is widely used in tactical intelligence, signaling, and other fields. As shown in Figures 7 and 8, the Cypher UAV designed by Sikorsky Company. Unmanned MAV aircraft designed by Honeywell



FIGURE 7: [Password] Unmanned helicopter.

International Company of America and "Golden Eye" produced by Aurora Flight Science Company of America. All UAVs will adopt this structural design.

The unmanned helicopter with a coaxial rotor blower is a new type of unmanned helicopter composed of rotor, duct body, and fan. Different from the annular ducted unmanned



FIGURE 8: Mini ducted fan drone.

helicopter, this helicopter uses the rotor as the main lift device, providing about 70%–80% lift, and the fan in the duct as the auxiliary lift system matches the torque generated by the rotor to realize heading control. The sample unmanned helicopter has the structural characteristics of both the coaxial rotor helicopter and annular ducted helicopter, so it not only retains some aerodynamic characteristics of these two types of helicopters but also has new flight modes and flight control problems that need further study.

3. Introduction of the Classical ADMM Algorithm

3.1. Brief Introduction of the Development of Classical ADMM Algorithm

3.1.1. *Dual Ascending Method.* We first give one of the most commonly used models:

$$\min f(x), \text{ s.t. } Ax = b, \quad (1)$$

where $x \in X$ is an optimization variable, $f: R^n \rightarrow R \cup \{+\infty\}$ is a convex function, A is a matrix of $R^{p \times n}$, $b \in R^p$ is a given vector, and X is a closed convex set in R^n .

The above optimization problem is a linear convex-convex optimization problem. In optimization theory, we do not have algorithms to solve constrained problems directly, but we have many algorithms to solve infinite optimization problems, so our idea is to transform a constrained problem into an unsolvable problem first. The simplest method is the double ascending method. First, according to the constraint condition of binary variable λ , the independent variable X and binary variable λ are updated by using the idea of substitution solution so that the original variable X and binary variable λ are optimal at the same time. The following is a detailed introduction to the steps of solving the optimization problem by Shuang Li's method. First, the Lagrangian function of the optimization problem is constructed as

$$L(x, \lambda) = f(x) - \lambda^T (Ax - b). \quad (2)$$

The dual function of formula (2) is given as

$$d(\lambda) = \inf_x L(x, \lambda) = -f^*(-A^T \lambda) - b^T \lambda, \quad (3)$$

where $\lambda \in R^p$ is a binary variable. The dual problem is given as

$$\max d(\lambda), \quad (4)$$

where $\lambda \in R^p$ also stands for a binary variable. Strong duality assumptions (although minimizing the initial problem $\min f(x)$ is equivalent to maximizing dual problem $\max d(\lambda)$) give the same optimal solution to the initial problem as the optimal solution to the dual problem. Assuming that the optimal solutions of the original optimization problem and the double optimization problem are x^* and λ^* , we have a strong double hypothesis $x^* = \operatorname{argmin}_x L(x, \lambda^*)$; that is, we can get the optimal solution x^* of the original problem through the optimal solution λ^* . In the double ascending method, assuming that the dual function $d(\lambda)$ is differentiable, its gradient $\nabla d(\lambda)$ can be estimated by the following method: first, the updated value is obtained, then $d(\lambda) = \inf_x L(x^{k+1}, \lambda) = f(x^{k+1}) + \lambda^T (Ax^{k+1} - b)$, then $\nabla d(\lambda) = Ax^{k+1} - b$, which is also called the remainder of the difference of difference constraint $Ax = b$. Therefore, the updating process of the Shuang Sheng method is

$$\begin{cases} x^{k+1} := \operatorname{argmin}_x L(x, \lambda^k) \\ \lambda^{k+1} := \lambda^k + \alpha^k (Ax^{k+1} - b), \end{cases} \quad (5)$$

where $\alpha^k > 0$ is the step size, and when the step size α^k is selected correctly, the double function $d(\lambda)$ rises continuously.

Note that the independent variable $x \in R^n$ and binary variable $\lambda \in R^p$ of the original problem are in different linear states, which means that the double ascending method alternately optimizes in two linear spaces R^n and R^p , does not intersect, and develops towards the optimal motion direction. A solution is coming. However, the double slope method also has some disadvantages: if the step size α^k is chosen correctly and the objective function $f(x)$ is strictly convex and strongly dual, both the independent variable x^k and the binary variable λ^k converge to the optimal point, and the original optimization problem and the double optimization problem can reach the optimal solution time at the same time. Unfortunately, many practical problems can not satisfy the assumptions of strict convexity and strong duality of the objective function $f(x)$ at the same time, so the Shuang-Li method is useless at this stage.

3.1.2. *Dual Decomposition Method.* Although the strict conditions of Shuang-Li method are not suitable for solving most practical problems, the Shuang-Li method has a particularly good feature worth exploring. If the objective function $f(x)$ is separable, we decompose the initial problem into many small problems, optimize these small problems, and then integrate them together to achieve full renewal, which is a double decomposition method. Nevertheless, let us take the optimization problem as an example and look at its decomposition form as

$$\min f(x) = \sum_{i=1}^N f_i(x_i), \text{ s.t. } Ax = \sum_{i=1}^N A_i x_i = b, \quad (6)$$

where the independent variable is decomposed into $x = (x_1, x_2, \dots, x_N)$, $x_i \in R^{n_i}$ is a component of the independent variable X , and accordingly the matrix A is decomposed into $A = (A_1, A_2, \dots, A_N)$ and satisfies $Ax \in \sum_{i=1}^N A_i x_i$. Accordingly, the Lagrangian function of formula (6) can be converted into

$$L(x, \lambda) = \sum_{i=1}^N L(x_i, \lambda) = \sum_{i=1}^N \left(f_i(x_i) + \lambda^T A_i x_i - \frac{1}{N} \lambda^T b \right). \quad (7)$$

In a given iterative process, due to the decomposition of the objective function $f(x)$, the x -part problem of (5) can be divided into the following N -part problems, and optimization is carried out at the same time as

$$\begin{cases} x_i^{k+1} := \operatorname{argmin}_x L_i(x_i, \lambda^k) \\ \lambda^{k+1} := \lambda^k + \alpha^k (Ax^{k+1} - b). \end{cases} \quad (8)$$

It can be seen that in formula (8), decomposition and integration operations are performed at each stage. For subproblems $i = 1, 2, \dots, N$ and x_i , simultaneous optimization can be realized independently. In the renewal stage of the binary variable λ , we integrate the decomposed constraint residuals $A_i x_i$ to form the total residuals $Ax^{k+1} - b$. Parallel updating of subproblems of the double decomposition method provides theoretical basis and ideas for the following problems.

3.1.3. Augmented Lagrange Multiplier Method. In order to reduce the assumption of the method and improve the applicability and practicability of the method, the following Lagrange coefficient method is added. The solution of adding Lagrange coefficient is to add quadratic addition term $(\beta/2)\|Ax - b\|_2^2$ to Lagrange function first and the addition delay of formula (1) is obtained as

$$L_\beta(x, \lambda) = f(x) - \lambda^T (Ax - b) + \frac{\beta}{2} \|Ax - b\|_2^2, \quad (9)$$

where $x \in X$ is still the variable to be optimized, and $\lambda \in R^p$ is the Lagrange coefficient. $\beta > 0$ is the penalty parameter of constraint, which is also called penalty coefficient. Let $\beta = 0$ be the general Lagrangian function $L_0(x, \lambda)$ in formula (9), where the additional term $\beta/2\|Ax - b\|_2^2$ plays a major guiding role in the iterative process because after introducing the added Lagrangian function, the optimal solution of formula (1) is transformed into the minimum solution of the extended Lagrangian function (9), which is far from the feasible range, then $\beta/2\|Ax - b\|_2^2$ is larger. The minimum solution of infinite problem (*) or the solution of each iteration x', y' certainly cannot gradually approach the feasible range of the original problem by the limit term $\beta/2\|Ax - b\|_2^2$. When x', y' becomes a realizable point, this realizable point x', y' is the optimal solution of the model. In

fact, the extended Lagrangian function $L_\beta(x, \lambda)$ can also be equivalent to the general Lagrangian function of the following optimization model in the form:

$$\min f(x) + \frac{\beta}{2} \|Ax - b\|_2^2, \text{ s.t. } Ax = b. \quad (10)$$

Obviously, equality (10) corresponds to equality (1) because for every possible solution X in equality (10), there is a penalty term. The dual function formula corresponding to formula (10) of the optimization problem is

$$d_\beta(\lambda) = \inf_x L_\beta(x, \lambda). \quad (11)$$

The introduction of quadratic penalty term $\beta/2\|Ax - b\|_2^2$ makes the dual function $d_\beta(\lambda)$ uniformly separable under the most relaxed conditions. The updating steps of solving the model by the Lagrange coefficient method are given as

$$\begin{cases} x^{k+1} := \operatorname{argmin}_x L_\beta(x, \lambda^k) \\ \lambda^{k+1} := \lambda^k + \beta(Ax^{k+1} - b). \end{cases} \quad (12)$$

The difference between the above formula (12) and Shuang Sheng method is, firstly, the additive Lagrange coefficient method introduces the quadratic addition term $\beta/2\|Ax - b\|_2^2$; secondly, in the double ascending method of α^k , the update step of binary variable λ is E , which is the variable to be redefined in each iteration. In the Lagrange coefficient method, the update step of λ is extended to become β , that is, a fixed value. The increased Lagrangian coefficient method makes up for the deficiency of the Shuang Lift method and converges under looser conditions (for example, when the objective function $f(x)$ does not strictly satisfy the convex attribute). Although the extended Lagrange coefficient method is more applicable, it also makes use of the decomposition property of the objective function $f(x)$, that is, the additive Lagrange method destroys the parallel solution property of the double-lift method and the double decomposition method. In daily multiplication, when the objective function $f(x)$ must be decomposable, the enlarged Lagrangian function $L_\beta(x, \lambda)$ cannot be decomposed, so it is impossible to optimize several smaller x_i -subproblems when solving x -subproblem.

Some scholars put forward the precision ADMM algorithm on the basis of the Shuang Lift method, double scattering method, and Lagrange coefficient method, which will be explained in detail in the next section.

3.2. Introduction to Classical ADMM Algorithms

3.2.1. Classical ADMM Algorithm. Classical ADMM algorithm inherits the advantages of Shuang Lift method, double scattering method, and Lagrangian coefficient method. Especially, because the objective function $f(x)$ of optimization problem is complex, the classical ADMM algorithm is particularly prominent in solving such problems. Next, we give the problem model and basic framework of the classical ADMM algorithm.

We consider the following forms of problem optimization:

$$\min_{x,y} f(x) + g(y), s.t. Ax + By = b, \quad (13)$$

where $x \in X, y \in Y$ is the optimization variable and $f: R \rightarrow R \cup \{+\infty\}, g: R^m \rightarrow R \cup \{+\infty\}$ is a convex function, and these initial problems can be transformed into the form of formula (13) after redefining the variables. For example, given $y = Ax$, the original problem $\min f(x) + g(Ax)$ can be transformed into (13), where $B = -1, b = 0$. In some problems, object functions have good properties such as strictly convex or squared convex functions or having a continuous Lipchitz gradient and so on.

For formula (13), we obtain its augmented Lagrangian function as

$$L_\beta(x, y, \lambda) = f(x) + g(y) - \lambda^T (Ax + By - b) + \frac{\beta}{2} \|Ax + By - b\|_2^2. \quad (14)$$

The basic idea of the classical ADMM algorithm is to obtain the extended Lagrangian penalty function and then solve the original problem by solving a series of subproblems on X and Y and some iterative division as

$$\begin{cases} y^{k+1} := \operatorname{argmin}_y L_\beta(x^k, y, \lambda^k) \\ x^{k+1} := \operatorname{argmin}_x L_\beta(x, y^{k+1}, \lambda^k) \\ \lambda^{k+1} := \lambda^k + \beta(Ax^{k+1} + By^{k+1} - b). \end{cases} \quad (15)$$

Replace the extended Lagrangian function in (15) with Algorithm 1:

Let $k = k+1$ go to step 2.

Compared with the method of adding Lagrange coefficients to update independent variables x and y simultaneously, each iteration of the classical ADMM algorithm can be divided into the following three steps: the first step is to solve the minimization problem related to updating variable y ; the second step is to solve the minimization problem related to updating variable X ; and the third step is to update the Lagrangian multiplier λ . In the updating step, λ is taken as the extended Lagrangian penalty parameter β . The classical ADMM algorithm considers that the objective functions F and G which are separated from the independent variable X . It allows the algorithm to be divided into two subproblems of a variable and alternately update variables X and Y , which are the origin of the inverse multiplication name. In addition, in the classical ADMM algorithm, the order of these two subproblems can be arbitrary: first, solve subproblem y -, and then solve subproblem x -, such as algorithm 1. First, the subproblem can be solved in inverse x -. The order of different solutions has no effect on the convergence of the algorithm. Although alternative upgrades require more steps than general upgrades, because it is easier to calculate the two subproblems of alternative upgrades, the classical ADMM converges faster than other methods, so it is more widely used.

3.2.2. Simplified Form of the Classical ADMM Algorithm. Here is another similar classic ADMM form, which is relatively simple and common in practical application fields. Let $r = Ax + By - b, u = 1/\beta\lambda$ be

$$\begin{aligned} & -\lambda^T (Ax + By - b) + \frac{\beta}{2} \|Ax + By - b\|_2^2 \\ & = \lambda^T r + \frac{\beta}{2} \|r\|_2^2 = -\frac{\beta}{2} \|r\|_2 + \frac{1}{\beta} \|\lambda\|_2^2 + \frac{1}{2\beta} \|\lambda\|_2^2 \\ & = -\frac{\beta}{2} \|r + u\|_2^2 + \frac{\beta}{2} \|u\|_2^2. \end{aligned} \quad (16)$$

Accordingly, the augmented Lagrange function is also equivalent to

$$L_\beta(x, y, \lambda) = f(x) + g(y) - \lambda^T (Ax + By - b) + \frac{\beta}{2} \|Ax + By - b\|_2^2 \quad (17)$$

$$= f(x) + g(y) - \frac{\beta}{2} \|r + u\|_2^2 + \frac{\beta}{2} \|u\|_2^2.$$

By the same token, the iteration of the subproblem is

$$\begin{cases} y^{k+1} := \operatorname{argmin}_y \left(g(y) + \frac{\beta}{2} \|Ax^k + By - b + u^k\|_2^2 \right) \\ x^{k+1} := \operatorname{argmin}_x \left(f(x) + \frac{\beta}{2} \|Ax + By^{k+1} - b + u^k\|_2^2 \right) \\ \lambda^{k+1} := \lambda^k + \beta(Ax^{k+1} + By^{k+1} - b). \end{cases} \quad (18)$$

The simplified form of formula (18) is exactly the same as the original form of formula (15). The simplified form of ADMM is often used in practical applications, but if we want to emphasize the role of binary variables, we must use the original form of ADMM.

3.2.3. Extended Form of the Classical ADMM Algorithm. If the objective function can be decomposed into N parts, the form is

$$\begin{aligned} & \min_{x_1, x_2, \dots, x_N} g_1(x_1) + g_2(x_2) + \dots + g_N(x_N) \\ & s.t. A_1 x_1 + A_2 x_2 + \dots + A_N x_N = b \\ & x_i \in X_i, i = 1, \dots, N, \end{aligned} \quad (19)$$

where $g_i(\cdot), i = 1, \dots, N$ is a convex function of $R^{n_i} \rightarrow R, x_i \in X, i = 1, \dots, N$ is a closed convex set of R^{n_i} , and $A_i \in R^{p \times n_i}, i = 1, \dots, N, b \in R^p$ is a given vector. It is easy to know that the extended Lagrangian function of formula (19)

is $L_\beta(x_1, x_2, \dots, x_N; \lambda) = \sum_{i=1}^N g_i(x_i) + \lambda^T (\sum_{i=1}^N A_i x_i - b) + (\beta/2) \|\sum_{i=1}^N A_i x_i - b\|_2^2$. Similar to the classical ADMM algorithm, we can get the update steps of the extended ADMM algorithm as

$$\begin{aligned} x_1^{k+1} &:= \operatorname{argmin} L_\beta(x_1, x_2^k, \dots, x_N^k; \lambda^k) \\ x_2^{k+1} &:= \operatorname{argmin} L_\beta(x_1^{k+1}, x_2, \dots, x_N^k; \lambda^k) \\ &\vdots \\ x_N^{k+1} &:= \operatorname{argmin} L_\beta(x_1^{k+1}, x_2^{k+1}, \dots, x_N; \lambda^k) \\ \lambda^{k+1} &:= \lambda^k + \beta(A_1 x_1^{k+1} + A_2 x_2^{k+1} + \dots + A_N x_N^{k+1} - b). \end{aligned} \quad (20)$$

In recent years, the ADMM algorithm, which can decompose the objective function into several parts or several subblocks, has become a hot research topic for many researchers, and the research results are of great significance. This provides a very powerful method for dealing with large-scale optimization models.

3.3. Convergence of the Classical ADMM Algorithm

3.3.1. Convergence of the Classical ADMM Algorithm. A typical model of the classical ADMM algorithm is an optimization problem whose objective function is two distinguishable variables. For the model in this chapter, the convergence of the classical ADMM algorithm has been obtained in many literatures. We use the following two assumptions to prove the convergence of the algorithm:

Suppose 1 function $f: R^n \rightarrow R \cup \{+\infty\}$, $g: R^m \rightarrow R \cup \{+\infty\}$ is a closed convex function.

The closed convex property of the function of Hypothesis 1 can also be described by the following equivalent property: A function $f(x)$ satisfies Hypothesis 1 if and only if its graph $\operatorname{epi} f(x) = \{(x, \lambda) \mid (x, \lambda) \in R^n \times R, f(x) \leq \lambda\}$ is a nonempty closed convex set.

Suppose 2 Lagrange function $L_0(x, y, \lambda)$ has stagnation point.

If Hypothesis 1 holds true, then subtasks x - and y - have optimal solutions. In addition, suppose 1 can become infinity when the function is nondifferentiable. Although the optimization problem is set under such loose conditions, the solution of its subproblem can still be found. This secondary programming task is obviously solvable. If Hypothesis 2 holds true, then the optimal solution x^*, y^*, λ^* can be obtained for the two problems mentioned above, and for any x, y, λ satisfying the constraint, the following inequality holds for $L_0(x^*, y^*, \lambda) \leq L_0(x^*, y^*, \lambda^*) \leq L_0(x, y, \lambda^*)$. According to assumptions 1 and 2, the Lagrange function $L_0(x^*, y^*, \lambda^*)$ is limited to each optimal solution x^*, y^*, λ^* . It can be concluded that x^*, y^* is the solution of (13), so $Ax^* + By^* = b$ and $f(x^*), g(y^*) < \infty$. Of course, it can also be concluded that λ^* is the optimal solution, and we do not make additional assumptions about matrices A, B and vector B in constraints nor do we require matrices A and B to have perfect permutation.

The following will give the convergence result of solving formula (13) with the classical ADMM algorithm:

Theorem 1. *In Hypotheses 1 and 2, the iterative generation sequence of the classical ADMM algorithm satisfies what as follows:*

- (1) *When $k \rightarrow \infty$ is the constrained residual set $r^k = Ax^k + By^k - b \rightarrow 0$, the residual converges, that is, the boundary point of the iterative sequence (x^k, y^k) is the feasible point of formula (13).*
- (2) *The objective function is convergent. When $k \rightarrow \infty$, the sequence $f(x^k) + g(y^k) \rightarrow p^*$; that is, the limit point p^* of the objective function sequence is the optimal solution of formula (13).*
- (3) *When $k \rightarrow \infty$ is a set of bivariate $\lambda^k \rightarrow \lambda^*$, the bivariate is convergent; that is, the boundary point of a set of bivariate variables is a double optimum.*

Generally speaking, the higher the accuracy of the classical ADMM algorithm, the slower the convergence speed. Especially in practical applications, we faced quite a lot of large optimization problems. If the accuracy is too high, the convergence speed of the classical ADMM algorithm is very slow. If we want to solve this large-scale optimization problem quickly, our method often meets the accuracy requirements of the algorithm and realizes the fast convergence of the algorithm, thus slowly appearing the inaccurate ADMM algorithm.

3.3.2. Optimal Conditions and Stopping Criteria of the Classical ADMM Algorithm. Generally, the optimization problem satisfies the following relationship as

$$\begin{cases} Ax^* + By^* - b = 0 \\ 0 \in \partial f(x^*) + A^T \lambda^* \\ 0 \in \partial g(y^*) + B^T \lambda^*, \end{cases} \quad (21)$$

and vice versa.

The above formula (21) is called the optimal condition of the classical ADMM algorithm. If x^*, y^*, λ^* is the optimum of formula (13), then formula (21) is satisfied; on the contrary, if there is x^*, y^*, λ^* satisfying (21), it is the best point of (13). In equation (21), the first line is called the initial problem feasibility condition; that is, the best point must satisfy the equality constraint of equation (12); the second and third lines are called dual-use conditions, where Operator ∂ represents the subdifferential or subgradient operators that is described in detail in the previous section.

Specific to each iteration, we have formula (22) defined by x^{k+1}

$$\begin{aligned} 0 &\in \partial f(x^{k+1}) + A^T \lambda^k + \beta A^T (Ax^{k+1} + By^{k+1} - b) \\ &= \partial f(x^{k+1}) + A^T \lambda^k + \beta A^T r^{k+1} \\ &= \partial f(x^{k+1}) + A^T \lambda^{k+1}. \end{aligned} \quad (22)$$

Step 1 Given the initial point $x^0 \in R^n, \lambda^0 \in R^p, \beta > 0, k = 0$
 Step 2 Calculate $y^{k+1} := \operatorname{argmin}_y L_\beta(x^k, y, \lambda^k)$
 Step 3 Calculate $x^{k+1} := \operatorname{argmin}_x L_\beta(x, y^{k+1}, \lambda^k)$
 Step 4 Calculate $\lambda^{k+1} := \lambda^k + \beta(Ax^{k+1} + By^{k+1} - b)$

ALGORITHM 1: Classical ADMM algorithm standalone.

Likewise, we have formula (23) by definition $y^{k+1} = \operatorname{argmin}_y L_\beta(x^k, y, \lambda^k)$ of y^{k+1} as

$$\begin{aligned} 0 &\in \partial g(y^{k+1}) + B^T \lambda^k + \beta B^T (Ax^k + By^{k+1} - b) \\ &= \partial g(y^{k+1}) + B^T (\lambda^k + \beta r^{k+1} + \beta A(x^k - x^{k+1})) \quad (23) \\ &= \partial g(y^{k+1}) + B^T \lambda^{k+1} + \beta B^T A(x^k - x^{k+1}). \end{aligned}$$

The above formula (23) can also be written as the corresponding form $\beta B^T A(x^k - x^{k+1}) \in \partial g(y^{k+1}) + B^T \lambda^{k+1}$, where $\beta B^T A(x^k - x^{k+1})$ is denoted as s^{k+1} , where s^{k+1} can be considered as a residue (double residue) of the double feasibility condition of formula (21). In formula (22), we still have the remaining $r^{k+1} = Ax^{k+1} + By^{k+1} - b$ for the original feasibility condition.

The simplest stop criterion is request $|f(x^k) + g(y^k) - p^*| \leq \varepsilon$, where p^* represents the optimal solution of the objective function and ε is the predetermined precision. But please note that this stop criterion uses a certain value of p^* , and we do not know the value of the optimal solution p^* , so we cannot use this criterion. In practical application, the most commonly used stopping criterion is that when the original residual r^k and the double residual s^k are less than the specified accuracy, the algorithm jumps out of the loop and terminates the iteration as

$$\|r^k\|_2 \leq \varepsilon^{pri}, \|s^k\|_2 \leq \varepsilon^{dual}, \quad (24)$$

where $\varepsilon^{pri} > 0, \varepsilon^{dual} > 0$ is the accuracy of the principal and dual feasibility conditions.

4. Experimental Analyses

4.1. Performance Comparison. In order to make the modeling of coaxial unmanned helicopter more convenient and accurate, we have done five experiments to compare the performance of ADMM, BCD, and ALM in decoupling ability, iterative updating ability, and convergence. The results are shown in Figures 9–11.

Looking at Figure 9, we can see that in terms of decoupling ability, ADMM is the best, followed by BCD and ALM; From Figure 10, we can conclude that ADMM is the best in terms of iterative update capability, followed by BCD and ALM. From Figure 11, we can conclude that ADMM is the best in terms of iterative update capability, followed by ALM and BCD. Therefore, in order to have higher accuracy in the next experiment, we choose the ADMM method.

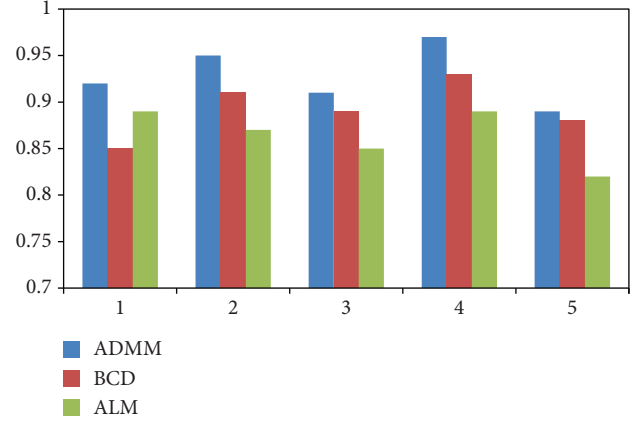


FIGURE 9: Decoupling ability.

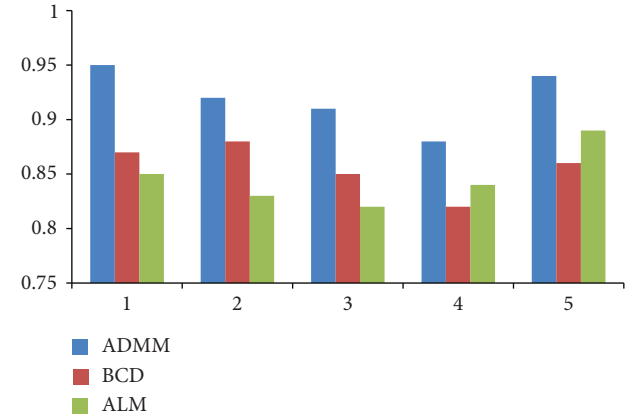


FIGURE 10: Iterative update capability.

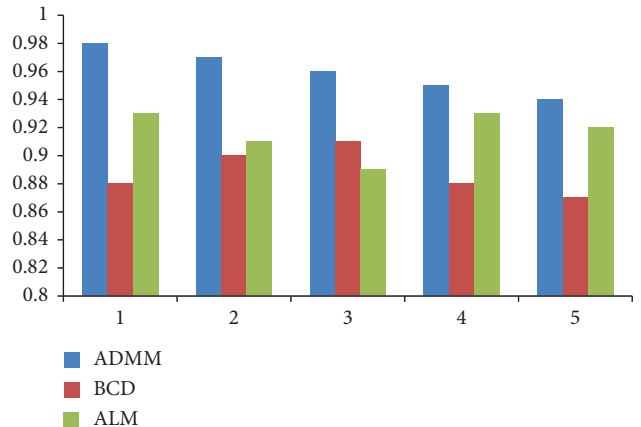


FIGURE 11: Convergence.

TABLE 1: Direct measurement parameters of the main smart wing.

Symbol	Physical meaning	Numerical value
STA_h	Pulp hub station	0.40 m
WL_h	Hub waterline	0.598 m
WL_h	Axis anteversion angle	0 rad
Ω	MR angular rate	190.5 rad/s
m_β	Main blade weight	0.18 kg
N_b	Number of main pulp blades	2
R	Plate radius	0.78 m
c	Chord length of main pulp	0.059 m
θ_t	Blade torsion	0 rad
K_l	Pitch-flap coupling rate	0

4.2. *Direct Measurement of Physical Parameters.* Most parameters can be measured directly, such as weight, length, angle, area, speed, and so on.

The weight of the helicopter rack can be weighed directly, but different tasks have different payloads, and the weight will also change, so consider the center of gravity below.

These directly measurable parameters are displayed in the helicopter assembly group.

It is assumed that all components of France and Italy are on the longitudinal axis of symmetry of the helicopter, so the longitudinal lines intersect, and it is shown in Tables 1–3.

The length of each control arm of the rotor head is measured separately, which is listed in Table 4. By measuring these lengths to determine the value of Bershiller coefficient, compared with other angle measurement methods, the estimation is more accurate.

In this case, gain can be obtained between the inclination changes of the stabilized wing tip as

$$K_f = \frac{L_0 L_7}{L_6 L_5} = 1.859. \quad (25)$$

Because there is no wind tunnel test condition, the frame is approximately a three-dimensional virtual plate, the vertical flow resistance coefficient is about 1, and only the windward side of the body axis is enough in the forward, transverse, and vertical directions. If the helicopter is equipped with shields and other components, the effective aerodynamic drag range within the block can be evaluated according to the relevant discussion of aerodynamic drag of various objects in the references, and it is shown in Table 5.

There are several parameters that are not easy to measure directly but can be estimated from the measured data, as shown in Table 6. The values of M_β , I_β , and I_β^{sb} have an important influence on the swinging dynamics, so it is advisable to divide the main blade and stabilizer bar with winglets into several homogeneous parts with regular geometric shapes, integrate them one by one, and then accumulate them to ensure the estimation accuracy. In the table, the dynamic pressure rates η_{hs} and η_{vf} of stabilizers are based on experience.

4.3. *Maneuverability Analysis of the Coaxial Unmanned Helicopter with the Blower.* It is known that the coaxial rotor blower-unmanned helicopter has introduced a new

TABLE 2: Direct measurement parameters of the tail rotor.

Symbol	Physical meaning	Numerical value
STA_{tr}	Tail hub station	1.325 m
WL_{tr}	Tail hub waterline	0.398 m
Ω_{tr}	TR angular rate	910.1 rad/s
θ_t^{tr}	Blade torsion	0 rad
N_{tr}	Number of tail pulp blades	2
R_{tr}	Plate radius	0.135 m
c_{tr}	Chord length of tail slurry	0.027 m
$k_{vf, tr}$	Double- v_t^{tr} occlusion factor	0.9

TABLE 3: Direct measurement parameters of the stabilizer bar.

Symbol	Physical meaning	Numerical value (m)
STA_{sb}	SB pulp hub station	0.40
WL_{sb}	SB hub waterline	0.563
c_{sb}	Aileron chord length	0.059
R_n	Pulp root separation from pulp hub	0.207
R_n	Pulp tip separation from pulp hub	0.312

aerodynamic structure, and its control mode and motion mode are quite different from those of traditional unmanned helicopters, which need to be studied and analyzed. Therefore, this paper chooses hovering mode as the trim mode and tests the maneuvering and motion characteristics of the unmanned helicopter based on the completely nonlinear mathematical model proposed above.

As shown in Figure 12, applying the step signal to the collective rise of the rotor produces a rotational angle, rotational angular velocity, and vertical velocity response. This is due to the increase in the collective rise of the rotor at constant speed, which leads to an increase in lift, which leads to vertical upward acceleration and velocity. Because the vertical downward direction is the positive direction of the $O_b Z_b$ axis in the body coordinate system, the vertical velocity response is a burden with the increase of collective ascent. The vertical speed finally approaches a stable value, which indicates that there is a first-order inertia relationship between the rise of the collective rotor and the vertical speed without the influence of fans. At the same time, the increase of collective distance increases the torque of unmanned helicopters. In the balance of reversing torque or external torque of unventilated helicopter, the unmanned helicopter produces steering angle, and the horizontal steering angle responds to directional motion. This shows that the vertical steering input of the unmanned monster helicopter is of course associated with the heading channel.

As shown in Figure 13, the longitudinal periodic pitch signal input of the rotor will cause pitch angle pitch angular velocity and linear velocity response in the $O_b X_b$ direction while it will also affect the roll angular velocity roll angle and linear velocity in the $O_b Y_b$ direction. The increase of rotor longitudinal periodic pitch leads to positive pitch angular velocity so that the pitch angle increases and the fuselage rises, resulting in the opposite speed to the $O_b X_b$ direction. The negative inclination angle reduces the inclination angle,

TABLE 4: Length of each operating stage of the rotor head and Bershiller coefficient.

Symbol	Physical meaning	Numerical value
L_0	SW turntable radius	0.020 m
L_1	MR pitch arm	0.032 m
L_2	Connecting rod of Bershiller mixer	0.015 m
L_3		0.017 m
K_b	Bell coefficient	0.322
L_4	Mixing force arm on SB	0.050 m
L_5	SB pitch force arm	0.024 m
L_6	Variable gain connecting rod of SB controlled by the slider	0.013 m
L_7		0.0029 m
K_h	Shearer coefficient	0.7324

TABLE 5: Direct measurement parameters of fuselage and stabilizer.

Symbol	Physical meaning	Numerical value
S_x^{prj}	Forward projection area	0.03 m ²
S_y^{prj}	Lateral projection area	0.11 ²
S_z^{prj}	Vertical projection area	0.06 m ²
STA_{hs}	HS station	1.035 m
WL_{hs}	HS waterline	0.418 m
STA_{vf}	VF station line	1.280 m
WL_{vf}	VF waterline	0.398 m
S_{hs}	Horizontal tail area	0.017 m ²
AR_{hs}	Horizontal tail aspect ratio	1.32
i_{hs}	Horizontal tail inclination	0 rad
S_{vf}	Horizontal tail area	0.011 m ²
AR_{vf}	Vertical tail aspect ratio	3.72
Λ_{vf}	Vertical tail sweep angle	0.4 rad
i_{vf}	Vertical tail inclination	0 rad

TABLE 6: Re-estimated parameters based on measurements.

Symbol	Physical meaning	Numerical value
M_β	Mass moment of main pulp relative to flapping hinge	0.869
I_β	Moment of inertia of main pulp around flapping hinge	0.0467
I_β^{sb}	Moment of inertia of auxiliary pulp relative to pulp hub	0.0034
η_{hs}	Effective dynamic pressure rate of horizontal tail	0.8
η_{vf}	Effective dynamic pressure rate of vertical tail	0.9

and the frame inclines to the left and sideslip occurs, as

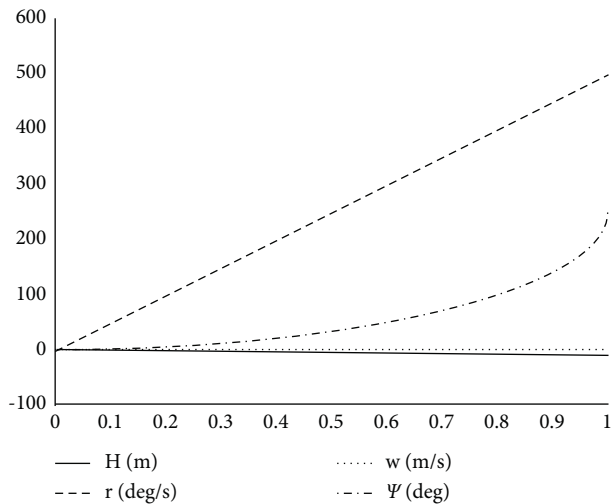


FIGURE 12: Rotor total pitch step response.

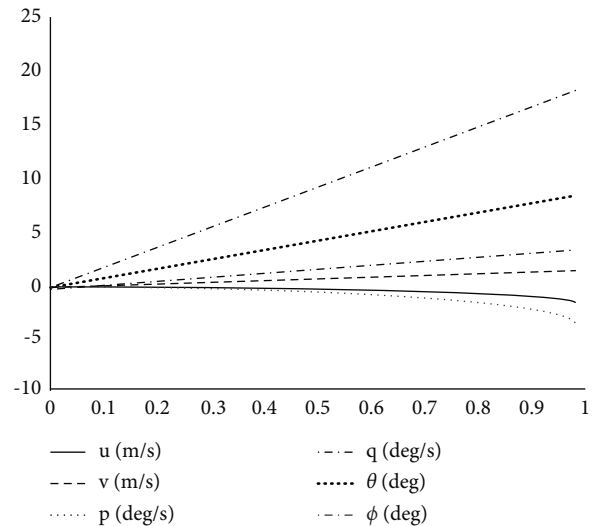


FIGURE 13: Longitudinal periodic variable pitch step response of the rotor.

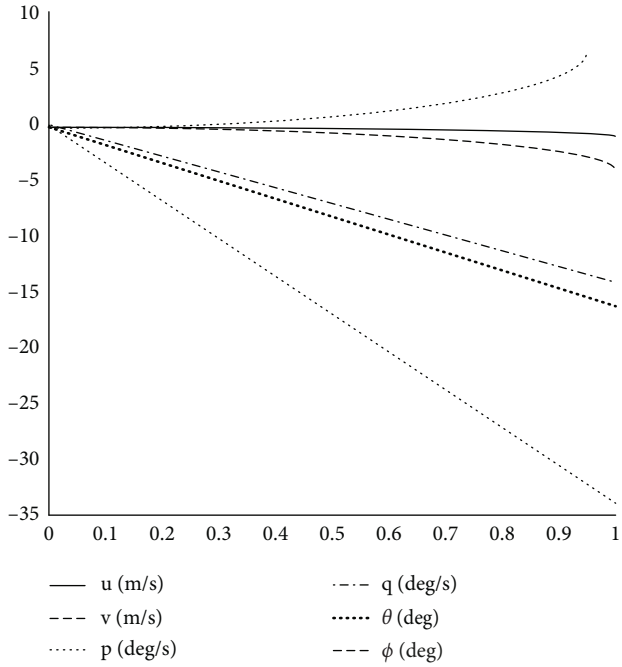


FIGURE 14: Rotor transverse periodic variable pitch step response.

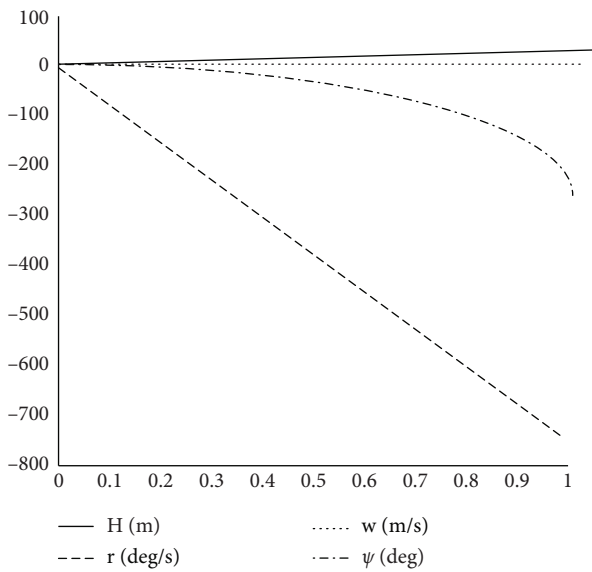


FIGURE 15: Variable pitch step response of the fan.

shown in Figure 14.

The structure of the unmanned helicopter with the coaxial rotor blower is completely symmetrical, so the unmanned model helicopter is basically the same in the $O_b X_b$ direction and $O_b Y_b$ direction. The signal input whose distance varies in the longitudinal period has the same dynamic characteristics.

As shown in Figure 15, applying a step signal to the fan pitch causes yaw angle, yaw angular rate, and vertical velocity response. Fan pitch change is the input signal of the heading channel, and the fan and rotor in ducted fuselage reverse coaxially. Controlling fan pitch change can offset the

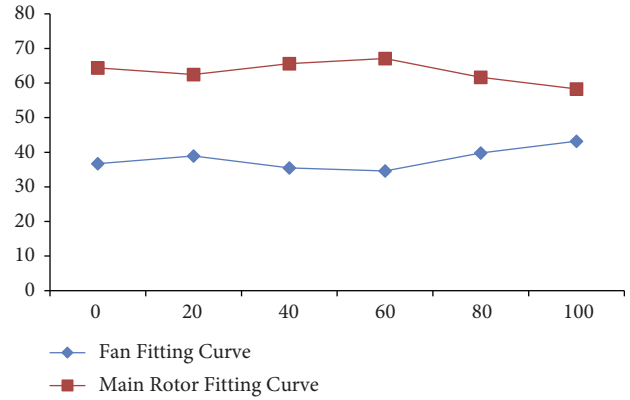


FIGURE 16: Effect of flight speed on lift distribution.

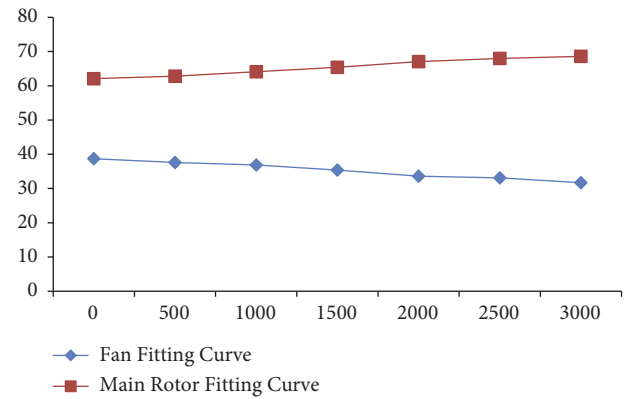


FIGURE 17: Effect of flight altitude on lift distribution.

antitorque of rotor rotation for fuselage and control the heading motion of the unmanned helicopter through the differential torque between them. Similar to the input signal of the vertical channel, the input signal of the heading channel will also have an impact on the vertical channel, but the effect is smaller than that of the total rotor distance, and it is shown in Figures 16 and 17.

5. Concluding Remarks

In this paper, a robust trajectory tracker based on feedback linearization is designed, which is used for the dynamic model of the coaxial unmanned helicopter. Combined with the existing aerodynamic modeling of the coaxial rotor system, a dynamic model which can reflect the aerodynamic disturbance coupling characteristics between coaxial helicopter rotors is established in this paper. In the altitude subsystem, the dynamic feedback linearization of the subsystem is firstly carried out by extending the state variables and analyzing the zero dynamic stability of the system. Then the pole placement of the disconnected subsystem is carried out, and the robust compensator is designed to improve the strength. Finally, the trajectory tracking is realized by designing the outer loop PD control. Simulation results shows that the designed program has good detachment characteristics and still has good tracking performance and robustness in the presence of various model uncertainties.

Data Availability

The experimental data used to support the findings of this study are available from the corresponding author upon request.

Conflicts of Interest

The authors declare that they have no conflicts of interest regarding this work.

Acknowledgments

This study was funded by the National Key Research and Development Project of China (No. 2021YFC3002101).

References

- [1] W. Shi, Q. Ling, K. Yuan, G. Wu, and W. Yin, "On the linear convergence of the ADMM in decentralized consensus optimization," *IEEE Transactions on Signal Processing*, vol. 62, no. 7, pp. 1750–1761, 2014.
- [2] B. Wahlberg, S. Boyd, M. Annergren, and Y. Wang, "An ADMM algorithm for a class of total variation regularized estimation problems," *IFAC Proceedings Volumes*, vol. 45, no. 16, pp. 83–88, 2012.
- [3] D. Davis and W. Yin, "Faster convergence rates of relaxed Peaceman-Rachford and ADMM under regularity assumptions," *Mathematics*, vol. 42, no. 3, 2015.
- [4] T. Lin, S. Ma, and S. Zhang, "On the global linear convergence of the ADMM with multi-block variables," *SIAM Journal on Optimization*, vol. 25, no. 3, 2014.
- [5] F. Wang, W. Cao, and Z. Xu, "Convergence of multi-block Bregman ADMM for nonconvex composite problems," *Science China Information Sciences*, vol. 61, no. 12, Article ID 122101, 2018.
- [6] M. Li, D. Sun, and K. C. Toh, "A convergent 3-block semi-proximal ADMM for convex minimization problems with one strongly convex block," *Asia Pacific Journal of Operational Research*, vol. 32, no. 04, Article ID 1550024, 2015.
- [7] H. Wang, D. Wang, and X. Niu, "Modeling and Hover Control of a Novel Unmanned Coaxial Rotor/Ducted-Fan Helicopter," in *Proceedings of the 2007 IEEE International Conference on Automation and Logistics*, Shandong, China, January 2007.
- [8] D. Schafroth, C. Bermes, S. Bouabdallah, and R. Siegwart, "Modeling, system identification and robust control of a coaxial micro helicopter," *Control Engineering Practice*, vol. 18, no. 7, pp. 700–711, 2010.
- [9] V. Duvvuri, S. Barissi, and N. Houshangi, "Modeling and simulation of an unmanned coaxial helicopter," *Proceedings of the IASTED International Conference on Robotics and Applications*, pp. 423–428, 2010.
- [10] T. Ishii, S. Suzuki, and G. Yanagisawa, "A303 Modeling of Fixed-Pitch Co-axial Rotor Unmanned Helicopter," in *Proceedings of the Dynamics & Design Conference The Japan Society of Mechanical Engineers*, 2011.
- [11] R. Mahony and T. Hamel, "Robust trajectory tracking for a scale model autonomous helicopter," *International Journal of Robust and Nonlinear Control*, vol. 14, no. 12, pp. 1035–1059, 2004.
- [12] C. F. Liu, J. Liu, and S. L. Wu, "Research on Dynamic Robust Compensation Decoupling Controller of Hydraulic Flight simulator," in *Proceedings of the 2008 Chinese Control and Decision Conference*, IEEE, Yantai, Shandong China, June 2008.
- [13] B. Bian and L. Wang, "A robust fuzzy PD inverse dynamics decoupling control of spherical motion mechanism with fuzzy linear extended state observer," *IEEE Access*, vol. PP4, no. 99, p. 1, 2021.
- [14] L. Chen and A. N. Jinwen, "EA/QFT Robust Control of Target Tracking System for Space Vehicle," in *Proceedings of the International Conference on Space Information Technology pt.2*, Shaanxi Xi'an 710072 China, 2005.
- [15] G. Jian, "Pressure observer based adaptive robust trajectory tracking control of a parallel manipulator driven by pneumatic muscles," *Journal of Zhejiang University-Science A: Applied Physics & Engineering*, vol. 8, no. 12, p. 10, 2007.

Research Article

Intelligent Identification of Coal Crack in CT Images Based on Deep Learning

Jinxia Yu,¹ Chengyi Wu ,^{1,2} Yingying Li ,^{2,3} and Yimin Zhang³

¹School of Computer Science and Technology, Henan Polytechnic University, Jiaozuo 454000, China

²State Key Laboratory Cultivation Base for Gas Geology and Gas Control, Henan Polytechnic University, Jiaozuo 454000, China

³School of Computer and Information Engineering, Luoyang Institute of Science and Technology, Luoyang 471023, China

Correspondence should be addressed to Yingying Li; liyinying@lit.edu.cn

Received 30 June 2022; Revised 30 July 2022; Accepted 22 August 2022; Published 23 September 2022

Academic Editor: Le Sun

Copyright © 2022 Jinxia Yu et al. This is an open access article distributed under the Creative Commons Attribution License, which permits unrestricted use, distribution, and reproduction in any medium, provided the original work is properly cited.

Automatic segmentation of coal crack in CT images is of great significance for the establishment of digital cores. In addition, segmentation in this field remains challenging due to some properties of coal crack CT images: high noise, small targets, unbalanced positive and negative samples, and complex, diverse backgrounds. In this paper, a segmentation method of coal crack CT images is proposed and a dataset of coal crack CT images is established. Based on the semantic segmentation model DeepLabV3+ of deep learning, the OS of the backbone has been modified to 8, and the ASPP module rate has also been modified. A new loss function is defined by combining CE loss and Dice loss. This deep learning method avoids the problem of manually setting thresholds in traditional threshold segmentation and can automatically and intelligently extract cracks. Besides, the proposed model has 0.1%, 1.2%, 2.9%, and 0.5% increase in Acc, mAcc, MioU, and FWIoU compared with other techniques and has 0.1%, 0.8%, 2%, and 0.4% increase compared with the original DeepLabV3+ on the dataset of coal CT images. The obtained results denote that the proposed segmentation method outperforms existing crack detection techniques and have practical application value in safety engineering.

1. Introduction

Coal is an important energy source for human society. The phenomenon of deformation and damage of coal and rock mass under load is common, which has a huge impact on the safety of mining engineering. The research on digital core technology based on industrial CT scanning technology is of great significance for the mining safety, and its basis is the high-precision segmentation of cracks in industrial CT scanning images. As the key technology of digital core, 3D reconstruction needs high-precision segmentation results to reflect the original topology of cracks. However, artificial segmentation of coal crack CT images undoubtedly takes a lot of time and energy. And, most of the existing auxiliary software is based on traditional threshold segmentation methods which are still impossible to get rid of the interference of noise even working with some image preprocessing methods. Therefore, intelligent

and automated segmentation of coal crack CT images is particularly important.

Digital images contain a lot of important information, which can be extracted in different ways in different fields. For example, it can be used in the field of encryption technology [1, 2], information security [3–6], in the field of industrial engineering [7], in the field of agriculture [8], and so on. Digital image processing technology includes many categories [9, 10], and image segmentation is one of them. Noise is one of the difficulties in the segmentation of coal crack images. In order to reduce the noise and enhance images, methods that were applied in the segmentation of crack include morphological filter [11], wavelet transforms [12, 13], anisotropic diffusion filter [14], and so on. However, many noises cannot be fundamentally removed by the traditional methods. Machine learning algorithms can achieve automatic crack detection and segmentation to a certain extent including structured forests [15, 16], minimal

path selection [17], support vector machine [18], etc. Nevertheless, most features in machine learning need to be identified by experts and hand-coded. Deep learning models have powerful learning ability which can automatically complete the tasks of classification, detection, and segmentation after training. Starting from FCN [19], many high-performance semantic segmentation models have emerged such as U-net [20], SegNet [21], and PSPNet [22]. These models are based on convolution operations, apply feature extraction networks as backbones, and incorporate multiscale semantic information to achieve pixel-by-pixel segmentation of images. Deep learning methods have been applied in different crack segmentation fields [23–25] nowadays.

In this work, we present an end-to-end coal crack CT image segmentation method based on the deep learning model DeepLabV3+ [26]. Compared with existing deep learning methods, postprocessing is unnecessary for our method. Besides, our method achieves better performance on some evaluation metrics. These advantages are meaningful for the subsequent 3D reconstruction work and the establishment of digital cores.

2. Related Work

All data in this paper comes from the tomograms of high-precision industrial CT during the fracturing experiment of coal samples. The CT scanning equipment is from the Nation Key of Natural Gas Geology and Natural Gas Control of the Henan University of Technology Laboratory which is a phoenix v|tome|xm high-resolution industrial X-ray μ CT scanner [27]. The equipment diagram and CT imaging principle are shown in Figure 1. Images collected by this equipment have many noise points in the coal matrix, and different samples may have different colors. CT image samples of coal cracks are shown in Figure 2. The datasets used for training in this experiment are cut from CT images obtained by the aforementioned platform at different sizes. The diversity of the crack structure is fully considered in the interception process to adapt to the segmentation of different images.

The high performance of deep learning in computer vision was first demonstrated in classification tasks. Many CNN models can provide good classification accuracy such as Vgg [28], ResNet [29], Xception [30], and so on. Some of them are applied as feature extractors in segmentation models. FCN replaces the fully connected layer in the classification model with deconvolution to upsample the pooled feature map to its original size, pioneered semantic segmentation. The application of deep learning in crack detection can be roughly divided into three types, methods based on classification [31], object detection [32], and semantic segmentation [33, 34]. Xue et al. [35] modified the last few deconvolution modules of FCN to adapt to the needs of crack segmentation. However, this FCN-based method may not be able to guarantee the accuracy of segmentation and maintain the original topological structure of the crack when facing the crack of complex structures.

DeepLabV3+ is a high-performance semantic segmentation model derived from DeepLabV1, V2, and V3 [36–38]. In view of the adverse effect of excessive downsampling on segmentation accuracy, this model proposed to use atrous convolution to reduce downsampling and enlarge the receptive field simultaneously. This model also applied atrous spatial pyramid pooling to capture and fuse multi-scale semantic information which is beneficial to improving the accuracy of segmentation. Besides, Encoder-Decoder architecture is used to recover pixels of features better. DeepLabV3+ achieves new state-of-the-art performance on PASCAL VOC 2012 dataset. However, compared with the public semantic segmentation dataset, the crack image dataset has the characteristics of smaller targets and unbalanced positive and negative samples. So we have made some improvements to the original model for these characteristics. The coal crack CT image segmentation method that we proposed has the following contributions:

- (1) Given that there are no publicly available datasets for research in this field, we established a dataset of coal crack CT images for our research. All original pictures come from a professional coal sample fracturing experimental platform and all labels are made by hand marking.
- (2) We modified DeepLabV3+ to adapt to the need for coal crack CT images by adjusting the OS of the backbone, adjusting the encoder-decoder module, and changing the rates of the ASPP module. The modified model achieves better performance than the original model under some authoritative evaluation indicators commonly used in semantic segmentation: PA, MPA, MIoU, and FWIoU.
- (3) A new loss function is defined by combining the CE loss and Dice loss. While adding contour factors to the prediction, the curve fluctuation of the Dice function in the training is alleviated.

3. Methodologies

3.1. Dataset. Since there is no open-source dataset for CT segmentation images of coal crack, we established a coal crack dataset manually. All these images were taken from the original coal fracturing experimental images in different sizes and different length-width ratios. All data were captured in images acquired by high precision industrial CT introduced before. It consists of 437 RGB images and their segmentation labels, including different crack shapes, complexities, and different background colors. Some representative images and their annotations are shown in Figure 3. These samples can reflect the complexity of crack morphology, noise situation, and background differences in the dataset to a certain extent.

Data augmentation is a technique widely used in deep learning. In supervised learning, fine data annotation is a time-consuming and energy consuming work. Data augmentation can expand the dataset so that the parameters learned during model training are more reliable and can effectively avoid overfitting. So we enhanced the coal crack

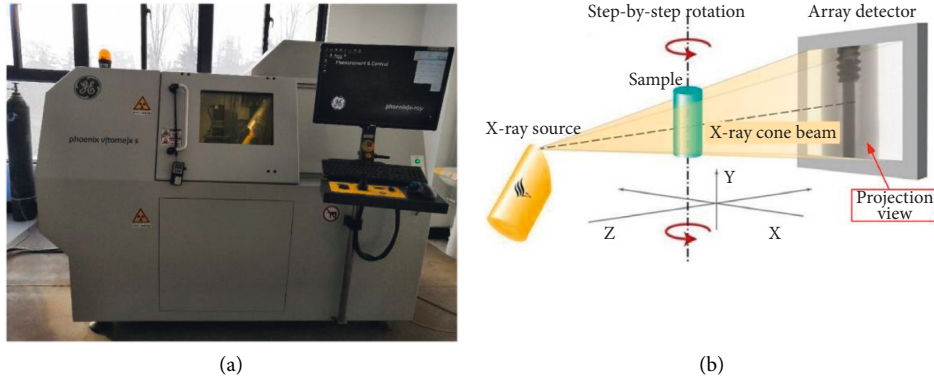


FIGURE 1: (a) High-precision industrial CT scanning equipment; (b) Schematic diagram of the scanning device.

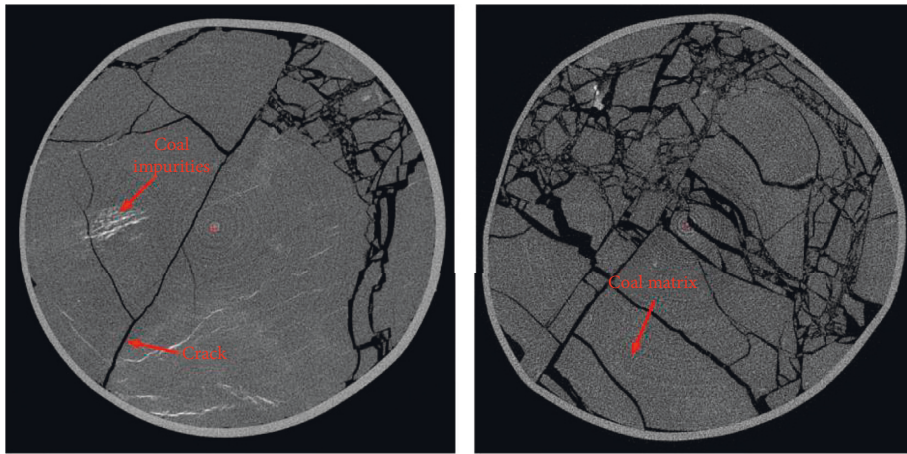


FIGURE 2: CT image samples of coal crack.

dataset to 5000 in different ways: rotation, flip and zoom. Angles of rotation were limited to -30 to 30 degrees, the flip direction is horizontal and the ratios of zoom were limited to 80% to 120% . Finally, after data augmentation, the training set contains 3500 images and the test set contains 1500 images.

3.2. Atrous Spatial Pyramid Pooling. Atrous convolution can be used to capture multiscale contextual information. The parameter can set different dilation rates of atrous convolution which can be regarded as the stride of the input signal we sample. The output of atrous convolution of a one-dimensional input signal with a filter of length is defined as follows:

$$y[i] = \sum_{k=1}^K x[i + r \cdot k]w[k]. \quad (1)$$

Combined with spatial pyramid pooling, ASPP is applied as a Multiscale information fusion module. The structure which is applied in the DeepLabV3+ model achieved multiscale information collection using four different rates of atrous convolutions (including image-level pooling). Different from the rates of (1, 6, 12, and 18) used in the original

DeepLabV3+, more kinds of combinations of rates were tried using to make the feature extractor more suitable for crack segmentation. As the OS (Output Stride) of the backbone was adjusted to 8 to reduce downsampling, a larger receptive field is required. We tried to make the enlargement of the receptive field follow the size of the feature map output from the backbone. And, the experiment proved that rates of (1, 12, 24, 36) can achieve a better performance. A more intuitive situation about ASPP can be seen in Figure 4.

3.3. Encoder-Decoder. The encoder-decoder structure is widely applied in the field of computer vision. As for the semantic segmentation field, the encoder gains semantic information from images with feature maps reducing as a feature extraction module. DeepLabV3+ model uses DeepLabV3 as the encoder block with some effective improvement. The decoder is applied to reconstruct the segmentation result by restoring the pixel and size of the feature map, at the same time, keeping the details of the original image as much as possible. DeepLabV3+ proposed a simple decoder as shown in Figure 4 and obtained a good effect practically. The first upsampling rate was adjusted to 2 as the OS of the backbone was changed to 8.

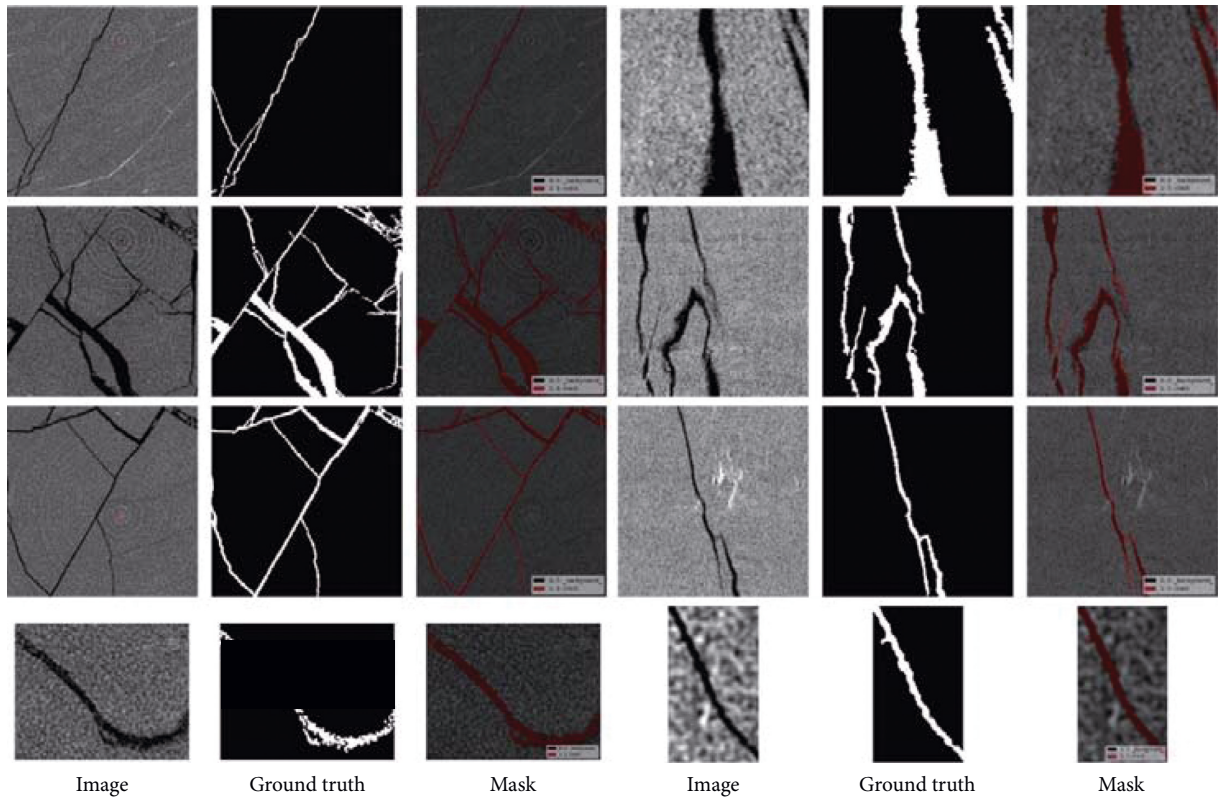


FIGURE 3: Some representative images in our datasets, their ground truth, and masks on original images. It shows that these pictures show that our dataset contains data of different sizes, different complexities, and different background color depths at the same time. Diversity allows the model trained on this dataset to adapt to most CT image environmental conditions.

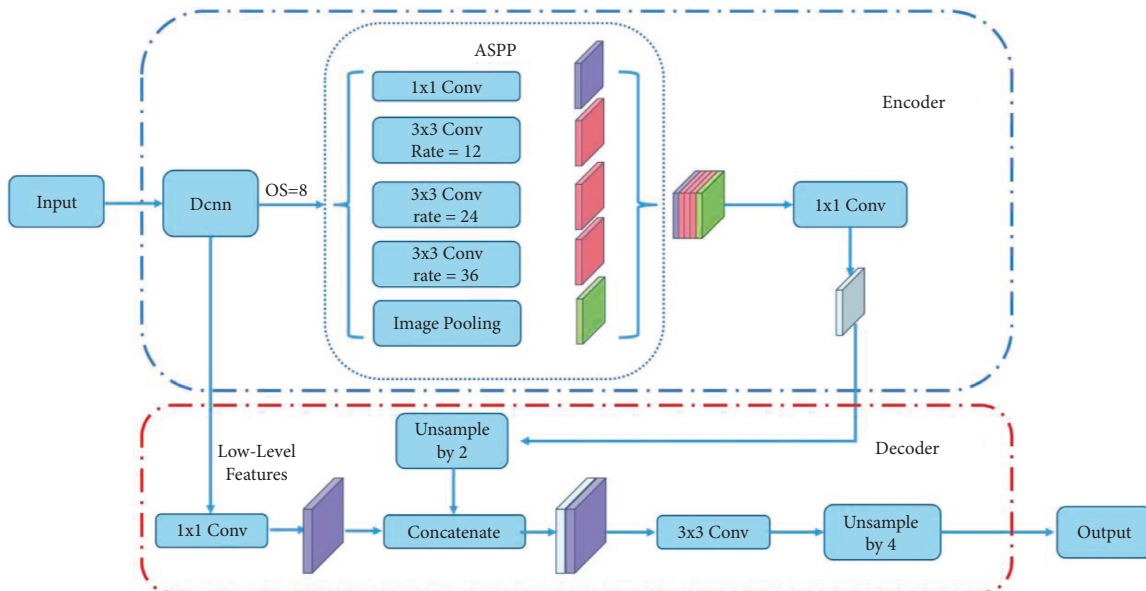


FIGURE 4: Modified DeepLabV3+ model structure. Compared with the original DeepLabV3+ architecture, the OS (output stride) was adjusted to 8, and rates of the ASPP module were adjusted to (1, 12, 24, 36). At the same time, the first upsampling rate is changed from 4 to 2 to restore image pixels to their original size.

3.4. *Adjusted Xception as Backbone.* Xception, as a high-performance convolution neural network is applied as the feature extractor of ordinary DeepLabV3+. This deep structure is developed based on the Inception model and based

entirely on depthwise separable convolution. Unlike conventional convolution, in depthwise separable convolution, each feature map channel only needs to perform an operation with each channel of the convolution kernel. This kind of

convolution can effectively reduce the number of parameters and computing costs, and by using this, Xception expanded the scale of the model and became state-of-the-art CNN architecture in classification tasks. The ordinary Xception has an OS = 32 so that it can adapt to the needs of classification tasks. But excessive pooling makes the feature maps too small so that the detailed information can be damaged. In order to get dense feature maps, the OS of 16 or 8 is desirable.

Different from the OS of 16 which performed better in natural scene datasets, crack images need a denser way to extract features because the targets of these images are tiny in most cases. For these small targets, downsampling has a particularly serious loss of accuracy. So the OS of 8 was used in this model, at the same time, the ASPP was adjusted to get a larger receptive field and the decoder also made corresponding adjustments. To achieve this goal, compared with the Xception structure in the DeepLabV3+ original text, we adjusted the stride of the third block of entry flow to 1, and correspondingly doubled the rate of the atrous convolution in the middle flow and the exit flow. The adjusted Xception structure is shown in Figure 5.

3.5. Loss Function. DeepLab series model apply the cross-entropy (CE) loss function which is widely applied in classification tasks to classify every single pixel. This loss function checks each pixel separately and compares the class prediction (the pixel vector in the depth direction) with the hot encoding target vector. The cross-entropy function can be formulated as follows:

$$L_{ce} = -\frac{1}{N} \sum_i \sum_{c=1}^M y_{ic} \log(p_{ic}), \quad (2)$$

where M refers to the number of categories, y_{ic} refers to the sign function (0 or 1), and p_{ic} refers to the predicted probability that the observed sample i belongs to category c . Thus, we can consider that the pixels in the image are learned equally with the cross-entropy loss function, and this kind of equality does not apply to the situation where the sample is extremely uneven. In coal crack CT images, the number of pixels corresponding to the crack is much smaller than that of the background. Taking the dataset we established as an example, the proportion of crack pixels in the whole image is less than 5%. Dice Loss [39] was proposed in 2016, designed to deal with scenarios where positive and negative samples are strongly imbalanced in semantic segmentation. Different from distribution-based cross-entropy loss, the Dice function is based on region and is used to calculate the similarity between two images. The Dice coefficient and Dice loss function can be formulated as follows:

$$dice = \frac{2|X \cap Y|}{|X| + |Y|}, \quad (3)$$

$$L_{dice} = 1 - \frac{2|X \cap Y|}{|X| + |Y|},$$

where X and Y refer to two different samples, they are ground truth and predict mask in segmentation tasks. In a

different way, the Dice coefficient and the loss function can be formulated as follows:

$$dice = \frac{2TP}{2TP + FP + FN}, \quad (4)$$

$$L_{dice} = 1 - \frac{2TP}{2TP + FP + FN}.$$

Where FP , FN refer to true positive, false positive, and false negative. However, although Dice loss can calculate the similarity of two contours, it may cause the gradient to change drastically, and the training is difficult so it is not credible to a certain extent sometimes. In this experiment, we did a weighted additive combination of CE loss and Dice loss to add contour features to the classification of pixels and avoid the shock of loss in training. The new loss function is formulated as follows:

$$L_{new} = \beta \cdot L_{ce} + L_{dice}, \quad (5)$$

where β is a weight coefficient for adjusting the proportion of CE function. It is a constant in the range $[0, 1]$, and the value of this article is 0.5. The experiment proved that this new loss function effectively improves the accuracy of crack segmentation compared to using the cross-entropy loss function alone.

4. Experiments

All experiments were done in the following environment: Intel (R) Xeon(R) Bronze 3204 CPU @ 1.90 GHz, 32 GB RAM, GPU Tesla V100, CentOS Linux release 7.6.1810. And experiments related to deep learning are completed under PyTorch 1.10.0. We compare the proposed method with existing representative algorithms to the performance of the model on the dataset we established and also compare the visual effects of these segmentation results.

4.1. Metrics. In order to evaluate our work, in addition to the visual effects of segmentation images, we introduced four authoritative evaluation indicators commonly used in semantic segmentation. All experiments are performed on the dataset we established.

Suppose k is the number of categories (background is excluded), p_{ij} indicates that the total number of pixels that are mispredicted. p_{ii} means, p_{ij} means FP and p_{ji} means FN . Four evaluations are

- (1) PA, which means the rate of the number of predicted right pixels to total pixels. It can be expressed as follows:

$$PA = \frac{\sum_{i=0}^k P_{ii}}{\sum_{i=0}^k \sum_{j=0}^k P_{ij}}. \quad (6)$$

- (2) MPA, which means the average pixel accuracy of each category. It can be expressed as follows:

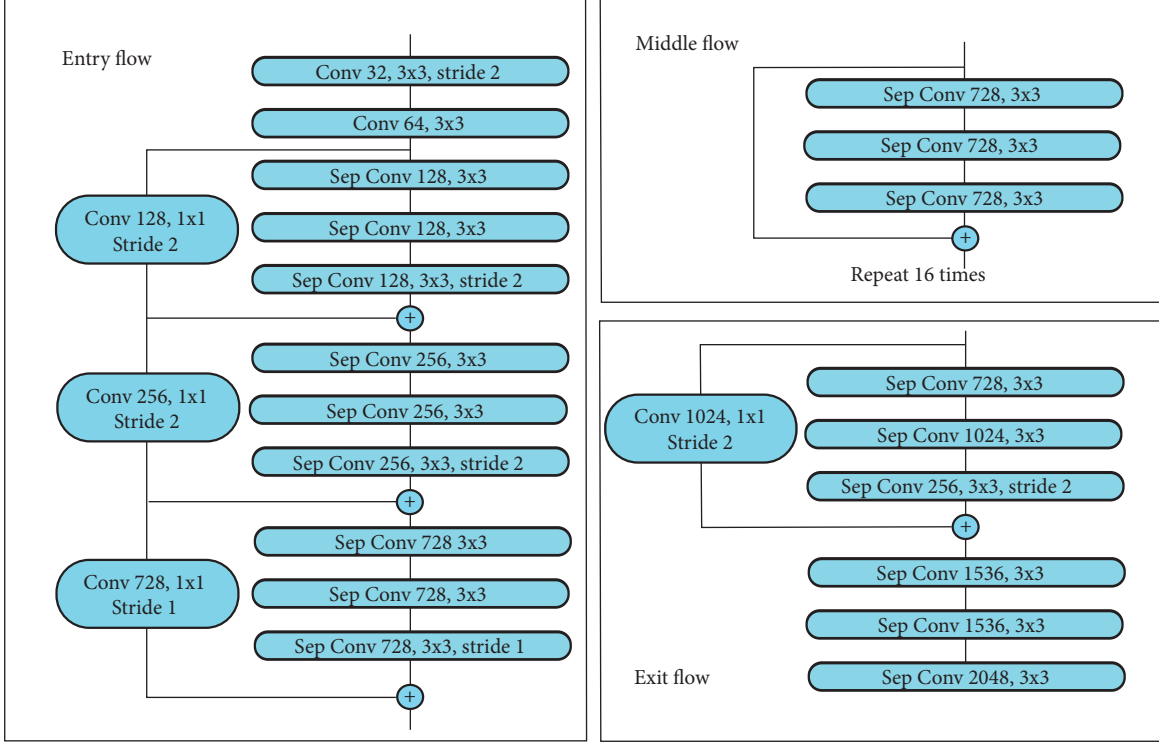


FIGURE 5: Modified Xception architecture. OS of the third block was adjusted to 1 to change the OS of the overall Xception to 8.

$$MPA = \frac{1}{k+1} \sum_{i=0}^k \frac{P_{ii}}{\sum_{j=0}^k P_{ij}}. \quad (7)$$

- (3) MIoU, which represents the IoU of each category. It can be expressed as follows:

$$MIoU = \frac{1}{k+1} \sum_{i=0}^k \frac{P_{ii}}{\sum_{j=0}^k P_{ij} + \sum_{j=0}^k P_{ji} - P_{ii}}. \quad (8)$$

- (4) FWIoU, which sets the weight for IoU of each class according to the frequency of its appearance. It can be expressed as follows:

$$FWIoU = \frac{1}{\sum_{i=0}^k \sum_{j=0}^k P_{ij}} \sum_{i=0}^k \frac{P_{ij} \sum_{j=0}^k P_{ij}}{\sum_{j=0}^k P_{ij} + \sum_{j=0}^k P_{ji} - P_{ii}}. \quad (9)$$

4.2. Ablation Experiments. To scrutinize the effectiveness of the methods we proposed, we conduct experiments with two different backbones which are used in the original DeepLabV3+. Hyperparameters used by these methods are shown in Table 1. When using the ResNet101 as the backbone, the model is trained by three following strategies: (1) DeepLabV3+-res, which is an unmodified DeepLabV3+ model applying ResNet101 [40] as the backbone. (2) DeepLabV3+-res-8 changes OS to 8 and ASPP rates to (1, 12, 24, 36) on the basis of DeepLabV3+-res. (3) DeepLabV3+-x-8-NL changes loss function to the new loss on the basis of DeepLabV3+-x-8. And, the experiment results are shown in Table 2. When

TABLE 1: Hyperparameters of six training strategies.

Batch size	LR	Epochs	LR scheduler	Weight decay	Momentum
16	0.007	100	Poly	$5e-4$	0.9

TABLE 2: Comparison of model modifications with the backbone of ResNet101.

Methods	Acc (%)	mAcc (%)	MIoU (%)	FWIoU (%)
DeepLabV3+-res	98.4	94.0	86.2	97.1
DeepLabV3+-res-8	98.5	94.5	87.1	97.4
DeepLabV3+-res-8-NL	98.5	95.1	88.5	97.5

using the Xception as the backbone, the model is trained by three following strategies: (1) DeepLabV3+-x, which is an unmodified DeepLabV3+ model applying Xception as the backbone. (2) DeepLabV3+-x-8 changes OS to 8 and ASPP rates to (1,12,24,36) on the basis of DeepLabV3+-x. (3) DeepLabV3+-x-8-NL changes loss function to the new loss on the basis of DeepLabV3+-x-8. Results are shown in Table 3. In order to more vividly reflect the advantages of our method, histograms were drawn in Figures 6 and 7.

It can be seen in Tables 2 and 3, adjusted the OS to 8 and using new loss improve all evaluation metrics. When the backbone is ResNet101, by our methods, the Acc, mAcc, MIoU, and FWIoU improved by 0.1%, 1.1%, 2.3%, and 0.4%. When the backbone is Xception, by our methods, the Acc,

TABLE 3: Comparison of model modifications with the backbone of Xception.

Methods	Acc (%)	mAcc (%)	MIoU (%)	FWIoU (%)
DeepLabV3+-x	98.5	94.6	87.4	97.3
DeepLabV3+-x-8	98.6	94.9	88.0	97.5
DeepLabV3+-x-8-NL	98.6	95.4	89.4	97.7

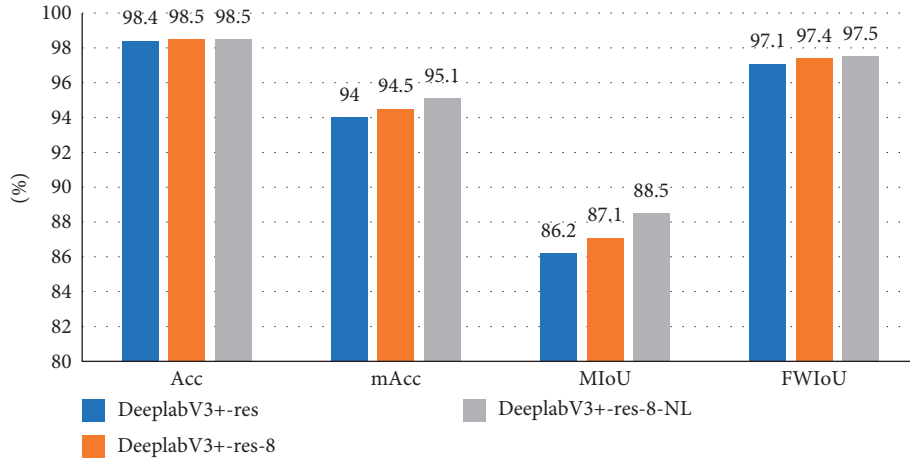


FIGURE 6: Histogram ablation experiment results with the backbone of ResNet101.

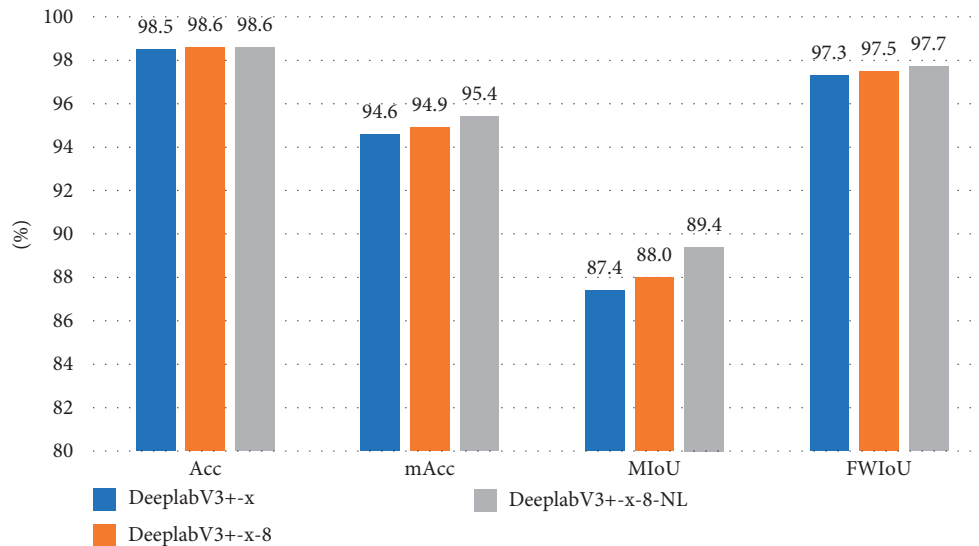


FIGURE 7: Histogram ablation experiment results with the backbone of Xception.

TABLE 4: Comparison of performance of our method and others.

Methods	Acc (%)	mAcc (%)	MIoU (%)	FWIoU (%)
Proposed method	98.6	95.4	89.4	97.7
FCN-32s-vgg16 [10]	97.6	85.4	76.7	93.3
PSPNet-res50 [12]	97.0	80.4	75.1	92.9
U-net-res50 [13]	98.5	94.2	86.5	97.2

mAcc, MIoU, and FWIoU improved by 0.1%, 0.8%, 2.0%, and 0.4%. Experimental results confirm the effectiveness of the proposed method.

4.3. *Comparing with Existing Methods.* We compare the proposed method in this paper with other three typical methods: (1) FCN, the most classic semantic segmentation

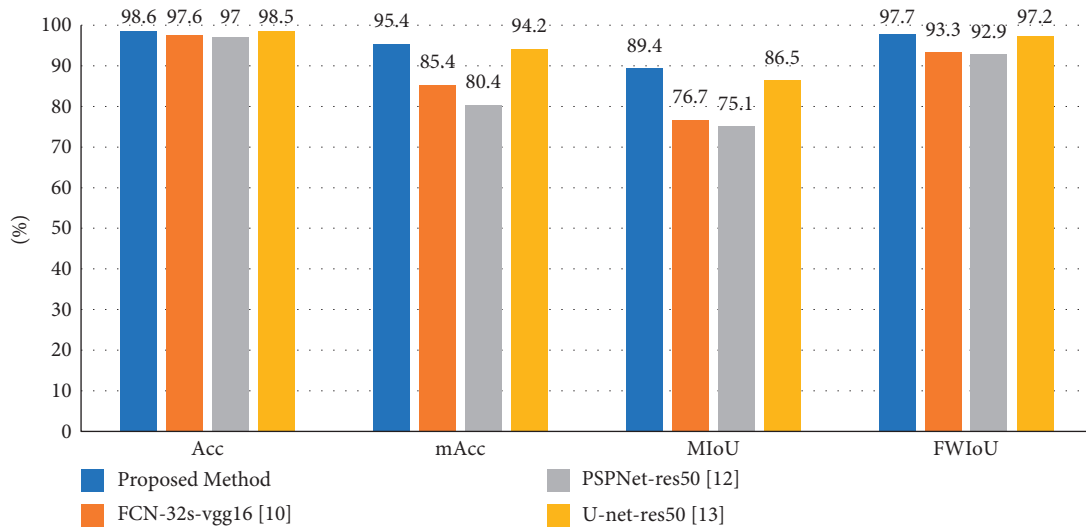


FIGURE 8: Histogram comparison of performance of our method and others.

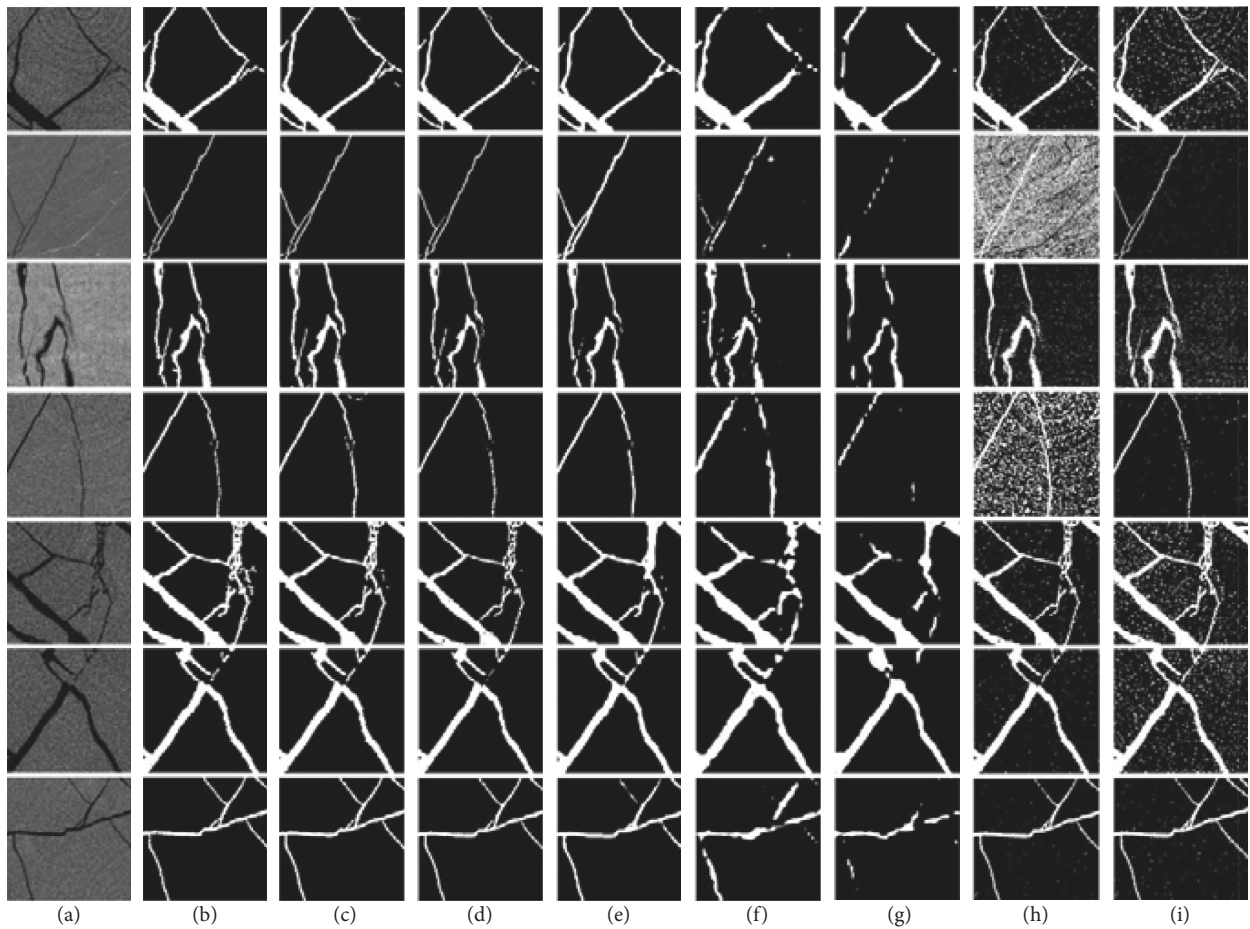


FIGURE 9: Visual effect comparison of prediction results of different methods. The columns are (a) original image, (b) ground truth, (c) our method, (d) DeepLabV3+-Xception, (e) U-net, (f) FCN32s-vgg16, (g) PSPNet, (h) Ostu, and (i) Max Entropy.

network. (2) U-net, the most widely used segmentation network in the medical field. (3) PSPNet, a very efficient model which applies a pyramid pooling module to fusion features on different levels. The feature extractors of all networks apply transfer learning techniques and are fine-tuned on our augmented dataset. Besides, all these models have trained 100 epochs with regular hyperparameters, and the convergence of these models was guaranteed. We also implement two different threshold segmentation methods on our test set to compare the segmentation effects between traditional methods and deep learning methods: (1) Otsu [41] (2) Max Entropy [42]. The two methods represent different automatic threshold determination methods.

A comparison of evaluation metrics of all these methods is shown in Table 4. As we can see, since the proportion of cracks in the images is very low, and the judgment error rate of image background pixels is low so that the total pixel accuracy of every method is not very different. However, the performance of different methods can still be judged from the remaining evaluation indicators. PSPNet and FCN may have good performance in semantic segmentation under natural conditions, but they do not perform well on the coal crack CT image dataset. U-net is designed to deal with medical images which have similarities with the images we used, so this model can have a nice performance. As the best performing comparison method, U-net achieved an Acc of 98.5%, mAcc of 94.2, MIoU of 86.5%, and a FWIoU of 97.2% which are 0.1%, 1.2%, 2.9%, and 0.5% lower than proposed method. A histogram comparison of the experimental results is shown in Figure 8.

Figure 9 shows a visual effect comparison of segmentation results of all methods. It can be seen that the method we proposed has a certain improvement in the dataset in this paper. Compared with the original DeepLabV3+, the ability to capture details has been improved and cracks whose pixel values are close to the background can be identified. Many locations that should be connected become disconnected during the segmentation process of other models, this problem is also alleviated by our method. Other deep learning methods even have a large number of separation cracks sticking together, which is caused by the insufficient segmentation performance. In addition, the shape and structure of cracks is not guaranteed. Experiments show that less downsampling and the addition of the Dice loss function allow the details to be effectively preserved and recovered. Comparing deep learning methods and traditional threshold segmentation methods, the noise problem is difficult to solve for threshold even though different thresholding methods are used. Although some deep learning methods are rough for object segmentation, they often do not misidentify noise.

5. Conclusions

In this paper, we propose a deep learning method to complete the CT image segmentation task of coal crack CT images. Since the target in the crack image is small, and downsampling can lose the accuracy to some extent, the OS of the backbone was proposed to be reasonably adjusted to reduce the loss of accuracy and adjusted the structure of

ASPP to adapt to this adjustment. In order to solve the problem of uneven sample distribution, CE loss and Dice loss were combined to define a new loss function. The experimental results show that our method is effective and has practical application value.

Nevertheless, the presented method can be improved in the following directions. First, scale-up datasets to accommodate more complex environments. And, more data will be added to this dataset which has more complex topologies and tiny targets. Moreover, we will define a new loss function according to the specific target proportion in the data set combined with probability mathematics which may be more adaptable to the needs of the field than the loss function in this paper.

Data Availability

The experimental data used to support the findings of this study are available from the corresponding author upon request.

Conflicts of Interest

The authors declare that there are no conflicts of interest regarding the publication of this paper.

Acknowledgments

The authors would like to thank the grants supported by the Support Plan of Scientific and Technological Innovation Team in Universities of Henan Province (Grant no. 20IRTSTHN013), the State Key Laboratory Cultivation Base for Gas Geology and Gas Control (Henan Polytechnic University) (Grant no. WS2020B13).

References

- [1] Z. Qu, S. Chen, and X. Wang, "A secure controlled quantum image steganography algorithm," *Quantum Information Processing*, vol. 19, no. 10, pp. 380–425, 2020.
- [2] Z. Qu, H. Sun, and M. Zheng, "An efficient quantum image steganography protocol based on improved EMD algorithm," *Quantum Information Processing*, vol. 20, no. 2, pp. 53–29, 2021.
- [3] Y. Tang, H. Lian, L. Li, X. Wang, and X. Yan, "A randomness detection method of ZigBee protocol in a wireless sensor network," *Sensors*, vol. 18, no. 11, p. 3962, 2018.
- [4] Y. Tang, J. Li, X. Yan, and Q. Zhao, "Edge-cloud-assisted multiuser forward secure searchable encryption (EMFSSE) scheme in the P2P networking environment," *Mobile Information Systems*, vol. 2021, pp. 2021–2114, 2021.
- [5] Z. Qu, Y. Huang, and M. Zheng, "A novel coherence-based quantum steganalysis protocol," *Quantum Information Processing*, vol. 19, no. 10, pp. 362–419, 2020.
- [6] Z. Qu, X. Liu, and S. Wu, "Quantum identity authentication protocol based on three-photon quantum error avoidance code," in *Proceedings of the 2019 International Conference on Internet of Things (iThings) and IEEE Green Computing and Communications (GreenCom) and IEEE Cyber, Physical and Social Computing (CPSCom) and IEEE Smart Data (Smart-Data)*, pp. 471–475, IEEE, Atlanta, GA, USA, July 2019.
- [7] Z. Luo, Y. Zhang, K. Wang, and L. Sun, "Detection of pine cones in natural environment using improved YOLOv4 deep

- learning algorithm,” *Computational Intelligence and Neuroscience*, vol. 2021, pp. 2021–12, 2021.
- [8] F. Dong and Y. Ma, “Railway traffic emergency management relying on image recognition technology in the context of big data,” *Computational Intelligence and Neuroscience*, vol. 2022, pp. 1–12, 2022.
- [9] Y. Tang, M. Zhao, and L. Li, “Secure and efficient image compression-encryption scheme using new chaotic structure and compressive sensing,” *Security and Communication Networks*, vol. 2020, pp. 1–15, 2020.
- [10] D. Khan, M. A. Muneer, Z. U. Nisa et al., “Effect of climatic factors on stem biomass and carbon stock of Larix gmelinii and Betula platyphylla in Daxing’anling Mountain of Inner Mongolia, China,” *Advances in Meteorology*, vol. 1, no. 10, 2019.
- [11] H. Oliveira and P. L. Correia, “Automatic road crack segmentation using entropy and image dynamic thresholding,” in *Proceedings of the 2009 17th European Signal Processing Conference*, Glasgow, UK, 24–28 August 2009.
- [12] S. Wu and Y. Liu, *A Segment Algorithm for Crack Detection*, Electrical & Electronics Engineering, 2012.
- [13] J. Zhou, “Wavelet-based pavement distress detection and evaluation,” *Optical Engineering*, vol. 45, no. 2, pp. 027007–027411, 2006.
- [14] D. Andrushia, N. Anand, and P. Arulraj, “Anisotropic diffusion based denoising on concrete images and surface crack segmentation,” *International Journal of Structural Integrity*, vol. 11, no. 3, pp. 395–409, 2019.
- [15] Y. Shi, L. Cui, Z. Qi, F. Meng, and Z. Chen, “Automatic road crack detection using random structured forests,” *IEEE Transactions on Intelligent Transportation Systems*, vol. 17, no. 12, pp. 3434–3445, 2016.
- [16] B. Nair, “Fast edge detection using structured forests,” *International Journal of Emerging Trends & Technology in Computer Science*, vol. 34, 2016.
- [17] R. Amhaz, S. Chambon, J. Idier, and V. Baltazart, “Automatic crack detection on two-dimensional pavement images: an algorithm based on minimal path selection,” *IEEE Transactions on Intelligent Transportation Systems*, vol. 17, no. 10, pp. 2718–2729, 2016.
- [18] G. Li, X. Zhao, K. Du, F. Ru, and Y. Zhang, “Recognition and evaluation of bridge cracks with modified active contour model and greedy search-based support vector machine,” *Automation in Construction*, JUN, vol. 78, , pp. 51–61, 2017.
- [19] E. Shelhamer, J. Long, and T. Darrell, “Fully convolutional networks for semantic segmentation,” *IEEE Transactions on Pattern Analysis and Machine Intelligence*, vol. 39, no. 4, pp. 640–651, 2017.
- [20] O. Ronneberger, P. Fischer, and T. Brox, *U-net: Convolutional Networks for Biomedical Image Segmentation*, Springer International Publishing, 2015.
- [21] V. Badrinarayanan, A. Kendall, and R. Cipolla, *SegNet: A Deep Convolutional Encoder-Decoder Architecture for Image Segmentation*, Entry, 2017.
- [22] H. Zhao, J. Shi, X. Qi, X. Wang, and J. Jia, *Pyramid Scene Parsing Network*, IEEE Computer Society, 2016.
- [23] Y. Liu, J. Yao, X. Lu, R. Xie, and L. Li, “DeepCrack: a deep hierarchical feature learning architecture for crack segmentation,” *Neurocomputing*, vol. 338, no. 21, pp. 139–153, 2019.
- [24] S. Wang, X. Wu, Y. Zhang, X. Liu, and L. Zhao, “A neural network ensemble method for effective crack segmentation using fully convolutional networks and multi-scale structured forests,” *Machine Vision and Applications*, vol. 31, no. 7–8, p. 60, 2020.
- [25] E. Protopapadakis, A. Voulodimos, A. Doulamis, N. Doulamis, and T. Stathaki, “Automatic crack detection for tunnel inspection using deep learning and heuristic image post-processing,” *Applied Intelligence*, vol. 343, 2019.
- [26] L. C. Chen, Y. Zhu, G. Papandreou, F. Schroff, and H. Adam, *Encoder-Decoder with Atrous Separable Convolution for Semantic Image Segmentation*, Springer, Cham, 2018.
- [27] Y. Li, H. Cui, P. Zhang, D. Wang, and J. Wei, “Three-dimensional visualization and quantitative characterization of coal fracture dynamic evolution under uniaxial and triaxial compression based on μ CT scanning,” *Fuel*, vol. 262, p. 116568, 2020.
- [28] K. Simonyan and A. Zisserman, “Very deep convolutional networks for large-scale image recognition,” *Computer Science*, vol. 22, p. 12866, 2014.
- [29] K. He, X. Zhang, S. Ren, and J. Sun, *Deep Residual Learning for Image Recognition*, IEEE, 2016.
- [30] F. Chollet, “Xception: deep learning with depthwise separable convolutions,” in *Proceedings of the 2017 IEEE Conference on Computer Vision and Pattern Recognition (CVPR)*, Honolulu, HI, USA, 21–26 July 2017.
- [31] Z. Lei, F. Yang, D. Zhang, and J. Z. Ying, “Road crack detection using deep convolutional neural network,” in *IEEE International Conference on Image Processing*, 2016.
- [32] G. Suh and Y. J. Cha, “Deep faster R-CNN-based automated detection and localization of multiple types of damage,” in *Sensors and Smart Structures Technologies for CivilMechanical, and Aerospace Systems*, 2018.
- [33] Y. Liu, J. Yao, X. Lu, R. Xie, and L. Li, “DeepCrack: a deep hierarchical feature learning architecture for crack segmentation,” *Neurocomputing*, vol. 338, no. 21, pp. 139–153, 2019.
- [34] E. Protopapadakis, A. Voulodimos, A. Doulamis, N. Doulamis, and T. Stathaki, “Automatic crack detection for tunnel inspection using deep learning and heuristic image post-processing,” *Applied Intelligence*, vol. 76, pp. 28–86, 2019.
- [35] X. Xue, “FCN-based intelligent identification and fractal reconstruction of pore-fracture network in coal by micro CT scanning,” *Chinese Journal of Rock Mechanics and Engineering*, vol. 39, no. 6, p. 19, 2020.
- [36] L. C. Chen, G. Papandreou, I. Kokkinos, K. Murphy, and A. L. Yuille, “Semantic image segmentation with deep convolutional nets and fully connected CRFs,” *Computer Science*, vol. 4, pp. 357–361, 2014.
- [37] L. C. Chen, G. Papandreou, I. Kokkinos, K. Murphy, and A. L. Yuille, “DeepLab: semantic image segmentation with deep convolutional nets, atrous convolution, and fully connected CRFs,” *IEEE Transactions on Pattern Analysis and Machine Intelligence*, vol. 40, no. 4, pp. 834–848, 2018.
- [38] L. C. Chen, G. Papandreou, F. Schroff, and H. Adam, *Rethinking Atrous Convolution for Semantic Image Segmentation*, IEEE, NEW JERSEY, 2017.
- [39] F. Milletari, N. Navab, and S. A. Ahmadi, “V-net: fully convolutional neural networks for volumetric medical image segmentation,” *2016 Fourth International Conference on 3D Vision (3DV)*, vol. 76, p. 65654, 2016.
- [40] K. He, X. Zhang, S. Ren, and J. Sun, *Deep Residual Learning for Image Recognition*, IEEE, NEW JERSEY, 2016.
- [41] N. Otsu, “A threshold selection method from gray-level histograms,” *IEEE Transactions on Systems, Man, and Cybernetics*, vol. 9, no. 1, pp. 62–66, 1979.
- [42] T. Pun, “A new method for grey-level picture thresholding using the entropy of the histogram,” *Signal Processing*, vol. 2, no. 3, pp. 223–237, 1980.

Research Article

Study on Personalized Recommendation Algorithm of Online Educational Resources Based on Knowledge Association

Ziqian Xu ¹ and Sheng Jiang ²

¹Huai'an Campus of Nanjing Forestry University, Nanjing, Jiangsu 210037, China

²School of Mechatronics and Information, Wuxi Vocational Institute of Arts and Technology, Yixing 214206, China

Correspondence should be addressed to Ziqian Xu; zqxu@njfu.edu.cn

Received 1 July 2022; Accepted 6 September 2022; Published 20 September 2022

Academic Editor: Le Sun

Copyright © 2022 Ziqian Xu and Sheng Jiang. This is an open access article distributed under the Creative Commons Attribution License, which permits unrestricted use, distribution, and reproduction in any medium, provided the original work is properly cited.

In order to overcome the problems of low accuracy, low recommendation efficiency, and low user satisfaction of educational resources recommendation algorithm, this paper proposes a personalized recommendation algorithm for online educational resources based on knowledge association. Firstly, online education resources are collected according to association rules. Secondly, firefly algorithm is used to classify online education resources. Then, the vector space function is constructed to filter the classified online education resources. Finally, the correlation between knowledge points is calculated by knowledge association theory, and the knowledge with the highest user interest is selected as the target recommendation resource to realize the personalized recommendation of online education resources. The resource recommendation accuracy of this method can reach 97%, the recommendation time is less than 5.0 s, and users are more satisfied with it, indicating that its recommendation effect is good.

1. Introduction

At this stage, Internet technology and information processing technology are developing at a rapid speed, making people enter the big data era. Information resources provide many conveniences for people's life and work [1]. People can use information technology to establish databases, access and apply various data resources, and realize data resource sharing [2]. Although big data technology has brought many conveniences to people's lives, with the enrichment of data resources and the increase of user information content requirements, how to obtain resources that meet their own requirements has become the main demand at present. This issue has also become a research hotspot in the field of resource application [3]. Due to the development of online education technology, the demand for online education resources is gradually increasing, and the recommendation of online education resources has become the focus of relevant researchers [4].

Reference [5] proposed a collaborative filtering and recommendation method for online learning resources based on learner model. Based on education and teaching theory, as well as taking the resource utilization status in the teaching platform as a reference, a learning resource recommendation model was established, in which the dynamic and static characteristics of learners were integrated, and the collaborative filtering method was used to improve the model so as to realize resource recommendation. The experimental results show that this method has a wide coverage and can effectively recommend most resources, but the accuracy of the recommendation results is not high. Reference [6] proposed a personalized learning resource recommendation method based on three-dimensional feature collaborative domination, constructed the matching relationship between learning resources and learners, constructed the learning resource recommendation model according to the relationship between them, optimized the model parameters using three-dimensional feature

collaborative matching method, and solved the model using particle swarm optimization algorithm to realize Learning Resource Recommendation. The experimental results show that this method has high recommendation efficiency. However, due to the lack of classification of resources, the adaptability between resources and users is not high, and there is a problem of low user satisfaction. Reference [7] proposed an online learning resource recommendation method based on multiobjective optimization strategy. Firstly, the objective function is established; that is, the learners' preference is the largest and the difficulty level is low. On the basis of meeting the above two objectives, the multiobjective particle swarm optimization algorithm is used to optimize and recommend online learning resources. The experimental results show that although this method can meet the needs of users it has the problem of low recommendation efficiency.

According to the above analysis, the existing methods not only have the problem of low accuracy of resource recommendation, but also have the problem of low recommendation efficiency, which affects the satisfaction of users. Therefore, a personalized recommendation algorithm for online education resources based on knowledge association is proposed. The specific research ideas of this paper are as follows.

Firstly, online education resource collection: Taking reliability, fault tolerance, and timeliness as standards, online education resources are collected according to association rules; Secondly, online education resources classification and online education resources filtering: Firefly algorithm is used to classify online education resources to improve the efficiency of resource recommendation and filter the online education resources by constructing vector space function classification.

Then, personalized recommendation of online educational resources: The correlation between knowledge points is calculated by knowledge association theory, and the knowledge with the highest user interest is selected as the target recommendation resource according to the measurement results so as to realize the personalized recommendation of online education resources.

Finally, the personalized recommendation effect of online education resources is verified by the accuracy of resource recommendation, the time of resource recommendation, and user satisfaction.

2. Personalized Recommendation Algorithm for Online Education Resources

2.1. Online Education Resource Collection. Because there are a large number of different types of educational resources in the network, in order to fully recommend online educational resources, first of all, we need to collect educational resources. This paper is mainly based on the theory of association rules. Association rules can not only reflect whether there is association between resources, but also describe the degree of association between resources [1, 8]. Understand the relationship between different educational resources,

clarify the attributes of various types of resources, and then mine the resources to collect online educational resources.

Based on the theory of association rules, association rules are described by $A \rightarrow B$. A and B represent itemsets, and there is no possibility of intersection between them; that is,

$$A \cap B = \emptyset. \quad (1)$$

Considering the need to protect some resources, it is necessary to effectively ensure the confidentiality and integrity of online education resources. In order to effectively avoid malicious dissemination and disclosure of online education resources, educational resources are collected based on the following principles [9].

2.1.1. Reliability. It is necessary to ensure that the online education resources collected through the network are accurate, true, and effective so as to effectively avoid misleading resource users.

2.1.2. Fault Tolerance. If some online education resources in the network are maliciously spread or leaked, it is necessary to cut off the propagation path in time and ensure that the transmission paths of other resources in the network can work normally so as to ensure the security of all online education resources and the reliability of online education resources' downloading, uploading, and other operations. At the same time, try to reduce the operation cost generated in the process of online education resource leakage prevention, such as storage space, network energy consumption, and so on.

2.1.3. Timeliness. Information resources in the network are changing rapidly, and users have high requirements for the efficiency of resource acquisition. Therefore, it is necessary to ensure a certain timeliness in resource acquisition so that users can obtain the most timely resource recommendation results.

Based on the above principles, the specific process of online education resource collection is given as shown in Figure 1.

According to the resource collection process in Figure 1, the online education resources obtained are represented by set U, $U = \{u_1, u_2, \dots, u_n\}$, where u_i represents the i educational resource and n represents the number of resource types.

Set the data change interval in the online education resource set as $[\alpha, \beta]$, and then set a threshold value K to judge the attributes of online education resources. The expression of threshold value K is

$$K = \sum_{k=1}^N H_k + S_k, \quad (2)$$

wherein H_k and S_k , respectively, represent the educational resources corresponding to the input and output target knowledge points and N represents the number of resources.

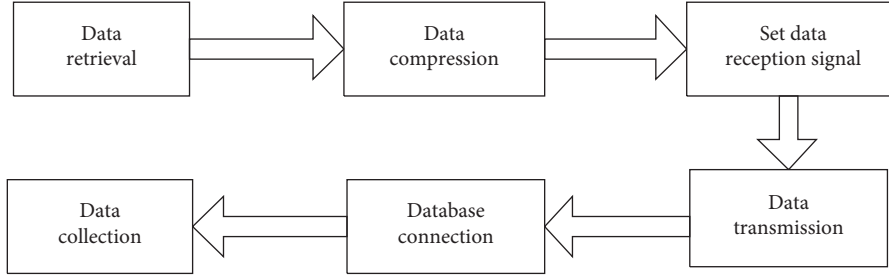


FIGURE 1: Flowchart of online education resource collection.

In order to clarify the application frequency of different education resource types, attribute values are given to different education resource types, and the attribute weights of education resources in set U are expressed in the form of matrix as follows:

$$W_k = \begin{bmatrix} w_{k11} & w_{k12} & w_{k1n} \\ w_{k21} & w_{k22} & w_{k2n} \\ w_{kn1} & w_{kn2} & w_{knm} \end{bmatrix}, \quad (3)$$

where m represents the resource attribute type. The specific calculation formula of the attribute weight of educational resources is

$$W_1 = \frac{(\max - W_k)}{(k - 1)}. \quad (4)$$

According to the attribute weights of different educational resources, the online educational resources are collected by comprehensively considering the threshold K ; namely,

$$U(A, B) = \sum_{i=1}^n K_i (A, B)^2, \quad (5)$$

where K_i represents resource coverage. To sum up, online education resources are collected.

2.2. Classification of Online Education Resources. In order to realize the omnidirectional recommendation of online education resources and further classify the resources, based on the resource collection results, this paper proposes a classification method of online education resources based on firefly algorithm so as to improve the efficiency of resource recommendation. Firefly algorithm is a heuristic optimization algorithm inspired by nature. The inspiration of the algorithm mainly comes from the flickering behavior of fireflies. The brightness of fireflies can be compared to a signal system to attract other fireflies and realize the clustering of fireflies [10, 11].

In order to successfully apply the firefly algorithm to the classification of resources, continuous variables must be converted into discrete variables. Therefore, the last two terms of formula (6) are converted into probability vectors by using logistic function. The logistic function is defined by the following formula:

$$P_{ij} = \frac{1}{1 + e^{\vartheta_{ij}}}, \quad (6)$$

where P_{ij} is the probability value of the j th dimension component of the feature vector represented by firefly i , wherein for ϑ_{ij} the function ensures that P_{ij} tends to 0 when ϑ_{ij} tends to positive infinity, and P_{ij} tends to 1 when ϑ_{ij} tends to negative infinity. The calculation formula of ϑ_{ij} is as follows:

$$\vartheta_{ij} = \beta_0 e^{-\gamma r_{ij}^2} (x_{kj} - x_{ij}) + \alpha \left(\text{rand} - \frac{1}{2} \right). \quad (7)$$

The position update rule of the i firefly during the iteration of the algorithm is as follows:

$$x_{ij}^{t+1} = \begin{cases} 1, & P_{ij} \geq \text{rand}, \\ 0, & P_{ij} < \text{rand}. \end{cases} \quad (8)$$

Based on the principle of the algorithm, online education resources are classified. Figure 2 shows the detailed operation steps of online education resources classification based on the firefly algorithm.

According to Figure 2, the detailed operation steps of online education resource classification are as follows:

- (1) Set the number of iterations to establish a solution space in which firefly individuals are randomly distributed.
- (2) Update the fluorescein values of different firefly individuals.
- (3) Calculate the neighborhood set of different firefly individuals, and the calculation formula is

$$F^2 = \exp \left[\frac{\left(|f_{i,j}|^2 \right)}{\left(|f_{i+1,j+1}|^2 \right)} \right]^2 \times f[a, b], \quad (9)$$

where $f_{i,j}$ represents the current neighborhood set; $f_{i+1,j+1}$ represents the next neighborhood set; and a and b represent subsets in the neighborhood set.

- (4) Calculate the probability that individuals i and j appear in the neighborhood set respectively:

$$\begin{cases} P(i) = A_{ij} - A_i, \\ P(j) = A_{ij} - A_j, \end{cases} \quad (10)$$

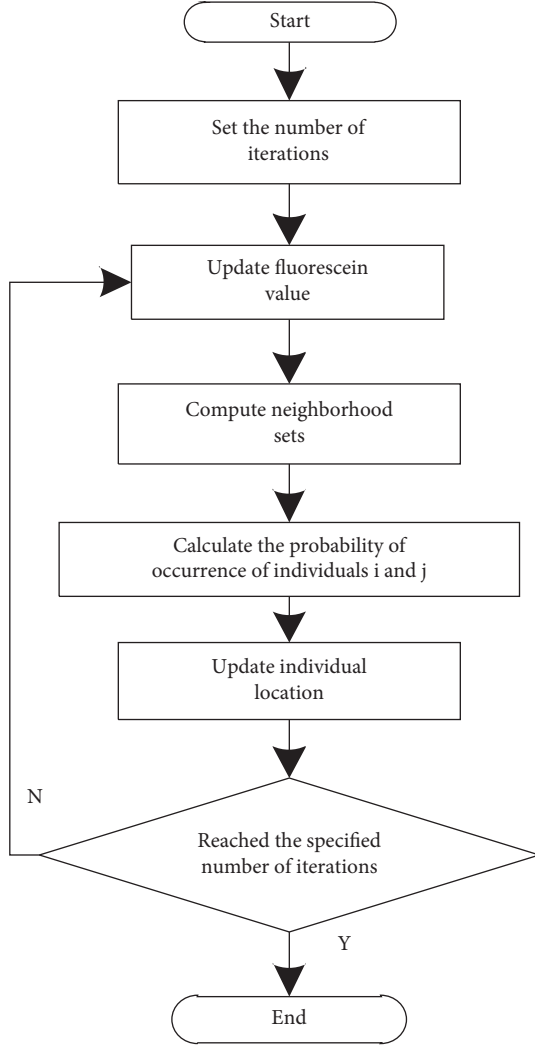


FIGURE 2: Classification flowchart of online education resources.

where A_{ij} represents the overall probability of occurrence of individual i and individual j ; A_i represents the probability of occurrence of individual i ; and A_j represents the probability of occurrence of individual j .

- (5) Calculate the probability that the target individual is selected, move the selected individual as the target, and update the position of the individual at the same time.
- (6) Judge whether the algorithm has reached the specified number of iterations, and if so, output the final result; that is, realize the classification of online education resources. If not, skip to step (2).

According to the above analysis, after fluorescein update and calculation of individual occurrence probability, we can obtain the probability of different education resources' appearance, will be able to distinguish between education resources together, form the same feature set, in accordance with the principle of the set U all education resources

classification processing, have access to education resources of different feature space vector, and realize the online education resources classification.

2.3. Online Education Resource Filtering. Based on the classification results of online education resources, further filter the resources. The purpose of this step is to avoid the impact of interference data on the effect of resource recommendation. In a broad sense, interference data refers to the data that does not meet the needs of users, repeated or wrong in the online education resource set. Recommending these data to users will not only affect the application effect of users on resources, but also affect the probability of useful resources being retrieved and recommended. Therefore, it is necessary to filter these resources [12]. This paper proposes an online education resource filtering method based on vector space function. Filtering resources using vector space function is mainly divided into two stages: training and filtering [13]. The training phase is to train the resource classification results to form a resource filter template. In the filtering stage, a filter board is mainly formed. The filter board is adjusted according to the user's feedback information to realize resource filtering.

According to the above analysis, firstly, the resource classification results obtained in Section 2.2 are trained to preliminarily screen out the invalid resources, and then the invalid resources are further screened out by taking the user's interest as a reference. Finally, the filtering and deletion process is realized to ensure the efficiency of educational resource recommendation. The educational resources in the network are not only diverse in content, but also constantly updated and iterated. It is very difficult to filter these resources. However, in order to recommend more comprehensive and accurate educational resources for users, it is necessary to preliminarily screen educational resources according to relevant standards.

Traditional filtering methods mainly reserve relevant resources according to users' interest points, while vector space functions provide users with resources with high interest and also remove the resources that users have no intention of establish a space vector model $S(\mu)$, whose expression is

$$S(\mu) = d_a + d_h + d_g + d_e + d_v. \quad (11)$$

Among them, d_a represents bad resources; d_h represents unbalanced resources; d_g represents duplicate resources; d_e represents special resources; and d_v represents effective resources.

Train the constructed spatial vector model: define ΔT as the time complexity, assuming that the model contains M nonvalid resources, form them into a document, and traverse the document to obtain the traversed document expression:

$$S'(\mu) = \frac{\sqrt{\sum_{k=1}^n \Delta T (e_i - e_k)^2 \times (g_i - g_k)^2}}{M}. \quad (12)$$

Among them, e_i and e_k , respectively, represent the state vector of valid resources and nonvalid resources in the document; g_i and g_k , respectively, represent the real distribution state of valid resources and nonvalid resources in the document.

Then, the goodness of fit of the distribution of ineffective resources in the document can be expressed as

$$F_{gk} = \omega_n^2 \times (e_k + g_k), \quad (13)$$

where ω_n^2 represents the sparsity of resources in the document. Under normal circumstances, as the F_{gk} value continues to increase, the filtering precision of educational resources also increases.

2.4. Personalized Recommendation of Online Educational Resources. The learner knowledge correlation function is constructed, and the learner knowledge correlation function is applied to the recommendation technology of basic content, and the content recommendation algorithm based on knowledge correlation is proposed. In this recommendation algorithm, the problem of learners' cold start is solved by considering the knowledge attribute information of learners. The knowledge correlation function is used to predict and modify the learning path of learners to solve the problem that the continuity and systematization of learning cannot be guaranteed. By introducing learning style, the problem of single interest in content recommendation is solved. Finally, solve the problem of knowledge trek and theme drift in the process of learning and improve learning interest and learning efficiency.

According to the filtering results of online education resources, the personalized recommendation algorithm of resources is designed. This paper proposes a personalized recommendation algorithm of online education resources based on knowledge association. Knowledge association can be divided into two types: the association between knowledge points and the association between learning resources and knowledge points. The following two knowledge association modes are specifically analyzed.

2.4.1. Correlation between Knowledge Points. The correlation between knowledge points means that the knowledge points of each subject are the basis of subject teaching. Although these knowledge points are divided in teaching research and practice, the knowledge points after the division are still related. This relationship can be divided into dependencies, siblings, and parent-child relationships.

2.4.2. Association between Learning Resources and Knowledge Points. At this stage, we mainly extract keywords from learning resources through semantic association technology and then calculate the association between keyword vectors and knowledge points so as to obtain the correlation between them.

The specific construction and updating steps of the learner knowledge resource association model are as follows:

Step 1. Obtain the domain knowledge attribute of the learner from the learner's personal information table, such as discipline, grade, major, and so on, and then obtain the root knowledge point set S_{K1} associated with the domain knowledge of the learner according to the association relationship between the knowledge in the knowledge base.

Step 2. Obtain the learner's learning behavior data from the learner's learning behavior information table and get the resource set S_R that the learner has learned after cleaning and filtering. Further, according to the association relationship between knowledge points and resources, the knowledge point set S_{K2} associated with S_R and the corresponding association weight W_i are obtained.

Step 3. After obtaining the knowledge point sets S_{K1} and S_{K2} , calculate the correlation weight between the knowledge point and the learner, wherein, if the knowledge point is not learned by the learner, the degree of association between the learner and the knowledge point is 0. On the contrary, the weight of the knowledge points and the learners is obtained by averaging the sum of the resources and the weights of the knowledge points.

Step 4. The updating of the association model of learners' knowledge resources mainly includes two situations: the change of learners' knowledge attribute information and the learners' learning of new learning resources. When these two situations occur, the above three steps are executed to obtain the latest knowledge set and association weight associated with the learner.

Based on the above theory, in order to realize the personalized recommendation of educational resources, the habit preference of learners is obtained from the needs of learners, the learning path of learners is mined, and the personalized recommendation of educational resources is realized in combination with knowledge association [14, 15].

First, establish a knowledge association model, select knowledge points Q_1 and Q_2 in the model, and calculate the weight of the two. The calculation formula is

$$\begin{cases} W(Q_1) = \frac{\delta_1(I - I_k)}{m_k}, \\ W(Q_2) = \frac{\delta_2(I - I_k)}{m_k}. \end{cases} \quad (14)$$

Among them, δ_1 and δ_2 represent the set of knowledge points; I represents the parent knowledge point; I_k represents the child knowledge point; and m_k represents the sum of the associated weights of the knowledge points.

The knowledge point set composed of knowledge points Q_1 and Q_2 is obtained by formula (8), and the similarity between them is calculated by formula (8):

$$S(Q_1, Q_2) = \frac{1 - (f_s + f_g)}{f_s}. \quad (15)$$

Among them, f_s represents the similarity relationship between resource attributes; f_G represents the similarity relationship between resource ontology.

Next, find the knowledge points related to learners' interest, measure the similarity between the knowledge points, and select the knowledge with the highest user interest as the target recommendation resource according to the measurement results. The measurement is mainly realized by calculating the cosine similarity between knowledge points:

$$S(Q_1, Q_2) = \cos \left[\frac{Q_1 \cdot Q_2}{|Q_1| \cdot |Q_2|} \right]. \quad (16)$$

Using formula (16) to get the similarity, recommend online education resources to learners, form a list of interest degrees, arrange the interest degrees in descending order, and then recommend education resources to learners in turn according to the arrangement results, and finally realize the personalized recommendation of online education resources. The personalized recommendation process of specific online education resources is shown in Figure 3.

Analysis of Figure 3 shows that online educational resources are collected according to the association rules, the firefly algorithm is used to classify the online educational resources, the classified online educational resources are filtered, the correlation between knowledge points is calculated by the knowledge association theory, and the user interest degree is selected. The highest knowledge is used as the target recommendation resource, and the personalized recommendation of online educational resources is completed.

3. Experimental Analysis

3.1. Experimental Design. There are two datasets used in this experiment:

- (1) *IntAddSub (Integer Addition and Subtraction) Dataset.* The dataset comes from an online learning platform and collects the real data of mathematics learning in grade 3 of a senior high school. The dataset mainly involves the function solving content in the senior high school mathematics of the people's education press, including 13 knowledge points. A total of 753 learners and 1056 exercises are collected. The time span is from February 23, 2021, to June 24, 2021. The data truly reflect the learning situation of learners. Personalized recommendation algorithm of online education resources based on knowledge association, which can personalized recommend online education resources to target learners
- (2) *FrcSub (Fraction Subtraction) Dataset.* This dataset is a public dataset. FrcSub collects exercise data on equation solving problems, which is often used by cognitive diagnostic models to validate the model's performance. The FrcSub dataset contains two parts of data: students' exercise scores and the relationship between exercise and knowledge points. It collects the score data of 536 learners on 20 exercises. Among

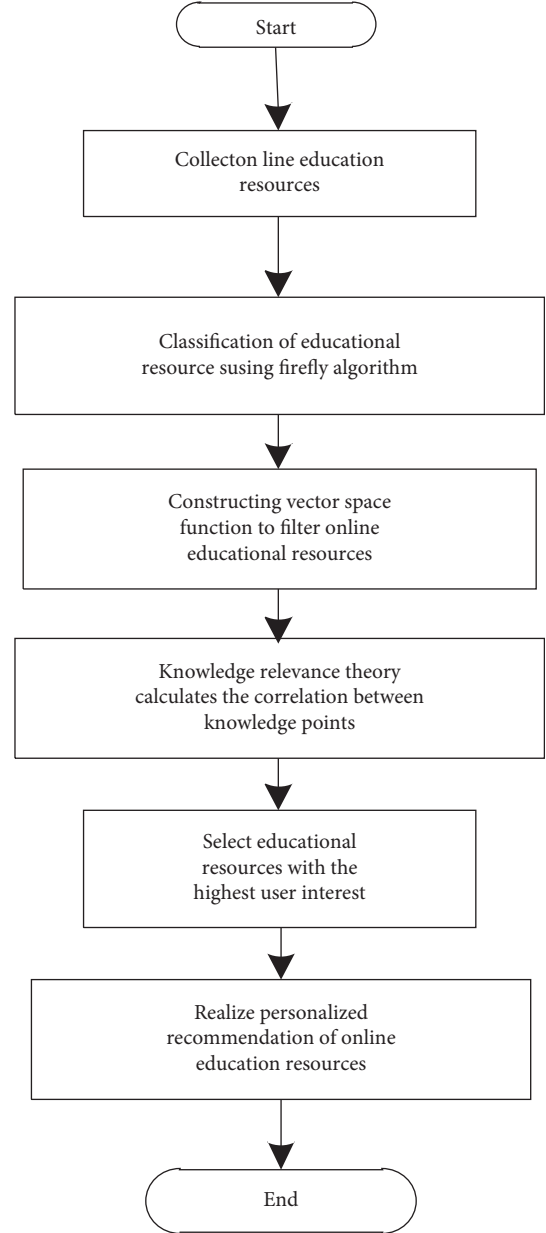


FIGURE 3: Personalized recommendation process of online educational resources.

them, 1 means that the exercise is answered correctly, and 0 means that the exercise is answered incorrectly. The relationship with knowledge points includes the investigation of 8 knowledge points in 20 exercises, among which, if the exercise examines the knowledge point, it is represented by 1; otherwise, it is represented by 0. The descriptive statistics of the two datasets are shown in Table 1.

On the basis of theoretical research, design experiments to verify the application performance of this method. Reference [5] method and reference [6] method are used as comparison methods to compare with this method. The specific experimental indicators are recommendation accuracy, recommendation efficiency, and user satisfaction.

TABLE 1: Dataset statistics.

Dataset	Number of learners	Number of exercises	Knowledge points
IntAddSub	753	1056	13
FrcSub	536	20	8

The data used in the experiment comes from the SQL Server database, in which the application statistics of online education of students in a university are extracted, including student resource retrieval data, resource download data, and resource submission data; based on the above data, the experimental research is carried out.

In this paper, recommendation accuracy, resource recommendation efficiency, and user satisfaction are selected as experimental evaluation indicators. The higher the calculation result, the better. On the contrary, the lower the calculation result, the worse.

3.2. Recommendation Effect Verification

3.2.1. Comparison of Online Educational Resources Recommendation Accuracy. In order to verify the effect of online education resource recommendation, reference [5] method, reference [6] method, and this method are used to verify the accuracy. The accuracy results of online education resource recommendation are shown in Figure 4.

As can be seen from Figure 4, compared with the traditional method, the online education resource recommendation accuracy of this method is significantly higher, always higher than 80%, and the maximum value reaches 97%. However, the online education resource recommendation accuracy of reference [5] method and reference [6] method is low. Among them, the maximum recommendation accuracy of reference [6] method is 78%, and the recommendation accuracy of reference [5] method is lower. It can be seen that this method has better recommendation effect and can provide more accurate resources for resource demanders. This is because this method uses firefly algorithm to classify online education resources and constructs vector space function to filter the classified online education resources, which effectively improves the accuracy of recommendation.

3.2.2. Comparison of Online Educational Resources Recommendation Efficiency. Recommendation efficiency describes the time consumed by resource recommendation. Therefore, under the same test conditions, the methods of reference [5], reference [6], and this paper are used to count the time consumed by resource recommendation. The results are shown in Table 2.

It can be seen from Table 2 that, during the testing process, the recommended time for resources of this method, reference [5] method, and reference [6] method has been increasing. Among them, the growth rate of this method is the smallest, and the recommended time is always controlled below 5.0s, which is far lower than the

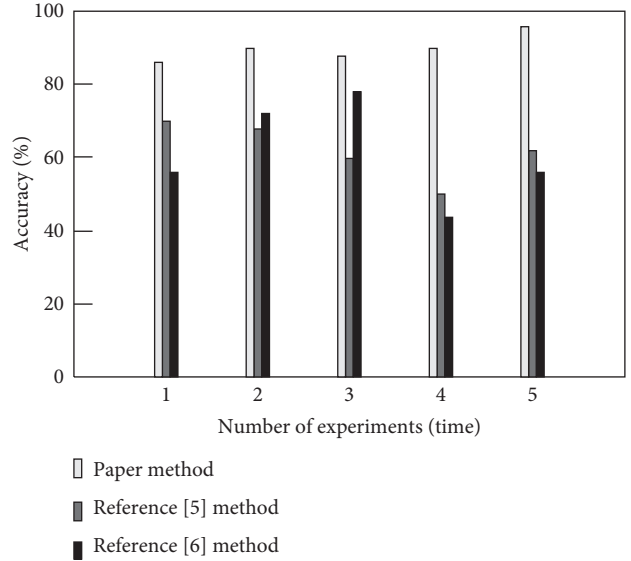


FIGURE 4: Recommendation accuracy of different methods.

recommended time of reference [5] method and reference [6], indicating that the recommended efficiency of this method is high. According to the above analysis, this method solves the problem of low recommendation efficiency of traditional methods and can provide users with educational resources faster. This is because this method uses association rules to collect online education resources and uses firefly algorithm to classify online education resources. The correlation between knowledge points is calculated by the knowledge association theory, and the knowledge with the highest user interest is selected as the target recommendation resource to effectively improve the recommendation efficiency.

3.2.3. Comparison of User Satisfaction. Online education resource recommendation is mainly for users, so users' satisfaction with the recommendation results is very important. By scoring the recommendation effect by 100 users, the users' satisfaction with the recommendation effect of the above method resources is tested. The test results are shown in Figure 5.

It can be seen from Figure 5 that, with the increase of the number of users, the average number of user scores gradually decreases. Through comparison, it can be seen that users are more satisfied with the recommendation effect of the method in this paper, and the score always remains above 80 points, [5] The satisfaction score of the method in [6] is basically below 80 points. It can be seen that users are more satisfied with the method in this paper, which also reflects the better recommendation effect of this method from the side. This is because this method uses firefly algorithm to classify online education resources. The correlation between knowledge points is calculated by the knowledge association theory, and the knowledge with the highest user interest is selected as the target recommendation resource, which effectively improves the user's satisfaction.

TABLE 2: Online educational resource recommendation efficiency of different methods.

Number of experiments/times	Online educational resource recommendation time/s		
	Reference [5] method	Reference [6] method	This paper method
1	1.6	3.1	2.9
2	2.0	4.9	3.5
3	3.1	5.2	4.7
4	3.4	6.9	5.0
5	3.5	7.1	6.3
6	4.0	8.1	7.1
7	4.2	8.9	7.5
8	4.5	9.8	8.2
9	4.8	10.2	8.8
10	4.9	11.1	9.0

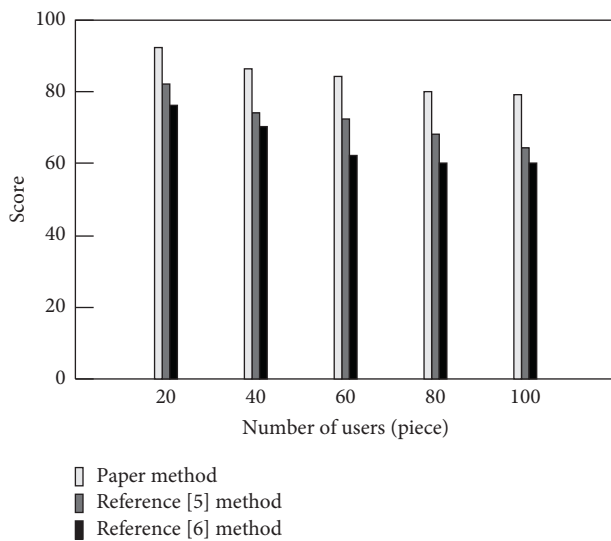


FIGURE 5: Users' satisfaction with different methods.

4. Conclusion

This paper proposes a personalized recommendation algorithm for online education resources based on knowledge association. Collect online education resources according to association rules, classify online education resources using firefly algorithm, filter the classified online education resources by constructing vector space function, calculate the correlation between knowledge points based on knowledge association theory, and select the knowledge with the highest user interest as the target recommendation resource according to the measurement results to realize the personalized recommendation of online education resources. The following conclusions are drawn through experiments:

- (1) The online educational resource recommendation accuracy of the method in this paper is significantly higher, always higher than 80%, and the maximum value can reach 97%.
- (2) The maximum resource recommendation accuracy rate of the method in this paper is 97%, the recommendation time is always controlled below 5.0 s, and the user's satisfaction with it is higher, indicating that its recommendation effect is better.

- (3) Users are more satisfied with the recommendation effect of the method in this paper, and the score is always above 80 points, which reflects the better recommendation effect of this method.

Under the method of this paper, the satisfaction of recommendation effect has been significantly improved, but the accuracy of education resources recommendation still needs to be further improved.

Data Availability

The data used to support the findings of this study can be obtained from the corresponding author upon request.

Conflicts of Interest

The authors declare that they have no conflicts of interest regarding the publication of this paper.

Acknowledgments

This work was supported by the Research Project of Educational Informatization in Jiangsu Province (Construction and Research of "Intelligent Educational Administration" Platform) (no. 20180067).

References

- [1] Q. Yuan, "Network education recommendation and teaching resource sharing based on improved neural network," *Journal of Intelligent and Fuzzy Systems*, vol. 39, no. 4, pp. 5511–5520, 2020.
- [2] Y. Han, "Educational resource online evaluation system based on neural network dynamic feedback algorithm[J]," *Journal of Intelligent and Fuzzy Systems*, vol. 38, no. 2, pp. 1–13, 2020.
- [3] J. Cao, "Mode optimization and rule management of intellectual property rights protection of educational resource data based on machine learning algorithm," *Complexity*, vol. 18, no. 4, pp. 1–12, 2021.
- [4] H. Yu and L. Sun, "Accurate recommendation algorithm of agricultural massive information resources based on knowledge map[J]," *Computer Simulation*, vol. 38, no. 12, pp. 485–489, 2021.
- [5] F. Liu, F. Tian, L. Xin, and L. Lin, "A collaborative filtering recommendation method for online learning resources

- incorporating the learner model,” *CAAI Transactions on Intelligent Systems*, vol. 16, no. 06, pp. 1117–1125, 2021.
- [6] H. Li, Z. Zhang, and P. Zhang, “Personalized learning resource recommendation method based on three-dimensional feature cooperative domination,” *Computer Science*, vol. 46, no. 01, pp. 461–467, 2019.
- [7] H. Li, L. Yang, and P. Zhang, “Method of online learning resource recommendation based on multi-objective optimization strategy,” *Pattern Recognition and Artificial Intelligence*, vol. 32, no. 04, pp. 306–316, 2019.
- [8] F. Alsolami, T. Amin, M. Moshkov, B. Zielosko, and K. Żabiński, “Comparison of heuristics for optimization of association rules,” *Fundamenta Informaticae*, vol. 166, no. 1, pp. 1–14, 2019.
- [9] G. Fan, Y. Dong, D. Chen, and F. Chen, “New method for forest resource data collection based on smartphone fusion with multiple sensors,” *Mobile Information Systems*, vol. 2020, no. 4, pp. 1–11, 2020.
- [10] I. Brajevic and J. Ignjatović, “An upgraded firefly algorithm with feasibility-based rules for constrained engineering optimization problems,” *Journal of Intelligent Manufacturing*, vol. 30, no. 6, pp. 2545–2574, 2019.
- [11] T. Toharudin, R. E. Caraka, R. C. Chen, and S. A. Bakar, “Some new construction of seasonal smooth support vector regression firefly algorithm in electrical load forecasting[J],” *Sylwan*, vol. 163, no. 11, pp. 314–321, 2019.
- [12] H. Xia, Y. Yang, F. Ding, A. Alsaedi, and T. Hayat, “Maximum likelihood-based recursive least-squares estimation for multivariable systems using the data filtering technique,” *International Journal of Systems Science*, vol. 50, no. 6, pp. 1121–1135, 2019.
- [13] R. C. Belwal, S. Rai, and A. Gupta, “Text summarization using topic-based vector space model and semantic measure,” *Information Processing & Management*, vol. 58, no. 3, pp. 102536–102542, 2021.
- [14] L. Wu, “Collaborative filtering recommendation algorithm for MOOC resources based on deep learning,” *Complexity*, vol. 2021, no. 46, pp. 1–11, 2021.
- [15] Z. Huang and P. Stakhiyevich, “A time-aware hybrid approach for intelligent recommendation systems for individual and group users,” *Complexity*, vol. 2021, no. 2, pp. 1–19, 2021.

Research Article

Style Transfer of Chinese Art Works Based on Dual Channel Deep Learning Model

Yan Tang 

College of Art of Jiujiang University, Jiujiang, Jiangxi Province 332005, China

Correspondence should be addressed to Yan Tang; 6060008@jju.edu.cn

Received 18 July 2022; Revised 8 August 2022; Accepted 17 August 2022; Published 20 September 2022

Academic Editor: Le Sun

Copyright © 2022 Yan Tang. This is an open access article distributed under the Creative Commons Attribution License, which permits unrestricted use, distribution, and reproduction in any medium, provided the original work is properly cited.

Aiming at the problems of style loss and lack of content in the style transfer of Chinese art works, this paper puts forward the style transfer technology of Chinese art works based on the dual channel deep learning model. On the basis of clarifying the technical principle of style transfer of art works, the image of art works is controlled and transformed based on the u-net network. The incomplete information in the restored image is filled, and the multiscale classification feature is used to calculate the color feature data items in the image. The sensitivity coefficient of color difference is calculated by using constraints, and the overlapping color discrimination and image segmentation of art images are realized. Poisson image editing is used to constrain the image spatial gradient to realize the style migration of art works. The experimental results show that this method can effectively avoid the problems of content error, distortion, and distortion in the process of art style migration, and has a better style migration effect.

1. Introduction

When appreciating the famous works of famous Chinese and foreign painters, we often hope to create a painting with a similar style. The emergence of image style transfer technology has helped people realize this wish [1]. People can convert any photo into any style of painting. In addition, in the era of the rise of a short video, various style filter effects are loved by people [2], and image style migration technology has been widely known by people. However, many image style migration methods can only target one style in a model, which is inefficient in an application.

Reference [3] proposes an example based image styling method based on the consistency of the target image during training. This method keeps the statistical data of neural response compatible with the data extracted from programmed sources and is widely used in video stylization, style conversion to panorama, face, and 3D models. Reference [4] mainly proposes improvements in the following two aspects: (1) adjust the structure of classical residual elements: convert the standard convolution into point convolution and depth convolution, and reduce the amount of computation while ensuring the convolution effect; (2)

simplify the loss network: the fourth and fifth layers of the model are highly consistent in structure, and the effect of style restoration and content reconstruction of these two layers is basically the same, which ensures the effect of style restoration and content reconstruction while reducing the amount of parameters. Reference [5] proposed an unsupervised image style migration method based on an image mask. In the experiment, cycleGAN architecture based on cyclic consistency is adopted, and a new generative model with a built-in image mask is designed by using the inception RESNET structure. Finally, the background of the image and the learned abstract features are automatically reorganized through unsupervised learning. Experiments show that the new method effectively separates and reorganizes the image background and abstract features, solves the problem of regional interference in the process of feature learning, and obtains considerable visual effect. Reference [6] in view of the difficulty of style extraction caused by the diversity of Mongolian clothing elements, large color differences, irregular patterns, and other characteristics, the method of combining K-means and a closed natural matting algorithm is used for image segmentation. The style and content of the image are extracted based on a neural network, and the resulting image is synthesized by image

reconstruction technology to realize the style transfer of Mongolian and Chinese clothing image. Aiming at the problem of serious artifacts in the output image, an improved image style migration algorithm is adopted. Transform the input parameter of the image into a local constraint, which can suppress the distortion of the image. Aiming at the problem of spatial inconsistency in the style transfer of real photos, smooth it to ensure the consistency of spatial style after style processing. This method greatly speeds up the operation speed. Reference [7] proposed a periodic consistency antagonistic domain adaptive method with four input channels for vegetation region segmentation based on an index. This method preserves the specific ratio between near infrared and RGB bands and improves the segmentation network performance of the target domain. Reference [8] proposes a style library composed of multiple convolution filter banks, and each filter bank explicitly represents a style. In order to convert the image into a specific style, the corresponding filter bank is operated on the intermediate features generated by a single automatic encoder. This method can obtain the same results as the single parameter setting method.

Based on the application of image style transfer technology in interior decoration design based on the ecological environment in reference [9], this paper proposes the style transfer of Chinese art works based on the dual channel deep learning model. The art work style transfer technology proposed this time refers to converting the style of an art work into an image similar to the style of the art work through learning (using the dual channel deep learning model). This paper mainly puts forward improvements in the following two aspects: first, adjust the lighting of art works; Secondly, based on the dual channel convolution transformation and control of the u-net network, the incomplete information in the restored image is filled to ensure the effect of style restoration and content reconstruction of art works while reducing the amount of parameters.

2. Art Style Transfer Technology

Using different styles of art works to express the semantic content of images, so the method of image processing is the transfer of style of art works [10]. That is, on the premise of retaining the central content and structure of the original image, an ordinary image is displayed in another art work style. For example, there are two images, one is the style image and the other is the content image. The style transfer of art works is mainly divided into the following steps:

Step 1: ensure that all the content and structure of the content image are preserved and then extract the main features of the style of the art work

Step 2: use the extracted features to reconstruct the features of the original content image

Step 3: perfectly combines the style of the style image and the content of the content image into a migration image, so as to obtain the output image

The implementation process of the above process is shown in Figure 1.

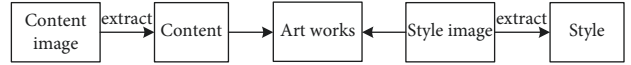


FIGURE 1: Flow chart of style transfer of art works.

2.1. Local Block Method of Double Threshold Image Based on Depth Convolution Neural Network

2.1.1. *Theoretical Analysis.* Full convolutional networks (FCNs) is a network model based on deep learning, which is widely used in image segmentation. FCN has the following advantages:

- (1) The convolution network training is realized by replacing the full connection layer with the convolution layer.
- (2) In order to achieve pixel level segmentation, all pixel features in the image are predicted and classified. However, for the images with complex visual environment, the sampling on the FCN network structure still adopts the simplest deconvolution method, resulting in the inability to recognize the detailed features of the image, the final segmented image contour is blurred and the adhesion is serious.

Therefore, mask r-cnn is proposed as an instance segmentation method, and the region of interest (ROI) is taken as the network branch of the deep convolution neural network to realize the instance segmentation of the target image. In order to preserve the accuracy of the target spatial position coordinates, the mask r-cnn network replaces the roipool operation with the roialign operation. Roialign can correct the misplaced layers of spatial quantization feature extraction. The bilinear difference keeps the spatial position accuracy between the input network and the output network unchanged, corresponding to the coordinate value on the ROI bin. The dependence between the judgment class and the output mask is minimized, and the average binary cross entropy loss is used to predict the binary mask separately for each target. This process reduces the competitiveness between categories and improves the efficiency of image segmentation.

Based on the mask r-cnn network structure, the network depth and width are optimized and adjusted, and the migration learning is carried out on the given training parameters. Based on the segmented target image, the optimal network parameters and network model are obtained by calculating the segmentation accuracy between different layers and different convolution kernels.

2.1.2. *Local Blocking of Double Threshold Image.* Based on the above-given theoretical analysis, this paper determines the optimal network model as the Pignet network structure and makes two optimization improvements on the mask r-cnn network structure in terms of the number of convolution layers and categories:

- (1) For different target areas in the image, the fourth stage of mask r-cnn network changes from 69 convolution layers to 12 layers, which can reduce the

feature loss on the one hand and the amount of convolution operation on the other hand.

- (2) The number of convolution layers in the last layer of the mask branch of mask r-cnn network is optimized and adjusted to Pignet and background. The specific structure is shown in Figure 2.

There are 44 convolution layers and five convolution layers, all of which adopt the Pignet structure. Each arc contains 3 convolution layers, $1 \times 1 \times 64$ layers indicate that the convolution kernel is 1×1 . Convolution layer with 64 channels. The residual learning structure reduces the number of parameters to a great extent, makes the calculation simpler and keeps the spatial position accuracy of the target unchanged. Through the arc part of the network diagram, the residual learning structure directly transmits the input information to the later layer, which also reduces some feature loss. The residual learning structure can also reduce the sliding step of each convolution layer from the original two pixels to one quarter, and the number of output channels increases continuously until 2048.

There are mainly two aspects of feature extraction in the Pignet backbone network structure: one is to analyze and process the feature map output by the network model conv4_12 convolution layer through the region proposal networks (RPN) [11] to extract the required feature information; on the other hand, it propagates forward to generate feature mapping, RPN can select the region of interest with the fastest speed.

The loss function L of the Pignet network is mainly composed of three parts: classification error L_{cls} , detection error L_{box} , and segmentation error L_{mask} . The calculation formula is shown as follows:

$$L = L_{cls} + L_{box} + L_{mask}. \quad (1)$$

Here, L_{cls} and L_{box} processes the full connection layer to predict the category of all regions of interest and the regression frame coordinate value of the target space. L_{mask} segment and mask the target image of each region of interest. Select the target image in which all regions of interest in the image are classified as pig, so that only the relative entropy error of pig needs to be considered when continuing to calculate the loss function generated by region segmentation. In order to avoid competition among classes, the background class is not considered when calculating the relative entropy error of pig class. L_{box} is mainly used to ensure that the position coordinates of the regression box of the target image do not deviate. L_{mask} is used to ensure the accuracy of the target image generation mask. Class branch predicts that the region of interest class is pig class, then L_{mask} only needs to predict pixels for pig class to ensure that the target image has clear contour and no adhesion, so as to ensure the accuracy of contour position coordinate information on different layer depths and realize accurate image segmentation. In this paper, the Pignet network model obtains two regions of interest from convolution calculation. L_{box} is used to predict the position coordinates of the target spatial regression frame. L_{mask} uses the combination of the

average binary cross entropy loss function and sigmoid function to separately predict the position coordinates of the target spatial regression frame to form a binary mask. The segmented image is represented by two different color masks and placed in two different layer depths. Even if more images are segmented, the Pignet model will form a corresponding binary mask for each segmented target.

2.2. Extraction of Light Component in Non-significant Area.

The multiscale Gaussian function can extract the illumination classification of different areas in the image by adjusting the adaptive parameters, so as to improve the quality of style migration of art works. The implementation process can be divided into the following steps:

Step 1: image acquisition: obtain the image of the art work to be migrated

Step 2: background removal: based on the HSI color space model, the i -component image is binarized according to the histogram selection threshold to form a binary mask image, and the two obtain the i -component image after removing the background through point multiplication

Step 3: construct multi-scale Gaussian function filter

Step 4: obtain the illumination component

Step 5: perform homogenization correction on the surface brightness of the i -component image after removing the background

There are pixel structures with various structures in the art works. When extracting the illumination component in the nonsignificant area, the multiscale Gaussian function is used to set adaptive parameters in the image area to correct the empirical parameters existing in the art works. The correction process can be expressed as follows:

$$I(x, y) = I \frac{\gamma(x, y)'}{\gamma(x, y)}. \quad (2)$$

Here, $I(x, y)$ represents the correction function formed, $\gamma(x, y)'$ represents the nonsignificant region extracted by bilateral filtering, and $\gamma(x, y)$ represents the light source point function in art works. According to the image processing experience and the original illumination parameters in the nonsignificant area, the empirical value is selected. There are many illumination levels in the nonsignificant image area. In order to deal with the weakening effect of different light and dark areas on the nonsignificant area, the illumination points are randomly selected for adaptive adjustment. In order to eliminate the influence of image noise on image details, the image structure with a linear structure is selected to process the image after adaptive processing, and the structure parallel to the linear structure is selected to be processed as a corrosion reflection component to eliminate the noise in the image. The processing process is shown as follows:

$$R_d = \frac{R \oplus H}{H}. \quad (3)$$

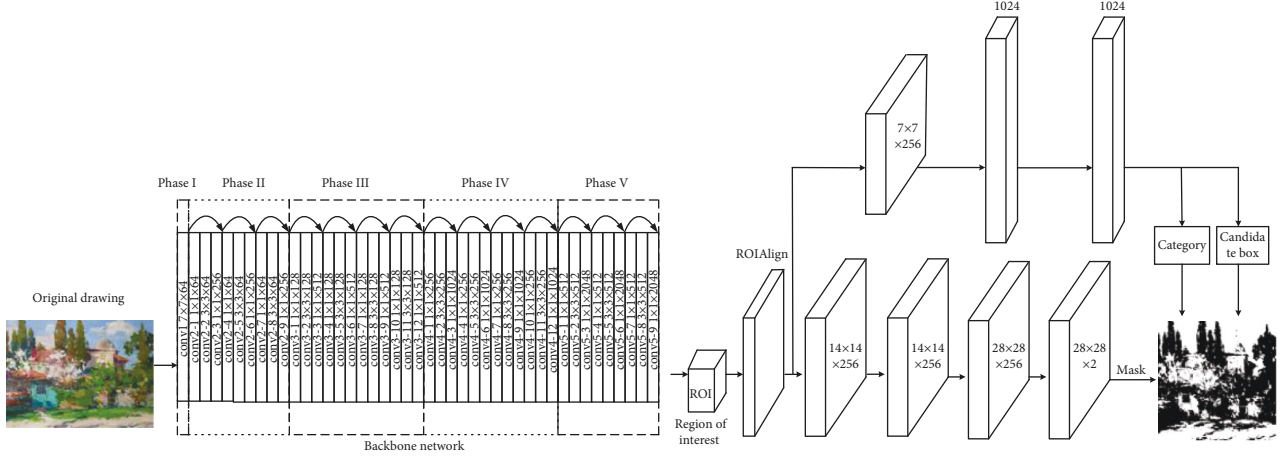


FIGURE 2: PigNet network structure.

Here, R_d represents the constructed denoising function, R represents the image expansion parameter, H represents the image structure parameter, and \oplus represents the image panoramic processing. After eliminating the noise in the image, divide the front and back scenes in the image structure, take the back scene image as the extraction object of the light component in the nonsignificant area and extract the light component by using the adaptive gamma function [12, 13]. The extraction process is shown as follows:

$$a = \frac{2R_d I(x, y)}{I_{\max}(x, y)}. \quad (4)$$

Here, a represents the extracted parameters, $I_{\max}(x, y)$ represents the maximum value of the image correction function, and the meaning of other parameters remains unchanged. In order to unify the dimension of the image illumination component, the above-extracted illumination component is linearly transformed by spatial image processing technology. The processing process is shown as follows:

$$g(x, y) = \frac{d-c}{b-a} [I(x, y) - a]. \quad (5)$$

Here, $g(x, y)$ represents the constructed linear function, abc and d represent the gray parameters of the illumination component, respectively, and the meaning of other parameters remain unchanged. After processing the illumination component in the image, the gray parameters in the image are divided according to the value size, and the gray level of small value is processed into a nonsignificant area [14]. For the image in this area, the image resolution is reconstructed by depth learning.

2.3. Poisson Image Editing Technology. The implementation process of Poisson image editing technology can be summarized as follows: assuming that the area occupied by the original image is Ω , according to the gradient of the original image and the boundary structure of the embedding position of the target image, the image pixel value of the transition region is constructed and seamlessly fused to the right

image. The image value of the right fusion part is unknown, and the energy function needs to be solved. That is, for an image, the macro significance is reflected in the texture features, so to make the two images integrate properly and seamlessly, it is necessary to make the texture of the fused part of the two images consistent. The texture is reflected in the gradient, so the gradient of the fused region should be consistent with that of the original image. The consistency of fused textures means that the variation difference between the inner and outer regions of the original image reaches a minimum; that is, the energy function takes a minimum.

The image used for the style transfer of art works is generally a fuzzy image. Logically, a fuzzy image is an image in which the contour of the object is not obvious and the gray change of the contour edge is not enough, resulting in a weak sense of hierarchy. In order to generate a clear image, we need to calculate the change rate of the image gray level and then obtain a clearer style transfer image. In the style transfer of art works, we should also pay special attention to not making the whole decoration look ambiguous. We should find the “change rate of image gray level” and then successfully fuse the source image with the target image. The image pixel construction diagram of the fusion area is shown in Figure 3.

In Figure 3, V represents the gradient field of the source image, u represents the source image of the art work, $\partial\Omega$ represents the boundary of the image, f^* represents the result of the combination of images other than Ω , Ω represents the area covered by the image, and f represents the image within Ω .

3. Realize the Style Transfer of Art Works

Due to the authenticity and complexity of the content in the style transfer process of art works, it is necessary to keep the consistency of the content image and the style as much as possible in the transfer process, so that there will be no error or distortion in the style transfer image content of art works [15, 16], which makes the effect after the transfer real and effective. The implementation process of style migration is shown in Figure 4.

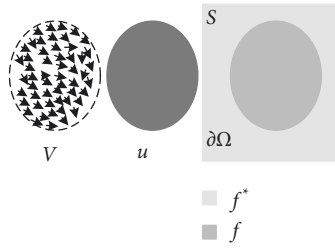


FIGURE 3: Schematic diagram of image pixel construction in fusion area.

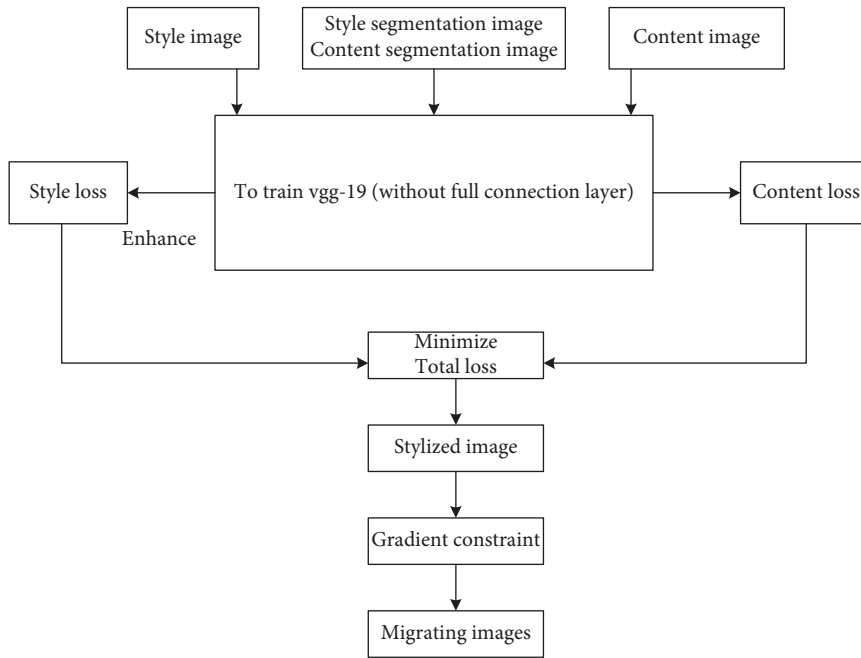


FIGURE 4: Style transfer process of art works.

According to the migration process shown in Figure 4, the migration process is analyzed in detail.

3.1. Image Segmentation of Art Works. The image segmentation technology of art works mainly through point by point convolution and pool layered recognition. After a series of processing of the image of art works, the final output feature vector of the image is clear and reliable, which is helpful to accurately distinguish the image category. Although the loss of pixels limits the pixel level classification, it does not affect the two-dimensional spatial information of the image. At this time, the full connection layer can be converted into a convolution layer, the original size of the image can be restored through deconvolution operation, and then each pixel can be classified one by one to realize the effective segmentation of the image of art works. This method is not limited by the size of the input image, reduces the repeated storage and convolution calculation of pixel blocks to a certain extent and improves the extraction efficiency of image features. In terms of data sets of different sizes, the image segmentation based on the u-net network [17, 18] has a good segmentation application effect.

The specific features of the u-net network include the following:

- (1) The image full connection layer can be transformed into a convolution layer in real time. The number of image convolution results output by the last convolution layer is equal to the number of image classification. For the image of art works, the parameter value of each coordinate point represents the probability corresponding to the pixel point and the relevant category, and the category to which the image feature belongs is the largest corresponding probability value.
- (2) When the input data in the image of art works passes through the pool layer, the output image features will be reduced to a certain extent. The size of the feature image obtained by the last down sampling will be reduced to 1/16 of the original image. On this basis, the restored image can be obtained by adding the deconvolution layer, recovering with the upper sampling, and fusing with the image after the change of the expansion path, and the size is the same as the original image.

- (3) The jump structure is added to the u-net network to extract the detailed features in the image of art works. At the same time, the semantic features are extracted through the network. After splicing and fusing the multiscale features, the image with complete and rich information is obtained.

Therefore, the u-net network is used for image segmentation of art works. The image of art works will produce color overlap in some special states. At this time, if only the color features in the image are used to judge the image information, it is easy to produce inaccurate boundary segmentation. Therefore, the data items in the image are calculated by using the multiscale classification features [19, 20].

$$D(a_u, \theta) = -1n(\gamma p_c(v'_u | a_u) + (1 - \gamma) p_s(v'_u)). \quad (6)$$

Here, Vu' represents the u -th color vertex in the adjacent pixel area in the target image, $a_u \in \{0, 1\}$ represents the correlation label between the foreground and the background in the image of art works, $p_c(v'_u | a_u)$ represents the constraint term of the color in the image background, $p_s(v'_u)$ represents the constraint term of the multi-scale classification feature on the image color, and γ represents the adjustment coefficient of the constraint term.

When the colors in the images of art works overlap, the multiscale classification feature plays a decisive role in the classification of graphics. Therefore, generally, the value of the adjustment coefficient γ will be relatively small. The specific calculation process is shown as follows:

$$\gamma = |P_c(v'_u | 1) - P_c(v'_u | 0)|^\beta \quad (\beta \in [0, 1]). \quad (7)$$

Here, β is the sensitivity coefficient to adjust the main color difference of the image, and the general value is set at 0.5. By calculating the shortest Euclidean distance between the vertex Vu' and the foreground seed and background seed in the image [21, 22], the degree of overlap of the main color distribution in the image can be obtained. The calculation method of Euclidean distance is shown in formulas (8) and (9):

$$d_u^F = \min \|I'_u - \theta_F\|, \quad (8)$$

$$d_u^B = \min \|I'_u - \theta_B\|. \quad (9)$$

In formulas (8) and (9), θ_F and θ_B represent the color values of foreground seed and background seed, respectively, and Iu' represents the vertex color value. After obtaining the above data, we can further obtain the color constraint value of the image of art works, as shown in the following formula:

$$P_c(v'_u | a_u) = \begin{cases} \frac{d_u^B}{d_u^F + d_u^B}, & \text{if } a_u = 1, \text{ and } d_u^F + d_u^B \neq 0, \\ \frac{d_u^F}{d_u^F + d_u^B}, & \text{if } a_u = 0, \text{ and } d_u^F + d_u^B \neq 0, \\ 0.5, & \text{if } d_u^F + d_u^B = 0. \end{cases} \quad (10)$$

The multiscale typing feature constraint is mainly determined by the eigenvalue S_{MP} . By adjusting the level variable eigenvalues in the foreground and background, the corresponding multiscale typing features are inversely increased. In this process, the adjustment is completed by adjusting the variable factor and the feature mean value is obtained. At this time, the foreground multi-scale typing eigenvalues, as shown in the following formula:

$$S'_{Fu} = \frac{P_c(v'_u | a_u) \times S_{MF}^2}{m}. \quad (11)$$

Here, m represents the mean value of typing characteristics. The calculated characteristic values of background multi-scale classification, as shown in the following formula:

$$S'_{Bu} = \frac{(1 - S'_{Fu})^2}{1 - m}. \quad (12)$$

The calculation formula of typing characteristic mean m , as shown in the following formula:

$$m = \frac{1}{n} \sum_{u=1}^n S'_{Bu}. \quad (13)$$

The constraint process of multi-scale segmentation between image foreground and background, as shown in the following formula:

$$\begin{cases} p_s(v'_u \in F) = \frac{S'_{Fu}}{S'_{Fu} + S'_{Bu}} \\ p_s(v'_u \in B) = \frac{S'_{Bu}}{S'_{Fu} + S'_{Bu}} \end{cases}. \quad (14)$$

In order to effectively improve the segmentation accuracy of the image of art works, the image area with a relatively high classification eigenvalue of the area with a relatively small area shall be subject to unified noise reduction. If $p_s(v'_u \in F) = 0.5$ and $A_u < A_{\text{avg}}$ conditions are met, then $p_s(v'_u \in F) = 0.5$ and A_{avg} represent the average area of the image. So far, the image segmentation of art works is completed.

3.2. Content Loss. For the image of art works, the style image is defined as s , the content image as C and the white noise image [23, 24], and it is input into the vgg-19 network to extract the style of the interior decoration art image through the low-level response, extract the content of the style migration image of art works through the high-level response and use the random white noise image as the initial input. In this way, we can make up for the deficiency of content feature map and white noise feature map, get many feature maps under the action of the convolution layer, and convert conv3_2, conv4_ The second layer is described as the content image of the style transfer of art works. An image is generated in the style transfer of art works, which is similar to the content image C in content design. The average loss function is introduced into the calculation of content loss,

and the calculation formula, as shown in the following formula:

$$L_{\text{coabut}}(c, g, l) = \frac{1}{2} \sum \|K_l(g) - K_l(c)\|^2. \quad (15)$$

Here, l represents the convolution layer and K_l represents the feature matrix of image g in the style transfer of art works.

Using the theory of error direction propagation, the gradient value of the generated image g in the style migration of art works is calculated and updated to the input image, so that the initial random image changes until the same response as the content image C appears in the style migration network of art works.

3.3. Enhanced Style Loss. Image style is expressed by the correlation between features. Art work style is texture information, which refers to calculating the relationship between features through Gram matrix, so as to capture the texture information of art work style migration image, and through conv2_1, conv1_1, conv4_1, conv3_1 conv5_1 as the style of the image, the gradient descent mode of the white noise image [25, 26] is used to match the image similar to the style of the art work. In addition, mark the segmented image in another channel and take it as the input mode to form the style loss for each semantic category. Use the segmented channel to enhance the algorithm of the convolutional neural network and form the style loss between the output image g and the style images through the calculation of function:

$$L_{\text{style}}(s, g, l, c) = \sum_{c=1}^c \frac{1}{2} \|G_{c,l}(g) - G_{c,l}(s)\|^2. \quad (16)$$

Here, $G_{c,l}$ represents the operation mode of Gram matrix, that is, the inner product between the style transfer graphs of art works and c represents the number of semantic segmentation mask categories in the style transfer of art works.

The loss function of art style migration image, as shown in the following formula:

$$L_{\text{total}} = \alpha L_{\text{content}} + \beta L_{\text{style}}. \quad (17)$$

After the minimization iteration of the loss function, the stylized image of art style transfer is obtained.

3.4. Poisson Image Editing Constraint Image Spatial Gradient.

In order to generate a clear style transfer effect in the style transfer of art works, take the style transfer image of art works after style processing as the input, then the gradient field of the content image can be expressed, as shown in the following formula:

$$g(x, y) = \nabla c(x, y). \quad (18)$$

While constraining the image spatial gradient, it also needs to meet the following requirements, as shown in the following formula:

$$L^* = \min \int_{\Omega} \|\nabla F - g\|^2 + (F - C_s)^2. \quad (19)$$

Based on the objective function of spatial gradient constraint, the Poisson equation is established, as shown in the following formula:

$$F(1 - \lambda \nabla^2) = C_s - \lambda \nabla g. \quad (20)$$

Here, λ represents the relative weight between the control content image and the style image.

To sum up, the style transfer steps of art work style transfer image are summarized as follows:

Step 1: input the art style migration style image, art style migration content image, and their segmented images into the trained vgg-19 network, initialize the white noise map of image pixels, and input them into the vgg-19 network together.

Step 2: conv3 in vgg-19 network_Layer 2 and conv4-2, extract the content feature matrix of the art work style migration content image and calculate the content loss value between the image pixel white noise image and the content image.

Step 3: conv1 in vgg-19 network_1st floor, conv2-1 floor, conv3_Layer 1, conv4-1, and conv5-1, extract the style feature matrix of the style transfer image of the art work, take the color marked segmented image as another channel of the style transfer of the art work, connect all the segmented channels, and calculate the enhanced style loss value of the image pixel white noise image and the style image.

Step 4: calculate the total loss function in terms of content loss and style loss of the style migration image of art works used for training.

Step 5: by training the style transfer image of art works, the white noise gradient of image pixels can be reduced, so as to minimize the total loss function. After several iterative calculations, the total loss function is adjusted to obtain the stylized image of interior decoration art; Poisson image editing technology is used to constrain the gradient of stylized images, and the migration effect picture of image content with both art work style migration style and art work style migration content is obtained.

According to the above process, complete the style transfer of art works.

4. Experimental Analysis

4.1. Experimental Data Set. In order to verify the practicality of the proposed style transfer method, 2200 art works of different styles are randomly selected from 15 groups of open art image data sets as pretraining data sets. And, input it into vgg-19 network model for pretraining to obtain model parameters. After setting the name of the image in 15 groups of open image data sets of art works, sort out the parameters of art works, as shown in Table 1.

TABLE 1: Parameters of art works data set prepared.

Artwork dataset name	Positive sample (%)	Size	Resolution (dpi)
Labeled faces in the wild	48273 (7.64)	640 × 480	100 million
MNIST-06	39390 (39.8)	1280 × 640	20 million
CIFAR-02	36640 (8.21)	640 × 480	100 million
AI-challneger-04	63605 (40.2)	1280 × 640	20 million
Pascal VOC-07	27001 (47.21)	640 × 480	100 million
COCO common objects dataset	75220 (4.1)	1280 × 640	20 million
CityScapes	51220 (46.9)	640 × 480	100 million
Lego bricks	19090 (38.67)	640 × 480	100 million
Visual genome	75904 (17.62)	640 × 480	100 million
VisualQA	72490 (25.05)	1280 × 640	20 million
MNIST-08	36257 (47.14)	640 × 480	100 million
KITTI-05	28284 (30.13)	1280 × 640	20 million
ApolloScape-02	33298 (18.37)	1280 × 640	20 million
TUM-08	68273 (1.9)	640 × 480	100 million

Using the data set of art works shown in Table 1, applying the parameters in the above table, the median difference method is used to calculate the regional gradient in the image. The numerical, as shown in the following formula:

$$\left\{ \begin{array}{l} G_x(i, j) = \frac{[V(i+1, j) - V(i, j)]}{2} \\ G_y(i, j) = \frac{[V(i, j+1) - V(i, j)]}{2} \\ gr(V(i, j)) = \sqrt{G_x(i, j)^2 + G_y(i, j)^2} \end{array} \right. \quad (21)$$

Here, $V(i, j)$ represents the pixel function of the art work, $gr(V(i, j))$ represents the amplitude value of the art work at the position of pixel (i, j) , $G_x(i, j)$ represents the horizontal gradient value of the image, and $G_y(i, j)$ represents the vertical gradient of the image. After the enhanced image is processed into regional gradient values, the gradient parameters in the data set are sorted out as the processing object, and the application performance of the proposed method is tested with reference [5] unsupervised image style migration technology based on image mask and reference [6] image style migration technology based on semantic segmentation.

4.2. Results and Analysis. In order to test the robustness of the proposed art work style migration technology, two art work scenes with different scenes are selected, and each scene selects different style types for migration and conversion. The results are shown in Figure 5. (from the Internet).

It can be seen from the migration results in Figure 5 that the content image corresponding to scene (a) belongs to the style of “lining people with objects,” and the corresponding style image belongs to the realistic style. A good migration effect can be generated between the content image and the style image; scene (b) is to test the style conversion effect of style migration images of art works with the same style and different contents. The corresponding style images and

content images belong to “lining people with objects,” but they can still produce a good migration effect.

Based on the above-given experimental preparation, the distortion parameters after image migration are defined by using the parameters obtained by the gradient processing; the numerical relationship is shown as follows:

$$D(v_1, v_2) = \sqrt{(v_1, v_2)^T \left(\frac{\Sigma_1 + \Sigma_2}{2} \right)}. \quad (22)$$

Here, v_1 and v_2 , respectively, represent the distortion vector of the image, Σ_1 and Σ_2 , respectively, represent the covariance value of the image, T represents the multivariate parameter in the image, and $D(v_1, v_2)$ represents the image distortion parameter. Corresponding to the numerical relationship constructed above, every three sets of art works data sets are processed into an independent variable. Finally, the image distortion parameter results after migration by the three methods are shown in Figure 6.

It can be seen from the experimental results shown in Figure 6 that 15 groups of open source images are integrated into 5 groups of image processing groups. Corresponding to the distortion parameter value relationship constructed above, the greater the calculated distortion value is defined, it means that the migrated image of this style migration technology has greater distortion. According to the values in Figure 6, the average distortion parameter obtained by the method of reference [5] is about 0.55, and the migrated image has great distortion. The average distortion parameter obtained by the method in reference [6] is 0.3, and the image migrated by this style migration technology produces less distortion. The average distortion parameter obtained by the proposed method is 0.15. Compared with the two comparison methods, the distortion parameter formed by the proposed style migration technology is the smallest, and the distortion generated by the actual migrated image does not affect the next image processing work.

In the above-given experimental environment, three methods are called to segment the nonsignificant region, and multiple overlapping measures are defined in the three methods. In the actual segmentation, when there is no overlap in the overlapping measures, it indicates that the

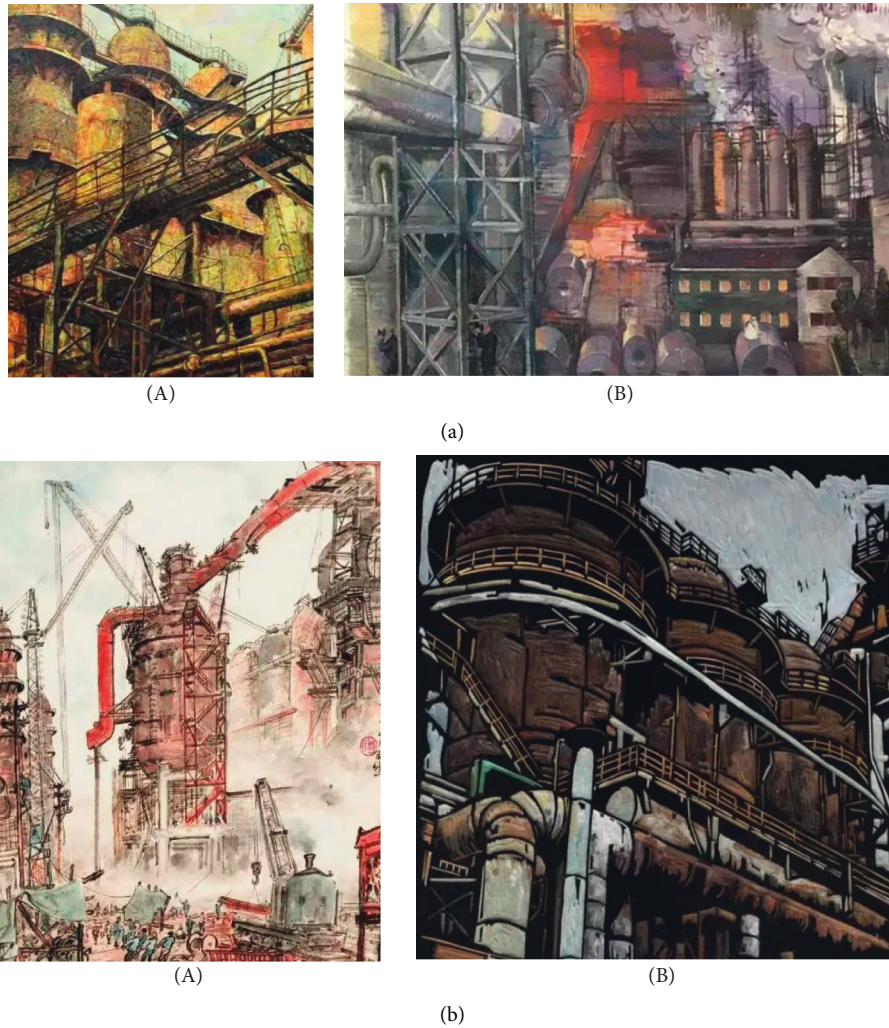


FIGURE 5: Style transfer of art works style transfer effect of art works (a) Premigration image (b) Post migration image.

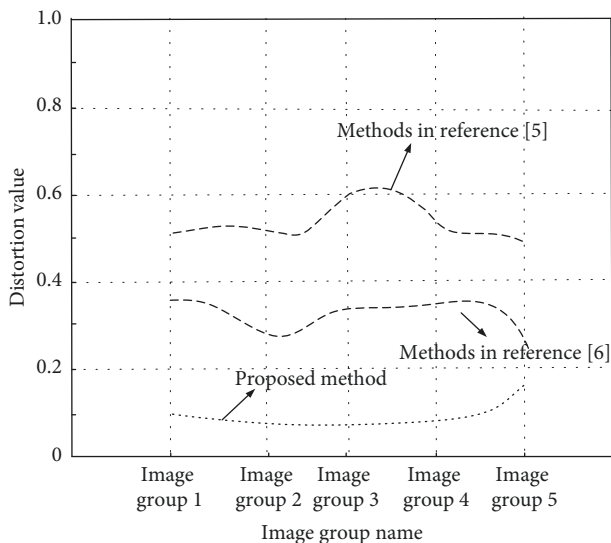


FIGURE 6: Distortion parameters generated by three methods.

image style migration technology can accurately segment the nonsignificant region, and the overlap degree of the three methods is defined. The numerical relationship is shown as follows:

$$I = \frac{A \times V(i, j)}{B} \tag{23}$$

Here, I represents the calculated overlap, A represents the significant area segmented by image style transfer technology, and B represents the nonsignificant area segmented by style transfer technology. Under the control of the above numerical relationship, sort out the art works data set prepared for the experiment, and sort out the overlap results generated by the three methods, as shown in Figure 7.

After the images participating in the experiment are divided into five groups of image groups, the average value of overlap in the image group is calculated according to the above-constructed overlap value relationship. It is defined that the closer the overlap value is to 1, it means that the significant area and nonsignificant area segmented by this style of migration technology overlap. According to the

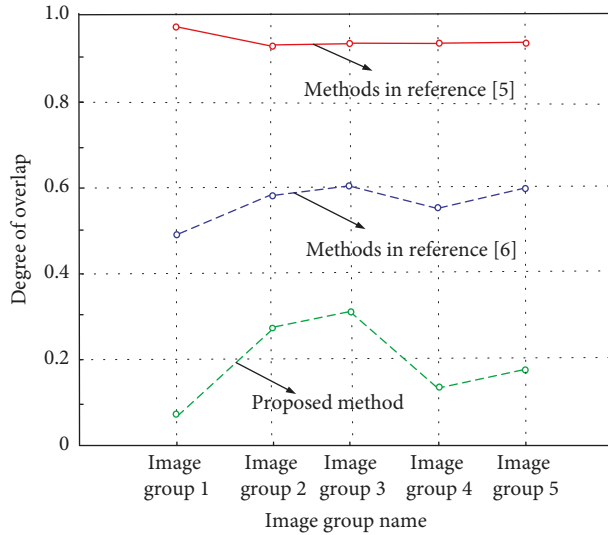


FIGURE 7: Overlap values generated by the three methods.

numerical relationship shown in Figure 7, the average overlap value obtained by the method of reference [6] is 0.9. There is a lot of overlap between the nonsignificant region and the significant region segmented by this style transfer technology, which has a great impact on enhancing the nonsignificant region. The average overlap obtained by the method of reference [5] is 0.5. The nonsignificant region segmented by this style of migration technology overlaps with the significant region, which has little impact on the process of image migration. The average overlap obtained by the proposed method is 0.2. Compared with the two comparison methods, the overlap between the nonsignificant region and the significant region actually segmented by the proposed method is small, which has little impact on the effect after migration.

Keeping the above-given experimental environment unchanged, the brightness of the art works processed by the three methods is stretched and processed into a light compensation process. After the stretching process of the same process, the gray level output by the three methods corresponds to the gray level output. The output gray level results are shown in Figure 8.

After the same illumination treatment, the art works prepared for the experiment are marked in order by comparing the gray level parameters of the output of the actual stretching enhanced image. It is defined that the larger the gray level parameter of the image output after migration, it indicates the loss of details of the image area after illumination compensation. According to the gray level parameter values sorted and calculated in Figure 8, when referring to the art works after migration according to the method of reference [6], the actual output gray level parameter is between 0.5 and 0.7, the actual output gray level parameter is the largest, and the nonsignificant area after migration loses the most details. The actual output gray level parameters of reference [5] method are between 0.4 and 0.5, the actual output gray level parameters are large, and the nonsignificant areas after migration lose more details. The

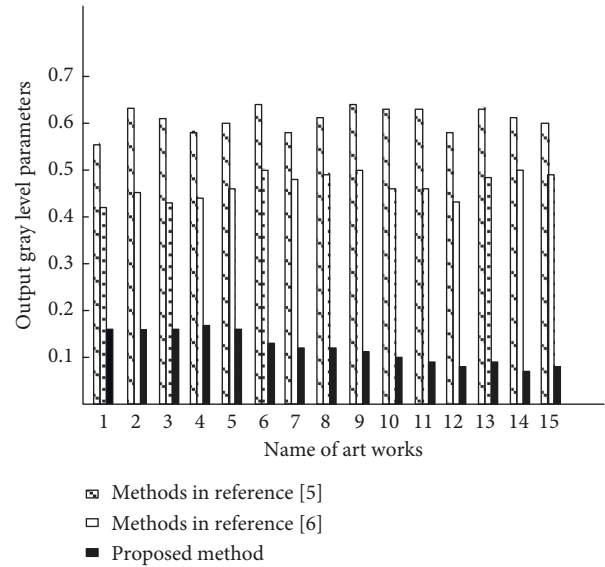


FIGURE 8: Gray level parameters output by three methods.

actual output gray level parameters of the proposed method are between 0 and 0.2. Compared with the two comparison methods, the output gray level parameters are the smallest, the details of the nonsignificant area of the migrated image are the least, and the quality of the migrated image is the best.

In conclusion, the experimental results prove the effectiveness of the proposed method. In the above tests, the average distortion parameter obtained by the proposed method is 0.15, the average overlap is 0.2, and the actual output gray level parameter is between 0 and 0.2. The test results of the three test indicators are low, which shows that the proposed art work style migration technology has very strong robustness and can achieve art work style migration. And this method can not only achieve a better migration effect but also will not make the style migration image of art works distorted.

5. Conclusion

Art works are an important tool of expression and communication in daily life and social life. However, with the changes of the times and the evolution of culture, the functions of the style of art works in reflecting cultural heritage, emotional appeal, visual beauty, as well as brand image, product information, industry characteristics, etc., have attracted more and more attention. Especially in recent years, with the vigorous development of digital carriers, digital design of art works has gradually become a daily demand of today's society and life. Therefore, aiming at the problems existing in the style image of art work style transfer, this paper proposes a style transfer technology of art work based on dual channel deep learning. Using the principle of art style migration technology and Poisson image editing technology, the style migration of art works is realized, so as to obtain a migrated image that can meet the modern style design. The experimental results show that the

proposed method has very strong robustness and can realize the style migration of art works. It can not only achieve a better migration effect but also will not make the style migration image of art works distorted.

Data Availability

The raw data supporting the conclusions of this article will be made available by the author, without undue reservation.

Conflicts of Interest

The author declares that there are no conflicts of interest regarding this work.

References

- [1] Z. Jinglei and H. Yawei, "Image-to-image Translation Based on Improved Cycle-consistent Generative Adversarial Network," *Journal of Electronics & Information Technology*, vol. 42, no. 5, pp. 1216–1222, 2020.
- [2] L. Huang, P. Wang, C. F. Yang, and H. W. Tseng, "Rapid Local Image Style Transfer Method Based on Residual Convolutional Neural Network," *Sensors and Materials*, vol. 33, no. 4, p. 1343, 2021.
- [3] D. Futschik, M. Kučera, M. Lukáč, Z. Wang, E. Shechtman, and D. Sykora, "STALP: Style Transfer with Auxiliary Limited Pairing," *Computer Graphics Forum*, vol. 40, no. 2, pp. 563–573, 2021.
- [4] X. Nan, D. Jin, Z. Bing, W. Xiaoyu, and Y. Lintao, "Research on Fast Image Style Transformation Based on Residual Network," *Computer Engineering and Applications*, vol. 56, no. 12, pp. 201–208, 2020.
- [5] K. Lengru and T. Shaohua, "Unsupervised image style transfer based on image mask," *Application Research of Computers*, vol. 37, no. 8, pp. 2552–2555, 2020.
- [6] L. Meili, Y. Chuanying, and S. Bao, "Research on Image Style Transfer Technology Based on Semantic Segmentation," *Computer Engineering and Applications*, vol. 56, no. 24, pp. 207–213, 2020.
- [7] F. Schenkel, S. Hinz, and W. Middelman, "Style transfer-based domain adaptation for vegetation segmentation with optical imagery," *Applied Optics*, vol. 60, no. 22, pp. F109–F117, 2021.
- [8] D. Chen, L. Yuan, J. Liao, N. Yu, and G. Hua, "Explicit Filterbank Learning for Neural Image Style Transfer and Image Processing," *IEEE Transactions on Software Engineering*, vol. 43, no. 7, pp. 2372–2387, 2020.
- [9] S. Liu, Y. Bo, and L. Huang, "Application of Image Style Transfer Technology in Interior Decoration Design Based on Ecological Environment," *Journal of Sensors*, vol. 2021, Article ID 9699110, 7 pages, 2021.
- [10] C. T. Lin, S. W. Huang, Y. Y. Wu, and S. H. Lai, "GAN-Based Day-to-Night Image Style Transfer for Nighttime Vehicle Detection," *IEEE Transactions on Intelligent Transportation Systems*, vol. 22, no. 2, pp. 951–963, 2021.
- [11] W. Jing-Kun, D. De-Rui, L. Wei, and W. Yong-Xiong, "Combining Feature Pyramid and Region Proposal Networks for Visual Object Tracking," *Journal of Chinese Computer Systems*, vol. 43, no. 1, pp. 117–123, 2022.
- [12] Y. Xian-feng, L. Xiao-lan, and G. Hong-jun, "Image Enhancement Algorithm Simulation Based on Improved Adaptive Gamma Transformation," *Computer Simulation*, vol. 37, no. 5, pp. 241–245, 2020.
- [13] W. Yu, H. Yao, D. Li, G. Li, and H. Shi, "GLAGC: Adaptive Dual-Gamma Function for Image Illumination Perception and Correction in the Wavelet Domain," *Sensors*, vol. 21, no. 3, p. 845, 2021.
- [14] Z. Hongyu, W. Jinming, and G. Zhenfei, "Image Enhancement Method based on Regional Saliency Recognition," *Communications Technology*, vol. 54, no. 7, pp. 1641–1646, 2021.
- [15] H. Li, H. Li, L. Xu, and X. Liu, "Distortion correction and image registration of ultralarge field of view near-eye display device," *Applied Optics*, vol. 59, no. 14, pp. 4422–4431, 2020.
- [16] M. K. Manhard, J. Stockmann, C. Liao et al., "A multi-inversion multi-echo spin and gradient echo echo planar imaging sequence with low image distortion for rapid quantitative parameter mapping and synthetic image contrasts," *Magnetic Resonance in Medicine*, vol. 86, no. 2, pp. 866–880, 2021.
- [17] C. Fafa, C. Mengteng, Y. Yunpeng, C. Baojia, X. Wenrong, and X. Nengqi, "A Segmentation Method Based on Dual Attention Mechanism and U-Net for Corrosion Images," *Journal of Xi'an Jiaotong University*, vol. 55, no. 12, pp. 119–128, 2021.
- [18] B. Olimov, K. Sanjar, S. Din, A. Ahmad, A. Paul, and J. Kim, "FU-Net: fast biomedical image segmentation model based on bottleneck convolution layers," *Multimedia Systems*, vol. 27, no. 4, pp. 637–650, 2021.
- [19] L. Liming, P. Renjie, F. Jun, and Y. Jiang, "Skin lesion image segmentation algorithm based on multi-scale feature fusion double U-Net," *Application Research of Computers*, vol. 38, no. 9, pp. 2876–2880, 2021.
- [20] C. Guozhong, L. Mengmeng, and W. Xiaoqin, "Integrating Height Features for Multi-scale Urban Building Type Classification from High-Resolution Remote Sensing Images," *Journal of Geo-Information Science*, vol. 23, no. 11, pp. 2073–2085, 2021.
- [21] B. R. Mosier and L. E. Bantis, "Estimation and construction of confidence intervals for biomarker cutoff-points under the shortest Euclidean distance from the ROC surface to the perfection corner," *Statistics in Medicine*, vol. 40, no. 20, pp. 4522–4539, 2021.
- [22] C. M. Chen, S. W. Liang, S. T. Chou, D. S. Hwang, U. K. Kim, and Y. C. Tseng, "Importance in the occurrence rate of shortest buccal bone marrow distance (<1 mm) for sagittal split ramus osteotomy," *Journal of the Formosan Medical Association*, vol. 120, no. 1, pp. 697–704, 2021.
- [23] Y. Zhang, J. Duan, Y. Jin, and Y. Li, "Discovering governing equation from data for multi-stable energy harvester under white noise," *Nonlinear Dynamics*, vol. 106, no. 4, pp. 2829–2840, 2021.
- [24] C. Qingjiang, S. Xiaohan, and C. Yuzhou, "Image denoising algorithm based on wavelet transform and convolutional neural network," *Journal of Applied Optics*, vol. 41, no. 2, pp. 288–295, 2020.
- [25] K. Tao, G. Zhe, and Y. Chuang, "Stochastic Gradient Descent Method of Convolutional Neural Network Using Fractional-Order Momentum," *Pattern Recognition and Artificial Intelligence*, vol. 33, no. 6, pp. 559–567, 2020.
- [26] W. Wu, X. Jing, W. Du, and G. Chen, "Learning dynamics of gradient descent optimization in deep neural networks," *Science China Information Sciences*, vol. 64, no. 5, pp. 150102–150115, 2021.

Research Article

Research on Movement Analysis and Guidance in Dance Learning Based on Data Mining

Guangle Yin  and Jing Liu

Music Academy, Henan Polytechnic, Zhengzhou 450046, China

Correspondence should be addressed to Guangle Yin; 36030@hnzj.edu.cn

Received 8 June 2022; Revised 1 August 2022; Accepted 26 August 2022; Published 19 September 2022

Academic Editor: Le Sun

Copyright © 2022 Guangle Yin and Jing Liu. This is an open access article distributed under the Creative Commons Attribution License, which permits unrestricted use, distribution, and reproduction in any medium, provided the original work is properly cited.

In dance, we must understand the essential meaning of dance movements from the inside and express them on the basis of dance. Therefore, in the process of developing new dance teaching methods, it is necessary to improve the basic education of dance students, so that they can express the emotions conveyed by dance through body language and movements, and improve dance expression ability. In this context, we made the research and reached the following conclusions: (1) the number of frames of different dance types is also different, and the number of frames to be learned is also increasing. The dance with the highest number of frames is Latin2, which has 3635 frames, and the dance with the highest number of frames that need to be learned is also Latin2, which requires 2519 frames to learn. (2) The data mining method is still the highest among the three methods, and the accuracy of the complete teaching method is 82%, which is the lowest among the three methods, and the accuracy of the decentralized teaching method is 87%. No matter in the test set or the mixed test set, the curve values of deep mining are very stable. First of all, human movements emphasize that in dance, the essential meaning of dance movements needs to be understood from the inside and expressed through the foundation of dance. Therefore, when developing new dance teaching methods, it is necessary to strengthen the basic dance training of students so that students can express the emotions conveyed by dance through body language and movements and improve their dance expression ability. We conduct research in this ecological environment. Different types of dance learning process using different frames, different types of dance in the algorithm transport have different recognition methods, using better and different algorithms can achieve the best performance. Both groups in the Hip Hop dance had a shorter average learning time than both groups in the Latin dance.

1. Introduction

For representing, processing, and extracting knowledge for a variety of applications from the ever-increasing accumulation of data, which made the pervasiveness of computers possible, perhaps inevitable, and built a general framework for inspection and classification methods. Provide simple examples to demonstrate the nature of representative feature selection methods, compare them using datasets with a combination of intrinsic properties according to the goal of selecting features, propose guidelines for using different methods in various situations, and identify areas of research new challenge venue. A reference for researchers in machine learning, data mining, knowledge discovery, or databases [1]. As the ability to track and collect large amounts of data

using current hardware technologies continues to improve, there has been interest in developing data mining algorithms that protect user privacy. A recently proposed technique addresses the privacy preservation problem by perturbing the data and reconstructing the distribution at the aggregation level to perform mining. This approach preserves privacy when accessing information implicit in the original attributes. The distribution reconstruction process naturally leads to some information loss, which is acceptable in many practical situations, and the algorithm is more efficient than currently available methods in terms of information loss levels. Specifically, it is demonstrated that the EM algorithm converges to a maximum-likelihood estimate of the original distribution based on perturbed data. When large amounts of data are available, the EM algorithm provides robust

estimates of the raw data [2]. Interest in mining time series data has exploded over the past decade. In this work, the following claims are made. Much of the utility of this work is small because the amount of improvement provided by the contributions is entirely the variance that can be observed by testing on many real-world datasets, or by changing minor implementation details. To illustrate the point, the most exhaustive time series experimental reimplementation ever performed [3]. When used with statistical methods, graphical models have many advantages in data modeling because the model encodes the dependencies between all variables, can easily handle missing data, and can be used to understand problems and predict consequences. The article discusses methods for building networks from prior knowledge and summarizes Bayesian statistical methods for improving these models using data [4]. Using soft computing provides a survey of the available literature on data mining. Classifications have been provided based on the different soft computing tools used and the data mining functions they implement and the data mining functions implemented and preference criteria selected by the model. The utility of different soft computing methods is highlighted. Generally fuzzy sets are suitable for dealing with problems related to pattern comprehensibility, mixed media information and human interaction, and can provide approximate solutions faster. Genetic algorithms provide efficient search algorithms to select models from mixed media data, pointing out some challenges to data mining and applications of soft computing methods are presented. An extensive bibliography [5] is also included. Girls showed a higher personal interest in dance than boys, but the two groups were equally interested. Although girls were not as physically active as boys, their skills/knowledge outcome indicators were higher than boys. It appears that gender has little effect on the motivational effect of situational interest, and the quality of classroom learning in girls may be higher than in boys due to higher personal interest. The findings suggest that situational interest may motivate all students, but it is necessary to enhance personal interest in order for them to engage in high-quality learning [6]. We emphasize generating augmented reality environments for individual dancers based on dance annotation analysis. We have introduced a new interactive technique for dance animations required for educational purposes. This approach opens up new possibilities for interactive dance observation, fast and slow motion, different perspectives, and multiple functions to support high interactivity between users and 3D dancers [7]. All people have the urge to express themselves through dance, which represents a unique opportunity to artificially capture human creative expression. In particular, the spontaneity and relative ease of moving with music without any overall planning suggests a natural link between temporal patterns and motor control [8]. Four preschool dance classes, including 32 children aged 3–6, were randomly assigned to pretend imagination and traditional instruction. Ratings were based on the speed at which new motor skills were learned, future recall of the skills, concentration on the task, and enjoyment during the task. It was found that children in the pretend imagination group had significantly

better visual fixation, engagement, and enjoyment of the task process, required less time for prompting and recall, and took less time to learn skills [9]. These multimedia applications need to store and retrieve different forms of media such as text, hypertext, graphics, still images, animation, audio, and video. Dance is one of the important cultural forms of a nation, and dance video is such a multimedia form. Archiving and retrieving the required semantics from these dance media collections are a crucial and demanding multimedia application [10]. In recent years, with the increase of work pressure, more and more people have begun to pay attention to national fitness, in order to improve personal physical and psychological quality. Square dancing is a sport suitable for all ages. It integrates fitness, a healthy heart, and a strong and handsome brain. It is the best way to communicate in fitness and is deeply loved by people. The current situation of residents' square dance was investigated, and the characteristics of square dance practitioners themselves and the characteristics of square dance were analyzed [11]. Track their movements using an optical motion capture system. Many pose and kinematic features are extracted from motion data. Findings indicated that the positive effects of proximity motivation were associated with higher movement speeds of the hands and head, as well as the extended posture of the hands. In addition, positive effects were also associated with higher-dimensional movements, suggesting an association with more complex and varied dance movements [12]. Chinese classical dance steps with unique aesthetics are closely related to traditional Chinese opera. Classical Chinese dance steps can be traced back to ancient women's foot binding, which had a great impact on the physiology and morphology of the dance steps [13]. Develop a method for automatic classification of the correctness of basic dance movements to support dance beginners in their self-practice outside the classroom. We first worked with dance professionals to design two basic dance moves, the waltz and the merengue. Acceleration and angular velocity data of the chest and pelvis were collected [14]. The article provides information on the health benefits of several dances. It mentions that dancing is a weight-bearing exercise that causes osteoblasts to grow. It added that dancing like boogie can enhance brain power, especially mental function and creativity. Furthermore, it mentions that dancing, including spinning, also burns calories, which is essential for a healthy heart [15].

2. Dance Learning

2.1. Status Quo of Dance Learning

2.1.1. Classroom Learning Mode Is Single. Because the basic level of dance of the students varies, it is difficult to carry out high-level teaching, and only the intermediate level can be unified and standardized. Students with a good foundation feel that it is "tasteless to eat, and it is a pity to abandon it," and repeating the content they have learned in the past feels a little dull and long; while students with a weak foundation are "dazzled" by the basic content and "hesitant" for the advanced content. In actual learning, teachers lead students

to count the beats and jump over and over again, and “fill-in” mechanical imitations cause students to lose their enthusiasm for autonomous learning. The grasp of dance style is submerged in form, which restricts students’ innovation and creativity.

2.1.2. Curriculum Setting Is Biased toward Professional Technical Training. Although the construction of dance teaching materials tends to be perfect, the curriculum covers a wide range, and professional theoretical courses such as Chinese dance history and Chinese folk dance culture have not been properly used in teaching. Just by simply sorting out and forcing memory, students cannot think about the connotation and value of their cultural system and bring them into the process of dance performance.

2.1.3. Lack of Distinctive Course Content Settings. The content and methods of dance course materials in advanced colleges have been tested by long-term teaching practice and tend to be stable, perfect, and self-contained. Different schools have different school-running characteristics. If the theory is blindly copied and the exploration of teaching practice is ignored, the content of the courses is similar, and there is a lack of regional targeting. In this way, the theory and practice of teaching are disconnected. For example, in the ethnic dance courses in the southwest region, if the advanced dance courses in other regions are set up step by step, there will be very few professional practice opportunities for students after graduation, which is not conducive to the study of ethnic culture and the inheritance of art in the southwest region. The teaching effect is maximized.

2.2. Problems in Dance Learning

2.2.1. The Lack of Exemplarity in Dance Education. If there is a need, there will be a market, and schools will slowly emerge to teach dance. Whether it is teaching, teachers, or educational institutions, the conditions are relatively comprehensive, and the social recognition is relatively high, but more and more dance schools are social institutions that lack education and teaching. In response to this problem, the head teacher asked teachers to train students according to the grade-level learning materials and prepare for the exams that the students will take. As the class progresses, children are the main source of students in dance schools. Students in this age group are special because they are more playful, have shorter attention spans, and do not understand many technical terms. Many teachers do not pay attention to the details of students’ physical and mental development. This creates a vicious circle. Finally, some dance schools only shout slogans and do not provide a good learning environment. The poor quality of teaching materials is not suitable for teachers. They always use a variety of teaching methods without caring about what each student’s dance really means.

2.2.2. The Teaching Method of Dance Education Is Not Systematic. The teachers of some dance schools are not of high quality and cannot arrange courses according to the learning ability of students of different age groups. In order to make learning more effective, they blindly teach students difficult dance moves, ignoring the rules of easy and difficult to learn. Exceeding a student’s physical capacity can affect not only his or her long-term physical development but also many potential risk factors. Others say learning to dance is difficult. Only strengthen the physical development of students. The intensity of the internship provides good grades but does not allow for dangerous movements that exceed the student’s physical endurance. Doing too much to achieve course goals in a short period of time may be detrimental to the healthy development of students. Additionally, many teachers are unable to teach students based on information about the learning process. For example, some students have poor physical fitness and poor dance skills; so teachers have to learn to be careful not to trust each other, so that students eventually lose confidence in learning dance. It is shown in Figure 1.

2.3. Measures to Solve the Problems Existing in the Current Dance Learning

2.3.1. Build an Excellent Team of Teachers. Everything related to education is inseparable from a good teacher. A good teacher must not only have good professional dance skills but also teach students moral education through language and action, that’s how you can become a really good dance teacher.

2.3.2. Pay Attention to Reasonable Arrangements for Teaching. Since most dance classes take place outside of school because of the need for concentration, teachers should give students enough time to learn about the teacher in class rather than just looking for a lot of knowledge. In addition, when explaining dance movements, teachers should try their best to explain in clear, clear, and easy-to-understand technical language to attract children’s attention and stimulate their interest in learning.

2.3.3. Strengthen the Construction of Hardware Facilities. It is necessary to strengthen the supervision of dance schools in all walks of life, and safety issues must be put in place in a timely manner, and dangerous accidents should be prevented as much as possible. Dance schools must determine that there is no income limit and no students will be admitted. This eliminates the need for quality teaching, liberating teachers, and increasing classroom efficiency.

2.3.4. Strengthen the Construction of Dance Teaching Materials. Whether it is the Children’s Palace or various extracurricular dance schools, the teaching materials need to be strengthened with the help of experts or experienced dance teachers to prepare the teaching materials for children’s physical and mental development. Know how to do

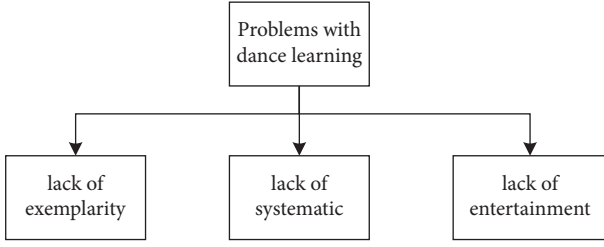


FIGURE 1: Problems in dance learning.

teaching tasks according to the actual situation of students in the classroom. Make a study plan and try to complete the study tasks correctly. Don't prepare for the exam. It is shown in Figure 2.

3. Data Mining Algorithms

3.1. Data Mining Algorithm Design. Create the subspace S required for data mining. Location is the value of the data function in the collection, and the data are in form $o \in D$. According to the data distribution characteristics of outliers, the nearest neighbors (O, S) of data elements can be expressed as also Subspace with uneven distribution. Regarding the nature of multidimensional data, it is clear that the focus of the subspace is the data object O , and the formula for calculating the probability distance is the following:

$$d_s = \frac{1}{I_d(o, s)}. \quad (1)$$

In the formula, distance is represented by d . If the data object is always in the middle of the excavation set, the mean or distance of the data can be calculated by formula:

$$\sigma(o, s) = \sqrt{\sum_{x \in s} d(o, s)^2}. \quad (2)$$

Since local discrete data have nonuniform distribution conditions, the properties of discrete data must be represented by an approximation between the density of discrete data and the standard distance.

$$\lambda = \frac{I_d}{\sigma(o, s)}. \quad (3)$$

The segregated asset is obtained from equation (3) and the result provides the desired distribution of segregated data within the region. Combined with the above feature search method, the data entropy information algorithm is used to extract the information needed to retrieve big data objects from the Internet. Observe the distribution of the given data x , and use the probability function of the p value to obtain the information element $E(x)$ of the data x :

$$E(x) = - \sum_{x \in x} p(x) \ln p(x). \quad (4)$$

Due to the differences in the detected data dimensions, it will have a certain negative impact on the results of IoT big data mining, so it is necessary that the detected data are processed according to the standard format, as shown in

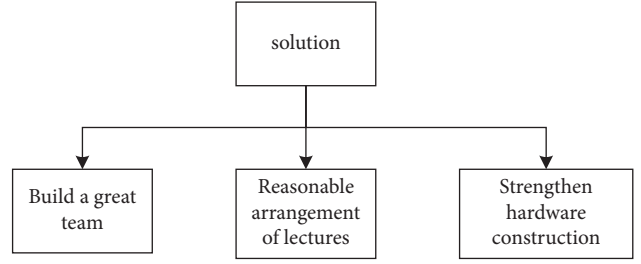


FIGURE 2: Measures to solve the problems existing in current dance learning.

$$\alpha = \frac{\alpha - \alpha_1}{Y_\alpha}. \quad (5)$$

The result of data normalization should be calculated based on the average attribute of the received data and the data standard deviation attribute. The calculation process uses standard deviation to increase the relevance of the data properties and to ensure the accuracy of the data retrieval.

The overall results of data processing should be calculated according to the method, the nature of the data observed, and the standard deviation of the data characteristics. The calculation process uses the standard deviation to make data attributes more important to the accuracy of data mining. In addition, mean deviations from known data characteristics can also be used to obtain standard data processing results. The calculation formula is the following:

$$\alpha_i = \frac{\alpha - \alpha_1}{G_a}. \quad (6)$$

The purpose of improving the anti-interference performance of the algorithm is achieved through the above formula, and the calculation formulas of the data attribute average α , the data attribute standard deviation Y_a , and the data attribute average deviation G_a are the following:

$$\alpha_1 = \sum_m \alpha \frac{1}{m},$$

$$G_a = \sum_m \frac{\alpha - \alpha_1}{m}, \quad (7)$$

$$Y_a = \sqrt{\sum_m \frac{(\alpha - \alpha_1)^2}{m}}.$$

In the formula, the number of iterations is m . After the data standardization is completed, artificial intelligence technology is applied to the processed data to obtain certain data mining results.

3.2. Realize Intelligent Data Mining. Neural network technology, an important branch of artificial intelligence technology, is used to carry out big data mining on the Internet of Things. The BP neural network with three-layer transmission structure is used as the main structure, and the normalized data are distributed into the neural network.

Due to the particularity of the neural network structure, the average value of the information entropy of the data is E :

$$\begin{aligned}\omega &= \frac{1 - H_i}{\sum_{i=1}^E H_i}, \\ \theta_1 &= u\theta_1 + (1 - u)\theta_2, \\ \theta_2 &= u\theta_2 + (1 - u)\theta_1.\end{aligned}\quad (8)$$

The two data in the formula and θ_1, θ_2 are linearly combined. The constant range of U is from 0 to 1, and the value range is narrowed according to the actual situation. If the constant value is fixed, it means that the hybridization operator is not constant during the calculation process. Since the constant value changes with the number of iterations, the average performance of the hybrid operator can be improved, and thereby realizing the integration of IoT big data.

$$v_k = v_k = \Delta(t, v_k - LB). \quad (9)$$

The data change value is generated from the left and right neighbors LB and UB of the variable k and the return value of the function. As the algebraic t increases, the value of the data change is likely to approach 0. Based on the above steps, a general operator search is performed on the dataset to create an IoT data view that meets the needs of data mining. In all the above processing steps, an IoT data mining algorithm based on artificial intelligence technology is developed.

3.3. Federated Average Algorithm. A unified learning algorithm distributes learning tasks to different devices to learn local model updates and, occasionally, interacts with a central server to coordinate learning objectives around the world. Unlike traditional machine learning methods, blended learning requires centralizing training models on a computer or data center so that each client device can use a local training data set to update the model. Federated learning is defined to solve the minimum loss of an objective function according to a formula.

The unified learning algorithm distributes learning tasks to different devices to learn local model updates and communicates with a central server from time to time to coordinate global learning goals. Unlike traditional machine learning approaches, blended learning requires training models to be centralized on a computer or data center so that each client device can use a local training dataset to update the model. Equation analysis is defined as the concentration of the dataset in a set of loss functions, which determine the solution to which Equation (10) is applied to the k samples of the dataset. The built-in analysis algorithm uses the generic, $n = \sum_k n_k, p_k = n_k/n$ algorithm trained on all k multifunctional devices in the dataset.

$$\min f(\omega) = \frac{1}{n} \sum_{k=1}^k n_k F_k(\omega) = \sum_{k=1}^k p_k(\omega). \quad (10)$$

The local prediction loss function for each client device k along the model parameters is $F_k(\omega)$. As shown in Equation

(11), when different local optima are computed they are combined to achieve an overall minimization of the learning loss:

$$F_k(\omega) = \frac{1}{n_k} \sum_{i \in n_k} f(x_k, \omega). \quad (11)$$

This will improve common patterns in connected learning systems. To solve the objective equation, FedAvg first randomly selects k units from a subset of system units at each computational iteration, and then uses a combined FedSGD optimization method to globally implement each selected unit, computing the location of the global state and local data.

During the calculation process, local search and global search are continuously amplified according to P1 and P2 points, which correspond to both yin and yang. If point P2 is better than point P1 the two points are exchanged, and the sympathy algorithm agrees. Yin and yang have repetitions according to P1 and P1 points. P2 exploration optimization is expected to achieve a balance between local development and global exploration, which is a balance of yin and yang. In this particular implementation, the yin–yang balance optimization algorithm typically consists of two steps: updating the solution based on the collection set and updating the solution based on the hypersphere the main content of these two terms is given as follows:

$$\begin{aligned}g_k &= \Delta F_k(\omega_k), \\ \forall k, \omega_{t+1}^k &\leftarrow \omega_t - \eta g_k.\end{aligned}\quad (12)$$

In each of the update round, the server collects training data from all devices participating in that training round of the pattern and calculates the weighted average system update pattern according to equation (13), where η represents the training learning rate:

$$\omega_{t+1} \leftarrow \omega_t \eta \sum_{k=1}^k. \quad (13)$$

The number of elements in the FedAvg algorithm plays a crucial role in the speed of convergence and the accuracy of predictions. Some people suggest adding the stack size to some value to approximate disk. When installing a large compressed package, each device can speed up the calculation of the same amount of data, improve the convergence speed of the system, reduce the number of iterations, and keep the training of the system at a high enough level of accuracy. In the calculation process, the local search and global search based on points P1 and P2 are continuously strengthened, which corresponds to both yin and yang. If point P2 is better than point P1, then these two points are exchanged, and the sympathetic algorithm corresponding to yin and yang is repeated based on points P1 and P1. The optimization search of P2 is expected to achieve a balance between local development and global search, corresponding to the balance of yin and yang. In the specific implementation, the yin–yang balance optimization algorithm mainly includes two stages: solution update based on archive set and solution update based on hypersphere. The main

contents of these two stages are given below. To update the search radius, the calculation method is as follows:

$$\begin{aligned}\delta_1 &= \delta_1 - \left(\frac{\delta_1}{\alpha}\right), \\ \delta_2 &= \delta_2 + \left(\frac{\delta_2}{\alpha}\right).\end{aligned}\quad (14)$$

4. Research on Action Analysis and Guidance of Data Mining in Dance Learning

4.1. Performance Test of Data Mining in Dance Movement Learning. To test the optimal performance of the data mining methods proposed in this dance review article, the models proposed in this article have been experimentally improved and research methods have been applied with subsequent tests and trials to make a complete and decentralized learning approach. Test kits are used to assess the generality of the final sample, and the hybrid test set meets the modern criteria of the model and is first used to assess the model's ability to write test results. Experimental data of different samples of the test group and the mixed test group are shown in Figure 3.

From the data in Figure 3, we can see that after performing a series of tests, the accuracy of the distributed learning method can be 89%, the accuracy can increase to 91%, and the accuracy can increase to 92% using data mining technology. The accuracy can increase to 93%, which is the highest value in the three test models. The complete teaching method has an accuracy rate of 85%, and the lowest of the three models. We can also see that the curve values of data mining technology are very stable, and the curve value of the decentralized teaching method remains around 0.90. The curve value of data mining is also always kept at 0.97, and the curve value of the complete teaching method is lower.

The data in Figure 4 and Table 1 shows that the performance of all three models decreases slightly after passing the mixed test series, but the data mining method proposed in the paper is still the highest of the three. The depth extraction curve is very stable whether it is a test series or a mixed test series.

4.2. Research on Movement Analysis and Guidance in Dance Learning. Based on the three aspects of human body structure, movement direction, and movement effect, the dance movement is reconstructed, the continuity and periodicity of dance movement data are determined, and a short and easy-to-understand language is developed to formally describe the MDL and application of dance movement. The structure of the MDL can be adjusted. As a description, language captures an individual's three-dimensional skeletal hierarchy, which is then described based on quantitative assessments of dance movements and biomechanical parameters (Tables 2 and 3). The action analyzes the spatial orientation of the human body, calculates the parameters of the movement characteristics from the key frame data, uses the description language to determine the



FIGURE 3: Data analysis on the test set.

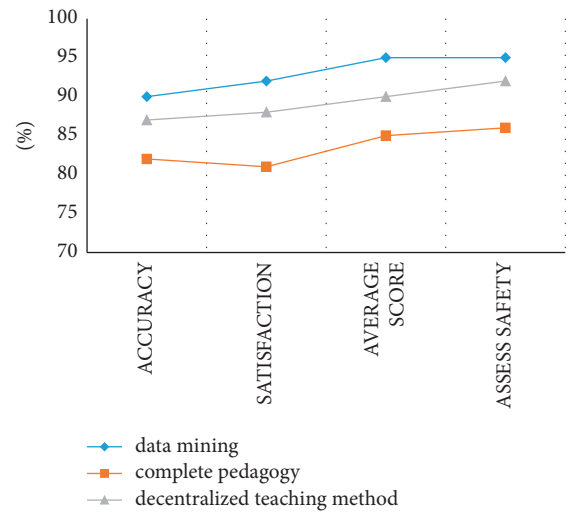


FIGURE 4: Data analysis on hybrid experience.

movement trajectory of the human body, determines the correlation between the human body coordinates, and the spatial direction of the environment, and determines the description language to the human body movement trajectory.

There are many types of basic movements in dance learning, such as kicking the swallow, chest and waist, squatting, lowering the waist, stepping down, and rubbing the floor. The number of movements for dance learning needs to be systematically trained: 8 times/group of kicking swallows for a total of 5 groups; 10 times for chest and waist/group for a total of 3 groups; 15 times for squatting/group for a total of 3 groups; 5 times for lower back/group A total of 4 groups were completed; a total of 3 groups were completed under the span of 30 s/group; a total of 5 groups were completed by rubbing the floor 20 times/group.

From the data in Figure 5 and Table 4, we can see that the number of frames for different dance types is also different, and the number of frames to be learned is also increasing. The dance with the highest number of frames is Latin2, which has 3635 frames, and the dance with the highest number of frames that needs to be learned is also Latin2, which requires 2519 frames to learn. The dance with the

TABLE 1: The performance of each method on the mixed test set.

Method	Accuracy (%)	Satisfaction (%)	Average score (%)	Assess safety (%)
Data mining	90	92	95	95
Complete pedagogy	82	81	85	86
Decentralized teaching method	87	88	90	92

TABLE 2: MDL action description description.

Main content	Variable type	Variable name	Variable description
Basic information	RATE	m_rate	Action collection frequency
Structure	BODY	m_body	Body parts
Position	LEVEL	m_level	Horizontal orientation
Power effect	BEND_LEG	m_legbending	The degree of bending of the legs

TABLE 3: Movement analysis in dance learning.

Dance moves	Number of actions	Number of action groups
Kick the swallow	8 times/set	5 groups
Chest and waist	10 times/set	3 groups
Squat	15 times/set	3 groups
Waist	5 times/set	4 groups
Down span	30 s/set	3 groups
Rub the ground	20 times/set	5 groups

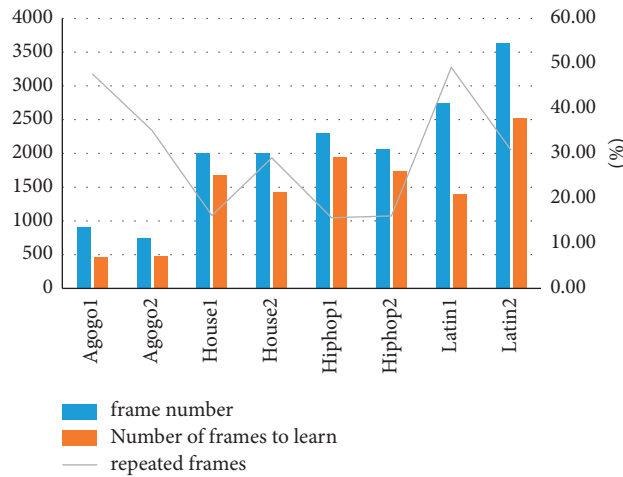


FIGURE 5: Number of repeating frames in dance.

TABLE 4: Number of repeated frames in dance.

Dance moves	Frame number	Number of frames to learn	Repeated frames (%)
Agogo1	903	472	47.70
Agogo2	740	480	35.10
House1	2008	1682	16.20
House2	2010	1427	29
Hiphop1	2300	1939	15.70
Hiphop2	2069	1736	16.10
Latin1	2738	1393	49.10
Latin2	3635	2519	30.70

highest number of repeated frames is Latin1 with 49.10% of repeated frames, and the dance with the lowest number of repeated frames is Hiphop1 with 15.70% of repeated frames.

A total of students, including girls and boys, participated in our user survey. None of them had ever studied dance. We invite them to learn two dances, dance and dance. These

TABLE 5: Grouping of students.

Dance	Group	Learning method	Number of students
Latin	Control	Browse freely	20
	Treatmentl	First stage course	20
Hip hop	Control	Browse freely	20
	Treatmentl	First stage course	20

TABLE 6: Statistics of learning time of control group and treatmentl group.

Dance	Group	Number of students	Ceaverage study time	Variance
Latin	Control	20	71.95	10.1
	Treatmentl	20	60.95	8.48
Hip hop	Control	20	97.4	7.56
	Treatmentl	20	84.7	10.8

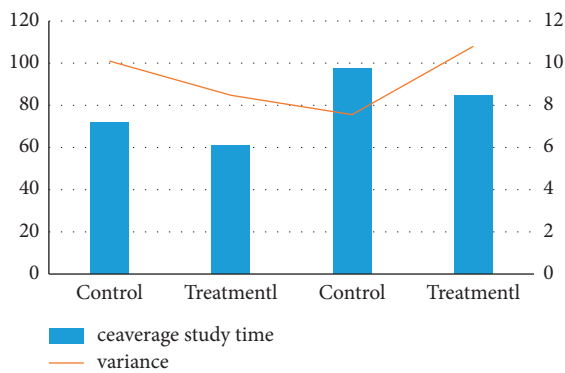


FIGURE 6: Statistics of the learning time of the control group and the treatmentl group.

TABLE 7: *t*-Test results of learning time in control group and treatmentl group.

Group	Ceaverage study time	Variance
Control	71.95	10.1
Treatmentl	60.95	8.48
Control	97.4	7.56
Treatmentl	84.7	10.8

students were divided into two groups, group and group study using the free-view method, and group study in the first stage of the course, as shown in Tables 5 and 6.

From Figure 6 and Table 5, we see that the groups of students who learned to dance reported the average time spent (in minutes). The average learning time of the two groups of hip hop was 71.95 and 60.95, respectively, while the average learning time of the Latin group was 94.4 and 84.7, respectively. It can be seen that the average learning time of the two groups in hip hop dance is shorter than that of the two groups in Latin dance.

From the data in Table 7, it can be seen that the learning data of the two groups are very different (Hip hop: $T = 3.74$, $P = 0.0006$; Latin: $T = 4.3$, $P < 0.0001$). Therefore, we believe that the first stage of dance teaching two this dance is more effective than the free-view method, so it works well.

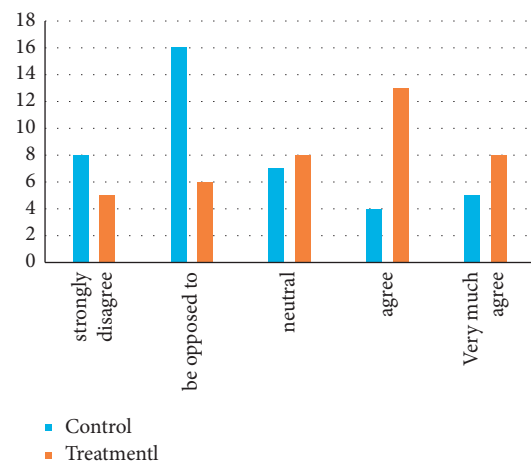


FIGURE 7: Comparison of control group and treatmentl group.

Given the data of the two groups of students on the questionnaire question “I think this system can help me learn dance,” from the experimental data in Figure 7, we can see that the proportion of those who hold opposing opinions is the largest in the control group. 16 people. In the Treatmentl group, the maximum proportion of people who agree with it reaches 13 people. It can be seen that there are more people in the control group who disagree with the Treatmentl group.

5. Conclusion

There is no direct connection between human movement and dance. In dance, the focus is on the movements of the people. The importance of dance moves must be understood from within and manifested on the basis of dance. Therefore, when developing new dance teaching methods, students need to improve their basic dance practice so that they can express the emotions conveyed by dance through body language and movements. In order to achieve the increase of dance performance. The goal of dance itself is to use the students’ internal motor activities to enable them to achieve a double improvement in movement and expression.

Data Availability

The experimental data used to support the findings of this study are available from the corresponding author upon request.

Conflicts of Interest

The authors declared that they have no conflicts of interest regarding this work.

References

- [1] R. S. Parpinelli, H. S. Lopes, and A. A. Freitas, "Data mining with an ant colony optimization algorithm," *IEEE Transactions on Evolutionary Computation*, vol. 6, no. 4, pp. 321–332, 2002.
- [2] S. K. Pal, V. Talwar, and P. Mitra, "Web mining in soft computing framework: relevance, state of the art and future directions," *IEEE Transactions on Neural Networks*, vol. 13, no. 5, pp. 1163–1177, 2002.
- [3] E. Frank, M. Hall, L. Trigg, and I. H. HolmesWitten, "Data mining in bioinformatics using Weka," *Bioinformatics*, vol. 20, no. 15, pp. 2479–2481, 2004.
- [4] Q. Yang and X. Wu, "10 challenging problems in data mining research [j]," *International Journal of Information Technology and Decision Making*, vol. 5, no. 04, 2006.
- [5] T. Hastie, R. Tibshirani, and J. H. Friedman, "The elements of statistical learning: data mining, inference and prediction. By [J]," *The Mathematical Intelligencer*, vol. 27, no. 2, pp. 83–85, 2009.
- [6] B. Shen, A. Chen, H. Tolley, and K. A. Scrabis, "Gender and interest-based motivation in learning dance," *Journal of Teaching in Physical Education*, vol. 22, no. 4, pp. 396–409, 2003.
- [7] F. Ofli, E. Erzin, Y. Yemez, and A. M. Tekalp, "Learn2Dance: learning statistical music-to-dance mappings for choreography synthesis," *IEEE Transactions on Multimedia*, vol. 14, no. 3, pp. 747–759, 2012.
- [8] T. J. Sacha and S. W. Russ, "Effects of pretend imagery on learning dance in preschool children," *Early Childhood Education Journal*, vol. 33, no. 5, pp. 341–345, 2006.
- [9] J. Batcheller, "Learning how to dance: courageous followership," *Nurse Leader*, vol. 10, no. 2, pp. 22–24, 2012.
- [10] Y. Wang and Q. Liu, "Effects of game-based teaching on primary students' dance learning," *International Journal of Game-Based Learning*, vol. 10, no. 1, pp. 19–36, 2020.
- [11] S. Saarikallio, G. Luck, B. Burger, and P. ThompsonToiviainen, "Dance moves reflect current affective state illustrative of approach-avoidance motivation," *Psychology of Aesthetics, Creativity, and the Arts*, vol. 7, no. 3, pp. 296–305, 2013.
- [12] H. Wulff and R. Martin, "Critical moves: dance studies in theory and politics," *Contemporary Sociology*, vol. 28, no. 6, p. 707, 1999.
- [13] K. D. Jong, M. Amorim, and P. J. Fonseca, "Singing and dancing fish: females pay more attention to males' dance moves when it is noisy [J]," *Frontiers for Young Minds*, vol. 7, p. 110, 2019.
- [14] H. Lee, "A study on analysis system on dance moves by applying munmyoilmu demonstrative illustrations [J]," *The Journal of Korean Dance*, vol. 30, no. 2, pp. 1–20, 2012.
- [15] C. Fontanesi and J. F. X. DeSouza, "Beauty that moves: dance for Parkinson's effects on affect, self-efficacy, gait symmetry, and dual task performance," *Frontiers in Psychology*, vol. 11, Article ID 600440, 2020.

Research Article

Efficient Lattice-Based Ring Signature Scheme without Trapdoors for Machine Learning

Qing Ye , Yongkang Lang , Zongqu Zhao , Qingqing Chen , and Yongli Tang 

School of Software, Henan Polytechnic University, Jiaozuo 454000, China

Correspondence should be addressed to Zongqu Zhao; zhaozong_qu@hpu.edu.cn

Received 30 June 2022; Accepted 11 August 2022; Published 19 September 2022

Academic Editor: Le Sun

Copyright © 2022 Qing Ye et al. This is an open access article distributed under the Creative Commons Attribution License, which permits unrestricted use, distribution, and reproduction in any medium, provided the original work is properly cited.

Machine learning (ML) and privacy protection are inseparable. On the one hand, ML can be the target of privacy protection; on the other hand, it can also be used as an attack tool for privacy protection. Ring signature (RS) is an effective way for privacy protection in cryptography. In particular, lattice-based RS can still protect the privacy of users even in the presence of quantum computers. However, most current lattice-based RS schemes are based on a strong trapdoor like hash-and-sign, and in such constructions, there is a hidden algebraic structure, that is, added to lattice so that the trapdoor shape is not leaked, which greatly affects the computational efficiency of RS. In this study, utilizing Lyubashevsky collision-resistant hash function over lattice, we construct an RS scheme without trapdoors based on ideal lattice via Fiat–Shamir with aborts (FSwA) protocol. Regarding security, the proposed scheme satisfies unconditional anonymity against chosen setting attacks (UA-CSA), which is stronger than anonymity against full key exposure (anonymity-FKE), and moreover, our scheme satisfies unforgeability with respect to insider corruption (EU-IC). Regarding computational overhead, compared with other RS schemes that satisfy the same degree of security, our scheme has the highest computational efficiency, the signing and verification time costs of the proposed scheme are obviously better than those of other lattice-based RS schemes without trapdoors, which is more suitable for ML scenarios.

1. Introduction

Machine learning (ML) and privacy protection are inextricably linked. On the one hand, ML itself requires privacy protection, i.e., the training datasets and models in ML systems should not be disclosed. On the other hand, ML can also be an attack tool for privacy protection, and how to protect users' sensitive information is a challenging task under the increasingly powerful ML technology.

Ring signature (RS), introduced by Rivest et al. [1] in 2001, is an effective technique for privacy protection in cryptography, which on the one hand enables the recipient of the data to believe that the source of the data is reliable, and on the other hand, obscures the identity of the data owner so that the recipient cannot be sure who is the real owner of the data. In an RS scheme, each user has a public key, and the signer can autonomously collect user's public keys to form a ring without the permission or assistance of other users (where the signer is contained in the set of ring

members), and the verifier only knows that the signature was generated under the ring, but is unsure which member's private key is used as the signing key. Due to the anonymity of RS, it is widely used in fields such as e-voting, anonymous membership authentication, and anonymous tip-off.

Since the seminal work of [1], the research on RS has been unprecedentedly active. A general framework for constructing 1-out-of- n signature schemes was introduced by Abe et al. [2], which can use different types of keys to construct signatures based on integer decomposition and discrete logarithm problems. After that, many RS schemes along with their associated authentication schemes [3–10] have been proposed. However, the security definitions of these RS schemes are weak, i.e., they have not considered for certain realistic attacks. Bender et al. [11] proposed new definitions of anonymity and the unforgeability of RS to cover these attacks. Bender et al. [11] divided anonymity into three levels according to the degree of security, where the strongest version is anonymity against full key exposure

(Anonymity-FKE), i.e., even if adversary is given the private keys of all ring members, the adversary is still unable to guess who is the genuine signer of the given RS. Regarding existential unforgeability, there are also three levels: unforgeability against fixed-ring attacks (EU-FRA), unforgeability against chosen-subring attacks (EU-CSA), and unforgeability with respect to insider corruption (EU-IC). Based on EU-CSA, the strongest EU-IC means the adversary cannot succeed in forging a signature, even if the adversary is allowed to obtain the private keys of ring members via asking a corruption oracle.

Most previous RS schemes [1–7, 9–11] are constructed under the assumptions of classical number theory, which are hardly resistant to quantum attacks [12]. In 1996, Ajtai [13] introduced the algebraic structure of lattice into cryptographic schemes. In the postquantum era, the new cryptosystem based on lattice has become a focus of research due to its merits of high asymptotic efficiency, simple operation, parallelizability, resistance to quantum attacks, and enjoying the average-to-worst reduction. The development of lattice-based provably secure encryption has developed rapidly and has made great progress [14–18], while lattice-based digital signature has experienced a tortuous and bumpy process in the earlier years. First, Goldreich et al. [19] made an attempt at a lattice-based signature, then NTRU signature was proposed by Hoffstein et al. [20], and it was repaired and enhanced in [21, 22]. However, these digital signature schemes [19, 20, 22] on lattice failed to be proved secure under the attacks of [23, 24]. To date, provably secure signature schemes on lattice can be divided into two main branches: schemes with trapdoors and without trapdoors. Digital signature schemes with trapdoors started from the “hash-and-sign” signature scheme constructed by Gentry et al. [25] based on SIS assumption, which is also the first lattice-based signature scheme, that is, provably secure. and Peikert [26] improved the structure of trapdoors, that is, proposed by [27], proposed the concept of G trapdoors on lattice, and remarkably improved the computational efficiency of trapdoor generation algorithm on lattice. A digital signature scheme on an ideal lattice was proposed by Ducas and Micciancio [28], and its trapdoor is constructed utilizing the technique of [26]. These trapdoors are deemed to be very suitable for lattice-based signature schemes, but the lattice is added with a hidden algebraic structure, which significantly affects the efficiency of signature schemes and is a payment that has to be considered. Digital signature schemes on lattice without trapdoors are mainly based on Stern’s zero-knowledge proofs. Although the Stern-type protocol is powerful, the soundness error of a single execution of the protocol is $2/3$. Such protocol needs to be repeated many times so that the soundness error drops to a negligible value, so it is difficult to further improve their efficiency. To the best of our knowledge, only Lyubashevsky signature schemes [29, 30] without trapdoors are constructed not based on the Stern-type protocol, but on the Fiat–Shamir with aborts (FSwA) protocol, via which a very efficient digital signature scheme on lattice could be constructed.

Similar to a digital signature over lattice, lattice-based (linkable) RS can also be mainly divided into two branches,

i.e., with trapdoors and without trapdoors. Lattice-based RS schemes with trapdoors have been extensively studied [31–36]. Notice that these lattice-based RS schemes with trapdoors, although are progressing about storage overhead, cannot always avoid the drawbacks brought by the structure of hash-and-sign, and the computational efficiency cannot be enhanced to a satisfactory level. Lattice-based RS schemes without trapdoors can be classified into membership proofs-based schemes and FSwA-based schemes. Several RS schemes [37–40] based on membership proofs have been proposed. Such RS schemes usually first construct a membership proof which is generally a zero-knowledge proof and then construct an RS scheme based on this proof. The efficiency of these RS schemes directly depends on that of underlying zero-knowledge proofs, which have the advantage that the signature length is usually $O(\log N)$, where N is the ring size, whereas the disadvantage is also obvious, i.e., the large and complex zero-knowledge proofs lead to low computational efficiency, and the length of RS could be large when N is small. (Linkable) RS schemes [41–44] based on FSwA are rather efficient in terms of computational efficiency, with the drawback that the signature length is common $O(N)$, yet it is very suitable in small-scale scenarios. For RS on lattice, several schemes [37–40] can satisfy the strongest Anonymity-FKE and EU-IC defined by Bender et al. [11]. In fact, Aguilar Melchor et al. [41] defined stronger anonymity, i.e., unconditional anonymity against chosen setting attacks (UA-CSA), and inspired by Lyubashevsky signature scheme [29], Aguilar Melchor et al. [41] constructed two RS schemes (AM1 and AM2) utilizing lattice-based collision-resistant hash function $h \in \mathcal{H}(D, D_x, m)$ [45], both of which can achieve UA-CSA for anonymity; regarding unforgeability, AM1 and AM2 satisfy EU-CSA and EU-IC, respectively. However, we deem that Aguilar Melchor et al. do not make good use of $h \in \mathcal{H}(D, D_x, m)$ in transforming Lyubashevsky digital signature [29] into RS, which causes the storage and computational overheads of both schemes of Aguilar Melchor et al. [41] to be large. In this work, via the FSwA protocol, we redesign an RS scheme on lattice without trapdoors using $h \in \mathcal{H}(D, D_x, m)$ again, the main contributions are as follows:

- (1) Different from the RS schemes of Aguilar Melchor et al. [41] on lattice, in our key generation algorithm, the input value of $h \in \mathcal{H}(D, D_x, m)$ is taken as a user’s private key, the output value of $h \in \mathcal{H}(D, D_x, m)$ is taken as a public key, that is, relevant to the private key, which makes the length of a public key is reduced from a polynomial vector of m dimensions to a polynomial. Our signing algorithm is designed based on the framework of the RS scheme of Abe et al. [2], which is based on the discrete-log assumption, and the proposed scheme will be more concise and efficient.
- (2) Under the improved security model of Aguilar Melchor et al. [41], the proposed RS scheme is rigorously proven to be safe. Regarding anonymity, our scheme satisfies the strongest UA-CSA; in terms of unforgeability, our scheme satisfies the strongest

EU-IC. And under the random oracle model, the unforgeability of the proposed scheme could be reduced to the approximate shortest vector problem (SVP_γ) over ideal lattice.

- (3) Finally, with respect to performance and security, the proposed scheme is comprehensively compared with several schemes [37, 38, 40, 41]. The results show that compared with AM1 and AM2 of [41], the storage and computational overhead of our scheme are significantly reduced. In addition, compared with the computational overhead of other schemes, our scheme is remarkably superior, and is more suitable for ML applications.

2. Preliminaries

2.1. Notations. The symbol $[N]$ represents the abbreviation of the set $\{1, 2, \dots, N\}$. Let \mathbb{R} be the set of real numbers, \mathbb{R}^+ be the set of positive real numbers, and \mathbb{Z} be the set of integers. For a finite set S , the symbol $y \leftarrow S$ denotes a random uniform sampling from S . The upper-case letter X is the random variable denoting a signature, and $X \leftarrow \mathcal{F}$ denotes X as the output of the signature algorithm \mathcal{F} . Vectors and matrices are denoted by lower-case (e.g., \mathbf{x}) and upper-case (e.g., \mathbf{X}) letters in italic & bold, respectively. In this work, we construct a cryptographic scheme on ring $D = \mathbb{Z}_q[x]/(x^n + 1)$, where $(x^n + 1)$ is an irreducible polynomial, and all logarithms we use are base 2. \mathbb{Z}_q is the set of integers modulo q , elements in \mathbb{Z}_q are denoted by integers selected from the interval $[-q/2, q/2]$, and then the elements in D are represented by $n - 1$ degree polynomials whose coefficients are taken from \mathbb{Z}_q . For $a = \sum_i f_i x^i \in D$, the common norms of a are given as follow:

$$\begin{aligned} l_1: \|a\|_1 &= \sum_i |f_i|, \\ l_2: \|a\|_2 &= \left(\sum_i |f_i|^2 \right)^{1/2}, \\ l_\infty: \|a\|_\infty &= \max_i |f_i|. \end{aligned} \quad (1)$$

For a polynomial vector $\mathbf{a} = (a_1, a_2, \dots, a_m)$, where $a_1, a_2, \dots, a_m \in D$, m is a positive integer, and the infinite norm with respect to \mathbf{a} is defined as follows:

$$\|\mathbf{a}\|_\infty = \max_i \|a_i\|_\infty. \quad (2)$$

Additionally, we will use the following notations:

$$\begin{aligned} D_c &= \{g \in D: \|g\|_\infty \leq 1\}, \\ D_s &= \{g \in D: \|g\|_\infty \leq \sqrt{n} \log n\}, \\ D_x &= \{g \in D: \|g\|_\infty \leq mn^{1.5} \log n + n \log^2 n\}, \\ D_y &= \{g \in D: \|g\|_\infty \leq mn^{1.5} \log n\}, \\ D_z &= \{g \in D: \|g\|_\infty \leq mn^{1.5} \log n - n \log^2 n\}. \end{aligned} \quad (3)$$

The complexity of algorithms is measured using the standard asymptotic notations ω, O :

$$f(n) = \omega(g(n)) \text{ if } \lim_{n \rightarrow \infty} \frac{f(n)}{g(n)} = \infty, \quad (4)$$

$$f(n) = O(g(n)) \text{ if } \lim_{n \rightarrow \infty} \frac{f(n)}{g(n)} \neq \infty.$$

Use the symbol \tilde{O} to suppress poly-logarithmic factors, and for example, for any constant c and c' , $f(n) = O(n^c \log^c n)$, we have $f(n) = \tilde{O}(n^c)$.

2.2. Lattice and Ideal Lattice. Micciancio [46] first proposed the concept of cyclic lattice, which to a certain extent eliminated the drawbacks of big key size and operational inefficiency of cryptographic schemes on Euclidean lattice. Lyubashevsky and Micciancio [45] first proposed the definition of an ideal lattice, which is a lattice with a special algebraic structure and is a generalization of the cyclic lattice. In general, a Euclidean lattice is a subgroup of a group, and an ideal lattice is an ideal of a ring.

Definition 1 (lattice). Supposing matrix \mathbf{B} is composed of a set of linearly independent vectors $\mathbf{b}_1, \mathbf{b}_2, \dots, \mathbf{b}_m \in \mathbb{Z}^n$, then the integer lattice generated by \mathbf{B} is defined as:

$$\mathcal{L}(\mathbf{O}) = \{\mathbf{B}\mathbf{x} = \sum x_i \mathbf{b}_i: \mathbf{x} \in \mathbb{Z}^m\}, \quad (5)$$

$\mathbf{b}_1, \mathbf{b}_2, \dots, \mathbf{b}_m$ form a set of bases over $\mathcal{L}(\mathbf{B})$. In short, $\mathcal{L}(\mathbf{B})$ is a discrete additive subgroup in the n -dimensional real space \mathbb{R}^n .

Definition 2 (q -ary lattice). Given a prime q , positive integers m, n , for any matrix $\mathbf{A} \in \mathbb{Z}_q^{n \times m}$, the integer lattice, that is, m -dimensional full-rank is described as follows:

$$\Lambda^+(A) = \{\mathbf{u} \in \mathbb{Z}^m \text{ s.t. } \mathbf{A}\mathbf{u} = \mathbf{0} \pmod{q}\}. \quad (6)$$

Definition 3 (ideal lattice). Let f be a monic irreducible polynomial of degree n , the ideal $I \subseteq \mathbb{Z}[x]/(f)$, then an integer lattice $\mathcal{L}(\mathbf{B}) \subseteq \mathbb{Z}^n$ such that $\mathcal{L}(\mathbf{B}) = \{g \pmod{f}: g \in I\}$ is called an ideal lattice.

2.3. Hardness Assumption

Definition 4 (R-SIS_{q,m,β} problem). Given a randomly chosen vector $\mathbf{a} \in D^m$, find the vector $\mathbf{x} \in D^m$ such that $\mathbf{a}^T \cdot \mathbf{x} = 0$ satisfying $0 < \|\mathbf{x}\|_2 \leq \beta$, where q, m are positive integers, $\beta \in \mathbb{R}^+$.

Definition 5 (SVP_γ). Given a lattice $\mathcal{L}(\mathbf{B})$ and an approximation factor $\gamma \geq 1$, find a nonzero vector \mathbf{v} on lattice such that $\|\mathbf{v}\|_\infty \leq \gamma \|\mathbf{u}\|_\infty$ holds for any vector $\mathbf{u} \in \mathcal{L}(\mathbf{B})$.

2.4. Collision-Resistant Hash Functions and Bounding $\|ac \pmod{(x^n + 1)}\|_\infty$. Lyubashevsky and Micciancio [45] defined a family of collision-resistant hash functions on ideal lattice, which are efficient functions based on the hardness of worst-case lattice problems, and showed that finding

collisions for $h \in \mathcal{H}(D, D_x, m)$ is at least as hard as solving SVP_γ , where $\gamma = \tilde{O}(n^2)$.

Definition 6 (family of hash functions). For any integer m and set D_x , the family of hash functions $\mathcal{H}(D, D_x, m) = \{h_{\mathbf{a}}: \mathbf{a} \in D^m\}$, where a hash function $h_{\mathbf{a}}: D_x^m \rightarrow D$. On input polynomial vectors $\mathbf{b} = (b_1, b_2, \dots, b_m) \in D_x^m$, then $h_{\mathbf{a}}(\mathbf{b}) = \mathbf{a} \cdot \mathbf{b} = a_1 b_1 + a_2 b_2 + \dots + a_m b_m$. There are two homomorphic properties about $h \in \mathcal{H}(D, D_x, m)$ as follows:

$$\begin{aligned} h(\mathbf{x} + \mathbf{y}) &= h(\mathbf{x}) + h(\mathbf{y}), \\ h(\mathbf{x}c) &= h(\mathbf{x})c, \end{aligned} \quad (7)$$

where $\mathbf{x}, \mathbf{y} \in D^m$, $c \in D$.

Definition 7 (collision problem $\text{Col}(h, D_x)$). Given a function $h \in \mathcal{H}(D, D_x, m)$, find two distinct vectors $\mathbf{z}_0, \mathbf{z}_1 \in D_x$ such that $h(\mathbf{z}_0) = h(\mathbf{z}_1)$.

The following lemma shows that when D_x is some limited domain (e.g., a set of small norm polynomials), solving the $\text{Col}(h, D_x)$ problem is as hard as solving SVP_γ in the worst case on the lattice corresponding to the ideal $\text{in}D_x$.

Lemma 1 (see [29]). Let n be any power of 2, ring $D = \mathbb{Z}_q[x]/(x^n + 1)$, and define the set $D_x = \{g \in D: \|g\|_\infty \leq d\}$, where d is an integer. $\mathcal{H}(D, D_x, m)$ is a family of hash functions as in Definition 6 such that $m > \log q / \log 2d$ and $q \geq 4dmn^{1.5} \log n$. For any $h \in \mathcal{H}(D, D_x, m)$, if there exists a polynomial-time algorithm that solves $\text{Col}(h, D_x)$ with some non-negligible probability, then there exists a polynomial-time algorithm that can solve SVP_γ over ideal lattice, where $\gamma = 16dmn \log^2 n$.

In addition, we recall the following boundary Lemma to justify the security of the proposed scheme.

Lemma 2 (Lemma 2.11 in [47] applied to our setting). Let $a \leftarrow D_s$, c be the response returned by the random oracle H (i.e., $c \leftarrow D_c$), then

$$\Pr[\|ac\|_\infty \leq n \log^2 n] \geq 1 - 4ne^{-\log^2 n/8} = 1 - n^{-\omega(1)}. \quad (8)$$

2.5. Statistical Distance and Probabilistic Lemma. The difference between two probability distributions can be measured by the statistical distance, and in the security proof of the proposed RS scheme, we complete the proof of anonymity by using it.

Definition 8 (statistical distance). For random variables X_0 and X_1 that are defined on a countable set S , if the set S is discrete, then the statistical distance between X_0 and X_1 is described as

$$\Delta(X_0, X_1) = \frac{1}{2} \sum_{x \in S} |\Pr[X_0 = x] - \Pr[X_1 = x]|. \quad (9)$$

If the random variables X_0 and X_1 satisfy $\Delta(X_0, X_1) \leq n^{-\omega(1)}$, then X_0 and X_1 are statistically close.

Regarding statistical distances, there are the following common properties:

- (1) $\Delta(X_0, X_1) \geq 0$;
- (2) $\Delta(X_0, X_1) = \Delta(X_1, X_0)$.

In addition, to prove the convergence of our algorithms, the following probabilistic lemma will be used:

Lemma 3 (Corollary 6.2 in [47]). For any $s \in D_s^m$,

$$\Pr_{c \leftarrow D_c, \mathbf{u} \leftarrow D_y^m} [\mathbf{s}c + \mathbf{u} \in D_z^m] = \frac{1}{e} - o(1). \quad (10)$$

3. Definition of RS and Security Model

3.1. Definition of RS. Suppose there exist N members in the ring and each member U_i ($i \in [N]$) has a pair of keys, i.e., public key pk_i and private key sk_i , a RS scheme can be composed of four polynomial-time algorithms:

- (1) **Setup** (1^λ): Taking a security parameter λ as input, it outputs the public parameters pp .
- (2) **KeyGen** (pp): Taking the public parameters pp as input, it generates a pair of keys (pk, sk) , where pk and sk denote the public and private keys, respectively.
- (3) **Sign** (pp, L_{pk}, μ, sk_π): On input public parameters pp , ring L_{pk} , message μ and the private key sk_π of the signer U_π (require that its corresponding public key $pk_\pi \in L_{pk}$), it outputs an RS sig of U_π on the message μ under ring L_{pk} .
- (4) **Verify** (pp, L_{pk}, μ, sig): On input public parameter pp , ring L_{pk} , message μ and RS sig, if sig satisfies the verification conditions, it outputs 1; otherwise, it outputs 0.

3.2. Security Model. For the above algorithms, an RS scheme is called to be secure if it satisfies the following definitions: correctness, anonymity, and unforgeability.

Definition 9 (correctness). If the signer signs honestly, i.e., according to the algorithms in Section 3.1, the Verify algorithm will always output 1 with overwhelming probability, that is, equality (11) holds.

$$\Pr \left[\text{Verify}(pp, L_{pk}, \mu, sig) = 1 \left| \begin{array}{l} pp \leftarrow \text{Setup}(1^\lambda) \\ (pk_\pi, sk_\pi) \leftarrow \text{KeyGen}(pp) \\ pk_\pi \in L_{pk} \\ sig \leftarrow \text{Sign}(pp, L_{pk}, \mu, sk_\pi) \end{array} \right. \right] = 1 - \text{negl}(\lambda). \quad (11)$$

Bender et al. [11] proposed the security definitions of RS under different security degrees, among which the highest degree in terms of anonymity is anonymity-FKE. Based on anonymity-FKE, Aguilar Melchor et al. [41] proposed a stronger definition, namely UA-CSA. In this work, the

security proof of anonymity is based on the security model of UA-CSA.

Let's define a game between adversary \mathcal{A} and challenger S Under UA-CSA since all secrets are known, the adversary can effectively simulate the signature and corrupt oracles, so these two oracles are no longer provided in the game and the procedure in which S generates pp and (pk, sk) is not required, since they will be generated by the adversary instead. The game is as follows:

- (i) Suppose l is the upper bound of ring member size in the system, the adversary submits to a set of public parameters pp , ring $L_{pk} = \{pk_1, pk_2, \dots, pk_N\}$, two private keys sk_{i_0}, sk_{i_1} , message μ , where $N, i_0, i_1 \in [l]$.
- (ii) S randomly selects $b \leftarrow \{0, 1\}$, invokes $\text{Sign}(pp, L_{pk}, \mu, sk_{i_b})$ to generate the signature sig_{i_b} , and returns sig_{i_b} to \mathcal{A} .
- (iii) Adversary \mathcal{A} outputs a bit b' , and if $b' = b$, then \mathcal{A} wins the game.

The advantage of winning the game is denoted by,

$$Adv_{\mathcal{A}}^{\text{anon}} = \left| \Pr [b' = b] - \frac{1}{2} \right|. \quad (12)$$

Definition 10 (anonymity). An RS scheme satisfies UA-CSA if $Adv_{\mathcal{A}}^{\text{anon}}$ is negligible for any polynomial-time adversary \mathcal{A} .

Bender et al. [11] consider two cases when defining the strongest unforgeability EU-IC: (1) An adversary can trick some honest user into using the public keys that are adversarially generated to generate a signature. (2) The adversary can adaptively corrupt some ring members and obtain their keys. The strongest EU-IC with respect to RS is depicted by the game between adversary \mathcal{A} and challenger \mathcal{A}' as follows:

- (i) Setup phase: Given security parameter λ , \mathcal{A}' runs the KeyGen algorithm to generate the user's public/private key pairs, and sends public parameters pp and the maximum set of user's public keys $S = (pk_i)_{i \in [l]}$ to adversary \mathcal{A} .
- (ii) Query phase: \mathcal{A} is allowed to make adaptive queries to the signature oracle SO and the corrupt oracle CO .
 - (a) Signing query: \mathcal{A} submits to \mathcal{A}' the set of user's public keys L_{pk} , message μ and $\pi \in [l]$, where π is an index such that $pk_{\pi} \in L_{pk}$. On receiving (π, μ, L_{pk}) , \mathcal{A}' invokes the Sign algorithm to generate sig and send it to \mathcal{A} .
 - (b) Corruption query: \mathcal{A} submits $i (i \in [l])$ to access corrupt oracle CO , then \mathcal{A}' returns the relevant private key sk_i to \mathcal{A} .
- (iii) Forgery phase: \mathcal{A} outputs $(\mu^*, L_{pk}^*, \text{sig}^*)$, and we call \mathcal{A} gets the triumph if the below conditions are satisfied:
 - (a) Verify $(pp, L_{pk}^*, \mu^*, \text{sig}^*) = 1$;

- (b) \mathcal{A} never queried for the signature on (μ^*, L_{pk}^*) ;
- (c) $L_{pk}^* \subseteq S \setminus C$, where C is the set of corrupted users.

The advantage of \mathcal{A} winning the game is depicted as:

$$Adv_{\mathcal{A}}^{\text{forge}} = \Pr [\mathcal{A} \text{ wins the game}]. \quad (13)$$

Definition 11 (unforgeability). A RS scheme is said to satisfy EU-IC if $Adv_{\mathcal{A}}^{\text{forge}}$ is negligible for any polynomial-time adversary \mathcal{A} .

4. Lattice-based RS Scheme without Trapdoors

4.1. Construction

- (1) Setup (1^λ): Given security parameter λ , it outputs the public parameter $pp = \{n, d, q, m, H, h, D_s, D_c, D_x, D_y, D_z\}$, where integer $n > \lambda$ and is a power of 2, $d = \sqrt{n} \log n$, prime $q \geq 4(mn^{1.5} \log n)^2$, integer $m > \log q / \log 2d$, $H: \{0, 1\}^* \rightarrow D_c$ is a cryptographic hash function, h is randomly chosen from the family $\mathcal{H}(D, D_x, m)$, and the other parameters are defined in Section 2.1.
- (2) KeyGen (pp): Given public parameters pp , it picks $\mathbf{r} \leftarrow D_s^m$, then generates the public key $pk = h(\mathbf{r})$ and sets the private key $sk = \mathbf{r}$.
- (3) Sign ($pp, L_{pk}, \mu, sk_{\pi}$): Given public parameters pp , ring $L_{pk} = \{pk_1, pk_2, \dots, pk_N\}$, message $\mu \in \{0, 1\}^*$ and private key $sk_{\pi} = \mathbf{r}_{\pi}$ of member U_{π} , it runs as follows:
 - (i) Pick $\mathbf{u} \leftarrow D_y^m$, calculate $c_{(\pi \bmod N)+1} = H(L_{pk}, \mu, h(\mathbf{u}))$;
 - (ii) For $i = \pi + 1, \dots, N, 1, \dots, \pi - 1$:
 - (a) Choose $\mathbf{r}_{z,i} \leftarrow D_z^m$;
 - (b) Calculate $t_i = h(\mathbf{r}_{z,i}) - c_i pk_i$, $c_{(i \bmod N)+1} = H(L_{pk}, \mu, t_i)$.
 - (iii) Calculate $\mathbf{r}_{z,\pi} = \mathbf{u} + c_{\pi} \mathbf{r}_{\pi}$;
 - (iv) If $\mathbf{r}_{z,\pi} \notin D_z^m$, then return to step (i);
 - (v) Output the signature $\text{sig} = (c_1, (\mathbf{r}_{z,i})_{i \in [N]})$.
- (4) Verify ($pp, L_{pk}, \mu, \text{sig}$): Given public parameters pp , ring $L_{pk} = \{pk_1, pk_2, \dots, pk_N\}$, message $\mu \in \{0, 1\}^*$ and signature $\text{sig} = (c_1, (\mathbf{r}_{z,i})_{i \in [N]})$, it accepts the signature and outputs 1 only if sig satisfies the below conditions, otherwise it rejects the signature and outputs 0.
 - (i) For $i \in [N]$, $\mathbf{r}_{z,i} \in D_z^m$;
 - (ii) For $i \in [N]$, calculate $t_i = h(\mathbf{r}_{z,i}) - c_i pk_i$, $c_{i+1} = H(L_{pk}, \mu, t_i)$, and determine $c_1 = H(L_{pk}, \mu, t_N) = c_{N+1}$.

4.2. Correctness and Convergence of the Scheme

Theorem 1 (correctness). *The proposed RS scheme satisfies correctness.*

Proof. When sig is a signature generated according to the signature algorithm, then (a) in step (ii) and step (iv) of Sign ensure that $(\mathbf{r}_{z,i})_{i \in [N]}$ are elements in D_z^m . In addition, we have the following equations:

$$\begin{aligned} c_2 &= H(L_{pk}, \mu, t_1), \text{ where } t_1 = h(\mathbf{r}_{z,1}) - c_1 pk_1, \\ c_3 &= H(L_{pk}, \mu, t_2), \text{ where } t_2 = h(\mathbf{r}_{z,2}) - c_2 pk_2, \\ &\vdots \\ c_\pi &= H(L_{pk}, \mu, t_{\pi-1}), \end{aligned}$$

where $t_{\pi-1} = h(\mathbf{r}_{z,\pi-1}) - c_{\pi-1} pk_{\pi-1}$,

since $\mathbf{r}_{z,\pi} = \mathbf{u} + c_\pi \mathbf{r}_\pi \in D_z^m$, we have

$$\begin{aligned} c_{\pi+1} &= H(L_{pk}, \mu, t_\pi) = H(L_{pk}, \mu, h(\mathbf{r}_{z,\pi}) - c_\pi pk_\pi) \\ &= H(L_{pk}, \mu, h(\mathbf{u} + c_\pi \mathbf{r}_\pi) - c_\pi pk_\pi) \\ &= H(L_{pk}, \mu, h(\mathbf{u})), c_{\pi+2} \\ &= H(L_{pk}, \mu, t_{\pi+1}), \text{ where } t_{\pi+1} \\ &= h(\mathbf{r}_{z,\pi+1}) - c_{\pi+1} pk_{\pi+1}, c_{\pi+3} = H(L_{pk}, \mu, t_{\pi+2}), \end{aligned}$$

where $t_{\pi+2} = h(\mathbf{r}_{z,\pi+2}) - c_{\pi+2} pk_{\pi+2}$,

\vdots

$$\begin{aligned} c_1 &= c_{N+1} = H(L_{pk}, \mu, t_N), \text{ where } t_N \\ &= h(\mathbf{r}_{z,N}) - c_N pk_N. \end{aligned}$$

(14)

To sum up, the polynomial sequence $\{c_1, c_2, \dots, c_N\}$ in the verification process is equal to that in the signature process, so it must pass the verification of the Verify algorithm, and the proposed scheme is correct. \square

Theorem 2 (convergence). *Under the parameter settings of algorithm Setup, the expected runtime of the proposed scheme is $\tilde{O}(n)$, and algorithm Sign is expected to repeat no more than three times.*

Proof. The proposed RS scheme is made up of four algorithms: Setup, KeyGen, Sign and Verify. The Setup algorithm selects a hash function $h \in \mathcal{H}(D, D_x, m)$ (i.e., pick mn random numbers from $\{-(q-1)/2, -(q-1)/2+1, \dots, (q-1)/2\}$), the time for the step is negligible. The step of generating a single user's private/public keys in KeyGen is to randomly select a vector $\mathbf{r} \leftarrow D_s^m$, which simply involves randomly selecting mn numbers from the set

$\{-\sqrt{n} \log n, \dots, \sqrt{n} \log n\}$, and then calculating $pk = h(\mathbf{r})$, which takes $\tilde{O}(n)$ time according to Lemma 2.16 from [47]. The Sign algorithm is to randomly select a vector $\mathbf{u} \leftarrow D_y^m$ and $N-1$ vectors $\mathbf{r}_{z,i} \leftarrow D_z^m$, then calculate small polynomial multiplication $c_i pk_i$ and hash function $h \in \mathcal{H}(D, D_x, m)N$ times, and access random oracles N times. The time of Sign algorithm running once is $\tilde{O}(n)$ from [47], but if $\mathbf{r}_{z,\pi} \notin D_z^m$, then the operations of Sign need to be repeated again. Lemma 3 states that for any $\mathbf{r} \leftarrow D_s^m$, $\Pr_{\mathbf{u} \leftarrow D_y^m, c \leftarrow D_s} [\mathbf{u} + c\mathbf{r} \in D_z^m] = 1/e - o(1)$. Therefore, we will iterate Sign no more than three times and the runtime of Sign is also $\tilde{O}(n)$. Finally, the Verify algorithm needs to calculate small polynomial multiplication $c_i pk_i$ and function $h \in \mathcal{H}(D, D_x, m)N$ times, and access random oracles N times, thus the running time is also $\tilde{O}(n)$. \square

5. Security

5.1. Anonymity. Before proving the anonymity of the proposed scheme, we first give and prove the following lemma, which shows that for an adversary who has the ability to distinguish two ring signatures based on adversarially-chosen private keys and the corresponding c_π associated with the private keys, the statistical distance between the following two sets of random variables Y_0 and Y_1 is negligible.

Define two sets of random variables $Y_0 = (\alpha_i \in D_z^m; i \in [N], \beta)$ and $Y_1 = (\alpha_i \in D_z^m; i \in [N], \beta)$ that are obtained from the Sign algorithm with input $(pp, L_{pk}, \mu, sk_{i_0})$ and $(pp, L_{pk}, \mu, sk_{i_1})$, where the first N components of Y_b represent the first N outputs $(\mathbf{r}_{z,i})_{i \in [N]}$ of sig_{i_b} , and the $(N+1)$ -th component of Y_b represents c_π corresponding to sig_{i_b} , $b \leftarrow \{0, 1\}$. In addition, we use $Y_b^{(i)}$ to represent the i -th component of Y_b , $i \in [N+1]$, e.g., $Y_0^{(N+1)}$ represents c_π .

Lemma 4. *If Y_0 and Y_1 are random variables obtained from two legitimate signatures, and these two legitimate signatures are generated by private keys sk_{i_0}, sk_{i_1} which are adversarially-chosen, we have*

$$\Delta(Y_0, Y_1) = n^{-\omega(1)}. \quad (15)$$

Proof. First define a set $D_c(sk_{i_0}, sk_{i_1}) = \{d \in D_c : \|sk_{i_0} d\|_\infty, \|sk_{i_1} d\|_\infty \leq n \log^2 n\}$. According to Lemma 2, it is concluded that almost all elements of D_c are in $D_c(sk_{i_0}, sk_{i_1})$. Even if the private keys $sk_{i_0}, sk_{i_1} \in D_s$, $n \geq \lambda$ are chosen by the adversary, Lemma 2 will also guarantee that $|D_c(sk_{i_0}, sk_{i_1})|/|D_c| = 1 - n^{-\omega(1)}$, where $n^{-\omega(1)}$ is a negligible function. Then divide the statistical distance $\Delta(Y_0, Y_1)$ into two parts, we have formulas (16) and (17).

Next we will discuss $\Delta(Y_0, Y_1)$ in two steps, first to prove that formula (16) is negligible (Step 1), and then to prove that formula (17) is equal to zero (Step 2).

$$\begin{aligned} \Delta(Y_0, Y_1) &= \frac{1}{2} \sum_{\alpha_i \in D_s^m; i \in [N], \beta} |\Pr[Y_0 = (\alpha_i; i \in [N], \beta)] - \Pr[Y_1 = (\alpha_i; i \in [N], \beta)]|, \\ &= \frac{1}{2} \sum_{\alpha_i \in D_s^m; i \in [N], \beta \notin D_c(sk_{i_0}, sk_{i_1})} |\Pr[Y_0 = (\alpha_i; i \in [N], \beta)] - \Pr[Y_1 = (\alpha_i; i \in [N], \beta)]|, \end{aligned} \quad (16)$$

$$+ \frac{1}{2} \sum_{\alpha_i \in D_s^m; i \in [N], \beta \in D_c(sk_{i_0}, sk_{i_1})} |\Pr[Y_0 = (\alpha_i; i \in [N], \beta)] - \Pr[Y_1 = (\alpha_i; i \in [N], \beta)]|. \quad (17)$$

□

Step 1. Considering the case of $\beta \notin D_c(sk_{i_0}, sk_{i_1})$, generally, since

$$\begin{aligned} (17) &\leq \frac{1}{2} \sum_{\alpha_i \in D_s^m; i \in [N], \beta \notin D_c(sk_{i_0}, sk_{i_1})} |\Pr[Y_0 = (\alpha_i; i \in [N], \beta)]| \\ &\leq \frac{1}{2} \sum_{\beta \notin D_c(sk_{i_0}, sk_{i_1})} |\Pr[Y_0^{(N+1)} = \beta]| \leq \sum_{\beta \notin D_c(sk_{i_0}, sk_{i_1})} |\Pr[Y_0^{(N+1)} = \beta]|, \end{aligned} \quad (18)$$

and since for any $b \in \{0, 1\}$, the variable $Y_b^{(N+1)}$ is calculated by the hash function $H(L_{pk}, \mu, t_{\pi-1})$, where $t_{\pi-1} = h(\mathbf{r}_{z, \pi-1}) - c_{\pi-1}pk_{\pi-1}$, thus $\beta \in D_c$ and the probability that $Y_b^{(N+1)}$ is equal to the given value β is $1/|D_c|$. Note that even hash function $h \in \mathcal{H}(D, D_x, m)$ is adversarially chosen, it does not affect the probability that $Y_0^{(N+1)}$ is equal to a given β . Further, for each $\beta \notin D_c(sk_{i_0}, sk_{i_1})$, $\Pr[Y_0^{(N+1)} = \beta] = 1/|D_c|$, and since almost all elements of D_c are in $D_c(sk_{i_0}, sk_{i_1})$ from Lemma 2, it is evident that the probability of $\beta \notin D_c(sk_{i_0}, sk_{i_1})$ is negligible. And then we get

$$\begin{aligned} (17) &\leq \sum_{\beta \notin D_c(sk_{i_0}, sk_{i_1})} \frac{1}{|D_c|} \\ &= \frac{|D_c| - |D_c(sk_{i_0}, sk_{i_1})|}{|D_c|} \\ &= 1 - \frac{|D_c(sk_{i_0}, sk_{i_1})|}{|D_c|} = n^{-\omega(1)}. \end{aligned} \quad (19)$$

Step 2. To prove that the value of formula (17) is zero, it is only necessary to prove that each term in formula (17) is zero. Since the last component $Y_b^{(N+1)}$ of $Y_b^{(N+1)}$ is derived from a random oracle H , the probability that $Y_0^{(N+1)}$ and $Y_1^{(N+1)}$ are equal to a given value β is the same. Then it is only necessary to prove that the following equation about conditional probabilities holds:

$$\begin{aligned} &\Pr\left[(Y_0^{(i)}; i \in [N]) = (\alpha_i; i \in [N]) \mid Y_0^{(N+1)} = \beta\right] \\ &= \Pr\left[(Y_1^{(i)}; i \in [N]) = (\alpha_i; i \in [N]) \mid Y_1^{(N+1)} = \beta\right]. \end{aligned} \quad (20)$$

For any $b \in \{0, 1\}$, $Y_b^{(i)} = \alpha_i \in D_z^m$ if $i \in [N] \setminus i_b$, thus the probability that $Y_b^{(i)}$ is equal to a given value is $1/|D_z^m|$; if $i = i_b$,

$$\begin{aligned} \Pr\left[Y_b^{(i_b)} = \alpha_{i_b}\right] &= \Pr\left[\mathbf{u}_b + sk_{i_b}\beta = \alpha_{i_b}\right] \\ &= \Pr\left[\mathbf{u}_b = \alpha_{i_b} - sk_{i_b}\beta\right]. \end{aligned} \quad (21)$$

Since $\beta \in D_c(sk_{i_0}, sk_{i_1})$, $\alpha_{i_b} \in D_z^m$, we have $\|sk_{i_0}\beta\|_\infty, \|sk_{i_1}\beta\|_\infty \leq n \log^2 n$, $\|\alpha_{i_b}\|_\infty \leq mn^{1.5} \log n - n \log^2 n$, then $\|\alpha_{i_b} - sk_{i_0}\beta\|_\infty = \|\alpha_{i_b} - sk_{i_1}\beta\|_\infty \leq mn^{1.5} \log n$. Thus, the values of both $\alpha_{i_b} - sk_{i_0}\beta$ and $\alpha_{i_b} - sk_{i_1}\beta$ belong to the set D_y^m . And since $\mathbf{u}_0, \mathbf{u}_1 \leftarrow D_y^m$, $\Pr[\mathbf{u}_0 = \alpha_{i_b} - sk_{i_0}\beta] = \Pr[\mathbf{u}_1 = \alpha_{i_b} - sk_{i_1}\beta] = 1/|D_y^m|$.

In summary, for any $b \in \{0, 1\}$,

$$\Pr\left[Y_b^{(i)} = \alpha_i \mid Y_b^{(N+1)} = \beta\right] = \begin{cases} \frac{1}{|D_z^m|}, & i \in [N] \setminus i_b, \\ \frac{1}{|D_y^m|}, & i = i_b. \end{cases} \quad (22)$$

Therefore, it can be proved that equation (20) holds, i.e., the proof of the lemma is completed.

Suppose that in the game of anonymity in Section 3.2, pk_{i_0} and pk_{i_1} are adversarially generated according to the Setup algorithm, message μ and ring L_{pk} are also chosen by adversary. The challenger chooses $b \leftarrow \{0, 1\}$ and invokes

$\text{Sign}(pp, L_{pk}, \mu, sk_b)$ to generate a signature, and give it to the adversary. Define the random variable $X_{b,pp,sk_{i_b},\mu,L_{pk}}$ to represent the signature generated by the challenger, and the following theorem shows that the statistical distance between $X_{0,pp,sk_{i_0},\mu,L_{pk}}$ and $X_{1,pp,sk_{i_1},\mu,L_{pk}}$ is negligible.

Theorem 3 (anonymity). *The proposed scheme satisfies UA-CSA, i.e., for the adversary in Definition 10, $X_{b,pp,sk_{i_b},\mu,L_{pk}} \leftarrow \text{Sign}(pp, L_{pk}, \mu, sk_{i_b})$, $b \in \{0, 1\}$, we have*

$$\Delta\left(X_{0,pp,sk_{i_0},\mu,L_{pk}}, X_{1,pp,sk_{i_1},\mu,L_{pk}}\right) = n^{-\omega(1)}. \quad (23)$$

Proof. Regarding $X_{b,pp,sk_{i_b},\mu,L_{pk}}$, it is known from the signing process, $\mathbf{r}_{z,i} \leftarrow D_z^m$ if $i \neq i_b$, $\mathbf{r}_{z,i} = \mathbf{u} + c_i \mathbf{r}_i$ if $i = i_b$. By Lemma 3 and Theorem 2, we know that $\mathbf{r}_{z,i}$ is indistinguishable from a randomly selected vector in D_z^m . And since the first component c_1 in $X_{b,pp,sk_{i_b},\mu,L_{pk}}$ is from a random oracle, the statistical distance $\Delta(X_{0,pp,sk_{i_0},\mu,L_{pk}}, X_{1,pp,sk_{i_1},\mu,L_{pk}}) = n^{-\omega(1)}$ for an ordinary adversary \mathcal{A} . However, for an UA-CSA adversary, obviously, such an analysis is not rigorous enough. The following will focus on the verification process, whether the adversary can distinguish the two signatures based on adversarially-chosen private keys and c_π associated with the private keys.

Since the first component c_1 of $X_{b,pp,sk_{i_b},\mu,L_{pk}}$ is obtained by accessing a random oracle, and it is not directly related to the associated private key, thus the discussion with respect to c_1 is not necessary. We only need to prove that for an UA-CSA adversary, the statistical distance between the defined Y_0, Y_1 is negligible. By Lemma 4 it is known that $\Delta(Y_0, Y_1) = n^{-\omega(1)}$, thus for an UA-CSA adversary, the probability of winning the anonymity game is also negligible. That completes the proof. \square

5.2. Unforgeability. Before proving unforgeability, the following lemma is first given and proved.

Lemma 5. *Let $\mathbf{r}, \mathbf{r}' \leftarrow D_s$, $\mathbf{v}, \mathbf{v}' \leftarrow D_z$, $c, c' \leftarrow D_c$ and $c \neq c'$, if $\mathbf{v} - c\mathbf{r} = \mathbf{v}' - c'\mathbf{r}$, $\mathbf{r} \neq \mathbf{r}'$, then the following inequality holds:*

$$\|\mathbf{v} - c\mathbf{r}' - \mathbf{v}' + c'\mathbf{r}'\| \neq 0. \quad (24)$$

Proof. Assume that both $\mathbf{v} - c\mathbf{r} = \mathbf{v}' - c'\mathbf{r}$ and $\mathbf{v} - c\mathbf{r}' = \mathbf{v}' - c'\mathbf{r}'$ hold. By subtracting the two equations, we have $(\mathbf{r}' - \mathbf{r})(c' - c) = 0$. Since the equation holds in ring $\mathbb{Z}_q[x]/(x^n + 1)$, it does not directly deduce that $\mathbf{r}' = \mathbf{r}$ or $c' = c$ holds. Due to $\|\mathbf{r}'\|_\infty, \|\mathbf{r}\|_\infty \leq \sqrt{n} \log n$, $\|c'\|_\infty, \|c\|_\infty \leq 1$, then the absolute values of the coefficients of $\mathbf{r}' - \mathbf{r}$ and $c' - c$ are no more than $2\sqrt{n} \log n$ and 2, respectively. When $\mathbf{r}' - \mathbf{r}$ is multiplied by $c' - c$ in ring $\mathbb{Z}[x]/(x^n + 1)$, the absolute value of the coefficients of $(\mathbf{r}' - \mathbf{r})(c' - c)$ is no more than $4n^{1.5} \log n$. Since $q \gg 4n^{1.5} \log n$, if $(\mathbf{r}' - \mathbf{r})(c' - c) = \mathbf{0}$ holds in ring $\mathbb{Z}_q[x]/(x^n + 1)$, then it must also hold in ring $\mathbb{Z}[x]/(x^n + 1)$. And since $c \neq c'$, then it must have $\mathbf{r}' = \mathbf{r}$,

which is contradictory to the assumption, thus the lemma is proved. \square

Theorem 4 (unforgeability). *Under the random oracle model, if there exists a polynomial-time adversary \mathcal{A} who can validly forge a RS signature about the proposed scheme with probability ε , then for a random-chosen $h \in \mathcal{H}(D, D_x, m)$, there is a polynomial-time algorithm \mathcal{A}' that can obtain a solution to $\text{Col}(h, D_x)$ with probability at least $\varepsilon^2/2(\psi + 3N\zeta)$, where N , ζ and ψ are the number of ring members, the maximum times that \mathcal{A} accesses SO and directly accesses HO, respectively.*

Proof. Suppose there exists an EU-IC adversary \mathcal{A} who can validly forge a signature against the proposed scheme with non-negligible probability ε , then there exists a challenger \mathcal{A}' who can solve $\text{Col}(h, D_x)$ with non-negligible probability ε' .

Suppose the number of maximum ring members in the system is $l = l(\lambda)$, and given a hash function family $\mathcal{H}(D, D_x, m)$, \mathcal{A}' obtains an instance (h) from the $\text{Col}(h, D_x)$ oracle as an input. \mathcal{A}' maintains two lists L_1 and L_2 , which are initialized to be null. For $i \in [l]$, \mathcal{A}' honestly runs the Keygen algorithm to generate the key pair (pk_i, sk_i) , and stores the tuple (i, pk_i, sk_i) in list L_1 . \mathcal{A}' gives the public key set $S = \{pk_1, pk_2, \dots, pk_l\}$ to \mathcal{A} , and then \mathcal{A}' simulates oracles and responds to the queries from \mathcal{A} in the following manner:

Hash query HO: \mathcal{A} submits a set of ring members $L_{pk} = (pk_1, pk_2, \dots, pk_N) \subset S$, message $\mu \in \{0, 1\}^*$ and $t_i \in D$, \mathcal{A}' inquires the list L_2 , and if the tuple $(L_{pk}, \mu, t_i, c_{i+1})$ exists, \mathcal{A}' returns c_{i+1} to \mathcal{A} . Otherwise, \mathcal{A}' randomly selects $c_{i+1} \in D_c$ and returns it to \mathcal{A} , and adds $(L_{pk}, \mu, t_i, c_{i+1})$ to the list L_2 .

Signing query SO: \mathcal{A} submits an index π , a message $\mu \in \{0, 1\}^*$ and a set of ring members $L_{pk} = (pk_1, pk_2, \dots, pk_N)$ (which may contain some public keys generated by \mathcal{A} in an arbitrary way). Note that since \mathcal{A}' knows the private keys of all members in set S , and in general, \mathcal{A} will not query signatures about a user outside S , which is meaningless. \mathcal{A}' responds to this query by honestly running the Sign algorithm.

Corruption query CO: \mathcal{A} can make corruption query about any user U_i ($i \in [l]$). If \mathcal{A} makes a query on (i, pk_i) , \mathcal{A}' first obtains the tuple (i, pk_i, sk_i) by looking for the list L_1 , and then returns sk_i to \mathcal{A} .

Forgery phase: Suppose that after finishing the above queries, \mathcal{A} outputs a valid forgery $(\mu^*, L_{pk}^*, \text{sig}^*)$ with non-negligible probability, ε and \mathcal{A} did not ask for any signature on $(*, \mu^*, L_{pk}^*)$, where $L_{pk}^* \subseteq S \setminus C$ and C is the set of corrupted users.

Analysis. Define p as the maximum times HO is queried during \mathcal{A} 's attack. By Theorem 2, we know that it takes at most $3NH$ queries to produce a RS, and since \mathcal{A} can make SO queries at most ζ times, the value of p is at most $\psi + 3N\zeta$. Suppose that $\text{sig}^* = (c_1^*, (\mathbf{r}_{z,i}^*)_{i \in [N]})$ can pass the verification

of Verify, then in general, it can be assumed that for some j , we have $H(L_{pk}^*, \mu^*, h(\mathbf{r}_{z,j}^*) - c_j^* pk_j^*) = c_{j+1}^*$.

If \mathcal{A} did not query HO on $(L_{pk}^*, \mu^*, h(\mathbf{r}_{z,j}^*) - c_j^* pk_j^*)$, then the probability of producing c_{j+1}^* such that $H(L_{pk}^*, \mu^*, h(\mathbf{r}_{z,j}^*) - c_j^* pk_j^*) = c_{j+1}^*$ is only $1/|D_c|$. Hence, the probability that $c_{j+1}^* \in \{s_1, s_2, \dots, s_p\}$ is $1 - 1/|D_c|$, where $s_1, s_2, \dots, s_p \leftarrow D_c$ is the sequence of return values from HO . Further, the probability that \mathcal{A} succeeds in a forgery and $c_{j+1}^* \in \{s_1, s_2, \dots, s_p\}$ is at least $\varepsilon - 1/|D_c|$. Suppose $c_{j+1}^* = s_j$, then there are two cases: (1) s_j is a response to SO query (Case 1); (2) s_j is a response to HO query (Case 2). We first analyze Case 1. \square

Case 1. Suppose c_{j+1}^* appears during signing query, and suppose that the corresponding response \mathcal{A} obtains is the signature $\text{sig} = (c_1, (\mathbf{r}_{z,i})_{i \in [N]})$ (i.e., $c_{j+1}^* = H(L_{pk}^*, \mu^*, h(\mathbf{r}_{z,j}^*) - c_j^* pk_j^*)$). Then compare the signature forged by \mathcal{A} with the legitimate signature $\text{sig} = (c_1, (\mathbf{r}_{z,i})_{i \in [N]})$, we have

$$c_{j+1}^* = H(L_{pk}^*, \mu^*, h(\mathbf{r}_{z,j}^*) - c_j^* pk_j^*) = H(L_{pk}^*, \mu^*, h(\mathbf{r}_{z,j}) - c_j pk_j). \quad (25)$$

Then either $L_{pk}^* \neq L_{pk}$ or $\mu^* \neq \mu$ (or $\mathbf{r}_{z,j}^* \neq \mathbf{r}_{z,j}$), since if all three equations hold, this means the adversary simply outputs a signature that has already been asked. If at least one of $L_{pk}^* \neq L_{pk}$ and $\mu^* \neq \mu$ holds, it implies that a collision has occurred in H . Hence there is $L_{pk}^* = L_{pk}$, $\mu^* = \mu$ and $\mathbf{r}_{z,j}^* \neq \mathbf{r}_{z,j}$ with overwhelming probability, that is, $H(L_{pk}^*, \mu^*, h(\mathbf{r}_{z,j}^*) - c_j^* pk_j^*) = c_{j+1}^* = H(L_{pk}^*, \mu^*, h(\mathbf{r}_{z,j}) - c_j pk_j)$. Therefore either $h(\mathbf{r}_{z,j}^*) - c_j^* pk_j^* \neq h(\mathbf{r}_{z,j}) - c_j pk_j$, which implies there is a collision in H , or $h(\mathbf{r}_{z,j}^*) - c_j^* pk_j^* = h(\mathbf{r}_{z,j}) - c_j pk_j$, which implies there is $h(\mathbf{r}_{z,j}^*) = h(\mathbf{r}_{z,j})$. Then we find a collision for h , and since $\mathbf{r}_{z,j}, \mathbf{r}_{z,j}^* \in D_x^m \subset D_x^m$, we find a solution to $\text{Col}(h, D_x)$. Note that after HO is queried p times, the probability that a collision happens in H is no more than $p/|D_c|$, therefore, the probability of \mathcal{A} outputting a forgery as a solution to $\text{Col}(h, D_x)$ is at least,

$$\frac{\varepsilon - p}{|D_c|}. \quad (26)$$

Case 2. The next is to consider the case that s_j is obtained by \mathcal{A} calling HO . In this scenario, suppose that \mathcal{A}' runs \mathcal{A} with some randomness and \mathcal{A}' obtains a valid forgery $\text{sig}^* = (c_1^*, (\mathbf{r}_{z,i}^*)_{i \in [N]})$ of μ^* . Suppose that $s_1, \dots, s_p \leftarrow D_c$ is the sequence of response values from HO during this forgery. Then generate fresh random elements $s'_1, \dots, s'_p \leftarrow D_c$, and \mathcal{A}' runs \mathcal{A} with the same randomness and responds to \mathcal{A}' 's HO query with $s_1, \dots, s_{j-1}, s'_j, \dots, s'_p$, by forking lemma from [48], \mathcal{A}' will obtain another forged signature $\text{sig}' = (c_1', (\mathbf{r}_{z,i}')_{i \in [N]})$ on message μ^* and $s_j \neq s'_j$ with probability at least $(\varepsilon - 1/|D_c|) / ((\varepsilon - 1/|D_c|) / (\psi + 3N\zeta) - 1/|D_c|)$. Since the input of HO query is the same in both forgeries, we have $h(\mathbf{r}_{z,j}^*) - c_j^* pk_j^* = h(\mathbf{r}_{z,j}') - c_j' pk_j'$. By the homomorphic

properties of h in Definition 6, it follows that $h(\mathbf{r}_{z,j}^* - c_j^* \mathbf{r}_j^*) = h(\mathbf{r}_{z,j}' - c_j' \mathbf{r}_j')$. If $\mathbf{r}_{z,j}^* - c_j^* \mathbf{r}_j^* \neq \mathbf{r}_{z,j}' - c_j' \mathbf{r}_j'$ and $\mathbf{r}_{z,j}^* - c_j^* \mathbf{r}_j^*, \mathbf{r}_{z,j}' - c_j' \mathbf{r}_j' \in D_x^m$, then \mathcal{A}' finds a collision for h .

Next, we analyze the probability of $\mathbf{r}_{z,j}^* - c_j^* \mathbf{r}_j^* \neq \mathbf{r}_{z,j}' - c_j' \mathbf{r}_j'$. By Lemma 5.2 in [47], we know that there is a distinct private key \mathbf{r}_j' such that $\text{pk}_j = h(\mathbf{r}_j') = h(\mathbf{r}_j^*)$ with overwhelming probability. And by Lemma 5, if the private key \mathbf{r}_j^* satisfies $\mathbf{r}_{z,j}^* - c_j^* \mathbf{r}_j^* = \mathbf{r}_{z,j}' - c_j' \mathbf{r}_j'$, then for another private key \mathbf{r}_j , we have $\mathbf{r}_{z,j}^* - c_j^* \mathbf{r}_j^* \neq \mathbf{r}_{z,j} - c_j \mathbf{r}_j$. By Theorem 6.5 from [47], it is statistically impossible to distinguish which one of \mathbf{r}_j and \mathbf{r}_j^* is used by the signer, and thus the probability of $\mathbf{r}_{z,j}^* - c_j^* \mathbf{r}_j^* \neq \mathbf{r}_{z,j}' - c_j' \mathbf{r}_j'$ is at least $1/2 - n^{-\omega(1)}$. And for any response from HO , $s_i \in D_c$, then by Lemma 2, we have $\|\mathbf{r}_{z,j}^* - c_j^* \mathbf{r}_j^*\|_\infty, \|\mathbf{r}_{z,j}' - c_j' \mathbf{r}_j'\|_\infty \leq mn^{1.5} \log n$, i.e., $\mathbf{r}_{z,j}^* - c_j^* \mathbf{r}_j^*, \mathbf{r}_{z,j}' - c_j' \mathbf{r}_j' \in D_y^m \subset D_x^m$, which implies that \mathcal{A}' finds a solution to $\text{Col}(h, D_x)$.

From the above analysis, we know that the probability of \mathcal{A}' breaking $\text{Col}(h, D_x)$ via \mathcal{A} calling SO is at least $\varepsilon - p/|D_c|$, while the probability of \mathcal{A}' breaking $\text{Col}(h, D_x)$ via \mathcal{A} calling HO is at least,

$$\left(\frac{1}{2} - n^{-\omega(1)}\right) \left(\varepsilon - \frac{1}{|D_c|}\right) \left(\frac{\varepsilon - 1/|D_c|}{\psi + 3N\zeta} - \frac{1}{|D_c|}\right). \quad (27)$$

By comparing formulas (26) and (27), we have the inequality (26) > (27). Thus, the probability of \mathcal{A}' running \mathcal{A} to solve $\text{Col}(h, D_x)$ successfully is,

$$\varepsilon' \geq \left(\frac{1}{2} - n^{-\omega(1)}\right) \left(\varepsilon - \frac{1}{|D_c|}\right) \left(\frac{\varepsilon - 1/|D_c|}{\psi + 3N\zeta} - \frac{1}{|D_c|}\right). \quad (28)$$

6. Discussion

From Theorem 4, it is known that if an adversary succeeds in forging an RS against the proposed scheme, then the challenger can find a collision for a randomly chosen hash function $h_a(\cdot)$ in $\mathcal{H}(D, D_x, m)$. From [29], solving $\text{Col}(h, D_x)$ is equivalent to finding a vector $\mathbf{u} \in \Lambda_q^\perp(\mathbf{A})$ on lattice $\Lambda_q^\perp(\mathbf{A}) = \{\mathbf{u} \in \mathbb{Z}^{mn} \text{ s.t. } \mathbf{A}\mathbf{u} = 0 \pmod{q}\}$ satisfying $\|\mathbf{u}\|_\infty \leq 2(mn^{1.5} \log n + n \log^2 n)$ where $\mathbf{A} = [\text{Rot}(a_1) \parallel \text{Rot}(a_2) \parallel \dots \parallel \text{Rot}(a_m)] \in \mathbb{Z}_q^{n \times mn}$, a_i is the i -th component of \mathbf{a} , $i \in [m]$.

It was shown in [49] that in a reasonable amount of time, the algorithm for finding short vectors on a random lattice will generate a vector no less than 1.01^n times the shortest vector over the lattice. Furthermore, based on the experiments of [49], Micciancio and Regev [50] conduct experiments on lattices very similar to $\Lambda_q^\perp(\mathbf{A})$, and proves that the length of the shortest vector, which can be found on $\Lambda_q^\perp(\mathbf{A})$ by using the well-known lattice reduction algorithm, is $\|\mathbf{z}\|_2 \geq \min \left\{ q, 2^{2\sqrt{n \log q \log 1.01}} \right\}$ and the corresponding $\|\mathbf{z}\|_\infty$ at least,

$$\min \left\{ q, 2^{2\sqrt{n \log q \log 1.01}} \cdot \left(\frac{n \log q}{\log 1.01}\right)^{-1/4} \right\}. \quad (29)$$

TABLE 1: Parameter setting for our scheme.

Parameter	n	$q(\approx)$	m	The vector length needed to break	The shortest vector length that can be	Security level (bits)
				RS	found	
Recommended choice	128	2^{79}	16	$2^{18.4}$	$2^{19.2}$	80
	256	2^{43}	8	$2^{19.1}$	$2^{20.3}$	80
	512	2^{41}	5	$2^{20.1}$	$2^{29.6}$	128
	1024	2^{73}	8	$2^{22.4}$	$2^{59.9}$	192

TABLE 2: Comparison of storage overhead and security.

Scheme	Public key size	Private key size	Signature size	UA-CSA	EU-IC
[37]	$O(n \log q)$	$O(n \log n)$	$O(\log(Nn)n \log^2 n)$	Yes	Yes
[38]	$O(n \log q)$	$O(n)$	$O(\log^5 N n \log^2 n)$	Yes	Yes
[40]	$O(n \log q)$	$O(n)$	$O(\log N n \log(nq))$	Yes	Yes
AM1 of [41]	$O(n \log n \log q)$	$O(n \log n)$	$O(Nn \log n \log(n^{1.5} \log^2 n))$	Yes	No
AM2 of [41]	$O(\lambda n \log n \log q)$	$O(\lambda n \log n)$	$O(Nn \log n \log(n^{1.5} \log^2 n))$	Yes	Yes
Ours	$O(n \log q)$	$O(n \log(\sqrt{n} \log n))$	$O(Nn \log(n^{1.5} \log n))$	Yes	Yes

TABLE 3: Comparison of computational overhead at security level $\lambda = 128$.

Scheme	Key generation cost	Signature cost	Verification cost
[38]	$438T_{\text{poly-mul}}$	$60N + 9660T_{\text{poly-mul}}$	$6N + 96T_{\text{poly-mul}}$
AM1 of [41]	$21T_{\text{poly-mul}} + T_{\text{poly-inv}}$	$63NT_{\text{poly-mul}}$	$21NT_{\text{poly-mul}}$
AM2 of [41]	$\lambda(21T_{\text{poly-mul}} + T_{\text{poly-inv}})/2$	$63NT_{\text{poly-mul}} + T_v + T_c$	$21NT_{\text{poly-mul}}$
Ours	$5T_{\text{poly-mul}}$	$15NT_{\text{poly-mul}}$	$5NT_{\text{poly-mul}}$

TABLE 4: Comparison of approximate computational costs under ring size $N = 2^7$.

Scheme	Key generation cost	Signature cost	Verification cost
[38]	$438T_{\text{poly-mul}}$	$17340T_{\text{poly-mul}}$	$864T_{\text{poly-mul}}$
AM1 of [41]	$21T_{\text{poly-mul}} + T_{\text{poly-inv}}$	$8064T_{\text{poly-mul}}$	$2688T_{\text{poly-mul}}$
AM2 of [41]	$\lambda(21T_{\text{poly-mul}} + T_{\text{poly-inv}})/2$	$8064T_{\text{poly-mul}} + T_v + T_c$	$2688T_{\text{poly-mul}}$
Ours	$5T_{\text{poly-mul}}$	$1920T_{\text{poly-mul}}$	$640T_{\text{poly-mul}}$

Therefore, in order to make $\text{Col}(h, D_x)$ be intractable, we should set the parameters in such a manner that requires $2(mn^{1.5} \log n + n \log^2 n)$ to be smaller than formula (29). For example, $n = 512$, $q \approx 2^{41}$, then calculate $2(mn^{1.5} \log n + n \log^2 n) \approx 2^{20.1}$, while the infinite norm of the shortest vector $\|z\|_\infty$ that can be found by formula (29) is around $2^{29.6}$. Table 1 gives several sets of parameter settings and security levels for our scheme.

7. Efficiency

In this section, in respect of efficiency and security, we compare our scheme with five lattice-based RS schemes without trapdoors: the RS schemes of [37, 38, 40] and the two RS schemes AM1 and AM2 of [41]. The comparison results of storage overhead and computational overhead are listed in Table 2 and 3, respectively. λ is a security parameter, $n > \lambda$ is a power of 2, N is the number of ring members, and q is a large prime number. In estimating the computational efficiency of each scheme, we mainly focus on the relatively time-consuming operations, such as polynomial inversion and polynomial-polynomial multiplication, while ignoring

the less time-consuming operations such as polynomial-polynomial addition and cryptographic hash operation H . The notation $T_{\text{poly-inv}}$ denotes the computational overhead of running polynomial-polynomial multiplication in D once, $T_{\text{poly-mul}}$ denotes the computational overhead of running polynomial inversion once, normally $T_{\text{poly-inv}} > T_{\text{poly-mul}}$. T_v denotes the time spent in performing λ times sanity checks of parameters in the signing phase of AM2. T_c denotes the computational overhead of selecting a compliant signing key in the signing phase of AM2.

From Table 2, the signature size of [37, 38, 40] is $O(\log N)$, while the signature size of AM1, AM2 and ours is $O(N)$. Without loss of generality, $n \geq \sqrt{n} \log n$, thus compared with AM1, AM2, our scheme has smaller public/private key size and signature size.

These schemes [37, 38, 40] all use complex and bloated zero-knowledge proofs, and it is very difficult for us to calculate their computational overheads. Among these schemes [37, 38, 40], only the relatively concise scheme of [38] gives its computational overheads analysis. Therefore, we only compare the computational cost of [38, 41] and our scheme. We adopt the calculation method of efficiency in

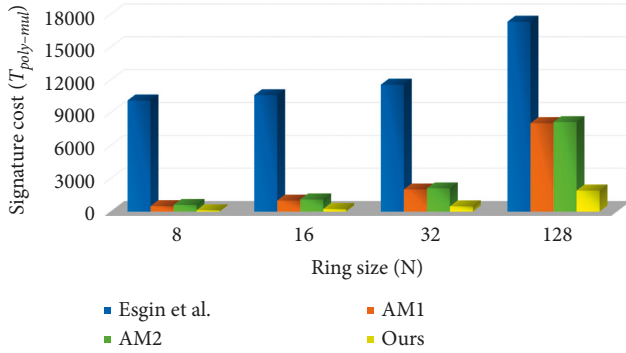


FIGURE 1: Comparison of computational overhead in the signing phase.

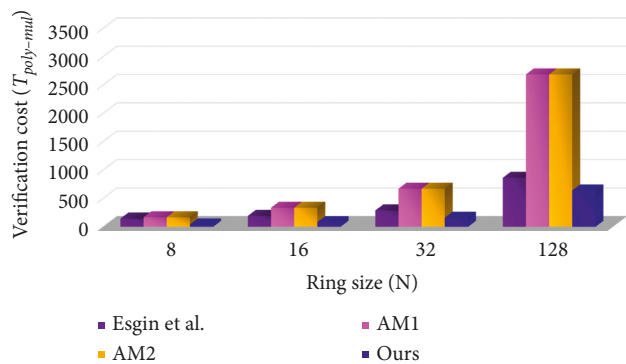


FIGURE 2: Comparison of computational overhead in the verification phase.

[38], and reduce the operations of KeyGen, Sign and Verify to polynomial-polynomial multiplication operations. To make the comparison results more intuitive, the parameters of [38, 41] and ours are set under the same security level $\lambda = 128$. Here, n in [38], AM, and ours are set to 256, 128, and 512, respectively; m in [38], AM, and ours are set to 15, 21, and 5, respectively. In terms of KeyGen, Sign and Verify, our scheme obviously has the smallest computational cost as shown in Tables 3 and 4.

To make the comparison results more intuitive, Figures 1 and 2 show the comparison between [38, 41] and ours in terms of computational overhead under different ring sizes.

8. Conclusions

Although lattice-based RS schemes are resistant to attacks by quantum computers, there still exists a big gap between them and the schemes that are based on traditional number-theoretic assumptions with respect to computational efficiency. To further boost the computational efficiency of RS on lattice, this work constructs a lattice-based RS scheme without trapdoors under the random oracle model. Based on a collision-resistant hash function on ideal lattice, our scheme is designed via the FSwA protocol. Our scheme avoids the use of trapdoors or sampling techniques that have high computational overhead and does not involve complex zero-knowledge proofs which are usually used in RS schemes without trapdoors. The proposed scheme is more concise

and efficient. Meanwhile, in terms of anonymity and unforgeability, our scheme is proven to satisfy the strongest UA-CSA and EU-IC, respectively. Next, we plan to investigate NTRU lattice-based RS scheme without trapdoors, which will be the first combination of NTRU lattice and RS without trapdoors.

Data Availability

The figures and tables used to support the findings of this study are included in the article.

Conflicts of Interest

The authors declare that they have no conflicts of interest.

Acknowledgments

This work was supported by the National Natural Science Foundation of China (61802117), the Support Plan of Scientific and Technological Innovation Team in Universities of Henan Province (201RTSTHN013), and the Youth Backbone Teacher Support Program of Henan Polytechnic University (2018XQG-10).

References

- [1] R. L. Rivest, A. Shamir, and Y. Tauman, "How to leak a secret," in *Proceedings of the 7th International Conference on the Theory and Application of Cryptology and Information Security*, pp. 552–565, Beijing, China, December, 2001.
- [2] M. Abe, M. Ohkubo, and K. Suzuki, "1-out-of-n signatures from a variety of keys," in *Proceedings of the 8th International Conference on the Theory and Application of Cryptology and Information Security*, pp. 415–432, Jeju Island, Korea, December, 2002.
- [3] E. Bresson, J. Stern, and M. Szydlo, "Threshold ring signatures and applications to ad-hoc groups," in *Proceedings of the 22nd Annual International Cryptology Conference*, pp. 465–480, California, USA, August, 2002.
- [4] F. G. Zhang and K. Kim, "Id-based blind signature and ring signature from pairings," in *Proceedings of the 8th International Conference on the Theory and Application of Cryptology and Information Security*, pp. 533–547, Queenstown, New York, December, 2002.
- [5] M. Naor, "Deniable ring authentication," in *Proceedings of the 22nd Annual International Cryptology Conference*, pp. 481–498, Santa Barbara, CA, USA, August, 2002.
- [6] D. Boneh, C. Gentry, and B. Lynn, "Aggregate and verifiably encrypted signatures from bilinear maps," in *Proceedings of the International Conference on the Theory and Applications of Cryptographic Techniques*, pp. 416–432, Zagreb, Croatia, May, 2003.
- [7] J. Herranz and G. Saez, "Forking lemmas for ring signature schemes," in *Proceedings of the 4th International Conference on Cryptology in India*, pp. 266–279, Jaipur, India, December, 2003.
- [8] J. K. Liu, V. K. Wei, and D. S. Wong, "Linkable spontaneous anonymous group signature for ad hoc groups," in *Proceedings of the 9th Australasian Conference on Information Security and Privacy*, pp. 325–335, Perth Australia, January, 2004.

- [9] B. Adida, S. Hohenberger, and R. L. Rivest, "Ad-hoc-group signatures from hijacked keypairs," in *DIMACS Workshop on Theft in E-Commerce*, Piscataway, NJ, USA, 2005, <https://citeseerx.ist.psu.edu/viewdoc/download?doi=10.1.1.73.4165&rep=rep1&type=pdf>.
- [10] J. Xu, Z. Zhang, and D. Feng, "A Ring Signature Scheme Using Bilinear Pairings," in *International Workshop on Information Security Applications*, vol. 3325, pp. 160–169, 2004.
- [11] A. Bender, J. Katz, and R. Morselli, "Ring signatures: stronger definitions, and constructions without random oracles," *Journal of Cryptology*, vol. 22, no. 1, pp. 114–138, 2009.
- [12] P. W. Shor, "Polynomial-time algorithms for prime factorization and discrete logarithms on a quantum computer," *SIAM Review*, vol. 41, no. 2, pp. 303–332, 1999.
- [13] M. Ajtai, "Generating hard instances of lattice problems," in *Proceedings of the 28th Annual ACM Symposium on Theory of Computing*, pp. 99–108, Pennsylvania USA, May, 1996.
- [14] O. Regev, "On lattices, learning with errors, random linear codes, and cryptography," *Journal of the ACM*, vol. 56, no. 6, pp. 1–40, 2009.
- [15] V. Lyubashevsky, C. Peikert, and O. Regev, "On ideal lattices and learning with errors over rings," in *Proceedings of the 29th Annual International Conference on the Theory and Applications of Cryptographic Techniques*, pp. 1–23, French Riviera, France, May, 2010.
- [16] R. Lindner and C. Peikert, "Better Key Sizes (And Attacks) for LWE-Based Encryption," *Cryptographers' Track at the RSA Conference*, pp. 319–339, Springer, San Francisco, CA, USA, 2011.
- [17] W. Susilo, P. Dutta, and D. H. Duong, "Lattice-based HRA-secure attribute-based proxy re-encryption in standard model," in *Proceedings of the 26th European Symposium on Research in Computer Security*, pp. 169–191, Darmstadt, Germany, October, 2021.
- [18] J. M. B. Mera, A. Karmakar, and T. Marc, "Efficient lattice-based inner-product functional encryption," in *Proceedings of the 25th IACR International Conference on Public-Key Cryptography*, pp. 163–193, Virtual Event, August, 2022.
- [19] O. Goldreich, S. Goldwasser, and S. Halevi, "Public-key cryptosystems from lattice reduction problems," in *Proceedings of the 17th Annual International Cryptology Conference*, pp. 112–131, Berlin, Heidelberg, August, 1997.
- [20] J. Hoffstein, J. Pipher, and J. H. Silverman, "An NTRU lattice-based signature scheme," in *Proceedings of the Annual International Conference on the Theory and Applications of Cryptographic Techniques*, pp. 211–228, Russia, May, 2001.
- [21] J. Hoffstein, N. Howgrave-Graham, and J. Pipher, "NTRU-Sign: Digital Signatures Using the NTRU Lattice," *Cryptographers' Track at the RSA Conference*, pp. 122–140, Springer, San Francisco, CA, USA, 2003.
- [22] Y. P. Hu, B. C. Wang, and W. C. He, "NTRUSign with a new perturbation," *IEEE Transactions on Information Theory*, vol. 54, no. 7, pp. 3216–3221, 2008.
- [23] P. Q. Nguyen and O. Regev, "Learning a parallelepiped: cryptanalysis of GGH and NTRU signatures," *Journal of Cryptology*, vol. 22, no. 2, pp. 139–160, 2009.
- [24] L. Ducas and P. Q. Nguyen, "Learning a zonotope and more: cryptanalysis of NTRUSign countermeasures," in *Proceedings of the 18th Annual International Conference on the Theory and Application of Cryptology and Information Security*, pp. 433–450, Tokyo, Japan, April, 2012.
- [25] C. Gentry, C. Peikert, and V. Vaikuntanathan, "Trapdoors for hard lattices and new cryptographic constructions," in *Proceedings of the 40th Annual ACM Symposium on Theory of Computing*, pp. 197–206, New York, USA, June, 2008.
- [26] D. Micciancio and C. Peikert, "Trapdoors for lattices: simpler, tighter, faster, smaller," in *Proceedings of the 31st Annual International Conference on the Theory and Applications of Cryptographic Techniques*, pp. 700–718, Cambridge UK, April, 2012.
- [27] J. Alwen and C. Peikert, "Generating shorter bases for hard random lattices," *Theory of Computing Systems*, vol. 48, no. 3, pp. 535–553, 2011.
- [28] L. Ducas and D. Micciancio, "Improved short lattice signatures in the standard model," in *Proceedings of the 34th Annual Cryptology Conference*, pp. 335–352, Santa Barbara, CA, USA, April, 2014.
- [29] V. Lyubashevsky, "Fiat-Shamir with aborts: applications to lattice and factoring-based signatures," in *Proceedings of the 15th International Conference on the Theory and Application of Cryptology and Information Security*, pp. 598–616, Tokyo, Japan, August, 2009.
- [30] V. Lyubashevsky, "Lattice signatures without trapdoors," in *Proceedings of the 31st Annual International Conference on the Theory and Applications of Cryptographic Techniques*, pp. 738–755, Cambridge UK, April, 2012.
- [31] Z. Brakerski and Y. T. Kalai, "A framework for efficient signatures, ring signatures and identity based encryption in the standard model," 2010, <http://eprint.iacr.org/2010/086>.
- [32] J. Wang and B. Sun, "Ring signature schemes from lattice basis delegation," in *Proceedings of the 13th International Conference on Information and Communications Security*, pp. 15–28, Beijing China, November, 2011.
- [33] Y. H. Zhang, Y. P. Hu, J. Xie, and M. Jiang, "Efficient ring signature schemes over NTRU lattices," *Security and Communication Networks*, vol. 9, no. 18, pp. 5252–5261, 2016.
- [34] G. M. Zhao and M. M. Tian, "A simpler construction of identity-based ring signatures from lattices," in *Proceedings of the 12th International Conference on Provable Security*, pp. 277–291, South Korea, October, 2018.
- [35] X. Y. Lu, M. H. Au, and Z. F. Zhang, "Raptor: a practical lattice-based (linkable) ring signature," in *Proceedings of the 17th Applied Cryptography and Network Security*, pp. 110–130, Bogota, Colombia, June, 2019.
- [36] Y. L. Tang, F. F. Xia, and Q. Ye, "Identity-based linkable ring signature on NTRU lattice," *Security and Communication Networks*, vol. 2021, Article ID 9992414, 17 pages, 2021.
- [37] B. Libert, S. Ling, and K. Nguyen, "Zero-knowledge arguments for lattice-based accumulators: logarithmic-size ring signatures and group signatures without trapdoors," in *Proceedings of the 35th Annual International Conference on the Theory and Applications of Cryptographic Techniques*, pp. 1–31, Vienna, Austria, May, 2016.
- [38] M. F. Esgin, R. Steinfeld, and J. K. Liu, "Lattice-based zero-knowledge proofs: new techniques for shorter and faster constructions and applications," in *Proceedings of the 39th Annual International Cryptology Conference*, pp. 115–146, Santa Barbara, CA, USA, August, 2019.
- [39] W. Beullens, S. Katsumata, and F. Pintore, "Calamari and falafi: logarithmic (linkable) ring signatures from isogenies and lattices," in *Proceedings of the 26th International Conference on the Theory and Application of Cryptology and Information Security*, pp. 464–492, Daejeon, November, 2020.
- [40] V. Lyubashevsky, N. K. Nguyen, and G. Seiler, "SMILE: set membership from ideal lattices with applications to ring signatures and confidential transactions," in *Proceedings of the*

- 41st Annual International Cryptology Conference, pp. 611–640, Virtual Event, August, 2021.
- [41] C. Aguilar Melchor, S. Bettaieb, and X. Boyen, “Adapting Lyubashevsky’s signature schemes to the ring signature setting,” in *Proceedings of the 6th International Conference on Cryptology in Africa*, pp. 1–25, Cairo, Egypt, July, 2013.
 - [42] W. A. Alberto Torres, R. Steinfeld, and A. Sakzad, “Post-quantum one-time linkable ring signature and application to ring confidential transactions in blockchain (lattice RingCT v1. 0),” in *Proceedings of the 23rd Australasian Conference on Information Security and Privacy*, pp. 558–576, Perth, WA, Australia, March, 2018.
 - [43] C. Baum, H. Lin, and S. Oechsner, “Towards practical lattice-based one-time linkable ring signatures,” in *Proceedings of the 20th International Conference on Information and Communications Security*, pp. 303–322, Lille, France, August, 2018.
 - [44] Z. Liu, K. Nguyen, and G. Yang, “A lattice-based linkable ring signature supporting stealth addresses,” in *Proceedings of the 24th European Symposium on Research in Computer Security*, pp. 726–746, Luxembourg, September, 2019.
 - [45] V. Lyubashevsky and D. Micciancio, “Generalized compact knapsacks are collision resistant,” in *Proceedings of the 33rd International Colloquium on Automata, Languages, and Programming*, pp. 144–155, Venice Italy, July, 2006.
 - [46] D. Micciancio, “Improved cryptographic hash functions with worst-case/average-case connection,” in *Proceedings of the 34th Annual ACM Symposium on Theory of Computing*, pp. 609–618, Dallas Texas USA, May, 2002.
 - [47] V. Lyubashevsky, *Towards practical lattice-based cryptography*, PhD Thesis, University of California, San Diego, 2008.
 - [48] M. Bellare and G. Neven, “Multi-signatures in the plain public-key model and a general forking lemma,” in *Proceedings of the 13th ACM Conference on Computer and Communications Security*, pp. 390–399, Berlin, Germany, May, 2006.
 - [49] N. Gama and P. Q. Nguyen, “Predicting lattice reduction,” in *Proceedings of the 27th Annual International Conference on the Theory and Applications of Cryptographic Techniques*, pp. 31–51, Istanbul, Turkey, April, 2008.
 - [50] D. Micciancio and O. Regev, “Lattice-based cryptography,” *Post-Quantum Cryptography*, pp. 147–191, 2009.

Research Article

Construction and Application of the Talent Training System in Colleges and Universities Based on the Fuzzy Analytic Hierarchy Process

Yan Yu ¹ and Jun Qiu ²

¹School of Economics and Management, Chong Qing Industry Polytechnic College, Chongqing 401120, China

²School Work Department QuZhou College of Technology, Quzhou 324000, China

Correspondence should be addressed to Jun Qiu; 112145@qzct.edu.cn

Received 15 April 2022; Revised 6 June 2022; Accepted 27 June 2022; Published 14 September 2022

Academic Editor: Le Sun

Copyright © 2022 Yan Yu and Jun Qiu. This is an open access article distributed under the Creative Commons Attribution License, which permits unrestricted use, distribution, and reproduction in any medium, provided the original work is properly cited.

At present, the competition among talents to seize jobs is becoming more and fiercer. How to stand out in the fierce competition for talents and seize market resources is a problem that every graduate must think deeply. Domestic research on the composition of the implementation elements of talent training in colleges and universities from the perspective of excellent school talent training has achieved fruitful results. Their measures and implementation ideas mainly include the following aspects: first, analyze the system of talent training in colleges and universities; second, analyze the teaching methods of college teachers; third, analyze the future development direction of talents. Taking a university as a pilot unit, this paper constructs a talent training system based on the combination method of fuzzy hierarchy, determines the training goal according to students' own ability, formulates the talent training scheme according to the goal, determines the rectangular array relationship between the training system and students' own ability requirements and attaches importance to practical teaching. The algorithm used in this paper firstly establishes a hierarchical structure model and then combines the relevant measures of AHP to sort the weights of indicators and finally calculates the entropy value by quoting entropy weight. We use the fuzzy method combined with hierarchical analysis to evaluate the five indexes of students' own influencing factors, such as learning attitude, basic knowledge, cooperation ability, development ability, and professional ability. It can be seen that the algorithm model is more accurate and the error value is the smallest. Compared with their combination method, the fuzzy evaluation method and the hierarchical analysis method are practical, and the fuzzy method combined with the hierarchical analysis combination method has more practical significance. Finally, the employment situation of graduates is compared and analyzed to further highlight the effectiveness of the model.

1. Introduction

Fuzzy map is generated by fuzzy membership function of each parameter in a suitable karst area, and the weight of each layer is assigned by the AHP method, and finally the final fuzzy-AHP map is generated [1]. For the popular Novel Coronavirus, fuzzy AHP is used to determine the weight of the existing criteria, and fuzzy TOPSIS is used to determine the safest area, that is ready to implement the new normal [2]. The competitive technology between China and Africa is transferred at any time, and the method in this paper is used to calculate the weight [3]. An appropriate proposed

framework was implemented using the fuzzy analytic hierarchy process in a palm oil industry in Indonesia to confirm its applicability and usefulness. Research shows that the environmental dimension is the most sustainable supplier standard, followed by the economic and social dimensions [4]. Taking Herat, Afghanistan as an example, the suitability of the GIS wind farm is evaluated by the fuzzy AHP multi-criteria method [5]. We combine the fuzzy analytic hierarchy process with the fuzzy mixed multi-criteria method and study the most influential and conflicting criteria in economy, service level, environment, society, and risk [6]. Our evaluation model of financial audit research in

the financial shared service mode is established by the fuzzy method combined with the hierarchical analysis combination method and order estimation methodology through similarity of solutions [7]. We use the fuzzy method and the hierarchical analysis combination method to find the optimal system of processing cigarette manufacturing [8]. We use the fuzzy method and the hierarchical analysis combination method to calculate the relative weights of relevant criteria. Finally, based on these weights, we use the ranking technology approaching the ideal solution to rank banks, and the results show that the major banks rank in the top three, respectively [9]. In the Craig–Harris method to measure the productivity level of farms, a fishbone diagram is used to analyze the reasons for productivity decline, and the fuzzy method combined with the class analysis combination method is proposed to improve productivity, which is based on the Craig–Harris method to measure productivity [10]. Researchers have developed and applied various standards and methods to find suitable rainwater harvesting sites and technologies. The main goal of the work is to use the fuzzy method combined with the hierarchical analysis combination method to assign weights to various standards involved in selecting suitable RWH sites in the Kandi subdivision of Murshidabad District, India [11]. Spectrum seems to be the lifeblood of wireless communication, and the fuzzy analytic hierarchy process seems to be an appropriate solution for spectrum allocation among SUs without interference between themselves [12]. Double-skin sickle (DSF) has been paid more attention by manufacturers in recent years because of its practical and aesthetic characteristics. In the previous research, our research group used the AHP method to evaluate DSF [13]. The fuzzy method combined with the hierarchical analysis and combination method is used to evaluate the quality of online commercial services, and the research results can be used by other e-commerce enterprises to improve the service quality according to the standards and sub-standards that experts think are important [14]. The supply chain adopted in medicine and medicine requires an orderly implementation plan for each strategic element of the pharmaceutical supply chain and uses the fuzzy method combined with the hierarchical analysis and combination method to minimize its weight on cost and time, so that decision makers can optimize the economy of PSC and create space [15]. In this paper, an extended FAHP model is proposed, in which two fuzzy comparison rectangular matrices are represented by a special class of fuzzy numbers. Then it is proved that a large number of FAHP methods can be simply written into the proposed E-FAHP structure [16]. We use the fuzzy method combined with hierarchical analysis to improve the understanding of the determinants of effective hotel websites and provide practical suggestions in order to formulate appropriate strategies to transform website visitors into customers [17]. In various cases of decision analysis, we adopt two popular methods: analytic hierarchy process (AHP) and fuzzy AHP. Both methods deal with random data, and the decision results can be determined by some criterion decision processes [18]. The purpose of this study is to assist the catering industry and credit card issuing banks

to establish performance evaluation indicators of marketing alliance by means of expert Delphi method, fuzzy method combined with hierarchical analysis, and balanced scorecard [19]. Fuzzy analytic hierarchy process (FAHP) is used to determine the weight of each sub-criterion according to the evaluation of experts. When there is no pairwise comparison of existing alternatives, we adjust to use sustainable development [20]. Fuzzy method combined with hierarchical analysis and ARAS-G is used to evaluate the performance of logistics in OECD countries [21]. Application of the fuzzy analytic hierarchy process and the TOPSIS method in cross-domain collaborative recommendation with fuzzy visual representation [22]. Researchers use the fuzzy method combined with hierarchical analysis to analyze the effective judgment of trademark infringement compensation cases in Beijing Intellectual Property Court in 2018 [23]. In the case study of an Indonesian sole manufacturer seeking to expand its business to the international market, the weights of the fuzzy method combined with the hierarchical analysis and combination method are adopted, and PROMETHEE is used to sort the schemes [24]. Fuzzy AHP and completely consistent implementation are used to rank the relative importance of these CSFs and their dimensions for continuous academic quality assurance and ABET certification [25].

2. The Necessity of Personnel Training in Undergraduate Colleges and Universities

2.1. Connotation of Personnel Training. To construct the talent training mode system in colleges and universities, the first point is to determine what system should be adopted to train talents. That is, through what kind of thinking mode and practical means to cultivate talents who conform to the development of the times. Therefore, to cultivate talents, we must first master the correct talent training system, so as to realize the terminal of talent training in the true sense for people's needs. The way of talent training is the professional knowledge, learning ability, future trend, and the way to achieve the ideal goal determined by the school for students. It collects and determines the characteristics that talents should have and also effectively embodies the educational philosophy and practice. Choose the appropriate way to realize the talent training mode and reference blueprint and cultivate talents with certain innovative ability. We can neither be subject to the traditional theoretical classroom teaching experience, blindly go with the flow, nor reform the training system that is arbitrarily enlarged to the whole school. Similarly, as the standard style of personnel training, it is formed by the integration and adjustment of many scientific theories, practical operations, and other factors, and many influencing factors together form a complex entity, which not only includes the theoretical chapters of personnel training but also reflects the reality of traditional educational practice training talents in recent years. This is a compound combination formed by the mutual influence and combination of many different links, and their multiple ideas together constitute the connotation of the current standardized talent training mode.

2.2. *Attach Importance to Vocational Education.* The implementation elements of vocational personnel training should pay attention to the cultivation of students' double-base ability. While improving vocational ability, we should uphold the sustainable development concept of lifelong learning and establish a training system in the field of vocational education that runs through from top to bottom and connects from left to right. Pave a smooth road for continuously improving professional quality and learning and development ability. This step is often realized through the school cultural education system. The school provides a basic place for students to cultivate and improve their professional ability. Only by receiving a certain period of school culture education and acquiring basic professional knowledge in school to meet the graduation requirements can students realize their personal value and further enhance their professional ability when they really go to work in the future. Vocational education is dominated by technical and professional characteristics, upholds the basic concepts of employment orientation, quality-oriented, unity of knowledge and practice, and lifelong development and cultivates students' vocational ability to meet the needs of social development.

2.3. *Education around Students.* Around the mode of students' education, the main object of talent education is the students who have received ordinary school education and have a certain knowledge base, and the training of vocational education talents at an undergraduate level is no exception. Students who graduated from ordinary high schools are also the main body of talent education. Therefore, we must adhere to the basic principle of "taking students as the main body and teachers as the leading factor". Talent education focuses on the basic teaching principles of the students' teaching mode, in order to explore the development laws of nature and society and constantly learn and pursue progressive learning. When formulating the implementation elements of personnel training, colleges and universities must pay attention to taking students as the main body, carry out education around students and accurately understand the training information fed back by students through the evaluation of teaching methods and students' questionnaire survey, which can also make schools clearly recognize their own shortcomings and correct them. We should not only take this measure but also formulate a personalized training mode for students, carefully understand the real needs of students and give full play to the leading role that school education can play in the process of personnel training. After the talent training mode has been tested in practice, we can get feedback by investigating the previous students' evaluation of the implementation of teaching content and the employment situation after graduation, so that the training mode can be continuously improved and the talent training mode can be continuously reformed. Realize the trinity consultation mechanism among schools, enterprises, and students. Both sides understand each other's pursuit of interests, so that the training of talents in schools is more

realistic, and the implementation elements of personnel training tend to be more ideal.

3. Fuzzy Analytic Hierarchy Process Algorithm

3.1. *Building a Hierarchical Model.* According to the analysis of their own needs, the goal, key impact factors, and program objects can be divided into goal level, method level, and program level according to their connection relationship, and the corresponding hierarchical structure diagram is constructed to form a hierarchical structure model.

3.1.1. *Constructing Judgment Matrices against Each Other.* According to the weights of the two factors, a judgment matrix is formed:

$$Judgment\ matrix = \left\{ \begin{array}{c} a_{11}, a_{12}, \dots, a_{1(n-1)}, a_{1n} \\ a_{21}, a_{22}, \dots, a_{2(n-1)}, a_{2n} \\ \dots, \dots, \dots, \dots, \dots \\ a_{n1}, a_{n2}, \dots, a_{n(n-1)}, a_{n(n-1)}, a_{nm} \end{array} \right\}. \quad (1)$$

3.1.2. *Single Layer Weight Calculation.* Multiply the factors of each row of matrix A to calculate the product as

$$M_i = a_{i1} * a_{i2} * \dots * a_{i(n-1)} a_{in}. \quad (2)$$

Calculate the root of N to the n th power, and the expression is as follows:

$$\bar{V} = \left[\sqrt[n]{N_1}, \sqrt[n]{N_2}, \dots, \sqrt[n]{N_{(n-1)}}, \sqrt[n]{N_n} \right]. \quad (3)$$

The weight vector of each factor is obtained by processing vector \bar{V} with the following normalization formula:

$$V_i = \frac{\bar{V}_i}{\sum_{i=1}^n \bar{V}_i}. \quad (4)$$

3.1.3. *Consistency Test of Matrix.* Calculate the maximum eigenvalue of matrix A as

$$\lambda_{\max} = \frac{1}{\sum_{i=1}^n (AV)_i / V_i},$$

$$(AV)_i = (V_1, V_2, V_3, V_4) \left\{ \begin{array}{c} A_{11}, A_{12}, A_{13}, A_{14} \\ A_{21}, A_{22}, A_{23}, A_{24} \\ A_{31}, A_{32}, A_{33}, A_{34} \\ A_{41}, A_{42}, A_{43}, A_{44} \end{array} \right\}. \quad (5)$$

Expressions for calculating consistency metrics is

$$C.I = \frac{\lambda_{\max} - n}{n - 1}. \quad (6)$$

According to the judgment matrices of different orders, the corresponding average random consistency index R.I. can be obtained by looking up the table, and finally the consistency ratio can be calculated by using it.

3.1.4. *Total Sort of All Hierarchies.* After sorting the importance and weight of the above single-level factors, all levels will be sorted in this way. The calculation method is as follows:

$$V_i^{(k)} = \sum_{j=1}^m p_{ij}^{(k)} w_j^{(k-1)}; i = 1, 2, 3, \dots, n. \quad (7)$$

In the same way, the consistency test of the total ranking is also carried out.

3.2. *Fuzzy Analytic Hierarchy Process.* The phase test of fuzzy matrix is established, and a matrix is defined as

$$R = (r_{ij})_{n \times n}. \quad (8)$$

The fuzzy complementary matrix of the matrix can be obtained by satisfying the following conditions:

If the formula satisfies: $0 \leq r_{ij} \leq 1$, ($i = 1, 2, \dots, n$; $j = 1, 2, \dots, n$), then fuzzy array R is a fuzzy complementary matrix.

The fuzzy consistent matrix can be obtained by satisfying the following conditions:

$$r_{ij} = r_{ik} - r_{jk} + 0.5. \quad (9)$$

3.3. *Index Scoring Weight Setting.* We use the fuzzy analytic hierarchy process to construct all indicators and calculate the basic steps of scoring weights as shown in Figure 1.

Construct fuzzy complementary judgment matrix, compare the importance of different influencing factors in pairs and transform it into fuzzy complementary judgment matrix as

$$R = \begin{Bmatrix} R_{11}, R_{12}, R_{13}, R_{14} \\ R_{21}, R_{22}, R_{23}, R_{24} \\ R_{31}, R_{32}, R_{33}, R_{34} \\ R_{41}, R_{42}, R_{43}, R_{44} \end{Bmatrix}. \quad (10)$$

The fuzzy complementary matrix is summed by rows, and the expression is

$$r_i = \sum_{j=1}^n r_{ij}, i = 1, 2, \dots, n. \quad (11)$$

Carry out mathematical transformation into the following formula:

$$r_{ij} = \frac{(r_i - r_j)}{2n + 0.5}. \quad (12)$$

For the neat fuzzy consistency matrix, the factor of each row of the matrix is multiplied by the power product method:

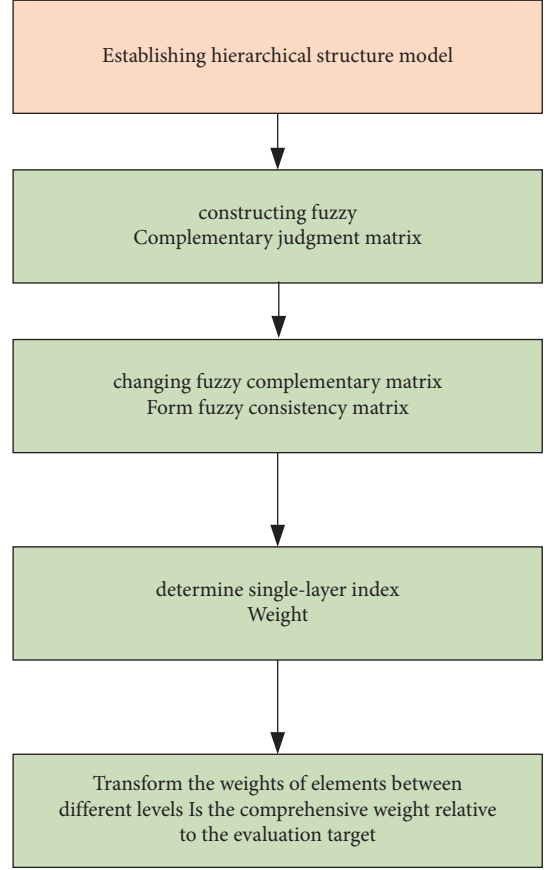


FIGURE 1: Weight setting steps of the bidding score.

$$R_i = r_{i1} \times r_{i2} \times \dots \times r_{i(n-1)} \times r_{in}. \quad (13)$$

Calculate the n th root of R_i as

$$\bar{R} = [\sqrt[n]{R_1}, \sqrt[n]{R_2}, \dots, \sqrt[n]{R_{n-1}}, \sqrt[n]{R_n}]. \quad (14)$$

Normalizing the above vectors as

$$R_i = \frac{\bar{R}_i}{\sum_{i=1}^n \bar{R}_i}. \quad (15)$$

Ranking vectors of fuzzy complementary judgment matrices as

$$w = (w_1, w_2, \dots, w_n)^T. \quad (16)$$

Its constraints are as follows:

$$w_i = \frac{\sum_{j=1}^n r_{ij} + n/2 - 1}{n(n-1)} \quad i = 1, 2, \dots, n. \quad (17)$$

Calculate the compatibility index of fuzzy judgment matrix: as

$$I(A, R) = 1/n^2 \sum_{i=1}^n \sum_{j=1}^n |r_{ij} - p_{ij}|. \quad (18)$$

3.4. *Triangular Fuzzy Number.* The relative importance of the two influencing factors is calculated. If W_1, W_2 are triangular fuzzy numbers, the probability degree of ($W_1 \geq W_2$) is defined as $V(W_1 \geq W_2)$.

TABLE 1: Basic information of respondents.

Category	Investigation items	Percentage proportion
Gender	Men	48%
	Women	52%
	Senior year	
Grade	Ken-ichi	20%
	Yanji	21%
	Yan san	25%
		34%
Areas of interest	Big data application	32%
	Finance	24%
	Construction engineering	20.8%
	Teacher training	20%
	Scientific research	3.2%

When

$$m_1 \geq m_2, V(W_1 \geq W_2) = 1. \quad (19)$$

When

$$m_1 \leq m_2, V(W_1 \geq W_2) = \begin{cases} \frac{l_2 - u_1}{(m_1 - u_1) - (m_2 - l_2)}, & l_2 \leq u_1, \\ 0, & l_2 > u_1. \end{cases} \quad (20)$$

The probability that the triangular fuzzy number W is greater than k triangular fuzzy numbers W_1 is defined as

$$V(W \geq W_1, W_2, \dots, W_k) = \min V(W \geq W_i) (i = 1, 2, \dots, n). \quad (21)$$

In order to introduce entropy weight into the model, several definitions are introduced below.

Set projection of all indicators as

$$P_{ij} = \frac{x_{ij}}{\sum_{i=1}^m x_{ij}}. \quad (22)$$

According to the information conclusion, the entropy value output by each index i is

$$E_i = k \sum_{i=1}^m P_{ij} \ln(P_{ij}), i = 1, 2, \dots, n, \quad (23)$$

$$k = (\ln m)^{-1}.$$

Deviation is

$$d_i = 1 - E_i (i = 1, 2, \dots, n). \quad (24)$$

4. Experimental Study

4.1. Basic Information of Research. In this experiment, the fuzzy analytic hierarchy process is used to investigate college students at different levels to better build a talent system in colleges and universities, involving basic information such as students' age, gender, grade, interest field, and school. The subjects of this survey are 200 students from 20 universities

in China, and their interest research fields are mainly concentrated in 5 fields. The investigation status are shown in Table 1.

Among the 200 respondents, we can see that the proportion of students majoring in scientific research is the least, and students are more inclined to study big data applications and financial fields. According to the fuzzy analytic hierarchy process studied in this paper, we carry out feedback analysis and statistics of the existing personnel training situation.

Whether the respondents in the five research fields are satisfied with the training system used by talents in schools today, the survey results are shown in Figure 2.

Continue to investigate whether the respondents in the five types of research fields recognize the teaching methods in colleges and universities today. The survey results are shown in Figure 3.

Finally, whether the respondents in the five research fields have a clear understanding of the future employment direction, the survey results are shown in Figure 4.

4.2. Model Comparison. In order to highlight the advantages of the fuzzy method combined with hierarchical analysis in the talent training system of colleges and universities, this paper studies and analyzes the students' self-influence indicators in the talent training system of five research fields together with the fuzzy average algorithm and the analytic hierarchy process.

$$MAE = \frac{1}{K} \sum_{K=1}^K |\hat{y}^k - y^{(k)}|,$$

$$RMSE = \sqrt{\frac{\sum_{K=1}^K (\hat{y}^k - y^{(k)})^2}{K}}, \quad (25)$$

$$R^2 = \frac{[\sum_{K=1}^K (y^k - \hat{y}_{Ave})(y^{(k)} - \hat{y}_{Ave})]^2}{\sum_{K=1}^K (\hat{y}^k - \hat{y}_{Ave}) \sum_{K=1}^K (y^{(k)} - \hat{y}_{Ave})}.$$

Fuzzy method combined with the class analysis method to evaluate students' self-learning attitude, basic knowledge,

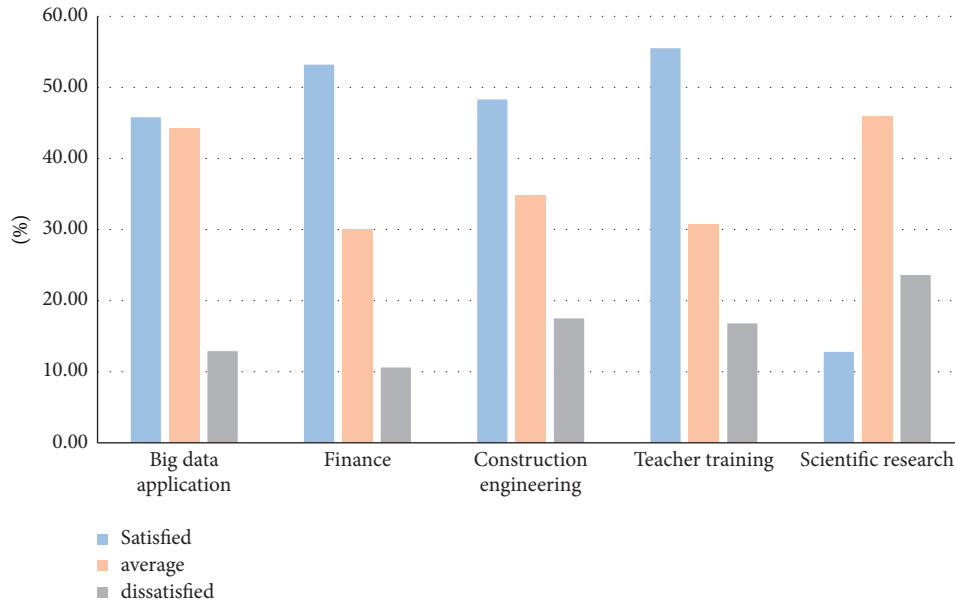


FIGURE 2: Students' satisfaction with the training system of colleges and universities.

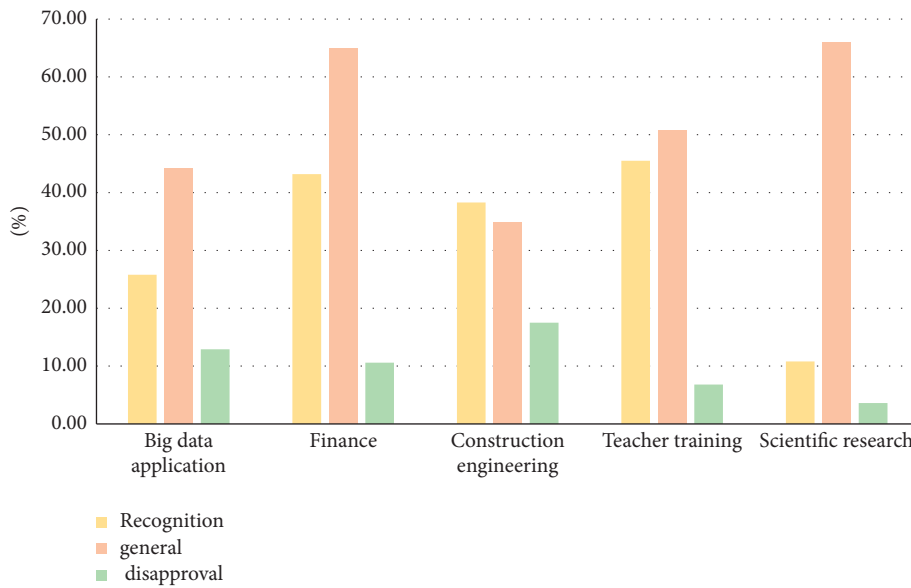


FIGURE 3: Students' recognition of teaching methods in colleges and universities.

cooperation ability, development ability, and professional ability. The research data are shown in Table 2.

Carry out histogram statistics on the data in the above table as shown in Figure 5.

Fuzzy evaluation method evaluates students' self-learning attitude, basic knowledge, cooperation ability, development ability, and professional ability. The research data are shown in Table 3.

Carry out histogram statistics on the data in the above table as shown in Figure 6.

Analytic hierarchy process (AHP) evaluates students' learning attitude, basic knowledge, cooperation ability, development ability, and professional ability. The research data are shown in Table 4.

Carry out histogram statistics on the data in the above table as shown in Figure 7.

4.3. Contrast Experiment. In view of the construction of the talent training system, this paper investigates the students in 5 fields in 20 universities, and use the fuzzy method combined with the hierarchy analysis combination method to construct and apply it. Finally, show whether the model is effective according to their employment situation and compare and analyze the fuzzy evaluation method and the analytic hierarchy process of constructing the talent training system with their combination method, as shown in Figure 8:

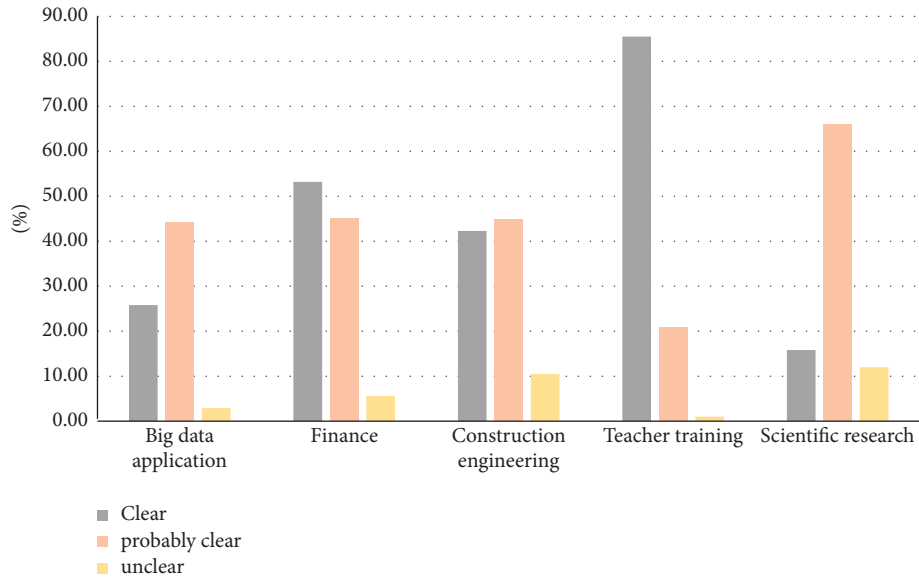


FIGURE 4: Students' clarity on the future development direction.

TABLE 2: Data of error, root mean square error, and determination coefficient of indicators.

Self-influence index	mae	rmse	R^2
Learning attitude	0.218	0.118	0.92
Basic knowledge	0.321	0.128	0.91
Cooperation ability	0.129	0.272	0.88
Development capacity	0.216	0.242	0.86
Professional ability	0.116	0.193	0.82

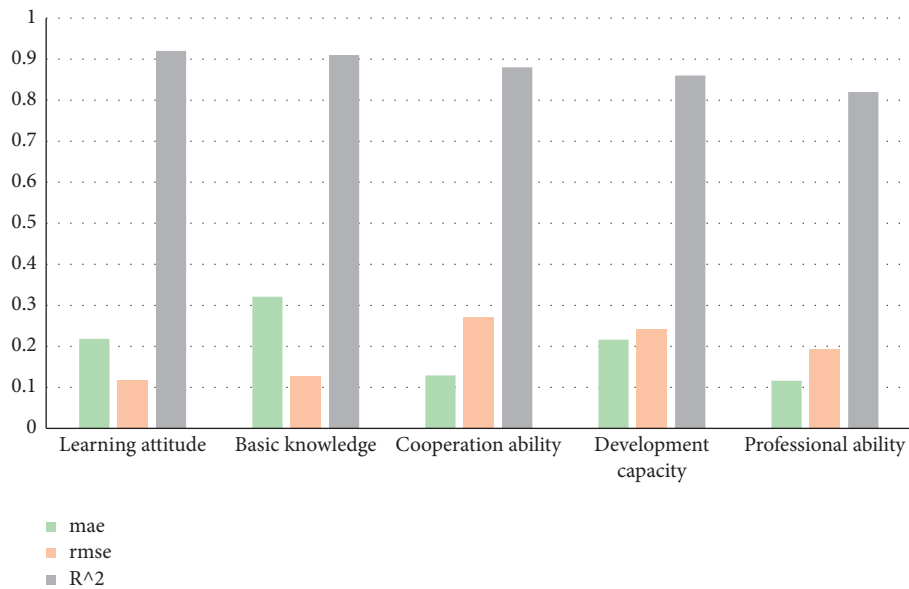


FIGURE 5: Performance analysis of the model on its own indicators.

TABLE 3: Data of error, root mean square error and determination coefficient of indicators.

Self-influence index	mae	rmse	R^2
Learning attitude	0.518	0.518	0.52
Basic knowledge	0.421	0.428	0.51
Cooperation ability	0.529	0.572	0.48
Development capacity	0.516	0.542	0.46
Professional ability	0.416	0.493	0.52

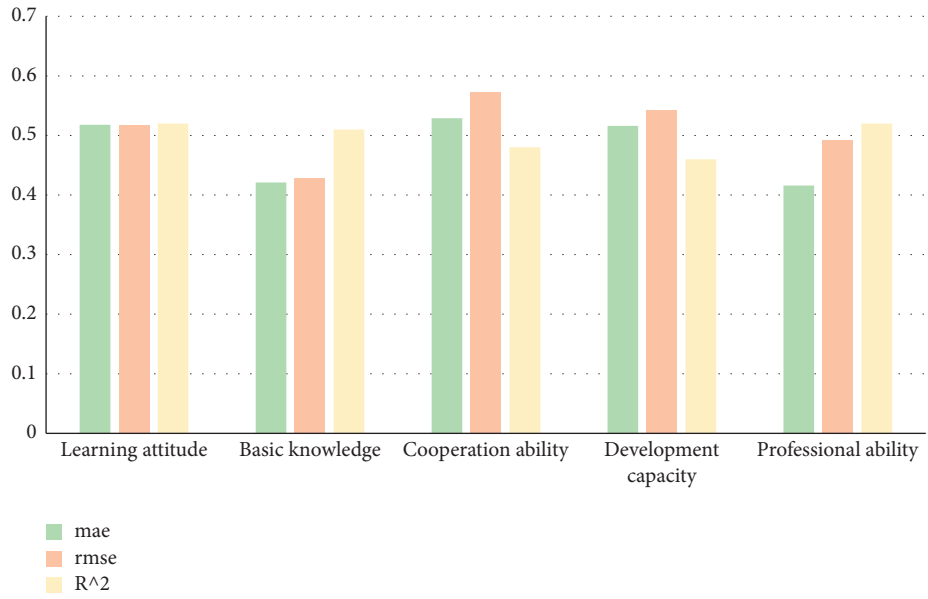


FIGURE 6: Performance analysis of the model on its own indicators.

TABLE 4: Data of error, root mean square error, and determination coefficient of indicators.

Self-influence index	mae	rmse	R ²
Learning attitude	0.428	0.448	0.56
Basic knowledge	0.532	0.318	0.65
Cooperation ability	0.424	0.432	0.66
Development capacity	0.383	0.382	0.58
Professional ability	0.325	0.323	0.59

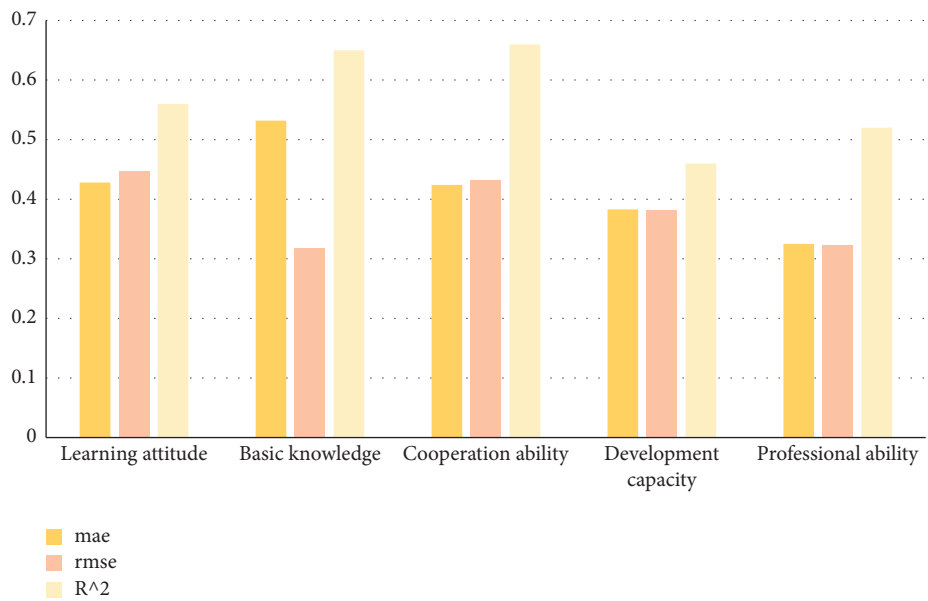


FIGURE 7: Performance analysis of the model on its own indicators.

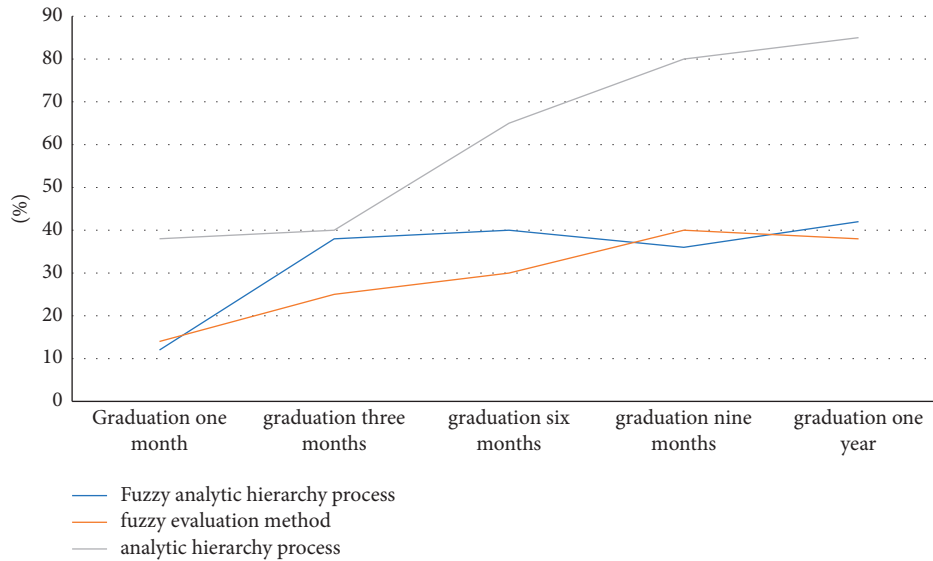


FIGURE 8: Employment situation under the talent training system of three models.

5. Conclusion

The construction of talent education and training system in colleges and universities needs a first-class education system with perfect functions, efficient operation, excellent service, and strong guarantee. Among them, it needs the joint efforts of teachers and students to become the winner in the talent market. Based on the fuzzy method combined with the class analysis and combination method, this paper has the following research results:

- (1) The proportion of students involved in scientific research is the least. We should encourage students to conduct scientific research and strengthen the motherland with the power of science.
- (2) Students in various research fields have low recognition of teachers' teaching methods, and teachers can change their inherent teaching thinking and mode in accordance with their aptitude.
- (3) Fuzzy analytic hierarchy process combined method is superior to the single fuzzy evaluation method and the analytic hierarchy process, and its root mean square error is the smallest, and its determination coefficient is closest to 1.
- (4) In the comparative experiment, the employment situation of students after graduation is used to test whether the talent training system in colleges and universities is effective, and the method advocated in this paper is superior to the other two methods.

Data Availability

The data used to support the findings of this study are available from the corresponding author upon request.

Conflicts of Interest

The authors declare that they have no conflicts of interest regarding this work.

Acknowledgments

This work was supported by the Special Planning Project of Vocational Education Research Institute in 2020 (VER202001).

References

- [1] M. Mokarram and P. Mohammadzadeh, "Prediction of karst suitable Area using fuzzy AHP method and dempster-Shafer theory," *Earth and Space Science*, vol. 8, no. 11, 2021.
- [2] E. Y. Utomo, T. Udjiani, and B. Surarso, "Application of Fuzzy AHP and Fuzzy TOPSIS methods for the new normal problem," *Journal of Physics: Conference Series*, vol. 1943, no. 1, pp. 1–8, 2021.
- [3] U. F. Iroegbu, M. A. Ushie, and B. P. Otiala, "A fuzzy AHP approach for technology transfer problems: a case study of Africa and China partnerships," *American Journal of Industrial and Business Management*, vol. 11, no. 06, pp. 646–663, 2021.
- [4] T. C. Kuo, M. Muniroh, and K. H. Fau, "An integrated Kano model, fuzzy analytical hierarchy process, and decision matrix for sustainable supplier selection in palm oil industries Indonesia, a case study," *Processes*, vol. 9, no. 6, p. 1078, 2021.
- [5] N. Suhrabuddin, K. Matci Dilek, and A. Uğur, "GIS-based wind farm suitability assessment using fuzzy AHP multi-criteria approach: the case of Herat, Afghanistan," *Arabian Journal of Geosciences*, vol. 14, no. 12, 2021.
- [6] C. N. Wang, N. A. T. Nguyen, T. T. Dang, and C. M. Lu, "A compromised decision-making approach to third-party logistics selection in sustainable supply chain using fuzzy AHP and fuzzy VIKOR methods," *Mathematics*, vol. 9, no. 8, p. 886, 2021.
- [7] S. Jiang, "Research on big data audit based on financial sharing service model using fuzzy AHP," *Journal of Intelligent and Fuzzy Systems*, vol. 40, no. 4, pp. 8237–8246, 2021.
- [8] G. Song, "Analysis of the information management system in the manufacturing process of cigarette enterprises using fuzzy AHP," *Journal of Intelligent and Fuzzy Systems*, vol. 40, no. 4, pp. 8257–8267, 2021.

- [9] M. R. Hassanzadeh and C. Valmohammadi, "Evaluation and ranking of the banks and financial institutes using fuzzy AHP and TOPSIS techniques," *International Journal of Operational Research*, vol. 40, no. 3, p. 297, 2021.
- [10] M. Kurniawan, S. Wijana, and E. O. Wilinda, "Application of Craig Harris and fuzzy analytical hierarchy process methods to improve chicken farming productivity at Jimny's farm," *IOP Conference Series: Earth and Environmental Science*, vol. 733, no. 1, Article ID 012042, 2021.
- [11] M. Chowdhury and P. K. Paul, "Identification of suitable sites for rainwater harvesting using fuzzy AHP and fuzzy gamma operator: a case study," *Arabian Journal of Geosciences*, vol. 14, no. 7, pp. 1–19, 2021.
- [12] K. R. Dhillip and V. Nagarajan, "Implementation and performance measure of fuzzy AHP for resource allocation in 5G," *Fluctuation and Noise Letters*, vol. 20, no. 02, 2021.
- [13] B. Esra, "Double skin façade assessment by fuzzy AHP and comparison with AHP," *Architectural Engineering and Design Management*, vol. 17, no. 1-2, pp. 110–130, 2021.
- [14] A. Ishak, R. Ginting, and W. Wanli, "Evaluation of e-commerce services quality using Fuzzy AHP and TOPSIS," *IOP Conference Series: Materials Science and Engineering*, vol. 1041, no. 1, Article ID 012042, 2021.
- [15] Shweta and D. Kumar, "Analysis of issues of generic medicine supply chain using fuzzy AHP: a Pilot study of Indian public drug distribution scheme," *International Journal of Pharmaceutical and Healthcare Marketing*, vol. 15, no. 1, pp. 18–42, 2020.
- [16] R. M. Javier, P. S. David, and G. B. Ana, "Extended fuzzy analytic hierarchy process (E-FAHP): a general approach," *Mathematics*, vol. 8, no. 11, p. 2014, 2020.
- [17] R. Baki, "Evaluating hotel websites through the use of fuzzy AHP and fuzzy TOPSIS," *International Journal of Contemporary Hospitality Management*, vol. 32, no. 12, pp. 3747–3765, 2020.
- [18] Md. Ashek Al Aziz, "A comparative study of AHP and fuzzy AHP method for inconsistent data [J]," *International Journal of Sciences: Basic and Applied Research*, vol. 54, no. 4, pp. 16–37, 2020.
- [19] J. Te Chiang, C. C. Chiou, S. C. Doong, and I. F. Chang, "Research on the construction of performance indicators for the marketing alliance of catering industry and credit card issuing banks by using the balanced scorecard and fuzzy AHP," *Sustainability*, vol. 12, no. 21, p. 9005, 2020.
- [20] D. M. Milošević, M. R. Milošević, and D. J. Simjanović, "Implementation of adjusted fuzzy AHP method in the assessment for reuse of industrial buildings," *Mathematics*, vol. 8, no. 10, p. 1697, 2020.
- [21] B. F. Yildirim and B. Adiguzel Mercangoz, "Evaluating the logistics performance of OECD countries by using fuzzy AHP and ARAS-G," *Eurasian Economic Review*, vol. 10, no. 1, pp. 27–45, 2020.
- [22] M. Zolkepli and T. N. Mohd, "Aris. Fuzzy AHP and TOPSIS in cross domain collaboration recommendation with fuzzy visualization representation," *International Journal of Machine Learning and Computing*, vol. 12, no. 6, 2020.
- [23] J. Liu, Y. Hu, and F. Wang, "A model for evaluating the influence factors in trademark infringement based on fuzzy analytical hierarchy process," *Journal of Intelligent and Fuzzy Systems*, vol. 38, no. 6, pp. 6777–6784, 2020.
- [24] E. Oey, Y. Sekiguchi, and Y. A. Nugroho, "Export country selection with fuzzy AHP and PROMETHEE - a case study of a shoe sole manufacturer," *International Journal of Business Excellence*, vol. 22, no. 2, p. 166, 2020.
- [25] N. Ahmad and A. Qahmash, "Implementing Fuzzy AHP and FUCOM to evaluate critical success factors for sustained academic quality assurance and ABET accreditation," *PLoS one*, vol. 15, no. 9, Article ID e0239140, 2020.

Research Article

Research on Monitoring of Gymnastics Facilities and Intelligent Optimal Distribution of Gymnastics Venues Based on Internet of Things

Hongbo Liu and Yuzhen Wang 

School of Physical Education, Henan Polytechnic University, Henan, Jiaozuo 454003, China

Correspondence should be addressed to Yuzhen Wang; wangyuzhen@hpu.edu.cn

Received 17 April 2022; Revised 30 July 2022; Accepted 9 August 2022; Published 9 September 2022

Academic Editor: Le Sun

Copyright © 2022 Hongbo Liu and Yuzhen Wang. This is an open access article distributed under the Creative Commons Attribution License, which permits unrestricted use, distribution, and reproduction in any medium, provided the original work is properly cited.

In view of the low level of gymnastics facilities monitoring and intelligent management of gymnastics venues, which cannot effectively manage gymnastics venues in real time, this paper proposes a method of gymnastics facilities monitoring and intelligent optimization distribution of gymnastics venues in the Internet of Things. This paper will build an information monitoring model, introduce a particle swarm optimization algorithm to participate in the location layout, and explore the actual effect of gymnastics and the Internet of Things. The research results show that (1) the system can measure the mechanical error of facilities and ensure that the controllable fault tolerance rate is less than 1%. (2) The quality of system monitoring is evaluated in accuracy, time, delay, and satisfaction, and the results are basically satisfactory, but the accuracy and time still need to be improved. (3) Using the evaluation system of sports facilities to test the temperature, humidity, facility pressure, and energy consumption suitable for gymnastics and to verify the injury tendency of athletes. When the damage tendency is between 70% and 100%, the actual damage rate is 1. (4) The speed of the PSO algorithm is faster than other methods, which is used to optimize the layout of gymnastics venues and has a certain role in promoting the construction of gymnastics venues. The system model designed in this paper performs well in gymnastics and needs to be further improved and optimized.

1. Introduction

The Internet of Things era breaks down the barrier between reality and virtuality and launches a great change in intelligent and efficient life. Under the background of the 5G network, all walks of life have entered a new stage of development by applying the Internet of Things, and at the same time, massive data information has been formed, and great progress has been made in connecting everything in the world. From the aspect of sports events and industry development, with the Internet of Things changing life, people's spiritual needs have become rich and diverse, and the attention to sports culture has increased. How to innovate and develop sports on the existing technology has become a new research topic. Gymnastics, as a sport with both aesthetics and mechanics, has high requirements for technology, venues, and facilities in order to avoid injuries to

athletes as much as possible. This paper will face the gymnastics, to build an intelligent Internet of Things system, which can be used for both teaching and scientific research and can also be used for sports events. The system model meets the monitoring requirements of gymnastics facilities and can also be connected with sports facilities through intelligent wearable devices to measure the physical condition of athletes. In addition, we should optimize the location and layout of gymnastics venues and strive for the most intelligent distribution layout.

Because the research on sports in China is still in the preliminary theoretical research stage, there are few references in the application field of the Internet of Things, and the experimental data are missing or incomplete. Therefore, in this case, we read a large number of experiments and cases using modern information technology for reference, so as to build the ideological line of the paper, and hope to fill in the

blank of this research by the content of this article. We use IoT to perceive sports resources for development and utilization and build the application architecture of related content [1]. Using the advantages of data mining and IoT, an intelligent sports health management system is constructed to control physical fitness [2]. H2T Internet of Things is used to monitor heart rate data, and NFC and mobile intelligent devices are used to build a sports evaluation platform [3]. This paper studies the overall structure and system functionality of an intelligent venue system and optimizes the design based on IoT [4]. We optimize various methods and technical routes, integrate them with a physical fitness test, and transform the original equipment and systems [5]. We organize the sensors and application principles of the Internet of Things and apply wearable devices to sports science [6]. This paper expounds the scope and main contents of sports facilities detection and puts forward prospects and suggestions for sports function detection [7]. Taking the public sports facilities of national fitness in Hebei Province as the object, this paper studies the resource allocation and service optimization [8]. We design a model to monitor the emission law of volatile pollutants in large stadiums and gymnasiums [9]. Combined with the concept of low carbon, we plan the resettlement, construction, and service quality of urban community sports facilities [10]. According to the experience and enlightenment of Finnish schools, referring to the result-oriented concept of sports quality monitoring, this paper studies the monitoring framework structure and system operation mechanism [11]. The intelligent management and monitoring system of sports training hall based on the Internet of Things is deeply analyzed and studied [12]. Based on automatic detection technology, sports machinery is detected and processed, and errors are analyzed [13]. Discrete wavelet transform (DWT) and random forest algorithm are used to construct sports injury training set, and the monitoring system of athletes' injury possibility is established [14]. Drawing lessons from the American experience, this paper analyzes the regional distribution characteristics and causes of venues in the four major sports leagues and provides theoretical and practical guidance for optimizing the layout [15]. The Internet of Things proposed in this paper is applied to the monitoring and management of gymnastics facilities, which can effectively improve the intelligence and utilization rate of sports venues. Compared with the application of other Internet of Things scenarios, it lacks the overall design and optimization. There are few application scenarios in sports venues, especially gymnastics venues, and the intelligent effect is not realized from the theoretical point of view and combined with artificial intelligence technology.

Applying Internet of Things technology in gymnastics venues can effectively improve the economic efficiency of venues. In this paper, we consider evaluating the quality of system monitoring in gymnastics venues in terms of accuracy, time, delay, and satisfaction, and the results are basically satisfactory, but the accuracy and time still need to be improved. Using sports facilities evaluation system, the temperature, humidity, facility pressure, and energy consumption suitable for gymnastics are tested to verify athletes' injury tendencies.

2. Theoretical Basis

2.1. Concept of Internet of Things Technology. International Organization for Standardization [16]: The technical term of this technology can be interpreted as "Internet of Things." It first appeared in AUTON-ER Research Center in 1999, which can realize intelligent identification and management and combine sensing devices with the Internet. Nowadays, IoT goes beyond the original traditional network and eliminates the communication restrictions between people. It belongs to a form of information sensing and network integration. It has broad prospects and is widely used in the interactive scenes of "IoT" in all walks of life, showing brand-new vigor and vitality. It uses sensing devices to connect to a network to promote information communication and data exchange between people and things, things and things; with the help of various computer technologies, the requirements of monitoring, identification, intelligent management, and positioning can be perfectly realized. It is worth noting that the Internet of Things industry is a new strategic industry, which still has great potential and room for transformation. The technical standards and commercial development related to it in China are still in the primary stage of development. People's concept of IoT is still vague, and the relatively sophisticated core depends on the introduction of foreign technology, so more efforts should be made in this respect.

Transducer/Sensor [17]: That is, a device can be used for detection. It can change the sensed measurement information into the required information by law and meet the requirements of data collection, storage, and recording. In the special network of IoT, the basic equipment plays a vital role in various sensors. Without sensors to realize automatic detection and control functions, objects cannot be anthropomorphic and have senses such as touch, taste, and vision, and human beings will lose a channel to obtain accurate and reliable information. In this paper, we will install different sensors in gymnastics facilities to detect pressure, temperature, gas, and other aspects in order to create a good suitable sports environment. Then, wearable intelligent sensors are installed on the athletes, which work together with the sensors on the facilities to monitor the physiological signals of the athletes and intelligently analyze the injury possibility of the athletes doing gymnastics based on environmental factors. The sensor hardware architecture realized in this paper can receive the sensor data sent by the microcontrol unit through communication technology and finally present a visual interface for easy viewing as shown in Figure 1.

2.2. DWT and Random Forest Algorithm. DWT [18]: It is called discrete wavelet transform. It can discretize the scale parameters and displacement parameters of the basic wavelet. According to the three-dimensional data collected by sensors, the acceleration data including X, Y, and Z directions are processed, and the characteristics can be processed and summarized by the computer after transformation. Each wavelet is scaled by translation, and the acceleration is

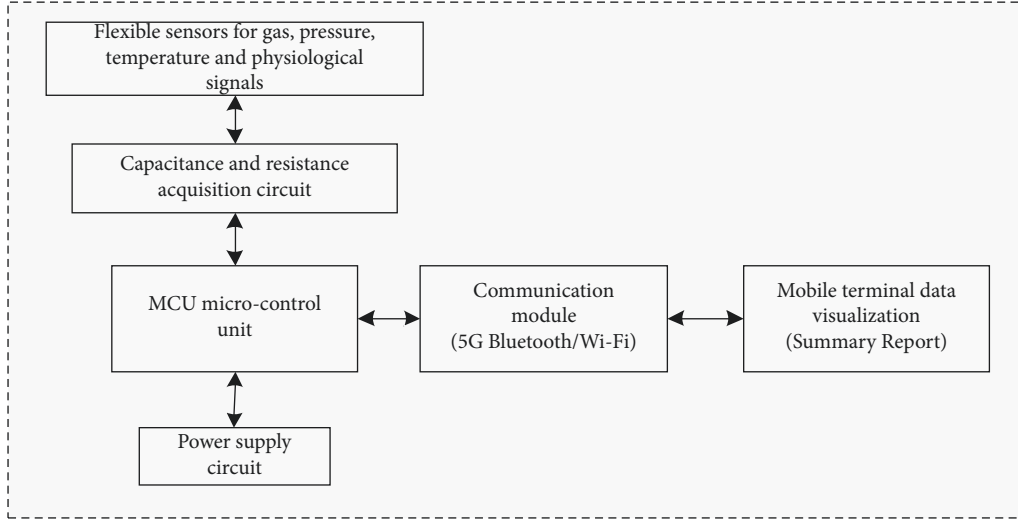


FIGURE 1: Display of sensor data monitoring structure.

replaced by a binary discrete wavelet. Formula (1) sets the total energy release in a period of time as E_1 and decomposes it into i levels, where A_i represents the approximate coefficient of wavelet; A_i^1 represents the result after transposition; D_i represents the actual coefficients of the wavelet. Formula (2) represents the energy ratio of approximate coefficients; formula (3) represents the energy ratio of coefficients in actual cases.

$$E_T = A_i A_i^T + \sum_{j=1}^i D_j D_j^T, \quad (1)$$

$$EDR_A = \frac{A_i A_i^T}{E_T}, \quad (2)$$

$$EDR_{D_j} = \frac{D_j D_j^T}{E_T}, j = 1, \dots, i. \quad (3)$$

This paper introduces how DWT transforms the original three-dimensional acceleration data into binary processable data. We also need to introduce classifiers in machine learning in order to automatically classify the activities of athletes efficiently and accurately so as to effectively monitor the sports situation of athletes and improve the success rate of exploring the possibility of injury. In this paper, the stochastic forest fusion algorithm with the statistical self-sampling method as the ideological root is adopted. A strong predictor [19] is composed of a plurality of weak decision-makers [20]. It has a good performance in practical application. The basic steps of the algorithm are as follows:

- (1) Bootstrap resampling is carried out on the original data to generate training sets, and then, a decision tree is formed

$$T(\theta): \{T(x, \theta_1)\}, \{T(x, \theta_2)\}, \dots, \{T(x, \theta_k)\}. \quad (4)$$

- (2) Achieve maximum prediction [21]
- (3) The observed value X belongs to leaf nodes and is not equal to zero, so the distribution weight is defined

$$\omega_i(x, \theta) = \frac{1\{X_i \in R_{l(x, \theta)}\}}{\{j: X_j \in R_{l(x, \theta)}\}}, i = 1, 2, \dots, n. \quad (5)$$

- (4) Set the sum of the weight values of a single decision tree as 1, and weigh the observed values of each dependent variable

$$\hat{\mu}(x) = \sum_{i=1}^n \omega_i(x, \theta) Y_i. \quad (6)$$

- (5) The predicted values shown in formula (6) are summed up, and the weights of formula (5) are combined to finally obtain the weights of each observed value

$$\omega_i(x) = \frac{1}{k} \sum_{i=1}^k \omega_i(x, \theta_i) Y_i. \quad (7)$$

Finally, the predicted value is obtained.

$$\hat{\mu}(x) = \sum_{i=1}^n \omega_i(x) Y_i. \quad (8)$$

2.3. Facility Site Selection and Site Layout

2.3.1. Address Selection of Site. The construction of gymnastics facilities belongs to the government construction project. Therefore, before formally optimizing the internal layout of the venue, we need to analyze the principle of venue location. Considering the principles of fairness, efficiency, integration, and networking, we should not only ensure the transportation convenience, benefits, facilities, and services of venues but also arrange facilities from the overall situation. Two classical models, P-center [22] and P-median [23], are selected.

(1) *Classical P-Center Model.* This model can embody the fairness principle of venue location and can find the

maximum and minimum distance from any demand point to the location. Let I be the number of demand points, where $i = \{1, 2, 3, \dots, I\}$; J is the number of candidate position points, where $j = \{1, 2, 3, \dots, J\}$; P is the number of newly added sites; d_{ij} is the distance between i and j . Get the mathematical expression of the model:

$$F_1 = \text{Min} \left\{ \text{Max} \sum_{j \in J} d_{ij} y_{ij} \right\} \forall i, \quad (9)$$

$$\text{st. } \sum_{j \in J} y_{ij} = 1, \quad \forall i, \quad (10)$$

$$y_{ij} \leq X_j, \quad \forall i, j, \quad (11)$$

$$\sum_{j \in J} X_j = P, \quad (12)$$

$$X_j \in \{0, 1\}, \quad \forall j, \quad (13)$$

$$y_{ij} \in \{0, 1\}, \quad \forall i, j. \quad (14)$$

Formula (9) refers to minimizing the length between the location points closest to the demand position. Formula (10) assigns each demand point to its nearest location. Formula (11) ensures that each candidate site is equipped with a facility site. Formula (12) indicates that there are P places in the candidate sites. Formulas (13) and (14) indicate binary constraints on variables.

(2) *Classical P-Median Model*. This model was first proposed in 1964 [24]. It mainly reflects the efficiency principle of site selection and calculates the shortest time from each demand point to the selected address. The mathematical expression of the model is obtained. Except for different objective functions, the constraint conditions of the model are the same as those of the P -center model, so it is not listed separately here.

$$F_2 = \text{Min} \sum_{j \in J} \sum_{i \in I} d_{ij} y_{ij}, \quad \forall i, j. \quad (15)$$

2.3.2. *Intelligent Optimal Distribution of Site*. Determining the position of objects [25] is the basis of all layout optimization problems. In this paper, the distribution of sports facilities in gymnastics venues can be simplified as a continuous space layout optimization problem. Taking a venue as an example, the length and width of the venue are H and K , respectively, so it is necessary to set up D sports facilities.

$$F = (f_1, f_2, \dots, f_D). \quad (16)$$

Set the total cost of moving sports facilities in the venue and make mathematical modeling. Solve the minimized objective function:

$$\min C = \sum_{s=1}^S \sum_{j=1}^D \sum_{k=1}^D P^S \cdot Q_{jk}^S \cdot D_{jk}, \quad (17)$$

$$D_{jk} = |x_j - x_k| + |y_j - y_k|$$

$$A_{jk} \cdot B_{jk} = 0.$$

3. Research on the Whole Model Framework

3.1. *Overall Functional Design*. In order to realize the construction of gymnastics venues and facilities, it is necessary to build a system engineering that can support the operation. The system is mainly used to monitor the environmental data of facilities, select the best venue address, and intelligently optimize the venue's spatial layout. The whole system is connected through the Internet of Things, and the system facilities are constructed through intelligent facilities, sensors, intelligent wearable devices, cloud management platform, and ArcGIS system. After completing a series of Internet infrastructures, the system automatically uploads the data of daily movement process to the cloud by using an automatic classification method and can quickly extract, cloud, classify, and exchange data through big data and cloud computing platform. Finally, we can view and use the results through the visual operation interface of the system. The specific design situation is shown in Figure 2.

3.2. *Mechanical Error Diagnosis of Gymnastics Facilities*. Our facilities and equipment for gymnastics are mainly electronic sports machinery. Due to the limitation of technical problems, it is difficult to control the quality of these machines in actual production and operation, so it is easy to cause inaccurate measurement results due to mechanical errors. In this section, we use some measures to detect and analyze the errors of sports facilities and strictly control the product quality of sports facilities. In order to achieve this step, we take the internal hardware circuit as the main research goal and extract error features. Where R is composed of different relative leakage resistors; C is the parallel equivalent of different relative ground capacitors. ω stands for frequency, and φ stands for the phase difference angle between error current and U_0 ; we can use $\tan \varphi$ to represent the mechanical error characteristics, as shown in the following formula :

$$\begin{cases} R = \frac{1}{3/r_0 + 1/r_L}, \\ C = 3C_0, \end{cases} \quad (18)$$

$$I_\delta = \frac{U_0}{R} + j\omega C_0 + \frac{U_0}{j\omega L} = I_R + j(I_C - I_L),$$

$$\tan \phi = \frac{(I_C - I_L)I_R}{I_C I_\delta} RC.$$

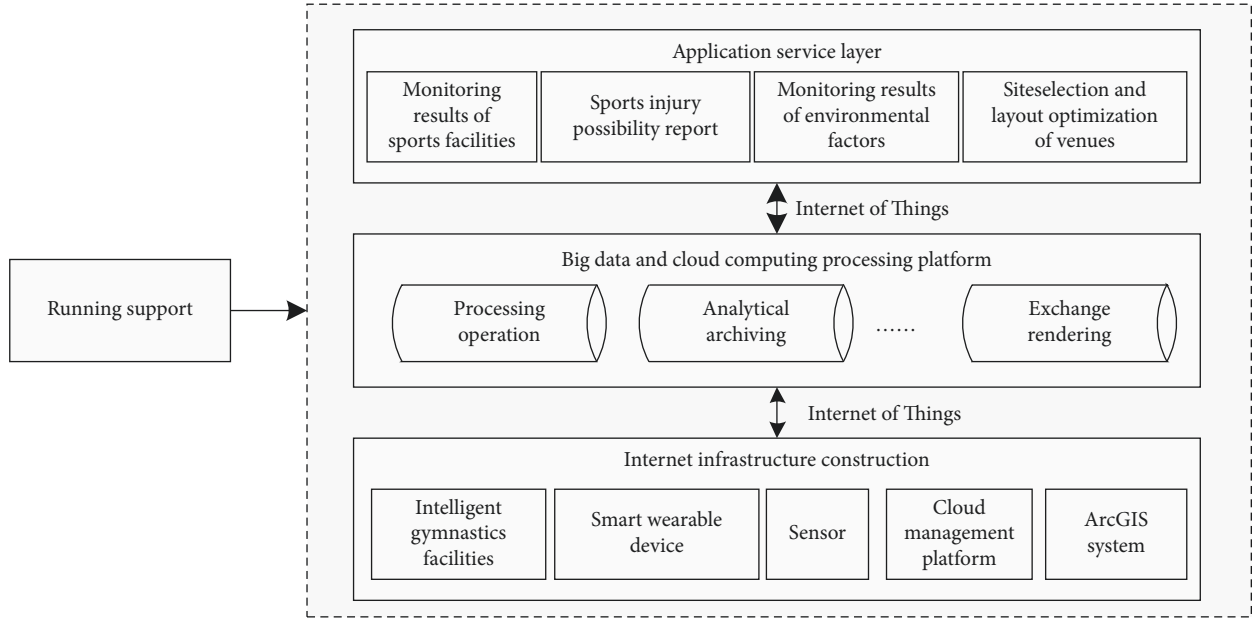


FIGURE 2: Overall architecture of monitoring and optimization facility system.

3.3. Damage Likelihood Monitoring. Based on DWT and random forest algorithm, a large-scale sports injury monitoring database is constructed by fusing the data collected by wearable smart devices and facility sensors. According to the motion monitoring results, various effective motion displacement curves are drawn, and the mechanical feedback of sports injuries is analyzed. Phase shift registration method is adopted.

$$\begin{aligned} x_i^*(t) &= x_i(t + \delta_i), \\ SSE &= \sum_{i=1}^N \int [x_i(t + \delta_i) - \mu(t)]^2 ds. \end{aligned} \quad (19)$$

Read the waveform until it does not change significantly, and get the activity classification. Look at the curve trend of eigenvalue and motion displacement, and discuss whether there is the possibility of injury.

$$SSE_{n-1} \leq SSE_n \approx SSE_{n+1}. \quad (20)$$

3.4. Location and Layout Optimization. Combining P -median and P -center models, considering the original gymnastics facilities, the location function is modified.

$$W = \alpha_1 F_1 + (1 - \alpha_1) F_2. \quad (21)$$

Gymnastics field layout problem needs to be in a certain internal space, and all the equipment and all kinds of resources are needed for gymnastics reasonable organization and layout. Venues need to determine the venues that meet all needs, and set up competition venues, warm-up venues, training venues, and competition platforms according to the level, scale, and athletes of competition or training. In order to ensure that athletes have good space and visual effects, there should be no direct natural light, and the

safe distance and space between edges should be guaranteed. Optimizing the layout of gymnastics venues with PSO intelligence is as follows:

$$P = (x_1, \dots, x_d, y_1, \dots, y_d),$$

$$V = (v_{x1}, \dots, v_{xd}, v_{y1}, \dots, v_{yd}),$$

$$F = \frac{1}{\sum_{s=1}^S \sum_{j=1}^D} \sum_{k=1}^D p^s \cdot Q_{jk}^s \cdot D_{jk} + Pe(i),$$

$$Pe(i) = 1/2 \left(t_1 \cdot (|h(i)| + h(i)) + t_2 \cdot \sum_{b=1}^4 (|g_b(i)| + g_b(i)) \right),$$

$$\omega = \omega_{\max} - \frac{\omega_{\max} - \omega_{\min}}{k_{\max}} \cdot k.$$

(22)

4. Experimental Analysis

4.1. Introduction of Experimental Environment. In this section, we show the software or hardware used in the experimental part as shown in Table 1.

4.2. System Monitoring Test

4.2.1. Mechanical Error Evaluation of Facilities. For all sports equipment, it is impossible to achieve 100% error-free production, and it can be qualified production within an error range. Especially for sports equipment, when the precise value is emphasized, the analysis of electro-mechanical error is also very important for the normal operation of the equipment. In this paper, the mechanical error

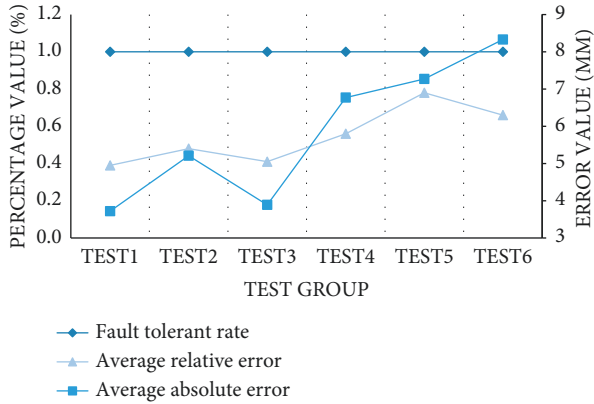


FIGURE 3: Monitoring results of facility accuracy error.

of our control facilities is less than 1% (i.e., fault tolerance rate), and if it exceeds this value, it will be deemed as unqualified. We set up six test groups and got the average relative error value of each group, the unit is millimeter, and the results are not more than 9 mm. Looking at the curve trend in the graph, we can find that the average relative error curve of facilities is below the fault tolerance curve. This means that the average relative error of all test groups is below 1%, which is within the qualified error range. Among them, the fifth test group has the highest error, which can reach 0.78%. The first test group has the lowest error, only 0.39%, as shown in Figure 3.

4.2.2. Monitoring Quality Evaluation. In this section, the main test system monitors the overall quality of the facility, for example, the accuracy of facility test results, the duration, and delay of use. Six kinds of gymnastics facilities that can be monitored are selected, numbered A~F. According to the curve trend in the figure, we can find that the monitoring time of the system is between 5 s and 10 s, and the overall time delay is less than 1.5 s. In terms of accuracy, the results of facilities E and F are all over 90%. Except for facility B, the accuracy is 77.80%, and the test results of other facilities A, C, and D are all between 80% and 90%. In addition, in order to evaluate and monitor sports facilities more professionally and comprehensively, three experts and scholars in related sports fields were invited to conduct a systematic satisfaction evaluation. It can be found that the satisfactory results are between 70% and 90%, and the overall effect is good. However, the monitoring results of A, B, and C facilities are 76.70%, 70.10%, and 78.45%, respectively. Experts think that these three gymnastics facilities still need to be improved as shown in Figure 4.

4.2.3. Evaluation of Monitoring Results. Usually, the temperature of gymnastics training venues is 22–23 degrees, and the humidity index is 22–38. Generally, it can be fine-tuned according to the actual weather conditions of the day. It is necessary to keep the indoor air of the site fresh and free from harmful gases or special gases causing human discomfort. We monitored the sports facilities of gymnastics

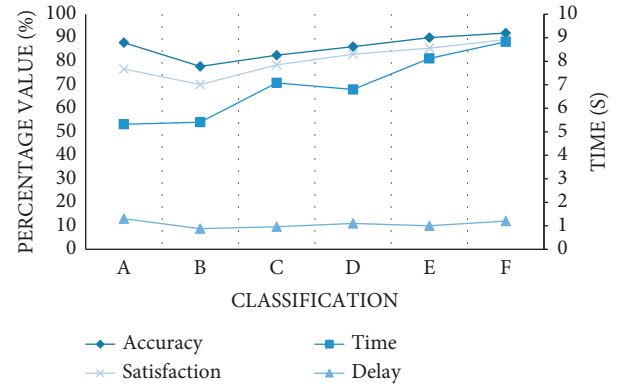


FIGURE 4: Overview of system quality.

venues 1 to 5 and summarized the following results as shown in Table 2.

Subsequently, through the monitoring of wearable intelligent devices, this paper counts the sports injury data of athletes under different gymnastics movements. Need to declare one point is because the gymnastics movement selected in this experiment belongs to more professional and difficult items, the data will be biased, resulting in a higher injury tendency. Let 7 athletes numbered A to G perform 6 gymnastics exercises on sports facilities. The controlled room temperature is 22 degrees, the air wettability is 35 degrees, the gas quality is good, the facility pressure detection and physiological signal detection devices can operate normally, and the energy consumption is in a general state. After testing, the system analyzes the possibility of damage according to the detected data. According to the curve, we find that the actual injury rate of athletes with an injury tendency between 70% and 100% is 100%, which proves the accuracy and effectiveness of monitoring and predicting effects as shown in Figure 5.

4.3. Results and Evaluation of Intelligent Layout Optimization

4.3.1. General Situation of Venue Facilities Selection Location. After selecting the appropriate gymnastics site, the system optimizes the distribution of the facilities intelligently. In this section, the final results are evaluated for three rounds. Score the site location evaluation, overall use efficiency, coverage demand points, layout cost, area utilization rate, and layout comfort and professional qualification. We can find that the location of the venue chosen in this paper is convenient and superior and can cover more demand points, and the use benefit can reach 74%. After optimizing the layout of facilities in the site, the distribution of facilities is more reasonable, with a professionalism of 100%, and both the area utilization rate and comfort are higher than 85% as shown in Figure 6.

4.3.2. Comparison of PSO Optimization Algorithms. In this paper, according to the global optimization, the PSO algorithm is used to plan and integrate all the internal resources or equipment in a given limited stadium to solve the

TABLE 1: Environment configuration.

Software or hardware conditions	Version or model
Microcontroller	ESP32-D0WDQ6, ATmega328P
Sensor	Sn3O4/RGO heterostructure, cotton/RGO/CN composites
Communication technology	5G
GIS technology	ArcGIS 10.5
WIMU	Wearable inertial measurement equipment
Software environment	Python 3.7.4
Aided design software	LabVIEW 2010

TABLE 2: Monitoring of gymnastics facilities.

Venue number	Temperature (degrees)	Wettability	Facility pressure	Gas mass	Physiological signal	Energy consumption
1	22.5	23	Normal	Good	Normal detection	General
2	21.8	35	Normal	Excellent	Normal detection	Larger
3	20.8	24	Normal	Good	Normal detection	General
4	23.1	36	Normal	Good	Normal detection	Smaller
5	22	30	Normal	Excellent	Normal detection	Smaller

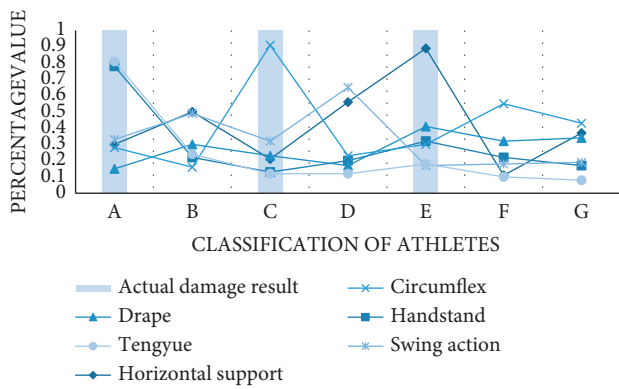


FIGURE 5: Damage monitoring.

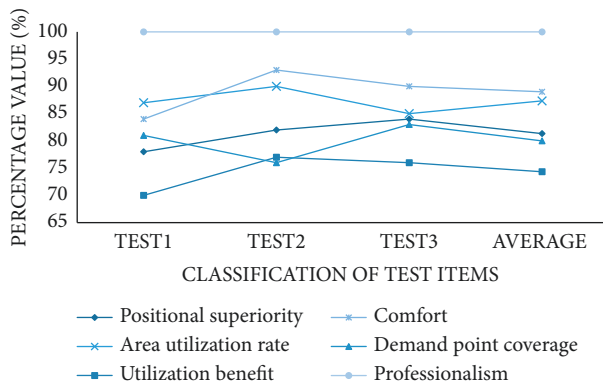


FIGURE 6: Rationality score for site layout optimization.

problem of site distribution. We add the FACOPT algorithm and genetic algorithm to compare the layout results. It can be found that the proposed method can obtain the optimal fitness value under the lower iteration times, and the shortest time is about 3.83 s as shown in Figure 7.

4.3.3. *Optimization Results of Continuous Spatial Distribution.* When optimizing the space of the site, there are usually many design schemes. In order to improve the

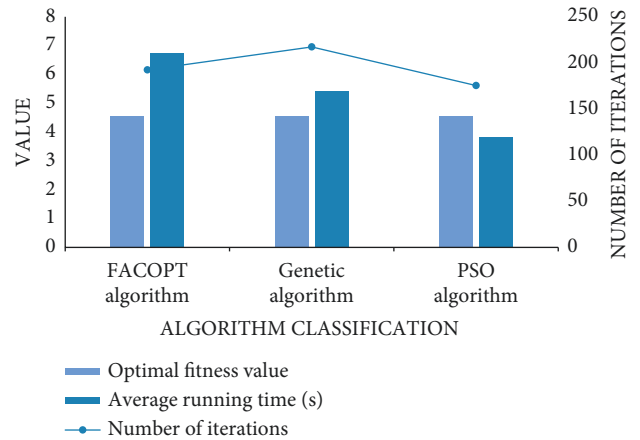


FIGURE 7: Comparison of different algorithms.

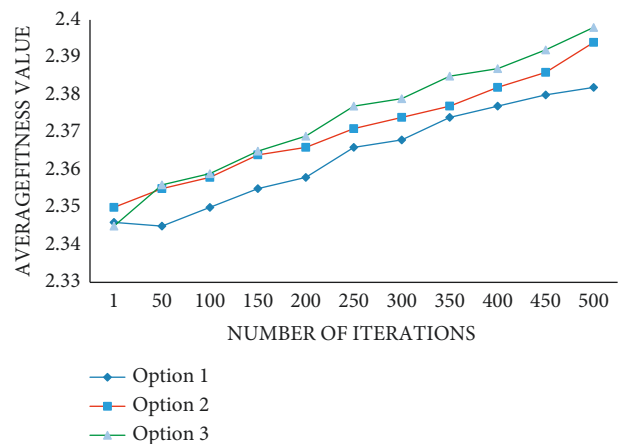


FIGURE 8: PSO optimization process of different schemes.

credibility and reliability of the results, we will go through 500 iterations of different schemes and observe their average fitness values. According to the curve in the figure, we can

know that with the increase in iteration times, the average fitness values of the three schemes also increase. Among them, the effect and advantage of scheme 3 are the most obvious as shown in Figure 8.

5. Conclusion

In this paper, flexible pressure, temperature, physiological signals, and other sensors are used to intelligently collect sports equipment data; wavelet transform and random forest algorithm are used to intelligently monitor gymnastics activities; ArcGIS system and particle swarm algorithm are used to optimize the layout of facilities. The final experimental results show that the application of GIS technology promotes the results of site selection and layout, and the model solution is efficient. Through the sensor data monitoring system, the equipment, environment, and athletes can be detected in real time. The Internet of Things can better improve the management efficiency of facilities and venues for China's sports industry and help to improve the overall level of competition. Although this paper has obtained good experimental data and research results but is affected by various factors and conditions, the research on this subject should be refined, further adjust the system environment and work, and put forward more stringent new requirements. The location of the venue selected in this paper is convenient and superior, which can cover more demand points, and the use efficiency can reach 74%. After optimizing the layout of facilities in the site, the distribution of facilities is more reasonable, the professionalism reaches 100%, and the area utilization rate and comfort are higher than 85%. FACOPT algorithm and genetic algorithm are to compare the layout results. The results show that the method can obtain the optimal fitness value with a low number of iterations, and the shortest time is about 3.83 s.

In the future, the following issues should also be considered: exploring cheap and effective sensor materials to reduce the use cost of Internet of Things technology, coordinating government departments to transform gymnastics venues, planning and construction from a more reasonable point of view; dynamically analyzing the optimal layout of gymnastics venues, site selection should be considered more thoroughly, facility types should be adapted to local conditions, and the layout should be clear according to the user groups and scale; smart wearable devices should be used together with smart devices of monitoring facilities to unify data specifications; learn from advanced technology and experience to further optimize the model algorithm, reduce a large number of complex calculation steps in training and testing, reduce the amount of calculation, and improve the calculation speed.

Data Availability

The experimental data used to support the findings of this study are available from the corresponding author upon request.

Conflicts of Interest

The authors declare that they have no conflicts of interest regarding this work.

Acknowledgments

This work was supported by the Annual Programme in Philosophy and Social Sciences in Henan Province in 2022—Research on the reformation and innovation of system for talent cultivation of integration of sports and education of dominant sports in China.

References

- [1] K. Qiao, G. Wang, and W. Sun, "Perceiving sports: application architecture of Internet of Things technology in sports field," *Journal of Wuhan Institute of Physical Education*, vol. 46, no. 1, pp. 5–13, 2012.
- [2] F. Deng and Y. Fan, "Research on intelligent sports health management system based on big data mining and Internet of things," *Henan Science and Technology*, vol. 40, no. 7, pp. 4–13, 2021.
- [3] T. T. Zhangqian, "Constructing the Internet of Things platform for physical education evaluation based on heart rate monitoring," *Hubei Sports Science*, vol. 37, no. 8, pp. 5–12, 2022.
- [4] T. Huang, "Research on intelligent stadium system based on Internet of things and its development trend," *Sports World, Academic Edition*, vol. 5, no. 08, pp. 172–173, 2018.
- [5] C. Xu, X. Yi, and F. Wang, "Theoretical research and analysis of intelligent military physical fitness evaluation model," *Educational Research*, vol. 4, no. 2, pp. 117–118, 2021.
- [6] H. F. Chang, Y.-S. Lee, and T. Y. Shiang, "Application of wearable technology in sports science," *China Sports Quarterly*, vol. 30, no. 2, pp. 121–127, 2016.
- [7] Y. Zhao and Y. Wang, "On the main contents and development of functional testing of sports facilities in China," *China Science and Technology Information*, vol. 2, no. 6, pp. 100–101, 2012.
- [8] Li Yan, Y. Liu, and W. Song, "Research on resource allocation and service optimization of public sports facilities for national fitness in Hebei Province," *Sports Time and Space*, vol. 5, no. 011, pp. 58–59, 2016.
- [9] X. Yan, "Design and research on dynamic monitoring model of volatile pollutants emission law in large stadiums," *Environmental Science and Management*, vol. 45, no. 8, pp. 5–14, 2020.
- [10] K. Tang, "Analysis of urban sports facilities planning based on low carbon concept—comment on research on urban community sports facilities planning and service quality," *Environmental Engineering*, vol. 39, no. 6, pp. 1–12, 2021.
- [11] Y. Jing, "Research on results-oriented school physical education quality monitoring structure and operation mechanism—Finnish experience and enlightenment," *Journal of Wuhan Institute of Physical Education*, vol. 54, no. 1, 2020.
- [12] H. Qian, "Optimization of intelligent management and monitoring system of sports training Hall based on Internet of things," *Wireless Communications and Mobile Computing*, vol. 2021, no. 2, pp. 1–11, 2021.
- [13] J. Cao, "Mechanical error analysis of sports based on automatic detection technology," *Adhesion*, vol. 44, no. 10, pp. 4–13, 2020.
- [14] Ma Dong, "Research on monitoring system of athletes' injury possibility based on DWT and random forest algorithm," *Journal of Natural Science of Hunan Normal University*, vol. 36, no. 4, pp. 6–13, 2020.
- [15] J. Zeng, J. Wang, and X. Cai, "Regional distribution characteristics and causes of stadiums and gymnasiums in the four

- major American sports leagues from 1960 to 1997--Also on the enlightenment to the optimal layout of stadiums and gymnasiums in China," *Journal of Wuhan Institute of Physical Education*, vol. 49, no. 2, pp. 6–15, 2015.
- [16] J. Hu and Li Wang, "Research on location optimization of urban public sports service facilities based on GIS," *Journal of Harbin Institute of Physical Education*, vol. 31, no. 4, pp. 6–13, 2013.
- [17] Y. Wang, "Research on site selection optimization of public sports facilities based on GIS," *Contemporary Sports Science and Technology*, vol. 9, no. 36, pp. 2–14, 2019.
- [18] Li Zheng and M. Cui, "Preliminary study on site selection planning of community public sports facilities," *Real Estate Guide*, vol. 21, no. 005, pp. 1–16, 2020.
- [19] R. Liu and H. Sun, "Research on the present situation and countermeasures of gymnastics injuries of college students in guiyang--taking guiyang university as an example," *Slam Dunk*, vol. 3, no. 15, pp. 33–35, 2021.
- [20] Xu Zhao, "Analysis of the relationship between sports measurement and evaluation in physical education," *Industry and Technology Forum*, vol. 20, no. 23, pp. 2–14, 2021.
- [21] Z. Zhang, Z. Song, and Y. Fan, "Research on key technologies of five-degree-of-freedom motion error measurement system," *Measurement Technology*, vol. 41, no. 3, pp. 7–12, 2021.
- [22] Y. He, "Research on architecture and key technologies of hybrid networking system," *Wireless Internet Technology*, vol. 18, no. 11, pp. 2–14, 2021.
- [23] Z. Tian and W. Kong, "Main cluster analysis of international physical fitness monitoring research based on CiteSpace," *Fujian Sports Science and Technology*, vol. 40, no. 6, pp. 5–12, 2021.
- [24] Yi Zhang, B. Guangyu, and S. Wu, "Design of a wearable multi-parameter cardiac activity monitoring device," *China Medical Equipment*, vol. 33, no. 3, pp. 4–13, 2018.
- [25] Y. Zhou, "Research on site selection and layout optimization of community public service facilities based on GIS," *Journal of the Hubei Institute of Socialism*, vol. 21, no. 2, pp. 4–14, 2020.

Research Article

SchizoGoogLeNet: The GoogLeNet-Based Deep Feature Extraction Design for Automatic Detection of Schizophrenia

Siuly Siuly ¹, Yan Li ², Peng Wen ³ and Omer Faruk Alcin⁴

¹Institute for Sustainable Industries & Liveable Cities, Victoria University, Melbourne, Australia

²School of Mathematics, Physics and Computing, University of Southern Queensland, Toowoomba, Australia

³School of Engineering, University of Southern Queensland, Toowoomba, Australia

⁴Department of Electrical and Electronics Engineering, Turgut Ozal University, Malatya, Turkey

Correspondence should be addressed to Siuly Siuly; siuly_1976@yahoo.com

Received 22 June 2022; Accepted 8 August 2022; Published 8 September 2022

Academic Editor: Abdul Rehman Javed

Copyright © 2022 Siuly Siuly et al. This is an open access article distributed under the Creative Commons Attribution License, which permits unrestricted use, distribution, and reproduction in any medium, provided the original work is properly cited.

Schizophrenia (SZ) is a severe and prolonged disorder of the human brain where people interpret reality in an abnormal way. Traditional methods of SZ detection are based on handcrafted feature extraction methods (manual process), which are tedious and unsophisticated, and also limited in their ability to balance efficiency and accuracy. To solve this issue, this study designed a deep learning-based feature extraction scheme involving the GoogLeNet model called “SchizoGoogLeNet” that can efficiently and automatically distinguish schizophrenic patients from healthy control (HC) subjects using electroencephalogram (EEG) signals with improved performance. The proposed framework involves multiple stages of EEG data processing. First, this study employs the average filtering method to remove noise and artifacts from the raw EEG signals to improve the signal-to-noise ratio. After that, a GoogLeNet model is designed to discover significant hidden features from denoised signals to identify schizophrenic patients from HC subjects. Finally, the obtained deep feature set is evaluated by the GoogLeNet classifier and also some renowned machine learning classifiers to find a sustainable classification method for the obtained deep feature set. Experimental results show that the proposed deep feature extraction model with a support vector machine performs the best, producing a 99.02% correct classification rate for SZ, with an overall accuracy of 98.84%. Furthermore, our proposed model outperforms other existing methods. The proposed design is able to accurately discriminate SZ from HC, and it will be useful for developing a diagnostic tool for SZ detection.

1. Introduction

Schizophrenia (SZ) is a devastating mental disorder and a progressive neurological disease that causes a significant impact on the quality of life of patients and their families, social environments, and healthcare systems [1]. This disorder affects a person’s perception of reality, social interactions, thought processes, and cognitive ability. Symptoms of SZ include hallucinations (hearing voices or seeing things that are not there), delusions (fixed, false beliefs), and thought disorders (unusual ways of thinking), as well as reduced expressions of emotions, reduced motivations to accomplish goals, difficulty in social relationships, motor impairments, and cognitive impairments

[2, 3]. SZ affects every 1 in 100 Australians and approximately 21 million people worldwide [4, 5]. It is associated with increased morbidity and mortality, and is the cause of disability and health costs worldwide [6]. SZ is treatable, but its treatment involves long-term medications, causing an extreme burden on healthcare systems and families. If the patients are not treated, SZ symptoms may be persistent which makes them disabled after a period of time. If early detection is possible, then patients can get timely treatments that can help those affected individuals and their families improve their lives [7]. Hence, there is a growing demand to develop an efficient and automatic diagnostic technique for the early detection of SZ patients from healthy control (HC) people.

Traditionally, the diagnosis of SZ is mainly performed through solely interviews and observations of patient behavior by a trained psychiatrist [8]. This diagnosis is a manual process that is time-consuming, burdensome, and subject to human errors and bias. Instead of this, recently, some imaging techniques, such as magnetic resonance imaging, computed tomography, positron emission tomography, and electroencephalography (EEG) have been introduced to diagnose SZ. Among these imaging techniques, currently, EEG has emerged as the reference standard for diagnosing SZ due to its high temporal resolution, noninvasiveness, and relatively low financial cost compared to other tests [2, 9]. EEG signals describe the electrical activity of the human brain recorded from the scalp via a set of electrodes. EEG recording generates a huge volume of data. Generally, this massive amount of data is analysed by visual inspection, which is time-consuming, error-prone, and reduces decision-making reliability. Thus, a computer-aided automatic data analysis system is required to make an accurate and reliable decision for the diagnosis of SZ.

1.1. Related Works. In recent years, many researchers have attempted to identify SZ from EEG data [10–18], but no efficient and reliable system has been developed yet for the reliable detection of SZ patients. Much research has been performed based on traditional handcrafted feature extraction methods, but they were inadequate in their ability to generate suitable performance for real-time applications. For example, Sabeti et al. [10] used autoregressive (AR) model coefficients, band power, and fractal dimension-based features for identifying SZ subjects. These features were fed to linear discriminant analysis (LDA), multiLDA, and adaptive boosting (AdaBoost) classifiers. An empirical mode decomposition (EMD) technique was introduced in [2] for the diagnosis of SZ from EEG signals to handle the behavior of nonstationary and nonlinear EEG signals. In [11], Ramos et al. employed power spectral density-based features in the maximum likelihood theory for classifying SZ and HC subjects.

Kaplan et al. [12] used spectral features, and the obtained features were classified using the “Kora-N” algorithm. A fast Fourier transformation (FFT)-based feature extraction process was reported by Buettner et al. in [13]. Finally, those features were used as input to a random forest (RF) classification method for identifying SZ and non-SZ. Approximate entropy, Shannon entropy, Kolmogorov complexity, and Lempel-Ziv complexity methods were proposed by Akar et al. in [14] for extracting features from EEG signals for identifying SZ. In their another work, Akar et al. [15] computed features using wavelet transformation (WT) and Welch power spectral density (PSD) methods for the detection of schizophrenia from EEG data. In [16], Li et al. used functional EEG networks to extract the inherent spatial pattern of the network (SPN) feature for brain states. The combined SPN features of the rest and task networks were used as the input to LDA and the support vector machine (SVM) to recognize SZ.

Only a few studies have been performed on deep learning for the detection of SZ using EEG data. In deep

learning, both the feature extraction and classification processes are conducted automatically, while traditional techniques require features to be extracted manually. Phang et al. [17] proposed a deep convolutional neural network (CNN) framework for the classification of SZ. In that model, the authors integrated the features from various domains and dimensions using different fusion strategies, and the model achieved 93.06% accuracy. An eleven-layered CNN model was introduced by Oh et al. in [18] to analyse the EEG signals for the diagnosis of schizophrenia. The model generated a classification accuracy of 81.26% for subject-based testing.

1.2. Motivations. Most of the existing research studies for SZ detection employ handcrafted feature extraction methods (e.g., WT, FFT, EMD, PSD, and entropy) before classification [10–16]. These feature extraction methods are manually chosen based on researchers’ expertise. The obtained performances of those methods are not satisfactory. The handcrafted feature extraction methods cannot form intellectual high levels of representations of EEG signals to discover deep concealed characteristics from data that can achieve better performance. This manual feature extraction process is time-consuming, labor-intensive, and has bias. Furthermore, if sizes of data are large, the method may not run properly and sometimes underperform.

As mentioned before, very few studies used deep learning methods for the detection of schizophrenia from EEG [17, 18]. The significant characteristic of deep learning is that the model can automatically extract effective features, which has certain advantages for large-scale data. The developed deep learning-based SZ detection methods are still limited in their ability to balance efficiency and accuracy. Hence, this study is motivated to introduce a new deep learning-based feature extraction scheme for automatic and efficient identification of SZ patients using EEG.

1.3. Objectives of This Study. The key objective of this study is to introduce a deep learning-based feature extraction scheme involving the GoogLeNet model called “SchizoGoogLeNet” for automatically and efficiently distinguishing schizophrenic patients from HC subjects using EEG data with improved performance. The reason for considering the GoogLeNet model in this study is that the GoogLeNet architecture has the ability to produce better performance than other deep learning models as it is designed to be a powerhouse with increased computational efficiency. This model trains faster than other network methods (e.g., AlexNet and VGGNet) and has fewer parameters and lower computational complexity than other models [19, 20]. Also, it has a relatively lower error rate than other deep learning methods.

To our knowledge, for the first time, GoogLeNet was introduced in SZ detection using EEG signals in this study. Our proposed “SchizoGoogLeNet” framework consists of several steps. First, this study employs an average filtering method to remove noise and artifacts from the raw EEG signals. Second, significant hidden features are extracted from EEG signals to identify schizophrenia patients from

HC subjects. Finally, a sustainable classification method for the obtained deep GoogLeNet features is explored. At this stage, deep learning and machine learning methods are tested for the obtained deep feature set. The performance of the proposed framework was tested using a publicly available EEG dataset.

1.4. Our Contributions. The main contributions of this work are summarized as follows: (1) For the first time, we introduce a GoogLeNet-based deep feature extraction scheme for automatic detection of SZ using EEG signals; (2) we investigate the impact of balance and unbalanced datasets on the proposed SZ detection model; (3) we discover a sustainable classifier for the obtained GoogLeNet deep feature set in a deep learning and machine learning environment; (4) we explore the performances of the deep feature set with a GoogLeNet classifier and several machine learning methods; (5) we achieve improved performances for our proposed model compared to those of the existing methods.

The rest of this paper is arranged as follows: The proposed methodology is described in Section 2. This section also provides the description of the data that is used in this study. Section 3 provides the experimental setup and the results with their corresponding discussions, followed by the conclusion in Section 4.

2. Proposed Methodology

This study proposes a GoogLeNet-based deep feature extraction scheme, “SchizoGoogLeNet,” for detecting SZ from EEG data automatically. Figure 1 graphically presents the general architecture of the proposed strategy. The proposed scheme involves four stages, such as data acquisition, removing noise and artifacts using average filtering, discovering deep features using GoogLeNet, and exploring sustainable classifiers for the obtained features. A detailed description of these steps is provided below.

2.1. Data Acquisition. This study used EEG data collected from 81 subjects, including 49 schizophrenia patients and 32 normal control persons, from the Kaggle data source. These data consist of EEG recordings of 14 female and 67 male subjects. The average age is 39 years, and the average education level is 14.5 years. The EEG data were recorded from 64 scalp sites and 8 external sites using a BioSemi active two system (<http://www.biosemi.com>). The data were continuously digitized at 1024 Hz and referenced offline to averaged earlobe electrodes. The details of the dataset can be seen online at <https://www.kaggle.com/broach/button-tone-sz> [21]. The description of the data is also available in [22].

2.2. Removing Noise and Artifacts Using Average Filtering. This section aims to introduce a technique for reducing noise and artifacts of EEG signals and improving the signal-to-noise-ratio (SNR) as the signal data are very noisy and often affected by artifacts. Due to noise, EEG signals have a low SNR that may lead to incorrect conclusions. The noise-

removing processes improve the data quality to create an appropriate model. In this study, we employ an average filter (AF) technique for removing noise and artifacts from EEG signals [23]. The reason for using this filtering is that it is simple, intuitive, and easy to implement for smoothing the signals and for dropping the amount of intensity variations that can reduce undesirable information from the signals.

In this study, we reduced noise smoothing of each signal (Sg) by the AF technique with a kernel size of $KS = 12$, and then, we sampled the smoothed signal considering an interval length $IL = KS = 12$ which is denoted as $\hat{S}g$. We selected the values of KS and IL using a trial and error procedure to make the final matrix with a size of around 200. After the filtering, the raw signal data become the input matrix in the feature extraction stage of the GoogLeNet model (discussed in the next step). Figure 2 shows an example of the pattern of a raw EEG signal and a filtered EEG signal. It is apparent from Figure 2 that the shape of the filtered signal is the same as that of the raw signal. As can be seen in Figure 2, the number of data points has been reduced while still keeping the shape of the original curve of the EEG signal.

$$\overline{Sg}(t) = \frac{1}{KS} \sum_{i=t-KS/2}^{t+KS/2} Sg(i). \quad (1)$$

$$\hat{S}g(t) = \sum_{i=0}^L \delta(i - t \cdot IL) \cdot \overline{Sg}(i). \quad (2)$$

2.3. Discovering Deep Features Using GoogLeNet. Technically, a feature represents a distinguishing property, a recognizable measurement, and a functional component obtained from a segment of a pattern [24]. Extracted features convey the most important information for the classification stage. Sometimes, traditional handcrafted features cannot convey meaningful information about the SZ detection due to manual choice of methods and also cannot handle big sizes of data. This section’s goal is to discover the significant feature set from EEG signals using the deep learning method that empowers efficiently the recognition of SZ from HC subjects. For this purpose, this study introduces the deep GoogLeNet-based architecture to extract representative features for identifying SZ from the denoised EEG signals automatically. To our knowledge, for the first time, GoogLeNet is employed in this study for the detection of SZ from EEG signals. GoogLeNet is a convolutional neural network (CNN)-based architecture designed by researchers at Google. It was the winner of ImageNet 2014, where it proved to be a powerful model.

The main objective of the GoogLeNet architecture is to achieve high accuracy with a reduced computational cost [19, 20]. The GoogLeNet model is constructed based on the inception architecture that introduced the new concept of the inception block in CNN, whereby it incorporates multiscale convolutional transformations using split, transform, and merge ideas [20]. A general strategy of the inception block is illustrated in Figure 3. The inception

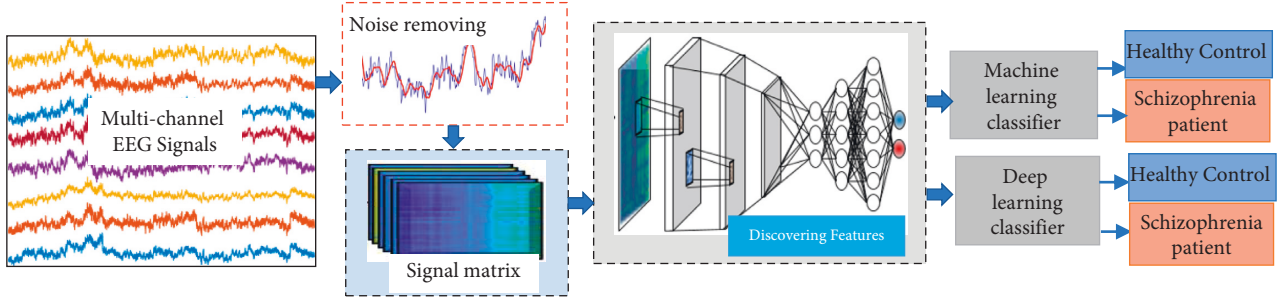


FIGURE 1: The overall architecture of the proposed “SchizoGoogLeNet” framework for automatic identification of SZ from EEG signals.

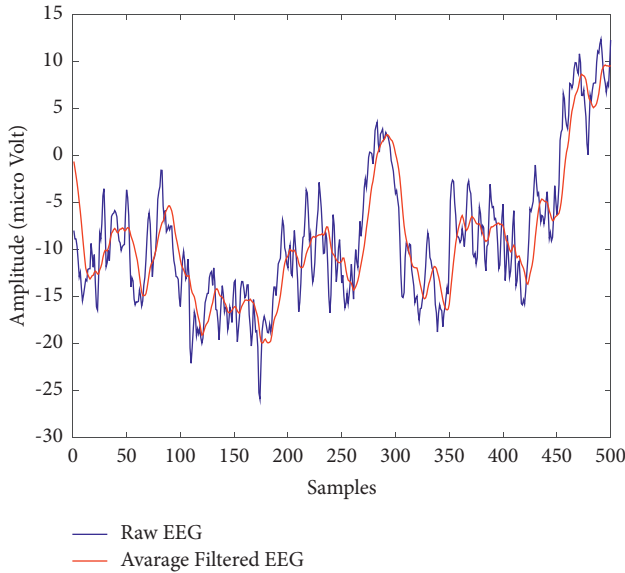


FIGURE 2: An illustration of the pattern of a raw EEG and filtered EEG signal.

module is different from other deep learning architectures where there is a fixed convolution size for each layer. In the inception module, 1×1 , 3×3 , and 5×5 convolutions and 3×3 max pooling perform in a parallel way at the input, and the output of these is stacked together to generate the final output. In the GoogLeNet model, conventional convolutional layers are replaced with small blocks. These blocks condense filters of different sizes (e.g., 1×1 , 3×3 , and 5×5) to capture spatial information at different scales, including both fine and coarse grain levels [19, 20]. As shown in Figure 3, multiple convolutions, with 1×1 filters, 3×3 filters, and 5×5 filters, and 3×3 max-pooling layers are organised in the GoogLeNet model.

The GoogLeNet model regulates the computations by adding a bottleneck layer of 1×1 convolutional filters before employing large-size kernels. 1×1 convolution is used to decrease the number of parameters (weights and biases) of the architecture. Furthermore, it uses sparse connections (not all the output feature maps are connected to all the input feature maps) to overcome the problem of redundant information and reduced costs by omitting feature maps that are not relevant [20]. Additionally, connection density is reduced by using global average pooling at the last layer

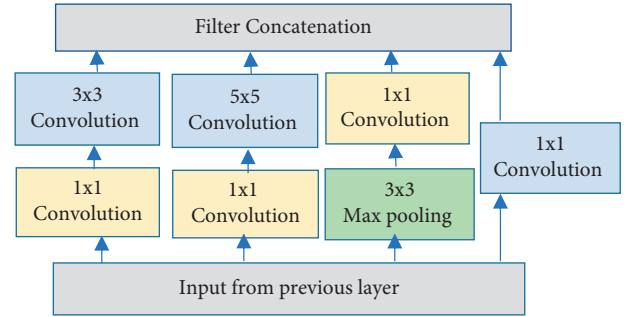


FIGURE 3: General architecture of the inception block.

instead of using a fully connected layer. These parameter tunings cause a significant decrease in the number of parameters [25].

In this study, we designed the structure of the GoogLeNet model for implementation of the SZ EEG database as illustrated in Table 1. This table presents layer-by-layer architectural details of the GoogLeNet model. “ 1×1 # 3×3 # 5×5 ” refers to various convolution filters used within the inception module. “ 3×3 reduce” and “ 5×5 reduce” symbolize the number of 1×1 filters in the reduction layer used before related convolution layers. The number of 1×1 filters in the projection layer after the built-in maximum pooling is shown in the “pool projection” column (denoted as “Pool proj”). “Max pool” stands for the maximum number of pooling layers. The purpose of these max-pooling layers is to downsample the input as it is fed forward through the network. All the convolution, reduction, and projection layers inside this architecture use rectified linear units (ReLUs) as their activation functions. This architecture is 22 layers deep without pooling (or 27 layers when we count pooling) [19, 20].

2.4. Exploring Sustainable Classification Method for Identifying Schizophrenia. This section’s aim is to discover a sustainable classifier for the obtained deep feature set to classify SZ and HC subjects and improve its performance. Unlike other deep learning models, GoogLeNet does not use fully connected (fc) layers for the final result of classification. Instead, the last convolutional map is subjected to channel-wise global average pooling, and the average activation values of each of the channels are used as the feature vector of the input image.

TABLE 1: Model architecture of GoogLeNet used in this study.

Layer	Patch size/stride	Depth	#1 × 1	#3 × 3 reduce	#3 × 3	#5 × 5 reduce	#5 × 5	Pool proj	Output size
Conv1	7 × 7/2	1							112 × 112 × 64
Max pool1	3 × 3/2	0							56 × 56 × 64
Conv2	3 × 3/1	2		64	192				56 × 56 × 192
Max pool2	3 × 3/2	0							28 × 28 × 192
Inception-3a		2	64	96	128	16	32	32	28 × 28 × 256
Inception-3b		2	128	128	192	32	96	64	28 × 28 × 480
Max pool3	3 × 3/2	0							14 × 14 × 480
Inception-4a		2	192	96	208	16	48	64	14 × 14 × 512
Inception-4b		2	160	112	224	24	64	64	14 × 14 × 512
Inception-4c		2	128	128	256	24	64	64	14 × 14 × 512
Inception-4d		2	112	144	288	32	64	64	14 × 14 × 528
Inception-4e		2	256	160	320	32	128	128	14 × 14 × 832
Max pool4	3 × 3/2	0							7 × 7 × 832
Inception-5a		2	256	160	320	32	128	128	7 × 7 × 832
Inception-5b		2	384	192	384	48	128	128	7 × 7 × 1024
Average pool5	7 × 7/1	0							1 × 1 × 1024
Dropout (40%)		0							1 × 1 × 1024
Fc		1							1 × 1 × 2
Softmax		0							1 × 1 × 2
Classification output									1 × 1 × 2

As can be seen in Table 1, the last four layers of our proposed architecture are as follows: a dropout layer set with a probability of 40% dropout, a fully connected (fc) layer, a softmax layer, and a classification output layer. The softmax layer is a final layer of the model that uses the softmax function, and an activation function is used to derive the probability distribution of a set of numbers within an input vector. The output of a softmax activation function is a vector in which its set of values represents the probability of a class or an event occurrence. The classification output layer is set to have the same size as the number of classes in the new dataset, which was two (e.g., SZ and HC) in our case. Before training GoogLeNet, training parameters were set after empirical evaluation. In our experiments, two parameters were used to access the performance of the networks: maximum epochs and batch size.

To determine an appropriate classifier for the obtained deep GoogLeNet feature set, this study also tested four machine learning classification methods: SVM, k-nearest neighbour (KNN), decision tree (DT), and linear discriminant analysis (LDA) for identifying SZ from HC subjects. The reason for the choice of these classifiers in this study is due to their popularity, simplicity, and effectiveness in implementation. They are also very powerful and fast learning algorithms that examine all their training inputs for classification. The description of these methods is available in [26–30].

2.5. Performance Evaluation Parameters. To fairly assess the performance of the proposed models, we computed all standard measurement parameters including the accuracy, sensitivity, specificity, positive predictive value, false alarm rate, F1-score, and the receiver operating characteristic curve (ROC) in this study. The descriptions of the mentioned measurements are available in [28, 31–35].

3. Experiments and Results

3.1. Experimental Setting. In this study, we performed all the experiments in MATLAB (2018b) on a PC with a six-core Intel i7 processor and 32 GB of memory. The server was equipped with an NVIDIA RTX 2060 GPU with 6 GB of memory. We run the GoogLeNet model in the MATLAB deep learning toolbox for our proposed design. As stated before, the dataset includes a total of 81 subjects, where 32 cases are normal control (with 3108 trials; 3072 samples per trial; 70 channels) and 49 cases are schizophrenia patients (with 4608 trials; 3072 samples per trial; 70 channels). In this study, we used all 70 channels' data for the proposed design. Here, we provide an example how we processed the raw EEG signal data of each subject and transformed the processed dataset for implementation in the experiments in this study. For example, for Subject 1, we had a dataset: 887808 × 70 (samples × channels), and we converted this dataset to a matrix sized 70 × 3072 × 289 (channels × window length × epoch) using the transpose process. Here, we obtained epoch = 289 dividing samples by window length (887808/3072). After the average filtering, the raw signal data matrix 70 × 3072 × 289 was moved to a reduced matrix size of 70 × 256 × 289. Afterward, the 70 × 256 × 289 matrix was resized to 224 × 224 × 3 × 289 to be compatible with the deep GoogLeNet input size for subject 1.

Following a similar process, for a total of 81 subjects, the whole dataset was transformed into an image matrix with a size of 224 × 224 × 3 × 23201 (height × weight × 3 symbolize color layer × image samples). The sizes of data for SZ and HC are 224 × 224 × 3 × 13975 and 224 × 224 × 3 × 9226, respectively, which shows that the sample points of SZ and the HC groups are not equal. Thus, we divided the dataset into two groups: balanced and unbalanced datasets to test the effect of equal and unequal sizes of sample points in SZ and HC categories. A balanced dataset is one that has the same

number of observations for each class in a classification dataset. An unbalanced dataset has the different number of observations for each class. Both SZ and HC categories in this study's balanced dataset have the same number of sample points; however, both categories in the unbalanced dataset have an unequal number of sample points. As seen in Table 2, the balanced dataset consists of 9226 sample points in each category of SZ and HC (including training, validation, and testing data), and total sample points for both categories are 18,452.

In the unbalanced dataset, the SZ category has 13,975 sample points and the HC category has 9,226 sample points (including training, validation, and testing data). The total sample point size for the unbalanced data is 23,201. Please note that the unbalanced dataset is the original dataset after data preprocessing. Thus, the balanced data size is $224 \times 224 \times 3 \times 18452$ (height \times weight \times 3 symbolize color layer \times image samples), and the unbalanced data size is $224 \times 224 \times 3 \times 23201$ (height \times weight \times 3 symbolize color layer \times image samples). Then, both datasets are divided into three parts: training, validation, and testing with a ratio of 70%, 10%, and 20%, respectively. The sizes of different parts of data are given in Table 2. In this study, the training dataset was used for the learning process in the proposed model, and the validation dataset was regarded as a part of the training set to tune the model. The validation set was used for tuning the parameters of the model and also for avoiding overfitting. Generally, the validation dataset helps provide an unbiased evaluation of the model's fitness. The testing dataset was used for the performance evaluation.

3.2. Feature Extraction Process and Hyperparameter Setting.

This section presents the process of how the features are extracted using the GoogLeNet model for the balanced and unbalanced datasets. Figure 4 shows the feature extraction process in the GoogLeNet model for the balanced dataset and unbalanced dataset. As seen in Figure 4, the proposed GoogLeNet model yields a deep feature set with a size of 18452×2 for the balanced dataset and 23201×2 for the unbalanced dataset. It means that two deep features are generated, including 18,452 sample points for the balanced dataset and 23,201 for the unbalanced dataset. In both datasets, two deep features are called deep feature1 and deep feature 2.

Figures 5 and 6 present the patterns of the distribution of the obtained two deep features (deep feature 1 and deep feature 2) for the balanced and unbalanced datasets through boxplots, respectively. As can be seen in both figures, the shape of the distribution in both schizophrenia and control groups are symmetrical and there are some outliers in each diagram. In both figures, it is observed that there is a significant difference between the central value of schizophrenia and control groups in both feature sets. The boxplot figures clearly demonstrate that there is a clear and significant difference in the values of the feature set in two groups that help in the efficient classification of schizophrenia and control.

To find the best model, the hyperparameters (e.g., the number of hidden units, the number of epochs, and the batch size) of the GoogLeNet model are optimized (tuned) by the training process. We run the data through the operations of the model, compare the resulting prediction with the actual value for each data instance, evaluate the accuracy, and adjust until we find the best values. We performed an extensive number of experiments to find appropriate values for different parameters. The configuration of hyperparameters of the proposed model is provided in Table 1. The table illustrates the layer-by-layer structural details of the proposed "SchizoGoogLeNet" model.

In this study, the SVM classifier with a linear kernel was used as an optimal kernel function after testing all the kernels (e.g., linear, polynomial, and radial basis kernels) because this kernel produced a better performance compared to others. The KNN classifier used the default distance metric "Euclidean distance" for the distance measure and $K=1$ in the model after several experimental evaluations. For DT and LDA classifiers, the parameter values are considered which have been used in MATLAB default parameter settings as there are no specific guidelines for setting the values of the parameters for these classifiers.

3.3. Results and Discussion. This section provides the experimental results that are achieved using 10-fold cross-validation through MATLAB. For both balanced and unbalanced datasets, we used the obtained deep feature set as an input to the softmax classifier of GoogLeNet (deep learning (DL) classifier) and also four popular machine learning (ML) classifiers (SVM, KNN, DT, and LDA), separately, to find an optimal classifier. Tables 3 and 4 present the overall performance results for our proposed approaches in terms of the sensitivity (SEN), specificity (SPE), accuracy (ACC), positive predictive value (PPV), and $F1$ -score for the balanced and unbalanced datasets, respectively.

As can be seen in Table 3, for the balanced dataset, the SVM classifier achieves the highest performances such as ACC (98.30%), SPE (98.27%), PPV (98.27%), and $F1$ -score (98.30%), and the LDA classifier produces the highest sensitivity value (98.53%). The lowest performances (e.g., ACC (94.28%), SEN (92.15%), SPC (96.42%), PPV (96.26%), and $F1$ -score (94.16%)) are obtained by the GoogLeNet classifier (DL classifier). For the unbalanced dataset, Table 4 reports that among the reported classifiers, the highest classification performances are attained by the SVM classifiers, which are 98.84% of ACC, 99.02% of SEN, 98.58% of SPE, 99.06% of PPV, and 99.04% of $F1$ -score. On the other hand, the lowest performance (e.g., ACC (95.09%), SEN (93.81%), SPC (97.02%), (PPV 97.95%), and $F1$ -score (95.83%)) are obtained by the GoogLeNet classifier like the balanced dataset.

In order to further assess, we also computed the false alarm rate (FAR) of the proposed classification models for the balanced and unbalanced datasets as shown in Figure 7. This figure also demonstrates that the SVM classifier produces better performance (a lower FAR indicates better

TABLE 2: The sizes of different parts of data.

Data	Category	Training data	Validation data	Testing data
Balanced	HC	$224 \times 224 \times 3 \times 6458$	$224 \times 224 \times 3 \times 922$	$224 \times 224 \times 3 \times 1846$
	SZ	$224 \times 224 \times 3 \times 6458$	$224 \times 224 \times 3 \times 922$	$224 \times 224 \times 3 \times 1846$
	Total	$224 \times 224 \times 3 \times 12916$	$224 \times 224 \times 3 \times 1844$	$224 \times 224 \times 3 \times 3692$
Unbalanced	HC	$224 \times 224 \times 3 \times 6458$	$224 \times 224 \times 3 \times 922$	$224 \times 224 \times 3 \times 1846$
	SZ	$224 \times 224 \times 3 \times 9782$	$224 \times 224 \times 3 \times 1397$	$224 \times 224 \times 3 \times 2796$
	Total	$224 \times 224 \times 3 \times 16240$	$224 \times 224 \times 3 \times 2319$	$224 \times 224 \times 3 \times 4642$

SZ = schizophrenia; HC = healthy control.

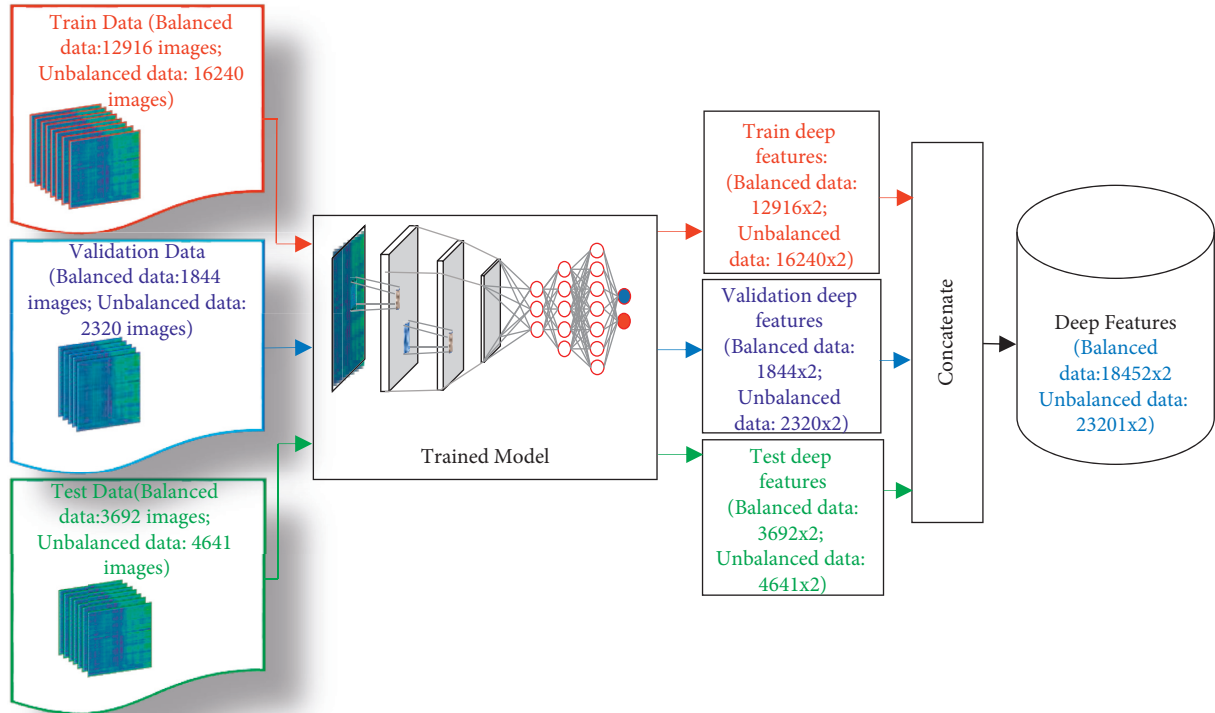


FIGURE 4: Feature extraction process in the proposed “SchizoGoogLeNet” model for the balanced and unbalanced dataset.

performance) with the obtained feature set than the GoogLeNet classifier (a higher FAR indicates lower performance). From Tables 3 and 4 and Figure 7, it is clearly apparent that the obtained feature set yields higher performance with ML classifiers than the DL classifier (e.g., GoogLeNet) for both balanced and unbalanced datasets. In both datasets, the SVM classifier is superior for the obtained deep feature set compared to other reported classifiers, and the GoogLeNet classifier with the same feature set achieved the worst performance.

Figure 8 and also Figure 7 show a comparison of the performances (in terms of ACC, SEN, SPE, and FAR) between the balanced and unbalanced datasets. The figures demonstrate that the performances of all classifiers are higher for the unbalanced dataset than those for the balanced dataset. The overall accuracy is increased by 3.75% for the unbalanced data and 4.02% for the balanced data for the ML-based classifier compared to the DL scheme. The

unbalanced dataset’s improved performance may be due to the fact that it is the original dataset, which includes all of the subjects’ data points. On the other hand, the balanced dataset was produced from the unbalanced dataset by eliminating some subjects. The performance was lower for the balanced dataset because some subjects’ data points had been eliminated. From the results, it can be considered that the obtained deep feature set with an SVM classifier is exceptional for the identification of SZ EEG signals from HC.

Figures 9(a) and 9(b) display an illustration of training and validation accuracy patterns for the deep GoogLeNet model in different iterations of the balanced and unbalanced datasets, respectively. For both datasets, the training accuracy and validation accuracy increase with the increase in the iteration numbers. It is notable that the accuracy of the training set does not deviate substantially from that of the validation set as observed in Figures 9(a) and 9(b). In the

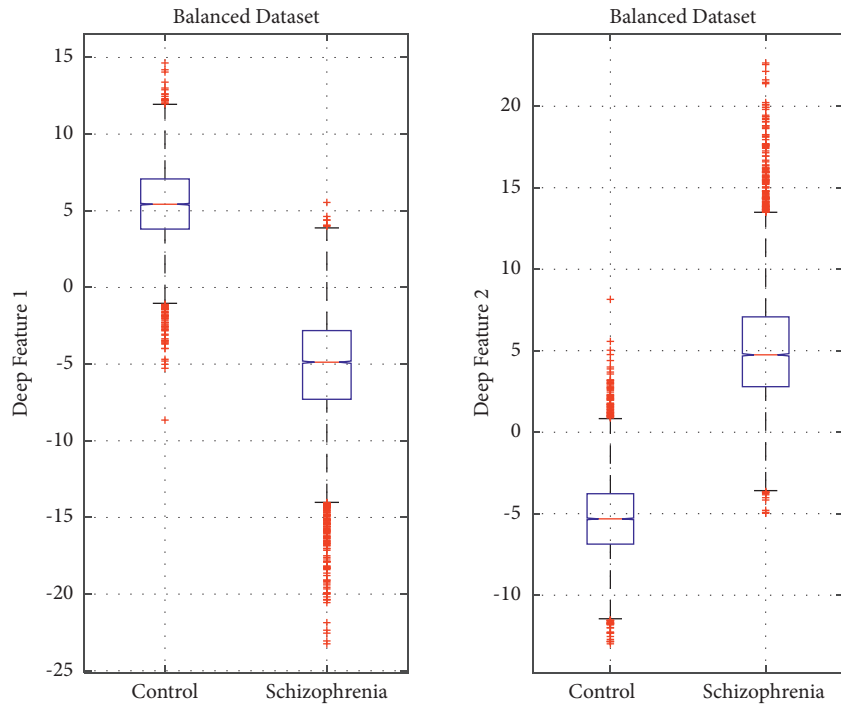


FIGURE 5: Distribution of two deep features for the balanced dataset.

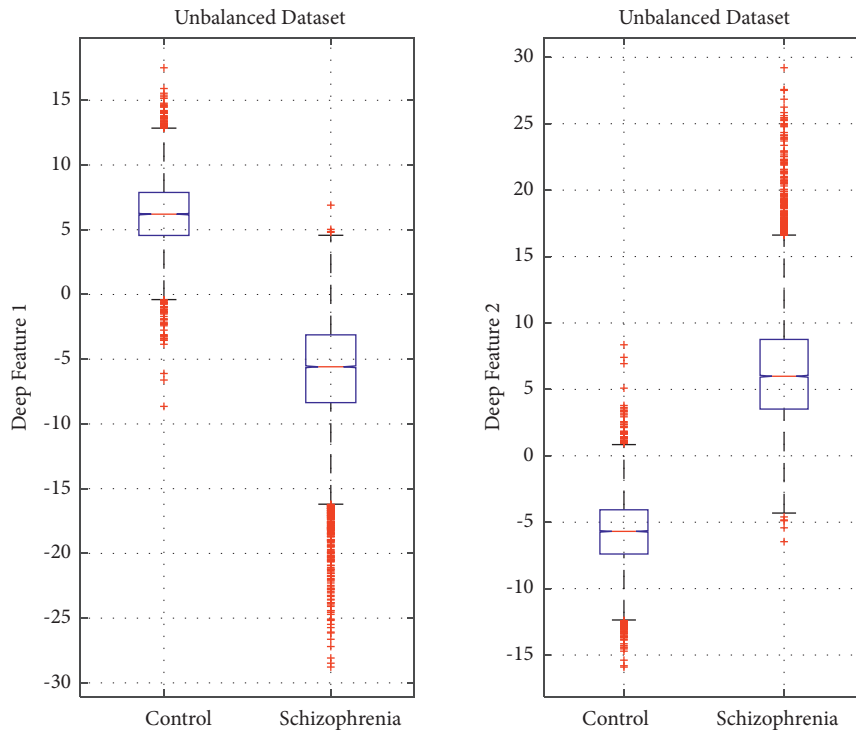


FIGURE 6: Distribution of two deep features for the unbalanced dataset.

TABLE 3: Overall performances of the proposed methods for the balanced dataset.

Classifier	Sensitivity (%)	Specificity (%)	Accuracy (%)	Positive predictive value (%)	F1-score (%)
GoogLeNet	92.15	96.42	94.28	96.26	94.16
SVM	98.33	98.27	98.30	98.27	98.30
KNN	97.29	97.27	97.28	97.27	97.28
DT	97.51	97.21	97.36	97.22	97.36
LDA	98.53	98.07	98.29	98.08	98.30

TABLE 4: Overall performances of the proposed methods for the unbalanced dataset.

Classifier	Sensitivity (%)	Specificity (%)	Accuracy (%)	Positive predictive value (%)	F1 score (%)
GoogLeNet	93.81	97.02	95.09	97.95	95.83
SVM	99.02	98.58	98.84	99.06	99.04
KNN	98.30	97.60	98.02	98.42	98.36
DT	98.55	97.62	98.18	98.43	98.49
LDA	99.13	98.18	98.75	98.80	98.97

Bold values represent highest performance.

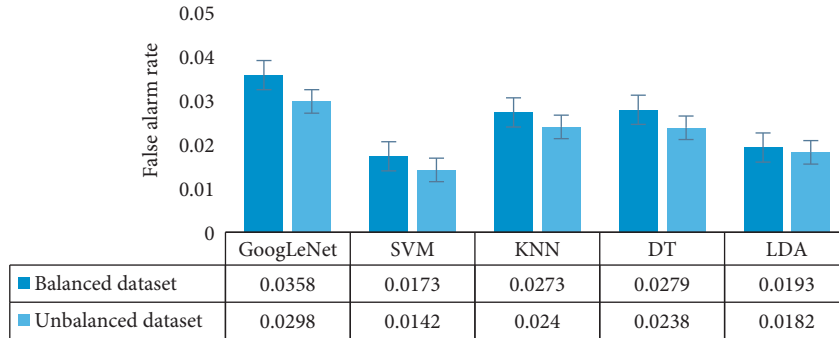


FIGURE 7: False alarm rate (FAR) for all of the reported classifiers for the balanced and unbalanced datasets.

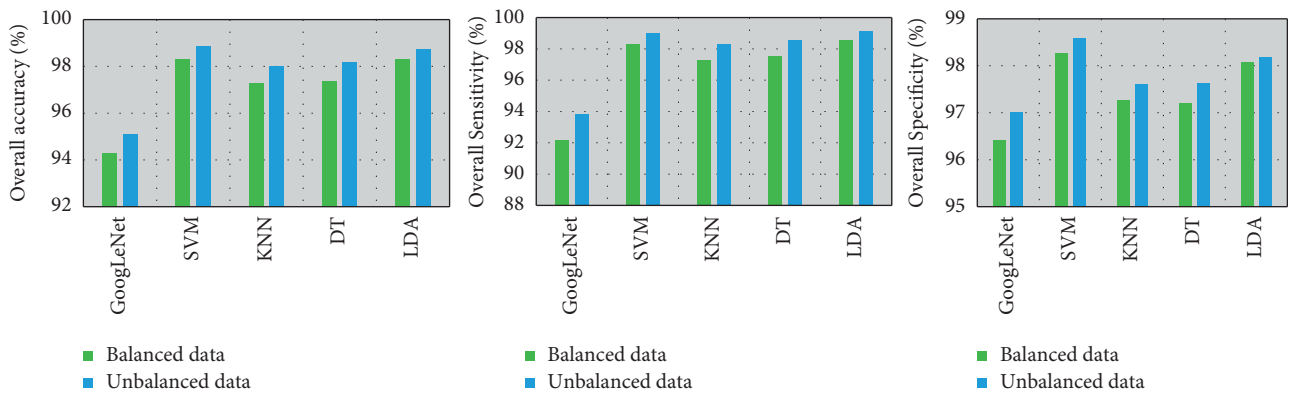


FIGURE 8: Comparison of performances between the balanced and the unbalanced datasets.

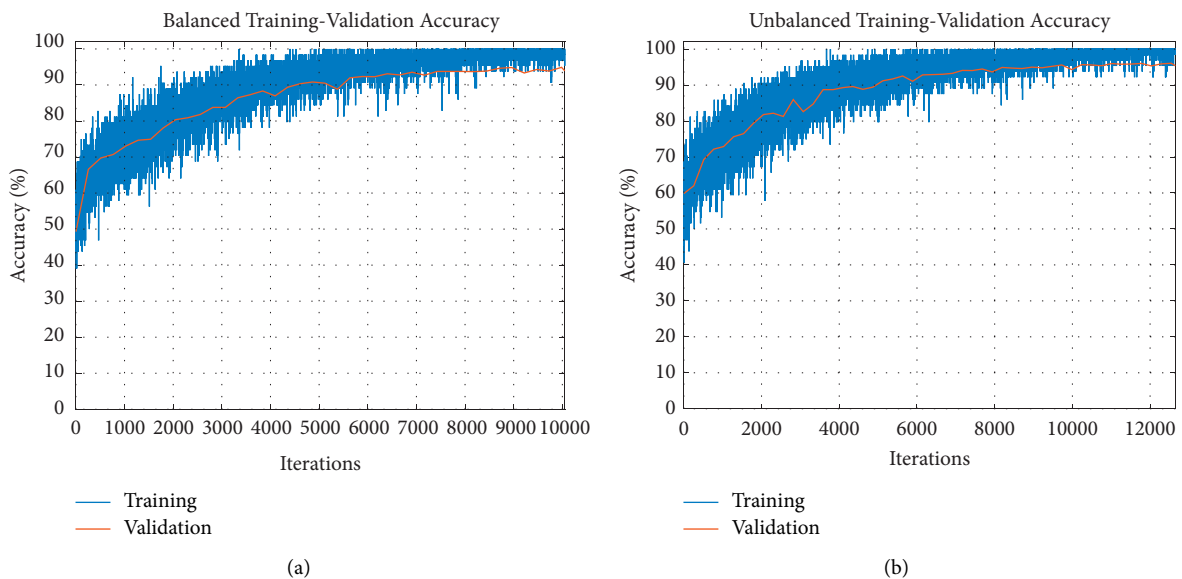


FIGURE 9: (a) Patterns of the training and validation accuracy of the GoogLeNet-based model for the balanced dataset. (b). Patterns of the training and validation accuracy of GoogLeNet-based model for the unbalanced dataset.

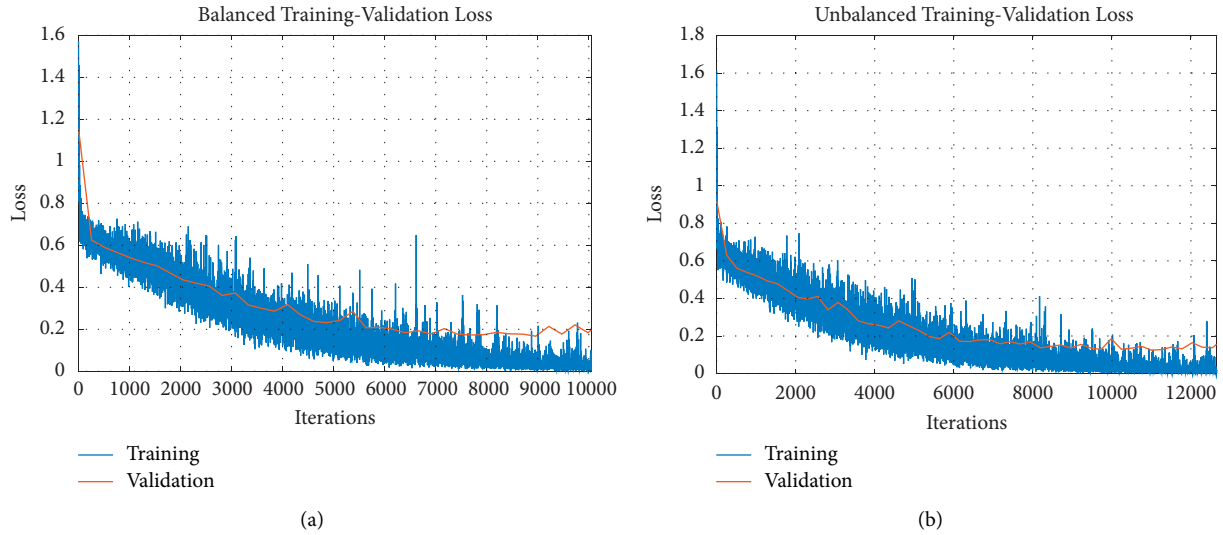


FIGURE 10: (a) Patterns of the training and validation loss information of the GoogLeNet-based model for the balanced dataset. (b). Patterns of the training and validation loss information of the GoogLeNet-based model for the unbalanced dataset.

training stage, the learning rate was set at 0.0001 and the batch number was one sample each time. The number of filters and kernel size was determined via the brute force technique.

The loss information of the training set and validation set with respect to different iterations is displayed in Figures 10(a) and 10(b) for the balanced dataset and unbalanced dataset, respectively. For both datasets, it is observed that the training loss and the validation loss decrease with the increase in the iteration numbers. The performance of the training set does not significantly diverge from that of the validation set, as shown in Figures 10(a) and 10(b).

To further assess the effectiveness of the GoogLeNet-based model, the ROC curves are drawn for different SZ detection models, where the input data were the deep feature set shown in Figures 11(a) and 11(b) for the balanced and unbalanced datasets, respectively. The corresponding performance measurements in every condition are shown in Table 5. Table 5 reports the area values under the ROC curve (AUC) for the reported classifiers. The AUC is the value of the area under the ROC curve that belongs to a value between 0 and 1 (a larger area indicates a better performance of the classifier). As can be seen in Table 5, the highest AUC is obtained by the SVM classifier, which is 0.9984 (close to 1) for the unbalanced dataset and 0.9973 for the balanced dataset. The KNN model produces the lowest AUC for both the balanced (0.9728) and the unbalanced (0.9795) datasets. Like the previous results, the results also indicate that the SVM classifier with the obtained deep feature set works better than other reported classifiers.

3.4. Comparative Analysis Report for Our Proposed Method with Existing State-of-the-Art Methods. A comparison of the prior EEG-based techniques used for SZ detection with our proposed model has been provided in Table 6. Until now, we found seven articles [2, 28, 35–39] in the literature for the

same database that we have used in this study. Table 6 shows the performance comparison of the proposed method with these published methods [2, 28, 35–39]. Kahre et al. [35] reported a method based on empirical wavelet transformation and SVM for the detection of SZ from EEG signals. Their method achieved an ACC of 88.70%, SEN of 91.13%, and SPE of 89.29. In [2], Siuly et al. introduced empirical mode decomposition (EMD)-based features with an ensemble bagged tree (EBT) for the detection of SZ using EEG signals. The ACC, SEN, and SPE scores of their method were 89.59%, 89.76%, and 89.32%, respectively. Guo et al. [38] reported a random forest (RF)-based machine learning algorithm for identifying schizophrenia patients from healthy control subjects using EEG signal data. In the designed plan, the author considered a number of features such as gender, age, education, and event-related potential (ERP) and the combination of the features.

RF yielded an accuracy of 81.1%. Khare et al. [36] introduced an automatic approach based on flexible tunable Q wavelet transform (F-TQWT) and a flexible least square support vector machine (F-LSSVM) classifier for the detection of SZ from EEG signals. The authors used the “Fisher score” method for the selection of the most discriminant channels. Their proposed method generated 91.39% accuracy, 92.65% sensitivity, and 93.22% specificity. In [37], Guo et al. proposed a scheme based on convolutional neural networks (CNNs) to characterize the difference in the distributed structure of data for identifying SZ from EEG. Their method achieved an accuracy of 92%. Khare et al. [38] designed a model involving a robust variational mode decomposition (RVMD) and an optimized extreme learning machine (OELM) algorithm. The experiment results reveal that the third mode’s chaotic features are responsible for generating the best performance (overall ACC of 92.30%). In [39], a time-frequency analysis-based convolutional neural network (CNN) model was proposed for identifying SZ from EEG signals by Khare and Bajaj. The authors used

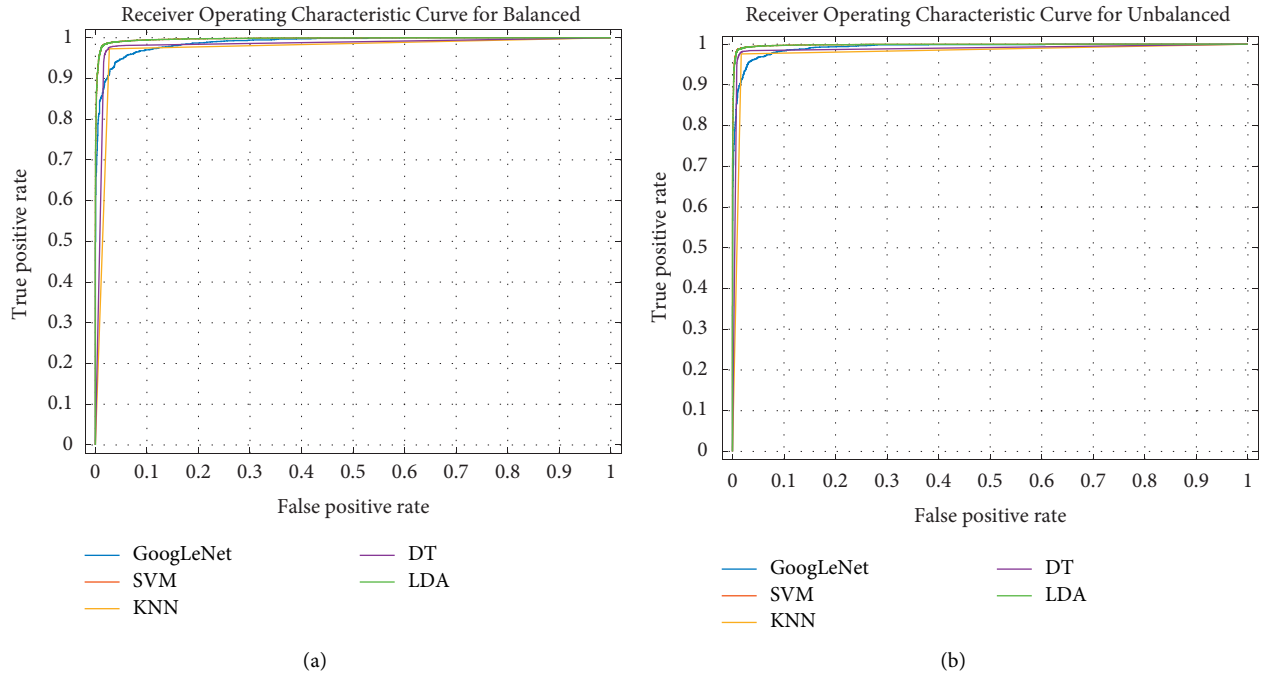


FIGURE 11: (a) The ROC curve for different classification models with the obtained deep feature set for the balanced dataset. (b) The ROC curve for different classification models with the obtained deep feature set for the unbalanced dataset.

TABLE 5: AUC values for the proposed SZ detection models.

Models	Balanced dataset	Unbalanced dataset
	Area under curve (AUC) values	Area under curve (AUC) values
GoogLeNet	0.9884	0.9923
SVM	0.9973	0.9984
KNN	0.9728	0.9795
DT	0.9815	0.9874
LDA	0.9973	0.9984

TABLE 6: The comparison of the proposed method with other methods for the same database.

Authors	Methods	ACC (%)	SEN (%)	SPE (%)
Khare et al. [35]	Empirical wavelet transformation with SVM	88.70	91.13	89.29
Siuly et al. [2]	EMD-based features with EBT	89.59	89.76	89.32
Guo et al. [38]	ERP features with RF	81.10	NA	NA
Khare and Bajaj [37]	F-TQWT-based scheme	91.39	92.65	93.22
Guo et al. [38]	Electrical marker with CNN	92.00	NA	NA
Khare et al. [38]	RVMD-based OELM method	92.93	97.15	91.06
Khare and Bajaj [39]	SPWVD-based TFR and CNN model	93.36	94.25	92.03
Proposed method	GoogLeNet-based deep features with an SVM model	98.84	99.02	98.58

*NA = not available.

Bold values represent the highest performance.

continuous wavelet transform, short-time Fourier transform, and smoothed pseudo Wigner–Ville distribution (SPWVD) techniques to obtain scalogram, spectrogram, and SPWVD-based time-frequency representation (TFR) plots for SZ detection. Their method achieved an overall accuracy of 93.36% using the SPWVD-based TFR and CNN model.

It is apparent from Table 6 that our proposed model yielded the highest performance scores with an accuracy of

98.84%, sensitivity of 99.02%, and specificity of 98.58%, compared to performance scores of the other existing methods. The achieved accuracy improvement of our proposed model is 17.74% better than the accuracy score of Zhang [28] and 10.14% better than the accuracy score of Khare et al. [35]. In the end, it can be concluded based on the experimental results that deep GoogleNet features of EEG signals with an SVM classifier could serve as an applicable

measurement to correctly discriminate between schizophrenics and HC subjects. [40].

4. Concluding Remarks

In this study, a GoogLeNet-based feature extraction scheme, called “SchizoGoogLeNet” is developed to efficiently identify SZ patients from HC subjects using EEG signal data. The proposed GoogLeNet model automatically extracted important hidden features which are advantageous for large-scale data. The obtained deep feature set was verified by the GoogLeNet classifier (DL classifier) and also four popular ML classifiers (e.g., SVM, KNN, DT, and LDA), separately. The performance of the proposed framework was evaluated on the benchmark SZ EEG database from Kaggle through extensive experimental evaluation. To check the effect of equal and unequal sample points in SZ and HC groups, we divided the dataset into two groups: balanced (the same number of sample points in SZ and HC) and unbalanced dataset (unequal sample points in SZ and HC) (original dataset). The experimental results show that the unbalanced set produces better performance compared to the balanced dataset. Among the reported classifiers, the SVM classifier with the obtained deep feature set yielded the highest performance (e.g., ACC 98.84%, SEN 99.02%, SPE 98.58%, PPV 99.06%, and F1-score 99.04%), while the lowest performances were obtained by the GoogLeNet classifier (e.g., ACC 95.09%, SEN 93.81%, SPC 97.02%, PPV 97.95%, and F1-score 95.83%). Moreover, our proposed model outperforms the existing methods. The findings of this study indicate that the obtained deep GoogLeNet features perform better with the SVM classifier in the SZ detection than the DL classifier (GoogLeNet classifier).

This study has some limitations, such as the fact that the study only considers two-class classification problems (SZ versus HC), while we intend to expand the application of the suggested approach to multiclass scenarios soon. Another flaw is that this study used a small SZ-based EEG dataset (81 total subjects: 49 schizophrenia (SZ) patients and 32 healthy control (HC) people). In the near future, we will broaden our method’s application to include huge clinical datasets.

Data Availability

The data can be obtained from the Kaggle website: <https://www.kaggle.com/broach/button-tone-sz>.

Conflicts of Interest

The authors declare that they have no conflicts of interest.

Acknowledgments

The authors would like to thank Kaggle EEG data collection team for the dataset: “EEG data from basic sensory task in Schizophrenia.” Funding for the data collection was supported by National Institute of Mental Health (Project Number: 5R01MH058262-16).

References

- [1] O. Baser, L. Xie, J. Pesa, and M. Durkin, “Healthcare utilization and costs of veterans health administration patients with schizophrenia treated with paliperidone palmitate long-acting injection or oral atypical antipsychotics,” *Journal of Medical Economics*, vol. 18, no. 5, pp. 357–365, 2015.
- [2] S. Siuly, S. K. Khare, V. Bajaj, H. Wang, and Y. Zhang, “A computerized method for automatic detection of schizophrenia using EEG signals,” *IEEE Transactions on Neural Systems and Rehabilitation Engineering*, vol. 28, no. 11, pp. 2390–2400, Nov 2020.
- [3] S. L. Oh, J. Vicnesh, E. J. Ciaccio, R. Yuvaraj, and U. R. Acharya, “Deep convolutional neural network model for automated diagnosis of schizophrenia using EEG signals,” *Applied Sciences*, vol. 9, no. 14, p. 2870, 2019.
- [4] Healthdirect, *Schizophrenia*, *Healthdirect*, <https://www.healthdirect.gov.au/schizophrenia> viewed 4 February 2020, 2018.
- [5] World Health Organization (Who), *Schizophrenia*, *WHO*, <https://www.who.int/news-room/fact-sheets/detail/schizophrenia> viewed 5 February 2020, 2019.
- [6] A. H. Mokdad, M. H. Forouzanfar, F. Daoud et al. “Global burden of diseases, injuries, and risk factors for young people’s health during 1990–2013: a systematic analysis for the global burden of disease study 2013,” *Lancet (North American Edition)*, vol. 387, no. 10036, pp. 2383–2401, 2016.
- [7] V. Jahmunah, S. Lih Oh, V. Rajinikanth et al., “Automated detection of schizophrenia using nonlinear signal processing methods,” *Artificial Intelligence in Medicine*, vol. 100, Article ID 101698, 2019.
- [8] C. Devia, R. Mayol-Troncoso, J. Parrini et al., “EEG classification during scene free-viewing for schizophrenia detection,” *IEEE Transactions on Neural Systems and Rehabilitation Engineering*, vol. 27, no. 6, pp. 1193–1199, 2019.
- [9] S. Siuly, O. F. Alçin, E. Kabir et al., “A new framework for automatic detection of patients with mild cognitive impairment using resting-state EEG signals,” *IEEE Transactions on Neural Systems and Rehabilitation Engineering*, vol. 28, no. 9, pp. 1966–1976, 2020.
- [10] M. Sabeti, R. Boostani, and T. Zoughi, “Using genetic programming to select the informative EEG-based features to distinguish schizophrenic patients,” *Neural Network World*, vol. 22, no. 1, pp. 3–20, 2012.
- [11] J. Ramos, L. F. Cerdán, M. A. Guevara, C. Amezcua, and A. Sanz, “Abnormal eeg patterns in treatment-resistant schizophrenic patients,” *International Journal of Neuroscience*, vol. 109, no. 1–2, pp. 47–59, 2001.
- [12] A. I. Kaplan, S. V. Borisov, and V. A. Zheligovskii, “Classification of the adolescent EEG by the spectral and segmental characteristics for normal,” *Zhurnal Vysshei Nervnoi Deiatelnosti Imeni I. P. Pavlova*, vol. 55, no. 4, pp. 478–486, 2005.
- [13] R. Buettner, D. Beil, S. Scholtz, and A. Djemai, “Development of a machine learning based algorithm to accurately detect schizophrenia based on one-minute EEG recordings,” in *Proceedings of the 53rd Hawaii International Conference on System Sciences*, 2020.
- [14] S. A. Akar, S. Kara, F. Latifoğlu, and V. Bilgiç, “Analysis of the complexity measures in the EEG of schizophrenia patients,” *International Journal of Neural Systems*, vol. 26, no. 02, Article ID 1650008, 2016.
- [15] S. A. Akar, S. Kara, F. Latifoğlu, and V. Bilgiç, “Wavelet-welch methodology for analysis of EEG signals of schizophrenia patients,” in *Proceedings of the 2012 Cairo International*

- Biomedical Engineering Conference (CIBEC) Cairo*, pp. 6–9, Egypt, December 20–21, 2012.
- [16] F. Li, J. Wang, Y. Liao et al., “Differentiation of schizophrenia by combining the spatial EEG brain network patterns of rest and task P300,” *IEEE Transactions on Neural Systems and Rehabilitation Engineering*, vol. 27, no. 4, pp. 594–602, 2019.
- [17] C.-R. Phang, F. Noman, H. Hussain, C. M. Ting, and H. Ombao, “A multi-domain connectome convolutional neural network for identifying schizophrenia from EEG connectivity patterns,” *IEEE J Biomed Health Inform*, vol. 24, no. 5, pp. 1333–1343, 2020.
- [18] S. L. Oh, J. Vicnesh, E. J. Ciaccio, R. Yuvaraj, and U. R. Acharya, “Deep convolutional neural network model for automated diagnosis of schizophrenia using EEG signals,” *Applied Sciences*, vol. 9, no. 14, p. 2870, 2019.
- [19] C. Szegedy, W. Liu, and Y. Jia, “Going deeper with convolutions,” in *Proceedings of the 2015 IEEE Conference on Computer Vision and Pattern Recognition (CVPR)*, pp. 1–9, 2015.
- [20] A. Khan, A. Sohail, U. Zahoora, and A. S. Qureshi, “A survey of the recent architectures of deep convolutional neural networks,” *Artificial Intelligence Review*, vol. 53, no. 8, pp. 5455–5516, 2020.
- [21] kaggle website, “Eeg data from basic sensory task in schizophrenia,” 2021, <https://www.kaggle.com/broach/button-tone-sz>.
- [22] J. M. Ford, V. A. Palzes, B. J. Roach, and D. H. Mathalon, “Did I do that? Abnormal predictive processes in schizophrenia when button pressing to deliver a tone,” *Schizophrenia Bulletin*, vol. 40, no. 4, pp. 804–812, 2014.
- [23] S. K. Khare, V. Bajaj, and U. R. Acharya, “SPWVD-CNN for automated detection of schizophrenia patients using EEG signals,” *IEEE Transactions on Instrumentation and Measurement*, vol. 70, p. 9, 2021.
- [24] Novel Egfr inhibitors attenuate cardiac hypertrophy, <http://pafit-phil.com/technically-a-feature-represents-a-distinguishing-property-a-recognizable-measurement-and/>, 2021.
- [25] Y. N. Dauphin, H. De Vries, and Y. Bengio, “Equilibrated adaptive learning rates for non-convex optimization,” *Advances in Neural Information Processing Systems*, pp. 1–10, 2015.
- [26] Y. L. Siuly and Y. Zhang, “EEG signal analysis and classification: techniques and applications,” *Health Information Science, Springer Nature*, US (ISBN 978-3-319-47653-7), Dec 2016.
- [27] M. N. A. Tawhid, S. Siuly, H. Wang, F. Whittaker, K. Wang, and Y. Zhang, “A spectrogram image based intelligent technique for automatic detection of autism spectrum disorder from EEG,” *PLoS One*, vol. 16, no. 6, Article ID e0253094, 2021.
- [28] M. T. Sadiq, H. Akbari, S. Siuly, A. Yousaf, and A. U. Rehman, “A novel computer-aided diagnosis framework for EEG-based identification of neural diseases,” *Computers in Biology and Medicine*, vol. 138, Article ID 104922, 2021.
- [29] V. Vapnik, *The Nature of Statistical Learning Theory*, Springer-Verlag, New York Inc, 2000.
- [30] T. Cover and P. Hart, “Nearest neighbor pattern classification,” *IEEE Transactions on Information Theory*, vol. 13, no. 1, pp. 21–27, 1967.
- [31] Y. Guo, G.-Q. Du, W.-Q. Shen, C. Du, P. N. He, and S. Siuly, “Automatic myocardial infarction detection in contrast echocardiography based on polar residual network,” *Computer Methods and Programs in Biomedicine*, vol. 198, Article ID 105791, 2021.
- [32] S. Taran, V. Bajaj, and S. Siuly, “An optimum allocation sampling based feature extraction scheme for distinguishing seizure and seizure-free EEG signals,” *Health Information Science and Systems*, vol. 5, no. 1, p. 7, 2017.
- [33] M. A. Alvi, S. Siuly, H. Wang, K. Wang, and F. Whittaker, “A deep learning based framework for diagnosis of mild cognitive impairment,” *Knowledge based System*, vol. 2022, 2022 (in press).
- [34] L. Farsi, S. Siuly, E. Kabir, and H. Wang, “Classification of alcoholic EEG signals using a deep learning method,” *IEEE Sensors Journal*, vol. 21, no. 3, pp. 3552–3560, 2021.
- [35] S. K. Khare, V. Bajaj, S. Siuly, and G. R. Sinha, “Classification of schizophrenia patients through empirical wavelet transformation using electroencephalogram signals,” in *Book: Modelling and Analysis of Active Biopotential Signals in Healthcare*, vol. 1, Publisher: IOP Science, 2020.
- [36] L. Zhang, “EEG signals classification using machine learning for the identification and diagnosis of schizophrenia,” in *Proceedings of the 2019 41st Annual International Conference of the IEEE Engineering in Medicine and Biology Society*, pp. 4521–4524, EMBC, 2019.
- [37] S. K. Khare and V. Bajaj, “A self-learned decomposition and classification model for schizophrenia diagnosis,” *Computer Methods and Programs in Biomedicine*, vol. 211, Article ID 106450, 2021.
- [38] Z. Guo, L. Wu, Y. Li, and B. Li, “Deep neural network classification of EEG data in schizophrenia,” in *Proceedings of the 2021 IEEE 10th Data Driven Control and Learning Systems Conference, DDCLS*, pp. 1322–1327, 2021.
- [39] S. K. Khare and V. Bajaj, “A hybrid decision support system for automatic detection of Schizophrenia using EEG signals,” *Computers in Biology and Medicine*, vol. 141, Article ID 105028, February 2022.
- [40] A. Kawala-Sterniuk, M. Podpora, M. Pelc et al., “Comparison of smoothing filters in analysis of EEG data for the medical diagnostics purposes,” *Sensors*, vol. 20, no. 3, p. 807, 2020.

Research Article

Interactive Design of Business English Learning Resources Based on EDIPT Multimodal Model

Xiaomei Yang and Shi Qi 

Fundamentals Department, Luxun Academy of Fine Arts, Shenyang 110816, Liaoning, China

Correspondence should be addressed to Shi Qi; qishi@lumei.edu.cn

Received 1 July 2022; Accepted 8 August 2022; Published 8 September 2022

Academic Editor: Le Sun

Copyright © 2022 Xiaomei Yang and Shi Qi. This is an open access article distributed under the Creative Commons Attribution License, which permits unrestricted use, distribution, and reproduction in any medium, provided the original work is properly cited.

Aiming at the problem that online video learning resources of business English are scattered and the learners are inefficient in acquiring learning resources, this paper designed a business English learning system based on the EDIPT model. In addition, aiming at the problem of multifeature fusion between low-level features and high-level semantic features in video scenes, this paper proposes a multi-modal video scene segmentation algorithm based on a deep network. By minimizing the square sum of distances in the time period, the shots are clustered, and finally, the semantic scene is obtained. The experimental results show that the algorithm has good performance in classification accuracy and can effectively segment video scenes, which is helpful for users to improve their comprehensive business English skills.

1. Introduction

Education makes human knowledge and civilization spread, and it is an important force to promote the development of human knowledge and civilization. With the development of science and technology and the increase of knowledge, the society needs more advanced and effective means of education. Using the network to spread knowledge is an effective way to spread knowledge. Among them, business English is an application-oriented major that teachers need to pay attention to the exercise of students' English, especially oral communication, so it is very important to build a good English learning environment [1, 2]. However, many colleges and universities are lack of a good business English learning environment, resulting in students cannot get effective English training. Normally, business English students in the development of oral practice are carried out in the simulation of business activities, the lack of daily teaching of business English oral exercise, so that students' oral English level cannot be effectively exercised and then affect the students' English level.

In the teaching design, the EDIPT design thinking model is widely recognized in the field of education from the

perspective of students. It is used to guide teaching practice and is conducive to the development of students' innovation ability and design thinking. Through the implementation of the design thinking process, Lin changed the current situation of single information technology works of junior high school students and provided a teaching model and activity design suitable for junior high school [3]. Yu introduced a foreign typical EDIPT design thinking model into a scratch classroom in primary school, guided scratch teaching according to the operation process of the EDIPT design thinking model, and designed learning activities to improve students' design thinking ability [4]. Design thinking is not only used to guide classroom teaching but also applied to practical teaching by many educational institutions outside school.

In addition, online video learning is an effective means for students to exercise their business English application ability. But at present, the retrieval of teaching video still relies on the TBVR form, which has the following problems [5, 6]. Firstly, the manual annotation only represents the staff's personal views on the video, which is too subjective and difficult to cover each person's grasp of the different focuses of the video; secondly, manual tagging requires staff

to make a brief summary after watching the video, but in the face of the explosive growth of massive video data, the time and labor cost of tagging are difficult to estimate; thirdly, the content in the video is abundant, so it is difficult to summarize it with simple words or phrases. For the above-given reasons, TBVR is not conducive to users to quickly find their interesting teaching video clips and knowledge points, and it is difficult to meet the needs of users. The semantic information based on a single modal analysis is always limited. While combining two or more modes for multimodal feature semantic analysis can obtain more abundant video semantic information, which is an effective method to extract video content.

Multimodal theory refers to the phenomenon that various senses interact with each other through language, image, sound, animation, and other elements [7]. However, multimodality can strengthen the communication of verbal meaning, and learners can effectively understand multiple knowledge signals. Cross thought that video information can promote the understanding of business English materials [8]. In particular, multimodal theory video resources are represented by images, sounds, and languages. Compared with single-mode learning resources, audio-visual learning resources can reduce the difficulty of business English learning. Most of the users' information comes from reading, listening, and writing in a business environment. A Révalo found that multimodal guidance can better promote learners' understanding of business English. Business English learning emphasizes scenario simulation and pays attention to the cultivation of communicative competence. In addition, the introduction of multimodal theory has a certain theoretical basis for the integration of business English videos [9].

Therefore, this paper extracts and analyzes the video learning resources of business English, introduces the EDIPT thinking model, and designs a business English learning system integrating multimodal information such as text, graphics, audio-visual, animation, and so on, so as to improve the comprehensive business English skills of users with different learning styles.

2. Design of Business English Learning System Based on EDIPT

2.1. EDIPT Design Thinking. The EDIPT design thinking model consists of five stages that can jump through the cycle: empathy, problem definition, conception, prototyping, and testing, as shown in Figure 1. Each stage includes stage objectives, implementation principles, specific methods, and tools. The specific stages and implementation process are as follows [10, 11].

The specific implementation process of the empathy stage: learners use What? How? Why? Empathy map, situational story method, and other tools, in-depth understanding of the user's environment, in-depth mining of the user's inner activities, to provide a foundation for targeted solutions. The specific implementation process of defining stage: learners use the POV problem definition method to state factual problems as operational problems, using the method of "how might we," we can ask questions in an open

way, decompose and think about the problems, and focus on innovative problems. In the stage of ideating, we can use the scaffold table to think about problems from the seven directions provided in the scamper table or from some selected directions and initially form the problem solution. The realization methods of the prototype stage include sketch drawing, pattern making, and demo design. The specific implementation process: learners can use the simplest tools such as paper and pen to draw sketches, show their own or group ideas, and achieve the goal of expressing ideas, presenting solutions, and quickly realizing creativity. The specific implementation process of the test: learners can use the "feedback capture grid graph" tool to collect and integrate user feedback information, sort out the highlights and problems of the prototype from the collected information, obtain constructive suggestions and further improvement ideas, so as to promote the generation of the best solution.

2.2. Teaching Model Design. The whole teaching model includes teaching process design, teaching evaluation design, teaching evaluation design, and teaching feedback design.

The learning mechanism is linear; learners need to complete all learning tasks, and then they can unlock the next video learning. Taking single video teaching as a cycle, the teaching process of this system belongs to cyclic teaching. In addition, learners complete the business English learning module in turn according to the set task objectives. In a single learning cycle, learners acquire business knowledge, improve oral communication, and strengthen other comprehensive business English skills. Video teaching is divided into seven indicators, namely, visual, listening, reading, speaking, testing, translation, and writing, to assess the teaching results. While each teaching task is set with a corresponding score.

2.3. Functional Design. By integrating high-quality business English video learning resources, users can improve the efficiency of acquiring learning resources, improve the learners' comprehensive learning ability of business English, create a microbusiness communication platform, and create a business communication circle. The business logic function of the system is divided into three functional modules: basic learning function, learning the main function, and learning auxiliary function. The main function of learning runs through the whole process of video learning and is the core function of the small program. The specific function design is shown in Figure 2.

2.3.1. Basic Learning Function. The basic learning functions include learning check-in, learning review, learning forwarding, video collection, and video like. Check-in design is a basic function commonly used by users, where learners get bonus points for daily check-in, and the points obtained by check-in are converted into scores in equal quantities. Users judge their current learning needs through video reviews, and their diagnostic learning evaluation strengthens their reflection on video learning.

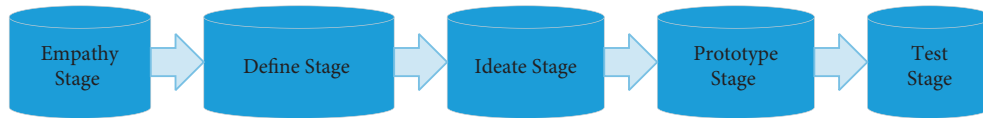


FIGURE 1: EDIPT design thinking model.

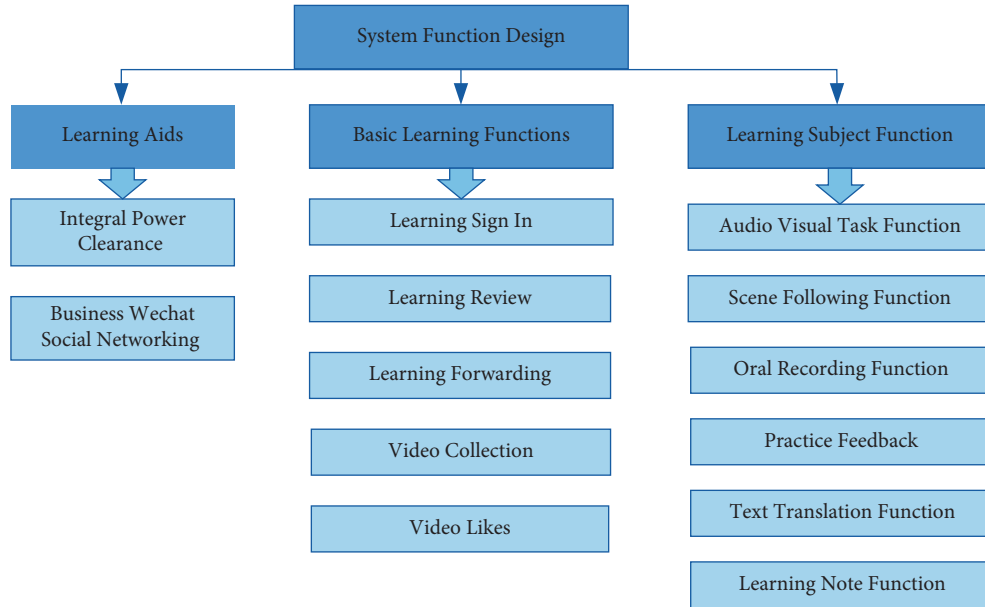


FIGURE 2: System function design.

2.3.2. *Learning Main Function.* The main functions of learning include audio-visual task function, scene following function, oral recording function, practice feedback function, text translation function, and learning note taking function. In the whole learning process, the task-driven teaching method promotes learners to complete video learning. For the key parts of the video content, blank out randomly and fill in the blanks with words. Subtitles are not set in the audio-visual task link. Text translation is attached in the learning link, and the learning note function is added.

2.3.3. *Learning Auxiliary Function.* The learning assistance function includes two parts: one is to help customs clearance with points and the other is to help the business microgroup to socialize. Redeem the points, add the points to the score, regenerate the score report, view the rating level, help the customs clearance, and unlock the next video learning. The score values of different task modules are recorded in the score report, and the video learning score must be greater than or equal to 90 points to pass the test.

2.4. *Design of Data Flow.* Because the system mainly uses user data and video data, the whole process includes three kinds of data flow. The first is that the user sends the behavior request to the system, and the system returns the processing results in the small control layer. The second way is to get the current data information, but it does not involve the change of database information, so it needs to access the

background server, where the user sends the access request to the client. After receiving the request, the client realizes C/S communication with the server. Finally, the server returns the business logic processing results to the client, and the client presents it to the user in the form of a page. The third one involves updating the data table information, where the user requests to update or query the data, and the client sends the event request to the server. During the process, the database server program will listen to the network request events, realize the communication between the model layer and the server by passing parameters, and update the information after data proofreading and validation, as shown in Figure 3.

3. Multimodal Video Scene Segmentation Algorithm

3.1. *Overall Design.* Because the above-given system is aimed at video learning resources, the semantic information based on single modal analysis is always limited. While combining two modes or more to carry out multimodal feature semantic analysis can obtain more abundant video semantic information, which is an effective method to extract video content. Therefore, the multimodal deep network method is adopted, where the video scene segmentation task is treated as a supervised time constrained clustering problem. Firstly, rich underlying features and semantic features are extracted from each shot; secondly, in order to obtain the similarity measure between shot features, these features are embedded

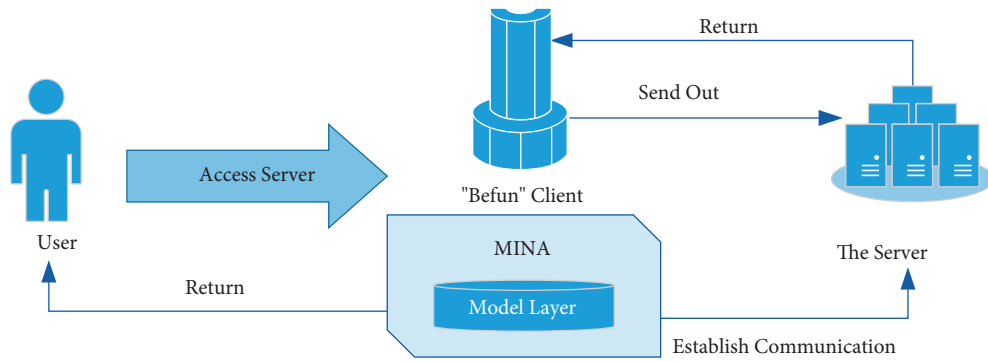


FIGURE 3: Design of data flow.

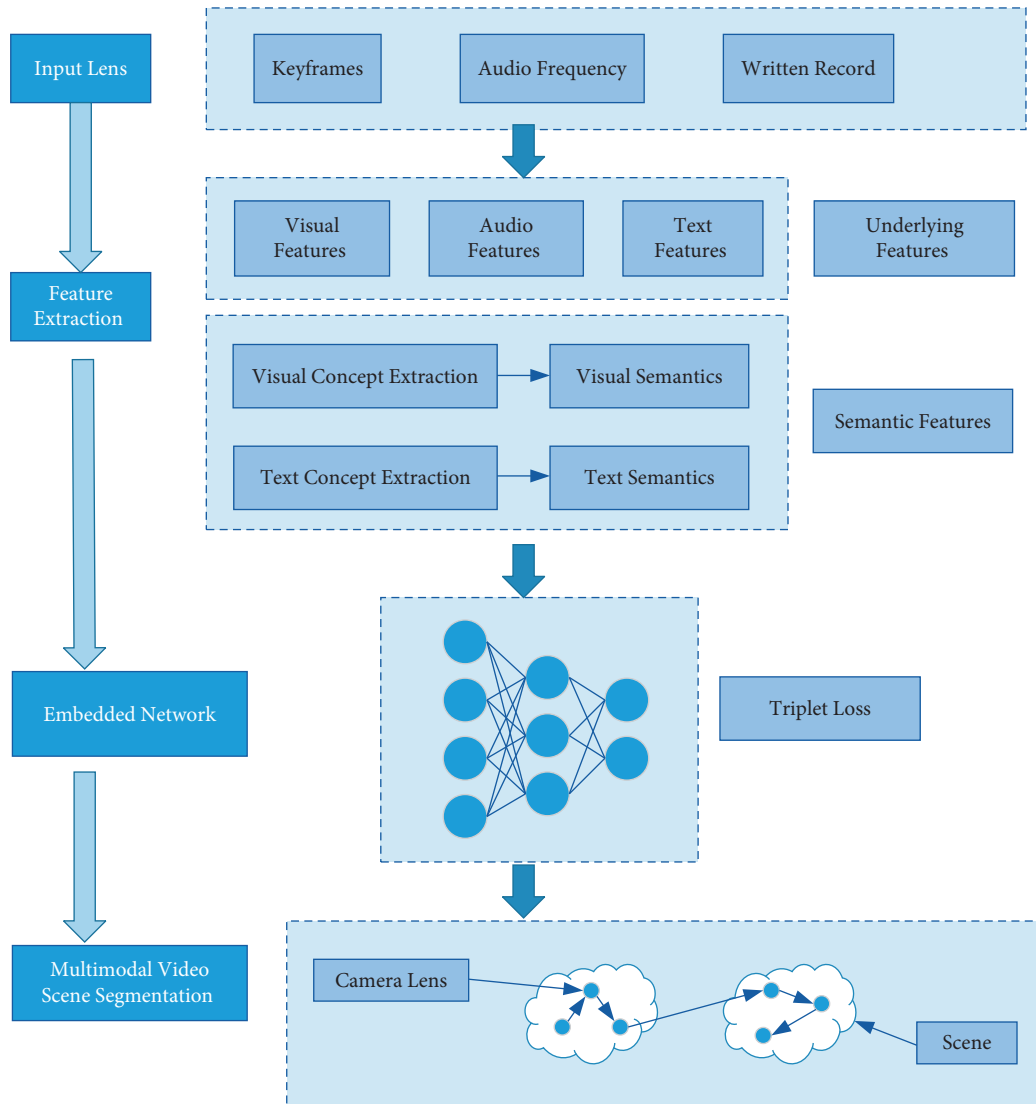


FIGURE 4: Overall algorithm framework.

in Euclidean space; finally, the optimal scene boundary is detected by minimizing the sum of squares of distances in the time period and use a penalty to automatically select the number of scenes. The overall framework is shown in Figure 4.

3.2. *Embed Deep Networks.* Considering that the shots in the same scene usually have the same content in the video stream, the scene segmentation problem is also considered as the problem of grouping adjacent shots together, which is to maximize the semantic consistency of similar shots. In

order to reflect the semantic similarity, it is necessary to calculate the distance between lens feature vectors X , so an embedding function $\varphi(X)$ is constructed, which can map a lens feature vector to the space where Euclidean distance has the required semantic properties. The distance matrix is

$$\left[\varphi(X_i) - \varphi(X_j) \right]^2 = [1 - \alpha_{i,j}], \quad (1)$$

where $\alpha_{i,j}$ is a binary function, indicating whether the scene X_i and X_j belong to the same scene, $i, j = 1, 2, \dots, N$.

The embedded function $\varphi(\cdot)$ makes the shots of a particular scene X_i closer to all shots of the same scene X_i^+ , rather than any other shots of any other scene X_i^- , so that the constraint can be carried out.

$$\varphi(X_i) - \varphi(X_i^+) < \varphi(X_i) - \varphi(X_i^-). \quad (2)$$

In order to improve the embedding ability, a triple depth network is designed, which is composed of three basic networks, where the same parameters are shared, and each parameter takes the scene descriptor as the input and calculates the required embedding function. Train the network loss of Triplet (X_i, X_i^+, X_i^-) through the Triplet loss function, and Hinge loss of Triplet is defined as follows:

$$L_i(w, \theta) = m(0, \varphi(X_i) - \varphi(X_i^+)^2 + (1 - \varphi(X_i) - \varphi(X_i^-))^2), \quad (3)$$

where w is the network weight; θ is the deviation. The total loss of N triples is given by the average loss of each triplet plus the L_2 regular term of the network weight to reduce overcompensation.

Therefore, the total loss of N triples can be defined as follows:

$$L(w, \theta) = \frac{5 \times 10^{-5}}{2} \|w\|^2 + \frac{1}{N} \sum_{i=1}^N L_i(w, \theta). \quad (4)$$

3.3. Multimodal Scene Segmentation. Because scenes need to be continuous in time, scenes with similar semantic content but far away in time should be distinguished. The task of video scene segmentation is treated as a supervised time constrained clustering problem; secondly, in order to obtain the similarity measure between shot features, these features are embedded in Euclidean space; finally, the optimal scene boundary is detected by minimizing the sum of squares of distances in the time period, and a penalty term is used to automatically select the number of scenes.

In order to obtain scene segmentation of video, shots are required to be as semantically consistent as possible. Inspired by K-means, cluster homogeneity can be described by the sum of square distances between cluster elements and their centroids, which is called within cells sum of squares (WSS) [12]. Therefore, the reasonable goal is to minimize the sum of squares within a group, that is, the sum of all WSS. While only minimizing the sum of squares within a group will lead to a trivial solution of only one scene in each sequence. Therefore, it is necessary to add penalty terms to

avoid over segmentation. Therefore, Formula (5) needs to be solved.

$$\min_{M, t_m} \sum_{m=0}^M WSS_{t_m, t_{m+1}} + C \cdot g(M, N), \quad (5)$$

where M is the number of change points of input video segmentation; t_m is the position of the m -th change point. t_0 and t_{M+1} are the beginning and end of the video respectively; $WSS_{t_m, t_{m+1}}$ is the sum of squares within the group of the m -th segment in the embedded space. $g(M, N) = M(\ln(N/M) + 1)$ is the standard punishment of Bayesian information, which is parameterized by the number of clips M and the number of scenes N in the videos. The C parameter is used to adjust the relative importance of the penalty. A higher penalty value of C would cause too many segments, so the choice of C value depends on the video. Adjust the C value by using a step size of 0.001, until the number of clusters is less than the number of scenes in the video.

The sum of the square distances between a set of points and its mean can be expressed as a function of the paired square distances between individual points. Therefore, the sum of squares within a group can be represented as scene segmentation.

$$WSS_{t_m, t_{m+1}} \triangleq \sum_{t=t_m}^{t_{m+1}-1} \varphi(X_t) - \mu_m^2 \quad (6)$$

$$= \frac{1}{2(t_{m+1} - t_m)} \sum_{i,j=t_m}^{t_{m+1}-1} \varphi(X_i) - \varphi(X_j)^2.$$

Among them, μ_m is the average value of each scene shot feature.

$$\mu_m = \frac{1}{2(t_{m+1} - t_m)} \sum_{t=t_m}^{t_{m+1}-1} \varphi(X_t). \quad (7)$$

In this way, clustering targets can be minimized using dynamic programming methods. First, $WSS_{r,r+d}$ is calculated for the starting point r and the duration d of each segment. Secondly, the optimal target values of $j \in [1, N]$ lenses and $M \in [0, N-1]$ change points are calculated iteratively to minimize the target, as shown in equation (8), where $D_{0,j} = WSS_{0,j}$. In the end, the optimal number of variation points was chosen as $M^* = M^* = \arg \min D_{M,N} + C \times g(M, N)$, and the optimal scene segmentation was reconstructed.

$$D_{M,j} = \min_{r=M, M+1, \dots, j-1} (D_{M-1,r} + WSS_{r,j}). \quad (8)$$

In the video scene segmentation algorithm, the input is the scene video stream, where the total number of video shots is N and the overall feature vector of the shot is X . The output is the scene boundary (lens number is S_i). The specific algorithm steps are as follows:

- (1) The input video frequency stream is segmented into shots, and the key frame of the shot is identified by calculating the average distance of all frames within

TABLE 1: Parameters of model training.

Training set	Epoch	Batch-size	Loss function	Number of iterations	Learning framework
8000	2	32	Cross entropy	2000	Keras

the shot. All shots and key frames after segmentation are numbered, namely, S_i and S_f .

- (2) According to Formulas (1) and (2), the visual concept feature vector $v(s)$ and text concept feature vector $t(s)$ of the lens are extracted respectively. Then, all of its features are connected in series to obtain its global eigenvector X .
- (3) Adopt a deep network to learn an embedding function $\varphi(X)$, embed video shot features in Euclidean space, and calculate the pair distance matrix between shots to get the similarity measure between shot features, and then get the semantic similarity between shots.
- (4) For each segment starting point r and segment duration d , calculate $WSS_{r,r+d}$.
- (5) Let $j \in [1, N]$, $M \in [0, N - 1]$, calculate an optimal target value containing j lenses and M change points to minimize the target $D_{M,j}$. If $r < N$, continue to Step (5). While if $r \dots N$, go to Step (6).
- (6) The optimal number of change points M^* is selected by calculation, and the lens number S_i of the corresponding scene boundary is output according to the location of the segmentation points, and the segmentation result of the video scene is finally obtained.

4. Experiment and Analysis

4.1. Model Training. The gradient descent method is used to optimize the algorithm, and the learning rate is taken as the default value of 0.01. Table 1 shows the specific parameter configuration of network training.

Figure 5 shows the influence of the number of iterations on the final experimental results. It can be seen that when the number of iterations is small, the number of learning is not enough, so the accuracy of the final result is insufficient. However, because the visual features are only one part of the basis of video scene segmentation, the results still have a certain accuracy. Then, with the increase of iterations, the value of F increases, and after 2 000 iterations, it is stable.

4.2. Analysis of Model Validity. In order to verify the effectiveness of the proposed algorithm for video scene segmentation, five kinds of standard teaching videos are selected from the school online (<https://www.icourse163.org/>). The total length of the video is 128'19", with 2760 lenses and 98 scenes. The details of the experiment are shown in Table 2.

Recall, Precision, and F were used to evaluate the performance of the algorithm; the calculation formula of them are as follows:

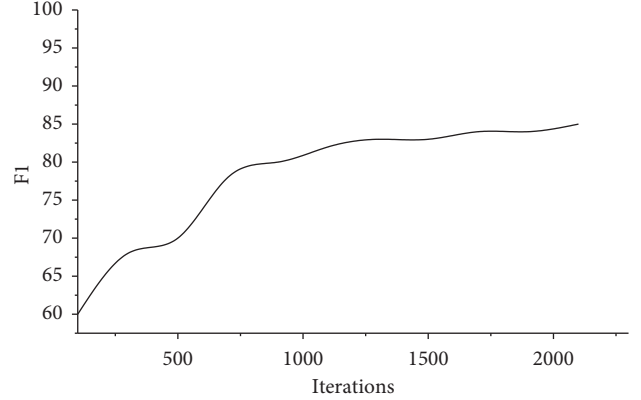


FIGURE 5: Results of model training.

$$\text{Recall} = \frac{n_c}{n_c + n_m} \times 100\% = \frac{n_c}{n_a} \times 100\%,$$

$$\text{Precision} = \frac{n_c}{n_c + n_f} \times 100\% = \frac{n_c}{n_d} \times 100\%, \quad (9)$$

$$F = \frac{2 \times \text{Precision} \times \text{Recall}}{\text{Precision} + \text{Recall}} \times 100\%,$$

where n_c is the total number of correct detected scenes; n_m is the total number of undetected scenarios; n_f is the total number of scenarios detected by errors; n_a is the total number of actual scenarios; n_d is the total number of detected scenarios. The proposed algorithm is compared with the NW algorithm [13] and STG algorithm [14], and the experimental results are shown in Figures 6 and 7.

From the data in the figure, we can see that the algorithm can construct video scene correctly. Compared with the NW algorithm and STG algorithm, the recall, precision, and F value of our algorithm are greatly improved. This is mainly because modesty only considers the combination of video underlying color features and NW algorithm, and the latter only integrates various visual and audio features in STG, the characteristics of temporal association and symbiosis between multiple modes in video data are not fully considered. We proposed a deep learning framework, where different low-level features from videos are extracted, and semantic concept features are combined with multi-modal semantic embedding space through triple deep network learning to segment videos into coherent scenes, thus effectively reducing the distance between low-level features and high-level semantics. Therefore, the scene segmentation effect achieved by our algorithm is better, and the algorithm is more universal for different types of videos.

4.3. System Testing. The response time of the system refers to the time spent by users when using the system. For the

TABLE 2: The details of the experiment.

Video clip	Duration	Number of lenses	Number of scenes
V1 Discovering business opportunities and establishment of a business	29'13"	390	23
V2 organizational structure & recruiting and training employees	292'21"	436	20
V3 employee motivation and corporate culture	30'06"	587	16
V4 production, product and marketing	27'19"	633	14
V5 financial management and financing	31'47"	714	25
Total	128'19"	2760	98

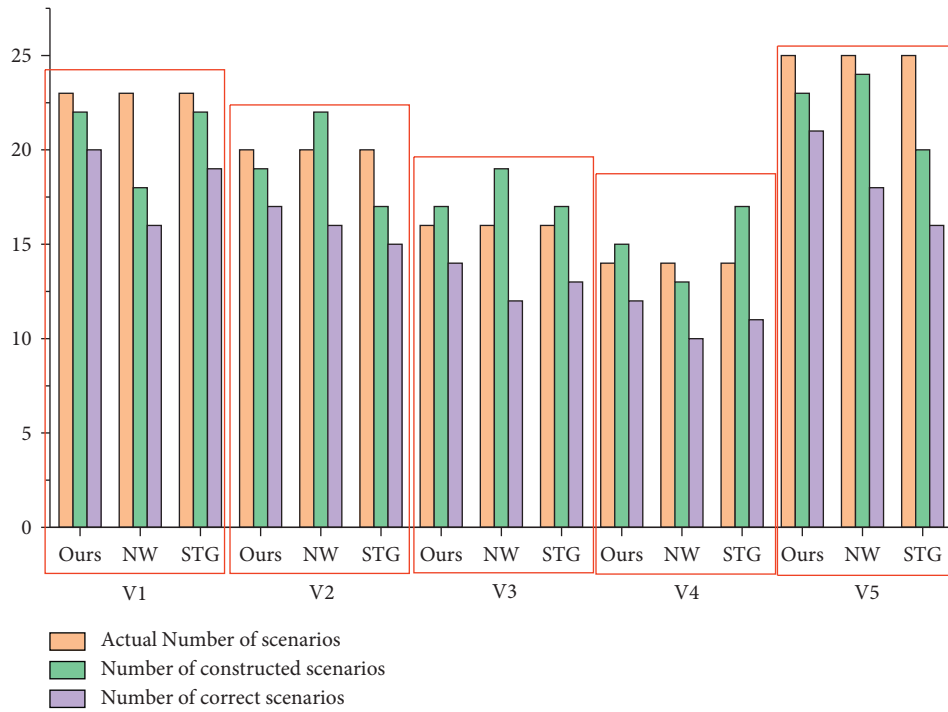


FIGURE 6: Comparison of scene construction.

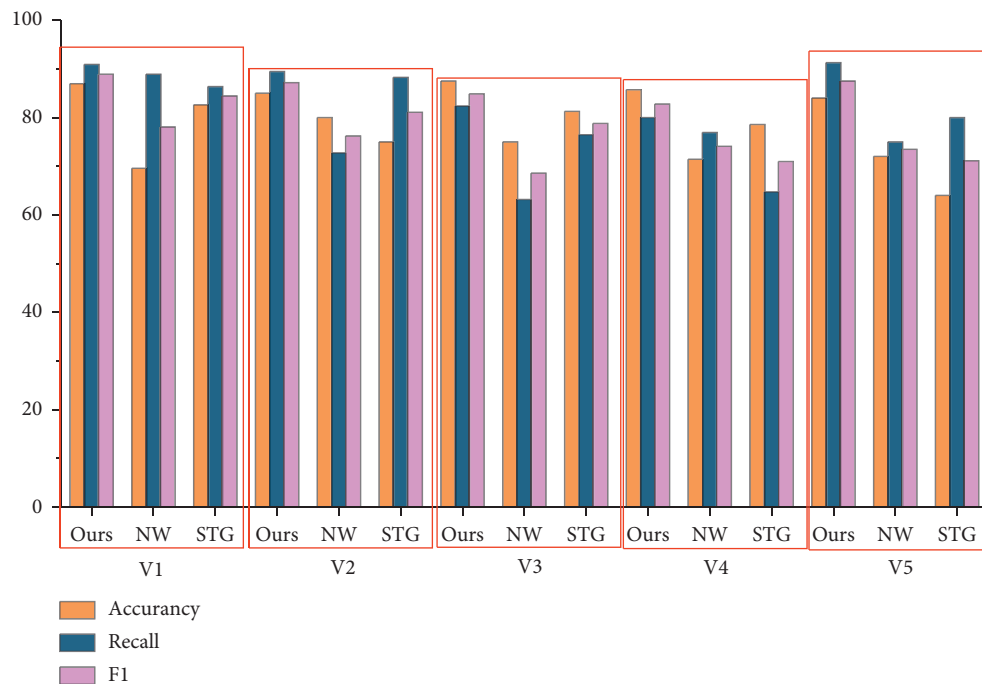


FIGURE 7: Comparison of model evaluation.

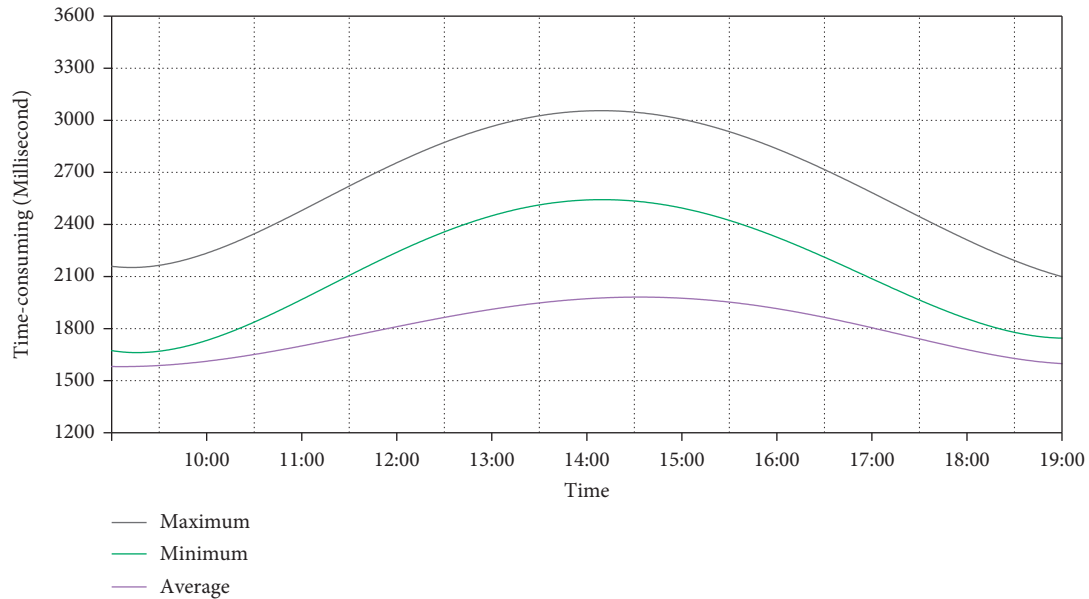


FIGURE 8: Response time of the system.

system, the response time is the time interval from clicking a page to displaying the page completely in the browser, which is divided into three parts, server response time, network response time, and client response time, respectively. The smaller the response time is, the faster the processing speed of the system is, and the shorter the waiting time of user operation is. Therefore, this paper tests the response time of the system, and the results are shown in Figure 8.

When users get a response between 2 and 5 seconds, the response speed of the system is considered to be good. When users get the response within 5 ~ 8 seconds, the response speed of the system is considered to be very slow, but it is still acceptable. It can be seen from Figure 8 that the peak value of the maximum response time curve of the system is about 3 seconds, indicating that the response time of the platform is very fast. In addition, the peak value of the minimum response time curve is only 1.5 seconds, and the response time of the platform is better. The peak value of the average response time curve of the system is about 2.5 seconds, and the average response time of the system is less than 3 seconds, which meets the actual needs.

5. Conclusion

This paper realizes the characteristic application of EDIPT design thinking and business English in the crossing field. With business English video learning resources as the carrier, a business English learning system is constructed, which solves the problem of learning integration of business English learning groups and opens the exploration mode of design thinking in the field of education. In addition, aiming at the multimodal video scene segmentation algorithm based on a deep network, this paper extracts rich underlying features and semantic concept features from each lens, which realizes fast segmentation of video scene and achieves good experimental results. Moreover, it solves the problem

of the “semantic gap” between video low-level e features and high-level semantics by multimodal feature fusion, making video scene segmentation more accurate and universal. In the following work, we will pay more attention to the functional test of the system, such as taking the form of the questionnaire.

Data Availability

The dataset can be accessed from the corresponding author upon request.

Conflicts of Interest

The authors declare that they have no conflicts of interest.

References

- [1] T. Xiao, “Problems and improvement measures in practical teaching of business English in Colleges and universities,” *Journal of Heilongjiang teachers’ development college*, vol. 41, no. 2, pp. 144–146, 2022, (in Chineses).
- [2] Q. Zhou, “Informatization teaching based on learning platform -- Taking Business English interpretation course as an example,” *Campus English*, vol. 15, pp. 9–11, 2022, (in Chineses).
- [3] L. Lin and S. Shen, “Concept connotation and training strategy of design thinking,” *Modern distance education research*, vol. 18, no. 6, p. 24, 2016 (in Chineses).
- [4] K. dong, *Research on Scratch Learning Activity Design in Primary School from the Perspective of Design Thinking*, Shandong Normal University, Shandong, (in Chineses), 2020.
- [5] K. Pelaez, *Latent Class Analysis and Random forest Ensemble to Identify At-Risk Students in Higher Education*, San Diego State University, San Diego, California, 2018.
- [6] H. Takeda, S. Yoshida, and M. Muneyasu, *Tag-based Video Retrieval with Social Tag Relevance Learning*, IEEE, in *Proceedings of the 2019 IEEE 8th Global Conference on Consumer*

- Electronics (GCCE)*, pp. 869–870, IEEE, Osaka, Japan, October 2019.
- [7] D. Zhang, “A comprehensive theoretical framework for multimodal discourse analysis,” *China foreign languages*, vol. 1, pp. 24–30, 2009, (in Chinses).
 - [8] J. Cross, “Comprehending news videotexts: the influence of the visual content,” *Language, Learning and Technology*, vol. 15, no. 2, pp. 44–68, 2011.
 - [9] B. Han, “Language testing, theory, practice and development,” *Foreign Language Teaching and Research*, vol. 1, 2001 (in Chinses).
 - [10] M. Qian, B. Zhao, and Y. Gao, “Exploring the training path of design thinking of students in educational technology,” in *Proceedings of the 2019 IEEE International Conference on Computer Science and Educational Informatization (CSEI)*, pp. 315–319, IEEE, Kunming, China, August 2019.
 - [11] W. Ge, H. Bai, and H. Ma, “Design thinking into the design of mixed curriculum and teaching intervention effect,” *Modern Educational Technology*, vol. 30, no. 7, pp. 42–49, 2020, (in Chinses).
 - [12] Q. Huang, H. Feng, and Li Liu, “Multimodal video scene segmentation optimization algorithm based on convolutional neural network,” *Computer application research*, vol. 39, no. 5, pp. 1595–1600, 2022, (in Chinses).
 - [13] V. Chasanis, A. Likas, and N. Galatsanos, “Scene detection in videos using shot clustering and sequence alignment,” *IEEE Transactions on Multimedia*, vol. 11, no. 1, pp. 89–100, 2009.
 - [14] P. Sidiropoulos, V. Mezaris, I. Kompatsiaris, H. Meinedo, M. Bugalho, and I. Trancoso, “Temporal video segmentation to scenes using high-level audiovisual features,” *IEEE Transactions on Circuits and Systems for Video Technology*, vol. 21, no. 8, pp. 1163–1177, 2011.

Research Article

Personalized Information Service System of Smart Library Based on Multimedia Network Technology

Juan Wang 

Library of Jiaxing University, Zhejiang Province, Jiaxing City 314001, China

Correspondence should be addressed to Juan Wang; wjhhs@zjxu.edu.cn

Received 23 May 2022; Revised 15 June 2022; Accepted 4 July 2022; Published 7 September 2022

Academic Editor: Le Sun

Copyright © 2022 Juan Wang. This is an open access article distributed under the Creative Commons Attribution License, which permits unrestricted use, distribution, and reproduction in any medium, provided the original work is properly cited.

Scientific and objective book quality evaluation and research on the value of books in the smart library are conducive to improving the reading needs of readers. However, it is difficult to obtain the important coefficient of the subjective and objective weight of the personalized information service index of the smart library at present, which has the problem of poor system performance. Therefore, a personalized information service system of the smart library based on multimedia network technology is designed. In multimedia network technology, the data collector module, data retriever module, and data memory module of the system hardware are designed. The Ethernet interface is connected through three buses to ensure the efficient operation of the system; according to the hardware, the software flow is introduced, which is divided into UI layer, logical business layer, and data access layer. On this basis, the application program is designed, all operation instructions follow the association rules, and the single-chip microcomputer is connected with the voice chip through the SPI serial port, so as to complete the design of the personalized information service system of the smart library. The experimental results show that the average absolute deviation of the designed system is small, the comprehensive performance is strong, and the update delay is kept within 0.6 s, which can improve the work efficiency.

1. Introduction

With the continuous development of society in recent years, the smart library, as the “concentration place” of books, is also the best place for readers to acquire knowledge and information in depth [1, 2]. Books make an important contribution to society and people’s acquisition of cultural knowledge and are also an important product of human civilization and development [3, 4]. Titles were there was a substantial growth in recent years, at the same time there were many behind the rapid growth of performance driven by economic interests of hidden trouble, the main performance for the quality of books has plummeted, and similar content in the books published, and follow the repeat publishing phenomenon everywhere so that the books are of variable quality [5]. Due to the continuous development of information and communication technology and the wide application of the Internet, the personalized information service system management of books in smart libraries has

become one of the main themes of the current library management reform and development [6, 7]. In this case, it is necessary to effectively design the personalized information service system in the smart library and establish a complete and scientific book quality evaluation index system in the smart library to identify the book quality in the smart library, so that more excellent books can stand out [8, 9].

Because the design method of the personalized information service system of the smart library has far-reaching development significance, it has also become a hot topic studied by experts and scholars, and has attracted extensive attention. Reference [10] proposes the role of media resource center in bringing novelty and creativity to Nigerian school library services. This article reveals the novelty of the functions of the center, especially in training qualified personnel to serve as librarians, media experts, reading teachers, and other school media personnel in Nigeria’s preschool, primary, and postprimary education institutions, as well as organizing programmes related to children’s

reading and library use in Nigeria. Reference [11] proposes to evaluate the impact of traditional and digital marketing practices on university library services and resources. Determine how digital and traditional marketing methods can raise awareness among users and make better use of library services and resources. Understand the role of library staff in university library marketing practice and technology in digital and traditional ways. Based on quantitative research methods, cross-sectional survey research methods were used for data collection.

Although the above methods have made some progress, the application of multimedia network technology is not particularly sufficient, so the design of the intelligent library personalized information service system is based on multimedia network technology. Multimedia network technology refers to the text-based data communication and the text-based communication technology, including file transfer, e-mail, remote login, network news, and e-commerce. The technology is a comprehensive, interdisciplinary technology. It integrates the computer technology, network technology, communication technology, and a variety of information science technology achievements and has become the world's fastest developing and the most dynamic high-tech. In multimedia network technology, the data collector module, the data retrieval module, and the data storage module of the system hardware are designed, and the Ethernet interface is connected by three buses to ensure the efficient operation of the system. According to the hardware analysis software process, it is divided into UI layer, logical business layer, and data access layer. On this basis, the application program is designed, all operation instructions follow association rules, and the MCU is connected with the voice chip through the SPI serial port, thus the personalized information service system of the smart library is designed. The application in the personalized information service system of the intelligent library has remarkable effects, and the designed system has high performance.

2. Personalized Information Service System of Smart Library under Multimedia Network Technology

In multimedia network technology, the data collector module, data retrieval module, and data memory module of the system hardware are mainly designed, and the Ethernet interface is connected through three buses to ensure the efficient operation of the system; according to the hardware, the software process is introduced, which is divided into UI layer, logic business layer, and data access layer; on this basis, the application program is designed, all operation instructions follow the association rules, and the single-chip microcomputer and the voice chip are connected through the SPI serial port, thus completing the design of the personalized information service system of the smart library.

2.1. Hardware Design of the Personalized Information Service System of Smart Library. The basic components of multimedia network technology are: CD-ROM with optical drive,

which is an important symbol of multimedia network technology system; It has the functions of A/D analog-to-digital conversion and D/A digital analog conversion, which can convert the analog signal and digital signal of voice to each other, so that the multimedia network technology has high-quality digital voice function; display with high definition [12, 13]. Under the multimedia network technology, the establishment of the personalized information service system of the smart library is the basis to ensure better service of resources. It can truly provide resources according to users' needs and enable users to obtain the richest resources, if allowed [14, 15]. The hardware function of the designed intelligent library personalized information service system is to use the client to feed back the data resources that customers need to retrieve and use the data collector module to collect library resources, and the data integrator will integrate and process the collected resources. The data searcher module will check and search the integrated data resources and finally feedback to the user by the data memory module [16]. The hardware structure of the personalized information service system of the smart library is shown in Figure 1.

The system hardware in Figure 1 applies multimedia network technology to share the resources of Smart Library. The system hardware adds a large number of embedded products to support various cloud classroom systems, improve teaching quality, and ensure students' learning efficiency [17].

2.1.1. Data Collector Module. The personalized information service system of the smart library designed in this paper can realize high-quality positioning collection, and compress the collected audio and video to meet the low-power requirements of the system [18, 19]. The internal chip of the collector is the GD32F103RCT6 chip, which was launched by Shenzhen Zhuocun Electronic Technology Co., Ltd. and has the characteristics of multifunctional multimedia application, which is convenient for collection, compression, and transportation [20, 21]. The GD32F103RCT6 chip consumes very low power. Generally, the chip can maintain normal acquisition work above 5V voltage. The acquisition speed under low voltage can also reach 10000 MIPS, and the acquisition speed under high voltage is higher [22, 23]. The acquisition capability fully meets the acquisition requirements of large-scale library digital resources, and the acquisition accuracy is much higher than that of other chips, with an accuracy of 10 bits or even more [24]. The power supply mode of the data collector module is dual power supply of internal and external interfaces, and the internal interface is connected to the external interface to ensure the continuous input of voltage [25]. The collector is automatically connected to the wireless network. After signal coding and synthesis, it is transmitted to the wireless network data terminal, stored in the terminal, and recorded on the hard disk. The collector structure is shown in Figure 2.

When collecting video signals, the collector in Figure 2 selects SCLK as the clock to record all signals, and the input video is one video. When collecting GPS signals, data

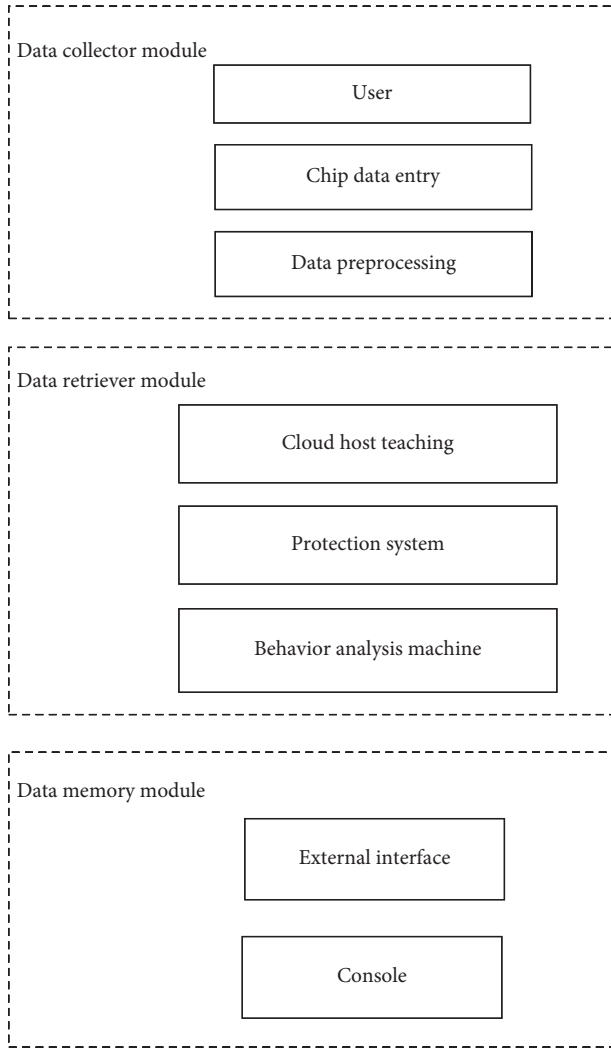


FIGURE 1: Hardware structure of the personalized information service system of smart library.

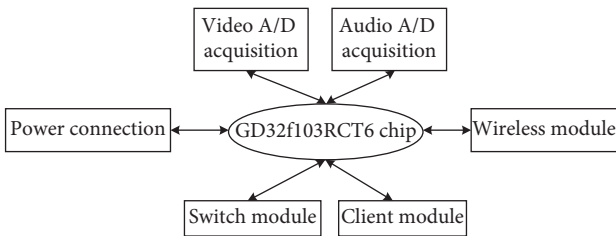


FIGURE 2: Collector structure.

transmission signals, RX data reception signals, and asynchronous signal interfaces are used as power interfaces, and the maximum baud rate supported is 2.56 Mbyte/s. When collecting, it is necessary to connect and receive personalized information service system signals. The positioning accuracy of GPS signals is very strong, and the error rate is less than 4 m, which can locate high-speed mobile signals [26, 27]. The signal collector is connected by PCI and HPI, and the bus interface is an Ethernet interface. The transceiver can send and receive 10 M~100 M personalized information service

data. In order to realize the simultaneous transmission of service data network, a wireless module is added in the system.

2.1.2. Data Retriever Module. The data searcher module is the core part of the hardware of the personalized information service system of the whole Smart Library. The searcher adopts the high-precision BAM6 chip developed by TRM Company in Norway. TRM fully analyzed the shortcomings and advantages of the previous two generations of BAM5 and BAM4 when developing the BAM6 chip. Therefore, this chip is significantly better than the previous two generations of chips in working time and retrieval efficiency [28]. The working delay time of the BAM6 chip is very short, only 10 minutes μ s. The rapid mode is used to control the retrieval speed, so the speed is very high. There are many retrieval interfaces inside. When the searcher runs, the interfaces will be connected together and work at the same time, which greatly reduces the working time, strengthens the retrieval ability, and retrieves more library digital resources [29]. The BAM6 chip requires the working voltage to be above 20 V and the data packet length of the chip is 45 B. It works under the multimedia network technology and the data retrieval rate is 80 Mb/s. However, in the low-voltage state, the chip will enter the automatic sleep mode and cannot start working.

2.1.3. Data Memory Module. In order to improve the storage efficiency of the hardware memory of the personalized information service system of the smart library, a flash memory with large storage range and low manufacturing cost is selected. A single-chip microcomputer is added to the memory to increase the storage capacity and reduce the floor area. The memory structure is shown in Figure 3.

There are three buses outside the memory, each bus is connected with an Ethernet interface, and different interfaces are connected with different signals [30]. The three wire buses are as follows:

Bus 1: connect signals in I/O mode, input and output in two-way way, and realize two-way exchange of data. The remark mode is I/O.

Bus 2: connect the signal in OUT mode, output the signal in one-way, and control the signal to enter.

Bus 3: connect the signal in BUSY mode, and the input mode is busy signal input.

2.2. Software Design of the Personalized Information Service System of Smart Library. In order to realize the software design of the intelligent library personalized information service system and complete the data receiving and processing, it communicates with the system terminal host computer through the wireless sensor network RS232 serial communication protocol of multimedia network technology. The gateway of the intelligent library personalized information service system uses socket process communication combined with a multithreading

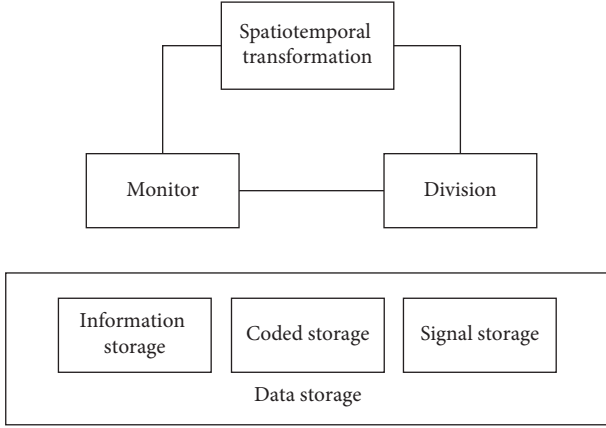


FIGURE 3: Memory structure.

mechanism to complete the communication with the intelligent library personalized information service system terminal host computer [31]. The software structure of the personalized information service system of the smart library is shown in Figure 4.

As shown in Figure 4, the specific contents of the system software are as follows:

- (1) The UI layer of the intelligent library personalized information service system based on multimedia network technology, that is, the user interface of the intelligent library personalized information service system, is mainly used to realize the organic interaction between the intelligent library personalized information service system and readers, including the design of book borrowing, return, query interaction, reader information management, user interface attribute configuration, and so on. The UI layer is connected with the logical business layer (UI layer service providing layer). The UI layer of the intelligent library personalized information service system based on multimedia network technology designed in this paper includes two parts: RFID tag reading and writing component and user page component using the ISO/IEC14443 protocol. The RFID tag reading and writing component using the ISO/IEC14443 protocol is essentially the interface part between the PC and the RFID RF terminal to realize the data reading and writing function of the RFID RF terminal. The design of UI layer interface components mainly includes the book borrowing management module, reader information management module, book ID information management module, and system parameter attribute setting [32].
- (2) The logical business layer of the intelligent library personalized information service system based on multimedia network technology: the main function is all logical operation and processing of readers and managers.
- (3) Data access layer of the intelligent library personalized information service system based on multimedia network technology: it provides services for all

logical operation and processing processes of readers and managers, and is mainly responsible for data access of the intelligent library personalized information service system database.

2.3. Application Design. The personalized information service system of the smart library connects the single-chip microcomputer with the voice chip through an SPI serial port, and all operation instructions must follow the association rules [33, 34]. All serial data transmission must be kept at a low level, and a high level should be used between two instructions. In order to ensure system security, a user authentication stage should be added in the process of application programming, and the system reminder function can be realized only through authorization.

In the implementation process, the layer-by-layer search iterative method is used to control the reminder function by calculating the confidence of association rules. The specific calculation contents are as follows:

$$D_{abc} = A_a \times B_b \times C_c. \quad (1)$$

In formula (1), A_a represents the total amount of all data in the personalized information service data item set, B_b represents the total amount of all data in the item set contained in the smart library database, and C_c represents the total amount of support corresponding to each subservers.

In the application structure, the storage and playback of reminder instructions are controlled by pressing the key to realize the reminder function. Therefore, the elimination of key jitter and key response are introduced [35, 36]. The key jitter time is determined by the equipment performance. The software delay is used to detect whether the key is really pressed, which effectively avoids the key jitter time.

In order to reduce the error, set F to represent the end value of the counter, so as to obtain the key cycle as follows:

$$Y_H = (F - C_s) \times T_z. \quad (2)$$

In formula (2), C_s represents the initial value of counting and T_z represents the clock cycle of a single-chip microcomputer. According to the key cycle shown in formula (2), the reminder time can be accurately mastered to avoid the delay problem of traditional system reminder.

When the system is started, the relevant reminder information is displayed on the display screen, and the pre-stored information is selected through the relevant keys of the keyboard. Under the multimedia network technology, the reminder instruction can be issued through the single-chip microcomputer controller of the hardware module to complete the design of the application program of the personalized information service system of the smart library.

3. Experimental Study

In order to test the actual working effect of the personalized information service system of the smart library based on multimedia network technology, an experiment is designed. The experimental environment is Intel(R) Pentium(R) 4, the

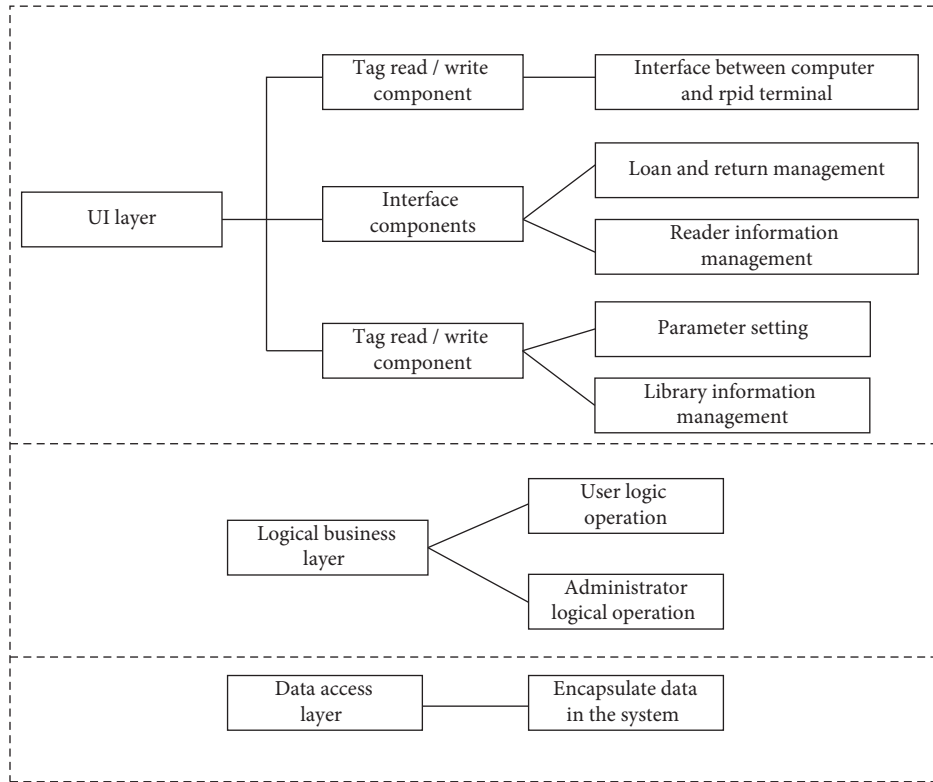


FIGURE 4: Software design of the personalized information service system of smart library.

CPU is 2.40 GHz, the memory is 1024 MB, and the operating system is Microsoft Windows XP SP3. Other experimental parameters are shown in Table 1.

According to the contents of Table 1, this paper uses the system in this paper, the system in reference [10] and the system in reference [11], respectively, to carry out the comparative experiment of intelligent library personalized information service system design. Three different methods are used to compare the accuracy of the personalized information service of the smart library. The average value of absolute deviation P_{JC} is used as the evaluation index of the accuracy of the personalized information service system. The average value of absolute deviation, i.e. the average deviation, refers to the average value of the absolute deviation of each measured value. The smaller the value, the better the effect of the personalized information service of the smart library. The calculation method is shown in

$$P_{JC} = \frac{\sum_{i \in S} |U_i - W_i|}{|S|} \quad (3)$$

In formula (3), $|S|$ represents the book quality evaluation data set, U_i represents the actual scoring value of readers on item i Book personalized information service scheme in the book quality evaluation data set, and W_i represents the predicted scoring value of readers on item i scheme given by the book personalized information service system. Compare the average absolute deviation (%) of three different methods for personalized information service of the smart library, and the results are shown in Figure 5.

Through the analysis of Figure 5, it can be seen that the average absolute deviation of the personalized information service of the smart library using the system in this paper is lower than that of reference [10] system and reference [11] system. This is mainly because in the process of designing the personalized information service system of the smart library using the system in this paper, high-quality positioning acquisition can be realized, and the collected audio and video can be compressed. Get the important coefficient of subjective and objective weight of each evaluation index of the personalized information service in the smart library, so that the average absolute error of the personalized information service in the smart library using this system is low.

In order to further verify the effectiveness of the designed system, it is necessary to comprehensively analyze the effects of different performance of the system, and compare and analyze the storage performance, operation difficulty coefficient, expansion performance, security performance, and integration performance, respectively. The comparison results are shown in Table 2.

It can be seen from Table 2 that the storage performance of the system in this paper is good, the operation difficulty coefficient is small, the expansion performance and security performance are good, and it has the ability of data sharing and integration at the same time. While the storage performance of reference [10] system is general, the operation difficulty coefficient is large, the expansion performance is good, but the security performance is poor, it does not have data sharing, and the integration ability is also poor. Reference [11] system has general storage performance, large

TABLE 1: Experimental parameter setting table.

Serial number	Entry name	Parameter content
1	Transmission signal	Audio signal, video signal, and GPS signal
2	Data line distance	1500 m
3	Input interface	TUB interface
4	Output interface	VUTR interface
5	Resolving power	One hundred and sixty \times 128 dpi
6	Operating hours	Usually 24 h
7	Power consumption	<1 W

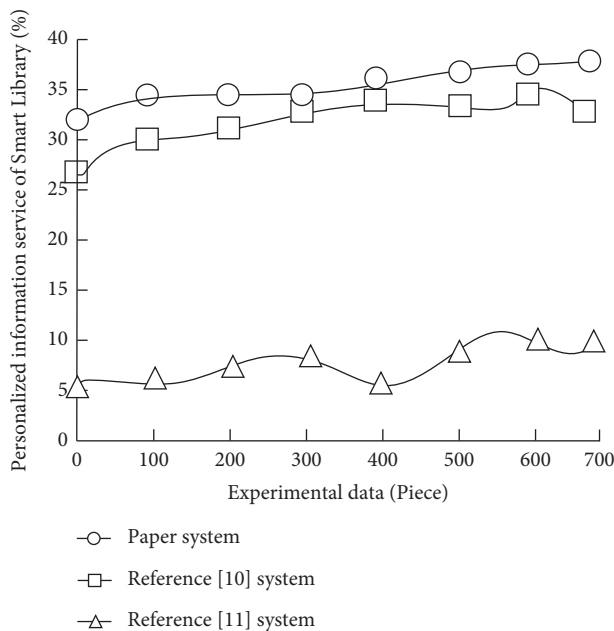


FIGURE 5: Comparison results of average absolute deviation of personalized information service of smart library under different methods.

operation difficulty coefficient, and poor expansion performance, but it has good security, data sharing, and general integration ability. Based on the traditional system, the designed system improves the storage performance of the system to make the storage performance of the designed system better.

Continue to explore the effects of the personalized information service system of the smart library based on multimedia network technology. The working frequency of the system is detected every 60 s, and there is no waiting time when readers query relevant book information. The time difference between the actual database update frequency and the corresponding book information update frequency of the designed system is defined as the update delay (s). The comparison results are shown in Figure 6.

According to Figure 6, compared with reference [10] system and reference [11] system, the book information refresh frequency of the personalized information service system of the smart library based on multimedia network technology designed in this paper can meet the practical requirements of the smart library. The system update delay is kept within 0.6 s, which can effectively realize multiple links such as on-board book inventory, return to the shelf, and query circulation, and greatly improve the work efficiency of the system.

To sum up, the designed system has good performance and realizes the intelligent inventory function and personalized service of personalized information service of the University Smart Library. With the help of the application of the personalized information service system of the University Smart Library, the work progress of the library and the work efficiency of librarians are greatly improved, which can better serve readers.

4. Discussion and Analysis

In terms of multimedia network technology, aiming at the development of personalized information service of the smart library, the countermeasures are as follows:

4.1. Improving the Management Mechanism of Personalized Information Service. Due to the lack of a macro-control mechanism in China's libraries, in order to coordinate and develop libraries and realize the common knowledge and sharing of information resources, China's higher education document guarantee system has been established. Strengthen the cooperation between the system and its member museums, improve the service level of higher education, and give full play to the maximum social and economic benefits. Strengthening the service consciousness and management means alone cannot meet the requirements of improving the service quality of the library. The cooperation between departments, the adjustment of structure, and the unification of the evaluation system are indispensable. Master the information needs of users, track and evaluate the service quality, pay attention to the feedback of user satisfaction, adopt incentive mechanism to stimulate the initiative of service personnel, and provide users with comprehensive and high-quality personalized information services. To develop the library personalized information service, the improvement of library personalized information service mechanism plays a very important role in the development of the smart library.

4.2. Strengthening the Construction of Information Service Resources

4.2.1. Strengthening the Content Construction of Information Resources. Establish a professional navigation database and a characteristic database. In order to cope with the rapid expansion and disorder of network information resources, the smart library should collect, sort, and classify the

TABLE 2: Comparison of different performance of different platforms.

Performance	Paper system	Reference [10] system	Reference [11] system
Storage performance	Preferably	Commonly	Commonly
Operation difficulty coefficient	Less	More	More
Extended performance	Preferably	Good	Poor
Safety performance	Preferably	Difference	Preferably
Data sharing	Have	No	Have
Integration performance	Preferably	Poor	Commonly

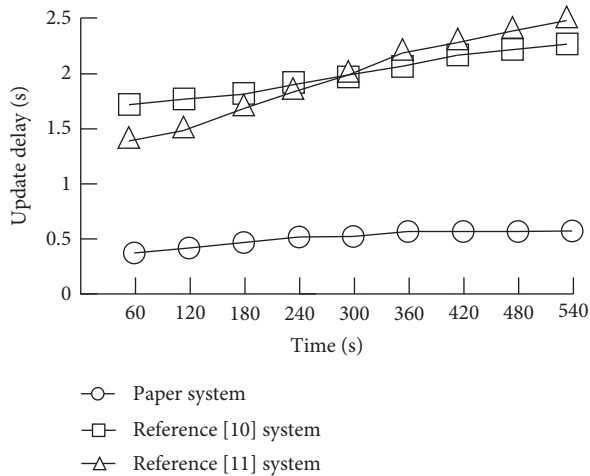


FIGURE 6: Book information update delay of the personalized information service system of smart library.

network information resources according to the specialty according to the characteristics of teachers and students, for the purpose of meeting users' learning and scientific research, highlight the professionalism of subject navigation, and establish professional navigation links. For the construction of information resources, the smart library is based on the careful investigation of databases at home and abroad. According to the professional setting of the university, the focus of scientific research and the information needs of users, combined with the library's collection resources, the smart library establishes a characteristic database according to a certain discipline, specialty, or local characteristics.

4.2.2. Strengthening the Organization and Integration of Information Resources. Resource integration and service integration are the main contents of information resource integration. Resource integration refers to the integrated information system formed by classifying and sorting the existing information resources. Service integration needs to build a personal information database, which includes the basic information of users and feedback information of users on services. Compared with traditional information services, in the organization of information resources, the new requirements of personalized information services are: the content should be targeted, clear, easy to understand, open, and flexible; in the navigation system, the classification should be detailed and reasonable; the user interface should be friendly; the evaluation ability and information navigation should be strong; and the cross-platform seamless

connection of information resource content should be realized. The library needs to sort out and classify the discrete electronic resources and establish a professional navigation database with a friendly interface, powerful functions, and comprehensive according to the needs of users.

4.2.3. Strengthening the Co-Construction and Sharing of Information Resources. In the school, each department will establish its own library reference room according to its own situation, which overlaps with the resource construction of the library, resulting in a low utilization rate and a waste of material and human resources. Therefore, strengthening the cooperation between reference room and library and jointly building and sharing information resources in the school is the main measure of information co-construction and sharing. Smart libraries can give full play to their respective advantages of document resources, which not only avoids the repeated construction of resources but also enriches the acquisition of users' information resources.

4.3. Changing the Service Concept and Improving the Quality of Service Personnel. The establishment of a humanistic care service concept of "people-oriented, user-first" is very beneficial to the active and effective development of personalized information services in the library. "People-oriented and service-oriented" refers to putting the needs of users in the first place, taking the completion of this goal as the fundamental purpose of the work, all for the sake of users and convenience, and providing users with maximized and optimized services. To meet the service needs of users, service personnel should have strong information analysis ability and language ability to answer various questions for users; we should broaden the scope of knowledge and strengthen learning, especially the relevant knowledge of library and information; master skilled information skills; be able to analyze, integrate, and summarize information; and master the sources and retrieval methods of various types of information. Only with these can service personnel improve the service level and provide users with obvious personalized information services. "Subject Librarian" is a kind of special personalized information service talent arising from the problems of low technical level, single knowledge, and poor information analysis ability of library service personnel. Subject librarian refers to the person that the library sets up to establish contact with a certain department or discipline specialty as the counterpart unit, build a bridge between the department, discipline specialty, and the library, communicate with each other, and actively collect and provide

document information services for users. This kind of service personnel needs to have a certain level of foreign language, be familiar with library business, be skilled in computer operation, have high educational background and professional title, profound cultural heritage and strong language ability, and be able to provide powerful help for teaching and scientific research.

4.4. Strengthening the Construction of Personalized Information Service Systems. To develop a personalized information service system, the library should have both rich system resources and rich system functions, and be able to provide comprehensive services. The designed system interface should be concise, intuitive, and clear-cut, and users should be able to make personalized customizations; it should be able to realize automatic integration with other resource systems, which not only saves users' time but also reduces users' use burden; and can protect user privacy. The measures to improve the personalized information service include the following: establishing a professional navigation system, building an effective information space, systematically organizing relevant information resources, providing users with a good retrieval interface, information customization, and information push. The system can provide users with selection services. Users can also select and manage information to realize their interactive functions. The problems encountered in use can be solved in time to improve the service quality.

To sum up, under the multimedia network technology, the smart library will encounter many problems in the process of building personalized information services. The smart library needs to improve its personalized service management mechanism, strengthen the construction of information resources, strengthen the construction of personalized information service system, and strengthen the research and training of user needs. While changing the service concept, library service personnel should also pay attention to the improvement of their own quality, improve the service quality, and make the library's personalized information service develop continuously.

5. Conclusions and Prospects

5.1. Conclusions

- (1) The average absolute deviation of the intelligent library personalized information service system based on multimedia network technology is lower than that of the reference system, which has a good effect. It can realize high-quality location collection and get the important coefficient of subjective and objective weight of each evaluation index of personalized information service a in smart library.
- (2) The system in this paper has good storage performance, low operation difficulty coefficient, good expansion performance, and security performance, as well as data sharing and integration ability.
- (3) The book information refresh frequency of the personalized information service system designed in this paper can meet the practical requirements of the smart library, and the system update delay is kept within 0.6 s, which effectively improves the working efficiency of the system. With the application of the personalized information service system of the university intelligent library, the progress of library work and the work efficiency of librarians have been greatly improved, and it can serve readers better.

5.2. Prospects. The personalized information service system of the smart library realizes the unattended of the library, uses the accurate positioning of multimedia network technology and the realization of self-help borrowing and returning books, reduces the labor intensity of the staff, and enables them to devote more energy to scientific research. However, in order to serve college teachers and students more perfectly, there are still a lot of problems to be solved in order to explore a more intelligent, personalized information service mode.

The further development of the personalized information service system of the smart library can use the mobile device library platform for subsequent docking on the basis of this information service system and realize a more efficient and intelligent library information service system through the construction of the mobile platform. For example, it can realize that the mobile device can receive an update of all library information, the system can automatically urge the return of books, etc. Interlibrary communication and information sharing can be achieved by relying on the mobile platform to improve the quality of interlibrary communication and information sharing. Relying on the advantages of multimedia network technology, we can popularize the installation and popularization scope of book borrowing and returning terminals, open library resources, break the constraints of time and space, and realize the possibility of systematic remote management and real-time circulation of books through the push of terminal points, so as to improve the circulation times in the book cycle.

The development of technology and the popularization of networks promote the development of library cause. In multimedia network technology, the personalized information service of the Smart Library continues to develop and progress with various changes. The specific contents are as follows:

- (1) Under the network environment, the information service of smart library is gradually open to the society from the closed state that only faces the teachers and students of the University. Each smart library will no longer "act in its own way," but build a network information platform and share information resources through networking.
- (2) The smart library is constantly changing its service mode due to the change of users' needs, changing from the traditional passive service mode to an active service, actively understanding the new trends of users, and adjusting the service content in time.

- (3) The service personnel of smart library are aware of the shortcomings of the traditional service concept, actively change their own service concept, and gradually establish a new concept of “people-oriented, user-first.”
- (4) The knowledge cultivation and ability of service personnel in Smart Library are constantly improving to adapt to the continuous development of personalized information service. In particular, the establishment of “Subject Librarian” is a prominent embodiment of talent training in personalized information service.
- (5) The strengthening of the awareness of training users by the smart library enables more users to master the ways and means of obtaining information and master the retrieval skills and tools, which is conducive to users to make better use of various resources in the library and improve the utilization rate of library information resources.

Data Availability

The raw data supporting the conclusions of this article will be made available by the author without undue reservation.

Conflicts of Interest

The author declares no conflicts of interest regarding this work.

Acknowledgments

This work was supported by Foundation Item Zhejiang Public Welfare Technology Application Research Project (LGG19E050017) and supported by Jiaxing Federation of Social Science, under No. JSKGH2014102.

References

- [1] D. Williams and C. Wavell, “The impact of the school library resource centre on learning,” *IASL Annual Conference Proceedings*, vol. 7, no. 11, pp. 803–806, 2021.
- [2] P. Moore, “Primary school children’s interaction with library media,” *IASL Annual Conference Proceedings*, vol. 27, no. 3, pp. 7–11, 2021.
- [3] A. D. Ewbank and J. Y. Kwon, “School library advocacy literature in the United States: a content analysis,” *IASL Annual Conference Proceedings*, vol. 2, no. 2, pp. 1–10, 2021.
- [4] R. Zhao, “Research on Library hybrid recommendation technology based on cloud computing platform,” *Modern electronic technology*, vol. 42, no. 23, pp. 145–149, 2019.
- [5] T. T. Yin and X. Y. Zeng, “Design and analysis of library collection resource recommendation model from the perspective of deep learning,” *Modern intelligence*, vol. 39, no. 4, pp. 103–124, 2019.
- [6] G. C. Ruan, F. Xie, and S. W. Tu, “Application Research on diversity of Library recommendation system based on word2vec,” *Library Journal*, vol. 39, no. 3, pp. 124–132, 2020.
- [7] Y. Q. Duan, Y. M. Liu, and S. Q. Cai, “Research on the influence of personalized recommendation users’ information adoption behavior in Digital Library -- the intermediary effect of information adoption intention,” *Modern intelligence*, vol. 39, no. 2, pp. 85–93, 2019.
- [8] Q. H. Wang, “Research on personalized fast recommendation algorithm of Library Based on data mining technology,” *Modern electronic technology*, vol. 42, no. 5, pp. 149–151, 2019.
- [9] F. Z. Ma and X. D. Li, “Re examining the multiple values of readers’ independent recommendation and purchase to resource construction -- Based on the analysis of readers’ recommendation data of Peking University Library,” *Journal of university library*, vol. 38, no. 1, pp. 57–62, 2020.
- [10] F. O. Oyewusi, “The role of abadina media resource centre in bringing novelty and creativity to school library services in Nigeria,” *IASL Annual Conference Proceedings*, vol. 2, no. 2, pp. 1–10, 2021.
- [11] N. Shah, S. Naeem, and R. P. Bhatti, “Assessing the impact of traditional and digital marketing practices on library services and resources in university libraries,” *Library Philosophy and Practice*, vol. 2021, no. 1, pp. 1–12, 2021.
- [12] P. Zhao, H. Zhou, C. Zhao et al., *Carbohydrate Polymers*, vol. 214, no. 5, pp. 44–52, 2019.
- [13] L. Wang, H. X. Yang, and N. Z. Sun, “Library book intelligent recommendation system based on wireless network technology,” *Modern electronic technology*, vol. 44, no. 13, pp. 85–89, 2021.
- [14] S. Rathee, A. Kumar, S. Kaushik, E. Kazimieras Zavadskas, A. Banaitis, and J. A. Garza-Reyes, “An mcda cause-effect factors model for the implementation of greenstone digital library software,” *Management Decision*, vol. 58, no. 11, pp. 2543–2564, 2020.
- [15] L. Bo, H. Li, Q. Guan, and Y. Liu, “Fine-grained sentiment analysis of university library social network platform based on CNN-BilstM-HAN Hybrid Neural Network,” *Journal of Agricultural Library and Information science*, vol. 34, no. 4, pp. 63–73, 2022.
- [16] X. J. Zhang, Y. H. Zhang, and F. Yang, “Research on document integrated retrieval method of digital library based on distributed structure,” *Electronic Design Engineering*, vol. 28, no. 12, pp. 35–38+43, 2020.
- [17] P. K. Kushwaha, S. P. Maurya, P. Rai, and N. P. Singh, “Prediction of petrophysical parameters using probabilistic neural network technique,” *Basics of Computational Geophysics*, vol. 1, no. 10, pp. 273–292, 2021.
- [18] H. Du, “Research on service mode and platform construction of smart library,” *Electronic Technology and Software Engineering*, vol. 7, no. 05, pp. 196–199, 2022.
- [19] J. I. A. N. Huang, “Fast retrieval of literature in smart library based on deep learning,” *Information & Technology*, vol. 12, no. 12, pp. 84–88+94, 2021.
- [20] Y. Yin, B. Zhang, and X. Shuai, “Based on seat for deep learning library management system design,” *Computer knowledge and technology*, vol. 12, no. 34, pp. 1–3, 2021.
- [21] X. Yang, “Personalized recommendation system for library bibliography based on collaborative filtering,” *Microcomputer application*, vol. 37, no. 09, pp. 169–171+175, 2021.
- [22] Y. Niu, L. Hui, and L. Zhao, “Pedestrian detection method based on the deep study in the library application,” *Journal of library journal*, vol. 40, no. 9, pp. 62–69, 2021.
- [23] B. Wang, “Research on library recommendation and borrowing based on big data,” *Information and computer (theoretical version)*, vol. 33, no. 17, pp. 150–152, 2021.
- [24] Y. Xiao, N. Li, and P. Xie, “Research on the application of machine learning in intelligent library,” *Journal of Shandong Library*, vol. 4, no. 04, pp. 63–67+71, 2021.

- [25] M. Tarhani, S. Sarkar, M. K. Eghbal, and M. Shadaram, "Efficient multicasting technique for elastic optical network," *IET Networks*, vol. 10, no. 1, pp. 34–42, 2021.
- [26] M. Yuan, "In wisdom library into the deep learning technology," *Journal of electronic and information technology*, vol. 5, no. 5, pp. 182–183, 2021.
- [27] C. Venkatesh Kumar and M. Ramesh Babu, "A novel hybrid grey wolf optimization algorithm and artificial neural network technique for stochastic unit commitment problem with uncertainty of wind power," *Transactions of the Institute of Measurement and Control*, vol. 4, no. 3, pp. 014233122110019–014233122110039, 2021.
- [28] F. Warsi, R. Khanam, S. Kamyra, and C. P. Suárez-Araujo, "An efficient 3D color-texture feature and neural network technique for melanoma," *Detection*, vol. 33, no. 1, pp. 121–136, 2021.
- [29] N. K. Singh, P. K. Gupta, and V. Mahajan, "Intrusion detection in cyber-physical layer of smart grid using intelligent loop based artificial neural network technique," *International Journal of Engineering, Transactions B: Applications*, vol. 34, no. 5, pp. 1250–1256, 2021.
- [30] X. W. Liu and X. Ma, "Simulation of sensitive information security retrieval in WLAN," *Computer Simulation*, vol. 37, no. 1, pp. 259–262, 2020.
- [31] F. Firdaus, S. Nurmaini, V. O. K. Putra et al., "Neural network technique with deep structure for improving author homonym and synonym classification in digital libraries," *TELKOMNIKA (Telecommunication Computing Electronics and Control)*, vol. 19, no. 4, pp. 1208–1217, 2021.
- [32] H. Kumar and S. Giri, "A new approach for solving the flow shop scheduling problem through neural network technique with known breakdown time and weights of jobs," *International Journal of Service Science, Management, Engineering, and Technology*, vol. 12, no. 1, pp. 77–96, 2021.
- [33] B. Mukunthan, "Efficient synergetic filtering in big data set using neural network technique," *International Journal of Computer Applications in Technology*, vol. 65, no. 2, pp. 134–144, 2021.
- [34] A. Jahani, S. Allahverdi, M. Saffariha, A. Alitavoli, and S. Ghiyasi, "Environmental modeling of landscape aesthetic value in natural urban parks using artificial neural network technique," *Modeling Earth Systems and Environment*, vol. 8, no. 1, pp. 163–172, 2021.
- [35] A. Dm, A. Skg, A. Rkt, B. Ms, and E. Uradc, "Automated accurate emotion recognition system using rhythm-specific deep convolutional neural network technique with multi-channel eeg signals," *Computers in Biology and Medicine*, vol. 34, no. 7, pp. 104–129, 2021.
- [36] R. Bhatia and N. Kaur, "Development of a faster region based convolution neural network technique for brain image classification," *Journal of Interdisciplinary Cycle Research*, vol. 8, no. 7, pp. 1216–1220, 2020.

Research Article

Using Pitch Feature Matching to Design a Music Tutoring System Based on Deep Learning

Jing Jiang 

College of Music and Dance, Zhengzhou Normal University, Zhengzhou 450044, China

Correspondence should be addressed to Jing Jiang; jiangjing@zznu.edu.cn

Received 27 May 2022; Accepted 10 August 2022; Published 6 September 2022

Academic Editor: Le Sun

Copyright © 2022 Jing Jiang. This is an open access article distributed under the Creative Commons Attribution License, which permits unrestricted use, distribution, and reproduction in any medium, provided the original work is properly cited.

It is a challenge for the current music teaching system to carry out teaching according to the difference of score difficulty and realize automatic grading. Therefore, identifying the difficulty of music score according to pitch is the key to individualize music teaching resources. This paper summarizes and analyzes the problem of pitch feature extraction in music teaching. In the pitch extraction, the audio signal is divided into frames, and the feature matching of high-pitched content in music teaching resources is realized by smoothing the pitch sequence. In addition, the pitch feature extraction algorithm in MIDI music score files is proposed, and the pitch feature matching model is constructed. Finally, a music tutoring system based on pitch feature matching is designed, including a music score learning tool, overall structure of system, and interaction between teachers and students. Tutoring strategies include three main functions: learning suggestions of knowledge points, skills in practice and training, and learning path adjustment. This study is helpful to further improve the music teaching model and realize intelligent and personalized music learning.

1. Introduction

With the rise of Internet teaching, the limitations of traditional teaching methods in time and space have been solved, and virtual teaching scenes and resources have been built by the network-based teaching platform, which makes the teaching behavior no longer confined to classrooms and classrooms. An intelligent learning guidance system uses artificial intelligence technology to simulate and learn the teaching methods of human teachers and furnishes them with customized learning ways and learning ideas as per the requirements of various students. In the educational experience, we can find out about their learning propensities and inclinations through language correspondence, conduct investigation, recreation, and so on and dynamically guide learners to master knowledge [1, 2]. In recent years, artificial intelligence (AI) technology has greatly promoted the development of intelligent tutoring system, formed a standardized structural framework, and produced many excellent products in computer foundation, language, medicine, mathematics, and other disciplines [3–5].

Musical Solfeggio is a course based on mastering the basic principles of music, which aims at cultivating students' abilities of reading music, singing music, memorizing music scores, recognizing music scores, and perceiving, analyzing, expressing, and imagining music. With the continuous development of the music education system, the teaching concepts of sight, singing, practice, and listening are constantly innovated. However, teaching and training in the classroom has been adopted for many years, which is not only wasteful, yet in addition, incredibly influences understudies' advantage in learning. Albeit increasingly more sight and sound apparatuses and showing programming are utilized in the study hall of solfeggio educating, they can help instructing, while the current internet-based courses and Internet learning stages just gives rich learning assets and different learning ways for students, and it can not meet the demand of intelligent teaching [6]. At the same time, the evaluation of students' ability and achievement is still done by teachers or experts, and the current scoring method can only evaluate the difference between singing performance and standard template. However, in the process of music

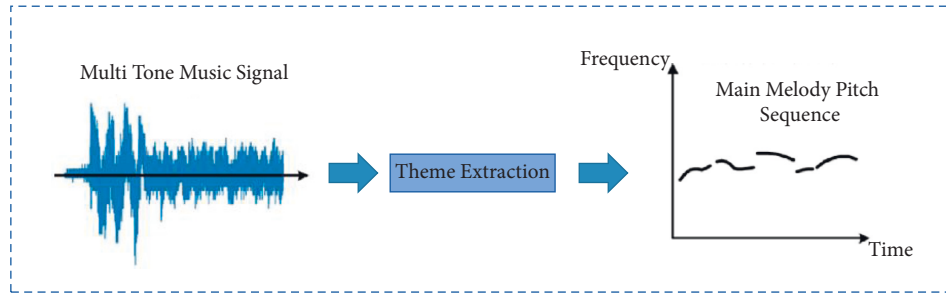


FIGURE 1: Pitch feature extraction process.

teaching, different music has different difficulty in singing, so there is a big error in the evaluation method that only considers the difference between template and performance [7]. In addition, the same problem as learning resources is that there is no uniform standard for the classification of music score difficulty level, and it depends on the subjective judgment of experts. In the evaluation of music teaching, the questions can only come from expert question banks or textbooks, while the individual inclination and expert level will influence the equilibrium of the trouble about the inquiries, which can not ensure the decency, exactness, and objectivity of the assessment [8, 9]. Therefore, it is also a challenge for the solfeggio teaching system to achieve automatic scoring according to the differences in score difficulty.

Therefore, this paper combines the characteristics of music, matches the characteristics of pitched content in music teaching resources, and designs an intelligent music tutorial system, which is helpful to further improve the music teaching model and realize intelligent and personalized music learning.

2. Research Basis of Pitch Feature Matching

2.1. Description of Pitch Features. Pitch is one of the most familiar note attributes, and intuitive understanding is the height of the note; as described in the previous chapter, the sound is composed of fundamental tone and overtone, and the part that determines the pitch of the sound is the fundamental tone. Physically, the vibration frequency, that is, Hertz, is used to describe the pitch of the sound. The pitch range recognized by human ears is about 20 to 20,000 Hz. Generally speaking, when people describe sounds, the higher the frequency, the higher the tone, which can be said to be a positive correlation [10].

According to the frequency, music can be divided into different pitches. The most commonly used method is the twelve-average law method, which divides an octave into twelve parts on average by a certain mathematical method of raising the power, which can improve the true performance of music and make the pitch reasonably distributed. In addition, the notation can be divided into numerical notation and alphabetic notation according to the different forms of notation symbols. The numeral notation uses numbers to indicate the pitch, and the short line under the numbers indicates the sound value, that is, the duration of notes; digital notation has the advantages of convenient

presentation and low learning difficulty. By using the law of twelve averages to divide the pitch, an octave can be divided into twelve points, each of which is called a semitone; similarly, an octave can be divided into six whole tones by the law of twelve averages.

2.2. Analysis of Pitch Feature Extraction. The research object of main melody extraction is polyphonic music composed of voice and one or more musical instruments. As shown in Figure 1, the target of main melody extraction is to extract the vocal pitch sequence defined as the main melody from such mixed audio signals.

Because the singing and accompanying note components have rich harmonic information, the harmonic characteristics of music signals can be fully utilized in the pitch estimation stage. When judging the pitch fundamental frequency, only the energy information of the fundamental frequency and its harmonic components plays a positive role, and other frequency energies are equivalent to noise here, which will interfere with the main melody extraction. However, due to the existence of harmonic characteristics, octave errors often appear in the main melody extraction results [11]. An octave error means that when the pitch is estimated, the pitch is mistakenly identified as one or more octaves different from the correct pitch, which makes it easy for people with healthy hearing to identify singing information from complex multisource music signals without being influenced by other accompaniments. However, it is extremely difficult to extract the main melody by computer, as shown in Figure 2, which is mainly caused by the following factors:

- (1) Multitone music signals are composed of the superposition of sound waveforms produced by all instruments in the recording. Many times these instruments are played at the same time. It is extremely difficult to separate the corresponding notes from different sound sources according to the frequency spectrum which is highly coupled and superimposed with the sound structure, and the later reverberation, echo, and other treatments will further increase the overlap of sound sources. Blurring the start and end time of the music signal makes spectrum separation more difficult.
- (2) Even if the fundamental frequency sequence of notes has been obtained, it is still necessary to judge which

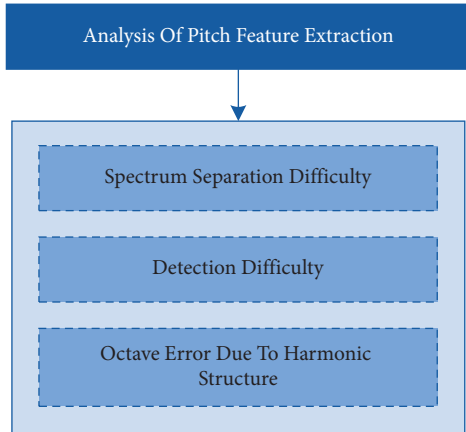


FIGURE 2: Problem analysis of pitch feature extraction.

pitches belong to melody and which belong to accompaniment. When the melody is singing but there is background harmony, it is more difficult to detect.

- (3) Because of the existence of harmonic structure, it is easy to produce octave errors.

For the existing methods, most methods based on pitch saliency have an unavoidable problem, that is, due to the harmonic characteristics of music signals, the algorithm can easily output the fundamental frequency of an octave before and after the correct melody pitch, resulting in octave errors. While the method based on source separation is more dependent on singing energy, for strong accompaniment, it is difficult for the model to correctly separate melody and accompaniment.

Therefore, this paper combines the characteristics of music and matches the characteristics of high-pitched content in music teaching resources based on the deep learning.

3. Pitch Feature Matching Based on Deep Learning

3.1. Deep Learning Theory. The purpose of deep learning is to establish a learning model similar to a brain neural network, which is a branch of machine learning. For machine learning algorithms, there are only one or two nonlinear feature structures. However, on complex problems, such as speech signal and image processing, these shallow structures have their limitations, while deep learning builds deep nonlinear structures, which can express richer information [12, 13]. In this paper, a fully connected layer neural network is adopted, as shown in Figure 3, it is a feedforward neural network with two hidden layers.

In order to make the network learn nonlinear characteristics and increase the complexity of the model, there is usually a nonlinear activation function between each layer this paper adopts the LRelu function, as shown in formula (1), which is a variant of ReLu.

$$\text{LRelu}(x) = \begin{cases} x, & x \geq 0, \\ 0.01x, & x < 0. \end{cases} \quad (1)$$

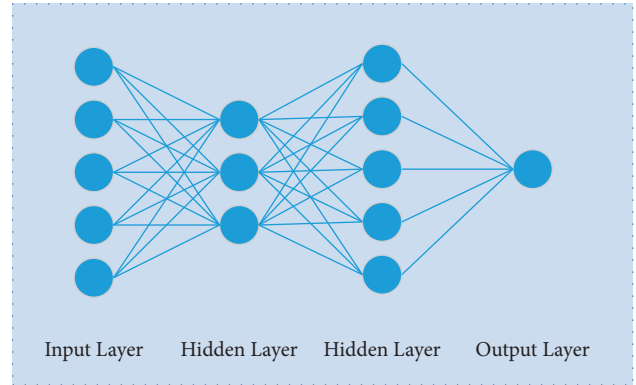


FIGURE 3: Fully connected neural network model.

The main melody extraction in this paper is actually the task of classifying pitches. In a neural network, for binary logistic regression, the output layer can be activated by sigmoid, and the real number field can be mapped to $0 \sim 1$ Range, this is the output probability of normal class. For multiclassification problems, the output layer can be activated by softmax, and its formula is as follows:

$$S_i = \frac{e^{z_i}}{\sum_{n=1}^N e^{z_n}}. \quad (2)$$

The training process of the neural network is a process of gradient iterative updating. Usually, the gradient descent method is used to find the optimal solution of the objective function, which makes the loss function smaller and smaller and makes the model learn the information of deep features from a large amount of data.

3.2. Feature Extraction Algorithm. In this study, the evaluation of music is based on the MIDI music score file, while MIDI uses pitch value and duration to describe notes in a music score, so it is necessary to extract pitch features and duration of solfeggio audio. The feature vector of music is usually obtained by the main melody, and MIDI files usually include multi-track accompaniment. It is very important to extract the main melody that can represent complete music information from a multitrack MIDI melody, whose extraction steps are shown in Figure 4.

3.2.1. Build Feature Vectors. Each note in the main melody corresponds to a characteristic point, which is described as follows:

$$v = \langle \text{Pitch}, \text{Time} \rangle, \quad (3)$$

where Pitch is the value of pitch, and the note value is derived from $0 \sim 127$; Time is the improvement of MIDI time, which represents the information of duration. The feature quantity corresponding to the main melody note sequence can be expressed as follows:

$$V = \{v_1, v_2, \dots, v_n\}. \quad (4)$$

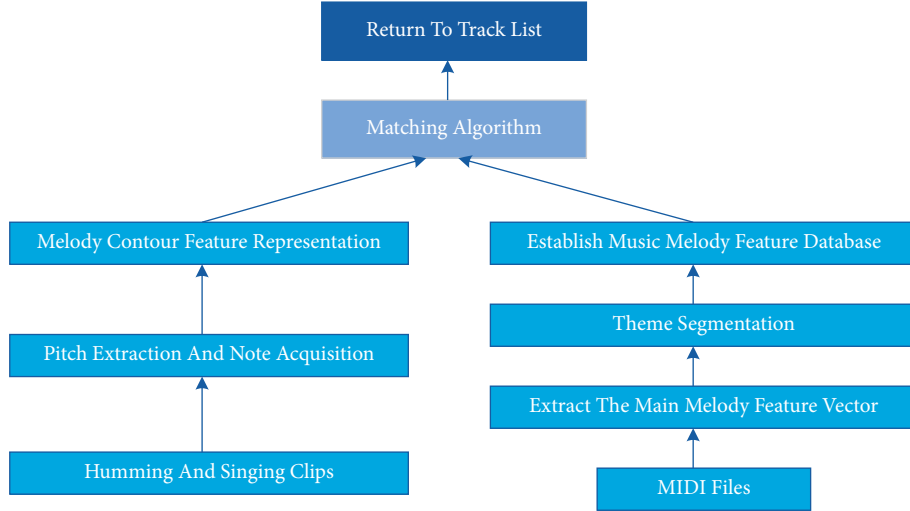


FIGURE 4: Steps of music feature extraction.

Among them, V is the sequence of note characteristic points of the whole music, n is the total number of notes.

Considering that there are phrases in music, the above vector can be further expressed as follows:

$$V = \{P_1, P_2, \dots, P_k\}. \quad (5)$$

Among them, V is the sequence of note characteristic points of the whole music, k is the total number of phrases.

$$P_i = \{v_{i1}, v_{i2}, \dots, v_{in}\}. \quad (6)$$

This feature vector can well express the melody and rhythm of the music.

3.2.2. Extraction of Pitch Pitch. The notes in each MIDI track are determined by two MIDI events: note on and note off. MIDI message: XX NN KK.XX represents the status byte, which determines 8 MIDI commands and 16 MIDI channels. The commonly used MIDI command 9x (X represents channel number) indicates that the note is on, and the data byte NN immediately following represents the pitch symbol (pitch), with a value of 1–127, and two consecutive notes are opened; the second note can be omitted to open the command 8x means off. KK means the key and release force (vel) value is 0~127. Command 9x followed by the key strength KK is 0, equivalent to note off. The Polyphony of music determines the simultaneous pronunciation of notes. In this paper, the value of the highest pitch note is selected according to the skyline algorithm, and the values of the remaining simultaneous notes are deleted.

According to the skyline algorithm, the notes with smaller pitch value can be removed and a MIDI event sequence can be obtained. The pitch stored in the MIDI file is expressed in hexadecimal. According to the MIDI note coding table, it is converted to a decimal system, and each value corresponds to the corresponding note. The pitch of a note is represented by the semitone value; the semitone and pitch frequency have the corresponding relationship expressed by the following formula:

$$\text{Pitch} = 69 + 12 * \log_2 \frac{f_0}{144}, \quad (7)$$

where 69 is the corresponding half-tone value of international standard A, f_0 represents the pitch frequency, and 144 is the frequency difference between two semitones.

3.2.3. Pitch Feature Matching. Assuming that each singer's goal is to sing the score accurately, the breaks should not last long and should be followed by a steady sub-sequence of pitches. In the pitch extraction, the audio signal is framed, and the pitch sequence obtained is also frame based. The breakpoint usually appears in the middle of two stationary signals, which only lasted 1–2 frames. Therefore, as shown in Figure 5, we can smooth the pitch sequence as follows:

- (1) The adjacent frames with equal pitch values in pitch sequence are regarded as a subsequence, and the number of frames is counted
- (2) After traversing the frame number of each pitch subsequence, the break point can be found where the frame number is between 1 and 2, and the pitch frame number before and after it is greater than 2
- (3) The pitch value corresponding to the breakpoint is set as the average pitch of the subsequences before and after the breakpoint
- (4) Median filter is used to optimize the pitch sequence

Assuming that the pitch sequences of the matching and template are respectively X and Y , where p represents pitch, t represents the number of frames, k is the number of subsequences with a continuous equal pitch in the sequence to be matched, and v is the number of notes in the template.

$$\begin{aligned} X & ((p_1, t_1), (p_2, t_2), (p_3, t_3), \dots, (p_k, t_k)), \\ Y & ((p_1, t_1), (p_2, t_2), (p_3, t_3), \dots, (p_v, t_v)). \end{aligned} \quad (8)$$

Replace frame matching with subsequence matching, then the calculation formula of distance is

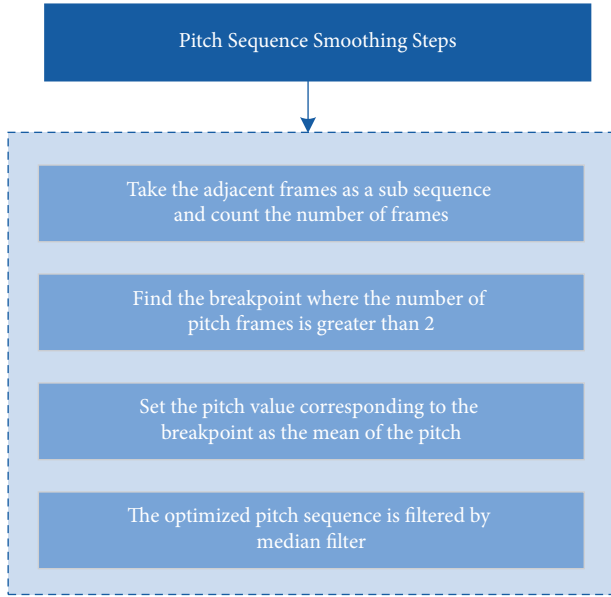


FIGURE 5: Steps of pitch sequence smoothing.

$$\text{dist}(x_i, y_j) = \sqrt{(p_i \cdot t_i - p_j \cdot t_j)^2}. \quad (9)$$

The formula of pitch path matching is as follows:

$$w(x_i, y_j) = m \left(\begin{array}{l} w(x_{i-1}, y_j) + \text{dist}(x_{i-1}, y_j) \\ w(x_{i-1}, y_{j-1}) + \text{dist}(x_{i-1}, y_{j-1}) \end{array} \right). \quad (10)$$

4. Design of Music Tutorial System Based on Pitch Feature Matching

4.1. Input of Musical Score. This research will be applied as a learning tool, to achieve the function by expanding the components, the following part mainly introduces the spectrum component that is difficult to realize. Considering that only the notes appearing in the music score need to be input in solfeggio practice, in order to reduce the difficulty of input and improve the fluency, there are two input methods in this paper.

4.1.1. Selective Input. Selective input means that the notes contained in the music score are provided in the input interface. After the user selects the input position, the system pops up the note selection interface, and the corresponding notes can be written into the staff and displayed.

4.1.2. Input by MIDI Symbol. In the MIDI standard, the pitch and duration of notes are respectively expressed by numerical values, in which the pitch value corresponds to the keys of a piano, and the pitch within each 8 degree is, respectively, expressed by 12 numerical values according to the 12-tone law. Because the range of voices that people can sing is limited, only 0–8 sound zones are provided, and the duration of notes is set by the time slider.

4.2. Overall Structure of the System. The music learning tutoring system includes a storage layer, strategy layer, and interaction layer. The storage layer is responsible for providing the databases needed by the system operation, including learner model base, knowledge model base, and learning resource base. The strategy layer is used for systematic decision-making and data analysis, it carries out personalized services such as learning resource push, resource management, intelligent learning guidance, learning effect statistics, and ability evaluation, with the data support of the strategy layer. And, then it analyzes students' learning process in real time, so as to dynamically construct and update their learning models; the interaction layer is the man-machine interface of the system, including system management, evaluation results display, learning progress display, ability level visualization, and interaction of learning process. The overall structure of the system is shown in Figure 6.

The interaction layer only directly accesses the storage layer to obtain data during data retrieval, and other interactions need to analyze the requirements through the strategy layer and then return the results to the interaction layer after making a decision.

4.2.1. Storage Layer. Learner model base: learner model base stores data of the learner model, including basic information of learners, solfeggio ability level, knowledge mastery, and learning history. Which provides the decision-making layer with the raw data needed for learning and analysis.

Knowledge model base: the knowledge model base is based on the knowledge model of solfeggio, including the main basic knowledge entities, solfeggio knowledge entities, and music knowledge entities.

Learning Resource Library: the resource library stores the examples, practice scores, and training scores needed in the learning process and establishes an index table according to the structure defined in the resource model, which facilitates the sorting and retrieval of resources.

4.2.2. Strategy Level. Ability evaluation: ability evaluation consists of two parts: evaluation strategy and evaluation algorithm. The evaluation strategy is the solfeggio scoring index and ability level calculation method, and the evaluation algorithm is a solfeggio scoring algorithm based on pitch characteristics proposed in Chapter 3. This module is responsible for evaluating learners' performance in exercises and tests, then dynamically update the data of the submodel of ability level and knowledge mastery in the learner model.

Learning tutor strategy: learning tutor strategy includes three main functions: learning suggestions of knowledge points, skills in practice and training, and learning path adjustment. The learning suggestions of knowledge points come from the attribute fields in the knowledge model; skill information is used to make the analysis of the difficulties and error-prone points contained in the current learning resources and then gives learning suggestions in combination with specific teaching methods; learning path adjustment refers to the degree of difficulty of adjusting learning

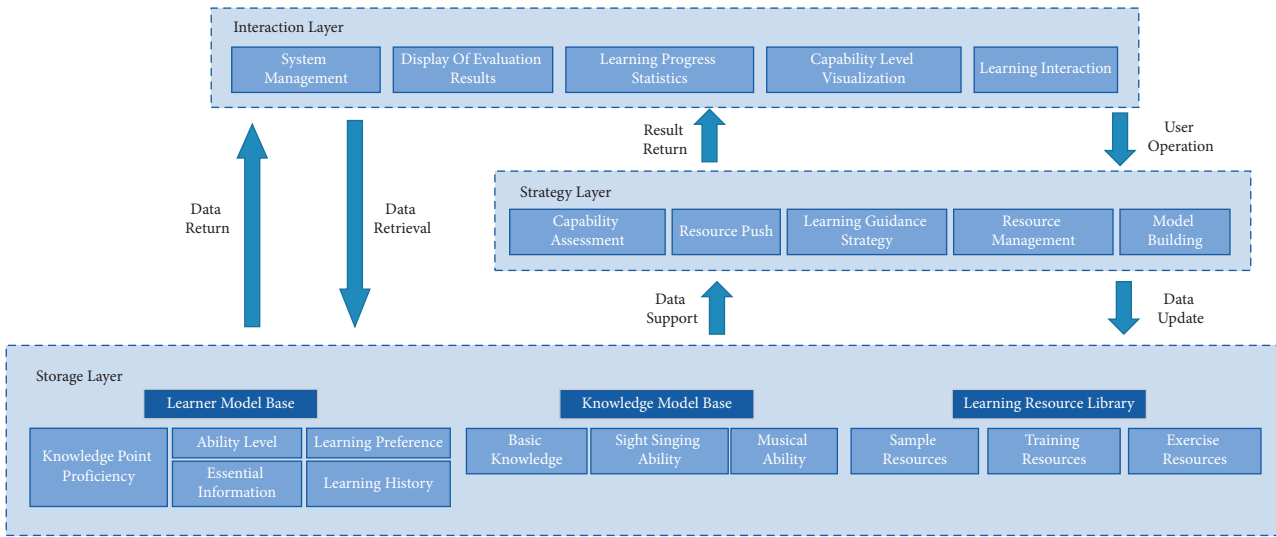


FIGURE 6: Overall structure of music tutorial system.

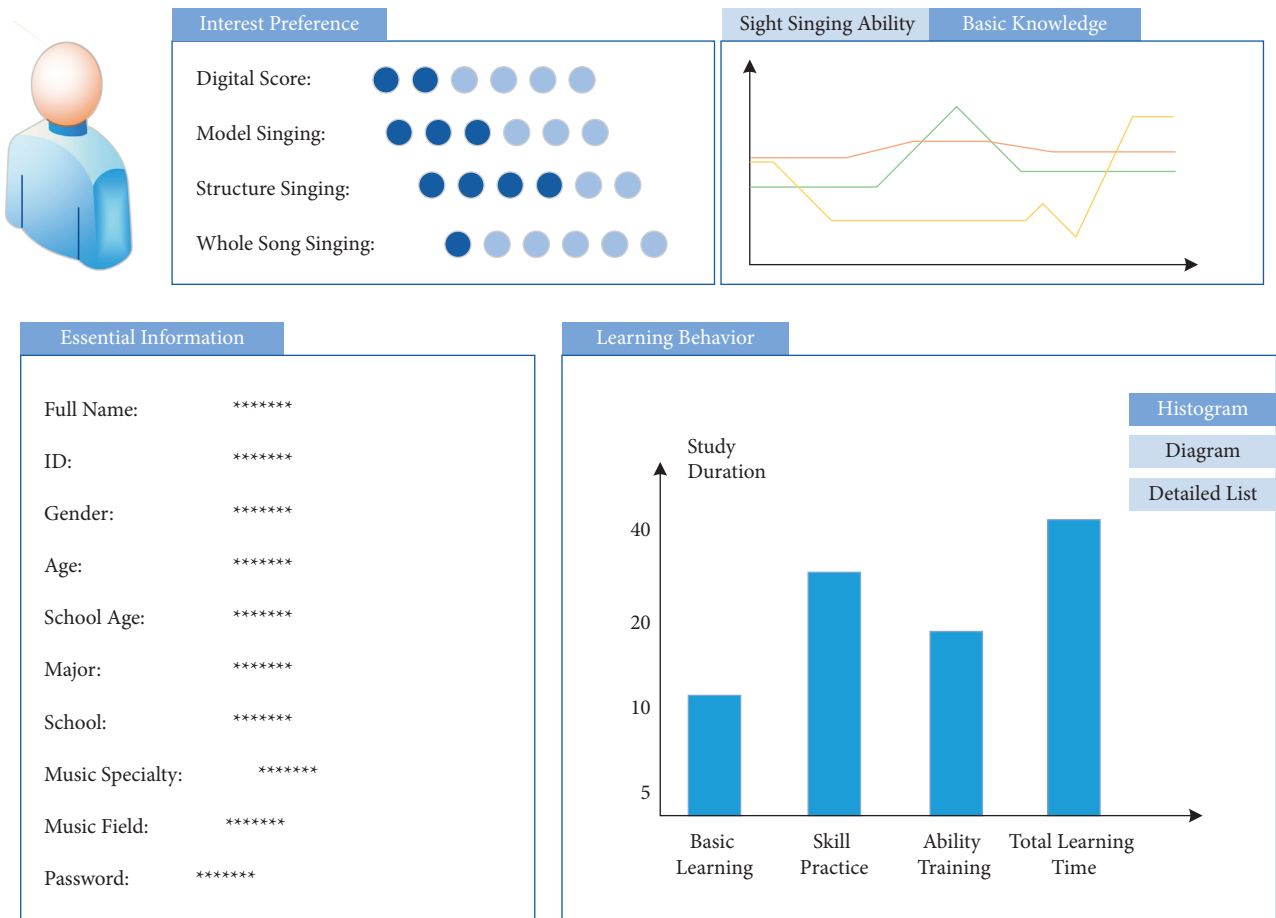


FIGURE 7: Learner interface.

resources after dynamically analyzing learners' learning effects. For example, when learners learn a certain knowledge well for many times, the system will adjust the difficulty coefficient of the next learning resource recommendation.

Resource management: resource management consists of two main functions: resource import and resource sorting.

Resource import is to provide learners with the function of customizing external resource import and online resource download; resource collation is to analyze the knowledge points and extract the difficulty features of the own resources or the resources imported by users, and it is also responsible for checking the validity of resource files.

Model construction: model construction mainly includes the learner model, the rules of knowledge point model construction, and the rules editing interface. Among them, rule editing is an interface to provide modification for the optimization of algorithms and models in the later system when there are enough user data.

4.2.3. Interaction Layer. System management: system management is the common functional interface of the system, including user registration, login, information modification, system settings, and other functions.

Data visualization: data visualization is mainly the display and comparative analysis of data such as evaluation results, ability level, and learning progress, which consists of visualization components and data control. Visualization components are mainly various commonly used chart controls, such as graphs, radar charts, and data tables. Data control includes data request, data structure transformation, data update, report generation, and printing and is mainly responsible for data generation and output to be displayed.

4.3. Design of Interaction between Teachers and Students. The learner model is the data entity of learners in the intelligent tutoring system, which records all kinds of information related to learners and stores them in the database. In order to let learners know their learning status in real time, the system needs to provide a visual user interface to present the learner model, as shown in Figure 7.

There are two kinds of music score files in this system: pictures and MIDI, so there are two kinds of music score display modes in each learning resource, which can be switched freely. The title bar of the component displays music score information such as range, bar number, interval number, note number, chord number, and the playing button of music score audio. To meet the learning preferences of different learners, the system provides a variety of learning modes, some of which need the assistance of special tools, such as music score input tools in dictation and musical note playing tools in singing.

5. Conclusion

The recognition and distinction of music difficulty is the key to realize the individualization of music teaching resources. Only by accurately recommending teaching resources with difficulty and the ability for learners, can they make effective use of resources, quickly master the knowledge and avoid the loss of learning interest. Therefore, this paper summarizes and analyzes the problem of pitch feature extraction in music teaching. By combining with the characteristics of music pitch, the features of high-pitched content in music teaching resources are matched based on deep learning. Then, the algorithm of pitch feature extraction in MIDI music score files is put forward, and the pitch feature matching model is constructed. Finally, a music tutoring system based on pitch feature matching is designed, including the design of music score learning tools, the overall structure of the system, and the interaction between teachers

and students, which is helpful to realize the individualized teaching of music solfeggio, and further improve the music teaching model and realize intelligent and personalized music learning.

Data Availability

The dataset can be accessed from the author upon request.

Conflicts of Interest

The author declares that there are no conflicts of interest.

References

- [1] S. Lian-xiu, *Research on the Construction of Dialogue Intelligent Tutoring System Based on Deep Learning [D]*Bohai university, China, 2021.
- [2] M. Zhou, Y. Ma, and F. Cen, "Review of application research of intelligent tutoring system," *Information and Computer (Theoretical Edition)*, vol. 33, no. 05, pp. 115–117, 2021.
- [3] Z. Cao, *Design of Intelligent Tutoring System Based on Deep Learning [D]*Beijing Jiaotong University, Beijing, 2020.
- [4] F. Guo, "Research and design of dynamic student model in intelligent teaching system [J]," *China Audio-visual Education*, vol. 1, pp. 119–123, 2011.
- [5] Q. Liu, L. Wu, M. Liu, W. Yezhu, and Z. Rongting, "Research status and development trend of intelligent tutor system [J]," *China Audio-visual Education*, vol. 10, pp. 39–44, 2016.
- [6] J. Salamon, J. Serrà, and E. Gómez, "Tonal representations for music retrieval: from version identification to query-by-humming," *International Journal of Multimedia Information Retrieval*, vol. 2, no. 1, pp. 45–58, 2013.
- [7] M. Liang, "Research on the reform of vocal music teaching in colleges and universities under the background of internet +[J]," *Curriculum and Teaching Methodology*, vol. 4, no. 4, 2021.
- [8] Y. Yang, "Research on the reform of vocal music teaching by computer multimedia technology[J]," *Journal of Physics: Conference Series*, vol. 2, p. 1992, 2021.
- [9] J. Shen, "Research on the innovation of college music teaching based on artificial intelligence technology [J]," *Food Research and Development*, vol. 42, no. 20, p. 243, 2021.
- [10] Li Qiang and F. Yu, "Improved melody extraction algorithm for pitch contour creation and selection [J]," *Computer Applications*, vol. 38, no. 08, pp. 2411–2415, 2018.
- [11] W. Jin, *Research and Application of Music Theme Extraction Algorithm [D]*Donghua University, Changning, 2021.
- [12] Y. Zhao, "Research on music score recognition based on deep learning [J]," *Microcomputer Applications*, vol. 37, no. 10, pp. 60–63, 2021.
- [13] A. Elbir and N. Aydin, "Music genre classification and music recommendation by using deep learning," *Electronics Letters*, vol. 56, no. 12, pp. 627–629, 2020.

Research Article

Evaluation of Enterprise Accounting Data Management Based on Maturity Model

Jun Xiang 

Accounting Institute of Wuhan College, Wuhan 430212, China

Correspondence should be addressed to Jun Xiang; 8530@whxy.edu.cn

Received 27 June 2022; Accepted 16 August 2022; Published 5 September 2022

Academic Editor: Le Sun

Copyright © 2022 Jun Xiang. This is an open access article distributed under the Creative Commons Attribution License, which permits unrestricted use, distribution, and reproduction in any medium, provided the original work is properly cited.

The study of enterprise management driven by accounting data has not only great strategic significance but also great practical value and distinctive characteristics of The Times. Although the macro evaluation of DCMM is strong, its objective operability is slightly weak. Therefore, based on the maturity model, this article establishes a three-level accounting data management (AAM) capability evaluation index system, divides the maturity level and key process domains, and constructs an AAM capability evaluation model. Through the evaluation of the accounting data management ability of the case enterprise, the evaluation value of the AAM ability is calculated, and the measurement of the AAM ability is completed, which is helpful to improve the data management ability of the enterprise scientifically and efficiently.

1. Introduction

At present, China's economic development has entered a "new normal," but economic development is closely related to the improvement of science and technology. With the nonstop improvement of science and innovation, information is a fundamental piece of it, which is rethinking the interaction and method of social administration and public key independent direction, an endeavor to board navigation, authoritative business cycle, and individual independent direction, and is becoming increasingly important for the development of modern enterprises and society [1]. Nowadays, accounting data is the top priority of data management and the huge commercial value, scientific research value, social management value, and the value of supporting scientific decision-making are being constantly recognized and developed. Scholars' research on AAM has gradually provided some improved overall ideas and strategies for optimizing AAM [2, 3]. However, at present, the domestic research is limited to a certain part of AAM or stays in the discussion of the relationship between the two, which cannot effectively combine the whole and part of AAM.

CMM (capability maturity model) refers to a staged description used by software development organizations to

define, implement, measure, control, and improve their software processes [4], which is divided into five grades to evaluate software contracting ability to improve software quality. In recent years, scholars have introduced the maturity model into data management for research, thereby forming a data management CMM. Literature [5] put forward the maturity model of enterprise information portals and evaluates the maturity of the case enterprise information portal. Literature [6] applied the maturity model to the measurement of the integration of industrialization and industrialization, which enriches the theoretical methods of evaluating the integration of industrialization and industrialization. Literature [7] applied the maturity model to the evaluation of multiproject management level of the construction unit. Literature [8] applied the maturity model to divide enterprise informatization maturity into five stages: informatization preparation, information system introduction, integration and sharing, enterprise extension, and decision support.

Although CMM has certain advantages compared with other data management capability models, it can be better applied to organizations in China. However, according to the published documents at present, DCMM (data capability maturity model) evaluation is strong in macro but slightly

weak in objective operability, and it does not classify the data. Moreover, there is no research on the combination of AAM and maturity in China at this stage. Therefore, aiming at the partial improvement of all aspects of AAM, this article establishes an evaluation model of AAM ability to promote the improvement of the overall ability, which has reference significance for the research of AAM among enterprises.

2. Theoretical Basis of Maturity Model

2.1. Overall Architecture. As shown in Figure 1, three capability domains of data capability maturity evaluation are defined: data strategy, data application, and data life cycle. The biggest difference between DCMM and other data management capability maturity models is that DCMM increases the data application capability domain. At the same time, data strategy and data life cycle are two indicators that run through the application.

2.2. Grading. Maturity is divided into five levels: initial level, managed level, steady level, quantitative management level, and optimization level [9, 10]. The positioning of each grade is shown in Figure 2:

Grade 1. Initial level: Organizations at this level are not aware of the importance of data to the organization, so they have not formed the consciousness of actively managing data. Data management within enterprises mainly runs through project management. No unified data management rules and procedures have been established within the enterprise, and the problems caused by the data lead to the low quality of customer service, which cost a lot of human resources to maintain the data.

Grade 2. Managed level: Organizations at this level realized the importance of data and began to manage data as an asset. Driven by the needs and strategies of the enterprise, the corresponding data management process was formulated, and the personnel within the organization were assigned to manage the data preliminarily, realizing and identifying the stakeholders of the data.

Grade 3. Robust level: Enterprises at this level regard data as an important asset that can improve performance. They have formulated organizational data management processes and policies to promote the standardization and standardization of data management. Data managers can manage across systems where the management of data can meet the requirements of the organization.

Grade 4. Quantitative management level: Enterprises at this level regard data as an important resource think that data management can enhance the competitiveness of enterprises and realize the promoting role of data in workflow and efficiency. All-round improvements have been made to the processes related to enterprise data management, performance indicators are set for relevant organizations, posts, personnel, etc., and they are regularly assessed so that the system and process can be

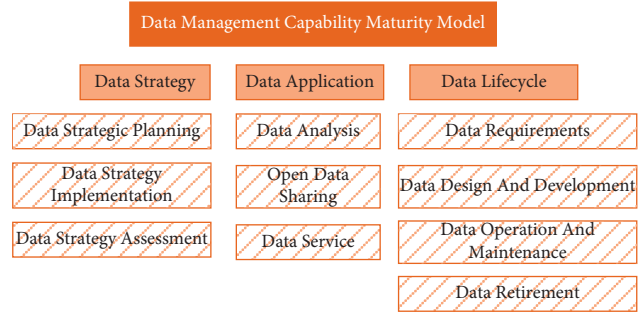


FIGURE 1: Architecture of DCMM.

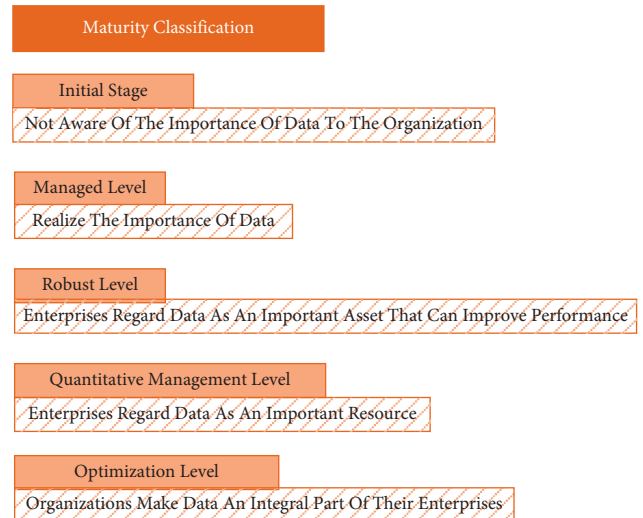


FIGURE 2: Grading of maturity.

optimized and improved according to the monitoring and analysis of data management, where data management is gradually becoming scientific and standardized.

Grade 5. Optimization grade: Organizations at this level regard data as an indispensable part of the enterprise. The policies and processes of AAM can be improved in real time according to the external environment and the current situation of the industry and are regarded as the benchmark of data management in the industry.

3. Enterprise AAM Evaluation Methods

3.1. Analytic Hierarchy Process. Analytic hierarchy process (AHP) is a multicriteria decision-making form combining quantitative and qualitative analysis. It is characterized in that based on analyzing the essence and internal relations of complex decision-making problems, a hierarchical structure model is constructed, and its process of complex problems is presented mathematically with less quantitative information. Through data to solve complex decision-making problems with multiobjectives, multicriteria, or no structural characteristics, the purpose of simplifying the decision-making scheme is achieved [11].

The general steps of AHP mainly include four steps. The first step is to build the hierarchical structure model; second,

construct the judgment matrix; third, obtain hierarchical single sorting and its consistency check; and finally implement hierarchical general ranking and its consistency check.

3.1.1. Establishment of a Hierarchical Structure Model.

The decision to solve the problem is divided into three levels, namely, the target level, the decision criterion level, and the decision scheme level. In the application of the AHP, the problem to be solved is to calculate the relative weight of the bottom layer to the top layer, so as to sort the schemes and measures at the bottom layer and choose the best scheme [12, 13].

3.1.2. Construction of a Comparative Judgment Matrix.

The construction of judgment matrix is to determine the weight of each criterion layer to the target layer by comparing each element with each other pairwise. The comparative judgment matrix of A is as follows:

$$A = (a_{ij})_{m \times n} = \begin{pmatrix} a_{11} & a_{12} & \cdots & a_{1n} \\ a_{n1} & \cdots & \cdots & \cdots \end{pmatrix}, \quad (1)$$

where the elements in A should meet the following requirements: $a_{ij} > 0$; $a_{ij} = 1/a_{ji}$; $a_{ii} = 1$.

3.1.3. Hierarchical Single Sort. Hierarchical single sort refers to evaluating all elements in pairs for an element in the previous layer and arranging the important order. The concrete calculation can be carried out according to the judgment matrix A , and the calculation can ensure that it can meet the characteristic root and characteristic vector conditions of $AW = \lambda_{ax}W$, where the largest feature root of A is λ_{ax} , and the normalized feature vector corresponding to λ_{ax} is W , and W_i is a component of W , which refers to the weight, and corresponds to the single ordering of its corresponding elements. Use the judgment matrix to calculate the weight of each factor a_{ij} to the target layer.

The calculation steps of the weight vector (W) and the maximum feature (λ_{ax}) are as follows.

First of all, take the product of the row elements according to equation (2) and then raise it to the n th power:

$$\vec{W}_i = \sqrt[n]{\prod_{j=1}^n a_{ij}}, \quad i, j = 1, 2, \dots, n. \quad (2)$$

Then, it is normalized into a ranking weight vector by formula (3), which is denoted as W (the element of W is the ranking weight of the relative importance of the factor in the same level to a factor of the previous level), then $W = (W_1, W_2, \dots, W_n)^T$ is the result of judging the hierarchical single ranking of the matrix.

$$W_i = \sum_{i=1}^n W_i. \quad (3)$$

Finally, determine the maximum characteristic root of the matrix by the following formula:

$$\lambda_{\max} = \frac{1}{n} \sum_{i=1}^n AW_i. \quad (4)$$

3.1.4. Consistency Inspection and Hierarchical General Sorting. If the n -order judgment matrix is B , the maximum characteristic root λ_{ax} can be obtained by the following methods:

$$BW = \lambda W. \quad (5)$$

The following consistency index CI is taken to test the consistency index of judgment:

$$CI = \frac{\lambda_{\max} - n}{n - 1}. \quad (6)$$

$CI = 0$ means that the judgment matrix is completely consistent and the larger the CI , the more serious the inconsistency of the judgment matrix.

Assuming that A is the target layer, the weight coefficients of m total ranking of factor levels are as follows: a_1, a_2, \dots, a_m ; B is the middle layer, and the weight coefficients of n hierarchical single sort of factors are as follows: $b_1^1 \cdots b_n^m$; therefore, the total ranking of layer B is calculated according to the following formula:

$$b_i = \sum_{j=1}^m a_j b_{ij}. \quad (7)$$

Set the B layer B_1, B_2, \dots, B_n On the upper layer (A Layer), the hierarchical ranking consistency index of factors A_j ($j = 1, 2, \dots, m$) is CI_j , the random consistency index is RI_j , and the consistency ratio of the hierarchical total sort is as follows:

$$CR = \frac{a_1 CI_1 + a_2 CI_2 + \cdots + a_m CI_m}{a_1 RI_1 + a_2 RI_2 + \cdots + a_m RI_m} = \frac{\sum a_i CI_i}{\sum a_i RI_i} = \frac{CI}{RI}. \quad (8)$$

When < 0.1 , it is considered that the overall ranking of the hierarchy has passed the consistency test; otherwise, it is necessary to readjust the element values of the judgment matrix and make the final decision according to the overall ranking of the decision-making level.

3.2. Fuzzy Analytic Hierarchy Process. The fuzzy comprehensive evaluation method is an overall decision based on a single decision of all factors involved in things, which is a comprehensive evaluation affected by multiple factors. In contrast, the fuzzy analytic hierarchy process (FAHP) is an improved AHP, which combines the above AHP with the fuzzy comprehensive evaluation method. It is a comprehensive qualitative and quantitative evaluation model, which is suitable for dealing with uncertain problems. It is widely used in system evaluation, system optimization, efficiency evaluation, and so on.

Generally speaking, the first step is to use AHP to determine the weight of each index in the model index system, and the second step is to use the fuzzy comprehensive evaluation method to comprehensively evaluate the grade so

as to effectively combine the two methods and obtain a more scientific evaluation result. The FAHP adopted in this paper is useful for studying the management ability of accounting data, which is applicable to determine the index weight, evaluate the maturity level, and establish the evaluation model of AAM ability.

4. Evaluation Model of Enterprise AAM Based on Maturity Model

4.1. Setting of Index System. The index system of the AAM capability evaluation model consists of three levels of indicators, including three competence domains (first-level indicators), eight competence items (second-level indicators), and 24 subcompetence items (third-level indicators). The weights of all levels of indicators in the AAM capability evaluation model are determined by AHP, and consistency tests are carried out in turn. The distribution of each indicator is shown in Figure 3.

4.1.1. Accounting Data Strategy. Generally speaking, accounting strategy is to combine accounting data technology, concept, framework, and strategic management so as to build an accounting data analysis platform and enhance the overall core strength and environmental adaptability. There are three competency items under the accounting data strategy, which are accounting data strategy planning, accounting data strategy implementation, and accounting data strategy evaluation.

4.1.2. Accounting Data Application. The application of accounting data is the process of mining effective information from accounting data using the method of accounting data analysis, providing users with auxiliary decisions, providing accounting data services, and maximizing the value of accounting data. There are three competency items in accounting data application: accounting data analysis, accounting data open sharing, and accounting data service.

4.1.3. Accounting Data Life Cycle. The accounting data life cycle is the whole process of accounting data from design, development, creation, migration, application, archiving, recycling, reactivation, and withdrawal. There are four competency items in the accounting data life cycle: accounting data demand management, accounting data design and development, accounting data operation and maintenance, and accounting data retirement.

4.2. Maturity Level Setting. The maturity level of the AAM capability evaluation model is divided into five levels: initial level, repeatable level, defined level, managed level, and optimized level. Each maturity level has its own function. Except for the first stage, all the other stages are constructed according to the same internal structure. Different maturity levels reflect different levels of AAM capabilities.

4.2.1. Initial Level. The initial level is characterized by passive management, and there is no initiative in AAM. The organization is not aware of the importance of AAM, and it is chaotic and disorderly as a whole, whose specific performance is that no standardized AAM policies, documents, plans, and processes have been formed. There is no formal AAM organization at the organizational level. There is no clear goal and practice. Moreover, there are no key process areas and key practices in this stage.

4.2.2. Repeatable Level. The repeatable level is the second stage of the accounting data management ability assessment model. Organizations in this stage initially realize the importance of accounting data management and begin to manage accounting data, but the scope of accounting data management is relatively limited. The definition of repeatable level is shown in Figure 4.

4.2.3. Defined Levels. The third level of the AAM evaluation model is the defined level, which means that the key process areas of repeatable level have been realized, whose specific performance is as follows: the relevant system and process of AAM are more perfect and standardized; it is able to carry out comprehensive AAM within the organization; the role of AAM personnel has been enhanced. The specific distribution is shown in Figure 5.

4.2.4. Managed Level. The fourth level of the AAM capability evaluation model is the managed level, which means that the key process areas of the defined level have all been realized. Specifically, it can optimize and update the systems and processes related to AAM; AAM is more systematic and professional, and its application in organizations is more standardized; AAM supports the decision-making of the organization and has made great progress. The specific distribution is shown in Figure 6:

4.2.5. Optimized Level. The highest level of the accounting management capability evaluation model is the optimization level, which means that the key process areas of the managed level have all been realized. The concrete performance is as follows: all the basic construction, manpower reserve, material resources, and other aspects of support are ready; through the long-term practice of AAM, the organization has accumulated a lot of experience and can make timely adjustments to the changes of the internal and external environment; the AAM culture is formed. The specific distribution is shown in Figure 7:

4.3. Calculation of Maturity Level

4.3.1. Fuzzy Evaluation Matrix. Before the fuzzy comprehensive evaluation of AAM ability, the evaluated fuzzy relationship should be expressed as a fuzzy evaluation matrix and then determine the evaluation set $A = \{A_1, A_2, \dots, A_n\}$, in which A_n indicates the grade of the evaluated index. Because the maturity level is divided into five levels, in the

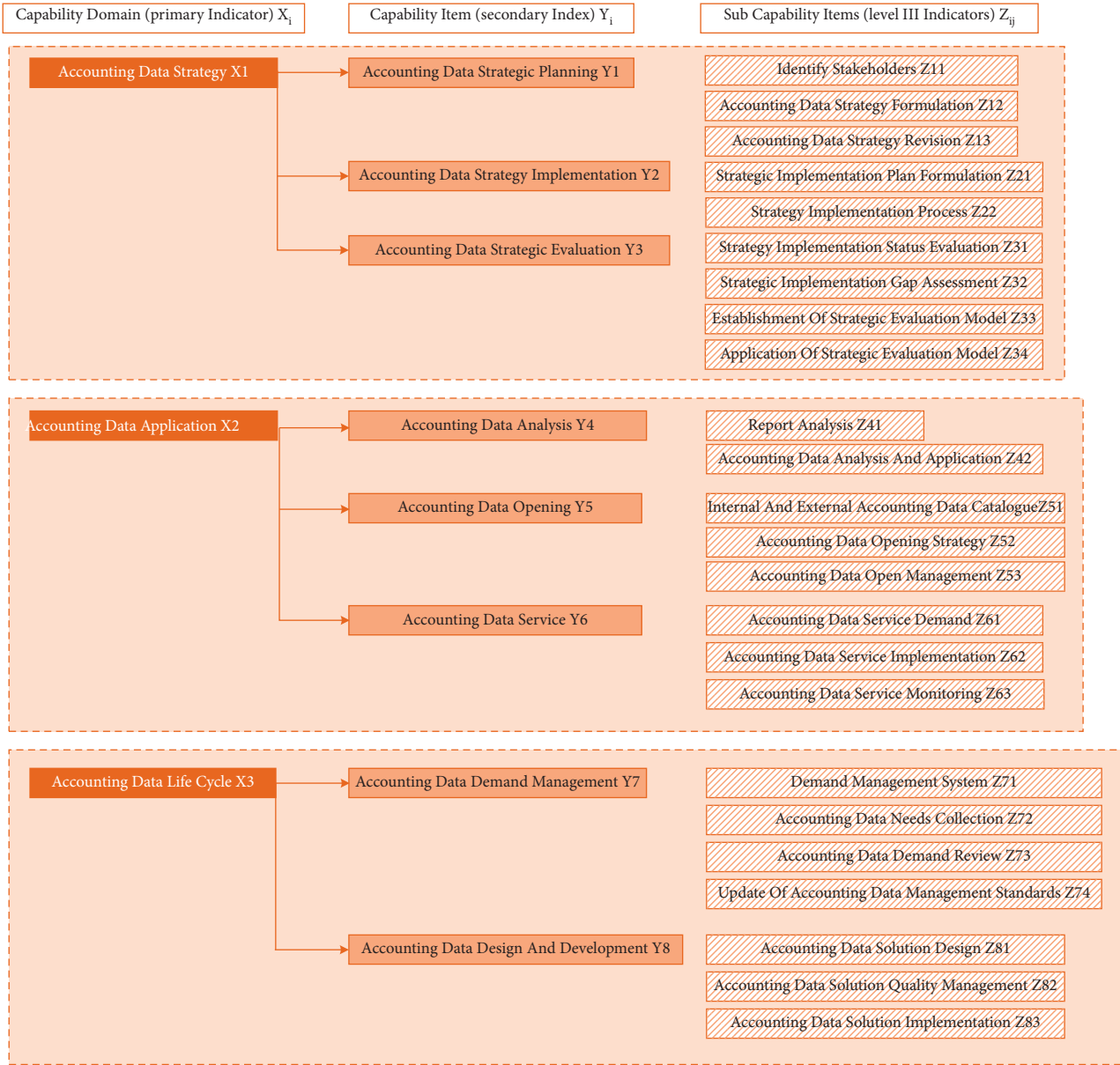


FIGURE 3: Distribution of index system.

evaluation set, $n = 5$, the fuzzy evaluation matrix with 5 columns is set as follows

$$P = \begin{pmatrix} P_{11} & P_{12} & P_{13} & P_{14} & P_{15} \\ P_{21} & P_{22} & P_{23} & P_{24} & P_{25} \\ \dots & \dots & \dots & \dots & \dots \\ P_{j1} & P_{j2} & P_{j3} & P_{j4} & P_{j5} \end{pmatrix}, \quad (9)$$

where element p_{jn} ($n = 1, 2, 3, 4, 5$) refers to the probability that all the three-level evaluation indexes Z_{ij} included by a certain second-level index Y_i get n -level times, respectively, in the scoring, namely, the membership degree p_{jn} of the measured index, which is expressed by the following formula:

$$p_{jn} = \frac{\text{The number of times the in dex } Z_{ij} \text{ was graded } n}{\text{Total grading times}}. \quad (10)$$

Note: the secondary indicators are the same in the same matrix Z_{ij} .

4.3.2. Fuzzy Evaluation Matrix. The weight matrix of all the three-level evaluation indexes Z_{ij} contained in a certain two-level index Y_i is set as $Z = (z_{i1}, z_{i2}, \dots, z_{ij})$, where Z_{ij} represents the weight of the corresponding three-level index Z_{ij} . Then, the fuzzy relationship evaluation matrix of indicators at all levels can be obtained by the calculation of the following formula:

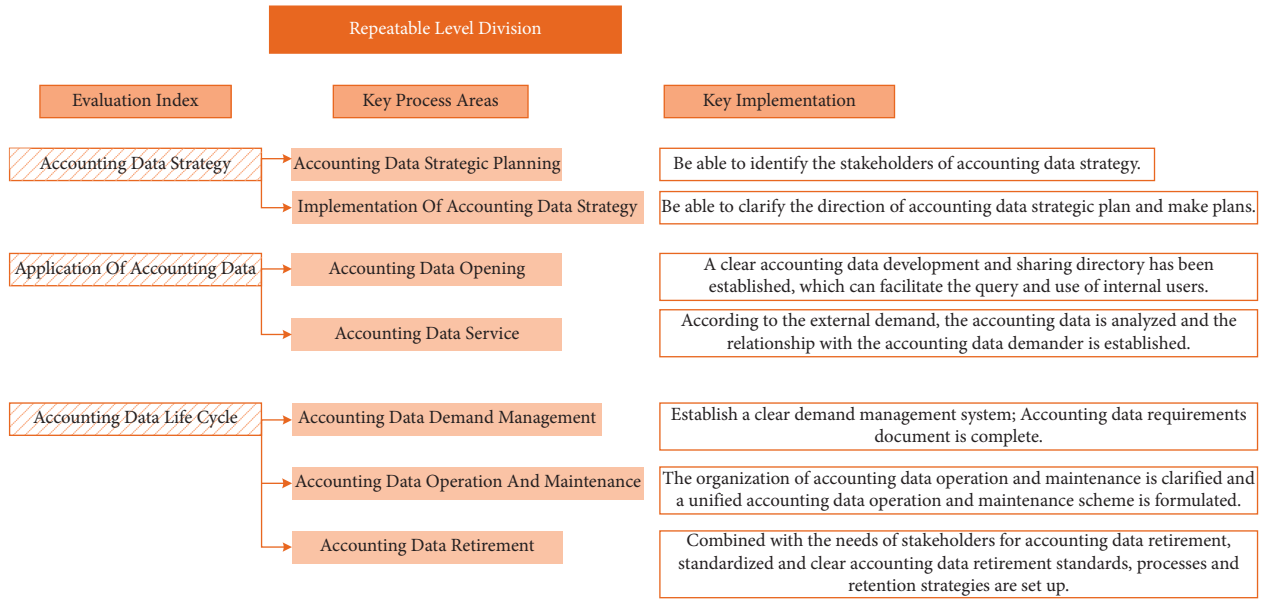


FIGURE 4: Division of repeatable level.

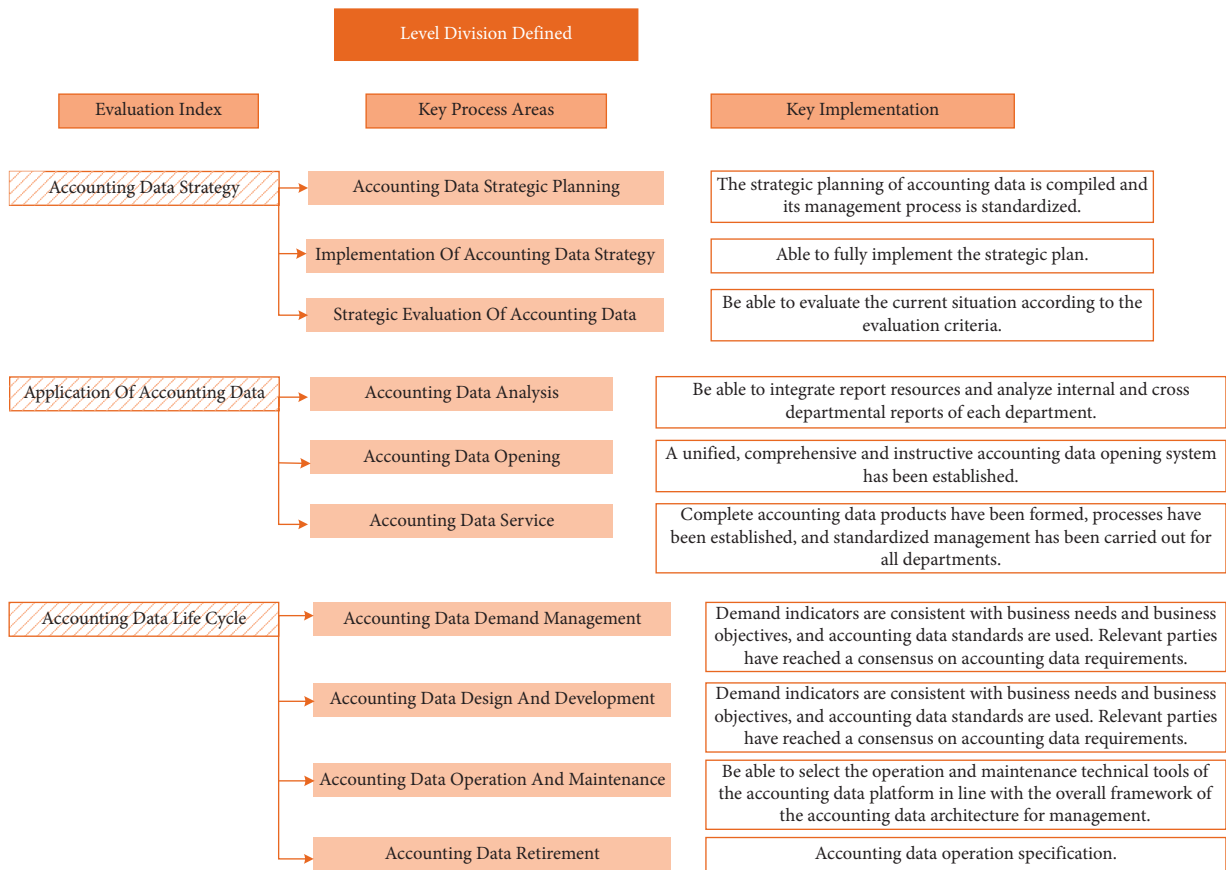


FIGURE 5: Division of defined level.

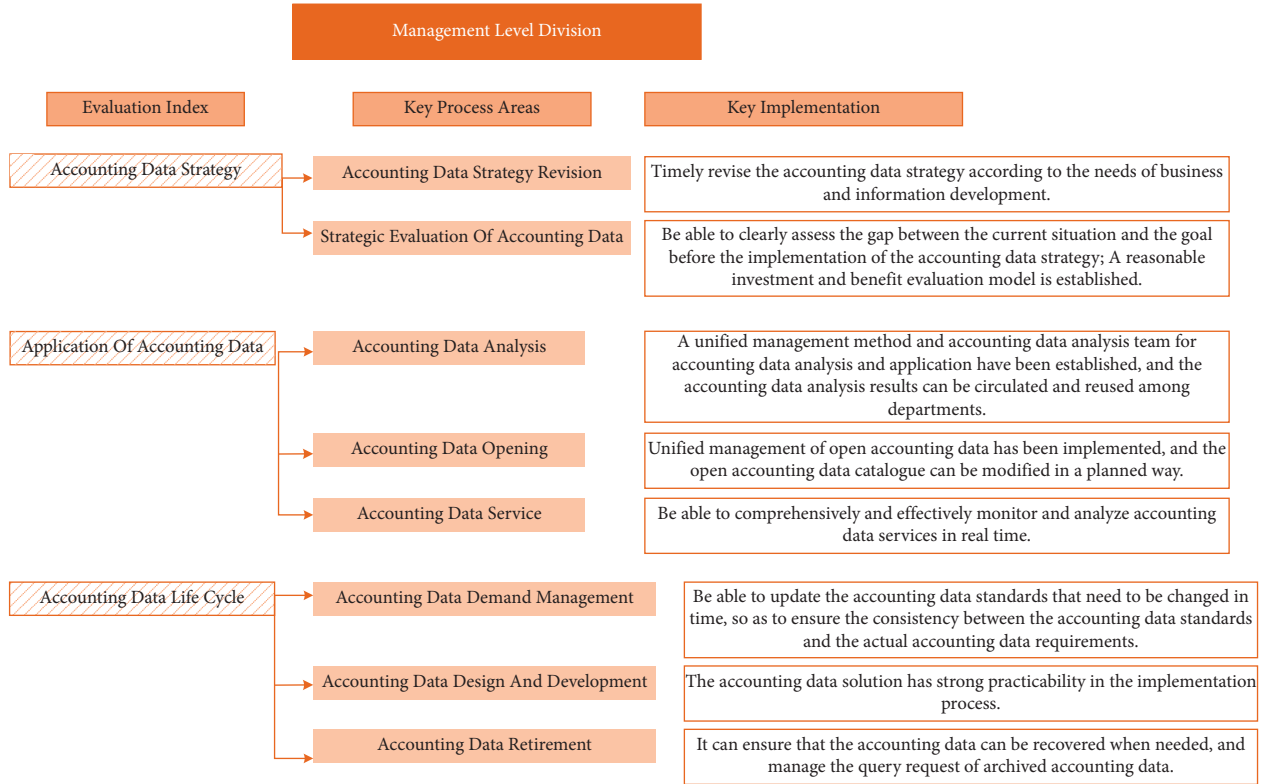


FIGURE 6: Division of managed level.

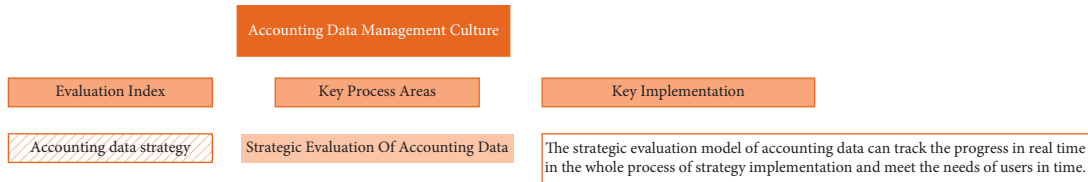


FIGURE 7: Division of optimized level.

$$M = (M_{ij})_{m \times n} = Z \times P. \quad (11)$$

4.3.3. *Determine the Maturity Level.* After the final fuzzy comprehensive evaluation result is obtained through the calculation in the previous section, the cascade of the enterprise's AAM ability can be calculated through the following formula:

$$L = M \times N. \quad (12)$$

Among them, $N = \{20, 40, 60, 80, 100\}$, $M = \{\text{Initial level, repeatable level, defined level, managed level, optimized level}\}$.

According to the calculation results of L , the maturity level of AAM ability to which each first-level index and the final result belong can be determined. At the same time, in the process of grade judgment, the maturity grade of AAM ability can be judged according to the principle of maximum membership degree, and the judgment result can be further proved.

5. Case Analysis

Through the evaluation of the accounting data management ability of the case enterprise, the evaluation value of the accounting data management ability is calculated, and the measurement of the accounting data management ability is completed, which is helpful in improving the data management ability of the enterprise scientifically and efficiently.

5.1. *Analysis of AAM.* The evaluation of Company A was conducted by questionnaire. The respondents are mainly stakeholders of AAM in enterprise A, including department heads, managers, experts, and AAM professionals. According to the scores of the respondents on the related indicators of Company A, the basic information of each capability domain of Company A can be obtained, and the results are shown in Tables 1–3.

According to the calculation formula mentioned above, it can be concluded that the fuzzy relation evaluation vector of each first-level index is as follows:

TABLE 1: Grading results of accounting data strategy.

First-level index	Second-level index	Third-level index	Grading				
			1	2	3	4	5
Accounting data strategy X1	Accounting data strategic plan Y1	Identify stakeholders Z11	1	5	11	13	0
		Strategy formulation Z12	0	3	12	14	1
		Revise strategy Z13	4	12	14	0	0
	Accounting data strategy implementation Y2	Implementation of strategic planning Z21	0	6	10	11	3
		Implementation process Z22	2	7	15	5	1
		Evaluation of strategic implementation status Z31	2	8	12	8	0
	Accounting strategy evaluation Y3	Implementation of strategic gap assessment Z32	0	7	9	12	2
		Establishment of strategic model Z33	6	15	7	2	0
		Evaluation model application Z34	5	16	7	2	0

TABLE 2: Grading results of accounting data application.

First-level index	Second-level index	Third-level index	Grading				
			1	2	3	4	1
Accounting data application X2	Accounting data analysis Y4	Analysis report Z41	0	0	10	15	5
		Analytical application Z42	0	1	9	11	9
	Accounting data opening Y5	Directory of Internal and External Accounting Data Z51	6	7	12	5	0
		Open strategy Z52	0	3	10	10	7
		Open management Z53	0	2	10	16	2
	Accounting data service Y6	Service Z61	4	11	14	0	1
		Implement service Z62	3	10	15	2	0
		Service Z63 monitoring	6	7	11	5	1

TABLE 3: Grading results of accounting data life cycle.

First-level index	Second-level index	Third-level index	Grading				
			1	2	3	4	1
Accounting data life cycle X3	Accounting data demand management Y7	Demand management system Z71	0	4	11	14	1
		Collect demand Z72	1	5	17	7	0
		Review requirements Z73	5	11	10	4	0
		Management standard update Z74	4	6	20	0	0
	Accounting data design and development Y8	Solution design Z81	0	5	21	4	0
		Solution Quality Management Z82	1	2	18	8	1
		Solution implementation Z83	0	1	7	21	1

$$\begin{aligned}
M_{x1} &= (0.0524 \ 0.2467 \ 0.3703 \ 0.2972 \ 0.0334), \\
M_{x2} &= (0.0619 \ 0.1548 \ 0.3763 \ 0.2778 \ 0.1292), \\
M_{x3} &= (0.0488 \ 0.1331 \ 0.4602 \ 0.3108 \ 0.0471).
\end{aligned} \quad (13)$$

By multiplying the weight vector composed of the weights of the first-level indexes with the above-mentioned first-level fuzzy relation evaluation matrix to obtain the final fuzzy relation evaluation vector, the following vector is obtained:

$$M_x = (0.0503 \ 0.1517 \ 0.3807 \ 0.3320 \ 0.0853). \quad (14)$$

According to the principle of maximum membership degree, the maximum value in the vector is the third value, i.e., 0.3807, which can preliminarily determine that the AAM ability of Company A is defined.

5.2. Comprehensive Evaluation of AAM. Calculate the final evaluation score and grade of Company A's AAM ability, and the comprehensive evaluation results of enterprise AAM ability are shown in Figure 8:

The evaluation value of Company A's accounting data strategy is 60.25. Although the corresponding maturity level is the "defined level," it is just entering the defined level, and there is still a big gap from the next level (managed level). Company A has not revised the accounting data strategy in time according to business and information development needs and cannot optimize the accounting data strategy in time. Before implementing the accounting data strategy, the gap between the present situation and the target cannot be clearly assessed. In addition, a reasonable investment and benefit evaluation model has not been established.

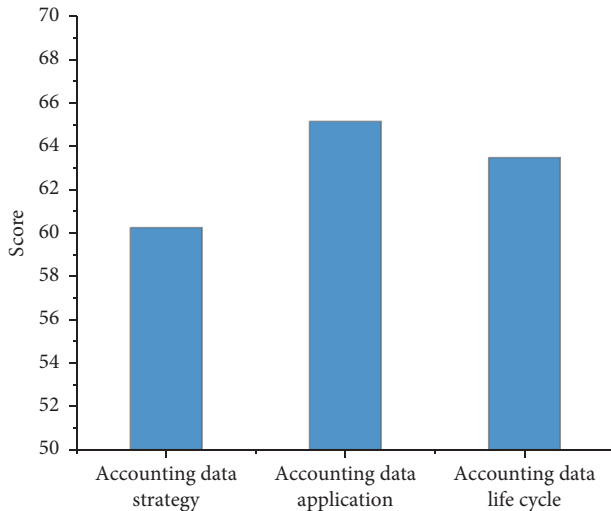


FIGURE 8: A Comprehensive evaluation of Company A's AAM ability.

The evaluation value of Company A's accounting data application is 65.152. The corresponding maturity level is the "defined level," and it is in the transitional stage between the defined level and managed level. It has not yet established a unified management method and accounting data analysis team for the application of accounting data analysis, and the results of accounting data analysis have not been circulated and reused among departments. In addition, we implement unified management of accounting data that has not yet been opened, which is failure to conduct comprehensive and effective monitoring and real-time analysis of accounting data services.

The evaluation value of the accounting data life cycle of Company A is 63.486. From the evaluation value, the corresponding maturity level is the "defined level," and it is in the transitional stage between the defined and managed levels. Specifically, the demand indicators are consistent with the business needs and business objectives, accounting data standards are used, and relevant parties have reached a consensus on accounting data needs. Moreover, the solution meets the demand for accounting data, and the design content is complete; and the operation of accounting data retirement is standard.

6. Conclusion

Based on the maturity model, this article establishes a three-level evaluation index system of AAM ability, divides the maturity level and key process areas, and constructs the evaluation model of AAM. In addition, Company A, which has some experience in AAM, is selected to evaluate the effectiveness of the model. The evaluation values of accounting data strategy, accounting data application, and accounting data life cycle of Company A are 60.25, 65.152, and 63.486, respectively, and its AAM ability belongs to the "defined level." The evaluation model of AAM ability established in this article can provide support for the research of AAM ability and provide guidance for the development of AAM ability evaluation.

Data Availability

The dataset can be accessed upon request.

Conflicts of Interest

The author declares that there are no conflicts of interest.

Acknowledgments

This work was supported by the Wuhan College Scientific Research and Innovation Platform Construction program "Research Center of Private Enterprise Value Evaluation and Creation," Project no. KYP202001.

References

- [1] Y. Chen, H. Wu, M. Dong, and X. Hu, "Analysis and suggestions on the evaluation effect of enterprise internal control—Based on the analysis of internal control evaluation report of China and the United States in 2008," in *Proceedings of the 2009 annual meeting of the audit committee of the Chinese Accounting Society*, pp. 52–60, 2009, in Chinese.
- [2] J. A. Wilson, L. Martinez-Urbe, and M. A. Fraser, "An institutional approach to developing research data management infrastructure," *International Journal of Digital Curation*, vol. 6, no. 2, pp. 274–287, 2011.
- [3] Y. Cui and W. Li, "Review of research data management progress," *Library Journal*, vol. 36, no. 1, pp. 12–19, 2017, in Chinese.
- [4] B. Li and B. Junzhi, "Data management capability maturity model," *Big Data*, vol. 3, no. 4, pp. 29–36, 2017, in Chinese.
- [5] P. Qinghua and J. Qinghua, "Research on comprehensive evaluation of enterprise information portal maturity," *Journal of Intelligence*, vol. 31, no. 2, pp. 93–97, 2012, in Chinese.
- [6] Z. Qian, *Research on the Cost and Benefit of Informatization in Construction Enterprises*, Henan University of Science and Technology, Luoyang, China, 2014, in Chinese.
- [7] C. Qiu, J. Zhang, and M. Shi, "Enterprise informatization maturity stage classification model," *Journal of Jilin University (Engineering and Technology Edition): Engineering Edition*, vol. 37, no. 4, pp. 976–980, 2007, in Chinese.
- [8] K. Wang, *Research on Informatization Application of Construction Enterprises in Shaanxi Province*, Xi'an University of Architecture and Technology, Xi'an, China, 2010, in Chinese.
- [9] L. Shen, X. Du, G. Cheng, and X. Wei, "Capability Maturity Model (CMM) method for assessing the performance of low-carbon city practice," *Environmental Impact Assessment Review*, vol. 87, Article ID 106549, 2021.
- [10] Y. Yan, Z. Tao, and Q. Lili, "Research on knowledge management maturity evaluation based on particle swarm optimization neural network," *Journal of Intelligence*, vol. 29, no. 5, pp. 124–128, 2010, in Chinese.
- [11] J. Du, R. Wu, and H. Pan, "Comprehensive evaluation of enterprise financial decision based on analytic hierarchy process," *Journal of Changchun University of Technology (Natural Science Edition)*, vol. 31, no. 6, pp. 110–114, 2018, in Chinese.
- [12] S. Kubler, J. Robert, W. Derigent, A. Voisin, and Y. Le Traon, "A state-of-the-art survey & testbed of fuzzy AHP (FAHP) applications," *Expert Systems with Applications*, vol. 65, 2016.
- [13] P. Hou, Y. Yao, and D. Zhang, "Research on strategic performance evaluation system of online travel service enterprises," *Enterprise economy*, vol. 41, no. 2, pp. 112–124, 2022, in Chinese.

Research Article

A Fast Data Transmission Method of Vehicle-Road Cooperative Communication Based on the Clustering Algorithm

Weifeng Wang ¹, Zijian Wang,² Yang Xu ³, Xinpeng Yao,² and Yulin Ma ⁴

¹College of Civil and Transportation Engineering, Hohai University, Nanjing 210098, China

²Shandong Key Laboratory of Smart Transportation (Preparation), Jinan 250101, China

³School of Engineering, Ocean University of China, Tsingtao 266100, China

⁴School of Mechanical Engineering, Anhui Polytechnic University, Wuhu 241000, China

Correspondence should be addressed to Yulin Ma; mayulin1983@163.com

Received 23 June 2022; Accepted 11 August 2022; Published 1 September 2022

Academic Editor: Le Sun

Copyright © 2022 Weifeng Wang et al. This is an open access article distributed under the Creative Commons Attribution License, which permits unrestricted use, distribution, and reproduction in any medium, provided the original work is properly cited.

In order to improve the security and stability of data transmission in vehicle-road cooperative communication and reduce the error rate of data transmission, a fast data transmission method based on the clustering algorithm is proposed. First, the multisensor information acquisition method of the vehicle networking is used to realize data acquisition and data structure analysis of the vehicle-road cooperative communication, and a data transmission channel model for vehicle-road cooperative communication is constructed. The interference suppression in the data transmission process of the vehicle-road cooperative communication is realized by the matched filter detection algorithm. Then, according to the symbol characteristic distribution of the vehicle-road cooperative communication channel, the baud interval equalization method is used to realize the piecewise equalization adjustment of data transmission for the vehicle-road cooperative communication. With the adaptive error compensation and channel fading suppression, the K-means clustering algorithm is used to carry out the coordinated adjustment to data packets during the rapid data transmission of the vehicle-road cooperative communication. Finally, the adaptive control of data transmission for the vehicle-road cooperative communication is carried out according to the dynamic distribution characteristics of the clustering center so as to reduce the influence of channel fading and intersymbol interference caused by channel spread. The simulation results show that the bit error rate of this method is kept at about 0.05, and the data transmission rate continues to increase, most of which remain above 0.95. This method has strong anti-interference ability for the rapid data transmission of vehicle-road cooperative communication, with lower communication bit error rate, less end-to-end time delay, and higher stability and accuracy of data transmission.

1. Introduction

With the development of vehicle networking technology and vehicular ad hoc network (VANET), people attach great importance to the research on the security and stability of data transmission in vehicle-road collaborative communication. With the channel balance control of vehicle-road collaborative communication, a data transmission method with high stability and strong anti-interference is adopted to realize the optimal control of vehicle-road collaborative communication and improve the collaborative control ability for the vehicle-road collaborative communication in data transmission. It is of great significance to study the rapid data

transmission method of vehicle-road cooperative communication in the design of mobile ad hoc network (MANET) for vehicle-road cooperative control and vehicle networking [1].

The data transmission of vehicle-road cooperative communication has the characteristics of nonstationarity and multipath so that the fast data transmission of vehicle-road cooperative communication is affected by intersymbol interference and multipath, and the output stability is not good. Thus, it is necessary to design a data transmission control model for vehicle-road cooperative communication to improve the stability of fast data transmission of the vehicle-road cooperative communication with channel equalization adjustment. At present, the fast data

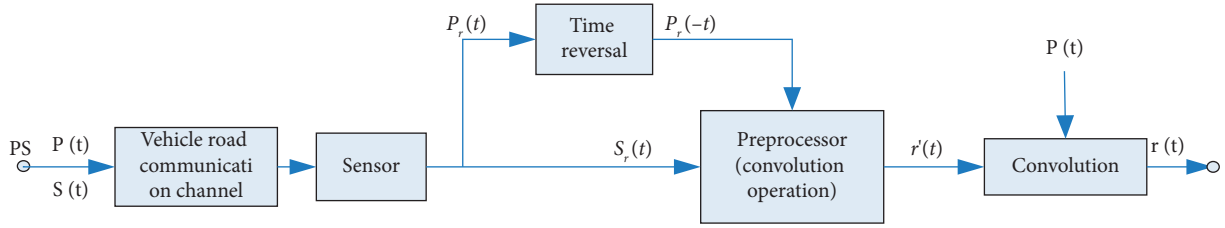


FIGURE 1: Structure model of data input and output of vehicle-road cooperative communication.

transmission methods of vehicle-road cooperative communication mainly include the data transmission control method of vehicle-road cooperative communication based on orthogonal frequency division multiplexing, the BPSK modulation method, the PSK modulation method, and so on [2–4]. Through time-frequency characteristic analysis and equalization control, the data transmission control of vehicle-road cooperative communication is realized. Reference [5] has proposed a method of vehicle-road cooperative communication and interference suppression based on the PTS-clipping algorithm. In the method, the piecewise fitting control method is used to design the channel equalization and suppress the intersymbol interference in the process of data transmission of vehicle-road cooperative communication, which improves the output signal-to-noise ratio and reduces the intersymbol interference, but the stability and real-time performance of this method are not good. Reference [6] has proposed a vehicle-road cooperative communication control method for the direct sequence spread spectrum. In this method, the direct sequence spread spectrum transmission method is used to transmit the data of vehicle-road cooperative communication in the spatial multipath channel, which reduces the output bit error rate, but the computational load is high. Reference [6] has proposed a vehicle-road cooperative communication control method based on matched filter detection. In this method, the interference suppression and filtering during data transmission of vehicle-road cooperative communication are analyzed by a matched filter detector, which improves the stability and real-time performance of data transmission of vehicle-road cooperative communication, together with error compensation, but the packet reception performance of this method is not good under the background of strong interference.

In view of the above problems, a fast data transmission method of vehicle-road cooperative communication based on clustering algorithm is proposed in this study. First, the multisensor information collection method of vehicle network is used to realize data acquisition and data structure analysis of vehicle-road cooperative communication. Then according to the symbol characteristic distribution of the vehicle-road cooperative communication channel, the baud interval equalization method is used to realize the piecewise equalization adjustment to data transmission for the vehicle-road cooperative communication. With the adaptive error compensation and channel fading suppression, the K-means clustering algorithm is used to carry out the coordinated adjustment of data packets during the rapid data transmission of the vehicle-road cooperative communication, and the Matlab simulation analysis method is used to realize

the fast data transmission of vehicle-road cooperative communication. The results demonstrate the superior performance of the proposed method in improving the control ability of vehicle-road cooperative communication.

2. Channel Model of Vehicle-Road Cooperative Communication and Signal Analysis

2.1. Channel Model. In order to realize fast data transmission and optimal control of vehicle-road cooperative communication based on the clustering algorithm, a channel model of vehicle-road cooperative communication is constructed based on routing protocol control and channel model equalization design of vehicle-road cooperative communication network. The single copy routing algorithm SimBet is used to reorganize the data transmission channel model of vehicle-road cooperative communication. With the passive time reversal mirror (PTRM) and BPSK modulation technology, the channel model of vehicle-road cooperative communication is established [6]. According to the attenuation of the data transmission bandwidth of the communication network, the weighted vector of the channel and the frequency component of the output signal are obtained. Through the convolution operation, the communication data transmission and equalization design are realized. The structure model of data input and output is shown in Figure 1.

According to the structure model of vehicle-road cooperative communication data input and output shown in Figure 1, the optimal distribution control of vehicle-road cooperative communication data time series is carried out based on the attenuation of communication network data transmission bandwidth. The vehicle network multisensor information collection method is used to realize the data acquisition and data structure analysis of vehicle-road cooperative communication. Assuming that the vehicle-road cooperative communication data signal is $p(t)$ and the cooperative communication data sequence of PS waiting for a period of time Tg to be transmitted is $S(t)$, the output processed by the reversal mirror is as follows after Wigner-Ville distribution detection and time reversal:

$$p_{ri}(t) = p(t) * h_i(t) + n_{pi}(t), \quad (1)$$

where $h_i(t)$ represents the attenuation coefficient of impulse response characteristic quantity $p(t)$ of vehicle-road cooperative communication data in the multipath channel. The channel equalization control of vehicle-road cooperative communication data transmission is carried out on a

continuous sliding window to obtain the symbol sequence of vehicle-road cooperative communication data $S_r(t)$ after matched filtering:

$$S_r(t) = S(t) * h(t) + n_s(t), \quad (2)$$

where $n_s(t)$ represents the interference noise on the data collection bandwidth of the vehicle-road collaborative communication, and the relevant matched filter detection output is obtained through a preprocessor $P_r(-t)$:

$$S_{r_i}(t) = S(t) * h'_i(t) + n_{si}(t), \quad (3)$$

where $h'_i(t)$ is the response function after filtering in $S(t)$, and the bandwidth of the data transmission array element sequence of vehicle-road cooperative communication is

$$\begin{aligned} r'_i(t) &= S_{r_i}(t) * p_{ri}(-t) \\ &= S(t) * p(-t) * h'_i(t) * h_i(-t) + n_{1i}(t), \end{aligned} \quad (4)$$

where $S(t)$ is the local signal, $S_{r_i}(t)$ is the multipath signal, $p_{ri}(-t)$ is power spectral density, and $n_{1i}(t)$ is the noise component. The signal component in the extended signal $r(t)$ of the vehicle-road cooperative communication in the spatial multipath channel is approximately the information signal waveform $S(t)$, and the output interference suppression component is

$$\begin{aligned} n_{1i}(t) &= S(t) * h'_i(t) * n_{pi}(-t) \\ &+ n_{si}(t) * p(-t) * h_i(-t) \\ &+ n_{si}(t) * n_{pi}(-t), \end{aligned} \quad (5)$$

where $n_{pi}(-t)$ represents the noise component on the p -th symbol sequence, and $n_{si}(t)$ represents the noise component on the s symbol sequences. According to the above processing, the data transmission channel model of vehicle-road cooperative communication is constructed, and the anti-interference design of signal transmission is realized by the matched filter detection algorithm.

2.2. Transmission Signal Analysis. In order to obtain the data transmission gain of vehicle-road cooperative communication, the subsection equalization adjustment of vehicle-road cooperative communication data transmission is realized. It is assumed that the vehicle-road cooperative communication data are transmitted to each node b_i , and the number of pulse frames for the impulse response of the channel is N_f , then the time required $T_{\text{spray}} = \max(t_i)$ for the diffusion stage is obtained by the auto-correlation matching filter detection. The extended signal of vehicle-road cooperative communication data output is

$$\begin{aligned} r(t) &= \sum_{i=1}^M r'_i(t) * p(t) \\ &= S(t) * p(t) * p(-t) * \sum_{i=1}^M h'_i(t) * h_i(-t) + \sum_{i=1}^M n_i(t), \end{aligned} \quad (6)$$

where $n_i(t)$ is also the noise interference term of the data transmission channel for vehicle-road cooperative

communication, $n_i(t) = n_{1i}(t) * p(t)$. The forwarding delay depends on the diffusion delay. Therefore, in the data transmission process of vehicle-road cooperative communication, the fuzzy function is introduced and the feature clustering algorithm is used. The clustering algorithm is a classic algorithm to solve the clustering problem, which is simple and fast. For dealing with large data sets, the algorithm maintains scalability and efficiency. When the cluster is close to Gaussian distribution, its effect is better. The fuzzy matching function of data transmission of vehicle-road cooperative communication is obtained as

$$\begin{aligned} H(t) &= \hat{h}(t) * p(t) * p(-t) \\ &= \left(\sum_{i=1}^M h'_i(t) * h_i(-t) \right) * p(t) * p(-t), \end{aligned} \quad (7)$$

where $\hat{h}(t)$ and $p(t) * p(-t)$ approximate the impulse response function $\delta(t)$; $p(t)$ and $p(-t)$ indicate the spectral components of the impulse response signal taken on the positive and negative sequences, respectively. $*$ is convolution operation. By the time-frequency analysis method and through calculation, $h'_i(t)$ is calculated through $h_i(t)$, and the signal components of the vehicle-road cooperative communication channel are processed by feature focusing, and the following result is obtained:

$$|s(f)| = A \sqrt{\frac{1}{2k} \{ [c(v_1) + c(v_2)]^2 + [s(v_1) + s(v_2)]^2 \}}, \quad (8)$$

where $A(t)$ is the amplitude of the vehicle-road cooperative communication signal, f_0 is the initial transmission frequency of the vehicle-road cooperative communication channel, $k = B/T$ is the BPSK modulation component of the vehicle-road cooperative communication, and B is the frequency modulation signal bandwidth. The spread spectrum algorithm is adopted to obtain the information flow of the output signal $a(t)$ in the delay time interval T_a . Accordingly, the data clustering algorithm is adopted to obtain the data transmission gain of the vehicle-road cooperative communication as follows:

$$E = \|x(t)\|^2 = \sum_j \sum_k |C_j(k)|^2 = \sum_j E_j, \quad (9)$$

where $x(t)$ is the time series of data transmission signal of vehicle-road cooperative communication, $C_j(k)$ is the data delivery delay, and E_j is the amplitude modulation parameter. According to the above channel and signal analysis, the baud interval equalization method is adopted to realize the piecewise equalization adjustment for data transmission of vehicle-road cooperative communication according to the symbol characteristic distribution of the vehicle-road cooperative communication channel [7].

3. Optimization of Fast Data Transmission in Vehicle-Road Collaborative Communication

3.1. Data Transmission Channel Equalization of Vehicle-Road Collaborative Communication. The channel equalization

model for vehicle-road cooperative communication is established by adaptive control of link forwarding protocol and baud interval equalization control [8]. In the process of forward and reverse driving, the time-frequency characteristic component of the vehicle-road cooperative communication signal received by the receiver is as follows:

$$s(t) = \cos[2\pi f_0 t + \pi\beta t^2 + \psi_0], \quad (10)$$

where f_0 and ψ_0 are the starting frequency and initial phase of the multipath channel of vehicle-road cooperative communication, respectively. The statistical characteristics of the units to be detected are estimated, and the spread spectrum allocation model of vehicle-road cooperative communication channel is constructed. The extended bandwidth loss is expressed as

$$X' = \sum_{v=1}^V b_v X_v, \quad (11)$$

where $\{b_v, v = 1, 2, \dots, V\}$ is the impulse weighting coefficient of the data transmission channel of vehicle-road cooperative communication and X_v represents the distance ambiguity parameter. $p(t)$ is introduced as the propagation attenuation coefficient. The multipath spectrum bandwidth of vehicle-road cooperative communication is W . By adopting the iterative learning and adaptive control methods, an equilibrium control mode for the multivehicle-road cooperative communication channel in multidimensional road network space is constructed [9], and the channel equilibrium adjustment output is as follows:

$$H(z) = Am \cdot \frac{1 + 2z^{-1} + z^{-2}}{(1 - \rho e^{j\phi} z^{-1})(1 - \rho e^{-j\phi} z^{-1})}, \quad (12)$$

where z is the transfer function of vehicle-road cooperative communication, A is the amplitude of path loss, and m is the intersymbol interference. Using pole estimation, the signal output $x(n)$ in the road network $\rho e^{\pm j\phi}$ is

$$x(n) = A \cos(0.3\pi n + \varphi) + v(n), \quad (13)$$

where φ is the output spread phase of vehicle-road cooperative communication and $v(n)$ is the intersymbol interference caused by path spread. By introducing the multiscale characteristics of channel transmission, data transmission control and adaptive adjustment are carried out based on man-machine interaction control [10].

3.2. Data Clustering of Vehicle-Road Collaborative Communication and Transmission Optimization. Based on data transmission channel equalization of vehicle-road cooperative communication, data clustering is carried out to vehicle-road cooperative communication, and the specific flow chart is shown in Figure 2.

With the adaptive error compensation and channel fading suppression, the K-means clustering algorithm is used to carry out coordinated adjustment to data packets during the rapid data transmission of the vehicle-road cooperative communication. The K-means clustering

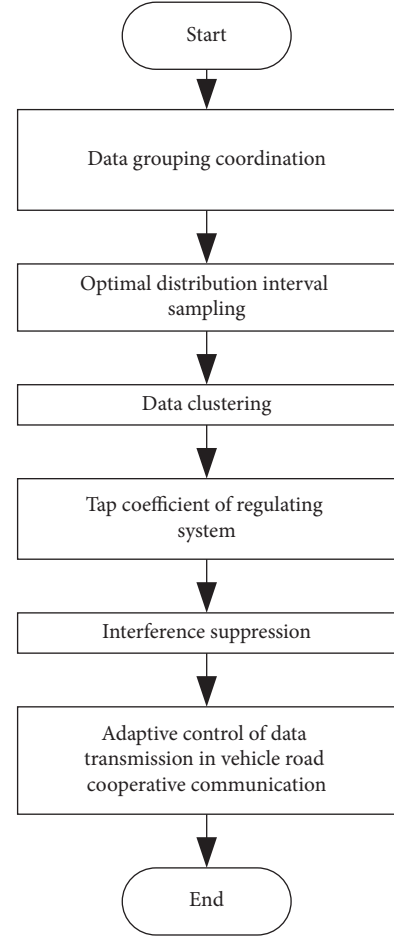


FIGURE 2: Flow chart.

algorithm is an iterative clustering analysis algorithm. This step is to divide the data into k groups, randomly select k objects as the initial clustering center, then calculate the distance between each object and each subclustering center, and assign each object to the nearest clustering center. According to the attenuation of communication network data transmission bandwidth, the optimal distribution interval sampling of vehicle-road cooperative communication data time series is carried out [11], and the clustering function is obtained as follows:

$$s(t) = \sum_i b_j \sum_{j=0}^{N_f-1} p(t - iT_s - jT_f - c_j T_c), \quad (14)$$

where b_j is the interference item of the vehicle-road cooperative communication data, T_s is the time sampling interval, and c_j is the transmission bandwidth of the vehicle-road cooperative communication data. Assuming that the similarity of the vehicle-road cooperative communication data is $h(n)$, the nonlinear equilibrium parameter is $n(n)$, the time domain loss is $\gamma(n)$, and the intersymbol interference is $\tilde{x}(n)$, then under the limited symbol rate, the channel aliasing and superposition are carried out by convolution $h'_i(t) * h_i(-t)$, and the data clustering is realized by the data K-means cluster shown in Figure 3.

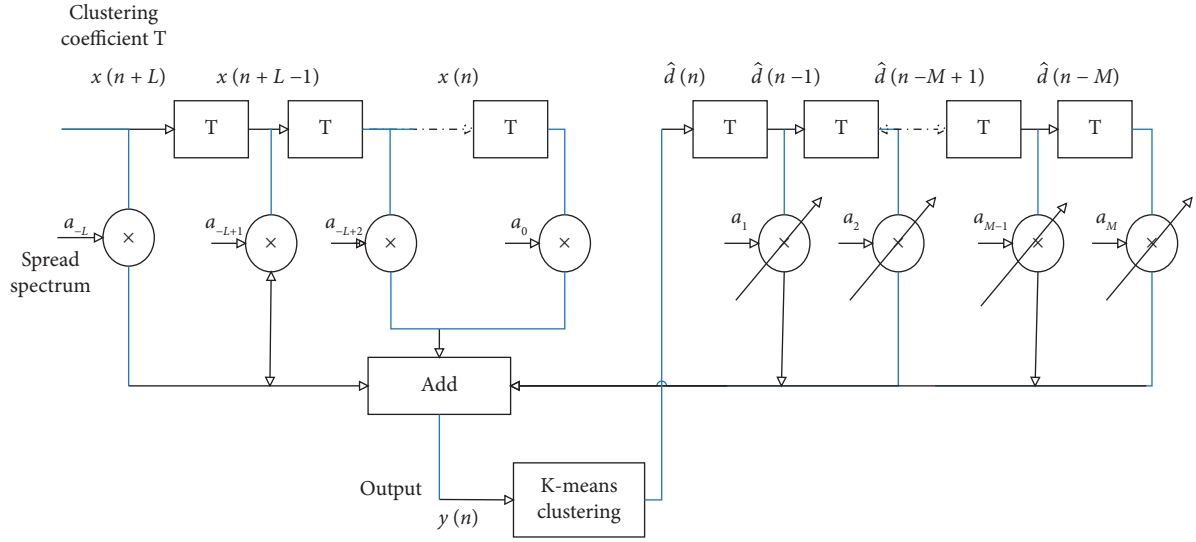


FIGURE 3: K-means clustering of data.

With the clustering result of vehicle-road cooperative communication data in Figure 3 as the output, the spectral component of communication data output is as follows:

$$\begin{aligned} S(n_j) &= (E_{\text{elec}} + E_{DF})l\delta + E_{Tx}(l, d_j) \\ &= (E_{\text{elec}} + E_{DF})l\delta + lE_{\text{elec}} + l\varepsilon_{fs}d_j^2 \quad (15) \\ &= [(E_{\text{elec}} + E_{DF})\delta + E_{\text{elec}} + \varepsilon_{fs}d_j^2]l, \end{aligned}$$

where E_{elec} is the superposition component of vehicle-road cooperative communication at the same time in the same phase, E_{DF} is the attenuation loss of multipath spread of vehicle-road cooperative communication, $E_{Tx}(l, d_j)$ is the channel impulse characteristic quantity of vehicle-road cooperative communication transmission, ε_{fs} is the frequency spectrum parameter, l is fuzzy information sequence, and d_j is the multipath component of detection signal. The tap coefficient of vehicle-road cooperative communication data transmission is adjusted, and the blind equalization method is adopted to suppress interference. The adaptive control of data transmission in vehicle-road cooperative communication is carried out according to the dynamic distribution characteristics of clustering centers so as to reduce the effects of channel fading and intersymbol interference caused by the channel spread spectrum [12].

4. Simulation Experiment

In the experiment, the distance between vehicles in the motorcade was kept at 24–100 m, and the upper speed line v_{max} was 120 km/h. RFID was used as the sensor in the motorcade, and 100 receiving array elements were set to form the transmission array of vehicle-road cooperative communication. The independent variable X of data transmission in vehicle-road cooperative communication indicated the distance between two nodes in the link establishment time. The vehicle driving can be divided into two situations: forward driving and reverse driving. The

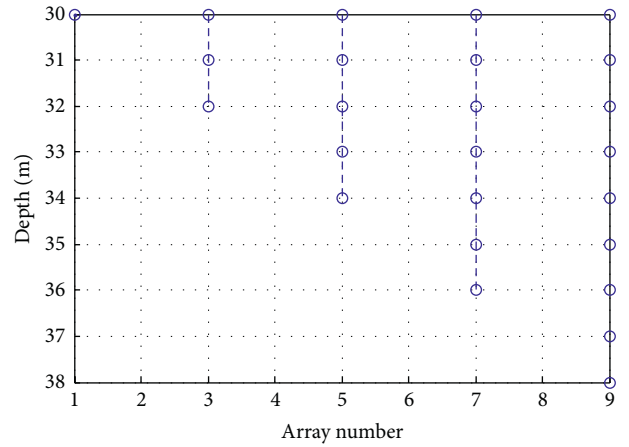


FIGURE 4: Distribution of transmission elements in vehicle-road cooperative communication.

communication range was $[0, 300)$, satisfying $0 \leq X < 300$. In vehicle-road cooperative communication, the symbol transmission rate was set at 1 k Baud. The maximum data transmission delay was set at 25 ms; the symbol distance was 100 m; the waiting time of vehicle-road cooperative communication data was $Tg = 100\text{ms}$; the signal-noise ratio was fixed at 10 dB; the number of snapshots was changed from 200 to 2000. According to the above simulation environment and parameter settings, the data transmission optimization simulation analysis of vehicle-road cooperative communication was carried out, and the distribution of transmission array elements of vehicle-road cooperative communication is shown in Figure 4.

According to the array element distribution in Figure 4, the signal transmission model for vehicle-road cooperative communication was constructed, and the output time series of vehicle-road cooperative communication data was obtained by taking the input signal-to-noise ratio of -10 dB , -5 dB , and 0 dB , respectively, as shown in Figure 5.

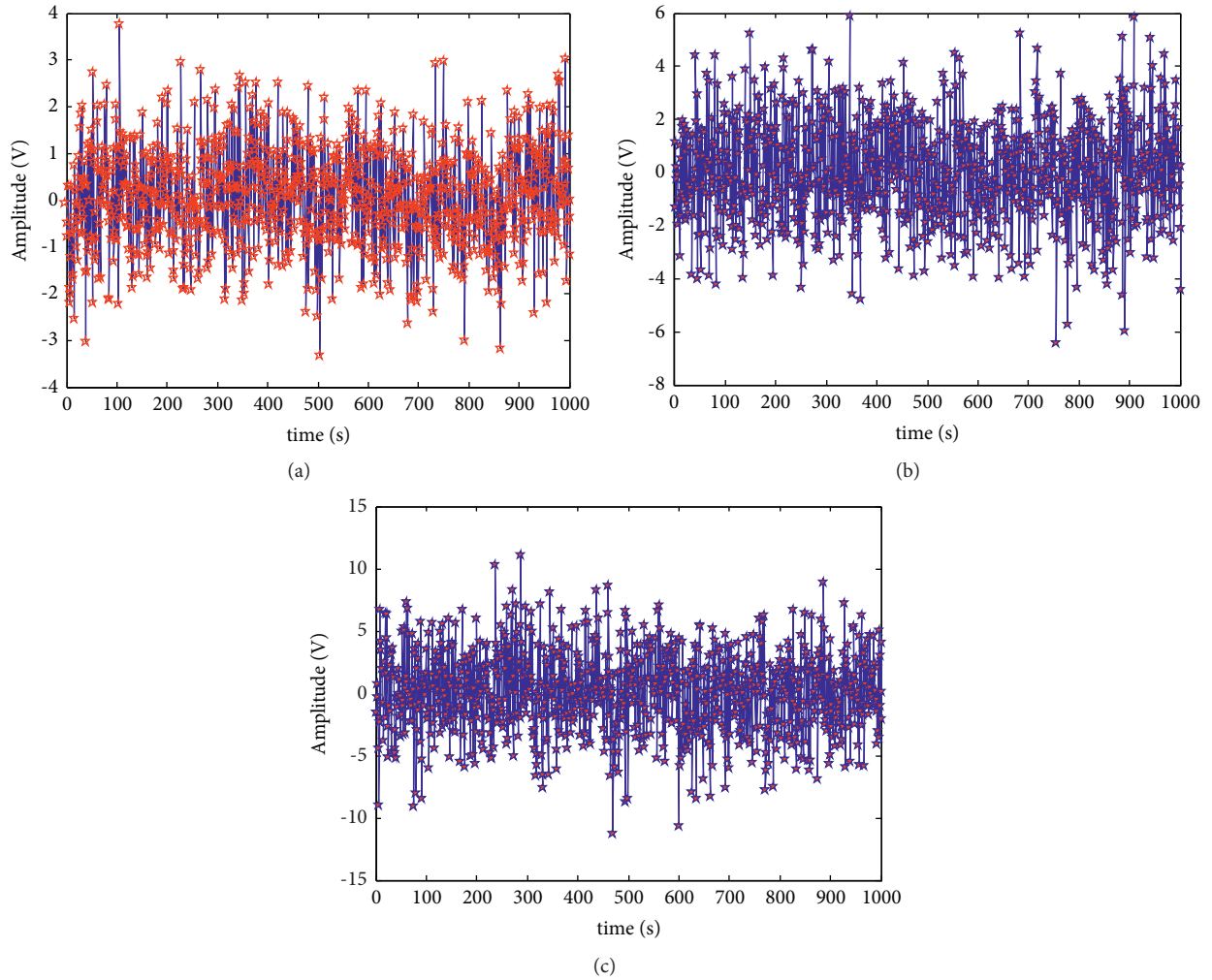


FIGURE 5: Output time series of vehicle-road cooperative communication data. (a) Transmission data sample 1 (SNR=0 dB). (b) Transmission data sample 2 (SNR=-5 dB). (c) Transmission data sample 3 (SNR=-10 dB).

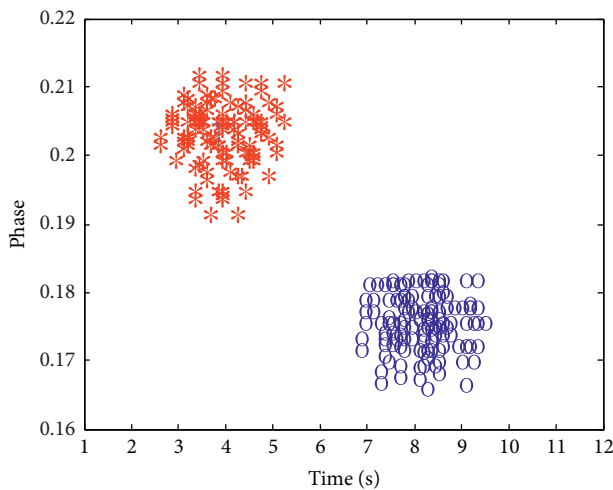


FIGURE 6: Data clustering results.

With the output time series of vehicle-road cooperative communication data shown in Figure 5 as a sample, the data were clustered. The clustering results are shown in Figure 6.

According to analysis of Figure 6, the method proposed in this paper has good clustering and strong segmentation detection ability. On this basis, the data transmission is realized, and the data transmission rate and bit error rate are tested. Data transfer rate is one of the important technical indicators to describe the data transmission system. It refers to the speed of information transmission on the communication line and the number of bits transmitted in unit time (usually one second). Ser (symbol error rate) is an index to measure the accuracy of data transmission within a specified time. $Ser = \text{error code in transmission} / \text{total number of transmitted codes} * 100\%$ [1]. If there is bit error, there is bit error rate. In addition, the bit error rate is also defined as the frequency used to measure the occurrence of errors. The research of bit error rate under specific conditions is of great

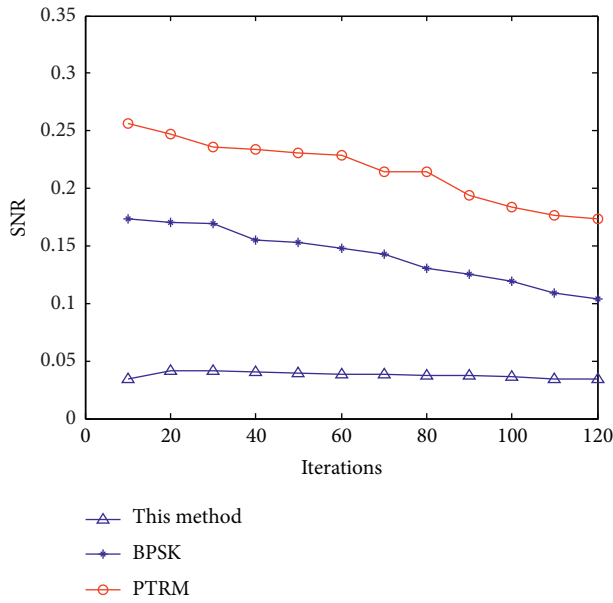


FIGURE 7: Bit error rate comparison.

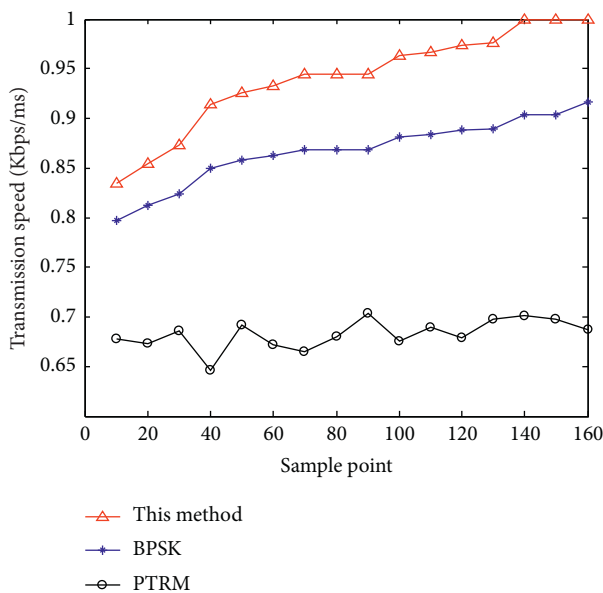


FIGURE 8: Comparison of data transmission rate.

significance to enhance the performance of wireless communication system and improve the quality of data transmission. The comparison results are shown in Figures 7 and 8. Through the analysis of the results in Figures 7 and 8, the bit error rate of the method proposed in this paper is maintained at about 0.05, the data transmission rate is above 0.8, and the data transmission rate continues to improve, most of which remain above 0.95. The bit error rate of BPSK and PTRM methods is above 0.1, and the data transmission rate of PTRM method is below 0.7. The results show that this method has strong anti-interference ability for the data transmission of vehicle-road cooperative communication, with low communication bit error rate, small end-to-end delay, high data transmission rate, high stability, and high accuracy.

5. Conclusion

The data transmission control model for vehicle-road cooperative communication is designed, which is used to improve the stability of fast data transmission of vehicle-road cooperative communication based on channel equalization adjustment. Accordingly, a fast data transmission method of vehicle-road cooperative communication based on the clustering algorithm is proposed in this paper. The single copy routing algorithm SimBet is used to reorganize the data transmission channel model for vehicle-road cooperative communication, and the data transmission channel model is thus constructed. The matched filter detection algorithm is used to realize the anti-interference design of signal transmission. According to the symbol characteristic distribution of the vehicle-road cooperative communication channel, the band interval equalization method is used to realize the segmented equalization control of the vehicle-road cooperative communication data transmission, and the channel equalization model is designed. The K-means clustering algorithm is used to carry out the coordinated adjustment to data packets during the rapid data transmission of the vehicle-road cooperative communication. According to the attenuation of communication network data transmission bandwidth, the optimal distribution interval sampling of vehicle-road cooperative communication data time series is carried out so as to improve the stability of data transmission. The test shows that the method proposed in this paper has a low bit error rate, with bit error rate kept at about 0.05, and has high data transmission rate and good stability [13].

Data Availability

The data used to support the findings of this study are available from the corresponding author upon request.

Conflicts of Interest

The authors declare that they have no conflicts of interest.

Acknowledgments

This work was supported by Open Project of Shandong Key Laboratory of Smart Transportation (Preparation).

References

- [1] T. A. N. G. Lun, Y. A. N. G. Xixi, S. H. I. Yingjie, and Q. Chen, "ARMA-Prediction based online adaptive dynamic resource allocation in wireless virtualized networks[J]," *Dianziyuxinxuebao*, vol. 41, no. 1, pp. 16–23, 2019.
- [2] H. Su, H. Liu, P. Shui, and Z. Bao, "Adaptive beamforming for nonstationary HF interference cancellation in skywave over-the-horizon radar," *IEEE Transactions on Aerospace and Electronic Systems*, vol. 49, no. 1, pp. 312–324, 2013.
- [3] A. Kumar, R. Pooja, and G. K. Singh, "Design and performance of closed form method for cosine modulated filter bank using different windows functions," *International Journal of Speech Technology*, vol. 17, no. 4, pp. 427–441, 2014.

- [4] R. Wang and Y. Xu, "Evaluation of security situation of communication network nodes based on grey correlation model," in *Proceedings of the 4th International Conference on Information Systems and Computer Aided Education*, pp. 2633–2638, New York, NY, USA, September 2021.
- [5] N. Rajapaksha, A. Madanayake, and L. T. Bruton, "2D space-time wave-digital multi-fan filter banks for signals consisting of multiple plane waves," *Multidimensional Systems and Signal Processing*, vol. 25, no. 1, pp. 17–39, 2014.
- [6] G. Zhan, Z. Huang, D. Ying, D. Ying, J. Pan, and Y. Yan, "Improvement of mask-based speech source separation using DNN[C]," in *Proceedings of the 10th International Symposium on Chinese Spoken Language Processing*, pp. 1–5, IEEE, Tianjin, China, October 2016.
- [7] Y. Luo, Z. Chen, and N. Mesgarani, "Speaker-independent speech separation with deep attractor network," *IEEE/ACM Transactions on Audio, Speech, and Language Processing*, vol. 26, no. 4, pp. 787–796, 2018.
- [8] Y. Han and D. Fang, "Lightweight coverage hole detection algorithm based on relative position of link intersections," *Journal of Computer Applications*, vol. 40, no. 9, pp. 2698–2705, 2020.
- [9] Z. H. Zou, X. Y. Gong, and X. J. Deng, "A coverage hole detection algorithm in wireless sensor networks based on the confident information coverage model[J]," *Journal of University of South China(Science and Technology)*, vol. 31, no. 1, pp. 32–38, 2017.
- [10] L. Nie, J. Zhang, and M. Hu, "Short-term traffic flow combination prediction based on CEEMDAN decomposition[J]," *Computer Engineering and Applications*, vol. 58, no. 11, pp. 279–286, 2022.
- [11] Z. Zhang, Y. Zhang, Improved FA optimizing LSTM time series prediction model[J]," *Computer Engineering and Applications*, vol. 58, no. 11, pp. 125–132, 2022.
- [12] X. Ren and L. Zhang, "Improved multi-primary-node consensus mechanism based on practical Byzantine fault tolerance[J]," *Journal of Computer Applications*, vol. 42, no. 5, pp. 1500–1507, 2022.
- [13] Y. Sun, Y. Xian, W. Wang, and S. M Naqvi, "Monaural source separation in complex domain with long short-term memory neural network," *IEEE Journal of Selected Topics in Signal Processing*, vol. 13, no. 2, pp. 359–369, 2019.

Research Article

Construction and Application of Farmers' Practical Teaching System in Vocational Education Based on Big Data Mining Technology

Wei Peng¹ and Zhibin Tang² 

¹Institute of Higher Vocational Education, Yueyang Vocational and Technical College, Yueyang, Hunan 414000, China

²College of Engineering and Design, Hunan Normal University, Changsha, Hunan 414000, China

Correspondence should be addressed to Zhibin Tang; tangzbin@hunnu.edu.cn

Received 13 June 2022; Revised 14 July 2022; Accepted 27 July 2022; Published 31 August 2022

Academic Editor: Le Sun

Copyright © 2022 Wei Peng and Zhibin Tang. This is an open access article distributed under the Creative Commons Attribution License, which permits unrestricted use, distribution, and reproduction in any medium, provided the original work is properly cited.

With the establishment and perfection of social market economy, China has made changes to the disadvantages of farmers' vocational education system, such as singleness, backward educational means, and backward levels. Compared to traditional forms of farming, problems related to lack of farming expertise, poor scientific and technological awareness, and weak labor skills are analyzed by applying big data mining technology to retrieve key issues in order to establish a professional education system. Data mining can meet the needs of farming knowledge and rapidly develop into an automatic information farming model, which is an effective way to maximize and enhance professional knowledge. The establishment of a professional education system will train most scientific research members and further enhance diversified labor productivity. The experimental summary of this paper is as follows: (1) the relevant data need to be predicted before and after, the predicted experimental data will effectively improve students' grades, which is beneficial to the development of practical teaching, and the pretreatment stage plays a substantial role. (2) Among the three algorithms, the adaptive function of genetic clustering algorithm is obviously better than the other two algorithms, and the adaptive curve is relatively stable. (3) The comprehensive assessment of the course divides students into three categories: poor students, medium students, and excellent students, among which poor students account for 30%, medium students account for 50%, and excellent students account for 20%. (4) The standardization of the education system has brought users a good learning mechanism, in which the teaching resources have been strengthened, and users have very high satisfaction with the evaluation of the whole system.

1. Introduction

Farmers' vocational education system is established on the level of economic system, which adapts to the development of market economy and will improve agricultural development economy. Adapt to the basic conditions of taking rural areas as the primary industry, and extend the professional technology to ideological education. The Internet plays a key and substantive role, and will adopt diversified educational models to teach farmers about planting methods. Because the allocation of teaching time in the whole period needs to be detailed, it is necessary to avoid the confusion of relevant information, which is a kind of

development and utilization of resources. Big data mining technology will retrieve and reserve the knowledge of farmers' professional education cognition, professional knowledge, technical training, and other personnel engaged in agricultural activities. School-running modes and means should be diversified, and school-enterprise cooperation, rural service, and other educational concepts serving the people should be implemented to run schools. This paper summarizes the innovation status of the pilot counties of new professional farmers and puts forward the theory of establishing and perfecting the policy system and giving full play to the role of the market [1]. In view of the confusion of the concept of new professional farmers, this paper re-

examines the basic concept and connotation of the times of new professional farmers [2]. This paper expounds the connotation and realistic needs of new-type professional farmers and the cultivation experience of foreign professional farmers, and puts forward some supporting policies and measures for perfecting the cultivation of new-type professional farmers [3]. Strengthen the policy orientation of cultivating new professional farmers, and construct a new professional farmer cultivation system that embodies the concept of lifelong learning [4]. The meaning of professional farmers: New professional farmers have a broad and narrow distinction, and have a more conscious sense of responsibility and broader responsibility requirements [5]. On the issue of cultivating new professional farmers, we can learn from the practice of the USA and introduce practical laws and regulations [6]. Vigorously strengthen system construction, promote the integration of industrial chain, and strengthen the education and training of agricultural practitioners [7]. Construct flexible practical curriculum system, implement flexible talent training scheme, and explore practical teaching assessment methods with vocational education characteristics [8]. This paper discusses the characteristics of vocational education with multiple purposes and comprehensive contents, and cultivates new teaching forms [9]. A practical teaching system suitable for agriculture and forestry majors has been established, which enriches and expands students' practical skills [10]. Based on the analysis of China's modern agricultural development perspective, this paper puts forward some suggestions on how to build a platform and other aspects of the reform of the training mode of agriculture-related professionals in secondary vocational schools [11]. This paper expounds how the experimental teaching demonstration center can better serve the experimental teaching and the cultivation of innovative talents, and give full play to the radiation role of the experimental teaching demonstration center [12]. In-depth thinking on the curriculum of agriculture-related majors provides scientific ideas for the development of rural secondary vocational education [13]. To better cultivate students' practical ability and innovative and entrepreneurial ability, we should carry out practical teaching reform from the aspects of teaching mode and teaching team [14]. Taking individualized experimental teaching as the content, the practical teaching system of microbiology is constructed to meet the individualized needs of different individuals [15].

2. Theoretical Overview of Big Data Mining Technology

Big data mining technology extracts useful information from data sets and makes use of it, which is expressed in the form of rules, concepts, laws, and patterns. It can effectively help decision-makers to analyze the current situation, find hidden relationships, and then predict possible behaviors. The basic process is shown in Figure 1.

The whole process is a continuous feedback process. For example, if a bad extraction is found in the process, or the expected results are not achieved, it is necessary to start over.

There are two influencing factors in quality selection: first, whether the effectiveness of its products can be brought into play in this process, whether key factors can be extracted, and whether it can be applied in the actual situation; second, if there are errors or improper options, the conversion is unsuccessful, which will depend on the goodness of the extraction results.

2.1. A Survey of Clustering Algorithms. Clustering is an easy-to-understand way to gather related activities. Through the research and analysis of things, people can recognize related laws. There are also small classifications in clustering projects. Classification is to classify the regular characteristics known in advance, and other categories are the results of human analysis and research. In biology, cluster analysis can be used to deduce the related habits of plants and animals, analyze genes, and obtain inherent survival rules. Correlation calculation can be roughly divided into three categories: classification of fuzzy relation, fuzzy algorithm of objective function, and fuzzy algorithm based on neural network.

Partition clustering refers to dividing related combined data sets into n groups, which makes the objective function partition level smaller. Hierarchy refers to merging or splitting related passing objects until all conditions are met. Strictly implement the conditions of partition, people can grasp the key points when dealing with problems, and each can reflect the actual problems, thus becoming the mainstream research of cluster analysis and making use of it.

2.1.1. K-Means Clustering Algorithm. K-means is the most classical clustering algorithm. Firstly, K objects are randomly selected, and each object represents a core. According to the distance between cores, similar type characteristics are assigned to one class for each subject. They are summarized as follows.

Nonlinear programming problem [16]: The classification algorithm is as follows:

$$\begin{aligned} \min J(W, P) &= \sum_{i=1}^k \sum_{j=1}^n d^2(x_j, p_i), \\ \text{s.t. } \omega_{ij} &\in \{0, 1\}, 1 \ll i \ll k, 1 \ll j \ll n. \end{aligned} \quad (1)$$

Among them,

$$W = [\omega_{ij}]_{k \times n}. \quad (2)$$

W is the partition matrix, which indicates that J samples belong to and do not belong to Class I , P is the cluster center, and D is the adaptation degree. The specific process is as follows:

Input: The number of clusters contains n object data sets.

Output: The value of the cluster.

The algorithm has good extensibility, and the difficulty of the algorithm can calculate the core quality results according

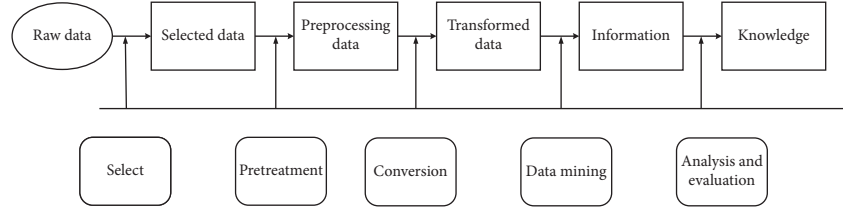


FIGURE 1: Basic process of data mining.

to the number of clusters generated in advance. His shortcomings are that we must realize the results of understanding spherical clusters, but also consider the choice of initialization, so as to achieve the optimal processing. Secondly, the sensitive response of noise to the algorithm is very strong.

2.1.2. Fuzzy C-Means Clustering. Fuzzy C-means (FCM) algorithm is an optimization algorithm based on K-means algorithm by introducing fuzzy matrix and dividing it. The objects considered in practice have not strict attributes, so they must be in the classification algorithm of fuzzy clustering. The algorithm is described as follows:

Mathematical programming problem [17] formula is as follows:

$$\begin{aligned} \min J(W, P) &= \sum_{i=1}^k \sum_{j=1}^k (\omega_{ij})^m, d^2(x_j, p_i), \\ \text{s.t: } \omega_{ij} &= \epsilon [0, 1], 1 \leq i \leq k, 1 \leq j \leq n, \\ \sum_{i=1}^k \omega_{ij} &= 1, 1 \leq j \leq n, \\ 0 < \sum_{i=1}^k \omega_{ij} &\leq n, 1 \leq j \leq n, \end{aligned} \quad (3)$$

where m represents the weighting index, and the algorithm is to find the fitness degree d of clustering center. Euclidean distance [18] formula is

$$d^2(x_j, p_i) = \left(\sum_{s=1}^l x_j(s) - p_i(s) \right)^{1/2}. \quad (4)$$

In order to realize the clustering center P of the minimum membership matrix of the objective function $J(W, P)$, it is necessary to cluster the fuzzy C of the mean value. The optimal solution of the objective function is the solution of the minimum value; that is, the center and membership degree are updated as follows:

$$\begin{aligned} \omega_{ij} &= \frac{1}{\sum_{c=1}^k (d_{ij}/d_{cj})^{2/(m-1)}}, \\ p_i &= \frac{\sum_{j=1}^n \omega_{ij}^m x_j}{\sum_{j=1}^n \omega_{ij}^m}. \end{aligned} \quad (5)$$

According to the above conditions, C-means can be modified repeatedly to achieve central clustering and

membership matrix. The specific algorithm flow is as follows in Figure 2.

Fuzzy C-means algorithm is a popular algorithm nowadays, which is not only simple, but also fast, because it has a fairly perfect theoretical system; secondly, it can be applied in many wide fields as a simple practical tool. However, there are still some shortcomings, such as sensitivity to initial points and local optimal clustering results, and improved points can be divided into any point and any class of different degrees of clustering.

2.2. Genetic Algorithm. Genetic algorithm is a search method with self-adaptation and organization ability, which draws lessons from the principles of natural evolution and development of biology. Its principle is that each individual has its corresponding fitness value, which can be used to measure the quality of an individual. By imitating the principle of survival of the fittest of animals and plants in nature, the classification is carried out according to the fitness value. Individual crossover operation is to form new individuals through the combination of individuals, so as to form excellent individuals, which is similar to the process of gene selection.

The general working steps are as follows:

- (1) The input parameter set is transformed into bit string structure.
- (2) Defining fitness function.
- (3) Confirming genetic strategy.
- (4) Calculating fitness value.
- (5) Optimize the operation to generate the next stage group.
- (6) Output decoding and return to optimization operation again; in order to understand the unique deterministic index of individual survival chance selection of population, its fitness value is non-negative, and the larger the result, the better. For a given optimization problem, the evaluation of the objective function is also non-negative, and the transformed coordinate direction is a positive correlation direction. This shows that the encoding of the initial population has a direction, different individual spaces have their own patterns, and its theory is rotation and gambling selection.

2.2.1. Genetic Clustering Algorithm. Genetic clustering algorithm divides all data elements corresponding to sample codes into a category, and this function is defined as

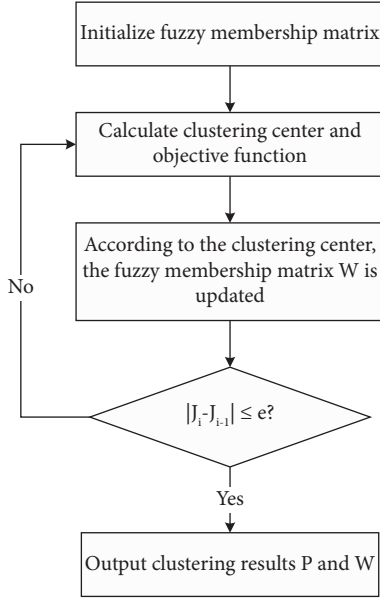


FIGURE 2: Basic flow of fuzzy C-means algorithm.

Euclidean distance, which can be randomly generated and obtained. Genetic operation can find the global optimal solution without the influence of outliers, which requires large data, more classifications, faster convergence, and stronger practicability. Its function expression is as follows: Adaptation function [19] is

$$\begin{aligned} \min J(W, P) &= \sum_{i=1}^k \sum_{j=1}^k (\omega_{ij})^m, \\ \text{s.t. } \omega_{ij} &\in [0, 1], \\ \sum_{i=1}^k \omega_{ij} &= 1, \\ 0 < \sum_{i=1}^k \omega_{ij} &\leq n, \end{aligned} \quad (6)$$

Through the definition of objective function, the minimum value is transformed into the maximum value. That is, the formula is

$$f = \frac{1}{J(W, P)}. \quad (7)$$

It needs to expand the coding form, and real coding is to directly define animal and plant genes through parameter problems. The clustering problem directly defines the center code.

Clustering center [20] expression is

$$P = (p_1, p_2, \dots, p_k)^T. \quad (8)$$

P represents a one-dimensional vector.

Gene string [21] expression is

$$I = \{p_{11}, p_{12}, \dots, p_{1m}, \dots, p_{k1}, p_{k2}, \dots, p_{km}\}. \quad (9)$$

Next, the genetic strategy is implemented, which includes selection operator, crossover operator, and mutation operator. The Group X for which the size is defined is

$$X = \{x_1, x_2, \dots, x_n\}. \quad (10)$$

Selection probability [22] is

$$p_s = \frac{f(x_i)}{\sum_{i=1}^n f(x_i)}, i = 1, 2, \dots, n. \quad (11)$$

Individual cumulative probability [23] is

$$p_s(x_i) = \sum_{j=1}^i p_s(x_j), i = 1, 2, \dots, n, j = 1, 2, \dots, i. \quad (12)$$

When selecting, the interval is $[0, 1]$, which obeys uniform distribution. When the individual x_i with cumulative probability p_s is selected to enter the classification center, the judgment result of random number $rand$ is as follows:

$$rand \leq p_s(x_i). \quad (13)$$

This means that the operator is selected. At present, the crossover operator has the mating forms of one-point crossover, uniform crossover, and multi-point crossover. When it obeys the uniform distribution, it can choose a crossover position, and the expression result is as follows:

$$a \in \{1, 2, \dots, m-1\}. \quad (14)$$

The exchange of gene strings at this position is as follows:

$$\begin{aligned} x_1 &= \{x_{11}, x_{12}, \dots, x_{1a}, x_{2(a+1)}, \dots, x_{2(m-1)}, x_{2m}\}, \\ x_2 &= \{x_{21}, x_{22}, \dots, x_{2a}, x_{1(a+1)}, \dots, x_{1(m-1)}, x_{1m}\}, \end{aligned} \quad (15)$$

In this way, the information exchange process between genes is completed, and new gene combinations are produced.

The validity function of clustering: the main requirement of analysis is that the similarity of categories is higher and there are more categories, so it can be measured from the compactness and separation of clustering.

Compactness definition [24] is

$$comp = \frac{1}{n} \sum_{i=1}^k \sum_{j=1}^n (\omega_{ij})^2 \cdot d^2(x_j, p_i). \quad (16)$$

Definition of separability [25] is

$$sep = (d_{\min})^2 = \min \|p_i - p_j\|^2. \quad (17)$$

The validity of clustering is directly proportional to compactness and conversely inversely proportional to separability. The greater the compactness value, the higher the classification similarity and the better the effect. On the contrary, the smaller the separation value, the better the clustering effect. Therefore, the validity function is defined as

$$S = \frac{\text{comp}}{\text{sep}} = \frac{\sum_{i=1}^k \sum_{j=1}^n (\omega_{ij})^2 \cdot d^2(x_j, p_i)}{n \min \|p_i - p_j\|^2}. \quad (18)$$

As a result, it is obvious that the maximized effectiveness S corresponds to the minimized comp, and the summary is the minimized objective function J . The requirement of analysis effectiveness is that the interior of classification is as similar as possible, and its exterior needs differentiation, which is to realize effective analysis of results by measuring the size of index.

3. Application of Algorithm Feature Module

Through the previous algorithm analysis, according to the strategy of genetic algorithm: selection, crossover, mutation, and a series of operations to produce new individuals, and then use fuzzy C-means for local optimization to speed up the algorithm. Its basic idea is as follows: firstly, encoding is done from randomly generated classification centers, and secondly, judging the termination condition: whether the maximum evolutionary algebra is reached. Otherwise, it is necessary to continue iteration, so that the maximum number of possible clusters can be judged, and then the transformation can be carried out. The application steps of adaptation are as follows in Figure 3.

The goal of feature analysis module is to group individuals into each group of features. Using the adaptive algorithm of this module to do system analysis can effectively reduce the irrationality of the initial cluster number, realize the evaluation and classification of individual overall features, and optimize the global parallelism of the system.

3.1. Data Collection and Preprocessing

3.1.1. Collect Data. Collect relevant useful data according to the experimental requirements, including the original historical data. For example, the curriculum content, basic information, education system, and teaching tasks included in this experiment are all original data.

3.1.2. Data Preprocessing

(1) Remove irrelevant items

If the basic features of the original data have no intuitive effect on this experimental analysis, they can be removed.

(2) Merging similar items

The practice of vocational education has relatively more performance assessment, which can be replaced by average performance in this system. There are still more practical training and theoretical study that can be comprehensively considered and merged.

(3) Numeralization

Convert the hierarchy of excellent, good, medium, and poor into 90, 75, 60, and 50 of the percentile system.

(4) Standardization

Through the unified processing in the preprocessing stage, the standard required by the data is adopted. If the corresponding table is used to express the students' course scores, the conclusions that are beneficial to the strategy analysis will be output.

3.2. Setting of Algorithm Parameters. Aiming at the problem of constructing the practical teaching system of vocational education in this paper, the clustering method is used to summarize and analyze, and the adaptive algorithm, fuzzy C-means algorithm, and genetic learning algorithm are provided. In order to reduce the workload and loss of classification and achieve global optimization, setting parameters have great influence on operation efficiency, which must be carefully considered. The setting parameters are as follows:

- (1) The maximum possible classification of data sets should not be less than 2 groups, and the best group number should be found between 2 and parameters.
- (2) The improvement of error accuracy is 0.01 by default.
- (3) Reducing the number of cycles of the algorithm and properly increasing the accuracy of parameters are helpful to improve the excellent classification.
- (4) Control the fuzzy degree of clustering process, too much classification is poor, and too little algorithm degenerates.

After setting the parameters, the system will automatically display the classification results and output relevant useful information. Set the unique parameters of genetic algorithm.

3.3. Clustering Analysis and Data Output. After clustering and parameters are set, you can view the proportion of various samples, the total scheme and variance of samples, the mean value of various types, standardization, and experimental results.

- (1) Sample ratio: Histogram, pie chart, and line chart can be used.
- (2) All kinds of variances of the total number of samples: histogram representation.
- (3) All kinds of mean values: rectangular coordinates represent abscissa courses and ordinate mean values.
- (4) The development of standardized curriculum implementation, expressed by curve.
- (5) Output the clustering results of each sample.

The output of effective function value avoids the oscillation phenomenon of genetic classification and analyzes the scores, preferred courses, and other related information of each educated person. On the one hand, the application of teaching system solves the arrangement of daily educational administration; on the other hand, it explores the effective use of clustering algorithm in student feature mining and gets good feedback.

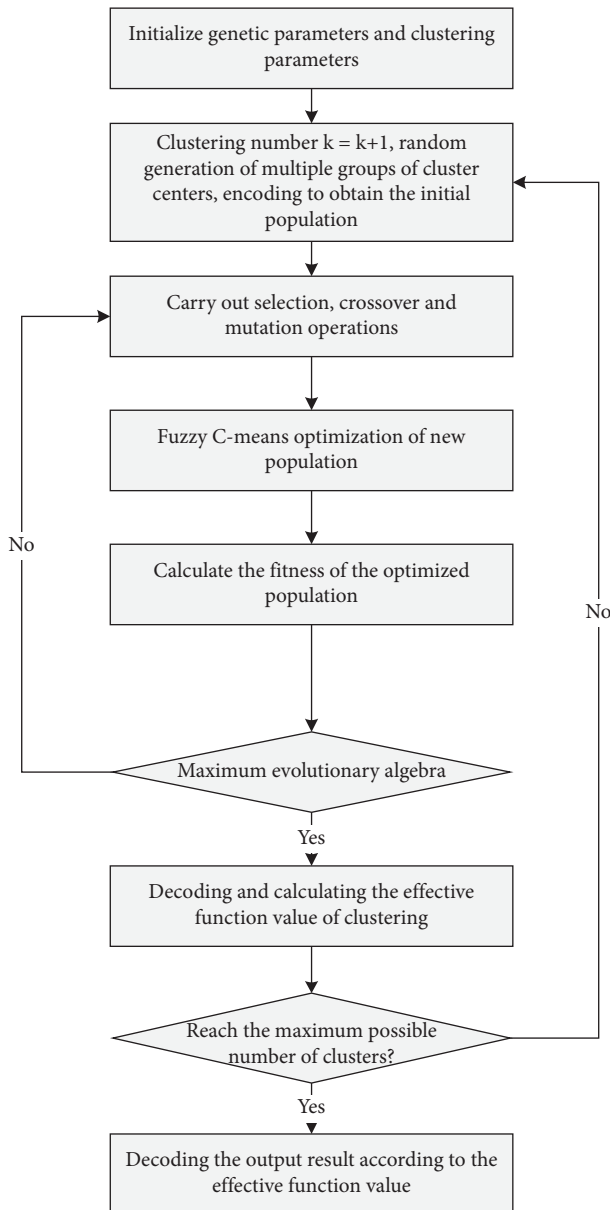


FIGURE 3: Flowchart of adaptive fuzzy C-means clustering algorithm.

4. Construction of Farmers' Practical Teaching System in Vocational Education

4.1. Comparative Analysis of Professional Farmers' Teaching Achievements before and after Data Preprocessing. According to the educational needs of farmers, the practical courses must be carried out, and the teaching tasks related to the needs must be conducive to the absorption of knowledge. Its technical economy, marketing, rural finance, etc., are all professional courses, and the efficiency and necessity of learning are analyzed before and after the prediction of achievement data sets. The results of the combination of theory and training are shown in Figure 4.

From the results in the figure, we can know that the results of relevant data preprocessing have been significantly improved, except for the course of marketing; accounting

course is the largest increase of 12% after prediction processing, which shows that this course has increased by 10 points, which is the effective improvement of data quality and the importance of preprocessing.

4.1.1. Output the Standardized Mean Value of Practical Courses. After the end of the semester, the practical course is to judge the student's learning situation. The practical course may be agricultural experiment, the development of planting technology and sowing, which all reflect the significance of the course arrangement. The arrangement of teaching tasks is judged by the number of course sections. C1, C2, and C3 represent the three dimensions of the evaluation criteria, and the standard results under the dimensions are as follows in Figure 5.

It can be seen from the results in the figure that the standard values of dimension C1 are all greater than 0, the standard results of C2 fluctuate around 0, and the evaluation results of dimension C3 are all less than 0, indicating that there are obvious differences in the evaluation results under the three dimensions. When the evaluation system is realized, the accuracy of the evaluation index is increased, the complicated work is reduced, and the learning efficiency is improved.

4.2. The Value of Educational Curriculum Adaptation Function of Related Algorithms. From the students' adaptation to the curriculum, we can get the degree of people's love for the curriculum and the rationality analysis of the number of school years. The previous three algorithms classify similar courses for better difference and plan the teaching arrangement for the next academic year from the students' adaptation. The experimental results are as follows in Figure 6.

From the numerical curve of fitness function, it can be clearly seen that genetic clustering algorithm is obviously superior to fuzzy C-means and K-means clustering algorithm, and has strong stationarity, while the other two kinds of algorithms have oscillation phenomenon. Genetic algorithm effectively avoids the fluctuation of average grades caused by the increase of the number of courses with the increase of evolutionary algebra, which will have a good preparation for teaching arrangement.

4.2.1. All Kinds of Mean Curves after Teaching Standardization. After the standardization of the teaching system, the work will be carried out efficiently with this system, which greatly improves the teaching quality and reduces the time for students to adapt to teachers' teaching habits. The 20-session cycle course of the semester is a standardized time, which can complete the work tasks of the whole semester. The following results in Figure 7 are obtained by analyzing the scores of three types of students.

Class I belongs to the overall level of poor, accounting for 30% of the total number, and the results are not idealized; Class II belongs to the medium level of learning, which has a certain mastery of basic knowledge and needs to strengthen learning, accounting for 50% of the total number; Class III belongs to top students, with excellent grades, accurate

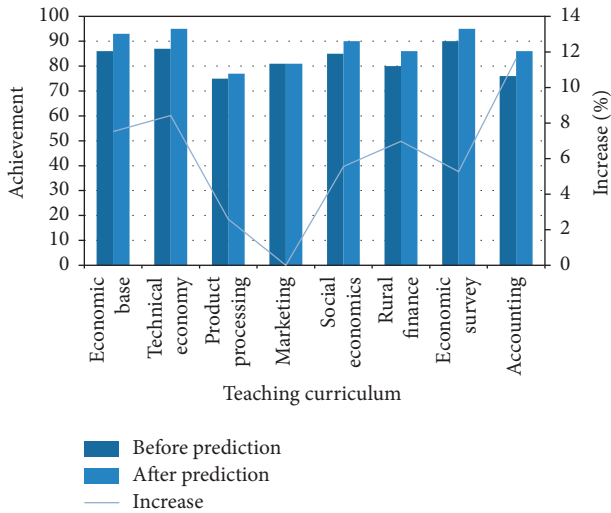


FIGURE 4: Comparative analysis of agricultural professional achievements before and after pretreatment.

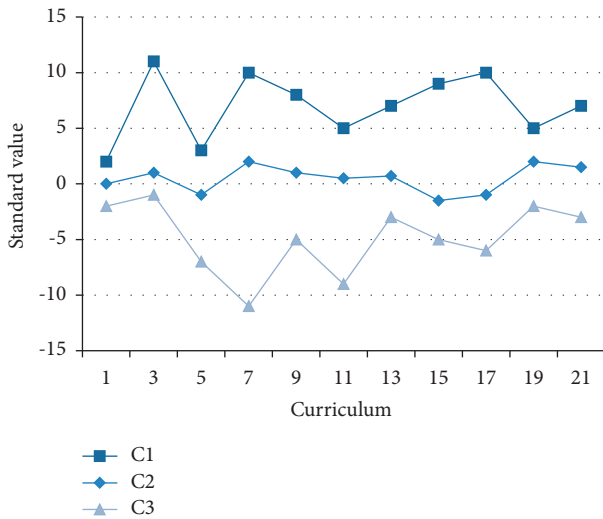


FIGURE 5: Average results of curriculum standardization.

mastery of knowledge and utilization, accounting for 20% of the total. Therefore, when carrying out professional skills training, we can strengthen innovative education and make technical ability develop in a balanced way.

4.3. Construction of Farmers' Practical Teaching System Based on Genetic Algorithm. Among the above three algorithms, genetic clustering algorithm is the best judgment for students to adapt to teaching, so according to the above results, it is determined to build a system with this algorithm. Teachers and students will have relevant key problems in the whole professional practice process, so this paper discusses the system evaluation. The experimental results are as follows in Figure 8.

It can be seen from the figure that the time spent on becoming a talent is the longest 8 ms in the whole test, because becoming a talent is a stage process that cannot be judged in a hurry, and difficult analysis is only a problem

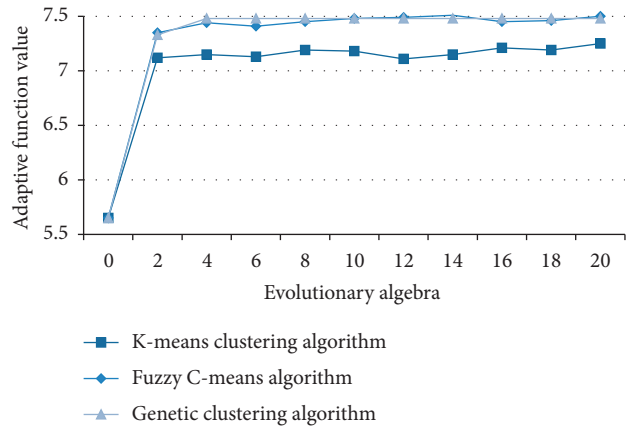


FIGURE 6: Evolutionary fitness curves of three clustering algorithms.

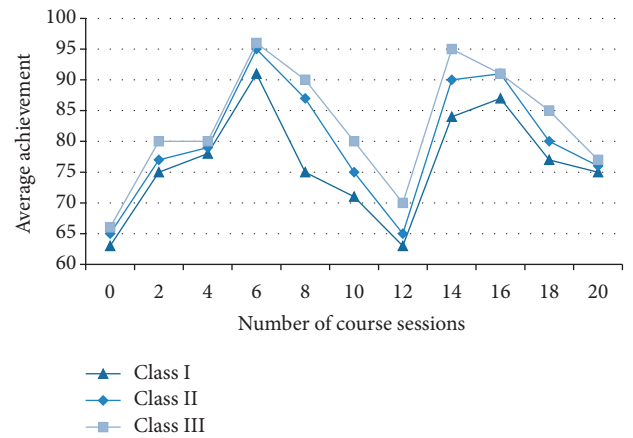


FIGURE 7: Average score curves of various algorithms.

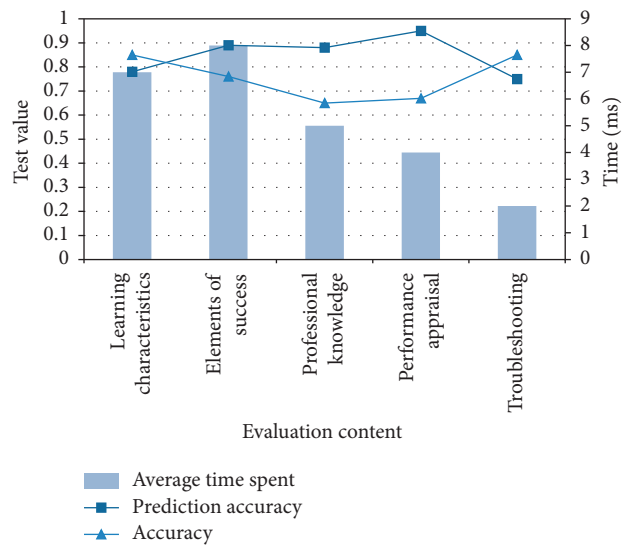


FIGURE 8: Experimental results of genetic algorithm.

concept, so it takes relatively little time. The accuracy measurement under the whole algorithm mechanism is relatively stable without large fluctuation. However, the prediction accuracy needs to be improved.

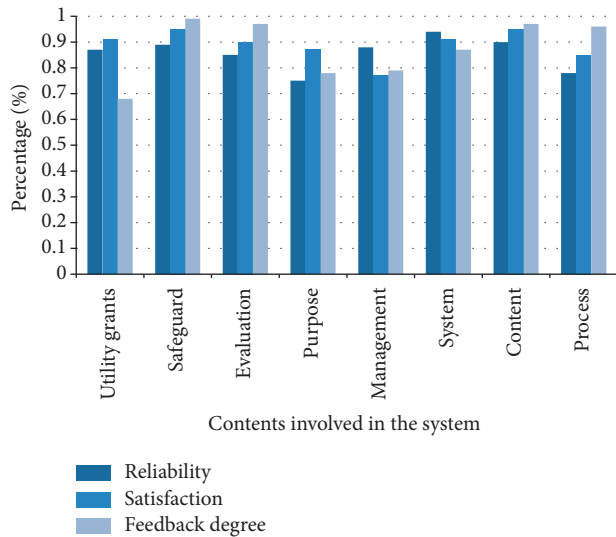


FIGURE 9: Questionnaire on the construction of teaching system.

4.4. Application of Vocational Teaching System. Promoting the professional agricultural teaching system will provide farmers with a good way to know the blind spots; instead of blindly judging by previous planting experience, it now relies on standardized planting techniques. Enhance people's learning efficiency and train a large number of comprehensive talents. The survey results of user use are as follows in Figure 9.

Taking the algorithm as the theoretical basis of the whole system, through the investigation of users' reliability, satisfaction, and feedback, it is known that the feedback degree of users to the situation of UGC is the lowest 68%, which shows that the rich cultural heritage under the system lies in it. However, there are also problems that the security system has not been satisfied by users, and it needs to be optimized and improved.

5. Conclusion

Farmers' vocational education system is a complete system, which needs comprehensive analysis from all aspects and multi-angle consideration of the synergy of the whole system factors. In building a feasible education system, we should establish relevant infrastructure conditions to teach professional education for every educated person. This paper uses big data mining technology to construct the whole system, database retrieval, and the rapid construction of the whole educational administration system and applies it to educators. The dissemination of agricultural knowledge through professional education has made obvious changes in planting skills, increased income, and diversified planting. Big data mining technology has greatly improved the way of education, provided a solid theory for professional education reform, and effectively analyzed the reform system. The experimental conclusions of this paper are as follows: (1) for the introduction of educational curriculum information, fuzzy mean is introduced through clustering algorithm to optimize the processing, which overcomes the slow running

problem of educational administration system. (2) The integration of peasant education in developing courses is studied, and data mining is used to analyze the influence of various educators' courses. (3) Explore the possible difficulties and conquering points in the whole learning process, so that people can understand knowledge more clearly. (4) Through comprehensive score prediction and analysis, the loopholes and optimization points in the education system are known, and the big data model is used as the basic theory to establish and optimize the system.

Experiments and Prospects: (1) The sparsity of data quantity and the authenticity of data will affect the accuracy of its results, and the quality of data sets should be greatly improved. (2) Because of the cultivation of professional knowledge in vocational education, more teachers and students resources should be mobilized to make use of. (3) With the continuous exploration of scientific research achievements, new teaching modes will inevitably appear, which is also the premise of promoting the reform of vocational education, and the continuous optimization of its system is also the basic work in the future. (4) To adapt to the specialized education mode, farmers should be regarded as the primary productive forces, but they should also learn modern mechanical work to adapt to the progress of the times.

Data Availability

The experimental data used to support the findings of this study are available from the corresponding author upon request.

Conflicts of Interest

The authors declared that they have no conflicts of interest regarding this work.

Acknowledgments

This work was supported by Hunan Philosophy and Social Science Fund Project, 2021, A study on the effect evaluation and promotion strategies of Hunan Vocational Colleges' participation in the cultivation of new-type professional farmers (award no. 21YBA302).

References

- [1] Z. Yan and Y. Cai, "Cultivation of new professional farmers: historical evolution and contemporary innovation [J]," *Vocational Education Forum*, vol. 15, no. 19, pp. 59–64, 2014.
- [2] H. Kang, "New professional farmers: concept discrimination and new interpretation of connotation [J]," *Contemporary Vocational Education*, vol. 19, no. 5, pp. 4–8, 2018.
- [3] Z. Guo and Q. Guo, "Research on cultivating new professional farmers [J]," *China Vocational and Technical Education*, vol. 4, no. 15, pp. 7–13, 2012.
- [4] H. Xu, "Cultivating new professional farmers: paths and measures [J]," *China Distance Education*, vol. 5, no. 11, pp. 70–73, 2012.

- [5] Q. Zhu, "Connotation, characteristics and status of new professional farmers [J]," *China Agricultural Information*, vol. 5, no. 17, pp. 16–18, 2013.
- [6] Y. Liu, J. young, and S. Meng, "Experience and enlightenment of cultivating new professional farmers in America [J]," *Agricultural Economic Issues*, vol. 162, no. 6, pp. 137–144, 2019.
- [7] J. Tan and J. O. E. Deng Junfeng, "French modern agriculture from the perspective of agricultural education and its enlightenment [J]," *China Agricultural Education*, vol. 17, no. 2, pp. 11–15, 2016.
- [8] J. Zhang, "Exploration of practical teaching reform of agriculture-related majors in higher vocational colleges [J]," *Education Review*, vol. 4, no. 10, pp. 112–114, 2014.
- [9] G. Wang, "On the teaching characteristics of field classroom [J]," *Vocational Education*, vol. 17, no. 4, pp. 55–57, 2018.
- [10] X. Jiang, "Exploration on practical teaching of "experiential crop growth cycle" for agriculture and forestry majors--taking the planting major of changsha vocational secondary school as an example [J]," *Journal of Yueyang Vocational and Technical College*, vol. 32, no. 1, pp. 72–74, 2017.
- [11] J. Han, X. Li, and X. Liu, "Reform of training mode of agriculture-related professionals in secondary vocational schools from the perspective of modern agriculture [J]," *Henan Agriculture*, vol. 9, no. 9, pp. 20–+29, 2016.
- [12] Z. Wang, "Research on management mode and operation mechanism of experimental teaching demonstration center in agricultural colleges [J]," *China Modern Education Equipment*, vol. 16, no. 23, pp. 30–32 +35, 2018.
- [13] D. Li, "Thoughts on the curriculum of agriculture-related majors in rural vocational education [J]," *Journal of Mudanjiang Institute of Education*, vol. 20, no. 5, pp. 37–50, 2015.
- [14] Z. Zhang, X. Gao, and Y. Li, "Research on the reform of practical teaching mode of pharmaceutical engineering major in local agricultural colleges [J]," *Jilin Agriculture*, vol. 24, no. 5, pp. 106–107, 2019.
- [15] Y. Wu, Y. Shi, and H. Xu, "Study on the construction of microbial practical teaching system in local applied agriculture-related colleges [J]," *Anhui Agricultural Sciences*, vol. 42, no. 10, pp. 3132–3134, 2014.
- [16] X. Zhuang, "From farmers to new professional farmers [J]," *Vocational Education Forum*, vol. 196, no. 10, pp. 23–28, 2015.
- [17] H. Li and F. Shi, "Comparative study on policies and systems of local modern vocational education system Construction [J]," *China Vocational and Technical Education*, vol. 25, no. 6, pp. 23–27, 2016.
- [18] Z. Tang and W. Shi, "Analysis of the development status and problems of rural vocational education [J]," *Vocational and Technical Education*, vol. 33, no. 28, pp. 60–65, 2012.
- [19] J. Xu and G. Li, "On the development status and countermeasures of agricultural vocational and technical education [J]," *Education and Teaching Forum*, vol. 6, no. 11, pp. 251–252, 2015.
- [20] T. Yan and L Zhang, J. Zhang, Exploration and thinking on the cultivation of new professional farmers-based on the investigation of dongxihu district in wuhan [J]," *Journal of Huazhong Agricultural University*, vol. 9, no. 3, pp. 35–41, 2017.
- [21] X. Liu, "Cultivation of new professional farmers from the perspective of modern agriculture; Realistic Dilemma and System Design [J]," *Vocational and Technical Education*, vol. 37, no. 13, pp. 60–64, 2016.
- [22] S. Zhu and S. Wang, "Thoughts on the cultivation of new professional farmers in China [J]," *Vocational Education Forum*, vol. 215, no. 27, pp. 56–60, 2016.
- [23] J. Liu and C. Chen, "Investigation and thinking on the present situation of farmers' education and training: an empirical analysis based on the people in 100 villages in China [J]," *Educational Research*, vol. 2015, no. 2, pp. 123–129, 2015.
- [24] Y. Hu and B. Wang, "Research on the difficulties and countermeasures of cultivating new professional farmers [J]," *Theory Monthly*, vol. 1549, no. 8, pp. 148–152, 2017.
- [25] L Zhang, J. Pan, and Y. Tan, "Thoughts on higher vocational colleges serving the cultivation of new professional farmers [J]," *Agricultural Economy*, no. 100, pp. 85–87, 2015.

Research Article

An English Flipped Classroom Teaching Model Based on Big Data Analysis

Wang Sa ¹, Li Dan,² Du Juan,¹ Yu Fei,¹ and Wang Wei ¹

¹School of Foreign Language, Beihua University, Jilin 132011, China

²School of Literature and Journalism, Yantai University, Yantai, Shandong 264005, China

Correspondence should be addressed to Wang Wei; wangwei@beihua.edu.cn

Received 9 May 2022; Revised 21 July 2022; Accepted 18 August 2022; Published 31 August 2022

Academic Editor: S. Venkatesan

Copyright © 2022 Wang Sa et al. This is an open access article distributed under the Creative Commons Attribution License, which permits unrestricted use, distribution, and reproduction in any medium, provided the original work is properly cited.

In order to improve the defect that the quality of English flipped classroom teaching cannot be quantitatively evaluated, an English flipped classroom teaching model based on big data learning analysis is proposed. In the English flipped classroom teaching mode, which applies the flipped classroom teaching mode, the classroom teaching links are changed, the preview feedback, joint answer and question between teachers and students, classroom teaching, and teachers' questions are taken as the key links of classroom teaching, and the teacher education and school management system are improved, so as to complete the reform of English flipped classroom teaching mode. The convolution neural network is used to extract the evaluation text features, mine the association rules of massive evaluation text data through the Apriori algorithm, determine the evaluation index of English flipped classroom teaching quality, and complete the evaluation of English flipped classroom teaching quality by using the decision tree method in big data analysis. The experimental results show that the proposed method can quantitatively evaluate the quality of English flipped classroom teaching by using the evaluation text, and the evaluation accuracy and recall rate are higher than 98%, which can realize the objective evaluation of English flipped classroom teaching quality.

1. Introduction

At present, many international conferences are communicated in English [1], and many materials are published in English. Even many letters and even broadcasts are inseparable from English. It can be seen that English is widely used [2, 3]. Therefore, in the new era of social development, English has gradually become the focus of attention and one of the important indicators of talent training in colleges and universities. In the information age, with the rapid development of information technology, on the one hand, it has brought new opportunities for college English teaching. On the other hand, it also makes college English teaching face new challenges. Therefore, it is a problem faced by major colleges and universities to establish an English flipped classroom teaching model in line with the development of the times under the background of informatization [4, 5].

Reference [6] uses the comparative method to analyze the two types of assessment: formative assessment and

summative assessment. The results show that the characteristics of formative evaluation include teachers' adaptability to the classroom and immediate feedback to teachers. As a high-risk evaluation, summative evaluation needs high standard control and safety to ensure its reliability and effectiveness. In [7], through one-on-one cooperation with speech and language therapy students, children participated in weekly activities aiming at promoting receptive and productive knowledge of 20 target words in secondary vocabulary categories. Reference [8] adopts an online format and carries out digital access through the school-oriented learning management system. Upon completion, teachers will receive a personalized report on their ability to assess teaching skills in nonuniversity teaching.

Considering that, at present, the evaluation of English flipped classroom teaching quality is mainly achieved through a small amount of data, and the evaluation results under the condition of small sample data have high limitations and one sidedness. Big data technology can

effectively improve this defect. Big data technology has transformed from sampling evaluation of English flipped classroom teaching quality to full data evaluation of English flipped classroom teaching quality. Mining teaching quality related information from massive data to improve the diversity of English classroom teaching quality evaluation [9]. Therefore, on the basis of clarifying the English flipped classroom teaching mode, this paper uses big data technology to evaluate the teaching quality of English flipped classroom.

2. Reform of English Flipped Classroom Teaching Mode

2.1. Changing Classroom Teaching Links. Under the traditional teaching mode, the low efficiency of traditional classroom teaching restricts the improvement of classroom teaching quality. At the same time, some students have relatively weak basic knowledge, weak learning ability, and low learning enthusiasm [10, 11]. In order to effectively improve classroom efficiency and improve students' knowledge level, it is urgent to reform classroom teaching. Therefore, we should change the traditional classroom teaching links. It is transformed into a teaching link of preview feedback, joint answer and question between teachers and students, classroom teaching, teachers' questions, students' oral training, classroom summary, and reflection, as shown in Figure 1.

Through preview feedback, teachers can quickly grasp the learning situation of students and help teachers explain in class. The main contents contained in preview feedback are shown in Figure 2.

First, the teacher organizes the students to have a group discussion [12], the team leader writes down the questions, and then the team leader asks the teachers. Through the above methods, the teachers can understand the students' learning situation and can also use these questions as a reference for subsequent classroom questioning and teaching. In the preview process, it is difficult for students to grasp the overall knowledge and logic, and it is inevitable that they will not fully understand the knowledge points and key points. Therefore, teachers need to check the lack of formulas, ask questions to students, make students' thinking active, and stimulate students' learning enthusiasm at the same time.

2.2. Improve Teacher Education and School Management System. The traditional teaching mode is that teachers teach according to textbooks. In the information age, teachers' teaching ability needs to be improved. At the same time, the traditional school management system is mainly managed by the school. Under the flipped classroom teaching mode [13], it not only puts forward higher requirements for teachers' ability but also puts forward higher requirements for school management.

In terms of improving the teacher education system, teachers are required to turn from the person who prepares the teaching plan to the video producer, from the lecturer on

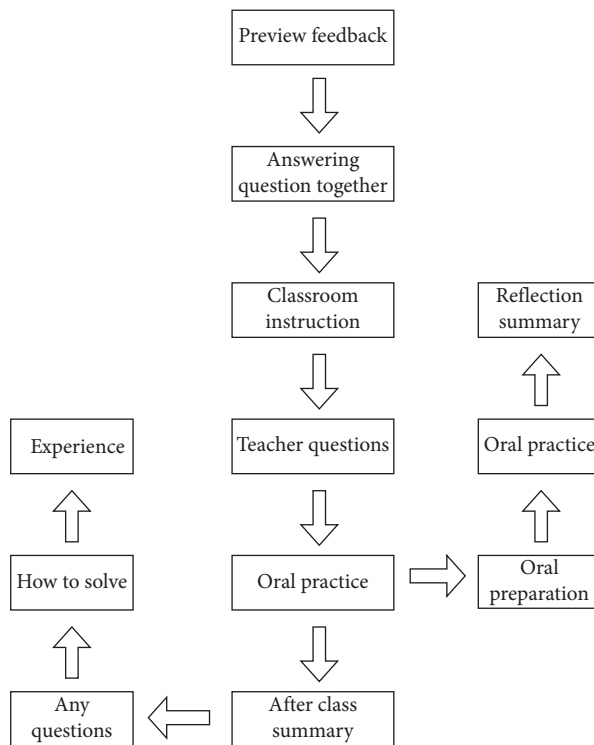


FIGURE 1: Process design of flipped classroom teaching.

the podium to the communicator among students, and from the outsider who internalizes students' knowledge to the guide in the classroom. The main teaching process of teachers in class is shown in Figure 3.

At the same time, the flipped classroom teaching mode pushes teachers and students to the front end of the network. Only by improving their ability in the information age can teachers better understand students and meet students' learning needs in the network environment [14, 15]. Through the above analysis, according to the requirements of English teaching, in order to improve the problem that the quality of English flipped classroom teaching cannot be quantitatively evaluated, the evaluation criteria of teachers' learning tasks are formulated according to Table 1.

Based on the analysis of the current school management system, parents are more dependent on the school management system. Because their right to participate in school management is limited, they will not take the initiative to fulfill their obligations to students' learning. The emergence of flipped classroom teaching mode divides the traditional teaching process into two parts, in class and after class [16, 17]; that is, the right to guide students' learning is pushed to parents. In order to better promote flipped classroom in China, innovate at the level of the school management system, tap the role of parents in the process of education and teaching, enable parents to give full play to their talents in the process of school running, and jointly promote the growth of students, so as to promote the application of flipped classroom teaching mode from the level of school management system.

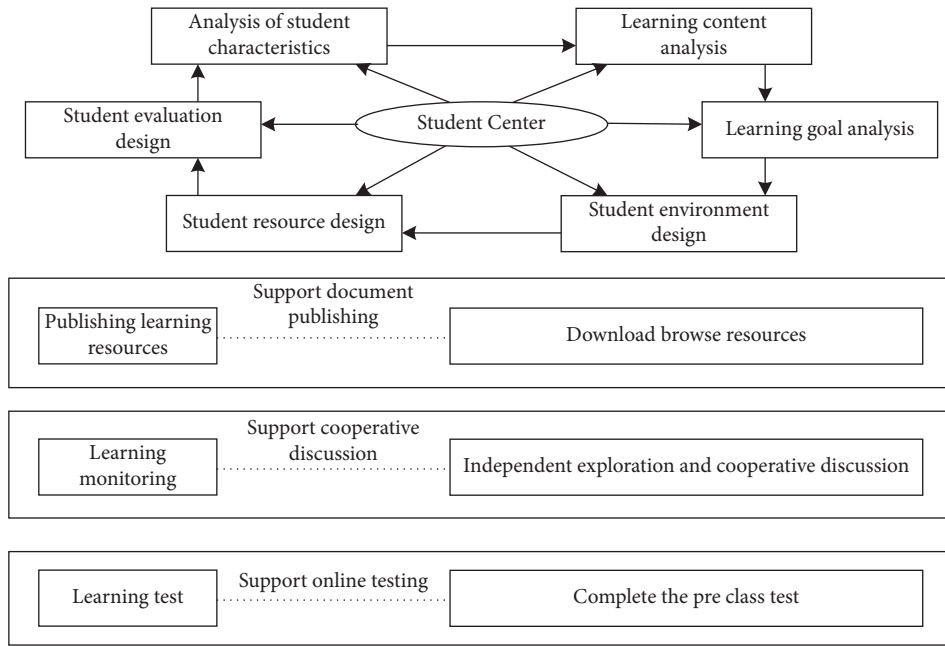


FIGURE 2: Design of learning activities in preview feedback stage.

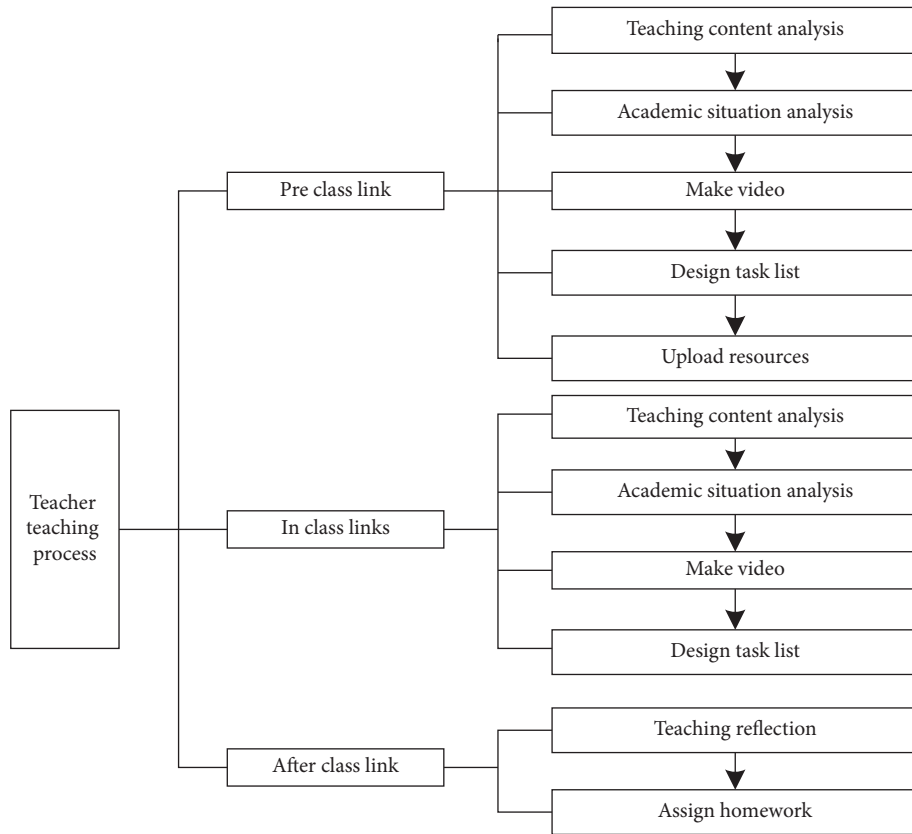


FIGURE 3: Teacher teaching process.

TABLE 1: Evaluation criteria for teachers' learning tasks.

Serial number	Project	Evaluation criteria	Weight (%)
1	Achieve the goal (Q1)	Internalizing knowledge and expanding ability (Q11)	10
2	Learning methods (Q2)	Ability to help students complete learning tasks (Q21)	10
3	Preview of classroom learning formula (Q3)	It is conducive to arousing students' enthusiasm to complete preclass tasks seriously (Q31)	10
4	Learning tasks (Q4)	Whether advanced homework is conducive to students' internalization of knowledge (Q41)	20
		Based on the cognitive level reached by "advanced," the difficulty is greater than that of advanced homework (Q42)	40
		Collaborative inquiry comes from real situations (Q43)	10
Total score		Comprehensive score	

3. Evaluation of English Flipped Classroom Teaching Quality Based on Big Data Technology

3.1. Evaluation Text Feature Extraction. The convolution neural network method is selected to extract the text features of English flipped classroom teaching quality evaluation. The convolution neural network automatically learns the input data features through convolution layer and pool layer. The training set is established by using the evaluation text, and all samples in the training set are marked by tags. After inputting the test dataset, the trained neural network is used to obtain the classification label of new samples [18]. Convolution neural network method not only has the characteristics of analyzing the context semantics of comment text and feature learning but also has the advantages of high noise resistance and high classification degree.

The feature structure of the evaluation text is extracted by convolution neural network, as shown in Figure 4.

As can be seen from Figure 4, the convolution neural network extraction and evaluation of text features mainly includes the following steps.

3.1.1. Data Preprocessing. Through data preprocessing, the useless comments of English flipped classroom teaching quality evaluation text are filtered, and the filtered evaluation text is divided into short sentences. Through data filtering, we can avoid noise interference in the process of evaluating the quality of English flipped classroom teaching. When using convolution neural network to classify text evaluation, it is necessary to deal with comments composed of many short essays.

3.1.2. Word Vector Training. Quantitatively transform the evaluation text, use the distribution formula word vector to represent the evaluation text, select a large-scale unsupervised method to train the distribution formula word vector so that the text that completes the quantitative transformation can reflect more grammatical information and semantics [19], and use the filtered evaluation text to realize the word vector training.

3.1.3. Model Training and Testing. Extract part of the data and set it as the training set to complete the classification training. Mark the added labels through the model, compare the labels marked by the model with the existing labels, and adjust the model parameters through the error of the comparison results.

3.1.4. Feature Extraction. The evaluation text represented by the word vector is input into the convolutional neural network, and the convolutional neural network outputs the corresponding label [20, 21]. Annotate the part of speech of the evaluation text, extract the nouns in the evaluation text, and obtain the feature word set. The tags forming the feature words are the same as those in the evaluation text.

3.2. Big Data Mining Technology. The same evaluation text contains multiple characteristic words, and the final evaluation index of English flipped classroom teaching quality needs to be determined by cluster analysis. Big data mining technology is to mine association rules with minimum confidence and minimum support in massive data [22]. Big data mining technology mining association rules mainly includes two parts: (1) mining frequent itemsets with minimum support in transaction database; (2) mining frequent itemsets used to generate association rules for English flipped classroom teaching quality evaluation. The Apriori algorithm is an important algorithm for mining frequent itemsets in data mining algorithms. This algorithm is used to obtain itemsets with support higher than the minimum support. The Apriori algorithm obtains $K+1$ itemsets by using K itemsets through a layer-by-layer search method.

B represents the transaction database, $I = \{I_1, I_2, \dots, I_m\}$ represents the itemset in the database, and I_i represents the elements in the itemset. $W = \{T_1, T_2, \dots, T_n\}$ and T_i , respectively, represent the transaction set and the elements contained therein and satisfy $T_i \subseteq T$. Identify all transactions T with separate labels. The length or dimension of itemset in massive data indicates the number of elements contained in the itemset. When the number of elements in the itemset is K , it indicates that the itemset is a K -itemset. Set up a random English flipped classroom teaching quality transaction database B and mine its frequent itemsets. The process is as follows:

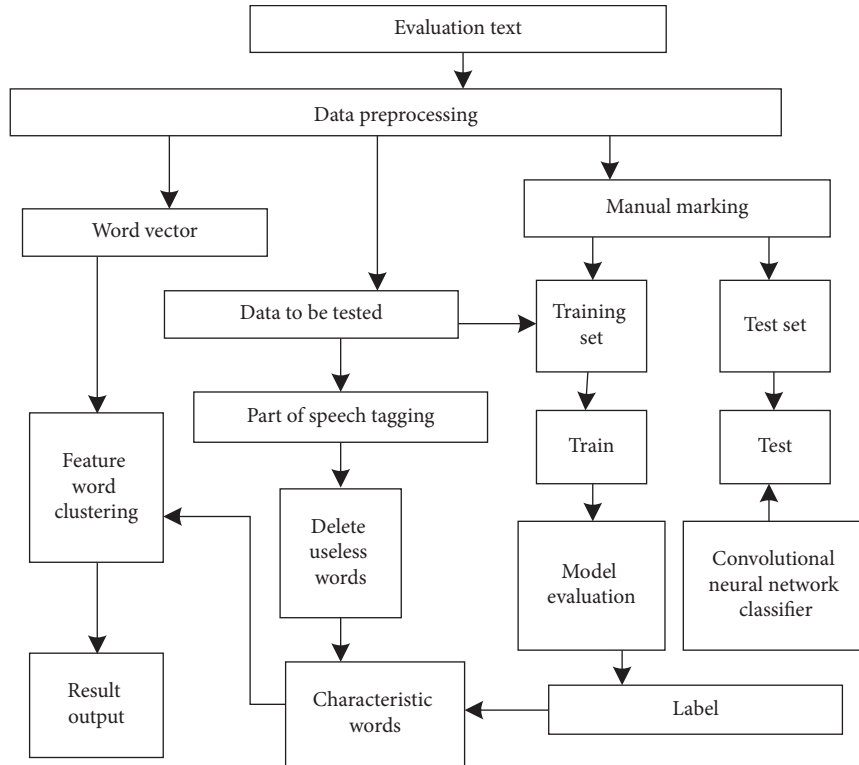


FIGURE 4: Structure diagram of evaluation text feature extraction.

- (1) Calculate all 1 itemsets, represented by C_1 , and search all common 1 itemsets greater than or equal to the set minimum support, represented by L_1 .
- (2) Use the common 1 itemset to obtain the candidate 2 itemsets, which are represented by C_2 . Search for all 2 itemsets greater than or equal to the set minimum support from the obtained 2 itemsets, which are represented by L_2 .
- (3) According to the above process, use the obtained common 2 itemsets to obtain the candidate 3 itemsets, which are represented by C_3 . Search for all three itemsets greater than or equal to the set minimum support from the obtained three itemsets, which are represented by L_3 .
- (4) Repeat the above process until higher dimensional frequent items cannot be obtained, and terminate the iteration.

It can be seen from the above process that the Apriori algorithm obtains the final frequent itemset through continuous iteration [23], and too many candidate sets are formed in the search process, which has high complexity and low operation efficiency. The Boolean matrix is introduced into the Apriori algorithm to make it suitable for massive big data mining. The massive database of big data is prone to excessive memory. The database needs to be segmented, and the segmented database will be scanned in segments. Suppose that there are N transaction databases that complete the

segmentation, which are represented by $\{B_1, B_2, \dots, B_N\}$. It can be seen that the number of Boolean matrices is N , which corresponds to the transaction database that completes the segmentation one by one. The process of obtaining frequent itemsets using the Apriori algorithm optimized by the Boolean matrix is as follows:

- (1) Set the number of copies of massive transaction database and determine the size of different copies. Initialize the loop variable to 1 and set the minimum support of the Apriori algorithm.
- (2) Read B_i in the transaction database and map it to the Boolean matrix R_i .
- (3) Calculate the local minimum support of R_i for B_i using formula (1):

$$\text{mins}_i = \min \frac{B_i}{|B|} \quad (1)$$

In formula (1), $|B_i|$ and $|B|$ represent the number of elements in the transaction database and the number of elements in the massive transaction database, respectively.

Obtain the corresponding row vector of the frequent itemset in B_i in the Boolean matrix R_i through the above formula, save the row vector obtained by searching, release the memory space of the Boolean matrix R_i update dataset, and obtain the updated matrix R_i .

- (4) Set $i = i + 1$, and when the $i \leq N$ condition is met, return to step (2) to repeat the iterative calculation. Otherwise, go to step (5).
- (5) Recombine the Boolean matrix R_i corresponding to all frequent itemsets in the transaction dataset B_i , and establish a new Boolean matrix, which is represented by $R = (R_1, R_2, \dots, R_N)^T$. Thirdly, search the minimum support of the new Boolean matrix, determine the corresponding row vector of the frequent itemset of the massive transaction database B , and obtain the frequent itemset that can finally evaluate the quality of English flipping classroom teaching.

3.3. *Realize the Evaluation of English Flipped Classroom Teaching Quality.* There are many commonly used algorithms for data mining, such as genetic algorithm, clustering algorithm, and Apriori algorithm [24]. Combined with the characteristics of English flipped classroom teaching quality evaluation, this paper uses the ID3 decision tree method to complete the data mining of teaching evaluation.

Decision trees can classify a large amount of data purposefully so as to obtain valuable potential information. The decision tree uses the sample attribute as the node, and the attribute value is the branch tree structure. The root node is the attribute with the largest amount of information in all samples, the middle node is the attribute with the largest amount of information in the root node, and the leaf node is the sample category value. In the ID3 algorithm [25], the entropy concept in information theory is applied to complete the selection of node attributes, and the decision tree is constructed through the attribute with maximum information gain, which ensures that the decision tree has the minimum number of branches and minimum redundancy.

The information entropy can be expressed as formula (2):

$$I(m) = \log_2 p(m_i). \quad (2)$$

In formula (2), $p(m_i)$ represents the proportion of samples with category m_i in the total samples. The information in the decision tree is binary coded [26], so the logarithm function is based on 2.

The conditional entropy of attribute A can be calculated by formula (3).

$$E(A) = p(m_i|v_j) \log_2 \left(\frac{1}{I(m)} \right). \quad (3)$$

In formula (3), $p(m_i|v_j)$ is the conditional probability of category m_i when the value of attribute A is v_j . The information gain of attribute A is calculated by formula (4):

$$\text{Gain}(A) = I(m)E(A). \quad (4)$$

In formula (4), $\text{Gain}(A)$ represents the coding information obtained from the branch of attribute A ; that is, the value of A causes the expected compression of information entropy.

To sum up, the ID3 algorithm realizes attribute selection through information gain. Therefore, the use of gain rate can be expressed as formula (5):

$$\text{Gain Ratio}(A) = \frac{\text{Gain}(A)}{\text{Split Info}(A)}. \quad (5)$$

Suppose D represents the training sample set, A represents an attribute in D , A contains n noncoincident values $\{v_1, v_2, \dots, v_n\}$, and D is divided into n subsets D_1, D_2, \dots, D_n ; then, the value of the training sample in D_i in A can be expressed as v_1 . The process of decision tree mining is to automatically construct a decision tree from the data of the training set through the above method and then judge any instance according to the obtained decision tree.

Taking the six evaluation contents in Table 1 as the sample data of evaluation indicators and training, the number of teachers participating in the evaluation is 1~6 to evaluate the quality of English flipped classroom teaching, and the results are divided into five grades as follows:

- (1) A: excellent, with a score of 90–100.
- (2) B: good, with a score of 80–89.
- (3) C: medium, with a score of 70–79.
- (4) D: pass, with a score of 60–69.
- (5) E: fail, score below 60.

The evaluation results of teachers are shown in Table 2.

It can be seen from Table 2 that the information entropy required by the sample can be expressed as formula (6):

$$I(S) = \frac{1}{6} \log_2 \left(\frac{1}{6} \right). \quad (6)$$

The information entropy of each attribute can be obtained through formula (6). The attribute with the largest information gain is taken as the node test attribute. The branch of the corresponding attribute value is constructed downward from the root node, and the ID3 decision tree algorithm is continued to be used for further division. If the path from the root node to the current node contains all attributes, the algorithm ends, and the whole process of comprehensive evaluation is completed.

4. Experimental Test

In order to verify the effectiveness of the designed English flipped classroom teaching quality evaluation model based on big data analysis, a teacher's English flipped classroom teaching course is selected as the test object, and the main data comes from the intelligent English flipped classroom teaching system. A total of 8795 people attended the English flipped classroom teaching. After the students completed the class, they did feedback on the evaluation text, deleted the useless evaluation text and garbage evaluation text, and collected a total of 8564 effective evaluation texts. The experimental tests were carried out by using the methods of papers [6, 7].

TABLE 2: Teacher evaluation results.

Number	Q11	Q21	Q31	Q41	Q42	Q43	Total
1	B	B	A	B	A	B	Good
2	B	A	B	B	B	A	Good
3	B	B	B	B	B	B	Good
4	C	B	C	C	C	C	Secondary
5	B	C	C	C	B	B	Secondary
6	A	A	A	B	A	A	Excellent

4.1. Model Inspection. The grid search method is selected to determine the hyperparameters. The results of the determined convolution neural network hyperparameters for extracting and evaluating text features are shown in Table 3.

According to the parameters determined in Table 3, the convolutional neural network is trained and tested by the tenfold cross-validation method. The convergence of the convolutional neural network is shown in Figure 5.

As can be seen from the experimental results in Figure 5, the convolutional neural network is used to extract the features contained in the evaluation text in this method, and the rapid convergence can be achieved only after about 15 times of network training. It shows that the convolutional neural network selected in this method has a high convergence speed and can improve the operational performance of the English flipped classroom teaching quality evaluation model.

4.2. Algorithm Performance Test. In order to make the comparative data more accurate, the comprehensive evaluation value given by several teaching supervision experts in many lectures is used as the verification basis of the accuracy of this method. The comparison data between the evaluation results obtained by using this method and the comprehensive evaluation results of several expert groups are shown in Table 4.

From the data in Table 4, it can be concluded that the evaluation results given by this method are close to those of the expert group. Therefore, it can be seen that the system is a feasible and reasonable teaching quality evaluation system.

The expert evaluation method is used as the standard to evaluate the quality of English flipped classroom teaching. This method is used to evaluate the evaluation accuracy and recall rate of English flipped classroom teaching quality in different evaluation text sizes. In order to intuitively show the evaluation effect of this method, this method is compared with the models in [6] and [7]. The comparison results are shown in Table 5.

From the data in Table 5, it can be concluded that using this method to evaluate the quality of English flipped classroom teaching has high evaluation accuracy and recall rate for different evaluation text sizes. Accuracy and recall rate are important evaluation indexes to evaluate the performance of machine learning methods. The evaluation accuracy and recall rate of this method are higher than 98%, which can meet the needs of big data English flipping classroom teaching quality evaluation. The evaluation accuracy and recall rate of the other two models decrease with

TABLE 3: Superparameter setting.

Superparametric index	Numerical results
Number of feature maps	100
L2 regularization coefficient	4
Convolution kernel size	(6,350), (7,350), (8,350)
Dropout scale	0.7
Batch value	9

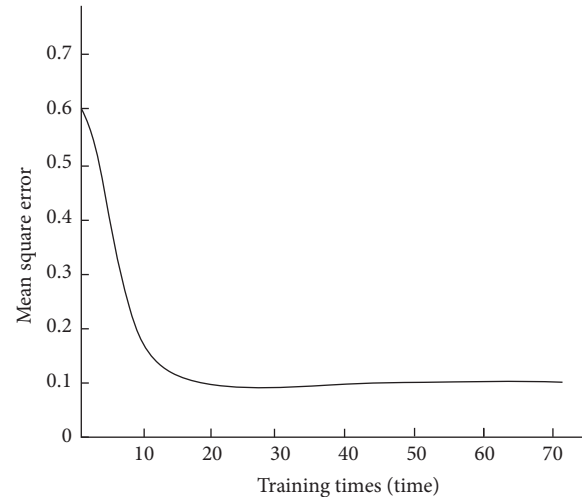


FIGURE 5: Convergence results of convolutional neural network.

the increase of the number of evaluation texts, indicating that the other two methods cannot adapt to massive data processing, and the operation level decreases when the amount of data increases.

4.3. Actual Verification. In the evaluation, the designed model text scoring standard is adopted, and the full score is 25 points. One class is selected to apply the teaching mode of this paper, and the remaining two classes are selected to adopt the traditional teaching mode. The average composition score data of the three classes are shown in Table 6.

According to the average composition score data of the three classes in Table 6, the average composition score of the experimental class is significantly higher, the average composition score of the control class 2 is in the middle, and the average composition score of the control class 1 is the lowest. It shows that the designed flipped classroom teaching mode of English writing is the most effective and can improve students' composition scores.

The comparison results of students' inquiry ability after learning the three methods are shown in Figure 6.

It can be seen from Figure 6 that the students' inquiry ability improved more after applying the design teaching mode, which is better than that of the students applying the comparative method.

The comparison results of students' innovation ability with the three methods are shown in Figure 7.

It can be seen from the analysis of Figure 7 that the innovation ability of students applying the design teaching mode is much higher than that in the past because, under the

TABLE 4: Comparison of evaluation results.

Sample number	Expert evaluation value	Evaluation value of this method	Expert evaluation results	The evaluation results of this method
1	62.88	62.79	Pass	Pass
2	72.34	72.46	Secondary	Secondary
3	84.57	84.57	Good	Good
4	93.67	94.11	Excellent	Excellent
5	77.31	77.31	Secondary	Secondary

TABLE 5: Comparison of evaluation results of different evaluation text sizes.

Evaluation text size (MB)	Paper method (%)		Reference [6] model (%)		Reference [7] model (%)	
	Accuracy	Recall	Accuracy	Recall	Accuracy	Recall
100	98.46	99.36	96.63	95.53	96.96	95.95
200	99.36	99.85	94.63	94.73	95.75	94.37
300	99.55	98.56	92.76	93.96	94.63	93.96
400	98.36	98.63	93.63	92.96	93.63	92.95
500	98.48	98.75	91.63	91.63	92.27	91.65
600	98.95	98.27	94.63	89.96	91.53	90.69
700	99.07	98.54	90.36	88.57	90.68	88.57
800	99.86	98.69	91.63	87.63	88.65	87.63
900	99.55	98.84	89.05	87.05	87.75	85.75
1000	98.76	98.45	88.75	85.75	86.63	84.72

TABLE 6: Average composition score data of three classes.

Composition	Average composition score		
	Experimental class	Control class 1	Control class 2
One	22	15	18
Two	23	16	17
Three	24	14	19
Four	22	15	18
Five	22	14	17

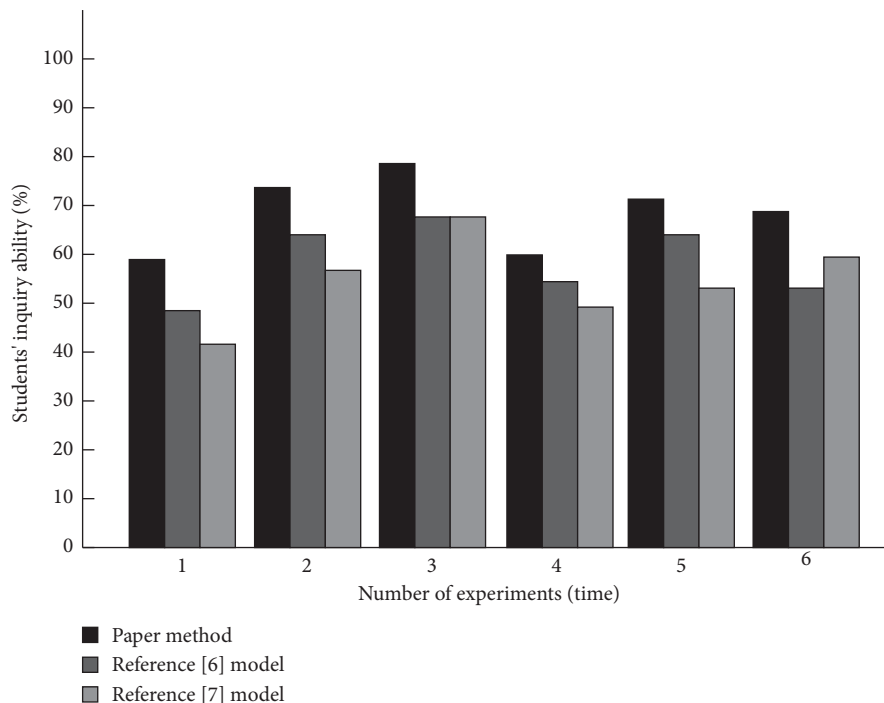


FIGURE 6: Comparison of students' inquiry ability.

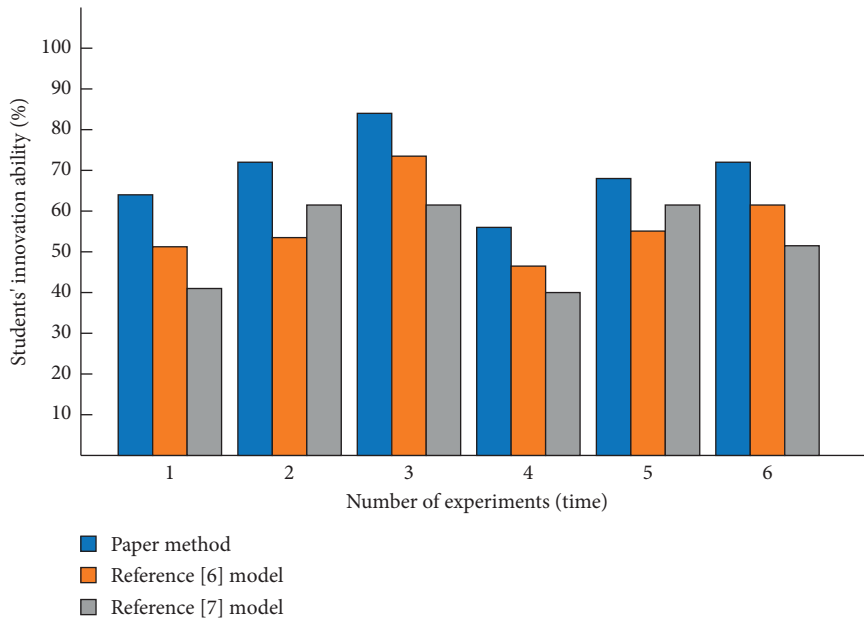


FIGURE 7: Comparison of students' innovation ability.

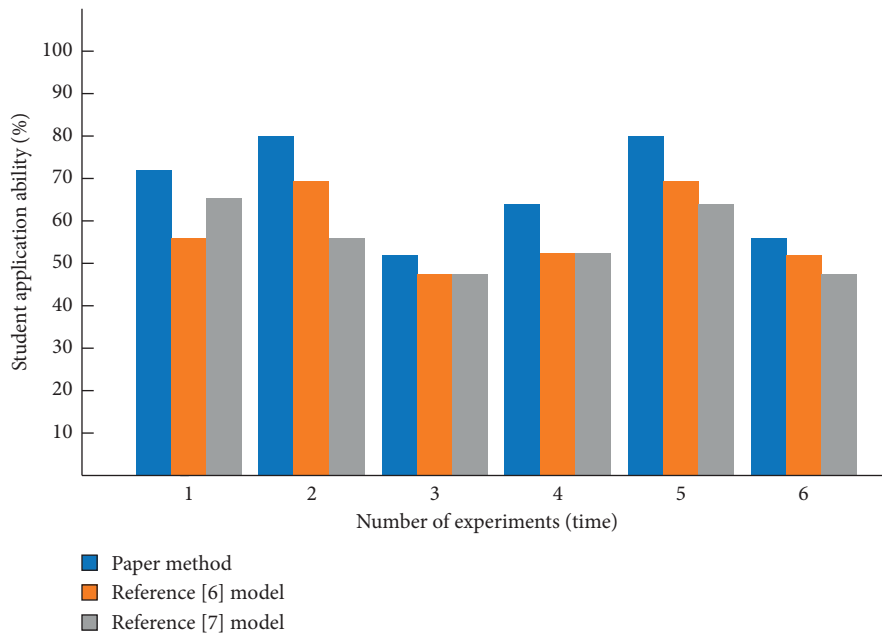


FIGURE 8: Comparison of students' application ability.

design teaching mode, students can experiment by themselves and strengthen their communication with teachers, so as to improve students' innovation ability. After the application of comparative teaching mode, although the students' innovation ability has improved, the improvement in innovation ability is not high.

The comparison results of students' application ability after applying the three methods are shown in Figure 8.

It can be seen from Figure 8 that the application ability of students after applying the traditional two systems is improved less, while the application ability of students after

applying the system designed this time is improved higher, which shows that students have accumulated small phenomena related to English in life and can connect their learned knowledge with practice.

The comparison results of students' satisfaction after applying the three methods are shown in Figure 9.

As can be seen from Figure 9, students' satisfaction is greatly improved after applying the designed English flipped classroom teaching mode because, in the flipped classroom teaching mode, students become the leaders in the classroom and stimulate students' curiosity. Although the satisfaction

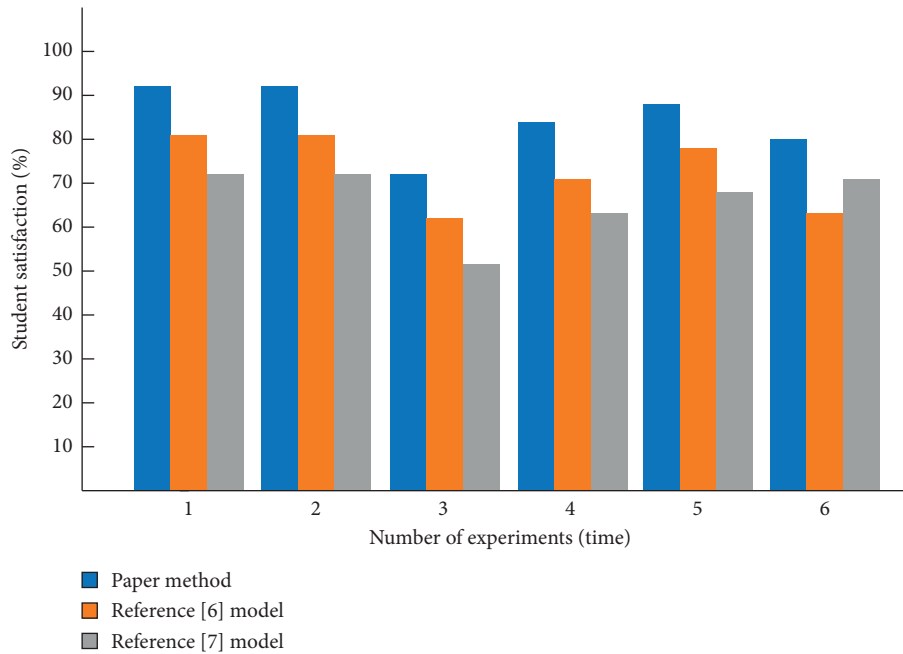


FIGURE 9: Comparison of students' satisfaction with teaching mode.

of students applying the comparative method has improved, it is lower than that of students applying the teaching mode designed this time.

Therefore, the above experiments can prove that the designed English flipped classroom teaching model can improve students' inquiry ability, innovation ability, and application ability, and students are more satisfied with the teaching model.

5. Conclusion

English flipped classroom teaching quality has high subjectivity, which is difficult to accurately quantify as a qualitative problem. The big data mining method is used to mine the massive data related to English flipped classroom teaching, determine the evaluation index of English flipped classroom teaching quality, and obtain the quantitative scoring results by using the determined evaluation index of English flipped classroom teaching quality. The use of big data technology provides theoretical support for the accurate evaluation of English flipped classroom teaching quality. Through the experimental verification, the evaluation accuracy and recall rate of the evaluation method studied are higher than 98%, which can realize the accurate evaluation of English flipped classroom teaching quality.

Data Availability

The raw data supporting the conclusions of this paper can be obtained from the corresponding author without undue reservation.

Conflicts of Interest

The authors declared that they have no conflicts of interest regarding this work.

Acknowledgments

This work was supported by the Jilin Province Philosophy and Social Science Fund Project: Research on Effective Foreign Language Teaching of Continuation Writing Based on Complex Dynamic System Theory (2021B214), the 2018 Jilin City Federation of Social Sciences Project (City Federation 18131) and the Social Science Research Program of the 13th Five-Year Plan from Jilin Provincial Education Office in 2019 (Humanities and Social Sciences): Research on the Construction and Application of Flipped College English Teaching Model Based on SPOC + Digital Resource Platform (JJKH20190678SK).

References

- [1] W. . Li, "Retraction Note: u," *Arabian Journal of Geosciences*, vol. 14, no. 22, p. 2313, 2021.
- [2] A. Prayoga, D. Irwansyah, and T. D. Harya, "Developing English learning materials for computer network engineering students at peripheral Indonesia," *EduLite Journal of English Education Literature and Culture*, vol. 6, no. 1, p. 28, 2021.
- [3] C. I. Branzila, "Online teaching English for Business and Economics in the time of pandemics," *Virgil Madgearu Review of Economic Studies and Research*, vol. 13, no. 2, pp. 27–36, 2020.
- [4] S. Teng, Z. Lian, and M. Jiang, "Research on the application of flipped classroom teaching in college English from the perspective of m based on WeChat public Platform," *Journal of Physics: Conference Series*, vol. 1992, no. 2, Article ID 022109, 2021.
- [5] E. A. Florence and T. Kolski, "Investigating the flipped classroom model in a high school writing course: action research to impact student writing achievement and engagement," *TechTrends*, vol. 65, no. 6, pp. 1042–1052, 2021.

- [6] H. Chen, "A contrastive analysis of classroom-based language assessments," *English Language Teaching*, vol. 13, no. 5, p. 110, 2020.
- [7] C. Dixon, J. Thomson, and S. Fricke, "Evaluation of an explicit vocabulary teaching intervention for children learning English as an additional language in primary school:[J]," *Child Language Teaching and Therapy*, vol. 36, no. 2, pp. 91–108, 2020.
- [8] C. Biencinto, M. García-García, E. Carpintero, P. Villamor, and S. Torrecilla, "Psychometric properties of the ProficiencyIn+E rubric: s," *Studies In Educational Evaluation*, vol. 70, no. 2, Article ID 101040, 2021.
- [9] Y. Zhou and Y. Cao, "Study about impact of big data technology on the diversity of ideological and political teaching methods," *Journal of Physics: Conference Series*, vol. 1852, no. 3, Article ID 032019, 2021.
- [10] S. Sartini, "Kahoot in maritime English teaching: its impact on nautical science cadet's oral reproduction and vocabulary," *English Language Teaching Educational Journal*, vol. 3, no. 1, p. 41, 2020.
- [11] T. M. Tan, S. M. Tan, T. W. Liew, and S. N. Kew, "Does speaker's voice enthusiasm affect social cue, cognitive load and transfer in multimedia learning," *Information and Learning Sciences*, vol. 121, no. 3/4, pp. 117–135, 2020.
- [12] S. Zu, Q. Zeng, and J. Zhang, "Investigation on the teachers' morality in universities: a comparative study of teacher-student evaluations," *Advances in Applied Sociology*, vol. 12, no. 03, pp. 53–68, 2022.
- [13] J. Y. Fan, Y. J. Tseng, L. F. Chao, S. L. Chen, and S. W. Jane, "Learning outcomes of a flipped classroom teaching approach in an adult-health nursing course: a quasi-experimental study," *BMC Medical Education*, vol. 20, no. 1, p. 317, 2020.
- [14] E. Ni, "Research on the autonomous learning mode in the environment of computer network technology," *Journal of Physics: Conference Series*, vol. 1578, no. 1, Article ID 012030, 2020.
- [15] C. Tan, "Using technology to support authentic learning approach in social studies education: a learning design for a social studies subject [J]," *Journal of Higher Education Research*, vol. 3, no. 1, pp. 69–75, 2022.
- [16] T. L. Sadiyah and K. A. N. Harmawati, "Analysis of reading difficulties for class III in elementary schools[J]," *Jurnal Sekolah Dasar*, vol. 6, no. 1, pp. 50–66, 2021.
- [17] J. H. M. Watanabe, F. Fitarelli, D. S. de Freitas et al., "Comparison of the facial profile attractiveness in Class III borderline patients after surgical or compensatory orthodontic treatment," *Journal of Clinical and Experimental Dentistry*, vol. 12, no. 4, pp. e348–e353, 2020.
- [18] Y. B. Zhang and K. Guo, "Text classification model based on fasttext and multi-feature fusion[J]," *Computer Simulation*, vol. 38, no. 7, pp. 461–466, 2021.
- [19] M. J. Mendoza, D. L. Velasco, C. A. Moreno, C. Parra, A. Carrillo-Ramos, and J. E. Gomez-Morantes, "Zeuss: a personalized tool for grammatical-construction learning," *International Journal of Web Information Systems*, vol. 16, no. 1, pp. 1–22, 2019.
- [20] M. O. Tamm, Y. Muhammad, and N. Muhammad, "Classification of vowels from imagined speech with convolutional neural networks," *Computers*, vol. 9, no. 2, p. 46, 2020.
- [21] S. Kamath, K. G. Karibasappa, A. Reddy, A. M. Kallur, B. B. Priyanka, and B. P. Bhagya, "Improving the relation classification using convolutional neural network," *IOP Conference Series: Materials Science and Engineering*, vol. 1187, no. 1, Article ID 012004, 2021.
- [22] T. Y. Prawira, S. Sunardi, and A. Fadlil, "Market basket analysis to identify stock handling patterns & item arrangement patterns using Apriori algorithms," *Khazanah Informatika Jurnal Ilmu Komputer dan Informatika*, vol. 6, no. 1, pp. 33–41, 2020.
- [23] W. Agustin and Y. Muharmi, "Penerapan data mining mamppgp," *Jurnal Teknologi Informasi dan Ilmu Komputer*, vol. 7, no. 2, p. 229, 2020.
- [24] C. Muralidharan and R. Anitha, "EDSAC–An efficient d shafer algorithm for classification to estimate the service, security and privacy risks with the service providers," *Wireless Personal Communications*, vol. 122, no. 4, pp. 3649–3669, 2021.
- [25] C. Si and W. Shi, "Establishment and improvement of financial decision support system using artificial intelligence and big data," *Journal of Physics: Conference Series*, vol. 1992, no. 3, Article ID 032082, 2021.
- [26] S. Seelothu and K. Rao, "A salient binary coding scheme for face and expression recognition from facial images," *International Journal of Intelligent Engineering and Systems*, vol. 14, no. 2, pp. 67–81, 2021.

Research Article

Detection and Analysis of Human Cells Based on Artificial Neural Network

Jun Yao and Hongji Yuan 

College of Computer Information and Engineering, Nanchang Institute of Technology, Nanchang 330044, China

Correspondence should be addressed to Hongji Yuan; yhj@nut.edu.cn

Received 16 May 2022; Revised 15 June 2022; Accepted 6 July 2022; Published 31 August 2022

Academic Editor: Le Sun

Copyright © 2022 Jun Yao and Hongji Yuan. This is an open access article distributed under the Creative Commons Attribution License, which permits unrestricted use, distribution, and reproduction in any medium, provided the original work is properly cited.

The detection and classification of histopathological cell images is a hot topic in current research. Medical images are an important research direction and are widely used in computer-aided diagnosis, biological research, and other fields. A neural network model based on deep learning is also common in medical image analysis and automatic detection and classification of tissue and cell images. Current medical cell detection methods generally do not consider that the yield is affected by other factors in the topological region, which leads to inevitable errors in the accuracy and generalization of the algorithm; at the same time, the current medical cell imaging methods are too simple to predict the classification markers, which affect the accuracy of cell image classification. This study introduces the concepts of two kinds of neural networks and then constructs a cell recognition model based on the convolution neural network principle and staining principle. In the experimental part, we developed three groups of experiments using the same equation as the experiment and tested the best cell recognition model proposed in this study.

1. Introduction

In this study, we propose a study to train neural network simulators using biosphere flux data collected by EURO-FLUX project to provide spatial and temporal estimates of European forest carbon flux on the continental scale. The novelty of this method is that the neural network structure is constrained and parameterized using traffic data, and a limited number of input driving variables are used [1]. In this study, a hybrid intelligent system based on past financial performance data is proposed, which combines a rough set method with neural network to predict enterprise failure. By comparing the traditional discriminant analysis and neural network method with our hybrid method, the effectiveness of this method is verified [2]. The artificial neural network method is used to predict short-term load of large-scale energy system. Different neuron combinations were used to test networks with one or two potential layers, and the prediction errors of the results were compared. When the neural network is divided into different load patterns, it can give a good load forecast [3]. The improved criteria of WG

and MPA are established and verified using the artificial neural network and traditional methods. A multicenter study was conducted on 240 WG patients and 78 MPA patients. Appropriately trained neural networks and CT can distinguish these diseases and perform better than LR [4]. The support vector machine (SVM) and artificial neural network (ANN) systems are applied to the drug/non-drug classification problem as an example of the binary decision-making problem in the early virtual compound filtering. The results show that compared with the artificial neural network, the solution obtained by support vector machine training has better robustness and smaller standard error [5]. In this study, a new method based on the artificial neural network is proposed to identify MHCII binding cores and binding affinities simultaneously. A new training algorithm is used for training, which allows the correction of deviations in training data caused by redundant binding kernel representations [6]. This study introduces the implementation of FANN, which is a fast artificial neural network library written by ANSIC. The results show that the speed of FAAN library is obviously faster than other libraries on the system

without floating-point processor, while the performance of FANN library on the system with floating-point processor is equivalent to other highly optimized libraries [7]. The purpose of this study was to determine whether circulating tumor cells were present in the blood of patients with large operable or locally advanced breast cancer before and after neoadjuvant chemotherapy and before and after preoperative neoadjuvant chemotherapy. After research, we concluded that in patients receiving neoadjuvant chemotherapy, CELLSEARCH system can detect circulating tumor cells in a low truncation range of 1 cell. Detection of circulating tumor cells is not associated with primary tumor response, but is an independent prognostic factor for early recurrence [8]. The pathological TNM stage is the best factor to judge the prognosis of non-small cell lung cancer. After isolating NSCLC patients by the size of epithelial tumor cells, cytological analysis was used to evaluate the presence of CTC in surgical patients [9]. In this study, a microbial electronic manipulation and detection lab-on-a-chip based on a closed dielectrophoresis cage combined with impedance sensing is proposed. This method is suitable for implementation in integrated circuit technology, which can not only operate and detect a single unit but also reduce the scale of the system [10]. Circulating tumor cells have long been considered to reflect the invasiveness of tumors. Therefore, many people have tried to develop analytical methods to reliably detect and enumerate CTCs, but such analytical methods have not been available until recently. This article reviews CTCs, especially the technical problems of its detection, the clinical results obtained so far, and the future prospects [11]. To determine the clinical application of immunoglobulin heavy chain gene rearrangement identification in multiple myeloma tumor cell detection, we investigated 36 consecutive newly diagnosed patients intending to receive high-dose chemotherapy in a research program. There is no consistent relationship between bone marrow MRD status and clinical course, and patients with negative PCR also have early recurrence [12]. Using yeast cells as a model system, a piezoelectric lead zirconate titanate-stainless steel cantilever beam was studied as a real-time cell detector in water. Under the experimental conditions, when the cell diffusion distance is less than the linear size of the adsorption area, the resonance frequency shift rate has a linear relationship with the cell concentration, and the resonance frequency shift rate can be used to quantify the cell concentration [13]. Although optical cell counting and flow cytometry devices have been widely reported, there is usually a lack of sensitive and effective nonoptical methods to detect and quantify large surface area cells attached to micro-devices. We describe an electrical method based on measuring cell count changes in the conductivity of the surrounding medium due to ions released by immobilized cells on the inner surface of the microfluidic channel [14]. Background of the diagnostic value and prognostic significance of circulating tumor cell detection in bladder cancer are still controversial. We conducted a meta-analysis to consolidate the current evidence of using CTC detection methods to diagnose bladder and other urothelial cancers and the association between CTC-positive and advanced and

remote diseases. Conclusion of CTC evaluation can confirm the diagnosis and differential diagnosis of bladder cancer [15].

2. Artificial Neural Network

2.1. RBF Neural Network. RBF neural network belongs to a kind of radial neural network. When there are enough nerve cells in the hidden layer, it can be designed as any continuous function infinitely. Local approximation, classification, and pattern recognition are all very good, and the learning and teaching time of the algorithm is very short. The mapping relation in RBF neural network is expressed as $f(x): R_n \rightarrow R_o$, as shown as follows:

$$y = f(x) = \sum_{i=1}^c \omega_i \varphi(\|x - c_i\|, \sigma_i) = \sum_{i=1}^c \omega_i \exp\left(-\frac{\|x - c_i\|^2}{2\sigma_i^2}\right), \quad (1)$$

where C is the number of neurons in the potential layer of the network, c_i is the center of radial basis function of each potential layer, the width is σ_i , and ω_i is the i th activation function and exit neuron. The neural network of RBF must be trained and learned to determine the radial basis center c_i , width σ_i , and weight ω_i between the potential layer and the output layer of neurons in each potential layer, to determine the mapping relationship between inputs.

To ensure that each activation function is not peaceful or too sharp, the activation function of latent neurons is regarded as a fixed radial basis function, and the center c_i of latent radial basis function is randomly selected from training. The radial basis function is defined as follows:

$$\varphi(x, c_i) = \exp\left(-\frac{k}{d_{\max}} \|x - c_i\|^2\right), \quad (2)$$

where K represents the number of neurons in the hidden layer and d_{\max} is the maximum distance between the two centers, and this formula shows that the width of neurons in the hidden layer is constant.

2.2. BP Neural Network. BP neural network is a multilayer feedback neural network with inverse error transmission. The learning process can be divided into signal transmission and error reverse transmission. A schematic diagram of BP neural network reverse transmission algorithm is shown in Figure 1.

From this, it can be deduced that the weight correction values are shown as follows:

$$\Delta\omega_{ji}(n) = \eta \times \delta_j(n) y_i(n), \quad (3)$$

$$\delta_j(n) = (d_j(n) - y_j(n)) \varphi_j \left(\sum_{i=0}^m \omega_{ji}(n) y_i(n) \right), \quad (4)$$

where M represents all the inputs that affect neuron J , η is the inverse error rate of learning, $\delta_j(n)$ is the local gradient, $y_i(n)$ is the output of neuron I , and Ψ is the activation function.

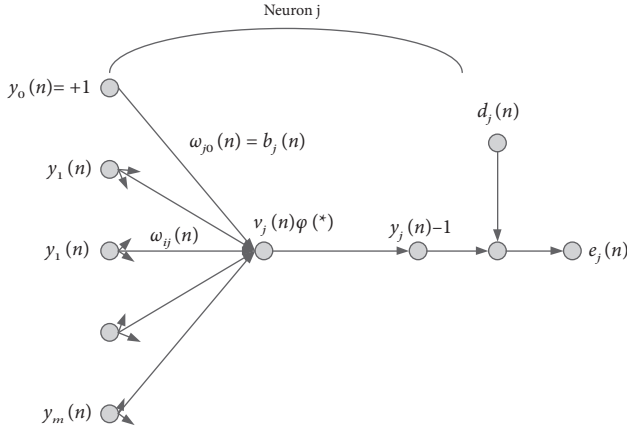


FIGURE 1: Schematic diagram of BP neural network reverse algorithm.

3. Research on Cell Image Detection

3.1. Construction of Cell Image Detection Network Model

3.1.1. Principle of Convolution Neural Network. The convolution neural network is based on the mathematical mapping in this study. It can learn the same mapping ability as this expression independently. It specializes in learning that needs to be practiced in a specific space, so this training can make it learn the mapping relationship between input and output. The process is shown as follows:

$$y = g(x; w_1, \dots, w_L),$$

$$= g_L(\cdot; w_L) \circ g_{L-1}(\cdot; w_{L-1}) \circ \dots \circ g_2(\cdot; w_2) \circ g_1(x; w_1), \quad (5)$$

where y represents output vector, x represents input vector, g represents CNN, g_L represents layer 1 CNN, w_L represents layer 1 g_L weight and bias vector, and \circ represents convolution operation.

A convolution neural network is usually composed of the following types (as shown in Figure 2). The convolution layer is used to separate important functions, the pooling layer is used to reduce the number of parameters and excessive matching, and the complete combination layer is usually used for network output after all convolution operations.

Input Layer: This layer is used to input data. In multi-dimensional data processing, because the input data are usually images, this study mainly introduces the input layer of objects placed in images. First, the image information is converted into function data and input into convolution neural network. The image structure is the embodiment of image information. In analysis, the CNN input layer keeps its original data when processing image information. Images are usually divided into black and white images and color images. When CNN analyzes different types of images, the inputs are different.

Convolution Layer: the convolution layer first detects each feature of the image locally and then performs local expansion processing at a higher level to obtain global information. The core of convolution operation is a mathematical operation, which usually represents discrete

convolution in convolution neural network. The convolution formula is as follows:

$$x_i^l = f\left(\sum_i w_{i,j}^{l-1,l} \circ x_i^{l-1} + b_j^l\right), \quad (6)$$

where x_i^l represents the i -level image of the i level, x_i^{l-1} represents the first to i -level images, \circ is the convolution operator, $w_{i,j}^{l-1,l}$ is the first to i -level images and $l-1$, b_j^l represents the offset of the j th feature corresponding to the l level, and F represents the activation function. The most common of these activation functions is the relay-type activation function, whose principle is shown as follows:

$$\text{Relu} = \max(0, x) = \begin{cases} x, & x \geq 0, \\ 0, & x < 0. \end{cases} \quad (7)$$

Pooling Layer: pooling layer is usually combined with the convolution layer, which is mainly used to reduce function scale, compare data, reduce the number of network parameters, reduce overmatching, and improve the tolerance of fault model. **Complete Combination Layer:** after processing several convolution layers and a pooling layer, the convolution neural network will be combined with the complete combination layer. **Output Layer:** the focus of the output layer of convolution neural network is to produce the desired results according to the situation. After calculation, different probability values are obtained from input to output.

3.1.2. Proposition and Construction of Cell Image Detection Model. Assuming that the time domain remains constant, Ω is defined as the state region of output Y , which is based on the finite state of the model. Suppose that the spatial constrained regression model g is used to test the known and has $y = g(\Omega; s(x))$ form, where $s(x)$ is an unknown parameter vector, and the result of the last layer of ordinary CNN is shown as follows:

$$y = f_L(x_{L-1}; w_L), \quad (8)$$

where x_{L-1} is the output of the network $(L-1)$ layer in the neural network and w_L is the weight of the last layer, which is output under the mapping of f_L . Based on the theoretical analysis of space constraints in this study, we need to extend the standard CNN to estimate $s(x)$ so that the last two layers (f_{L-1}, f_L) of the network are defined as follows:

$$s(x) = f_{L-1}(x_{L-2}; w_{L-1}), \quad (9)$$

$$y = f_L(\Omega; s(x)) = g(\Omega; s(x)), \quad (10)$$

where x_{L-2} is the output of the network $(L-2)$ layer and Formula (9) is the parameter estimation layer. According to the weight w_{L-1} , printing the image to obtain a parameter vector; Formula (10) is the spatial constraint layer, which belongs to the parameter vector in the regression model.

At the beginning of kernel image recognition, image plane $x \in R^{H \times W \times D}$, height H , width W , and feature number

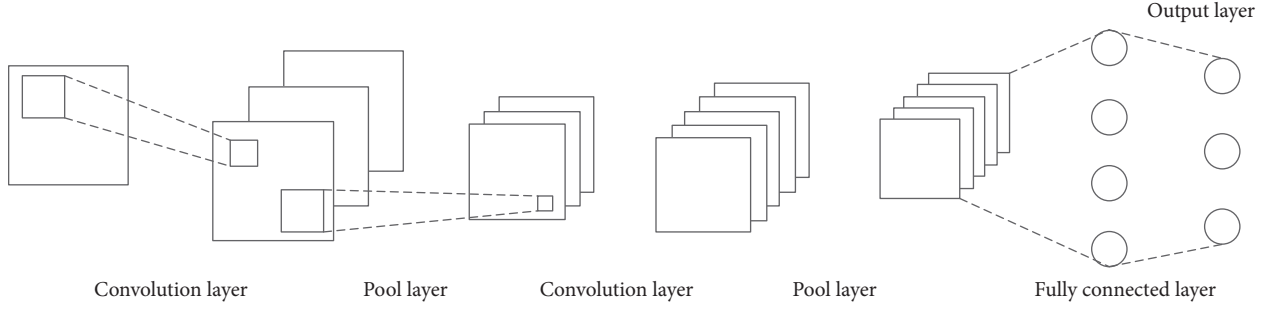


FIGURE 2: Basic structure diagram of convolution neural network.

D are given, and the goal is to detect the center point X of each kernel.

In this study, the Euclidean distance from the pixel to the core, i.e., $\|Z_j - Z_m^0\|_2$, is obtained when the core is detected, where Z_j and Z_m^0 represent the coordinates of y_j and the center coordinates of the m th core, respectively. The weight is reduced, i.e., normalized, and the regularized formula is shown as follows:

$$d = \frac{1}{2} \|Z_j - Z_m^0\|_2^2. \quad (11)$$

Let $\Omega = \{1, \dots, H'\} * \{1, \dots, w'\}$, and y is the spatial region. The j -th element is $j = 1, \dots, |\Omega|$. Equation (12) is defined as follows:

$$y_j = \begin{cases} 1 & \text{if } \forall m \neq m', \|Z_j - Z_m^0\|_2 \leq \|Z_j - Z_{m'}^0\|_2 \leq d, \\ \frac{1}{1 + \left(\|Z_j - Z_m^0\|_2^2 / d^2\right)} & \text{otherwise,} \end{cases} \quad (12)$$

where Z_j and Z_m^0 represent the coordinates of y_j and the center coordinate of the m th core of D , respectively, and Ω is a constant radius. It can be seen from the figure that the probability graph defined by Equation (12) has a maximum value near the center of each core Z_m^0 , and other places are

flat. Next, a prediction output \hat{y} generated from a space-constrained layer of the network is determined. Based on the known structure of the motion result probability graph described in Equation (12), we define the predicted output as Equation (13) of the J th element.

$$\hat{y}_j = g\left(Z_j; \hat{Z}_1^0, \dots, \hat{Z}_M^0, h_1, \dots, h_M\right), \quad (13)$$

$$= \begin{cases} 1 & \text{if } \forall m \neq m', \|Z_j - \hat{Z}_m^0\|_2 \leq \|Z_j - \hat{Z}_{m'}^0\|_2 \leq d, \\ \frac{1}{1 + \left(\|Z_j - \hat{Z}_m^0\|_2^2 / d^2\right)} & \text{otherwise,} \end{cases}$$

where $\hat{Z}_m^0 \in \Omega$ represents the center of the formula estimate, $h_M \in [0, 1]$ represents the height of the m th variable, and M represents the maximum number on \hat{y} . Because of the redundancy provided by $h_M = 0$ or $\hat{Z}_m^0 = \hat{Z}_{m'}^0, m \neq m'$, \hat{y} defined in this way will occur to allow the number of prediction cores to change from 0 to M . In the experiment, D in Formula (12) and Formula (13) is set to 4 pixels to provide sufficient support area for the probability mask.

Parameters $\hat{Z}_m^0 = (u_m, v_m)$ and h_m are estimated in a parameter estimation layer. X_{L-2} is made the output of the $(L-2)$ layer of the network. u_m, v_m, h_m are defined as follows:

$$u_m = (H' - 1) * \text{sigm}(W_{L-1, u_m} * X_{L-2} + b_{u_m}) + 1, \quad (14)$$

$$v_m = (W' - 1) * \text{sigm}(W_{L-1, v_m} * X_{L-2} + b_{v_m}) + 1, \quad (15)$$

$$h_m = \text{sigm}(W_{L-1, h_m} * X_{L-2} + b_{h_m}). \quad (16)$$

The purpose of formulas (14) and (15) is to show that the corresponding weights and deviations are output to the previous layer, then normalized, and then combined with the previous predictions to obtain a parameter estimate.

The importance of Formula (16) is that it is useful for the upper exit. After the corresponding weights and deviations are given, normalization is carried out to obtain the

estimated height of M variable, which fully integrates the spatial area position data. When $b_{u_m}, b_{v_m}, b_{h_m}$ and $W_{L-1,u_m}, W_{L-1,v_m}, W_{L-1,h_m}$ are vectors, the former represents deviation, the latter represents weighting, and $\text{sigm}(\cdot)$ represents the sigmoid function commonly used in convolution neural networks, which is often used to hide the output of neurons, and its value range is $(0, 1)$. It can specify a real number between $(0, 1)$; that is, it is used for normalization. The principle is shown as follows:

$$S(x) = \frac{1}{1 + e^x}, \quad (17)$$

where X represents the data after zero mean processing and $S(x)$ represents the data after normalization processing, and the learning method should use a loss function, as shown as follows:

$$l(y, \hat{y}) = \sum (y_j + \varepsilon)H(y_j, \hat{y}_j), \quad (18)$$

where ε is a small constant, which represents the ratio of nonzero probability pixels to the total number of zero probability pixels in the training input, and $H(y_j, \hat{y}_j)$ is the cross-entropy loss, which is specifically defined as follows:

$$H(y_j, \hat{y}_j) = -[y_j \log(\hat{y}_j) - (1 - y_j) \log(1 - \hat{y}_j)]. \quad (19)$$

Among them, when the actual values are $y_j = 1$ and $H(y_j, \hat{y}_j) = -\log(\hat{y}_j)$, when the predicted value of \hat{y}_j is closer to 1, $\log(\hat{y}_j)$ is closer to the maximum value of 1, and the minus sign indicates the minimum error value. When the predicted value of \hat{y}_j is closer to zero, $\log(\hat{y}_j)$ is closer to the negative. An infinite addition and subtraction sign indicates the maximum error value. When the actual values are $y_j = 0$ and $H(y_j, \hat{y}_j) = -\log(1 - \hat{y}_j)$, when the predicted value \hat{y}_j is closer to zero, $\log(\hat{y}_j)$ is closer to the maximum value 1, and the minus sign indicates the minimum error value, while when the predicted value \hat{y}_j is closer to 1, $\log(\hat{y}_j)$ is closer to the negative infinite addition and subtraction sign, which represents the maximum error value.

The detailed parameters of each convolution are shown in Table 1.

In Table 1, you can see that the input is an input attribute with a size of 27×27 , and the output attribute after the final network frame is 11×11 . To extract and merge all function information, the scroll window increment is always set to 1, and the trigger function uses relay-type trigger function evenly.

The network model structure mentioned in this article is shown in Figure 3.

F is the full interconnection layer, and these neurons in the full interconnection layer represent medical image information without spatial information; $S1$ is a new parameter estimation layer, and these neurons in the parameter estimation layer represent the estimated position information; $S2$ is the spatial constraint layer, L is the total number of layers in the network, and each neuron represents the medical image information with state parameter information.

3.2. Nuclear Image Preprocessing

3.2.1. *Coloring Principle of Stain.* The color deconvolution method is mainly based on the orthogonal transformation of the original RGB image, and according to the Beer-Lambert law, it is expressed as the relationship between the light intensity of the histological cell image and the staining matrix, as shown as follows:

$$I_C = I_{O,C} \exp(-Q * C_C), \quad (20)$$

where $I_{O,C}$ is the intensity of incident light radiated from the tissue cell image, I_C is the intensity of light passing through the tissue cell image, subscript C is the RGB three-channel identifier, Q is the dye color matrix, and C is the dye absorbance. It can be seen from Equation (10) that the intensity of transmitted light and dye content is relatively complex nonlinear relations. In the RGB color model, the light intensity of each pixel in the camera is I_R , I_G , and I_B , respectively. The optical density (OD) expression of each pixel is shown as follows:

$$\text{OD}_C = -\log_{10}\left(\frac{I_C}{I_{O,C}}\right) = Q * C_C. \quad (21)$$

It can be seen from Equation (21) that the optical density of each channel has a linear relationship with the absorption of light absorbent, so the optical density of each channel can be used to distinguish the color rendering effect of several dyes. The color effect of each point can be quantified by a 3×1 RGB three-channel optical density matrix. Using simple hematoxylin staining, the absorbance of R, G, and B channels was 0.18, 0.20, and 0.18, respectively. The size of the color matrix Q is related to the type of point, and each element of the matrix is proportional to the absorbance of each channel. For the three dyes R, G, B, the three-channel color system is defined as follows:

$$\begin{bmatrix} Y_{11} & Y_{12} & Y_{13} \\ Y_{21} & Y_{22} & Y_{23} \\ Y_{31} & Y_{32} & Y_{33} \end{bmatrix}. \quad (22)$$

Each row represents a dot, and each column represents the absorbance values of R, G, and B channels. In this data set, only two dyes are used for staining, and the corresponding chromosome systems of R, G, and B channels are shown as follows:

$$\begin{bmatrix} Y_{11} & Y_{12} & Y_{13} \\ Y_{21} & Y_{22} & Y_{23} \end{bmatrix}. \quad (23)$$

In the dyeing experiment, one dye was used to obtain the absorbance values of three RGB channels after dyeing with each dye. The dyeing formula for hematoxylin and eosin multiple dyeing is as follows:

$$\begin{bmatrix} 0.18 & 0.20 & 0.18 \\ 0.01 & 0.13 & 0.01 \end{bmatrix}. \quad (24)$$

TABLE 1: Design of parameter table of nuclear detection model based on spatial information.

Number of layers	Category	Filter size	Input/output dimensions
0	Input		$27 \times 27 \times 1$
1	conv1	$4 \times 4 \times 1 \times 36$	$24 \times 24 \times 36$
2	pooling1	2×2	$12 \times 12 \times 36$
3	conv2	$3 \times 3 \times 36 \times 48$	$10 \times 10 \times 48$
4	pooling2	2×2	$5 \times 5 \times 48$
5	Fully-connected1	$5 \times 5 \times 48 \times 512$	1×512
6	Fully-connected2	$1 \times 1 \times 512 \times 512$	1×512
7	sconv1	$1 \times 1 \times 512 \times 3$	1×3
8	sconv2		11×11

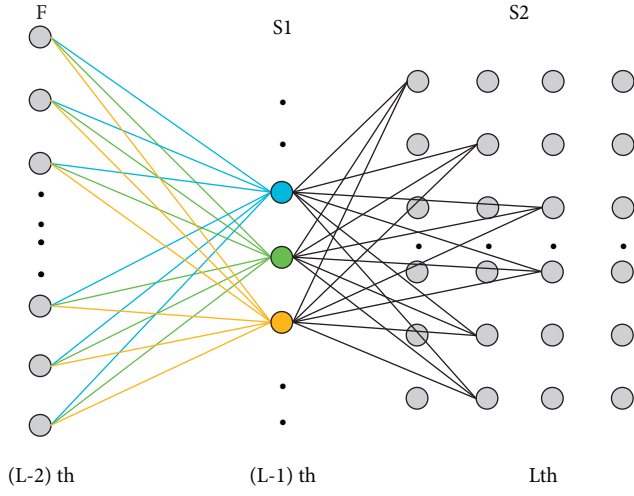


FIGURE 3: Structure of cell detection model.

3.2.2. Color Deconvolution. To make the color effect of each color in multicolor image stand out, RGB information must be transformed orthogonally. The purpose of orthogonal transformation is to make the color effect of each color independent of each other, to obtain the color effect of a dye. The transformed matrix must be normalized, and the normalization process for each dye is shown as follows:

$$\hat{Y}_{11} = \frac{Y_{11}}{\sqrt{Y_{11}^2 + Y_{12}^2 + Y_{13}^2}}, \quad (25)$$

$$\hat{Y}_{21} = \frac{Y_{21}}{\sqrt{Y_{21}^2 + Y_{22}^2 + Y_{23}^2}}. \quad (26)$$

The normalized optical density matrix A is shown as follows:

$$\begin{bmatrix} \hat{Y}_{11} & \hat{Y}_{12} & \hat{Y}_{13} \\ \hat{Y}_{21} & \hat{Y}_{22} & \hat{Y}_{23} \end{bmatrix}. \quad (27)$$

The $N \times 2$ matrix C is used to describe the color effect of two dyes on a pixel, and then, the optical density matrix $Y = AC$ of the image collected from the pixel is obtained. $C = A^{-1} Y$, and the color convolution matrix is then a pixel hint. Individual color effects can be determined according to the optical density and color moment of the image. The inverse of matrix $D = A^{-1}$ is obtained.

The color deconvolution matrix of the above H&E coloring method is shown as follows:

$$\begin{bmatrix} 1.88 & -0.07 & -0.60 \\ -1.02 & 1.13 & -0.48 \end{bmatrix}. \quad (28)$$

Multiple color images are separated by color deconvolution theory, and the separated images can be used for density and texture analysis.

The cell sample images were experimented according to H&E staining mode, and the experimental results are shown in Figures 4–6.

In the image of the isolated hematoxylin-stained component, the nucleus is blue, while in the image of the eosin-stained component, the cytoplasm and cytoplasm are pink. After color inversion of the pathological picture of this material, the separation result of nucleus and cytoplasm is very good. As shown in the above figure, the color deconvolution method can be used as an image preprocessing method in this study.

4. Comparative Experiment and Analysis

4.1. Comparative Experiment and Analysis of Cell Detection. In this section, we designed the same control group as the experimental group, tested SCNN and SR-CNNSSAE models, respectively, and tested the parameters according to the detection performance of CRCStoPhenotypes data set.

This section selects 100 cell images from the test data set and stores the accuracy, recovery rate, and F1 scores of the three experimental models when testing the images. Tables 2–4 compare the differences in the three experimental systems in three evaluation indexes in detail.

Table 2 shows that the maximum recovery rate of SCNN is 0.9076, which is 0.0546 and 0.2146 higher than SR-CNN and SSAE, respectively, same but improved compared with 0.16 SSAE; on average, SCNN still leads SR-CNN and SSAE. SCNN through the maximum recovery rate, minimum recovery rate, and average recovery rate of comparative analysis shows that the detection accuracy has been greatly improved. However, the mean square error of SCNN is larger than that of SR-CNN and SSAE, which shows that the stability is not as good as that of SR-CNN and SSAE, but the difference is very small, only 0.01, which is within the range of acceptable area.

It can be seen from Table 3 that in terms of accuracy, the highest accuracy of SCNN is 0.8883, and SR-CNN and SSAE are 0.0503 and 0.2163, respectively; SCNN has a minimum

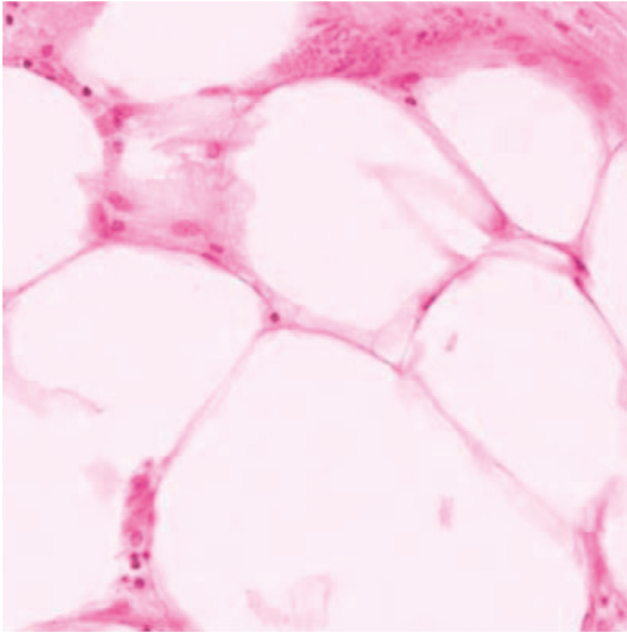


FIGURE 4: Sample image of H&E staining.

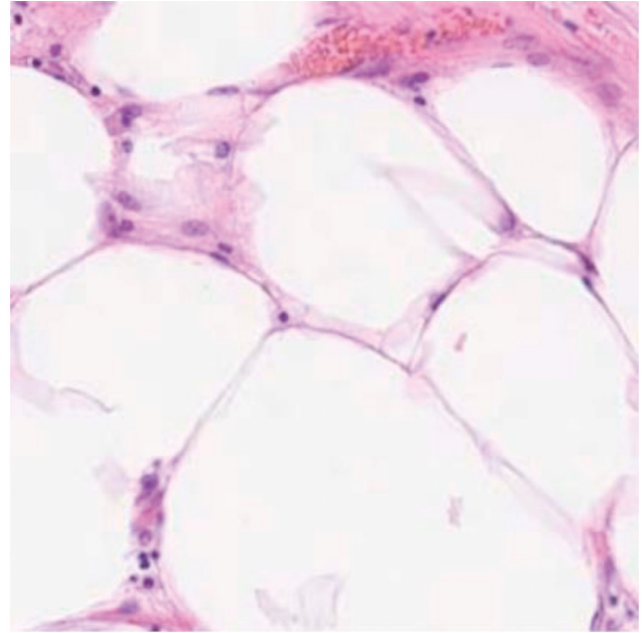


FIGURE 6: Eosin staining component image.

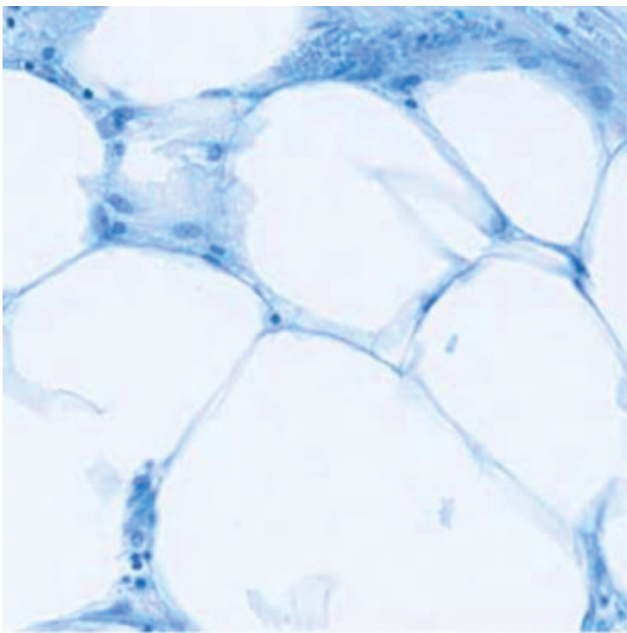


FIGURE 5: Images of hematoxylin staining components.

accuracy of 0.7002. In SR-CNN and SSAE, the minimum values are 0.6801 and 0.5141, respectively; in terms of average accuracy, SCNN and SR-CNN are basically the same, only 0.002 behind, which belongs to the normal statistical range and is obviously ahead of SSAE. The above three groups of comparative data show that SCNN has an excellent performance in accuracy. In terms of stability, the three experimental systems are basically the same, and they are all relatively stable.

It can be seen from Table 4 that the maximum F1 of SCNN is 0.836947, which is 0.009 and 0.173 higher than SR-CNN and SSAE, respectively. Based on SR-CNN, the

TABLE 2: Quantitative table of detection and evaluation indexes.

	SCNN	SR-CNN	SSAE
Maximum value	0.9076	0.8531	0.6932
Minimum value	0.7011	0.7011	0.5411
Mean value	0.8234	0.8039	0.6439
Mean square error	0.0363	0.0264	0.0264

TABLE 3: Quantitative table of detection and evaluation indexes.

	SCNN	SR-CNN	SSAE
Maximum value	0.8823	0.8321	0.6662
Minimum value	0.7002	0.6801	0.5141
Mean value	0.7811	0.7829	0.6169
Mean square error	0.0285	0.0264	0.0264

TABLE 4: Quantitative table of detection and evaluation indexes.

	SCNN	SR-CNN	SSAE
Maximum value	0.8369	0.8276	0.6638
Minimum value	0.7006	0.7102	0.5688
Mean value	0.8007	0.7929	0.6296
Mean square error	0.0159	0.0208	0.0194

TABLE 5: Experimental comparison results.

Method	Precision	Recall	F1 score
SCNN	0.781	0.823	0.802
SR-CNN	0.782	0.804	0.793
SSAE	0.617	0.644	0.63

minimum F1 of SCNN is 0.70065. On the basis of SSAE, it decreased by 0.009 and increased by 0.132. For average, F1 of SCNN improved by 0.008 on SR-CNN but significantly surpassed SSAE. The above three sets of comparative data

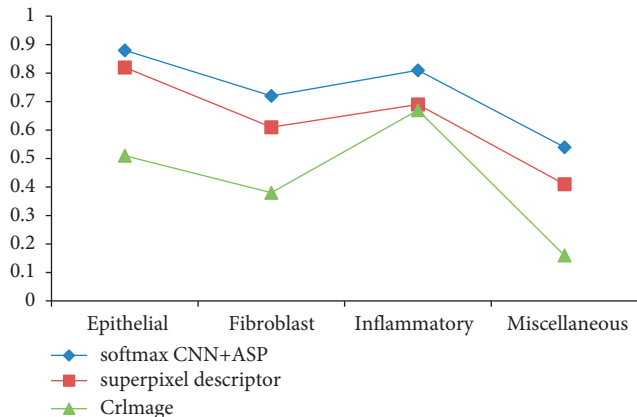


FIGURE 7: F1 scores were obtained by classifying different types of nuclei by three methods.

show that SCNN performed very well at F1. In terms of stability, the F1 score of SCNN in SR-CNN system is less than 0.005 and that in SSAE system is 0.001, which shows that this system is more stable.

The above analysis compares the detection performance differences in multiple cell images in detail from three indexes. Table 5 analyzes and compares the total indexes of the three experimental systems.

Table 5 shows that SCNN has better performance than SR-CNN and SSAE in terms of recovery rate and F1 score. Although it lags behind SR-CNN in accuracy, the difference is very small, which indicates that the experimental performance can be relied on.

Summarizing the above experimental results and comparative analysis, this section shows that the SCNN cell recognition model proposed in this study has better detection accuracy and stronger generalization ability, which shows that it is very important to add spatial information to the designed convolution neural network model.

4.2. Comparative Experiment and Analysis of Cell Classification. This section contains three sets of comparative experiments with the same experimental settings, which are designed to test the classification ability of the kernel classification model, the kernel classification model, and the kernel classification model proposed in this paper for the CRCHistoPhenotypes dataset. The parameters of the comparative test are the same as those of the classification test in Chapter 3.

The F1 scores in different core classifications are compared, and the reference methods are CRImage method and superpixel imaging method. The exact F1 score is shown in Figure 7.

As can be seen from Figure 7, the F1 score of the classification method based on adjacent set prediction proposed in this study is higher than that of the other two methods in the four categories, and the curve is more stable, indicating the best performance. See Table 6 for a detailed comparison.

TABLE 6: Quantitative table of F1 fraction of different nuclear classifications by three methods.

	Softmax CNN + ASP	Super-pixel descriptor	CRImage
Maximum value	0.875	0.817	0.672
Minimum value	0.538	0.395	0.156
Mean value	0.7342	0.625	0.427
Mean square error	0.1692	0.177	0.216

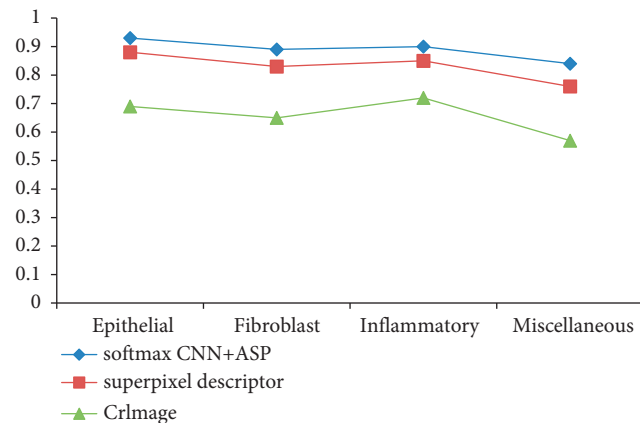


FIGURE 8: AUC values of four types of nuclear classification by three methods.

It can be seen from Table 6 that in terms of average F1, this method is obviously ahead of CRImage method in the super-pixel imaging method. The above three groups of comparative data show that the classification model based on adjacent set prediction in this study performs very well for F1 scores. In terms of stability, this method is 0.047 smaller than CRImage method, which shows that this model is more stable. In the same experimental environment, we combine SoftmaxCNN with a group of adjacent prediction methods, use CRImage method and superpixel imaging method to detect four different nuclei, and get the AUC values of different nuclei. See Figure 8 for details.

Figure 8 analyzes and compares the present model, the CRImage super-pixel imaging model, and the AUC metrics. Comparing these three curves, we can see that the model in this study has better AUC performance than the other two methods in the classification of four types of kernels. Table 7 compares the differences in AUC statistical data of the three experimental schemes in detail.

As can be seen from Table 7, the AUC of prediction-based adjacent set classification model for four different core types is 0.059 and 0.217 higher than that of super-pixel imaging method and CRImage method, respectively, the minimum value is 0.099 and 0.295 higher, and the average value is higher, more than 0.071 and 0.2435. The performance of this model is better, and the mean square error is less than 0.0208 and 0.0346, which shows that the model in this study is more stable in classifying cell images. After comparing the F1 fraction and AUC values obtained from

TABLE 7: Quantification table of AUC values of four nuclear classifications by three methods.

	Softmax CNN + ASP	Super-pixel descriptor	CRImage
Maximum value	0.946	0.887	0.729
Minimum value	0.836	0.737	0.541
Mean value	0.901	0.831	0.657
Mean square error	0.047	0.068	0.081

TABLE 8: Comparison of nuclear classification results of three methods.

Method	F1 score	Multi-class AUC value
Softmax CNN + ASP	0.784	0.917
Super-pixel descriptor	0.687	0.853
CRImage	0.488	0.684

different types of nuclei, the weighted integration of F1 fraction and AUC values was carried out and a detailed comparison was made. The specific numerical equations are shown in Table 8.

Table 8 shows that the combination of SoftmaxCNN and AdjacentSetPrediction is used to classify the kernel used in this study, which is nearly 1 percentage point higher than the F1 score of the other two kernel classification methods, which is more. It shows the superiority of the proposed model in nuclear classification of cell histology image classification based on adjacent set prediction. The multi-class AUC is at least 0.6 percentage points higher than that of SuperpixelDescripto method and 2 percentage points higher than that of CRImage method. The combination of SoftmaxCNN and adjacent force prediction is more than 90% in multiclass. The comparison results of AUC values show that the proposed method has better classification ability and stability in nuclear classification.

Based on the above experimental results and comparative analysis, this section demonstrates that the proposed nuclear classification model based on adjacent set prediction has better classification ability and stronger stability and proves that convolution neural network combined with adjacent set prediction model is effective.

5. Concluding Remarks

In this study, we propose a method to detect nuclei by combining spatial data. This method aims at detecting nuclei in histological cell images and constructing a spatial model of cell image detection, to solve the problem of missing topological input in the current model. Aiming at the problem of how to classify the nuclei in the enlarged image of human cells, a prediction mechanism based on adjacent sets is proposed, and a large classification model of human cell images is constructed by combining the convolution neural network system of linear regression. In recent years, the deep learning method is widely used, which provides a

theoretical basis for human cell image detection and classification combined with neural network model.

Data Availability

The experimental data used to support the findings of this study are available from the corresponding author upon request.

Conflicts of Interest

The authors declare that they have no conflicts of interest regarding this work.

Acknowledgments

This study was supported by the Application of Soft X-Ray Technology in Human Cell Pathology (grant no.: 20202BBGL73056).

References

- [1] D. Papale and R. Valentini, "A new assessment of European forests carbon exchanges by eddy fluxes and artificial neural network spatialization," *Global Change Biology*, vol. 9, no. 4, pp. 525–535, 2003.
- [2] B. S. Ahn, S. S. Cho, and C. Y. Kim, "The integrated methodology of rough set theory and artificial neural network for business failure prediction," *Expert Systems with Applications*, vol. 18, no. 2, pp. 65–74, 2000.
- [3] K. Y. Lee, Y. T. Cha, and J. H. Park, "Short-term load forecasting using an artificial neural network," *IEEE Transactions on Power Systems*, vol. 7, no. 1, pp. 124–132, 1992.
- [4] R. Linder, I. Orth, E. C. Hagen, F. J. van der Woude, and W. H. Schmitt, "Differentiation between Wegener's granulomatosis and microscopic polyangiitis by an artificial neural network and by traditional methods," *Journal of Rheumatology*, vol. 38, no. 6, pp. 1039–1047, 2011.
- [5] E. Byvatov, U. Fechner, and J. Sadowski, "Comparison of support vector machine and artificial neural network systems for drug/non-drug classification," *Journal of Chemical Information and Modeling*, vol. 5, no. 7, pp. 497–546, 2003.
- [6] M. Nielsen and O. Lund, "NN-align. An artificial neural network-based alignment algorithm for MHC class II peptide binding prediction," *BMC Bioinformatics*, vol. 10, no. 1, p. 296, 2009.
- [7] S. Nissen, "Implementation of a fast artificial neural network library (FANN)," *Report*, vol. 3, no. 4, pp. 54–98, 2003.
- [8] J. Y. Pierga, F. C. Bidard, C. Mathiot et al., "Circulating tumor cell detection predicts early metastatic relapse after neo-adjuvant chemotherapy in large operable and locally advanced breast cancer in a phase II randomized trial," *Clinical Cancer Research*, vol. 14, no. 21, pp. 7004–7010, 2008.
- [9] V. Hofman, C. Bonnetaud, M. I. Ilie et al., "Preoperative circulating tumor cell detection using the isolation by size of epithelial tumor cell method for patients with lung cancer is a new prognostic biomarker," *Clinical Cancer Research*, vol. 17, no. 4, pp. 827–835, 2011.
- [10] G. Medoro, N. Manaresi, A. Leonardi, L. Altomare, M. Tartagni, and R. Guerrieri, "A Lab-On-A-Chip for Cell Detection and manipulation," in *Proceedings of the Sensors, IEEE*, IEEE, Orlando, FL, USA, June 2002.

- [11] S. Sleijfer, J. W. Gratama, A. M. Sieuwerts, J. Kraan, J. W. Martens, and J. A. Foekens, "Circulating tumour cell detection on its way to routine diagnostic implementation," *European Journal of Cancer*, vol. 43, no. 18, pp. 2645–2650, 2007.
- [12] A. Swedin, S. Lenhoff, and T. Olofsson, "Clinical utility of immunoglobulin heavy chain gene rearrangement identification for tumour cell detection in multiple myeloma," *British Journal of Haematology*, vol. 103, no. 4, pp. 1145–1151, 2015.
- [13] J. W. Yi, W. Y. Shih, R. Mutharasan, and W. H Shih, "In situ cell detection using piezoelectric lead zirconate titanate-stainless steel cantilevers," *Journal of Applied Physics*, vol. 93, no. 1, pp. 619–625, 2003.
- [14] X. Cheng, Y. s. Liu, D. Irimia et al., "Cell detection and counting through cell lysate impedance spectroscopy in microfluidic devices," *Lab on a Chip*, vol. 7, no. 6, pp. 746–755, 2007.
- [15] P. Msaouel and M. Koutsilieris, "Diagnostic value of circulating tumor cell detection in bladder and urothelial cancer: systematic review and meta-analysis," *BMC Cancer*, vol. 11, no. 1, p. 336, 2011.

Research Article

Task Offloading and Resource Allocation Strategy Based on Deep Learning for Mobile Edge Computing

Zijia Yu , Xu Xu , and Wei Zhou 

School of Information Engineering, Suzhou University, Suzhou, Anhui 234000, China

Correspondence should be addressed to Zijia Yu; yuzj@ahszu.edu.cn

Received 14 June 2022; Revised 2 August 2022; Accepted 13 August 2022; Published 31 August 2022

Academic Editor: Le Sun

Copyright © 2022 Zijia Yu et al. This is an open access article distributed under the Creative Commons Attribution License, which permits unrestricted use, distribution, and reproduction in any medium, provided the original work is properly cited.

For the problems of unreasonable computation offloading and uneven resource allocation in Mobile Edge Computing (MEC), this paper proposes a task offloading and resource allocation strategy based on deep learning for MEC. Firstly, in the multiuser multiserver MEC environment, a new objective function is designed by combining calculation model and communication model in the system, which can shorten the completion time of all computing tasks and minimize the energy consumption of all terminal devices under delay constraints. Then, based on the multiagent reinforcement learning system, system benefits and resource consumption are designed as rewards and losses in deep reinforcement learning. Dueling-DQN algorithm is used to solve the system problem model for obtaining resource allocation method with the highest reward. Finally, the experimental results show that when the learning rate is 0.001 and discount factor is 0.90, the performance of proposed strategy is the best. Furthermore, the proportions of reducing energy consumption and shortening completion time are 52.18% and 34.72%, respectively, which are better than other comparison strategies in terms of calculation amount and energy saving.

1. Introduction

With the rise of computing-intensive applications and explosive growth of data traffic, users' requirements for the computing power and service quality of mobile devices are also increasing [1]. At present, cloud computing also faces many problems and challenges. Due to its resource-intensive architecture, mobile cloud computing imposes a huge additional load on the backhaul link of mobile networks [2, 3]. Thus, Mobile Edge Computing (MEC) technology is proposed, which physically integrates computing and storage resources into the edge of mobile network architecture [4, 5]. This not only effectively reduces the transmission delay but also solves the problems of high load and high delay caused by mobile cloud computing [6]. At the same time, MEC has the characteristics of distributed architecture, being at the edge of network, low latency, user location awareness, and network status awareness [7, 8]. However, deploying a large number of computing and storage devices at the edge of network for users

to choose and accessing neighboring service providers for edge computing will bring a series of complexities such as access and resource allocation strategy selection, user mobility management, and computing task migration problems [9].

In order to achieve the goal of short completion time and lower terminal energy consumption under delay constraint, this paper proposes a task offloading and resource allocation strategy based on deep learning for MEC. In order to shorten the completion time of computing tasks and minimize the energy consumption of all terminal devices while satisfying delay constraints, the proposed strategy is designed in a multiuser multiserver MEC environment, combined with computing model and communication model in system. Moreover, a new objective function is designed, which uses objective optimization to further reduce energy consumption and time delay. It uses Dueling-DQN algorithm to solve the optimization model to shorten completion time and minimize energy consumption of all terminal devices while meeting the delay constraints.

The remaining chapters of this paper are arranged as follows: Section 2 introduces the relevant research work on mobile task unloading. Section 3 introduces the system model. Section 4 introduces the new computing offload method based on improved DQN. In Section 5, simulation experiments are designed to verify the performance of the proposed model. Section 6 is the conclusion.

2. Related Work

In MEC network, computation offloading may occur in three types: full offloading, partial offloading, and local processing [10]. An important research hotspot in the field of computation offloading is computation offloading decisions. Generally speaking, the offloading goal mainly focuses on minimizing the overall delay or minimizing energy consumption for user devices while meeting the minimum delay requirements [11]. Reference [12] proposed a distributed task offloading strategy for low-load base station groups in MEC environment. It selects the best MEC node offloading amount by game equation on the basis of quantifying offloading cost and delay. But it is not suitable for high-load application environments. In reference to the problem of unbalanced computing resources on the edge server in vehicle edge computing network, [13] proposed a load balancing task offloading scheme based on software-defined network. This solution can effectively reduce delay and improve the efficiency of task offloading processing. However, the processing method used has poor performance, which affects the distribution efficiency. Reference [14] used greedy selection to design a maximum energy-saving priority algorithm to achieve optimal offloading of computing tasks on mobile devices, but it does not consider the delay constraints of task offloading. Reference [15] combined long short-term memory (LSTM) and candidate network set to improve the deep reinforcement learning algorithm and used this algorithm to solve the problem of offloading dependency of multinode and mobile tasks in large-scale heterogeneous MEC. But they ignore the optimal allocation problem of computing resources.

Similar to computation offloading, resource allocation is also one of the core issues in MEC [16]. In MEC network, technologies such as content caching and ultradense deployment are introduced, and multiple resources are deployed to mobile network edge according to the specific needs of users. This can further ensure the quality of service and greatly increase system capacity [17]. However, due to objective reasons such as physical volume and power consumption, the mobile network edge has limited computing resources, storage cache capacity, and spectrum resources. How to allocate multiple resources and improve the system service efficiency has a huge effect on the improvement of MEC network system performance [18]. Reference [19] proposed a time average computation rate maximization (TACRM) algorithm, which allows joint allocation of radio resources and calculation resources. However, the overall performance and task requirements of devices were not considered comprehensively in the allocation process, and the allocation efficiency still needs to be improved. Reference

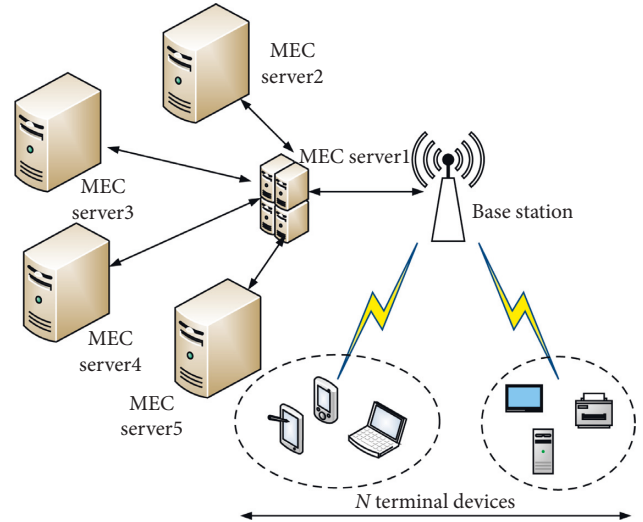


FIGURE 1: System model diagram.

[20] comprehensively considered factors such as CPU, hard disk space, and required time and distance and proposed a comprehensive utility function for MEC resource allocation to achieve the optimal allocation of resources in MEC and cloud computing. However, this function considers many factors, which will seriously affect the efficiency of allocation in real applications. Reference [21] designed a two-layer optimization method for MEC, which uses pruning candidate modes to reduce the number of unfeasible offloading decisions. Through ant colony algorithm to achieve the upper-level optimization, the resource allocation effect is better. However, the server computing resource constraints and task delay constraints are not considered, and the overall timeliness is not good. Reference [22] constructed a low-complexity advanced branch model, which can be used for resource scheduling in large-scale MEC scenarios.

Due to the lack of powerful processing algorithms, the overall efficiency and performance are not ideal. To this end, comprehensively considering the task offloading and resource allocation problem, a deep learning-based MEC task offloading and resource allocation strategy is proposed to coordinate and optimize the allocation and offloading between computing resources and computing tasks, which improves the comprehensive computing efficiency of MEC.

3. System Model

The system model is a multiuser multiserver application scenario, in which there are N terminal devices and M MEC servers. The base station is used to provide communication resources for user equipment. Each base station is connected to an edge computing server through optical fiber, through the wireless communication link to connect to MEC server to calculate task data of offloading terminal devices, as shown in Figure 1. It is assumed that each terminal device can perform offloading computations or local calculations for its own execution tasks. And when offloading, the task can only be offloaded to one MEC server for calculation, and each terminal device is within the range of wireless

connection. However, the computing power of each MEC server is limited; it cannot accept the offloading request of each terminal at the same time.

The collection of terminal devices is $U = \{1, 2, \dots, n, \dots, N\}$, the collection of MEC server is $H = \{1, 2, \dots, m, \dots, M\}$, and the collection of all tasks is G . Each terminal device n has a calculation-intensive task G_n to be processed, which specifically includes the data D_n (code and parameters) required for computing task G_n , the CPU workload ϕ_n required for computing task G_n , and the completion time of task G_n . The extension constraint is τ_n , namely, $G_n \cong (D_n, \phi_n, \tau_n)$. The set of offloading decisions for each G_n is $X = [x_1, x_2, \dots, x_n, \dots, x_N]$.

When $x_n = \{0, 1, \dots, m, \dots, M\}$, and $x_n = 0$ is local offloading, the rest means offloading G_n to m MEC servers.

3.1. Communication Model. In the computation offloading problem, two links are mainly studied: wireless link from terminal devices to MEC and the wired link from MEC to cloud in the core network. In the wireless link, Finite-State Markov Channel (FSMC) model based on fading characteristics is used. FSMC model has a wide range of applications in wireless networks [23, 24].

The channel is divided into nonoverlapping intervals through the division of channel-related parameter ranges, and each interval of selected parameters represents a state in FSMC model. The relevant parameter used in FSMC may be Signal-to-Noise Ratio (SNR) amplitude of received signal at the receiving end or collected energy. SNR can be selected as a parameter that composes SNR model [25]. The SNR of receiving end is divided into K levels, and each level is associated with a state of Markov chain. The block fading channel is considered to be that the SNR of receiving end is a constant within a period of time but will change according to Markov transition probability between different periods. Assume that random variable γ is the SNR of receiving end of terminal device n . That is, γ can be improved according to Markov chain of finite states, and all its states can be expressed as $\kappa = \{1, 2, \dots, K\}$. The realization of random variable γ of terminal device n in the time period t is represented as $\Gamma(t)$, specifically expressed as

$$\Gamma_n(t) = k, \text{ if } \gamma_n(t) \in [h^{i-1}, h^k), \quad (1)$$

where $k \in \kappa = \{1, 2, \dots, K\}$ and $h^0 = 0 < h^1 < h^2 < \dots$. Let $\rho_{s'_n, s''_n}(t)$ denote the probability of state $\Gamma_n(t)$ transitioning from state s'_n to state s''_n in the time period t . The $K \times K$ channel state transition probability matrix of terminal device n is denoted as $\Phi_n(t) = [\rho_{s'_n, s''_n}(t)]_{K \times K}$, where $\rho_{s'_n, s''_n}(t) = \Pr(\Gamma_n(t+1) = s''_n | \Gamma_n(t) = s'_n)$, $s'_n, s''_n \in \kappa$.

In practical applications, the transfer matrix can be observed and measured from wireless environment in the past. In addition, it is considered that $\{\Gamma_n(t), 1 \leq t \leq T\}$ exists independently for terminal device n . Based on FSMC channel model, $\Gamma_{n,m}$ is used here to represent SNR between terminal device n and MEC server m . Since there is no interference between terminal devices, its channel efficiency can be expressed as $\vartheta_{n,m} = \log_2(1 + \Gamma_{n,m})$. Considering that the bandwidth W_m of MEC server m is divided into W_m/B_m ,

the bandwidth of each channel is B_m . Assuming that each user is allocated at most one channel, the transmission rate from terminal device n to MEC server m can be expressed as

$$v_{n,m}(t) = B_m \vartheta_{n,m}(t). \quad (2)$$

The subchannel owned by MEC server m has certain restrictions on receiving W_m/B_m ; that is, the bandwidth allocated by MEC server m to all connected users cannot exceed the total bandwidth of MEC server m . Besides, MEC server is limited by cache and computing capacity. On the one hand, MEC server can only handle a limited number of tasks; on the other hand, the load that MEC server can handle is also limited (such as the number of computing tasks). Therefore, some tasks will be further offloaded to the core network to be processed by the core network. Use $g_u(t) \in \{0, 1\}$ to represent the computation offloading decision indicator, which is used to indicate the way the server provides services. Among them, $g_n(t) = 0$ means that the terminal device n is processed by connected MEC server for computing tasks. And $g_n(t) = 1$ indicates that the task will be further offloaded to core network for processing by connected MEC server.

In order to further offload tasks to cloud, the wired backhaul link from MEC server to core network is considered. Assuming that the backhaul link capacity of network is Z (in bits per second), the backhaul link capacity allocated by MEC server m is Z_m . Then, the following restrictions must be met:

$$\begin{aligned} \sum_{n=1}^N g_n(t) \theta_{n,m}(t) \bar{\omega}_{n,m}(t) &\leq Z_m, \\ \sum_{m=1}^M \sum_{n=1}^N g_n(t) \theta_{n,m}(t) \bar{\omega}_{n,m}(t) &\leq Z, \end{aligned} \quad (3)$$

where $\theta_{n,m}$ is the connection between terminal device n and MEC server m and $\bar{\omega}_{n,m}$ is the transmission rate between terminal device n and MEC server m .

The sum of the rates of offloading computation tasks to the terminal device of core network by MEC server m cannot exceed the backhaul capacity of MEC server m . And the sum of speeds of all terminal devices processing computing tasks in the cloud cannot exceed the total backhaul capacity of system.

3.2. Calculation Model. If G_n is processed locally, use T_n^L to represent the time when G_n is executed locally, which is specifically defined as

$$T_n^L = \frac{\phi_n}{f_n^L}, \quad (4)$$

where workload ϕ_n is the total number of CPU cycles required to complete G_n and f_n^L is the local computing power of terminal device n (i.e., the number of CPU cycles executed per second).

Use E_n^L to represent the energy consumption of devices executed locally by G_n , which is defined as follows:

$$E_n^L = \phi_n \times e_n, \quad (5)$$

where e_n is terminal device n to calculate the energy consumption per unit of CPU cycle, $e_n = (f_n^L)^2 \times 10^{-27}$.

If G_n is processed at the edge, delay T_n^O and device energy consumption E_n^O under G_n edge execution should be calculated from three parts: data upload, data processing, and data return [26]. The specific calculation is as follows.

First, terminal device n uploads data G_n to the corresponding MEC server by wireless channel. Let T_n^I be the time when device n uploads G_n data, which is defined as

$$T_n^I = \frac{D_n}{v'}, \quad (6)$$

where D_n is the data size of G_n and v' is data upload rate in the system model (i.e., the amount of data uploaded per second).

Then, the energy consumption E_n^I of terminal device n uploading data is

$$E_n^I = T_n^I \times P', \quad (7)$$

where P' is the uplink transmission power of terminal device n .

Then, MEC allocates computing resources for calculation after receiving processed data. Use T_n'' to represent the time when the offloading data is calculated in MEC server, which is defined as

$$T_n'' = \frac{\phi_n}{f_{nm}^O}, \quad (8)$$

where f_{nm}^O are the computing resources allocated by m MEC servers for G_n offload execution (i.e., the number of CPU cycles executed per second). When G_n is unloaded to the local or other MEC server, f_{ij}^O is zero and serves as a constraint in the model, namely,

$$f_{nm}^O = 0, x_n \neq m. \quad (9)$$

At this time, terminal device n has no computing task and is in a waiting state and generates idle energy consumption. Suppose P_n^I is the idle power of terminal device n , then the idle energy consumption E_n'' of terminal device n under offloading computation is

$$E_n'' = T_n'' \times P_n^I. \quad (10)$$

Finally, MEC server returns the calculation result to terminal device n . The calculation result during backhaul is small and downlink rate is high, so the time delay and energy consumption when terminal device is received are ignored. Therefore, delay T_n^O under G_n edge execution is the sum of transmission delay T_n^I and the calculation delay T_n'' of MEC server, namely,

$$T_n^O = T_n^I + T_n''. \quad (11)$$

The device energy consumption E_n^O under G_n edge execution is the sum of upload energy consumption E_n^I of device n and the idle energy consumption E_n'' of device n waiting for G_n to complete calculation on MEC server, namely,

$$E_n^O = E_n^I + E_n''. \quad (12)$$

In summary, the time delay T_n and energy consumption E_n of the entire calculation process of task G_n in terminal device n are

$$T_n = \begin{cases} T_n^L, & x_n = 0, \\ T_n^O, & x_n \neq 0, \end{cases} \quad (13)$$

$$E_n = \begin{cases} E_n^L, & x_n = 0, \\ E_n^O, & x_n \neq 0. \end{cases}$$

Note that T_n and f_{nm}^O should meet the following restrictions:

$$T_n \leq \eta_n, \quad (14)$$

$$T_n \leq \eta_n.$$

The time delay constraint η_n of G_n is that computing power is twice 1.4GHz. F_m is the overall computing resources of MEC server m ; that is, the sum of computing resources allocated by each G_n that is offloaded to MEC server m should not exceed F_m .

3.3. Problem Model. The purpose of this paper is to jointly optimize offloading decision-making and resource allocation scheme in the multiuser multi-MEC server scenario, considering the limited computing resources and time delay constraint of computing tasks. This allows all computing tasks to shorten the completion time and minimize energy consumption of all terminal devices while meeting the delay constraints and extend the use time of terminal devices [27, 28]. Thus, the system objective function Ψ is defined as

$$\Psi = \sum_{n=1}^N E_n + 10 \times \sum_{n=1}^N \frac{T_n}{\eta_n}. \quad (15)$$

(T_n/η_n) is the ratio of completion time G_n to the delay constraints. According to the calculation results of simulation experiment, the difference between $\sum_{n=1}^N E_n$ and $\sum_{n=1}^N (T_n/\eta_n)$ is a decimal order of magnitude. Therefore, to ensure that the two are of the same order of magnitude and optimized together, $\sum_{n=1}^N (T_n/\eta_n)$ is multiplied by a factor of 10. The objective function Ψ minimizes the ratio of overall energy consumption of terminal devices to the task execution time and delay constraints by solving the optimal offloading decision and resource allocation plan to achieve research purpose. The overall problem model is as follows:

$$\begin{aligned}
 & \min_{x,f} (\Psi), \\
 & X = [x_1, x_2, \dots, x_n, \dots, x_N], \\
 & X = [x_1, x_2, \dots, x_n, \dots, x_N], \\
 & y_n = \begin{cases} f_n^L, x_n = 0, \\ f_{nm}^O, x_n = m, \end{cases} \\
 & \text{s.t.} \\
 & C_1: x_n \in \{0, 1, \dots, m, \dots, M\}, \forall n \in U, \\
 & C_2: y_n > 0, \forall n \in U, \\
 & C_3: f_{nm}^O = 0, x_n \neq m, \\
 & C_4: T_n \leq \eta_n, \forall n \in U, \\
 & C_5: \sum_{n=1}^N f_{nm}^O \leq F_m, \forall m \in H, \\
 & C_6: \begin{cases} \sum_{n=1}^N g_n(t) \theta_{n,m}(t) \omega_{n,m}(t) \leq Z_m, \\ \sum_{m=1}^M \sum_{n=1}^N g_n(t) \theta_{n,m}(t) \omega_{n,m}(t) \leq Z, \end{cases}
 \end{aligned} \tag{16}$$

where X is the task offloading decision amount and Y is the calculation resource allocation amount. Constraints C_1 , C_2 , and C_3 indicate that each task G_n can only be offloaded to the local or one of MEC servers for calculation. C_4 represents the constraint of task completion delay, and C_5 and C_6 represent the constraint that allocated computing resources should meet.

4. New Computation Offloading Method Based on Improved DQN

4.1. Multiagent Reinforcement Learning Algorithm. The multiagent reinforcement learning system is shown in Figure 2, where multiple agents act at the same time. Under the joint action, the entire system will be transferred, and each agent will be rewarded immediately [29, 30].

For multiagent reinforcement learning, it is first necessary to establish a Markov game model. Markov game can be described by a multigroup $(n, S, A_1, \dots, A_n, R_1, \dots, R_n)$. Among them,

- (1) n is the number of agents; that is, N is the number of terminal devices. S is the system state, which generally refers to the joint state of multiple agents, that is, the joint state of each agent. The terminal device shares the current load status of edge computing servers, which can be expressed as

$$LD(t) = [LD_1(t), LD_2(t), \dots, LD_m(t)], \tag{17}$$

where LD_m is the load of MEC.

- (2) R_i is the instant reward function of each agent. That is, in current state s , after joint action (A_1, \dots, A_n) taken by multiple agents, the reward is obtained in the next system state \hat{s} .

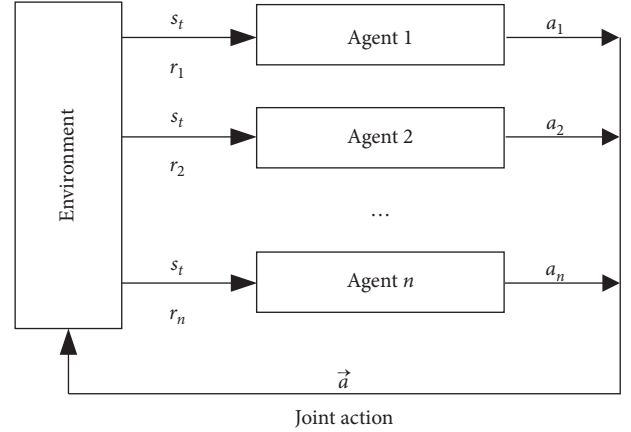


FIGURE 2: Multiagent reinforcement learning system.

The reward function completely describes the relationship between multiple agents. When the reward function of each agent is the same, that is, $R_1 = R_2 = \dots = R_n$, it means that the agent is a complete cooperative relationship. When there are only two agents and reward function is opposite, that is, $R_1 = -R_2$, it means that the agents are in perfect competition. When the return function is between the two, it is a mixed relationship between competition and cooperation.

4.2. Problem Description and Modeling

4.2.1. Network Status. $S = \{s(t)\}$ represents the network state space, where $s(t)$ represents the network state at time period t , and improvements are made in the entire time period T . The network status consists of SNR of each terminal device and cache status of each MEC server. $s(t)$ can be defined as

$$\begin{aligned}
 s(t) = & (\Gamma_1(t), \dots, \Gamma_n(t), \dots, \Gamma_N(t), \\
 & \psi_1(t), \dots, \psi_m(t), \dots, \psi_M(t)),
 \end{aligned} \tag{18}$$

where $\Gamma_n = \{\Gamma_{n,m}, m \in M\}$ represents SNR between user terminal device n and all MECs. $\psi_m(t) = \{\varphi_{k,m}, k \in K\}$ represents the cache status of MEC servers.

4.2.2. Network Behavior. The intelligent agent needs to determine the attachment relationship between the terminal device and MEC server in each time period. That is the determination of the terminal device's computing offload, the allocation of computing resources, and the service cache policy of each MEC server. Thus, each executable action of terminal devices in the time period t can be defined as follows:

$$\begin{aligned}
 a(t) = & (A_1(t), \dots, A_n(t), \dots, A_N(t), \\
 & G_1(t), \dots, G_n(t), \dots, G_N(t), \\
 & \psi_1(t), \dots, \psi_m(t), \dots, \psi_M(t)),
 \end{aligned} \tag{19}$$

where $A_n(t) = \{a_{n,m}(t), m \in M\}$ represents the attachment indicator of terminal device n and $G_n(t)$ represents the calculation and offloading decision of terminal device n .

4.2.3. Reward Function. The goal is to maximize total benefit of system, but the reward function should be set to current benefit of system. First calculate the system leased spectrum and backhaul resources and allocate them to terminal devices part of the revenue. The unit price of spectrum leased from MEC server m is set to δ_m per Hz, and the unit price of backhaul link from MEC server m to core network is set to σ_m per bps. Corresponding to this, the calculation data is transmitted to MEC server corresponding to terminal device n and backhaul link from MEC server to the core network is used for charging. The unit price is defined as α_n per Hz and β_n per bps. Therefore, by summarizing this part of the income and expenditure, part of income for leased spectrum and backhaul resources obtained by terminal device n can be obtained:

$$R'_n(t) = \alpha_n \sum_{m=1}^M a_{n,m}(t) B_m + \beta_n g_n(t) \sum_{m=1}^M a_{n,m}(t) R_{n,m}(t) - \sum_{m=1}^M \delta_m a_{n,m}(t) B_m - g_n(t) \sum_{m=1}^M \sigma_m a_{n,m}(t) R_{n,m}(t). \quad (20)$$

Then, calculate the profit obtained by terminal devices from allocating computing resources. On the one hand, when MEC side performs computing tasks, it needs to pay communication company for the loss of processing computing tasks and define the unit price of MEC server m energy consumption as χ_m . On the other hand, the terminal device needs to pay a certain price for the server on MEC side, and computing resource allocated for each unit computing task is set to ζ_n . Therefore, the benefit obtained by allocating computing resources to terminal device n can be calculated as

$$R''_n(t) = (1 - d_n(t)) \sum_{m=1}^M \alpha_{n,m} \frac{\zeta_n F_{n,m}(t)}{L_{u_n} - \chi_m E_{n,m}^{MEC,e}(t)}. \quad (21)$$

The amount of computing resources allocated to each unit computing task by the above formula has a very important impact on the completion time of computing task. Thus, the service cache cost mainly includes two parts: the cost of replacing type of cache supported on MEC side, and the cost of caching specific services on MEC server. Define the unit price of replacing cache type on MEC server m as ξ_m for each service type, and the unit price for caching services on MEC server is ξ_m per storage space. In order to increase the benefits of cache, the business type is quantified by weak backhaul from MEC server to the core network, which will be used to measure the cost of users. The benefits obtained by executing the cache service on MEC server m can be expressed as

$$R''_m(t) = \sum_{n=1}^N \beta_n (1 - g_n(t)) R_{n,m}(t) - \xi_m |I[\psi_m(t) - \psi_m(t-1)] - c_m \kappa |\psi_m(t)|, \quad (22)$$

where $|\psi_m(t)|$ represents the number of nonzero elements, $I[\cdot]$ is an auxiliary function, and when $x > 0$, $I(x) = 1$;

otherwise, $I(x) = 0$. The instant reward is designed as the total income of MVNO of all current users of system during the time period t , namely,

$$r(t) = \sum_{n=1}^N (R_n(t) + R''_n(t)) + \sum_{m=1}^M R''_m(t). \quad (23)$$

Here the long-term return $\mathfrak{R}(t)$ is expressed as

$$\mathfrak{R}(t) = \sum_{t=1}^T \epsilon r(t), \quad (24)$$

where $\epsilon \in [0, 1)$ is the discount rate of future earnings weights. When ϵ approaches 1, the system will pay more attention to long-term benefits, and when ϵ approaches 0, the system will pay more attention to short-term benefits.

4.3. Dueling-DQN. DQN is an effective reinforcement learning algorithm, which can make the agent learn good experience from the interaction with environments [31–33]. At the same time, according to DQN learning mechanism, there are improvements to DQN algorithm in different aspects. In DQN, due to the error in the Q estimated value itself, $\max_a Q$ process can be seen according to the expression. It is equivalent to putting forward the largest error, which also leads to the problem of overestimation. Double-DQN is an effective improved algorithm for this problem. In Double-DQN algorithm, the update form of $\hat{Q}(S)$ is changed to

$$\hat{Q}(s) = R(s) + \lambda \cdot \hat{Q}\left(\hat{s}, \max_a Q_{\text{eval}}(\hat{s}, a; \alpha); \alpha^-\right), \quad (25)$$

where λ is the discount factor.

The Double-DQN algorithm takes advantage of double neural network and uses two neural networks to learn at the same time, effectively avoiding the overestimation problem caused by error amplification.

Dueling-DQN is also an improvement to DQN algorithm. Compared with previous algorithms, Dueling-DQN algorithm learns faster and has better results. Compared with DQN algorithm, Dueling-DQN retains most of the learning mechanism, and the only difference is the improvement of neural network, as shown in Figure 3.

In the traditional DQN algorithm, the output result is Q value corresponding to each action. In Dueling-DQN algorithm, the output is expressed as a combination of two parts: the value function and advantage function [34]. Among them, value function refers to the value of a certain state, and advantage function refers to the advantage obtained by each action on the state. Therefore, in Dueling-DQN algorithm, Q value problem in DQN can be reexpressed as the following form:

$$Q(s, a; \alpha, \omega_1, \omega_2) = V(s; \omega, \omega_2) + \ell(s, a; \omega, \omega_1) - \frac{1}{|\mathcal{L}|} \sum_{a'} \ell(s, a'; \omega, \omega_1), \quad (26)$$

where $V(\cdot)$ and $\ell(\cdot)$ are the value function and advantage function, respectively, and ω is the parameter of neural

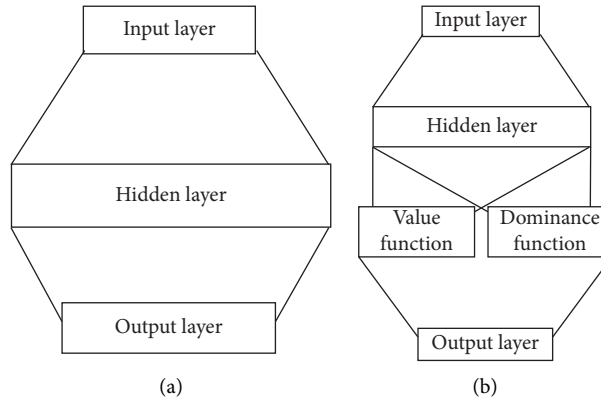


FIGURE 3: Comparison between DQN algorithm and Dueling-DQN algorithm. (a) DQN. (b) Dueling-DQN.

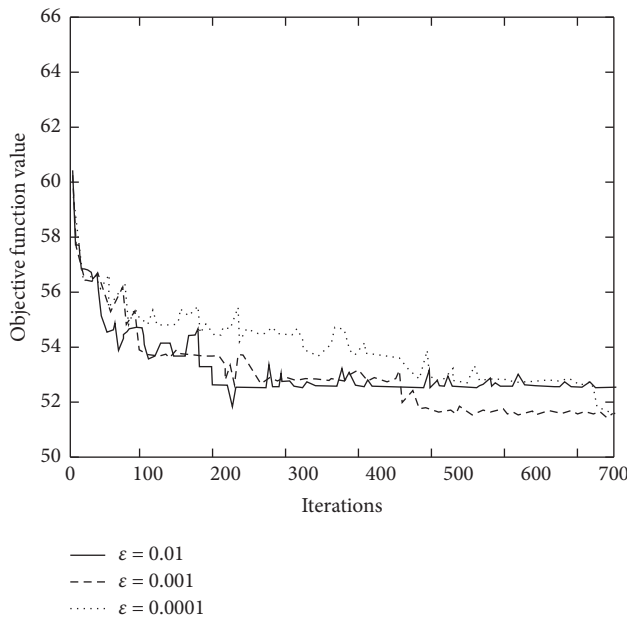


FIGURE 4: Convergence of the proposed algorithm under different learning rates.

network convolutional layer. ω_1, ω_2 are the parameters of two control flow layers, respectively. The latter item of the plus sign centralizes the advantage function in order to solve the uniqueness problem of Q value.

5. Experimental Results and Analysis

The specific simulation parameters are as follows.

Assume that the computing power of each device n is 1.5 GHz, the uplink transmission power is 800 mW, the idle power is 100 mW, and the upload rate is 2.5 Mb/s. $M = 4$ and overall computing capacity of each MEC server is 6 GHz, 5 GHz, 3 GHz, and 1 GHz, respectively. The data D_n in task G_n obeys uniform distribution of (600, 1200), and the unit is k bits. The workload ϕ_n obeys uniform distribution of (1000, 1500), and the unit is Megacycles.

For the parameters of Dueling-DQN algorithm, set the learning rate ϵ to 0.001 and discount coefficient λ to 0.90. The

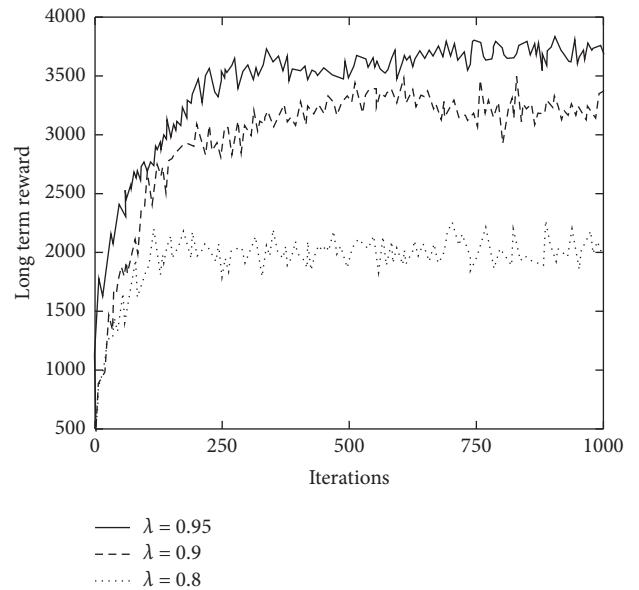


FIGURE 5: System long-term rewards with different discount rates.

size of experience replay set is 3000, and the number of randomly sampled samples is 40.

5.1. Parameter Analysis

5.1.1. Learning Rate Analysis. The learning rate of the algorithm will have a great impact on the performance of the proposed strategy. Therefore, three different learning rates ϵ of 0.01, 0.001, and 0.0001 are selected to compare the convergence of improved DQN algorithm, as shown in Figure 4.

5.1.2. Discount Factors Analysis. Similarly, the influence of discount factor on improved DQN algorithm is shown in Figure 5, where the discount factor takes values 0.8, 0.9, and 0.95.

It can be seen from Figure 5 that as the discount factor increases, the long-term reward is continuously increasing. When λ is 0.95, the long-term reward is 3700 when it is

stable. Because the discount factor will affect behavior selection strategy, that is to say, a larger discount factor will cause system to pay more attention to long-term benefits, and a lower discount factor will cause system to pay more attention to current benefits, a higher discount factor will often lead to greater long-term benefits. However, in actual use, using an overly high discount factor does not have corresponding benefits. This is because the system in reality is more changeable, and too much emphasis on future benefits will lead to excessive calculations and excessive losses in the system, which often requires a trade-off.

5.2. Optimization Comparison under Different Objective Functions. For multiobjective optimization problems that reduce time delay and energy consumption, the weighted sum of task execution time delay and terminal execution energy consumption is usually used as the objective function to solve problem, and the calculation is as follows:

$$\Psi' = \frac{\sum_{n=1}^N (\omega_t \times T_n + (1 - \omega_t) \times E_n)}{N}, \quad (27)$$

where ω_t is the weight coefficient of execution delay and $1 - \omega_t$ is the weight coefficient of execution energy.

Comparing (22) with the proposed objective function (13) to optimize the delay and energy consumption, the number of terminal devices is 12. Considering that the goal of the proposed strategy is to shorten time delay and reduce energy consumption while satisfying the time delay constraints, therefore, the values of ω_t are, respectively, 0.8, 0.6, and 0.4, and the joint experiments of Energy Reduced Scale (ERS) and Time Reduced Scale (TRS) are carried out, as shown in Table 1.

It can be seen from Table 1 that when ω_t is 0.8 and 0.6, the control strategy pays more attention to the optimization of time delay, and when ω_t is 0.4, optimization results pay more attention to the optimization of energy consumption. However, the optimization result of the proposed objective function is the best, and ERS and TRS are 52.18% and 34.72%, respectively, which can shorten time delay and reduce energy consumption under the time delay constraints.

When computing task is 150, comparing control strategies under the four objective functions with the random offloading strategy, the results of ratio of the time delay and energy consumption reduction are shown in Table 2.

It can be seen from Table 2 that delay and energy consumption optimization effect of the proposed optimization target is better, and the reduction ratio of delay and energy consumption is 2.58% and 30.67%, respectively, because the optimization objective of the proposed strategy comprehensively considers the offloading decision and resource allocation plan of joint optimization system when the computing resources are limited and computing tasks have time delay constraints. This allows all computing tasks to shorten completion time and minimize the energy consumption of all terminal devices while meeting the delay constraints. This demonstrates the effectiveness of the proposed objective function.

TABLE 1: Comparison results of optimization for different objective functions.

Objective function	ERS (%)	TRS (%)
$\omega_t = 0.4$	48.71	27.96
$\omega_t = 0.6$	41.85	31.38
$\omega_t = 0.8$	31.03	32.56
Formula (13)	52.18	34.72

TABLE 2: Comparison results of optimization for four objective functions.

Objective function	Delay reduction ratio (%)	Energy consumption reduction ratio (%)
$\omega_t = 0.4$	1.25	23.29
$\omega_t = 0.6$	1.97	21.16
$\omega_t = 0.8$	2.03	19.98
Formula (13)	2.58	30.67

5.3. Performance Comparison with Other Algorithms. In order to demonstrate the performance of the proposed strategy, compare it with [12], [19], and [14] in terms of objective function value, calculation amount, and time saving. Li and Jiang [12] proposed a distributed task offloading strategy, which selects the best MEC node offloading amount by game equation on the basis of quantifying offloading cost and delay. Reference [14] used the greedy selection algorithm to design the maximum energy-saving priority algorithm and energy priority strategy to achieve optimal offloading of computing tasks on mobile devices. Reference [19] used the time average calculation rate maximization algorithm to jointly and efficiently allocate radio resources and computing resources.

5.3.1. Algorithm Comparison under Different Cumulative Tasks. In the experiment, objective function value results of the four strategies are shown in Figure 6 for different accumulations of computing tasks.

It can be seen from Figure 6 that the value of objective function is gradually increasing with the increase of cumulative number of tasks for the four offloading strategies. However, the proposed strategy has a relatively lower objective function value than other strategies. That is, the energy consumption and delay are relatively small. For example, when the number of tasks is 180, the objective function value is only 298. Since the proposed strategy considers computation offloading and resource allocation comprehensively, improved deep learning algorithm is used for optimization, and delay and energy consumption are minimized. Reference [19] only matched computing resources but did not rationally optimize the task offloading scheme and computing resource allocation scheme, resulting in high task execution time delay and energy consumption. References [12] and [14] both used corresponding algorithms for optimization to achieve better resource allocation and task offloading. But their analysis of time delay is less, so the performance needs to be strengthened.

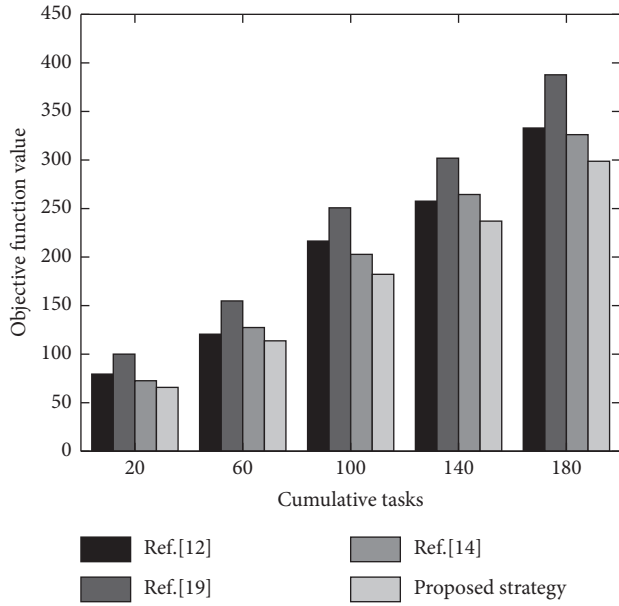


FIGURE 6: Comparison results of offloading strategies under different cumulative number of tasks.

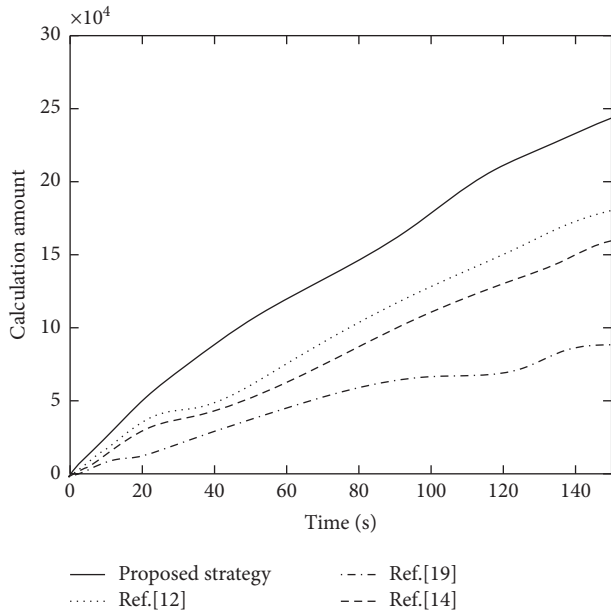


FIGURE 7: Comparison results of the computation number of offloading tasks under different offloading strategies.

5.3.2. Computation Number Comparison of Offloading Tasks under Different Offloading Strategies. Under four different computation offloading strategies, the comparison results of the computing number of offloading tasks on terminal device side are shown in Figure 7. Vertical axis represents the total calculation number of tasks performed by all terminal devices to perform calculation and offloading. The calculation number of tasks is used to represent the amount of calculation services provided by MEC server. Therefore,

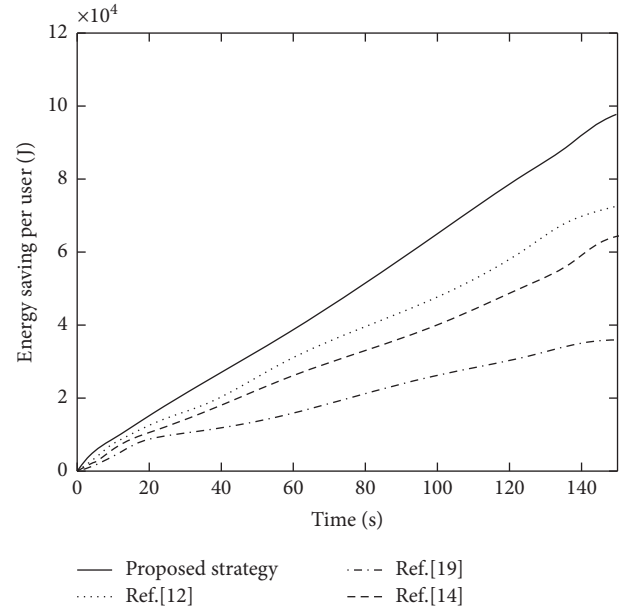


FIGURE 8: Comparison results of energy saving per unit terminal device under different offloading strategies.

the evaluation indicators in the figure also represent the benefits of computing terminal devices in the offloading mode.

It can be seen from Figure 7 that as time increases, computing tasks continue to increase, and the amount of task calculations also increases. However, the calculation amount of the proposed strategy is significantly better than other comparison strategies. Taking the simulation time of 140 s as an example, compared with [12], [19], and [14], the proposed strategy has increased by 11.54%, 20.83%, and 152.72%, respectively. It can be argued that the proposed strategy is the best compared to task offloading. It uses Dueling-DQN algorithm to process task offloading and resource allocation models, and its optimization performance is better than the greedy selection algorithm in [14] and the game equation model in [12].

5.3.3. Energy-Saving Comparison of per Unit Terminal Devices. Under four different computation offloading strategies, the comparison of energy consumption saved by each terminal device by computation offloading on average is shown in Figure 8. In the local calculation model, all energy consumption is generated by local calculations. In the computation offloading mode, the energy consumption is communication energy consumption caused by upload tasks. For the task of performing computation offloading, the difference between the two is energy saving.

It can be seen from Figure 8 that, compared with other comparison strategies, the proposed strategy has the largest energy-saving rate, which is close to 10×10^4 J; this also means the least energy consumption. Aiming at the over-estimation problem in DQN, the proposed strategy uses Dueling-DQN algorithm for optimization. And it designs the system benefits and resource consumption as rewards and

losses, which improves the efficiency and rationality of task offloading and resource allocation by optimizing problem solution. Reference [19] only used the time average calculation rate maximization algorithm to efficiently allocate computing resources. The optimization algorithm is more traditional and has poor performance. Thus, the overall energy saving is not high. Reference [12] used the game equation model to optimize task offloading strategy but does not realize the rationalization of resource allocation. Therefore, the maximum energy saving is 710×10^4 J. Reference [14] used greedy selection algorithm to design an optimal energy-saving strategy but did not consider server computing resource constraints and task delay constraints. Therefore, the overall performance is not as good as the proposed strategy.

6. Conclusion

MEC server has limited computing resources and computing task has delay constraint. How to shorten completion time and reduce terminal energy consumption under the delay constraints becomes an important research issue. To solve this problem, this paper proposes a task offloading and resource allocation strategy based on deep learning for MEC. In the multiuser multiserver MEC environment, a new objective function is designed to construct mathematical model. In combination with deep reinforcement learning, the partially improved Dueling-DQN algorithm is used to solve the optimization problem model, which can reduce the completion time of computing tasks and minimize energy consumption of all terminal devices under the delay constraints. The proposed strategy is demonstrated by experiments based on Python platform. The experimental results show that when learning rate is 0.001 and discount factor is 0.90, the energy saving is close to 10×10^4 J, which is better than other comparison strategies. In terms of calculation amount, it increased by 11.54%, 20.83%, and 152.72%, respectively.

In practice, different users have different concerns about service quality. Therefore, we can refer to the different needs of users when making computation and offloading decisions in the following research. It can assign a certain weight to the factors affecting the quality of service and combine the task priority for scheduling.

Data Availability

The data used to support the findings of this study are included within the article.

Conflicts of Interest

The authors declare that there are no conflicts of interest regarding the publication of this paper.

Acknowledgments

This work was supported by Key Disciplines of Computer Science and Technology (2019xjzdxk1) and New Engineering Pilot Project (szxy2018xgk05).

References

- [1] W. P. Peng, Z. Su, C. Song, and J. Zongpu, "Research on adaptive dual task offloading decision algorithm for parking space recommendation service," *The Journal of China Universities of Posts and Telecommunications*, vol. 26, no. 06, pp. 33–45, 2019.
- [2] K. Wang, X. F. Wang, X. Liu, and A. Jolfaei, "Task offloading strategy based on reinforcement learning computing in edge computing architecture of internet of vehicles," *IEEE Access*, vol. 8, no. 6, pp. 173779–173789, 2020.
- [3] J. Wang, J. Hu, G. Min, A. Y. Zomaya, and N. Georgalas, "Fast adaptive task offloading in edge computing based on meta reinforcement learning," *IEEE Transactions on Parallel and Distributed Systems*, vol. 32, no. 1, pp. 242–253, 2021.
- [4] Y. Sun, X. Guo, J. Song et al., "Adaptive learning-based task offloading for vehicular edge computing systems," *IEEE Transactions on Vehicular Technology*, vol. 68, no. 4, pp. 3061–3074, 2019.
- [5] X. Liu, J. Yu, J. Wang, and Y. Gao, "Resource allocation with edge computing in IoT networks via machine learning," *IEEE Internet of Things Journal*, vol. 7, no. 4, pp. 3415–3426, 2020.
- [6] R. Wang, Y. Cao, A. Noor, T. A. Alamoudi, and R. Nour, "Agent-enabled task offloading in UAV-aided mobile edge computing," *Computer Communications*, vol. 149, no. 5, pp. 324–331, 2020.
- [7] W. Zhan, C. Luo, G. Min, C. Wang, Q. Zhu, and H. Duan, "Mobility-aware multi-user offloading optimization for mobile edge computing," *IEEE Transactions on Vehicular Technology*, vol. 69, no. 3, pp. 3341–3356, 2020.
- [8] Z. Wei, J. Pan, Z. Lyu, J. Xu, L. Shi, and J. Xu, "An offloading strategy with soft time windows in mobile edge computing," *Computer Communications*, vol. 164, no. 8, pp. 42–49, 2020.
- [9] R. Zhang, P. Cheng, Z. Chen, S. Liu, Y. Li, and B. Vucetic, "Online learning enabled task offloading for vehicular edge computing," *IEEE Wireless Communications Letters*, vol. 9, no. 7, pp. 1–932, 2020.
- [10] Q. Zhang, L. Gui, F. Hou, J. Chen, S. Zhu, and F. Tian, "Dynamic task offloading and resource allocation for mobile edge computing in dense cloud RAN," *IEEE Internet of Things Journal*, vol. 7, no. 4, pp. 3282–3299, 2020.
- [11] J. Zhang, H. Guo, and J. Liu, "Adaptive task offloading in vehicular edge computing networks: a reinforcement learning based scheme," *Mobile Networks and Applications*, vol. 25, no. 5, pp. 1736–1745, 2020.
- [12] Y. Li and C. Jiang, "Distributed task offloading strategy to low load base stations in mobile edge computing environment," *Computer Communications*, vol. 164, no. 2, pp. 240–248, 2020.
- [13] J. Zhang, H. Guo, J. Liu, and Y. Zhang, "Task offloading in vehicular edge computing networks: a load-balancing solution," *IEEE Transactions on Vehicular Technology*, vol. 69, no. 2, pp. 2092–2104, 2020.
- [14] F. Wei, S. Chen, and W. Zou, "A greedy algorithm for task offloading in mobile edge computing system," *China Communications*, vol. 15, no. 11, pp. 149–157, 2018.
- [15] H. Lu, C. Gu, F. Luo, W. Ding, and X. Liu, "Optimization of lightweight task offloading strategy for mobile edge computing based on deep reinforcement learning," *Future Generation Computer Systems*, vol. 102, no. 3, pp. 847–861, 2020.
- [16] L. Li and H. Zhang, "Delay optimization strategy for service cache and task offloading in three-tier architecture mobile edge computing system," *IEEE Access*, vol. 8, no. 9, pp. 170211–170224, 2020.

- [17] X. Zhang, J. Zhang, Z. Liu, Q. Cui, X. Tao, and S. Wang, "MDP-based task offloading for vehicular edge computing under certain and uncertain transition probabilities," *IEEE Transactions on Vehicular Technology*, vol. 69, no. 3, pp. 3296–3309, 2020.
- [18] F. Wang, J. Xu, and S. Cui, "Optimal energy allocation and task offloading policy for wireless powered mobile edge computing systems," *IEEE Transactions on Wireless Communications*, vol. 19, no. 4, pp. 2443–2459, 2020.
- [19] C. Li, W. Chen, J. Tang, and Y. Luo, "Radio and computing resource allocation with energy harvesting devices in mobile edge computing environment," *Computer Communications*, vol. 145, no. 09, pp. 193–202, 2019.
- [20] Z. Ali, S. Khaf, Z. H. Abba, G. Abbas, and L. Jiao, "A Comprehensive Utility Function for Resource Allocation in Mobile Edge Computing," *arXiv preprint arXiv:2012.10468*, vol. 66, no. 2, pp. 1461–1477, 2020.
- [21] P. Q. Huang, Y. Wang, K. Wang, and L. Zhi-Zhong, "A bilevel optimization approach for joint offloading decision and resource allocation in cooperative mobile edge computing," *IEEE Transactions on Cybernetics*, vol. 50, no. 10, pp. 1–14, 2019.
- [22] Y. Liu, Y. Li, Y. Niu, and D. Jin, "Joint optimization of path planning and resource allocation in mobile edge computing," *IEEE Transactions on Mobile Computing*, vol. 19, no. 9, pp. 2129–2144, 2020.
- [23] Y. A. Lei, A. Cz, B. Qy, W. Zou, and A. Fathalla, "Task offloading for directed acyclic graph applications based on edge computing in Industrial Internet-ScienceDirect," *Information Sciences*, vol. 540, no. 7, pp. 51–68, 2020.
- [24] X. F. He, R. C. Jin, and H. Y. Dai, "Peace: privacy-preserving and cost-efficient task offloading for mobile-edge computing," *IEEE Transactions on Wireless Communications*, vol. 19, no. 3, pp. 1814–1824, 2020.
- [25] B. Gu and Z. Zhou, "Task offloading in vehicular mobile edge computing: a matching-theoretic framework," *IEEE Vehicular Technology Magazine*, vol. 14, no. 3, pp. 100–106, 2019.
- [26] T. Alfakih, M. M. Hassan, A. Gumaei, C. Savaglio, and G. Fortino, "Task offloading and resource allocation for mobile edge computing by deep reinforcement learning based on SARSA," *IEEE Access*, vol. 8, no. 5, pp. 54074–54084, 2020.
- [27] Y. Pan, M. Chen, Z. Yang, N. Huang, and M. Shikh-Bahaei, "Energy-efficient NOMA-based mobile edge computing offloading," *IEEE Communications Letters*, vol. 23, no. 2, pp. 310–313, 2019.
- [28] Y. L. Jiang, Y. S. Chen, S. W. Yang, and C. H. Wu, "Energy-efficient task offloading for time-sensitive applications in fog computing," *IEEE Systems Journal*, vol. 13, no. 3, pp. 2930–2941, 2019.
- [29] X. Xu, Q. Liu, Y. Luo et al., "A computation offloading method over big data for IoT-enabled cloud-edge computing," *Future Generation Computer Systems*, vol. 95, no. 06, pp. 522–533, 2019.
- [30] C. Shu, Z. Zhao, Y. Han, G. Min, and H. Duan, "Multi-user offloading for edge computing networks: a dependency-aware and latency-optimal approach," *IEEE Internet of Things Journal*, vol. 7, no. 3, pp. 1678–1689, 2020.
- [31] S. Hu and G. Li, "Dynamic request scheduling optimization in mobile edge computing for IoT applications," *IEEE Internet of Things Journal*, vol. 7, no. 2, pp. 1426–1437, 2020.
- [32] J. Zeng, J. Sun, B. Wu, and X. Su, "Mobile edge communications, computing, and caching (MEC3) technology in the maritime communication network," *China Communications*, vol. 17, no. 5, pp. 223–234, 2020.
- [33] Q. Lin, F. Wang, and J. Xu, "Optimal task offloading scheduling for energy efficient D2D cooperative computing," *IEEE Communications Letters*, vol. 23, no. 10, pp. 1816–1820, 2019.
- [34] X. Xu, C. He, Z. Xu, L. Qi, S. Wan, and M. Z. A. Bhuiyan, "Joint optimization of offloading utility and privacy for edge computing enabled IoT," *IEEE Internet of Things Journal*, vol. 7, no. 4, pp. 2622–2629, 2020.

Research Article

Text Analysis and Policy Guidance of Emotional Intonation of Enterprise Management Based on Deep Learning

Ni Yang and Jing Qiu 

School of Accounting, Guizhou University of Finance and Economics, Guiyang 550025, China

Correspondence should be addressed to Jing Qiu; jingq@mail.gufe.edu.cn

Received 28 June 2022; Revised 27 July 2022; Accepted 11 August 2022; Published 30 August 2022

Academic Editor: Le Sun

Copyright © 2022 Ni Yang and Jing Qiu. This is an open access article distributed under the Creative Commons Attribution License, which permits unrestricted use, distribution, and reproduction in any medium, provided the original work is properly cited.

In the context of global science and technology, all countries pay more and more attention to the text analysis of emotional intonation, and the emotional intonation text analysis and policy orientation of enterprise management in major international and domestic enterprises have also changed from shallow to deep. In the twenty-first century, with the rapid development of human society, people's demand for living standards and material needs increases rapidly, and employees' awareness and needs for work are constantly changing. At present, there is the problem of emotional intonation text analysis error in the management of the enterprise, and the task and emotional transmission command are not clear and thorough. It is necessary to reasonably use deep-learning-related algorithms, especially convolutional neural network and other algorithms, to study the emotional intonation text analysis and policy guidance of the enterprise management. Aiming at the forefront of deep learning development, the latest deep learning technologies are constantly introduced. The research field of emotional intonation text analysis and policy orientation of enterprise management is focused. Through simulation experiment, the characteristics of emotional intonation text analysis and policy orientation research of different enterprise management are compared and analyzed, so as to further improve the emotional intonation text analysis and policy orientation of deep learning for enterprise management.

1. Introduction

Can Chinese capital market investors understand the management's "commitment"? This paper uses LSM deep learning technology to analyze the management response in the annual performance briefing of Chinese listed companies and discusses the actual semantics of management. The results show that investors can understand the true semantics of management, and the capital market gives a positive response to the positive semantics and gives a more timely and meaningful negative response to the negative semantics. Starting from a three-factor model, we further investigate whether management semantics is a factor in the investor stock trading strategy, but there is no evidence that investors use management semantics as a factor in the trading strategy. On the one hand, this study shows that nonfinancial disclosure channels such as performance briefing are valuable, verifying the perspective theory of

behavioral economics; on the other hand, it is worth extending to other areas of text analysis for future application of [1]. With the development of deep learning, more and more neural network-based algorithms are used for classifying text sensation, and the accuracy of classification is constantly improved. If we blindly pursue accuracy and go deep into the network level, it will bring huge obstacles to the reaction performance in real application scenarios. By studying techniques such as integrated representation of texts, we can further grasp the main features of the text in the classification logic based on the current FastText models. A novel weight-based WDFM model is presented for classifying lighter text immunity, achieving high accuracy while ensuring the simplicity of the model and better solving the classification task of text immunity. To solve the problem of employee behavior analysis in key positions, a video-based behavior analysis method is proposed. Multipostural sampling employee behavior records were created, formed by

the YOLOv3 network, yielding a behavior detection model [2]. The proposed behavior analysis algorithm is combined with the behavior detection model. Based on the behavior analysis algorithm and the similarity and brightness characteristics of the image, the evaluation results of mobile phone shutdown, sleep, and game events are presented. The experimental results show that the product data group has high recognition accuracy in identifying employee behavior and behavior analysis, which can handle in real time [3].

Emotional text analysis mainly uses text extraction technology to analyze emotional processing, and identifying the tendency of subjective text is a positive, negative, and neutral process. This classification of text emotion particles is insufficient, incomplete, too rigid, and violent, which not only effectively reflects the intensity and size of different emotion particles in the text but also requires extensive manual annotation. We verify the effectiveness of emotion word carrier and improve the accuracy of text emotion classification [4]. Through a sample survey of nonfinancial enterprises that issued bonds in China's stock market in 2017, this paper studies the influence of accounting text intonation on bond communication, establishes an emotional dictionary for China's financial market, and quantifies the direction intonation by using text extraction technology. The study shows that management's positive tone can significantly reduce the credit spread of bonds. The management tone has a less negative relationship with the bond interest rate difference. In addition, the bond market is more sensitive to the tone of state-owned and small-business management [5]. Selecting listed companies from 2008 to 2019, through management analysis and discussion text analysis, this paper studies the constraints and impact mechanism of management emotional voice signals on corporate financing; the results show that management of positive net tone may have signal conduction effect, alleviate enterprise financing constraints, by expanding equity financing channels to achieve this effect, attract the attention of investors, is the management emotional influence to financing bottleneck mechanism. The results of the heterogeneous effects of speech tampering strategies show that investors cannot effectively identify text readability strategies and positive speech bias strategies, while speech splitting strategies are fully understood by investors, leading to differences in the emotional voices of people at different levels of management in reducing financial constraints. Expand the voice. This paper confirms that management can effectively use the emotional sound in the text to exert the signal transmission effect and guide the market to achieve its ideal goal [6].

If the hardware is the body of the company, the software is the blood of the company; the invisible emotion and emotion cannot be touched but really exist in the company that is the "gas" of the company. On the contrary, mismanaged corporate emotions and emotions, creating a healthy entrepreneurial spirit, and psychological and emotional air are major issues that managers cannot face up to and think about. Traditional management theory holds that human feelings have an influence on the realization of organizational goals in [7]. The development and evolution of

network public opinion between the COM incident on June 6 and the Hyderabad incident were compared, and the ways of emotional development of netizens were revealed through the collection and analysis of microblog data, especially the emotional analysis of microblog text. Comparing the gains and losses of the two online incidents to deal with these events, we summarize the strategy of enterprises to effectively deal with the network public opinion, which will help enterprises to deal with the public opinion crisis online [8].

In the 1980s, emotion management as a management model was proposed by many experts and scholars. In the twenty-first century, with the rapid development of human society, people's demand for living standards and material needs increases rapidly, and employees' awareness and needs for work are constantly changing. This paper briefly introduces the concept and significance of emotion management, summarizes the main factors affecting employees "emotions, analyzes the current situation of employees" emotions in the chemical industry, and puts forward some suggestions for emotion management [9]. Based on the on-site interviews and two questionnaires of 28 middle and senior managers, as well as the analysis of exploratory factors and confirmed factors, this paper formulated the scale to measure the emotional connection of managers in the transformation process of local enterprises in China. The results show that managers' emotional attachment consists of three factors: attachment to life, attachment to work and situation, and attachment to life that are positively related to attachment to work. They also have a positive relationship with context-binding. The research content not only illuminates the emotional culture of the organization but also provides a new way to promote the transformation of enterprises through emotional strategies [10].

Structural and functional analysis of managers' trust found that managers need to handle three trust relationships in their careers: subordinate trust, supervisor trust, and colleague trust. These three trusts lead to superior support, subordination, and peer cooperation, which is conducive to improving the personal performance of business operators. In modern enterprise management, the emotional contribution of employees to enterprise development is very important. This paper discusses the concept of emotion management and its role and position in human resource management [11]. By utilizing the "emotional talent" of employees, we can grasp the emotional management method in management practice, promote the emotional investment of employees, and ensure the continuous success of [12]. With the increasing popularity of online review and suggestion systems, emotion analysis has gradually become an important academic research task that has attracted the attention of many scholars in recent years. The traditional method to solve the problem of text emotion analysis is mainly based on the emotional dictionary or shallow knowledge, and the feature extraction and classification are conducted through regression and classification schemes. However, due to the short and clear features of the annotated text, a large number of unknown words make these methods have data scarce and ignore the problem of word tracking. Starting from these methods, deep learning methods are

used to analyze the mood of comment text, and we can find a deep understanding of human emotional expression mode through comparative combination experience [13].

In recent years, public opinion sentiment analysis has become one of the most popular topics in the NLP space. The sentiment analysis and emotional trend assessment of these public opinion data provide important support for the company government to make strategic decisions. At present, the supervised plane automatic learning algorithm model is widely used in emotion analysis research. The manual annotation process is lengthy, and the annotation results often do not reflect the real situation of the data. This paper expounds on the current situation of emotional word analysis, discusses the emotional analysis of public opinion data by using deep learning and fusion methods, summarizes the shortcomings and challenges of Chinese emotional analysis, and looks forward to the future [14]. Some scientists say that deep learning algorithms are a gem in the crown of artificial intelligence. By applying deep neural network (DNN) models, deep learning has become the closest intelligent learning method to the human brain. Not only Google, Baidu, and other companies participate in the application research of in-depth learning but also e-commerce giants such as Jingdong and Ali join the competition. This paper introduces the in-depth study of e-commerce in China [15].

2. Deep-Learning-Related Algorithms

2.1. Artificial Neural Network. Artificial neural networks are the foundation of deep learning, simulating human brain models. Neuron is the basic computational unit of deep learning model [16]. The neuron output formula is

$$y = f\left(\sum_{i=1}^n w_i x_i - \theta\right), \quad (1)$$

where f represents the activation function. Commonly used activation functions are the Sigmoid activation function, the Tanh activation function, and the ReLU activation function. The respective representation formulas are as follows:

$$\begin{aligned} f(z) &= \frac{1}{1 + \exp(-z)}, \\ f(z) &= \frac{e^z - e^{-z}}{e^z + e^{-z}}, \\ f(z) &= \max(0, z). \end{aligned} \quad (2)$$

2.2. Circular Neural Network and Long-and Short-Term Memory Network. The recurrent neural network can handle the time-series data well. The simplest recurrent neural network formula is as follows:

$$\begin{aligned} o_t &= g(V \bullet S_t), \\ S_t &= f(U \bullet X_t + W \bullet S_{t-1}). \end{aligned} \quad (3)$$

However, as the input increases, the standard RNN decreases the perception ability of the data nodes, resulting in the gradient disappearance and gradient dispersion phenomenon. To address this problem, the transformation function is defined as follows:

$$\begin{aligned} i_{(t)} &= \sigma(W_{xi}^T \cdot x_{(t)} + W_{hi}^T \cdot h_{(t-1)} + b_i), \\ g_{(t)} &= \tanh(W_{xg}^T \cdot x_{(t)} + W_{hg}^T \cdot h_{(t-1)} + b_g), \\ f_{(t)} &= \sigma(W_{xg}^T \cdot x_{(t)} + W_{hf}^T \cdot h_{(t-1)} + b_f), \\ c_{(t)} &= i_{(t)} \otimes g_{(t)} + f_{(t)} \otimes c_{(t-1)}, \\ o_{(t)} &= \sigma(W_{xo}^T \cdot x_{(t)} + W_{ho}^T \cdot h_{(t-1)} + b_o), \\ h_{(t)} &= o_{(t)} \otimes \tanh(c_{(t)}), \end{aligned} \quad (4)$$

where σ is the sigmoid activation function.

2.3. Support Vector Machine. The core idea of the SVM algorithm that is fast and reliable is to find an optimal classification hyperplane [17] in high-dimensional space. In linearly separable samples, the formula for defining the hyperplane is

$$w^T x + b = 0. \quad (5)$$

The distance from any point in the sample to the optimal plane is

$$r = y_0 \left(\frac{w}{\|w\|} x_0 + \frac{b}{\|w\|} \right). \quad (6)$$

Any training data satisfies the following formula:

$$y_0 (w^T x_0 + b) \geq 1. \quad (7)$$

So the SVM solves the constrained optimization problem as follows:

$$\begin{aligned} \min_{w,b} & \frac{1}{2} \|w\|^2, \\ \text{s.t.} & y_i (w^T x_i + b - 1) \geq 0 \quad i = 1, 2, \dots, N. \end{aligned} \quad (8)$$

Cross-validation methods and prior knowledge can be used to select the kernel functions that meet the data distribution. The following are the four common kernel functions:

$$\begin{aligned} (1) \text{ Linear kernel function} \\ K(x, x_i) &= x \cdot x_i. \end{aligned} \quad (9)$$

$$\begin{aligned} (2) \text{ Polynomial kernel function} \\ K(x, x_i) &= ((x \cdot x_i) + b)^d. \end{aligned} \quad (10)$$

$$\begin{aligned} (3) \text{ Gaussian kernel function} \\ K(x, x_i) &= \exp\left(-\gamma \|x - x_i\|^2\right). \end{aligned} \quad (11)$$

$$(4) \text{ Sigmoid kernel function}$$

$$K(x, x_i) = \tanh(\gamma x \cdot x_i + b). \quad (12)$$

2.4. Logical Regression. The logic regression algorithm is very simple and practical, belongs to the generalized linear regression model, and is often used to solve the binary classification problem [18]. The basic mathematical formula is as follows:

$$g(x) = \frac{1}{1 + e^{-x}}. \quad (13)$$

Mathematical expression model of logistic regression is as follows:

$$h_{\theta}(x) = g(\theta^T x) = \frac{1}{1 + e^{-\theta^T x}}. \quad (14)$$

For binary classification problems, the logistic regression formula can be simplified as follows:

$$p(y = 1|x; \theta) = \frac{1}{1 + e^{-\theta^T x}}, \quad (15)$$

$$p(y = 0|x; \theta) = 1 - \frac{1}{1 + e^{-\theta^T x}}.$$

For a single sample, the model assumes a unity of

$$P(y|x; \theta) = \left(\frac{1}{1 + e^{-\theta^T x}} \right)^y \left(1 - \frac{1}{1 + e^{-\theta^T x}} \right)^{1-y}, \quad (16)$$

where $y \in \{0, 1\}$.

3. Text Analysis of Emotional Intonation

Text emotion analysis is one of the studies of natural language processing. Pang et al., in 2002, has been widely studied and applied in data exploration, information search, text search, and other fields. As textual emotion analysis plays an important role in society and the economy, it transforms into an interdisciplinary research topic. In recent years, high-level academic conferences at home and abroad have produced many excellent research results. In China, Internet companies such as Baidu and Ali have provided users with a text sentiment analysis API to help users quickly deploy online applications and reduce development costs. Lip, in 2012, introduced the emotional analysis in detail. According to the research method, the text emotion analysis method can be divided into supervised and unsupervised methods. In foreign countries, the research of English text emotional analysis is gradually mature. The main methods of text sentiment analysis can be divided into sentiment dictionary based sentiment analysis method, sentiment analysis method based on traditional machine learning and sentiment analysis method based on deep learning. The method uses processed and labeled data to form a classifier and then uses a classifier to assess the emotional trend [19] of unlabeled data.

The emotional dictionary mainly consists of emotional polarity or emotional intensity. There are three common methods to create emotional dictionaries: methods based on

manual annotation, methods based on existing dictionaries, and methods [20] based on body statistics. The research on the construction of emotion dictionaries abroad started earlier, among which SentiWordNet is the most seriously affected English emotion dictionary. In China, the research on the Chinese emotion dictionary started relatively late. Founded by Dong Zhendong and Dong Qiang, HowNet was a widely used emotional dictionary in early China. Manual creating emotional dictionaries requires a lot of manpower and material resources, and their effects vary by field, so researchers tend to create emotional dictionaries automatically. Hu cites emotionally inclined words as opening phrases and generates a general emotional dictionary through constant iterations. Emotional polarity reverses only when words change. Huang et al. first mark the emotional polarity of high-frequency words in the main text of a specific domain and then use connectors to evaluate the emotional polarity between words to generate a domain-specific emotion dictionary. Due to the few Chinese knowledge bases, most domestic scholars will combine different methods of [21] when automatically compiling the Chinese sentiment dictionary. Zhou Yongmei adopted the Chinese-English translation method, searched for the English words translated by the HowNet dictionary in the SentiWordNet dictionary, calculated the average emotional intensity of all the words, and finally generated the Chinese emotional dictionary. Wang Changhou et al. used the model-based paddle method to extract emotional words, through which they collected a large number of words not included in the traditional emotional dictionary.

This is a popular research method that applies traditional machine learning methods to text emotion analysis. It can learn training data sets to extract functions and generate a text emotion analysis model [22]. Experience has shown that analyzing text sensation using SVMs is effective. Zhang adopted the Bayesian algorithm weighted SME TF-DF own value, applied it to the emotional analysis of the course evaluation text, and achieved good results. Chiong et al. analyzed the text sense of new finance using an SVM-based approach and used a particle test optimization algorithm to optimize the parameters. Huang et al. used the Stanford method to support the voice-dependent support vector machine to analyze financial information, with good results. Liu Siye et al. introduced the keywords of facial expression to expand the text characteristics of tourists' microblog and adopted the maximum entropy model to achieve good results.

In the early 1990s, the development of scientific and industrial deep learning was directly suspended due to the problem of gradient disappearance in the BP algorithm. Until 2006, Hinton, the father of deep learning, has always proposed the weight initialization scheme through the fine adjustment of unsupervised training and supervised training, thus solving the problem of gradient disappearance in the process of deep network formation. The emotional dictionary method and traditional machine learning method have produced many excellent research results in the research of emotional text analysis, but a large labor cost of [23] is needed early in the data processing process.

Deep learning is a machine learning technique based on a set of self-learning algorithms and deep neural networks. In recent years, with the rapid development of technology, the research and application of in-depth learning have also undergone great changes. Compared with traditional machine learning methods, deep learning reduces artificial factors, has deeper model depth, mimics the mechanism by which the human brain processes data, and is able to deeply extract data features. A convolutional neural network is a special neural network that has achieved very good [24] in the field of computer vision. The convolutional layer of the convolutional neural network can extract the local features very well. Six sets of data were used for experimental comparison, demonstrating that TextCNN is effective for some simple text classification tasks. Yu et al. have studied the problem of cross-domain sentence fitting analysis, designing a model involving two distinct networks of convolutional neurons that learn two hidden feature representations from labeled and unlabeled data. The emotional classification, using low-monitoring convolutional neural networks, was performed by Guan et al. The framework consists of two stages: the first is to learn the representation of a sentence, which is not adequately monitored, and the second is to perfect the sentences with labels. Zhao et al. proposed a text sentiment classification method by using the underlying contextual semantic relations and statistical features of co-occurring words on Twitter, combined with a powerful neural network.

Long-term memory networks contribute to natural language modeling, which is important for computer processing and computer processing natural language, deep into the semantic comprehension level [25]. Twitter emotions were classified using long, short-term memory networks. Huang et al. suggest encoding syntactic knowledge into long- and short-term tree memory networks to improve the expression of sentences and phrases. Learning emotion intensity using long- and short-term bidirectional memory networks. Long- and short-term memory networks of language regulation for textual emotion analysis were proposed by Qian et al. This model combines emotional dictionaries, negative words, and intensity words and more accurately captures feelings in sentences. Fu et al. introduced a dictionary-modified LSM model that uses the emotion dictionary to train a word sense classifier to maintain the emotional integration of each word and address the problem that word integration contains more semantic information than emotional information. Lu et al. used the word integration model CBOW to capture word semantic features in microblog text sentiment analysis and extract deep sequence word vector features using stacking BiLSTM.

4. Example Analysis

4.1. Experimental Preparation. Based on the experiment designed for the emotion intonation analysis of enterprise management based on deep learning, we should first collect and classify the emotion tendency data and then analyze it. The experimental environment and configuration adopted in this article are shown in the following Table 1.

TABLE 1: Experimental environment and configuration.

Experimental environment	Configuration information
Operating system	Windows10 (64 bit)
Processor	Intel® Core™ i7-4790, 3.6 GHz
Internal storage	16 GB
Programming language	Python 3.6
Deep learning framework	TensorFlow 1.13
Partition tool	Jieba, PkuSeg

Based on the management staff, a comprehensive happiness questionnaire was specially designed as the measurement questionnaire of this study, and the emotional text analysis of the enterprise management personnel was used in two modules and nine dimensions. It is shown in Figure 1 and Table 2.

Descriptive statistics, factor analysis, correlation analysis, and regression analysis were used in this study. With the enterprise managers, the enterprise managers of all levels in Chengdu, Shenzhen, Xiamen, and Wuhan were investigated. The enterprises mainly include finance, logistics, construction, and other aspects. The sample was selected in April 2022. A total of 300 questionnaires were distributed through the Internet, and 237 valid questionnaires were collected. The sample is provided in Table 2.

4.2. Statistical Results of the Scale. In the general happiness questionnaire, the happiness index scores ranged between 4.91 and 1.628, with the highest proportion being “mean” (see Figure 2). The lowest scores were negative emotions (2.42, 0.96), and the highest scores were self-worth (5.25, 68.4). Besides negative emotions, other dimensions were scored between 3.91 and 5.68 (see Figure 2).

Figure 3 shows that the values for all well-being dimensions are type V, and the lowest point is negative effect. Understandably, Figure 4 respondents’ happiness, Figure 5, in all aspects are positive and high.

4.3. Analysis and Comparison of Experimental Results

4.3.1. Mean Comparison of Each Dimension

- (1) According to the survey results of the psychological authorization scale, the average of the four dimensions of psychological authorization is shown in Figure 4, where the autonomy dimension has the highest score of $4.42 + 0.79$; self-efficacy and work impact are the lowest, 3.71 ± 0.76 and 3.71 ± 0.90 , respectively. It can be seen that the mean for each dimension is between “uncertain” and “very consistent.”
- (2) According to the survey results of the integrity management scale, the average score of the five dimensions of integrity management is shown in Figure 5. We can see that integrity and selflessness have the highest score of $5.17 + 0.91$, while subordinates have the lowest score of $4.59 + 0.93$. The various dimensions of integrity management were scored between 4.59 ± 0.93 and 5.17 ± 0.91 , namely between “slightly consistent” and “fully consistent.”

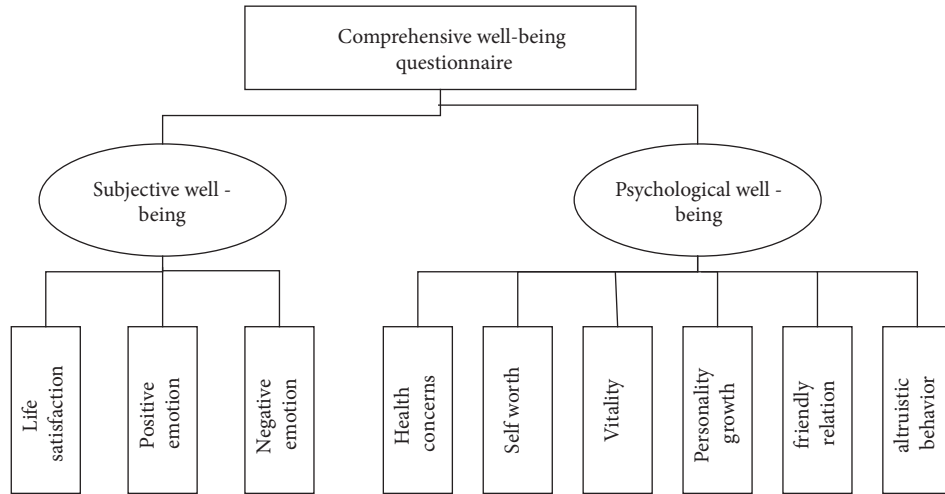


FIGURE 1: The comprehensive happiness questionnaire.

TABLE 2: Description of the sample situation.

Demographic variables	Encoding	Class	Number of people	Percentage (%)	Cumulative percentage (%)
Sex	0	Man	158	66.7	66.7
	1	Woman	79	33.3	100
Education level	1	Specialist below	18	7.6	7.6
	2	Junior college education	53	22.4	30
	3	Undergraduate course	149	62.9	92.8
	4	Master's degree or above	17	7.2	100
Working life	1	1-3 Years	26	11	11
	2	3-5 Years	107	45.1	56.1
	3	5-10 Years	69	29.1	85.25
	4	More than 10 years	35	14.8	100
Position	1	Grassroots management personnel	62	26.1	26.1
	2	Middle management	142	59.9	86.1
	3	Senior management staff	33	13.9	100

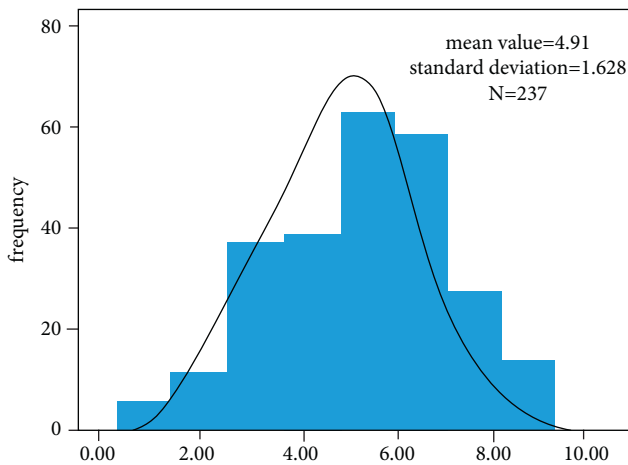


FIGURE 2: Distribution of the happiness index.

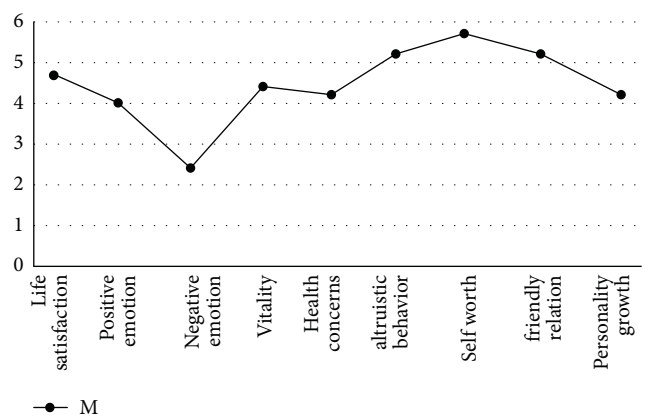


FIGURE 3: Mean average of each dimension of happiness.

4.4. Experimental Summary

4.4.1. Innovation of This Experiment

- (1) As a questionnaire compiled by domestic scholars, the comprehensive happiness questionnaire has high

reliability and validity and has been verified in different groups. However, the questionnaire was not applied to business managers prior to this study. In this study, the volume was used for the first time for business managers to conduct qualitative and quantitative analysis, resulting in good credit validity

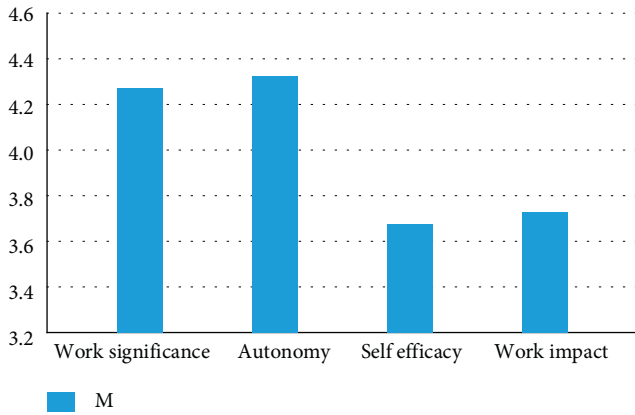


FIGURE 4: Bar chart of the average value of all dimensions of psychological authorization.

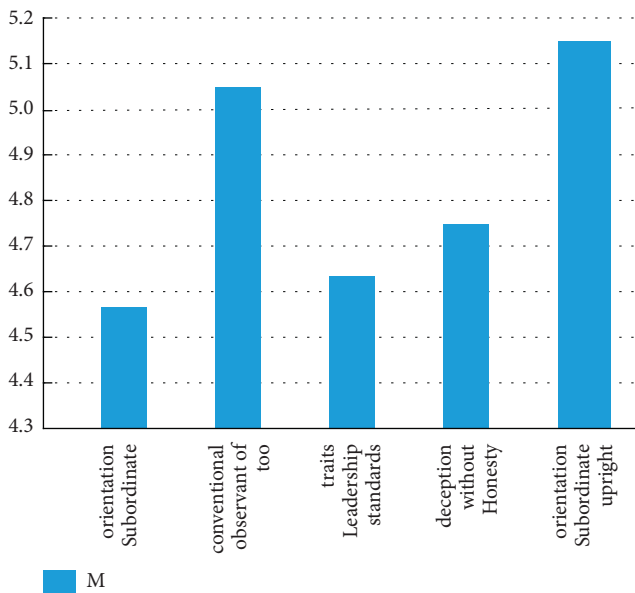


FIGURE 5: Bar chart of the mean of each dimension.

and expanding the scope of the comprehensive well-being questionnaire.

- (2) According to the results of this study, the purpose is to adjust the psychological empowerment of management, improve the well-being of enterprise managers, and stimulate their potential through the intermediary variables of well-being. In order to improve the manager’s ability of honesty management and manage the enterprise and staff better, the theory of honesty management and the theory of humanistic management are expanded.

4.4.2. Limitations of This Experiment

- (1) Due to time, resources, and financial constraints, the sampling range of this paper is very limited, and the representativeness of the sample data needs to be further tested by more researchers. Because the mechanisms of happiness are very complex and the

influencing factors are also very complex, they are greatly influenced by regional and economic conditions. Therefore, it is suggested that future studies can expand the regional range of the sample and increase the volume.

- (2) This study focuses on model building and the surface analysis of demographic variables. Furthermore, this study only collected and analyzed data on demographic variables from four aspects: gender, education, years of work, and position. Other demographic variables may differ significantly. No more research was done in this paper due to energy and condition limitations, which require further discussion by later researchers.

5. Conclusion

In view of the emotional intonation text analysis and policy orientation of enterprise management, the technical methods of the deep learning are preliminarily introduced, but more in-depth research is still needed. The application of deep learning method, especially the network neural method; has just started in the field of emotional intonation text analysis and policy orientation of enterprise management; and faces many uncertainties and challenges, but the application prospect is broad.

- (1) Aiming at the forefront of deep learning development, the latest deep learning technologies are constantly introduced. The research field of emotional intonation text analysis and policy orientation of enterprise management is focused. Through simulation experiment, the characteristics of emotional intonation text analysis and policy orientation research of different enterprise management are compared and analyzed, so as to further improve the emotional intonation text analysis and policy orientation of deep learning for enterprise management.
- (2) In the face of doubts about emotional intonation text analysis and policy-oriented research, conduct the interpretability research of deep learning. Based on domain knowledge, an interpretable deep learning model is established to promote the development of crossover research between emotional intonation text analysis and policy-oriented research in the field and the field of deep learning research.
- (3) Enterprise management can not only improve the enthusiasm of enterprise management but also bring positive impact on the health of employees by using emotional tone text analysis and policy-oriented research and analysis to select the optimal scheme.

Data Availability

The experimental data used to support the findings of this study are available from the corresponding author upon request.

Conflicts of Interest

The authors declared that they have no conflicts of interest regarding this work.

References

- [1] Yang and Ma Beili, "Can investors understand the "string voice" of management—," *LSTM Deep Learning Study based on management semantic research*, vol. 6, pp. 63–72, 2021.
- [2] H. Sun, "Based on deep learning," *Computer Programming Skills and Maintenance*, vol. 2022, no. 3, p. 4, 2022.
- [3] Y. Xu, H. Song, H. Liang, J. Hou, and Z. Dai, "Personnel behavior analysis system based on deep learning," *Computer Engineering and Application*, vol. 57, no. 2, p. 1, 2021.
- [4] C. Nan, J. Chen, and P. Lu, "Research and analysis based on deep learning [J]," *Computer Science and Application*, vol. 8, no. 5, p. 18, 2018.
- [5] Y. Xiao, D. Wu, and S. Pang, "Effect of text-mining-based management tone on corporate bond credit spreads," *Economic Theory and Economic Management*, vol. 12, no. 3, p. 14, 2020.
- [6] J. Qiu and Y. Ni, "Emotional intonation signal transmission and enterprise financing constraints," *Journal of Zhongnan University of Economics and Law*, vol. 13, no. 5, p. 14, 2021.
- [7] C. Zhou, "Manager: manage the emotions and emotions of the enterprise well," *Hebei Enterprise*, vol. 16, no. 6, p. 1, 2006.
- [8] Y. Zhang and oling Deng, "Comparative research on enterprise network public opinion coping strategies based on text emotion analysis," *E-commerce*, vol. 9, no. 5, p. 4, 2019.
- [9] J. Niu, Z. Liu, Y. Xu, and so on, "Analysis of enterprise emotion Management," *Sme Management and Technology*, vol. 12, no. 22, p. 2, 2011.
- [10] X. Han, "Development of managers' emotional attachment scale in the process of transformation and reform of Chinese local enterprises," *Human Resources Development in China*, vol. 21, no. 11, p. 9, 2016.
- [11] Z. Yang, "Structure and functional analysis of the trust relationship of business managers," *Entrepreneur world: Next ten days Magazine*, vol. 15, no. 8, p. 1, 2011.
- [12] G. Liu and W. Gao, "A brief analysis on emotional management in modern enterprise management," *Journal of Gansu University of Administration*, vol. 12, no. 2, p. 3, 2004.
- [13] H. Wang and X. Jin, "Emotion analysis of Chinese E-commerce comments based on deep learning," *Information and communication*, vol. 15, no. 3, p. 3, 2018.
- [14] K. Kou, C. Fang, and Y. Li, "Research on emotion analysis based on deep learning and integration methods," *Computer Programming Skills and Maintenance*, vol. 21, 2016.
- [15] N. Zhang, "Deep learning application and the latest progress of Chinese e-commerce enterprises," *China Management Informatization*, vol. 12, no. 1, p. 2, 2017.
- [16] C. Li and X. Li, "Chen Xuefeng and its relationship with staff working attitude," *Psychology Journal*, vol. 9, no. 38, 2006.
- [17] C. Li, B. Tian, and time survey, "Transformational leadership and employee working attitude: the intermediary role of psychological authorization," *Psychology Journal*, vol. 38, no. 2, 2006.
- [18] D. H. Hubel and T. N. Wiesel, "Receptive fields, binocular interaction and functional architecture in the cat's visual cortex," *The Journal of Physiology*, vol. 160, no. 1, pp. 106–154, 1962.
- [19] Y. Bengio, R. Ducharme, and P. Vincent, "A neural probabilistic language model," *Journal of Machine Learning Research*, vol. 3, pp. 1137–1155, 2003.
- [20] Y. Lecun, L. Bottou, Y. Bengio, and P. Haffner, "Gradient-based learning applied to document recognition," *Proceedings of the IEEE*, vol. 86, no. 11, pp. 2278–2324, 1998.
- [21] r S. Hochreite and J. Schmidhuber, "Long short-term memory," *Neural Computation*, vol. 9, no. 8, pp. 1735–1780, 1997.
- [22] P. D. Turney and M. L. Littman, "Measuring praise and criticism: inference of semantic orientation from association," *ACM Transactions on Information Systems*, vol. 21, no. 4, pp. 315–346, 2003.
- [23] H. Peng, E. Cambria, and A. Hussain, "A review of sentiment analysis research in Chinese language," *Cognitive Computation*, vol. 9, no. 4, pp. 423–435, 2017.
- [24] A. Go, R. Bhayani, and L. Huang, "Twitter sentiment classification using distant supervision," *CS224N Project Report, Stanford*, vol. 1, no. 12, p. 2009, 2009.
- [25] C. Troussas, M. Virvou, and E. Alepis, "Comulang: towards a collaborative e-learning system that supports student group modeling," *SpringerPlus*, vol. 2, no. 1, p. 387, 2013.

Retraction

Retracted: Artificial Intelligence-Based Recommendation and Application of Public Services in Smart Cities

Computational Intelligence and Neuroscience

Received 3 October 2023; Accepted 3 October 2023; Published 4 October 2023

Copyright © 2023 Computational Intelligence and Neuroscience. This is an open access article distributed under the Creative Commons Attribution License, which permits unrestricted use, distribution, and reproduction in any medium, provided the original work is properly cited.

This article has been retracted by Hindawi following an investigation undertaken by the publisher [1]. This investigation has uncovered evidence of one or more of the following indicators of systematic manipulation of the publication process:

- (1) Discrepancies in scope
- (2) Discrepancies in the description of the research reported
- (3) Discrepancies between the availability of data and the research described
- (4) Inappropriate citations
- (5) Incoherent, meaningless and/or irrelevant content included in the article
- (6) Peer-review manipulation

The presence of these indicators undermines our confidence in the integrity of the article's content and we cannot, therefore, vouch for its reliability. Please note that this notice is intended solely to alert readers that the content of this article is unreliable. We have not investigated whether authors were aware of or involved in the systematic manipulation of the publication process.

Wiley and Hindawi regrets that the usual quality checks did not identify these issues before publication and have since put additional measures in place to safeguard research integrity.

We wish to credit our own Research Integrity and Research Publishing teams and anonymous and named external researchers and research integrity experts for contributing to this investigation.

The corresponding author, as the representative of all authors, has been given the opportunity to register their agreement or disagreement to this retraction. We have kept a record of any response received.

References

- [1] J. Zhou, "Artificial Intelligence-Based Recommendation and Application of Public Services in Smart Cities," *Computational Intelligence and Neuroscience*, vol. 2022, Article ID 8958865, 10 pages, 2022.

Research Article

Artificial Intelligence-Based Recommendation and Application of Public Services in Smart Cities

Jin Zhou ^{1,2}

¹School of Public Administration, Sichuan University, Chengdu 610065, China

²Hubei Minzu University Library, Hubei, En'shi 445000, China

Correspondence should be addressed to Jin Zhou; 2006024@hbmzu.edu.cn

Received 16 June 2022; Revised 29 July 2022; Accepted 10 August 2022; Published 30 August 2022

Academic Editor: Le Sun

Copyright © 2022 Jin Zhou. This is an open access article distributed under the Creative Commons Attribution License, which permits unrestricted use, distribution, and reproduction in any medium, provided the original work is properly cited.

With the promotion and application of information technology, smart cities based on artificial intelligence have become the best choice for the government to solve urban problems, connect urban citizens, and provide quality public services. From the initial information city and digital city to the current smart city, the construction of smart cities has undergone profound changes with five major characteristics: big data, intelligence, innovation, interaction, and integration, and Internet giants have emerged in the field of public services in smart cities. Internet giants are emerging in the construction of public service platforms for smart cities, and traditional smart city construction enterprises are also expanding various forms of urban operation services through the form of “Internet+”. Nevertheless, there is still a gap between the quantity and quality of China’s smart cities compared with developed countries, and there is a need to build a number of pilot smart cities characterized by the linkage of artificial intelligence technology and public services, easy to promote, and sustainable development. The smart city construction model with public services as the core has research value and has the possibility of becoming the mainstream development in the future. Therefore, exploring the organic combination of AI technology and urban public services is the key to answer whether AI technology can promote the improvement of urban public services.

1. Introduction

China’s urbanization process is accelerating, the level of economic development is rapidly increasing, the urban population is constantly coming in and expanding, and residents’ requirements for daily life and public services are also increasing [1]. Under such circumstances, the traditional public service model is increasingly unable to adapt to these changes [2]. In the face of the growing population size and the increasing requirements for living experience, the contradiction between insufficient urban carrying capacity and low level of public services has forced the need for rapid transformation in the construction of urban public service facilities. Smart cities are undoubtedly a powerful means to break this bottleneck [3]. SmartCity is an intelligent self-awareness, self-adaptation, and self-optimization based on comprehensive perception and interconnection of ubiquitous information using new-generation information technology to achieve

seamless connection and cooperative linkage among people, things, and urban functional systems, so as to make intelligent responses to urban service demands, such as people’s livelihood, environmental protection, public safety, urban functions and business activities, and form a safe, convenient, efficient, and green city with sustainable endogenous power. It can form a safe, convenient, efficient, and green city form with sustainable endogenous power [4]. It can make the services and facilities in the city make intelligent and rapid responses to better perform their functions and guarantee the development of people’s livelihood [5]. Public service facilities, which are the concrete manifestation of the city’s services for its residents, are the means of expression of all aspects of the city’s functions [6]. Whether they are truly organically combined with modern information means, scientific planning and innovation, and ultimately meet the requirements of intelligent services, is the biggest criterion to measure whether a smart city is truly built.

For the construction of urban public service facilities, the main issues to be considered are the rational allocation of space and the correspondence between functions and needs, so when using the theory of smart cities for construction, these issues should also be considered, and on this basis, a more “intelligent” model and thinking should be used to deal with problems, introduce new technologies, and bring wisdom into play [7]. After setting this basic direction, it is necessary to consider various factors, such as input, efficiency, effectiveness and balance. For example, when planning the space, it is necessary to ensure the maximum representation of functions, but also to take care not to take resources from other areas and to ensure the overall coordination and science of urban planning. When designing the specific locations and configurations of various service facilities, the degree of residents’ demand for different services should be actually investigated so that the response speed and priority of the service facilities meet the actual needs, such as appropriately increasing the number and density of some services with high pedestrian flow and urgent demand [8]. In addition, when designing and planning, it is also necessary to apply a developmental perspective as much as possible and introduce innovative means and technologies so that traditional public service facilities can be infused with new vitality, keep up with the times, and strive to meet the gradually growing individualized needs of residents. In this way, it is also expected to enhance the residents’ sense of identity and life experience in the city, pull the development of the city, and improve the overall development level and comprehensive strength of the city.

The construction of smart cities is also inseparable from the application of big data. Through data collection and macro analysis of city residents, we can summarize the demand and intensity of various public service facilities and residents’ tendency to choose them to help make more reasonable planning and settings [9]. By applying various perception-based technologies and location identification systems to draw precise point-to-point planning maps and incorporate detailed information of residents in real time, we can gain a deeper and more comprehensive understanding of residents’ daily needs and living habits and improve the efficiency of public service facilities in a targeted manner.

At present, the construction and development of smart cities suffer from the lack of regional characteristics, insufficient development planning, unbalanced construction and application, imitation over R&D, and difficulty in integrating resources, while the research on smart cities emphasizes technology over application, the disconnection between high-tech and application services, and the deviation between concept and practice. How to plan urban public service facilities scientifically and effectively, and how to apply wisdom technology to public services in combination with social needs are the key points and difficulties of smart city construction, which is also the main theme of this paper.

2. Related Work

Since the theory of “smart city” was proposed, it has been discussed and analyzed by various parties, and the

theoretical system is becoming more and more enriched and mature, and the basic connotation is changing [10, 11]. At present, the discussions and concerns about smart cities are mainly focused on the technical level and the policy level: at the technical level, the concern is about the technology to be introduced and its feasibility; at the policy level, the discussion is about the government’s attitude and guidance, and the presence of democratic forces is considered [12]. In addition, many scholars in China have been committed to constructing and filling the basic framework of smart city theory, trying to explore deeper connotations, combining local characteristics or even local features, and constructing a comprehensive and detailed theory from which all places can learn and form a system that truly fits our national conditions [13].

Technology has always been the focus of attention, and although the combination of information technology and urban construction is not a new concept, how to use it skillfully and rationally needs to be explored in depth [14]. At present, smart cities are applied to a variety of technical means, of which the supporting technologies mainly include cloud computing, information collection and integration, artificial intelligence identification, etc. And with the continuous development of information technology and frequent results, more new technologies are bound to be applied to the construction of smart cities [15]. At present, several cities in China have incorporated the construction of smart cities into their development plans, and the applicable technologies will be different for these cities with different development directions and human geographic connotations [16]. How to use the technology comprehensively according to their own characteristics and realize the maximum value of the technology is also a problem that needs to be faced directly [17].

The smooth construction and development of smart cities cannot be achieved without the support and guidance of policies [18]. In this regard, relevant departments and experts have studied and discussed the policies. Smart cities involve economy, people’s livelihood, humanities, environment, etc., which cannot be favored over others, otherwise, it will easily cause unbalanced and unstable conditions, which is the reason why policy forces are needed to intervene. The policy research should start from the position of each resident, close to the people’s life, and try to achieve real benefit to the people.

In the context of artificial intelligence, it is of great importance how to better recommend and apply public services in smart cities, in which effective intelligent recommendation algorithms are necessarily needed. The basic idea of recommendation system, as a tool to facilitate people to quickly and accurately locate the items they are interested in among a large number of item choices in the era of big data, is to extract the characteristics of users and items from their historical data by building a model, and to recommend items to users in a targeted manner using the trained model [19]. Research on applying reinforcement learning to recommender systems has received increasing attention. The first exploratory model that applies deep reinforcement

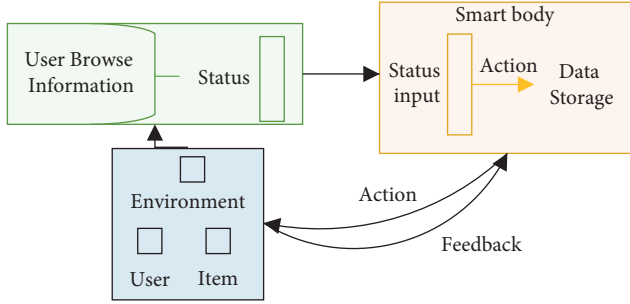


FIGURE 1: Schematic diagram of deep reinforcement learning-based recommendation system.

learning to recommender systems is DRN [20], which constructs a basic framework for recommender systems, and the block diagram is shown in Figure 1.

In such a reinforcement learning framework, the learning process of the model can be iterated continuously, and the iterative process has the following main steps.

- (1) Initialize the recommendation system (intelligent body)
- (2) The recommendation system performs news ranking (action) based on the current collected data (state) and pushes it to the website or app (environment)
- (3) The user receives a list of recommendations and clicks or ignores (feedback) a recommendation result
- (4) The recommendation system receives the feedback and updates the current state or updates the model-by-model training
- (5) Repeat step 2

There have been many research results about deep reinforcement learning-based recommender systems, such as

the literature [21] and others applied DQN to social networks. Applied DQN to a trust recommendation system based on social networks, applied to an intelligent body to learn the dynamic representation of trust between users and recommend users based on that trust value; literature [22] applied DDQN to recommendation suggestions, solving the problems of low recommendation accuracy, slow speed, and cold start; literature [23] applied DDPG algorithm to stored recommendations, solving the problem of sparse user data. The literature [24] applied the Actor-Critic algorithm to list-based recommendation, solving the problem that the traditional recommendation model can only model the recommendation process as a static process. The above research results and the numerous studies not listed above use the nature of reinforcement learning itself to solve the recommendation problem, and rarely consider the problem from the recommendation perspective.

3. Practical Scheme

By dividing the basic public service items, the dimensions of measuring the level of public services in smart cities were classified as public education (PE), social security (SC), medical health (MHC), housing security (HC), public culture (PC), and social services (SS). The smart city pilot started in 2013, so the panel data of 31 provinces (regions and cities) in China from 2014 to 2018 were selected for the empirical study. The data were obtained from China Statistical Yearbook, China Science and Technology Statistical Yearbook, and National Housing Fund Report from 2014 to 2018. In order to exclude the influence of factors, such as interaction terms and reveal the relationship between AI technology and public service level, control factors are added and a panel data model is constructed:

$$\begin{aligned}
 PE_{ti} &= \alpha_0 + \beta_1 DI_{ti} + \beta_2 DO_{ti} + \beta_3 GDP_{ti} + \beta_4 FDI_{ti} + \beta_5 INF_{ti} + \beta_6 PS_{ti} + \epsilon_{ti}, \\
 SC_{ti} &= \alpha_0 + \beta_1 DI_{ti} + \beta_2 DO_{ti} + \beta_3 GDP_{ti} + \beta_4 FDI_{ti} + \beta_5 INF_{ti} + \beta_6 PS_{ti} + \epsilon_{ti}, \\
 MHC_{ti} &= \alpha_0 + \beta_1 DI_{ti} + \beta_2 DO_{ti} + \beta_3 GDP_{ti} + \beta_4 FDI_{ti} + \beta_5 INF_{ti} + \beta_6 PS_{ti} + \epsilon_{ti}, \\
 HC_{ti} &= \alpha_0 + \beta_1 DI_{ti} + \beta_2 DO_{ti} + \beta_3 GDP_{ti} + \beta_4 FDI_{ti} + \beta_5 INF_{ti} + \beta_6 PS_{ti} + \epsilon_{ti}, \\
 PC_{ti} &= \alpha_0 + \beta_1 DI_{ti} + \beta_2 DO_{ti} + \beta_3 GDP_{ti} + \beta_4 FDI_{ti} + \beta_5 INF_{ti} + \beta_6 PS_{ti} + \epsilon_{ti},
 \end{aligned} \tag{1}$$

$$\frac{1}{n} \sum_{i=1}^n \text{Ave_Reward}_i, n,$$

where PE_{ti} denotes the level of public education in city i ($i = 1, 2, \dots, n$) in year t , SC_{ti} denotes the level of social security in city i in year t , MHC_{ti} denotes the level of health care in city i in year t , HC_{ti} denotes the level of housing security in city i in year t , PC_{ti} denotes the level of public culture in city i in year t , SS_{ti} denotes the level of social services in city i in year t , DI_{ti} denotes the AI technology input of city i in year t , DO_{ti} denotes

the AI technology output of city i in year t , GDP_{ti} denotes the economic level of city i in year t , FDI_{ti} denotes the openness level of city i in year t , INF_{ti} denotes the infrastructure level of city i in year t , PS_{ti} denotes the population size of city i in year t , and ϵ_{ti} is a random disturbance term.

Public education (PE) is measured by the pupil–teacher ratio in elementary schools. With the popularization of

TABLE 1: Descriptive statistics of each variable.

Variable name	Sample size	Mean value	Standard error	Min	Maximum value
PE	155	16.187	2.35	12.13	18.99
SC	155	3.197	0.65	1.32	4.51
MHC	155	8.933	2.06	5.39	18.21
HC	155	545.798	445.21	42.12	2293.69
PC	155	0.699	0.55	0.28	3.28
SS	155	28.798	10.05	8.31	65.21
DI	155	0.245	0.21	0	1.00
DO	155	0.205	0.23	0	1.00
GDP	155	0.279	0.19	0	1.00
FDI	155	0.152	0.21	0	1.00
INF	155	0.556	0.23	0	1.00
PS	155	0.387	0.28	0	1.00

quality education, the teacher–student ratio has become an important criterion for the improvement of educational strength. Social Security (SC) is measured by the urban registered unemployment rate. With the development of the economy, the role of unemployment insurance in preventing unemployment and promoting employment is becoming more and more important, and has become a booster and safety valve for economic development and social stability. Medical Health Care (MHC) is measured by the number of beds in medical and health institutions per 1,000 people. With the development of modern economy, the residents’ demand for medical and health resources allocation is getting higher and higher, and the number of medical and health institution beds in a region represents the intensity of medical and health security in that region. Housing security (HC) is measured by the amount of CPF contributions. The value-added income of the CPF provides a source of funds for the construction of low-cost housing and supports low-income families in solving their housing problems, reflecting the special function of housing security. Public culture (PC) is measured by the number of books per capita in public libraries. In terms of equalization, standardization, digitalization, and socialization, libraries have always led the development of public cultural services. Social services (SS) are measured by the number of elderly beds per 1,000 elderly people. “The 13th Five-Year Plan points out that the number of social service beds for the elderly can be used as the basis for judging the assistance and welfare subsidies for the elderly.

Artificial intelligence investments are based on trading logic and mathematical models given to computers by computer programmers. Computers are programmed to capture investment opportunities across the market and put them into practice, and all trading moves are made based on models, algorithms, and logic that can overcome human weaknesses, such as greed, fear, and fluke. Investment in artificial intelligence (DI) is measured by the intensity of investment in research and experimental development (R&D) in each region. Capital is the blood of innovation activities and is an important link to continuously support the development of innovation in the digital economy. R&D investment intensity can better measure the R&D capital investment in digital information technology. Artificial intelligence technology output (DO) is measured by the number

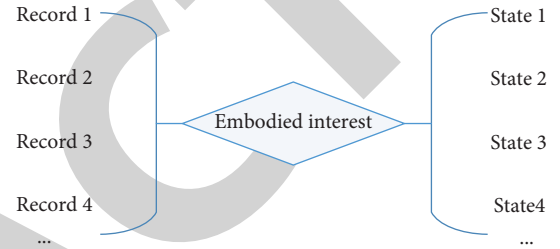


FIGURE 2: Sketch of state generation.

of patent applications per 10,000 people in each region. Patent data can better reflect technological innovation and better demonstrate the level of AI technology in cities.

Economic level (GDP), measured by per capita gross regional product; openness level (FDI), measured by foreign fixed asset investment; infrastructure (INF), measured by per capita urban road area; and population size (PS), measured by the number of population at the end of each year, are given in Tables 1–3.

This section introduces the proposed model for Smart City Recommendation (SCR), which uses user interests as the states seen by the intelligences in deep reinforcement learning as a way to accomplish the intelligent recommendation task. To capture the long-term interest of users, this paper uses a long- and short-term memory network (LSTM) with state enhancement units to learn the browsing records of users over a longer period of time, and retention ratios in the network through three gating units.

We use the attention mechanism as the base model for extracting users’ short-term interests. It is assumed that the user’s short-term interest can be extracted from three consecutive browsing records (item1, item2, and item3), which are coded to form vector γ . After that, the three vectors are calculated as respective Queries vector, Keys vector, and Values vector according to different parameters W_{Qi}, W_{Ki}, W_{Vi} ($i = 1, 2, 3$) and combined into a matrix form, and then the following formula is used to calculate the self-attentive value of each record is calculated by the following formula.

$$Z * = \text{softmax}\left(\frac{Q \times K^T}{\sqrt{d_k}}\right), \quad (2)$$

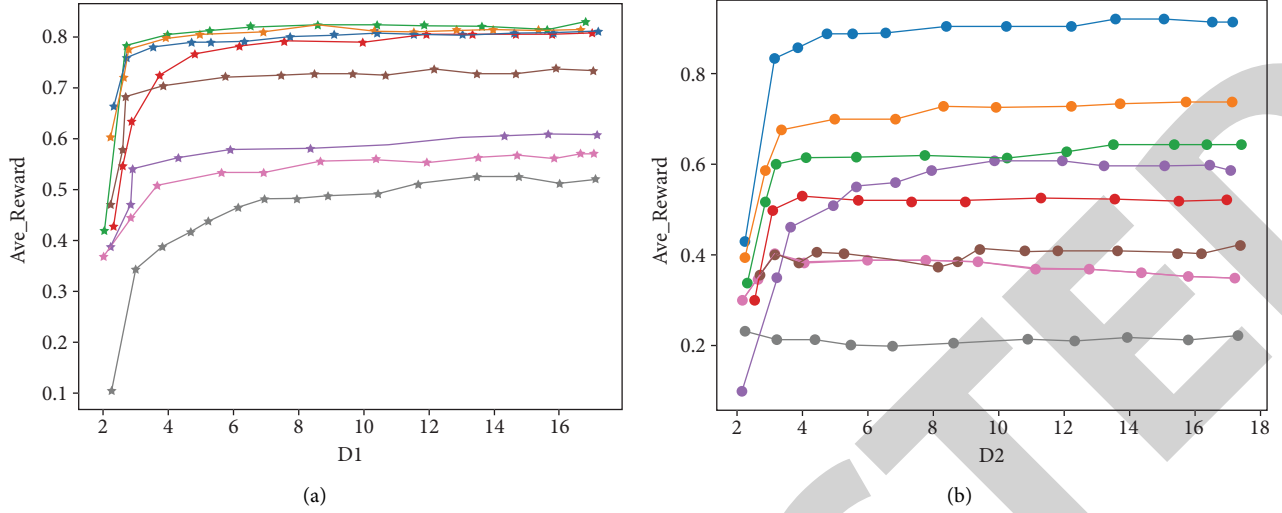
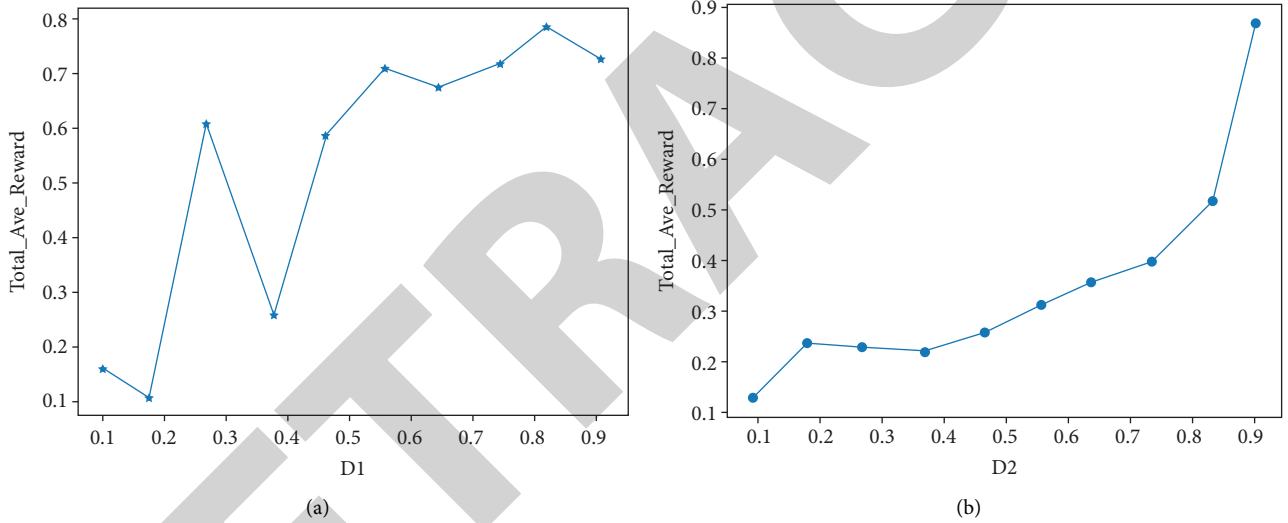


FIGURE 3: Ave_Reward trend graph.


 FIGURE 4: Trend of total_ave_reward value for different values of γ .

where Q, K, V are the matrices based on X_1, X_2, X_3 vectors combined as Queries vector, Keys vector, and Values vector, respectively, and d_k is the length of a browsing record. Z^* is the matrix of the final calculated vector of short-term interests of the user reflected by each item.

The final short-term interest of the user is achieved by directly summing the user short-term interest vectors reflected by each item, i.e.,

$$\text{shortinterest} = Z_1 + Z_2 + Z_3 + \dots + Z_n. \quad (3)$$

The Z_i in the equation represents the user's short-term interest reflected by the i th browsing record. i has a temporal characteristic, i.e., the larger i is, the closer it is to the current moment, and Z_i the closer the interest expressed is to the user's current interest. Careful consideration reveals that when multiple Z_i 's are superimposed, the trend of current user short-term interest is diluted as Z_i 's are superimposed. To solve this problem, this paper improves short interest by

adding weights to the short-term interests expressed by each browsing record in order, and the more backward the time, the greater the weight assigned to the user's short-term interests, as expressed by the formula

$$\text{shortinterest} = \frac{1}{n}Z_1 + \frac{2}{n}Z_2 + \frac{3}{n}Z_3 + \dots + Z_n. \quad (4)$$

The final model is called T -self-attention, and the weight of the interest vector in the short-term interest composition is assigned in time sequence. By embedding the long and short-term interest extraction module into the Actor network of the DDPG algorithm, the purpose of updating the parameters of the long- and short-term interest extraction module network while training the Actor network is achieved, and an improvement of the Actor network is shown next. The pseudocode of the algorithm of SCR is given in Algorithm 1.

TABLE 2: Basic regression analysis.

Public services	Model	DI		DO		Fixed effects	Time effect	Control variables	N	R ²
Public education	1	-4.029	(2.268)	0.153	(1.325)	√	×	×	155	0.049
	2	-5.055	(0.569)	-1.195	(1.387)	√	√	×	155	0.103
	3	-5.348	(2.446)	-0.352	(1.396)	√	×	√	154	0.069
	4	-5.987	(2.568)	-0.935	(1.558)	√	√	√	154	0.129
Social security	5	-1.921	(1.281)	-0.093	(0.265)	√	×	×	155	0.061
	6	-1.202	(1.178)	0.510	(0.389)	√	√	×	155	0.151
	7	-0.857	(0.935)	1.754	(0.558)	√	×	√	154	0.269
	8	-0.635	(0.976)	1.727	(0.597)	√	√	√	154	0.289
Health care	9	7.267	(3.825)	0.907	(0.955)	√	×	×	155	0.051
	10	5.854	(3.789)	-2.062	(1.263)	√	√	×	155	0.188
	11	6.395	(4.223)	-1.358	(1.989)	√	×	√	154	0.071
	12	6.236	(3.512)	-1.598	(1.539)	√	√	√	154	0.223
Housing	13	485.002	(386.698)	1694.899	(230.699)	√	×	×	155	0.739
	14	101.899	(435.698)	1357.400	(268.000)	√	√	×	155	0.798
	15	62.001	(435.199)	555.200	(286.000)	√	×	√	154	0.855
	16	25.031	(424.899)	599.100	(283.000)	√	√	√	154	0.859
Public culture	17	0.212	(0.285)	0.868	(0.145)	√	×	×	155	0.738
	18	-0.115	(0.283)	0.539	(0.142)	√	√	×	155	0.798
	19	0.035	(0.302)	0.435	(0.161)	√	×	√	154	0.855
	20	-0.062	(0.289)	0.469	(0.129)	√	√	√	154	0.865
Social services	21	-4.359	(19.798)	8.779	(10.188)	√	×	×	155	0.659
	22	6.987	(25.268)	9.899	(13.872)	√	√	×	155	0.789
	23	-25.599	(18.982)	23.835	(12.599)	√	×	√	154	0.755
	24	-16.029	(19.525)	15.001	(14.232)	√	√	√	154	0.132

TABLE 3: Heterogeneity regression results.

Public services	Category	DI		DO		N	R ²
Public services	A	-3.321	(3.159)	0.122	(2.155)	55	0.299
	B	-11.563	(4.712)	-1.456	(3.652)	50	0.367
	C	-5.698	(6.312)	-10.799	(5.235)	49	0.451
	East	-2.156	(3.038)	-0.195	(2.659)	60	0.191
	Central	-10.179	(9.068)	-8.985	(7.334)	45	0.412
	West	-10132	(5.556)	-3.178	(2.894)	49	0.468
Social security	A	-2.049	(0.953)	0.522	(0.688)	55	0.293
	B	2.036	(1.478)	1.623	(0.915)	50	0.595
	C	-6.599	(3.523)	2.998	(0.820)	49	0.645
	East	-0.152	(1.132)	1.293	(0.652)	60	0.265
	Central	0.323	(2.598)	2.187	(0.126)	45	0.371
	West	-5.236	(2.239)	1.789	(1.569)	49	0.525
Health care	A	9.156	(1.650)	-5.123	(1.002)	55	0.253
	B	2.968	(5.469)	-1.489	(2.006)	50	0.372
	C	9.367	(19.185)	-11.321	(15.865)	49	0.521
	East	7.152	(3.339)	-2.789	(3.422)	60	0.820
	Central	-0.705	(5.525)	-13.569	(4.335)	45	0.453
	West	16.598	(12.635)	-3.155	(5.985)	49	0.203
Housing	A	44.003	(486.200)	-563.651	(280.400)	55	0.429
	B	-39.598	(345.900)	-116.987	(230.400)	50	0.719
	C	539.251	(398.200)	68.487	(328.200)	49	0.235
	East	666.798	(575.600)	356.000	(515.300)	60	0.968
	Central	1298.362	(420.400)	522.400	(288.600)	45	0.897
	West	-122.000	(415.200)	470.000	(265.400)	49	0.921
Public culture	A	0.036	(0.449)	0.022	(0.142)	55	0.893
	B	0.061	(0.272)	-0.055	(0.188)	50	0.926
	C	-0.698	(0.345)	-2.179	(0.455)	49	0.906
	East	0.309	(0.455)	0.279	(0.195)	60	0.896
	Central	0-0.049	(0.355)	-0.035	(0.295)	45	0.897
	West	-0.255	(0.519)	-0.263	(0.196)	49	0.793
Social services	A	7.186	(25.325)	1.059	(12.725)	55	0.879
	B	-37.269	(23.805)	34.100	(17.655)	50	0.931
	C	187.399	(117.825)	46.168	(77.165)	49	0.756
	East	-15.598	(21.155)	16.239	(10285)	60	0.425
	Central	18.459	(36.825)	-49.179	(30.958)	45	0.498
	West	91.897	(135.895)	58.235	(35.889)	49	0.620

Input: user history browsing records
Random initialization of Critic network $Q(s, a \theta^Q)$ and Actor network $\mu(s \theta^\mu)$
Network parameters θ^Q, θ^μ
Initialize the network parameters $\theta^{Q'} \leftarrow \theta^Q, \theta^{\mu'} \leftarrow \theta^\mu$ for the target network Boo Q', μ' .
Initialize the LSTM network parameters
Initialize the T -self-attention network parameters
Initialize the T -self-attention network parameters
For episode = 1, Mdo for action exploration initialization
Random process N
Randomly select user u
Get the current browsing history of user u and the browsing history of the next moment
For $t = 1$ to T do
Based on the current browsing record R_c , the current moment status s_t is generated by Algorithm 2
Based on the next browsing record R_n , the next moment s_{t+1} is generated by Algorithm
Generate action based on Evaluation-Actor and noise $a_t = \mu(s_t \theta^\mu) + N_t$
Execute the action a_t Get the return r_t
Calculating TD-error target values $y_t = r_t + \gamma Q'(s_{t+1}, \mu'(s_{t+1} \theta^{\mu'})) \theta^{Q'}$
Based on loss $L = 1/n \sum_i (y_i - Q(s_i, a_i \theta^Q))^2$
Update Critic Network
Update actor policy with sampling policy gradient: $\nabla_{\theta'} J \approx 1/N \sum_i \nabla_a Q(s, a \theta^Q) _{s=s_i, a=\mu(s_i)} \nabla_{\theta'} \mu(s \theta^\mu) _{s=s_i}$
Update the target network parameters by soft copy. $\theta^{Q'} \leftarrow \tau \theta^Q + (1 - \tau) \theta^{Q'}$
$\theta^{\mu'} \leftarrow \tau \theta^\mu + (1 - \tau) \theta^{\mu'}$
Output: predicted ratings

ALGORITHM 1: SCR algorithm.

TABLE 4: Comparison of experimental results.

Algorithm	Dataset 1		Dataset 2	
	Ave_RMSE	Ave_MAE	Ave_RMSE	Ave_MAE
SCR	0.3992	0.2288	0.2776	0.1115
DDPG + RLSTM	0.4580	0.2616	0.5222	0.4085
DDPG + LETM	0.5892	0.4659	0.5568	0.4439
DDPG + T _self_attention	0.5762	0.4025	0.4486	0.2826
DDPG + self_attention	0.5965	0.44259	0.5356	0.3636
DDPG + RLSTM + self_attention	0.4025	0.2419	0.8552	0.1818
DDPG + LSTM + T _self_attention	0.4036	0.2358	0.6658	0.2860
DDPG + LSTM + self_attention	0.4478	0.2886	0.6829	0.3259
KNNBasic	0.9228	0.7476	0.6658	0.4201
KNNWithMeans	0.9320	0.7386	0.9886	0.7325
KNNBaseline	0.8958	0.7066	0.9335	0.7136
SVD	0.8830	0.6856	0.9258	0.7022
SVD++	0.8622	0.9728	0.9225	0.7268
NMF	0.9216	0.7352	0.9680	0.7698

4. Case Study

In order to prove the effectiveness of our scheme, we have experimented and analyzed it on a dataset. In this paper, the following rules are followed in both training and testing phases: the user browsing sequence is denoted as: $S_u = (I_1, I_2, I_3, \dots, I_{|S_u|})$, where I_i denotes the i -th record of the item viewed by the user. The first $0.8 * |S_u|$ of each user's browsing records are used as the training set, and the remaining data are used as the test data. During training, the browsing records in the training set are input into the model in order of users, and for each record, the model predicts the rating of the recommendations contained in the record, and

the reward value is calculated based on the difference between the real rating and the predicted rating and fed back to the intelligence, and the algorithm optimizes the model based on the reward value. The operations during testing are similar to those during training, but there is no model optimization operation.

- (1) Action space: in this paper, the original scores are normalized to map the range of values to the interval $[0, 1]$, which becomes $(0, 0.25, 0.5, 0.75, 1)$. Meanwhile, the results are mapped to the $[0, 1]$ interval using the sigmoid activation function at the fully connected layer of the algorithm using the

TABLE 5: Boost values of SCR and module combination algorithm on Ave_RMSE.

	KNNBasic	KNNWithMeans	KNNBasicline	SVD	SVD++	NMF	
D1	SCR	0.5225	0.5288	0.4958	0.4873	0.4562	0.5216
	DDPG + RLSTM	0.4848	0.4820	0.4562	0.7592	0.4212	0.4879
	DDPG + LETM	0.3258	0.3352	0.3568	0.2252	0.3210	0.3215
	DDPG + T_self-attention	0.3465	0.3525	0.2365	0.6582	0.3242	0.4521
	DDPG + self-attention	0.3288	0.3355	0.1598	0.7830	0.2826	0.4663
	DDPG + RLSTM + self-attention	0.5220	0.5268	0.2256	0.1259	0.2789	0.3221
	DDPG + LSTM + T_self-attention	0.5122	0.5255	0.3558	0.2525	0.2345	0.5124
	DDPG + LSTM + self-attention	0.4680	0.4820	0.7035	0.3251	0.2325	0.5110
D2	SCR	0.7535	0.7078	0.6524	0.3256	0.2451	0.3654
	DDPG + RLSTM	0.4568	0.4258	0.4125	0.2564	0.3214	0.3219
	DDPG + LETM	0.4256	0.3865	0.3254	0.6871	0.4004	0.2598
	DDPG + T_self-attention	0.5325	0.5226	0.4687	0.3252	0.6587	0.3987
	DDPG + self-attention	0.4452	0.4226	0.1036	0.2520	0.2335	0.4210
	DDPG + RLSTM + self-attention	0.1569	0.1298	0.7255	0.3210	0.5632	0.2113
	DDPG + LSTM + T_self-attention	0.3250	0.2826	0.3652	0.1020	0.1235	0.1558
	DDPG + LSTM + self-attention	0.3055	0.2678	0.5529	0.2325	0.2558	0.2864

floating-point data with continuity generated each time as the action, i.e., the predicted recommendation scores. Therefore, the action space of this model is a continuous space in the interval of $[0, 1]$.

- (2) State space: the user browsing records are treated as an observation, and the extracted interests are used as states after interest extraction by the long-term interest and short-term interest extraction modules in chronological order. The brief process is shown in Figure 2.
- (3) Reward function: when designing the reward function, this paper uses the difference between the predicted score and the real score as the criterion to guide the optimization direction of the intelligent body. The specific design approach is as follows:

$$\text{Reward} = e^{-(\text{abs}(\text{pre_score} - \text{real_score}))}, \quad (5)$$

where pre_score indicates the predicted score, real_score indicates the real score, and abs indicates that the absolute value sign is taken. The reward function can be interpreted as follows: the larger the gap between the predicted score and the real score, the smaller the reward obtained by the intelligence, and the smaller the gap the larger the reward obtained.

In this paper, the performance of the algorithm is observed mainly through the trend of the rewards obtained by the intelligences to observe whether the algorithm eventually converges. In testing the convergence of the algorithm, because the test results of a single user are contingent and do not reflect the overall performance of the algorithm, this paper collects the rewards obtained by the intelligences of each record of each user during the test and reflects the convergence of the algorithm by calculating the mean value of the collected data. Thus, the final rewards used for testing take the form of

$$\text{Ave_reward} = \frac{\sum_i \sum_j r_{ij}}{N}. \quad (6)$$

The effectiveness of the algorithm is tested using the root mean square error (RMSE) and the mean absolute error (MAE), which are common test metrics for rating classification algorithms. The RMSE and MAE are expressed as

$$\text{RMSE} = \sqrt{\frac{1}{m} \sum_{i=1}^m (y_i - \hat{y}_i)^2}, \quad (7)$$

$$\text{MAE} = \frac{1}{m} \sum_{i=1}^m |y_i - \hat{y}_i|.$$

4.1. Experimental Results and Analysis

4.1.1. Overall Performance Comparison. Therefore, after the analysis of Tables 4–6, the performance of the deep reinforcement learning algorithm based on the extraction of public service infrastructure. The specific results are given in Tables 4–6.

4.1.2. Analysis of Algorithm Convergence. This part of the experiment mainly collects the Reward value Reward that the intelligent body can obtain after each prediction recommendation score when the algorithm is tested, as well as the RMSE and MAE values that can be obtained for each round of prediction, and analyzes the convergence of the algorithm by observing the trend of the values of these evaluation indexes. Also, in order to evaluate the convergence of the algorithm as a whole, this paper analyzes the algorithm by observing the trend of the average return Ave_Reward in each round. Figure 3 shows the trend graph of the Ave_Reward values of the DDPG-LA algorithm and the combined algorithm of each module with increasing number of training sessions on both data sets.

From Figure 3, it can be seen that the overall results of all algorithms tested on the dataset are better.

TABLE 6: Lift values of SCR and module combination algorithm on Ave_MAE.

		KNNBasic	KNNWithMeans	KNNBasicline	SVD	SVD++	NMF
D1	SCR	0.4886	0.8098	0.4776	0.4568	0.4432	0.4862
	DDPG + RLSTM	0.4650	0.4886	0.4446	0.4250	0.4112	0.4620
	DDPG + LETM	0.2525	0.2692	0.2456	0.2268	0.2032	0.2556
	DDPG + T_{self} -attention	0.3256	0.3365	0.3005	0.2826	0.2688	0.3228
	DDPG + self-attention	0.3001	0.3225	0.2687	0.2642	0.2545	0.2788
	DDPG + RLSTM + self-attention	0.4865	0.5065	0.4856	0.4652	0.2459	0.4825
	DDPG + LSTM + T_{self} -attention	0.4935	0.5225	0.4826	0.4515	0.4340	0.4896
	DDPG + LSTM + self-attention	0.4358	0.4488	0.4268	0.4525	0.4368	0.4456
D2	SCR	0.6612	0.6325	0.6258	0.3898	0.3958	0.6548
	DDPG + RLSTM	0.3632	0.3342	0.3445	0.6352	0.6098	0.3588
	DDPG + LETM	0.3330	0.3095	0.3026	0.3280	0.3112	0.3128
	DDPG + T_{self} -attention	0.5220	0.4882	0.4682	0.3002	0.2001	0.4858
	DDPG + self-attention	0.488	0.3952	0.3846	0.2966	0.1987	0.3987
	DDPG + RLSTM + self-attention	0.0044	-0.0196	-0.0352	-0.0320	-0.4680	-0.0106
	DDPG + LSTM + T_{self} -attention	0.2090	0.1849	0.1568	0.1822	0.1562	0.1952
	DDPG + LSTM + self-attention	0.1826	0.1658	0.1423	0.1552	0.1283	0.1658

4.1.3. *Comparative Analysis of Discount Factor γ* . In the experimental process to get the best experimental results, this paper tries various different discount factor values and visualizes the effect of each discount factor through the final results. And by comparing the height of the curves, it is found that the height of the curve changes with the value of γ from small to large, and the trend of this correlation is shown in Figure 4.

The Total_Ave_Reward value represents the average of the average Reward for each round of testing at different γ values, i.e.,

$$\frac{1}{n} \sum_{i=1}^n \text{Ave_Reward}_i, \quad (8)$$

where n denotes the number of test rounds. Figure 4 shows that different discount factors have an effect on the final convergence of the algorithm and are positively correlated.

5. Conclusion

The needs of social development, the support of national policies, and the support of information technology have created a very favorable environment for the development of smart cities and become a strong impetus for the smooth development of smart cities. In practice, construction planners tend to pay too much attention to the input of technology and its effect to meet expectations, while ignoring the inner needs of thousands of city dwellers, that is, ignoring the essence of "service." Before making a decision, a comprehensive and large-scale survey should be conducted to identify the needs of the residents, and on this basis, a plan should be designed to make the city a livable place that is recognized by the people through artificial intelligence-based methods, rather than operating according to the criteria that the decision makers have in mind. The concept of smart cities continues to rise in popularity, with more and more voices participating in the discussion, and it is normal for misconceptions and deviations to occur, but as decision makers and builders, it is important to clearly understand

where the original intention of developing smart cities lies, to think about its essence and connotation in an environment where the heat remains high, and to make decisions that are truly relevant.

Data Availability

The experimental data used to support the findings of this study are available from the corresponding author upon request.

Conflicts of Interest

The author declares that there are no conflicts of interest.

References

- [1] D. Thakker, B. K. Mishra, A. Abdullatif, S. Mazumdar, and S. Simpson, "Explainable artificial intelligence for developing smart cities solutions," *Smart Cities*, vol. 3, no. 4, pp. 1353–1382, 2020.
- [2] A. B. Kanase-Patil, A. P. Kaldate, S. D. Lokhande, H. Panchal, M. Suresh, and V. Priya, "A review of artificial intelligence-based optimization techniques for the sizing of integrated renewable energy systems in smart cities," *Environmental Technology Reviews*, vol. 9, no. 1, pp. 111–136, 2020.
- [3] L. D. Radu, "Disruptive technologies in smart cities: a survey on current trends and challenges," *Smart Cities*, vol. 3, no. 3, pp. 1022–1038, 2020.
- [4] E. Miller, "Networked and integrated sustainable urban technologies in Internet of Things-enabled smart cities," *Geopolitics, History, and International Relations*, vol. 12, no. 2, pp. 30–36, 2020.
- [5] K. Wade, J. Vrbka, N. A. Zhuravleva, and V. Machova, "Sustainable governance networks and urban Internet of Things systems in big data-driven smart cities," *Geopolitics, History, and International Relations*, vol. 13, no. 1, pp. 64–74, 2021.
- [6] C. E. Jimenez-Gomez, J. Cano-Carrillo, and F. Falcone Lanas, "Artificial intelligence in government," *Computer*, vol. 53, no. 10, pp. 23–27, 2020.
- [7] R. Lowe, "Networked and integrated sustainable urban technologies in Internet of Things-enabled smart city

Research Article

Prediction and Evaluation Method of e-Commerce Service Satisfaction Based on Intelligent Computing Method

Fang Tu¹ and Bo Tu ²

¹Jiangxi Engineering Vocational College, Jiangxi Open University, Jiangxi 330046, China

²School of Art East Jiao Tong University, East China Jiaotong University, Jiangxi 330013, China

Correspondence should be addressed to Bo Tu; tubo@ecjtu.edu.cn

Received 10 June 2022; Revised 20 July 2022; Accepted 2 August 2022; Published 30 August 2022

Academic Editor: Le Sun

Copyright © 2022 Fang Tu and Bo Tu. This is an open access article distributed under the Creative Commons Attribution License, which permits unrestricted use, distribution, and reproduction in any medium, provided the original work is properly cited.

Among the many service industries, e-commerce, which is based on the Internet and relies mainly on platforms and third-party transaction models, has developed rapidly. All localities have actively deployed their regional e-commerce development strategies to improve the core competitiveness of the regional economy. The rapid development of e-commerce provides a favorable development environment and construction environment for the spatial agglomeration of e-commerce service industry. We use the intelligent computing method to calculate the e-commerce service degree prediction experimental results that show that according to the curves of the three algorithms, we can also see that the curve values of the intelligent computing and fuzzy statistical algorithm models are very stable and the experimental results are also very stable. It shows that the performance of the intelligent computing algorithm is the most superior; the second-level indicators are the after-sales service of the merchant, the popularity of the merchant, and the attitude of the merchant's customer service; in the establishment of the logistic satisfaction evaluation index system, we found that the logistic satisfaction is the first-level indicator; the secondary indicators are the speed of logistics, the safety of logistics, the service attitude of logistics, and the price of logistics; after running on the test set, the model accuracy rate of the fuzzy statistical algorithm is 89.12%, and the accuracy rate can reach 89.56%. The accuracy rate of the intelligent algorithm can reach 92.46%, and the accuracy rate can reach 93.27%, which is the one with the highest index value among the three experimental models. Among the many service industries, e-commerce, which is based on the Internet and relies on platforms and third-party transaction models, is developing rapidly. All localities have actively deployed their regional e-commerce development strategies to improve the core competitiveness of the regional economy. The rapid development of e-commerce provides a favorable development environment and construction environment for the spatial agglomeration of e-commerce service industry.

1. Introduction

While users are using such huge multimedia data more and more, more and more people are using cloud computing technology. It is necessary to effectively manage big data and consider the transmission efficiency of multimedia data of different qualities. A variable allocation algorithm is required for this. This study proposes a method to design a MapReduce scheme applying the FP-growth algorithm, which is a data mining method based on the IaaS (infrastructure as a service) stage of the Hadoop platform, including CPU, network, and storage. The method is then used to allocate resources using this scheme [1]. This study is

devoted to applying evolutionary algorithms, gradient methods, and artificial neural networks to the problem of mechanical structure recognition. A dedicated intelligent computing technology (ICT) for global optimization is proposed. ICT is based on a two-phase strategy. The first stage adopts an evolutionary algorithm as a global optimization method. The second stage adopts a special local method combining gradient method and artificial neural network. The proposed technique has many advantages. The key issue of the proposed method is the application of artificial neural networks to compute sensitivity analysis [2]. This study proposes to use the quality prediction method to develop a cloud computing-based intelligent manufacturing

scheduling system. A CBIMS continuously builds a variety of different production line layout modes. We use a cloud database for data decentralization and storage, and the scheduling engine contains a sequence scoring system for products, an optimized layout system, and a monitoring system for all available resources [3]. Big data fusion intelligence is the core issue of data science and engineering. This study will first analyze the connotation of big data fusion from the perspective of complex systems. The new research perspective of deep learning technology and the new technology trend of granular processing in data fusion are analyzed, and finally, the architecture of particle computing and processing used to build an intelligent big data integration model for complex system intelligence research is discussed. The research of this subject is a meaningful research and development method in system management and control [4]. According to previous studies, robot walking can only be achieved in prespecified spaces and prespecified actions. In this study, a walking system for a bipedal robot uses fuzzy systems and neural networks to overcome these limitations. The system enables bipedal walking in a variety of environments and more complex obstacles. To do this, a walking robot should recognize its surroundings and determine its movements. In the proposed system, the robot uses neural networks to dynamically generate the walking path of each of its joints as it encounters new obstacles, such as stairs, and maintains walking stability thanks to the control system. The walking stability is maintained by controlling the closed-loop fuzzy control system of the lumbar joint [5]. This article was prepared with financial support from the UK Government's Department for International Development, funding a B2B e-commerce research project in developing countries. The authors draw on comments from Robin Mansell, John Humphrey, and Hubert Schmitz in previous publications in which they collaborated on this research project. Any errors or omissions are the sole responsibility of the authors [6]. We recommend designing an intelligent agent to improve the accessibility of e-commerce applications and websites for the visually impaired. An important feature of this design is the use of information presentation techniques, especially conceptual structures that accurately capture and represent the navigational semantics of each document. It allows users to express high-level navigation destinations using design techniques to achieve these goals. In practice, complex parts of HTML documents are traversed by proxy servers on behalf of visually impaired users [5]. As an emerging network technology, cloud computing provides new methods and means for the construction of e-commerce service system. The author discusses the operation mechanism of the service platform from four aspects: the distributed storage of resources, the coordination of service subjects, and the multiparty interaction between services and security, aiming to promote the rapid development of e-commerce in the cloud computing environment [7]. This study firstly extends log4j and then applies the log file distribution function of log4j to the e-commerce service system. In this way, all log information can be avoided centrally interspersed in a single log file, and log information of different

concerns can be effectively dispersed, which is convenient for monitoring and analyzing the running status of the e-commerce service system [8]. Whereas traditional marketing is product-centric, e-commerce marketplaces focus exclusively on customers. The challenge of e-commerce is to really capture the interest of the Internet user and tailor the answer to his requirements that helps the business to target the right customer with the right product or service. To address these issues, the system analyzes the property marketing of online businesses to connect advertisements to target customer groups. Through an agent-based architecture and obfuscation techniques, the system provides simple support for e-commerce market intermediaries [9]. First, a multinomial logit (MNL) model was constructed to reveal the influence of individual attributes, family attributes, and safety hazards on residents' travel satisfaction and to clarify the influencing factors. Then, with significant factors as independent variables, a tourism satisfaction evaluation model based on support vector machine is constructed. The results show that the following factors have a significant impact on residents' travel satisfaction: age, work, education level, number of cars, income, living area, and hidden safety hazards of people, vehicles, roads, and environment [10]. This article conducts a comprehensive and effective survey and data collection on the current situation of geriatric nursing with questionnaires and establishes an evaluation index system that influences the satisfaction of geriatric nursing services with the SERVQUAL model. Based on this, this article analyzes one-dimensional data into two-dimensional data, uses extensive computer vision research, and then uses the educated online model as an effective analysis tool to provide possible predictive outcomes to improve the health care of proposed retirees [11]. Even if neural language models encode these constraints, we design an extensible test suite to address different aspects of utterance and dialogue coherence. Unlike most previous coherence assessment studies, we address language-specific devices beyond sentence order perturbations, allowing for a more fine-grained analysis of what constitutes coherence and what neural models trained on language modeling goals actually encode. This paradigm is equally applicable to assessing the quality of language that contributes to the concept of coherence [12]. The job responsibilities of teachers have changed significantly in recent years, and now more than ever, there is an urgent need for high-quality teachers to achieve the goals of ESD, especially in developing countries. This timely study examined professional and nonprofessional teachers' assessment competencies and their satisfaction [13]. Job satisfaction is one of the most important variables in student standards. We compare, but are not limited to, a number of employee-related variables, including performance, organizational commitment, and core concepts. The results provide documentation of the structural impact and identify two-thirds. The unique effect was found to be the strongest predictor of job satisfaction, despite the use of the satisfaction measure. Further developments are needed to structure the impact, knowledge, and components of these factors and evaluations of job satisfaction predictions [14].

2. Research on e-Commerce Services

2.1. Deep Docking between e-Commerce Services and Individual Consumers. e-commerce relies on online system platforms to provide users with services of different types and natures. Whether it is purchasing physical products, recharging games in virtual space, or even making lists for fans on specialized service websites, they can all be regarded as the category of e-commerce services. In the era of big data, people in the industry need to expand their management concepts, should not focus on traditional commodities, logistics, and other services, and should summarize all transaction behaviors based on the Internet platform into the e-commerce service system. In the future, enterprises should deeply infiltrate e-commerce into individual consumers, emphasizing individualized services for consumers. Every ordinary consumer is the service object of e-commerce enterprises. Organizations must provide accurate and proactive customer service through scientific analysis of big data. Organizations must also innovate and improve service models in daily consumption and self-satisfaction, such as when consumers buy clothes. They only enjoy the personalized service of premium members; that is, online or offline designers can provide consumers with unique clothing designs. It cannot only enrich the service content but also bring users the ultimate enjoyment and service, so that they can feel the respect and attention from the enterprise. The groups of e-commerce services are shown in Figure 1. The scope of sub-business is very wide and generally can be divided into business-to-business, or business-to-consumer, or two. There is also a consumer-to-consumer model that is growing in stride. As the number of Internet users in China grows, the method of using the Internet to purchase and pay with a debit card is becoming increasingly popular. Market share is also growing rapidly. e-commerce sites are slowly evolving. The most common security mechanisms for e-commerce are SSL (secure socket layer) and SET (secure electronic transaction protocol).

2.2. Innovation Strategy of the e-Commerce Service Model. Today, the Internet provides global connectivity. Through the network, customers can bypass distance restrictions and provide consulting and consumption services to global merchants at any time. Despite the growing share of the e-commerce market, the influx of anonymous users has created many problems for the company. With the development of data technology, marketers can accurately identify anonymous shoppers and recommend products that satisfy customers' purchasing power by examining their attention and enthusiasm for purchasing. This not only saves consumer consultation time but also helps merchants avoid the cost of moving unnecessary merchandise. Based on this, providing these services is not enough—e-commerce companies need to improve service specifications and find market gaps from data analysis to service development.

As the online shopping model becomes more and more popular, e-commerce models such as Taobao, Pinduoduo, and Tmall Suning Tesco have shown positive growth. People have a wider choice of shopping routes, and the logistic requirements for these online shopping businesses are also

greater. E-commerce businesses not only need to serve customers and recommend products but also need to enhance transportation and logistics. For example, consumers may want to buy their favorite fruit online, but the delivery time is too long and they miss the coldest moment, which naturally makes customers happy. Therefore, enterprises need to evaluate the nature of products purchased by consumers; data technology is used to select the most suitable transportation method to effectively improve logistic efficiency.

Due to the unstable market, e-commerce companies should not copy others' words along the way, and if they see an advantage over other companies, they do not copy them. You will only look ridiculous and never go the way of a market economy. Electronics companies not only focus on this fact in business operations but also make similar mistakes in the field of services. In the era of big data, e-commerce companies can use real-time market analysis to predict future market trends and fine-tune their service models. The e-commerce innovation strategy is shown in Figure 2.

2.3. Suggestions for Improving e-Commerce Services

2.3.1. Building a Multilingual Service Platform. Intensification and integration are the focus of cross-border e-commerce service innovation. Cross-border transfers include multilingual communication and customs documentation to complete logistics and distribution; multiple currency changes and multilingual payment instructions are required. A multilingual service platform is established to solve language translation problems.

2.3.2. Providing Full Logistic Services. Cross-border logistic services can improve cross-border e-commerce, making it easier for local consumers to search for information in other countries and buy high-quality, affordable products. Logistic services are provided throughout the process, greatly enhancing cross-border e-commerce opportunities. For example, overseas warehousing and logistic providers bear development costs; speed will combine various transportation methods to meet the needs of different suppliers, including security and after-sales service. The delivery and delivery time of all logistic service products are shortened, and customers with a one-stop solution are provided. It includes product tracking service. Cargo visibility service is a local and international logistic information platform that connects importing companies to provide real-time cargo information. The service aims to accurately understand market demand, help cross-border e-commerce companies to accurately locate goods, and distribute popular science vehicles to increase capacity.

2.3.3. Strengthening Omni-Channel Management. Massive mobile Internet applications have created multi-channel channels in the network, expanding the scope of no application boundaries, integrating online and offline, and taking multichannel channels as the development goal. Overseas "tentacles" (such as opening foreign experience stores and opening foreign warehouses through display

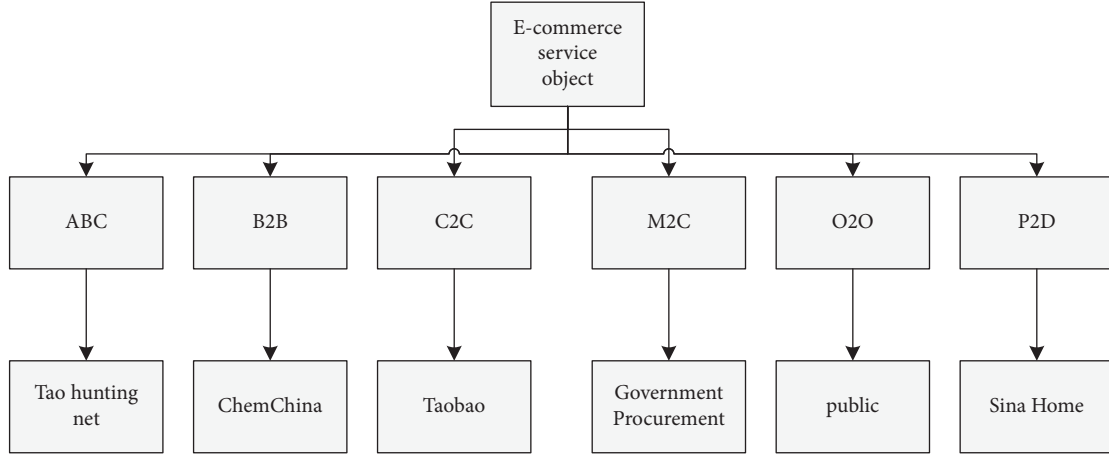


FIGURE 1: e-commerce service groups.

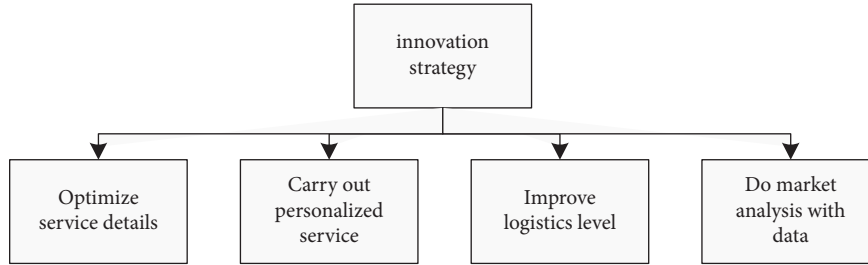


FIGURE 2: e-commerce innovation strategy.

business) are created to shorten the distance with customers; experience services combined with online product information are provided; customer trust, discounts, and promotions are built; and it is inspiring. Consumption provides value-added services for enterprises. The proposed model of e-commerce service is shown in Figure 3.

3. Intelligent Computing Algorithm

3.1. Federated Average Algorithm. In traditional machine learning methods, feature extraction needs to capture unique features based on images and unique detection purposes, such as HOG features that emphasize the outline of objects and Haar features that focus on light and dark contrast. After the features are described, they are sent to the machine learning algorithm for classification, such as SVM and AdaBoost, and then determine the classification of objects. The image detection and recognition tasks are completed by performing the sliding frame operation on the image or substituting the above process into the preprocessed ROI frame.

Centralized learning algorithm, distributed learning across devices, learns local model updates and occasionally interacts with a central server to coordinate global learning objectives. Unlike traditional machine learning methods, blended learning requires training models to be centralized on a computer or data center so that each client device can use a local training dataset to update the model. Federated learning is defined as solving the minimization of the objective loss function according to equation (1), where K is the

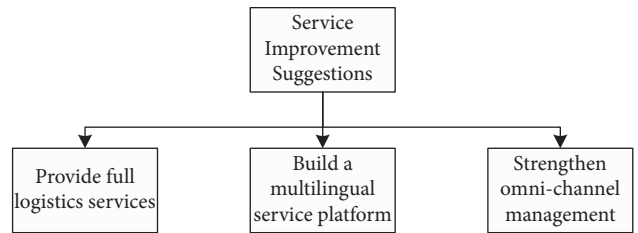


FIGURE 3: e-commerce service suggestion.

total number of client devices and n_k is the number of samples in the dataset on the client device k . The combinatorial learning algorithm uses the shared dataset as $n = \sum_k n_k$ and $p_k = n_k/n$. It is expressed as the proportion of the total set of algorithm training data for each device k .

The data of horizontal federated learning are divided horizontally, and the data schemas of the participants are consistent and have the same characteristics. This is the most mature direction of federated learning at present. The federated learning first proposed and implemented by Google can be regarded as horizontal federated learning, except that the participants are its APP clients.

$$\min f(\omega) = \frac{1}{n} \sum_{k=1}^K n_k F_k(\omega) = \sum_{k=1}^K p_k(\omega). \quad (1)$$

The local prediction loss function trained by the model parameters for each client device k is $F_k(\omega)$, as shown in equation (2). By computing multiple local optima, it is aggregated to achieve global learning loss minimization.

Centralized learning algorithm, distributed learning across devices, learns local model updates and occasionally interacts with a central server to coordinate global learning objectives. Unlike traditional machine learning methods, federated learning requires training models to be centralized in a data center on a machine or computer, allowing each client device to use a local training dataset for model updates. Federated learning is defined to solve the objective loss function minimization.

$$F_k(\omega) = \frac{1}{n_k} \sum_{i \in n_k} f(x_k, \omega). \quad (2)$$

This will improve common patterns in connected learning systems. To solve the objective equation (1), FedAvg first randomly selects k units from a subset of system units at each computation iteration and then uses a combined FedSGD optimization method to globally implement each selected unit, computing the sum of the global state and local data.

$$\begin{aligned} g_k &= \Delta F_k(\omega_k), \\ \forall k, \omega_{t+1}^k &\leftarrow \omega_t - \eta g_k. \end{aligned} \quad (3)$$

In each round of the update round, the server collects training data from all devices participating in that training round of the pattern and calculates the weighted average system update pattern according to equation (4), where η represents the training learning rate.

$$\omega_{t+1} \leftarrow \omega_t \eta \sum_{k=1}^k 1. \quad (4)$$

The number of elements in the FedAvg algorithm plays a crucial role in the speed of convergence and the accuracy of predictions. Some people suggest adding the stack size to some value to approximate disk. When installing a large compressed package, each device can speed up the calculation of the same amount of data, improve the convergence speed of the system, reduce the number of iterations, and keep the training of the system at a high enough level of accuracy.

3.2. Balanced Optimization Algorithm. In the equilibrium optimization algorithm, two points P_1 and P_2 are used within a hypersphere of radius of 1 for local development and global exploration, respectively. The search radius δ_1 based on point P_1 will become smaller and smaller, which has the meaning of shrinking inward, corresponding to the yin, while the search radius δ_2 based on the point P_2 will become larger and larger. It has a sense of outward expansion, which is consistent with any Yang pair. In an intelligent optimization algorithm, local development and global exploration are both complementary and competitive, corresponding to yin-yang mutual root and yin-yang opposition, respectively. In the calculation process, the local search and global search based on points P_1 and P_2 are continuously strengthened, which corresponds to both yin and yang. If point P_2 is better than point P_1 , then these two points are exchanged, and the

sympathetic algorithm corresponding to yin and yang is repeated based on points P_1 and P_1 . The optimization search of P_2 is expected to achieve a balance between local development and global search, corresponding to the balance of yin and yang. In the specific implementation, the yin-yang balance optimization algorithm mainly includes two stages: the solution update based on the archive set and the solution update based on the hypersphere. The main contents of these two stages are given below. The search radius δ_1 and δ_2 are updated, and the calculation method is as follows:

$$\begin{aligned} \delta_1 &= \delta_1 - \left(\frac{\delta_1}{\alpha}\right), \\ \delta_2 &= \delta_2 + \left(\frac{\delta_2}{\alpha}\right), \end{aligned} \quad (5)$$

where α represents the scaling factor. In this stage, P_1 is the center, δ_1 is the radius, P_2 is the center, and δ_2 is the radius to perform local search and global search in the hypersphere. According to the algorithm design, these two searches use the same solution update equation. For the convenience of expression, let P and δ denote the search center and radius. Before updating the solution, firstly 2D identical points P are generated, denoted by $NP_1, NP_2, \dots, NP_{2D}$, respectively, and then the update operation on these 2D points is performed. In the algorithm, one component or all components of a point can be updated. A component update equation for a point is as follows:

$$\begin{aligned} NP &= P^j + \delta \times \frac{r}{\sqrt{2}}, \\ NP &= P^j + \delta \times \frac{r}{\sqrt{2}}, k = D + 1, D + 2, 2D. \end{aligned} \quad (6)$$

Among them, NP represents the NP component of point j ; P^j represents the P component of point r ; and r represents the random number between 0 and 1. When updating all components of the point, $2D \times D$ is also used. Binary matrix B requires each binary string of the matrix to be unique, and the updated equation for all components of points is as follows:

$$\begin{aligned} NP_k &= P^j + \delta \times r, B_k^j = 1, \\ NP &= P^j - \delta \times r, B_k^j = 0, \end{aligned} \quad (7)$$

where B_k^j represents the matrix element at row k and column j . In the algorithm, one of the above two update methods is selected with a probability of 50%. It has the characteristics of strong fine-tuning ability and applies wavelet to the learning of these elite solutions. Let X be an elite solution in the file set, and the new solution after learning through the wavelet elite solution is X^* . The specific method is as follows:

$$X^* = \gamma X + r(L + U). \quad (8)$$

Among them, γ is the wavelet function value; r is a random number between 0 and 1; and U and L are the upper and lower bounds of the variable X . Because the Morlet wavelet has excellent time-frequency characteristics and

dynamic characteristics, it is a typical representative of the dynamic change space of wavelet function, this study will use the Morlet wavelet in the calculation of equation (8), and its calculation method is as follows:

$$\begin{aligned} \gamma &= \frac{1}{\sqrt{a}} \exp\left(1\left(\frac{\Phi}{2}\right)^2\right) \cos\left(5\left(\frac{\Phi}{2}\right)\right), \\ a &= \exp\left(-\ln g \times \left(1 - \frac{t}{T}\right)^\xi\right) + \ln g. \end{aligned} \quad (9)$$

Among them, g represents the upper bound of a ; t represents the current number of iterations of the algorithm; T represents the maximum number of iterations; ξ represents the shape parameter. In the algorithm, the elite solution retained in the archives is compared with the new solution learned by adopting the wavelet elite solution, and the best two solutions to P_1 and P_2 are assigned, respectively. In addition, if these elite solutions are local optimal solutions, the learning of these solutions can also jump out of the local extreme points to avoid premature convergence of the algorithm.

g represents the upper bound of a ; t represents the current number of iterations of the algorithm; T represents the maximum number of iterations; ξ represents the shape parameter. In the algorithm, the elite solution retained in the archives with the new solution learned by adopting the wavelet elite solution is compared, and the best two solutions to P_1 and P_2 , respectively, are assigned.

3.3. Lightweight MobileNet-SSD Model Construction. To adapt to the computing power limitation of embedded devices, this study constructs the MobileNet-SSD network, adopts the lightweight MobileNet feature extraction network, combines it with the SSD detection network, and replaces the backbone network VGG-16 in the SSD with MobileNet, which greatly reduces the memory usage. Then, patches of different scales and aspect ratios are placed a priori on the feature maps of different scales, and the predicted boundary patches are based on the previous patch. The size of the previous image depends on the scale and aspect ratio. The rules for scaling the previous frame in different target maps are as follows:

$$S_k = S_{\min} + \frac{S_{\max} - S_{\min}}{M - 1} (k - 1), \quad k \in [1, m]. \quad (10)$$

In the formula, the K th feature map of S_k shows the relationship between the size of the previous frame and the feature map; S_{\min} and S_{\max} represent the maximum and minimum values, respectively; m represents the number of map features. From equation (10), it can be seen that as the map feature size decreases, the scale of the previous field increases linearly. This article predefines the aspect ratio of the box according to the prior configuration rules of the SSD box:

$$a_r \in \left\{1, 2, 3, \frac{1}{2}, \frac{1}{3}\right\}. \quad (11)$$

In the formula, a_r is the aspect ratio of the prior frame. According to the aspect ratio and the scale of the a priori

frame, the width and height of the prior frame are calculated, and the calculation formula is as follows:

$$\begin{aligned} w_k^a &= s_k \sqrt{a_r}, \\ h_k^2 &= \frac{s_k}{\sqrt{a_r}}, \end{aligned} \quad (12)$$

where w_k^a and h_k^2 are the width and height of the prior frame, respectively. The loss of the whole process is divided into two parts, the weighted sum of the position loss and the confidence loss, that is, the loss function. The input sample x is defined, and then, the loss function is defined as follows:

$$L(x, c, l, g) = \frac{1}{n} (L_{\text{conf}}(x, c)) + \alpha L_{\text{conf}}(x, c, l, g), \quad (13)$$

$$Pe(Q(K + 1)) = S_i Q(k) = s_j.$$

In the formula, c is the trust value of the trust class; l is the predicted value of the associated box position corresponding to the previous box; g is the position parameter of the actual object; and N is the number of positive samples in the previous field. Finally, non-maximum suppression (NMS) is used to reduce the number of negative samples. Since multiple multiscale feature maps will generate a large number of prior frames, which contain a large number of redundant and overlapping samples, resulting in redundant computation, NMS can be used to perform iterations the traversal-elimination process filters the a priori boxes, which can effectively improve the network performance.

4. Prediction and Evaluation of e-Commerce Services

4.1. e-Commerce Service Evaluation Index of Intelligent Computing. We summarized the questions in the questionnaire and came up with 10 secondary indicators. These include the secondary indicators of the customer service index system, the popularity and satisfaction of customer service attitudes, the speed, safety, attitude, price, and other indicators of secondary logistic services. By analyzing the indicator system, we are satisfied with the logistics of Shentong. Some categories are listed in Tables 1 and 2.

Among them, in the establishment of the merchant satisfaction evaluation index system, the first-level index is the merchant's satisfaction, and the second-level indicators are the merchant's after-sales service, the merchant's reputation, and the attitude of the merchant's customer service; in the establishment of the logistic satisfaction evaluation index system, we found that the satisfaction of logistics is the first-level indicator, and the second-level indicators are the speed of logistics, the safety of logistics, the service attitude of logistics, and the price of logistics.

When establishing an index system to measure seller satisfaction, the survey questions are summarized into first-level indicators, and the second-level indicators are salesperson service, salesperson popularity, and salesperson attitude. Dealer customer service: when establishing the logistic satisfaction index system, we found that logistic

TABLE 1: Establishment of the evaluation index system of merchant satisfaction.

First-level indicator	Secondary indicators	Symbol
Merchant satisfaction	After-sales service	H1
	Reputation	H2
	Customer service attitude	H3

TABLE 2: Establishment of the evaluation index system of logistic satisfaction.

First-level indicator	Secondary indicators	Symbol
Logistic satisfaction	Logistic speed	T1
	Safety	T2
	Service attitude	T3
	Logistic price	T4

satisfaction is the first-level indicator, and the second-level indicators are logistic speed, logistic safety, service logistic ratio, and logistic price. The data collected can be used to assess customer satisfaction with services, popularity, customer service, logistic speed, security, and service and trade logistic prices. “Very satisfied” represents 5 points, “satisfied” represents 4 points, “generally satisfied” represents 3 points, “dissatisfied” represents 2 points, and “very dissatisfied” represents 1 point; the 5-year total score of each indicator is calculated on the basis of annual satisfaction. By calculation, we get Figure 4.

Through the analysis of Figure 4, we find that the membership degree also increases with the increase in the year, which indicates that the evaluation of the e-commerce service is getting better and better each year. Through the increase in the year, we also find that the weighted average satisfaction has been increasing the rate of increase and membership increase in 2019–2020 is the fastest, indicating the highest e-commerce satisfaction in this year.

4.2. Prediction of e-Commerce Service Satisfaction Based on Intelligent Computing. It can be seen from the following figure that there is not much difference between the predicted value and the actual value, indicating that the e-commerce service satisfaction prediction is effective. In 2018, the actual comprehensive score of service satisfaction was 2.8, the prediction of polynomial fitting was 2.9, and the prediction of Gaussian curve fitting was 2.98; in 2019, the actual comprehensive score of service satisfaction was 3.2, the prediction of polynomial fitting was 3.26, and the prediction of Gaussian curve fitting was 3.2. The forecast is 3.3; the actual comprehensive score of service satisfaction in 2020 is 3.9, the polynomial fitting forecast is 3.81, and the Gaussian curve fitting forecast is 3.86; in 2021, the actual comprehensive score of service satisfaction is 4.5, and the polynomial fitting forecast is 4.56. Gaussian curve fit predicts 4.44, as shown in Figure 5.

The model can help e-commerce service platforms to quickly judge the indicators that affect satisfaction. Through the gradual regression results of the satisfaction prediction model, the improvement of indicators such as after-sales service, customer service attitude, and logistic speed, safety,

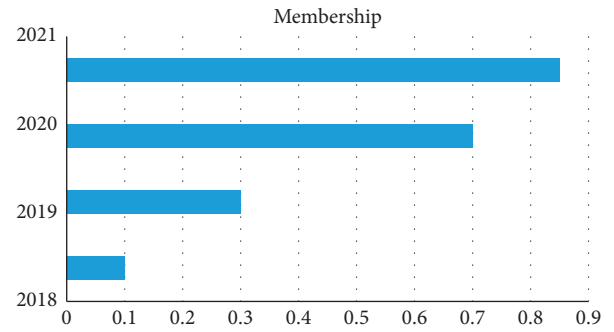


FIGURE 4: Weighted average satisfaction.

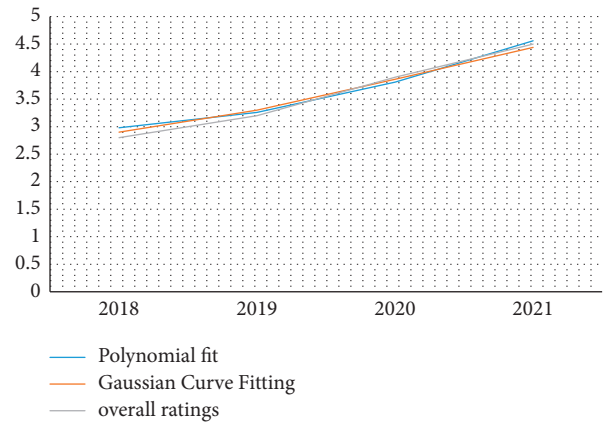


FIGURE 5: Fitting comparison between actual and predicted values of e-commerce service satisfaction.

service attitude, and logistic price can be obtained. It can improve service satisfaction. The fitting result of stepwise regression analysis is $R^2 = 0.9996$, indicating that the model has a high degree of fit, as shown in Table 3.

4.3. Comparison of Service Accuracy under Intelligent Computing. In this article, we use the intelligent computing method to calculate the e-commerce service satisfaction evaluation, which improves the accuracy of the effect evaluation. In order to obtain the evaluation of e-commerce service satisfaction under intelligent computing, the intelligent computing method is compared with other computing methods in accuracy. We conducted a comparison test, and the comparison results are shown in Figure 6:

According to the experimental data of the figure, we can know that the evaluation accuracy of the algorithm after intelligent calculation is the highest among the three methods. When the number of times reaches 40, the evaluation accuracy of the intelligent algorithm can reach about 0.9, and when the number of times reaches 30, in the three methods the accuracy of the algorithm is the closest to around 0.5.

4.4. Performance Test. The performance advantages of the intelligent algorithm technology model proposed in the article are tested. The test will test the models of the three algorithms proposed in the article. The smart algorithm is an

TABLE 3: Stepwise regression analysis results of the service satisfaction prediction model.

Secondary indicators	Analysis results		
	Correlation coefficient	P value	Saliency
After-sales service	0.273	0.03	Significant
Reputation	0.028	0.105	Not obvious
Customer service	0.309	0.0169	Not obvious
Logistic speed	0.021	0.0298	Not obvious
Safety	0.0294	0.0076	Not obvious
Service attitude	0.243	0.0243	Not obvious
Logistic price	0.225	0.0345	Not obvious
Fitting results	Intercept = 1.154	$R^2 = 0.9996$	

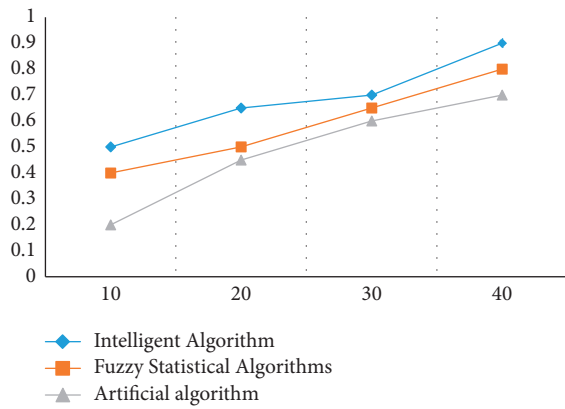


FIGURE 6: Comparison of evaluation accuracy.

TABLE 4: Performance of each model on the test set.

Model	Accuracy (%)	Accuracy (%)	Score (%)
Fuzzy statistical algorithm model	89.12	89.56	90.48
Intelligent algorithm model	92.46	93.27	93.45
Artificial algorithm model	85.45	85.43	86.18

ambiguous statistical algorithm and the pseudo-algorithm model runs on a test suite and an integrated test suite, respectively. The test suite is used to evaluate the general capabilities of the final model. A set of hybrid tests is used to tune the model's hyperparameters, and initially, the model's capabilities are evaluated. The results of the tests are recorded to verify the validity of the three sample ratings. A curve according to the test results is drawn.

According to the data in the table and graph, we can conclude that after running on the test set, the model accuracy rate of the fuzzy statistical algorithm can reach 89.12%, the accuracy rate can reach 89.56%, the accuracy rate of the intelligent algorithm can reach 92.46%, and the accuracy rate can reach 92.46%. It reaches 93.27%, which is the highest index value among the three experimental models. The accuracy of the artificial model is 75.14%, which is the lowest among the three systems, and the fuzzy statistical

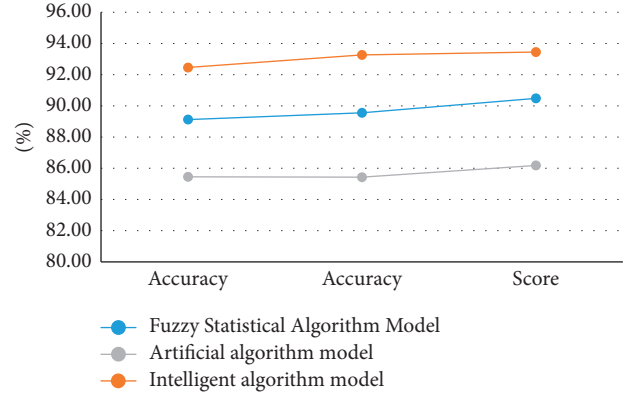


FIGURE 7: Curve of the test set.

TABLE 5: Performance of each algorithm on the mixed test set.

Model	Accuracy (%)	Accuracy (%)	Score (%)
Fuzzy statistical algorithm model	87.88	87.12	88.96
Intelligent algorithm model	90.12	90.24	90.29
Artificial algorithm model	82.14	82.47	82.64

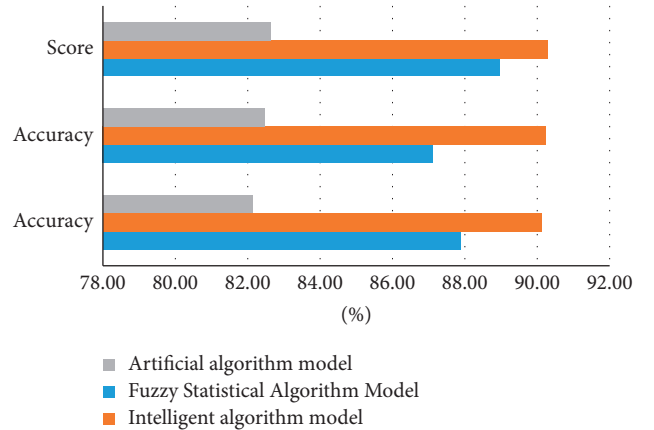


FIGURE 8: Performance on the mixed test set.

model is in the middle state. According to the curves of the three algorithms, we can also see that the curve values of the intelligent computing and fuzzy statistical algorithm models are very stable, and the experimental results also show that the performance of the intelligent computing algorithm is the best, as shown in Table 4 and Figure 7.

According to the data in Table 5 and Figure 8, after running the hybrid test package, the performance of the three models decreases somewhat, but the performance of the smart computer model is still high. In three models, the accuracy rate of the fuzzy statistical algorithm is 87.25%, and the accuracy rate of the intelligent computer algorithm is 90.12%. According to the performance of the three algorithms, it can be seen that the intelligent computer algorithm is very stable and always at 0.95, whether it is a test set or a mixed test set. The experimental results also show that the model validation accuracy of the intelligent computing algorithm is very high.

5. Conclusion

Through the comparison of algorithms and experiments, we can conclude that the current e-commerce services are facing severe postgraduate entrance examinations, and more and more e-commerce platforms are facing the risk of bankruptcy. In the face of these risks, government departments should introduce corresponding measures, such as introducing corresponding policies to reduce the taxation of merchants; the government should relax the corresponding import and export of goods. Our experiments in the fourth part can be concluded that, after running on the test set, the model accuracy rate of the fuzzy statistical algorithm can reach 89.12%, the accuracy rate can reach 89.56%, the accuracy rate of the intelligent algorithm can reach 92.46%, and the accuracy rate can reach 93.27%, which is one of the highest index values in the experimental model.

Data Availability

The experimental data used to support the findings of this study are available from the corresponding author upon request.

Conflicts of Interest

The authors declare that they have no conflicts of interest regarding this work.

Acknowledgments

This study was supported by the Research on the Service Model of “Cultivation of Live Broadcast e-commerce Professionals in Colleges and Universities+Rural Economic Development” under the Background of Rural Revitalization (JKND2106).

References

- [1] R. G. Kaplinsky, “Unequalisation: What can Be learned from value chain analysis,” *Journal of Development Studies*, vol. 37, no. 2, pp. 117–146, 2000.
- [2] L. Seongu and Heejun, “Intelligent Walking of a Biped Robot Using Soft-Computing Method,” *Information and Control Symposium*, vol. 18, pp. 312–314, 2006.
- [3] W. Deng, C. Rong, and X. Yang, “An intelligent fault diagnosis method based on soft computing and expert system,” *International Journal of Engineering Intelligent Systems for Electrical Engineering & Communications*, vol. 18, no. 2, pp. 77–84, 2010.
- [4] J. Choi, C. Choi, K. Yim, J. Kim, and P. Kim, “Intelligent reconfigurable method of cloud computing resources for multimedia data delivery,” *Informatica*, vol. 24, no. 3, pp. 381–394, 2013.
- [5] E. Pontelli and T. C. Son, “Designing intelligent agents to support universal accessibility of E-commerce services [J],” *Electronic Commerce Research and Applications*, vol. 2, no. 2, pp. 147–161, 2004.
- [6] M. Pushpalatha and A. V. Kathiravan in *Proceedings of the 2014 international conference on intelligent computing applications—an exclusive WS-ranking method for ranking of web blogs using W*, pp. 392–396, IEEE, Coimbatore, India, June 2014.
- [7] J. Xu, V. N. Hsu, and B. Niu, “The impacts of markets and tax on a multinational firm’s procurement strategy in China,” *Production and Operations Management*, vol. 27, no. 2, pp. 251–264, 2018.
- [8] W. Z. Liu, Q. Y. Tao, Q. He, and L. J. Yu, “Application of Log4j in E-commerce services,” *Applied Mechanics and Materials*, vol. 635–637, pp. 1517–1521, 2014.
- [9] V. Loia, S. Senatore, and M. I. Sessa, “Customized advertising in E-commerce services provision,” *è-è*, vol. 9, no. 4, pp. 355–363, 2008.
- [10] Z. Xu, C. Shao, S. Wang, and C. Dong, “Analysis and prediction model of resident travel satisfaction,” *Sustainability*, vol. 12, no. 18, p. 7522, 2020.
- [11] J. Gao, J. Song, and L. Han, “Research on analysis and prediction of elderly medical satisfaction based on convolutional neural network,” *Journal of Physics: Conference Series*, vol. 1944, no. 1, Article ID 012013, 2021.
- [12] H. Kook and Lee, “Prediction and evaluation of indoors noise level of exhibition room in museum by road traffic noise,” *Journal of Korean Society of Environmental Engineers*, vol. 32, no. 8, pp. 787–794, 2010.
- [13] Y. Chen, Y. Liu, and M. Zhang, “Predicting User Satisfaction in SERPs with Mouse Movement Information,” *IEEE Transactions on Knowledge & Data Engineering*, vol. 7, 2017.
- [14] A. Monika, “Wisdom and life satisfaction in old age,” *J Gerontol B Psychol, Soc*, vol. 12, pp. 15–27, 1997.

Research Article

Application of Convolutional Neural Network in Motor Bearing Fault Diagnosis

Shuiqin Zhou, Lepeng Lin, Chu Chen, Wenbin Pan, and Xiaochun Lou 

Fair Friend Institute of Intelligent Manufacturing, Hangzhou Vocational and Technical College, Hangzhou 310018, China

Correspondence should be addressed to Xiaochun Lou; 1998010149@hzvtc.edu.cn

Received 10 May 2022; Revised 11 June 2022; Accepted 22 July 2022; Published 28 August 2022

Academic Editor: Le Sun

Copyright © 2022 Shuiqin Zhou et al. This is an open access article distributed under the Creative Commons Attribution License, which permits unrestricted use, distribution, and reproduction in any medium, provided the original work is properly cited.

In the field of mechanical and electrical equipment, the motor rolling bearing is a workpiece that is extremely prone to damage and failure. However, the traditional fault diagnosis methods cannot keep up with the development pace of the times because they need complex manual pretreatment or the support of specific expert experience and knowledge. As a rising star, the data-driven fault diagnosis methods are increasingly favored by scholars and experts at home and abroad. The convolutional neural network has been widely used because of its powerful feature extraction ability for all kinds of complex information and its outstanding research results in image processing, target tracking, target diagnosis, time-frequency analysis, and other scenes. Therefore, this paper introduces a convolutional neural network and applies it to motor-bearing fault diagnosis. Aiming at the shortcomings of fault signal and convolutional neural network, a large-scale maximum pooling strategy is proposed and optimized by wavelet transform to improve the fault diagnosis efficiency of motor bearing under high-voltage operation. Compared with other machine learning algorithms, the convolution neural network fault diagnosis model constructed in this paper not only has high accuracy (up to 0.9871) and low error (only 0.032) but also is simple to use. It provides a new way for motor bearing fault diagnosis and has very important economic and social value.

1. Introduction

With the development of the economy, mechanical equipment is developing towards large-scale and integration, and the structure is becoming more and more complex, such as high-speed railway, aviation aircraft, nuclear power plant, and so on. These equipment put forward high requirements for reliability. If mechanical faults cannot be diagnosed in time, it may lead to machine shutdown, economic losses, and even accidents [1, 2]. Therefore, the research on mechanical fault diagnosis is of great significance.

Rolling bearing is an important part of rotating machinery. It plays an important role in supporting the high-precision rotation of the mechanical rotating body. It is a key component prone to damage [3]. Different electric rotating machinery and equipment often work in various complex working environments, and the uncertain change of working environment can easily lead to different types of damage to rolling bearing, such as high temperature, high heat, high

speed, overload load, and so on. If these factors are not controlled in time, they will greatly affect the working life of bearing [4]. As the key parts of most rotating machinery and equipment, once the rolling bearing fails, the replacement of maintenance goods is not timely, which is likely to lead to the paralysis of the whole power unit and even the scrapping of the equipment, resulting in major accident casualties and huge loss of economic property [5, 6].

In recent years, with the rise of computer technology, in order to more accurately and quantitatively describe the performance indexes of electromechanical equipment, many scholars are committed to the research of information diagnosis technology of motor bearing fault. By introducing dyadic discrete wavelet transform, Chen et al. realized the automatic selection of weight factors in the network and then realized the automatic acquisition of bearing fault characteristics [7]. Tan et al. used the public data set of bearing fault of Case Western Reserve University in the United States for diagnosis. The final results showed that this

method performed significantly better than the traditional BP neural network [8–10]. Li et al. proposed a bearing fault diagnosis technology combining CNN and wavelet time-frequency map by using a convolution network for excellent feature extraction and generalization performance of data. Relevant experiments were carried out using fault data sets. The results show that this method can effectively classify bearing fault types [11–13]. Han et al. developed a bearing fault classification model based on a deep neural network (DNN). The feature of this method is to directly extract the features of the original fault data and use it as the feature input of the deep neural network model to realize the diagnosis of fault data [14, 15]. Aiming at the problem of manual acquisition of fault characteristics in traditional fault diagnosis, Lu et al. proposed a bearing fault diagnosis method based on a deep self-coding network and carried out experiments under the network model. The results show that this method can effectively diagnose the fault data [16–18]. David et al. proposed a novel network model LAMSTAR and then used the proposed lamstar model to classify the bearing fault signals. Under this method, the equipment is tested at different speeds, and finally, the fault identification accuracy is more than 96% [19–23].

It can be seen from the above research that at present, the CNN fault diagnosis model has been widely used in motor bearing fault diagnosis, and the accuracy of bearing fault diagnosis has gradually improved with the deepening of research. However, many studies also found that when the machine works, because the load often changes greatly and the speed will change within a certain range, it is difficult for the conventional method to be robust to the load and speed at the same time. In addition, the acquisition of training samples is very difficult, and the weak generalization ability in the case of small samples also limits the development of these fault diagnosis methods. The strategy of weight summation and large-scale maximum pooling is proposed to solve the translation invariance of features and enhance the generalization ability of small samples. Improve the practical application ability of the CNN motor bearing fault diagnosis model in bearing fault diagnosis.

2. Basic Theory of CNN

2.1. Basic Structure of CNN. The CNN is generally composed of three neural network layers: convolutional layer, pooling layer, and fully connected layer, as well as an output layer (softmax and other classifiers). Its essence is a multilayer perceptron (MLP) neural network. Each layer is composed of multiple two-dimensional plane blocks, and each plane block is composed of multiple independent neural elements, as shown in Figure 1.

2.1.1. Convolutional Layer. The convolutional layer is partially connected with the neurons of the upper layer through the local receptive field. The neurons in the same local receptive field are associated with the corresponding pixels in the image area with fixed two-dimensional plane coding information, forcing the neurons to extract local features.

Many groups of different neurons are distributed at each position of each layer, and each group of neurons has a set of input weights. These weights are associated with the neurons in the rectangular block of the previous neural network, that is, shared weights, which reduces the number of weights and the complexity of the network model. Convolutional layer plays an important role in feature extraction in CNN. The observation features obtained by the local sensing domain method are independent of translation, scaling, and rotation. Its weight-sharing structure reduces the number of weights and further reduces the complexity of the network model.

2.1.2. Pooling Layer. The pooling layer is a feature mapping layer. Different continuous ranges in the convolution feature map are selected as the pooling area, and then the maximum or average value of the feature is taken as the feature of the pooling area, so as to reduce the dimension of the feature vector, realize the local average and sampling, and reduce the sensitivity of the feature mapping output to translation, rotation, scaling, and other forms of transformation. The pooling layer usually follows the convolutional layer, which forms a structure of twice feature extraction, so that the network has good distortion tolerance in the identification of input samples.

2.1.3. Fully Connected Layer. The fully connected layer is a structure in which the neurons in this layer and the neurons in the upper layer are connected in pairs, but the neurons in this layer are not connected. It is equivalent to the hidden layer in the multilayer perceptron (MLP). The local feature information is used as the input of the output layer (softmax and other classifiers), and then the convolutional layer is no longer connected. Because after passing through the fully connected layer, the image feature has been reduced from two-dimensional information to one-dimensional information, and the two-dimensional convolution operation cannot be carried out.

2.1.4. Output Layer (Softmax Classifier). Softmax classifier is the generalization of the logistic regression model in multicategory classification. It can predict the possibility (the number of types of sample labels), but here, it is required that the label of each sample must be unique. If it is a multilabel sample, the softmax model is not applicable. Assuming that the input feature is marked as $x^{(i)}$ and the sample label is marked as $y^{(i)}$, which constitutes the training set $S = \{(x^{(1)}, y^{(1)}), (x^{(2)}, y^{(2)}), \dots, (x^{(m)}, y^{(m)})\}$ of supervised learning at the classification level, the forms of hypothesis function $h_{\theta}(x)$ and logistic regression cost function are as follows:

$$h_{\theta}(x) = \frac{1}{\sum_{j=1}^k e^{\theta_j^T x^{(i)}}} \begin{bmatrix} e^{\theta_1^T x^{(i)}} \\ e^{\theta_2^T x^{(i)}} \\ \vdots \\ e^{\theta_k^T x^{(i)}} \end{bmatrix}, \quad (1)$$

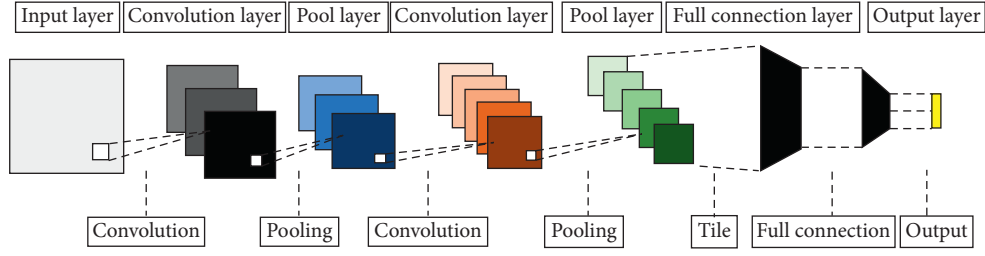


FIGURE 1: Classic structure of CNN.

where $\theta_1, \theta_2, \dots, \theta_k$ is the learnable parameter of the model and $1/\sum_{j=1}^k e^{\theta_j^T x^{(i)}}$ is the normalized term.

$$J(\theta) = -\frac{1}{m} \left[\sum_{i=1}^m \sum_{j=1}^k 1\{y^{(i)} = j\} \ln \frac{e^{\theta_j^T x^{(i)}}}{\sum_{l=1}^k e^{\theta_l^T x^{(i)}}} \right], \quad (2)$$

where $1\{\cdot\}$ is an indicative function, that is, when the value in braces is true, the result of the function is 1; otherwise, the result is 0.

The optimal solution of softmax's cost function is usually solved by iterative algorithms such as random gradient descent method (SGD), Newton method, and quasi-Newton method (L-BFGS).

2.2. Error Propagation of CNN. The convolution neural network adopts error backpropagation and then is optimized by gradient descent method (or conjugate gradient method, L-BFGS method). Residual δ is defined as the influence of the node on the error of the final output value, so residual δL of output layer L is

$$\delta^L = f'(z^L) \odot (y^n - \sigma^n), \quad (3)$$

where \odot represents point-by-point product. Therefore, the weight and bias gradient of the output layer, respectively, are

$$\begin{cases} \frac{\partial E}{\partial \mathbf{W}^L} = \mathbf{x}^{L-1} (\delta^L)^T, \\ \frac{\partial E}{\partial \mathbf{b}} = \delta^L. \end{cases} \quad (4)$$

The convolutional layer is followed by a lower sampling layer, so the upper sampling is required first when calculating its residual.

$$\delta_j^l = \beta_j^{l+1} (f'(z_j^l) \odot \text{up}(\delta_j^{l+1})), \quad (5)$$

where $\text{up}(\cdot)$ indicates upsampling operation. For maximum pooling, copy the residual in layer $l+1$ to the position corresponding to the maximum in layer l and fill the positions of other elements with zero. Summing all elements in the error signal δ_j^l is the gradient of bias in the convolutional layer.

$$\frac{\partial E}{\partial b_j} = \sum_u (\delta_j^l)_u. \quad (6)$$

Considering that the convolution kernel k_{ij}^l is connected with many shared weights, the region corresponding to the convolution kernel k_{ij}^l in the convolution process needs to be considered when calculating its gradient through backpropagation.

$$\frac{\partial E}{\partial k_{ij}^l} = \sum_u (\delta_j^l)_u (p_i^{l-1})_u, \quad (7)$$

where $(p_i^{l-1})_u$ represents the area multiplied by convolution kernel k_{ij}^l in the convolution process in layer x_i^{l-1} .

For the lower sampling layer where the next layer is connected with the convolutional layer, the shared weight needs to be considered when calculating the residual.

$$\delta_j^l = \sum_u (\delta_j^{l-1})_u (q_i^{l-1})_u, \quad (8)$$

where $(q_i^{l-1})_u$ represents the weight in the corresponding convolution kernel k_{ij}^l .

After the gradient is calculated by the above method, the convolution kernel, bias, and the fully connected parameters of the last layer are updated to realize the automatic learning of the convolution kernel, so as to complete the expression and recognition of the signal.

3. CNN Fault Diagnosis Model

3.1. Basic Model of CNN Fault Diagnosis. The idea of the basic model structure of CNN in this paper is shown in Figure 2.

3.2. Basic Idea of CNN Fault Diagnosis. The idea of bearing fault diagnosis in this paper is shown in Figure 3.

3.3. CNN Fault Diagnosis Model Optimization. CNN's unique topology makes it invariant to feature translation and scaling although CNN has been proved to have good application effects in many fields, such as digital recognition, face recognition, voice recognition, pedestrian diagnosis, and so on. However, there are great differences between motor bearing fault diagnosis and the above problems, and the traditional CNN model is difficult to be effectively applied. Therefore, in the application of motor bearing fault diagnosis, in order to accurately diagnose the rolling bearing fault and reduce the impact of rolling bearing fault on equipment operation, the combination of wavelet packet transform analysis and convolutional neural

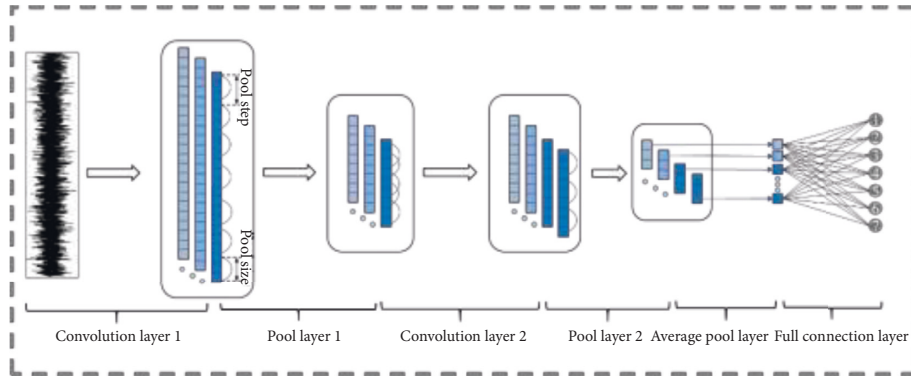


FIGURE 2: Basic model structure of CNN.

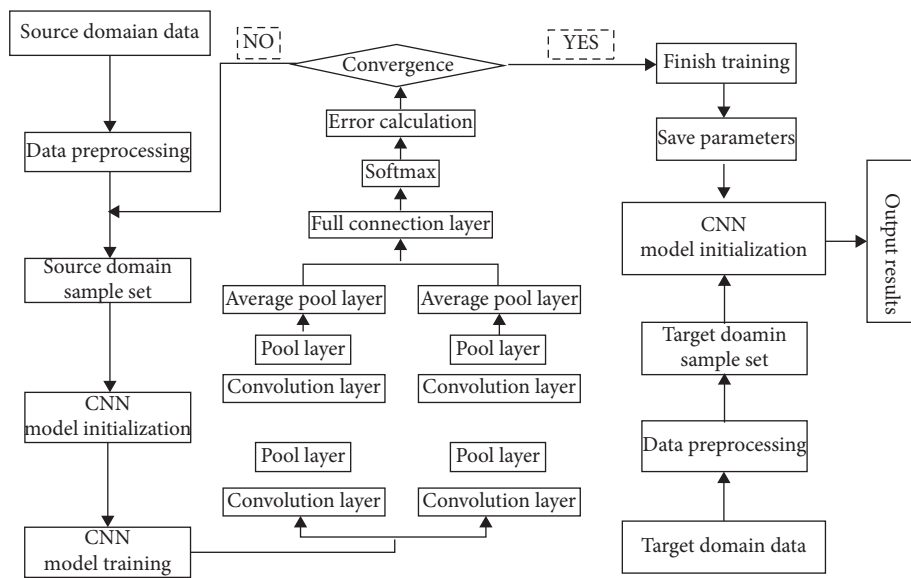


FIGURE 3: CNN bearing fault diagnosis idea.

network is proposed to optimize the motor rolling bearing fault diagnosis model. The optimization steps are as follows:

Step 1. Denoise the bearing vibration signal through wavelet packet transform and analyze the signal in the time domain and the frequency domain by wavelet packet analysis method. The three-layer decomposition process of the wavelet packet is shown in Figure 4.

Step 2. Extract the eigenvalues of the denoised signal with the eight characteristics of the signal as indicators and diagnose the bearing fault a priori through the time domain and frequency domain information map.

Step 3. Taking the extracted eigenvalues as samples, the bearing fault category is classified and diagnosed by a convolution neural network model.

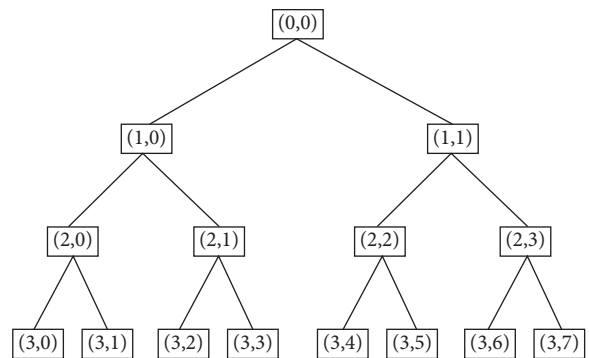


FIGURE 4: Tree structure of wavelet packet decomposition.

4. Experimental Process

The vibration signal of the rolling bearing is collected through the rolling bearing fault simulation test bed. Firstly, the collected signal is processed by wavelet packet transform, and the noise signal is eliminated to facilitate

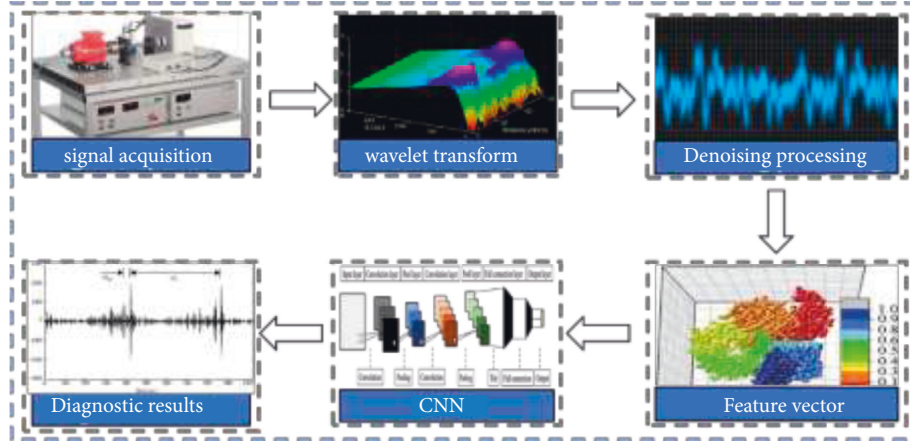


FIGURE 5: Fault diagnosis flow chart after wavelet transform.

the subsequent diagnosis. Then extract the fault feature information, input the obtained feature vector into CNN for training and testing, and finally diagnose the fault category through CNN. The specific process is shown in Figure 5.

4.1. Data Acquisition. The experimental data come from the comprehensive mechanical fault simulation experimental platform. The experimental platform is shown in the first figure of Figure 5. The platform mainly includes five parts: engine, governor, rotor, shaft, and rolling bearing. The rolling bearing with a fault diameter of 0.3 mm is selected as the experimental object, and the sensor is arranged at the end of the fault bearing.

The experiment collects a variety of fault data at 10 Hz, 20 Hz, and 40 Hz. The data types include the faults of the outer ring, the inner ring, and rolling element and the data of normal bearing. Set the sampling frequency to 1 kHz, take the sampling time for 3 min, and finally pass the data collected by the sensor through MATLAB 2016b[®] (The MathWorks, Inc, Natick, MA, USA) software conversion to save the mat file. After that, the signal is effectively cut. According to the sampling frequency, every 1,024 sampling points are selected as a whole fault sample. The four data types under each working condition are 100 samples, except for 300 normal signal samples. Finally, the sum of the four fault type sample data under each working condition is 600. Then the data is preprocessed and divided into two groups: one is used for model training, which is called the training set, and the other group is used for model testing, which is called the test set.

4.2. Data Preprocessing. The data preprocessing process mainly is as follows: using data window shift technology to enhance the original time-domain vibration signal and generating training and test sample sets. The “single heat” coding method is used to label the fault type, and then all the data in the training and test set are standardized.

4.2.1. Data Enhancement. To realize the high recognition rate of deep learning fault diagnosis, a large number of data samples are needed as support, and the correlation between the fault vibration signal of the rolling bearing cage and the

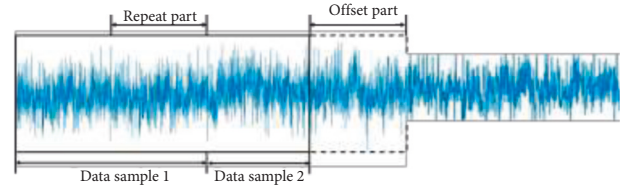


FIGURE 6: Overlapping sample segmentation.

adjacent time series signal is retained. In this paper, a data window shift technique is proposed to segment overlapping samples to achieve data enhancement. The division method is shown in Figure 6. This method can preserve the continuity and periodicity between time series signals, avoid the problem that equal distance sampling is difficult to express all the information characteristics of signals, greatly increase the total number of samples input to network training, and give full play to the powerful learning ability of the model.

As can be seen from Figure 6, if the total length of vibration signal data in fault state is L , the length of the sample is l , and the vibration signal is divided by a certain offset m , the data length of the overlapping part is $l - m$.

- (1) Number of divisible samples under current signal length D :

$$D = \left\lfloor \frac{L - l}{m} + 1 \right\rfloor, \quad (9)$$

where $\lfloor \cdot \rfloor$ is the downward rounding operator.

Expansion multiple of the sample set after data enhancement β :

$$\beta = \frac{l(L - l + m)}{Lm}. \quad (10)$$

- (2) Position x_i of the i segmented sample in the vibration signal data.

$$x_i = L[(i - 1) \times m + 1] : (i - 1) \times m + l, i \in [1, D], \quad (11)$$

where B is the split sample, and sample data sets of different sizes can be obtained by setting the corresponding offset M .

4.2.2. Data Standardization. In order to improve the convergence speed and accuracy of the model in deep learning, the sample set is usually standardized and preprocessed. The standardized formula is as follows:

$$\bar{x} = \frac{x - x_{\text{mean}}}{x_{\text{std}}} \quad (12)$$

Where x_{mean} is the mean value of sample data, x_{std} is the standard deviation of sample data, and x is the result after standardization.

At present, formula (12) is one of the most commonly used methods in big data normalization processing. Compared with other data normalization processing formulas, this formula has a better processing effect. Using this formula can also greatly improve the convergence speed and accuracy of the model.

After data standardization, the gradient explosion during model training can be prevented, and the reliability of the results can be guaranteed.

4.2.3. Time-Frequency Analysis Based on Wavelet Transform.

In the time-frequency analysis of unstable signals, a wide window is needed to analyze the low-frequency signals in the low-frequency region. On the contrary, a narrow window is needed in the high-frequency region to obtain high-precision amplitude information. However, in the fast Fourier transform, the shape of the window function is fixed. When analyzing the nonstationary signal, there is no adaptability for the signals with different time intervals. Therefore, the fast Fourier transform has some limitations. In order to solve this limitation, the Morlet mother wavelet is introduced into the time-frequency analysis in this paper. Its window area is fixed. It can change the length and height of its window according to the high- and low-frequency characteristics of the signal to adapt to the signal characteristics and ensure the accuracy of time-frequency analysis, its unique multi-resolution characteristics, and the advantages of time-frequency localization, which can well meet the needs of practical engineering. The time-frequency analysis results of the Morlet wavelet are shown in Figure 7. It can be seen from the figure that the Morlet wavelet has a relatively concentrated energy distribution of signal, better frequency resolution at high frequency, more accurate time positioning, and slightly better time-frequency focusing. When this kind of time-frequency analysis method is applied, it not only can reduce the burden of time-frequency analysis but also can effectively improve the learning efficiency and diagnosis accuracy of convolutional neural networks.

4.3. Establishment of CNN Model Based on Bearing Fault Detection in This Paper. The convolutional layer is a supervised deep learning network, which can extract the fault features in the rolling bearing signal by scanning the

convolution kernel on the axis of the image. Usually, a convolutional layer has one or more convolutional nuclei. The neurons of two adjacent convolutional layers are connected with each other. The number of connected neurons is related to the size of the convolution nucleus. By scanning the features, the convolution kernel can take the input data as a matrix, multiply and sum the values in the matrix, and finally superimpose all deviations as follows:

$$\begin{aligned} Z^{l+1}(i, j) &= [Z^l \omega^{l+1}](i, j) + b \\ &= \sum_{k=1}^{K_l} \sum_{x=1}^f \sum_{y=1}^f [Z_k^l(s_0 i + x, s_0 j + y) \omega_k^{l+1}(x, y)] + b, \\ &\cdot (i, j) \in \{0, 1, \dots, L_{l+1}\} = \frac{L_l + 2p_0 - f}{s_0} + 1, \end{aligned} \quad (13)$$

where b is the deviation in neurons; Z^l and Z^{l+1} are the input part and the output part of layer $l + 1$ convolutional layer, respectively; L_{l+1} is the size of the output part Z^{l+1} ; $Z(i, j)$ is the pixel of time-frequency spectrum after wavelet transform; K is the number of channels of the map (the time-frequency map used in this paper is an RGB image, and the number of channels is 3); f , s_0 , and p_0 are the parameters of convolution neural network layer, where f is the size of convolution kernel, s_0 is the step size of convolution operation, and p_0 is the size of padding pixels.

Among them, the activation function used by each convolutional layer is ReLU activation function, and its expression and function image are shown in Figure 8.

After extracting fault features in the convolutional layer, a pooling layer is often needed to filter the extracted fault information and the useless features. The pooling function of the pooling layer is usually preset, which can reduce the dimension of the output of the convolutional layer and make the data compact. This paper selects the maximum pooling layer in the pooling layer, which is used to reduce the estimation mean deviation caused by errors in the training process of the convolutional layer. Generally, the maximum pooling layer is set after the convolutional layer, and the output characteristics of the convolutional layer are maximized by obtaining the maximum value of the feature points. Mathematically, the l -th feature map y_n^l of the n -th pooling layer can be expressed as follows:

$$y_n^l = \text{pool}(y_n^l, p, s), \quad (14)$$

where y_n^l is the n -th input mapping, that is, the n -th input mapping of the previous convolutional layer; $\text{pool}()$ is the maximum pool equation; p is the maximum pool size; and s is the step size of the maximum pool.

The CNN architecture constructed in this paper is shown in Figure 9. In the proposed CNN model, four different convolution paths are used to learn the representation from the input sensor data. Each convolution module is composed of two parts: two-dimensional convolutional layer and maximum pooling layer. These convolutional layers and maximum pooling layers are arranged in parallel, and four

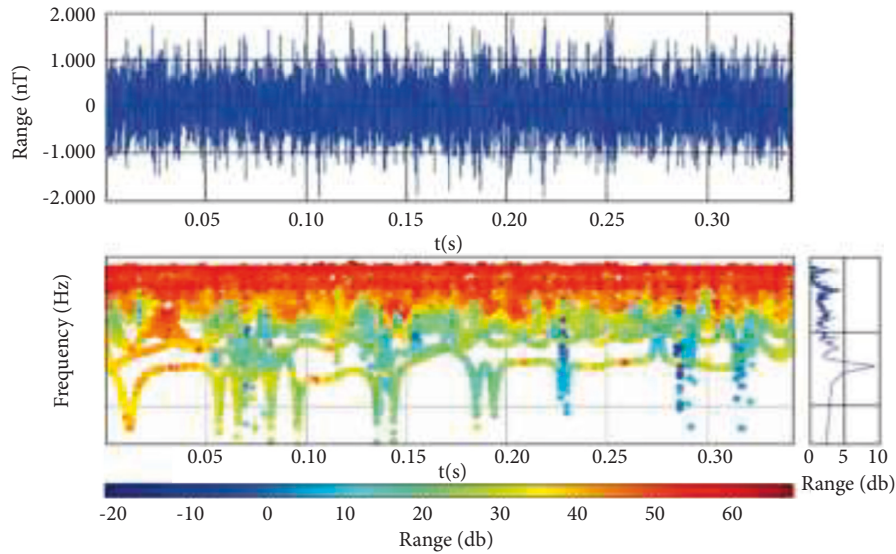


FIGURE 7: Morlet mother wavelet transform.

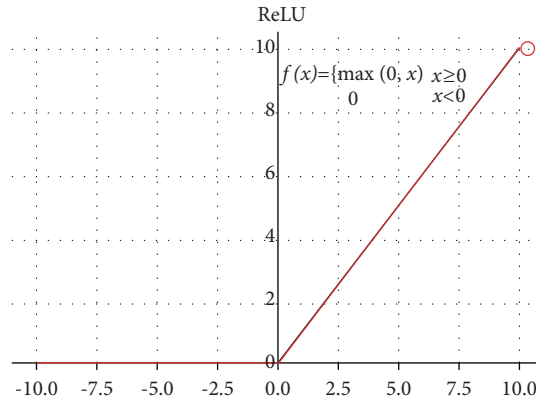


FIGURE 8: ReLU activation function.

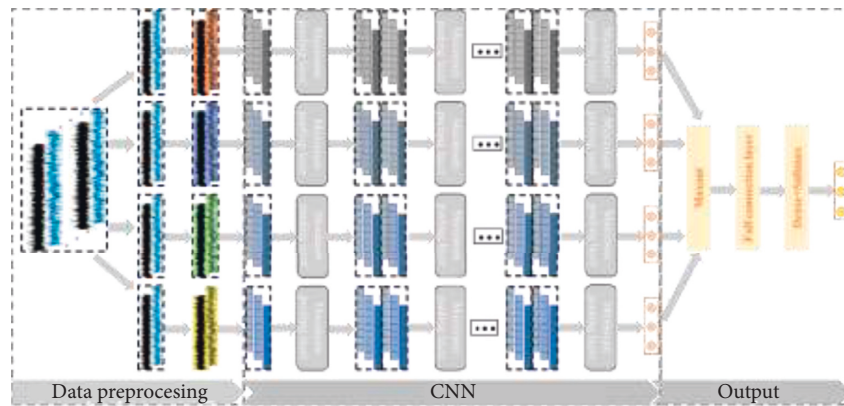


FIGURE 9: CNN model framework.

different convolution kernel sizes are used to extract the fault features at different speeds. In feature learning, there is no interaction between the four convolution paths, and the fault information is extracted independently from the convolutional layers with different convolution kernel sizes, so as to

ensure the integrity of feature extraction. In addition to using different convolution kernel sizes, the four convolution paths are the same in network structure. Each convolution path is constructed by stacking one convolutional layer plus one maximum pooling layer five times. After each

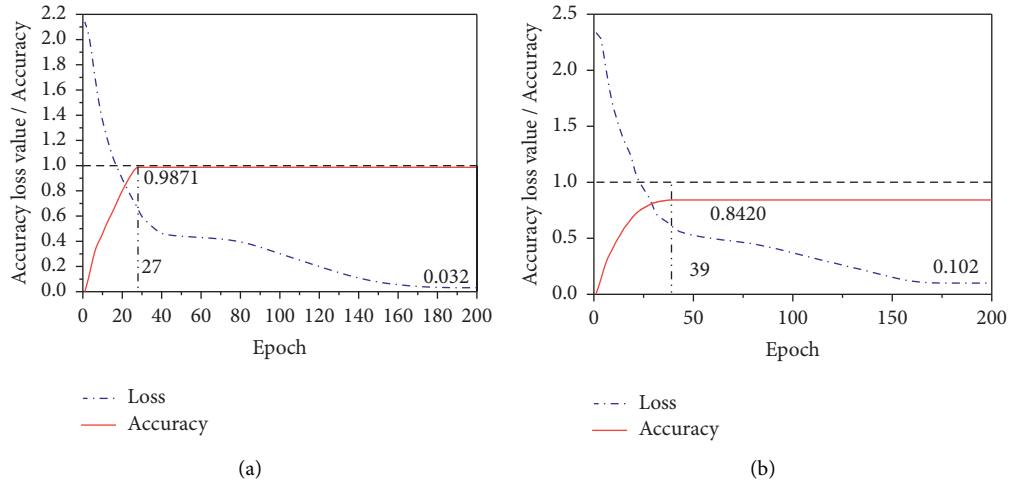


FIGURE 10: CNN training convergence curve: (a) CNN after wavelet transform and (b) CNN.

convolution path, an attention module is added to learn the weight of each channel, suppress useless feature information, emphasize fault-related information, and then flatten these learned features into a one-dimensional vector through the flatten layer. Finally, the four vectors are combined and input into the classification module for classification.

5. Analysis of Experimental Results

5.1. Performance Evaluation of Wavelet Transform. After the network is constructed, the classification prediction results are obtained after 200 times of iterative training, as shown in Figure 10. Figure 10(a) shows the training convergence curve of the CNN after wavelet transform, and Figure 10(b) shows the training convergence curve of the CNN without wavelet transform. Comparing the two figures, it can be found that the network errors of the two models gradually decrease with the increase of epoch. After 27 iterations of the CNN through wavelet transform, the network fully converges. At this time, the network accuracy reaches the best accuracy of 98.71%, and the loss is only 0.032. However, the CNN without wavelet transform needs 40 iterations to converge. At this time, the network accuracy is only 0.8420, but the error is 0.102. It can be seen that compared with the traditional CNN fault detection model, the result of training the network by preprocessing the data through wavelet transform converges faster, and the accuracy is greater than that of training the network without wavelet transform. It shows that the nonstationary original data can be processed through wavelet transform, which reduces the time of network feature extraction and improves the network accuracy.

5.2. Model Generalization and Robustness Verification. It can be seen from Section 4.1 that the CNN model optimized by wavelet transform has high accuracy in detecting the original test set. In order to further verify the generalization ability of the model, build a new test set, input it into the CNN model

and count its classification results to obtain the confusion matrix of the test data, and use column summary and row summary to display the accuracy and recall of each class. The results are shown in Figure 11. It can be seen that the CNN model optimized by wavelet transform has a strong generalization ability, and the deep features of the whole original signal can be obtained through less sample learning.

In order to verify the feature extraction ability of the method proposed in this paper, t-SNE dimensionality reduction technology is used to visualize the image features extracted from the traditional CNN model and the last hidden layer of the optimized CNN model proposed in this paper, as shown in Figure 12. The left figure is the CNN fault data feature visualization image after wavelet optimization, and the right figure is the fault data visualization image of the traditional CNN model. It can be seen from Figure 12 that both methods have efficient feature extraction performance for image data, and the fault features representing each fault type have obvious separability in space. However, in terms of spatial clustering, CNN optimized by wavelet transform is obviously better than the traditional CNN model. For example, the features representing the slight damage of the inner ring are distributed in different spatial positions in the feature space of the traditional CNN model, while they are distributed in similar spatial positions in the feature space of the optimized CNN model. The characteristics representing the severe damage of the inner ring also show more dense clustering in the feature space of the optimized CNN model. It further verifies the detection accuracy of the model proposed in this paper for the fault category of rolling bearing.

Because the above verification only tests a group of fault data and cannot represent the detection accuracy of all faults, in order to further verify the feasibility of the method proposed in this paper, the vibration signals and normal vibration signals of 10 different fault positions and different fault degrees at different bearing positions with the measurement speed of 1,797 r/min and the sampling frequency of 12 kHz are selected as the research object. The collected experimental sample data are shown in Table 1.

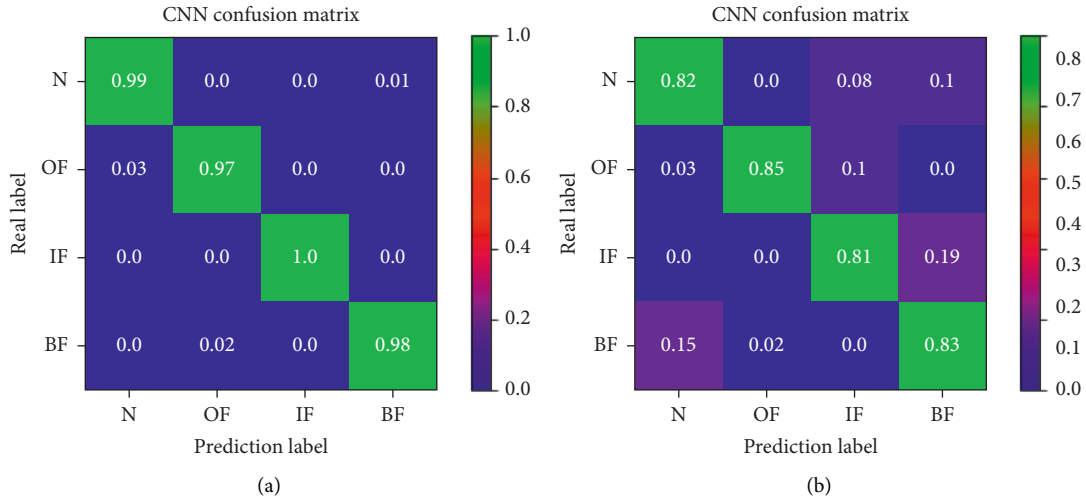


FIGURE 11: CNN training convergence curve: (a) CNN after wavelet transform and (b) CNN.

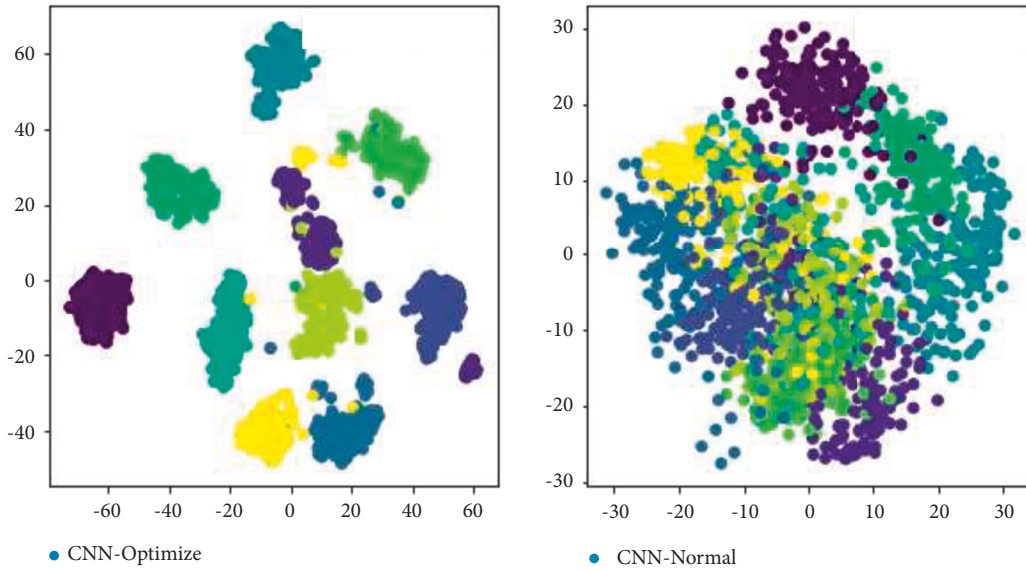


FIGURE 12: Features visualization for faulty data.

TABLE 1: Experimental sample data.

Test number	Detection position	Damage diameter (mm)	Training/validation samples	Test sample
1	Inner	0.3105	1,600/400	400
2	Outer	0.2987	1,600/400	400
3	Roller	0.4136	1,600/400	400
4	Roller	0.2254	1,600/400	400
5	Normal	0.0000	1,600/400	400
6	Roller	0.3512	1,600/400	400
7	Inner	0.3528	1,600/400	400
8	Normal	0.0000	1,600/400	400
9	Outer	0.2911	1,600/400	400
10	Outer	0.3019	1,600/400	400

Figure 13 intuitively shows the fault detection accuracy of the two models in 10 tests. From Figure 10, it can be seen that the CNN algorithm applied to wavelet optimization proposed in this paper has the highest detection accuracy of

bearing fault, the smallest numerical fluctuation, and the best stability, which is basically more than 0.95, while the detection accuracy of bearing fault applied to traditional CNN model algorithm is not only lower than that of the

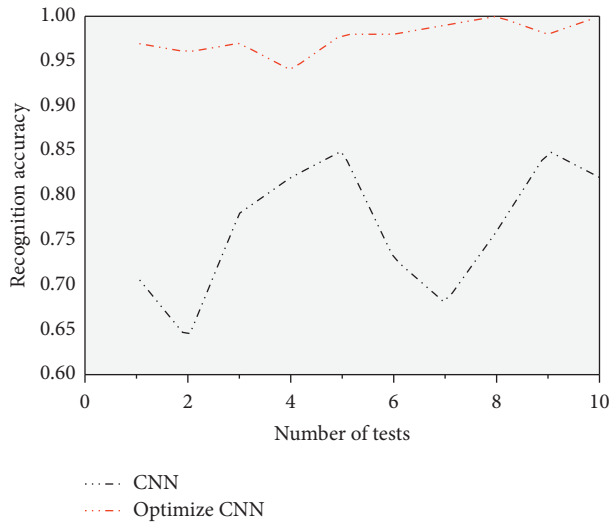


FIGURE 13: Recognition accuracy of different models.

optimized model but also fluctuates greatly, and the lowest accuracy is only 0.63, The highest is only 0.85, but the accuracy difference between the two is 34.92%. Thus, the reliability of the optimized CNN model in bearing fault detection is verified again.

6. Conclusion

Aiming at the problem that the bearing fault information is difficult to extract completely and the label data samples are insufficient under variable working conditions, this paper proposes a fault detection method based on a convolutional neural network combining wavelet transform and maximum pooling strategy. In this method, the bearing signals at different speeds are used as the input of the fault diagnosis network to integrate the complete fault information. Firstly, the optimized CNN model is constructed by four parallel convolutional neural networks combined with a wavelet transform. Then, after the original data is processed by data enhancement, the time-domain signal is transformed by wavelet transform to obtain the two-dimensional time-frequency spectrum of the fault signal, which is used as the input of the network. Finally, the learned model is used to diagnose and identify the test data. Using the bearing fault data at different speeds to verify the proposed optimized CNN model, it can be concluded that this method has the following advantages:

- (1) Wavelet transform preprocessing of fault data can reduce the influence of redundant background noise in the data, and when the one-dimensional fault time-domain signal is converted into a two-dimensional fault, the frequency energy spectrum can give better play to the feature extraction function of convolutional neural network.
- (2) The optimized convolution neural network can select different convolution parameters according to different frequency conversions to extract more complete fault features and highlight fault information.

The convolution neural network fault diagnosis model constructed in this paper not only has high accuracy (up to 0.9871) and low error (only 0.032) but also is simple to use, providing a new way for motor bearing fault diagnosis.

- (3) The data enhancement method can effectively expand the data set and can effectively improve the convergence speed and accuracy of the network while expanding the data set.

Data Availability

The experimental data used to support the findings of this study are included within the article.

Conflicts of Interest

The authors declare that there are no conflicts of interest regarding the publication of this paper.

Authors' Contributions

Shuiqin Zhou and Xiaochun Lou conceived the idea of this manuscript. And Shuiqin Zhou and Lepeng Lin developed this theory and performed the computations. Shuiqin Zhou, Chu Chen, and Wenbin Pan verified the results and completed the written work. All the authors read and approved this final manuscript.

Acknowledgments

This study was supported by the Public Technology Research Project of Zhejiang Province (LGN19C020003) and the Project of Hangzhou Science and Technology Bureau (20201203B116/20201203B97).

References

- [1] J. J. Callaghan, E. A. Salvati, P. M. Pellicci, P. D. Wilson, and C. S. Ranawat, "Results of revision for mechanical failure after cemented total hip replacement, 1979-1982. A two to five-year follow-up. J Bone Joint Surg 67-A:1074-1085," *The Journal of Bone and Joint Surgery*, vol. 67, no. 7, pp. 1074-1085, 1985.
- [2] M. M. Nagl and W. T. Evans, "The mechanical failure of oxide scales under tensile or compressive load," *Journal of Materials Science*, vol. 28, no. 23, pp. 6247-6260, 1993.
- [3] J. Zheng, J. Cheng, and Y. Yang, "A rolling bearing fault diagnosis approach based on LCD and fuzzy entropy," *Mechanism and Machine Theory*, vol. 70, pp. 441-453, 2013.
- [4] T. A. Harris and J. I. McCool, "On the accuracy of rolling bearing fatigue life prediction," *Journal of Tribology*, vol. 118, no. 2, pp. 297-309, 1996.
- [5] B. Muruganatham, M. A. Sanjith, B. Krishnakumar, and S. Murty, "Roller element bearing fault diagnosis using singular spectrum analysis," *Mechanical Systems and Signal Processing*, vol. 35, no. 1-2, pp. 150-166, 2013.
- [6] D. S. Chandra and Y. S. Rao, "fault diagnosis of a double-row spherical roller bearing for induction motor using vibration monitoring technique," *Journal of Failure Analysis and Prevention*, vol. 19, no. 4, pp. 1144-1152, 2019.

- [7] G. Chen, "Feature extraction and intelligent diagnosis of early faults of rolling bearings," *Journal of Aeronautics*, vol. 30, no. 2, p. 6, 2009.
- [8] B. Aka, A. Yz, and C. Cpg, "Bearing defect size assessment using wavelet transform based Deep Convolutional Neural Network (DCNN)," *Alexandria Engineering Journal*, vol. 59, no. 2, pp. 999–1012, 2020.
- [9] H. H. Tang, Z. Q. Liao, Y. Kobayashi, T. Masaru, and P. Chen, "Intelligent fault diagnosis for low-speed roller bearings based on stacked auto-encoder," *International Journal of COMA-DEM*, vol. 22, no. 4, pp. 45–50, 2019.
- [10] S. Liu, Y. Liu, Y. Gu, and X. Xu, "Method of extracting gear fault feature based on stacked autoencoder," *Journal of Engineering*, vol. 2019, no. 23, Article ID 9101, pp. 8765–8769, 2019.
- [11] P. Li, H. Yuan, Y. Wang, and X. Chen, "Pumping unit fault analysis method based on wavelet transform time-frequency diagram and CNN," *International Core Journal of Engineering*, vol. 6, no. 1, pp. 182–188, 2020.
- [12] J. Yuan, T. Han, J. Tang, and L. An, "An approach to intelligent fault diagnosis of rolling bearing using wavelet time-frequency representations and CNN," *Machine Design and Research*, 2017.
- [13] J. Guo, X. Liu, S. Li, and Z. Wang, "Bearing intelligent fault diagnosis based on wavelet transform and convolutional neural network," *Shock and Vibration*, vol. 2020, no. 19, Article ID 6380486, pp. 1–14, 2020.
- [14] S. Han, S. Oh, and J. Jeong, "bearing fault diagnosis based on multiscale convolutional neural network using data augmentation," *Journal of Sensors*, vol. 2021, no. 1, Article ID 6699637, pp. 1–14, 2021.
- [15] N. B. Thamba, A. Aravind, A. Rakesh, and M. Jahzan, "Application of EMD ANN and DNN for self-aligning bearing fault diagnosis," *Archives of Acoustics Journal of Polish Academy of Sciences*, vol. 43, no. 2, 2018.
- [16] W. Lu, X. Wang, C. Yang, and T. Zhang, "A novel feature extraction method using deep neural network for rolling bearing fault diagnosis," in *Proceedings of the 27th Chinese Control and Decision Conference (2015 CCDC)*, IEEE, Qingdao, China, May 2015.
- [17] H. J. Kang, M. J. Kim, K. B. Chu, S. H. Lee, E. K. Moon, and F. S. Quan, "Passive iarii," *Vaccines, Machines*, vol. 9, no. 5, p. 425, 2021.
- [18] D. Miki and K. Demachi, "Weakly supervised deep neural network for bearing fault diagnosis," in *Proceedings of the 2020 International Conference on Nuclear Engineering collocated with the ASME 2020 Power Conference*, New York, U.S.A, August 2020.
- [19] M. He and D. He, "Deep learning based approach for bearing fault diagnosis," *IEEE Transactions on Industry Applications*, vol. 53, no. 3, pp. 3057–3065, 2017.
- [20] J. Shi, M. Liang, D. S. Neculescu, and Y. Guan, "Generalized stepwise demodulation transform and synchrosqueezing for time-frequency analysis and bearing fault diagnosis," *Journal of Sound and Vibration*, vol. 368, pp. 202–222, 2016.
- [21] I. Rashedul, K. S. Ali, and K. J. Myon, "Discriminant feature distribution analysis-based hybrid feature selection for online bearing fault diagnosis in induction motors," *Journal of Sensors*, vol. 2016, Article ID 7145715, pp. 1–16, 2015.
- [22] L. Zhao, W. Yu, and R. Yan, "Rolling bearing fault diagnosis based on CEEMD and time series modeling," *Mathematical Problems in Engineering*, vol. 2014, Article ID 101867, pp. 1–13, 2014.
- [23] M. Bonforte and J. L. Vazquez, "Global positivity estimates and Harnack inequalities for the fast diffusion equation," *Journal of Functional Analysis*, vol. 240, no. 2, pp. 399–428, 2006.

Research Article

Intelligent Optimization Method of Resource Recommendation Service of Mobile Library Based on Digital Twin Technology

Shanshan Shang ¹, Zikai Yu,² Aili Geng,¹ Xiuxiu Xu,¹ Huizhen Ma,¹ and Guozhong Wang³

¹Library, Shanghai University of Engineering Science, Shanghai 201620, China

²Assembly Department, Shanghai Aerospace Equipments Manufacturer Co., Ltd., Shanghai 200245, China

³Institute of Artificial Intelligence Industry, Shanghai University of Engineering Science, Shanghai 201620, China

Correspondence should be addressed to Shanshan Shang; 91130001@sues.edu.cn

Received 23 June 2022; Revised 18 July 2022; Accepted 2 August 2022; Published 27 August 2022

Academic Editor: Le Sun

Copyright © 2022 Shanshan Shang et al. This is an open access article distributed under the Creative Commons Attribution License, which permits unrestricted use, distribution, and reproduction in any medium, provided the original work is properly cited.

In order to improve the Resource Recommendation and sharing ability of mobile library, an intelligent optimization model of Mobile Library Resource Recommendation Service Based on digital twin technology is proposed. Build the association rule feature distribution set of mobile library resource recommendation service, carry out text information retrieval in the process of Mobile Library Resource Recommendation and sharing, carry out semantic correlation feature registration according to the retrieval preference of mobile library reading user object, establish the association rule data set of mobile library reading user object preference for mobile library Resource Recommendation and sharing, carry out feature block processing, and analyze the library reader preference. Complete the collaborative filtering recommendation of Mobile Library Resource Recommendation sharing. The simulation results show that the collaborative recommendation under the intelligent optimization mode of mobile library resource recommendation service using this method has high accuracy and good confidence level, which improves the intelligent level of Mobile Library Resource Recommendation and user satisfaction.

1. Introduction

As a place with strong professional scholarship and comprehensive scientific research, mobile library has provided a huge development space for discipline teaching, cultural exchange, scientific research and application technology in Colleges and universities [1, 2]. In order to enable the library to play a greater social role, improve its social value of information services and the quality of information service products, considering how to improve the sociality of services is also an important opportunity for the quality improvement and career development of library staff [3, 4]. The research on Collaborative Recommendation Algorithm under the intelligent optimization model of mobile library resource recommendation service is of great significance in the construction of digital library. The related research on intelligent optimization model and fusion scheduling algorithm of mobile library resource recommendation service has attracted great attention.

Reference [5] takes the public library in Matara District of Sri Lanka as an example, and puts forward the research on mobile library services of public libraries. The main purpose of this research is to investigate the application, practice, and challenges of mobile library services provided by public libraries. The survey method is used as the data collection method. The library does not collect books separately for the mobile library service, and the mobile library has fewer books. The mobile library identifies school-age children as its target audience, and most people use the vehicles of management institutions to transport books and provide services. Research shows that no library provides this service to people in hospitals and prisons, and the vehicles allocated to mobile libraries lack the necessary facilities. Increasing financial support, the number of books collected, publicity plans, and improving transportation facilities can be used as suggestions. Reference [6] proposes a mobile library Resource Recommendation Algorithm Based on data mining, which uses block fusion clustering analysis and data mining

algorithm combined with particle swarm optimization to analyze the personalized demand feature categories of users for mobile library resources, and realizes mobile library resource recommendation according to the identification of typed parameters. This method has poor recommendation performance in complex environments.

In view of the above problems, this paper proposes an intelligent optimization model of Mobile Library Resource Recommendation Service Based on digital twin technology. Combined with the filter detection method, it realizes the analysis of Library Readers' preference, realizes the collaborative matching of Mobile Library Resource Recommendation sharing and reading user object preference, and completes the collaborative filtering recommendation of Mobile Library Resource Recommendation sharing. Finally, simulation experiments are carried out to show the superior performance of this method in improving the collaborative recommendation ability under the intelligent optimization model of mobile library resource recommendation service.

2. Theoretical Method of Digital Twinning Technology

Digital twin technology is an integrated system composed of data, models, and analysis tools. It can not only describe the state of aircraft fuselage in the whole life cycle but also make operation and maintenance decisions (including real-time diagnosis and future prediction) for the whole fleet and single fuselage based on uncertain information [7, 8].

Digital twinning is a virtual entity that creates physical entities digitally. It makes full use of data such as physical model, sensor update and operation history [9, 10], integrates multi-disciplinary, multi-physical, multi-scale and multi-probability simulation processes, and completes mapping in virtual space, thus reflecting the whole life cycle process of the corresponding physical equipment [11, 12]. By digitizing all elements of the physical world, such as people, things, and events, a corresponding "virtual world" will be recreated in cyberspace, forming a pattern of coexistence of physical world and digital world in the information dimension [13, 14]. The dynamics of the physical world are fed back to the digital world accurately and in real time through sensors [15]. Digitization and networking can realize the goal of turning reality into reality, networking and intelligence can realize the goal of turning reality into reality, and through virtual-real interaction and continuous iteration, the best and orderly operation of the physical world can be realized. It is the core element of digital twinning. It originates from physical entities, virtual models, and service systems, and at the same time, it is integrated into each part after integration, which promotes the operation of each part [16–18]. Therefore, data acquisition is the basis of digital twinning. To read the equipment data from the control system, it is necessary to clean the native data through data format analysis, data structure redefinition, data logic redefinition, etc., and then extract the key and effective parts from the data and output them. Twin data include data related to physical entities, virtual models, service systems, domain knowledge, and their fusion data, and is constantly

updated and optimized with the production of real-time data. Twin data are the core driver of digital twin operation. The above four parts are connected pairwise to enable effective real-time data transmission, thus realizing real-time interaction to ensure consistency and iterative optimization among the parts. Digital twinning technology supports the open communication standard OPCUA and API custom protocol access, which can ensure the stability of data transmission, reduce the delay of data transmission, realize the high speed, high reliability, and high adaptability of edge data acquisition, and provide an important foundation for subsequent digital twinning applications. The digital function architecture is shown in Figure 1.

It can be seen from Figure 1 that the digital twin functional architecture is a simulation process that makes full use of the physical world, information dimensions and other information to map and feedback each other, integrates multi-disciplinary, multi-physical quantities, multi-scale and multi-probability, and completes the mapping in the virtual space, so as to reflect the whole life cycle process of the corresponding real equipment. Digital twinning is a concept that transcends reality and can be regarded as a digital mapping system of one or more important and interdependent equipment systems.

3. Information Retrieval and Information Extraction of Mobile Library Resource Recommendation

3.1. Overall Structure and Information Retrieval of Mobile Library Resource Recommendation. In order to realize the optimization design of intelligent optimization model of mobile library resource recommendation service based on digital twin technology, firstly, the information retrieval model of mobile library resource recommendation sharing is constructed, and the personalized preference judgment model of mobile library resource recommendation is established. This paper analyzes the local relationship between users and the library, and then explores the diversity of users' preferences. Hidden factor analysis is a model-based collaborative filtering method, which defines the recommendation problem as the behavior matrix between sparse users and libraries. Assuming the low-rank matrix, the low-rank approximation of the matrix is performed to realize the learning task of implicit representation [19]. The hidden factor analysis method based on matrix approximation can effectively estimate the global structure of users' personalized preference judgment. Split the original behavior matrix into multiple sub-matrices, where each sub-matrix contains the relevance of users, projects, and ratings. The recommended method expression based on matrix approximation is

$$V_m = \frac{C_m \times \chi}{\rho}. \quad (1)$$

In formula (1), C_m represents the set of fitting real score items, χ represents the number of users, and ρ represents the parameter of loss items. Implicit representation of user preference diversity by low-rank matrix approximation:

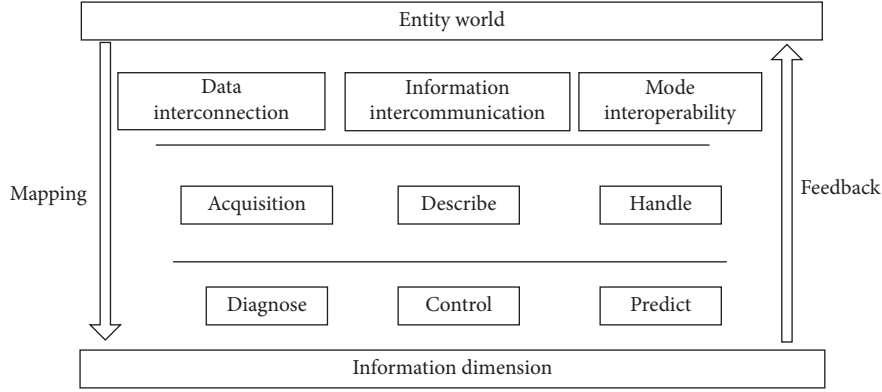


FIGURE 1: Digital twin functional architecture.

$$Q = \sum V_m \times g \times (1 - j). \quad (2)$$

In formula (2), g represents the preference weight of the user, and j represents the option of fitting the scoring items. Two-stage separated local low-rank matrix approximation is used to weight the results of user preference diversity:

$$H_i = \frac{[Z(x_i) - Z(x_i + h)]^2}{Q}. \quad (3)$$

In formula (3), Z represents the superposition of non-linear fitting functions, x_i represents the item score of the i -th user, and h represents the dependence of missing data. The global low-rank matrix approximation method can effectively obtain the overall characteristics of user preference diversity. According to the correlation analysis of users, items, and ratings, the model factors of personalized distribution of mobile library resources are established, and the tag form of mobile library resource recommendation is obtained: $G = (V, E, C)$. Where V represents the nearest neighbor set of graph model nodes recommended by mobile library resources, and the RFID tag of each node represents the number of items of mobile library resources; E represents the edge set of the distribution domain of mobile library resources, and represents the distribution sequence of user parameters of mobile library resources; Indicates the user's interest in different mobile library resources. Using the method of knowledge map modeling analysis, combined with personalized feature preferences, this paper establishes the user preference typing parameters of mobile library resource recommendation, analyzes the click and collection distribution characteristics of mobile library resource user U in a period of time, optimizes the collection management of library resources by combining video monitoring equipment, realizes the integration and information transmission of library resource information in the network layer, and constructs the library information management database in the application layer. SQL database is used to build the local database of library resource information management, artificial intelligence algorithm is used to manage and optimize the scheduling of information, and man-machine interaction is carried out in the application layer to realize the information retrieval and intelligent service of mobile library resource recommendation and sharing [20]. The

information retrieval and intelligent service mode of mobile library resource recommendation and sharing designed in this paper is shown in Figure 2.

According to the distribution structure model of mobile library resources recommendation and sharing resources shown in Figure 2, the phase space reconstruction method is adopted to reconstruct and extract the features of library resources under the intelligent service mode. Phase space reconstruction is a method to recover and describe the motive power system from the known time series. Using takens' delay embedding theorem, the infinite and noiseless dimension factors are embedded into the phase space. Multi-dimensional phase space vector is constructed by different delay times of one-dimensional time series. Reconstruct a phase space from one-dimensional chaotic time series, which is the same as the power system in topological sense, and judge, analyze, and predict the chaotic time series in the phase space. The recommendation module is established by using typed parameter analysis and category similarity feature analysis, and the workflow of mobile library resource recommendation based on digital twin technology is shown in Figure 3.

According to the distributed structure model of mobile library resource recommendation and sharing resources shown in Figure 3, the phase space reconstruction method is used to reconstruct and extract the features of library resources under the intelligent service mode, and the recommendation module is established by using the typed parameter analysis and category similarity feature analysis [21]. The workflow of mobile library resource recommendation based on digital twin technology is shown in Figure 4.

Establish the resource distribution attribute set $i \in S_s$ under the intelligent optimization model of mobile library resource recommendation service, and use semantic extraction method to retrieve the information of mobile library resource recommendation sharing. The semantic feature distribution mapping satisfies

$$\alpha^T Q \alpha = \sum_{i=1}^n \sum_{j=1}^n \alpha_i \alpha_j Q_{ij} \geq 0. \quad (4)$$

In formula (4), α_i is the satisfaction parameter of mobile library resource recommendation, α_j is the reliability parameter of mobile library resource recommendation, Q_{ij} is

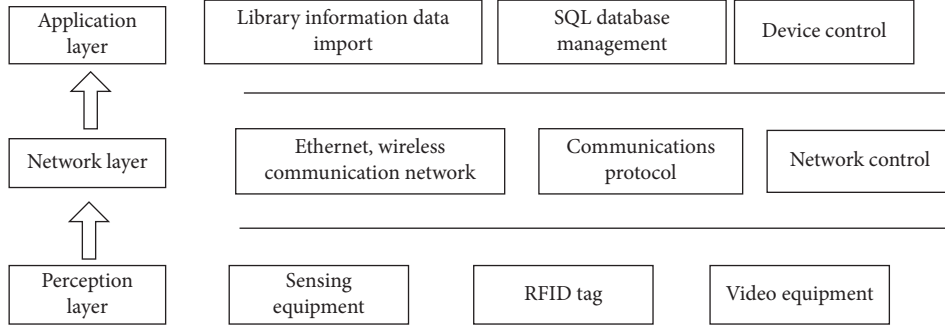


FIGURE 2: Information retrieval and intelligent service structure system of resource recommendation and sharing in mobile library.

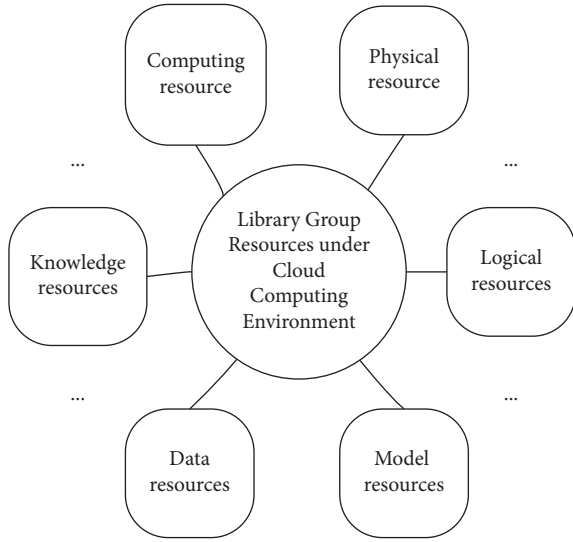


FIGURE 3: Resource distribution structure model of resource recommendation and sharing in mobile library.

the personalized feature matching parameter, and the trust relationship of library resources under the intelligent service mode is expressed $A \rightarrow B$ and $B \rightarrow C$. According to the above analysis, the semantic extraction method is used to search the information of mobile library resource recommendation and share, extract the semantic correlation features of mobile library resource recommendation, and filter and recommend the information of mobile library resource recommendation and share.

3.2. Semantic Relevance Feature Extraction. The semantic extraction method to retrieve information of mobile library resource recommendation and sharing is used, semantic correlation features of mobile library resource recommendation is extracted, a big data statistical analysis model of mobile library resource recommendation and sharing is constructed [22]. The specific process is shown in Figure 5.

Association rules under the intelligent optimization model of mobile library resource recommendation service is scheduled according to the attribute features of library resources, analyzes the distribution feature values of multi-source data recommended by mobile library resources [23], and it makes fuzzy matching according to user preference

scores in the recommended cache area, The details are shown in Table 1:

The tag category parameters are established, and the personalized features of mobile library resources are mined by using the feature registration algorithm, and the iterative formula of semantic correlation feature reconstruction of mobile library resources recommendation and sharing is obtained as follows:

$$x_i^{(k+1)} = (1 - \omega)x_i^{(k)} + \frac{\omega}{a_{ni}} \left(b_i - \sum_{j=1}^{i-1} a_{ij}x_j^{(k+1)} - \sum_{j=i+1}^n a_{ij}x_j^{(k)} \right), \quad (5)$$

$$i = 1, 2, \dots, n,$$

$$k = 1, 2, \dots, n.$$

In formula (5), ω is a weighted learning parameter, $x_i^{(k)}$ and $x_j^{(k)}$ represent personalized knowledge map and project distribution parameters of mobile library resources, respectively, and a_{ij} is a fuzzy matching degree. According to the part-of-speech tagging and part-of-speech filtering results of book information, the discrete scheduling feature distribution set of collaborative filtering of library resources is established as follows:

$$S_b = \sum_{i=1}^c p_i (\vec{m}_i - \vec{m}) (\vec{m}_i - \vec{m})^T. \quad (6)$$

In formula (6), $\vec{m} = \sum_{i=1}^c p_i \vec{m}_i$ is the difference between positive samples and negative samples, p_i is the recommended reliability probability magic parameter, and fuzzy clustering is carried out according to the matching results of semantic features of library resources under the intelligent service mode. The semantic ontology concept set of library resources under the intelligent service mode is as follows:

$$J(\vec{X}_j) = \frac{y_j^T S_b y_j}{\lambda_j}, \quad j = 1, 2, \dots, l. \quad (7)$$

In formula (7), y_j is the correlation entropy, λ_j is the recommended reliability characteristic value, and S_b is the similarity between recommended combinations. Using

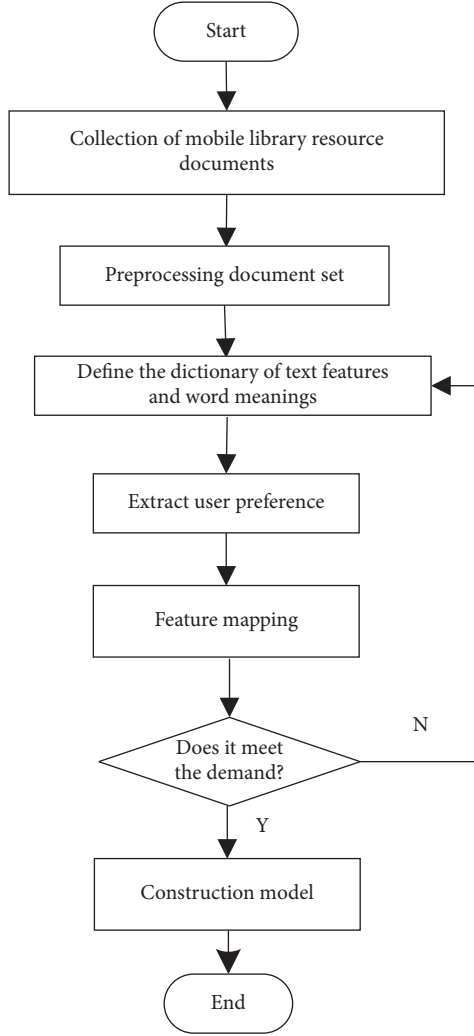


FIGURE 5: Process of building model.

TABLE 1: Resource recommendation label attribute allocation matrix of mobile library.

Item	Attribute 1	Attribute 2	Attribute j	Attribute m
Item 1	LI ₁₁	LI ₁₂	LI _{1j}	LI _{1m}
Item 2	LI ₂₁	LI ₂₂	LI _{2j}	LI _{2m}
.....
Item i	LI _{i1}	LI _{i2}	LI _{ij}	LI _{im}
.....
Item n	LI _{n1}	LI _{n2}	LI _{nj}	LI _{nm}

$$W_k = [w_{0k}, w_{1k}, \dots, w_{lk}]^T. \quad (11)$$

In formula (11), w_{0k} is the weighting coefficient of the k th node under the joint constraint of user set and item set, w_{1k} is the weighting coefficient of the next node, and w_{lk} is the weighting coefficient of terminal i at time t .

The mining results of reading user object preference information of mobile library in the process of resource recommendation and sharing of mobile library are as follows:

$$\text{Recall}(X, Y) = \frac{P(X \cap Y)}{P(X) + P(Y) - P(X \cap Y)}, \quad (12)$$

$$\text{Overload}(X, Y) = \frac{P(X \cap Y)}{\min(P(X), P(Y))}, \quad (13)$$

$$\text{Time}(X, Y) = \frac{2P(X \cap Y)}{P(X) + P(Y)}. \quad (14)$$

In formulas (12)–(14), $P(X)$ and $P(Y)$ represent the probability density function of the fusion of library information resource recommendation and mobile library reading user object preference under the intelligent service mode, X and Y are the concept sets of library information resource distribution, and $P(X \cap Y)$ is the joint cross distribution set. According to the above analysis, the object preference information mining and text information retrieval of mobile library readers are realized, and the resource recommendation and sharing collaborative filtering recommendation design of mobile library is carried out according to the matching results of the two features.

4.2. Mobile Library Resource Recommendation and Sharing Optimization. Establish a data set of association rules for reading users' preferences of mobile library resources recommendation and sharing [26], and use digital twin matching method to block features [27]. The association rules structure model of mobile library resources recommendation and sharing is as follows:

$$X = [s_1, s_2, \dots, s_K] = \begin{bmatrix} x_1 & x_2 & \dots & x_K \\ x_{1+\tau} & x_{2+\tau} & \dots & x_{K+\tau} \\ \dots & \dots & \dots & \dots \\ x_{1+(m-1)\tau} & x_{2+(m-1)\tau} & \dots & x_{M+(m-1)\tau} \end{bmatrix}. \quad (15)$$

In formula (15), $K = N - (m - 1)\tau$ represents the embedding dimension of mobile library resources search, τ is the time delay, m is the number of layers of semantic relations of mobile library resources, and $s_i = (x_i, x_{i+\tau}, \dots, x_{i+(m-1)\tau})^T$ is called the semantic ontology feature sequence of mobile library resources. The project scoring item $v \in N_u$ is introduced. According to the scoring distribution of mobile library resource users' items, the classification distribution law of mobile library resource labels is as follows:

$$\bar{R}_{ik} = \sum_{j \in N_u} C_{i,j}^* R_{jk}. \quad (16)$$

In formula (16), \bar{R}_{ik} represents the evaluation value of user u_i 's satisfaction with the recommended mobile library resources. The credibility level of R_{jk} library readers u_j to recommended mobile library resources is indicated. Combined with K-means clustering method, library readers'

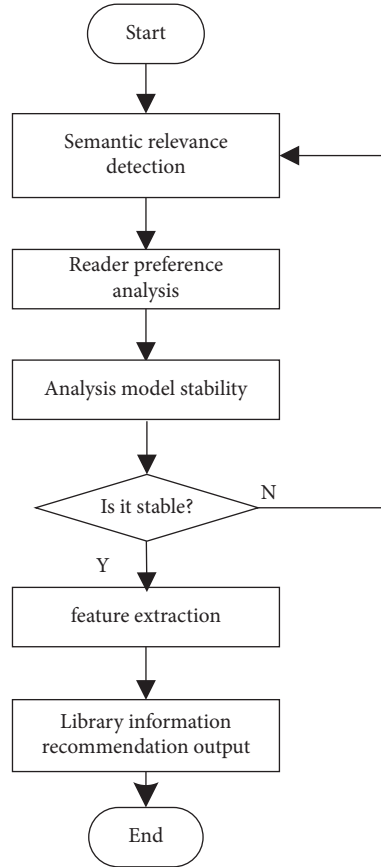


FIGURE 6: Implementation process of the algorithm.

TABLE 2: Fuzzy decision parameters of resource recommendation and sharing in mobile library.

X Value	Y Value	Fuzzy closeness vector Q_1, Q_2, Q_3, Q_4, Q_5	Priority order of recommendation and sharing of mobile library resources
821.404	417.343	0.334	$Q_4 > Q_1 > Q_3 > Q_2 > Q_5$
262.254	359.380	0.504	$Q_3 > Q_2 > Q_1$
89.749	887.285	0.480	$Q_4 > Q_1 > Q_3 > Q_2 > Q_5$
479.380	396.897	0.118	$Q_4 > Q_1 > Q_3 > Q_2 > Q_5$
149.439	381.151	0.328	$Q_4 > Q_1 > Q_3 > Q_2 > Q_5$
233.175	707.076	0.869	$Q_4 > Q_1 > Q_3 > Q_2 > Q_5$
519.723	150.878	0.810	$Q_4 > Q_1 > Q_3 > Q_2 > Q_5$

preference analysis is realized, and the trust value of library resource recommendation under intelligent service mode is obtained:

$$ITrust_{a \rightarrow c} = \frac{\sum_{b \in adj(a,c)} DTrust_{a \rightarrow c} \times (DTrust_{a \rightarrow c} \times \beta_d)}{\sum_{b \in adj(a,c)} DTrust_{a \rightarrow b}} \quad (17)$$

In formula (17), $Trust_{a \rightarrow b}$ represents the trust degree of recommended choices A to B , and has a similar concept. $Trust_{b \rightarrow c}$ is the domain ontology parameter. According to the scoring results of N mobile library resource users, the typed list parameter analysis is adopted. The digital twin matching method is used to block the features, and the K-means clustering method is used to realize the library reader preference analysis, so as to realize the collaborative matching of mobile library resource

recommendation sharing and reading user object preference, and complete the collaborative filtering recommendation of mobile library resource recommendation sharing. The iterative formula of collaborative filtering recommendation of library resources under intelligent service mode is obtained as follows:

$$x_i(k+1) = x_i(k) + s \left(\frac{x_j(k) - x_i(k)}{\|x_j(k) - x_i(k)\|} \right) \quad (18)$$

In formula (18), $\|\vec{x}\|$ represents the norm of \vec{x} , the preference feature of reading user objects in mobile library is $P_{ij}^{best}(k)$, and the iteration step is S . To sum up, the collaborative filtering recommendation of resource recommendation and sharing of mobile library is realized, and the intelligent optimization model of resource recommendation service of mobile library is optimized according to the

TABLE 3: User parameter configuration.

User list	Preference level	Contribution degree	Similarity level
1	0.166	0.166	5.3428
2	0.167	0.204	7.4065
3	0.169	0.146	4.8596
4	0.177	0.161	1.0726
5	0.171	0.187	1.5970
6	0.176	0.174	7.9761
7	0.171	0.187	1.6630
8	0.176	0.177	6.2025
9	0.173	0.207	6.3593
10	0.174	0.186	3.0750

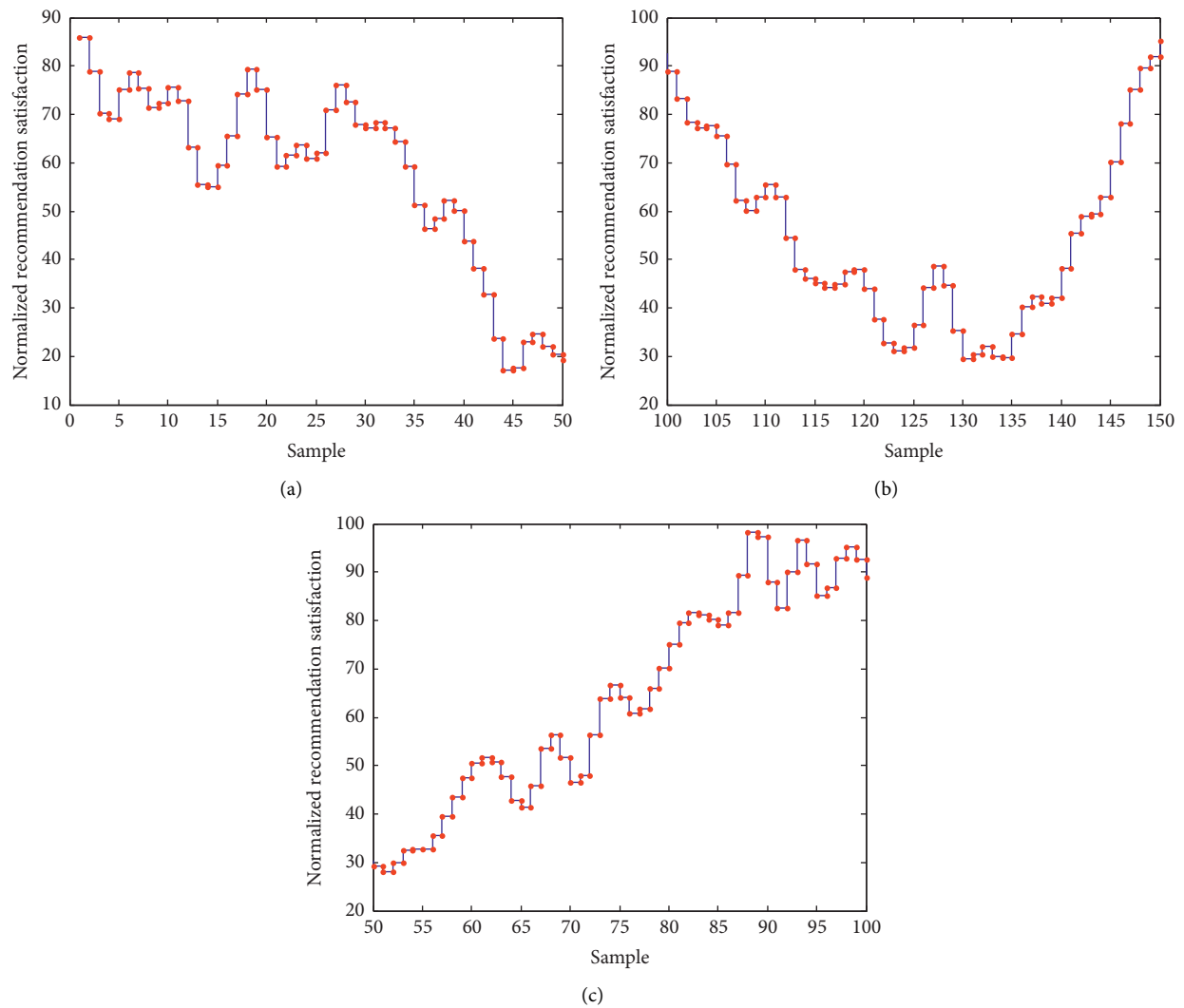


FIGURE 7: Satisfaction distribution of resource recommendation of mobile library. (a) Evenly distribution (b) Differential distribution. (c) Optimal distribution.

optimization design of fusion scheduling algorithm. The implementation process is shown in Figure 6.

5. Simulation and Result Analysis

In order to test the application performance of this method in collaborative filtering recommendation of mobile library

resource recommendation sharing, an experimental analysis was carried out, and a simulation test was carried out by combining Matlab and C++ programming software. The sample size of information sampling of library resources in intelligent service mode is 2000, the test set size of reading user's preference information distribution in mobile library is 400, and the initial statistic value of intelligent optimization

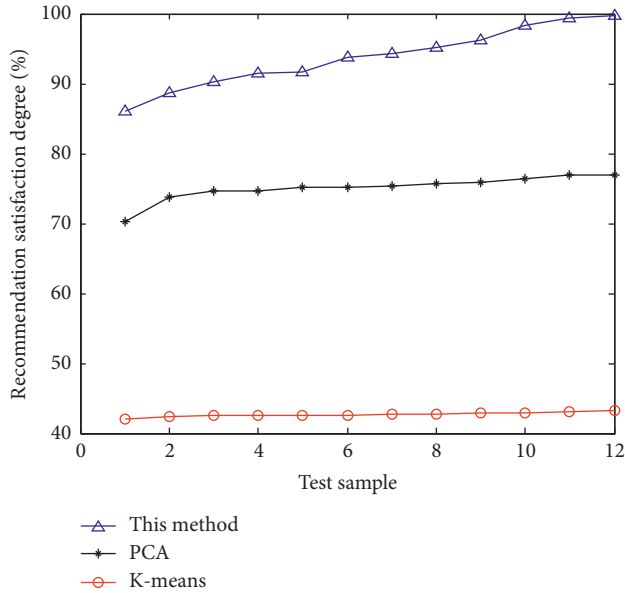


FIGURE 8: Comparative test of resource satisfaction of mobile library.

model of mobile library resource recommendation service is $\hat{\delta}_0 = -15$. The number of users is set to 20,000, and 1,500 users are randomly generated as the test set and 200 users as the training set. The recommended parameters $\lambda_1 = 1, \lambda_2 = 1, c_1 = 2, c_2 = 2$ are adaptively and collaboratively filtered, and the distribution of fuzzy decision parameters for resource recommendation and sharing of mobile library is shown in Table 2. See Table 3 for user parameter configuration.

According to the above parameter design results, the collaborative filtering recommendation of mobile library resource recommendation sharing is carried out, and the semantic relevance feature registration is carried out according to the retrieval preference of reading user objects in mobile library, and the user object preference association rule data set pushed by mobile library resources is established. The confidence level distribution weight is set to 1.25, and the mean square error is set to 0.031. The satisfaction level distribution of the recommendation is shown in Figure 7.

According to the analysis of Figure 7, the satisfaction level of mobile library resource recommendation by this method is high, among which the average satisfaction level of recommendation in the optimal state is 95.1%, and the recommendation satisfaction level is higher in the confidence range of $P < 0.01$. The reason is that this method extracts semantic correlation features, which is conducive to improving the satisfaction of mobile library resource recommendation.

The resource holding level of mobile library resources recommended by different methods is tested, and the comparison results are shown in Figure 8.

After analyzing Figure 8, it is found that the adaptability and preference satisfaction level of mobile library resources recommended by this method are high, which improves the user's satisfaction level with mobile library resources. Because of the small number of iteration steps, it can be seen that this method has a good optimization management ability. The

reason is that this method is conducive to improving the adaptability and preference satisfaction of mobile library reading user object preference information mining and text information retrieval in the research process.

To sum up, using the intelligent optimization method of Mobile Library Resource Recommendation Service Based on digital twin technology to recommend mobile library resources has a high level of satisfaction, and the average satisfaction of recommendation in the optimal state is 95.1%; It can improve users' satisfaction with mobile library resources and has better optimization management ability.

6. Conclusion and Prospect

6.1. Conclusion. This paper proposes an intelligent optimization model of Mobile Library Resource Recommendation Service Based on digital twin technology. To realize the collaborative matching between the recommendation and sharing of mobile library resources and the preferences of reading users, the following conclusions are obtained through the research:

- (1) The method in this paper has good registration for Mobile Library Resource Recommendation and sharing
- (2) Using this method to recommend mobile library resources has a high level of satisfaction
- (3) Using this method to recommend mobile library resources has a high level of adaptability and preference satisfaction

6.2. Prospect. Further research is still needed for the next step:

- (1) Each mobile library has its own characteristics, and does not fully use all the models and mechanisms of library resource aggregation and services. Only by properly improving and perfecting the methods and technologies of resource aggregation in combination with the characteristics, advantages and disadvantages of specific libraries, can we realize the deep aggregation and innovative services of mobile library resources on the basis of reflecting the characteristics of the library.
- (2) The lack of systematic understanding of mobile library resource aggregation and innovative services, the combination of resource aggregation and innovative services, enhances the integrity and systematicness of the research itself in the process of research from a certain angle, thus strengthening the service effect of resource aggregation and innovative services on user resource retrieval and knowledge acquisition, which needs to be further studied in the future.

Data Availability

The raw data supporting the conclusions of this article will be made available by the authors, without undue reservation.

Conflicts of Interest

The authors declare that they have no conflicts of interest regarding this work.

References

- [1] F. M. Temim, K. T. Omopupa, and F. O. Ajani, "Users' education as correlates of library resources utilization by undergraduates' in selected universities in k state," *Record and Library Journal*, vol. 7, no. 1, pp. 76–91, 2021.
- [2] Z. Yan, W. Ding, and X. Wang, "Design of library seats management system based on image recognition," *Electronics Test*, vol. 27, no. 4, pp. 19–20, 2020.
- [3] H. Yu, "Application of algorithm of fast mining maximal frequent itemsets in library management," *Computer and Modernization*, vol. 27, no. 6, pp. 68–72, 2020.
- [4] L. I. Jun, H. Liu, and L. Zhu, "Research on association rule data mining based on improved K-means algorithm," *Journal of Chinese Computer Systems*, vol. 42, no. 1, pp. 15–19, 2021.
- [5] R. A. P. S. Senevirathna, "A study on the mobile library services in the public libraries: with reference to the public libraries in Matara District, Sri Lanka," *Sri Lanka Library Review*, vol. 35, no. 2, pp. 18–35, 2021.
- [6] Y. Gu, X. Gu, and J. Wu, "Service quality evaluation via mining unbalanced network reviews," *Journal of Chinese Computer Systems*, vol. 42, no. 2, pp. 354–361, 2021.
- [7] L. Xu, R. Li, and G. Wang, "Research on K-truss community search algorithm for temporal networks," *Journal of Frontiers of Computer Science & Technology*, vol. 14, no. 9, pp. 1482–1489, 2020.
- [8] H. Wang, H. Wang, and C. Zheng, "Design of dynamic early warning system for overdue borrowing information in library," *Modern Electronics Technique*, vol. 44, no. 8, pp. 58–62, 2021.
- [9] S. Yu and S. Li, "Distributed multi-module retrieval simulation of library electronic resource information," *Computer Simulation*, vol. 37, no. 6, pp. 439–442, 2020.
- [10] N. A. Oche, "Observance of COVID 19 protocols and effective use of library resources and services in the state universities in north central, Nigeria," *American Journal of Information Science and Technology*, vol. 5, no. 1, pp. 12–18, 2021.
- [11] Y. Huo, "Prototype system of RFID internet of things clustering analysis based on big data," *Microcontrollers & Embedded Systems*, vol. 20, no. 11, pp. 17–20, 2020.
- [12] R. Jiang, "Research on online recommendation algorithm of university library based on data mining," *China Computer & Communication*, vol. 32, no. 23, pp. 50–52, 2020.
- [13] W. Marsolek, K. Barrick, and S. J. Brown, "Two years in the making: library resources for transgender topics," *Journal of eScience Librarianship*, vol. 10, no. 1, pp. 1188–1126, 2021.
- [14] J. Shi, X. Liu, and T. Liu, "Method of digital twin logic model oriented to production line simulation," *Computer Integrated Manufacturing Systems*, vol. 28, no. 2, pp. 442–454, 2022.
- [15] T. Liu, P. Zhang, and Y. Liu, "Fast approach for modelling human digital twin in workshop based on enhanced visual detection," *Computer Integrated Manufacturing Systems*, vol. 27, no. 2, pp. 545–556, 2021.
- [16] Y. Oloyede, "A survey of users' satisfaction with library resources and services at mountain top university library, Nigeria," *Library Philosophy and Practice*, vol. 2690, no. 1, pp. 1–14, 2021.
- [17] Z. Pan, J. Gao, R. Wang, Q. Yuan, R. Fan, and L. She, "Digital twin registration technique of spatial augmented reality for tangible interaction," *Journal of Computer-Aided Design & Computer Graphics*, vol. 33, no. 5, pp. 655–661, 2021.
- [18] F. Tao, C. Zhang, and Q. Qi, "Digital twin maturity model," *Computer Integrated Manufacturing Systems*, vol. 28, no. 5, pp. 1267–1281, 2022.
- [19] X. Yu and H. Zhang, "Low-rank matrix factorization recommendation model based on double regularization mechanism," *Application Research of Computers*, vol. 37, no. 4, pp. 977–981, 2020.
- [20] L. Zhang, "Simulation research on the integration and sharing of public library resources under cloud computing," *Computer Simulation*, vol. 37, no. 5, pp. 416–419, 2020.
- [21] Z. Yuan, X. Lu, and J. Huang, "Data compression technology of wireless sensor network based on multi-dimensional phase space re-construction," *Journal of Information Technology*, vol. 29, no. 4, pp. 85–89, 2022.
- [22] G. Fu, "The classified search method of library electronic resources based on Top-k query algorithm," *Electronic Design Engineering*, vol. 29, no. 16, pp. 173–176, 2021.
- [23] Z. Tian, X. Wu, X. Xie, J. Xu, and J. Lu, "Real-time analysis model for short texts with relationship graph of domain semantics," *Data Analysis and Knowledge Discovery*, vol. 4, no. 01, pp. 239–247, 2020.
- [24] K. Hui, Y. Ji, J. Wang, and H. He, "Collaborative filtering algorithm based on deep neural support vector autoregression," *Computer Engineering and Design*, vol. 41, no. 5, pp. 1308–1313, 2020.
- [25] W. Xu, Y. Yang, and C. Zhang, "Incorporating entity context features for deep text semantic matching," *Journal of Wuhan University (Natural Science Edition)*, vol. 66, no. 5, pp. 483–494, 2020.
- [26] Z. Xiong, B. Wang, and R. Tao, "An association rule mining reduction algorithm based on determining prime attributes," *Computer Engineering and Science*, vol. 43, no. 4, pp. 738–745, 2021.
- [27] S. Gao, "Commercial application of XR and digital twin technology in smart city," in *Proceedings of the 2021 3rd International Symposium on Smart and Healthy Cities (ISHC)*, pp. 84–89, Toronto, ON, Canada, December 2021.

Research Article

Trusted Data Analysis and Consensus Mechanism of Product Traceability Based on Blockchain

Yang Kang, Qiang Li , and Yuanyong Liu

College of Artificial Intelligence, Chongqing University of Arts and Sciences, Yongchuan 402160, Chongqing, China

Correspondence should be addressed to Qiang Li; 20160050@cqwu.edu.cn

Received 28 June 2022; Revised 20 July 2022; Accepted 29 July 2022; Published 27 August 2022

Academic Editor: Le Sun

Copyright © 2022 Yang Kang et al. This is an open access article distributed under the Creative Commons Attribution License, which permits unrestricted use, distribution, and reproduction in any medium, provided the original work is properly cited.

As a decentralized, distributed system between functional and benefit management functions, blockchain is effective for financial transaction data security, data tracking and antitampering, product tracking, and access control. In this context, we have conducted experimental research on the blockchain product traceability trusted data analysis consensus mechanism and reached the following conclusions. (1) There are decentralization, irreversible tampering, traceability, and openness through the blockchain's own information and other functions so that a series of processes from raw material production, transportation, and logistics sales are well documented. (2) Under the same network environment, if the number of matches in the system increases, the average matching time consumed by the original engine is greater than the average matching time on the optimized engine. For example, taking 10% of Byzantine nodes in the system, the number of consensus increases, the average ITPBFT consensus time is about 5.74 s, and the average consensus time of the PBFT consensus mechanism is about 6.13 s. As a decentralized distributed data management system through nodes, blockchain is widely used in financial transactions, copyright protection, and product areas such as tracking and access control. In this regard, we conducted an experimental study of the consensus mechanism to analyze reliable data on the traceability of blockchain products and came to the conclusion of the experiment.

1. Introduction

Driven by the recent surge in interest in blockchains, it was investigated whether they would be ideal for the Internet of Things (IoT). Blockchain supports networks where untrusted participants communicate together in a verifiable manner without a trusted broker. We study the operation of this mechanism and evaluate smart contract scenarios which are in the blockchain and allow you to automate multistage processes. Then, we move into the IoT field and describe how the combination of blockchain and IoT can facilitate sharing of services and resources and create a market for interoperable services [1]. The performance of a probabilistic proof-of-work- (PoW-) based consensus structure, also known as a blockchain, is not a major concern. It is a success story despite its consensus latency of around hours, and the theoretical maximum throughput is only 7 transactions per second. The current situation is very different and the poor performance scalability of the initial PoW blocks no longer makes sense. In particular, platform trends support the

implementation of randomly distributed applications across block structures, and the need for better performance has entered the realm of database replication protocols [2]. Blockchain is a distributed transaction and information management technology first developed for the Bitcoin cryptocurrency. Interest in blockchain technology has grown since the idea was proposed in 2008. Interest in blockchain lies in the fact that its key features ensure security, anonymity, and data integrity without third-party control. This makes it an interesting area of research, especially in terms of technical issues and limitations [3]. Block chains are a new cryptographic and IT application to solve an old financial reporting problem and can lead to extensive changes in corporate governance. Many major financial players have already started investing in the new technology, with exchanges proposing the use of block chain as a new way to trade in company shares and track ownership. The effects of these changes on directors, institutional investors, minority shareholders, auditors, and other parts of the corporate governance system are reviewed. The lower costs,

higher liquidity, more detailed information, and ownership transparency offered by blockchain can significantly improve the balance of power between these groups [4]. The main advantages of blockchain are decentralization, time series data, shared services, programmability, and security, making it particularly suitable for building programmable monetary systems, financial systems, and even macrosocial systems. The basic model of the blockchain system is proposed, and the principles, technologies, methods, and applications of the blockchain and related Bitcoin systems are discussed. We also discuss smart contracts and their applications and show future trends in a blockchain parallel society. It provides useful guidance and reference for future research work [5]. At present, several Chinese departments have invested a lot of money and effort in setting up proper food control systems. As a research team that has developed and applied traceability systems for several years, this article presents methods to achieve effective traceability and highlights the importance of traceability systems. The scientific elements of the proposed traceability system will be used to explore the usefulness of analytical data and the development of a food safety assessment system. The above methods can be used to produce useful and effective information to improve corporate governance [6]. Logistics helps companies optimize the entire enterprise supply chain from one source to another to achieve their strategic goals. Traceability has become one of the integrated components of supply chain management, supply chain monitoring, and data monitoring at various points at the beginning and end of a product. Depending on their role, all participants in the supply chain have different goals for implementing monitoring solutions [7]. Blockchain technology is a distributed ledger that allows you to transfer data seamlessly, securely, and reliably. The benefits of introducing blockchain technology to manage and control PSA products in the supply chain include decentralized management, security, tracking capabilities, and verified operational planning [8]. Elaborated through the required performance analysis with data traceability. The implementation of the proposed EWRDN service for sexual functionality is the main contribution of this work. A trusted authoritative service coordination is also introduced to operate the proposed service. The results show that the proposed service synergy can provide the traceability function of data and experimentally defends against most experienced data security threats. Additionally, the EWRDN service has been shown to provide two different data compression qualities as a differentiated quality service. It has been shown that in EWRDN coordination, a fixed compression recovery rate has been achieved [9]. There is a traceability link between each new requirement and the objects predicted to change in the design object model. When asked, they claimed they were confident that the correct number of objects would be changed, but they were less sure what was needed number of hours worked. Analysis of impact analysis shows that predictions for individual objects are often nearly correct, but the number of objects actually changed is often larger than the number of objects predicted [10]. The multiterminal controllable security intelligent system not only adopts the proprietary protocol to

fight against wireless network intrusion and system vulnerability mining program to realize the secure encrypted transmission of multiterminal data exchange but also establishes a consensus environment and uses the consensus mechanism to record and verify the security status of the access device to ensure the security of the system. The system reduces the cost of establishing a security architecture and the requirements for computing power and can better cope with the frequent occurrence of security incidents [11]. The current architecture of the risk scoring system is highly centralized, which can lead to issues such as data loss, bias, and decentralization. Along with blockchain technology, it has the features of decentralization, security and reliability, integrated service, and consistency. A new architecture of a blockchain-based risk assessment system and an enhanced DPOS-based consensus mechanism algorithm is proposed [12]. Strengthening the management and support of non-consensus basic research is conducive to promoting the original innovation of basic research, and local science and technology departments are increasingly interested in exploring the management mechanism of nonconsensus basic research. Combined with management experience, policy recommendations are put forward from two aspects: the establishment of nonconsensus basic research special funds and the design of nonconsensus project selection mechanism, to provide certain theoretical guidance for the management practice of nonconsensus basic research in the future [13]. The blockchain and D-IoT equivalent architectures are based on a master-slave multichain. The integrated equivalent architecture provides key applications of blockchain technology as a unified mechanism and smart contract in D-IoT. The broad perspective for blockchain deployment in D-IoT is explored [14]. There are several general consensus algorithms in blockchain technology. They differ in the complexity of calculating fault tolerance and fault tolerance. The implementation, consistency, scalability, and efficiency of blockchain consensus mechanisms require further refinement and improvement. Mechanisms for code approval and implementation of Bitcoin, Ethereum, and Hyperledger are reviewed, discussed, and proposed in [15].

2. Trusted Data Analysis of Product Traceability of Blockchain

2.1. Blockchain Technology

- (1) Decentralization: the blockchain uses peer-to-peer technology to store data, using distributed accounting and storage. All nodes have equal rights and obligations
- (2) Security: information security cannot be tampered with
- (3) History: any transaction records will be stored in the database
- (4) Collective maintenance: in an open system, private information in transactions is encrypted, and all nodes with maintenance functions are jointly maintained. Anyone can query each blockchain data

through an open interface, so the entire system information is highly transparent

Blockchain technology is considered the key technology most likely to power the fifth wave of disruption. It is a distributed ledger technology consisting of distributed databases, encryption algorithms, consensus mechanisms, and smart protocols. Based on the characteristics of openness, transparency, decentralization, and nontampering of blockchain data, it has received more and more attention, and it has gradually become materialized from the concept, from the initial application of financial currency to applications in various fields.

Encryption Algorithm. The encryption algorithm is the cornerstone of the blockchain. Blockchain uses hash algorithms and asymmetric encryption technology to ensure the irreversibility and security of blockchain technology. Hash algorithms, also known as secure hash algorithms, are widely used in many encryption technologies, including blockchain technology. It maps data of any length to a fixed-length hash queue according to certain rules. Algorithms, the most common being the SHA-1, SHA-2, and SHA-3 families, MD5, etc.

Consensus Mechanism. The consensus mechanism is the key blockchain mechanism. The blockchain consensus mechanism introduces Basic Certificate (PoW), Proof of Contribution (POS), Delegated Proof of Contribution (DPOS), Practical Byzantine Error Resistance (PBFT), etc. to adapt to the consensus system of each platform. The consensus mechanism is used to solve the consensus problem of distributed systems. It first appeared in 1975, and the blockchain consensus mechanism was the proof-of-work mechanism proposed by Satoshi Nakamoto in Bitcoin core.

Smart Contract. A smart contract is essentially a computer protocol that allows the blockchain application platform to operate automatically and unconditionally according to the proposed contract terms, thereby replacing the uncertainty of manual calculations and operations used in traditional business practices to perform contracts. It greatly improves the interaction and circulation of information nodes. Smart contracts have a certain ability for independent judgment and self-execution. Because they are based on programming languages, they do not need to rely on third parties or centralized institutions and cannot be intervened by humans, so they have high efficiency and accurate and strong execution capabilities. The technical types of blockchain are shown in Figure 1.

2.2. Blockchain Product Traceability. With the continuous improvement of material living standards, product updates and iterations have become more and more frequent, resulting in the emergence of many electronic foundry companies, small workshops, etc., which have threatened the safety of electronic use. The trust mechanism between consumers and consumers has not been perfected. The main raw materials, parts, production, processing, assembly, supply,

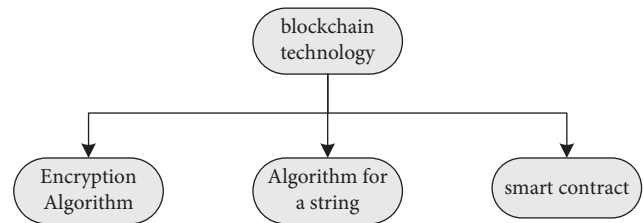


FIGURE 1: Blockchain technology.

and all aspects of logistics involved in the production of products will involve many supply chains, distributors, software and hardware companies, and so on. The traceability of the product cannot be fully maintained and guaranteed at all. A series of processes that make products from raw material production, transportation, and logistics sales are well documented. Compared with other traditional traceability methods, the advantages of blockchain traceability can be roughly summarized into the following three basic aspects:

- (1) **Multiparty confirmation:** use blockchain features such as decentralization, irreversibility, and traceability to support product trust, encourage more participants in the supply chain to jointly collect and maintain product information, and increase system trust.
- (2) **Traceability and accountability:** the blockchain adopts distributed ledger technology to ensure that data records cannot be tampered with, making commodity information and transaction information transparent, authentic, and traceable. Consumers can view product information and eliminate the problem of fake and inferior products. Enterprises can effectively and quickly trace the cause and source of electronic product problems and quickly recall all problematic products to reduce financial losses.
- (3) **Hacker data warehouse of all parties:** when these data are packaged and stored in blocks, supply chain participants jointly maintain their own data sources, which can realize information disclosure. All parties can query the process information through the system to ensure that all participants find out the problems in their operation in time, which helps to improve the management efficiency of the entire supply chain. The advantages of blockchain product traceability are shown in Figure 2.

2.3. Product Traceability Method. The blockchain approach to product tracking involves each merchant and consumer registering an address before using the system. More event information for this address is as follows. When selling an item, the seller must provide the system with information about the transaction. When consumers buy a product, they can verify the product through the QR code in the system before purchasing. The first level of the system is Consumer, Outstanding Supplier, and Production Log in to create a public/private key pair and use the revocation script and personal information to register and authenticate to the

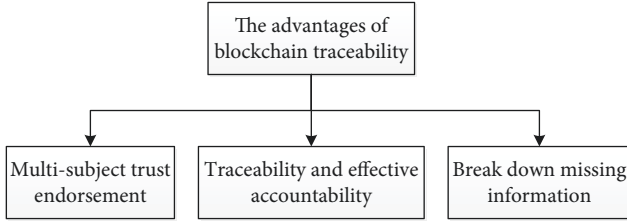


FIGURE 2: The advantages of blockchain traceability.

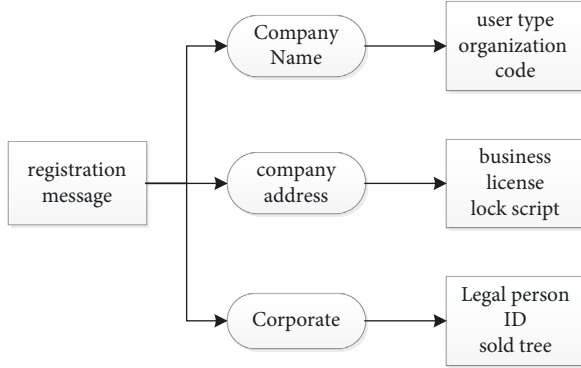


FIGURE 3: Registration information data structure.

system, as shown in Figure 3 to add information to the registration: company name, address, corporate legal entity, etc. The registration node sends registration information, and other nodes cache the registration information after receiving the message, making a smart trade. Registration information is collected in blocks awaiting approval if the message conforms to all terms of the smart agreement. If the message does not meet all the requirements of the smart contract, the message is removed from the cache. Review intelligence logs to ensure that information provided by controllers is the property of individuals and to prevent attackers from maliciously recording information about others. Check the contents of the “Authentication Information” field of the registration information. Registration information performs three functions: first, to inform consumers of the legitimacy of transactions, second, to trace incidents involving commodities, and third, to prevent manufacturers from releasing counterfeit products. It returns success if all conditions are true and returns an error if any test fails.

3. Blockchain Algorithms

3.1. Adaptive PoW Algorithm

- (1) The node monitors the data records of the entire network, and the data records that pass the basic legality verification will be temporarily stored.
- (2) After finding a reasonable random number, generate block information, first enter the block header information, and then the data record information.
- (3) The newly generated block is broadcasted to the outside after receiving the order. After other nodes

have passed the verification, they will be connected to the blockchain, and the height of the main chain will be increased by one. Then, all nodes will switch to the new block and continue to perform workload proof and block. Production.

To improve the efficiency of end node transactions on the local network, end nodes use a handshake protocol called an adaptive handshake algorithm. The algorithm dynamically adjusts the complexity of implementing the PoW algorithm according to the behavior of end nodes. At the same time, the security risk in the local network is reduced by reducing the complexity of the PoW algorithm. The correct operation of the A-PoW algorithm depends on the results of the local network node edge verification mechanism checks. The following describes how the node bounds checking mechanism works. We describe how edge nodes calculate the contribution of the corresponding node based on the behavior of the node under test. We create nodes in a variety of ways and ultimately ensure that the node’s input value calculation formula effectively and accurately represents the node’s contribution to the input blockchain. We calculate node contribution using the following formula:

$$C_i = \lambda_1 C_i^P + \lambda_2 C_i^N. \quad (1)$$

To study the influence of different types of transactions on the contribution amount, C_i^N represents the influence of malicious behavior on the contribution value, λ_1 and λ_2 represent the weight of these two effects, and the formula can be expressed as

$$C_i^P = \sum_{k=1}^n T_1(t) * a(b). \quad (2)$$

Among them, n is the number of events published by the entire node in unit time, $T_1(t)$ is a function of time damping, its value gradually decreases with time, and when the importance is greater, $T_1(t)$ can be expressed as

$$T_1(t) = N_0 e^{-a(t+1)}, \quad (3)$$

$$a = \frac{1}{m} \ln \left(\frac{N_{\text{INIT}}}{N_{\text{FINISH}}} \right), \quad (4)$$

$$l = \frac{1}{a} \ln \left(\frac{N_0}{N_{\text{init}}} \right), \quad (5)$$

N_0 in formula (3) is the initial value of the function, a is called an exponential decay variable, and l is the inversion to the left, so the value of $T_1(t)$ can be calculated from any position instead of N_0 . According to equations (4) and (5), the decay function of N_{init} begins to decrease and decreases to N_{finish} after m unit time. $A(b)$ represents the actual impact on the payment amount. When the host requests authentication, if there are pending events, $a(b)$ has the value N ; otherwise, $a(b)$ has the value $-N$. Therefore, the payment calculation formula encourages nodes to actively look at these “pending” events. The impact factor of the detected harmful payment behavior can be expressed as

$$C_I^N = \sum_{k=1}^n T_2(i) * \beta(b). \quad (6)$$

The system assumes relatively no malicious activity. Harmful activity detected during this check affects not only the number of attachments calculated at this time but also the number of attachments in the future. As shown in the formula, $T_2(i)$ is a function of temporary damping, which can be written as

$$T_2(i) = 0.8^i, \quad (7)$$

where $B(b)$ in the C_I^N calculation formula represents the degree of damage caused by malicious behavior. Assuming that in the current system, the threshold for publishing transactions through terminal nodes is M , and the number of transactions performed during this analysis T period is N , then $\beta(b)$ can be expressed as

$$\beta(b) = \begin{cases} 0, & N < M, \\ K * (N - M), & N > M. \end{cases} \quad (8)$$

If the number of errors is below the threshold, there is no penalty. If the trading volume exceeds 10%, the value of k is relatively large. If the additional transaction volume does not exceed 10%, the edge node considers this to be an acceptable margin of error. Therefore, the value of k is relatively small. Meanwhile, $T_2(t)$ is a function that is repeatedly decomposed in control events. Formula (1) is the number of breakpoints between the malicious activity's breakpoint and the current breakpoint.

3.2. Affinity Propagation Clustering Algorithm. Since the number of game participants and the number of solutions have a great influence on the complexity of the game, in order to solve this problem, this paper firstly organizes the data and regards the clustering of the game as a category of participants, which not only simplifies the game process. At the same time, the original structure and function of the data are preserved. If participants rely on clusters, they will not be penalized if the number falls below a threshold. When the trading volume exceeds 10%, the value of k is relatively large. If the number of transactions exceeds 10%, the edge node is considered to have an error range. So, the value of k is relatively small. Meanwhile, $T_2(t)$ is a function that is repeatedly decomposed in checkpoint events. The i formula represents the breakpoint between the malicious behavior and the current breakpoint (the number of breakpoints between intervals). That is, the longer the malicious behavior is, the lower the $T_2(t)$ is. The result is to observe the data characteristics of each cluster and further analyze a specific set of clusters to make decisions. The silhouette factor provides a nice scoring function to determine the best score. The silhouette coefficient is one of the commonly used performance metrics to evaluate cluster cohesion and separation, defined as follows:

$$s(i) = \frac{b(i) - a(i)}{\max\{b(i) - a(i)\}}. \quad (9)$$

The higher the silhouette factor, the better the clustering effect. The quality of the grouping is evaluated by silhouette

coefficients corresponding to different reference values. We choose a Nash equilibrium solution and find the best path. This paper captures the best idea of finding the optimal solution, uses the advanced particle swarm algorithm to achieve the optimal global resource allocation, and develops and solves the Nash equilibrium solution for various industries. The position of each particle in the algorithm represents the situation of an investment company. Using this algorithm, we display the origin of all particles in $[0, 1]$ and determine the origin of the particle.

$$N_{X,Y} = \frac{N_{\max} - N_{\min}}{O_{\max} - O_{\min}} \times (O_{x,y} - O_{\min}) + N_{\min}. \quad (10)$$

The optimal idea is used to find the optimal solution, the improved particle clustering algorithm is used to obtain the overall optimal distribution of resources, and the Nash equilibrium solution is designed and opened for each type of industry. The position of each particle in the algorithm represents the situation in which the investment company operates. The starting positions of all particles in the algorithm are plotted on $[0, 1]$, and the initial positions of the particles are determined.

In the game situation, the strategy selected by the player optimally matches the strategies of other players. In the game scenario, the strategy selected by the player corresponds well with the strategies of other players. Therefore, the particle in the optimal state is the Nash equilibrium in the game, according to the definition and properties of N_{ash} equilibrium. The game strategic planning based on n -person limited refusal to cooperate is as follows:

$$u_i = \max\{\text{sreg}_i - (E(x) - E_{\text{avg}}), 0\}. \quad (11)$$

If the mixed situation according to equation (11) is a Nash equilibrium solution, u_i can obtain the minimum value of 0, and when the mixed situation is a non-Nash equilibrium solution, u_i can obtain a larger value. In order to evaluate the Nash equilibrium solution and obtain an approximate Nash equilibrium solution, this article will develop the fitness function in the investment board game scenario:

$$f(x) = \min u_i, \quad i \in (1, 2, \dots, n). \quad (12)$$

In the game strategy combination space, the smaller the condition of $f(x)$ is, the closer the enterprise profit is to the equilibrium value. The compaction rate method selects the global optimal position and guides the particles to search the sparse area, so that it does not fall into the local optimum, improves the understanding of variability, and finally adheres to the game balance for adaptation. This method takes time. As the data accumulates or the complexity increases on a large scale, the performance of the algorithm degrades. In intelligent algorithms, the data processing capacity is limited and the accuracy is insufficient. In this paper, the gravity search algorithm is used to improve the particle flow algorithm to improve the overall optimization ability. GSA is a new heuristic method. The motion of particles follows the laws of dynamics. Particles move toward particles with higher mass, and particles with higher mass are in the best

position to obtain the optimal solution to the problem. Learning the value of the particle state function determines each particle's mass and force, calculates acceleration, and updates velocity and position. The steps to calculate these parameters are as follows:

$$m_i(t) = \frac{\text{fit}_i(t) - \text{worst}(t)}{\text{best}(t) - \text{worst}(t)},$$

$$M_i(t) = \frac{m_i(t)}{\sum_{l=1}^N m_l(t)}. \quad (13)$$

Calculate gravity. The gravitational force of particle j on particle i is

$$F_{ij}(t) = G(t) \frac{M_{pi}(t) \times M_{aj}(t)}{R_{ij}(t) + \varepsilon} (x_j(t) - x_i(t)). \quad (14)$$

The gravity detection algorithm is used to improve the particle swarm algorithm to improve global optimization capabilities. GSA is a new research method. The movement of particles obeys the laws of kinetics. Particles move in the direction of the particles with the greatest force, and the most powerful particles are in the best position to obtain the best solution to the problem. By evaluating the value of the particle's fitness function, the force and strength of each particle are determined, the acceleration is calculated, and the speed and position are updated.

In the formula, $G(t)$ represents the value of the gravitational constant, $M_{pi}(t)$ represents the inertial mass of the acted particle i , M_{aj} represents the inertial mass of the acting particle j , and ε is a small constant to avoid the denominator being 0. The net force is then applied to part i .

$$F_I(t) = \sum_{j=1}^N \text{rand} \times F_{ij}(t), \quad (15)$$

where rand is the reference value for calculating acceleration. According to the law, the acceleration of particle i is

$$a_i(t) = \frac{F_I(t)}{M_i(t)}. \quad (16)$$

In this paper, the particle swarm algorithm is used to solve the Nash equilibrium solution, and the clustering distance calculation method is used to control the particle search process.

3.3. Homomorphic Encryption Algorithm. Encryption algorithms can achieve additive homomorphic properties, which can meet the needs of many privacy-preserving applications. In particular, the Payet encryption algorithm can be composed of three parts, namely, key generation, data encryption, and data decryption. Generate the key: according to the specified security parameter k , first select two sufficiently large prime numbers, where the sum of these two prime numbers is k , and then calculate the RSA modulus N . Define a function.

$$L(\mu) = \frac{\mu - 1}{N}. \quad (17)$$

Then, choose a suitable generator, and use the above parameters to calculate. Finally, the formula in the Payet encryption algorithm is obtained. $p_k = (N, g)$, and its corresponding formula $m \in Z_N$. Data encryption: according to the given message $m \in Z_N$, choose a random number $r \in Z_N^*$, so the file can be calculated by the following formula:

$$c = E(M) = g^m \cdot r^n \text{mod} N^2. \quad (18)$$

Data decryption: according to the ciphertext $C \in Z_N^*$ calculated above, the corresponding ciphertext m before encryption can be calculated by the following formula:

$$m = D(C) = L\left(C^{\text{mod} N^2}\right). \quad (19)$$

It should be noted that the Payet encryption algorithm is semantically secure and can resist multiple plaintext attacks, and its accuracy and security can be verified.

4. Research on Consensus Mechanism of Product Traceability Trusted Data Analysis of Blockchain

4.1. Analysis of Product Traceability under Different Blockchain Algorithms. This paper examines the time between transaction validation and block generation and compares the PoVT proposed in CDBFT to the PBFT used in Hyperledger Fabric. The initial total number of nodes in the system is fixed at 10, and the number of transfers per block is 1 to 500. It is shown in Table 1.

In Figure 4, the required time is shown as a function of the number of events in the block. The comparison shows that for multiple simultaneous 100 events, PBFT lasts 200 ms, CDBFT lasts 120 ms, and PoVT lasts 80 ms. Correspondingly, for 30 events, the PBFT gain time is 600 ms, the CDBFT is 350 ms, and the PoVT is about 210 ms. As the number of simultaneous events increases, so does the confirmation time for all three. However, the computation time oT is higher than PBT and CDBFT.

Figure 5 compares the time required to complete a transaction under two different scenario changes. The horizontal axis represents the number of events in each block and the number of participants in the corresponding consensus. In the consensus algorithm proposed in this paper, each session has 20 consensus nodes and 100 events. PBFT acceptance time increases significantly (200 ms), CDBFT takes 100 ms, and PoVT takes only 80 ms. From the analysis point of view, PoVT takes less time to complete the transaction. PBFT reaches consensus through a full three-step broadcast, while the CDBFT system takes a long time to calculate voting fees, fines, and the credit evaluation process. If 100% of the nodes participate in the consensus process, the time required will gradually increase. The solution proposed in this paper is to achieve consensus by selecting multiple nodes and reducing the amount of communication, which can effectively reduce the communication cost.

TABLE 1: Number of block products under different algorithms.

Number of product transactions	0	100	200	300	400	500
PBFT	0	200	300	550	800	1000
CDBF	0	80	90	150	280	390
PoVT	0	90	145	300	400	550

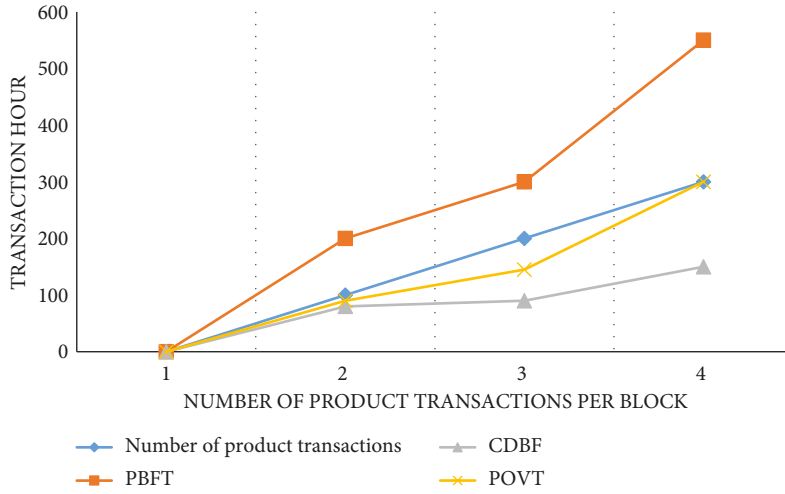


FIGURE 4: Time changes of PoVT algorithm when the node is fixed.

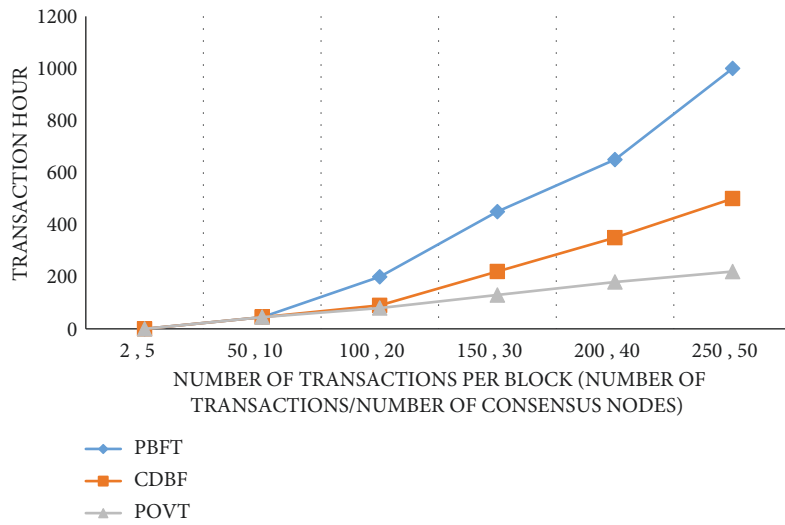


FIGURE 5: Time changes of PoVT algorithm when the number of nodes and transactions is variable.

In Figure 6, we see the importance of ensuring the performance required to achieve optimal transaction rates, as consensus must be formed when a particular block is delivered. Bandwidth requirements are measured by varying the number of simultaneous events per second and the number of participating nodes. Bandwidth requirements increase with the number of simultaneous events, not directly with the number of IoT nodes. In traditional blockchains, this demand is quasi-linear and proportional to the increase in transaction volume.

4.2. *Product Traceability Trusted Data Analysis.* We can conclude that the method in this article analyzes the reliable data of product traceability, and the accuracy of the effect evaluation is high. The experiment also conducts a reliability test of the method presented in the article and compares it with the statistically ambiguous method and the digital game method. The results are shown in Figure 7.

From the experimental data in Figure 7, we can know that the reliability of reliable traceability tracking is highest among the three methods. The number of iterations can be up to 50, the confidence level can be up to 1, and the number

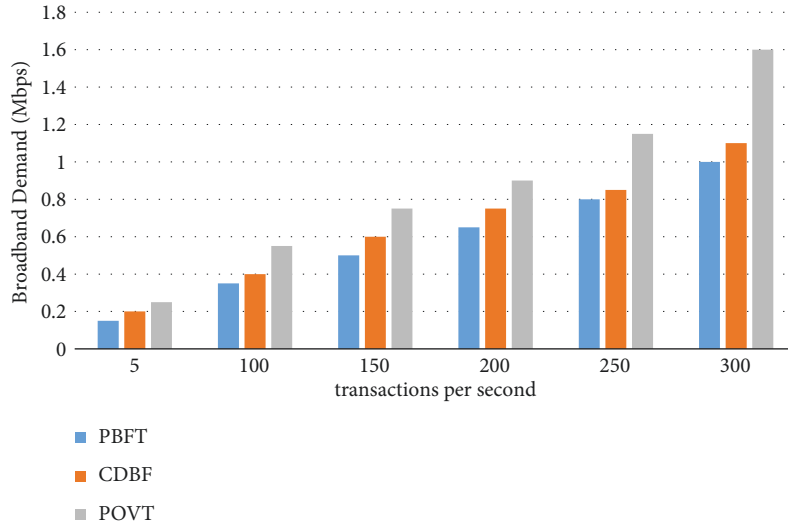


FIGURE 6: Changes in bandwidth demand as the number of concurrent transactions increases.

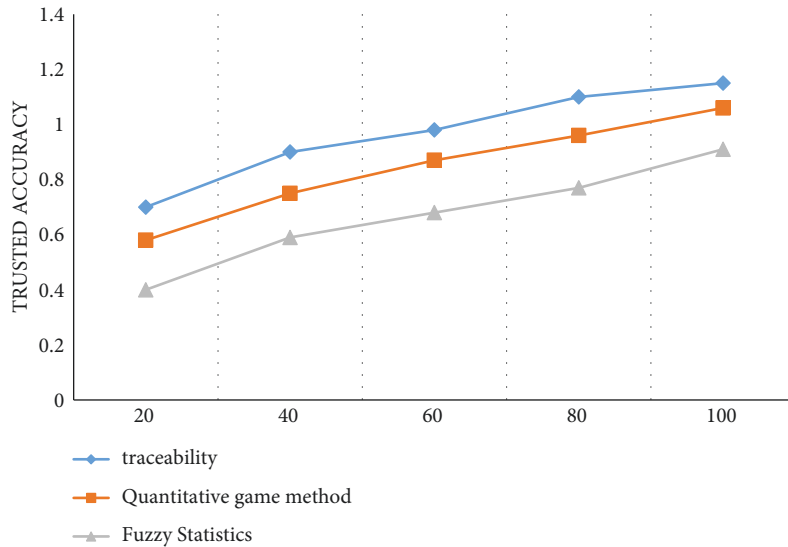


FIGURE 7: Credibility comparison test.

of iterations of obscure statistical methods with quantitative estimates can be up to 80. Up to 90 repetitions of game mods, reliability can reach 1.

4.3. Research on Consensus Mechanism of Blockchain Product Traceability. The security of blockchain consensus protocols is often related to feasibility. The security evaluation of the consensus protocol proposed in this paper is carried out in terms of durability and performance.

It can be seen from Table 2 that the selection times of each node are not related to each other, the maximum error rate can be allowed in the design, and the selection times of each node are roughly the same, which are all possible events. That is, all nodes are selected approximately the same number of times in each cycle. Also, the maximum number of selection errors does not depend on the total number of nodes. In terms of consensus effectiveness, the experiment

TABLE 2: Statistical table of data related to node election in four cases.

Number of elections	Trend line function	Maximum number of errors	Maximum error rate (%)	R.R
10000	$Y = 400$	13	3.35	0.0078
10000	$Y = 200$	11	5.50	0.0015
10000	$Y = 133.3$	9.3	6.97	0.0026
10000	$Y = 100$	6	6	0.0017

mainly estimates and evaluates the average consensus time of these two mechanisms, and the average consensus time is shorter and the consensus efficiency is higher. The test graph environment selects 10%, 20%, and 30% of Byzantine nodes in the network. The number of system nodes n is 52, the number of hits is increased to 2000, and the corresponding number t is 1500. Under certain conditions, the number of

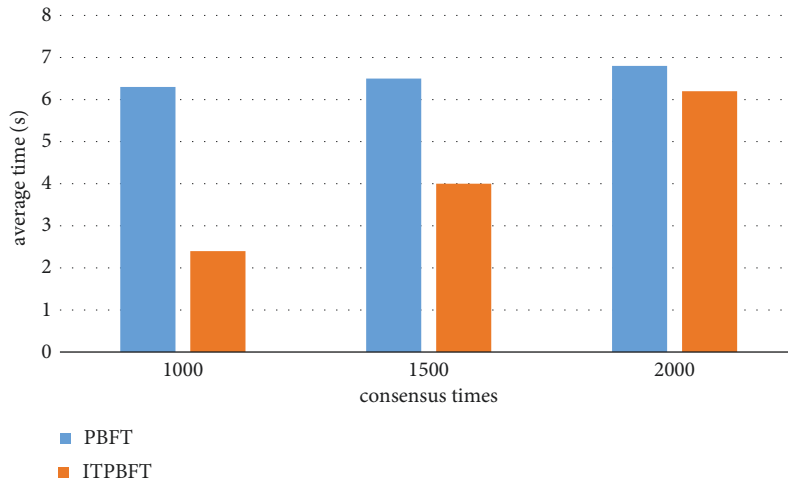


FIGURE 8: Average consensus time when the number of consensus increases.

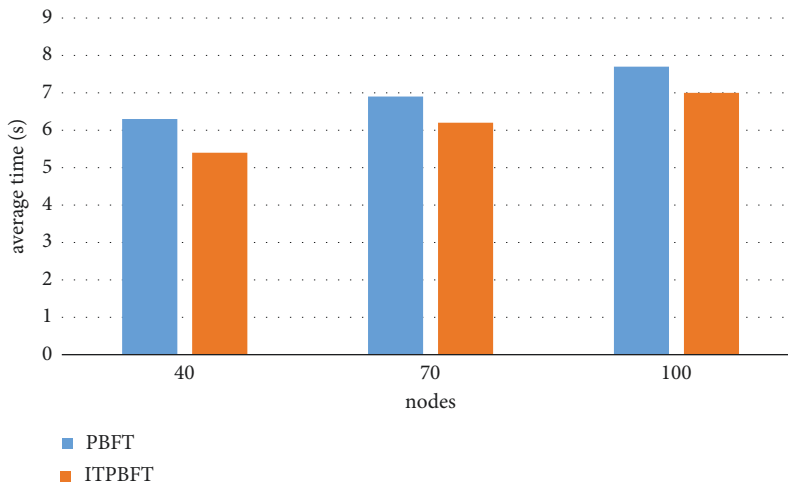


FIGURE 9: Average consensus time when nodes are incremented.

TABLE 3: Average consensus schedule with increasing consensus times.

Mechanism	1000	1500	2000
PBFT	6.3	6.5	6.8
ITPBFT	2.4	4	6.2

TABLE 4: Average consensus time when nodes are incremented.

Mechanism	40	70	100
PBFT	6.3	6.9	7.7
ITPBFT	5.4	6.2	7

system nodes increases to 100. We compare the consensus performance of the two mechanisms under different conditions, check the consensus number, the number of nodes, and other factors, repeat the experiment 100 times, and run the average test results. The results are shown in Figures 8 and 9.

In Tables 3 and 4, the following are experimental results for network environments with 10%, 20%, and 30% Byzantine nodes. According to the test results, the average consensus time of the main mechanism under the same network environment is higher than the average consensus time of the optimized mechanism in the system. For example, the number of Byzantine nodes in the system has increased by 10%, and the average repair time of ITPBFT is about 5.74 seconds. The average fitting time of the PBFT consensus engine is about 6.13 seconds; in addition, as the number of nodes in the system increases, the average consensus time used by the original engine is also higher than that of the optimized engine. The consensus efficiency of the optimized engine has been significantly improved compared to the original engine. For example, by using 10% of Byzantine nodes in the system, the optimization engine can increase consensus efficiency by about 4.7%. With the gradual growth of Byzantine Online, the improvement of consensus performance has become more and more obvious. There are 30% Byzantine nodes in the system. By increasing the consensus, the optimization engine can improve

the consensus efficiency by about 18.5%; as the number of nodes increases, the optimization engine can improve by nearly 16% compared to the original engine. The test results show that although the approval efficiency of the two mechanisms decreases with the increase of the number of approvals and the number of nodes, the optimization engine can improve the approval efficiency and reduce the approval time.

5. Conclusion

As a distributed information system supported by nodes, blockchain is widely used in the fields of transaction, copyright protection, product control, and access control. The emergence of platforms such as Ethereum and Hyperledger has promoted the rapid development of blockchain technology. Although blockchain technology is popular, high-power consumption and poor performance also affect the development of blockchain. The consensus mechanism is the core of blockchain technology: it is the basic mechanism for nodes to sequence events during model implementation, ensuring that nodes reach a consistent and secure network during delivery.

Data Availability

The experimental data used to support the findings of this study are available from the corresponding author upon request.

Conflicts of Interest

The authors declared that they have no conflicts of interest regarding this work.

Acknowledgments


This work was sponsored in part by the Innovation and Entrepreneurship Demonstration Team of Yingcai Program of Chongqing, China (Grant no. CQYC201903167), Science and Technology Research Project of Chongqing Education Commission (Grant no. KJQN202001342), and Technical Innovation and Application Development Special Project of Chongqing (Grant no. cstc2020jscx-sbqwX0015).

References

- [1] K. Christidis and M. Devetsikiotis, "Blockchains and smart contracts for the Internet of Things," *IEEE Access*, vol. 4, pp. 2292–2303, 2016.
- [2] M. Vukoli, "The quest for scalable blockchain fabric: proof-of-work vs. BFT replication," *International Workshop on Open Problems in Network Security*, vol. 10, no. 6, pp. 101–189, 2016.
- [3] J. Yli-Huumo, D. Ko, S. Choi, and K. ParkSmolander, "Where is current research on blockchain technology?-A systematic review," *PLoS One*, vol. 11, no. 10, Article ID e0163477, 2016.
- [4] D. Yermack, "Corporate governance and blockchains," *Social Science Electronic Publishing*, vol. 21, no. 1, pp. 7–31, 2015.
- [5] Y. Yuan and F. Y. Wang, "Blockchain: the state of the art and future trends," *Acta Automatica Sinica*, vol. 32, no. 22, p. 61, 2016.
- [6] M. Yan, J. Liu, and Y. Lin, "Research and exploration of the key elements of food safety data analysis system based on the food safety traceability system," *IEEE in Proceedings of the 2014 9th international conference on computer science & education (ICCSE)*, vol. 10, no. 6, pp. 101–189, Vancouver, BC, August 2014.
- [7] D. K. Mishra, S. Henry, and A. Sekhari, "Traceability as an integral part of supply chain logistics management: an analytical review," 2018, <https://arxiv.org/abs/1811.06358>.
- [8] N. Zawawi, M. Hamdy, and R. Ghary, "Realization of a data traceability and recovery service for a trusted authority service co-ordination within a Cloud environment," *Soft Computing*, vol. 1, no. 6, pp. 54–59, 2016.
- [9] U. Förstner, "Traceability of sediment analysis," *Trac Trends in Analytical Chemistry*, vol. 23, no. 3, pp. 217–236, 2004.
- [10] M. Habib, F. Muhammad, and S. L. Abir, "Chemometrics methods for specificity, authenticity and traceability analysis of olive oils: principles, classifications and applications," *Foods*, vol. 5, no. 4, p. 77, 2016.
- [11] J. Zhang, H. Zhao, and J. University, "Implementation of multi-terminal security intelligent housekeeper control system based on consensus mechanism," *Journal of Information Security Research*, vol. 37, no. 3, pp. 197–206, 2019.
- [12] Y. Zhao, S. Zhang, and M. Yang, "Research on architecture of risk assessment system based on block chain," *Comput. Mater. Continua*, vol. 12, no. 6, pp. 812–832, 2019.
- [13] R. U. Xiao-Xiao, L. I. Zhi-Lan, and B. O. Discipline, "Funding policy research on non-consensus basic research," *Scientific Management Research*, vol. 13, no. 20, pp. 34–56, 2018.
- [14] Y. Sun, J. Yang, W. Chen, and G. XuGong, "Research on typical architecture and application of distribution Internet of Things based on blockchain," *Journal of Physics: Conference Series*, vol. 1621, no. 1, Article ID 12095, 2020.
- [15] X. Zhu, "Research on blockchain consensus mechanism and implementation," *IOP Conference Series: Materials Science and Engineering*, vol. 569, no. 4, Article ID 42058, 2019.

Research Article

Web Log Analysis and Security Assessment Method Based on Data Mining

Jingquan Jin¹ and Xin Lin² 

¹Computer Department, Anhui Post and Telecommunication College, Hefei 230031, China

²Department of Information Technology, Anhui Vocational College of City Management, Hefei 230011, China

Correspondence should be addressed to Xin Lin; 2020025@cua.edu.cn

Received 21 June 2022; Revised 20 July 2022; Accepted 29 July 2022; Published 25 August 2022

Academic Editor: Le Sun

Copyright © 2022 Jingquan Jin and Xin Lin. This is an open access article distributed under the Creative Commons Attribution License, which permits unrestricted use, distribution, and reproduction in any medium, provided the original work is properly cited.

Web content mining describes the classification, clustering, and attribute analysis of a large number of text documents and multimedia files on the web. Special tasks include retrieval of data from the Internet search engine tool W; structured processing and analysis of web data. Today's blog analysis has security concerns. We do experiments to investigate its safety. Through experiments, we draw the following conclusions: (1) Web log extraction can use efficient data mining algorithms to systematically extract logs from web servers, then determine the main access types or interests of users, and then to a certain extent, based on the discovered user patterns, analyze the user's access settings and behavior. (2) No matter in the test set or the mixed test set, the curve value of deep mining is very stable, the curve value has been kept at 0.95, and the curve value of fuzzy statistics method and quantitative statistics method is stable within the interval of 0.90–0.95. The results also show that the data mining method has the highest identification accuracy and the best security performance. (3) Web usage analysis requires data abstraction for pattern discovery. This data abstraction can be achieved through data preprocessing, which introduces different formats of web server log files and how web server log data is preprocessed for web usage analysis. One of the most critical parts of the web mining field is web log mining. Web log mining can use powerful data mining algorithms to systematically mine the logs in the web server and then learn the user's access or preferred interests and then conduct a certain degree of user preferences and behavior patterns according to the discovered user patterns. Based on the above analysis, the current web log analysis is faced with security problems. We conduct experiments to study to verify the security performance of web logs and draw conclusions through experiments.

1. Introduction

Methods developed since the 1970s to represent, process, and extract knowledge for a variety of applications from the ever-increasing accumulation of data have made the pervasiveness of computing possible, perhaps inevitable, and have built a system for examining and a general framework for classification methods. Provide simple examples to demonstrate the nature of representative feature selection methods, compare them using datasets with a combination of intrinsic properties according to the goal of selecting features, propose guidelines for using different methods in various situations, and identify areas of research new challenge venue. There is a reference for researchers in

machine learning, data mining, knowledge discovery, or databases [1]. As the ability to track and collect large amounts of data using current hardware technologies continues to improve, there is a lot of interest in developing data mining algorithms that protect users. Recently proposed approaches have addressed data protection issues by aggregating data and restoring aggregation level distributions for data mining. This technology protects the confidentiality of the information contained in the original mark. Of course, rebuilding a distribution will result in an acceptable loss of information in many real situations. The algorithm is better in terms of data loss levels than currently available methods. In particular, the EM algorithm has been shown to satisfy the maximum likelihood method of the

initial distribution in noise-based estimation. When large amounts of data are available, the EM algorithm provides a reliable estimate of the raw data [2]. Interest in mining time series data has exploded over the past decade. In this work, the following claims are made. Much of the utility of this work is small, because the amount of improvement provided by the contributions is entirely the variance that can be observed by testing on many real-world datasets or by changing minor implementation details. To illustrate this point, the most exhaustive time series experiment ever performed has been reimplemented [3]. The Bayesian network is a graphical model that encodes probability relationships between variables of interest. When used in statistical methods, the model has many advantages in data modeling because it encodes relationships between all variables, facilitates the processing of missing data, and can be used to understand problems and predict results. This article describes the construction of the Bayesian network based on historical data and summarizes Bayesian statistical methods for using the data to improve these models [4]. The use of soft-computing provides an overview of the available data mining literature. Classifications were made based on the various software computing tools used and the data mining activities they performed, as well as the data mining activities performed and the preference criteria selected of the model. The utility of various soft computation methods is emphasized. In general, fuzzy sets are useful for solving problems related to image comprehension, mixed-media information, and human interaction and can provide approximate solutions more quickly. Genetic algorithms provide efficient search algorithms for selecting models from mixed-media data, pointing out specific problems for data mining, and applications of soft-computing techniques are presented in extensive bibliography [5]. Access blogs through business services and academic research are usually limited to the content of web posts. In this paper we provide a large-scale study of blogging and its relationship to posts. Using a large-scale comment corpus, we estimate the large number of comments in the blogosphere; analyze the relationship between blog popularity and comment patterns; and measure the contribution of comment content to various aspects of our blog visits [6]. Several systems have been developed to provide statistical analysis of World Wide Web usage logs. These programs typically report the number of files used and the number of times the site was used by the site, and some programs even provide time-of-request analysis. However, these programs are not interactive and cannot see the local database. The Internet is designed to provide database administrators and designers with graphical representations and templates for accessing local databases. In other words, by incorporating the network path paradigm into interactive software, users can not only view documents in the database, but also contact users by requesting documents from the database [7]. It presents the methods and analysis used in the ongoing, three-year Excite research project, which aims to examine the search nature of major Internet search engines. This article starts with general information about the web, unique and attractive views of users searching the web, and the impact of the web. The main

content of this article discusses the structures and methods used so far in material analysis and concludes with conclusions and expectations for future network research [8]. Web usage analysis or web usage analysis or web log extraction or clickthrough rate analysis is the process of extracting useful information from web server logs, database logs, user requests, client-side cookies, and user profiles to test the performance of web users. Internet usage analysis requires data abstraction to find patterns. This data abstraction can be achieved by data preprocessing, which adopts different web server log file formats and how the web server log data is preprocessed to analyze network usage [9]. Log files are maintained in communication between web browsers and web servers generated by real users accessing content associated with dynamic hyperlinks. These log files represent past user access to content and are used to generate web crawler access. This approach allows crawlers to accurately simulate real users, leading to the ability of legacy bots to automatically access everything a real user can access [10]. A method of evaluating an organization's information security policies and practices, including identifying risks associated with information security policies and practices, collecting information about information security policies and practices, using a security due date assessment matrix, generating ratings from the collected information, and correlating information with information risks associated with security policies and exercises, is to use ratings to generate a list of corrective actions, execute the list of corrective actions to create new security information policies and exercises, and monitor new security information policies and exercises [11]. Ecological security is a challenging issue for human survival and development. Cities are efficient and interactive human activities, resource shortages prevent further urban development, and ecological refugees and environmental health issues affect human survival. Urban ecological security is threatening the sustainable development of cities. There is an urgent need to appreciate urban sustainability. There is an urgent need to appreciate that urban ecological security and urban ecological security assessment are the most important issues. Through the assessment, decision makers can obtain more information about the current status of urban ecological security so that they can issue rational strategies to solve the problem. People can obtain information in time and then take decisive action to protect themselves [12]. Security analysis is a complex system development. The latest security scanning tools are only used to scan and detect vulnerabilities in network systems. Systems engineering thinking and techniques are applied to a comprehensive cybersecurity analysis. An artificial neural network model for safety analysis has been proposed, and computer simulation experiments have been carried out. The results show that the model can be effectively used to comprehensively evaluate the network security level. The overall assessment of the security status of computer networks provides new ideas and methods [13]. Security assessment is a complex system engineering. Through the hierarchical analysis process, various factors affecting network security are deeply studied, and a comprehensive network security ranking index system is

established. A security assessment is proposed, which provides a new idea and method for the overall assessment of computer network security status [14]. Network security analysis is a complex system design. The latest security analysis tools are only used to scan and detect security vulnerabilities in network systems. Comprehensive analysis of system design and techniques applied to cybersecurity is done. Build a comprehensive evaluation index system for network security. An artificial neural network model for safety assessment is proposed, and computer simulation experiments are carried out. The results show that the model can be effectively used to comprehensively evaluate the network security level. The overall assessment of the security status of computer networks provides new ideas and methods [15].

2. Web Log Analysis under Data Mining

2.1. Overview of Web Log Mining. Web mining is one of the most important components of the web mining industry. The web systematically extracts logs from web servers using powerful data mining algorithms to obtain information about user availability or priority of interest and is based in part on detected user patterns. Evaluate your website, adjust its topology, improve system performance, improve your website experience, provide intelligent personalization, and increase user loyalty. Internet communication is usually done through a web server architecture. The server for each site generates logs, the web client generates log files for clients accessing multiple sites, the proxy server generates log files for multiple users accessing multiple sites through a proxy, and the web server generates journal log files. Log files for multiple users using the site. Therefore, recording user habits can also capture user habits from three perspectives: network client, proxy server, and web server. Since the log information of the three nodes is different, the available user information is also different. Currently, two main aspects of the weblog algorithm are being analyzed, pattern sequence analysis algorithms and clustering algorithms. Customer usage patterns and agency buying should start online. Periodic pattern analysis algorithms are usually chosen to analyze the user's desired path, capture the content of interest to the user, and use an intelligent search engine to improve performance. Server-side clustering algorithms are commonly used to aggregate log data generated by all users visiting a website and create blogs that evaluate user behavior based on the clustering results. Finally, in this article, we will look at campus website logs to determine patterns of visitors. Therefore, it was decided to use a clustering algorithm to extract server-side access patterns.

2.2. Web Log Mining Process. In general, the journal launch process is divided into four steps: collecting journals, defining journals, defining templates, and modifying templates. (1) This article also uses this type of logs to review work, and there are ways to collect logs using

JavaScript scripts on our web page. (2) Log preprocessing phase after the general data exploration phase; initial data preprocessing will be performed in this phase. The log data source is irregular, impure, invalid data. Raw logs are used to cover data processing. It is converted into a format suitable for intelligence assessment, stored in a single format, and then continuously assessed. (3) Use a variety of data mining algorithms according to other business needs, mainly covering cluster analysis, association recommendation, path and intelligent sequence data analysis, etc. (4) Model analysis step: This step is the process of defining and analyzing data mining, which makes the generated model easy to understand. In the case of solving fundamental problems, theoretical theory is based on the definition of strategies. The web log mining process is shown in Figure 1.

2.3. Web Data Mining Classification and Development Design Focus. Web content mining involves classifying, grouping, and analyzing connections between multiple text and multimedia files on the Internet. Specific tasks include retrieving information from W search engines on the Internet; structuring and analyzing network data; page content analysis based on HTML technical standards and efficient data analysis. The implementation methods of web content extraction are mainly divided into direct document content decompression object; search engine query data retrieval object. According to different data mining objects, online content decompression includes two categories: online document decompression and media decompression. Web analysis is basically the process of searching and refining information about the structure and informational associations of pages on the World Wide Web. Its traditional implementation is as follows: First, the topology structure of the World Wide Web is analyzed using graph theory and transformed into a directed graph model. Each web page acts as a structural cue for a directed graph, with each edge of the graph representing links between different web pages. Examining the network structure can capture the necessary elements of directed graphs transformed from the World Wide Web to objects and extract valuable information from them. The purpose of a preliminary analysis of the site structure is to support search engines and provide users with valid information on the man pages. The object of web data mining research is shown in Figure 2.

Web content mining refers to the classification, clustering, and association analysis of a large number of text documents and multimedia files on the web. The specific tasks include extracting data information from the W search engine tool in the Internet; performing structured processing and analysis on network information; analyzing the page content based on HTML technical standards and mining the effective data information.

Pure log mining analysis extracts the access records stored by the server when users access network resources. The information stored in the web log includes the user's access method, access date and time, user query, user's

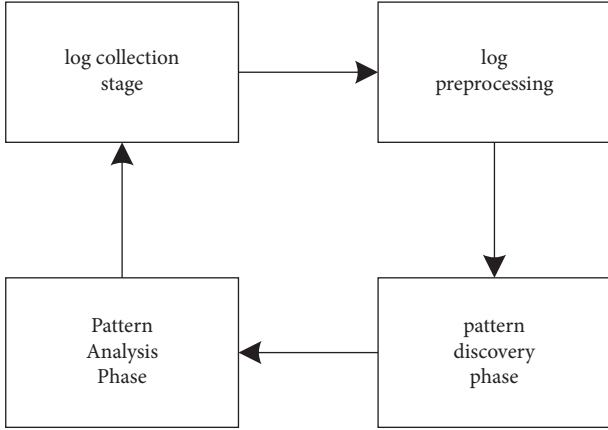


FIGURE 1: Web log mining process.

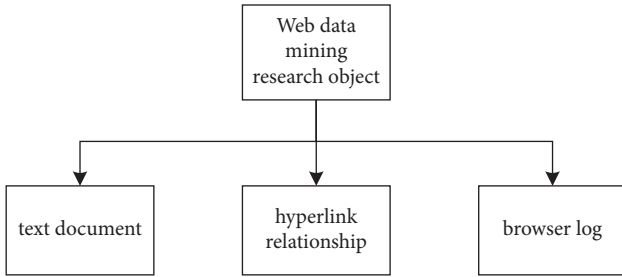


FIGURE 2: Web data mining research objects.

smart address, etc. Statistical analysis of this information allows us to examine the relationship between this information so that we can still find some key characteristics of user behavior. The key points of the development and design of network log extraction technology are as follows: (1) Before data mining, the target data must be pre-processed to meet the requirements of data mining and retrieval and to improve the level of efficient use of data. (2) OLAP can be used to perform multilevel analysis on the web log database to determine the N most popular web pages that will be opened when N users open web pages, so that users can understand their usage preferences and lay a foundation for this, so as to tap potential demand and market development.

3. Web Log Analysis under Data Mining Algorithm

3.1. Data-Based Mining Model. When performing data analysis based on historical data, data analysis can be carried out from a mathematical point of view and in accordance with the idea of time series analysis. When analyzing historical data, the algorithm used in this paper is support vector machine. Define a training set (X_i, Y_i) of number n and a nonlinear map $\psi(X)$ as

$$\{(X_i, Y_i) | i = 1, 2, \dots, n\},$$

$$\psi(X) = (\varphi(x_1), \varphi(x_2), \dots, \varphi(x_n)). \quad (1)$$

The two complete the mapping from the sample input space to high-dimensional features by a linear regression function:

$$f(x_t) = \omega^T \varphi(x_t) + b. \quad (2)$$

Among them, ω is the weight vector in the high-dimensional space, and b is the bias of the model. The ultimate goal of the SVM algorithm is to minimize the structural risk, that is, to find the optimal ω and b . During the calculation of model parameters, SVM is usually based on the principle of structural risk minimization:

$$\min J = \frac{1}{2} \omega^2 + c \sum_{i=1}^n (\xi_i + \xi_l) \quad (3)$$

$$s.t \{ y_i - \omega^T \varphi(x_i) - b \leq \varepsilon + \xi_i.$$

Among them, c is the regularization coefficient in the optimization process, and ξ_i, ξ_l is the relaxation factor to adjust the structural risk. When solving the optimization problem, this paper uses the Lagrange function, and its basic process is as follows:

$$L = \frac{1}{2} \omega^2 + c \sum_{i=1}^n (\xi_i + \xi_l) - \sum_{i=1}^n \bar{\alpha}_i. \quad (4)$$

According to the optimization algorithm there are

$$\frac{\partial L}{\partial \omega} = 0 \longrightarrow \omega = \sum_{i=1}^n (\alpha_l - \alpha_i) \varphi(x_i). \quad (5)$$

At this point, the kernel function that defines the heap function used in the optimization process is

$$k(x_i, x_j) = \varphi(x_i)^T \varphi(x_j). \quad (6)$$

Finally, the prediction formula of the model can be obtained:

$$f(x) = \sum_{i=1}^n (\alpha_l - \alpha_i) K(x_i, x_j) + b. \quad (7)$$

Among them, $k(x_i, x_j)$ is the radial basis function used in the model prediction, and its form is as follows:

$$k(x_i, x_j) = \exp \left[\frac{-x_i - x_j}{2\sigma^2} \right]. \quad (8)$$

3.2. Realize Intelligent Data Mining. Use neural network technology, an important branch of artificial intelligence technology, to achieve the goal of big data mining in the Internet of Things. A BP neural network with a three-layer transmission structure is used as the main structure, and normalized data is inputted into the neural network. Due to the peculiarities of the structure of the neural network, to replace the weight of the connection between the input and intermediate layers of the network W , the average information-information entropy E is used. The formula for calculating the weight:

$$\omega = \frac{1 - H_i}{\sum_{i=1}^E H_i}. \quad (9)$$

In the formula, the calculation result of the connection weight of the neural network is obtained through the entropy value of the i -th dimension attribute of the data. A genetic learning step is added to design a classifier with the network nonlinear classification ability and network structure as the core. Through the optimization of the genetic learning algorithm, the data that meets the mining requirements is output. The improvement of this artificial intelligence technology method, while ensuring the nonlinear ability, is connected with the previous processing method to ensure the accuracy of data mining. The genetic algorithm is integrated in the data mining process, and it is necessary to complete the modification of the hybridization operator and the mutation operator on the data input to the neural network. The calculation of the hybridization operator is expressed as a linear combination, expressed as:

$$\begin{aligned} \theta_1 &= u\theta_1 + (1-u)\theta_2, \\ \theta_2 &= u\theta_2 + (1-u)\theta_1. \end{aligned} \quad (10)$$

In the formula, θ_1 and θ_2 are the two data pieces of linear combination, and the value range of the constant U is between 0 and 1, and the value range is narrowed according to the actual situation. When the constant value is in a fixed state, it means that the hybridization operator in the calculation process is inconsistent. When the constant value changes with the number of iterations, the average performance of the hybridization operator can be improved, so that the IoT big data can be gradually mixed. In the modification of mutation operator in data mining, each random data C may have a certain probability of mutation, and the value V_k after one mutation of the data is randomly expressed as

$$v_k = v_k + \Delta(t, v_k - LB). \quad (11)$$

Generate data variation values based on the left and right neighbors LB and UB of variable k and the return value of the function. The value of data variation tends to be infinitely close to 0 as the algebraic t increases. Based on the above operations, the overall search of the operator in the data set is completed, and the IoT data information that meets the data mining requirements is output. Through all the above processing steps, the design of the IoT big data mining algorithm based on artificial intelligence technology is realized.

3.3. Data Mining Based on Influencing Factors. In the data analysis based on influencing factors, this paper introduces the Gray Wolf Optimal Algorithm (GWO) in the field of data mining. The GWO algorithm is an optimization algorithm based on the gray wolf population hierarchy and

group predation behavior. The principle is described in mathematical language as follows: For a gray wolf population, its number is M , and the search space is k , and for the gray wolf individual numbered i , its position can be described as

$$x_i = (x_1, x_2, \dots, x_k), \quad (12)$$

(13) and (14) give the process of wolves surrounding their prey:

$$D = |C \cdot x_p(t) - x(t)|, \quad (13)$$

$$x(t+1) = x_p(t) - A \times D. \quad (14)$$

Among them, D is the distance between the wolf and the prey in the wolf pack, $x(t)$ is the individual position of the gray wolf after iteration, and A and C are the parameter vectors of the model. The calculation method is as follows:

$$\begin{aligned} A &= 2ar_1 - a, \\ c &= 2r_2. \end{aligned} \quad (15)$$

When rank α, β, δ is close to the prey in the gray wolf group, the position of the prey can be estimated at this time, and the gray wolf group will iteratively update the position according to α, β, δ . Combined with the application scenarios in this paper, the common gray wolf optimization algorithm has a local optimum in the iterative process. Therefore, dynamic evolution operators and nonlinear convergence factors are introduced into the traditional gray wolf algorithm to improve the performance of the algorithm. After introducing the dynamic evolution operator, the wolf population combines the position of α, β, δ to update the position. At this point, the location update method can be rewritten as

$$\alpha = 2 - (e^{1/t} - 1) \cdot \frac{2}{(e - 1)}. \quad (16)$$

Differential evolution algorithm is used in this paper when making evolution improvements to the improved gray wolf algorithm. The algorithm includes three steps of mutation, crossover, and selection. First, the population is initialized:

$$x_{ij}(0) = x_{ij}^L + \text{rand}(0, 1)(x_{ij}^U - x_{ij}^L). \quad (17)$$

Mutate N initial populations on a random search space:

$$V_i(t+1) = x_{r_1}(t) + F[x_{r_2}(t) - x_{r_3}(t)]. \quad (18)$$

Then perform a crossover operation to improve the diversity of the population:

$$U_{ij}(t+1) = X_{ij}(t+1). \quad (19)$$

Based on the greedy algorithm, the individual with better evolution is selected as the new generation individual:

$$X_{ij}(t+1) = U_i(t+1), f[U_i(t)] \leq f[X_i(t)]. \quad (20)$$

TABLE 1: Web log security assessment.

Log model	Coverage (%)	Accuracy (%)	Recall (%)	Safety score (%)
Web log	81	93	44	94
Normal log	70	83	57	82

4. Web Log Analysis and Security Assessment under Data Mining

4.1. *Web Log Security Assessment.* In order to test the security performance of web logs, we collected the following data to evaluate the data coverage, accuracy, and recall to obtain the experimental results. The experimental results are shown in Table 1 and Figure 3.

According to the experimental data in the above chart, we can conclude that the accuracy rate and security score of web logs have reached more than 90%, and the coverage rate has reached 81%, and the recall rate is only 44%, while the accuracy rate and security score of ordinary logs have only reached about 80%, and the coverage rate is only 70%, and the recall rate reaches 57%. Through comparative experiments, we can see that web logs are more stable than ordinary logs in terms of coverage accuracy and security score.

4.2. *Overview of Web Log Hotspots and Trend Analysis.* We have made comprehensive statistics on the hot issues mentioned in the web logs and counted the overall traffic, monthly hot spots, and the highest visiting days and traffic. The data obtained are shown in Table 2 and Figure 4.

As can be seen from the above figure, the number of visits was the highest in the fifth week, and the number of visits this week reached 99,473. The least week was the first week, with 87,655 visits. From the trend point of view, the fluctuation of the number of visits is dominated by a continuous upward trend, with a slight increase in the number of abnormal weekly visits.

4.2.1. *Web Log Hotspot Query Type.* As shown in Figure 5 above, the largest query type was sales, which accounted for 33% of the total; by contrast, intermediaries had the lowest share, accounting for less than 20% of the total. This is followed by Ajax pages at 17% to 29%, followed by Ajax pages at 18% to 22%. In terms of trends, the sales page has maintained a high level of attention for a long time, while the data on the intermediate pages is scattered and incomplete, making it difficult to build a stable trend.

4.2.2. *Visits of Web Logs during Hot Spots.* As can be seen from Figure 6 above, the hot spots browsed by users are all concentrated in the noon and June period, the frequency of visits reaches the highest and its proportion reaches about 15%, and the time period with the lowest visit frequency is 3. During the month, it accounted for about 7%. From the above figure, we can see that the time period of hotspot access is always fluctuating, and there is no stable trend.

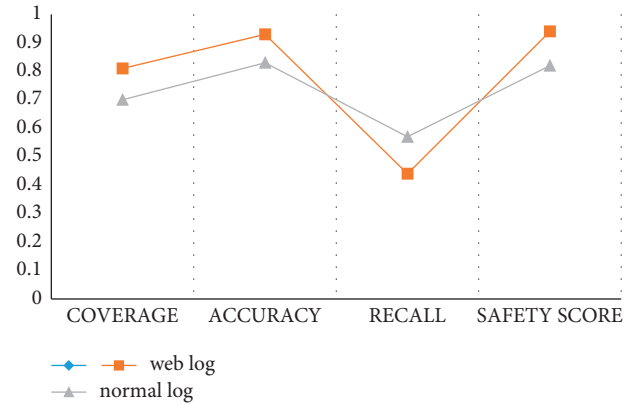


FIGURE 3: Web log security assessment.

TABLE 2: Weekly visits.

	First	second	Third	Fourth	Fifth
Weekly visits	87655	87898	88242	89883	99473

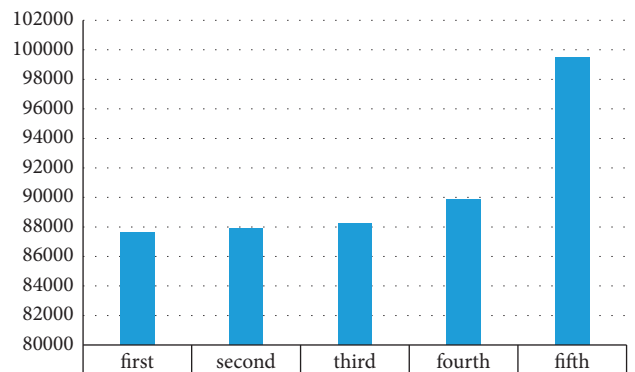


FIGURE 4: Week visits.

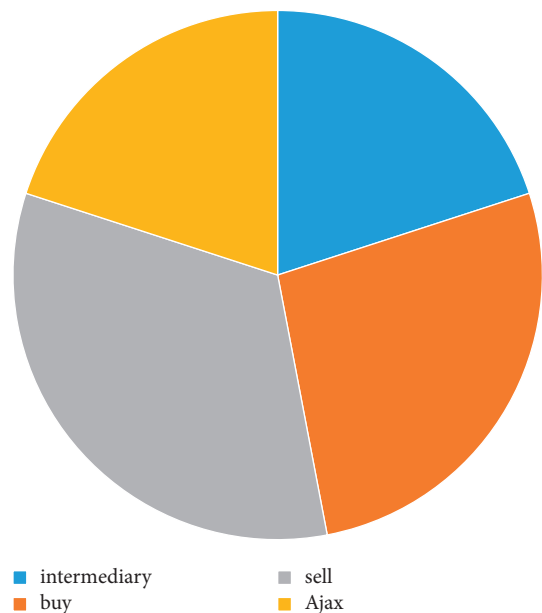


FIGURE 5: Hotspot query types.

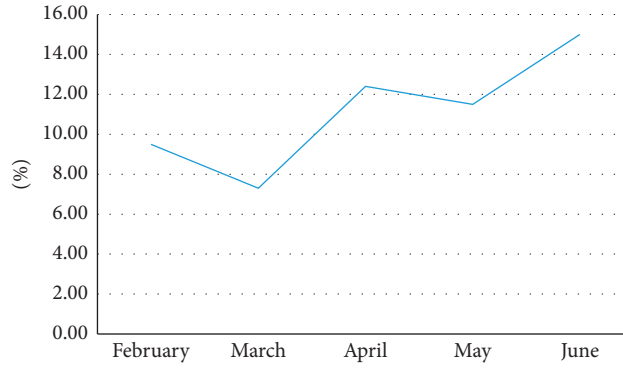


FIGURE 6: Visits during hotspots.

4.3. *Data Mining Accuracy Comparison.* According to the experimental results, we can conclude that the data mining method used in this paper is relatively high in terms of experimental results and accuracy. The statistical method was compared, and the comparison results are shown in Figure 7.

According to the experimental data of the graph, we can know that the evaluation accuracy of the data mining method is the highest among the three methods. When the number of iterations reaches 50, the evaluation accuracy can reach 1, and when the number of iterations of the fuzzy statistical method is 80. When the number of iterations of the game method is 90, the evaluation accuracy can reach 1.

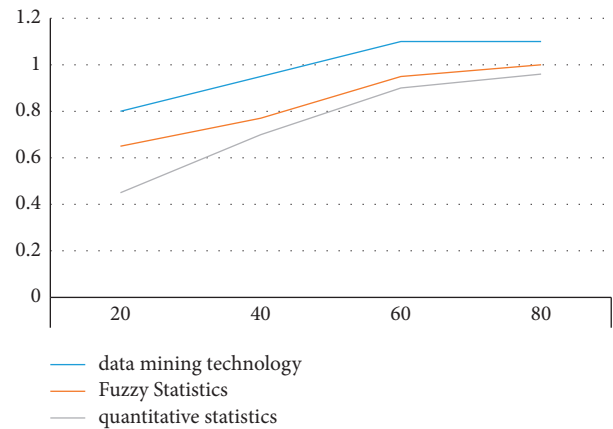


FIGURE 7: Evaluation accuracy comparison test.

4.4. *Performance Test and Safety Evaluation Test.* In order to test the superiority of the performance based on the data mining technology proposed in the paper, after the model proposed in the paper is improved, the fuzzy statistics method and the quantitative statistics method are, respectively, run on the test set and the mixed test set. The test set is used to evaluate the generalization ability of the final model, and the mixed test set is used to tune the model’s hyperparameters and to make an initial evaluation of the model’s ability. Record the experimental results to verify the advantages of the three methods, and draw graphs based on the experimental results. The experimental data of different models on the test set and the mixed test set are shown in Table 3 and 4.

According to the data in the table and Figure 8, we can conclude that, after running on the test set, the accuracy rate of quantitative statistics method can reach 89%, the accuracy rate can reach 91%, and the accuracy rate through data mining technology can reach 92.%. The accuracy rate can reach 93%, which is the highest index value among the three experimental models. The accuracy rate of fuzzy statistics method is 85%, which is the lowest among the three models. According to the curves of the three models, we can also see that the curve values of the data mining technology are very stable, the curve value of the quantitative statistics method is kept at about 0.90, and the curve value of the data mining method is also always kept at 0.97. The curve value of the statistical method is lower, and the experimental results also

TABLE 3: The performance of each model on the test set.

Method	Accuracy (%)	Accuracy (%)	Score (%)
Data mining	92	93	95
Fuzzy statistics	85	82	83
Quantitative statistics	89	91	90

show that the performance of the data mining technology is the best and the security performance is also the best.

According to the data in Table 4 and Figure 9, we can conclude that, after running on the mixed test set, the performance of the three models has decreased to a certain extent, but the data mining method proposed in the article is still the highest among the three methods. One, the accuracy rate of quantitative statistics method is 87%, and the accuracy rate of fuzzy statistics method is 90%. According to the curves of the three algorithms, we can also see that the curve value of deep mining is very stable, whether in the test set or the mixed test set, the curve value has been kept at 0.95, and the curve of the fuzzy statistical method and the quantitative statistical method values stabilized within the range 0.90–0.95. The experimental results also show that the data mining method has the highest recognition accuracy and the best security performance.

TABLE 4: The performance of each method on the mixed test set.

Method	Accuracy (%)	Accuracy (%)	Score (%)
Quantitative statistics	87	88	90
Data mining	90	92	95
Fuzzy statistics	82	81	85

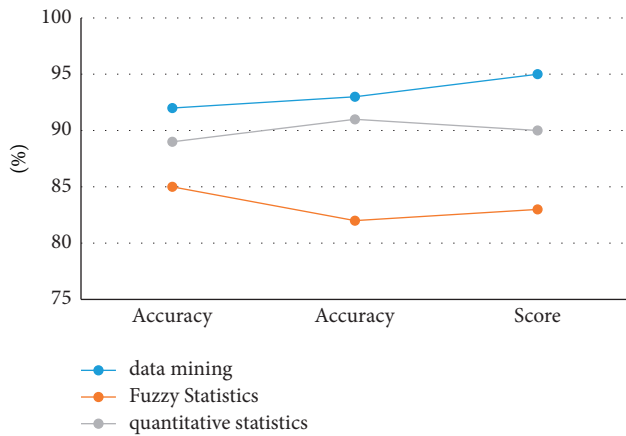


FIGURE 8: Curves on the test set.

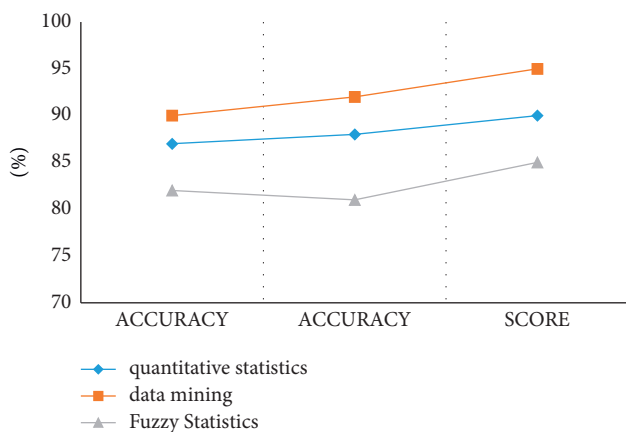


FIGURE 9: Curves on the mixed test set.

5. Conclusion

One of the most important parts of the web indexing arena is the indexing of your blog. Web log extraction can use powerful data mining algorithms to systematically manage our logs on web servers and then learn accessibility or user preferences, in part based on settings and usage patterns. Website analytics and interactive website experience will be enhanced, and intelligent personalization will be provided to increase user loyalty. Through the analysis of the web log of data mining, we can also find that the curve value of deep mining is very stable no matter in the test set or the mixed test set, the curve value has been kept at 0.95, the curve value of fuzzy statistics method and quantitative statistics method is stable within the range of 0.90–0.95. The experimental results also show that the data mining method has the highest recognition accuracy and the best security performance.

Data Availability

The experimental data used to support the findings of this study are available from the corresponding author upon request.

Conflicts of Interest

The authors declare that they have no conflicts of interest regarding this work.

References

- [1] R. S. Parpinelli, H. S. Lopes, and A. A. Freitas, "Data mining with an ant colony optimization algorithm," *IEEE Transactions on Evolutionary Computation*, vol. 6, no. 4, pp. 321–332, 2002.
- [2] S. K. Pal, V. Talwar, and P. Mitra, "Web mining in soft computing framework: relevance, state of the art and future directions," *IEEE Transactions on Neural Networks*, vol. 13, no. 5, pp. 1163–1177, 2002.
- [3] E. Frank, M. Hall, L. Trigg, G. Holmes, and I. H. Witten, "Data mining in bioinformatics using Weka," *Bioinformatics*, vol. 20, no. 15, pp. 2479–2481, 2004.
- [4] Q. Yang and X. Wu, "10 challenging problems in data mining research," *International Journal of Information Technology and Decision Making*, vol. 5, no. 04, 2006.
- [5] T. Hastie, R. Tibshirani, and J. H. Friedman, "The elements of statistical learning: data mining, inference and prediction. By," *The Mathematical Intelligencer*, vol. 27, no. 2, pp. 83–85, 2009.
- [6] M. Thelwall, "Handbook of research on web log analysis," *Journal of the Association for Information Science & Technology*, vol. 60, no. 9, p. 1943, 2010.
- [7] B. J. Jansen and A. Spink, "Methodological approach in discovering user search patterns through web log analysis," *Bulletin of the American Society for Information Science and Technology*, vol. 27, no. 1, pp. 15–17, 2000.
- [8] C. C. Yang and T. D. Ng, "Terrorism and Crime Related Weblog Social Network: Link, Content Analysis and Information Visualization," in *Proceedings of the Intelligence & Security Informatics*, pp. 55–58, IEEE, New Brunswick, NJ, USA, May 2007.
- [9] S. Malik and E. Koh, "High-volume hypothesis testing for large-scale web log analysis," *ACM*, in *Proceedings of the 2016 CHI Conference Extended Abstracts on Human Factors in Computing Systems*, pp. 1583–1590, New York, NY, U S A, May 2016.
- [10] Y. Q. Wei, G. G. Zhou, D. Xu, and Y. Chen, "Design of the web log analysis system based on hadoop," *Advanced Materials Research*, vol. 926, pp. 2474–2477, 2014.
- [11] X. Q. Shi and Z. Y. Ouyang, "Urban eco-security and its dynamic assessment method [J]," *Acta Ecologica Sinica*, vol. 25, no. 12, pp. 3237–3243, 2005.

- [12] R. A. Schlueter, "A voltage stability security assessment method," *IEEE Transactions on Power Systems*, vol. 13, no. 4, pp. 1423–1438, 1998.
- [13] X. Jia, Y. Cai, C. Li, X. Wang, and L. Sun, "An improved method for integrated water security assessment in the Yellow River basin, China," *Stochastic Environmental Research and Risk Assessment*, vol. 29, no. 8, pp. 2213–2227, 2015.
- [14] H. Yuan, "A network security risk assessment method based on immunity algorithm," *Advanced Materials Research*, vol. 108-111, pp. 948–953, 2010.
- [15] L. Hang, A. Bose, and V. Venkatasubramanian, "A fast voltage security assessment method using adaptive bounding [J]," *IEEE Transactions on Power Systems*, vol. 15, no. 3, pp. 1137–1141, 2000.

Research Article

Deep Learning-Based Correlation Analysis between the Evaluation Score of English Teaching Quality and the Knowledge Points

Yuanyuan Li 

Foreign Language School, Suzhou Vocational University, Suzhou 215104, China

Correspondence should be addressed to Yuanyuan Li; 00986@jssvc.edu.cn

Received 14 April 2022; Revised 9 May 2022; Accepted 12 July 2022; Published 25 August 2022

Academic Editor: Le Sun

Copyright © 2022 Yuanyuan Li. This is an open access article distributed under the Creative Commons Attribution License, which permits unrestricted use, distribution, and reproduction in any medium, provided the original work is properly cited.

As one of the three main courses from primary school to senior high school, improving the quality of English teaching in and out of class has become the top priority of colleges and universities. English knowledge points are complex, and domestic scholars have studied vocabulary knowledge and grammatical awareness from various perspectives, but there is still a lack of research on the correlation between vocabulary knowledge, grammatical awareness, and cloze test scores of senior high school students. Therefore, this paper carries out empirical research from the depth of English vocabulary, English grammar, reading comprehension, cloze test, and composition, aiming at exploring the relationship between teaching quality and English knowledge points. Classroom teaching quality evaluation is the basic content of education quality evaluation, which not only needs to evaluate the effect of class hours but also needs a student's long-term learning effect. In order to improve the quality of classroom English teaching, enrich the content of classroom English, and ultimately make the quality of students' learning to a higher level, the combination model of the teaching quality evaluation index is established by combining the decision tree with the knowledge point rule association method and the evaluation results are verified by association rule analysis. This paper selects the effective indicators that affect the evaluation of English teaching quality, determines the weight of the indicators by using the analytic hierarchy process, effectively constructs the combination model of the decision tree and rule association method, and establishes the evaluation model of students' English learning ability in the classroom. Taking students as the main object and combining them with the requirements of digital teaching, the evaluation index system is formed, the index weight is determined by using the analytic hierarchy process, and the classroom teaching quality evaluation model based on the decision tree and English knowledge point correlation analysis is constructed to truly reflect the teaching level of teachers, and the correlation analysis is carried out between English teachers' own quality and students' learning effects and knowledge points. By testing the model performance of English vocabulary depth, reading comprehension, grammar, writing, and other knowledge points, we can well evaluate and analyze students' mastery of English learning and the correlation of English knowledge points.

1. Introduction

English is the most common language in the world, and its importance goes without saying. In order to evaluate the quality of English teaching in schools and study the correlation between teaching quality and English knowledge points, we have constructed a combined evaluation system of the decision tree and rule association analysis of knowledge points. This paper expounds that this method is efficient in detecting large error data in fringe images [1] and uses artificial intelligence technology to evaluate the quality of surgery in medicine [2]. It expounds the anatomical analysis

of the components of kidney stones by the deep learning method [3]. In order for the leaders of colleges and universities to do a better job in teaching management and reduce unnecessary management problems, literature [4] fully demonstrates the effectiveness of teaching evaluation for students in colleges and universities under the background of intelligent computing. Using big data related knowledge to study the evaluation system of college physical education can not only promote the implementation of college physical education evaluation but also effectively improve the quality of college physical education [5]. It takes the quality of graduates as the core content, establishes a result-oriented

evaluation system of teaching quality in colleges and universities, and finds that the academic level and the level of competition in choosing jobs are two quantitative levels reflecting the quality of graduates [6]. It mainly puts forward some measures to construct the evaluation system of college English teaching from the key point of constructing the evaluation system of junior and senior high school English teaching based on online learning platform [7]. Through a scientific and complete teaching evaluation system, we can optimize the physical education teaching process to a certain extent, promote the effective realization of physical education teaching objectives, and improve the quality and efficiency of physical education in colleges and universities [8]. It expounds the development of task-based learning as the center of the English teaching evaluation model and cultivates the English writing ability and creative thinking of Thai sixth grade students [9]. It mainly explores the multidimensional teaching evaluation system of local universities under the background of transformation [10]. It discusses how higher education institutions apply the questionnaires used in our research to diversity management [11]. It implements gauge teaching evaluation from the perspective of students and teachers [12]. There are considerable problems in the hypothesis of students' evaluation to measure the teaching effect, especially in the system where problem-based learning is the main teaching idea. It determines a working hypothesis; that is, students do not use teaching ideas as the main motivation to evaluate employees, which leads to an abnormal incentive [13]. This study assessed the effectiveness of focused educational practice designed for teachers in multiple professional departments, which have a large number of elderly patients, and became a geriatrics-based teacher development plan [14]. This paper explores the diversity of evaluation methods and exerts the positive functions of evaluation, detection, stimulation, and development. By expanding evaluation ideas, emphasizing performance evaluation, realizing immediate evaluation, and carrying out special evaluation, the evaluation function can be repositioned [15]. The paper verifies the effectiveness and practicability of our method through an intuitive multimedia teaching evaluation example [16]. The analysis results of this paper may provide some theoretical basis and reference for the research of history teaching methods and also provide relevant information for overseas Chinese modern history research institutions to understand the learning situation of Chinese history in this period [17]. On the basis of continuous development and improvement of teaching evaluation, this paper explores the refined management of undergraduate teaching [18]. Teaching evaluation is an important part of curriculum teaching, which is beneficial for teachers to get feedback, improve the teaching quality, and maintain the teaching foundation. It is an effective measure for students to find the most suitable learning method, correct learning habits, and improve learning efficiency [19]. The fuzzy comprehensive evaluation of the cloud system is studied, and finally the experimental verification is carried out by an example [20]. The purpose of this study is to analyze the relationship between learning styles and academic achievements of accounting science students combined with teachers' evaluation [21]. It examines the evaluation degree of

teachers' own teaching behavior management practice, as measured by the evaluation system of classroom learning strategies [22]. The teaching evaluation method proposed in this study is helpful to fully reflect the quality of classroom teaching and guide students' professional development [23]. In this paper, we propose two vocabulary-based methods, especially knowledge-based and machine learning-based methods, to automatically extract opinions from short comments [24]. This structured process produces an evidence-based and systematically developed EM teacher evaluation tool, which can provide teachers with real-time operational feedback and support improved clinical teaching [25].

2. Construction of the Index System of the English Teaching Quality Evaluation Model

2.1. Indicator Construction. The evaluation of English teaching quality from primary school to senior high school is a nonstatic process involving many variables and influencing factors. The evaluation system of English teachers' classroom teaching quality needs to reflect and exclude teachers' own influencing factors, such as teachers' teaching concepts, teaching attitudes, teaching methods, and educational effects. It is also necessary to take into account the factors of students who directly participate in teaching. Students can directly feel teachers' own teaching quality and students' learning effects during the whole feeling process of participating in classroom teaching. The innovation and diversification of information-based foreign language teaching methods require the cultivation of students' intrinsic motivation and self-efficacy and the effective integration of information technology and foreign language teaching. Finally, it establishes the initial index content composed of four most important indexes and fifteen more important indexes: "curriculum goal, classroom teaching, teaching effect, and teaching expansion."

- (1) The index of "curriculum goal" is the direction and soul of the curriculum, which determines the overall quality of personnel training. It aims to reflect the applicability of teaching content and cultivates the matching degree of knowledge and skills that students need to achieve through curriculum study.
- (2) The index of "classroom teaching" reflects the main forms and key links of English teaching from primary school to senior high school, including the effectiveness of English classroom teaching activities in cultivating knowledge depth and learning ability, the rationality of classroom teaching time and content arrangement, and the breadth and depth of information resources use under the background and environment of the digital age.
- (3) The "Teaching effect" reflects the effectiveness measurement index after the teaching process, especially reflects the advancement of foreign language teaching supported by information technology and its promotion to the teaching effect.

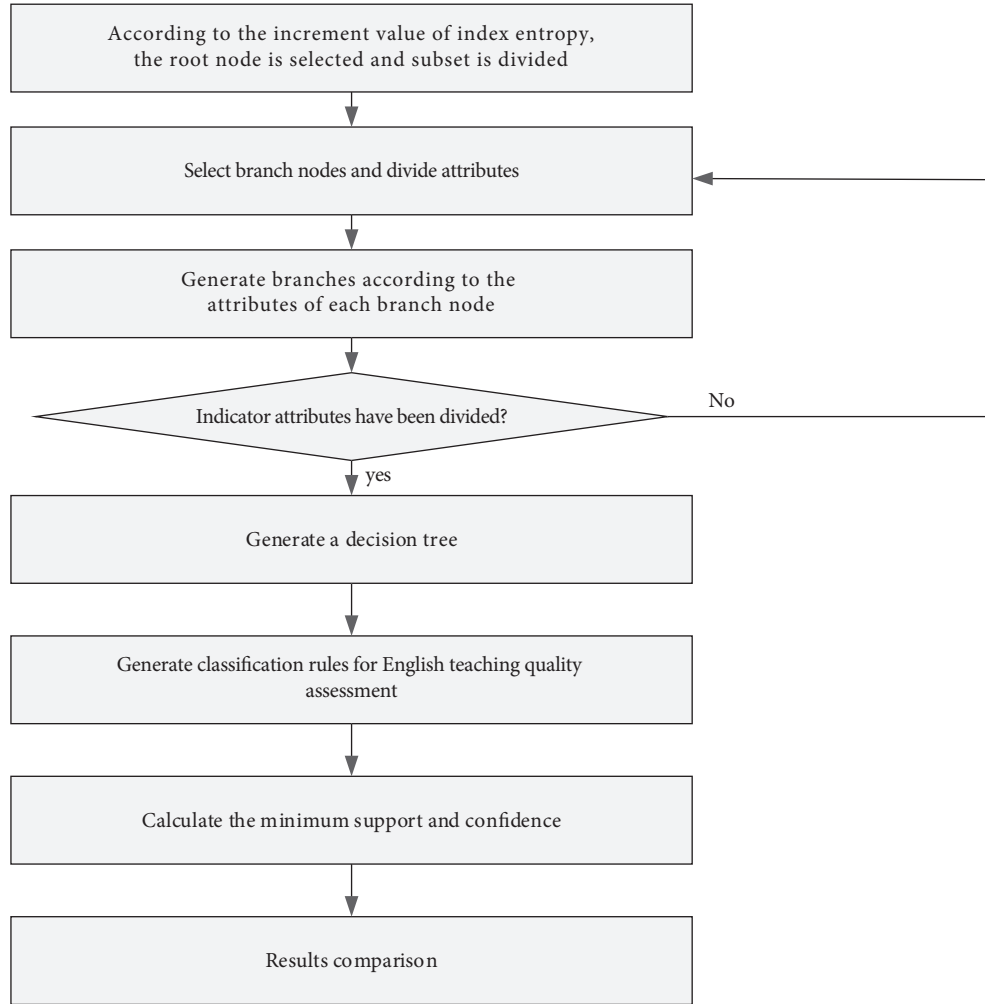


FIGURE 1: Evaluation process.

- (4) “Teaching expansion” refers to the teaching methods outside the classroom, which are carried out around the curriculum objectives under the support of information technology. The design and effect evaluation of extracurricular learning content to assist classroom teaching and enrich related courses, including the diversification of extracurricular learning resources and assessment contents and methods, the abundance of resources provided online and offline, and the effectiveness of promoting college English learning.

2.2. Teaching Evaluation Process. The evaluation process is the selection of teaching quality and teachers’ own quality evaluation indicators from two aspects; one is the relevant data of teachers, and the other is the related factors of teaching schedule and teaching links. Obtain the English teaching evaluation data package from the educational administration platform, initialize the data according to indicators, generate samples to be evaluated, calculate entropy increment values of all indicators to generate a decision tree, and verify the classification rules of English teaching quality

evaluation generated by the decision tree by the association rules method. In this, the specific steps for verifying the decision tree and association rule combination model are shown in Figure 1.

3. Description of the Algorithm

3.1. Decision Tree and Knowledge Point Association. The decision tree is mainly composed of roots, branches, and leaves. The calculation method of expected entropy is as follows:

$$I(s_1, s_2, s_3, \dots, s_m) = - \sum_{i=1}^m \frac{s_i}{s} \log_2 \frac{s_i}{s}. \quad (1)$$

Let the expected expression of an attribute A of the sample be

$$E(A) = \sum_{j=1}^m \frac{s_{ij} + s_{2j} + \dots + s_{mj}}{s} I(s_{ij}, s_{2j} + \dots + s_{mj}). \quad (2)$$

For the subset Is_j is defined as follows:

$$I(s_{ij}, s_{2j} + \dots + s_{mj}) = - \sum_{i=1}^m \frac{s_{ij}}{s_j} \log_2 \frac{s_{ij}}{s_j}. \quad (3)$$

Expected Entropy Gain of A to S is

$$\text{Gain}(A) = I(s_{ij}, s_{2j} + \dots + s_{mj}) - E(A). \quad (4)$$

The gain rate is expressed as

$$\text{Gain}(A) = \frac{\text{Gain}(A)}{\text{splitinfo}(s)}, \quad (5)$$

$$\text{splitinfo}(s) = \sum_{i=1}^m \frac{s_i}{|s|} \times \log_2 \frac{s_i}{|s|}.$$

3.2. Correlation Analysis of Knowledge Points. Suppose that the number of items in all sets D is D , X is an item set in D , and the number of item sets in D is count, then the support degree of X is

$$\text{support}(X) = \frac{\text{count}(X \subseteq D)}{|D|}. \quad (6)$$

Let any two item sets X and Y in D satisfy the condition $X \subset D$, $Y \subset D$, they are independent of each other, and the probability that they appear at the same time in D can also be expressed by support:

$$\text{support}(X \Rightarrow Y) = \frac{\text{count}(X \cap Y)}{|D|}. \quad (7)$$

In addition to calculating support, reliability can also be used to measure the relationship between X and Y :

$$\text{confidence}(X \Rightarrow Y) = \frac{\text{support}(X \Rightarrow Y)}{\text{support}(X)}. \quad (8)$$

It can also be measured by the degree of improvement:

$$\text{lift}(X \Rightarrow Y) = \frac{\text{confidence}(X \Rightarrow Y)}{\text{support}(X)}. \quad (9)$$

3.3. RCNet Model. RCNet consists of four parts, namely, the output layer, bidirectional GRU layer, attention layer, and prediction layer. In this, GRU is selected to learn the calculation formula of remote dependency of the whole input sequence as follows:

$$\begin{aligned} z_n &= \sigma_g(w_z x_n + u_z h_{n-1} + b_z), \\ r_n &= \sigma_g(w_r x_n + u_r h_{n-1} + b_r), \\ \hat{h}_n &= \varnothing_h(w_h x_n + u_h (r_n * h_{n-1} + b_h), \end{aligned} \quad (10)$$

$$\text{GRU}(h_{n-1}, x_n) = (1 - z_n) * h_{t-1} + z_n * \hat{h}_n.$$

The hidden layer vector of the bidirectional GRU is calculated as follows:

TABLE 1: Quantitative statistics of text length.

Statistical parameters	Quantity
Content and text length of English test questions	53003
Length of English text	11393
Length of question text	3291
Length of option text	9132

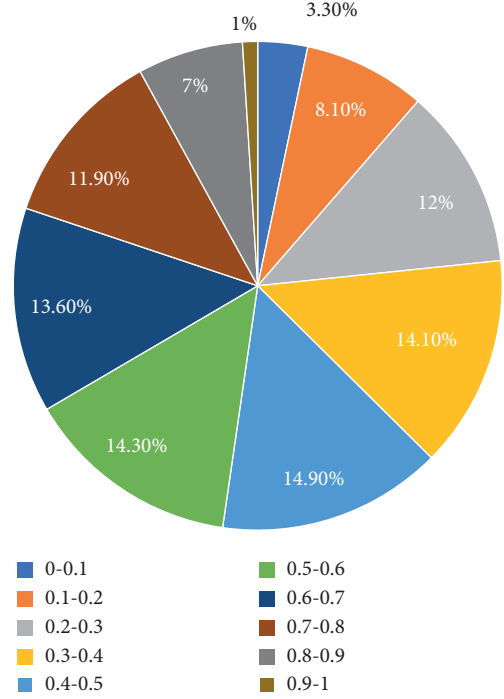


FIGURE 2: Difficulty distribution of test questions.

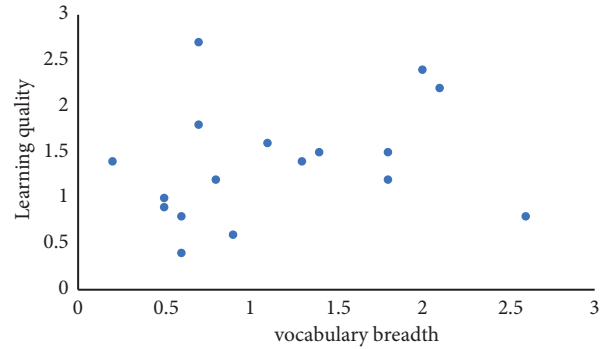


FIGURE 3: Scatter plot of English learning quality and vocabulary breadth knowledge level.

$$\begin{aligned} \vec{h}_n &= \text{GRU}(\vec{h}_{n-1}, x_n), \\ \overleftarrow{h}_n &= \text{GRU}(\overleftarrow{h}_{n-1}, x_n), \\ h_n &= [\vec{h}_n, \overleftarrow{h}_n]. \end{aligned} \quad (11)$$

The N word vectors are fused into

TABLE 2: The actual value and evaluation value of teaching quality evaluation.

Weight	Evaluation value	Actual value
K11	0.78	0.69
K12	0.82	0.80
K32	0.81	0.83
K31	0.79	0.87
K35	0.88	0.89
K41	0.83	0.88
K43	0.91	0.90

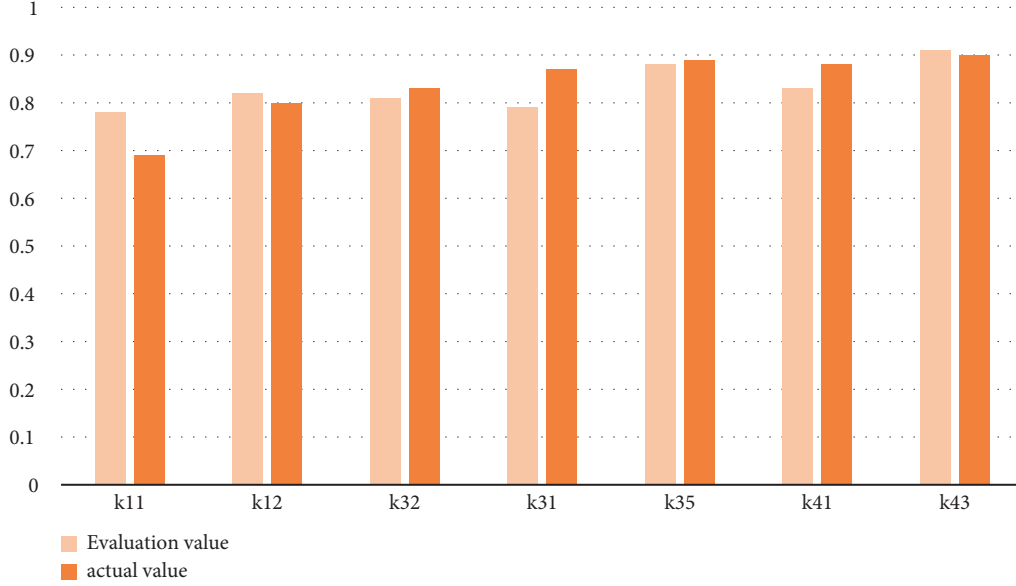


FIGURE 4: Comparison between the actual value and the evaluation value.

$$\bar{Q}_i = \text{avg}(h_1, h_2, \dots, h_N) \in R^{2u}. \quad (12)$$

In the further calculation, the influence of TC and TQ tail is eliminated by the mask method, namely,

$$G(i, j) = \begin{cases} H_C(i)^T H_Q(j), & i < |TC|, < |TQ| \\ 0, & i \geq |TC| \text{ or } j \geq |TQ|. \end{cases} \quad (13)$$

After obtaining the paired matching matrix, the attention layer applies the softmax function to each column in G to obtain the probability distribution of each column, wherein when considering a single test word, each column in the matrix represents a separate text-level attention, the text-level attention of the n th word is as follows:

$$a(n) = \text{soft max}(G(1, n), \dots, G(|TC|, n)). \quad (14)$$

Calculate reverse attention; that is, for words in the n th chapter, calculate the importance distribution of test words to indicate which test words are more important for individual words in the chapter. The attention mechanism will gradually implement the softmax function and apply it to each pair of matching matrices to obtain the attention of English test questions with different difficulties:

$$\beta(n) = \text{soft max}(G(n, 1), \dots, G(n, |TQ|)). \quad (15)$$

Get the average attention at the test level as follows:

$$\beta = \frac{1}{|TC|} \sum_{N=1}^{|TC|} \beta(n). \quad (16)$$

Explicitly understand the contribution of each test word, vote according to the importance of each test word, and output the final text-level attention weight as the text-level attention vector as follows:

$$CA_i = a^T \beta. \quad (17)$$

The expression for predicting the difficulty of English test questions is as follows:

$$\tilde{P} = \text{Sigmoid}(W_2 \cdot o_i + b_2). \quad (18)$$

Training model expression is as follows:

$$J(\theta) = \sum_{T_i, Q_i, Q_j} ((P_i^t - P_j^t) - (\tilde{P}_i^t - \tilde{P}_j^t))^2 + \lambda_\theta \theta_M^2,$$

$$\text{RMSE} = \sqrt{\frac{1}{m_i} \sum_{j=1}^{m_i} (P_{ij} - \bar{R}_{ij})^2}, \quad (19)$$

$$R^2 = 1 - \frac{\sum_{j=1}^{m_i} (P_{ij} - \bar{R}_{ij})^2}{\sum_{j=1}^{m_i} (R_i - \bar{R}_{ij})^2}.$$

TABLE 3: Comparison of learning effects of knowledge points.

Category of knowledge points	Learning effect (%)	Teaching effect (%)
Vocabulary depth	82	82
Grammar	88	76
Reading comprehension	79	79
Cloze	78	80
Writing	82	83

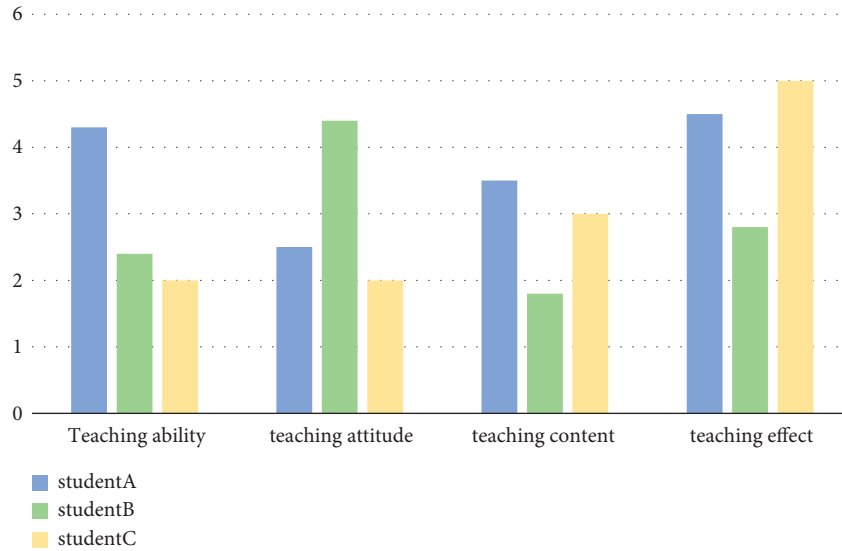


FIGURE 5: Comparison of vocabulary depth teaching quality.

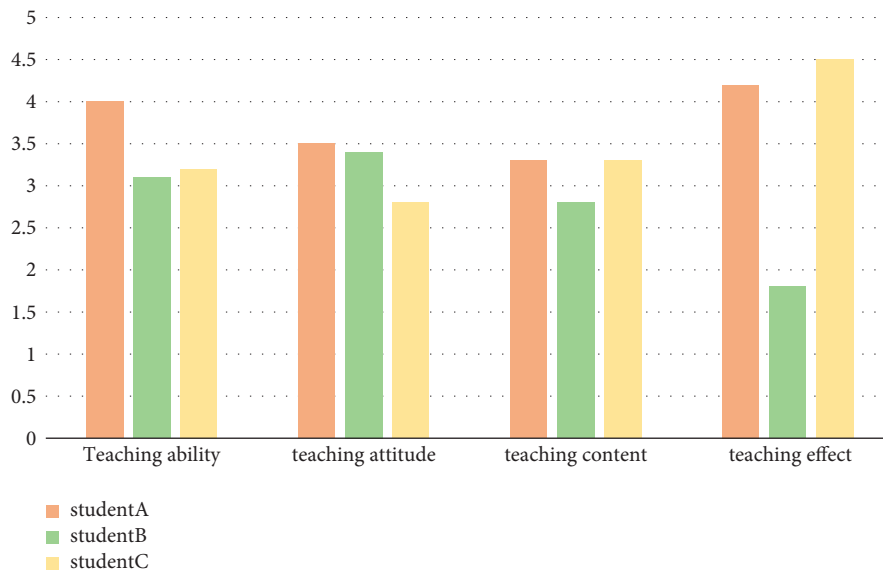


FIGURE 6: Comparison of grammar teaching quality.

4. Experiment

4.1. Simulation Experiment

4.1.1. Data Set Introduction. The sample data set adopted in this experiment is the English test results and answer records

from many middle schools in China from 2014 to 2021. Each data include five fields: English test content, question, correct option, wrong option, and test difficulty. The statistical results are shown in Table 1.

The difficulty of the experimental data set is tested, and the uniformity of the difficulty distribution of the test

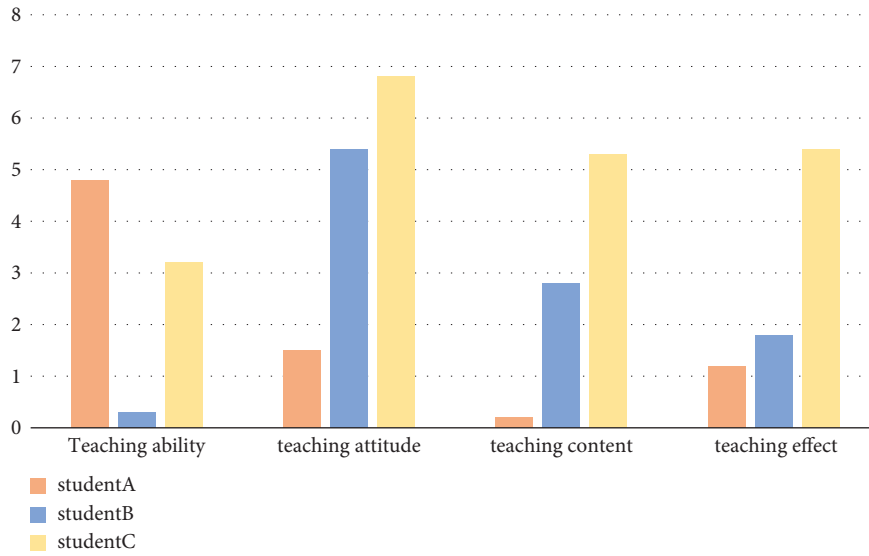


FIGURE 7: Comparison chart of reading comprehension teaching quality.

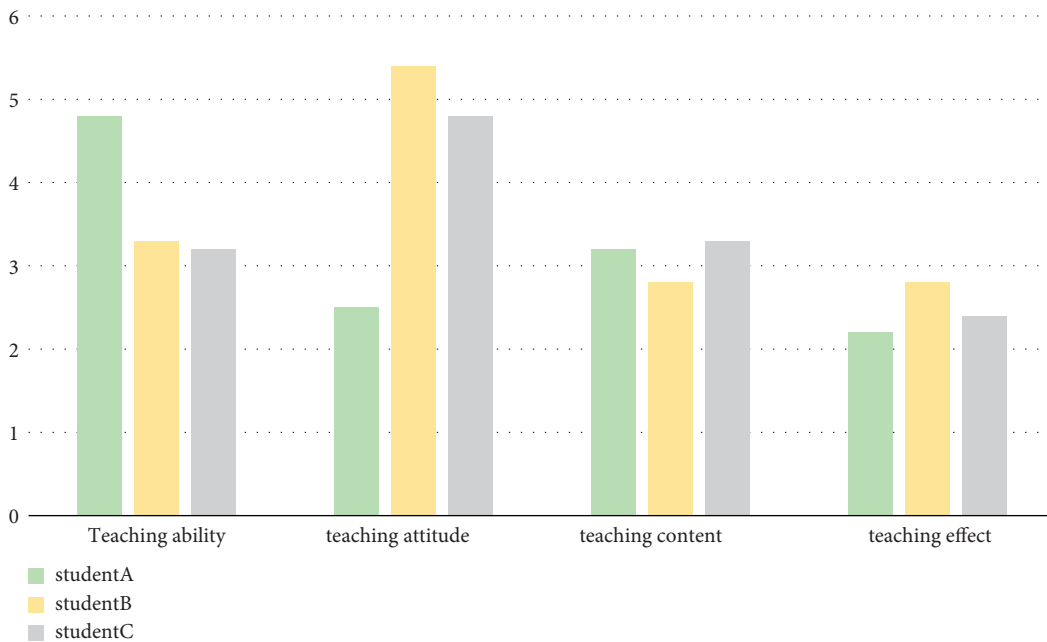


FIGURE 8: Comparison of cloze teaching quality.

questions is distributed by the classical measurement theory difficulty of 0–1, as shown in Figure 2.

4.2. *Experimental Research.* The correlation between the quality of English teaching and the breadth and depth of vocabulary is analyzed. This question verifies the correlation between English teaching quality, vocabulary breadth knowledge, and vocabulary depth knowledge. It is necessary to check whether there are singular values in the whole data so as to analyze whether there is a curve relationship between the data. Therefore, before testing the correlation coefficient,

we draw scatter charts on the relationship between the teaching quality of English learning and vocabulary breadth knowledge and vocabulary depth knowledge as shown in Figure 3.

The effectiveness of the index system of the traditional English classroom teaching quality evaluation model is to ensure students’ trust in the evaluation results of college English classroom teaching quality. The purpose of training the students before the evaluation is to let them know the purpose and significance of the evaluation and to guide students to deepen their familiarity with the indicators and grading standards. Finally, the scoring results are collected,

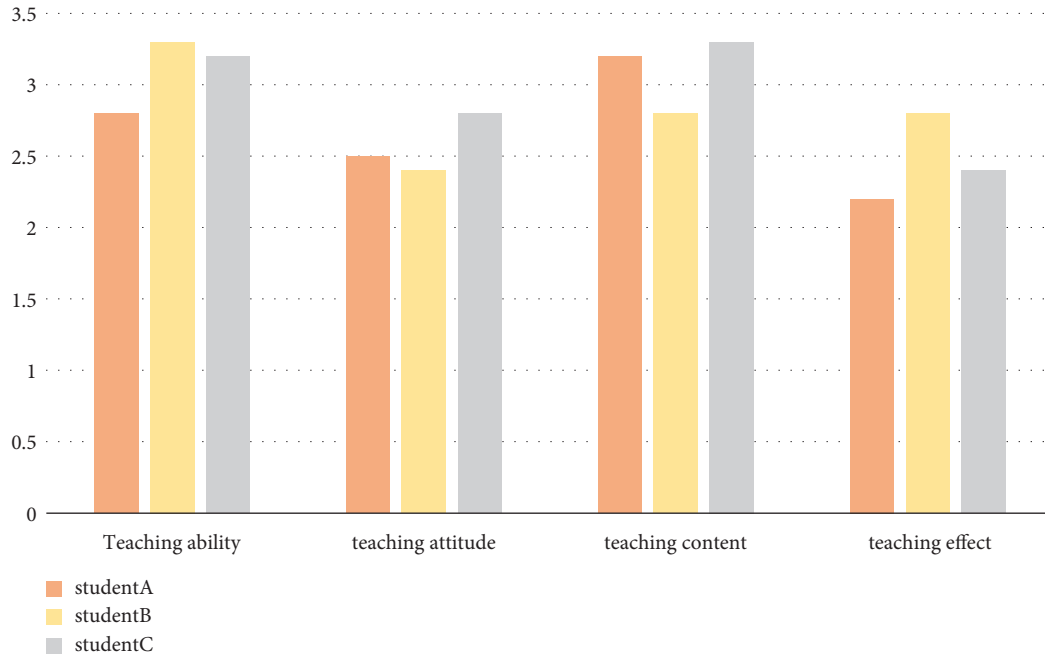


FIGURE 9: Comparison of English writing teaching quality.

TABLE 4: Performance comparison of knowledge points.

Category of knowledge points	Accuracy	Precision	Recall	F1	AUC
Vocabulary depth	0.813	0.861	0.891	0.791	0.815
Grammar	0.824	0.854	0.882	0.832	0.824
Cloze	0.841	0.860	0.883	0.814	0.803
Reading comprehension	0.852	0.866	0.873	0.853	0.815
Writing	0.887	0.871	0.838	0.856	0.887

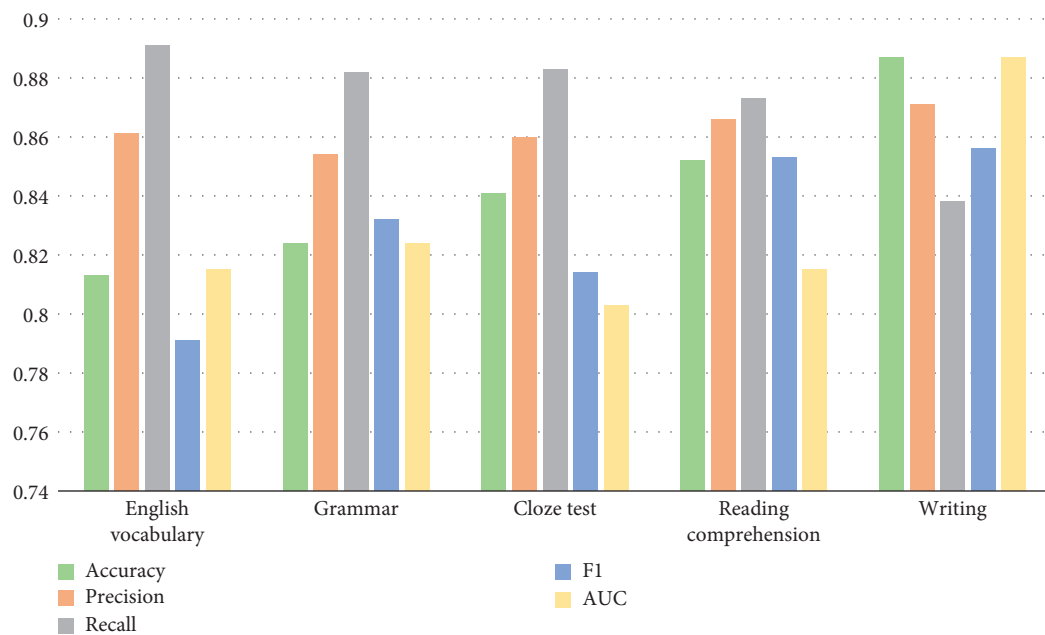


FIGURE 10: Comparison between teaching quality and English knowledge points.

and according to the students' scoring data, the actual scores of teaching quality evaluation are calculated. The results are shown in Table 2.

The above data are counted into tables as shown in Figure 4.

4.3. Model Comparison. For English learning vocabulary depth, grammar, reading comprehension, cloze, writing, and other knowledge points, student-centered teaching quality evaluation uses their mastery to evaluate teachers' English teaching quality. Based on the above index standards, we use the decision tree method under deep learning to study and evaluate English teaching quality evaluation. The experimental data are given in Table 3.

Three senior high school students were selected to evaluate the teaching ability, teaching attitude, teaching content, teaching methods, and teaching effect of English teachers as the quality indicators of English classroom teaching and to evaluate the quality of each English learning knowledge point.

The combination model of the decision tree and knowledge point association rule mining is used to evaluate the teaching quality of English vocabulary depth, as shown in Figure 5.

The combination model of the decision tree and knowledge point association rule mining is used to evaluate the teaching quality of English grammar, as shown in Figure 6.

The combination model of the decision tree and knowledge point association rule mining is used to evaluate the teaching quality of English reading comprehension, as shown in Figure 7.

The combination model of the decision tree and knowledge point association rule mining is used to evaluate the teaching quality of the English cloze test, as shown in Figure 8.

The combination model of the decision tree and knowledge point association rule mining is used to evaluate the teaching quality of English writing ability as shown in Figure 9.

4.4. Contrast Experiment. The decision tree model and rule mining association combination model proposed in this paper are tested in terms of model performance, and different English knowledge points are compared, as shown in Table 4.

The comparison table between teaching quality and English knowledge points is counted into a bar chart, as shown in Figure 10.

5. Conclusion

We analyze the relationship between the effective evaluation of teaching quality in the college English classroom and knowledge points and propose a combined model based on the decision tree and rule association analysis of English knowledge points to evaluate teaching quality in English classrooms. Through the combination model of the two

methods to evaluate the teaching quality in the classroom, the evaluation results of teaching quality after evaluation are obtained, which shows that this method is effective and has strong applicable value for the evaluation of English teaching quality in the classroom. The results are as follows:

- (1) In the difficulty test of English, the difficulty distribution of test questions is relatively uniform. In the difficulty interval of classical measurement theory from 0 to 1, the proportion of test questions in each difficulty interval with a difficulty interval of 0.1 is about 10%.
- (2) By comparing the actual values of different weights of English teaching indicators with the evaluation values, we can see that the evaluation performance of this model is good.
- (3) The limitations of the decision tree model combined with rule association analysis can greatly improve the evaluation level of English teaching quality inside and outside the classroom and study and analyze the relevance of English knowledge points.

Data Availability

The experimental data used to support the findings of this study are available from the corresponding author upon request.

Conflicts of Interest

The author declares no conflicts of interest regarding this work.

References

- [1] W. Z. Ji, "A structured light image quality evaluation method based on no-reference quality assessment," *Journal of Physics: Conference Series*, vol. 1914, no. 1, 2021.
- [2] T. Bucher, "Artificial intelligence-assisted surgical quality assessment: hype or hope?" *Journal of the American College of Surgeons*, vol. 232, no. 6, pp. 971-972, 2021.
- [3] L. Stone, "Assessing kidney stone composition using deep learning," *Nature Reviews Urology*, vol. 17, no. 4, pp. 192-193, 2020.
- [4] H. Xiang, "The effectiveness of students' teaching evaluation of colleges and universities in the context of big data," *Scientific Journal of Intelligent Systems Research*, vol. 3, no. 4, 2021.
- [5] Z. Cao, "Reform of physical education teaching evaluation in general colleges," *Frontiers in Educational Research*, vol. 40, no. 20, 2021.
- [6] B. Li, Y. Fei, and H. Liu, "An artificial intelligence based model for evaluation of college students' ability and characteristics through teaching evaluation," *Journal of Intelligent and Fuzzy Systems*, vol. 40, no. 2, pp. 3397-3407, 2021.
- [7] X. Chen, "Analysis on the construction of college English teaching evaluation system based on online learning platform," *Advances in Higher Education*, vol. 4, no. 10, 2020.
- [8] W. Li, "The status quo and improvement methods of college physical education evaluation," *Lifelong Education*, vol. 9, no. 7, 2020.

- [9] S. Phetaree, S. Terdsak, S. Somprasong, and A. Sirisak, "Development of the English teaching evaluation model focusing on task-based learning to develop English writing ability and creative thinking in Language for sixth grade students in Thailand," *Educational Research and Reviews*, vol. 15, no. 7, pp. 377–384, 2020.
- [10] K. Yu, "Construction of multidimensional teaching evaluation system in local universities under the background of transformation," *Advances in Higher Education*, vol. 4, no. 3, 2020.
- [11] E. Braun, A. Spexard, A. Nowakowski, and B. Hannover, "Self-assessment of diversity competence as part of regular teaching evaluations in higher education: raising awareness for diversity issues," *Tertiary Education and Management*, vol. 26, no. 2, pp. 171–183, 2020.
- [12] G. Abbs and S. B. Qutoshi, "Implementation of rubrics in assessment of teaching from students' and teachers' perspectives," *International Journal of Innovative Technology and Exploring Engineering*, vol. 9, no. 4, pp. 83–88, 2020.
- [13] S. J. F. J. Claessens, "The role of student evaluations in a PBL centred law curriculum: towards a more holistic assessment of teaching quality," *The Law Teacher*, vol. 54, no. 1, pp. 43–54, 2020.
- [14] C. A. A. Jones, "360-degree assessment of teaching effectiveness using a structured-videorecorded observed teaching exercise for faculty development," *Medical education online*, vol. 24, no. 1, 2019.
- [15] K. Lv, "The function orientation and mode diversity of classroom teaching evaluation in primary and secondary schools," *Frontiers in Educational Research*, vol. 2, no. 8, 2019.
- [16] P. Liu, H. Cui, Y. Cao, X. Hou, and L. Zou, "A method of multimedia teaching evaluation based on fuzzy linguistic concept lattice," *Multimedia Tools and Applications*, vol. 78, no. 21, pp. 30975–31001, 2019.
- [17] H. Zhou, "Teaching evaluation of modern Chinese history courses for different majors," *History Research*, vol. 7, no. 2, pp. 27–31, 2019.
- [18] J. Qiu, "Research on the problems and countermeasures of undergraduate teaching fine management based on teaching evaluation," *Frontiers in Educational Research*, vol. 2, no. 6, 2019.
- [19] G. Guihang and C. Chen, "The analysis of the problems in business English teaching assessment system and suggestions for improvements," *English Language Teaching*, vol. 12, no. 8, p. 44, 2019.
- [20] Yi Yang and Y. Song, "Research on the performance assessment of teaching cloud platform based on fuzzy comprehensive evaluation," *Journal of Physics: Conference Series*, vol. 1213, no. 4, 2019.
- [21] S. Antonieta Lizote, "Learning styles, academic performance and teaching evaluation," *Revista Catarinense da Ciência Contábil*, vol. 18, no. 0, 2019.
- [22] J. Lekwa, L. A. Reddy, C. M. Dudek, and A. N. Hua, "Assessment of teaching to predict gains in student achievement in urban schools," *School Psychologist*, vol. 34, no. 3, pp. 271–280, 2019.
- [23] J.-wei Jia, Ke-li Jiao, and X.-jun Jiao, "Teaching evaluation on a WebGIS course based on dynamic self-adaptive teaching-learning-based optimization," *Journal of Central South University*, vol. 26, no. 3, pp. 640–653, 2019.
- [24] Q. Lin, Y. Zhu, S. Zhang, P. Shi, Q. Guo, and Z. Niu, "Lexical based automated teaching evaluation via students' short reviews," *Computer Applications in Engineering Education*, vol. 27, no. 1, pp. 194–205, 2019.
- [25] D. Erin, "Development of a clinical teaching evaluation and feedback tool for faculty," *Western Journal of Emergency Medicine*, vol. 20, no. 1, pp. 50–57, 2019.

Research Article

Deep Learning Algorithm for Online College Physical Education Teaching with Flipping Classroom

Zhengqiang Chen 

Basic Teaching Department, Zhejiang Tongji Vocational College of Science and Technology, Hangzhou 311231, China

Correspondence should be addressed to Zhengqiang Chen; z20520040603@zjtongji.edu.cn

Received 20 May 2022; Revised 28 June 2022; Accepted 6 July 2022; Published 24 August 2022

Academic Editor: Le Sun

Copyright © 2022 Zhengqiang Chen. This is an open access article distributed under the Creative Commons Attribution License, which permits unrestricted use, distribution, and reproduction in any medium, provided the original work is properly cited.

In view of the inability to accurately analyze the application of deep learning in college physical education teaching design from the perspective of flipping classroom, this paper puts forward an improved deep learning method based on the integration of flipping classroom vision and deep learning, which can reduce the design ability of physical education teaching design in college physical education teaching design and improve the level of college physical education teaching design. Firstly, the initial data set is established by using the theory of flipping classroom horizon, so that the data meet the requirements of normal distribution and reduce the differences between teaching data; Then, the physical education teaching design is divided into different subdesigns by using the theory of flipping classroom horizon. Find the best design result in this domain in each subinstructional design; Finally, under the guidance of the theory of flipping classroom horizon, each subdesign realizes the optimal allocation of teaching resources. MATLAB simulation shows that under the conditions of initial design scheme and teaching resources setting, the improved deep learning method can improve the accuracy of physical education teaching design and shorten the convergence time of design, which is superior to the original deep learning method. Therefore, the deep learning method is used to analyze the instructional design of college physical education, which has a good design effect and is suitable for the instructional design of college physical education.

1. Introduction

With the continuous improvement of physical education teaching level, the requirements of instructional design are becoming more and more strict, and it presents a complicated direction of development Yu, and Zhu [1], so it is particularly important to study physical education instructional design under complex conditions. The key to the allocation of teaching resources in physical education teaching design is to judge the types of resources and design requirements Yin [2]. The theory of flipping classroom horizon can not only adjust the dynamic relationship between teaching content and resources but also solve the selection of physical education teaching design under multiple horizons, which is the main theory of physical education teaching design at present Xiao et al. [3]. Flipping the classroom horizon can make teachers realize the significance of preview and its importance to physical education. Flipping classroom

takes students as the main core, which can give full play to students' initiative and change the center of traditional teaching. Relatively speaking, flipping the classroom can distinguish the primary and secondary of teaching, so that students can study deeply according to their own interests. Therefore, flipping classroom plays a very important role in physical education teaching design. Literature research shows that the theory of flipping classroom horizon classifies physical education teaching design, shortens the design time and improves the overall level of design. However, in the process of design classification by flipping classroom horizon theory, the complexity of design will affect the judgment of conditions and the final design result Webb et al. [4]. Some scholars have put forward the deep learning method. Although the deep learning method can realize the selection of design schemes, it is suitable for the conditions with less design requirements. Although there are many researches on flipping classroom by scholars at home and abroad, there are

TABLE 1: Complexity of physical education teaching design requirements from the perspective of flipping classroom.

Classification	Instructional design in colleges and universities		Physical education teaching design	
	Technical production	Content modification	Production innovation	Policy selection
Football	4.12	20.62	36.08	43.30
Tennis	38.14	42.27	21.65	18.56
Volleyball	9.28	10.31	29.90	15.46
Swimming	6.19	9.28	17.53	4.12
Yoga	7.22	22.68	36.08	23.71
Fitness	23.71	23.71	25.77	30.93
Martial arts	11.34	45.36	8.25	12.37
100 meters	41.24	44.33	20.62	30.93
500 meters	7.22	16.49	43.30	4.12
High jump	29.90	28.87	15.46	6.19
Long jump	15.46	20.62	10.31	22.68
Shot put	15.46	44.33	42.27	15.46
Javelin	18.56	12.37	39.18	8.25

few researches on other methods from the perspective of flipping classroom, and deep learning methods can better promote the improvement of physical education teaching design level. At present, scholars at home and abroad have little research on deep learning from the perspective of flipped classroom, especially the actual case analysis. Under changeable and complex conditions, the overall design ability of the design scheme is greatly reduced Wang and Wang [5]. Therefore, some scholars put forward the theory of flipping classroom horizon and improving deep learning, as shown in Table 1.

It can be seen from Table 1 that the complexity of college physical education teaching design is high from the perspective of flipping classroom. However, to a certain extent, it also shows the need of intelligent algorithm for college physical education teaching design. Among them, shooting, martial arts, 100 meters, and high jump need intelligent algorithms to achieve intelligent management and analysis. At the same time, some scholars have studied the integration of deep learning method and flipped classroom horizon theory, and found that the flipped classroom horizon theory can reduce the complex design requirements and improve the reliability of physical education teaching design Umezawa et al. [6]. Based on this, this paper puts forward an improved deep learning method based on the integration of deep learning and flipping classroom horizon theory, designs physical education under complex conditions, and verifies the effectiveness of the design. At present, there is a dynamic relationship between design difficulty and standard in college physical education teaching design, as shown in Figure 1.

As can be seen from Figure 1, there is a positive correlation between physical education teaching design and standards, so it is necessary to strengthen the difficulty analysis of physical education teaching design to meet the design standards and requirements Trpkovska et al. [7].

To sum up, there are many researches on flipping classroom horizon, which can provide support for deep learning and better promote the improvement of college physical education teaching design level. At the same time, the integration of deep learning and physical education teaching design requires more reasonable adjustment. Flipping the classroom

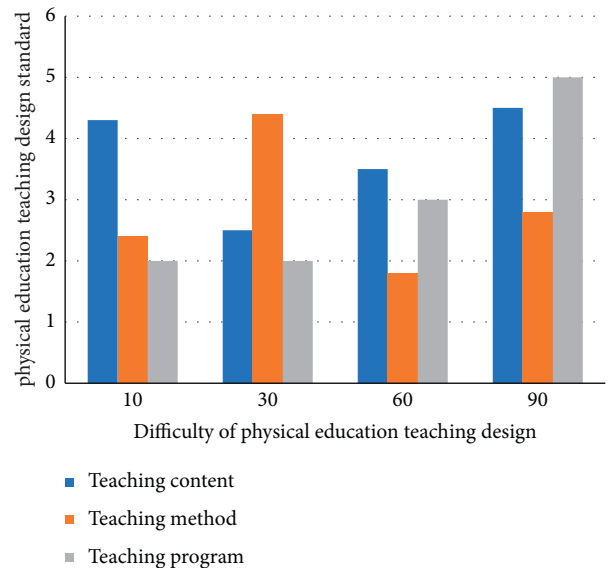


FIGURE 1: Relationship between difficulty and standard in physical education teaching.

can provide preview in the early stage and discussion in the later stage, and realize a series of teaching optimization. At present, the research of physical education teaching design is developing in the direction of intelligence, and turning over the classroom horizon lays the foundation for this development, which is also the focus of future research.

2. Related Concepts

2.1. Flip the Classroom Horizon Theory. The theory of flipping classroom horizon was first put forward by Eric Mazur in 1990s, which is based on peer teaching method. Compared with the traditional teaching mode, the theory of flipping classroom horizon not only pays attention to information transmission, but also deepens the understanding of knowledge Tang, and Wang [8]. The theory of flipping classroom horizon requires students to teach themselves the course content after class and interact in the form of “asking questions-thinking-answering” in class. According to the

proportion of students' correct answers, teachers should adjust their teaching contents J. Song, and Kapur [9], so as to deepen students' understanding of knowledge and make them understand the key points and difficulties of teaching. However, flipping classroom is the best combination put forward from the perspectives of teachers, teaching, and students, which has the characteristics of sparsity and integration, and can be designed dynamically in physical education. The theory of flipping classroom horizon needs to construct core functions and analyze the experience and requirements in physical education teaching design in order to improve the accuracy of the design scheme Soler et al. [10].

Theorem 1. *Assuming a collection of physical education instructional design schemes, $T = (\{d_i \forall b_i, i = any\})$ arbitrary physical education instructional design $q_i \in [-\infty, +\infty]$, innovative instructional design $b_i \in [1, 100]$, and adopted design methods $K(d_i \Rightarrow q_i \Leftarrow b_i)$. The resource allocation function matches the teaching resources with the educational requirements $L(x_i \Leftrightarrow y_i \Leftarrow z_i)$, and the sports design scheme makes the scheme optimal Y_f . The calculation is shown in formula.*

$$Y_f = w \times f(d_i \Rightarrow q_i \Leftarrow b_i) \Leftarrow \lambda. \quad (1)$$

Among them, w is the allocation condition of different resources and λ is the teaching resource. When $\sum Y_f \approx \infty$, the number of physical education teaching design classifications was the largest, the classification interval was the largest, and the design was more difficult; when $w=1$, the design was the most innovative.

Theorem 2. *If the deviation of physical education teaching design ξ_i is between $[-1, 1]$, it means that physical education teaching design is reasonably optimized, otherwise, it should be re-optimized, and the optimal scheme Y_f calculation is shown in formula.*

$$\begin{cases} \min Y_f = w \cdot K(d_i, q_i, b_i) \quad \forall C \sum \xi_i, \\ w \cdot K(d_i, q_i, b_i) \approx 1. \end{cases} \quad (2)$$

Among them, C is deviation, which reflects the deviation between physical education teaching design and design conditions Sofya, and Sahara [11].

Theorem 3. *If the resource allocation function $K(d_i \Rightarrow q_i \Leftarrow b_i) = \sum \varphi(d_i) \Leftrightarrow \sum \varphi(q_i)$, the matching function $L(x_i, y_i, z_i)$ is calculated as shown in the following formula:*

$$\begin{cases} \max L(a) = \sum a_i \Leftrightarrow \sum a_{ij} q_{ij}, \\ \sum a_i = dx_i \Leftrightarrow q_i. \end{cases} \quad (3)$$

Among them, flipping the deviation coefficient C in the theory of classroom horizon is the key to the implementation of deep learning method Shim et al. [12].

2.2. Improve the Deep Learning Method

2.2.1. Deep Learning Can Realize the Optimization of Large-Scale Physical Education Teaching Design by Simulating Artificial Behavior, Including Leading, Assisting, and Adjusting. During initialization, the number of PE instructional design and instructional design innovation schemes is the same, and the matching of different PE instructional designs represents the optimal solution. Firstly, the initialization of physical education teaching design and physical education teaching design are randomly generated, and the physical education teaching design is judged near the scheme with better fitness scheme Luo and Zhu [13], and the "poor" scheme is eliminated by comparison, about 1/2 of the number; Then, the auxiliary scheme uses roulette strategy to judge the best scheme, gives corresponding weights, and carries out greedy judgment around the optimal scheme to generate a 1/2 scheme. Finally, the physical education teaching design that does not conform to the teaching resources needs to be abandoned, and the physical education teaching design should be judged in other directions [14].

Assuming that the initial number of physical education teaching design and innovative schemes is n , and the random matching of physical education teaching design is $L = (x_i, y_i, z_i)$, x_i, y_i represent plane coordinates and z_i represents difficulty, then the initial matching calculation of physical education teaching design is shown in formula:

$$L_i(x_i, y_i, z_i) = w \cdot K(d_i \Rightarrow q_i \Leftarrow b_i) K \left\{ (x_{j \max}, y_{j \min}, z_{j \min}) \rightarrow L(0, 1) \right\} \quad (4)$$

where, x_i, y_i , and z_i are any matching resources $x_{j \max}$ is the scheme with the greatest complexity, $y_{j \min}$ and $z_{j \min}$ the sum is the scheme with the smallest complexity. $L(0, 1)$ is a random number in the range of $[0, 1]$.

The improvement scheme is to randomly allocate physical education teaching resources and make cross judgment among resources to realize the renewal of physical education teaching design. Under the constraint of fitness, the optimal resource matching is obtained by using the most complex conditions, and the calculation is shown in formula:

$$\Delta L_i(x_i, y_i, z_i) = w \cdot K(d_i, q_i, b_i) \Leftrightarrow \int \varphi_{ijz} \frac{(\Delta x_{io} \Rightarrow \Delta y_{io} \Leftarrow \Delta z_{io})}{\sum \lambda \cdot K(d_i \Rightarrow q_i \Leftarrow b_i)} \quad (5)$$

Among them, $o, i \in [0, n]$, $\varphi_{ijz} \in (-2, 1)$.

The auxiliary scheme p_i is to adjust the physical education teaching design by probability method, and judge the neighborhood of the better physical education teaching design to obtain the optimal design result, which is calculated as shown in formula:

$$p_i = \frac{K(b_i)}{\sum_{i,j,k}^n [K(\Delta d_{io} \Rightarrow \Delta q_{io} \Leftarrow \Delta b_i)]} \quad (6)$$

Among them, $F(\cdot)$ is a moderate function with different complexity.

If the physical education teaching design has not got the optimal solution after circular adjustment, the complexity will be reduced, and then the physical education teaching design will be judged.

2.2.2. Dynamic Optimization of Physical Education Teaching Design.

In the preliminary analysis, physical education teaching design can not guarantee the whole design, which may increase the subjectivity of the design and reduce the overall effect of the design. Therefore, in the process of physical education teaching design, we should try our best to expand the use of teaching resources and constantly adjust teaching resources. Some scholars adjust teaching resources ρ linearly to reduce the randomness in the selection of teaching resources, but there is still “partial subjectivity” in the selection of teaching resources. In order to make up for the above shortcomings, the adjustment factor ν is introduced in this paper, and the calculation is as shown in formula:

$$\rho = \min \sum \Delta \nu_i \Rightarrow \log e^{-F(x_i, y_i, z_i) / \sum F(x_i, y_i, z_i)}. \quad (7)$$

Among them, $\Delta \nu_i$ is i times dynamic adjustment and $F(x_i \Rightarrow y_i \Leftarrow z_i)$ is i times update function Gayef [15]. The matching function between teaching resources and teaching design can be obtained from formulas (6) and (7), and the calculation is shown in formula

$$\Delta L(x_i, y_i, z_i) = w \cdot K(d_i, q_i, b_i) + \nu_{ijz} K(\Delta d_{ik}, \Delta q_{ik}, \Delta b_{ik}). \quad (8)$$

It can be seen from formula (8) that the complexity of $(F(x_i, y_i, z_i) / \sum F(x_i, y_i, z_i)) = 1$ and $\nu = 1$ is the smallest and the complexity of time and time is the largest in preliminary analysis. In order to reduce the “subjectivity” in instructional design, we should keep the diversity of teaching resources. In the final judgment of instructional design $(F(x_i, y_i, z_i) / \sum F(x_i, y_i, z_i)) = 1$, ν harmony plays an important role, which can not only reduce the complexity of design but also improve the processing ability of design resources and play the role of deep learning method. The result is shown in Figure 2.

As can be seen from Figure 2, the dynamic adjustment of physical education teaching design can accurately carry out the overall design, and the teaching design and teaching resources can be matched. This shows that the dynamic adjustment of physical education teaching design can meet different complexities and improve the effect of teaching design Fang and Jiang [16]. At the same time, the number of physical education teaching designs is relatively uniform, and the adjustment degree is relatively average, which shows that deep learning can achieve the balance of physical education teaching design. Under the condition of ensuring the requirements of physical education teaching design, the analysis of physical education teaching should be carried out to the greatest extent, and the adjustment level of teaching design should be ensured.

2.2.3. Introduction of Flip Classroom Horizon Factor.

When a certain physical education teaching design has been adjusted many times and meets the best standard, leading to flip the classroom horizon factor can make the teaching design more in line with “asking-thinking-answering” and get a new solution. Because of the randomness of deep learning method, “subjectivity” has great influence, which will reduce the objectivity of design and do not meet the relevant requirements. In order to reduce the probability of “subjectivity” in physical education teaching design and meet the requirements of different complexities. The “flip class horizon factor” can be introduced by probability density calculation, which is shown in formula:

$$L(x_i) = \frac{\lim_{\delta x \rightarrow 0} (F(x_i, y_i, z_i) / \sum F(x_i \Rightarrow y_i \Leftarrow z_i))}{\pi \sum_{i,k=1}^{+\infty} |K(\Delta x_{ik} \Rightarrow \Delta y_{ik} \Leftarrow \Delta z_{ik})|^2}. \quad (9)$$

If the educational design meets the sum of $\lim_{x \rightarrow 0} (F(x_i, y_i, z_i) / \sum F(x_i, y_i, z_i)) \approx 1$ and $F(x_i \Rightarrow y_i \Leftarrow z_i) = 1$ it shows that the physical education teaching design is the best, otherwise the design does not meet the requirements Fan, and Meng [17].

2.3. Analysis of Physical Education Teaching Design from the Perspective of Flipping Classroom

2.3.1. Optimization Model of Physical Education Teaching Design from the Perspective of Flipping Classroom.

Rationality judgment of physical education teaching design from the perspective of flipping classroom Collins [18], it is the main index to measure the deep learning method. From formula (8), it can be seen that in the early stage of physical education teaching design, great attention is paid to the overall utilization of teaching resources, and in the later stage of design, attention is paid to the utilization of local teaching resources, so different design strategies should be adopted in different stages of physical education teaching design. At present, besides the improved deep learning method proposed in this paper, there are other dynamic optimization models.

- (1) The adjustment strategy of specific instructional design is calculated as shown in formula:

$$\Delta L_i(x_i) = \sum_t \Delta L_{i-1}(x_i \Rightarrow y_i \Leftarrow z_{i-1}) \forall [p \cdot K(\Delta d_{ik}, \Delta q_{ik}, \Delta b_{i-1k})]. \quad (10)$$

- (2) The adjustment strategy of the whole instructional design is calculated as shown in formula:

$$\Delta L_i(x_i) = \sum_t \Delta L_{i-1}(x_{i-1} \longrightarrow y_{i-1} \Leftarrow z_{i-1}) \forall [g \cdot \max K(\Delta d_{i-1k}, \Delta q_{i-1k}, \Delta b_{i-1k})]. \quad (11)$$

- (3) The adjustment strategy of teaching resources is calculated as shown in formula:

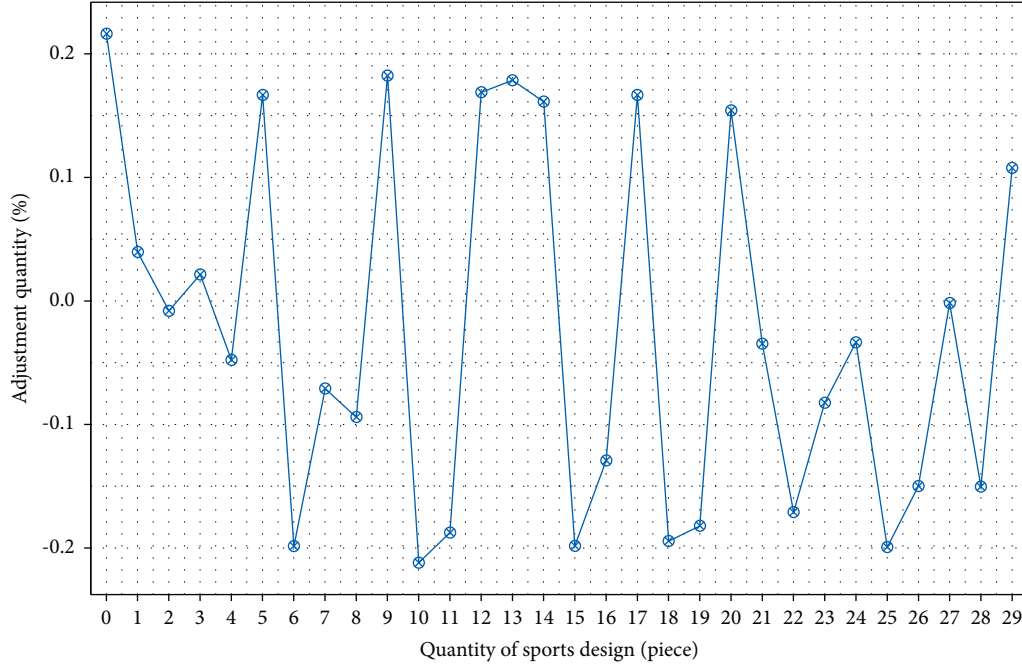


FIGURE 2: Dynamic adjustment results of physical education teaching resources.

$$\Delta L_i(x_i) = \sum_{i=1, t}^{n/2} \Delta L_{i-1}(x_i \Rightarrow y_i \Leftarrow z_{i-1}) \forall [\max K(g) \quad \forall \max K(p)]. \quad (12)$$

- (4) The adjustment strategy of multiview instructional design is calculated as shown in formula:

$$\Delta L_i(x_i) = \sum_t \Delta L_{i-1}(x_{i-1} \longrightarrow y_{i-1} \Leftarrow z_{i-1}) \cdot F(x_{i-1}, y_{i-1}, z_{i-1}) \forall K(\Delta d_{i-1k} \longrightarrow \Delta q_{i-1k} \Leftarrow \Delta b_{i-1k}). \quad (13)$$

Among them, T is the time designed for physical education.

In this paper, the deep learning method is improved in two aspects: on the one hand, the physical education teaching design is constantly adjusted. Under the constraint of weight and threshold, we choose randomly from five strategies and complete many adjustments of physical education teaching design. In the later period of physical education teaching design, the use of physical education teaching resources is gradually reduced, and small-scale design adjustment is carried out to keep the diversity of design and improve the overall design ability. On the other hand, we should balance the relationship between physical education teaching design and resources, and integrate renewal coefficient, Δv_i moderate function $F(x_i, y_i, z_i)$ and Lagrangian multiplier function to carry out physical education teaching design more quickly.

2.3.2. Complexity Adjustment of Physical Education Teaching Design from the Perspective of Flipping Classroom. The complexity of physical education teaching design is the key to realize dynamic optimization. This paper based on the complexity optimization of physical education teaching design from the perspective of flipped classroom can further improve the design effect. Different physical education teaching design complexities adopt different optimization strategies. The physical education teaching design is randomly divided into five subclasses, each subclass represents the scope of physical education teaching design in No. 1 Middle School. In each iteration process, different schemes will be randomly selected from subclasses. After each subclass is adjusted, the fitness and resource utilization of physical education teaching design in different sub-classes is compared, and the overall optimal matching design is recorded; other subclasses gather to the optimal matching design to improve the level of the optimal physical education teaching design.

2.4. Flip the Steps of Physical Education Teaching Design from the Perspective of Classroom. The basic idea of deep learning method from the perspective of flipping classroom is to use various strategies to optimize physical education teaching design, improve the utilization rate of teaching resources, obtain the overall optimal design scheme, and meet the requirements of design complexity. The implementation steps of physical education teaching design from the perspective of flipping classroom in this paper are shown in the Figure 3:

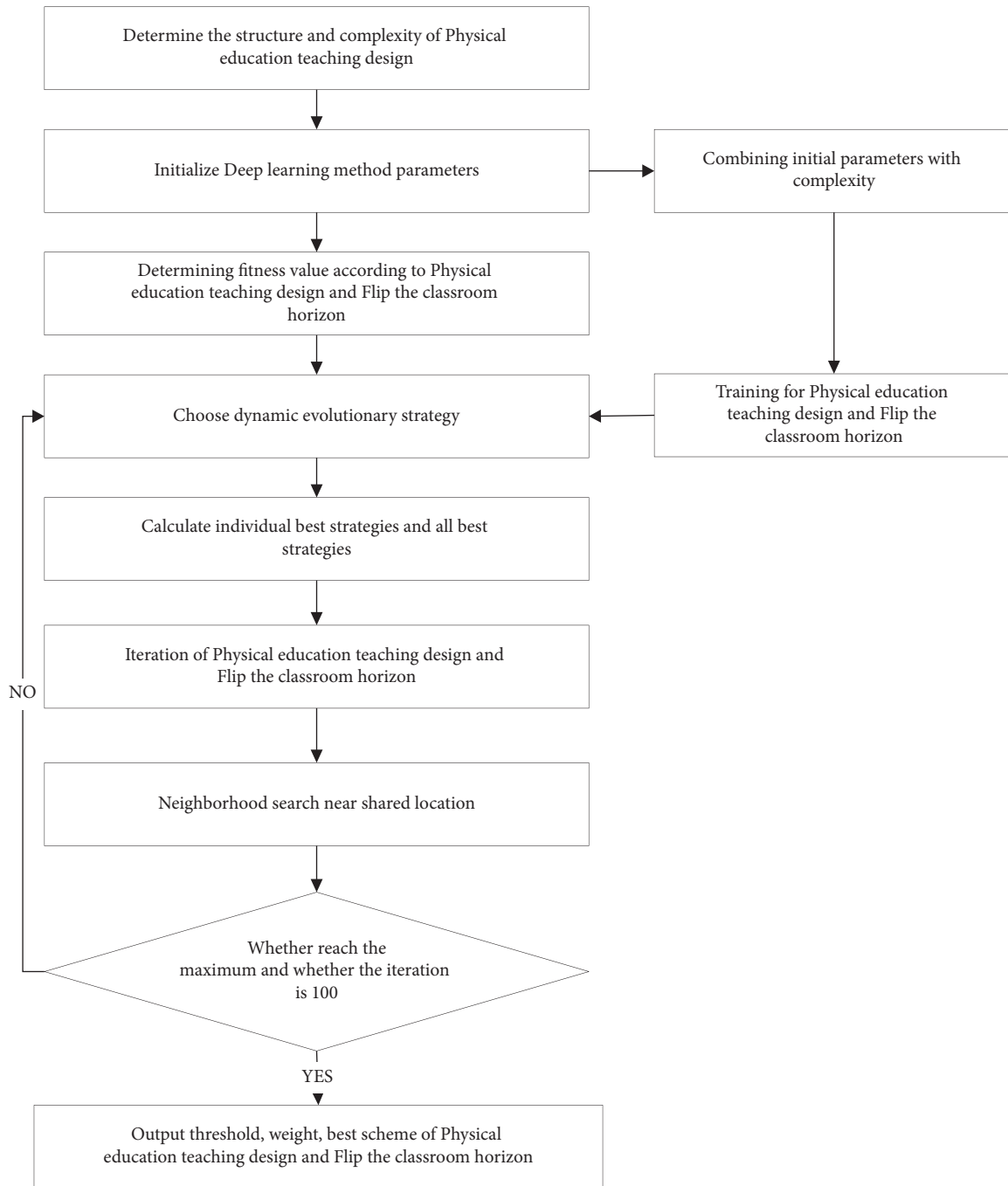


FIGURE 3: Implementation flow of improved deep learning method.

Step 1: Determine the structure and complexity of physical education teaching design. According to the actual design requirements, determine the steps of physical education teaching design, generally speaking, the complexity of physical education teaching design.

Step 2: Initialize the physical education teaching design. According to the relevant instructional design

parameters, the physical education instructional design is initialized. The number of physical education teaching designs $n = 120$, and the number of iterations $m = 100$.

Step 3: Determine the fitness function. Using the theory of flipping classroom horizon, the physical education teaching design scheme is randomly produced, and

TABLE 2: Results of different test functions.

Function	Method	Minimum value	Maximum value	SD	Global optimal design	Local optimal design
Utilization rate of teaching resources	Deep learning method	38.14	48.45	3.72E-05	97.94	1
	Improve deep learning methods	35.05	46.39	5.18E-05	96.91	3
Student satisfaction rate	Deep learning method	47.42	45.36	4.73E-05	96.91	2
	Improve deep learning methods	40.21	55.67	5.07E-05	97.94	1
Feedback rate of teaching	Deep learning method	47.42	51.55	4.17E-05	97.94	2
	Improve deep learning methods	31.96	50.52	3.94E-05	98.97	3
Students' thinking situation	Deep learning method	40.21	50.52	4.39E-05	97.94	1
	Improve deep learning methods	45.36	56.70	4.28E-05	98.97	2

combined with teaching materials, the initial weight w and complexity λ are obtained, that is $w = 0.32$, $\lambda = 0.62$. Through formulas (3)–(7), the physical education teaching design is improved, and the fitness scheme of each physical education teaching design is obtained.

Step 4: The whole and local optimal matching of instructional design. The initial physical education teaching design is divided into five subclasses, and the fitness degree is obtained, and the corresponding local matching and overall optimal matching are calculated.

Step 5: Update iteration of physical education teaching design. According to the requirements of physical education teaching design, the five subclasses dynamically adjust the flipping classroom horizon factor, randomly select strategies from the five subclasses, and integrate the flipping classroom horizon factor C according to formulas (2) and (7).

Step 6: Dynamic optimization of each subclass. After optimizing the local physical education instructional design, the overall optimal design is selected, and the instructional design is shared with other subclasses, and the neighborhood optimal instructional design scheme is adjusted.

Step 7: Judge whether the physical education teaching design reaches the maximum iteration value M . If it is not reached, repeat steps 1–5, otherwise stop iterative calculation and return to the best physical education teaching design and complexity.

3. Empirical Case Analysis

3.1. Model Performance Analysis. In order to further judge and improve the deep learning method, four tests were conducted, namely, the utilization rate of teaching resources, the satisfaction rate of students, the feedback rate of teaching, and the thinking situation of students. The test process is as follows.

- (a) The utilization function of teaching resources is calculated as shown in formula:

$$f(x) = \sum_{i=1}^n \frac{x_i^2}{10} \cdot \cos(2\pi x_i) + \xi' \quad (14)$$

- (b) The student satisfaction rate function is calculated as shown in formula:

$$f(x) = \left| \sum_{i=1}^n x_i^2 \right| \quad (15)$$

- (c) The feedback rate function of teaching is calculated as shown in formula:

$$f(x) = \left\{ e^{(1/n) \sum_{i=1}^n \cos(2\pi x_i)}, 1 - \lim_{x \rightarrow 0} e^{(x_i/5)\sqrt{1/n}} \right\} \quad (16)$$

- (d) The student's thinking function is calculated as shown in formula:

$$f(x) = \sum_{i=1}^n \frac{x_i^2}{100} \pm \prod_{i=1}^n \left| \cos\left(\frac{x_i}{\sqrt{i}}\right) \right| \quad (17)$$

In this paper, the parameters of physical education teaching design are set: the total number of physical education teaching resources is 50, the iteration times are 120, and each teaching design is analyzed independently. The results of the four test functions are shown in Table 2.

It can be seen from Table 2 that the improved deep learning method is superior to the deep learning method, and its overall optimal design and theoretical optimal design Chew et al. [19]. The maximum value of improved deep learning is less than deep learning, while the minimum value is greater than deep learning, and the global design value of improved deep learning is greater than deep learning, so the improved deep learning method is better, the overall result is more reasonable, and it can promote the development of physical education teaching design. Moreover, the analysis scope, resource matching rate and analysis error of the improved deep learning method are smaller than those of the deep learning method. In order to reflect the test results of the test function in 4 more intuitively, the following convergence curves are given, as shown in Figure 4.

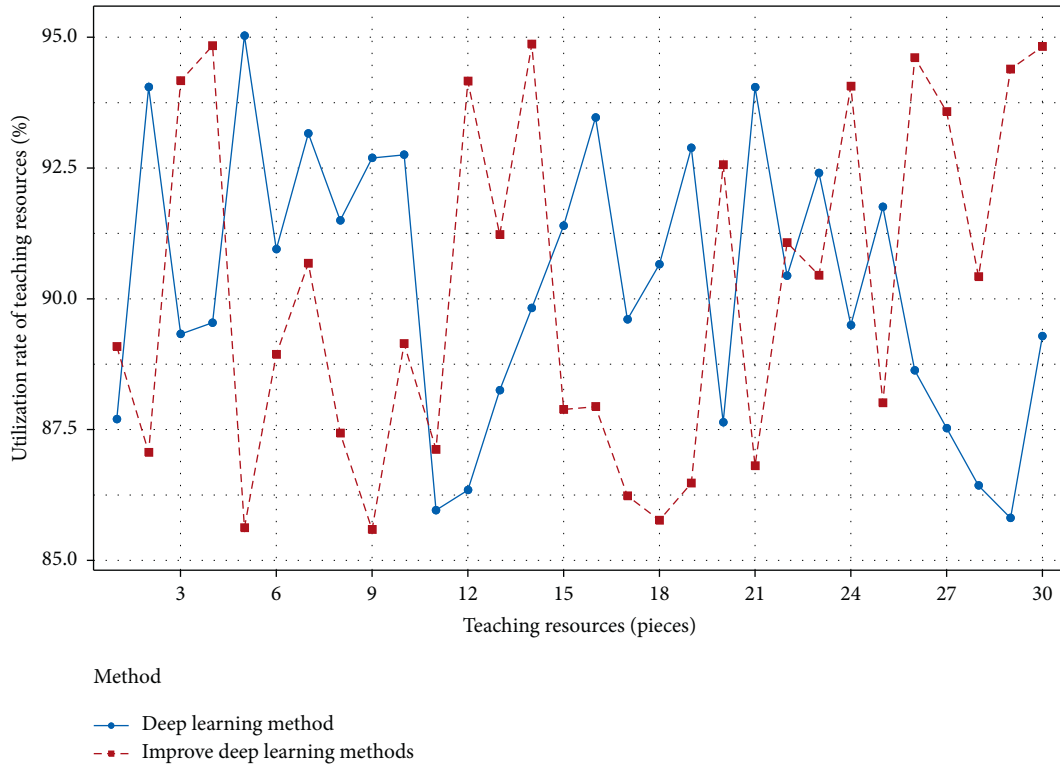


FIGURE 4: Convergence curve of the best scheme for selecting the test function of teaching resource utilization rate.

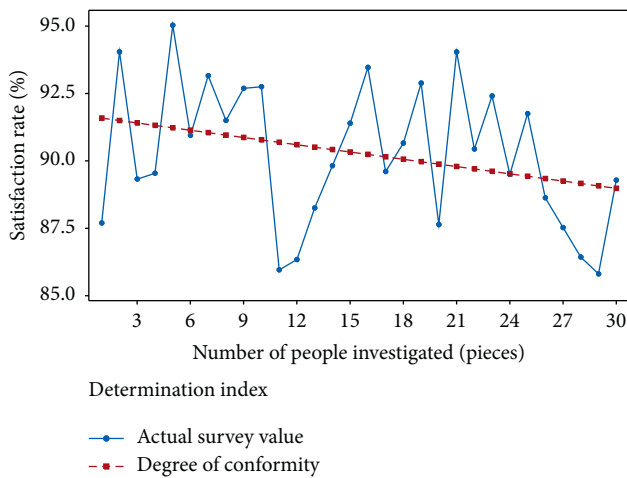


FIGURE 5: Satisfaction rate test of improved deep learning methods.

It can be seen from Figure 4 that the resource utilization rate of the improved deep learning method is higher than that of the deep learning method, and the change range is relatively large, which makes the processing more difficult. In Figure 4, the number of inflection points of improving deep learning is less than that of deep learning, and the method of improving deep learning is more stable, which makes the college physical education teaching design more scientific and can comprehensively improve the level of physical education teaching design. The result is shown in Figure 5.

It can be seen from Figure 5 that the design satisfaction rate of the improved deep learning method is concentrated

between 40% and 90%, which shows that the overall effect of the satisfaction rate is high and meets the requirements of physical education teaching design.

The data in Figure 5 are scattered, but the overall distribution is relatively concentrated. Therefore, improving deep learning can optimize the physical education teaching design, and the optimization effect is relatively stable. In the optimization process, the results show scattered distribution, which meets the requirements of objective normal distribution. The result is shown in Figure 6.

It can be seen from Figure 6 that the feedback rate of the improved deep learning method is significantly higher than that of the deep learning method, which shows that flipping the classroom horizon can improve the feedback rate of students and the level of physical education teaching design. The result is shown in Figure 7.

It can be seen from Figures 4–7 that the improved deep learning method has faster calculation speed and better stability, which is superior to the deep learning method. Therefore, the improved deep learning method is suitable for the analysis of college physical education teaching design, and the design process is more stable.

3.2. Design and Treatment of Actual Cases. In this paper, football, tennis, swimming, high jump, and other types are selected as research objects, and the collection time was from January 2021 to January 2022. A total of 402 lesson plans were collected, and the class hours were 1023 hours. According to the requirements of the Ministry of Education for physical education, the above-mentioned physical

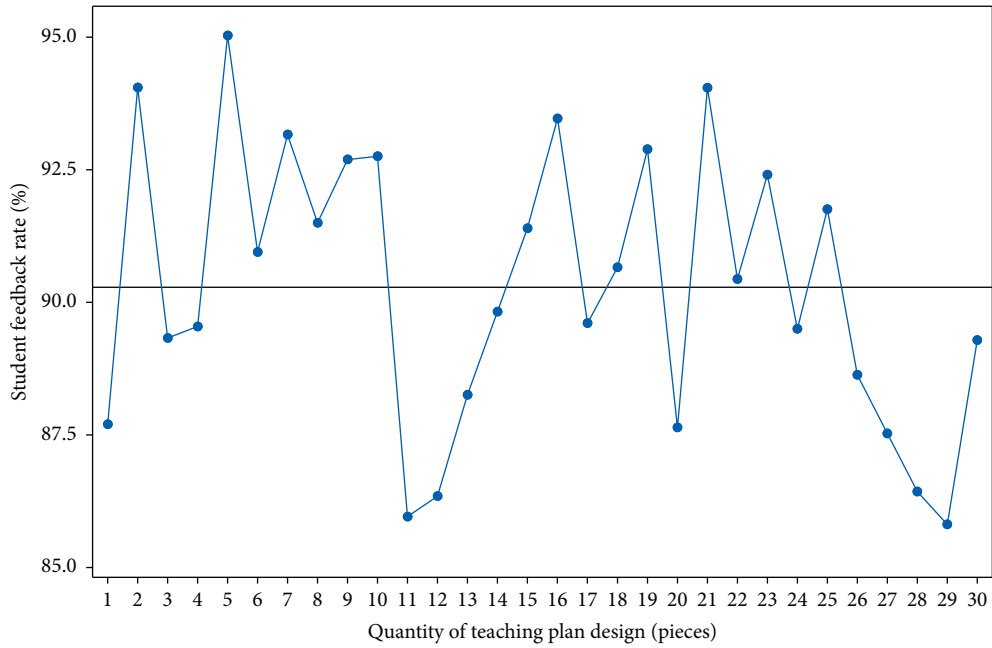


FIGURE 6: feedback rate test of teaching with different functions.

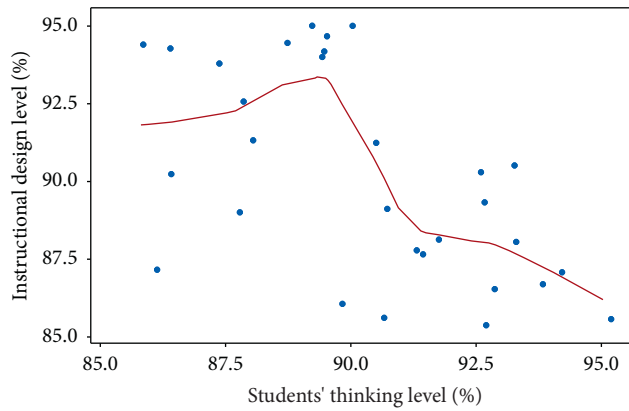


FIGURE 7: Students' thinking levels of different functions.

TABLE 3: Types and proportion of physical education teaching design.

Design type	Quantity of physical education teaching design (pieces)	Proportion (%)
Ask questions-think	99	24.63
Ask-think-answer	110	27.36
Ask-think-answer	91	22.64
Ask-think-answer-feedback	102	25.37

education design is divided into four categories: question-thinking, thinking-answering, question-thinking-answering, question-thinking-answering-feedback. The results are shown in Table 3. This paper verifies the accuracy of the analysis results according to theoretical judgment and actual detection methods. In order to avoid too many subjective factors in physical education teaching design, DETEL function is called to eliminate the design, which makes the physical education teaching design meet the relevant conditions. The results are shown in Table 3.

The physical education teaching design is trained by dichotomy, the first half is the research object, the second half is the analysis object, and the overall results are compared.

3.3. *Final Research Results.* According to the research conditions of physical education teaching design, the structure of physical education teaching design collection is determined as: structural design-semi-structural design-non-structural design, which meets the analysis

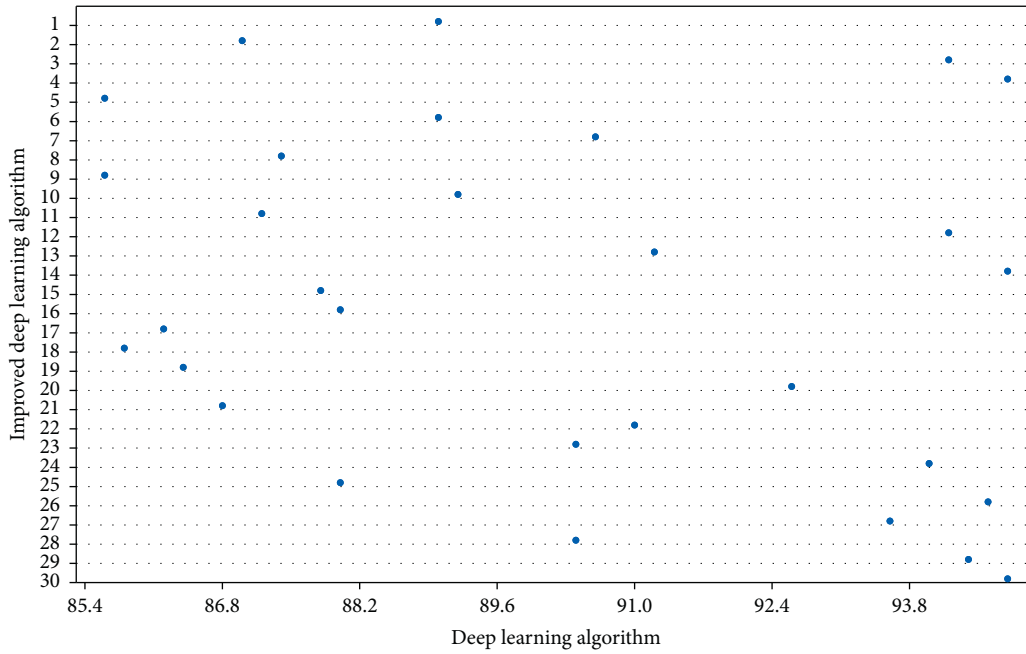
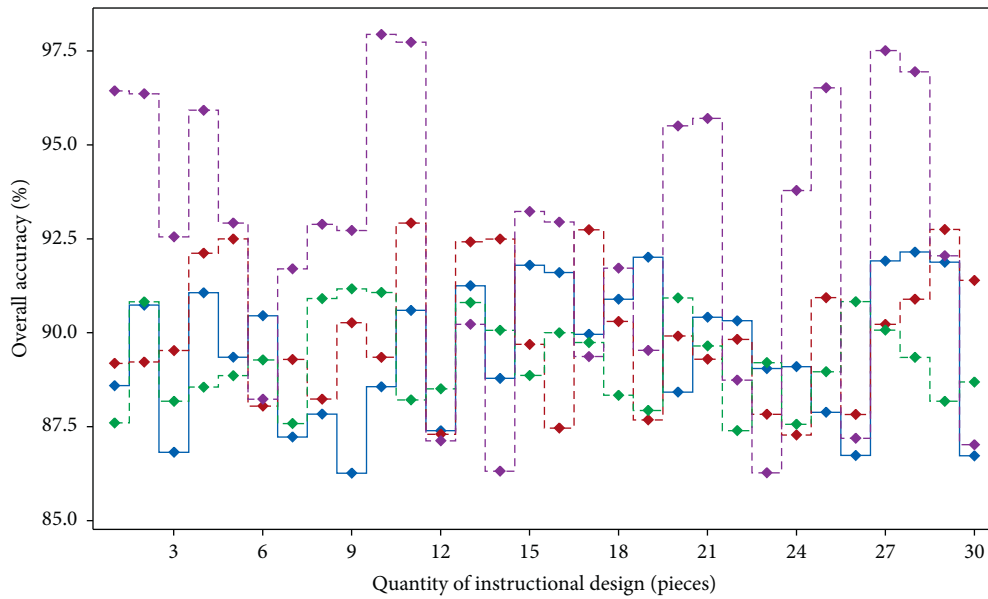


FIGURE 8: Classification results of complex physical education teaching design.



Different algorithms

- ◆ Flip classroom method
- ◆ Deep learning method
- ◆ General instructional design method
- ◆ Improve deep learning methods

FIGURE 9: Comparison of overall accuracy of different methods.

TABLE 4: Overall accuracy of different design types.

Design type	Improve deep learning methods	Deep learning method	Flip classroom method	General instructional design method
Ask questions-think	93.94	91.97	91.97	91.90
Ask-think-answer	97.91	96.90	92.91	91.91
Ask-think-answer	98.92	98.92	92.97	91.92
Ask-think-answer-feedback	98.93	97.93	97.92	92.91

requirements of improving deep learning methods. In this paper, the classification results of physical education teaching design by improving deep learning method are proposed, as shown in Figure 8.

Through comparative analysis, we can see that the classification of the improved deep learning method is discrete, which is closer to the actual situation, while the classification of the deep learning method is concentrated and cannot meet the needs of actual classification. In addition, the classification of improved deep learning method is not affected by complexity, while the classification of deep learning method is obviously affected by complexity, and becomes more concentrated with the increase in complexity.

The reason is that the improvement of deep learning method adds the theory of changing classroom horizon, and establishes a mapping among questioning, thinking, answering, and feedback, which makes the physical education teaching design more in line with the requirements. At the same time, fitness function is used to adjust physical education teaching design. In order to further prove the effectiveness of the model proposed in this paper, other comparative models are introduced for comparative analysis, and the results are shown in Figure 9.

It can be seen from the above figure that the fitness value of the improved deep learning method is the highest and reaches the limit at the earliest. Under the same complexity, the improved deep learning method has higher stability; The second is the deep learning method. The reason is that the theory of flipping classroom horizon reduces the influence of complexity on physical education teaching design; Different optimization strategies improve the accuracy of design, which is consistent with related research [19]. From the aspect of physical education teaching design types, this paper analyzes the accuracy of different deep learning methods, and the results are shown in Table 4.

It can be seen from the above table that improving the deep learning method can not only improve the efficiency of physical education teaching design but also keep the accuracy unchanged with the change of design type. The main reason is that the dynamic analysis of physical education teaching design from the perspective of classroom makes the time of physical education teaching design shorter and more flexible. Therefore, flipping the classroom horizon theory can not only reduce the impact of complexity on the results but also meet the requirements of different design types.

4. Conclusion

This paper puts forward an improved deep learning method based on the theory of flipping classroom horizon, which optimizes the physical education teaching design by setting teaching resources, weights, and designing strategies. The improved deep learning method constructed in this paper can classify the physical education teaching design discretely which makes the physical education teaching design more in line with the actual requirements. MATLAB simulation

results show that the deep learning method constructed in this paper has high design accuracy, the accuracy is concentrated in 90~98%, the single design quantity is relatively stable, accounting for about 3~4% of the total, the overall convergence is relatively short, and the convergence is carried out between 10 and 20 iterations, which can deal with physical education teaching design with complexity less than 45%, and the global optimal value is 2~3, the results are consistent with related studies. However, in the analysis of complexity, there are still deficiencies, future research in-depth analysis, to further improve the requirements of college physical education teaching design.

Data Availability

The experimental data used to support the findings of this study are available from the corresponding author upon request.

Conflicts of Interest

The authors declared that they have no conflicts of interest regarding this work.

References

- [1] Z. G. Yu and Q. Zhu, "Schema theory-based flipped classroom model assisted with technologies," *International Journal of Information and Communication Technology Education*, vol. 15, no. 2, pp. 31–48, 2019.
- [2] H. T. Yin, "Flipped classroom and its application to college English teaching," *Advances in Social Science Education and Humanities Research*, vol. 2, no. 2, pp. 238–242, 2017.
- [3] N. Xiao, D. Thor, and M. X. Zheng, "Student preferences impact outcome of flipped classroom in dental education: students favoring flipped classroom benefited more," *Education Sciences*, vol. 11, no. 4, p. 150, 2021.
- [4] R. Webb, D. Watson, C. Shepherd, and S. Cook, "Flipping the classroom: is it the type of flipping that adds value?" *Studies in Higher Education*, vol. 46, no. 8, pp. 1649–1663, 2021.
- [5] F. Wang and H. J. Wang, "The impact of the EFL flipped classroom teaching model (FCTM) on student engagement," vol. 2, no. 2, pp. 508–514, 2017.
- [6] K. Umezawa, T. Ishida, and M. Nakazawa, "Evaluation by questionnaire on grouped flipped classroom method," *Proceedings of the 2018 IEEE 10th International Conference on Engineering Education (ICEED)*, vol. 2, no. 3, pp. 83–88, IEEE, Kuala Lumpur, Malaysia, November 2018.
- [7] M. A. Trpkovska, L. A. Bexheti, and B. Cico, "Enhancing flipped classroom model implementation," *Proceedings of the Mediterranean Conference on Embedded Computing*, pp. 480–483, IEEE, Bar, Montenegro, June 2017.
- [8] P. R. Tang and L. Wang, "The construction and practice of the flip classroom in the background of rain classroom," vol. 7, no. 2, pp. 529–532, 2018.
- [9] Y. J. Song and M. Kapur, "How to flip the classroom - "productive failure or traditional flipped classroom"

- pedagogical design?" *Educational Technology & Society*, vol. 20, no. 1, pp. 292–305, 2017.
- [10] M. Soler, M. Bentabol, A. P. Lopes, and C. Rocio, "Looking for students' enthusiasm: flipped classroom," *ICE Proceedings*, vol. 2, no. 3, pp. 888–895, 2018.
- [11] R. Sofya and R. Sahara, "Optimization of flipped classroom using google classroom to improve student learning outcomes," *AEBMR-Advances in Economics Business and Management Research*, vol. 9, no. 2, pp. 407–412, 2020.
- [12] K. J. Shim, S. Gottipati, and Y. M. Lau, "Flip & slack - active flipped classroom learning with collaborative slack interactions," vol. 2, no. 3, pp. 121–131, 2021.
- [13] Y. Luo and H. G. Zhu, "Study on MOOC flip classroom," pp. 358–361, 2018.
- [14] W. W. Liu, "College English flipped classroom in applied undergraduate colleges based on rain classroom," vol. 8, no. 2, pp. 1223–1228, 2018.
- [15] A. Gayef, "Flipped classroom in medical education," *INTED Proceedings*, vol. 7, no. 8, pp. 3484–3491, 2020.
- [16] Q. H. Fang and J. B. Jiang, "An empirical study on influence of flipped classroom on college English listening and speaking classroom environment," *ACSR-Advances in Computer Science Research*, vol. 9, no. 7, pp. 372–380, 2017.
- [17] G. G. Fan and F. Meng, "Research on the new mode of MOOC and flipping classroom teaching method in classroom teaching of "network database," *Advances in Social Science Education and Humanities Research*, vol. 8, pp. 784–789, 2018.
- [18] B. V. C. Collins, "Flipping the precalculus classroom," *International Journal of Mathematical Education in Science & Technology*, vol. 50, no. 5, pp. 728–746, 2019.
- [19] E. Chew, L. J. N. Jones, and S. Wordley, "Flipping or flapping?" investigating engineering students' experience in flipped classrooms," *On the Horizon*, vol. 26, no. 4, pp. 307–316, 2018.

Research Article

Time Series Data Prediction and Feature Analysis of Sports Dance Movements Based on Machine Learning

DongXia Zheng  and **Yi Yuan** 

College of Physical Education, Hunan University of Science and Technology, Xiangtan 411201, China

Correspondence should be addressed to DongXia Zheng; 1170068@hnust.edu.cn

Received 13 June 2022; Revised 14 July 2022; Accepted 25 July 2022; Published 24 August 2022

Academic Editor: Le Sun

Copyright © 2022 DongXia Zheng and Yi Yuan. This is an open access article distributed under the Creative Commons Attribution License, which permits unrestricted use, distribution, and reproduction in any medium, provided the original work is properly cited.

Sports dance is a competition project and a kind of sports, with the characteristics of being smooth, generous, leisurely, and comfortable, dance steps, smooth movements, and flowing clouds, and it can give full play to the indoor space. In the light of the new era, sports dance is also playing an increasingly important role. Through the time series data and feature analysis of dance sports movements through machine learning, the internal information is mined to find the trends and laws. Machine learning in the era of big data is widely used in research as the main tool for data analysis and mining. The key difficulty of data mining has always been time series data. Machine learning refers to a method of using the resulting data in a computer to derive a certain model and then using this model to make predictions. The core is “using algorithms to parse data, learn from it, and then make decisions or predictions about new data.”

1. Introduction

This paper is based on how machine learning analyzes the time series data prediction and characteristics of dance sport movements. The process of machine learning is similar to the learning process of human beings, such as people learning mathematical theoretical models to establish logical thinking skills, analyzing and predicting things [1]. For example, chatbots—chatbots is one of the earliest forms of learning that allows humans and machines to communicate and dialogue, from which to fill the communication gap between humans and technology. For example, machines can act according to human demands or requirements [2]. The earliest is to write scripts, put the script in the machine to compile and run so that these machines have a chat function, and the script code run by the machine will make the machine recognize and let the machine according to what keywords to take what action. But there is another member of the AI family, the acceptance of machines and the use of language recognition (NLP) [3]. Let us take the interactivity and productivity generated by chatting with machines to the next level [4]. The new generation of

chatbots can more effectively handle the needs of users and move forward like human-to-human communication [5]. Machine learning’s algorithms are used in a wide variety of digital assistants, and this technology can be applied to the new B2C and C2C to find ways to update the traditional way of chatting with robots [6]. Communicating with robots is one of the most widely used machine learning applications in the commercial world [7]. Some AI assistant scripting languages can analyze when relevant questions need to be asked and when to ask questions and demands from humans identification classification [8]; multimedia live platform chatbots can satisfy users’ use, search, and pass good music to friends and family, and at the same time, they can also enjoy the relevant music recommended by AI robots according to their personal preferences for us to enjoy [9]; during the rush hour of traffic jam, we need to take a taxi. Then you can take a taxi online through the relevant software, use the relevant software or other platforms or related request services, and receive the basic information of the driver and related vehicles that come to pick us up, such as the license plate number, color, and model of the vehicle [10]. Machine learning is also used in organizational

structures, and sophisticated learning and neural networks help them analyze images [11]. Machine learning-related technologies like this which have a high breadth of applications in social media sites want to put signs on photos of other media sites, as well as road cameras and store monitoring [12]. Groups that maintain safety such as Sky Eye conduct real-time monitoring, detection, and identification of criminal behavior; later, driverless cars are driven on smooth and wide roads. Retail investors also have many applications in various aspects such as the classification of images and the recognition and analysis of images. For example, install cameras in warehouses, connect the cameras to the computer, use the computer's visual system and the self-learning system to scan the relevant items on the current shelves, and identify and determine whether there are items that are misplaced, random, or out of stock; you can also use the scanner to scan the goods taken out of the shopping cart using image recognition technology to make the goods be identified one by one. This reduces the loss of sales formed in an unintentional state; it can also be used to use image recognition in the computer through cameras, surveillance, sky eyes, and other devices to analyze whether there is suspicious activity or illegal and criminal behavior (such as smoking on high-speed rail or carrying unauthorized dangerous goods or equipment) [13]. Although most of the machine learning is highly specialized for a certain need, most merchants still try the highly specialized technology of machine learning to shorten the business process, making it easy and fast to optimize the process of collaborative processing of daily business, especially financial transactions and software development such as banks, securities companies, and other related financial transactions [14]. From the early days to the present, the most widely used applications are in the financial organization, IM, and companies' business processes, as well as software development and testing. Most departments, such as VCs and operations, are using machine learning techniques to improve the efficiency of their own departments, thereby creating more value for the company [15]. Because human energy is always limited, machine learning techniques can be used to reduce work cycles, reduce errors, and speed up work efficiency. In machine learning, we can give it a time to form a cycle according to the time we set, automatically troubleshoot errors, detect problems, and give problems to the relevant technicians in a cycle, so that we can reduce the effort on it, thereby reducing unexpected problems and interference caused by unplanned work [16]. In addition, in software testing, machine learning techniques can be added to black and white box testing and automated testing, which greatly improves the speed of software testing so that software development is faster and cheaper. Sometimes we need to extract structured critical data in documents that cannot be extracted directly, because not all data is structured and stored in unstructured and semistructured formats; that is, we need to apply NLP's machine learning technology to help us extract key structured data in related documents [17]. Experts say applying machine learning-related techniques to understand documents is a great opportunity for all aspects of life. Companies can do this, from tax returns to invoices to

statutory contracts, all of which can improve efficiency and accuracy and free the work force [18] from positions that are seen as day-to-day work. Most of the smartphone's capabilities also come from machine learning. For example, voice assistants, from setting alarm clocks to finding language assistants in restaurants to decoding facial recognition phones, Apple's Siri, Xiaomi's Little Love, and Google Assistant, establish a dance sport movement time series data prediction and feature analysis based on machine learning to explore the characteristics of them for overall development.

2. Machine Learning for Sports Dance Movement Cognition

2.1. Obtain Sports Dance Movement Data. From the appearance of people, it is composed of several parts: head, neck, body, limbs, and so forth, of which the skin is on the surface of the body, and the subcutaneous tissue, muscles, and bones are below the skin. Composed of 206 bones, it can complete a variety of types, as well as uses of complex shapes; based on this physical test structure, people can complete a variety of actions; through the brain's thinking coordination, the human body in the completion of different movements reflects a strong coordination, so the study of sports dance is to make the AI system like a person have the abilities of learning, reasoning, and thinking; according to the content learned, knowledge judges what is actually going on online and predicts what will happen, hence the research on sports dance movements and intelligent control, human-computer interaction, AI, and other fields of research hotspots [19]. The capture of dances in sport includes contact and no contact in equipment, electromagnetic, inertial, machine, and optical terms, which record the movements through specific man-machine instruments, and the noncontact type includes a monocular RGB-D camera or a monocular RGB camera and a depth camera.

2.2. Dance Sport Movement Data Files. The dance sport movement acquisition system stores the acquired data to capture the movements in a file as BVH, which is parsed out after the action capture, which is the general format of the animation characteristic file through the human body function. It is well supported on many well-known animation software programs (flash, TV Painter, Blender3D) [20]. The representation of the human body therein is the skeleton model in the picture above, which is then expressed through the structure of the tree. BVH contains data on the movement of limb joints of characters performing dance sport movements.

3. Machine Learning Time Series Data Prediction Algorithm Implementation

3.1. Wavelet Transform. The basic solution of the wavelet transform (WT) is to represent the action signal as a set of wavelets, which can obtain information about the time and frequency domain of the action signal. The two most commonly used types of wavelet transform in WT include

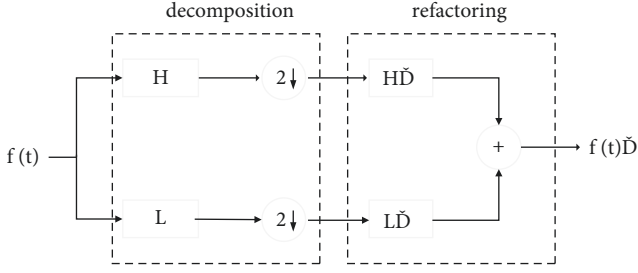


FIGURE 1: Disassembly and reconstruction of discrete wavelet transforms.

the continuous wavelet transform (CWT) and the discrete wavelet transform (DWT) [21].

Continuous wavelet transforms are expressed as follows:

$$W_{s,\tau}(t) = \int_{-\infty}^{\infty} f(t) \psi_{s,\tau}^*(t) dt, \quad (1)$$

$$\psi_{s,\tau}(t) = \frac{1}{\sqrt{|s|}} \psi\left(\frac{t-\tau}{s}\right). \quad (2)$$

$\psi_{s,\tau}^*(t)$ is called a base wavelet or a mother wavelet; it is called a scaling factor (or scale); τ is the $\psi_{s,\tau}^*(t)$ conjugate of the translation factor. When the harmony can be continuously changed, the wavelet change at this time is called the continuous wavelet transform $\psi_{s,\tau}(t)st$ CWT. Due to the complexity of the calculation of the continuous wavelet transform and the high degree of redundancy, it is not suitable for practical applications. Therefore [22], the DWT is obtained by discretizing the scaling factor in the CWT. Bring it in (2) ($s = s_0^m \tau = n^{\tau_0 s_0^m} m, n \in \mathbb{Z}$) to get discrete wavelets:

$$\psi_{m,n}(t) = \frac{1}{\sqrt{|s_0^m|}} \psi(s_0^m t - nb_0), \quad m, n \in \mathbb{Z}. \quad (3)$$

The discrete wavelet transform is

$$W_{s,\tau}(t) = \int_{-\infty}^{\infty} f(t) \psi_{s,\tau}^*(t) dt = \frac{1}{\sqrt{|s_0^{-m}|}} \int_{-\infty}^{\infty} f(t) \psi^*(s_0^{-m} t - nb_0) dt. \quad (4)$$

The decomposition process of DWT is equivalent to going through a high-pass filter and a low-pass filter, followed by using a binary decimation algorithm for downsampling. The DWT decomposition and reconstruction process is shown in Figure 1. H and L are decomposition filters, where H is a high-pass filter and L is a low-pass filter; after decomposition, a downsampling operation is required. H' , L' is a reconstruction filter; likewise, H' is a high-pass filter and L' is a low-pass filter.

3.2. Static Wavelet Transform. Since the discrete wavelet decomposition uses a binary decimation algorithm to downsample the action, the wavelet coefficient will be reduced by one-half after each decomposition, so the details of the original action will be lost in each decomposition. The stationary wavelet transform (SWT) that removes the

downsampling and upsamples the filter solves this problem. The SWT decomposition reconstruction process is shown in Figure 2, in which the output components of the high-pass filter and the low-pass filter are no longer downsampled, but the upper filter is upsampled to obtain a decomposition of the high-pass filter and low-pass filter in each step [23]. The detail and approximate components after each decomposition of the static wavelet are the same as the length of the original action signal, which ensures that the characteristics of the movement are preserved to the greatest extent possible and are also conducive to the analysis and study of sports dance movements.

The single-step multiscale static wavelet decomposition process of the action signal is similar to the single-step multiscale discrete wavelet decomposition process, as shown in Figure 3.

3.3. ERD Models. The ERD model was proposed by Frigidaria [24]. It is an encoder-loop unit-decoder (ERD) model used to identify and predict human posture in video and motion capture [25]. The main way it runs is to obtain a new prediction frame by continuously putting the prediction frame of the previous step into the model, so as to achieve the effect of multiframe prediction; the specific method he achieves is to encode the human action data through the fully connected network and put it into the recurrent neural network to predict the next action state according to the memory information of the previous time, and then the obtained data vector is decoded through the corresponding full connection layer, obtain the action data, and reconstruct the action through a certain reconstruction method to obtain the prediction result. Its main structure is shown in Figure 4.

3.4. Conversion between Dance Sport Movement Data and Trainable Data. Since the sports dance action data recorded in the dataset is in the form of quaternions, the rotation amplitude of one of the movements consists of four numbers between -1 and 1 , and the continuity in the number value is not strong, so the original movement data needs to be processed to a certain extent.

That is, it proposes exponential mapping of raw data, which can effectively avoid data discontinuities and Vientiane knot locks [26]. The process is as follows:

$$\theta = r_2,$$

$$r'x = \begin{bmatrix} 0 & -r'[2] & r'[1] \\ 0 & 0 & -r'[0] \\ 0 & 0 & 0 \end{bmatrix},$$

$$r'x = r'x - r'X^T, \quad (5)$$

$$\text{rotationmat} = \begin{bmatrix} 1 & 0 & 0 \\ 0 & 1 & 0 \\ 0 & 0 & 1 \end{bmatrix} + \sin \theta * r'x$$

$$+ (1 - \cos(\theta)) * r'x \cdot (r'x).$$

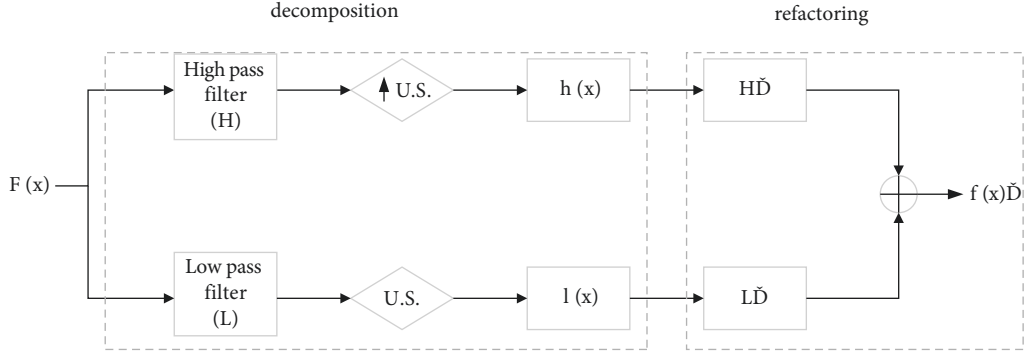


FIGURE 2: Static wavelet decomposition reconstruction.

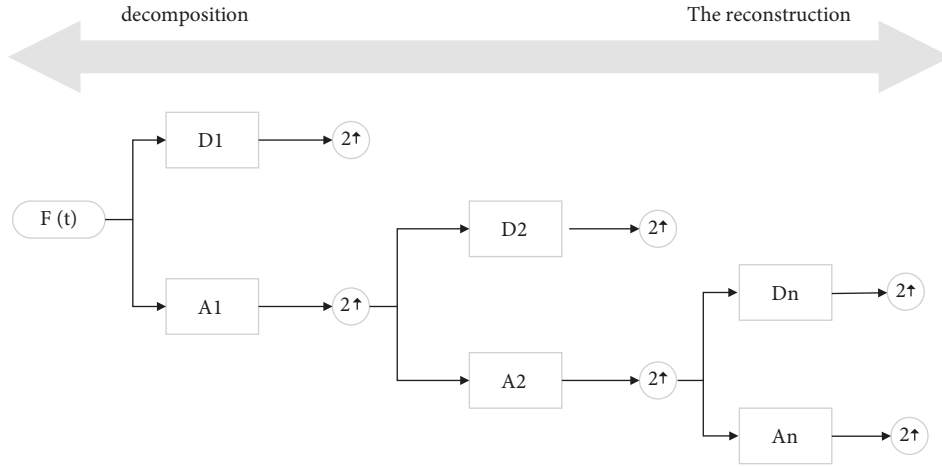


FIGURE 3: Single-step multiscale SWT decomposition process.

To find the rotation matrix rotationmat , where rotationmat is the original exponential mapping matrix, according to the rotation r matrix to find the rotation quaternion, the process is as follows:

$$\text{rotdiff} = R - R^T,$$

$$r0 = [-\text{rotdiff}[1, 2] \text{rotdiff}[0, 2] \text{rotdiff}[0, 1]],$$

$$\sin \theta = r_2,$$

$$r0 = \frac{r}{r_2},$$

$$\cos \theta = \frac{\text{trace}(R) - 1}{2}, \quad (6)$$

$$\theta = \arctan\left(\frac{\sin \theta}{\cos \theta}\right),$$

$$\begin{aligned} \text{quaternion} = & \left[\cos\left(\frac{\theta}{2}\right) r0[0] * \sin\left(\frac{\theta}{2}\right) r0[1] \right. \\ & \left. * \sin\left(\frac{\theta}{2}\right) r0[2] * \sin\left(\frac{\theta}{2}\right) \right] \end{aligned}$$

In the above equation, R is the rotation matrix, which eventually yields quaternion.

Due to the particularity of the heel node, if it controls the rotation mode and angle of the entire human body, we hope that the human body can have a certain stability, so the human root node is unchanged for the translation of the ground plane and for the rotation of gravity perpendicular to the ground (assuming that the ground surface is horizontal).

4. Case Studies

4.1. Comparative Experiments. The experiment selected 30 personnel for dance steps, outer dance steps, preparatory outside dance steps, reflexive movements, reflexive action positions, lifting, swinging, and other 7 kinds of sports dance movements in the same time and place to complete the experiment; the experiment does not constrain the behavior habits of the testers; participating students who take the test only need to complete the experiment in their own way. In this comparative experiment, the first adopts the traditional human movement pattern information collection method, and the second adopts the motion pattern recognition method of the accelerator and the sensor. There is a sports dance movement A, a dance step T, an outer dance step N, a preparatory outer dance step W, and a reflexive movement A. The experimental results of the reflexive action position of F lifting and descending to H and swinging to M are shown in Tables 1 and 2.

According to Tables 1 and 2, we can conclude that the difference between the dance steps and several other

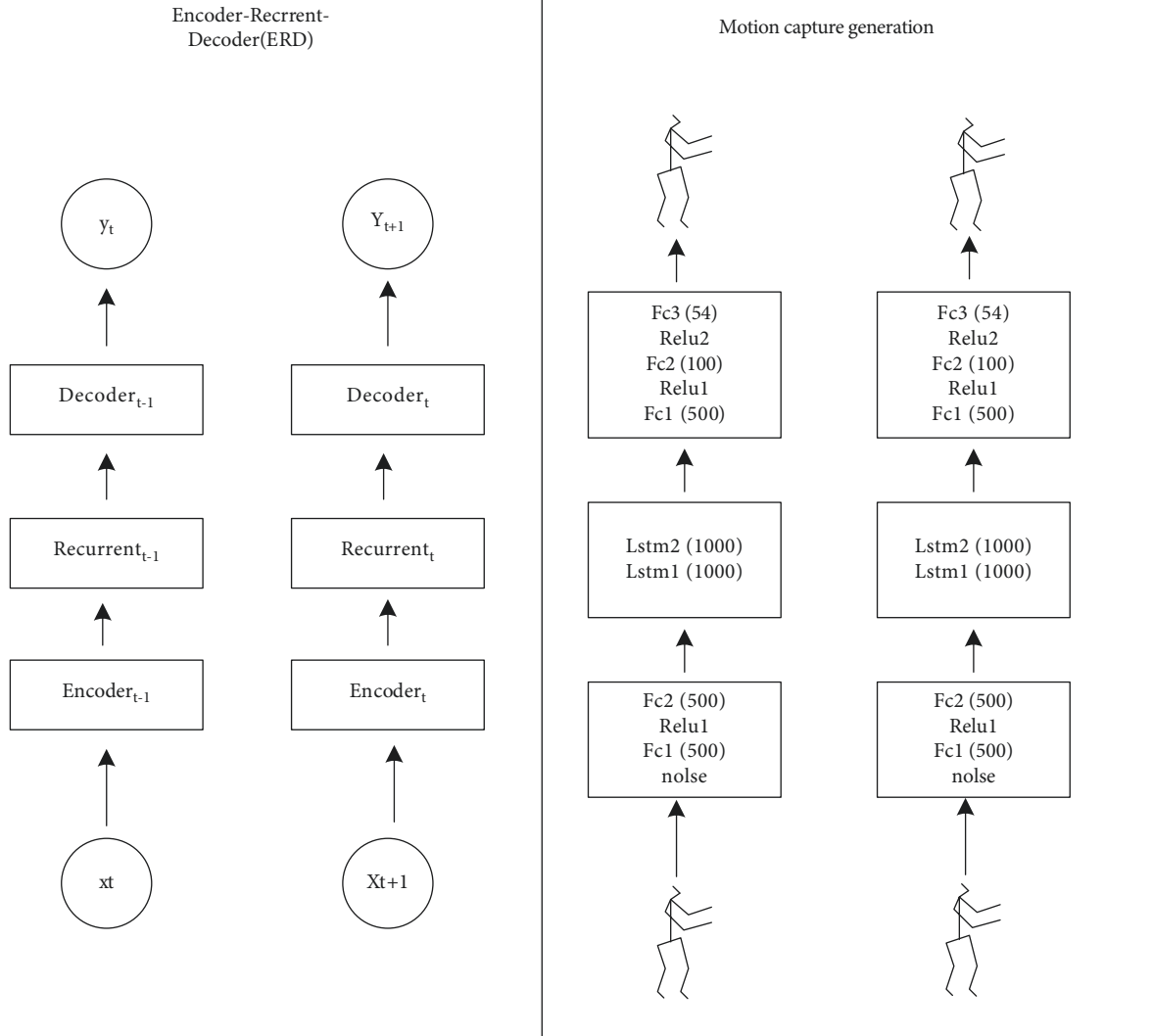


FIGURE 4: ERD model.

TABLE 1: Confusion matrix of the first set of dance sport movements.

A	T	N	W	U	F	H	M
T	190	4	2	1	2	1	0
N	1	180	7	5	7	0	0
W	0	7	81	5	6	0	1
U	0	6	7	83	4	0	0
F	2	6	3	2	87	0	0
H	5	0	0	0	3	92	0
M	5	1	0	1	0	0	93

movements is very high, so the recognition is 100%; the difference between the reflex and reflexive action positions is very small, so its recognition is very low. Specific parameters are identified as shown in Table 3.

As can be seen from Figure 5, traditional recognition technology can identify a variety of action patterns, and its recognition accuracy is balanced at 90.1%. The recognition of reflexive action and reflexive action position is low. When integrated with the accelerometer, its recognition accuracy can be balanced to 94.3%. Compared with the

TABLE 2: Confusion matrix of the second set of dance sport movements.

A	T	N	W	U	F	H	M
T	194	3	1	1	1	0	0
N	1	188	5	3	3	0	0
W	0	3	90	4	3	0	0
U	0	4	3	91	2	0	0
F	0	3	2	2	93	0	0
H	3	2	0	0	1	94	0
M	3	1	0	0	1	0	95

TABLE 3: Statistical table of identification results.

Mode	T (%)	N (%)	W (%)	U (%)	F (%)	H (%)	M (%)
The first group	100	95	90	81	83	87	92
The second group	100	97	94	90	91	93	94

previous recognition accuracy, its recognition accuracy is balanced upward by 4.2 percentage points, and the result is better.

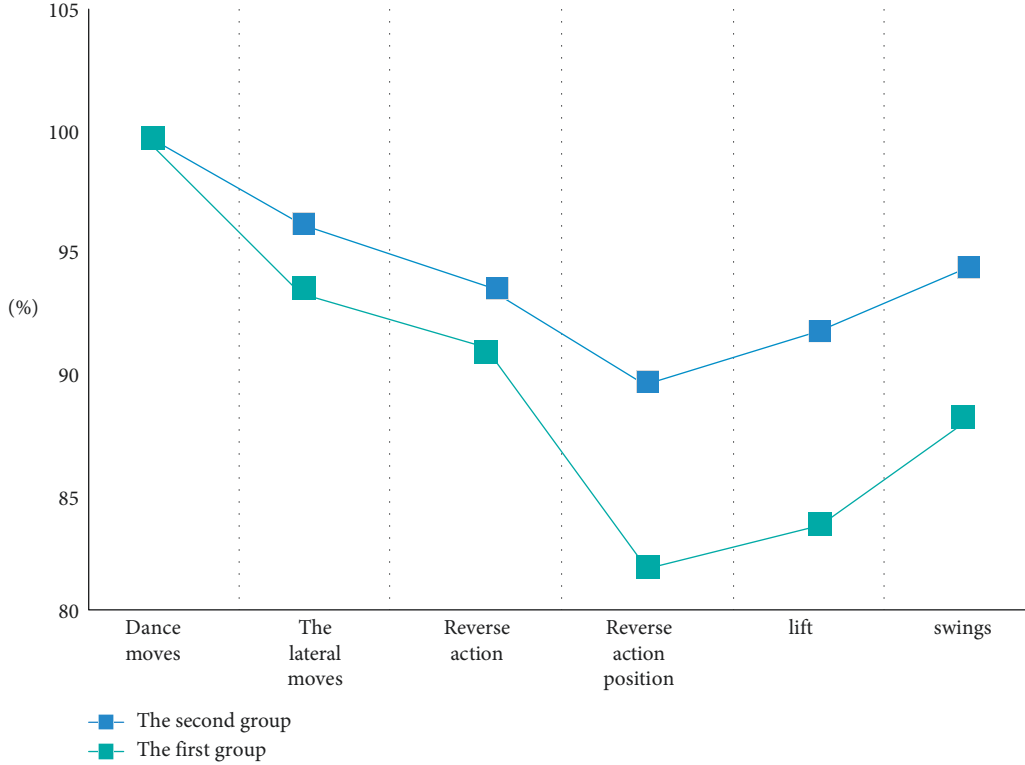


FIGURE 5: Statistical chart of recognition results.

TABLE 4: Student physical condition statistics.

	General groups	Training group	<i>P</i> value	<i>T</i> value
Height (cm)	175 2.00 ±	175 1.41 ±	1.100	-0.150
Weight (kg)	70.10 2.61 ±	70.10 2.17 ±	0.978	-0.087
Age	16.6 0.51 ±	17 0.00 ±	0.701	-2.049

40 students were selected to test the standard degree of sports dance movements, and they were divided into two groups; that is, the regular group completed the experiment according to their own behavior, and the training group conducted sports dance movement analysis and teaching. The two sets of results are then compared and analyzed. Because the height, weight, and age of the students participating in the test are basically the same, the *P* value is greater than 0.06, so the elements related to the body will not affect the experimental results. Their situation is shown in Table 4.

From Table 5 and Figure 6, it can be seen that the indicators of the conventional group and the training group are basically the same, and after the *t*-test is carried out on both groups, *P* is above 0.05, which depends on the initial situation of the two groups.

From Table 6 and Figure 7, it can be seen that, under the same initial conditions, the sports dance indicators of the trained students can be improved.

Throughout the dance movements, the angle and speed of each movement change periodically. After making appropriate modifications to the movement predictions of the time series data, the comparison curve of the angle and speed of the movements during the process of performing the dance sport movements is shown in Figure 8.

4.2. Data Processing. The experiments set the mean and variance of the prediction accuracy as *p* and $p(1-p)$, respectively. Due to different experiments, the prediction reversibility of the algorithm is now statistically zero, so the correct random variable with a mean of *p* is *f*, and its variance decreases as $p(1-p)/N$ with the increase of the repeated simulation experiment coefficient *N*, and when $N > 100$, it is close to the normal distribution. This makes it possible to construct a positive-tyrannous random variable:

$$\frac{f - p}{\sqrt{p(1-p)/N}} \quad (7)$$

The following equation is then passed with the confidence level *c* determined:

$$P \left[-z < \frac{f - p}{\sqrt{p(1-p)/N}} < z \right] = 2 * (1 - c). \quad (8)$$

z values can be extrapolated from a probability table. The true value *p* can be obtained using the calculation method of probability theory, with the interval boundary value *c* of the probability approaching *f*.

$$p = \frac{\left(f + z^2/2N \pm \sqrt{f/N - f^2/N + z^2/4N^2} \right)}{(1 + z^2/N)}. \quad (9)$$

± gives two values, the upper and lower bounds of the confidence.

When collecting data, the duration of each action is relatively short, and it cannot correspond well to the data

TABLE 5: Evaluation results of regular dance sport training indicators.

Test the content	General groups	Training group	P value	T value
Quick squats	11.0	13.0	0.512	-0.673
Wave speed ball pilates	41.0	43.0	0.378	0.911
Pick up	9.5	14.5	0.611	-0.521
Variable speed running (s)	5.5	5.1	0.685	0.414
Long Jump (m)	1.9	2.3	0.920	0.102
Push-ups (times)	25.0	50.0	0.081	-1.880
Accelerate run (s)	18.2	17.5	0.495	-0.701
Repeatedly crossed (times)	40.0	44.0	0.262	1.168
Russian rotation (min)	4.59	4.35	0.887	-0.144

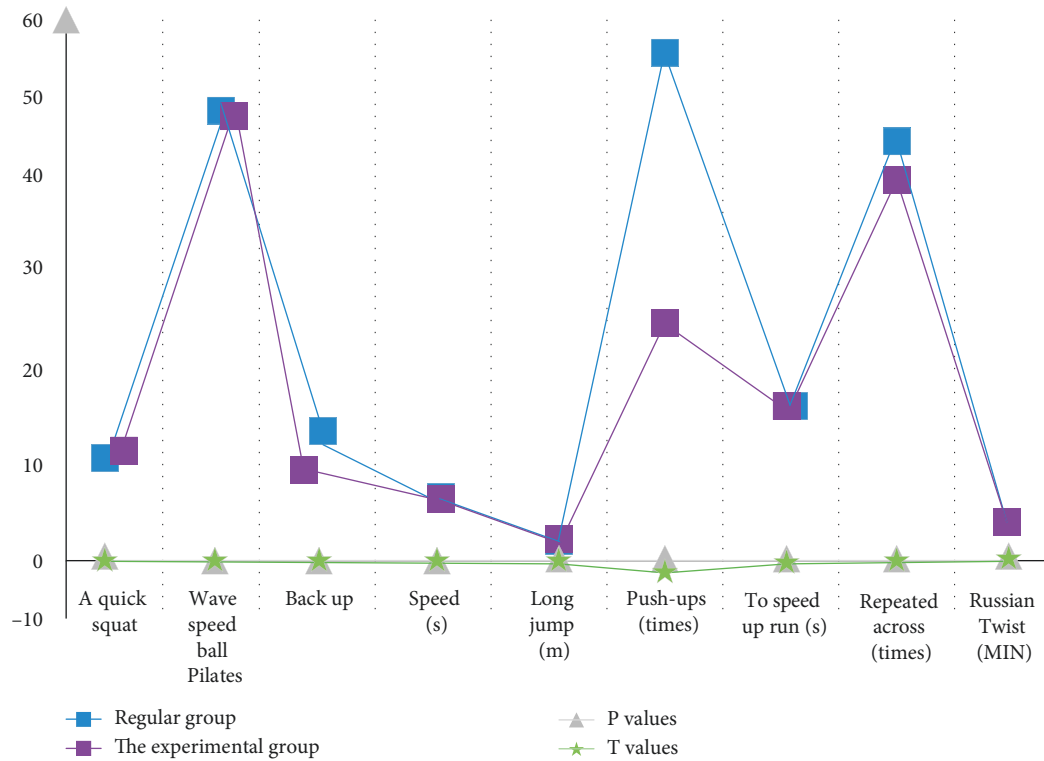


FIGURE 6: Evaluation results of preteaching SPI training indicators.

TABLE 6: Evaluation results of sports dance indicators in the training group.

Test the content	General groups	Training group	P value	T value
Quick squats	13.0	15.0	0.003	-3.578
Wave speed ball pilates	42.0	44.0	0.192	-1.372
Pick up	12.1	15.3	0.009	-3.026
Variable speed running (s)	4.6	4.2	0.000	5.062
Long Jump (m)	2.1	2.5	0.028	-2.456
Push-ups (times)	44.0	52.0	0.086	-1.864
Accelerate run (s)	18.9	17.1	0.018	2.677
Repeatedly crossed (times)	42.0	46.0	0.010	-2.973
Russian rotation (min)	4.4	4.36	0.335	0.998

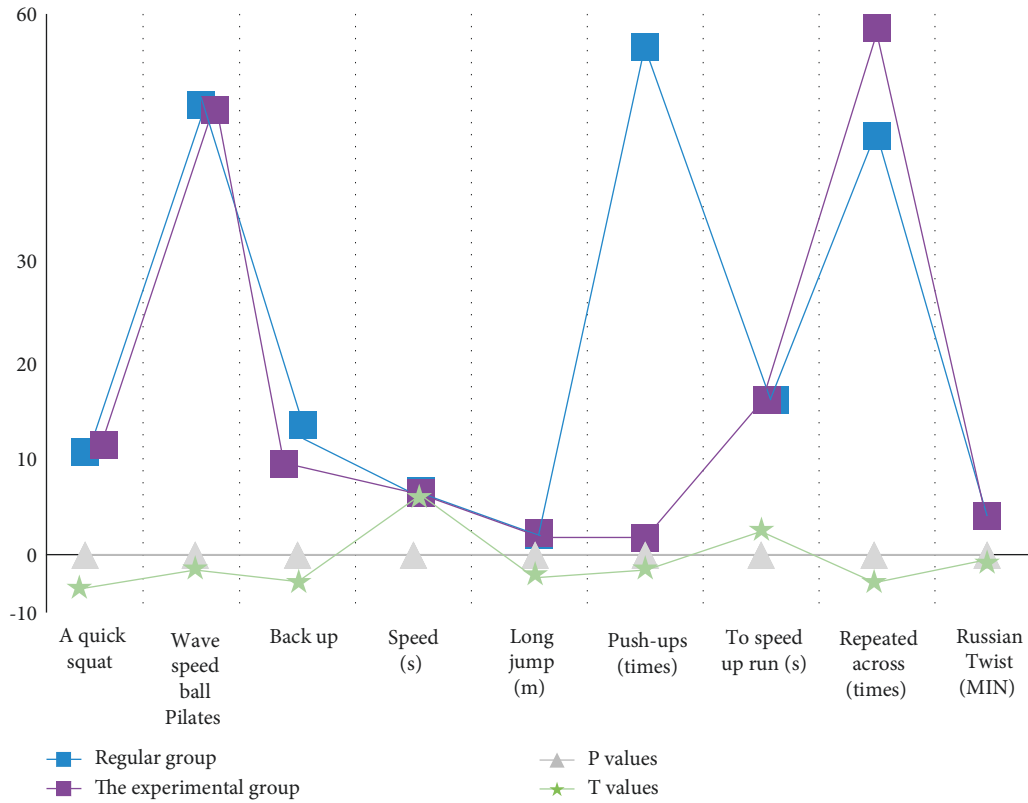


FIGURE 7: Statistics on the evaluation results of posttraining sports dance training indicators.

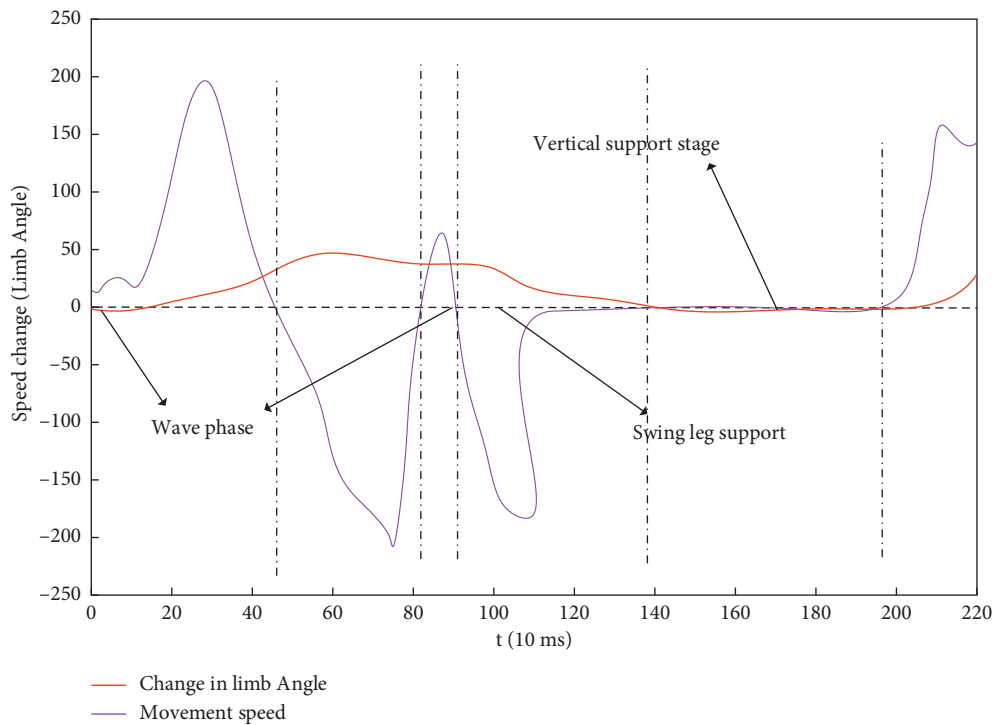


FIGURE 8: Movement angle/movement speed change curve during the dance sport movement process.

obtained individually, so, by obtaining several pieces of action cycle data, clustering is divided, and the results and data are analyzed by curve comparison to determine the

action period to which the data belongs. As shown in Figures 9 and 10, the clustering results correspond to the two-dimensional three-point plot of the action.

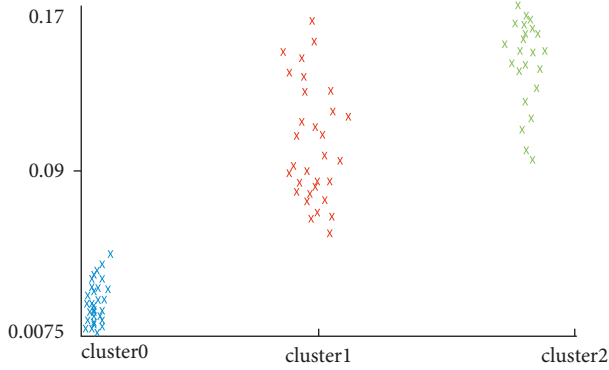


FIGURE 9: The correspondence between clustering results (horizontal axis) and action (number axis).

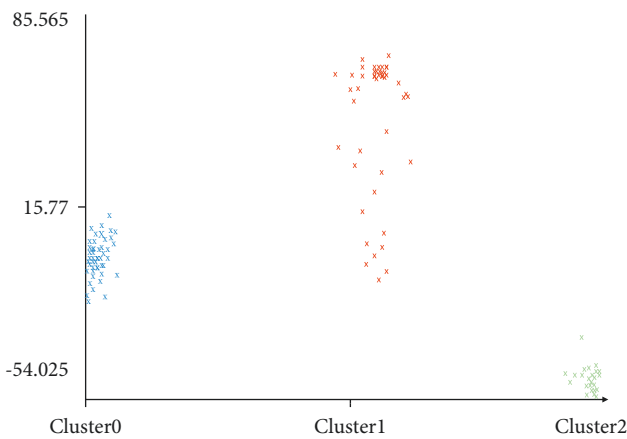


FIGURE 10: The correspondence between the clustering results and the action angle.

TABLE 7: Category II prediction confusion matrix.

		Prediction class	
		Dance sport moves (T)	Stationary (F)
Real class	Action (T)	Right (affirmatively)	Error (negation)
	Stationary (F)	Error (affirmation)	Right (negative)

TABLE 8: Three types of projected cost matrices.

		Prediction class		
		a	b	c
Real class	a	0	1	1
	b	1	0	1
	c	1	1	0

Table 1 shows the type II prediction confusion matrix. For one class, for example, the “Dance Sport” class in Table7, set to T the correct class, and the other is the negative class F, so that the true positive (TP), true negative (TN), false positive (FP), and false negative (FN) are verified. So, the correct rate of classification of an action is

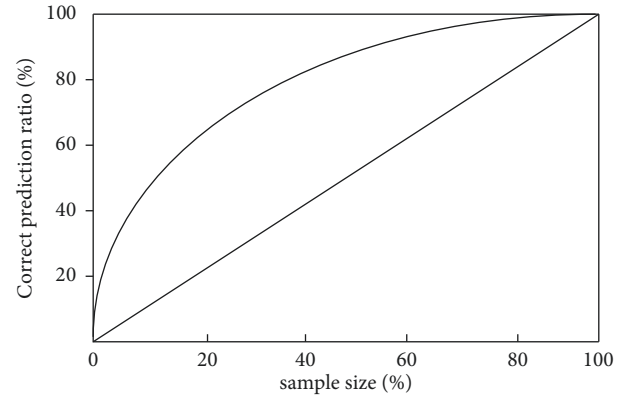


FIGURE 11: Assuming an ascending chart.

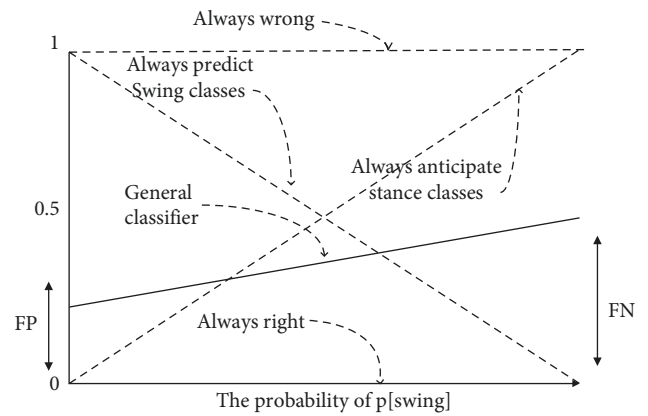


FIGURE 12: The effect of probability classification on sports movements of the sample class.

$$\text{Kappa} = \frac{TP + TN}{TP + TN + FP + FN} \tag{10}$$

The maximum value is 1, and the action is the best.

Table 8 shows the cost matrix of the three classification projections. The cost matrix represents the cost caused by prediction error and correctness, the correct cost is 0 and the cost of error is 1, so the cost of the resulting statistical error is the number of errors, as shown in Table 8.

The first thing we need to consider for different movement performances is the rising chart, which represents the total number of students testing SCORP movements and the proportion of students practicing SCORP, and the vertical axis represents the correct prediction rate, as shown in Figure 11.

The cost curve is an action corresponding to a straight line, the purpose of which is that the action changes with the distribution of the class, as shown in Figure 12; the horizontal axis represents the probability of a certain class of samples in the training sample, and the vertical axis represents the expected error. Predictions made for only one of these types are represented by two diagonal lines, decisions are always erroneously represented by horizontal dotted lines, and horizontal lines indicate that predictions are always correct.

TABLE 9: Numerical projection indicators.

Performance measurement	Formula
Mean square error	$(p_1 - a_1)^2 + \dots + (p_n - a_n)^2/n$
Root mean square error	$\sqrt{(p_1 - a_1)^2 + \dots + (p_n - a_n)^2/n}$
Average absolute error	$ p_1 - a_1 + \dots + p_n - a_n /n$
Relative square error	$(p_1 - a_1)^2 + \dots + (p_n - a_n)^2 / (a_1 - \sigma)^2 + \dots + (a_n - \sigma)^2$
Relative square root error	$\sqrt{(p_1 - a_1)^2 + \dots + (p_n - a_n)^2 / (a_1 - \sigma)^2 + \dots + (a_n - \sigma)^2}$
Relative absolute error	$ p_1 - a_1 + \dots + p_n - a_n / a_1 - \sigma + \dots + a_n - \sigma $

P is the predicted value and a is the true value: $\sigma + 1/n \sum_i a_i$

TABLE 10: Action comparison indicators.

Index	Definition	Significance
Kappa statistic	—	Close to 100% is best
TP rate	Correct proportions	Close to 1 is best
Accuracy rate precision	$TP/TP + FP * 100\%$	Close to 1 is best
Feedback rate recall	TP	Close to 1 is best
F-measure	$2 * TP/2 * TP + FP + FN$	Close to 1 is best
ROC area	—	Close to 1 is best

TABLE 11: Dance sport movement model recognition accuracy.

	1 (%)	2 (%)	3(%)	4 (%)	5 (%)	6 (%)	7 (%)	8 (%)
Multisensor motion analysis model	98	98.1	98.2	98.4	98.5	98.6	98.6	99
Support vector machine motion analysis model	97	97.2	97.4	97.6	97.7	97.8	97.9	98
Decision tree motion analysis model	96	96.2	96.3	96.4	96.4	96.5	96.7	96.8

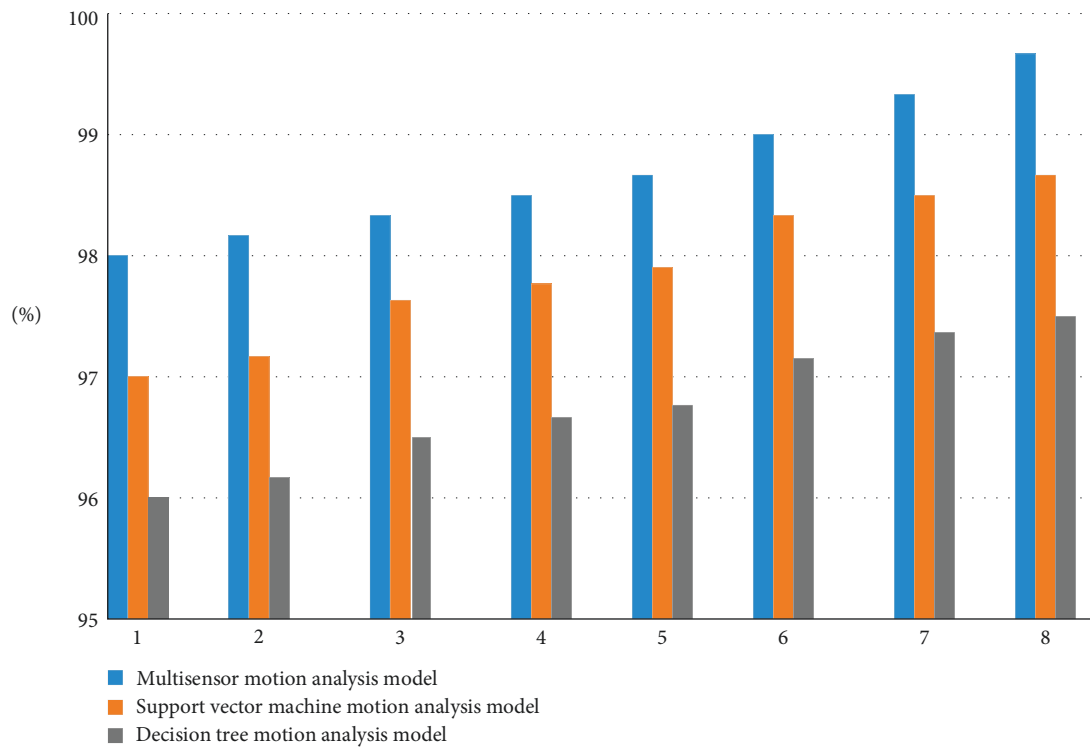


FIGURE 13: Dance sport movement model recognition accuracy.

Weka simulation analysis will also use the working metrics in numerical forecasting to identify and propose each indicator, as shown in Tables 9 and 10.

4.3. Data Results Analysis. According to the experiment, the model of the article is compared with the performance of the support vector machine and the decision tree motion analysis model, and the results of three different models are observed from different aspects of accuracy and page response, and the specific experimental data are shown in Table 11.

As shown in Table 11, 8 images were taken at different distances on the same circuit board; the closest one was set as the template, and the remaining 7 groups of different images were tested to calculate the matching accuracy of various models. The method of detecting the response time of different models is to increase the number of tests and observe the average response time of different models.

As can be seen from Figure 13, among the 8 image samples used in our experiment, the multisensor motion analysis model has the highest accuracy, followed by the vector machine motion analysis model and the decision tree motion analysis model.

5. Conclusion

This paper mainly studies the use of machine learning to predict the timing data of sports dance movements and applies wavelet deformation and static wavelet variation based on the characteristics of time series data in the implementation of the algorithm. Through the implementation of the algorithm of time series data prediction, and then through the acquisition of the action data analysis model, the acquired data is transformed, and then the characteristics of the action are learned, including the encoder-loop unit-decoder (ERD) model. Then, a comparative experiment was conducted to verify this method, and the data collected were analyzed and processed to obtain the advantages of time series data prediction and feature analysis of dances in sport based on machine learning. That is, the action time series data prediction of machine learning is suitable for sports dance moves. However, due to the fact that the structure used does not have a higher level of supervision, the effect is not ideal in some aspects, although some results have been achieved here, but further research can be carried out, for example,

- (1) studying using seq2seq structure;
- (2) a combination of time and space studied using structure-run, a corresponding spatial attention model;
- (3) deeper use of Python and Unity3D for research.

Data Availability

The experimental data used to support the findings of this study are available from the corresponding author upon request.

Conflicts of Interest

The authors declare that they have no conflicts of interest regarding this work.

Acknowledgments

This paper is supported by the Key Project of Teaching Reform in Universities of Hunan Province (HNJG—2021—0106).

References

- [1] M. J. Alizadeh, M. R. Kavianpour, O. Kisi, and V. Nourani, "A new approach for simulating and forecasting the rainfall-runoff process within the next two months," *Journal of Hydrology*, vol. 548, no. 1, pp. 588–597, 2017.
- [2] K. Wang, L. Lin, J. Lu, C. Li, and K. Shi, "PISA: pixelwise image saliency by aggregating complementary appearance contrast measures with edge-preserving coherence," *IEEE Transactions on Image Processing*, vol. 24, no. 10, pp. 3019–3033, 2015.
- [3] Y. Zhao, H. Cheng, and R. Chen, "multi-saliency aggregation-based approach for insulator flashover fault detection using aerial images[J]," *Energies*, vol. 11, no. 2, p. 340, 2018.
- [4] H. A. Ehrenfeucha and A. Kearns, "A general lower bound on the number of examples needed for learning[J]," *Information and Computation*, vol. 82, no. 3, pp. 247–261, 1989.
- [5] R. K. O. H. A. V. I. Bauere, "An empirical comparison of voting classification algorithms: bagging, boosting, and variants[J]," *Machine Learning*, vol. 36, no. 1-2, pp. 105–139, 1999.
- [6] Y. Freund and R. E. Schapire, "A decision-theoretic generalization of on-line learning and an application to boosting," *Journal of Computer and System Sciences*, vol. 55, no. 1, pp. 119–139, 1997.
- [7] R. Avnimelech and N. Intrator, "Boosting regression estimators," *Neural Computation*, vol. 11, no. 2, pp. 499–520, 1999.
- [8] Y. Lecun, L. Bottou, Y. Bengio, and P. Haffner, "Gradient-based learning applied to document recognition," *Proceedings of the IEEE*, vol. 86, no. 11, pp. 2278–2324, 1998.
- [9] D. H. Hubel and T. N. Wiesel, "Receptive fields of single neurons in the cat's striate cortex," *Journal of Physiology*, vol. 148, no. 3, pp. 574–591, 1959.
- [10] K. F. U. K. U. S. H. I. MA. Noncognition, "A self-organizing neural network model for a mechanism of pattern recognition unaffected by shift in position," *J. Biological cybernetics*, vol. 36, no. 4, pp. 193–202, 1980.
- [11] Y. Lecun, Y. Bengio, and G. Hinton, "Deep learning," *Nature*, vol. 521, no. 7553, pp. 436–444, 2015.
- [12] A. Graves and J. Schmidhuber, "Framewise phoneme classification with bidirectional LSTM and other neural network architectures," *Neural Networks*, vol. 18, no. 5-6, pp. 602–610, 2005.
- [13] S. Hochreiter and J. Schmidhuber, "Long short-term memory," *Neural Computation*, vol. 9, no. 8, pp. 1735–1780, 1997.
- [14] J. S. Zhang and X. C. Xiao, "Predicting chaotic time series using recurrent neural network," *Chinese Physics Letters*, vol. 17, no. 2, pp. 88–90, 2000.
- [15] P. Werbos, "Backpropagation through time: what it does and how to do it," *Proceedings of the IEEE*, vol. 78, no. 10, pp. 1550–1560, 1990.

- [16] Z. I Wang, Y. C. Li, and R. Shen, "Correction of soil parameters in calculation of embankment settlement using a BP network back-analysis model," *Engineering Geology*, vol. 91, no. 2-4, pp. 168-177, 2007.
- [17] M. Han, R. Zhang, and M. Xu, "Multivariate chaotic time series prediction based on ELM-PLSR and hybrid variable selection algorithm," *Neural Processing Letters*, vol. 46, no. 2, pp. 705-717, 2017.
- [18] C. Rehman, A. Hosni, and M. Bleyer, "Fast cost-volume filtering for visual correspondence and beyond[J]," *IEEE Transactions on Pattern Analysis and Machine Intelligence*, vol. 35, no. 2, pp. 504-511, 2013.
- [19] F. Y. Wang, "A big-data perspective on AirNet, merton. And an-allistics intelligence," *IEEE Intelligent Systems*, vol. 27, no. 5, p. 2, 2012.
- [20] F. Angiulli, "Hart Pithed Condensed Nearest Neighbor Ulexite," *Trans on In-formation Theory*, vol. 14, no. 3, p. 515, 1968.
- [21] Brighton Hellas Chavannes, "Instance selection for instance-based learning algorithms," *Data Mining and Knowledge Discovery*, vol. 6, no. 2, p. 153, 2002.
- [22] Y. Li and L. Maguire, "Selecting critical patterns based on local geometrical and statistical information.,Maguire selecting critical patterns based on local geo-metrical and statistical information view," *IEEE Transactions on Pattern Analysis and Machine Intelligence*, vol. 33, no. 6, pp. 1189-1201, 2011.
- [23] J. Quevedo and O. Bohemond Alu aces, "A simple and efficient method for VariableR asking according to their usefulness for learning," *Computational Statistics & Data Analysis*, vol. 52, no. 1, pp. 578-595, 2007.
- [24] M. Pal and G. M. Foody, "Feature selection for classification of hyper-spectral data by SVM," *IEEE Transactions on Geoscience and Remote Sensing*, vol. 48, no. 5, pp. 2297-2307, 2010.
- [25] Y. J. Sun, "Todorovich goodison slocan-learning-based features election for high-dimensional data analyssa," *Trans on Pat-tern Analysis and Machine Intelligence*, vol. 32, no. 9, p. 1610, 2010.
- [26] A. O. Franco-Arciga and J. A. Carrasco-Ochoa, "Sánchez-díaz gretel building fast decision trees from large training sets," *Intelligent Data Analysis*, vol. 16, no. 4, p. 649, 201.

Research Article

Efficiency Evaluation and Influencing Factors Analysis of Logistics Industry based on Multiobjective Intelligent Computing

Tingyan Zhou  and Wenxing Li

School of Economics and Management, Beijing Jiaotong University, Beijing 100044, China

Correspondence should be addressed to Tingyan Zhou; zhouty@bjtu.edu.cn

Received 30 May 2022; Revised 30 June 2022; Accepted 15 July 2022; Published 23 August 2022

Academic Editor: Le Sun

Copyright © 2022 Tingyan Zhou and Wenxing Li. This is an open access article distributed under the Creative Commons Attribution License, which permits unrestricted use, distribution, and reproduction in any medium, provided the original work is properly cited.

In logistics industry of 12 provinces along China's new western land-sea corridor from 2010 to 2019, this research employed three-stage SBM model that considers undesirable output to measure logistics industrial efficiency and the panel Tobit model to investigate variables impacting logistics efficiency. The study found that after controlling for environmental variables and statistical noise, the logistics industrial efficiency in China's new western land-sea corridor has improved, and the logistics sector efficiency of each province has spatial variability. Generally speaking, the south part goes up and the north part goes down; industrial structure, logistics transportation intensity, and economic development have a favorable influence on logistics sector efficiency. The urbanization rate, government support level, level of infrastructure, and degree of openness all have a negative influence on efficiency. Finally, relevant policy considerations such as logistics transport intensity, pure technical efficiency, scale efficiency, and external environment are proposed.

1. Introduction

From the mid-1990s to the present, as the economy develops, the logistics industry has developed rapidly. Logistics is an important strategic sector whose development is inseparable from the dynamics of other businesses. Despite China's logistics industry has developed rapidly, due to the continuous improvement of distribution capabilities, the proportion of total social logistics costs as a percentage of GDP has dropped from 18.0% in 1991 to 14.6% in 2017, the proportion remains significantly higher than in industrialized nations like Europe and the United States. The current situation is still a real problem for China's trade [1]. Most earlier studies on the relationship between logistics and economic returns produced biased results regardless of social and environmental concerns. However, the spatial temporal variations in China logistics efficiency are examined with undesired outcomes as well as the impact of other external factors, and the results show that the China's logistics is less efficient but will only improve over time [2].

The growth of the logistics industry of China's new western land-sea corridor will benefit the economy of western China and its surrounding countries, and the new western land-sea corridor may have fostered trade partnerships with other countries, boosting regional growth in western China and Southeast Asia [3]. Therefore, following a comprehensive assessment by a multisector computer model, this paper aims to evaluate system efficiency of the sustainable logistics industry based on combining inputs and desired and undesired outputs.

2. Literature Review

In regional logistics industry efficiency measurement methods, Data Envelope Analysis (DEA) has become the main method, which does not require to define certain production functions and process measurement data, nor specify the weights of the input-output indicators. Markovits-Somogyi and Bokor used the new DEA-PC method (pairwise comparison) to assess logistics efficiency in 29 European nations, and the results were analyzed by

using Logistics Performance Index (LPI) [4]. Zahran et al. evaluated the efficiency of port taxation by using DEA and assessed their income generation mechanisms in terms of efficiency [5]. Lei et al. used the DEA-Malmquist approach to conduct an empirical research of the technical growth of 49 Chinese listed logistics enterprises from 2008 to 2017 [6]. Fried et al. proposed a three-stage DEA to reduce the impact of environment and statistical noise on decision-making units, with the positive objective of reflecting efficiency measurement result [7]. Qin used a three-stage DEA to quantify logistics efficiency in the 9 + 2 urban agglomeration of Guangdong, Hong Kong, and Macao from 2012 to 2018 and concluded that the impact of logistics sector fixed asset investment and the transportation network density on efficiency is extremely important [8].

In order to overcome the bias caused by the radial DEA, slack based measure (SBM) is presented, which considers not only slack variables but also desirable and undesirable outputs to improve efficiency measurement accuracy [9]. Wang and Liu used panel data from the Yangtze River Economic Zone logistics industry between 2005 and 2014 to quantify logistics sector efficiency with the Super-SBM accounting for undesirable output, and the results indicate that measuring logistics efficiency with undesirable output is close to the real distribution process [10]. Feng et al. used panel data of 17 Chinese port listed companies between 2010 and 2015, an empirical analysis is conducted with the SBM model, and conclusions were drawn on their overall operational efficiency [11]. Liu and Sun used the panel data from China's logistics sector between 2004 and 2014 to calculate the Super-SBM and Malmquist models with undesired output and concluded that the total factor productivity with undesired output is more realistic [12]. Ma et al. utilized a three-stage SBM to examine the logistics sector efficiency in Northeast China and six provinces in the "Yangtze River Delta" area from 2011 to 2015, which revealed that the logistics industry's technological efficiency and scale efficiency are higher in the "Yangtze River Delta" area than in the Northeast, and the small size of the logistics industry in the Northeast causes poor efficiency [13].

Some researchers have conducted relevant studies on the elements impacting logistics sector efficiency, and the research methods are mainly divided into three categories: (1) combine DEA and Tobit models to examine specific aspects of logistics efficiency. Zhou et al. analyzed Chinese 3PL enterprises efficiency using DEA and used multiple regression analysis to investigate the factors influencing 3PL efficiency [14]. Wang et al. analyzed China's road logistics efficiency and the elements that influence it and found that the central region has the highest road logistics efficiency and the western region has the lowest, but some western provinces have higher road logistics efficiency, and the level of regional informatization and road logistics resource utilization have the greatest influence on China's road logistics efficiency [15]. Gong et al. examined the effectiveness of China's logistics sector in 2017 and concluded that while there are significant disparities in logistics efficiency among areas, the amount of regional economic growth has minimal

impact on logistics efficiency [16]. (2) Combine three-stage DEA and Tobit model to assess various aspects affecting logistics efficiency. Wong et al. utilized three-stage DEA to examine the efficiency of 77 logistics companies in Singapore and Malaysia between 2012 and 2013, and the Tobit model to examine the elements that impact logistics efficiency [17]. Zhang et al. analyzed the logistics sector efficiency of 19 provinces in the Yangtze River Reserve from 2013 to 2017, concluding that scale efficiency is a key factor influencing total efficiency [18]. (3) Combine SBM and Tobit model to examine the specific aspects affecting influencing logistics efficiency. Tian et al. studied the efficiency and its influencing factors of 90 fresh produce e-commerce enterprises in China from 2016 to 2017 and found that the overall technical efficiency of fresh produce e-commerce enterprises was low, and there was a significant positive effect of IT talent share structure, relationship with partners and logistics infrastructure level on the technical efficiency of fresh produce e-commerce enterprises, while there was a significant negative effect of information technology level [19]. Cao and Deng conducted an empirical analysis on the Yangtze River Economic Zone's logistics efficiency between 2007 and 2016 and analyzed the factors affecting logistics efficiency [20].

Therefore, previous research mostly focuses on the radial DEA or nonradial SBM for assessing the efficiency of logistics industry, without taking into account the influence of environment and statistical noise. Although the three-stage DEA reduces the influence of environmental factors and statistical noise, it ignores undesirable output and cannot guarantee the objectivity of efficiency measurement results. In addition, few studies have been conducted to systematically assess the logistics sector efficiency in China's new western land-sea corridor as the research topic. On this basis, this paper is extended as follows: (1) in the research method, considering the undesirable results, a three-stage SBM model is developed to calculate the logistics sector efficiency, and a panel Tobit model can be used to discuss the main influences elements on logistics sector efficiency. (2) In the research content, from 2010 to 2019, the panel data of logistics industry input-output indicators from 7 provinces, 4 autonomous regions, 1 municipality (henceforth referred to as 12 provinces) along China's new western land-sea corridor are selected for empirical analysis to identify the important influencing factors.

3. Research Design

3.1. Measure Model

3.1.1. Three-Stage SBM Model. The first stage: slack-based measure (SBM) considering undesirable output.

Suppose there are n decision making units (DMU), each unit has x input indicators, y^g desirable output indicators, and y^b undesirable output indicators, assuming matrices $X = [x_1, \dots, x_n] \in R^{m \times n}$, $Y^g = [y_1^g, \dots, y_n^g] \in R^{s_1 \times n}$, $Y^b = [y_1^b, \dots, y_n^b] \in R^{s_2 \times n}$, and $X > 0$, $y^g > 0$ and $y^b > 0$. The equation is as follows:

$$\rho = \min \frac{1 - 1/m \sum_{i=1}^m s_i^- / x_{i0}}{1 + 1/s_1 + s_2 (\sum_{r=1}^{s_1} s_r^g / y_{r0}^g + \sum_{r=1}^{s_2} s_r^b / y_{r0}^b)}$$

$$\text{subject to } \begin{cases} x_0 = X\lambda + s^- \\ y_0^g = Y^g\lambda - s^g \\ y_0^b = Y^b\lambda + s^b \\ s^- \geq 0, s^g \geq 0, s^b \geq 0, \lambda \geq 0. \end{cases} \quad (1)$$

In the above formula: ρ is the efficiency, and $0 \leq \rho \leq 1$; $s^- \in R^m$ is the input slack variable; $s^g \in R^{s_1}$ is the desirable output slack variable; $s^b \in R^{s_2}$ is the undesirable output slack variable; $\lambda \in R^n$ is the weight variable.

The second stage: stochastic frontier analysis(SFA)

The equation is measured as follows by using SFA:

$$s_{ni} = f^n(z_i; \beta^n) + v_{ni} + \mu_{ni}, n = 1, \dots, N, i = 1, \dots, I. \quad (2)$$

Among them, s_{ni} is the slack variable of item n of the i DMU's input; $f^n(z_i; \beta^n)$ is the influence of environmental variables on s_{ni} ; $z_i = (z_{1i}, z_{2i}, \dots, z_{ki})$ is the k environmental variables; β^n is the environmental variables coefficient; v_{ni} is the statistical noise; μ_{ni} is the managerial inefficiency.

Using the results of SFA to alter the input variables, all decision-making units are modified to the similar situations, the equation is as follows:

$$x_{ni}^A = x_{ni} + [\max(f(z_i; \hat{\beta}^n)) - f(z_i; \tilde{\beta}^n)] + [\max(\hat{v}_{ni}) - \tilde{v}_{ni}], n = 1, \dots, N, i = 1, \dots, I, \quad (3)$$

where: x_{ni}^A is the modified input variable, x_{ni} is the original input variable before modification. $[\max(f(z_i; \hat{\beta}^n)) - f(z_i; \tilde{\beta}^n)]$ represents the adjustment for external environmental influences, and $[\max(\hat{v}_{ni}) - \tilde{v}_{ni}]$ represents the adjustment for statistical noise.

The third stage: after adjusting the input variables, carry out the SBM model analysis.

The adjusted input variable x_{ni}^A obtained by formula (3) is used to replace the original input x_{ni} before adjustment, and the first-stage SBM is proposed again to assess the efficiency to obtain the real efficiency after excluding external environmental influences and statistical noise.

3.1.2. Panel Tobit Model. Since the logistics sector efficiency assessed by the SBM in the third stage is in the $[0,1]$ interval, which is not a normal distribution, it does not meet the assumption requirements of OLS for the normal distribution of the explained variables. Therefore, taking the logistics industry efficiency calculated by three-stage SBM model as the dependent variable, and various impacting factors on the logistics industry efficiency are used as independent variables, the equation is as follows:

$$y_i = \begin{cases} y_i^* = X_i' \beta + u_i, & y_i^* > 0, \\ 0, & y_i^* \leq 0, \end{cases} \quad (4)$$

where y_i is the efficiency; y_i^* is the potential dependent variable; X_i' is the independent variable; β is the coefficient; u_i is the statistical noise, $u_i \sim (0, \sigma^2)$

Substitute the variables in Table 1 into formula (4) to construct a panel Tobit model:

$$y_{it} = \beta_0 + \beta_1 X1_{it} + \beta_2 X2_{it} + \beta_3 X3_{it} + \beta_4 X4_{it} + \beta_5 X5_{it} + \beta_6 X6_{it} + \beta_7 X7_{it} + u_{it}. \quad (5)$$

Among them, y_{it} is the logistics industry efficiency; β_0 is a constant term; $\beta_1, \beta_2, \dots, \beta_7$ is the regression coefficient; u_{it} is the statistical noise; $X1_{it}$ is the urbanization rate; $X2_{it}$ is the government support level; $X3_{it}$ is the infrastructure level; $X4_{it}$ is the industrial structure; $X5_{it}$ is the degree of openness; $X6_{it}$ is the logistics transportation intensity; $X7_{it}$ is the economic development; i is the province; t is the time.

3.2. Indicator System. This paper selects indicators of the logistics industry and provides a suite of research indicator systems to assess the efficiency and influencing factors of the logistics sector in China's new western land-sea corridor, as indicated in Table 1.

3.2.1. Input Indicator. Use labor force, capital, and energy as input indicators.

The work force is calculated by adding the total population employed in urban logistics units, urban private logistics firms, and individual logistics sector employees.

The capital stock formula is as follows:

$$K_{it} = K_{it-1} \times (1 - \delta) + \frac{I_{it}}{P_{it}}. \quad (6)$$

Among them, K_{it} and K_{it-1} represent the logistics industry's capital stock in i province in period t and $t - 1$, respectively; K_{i0} represents the logistics industry's capital stock in i province in its base period, divided by 10% of the fixed asset investment in 2010(2010 as the base period); δ represents the capital depreciation rate, which is taken as 9.6% [21]; I_{it} represents the fixed asset investment amount of t period of i province; P_{it} represents the price index of fixed asset investment of t period of i province.

The formula for calculating energy is as follows:

$$E = \sum_{i=1}^{11} (M_i \times P_i). \quad (7)$$

Among them, E represents the total energy consumption of energy after the conversion to standard coal of various types of energy; M_i is the various types of energy involved in the logistics industry; P_i is the reference coefficient for the conversion to standard coal of the i energy.

TABLE 1: Efficiency measurement and influencing factor index system of logistics industry.

Indicator type	Metric name	Metric definitions	Unit
Input	Labor force	People employed in urban units in the logistics industry	10,000 people
	Capital	Logistics industry total social fixed asset investment	100 million yuan
	Energy	Logistics industry energy consumption	10,000 tons of standard coal
Desirable output	Value added	Logistics industry value added	100 million yuan
Undesirable output	CO ₂ emissions	CO ₂ emissions from the logistics industry	10,000 tons
Environmental variables	Economic condition	Gross domestic product (GDP)	100 million yuan
	Computerization development level	The mobile phone users at the end of the year	10,000 households
	Industrial market structure	The amount of registered legal entities in the logistics sector	Piece
	Import and export	Total import and export	Billion dollars
Influencing factors	Urbanization rate	Urban population/total population	%
	Government support level	Financial expenditure of the logistics industry/fiscal general budget expenditure	%
	Infrastructure level	Length of transportation route/land area	km/km ²
	Industrial structure	Added value of tertiary industry/GDP	%
	Degree of openness	Total import and export/GDP	%
	Logistics transportation intensity	Total turnover of the logistics industry/GDP	Tons of km/yuan
	Economic development	Real GDP per capita	Chinese yuan/person

3.2.2. *Output Indicator.* Value added and carbon dioxide emissions are used as output indicators. Value added represents the desirable output and is processed by using the GDP deflator (2010 as the base period). Carbon dioxide emissions represent undesirable output and are computed as the sum of the logistics industry's energy consumption with the emission factors provided by IPCC 2006 Guidelines.

3.2.3. *Environmental Variables.* Complex environmental factors affect the efficiency of the logistics industry, but they are independent of the logistics industry itself. Four indicators are selected as environmental variables: economic condition, computerization development level, industrial market structure, import and export. Considering the availability of relevant indicators and the requirements of indicator selection, GDP is selected as the surrogate variable for economic condition, the mobile phone users at the end of the year is selected as the surrogate variable for computerization development level, the amount of registered legal entities in the logistics sector is selected as the surrogate variable for industrial market structure, and total import and export is selected as the surrogate variable for import and export.

3.2.4. *Influencing Factors.* Seven factors influencing logistics sector efficiency are selected: urbanization rate, government support level, infrastructure level, industrial structure, logistics transportation intensity, degree of openness, and economic development.

- (1) Urbanization rate (X1): with the development of spatial structure and economic structure, the strong agglomeration of industries and population in the

urbanization process and the change in distribution cost of logistics industry will affect the agglomeration of logistics industry. This paper describes the urbanization rate in terms of the share of urban population to overall population in each province.

- (2) Government support level (X2): the government can improve logistics infrastructure by providing effective logistics development strategies and financial support. At the same time, ineffective government intervention has also delayed the improvement of logistics competitiveness to a certain extent. This article reflects the level of government support through the ratio of logistics industry fiscal expenditure to the general budget expenditure of each province.
- (3) Infrastructure level (X3): the construction of transportation infrastructure network can improve the service capacity of the logistics sector. The ratio of the sum of railroad mileage, inland waterway mileage, and road mileage of each province to the area of each province is chosen to reflect the degree of infrastructure in each province.
- (4) Industrial structure (X4): the service demand for logistics industry in the tertiary industry exceeds that in the secondary sector, and the logistics sector demand composition is constantly changing. This paper selects the proportion of tertiary sector added value to GDP in each province to represent the industrial structure.
- (5) Degree of openness (X5): the expansion of the degree of openness can improve the level of local logistics technology and management, which in turn affects the logistics industry efficiency. The ratio of total exports and imports to GDP in each province is selected to represent the level of openness.

- (6) Logistics transportation intensity (X6): this paper selects the ratio of the total logistics turnover to the GDP of each province to represent the logistics transportation intensity.
- (7) Economic development (X7): the development of regional economy can provide relevant supporting facilities, human resources, scientific and technological foundation for the logistics industry, which in turn effects the logistics sector efficiency. This study utilizes real GDP per capita to assess the economic progress of each province.

3.3. Data Analysis. This paper selects the transportation, warehousing, and postal industries of 12 provinces along China's new western land-sea corridor between 2010 and 2019 as the research object to study the logistics industry. Tibet is excluded from the research scope owing to lack of statistics data. All research data came from the National Bureau of Statistics' website and the China Energy Statistical Yearbook (see Table 2 for details).

The correlation test of input and output indicators of logistics industry was carried out by stata16, the correlation coefficients are positive and pass the test at 1% significance level, which indicates that the indicators are reasonably chosen. Table 3 displays the results.

4. Three-Stage SBM Model Results and Analysis

4.1. The First Stage. Based on the input-oriented SBM, MaxDEA Pro8 is used to assess the logistics sector efficiency in China's new western land-sea corridor between 2010 and 2019, as shown in Table 4. Technological efficiency, pure technological efficiency, and scale efficiency have averages of 0.71, 0.84, and 0.85, respectively, all of which do not reach DEA effectiveness. By province, the logistics industry's uneven development is more prominent, and its efficiency level varies greatly. The top three logistics industry efficiency averages are Ningxia, Inner Mongolia, and Shaanxi, all above 0.9, close to the frontier of efficiency levels. The bottom three logistics industry efficiency averages are Hainan, Qinghai, and Sichuan, which are all below 0.6. Among them, the explanation for Sichuan and Qinghai's poor average technical efficiency is low scale efficiency, while the low technical efficiency in Hainan is due to the low pure technical efficiency. Only five provinces have an average technical efficiency of more than 0.71, namely Ningxia, Inner Mongolia, Shaanxi, Gansu, and Guizhou, most of which are located in the northern portion of the new western land-sea corridor.

4.2. The Second Stage. Based on the SFA, the explained variables are the input slack variables collected in the first stage, as well as four environmental elements, namely, GDP, the mobile phone users at the end of the year, the amount of registered legal entities in the logistics sector, and total import and export are used as explanatory variables, and the frontier4.1 is used to examine whether environmental factors have a considerable influence on input slack variables. Table 5 displays the results.

From Table 5, it can be concluded that:

Economic condition: the economic condition represented by GDP is negatively associated with all three slack factors and passes the significance test. It shows that improving economic conditions can minimize input redundancy of capital stock, employees, and energy consumption, and reasonable deploy of resources to increase the overall logistics business efficiency.

Computerization development level: the level of computerization represented by the mobile phone users at the end of the year is positively correlated with the slack variables "fixed assets" and "energy consumption," and negatively correlated with the slack variable "employees," all of which pass the test at the 1% statistical significance. It demonstrates that an increase in phone users at year end can result in increase in input redundancy of capital stock and energy consumption, resulting in inefficient allocation of capital and energy, while reducing the redundancy of employee input and making the employee input more reasonable.

Industrial market structure: the industrial market structure, represented by the amount of registered legal entities in the logistics sector, is positively correlated with the slack variable of energy consumption and negatively correlated with the slack variable of capital stock, both of which pass the test at the 1% significance level. There is no significant relationship with the slack variable of employees. This shows that the increase in the number of registered legal entities in the logistics sector may lead to inefficient energy consumption and more rational allocation of capital.

Import and export: total imports and exports is positively correlated with the slack variable of employees and energy consumption, and they pass the 1% significance test. It indicates that increasing import and export can lead to redundancy of employees and energy consumption, resulting in unreasonable input of employees and inefficient use of energy in the logistics industry.

4.3. The Third Stage. The second stage's modified input variables and the first stage's initial outputs are fed to the SBM of the first stage for calculation and give the real logistics industry efficiency. Table 6 displays the results.

The third-stage logistics industry efficiency in different provinces is shown in Figure 1:

By province, there are obvious disparities in the logistics sector efficiency before and after the adjustment of each province. Inner Mongolia and Shaanxi's logistics sector efficiency always remains at the forefront. The technical efficiency in Ningxia, Hainan, Qinghai, Gansu, and Guizhou declines, and the technical efficiency of Chongqing, Guangxi, Sichuan, Yunnan, and Xinjiang improves. This shows that the first-stage SBM does not consider the impact of environmental factors and statistical noise; it is

TABLE 2: Descriptive statistics of the efficiency measurement and influencing factors.

Indicator type	Metric name	Sample size	Average value	Standard deviation	Minimum	Maximum
Input	Labor force (100 million yuan)	120	7893.05	5676.19	1188.36	29314.7
	Capital (10,000 people)	120	342.86	259.79	46.5	1175.5
	Energy (10,000 tons of standard coal)	120	728.79	391.62	110.77	1715.84
Desirable output	Value added (100 million yuan)	120	533.16	330.82	70.7	1473.1
Undesirable outputs	CO ₂ emissions (10,000 tons)	120	1793.21	958.19	285.35	4083.73
	Economic condition (100 million yuan)	120	10829.42	8099.97	1144.2	43169.27
Environment elements	Computerization development level (10,000 households)	120	2670.01	1800.94	290.3	9443.5
	Industrial market structure (piece)	120	5623.53	4161.65	471	19283
	Import and export (billion dollars)	120	241.01	235.78	5.45	984.01
Influencing factors	Urbanization rate (%)	120	0.5	0.07	0.34	0.67
	Government support level (%)	120	0.08	0.02	0.04	0.16
	Infrastructure level (km/km ²)	120	0.62	0.46	0.09	2.20
	Industrial structure (%)	120	0.51	0.05	0.35	0.63
	Degree of openness (%)	120	0.12	0.09	0.01	0.44
	Logistics transportation intensity (tons km/yuan)	120	0.26	0.14	0.06	0.65
	Economic development (yuan/person)	120	35137.26	12264.26	12882.00	71333.96

TABLE 3: Pearson correlation analysis on input-output indicators.

Input-output indicators	Logistics industry total social fixed asset investment	People employed in urban units in the logistics industry	Logistics industry energy consumption
Logistics industry value added	0.873***	0.815***	0.874***
CO ₂ emissions from the logistics industry	0.870***	0.712***	0.998***

Note.*** means significant at the 1% level.

TABLE 4: First-stage logistics industry efficiency.

Province	Technical efficiency	Ranking	Pure technical efficiency	Ranking	Scale efficiency	Ranking
Inner Mongolia	0.913	2	1	1	0.913	3
Guangxi	0.656	7	0.752	9	0.879	8
Hainan	0.581	10	0.699	10	0.825	10
Chongqing	0.685	6	0.831	6	0.847	9
Sichuan	0.532	12	0.817	8	0.671	11
Guizhou	0.740	5	0.817	7	0.907	5
Yunnan	0.615	9	0.669	12	0.901	6
Shaanxi	0.855	3	0.956	4	0.899	7
Gansu	0.796	4	0.882	5	0.908	4
Qinghai	0.544	11	0.972	3	0.560	12
Ningxia	0.961	1	1	1	0.961	1
Xinjiang	0.645	8	0.688	11	0.931	2
Maximum	0.961		1		0.961	
Minimum	0.532		0.669		0.560	
Average	0.71		0.84		0.85	

Note. Provincial averages for technical efficiency, pure technical efficiency, and scale efficiency range from 2010 to 2019.

responsible for underestimating the logistics sector efficiency in some provinces with better environment. The logistics sector efficiency in better-off provinces cannot objectively reflect the real level of logistics industry efficiency. Environmental variables in different provinces have different effects on the technical efficiency of the logistics industry. After controlling for environmental factors and statistical noise, the largest changes in technical efficiency

rankings include Sichuan (up 6 places) and Ningxia (down 8 places); the largest changes in pure technical efficiency rankings include Hainan (up 4 places), Chongqing, Sichuan, and Guizhou (down 2 places); and the largest changes in scale efficiency rankings include Chongqing (up 6 places) and Ningxia (down 9 places). Among them, the technical efficiency improvement areas are Sichuan, Yunnan, Chongqing, Guangxi, Guizhou, Inner Mongolia, Shaanxi,

TABLE 5: SFA regression results in the second stage.

Variable	Slack variable in capital stock	Employee slack variable	Slack variable in energy consumption
Constant term	-550.08 (-1.58)	12.75 (0.9)	8.63 (0.5)
GDP	-12170.52***(-15.18)	-421.26*(-1.74)	-2824.5***(-6.7)
The mobile phone users at the end of the year	78220.58***(177.01)	-599.99***(-2.74)	2161.98***(5.13)
The amount of registered legal entities in the logistics sector	-1778.34***(-4.29)	-415.43(-0.71)	3468.94***(4.95)
Total import and export	296.32(0.34)	415.78***(6.41)	231.79***(3.01)
Sigma-squared	6601762.7***(2627652.00)	13050.99***(66.78)	36212.3***(6556.07)
Gamma	0.53***(7.65)	0.58***(10.71)	0.73***(20.83)
Log likelihood function	-1076.76	-717.98	-740.05
LR test of the one-sided error	34.03***	31.77***	57.28***

Note. *, **, *** indicate significant at 10%, 5%, and 1%, respectively, with the *t*-value enclosed in brackets.

TABLE 6: Third-stage logistics industry efficiency.

Province	Technical efficiency	Ranking	Pure technical efficiency	Ranking	Scale efficiency	Ranking
Inner Mongolia	1	1	1	1	1	1
Guangxi	0.904	4	0.976	7	0.926	4
Hainan	0.401	11	0.979	6	0.409	11
Chongqing	0.917	3	0.961	8	0.953	3
Sichuan	0.792	6	0.931	10	0.860	6
Guizhou	0.704	7	0.955	9	0.738	7
Yunnan	0.795	5	0.899	12	0.886	5
Shaanxi	0.969	2	0.984	5	0.985	2
Gansu	0.701	8	0.989	4	0.708	9
Qinghai	0.259	12	0.997	3	0.259	12
Ningxia	0.697	9	1	1	0.697	10
Xinjiang	0.665	10	0.921	11	0.723	8
Maximum	1		1		1	
Minimum	0.259		0.899		0.259	
Average	0.734		0.966		0.762	

Note. Provincial averages for technical efficiency, pure technical efficiency, and scale efficiency range from 2010 to 2019.

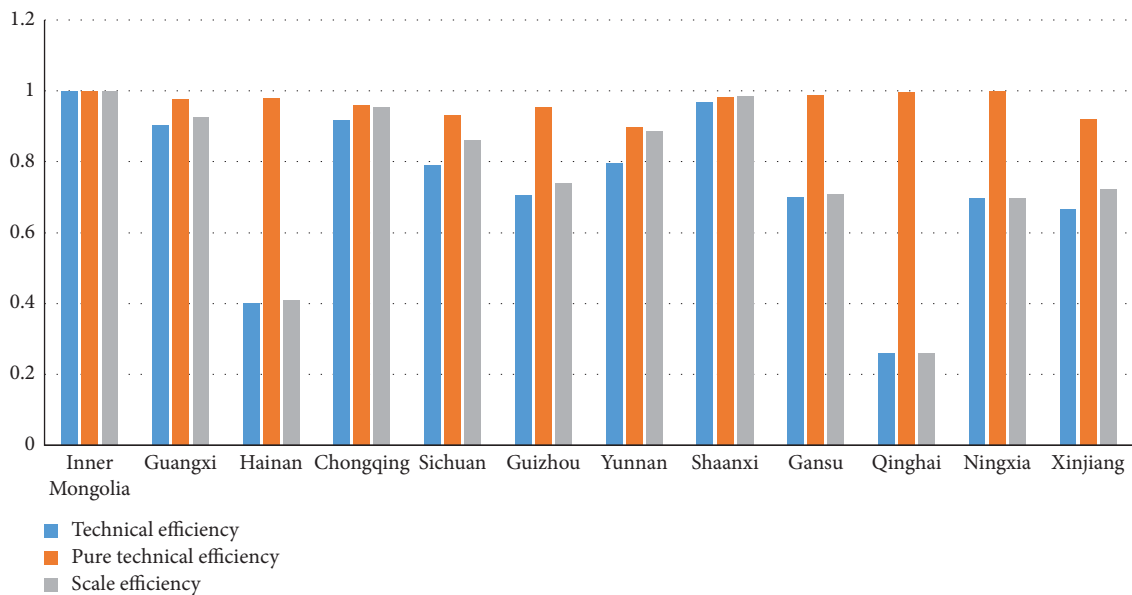


FIGURE 1: Third-stage logistics industry efficiency.

and the pure technical efficiency areas are Hainan, Guangxi, Gansu, maintaining the original ranking of Inner Mongolia, Yunnan, Qinghai, Ningxia, and Xinjiang, and scale efficiency

ranking changes in Chongqing, Sichuan, Guangxi, Inner Mongolia, and Yunnan were the provinces with the highest efficiency levels, and Qinghai maintains the original ranking.

TABLE 7: Regression results of influencing factors on logistics industry efficiency.

y_{it}	Coef.	Std. Err.	z	$P > z$
Urbanization rate	-3.5985***	1.121	-3.21	0.001
Government support level	-0.4964	0.588	-0.84	0.398
Infrastructure level	-0.3267*	0.187	-1.75	0.081
Industrial structure	0.5721	0.467	1.23	0.22
Degree of openness	-0.5664*	0.305	-1.86	0.063
Logistics transportation intensity	1.0097***	0.192	5.25	0
Economic development (take logs)	0.5113***	0.169	3.02	0.003
Constant term	-2.9876**	1.247	-2.4	0.017
Log likelihood	34.2272			
Prob > chi2	0			

Note. *, **, *** indicate significant at 10%, 5%, and 1%, respectively.

The average technical efficiency in Guangxi has adjusted from 0.656 to 0.904, mainly due to pure technological efficiency improvement. Chongqing's average technological efficiency has increased from 0.685 to 0.917, mainly due to the improvements in both pure technological efficiency and scale efficiency. Qinghai and Ningxia's technological efficiency have decreased from 0.544 to 0.961 before adjustment to 0.259 and 0.697 after adjustment, respectively. The pure technical efficiency of the two provinces has been at the production frontier, so the reduction in technical efficiency is mostly related to the reduction in scale efficiency. The phenomenon of high technical efficiency in the first stage is partly due to external environmental variables. Hainan, Guizhou, Gansu, and Xinjiang have improved their pure technological efficiency, while their scale efficiency has declined, leading to a slight drop in logistics industry efficiency, showing that external environmental variables have not significantly driven the logistics sector development. The average technical efficiency of 6 provinces of Inner Mongolia, Shaanxi, Chongqing, Guangxi, Yunnan, and Sichuan exceeds 0.734, most of which are located in the southern half of the new western land-sea corridor.

5. Analysis of Influencing Factors

Panel Tobit model regression is performed by Stata16, and the results are shown in Table 7.

- (1) The effect of urbanization rate: the urbanization rate has significantly negatively correlated with the logistics sector efficiency. If the proportion of urban population to the total population in each province increases by 1 unit, the efficiency of the logistics sector will decrease by 3.5985, which means that the logistics industry's efficiency cannot be significantly improved as the urban population grows. Although the provinces of the new western land-sea corridor are accelerating the process of new urbanization, it will take a long time to push the growth of regional large logistics hubs and intracity logistics systems.
- (2) The influence of government support level: the degree of government funding has no obvious negative impact on logistics business efficiency. If the share of fiscal expenditure on the logistics sector in the

general budget expenditure of each province increases by 1 unit, the efficiency of the logistics sector will decrease by 0.4964, indicating that there is no positive relationship between the government's fiscal expenditure on logistics industry and logistics business efficiency. Despite significant investments in logistics infrastructure by local governments, the logistics business in various provinces remains unequal.

- (3) The impact of infrastructure level: the transportation infrastructure network has a considerable negative impact on the logistics sector efficiency. If the share of the length of transport lines to the national territory in each province increases by 1 unit, the logistics sector efficiency will decrease by 0.3267. It shows that the increase in infrastructure construction cannot considerably enhance logistics sector efficiency. The convenient transport infrastructure network can help the logistics sector more efficient, but the redundant construction of the transport infrastructure will waste logistics resources.
- (4) The effect of industrial structure: the impact of industrial structure on logistics sector efficiency is not significant. If the share of value added in the services sector to GDP in each province increases by 1 unit, the efficiency of logistics industry will increase by 0.5721. This suggests that the industrial structure will lead to an increase in the efficiency, but the impact is not prominent. The development of the service sector contributes to service innovation in the logistics sector, the continuous satisfaction of different logistics services needs, and the continuous optimization of the resource allocation.
- (5) The impact of the degree of openness: the degree of openness has a considerable adverse influence on the logistics sector efficiency. If the share of total import and export to GDP of each province increases by 1 unit, the logistics sector efficiency will decrease by 0.5664. The majority of new western land-sea corridor is located in China's interior and its openness to the outside world is not high, which affects the flow of production factors and leads to the decrease of logistics sector efficiency.

- (6) The impact of logistics transportation intensity: logistics transportation intensity has a strong positive influence on logistics sector efficiency, when the ratio of total logistics turnover to GDP in each province increases by 1 unit, logistics sector efficiency increases by 1.0097. It indicates that the growth of logistics sector along the new western land-sea corridor should increase the value added while decreasing energy consumption of logistics industry by improving transportation intensity.
- (7) The influence of economic development: the economic development of each province has a substantial positive impact on the logistics sector efficiency, when each province's GDP per capita increases by 1%, the logistics sector efficiency increases by 0.5113%, implying that economic development leads to the improvement of logistics efficiency. Provinces with high level of economic development have a stable industrial base and sound industrial structure, which in turn promote the improvement of logistics industry efficiency.

6. Conclusion and Suggestion

Based on the growth of the logistics sector in 12 provinces of China's new western land-sea corridor from 2010 to 2019, this paper has introduced a three-stage SBM model considering nonradial, nonoriented, and undesirable output to make quantitative analysis of logistics efficiency and analyzes the influencing factors of logistics efficiency by using panel Tobin model and gets the following conclusions:

First, there are spatial variability of the logistics industry efficiency among provinces. From 2010 to 2019, except for Inner Mongolia, where the logistics sector's adjusted efficiency was at the production frontier. The logistics sector's efficiency in other provinces was uneven. The adjusted logistics sector efficiency of Shaanxi and Chongqing remains stable, while the logistics sector efficiency of Qinghai, Xinjiang, and Hainan was weak.

Second, the influence of environmental variables on logistics sector efficiency is diverse. Economic condition, computerization development level, industrial market structure, and import and export have a significant influence on logistics sector efficiency. There seem to be significant differences in logistics sector efficiency before and after adjustment.

Third, the panel Tobit model regression results indicate that industrial structure, logistics transportation intensity and economic development have positive effects on logistics sector efficiency, while urbanization rate, government support, infrastructure level, and degree of openness have negative effects on logistics business efficiency. Urbanization rate, infrastructure level, degree of openness, logistics transportation intensity, and economic development have significant effects on logistics industry efficiency, while government support and industrial structure have little effects on logistics industry efficiency.

In light of the findings, the following proposals are made in this paper:

The first is to improve current logistics transportation intensity of China's new western land-sea corridor. Promote the development of multimodal transit and land-sea intermodal transportation by railroad, highway, and waterway; support inland transport to speed up the adjustment of the transport structure; and increase the proportion of railway and waterway cargo transportation to the total freight volume. Rail and river transport for bulk transport has significantly reduces the cost of transporting raw materials, freight, and port transportation promote and facilitates the development of railway container distribution centers through rail-sea combined transportation and international trains, and strengthen intracorridor and cross-corridor cooperation. Ensure the smooth flow of the Southbound international railway and sea transport; promote the development of ports; improve the service level; formulate practical customs policies; and improve the comfort of pass customs.

The second is to improve the pure technological efficiency and scale efficiency of the logistics sector in the new western land-sea corridor. Make full use of the opportunity of creating "new infrastructure"; implement digital and intelligent logistics systems; expand the scope of information exchange; and improve the capabilities of logistics enterprises. Establish intelligent logistics industrial park; combine logistics with production factor policies; and develop the scale and benefits of logistics industrial parks.

Third, create a good external environment for logistics development in China's new western land-sea corridor. Considering the heterogeneity among environmental variables in different provinces, the change of environmental variables leads to significant changes in logistics efficiency in different provinces. All provinces should combine their own advantages, take enterprises as the main body under the leadership of the state, plan and standardize logistics industry growth, formulate and improve the logistics sector strategy, and promote the growth and introduction of green technology.

Data Availability

The experimental data used to support the findings of this study are available from the corresponding author upon request.

Conflicts of Interest

The authors declared that they have no conflicts of interest regarding this work.

References

- [1] Z. G. Chen, J. H. Du, and H. Li, "Industrial influence effect of logistics industry and its policy enlightenment-empirical study based on panel data of 35 large and medium-sized cities in China," *China Business And Market*, vol. 32, no. 12, pp. 31–40, 2018.
- [2] L. Tan, Q. Wu, and Q. Li, "A panel analysis of the sustainability of logistics industry in China: based on non-radial

- slacks-based method,” *Environmental Science and Pollution Research*, vol. 26, no. 10, 2019.
- [3] X. N. Cong, “Effect of the new western land-sea corridor and corresponding regional cooperation mechanism,” *Chinese Soft Science*, vol. 36, no. 02, pp. 65–78, 2021.
- [4] R. Markovits-Somogyi and Z. Bokor, “Assessing the logistics efficiency of European countries by using the DEA-PC methodology,” *Transport*, vol. 29, no. 2, pp. 137–145, 2014.
- [5] S. Z. Zahran, J. B. Alam, A. H. Al-Zahrani, Y. Smirlis, S. Papadimitriou, and V. Tsioumas, “Analysis of port authority efficiency using data envelopment analysis,” *Maritime Economics & Logistics*, vol. 19, no. 3, pp. 518–537, 2017.
- [6] X. Q. Lei, J. J. Yang, J. B. Zou, and Me Zhuang, “Research on the impact of logistics technology progress on employment structure based on DEA-malmquist method,” *Mathematical Problems in Engineering*, vol. 2020, no. 12, Article ID 7064897, 10 pages, 2020.
- [7] H. O. Fried, C. A. K. Lovell, S. S. Schmidt, and S. Yaisawarng, “Accounting for environmental effects and statistical noise in data envelopment analysis,” *Journal of Productivity Analysis*, vol. 17, no. 1/2, pp. 157–174, 2002.
- [8] W. Qin, “Spatial-temporal evolution and improvement path of logistics industry efficiency in Guangdong-HongKong-Macao Greater Bay Area,” *China Business And Market*, vol. 34, no. 09, pp. 31–40, 2020.
- [9] K. Tone, “Dealing with Undesirable Outputs in DEA: A Slacks-Based Measure (SBM) approach,” *GRIPS Research Report Series*, vol. 2003, 2003.
- [10] Y. H. Wang and Q. Liu, “Research on logistics efficiency measurement of Yangtze River Economic Belt based on super-SBM model,” *East China Economic Management*, vol. 31, no. 05, pp. 72–77, 2017.
- [11] F. Feng, L. Chen, and H. Huang, “Research on the measurement and promotion path of the efficiency of China’s port listed companies—based on SBM-DEA model,” *China Business And Market*, vol. 31, no. 06, pp. 106–112, 2017.
- [12] Z. Y. Liu and X. L. Sun, “Spatial and temporal evolution of green total factor productivity in China’s logistics industry and causes analysis,” *Soft Science*, vol. 32, no. 04, pp. 77–81+114, 2018.
- [13] M. Ma, L. Tang, and Y. Liu, “Comparison of logistics industry efficiency between Northeast and Yangtze River Delta regions,” *Journal of Beijing University of Technology*, vol. 18, no. 03, pp. 54–60, 2018.
- [14] G. Zhou, H. Min, C. Xu, and Z. Cao, “Evaluating the comparative efficiency of Chinese third-party logistics providers using data envelopment analysis,” *International Journal of Physical Distribution & Logistics Management*, vol. 38, no. 4, pp. 262–279, 2008.
- [15] C. H. Wang, J. Zhang, and Y. Ding, “Efficiency measurement of China’s road transport logistics and the determinants analysis,” *Journal of Applied Sport Management*, vol. 37, no. 02, pp. 318–328, 2018.
- [16] Y. L. Gong, J. X. Wang, and F. Y. Feng, “A study on the measurement of regional logistics efficiency and its influencing factors—based on DEA and Tobit model,” *Jiangxi Social Sciences*, vol. 39, no. 10, pp. 72–80, 2019.
- [17] W. P. Wong, K. L. Soh, C. L. Chong, and N. Karia, “Logistics firms performance: efficiency and effectiveness perspectives,” *International Journal of Productivity and Performance Management*, vol. 64, no. 5, pp. 686–701, 2015.
- [18] Y. N. Zhang, Z. Q. Liu, and H. X. Ouyang, “A comprehensive study on the efficiency of the regional logistics industry in a low carbon environment—an empirical analysis based on 19 provinces in Yangtze River protection area,” *Modernization of Management*, vol. 40, no. 02, pp. 33–40, 2020.
- [19] G. Tian, M. Zhang, and Z. W. Li, “The technical efficiency and its influencing factors of fresh agricultural product e-suppliers: an empirical study based on improved DEA method and Tobit model,” *Journal of Hunan Agricultural University*, vol. 19, no. 05, pp. 80–87, 2018.
- [20] B. R. Cao and L. J. Deng, “Influencing factors of logistics industry growth efficiency in Yangtze River Economic Belt,” *Economic Geography*, vol. 39, no. 07, pp. 148–157, 2019.
- [21] J. Zhang, G. Y. Wu, and J. P. Zhang, “The estimation of China’s provincial capital stock:1952–2000,” *Economic Research Journal*, vol. 39, no. 10, pp. 35–44, 2004.

Research Article

Lightweight Deep Learning Model for Marketing Strategy Optimization and Characteristic Analysis

Yang Su , Chonghong Wang, and Xuejiao Sun

Yantai Institute of Technology, School of Economics and Management, Yantai 264005, China

Correspondence should be addressed to Yang Su; suyang@yitsd.edu.cn

Received 5 May 2022; Revised 12 July 2022; Accepted 18 July 2022; Published 23 August 2022

Academic Editor: Le Sun

Copyright © 2022 Yang Su et al. This is an open access article distributed under the Creative Commons Attribution License, which permits unrestricted use, distribution, and reproduction in any medium, provided the original work is properly cited.

The business model of traditional market is declining day by day, and people's consumption cognition has risen to a new level with the leap in science and technology. Enterprises need to adjust and optimize their marketing strategies in time according to the new consumption characteristics, so as to smoothly adapt to the environmental changes in the Internet age. This paper briefly analyzes the relationship between sales development and psychology and constructs a fusion model that can predict preferences with the help of neural network structure of the deep learning method. Describe user portraits and characteristics, analyze users' purchasing behavior and credit literacy, and push related products combined with a hash algorithm to achieve accurate e-commerce marketing purposes. The results show that (1) the model constructed in this paper and five different models are used for multi-modal recognition analysis: the accuracy is 79.56%, the recall rate is 77.43%, F1 is 0.785, and the error value can be reduced to about 0.18 by epoch iteration; the model is superior and has great use value. (2) Using the model to extract user attribute features and predict certain preferences, 13 topics and weight ratios are obtained for users of a certain platform, and the portrait model of each user is constructed. (3) According to the portrait optimization, 8 different marketing strategies are obtained, and the marketing effect is remarkable, fluctuating between 69% and 82%, and the income situation is also satisfactory. The final model design is reasonable and the data performance is good, which provides an intelligent and efficient dynamic strategy service for enterprises.

1. Introduction

In the era of information explosion, the way of computer communication technology has changed, and people can complete the whole process of challenging, pricing goods or services without going out on the material platform and interconnected financial service. It is also a big challenge for each attempt to move the market. Consumers have more information channels. They no longer pay more attention to the sales promotion of merchants but pay more attention to the sexual price and sufficient demand for goods themselves. They also tend to pursue new things and expect 24-hour all-round service. Due to the shift of the focus of purchasing characteristics, which drives the shift of marketing focus, enterprises need to cater to the psychology of users and formulate different strategies for different users. However, relying solely on the strength of enterprise decision-making

and marketing personnel cannot cope with the massive user data, and it is easy to miss the market outlet and lose the opportunity to expand the reputation and influence of enterprises. Therefore, adhering to the concept of innovation and development, we collect relevant information for reference.

Design a multi-level network structure model, according to the data-driven and key characteristics of the development of gas station marketing strategy, and forecast oil sales [1]. Using the PaaS platform of Kubernetes container to construct TensorFlow container, unified resource scheduling management, and API access control service architecture [2]. Using stuttering word segmentation algorithm, SIFT method, PGBN deep learning model, and Gibbs up-down sampling method, an accurate marketing push is realized [3]. DCNN is used to extract feature vectors, regression analysis method is used to evaluate face value, and personalized products and services are output [4]. Based on the deep

learning of Maker Space as the carrier, the marketing major designs experimental teaching [5]. This paper studies the formation mechanism of marketing dynamic capability of international enterprises from the perspective of knowledge [6]. Combined with the characteristics and teaching experience of marketing specialty, this paper explores [7]. Neural marketing based on brain waves, combined with five 3D CNN and multi-layer LSTM prediction models, predicts consumers' preference for products [8]. By establishing a fusion model, artificial feature screening, and tree model for various machine learning algorithms, new ideas are provided for judging users' financial consumption behavior [9]. Test the combination form and effectiveness of graphic information, and explore the influence of consumer behavior and brand relationship [10]. Provide personalized recommendation service for consumers through multi-source big data recommendation system [11]. Using DCNN to learn binary hash coding, large-scale image retrieval is completed in low-dimensional Hamming space [12]. Logistic equations and particle swarm optimization algorithms are introduced to evolve and predict the time series of Internet communication behavior [13]. Based on the three mobile Internet portals of WeChat, Weibo, and APP, this paper studies the optimization of marketing strategy on railway lines [14]. CiteSpace software analyzes business intelligence at home and abroad, and measures management decisions and technology applications [15].

Based on the description of the above literature, this topic has a large number of theoretical basis and experimental ideas that can be used for reference. Change the marketing strategy into online mode, read the text, images, audio, and other contents of the network, and deal with the relevance of dynamic data with the help of business characteristics and users' consumption habits. Describe the user consumption portrait, and build a prediction model with mixed DCNN and LSTM neural network structure. In addition, a recommendation framework based on deep hash is introduced as a supplement, hoping to bring users a better experience and achieve more accurate marketing methods than traditional methods.

2. Theoretical Basis

2.1. Marketing Strategy. Marketing Strategy [16]; this kind of enterprise activity is mainly organized and operated in a planned way for the market, and obtains sales volume, purchasing power information, and industry prestige value according to various needs and past experience of certain target customers, including comprehensive strategies such as price, promotion, channel, and public relations. Marketing is a means that people, who receive news accept and appreciate the products, services, and benefits introduced and promoted by enterprises. Its main purpose is to make products accepted by consumers, provide customers with satisfactory goods or required services, improve the purchase and use effect, and at the same time establish a brand effect. Because this is a dynamic and changing process, decision-makers need to adjust, create and make plans repeatedly with the changes in the market. Use the 4P principle [17]; according

to the actual situation, we should optimize the strategic policy, selectively capture the target market, enhance the competitiveness, and strive to obtain the best economic results with the least input cost in the big environment. Focusing on the seven characteristics of marketing, such as purpose, foresight, uncertainty, systematicness, creativity, debugging, and dynamics, we can carry out effective marketing according to the types and characteristics of different markets.

2.2. Overview of Deep Learning. The realization of AI is inseparable from the application of deep learning (DL), which belongs to the extension of machine learning (ML) in AI field. It comes from researchers' exploration of ANN, that is, simulating and approximating biological neural networks. DL can be simply understood as feature learning or representation learning. Through multi-level processing, DL represents features from low level to the high level and completes complex learning tasks such as classification and recognition. Taking the deep learning structure of multi-layer perceptron as an example, it is composed of multiple hidden layers, which can solve the problem of linear indivisibility of a single layer. DL [18] is a general name for a class of pattern analysis methods; it mainly involves CNN [19], Autoencoder [20], and DBN [21]. In recent years, in order to have a deeper understanding of the characteristics and practical applications of DL, researchers have chosen to combine the three methods, which not only increase the parameters but also increase the training difficulty of the model. However, compared with the traditional models, these new fusion models have achieved excellent performance. This paper trains the hybrid network model of DCNN and LSTM to deal with complex transactions.

2.3. Deep Convolution Neural Network. Convolution neural network is a kind of feedforward neural network [22]. It is a hierarchical structure, and each convolution layer contains a certain number of convolution kernels. When the convolution layer and the pooling layer interact with each other, the features of the entered data are extracted, the data features are mapped and the output dimension size is reduced. Scholars represented by LeCun designed and trained the classical LeNet-5 model based on the principle of neural cognitive machine and BP algorithm. As the most classical CNN structure, many subsequent works need to improve this model to achieve. Using DCNN of VGGnet series and using multiple nonlinear feature extraction stages to automatically learn hierarchical representation, the computation can be greatly reduced. The operation process of convolution layer convolution is as follows:

$$y_n^l = f \left(\sum_{\forall m} (y_m^{l-1} * c_{n,m}^l) + b_n^l \right). \quad (1)$$

After complex neuron calculation, DCNN needs to be judged by activation and function, and then can output recognition results, which can improve the recognition ability of neural network. Therefore, our formulas (2)–(4),

respectively, introduce the three commonly used activation functions of Sigmoid, ReLu, and tanh, which can solve the problem of gradient disappearance.

$$f(x) = \frac{1}{1 + e^{-x}}, \quad (2)$$

$$\text{ReLu}(x) = \max(0, x), \quad (3)$$

$$f(x) = \frac{e^x - e^{-x}}{e^x + e^{-x}}. \quad (4)$$

The calculation form of convolution layer is introduced.

$$\begin{aligned} y_j^l &= f(z_j^l), \\ z_j^l &= \sum_{vm} y_i^{l-1} * c_{ij}^l + b_j^l. \end{aligned} \quad (5)$$

Weights [23] and thresholds [24] are obtained by random gradient descent method.

$$c_{ij}^l = c_{ij}^l + \alpha \frac{\partial L(c_{ij}^l)}{\partial c_{ij}^l}, \quad (6)$$

$$b_j^l = b_j^l + \alpha \frac{\partial L(b_j^l)}{\partial b_j^l}.$$

2.4. Long-Term and Short-Term Memory Neural Network. LSTM model is a special RNN [25]. It makes some changes in the neuron structure of RNN and introduces memory units to solve the problem of gradient explosion and disappearance that traditional RNN cannot avoid. Gradient learning algorithm is introduced into the network structure of LSTM, and a processor is added to judge whether information is useful or not, which includes three gates: input, forgetting, and output. In addition, it also has a memory unit that can improve the ability to process long sequence data. First of all, LSTM needs to decide the information to be discarded in the cell state, and view $h_{t-1}x_t$ through the forgetting gate to output the 0–1 vector, as shown in Formula (7). Then the information of the cell state is updated by the input gate and tanh to obtain Formulas (8) and (9). After updating the new unit information C_t , the output state characteristics are judged, and the vectors between $[-1, 1]$ are obtained by sigmoid and tanh. Finally, the RNN unit is output, and the vector is multiplied by the judgment condition to obtain a Formulas (12) and (11).

$$f_t = \sigma(W_f \bullet [h_{t-1}, x_t] + b_f), \quad (7)$$

$$i_t = \sigma(W_i \bullet [h_{t-1}, x_t] + b_i), \quad (8)$$

$$C_t = \tanh(W_c \bullet [h_{t-1}, x_t] + b_c), \quad (9)$$

$$o_t = \sigma(W_o [h_{t-1}, x_t] + b_o), \quad (10)$$

$$h_t = o_t * \tanh(C_t). \quad (11)$$

Attention mechanism can solve the capacity problem and long-term dependence problem of coding vector, effectively shorten the distance of information transmission and reduce unnecessary steps. So, the LSTM model is optimized. After input $x = \{x_1, x_2, \dots, x_n\}$, the attention mechanism is introduced when the hidden layer outputs vector h . According to the encoder output and attention probability, the average value is calculated after addition. Where A_i stands for the probability of attention; matrix parameters are represented by w, W, U ; b is the biased vector; tanh is a hyperbolic tangent function.

After introducing the attention mechanism, the related calculations are as follows:

$$A_i = \frac{\exp(f(\bar{h}, h_i))}{\sum_j \exp(f(\bar{h}, h_j))},$$

$$f(\bar{h}, h_i) = w^T \tanh(W\bar{h} + Uh_i + b), \quad (12)$$

$$V = \sum_{i=0}^t A_i h_i.$$

2.5. Binary Hash Algorithm. A binary hash layer is introduced to construct an independent hash function. When the feature passes through this layer, the hash code can be obtained. Then, the hash code passes through the loss layer to obtain the optimized parameters calculated by the loss function. Hash codes can be expressed as

$$(h_1, h_2, \dots, h_q)^T = (\text{sign}(Wx))^T. \quad (13)$$

Sub features that can enter the full connection layer are obtained from the slice layer.

$$f_i(x^{(i)}) = W_i x^{(i)}, i = 1, 2, \dots, q. \quad (14)$$

The activation layer maps the one-dimensional value output by each block.

$$\tanh(v^{(i)}) = \frac{1 - e^{\beta v^{(i)}}}{1 + e^{\beta v^{(i)}}}, i = 1, 2, \dots, q, \quad (15)$$

$$v^{(i)} = f_i(x^{(i)}).$$

Enter the merging layer and represent vectors.

$$s = (v^{(1)}, v^{(2)}, \dots, v^{(q)})^T. \quad (16)$$

Enter the thresholding layer.

$$g(s^{(i)}) = \begin{cases} 1, & s^{(i)} \geq 0, \\ -1, & s^{(i)} < 0. \end{cases} \quad (17)$$

The quantization error loss is added to the objective function.

$$L_q = \frac{1}{2} \|h - s\|_2^2. \quad (18)$$

Combined with SoftMax, the overall loss function is obtained.

$$L_T = L_s + \lambda L_q. \quad (19)$$

3. Design and Implementation of 3 System Model

3.1. User Portrait Model. The characteristics of the times make more and more people active on the Internet. People use but are not limited to words, pictures, videos, and other ways to record their lives and work in this online world and express their preferences freely and fully. Social activity data on the Internet will record a person's interests, behavior habits, psychological state, and other personal attributes. Major small and medium-sized enterprises should seize the opportunity, open up their thinking, and realize accurate marketing according to the distinctive personal characteristics of Internet users. Adjust the original strategy, carry out personalized analysis and feature optimization of products, and mine the value hidden in the data.

In view of the universality and practicability of the user portrait model, this paper also adds this mining method, which classifies users and labels them according to the features extracted from the DL model, so as to facilitate more detailed consumption analysis. First of all, we need to collect the user's basic data, and then preprocess the user's text data source and picture data source. Finally, the attributes are abstracted by a genetic algorithm, Bayesian algorithm, and neural network algorithm, and the useable user portrait is successfully established.

The hierarchical structure of portrait construction is as follows:

$$\left\{ \begin{array}{l} \Theta_j^{(T)} : \text{Gam} \left(r, \left(\frac{1}{c_j^{(T+1)}} \right) \right), \\ \Theta_j^{(T)} : \text{Gam} \left(\left[\begin{array}{l} \phi_w^{(t+1)} \phi_{w-j}^{(t+1)} \\ \phi_v^{(t+1)} \phi_{v-j}^{(t+1)} \end{array} \right], \left(\frac{1}{c_j^{(t+1)}} \right) \right), \\ \Theta_j^{(1)} : \text{Gam} \left(\left[\begin{array}{l} \phi_w^{(2)} \phi_{w-j}^{(2)} \\ \phi_v^{(2)} \phi_{v-j}^{(2)} \end{array} \right], \left(\frac{p_j^{(2)}}{(1 - p_j^{(2)})} \right) \right). \end{array} \right. \quad (20)$$

After simplification and derivation, we can get the following formula:

$$\left\{ \begin{array}{l} w_j^{(t)} : \text{Pois}(-\phi_w^{(t)} \theta_{w-j}^{(t)}, \ln(1 - p_j^{(t)})), \\ v_j^{(t)} : \text{Pois}(-\phi_v^{(t)} \theta_{v-j}^{(t)}, \ln(1 - p_j^{(t)})). \end{array} \right. \quad (21)$$

3.2. Preference Recommendation and Strategy Adjustment. Traditional marketing methods cannot meet the needs of Internet users, and cannot play a very good role in publicity,

but greatly increase costs, while achieving little effect. In order to improve the loyalty and satisfaction of users and achieve the predetermined sales volume and reputation, recommending the relevant preferences of users is the key. The preference here means that users have a good impression of specific goods or services, and are more inclined to buy trusted brands or trademark products when consuming, that is, consumption preference. Such users will buy repeatedly under the influence of subconscious habits. In addition, users are no longer limited to ordinary and popular standard goods after having a variety of choices. They are easily influenced by their own psychology, environment, and culture, and have a strong willingness to choose products that can satisfy their individualized pursuit. The previous experimental design has laid the foundation for our preference recommendation. We can analyze the user's love and habit of a certain kind of product or a certain kind of service, and turn this market information that can be mastered into the core of marketing strategy.

- (1) For consumers, who care about the price and practicality of goods or services, take affordable promotion as the marketing strategy, and push full reduction activities, coupons, and discounted goods for these people. They cannot control their desire to buy, and they cannot help buying more goods or services.
- (2) Not everyone measures the value of goods by cost performance, and there are also main buyers who, pay more attention to new things. They do not care about the amount of money, but pay attention to the trend of the times, the style and novelty of goods. They can pay generously for a service that has only become popular in society, just to satisfy the novelty of the moment; you can also snap up a small commodity because of its limited sales. Therefore, aiming at this part of consumers, we should constantly update and focus on the marketing of new models and early adopters.
- (3) For people, who go to work and study, due to the limitation of time and space, they cannot participate in offline shopping experience activities anytime and anywhere. They need convenient, fast and simple shopping choices, and can enjoy centralized customer service and after-sales service at any time.

3.3. Framework of Hybrid Model. The model of this paper is based on DCNN and LSTM neural network with an attention mechanism, which also introduces a binary hash layer so that the overall processing ability of the model is higher. According to the performance of users on the Internet, collect basic data, then preprocess the text and pictures, and transmit them to DCNN + LSTMATTENTION model to find various hidden user characteristics. According to the information characteristics of these users, the user portrait model is constructed, and the marketing strategy is optimized and adjusted. In order to better cater to consumers' ideas, analyze decision-making behavior, search

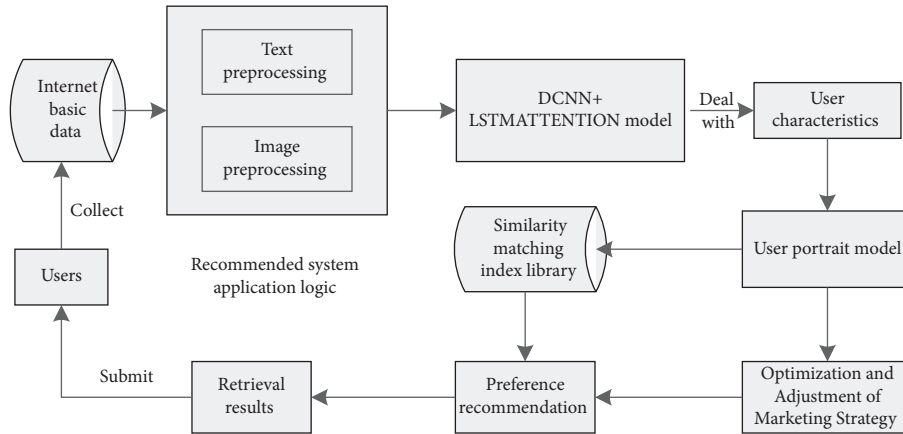


FIGURE 1: Schematic diagram of DL-based hybrid model.

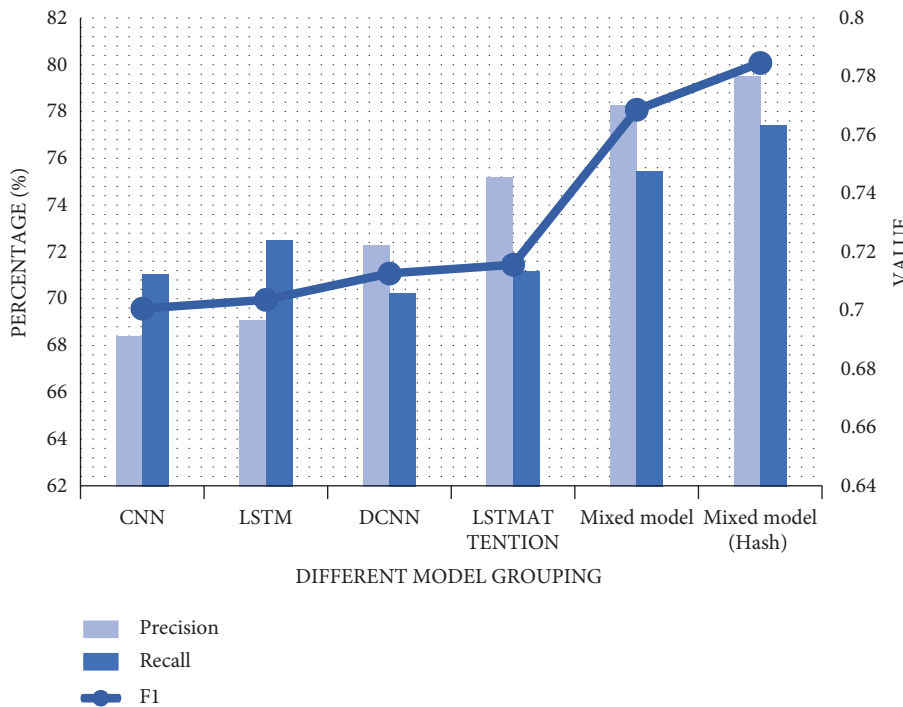


FIGURE 2: Comparison of multi-modal recognition results.

the index database of similarity matching, recommend preferred products that meet consumers’ interests, and make the adjusted marketing strategy play a role. Finally, the retrieval results are submitted to users for use, which directly affects the transactions of consumer customers as shown in Figure 1.

4. Experimental Analysis

4.1. Performance Results of the Model. In this section of the experiment, we will explain the reasons for choosing the hybrid model. By identifying and detecting the graphic text of consumer shopping, we record the three indicators identified by multimodality respectively. In order to highlight the superiority of this model, CNN, LSTM, DCNN, LSTMATTENTION, basic hybrid model (DCNN + LSTMATTENTION), and mature hybrid model with hash

layer are compared. The recognition accuracy of CNN model is 68.42%, the recall rate is 71.08%, and the F1 score is about 0.701. LSTM and its value fluctuate between 1% and 2%, and their performance is roughly the same. The performance of DCNN and LSTMATTENTION models is slightly better than the first two models, with accuracy of 72.31% and 75.22%, respectively, and there is still room for optimization and improvement. The data of the common hybrid model performs well. After adding Hash, the accuracy of the fusion model is as high as 79.56%, the recall rate rises to 77.43%, and the equilibrium F score reaches 0.785. The larger the value, the better the model as shown in Figure 2.

After testing the above indexes, the error values of each model are analyzed. With the increase of the number of an epoch, the weight of the model is set to undergo repeated update iterative training. With the increase of epoch, their

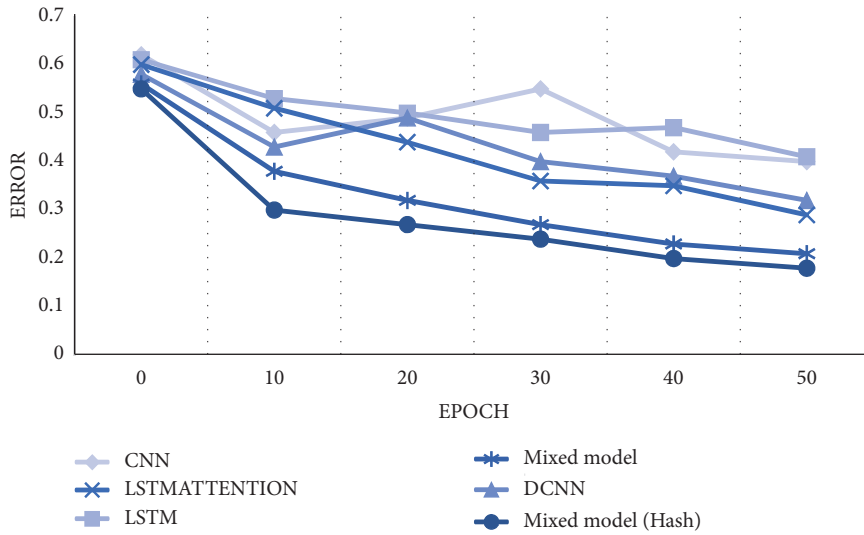


FIGURE 3: Comparative analysis of errors.

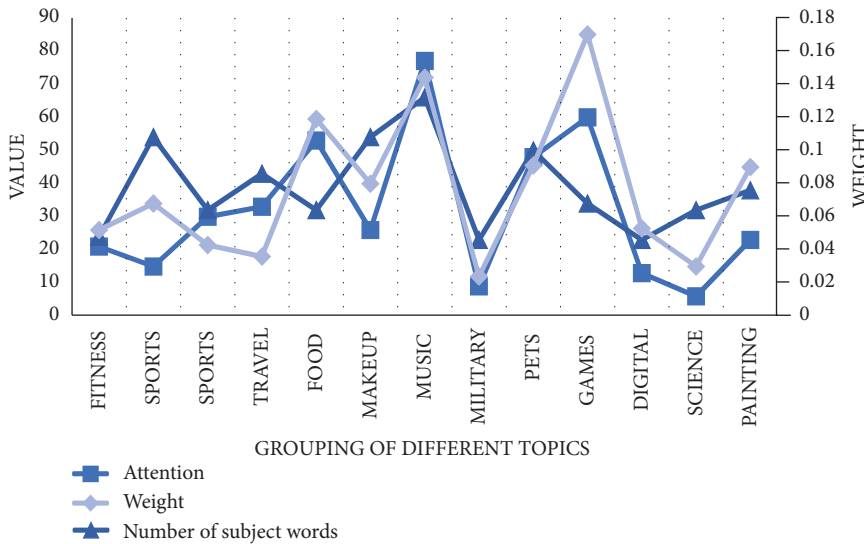


FIGURE 4: Weight information for part of the topic.

diversity becomes stronger and stronger, and the curves transition from the initial nonfitting state to the fitting state. The method in this paper not only reduces the weight parameters but also reduces the prediction error of the model. After 50 updates, its error value can be reduced to about 0.18. Compared with other models, the error value of this model does not appear high or low, and its dynamic performance is obviously better than other basic network models. Finally, we can find that the performance of the model designed by this method is better than that of other single models and common mixed models, and the effect is satisfactory as shown in Figure 3.

4.2. Preference Prediction Analysis. First of all, we collect the basic data of users' Internet, and after processing the model, we can determine the topic content and its weight bias that

users prefer. Most subject words under each topic will have different characteristics, which are identifiable and unique, and can well distinguish the personal attributes of different users from their corresponding hobbies. Confirming these themes can better assist the construction of users' portraits and strive to create a database of one person and one portrait. A total of 1000 active users of a certain platform were randomly selected, the data containing text pictures were crawled as the original data, and 13 topics with a high topic degree were obtained, each topic had 20~70 subject words as shown in Figure 4.

Three users who volunteered to participate in the experimental test were selected, the training data set was processed and constructed, and their different preferences were predicted by portraits. It is obvious that they have different tendency distribution in theme preference, which proves that they pay close attention to and have a strong

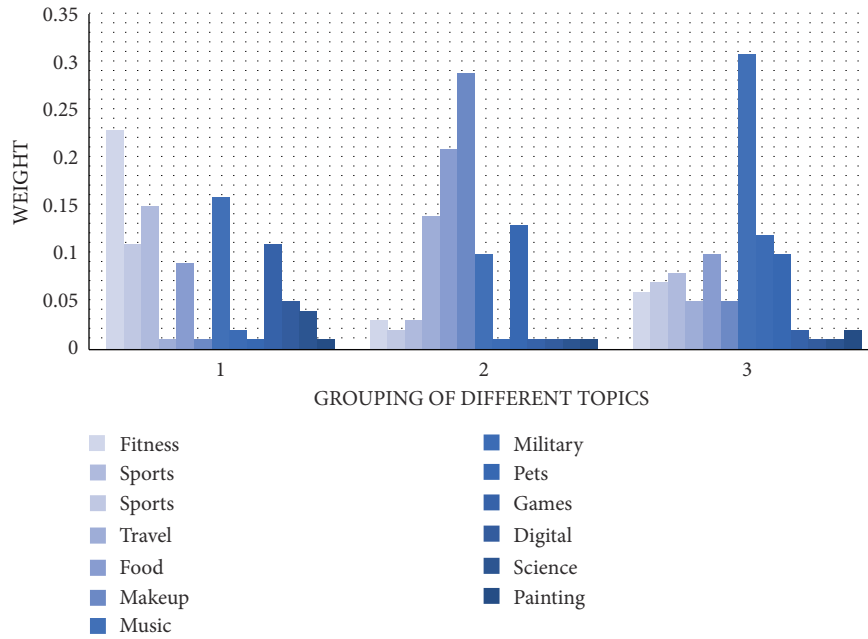


FIGURE 5: Preference prediction of user portrait.

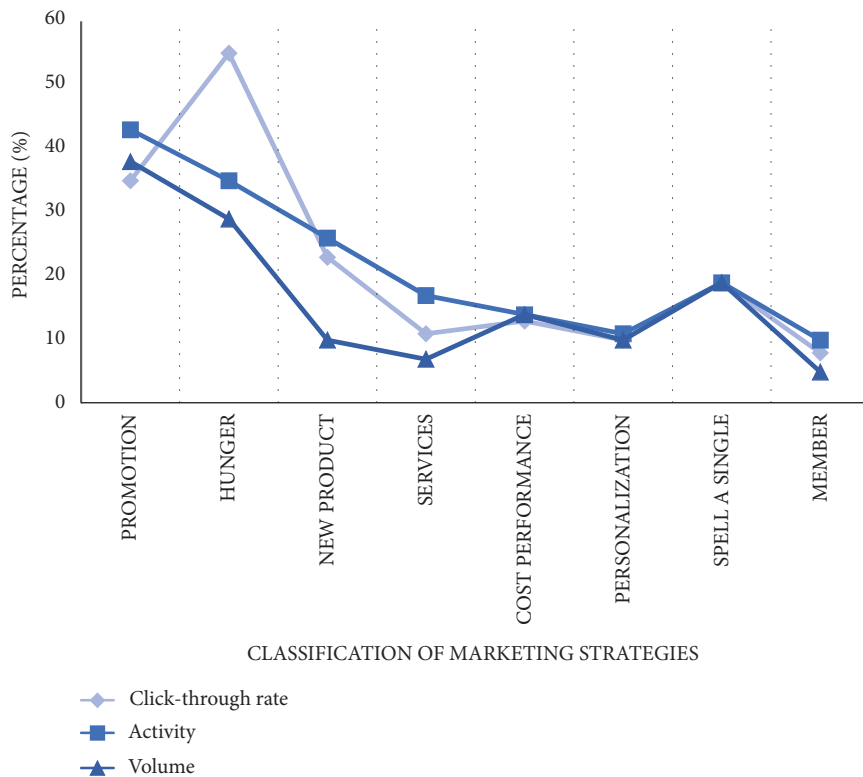


FIGURE 6: Marketing strategy optimization.

interest in a certain kind or several themes in daily life. We can clearly see that the first user prefers topics such as physical fitness, followed by music. The second user focused on travel, food, and beauty, and was interested in music and pets. The last user is interested in music, with a weight ratio as high as 31%, and pays attention to food, military affairs, and pets as shown in Figure 5.

4.3. Analysis of Marketing Strategy and Recommendation Effect. After using network and model to extract users' attributes effectively, enterprises can adjust different markets and optimize marketing strategies for different types of users. We analyzed and counted the increased percentage points of 8 adjusted marketing strategies, and compared the click-through rate, activity, and turnover of goods or services with

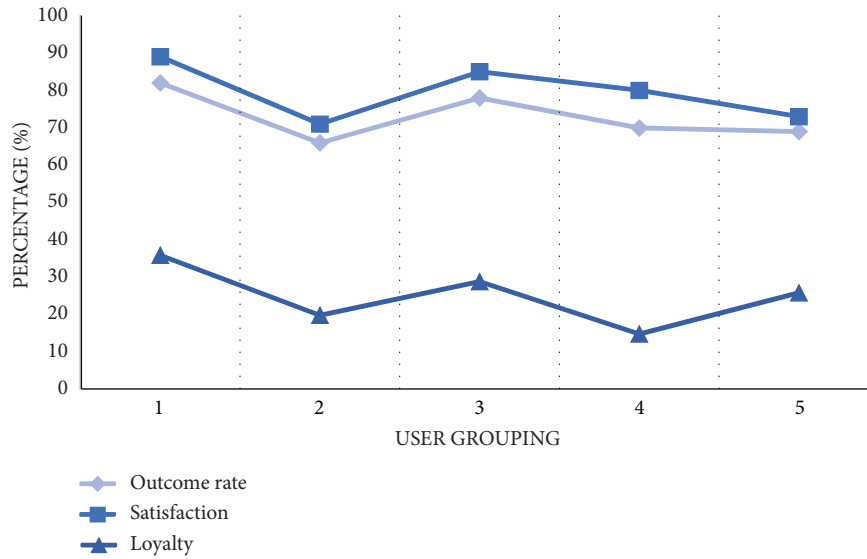


FIGURE 7: Recommended effect feedback.

the data of traditional marketing models. From the curve trend in the figure, we can find that preferential promotion and hunger marketing have the best effect, and the click-through rate and activity have increased by more than 20%. Secondly, the new product launch and group purchase/spelling strategy bring considerable benefits. Other strategies have increased to varying degrees, which proves that the adjusted and optimized model is very practical as shown in Figure 6.

After adjustment, this section also needs to evaluate the effect of the optimized strategy. Recycling five groups of users (10 people in each group) in the marketing achievement rate, consumer satisfaction, and brand loyalty of these three indicators of evaluation. According to these data, we can evaluate the actual effect and true value of the model after use, so as to carry out feedback and correction work. Because of different marketing strategies and individual differences, the index value of each group fluctuates to a certain extent. From the perspective of marketing results, the values of the five groups are between 69% and 82%, which has good results; consumer satisfaction is between 70% and 90%. However, brand loyalty needs long-term accumulation of word of mouth, so it is generally low, which needs further testing and research as shown in Figure 7.

5. Conclusion

Traditional marketing relies on the investment of manpower and capital and needs a large number of advertisements to put into the market, so as to arouse customers' desire to buy, establish the image of products, and make them deeply rooted in the hearts of the people. Customers can only choose the products and services provided by merchants or enterprises within a certain range, ignoring their different feelings. However, due to the rise of e-commerce, consumers are more willing to choose products with personality signs, low cost and good quality, and guaranteed after-sales service. Traditional marketing strategy in this online shopping trend does not have much effect, enterprises need an optimization

model that can constantly adjust marketing strategy. Based on this research background, the experiment in this paper takes the Internet as the basic business environment and enriches the field of personalized recommendation from all aspects and angles. Combining the purpose of the previous sale with the existing demand, we will promote e-commerce marketing that is accurate to everyone. Customers can enjoy high-quality services and fully meet individual needs. Enterprises also exceed their marketing objectives while expanding their influence, which has certain practical value. In this paper, combined with multi-modal data, the experiment based on a deep learning model can be done, and the completion and accuracy of the results are satisfactory. Because the research of deep learning is still in the development stage, there are many places that need to be further revised and improved in this experiment. In addition to the challenges faced by the fusion model algorithm, future research work should focus on the dynamic development process of marketing strategy facing the market. At present, the push function of marketing is relatively simple, which is only for the products that users are interested in. It can also appropriately enhance the broadcasting of online advertisements and send a variety of preferential policies for promotions and discounts to attract more customers. There is still a lack of inspection and analysis of overall operation defects, so as to ensure the normal operation of equipment in actual deployment. More data sets and features are still needed for testing, and the variability of parameters in different scenarios is worth exploring.

Data Availability

The experimental data used to support the findings of this study are available from the corresponding author upon request.

Conflicts of Interest

The authors declare that they have no conflicts of interest regarding this work.

References

- [1] Lu Chenhui, F. Shuo, Y. Aihua, and Y. Xiaojun, "Research on Sales Forecast and Marketing Strategy Application of Gas Station Based on Deep Learning," *Journal of Zhengzhou University (Engineering Edition)*, vol. 43, no. 1, pp. 1–6, 2022.
- [2] H. Xiaopei, S. Xinghua, L. Yong, and W. Weiwei, "Design and implementation of deep learning platform for railway passenger transport marketing based on Kubernetes," *Railway Computer Application*, vol. 30, no. 1, pp. 57–61, 2021.
- [3] S. Cuihua and X. Ting, "Design and simulation of precision marketing push algorithm based on deep learning," *Modern Electronic Technology*, vol. 43, no. 22, pp. 144–147, 2020.
- [4] Wu Anbo, Ge Chenchen, S. Linhui, Z. Yun, and L. Gang, "Yan value estimation and e-commerce precision marketing based on deep learning," *Industrial Engineering & Management*, vol. 24, no. 06, pp. 124–131, 2019.
- [5] J. Yan, "Deep learning design of experimental teaching for marketing major based on maker space," *Journal of Chengdu Institute of Technology*, vol. 21, no. 04, pp. 56–59, 2018.
- [6] Z. Xun and P. Jisheng, "Research on the formation mechanism of marketing dynamic capability of international enterprises: from the perspective of knowledge," *Journal of Hohai University (Philosophy and Social Sciences Edition)*, vol. 19, no. 03, pp. 28–35, 2017.
- [7] W. Lirong, "Excavating interactive function, promoting deep learning and improving teaching effectiveness-Discussion on the application of interactive teaching mode in marketing teaching," *Journal of Guangxi Political Science and Law Management Cadre College*, vol. 27, no. 06, pp. 112–115, 2012.
- [8] J. Zhongxing and L. Dong, "Deep learning neural network model for consumer preference prediction," *Computer Applications*, vol. 39, no. 07, pp. 1888–1893, 2019.
- [9] Z. Puyang, "Application of deep learning algorithm in financial consumer behavior research," *Technology and Market*, vol. 27, no. 7, p. 4, 2020.
- [10] L. Lei, Y. Chunling, and Z. Ping, "The influence of graphic information on consumer interaction behavior and brand relationship," *Management Science*, vol. 31, no. 1, p. 11, 2018.
- [11] Y. Kai, T. Ping, and C. Yuxin, "Research on the effect of personalized recommendation system based on multi-source big data," *Management Science*, vol. 31, no. 5, p. 13, 2018.
- [12] P. Tianqiang and L. Fang, "Image retrieval method based on deep convolution neural network and binary hash learning," *Journal of Electronics and Informatics*, vol. 38, no. 08, pp. 2068–2075, 2016.
- [13] T. He, Z. Hai, and W. Jinfu, "Time series evolution and prediction of Internet communication behavior," *Journal of Communication Science*, vol. 39, no. 6, p. 11, 2018.
- [14] T. Yaming, "Research on railway mobile Internet marketing strategy," *Railway Computer Application*, vol. 26, no. 6, p. 4, 2017.
- [15] X. Wenlong, W. Zhenhao, and C. Hao, "Analysis of research trends and development trends of business intelligence and big data analysis at home and abroad," *Science and Technology and Economy*, vol. 33, no. 6, pp. 66–70, 2020.
- [16] D. Silver, J. Schrittwieser, and K. Simonyan, "Mastering the game of Go without human knowledge," *Nature*, vol. 550, no. 7676, pp. 354–359, 2017.
- [17] L. Tingting, Z. Wendong, and L. Guangyi, "Research progress of text classification based on deep learning," *Power Information and Communication Technology*, vol. 16, no. 3, 2018.
- [18] Li Guoliang and X. Zhou, "Overview of AI-oriented data management technology," *Journal of Software Science*, vol. 32, no. 01, pp. 21–40, 2021.
- [19] W. Li, X. Wenjian, L. Peng, Z. Zhibin, and Z. Yonggang, "Research on the evolution of information system architecture based on business middle station," *Telecommunication Engineering Technology and Standardization*, vol. 33, no. 11, 2020.
- [20] Xu Chunxia and Ma Litao, "Predicting GDP by uncertain delphi method," *Practice and Understanding of Mathematics*, vol. 44, no. 11, pp. 140–146, 2014.
- [21] L. Jianwei and L. Yuan, "Luo Xionglin. Research progress of deep learning," *Computer Application Research*, vol. 31, no. 07, pp. 1921–1930, 2014.
- [22] W. Xianqing and L. Shaohui, "Research on the influence of artificial intelligence on consumption and shopping experience in the new retail environment—based on the perspective of commercial retail reform and reconstruction of people and goods yard system," *Business and Economic Research*, vol. 4, no. 17, pp. 5–8, 2018.
- [23] G. Dandan, C. Bo, and C. Yulai, "SAR image target recognition method based on PGBN model," *Journal of Electronics and Informatics*, vol. 38, no. 12, pp. 2996–3003, 2016.
- [24] T. Chen, H. Yin, and H. Chen, "Online sales prediction via trend alignment-based multitask current neural networks," *Knowledge and Information Systems*, vol. 62, no. 7, pp. 1–29, 2020.
- [25] A. Sayl, I. Ozturk, and M. Ustunel, "Brand legal analysis system using K-Means algorithm," *Journal of Engineering Technology and Applied Sciences*, vol. 1, no. 3, pp. 107–126, 2016.

Research Article

The Intervention of Data Mining in the Allocation Efficiency of Multiple Intelligent Devices in Intelligent Pharmacy

Xiaohua Li, Benren Tan , Jinkun Zheng, Xiaomei Xu, Jian Xiao, and Yanlin Liu

The Affiliated Yuebei People's Hospital of Shantou University Medical College, Shaoguan 512026, Guangdong, China

Correspondence should be addressed to Benren Tan; tanbenren@126.com

Received 31 May 2022; Revised 20 July 2022; Accepted 29 July 2022; Published 22 August 2022

Academic Editor: Le Sun

Copyright © 2022 Xiaohua Li et al. This is an open access article distributed under the Creative Commons Attribution License, which permits unrestricted use, distribution, and reproduction in any medium, provided the original work is properly cited.

With the wide application of artificial intelligence and big data technology in the medical field, the problems of high cost and low efficiency of traditional pharmacy management were becoming more and more obvious. Therefore, this paper proposed to use data mining technology to design and develop the dispensing process and equipment of intelligent pharmacy. Firstly, it summarized the existing data mining technology and association rule methods and expounded its application value in the related fields. Secondly, the data standard and integration platform of dispensing in intelligent pharmacy were established. Web service technology was used to design the interactive interface and call it to the intelligent device of pharmacy. Finally, an intelligent pharmacy management system based on association rule mining was constructed through the data mining of intelligent pharmacy equipment, in order to improve the intelligence and informatization of modern pharmacy management. For the emergency dispensing process of intelligent equipment failure, data mining was used to optimize the intelligent pharmacy equipment and dispensing process and change the pharmacy management from traditional prescription to patient drug treatment, so as to improve the dispensing efficiency of intelligent pharmacy equipment. Through the systematic test and analysis, the results showed that through the real-time risk prevention and control, the formula accuracy and operation speed of the intelligent dispensing machine were improved and the dispensing time was shortened. Through intelligent drug delivery, the unreasonable drug use of patients was reduced, the safety and effectiveness of clinical drug use were ensured, and the contradiction between doctors and patients was reduced. This study can not only optimize the medical experience of patients and provide patients with more high-quality and humanized pharmaceutical technical services but also provide some support for the intelligent management of modern hospitals.

1. Introduction

In recent years, with the rapid development of artificial intelligence and big data technology, the automation and intelligent management level of hospital pharmacies has been rising, and intelligent pharmacies have been used in some hospitals one after another. Compared with the traditional hospital pharmacy mode, the intelligent pharmacy service mode changes the traditional guarantee of drug supply into focusing on strengthening the pharmaceutical professional and technical services and participating in the dynamic management of clinical medication, so as to improve the management level of hospital pharmacy to a new level [1, 2]. In July 2018, the National Health Commission and the State Administration of Traditional Chinese

Medicine issued relevant documents and encouraged qualified medical institutions to promote the construction of smart pharmacy, so as to realize the seamless connection between prescription system and pharmacy dispensing system, so as to facilitate people to take medicine in time.

The construction of intelligent pharmacy mainly involves relevant intelligent equipment, database software, and interface technology. It needs to integrate different software and hardware technologies, which has the characteristics of diversity and cross platform [3]. In the construction planning of hospital information system, the business module of the hospital is generally considered, while the overall planning of medical industry information system is less. Due to the lack of effective top-level design and standard specification requirements, there are great differences in database

types and data formats involved in different information systems. At the same time, there are some problems in the construction of business information system of functional departments, such as insufficient function integration and different data interface standards, which leads to the widespread phenomenon of information island [4]. Traditional medicine management has seriously hindered the sharing of medical information and the improvement of medical service level, restricted the data sharing and resource utilization and allocation efficiency of intelligent pharmacy management information, and affected the time of taking and waiting for drugs and the quality of pharmaceutical care.

Research shows that some developed countries have effectively improved work efficiency and reduced deployment errors and labor intensity by realizing the automatic and intelligent management of pharmacies [5]. From the development trend of modern pharmaceutical industry, improving the overall application efficiency of intelligent pharmacy system and the accuracy of prescription review has become an inevitable trend of pharmacy management and development. At present, people have made a preliminary study on the intelligent efficiency of the same brand of equipment. Some people apply data mining to the market analysis, sales prediction, and intelligent drug preparation of automated pharmacies, which provides a basis for the establishment of the working mode of the automatic dispensing system of large-scale comprehensive outpatient pharmacies [6]. It is known from the existing research that the existing achievements have not conducted in-depth research on the unification of various intelligent device interfaces and data standards in the intelligent pharmacy, as well as the deployment and dispensing of various devices. Therefore, the existing intelligent drug management is still difficult to meet the needs of practical application. Therefore, this paper proposed to use data mining to study the deployment efficiency and intervention function of various intelligent devices in intelligent pharmacy, in order to provide theoretical reference for improving the modern management level and service function of intelligent pharmacy.

2. Related Works

With the gradual standardization of drug management under the situation of medical reform, in order to improve the capital turnover rate and reduce the cost, the hospital has adjusted the drug reserve of pharmacy accordingly. The hospital has optimized the types, quantity, and reserves of drugs, and tried to keep the balance of the use and management of drugs in stock. Through market analysis and sales forecast, some people use data mining to analyze drug sales data and inventory, and increase or decrease relevant drugs in real time, so as to maintain a dynamic balance of inventory [7, 8]. Through the given pharmacy inventory and sales data, the information is analyzed by using data mining technology, and the results are fed back to the drug warehouse, so as to effectively prevent the extrusion or shortage of drug inventory, which can not only meet the clinical needs, but also reduce the cost.

Outpatient medicine has a certain randomness. As a part of it, outpatient pharmacy should not only meet the needs of patients, but also ensure the standardized management of internal personnel. Some people use data mining technology to analyze the service information of outpatient pharmacy, and provide support for outpatient pharmacy service by evaluating the cost and risk of pharmacy. At the same time, according to the correlation degree of different links in the pharmacy service process, association rules are used to optimize relevant service matters, so as to reduce the waiting time of patients [9]. By optimizing the workflow of outpatient pharmacy, we can not only improve the allocation efficiency of drugs, but also reduce the waiting time of patients, so as to improve the service quality and level of pharmacy.

In modern intelligent pharmacy management, different types of drugs have certain differences in access efficiency. Generally, there may be some time differences when accessing the drugs in different storage locations [10]. Especially when the type and quantity of drugs change, the storage position of drugs needs to be adjusted. At the same time, the randomness of patients' demand for drugs should be fully considered in the design of pharmacy storage space. For example, patients may put forward the demand for different drugs. According to the dispensing characteristics of pharmacies, some scholars used data mining to analyze drug data and prescription information, and designed drug storage according to the batch number, distance, and relevance of drugs, and achieved certain results.

Data mining is widely used in the field of hospital pharmacy and its management [11, 12]. From the existing research results, compared with the traditional manual inference and experience, using data mining to manage the intelligent pharmacy is not only more efficient, but also more reliable. Intelligent pharmacies have high requirements for fine management and dispensing efficiency of drugs. The management of intelligent pharmacy needs the support of various intelligent devices [13]. For example, as a part of the dispensing machine, the intelligent medicine cabinet can effectively improve the efficiency and accuracy of drug dispensing only by tapping the design and functional potential of the medicine cabinet. The research shows that only by creating certain conditions for the use of intelligent medicine cabinet, can it give full play to its due effect. For example, intelligent medicine cabinet is not suitable for the storage of refrigerated drugs. Therefore, it is still difficult to obtain reliable results from drug data by using traditional data mining methods.

3. Data Mining Theory

3.1. Data Mining Method. According to the massive data provided by data warehouse and other data sources, data mining extracts the required relevant knowledge by means of mining calculation or knowledge discovery, so as to provide the basis for decision-making and analysis for relevant departments or personnel. For different research purposes, researchers' understanding of data mining may be different. Some scholars believe that the content or process

of data mining and database knowledge discovery (KDD) is similar, while others believe that data mining belongs to a stage of knowledge discovery, and there are obvious differences between data mining and knowledge discovery in related connotation. This paper mainly understands data mining from the broad concept and divides it into different stages, such as data acquisition, pro-processing, data analysis, and knowledge representation.

At present, the content of data mining generally includes descriptive objects or predictive objects. Descriptive objects mainly use certain data mining algorithms to explore the correlation between data. The results explored from descriptive information need to be further verified by relevant data. Predictive data is mainly used to predict possible future events based on known phenomena, which has strong purpose. It can be seen that the descriptive information reflects the hidden law within the data, while predictive data reflects the possible results in the future.

Different from the existing data analysis methods, data mining adopts automatic statistics and analysis methods, which can not only find out the valuable information inside the data, but also predict the future development trend or change law through the obtained useful information. Data mining can analyze the correlation of massive data, which is more efficient than the traditional analysis methods. At the same time, data mining can use clustering algorithm to realize the statistical analysis of discrete data and obtain the relationship between discrete information. In addition, data mining generally processes the relevant knowledge or information under unknown conditions and obtains the results, which is completely different from the traditional data analysis methods. With the development of related technology, the analysis object of data mining is no longer limited to structured data, but extended to almost any type of data processing, such as semi-structured or unstructured data information, which provides powerful conditions for making relevant decisions in different fields.

Fayyad model and CRISP-DM model are generally adopted in the process of data mining [14, 15]. Fayyad model is divided into nine different stages: data preparation and selection, data dimensionality reduction and transformation, knowledge evaluation, and so on. The model has no specific data source and result destination in the whole process from the beginning of data processing to the final result, so its application is not strong. Different from Fayyad model, CRISP-DM model combines the specific application environment. CRISP-DM model gives a more detailed description of the data to be processed, that is, data source and selection. At the same time, it also gives application reference for the output results of the model, so as to ensure the integrity of data source, data processing, and application results. As shown in Figure 1, the basic working process of data mining is described.

In the process of data mining, the tasks to be processed mainly include data classification analysis, cluster analysis, and association analysis. Data classification mainly analyzes and processes different data to obtain the common attribute information between data, and then attribute it to different classification models [16]. Clustering mainly adopts

unsupervised learning method, and uses the similarity of data to divide classes, and then classifies different data into different categories according to their attributes. Association mainly explores the internal relationship according to the attribute information between different data, so as to find the correlation between data. In practical application, parameters such as support and confidence are generally used to evaluate the correlation between different data.

3.2. Association Rule Mining. Association rule method is a part of data mining technology. This method is often used to deal with the internal relationship between things. It has certain stability and flexibility, and is not limited to the treatment of dependent variables. Therefore, it can provide effective support for the application of data mining in related fields [17, 18].

According to the existing research, the basic methods for association rules are as follows:

- (1) If P and Q are disjoint data item sets in database M , that is, $P, Q \subseteq M, P \cap Q = \Phi$, then association rules can be expressed as implication in the following form:

$$R: P \longrightarrow Q. \quad (1)$$

- (2) If the support of rule Q is expressed by S , S means that $S\%$ of transactions in M contain $P \cup Q$, and the support can be expressed by $Sup(R)$, which is as follows:

$$\begin{aligned} Sup(R) &= S \cdot M \cdot 100\%, \\ S &= Sup(R), P \cup Q \subseteq M. \end{aligned} \quad (2)$$

- (3) If the confidence of rule Q is represented by T , then T means that $T\%$ of the transactions in M and N that support P also support Q . The confidence can be expressed by $Con(R)$, which is defined based on conditional probability as follows:

$$Con(P \longrightarrow Q) = p\left(\frac{Q \subseteq N}{P \subseteq M}\right), \quad (3)$$

$$p\left(\frac{Q \subseteq N}{P \subseteq M}\right) = \frac{p(Q \subseteq N \cap P \subseteq N)}{p(P \subseteq N)}, \quad (4)$$

$$\frac{p(Q \subseteq N \cap P \subseteq N)}{p(P \subseteq N)} = \frac{Sup(P \cup Q)}{Sup(P)}. \quad (5)$$

According to the above equations (3) to (5), the following relationship can be obtained:

$$Con(P \longrightarrow Q) = \frac{Sup(P \cup Q)}{Sup(P)}. \quad (6)$$

If $MinSup$ represents the minimum support and $MinCon$ indicates the minimum confidence, when $Sup(R) \geq MinSup$ and $Con(R) \geq MinCon$, Q can be considered as a strong association rule. It can be described as follows:

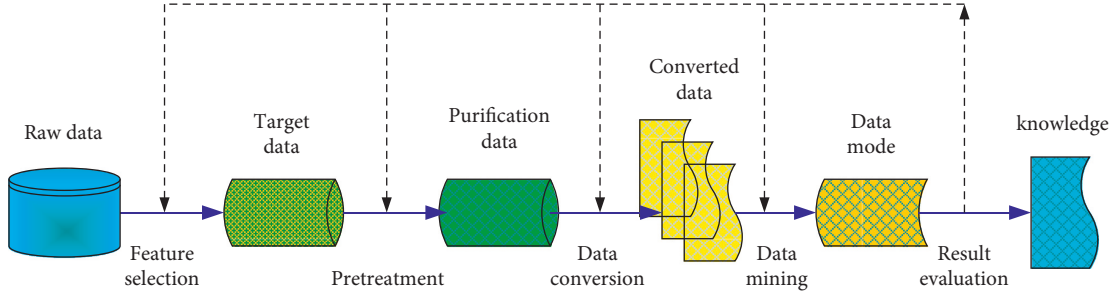


FIGURE 1: The basic working process of data mining.

$$R: P \Rightarrow Q. \quad (7)$$

Support is mainly used to reflect the effectiveness of association rules, while confidence is used to describe the credibility of association rules. Generally speaking, the mining of association rules should meet the minimum support threshold of user needs in order to reflect the minimum association between projects. At the same time, the confidence of mining rules should reach the lowest threshold, so that the reliability of mining rules should also reach the lowest. Therefore, the mining of association rules should reach the minimum support and minimum confidence, that is, the mining of association rules should meet the following conditions:

$$\begin{aligned} \text{Sup}(P \cup Q, M) &\geq \text{MinSup}, \\ \text{Con}(P \Rightarrow Q) &\geq \text{MinCon}. \end{aligned} \quad (8)$$

According to the existing research, item set refers to the set of items, and i -item set refers to the item set containing i items. The sum of the number of transactions that contain the item set is called the frequency of the item set, also known as the support rate of the item set. If the item set is greater than the minimum support, it can be called a frequent item set. D_i represents the sum of all frequent i -item sets.

Mining association rules mainly include finding frequent item sets and obtaining strong association rules through frequent item sets. When searching for frequent item sets, the frequency of item sets cannot be less than the minimum support. In order to obtain strong association rules, it is necessary to ensure that the rules are greater than the minimum support and minimum confidence.

Association rule mining methods can be classified from different angles. Firstly, in terms of the types of variables handled by association rules, association rule mining methods can be divided into Boolean and numerical types [19]. Boolean association rules mainly deal with discrete objects. This method only considers the existence of data items without knowing the number of data items. Numerical association rules mainly deal with the relationship between data items. The data item set processed by this method contains at least one data item belonging to numerical type. Secondly, from the data abstraction level processed by association rules, association rule mining methods can be divided into single-level association mining and multi-level association mining. The data items processed by the single-

level association mining method belong to the same level, while the data items processed by the multi-level association mining method may belong to different levels. In addition, according to the data dimension processed by association rules, association rule mining methods can be divided into single-dimensional association mining and multi-dimensional association mining. If the attribute of the processed data item is single, the association rule mining is single-dimensional association mining. If the attribute of the processed data item is multiple, the association rule mining is multi-dimensional association mining. The object processed by the single-dimensional association mining method is the relationship between single attributes, while the object processed by the multi-dimensional association mining method is the relationship between multiple attributes.

3.3. Association Rule Algorithm. Apriori algorithm can be used to get the required frequent item sets and obtain the corresponding association rules. Apriori algorithm mainly finds all frequent item sets through two different stages. Apriori algorithm forms the preliminary item set with the length of $i + 1$ from the frequent item set with the length of i through the layer-by-layer iterative method, and then forms the frequent item set with the length of $i + 1$, so as to obtain the corresponding association rules [20].

After setting the minimum support, start running the Apriori algorithm. First, calculate the support of each item one by one through scanning to form a frequent 1-item set, and then traverse i times until the obtained frequent item set is empty, and then stop the algorithm. The running process of Apriori algorithm is shown in Figure 2.

Apriori algorithm needs to scan the database many times in the process of data mining, which brings a large workload to the input and output of data. Moreover, Apriori algorithm may produce a large number of pre-selected item sets in the running process, which increases the running time and memory overhead of the algorithm to a certain extent. Therefore, FP-tree algorithm can be used, which can effectively obtain the association rules by generating frequent item sets [21, 22].

In order to improve the efficiency of obtaining the association rules, some people improve FP-tree algorithm and propose FP-growth algorithm. When using this algorithm, firstly, the database is scanned once, and the generated frequent item sets are added to the frequent pattern tree. Then, the association information between item sets remains

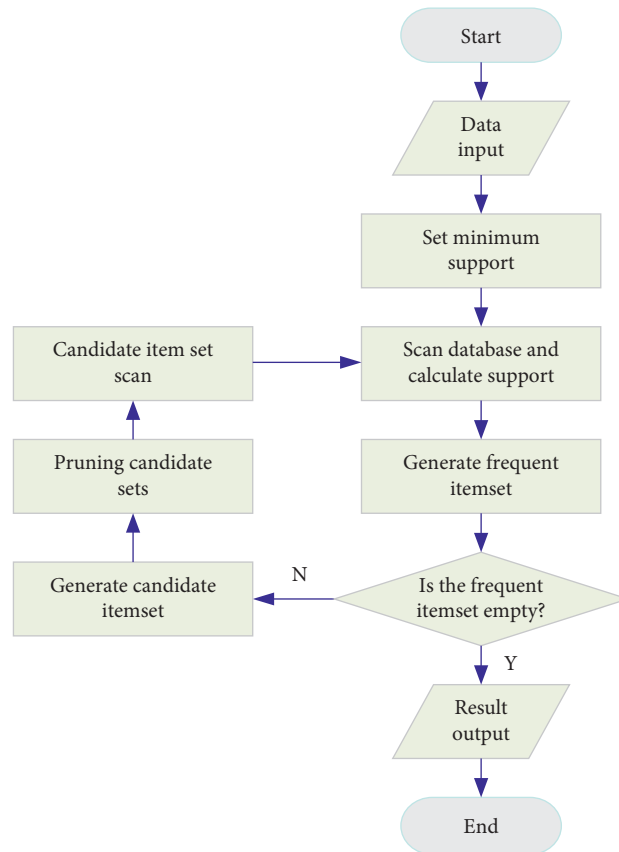


FIGURE 2: The running process of apriori algorithm.

unchanged. Then, the generated FP-growth is divided into different condition trees, and each condition tree corresponds to a frequent item set. Finally, the condition trees are mined in turn. FP-growth algorithm can be effectively applied to different rules, and it is better than the other algorithms in efficiency.

4. Deployment of Multiple Intelligent Devices in Intelligent Pharmacy

4.1. *Construction of the Data Integration Platform for the Intelligent Pharmacy System.* Web service is an Internet-based development model proposed by Microsoft [23]. It provides services for other applications through web communication protocol and open standards of information format (HTTP, XML, and soap). The integrated platform involves software suppliers such as his system (Beijing Donghua, cache database, and software architecture B/S), Tangshan automatic medicine dispenser system (Japan, SQL Server database, and software architecture C/S), medicine taking and reporting machine system (Great Wall, MySQL database, and software architecture C/S), Weilehitz whole box dispensing consis system (Shanghai, SQL database, software architecture is dbo), and Shenzhen weisi'an drug intelligent management system. The system interface technologies include Webservice, XML, Webservice + XML.

After data mining the information stored by various intelligent devices, the format and interactive content of

pharmacy data information can be further unified, and the corresponding interface program can be developed. Collect the interface documents of all intelligent devices and establish a unified pharmacy dispensing database. The main data tables are as follows:

- (1) *Basic Data Sheet of Drug Information.* This table mainly includes drug code, alias, trade name, English name, category, dosage form, specification, minimum specification, packaging unit, large packaging unit, packaging conversion factor, dose unit, minimum unit dose, dose conversion factor, drug price, manufacturer, manufacturer code, approval number/registration certificate number, storage conditions, storage type, and stop sign.
- (2) *Pharmacy Drug Storage Location Data Sheet.* This table mainly includes drug number, storage location information, drug batch, drug batch number, production date, expiration date, and storage location inventory quantity.
- (3) *Hospital Department Basic Data Sheet.* This table mainly includes department number, department name, and department category.
- (4) *Pharmacist Basic Information Data Sheet.* This table mainly includes pharmacist number, pharmacist job number, department number, pharmacist name, professional title, and job category.

- (5) *Prescription Information Data Sheet*. This table mainly includes prescription time, prescription number, patient name, medical card number, invoice number, patient type, patient birth date, patient gender, patient identity, medical insurance type, prescription attribute, prescription type, diagnostic information, prescription remarks, number of doses, expenses, paid in expenses, billing department number, billing department name, prescribing doctor, dispensing priority, drug name, drug specification, manufacturer number and manufacturer name, drug packaging specification, drug packaging unit, drug dose, dose unit, drug usage, drug dosage, supplementary usage, prescription details, and remarks.
- (6) *Prescription Window Information and Screen Call Information Data Sheet*. This table mainly includes dispensing window, dispensing time, dispensing man number, dispensing person's name, call number display information, drug return time, quantity, drug return person's name, and work number and other information.

In order to meet the various needs of pharmacies, intelligent pharmacy equipment and its control system can be used to improve the prescription allocation efficiency and information management level of modern hospitals. The intelligent pharmacy uses semi-automatic equipment to receive the electronic prescription provided by the hospital management system. Through data mining and information association processing, it compares the drug information stored in the upper computer, sends relevant instructions to the lower computer through the data bus, allocates the drugs required by the patients to the drug outlet, reminds relevant personnel to extract the corresponding drugs, and then transmits them to the patients from the drug distribution window after verification.

The intelligent pharmacy control system is mainly composed of upper computer control and lower computer control. Its control system and distribution are shown in Figure 3.

In the intelligent pharmacy control system, the upper computer system mainly receives and processes the prescription information from the hospital by using the data mining method, obtains the drug distribution in the dispensing prescription by associating the data, and then sends instructions to the lower computer system. Then, allocate the corresponding bin to the medicine outlet for relevant personnel to take medicine for dispensing, and receive the feedback message from the lower computer at the same time. When the drug treatment is finished, send the prescription to the window, and return the prescription to the patient after the relevant personnel check the dispensing prescription. The lower computer system mainly receives the instructions from the upper computer system and processes them through data mining. Then, send the instruction to the corresponding intelligent device, transfer the instruction to the drug outlet through the corresponding bin of the device, and display the corresponding instruction and drug

information on the man-machine interface board for the staff to take the medicine. When the above operations are completed, the results are transmitted to the upper computer system to feed back relevant information.

4.2. Intelligent Pharmacy Management System Based on Association Rule Mining. Association rule mining for medicine is mainly based on the prescription drug information provided by the hospital database to mine the information hidden between drugs with certain association. Because the hospital medical database stores a large amount of information occurring in the medical process, including clinical medical diagnosis information and medical management information, the medical data information has a wide range of sources and a large scale. Medical data information usually has certain characteristics. Medical data usually show some heterogeneity and complexity, and medical academic language is relatively rich, which brings some difficulties to the processing of medical information by data mining. Medical data has certain privacy, that is, the privacy of patients. In the process of data mining, we should not only protect the privacy of patients, but also ensure the security of relevant data. Medical data has certain diversity, that is, the establishment of medical database is based on medical experimental observation, doctor diagnosis, and communication between doctors and patients. Therefore, medical data have various forms, which is also the characteristic of medical data different from other types of data information. Medical data has certain relevance, that is, the data in cases may be related to each other. For example, there is often correlation between symptoms, therapies, prescriptions, and drugs, which can be explored by association rule mining. Medical data has certain repeatability, that is, the case data stored in the medical database will inevitably have some duplicate information. Association rule mining method can be used to find the hidden rules in the data. It can be seen that although a large number of medical data are diverse and complex intertwined, on the basis of data pre-processing, association rules can be used to mine the internal laws of medical data.

Considering that the purposes of data mining may be different in practical application fields, the process of data mining is related to specific application fields. For medical data mining, mainly according to the medical information resources stored in the hospital database, the data mining algorithm is used to mine the knowledge with certain correlation between the data. The specific mining process of medical data is as follows:

First of all, make relevant preparations and clarify the main objectives and work steps of medical data mining. On the basis of mastering the characteristics of medical data, pre-process the information stored in medical database with standardization and structure, so as to provide effective guarantee for the mining of association rules. Secondly, according to the goal of medical data mining, appropriate data mining algorithms are used to obtain the required information, and the mining results are analyzed and evaluated. Finally, test the results, decide whether to further

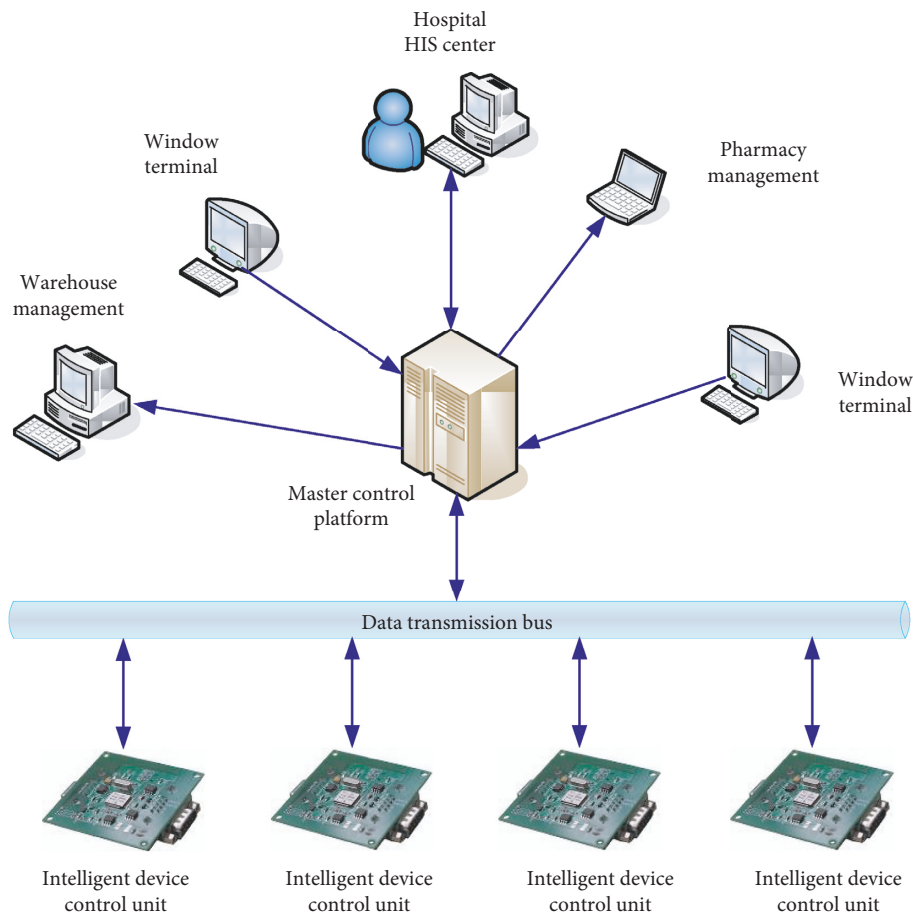


FIGURE 3: Structure and distribution diagram of the intelligent pharmacy control system.

mine the medical data according to the feedback results, and apply the final data mining results to the actual system.

As shown in Figure 4, it reflects the framework of intelligent pharmacy management system based on association rule mining.

4.3. Optimization of the Intelligent Pharmacy Management System. Based on the constructed data integration platform and intelligent pharmacy, the original dispensing process of pharmacy can be further optimized, and the integrated platform and unified data standard can be developed. At the same time, the dispensing process of outpatient prescriptions and emergency prescriptions can be improved by using the standard interface provided by intelligent devices, as shown in Figures 5 and 6.

Considering that various devices in the intelligent pharmacy may fail during use, the emergency dispensing process in case of failure of intelligent devices in the pharmacy is optimized through the construction of data integration platform.

5. System Test and Result Analysis

5.1. System Integration. In 2018, the outpatient pharmacy of our hospital carried out the transformation and construction of intelligent pharmacy, and introduced the first fully automatic integrated dispensing machine, intelligent medicine rack, transportation track, and other intelligent and automatic advanced equipment of pharmacy in Japan. The his system is connected with the pharmacist workstation, which realizes the preliminary intellectualization and automation of drug dispensing in the hospital, and changes the existing mode of manual dispensing and distribution of drugs in the hospital pharmacy. In 2021, weilehitz (Shanghai) was introduced to integrate intelligent equipment such as dispensing machine, and an integrated platform was built by using web service technology to integrate all kinds of servers, high-performance processors, and medical databases through the development and management environment system. According to the prescription data characteristics of various intelligent devices in intelligent pharmacy, data mining technology is used to analyze the relevant

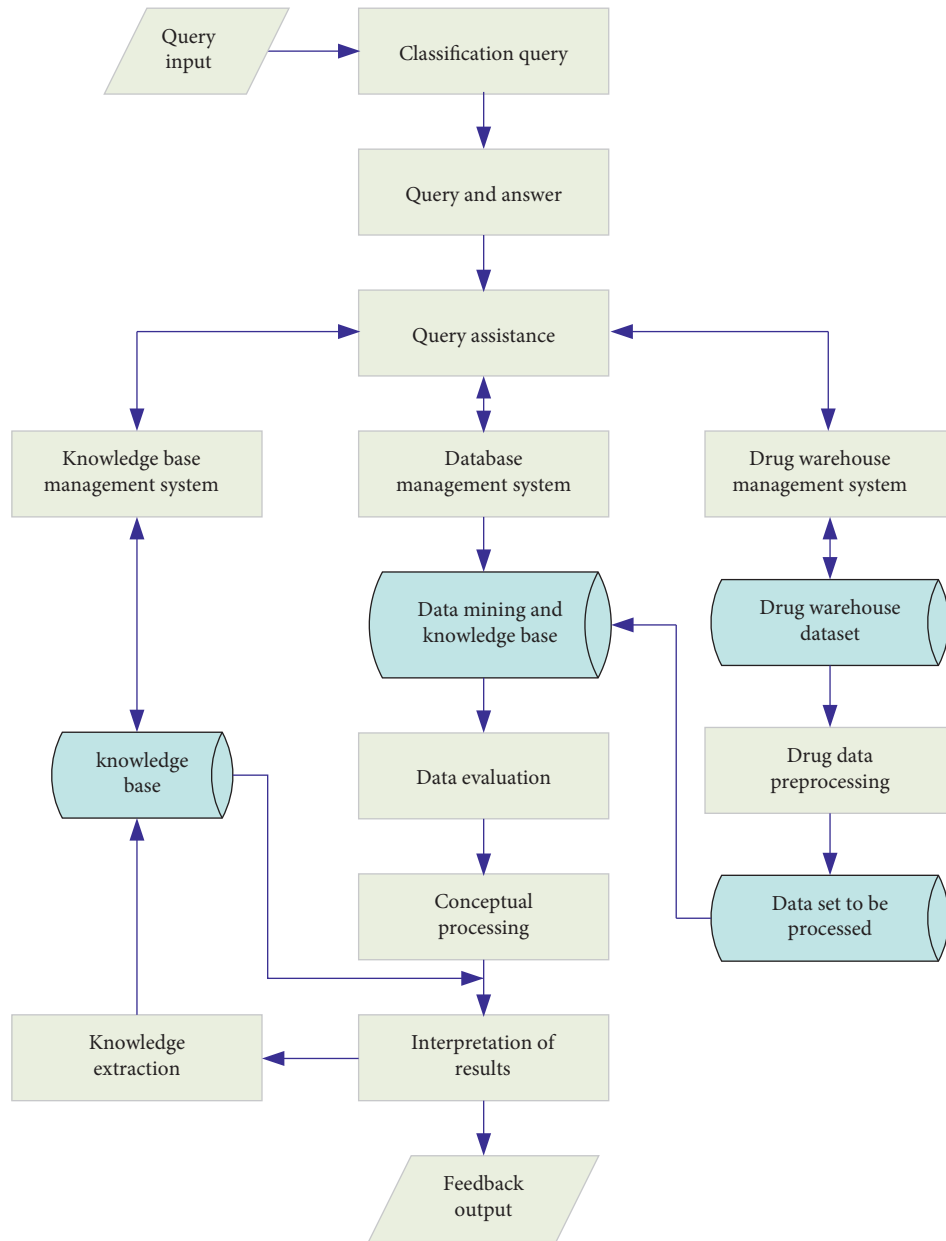


FIGURE 4: The framework of intelligent pharmacy management system based on association rule mining.

information, so as to improve the intelligent degree, dispensing efficiency, dispensing speed, and quality of pharmacy.

5.2. Result Analysis

5.2.1. Comparative Analysis of Equipment Faults. The equipment failures and errors of the dispensing machine from July to September 2020 were statistically analyzed. The main problems occurred in the whole machine drug receiving basket, drug delivery, drug delivery receiving basket,

transmission process, drug lifting, machine restart, drug filling, and other links. In view of various problems, the replacement or transformation and upgrading of relevant equipment were carried out, and the faults and errors of the optimized intelligent pharmacy equipment were statistically analyzed from July to September 2021. The results showed that the failure rate of the system was reduced by 45.27% on average, which effectively improved the operation stability of intelligent pharmacy. The comparison results of faults and errors before and after optimization of intelligent pharmacy equipment are shown in Table 1.

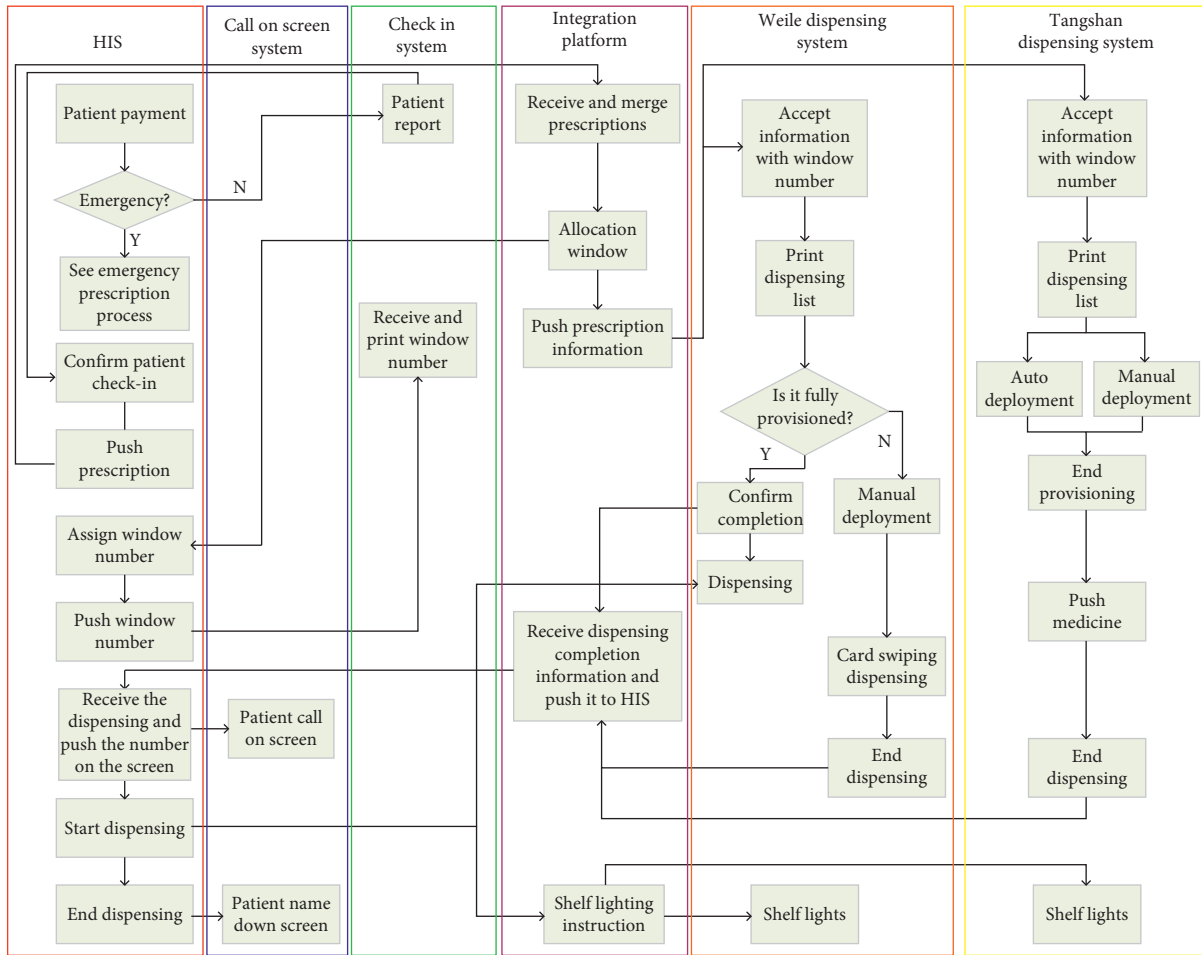


FIGURE 5: Outpatient prescription dispensing process after system optimization.

5.2.2. *Analysis of Allocation Efficiency.* From July to September 2020, the medical data sent by HIS system received by the dispenser every day were mined and analyzed, and the difference between the prescription payment time of patients in the outpatient department and the dispensing processing time of the dispenser was compared. As shown in Figure 7, it was the average waiting time of patients before building the data platform. Through data mining and association rule processing, the main reasons for the delay of dispensing machine were obtained. These factors mainly included the slow dispensing speed of the dispenser itself, the lack of drugs, the blockage of the dispensing basket due to the failure of the dispensing personnel to take drugs in time at the peak, and the blockage of the transportation of the medicine basket due to the failure of the dispensing personnel to take drugs in time. In addition, the deployment delay may also be caused by the networking delay of drug dispensers, drug errors, basket string, etc.

Aiming at the problem of dispensing delay of dispensing machine, this paper used data mining to analyze the prescription data of various intelligent devices in intelligent pharmacy, adopts data integration management, and optimized the dispensing machine and other intelligent devices in pharmacy. Then, the medical data were mined and analyzed from July to September 2021, and the waiting time of patients was compared. As shown in Figure 8, it was the average waiting time of patients after building the data platform. According to the comparison results of the average waiting time of patients before and after the construction of the data platform, it was known that the intelligent pharmacy after the construction of the data platform can significantly improve the dispensing efficiency, dispensing speed, and quality.

Through the construction of data integration platform and prescription data mining, the use of various intelligent devices in the pharmacy had been optimized, the dispensing

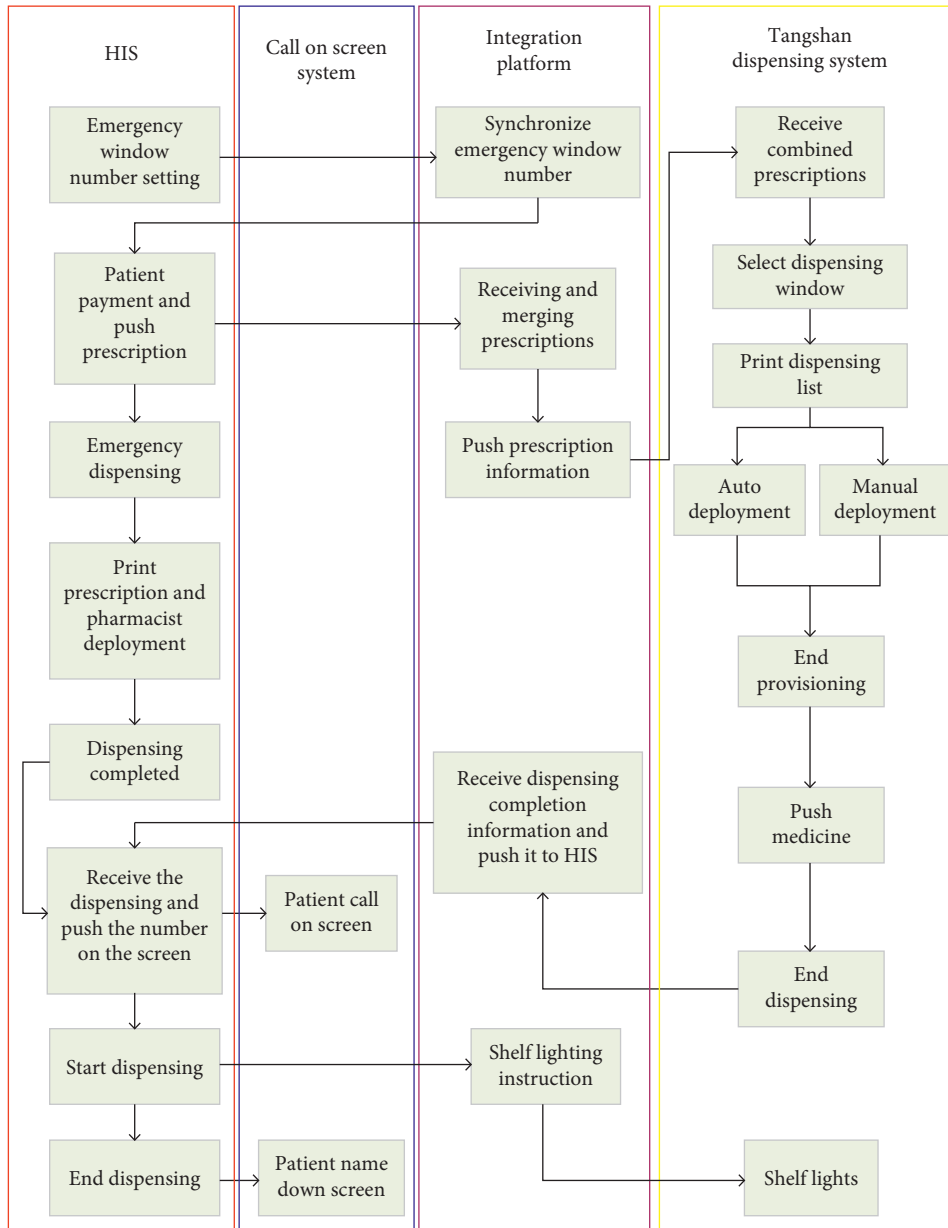


FIGURE 6: Emergency prescription dispensing process after system optimization.

TABLE 1: Comparison results of faults and errors before and after optimization of intelligent pharmacy equipment.

Fault type	2020			2021		
	July	August	September	July	August	September
Machine drug receiving basket	135	58	39	107	32	12
Drug delivery	78	52	43	38	26	5
Drug delivery receiving basket	97	36	41	63	18	14
Transmission process	59	57	38	25	23	9
Drug lifting	76	47	44	39	15	13
Machine restart	73	56	47	42	23	7
Drug filling	54	42	35	21	14	8
Other links	42	39	47	14	12	6

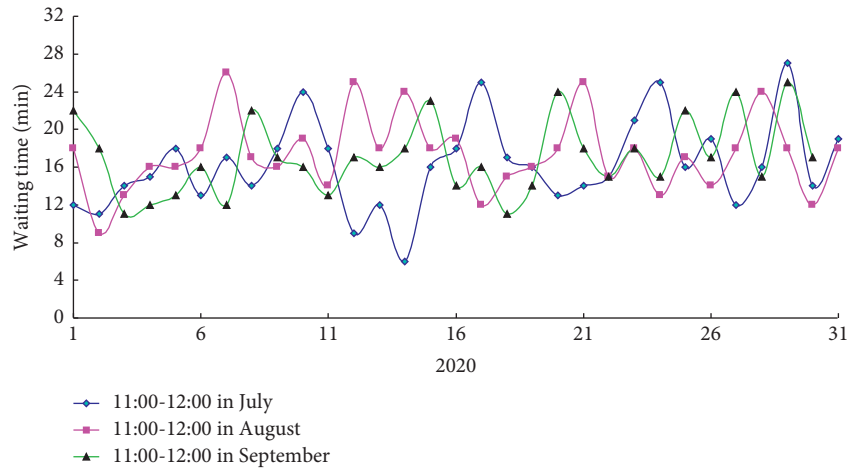


FIGURE 7: Average waiting time of patients before building the data platform.

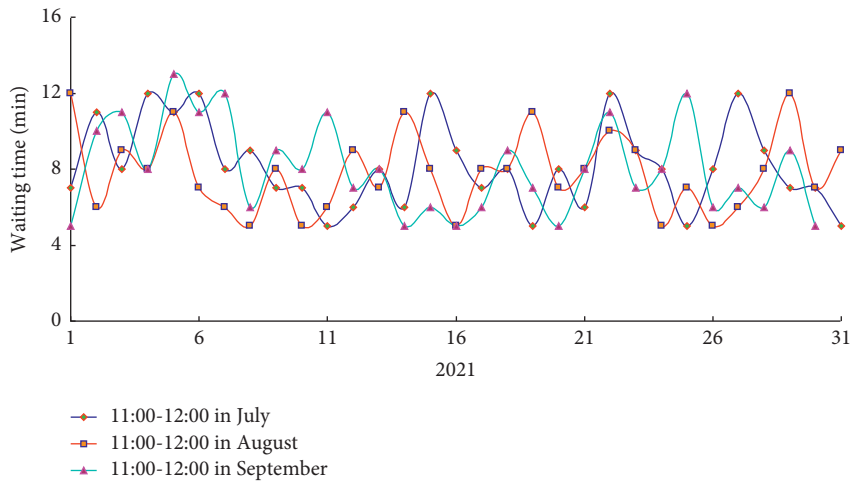


FIGURE 8: Average waiting time of patients after building the data platform.

efficiency of the pharmacy had been improved, and the waiting time of patients in peak hours had been shortened.

6. Conclusion

This paper studies the design and development of intelligent pharmacy, and establishes the dispensing data standard and integration platform of intelligent pharmacy. Web service technology is used to design the interactive interface, which can be called by various intelligent devices. It is also used to standardize the emergency dispensing process of various intelligent equipment failures, optimize the intelligent pharmacy equipment and dispensing process by using data mining, and improve the dispensing efficiency of intelligent pharmacy equipment. Through the data mining of intelligent pharmacy equipment, the intellectualization and informatization of modern pharmacy management are improved. Change the pharmacy management from traditional prescription based to patient-centered drug treatment. Through real-time risk prevention and control, the formula accuracy and operation speed of the intelligent dispensing

machine are improved, and the dispensing time is shortened. Through intelligent drug delivery, the unreasonable drug use of patients is reduced, the safety and effectiveness of clinical drug use are ensured, and the contradiction between doctors and patients is reduced. The research results obtained in this paper can not only reflect the professional technical value of pharmacists and change the pharmaceutical care mode, but also optimize the medical experience of patients, so as to provide patients with more high-quality and humanized pharmaceutical technical services. This study can provide some reference for modern hospital intelligent management and its economic and social benefits.

Data Availability

The labeled data set used to support the findings of this study is available from the corresponding author upon request.

Conflicts of Interest

The authors declare are no conflicts of interest.

Acknowledgments

The research was supported by Guangdong Medical Research Fund Project (B2019244), Shaoguan Science and Technology Bureau Project (2019sn132), and Shaoguan Health and Family Planning Research Project (Y19048).

References

- [1] Y. F. Xu and L. X. Wang, "Discussion on the pharmacy service under the background of new medical reform," *World Latest Med. Inf.* vol. 17, no. 29, pp. 99–100, 2017.
- [2] K. B. Yu, "How to Improve the Quality of traditional Chinese medicine decoction of basic level hospital," *China Health Ind.* vol. 16, no. 3, pp. 20–22, 2019.
- [3] C. Yu and H. L. Liu, "Research and development of information platform based on distribution and quality control of traditional Chinese medicine decoction pieces," *China Med. Educ. Technol.* vol. 30, no. 1, pp. 98–100, 2016.
- [4] D. Martín, R. Alcarria, Á. Sánchez-Picot, and T. Robles, "An ambient intelligence framework for end-user service provisioning in a hospital pharmacy: a case study," *Journal of Medical Systems*, vol. 39, no. 10, pp. 116–210, 2015.
- [5] M. K. Cor and M. J. Peeters, "Using generalizability theory for reliable learning assessments in pharmacy education," *Currents in Pharmacy Teaching and Learning*, vol. 7, no. 3, pp. 332–341, 2015.
- [6] J. Verdasca, F. A. Costa, C. Ramos, R. Murteira, and A. Miranda, "The South Region Cancer Registry: an evaluation of its exhaustiveness in a cohort of lung cancer patients," *Thoracic Cancer*, vol. 10, no. 2, pp. 330–334, 2019.
- [7] C. Donnelly, V. Cairnduff, J. J. Chen et al., "The completeness and timeliness of cancer registration and the implications for measuring cancer burden," *Cancer Epidemiology*, vol. 49, pp. 101–107, 2017.
- [8] X. f. Zhao, C. Yun, X. g. Liu, and W. Wang, "Optimization for scheduling of auto-pharmacy system," *Computer Engineering*, vol. 200, pp. 193–195, 2009.
- [9] R. L. Mador and N. T. Shaw, "The impact of a Critical Care Information System (CCIS) on time spent charting and in direct patient care by staff in the ICU: a review of the literature," *International Journal of Medical Informatics*, vol. 78, no. 7, pp. 435–445, 2009.
- [10] Ó. Álvarez-Machancoses and J. L. Fernández-Martínez, "Using artificial intelligence methods to speed up drug discovery," *Expert Opinion on Drug Discovery*, vol. 14, no. 8, pp. 769–777, 2019.
- [11] S. Rodriguez, C. Hug, P. Todorov et al., "Machine learning identifies candidates for drug repurposing in Alzheimer's disease," *Nature Communications*, vol. 12, no. 1, pp. 1033–1113, 2021.
- [12] A. W. McMahon and G. Dal Pan, "Assessing drug safety in children—the role of real-world data," *New England Journal of Medicine*, vol. 378, no. 23, pp. 2155–2157, 2018.
- [13] S. Schneeweiss, "Learning from big health care data," *New England Journal of Medicine*, vol. 370, no. 23, pp. 2161–2163, 2014.
- [14] T. Egualé, D. L. Buckeridge, A. Verma et al., "Association of off-label drug use and adverse drug events in an adult population," *JAMA Internal Medicine*, vol. 176, no. 1, pp. 55–63, 2016.
- [15] H. Salmasian, T. H. Tran, H. S. Chase, and C. Friedman, "Medication-indication knowledge bases: a systematic review and critical appraisal," *Journal of the American Medical Informatics Association*, vol. 22, no. 6, pp. 1261–1270, 2015.
- [16] R. J. J. Bepko, J. R. Moore, and J. R. Coleman, "Implementation of a pharmacy automation system (robotics) to ensure medication safety at norwalk hospital," *Quality Management in Health Care*, vol. 18, no. 2, pp. 103–114, 2009.
- [17] S. W. Collins, "Knowledge clusters and the revitalization of regional economies in Japan: a case study of the biomedical industry in Kobe," *Prometheus*, vol. 26, no. 1, pp. 111–122, 2008.
- [18] Z. V. Meshcheryakova, "Medical cluster in the health care system of the region as an innovative model of integration of subjects of public-private partnership," *Econ. Bus. Theory Pract.* vol. 3, pp. 43–45, 2017.
- [19] J. Sankaranarayanan, L. J. Murante, and L. M. Moffett, "A retrospective evaluation of remote pharmacist interventions in a Tele-pharmacy service model using a conceptual framework," *Telemedicine and e-Health*, vol. 20, no. 10, pp. 893–901, 2014.
- [20] K. L. James, D. Barlow, A. Bithell et al., "The impact of automation on workload and dispensing errors in a hospital pharmacy," *International Journal of Pharmacy Practice*, vol. 21, no. 2, pp. 92–104, 2013.
- [21] R. J. Hodes and N. Buckholtz, "Accelerating medicines partnership: alzheimer's Disease (AMP-AD) Knowledge Portal aids Alzheimer's drug discovery through open data sharing," *Expert Opinion on Therapeutic Targets*, vol. 20, no. 4, pp. 389–391, 2016.
- [22] X. Zhang, D. Meiser, Y. Liu, B. Bonner, and L. Lin, "Kroger uses simulation optimization to improve pharmacy inventory management," *Interfaces*, vol. 44, no. 1, pp. 70–84, 2014.
- [23] D. Martín, D. López-de-Ipiña, A. Alzua-Sorzabal, C. Lamsfus, and E. Torres-Manzanera, "A methodology and a web platform for the collaborative development of context-aware systems," *Sensors*, vol. 13, no. 5, pp. 6032–6053, 2013.

Research Article

Analysis of Teaching Tactics Characteristics of Track and Field Sports Training in Colleges and Universities Based on Deep Neural Network

Wei Wang 

Sports Department, Wuhu Institute of Technology, Anhui Wuhu 241003, China

Correspondence should be addressed to Wei Wang; wangw@whit.edu.cn

Received 23 May 2022; Revised 23 June 2022; Accepted 12 July 2022; Published 21 August 2022

Academic Editor: Le Sun

Copyright © 2022 Wei Wang. This is an open access article distributed under the Creative Commons Attribution License, which permits unrestricted use, distribution, and reproduction in any medium, provided the original work is properly cited.

In the analysis of the teaching tactical characteristics of track and field sports training in colleges and universities, the teaching tactical characteristics are not quantified, which leads to the low key degree of determining the influencing factor indicators in colleges and universities, and the error in the evaluation of the teaching tactical characteristics of track and field sports training is large. Therefore, this paper designs a method to analyze the tactical characteristics of college track and field sports training teaching based on deep neural network. Firstly, by analyzing the current situation of track and field sports training teaching in colleges and universities, it determines the areas that need to be improved in teaching. Then, by determining the factors of teaching environment, the core competitiveness of track and field teams, and the teaching ability of track and field coaches, these factors are determined as the key characteristics, the data basis is analyzed, and the unified data quantitative processing is carried out to determine the key factor indexes affecting the analysis of tactical characteristics. Finally, the deep neural network is introduced to construct the evaluation model of the tactical characteristics of college track and field sports training teaching, and the characteristic analysis results are further modified with the help of cascade noise reduction self-encoder to complete the analysis of the tactical characteristics of college track and field sports training teaching. The experimental results show that the proposed method can effectively analyze the teaching tactical characteristics of track and field sports training in colleges and universities and improve the performance of the evaluation of the teaching tactical characteristics of track and field sports training.

1. Introduction

College track and field training is an important part of school physical education. Track and field is one of the key items of school physical education teaching and after-school training. It has the advantage of talent concentration and wide popularity [1, 2]. Track and field training is the basic training stage of track and field. It is the key stage to develop sports quality, learn and master track and field technology, and improve track and field ability. Paying attention to and strengthening track and field training is an important link to improve the overall training level of track and field [3]. Track and field sports play a positive role in realizing the knowledge, technology, and skills of sports in college physical education and improving students' physical and psychological quality and social adaptability. However, in

the process of deepening the reform of physical education teaching in colleges and universities, it is found that the number of students participating in track and field is becoming less and less, and the students' understanding of the value of participating in track and field is becoming less and less. The school also makes track and field teaching more and more marginalized because of the students' weak awareness of track and field teaching [4]. At the same time, track and field teaching pursues the integrity and systematization of competitive events too much and only pays attention to the teaching of technical actions in running, jumping, throwing, and other events, and the teaching means are single. It can not develop students' relevant physical quality around a certain event, so students' subjectivity and creativity are difficult to play. Only by making the track and field teaching concept clear and the goal clear and paying attention to a

series of problems such as teaching content, teaching methods, and textbook selection, can the track and field teaching reform in colleges and universities not be in a chaotic and fuzzy state and can a clear main line be provided for the reform and development of track and field teaching in colleges and universities [5, 6].

How to cultivate track and field sports talents who can shoulder the historical mission and have practical ability and innovation ability, constantly keep pace with the times, improve track and field sports training tactics, implement effective training tactics, and improve the quality of track and field training has become the top priority to be solved by China's colleges and universities of physical education [7]. Therefore, relevant researchers have made a lot of analysis on the tactical characteristics of track and field training in colleges and universities. Literature [8] designed a simulation training method and studied its application in track and field training tactics. In this technology, in order to ensure that athletes can play a better level in the competition, coaches should not only strengthen the training of their physical quality, but also let them fully master and use sports technology, which is a vital way and means in training. Once the psychological and special situation handling skills training is ignored, it will affect the normal competition of athletes and even lead to the loss of the competition. Therefore, this paper mainly analyzes the main advantages and characteristics of track and field simulation training and puts forward the specific application of simulation training method in track and field situation. It aims to promote athletes to have a good psychological and physical state in the process of competition, so as to give full play to their best potential and level and finally win the ideal results. This study pointed out the psychological characteristics and sports characteristics of training technology but did not effectively quantify the detailed tactical characteristics and indicators. Literature [9] analyzes the influencing factors of physical fitness training in track and field sprint events. Take this as the research basis to improve the quality of training tactics. This paper points out that, with the rapid development of track and field sprints in China, the requirements for sprinters' competition skills and tactical level are becoming higher and higher. How to improve the quality of track and field sprinters' training plan and how to quickly enhance the physical quality of track and field sprinters have become the most concerned topic in the field of track and field sprinters' training. Physical training is an important basis for all skill training. In order to make sprinters give full play to their potential and win the sprint competition, physical training is the most indispensable and important factor. This paper will deeply analyze and explore the influencing factors and related contents of physical fitness training in track and field sprint. However, this article is highly theoretical and needs to further expand the main technical characteristics of the research.

In view of the shortcomings in the above analysis of the teaching tactical characteristics of track and field sports training, this paper designs an analysis method of the teaching tactical characteristics of track and field sports training in colleges and universities based on the deep neural

network algorithm to complete the analysis of the teaching tactical characteristics of track and field sports training in colleges and universities. The main technical route of this paper is as follows:

Step 1: by analyzing the current situation of track and field sports training teaching in colleges and universities, determine what needs to be improved in teaching.

Step 2: by determining the factors of teaching environment, the core competitiveness of track and field teams, and the teaching ability of track and field coaches, these factors are determined as the key characteristics, the data basis is analyzed, and the unified data quantitative processing is carried out to determine the key factor indicators affecting the analysis of tactical characteristics.

Step 3: introduce the deep neural network to construct the evaluation model of the tactical characteristics of college track and field sports training teaching, and further modify the characteristic analysis results with the help of the cascade noise reduction self-encoder to complete the analysis of the tactical characteristics of college track and field sports training teaching.

Step 4: conduct experimental analysis. Taking a university as an example, the effectiveness of the proposed analysis method is verified.

2. Current Situation of Track and Field Physical Training Teaching in Colleges and Universities and the Determination of Influencing Factors and Indicators of Tactical Characteristics

2.1. Analysis on the Current Situation of Track and Field Physical Training Teaching in Colleges and Universities

2.1.1. *The Meaning of Track and Field Training Is Vague.* The goal of track and field teaching in colleges and universities is to enhance students' physical qualities, help students form good physical exercise habits, and establish correct health awareness. However, in the actual teaching and training, many teachers pay too much attention to the cultivation of students' track and field skills, and take the learning results of track and field skills as the standard to measure students, but they lack accurate positioning for the cultivation of students' fitness consciousness and exercise consciousness. Due to the overemphasis on the integrity and technicality of track and field events in teaching activities and the neglect of students' acceptance ability, students' interest in track and field training is not high [10].

2.1.2. *The School Pays Less Attention to the Teaching Value of Sports Track and Field.* As a special field, the school field is a space with its own logic and inevitability composed of various objective relations including organization and system. Its interior follows its own unique logic, operation rules, and development track and has a restrictive effect on the

survival and development of school leaders and track and field teachers in the field. School field is a realistic factor that affects the value orientation of track and field teaching in colleges and universities. It is mainly reflected in the fact that the school field has more and more successfully made people learn fast, learn more, and learn well, but it has caused the forgetting of the meaning of “learning,” which is not used by people, makes people subordinate to “learning,” is trapped by “learning,” and suppresses the perfection and harmonious generation of people. Track and field classroom teaching is based on rational knowledge. The real life, quality of life, and life value of teachers and students are usually ignored, forgetting the humanistic care for teachers and students and the improvement of human nature [11].

2.1.3. The Organization Form of Track and Field Teaching Is Single. The organizational form of track and field teaching in colleges and universities is relatively single. Teachers often do demonstration actions, then explain step by step, and learn to imitate and practice repeatedly. In this form of teaching organization, teachers are the main body of classroom teaching, and students can only passively accept teachers’ knowledge indoctrination, so students’ learning enthusiasm is greatly affected. In addition, many teachers only pay attention to how much they have taught but ignore how much students have learned. As long as their teaching tasks are completed, they think they have achieved the purpose of teaching.

2.1.4. The Influence of the Inertia of Power Field on the Occupation of Track and Field Teaching Skills. As an objective social existence, the behavior and thought of educators and other educational participants are affected by the right field, and anyone’s survival and development are in a certain right field. Zimmer, a famous sociologist, pointed out that, in any situation of social interaction, people may have the difference between superior position and inferior position. He called this form of social relations with the advantages and disadvantages of position and position as “domination”; that is, the dominant person has the ability and opportunity to influence, decide, and control the inferior person. Looking at the track and field teaching environment of physical education departments in colleges and universities from the field of power, as long as we understand the power of the “test baton,” we can understand why the first place of skills is virtual, and only the students’ track and field standard score is real [12].

2.2. Determination of Influencing Factors and Indexes of Teaching Tactics of Track and Field Sports Training in Colleges and Universities. In order to more effectively highlight the effectiveness of this analysis method, first quantify the data on track and field sports training teaching characteristics in colleges and universities, convert it into certain data, and more intuitively analyze the tactical characteristics of track and field sports training teaching in colleges and universities. In the teaching of track and field sports in colleges and

universities, the teaching environment is the key to the tactical characteristics of track and field sports training and teaching in colleges and universities. Therefore, this paper determines the important indicators affecting the track and field teaching environment in colleges and universities and effectively quantifies them [13].

Taking the element structure system of track and field teaching environment in colleges and universities as the basis, according to the establishment principles of the evaluation system and drawing on previous research experience, this paper summarizes, divides, and compares the important indicators affecting the track and field teaching environment in colleges and universities, forms the conceptual indicators of track and field teaching environment in colleges and universities, and finally constructs the evaluation index system of track and field teaching environment in colleges and universities. The specific contents are shown in Figure 1.

According to the abovementioned evaluation index system of track and field teaching environment in colleges and universities, this teaching strategy is quantitatively analyzed. Because the track and field teaching environment is the main influencing factor, it can not directly transform the data. Therefore, with the help of coefficient of variation, the influencing factors are studied quantitatively. The coefficient of variation is the ratio of the standard deviation of the index to the weighted average. If the coefficient of variation is small, it means that the expert evaluation results are not dispersed or the degree of dispersion is small [14]. Generally, the coefficient should be less than the standard of 0.25. If it is more than or equal to, it means that the index lacks coscheduling. The calculation formula of the influencing factor index is

$$R_r = \frac{A_i}{v_i}. \quad (1)$$

Among them, R_r represents the coefficient of variation of track and field teaching environment factors. The smaller the value, the higher the coordination degree of the teaching environment on tactics. A_i represents the standard deviation of teaching environment influencing factors, and v_i represents the arithmetic mean of environmental factors.

In order to minimize the influence of the teaching environment of university track and field on the teaching tactics, the coordination coefficient is introduced to balance it. The meaning of the coordination coefficient is whether there is a large difference between the recommendations in the expert group. The accounting of the coordination coefficient can obtain the degree of expert coordination of the index. The coordination coefficient is represented by W , and the value is between 0 and 1. Use consistency test; if $P > 0.05$, the evaluation made by experts does not have strong credibility and the result is invalid; if $P < 0.05$, it has certain credibility and can be used. The calculation formula is

$$P = \frac{W}{\sum R_r}. \quad (2)$$

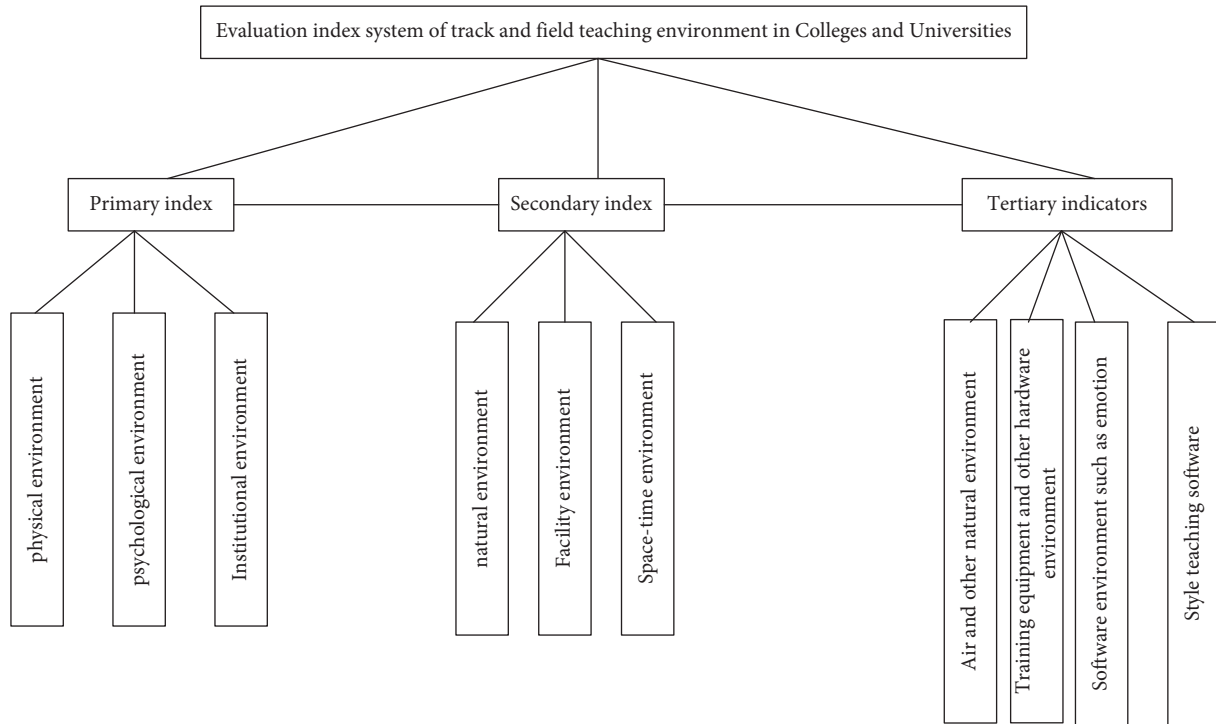


FIGURE 1: Evaluation index system of track and field teaching environment in colleges and universities.

According to the above calculation, the influence degree of track and field teaching environmental factors in colleges and universities is determined, which is regarded as a key factor affecting the characteristics of sky landing teaching tactics. In addition, it also includes other influencing factors, which also need to be quantified one by one.

Core competitiveness is the integration of various advantageous resources that have been continuously optimized and improved to form their own unique and difficult to imitate form. Its core competitiveness is not only different from its general competitiveness, but also related. The core competitiveness of high-level track and field teams is finally formed in the general competitiveness. It goes beyond the general competitiveness [15], so that it can maintain a stable, leading position and advantage in the field of track and field competition for a long time. The biggest feature of this difference is that it is not easy to be imitated by competitors and can form its own unique competitive advantage. Therefore, to analyze the elements of the core competitiveness of high-level track and field teams, we should extract the most core factors from many “seemingly” general competitiveness elements, because these factors are most likely to play a vital and irreplaceable role in the formation of the core competitiveness of high-level track and field teams in colleges and universities [16]. The schematic diagram of competitive core strength of college track and field teams is shown in Figure 2.

By analyzing Figure 2, it can be found that the current model has the following important characteristics: first, integrity. The model reflects the main components of the core competitiveness of excellent high-level track and field teams, and the content system is relatively complete. The

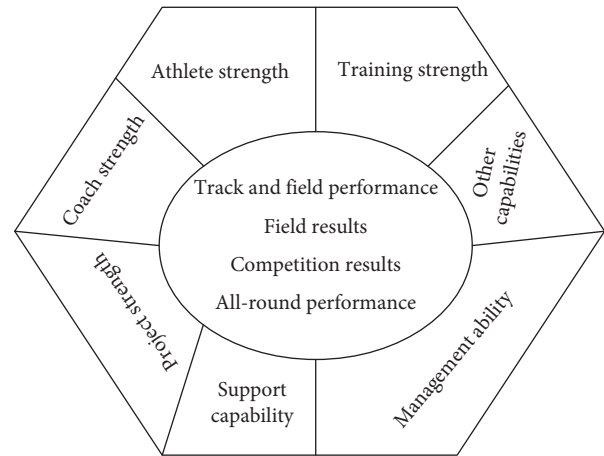


FIGURE 2: Schematic diagram of influencing factors of core competitiveness of college track and field teams.

second is scientific. The construction basis of this model is in line with the purpose and law of high-level track and field teams, the basic theory of core competitiveness construction, and the reality of running high-level track and field teams. It is highly scientific. The third is hierarchy, which is divided into three interrelated levels according to the relationship with competitive performance, reflecting the hierarchical principle of system theory, with rigorous logic and clear hierarchy. The fourth is the development and variability. This model expresses the meaning of the continuous operation of various elements of core competitiveness around the “expression of competitive achievements” and suggests that the composition of core competitiveness will change

with time and team running conditions. Only when the joint force of these elements can bring competitive advantages to the sports team, can the status of core competitiveness of various elements be stabilized; otherwise it may fall into the ranks of general competitiveness. Therefore, it has development and variability. In the quantification of the influencing factors, the importance of an aspect of the previous level is compared according to the factors in the same level, and the pairwise comparison judgment matrix is completed [17]. When the above layer factors are regarded as standards, the comparative standard b_{ij} can be adopted to represent the importance of competitiveness influencing factors. The judgment matrix composed is

$$B = \sum_{i=1, j=1} b_{ij}. \quad (3)$$

The constructed judgment matrix is tested, and the consistency and randomness of the matrix are tested. The following results are obtained:

$$C = \frac{c_i}{\eta_i}, \quad (4)$$

$$c_i = \frac{\lambda \max - k}{k - 1}, \quad (5)$$

where η_i represents the average random consistency criterion and c_i is a constant.

In the analysis of the tactical characteristics of track and field teaching in colleges and universities, the teaching ability of teachers, that is, coaches in track and field training, is also the key factor affecting the tactical characteristics. When evaluating the teaching ability of track and field coaches, we need to reflect their ability level through multiple indicators. The first step of this study is to classify the collected indicators. The second step is to screen and integrate the indicators with the same connotation and overlapping contents and rename them. On the basis of formulating the primary indicators, the Delphi method (the first round of expert questionnaire) is used to determine the candidate indicators of track and field coaches' teaching ability. Then make statistics of the feedback and further sort out and screen the corresponding indicators to determine the teaching ability index system of track and field coaches. The process is shown in Figure 3.

The contents of the teaching ability indicators of track and field coaches are shown in Table 1.

According to the abovementioned factors affecting the characteristics of track and field teaching tactics in colleges and universities, that is, the factors of teaching environment, the core competitiveness of track and field teams, and the teaching ability of track and field coaches, these factors are determined as the data basis of key characteristic analysis and unified data quantitative research [18]. The set of factors affecting the evaluation objectives is determined as follows:

$$E = \{e_1, e_2, \dots, e_n\}. \quad (6)$$

The comment set for establishing impact assessment objectives is

$$U = \{u_1, u_2, \dots, u_n\}. \quad (7)$$

Calculate the weight of each evaluation factor and the objective vector of impact assessment is

$$Q = \{q_1, q_2, \dots, q_n\}. \quad (8)$$

Using analytic hierarchy process to calculate the weight vector: carry out single factor fuzzy evaluation and determine the fuzzy relationship matrix; combined with the single factor evaluation vector of membership degree, complete the construction of multi-index comprehensive evaluation vector, and obtain

$$H_i = V \sum_{i=1}^n (E, U, Q). \quad (9)$$

According to formula (9), the results of fuzzy comprehensive evaluation are analyzed, and the quantitative influencing factors of track and field teaching tactical characteristics are taken as the key indicators of subsequent characteristic analysis. On this basis, the analysis of track and field teaching tactical characteristics in colleges and universities is improved.

3. Design of Evaluation Model of Teaching Tactics Characteristics of Track and Field Physical Training in Colleges and Universities Based on Deep Neural Network

3.1. Determination of Teaching Tactics Characteristics of Track and Field Physical Training in Colleges and Universities. Among the tactical characteristics of track and field teaching in colleges and universities, the characteristic of speed change is the external form of tactical application. The smooth implementation of tactics is reflected by athletes through the whole process of speed distribution and speed saving. Therefore, it can be said that the characteristics of speed change are the basis of tactical application. The main features are the following teaching tactics.

3.1.1. Leading Tactics. According to the different positions of athletes in the competition, the tactics can be divided into leading walking tactics and following walking tactics. The leading walking strategy refers to the strategy that athletes start walking at a faster speed at the beginning of the game, strike first, try their best to get rid of the opponent's follow, open the distance with the opponent, and lead all the way through the whole process [19]. The advantage of this tactic is that it can give full play to the physical, tactical, and psychological advantages of athletes without interference from opponents. It is suitable for athletes with good speed endurance, strong ability to walk at high speed for a long time, and special strength. The disadvantage is that the tactical speed changes greatly, the physical energy consumption is much, and the use is too risky. Therefore, it is not recommended to use it by ordinary athletes. If it is used blindly, it will often lead to the second half or final rush due to unreasonable physical distribution.

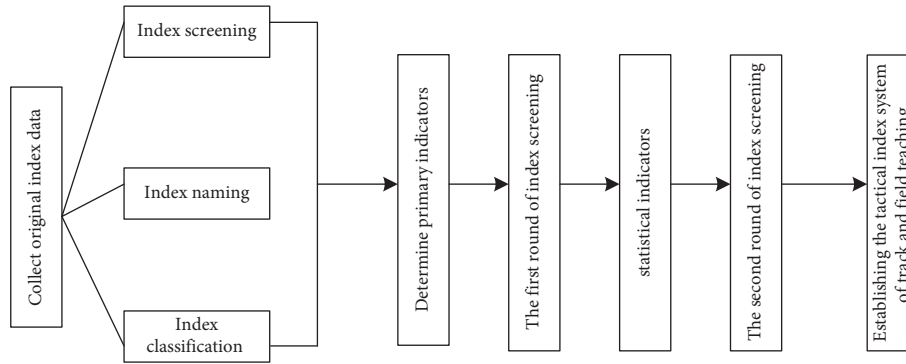


FIGURE 3: Process of teaching ability index system of track and field coaches.

TABLE 1: Contents of coaching ability indicators of track and field coaches.

Teaching ability	Content
Personal experience	Age, educational background, sports level, years, post training, etc.
Training ability	Diagnostic ability, prediction ability, designated plan ability, recovery ability, stimulation means, etc.
Teaching ability	Action modeling, explanation ability, sports equipment ability, learning ability
Competition guidance ability	Specify the program ability, organization and arrangement ability, and adjustment ability
Organization and management ability	Daily training and management, conflict resolution, etc.
Scientific research and innovation ability	Postgame summary, reflection ability, scientific research ability, etc.

In the stabbing stage, the physical strength is overdrawn, resulting in the situation of being surpassed by the opponent.

3.1.2. *Follow Tactics.* Following tactics refers to the tactics that athletes use faster speed to quickly seize a favorable position at the beginning of the competition, closely follow an athlete who is roughly consistent with their own rhythm and pace, and in the final sprint stage, attack later and surpass the follower or even the leader with the advantage of their own sprint ability. The advantage of using this tactic is that athletes only need to concentrate on following the followers, which not only reduces their psychological pressure, but also causes greater psychological pressure to the followers. In addition, from the perspective of hydrodynamics, compared with the follower, the follower resists certain air resistance because the follower leads in front, which makes the follower walk more labor-saving and less physical consumption. It is suitable for athletes with good speed and strong sprint ability, as well as competition in bad weather such as wind and rain [20]; its disadvantage is that the follower’s speed rhythm is easily disturbed by the follower. It is easy to put the follower in a passive position on the competition field.

3.1.3. *Uniform Velocity Tactics.* According to the speed changes of athletes in the competition, tactics can be divided into constant speed tactics and variable speed tactics. Uniform speed tactics refers to the tactics that athletes start and walk at a relatively uniform speed from the beginning of the game and maintain this speed to complete the whole process. The advantage of this tactic is that athletes can

determine the speed and rhythm according to their own competitive ability, and the physical consumption is small. It is suitable for athletes who create their best sports performance.

3.1.4. *Variable Speed Tactics.* Variable speed tactics refers to the tactics that athletes occupy a favorable position at a relatively fast speed at the beginning of the game, constantly adjust their physical fitness through speed control and rhythm changes, interfere with the opponent as much as possible, get rid of the opponent, and win the game. The advantage of this tactic is that it can not only disrupt the opponent’s speed change rhythm and break the functional balance of its internal organs and systems, but also cause greater psychological pressure on the opponent. It is suitable for athletes with high speed and endurance. Its disadvantage is that it consumes a lot of physical energy for athletes. If you cannot reasonably distribute your physical strength, it is easy to cause your own physical weakness.

3.2. *Evaluation Model of Teaching Tactics Characteristics of Track and Field Sports Training in Colleges and Universities.* According to the above extracted quantitative indicators of the influencing factors of the teaching tactical characteristics of college track and field sports training, in order to realize the analysis of the teaching tactical characteristics of college track and field sports training, this paper introduces the deep neural network algorithm [21] to construct the evaluation model of the teaching tactical characteristics of college track and field sports training and takes the quantitative indicators of the influencing factors of the teaching tactical

characteristics of college track and field sports training as the input data of the neural network, in order to complete the analysis of the teaching tactical characteristics of track and field sports training in colleges and universities.

3.2.1. Theoretical Basis of Deep Neural Network Algorithm. Deep neural network is an important branch of machine learning. Deep learning method has the ability to extract abstract features. Compared with machine learning, it does not need to extract features manually but automatically extracts basic features from samples. Then, some more advanced features are extracted layer by layer, such as lines, local structure, and so on. Finally, effective fitting results are obtained by updating model parameters similar to machine learning. The basic neural network structure is shown in Figure 4.

In Figure 4, the circle in the graph represents a neuron, x_i represents the i th input signal, z_{ij} represents the weight of the signal effect on the neuron j to simulate the strength of the synapses, μ_{ij} represents a threshold, and $y(x)$ represents the activation function after the neuron reaches the threshold, requiring that its nonlinearity is differentiable. The last current layer i th output signal t_i may be expressed as follows:

$$t_i = y\left(\sum_{i=1}^n z_{ij}x_i + \mu_{ij}\right). \quad (10)$$

The neural nodes in each layer of the traditional network model are connected with each other. As the learning task becomes more and more complex, the performance of hardware equipment shows a certain bottleneck. The amount of network parameters is limited, the neuron layer cannot be further deepened and widened, and the learning ability of the model is limited. In addition, in the field of computer vision, the fully connected network can not use the location information between pixels, which also limits the learning ability of the network to a certain extent. The emergence of deep neural network solves the above problems well [22].

3.2.2. Evaluation on Teaching Tactics of Track and Field Sports Training. With its excellent characteristic learning ability, deep neural network has become one of the most far-reaching achievements in the field of deep learning. For one of the neural network layers, the output characteristic formula is

$$x_j^l = f\left(\sum_{i=1}^n x_j^{l-1} \times w_{ij} + \beta_{ij}\right), \quad (11)$$

where w_{ij} represents the ensemble of neurons in the input layer, x_j^l represents the output of the i neuron, also the input in layer 1, and β_{ij} is the bias of the j input in layer 1.

Taking the tactical characteristic index data of track and field teaching in colleges and universities as the basic data of initial training in deep neural network, an appropriate loss function is determined to measure the error between the

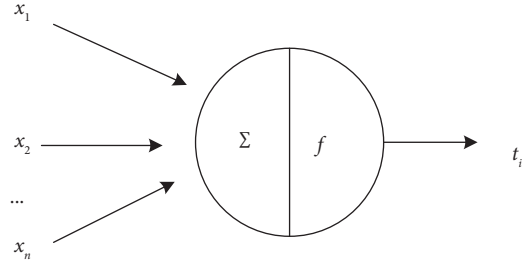


FIGURE 4: Structure diagram of basic neural network.

output of deep neural network and the original data [23, 24], and the following results are obtained:

$$W = \sum \frac{1}{2} \|s_i - y\|_2^2, \quad (12)$$

where s_i represents the network output value, and y represents the sample label value. The network output with the sample labels was fitted by the algorithm to minimize the error.

The multilayer perceptron in the deep neural network further defines the error of the value of track and field teaching tactical characteristics output by the output layer as

$$\varphi_i = \frac{\partial w}{\partial s_i} H f'(s_i), \quad (13)$$

where φ_i represents the inactive output; H is the product of Hadama (Hadamard), and f' represents the derivative of the activation function, producing different types depending on the selected activation function.

Then, the gradient descent method [25] is used to update the result value of the tactical characteristics of track and field teaching in colleges and universities, and the following results are obtained:

$$\Delta\varphi_i = -\chi \frac{\partial w}{\partial s_i}, \quad (14)$$

where χ represents the learning rate. Through this method, the deep neural network parameters are iteratively updated to solve the target threshold, that is, the key value to determine the tactical characteristics of track and field teaching.

Because the characteristic of track and field teaching tactics is an abstract concept, it can not be output intuitively. Therefore, according to the output results of deep neural network, an unsupervised method is used to extract the key tactical characteristics from a large number of track and field tactical characteristics data. In this paper, the cascade noise reduction self-encoder is introduced to effectively extract the key features of the tactical characteristics of track and field teaching. The basic mode of the cascade noise reduction self-encoder [26] is shown in Figure 5.

Through cascade noise reduction, the input of the self-encoder network is the result of noise distortion of the original data. The training process does not need any manually labeled data labels, and the target label is the pure original data itself. The criterion of network training is to

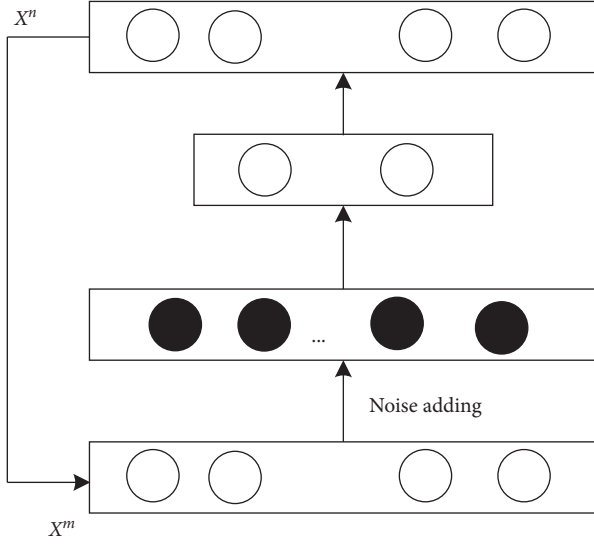


FIGURE 5: Basic mode of stacked noise reduction self-encoder.

minimize the difference between the output of the network and the pure original data, that is, the reconstruction loss. Suppose that m track teaching tactical characteristics quantify the training sample data set $x = \{x^1, x^2, \dots, x^m\}$ as network input, where c represents a pure original sample, while x^n represents the noise distortion result of the original sample x^m . For a typical noise reduction autoencoder structure, the bottom-up process is usually called the encoding process, while the top-down process is known as the decoding process.

If d and d' represent the weight matrix of the uplink and downlink encoder, and b and b' represent the bias of the corresponding nodes, the objective function of the learned regularity term of a noise-reducing self-encoder is expressed as

$$\min \varepsilon = \eta \sum_{i=1}^m \|x^n - x^m\|_2^2 + \nu(d^2) + \|d'\|^2, \quad (15)$$

where ε represents the set of all parameters to be learned in the network; ν is a nonlinear excitation function, and η is the weight factor of the parametric regular term used to balance the reconstruction loss and the weight penalty.

According to the characteristic data of track and field teaching tactics after noise reduction self-encoder training, input it into the constructed depth neural network. When the number of samples is enough, these samples can really reflect the characteristics of track and field teaching tactics. The output results of the final track and field teaching tactics evaluation are as follows:

$$Y(x^n) = \sum_{i=1}^n r \delta_i (x^n - x^m). \quad (16)$$

Among them, $Y(x^n)$ represents the analysis result value, and δ_i represents the deviation coefficient of the output characteristics of teaching tactics.

4. Experimental Analysis

4.1. Experimental Scheme Design. In order to verify the effectiveness of the proposed method, an experimental analysis is carried out. In the experiment, the 20-kilometer walking race held by a university was taken as the research object, and 12 male athletes were selected as the research object. These 12 contestants were contestants in different classes of the same grade, aged between 18 and 19 years, and their physical qualities were relatively similar. In the 20-kilometer walking race, the characteristics of the speed change in the first and second half of the race are analyzed, and the feasibility of the analysis method in this paper is analyzed. Before the game, under the guidance of the coach, the training has been carried out for three months. The 12 people are divided into two groups. One group is the experimental group. Six players in this group compete in the tactics formulated by the coach, and the other group compete in accordance with their own training methods. Investigate the importance of the first and second half of the 20 km race walking race, as shown in Table 2.

According to the experimental scheme designed above, the effective analysis of the characteristics of teaching tactics is carried out. In the experiment, taking the analysis method of this paper, the method of [8], and the method of [9] for the 20 km race walking competition as the research object, analyze the error of different methods on the tactical analysis and the key degree of the influencing factors determined by the tactical characteristics as the experimental object, summarize the experimental data, and complete the experimental analysis.

4.2. Analysis of Experimental Results. In the experiment, firstly, the proposed method is analyzed. In the 20-kilometer race walking competition, the group using coach teaching tactics and the group without teaching tactics are used to determine the results of the 12 athletes. Among them, No. 1–6 are the athletes without coach teaching tactics, and 7–12 are the athletes under coach tactics. The 12 athletes complete the speed analysis of the 20-kilometer race walking competition. The results are shown in Table 4.

By analyzing the experimental results in Table 4, it can be seen that the shortest time spent by athletes No. 1–6 in the 20 km race walking competition is about 30.25 min, that of athletes No. 7–12 in the 20 km race walking competition is about 29.54 min, that of athletes No. 1–6 in the 20 km race walking competition is more than 30 min, and for athletes No. 7–12 in the 20 km race walking competition, two athletes spend less than 30 min, and the overall time is lower than that of athletes No. 1–6. It can be seen that the athletes using teacher tactics achieve better results, which verifies the feasibility of the proposed method.

The experiment further analyzes the error of the analysis method of this paper, the method of [8], and the method of [9] on the characteristics of teaching tactics in this race walking competition. The results are shown in Figure 6.

By analyzing the experimental results in Figure 6, it can be seen that there are some differences in the error of

TABLE 2: Investigation on the importance of the first and second half of the 20 km race walking race.

	The first-half result is even more important	The result in the second half is even more important	The first- and second-half results are equally important
Trainer	3	1	0
Percentage	75%	25%	0

The average speed (M/s) of 12 participating men in 20 km race walking is set as shown in Table 3.

TABLE 3: Average speed of participating men in 20 km race walking (m/s).

Number	Segmental average speed (km)					
	0-2	2-4	4-6	6-12	12-16	16-20
1	3.95	4.12	4.16	4.35	4.38	4.43
2	3.95	4.12	4.17	4.35	4.35	4.43
3	3.96	4.13	4.18	4.35	4.35	4.42
4	3.96	4.14	4.17	4.32	4.36	4.41
5	3.95	4.13	4.16	4.32	4.39	4.40
6	3.95	4.12	4.15	4.33	4.35	4.40
7	3.96	4.12	4.16	4.34	4.32	4.43
8	3.94	4.13	4.16	4.33	4.36	4.39
9	3.94	4.15	4.17	4.34	4.36	4.35
10	3.95	4.16	4.18	4.35	4.38	4.32
11	3.94	4.17	4.19	4.35	4.35	4.33
12	3.94	4.17	4.19	4.35	4.35	4.33

TABLE 4: Analysis of 20 km race walking results.

Number	Result (min)	Number	Result (min)
1	30.25	7	29.54
2	32.15	8	30.21
3	33.21	9	29.65
4	33.22	10	30.12
5	31.25	11	30.14
6	30.45	12	30.54

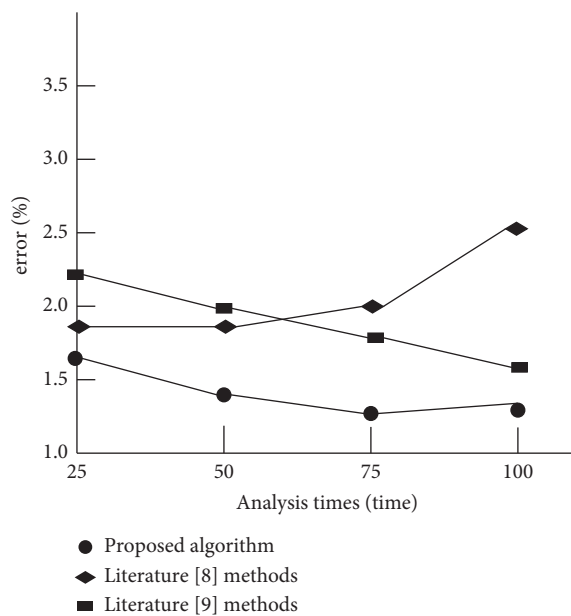


FIGURE 6: Comparison of analysis error results of different analysis methods.

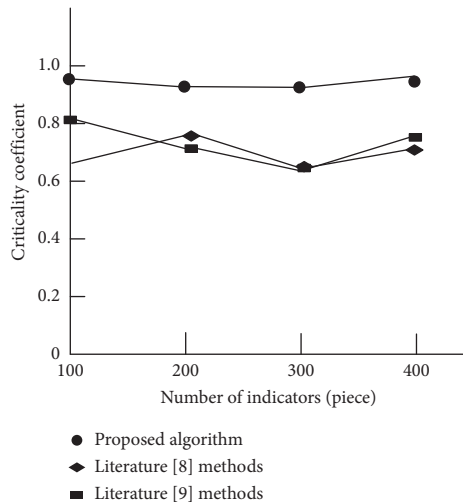


FIGURE 7: Analysis of key degree results of influencing factors determined by teaching tactics characteristics of different analysis methods.

analyzing the characteristics of teaching tactics in this race walking competition by using the analysis methods of this paper, of [8], and of [9]. Among them, the analysis error of this method is low and is always lower than 1.8%, while the error of the two methods is high, which verifies the feasibility of the proposed method.

The experiment further analyzes the key degree of the analysis method of this paper, the method of [8], and the method of [9] on the influencing factors determined by the characteristics of teaching tactics in this race walking competition. The results are shown in Figure 7.

By analyzing the experimental results in Figure 7, it can be seen that the key degrees of the influencing factors determined by the analysis method of this paper, the method of [8], and the method of [9] in this race walking competition are different. With the change of the number of indicators, the curve trend of the three methods has changed to some extent. Among them, the key coefficient of the influencing factors determined by the teaching tactical characteristics of the proposed method is higher and always higher than 0.9. Compared with the other two methods, the key coefficient is lower, which verifies the feasibility of the proposed method.

5. Conclusion

This paper designs a method to analyze the tactical characteristics of college track and field sports training teaching based on deep neural network. By analyzing the current situation of track and field sports training teaching in colleges and universities, this paper determines the key characteristics of teaching tactics. By determining the factors of teaching environment, the core competitiveness of track and field teams, and the teaching ability of track and field coaches, these factors are determined as the key characteristics, the data basis is analyzed, and the unified data quantitative processing is carried out to determine the key factor indexes affecting the analysis of tactical characteristics. This paper introduces the deep neural network to

construct the evaluation model of the tactical characteristics of college track and field sports training teaching and further modifies the characteristic analysis results with the help of cascade noise reduction self-encoder to complete the analysis of the tactical characteristics of college track and field sports training teaching. The experimental results show that the proposed method can effectively analyze the teaching tactical characteristics of track and field sports training in colleges and universities and improve the performance of the evaluation of the teaching tactical characteristics of track and field sports training.

Data Availability

The raw data supporting the conclusions of this article will be made available by the author, without undue reservation.

Conflicts of Interest

The author declares that there are no conflicts of interest regarding this work.

Acknowledgments

This work supported by Key Project of Quality Engineering Teaching Research in Universities of Anhui Province in 2020: Research on Sports Club System Teaching Innovation in Higher Vocational Colleges under the Background of Double High Construction (2020JYXM2177); 2020 Quality Engineering Online Course Project of Anhui Colleges and Universities: Tennis (2020MOOC556); 2018 Education Research Project of Anhui Vocational and Adult Education Society: Vocational Demand-Oriented Research on Higher Vocational Physical Education Curriculum Construction (AGZ18066); Key Project of Quality Engineering Teaching Research in Universities of Anhui Province, 2018: Empirical Research on the Influence of Sports Course Club System on College Students' Physical Quality Based on Cyclic Neural Network (2018JYXM1316).

References

- [1] N. Kasai, F. Tanji, A. Ishibashi et al. vol. 15, no. 7, pp. 1–11, 2021.
- [2] N. Pollock, S. Kelly, J. Lee, and B. Stone, "A 4-year study of hamstring injury outcomes in elite track and field using the British Athletics rehabilitation approach," *British Journal of Sports Medicine*, vol. 10, no. 3, pp. 791–802, 2021.
- [3] Z. Bing and C. Meschede, "Indirect and direct training of spiking neural networks for end-to-end control of a lane-keeping vehicle," *Neural Networks*, vol. 121, no. 1, pp. 21–36, 2020.
- [4] F. Zihao, "Complementing of sports training and PHYSICAL education," *Science and Technology Information*, vol. 20, no. 6, pp. 248–250, 2022.
- [5] N. Xinmiao, "ZHANG xin 'an, CAO lihua. Application of motion capture technology in sports field," *Sports Science and Technology*, vol. 42, no. 04, pp. 52–56, 2021.
- [6] L. Jinghua, "Design of sports training support System based on VR Technology," *Automation Technology and Application*, vol. 40, no. 02, pp. 108–111, 2021.

- [7] W. M. Adams, Y. Hosokawa, and D. J. Casa, "Preseason heat safety in secondary school athletics," *Journal of Athletic Training*, vol. 56, no. 4, pp. 349–351, 2021.
- [8] W. Mengnan, "Chen kanggui. Application of inertial motion capture technology in sports training: a case study of badminton teaching," *Contemporary Sports Technology*, vol. 10, no. 11, pp. 37–40, 2020.
- [9] X. jiaqin, *Application of simulation training method in track and field training [J] Sporting goods and technology*, vol. 15, no. 1, pp. 2–8, 2020.
- [10] Q. Ling, "Analysis on Influencing Factors of physical fitness training in track and field sprint," *Sports fashion*, vol. 15, no. 3, pp. 58–59, 2021.
- [11] S. Longo, E. Cè, A. V. Bisconti et al., "The effects of 12 weeks of static stretch training on the functional, mechanical, and architectural characteristics of the triceps surae muscle–tendon complex," *European Journal of Applied Physiology*, vol. 121, no. 1, pp. 102–110, 2021.
- [12] A. N. Marshall, T. Mcleod, and K. C. Lam, "Characteristics of injuries occurring during cross-country: a report from the athletic training practice-based research network," *Journal of Athletic Training*, vol. 13, no. 18, pp. 90–99, 2020.
- [13] J. A. Drake, L. P. Diggs, S. P. Martin et al., "Characteristics of matriculants to thoracic surgery residency training programs," *The Annals of Thoracic Surgery*, vol. 19, no. 08, pp. 65–72, 2020.
- [14] J. Zhao, Y. Wang, D. Zhao, Z. Lizhen, C. Peijie, and X. Xin, "Integration of metabolomics and proteomics to reveal the metabolic characteristics of high-intensity interval training," *Analyst*, vol. 145, no. 5, pp. 12–19, 2020.
- [15] R. Ali, R. Wharton, L. Li, and J. Waterman, "932Delivering excellence in orthopaedic training - a five year qualitative study of characteristics valued by trainees voting for trainer of the year," *British Journal of Surgery*, vol. 9, no. 17, pp. 675–682, 2021.
- [16] J. Lévesque, H. Rivaz, A. Rizk, S. Frenette, M. Boily, and M. Fortin, "Lumbar Multifidus Muscle Characteristics, Body Composition, and Injury in University Rugby Players," *Journal of Athletic Training, Body Composition, and Injury in University Rugby Players*, vol. 55, no. 10, pp. 1116–1123, 2020.
- [17] S. Alya Ev, M. Shahriari, D. Pardo et al., "Modeling extra-deep EM logs using a deep neural network," *Geophysics*, vol. 86, no. 3, pp. 1–47, 2021.
- [18] Z. Junya, "Zhang qiang, dai Yue. An intelligent walking robot construction method based on physiological neural network [J]," *Chinese Journal of Medical Physics*, vol. 39, no. 4, pp. 493–497, 2022.
- [19] Mu Haifang, G. Kai, and B. Hu, P. I. D. Fuzzy and N. Network, *Impedance Control for Upper Limb of Rehabilitation Robot*, Journal of Jining University, vol. 43, no. 2, , pp. 89–92+97, Wuhan, 2022.
- [20] L. Xiao, "Design of a machine learning framework for sports outcome prediction," *Automation technology & application*, vol. 38, no. 09, pp. 59–62+87, 2019.
- [21] S. Lee and I. Kim, "DVCKmet: a deep neural network model for dense video captioning," *IET Computer Vision*, vol. 15, no. 2, pp. 1089–1094, 2021.
- [22] B. Alhnaity, S. Kollias, G. Leontidis, J. Shouyong, S. Bert, and P. Simon, "An autoencoder wavelet based deep neural network with attention mechanism for multi-step prediction of plant growth," *Information Sciences*, vol. 56, no. 1, pp. 176–182, 2021.
- [23] X. Yang, W. Ni, W. Yan et al., "3-D electromagnetic-model-based absolute attitude estimation using a deep neural network," *Remote Sensing Letters*, vol. 12, no. 10, pp. 1015–1024, 2021.
- [24] Y. Lee, Y. C. Fang, and C. H. Tien, "Deep neural network for coded MaskCryptographical imaging," *Applied Optics*, vol. 60, no. 6, pp. 971–978, 2021.
- [25] Z. Renjun and w. Wang, "Simulation of network traffic prediction model based on deep neural network," *Computer simulation*, vol. 38, no. 6, p. 5, 2021.
- [26] R. M. Dibiase, R. Salas, C. E. Gamaldo et al., "Training in neurology: implementation and evaluation of an objective structured clinical examination tool for neurology post-graduate trainees in lusaka, Zambia," *Neurology*, vol. 12, no. 08, pp. 3465–3471, 2021.

Research Article

Intelligent Evaluation of Public Sports Service Based on Intuitionistic Fuzzy Set Theory

Yu Shao ¹ and Rong Bo ²

¹Department of Leisure Sport, Shanghai University of Sport, Shanghai 200438, China

²Institute of Physical Education, Central South University of Forestry and Technology, Changsha 410004, Hunan, China

Correspondence should be addressed to Rong Bo; t20071571@csuft.edu.cn

Received 20 April 2022; Revised 18 June 2022; Accepted 14 July 2022; Published 21 August 2022

Academic Editor: Le Sun

Copyright © 2022 Yu Shao and Rong Bo. This is an open access article distributed under the Creative Commons Attribution License, which permits unrestricted use, distribution, and reproduction in any medium, provided the original work is properly cited.

At this stage, in the research process of sports public service efficiency evaluation and analysis, due to the use of accurate data analysis methods, there are problems of low evaluation reliability and low analysis speed. Based on this, this paper studies the application of an information strategy based on the intuitionistic fuzzy data matching method in the evaluation and analysis of sports public service efficiency. The efficiency evaluation and analysis model of sports public service based on the intuitive fuzzy information algorithm is established. According to the characteristics of different types of sports public service, different types of data analysis methods are used to evaluate the efficiency, and the optimization of the efficiency analysis model of sports public service is realized according to the service demand and data type of different sports events. Finally, an experiment is designed to quantitatively evaluate the accuracy, stability, and reliability of the sports public service analysis model. The results show that the efficiency intelligent evaluation and analysis model based on the intuitive fuzzy information algorithm can effectively select the optimal sports public service evaluation countermeasures and rules according to the characteristics and data types of different sports events, realize the multi-dimensional accuracy classification of different types of sports events, and effectively improve the reliability of sports public service efficiency evaluation.

1. Introduction

Implementing the national strategy of nationwide fitness is the basic task of promoting healthy China to build a sports power. In order to optimize the transformation of government service functions, we will vigorously promote the development of public services for national fitness, so that the grass-roots people can enjoy the fruits of sports development and enhance their sense of gain and happiness. It is particularly important to improve the public sports service system and improve the efficiency of public sports service. Therefore, it is necessary to evaluate the efficiency of public sports services, explore the relevant influencing factors, solve the practical problems of the current reform and development of sports, and put forward effective paths for reference. The evaluation and analysis of sports public service efficiency has important practical significance for the improvement of

public service [1]. At this stage, due to different types of sports and different service contents, it is easy to have a variety of inefficient services, which will affect the experience of public users [2]. Although there are many researches on the efficiency evaluation of sports public service at this stage, there are still no good migration application research results, and many methods still need to be analyzed in combination with the problems existing in the public service of specific sports types [3]. Therefore, in order to better develop a more targeted evaluation system based on different types of sports public service strategies, it is necessary to combine the intuitive fuzzy information algorithm to realize high-quality analysis and customized evaluation of different sports events [4].

Based on this background, this paper studies the application of the intuitionistic fuzzy information algorithm in intelligent analysis of sports public service efficiency

evaluation, which is mainly divided into four chapters. The first chapter briefly introduces the application background of sports public service efficiency evaluation and intuitionistic fuzzy information algorithm and the chapter arrangement of this study. The second chapter introduces the research status of the efficiency evaluation model of sports public service and summarizes the shortcomings of the current research. The third chapter constructs the evaluation and analysis model of sports public service efficiency based on the intuitive fuzzy information algorithm. Through the disturbing intelligent analysis of different types of sports service data, it realizes the high-intensity representation of its internal relevance and carries out centralized control according to its internal error to improve the accuracy of the model. Chapter 4 tests the innovative characteristics of different types of data groups of the intelligent analysis sports public service efficiency evaluation model constructed in this paper and realizes the accuracy verification and analysis of the sports public service efficiency model by analyzing the error degree of the efficiency evaluation process of different types of sports public services. The experimental results show that compared with the traditional sports public service analysis and matching model of database modular analysis and processing, the sports public service efficiency evaluation and analysis model based on the intuitive fuzzy information algorithm proposed in this study has better use value and lower error rate.

The innovation of this paper is to propose an efficiency evaluation and analysis model of sports public service based on the intuitionistic fuzzy information algorithm. The model can evaluate the accuracy of different data groups according to the intelligent degree of sports public service efficiency evaluation types corresponding to different types of sports events and the efficiency analysis according to the intelligent classification effect of data, in order to improve its internal data accuracy.

2. State of the Art

At present, many mathematicians have carried out a lot of research according to the efficiency of sports public service, mainly focusing on service data group, innovative group analysis, and efficient intelligent matching and tracking [5]. Researchers Crothers and others adopted different matching strategies and data analysis stability thinking for different databases according to different types of sports, so as to realize intelligent and stable tracking of different data groups, and their internal data relevance has good analysis and fuzzy rules, so they can better complete the efficiency analysis of different sports public services. However, more parameters need to be checked [6]. Ni and other scholars adopted different types of data group classification ideas for different sports public service methods from the differences of service strategies and service methods of different types of sports, tree thinking strategy, and grid management thinking at marriage [7]. In the process of analyzing the efficiency evaluation of sports public service, Zhao and other scholars found that different types of sports have different sets of data centers, so they adopted a source efficient attack model to

realize targeted analysis and intelligent matching and tracking of data groups [8]. According to the characteristics of fuzzy information processing system, Rahimian and other scholars intelligently analyze different types of sports public service methods, classify different data, and use repair sparsity algorithm for in-depth analysis [9]. Simone and other scholars adopted an intelligent adaptive allocation strategy for sports events according to different types of sports service thinking. The experimental results show that this strategy can carry out feature recognition and intelligent analysis according to its internal differences and can be used for optimal matching analysis of different types of strategy groups [10]. Wu and other scholars conducted targeted analysis on the service efficiency of different sports events according to the differentiated characteristics of power points of sports events, discussed their internal relevance of sports events and evaluated their efficiency, and proposed a sports public service analysis model based on multi-dimensional innovation matching identification [11]. Relying on different types of high-end sports public service databases, Yang and other scholars classify the efficiency of sports public service for different types of sports events and put forward a sports public service analysis model that can match high-value data [12]. In the process of studying the efficiency evaluation of sports public service, Pradeep and other scholars found that different types of efficiency analysis problems need different methods for stability matching. Therefore, they proposed a high-intensity and multi type collaborative sports public service analysis and efficiency stability evaluation system. The system can effectively improve the service efficiency and data accuracy of different types [13].

To sum up, it can be seen that the current commonly used intelligent analysis models for sports public service efficiency evaluation cannot efficiently complete the quantitative analysis of high-precision data of sports events and need to classify and analyze the innovation of different model data. Therefore, there is the possibility of further research on the efficiency and stability of data analysis [14–16]. On the other hand, in the research on the differentiation of sports public service efficiency evaluation, there are few research results combined with the intuitive fuzzy information algorithm and few unified analysis combined with the fuzzy information strategy [17–19]. Therefore, it is of great significance to carry out the model analysis and research based on the fuzzy information algorithm applied to the efficiency evaluation of sports public service.

3. Methodology

3.1. Analysis of Intelligent Analysis Model for Efficiency Evaluation of Sports Public Service. Intuitionistic fuzzy information theory adopts the discrete processing technology of data group and multi-dimensional data matching and tracking strategy to realize data analysis and processing and intensity matching to varying degrees [20]. The current data analysis types have different degrees of error, which is because the parameters set by different data analysis types have many differences. Therefore, in the process of solving

specific problems, the differences of parameters are very different, which will affect the final data operation results [21]. Intuitionistic fuzzy information algorithm is mainly used to quantitatively analyze the targeted data of different sports public service efficiency and evaluation in solving the problem of sports public service efficiency evaluation. Through the value matching of different data groups, it can classify different types of data groups and then realize the high-accuracy analysis of different service efficiency [22]. The thinking process of data operation is shown in Figure 1. On the other hand, in the process of differential analysis of different types of sports public service projects, there will be great differences in their internal data matching degree and value analysis strategy, so there will be obvious differences in their internal data analysis intensity, and there is great uncertainty in their internal data accuracy [23]. In the process of adopting diversified data analysis dimension strategy for the data type of sports public service efficiency evaluation, the value degree will be matched according to its internal "Anjian performance," so as to realize the classification and quantitative research of the data group [24]. By using the intuitionistic fuzzy information algorithm and computer network analysis technology, the difference characteristics of its internal data types can be well analyzed, especially in value matching and stability strategy [25].

3.2. The Process of Establishing the Efficiency Evaluation Model of Sports Public Service. After the analysis and intelligent evaluation of different types of sports public service efficiency, high-precision quantitative analysis and stability solution can be realized according to its external relevance and internal matching. Usually, the quantitative analysis of sports public service mainly adopts common statistical analysis. However, it is difficult to obtain data related to sports public services or because they are often mixed with public services. Therefore, the relevant statistical analysis is difficult, even difficult to carry out. Compared with a large number of mathematical models and quantitative analysis methods and means in the fields of economy, management, education, and so on, it is not common to adopt similar methods in the field of sports public service.

Therefore, after the simulation analysis of different types of sports public service efficiency strategies combined with the fuzzy information classification algorithm, the data simulation analysis process based on computer intuitive fuzzy high latitude value analysis strategy is shown in Figure 2.

It can be seen from Figure 2 that for the sports public service efficiency evaluation data sets with different value analysis matching strategies, the evaluation scores of different types of sports public services are different because different types of fuzzy information data analysis networks and intuitive fuzzy algorithms are in the process of high-precision analysis of the data group. Eight dimensional matching classification will be carried out according to the accuracy of its data group to realize the classified processing of different service events, and then value analysis will be carried out according to its internal error, and its efficiency

will be evaluated. In this process, the corresponding evaluation function $P(x)$ and efficiency function $G(x)$ can be expressed as $h_c = 1/M \times N \sum_{i=0}^{M-1} \sum_{j=0}^{N-1} \delta(f_{ij} - c)$.

$$P(x) = \frac{8 \sum_{i=1}^n (x_i^2 + x_{i-1}^2/2)}{3x_{i-1}^2 + 5x_{i-2}^2}, \quad (1)$$

$$G(x) = \frac{\sqrt{\sum_{i=1}^n (x_i^2 + x_{i-1}^2/2)/3x_{i-1}^2 + 4x_{i-2}^2}}{8\sqrt{x_i^2 + x_{i-2}^2}}. \quad (2)$$

The solution expression $L(x)$ of the eigenvector corresponding to different public sports service data groups is

$$L(x) = \sqrt{\frac{\lim_{x \rightarrow \infty} \sqrt{G(x)^2 + P(x)}}{\lim_{x \rightarrow 0} \sqrt{G(x)^2 + rP(x)}}}, \quad (3)$$

where r is the high-value response value of public service efficiency evaluation, which is converted into the classified value parameter of high latitude, then the corresponding discrete function $R(x)$ formula is expressed as

$$R(x) = \frac{\lim_{x \rightarrow \infty} G(x_k) + x_k}{L(x_k)}, \quad (4)$$

where x_k represents the low latitude parameter of public sports service. Complete different types of arrays and the corresponding combination strategy formula is

$$R(x_{k+1}) = \frac{\sqrt{R(x_k)^2 + L(x_k)^2}}{L(x_{k-1})}. \quad (5)$$

After discarding the correlation degree of its internal data type, with the help of the intuitive fuzzy strategy, its corresponding efficiency classification function is

$$U(x_k) = 8 \sqrt{\frac{\sqrt{R(x_k)^2 + L(x_k)^2}}{8R(x_k) + 3L(x_{k-1})}}, \quad (6)$$

where x is the high-intensity-type parameter group of the intuitionistic fuzzy classification. After completing this link, the corresponding high-value degree function analysis results are shown in Figure 3.

According to the results of Figure 3, after classifying the efficiency evaluation data of sports public service by using the intuitive fuzzy information algorithm, different types of arrays have great change intensity, and their efficiency is also different and multidimensional. In essence, public service efficiency is a production efficiency problem within the public service system. Most of the current research methods use the nonparametric method to determine the frontier production function, that is, the data envelopment analysis (DEA) method for research evaluation. It is a nonparametric linear mathematical programming method for convex efficient frontier estimation. At present, this method has been widely used in the efficiency evaluation and research of various industries and fields. This is because different types

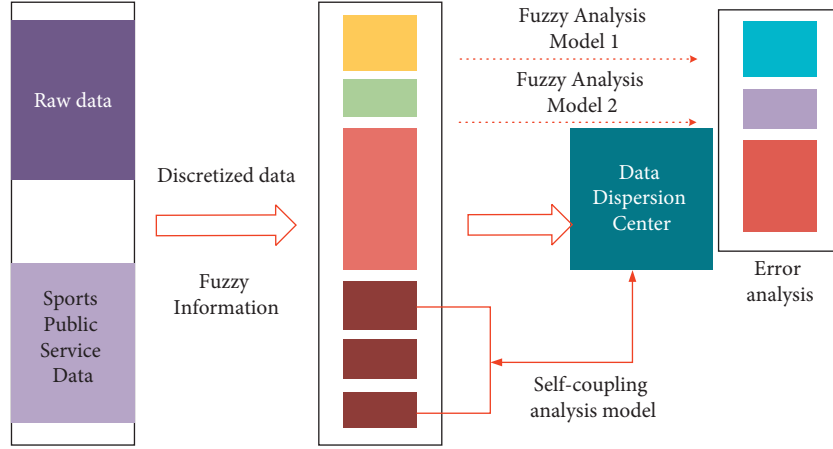


FIGURE 1: Data operation and processing process of intuitionistic fuzzy information algorithm.

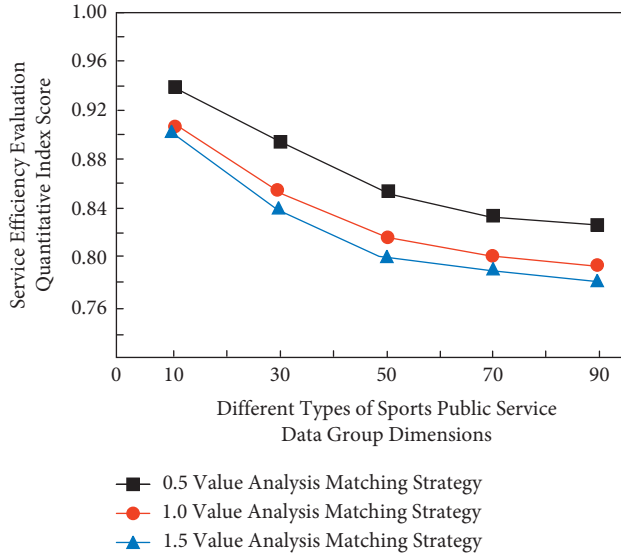


FIGURE 2: Data simulation analysis process based on computer intuitive fuzzy high latitude value analysis strategy.

of fuzzy information analysis algorithms can realize high-dimensional classification and evaluation analysis of data according to super-precision function group. Then it realizes the quantitative representation and value matching analysis of the efficiency evaluation of sports public service.

Set the basic analysis value of the sports public service efficiency of the corresponding intuitive fuzzy information in this study as 0.1, and the simulation analysis results are shown in Figure 4.

It can be seen from Figure 4 that when characterizing and intensity matching analysis of sports public service efficiency evaluation data, the internal relevance data groups also have different types of value analysis strategies because different types of data groups need to carry out value matching and dimension correspondence in combination with the types of data groups in value analysis. At this time, the corresponding intuitionistic fuzzy information function can be expressed as

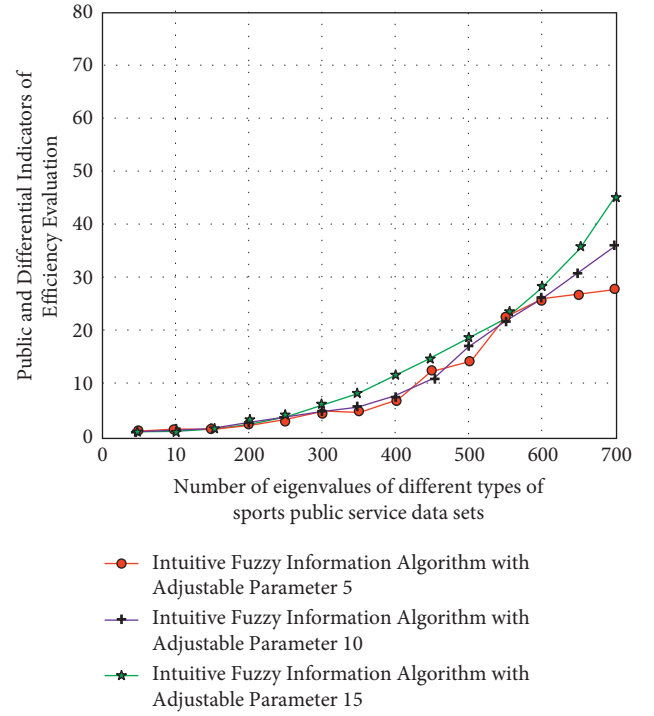


FIGURE 3: Analysis results of high-value function based on intuitive fuzzy evaluation algorithm.

$$r(x) = \sqrt{\frac{w\sqrt{x} + bx}{w + b}}. \quad (7)$$

The corresponding application restrictions are

$$\frac{x_i[h(x) + n]}{w\sqrt[3]{w} + r\sqrt[3]{b}} \geq \frac{x_i[h(x) - n(x)]}{w\sqrt[3]{w} + r\sqrt[3]{b}}. \quad (8)$$

Under the intuitionistic fuzzy analysis algorithm, the corresponding truth function is $T(x)$:

$$T(x) = \sum_{i=1}^n rx_i + b(x), \quad (9)$$

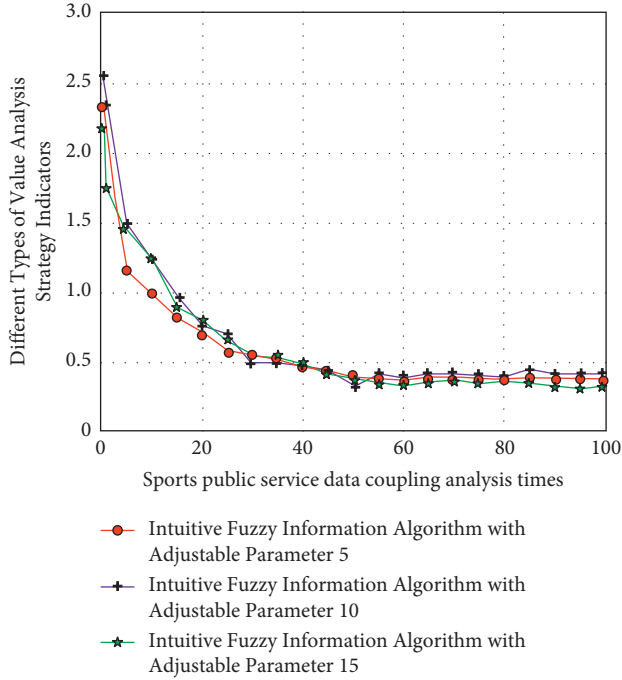


FIGURE 4: Simulation analysis results of sports public service efficiency indicators based on intuitionistic fuzzy information.

where $b(x)$ represents the truth value correspondence analysis function, w is the real array of sports public service efficiency evaluation, and b is the two-dimensional editing number of sports public service efficiency evaluation data group.

In order to improve the accuracy of its evaluation efficiency, it is also necessary to add the necessary conditions for significance classification:

$$\frac{x_i [h(x) + n] - x_{i-1}}{b\sqrt{x_i}} > b\sqrt{x_{i-1} + x_i}. \quad (10)$$

Under this significant condition, the formula corresponding to the collimation function $\beta(w, x)$ is

$$\beta(w, x) = \frac{\sqrt{\|w^2\|^3 + 2/3(K - x \sum_{i=1}^n x_i)}}{b(w, x)}, \quad (11)$$

where K represents the standard threshold function of intuitionistic ambiguity.

In order to further improve the standardization of fuzzy information, the gradient function $H'(x)$ of the judgment function in different dimensions is

$$H'(x) = \frac{\sqrt{|\sum_{i=1}^n a_i x_i (x_i \times x) + b(x_i \times x)|}}{H'(x-1)}, \quad (12)$$

$$H''(x) = \frac{\sqrt{|\sum_{i=1}^n a_i x_i (x_i \times x) + b(x_i \times x)|}}{H''(x-1)}, \quad (13)$$

$$H'''(x) = \frac{\sqrt{|\sum_{i=1}^n a_i x_i (x_i \times x) + b(x_i \times x)|}}{b(x_i)H''(x-1)}. \quad (14)$$

After quantitative evaluation, the corresponding public service efficiency analysis function is

$$Z(x_j, x_i) = \frac{\lim_{\delta x \rightarrow 0} \sqrt{|\sum_{i=1}^n a_i x_i (x_i \times x) + b(x_i \times x)|} / b(x_i) H''(x-1)}{|x_i - x_j|}, \quad (15)$$

where a_i represents data groups of different groups. At this time, the corresponding fuzzy information analysis results under different differentiation conditions are shown in Figure 5.

It can be seen from Figure 5 that when the efficiency evaluation of sports public service normalizes and analyzes different sports, the corresponding numerical changes are also quite different, but there are some regular and stable changes in local data. This is because the internal relevance is very different under the analysis of the intuitive fuzzy information algorithm. Therefore, the corresponding standardized single factor has good universality and stability.

4. Result Analysis and Discussion

4.1. Experimental Design of Sports Public Service Efficiency Evaluation Model Based on Intuitionistic Fuzzy Information Algorithm. During the experiment, in order to further confirm the credibility and feasibility of the sports public service efficiency evaluation model proposed in this study in dealing with unknown problems, it is necessary to carry out the authenticity data analysis experiment. The fuzzy evaluation analysis strategy used in this experiment is a multi-dimensional method combining fuzzy information processing and intelligent normalization strategy. In the process of analyzing different types of sports public service data groups, this method has high accuracy and periodicity in its internal relevance evaluation and value analysis. Specifically, the research selects quantifiable public service input and output variables. Generally speaking, to study the efficiency of public services between regions, we need to take all public services or some major public service projects provided by local governments as the research object to comprehensively investigate their efficiency. Here, we generally choose two main basic public service items, medical care and education, as samples for research. In terms of variable selection, in order to make the input-output data of various regions comparable, we all choose the per capita index for investigation. In terms of public service input variables, we select the per capita public service expenditure in each region, which represents the resources consumed by each region to provide public services. In terms of output variables, we selected three indicators from the fields of health care and education to reflect their comprehensive output.

Therefore, its internal data groups have good service characteristics and value types. Figure 6 is the preliminary experimental results based on the intuitive fuzzy information algorithm analysis model.

In the experimental results in Figure 6, it can be found that under the analysis of different types of intuitive fuzzy

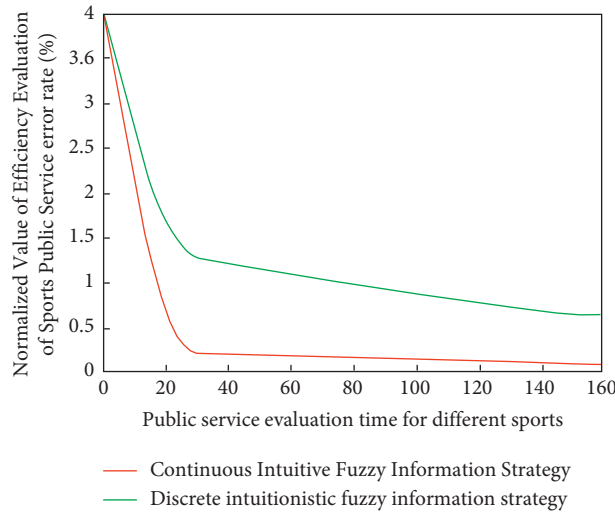


FIGURE 5: The corresponding fuzzy information analysis results under different differentiation conditions.

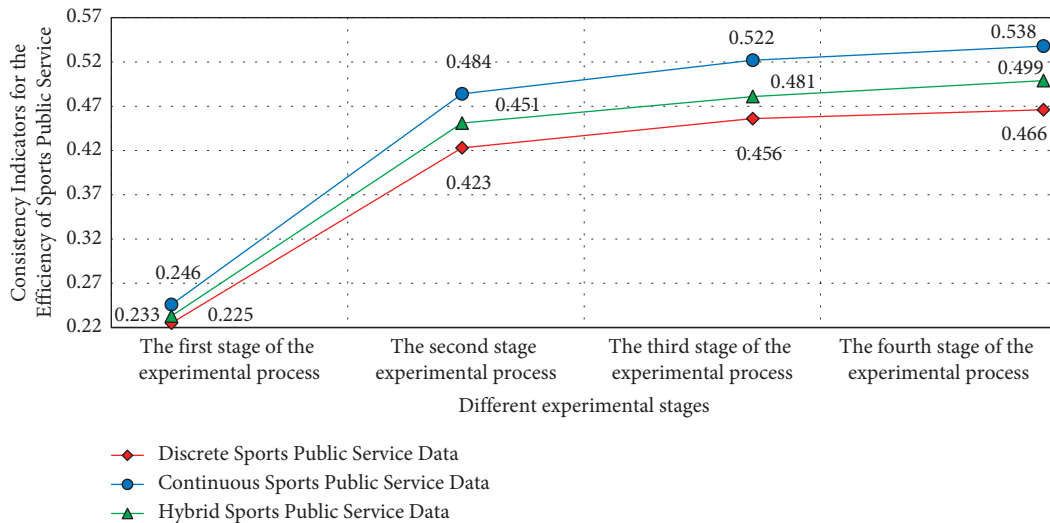


FIGURE 6: Preliminary experiment results of computer chaos algorithm analysis model.

information algorithms, the internal differences in data reliability and stability of different sports public service data groups are obvious, and the results have high variability and consistency in the process of discretization of sports service behavior. This result is also in line with the experimental expectations. This is because under the intuitionistic fuzzy information analysis strategy, the data calculation efficiency of the corresponding sports public service efficiency evaluation model is improved, and its internal data group and reliability will also change, which leads to higher differences in its internal relevance and matching tracking rate.

4.2. Experimental Results and Analysis. This paper evaluates the residents' satisfaction with sports public service and constructs the evaluation index system. At present, the evaluation index of sports public service should be determined from the dimensions of the construction of national fitness facilities,

the construction of national fitness organizations, the development of national fitness activities, and the guidance service of national fitness. In the sports public service efficiency evaluation and analysis model based on fuzzy information processing algorithm proposed in this study, the commonly used evaluation index is used as the necessity reference strategy. If the error analysis is not carried out, the reliability of the results of the corresponding high-precision efficiency evaluation model will be reduced. Therefore, its internal relevance and data thinking coupling have different value analysis strategies, which will be directly related to the analysis accuracy of sports public service efficiency evaluation. The experimental analysis results are shown in Figure 7, in which the horizontal axis is the number of experimental analysis and the vertical axis is the quantitative characterization function value of the fuzzy evaluation index.

As can be seen from Figure 7, when analyzing different types of data groups, the experimental group using

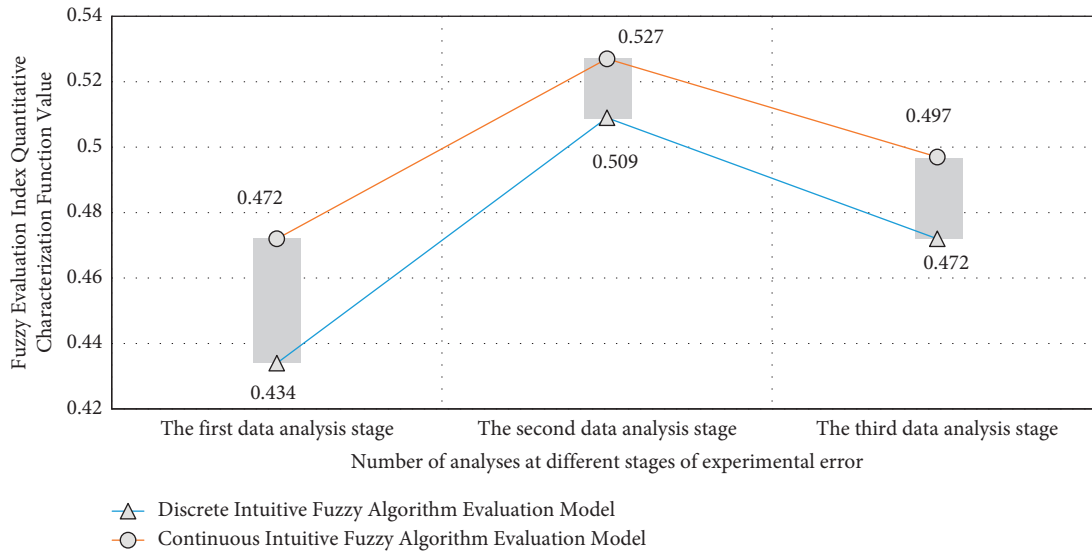


FIGURE 7: Final experimental analysis results in computer monitoring mode.

intuitionistic fuzzy strategy has the lowest error degree of corresponding data results, and its corresponding efficiency evaluation parameters are also the highest. This is because after adopting the fuzzy information processing algorithm and intuitionistic fuzzy analysis strategy, the matching degree of the corresponding data analysis and the value degree of the disturbing error function will show the characteristics of strong pertinence and high efficiency. Therefore, when the difference of the corresponding different function types in the analysis process is large, the accuracy and value degree of the corresponding evaluation and analysis vector will have good reliability and stability, and its internal relevance vector group will also have a coupling effect with the internal matching degree of the value function, resulting in higher accuracy and value matching degree in its evaluation of the efficiency of sports public service. Therefore, its evaluation results can improve the accuracy by at least 33% and be more convincing.

5. Conclusion

This paper studies the application of information strategy based on the intuitionistic fuzzy data matching method in the evaluation and analysis of sports public service efficiency. An evaluation and analysis model of sports public service efficiency based on the intuitionistic fuzzy information algorithm is established. According to the characteristics of different types of sports public service, different types of data analysis methods are used to evaluate its efficiency, and according to the service needs and data types of different sports events, the optimization of the efficiency analysis model of sports public service is realized. Finally, an experiment is designed to quantitatively evaluate its accuracy, and the stability and reliability of the sports public service analysis model. The results show that the effectiveness intelligent evaluation analysis model based on the intuitionistic fuzzy information algorithm can effectively select the

optimal sports public service evaluation countermeasures and rules according to the characteristics and data types of different sports events, realize the multi-dimensional and accurate classification of different types of sports events, and effectively improve the reliability of sports public service efficiency evaluation.

However, this paper only focuses on the evaluation strategy of the efficiency of sports public service, so there is still room for improvement. We can conduct in-depth research on the scope of application and regional differences of the efficiency evaluation model of sports public service.

Data Availability

The data used to support the findings of this study are available from the corresponding author upon request.

Conflicts of Interest

The authors declare that they have no conflicts of interest.

References

- [1] Z. J. Zhang, G. Y. Song, T. Zheng, Q. Ni, H. Feng, and H. Zhang, "The presence of a preoperative high-grade J-sign and femoral tunnel malposition are associated with residual graft laxity after MPFL reconstruction," *Knee Surgery, Sports Traumatology, Arthroscopy*, vol. 29, no. 4, pp. 1183–1190, 2021.
- [2] Z. J. Zhang, H. Zhang, G. Y. Song, T. Zheng, Q. Ni, and H. Feng, "Increased femoral anteversion is associated with inferior clinical outcomes after MPFL reconstruction and combined tibial tubercle osteotomy for the treatment of recurrent patellar instability," *Knee Surgery, Sports Traumatology, Arthroscopy*, vol. 28, no. 7, pp. 2261–2269, 2020.
- [3] J. S. Eriksson, B. Ekblom, L. V. Kallings et al., "Active commuting in Swedish workers between 1998 and 2015—trends, characteristics, and cardiovascular disease risk," *Scandinavian Journal of Medicine & Science in Sports*, vol. 30, no. 2, pp. 370–379, 2020.

- [4] M. A. Azimifar, Z. Salmasi, A. Doosti, N. Babaei, and M. Hashemi, "Evaluation of the efficiency of modified PAMAM dendrimer with low molecular weight protamine peptide to deliver IL-12 plasmid into stem cells as cancer therapy vehicles," *Biotechnology Progress*, vol. 37, no. 4, Article ID e3175, 2021.
- [5] N. Hertel, "Distinguished public service Award: Presented to MICHAEL BOYD by the health Physics Society," *Health Physics*, vol. 119, no. 6, pp. 671-672, 2020.
- [6] A. Bottle and J. Browne, "Outsourcing care to the private sector: some reassuring evidence on patient outcomes," *BMJ Quality & Safety*, vol. 31, no. 7, pp. 486-488, 2022.
- [7] Q. K. Ni, G. Y. Song, Z. J. Zhang, T. Zheng, Y. W. Cao, and H. Zhang, "Posterior tibial slope measurements based on the full-length tibial anatomic axis are significantly increased compared to those based on the half-length tibial anatomic axis," *Knee Surgery, Sports Traumatology, Arthroscopy*, vol. 30, no. 4, pp. 1362-1368, 2021.
- [8] B. Zhao, Y. Ren, D. Gao, L. Xu, and Y. Zhang, "Energy utilization efficiency evaluation model of refining unit Based on Contourlet neural network optimized by improved grey optimization algorithm," *Energy*, vol. 185, pp. 1032-1044, 2019.
- [9] M. Rahimian, A. Dejamkhooy, M. Hosseinpour, and Y.-V. Ali, "Efficiency improvement and reliability evaluation of small-scale PMSG-based wind energy conversion system using back-to-back T-type converter," *Electrical Engineering*, vol. 103, pp. 1-13, 2021.
- [10] A. Simone, M. D. Di, R. Stefano, and L. Vittorio, "DDT - Drug Discovery Tool: a fast and intuitive graphics user interface for docking and molecular dynamics analysis," *Bioinformatics*, vol. 35, no. 24, p. 24, 2019.
- [11] P. Wu, J. Ma, and X. Guo, "Efficiency evaluation and influencing factors analysis of fiscal and taxation policies: a method combining DEA-AHP and CD function," *Annals of Operations Research*, vol. 309, no. 4, pp. 1-21, 2021.
- [12] J. Yang and B. Chen, "Energy efficiency evaluation of wastewater treatment plants (WWTPs) based on data envelopment analysis," *Applied Energy*, vol. 289, no. 2, Article ID 116680, 2021.
- [13] S. Pradeep, A. Muhammad, Q. Abdul, and P. Kannoja, "Simultaneous analytical efficiency evaluation using an HPTLC method for the analysis of Syringic Acid and Vanillic Acid and their Anti-Oxidant Capacity from Methanol Extract of *Ricinus communis* L. And *Euphorbia hirta* L.," *Journal of AOAC International*, vol. 104, no. 4, p. 4, 2020.
- [14] J. He, J. Cheng, and I. M. C. Lo, "Green photocatalytic disinfection of real sewage: efficiency evaluation and toxicity assessment of eco-friendly TiO₂-based magnetic photocatalyst under solar light," *Water Research*, vol. 190, Article ID 116705, 2020.
- [15] Z. Chen, L. Zhang, J. You, J. Wang, and G. Chen, "Evaluation of efficiency and safety of oral corticosteroid therapy in children patients with exacerbations of asthma: a protocol for systematic review and meta-analysis," *Medicine*, vol. 100, no. 24, Article ID e26250, 2021.
- [16] S. Tiwari, S. Basu, T. M. Undeland, and O.-M. Midtgard, "Efficiency and conducted EMI evaluation of a single-Phase power factor Correction Boost converter using State-of-the-Art SiC Mosfet and SiC Diode," *IEEE Transactions on Industry Applications*, vol. 55, no. 6, pp. 7745-7756, 2019.
- [17] A. J. Fisher, M. M. Keeley, J. M. Lane, and P. Y. Furlan, "Spectroscopic evaluation of Removal efficiency for a Pharmaceutical Pollutant in water using a Magnetite-Activated Carbon Nanocomposite," *Journal of Chemical Education*, vol. 96, no. 4, pp. 751-755, 2019.
- [18] W. Xu, Y. Cao, and B. Liu, "Strength efficiency evaluation of cemented tailings backfill with different stratified structures," *Engineering Structures*, vol. 180, pp. 18-28, 2019.
- [19] C. Price, S. Mccarthy, A. Bate, and P. McMeekin, "Impact of emergency care centralisation on mortality and efficiency: a retrospective service evaluation," *Emergency Medicine Journal*, vol. 37, no. 4, pp. 180-186, 2020.
- [20] M. Bonanno, K. Müller, B. Bensmann, R. Hanke-Rauschenbach, R. Peach, and S. Thiele, "Evaluation of the efficiency of an elevated temperature proton exchange membrane water electrolysis system," *Journal of the Electrochemical Society*, vol. 168, no. 9, Article ID 094504, 2021.
- [21] X. Yao, W. Liu, W. Zhu et al., "Near-infrared fluorescent chemodosimeter for real-time *in vivo* evaluation of H₂S-release efficiency of prodrug," *Chemical Communications*, vol. 56, no. 58, pp. 8111-8114, 2020.
- [22] P. H. Robinson, "Impacts of feeding monensin sodium on production and the efficiency of milk production in dairy cows fed total mixed rations: evaluation of a confounded literature," *Canadian Journal of Animal Science*, vol. 100, no. 3, pp. 391-401, 2020.
- [23] S. Pokhrel, L. Amiri, A. Zueter et al., "Thermal performance evaluation of integrated solar-geothermal system; a semi-conjugate reduced order numerical model," *Applied Energy*, vol. 303, Article ID 117676, 2021.
- [24] X. Ca, W. Zeng, M. Wu, X. Guo, and W. Wang, "Hybrid analytical framework for regional agricultural water resource utilization and efficiency evaluation," *Agricultural Water Management*, vol. 231, Article ID 106027, 2020.
- [25] M. W. Fan, C. C. Ao, and X. R. Wang, "Comprehensive method of natural gas pipeline efficiency evaluation based on energy and big data analysis," *Energy*, vol. 188, Article ID 116069, 2019.

Research Article

Nonlinear Dynamic Response Analysis of a Three-Stage Gear Train Based on Lightweight Calculation for Edge Equipment

Dongdong Ren, Yangwu Yao , Huiyuan Wang , Huixian Qu, and Guoqiang Wang

College of Mechanical and Electrical Engineering, North University of China, Taiyuan 030051, China

Correspondence should be addressed to Yangwu Yao; 2016123632@jou.edu.cn

Received 15 June 2022; Accepted 27 July 2022; Published 21 August 2022

Academic Editor: Le Sun

Copyright © 2022 Dongdong Ren et al. This is an open access article distributed under the Creative Commons Attribution License, which permits unrestricted use, distribution, and reproduction in any medium, provided the original work is properly cited.

Bevel gears are widely used in aerospace transmission systems as well as modern mechanical equipment. In order to meet the needs and development of aerospace, high-speed dynamic vehicles, and various defense special equipment, higher and higher requirements are made for the high precision and stability of gear transmission systems, as well as the prediction and control of noise and vibration. Considering the nonlinear factors such as comprehensive gear error and tooth side clearance, a dynamic model of the three-stage gear transmission system is established. The relevant physical parameters, geometric parameters, and load parameters in the gear system are considered random variables to obtain the stochastic vibration model. When the random part of the random parameters is much smaller than the deterministic part, the vibration differential equation is expanded into a first-order term at the mean of the random parameter vector according to the Taylor series expansion theorem, and the ordering equation is solved numerically. Based on the improved stochastic regression method, the nonlinear dynamic response analysis of the three-stage gear train is carried out. This results in a relatively stable system when the dimensionless excitation frequency is in the range of 0.716 to 0.86 and the magnitude of the dimensionless integral meshing error is < 1.089 .

1. Introduction

Gearing systems are widely used in various types of machinery and equipment, and ensuring the smoothness and accuracy of the transmission process has always been the goal of industrial production [1]. With the development of wind turbine drive train power towards the megawatt level, the accuracy of the dynamic response analysis of the three-stage gearbox drive train model has been increasing. Therefore, the study of the coupled nonlinear dynamic characteristics of large generator gearboxes under variable loads, and then provide important theoretical value and practical engineering significance for the design of three-stage gearboxes [2]. In recent years, many domestic and foreign scholars have conducted in-depth studies on the performance research methods and dynamics models of three-stage gearbox drive systems, and have made certain achievements [3, 4, 5]. The coupled nonlinear dynamics model of the gear-rotor-bearing-box of a large three-stage gearbox with multi-stage planetary gearing was established

under the combined effect of internal and external load excitation, and the vibration response analysis of the three-stage gearbox was carried out by using the modal superposition method. Reference [6] accurately modeled the gearbox drive train of a large wind turbine and studied its drive train under variable wind loads. Reference [7] established a bending-torsion coupled dynamics model of a megawatt-class wind turbine gearbox drive train and calculated the structural sketch of the three-stage gearbox drive train using the fourth-order Runge-Kutta method.

Wind turbine gearboxes can be configured in different types, such as three-stage fixed shaft gear systems, planetary gear systems, and planetary and parallel shaft gear systems. The form of transmission mechanism used in the three-stage gearbox depends on the capacity requirements of the three-stage unit. The development of offshore three-stage technology and the need to reduce the cost of three-stage have strongly promoted the development of large single-capacity three-stage units. Three-stage planetary gearboxes are widely used in high-power double-fed three-stage gearboxes

because of their strong load-bearing capacity, large speed increase ratio, and compact structure. Compared with single-stage planetary gearboxes, three-stage planetary gearboxes are more susceptible to vibration and noise and failure due to interstage coupling and three-stage transmission of torque [8]. Therefore, it is important to analyze the dynamic characteristics of three-stage planetary gear trains. A series of research results have been obtained for the analysis of the dynamics of a three-stage planetary gear train in three-stage gearboxes.

The dynamics of a single pair of a gear pair system has been studied more systematically. In [8], a time-varying nonlinear dynamics model was established, and the effect of side clearance on the meshing state and its frequency response characteristics was considered [9]. The parameters of the single-stage spur gear system are studied in detail, and the effects of parameter variations on the dynamic characteristics are presented. In [10], an approximate analytical solution of the three-stage nonlinear gear train was carried out using the harmonic balance method, and the effect of the variation of key parameters on the system response was analyzed [11]. The dynamic simulation technique of a three-stage gear train considering only the time-varying meshing stiffness was studied [12]. The nonlinearities of the intermediate shaft system and the idler system with time-varying meshing stiffness are investigated, and the analytical and numerical solutions are compared. In [13], the dynamic characteristics of the three-stage idler system with nonlinear parameter excitation are presented, and the periodic steady-state solutions are obtained by both analytical and numerical methods.

Tooth surface errors are unavoidable in the gear manufacturing process. In this paper, a modified stochastic regression method is used to solve the system of vibration differential equations for a three-stage gear train, and the effects of the changes of the integrated dimensionless excitation frequency and the integrated meshing error on the dynamic response of the system are analyzed. It is found that the system is in a relatively stable state when the dimensionless excitation frequency is in the range of 0.716–0.86 and the magnitude of the integrated dimensionless meshing error is <1.089 .

2. Related Work

In order to meet the practical needs of low speed and a heavy load and a large transmission ratio, the study of the dynamics of the gear transmission system is becoming a hot spot for engineering applications and academic research. According to the research focus, [14] used the finite element method, the centralized parameter method, and the experimental modal analysis method, respectively. In [15], the finite element model and the centralized parametric model of the gear set were established, and the results of the two models were compared and analyzed, and the results of the two models were found to be consistent. In [16], the dynamic characteristics of the system under different fixation methods of the solar wheel were analyzed. In [17], the vibration model of the planetary gear was developed by the

centralized parameter method considering the meshing phase relationship, and the modalities and vibration modes of the system were calculated for different modalities. In terms of nonlinear dynamics of planetary gear sets, [18] analyzed the dynamics of planetary gears under changing meshing stiffness by using rectangular waves to represent the time-varying meshing stiffness of the gear teeth. In [19], the effect of manufacturing errors on the nonlinear dynamics of planetary gears were studied, and the differences in the dynamics of the system under normal conditions, in the presence of tooth profile errors, and when centrifugal forces were considered and compared. In [20], the dynamics of planetary gears under strong nonlinear factors with multiple clearances is considered, and it is important to note that the analytical solution of the system vibration differential equations is obtained by the harmonic balance method, which is a typical application of the approximate analytical solution method under strong nonlinear factors. The study of the concentrated mass model of planetary gear sets focuses on the pure torsional vibration model and the meshing coupling model. Theoretical tooth surface and real tooth surface STE are introduced into the dynamics model in the form of discrete points, and the effects of real tooth surface STE and theoretical tooth surface STE on the dynamics performance of the curved bevel gear pair are compared and analyzed.

3. Complex Modal Structural Systems

The basic equation for the vibration of a gear system and the complex modal forced vibration equation for an N -dimensional linear system can be expressed as

$$M\ddot{X} + C\dot{X} + KX = Q(t), \quad (1)$$

where M , C , and K denote the $N \times N$ order mass matrix, damping matrix, and stiffness matrix, respectively, X and $Q(t)$ denote the generalized displacement vector and external excitation, respectively, $M\dot{X}$ denotes the generalized velocity vector and $C\dot{X}$ denotes the generalized acceleration vector. The free vibration equation of the complex modal structural system can be expressed as

$$M\ddot{X} + C\dot{X} + KX = 0. \quad (2)$$

It may be assumed that, $X = xe^{\lambda t}$ by substituting into (2), the corresponding right eigenvalue problem is obtained as follows:

$$(M\lambda^2 + C\lambda + K)x = 0. \quad (3)$$

The corresponding concomitant eigenvalue problem is $(M\lambda^2 + C\lambda + K)^T y = 0$, and the left eigenvalue equation is obtained by transposing the concomitant eigenvalue equation as follows:

$$y^T (M\lambda^2 + C\lambda + K) = 0, \quad (4)$$

where the vectors x and y denote the right and left eigenvalues, respectively, and λ denotes the eigenvalue of the vibration equation.

To simplify the above representation, a right state vector u is introduced to replace x , satisfying $u = \lambda x / x = Tx$, where T is the state transition matrix and can be expressed as $T = \lambda I / I$. Similarly, another left state vector v is used instead of y , satisfying $V = \lambda Y / Y$. Thus, (3) and (4) can be rewritten as

$$\begin{aligned} (A\lambda + B)u &= 0, \\ v^T(A\lambda + B) &= 0. \end{aligned} \quad (5)$$

Among them

$$A = \begin{bmatrix} 0 & M \\ M & C \end{bmatrix}, B = \begin{bmatrix} -M & 0 \\ 0 & K \end{bmatrix}. \quad (6)$$

After the state transformation, (6) can be rewritten as

$$(A\lambda + B)u = 0. \quad (7)$$

$$v^T(A\lambda + B) = 0. \quad (8)$$

(7) and (8) have the same eigenvalues and can be derived from the following equation:

$$\det(A\lambda + B) = 0. \quad (9)$$

(8) is an algebraic equation with $2N$ eigenvalues in the complex domain, which can be expressed as $\lambda_i (i = 1, 2, \dots, N)$.

A and B can be expressed as

$$\begin{cases} A = A_0 + \varepsilon A_1, \\ B = B_0 + \varepsilon B_1. \end{cases} \quad (10)$$

4. Matrix Ingestion Method for Complex Modal Structural Vibrations

Since the non-diagonal of the consistent mass matrix contains non-zero elements, when vectorial finite elements are used for dynamic analysis, the consistent mass matrix is often replaced by the concentrated mass matrix in order to reduce computational effort and storage space. The most common method of constructing a centralized mass matrix is to distribute the mass of a cell equally among the connected nodes. When the mass of the unit or the internal nodes are not uniformly distributed, a higher-order difference function is used for mass distribution.

For the rod system structure, the elements on the main diagonal of each row of the centralized mass matrix element on each row of the consistent mass matrix is the sum of all elements in the corresponding row of the consistent mass matrix, i.e.,

$$M_1^c = \text{diag}(M_c^c \cdot J_n), \quad (11)$$

where $\frac{1}{M}$ is the concentrated mass matrix. $\frac{c}{M}$ is the consistent mass matrix. J_n is the n th-order square matrix composed of 1. Substituting equation (5) into (6) further simplification yields

$$M_1 = \left(\frac{1}{2}\right) \text{diag}(C^T \hat{m} C) \otimes I_3. \quad (12)$$

In practical engineering, the variation of structural parameters is reflected in the variation of the mass matrix. Considering the small perturbations of the parameters around their mean values, the mass matrix can be expressed as

$$\begin{aligned} \{M &= M_0 + \varepsilon M_1, \\ \{C &= C_0 + \varepsilon C_1 \\ K &= K_0 + \varepsilon K_1. \end{aligned} \quad (13)$$

According to the matrix regression method, the eigenvalues and eigenvectors of a complex modal structural vibration system can be expanded into the form of a regression series:

$$\begin{aligned} \{\lambda^i &= \lambda_0^i + \varepsilon \lambda_1^i + \varepsilon^2 \lambda_2^i + \dots u^i \\ &= u_0^i + \varepsilon u_1^i + \varepsilon^2 u_2^i + \dots \{v^i \\ &= v_0^i + \varepsilon v_1^i + \varepsilon^2 v_2^i + \dots x^i \\ &= x_0^i + \varepsilon x_1^i + \varepsilon^2 x_2^i + \dots y^i \\ &= y_0^i + \varepsilon y_1^i + \varepsilon^2 y_2^i + \dots \end{aligned} \quad (14)$$

Substituting (11) and (13) into (12), we get

$$\begin{aligned} (A_0 + \varepsilon A_1)(\lambda_0^i + \varepsilon \lambda_1^i + \varepsilon^2 \lambda_2^i + \dots) \\ + (B_0 + \varepsilon B_1)(u_0^i + \varepsilon u_1^i + \varepsilon^2 u_2^i + \dots) = 0. \end{aligned} \quad (15)$$

Similarly, substituting equations (12) and (13) into (14) gives

$$(v_0^i + \varepsilon v_1^i + \varepsilon^2 v_2^i + \dots)^T \left(\begin{matrix} (A_0 + \varepsilon A_1) \\ (\lambda_0^i + \varepsilon \lambda_1^i + \varepsilon^2 \lambda_2^i + \dots) \end{matrix} \right) + (B_0 + \varepsilon B_1) = 0. \quad (16)$$

Expanding (15) and ignoring the terms of $O(\varepsilon^2)$, comparing the coefficients of the same power of ε on the left and right sides of the equation yields

$$\begin{aligned} \varepsilon^0: (A_0 \lambda_0^i + B_0) u_0^i &= 0, \\ \varepsilon^1: (B_0 + \lambda_0^i A_0) u_1^i + B_1 u_0^i + \lambda_0^i A_1 u_0^i + \lambda_1^i A_0 u_0^i &= 0, \\ \varepsilon^2: (B_0 + \lambda_0^i A_0) u_2^i + (B_1 + \lambda_0^i A_1) u_1^i + \lambda_1^i A_0 u_1^i \\ &+ \lambda_1^i A_1 u_0^i + \lambda_2^i A_0 u_0^i &= 0, \end{aligned} \quad (17)$$

where ε is a small parameter and has $\varepsilon = 0$ for the original system; M_0, C_0, K_0 denotes the mean values; and $\varepsilon M_1, \varepsilon C_1, \varepsilon K_1$ denotes the first-order regression term of M_0, C_0, K_0 , respectively. Further, the same operation of (13) and (14) for (17) gives

$$\begin{aligned}
\varepsilon^0: \begin{pmatrix} A \\ 0 \end{pmatrix} + B_0 \Big) T v_0^i &= 0, \\
\varepsilon^1: \begin{pmatrix} B \\ 0 \end{pmatrix} + A_0 \Big) T v_1^i + \begin{pmatrix} B \\ 1 \end{pmatrix} + A_1 + A_0 \Big) T v_0^i &= 0, \\
\varepsilon^2: \begin{pmatrix} B \\ 0 \end{pmatrix} + A_0 \Big) T v_2^i + \begin{pmatrix} B \\ 1 \end{pmatrix} + A_1 \Big) T v_1^i + \lambda_1^i A_0^T v_1^i \\
+ \lambda_1^i A_1^T v_0^i + \lambda_2^i A_0^T v_0^i &= 0,
\end{aligned} \tag{18}$$

where λ_1^i and λ_2^i represent the first-order and second-order registers of the i th eigenvalue, respectively. In addition, the first-order and second-order registers of the left eigenvector and the first-order and second-order registers of the right eigenvector can also be found by (15).

Expanding u_1^i on the original right state eigenvector u_0^s yields

$$u_1^i = \sum_{s=1}^{2N} h_{is}^1 u_0^s. \tag{19}$$

Substituting (17) into (18) yields

$$(B_0 + \lambda_0^i A_0) \sum_{s=1}^{2N} h_{is}^1 u_0^s + (B_1 + \lambda_0^i A_1) u_0^i + \lambda_1^i A_0 u_0^i = 0. \tag{20}$$

The left multiplication of (19) by v_0^{sT} has

$$\begin{aligned}
v_0^{sT} (B_0 + \lambda_0^i A_0) \sum_{s=1}^{2N} h_{is}^1 u_0^s + v_0^{sT} (B_1 + \lambda_0^i A_1) \\
u_0^i + v_0^{sT} A_0 u_0^i \lambda_1^i = 0.
\end{aligned} \tag{21}$$

Considering the modal orthogonal normalization conditions expressed in (14) and (15), (20) can be reduced to

$$h_{is}^1 (\lambda_0^i - \lambda_0^s) + v_0^{sT} (B_1 + \lambda_0^i A_1) u_0^i + \lambda_1^i \delta_{is} = 0. \tag{22}$$

Only if $s = i$, then $\lambda_0^i = \lambda_0^s$ can be obtained from (22)

$$\lambda_1^i = -v_0^{iT} (B_1 + \lambda_0^i A_1) u_0^i. \tag{23}$$

(20) can be further rewritten as

$$\lambda_1^i = -y_0^{iT} \left((\lambda_0^i)^2 M_1 + \lambda_0^i C_1 + K_1 \right) x_0^i. \tag{24}$$

5. Uncertainty Propagation Analysis of Random Complex Eigenvalues

The mass matrix, damping matrix, and stiffness matrix of real engineering structures are generally considered as stochastic structural parameters due to the variation of raw material properties of gears, manufacturing errors, and loading environment. In this paper, the matrix regression method is introduced to the eigenvalue analysis of complex modal structures with stochastic parameters,

and also provides a basis for uncertainty propagation analysis of asymmetric systems. Considering the stochastic nature of the structural parameters, the stiffness matrix K , the mass matrix M , the damping matrix C , the complex eigenvalues λ_r , the left complex eigenvector y , and the right complex eigenvector x can be expressed in the following form:

$$\begin{cases} K = K_d + \varepsilon K_r, M = M_d + \varepsilon M_r, C = C_d + \varepsilon C_r, A = A_d + \varepsilon A_r, \\ B = B_d + \varepsilon B_r, \lambda^i = \lambda_d^i + \varepsilon \lambda_r^i, y^i = y_d^i + \varepsilon y_r^i, x^i = x_d^i + \varepsilon x_r^i, \end{cases} \tag{25}$$

where ε is a small parameter, $K_d, M_d, C_d, A_d, B_d, \lambda_d^i, y_d^i, x_d^i$ and $K_r, M_r, C_r, A_r, B_r, \lambda_r^i, y_r^i, x_r^i$ are the deterministic and random components of K, M, C , and $A, B, \lambda^i, y^i, x^i$, respectively. Also, it is assumed that the mean value of $K_r, M_r, C_r, A_r, B_r, \lambda_r^i, y_r^i, x_r^i$ is zero.

6. Numerical Solution of the Model

In this paper, we solve the differential equations of the system in terms of the magnitudes and vibrations, and briefly compare the results of the two numerical integration methods. Given the initial values of the system vibration, the first 800 transient response periods are omitted, and the dynamic response of the system is programmed in MATLAB to analyze the effect of the variation of excitation frequency, mesh damping ratio, and tooth side clearance on the bifurcation characteristics of the system. The basic parameters of the two-stage planetary gear train of the three-stage gearbox are as follows: rated power $P = 2500$ kW, normal speed range 16r/min~21r/min, transmission ratio $i_1 = 5.25$, $i_2 = 5.28$, number of teeth of the first stage $Z_s = 31$, $Z_{pi} = 47$, $Z_r = 125$, number of planetary wheels $N_1 = N_2 = 3$, and the basic parameters of each gear are shown in Table 1.

The presence of static transmission error can aggravate the meshing shock of the gear teeth and cause abnormal vibration of the system, therefore, this paper discusses the effect of the integrated meshing error on the bifurcation characteristics of the system.

The kinetic analysis of the solution results by the global bifurcation diagram and maximum Lyapunov exponent (LLE) is shown in Figures 1 and 2. Given the dimensionless excitation frequency $\Omega_m^1 = 0.86$, the mesh damping ratio $\xi = 0.07$ and the tooth side clearance $b = 1$, the effect of the integrated meshing error on the dynamic characteristics of the system is discussed with the dimensionless integrated meshing error magnitude E as the bifurcation parameter (for simplicity, the image coordinates $x_{spi}^{(1)}$ are denoted as $x_{spi}^{(1)}$ and $E_{spi}^{(1)}$ as E). According to Figure 1, the three-stage planetary gear system has a rich nonlinear dynamic behavior when the magnitude of the integrated dimensionless meshing error is used as the bifurcation parameter. Combined with Figure 2, it is found that the system is relatively stable at low values of the integrated meshing error, when LLE is negative, and it is clear that the system enters the chaotic response as a multiperiodic bifurcation.

TABLE 1: Basic parameters of a three-stage gear train.

	Planet carrier C	Sun wheel S	Planetary gear p	Inner ring gear r
<i>First stage planetary gear train</i> (number of planetary gears $N_1 = 3$)				
Radius of base circle R_b /(m)	0.471	0.196	0.243	0.683
Mass M /(kg)	2042.9	345.0	388.3	410.3
Moment of inertia im /(kg m^2)	462.56	7.63	16.26	226.58
Average meshing stiffness kel /(n/M)	—	—	1.31×10^{10}	1.49×10^{10}
Stiffness variation amplitude kal /(n/M)	—	—	4.97×10^9	5.12×10^9
<i>First stage planetary gear train</i> (number of planetary gears $N_2 = 3$)				
Radius of base circle R_b /(m)	0.351	0.133	0.194	0.157
Mass M /(kg)	1212.6	132.4	176.6	81.6
Moment of inertia im /(kg m^2)	151.76	1.30	5.13	26.66
Average meshing stiffness kel /(n/M)	—	—	2.62×10^{10}	2.54×10^{10}
Stiffness variation amplitude kal /(n/M)	—	—	7.54×10^9	3.23×10^9

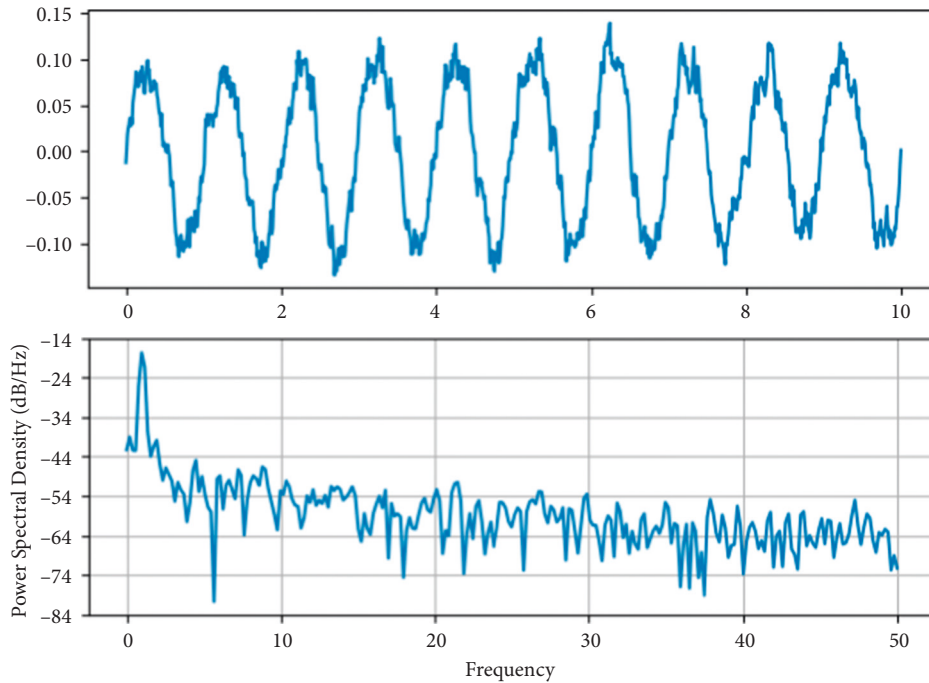


FIGURE 1: System under the variation of the integrated meshing error.

The dynamics of the two-stage planetary gear and the one-stage parallel shaft gear system are further verified and analyzed by combining the phase trajectory diagram and the Poncelet cross section diagram with the aid of the time history diagram and the spectrum diagram, as shown in Figure 3. When the dimensionless integrated meshing error value $E_{spi}^{(1)} = 0.05$, the system is in a single-cycle motion state, the time history graph is close to a sinusoidal curve, the vibration amplitude between cycles is basically the same, the phase trajectory line is an elliptical closed curve, the Poincaré diagram is a single point and the fundamental frequency signal in the spectrum is very prominent at this time, indicating that the system is in a typical single-cycle state.

With the increase of the integrated meshing error, when 0.779, as shown in Figure 4, the time course diagram changes periodically with two amplitudes as one cycle, the phase trajectory line is concave from one elliptic curve to two elliptic curves, the Poincaré cross-sectional diagram splits from one single point to two single points, and the FFT spectrum is shown as octave components, indicating that the system is in a two-cycle motion state. Combining Figures 3 and 4, it can be found that the motion state of the system splits and changes from single-cycle to two-cycle and four-cycle with the increase of the magnitude of the integrated dimensionless mesh error. At the integrated dimensionless meshing

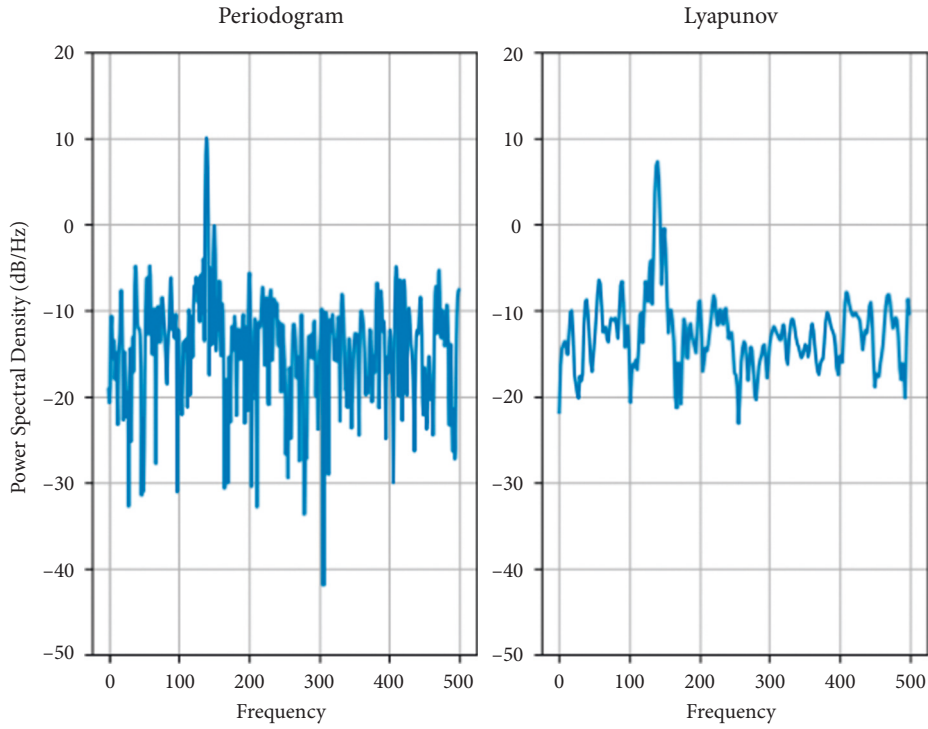


FIGURE 2: Plot of the maximum Lyapunov exponent of the system under the variation of the integrated error.

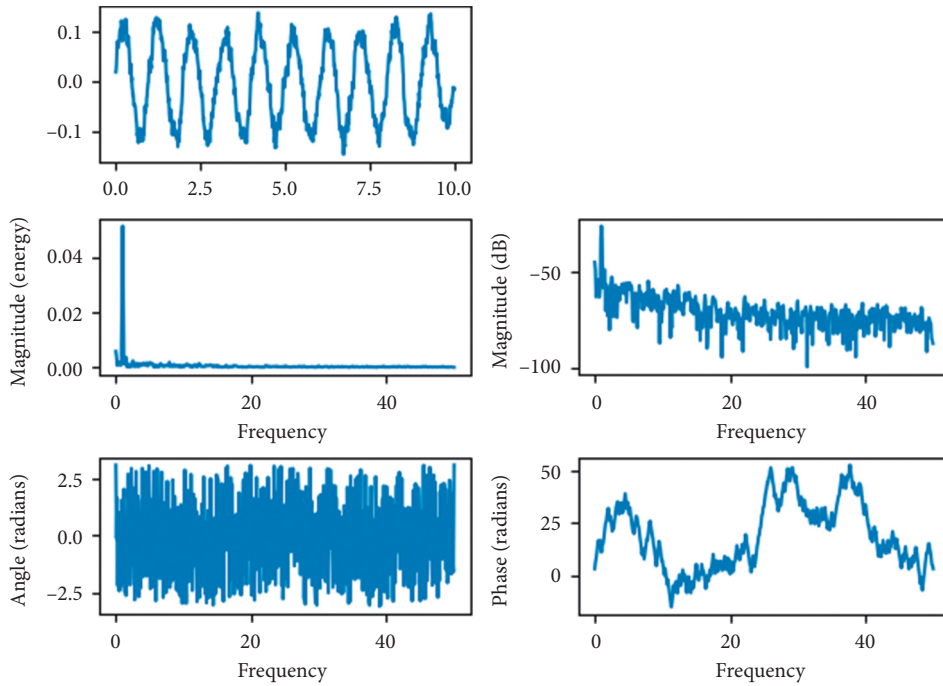


FIGURE 3: Dynamics of the system at $E = 0.05$.

error (1) $E_{spi}^{(1)} = 1.259$, strange attractors appear in the cross-sectional plot of Poincaré, indicating that the system enters the chaotic state through multi-cycle bifurcation at this time. When (1) $E_{spi}^{(1)}$ reaches 0.939, the system bifurcates from the two-cycle state to the two-

cycle state with an LLE value of -0.001713. Therefore, the “negative pole” that appears in the plot of the maximum Lyapunov exponent of the system under the change of the integrated mesh error can characterize the dynamics of the two-cycle bifurcation, as shown in Figure 5.

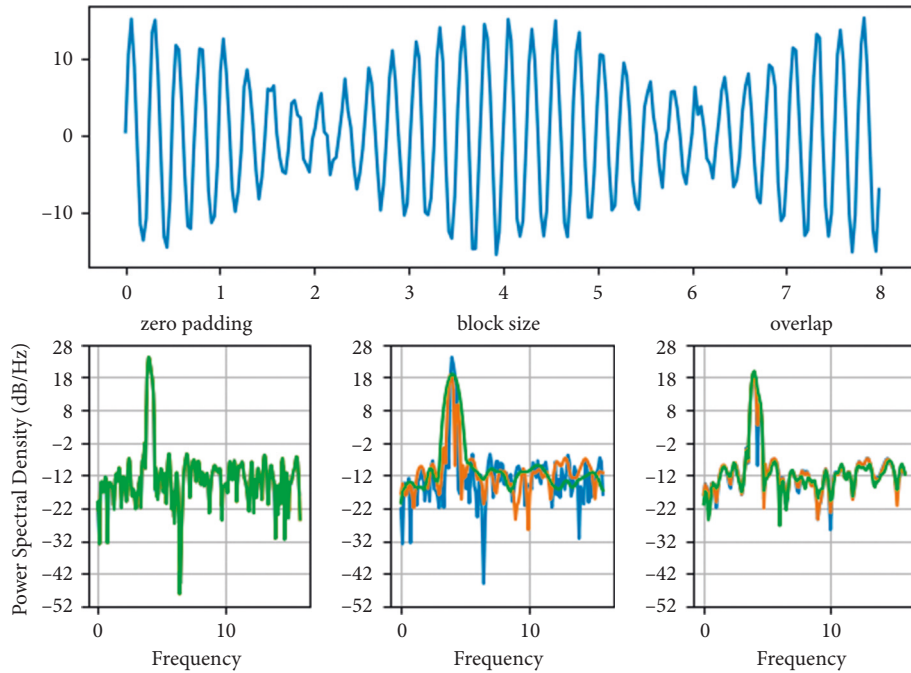


FIGURE 4: Dynamics of the system at $E = 0.779$.

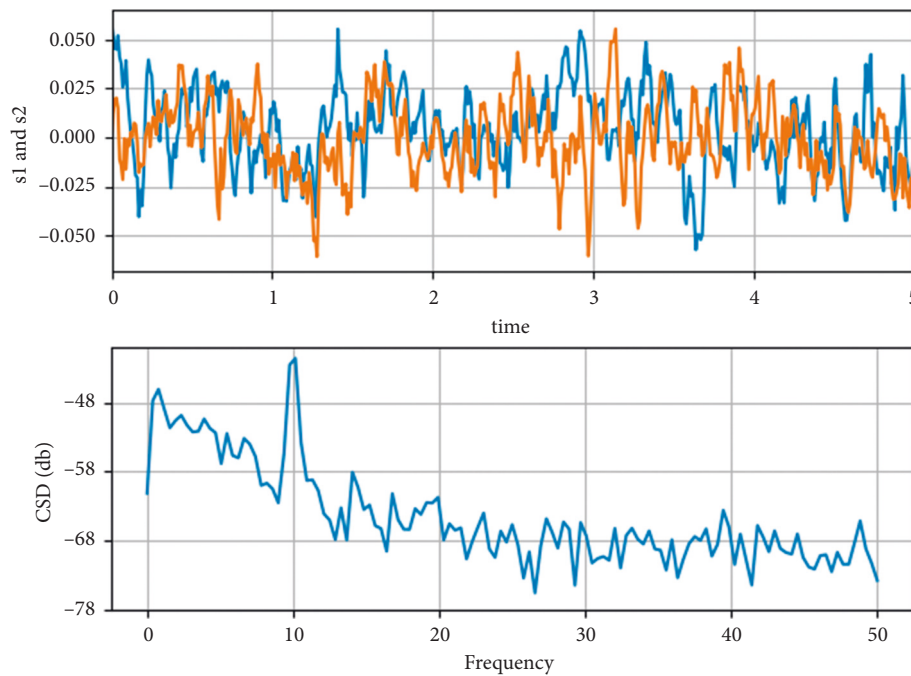


FIGURE 5: Dynamics of the system at $E = 0.956$.

7. Conclusion

In this paper, a modified stochastic regression method is used to solve a system of vibration differential equations for a three-stage gear train, and the effects of changes in the integrated dimensionless excitation frequency and the integrated meshing error on the dynamic response of the system are analyzed. A new static no-load transmission error model is established, which has its unique advantages in the

fault diagnosis of gears. The model no longer requires tooth surface equations, avoiding the difficulty of merging tooth surface errors into tooth surface equations. The effect of the static unloaded transmission error of the real tooth surface on the dynamic characteristics of the bevel gear is analyzed. The model is also applicable to other types of gears. The global bifurcation diagram, Poincaré cross section diagram, and phase trajectory diagram are used as the main basis, and the time history diagram and the spectrum diagram are used

as auxiliary tools to determine the range of bifurcation parameters when the three-stage gearing system is in a relatively stable state. It is found that the system is in a relatively stable state when the dimensionless excitation frequency is in the range of 0.716–0.86 and the magnitude of the dimensionless integrated meshing error is < 1.089 .

Data Availability

The data used to support the findings of this study are available from the corresponding author upon request.

Conflicts of Interest

The authors declare that they have no conflicts of interest regarding this work.

References

- [1] G. Wojnar, R. Burdzik, A. N. Wiecek, and L. Konieczny, "Multidimensional data interpretation of vibration signals registered in different locations for system condition monitoring of a three-stage gear transmission operating under difficult conditions," *Sensors*, vol. 21, no. 23, p. 7808, 2021.
- [2] R. Wang, S. Lu, and W. Feng, "A three-stage optimization methodology for envelope design of passive house considering energy demand, thermal comfort and cost," *Energy*, vol. 192, p. 116723, 2020.
- [3] H. Li, H. He, J. Shan, and J. Cai, "Innovation efficiency of semiconductor industry in China: a new framework based on generalized three-stage DEA analysis," *Socio-Economic Planning Sciences*, vol. 66, pp. 136–148, 2019.
- [4] W. Cao, J. Ni, B. Jiang, and C. Ye, "A three-stage parameter prediction approach for low-carbon gear hobbing," *Journal of Cleaner Production*, vol. 289, p. 125777, 2021.
- [5] M. Saritaş, Ö. Gölbol, and P. Yayla, "Finite element stress analysis of three-stage gear box," *Ömer Halisdemir Üniversitesi Mühendislik Bilimleri Dergisi*, vol. 10, no. 2, pp. 784–790, 2021.
- [6] N. Shen, H. Liao, R. Deng, and Q. Wang, "Different types of environmental regulations and the heterogeneous influence on the environmental total factor productivity: empirical analysis of China's industry," *Journal of Cleaner Production*, vol. 211, pp. 171–184, 2019.
- [7] R. Hu, K. Chen, W. Chen, Q. Wang, and H. Luo, "Estimation of construction waste generation based on an improved on-site measurement and SVM-based prediction model: a case of commercial buildings in China," *Waste Management*, vol. 126, pp. 791–799, 2021.
- [8] Y. Zhu, G. Li, S. Tang, R. Wang, H. Su, and C. Wang, "Acoustic signal-based fault detection of hydraulic piston pump using a particle swarm optimization enhancement CNN," *Applied Acoustics*, vol. 192, Article ID 108718, 2022.
- [9] C. P. Tan, A. Garg, L. Gao, S. Singh, and X. Meijuan, "Multi-objective optimisation framework of genetic programming for investigation of bullwhip effect and net stock amplification for three-stage supply chain systems," *International Journal of Bio-Inspired Computation*, vol. 16, no. 4, pp. 241–251, 2020.
- [10] J. L. Gomez, I. Khelif, A. Bourdon, H. André, and D. Rémond, "Angular modeling of a rotating machine in non-stationary conditions: application to monitoring bearing defects of wind turbines with instantaneous angular speed," *Mechanism and Machine Theory*, vol. 136, pp. 27–51, 2019.
- [11] A. Blanco-Rodríguez, V. F. Camara, F. Campo et al., "Development of an electronic nose to characterize odours emitted from different stages in a wastewater treatment plant," *Water Research*, vol. 134, pp. 92–100, 2018.
- [12] R. Gao, L. Liu, X. Liu et al., "An overview of ML-based applications for next generation optical networks," *Science China Information Sciences*, vol. 63, no. 6, Article ID 160302, 2020.
- [13] V. Inturi, G. R. Sabareesh, and V. Sharma, "Integrated vibro-acoustic analysis and empirical mode decomposition for fault diagnosis of gears in a wind turbine," *Procedia Structural Integrity*, vol. 14, pp. 937–944, 2019.
- [14] H. Zhao, C. Liu, Z. Dong, R. Huang, and X. Li, "Design and optimization of a magnetic-g geared direct-drive machine with V-shaped permanent magnets for ship propulsion," *IEEE Transactions on Transportation Electrification*, vol. 8, no. 2, pp. 1619–1633, 2022.
- [15] X. Liu, H. Huang, and J. Xiang, "A personalized diagnosis method to detect faults in gears using numerical simulation and extreme learning machine," *Knowledge-Based Systems*, vol. 195, Article ID 105653, 2020.
- [16] X. Zhang, X. Tang, and W. Yang, "Analysis of transmission error and load distribution of a hoist two-stage planetary gear system," *Proceedings of the Institution of Mechanical Engineers - Part K: Journal of Multi-body Dynamics*, vol. 233, no. 1, pp. 3–16, 2019.
- [17] C. Wang, "Analysis of modal transition and coincidence degree variation instabilities of wind turbine planetary gear system," *International Journal of Pattern Recognition and Artificial Intelligence*, vol. 33, no. 04, Article ID 1959012, 2019.
- [18] I. Vamsi, G. R. Sabareesh, and P. K. Penumakala, "Comparison of condition monitoring techniques in assessing fault severity for a wind turbine gearbox under non-stationary loading," *Mechanical Systems and Signal Processing*, vol. 124, pp. 1–20, 2019.
- [19] H. Yang, X. Li, J. Xu, Z. Yang, and R. Chen, "Dynamic characteristics analysis of planetary gear system with internal and external excitation under turbulent wind load," *Science Progress*, vol. 104, no. 3, Article ID 003685042110356, 2021.
- [20] H. Chen and X. A. Chen, "Recirculation of parallel-connected planetary gear trains," *Chinese Journal of Mechanical Engineering*, vol. 35, no. 1, pp. 27–11, 2022.

Research Article

Prediction and Estimation of River Velocity Based on GAN and Multifeature Fusion

Yan Wang,¹ Weiwei Chen ,^{1,2} and Yulan Wang³

¹School of Artificial Intelligence, Xi'an Aeronautical Polytechnic Institute, Xi'an 710089, China

²School of Information Engineering, Chang'an University, Xi'an 710064, China

³Department of Mathematics and Physics, Hebei University of Architecture, Zhangjiakou 075000, China

Correspondence should be addressed to Weiwei Chen; 2014024010@chd.edu.cn

Received 27 May 2022; Revised 22 June 2022; Accepted 15 July 2022; Published 21 August 2022

Academic Editor: Le Sun

Copyright © 2022 Yan Wang et al. This is an open access article distributed under the Creative Commons Attribution License, which permits unrestricted use, distribution, and reproduction in any medium, provided the original work is properly cited.

The necessity of predicting and estimating river velocity motivates the development of a prediction method based on GAN image enhancement and multifeature fusion. In this method, in order to improve the image quality of river velocity, GAN network is used to enhance the image, so as to improve the integrity of image data set. In order to improve the accuracy of prediction, the image is extracted and fused with multiple features, and the extracted multiple features are taken as the input of CNN, so as to improve the prediction accuracy of convolution neural network. The results show that when the velocity is 0.25 m/s, 0.50 m/s, and 0.75 m/s, the accuracy of improved method can reach 85%, 90%, and 92%, which are higher than SVM, VGG-16, and BPNET algorithms. The above results indicate that the improvement has certain positive value and practical application value.

1. Related Work

China has abundant water resources, but it is also threatened by catastrophic flooding. However, due to the limitations of field environmental factors and the increase of data volume, using the traditional manual measurement for river velocity not only has great constraints, but also faces serious personnel threats. With the maturity of modern image acquisition technology and the wide application of artificial intelligence algorithm, how to use noncontact equipment for river monitoring has become the focus of current thinking and research.

It is found that the texture features of river channel image have a certain mapping relationship with the flow velocity, but the features are relatively single. If the traditional contact real-time monitoring is used, its accuracy will be greatly affected. To solve this problem, Tauro F et al. proposed a nonlinear learning fluid prediction method, so as to provide reference for fluid velocity prediction [1]. Ghoulami et al. [2] proposed a new CRBFNN model for the problem of river flow velocity. Through the model, the river flow velocity of 60° and 90° was predicted. The results showed

that the model was more suitable for the prediction of bend flow velocity of 60° [2]. Khuntia et al. [3] proposed to use multivariate regression to analyze and predict the river velocity and found that the machine learning algorithm performed better than the traditional Shiono and Knight methods [3]. Based on particle tracking velocimetry, Eltner et al. [4] collected and estimated River images. The results show that the deviation of this method is between 4% and 5% [4]; Zhang et al. [5] used the reflection technology of BeiDou system to inverse the river velocity and then obtained the river velocity with small error [5].

All the above studies focus on fluid velocity prediction, but its accuracy needs to be further improved. In view of the above problems, some scholars also proposed to process the collected water flow images. For example, Gulrajani et al. [6] proposed to introduce gradient punishment mechanism into the WGAN algorithm to better improve the WGAN algorithm [5]. David proposed an image processing technology based on the BEGAN algorithm to solve the contradiction between picture type and generation [6].

The above research shows that this paper proposes a flow image processing and velocity prediction method based on

GAN algorithm and CNN algorithm, which takes the Yellow River flow image as the object. Meanwhile, the feasibility of the construction method is verified.

2. The Basis of Convolutional Neural Network Algorithm

Convolutional neural network has been widely used in classification problems. The characteristics of the convolutional neural network are reflected in translation invariance, feature extraction, and so on. Moreover, it has the characteristics of weight sharing and local connection. The structure is divided into multiple layers, including input, output, and convolution layer. And each layer has different functions. In the different layer structure, the calculation methods are different to some extent. The basic structure of the network is shown in Figure 1.

The convolution layer needs to carry out convolution processing for the upper feature maps or input information. In this process, some learnable convolution kernel and activation function should be used to obtain the corresponding output results. The formula is shown below [7–9]:

$$\begin{aligned} x_j^l &= f(u_j^l), \\ u_j^l &= \sum_{i \in M_j} x_j^{l-1} * k_{ij}^l + b_j^l, \end{aligned} \quad (1)$$

where l represents the convolution layer; $f(\cdot)$ represents the activation function of l ; x_j^l represents the output of channel j in l ; u_j^l represents the net activation of channel j in l , and, specifically, it is obtained by the convolution layer $l-1$ of the output feature map with l convolution and then adding b_j^l . k_{ij}^l represents the convolution kernel weight matrix, whose size is generally $1 * 1$, $3 * 3$, $5 * 5$, etc. M_j represents the set of input feature maps.

The pooling layer is divided into two types: maximum pooling and average pooling, which is divided according to the input feature graph. Then, the dividing matrix block pixels are processed by sliding window. This layer is also called the downsampling layer, and the formula is shown as follows [10–12]:

$$\begin{aligned} x_j^l &= f(u_j^l), \\ u_j^l &= \beta_j^l \text{down}(x_j^{l-1}) + b_j^l. \end{aligned} \quad (2)$$

Here, $\text{down}(\cdot)$ represents the pooling function to realize the function of narrowing the input feature map; β represents the weight coefficient of pooling layer; u_j^l represents net activation, which means that it is necessary to combine the previous layer output feature map with the current layer pooling function, and then add b_j^l .

For convolutional neural network, the features of input information can be extracted in the execution, specifically using the convolution and pooling repeated superposition. The convolution is divided into two parts: high level and low level. The former mainly extracts image semantic information, and so on. The latter extracts details, such as image edge information. Combined with the previous analysis, it

can be seen that the characteristics of convolutional neural network include weight sharing and local connection, among which the weight sharing can effectively reduce the parameters, because the neurons weight on each feature mapping surface is consistent. The local connection means that the input of each neuron is connected with the local acceptance domain of the previous layer. In this way, the local features can be extracted. Meanwhile, the location relationship with other features can be clarified.

3. Flow Rate Classification Network Based on Multifeature Fusion

3.1. Multifeature Fusion. Traditional classification methods can achieve higher accuracy by deepening the network depth or broadening the network width of the classification model, namely, increasing the number of convolution layers or adding more feature map dimensions to the single convolution layer. However, the direct result of increasing the number of convolution layers is that the network parameters and computational complexity will greatly increase, and the training process will consume a lot of hardware and software resources. In addition, the increase of model layers can just improve the classification effect of the network within a certain range. When the number of layers increases to a certain depth, the gradient disappearance may occur during the backpropagation [13]. And the feedback information of shallow convolution cannot be obtained to adjust the weight size. Therefore, too deep structure will lead to performance degradation of the classification network. Taking the above considerations into account, this chapter proposes a multifeature fusion mechanism.

Figure 2 shows that, without increasing the network depth and spatial parameters, the learning robustness of the classification model for target data can be improved.

The feature maps of multiple convolution middle layers are fused. Under the normal use of data semantic information obtained by deep convolution, the local detail features reinforce information obtained by shallow convolution. The classification goal of higher accuracy can be achieved [14–17]. The calculation method is shown as follows:

$$L_n = \text{Concat}(L_k, L_p, L_q). \quad (3)$$

It can be seen from the formula that k , p , q represent the number of convolution layers of fusion output; L_n represents the output feature map of the convolution layer n . The output of each convolution layer is multichannel feature map, and the size is the same. But the size is directly related to the number of convolution layers, which are negatively correlated. In the multiscale fusion, the size of the feature map needs to be adjusted first, which means that the nearest neighbor interpolation method is used for upsampling, and then splicing. So, the multilevel feature map fusion can be achieved.

3.2. Classification Network Structure. As shown in Figure 3, VGG-16 is adjusted and applied to image recognition. The classification model consists of one input layer and five

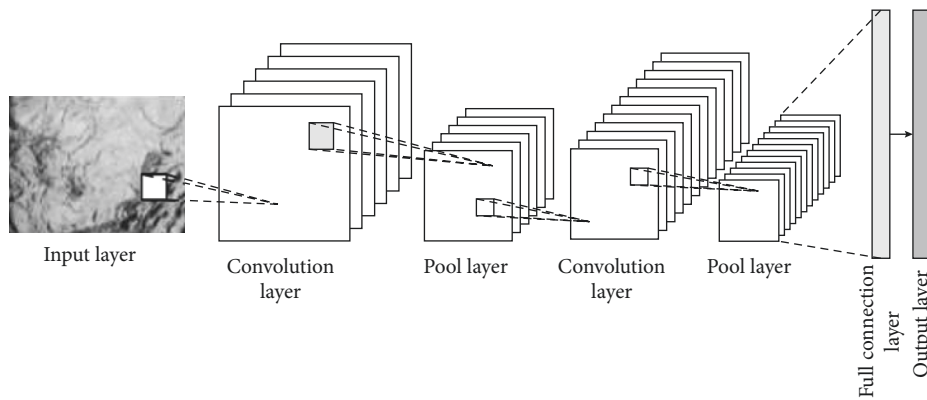


FIGURE 1: Structure of CNN.

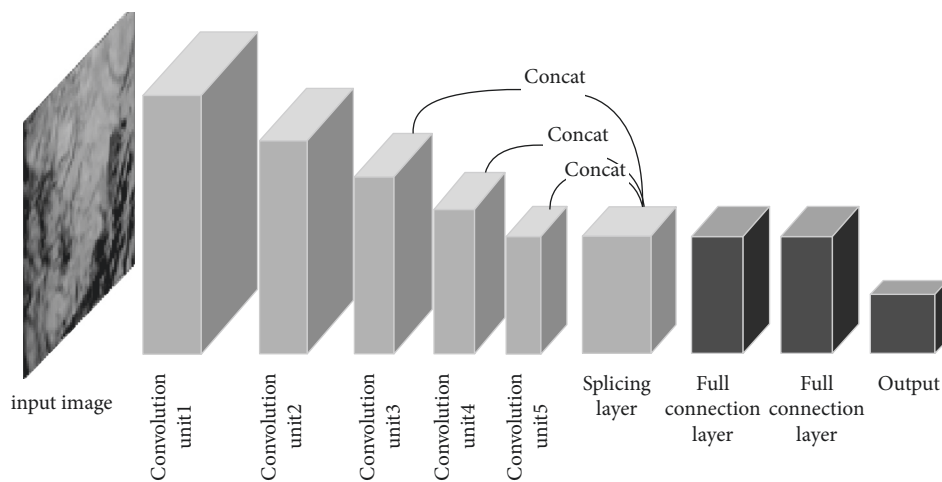


FIGURE 2: Diagram of multifeature fusion.

convolutional processing units. Each unit contains two to three unequal convolution layers, a single pooling layer, two full connection layers, a Dropout layer, and a feature fusion layer [18–22]. The feature fusion mechanism is introduced to upsample the flow feature map output from convolution C5_2 layer. Then fuse it with the feature map output from convolution C3_3 layer and convolution C4_3 layer to form the feature fusion layer. In this network, the 3×3 small convolution kernels are stacked to increase the depth of the model, and multiple Rectified Linear Units (ReLU) are added, which can reduce the computational complexity in the classification and recognition process. Apart from that, it can alleviate the overfitting problem to some extent. Before training the network, the multitype images generated by model learning in Chapter 2 and Chapter 3 are mixed with real samples. 70% of the data are randomly selected as the training set, and the rest as the test set. Dropout mechanism is added after the full connection layer of the classification network to alleviate the problem of overfitting during training.

The use of feature fusion mechanism has certain advantages, so that the underlying features on classification decision-making is strengthened. It is easy to identify the image with no significant difference in detail features. So, it has higher robustness. Even if the error between the training

set and the test set is large, the higher recognition accuracy can still be achieved.

4. Experiment and Analysis

4.1. Experimental Subjects. In this paper, a section of the Yellow River is analyzed as an example. The precipitation in this section basically stays within 1800 to 2000 mm, and there are significant changes. The precipitation is mainly concentrated in summer, and there are many rainstorms. It is easy to cause mountain floods and other disasters. Therefore, it is necessary to monitor and analyze the flow velocity of each tributary in this region which is as follows in Figure 4.

4.2. Flow Image Acquisition. The professional camera devices are set up on both sides of boundary card river to collect water images. And the collected images are transmitted through wireless equipment. Install cameras at an appropriate position in the building and set the frame rate to 60 fps at an appropriate spacing. In addition to capturing images of the river, information such as weather and velocity values should also be recorded. The specific solution is shown in Figure 5.

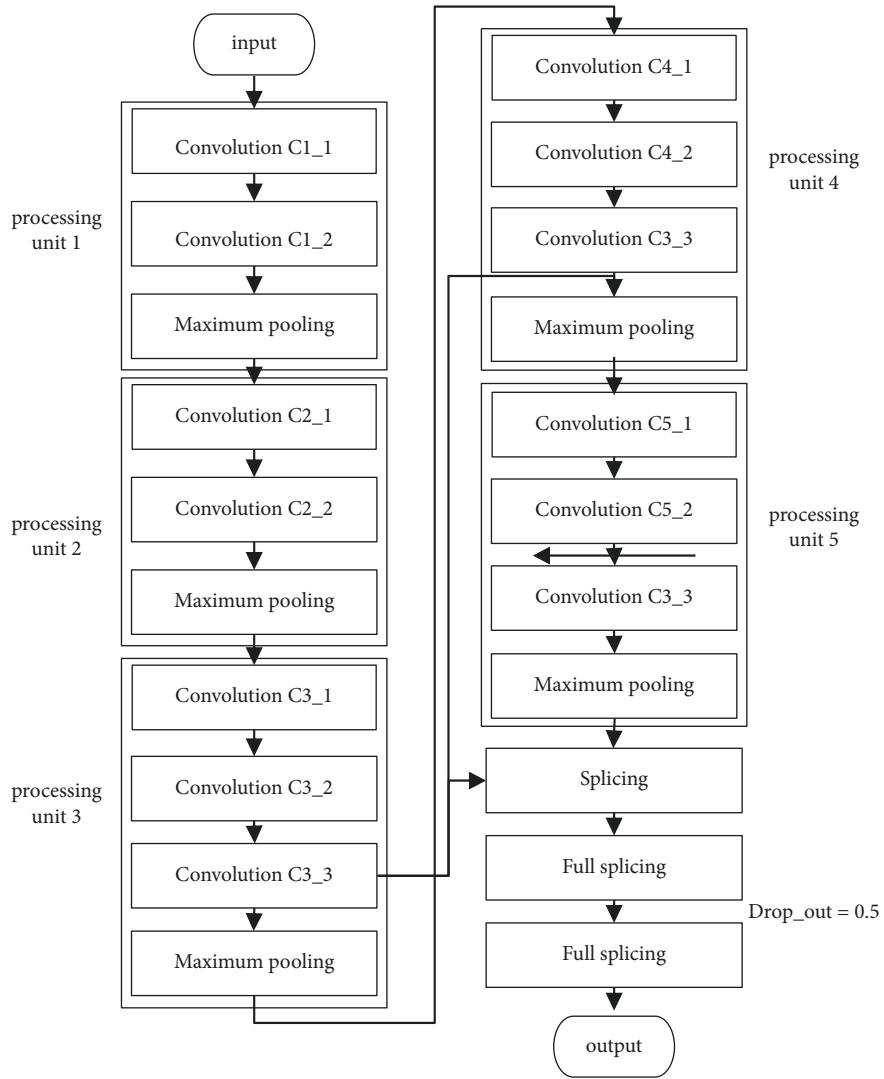


FIGURE 3: Classification network structure.



FIGURE 4: General River and tributary map.

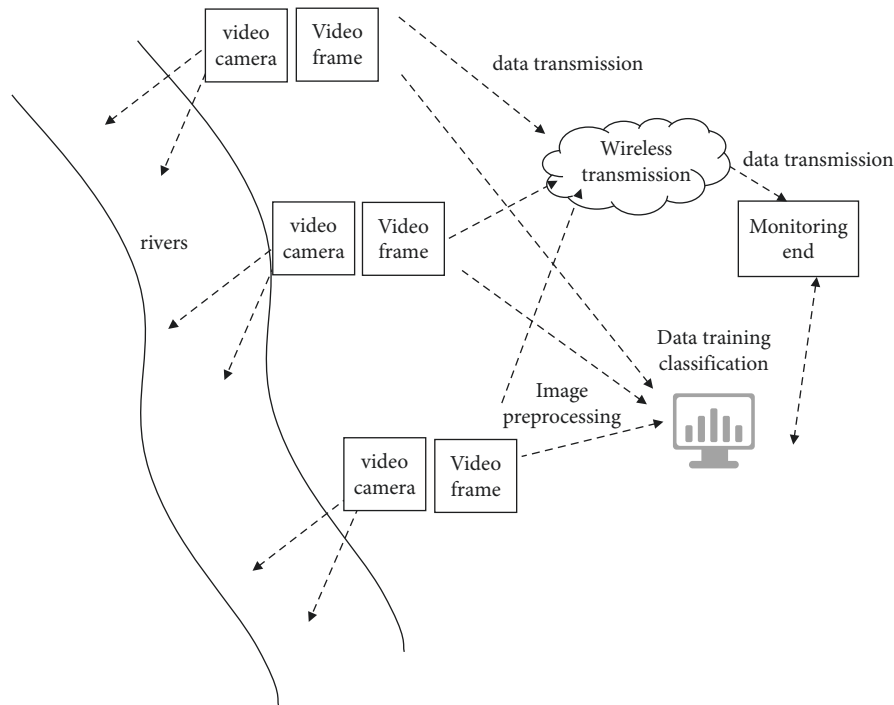


FIGURE 5: Water flow image acquisition scheme.

Many modules are involved in the river image acquisition, including video acquisition and wireless transmission module. The image acquisition and transmission functions are completed as a result of each module's effective cooperation. In the video acquisition module, the function camera with high performance is used to collect images according to the set parameters. The data transmission module realizes the video transmission function, which adopts the Unicom CDMA network. In addition to the above part, it also includes the central monitoring platform. The monitoring terminal can use different access methods. First is to automatically record and update the monitoring position of the image, and second is to query the current record of the image.

During image acquisition, not only the current average velocity is recorded, but also the velocity at both sides of the same time and middle positions is compared, so as to meet the requirements of hierarchical estimation. After the collection is completed, the professional software is used for video interception. So, the training sets can be obtained, totaling 8000 pieces, 1000 pieces for each power station. The classification interval is set, then the flow rate images were clipped. Therefore, the images with the same flow rate are classified based on the flow rate label. The flow rate resolution designed in this study is 0.5 m/s, which is totally divided into five flow rate intervals.

4.3. Experimental Platform Configuration. The experimental platform is set up, and the computing platform uses the Dawn W580-G20 server, Nvidia Tesla k8/0 computing card, dual processor architecture, and 480 GB/S video memory bandwidth. The computing performance is higher, which meets the requirements of this paper.

4.4. Image Processing. In order to enhance the completeness of data and improve the robustness of Figure 3 network, it is proposed to process the collected water flow image data before prediction. Based on GAN and current models, the relatively real pseudo samples can be obtained. But there are some problems with GAN. First, the diversity of sample generation cannot be guaranteed. Second, the training process is difficult [23, 24]. Third, the discriminator is stronger than the generator in the initial stage, so it is difficult for them to achieve a balance in the adversarial training. To solve the problem, David et al. designed a boundary-balanced generative adversarial network. In this network, a new loss function is set up and an autoencoder is introduced. Meanwhile, the GAN is able to learn the texture features directly from raw data, without modeling. Thus, it is consistent with the real data to the maximum extent available. However, as the BEGAN described earlier did not set generator constraints, the fitting effect is affected to some extent. In this study, the above problems are analyzed, and a method based on conditional boundary balance generative adversarial network is designed. Conditional label information has been added to this method to guide the direction in which the data flow is generated. At the same time, the reliability of the generated image is verified to ensure that the generated image meets the higher quality requirements.

4.4.1. Image Generation of Basic Label Information. To study the image generation strategy based on label information, firstly, the samples containing labels need to be extracted. Then, the conditional information is added in the boundary balance network to guide the image output based on

category information. In the design, the label information y is added to the input of the generator and spliced with the sampled noise z . So, the corresponding category's images are generated under guidance. The basic form of the objective function is shown below [25]:

$$\min_G \max_D V(D, G) = E_{x \sim p_{\text{dova}}}(x) [\log D(x|y)] + E_{z \sim p_z(z)} [\log(1 - D(G(z|y)))] \quad (4)$$

where $D(x|y)$ represents the probability of judging that the input image belongs to the real sample, while $D(G(x|y))$ represents the probability after the generator mapping. The loss function is as follows:

$$\text{Loss}(s) = |s - D(s)|^l, \quad l \in 1, 2. \quad (5)$$

In the formula, s represents the sample through autoencoder, and l represents the l_1 or l_2 norm.

In the algorithm, the discriminator and generator have different functions, which can minimize the reconstruction errors of real image and generated image, respectively. Bulldozer distance (EM) is introduced to fit the loss distribution of the autoencoder. The specific formula is as follows:

$$W(\mu_1, \mu_2) = \inf_{\gamma \in (\mu_1, \mu_2)} E_{(x_1, x_2) \sim \gamma} [\|x_1 - x_2\|], \quad (6)$$

Here, μ_1 and μ_2 represent the loss distribution of real data and generated data respectively, while $W(\mu_1, \mu_2)$ represents the set of all possible joint distributions of both of them.

4.4.2. Generate Image Verification Mechanism. This part designs a verification module, which is added into D to identify the extracted image features. The input data is processed based on the nonlinear method and inputs the results in Softmax layer, where the probability of the category can be calculated. The probability formula of an output sample belonging to category i is shown as follows:

$$y_i = \frac{e^{a_i}}{\sum_{k=1}^C e^{a_k}}, \quad \forall i \in 1, \dots, C. \quad (7)$$

It can be seen from the formula that C represents the number of categories to be predicted. The full connection layer output a_1, a_2, \dots, a_c can get the corresponding probability distribution by the Softmax layer processing. The loss function is cross entropy, and the specific formula is as follows:

$$\text{Loss} = - \sum_{k=1}^n \sum_{i=1}^C t_{ki} \log(y_{ki}). \quad (8)$$

The above formula revealed that n represents the number of samples; k stands for some sample; i stands for category; t_{ki} is the probability of k real categories; y_{ki} is the probability that the model pair k belongs to i .

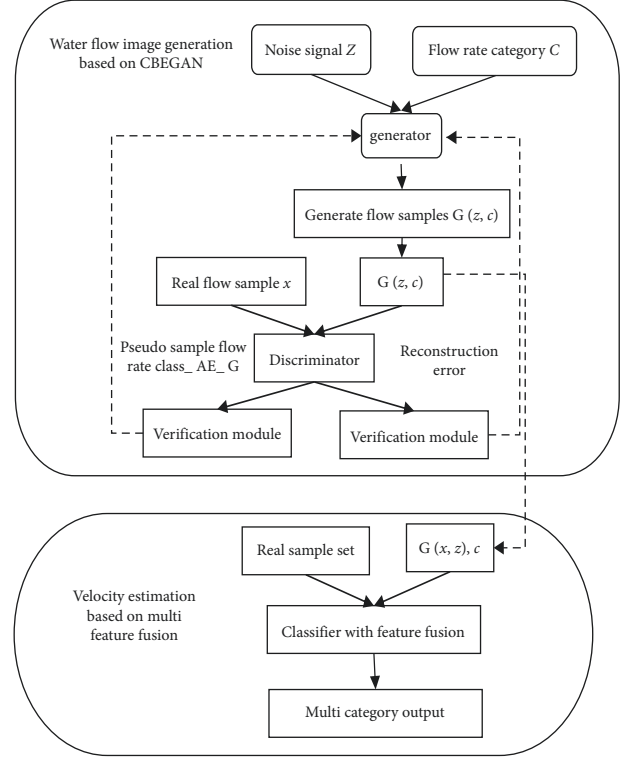


FIGURE 6: Proposed model based on GAN.

4.4.3. The Overall Model Construction. Combined with the above design, the flow velocity estimation model is constructed as shown in Figure 6.

where the whole model is divided into several parts, including three modules, namely, flow image generation, fogging, and velocity estimation. The design of each module is as follows:

Step 1: Collect the video of water flow in this area, which can be divided into two weather conditions. The first is fog blocking, and the second is no blocking, namely, normal illumination. During recording, it is necessary to record the velocity on both sides and in the center of the river, and the flow rate should be determined. Except for the above operations, the appropriate cropping and other operations are required to support the subsequent processing.

Step 2: First of all, the real sample is constructed, which means that the small flow data obtained in the previous step is corresponding to the flow velocity interval. Then, the discriminator and generator are constructed. Meanwhile, the uniform noise signals are input into the generator, and the mixed generated samples and real samples are input into the discriminator.

Step 3: To verify the reliability of the generated flow image, in this process, the classifier with the same structure as the discriminator is used to analyze the flow velocity category. Hence, the optimal model weight is determined on this basis.

Step 4: To generate the flow images, the key part of this step is the CBEGAN network.

Step 5: To generate the data set, normalize the generated samples in the fourth and sixth steps, mix the generated samples and original samples in a random way, and then divide them into training set and test set, which account for 70% and 30%, respectively.

Step 6: To build CNN, input the training set into the designed classification network. So, the recognized flow category can be obtained. Then the verification can be achieved through the test set. During the test, the input image is clipped with the same size, and the output results are weighted and averaged. Finally, the current time flow rate can be obtained.

4.5. Result Analysis

4.5.1. Image Generation Quality Verification

(1) *Verification Mechanism Results Analysis.* The results of verification mechanism are analyzed, and the accuracy curve and category label loss function are shown in Figures 7 and 8 respectively. According to the information in the figure, the quality stability of generated images in the initial stage of training is low, which is related to the training imbalance. And it corresponds to a higher loss function value. When the iterations increase, the adversarial network becomes stable, and the probability of accurate classification increases gradually. For the average accuracy of 0.95, the probability of generating the corresponding category flow image is significantly improved after adding the label information.

(2) *Image Generation Quality.* The results in Figure 9 show that the recognition accuracy of naive GAN and CGAN models is consistent, because the latter is the result of a slight improvement of the former. The classification accuracy obtained by the BEGAN model is significantly higher, because it improves the naive GAN greatly. However, the CBEGAN model designed a special validation module to constrain the flow of generated network data by the loss function. Thus, the higher accuracy is achieved relative to the BEGAN model.

It can be seen that CGAN is difficult to compute unlabeled data efficiently with unsupervised input. Compared with the naive GAN, the generation sample accuracy of BEGAN model is higher, which is related to the self-encoder that exists. The CBEGAN model designed in this study can transfer learning information to the model and then realize the adjustment of weight parameters.

Comparing the GAN network with conditional and unconditional input, it is found that the accuracy of the former generated sample is higher. It is mainly related to the mitigation of the freedom problem in training, which improves the quality of the generated sample.

(3) *Quality Analysis of Generated Image.* In image quality analysis, there are 5 different flow rate levels, namely, 0.5, 1, 1.5, 2, 2.5, and the unit is m/s. After the data set is

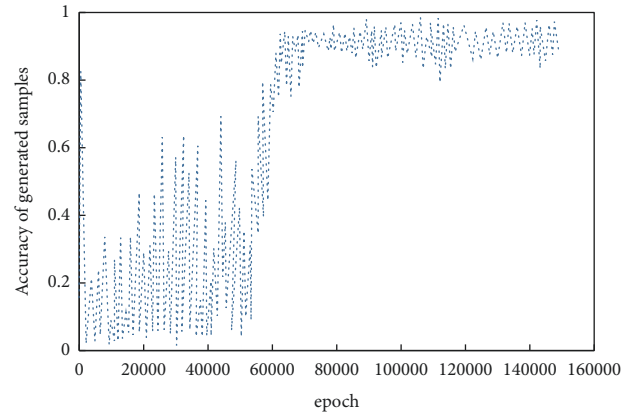


FIGURE 7: Accuracy of generated image.

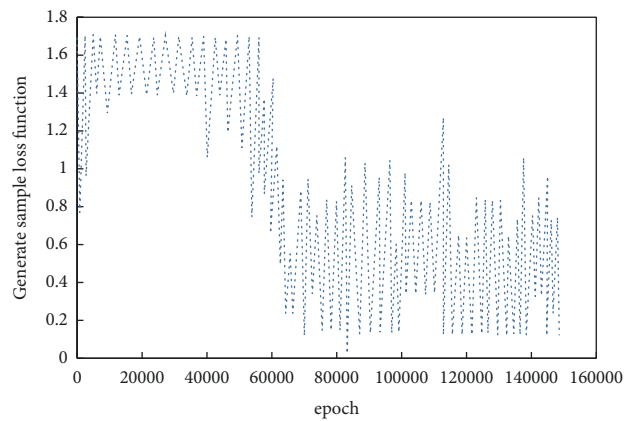


FIGURE 8: Loss function value of generated image.

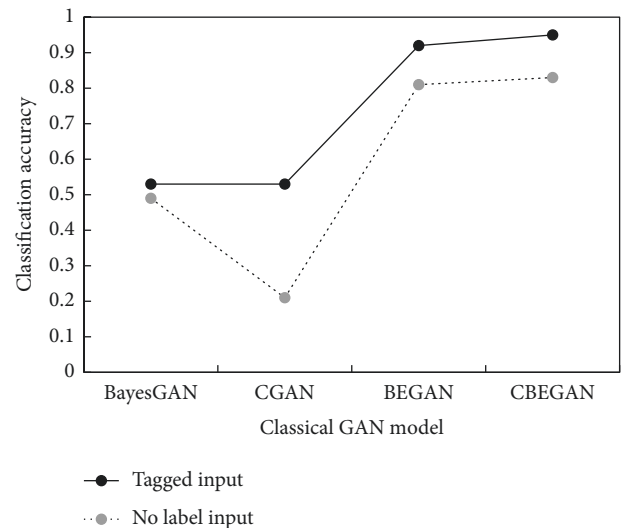


FIGURE 9: The effect of image generation under different models.

established, it is calculated by the SIM indicator. The formula is as follows:

$$SSIM(x, y) = I(x, y) * c(x, y) * s(x, y), \quad (9)$$

Here, x and y belong to two images, and $l(x, y)$, $s(x, y)$, and $c(x, y)$ are the brightness, structural similarity, and contrast of images in turn.

The above indexes can be used to analyze the image distortion. If the index is large, it means that the quality of the generated image is higher. The SSIM calculation results of different methods are shown in Figure 10.

The information above shows that, compared with GAN, CGAN, and BEGAN, the structural similarity of the algorithm was improved by 0.25, 0.14, and 0.05, respectively. So, the improvement effect was significant compared with the two front algorithms. Compared with the third model, the labeled mechanism can also improve the quality of the generated image, which proves the feasibility of the proposed algorithm.

Here are two images of three-channel X and Y . The size of them is $m * n$. The formula of MSE is as follows:

$$MSE = \frac{1}{m * n} \sum_k \sum_{i=0}^{m-1} \sum_{j=0}^{n-1} (x(i, j, k) - y(i, j, k))^2. \quad (10)$$

In the formula, k represents the number of channels.

In this study, the peak signal-to-noise ratio (PSNR) index is also introduced for evaluation, and its formula is as follows:

$$PSNR = 10 * \lg \left(\frac{MAX^2}{MSE} \right). \quad (11)$$

The above formula shows that the MAX represents the maximum color value of image points, which is 255. Figure 11 lists the calculation results of each method.

The results show that the PSNR index of CGAN is significantly higher than that of GAN, which verifies the positive role of the labeled mechanism. Compared with CGAN, the PSNR of BEGAN is improved again, which verified that improving loss function can improve the image quality.

Compared with other methods, the algorithm designed in this paper has some advantages in the peak signal-to-noise ratio, but the overall PSNR is low. It is presumed to be related to the image compression caused by the autoencoder. The relevant studies are needed to further improve the quality of the generated image.

4.5.2. Analysis of Multifeature Fusion Effect. The adversarial network generated samples are mixed with the real samples. Then the VGG-16 model is adjusted using the transfer learning method. The unsampling and other processing are carried out for the obtained feature maps. After adjusting to a consistent size, the deep semantic and shallow detail information is fused and unified input to the full connection layer. After completing the above operations, the feature fusion network is compared with the untreated network. The training data are uniformly normalized, and the iterative recognition rate and other information are recorded. The final results are shown in Figures 12 and 13.

The information in Figure 11 shows that, compared with the unfused model, the fused model achieves higher

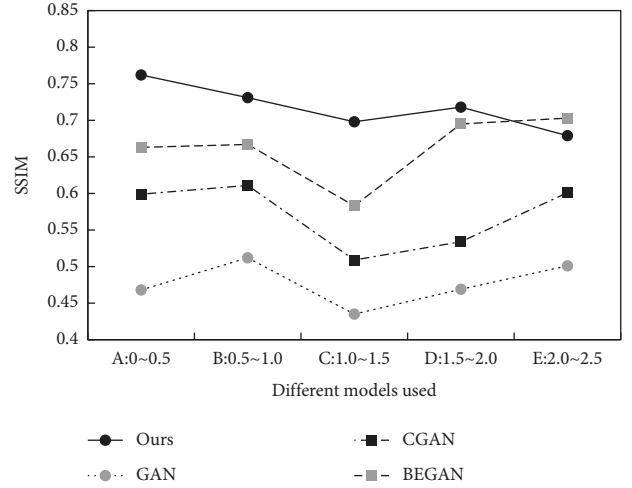


FIGURE 10: Comparison of different methods of SSIM.

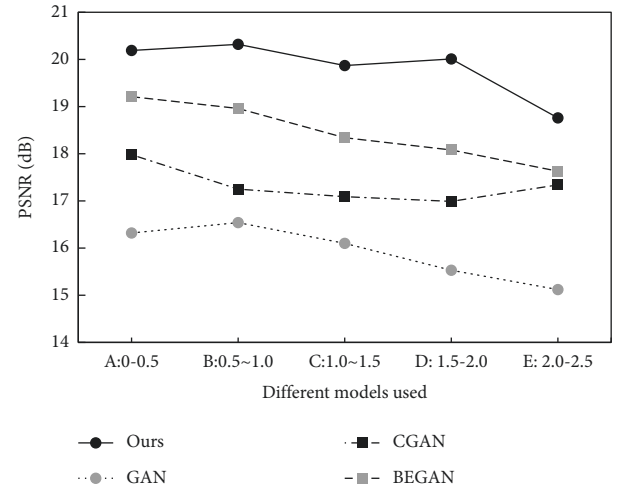


FIGURE 11: Comparison of different methods of PSNR.

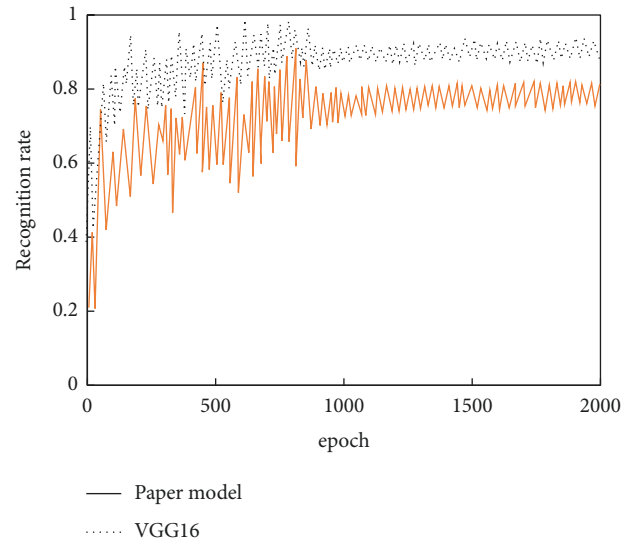


FIGURE 12: Recognition rate comparison of proposed model and VGG-16.

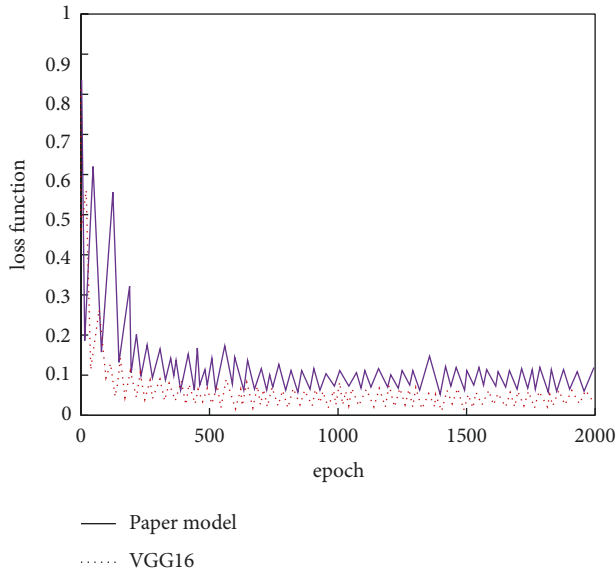


FIGURE 13: Loss function of proposed model and VGG-16.

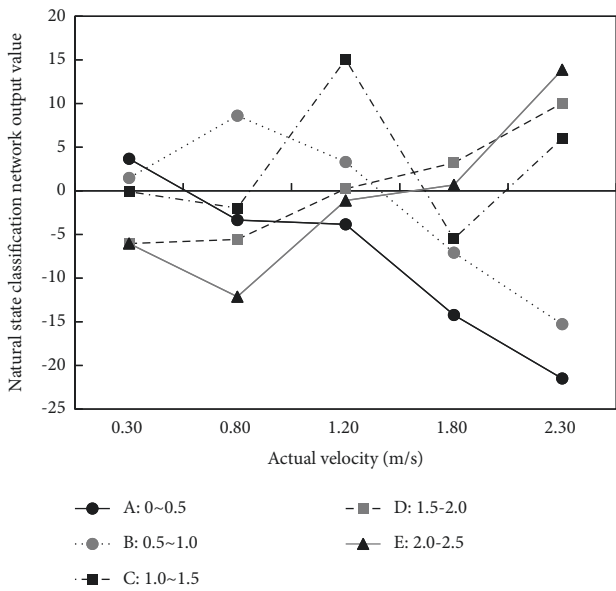


FIGURE 14: Output of model in normal state.

recognition accuracy under the condition of the same iterations, which has basically converged around 800 times. Combined with the above analysis, it can be seen that the feature fusion method can be adopted for the feature recognition problem with insignificant difference, which is helpful to enhance the effect.

4.5.3. Flow Rate Estimation Analysis in Natural State. It is necessary to select appropriate test set data in natural state flow rate analysis. Here, the original A-E sample data are selected. In addition, the images without flow rate labels are used to uniformly input into the classification network for processing. The result is as shown in Figure 14. The information in the table shows that the predicted classification

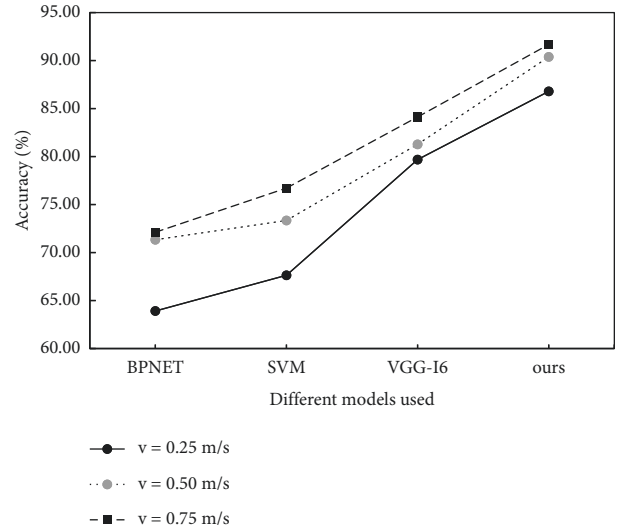


FIGURE 15: Comparison of recognition rate in normal state.

results are basically consistent with the real flow rate levels, which verifies the validity of the model.

Here, when different images are input, the higher the network output result is, the higher the probability of the category is. For the images with different flow velocity intervals, the differentiation is different. The differentiation of B and C images is higher, and the degree of A and D images is lower. For E image, it is found that the category similarity has a certain influence on the discrimination.

The difference of recognition accuracy is analyzed based on different methods, as shown in Figure 15. The same data set is used in the verification, and the velocity resolution of multiple groups, respectively, is set as 0.25, 0.5 and 0.75, and the unit is m/s.

5. Conclusion

In summary, it can be seen that the prediction of river flow image velocity can be effectively realized through the enhancement of river image and multifeature fusion combined with convolutional neural network. The results show that the method has obvious advantages, which is not only in the accuracy of speed prediction, but also in the loss function of the algorithm itself. Through the research, the problem of single feature of river image and the problem of traditional manual real-time acquisition are changed, and the information ability of river disaster early warning is greatly improved.

Data Availability

The experimental data used to support the findings of this study are available from the corresponding author upon request.

Conflicts of Interest

The authors declare that they have no conflicts of interest.

References

- [1] F. Tauro, S. Grimaldi, and M. Porfiri, "Unraveling flow patterns through nonlinear manifold learning," *PLoS One*, vol. 9, no. 3, Article ID 91131, 2014.
- [2] A. Gholami, H. Bonakdari, A. H. Zaji, and A. A. Akhtari, "An efficient classified radial basis neural network for prediction of flow variables in sharp open-channel bends," *Applied Water Science*, vol. 9, no. 6, p. 145, 2019.
- [3] J. R. Khuntia, K. Devi, and K. K. Khatua, "Prediction of depth-averaged velocity in an open channel flow," *Applied Water Science*, vol. 8, no. 6, p. 172, 2018.
- [4] A. Eltner, H. Sardemann, and J. Grundmann, "Technical Note: flow velocity and discharge measurement in rivers using terrestrial and unmanned-aerial-vehicle imagery," *Hydrology and Earth System Sciences*, vol. 24, no. 3, pp. 1429–1445, 2020.
- [5] Y. Zhang, Z. Yan, S. Yang et al., "Research on shore-based river flow velocity inversion model using GNSS-R raw data," *Remote Sensing*, vol. 14, no. 5, p. 1170, 2022.
- [6] I. Gulrajani, F. Ahmed, M. Arjovsky, V. Dumoulin, and V. Dumoulin, "Improved training of wasserstein gans," in *Proceedings of the Advances in Neural Information Processing Systems*, pp. 5767–5777, New York, NY, USA, July 2017.
- [7] D. Berthelot, T. Schumm, and L. Metz, "BEGAN: boundary equilibrium generative adversarial networks," 2017, <https://arxiv.org/abs/1703.10717?context=stat#:~:text=We%20propose%20a%20new%20equilibrium,generator%20and%20discriminator%20during%20training>.
- [8] N. K. Senthil Kumar and N. Malarvizhi, "Bi-Directional LSTM–CNN combined method for sentiment analysis in part of speech tagging (PoS)," *International Journal of Speech Technology*, vol. 23, pp. 1–8, 2020.
- [9] N. Zheng, S. Yupeng, R. Weicong, and K. Yuyong, "Effects of skip connections in CNN-based architectures for speech enhancement," *Journal of Signal Processing Systems*, vol. 92, pp. 1–10, 2020.
- [10] V. V. Shankar, K. Varun, and D. Umesh, "Heart disease prediction using CNN algorithm," *SN Computer Science*, vol. 1, no. 3, pp. 88–92, 2020.
- [11] A. Mehmood, M. A. Khan, M. Sharif et al., "Prosperous Human Gait Recognition: an end-to-end system based on pre-trained CNN features selection," *Multimedia Tools and Applications*, pp. 1–21, 2020.
- [12] F. Hardalac, H. Yasar, A. Akyel, and U. Kutbay, "A novel comparative study using multi-resolution transforms and convolutional neural network (CNN) for contactless palm print verification and identification," *Multimedia Tools and Applications*, vol. 79, no. 31-32, Article ID 22929, 2020.
- [13] P. Doke and D. Shrivastava, "Using CNN with Bayesian optimization to identify cerebral micro-bleeds," *Machine Vision and Applications*, vol. 31, no. 5, pp. 48–54, 2020.
- [14] Y. Kurmi, V. Chaurasia, N. Ganesh, and A. Kesharwani, "Microscopic images classification for cancer diagnosis," *Signal, Image and Video Processing*, vol. 14, no. 4, pp. 665–673, 2020.
- [15] H. S. Pannu, S. Ahuja, N. Dang, S. Soni, and A. K. Malhi, "Deep learning based image classification for intestinal hemorrhage," *Multimedia Tools and Applications*, vol. 79, no. 29-30, Article ID 21941, 2020.
- [16] D. Li, L. Deng, and Z. Cai, "Research on image classification method based on convolutional neural network," *Neural Computing & Applications*, pp. 1–11, 2020.
- [17] Y. Zhang, Y. Chen, C. Wang et al., "Prodconn - protein design using a convolutional neural network," *Biophysical Journal*, vol. 118, no. 3, pp. 43a–44a, 2020.
- [18] S. Srivastava, "Detection of ovarian cyst in ultrasound images using fine-tuned VGG-16 deep learning network," *SN Computer Science*, vol. 1, no. 6, pp. 121–155, 2020.
- [19] V. Kudva, K. Prasad, and S. Guruvare, "Hybrid transfer learning for classification of uterine cervix images for cervical cancer screening," *Journal of Digital Imaging*, vol. 33, no. 3, pp. 619–631, 2020.
- [20] J. Jian, F. Xiong, W. Xia et al., "Fully convolutional networks (FCNs)-based segmentation method for colorectal tumors on T2-weighted magnetic resonance images," *Australasian Physical & Engineering Sciences in Medicine*, vol. 41, no. 2, pp. 393–401, 2018.
- [21] S. Srivastava, "A novel deep learning framework approach for sugarcane disease detection," *SN Computer Science*, vol. 1, no. 12, pp. 497–502, 2020.
- [22] T. Zhou, D.-P. Fan, M.-M. Cheng, J. Shen, and L. Shao, "RGB-D salient object detection: a survey," *Computational Visual Media*, vol. 7, no. 1, pp. 37–69, 2021.
- [23] C. Yan, G. Pang, X. Bai et al., "Beyond triplet loss: person re-identification with finegrained difference-aware pairwise loss," *IEEE Transactions on Multimedia*, vol. 24, pp. 1665–1677, 2022.
- [24] X. Ning, P. Duan, W. Li, and S. Zhang, "Real-time 3D face alignment using an encoder-decoder network with an efficient deconvolution layer," *IEEE Signal Processing Letters*, vol. 27, pp. 1944–1948, 2020.
- [25] X. Ning, F. Nan, S. Xu, L. Yu, and L. Zhang, "Multi view frontal face image generation: a survey," *Concurrency and Computation: Practice and Experience*, vol. 3, 2020.

Research Article

Optimized Deep Neural Network and Its Application in Fine Sowing of Crops

Bing Li  and **Jiyun Li**

College of Modern Information Technology Henan Polytechnic, ZhengZhou 450018, China

Correspondence should be addressed to Bing Li; 25015@hnzj.edu.cn

Received 31 May 2022; Revised 15 July 2022; Accepted 25 July 2022; Published 21 August 2022

Academic Editor: Le Sun

Copyright © 2022 Bing Li and Jiyun Li. This is an open access article distributed under the Creative Commons Attribution License, which permits unrestricted use, distribution, and reproduction in any medium, provided the original work is properly cited.

Winter wheat is one of the most important food products. Increasing food demand and limited land resources have forced the development of agricultural production to be more refined and efficient. The most important part of agricultural production is sowing. With the promotion of precision agriculture, precision seeding has become the main component of modern agricultural seeding technology system, and the adoption of precision seeding technology is an important means of large-scale production and cost saving and efficiency enhancement. However, the current sowing technology and sowing equipment cannot meet the requirements of wheat sowing accuracy. In this context, a differential perturbation particle swarm optimization (DPPSO) algorithm is proposed by embedding differential perturbation into particle swarm optimization, which shows fast convergence speed and good global performance. After that the DPPSO is used to optimize the convolutional neural network (CNN) to build an optimized CNN (DPPSO-CNN) model and applied to the field of crops fine sowing. Finally, the experimental results show that the proposed method not only has a faster convergence rate but also achieves better wheat seeding performance. The research of this paper effectively improves the accuracy and uniformity of wheat seeding and lay a foundation for improving wheat yield per unit area and promotes the intelligent development of agriculture in the future.

1. Introduction

Food security is an important strategic issue concerning China's economic development and social stability. As a country with a large population in the world, China should attach great importance to food security at all times [1, 2]. Since the beginning of the new century, the central government has successively issued no. 1 documents, which have made great achievements in agriculture and rural areas. In 2020, China's grain and other agricultural products will have a bumper harvest, and the total grain output will reach 1,339 billion Jin. At the same time, it is very difficult for farmers to feed their families only by growing grain without relying on sideline work or migrant work, and a large number of agricultural labor force has flooded into the cities, and China's food security depends on the left-behind people who struggle to make a living by growing grain, and it is increasingly unsustainable [3, 4].

China is a big agricultural country, and wheat is one of the most important grain crops in China. The population whose staple food is wheat accounts for about 1/3 of the world's total population. Therefore, ensuring high and stable wheat yield is of great significance to food security. Agricultural production is a necessary condition for the survival and development of human society, closely related to social stability and economic development, and is the most important social production activities of human beings [5]. The development of wheat industry is directly related to food safety and social stability in China. The annual consumption of wheat products accounts for about 20% of the total food consumption in China [6].

As the key link of wheat production, sowing affects the growth and development of wheat, and ultimately affects the yield of wheat [7]. In the process of wheat production, there are mechanical drill sowing, broadcast sowing, and set sowing, etc. In the actual production, due to the contradiction between rice-wheat rotation system and wheat

seeding in South China, the production is mainly based on artificial broadcast sowing and extensive management, which increases the yield of wheat. Strengthening the research on new variety breeding and cultivation technology has a significant impact on the development of wheat productivity. The first is the success of wheat breeding, and the corresponding wheat breeding agronomy needs corresponding farming tools. Second, uniform plant distribution will increase the yield, which indicates the direction for the study of precision seeding in a plot. Precision sowing needs to be applied to the original seed quantity, quality, and other indicators to control, so as to complete the control of seeding quantity and quality to achieve the purpose of precision sowing [8]. Precision seeding device can complete the precise seeding process, but precision seeding is a complex organic combination, including the precise control of seeding depth and seeding position. Although the consistency of seeding depth can be achieved by seeding machine, the cost is too high. To sum up, precision sowing is the result of multiple factors, and a single analysis of seed metering device is not comprehensive. Therefore, it is necessary to combine machine-learning methods to increase the description of iodine excess in the sowing process, which is of great significance to promote precision sowing.

Compared with western developed countries, China's wheat production mode is relatively backward, mainly in the traditional way of planting, sowing, and fertilization according to artificial experience [9]. Planting closely can lead to crowding of crop seedlings and insufficient light, thus increasing the labor density. . Too little sowing will lead to inadequate land use and affect crop yield. Therefore, the realization of precision sowing and application of crops and the promotion of precision agriculture are not only of great significance to improve crop yield and reduce production costs, but also imperative. Precision agriculture is a modern agricultural production system based on modern information and space technology, which is based on remote sensing technology, geographic information system, and global positioning system to achieve precise agricultural operations [10, 11]. According to the specific conditions of each unit inside the farmland area, the soil nutrition information and the spatial status of productivity, the rational use of crop input determine the production target.

At present, the acquisition of crop growth information technology with high accuracy, high speed, high density, and low cost is still the biggest obstacle to the implementation of precision agriculture [12]. The traditional method of field sampling is to understand wheat-sowing situation, but due to the large manpower and material resources consumption of sampling and experiment, the amount of information collection and sampling cost is contradictory. Traditional precision agriculture variable implementation to obtain target data time-consuming, high cost, and time lag, cannot reflect the real-time sowing of wheat. Deep learning technology can provide timely information for agricultural production decision-making and management and provide new approaches and methods for crop growth, quality, and yield monitoring and regional management. Deep learning technology is an important means to collect physical and

chemical data of ground objects and their spatio-temporal change information [13, 14]. It has been widely used, especially with the development of hyperspectral remote sensing technology. Because it can measure the main information needed for wheat seeding and fully display its growth characteristics, it can obtain more abundant information than the conventional method, so as to realize the fine monitoring of wheat seeding. To sum up, wheat fine sowing benefits the country and the people, and the development of deep learning brings convenience to the evaluation and analysis of seeding effect. On this basis, it is of great significance to analyze wheat growth and spatial variation [15].

2. Related Work

The water consumption of wheat from sowing to overwintering was mainly distributed in the shallow soil layer of 60 cm. The water-consuming layer moved from shallow layer to deep layer as the temperature increased from rising stage to mature stage. The water use efficiency decreased with the increase of planting density. If the sowing rate is too high or too low, the soil water storage in the early stage will be overused and the water consumption of winter wheat will be reduced throughout the growth period [16, 17]. If the amount of sowing, the number of basic seedlings in the early stage, and the total tiller number and leaf area index were large too large, then all these factors lead to the decrease of leaf area in the middle and late stage than that in the low sowing. When the amount is small, the population per unit area is insufficient, resulting in low dry matter quality. The tillering capacity and material production capacity of wheat decreased when the amount of sowing was large, and finally the grain quality decreased [18].

With the increase of sowing amount, the number of grains per spike and 1000-grain weight of wheat decreased gradually over the small sowing amount, while the number of ears increased gradually with the sowing amount, and the number of ears was the highest under the large sowing amount. Under the condition of high sowing amount, the yield did not increase but decreased slightly with increasing sowing amount. The main effect of sowing rate on yield was panicle number, followed by grain number per panicle and 1000-grain weight. Increasing sowing amount could effectively increase panicle number, but grain number per panicle weight decreased, and the positive effect of increasing panicle number was greater than the negative effect of decreasing grain number per panicle weight. Nitrogen absorption efficiency and nitrogen production efficiency increased with the increase of sowing amount. With the increase of planting density, the assimilate transport decreased before anthesis, but the accumulation of assimilate and its contribution rate to grain increased after anthesis due to the influence of soil moisture and sunlight, and finally increased protein content. Medium and low sowing rate can not only increase the yield but also significantly increase the content of starch and protein in grain, so that the grain yield and quality can be improved synchronously. Suitable medium sowing amount could increase protein content at

maturity stage, and before the suitable sowing amount, protein content gradually increased with the increase of sowing amount and decreased when the suitable sowing amount exceeded [19, 20].

The appearance characteristics of granular fertilizer and wheat seed are similar, so the existing control system of granular fertilizer application amount has important reference significance to the research and development of wheat seeding amount control system. It can be seen from the current situation of foreign research that some seeding quantity control systems are still controlled by open-loop system, and even closed-loop system is controlled by indirect seeding quantity. In actual sowing operations, there is no breakthrough in the technology of accurate monitoring of large flow sowing quantity of wheat [21]. Therefore, in the process of literature research, there is no sowing quantity control system that can feedback the actual sowing quantity. Through the literature review, it can be seen that the domestic seeding quantity control system is mainly an open-loop system. If the friction between the seeding shaft and the machine and tools is large or there is an installation error, there is an error between the rotation speed of the seeding shaft and its theoretical value, and the rotation speed of the seeding shaft is not uniform within one week which will seriously affect the accuracy of seeding uniformity and seeding amount [22].

According to domestic and foreign practical experience, the advanced agricultural technology depends on the progress of agricultural production machinery. The current pattern of wheat precision sowing in China is also the most recognized by farmers [23, 24]. After that, the speed of seed wheel is controlled by the intelligent speed regulation system, so as to achieve uniform sowing of wheat seed. In this process, it is often necessary to have a fixed power source to provide power for the seed feeder, and the common power source is the ground wheel. However, due to the special properties of ground wheel drive, it has certain requirements on the size of seed besides the loss of seed and ridging, and only the wheat seeds that meet the requirements can be precisely sown. In particular, the poor stability of the power source has always limited the accuracy of seeding, so it is easy to form the instability of plant spacing, and serious shortcomings will also appear in ridging and lumps of seedlings. In the actual production process, due to the consideration of cost, the intelligent precision control system of this type of seeder is often missing, resulting in the adjustment of seeding quantity that is not accurate and cannot meet the most basic precision seeding requirements. At present, air-suction seeder is mainly oriented to large seeds, such as beans, cotton, which is generally economic crops and mainly applied to corn in the field of food crops [25, 26]. However, because wheat belongs to small seeds, air-suction seeder is not suitable for large seeds, and the existing small-seed seeder is mainly used for rapeseed, pepper, and other cash crops, so the type and number of air-suction seeder suitable for wheat are not very common.

The research on precision sowing in agricultural developed countries abroad is earlier, which can be traced back to the middle of the last century. Precision sowing can not

only save seeds but also improve the quality of sowing, thus playing an important role in improving crop yield. Therefore, precision sowing has become the development trend of the sowing industry once it came into being. The same type of precision planter is divided into different series to meet the requirements of different rows, spacing, and traction power. For example, the NC model of MONOSEM precision planter in the United States can realize 4–12 rows of simultaneous seeding. The spacing between rows is 35–80 cm and can realize the simultaneous sowing of 6–24 rows. The line spacing is 45–50 cm, and different types of fine seeding machine can meet the requirements of different ground conditions, soil conditions, and crops by replacing different structures or specifications of the working parts. Precision seeding is divided into mechanical type and pneumatic type. Compared with mechanical type, pneumatic type seed metering device pushes the seeds forward by the force of airflow [27, 28]. It has the advantages of fast seed dividing speed and noninjury and can realize the sowing of different seeds through the replacement of the seed metering plate, with high versatility. In the 1980s, the agricultural developed countries represented by the United States focused their attention on the research of pneumatic precision seeder, and it has been widely used. With the development of research, many modern technologies have been applied to precision seeding machines. In the 1990s, Japan developed a seeder that could be controlled by solenoid valve and developed an electronically controlled precision seeder. The precision seeder has high precision and can control the amount of seeding in real time, which greatly improves the sowing efficiency. This study not only broadens the research idea for the researchers of wheat fine seeding but also has great significance for the development of wheat industry, since the CNN model proposed in this paper is a typically deep learning model, and it can effectively deal with big data situations. The main contributions of this paper are the following:

- (1) DPPSO-CNN is applied in the field of fine sowing of crops for the first time in this paper.
- (2) The method in this paper not only has solid theoretical foundation but also has broad application prospect.

3. Optimized CNN for Fine Sowing of Crops

3.1. Deep CNN Model Introduction. In recent years, CNN model is often used to solve complex image recognition problems [29, 30]. Based on the traditional full-connection layer neural network, CNN adds convolution layer and pooling layer to form the deep CNN model, which is shown in Figure 1. As Figure 1 only shows the schematic diagram of CNN algorithm in this paper, it is impossible to know how many convolutional layers and pooling layers there are. In the algorithm of this paper, we set two layers of pooling layer and two layers of convolution layer, respectively.

The function of the convolution layer lies in the extraction of image features. The essence of the convolution kernel is a filter matrix, which can produce many different

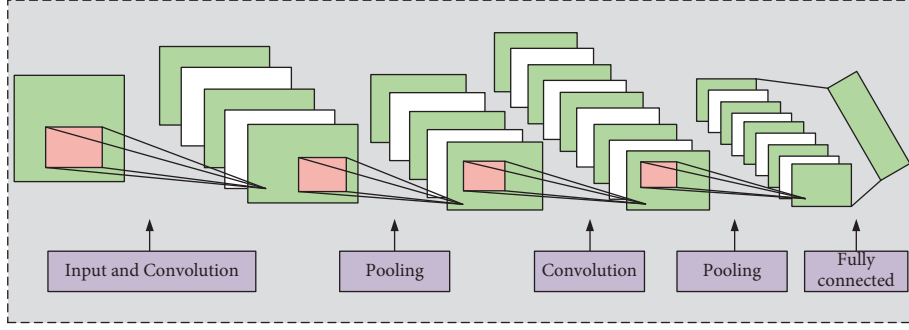


FIGURE 1: The typical schematic diagram of CNN.

effects on the original image. The calculation process of convolution is as shown in equation (1):

$$\text{CONV}_{(ij)} = \sum_i^{m-1} \sum_j^{n-1} u_{ij} \times w + b \quad (1)$$

$$(i = 1, 2, \dots, m-1; j = 1, 2, \dots, n-1),$$

where, u_{ij} is the input image, m and n are the sizes of the input image, w is the size of the convolution kernel, and b is the bias constant of the convolution kernel. $\text{CONV}_{(ij)}$ is the characteristic graph output after convolution operation.

CNN adds an activation function layer to the network and analyzes the model better by adopting the feature mapping method of nonlinear function. Then, the mathematical expression of common activation function is introduced one by one. The mathematical expression of sigmoid function is

$$f(x) = \frac{1}{1 + e^{-x}}. \quad (2)$$

Since formula (1) is an almost function, the value range of its independent variables is the whole real number, and the range of its dependent variables is $[-1,1]$. The mathematical expression of tanh function is

$$f(x) = \frac{e^x - e^{-x}}{e^x + e^{-x}}. \quad (3)$$

The mathematical expression of ReLU function is

$$f(x) = \max(0, x). \quad (4)$$

The full name of ReLU function is rectified linear unit. The function is one of the commonly used activation functions, which are characterized by low-computational complexity and no exponential operation. However, it is worth explaining that ReLU function has certain defects in the calculation process. When the data passes through the negative range of ReLU function, the output value is equal to 0. The Leaky-ReLU function can solve the above problem.

$$f(x) = \begin{cases} x, & x \geq 0, \\ \alpha x, & x < 0. \end{cases} \quad (5)$$

Therefore, the efficiency of the entire network operation can be improved to a certain extent. The corresponding equations of Sig and Tanh are as follows:

$$\begin{cases} \text{sig}(x) = \frac{1}{1 + \exp(-x)}, \\ \text{tanh}(x) = \frac{\exp(x) - \exp(-x)}{\exp(x) + \exp(-x)}, \end{cases} \quad (6)$$

$$h_{w,b}(x_i) = \begin{bmatrix} p(y_i = 1|x_i; w, b) \\ p(y_i = 2|x_i; w, b) \\ p(y_i = 3|x_i; w, b) \\ \dots \\ p(y_i = n|x_i; w, b) \end{bmatrix} \quad (7)$$

$$= \frac{1}{\sum_{j=1}^n e^{w_j x_i + b_j}} \begin{bmatrix} e^{w_1 x_i + b_1} \\ e^{w_2 x_i + b_2} \\ e^{w_3 x_i + b_3} \\ \dots \\ e^{w_n x_i + b_n} \end{bmatrix}.$$

The output layer adopts softmax function to normalize, and the probability value in the corresponding category is shown in equation (7). In the classification tasks, i is the cross entropy (CE) loss function that is often used to evaluate the gap between predicted value and true value. The CE formula is as follows:

$$\text{loss} = -\frac{1}{m} \sum_{j=1}^m \sum_{i=1}^n y_{ji} \log(\hat{y}_{ji}), \quad (8)$$

where \hat{y}_{ji} is the predicted value and y_{ji} is the real value. The error calculated from the CE function needs to be calculated by back propagation, so as to realize the newer back propagation of model parameters. The original form of the gradient descent method is shown in equation (9):

$$\theta := \theta - \alpha \frac{\partial}{\partial \theta} J(\theta). \quad (9)$$

In the experiments in the following sections, this paper also verifies that the use of Adam has faster convergence than SGD. The mathematical expression of a common Adam optimizer is given as follows:

$$\begin{aligned} m_t &= \beta_1 m_{t-1} + (1 - \beta_1) g_t, \\ v_t &= \beta_2 v_{t-1} + (1 - \beta_2) g_t^2. \end{aligned} \quad (10)$$

Therefore, the updating rule of gradient descent is as follows:

$$\theta_{t+1} = \theta_t - \frac{\alpha}{\sqrt{v_t + \epsilon}} m_t. \quad (11)$$

3.2. Optimized CNN Model. It is worth noting that differential perturbation is used in this paper to optimize the CNN model, but other optimization algorithms are feasible in this theory, but they are not optimal choices. Particle swarm optimization (PSO) is simple and easy to solve, but it is prone to local extreme points, low accuracy, slow convergence, and stagnation. In this section, the differential perturbation is introduced into the PSO to form the differential perturbation particle swarm optimization (DPPSO) algorithm, which makes use of the advantages of fast convergence speed and good global performance of difference, overcomes the shortcomings of low precision and local optimal caused by PSO, and builds an optimized CNN model. The multiobjective optimization model is

$$\begin{aligned} \min f_1(x_1, x_2), \\ \max f_2(x_1, x_2). \end{aligned} \quad (12)$$

s.t.

$$\begin{aligned} p_1 &< g_1(x_1, x_2) < q_1, \\ p_2 &< g_2(x_1, x_2) < q_2, \\ p_3 &< g_3(x_1, x_2) < q_3, \\ p_4 &< g_4(x_1, x_2) < q_4. \end{aligned} \quad (13)$$

and

$$\begin{aligned} 120 &< x_1 < 180, \\ 120 &< x_2 < 180, \end{aligned} \quad (14)$$

where f_1 represents energy consumption target, f_2 represents the output target $g_{\{1\}}, g_{\{2\}}, g_{\{3\}}, g_{\{4\}}$ $g_1(x_1, x_2), g_2(x_1, x_2), g_3(x_1, x_2), g_4(x_1, x_2)$ represent the packaging quality of four indicators: crushing strength, wear strength, drop strength, compressive strength, respectively. It is worth noting that the DPPSO algorithm used in this paper optimizes network parameters to obtain better model performance.

Based on the above discussions, the optimized deep neural network and its application in fine sowing of crops is shown in Figure 2. It mainly includes data preprocessing, CNN model training, and parameter optimization based on DPPSO model, and finally obtains the optimal model performance.

4. Experimental Results and Analysis

4.1. Experimental Data Introduction. This area belonged to semiarid and semihumid winter wheat growing. The experimental site was a hilly dry land with an average annual

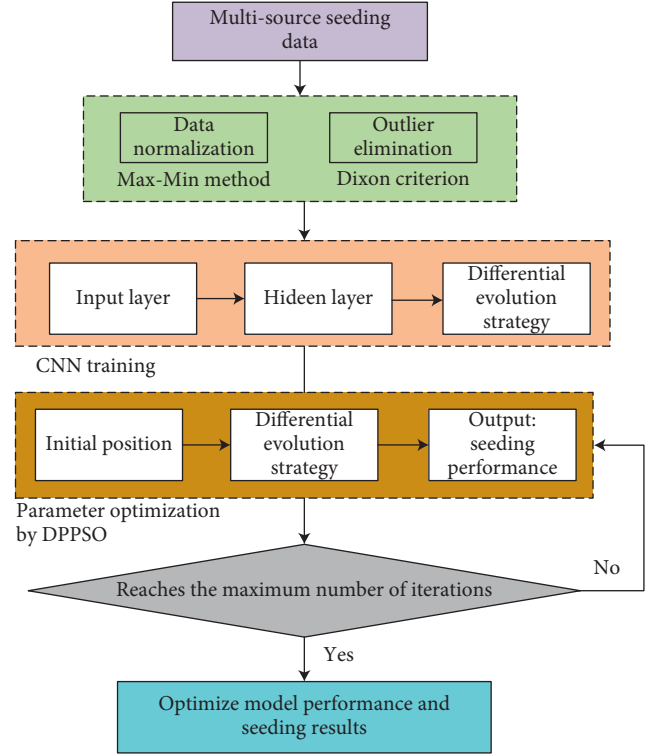


FIGURE 2: The framework of the proposed method in this paper.

rainfall of about 450 mm. The test field was flat and has one cropping system in a year, and the soil was medium alkaline clay loam. The water storage in the test area was mainly natural precipitation, which was concentrated in October and November of 2019. The experimental variety Linfeng no. 3 was provided by the County Agricultural Committee. The experiment used a two-factor experimental design. Furrow sowing (FS) was the main sowing area, and furrow sowing (FS), wide drilling sowing (WDS), and conventional drilling sowing (CDS) were the main sowing methods.

In addition, this study referred to the following data sources: China Rural Statistical Yearbook (1998–2019), China Statistical Yearbook (19982020), and National Agricultural Product Cost–Benefit Data Collection (1998–2020). Excel 2019 software and DPS7.05 software were used for statistical collation of data, Excel 2019 software was used for plotting, and least significant difference (LSD) method was used for significance test of difference, reaching significance level $\alpha = 0.05$.

4.2. Experimental Results Analysis. In order to demonstrate the universality of the proposed method, change curves of different activation functions of CNN model are presented in Figure 3. They all have the following common characteristics: (1) differentiability: this property is a prerequisite when using gradient-based optimization algorithms to optimize models. (2) Monotonicity: when the activation function meets the monotonicity, the single-layer network is guaranteed to be convex so that the subsequent convex optimization operations can be carried out. But in this case,

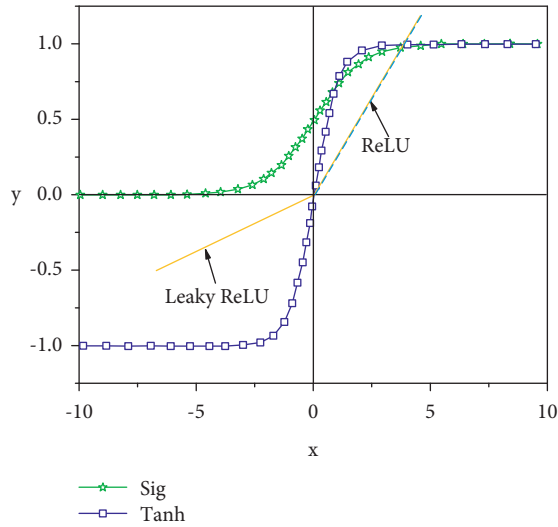


FIGURE 3: Different activation functions curves of CNN model.

the learning rate usually needs to be set to a small value, which inevitably increases the training time.

In order to verify the training performance of the model, different parameter updating methods are presented, as shown in Figure 4. The left is the batch gradient descent (BGD) algorithm, which refers to the calculation error every time, the gradient is obtained by the same batch as a whole, and the parameters are constantly updated until the error is zero or within the allowed range. The right is the stochastic gradient descent (SGD) algorithm, which means that the training of each sample is updated once, and the data order needs to be shuffled before each cycle. From Figure 4, we know that a big problem of BGD is that the whole data set needs to be scanned in each iteration of gradient calculation. Therefore, when the data volume is large, it inevitably leads to a large amount of calculation and low efficiency, while SGD only needs to take one sample point in each iteration of gradient calculation, so it has computational advantages. Second, since the gradient calculated by SGD is very different from the real negative gradient, it is not very stable, which also explains one of the advantages of SGD, which can jump out of the local optimal solution, so as to find the real global optimal solution. This is especially important in deep learning, where objective functions tend to be nonconvex. In conclusion, SGD model not only runs faster than BGD model in training time. In addition, SGD model solves the problem that BGD model can easily fall into local optimum. Hence, the SGD is used to update the model parameters in this paper.

In order to verify the effective control of the proposed method on wheat sowing range and sowing quantity, according to the determination method of seeding uniformity recorded in national standard GB/T 9478–2005, after the seeding operation is completed, a total of 30 sections of 10 cm were taken, and the number of seed particles in each section was counted, as shown in Figure 5. Sowing uniformity was calculated for each level of combination seeding operation. It can be seen from the

figure that the relative frequency distribution of wheat grain number in each subsection presents positive distribution. The experimental results were analyzed uniformly under the same theoretical sowing rate per hectare. Specifically, when the number of seeds is 50–60, both the sowing range and the sowing rate are the highest, so the result can be considered as the optimal sowing amount per unit area.

Figure 6 shows the computational efficiency and actual complexity of the proposed method. As can be seen from the figure, the computational complexity and efficiency of the proposed method increase first and then decrease with the increase of iterations. In other words, the computational efficiency of the method in this paper reaches the maximum after iteration at 1000 hours. Therefore, the proposed method has a large model fault tolerance rate, which can ensure good model performance within 1000 iterations. It also indirectly shows that the method proposed in this paper has good generalization and extensibility.

Because BP neural network is a shallow model, RNN is a classic deep learning model, and the method in this paper is based on CNN model. Hence, they are selected as the comparison algorithms and the simulation results are presented in Figure 7. As can be seen from the figure, the convergence rates of the four methods all were tended to increase first with the increase of data volume, but with the further increase of data volume, the convergence rate of BP neural network showed a downward trend, indicating that BP neural network is not suitable for processing a large amount of wheat sowing data in this paper. In contrast, the convergence rate of RNN and CNN models generally keeps increasing with the increase of data volume at any time. The main reason is that both methods are deep neural networks with the ability to process big data. However, the convergence rate of these two methods is still not as high as that of PSO-CNN in this paper, which shows the effectiveness and practicability of the method proposed in this paper.

Figure 8 shows the relationship between sowing accuracy and iteration times of different methods. We can figure out from the figure whether with the increase of iteration number, the sowing accuracy of the three methods shows an increasing trend. When the iteration number is 600, the three models all reach the highest classification accuracy, which is 81%, 87%, and 98%, respectively. Therefore, the PSO-CNN model in this paper achieves the highest classification accuracy. In addition, even when the number of iterations is small, the proposed method also has the best model performance and achieves the highest classification accuracy throughout the training process, which demonstrates the effectiveness of the proposed method in wheat seeding monitoring.

To better demonstrate the effectiveness of the proposed method, the monitoring results of CNN and PSO-CNN are shown in Figure 9. Specifically, it can be seen from Figure 9(b) that PSO-CNN method not only achieved the lowest omission ratio of 18.88% but also detected abnormal sowing at the 163rd sampling point with a detection delay of 2, while the corresponding delay numbers of CNN method

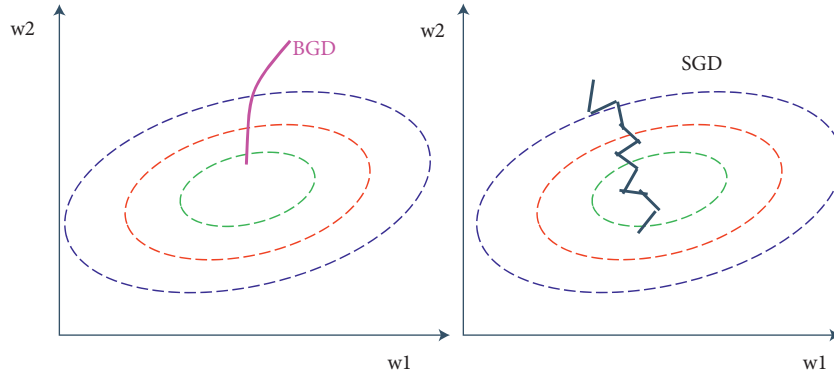


FIGURE 4: BGD vs. SGD.

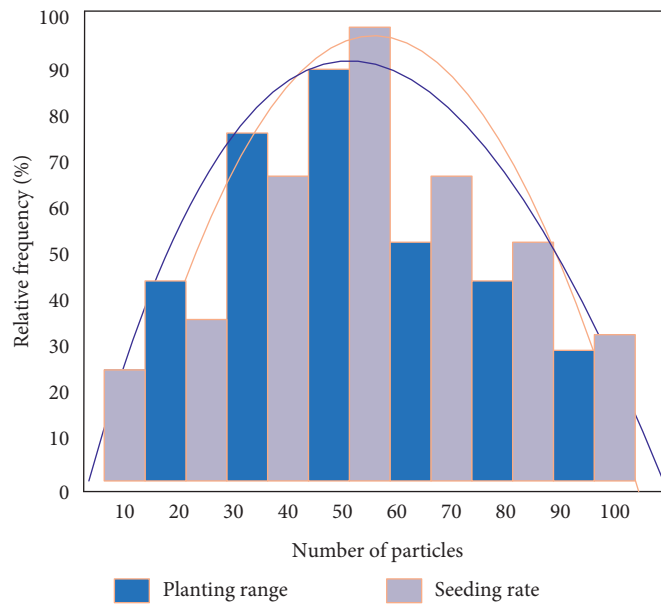


FIGURE 5: Distribution of sowing quantity and sowing area.

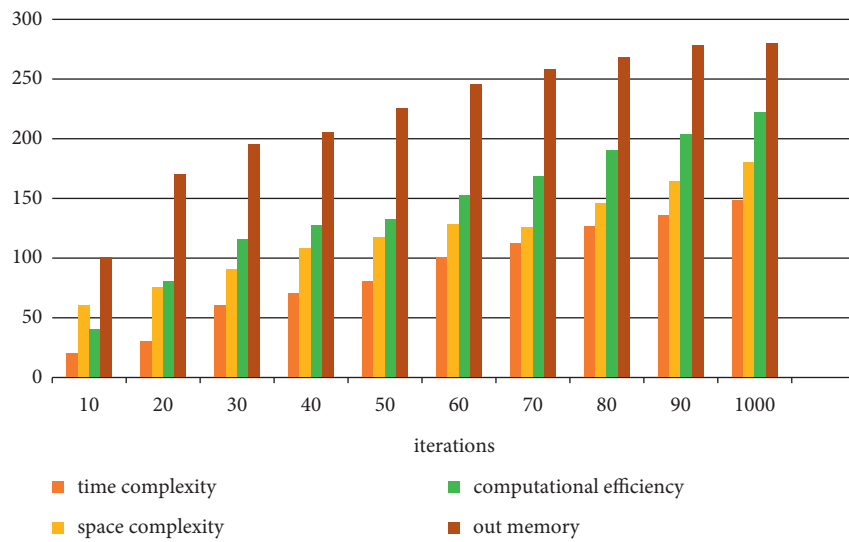


FIGURE 6: The computational efficiency and actual complexity of the proposed method.

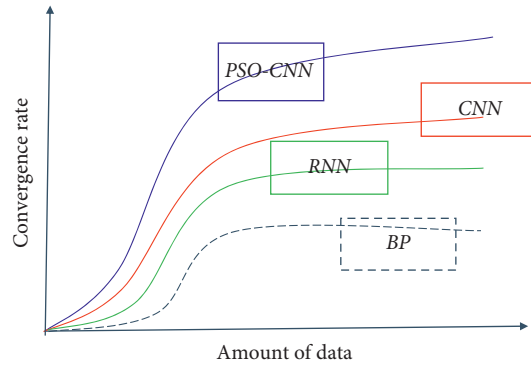


FIGURE 7: Comparison of convergence speed between different methods.

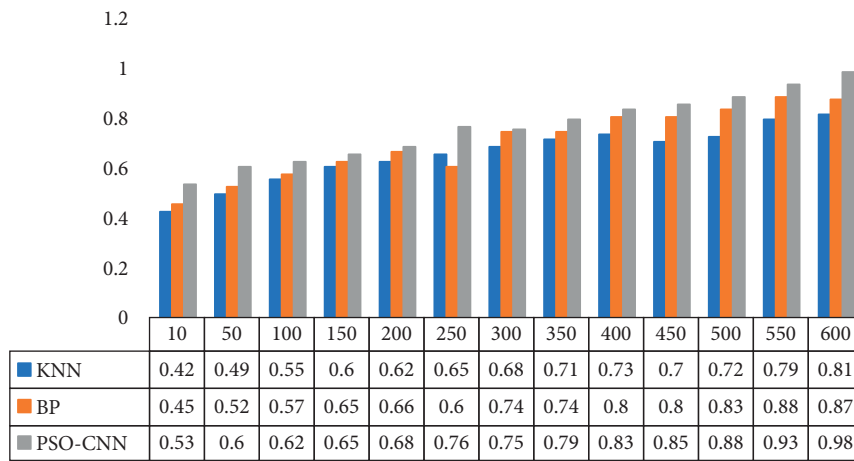


FIGURE 8: Comparison of sowing accuracy of different methods.

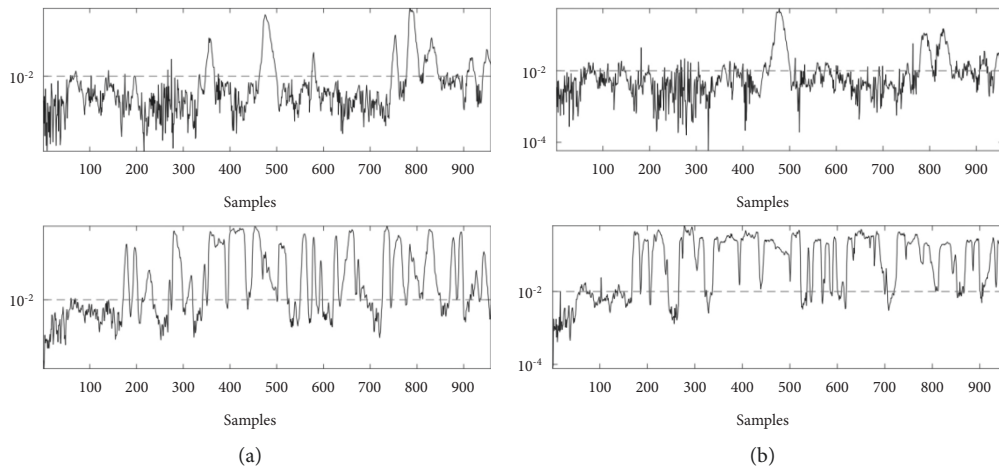


FIGURE 9: Monitoring accuracy of wheat seeding by (a) CNN, (b) PSO-CNN.

were 24, respectively. It shows that the method presented in this paper can detect the sowing error quickly. In addition, when the error is detected, the statistical curve corresponding to the PSO-CNN model rarely falls below the

threshold line, while the statistical curve corresponding to the CNN method always falls back to different degrees, resulting in a high failure rate, which further demonstrates the stability and persistence of the proposed method.

5. Conclusions

Sowing is a key link in wheat production. The performance of seeding machine directly affects the growth and yield of crops. With the promotion of precision agriculture and the development of precision seeding technology, precision seeding has become the main component of modern agricultural seeding technology system. Adopting precision seeding technology is an important means of large-scale production and realizing cost-saving and efficiency enhancement. The online precision measurement of seeding amount is the key to realize precision seeding and precise control and also the basis of realizing precision seeding in real sense.

In view of the shortcomings of the existing methods, this paper proposed an optimized deep learning model PSO-CNN, which not only achieved better model convergence rate and model parameters but also effectively improved the sowing accuracy and sowing range of wheat showing strong theoretical value and application potential. This work is helpful to realize the fine sowing of wheat and improve the level of agricultural automation. Although the method proposed in this paper has achieved good results, the research in this paper does not consider the effects of planting weather and soil in the process of agricultural sowing. This will be the focus of future research.

Data Availability

The experimental data used to support the findings of this study are available from the corresponding author upon request.

Conflicts of Interest

The authors declared that they have no conflicts of interest regarding this work.

Acknowledgments

This study was supported by Science and Technology Project of Henan Province (Project No. 222102110269) and Project Support for Key Scientific Research Projects of Henan Provincial University (Project No. 22A520031).





References

- [1] K. Cui and S. P. Shoemaker, "Public perception of genetically-modified (gm) food: a nationwide Chinese consumer study," *Npj Science of Food*, vol. 2, no. 1, pp. 10–12, 2018.
- [2] G. Q. Huang and F. S. Tsai, "Social innovation for food security and tourism poverty alleviation: some examples from China," *Frontiers in Psychology*, vol. 12, p. 614469, 2021.
- [3] J. Yu and Q. Han, "Food security of mariculture in China: e," *Marine Policy*, vol. 115, p. 103892, 2020.
- [4] L. Chen, J. Chang, Y. Wang et al., "Disclosing the future food security risk of China based on crop production and water scarcity under diverse socioeconomic and climate scenarios," *Science of the Total Environment*, vol. 790, p. 148110, 2021.
- [5] M. Pu and Y. Zhong, "Rising concerns over agricultural production as COVID-19 spreads: I," *Global Food Security*, vol. 26, p. 100409, 2020.
- [6] H. Gao, C. Yan, Q. Liu, W. Ding, B. Chen, and Z. Li, "Effects of plastic mulching and plastic residue on agricultural production: a meta-analysis," *Science of the Total Environment*, vol. 651, pp. 484–492, 2019.
- [7] A. Maresma, A. Ballesta, F. Santiveri, and J. Loveras, "Sowing date affects maize development and yield in irrigated mediterranean environments," *Agriculture*, vol. 9, no. 3, p. 67, 2019.
- [8] L. Mack, S. Munz, F. Capezzone et al., "Sowing date in Egypt affects chia seed yield and quality," *Agronomy Journal*, vol. 110, no. 6, pp. 2310–2321, 2018.
- [9] E. Švamberková, J. Doležal, and J. Lepš, "The legacy of initial sowing after 20 years of ex-arable land colonisation," *Oecologia*, vol. 190, no. 2, pp. 459–469, 2019.
- [10] D. I. Herman, C. Weerasekara, L. C. Hutcherson et al., "Precise multispecies agricultural gas flux determined using broadband open-path dual-comb spectroscopy," *Science Advances*, vol. 7, no. 14, Article ID eabe9765, 2021.
- [11] Z. Yan and H. Jingtao, "The precise positioning algorithm optimization base on PSO-PF for agricultural machinery navigation system Journal of physics: conference series," *Journal of Physics: Conference Series*, vol. 1213, no. 4, Article ID 042068, 2019.
- [12] X. Z. Lin, C. X. Lin, X. Wang, J. Xue, and E. Zheng, "Precise positioning of agricultural vehicles under static conditions via artificial intelligence algorithms," *International Agricultural Engineering Journal*, vol. 27, no. 4, pp. 248–254, 2018.
- [13] M. Coccia, "Deep learning technology for improving cancer care in society: new directions in cancer imaging driven by artificial intelligence," *Technology in Society*, vol. 60, p. 101198, 2020.
- [14] M. Yamada, Y. Saito, H. Imaoka et al., "Development of a real-time endoscopic image diagnosis support system using deep learning technology in colonoscopy," *Scientific Reports*, vol. 9, no. 1, pp. 14465–14469, 2019.
- [15] S. Verma, N. Kumar, A. Verma, H. Singh, K. H. M. Siddique, and N. P. Singh, "Novel approaches to mitigate heat stress impacts on crop growth and development," *Plant Physiology Reports*, vol. 25, no. 4, pp. 627–644, 2020.
- [16] F. Feng, Y. Li, X. Qin, Y. Liao, and K. H. M. Siddique, "Changes in rice grain quality of indica and japonica type varieties released in China from 2000 to 2014," *Frontiers of Plant Science*, vol. 8, p. 1863, 2017.
- [17] A. Ozturk, E. Erdem, M. Aydin, and M. M. Karaoglu, "The effects of drought after anthesis on the grain quality of bread wheat depend on drought severity and drought resistance of the variety," *Cereal Research Communications*, vol. 50, no. 1, pp. 105–116, 2022.
- [18] Q. Liu, H. Ma, X. Lin, X. Zhou, and Q. Zhao, "Effects of different types of fertilizers application on rice grain quality," *Chilean Journal of Agricultural Research*, vol. 79, no. 2, pp. 202–209, 2019.
- [19] Z. Dong, X. Zhang, J. Li et al., "Photosynthetic characteristics and grain yield of winter wheat (*Triticum aestivum* L.) in response to fertilizer, precipitation, and soil water storage before sowing under the ridge and furrow system: a path analysis," *Agricultural and Forest Meteorology*, vol. 272–273, pp. 12–19, 2019.
- [20] H. Wang, F. Ke, H. Wang, and Y. Zhao, "Effects of sowing time, density and fertilizer application on the economic characters of Zhuoyou 058," *Agricultural Biotechnology*, vol. 8, no. 3, pp. 54–63, 2019.

- [21] Ł. Gierz, W. Kruszelnicka, M. Robakowska et al., "Optimization of the sowing unit of a piezoelectrical sensor chamber with the use of grain motion modeling by means of the discrete element method. Case study: rape seed," *Applied Sciences*, vol. 12, no. 3, p. 1594, 2022.
- [22] O. Matsera, "Comparative evaluation of quality properties of winter rapeseed depending on the level of fertilizers and sowing date," *Agriculture and Forestry*, no. 1, pp. 108–118, 2020.
- [23] K. Romanekas, D. Steponavičius, A. Jasinskas et al., "How to analyze, detect and adjust variable seedbed depth in site-specific sowing systems: a case study," *Agronomy*, vol. 12, no. 5, p. 1092, 2022.
- [24] A. Muscalu, C. Tudora, L. Vlăduțoiu, C. Vlad, and A. Dorogan, "Precision sowing of vegetable seeds using electrically operated distribution devices[C]/E3S Web of Conferences," in *Proceedings of the 10th International Conference on Thermal Equipments, Renewable Energy and Rural Development (TE-RE-RD 2021)*, vol. 286, Article ID 03015, Les Ulis, France, July 2021.
- [25] M. M. Onakpa, A. A. Njan, and O. C. Kalu, "A review of heavy metal contamination of food crops in Nigeria," *Annals of global health*, vol. 84, no. 3, pp. 488–494, 2018.
- [26] S. Savary, L. Willocquet, S. J. Pethybridge, P. Esker, N. McRoberts, and A. Nelson, "The global burden of pathogens and pests on major food crops," *Nature ecology & evolution*, vol. 3, no. 3, pp. 430–439, 2019.
- [27] X. Gao, T. Cui, Z. Zhou et al., "DEM study of particle motion in novel high-speed seed metering device," *Advanced Powder Technology*, vol. 32, no. 5, pp. 1438–1449, 2021.
- [28] E. J. Ibrahim, A. D. Elfadil, and A. D. Abdallah, "Laboratory and field investigation comparison for seed distribution accuracy of a multi-rows pneumatic plate metering device," *Asian Journal of Agriculture and Food Sciences*, vol. 10, no. 2, 2022.
- [29] A. Kumar, G. Vashishtha, C. P. Gandhi, Y. Zhou, A. Glowacz, and J. Xiang, "Novel convolutional neural network (NCNN) for the diagnosis of bearing defects in rotary machinery," *IEEE Transactions on Instrumentation and Measurement*, vol. 70, pp. 1–10, 2021.
- [30] Z. Wang, W. Zhao, W. Du, N. Li, and J. Wang, "Data-driven fault diagnosis method based on the conversion of erosion operation signals into images and convolutional neural network," *Process Safety and Environmental Protection*, vol. 149, pp. 591–601, 2021.

Research Article

Video Image Moving Target Recognition Method Based on Generated Countermeasure Network

Zilong Li ^{1,2,3}, DaiHong Jiang ¹, Hongdong Wang ¹ and Dan Li ¹

¹School of Information Engineering, Xuzhou University of Technology, Xuzhou 221018, China

²School of Computer Science & Technology, China University of Mining and Technology, Xuzhou 221116, China

³Post-Doctoral Research Center, Onnes Power Technology Co.Ltd., Xuzhou 221003, China

Correspondence should be addressed to Zilong Li; zilongli@36haojie.com

Received 16 May 2022; Accepted 19 July 2022; Published 19 August 2022

Academic Editor: Le Sun

Copyright © 2022 Zilong Li et al. This is an open access article distributed under the Creative Commons Attribution License, which permits unrestricted use, distribution, and reproduction in any medium, provided the original work is properly cited.

In order to improve the accuracy of video image moving target recognition and shorten the recognition time, a video image moving target recognition method based on a generation countermeasure network is proposed. Firstly, the image sensor is used to collect the video image and obtain the video image sequence. The Roberts operator is used for edge detection and Gaussian smoothing of the video image. Secondly, the normalization method is used to extract the key features of moving targets in video images. Finally, training is carried out alternately to generate the countermeasure network model, and the video image moving target recognition sample results are output according to the training results to realize the video image moving target recognition. The experimental results show that the highest recognition accuracy of the proposed method is 98.1%, and the longest recognition time is only 5.7 s, indicating that its recognition effect is good.

1. Introduction

Vision is the most direct way for people to get information. Images are the main way for humans to visually obtain information, and images can vividly and vividly describe the dynamic state of images and can convey information more intuitively and specifically [1–3]. With the advancement of science and technology, the development of computer vision technology has gradually made up for and improved the ability of people's vision that they do not have. Among these data, images and videos are important information carriers for computer vision systems. Recognition of moving objects is the key technology of visual analysis of moving objects, and it is also the most basic problem. It usually extracts moving images from the background and preprocesses them [4–6]. When performing target recognition, it is necessary to effectively detect the target and to classify and preprocess it to facilitate subsequent processing. In each frame of video, each independent moving object or region of interest to the user can be quickly and accurately identified and positioned

to the next node. Therefore, it is of great significance to identify moving objects in video images.

At present, scholars in related fields are studying the recognition of moving objects in video images. Reference [7] proposed a video moving object recognition method based on hierarchical modeling and alternating optimization. Based on the observation that foreground and background are two sides of the same coin, treat them as equivalent unknown variables and pose a joint estimation problem called hierarchical modeling and alternating optimization. For the background, it is decomposed into low and high frequency components in time. For the foreground, a Markov random field is constructed as the axis at low spatial resolution. Based on the hierarchical extension of the two models, under a unified framework called the alternating direction multiplier method, the joint estimation is improved to realize video moving target detection and recognition. Experimental results show that this method can generate more discriminative backgrounds and has better robustness to noise, but there is a problem of low recognition accuracy. Reference [8] proposed

a moving target recognition method in a high dynamic scene of a visual prosthesis. A new unsupervised moving target segmentation model is constructed to automatically extract moving targets in high dynamic scenes. The model utilizes foreground cues with spatiotemporal edge features and background cues with boundary priors to generate proximity maps of moving objects in dynamic scenes according to a manifold ranking function. At the same time, foreground and background cues are ranked, and moving objects are extracted through the integration of the two ranking maps. Experimental results show that this method can evenly highlight moving objects in high dynamic scenes and maintain a good boundary, but there is a problem of long recognition time. Reference [9] proposed a moving target recognition method based on sparse and robust principal component analysis of spatiotemporal structure in complex scenes. The algorithm spatially and temporally regularizes the sparse components in the form of the graph Laplacian. Each Laplacian corresponds to a multifeature map constructed over superpixels in the input matrix. The sparse components are used as eigenvectors for the spatial and temporal graph Laplacian while minimizing the robust PCA objective function. A novel objective function is obtained for separating moving objects in complex backgrounds. The proposed objective function is solved using a linear alternating directions method with multiplier-based batch optimization. In addition, an online optimization algorithm for real-time applications is also proposed. Batch and online solutions are evaluated using six publicly available datasets containing most of the above-given challenges. The experimental results show that the algorithm has higher performance, but there is a problem of poor recognition effect.

In order to solve the problems of low recognition accuracy of video images, long recognition time, and poor recognition improvement in traditional methods, this paper proposes a video image moving target recognition method based on a generative adversarial network. The specific technical route studied in this paper is as follows:

Step 1: collect a real-time image through an image sensor to obtain a video image sequence, preprocess the collected video image sequence, use the Roberts operator to perform edge detection on the video image, and perform Gaussian smoothing on the video image at the same time

Step 2: according to the video image preprocessing result, after the feature vector of the video image moving target is obtained by using the normalization processing method, the key features of the video image moving target are extracted

Step 3: train the generative adversarial network model through interactive training, identify the video image moving target according to the training result and the key features of the moving target, and output the moving target recognition sample, thereby realizing the video image moving target recognition

Step 4: comparing the proposed method with the method of reference [7] and the method of reference [8], the experimental results and conclusions are drawn

2. Design of Video Image Moving Target Recognition Method

2.1. Video Image Preprocessing. The object of video image moving target recognition is video image sequence, which is also called video sequence and dynamic image [10, 11]. A video image sequence is a series of video images with a certain or assumed relative order acquired by an image sensor, and the time interval between two adjacent two pictures is given. The video image sequence can generally be expressed as follows:

$$Q = \{q(e, r, w_0, e, r, w_1, \dots, e, r, w_{N-1})\}. \quad (1)$$

Or,

$$Q = \{q_k(e, r)\}_{k=1}^N. \quad (2)$$

In formulas (1) and (2), $w_i, i = 0, 1, \dots, N - 1$ is the moment when the frame of video image is acquired, e, r is the direction of the sensor in the imaging interval, k is the frame sequence, and N is the total number of frames of the video image sequence.

Due to the restriction of the acquisition environment and the influence of random interference and other factors, the effect of recognizing the moving target of the video image is not good, and it needs to be preprocessed. It consists of two steps: edge detection and smooth noise reduction.

2.1.1. Video Image Edge Detection. There are many operators for edge detection, and the fixed template is convolved to obtain the edge of the image. Select Roberts operator [12] to complete video image edge detection.

The video image gradient and the first-order derivative operator correspond to each other. Assuming that the video image function is expressed as $Q(u, o)$, its gradient is defined as follows:

$$\nabla Q(u, o) = (U_u, U_o) = \begin{pmatrix} \alpha u - \alpha o \\ \alpha u + \alpha o \end{pmatrix}. \quad (3)$$

In formula (3), U_u and U_o represent the gradients at pixels u and o of the video image, respectively, and α is a vector factor. Then, the magnitude of this vector is as follows:

$$\beta = |\nabla Q(u, o)| = \frac{U_u^2}{U_o^2}. \quad (4)$$

For ease of calculation, the magnitude can be expressed in the following different ways:

$$\begin{cases} \beta = \max(U_u, U_o) \\ \beta = |U_u| + |U_o| \end{cases} \quad (5)$$

Using Roberts operator, the process of realizing video image edge detection is described as follows:

$$Y(u, o) = \beta [P(u, o) - P(u + 1, o + 1) + P(u + 1, o)]. \quad (6)$$

In formula (6), $Y(u, o)$ and $P(u, o)$, respectively, represent the gray value of the pixel point (u, o) before and after the edge detection of the video image.

2.1.2. Gaussian Smoothing of Video Image. In the process of edge detection, the noise will cause the edge contour curve of the video image to be not smooth enough, which reduces the description accuracy of the edge contour curve of the video image. To this end, for video images, Gaussian smoothing is also required [13–15]. Assuming that the contour curve of the video image is represented as A , and $A(i)$ is the set of all pixels on the contour curve of the video image, there are

$$A = \{A(i) = (u(i), o(i))\}. \quad (7)$$

In formula (7), $u(i), o(i)$, respectively, represents the pixel points on the contour curve of the video image after Gaussian smoothing.

Using formula (7), all pixels in the outline of the video image can be traversed to achieve smoothing. After edge detection and smoothing, the video image quality is improved.

2.2. Extraction of Key Features of Moving Objects in Video Images. Based on the video image preprocessing results, the key features of moving objects are extracted. In order to improve the accuracy of video image moving target recognition, after normalizing the video image moving target feature vector, the key features of the video image moving target are extracted. The normalization processing method does not require geometric correction of moving objects in video images and can achieve a higher feature recognition rate, reduce the complexity of key feature extraction of objects, and basically eliminate the influence of changes in moving objects in images on feature extraction results., with high application value.

- (1) Normalization of video image moving target feature vector [16, 17]: the depth value of a video image moving target pixel and its neighboring pixels is regarded as the video image moving target feature. Then, the feature vector expression of the video image moving target is as follows:

$$S(u, o) = \frac{[D(u-1, o-1), D(1-u, 1-o)]}{[D(u, o+1), D(u+1, o)]}. \quad (8)$$

In formula (8), $D(u, o)$ is the depth value of the pixel point (u, o) of the video image. Perform the following normalization processing on all video image moving target feature vectors:

$$S'(u, o) = \frac{S(u, o)}{S(u, o)}. \quad (9)$$

In formula (9), $S'(u, o)$ represents the normalized video image moving target feature vector.

After the above-given processing, the key parts of the video image are effectively preserved, thereby reducing the complexity of feature extraction for moving objects in the video image.

- (2) Extraction of key features of moving objects in video images: after the feature vector of moving objects in video images is normalized, redundant features in

moving objects in video images are removed. According to the shape of the moving target area of the video image, the key feature points of the moving target of the video image are determined, and the key lines are drawn from this point as the center. The specific operation process is described by the following formula:

$$\gamma = \prod_{n=5}^F \left[\frac{g_n - g_1}{\sqrt{(g_n - g_1)^2 + (g_n - g_1)}} \right] + \left| \frac{g_{n-1} - g_1}{\sqrt{(g_{n-1} - g_1)^2 + (g_{n-1} - g_1)}} \right|^2. \quad (10)$$

In formula (10), g_n represents the image moving target key point, n is the number of video image moving target key points, and F is the video image moving target key feature point set. After the above process, the key features of the video image moving target are effectively extracted, which lays a foundation for the video image moving target recognition.

2.3. Realization of Video Image Moving Target Recognition. The establishment of a generative adversarial network is based on game theory, which includes two aspects, namely, the generative model and the discriminative model [18–20]. By establishing a generative adversarial network model, using the interactive training generative adversarial network model, optimizing the discriminant network and the generator network, and outputting the video image moving target recognition sample results, the video image moving target recognition is realized. Compared with traditional methods, the generative adversarial network has the following advantages: in principle, the generative adversarial network can approach any probability distribution gradually and can be considered as a nonparametric production modeling method. If the discriminator is well trained, the generator can learn the distribution of training samples perfectly. In the generation countermeasure network training, the reconstruction loss weighting coefficient is set to 0.999, and the countermeasure loss weighting coefficient is set to 0.001.

The objective function of the generative adversarial network model used to realize the recognition of moving objects in video images is derived as follows:

$$\min_L \max_K J(K, L) = Z_{x \sim c_d(x)} \times [\lg(K(x))] + Z_{h \sim c_h(h)} \times [\lg(1 - K(L(h)))] \quad (11)$$

In formula (11), x is the video image, $J(K, L)$ is the generative adversarial network model function, and K, L is the discriminative model and the generative model. $Z_{x \sim c_d(x)}$ refers to the expected value of the actual data after passing through the discriminator, $x \sim c_d(x)$ means that x is subject to the actual data distribution, and $K(x)$ is the discriminator.

$Z_{h \sim c_h(h)}$ refers to the expected value of random data after the generator and discriminator, $h \sim c_h(h)$ refers to the sampling distribution of the randomly generated video image moving objects, and $L(h)$ refers to the generator.

In the training of the discriminator network and the generator network, the alternate training method is adopted, which is optimized, and the corresponding training steps are given:

Step 1: pretrain the generative adversarial network initial discriminator network.

Step 2: input the moving target of the video image to be trained into the discriminator network to obtain the mask δ .

Step 3: extract ε moving target samples from training real video images and their corresponding masks δ_ε . Input ε real video image moving target samples into the discriminator. Input the ε real video image moving target samples and the corresponding mask δ_ε into the generator, generate the realistic video image moving target samples, and input the realistic video image moving target samples into the discriminator.

Step 4: calculate the discriminator loss function according to the discriminant situation:

$$G^D = \frac{1}{\varepsilon} [-\lg(K(x)) - \lg(1 - K(L(h, \delta_\varepsilon)))] \quad (12)$$

Step 5: the discriminator network parameters are updated by the Adam gradient descent algorithm:

$$\theta_d = \text{Adam}(\delta_\varepsilon(G^D), \theta_d) \quad (13)$$

Step 6: according to the discriminant situation, calculate the generator loss function:

$$G^H = \frac{1}{\varepsilon} [\lg(1 - K(L(h, \delta_\varepsilon)))] \quad (14)$$

Step 7: the generator network parameters are updated by the Adam gradient descent algorithm:

$$\theta_h = \text{Adam}(\delta_\varepsilon(G^H), \theta_h) \quad (15)$$

Step 8: repeat step 3 until the upper limit of the number of iterations or the generative adversarial network is close to the Nash equilibrium, and the result of the output video image moving target recognition sample is:

$$\mu = (G^D \times \theta_d) - (G^H \times \theta_h) \quad (16)$$

According to the above-given analysis, the method in this paper first collects the video image through the image sensor and uses the Roberts operator to preprocess the video image to obtain the results of edge detection and Gaussian smoothing. On this basis, the key features of moving objects in video images are obtained by normalized processing, and the recognition of moving objects in video images is realized by using the generative adversarial network to output the sample results of moving objects in video images.

TABLE 1: Parameter settings of the experimental test platform.

Name	Specific parameters
CPU	i7-6770K@4.00 GHz
Hard disk	1 TB SSD
Graphics card	AMD
Memory	8G
Operating system	Windows 10

Through the above-given process, the recognition of moving objects in video images based on the generative adversarial network is realized.

3. Experimental Analysis

3.1. Experimental Design. In order to verify the effectiveness of the video image moving target recognition method based on a generative adversarial network, experimental tests are carried out.

- (1) Experimental hardware environment: the experimental test platform is 64 bit Ubuntu14.04, and the specific parameters of the platform are shown in Table 1.
- (2) Source of experimental data: the images used in this paper are all from the VOC2007 public dataset, which includes 20 different types of video images. Among them, including 5011 pictures and 4952 video images, 50 video image moving objects are selected from this dataset as experimental data to identify the video image moving objects. In order to improve the accuracy of the experimental results, it is necessary to ensure the consistency of the image sample specifications used in the experiment, and to process the samples through MATLAB software.
- (3) Experimental indicators: in the experiment, the video image moving target recognition effect, recognition accuracy, recognition time, target recognition quantity, and recognition rate are analyzed as performance indicators.
- (4) In the experiment, the method of reference [7], the method of reference [8], and the proposed method were used to compare and verify the effectiveness of the proposed method.

3.2. Testing and Analysis of Performance Indicators. Two video images were selected for recognition in the experimental data set to verify the recognition effect of the proposed method on moving objects. By comparing the method of reference [7], the method of reference [8], and the proposed method, the recognition effects of different methods on moving objects in video images are obtained, as shown in Figure 1 and Figure 2.

According to Figure 1, it can be seen that the recognition result of the video image moving target obtained by the method of reference [7] is too dark, and the recognition effect is not good due to too much noise interference. The video image moving target recognition result obtained by

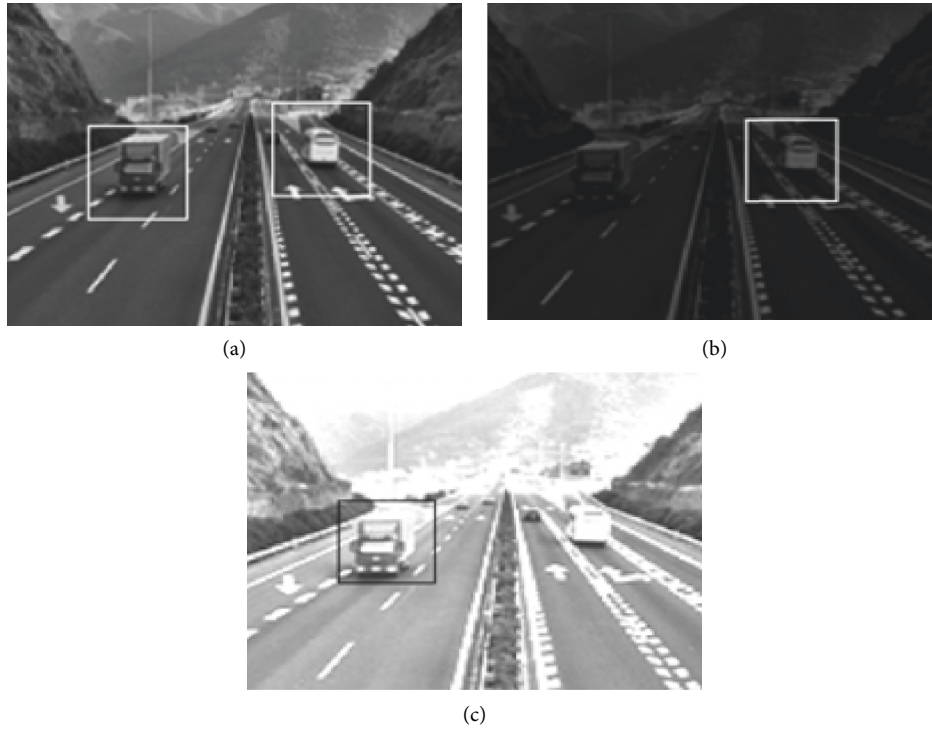


FIGURE 1: Image 1 recognition effect. (a) The proposed method. (b) Reference [7] method. (c) Reference [8] method.



FIGURE 2: Image 2 recognition effect. (a) The proposed method. (b) Reference [7] method. (c) Reference [8] method.

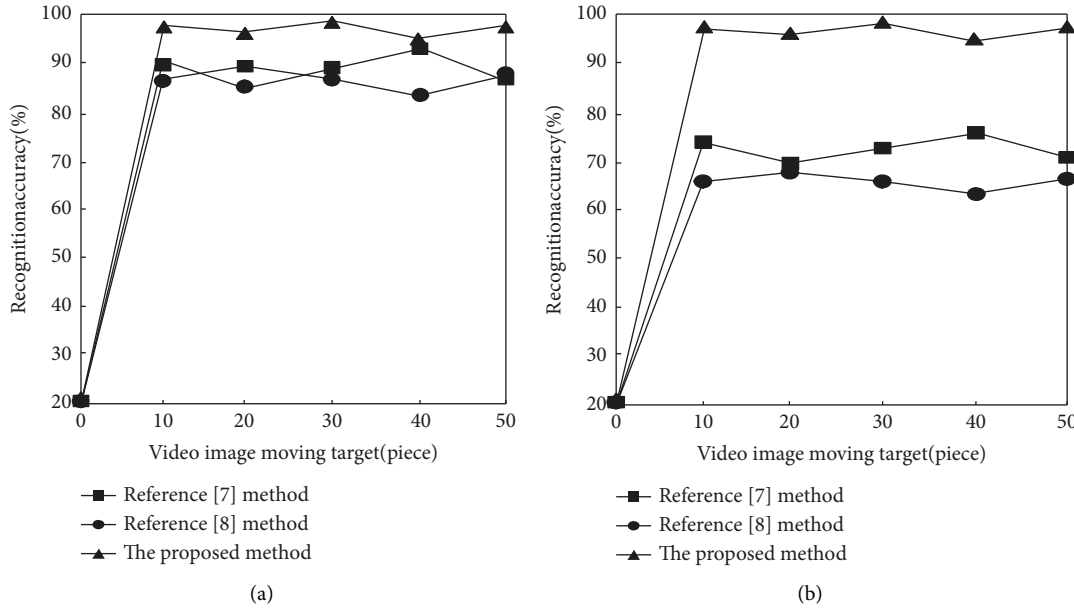


FIGURE 3: Video image moving target recognition accuracy of different methods. (a) Unobstructed. (b) Partial occlusion.

the method of reference [8] is too bright, and the recognition effect is also poor because the edge is not clear enough. In addition, both methods are not good at identifying moving objects. However, the proposed method recognizes moving objects and obtains good results, with moderate brightness, low noise, and clear edges of moving objects. It can be seen from this point that the proposed method is effective and the recognition effect is better.

It can be seen from Figure 2 that when the proposed method is used to identify the moving target in image 2, the head, hands, legs, and footsteps of the athlete in the image can be effectively identified, and the movements are independent of each other and do not appear to identify problems with confusing results. In the recognition method of reference [7], some head movements and footsteps are missing, and the recognition results are not comprehensive enough. The method of reference [8] has the problem of confusion in recognition and recognizes the actions of different moving subjects as one part. It can be seen from the above analysis that the proposed method has a better recognition effect.

To further verify the accuracy of the video image moving target recognition of the proposed method, the method of reference [7], the method of reference [8], and the proposed method are used to compare, and the accuracy of video image moving target recognition of different methods is shown in Figure 3.

According to Figure 3(a), it can be seen that the difference between the recognition accuracy of video images of the three methods is small. The recognition accuracy of the proposed method is compared with the method in reference [7] and reference [8]. There are certain advantages, but the advantages are not obvious.

According to Figure 3(b), when there are 50 moving objects in the video image, the average video image moving target recognition accuracy of the method of reference [7] is

82.9%, and the average video image moving target recognition accuracy of the method of reference [8] is 66.2%. The average video image moving target recognition accuracy of the proposed method is as high as 98.1%. It can be seen that the proposed method has a high accuracy of video image moving target recognition. This is because the proposed method uses the normalization processing method to extract the moving target features of the video image. This method does not require geometric correction of the moving target in the video image but also achieves a high feature recognition rate and reduces the time required for the extraction of key features of the target. Complexity, which is beneficial to improve the accuracy of target recognition.

On this basis, the proposed method is further verified for the recognition time of moving objects in video images. Comparing the method of reference [7] and the method of reference [8] with the proposed method, the recognition time of moving objects of different methods is obtained, as shown in Table 2.

According to Table 2, with the increase of moving objects in video images, the recognition time of moving objects in video images by different methods increases. When there are 50 moving objects in the video image, the recognition time of the method of reference [7] is 12.5 s, and that in the method of reference [8] is 14.4 s. The time for the proposed method to recognize moving objects in video images is only 5.7 s. It can be seen that the proposed method has a short time for the recognition of moving objects in video images. This is because the proposed method preprocesses the video image before target recognition, which is conducive to more efficient target recognition.

There may be a large number of moving targets in the video image, and whether these targets can be comprehensively recognized is also a key indicator to verify the proposed method. Comparing reference [7] method and reference [8] method with the proposed method, the number

TABLE 2: Video image moving target recognition time by different methods.

Video image moving target (piece)	The proposed method (s)	The method of reference [7] (s)	The method of reference [8] (s)
10	1.2	4.1	6.5
20	2.5	6.8	8.3
30	3.6	8.6	10.8
40	4.8	10.3	12.7
50	5.7	12.5	14.4
60	6.0	13.1	15.4
70	6.5	14.6	16.3
80	6.9	15.2	17.0
90	7.2	16.7	17.6
100	7.4	17.9	18.3

TABLE 3: Comparison results of target recognition number of different methods.

Video image number	The proposed method	The method of reference [7]	The method of reference [8]
1	35	27	34
2	41	38	36
3	29	26	26
4	24	21	19
5	31	25	27
6	34	30	30
7	40	34	35
8	27	22	23
9	26	23	20
10	33	28	28

of moving targets recognized by different methods is obtained, and the results are shown in Table 3.

It can be seen from the data in Table 3 that when the proposed method is used for target recognition on 10 video images, the number of recognized targets is significantly higher than that of reference [7] method and reference [8] method. Taking image 5 as an example, the proposed method identified 31 targets, reference [7] method identified 25 targets, and reference [8] method identified 27 targets; taking image 8 as an example, the proposed method identified 27 targets, 22 targets were identified by reference [7] method, and 23 targets were identified by reference [8] method. By comparison, it can be seen that the number of targets identified by the proposed method is more, indicating that the identification results of this method are more comprehensive. This is because the method uses the normalization processing method to extract the key features of moving objects in video images, which is beneficial to improve the comprehensiveness of object recognition.

Finally, the target recognition rate is used as the experimental index to compare the moving target recognition effects of reference [7] method, reference [8] method, and the proposed method. The results are shown in Figure 4.

According to Figure 4, with the increase of the number of experiments, the recognition rate of reference [7] method, reference [8] method, and the proposed method shows a rapid upward trend, but the recognition rate of the proposed method is always higher than that of reference [7] method and reference [8] method. The highest recognition rate of the

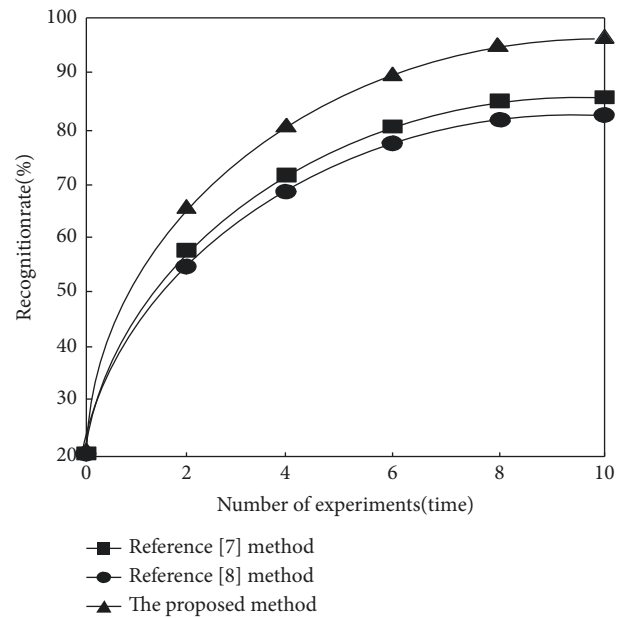


FIGURE 4: Comparison results of recognition rates of different methods.

proposed method is 95%, which is increased by 11% and 13% respectively compared with reference [7] method and reference [8] method. It can be concluded that the recognition effect of the proposed method is better, which further verifies its application value.

4. Conclusion

In order to effectively improve the accuracy of video image moving target recognition, ensure the recognition effect, and shorten the recognition time, a method for video image moving target recognition based on the generative adversarial network is proposed. The main innovations of this method are as follows:

- (1) A video image acquisition method based on an image sensor is adopted to acquire a video image sequence.
- (2) Select the Roberts operator to detect the edge of the video image, use Gaussian smoothing, and then standardize it to obtain the key features of the moving target.
- (3) By establishing a generative adversarial network model, training it, optimizing the discriminant and generator networks respectively, and outputting the sample results of video image moving target recognition to realize video image moving target recognition.
- (4) The experimental results show that the proposed method has a good recognition effect, with moderate brightness, low noise, and clear moving target edges. The recognition accuracy rate reaches 98.1%, and the recognition time is only 5.7 s.

Data Availability

The data used to support the findings of this study are available from the corresponding author upon request.

Conflicts of Interest

The authors declare that they have no conflicts of interest.

Acknowledgments

This work was supported by Scientific Research Project of Xuzhou University of Technology (Grant no. XKY2019107), Science and Technology Project of Construction System, Jiangsu Province, China (Grant no. 2018ZD077), Natural Science Foundation of the Higher Education Institutions of Jiangsu Province, China (Grant no. 20KJB170023), and Xuzhou Science and Technology Planning Project (Grant no. KC21303).

References

- [1] W. Cao, "Applying image registration algorithm combined with CNN model to video image stitching," *The Journal of Supercomputing*, vol. 77, no. 12, pp. 13879–13896, 2021.
- [2] L. Zhang, "Feature mining simulation of video image information in multimedia learning environment based on BOW algorithm," *The Journal of Supercomputing*, vol. 76, no. 9, pp. 6561–6578, 2020.
- [3] L. Pan, Y. Dai, M. Liu, F. Porikli, and Q. Pan, "Joint stereo video deblurring, scene flow estimation and moving object segmentation," *IEEE Transactions on Image Processing*, vol. 29, no. 3, pp. 1748–1761, 2020.
- [4] M. Ma and H. Song, "Effective moving object detection in H.264/AVC compressed domain for video surveillance," *Multimedia Tools and Applications*, vol. 78, no. 24, pp. 35195–35209, 2019.
- [5] C. M. Patil and Y. N. Sunitha, "A review of the multiple object detection, tracking and recognition in video surveillance systems using different approaches," *Restaurant Business*, vol. 118, no. 7, pp. 34–43, 2019.
- [6] G. Balamurugan and J. Ja Yabharathy, "A study on moving object recognition for video surveillance applications," *Journal of Advanced Research in Dynamical and Control Systems*, vol. 11, no. 1, pp. 157–167, 2019.
- [7] L. Li, Q. Hu, and X. Li, "Moving object detection in video via hierarchical modeling and alternating optimization," *IEEE Transactions on Image Processing*, vol. 28, no. 4, pp. 2021–2036, 2019.
- [8] F. Guo, Y. Yang, Y. Xiao, Y. Gao, and N. Yu, "Recognition of moving object in high dynamic scene for visual prosthesis," *IEICE - Transactions on Info and Systems*, vol. E102.D, no. 7, pp. 1321–1331, 2019.
- [9] S. Javed, A. Mahmood, S. Al-Maadeed, T. Bouwmans, and S. K. Jung, "Moving object detection in complex scene using spatiotemporal structured-sparse RPCA," *IEEE Transactions on Image Processing*, vol. 28, no. 2, pp. 1007–1022, 2019.
- [10] S. Zebhi, S. Almodarresi, and V. Abootalebi, "Converting video classification problem to image classification with global descriptors and pre-trained network," *IET Computer Vision*, vol. 14, no. 8, pp. 614–624, 2020.
- [11] A. Brifman, Y. Romano, and M. Elad, "Unified single-image and video super-resolution via denoising algorithms," *IEEE Transactions on Image Processing*, vol. 28, no. 12, pp. 6063–6076, 2019.
- [12] N. Albdour and N. Zanoon, "A steganographic method based on Roberts operator. Jordan journal of electrical engineering," *All rights reserved-Volume*, vol. 6, no. 3, pp. 266–273, 2020.
- [13] B. Khagi, K. H. Lee, K. Y. Choi, J. J. Lee, G. R. Kwon, and H. D. Yang, "VBM-based alzheimer's disease detection from the region of interest of T1 MRI with supportive Gaussian smoothing and a bayesian regularized neural network," *Applied Sciences*, vol. 11, no. 13, pp. 6175–6182, 2021.
- [14] R. Hostettler and S. Särkkä, "Rao-blackwellized Gaussian smoothing," *IEEE Transactions on Automatic Control*, vol. 64, no. 1, pp. 305–312, 2019.
- [15] L. B. White and F. Carravetta, "State-space realizations and optimal smoothing for Gaussian generalized reciprocal processes," *IEEE Transactions on Automatic Control*, vol. 65, no. 1, pp. 389–396, 2020.
- [16] S. K. Johal and R. Mohana, "Effectiveness of normalization over processing of textual data using hybrid approach sentiment analysis," *International Journal of Grid and High Performance Computing*, vol. 12, no. 3, pp. 43–56, 2020.
- [17] J. M. Jo, "Effectiveness of normalization pre-processing of big data to the machine learning performance," *The Journal of the Korea institute of electronic communication sciences*, vol. 14, no. 3, pp. 547–552, 2019.
- [18] Y. Zhai, R. Sun, and F. Shao, "Multi-view gait recognition using generative adversarial network," *Computer Simulation*, vol. 37, no. 08, pp. 446–451, 2020.
- [19] H. Wu, "A summary of Research progress of generative countermeasure network," *Industrial Control Computer*, vol. 32, no. 7, pp. 70–71, 2019.
- [20] S. Liu, B. Zhang, Y. Liu et al., "Unpaired stain transfer using pathology-consistent constrained generative adversarial networks," *IEEE Transactions on Medical Imaging*, vol. 40, no. 8, pp. 1977–1989, 2021.

Research Article

Gear Fault Diagnosis and Life Prediction of Petroleum Drilling Equipment Based on SOM Neural Network

Lin Zhu Lu,¹ Jie Liu ,² Xin Huang,¹ and Yongcai Fan³

¹College of Petroleum and Chemical Engineering, Jingzhou University, Jingzhou 434000, Hubei, China

²School of Chemistry and Chemical Engineering, Huanggang Normal University, Jingzhou 438000, Hubei, China

³Jingzhou University, Admissions and Employment Department, Jingzhou 434000, Hubei, China

Correspondence should be addressed to Jie Liu; liujie5856@hgnu.edu.cn

Received 23 May 2022; Accepted 11 July 2022; Published 18 August 2022

Academic Editor: Le Sun

Copyright © 2022 Lin Zhu Lu et al. This is an open access article distributed under the Creative Commons Attribution License, which permits unrestricted use, distribution, and reproduction in any medium, provided the original work is properly cited.

In order to solve the problem that variable working conditions and fault types cannot be diagnosed in gear fault diagnosis of petroleum drilling equipment, four kinds of faults, namely, gear broken tooth, gear crack, gear pitting, and gear wear, are studied in this paper. Based on the SOM neural network algorithm, an intelligent diagnosis model of gear fault is proposed, and the PCA method is used to reduce data dimension and fuse features. The state index of life prediction is determined, and the remaining service life prediction of gear transmission system is predicted based on exponential degradation model. The results show that the accuracy of the SOM model for fault diagnosis is high, and the bearing in gearbox can be replaced or repaired in advance according to the residual life curve, so as to achieve the purpose of predictive maintenance.

1. Introduction

With the manufacturing industry entering the “industry 4.0” era, modern mechanical equipment has absorbed the new technology of modern science and technology development, and the degree of automation of mechanical equipment has become higher. At the same time, the structure of equipment has become more complex. Therefore, higher requirements have been put forward for the safety, reliability, and maintainability of the equipment in the operation process [1, 2]. Fault diagnosis technology plays an important role in ensuring the reliability, safety, and maintainability of equipment operation.

The key transmission equipment of petroleum drilling equipment is the key part to ensure the normal operation and power transmission of the whole equipment system. However, affected by the bad working environment, heavy load, high speed, and other working conditions, some typical parts of petroleum drilling and production equipment, such as gears and rolling bearings, are prone to various types of failures, which will affect the safety and reliability of the whole petroleum drilling system. At least, it will lead to the

decline of product or service quality and even cause huge economic losses and casualties. Monitor the condition of large-scale key gear transmission equipment in the petroleum industry, timely handle the faults in the operation of petroleum equipment, and ensure the safe operation of the equipment. At the same time, predicting the future operation trend and remaining service life of the equipment and carrying out equipment maintenance in advance can save maintenance costs, improve economic benefits of enterprises, avoid accidents, and ensure personnel safety [3, 4].

In the process of fault diagnosis of mechanical equipment, after obtaining equipment information, equipment fault is judged by simple time domain signal in the early stage. With the development of diagnosis technology, this simple diagnosis method cannot meet the development needs, and then more reliable and accurate modern signal processing and feature extraction methods are derived [5]. But as the amount of data storage increases, the amount of data to be processed and the corresponding feature dimension increase, these factors will make the fault database rich, but also weaken the information redundancy, data processing, and computing capacity [6]. In addition, the

application of fault diagnosis in petroleum field is too few, the main research results are also mainly focused on fault diagnosis and analysis under fixed working conditions. Although the structure and principle of the petroleum gear transmission system are the same, the operation conditions of the heavy petroleum gear transmission system are complex, and there are problems of variable speed and variable load, which will increase the difficulty of fault diagnosis [7, 8]. The research on fault prediction and remaining service life prediction of petroleum drilling equipment is relatively less. Moreover, it is also found that the fault diagnosis method based on machine learning and remaining service life prediction of equipment are the development trend of petroleum drilling and production equipment [9, 10].

In order to solve the problem that variable working conditions and fault types cannot be diagnosed in the gear fault diagnosis of petroleum drilling equipment, four kinds of faults, namely, gear broken tooth, gear crack, gear pitting, and gear wear, are studied in this paper. Therefore, in view of the limitations of existing fault diagnosis methods in heavy petroleum gear fault diagnosis, this paper studies the unsupervised machine learning algorithm based on SOM for heavy petroleum gear fault diagnosis under complex working conditions.

2. Fault Classification of Transmission System

As the key transmission equipment of petroleum drilling and production equipment, a heavy petroleum gearbox is the key part to ensure the normal operation of the whole equipment system and transfer power. The components of gear transmission system include gears, bearings, and shafts. According to the statistics in literature [11], the gear and bearing account for 79% of failure parts. Gear failure mainly includes gear broken and crack, gear pitting, gear wear, tooth surface gluing, and tooth profile error caused by manufacturing and installation. As shown in Figure 1, this paper selects four kinds of faults: gear broken, gear crack, gear pitting, and gear wear.

2.1. Gear Broken. Gear broken tooth is a serious fault in gear fault. In the process of gear meshing, when the overload impact and pulse cyclic stress occur, the gear will be broken, which can be divided into two forms: overload and fatigue. The first is the tooth fracture caused by overload, which is mainly due to improper assembly. In the process of operation, the load is concentrated at one end of the gear, or the sudden stop and reversing of the gear cause impact overload, resulting in tooth fracture. The second is fatigue fracture, which is mainly caused by improper design, poor assembly, excessive or unbalanced load, stress concentration caused by surface defects of gear teeth, etc.

2.2. Gear Wear. Gear wear is common in gear failure. The wear is mainly divided into normal wear, medium wear, abrasive wear, interference wear, and corrosion wear. If the degree of wear does not affect the normal operation of the

gear, it is generally called normal wear. Moderate wear is mainly caused by high load on the teeth. In general, the service life of the driving gear will be reduced from large to small. When the sliding of the gear meshing dividing circle is blocked, it will lead to excessive wear of the gear, which shows that the working state becomes bad, the tooth profile changes, and in serious cases, it will cause pitting corrosion and plastic deformation. When there are external particles into the gear meshing surface, it will lead to abrasive wear.

2.3. Gear Crack. Gear crack is an early phenomenon of gear fatigue fracture. When the petroleum film of the gear is damaged, the local stress concentration will be caused at the crack. Under the action of cyclic stress, the crack will slowly expand and eventually cause the crack to fracture. This process can be monitored and predicted where the crack appears as tearing crack on the sliding direction of the tooth surface or the appearance is a ridge shape.

2.4. Gear Pitting. The pitting corrosion of gears can be divided into early pitting and destructive pitting. When the surface of the gear is locally convex and bears a large load, or is affected by the high-frequency variable stress, the early pitting corrosion of the gear will be caused, which generally occurs on the surface of the tooth root near the dividing circle of the gear. When the hardness of the gear surface is low, the viscosity of lubricating petroleum is low, and when the dynamic load caused by local pitting corrosion increases, the destructive pitting corrosion of gear will be caused, which is characterized by the destruction of profile and the large size of pitting corrosion. The pitting formed by destructive pitting often becomes the fatigue source and eventually leads to the fatigue fracture of gear.

3. Fault Diagnosis of Transmission System based on Neural Network

3.1. Self-Organizing Maps (SOM) Neural Network Algorithm. SOM neural network realizes the ordered mapping from high-dimensional distribution to low-dimensional regular grid, which is often used as dimensionality reduction of data features. The output neurons of the SOM network compete with each other to be activated, so only one winning neuron is output at each time. As shown in Figure 2, in the self-organizing map, neurons are placed on the network nodes. Usually, the mesh is one-dimensional or two-dimensional, while the SOM network is different from the BP network in that it only contains input layer and competition layer. Since there is no hidden layer, the SOM network can keep the original topological structure of output layer data, which is a typical feature of the SOM network.

The formation process of SOM can be divided into four stages.

The first stage: initialization, the initial connection weights are randomly initialized and the smaller weights are selected.

The second stage of their numerical competition is called the numerical discrimination of neurons.

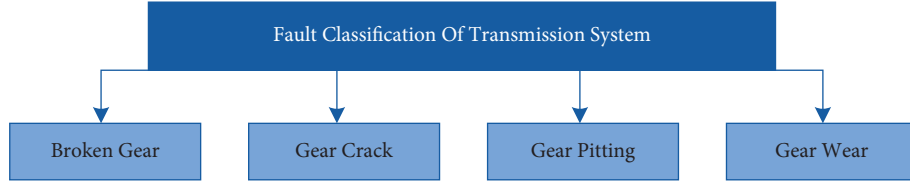


FIGURE 1: Fault classification of the transmission system.

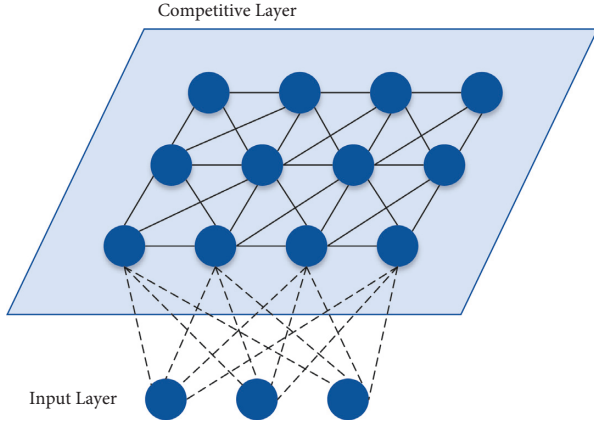


FIGURE 2: SOM network structure.

The third stage: cooperation, the winning neuron determines the spatial location of the topological neighborhood of the excited neuron, thus providing the basis for the cooperation of adjacent neurons.

The fourth stage: adaptation, in which the excitatory neurons increase their discriminant function value about the input pattern through the proper adjustment of their synaptic weights, and the response of the winning neurons to the later similar input patterns is enhanced. Based on the formation process of SOM, the algorithm steps of feature mapping are as follows [12]:

- (1) The weight vector W_j is initialized randomly and the smaller weight is selected
- (2) A sample $X = (x_1, x_2, x_3, \dots, x_m)^T$ is randomly selected from the input space to the input layer
- (3) The distance between the weight vector of each neuron and the input vector is calculated, its calculation formular is as follows:

$$d_j = \|X - W_j\| = \sqrt{\sum_{i=1}^m (x_i(t) - w_{ij}(t))^2}, \quad (1)$$

where w_{ij} is the weight between i neuron at the input layer and j neuron at the mapping layer. Through calculation, a neuron with the minimum distance is obtained, which is called the winning neuron and denoted as j^* , that is, a certain unit k is determined, such that $d_k = \min_j(d_j)$ for any j . And the set of adjacent neurons is obtained.

- (4) Modify the weights of output neurons and their adjacent neurons

$$\Delta w_{ij} = w_{ij}(t+1) - w_{ij}(t) = \eta(t)(x_i(t) - w_{ij}(t)), \quad (2)$$

where r is a constant greater than 0 and less than 1, which gradually decreases to 0 as time changes.

$$\eta(t) = \frac{1}{t} \text{ or } \eta(t) = 0.2 \left(1 - \frac{t}{10000}\right). \quad (3)$$

- (5) Calculate the output

$$o_k = f\left(\min_j \|X - W_j\|\right), \quad (4)$$

where $f(*)$ is generally 0~1 function or other nonlinear functions.

3.2. Signal Extraction. Before the fault intelligent diagnosis of heavy petroleum gear, it is necessary to complete the feature extraction of fault vibration signal due to the fact that the internal parts of the heavy petroleum gearbox are coupled with each other under actual working conditions, and the load under variable working conditions is complex and changeable. In order to obtain more useful fault feature information, based on the time domain feature extraction of the original signal, the modulation information affecting the sideband in different faults is extracted, and the high-frequency characteristics are filtered out by Hilbert envelope spectrum method, The modulation frequency information affecting the sideband is extracted from the low frequency signal, and then the feature set is formed with the time domain index characteristics of the original vibration signal, which is used as the data sample of the subsequent intelligent fault diagnosis algorithm.

3.2.1. Extraction Device. The vibration data used is from the QPZZ-II rotating machinery vibration analysis and fault diagnosis test platform [13]. The data has the characteristics of various loads and variable speed. In order to collect vibration signals, nine sensors are installed in the gearbox box, and the installation position diagram is shown in Figure 3.

In order to collect vibration signals, nine sensors are installed in the gearbox box, and the installation position diagram is shown in Figure 3, where X is the radial horizontal direction and Y is the radial vertical direction. The measurement position and type of each channel are shown in Table 1.

In the experiment, the input and output frequencies of the gearbox are 5120 Hz and 880 rpm, respectively. The sampling time of each state is 10 s. The vibration signals collected by sensors 2–9 are selected. Combined with speed and gearbox related result parameters, two-stage meshing

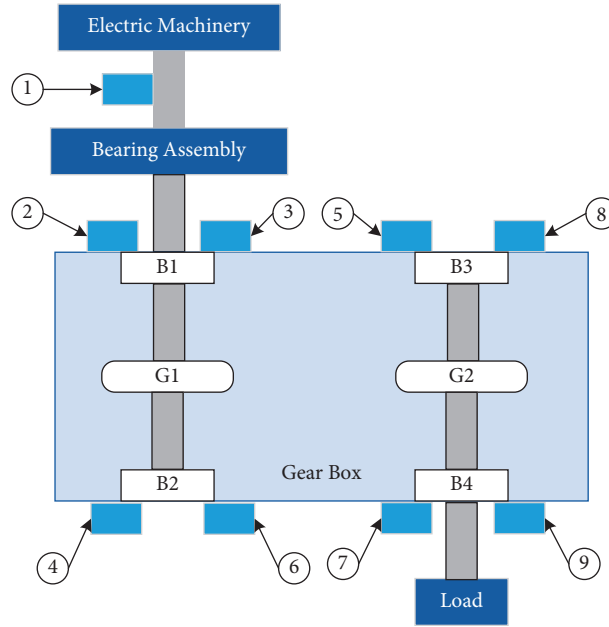


FIGURE 3: Installation position of sensors.

TABLE 1: Measurement position and type of sensors.

Serial number	Channel	Type	Position
1	TACH1	Speed, photoelectric	Input shaft
2	CH1	Displacement	Input shaft X direction displacement
3	CH2	Displacement	Y direction displacement of input shaft
4	CH3	Acceleration	Input shaft motor side bearing Y direction
5	CH4	Acceleration	Output shaft motor side bearing Y direction
6	CH5	Acceleration	Input shaft load side bearing Y direction
7	CH6	Acceleration	Output shaft load side bearing Y direction
8	CH7	Acceleration	Output shaft motor side bearing X direction
9	CH8	Magnetolectric acceleration	X direction of bearing on load side of output shaft

frequency and fault characteristic frequency of each gear can be obtained, as shown in Table 2.

3.2.2. Sample Extraction. Under the QPZZ-II rotating machinery vibration analysis and fault diagnosis test platform, gear normal, broken teeth, pitting corrosion, and wear data are analyzed. Gear fault features are extracted from time domain, where the state can be divided into normal, broken gear, pitting, and abrasion. Eight features are selected, namely, kurtosis, RMS, ShapeFactor, MarginFactor, peak-to-peak value, waveform factor, margin factor, and energy value under the envelope frequency signal. Four samples are selected for each fault type, and a total of 16 groups of samples are selected to form SOM adaptive network learning samples. The characteristic number of envelope spectrum signal is 8, which makes up $16 \times$. The matrix of 8 is used as the data sample of energy algorithm, as shown in Table 3.

3.3. Fault Diagnosis. The SOM algorithm belongs to an unsupervised algorithm. The difference between the supervised algorithm and unsupervised algorithm is that the supervised algorithm requires input data and corresponding

TABLE 2: Characteristics of gear fault.

	G1	G2
Speed (rpm)	880	880
Meshing frequency (Hz)	806	806
Gear shaft rotation frequency (Hz)	14.67	10.75
Modulus	2	2
Number of teeth	55	75

label, while the unsupervised algorithm does not need corresponding label of input data, so it has self-learning ability and explores the internal structure of unknown data. Combined with the SOM network algorithm, the flow chart of fault diagnosis is shown in Figure 4.

Different from the supervised algorithm, the SOM network algorithm should design the number of competition layer neurons and network topology before training, and the number of output neurons will also be the final classification results. In this paper, each input is connected to $8 \times$. There are 64 neurons in the hexagonal grid. A two-dimensional output layer composed of 64 neurons is selected, and the index value ranges from 1 to 64. The competitive position of neurons is shown in Figure 5.

TABLE 3: Sample data of SOM algorithm.

Working condition	Number	1	2	3	4	5	6	7	8
Normal	1	4.8204	5.4538	1.3249	1.6298	22.7901	1.7988	11.9818	776444.4
	2	4.9564	3.9660	1.2248	1.5282	10.2257	4.5461	11.5586	74443.0
	3	3.3134	3.5523	1.2034	0.9806	5.0575	10.2814	15.9342	11443.0
	4	5.8960	3.7342	1.1651	1.9874	0.1924	7.3950	17.6332	17344.2
Broken gear	5	7.0881	3.8081	1.3260	3.1636	15.4171	3.5039	7.1462	154360.0
	6	4.1284	5.7812	1.2990	1.7334	21.1364	3.1244	5.1195	288630.0
	7	4.0225	3.7241	1.2631	2.1591	11.2343	3.7386	9.4664	92477.0
	8	3.8737	3.9982	1.2519	1.6157	12.1311	3.9084	9.9526	105970.0
Pitting	9	18.4485	4.2961	1.3399	6.5161	32.5243	4.7026	17.3040	161890.0
	10	13.8548	5.2683	1.4125	3.6196	28.1052	3.2914	10.1228	362930.0
	11	15.6913	4.2410	1.3865	4.7952	21.6414	3.8384	16.4008	201850.0
	12	21.7750	4.2334	1.3950	6.2305	22.8853	4.2299	21.3788	192410.0
Abrasion	13	2.6554	6814.4	1.0001	0.0001	40.2643	4710.3	17.8188	221550.0
	14	2.5848	6827.7	1.0001	0.0001	37.0109	4819.0	16.9743	208020.0
	15	2.6557	6835.2	1.0001	0.0001	32.9251	5019.1	16.2253	197220.0
	16	1.7965	6693.4	1.0001	0.0001	34.0624	5176.3	17.7266	217170.0

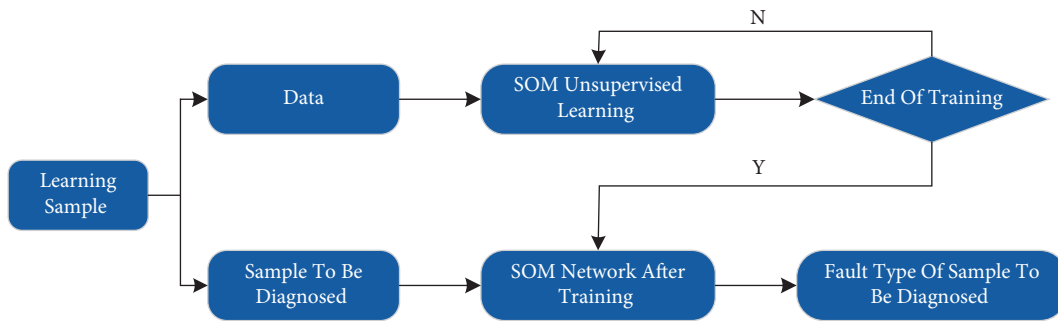


FIGURE 4: Fault diagnosis process of the SOM network.

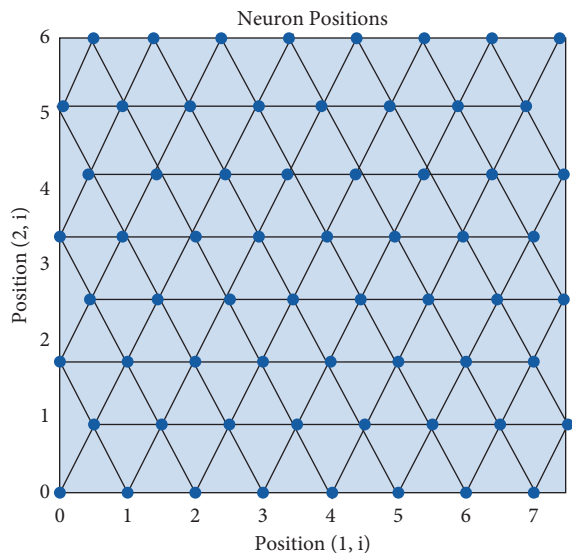


FIGURE 5: Location of neurons in the competitive layer.

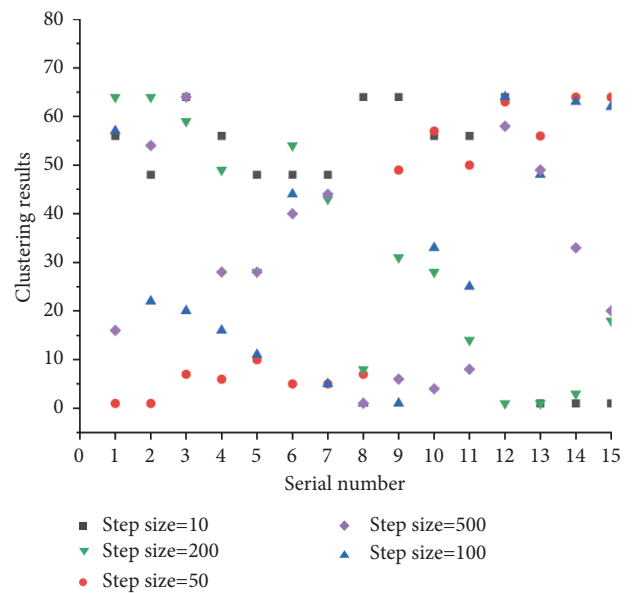


FIGURE 6: Clustering results of the model.

3.4. Result Analysis

3.4.1. Results of Model Training. As shown in Figure 6, when the number of training steps is 10, the number 1 and 5 of fault causes are divided into one category; 2, 6, and 7 are

divided into one category; 3, 9, and 10 are divided into one category; and 13, 14, and 15 are divided into one category. It can be seen that the SOM network can classify the samples in the case of few training steps, but this classification is not

accurate enough. When the number of training steps is increased, the accuracy of classification is also increased, and the SOM network has been able to accurately classify each sample when the number of training steps is increased to 100. However, when the number of training steps continues to increase, it has no effect on the classification results. For example, when the number of steps is 200 and 500, the improvement of training steps has no effect on the accuracy of the results. On the contrary, it will increase the training time.

3.4.2. Results of Sample Diagnosis. Through the comparison of different training times of the SOM model, in order to exclude the influence of too few or too many training steps on the results, the training times of the model are selected as 200, and the test set data numbered 4, 8, 12, and 16 are classified with the SOM network completed by training. The results are shown in Table 4.

Comparing the diagnosis results in Table 4 with the results of 200 training steps in Figure 6, it is found that the SOM network can diagnose the fault types corresponding to the data to be tested, and the accuracy rate reaches 75%.

4. Life Prediction of Equipment

4.1. Prediction Steps. The process steps of residual life prediction of rolling bearing based on the degradation model are as follows:

- Step 1: collect the original vibration signal of rolling bearing with sensor
- Step 2: extract and calculate the eigenvalues by using vibration signal processing and analysis technology and smooth the extracted features
- Step 3: divide the training set and take the early data of the data set as the training data
- Step 4: evaluate the features, use PCA technology to reduce the dimension of the data, and perform data fusion
- Step 5: select the status index
- Step 6: fitting the degradation model of the remaining service life of the training data to obtain the fitting degradation model
- Step 7: use the fitting degradation model to predict the residual life

4.2. State Index Selection. The extraction of the original vibration signal of rolling bearing is the same as before, so the selection of state index is directly described. Among the first six features with large monotonicity, only the peak-to-peak value has better monotonicity. However, if only it is selected as the state index, the information of original data will be lost and error analysis will be caused. Therefore, PCA is used to analyze and fuse multiple features extracted from original data, and the largest principal component is taken as the indicator of state. Through the PCA analysis of vibration signal, the state index is obtained as shown in Figure 7. The

TABLE 4: SOM diagnosis results.

	Normal	Broken gear	Pitting	Abrasion
Serial number to be tested	1	5	9	13
Diagnosis results	59	30	8	1

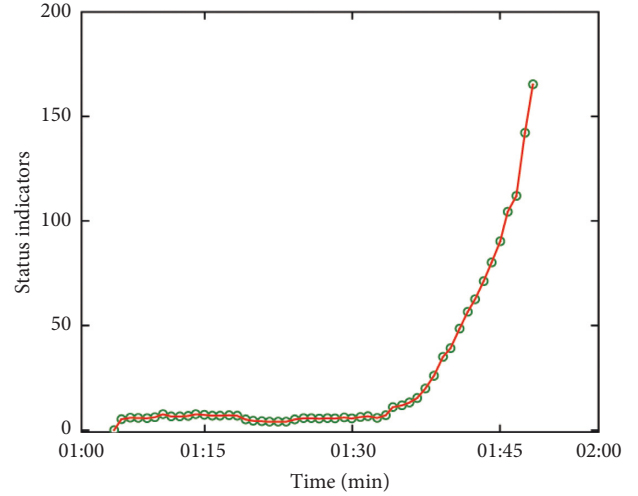


FIGURE 7: Status indicators.

value of state index increases gradually with time, and it can be seen from the growth trend that the state index has a monotonic increasing trend, which can be used to fit the degradation model.

4.3. Prediction Results. When the state index is selected, the exponential degradation model is used to fit the residual life degradation model of bearing. The model can predict the remaining service life of bearing in real time. The exponential degradation model predicts the remaining service life according to its prior parameters and measured values:

The parameter values are defined as follows:
 $E(\theta) = 1$, $\text{Var}(\theta) = 10^6$, $E(\beta) = 1$, $\text{Var}(\beta) = 10^6$.

The exponential degradation model also provides a function to evaluate the slope. Once the slope of the state index changes significantly, the model will forget the previous observation results and reestimate based on the original prior value. When the slope detection value is adjusted continuously in the model fitting, the final value is 0.025 that the model has the best effect. The degradation model obtained by fitting is shown in Figure 8.

After the model fitting is completed, the life prediction of the data is carried out, and the remaining service life of the bearing is predicted by comparing the threshold value of the input measured value with the final failure threshold value. The residual life curve is shown in Figure 9.

The actual life curve (blue) and predicted life curve (red) show that the slope of input state index changes at 37 min. Before that, the change of slope cannot be detected in this time

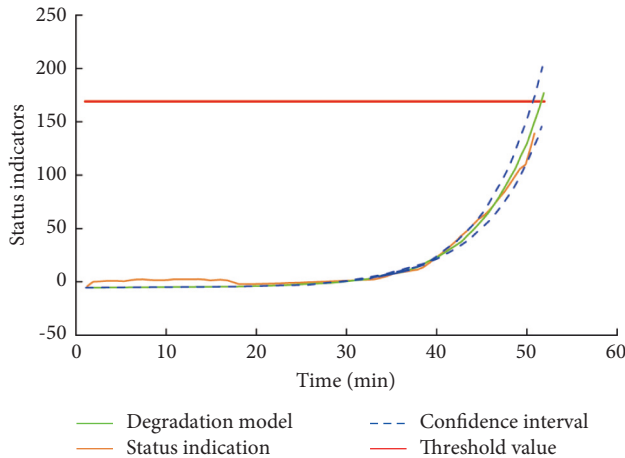


FIGURE 8: Degradation model.

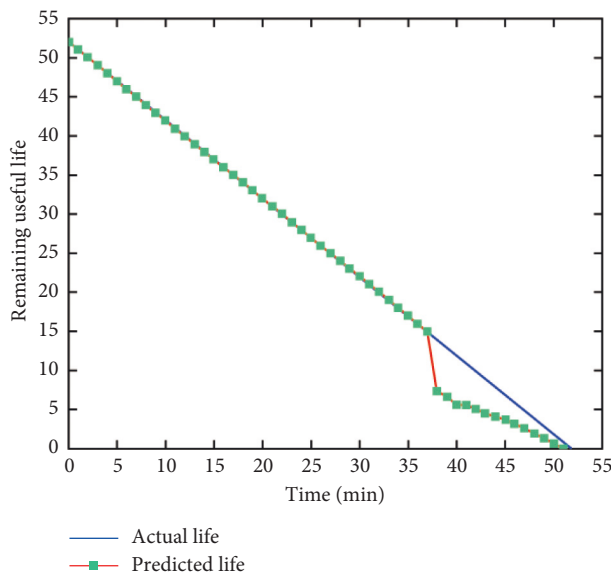


FIGURE 9: Residual life curve of equipment.

area because the change of state index is not obvious. After 37 min, the life curve changes obviously, and the life is 0 at 51 min, reaching the failure threshold one day earlier than the actual life. According to the predicted residual service life curve, the equipment can be maintained in advance and the bearing can be replaced to prevent accidents.

5. Conclusion

In view of the limitations of the existing fault diagnosis methods in gear fault diagnosis of heavy petroleum drilling, this paper proposes a gear fault intelligent diagnosis model based on the SOM neural network algorithm. Under this model, the data not entered into the label are classified. 16 groups of data samples are selected and 8 characteristic indexes are selected. Experimental results show that the accuracy rate of fault classification is 75%. In addition, based on the degradation model, the remaining useful life of drilling equipment is predicted. The results show that the

obvious change of slope can be detected at 37 min, which verifies the effectiveness of the exponential degradation model. The bearing in gearbox can be replaced or repaired in advance according to the residual life curve, so as to achieve the purpose of predictive maintenance.

Data Availability

The dataset can be accessed upon request.

Conflicts of Interest

The authors declare that they have no conflicts of interest.

References

- [1] Z. He, H. Cao, Y. Zi, and B. Li, "Development and thinking of operational reliability evaluation of mechanical equipment," *Journal of mechanical engineering*, vol. 50, no. 2, pp. 171-186, 2014.
- [2] G. Hu, "Countermeasures for sustainable development of petroleum drilling and production equipment manufacturing enterprises," *China market*, vol. 14, no. 2, pp. 68-69, 2016.
- [3] C. Rong, "Petroleum drilling and production machinery equipment fault monitoring and diagnosis technology," *Chemical management*, vol. 9, no. 27, pp. 209-210, 2017.
- [4] R. Gasch, "Dynamic behaviour of the Laval rotor with a transverse crack," *Mechanical Systems and Signal Processing*, vol. 22, no. 4, pp. 790-804, 2008.
- [5] B. Lei, C. Jiang, and L. Hou, "Automatic petroleum equipment fault monitoring method based on external random Automation technology and application," vol. 40, no. 7, pp. 125-128+155, 2021.
- [6] A. K. S. Jardine, D. Lin, and D. Banjevic, "A review on machinery diagnostics and prognostics implementing condition-based maintenance," *Mechanical Systems and Signal Processing*, vol. 20, no. 7, pp. 1483-1510, 2006.
- [7] Z. Feng, F. Chu, and M. Zuo, *The Principle of Complex Non-stationary Signal Analysis Method for Mechanical System and its Application in Fault Diagnosis*, Science Press, Beijing, China, 2018.
- [8] L. Wang, *Research on Variable Scale Demodulation and Vibration Feature Extraction Algorithm of Gearbox Gear Fault Vibration Signal*, Chongqing University, Chongqing, China, 2018.
- [9] L. Han and D. Xiao, "Overview of data driven fault diagnosis methods," *Control and decision making*, vol. 25, no. 1, pp. 3-11+18, 2011.
- [10] J. Wang, Y. Liang, Y. Zheng, R. X. Gao, and F. Zhang, "An integrated fault diagnosis and prognosis approach for predictive maintenance of wind turbine bearing with limited samples," *Renewable Energy*, vol. 145, pp. 642-650, 2020.
- [11] C. Peng, *Research on Gearbox Fault Diagnosis Instrument Based on Vibration Signal Analysis*, Chongqing University, Chongqing, China, 2011.
- [12] X. Wang, *Matlab Neural Network Analysis of 43 Cases*, Beijing University of Aeronautics and Astronautics Press, Beijing, China, 2013.
- [13] Z. Meng, Y. Wang, and M. G. Hu, "fault feature extraction method of gear based on improved local mean decomposition and instantaneous energy distribution-sample entropy," *Journal of Mechanical Engineering*, vol. 52, no. 5, pp. 169-176, 2016.

Research Article

Identification of Sports Athletes Psychological Stress Based on K-Means Optimized Hierarchical Clustering

Jun Huang 

School of Competitive Sports, Shandong Sport University, Rizhao 276800, China

Correspondence should be addressed to Jun Huang; huangjun@sdpei.edu.cn

Received 27 May 2022; Accepted 19 July 2022; Published 18 August 2022

Academic Editor: Le Sun

Copyright © 2022 Jun Huang. This is an open access article distributed under the Creative Commons Attribution License, which permits unrestricted use, distribution, and reproduction in any medium, provided the original work is properly cited.

In order to solve the problem, the psychological identification of athletes in professional competition pressure is difficult. This paper first analyzes the sources of athletes' psychological pressure based on the hierarchical clustering method, and then divides the weights of the sources of psychological pressure, quantitatively scores them and constructs an identification model of athletes' psychological pressure. Then, the clustering process is optimized based on the K-Means algorithm, and its effectiveness is verified. Finally, the psychological stress of 10 players in a football club was analyzed. The results show that the model effectively and reasonably reflects the influence of pressure sources on the athletes' competitive state during the competition, which provides a basis for the decision-making of relief about athletes' stress.

1. Introduction

Competitive sport is a highly stressed profession that high-level athletes often lose in major competitions. With the professionalization of sports and the improvement of athletes' psychological requirements, it is an inevitable trend to relieve the pressure before competition. Therefore, it is very important to identify the stress sources of athletes in sports competitions. Psychological counseling is generally to evaluate the athletes' psychological state by consulting professionals or using some questionnaires [1, 2], where professionals divide the results given by athletes into three grades: high, medium, and low. Different grades give different psychological analysis, and generally, athletes' psychology only needs to be roughly classified according to grades [3]. To alleviate the chronic stress of athletes, team doctors and psychologists need to intervene through investigation and interviews where athletes' thoughts can be understood, and the types of stress can be identified through professional psychological analysis. In the past, the research conclusions often focused on the coping strategies of athletes in a specific event, or on a certain element or link in the coping process, so it is impossible to effectively analyze the overall psychological situation [4, 5]. When the number of athletes increases, psychologists cannot effectively make

personalized judgments according to their personal situation, which is inefficient and the coping strategies and results are not ideal.

The work required for stress relief includes information collection of athletes, identification of stress sources, evaluation of sports psychological state, and formulation of strategies, among which the identification of stress sources generally includes training activity test, team doctor inquiry, real-time evaluation, and self-explanation [6]. For the work of relieving athletes' precompetition stress, source identification is the most basic and the most difficult part to implement, which is determined subjectively by the experience of team doctors, whose uncertainty is high. In the process of identifying the source of athletes' stress, because athletes' own experiences are different and their psychological feedback is different, it is particularly important to deal with the collected psychological index data reasonably. Hierarchical clustering method is a common method in the field of data mining. By grouping data samples, it can quickly summarize the common points of different cluster information and then identify the core information. In addition, it is simple, clear-thinking, and can effectively deal with big data sets, so it has been applied in many fields. However, from the perspective of identifying athletes' stress sources,

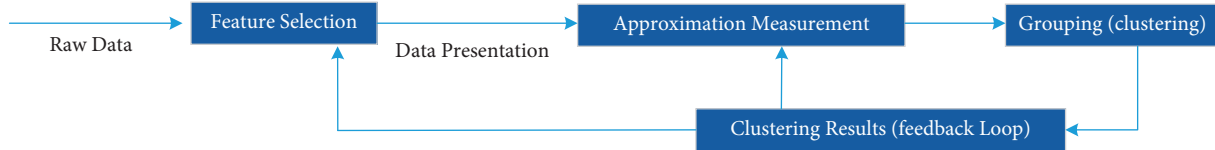


FIGURE 1: The process of the clustering algorithm.

the judgment chain of the hierarchical clustering method is still insufficient to deal with relevant data [7, 8].

In order to help psychological experts provide scientific suggestions, this paper carries out automatic simulation from the aspect of data mining, analyzes athletes' psychological pressure by using the clustering algorithm and effectively reflects the influence of pressure sources on the athletes' competitive state in the process of competition, which offers a basis for the formulation of decisions to athletes' stress relief.

2. Identification of the Athletes' Psychological Pressure Based on the Hierarchical Clustering Method

2.1. Clustering Algorithm. Clustering analysis is one of the main methods of data mining, which is used to divide a large number of datasets into several clusters. Typical clustering mainly includes the processes of raw data preparation, feature extraction, proximity measurement, clustering or grouping, and clustering result evaluation [9]. Figure 1 depicts the typical sequence of the first three steps, which includes a feedback route; among them, the output of grouped results will affect the extraction of data features and the calculation of its similarity:

- (1) Primary data preparation. It means preparing data, including processed valid data, number, quantity, type and scale of valid data, standardization, and dimension reduction of data features.
- (2) Feature extraction. Extracting the most effective feature subset from the original feature set to form a new dataset. Therefore, feature extraction is a method of converting the original feature subset into a more significant new feature subset to make the clustering effect more obvious.
- (3) Proximity measurement defines the distance function between pairs of data, which is used to measure the similarity between data;
- (4) Clustering or grouping. For grouping or clustering, you can use a variety of clustering algorithms, such as hard clustering (giving a clear division result) or fuzzy clustering (giving the membership degree of each data in the cluster), and hierarchical clustering algorithm.
- (5) Evaluation of clustering results. Evaluate whether the clustering results are valid by measuring the matching degree of clusters to data or by measuring the matching degree of clusters to benchmarks. The main evaluation methods are the object matching degree and related test evaluation.

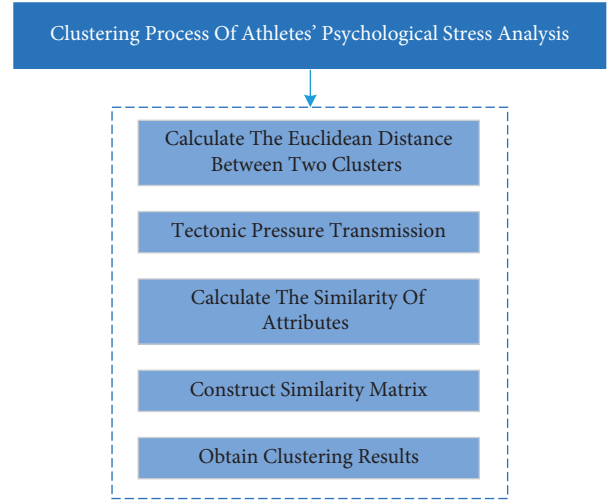


FIGURE 2: Clustering process of athletes' psychological stress analysis.

2.2. Hierarchical Clustering Algorithm. Hierarchical clustering method is a common method to test abnormal data in samples which firstly standardizes multidimensional datasets and then aggregates data categories according to different levels, so that data subsets at different levels have certain similarities, while the gaps between subsets are relatively obvious [10]. According to the difference of hierarchical decomposition methods, it can be further divided into two categories: condensation and classification. Condensation clustering method takes each unit object as an independent cluster and then merges the nearest cluster in turn until the basic conditions set by the system are met or all objects are merged into one cluster. The rule of classification clustering is to treat all units of objects as a cluster and divide each cluster by iteration until the basic conditions set by the system are met or each object is divided into a cluster. Therefore, this method is also called the top-to-bottom clustering method.

2.3. Cluster Analysis Model. In contrast, the operation process of the aggregation clustering method is simpler, which is more suitable for the analysis of the athletes' psychological state. Therefore, this paper adopts this method. The specific clustering process is shown in Figure 2:

- (1) Calculate the Euclidean distance between two clusters as

$$d(i, j) = \sqrt{\sum_{i=1}^m (x_{il} - x_{jl})^2}, \quad (1)$$

where $d(i, j)$ represents the distance between x_i and x_j , which are composed of m attributes; x_{il} and x_{jl} represent the l th attribute value of x_i and x_j , respectively.

(2) Construct pressure transmission.

The clustering method based on Euclidean distance is efficient, but the Euclidean distance is not transitive, that is, through $d(i, j) > t$ and $d(j, k) > t$, $d(i, k) > t$ cannot be directly deduced. In identification of athletes' stress, it is necessary to distinguish the pressure by ordinal utility theory, so that the transmission of pressure must be ensured.

Assuming that n object samples for $\{u_1, u_2, \dots, u_n\}$, and each object is m attributes which are set as $\{a_1, a_2, \dots, a_m\}$, and the i th object has the property of $u_i = \{x_{i1}, x_{i2}, \dots, x_{in}\}$. Then the distance between x_{ik} and x_{jk} of the k th attribute of u_i and u_j is

$$d_k(i, j) = \frac{|x_{ik} - x_{jk}|}{a_{k \max} - a_{k \min}}. \quad (2)$$

Among them, $a_{k \max}$ and $a_{k \min}$, respectively, represent the maximum and minimum values of the k th attribute a_k of each object.

(3) Calculate the similarity of attributes.

The similarity of each attribute of object u_i and u_j is

$$d(i, j) = \frac{\sqrt{\sum_{l=1}^m d_k^2(i, j)}}{m}, \quad (3)$$

where, $d(i, j)$ represents the distance between x_i and x_j , which are composed of m attributes; x_{il} and x_{jl} represent the l th attribute value of x_i and x_j , respectively.

$$s(i, j) = 1 - d(i, j), \quad (4)$$

where, $d(i, j)$ represents the distance between x_i and x_j .

(4) Construct similarity matrix.

The transitive closure $T = T(R)$ of similarity matrix S is obtained by the quadratic method in fuzzy mathematics.

(5) Obtain a clustering result.

The corresponding clustering results can be obtained by establishing the system clustering graph based on T and setting a threshold value for interception.

2.4. Identification of Athletes' Psychological Pressure. The psychological conditions of athletes in different categories of events are selected as basic samples, and the scores of psychological pressures are taken as attributes. The above clustering analysis model is used to analyze the psychological pressures of athletes, so as to identify the clustering results of various pressures. The formula of identification is

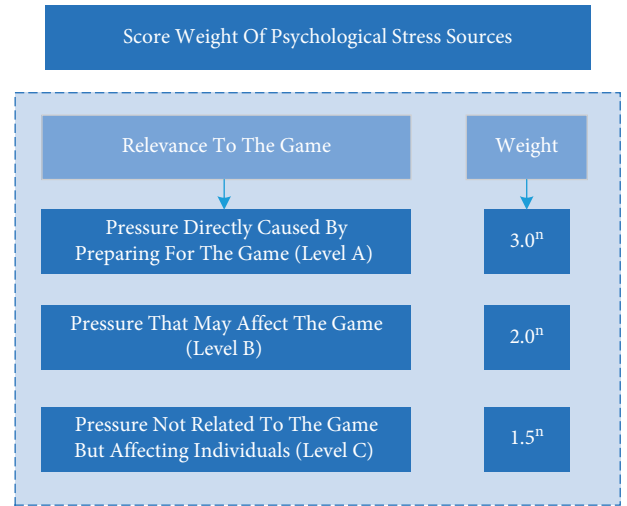


FIGURE 3: Score weight of psychological stress sources.

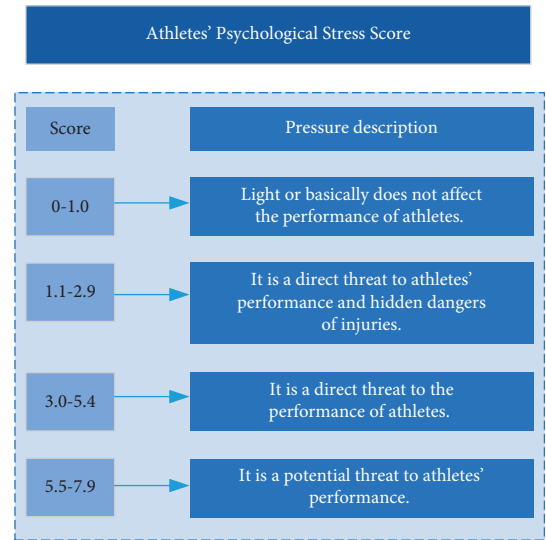


FIGURE 4: Score of athletes' psychological stress.

$$Q = \frac{(\sum_{i=1}^m w_i e_i)}{\sum_{i=1}^m w_i}, \quad (5)$$

where m represents the type of pressure source, w_i represents the score weight from sources of category i , which is directly related to its impact on performance. The stronger the correlation between psychological stress and the performance of the field, the higher the weight, otherwise, the lower the weight. According to "Psychological Instruction Manual for Active Athletes," the weights are distributed and calculated in the form of index. The results are shown in Figure 3:

Among them, n represents the repeated times of the same kind of pressure in different athletes' psychological information.

The description of athletes under different psychological stress scores is shown in Figure 4:



FIGURE 5: Optimization process based on K-Means.

3. Optimized Model of Athletes' Psychological Stress Based on the K-Means Algorithm

3.1. *Optimization Process.* Because the amount of data is small, and there are many features of them, if only a clustering algorithm is used, the discrimination between data will be low. In order to obtain better initial center and time complexity, the above model is improved in a hierarchical way.

Assuming that $X = \{x_1, x_2, \dots, x_n\}$ is the data of n r -dimensional spaces. Firstly, the algorithm uses a contour coefficient to determine the approximate number of clusters. After hierarchical clustering is used to reach this level, the number of clusters and the initial center of iteration are locally adjusted, thus greatly saving the computation for clusters with more levels. In addition, when adjusting the initial center locally, the evaluation standard of intra-class similarity is adopted, the cluster with the lowest similarity is decomposed into two new clusters. In this way, the clusters with insufficient cohesion but mistakenly classified into one class can be adjusted locally, which makes the selection of initial center more reasonable and convenient for operation. The specific implementation steps are shown in Figure 5:

- (1) Data processing is carried out on the original data, and the contour coefficient is calculated. The maximum K is taken as the initial value.
- (2) Two adjacent clusters are combined by using the aggregation hierarchical clustering algorithm to form a new cluster.
- (3) The mean values of two cluster centers at the same level on the new cluster center after merging are calculated.

TABLE 1: Experimental data set.

	Size of dataset	Number of clusters
Iris	150	3
Breast cancer	300	2
Abalone data	4000	30

- (4) Repeat step (2) and step (3) until $(K - R)(0 < = R < K - 2)$ cluster (if $k = 2$, then $R = 0$).
- (5) Calculate the intra-cluster similarity of all the divided clusters, respectively.
- (6) Select the cluster with the smallest similarity in the cluster, that is, the cluster with the largest class radius, decompose the cluster and find out the sample point x_{i1} farthest from the center c_i of the class, and then select the sample point x_{i2} farthest from x_{i1} in the class.
- (7) x_{i1} , x_{i2} and other cluster centers are used as new cluster centers to make K-Means clustering again.
- (8) If the centroid changes, return to step (6), otherwise, the algorithm ends and the result is output.

It can be seen that from step (1) to step (4), the hierarchical clustering algorithm is used to cluster the original data; while from step (5) to step (6), K-Means clustering is started where the number of clusters is reselected according to the number of clusters roughly calculated by the previous hierarchical clustering algorithm, and the initial clustering center of the K-Means algorithm is selected according to hierarchical clustering. Finally, K-Means algorithm is used for secondary clustering from steps (7) to (8).

3.2. Validation of the Model

3.2.1. *The Validation Environment.* In order to verify the effectiveness of the improved algorithm, Iris data, Breast Cancer data, and Abalone data in the UCI database are selected for verification. The size of the dataset and the number of clusters are shown in Table 1.

The experiment is tested on a PC (2.4 GHz Intel CPU, 2G memory, windows7 system). The programming language is R language, which is an open source language and the operating environment for statistical analysis and drawing. But it has stronger statistical analysis and data operation (especially in vector and matrix operation) functions than C language. Therefore, in this paper, the algorithm is implemented with its powerful extended language package and function of matrix calculation [11, 12].

3.2.2. *Validation Results.* The results of clustering are compared from the aspects of operation efficiency and the aggregation degree. The comparison of CPU runtime under different models is shown in Figure 6.

It can be seen from the data that with the increase in datasets, the CPU run time increases significantly. This is because the improved algorithm uses the contour coefficient to predict the value of K in advance, and only performs

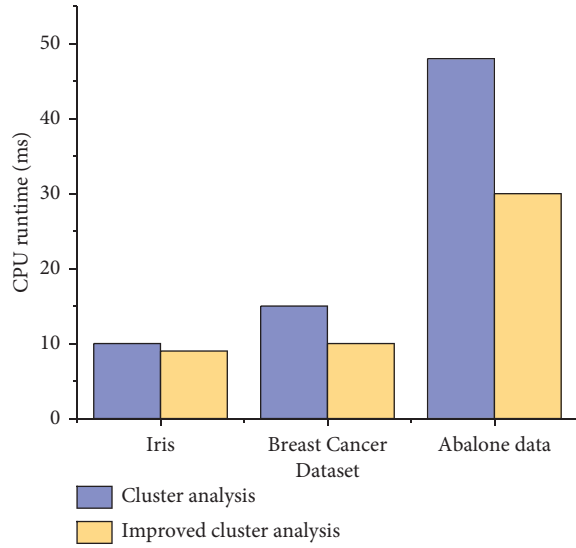


FIGURE 6: Comparison of CPU run time of different algorithms.

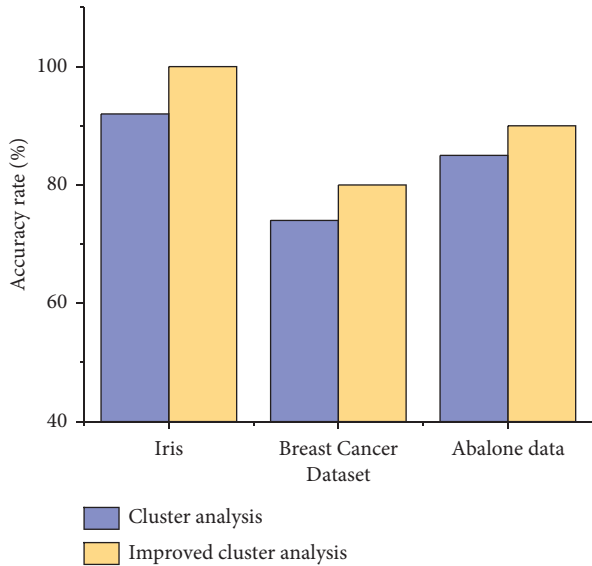


FIGURE 7: Comparison of accuracy under different algorithms.

small-scale optimization near the K value, which effectively reduces the time complexity of the algorithm.

In addition, in order to represent the clustering degree of the cluster, we evaluate the effectiveness of the algorithm through the accuracy rate, and the results are shown in Figure 7.

The accuracy of the improved clustering algorithm is higher than that of the traditional clustering algorithm, which shows that the efficiency and accuracy of the improved algorithm are significantly strengthened for small sample datasets.

4. Case Analysis

4.1. Index Selection. Taking the players in a football club as the research object where 10 players of different ages were

randomly selected for psychological stress analysis. The participants were evaluated with the stress perception scale and the psychological stress tolerance test. The original test data were standardized as the score data of [0, 10] by using the linearization processing, then the identification model of athletes' psychological pressure in Section 4 can obtain the data of psychological stress of athletes in the club, as shown in Table 2.

There are two types of pressure sources [13]: acute pressure and chronic pressure. In specific application, the pressure sources can be further subdivided, and then the corresponding analysis is conducted by using the clustering method, so as to provide reference for the team to relief athletes' pressure.

4.2. Analysis of Athletes' Psychological Pressure. Taking the score data of athletes' psychological pressure under different factors into the algorithm mentioned above, the transfer closure matrix T of each influencing factor can be calculated as follows:

$$T_1 = [1, 0.8, 0.9, 0.9, 0.8, 0.9, 0.9, 0.9, 0.9]^T$$

$$T_2 = [0.9, 1, 0.9, 0.8, 0.8, 0.8, 0.8, 0.8, 0.8]^T$$

$$T_3 = [0.9, 0.9, 1, 0.9, 0.8, 0.9, 0.8, 0.8, 0.8]^T$$

$$T_4 = [0.9, 0.9, 0.9, 1, 0.9, 0.9, 0.9, 0.8, 0.8]^T$$

$$T_5 = [0.9, 0.9, 0.9, 0.9, 1, 0.9, 0.9, 0.8, 0.8]^T$$

$$T_6 = [0.9, 0.9, 0.9, 0.9, 0.9, 1, 0.9, 0.9, 0.8]^T$$

Therefore, the system clustering diagram of this model is shown in Figure 8:

According to the transitive closure T , it is necessary to take 0.90 as the threshold value of the system clustering diagram. Thus, A1 and A2 are combined into a cluster, A4 and A5 are combined into a cluster, and A3 and A6 are formed into a cluster, respectively. Therefore, the psychological pressure of athletes in the club is shown in Table 3.

It can be seen from the above data that 67.87% of athletes' pressure comes from the outside, which is chronic pressure; while 32.13% of them comes from competitions, which is acute pressure. Generally speaking, athletes cannot fully concentrate in the game, and they are easy to be affected by off-site factors. To deal with a large proportion of off-site pressure, the organizers need to assist the team operators to introduce professional psychologists for counseling, so that athletes can focus on the competition.

Through the analysis of the example shows that the athletes clustering algorithm can realize effective pressure source identification, through the study of the automatic classification of athletes psychological pressure information, based on individual rating of athletes get event athletes overall pressure source, for the organizers to provide guidance for alleviating the psychological pressure of the athletes.

Athletes A2, A3, A6, and A9 have less pressure on training and life, which indicates that they have better control of tenacity, lower confidence, and enthusiasm in engagement. In addition, their overall relationship with coaches is better, but it is poor in terms of complementarity

TABLE 2: Psychological pressure scores of athletes under different factors.

Athletes	M1 training	M2 life	Developing M3	M4 family	M5 social networking	M6 score
A1	7.44	4.56	4.48	7.98	3.45	7.89
A2	3.15	7.38	7.26	5.01	6.38	5.06
A3	4.61	3.80	3.86	8.93	3.60	8.43
A4	7.05	4.55	8.78	4.44	4.43	6.61
A5	3.19	4.94	3.15	6.27	7.07	5.65
A6	8.42	8.29	4.55	3.72	7.31	5.61
A7	8.05	3.16	8.26	8.08	4.61	5.46
A8	8.68	6.63	5.90	6.10	6.53	6.53
A9	8.77	7.84	7.34	5.88	4.92	8.81
A10	7.87	3.13	8.98	8.36	6.53	7.68

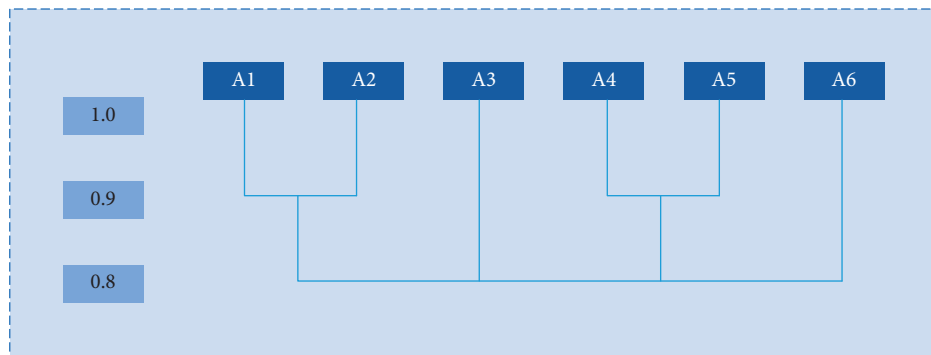


FIGURE 8: System cluster diagram.

TABLE 3: Analysis of athletes' psychological pressure.

Athletes	Stress score	Relevance
A1	0.6	B
A2	1	B
A3	1	A
A4	0.7	C
A5	0.7	B
A6	1	C
A7	0.8	A
A8	0.6	A
A9	1	B
A10	0.7	C

that mainly refers to the state of athletes under the guidance. The overall stress level of these athletes is relatively low which shows that they have better psychological quality, higher happiness, and social support.

5. Conclusion

In this paper, an analysis model of athletes' psychological pressure is constructed by the clustering algorithm, and the source of athletes' psychological pressure is identified quantitatively. The validation results show that the optimized psychological pressure analysis model can effectively reduce the time complexity of the algorithm, improve its operation efficiency and accuracy, and can better adapt to the test of psychological stress. In addition, the result of case analysis shows that the overall stress level of athletes A2, A3, A6, and A9 is relatively low, which indicates that they have

better psychological quality, higher happiness, and social support. To sum up, the model realizes the automatic evaluation of athletes' pressure and can be used as an assistant tool for team doctors or psychologists. From a practical point of view, the pressure source identification tool constructed in this paper is practical in large-scale competitions, and the identification of athletes' pressure sources can help each team to pretest athletes' psychological pressure, and then make targeted adjustments, which is conducive to maximizing athletes' potential for competition.

Data Availability

The dataset is available from the corresponding author upon request.

Conflicts of Interest

The authors declare that they have no conflicts of interest.

References

- [1] P. Zhou and X. Zhao, "Research on the factors influencing the Psychological change of middle school football players and its regulation Methods," *Youth Sports*, vol. 14, no. 03, pp. 57-58, 2022.
- [2] J. Zaragoza, G. Tinsley, S. Urbina et al., "Effects of acute caffeine, theanine and tyrosine supplementation on mental and physical performance in athletes," *Journal of the International Society of Sports Nutrition*, vol. 16, no. 1, p. 56, 2019.

- [3] S. Yang, *Mental Health Status and Intervention of High-Level Athletes*, Shanghai Institute of Physical Education, Shanghai, China, 2015.
- [4] C. Chen, J. Li, and Y. Wang, "Comparative study on stressors and coping styles of athletes in different events," *China Sports Science and Technology*, vol. 45, no. 1, pp. 46–50, 2009.
- [5] K. Benrabah, M. Bennadja, and K. M. Fayçal, "The level of community cohesiveness under psychological pressure and control center for emerging football players U17," *Acta Facultatis Educationis Physicae Universitatis Comenianae*, vol. 60, no. 1, pp. 44–54, 2020.
- [6] S. Shen, "Analysis of the correlation between social support emotion coping and psychological fatigue of basketball players," *Journal of Wuhan Institute of Physical Education*, vol. 49, no. 11, pp. 76–81, 2015.
- [7] J. He, "Application of fuzzy matter-element clustering method in physical education teaching evaluation," *Sports Science Research*, vol. 16, no. 01, pp. 72–75, 2012.
- [8] H. Xu, "Identification of stress sources of basketball players based on Hierarchical system clustering," *Journal of Dali University*, vol. 5, no. 12, pp. 75–79, 2020.
- [9] J. Yang, "A survey of clustering analysis algorithms for data mining," *Communication World*, vol. 33, no. 16, p. 291, 2017.
- [10] T. Kono and S. Katsura, "Clarification of fundamental motion using hierarchical clustering and graph theory," *IEEJ Journal of Industry Applications*, vol. 5, no. 2, pp. 108–116, 2016.
- [11] Q. Zhang and Y. Liu, "Overview of runtime verification technology of C language memory security," *Modern Information Technology*, vol. 5, no. 23, pp. 84–87, 2021.
- [12] L. Research, "On the role of good psychological quality in basketball matches [J]," *Contemporary Sports Science and Technology*, vol. 8, no. 19, pp. 1–3, 2018.
- [13] Ju Gan, "An empirical study on the influence of "HISRT+LBFRT" comprehensive training on the explosive force of male basketball players in Chinese universities," *Journal of Shenyang Sport University*, vol. 38, no. 1, pp. 116–122, 2019.

Retraction

Retracted: Data Sharing Method of College Dance Teaching Resource Database Based on PSO Algorithm

Computational Intelligence and Neuroscience

Received 25 July 2023; Accepted 25 July 2023; Published 26 July 2023

Copyright © 2023 Computational Intelligence and Neuroscience. This is an open access article distributed under the Creative Commons Attribution License, which permits unrestricted use, distribution, and reproduction in any medium, provided the original work is properly cited.

This article has been retracted by Hindawi following an investigation undertaken by the publisher [1]. This investigation has uncovered evidence of one or more of the following indicators of systematic manipulation of the publication process:

- (1) Discrepancies in scope
- (2) Discrepancies in the description of the research reported
- (3) Discrepancies between the availability of data and the research described
- (4) Inappropriate citations
- (5) Incoherent, meaningless and/or irrelevant content included in the article
- (6) Peer-review manipulation

The presence of these indicators undermines our confidence in the integrity of the article's content and we cannot, therefore, vouch for its reliability. Please note that this notice is intended solely to alert readers that the content of this article is unreliable. We have not investigated whether authors were aware of or involved in the systematic manipulation of the publication process.

Wiley and Hindawi regrets that the usual quality checks did not identify these issues before publication and have since put additional measures in place to safeguard research integrity.

We wish to credit our own Research Integrity and Research Publishing teams and anonymous and named external researchers and research integrity experts for contributing to this investigation.

The corresponding author, as the representative of all authors, has been given the opportunity to register their agreement or disagreement to this retraction. We have kept a record of any response received.

References

- [1] X. ZhuGe and H. Cao, "Data Sharing Method of College Dance Teaching Resource Database Based on PSO Algorithm," *Computational Intelligence and Neuroscience*, vol. 2022, Article ID 2162981, 9 pages, 2022.

Research Article

Data Sharing Method of College Dance Teaching Resource Database Based on PSO Algorithm

Xulong ZhuGe¹ and Haibin Cao² 

¹*School of Preschool Education, Linyi Vocational College, Linyi 276000, China*

²*Jiangsu Normal University Academy of Music, Jiangsu, Xuzhou 221116, China*

Correspondence should be addressed to Haibin Cao; 18409009@masu.edu.cn

Received 23 May 2022; Revised 14 June 2022; Accepted 4 July 2022; Published 17 August 2022

Academic Editor: Le Sun

Copyright © 2022 Xulong ZhuGe and Haibin Cao. This is an open access article distributed under the Creative Commons Attribution License, which permits unrestricted use, distribution, and reproduction in any medium, provided the original work is properly cited.

Aiming at the problems of long sharing time, low accuracy, recall, and F1 value in the traditional data sharing method of college dance teaching resource database, a data sharing method of college dance teaching resource database based on PSO algorithm is proposed. Multiple regression KNN method is used to eliminate the data noise of college dance teaching resource database, so as to obtain the missing value and complete the filling of incomplete data of college dance teaching resource database. Taking the preprocessed data as the basic element of transmission object statistics and analysis, establish the data transmission self-service channel of college dance teaching resource database, calculate the similarity of the data according to the unequal length sequence, and use the partial least square method to complete the feature extraction of the resource database data. According to the feature extraction results, particle swarm optimization algorithm is adopted to share the data of college dance teaching resource database. The simulation results show that the accuracy, recall, and F1 value of the data sharing method of college dance teaching resource database based on PSO algorithm are high, and the sharing time is short.

1. Introduction

With the development of information technology in China and the global trend towards interconnection, information resources have received unprecedented attention and are listed as equally important strategic resources as energy resources and material resources. Information resources are of great significance to promote socioeconomic and social development because of their unique characteristics of easy sharing, unlimited dissemination, reuse, and zero pollution [1]. Since entering the twenty-first century, the application of information technology in education and teaching has attracted more and more attention. The degree of educational informatization also occupies an important position in the measurement of national educational modernization. Improving the quality of higher education is not only the need of the development law of higher education itself, but also the need of building an innovative country. Through unremitting efforts, China has made certain achievements in

the construction of educational information infrastructure. Educational informatization has been incorporated into the overall development of national informatization, and the application of informatization in education has been qualitatively improved. Among them, educational informatization in colleges and universities is an extremely important one [2].

How to fully and effectively develop and utilize teaching resources, turn disadvantages into advantages, enhance professional school running characteristics, improve education and teaching quality, and cultivate qualified dance professionals is an important issue in front of us. At present, the development of multimedia technology is changing with each passing day. We rely more and more on multimedia technology in our daily life and work. There are more and more dance videos. Through multimedia, college dance teaching is digitized, and the way of expression is more and more intuitive, both in content and in information [3, 4]. In addition, due to the development and popularization of

network and computer, many video websites, such as iqiyi, Tudou, Tencent, Sohu, and Youku, have many university dance teaching resource databases on these websites, but how to manage these videos has become the key research direction of multimedia information experts [5]. The composition of college dance teaching resource database is very complex, with a large amount of information, which is very different from the general form of text information processing. How to import high-definition dance videos into the video website resource database and let students share the data in the college dance teaching resource database is an urgent problem to be solved [6, 7].

Reference [8] puts forward the storage and sharing method of digital media materials through MVC mode, and [9] puts forward the information-based teaching resource sharing method through multimedia technology. However, the accuracy, recall, and F1 value of the above two methods for teaching resource data sharing are low, resulting in poor sharing effect and short time of teaching resource sharing, resulting in low sharing efficiency. In view of the problems existing in the above methods, this paper proposes a data sharing method of college dance teaching resource database based on PSO algorithm. PSO is the abbreviation of particle swarm optimization algorithm. It is a random optimization technology based on population. Particle swarm optimization simulates the swarm behavior of insects, herds, birds, and fish. These groups look for food in a cooperative way. Each member of the group changes its search mode by learning its own experience and the experience of other members. By collecting the data of college dance teaching resource database and processing the collected data, the data of college dance teaching resource database is shared through PSO algorithm according to the processing results. The experimental results show that this method can share the data of college dance teaching resource database quickly and accurately, and it lays a foundation for improving the quality of dance teaching in colleges and universities.

2. Data Sharing Method of College Dance Teaching Resource Database Based on PSO Algorithm

2.1. Data Preprocessing of Dance Teaching Resource Database in Colleges and Universities. Since the inventory of dance teaching resources in colleges and universities is in incomplete data, this paper uses multiple regression KNN method to fill in the incomplete data of dance teaching resource database in colleges and universities [10–12], and the steps are as follows:

First, initialize the data of college dance teaching resource database, and calculate the classification interval in college dance teaching resource database. The expression is as follows:

$$F = \frac{e \cdot x_i + bg}{s}. \quad (1)$$

In formula (1), e represents the interval value between data and data in the dance teaching resource database

of colleges and universities, b represents the optimal classification function, s represents the objective function of classification, and x_i represents the discriminant function of the i -th data [13].

Second, calculate the Euclidean distance between the target data in the college dance teaching resource database and all data records in the complete value data matrix, and its expression is as follows:

$$d_i = \sqrt{(z_i - o)^t (z_i - o)}. \quad (2)$$

In formula (2), z_i represents the nearest neighbor parameter of the i -th nearest neighbor, and o represents the target data.

Third, the Euclidean distance is calculated through the above process [14]. The data record with the smallest Euclidean distance is selected as the nearest neighbor of the target data and stored in the response position of the data matrix. Fourth, select the data record with the smallest nearest Euclidean distance from each target data from the complete value data matrix and store it in the data group; Fifthly, initialize the nearest neighbor importance of each target data nearest neighbor, and its expression is as follows:

$$R = \frac{F}{d_i(z_i, B)}. \quad (3)$$

In formula (3), R represents the importance of nearest neighbors and B represents the judgment parameter of data importance [15].

Sixth, eliminate the nearest neighbor noise of the target data. The specific judgment criteria are as follows:

$$W = \frac{M}{R/d(x, x_i)}. \quad (4)$$

In formula (4), V represents the noise judgment result of the i nearest neighbor of the target data record, and M represents the noise elimination parameter [16].

Judge the nonnoise nearest neighbor of the target data according to the above calculation, eliminate the nearest neighbor noise, and obtain the missing value. On this basis, map the data from the original feature space to a new feature space through an appropriate nonlinear function, and its expression is

$$w^* = \sum_i^{i=1} W \alpha_i^* y_i x_i. \quad (5)$$

In formula (5), y_i represents the discriminant function and α_i^* represents the set threshold.

Seventh, based on the completion of the above data space mapping, the incomplete data of college dance teaching resource database is estimated and filled according to the missing value [17]. In the process of processing, it should be noted that, in most cases, the component data in the database is different; that is, each

row of data in the database is different data, which is expressed as

$$Q = \begin{pmatrix} x_{11} & x_{12} & \cdots & x_{1D} \\ x_{21} & x_{22} & \cdots & x_{2D} \\ \vdots & \vdots & \ddots & \vdots \\ x_{n1} & x_{n2} & \cdots & x_{nD} \end{pmatrix}. \quad (6)$$

The above matrix is the observation matrix, n represents the number of rows, that is, the sample size, and D represents the number of columns, that is, the number of parts of the component data [18].

Since the fixed sum of each observation value in the data is different, in order to fill the accuracy, set the adjustment factor, which is expressed as

$$f_{lj} = \frac{V}{w^* Qc * x_{jk}}. \quad (7)$$

In formula (7), x_{jk} represents the equilibrium component of different observed values, c represents the adjustment factor, and V represents the missing value. Through the above process adjustment, the consistency of component data in college dance teaching resource database can be ensured [19]. Finally, the incomplete information of college dance teaching resource database is filled, and its expression is

$$\bar{g} = \sum_k^{i=1} \frac{w_i}{x f_{lj}}. \quad (8)$$

In formula (8), x represents the value of the nearest neighbor response position, and $\sum_k^{i=1} w_i$ represents the missing data judgment parameter.

Continue to iterate the above steps until all the incomplete data in the dance teaching resource database of colleges and universities are filled, so as to complete the filling of the incomplete data in the dance teaching resource database of colleges and universities through the above process [20].

2.2. Establishment of Data Transmission Self-Service Channel.

The preprocessed college dance teaching resource database data can be used as the basic element of transmission object statistics and analysis and can also be used as the collection object and statistical caliber of transmission self-service channel [21]. Users can collect from any number of angles and define the data object of college dance teaching resource database according to the occurrence of the preprocessed college dance teaching resource database data, as shown in Table 1.

According to Table 1, according to the definition of dance teaching resource objects in colleges and universities, the transmission object categories are divided. Each transport unit can use these transport object definitions, but only the data belonging to the respective transport unit can be seen. For the cross-domain data center, the expression form

of the dance teaching resource catalog is not important, and the openness and detailed content are the standards to measure the quality of data [22]. The relative value of dance teaching resources lies in its openness. While ensuring the security of dance teaching resources, the public should be aware of the dance teaching resource database data. The sharing of dance teaching resource database data is built on the openness of data. If there is no flow, the value of data will be generated at a very slow speed. Therefore, on the basis of data security, the catalogue of dance teaching resources in colleges and universities should be open to stakeholders and value creators [23]. Therefore, the data transmission interface is described according to the data transmission object definition of college dance teaching resource database, as shown in Table 2.

According to the format in Table 2, set up the self-service channel interface for the data transmission of the university dance teaching resource database. By mobilizing the university dance teaching resource object to define the category, after the module receives the data of the teaching resource database, call the back-end interface, and update the records in the data transmission of the teaching resource database. Finally, the index module is called to complete the establishment of the data transmission self-service channel of the dance teaching resource database in colleges and universities [24].

2.3. Feature Extraction Method of Resource Database Data.

The data similarity problem in the university dance teaching resource database is transformed into the measurement problem of data. The unequal length sequence query matrix in the university dance teaching resource database is set as C , the reference matrix is marked with K , and the measurement value is marked with α . The corresponding relationship between the matrices is as follows:

$$|C_i| < |K_i|. \quad (9)$$

In the formula, K_i and K_i both represent unequal length sequences of college dance teaching resource database data. According to the unequal length sequence relationship obtained above, the data of college dance teaching resource database is traversed and slid along the window units with a long sequence by using the sliding window theory. Set K_i as the corresponding sequence of C_i , and the subsequence acquisition results between them are as follows:

$$\begin{cases} Z(Q)_j = Q_i(j, j + |C_i| - 1), \\ j = 1, 2, \dots, |Q_i| - |C_i| + 1. \end{cases} \quad (10)$$

In the formula, $Z(Q)_j$ represents the acquired subsequence window, $K_i(j, j + |C_i| - 1)$ represents the j subsequence in the window, $|C_i|$ represents the window length, and i and j are nonzero constants [25].

Based on the above calculation results, calculate the sequence sliding similarity of the window corresponding to the dance teaching resource database data in colleges and universities. The process is as follows:

TABLE 1: Definition of data transmission object of dance teaching resource database in colleges and universities.

Object category	Object description	Object type	Object mode
10	Dance teaching resources in colleges and universities	User	List
A	A	User	Descriptive text
BESTACT	Activity	User	List
CESTCATE	Category	User	List
BESTPLAM	Platform	System	List
Exp	Dance species	System	List
PROJECET	Theme	User	Descriptive text
SQL	Number of resources	System	List
BESTSEAS	Project	User	List

TABLE 2: Data transmission interface information of dance teaching resource database in colleges and universities.

Format	Interface type	Null value allowed	Describe the results
AAM	String	No	File name
AAS	List	No	Information package
ABF	String	Yes	Binary font
ABK	List	No	Backup files

$$S_{ei}(C_i, Z(C_i)_j) = 1 - \frac{(D_{ij}(C_i, Z(C_i)_j))}{D_{\max}}. \quad (11)$$

In the formula, $S_{ei}(C_i, Z(C_i)_j)$ represents the sliding similarity vector of the data sequence of the university dance teaching resource database, $(D_{ij}(C_i, Z(C_i)_j))$ represents the distance between the reference sequence C_i and the sliding sequence, and D_{\max} represents the maximum distance.

Based on the similarity of the data of college dance teaching resource database obtained above, the partial least square method is used to complete the feature extraction of college dance teaching resource database [26].

It is set that there are m pairs of data samples in the college dance teaching resource database B , marked in the form of (P, Q) , and $(P, Q) = \{(p, q)\}_{i=1}^m \in R$. The mapping direction of the college dance teaching resource database is expressed in β and χ . The mapping projection is as follows:

$$\begin{cases} p^* = P\beta, \\ q^* = Q\chi. \end{cases} \quad (12)$$

In the formula, p^* and q^* , respectively, represent the mapped projection area of dance teaching resource database in colleges and universities. Based on the above calculation results, the maximization function criterion of college dance teaching resource database is established. The process is as follows:

$$J_{\text{pls}}(\beta, \chi) = \frac{(\beta^T H_{p,q} \chi)^2}{[\beta^T \beta][\chi^T \chi]}. \quad (13)$$

In the formula, $J_{\text{pls}}(\beta, \chi)$ represents the criterion function of the established college dance teaching resource database, $H_{p,q}$ represents the covariance matrix, and T represents the function coefficient. According to the above criterion function, formulate the corresponding data

orthogonal constraints, mark the $\beta_k^T \beta_i = \chi_k^T \chi_i = 0$ form, and use the Lagrange multiplier to convert the feature extraction problem of the data of the university dance teaching resource database into the equation form. The process is as follows:

$$\begin{cases} H_{p,q} H_{q,p} \beta = \delta^2 \beta, \\ H_{q,p} H_{p,q} \chi = \delta^2 \chi. \end{cases} \quad (14)$$

In the formula, $\delta^2 \beta$ and $\delta^2 \chi$ represent the characteristic equation of transformation. Set the mapping vector of the university dance teaching resource library as r , the number of relative mapping vectors does not exceed group d ($\leq r$), set the nonzero eigenvalue of the university dance teaching resource library as δ_j^2 , use onipils algorithm to complete the optimal mapping area of the first pair of mapping data vectors in the University Dance Teaching Resource Library, and obtain the irrelevant constraints of the data mapping vector. The process is as follows:

$$\begin{cases} \beta_{k+1}^T H_p \beta_i = \chi_{k+1}^T H_q \chi_i = 0, \\ i = 1, 2, \dots, k. \end{cases} \quad (15)$$

In the formula, H_p represents the data variance value in the β direction, H_q represents the covariance difference in the χ direction, T represents the function coefficient, and k and i represent the vector parameters, respectively.

Integrate the mapping parameters of the university dance teaching resource database data into D_p and D_q forms, and complete the solution and calculation of the characteristic equation of the university dance teaching resource database data according to the above calculation results. The results are as follows:

$$\begin{cases} FH_{p,q} H_{q,p} \beta_{k+1} = \delta \beta_{k+1} \times F \times I, \\ LH_{q,p} H_{p,q} \chi_{k+1} = \delta \chi_{k+1} \times L \times I. \end{cases} \quad (16)$$

In formula (16), $\delta \beta_{k+1}$ and $\delta \chi_{k+1}$ represent the calculation results of the data characteristics of the dance teaching resource database in colleges and universities, F and L represent the equation parameters, and I represents the constant coefficients. Finally, according to the calculation results of the data characteristic equation of the university dance teaching resource database, the data characteristic vector value of the university dance teaching resource database is extracted to provide important information for the

data sharing of the university dance teaching resource database.

2.4. Data Sharing of Dance Teaching Resource Database in Colleges and Universities

2.4.1. PSO Algorithm. Particle swarm optimization (PSO) algorithm is proposed by Kennedy and Eberhart. Its algorithm idea is to study and simulate the foraging behavior of birds. The bird in the bird group is compared to the particle in the particle group, which represents the candidate solution of the problem. The flight space of birds corresponds to the search space of particle group, and the process of birds looking for food corresponds to the process of looking for the optimal solution. All particles are randomly assigned to the search space as the initial state of the algorithm. The total number of particles is recorded as N and the dimension of the search space is recorded as D . Each particle includes a D -dimensional velocity vector $V_i = (v_{i1}, v_{i2}, \dots, v_{iD})$ and a D -dimensional position vector $X_i = (x_{i1}, x_{i2}, \dots, x_{iD})$. By learning from its own individual extreme value $pbest_i = (p_{i1}, p_{i2}, \dots, p_{iD})$ and the global extreme value $gbest_i = (g_1, g_2, \dots, g_D)$ of the population, the particle velocity and position are updated until the optimal solution is found. The speed and position of particles are updated as follows:

$$\begin{aligned} V_i^{t+1} &= wV_i^t + C_1 * \text{Rand}_1() \times (pbest_i - X_i^t) \\ &\quad + C_2 * \text{Rand}_2() \times (gbest_i - X_i^t), \quad (17) \\ X_i^{t+1} &= X_i^t + V_i^{t+1}. \end{aligned}$$

In the formula, V_i^t, V_i^{t+1} represents the velocity of the i -th particle in the t -th and $t+1$ -th iterations, respectively; w represents the inertia weight, which is the coefficient to maintain the original speed; X_i^t, X_i^{t+1} represents the position of the i -th particle in the t -th and $t+1$ -th iterations, respectively; C_1 is the weight of the particle to learn its own individual extreme value, indicating the particle's understanding of itself, which is usually assigned as 2; C_2 is the weight of the particle to learn the global extreme value of the population, which indicates the particle's understanding of the whole population. It is usually assigned as 2; $\text{Rand}_1(), \text{Rand}_2()$ is the random number in the interval (0, 1); $pbest_i$ is the individual extreme value of the i -th particle, which is the historical optimal value found by the particle, also known as individual optimal; $gbest_i$ is the global extremum of particle swarm, which is the group optimal value found by the whole particle swarm, also known as global optimal.

2.4.2. Data Sharing Based on PSO Algorithm. The particle swarm optimization algorithm is adopted for fuzzy iteration and adaptive learning in the process of data sharing of college dance teaching resource database, and the particle swarm mutation optimization control model for data sharing of college dance teaching resource database is established. The tightness index of data sharing of college

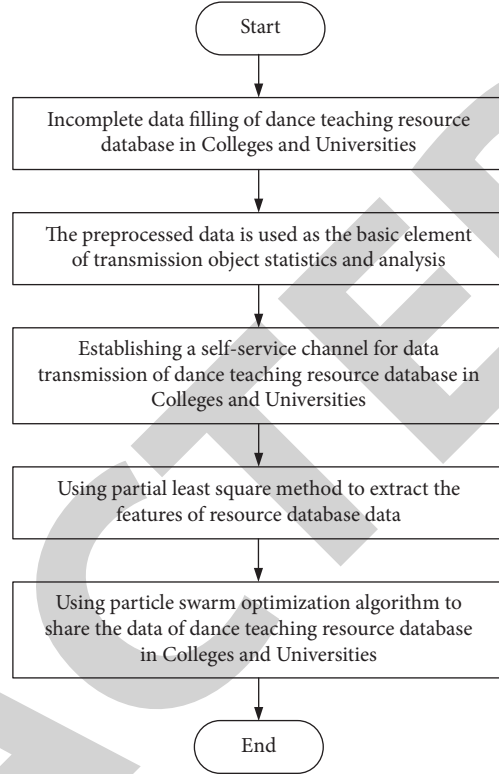


FIGURE 1: Specific flow chart of data sharing method of college dance teaching resource database based on PSO algorithm.

dance teaching resource database is (RT_1, RT_2) . The k associated node is selected for particle swarm evolution of data sharing of college dance teaching resource database, Statistical probability distribution of data sharing particle swarm variation in college dance teaching resource database:

$$p_D = k \frac{4}{3} \pi R X_i^{t+1}. \quad (18)$$

In the formula, R is the particle swarm variation dimension of university dance teaching resource database data sharing. The quantitative feature decomposition of university dance teaching resource database data sharing is carried out by using individual extreme value iteration technology, and the following results are obtained:

$$R_k = F_{Z_{\min}} p_D. \quad (19)$$

Using the adaptive optimization technology, the redundant individual search for the data sharing of the university dance teaching resource database is carried out, and the variation individual extreme value $F_{Z_{\min}}$ of the university dance teaching resource database data is obtained. According to the individual differences in the process of particle swarm evolution, the shortest link iteration technology is adopted to obtain the feature mining output of the university dance teaching resource database data:

$$S(x) = \frac{F_{Z_{\min}}}{R_k}. \quad (20)$$

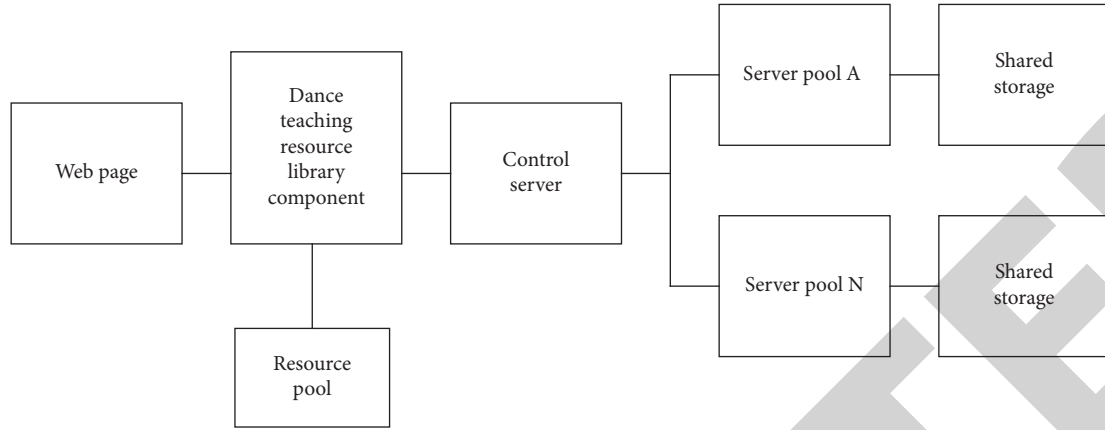


FIGURE 2: Physical architecture of teaching resource database.

TABLE 3: Experimental parameter setting.

Name	Parameter
The server	Intel Xeon processor e5430266ghz, ddr3-1336mhz SSD500G
Client	Intelcpu3. 06 GHz, memory above 2G, hard disk
Server operating system	Windows2008R2
Client operating system	Win7
Database	Oracle
Database server	192.168. 44.254
Test tools	Mercury loadrunner6
Accuracy	95-100%
Recall	95-100%
F1 value	0.95-1

To sum up, PSO algorithm is used to design the data sharing of dance teaching resource database in colleges and universities.

Let s_k and a_k be the characteristic quantity of association rule information of college dance teaching resource database data, and the visual characteristic quantity of each particle in the search space is $\phi(w)$. Randomly select z uniform college dance teaching resource database data visual analysis nodes to locate the optimal location of college dance teaching resource database data sharing, and obtain the optimal location distribution:

$$p_z = \phi(w)a_k(1 - s_k). \quad (21)$$

The improved inertia weight analysis method is adopted to carry out the sharing scheduling of college dance teaching resource database data. The particle is near the optimal particle. The optimal characteristic of the adaptation function of college dance teaching resource database data is extracted, and c_1, c_2 is set as the initial value to obtain the optimized data sharing output result:

$$\alpha = \frac{c_1 + c_2}{p_z}. \quad (22)$$

According to the individual differences of particle swarm optimization, the classification and reorganization in the process of data sharing of college dance teaching resource database are carried out. The data visual sharing design of

college dance teaching resource database is carried out by using particle swarm optimization algorithm and association mining method.

To sum up, the specific flow of the data sharing method of college dance teaching resource database based on PSO algorithm proposed in this paper is shown in Figure 1.

According to Figure 1, it is necessary to complete the incomplete data filtering of the university dance teaching resource database, and then the preprocessed data is used as the basic element for the statistics and analysis of the transmission object, so as to build a self-service channel for the data transmission of the university dance teaching resource database. Finally, the partial least square method is used to extract the characteristics of the resource database data, and complete the data sharing of the university dance teaching resource database based on the particle swarm optimization algorithm, so as to realize the process.

3. Simulation Experiment Analysis

In order to verify the effectiveness of the data sharing method of college dance teaching resource database based on PSO algorithm in practical application, a college dance teaching resource is selected as the experimental object for a simulation experiment analysis. The physical structure of college dance teaching resource library is shown in Figure 2.

Under the above environment, set the experimental parameters, as shown in Table 3.

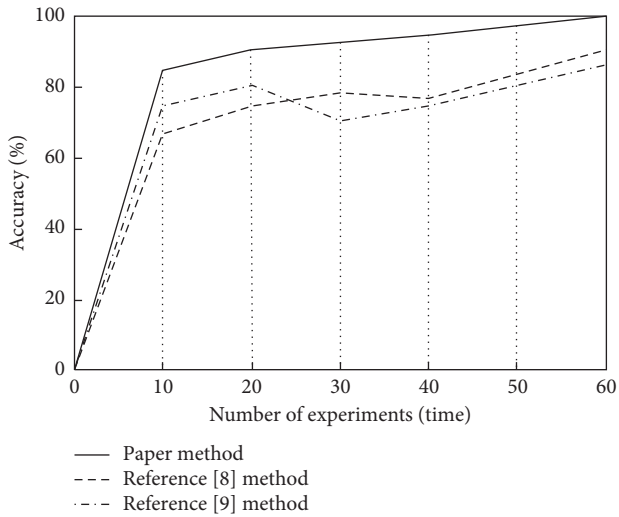


FIGURE 3: Accuracy comparison results.

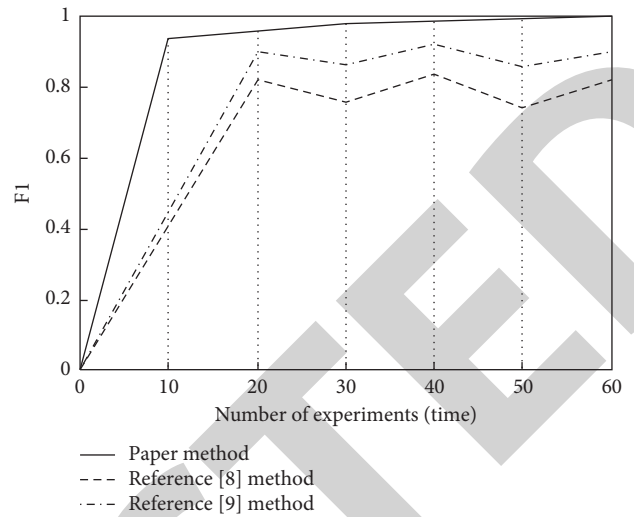


FIGURE 5: F1 value comparison results.

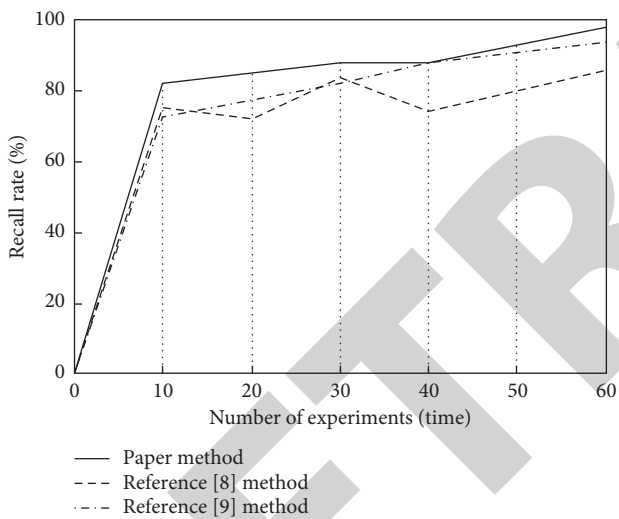


FIGURE 4: Comparison results of recall rate.

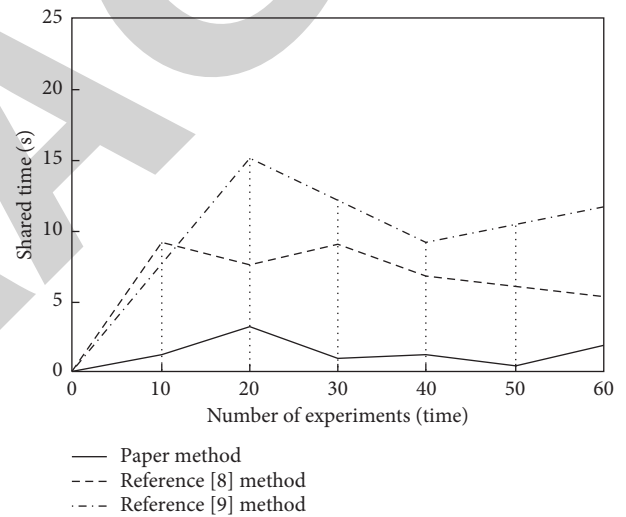


FIGURE 6: Comparison results of data sharing time of dance teaching resource database in colleges and universities.

This paper selects the accuracy rate, recall rate, and F1 value as the experimental indicators and uses the data sharing method of college dance teaching resource database based on PSO algorithm and [8] and [9] to carry out the experimental test. The test results are shown in Figures 3–5.

According to Figure 3, the accuracy of the data sharing method of college dance teaching resource database based on PSO algorithm proposed in this paper can reach 100%, and the recall rate and F1 value are high, while the accuracy, recall rate, and F1 value of [8] and [9] are not ideal. The reason is that the algorithm in this paper establishes a data transmission self-service channel and takes the pretreated college dance teaching resource database data as the basic element for the statistics and analysis of transmission objects. Users can collect from any number of angles according to the occurrence of the pretreated college dance teaching resource database data. Set up the self-service channel

interface for the data transmission of the university dance teaching resource database. By mobilizing the university dance teaching resource object to define the category, after the module receives the teaching resource database data, call the back-end interface, operate the records in the data transmission of the teaching resource database, and finally call the index module, which is conducive to improving the performance to a certain extent.

In order to further verify the effectiveness of this method, the data sharing method of college dance teaching resource database based on PSO algorithm, [8] and [9] proposed in this paper are used to compare and analyze the data sharing time of college dance teaching resource database. The comparison results are shown in Figure 6.

According to Figure 6, the data sharing time of university dance teaching resource database based on PSO algorithm proposed in this paper is within 4S, which is shorter than

that of university dance teaching resource database in [8] and [9]. The reason is that this algorithm proposes data sharing based on PSO algorithm, adopts particle swarm optimization algorithm to carry out fuzzy iteration and adaptive learning in the process of data sharing of university dance teaching resource database, and establishes a particle swarm mutation optimization control model for data sharing of university dance teaching resource database, which is conducive to reducing the sharing time.

To sum up, the research algorithm has good performance. Taking the resource sharing platform as the integration of college dance teaching resource library, the new development of teachers' and learners' autonomous learning ability, research ability, and cooperation ability has been strengthened, and teaching resources have attracted more and more attention.

4. Conclusion

This paper designs the data sharing method of dance teaching resource database in colleges and universities through PSO algorithm. It is best to verify the effectiveness and practicability of this method through experimental comparison. Taking the resource sharing platform as the integration of dance teaching resource library in colleges and universities and strengthening the new development of autonomous learning ability, research ability, and cooperation ability of teachers and learners, teaching resources have attracted more and more attention and have good performance.

The data sharing method of university dance teaching resource database based on PSO algorithm designed in this study has preliminarily realized the basic functions designed in advance, but due to the limitation of technology level and time, the method still has many shortcomings. Through reflection and summary of the whole development and trial operation process, the following two shortcomings are highlighted, which are also the direction for improvement in the future:

- (1) Although corresponding support is provided for various activities using the teaching resource sharing method, sufficient personalized support is not provided for the individual differences of users. Therefore, how to provide adequate personalized support is a key direction of follow-up research.
- (2) There is no strong support for different types of dance teaching resources in universities. This is another focus of the subsequent development of this method. In the future study and work, I will continue to study and discuss the above problems, so as to further develop and improve the teaching resource sharing method theory and teaching resource sharing platform in colleges and universities.

Data Availability

The raw data supporting the conclusions of this article will be made available by the authors, without undue reservation.

Conflicts of Interest

The authors declare that they have no conflicts of interest regarding this work.

References

- [1] J. Ma, "Design of multimedia sharing system for multi-node networked intelligent teaching," *Modern electronic technology*, vol. 42, no. 14, pp. 157–160, 2019.
- [2] S. Yao, D. Li, A. Yohannes, and H. Song, "Exploration for network distance teaching and resource sharing system for higher education in epidemic situation of COVID-19," *Procedia Computer Science*, vol. 183, no. 1, pp. 807–813, 2021.
- [3] S. Hu, Y. Liu, and S. Wang, "Teaching exploration of case-based data modeling optimization for database system," *Open Journal of Social Sciences*, vol. 8, no. 3, pp. 514–521, 2020.
- [4] F. Zhao, "Research on distributed multi-spatial database information remote sharing method," *China Computer & Communication*, vol. 31, no. 17, pp. 146–147, 2019.
- [5] K. A. . Cooper, "Data sharing attitudes and practices in the plant sciences: results from a mixed method study," *Journal of Agricultural & Food Information*, vol. 18, no. 8, pp. 37–58, 2021.
- [6] L. Yin, J. Feng, S. Lin, and Z. Cao, "A blockchain-based collaborative training method for multi-party data sharing in Space-Ground Integrated Network," *Computer Communications*, vol. 173, no. 6, pp. 28–32, 2021.
- [7] K. M. Merz, R. Amaro, Z. Cournia et al., "Editorial: method and data sharing and reproducibility of scientific results," *Journal of Chemical Information and Modeling*, vol. 60, no. 12, pp. 5868–5869, 2020.
- [8] W. Ren, "Design of digital media data storage and sharing system based on MVC mode," *Electronic Design Engineering*, vol. 28, no. 4, pp. 118–122, 2020.
- [9] Y. Shi and J. Zhang, "Design of information-based teaching resources sharing system based on multimedia technology," *Modern Electronics Technique*, vol. 44, no. 20, pp. 32–36, 2021.
- [10] Li Xi, "Design of MOOC idea based teaching resource sharing system for digital film and television production," *Modern Electronics Technique*, vol. 43, no. 16, pp. 115–118, 2020.
- [11] Y. Fan and M. Liu, "Design and research of online education course resource sharing based on cloud platform," *Modern Electronics Technique*, vol. 43, no. 1, pp. 175–178, 2020.
- [12] L. Chen, B. Wutong, and Y. Zhiqiang, "A secure and privacy-preserving watermark based medical image sharing method," *Chinese Journal of Electronics*, vol. 29, no. 5, pp. 31–37, 2020.
- [13] G. S. Kumar, D. R. Jegadeesan, A. Pravalika, G. Varsha, and N. Ramyasai, "Energy efficient data sharing method using lightweight algorithm for mobile cloud environment," *SSRN Electronic Journal*, vol. 6, no. 3, pp. 167–173, 2019.
- [14] K. R. Abirami, K. P. Ajaye, R. B. L. Amrriish, and N. A. Arun, "Efficient method for storing health record in cloud using integrity auditing and data sharing," *Journal of Physics: Conference Series*, vol. 1916, no. 1, Article ID 012191, 2021.
- [15] F. Liu, Y. Yang, and Y. Du, "Study on the building of network sharing system for the database of genuineness of Chinese medicinal materials," *Journal of Medical Informatics*, vol. 42, no. 7, pp. 62–67, 2021.
- [16] W. Huizeng and Y. Guo, "Overall structure design and application of provincial public credit information sharing platform database," *Information & Systems Engineering*, vol. 6, no. 1, pp. 29–30, 2019.

Retraction

Retracted: Construction and Analysis of Indicators of the Labor Education System Based on the Gray Correlation Degree Model

Computational Intelligence and Neuroscience

Received 25 July 2023; Accepted 25 July 2023; Published 26 July 2023

Copyright © 2023 Computational Intelligence and Neuroscience. This is an open access article distributed under the Creative Commons Attribution License, which permits unrestricted use, distribution, and reproduction in any medium, provided the original work is properly cited.

This article has been retracted by Hindawi following an investigation undertaken by the publisher [1]. This investigation has uncovered evidence of one or more of the following indicators of systematic manipulation of the publication process:

- (1) Discrepancies in scope
- (2) Discrepancies in the description of the research reported
- (3) Discrepancies between the availability of data and the research described
- (4) Inappropriate citations
- (5) Incoherent, meaningless and/or irrelevant content included in the article
- (6) Peer-review manipulation

The presence of these indicators undermines our confidence in the integrity of the article's content and we cannot, therefore, vouch for its reliability. Please note that this notice is intended solely to alert readers that the content of this article is unreliable. We have not investigated whether authors were aware of or involved in the systematic manipulation of the publication process.

Wiley and Hindawi regrets that the usual quality checks did not identify these issues before publication and have since put additional measures in place to safeguard research integrity.

We wish to credit our own Research Integrity and Research Publishing teams and anonymous and named external researchers and research integrity experts for contributing to this investigation.

The corresponding author, as the representative of all authors, has been given the opportunity to register their agreement or disagreement to this retraction. We have kept a record of any response received.

References

- [1] L. Huang, "Construction and Analysis of Indicators of the Labor Education System Based on the Gray Correlation Degree Model," *Computational Intelligence and Neuroscience*, vol. 2022, Article ID 2281469, 8 pages, 2022.

Research Article

Construction and Analysis of Indicators of the Labor Education System Based on the Gray Correlation Degree Model

Ling Huang 

College of Marxism of Hunan Biological and Electromechanical Polytechnic, Changsha 410000, China

Correspondence should be addressed to Ling Huang; huangling@hnbemc.edu.cn

Received 21 April 2022; Accepted 8 June 2022; Published 12 August 2022

Academic Editor: Le Sun

Copyright © 2022 Ling Huang. This is an open access article distributed under the Creative Commons Attribution License, which permits unrestricted use, distribution, and reproduction in any medium, provided the original work is properly cited.

Labor education is a complex concept whose value is not only the sum of labor + education. It plays an extremely important role in the growth education of students. Its fundamental purpose is to cultivate students' good technical literacy, improve their practical skills, and form innovative thinking. The monitoring data show that the path of labor education in schools is good, but there are also problems such as unbalanced development of labor practice, insufficient leading role of schools, insufficient basic role of families, and serious lack of social support. Responsibility index, learning motivation, motor health, and self-awareness are significantly and positively correlated with labor practice index. Based on the gray relationship theory, this paper selected relevant data of Chinese students, calculated the comprehensive gray relationship degree between each factor and students' labor education level, and analyzed the variables; the new connotation of education, the construction of labor education evaluation index system, and the construction of labor education support system were studied.

1. Introduction

Labor education means organizing students to learn certain technical knowledge of labor and to participate in certain labor activities so that they can acquire the viewpoint of labor, develop labor habits, understand the basic principles of modern production technology, and master the corresponding basic skills so that they can use them in the future [1], engage in educational activities, and lay the foundation for various occupations [2, 3]. The current labor education in colleges and universities can be analyzed from the perspective of colleges and students [3–5]. The following problems exist: lack of labor education courses in colleges and universities and lack of conducting labor education courses as basic courses in universities; but, few schools actually include labor education in their course syllabus [6]. Even if the school reluctantly opens the door to this course and the teacher does not say so, it is painful for both teachers and students to offer this course [7]. Students are not aware of labor education; most students grow up in the context of examinations and still have a utilitarian purpose of education after the university. Students have been immersed in the

frenzy of textual research, neglecting the development of their own interests and creative consciousness and lacking the awareness of actively improving their practical skills [8].

From basic education to higher education, we have emphasized the all-round development of students. However, in terms of concrete implementation, we have been following a talent development route that emphasizes achievement at the expense of ability [9]. Labor education is a bridge between students' learning and employment. Students can acquire relevant practical skills through labor education to prepare for their future employment [10–12]. Schools are an important platform for implementing labor education. First, schools should invite vocational and labor education talents to popularize labor education for all teachers so that college teachers can understand labor education objectively and change old concepts [13]. Secondly, schools should cooperate with enterprises and select outstanding talents from enterprises to provide relevant practical courses for students in schools, which can not only enrich students' campus life but also exercise their practical skills and give them a comprehensive understanding of labor education. Finally, schools should develop corresponding

labor education bases according to local characteristics, which can not only establish the school brand but also provide students with sufficient training opportunities [14–16].

Labor education is closely related to each of us, and it permeates all aspects of our lives [17].

In this paper, we monitored two aspects: the development of students' labor education in school and at home and students' labor concepts, labor dynamics, and labor habits, including four dimensions of self-service, homework, in-school labor, and out-of-school labor [18]. It can be seen that the gap between urban and rural areas and disciplines is not very large in terms of support for labor education in schools. Urban teachers are slightly higher than rural teachers in counties and villages, and math and science teachers are slightly higher than Chinese teachers. Parents generally believe that labor education can promote the healthy development of their children. When asked if students'

participation in labor is a good exercise, 65.2% of parents strongly agreed and 24.4% agreed. Parents are very satisfied with the current state of education in their schools, and 84% of parents say they are relatively satisfied or very satisfied. Also, comparing urban and rural data, there was no significant difference between urban and rural parents [19].

2. Gray Relational Analysis

2.1. Calculation of Gray Absolute Relevance Degree. First, determine the reference sequence X_0 and the comparison sequence X_i according to the specific problem of the study:

$$\begin{aligned} X_0 &= (x_0(1), x_0(2), \dots, x_0(n)), \\ X_i &= (x_i(1), x_i(2), \dots, x_i(n)), \quad (i = 1, 2, \dots, m). \end{aligned} \quad (1)$$

Next, find the zeroed image of the starting point of the reference sequence and the comparison sequence:

$$\begin{aligned} X_0^0 &= (x_0^0(1), x_0^0(2), \dots, x_0^0(n)) = (x_0(1) - x_0(1), x_0(2) - x_0(1), \dots, x_0(n) - x_0(1)), \\ X_i^0 &= (x_i^0(1), x_i^0(2), \dots, x_i^0(n)) = (x_i(1) - x_i(1), x_i(2) - x_i(1), \dots, x_i(n) - x_i(1)). \end{aligned} \quad (2)$$

Finally, find the gray absolute correlation degree ε_{0i} of the reference sequence X_0 and the comparison sequence X_i :

$$\varepsilon_{0i} = \frac{1 + |S_0| + |S_i|}{1 + |S_0| + |S_i| + |S_i - S_0|}. \quad (3)$$

Here,

$$\begin{aligned} |S_0| &= \int_1^n X_0^0 dt \\ &= \left| \sum_{k=2}^{n-1} x_0^0(k) + \frac{1}{2} x_0^0(n) \right|, \\ |S_i| &= \int_1^n X_i^0 dt \\ &= \left| \sum_{k=2}^{n-1} x_i^0(k) + \frac{1}{2} x_i^0(n) \right|, \end{aligned} \quad (4)$$

$$|S_i - S_0| = \left| \sum_{k=2}^{n-1} (x_i^0(k) - x_0^0(k)) + \frac{1}{2} (x_i^0(n) - x_0^0(n)) \right|.$$

2.2. Calculation of Gray Relative Correlation Degree. First, find the initial value of X_0 and X_i as X_0' and X_i' :

$$\begin{aligned} X_0' &= \frac{X_0}{x_0(1)} = \left(\frac{x_0(1)}{x_0(1)}, \frac{x_0(2)}{x_0(1)}, \dots, \frac{x_0(n)}{x_0(1)} \right), \\ X_i' &= \frac{X_i}{x_i(1)} = \left(\frac{x_i(1)}{x_i(1)}, \frac{x_i(2)}{x_i(1)}, \dots, \frac{x_i(n)}{x_i(1)} \right). \end{aligned} \quad (5)$$

Next, find the zeroing image of the starting point of X_0' and X_i' .

Finally, find the relative correlation degree r_{0i} between X_0' and X_i' .

$$r_{0i} = \frac{1 + |S_0'| + |S_i'|}{1 + |S_0'| + |S_i'| + |S_i' - S_0'|}. \quad (6)$$

2.3. Finding the Gray Comprehensive Correlation Degree. $\rho_{0i} = \theta \varepsilon_{0i} + (1 - \theta) r_{0i}$, where $\theta \in [0, 1]$. (6) is generally acceptable when $\theta = 0.5$. If we pay more attention to the relationship between absolute quantities, it can be larger. If you pay more attention to the rate of change, θ can be smaller.

3. Data Collection

Student labor practice mainly includes on- and off-campus labor organized by the school, as well as student self-service and housework. As shown in Figure 1, the survey found that junior high school students have relatively good on-campus labor practices and weaker off-campus practices, self-service is relatively good, and housework is relatively weak. In terms of self-service and housework, students in private migrant schools are significantly stronger than students in other schools, but there is no significant difference in labor practices inside and outside the school. In different regions and gender dimensions, the labor practices of students are basically similar.

Table 1 further analyzes the students' participation in labor practice activities organized by the school and presents the types and frequencies of students' participation in labor practice both inside and outside the school.

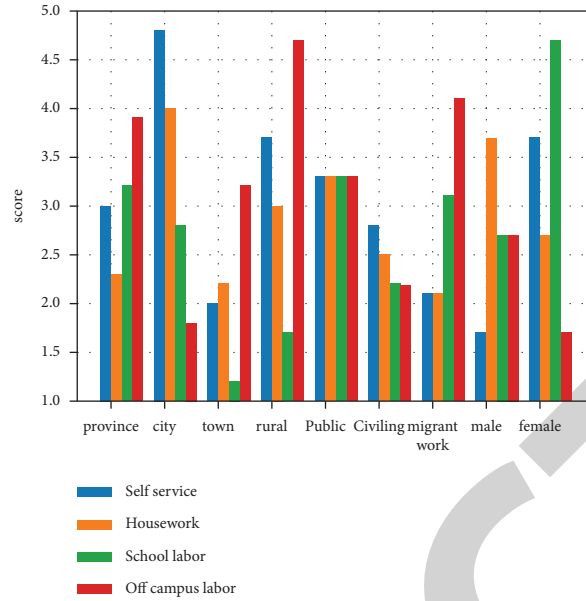


FIGURE 1: Structural characteristics of labor practice of junior middle school students in Zhejiang province.

TABLE 1: The situation of students participating in labor practice.

		No	Annually	Once a semester	Once a month	Once a week
School labor practice	Frequency	2.4%	1.2%	8.1%	26.7%	61.9%
	Type (multiple choices)	Practice-based learning	Various service posts of the school	Professional postexperience activities	other	
		42.4%	51.6%	18.9%	39.1%	
Off-campus labor practice	Frequency	Never	1~2 times	3~6 times	6~10 times	More than 10 times
	Type (multiple choices)	Community convenience and public welfare services	Cultural publicity activities	Environmental voluntary activities	Caring and serving others	Other
		25%	55.4%	16.4%	2.1%	1.5%
		22.6%	23.4%	32.9%	31%	52.9%

The data show that the frequency of students' on-campus labor practice is relatively high, and the proportion of students participating in on-campus labor practice once a week is 61.8%. Although the types of students' off-campus labor practice are relatively rich, the frequency is generally low. 24.9% of the students have never participated in off-campus labor practice, and less than 20% of the students have participated three or more times. Junior high school should be the initial stage of career experience, and 18.6% of students have participated in career experience activities. In addition, 38.8% and 52.8% of students have participated in "other" on-campus and off-campus labor practices other than the options, respectively, which shows that the types of labor practices are quite diverse.

Junior high school students have strong self-service ability, and 62.1% of the students take the initiative to organize their daily life and school supplies at least three times a week. Junior high school students participate better in housework. Table 2 presents the frequency of students doing housework in different regions and genders. 40% of students said they do housework at least three times a week, and 39.4% said they do housework once or twice a week. Among

the students who do housework every day, towns and villages account for the highest proportion (19.2%). In terms of gender, boys who do housework at least three times a week account for 41.9%, 3.9% points higher than girls. Most of the students who do not do housework are urban students or boys. It can be seen that the participation in housework of rural students in townships and villages is better than that of students in the county and urban areas.

The data in Table 3 show that 5.6% of the students do the "cooking" housework every day on weekends, 26.8% of the students do the "cooking" housework once or twice a month, and 39.4% of the students basically do not do the "cooking" housework.

The monitoring data show that the labor education path of junior high schools in Zhejiang province is sound. Figure 2 presents school labor education implementation from teacher questionnaires.

As can be seen from Figure 2, among the compulsory courses for labor, technology, and comprehensive practice activities in schools, 1-2 times a week accounted for 30.9% and 1-2 times every two weeks accounted for 17.6%. Schools carry out sanitation, green planting, class activities with the theme

TABLE 2: Frequency of housework for students in different regions and genders in the province.

		Do it every day (%)	Four times on Wednesday (%)	Twice a week (%)	Once or twice a month (%)	Basically not (%)
Whole province		15.6	24.4	39.5	12.4	8.4
Regional nature	City	12.96	22.3	40.4	15.1	9.8
	County town	12.5	22.6	41.5	14.3	8.9
	Rural township	19.3	26.4	37.6	9.8	7.4
Gender	Male	17.3	24.7	36.7	12.2	9.5
	Female	14.1	23.9	42.3	12.6	7.4

TABLE 3: Frequency of students doing “cooking” housework on weekends.

	Never or hardly (%)	Once or twice a month (%)	Once or twice a week (%)	3 or 4 times a week (%)	Every day or almost every day (%)
Whole province	39.5	26.9	22.6	5.7	5.7

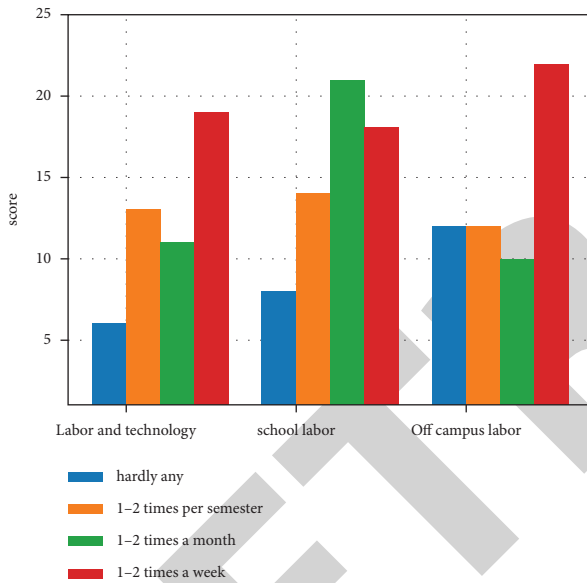


FIGURE 2: Distribution of school labor practice activities.

of labor education, clubs, interest groups, and other on-campus labor more frequently. In terms of the frequency of teachers organizing students to carry out on-campus labor, 1-2 times a week accounted for 30.2%, at least once a month accounted for 40.2%. The school also offers labor practice expansion elective courses such as housekeeping, cooking, handicraft, and gardening to enrich the course content. The frequency of offering these courses is 1-2 times a week, accounting for 21.9%, and 1-2 times every two weeks, accounting for 14.5%. The school promotes and evaluates the effectiveness of home labor education in the form of homework assignments. The frequency of homework assignments for students is 16.5% once or twice a week and 15.1% is once or twice every two weeks. The frequency of off-campus labor practices such as public welfare activities, voluntary services, research trips with labor education as the theme, and social practice organized by schools is relatively low, accounting for 57.4% once or twice per semester and

9.1% once or twice a week. This shows that although the school can carry out labor practice education normally, its frequency is relatively low and the content is single. It is urgent to build a scientific labor education curriculum system and explore diversified labor education practice paths.

The data in Table 4 show that among teachers who arrange homework once or twice a week, the proportions of urban, county, and township and rural teachers are 18.9%, 16.9%, and 14.5%, respectively. It can be seen that urban teachers' homework assignments are better than county teachers, and county teachers are better than township and rural teachers.

4. Results and Analysis

According to the calculation result of the gray correlation degree, the correlation degree of each factor is compared in pairs and the judgment matrix is constructed. Scales 1, 3, 5, 7, and 9 are used to indicate that factor X_i is equally important, slightly important, clearly important, strongly important, and extremely important compared to factor X_j , while scales 2, 4, 6, and 8 indicate the difference between the above judgments. After the judgment matrix is constructed, use the following formula to calculate its influence:

$$\lambda_{\max} = \frac{1}{n} \frac{(BW)_i}{W_i}. \quad (7)$$

Here, λ_{\max} represents the largest eigenvalue of the judgment matrix B ; W represents the normalized eigenvector corresponding to λ_{\max} ; W_i represents the influence of the ranking of the constituent factors; and n represents the dimension of the judgment matrix B . In order to check the consistency of the judgment matrix B , the consistency index CI needs to be calculated and the corresponding calculation formula is as follows:

$$CI = \frac{\lambda_{\max} - n}{n - 1}. \quad (8)$$

TABLE 4: Frequency of homework assignments.

	Never or hardly (%)	Once or twice a month (%)	Once or twice a week (%)	3 or 4 times a week (%)	Every day or almost every day (%)
City	13.12	32.2	21.3	14.8	18.7
County town	16.2	30.2	21.6	15.6	17.1
Rural township	17.9	31.2	21.2	15.3	14.7

We compare CI with the average random consistency index RI to test whether the judgment matrix B is consistent. For matrices of orders 1 to 16, the values of RI are listed in Table 5.

The first-order and second-order judgment matrices are completely consistent. Starting from order 3, the random consistency ratio of the judgment matrix needs to be calculated: $CR = (CI/RI)$. When $CR < 0.1$, it is considered that the judgment matrix has satisfactory consistency; otherwise, the judgment matrix is readjusted.

As shown in Table 6, the correlation analysis was made between the labor practice index and monitoring indexes, such as sense of responsibility, learning motivation, sports health, self-cognition, family education, teacher-student relationship, parent-child relationship, hobbies, parent participation, and peer relationship. It shows that there is a significant positive correlation between each monitoring index and the labor practice index and the labor practice index has the highest correlation with the sense of responsibility index.

Responsibility refers to the process by which students take responsibility for themselves, others, collectives, and society by performing certain normative behaviors, including fulfilling obligations, duties, and other requirements. On the one hand, students with a strong sense of responsibility often participate in more labor practices; on the other hand, labor practice activities are just a good carrier to enhance students' sense of responsibility and develop courage and perseverance [20–22].

It can be seen from Figure 3 that with the improvement of the level of responsibility index, the score of labor practice index is getting higher and higher and the two sub-dimensions also have similar conclusions. The labor practice index scores for each level of "citizen responsibility" are higher than those of "self-responsibility." It can be seen that the awareness of civic responsibility has a relatively large impact on labor practice.

It can be seen from Figure 4 that with the improvement of family education level, the score of labor practice index is getting higher and higher and the three subdimensions also have similar conclusions. The labor practice index scores corresponding to each level of "democracy and respect" are higher than those of "affirmation and encouragement" and "independence training." It can be seen that the family education method of "democracy and respect" has a relatively large impact on labor practice.

As can be seen from Figure 5, from the perspective of the relationship between participation in various types of

regular on-campus labor practice activities organized by the school and students' sense of responsibility, the scores of students' sense of responsibility index who participated in on-campus activities were much higher than those who did not participate in on-campus activities and participating in vocational postexperience activities was more helpful in the formation of a sense of responsibility.

As can be seen from Figure 6, from the perspective of the relationship between participation in various types of regular off-campus labor practice activities organized by the school and students' sense of responsibility, students who participated in off-campus activities scored much higher than those who did not participate in off-campus activities and participated in community-friendly public welfare services or cultural activities. Publicity activities are more conducive to the formation of a sense of responsibility.

Labor education has the comprehensive educating value of cultivating morality, enhancing intelligence, strengthening body, and nurturing beauty, and it is of great significance to fully tap its hidden value of promoting the healthy growth of students. In fact, labor education must not only be presented at the material level but also must be sublimated at the spiritual level and attention should be paid to cultivating students' labor literacy. For example, in the process of doing housework, students learn to manage their own time, coordinate the relationship between housework and study, and do things in a short time and efficiently. Students undertake housework as much as they can, cultivate their sense of independence and the ability to overcome difficulties, appreciate the hardships of labor, cherish the fruits of labor more, feel the joy of labor, and form a positive attitude towards labor.

5. Countermeasures and Suggestions

Based on the monitoring results and the analysis of the current situation of labor education in Zhejiang province, the following three suggestions are put forward for the comprehensive promotion of labor education for junior high school students.

5.1. Endowing Labor Education with New Connotation.

Monitoring data show that labor education has a positive effect on the formation of students' "responsibility"; some studies have also shown that "responsibility" and "learning motivation" have a significant positive effect on students' academic performance. It can be seen that it is necessary to give the original labor education a new connotation.

TABLE 5: Average stochastic consistency indicators RI.

Orders	1	2	3	4	5	7	8	9	10	11	12	13	14	15	16
RI	0	0	0.53	0.88	1.13	1.25	1.37	1.42	1.46	1.51	1.54	1.57	1.59	1.60	1.62

TABLE 6: Relationship between monitoring index and labor practice index.

Index	Correlation coefficient
Responsibility index	0.352
Learning motivation index	0.278
Exercise health index	0.257
Self-cognition index	0.255
Family education index	0.219
Self-cognition index	0.256
Family education index	0.219
Teacher-student relationship index	0.215
Parent participation index	0.207
Peer relationship index	0.173

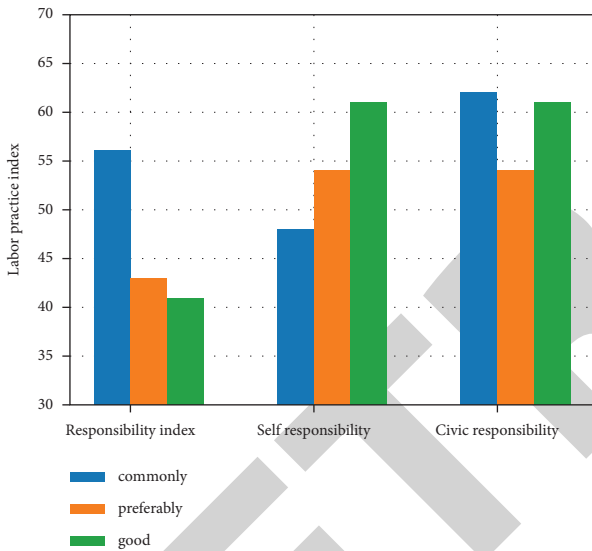


FIGURE 3: Responsibility index.

It can be seen that in terms of standpoint, it is necessary to fully realize the combination of the “substance” rather than “form” of education and productive labor. In terms of content, it embodies a developmental view of education, emphasizing leisure education and consumer education. In terms of function, it emphasizes labor. The existential value of the individual is to endow the individual with a sense of value and meaning of self-existence in labor education, enrich their relationship attributes, and enhance their aesthetic personality; in practice, it should cultivate students' correct labor concepts and attitudes and build an integrated and open labor education practice system. This kind of labor education focuses on the cultivation of labor literacy and cannot be simply understood as the establishment of labor classes. Morality, intelligence, physique, beauty, and labor mentioned in the educational policy are all concepts of literacy, and they do not correspond to specific disciplines; that is, it cannot be said that “morality” corresponds to the

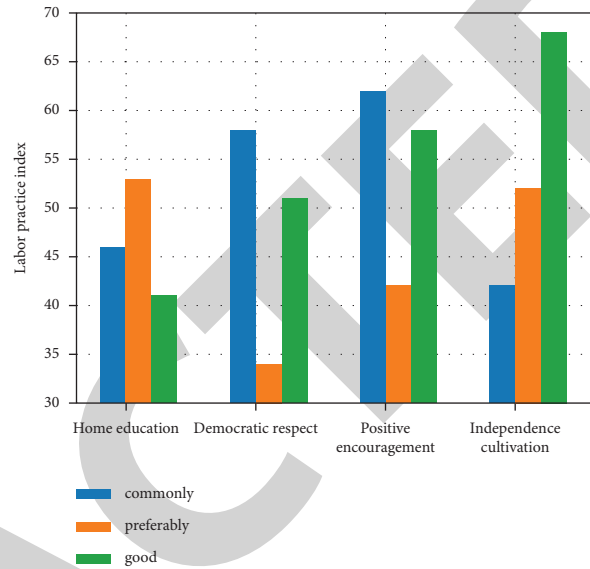


FIGURE 4: Labor practice index scores under different family education levels.

discipline of moral education and “physical” cannot be regarded as a physical education class. In the same way, students' labor literacy is not only cultivated in labor classes but also in the daily care of home and school, the sanitation rotation of the class, the layout of the environment, the physical measurement and field investigation of subject teaching, the practical activities of various comprehensive practice courses and the cultivation function of labor literacy [23, 24].

Junior high school students are in adolescence, and their growing physical maturity prompts them to seek independence psychologically, gradually reduce their dependence on their parents, and hope to get rid of their parents' “control.”

However, they also face many challenges and problems in their studies and life and still need the support, companionship and guidance of their parents. Therefore, parents need to change their educational roles, adjust their parenting methods, give their children trust and understanding, provide timely help and guidance, infiltrate the cultivation of sense of responsibility in labor education, and stimulate children's learning motivation.

5.2. *Constructing the Labor Education Evaluation Index System.* Schools should incorporate labor education into their teaching plans, set up labor courses, cultivate labor literacy, continuously improve labor education programs and security systems, and implement refined labor education evaluations. According to the “opinions,” a labor education evaluation index system with regional characteristics is formulated. For example, curriculum settings generally

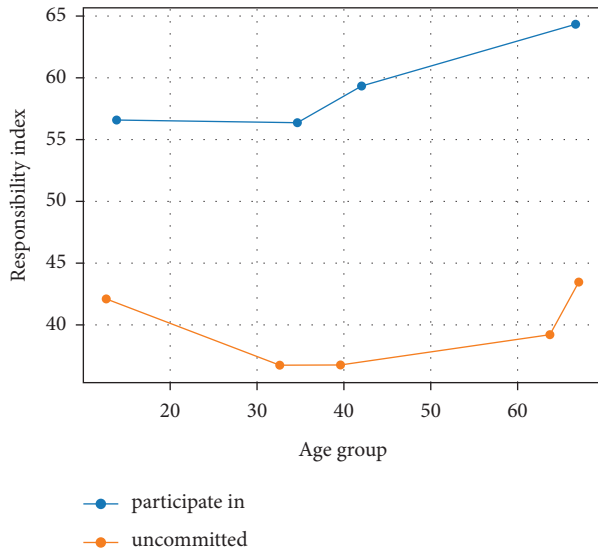


FIGURE 5: Relationship between different types of on-campus labor practices and sense of responsibility.

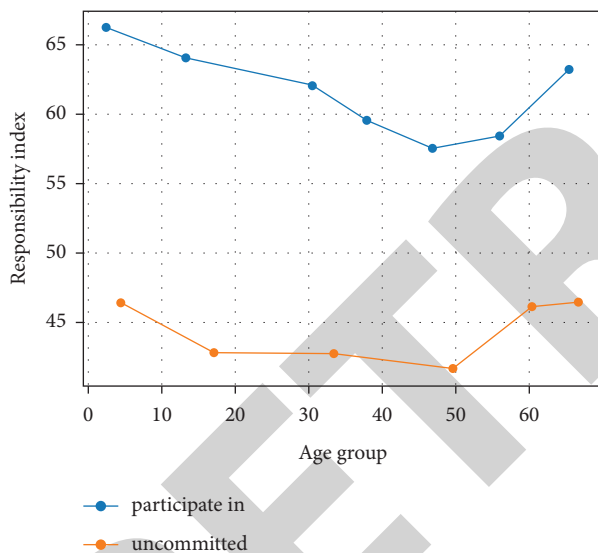


FIGURE 6: The relationship between different types of off-campus labor practices and sense of responsibility.

include labor compulsory courses, labor development courses, labor weeks, and subject penetration. Teaching implementation includes teaching content, teaching form, teaching resources, and teaching evaluation. The guarantee mechanism includes system guarantee, teacher guarantee, funding investment, and safety. Labor literacy includes labor concepts, labor knowledge and skills, labor habits, and labor practice capabilities. Curriculum settings can also draw lessons from mature foreign experience. For example, Japan's labor courses include home economics, lunch education, and field education; Germany's labor courses include technology, economics, home economics, and vocational skills; Finland's labor courses include handicraft, home economics, programming courses, and comprehensive courses.

At the same time, the results of students' usual labor are included in the personal comprehensive quality evaluation and the education supervision department incorporates the results of school labor education into the school's developmental assessment to promote the effective achievement of labor education goals.

5.3. Construction of the Labor Education Support System. Labor education must permeate the moral, intellectual, physical, and aesthetic education in schools and cannot be done without the operation and social support of the home and school. Therefore, it is necessary to strengthen the cooperation between school, family, and society to carry out labor education and ensure the effective implementation of labor education. Teachers should make full use of the special activity classroom as the main post to educate students about labor so that they can form correct labor values; they should praise students in the class who love labor and have strong labor skills and encourage other students to follow them. Schools should carry out relevant activities to stimulate students' interest in labor, such as organizing tree planting festivals and small production competitions, which not only help transform passive labor into conscious labor but also improve students' ability to use their hands and brains.

Data Availability

The experimental data used to support the findings of this study are available from the author upon request.

Conflicts of Interest

The author declares that there are no conflicts of interest regarding this work.

Acknowledgments

This work was supported by the Scientific Research Fund of Hunan Provincial Education Department (Grant no. 21C1252).

References

- [1] T. Ahmad, H. Chen, Y. Guo, and J. Wang, "A comprehensive overview on the data driven and large scale based approaches for forecasting of building energy demand: a review," *Energy and Buildings*, vol. 165, pp. 301–320, 2018.
- [2] S. B. Tsai, Y. Xue, J. Zhang et al., "Models for forecasting growth trends in renewable energy," *Renewable and Sustainable Energy Reviews*, vol. 77, pp. 1169–1178, 2017.
- [3] H. Luo, C. Xiong, W. Fang, P. E. Love, B. Zhang, and X. Ouyang, "Convolutional neural networks: computer vision-based workforce activity assessment in construction," *Automation in Construction*, vol. 94, pp. 282–289, 2018.
- [4] Z. Jiang, Z. Ding, H. Zhang, W. Cai, and Y. Liu, "Data-driven ecological performance evaluation for remanufacturing process," *Energy Conversion and Management*, vol. 198, Article ID 111844, 2019.
- [5] M. Yazdani, C. Kahraman, P. Zarate, and S. C. Onar, "A fuzzy multi attribute decision framework with integration of QFD

Retraction

Retracted: Design and Optimization of Aesthetic Education Teaching Information Platform Based on Big Data Analysis

Computational Intelligence and Neuroscience

Received 25 July 2023; Accepted 25 July 2023; Published 26 July 2023

Copyright © 2023 Computational Intelligence and Neuroscience. This is an open access article distributed under the Creative Commons Attribution License, which permits unrestricted use, distribution, and reproduction in any medium, provided the original work is properly cited.

This article has been retracted by Hindawi following an investigation undertaken by the publisher [1]. This investigation has uncovered evidence of one or more of the following indicators of systematic manipulation of the publication process:

- (1) Discrepancies in scope
- (2) Discrepancies in the description of the research reported
- (3) Discrepancies between the availability of data and the research described
- (4) Inappropriate citations
- (5) Incoherent, meaningless and/or irrelevant content included in the article
- (6) Peer-review manipulation

The presence of these indicators undermines our confidence in the integrity of the article's content and we cannot, therefore, vouch for its reliability. Please note that this notice is intended solely to alert readers that the content of this article is unreliable. We have not investigated whether authors were aware of or involved in the systematic manipulation of the publication process.

Wiley and Hindawi regrets that the usual quality checks did not identify these issues before publication and have since put additional measures in place to safeguard research integrity.

We wish to credit our own Research Integrity and Research Publishing teams and anonymous and named external researchers and research integrity experts for contributing to this investigation.


The corresponding author, as the representative of all authors, has been given the opportunity to register their agreement or disagreement to this retraction. We have kept a record of any response received.

References

- [1] X. Wu and H. Gu, "Design and Optimization of Aesthetic Education Teaching Information Platform Based on Big Data Analysis," *Computational Intelligence and Neuroscience*, vol. 2022, Article ID 5109638, 9 pages, 2022.

Research Article

Design and Optimization of Aesthetic Education Teaching Information Platform Based on Big Data Analysis

Xingxing Wu^{1,2} and Hai Gu³ 

¹School of Finance, Jiangxi Institute of Economic Administrators, Nanchang 330088, China

²School of Art, Mokwon University, Daejeon 35349, Republic of Korea

³Department of IT Engineering, Mokwon University, Daejeon 35349, Republic of Korea

Correspondence should be addressed to Hai Gu; guhainit@163.com

Received 13 May 2022; Accepted 17 July 2022; Published 11 August 2022

Academic Editor: Le Sun

Copyright © 2022 Xingxing Wu and Hai Gu. This is an open access article distributed under the Creative Commons Attribution License, which permits unrestricted use, distribution, and reproduction in any medium, provided the original work is properly cited.

In the process of promoting school aesthetic education, some schools have some problems, such as insufficient construction of campus aesthetic education environment, lack of aesthetic thinking in various disciplines, and so on. In view of these problems, combined with the concept of the flipped classroom and the characteristics of artificial intelligence task-driven teaching, taking PHP, HTML + CSS + JS, and other development technologies as the main development technologies, and relying on the flipped classroom teaching mode of network learning space, this paper constructs an artificial intelligence core course website as a teaching platform for graduate teaching and undergraduate extended learning. The platform seeks the optimal solution of multiple combination optimization based on a genetic algorithm effectively improves the teaching quality of artificial intelligence courses and students' learning efficiency.

1. Introduction

Aesthetic education enhances aesthetic qualities, cultivates sentiment, warms the soul, stimulates innovation and creativity, and is an indispensable element in the overall development of students [1].

Aesthetic education informatization refers to the process of teachers incorporating modern information technology in the top-level system design, campus culture enhancement, teacher training, teaching platform construction, resource development, and implementation of teaching activities to accelerate the modernization of aesthetic education [2–4].

This document clarifies the why, what, and how of school aesthetic education in the new era, strengthening the nurturing function of school aesthetic education, which is an important model for guiding the whole society to value aesthetic education and creating a social atmosphere that jointly promotes the development of school aesthetic education [5]. Teachers should attach importance to aesthetic education and make it permeate and permeate all aspects of

education and teaching. Information technology is a booster for improving the quality of education, and promoting aesthetic education with information technology is the direction and trend of education development and a necessary stage of education modernization [6]. At present, information technology in aesthetic education has become a new area of research in the field of aesthetic education, and its research is on the rise [7].

Aesthetic education is an important part of school education, and the construction of the campus environment is very important for cultivating students' aesthetic thinking. The campus environment can be a visual representation of a school's understanding and interpretation of aesthetic education [8]. However, some primary and secondary schools have a single style of campus environment construction and do not pay attention to the importance of the campus environment to the cultivation of students' aesthetic thinking, lacking an environmental design that reflects the unique local humanities, beautification style, and the core concept of campus culture [9].

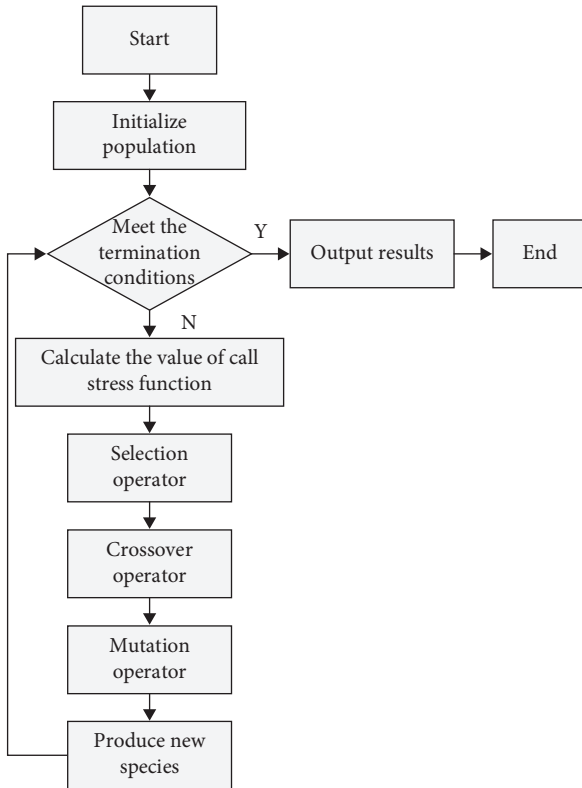


FIGURE 1: Flow chart of a traditional genetic algorithm.

The most pressing need in aesthetic education is the issue of teacher development. Nationally, there is still a considerable shortage of teachers for aesthetic education in terms of quantity, and even more so in terms of quality. [10] Interviews with some teachers and students revealed that there is a serious shortage of teachers with an arts background in some schools, so schools are lowering the bar when recruiting, which in turn leads to overall low quality of art teachers. In terms of curriculum arrangement, art and music courses are often taken up or switched at will by the main teachers, which leads to a lack of assurance in terms of class time and teaching quality in the Aesthetic Education curriculum [11].

Our schools have not invested enough in the infrastructure and teaching resources for Aesthetic Education's information-based teaching activities, and there is a general problem of low popularity and small scale. Although teaching resources in the information age have been greatly enhanced in terms of quantity, quality, and content, some teachers fail to select appropriate resources to make them fit with classroom teaching content when making use of the abundant teaching resources. At the same time, the construction of regional educational resource banks is in its infancy, and the use of information resources for the teaching of Aesthetic Education in Chinese primary schools is still far from the goal of abundant and effective use of resources [12].

Artificial Intelligence is a core course in the discipline of computer application technology. Through the study and practical application of this course, students can be trained to master the basic theories, cutting-edge technologies, and the ability to do things on their own and to be innovative

[13]. Students are required to have a basic understanding of the classical algorithms and reasoning mechanisms of artificial intelligence theory and to develop intelligent systems based on the main research content after completing the basic theory and experimental teaching courses [14]. This requires a wide range of knowledge, deep basic theories, and strong practical skills in the teaching of AI courses [15–17].

In this paper, relying on the flipped classroom teaching mode of the online learning space, combined with the actual teaching cases based on the task-driven teaching mode, a website of artificial intelligence core courses is constructed as a teaching platform for postgraduate teaching and undergraduate extended learning, which effectively improves the artificial intelligence courses. Teaching quality and student learning efficiency.

2. Artificial Intelligence Web-Based Teaching Platform Positioning and Related Technologies

2.1. Online Teaching Platform Positioning. The construction of an online teaching platform for core courses in artificial intelligence mainly includes a flipped teaching concept, course content based on a task-driven teaching model, and an interactive and shared online platform. These two are complementary and mutually reinforcing. Secondly, mature network technology is needed to build the platform framework, so that the best course content can be displayed on the network platform, thus realizing the purpose of sharing and applying course resources [18]. In this paper, the teaching cases of AI core course teams in the past ten years are collected and collated, and an online teaching platform based on the flipped classroom teaching model is constructed.

2.2. Web-Based Teaching Platform Related Technologies. PHP is a server-side scripting language; MySQL is the most widely used Web database today. PHP and MySQL are a natural pair, and the combination of the two can be used to achieve many powerful features in web development. CSS makes it easy to control the appearance of a website's interface, making it easy to create web pages. CSS is also a great solution to the problem of page layout, making web pages smaller and faster to download [20].

3. Introduction to Traditional Genetic Algorithms and Hierarchical Decision Model

Genetic algorithms, or GA for short, are computational models that combine biological evolution and genetics. They can mathematically model the natural evolutionary process of organisms, corresponding the process of problem solving to the selection, crossover, and mutation of chromosomal genes during biological evolution and are thus used to find the optimal solution for multi-combination optimization.

The specific flow chart of the traditional genetic algorithm is shown in Figure 1.

The algorithmic components of a traditional genetic algorithm (GA) include chromosome encoding (containing

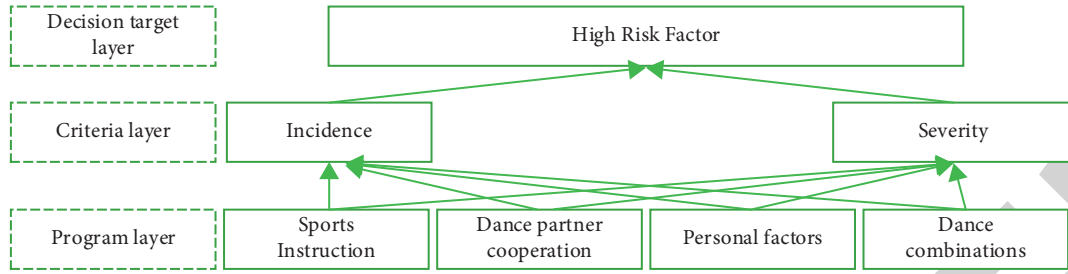


FIGURE 2: Hierarchical decision model for high-risk factors.

TABLE 1: Electronic lesson plan datasheet.

Field name	Field identification	Field type
Title	Title	System field
Specialfield	Special properties	System field
Titlepic	Title picture	System field
Newstime	Release time	System field

TABLE 2: Fash system datasheet.

Field name	Field identification	Field type
Title	Title	System field
Specialfield	Special properties	System field
Newstime	Release time	System field
Titlepic	Title picture	System field
Flashwriter	Author	VARCHAR (30)
E-mail	Author e-mail	VARCHAR (80)
Star	Work level	TIV NYINT(1)
Filesize	File size	VARCHAR (16)
Flashurl	Flash address	VARCHAR (255)
Width	Flash width	VARCHAR (12)
Height	Flash height	VARCHAR (12)
Flashsay	Introduction to works	Text

the initialized population), fitness functions, and genetic operators (selection, crossover, variation). The traditional genetic algorithm firstly encodes and randomly generates an initial population, then conducts individual evaluation, and selection, determines whether to output, followed by random crossover and mutation operations and finally turns to individual evaluation to start a new cycle.

In order to establish a systematic risk assessment system for sports injuries, it is necessary to decompose the decision object based on the idea of the decomposition method and build a hierarchical model accordingly. According to the above-mentioned points, the hierarchical analysis model is constructed as shown in Figure 2.

The basic level of the model: decision target refers to the final derived result; criterion layer is the criteria for the model judgment to make a decision; program layer refers to each specific program limited by the decision target and criterion layer. In the model, the highest risk factor is used as the target: severity and incidence as the criterion; four types of risk: sports instruction, partner cooperation, personal factors, and sports combination as the alternative. Next, a comparison matrix is constructed and solved, and finally the highest risk category is determined in a logical way, and those risk exposures with higher incidence and more severe consequences are identified and focused on [21–25].

The relative importance of the above-given four factors was compared between the two under the constraints of the criterion level. The importance ratings of coaches and athletes on the seven major exposures of the four risk categories were first arithmetically averaged in terms of categories and then weighted in terms of the ratio of the number of coaches and athletes participating in the study to obtain the final values of the matrix factors, and the judgment matrix was constructed.

The fourth-order matrix A formed is as follows (A_{ij} is the ratio of importance between risks ij , $A_{ji} = 1/A_{ij}$):

$$A = \begin{bmatrix} 1.00 & 4.00 & 7.00 & 9.00 \\ 0.25 & 1.00 & 4.00 & 6.00 \\ 0.14 & 0.25 & 1.00 & 3.00 \\ 0.11 & 0.16 & 0.33 & 1.00 \end{bmatrix}. \quad (1)$$

To achieve the sports training injury risk assessment model, the big data fusion scheduling method is used for big data information sampling of sports training injury risk assessment, combined with the statistical information mining method for sports training injury risk assessment, dividing the level of sports training injury risk assessment $X^{(0)}$, into N levels, as $X^{(1)}, X^{(2)}, \dots, X^{(N)}$, i.e. $X^{(0)} = \cup_{i=1}^N X^{(i)}$, with fuzzy feature distributed mining method for statistical analysis and optimal assessment of sports training injury risk, establishing a big data analysis model for sports training injury risk assessment, adaptive learning for sports training injury risk assessment, and obtaining a statistical function for sports training injury risk assessment as.

The above-given equation is a big data fusion model of sports training injury risk assessment for quantitative analysis of sports training injury risk assessment [26, 27], and the correlation distribution relationship of the constraint covariate set R^N, X^N of sports training injury risk assessment is established as follows.

Combining the autocorrelation feature matching method for sports training injury risk assessment big data sampling, according to the sampling results for sports training injury risk optimization evaluation and decision making. The feature matching function of sports training injury risk is established, $\{x(t_0 + i\Delta t)\}$, $i = 0, 1, \dots, N - 1$. The optimization-seeking trajectory of machine learning is as follows.

The fuzzy parametric identification of sports training injury risk assessment is carried out by using output stability gain assessment and the fuzzy decision method is constructed as follows.

TABLE 3: Sports training risk factors category statistics.

No.	Risk factor category	Frequency	Cumulative percentage (%)
A-a	Student movement behavior risk	162	20.12
C-b	Sports equipment risk	148	39.69
C-a	Activity venue risk	139	55.36
A-b	Student self-management risk	125	71.03
B-a	School safety management risk	100	82.55
D-b	Man-made environment risk	75	92.36
B-b	School medical supervision risk	35	96.77
D-a	Natural environment risk	28	100

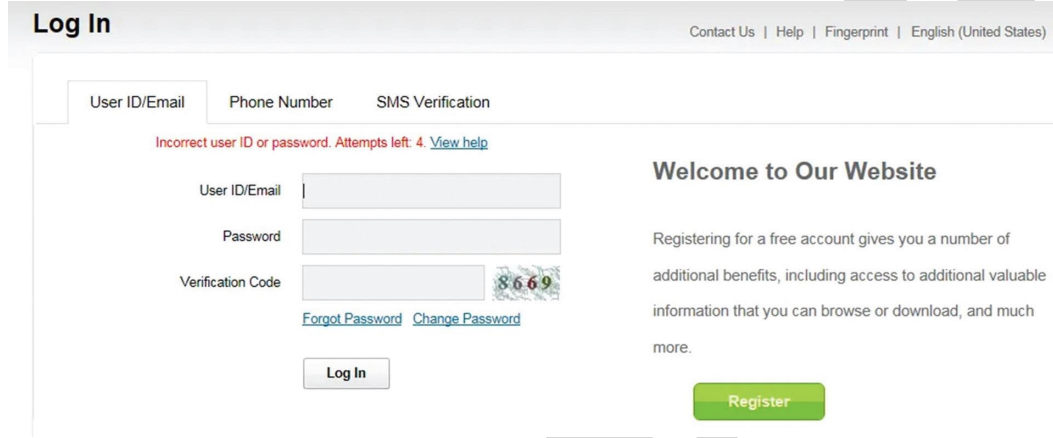


FIGURE 3: System login interface.



FIGURE 4: Website home page.

In the following equation, λ represents the fuzzy distribution factor of the big data for sports training injury risk assessment, combined with the statistical feature analysis method for sports training risk assessment. The sports training injury risk assessment is obtained as follows:

$$\sum_{s_c \in S^2} p\{C_k^i / A_k^i B_k^b\} p\{A_{k+1}^j / A_k^i B_k^b C_k^i\} \quad (2)$$

The linear fit equation for the risk assessment of physical training injuries is

$$P_{id}^{new} = \begin{cases} p_{id} + m() (X_{max} - p_{id}) & \text{if } m() > 0 \\ p_{id} + m() (p_{id} - X_{min}) & \text{if } m() \leq 0 \end{cases} \quad (3)$$

The similarity analysis method is used for adaptive assessment of sports training injury risk, and the fuzzy control in the process of sports training injury risk assessment is as follows:

$$SL_i = \begin{cases} L_i & \text{if } i = 1 \\ N_{ew} & \text{otherwise} \end{cases} \quad (4)$$

The association rule distribution function for sports training injury risk assessment is M_h , and the joint association rule mining method is used to obtain a finite dataset of association dimensional distribution for sports training injury risk assessment.

$$X = \{x_1, x_2, \dots, x_n\} \subset R^2 \quad (5)$$

Among them, the sports training injury risk assessment contains n samples, and the expert system analysis model of sports training injury risk assessment is established, and the control sample function is obtained as $x_i, i = 1, 2, \dots, n$, and the feature quantity of sports training injury risk assessment is obtained by combining the hierarchical gray-scale correlation analysis method p_q , and the quantitative relationship of sports training injury risk assessment is as follows.

To sum up, the analysis, to achieve the optimization of sports training injury risk and improve sports training injury risk control.

4. Overall Design of the Artificial Intelligence Web-Based Teaching Platform

4.1. Overall Design of the Web-Based Teaching Platform. The Artificial Intelligence Network Teaching Platform, with its efficient, remote, and resource-sharing features, allows advanced and rich course resources to be shared on the Internet, enabling teachers and students to download and

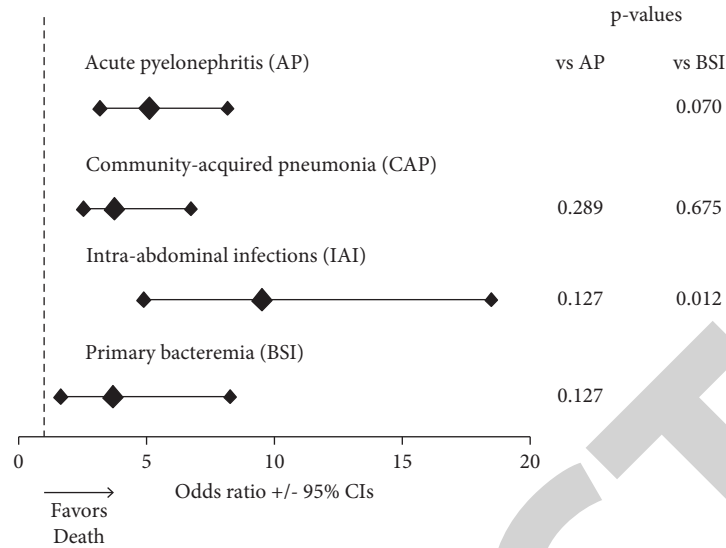


FIGURE 5: Interaction process of micro class.

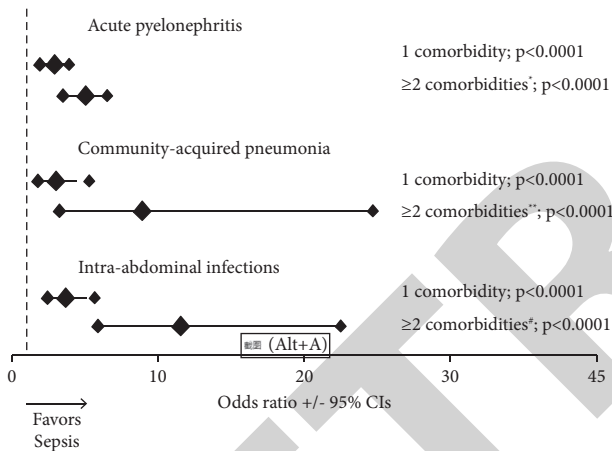


FIGURE 6: Grass damage diagnosis and treatment system.

share electronic resources such as teaching contents and cases, microlessons and courseware, and scientific research results and papers. Students can rely on the flipped classroom teaching model in the online learning space to customize and personalize their learning or rely on the teaching platform for interactive and shared communication and as a supplementary teaching tool to traditional teaching.

4.2. Design of the Database. To design an effective database, a systems engineering perspective is required. As the website is an AI web-based teaching platform, it has a wide range of course resources and therefore a large number of corresponding data sheets, including article system Data Sheet; Downloading system Data Sheet; Electronic lesson plans Data Sheet; FLASH System Data Sheet; Classified information Sheet; Electronic lesson plans Data Sheet. The electronic lesson plans Data Sheet; the FLASH System Data Sheet; the Classified information Sheet; the Photo System Data Sheet, etc. The electronic lesson plans and FLASH System Data Sheet are shown in Tables 1 and 2.

4.2.1. Electronic Lesson Plan Data Sheet. The Electronic lesson plans Data Sheet is an information management tool for electronic lesson plans, which includes: title, special attributes, title image, and release time information. The corresponding fields are shown in Table 1.

4.2.2. FLASH System Data Sheet. The FLASH System Data Sheet is the information management for FLASH files, including Title, Special Attributes, Author, FLASH Address, FLASH Width, and FLASH Height. The corresponding fields are shown in Table 2.

5. Functional Implementation of a Web-Based Platform for Artificial Intelligence Courses

5.1. Experiments. Pareto analysis was applied to assess the overall risk factors of sports training, and the results of the overall risk assessment of sports training were obtained, as shown in Table 3.

The artificial intelligence course network teaching platform is divided into the following six functional modules:

Course introduction: provide users with course introduction and courseware materials.

Teaching team: briefly introduce the teaching team of the course website, so that users can have a certain understanding of the teachers of the website.

Teaching achievements: the teaching achievements module is a platform for teachers' achievements display and sharing. Users can browse teachers' teaching achievements on the website, such as teachers' papers, certificates, and projects.

Teaching resources: including teaching resources such as course content based on flipped teaching concepts (WeChat, PPT, WeChat platform, etc.), course cases, and syllabus based on task-driven teaching mode. Users

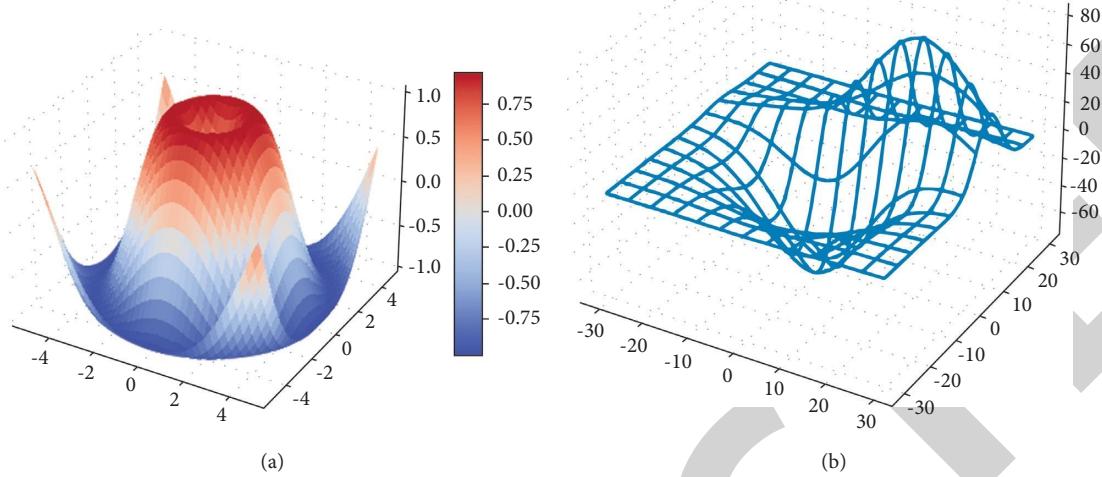


FIGURE 7: Utilisation of learning resources.

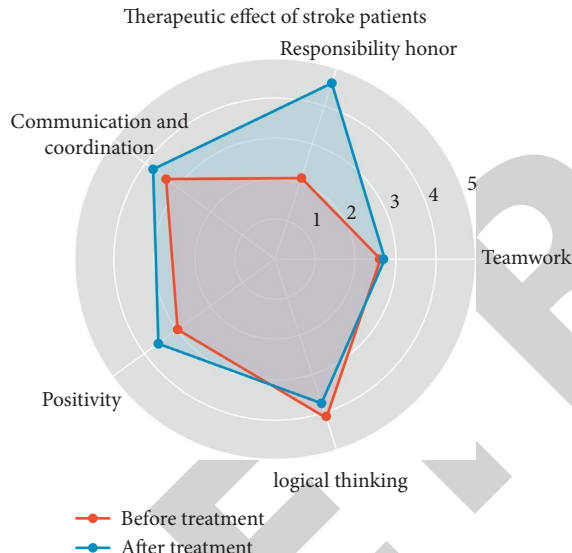


FIGURE 8: Radar chart of school resources and student status.

can freely choose the required materials for browsing and learning.

Learning garden: the learning garden is a display platform for scientific papers and excellent homework and a platform for interactive communication between teachers and students, providing users with reference materials for learning and reference.

Data download: it mainly completes the function of uploading and downloading electronic resources. The courseware includes relevant videos, a question bank, and courseware.

5.2. Platform Implementation. According to the function of the platform, it realizes six modules: course introduction, teaching team, teaching results, teaching resources, learning garden, and data download. Different modules correspond

to different pages, with simple structure and clear content. The function menu of the website is expanded in the form of a single row list, which makes the whole page appear orderly, concise, and clear. Users can easily browse the content of the website according to their needs and introduce the implementation process of the platform with the login interface and teaching resource module of the website.

5.2.1. Login Operation. This module is the system login interface. Its function is to detect whether the login user is legal and prevent illegal users from invading the system by verifying their user name and password. The system shall automatically judge the correctness of the user name and password entered. If the login is normal, the system shall record the current user name so that other operations can be assigned with appropriate permissions. The system login interface and website home page are shown in Figures 3 and 4.

5.2.2. Teaching Resource Module. The teacher resource module is the main functional module of the course platform. The module includes: teaching cases, teaching content, teaching video, teaching calendar, microclass, and PPT. Administrators release teachers' teaching videos and other teaching content to provide users with browsing and learning resources. After users select the required course resources and download them, they can view the course resources such as the course content and teaching cases [21, 22].

(1) Course Content Module. In the course content module, the teaching platform integrates the microcourse and diagnosis and treatment system of flipped classroom concept [23]. The flipped classroom is a new teaching model, which is composed of three basic elements: technical elements (mainly microvideo), process elements (before class-in class-after class), and environmental elements (intelligent diagnosis learning system). Flipped classroom focuses on the

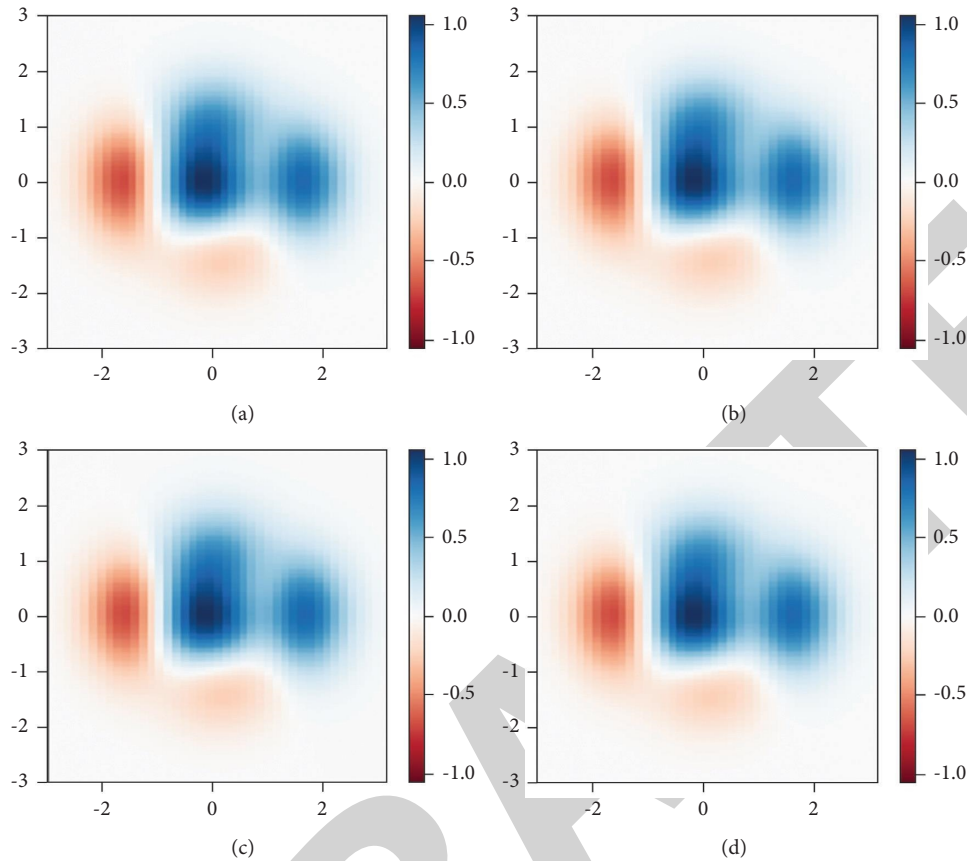


FIGURE 9: School teaching platform conversion matrix.

whole process of teaching activities, focuses on the teaching interactive behavior of teachers and students supported by a multimedia environment, and focuses on the active awakening of students' innovative spirit [24]. Based on this new concept of "flipped classroom," this paper designs the teaching design process and mode based on the public platform, as well as how to carry out the learning and interactive process of the micromobile course based on the WeChat public platform and develops the microcourse of principles of artificial intelligence based on the WeChat public platform and the corn pest diagnosis and treatment system in smart agriculture, as shown in Figures 5 and 6.

Figure 5 shows the characteristics of the flipped classroom. Teachers and students use multimedia technology to interact and communicate in time in the classroom. This teaching method plays a very good role in cultivating students' autonomous learning ability, autonomous problem discovery, and problem-solving ability. Figure 6 is the interface of the grass damage diagnosis and treatment system. The system is the application of artificial intelligence in grass damage diagnosis and treatment. Students can learn independently after class and diagnose grass damage by themselves [25–27].

6. Effectiveness of Aesthetic Informatics

Campus culture has a subtle effect on teachers and students, influencing both their values and the learning atmosphere on

campus. An information-based campus environment can enhance the breadth and depth of campus culture communication, break the constraints of time and space, enhance the attractiveness of campus culture, stimulate students' curiosity and creativity, and improve the efficiency of campus culture construction. Firstly, schools should actively use information technology to promote communication between students and the outside world and to stimulate their imagination and creativity in beauty. As shown in Figure 7 for its 3D distribution of resource use, schools use the network to share campus aesthetic culture resources, which can create a campus culture building platform for teachers, students, and parents to participate in, bringing individual campus culture in line with popular culture. Schools should use new media technology to create an information-based aesthetic environment for students, such as providing them with brightly colored pictures, pleasant music, lively animations, and virtual simulation images so that they can perceive the charm of campus aesthetic culture in many ways.

Schools should train teachers in all subjects at the generalist level of aesthetic education, set out beauty design requirements for teaching design and courseware, regulate teachers' teaching language and processes in terms of beauty, and integrate aesthetic education organically into the teaching of all subjects. As shown in the radar diagram of the functions of different resources in schools in Figure 8, the practice of specialized courses in aesthetic education should be increased so that students can perceive first-hand what is

around them. Schools can also try to integrate humanistic customs and local characteristics of landscape resources from around the world; for example, by offering a weekly practical lesson on aesthetic education and allowing teachers to take students outside for viewing and learning. Such a teaching approach that combines aesthetic education with local natural and humanistic landscapes can broaden the scope of aesthetic education, allowing students to appreciate the beauty of their hometowns and lives while enriching their own aesthetic world and enhancing their own aesthetic sensibilities.

Exploring information technology to facilitate cooperation between home, school, and society Aesthetic education in the new era requires schools to co-ordinate and integrate social resources to implement the goal of enhancing students' aesthetic abilities in a home-school approach. With the increasing improvement of the school's information technology hardware construction and the increasing awareness of information technology, the learning effect of different campus websites, as shown in Figure 9, which can release school information or communicate with parents and society. Schools should pay full attention to and make use of the social resources around them, using information technology as a medium to design feasible aesthetic education collaborative projects to benefit students.

7. Conclusions

In the process of promoting aesthetic education, as the main body, the school has many shortcomings. Schools should strive to find strong and feasible initiatives in terms of system construction, teaching methods, teachers, digital resources, and improvement of conditions to find a breakthrough and anchor point for information-based aesthetic education and enhance students' aesthetic literacy. This paper combines the teaching objectives of the AI course and the characteristics and steps of the task-driven teaching method to develop an online teaching platform for the core AI course, which breaks the time and space limitations of the traditional teaching mode and enables teachers and students to learn and communicate anytime and anywhere, rather than being confined to the classroom. This provides a new mode of learning for the core AI course and has a positive effect on students' learning [19].

Data Availability

The experimental data used to support the findings of this study are available from the corresponding author upon request.

Conflicts of Interest

The authors declare that they have no conflicts of interest regarding this work.

Acknowledgments

This work was supported by the General research projects of Humanities and Social Sciences in Colleges and Universities

of Jiangxi Province in 2019 (Grant no. SZZX1901) and the 2019 General Research Project of Jiangxi Institute of Economics Administrators (Grant no. 2019YB034).

References

- [1] Y. Pan and L. Zhang, "Roles of artificial intelligence in construction engineering and management: a critical review and future trends," *Automation in Construction*, vol. 122, Article ID 103517, 2021.
- [2] F. Kong, "Application of artificial intelligence in modern art teaching," *International Journal of Emerging Technologies in Learning (ijET)*, vol. 15, no. 13, pp. 238–251, 2020.
- [3] X. Xie, X. Pan, F. Shao, W. Zhang, and J. An, "MCI-Net: multi-scale context integrated network for liver CT image segmentation," *Computers & Electrical Engineering*, vol. 101, Article ID 108085, 2022.
- [4] O. I. Abiodun, A. Jantan, A. E. Omolara, K. V. Dada, N. A. Mohamed, and H. Arshad, "State-of-the-art in artificial neural network applications: a survey," *Heliyon*, vol. 4, no. 11, Article ID e00938, 2018.
- [5] R. Sil, A. Roy, B. Bhushan, and A. K. Mazumdar, "Artificial intelligence and machine learning based legal application: the state-of-the-art and future research trends," in *Proceedings of the 2019 International Conference on Computing, Communication, and Intelligent Systems (ICCCIS)*, pp. 57–62, IEEE, Greater Noida, India, 2019, October.
- [6] T. Yigitcanlar, K. C. Desouza, L. Butler, and F. Roozkhosh, "Contributions and risks of artificial intelligence (AI) in building smarter cities: insights from a systematic review of the literature," *Energies*, vol. 13, no. 6, p. 1473, 2020.
- [7] Y. Lu, "Artificial intelligence: a survey on evolution, models, applications and future trends," *Journal of Management Analytics*, vol. 6, no. 1, pp. 1–29, 2019.
- [8] X. I. E. Tao, C. Zhang, and Y. Xu, "Collaborative parameter update based on average variance reduction of historical gradients," *Journal of Electronics and Information Technology*, vol. 43, no. 4, pp. 956–964, 2021.
- [9] Z. H. A. N. G. Zhengwan, Z. H. A. N. G. Chunjong, L. I. Hongbing, and X. I. E. Tao, "Multipath transmission selection algorithm based on immune connectivity model," *Journal of Computer Applications*, vol. 40, no. 12, p. 3571, 2020.
- [10] A. Mosavi and A. R. Varkonyi-Koczy, *Integration of machine learning and optimization for robot learning*, pp. 349–355, Springer, Cham, 2017.
- [11] T. Ahmad, D. Zhang, C. Huang et al., "Artificial intelligence in sustainable energy industry: status Quo, challenges and opportunities," *Journal of Cleaner Production*, vol. 289, Article ID 125834, 2021.
- [12] A. Gupta, Y. S. Ong, and L. Feng, "Insights on transfer optimization: because experience is the best teacher," *IEEE Transactions on Emerging Topics in Computational Intelligence*, vol. 2, no. 1, pp. 51–64, 2018.
- [13] H. Salehi and R. Burgueño, "Emerging artificial intelligence methods in structural engineering," *Engineering Structures*, vol. 171, pp. 170–189, 2018.
- [14] J. E. Auerbach, A. Concordel, P. M. Kornatowski, and D. Floreano, "Inquiry-based learning with robogen: an open-source software and hardware platform for robotics and artificial intelligence," *IEEE Transactions on Learning Technologies*, vol. 12, no. 3, pp. 356–369, 2019.

Research Article

Personalized Recommendation Algorithm for Movie Data Combining Rating Matrix and User Subjective Preference

Chang Liu 

Zhewen Pictures Group Co.,Ltd, Hangzhou 31000, China

Correspondence should be addressed to Chang Liu; zwoc@zhewenpictures.com

Received 7 June 2022; Revised 28 June 2022; Accepted 6 July 2022; Published 9 August 2022

Academic Editor: Le Sun

Copyright © 2022 Chang Liu. This is an open access article distributed under the Creative Commons Attribution License, which permits unrestricted use, distribution, and reproduction in any medium, provided the original work is properly cited.

The film industry has also caught the fast train of Internet development. Various movie resources have come into view. Users need to spend a lot of time searching for movies they are interested in. This method wastes time and is very bad. The article proposes an NMF personalized movie recommendation algorithm, which can recommend movies to users based on their historical behavior and preference. The research results of the article show the following: (1) the experiment counts movie reviews of different users in the same time span. The results show that 48.42% of users have only commented on a movie once, 79.76% of users have posted less than or equal to 5 comments, and 89.92% of user reviews have posted less than or equal to 10 times. (2) In the comparative experiments of the NMF algorithm in different dimensions, the effect of the NMF-E algorithm is much better than that of the NMF-A algorithm. The accuracy, recall, and $F1$ value of the NME-E algorithm are all 3 types. The experimental results show that the NME-E algorithm is the best among all algorithms. (3) In the experiment to test the effectiveness of the NMF personalized recommendation algorithm, comparing the experimental results, the MAE value of the improved NMF personalized recommendation algorithm is lower than that of the unimproved algorithm. When the number of neighbors is 10, the highest value of the improved MAE of the previous algorithm is 0.837. After the improved algorithm, the MAE value is the highest (0.83), and the MAE value has dropped by 0.007, indicating that the error is smaller after the improved algorithm, and the result of recommending movies is more accurate. The recall value of the four algorithms will increase as the number of neighbors increases. Among them, the recall value of the NMF algorithm proposed in the article is the highest among several algorithms. The highest value can reach 0.200, which is higher than the highest value of other algorithms. It shows that the recommendation effect of NMF algorithm is the best. (4) According to the results of the questionnaire, after using the NMF personalized recommendation algorithm, users' satisfaction increased from 20% to 50%, an increase of 30%, and their dissatisfaction decreased from 15% to 8%, a decrease of 7%. Relative satisfaction increased from 52% to 55%, an increase of 3%, satisfaction increased from 35% to 60%, an increase of 25%, and dissatisfaction decreased from 40% to 20%, a decrease of 20%, indicating that the algorithm can meet the requirements of most people.

1. Introduction

With the rapid development of the information age, we will be faced with very complex digital and networked data. How users choose effective information from the tedious information, personalized recommendation algorithms can help users filter out the information they want and solve the needs of the vast majority of people. The film industry in China has also been developing rapidly in recent years. There are many movies released every year. The personalized recommendation of movie data can effectively solve the different needs

of users. There are many types of movies released every year in our country. When faced with so many movies, users will inevitably be at a loss and do not know how to choose. Literature [1] proposed a new cross-space affinity learning algorithm on different spaces with heterogeneous structures. The algorithm records and saves the record of the movie watched by the user, as well as the record of the comment. According to the user's comment, the user's movie hobby can be calculated. The article also compares the performance of the algorithm with the benchmark movie recommendation set, and the results show that the algorithm proposed

in the article has advantages. Literature [2] focuses on how to design a reliable and highly accurate movie recommendation algorithm. Literature [3] proposed an improved deep reinforcement learning algorithm to recommend movies. Literature [4] proposed an efficient privacy protection collaborative filtering algorithm based on differential privacy protection and time factors. Literature [5] discussed the problems of traditional collaborative filtering algorithms and proposed improvements. Literature [6] introduced virtual prediction items in a relatively sparse rating database. Literature [7] is combining collaborative filtering and association rules to accurately improve user recommendations. Literature [8] proposed a hybrid collaborative filtering algorithm based on user preferences and item characteristics. Literature [9] is inspired by the user-item rating matrix of the network and introduces an improved algorithm that combines the similarity of items with the dynamic resource allocation process. Aiming at the problem of insufficient demand mining for movie recommendation systems, literature [10] proposed a personalized movie recommendation system based on the collaborative filtering algorithm. Literature [11] proposed a spark-based matrix factorization recommendation algorithm, which uses spark memory computing and parallel data processing. Literature [12] focuses on the application of the latent factor model in the movie recommendation system and improves the latent factor model to overcome its shortcomings that it cannot give recommendation explanation. Literature [13] proposed a distributed collaborative filtering recommendation algorithm. Literature [14] researched using the concept of data warehouse to create a movie recommendation system. Literature [15] introduced the theory of semantic computing to label the semantic tags in movie clips and candidate advertisements.

2. Research on Personalized Movie Recommendation Technology

2.1. Research Background and Significance. This paper considers the introduction of other important movie information under the framework of collaborative filtering algorithm and combined with scoring data for hybrid recommendation [16]. It is worth noting that there is a kind of rich and valuable information on movie websites-movie reviews, but this kind of information is often ignored. Movie sites do hope that users can give more and more detailed reviews because considering that when users decide whether to watch a movie, the movie reviews given by other users will provide them with reference opinions, and a large number of movie reviews can improve users' perceptions. The level of interaction between users, thereby, potentially increases user stickiness. Generally, users always express the points or aspects that they care about most in their reviews of a certain movie, and these aspects often reflect the user's potential preference for the movie. A general rating can only indicate whether a user likes the movie or not, but it cannot give a specific reason why the user likes or hates the movie [17]. The user's specific evaluation of the movie is shown in Table 1.

2.2. Current Status of Movie Recommendation Research. Since review information is user-generated content, which contains the opinions and emotions of the reviewer, it is worth digging deeper to describe the "unique attributes" of users by using the review text. However, in the field of movie recommendation, film reviews should be digging. Relatively speaking, there are still very few studies. From the perspective of the recommendation field as a whole, some researchers have realized the rich information contained in text reviews and the value contained therein, but most of the researches use topic models to directly extract the topic distribution of text reviews without considering to the emotional factor in the comments. The user's film reviews actually reflect the user's likes and dislikes of a movie from certain angles. The previous research mixed texts with different emotional tendencies for analysis and could not fully extract the user's favorite and dissatisfied aspects of the movie. The use of sentiment analysis is to refine and divide the reviews and extract the user's satisfaction and dissatisfaction with the movie, which is the significance of mining reviews [18].

2.3. Personalized Recommendation Process. It can be regarded as first data collection of movie information evaluated by users, combined with user's movie reviews for sentiment analysis, and then imported into the NMF personalized recommendation model. The model will predict the movies that the user may like based on the user's historical behavior information and the supervisor's preference. Sort the movies according to the degree of preference. The first one is the one that the user may be most interested in, and then the list is recommended to the user. The basic flow chart is shown in Figure 1.

3. Research on the Recommendation Algorithm of Scoring Matrix and User Supervisor Preference

3.1. User Subjective Preference Recommendation Algorithm. The recommended algorithm steps are shown in Figure 2.

Construct a user movie rating table, as shown in Table 2.

I_u is a collection of movies rated by user u , and I_v is a collection of movies rated by user v [19]; user similarity is

$$\text{sim}(u, v) = \frac{|I_u \cap I_v|}{|I_u \cup I_v|} \quad (1)$$

Recommended results:

$$\bar{r}_{ui} = \sum_{j \in S(j,k) \cap N(u)} \text{sim}(i, j) r_{uj}. \quad (2)$$

$N(u)$ is a collection of movies rated by the user u , and $S(j, k)$ is a collection of movies j similar to K movie collections [20].

The formula for calculating the degree of preference between user u and other movies v is

TABLE 1: User evaluation form.

User ID	Time	Comment	score
68547261 (A)	2018-02-23 17:47:06	Watching "Interstellar," the initial surprise comes from music. The first climax of the film is the appearance of the song called comfield chase. Perhaps the reason why this song became the core of the film is this kind of senseless spirit of exploration. Director Nolan said after listening to this piece: My movie is ready for shooting. Hans Zimmer's soundtrack makes this film the uncrowned king in many people's hearts.	4
58691048 (B)	2019-02-12 23:55:04	Why can this science fiction movie stand out and be included in the history of film and television? Interstellar is a real hard science fiction movie. The movie incorporates the concept of five-dimensional space. This is a film that fully uses the concept of time and space. Its script is more based on data theories and formulas to support the development of the entire plot. Compared with other movies with no scientific basis, it is judged high.	5
78651562 (C)	2018-10-25 9:53:09	"Interstellar," Nolan is another magical film, and it should be the greatest science fiction film. Leaving aside the science fiction elements in the movie, after all, I do not understand [covering face]. From a human point of view, Nolan always likes to put the complexity of human nature in front of people, facing the instinct to survive, calling him the Earth. The hopeful professor Mann has become another Harvey Dante, with a feeling of DK series.	5
78961310 (D)	2014-11-16 00:49:28	Anne Hathaway said, I love him, but that does not mean I'm wrong. Love is something that humans cannot understand. It may be given to us by more advanced creatures. Although we think it is sensibility, it may be the highest level of wisdom. Anne Hathaway's short hair is very beautiful, like a smart and stubborn little boy, with human wisdom and love, who would not love her?	4

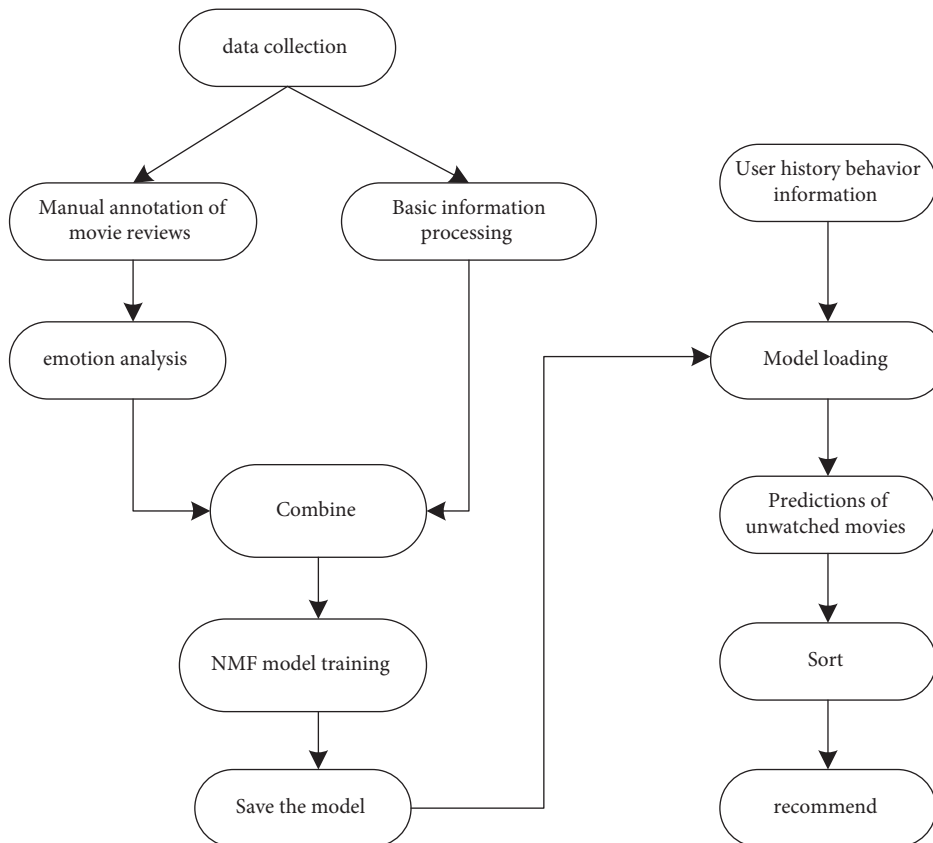


FIGURE 1: Flowchart of personalized recommendation.

$$S(u, v) = \sum_{V \in N(u)} \cos(R(:, v)^T, R(:, v)). \quad (3)$$

Common mixed recommendation models are shown in Table 3:

Build user characteristics such as in Table 4.

Calculate user G 's preference for your teenage movie:

$$r = \frac{1}{n} \sum_{i=1}^n (x_i - ave). \quad (4)$$

Movies users may like

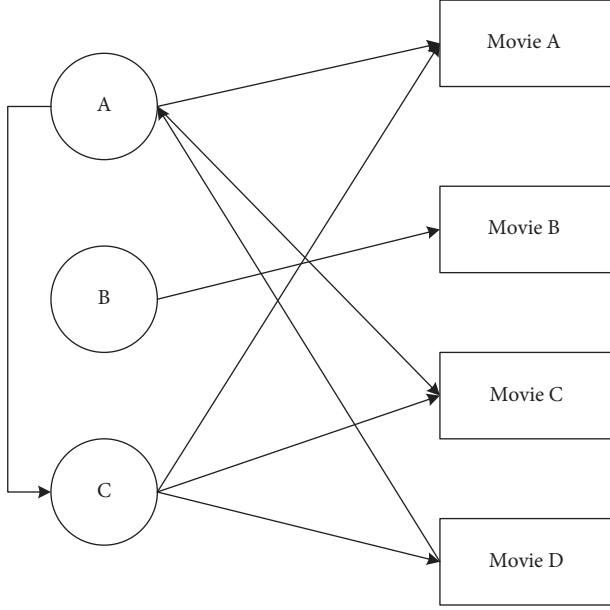


FIGURE 2: Overview of user recommendation algorithm.

TABLE 2: User rating matrix.

User	Movie A	Movie B	Movie C	Movie D	Movie E
A	3	4	0	3.5	0
B	4	0	4.5	0	3.5
C	0	3.5	0	0	3
D	0	4	0	3.5	3

$$\cos(U, I) = \frac{\sum U_a \times I_a}{\sqrt{\sum U_a^2} \times \sqrt{\sum I_a^2}} \quad (5)$$

Error value of movie prediction:

$$\text{MAE} = \frac{\sum_{u,i \in T} |r_{ui} - \bar{r}_{ui}|}{N} \quad (6)$$

Movie recommendation accuracy rate:

$$\text{RMSE} = \frac{\sqrt{\sum_{u,i \in T} (r_{ui} - \bar{r}_{ui})^2}}{N} \quad (7)$$

Movie ranking prediction:

$$\text{Precision} = \frac{\sum_{u \in U} |R(u) \cap T(u)|}{\sum_{u \in U} |R(u)|} \quad (8)$$

3.2. Score Matrix Recommendation Algorithm. In the recommendation system, $U^m = \{u_1, u_2, \dots, u_m\}$ represents the user level, $I^n = \{i_1, i_2, \dots, i_n\}$ represents the movie set, and $R^{m \times n}$ represents the $m \times n$ -dimensional rating matrix [21] as shown in Table 5.

The similarity between users is expressed as

$$\text{PCC_sim}(a, b) = \frac{\sum_{p \in P} (r_{a,p} - \bar{r}_{a,p})(r_{b,p} - \bar{r}_{b,p})}{\sqrt{\sum_{p \in P} (r_{a,p} - \bar{r}_{a,p})^2} \sqrt{\sum_{p \in P} (r_{b,p} - \bar{r}_{b,p})^2}} \quad (9)$$

Among them, P represents the collection of movies that users a and b have rated together, and $\bar{r}_{a,p}$ and $\bar{r}_{b,p}$ represent the average ratings of users and based on the common movie collection P , respectively.

Cosine similarity:

$$\text{Cos_sim}(a, b) = \frac{\vec{a} \cdot \vec{b}}{|\vec{a}| * |\vec{b}|} \quad (10)$$

The formula can also be written as

$$\text{Cos_sim}(a, b) = \frac{\sum_{p \in P} r_{a,p} * r_{b,p}}{\sqrt{\sum_{p \in P} r_{a,p}^2} \sqrt{\sum_{p \in P} r_{b,p}^2}} \quad (11)$$

Select the first K similar users to rate the unreviewed movie collection [22]; the calculation formula is

$$\text{pre}(a, p) = \bar{r}_a + \frac{\sum_{b \in NN} \text{sim}(a, b) * (r_{b,p} - \bar{r}_b)}{\sum_{b \in NN} \text{sim}(a, b)} \quad (12)$$

User u 's rating calculation formula for unrated movie p :

$$\text{pre}(u, p) = \frac{\sum_{i \in NN} \text{sim}(i, p) * r_{u,i}}{\sum_{i \in NN} \text{sim}(i, p)} \quad (13)$$

3.3. NMF Personalized Recommendation Algorithm. The NMF personalized recommendation algorithm combining the scoring matrix and the user's subjective preference is to extract and generate each user's comment [23] and calculate the weight, as shown in Table 6:

\bar{r}_i Is the average rating of user u_i on the movie.

Calculate the interest topics of a user's single movie review:

$$\theta_{ij} = \alpha_p \cdot \theta_{p-i,j} + \alpha_N \cdot \theta_{N-i,j} \quad (14)$$

The formula for calculating the overall interest distribution of users is

$$\theta_i = \frac{\sum_{j \in I} \theta_{ij}}{|I_i|} \quad (15)$$

The following formula measures the similarity between users:

$$D_{KL}(\theta_a \| \theta_b) = \sum_i \theta_a(i) \ln \frac{\theta_a(i)}{\theta_b(i)},$$

$$\vec{M} = \frac{1}{2} (\theta_a + \theta_b), \quad (16)$$

$$D_{JS}(\theta_a \| \theta_b) = \frac{1}{2} \left(D_{KL}(\theta_a \| \vec{M}) + D_{KL}(\theta_b \| \vec{M}) \right),$$

$$\text{sim}(a, b) = 1 - D_{JS}(\theta_a \| \vec{M}).$$

Average the topic distribution of all film reviews:

TABLE 3: Common mixed recommendation models.

Mixed way	Description
Weighted	The calculation results of multiple recommendation techniques are weighted and mixed to generate recommendations
Switching	The calculation results of multiple recommendation techniques are weighted and mixed to generate recommendations
Cascade	The cascading technology constructs the order of preference between different projects in the iterative refinement process
Combined	At the same time, multiple recommendation techniques are used to give multiple recommendation results to provide users with reference
Feature combination	The features generated by a specific recommendation technique are input to another recommendation technique
Increasing features	The output of the former recommended method is used as the input of the latter recommended method
Meta-level mixing	An internal model generated by one recommendation technique is used as an input for another recommendation technique

TABLE 4: User rating matrix.

User	Young you	Wolf warriors 2	Me and my motherland
User F	3	4	5
User G	—	3	6

TABLE 5: User-movie collection rating matrix.

User-movie collection	i_1	i_2	\dots	i_j	\dots	i_n
u_1	r_{11}	r_{12}	\dots	r_{1j}	\dots	r_{1n}
u_2	r_{21}	r_{22}	\dots	r_{2j}	\dots	r_{2n}
\dots	\dots	\dots	\dots	\dots	\dots	\dots
u_i	r_{i1}	r_{i2}	\dots	r_{ij}	\dots	r_{in}
\dots	\dots	\dots	\dots	\dots	\dots	\dots
u_m	r_{m1}	r_{m2}	\dots	r_{mj}	\dots	r_{mn}

$$\theta_j = \frac{\sum_{i \in U_j} \theta_{ij}}{|U_j|}. \quad (17)$$

Predict the distance between the user and the movie according to U, V :

$$\begin{aligned} U_u &= U_u - \alpha \frac{\partial L}{\partial U_u}, \\ V_i &= V_i - \alpha \frac{\partial L}{\partial V_i}, \\ b_u(u) &= b_u(u) - \alpha \frac{\partial L}{\partial b_u(u)}, \\ b_i(i) &= b_i(i) - \alpha \frac{\partial L}{\partial b_i(i)}, \end{aligned} \quad (18)$$

in

$$\begin{aligned} \frac{\partial L}{\partial U_u} &= -\sum_{i=1}^n I_{ui} T_{ui} (Y_{ui} - \bar{d}_{ui}) \times \frac{1}{D_{ui}} (U_u - V_i) + \lambda U_u, \\ \frac{\partial L}{\partial V_i} &= -\sum_{u=1}^m I_{ui} T_{ui} (Y_{ui} - \bar{d}_{ui}) \times \frac{-1}{D_{ui}} (U_u - V_i) + \lambda V_i, \\ \frac{\partial L}{\partial b_u(i)} &= -\sum_{i=1}^n I_{ui} T_{ui} (Y_{ui} - \bar{d}_{ui}) + \lambda b_u(i), \\ \frac{\partial L}{\partial b_i(u)} &= -\sum_{u=1}^m I_{ui} T_{ui} (Y_{ui} - \bar{d}_{ui}) + \lambda b_i(u). \end{aligned} \quad (19)$$

4. Simulation Experiment

4.1. Data Set Characteristics. The experiment selected a real user evaluation album with a time span of 2016.9.1–2017.1.14. The experiment recorded the ID of each user, the content and value of the rating, and the time of the rating. The experiment was carried out on each user who scored. Statistics on the total number of comments has been made. The results show that 48.42% of users have only commented on the movie once, 79.76% of users have commented less than or equal to 5 times, and 89.92% of users have commented less than or equal to 10 times. The results are shown in Tables 7 and 8.

4.2. Evaluation Criteria. The evaluation criteria are shown in Table 9.

4.3. Experimental Results and Analysis. The experiment compares the NMF personalized recommendation algorithm in different dimensions to verify the rationality and performance superiority of the algorithm. An algorithm in the experiment is to only collect user movie reviews without any analysis. This algorithm is called NMF-E for short. The second algorithm ignores the influence of some negative reviews in movie reviews on user interest topics, and only considers positive movie reviews. This algorithm is referred to as NMF-A for short. The experimental comparison results are shown in Figures 3–5:

According to the results of the comparative experiment, we can find that the NMF-E algorithm, which does not do any sentiment analysis on the movie reviews posted by users, is better than ignoring the impact of some negative reviews in movie reviews on user interest topics and only takes into account the positive reviews. The effect of the NMF-A algorithm of the movie review is much better. The accuracy, recall, and $F1$ value of the NMF-E algorithm are the highest among the three algorithms. The accuracy and $F1$ value will decrease as the number of movies recommended by the user increases, and the recall rate will follow the user recommendation. The number of movies decreases as the number of movies increases.

TABLE 6: Weights of topic vectors.

	High score ($r_{ij} > \bar{r}_i$)	Low score ($r_{ij} > \bar{r}_i$)
Forward document weight	$\alpha_p = 1/1 + e^{-(r_{ij} > \bar{r}_i)}$	$\alpha_p = 1/1 + e^{r_{ij} - \bar{r}_i}$
Negative document weight	$\alpha_N = 1/1 + e^{r_{ij} - \bar{r}_i}$	$\alpha_N = 1/1 + e^{-(r_{ij} > \bar{r}_i)}$

TABLE 7: Evaluation record template.

User ID	Time	Movie IDmmcl	Score	Comment
61719620	2016-01-14 13:41:34	10577869	5	Love movie I really like! we met in the dark, of course we love each other, family feelings, family trivial matters, everything is so beautiful... Remember the English accent? The hostess is so beautiful! male starring in sunglasses, handsome! It's worth watching again anyway

TABLE 8: Statistics of user evaluation times.

Number of comments	User number	Percentage (%)
1	237209	48.42
≤ 5	390775	79.76
≤ 10	440539	89.92

4.4. Model Performance Testing. In order to test the effectiveness of the NMF personalized recommendation algorithm, we selected more than 100,000 comments on more than 1,000 movies from more than 900 users, and each user has more than 20 comments on the movie. In order to improve the accuracy of the NMF algorithm and find the most suitable decomposition dimension value, we can conclude from the data in the graph that the value of MAE will first decrease and then increase as the decomposition dimension increases. When the decomposition dimension value is at 6 o'clock, the value of MAE is the lowest. The value of MAE represents the accuracy of the algorithm for personalized recommendation of movies according to the user's preferences, and the recall value is reflected in the recommended movie results, the proportion of users who are really interested in the movie [24]. Among them, the value of MAE is small, indicating that the error of the algorithm is lower, and the value of recall is larger, indicating that the proportion of users who are really interested is more. The relationship between the decomposition dimension and MAE is shown in Figure 6.

After improving the NMF personalized recommendation algorithm, we compare it with the traditional NMF algorithm. Under the condition that the adjacent numbers of the variables are set to 10, 20, 30, 40, and 50, respectively, we compare the MAE values of the two different algorithms. The experimental data is shown in Figure 7:

From the data in the figure, we can conclude that the MAE value of the improved NMF personalized recommendation algorithm is lower than that of the unimproved algorithm. When the number of neighbors is 10, the highest MAE value of the algorithm before the improvement is 0.837. After the algorithm is improved, the MAE value is the highest value is 0.83, and the MAE value has dropped by 0.007, indicating that the error is smaller

after the improved algorithm, and the result of recommending movies is more accurate. In order to further test the effectiveness of the NME algorithm, we compared with 3 other different algorithms and observed their MAE value and recall value. The details are shown in Tables 10 and 11.

From the data in Figure 8, we can conclude that the MAE values of the four algorithms will change with the fluctuation of the number of neighbors. When the number of neighbors is small, the MAE value of the NMF algorithm and the Jaccard algorithm fluctuates greatly. The NMF personalized recommendation algorithm proposed in the article among the four algorithms has the smallest MAE value regardless of the number of neighbors. When the number of neighbors is 10, the MAE value is the largest, and the maximum value is 0.783. The MAE value of the CEHPI algorithm is the largest among the four algorithms. The NCF and Jaccard algorithms are between the two algorithms. The experimental data further shows that the prediction accuracy of the NMF personalized recommendation algorithm proposed in the article is the highest among the four algorithms.

According to the data in Figure 9 and Table 11, we can conclude that the recall value of the four algorithms will increase as the number of neighbors increases. The recall value of the NMF algorithm proposed in the article is the highest among several algorithms, and the highest value can reach 0.200, both high and the highest value of other algorithms. The recall value of the Jaccard algorithm is the lowest among several algorithms, the lowest value is 0.100, and the CEHPI and NCF algorithms are somewhere in between.

4.5. Satisfaction Survey of Recommendation Results. In order to study the user's satisfaction after using the NMF personalized recommendation algorithm, the experiment took the form of questionnaire. The specific data is shown in Figure 10:

According to the data in Figure 10, after using the NMF personalized recommendation algorithm, the user's degree of satisfaction increased from 20% to 50%, an increase of 30%, and the degree of dissatisfaction decreased from 15% to 8%, a decrease of 7%. Relative

TABLE 9: Evaluation criteria table.

	Metrics	Formula
Accuracy	The accuracy measurement standard refers to the ratio of the number of hit movies to the number of recommended movies. The larger the index value, the more accurate the recommendation result.	$Precision = hits_u / recset_u$
Recall rate	The recall rate standard refers to the ratio of the number of hit movies to the theoretical maximum number of hits. The larger the index value, the more accurate the recommendation result.	$Recall = hits_u / testset_u$
F1 measurement	The F1 measurement index can effectively balance the accuracy rate and the recall rate by favoring the smaller value. The larger the index value, the more accurate the recommendation result.	$F1 = 2 \times precision \times recall / (precision + recall)$

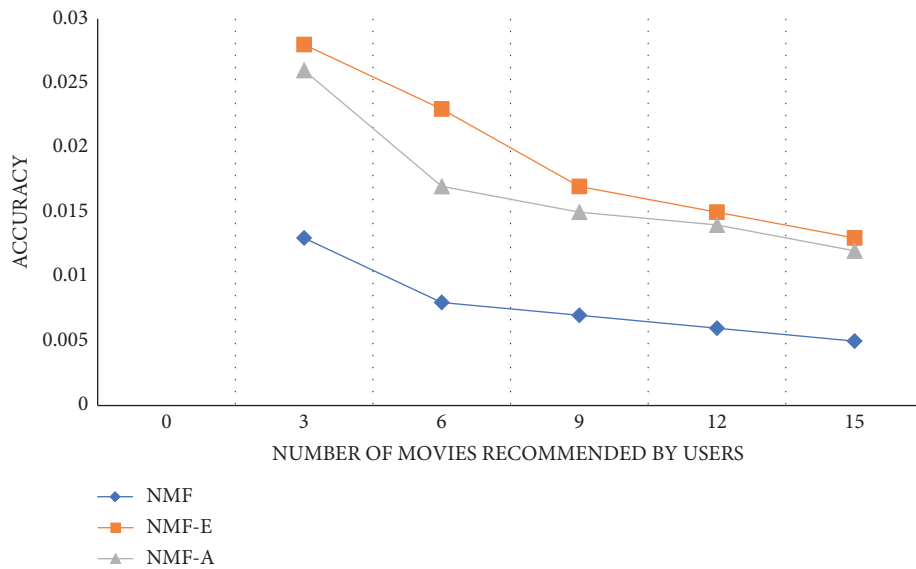


FIGURE 3: Accuracy curve.

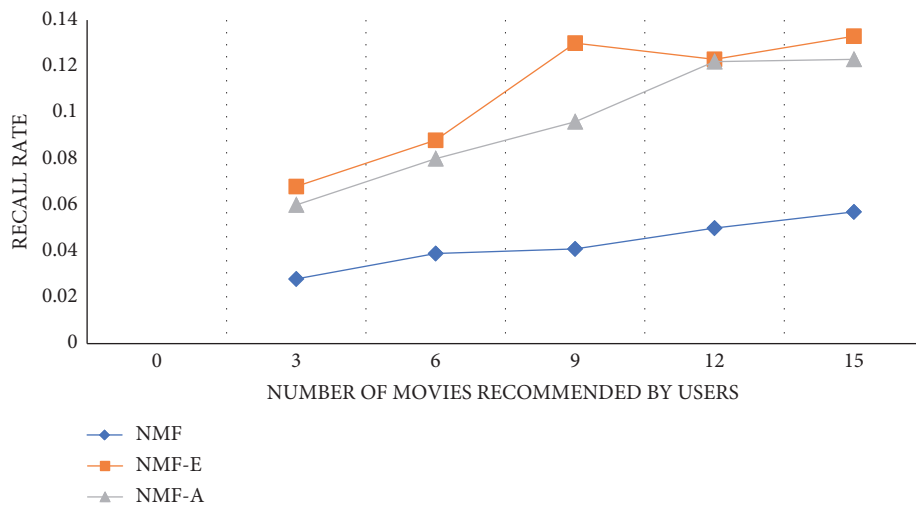


FIGURE 4: Recall rate curve.

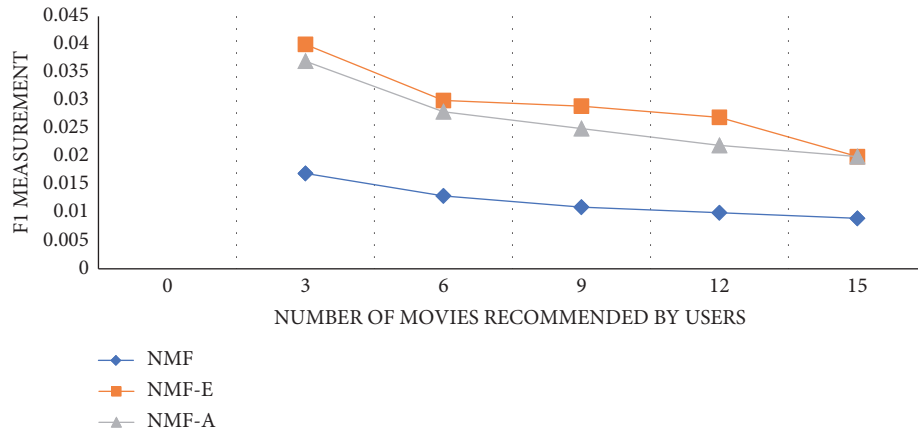


FIGURE 5: F1 measurement value curve.

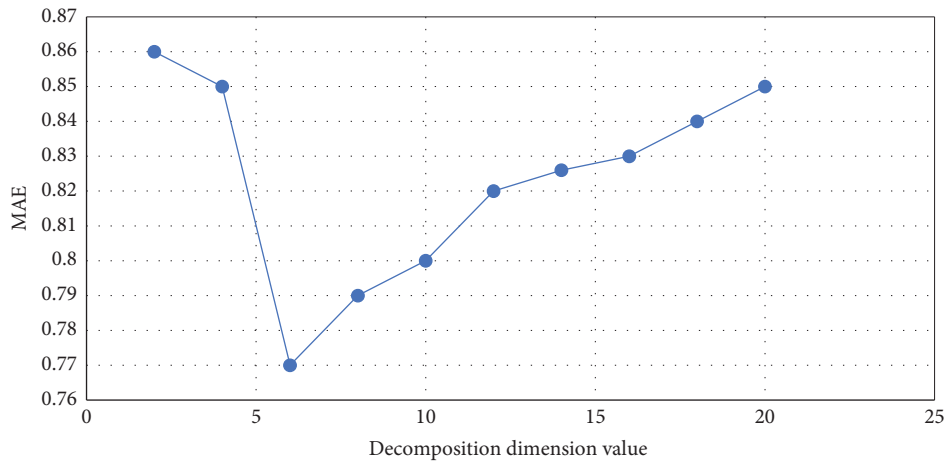


FIGURE 6: Relationship between decomposition dimension and MAE value.

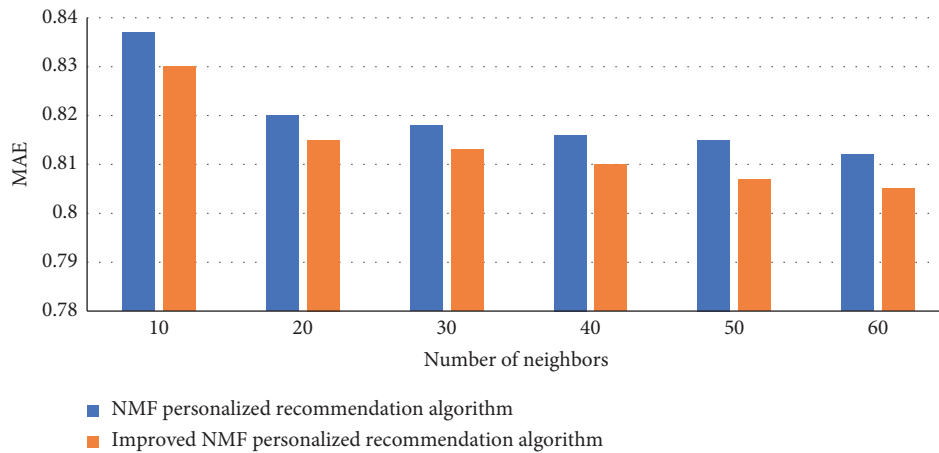


FIGURE 7: Improved algorithm performance comparison chart.

TABLE 10: MAE values of different algorithms.

Algorithm	5	10	15	20	25	30	35	40	45	50
NMF personalized recommendation algorithm	0.762	0.783	0.770	0.771	0.772	0.774	0.775	0.775	0.776	0.776
Jaccard personalized recommendation algorithm	0.815	0.790	0.790	0.791	0.795	0.797	0.802	0.803	0.804	0.809
CEHPI personalized recommendation algorithm	0.837	0.820	0.819	0.816	0.810	0.806	0.800	0.799	0.796	0.795
NCF personalized recommendation algorithm	0.810	0.791	0.790	0.790	0.785	0.784	0.783	0.782	0.780	0.779

TABLE 11: Recall values of different algorithms.

Algorithm	5	10	15	20	25	30	35	40	45	50
NMF personalized recommendation algorithm	0.042	0.058	0.100	0.130	0.157	0.184	0.185	0.188	0.776	0.200
Jaccard personalized recommendation algorithm	0.024	0.030	0.042	0.051	0.063	0.080	0.090	0.095	0.804	0.100
CEHPI personalized recommendation algorithm	0.024	0.031	0.051	0.060	0.073	0.110	0.115	0.117	0.796	0.120
NCF personalized recommendation algorithm	0.030	0.050	0.073	0.091	0.120	0.160	0.172	0.176	0.780	0.190

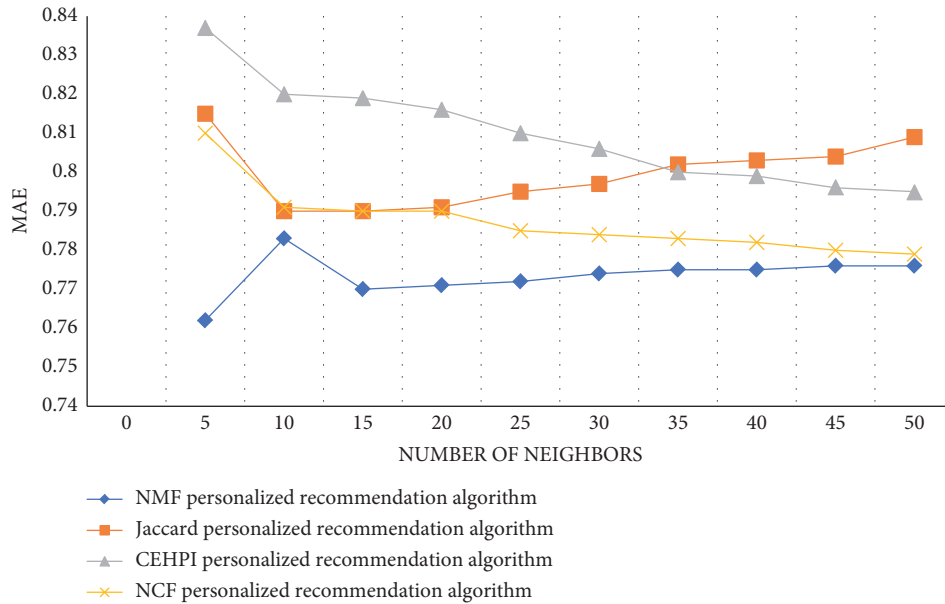


FIGURE 8: MAE values of different algorithms.

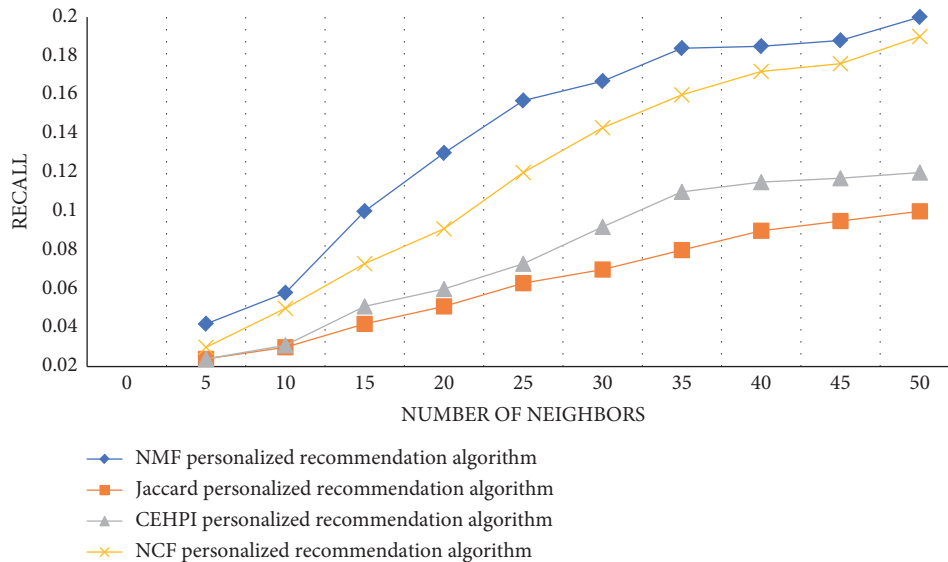


FIGURE 9: Recall values of algorithms.

satisfaction increased from 52% to 55%, an increase of 3%, satisfaction increased from 35% to 60%, an increase of 25%, and dissatisfaction decreased from 40% to 20%, a decrease of 20%. The experimental results prove that the

NMF personalized recommendation algorithm can provide users with effective decision support, improve user satisfaction, and promote the long-term development of the film industry.

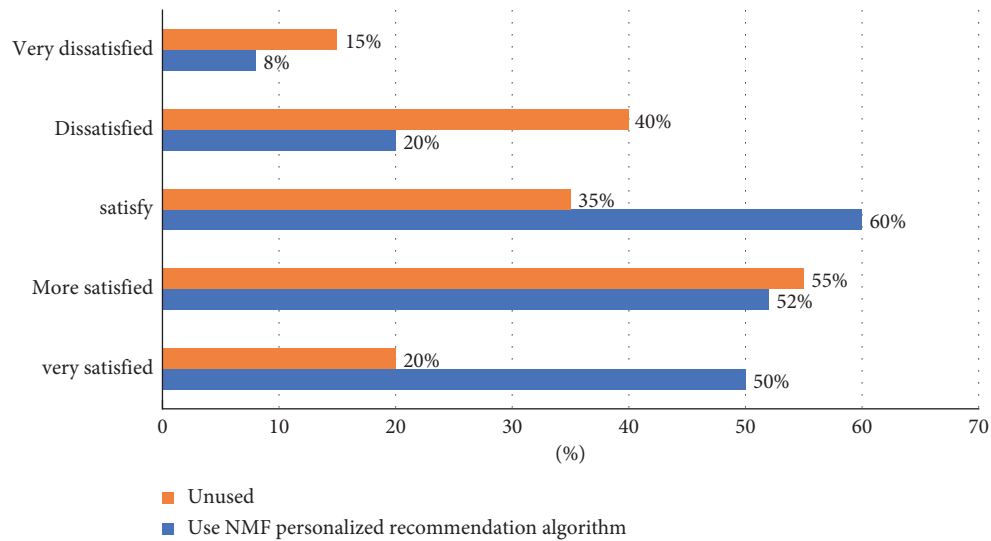


FIGURE 10: User satisfaction survey.

5. Conclusion

Movie reviews are important information that directly reflects the subjective feelings of users. According to user reviews, we can know the theme of the movie and the user's viewing experience. The article combines the scoring matrix and the personalized recommendation algorithm of movie data preferred by the user's supervisor and proposes an NMF personalized recommendation model. When users are faced with dazzling movie data, users no longer have to spend a lot of time searching for movies they are interested in. While the system meets the diverse needs of users, it also promotes the long-term development of the film industry [25]. According to the effective survey results, there are still some users whose satisfaction with the personalized recommendation model needs to be improved. Therefore, the performance of the personalized recommendation model should be continuously improved. This is the invincibility of the Chinese film industry in the face of increasing business competition.

Data Availability

The data used to support the findings of this study are available from the corresponding author upon request.

Conflicts of Interest

The author declares that there are no conflicts of interest.

References

- [1] J. Tang, G. J. Qi, L. Zhang, and C. Xu, "Cross-space affinity learning with its application to movie recommendation," *IEEE Transactions on Knowledge and Data Engineering*, vol. 25, no. 7, pp. 1510–1519, 2013.
- [2] T. Zhou, L. Chen, and S. Jian, "Movie recommendation system employing the user-based CF in cloud computing[C]," in *Proceedings of the 2017 IEEE international conference on computational science and engineering (CSE) and IEEE international conference on embedded and ubiquitous computing (EUC)*, vol. 12, no. 01, pp. 11–19, IEEE, Manhattan, NY, USA, 2017.
- [3] Q. Zhou, "A novel movies recommendation algorithm based on reinforcement learning with DDPG policy[J]," *International Journal of Intelligent Computing and Cybernetics*, vol. 12, no. 02, pp. 21–31, 2020.
- [4] C. Yin, L. Shi, R. Sun, and J. Wang, "Improved collaborative filtering recommendation algorithm based on differential privacy protection," *The Journal of Supercomputing*, vol. 76, no. 7, pp. 5161–5174, 2020.
- [5] Z. Yu, Y. Fang, and Y. Zhang, "The research of modified collaborative filtering recommendation algorithm[C]," in *Proceedings of the international conference on information technology in medicine & education*, vol. 14, no. 12, pp. 21–26, IEEE, Manhattan, NY, USA, 2016.
- [6] M. Saeed and E. G. Mansoori, "Lupus pathobiology based on genomics," *Immunogenetics*, vol. 69, no. 1, pp. 1–12, 2017.
- [7] Z. Wang and Z. Moudi, "Hybrid algorithm for precise recommendation for the classifications of movie reviews[C]," in *Proceedings of the new strategic thinking: green, innovation and sharing-2017 International Conference on Strategic Management (2017ICSM)*, vol. 12, no. 22, pp. 45–51, Chengdu, China, 2017.
- [8] L. Hu, G. Song, Z. Xie, and K. Zhao, "Personalized recommendation algorithm based on preference features," *Tsinghua Science and Technology*, vol. 19, no. 3, pp. 293–299, 2014.
- [9] H. Chen, M. X. Gan, and M. Z. Song, "An improved recommendation algorithm based on graph model," *Applied Mechanics and Materials*, vol. 380–384, no. 12, pp. 1266–1269, 2013.
- [10] Y. E. Liang, "Design of movie recommendation system based on collaborative filtering algorithm[J]," *Modern Computer*, vol. 14, no. 12, pp. 14–25, 2018.
- [11] F. F. Zheng, W. P. Huang, and G. U. Meng zheng, "Recommendation Algorithm with Matrix Factorization Method Based on Spark," *Computer Application*, vol. 08, no. 12, pp. 101–109, 2015.
- [12] W. Liu, B. Wang, and D. Wang, "Improved latent factor model in movie recommendation system[C]," in *Proceedings of the International Conference on Intelligent Autonomous Systems*, vol. 04, no. 12, pp. 24–29, Xiamen, China, 2001.

- [13] K. Y. Lin, J. Wang, and M. Wang, "A hybrid recommendation algorithm based on hadoop[C]/international conference on computer science & education," *Social Science & Medicine*, vol. 100, no. 02, pp. 21–29, 2014.
- [14] W. Jakkhupan and S. Kaj kahaeng, "Movie recommendation using OLAP and multidimensional data model[C]," *International Conference on Computer Information Systems & Industrial Management*, vol. 12, no. 12, pp. 11–19, 2016.
- [15] Y. Wang, Le Sun, and S. Subramani, "CAB: Classifying arrhythmias based on imbalanced sensor data," *KSII Transactions on Internet & Information Systems*, vol. 15, no. 7, pp. 2304–2320, 2021.
- [16] C. A. Gomez-Urbe and N. Hunt, "The netflix recommender system," *Acm Transactions on Management Information Systems*, vol. 6, no. 4, pp. 1–19, 2016.
- [17] G. Adomavicius and A. Tuzhilin, "Toward the next generation of recommender systems: a survey of the state-of-the-art and possible extensions," *IEEE Transactions on Knowledge and Data Engineering*, vol. 17, no. 6, pp. 734–749, 2005.
- [18] G. Chen, J. Qi, C. Tang, Y. Wang, Y. Wu, and X Shi, "Analysis and research of key genes in gene expression network based on complex network," *Complexity*, vol. 2020, pp. 1–12, 2020.
- [19] X. Zhao, Z. Niu, w Chen, C. Shi, K. Niu, and D Liu, "A hybrid approach of topic model and matrix factorization based on two-step recommendation framework," *Journal of Intelligent Information Systems*, vol. 44, no. 3, pp. 335–353, 2015.
- [20] Z. Zhou, Q. Yang, and H. Lu, "Social-Aware movie recommendation via multimodal network learning [J]," *IEEE Transactions on Multimedia*, vol. 20, no. 2, pp. 430–440, 2018.
- [21] J. A. Konstan and J. Riedl, "Recommender systems: from algorithms to user experience," *User Modeling and User-Adapted Interaction*, vol. 22, no. 1-2, pp. 101–123, 2012.
- [22] J. Herlocker, J. A. Konstan, and J. Riedl, "An empirical analysis of design choices in neighborhood-based collaborative filtering algorithms," *Information Retrieval*, vol. 5, no. 4, pp. 287–310, 2002.
- [23] F. Alyari and N. Jafari Navimipour, "Recommender systems," *Kybernetes*, vol. 47, no. 5, pp. 985–1017, 2018.
- [24] Z. Qu, H. Zheng, and M. Zheng, "An efficient quantum image steganography protocol based on improved EMD algorithm," *Quantum Information Processing*, vol. 20, no. 2, pp. 53–29, 2021.
- [25] Y. Deldjoo, M. Elahi, P. Cremonesi, F. Garzotto, P. Piazzolla, and M. Quadrana, "Content-based video recommendation system based on stylistic visual features," *Journal on Data Semantics*, vol. 5, no. 2, pp. 99–113, 2016.

Research Article

Antioclusion Visual Tracking Algorithm Combining Fully Convolutional Siamese Network and Correlation Filtering

Xiaomiao Tao , **Kaijun Wu** , **Yongshun Wang**, **Panfeng Li**, **Tao Huang**,
and **Chenshuai Bai**

School of Electronic and Information Engineering, Lanzhou Jiaotong University, Lanzhou 730070, China

Correspondence should be addressed to Xiaomiao Tao; taoxm@mail.lzjtu.cn

Received 9 May 2022; Revised 23 June 2022; Accepted 30 June 2022; Published 9 August 2022

Academic Editor: Le Sun

Copyright © 2022 Xiaomiao Tao et al. This is an open access article distributed under the Creative Commons Attribution License, which permits unrestricted use, distribution, and reproduction in any medium, provided the original work is properly cited.

Machine learning only uses single-channel grayscale features to model the target, and the filter solution process is relatively simple. When the target has a large change relative to the initial frame, the tracking effect is poor. When there is the same kind of target interference in the target search area, the tracking results will be poor. The tracking algorithm based on the fully convolutional Siamese network can solve these problems. By learning the similarity measurement function, the similarity between the template and the target search area is evaluated, and the target area is found according to the similarity. It adopts offline pre-training and does not update online for tracking, which has a faster tracking speed. According to this study, (1) considering the accuracy and speed, the target tracking algorithm based on correlation filtering performs well. A sample adaptive update model is introduced to eliminate unreliable samples, which effectively enhances the reliability of training samples. With simultaneous changes in illumination and scale, fast motion and in-plane rotation IPR can still be maintained. (2) Determined by calculating the Hessian matrix, in the Struck function, Bike3 parameter adjustment can achieve fast tracking, and Boat5 ensures that the system stability is maintained in the presence of interference factors. The position of the highest scoring point in the fine similarity score map of the same size as the search image is obtained by bicubic interpolation as the target position. (3) The parallax discontinuity caused by the object boundary cannot be directly processed as a smooth continuous parallax. The MeanShift vector obtained by calculating the target template feature and the feature to be searched can increase the accuracy by 53.1%, reduce the robustness by 31.8%, and reduce the error by 28.6% in the SiamVGG algorithm.

1. Introduction

The tracking algorithm based on the fully convolutional Siamese network (SiameseFC) uses the Siamese network structure to build a tracking framework, which transforms the tracking problem into a similarity measurement problem between sample images and target search regions. The algorithm includes the target sample image, the target search area image, and the CNN network. According to the similarity measurement function, the output features of the upper half and the output features of the lower half are convolved to obtain the similarity, and then the maximum similarity is taken out. Position the maximum similarity and map it back to the original image, and finally use it as the tracking prediction result. By learning the similarity

measurement function, the similarity between the template and the target search area is evaluated, and then the target area is found according to the similarity [1–3]. The method of offline pretraining and no online update is used for tracking. Although it has a faster tracking speed, since the target template is not updated online, when the target changes greatly from the initial frame, the tracking effect is poor. The problem of solving the filter is transferred from the time domain to the frequency domain by using the cyclic structure and the Fourier transform. FCNT obtains the filter by multiplying the counterpoints in the frequency domain. When the target search area has the same interference of the target, the tracking result will be poor. Only single-channel grayscale features are used to model the target [4–7]. Although the filter solution process is relatively simple, the

tracking effect is poor. It is mainly composed of a recurrent neural network. The algorithm has abstraction for feature extraction module selection, such as minimum output square error and traditional pixel features used by the MOSSE filter. In the field of single-target tracking, the Siamese network framework takes a target template patch z (Template patch) and a search area block x (Search patch) as input, where z represents the target object, and x is the larger search area in subsequent video frames. Similar feature maps obtain the classification branch result CIs through CNN and determine the categories of different pixel positions. The KCF algorithm for multichannel HOG features is proposed, and the tracking effect is significantly improved, but the algorithm uses low-dimensional data to represent high-dimensional features when processing multichannel sample features, and the feature information will be lost. The regression branch result Reg is obtained, and the precise position of the tracking target is determined. The tracking algorithm implements the tracking network through classification tasks and regression tasks in the training phase. It is worth noting that the size of z is larger than that of the target template block z extracted by the Siamese network tracking algorithm. The generative model pays more attention to the description of the target, and the discriminative model pays attention to the classification of the target and the background. The generative modeling is time-consuming and fails to consider the background information. The tracking algorithm based on discriminant correlation filtering performs template matching and background discrimination at the same time. After obtaining the tracking model, the feature responses are obtained [8, 9]. In the visual system, geometric features are the main mechanism for humans to recognize or track objects. When the target is deformed, the depth image features can be used as effective information to assist the visual tracking task, which brings new research directions to visual tracking. The traditional discriminative correlation filtering tracking algorithm solves the regression through the samples generated by the closed-form solution loop in the Fourier domain. Deep learning-based discriminative correlation filtering methods use stochastic gradient descent or conjugate gradient methods to avoid boundary effects. A multicue pedestrian detector and an online detector are jointly used to learn individual object models, incorporating visible light and depth data in the same decision framework. Using RGBD features to build a more stable and more discriminative model, it can effectively identify the target area from the background. When visible light changes in illumination and occlusion, the robustness of the model decreases. The essence of image formation is actually a process of projection [10–13]. It can deal with the change of illumination in visual tracking, and the three-dimensional information of the object is lost in the process. How to restore the three-dimensional information has become the main content of binocular stereo vision research. Based on RGBD data for visual tracking task, a special occlusion template set is designed to supplement the existing dictionary to deal with different occlusion situations. Finally, a depth-based occlusion detection strategy is proposed to determine the template update time. The two-dimensional

appearance model and three-dimensional distribution model of the target are simultaneously constructed using visible light and depth images, and the visual tracking task is divided into three parts: detection, learning, and segmentation. The detection and segmentation part uses the above two models to locate the target, and the learning part is used to estimate detections, segmentation errors, and update the target model. The eyes send the collected two-dimensional images to the brain for calculation and processing, and finally form a three-dimensional image of the objective object. The binocular parallax is based on this principle, and the binocular camera is used to obtain two images, one is called the reference image, and the other is called the target map, and the disparity is calculated based on the position difference between the corresponding points in the reference map and the target map. This binocular camera is composed of two monocular cameras with the same parameters on the same horizontal line, and it is used to shoot objects in the real world. Taking multiple photos from different perspectives ensure that the effects of large differences between two photos taken in the same scene due to differences in camera performance and distortion are eliminated. In the test sequence, the result of camera calibration will have a significant impact on the accuracy of subsequent stereo matching, which is an indispensable step in the binocular stereo vision system. In the process of image acquisition, due to the influence of camera distortion, shooting angle, and light and other factors, the collected image may appear partially distorted. On the corrected image pair, after the disparity map of the two images is output in the previous step, the depth information can be determined by combining the internal and external parameters of the camera and the geometric relationship, so as to obtain its real coordinates in the real space, and finally realize the 2D image to 3D scene output update target. The advantage of particle filter is that it has better modeling ability in nonlinear environment, so it performs well in the field of target tracking. The discriminant model directly obtains the decision function from the limited data and directly learns the conditional probability distribution from the perspective of probability. The sparsity of target candidates is achieved using the least squares method. By splicing visible light and thermal infrared features together, both thermal infrared features and visible light features may exist as noise, thermal infrared features in thermal crossover or visible light features in dark conditions, etc. From a machine learning perspective, discriminative tracking is essentially a regression or classification problem [14, 15]. The background information of the image is introduced into the discriminative model. Modeling the object appearance usually uses sparse or low-rank theory to learn the representation coefficients of the features, taking into account the background noise. Some algorithms will use the target and background of recent frames to update the target model at regular intervals during the tracking process. Compared with the generative model, the discriminant has higher robustness to the interference of external factors and its own deformation. Therefore, the input target features should be comprehensively analyzed to greatly improve the robustness of target modeling. The previous algorithms for

constructing the target appearance representation usually directly input the target original features without decomposing them to obtain the target appearance model.

2. Siamese Network Class Tracking Algorithm

2.1. The Principle of Binocular Stereo Vision. Epipolar constraint is one of the most critical constraints in stereo matching. The line segment connecting the optical center of the camera is called the baseline. Abstract function represents the similarity score. But in the case of binocular cameras, a point in the real scene will form two different images on the image plane of the left camera and the image plane of the right camera, respectively. According to the position offset between the two images, plus the camera model and the geometric relationship between them, the depth information of the point can be calculated as shown in Figure 1.

2.2. RGBT-Based Visual Tracking Technology. Depth information can provide valuable features to assist trackers in predicting target locations when dealing with visual tracking tasks. It can not only increase the training speed but also solve the gradient vanishing problem of the sigmoid function. The depth sensor is limited by a limited range, and in practical applications, the RGBD visual tracking algorithm has many limitations. The depth sensor only collects the distance between the scene and the image collector, and it cannot correctly distinguish targets with the same distance, as shown in Figure 2. In recent years, visual tracking based on visible light modality has developed rapidly, and a large number of labeled datasets have been proposed for training models. The visual tracking technology based on RGBT was developed relatively late, and a dataset with ground-truth registration of visible light and thermal infrared was constructed. Dropout is used to alleviate over fitting. The training set is isolated from the test set of target tracking, the test results of the algorithm are more credible, and the ILSVRC dataset is established for the video target detection problem. The background between different frames is linearly correlated, and the moving target appears relatively sparse, so the model of the target appearance is usually based on the theory of sparse representation. Sparse representation to multimodal data fusion is applied, and visible light and thermal infrared reference templates are updated in a jointly optimized way for visual tracking tasks.

3. Algorithm Model

3.1. SiamVGG Algorithm [16–20]. Fully convolutional Siamese network

$$\text{dist}(X, Y) = \sqrt{\sum_{i=1}^n (x_i - y_i)^2}. \quad (1)$$

Tracking algorithm

$$\text{sim}(X, Y) = \cos \theta = \frac{x \bullet y}{\|x\| \bullet \|y\|}. \quad (2)$$

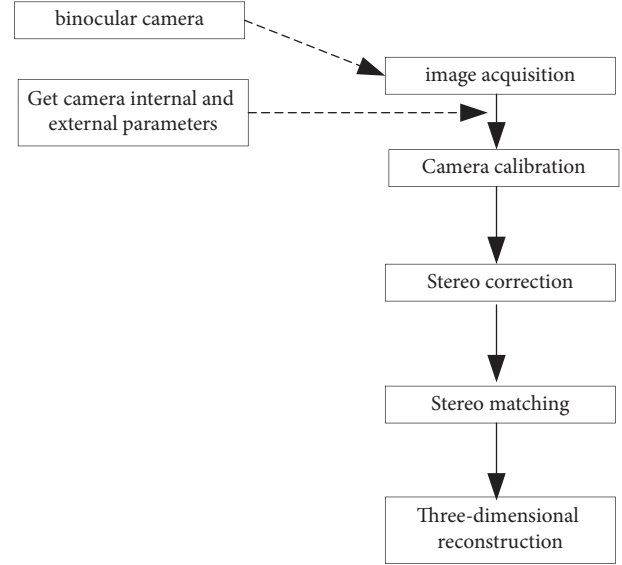


FIGURE 1: Binocular stereo vision system.

Sample image

$$\text{output} = \sum_{i=1}^m \sum_{j=1}^n I_{i,j} \times K_{i,j} + b. \quad (3)$$

Target search area

$$o = \left\lfloor \frac{i + 2p - k}{s} \right\rfloor + 1. \quad (4)$$

$$\mu_B \leftarrow \frac{1}{m} \sum_{i=1}^m x_i. \quad (5)$$

Similarity

$$\sigma_B^2 \leftarrow \frac{1}{m} \sum_{i=1}^m (x_i - \mu_B)^2. \quad (6)$$

$$x_i \leftarrow \frac{x_i - \mu_B}{\sqrt{\sigma_B^2 + \varepsilon}}. \quad (7)$$

Predicted location

$$y_i \leftarrow \gamma x_i + \beta. \quad (8)$$

$$y = \frac{1}{1 + e^{-x}}. \quad (9)$$

Offline pretraining

$$y = \max(0, x). \quad (10)$$

$$H(x) = F(x) + x. \quad (11)$$

Loop structure

$$f(z, x) = \varphi(z) * \varphi(x) + b. \quad (12)$$

$$l(y, v) = \log(1 + \exp(-yv)). \quad (13)$$

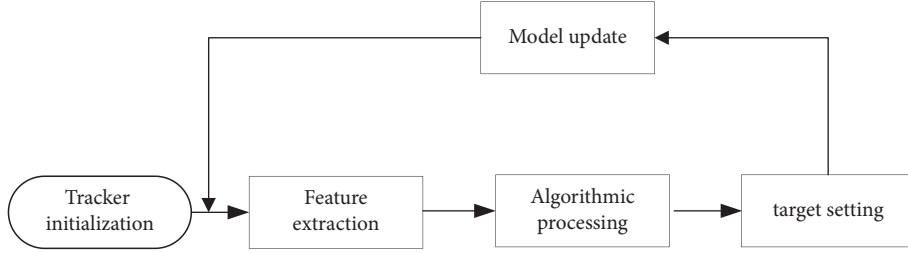


FIGURE 2: Visual tracking algorithm framework.

3.2. SA-Siam Algorithm [21–23].

$$L(y, v) = \frac{1}{D} \sum_{u \in D} (l(y(u), v(u))). \quad (14)$$

MOSSE filter

$$y(u) = \|u - c\| \leq R. \quad (15)$$

Multichannel HOG features

$$V_{\text{CLE}} = \sqrt{(x_A - x_G)^2 + (y_A - y_G)^2}. \quad (16)$$

KCF algorithm

$$IoU = \frac{B_A \cap B_G}{B_A \cup B_G}. \quad (17)$$

2D appearance model

$$\Phi(i) = \frac{1}{N_{\text{rep}}} \sum_{i=1}^{N_{\text{rep}}} \Phi(i, k). \quad (18)$$

3.3. ECO Algorithm [24–27].

$$\rho_A(i) = \frac{1}{N_{\text{valid}}} \sum_{i=1}^{N_{\text{valid}}} \Phi(i). \quad (19)$$

Return branch result Reg

$$\rho_R(i) = \frac{1}{N} \sum_{k=1}^{N_{\text{rep}}} F(i, k). \quad (20)$$

3D distribution model

$$\phi_{N_s} = \frac{1}{N_s} \sum_{i=1}^{N_s} \phi_{N_c}. \quad (21)$$

Classification task

$$\phi = \frac{1}{N_{hi} - N_{lo}} \sum_{N_s=N_{lo}}^{N_{hi}} \phi_{N_s}. \quad (22)$$

Return task

$$x' = \rho(x; M). \quad (23)$$

Visual system

$$M_i = F_{ap} \left(\frac{\partial J}{\partial F_i} \right). \quad (24)$$

Light change

$$L = \sum_{i,j} \|Y(i, j) - W * X_{i,j}\|^2 + \lambda \|W\|^2. \quad (25)$$

Closed loop

$$f(z, x) = \sum_{i,j} \varphi(z) * \varphi(x) + bI. \quad (26)$$

$$R = \arg_T \min \|T * X - Y\|^2 + \lambda \|T\|^2. \quad (27)$$

4. Simulation Experiment

4.1. Generative Models. In generative models, statistical models are usually generated from a probabilistic perspective, using past information to train a joint probability distribution, and modeling the posterior probability to predict the categories of candidate targets, as shown in Table 1 and Figures 3 and 4. Consider IV = 14, SV = 13, OCC = 15, and DEF = 3 in terms of accuracy and speed. The performance of the target tracking algorithm based on correlation filtering is relatively good. MB = 11, FM = 4, and IPR = 3.93. Most of the current tracking algorithms select the target as the center to cut out a fixed proportion of the area to be searched. The generative model uses the historical frame information to characterize the target and finds the candidate target with the smallest reconstruction error as the new target. OPR = 1.41, OV = 1.94, BC = 1.1, and LR = 1.97. Whether the search locale is set properly has a lot to do with the correct tracking. Depending on the sample size, the central target is cyclically shifted to obtain a set of positive and negative samples. Due to the existence of negative samples, the correlation filter can distinguish the target and the background well. Considering the background information and the diversity of changes in the target's own appearance, the results obtained by applying multiple trackers in the target decision-making layer are used as the final result. The sample adaptive update model is introduced to eliminate unreliable samples and effectively enhance the reliability of training samples. The illumination change IV = 10, the scale change SV = 10, the occlusion OCC = 13, the deformation DEF = 11, and the motion blur MB = 4.

TABLE 1: Generative models.

IV	SV	OCC	DEF	MB	FM	IPR	OPR	OV	BC	LR
14	13	15	3	11	4	3.93	1.41	1.94	1.1	1.97
14	18	16	9	10	11	2.27	4	2.24	1.07	1.21
11	18	19	15	16	3	4.19	4.6	3.32	1.95	1.56
10	12	15	16	1	14	1.53	3.63	4.34	1.67	1.76
10	10	13	11	4	15	1.96	2.2	1.43	1.25	1.74
12	17	12	13	1	16	3.36	4.11	2.87	1.21	1.94
16	18	18	16	11	11	3.05	1.56	2.36	1.05	1.15
12	11	16	11	5	14	2.08	4.66	1.81	1.17	1.34
16	16	13	5	1	7	2.78	1.45	1.73	1.27	1.05
11	14	19	16	16	6	4.83	3.33	3.48	1.87	1.9

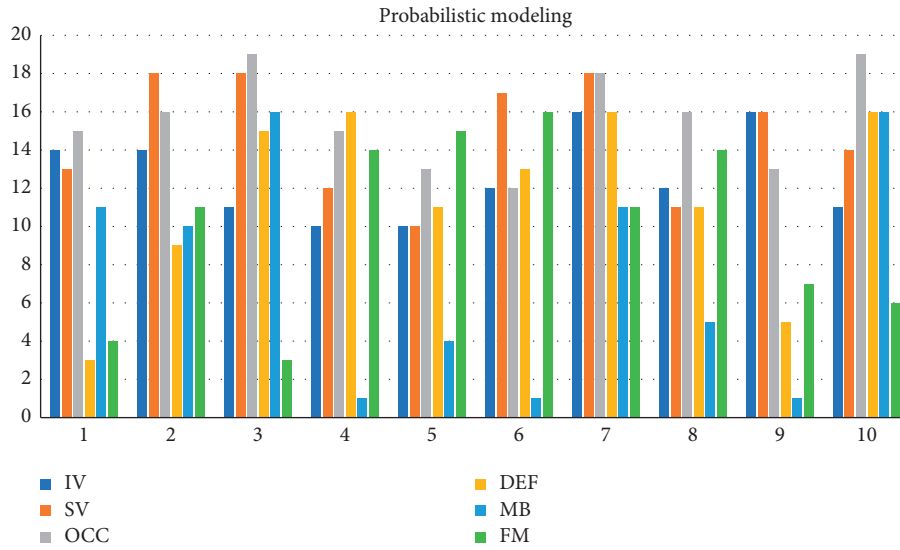


FIGURE 3: Probabilistic modeling.

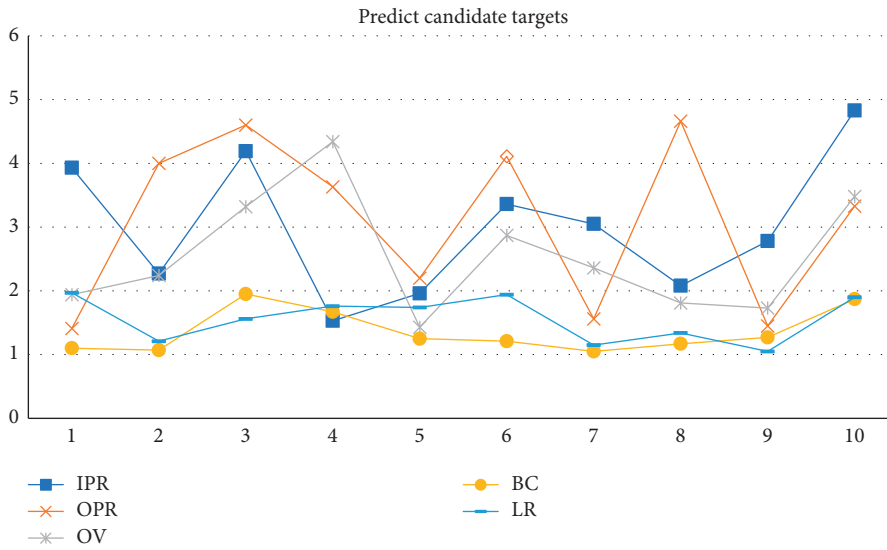


FIGURE 4: Predicting candidate targets.

Rapid motion FM = 15, in-plane rotation IPR = 1.96, out-of-plane rotation OPR = 2.2, target out-of-view OV = 1.43, background interference BC = 1.25, and low-resolution LR = 1.74.

4.2. *Kernel Function.* The target image is obtained, the depth feature of the template image is calculated by the feature extraction network, and the search image is obtained during subsequent continuous tracking. Depth features are

TABLE 2: Tracking success rate.

	Struck	SAMF	MUSTER	KCF	Srdcf	CFNet
Bike3	6.9	15.7	19.4	12.2	13.9	14.1
Boat5	16.6	74.7	85.1	23.2	48.6	36
Building5	99.3	96.9	97.3	89	97.5	21.6
Car15	42.4	3	8.5	2.3	44.4	45.8
Person21	31.2	0.6	51.3	0.6	30.8	18.6
Truck2	42.9	86.1	48.9	39.2	70.5	88.2
Uav4	6.3	1.9	3.8	1.3	7.6	2.8
Wakeboard2	3.1	3.3	5.3	4.9	4.5	6.4
car1_s	18.4	18.4	18.4	18.4	23.2	10.6
Person3_s	30.2	46.5	46.1	30	69.5	25.1

computed through the same feature extraction network, as shown in Table 2 and Figure 5. The feature extractor uses the VGGNet deep network, and then maps the feature maps of different layers to the continuous confidence map in the spatial domain, and finally the center position of the target is determined by calculating the Hessian matrix. In the Struck function, Bike3 = 6.9, Boat5 = 16.6, and Building5 = 99.3. A fine similarity score map of the same size as the search image is obtained by bicubic interpolation Car15 = 42.4, Person21 = 31.2, Truck2 = 42.9, Uav4 = 6.3, Wakeboard2 = 3.1, car1_s = 18.4, and Person3_s = 30.2. The position of the highest scoring point is the target location. By analyzing and calculating the similarity and correlation of adjacent video frames, the estimation of the target position state is realized. The disadvantage of the C-COT algorithm is that the amount of computation and data is very large when training with the VGGNet deep network, which makes it difficult to meet the real-time requirements of target tracking. The assumptions of the method based on optical flow are two points: one is that the brightness of the target is constant when moving, and the other is that the gap between the adjacent video frames is small.

4.3. Parallax Continuity Constraint. Calculate the pixel feature value probability of the target and the frame to be searched to obtain the template and the feature model to be searched. According to the constraint rule that parallax has continuity, the parallax on the surface of this object is considered to be continuous and smooth, as shown in Table 3 and Figure 6. In the HA-SiamVGG calculation template, $A = 0.537$, $R = 0.309$, and $EAO = 0.313$. The parallax discontinuity caused by the object boundary cannot be directly processed as a smooth continuous parallax, due to the different shooting angles and the influence of the front and rear occlusion of the object. That is, the mapping point of a point in the space on the left and right image planes is unique. The target frame of the area to be searched is iterated continuously along the vector direction closest to the target in the first frame, and the convergence result is finally obtained through continuous iteration to locate the target. The pixel regions generated by the projection of the same object under different shooting angles must have consistent or similar properties. Due to the influence of the camera's photosensitive components, the surrounding environment, and noise, when the pixels in the same space are mapped to

the two-dimensional image, the gray value of the pixels will be different. Similarity constraints should be used to make their corresponding matching points have similar properties. Difficult samples in network training are added, data augmentation to solve the spatial location bias of training is used, and the generalization ability of the model is improved.

4.4. Siamese Region Candidate Network Tracking Algorithm.

The confidence of the classified samples is obtained by correlation filtering, and then the target is tracked. The use of signal operations such as fast Fourier transform and dot product greatly improves the real-time performance of target tracking. The depth features are extracted through the same feature extraction network in SiamFC, and the classification branch depth feature map and the regression branch depth feature map are obtained through the RPN network, as shown in Table 4 and Figure 7. Optical flow refers to the use of images to represent the speed of motion, and each pixel is given a speed vector including size and direction. The motion state of the target is judged by the displacement change of the pixels in the adjacent frame images, so as to realize the tracking of the target. The correlation calculation with the template feature is performed to obtain the result feature map of the classification branch and the regression score. It needs to meet the time continuous or the target moves slowly, so the scope of application is small. The MeanShift algorithm is based on the probability density distribution, uses color features to describe the target, and iteratively finds the local optimum along the gradient ascending direction, that is, the position of the target. SiamFC searches based on the scale pyramid method. The calculation of depth features at each scale is time-consuming, and the tracking speed is slow. The introduction of the RPN structure enables SiamRPN to avoid time-consuming multiscale calculations and replace it with bounding box regression, which improves the tracking speed. The algorithm calculates the probability distribution of color features within the target and candidate regions, respectively. The Kalman filter tracking model is used to model the motion as a linear system. The motion state of the target in the current frame depends on the state of the previous frame. The filter is divided into two parts: prediction and observation. Calculate the observed values (speed, acceleration, etc.), and synthesize the observed state and the predicted state to obtain the optimal state estimate. It

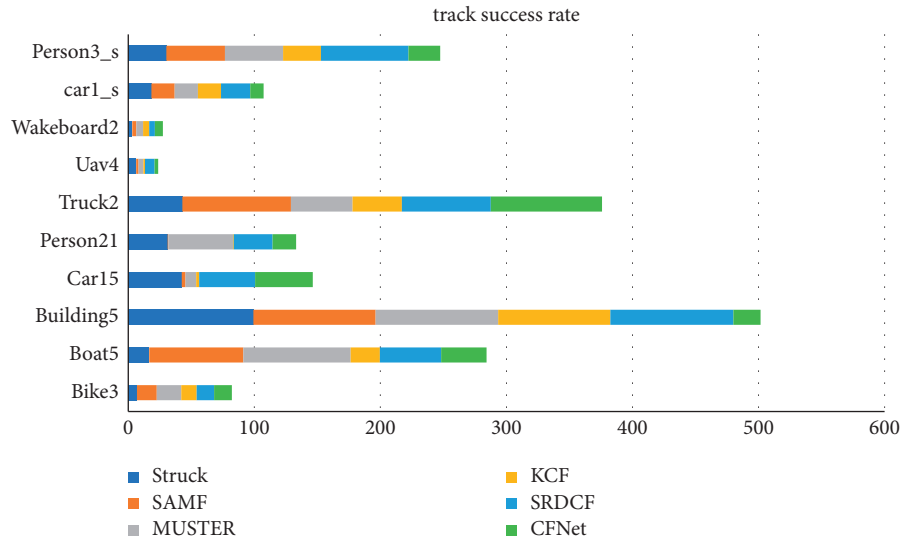


FIGURE 5: Tracking success rate.

TABLE 3: Comparative evaluation results.

	A	R	EAO
HA-SiamVGG	0.537	0.309	0.313
SiamVGG	0.531	0.318	0.286
SA-Siam	0.533	0.337	0.286
ECO	0.484	0.276	0.28
MCCT	0.532	0.318	0.274
SiamDW	0.538	0.398	0.27
SiamFC	0.503	0.585	0.187

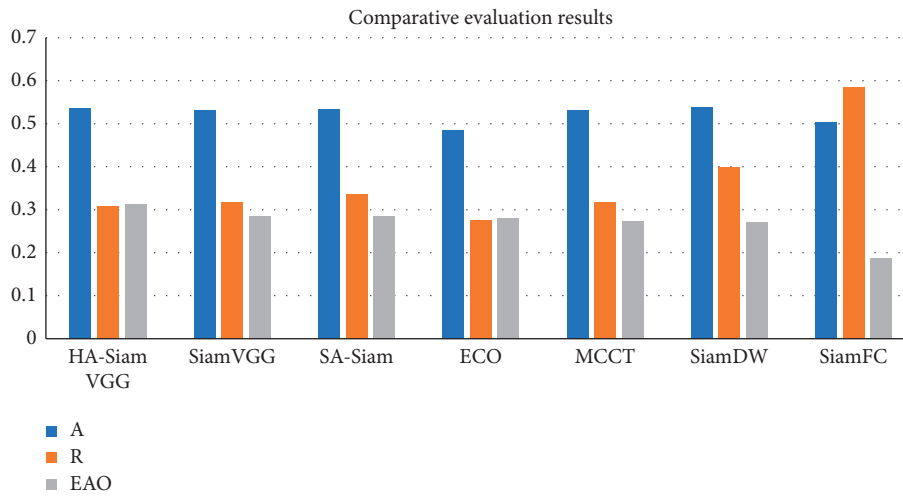


FIGURE 6: Comparative evaluation results.

TABLE 4: Comparison of algorithm accuracy values.

	FM	BC	MB	DEF	IV	IPR	LR	OCC	OPR	OV	SV
HA-SiamVGG	0.878	0.836	0.916	0.873	0.905	0.922	0.996	0.833	0.887	0.839	0.892
DaSiamRPN	0.817	0.856	0.816	0.877	0.868	0.889	0.942	0.811	0.877	0.72	0.852
ATOM	0.851	0.827	0.839	0.854	0.881	0.881	0.993	0.832	0.867	0.821	0.876
ACT	0.791	0.881	0.79	0.826	0.86	0.867	0.943	0.799	0.837	0.707	0.841
C-RPN	0.832	0.823	0.831	0.831	0.875	0.89	0.927	0.764	0.865	0.777	0.854
SiamDW	0.808	0.762	0.841	0.765	0.795	0.823	0.902	0.8	0.83	0.78	0.818
SiamFC	0.743	0.69	0.705	0.69	0.736	0.742	0.9	0.722	0.756	0.669	0.735

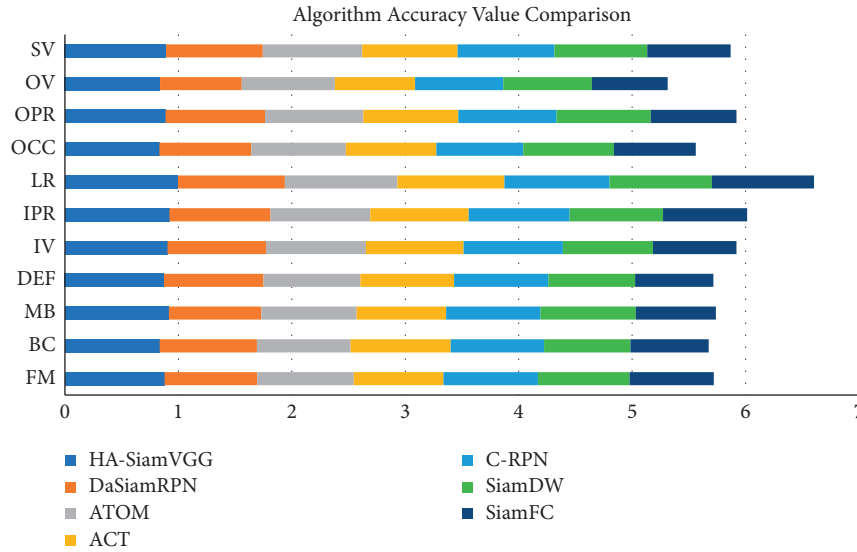


FIGURE 7: Comparison of algorithm accuracy values.

is not sensitive to the change of the appearance of the target but has higher requirements on the selection of the motion model and the matching of the noise covariance, and the effect becomes worse when the motion speed is fast.

5. Conclusion

Traditional image acquisition refers to the process of image acquisition of objects in the real scene, while binocular stereo vision uses a binocular camera to achieve this process. Although machine learning has a faster tracking speed, its shortcomings are also obvious. The disadvantages of machine learning are that it takes a lot of time to make machine programs, and the demand for data is huge. Results may be satisfactory, but a fully automated system requires extensive research and analysis. The backups and servers required to maintain and record the acquired data keep piling up, making it increasingly costly. Since the target template is not updated online, when the target changes greatly from the initial frame, the tracking effect is poor. When there is the same kind of target interference in the target search area, the tracking results will be poor. Only single-channel grayscale features are used to model the target, and the filter solution process is relatively simple. The tracking algorithm based on the fully convolutional Siamese network can solve these problems. By learning the similarity measurement function, the similarity between the template and the target search area is evaluated, and the target area is found according to the similarity. It adopts offline pretraining and does not update online for tracking, which has a faster tracking speed. According to this study: 1. Considering the accuracy and speed, IV = 14, SV = 13, OCC = 15, and DEF = 3. The performance of the target tracking algorithm based on correlation filtering is relatively good. MB = 11, FM = 4, and IPR = 3.93. Most of the current tracking algorithms select the target as the center to cut out a fixed proportion of the area to be searched. The generative model uses the historical frame information to characterize the target, and finds the

candidate target with the smallest reconstruction error as the new target. OPR = 1.41, OV = 1.94, BC = 1.1, and LR = 1.97. The sample adaptive update model is introduced to eliminate unreliable samples and effectively enhance the reliability of training samples. The illumination change IV = 10, the scale change SV = 10, the occlusion OCC = 13, the deformation DEF = 11, and the motion blur MB = 4. Fast motion FM = 15, in-plane rotation IPR = 1.96, out-of-plane rotation OPR = 2.2, target out-of-view OV = 1.43, background interference BC = 1.25, and low-resolution LR = 1.74.2 are determined by calculating the Hessian matrix. In the Struck function, Bike3 = 6.9, Boat5 = 16.6, and Building5 = 99.3. A fine similarity score map of the same size as the search image is obtained by bicubic interpolation Car15 = 42.4, Person21 = 31.2, Truck2 = 42.9, Uav4 = 6.3, Wakeboard2 = 3.1, car1_s = 18.4, and Person3_s = 30.2, and the position of the highest scoring point is the target location. 3. In the HA-SiamVGG calculation template, $A = 0.537$, $R = 0.309$, and $EAO = 0.313$. The parallax discontinuity caused by the object boundary cannot be directly processed as a smooth continuous parallax, due to the different shooting angles and the influence of the front and rear occlusion of the object. The target template feature is calculated, and the MeanShift vector obtained by the feature is to be searched. In the SiamVGG algorithm, $A = 0.531$, $R = 0.318$, and $EAO = 0.286$. The visual tracking algorithm is still an active research direction in the field of computer vision. Although detection algorithms have achieved good results, there is still a certain gap in the application in real scenes, and the basic task of target detection is still very challenging. There is great potential and space for improvement.

Data Availability

The experimental data used to support the findings of this study are available from the corresponding author upon request.

Conflicts of Interest

The authors declared that they have no conflicts of interest regarding this work.

References

- [1] D. Park, S. Kim, and H. Kwon, "Host-based intrusion detection model using Siamese," *The Network Journal*, vol. 1828, no. 1, Article ID 012044, 2021.
- [2] N. Javaid, N. Jan, and M. U. Javed, "An adaptive synthesis to handle imbalanced big data with deep siamese network for electricity theft detection in smart grids," *Journal of Parallel and Distributed Computing*, vol. 153, pp. 44–52, 2021.
- [3] X. Hu, H. Liu, Y. Chen, Y. Hui, Y. Liang, and X Wu, "Siamese network object tracking algorithm combining attention mechanism and correlation filter theory," *International Journal of Pattern Recognition and Artificial Intelligence*, vol. 36, no. 01, 2022.
- [4] Y. Cui and H. Ren, "Research on visual tracking algorithm based on Peak Sidelobe Ratio [J]," *IEEE Access*, vol. 95, no. 7, Article ID 116293, 2021.
- [5] M. Li, W. Sun, X. Du, X. Zhang, and L Yao, "Ship classification by the fusion of Panchromatic image and multi-spectral image based on Pseudo Siamese LightweightNetwork," *Journal of Physics: Conference Series*, vol. 1757, no. 1, Article ID 012022, 2021.
- [6] H. Jiao and G. Chen, "Global self-localization of redundant robots based on visual tracking [J]," *International Journal of System Assurance Engineering and Management*, vol. 46, pp. 1–9, 2021.
- [7] J. He, C. Shen, Y. Chen, Y. Huang, and J. Wu, "FPSN-FNCC: an accurate and fast motion tracking algorithm in 3D ultrasound for image-guided interventions," *Physics in Medicine and Biology*, vol. 66, no. 15, Article ID 155012, 2021.
- [8] N. Fan, X. Li, Z. Zhou, Q. Liu, and Z He, "Learning dual-margin model for visual tracking," *Neural Networks*, vol. 140, no. 7, pp. 344–354, 2021.
- [9] C. Wu, H. Chen, B. Du, and L Zhang, "Unsupervised change detection in multitemporal VHR images based on deep Kernel PCA convolutional mapping network," *IEEE Transactions on Cybernetics*, vol. 13, no. 23, pp. 1–15, 2021.
- [10] W. Liao, D. Yang, and Y. Wang, "Fault diagnosis of power transformers using graph convolutional," *network [J]*, vol. 7, no. 2, p. 9, 2021.
- [11] Y. K. Kai and P. Rajendran, "A descriptor-based Advanced feature detector for improved visual tracking [J]," *Symmetry*, vol. 13, no. 8, p. 1337, 2021.
- [12] D. M. Shi and X. Chen, "Research on visual object tracking algorithm based on improved twin network [J]," *Journal of Physics: Conference Series*, vol. 1966, no. 1, Article ID 012006, 2021.
- [13] S. Lin, Y. Wang, and L. Zhang, "MDF-SA-DDI: predicting drug–drug interaction events based on multi-source drug fusion, multi-source feature fusion and transformer self-attention mechanism [J]," *Briefings in Bioinformatics*, vol. 42, no. 5, p. 5, 2021.
- [14] Z. Y. Gong, C. R. Qiu, B. Tao, H. Bai, Z. Yin, and H. Ding, "Tracking and grasping of moving target based on accelerated geometric particle filter on colored image," *Science China Technological Sciences*, vol. 64, no. 4, pp. 755–766, 2021.
- [15] T. Lagache, A. Hanson, and J. E. Pérez-Ortega, "Tracking calcium dynamics from individual neurons in behaving animals [J]," *PLoS Computational Biology*, vol. 15, p. 17, 2021.
- [16] H. Lee, K. S. Lee, and J. Kim, "Local similarity Siamese network for urban land change detection on remote sensing images [J]," *Journal of Selected Topics in Applied Earth Observations and Remote Sensing*, vol. 23, pp. 1–13, 2021.
- [17] L. Liu, L. Huang, F. Yin, and Y Chen, "Offline Signature Verification using A region based deep Metric learning network," *Pattern Recognition*, vol. 118, no. 1, Article ID 108009, 2021.
- [18] F. Tokuda, S. Arai, and K. Kosuge, "Convolutional neural network-based visual Servoing for Eye-to-Hand Manipulator [J]," *IEEE Access*, vol. 14, pp. 56–72, 2021.
- [19] P. Reinartz, "Multiple pedestrians and Vehicles tracking in Aerial imagery using a convolutional neural network [J]," *Remote Sensing*, vol. 15, p. 13, 2021.
- [20] J. Suto, "Real-time Lane line tracking algorithm to Mini Vehicles [J]," *Transport and Telecommunication Journal*, vol. 22, no. 4, pp. 461–470, 2021.
- [21] Y. Cui, D. Guo, Y. Shao et al., "Joint classification and regression for visual tracking with fully convolutional Siamese networks [J]," *International Journal of Computer Vision*, vol. 130, no. 2, pp. 550–566, 2022.
- [22] R. W. Robinson, "Health assessment of eucalyptus trees using Siamese network from Google Street and ground truth images [J]," *Remote Sensing*, vol. 19, p. 13, 2021.
- [23] D. Peng, L. Bruzzone, Y. Zhang, H. Guan, and P. He, "SCDNET: a novel convolutional network for semantic change detection in high resolution optical remote sensing imagery," *International Journal of Applied Earth Observation and Geoinformation*, vol. 103, Article ID 102465, 2021.
- [24] H. Fan, J. Ren, and J. Yang, "Osteoporosis prescreening using panoramic radiographs through a deep convolutional neural network with attention mechanism [J]," *Dentomaxillofacial Radiology*, vol. 13, no. 2, pp. 50–76, 2021.
- [25] X. Yang, S. Yang, and X. Lian, "Transfer learning via multi-scale convolutional neural layers for human–virus protein–protein interaction prediction [J]," *Bioinformatics*, vol. 28, no. 24, p. 24, 2021.
- [26] S. Bakshi and S. Rajan, "Fall event detection system using inception-Densenet inspired sparse siamese network [J]," *Sensor Letters*, vol. 20, no. 12, pp. 123–148, 2021.
- [27] Z. Li, C. Hu, K. Nai, and J. Yuan, "Siamese target estimation network with AIoU loss for real-time visual tracking," *Journal of Visual Communication and Image Representation*, vol. 77, no. 6, Article ID 103107, 2021.

Retraction

Retracted: Application of Intelligent Image Matching and Visual Communication in Brand Design

Computational Intelligence and Neuroscience

Received 25 July 2023; Accepted 25 July 2023; Published 26 July 2023

Copyright © 2023 Computational Intelligence and Neuroscience. This is an open access article distributed under the Creative Commons Attribution License, which permits unrestricted use, distribution, and reproduction in any medium, provided the original work is properly cited.

This article has been retracted by Hindawi following an investigation undertaken by the publisher [1]. This investigation has uncovered evidence of one or more of the following indicators of systematic manipulation of the publication process:

- (1) Discrepancies in scope
- (2) Discrepancies in the description of the research reported
- (3) Discrepancies between the availability of data and the research described
- (4) Inappropriate citations
- (5) Incoherent, meaningless and/or irrelevant content included in the article
- (6) Peer-review manipulation

The presence of these indicators undermines our confidence in the integrity of the article's content and we cannot, therefore, vouch for its reliability. Please note that this notice is intended solely to alert readers that the content of this article is unreliable. We have not investigated whether authors were aware of or involved in the systematic manipulation of the publication process.

Wiley and Hindawi regrets that the usual quality checks did not identify these issues before publication and have since put additional measures in place to safeguard research integrity.

We wish to credit our own Research Integrity and Research Publishing teams and anonymous and named external researchers and research integrity experts for contributing to this investigation.

The corresponding author, as the representative of all authors, has been given the opportunity to register their agreement or disagreement to this retraction. We have kept a record of any response received.

References

- [1] M. Liu and W. Zhong, "Application of Intelligent Image Matching and Visual Communication in Brand Design," *Computational Intelligence and Neuroscience*, vol. 2022, Article ID 5964851, 9 pages, 2022.

Research Article

Application of Intelligent Image Matching and Visual Communication in Brand Design

Ming Liu ¹ and Wenyan Zhong²

¹*School of Communication and Design, Longyan University, Longyan 364000, China*

²*Department of Design, Hainan Vocational University of Science and Technology, Haikou 571126, China*

Correspondence should be addressed to Ming Liu; 82013059@lyun.edu.cn

Received 22 April 2022; Accepted 15 June 2022; Published 5 August 2022

Academic Editor: Le Sun

Copyright © 2022 Ming Liu and Wenyan Zhong. This is an open access article distributed under the Creative Commons Attribution License, which permits unrestricted use, distribution, and reproduction in any medium, provided the original work is properly cited.

In this paper, from the perspective of improving the visual communication of brand design, image texture intelligent matching processing is needed, proposing a brand design texture intelligent matching method based on visual communication, constructing a brand design texture intelligent information acquisition model under visual communication, using automatic image imaging technology for texture imaging and feature segmentation of brand design, and extracting typical brand design and ethnic design language of texture histogram, texture segmentation, and automatic matching under visual communication according to histogram distribution, brand design texture information enhancement and optimization detection by regularized feature fusion method, extraction of edge contour feature points of brand design, and texture matching with the extracted edge contour feature points of decorative patterns as input statistics. The adaptive performance of texture matching for a brand design using this method is better, and the texture discrimination ability is stronger, which improves the application research of better reflecting brand design in modern visual communication design and promotes the innovative combination of traditional cultural elements and modern design.

1. Introduction

The concept of visual packaging design is to give the audience visual and psychological cognition from words, graphics, and colors [1]. It establishes the logo, color, and labeling and is used for identification shorthand. For consumers, brand perception is the most beneficial tool to judge and distinguish similar products. The brand is used to reduce the time to choose [2].

A dazzling visual packaging war was staged between TV stations and channels. In the midst of the audiovisual inundation but can not help but disappoint some people. The form does not focus on positioning but only seeks to obtain gorgeous visual effects [3]. In the competition of brand media, not only the formal beauty should be pursued but also the connotation of the theme and the brand effect should be added [4]. The impact of digital packaging on the brand of television media and the important role of brand

image [5]. Through the analysis and systematic elaboration of the packaging process. Misconceptions, drawbacks, and successful columns are taken as the focus of the analysis. To explore the role of media packaging and excellent columns for brand building [6]. Learn from successful packaging and make the production team brand conscious as well through brand awareness implantation [7]. It is important to consider not only positioning, style, and innovation, but also brand awareness in production [8].

Speaking of packaging seems to know what he means, and it has a lot in common with the usual packaging of products. Packaging is also borrowed for the packaging of products. And, the definition of TV packaging is the specification and strengthening of the audiovisual elements of the channel, column, and TV station image as a whole [9]. Packaging design prerequisites are to solve the audience for their channel and the initial recognition of the column and program identification superior poor choice. Such as a channel to broadcast a new TV

series in prime time, before the broadcast to be after the packaging design to edit out the exciting images of the TV series, story conflict, in the postvisual design as a TV series promotional video [10]. Publicity to the audience, this is not the era of good wine is not afraid of the alley, is the need for active marketing and self-promotion of the times [11]. For the status of their own brand, the establishment of personality characteristics is the audience to establish their own channel media must mean of recognition [12].

Packaging is an important part of media brand building. In an era of excessive selectivity, you are successful if you catch the audience's eye, while hasty conversion is your undoing. For viewers to choose you, an initial understanding of you is essential. In addition to the full publicity on the TV screen [13]. This is not enough, in the development of the network today, the popularity of smart phones, tablets, the network, and cell phone platform publicity when it is the way to go. TV media need to actively promote the network if they want to break through [14]. By bringing PPS videos close to other smart-phones and tablets so that they are no longer limited by space, the visual packaging design of the media is the most direct means of publicity for each platform [15].

This is not conducive to the interests of the channel itself, so it is generally more stable, and if there are changes, they are modified and improved in the initial design [16]. We try to keep the original features and optimize only in terms of beautification. For example, the image logo of Phoenix TV is two phoenixes flying together. This logo leaves a deep impression, and whenever you see this logo you will clearly identify this Phoenix TV. Excellent LOGO image will make the audience remember deeply and penetrate into the audience's mind. A fixed memory is formed. When choosing a channel, based on the label viewers will quickly choose what frequency to see [17]. What programs are available on the channel and which ones do they like. Through tags, viewers can establish a connection. The label is in the upper left corner of the screen, which has become an inherent pattern in the media, as a necessary element that is inherent on the TV screen in addition to being fixed on the screen. There is a digital visual design of dynamic video often referred to as logo rendering that scrolls between programs in the channel [18]. When creating the logo image, attention should be paid to simplicity and clarity, outstanding features, reflecting modernity and design, incorporating regional culture, and enhancing viewability and locality [19]. In the channel, the interpretation of LOGO can enhance the sense of coherence between programs, make the rhythm and paragraphs more compact, and fill the gap between programs and advertisements. In media packaging, dynamic LOGO interpretation and image logo design are the cornerstones of tonality and make the features more prominent [20].

2. Image Acquisition and Preprocessing of Brand Texture Patterns

2.1. Image Acquisition of Brand Texture Pattern. In order to realize the intelligent matching of brand design texture based on visual communication, firstly, the 3D image reconstruction method is used for visual information acquisition of brand

texture pattern, and the multimedia digital information reconstruction method is used for intelligent matching of brand design texture, visual feature sampling, and the intelligent matching of brand design texture in the texture distribution area of the image; the image feature reconstruction space technique is used to read the 3D of brand design texture data feature volume, and form the raw file of brand design texture, the brand design texture PBO (OpenGL pixel cache object) is built according to the spatial feature sampling technique, and the image is stored in device memory, the brand design texture information is read, and the brand design texture matching is performed according to the brand design data information in device memory. According to the above-given design idea, it is assumed that the pixel set distribution of brand texture pattern is n , and the amount of label category information features of the output brand texture pattern is $P(1) = [1 - L^{-1}]m - 1$. According to the size and texture complexity of the brand design, the brand texture point pair matching is performed to get the brand texture pattern texture distribution.

$$E_m^{ij} = \sum_{k=0}^{255} e_{mk}^{ij}, \quad (1)$$

where E_m^{ij} is the color information of column j of row i in the m th image of the 3D branded texture pattern data sampling sequence.

$$e_{mk}^{ij} = \begin{cases} -p_k \log(p_k) & p_k \neq 0 \\ 0 & p_k = 0 \end{cases}. \quad (2)$$

Here, e_{mk}^{ij} for the 2×2 brand design edge information.

Combining the pixel frame distribution for texture alignment, the brand texture pattern information is fused using k th order moment feature statistics for the pixel points on each scale $\sigma_l^{(n)} (1, 2, \dots, n)$, and one sampling point is taken in each subinterval to obtain the grayscale histogram of the brand texture pattern.

$$P_k = \frac{n_k}{\sum_{i=0}^{255} n}. \quad (3)$$

For N brand design labels, the information fusion expression for the color, texture, shape, and other features of the brand texture pattern is

$$c(x, y) = [\Delta x \quad \Delta y] \begin{bmatrix} \sum_W I_x^2 & \sum_W I_x I_y \\ \sum_W I_x I_y & \sum_W I_y^2 \end{bmatrix} \begin{bmatrix} \Delta x \\ \Delta y \end{bmatrix}. \quad (4)$$

The intelligent information acquisition model of brand design texture under visual communication is constructed, and the automatic image imaging technology is used for texture imaging and feature segmentation of brand design, and the average energy of the window is examined, and the neighborhood frame intensity at the spatial scale of brand design texture at (x, y, σ) is

$$H = \begin{bmatrix} L_{xx}(x, \sigma) L_{xy}(x, \sigma) \\ L_{xy}(x, \sigma) L_{yy}(x, \sigma) \end{bmatrix}, \quad (5)$$

where $L_{xx}(x, \sigma)$ is the brand design texture convolution, L_{xy} and L_{yy} have similar meanings. According to the fusion result of the edge pixel set of brand design, the multidimensional feature space reconstruction method is implemented for brand texture pattern information collection, and the edge energy value of the regional distribution pixel points $p(i, j)$ of brand design is obtained, which is used as the data input basis for intelligent matching and feature extraction of brand design texture.

2.2. Brand Design Feature Segmentation. The automatic image imaging technology is used for texture imaging and feature segmentation of the brand design, and the texture histogram of the brand design is extracted. According to the known pixel points x of the brand texture pattern, the maximum intensity of the texture distribution of the brand texture pattern is obtained to satisfy $I(x) = 1$, and the regional template matching the value of the brand image is determined as follows:

$$I_{\text{total}} = \frac{L_{\text{total}}}{\rho_{SRm} |S_{SR}|} \quad (6)$$

$$= \frac{\sum_{i=1}^M \sum_{m=1}^{|S_{SR}|} (\lambda_i P_{im} T_{SRm} / \rho_{SRm})}{|S_{SR}|}$$

The adaptive chunking feature matching method is used to determine the priority coefficients of the branded texture pattern output, and the dyadic geometric relationship of the output branded texture pattern is described by the following equation:

$$P = \sum_{i=1}^M \left(\lambda_i \cdot \frac{\sum_{m=1}^{|S_{SR}|} P_{im} T_{SRm}}{\sum_{m=1}^{|S_{SR}|} \lambda_{SRm}} \right). \quad (7)$$

The template alignment of the branded texture pattern is performed using the texture intelligent matching method, and the template alignment function is constructed as follows:

$$\text{STFT}(t, f) = \int_{-\infty}^{\infty} x(\tau) h^*(\tau - t) e^{-j2\pi f \tau} d\tau. \quad (8)$$

Using the pixel difference between the two branded texture patterns K_m and the spatial distribution pixel level s , the branded texture matching window is

$$d_{mn}^{ij}(x, y) = \begin{cases} \frac{\sum_{k=-s}^{+s} |\theta_m^{ij}(x+k, y+k) - \theta_n^{ij}(x+k, y+k)|}{(2s+1)^2}, & m \neq n, \\ 0, & m = n, \end{cases} \quad (13)$$

where m, n are the image projection numbers of the brand texture pattern in 3D; i, j are the feature matching points of

$$\text{SPEC}(t, f) = |\text{STFT}(t, f)|^2. \quad (9)$$

Using the adaptive chunking technique, a brand design texture template matching window of 2^l times the length and width is created, and the brand design texture distribution function is described as follows:

$$U(x) = 1 - \tilde{t}'(x)$$

$$= \omega \tilde{U}(x) \quad (10)$$

$$= \omega \min_{c \in \{r, g, b\}} \left(\min_{y \in \Omega(x)} \left(\frac{I^c(y)}{A} \right) \right).$$

The brand design texture segmentation is performed by means of a two-dimensional function expression, and the schematic diagram of the implementation process is shown in Figure 1.

3. Brand Design Texture Intelligent Matching Optimization

3.1. Texture Histogram Extraction of Brand Design. Based on the above-mentioned construction of the intelligent information collection model of brand design texture under visual communication, the intelligent matching of brand design texture is carried out, and a method of intelligent matching of brand design texture based on visual communication is proposed. With the feature points of edge texture distribution as the center, the fuzzy feature distribution function of the brand texture pattern is calculated in the irregular texture distribution triangle region W_{mE}^{ij} . The initial pixel set of the brand design is described as follows:

$$L(a, b_m) = \sum_{V_m \in P_{res}^n} \in \sum_{P_{rtue}} \frac{|V_m \cap V_n|}{|V|} \log \left(\frac{|V| |V_m \cap V_n|}{|V_m| |V_n|} \right). \quad (11)$$

The scale function of the distribution of feature points of the brand design is obtained and expressed as follows:

$$W_{mE}^{ij} = \frac{E_m^{ij}}{\sum_{m=1}^N E_m^{ij}}. \quad (12)$$

Within the grayscale neighborhood of the brand design, the spatial distribution of texture-matched clusters with center lengths of

the brand texture pattern; θ is the regional rotation angle of the brand texture pattern.

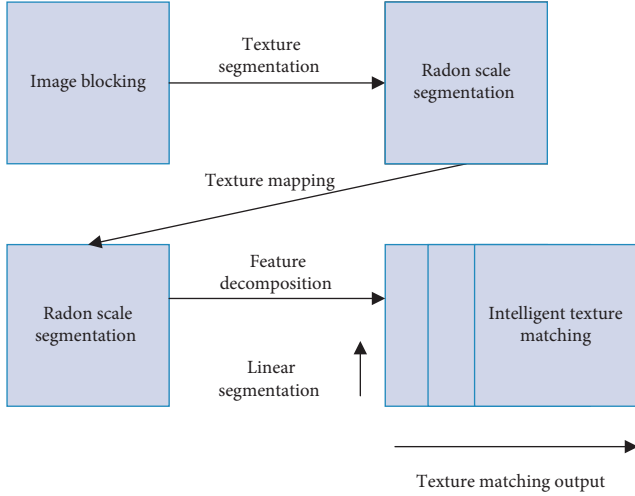


FIGURE 1: Schematic diagram of the implementation process of brand design texture segmentation.

The Taubin smoothing operator is used to reconstruct the brand texture pattern in 3D, and the main directional feature components of the edge contour of the brand texture pattern are noted as follows:

$$D_{mn}^{ij}(x, y) = \begin{cases} 1, & d_{mn}^{ij}(x, y) \geq \text{median}(d_{mn}^{ij}(x, y)), \\ 0, & \text{others,} \end{cases} \quad (14)$$

where $\text{median}()$ is the median operation expression, and the texture matching value W_{mD}^{ij} is obtained according to the sparsity of the boundary pixel points of the brand design.

$$W_{mD}^{ij} = \begin{cases} 1, & n_{mD}^{ij} < \alpha, \\ 0, & \text{others,} \end{cases} \quad (15)$$

where n_{mD}^{ij} is the set of edge pixels of the brand design; α is the ratio of the number of all pixels, set at 5%.

3.2. Visual Communication of Brand Design. Constructing the texture activity contour component of the brand design in the 4×4 subgrid region, setting h as the edge pixel set of the brand design, using the adaptive chunking feature matching method for window template matching, and using w_i as the weighting vector within the $N \times N$ window, the center pixel set and edge pixel set of the brand design is expressed as follows:

$$\begin{aligned} I_{if}(x, y) &= I^* G(x, y, \sigma_i), \\ I_{iv}(x, y) &= I^* \text{stdfilt}(x, y, w_i), \\ S_{gif}(x, y) &= -\log(P_{if}(x, y)), \end{aligned} \quad (16)$$

where $G(x, y, \sigma_i)$ is the multichromatic set of the brand design, and the texture matching hierarchy function of the brand design is calculated at each scale $\sigma_1^{(n)}(1, 2, \dots, n)$ of the brand design.

$$L(a, b_m) = \log\left(\frac{|V||V_m \cap V_n|}{|V_m||V_n|}\right). \quad (17)$$

According to the feature segmentation of the edge contour feature points of the image, the fusion feature distribution of the decorative pattern is obtained as follows:

$$f_R(z) = \begin{pmatrix} f_x(z) \\ f_y(z) \end{pmatrix} = \begin{pmatrix} h_x * f(z) \\ h_y * f(z) \end{pmatrix}, \quad (18)$$

where $f(z)$ is the texture feature component of the brand design and $*$ is the convolution operation.

The amount of edge information features of the brand design is calculated, and the optimized brand design feature extraction output is obtained as follows:

$$E_{int}(vi) = \frac{1}{2}(\partial i |d - |vi - vi - 1||^2 + \beta i |vi - 1 + 2vi + vi + 1|^2), \quad (19)$$

where

$$d = \frac{1}{n} \sum_{i=0}^{n-1} |vi - vi - 1|. \quad (20)$$

Let I_x be the chunked feature matching set of the brand design, where $x = P, N$, The activity profile of the brand design is

$$\begin{aligned} S_c &= [S_0, \dots, S_{Q-1}]_{\text{binary}} = \left[\sum_i^{Q-1} S_i \times 2^i \right]_{\text{Dec}}, \\ S_i &= \sum_j^{W \times W} I_x^j, \end{aligned} \quad (21)$$

where Q is the edge scale of the brand design; W is the amount of weak edge features.

The regularized feature fusion method is used for brand design texture information enhancement and optimal detection, and the output texture intelligent matching map is obtained as follows:

$$w(i, j) = \frac{1}{Z(i)} \exp\left(-\frac{d(i, j)}{h^2}\right), \quad (22)$$

where $Z(i) = \sum_{j \in \Omega} \exp(-d(i, j)/h^2)$ is the symbolic distance function of brand design feature extraction, and let H_x, H_y be the wavelet feature solution of multiresolution brand design, respectively, to obtain the chromatographic distribution matrix of the image as follows:

$$C = O^T O \begin{bmatrix} \sum H_x(t) H_x(t) & \sum H_x(t) H_y(t) \\ \sum H_y(t) H_x(t) & \sum H_y(t) H_y(t) \end{bmatrix}. \quad (23)$$

Using the extracted edge contour feature points of the decorative pattern as input statistics for texture matching, the texture matching output is obtained as follows:

$$O = USV^T, \quad (24)$$

where U is the matrix of pixel training sample set of brand design in $N \times N$ dimensions, and in summary analysis, the intelligent matching of brand design texture based on visual communication is achieved [21, 22].

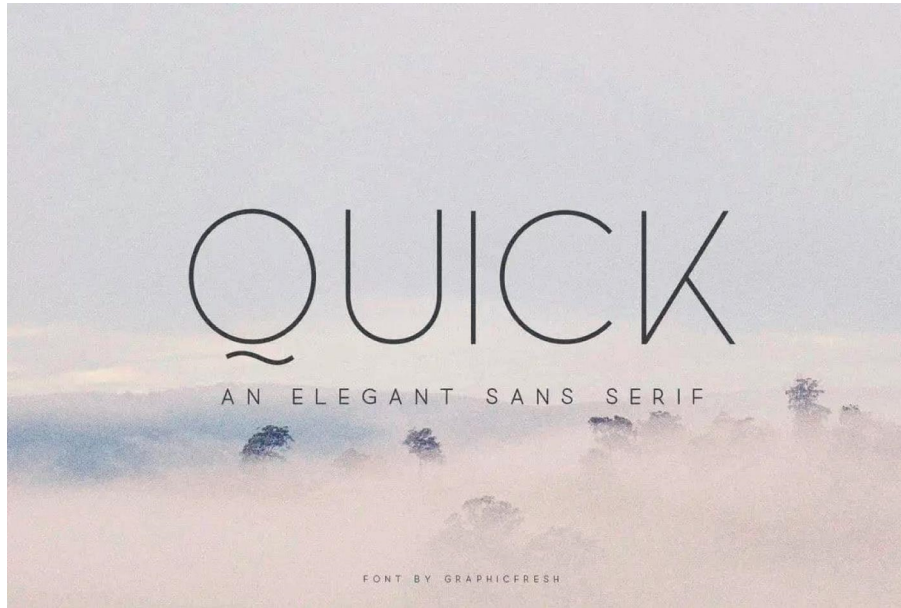


FIGURE 2: Brand image.

4. Brand Design Effect

There are many different forms of design in digital visual design packaging. Among the many variations, there are also fixed patterns. For modular packaging, the first and foremost is the channel promo. It has many styles, such as brand presenter image propaganda and regional cultural elements propaganda. There are also abstract picture combinations, national elements of traditional painting art, and post-modern three-dimensional post-technology synthesis style show. CCTV's "power of brand" is of great significance to the channel's promotional video. Delicate production, from ancient to the contemporary use of elements: interspersed, ink, ink splash, the use of techniques. It has to be said that it is deeply appealing. The creative form is based on the style of Chinese ink and wash, with the regional landmarks of Greater China. To witness the rise of China and the road to the realization of the Chinese dream. This not only represents the brand of the channel media. It also reflects the disgusted Chinese culture and the rise of the nation. It is a window to the world to declare our dream and the belief to achieve it. It further establishes the cultural communication concept of CCTV and its own brand image. As shown in Figure 2.

Various different channels and different columns in their promotional video production methods also have a lot of different strategies. Such as CCTV's windmill column have mostly children as the audience. Then, it is the pursuit of fantasy, science fiction, and childlike. His style of production, can not be limited to the host of the promo class. More to join the digital technology now three-dimensional animation effects, to produce a fantastic and bizarre fairy tale world to make it more attractive. Fully demonstrate the whimsical mode of thinking of children. In combination with specific channel call signs, etc., such as the CCTV13 news channel, its promos, and headlines

are mostly in the image of reporters and hosts for real-time interview documentary. The picture switches quickly, which makes the content more realistic, comprehensive, and global [23, 24].

In short, each program has its own positioning and presentation. It is the best to seize its own characteristics and find the suitable form of expression as shown in Figure 3.

A place of water and soil nurtures a place of people. This is also true for television media. However, this is also true for digital visual design. The characteristics of the region's packaging can always resonate with the region. For example, in the packaging design of Jinan TV, the application elements always revolve around the characteristics of the spring city. With water and springs, plus the city flower of Jinan. It not only reflects the regional characteristics. Also, for the city to make favorable publicity. For other provinces and cities, according to the different geographical location, cultural background, and ethnic folklore to package themselves to establish a unique style. In the design of highlighting the personality and regional characteristics, folk culture is one of the inevitable choices of the principle of characteristics as shown in Figure 4.

5. Experimental Results and Analysis

In order to verify the overall effectiveness of the self-matching method of significant image feature weights based on visual communication. The hardware environment during the test was an AMDA6-36702.70 GHz CPU, and the computer's memory was 2G The operating system is MatlabR2010b [25].

The time used to match the image feature weights by the three different methods was compared, and the test results of the three different methods are shown in Figure 5.

Analysis of Figure 5 shows that the matching time used in multiple iterations is less than 3 s when the significant



FIGURE 3: Brand image.

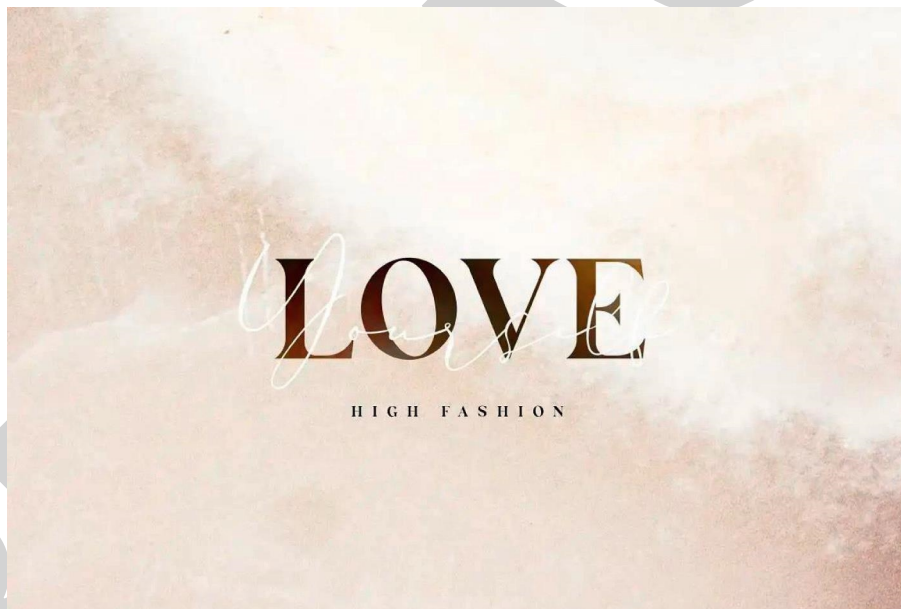


FIGURE 4: Cultural image.

image feature weight self-matching method based on visual communication is used to match the image feature weights; analysis of the matching time used in multiple iterations fluctuates around 5 s when the image feature weight self-matching method based on median filtering and the image feature weight self-matching method based on percolation filter are used to match the image feature weights. The matching time used in multiple iterations fluctuates around 5 s when matching. The test results show that the self-matching method of significant image feature weights based on visual communication takes less time to match the image feature weights because the self-matching method of significant image feature weights based on visual

communication uses the linear combination of filter functions to represent the response of the filter, which reduces the number of convolution operations, decreases the amount of operations, and shortens the time used for self-matching the image feature weights, verifying that the self-matching method of significant image feature weights based on visual communication. It is verified that the matching efficiency of the significant image feature weight self-matching method based on visual communication is high.

The image feature weight self-matching method based on the percolation filter are tested, and the matching accuracy of the three different methods is shown in Figure 6.

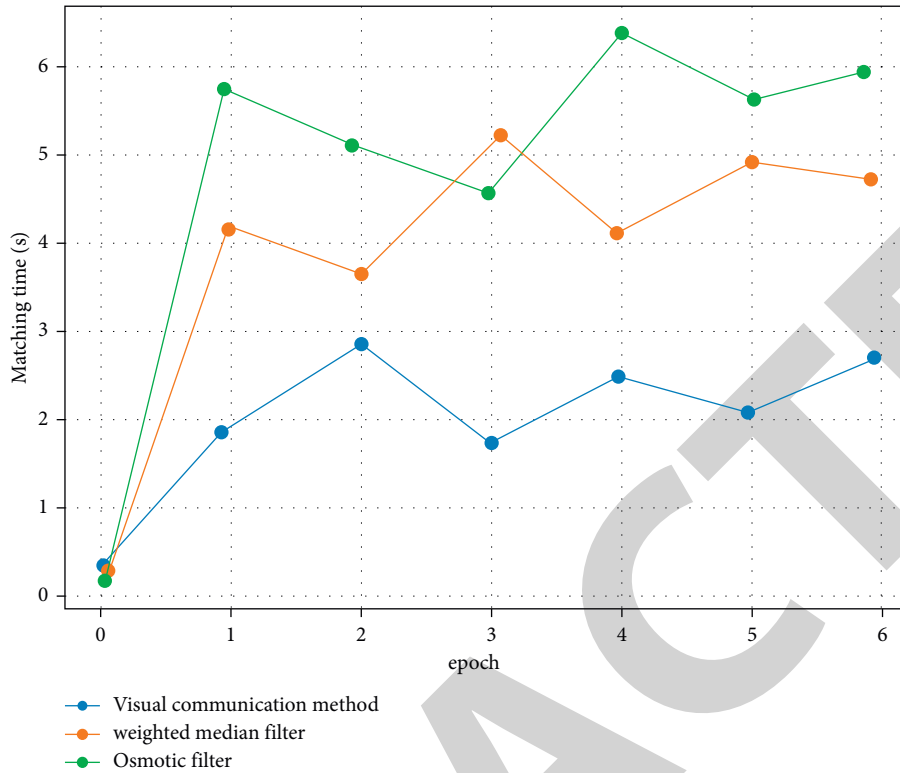


FIGURE 5: Matching time of three different methods.

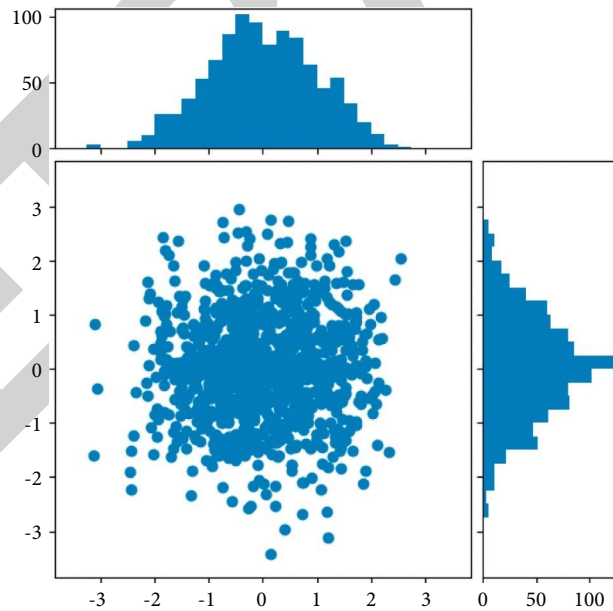


FIGURE 6: Matching accuracy of three different methods.

According to the analysis of Figure 6, the matching accuracy is around 90% in multiple iterations. According to the analysis of Figure 6, the matching accuracy of the self-matching method based on the median filter fluctuates around 80% in multiple iterations. According to the analysis of Figure 6, the matching accuracy of the self-matching

method based on an osmotic filter fluctuates around 70% in multiple iterations.

According to the above-given analysis, the matching accuracy of the self-matching method based on visual communication is higher than that of the self-matching method based on median filter and the self-matching

method based on an osmotic filter. Because the self-matching method of significant image feature weight based on visual communication constructs a controllable filter to extract image features, reduces repeated convolution operations, solves the problem of poor subjective visual effect caused by human eye sensitivity, realizes the matching of image feature weight through the ratio method, and improves the matching accuracy of the method.

6. Conclusion

The significance of digital packaging lies in the promotion of the brand. In the process of packaging, publicity, and communication, make the potential output of media concept culture. The audience is unconsciously affected. Digital packaging only beautifies and conveys. Based on the application of the image matching method and visual communication in brand design, this paper is an effective platform to establish a brand and expand the business. At the same time, promote their own value and enhance the brand image of the media.

Data Availability

The experimental data used to support the findings of this study are available from the corresponding author upon request.

Conflicts of Interest

The authors declare that they have no conflicts of interest regarding this work.

References

- [1] C. Yu, "Retracted article: climate environment of coastline and urban visual communication art design from the perspective of GIS," *Arabian Journal of Geosciences*, vol. 14, no. 4, p. 310, 2021.
- [2] F. Wang, J. Lv, G. Ying, S. Chen, and C. Zhang, "Facial expression recognition from image based on hybrid features understanding," *Journal of Visual Communication and Image Representation*, vol. 59, pp. 84–88, 2019.
- [3] S. Venkatraman, M. Alazab, and R. Vinayakumar, "A hybrid deep learning image-based analysis for effective malware detection," *Journal of Information Security and Applications*, vol. 47, pp. 377–389, 2019.
- [4] F. Baek, I. Ha, and H. Kim, "Augmented reality system for facility management using image-based indoor localization," *Automation in Construction*, vol. 99, pp. 18–26, 2019.
- [5] Y. Bai, "Target detection method of underwater moving image based on optical flow characteristics," *Journal of Coastal Research*, vol. 93, no. sp1, p. 668, 2019.
- [6] X. Huang, J. Sang, and C. Xu, "Image-Based personality questionnaire design," *ACM Transactions on Multimedia Computing, Communications, and Applications*, vol. 18, no. 4, pp. 1–20, 2022.
- [7] S. N. Chandrasekaran, H. Ceulemans, J. D. Boyd, and A. E. Carpenter, "Image-based profiling for drug discovery: due for a machine-learning upgrade?" *Nature Reviews Drug Discovery*, vol. 20, no. 2, pp. 145–159, 2021.
- [8] S. Anayat, A. Sikandar, S. Abdul Rasheed, and S. Butt, "A deep analysis of image based video searching techniques," *International Journal of Wireless and Microwave Technologies*, vol. 10, no. 4, pp. 39–48, 2020.
- [9] E. Shahid and Q. A. Arain, "Indoor positioning: an image-based crowdsourced machine learning approach," *Multimedia Tools and Applications*, vol. 80, no. 17, pp. 26213–26235, 2021.
- [10] P. Sérout, R. Campiche, S. Gougeon, M. Chereh, A. V. Rawlings, and R. Voegeli, "An image-based mapping of significance and relevance of facial skin colour changes of females living in Thailand," *International Journal of Cosmetic Science*, vol. 42, no. 1, pp. 99–107, 2020.
- [11] C. Morgan, T. M. Fajardo, and C. Townsend, "Show it or say it: how brand familiarity influences the effectiveness of image-based versus text-based logos," *Journal of the Academy of Marketing Science*, vol. 49, no. 3, pp. 566–583, 2021.
- [12] D. Wu, C. Zhang, L. Ji, R. Ran, H. Wu, and Y. Xu, "Forest fire recognition based on feature extraction from multi-view images," *Traitement du Signal*, vol. 38, no. 3, pp. 775–783, 2021.
- [13] Q. Sun and Q. Wu, "Feature space fusion classification of remote sensing image based on ant colony optimisation algorithm," *International Journal of Information and Communication Technology*, vol. 20, no. 2, p. 164, 2022.
- [14] R. Rout, P. Parida, Y. Alotaibi, S. Alghamdi, and O. I. Khalaf, "Skin lesion extraction using multiscale morphological local variance reconstruction based watershed transform and fast fuzzy C-means clustering," *Symmetry*, vol. 13, no. 11, p. 2085, 2021.
- [15] R. Surendran, O. Ibrahim Khalaf, and C. Andres Tavera Romero, "Deep learning based intelligent industrial fault diagnosis model," *Computers, Materials & Continua*, vol. 70, no. 3, pp. 6323–6338, 2022.
- [16] I. Lukonin, M. Zinner, and P. Liberali, "Organoids in image-based phenotypic chemical screens," *Experimental & Molecular Medicine*, vol. 53, no. 10, pp. 1495–1502, 2021.
- [17] K. Bakour and H. M. Ünver, "DeepVisDroid: android malware detection by hybridizing image-based features with deep learning techniques," *Neural Computing & Applications*, vol. 33, no. 18, pp. 11499–11516, 2021.
- [18] F. M. A. Abd-AlGalil, S. P. Zambare, and A. M. A. Mashaly, "First record of *Chrysomya saffrana* (Diptera: Calliphoridae) of forensic importance in India," *Tropical Biomedicine*, vol. 33, no. 1, pp. 102–108, 2016.
- [19] G. Cai, Y. Fang, J. Wen, S. Mumtaz, Y. Song, and V. Frascolla, "Multi-carrier M-ary DCSK system with code index modulation: an efficient solution for chaotic communications," *IEEE Journal of Selected Topics in Signal Processing*, vol. 13, no. 6, pp. 1375–1386, 2019.
- [20] J. Wang, X. Wang, P. Zhang et al., "Correction of uneven illumination in color microscopic image based on fully convolutional network," *Optics Express*, vol. 29, no. 18, p. 28503, 2021.
- [21] C. Zhao, H. Yang, X. Li, R. Li, and S. Zheng, "Analysis and application of martial arts video image based on fuzzy clustering algorithm," *Journal of Intelligent and Fuzzy Systems*, vol. 40, no. 4, pp. 6339–6347, 2021.
- [22] P. S. Tandel and S. Dubey, "Sign Language recognition using image-based hand gesture recognition techniques," *VIVA*

Research Article

An Improved Logistic Regression Method for Assessing the Performance of Track and Field Sports

Songling Zheng  and Xi Man

Institute of Physical Education, Inner Mongolia Normal University, Hohhot 010020, China

Correspondence should be addressed to Songling Zheng; zhsl2020@imnu.edu.cn

Received 1 June 2022; Revised 22 June 2022; Accepted 6 July 2022; Published 2 August 2022

Academic Editor: Le Sun

Copyright © 2022 Songling Zheng and Xi Man. This is an open access article distributed under the Creative Commons Attribution License, which permits unrestricted use, distribution, and reproduction in any medium, provided the original work is properly cited.

Track and field is an important part of sports. Track and field athletes are an important reserve force for the development of national sports. An accurate assessment of track and field athletes' performance can help them develop more appropriate training programs and improve their performance. In order to assess the performance of track and field athletes better, this paper proposes an improved logistic regression method. Firstly, this method uses factor analysis to reduce the data dimensions of the factors that affect the performance of track and field athletes, and uses the principal component analysis to select common factors and their corresponding values. Then, according to the common factors, a binary logistic regression model is established to evaluate the performance of track and field athletes. Experiments show that the method can effectively evaluate the performance of track and field athletes and is suitable for athletes of different track and field sports. It has high accuracy, fast evaluation efficiency, and good universality of performance evaluation. For different numbers of athletes, the proposed method has a lower error evaluation index, higher evaluation accuracy, and better evaluation quality. Compared with the other two methods, the proposed method has the shortest evaluation time and is more effective for the performance evaluation of track and field athletes.

1. Introduction

Athletes are an important reserve force for the development of national sports, and the accurate assessment of athletes' performance can develop more applicable training plans for them and improve their performance [1]. In addition to a complete training system, an objective and fair assessment evaluation system is particularly important for training athletic sports talents. An objective evaluation system of track and field sports performance aims to explore the potential of track and field athletes and is conducive to the national selection of more suitable track and field sports talents [2]. Constructing an evaluation model reflects the objective training effects of track and field athletes, finds the strengths and weaknesses of track and field athletes themselves, and then promotes track and field training reform and maximizes the effects and benefits of the sports training reform. At the same time, the feedback information from the model can also promote track and field athletes to clearly

recognize their training situation in the future training process and continuously adjust their training status to achieve the highest training efficiency. This can also serve as a guideline for track and field athletes' career planning.

Factors such as training intensity and track and field athletes' own physical quality can directly affect their performance. Accurately understanding the changing characteristics of track and field athletes' performance can ensure their better performance [3]. This makes it very important to assess track and field athletes' performance. The assessment of track and field athletes' performance is an important part of the athletes' training activities. This work plays a role in diagnosing, regulating, and strengthening the training process of track and field athletes, as well as making value judgments about the effectiveness of their training [4]. The evaluation of the training effectiveness of track and field athletes should be an evaluation of the training effect and training process. The evaluation should not only emphasize the function of screening and selection, but also strengthen

the function of motivation and development [5]. What should we do in the evaluating the training performance of track and field athletes to achieve the purpose of cultivating the training interest of track and field athletes, stimulating the subjective initiative of track and field athletes, and meeting the psychological needs of athletes is directly related to the functional orientation of track and field athletes' training and the realization of training goals. This is a problem that needs to be solved urgently at present.

Athletic athlete performance assessment is not only a test of sports training effects, but also a comprehensive judgment of athletes' sports ability. Whether the assessment is comprehensive, objective and fair, and truly reflects an athlete's actual level in sports [6] is often an concern of the athletes. Therefore, it is particularly important to construct a diversified performance assessment system. The diversification of the assessment system is reflected in the diversification of the assessment content. Athletic performance assessment should not be limited to physical fitness and motor skills, but also include training attitude, physical exercise, training participation, and competition winning together. The assessment should cover various factors such as cognition, emotion, cooperation, learning, and practice of the athletes [7]. The diversification of the assessment system is also reflected in the setting of dual subjects of assessment. They are the summative assessment made by the coach as the main body relying on the assessment results of training programs and the formative assessment made by the athlete as the main body with training activities as the main content [8]. By constructing a diversified track and field athletes' performance assessment system, it further broadens the dimensions and connotations of track and field athletes' performance assessment, which is of practical significance to improve the fairness and comprehensiveness of track and field athletes' performance assessment, enhance track and field athletes' participation and dominance in the process of performance formation, and help track and field athletes understand themselves, discover themselves, and transform themselves more objectively.

The regression model is a predictive model that studies the dependent and independent variables and integrates various possible influencing factors to assess athletes' performance and training effects through multiple regression models [9]. The research methodology in this paper takes the factors affecting the training performance of track and field athletes as the object of study, selects the factors affecting the assessment of track and field athletes' performance as the target variable, and establishes a logistic regression model. In this paper, the historical performance of track and field athletes was selected as the dataset. Among the assessment variables were competition ranking, competition time, age, gender, training duration, BMI, and blood pressure. First, factor analysis is carried out on the evaluation indicators to reduce the dimension of the data, eliminate the correlation between the data, and determine the final indicators. Then, a logistic regression model was established based on the final indicators. Finally, the assessment effects of the models were compared. Compared with the other methods, the method in this paper can achieve high-quality assessment of track

and field athletes' performance, which is very important for their training planning. Accurate assessment of track and field athletes' performance can help them understand themselves and training planning, which is good to improve their performance and make them better and better.

This paper has the following innovative points.

- (1) The factors affecting track and field athletes' performance are multiple. In order to effectively conduct track and field athletes' performance assessment, this paper simplifies the data and influencing factors by the factor analysis method. Discarding secondary factors and selecting primary factors as evaluation variables allows for a more simplified and efficient operation of the algorithm.
- (2) The common factors affecting the performance of track and field athletes were selected using the principal component analysis, and classified and assigned different weight values according to the degree of influence, which can improve the accuracy of the evaluation.

This paper mainly consists of five parts; the first is the introduction, the second is the state of the art, the third is the methodology, the fourth is the experiment and analysis, and the fifth is the conclusion.

2. State of the Art

2.1. Research Status. At present, with the deepening of the concept of "Internet Plus," information technology has been widely used in sports training activities. A large number of scholars have conducted in-depth research on sports performance assessment models and constructed many assessment models. Under the guiding principles of advancement and comprehensiveness, the literature [10] established indicators such as training hours to improve the quality of sports training and to promote further the internalization of athletes' knowledge. The literature [11] established an evaluation model from three aspects of the basic needs theory. The model used hierarchical analysis to analyse the indicator weights and found that the greatest weight was given to the autonomy needs and the least weight to the competence needs. When summarizing the methodological studies on the quantification of performance evaluation in universities, hierarchical analysis was found to be the most representative, but it is very difficult to test whether the judgment matrix is consistent when studying real-world problems and it is difficult to truly reflect the fuzzy nature of human evaluation [12]. Therefore, the literature [13] addresses the shortcomings of expert scoring in the hierarchical analysis method and integrates the principles of fuzzy mathematics to establish a mathematical model to evaluate the training quality more objectively. The literature [14] established an evaluation system from three aspects: training platform, coaches, and athletes. The method is based on AHP to determine the index weights and introduces a fuzzy comprehensive evaluation model for the differences that exist between the consistency of judgment matrix and the consistency of human brain thinking. This

provides a new perspective for athlete training quality assessment. With the continuous improvement of the fuzzy complementary judgment matrix theory, the literature [15] established athlete satisfaction indicators. The theory indicates that the influence of personal factors on the index system is the highest and the influence of gymnasium factors is the lowest, which provides a more scientific and reasonable reference basis for athlete training strategies. The literature [16] investigated the athlete performance prediction method integrating knowledge mapping and collaborative filtering to establish a training knowledge map depicting training information. The algorithm calculates the similarity of training at the knowledge level by the neighbour node-based method and the knowledge graph-based learning method, and integrates the obtained similarity into the collaborative filtering performance prediction framework to obtain athlete performance prediction results. The literature [17] investigates a two-way attention-based mechanism for athlete performance prediction model. The model obtains the attention scores of different attribute features on the first stage and second stage competition performance through two attention calculations, and combines the multi-feature fusion approach to obtain the competition performance prediction results. The historical data-driven prediction method is implemented by historical data. There are many historical data-driven prediction methods such as hidden Markov models, chaotic prediction, and support vector machines [18]. Support vector machines have the advantage of small sample learning and high learning ability in prediction, and hence they are also used to study the historical data-driven athlete performance estimation method. This method uses the KNN algorithm to pre-process the historical performance of athletes to remove the effect of distracting data and classify the data accurately. It uses support vector institutions to build regression prediction models and introduces Lagrangian functions for data transformation to avoid data operations from getting localized [19]. The support vector regression prediction model parameters are optimized using the particle swarm algorithm to reduce the interference of input quantity noise and reduce the complexity of the computation. These evaluation models are built according to different application scenarios and are important for promoting the scientific training of athletes.

2.2. Factor Analysis Method. Factor analysis is a technique to reduce the dimensionality and simplify the data. It explores the underlying structure of the observed data by examining the internal dependencies among many variables and represents the underlying data structure with a few “abstract” variables. These abstract variables are called “factors.” By discarding secondary factors and selecting primary factors as evaluation variables, the model is made more simplified and the efficiency of the algorithm operation is improved. This reflects the main information of the original set of variables. The original variables are observable explicit variables, while the factors are generally unobservable latent variables. The common factors in factor analysis are common influences

that are not directly observable but exist objectively. Each variable can be expressed as a linear function of the common factor and the sum of the special factors [20]. Its mathematical model can be expressed as

$$\begin{pmatrix} i_1 \\ i_2 \\ \vdots \\ i_u \end{pmatrix} = \begin{pmatrix} g_{11} & L & g_{1u} \\ g_{21} & \cdots & g_{2u} \\ \vdots & & \vdots \\ g_{u1} & \cdots & g_{uu} \end{pmatrix} \begin{pmatrix} F_1 \\ F_2 \\ \vdots \\ F_w \end{pmatrix} + \begin{pmatrix} \varepsilon_1 \\ \varepsilon_2 \\ \vdots \\ \varepsilon_w \end{pmatrix}. \quad (1)$$

That is, $I = GF + \varepsilon$, where $I = (i_1, i_2, \dots, i_u)^N$ is an observable u -dimensional random vector. Each component represents an indicator or vector. F in $F = (F_1, F_2, \dots, F_w)^N$ is an w -common factor variable. w is less than or equal to u . It is the factor that appears in the expressions of each original observed variable, which are mutually independent unobservable theoretical variables. Matrix G is called the factor loading matrix. g_{xy} is called the factor loading. It represents the correlation coefficient between the x -th original variable and the y -th public factor variable. The larger g_{xy} indicates the stronger correlation between the public factor F_y and the original variable I . ε is a special factor. It represents the part of the original variables that cannot be explained by the common factor variables, which is equivalent to the residual part in the multiple linear regression analysis.

Factor analysis utilizes the idea of dimensionality reduction, starting from the study of the dependencies within the correlation matrix of the original variables, and groups the original variables according to the magnitude of the correlation, making the correlation between variables within the same group high and the correlation between variables in different groups low [21]. Each group of variables represents a basic structure and is represented by an unobservable composite variable. This underlying structure is called the common factor. Capturing these main factors can help us analyse and interpret complex problems.

3. Methodology

3.1. Regression Models

3.1.1. Regression Model Where the Dependent Variable Is a Qualitative Variable. (1) *Qualitative variables* The dependent variable takes only two outcomes. $j=0$ means that the event did not occur. $j=1$ means that the event occurred. Consider the following expression for a simple linear regression model.

$$\begin{aligned} j_x &= \beta_0 + \beta_1 i_x + \varepsilon_x, \\ E(j_x) &= \beta_0 + \beta_1 i_x. \end{aligned} \quad (2)$$

Since j_x is a Bernoulli random variable of type 0 to 1, the following probability expression is obtained:

$$\begin{aligned} U(j_x = 1) &= \pi_x, \\ U(j_x = 0) &= 1 - \pi_x. \end{aligned} \quad (3)$$

According to the definition of discrete random variable expectation, the following function is obtained:

$$E(j_x) = 1(\pi_x) + 0(1 - \pi_x) = \pi_x. \quad (4)$$

Thus, $E(j_x) = \pi_x = \beta_0 + \beta_1 i_x$.

(2) *Error term* The error term $\varepsilon_x = j_x - (\beta_0 + \beta_1 i_x)$ can only take two values for a dependent variable, i.e., 0 or 1. Its expression is as follows:

$$\begin{aligned} j_x = 1, \varepsilon_x &= 1 - (\beta_0 + \beta_1 i_x) = 1 - \pi_x, \\ j_x = 0, \varepsilon_x &= -(\beta_0 + \beta_1 i_x) = -\pi_x. \end{aligned} \quad (5)$$

The error term is a two-point discrete distribution, and thus it cannot be assumed to be a normal error regression model.

Zero-mean heteroskedasticity means that the error term is zero-mean and its variances are not equal, and the expressions are as follows:

$$D(\varepsilon_x) = D(j_x) = \pi_x(1 - \pi_x) = (\beta_0 + \beta_1 i_x)(1 - \beta_0 - \beta_1 i_x). \quad (6)$$

If a multiple linear regression equation is used to analyse the quantitative relationship between the dependent variable and the independent variable, the relationship function is expressed as follows:

$$j = \beta_0 + \beta_1 i_1 + \beta_2 i_2 + \dots + \beta_w i_w. \quad (7)$$

(3) The left side of the equation j takes 0 or 1, and the right side of the equation can take any real number; the left and right sides do not correspond to each other in terms of the range of values. Therefore, multiple linear regression cannot be used for fitting the dependent variable as a qualitative variable.

3.1.2. Logistic Regression Model. The logistic function has the form [22].

$$f(i) = \frac{e^i}{1 + e^i} = \frac{1}{1 + e^{-i}}. \quad (8)$$

The range of values of its independent variable is $(-\infty, +\infty)$ and the range of values of the function is $(0, 1)$.

The dependent variable j itself takes only two discrete values of 0 or 1. It is not suitable as the dependent variable in the regression model, such that

$$\begin{aligned} \pi_x &= f(i_x) = \frac{1}{1 + \exp(-(\beta_0 + \beta_1 i_x))}, \\ \ln\left(\frac{\pi_x}{1 - \pi_x}\right) &= \beta_0 + \beta_1 i_x, \end{aligned} \quad (9)$$

where π_x is the probability that the random variable j takes 1, and its value varies continuously in the interval $[0, 1]$; thus, π_x can be used as the dependent variable instead of j .

Let j be a variable of type 0 to 1, and t sets of observations be $(i_{x1}, \dots, i_{xu}, j_x)$, where j_1, j_2, \dots, j_t is a random variable that takes the value 0 or 1. The expression for the expected value is as follows:

$$E(j_x) = \pi_x = f(\beta_0 + \beta_1 i_{x1} + \dots + \beta_u i_{xu}). \quad (10)$$

The expression of the function for the logistic regression model [23] is as follows:

$$\pi_x = f(i_x) = \frac{e^{\beta_0 + \beta_1 i_{x1} + \dots + \beta_u i_{xu}}}{1 + e^{\beta_0 + \beta_1 i_{x1} + \dots + \beta_u i_{xu}}}. \quad (11)$$

Thus, j_x is a random variable of type 0 to 1 with mean $\pi_x = f(\beta_0 + \beta_1 i_{x1} + \dots + \beta_u i_{xu})$; and the probability function is

$$\begin{aligned} U(j_x = 1) &= \pi_x, \\ U(j_x = 0) &= 1 - \pi_x. \end{aligned} \quad (12)$$

The random probability of j_x can be defined as:

$$U(j_x) = \pi_x^{j_x} (1 - \pi_x)^{1 - j_x}, \quad j_x = 0, 1; \quad x = 1, \dots, t. \quad (13)$$

The likelihood function of j_1, j_2, \dots, j_t is thus

$$L = \prod_{x=1}^t U(j_x) = \prod_{x=1}^t \pi_x^{j_x} (1 - \pi_x)^{1 - j_x}. \quad (14)$$

The likelihood function is taken logarithmically and the following expression can be obtained:

$$\begin{aligned} \ln L &= \sum_{x=1}^t [j_x \ln \pi_x + (1 - j_x) \ln(1 - \pi_x)] \\ &= \sum_{x=1}^t \left[j_x \ln \frac{\pi_x}{1 - \pi_x} + \ln(1 - \pi_x) \right]. \end{aligned} \quad (15)$$

Bringing equation (2.14) into the equation gives the expression

$$\ln L = \sum_{x=1}^t \left[j_x (\beta_0 + \beta_1 i_{x1} + \dots + \beta_u i_{xu}) - \ln(1 + \exp(\beta_0 + \beta_1 i_{x1} + \dots + \beta_u i_{xu})) \right]. \quad (16)$$

The maximum likelihood estimation yields the estimate $\hat{\beta}_0, \hat{\beta}_1, \dots, \hat{\beta}_u$ of $\beta_0, \beta_1, \dots, \beta_u$.

3.2. Prediction Model

3.2.1. Data Processing. The data taken in this paper are from the historical performance of athletes in a sports school. They mainly contain factors such as competition ranking, competition sports time, age, gender, training hours, and physical fitness at all levels of events. The dataset contains data related to 100 athletes. The dataset consists of training predictor variables and one target variable for track and field sports. The predictor variables include athletic athletes' competition ranking, competition time, age, gender, training time, BMI, and blood pressure, and the variable descriptions are shown in Table 1. The goal of the dataset is to predict athletic athletes' performance based on certain parameter measures contained in the dataset.

The process of data cleaning requires the consideration of the following effects.

- (1) Duplicate or irrelevant data.
- (2) Mislabelled data or multiple occurrences of the same label.

TABLE 1: Variable declaration.

I_1	Competition ranking
I_2	Race time
I_3	Age
I_4	Gender
I_5	The training time
I_6	BMI
I_7	Blood pressure

(3) Missing or empty data points.

(4) Outlier values.

The data are a standard database, and hence there is no duplicate or irrelevant data and no vacant data points have been checked. Since blood pressure, age, and body mass index cannot be 0 in general, and 0 is an abnormal data point, the rows with 0 values in each feature of blood pressure, age, and body mass index were filtered out. There were 724 valid data left after processing.

3.2.2. Factor Analysis

(1) *Applicability Test of Factor Analysis.* The results of the KMO and Bartlett's sphericity tests on the data of track and field athletes using SPSS software are shown in Table 2. It is generally considered that if the KMO measure is greater than 0.5, then factor analysis can be performed. The significance of $p=0$ indicates that there is a certain correlation between the original variables, and the conditions for factor analysis are available.

(2) *Extraction of Common Factors.* Factor analysis was performed on the data, and the extraction of principal components was performed by principal component analysis. Classifying them according to the degree of influence and assigning different weight values improves the assessment accuracy. Under the principle of eigenvalue of 1, three principal factors were retained, i.e., the seven variables were grouped into three categories. This reduces the amount of operations, but categorization causes information loss, and the amount of information retained is 64.49%, and the amount of information lost is large; thus, a common factor is added to make the amount of information lost reside within an acceptable range. The following variance interpretation Table 3 shows that each principal component contains the total variance of each original variable, and the improved retained information is 77.08%.

(3) *Public Factor Naming.* The original factor loading matrix was rotated by extracting the four public factors and performing maximum variance orthogonal rotation to obtain the variance maximum orthogonal rotation matrix, as shown in Table 4.

Based on the rotated component matrix, the four common factors can be named. The first factor Z1 has large loadings on the gender and age indicators. The second factor Z2 has larger loadings on the race ranking and race time indicators. The third factor Z3 has a large loading on BMI and

training duration. The fourth factor Z4 has a larger loading on blood pressure. It can be found that the evaluation indexes corresponding to Z1 are indirect influence data. The evaluation indexes corresponding to Z2 are race performance-related data. The evaluation indexes corresponding to Z3 are other physical data. Z4 represents blood pressure. They are named as indirect factors, competition performance, physical quality, and blood pressure, respectively.

3.2.3. Binary Logistic Regression

(1) *Hosmer-Lemeshaw test.* The original hypothesis H0: the model fits well with the observations. The results are shown in Table 5 $p=0.279 > 0.05$; the original hypothesis is accepted and the regression model can fit the data well.

$$\text{Logit}U = -0.82 + 0.65k_1 + 0.86k_2 + 0.67k_3 + 0.38k_4, \quad (17)$$

(2) As shown in Table 7, the significant p -values are all 0, indicating that BMI, age, gender, and training duration have highly significant effects on the performance of track and field athletes. The effects were ranked from the highest to the lowest: BMI > age > gender > training duration.

(3) As shown in Table 7, the significant p -values are all 0, indicating that BMI, age, gender, and training duration have highly significant effects on the performance of track and field athletes. The effects were ranked from the highest to the lowest: BMI > age > gender > training duration.

(4) The accuracy is shown in Table 6, with an accuracy of 74.9%, which indicates that the model predicts more accurately.

(5) From the regression analysis of multiple factors, a binary logistic regression equation was established. where $U = \beta_0 + \beta_1 i_1 + \beta_2 i_2 + \dots + \beta_w i_w$.

4. Result Analysis and Discussion

Using track and field athletes of a sports school as the experimental subjects, 10 groups of 200m sprinters were randomly selected as the research subjects. The evaluation results are shown in Figure 1. According to Figure 1, the method of this paper can effectively evaluate the performance of 200m sprinters, and the estimated value is very close to the actual value. The experiment proves that the method in this paper can accurately estimate the performance of track and field athletes and has a high accuracy of track and field athletes' performance assessment results.

The athletes of 10 types of track and field sports were randomly selected in this sports school to verify the generality of this paper's method. Using the method of this paper, the athletes' performance of these 10 types of track and field sports was evaluated and compared with the actual values, and the evaluation accuracy of the 10 types of track and field sports is shown in Figure 2. According to Figure 2, it can be seen that for different types of track and field sports, the method in this paper can accurately assess the performance of track and field athletes, and the estimation accuracy is basically maintained at more than 96%. The experiment proves that the method in this paper has good generality and a high estimation accuracy for different types of track and field sports.

TABLE 2: KMO and Bartlett's test.

KMO sampling suitability quantity	0.592
Bartlett sphericity test	The approximate chi-square Degrees of freedom Significant
	952.82 26 0

TABLE 3: Total variance explained.

Composition	Total	Percentage of variance of initial eigenvalue	Cumulate %	Total	Load square and percent variance	Cumulate %	Total	Rotational load square and percent variance	Cumulate %
1	1.98	28.28	28.28	1.98	28.28	28.28	1.70	24.41	24.41
2	1.53	21.90	50.19	1.53	21.90	50.19	1.35	19.35	43.77
3	1.00	14.29	64.49	1.00	14.29	64.49	1.30	18.70	62.48
4	0.88	12.58	77.08	0.88	12.58	77.08	1.02	14.60	77.08
5	0.65	9.33	86.41						
6	0.54	7.77	94.19						
7	0.40	5.80	100.00						

TABLE 4: Rotated factor matrix and score matrix.

Variable	Indicators	Rotation factor matrix				Factor scoring matrix			
		1	2	3	4	1	2	3	4
I_1	Competition ranking	0.846	-0.018	0.008	-0.001	0.519	-0.028	-0.116	0.044
I_2	Race time	0.868	0.077	0.113	0.011	0.516	0.029	-0.048	0.035
I_3	Age	-0.155	0.855	-0.035	0.123	-0.096	0.674	-0.149	-0.031
I_4	Gender	0.278	0.748	0.231	0.001	0.124	0.561	0.032	-0.129
I_5	The training time	-0.146	0.207	0.798	0.173	-0.205	0.010	0.650	0.090
I_6	BMI	0.334	-0.044	0.773	-0.108	0.083	-0.1465	0.612	-0.127

TABLE 5: Hosmer-Lemeshaw test.

Chi-square	Degrees of freedom	Significant
9.806	8	0.278

TABLE 6: Prediction accuracy.

	Assessment of conformity		Accuracy rate
	0	1	
Actual qualification	0	412	64
	1	118	132
Overall percentage			74.9

Comparing the method of this paper with the methods in the literature [16] and literature [17] clearly indicates that the assessment of athletes' performance of the above-mentioned 10 types of track and field sports was implemented at the same time. The evaluation accuracy and evaluation efficiency of the three methods were tested by comparing, among which literature [16] is a student performance prediction method integrating knowledge mapping and collaborative filtering, and literature [17] is a student performance prediction model based on a two-way attention mechanism. The performance of 100 athletes in each type of track and field sports was selected for testing and the average value was taken to enhance the credibility of the experiment. The accuracy and assessment efficiency of the three methods for

assessing athletes' performance in the 10 types of track and field sports are shown in Figures 3 and 4. According to Figure 3, it can be seen that for athletes of different types of track and field sports, the assessment accuracy of athletes' performance of this paper's method is significantly higher than the remaining two methods, and the average assessment accuracy of this paper's method is 97.7%, the average assessment accuracy of literature [16] is 81.8%, and the average assessment accuracy of literature [17] is 86.5%. The experiment proves that when assessing the performance of athletes in different types of track and field sports, the method in this paper has the highest assessment accuracy, which significantly reduces the estimation error of athletes' performance and increases the credibility of the assessment results at the same time.

According to Figure 4, for athletes of different types of track and field sports, the evaluation time of this paper's method is significantly lower than the remaining two methods, and the evaluation time of this paper's method is always maintained within 20s with less variation, while the estimation time of the remaining two methods is more variable and less stable. This is due to the fact that the algorithm in this paper introduces factor analysis to optimize the parameters affecting the evaluation, which reduces the computational parameters and decreases the computational effort. The experiment proves that the evaluation time of this paper's method is the least and the athlete's performance evaluation is more efficient.

TABLE 7: Logistic regression analysis.

	B	Standard error	Wald	Degree of freedom	Significance	Exp (B)	95% confidence interval of EXP (B)	
							Lower limit	Upper limit
Gender	0.65	0.09	51.66	1	0	1.92	1.61	2.3
BMI	0.86	0.1	75.36	1	0	2.38	1.96	2.9
Age	0.67	0.09	49.18	1	0	1.97	1.63	2.38
Training time	0.38	0.09	17.32	1	0	1.47	1.22	1.76
Constants	-0.82	0.09	76.33	1	0	0.43		

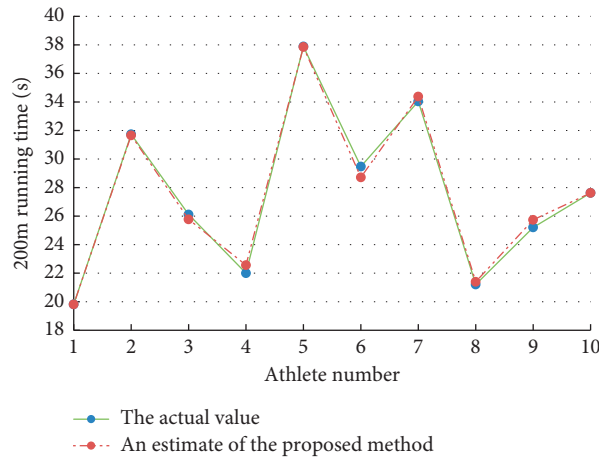


FIGURE 1: Performance evaluation results of the 10 groups of 200m sprinters.

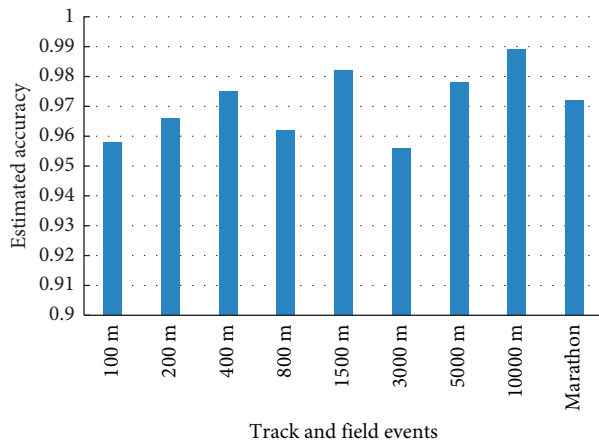


FIGURE 2: Estimation accuracy of the performance of the 10 track and field sports.

Taking 200m sprinters’ performance as an example, the accuracy of the performance assessment of the three methods was tested with different numbers of athletes. The accuracy of the three methods was evaluated by the Mean Absolute Percentage Error (MAPE), an error evaluation index. The results of the error evaluation index tests for the three methods with different numbers of athletes are shown in Figure 5. According to Figure 5, the MAPE values of all three methods increased with the increasing number of athletes. Generally, if the MAPE value is lower than 10, it indicates that the evaluation accuracy of the evaluation methods is higher. With different numbers of athletes, the

MAPE values of this paper are significantly lower than those of the remaining two methods. The MAPE value of this method always stayed within 6, and the MAPE value of the other two methods was lower than 10 only when the number of athletes was less than 200. When the number of athletes was more than 200, the MAPE values of the other two methods were greater than 10.

The experiment proves that the MAPE value of this paper method is the lowest when the number of athletes is different. This indicates that the evaluation value of this paper’s method is closest to the actual value, with a higher evaluation accuracy and high evaluation quality.

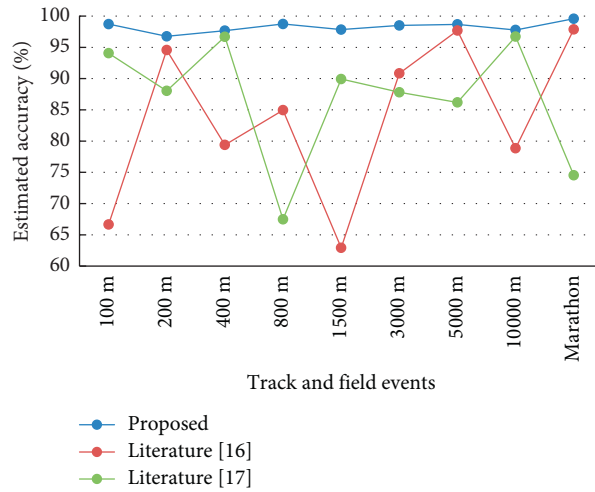


FIGURE 3: Evaluation accuracy of the three methods.

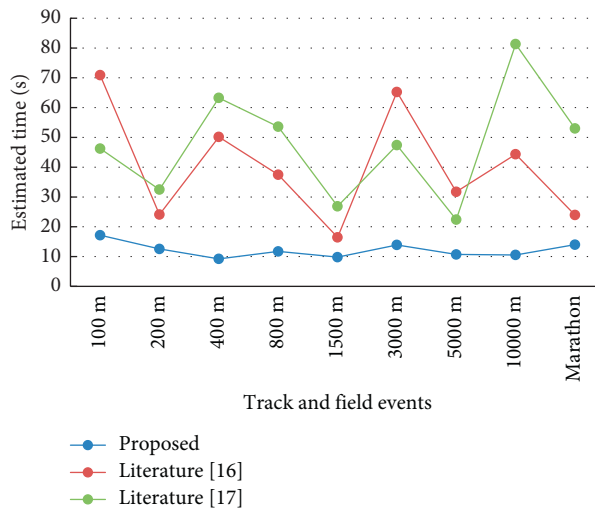


FIGURE 4: Evaluation efficiency of the three methods.

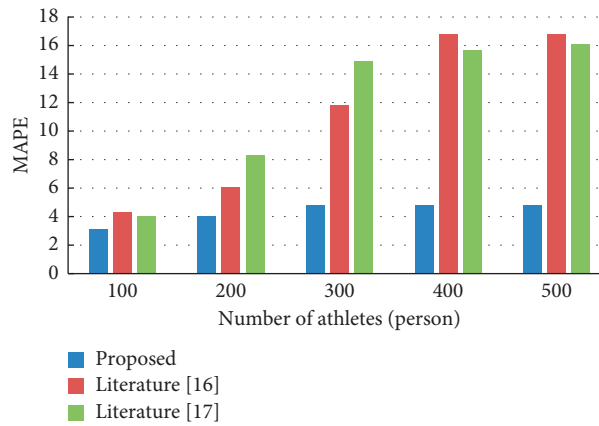


FIGURE 5: Comparison of the error evaluation indexes of the three methods.

5. Conclusion

Based on the model obtained in this paper, the performance of track and field athletes can be effectively evaluated. The main objective of this paper is to evaluate the performance of track and field athletes using a logistic regression model. The method adopts the idea of factor analysis, reduces and simplifies the data, and improves the evaluation effect. The experiments show that the method can accurately estimate the performance of track and field athletes and has a high accuracy of track and field athletes' performance assessment. At the same time, the method has good generality for track and field athletes' performance evaluation, less evaluation time, and higher evaluation efficiency. Overall, the method in this paper can achieve high-quality athlete performance assessment, which is very important for athletes' training planning. The accurate estimation of athletes' performance can help improve their performance and make them better by understanding the training planning they need. Therefore, we study the historical data-driven athlete performance estimation method to improve the accuracy and estimation efficiency of athlete performance estimation, provide more valuable information for athlete training planning, and develop better athletes for the country. However, the good experience of using this method requires a large amount of track and field athletes' historical competition performance data, and the effectiveness of the evaluation for individual track and field athletes' performance is yet to be verified. The experimental data are all track and field athletes' performance, and the generality of the prediction for other non-track and field sports is also yet to be verified. The next step will be to further explore the effectiveness of the model in evaluating the performance of athletes in a wider range of sports, to verify the generality of the model in evaluating athletes' performance, and to expand the scope of the application.

Data Availability

The labeled dataset used to support the findings of this study is available from the corresponding author upon request.

Conflicts of Interest

The author declares no competing interests.

Acknowledgments

This study was sponsored by Inner Mongolia Natural Science Foundation of China, Grant 2021MS03018, & High-Level talent Scientific Research Start-Up Foundation of Inner Mongolia Normal University, Grant 2019YJRC060.

References

- [1] K. Lindberg, P. Solberg, B. R. Rønnestad et al., "Should we individualize training based on force-velocity profiling to improve physical performance in athletes?" *Scandinavian Journal of Medicine & Science in Sports*, vol. 31, no. 12, pp. 2198–2210, 2021.
- [2] C. E. Thomas, P. B. Gastin, G. Abbott, and L. C. Main, "Impact of the talent development environment on the wellbeing and burnout of Caribbean youth track and field athletes," *European Journal of Sport Science*, vol. 21, no. 4, pp. 590–603, 2021.
- [3] R. Rico, C. B. Gibson, M. Sánchez-Manzanares, and M. A. Clark, "Building team effectiveness through adaptation: team knowledge and implicit and explicit coordination," *Organizational Psychology Review*, vol. 9, no. 2-3, pp. 71–98, 2019.
- [4] N. Pollock, S. Kelly, J. Lee et al., "A 4-year study of hamstring injury outcomes in elite track and field using the British Athletics rehabilitation approach," *British Journal of Sports Medicine*, vol. 56, no. 5, pp. 257–263, 2022.
- [5] M. Paais, J. R. Pattiruhu, "Effect of motivation, leadership, and organizational culture on satisfaction and employee performance," *The Journal of Asian Finance, Economics and Business*, vol. 7, no. 8, pp. 577–588, 2020.
- [6] A. C. Jeffries, L. Wallace, A. J. Coutts, S. J. McLaren, A. McCall, and F. M. Impellizzeri, "Athlete-reported outcome measures for monitoring training responses: a systematic review of risk of bias and measurement property quality according to the cosmin guidelines," *International Journal of Sports Physiology and Performance*, vol. 15, no. 9, pp. 1203–1215, 2020.
- [7] S. Costa, G. Santi, S. di Fronso et al., "Athletes and adversities: athletic identity and emotional regulation in time of COVID-19," *Sport Sciences for Health*, vol. 16, no. 4, pp. 609–618, 2020.
- [8] A. Tomiak, H. Braund, R. Egan et al., "Exploring how the new entrustable professional activity assessment tools affect the quality of feedback given to medical oncology residents," *Journal of Cancer Education*, vol. 35, no. 1, pp. 165–177, 2020.
- [9] S. Del Rosso, D. Pinho Souza, F. Muñoz, D. G. Behm, C. Foster, and D. Boullosa, "10 km performance prediction by metabolic and mechanical variables: influence of performance level and post-submaximal running jump potentiation," *Journal of Sports Sciences*, vol. 39, no. 10, pp. 1114–1126, 2021.
- [10] A. J. Sturges, Z. Huysmans, W. Way, and A. Goodson, "Examining the role of high school athletic directors in promoting leadership development in high school student-athletes," *Journal for the Study of Sports and Athletes in Education*, vol. 14, no. 1, pp. 58–81, 2020.
- [11] M. Vansteenkiste, R. M. Ryan, and B. Soenens, "Basic psychological need theory: advancements, critical themes, and future directions," *Motivation and Emotion*, vol. 44, no. 1, pp. 1–31, 2020.
- [12] H. Zhang, X. He, and H. Mitri, "Fuzzy comprehensive evaluation of virtual reality mine safety training system," *Safety Science*, vol. 120, pp. 341–351, 2019.
- [13] W. Li, G. Xu, Q. Xing, and M. Lyu, "Application of improved AHP-BP neural network in CSR performance evaluation model," *Wireless Personal Communications*, vol. 111, no. 4, pp. 2215–2230, 2020.
- [14] A. Rizvandi, M. Taghipour Gharbi, and M. Esmaeili, "The evaluation of performance indicators of coaches in football development[J]," *Journal of Humanities Insights*, vol. 3, no. 04, pp. 246–252, 2019.
- [15] X. Huang, X. Ma, and Q. Zhang, "Effect of building interface form on thermal comfort in gymnasiums in hot and humid climates," *Frontiers of Architectural Research*, vol. 8, no. 1, pp. 32–43, 2019.
- [16] I. Fernández-Tobías, I. Cantador, P. Tomeo, V. W. Anelli, and T. Di Noia, "Addressing the user cold start with cross-domain collaborative filtering: exploiting item metadata in matrix

- factorization,” *User Modeling and User-Adapted Interaction*, vol. 29, no. 2, pp. 443–486, 2019.
- [17] M. Qiu, B. Thuraisingham, M. Daneshmand, H. Ning, and P. Barnaghi, “Special issue on robustness and efficiency in the convergence of artificial intelligence and IoT,” *IEEE Internet of Things Journal*, vol. 8, no. 12, pp. 9460–9462, 2021.
- [18] J. S. Raj and J. V. Ananthi, “Recurrent neural networks and nonlinear prediction in support vector machines,” *Journal of Soft Computing Paradigm (JSCP)*, vol. 1, no. 1, pp. 33–40, 2019.
- [19] Z. Tian, Y. Ren, and G. Wang, “An application of backtracking search optimization-based least squares support vector machine for prediction of short-term wind speed,” *Wind Engineering*, vol. 44, no. 3, pp. 266–281, 2020.
- [20] X. Wang, Y. Liu, F. Wang, J. Wang, L. Liu, and J. Wang, “Feature extraction and dynamic identification of drivers’ emotions,” *Transportation Research Part F: Traffic Psychology and Behaviour*, vol. 62, pp. 175–191, 2019.
- [21] M. Espadoto, R. M. Martins, A. Kerren, N. S. T. Hirata, and A. C. Telea, “Toward a quantitative survey of dimension reduction techniques,” *IEEE Transactions on Visualization and Computer Graphics*, vol. 27, no. 3, pp. 2153–2173, 2021.
- [22] R. Gupta, R. Pachauri, and A. K. Singh, “Image encryption method using dependable multiple chaotic logistic functions,” *International Journal of Information Security and Privacy*, vol. 13, no. 4, pp. 53–67, 2019.
- [23] T. Denoeux, “Logistic regression, neural networks and Dempster-Shafer theory: a new perspective,” *Knowledge-Based Systems*, vol. 176, pp. 54–67, 2019.

Research Article

Traffic Flow Prediction and Analysis in Smart Cities Based on the WND-LSTM Model

SuYuan Ma ¹ and MingYe Zhao ²

¹*School of Marxism, Guangzhou University of Chinese Medicine, Guangzhou 510006, China*

²*Business School of International Medicine, China Pharmaceutical University, Nanjing 210009, China*

Correspondence should be addressed to MingYe Zhao; 3220040596@stu.cpu.edu.cn

Received 15 April 2022; Accepted 8 June 2022; Published 2 August 2022

Academic Editor: Le Sun

Copyright © 2022 SuYuan Ma and MingYe Zhao. This is an open access article distributed under the Creative Commons Attribution License, which permits unrestricted use, distribution, and reproduction in any medium, provided the original work is properly cited.

Aiming at the problem that the road traffic flow in intelligent city is unevenly distributed in time and space, difficult to predict, and prone to traffic congestion, combined with pattern recognition and big data mining technology, this paper proposes a research method to analyze and mine the daily travel patterns of urban vehicles. This paper proposes a WND-LSTM model, which mainly includes data preprocessing, data modelling, and model implementation, to analyze the similarity of travel patterns in seasonal changes. Combining the data mining results with the data mining results, the daily travel model of road traffic vehicles in intelligent city is established. The results of the case study showed that the WND-LSTM model outperformed ARIMA (88.48%), LR (65.79%), SVR (70.46%), KNN (68.21%), SAEs (66.95%), GRU (68.43%), and LSTM (70.41%) in MAPE, respectively, with an average accuracy improvement of 71.25% (MAPE of 0.651%).

1. Introduction

At present, with the rapid development of the global economy, the quality of life in a country is booming, especially the rapid changes in clothing, food, housing, and transportation, and the number of household cars is increasing year by year [1]. The urban motor vehicle ownership rate is growing at a rate of no less than 11.5% per year [2]. Despite the rapid development planning of cities and towns in China, the construction of transportation facilities is far from catching up with the rapid growth of vehicles. With the continuous popularization of people's means of transportation, the problems of traffic congestion and traffic pollution are becoming more and more serious [3]. The traditional urban transportation system is facing severe challenges because it seriously restricts the quality of life of citizens.

Consistent with today's urban traffic planning ability, how to optimize the road network capacity and improve the decision-making ability has always been the most difficult problem in traffic management [4]. As one of the core

contents of smart city, its goal is to create a modern, efficient, and stable traffic management system by using the technology of cutting-edge fields (computer information, automation, and artificial intelligence) so as to maximize the road capacity, alleviate or even maximize the road capacity, alleviate or even solve the problem of traffic congestion, and make all citizens live in a stable and orderly environment [5]. As the core element of intelligent transportation system (ITS), the research on transportation network operation mode and people's daily travel behavior can provide real and reliable data information for decision-makers so as to effectively deploy transportation network resources [6].

Today, we are in the age of big data. Data has permeated every industry and every function and has become an important factor in production [7]. As a fundamental part of ITS, the accuracy of traffic flow information collection is particularly important. A wide range of traffic flow information collection technologies such as laser sensing, GPS positioning information microwave detection, geomagnetic coil detection, and camera recording are widely used in this field, and these sensors can be found almost everywhere,

generating huge amounts of real-time traffic data information all the time, with information volumes of up to petabytes [8]. The question of how to fully exploit the “gold” of this data has been met with great enthusiasm by a wide range of knowledgeable people [9]. Big data mining method can use high-speed computer cluster or server cluster to process massive original traffic video data, carry out information mining, extract valuable rule information in a short time, and realize the knowledge transformation of data. Big data technology combines high-speed computing power and powerful storage capacity and will play a key role in reasonably allocating traffic network resources and avoiding various traffic problems [10].

Image recognition and big data mining are widely used artificial intelligence technologies. At present, they are playing a great role in promoting a wide range of industries, including government functions, medical care, industry, commerce, and military. However, the author found that their application in the field of transportation still has great potential. Based on the above background, this paper aims to combine a new perspective with the road network, use the massive traffic data generated by the well-equipped monitoring system in the traffic road network, and use the Hadoop big data processing framework, combined with K -means clustering algorithm and Δ Apriori association algorithm, from the perspective of data feature selection, obtains license plate information through image recognition, mines traffic flow model, and transforms big data into small data. Data are selected from the perspective of data characteristics, big data are converted into small data, and traffic network operation model is established [1]. This allows more targeted data and significantly reduces redundant data, so it has the advantages of cost-effectiveness and efficiency. Based on the traffic flow model and the accurate space-time mode of each vehicle, the designed route guidance algorithm provides real-time and effective route planning services for end users, allows each vehicle to find the route that best meets its requirements at the lowest user cost, reduces the concentrated load on the road, and reduces the causes of traffic congestion to a certain extent. This reduces the causes of traffic congestion, reduces the pressure of traffic management departments, and saves the waste of human and material resources [11].

2. Related Work

Since the turn of the century, computer information technology has developed rapidly, and the era of big data has arrived. Once the concept of big data mining methods was introduced, it has contributed to huge changes in a large number of traditional industries, such as energy, health care, and services, and has promoted the development of many industries. Many experts and scholars are also using the current hot big data analysis methods to solve transportation problems. Reference [12] modelled the public transport system based on discrete choice in terms of the impact of comfort and other aspects on passengers’ choice of travel mode, and [13] modelled the urban public transport system

based on Neighborhood search algorithm. A group intelligence model-based approach is proposed in [14] for open-ended route planning. Deletion algorithm and Ms algorithm are proposed for the shortest path problem, respectively, by [15]. In [16], a model for rail transit path selection is developed based on the Logit model. The model clustering analysis is applied in [17] for efficient detection of the forward speed of the traffic within the detection range. In [18], it is proposed to combine road intersection vehicle data, traffic facility data and traffic accident data with the help of establishing a GIS platform for accident analysis and detection. Reference [19] designed an Android-based GIS online navigation system. In [14], in order to solve the parameter convergence problem, weights’ calculation is added to the particle swarm algorithm, and the right of way is dynamically adjusted according to the roadway load change by combining the discrete selection of fuzzy rules. Reference [15] ensembles neural networks and Bayesian methods for predicting short-time traffic. Reference [16] applies multiprediction models to the field of road section load research. Reference [17] proposed a dynamic stochastic shortest path optimisation method to provide guidance on vehicle path optimisation through stochastic meritocratic planning.

3. WND-LSTM Model

3.1. Model Overview. As shown in Figure 1, our proposed WND-LSTM model mainly consists of three parts: data preprocessing, data modelling, and model implementation. Firstly, in the data preprocessing, the MapReduce parallel processing framework is used to process large-scale taxi GPS track data on the Hadoop distributed computing platform to achieve data extraction, data statistics, and data integration; secondly, the distributed WND-LSTM model is built on Hadoop, and the LSTM model is weighted with time windows and normal distributions. Finally, the WND-LSTM model was executed on MapReduce using Mapper, Combiner, and Reducer functions to improve the efficiency and scalability of the model predictions.

In addition, to address the storage and computational issues that exist when using independent learning models to handle large data of traffic, we introduce a generic MapReduce framework distributed modelling architecture for traffic flow prediction (MF-TFF) in the proposed WND-LSTM model [18].

3.2. Data Preprocessing. As the taxi GPS track data is not only spatiotemporally correlated and nonlinear, but also has the characteristics of huge data volume, variety, high value, low density, and fast speed, it is necessary to do data preprocessing work on the original GPS track data. In this paper, we extracted taxi GPS track point record data from the target road section for data preprocessing respectively. The specific process is shown in Figure 2. The data preprocessing process on MapReduce consists of three main tasks.

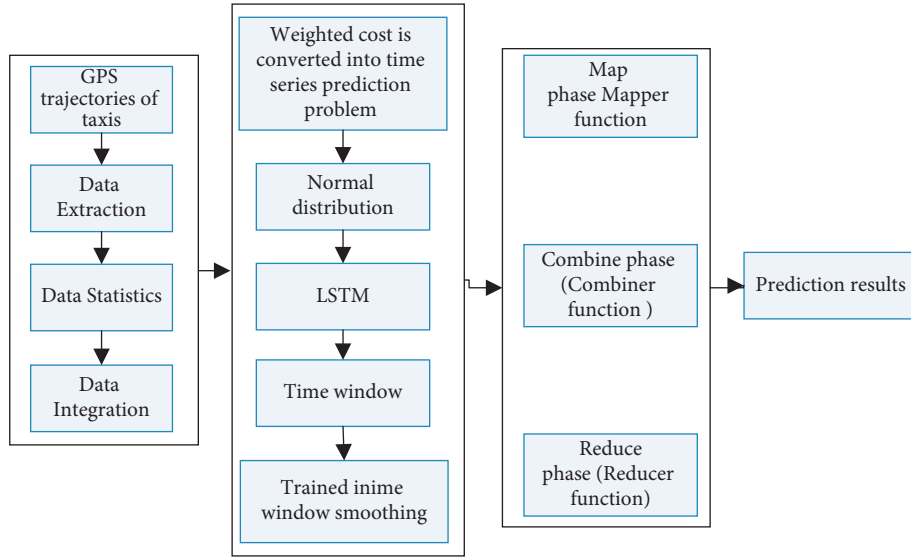


FIGURE 1: WND-LSTM model framework.

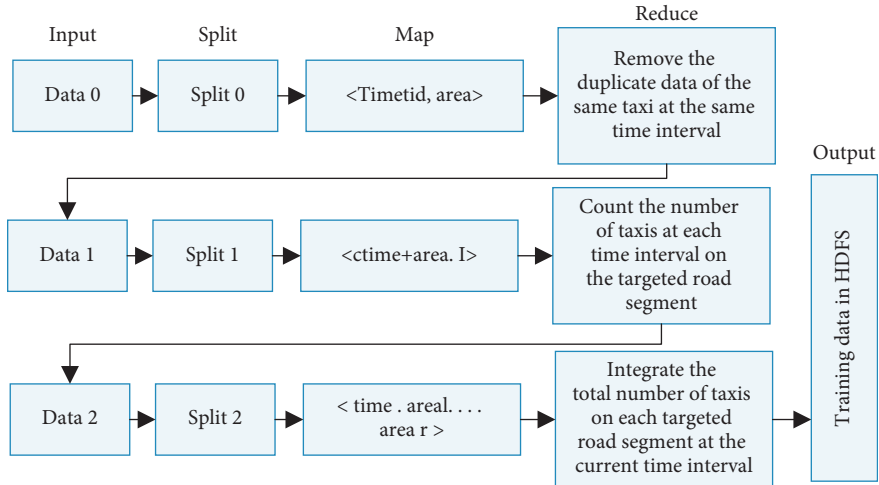


FIGURE 2: MapReduce-based data preprocessing process.

3.2.1. *Task 1: Data Extraction.* Extract the taxi vehicles present in the area of interest on the same day via GPS. Define a key-value pair $\langle \text{key1}, \text{value1} \rangle$ in the first Map task, where key1 represents the time and vehicle ID and value1 represents the number of the area location. Input to the Reduce task, in the Reduce stage, by sorting the time and vehicle number, remove the duplicate data of the same vehicle at the current time, and write to HDFS; see Algorithm 1 for details.

3.2.2. *Task 2: Data Statistics.* Count the number of taxis in each road section every five minutes, read in the information saved in the previous task in the second Map task, and define the key values. In the second Map task, the information saved in the previous task is read in and the key-value pair $\langle \text{key2}, \text{value2} \rangle$ is defined, with key2 representing the time and area number and value2 being entered as count 1. The database may be missing data for the current time point

due to the absence of vehicle information at a certain time point in the previous task. Therefore, a key-value pair $\langle \text{keys}, \text{values} \rangle$ needs to be added to the database at this point in time as a marker to ensure that the number of taxis at this point in time is not missing. As a marker for this moment in time, ensuring that each day has a fixed point in time.

3.2.3. *Task 3: Data Integration.* In the third Map task, the number of taxis counted in the second task is read in, and the key-value pair $\langle \text{key3}, \text{value3} \rangle$ is defined, where the time point is used as key3 and value3 represents the number of taxis counted in each road section.

3.3. *Model Construction.* The LSTM model has a unique structure that not only inherits the general characteristics of RNNs, but also solves the problem of gradient explosion and gradient disappearance when the values are too large or too small. The structure of the LSTM consists of an input layer,

an implicit layer, and an output layer, which also contains a memory cell. The LSTM is structured as an input layer, an implicit layer, an output layer, a memory cell, and three gating units: an input gate, an output gate, and a forgetting gate, which are used to control the flow of information in the input and memory cells, allowing the LSTM to better remember useful information and handle long-term time-dependent relationships.

In an LSTM network, assuming an input $x = (x_1, x_2, \dots, x_t)$ time series, a time series of $h = (h_1, h_2, \dots, h_t)$ in the implicit layer and a time series of $y = (y_1, y_2, \dots, y_t)$ in the output layer, the calculation can be performed by the following equation:

$$\begin{aligned} y &= W_{hy}h_y + b_y, \\ h_t &= H(W_{xh}x_t + W_{hh}h_{t-1} + b_h), \end{aligned} \quad (1)$$

where the implicit layer function of the LSTM can be obtained by the following equation:

$$\begin{aligned} i_t &= \sigma(W_{xi}x_t + W_{hi}h_{t-1} + W_{ci}c_{t-1} + b_i), \\ f_t &= \sigma(W_{xf}x_t + W_{hf}h_{t-1} + W_{cf}c_{t-1} + b_f), \\ c_t &= f_t c_{t-1} + i_t g(W_{xc}x_t + W_{hc}h_{t-1} + b_c), \\ o_t &= \sigma(W_{xo}x_t + W_{ho}h_{t-1} + W_{co}c_{t-1} + b_o), \\ h_t &= o_t h(c_t), \end{aligned} \quad (2)$$

where i , o , f , and c represent the input gate, output gate, forgetting gate, and memory cell, respectively, W is the weight matrix, b is the bias vector, and σ is the activation function.

In this work, as a result of simply using the traffic flow sequences upstream and downstream and at each bifurcation intersection to participate in the training, which does not consider the impact of each intersection on the current roadway in the time axis, thus proposing a relatively novel weighting method. A relatively novel weighting method is proposed to improve the prediction accuracy of short-time traffic flow. The LSTM is weighted to find the cost by using the characteristics of normal distribution and time window smoothing, and the cost is transformed into a time series. The problem of predicting traffic flow in a series of single variables over time is used to predict the state of the variables at the current moment.

Therefore, the MapReduce parallel computing framework on Hadoop optimises the traditional LSTM neural network. Firstly, the LSTM neural network is weighted to find the cost using a time window and normal distribution, and the cost is used as a time series prediction problem to form a time-dependent single variable series to predict the state of the variable at the current moment; secondly, on the Hadoop distributed computing platform with large data of taxi trajectories, we can obtain the traffic with time series by the above data preprocessing method. Finally, based on the obtained traffic sequence dataset, we select the target road section and then use WND-LSTM to build a traffic flow prediction model, which consists of the following three steps.

Step 1. The horizontal intersection section is considered as a network diagram, and V_t^i is defined as the traffic flow value collected from the target section at time t . Using the traffic flow sequence at time t to predict the traffic flow at time $t+1$ V_{t+1}^i , with a sampling interval of 5 minutes, the traffic flow sequence can be expressed as $O_i = \{V_1^i, V_2^i, \dots, V_n^i\}t$, where $i = 1, 2, R$ ($n = 288$), and the predicted traffic flow of any target road is predicted by the current moment of the road section and the related intersection, using the LSTM recurrent neural network. If section i junction is used as the predicted junction, the prediction model inputs and outputs are

$$\begin{aligned} X &= (O_1, O_2, \dots, O_R), \\ Y &= (O_{t+1}^i). \end{aligned} \quad (3)$$

Step 2. A normal distribution is one in which the random variable x follows a normal distribution with a mathematical expectation of μ and a variance of σ^2 , denoted as $N(\mu, \sigma^2)$. The probability density function is the expectation of the normal distribution μ that determines its location (centre line) and its standard deviation σ that determines the magnitude of the distribution. Since it is clearly not reasonable to simply use the traffic flow sequences upstream and downstream and at each bifurcation to participate in the training and does not take into account the influence of each intersection on the current roadway in the time axis, the WND-LSTM uses the idea of a normal distribution to weight the cost of each road segment and then uses the cost as a time series prediction problem to form a single variable sequence over time to predict the state of the variable at the current moment, which allows for artificial control purposes. The mean value of the normal distribution is the target road section, where the empirical value is 0.6 (which can be any reasonable value) and x is the discrete value of the traffic volume on each road section.

$$f(x) = \frac{1}{\sqrt{2\pi}\delta} \exp\left(-\frac{(x-\mu)^2}{2\delta^2}\right). \quad (4)$$

Step 3. Based on the above steps, the traffic flow on the target roadway at time t of the day is selected as V_t^i , and $V_{t-1}^i, V_{t-2}^i, V_{t-3}^i$ of the current historical moment is taken by window smoothing, and a window of size 4 is formed and fed into the training, in the following form:

$$V = \begin{bmatrix} V_1 \\ V_2 \\ \vdots \\ V_{n-3} \end{bmatrix} = \begin{bmatrix} v_1 & v_2 & v_3 & v_4 \\ v_2 & v_3 & v_4 & v_5 \\ \vdots & \vdots & \vdots & \vdots \\ v_{n-3} & v_{n-2} & v_{n-1} & v_n \end{bmatrix}. \quad (5)$$

4. Experimental Results and Analysis

4.1. Experimental Environment. The experimental environment was built on a Hadoop cluster with a MapReduce framework and ArcGIS platform, where the base hardware

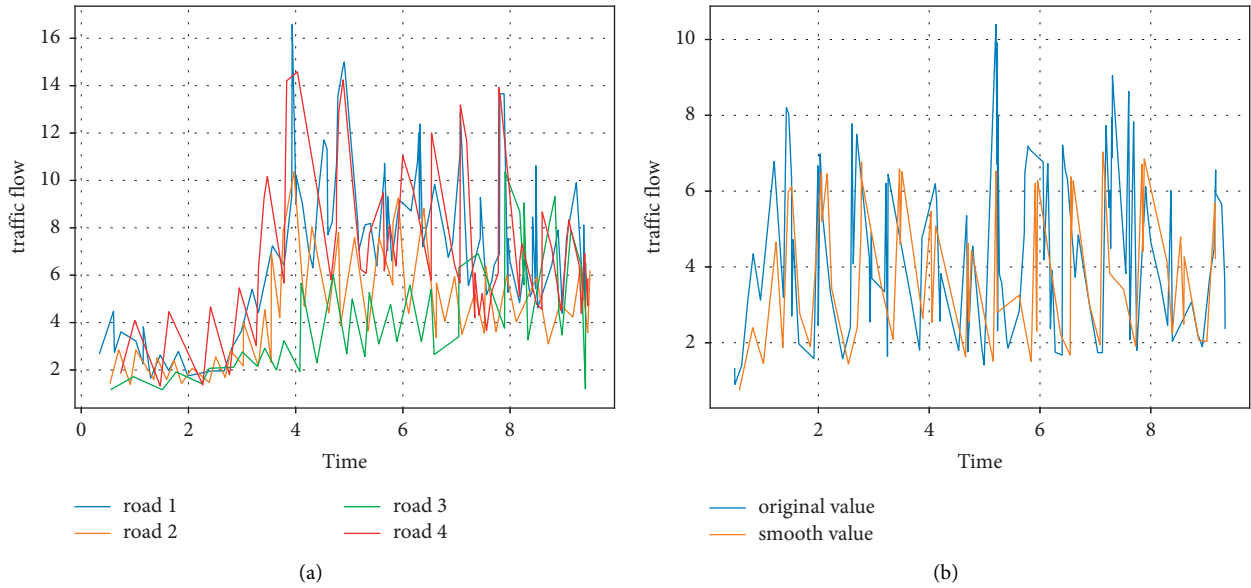


FIGURE 3: Experimental data smoothing. (a) Traffic flow on 4 road sections. (b) Kalman filter smoothing.

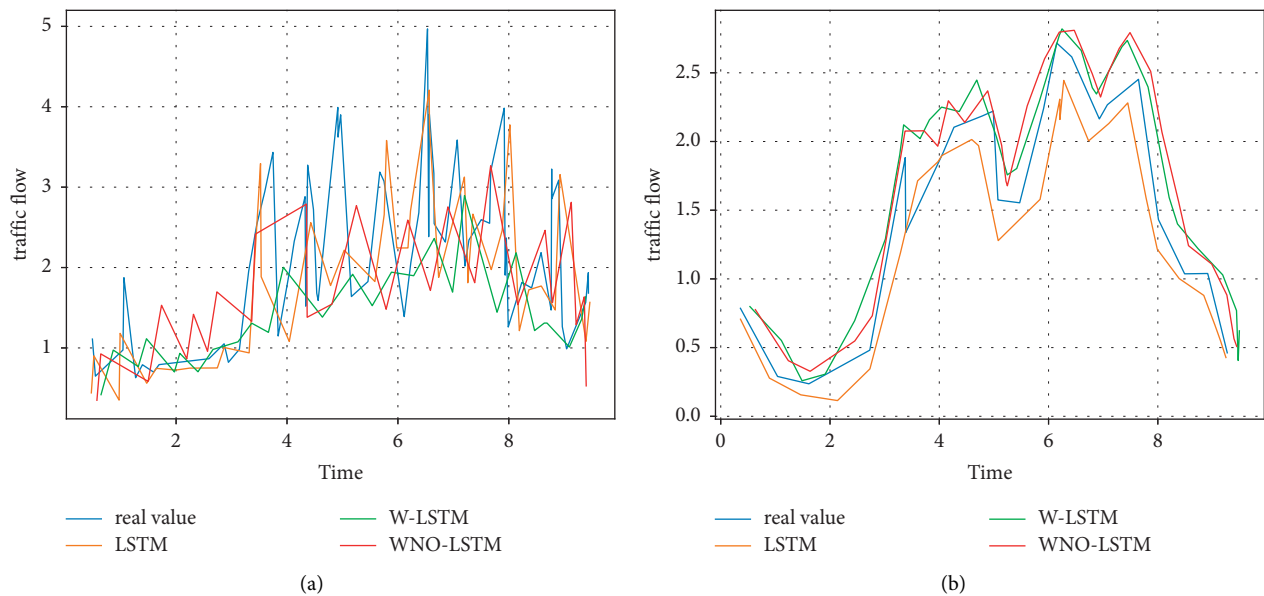


FIGURE 4: LSTM, W-LSTM, ND-LSTM, and WND-LSTM smoothing treatments.

was an HP Z400 workstation with an Intel Xeon 3500 CPU and ECC and DDR3 8.0 GB RAM. We ran all experiments with Hadoop 3.1.1 using Java, Python on Ubuntu 18.64 OS [20, 21].

4.2. Experimental Data. We used real taxi GPS trajectory data (approximately 25 GB) as the experimental data for this case study, which was produced from November 5 to November 18, 2021, in Beijing via 12,000 taxis.

These data consisted of 968 million GPS trajectory points, forming a visible traffic network map of Beijing, China, as shown in Figure 3(a).

In this experiment, we selected datasets from the above datasets for weekdays (November 5 to November 18, 2012) and also divided the datasets into five groups according to 1 day, 3 days, 6 days, 10 days, and 14 days in order to verify scalability, where 168 data were selected as the test set and the rest as the training set at 1 day, and 1 day was selected as the test set and the rest as the training set for all 3 days, 6 days, 10 days, and 14 days [22].

In particular, using the method described in the text, the above dataset was preprocessed based on MapReduce, and the traffic flows of the four road sections are shown in Figure 3(a). In addition, to make the experimental data valid, we used KF filtering to smoothen the set of the counted data

TABLE 1: Comparison of evaluation metrics for LSTM, W-LSTM, ND-LSTM, and WND-LSTM models.

Days		MOSES			
		ND-LSTM	W-LSTM	LSTM	WND-LSTM
1 day	MAPE	6.324	3.195	6.122	2.159
	MAE	0.108	0.055	0.137	0.056
	RMSE	0.147	0.066	0.184	0.372
	ME	0.374	0.131	0.368	0.372
3 days	MAPE	5.579	2.973	5.587	1.793
	MAE	0.144	0.081	0.145	0.053
	RMSE	0.202	0.146	0.275	0.102
	ME	0.612	0.581	1.072	0.412
6 days	MAPE	1.268	1.894	2.756	0.194
	MAE	0.015	0.029	0.044	0.012
	RMSE	0.018	0.036	0.059	0.015
	ME	0.041	0.109	0.164	0.039
10 days	MAPE	4.305	1.931	2.988	0.715
	MAE	0.056	0.035	0.045	0.015
	RMSE	0.064	0.004	0.054	0.018
	ME	0.121	0.135	0.141	0.048
14 days	MAPE	1.223	2.095	2.200	0.651
	MAE	0.016	0.032	0.03	0.014
	RMSE	0.02	0.042	0.037	0.014
	ME	0.045	0.114	0.105	0.044

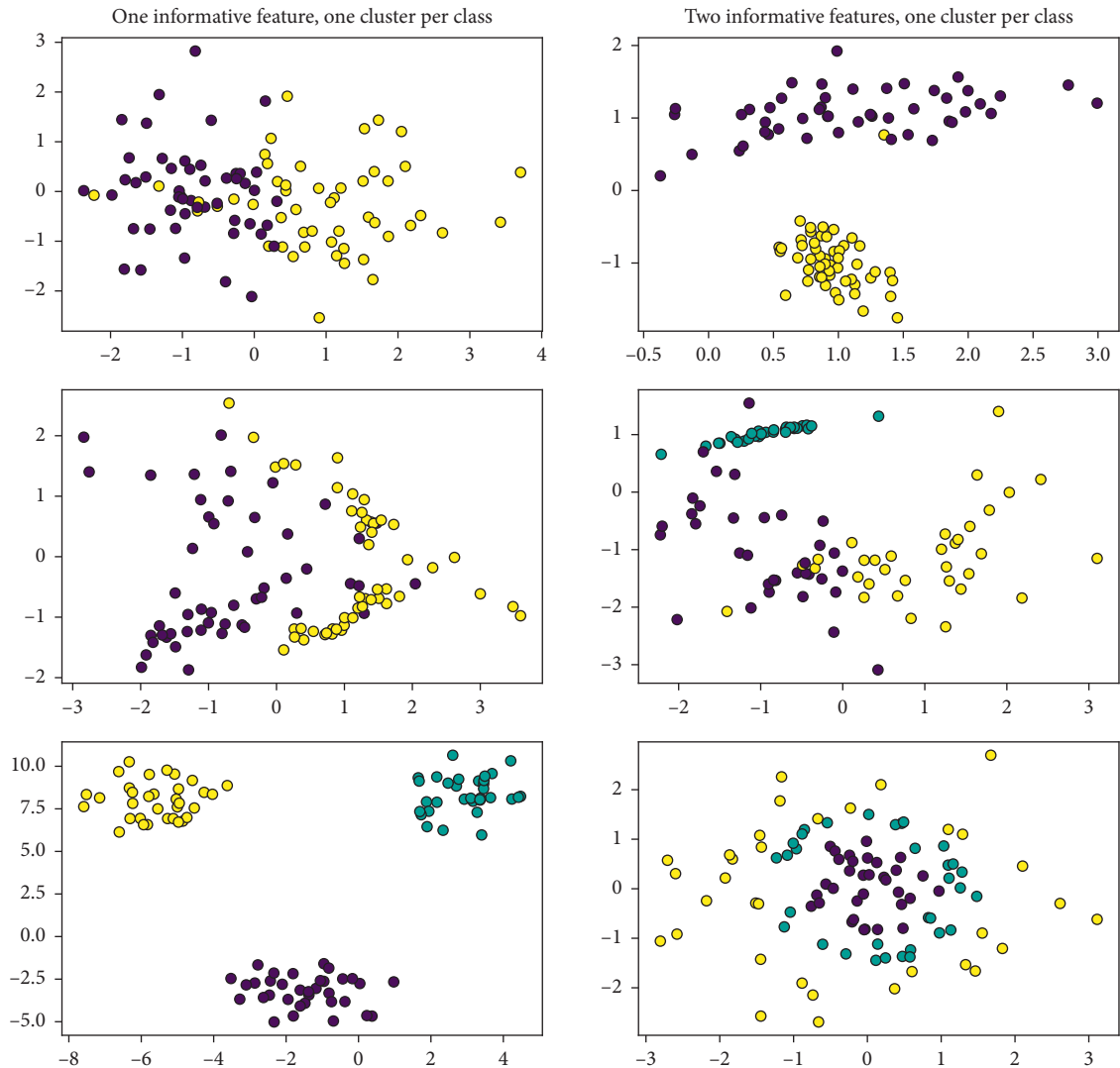


FIGURE 5: LSTM, W-LSTM, ND-LSTM, and WND-LSTM evaluation metrics.

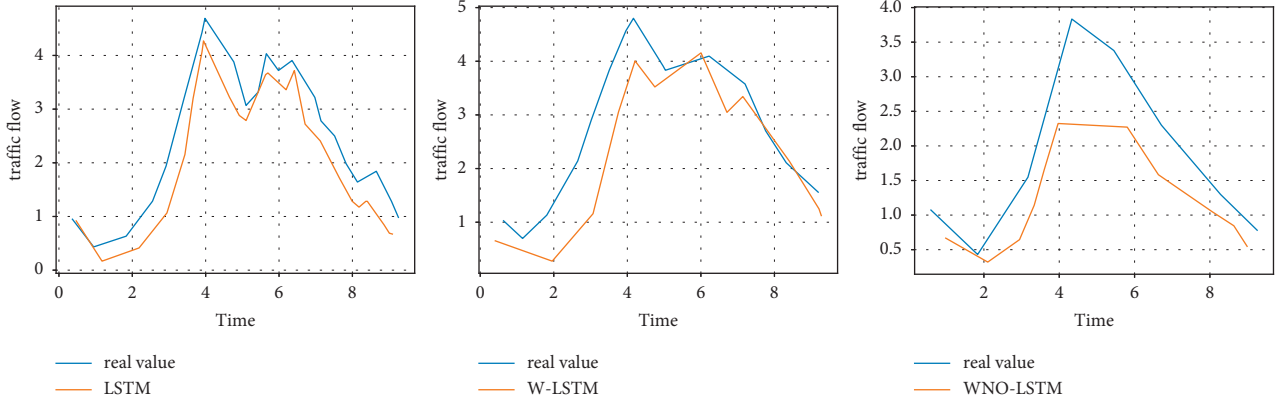


FIGURE 6: Comparison of prediction results of different models on the same dataset.

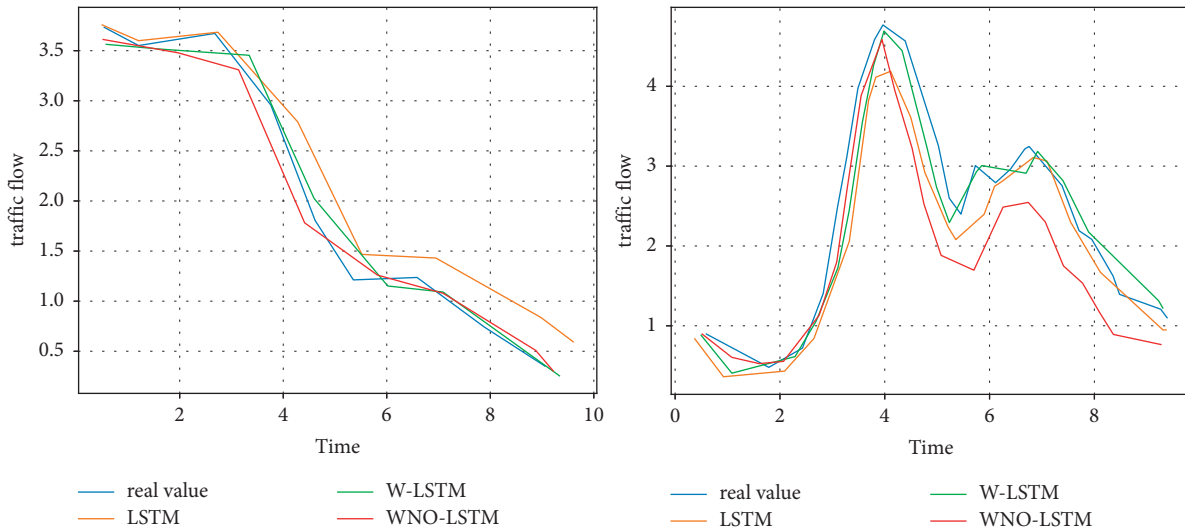


FIGURE 7: Prediction results of LSTM, W-LSTM, and WND-LSTM models for different datasets.

and normalised the data to between $[0, 1]$ by the Min-MaxScaler function, as shown in Figure 3(b).

4.3. Performance Assessment. In general, the more hidden layers a neural network has, the deeper the model is, and the better the representation and learning ability of the model, but it also leads to gradient loss and increases the difficulty of training. In this experiment, the model is trained on a limited dataset. The first part is an input layer of dimension 11, the second part is an LSTM hidden layer of dimension 64, and the third part is an output 1 vector, with batch taken as 1 (grid search) and 100 iterations using a sigmoid optimiser [23].

To evaluate the prediction accuracy of the proposed WND-LSTM model in terms of time windows and normal distribution, we compared it with LSTM, W-LSTM (LSTM with time window smoothing), and ND-LSTM (LSTM with normal distribution).

With the same experimental dataset, we used KF for data smoothing based on similar traffic flow characteristics and,

in particular, for experimental results with the same trend, we chose a dataset of 14 days due to spatial constraints [24], as shown in Figure 4. More importantly, we compared the MAPE values of LSTM, W-LSTM, ND-LSTM, and WND-LSTM, presenting the values of MOEs (MAPE, MAE, RMSE, and ME) for LSTM, W-LSTM, ND-LSTM, and WND-LSTM, respectively, as shown in Table 1 and Figure 5.

Table 1 reports the MOEs for the five datasets of the four LSTM methods, and it can be seen that the MAPE of the WND-LSTM method is lower than that of the other methods. The MAPEs of the WND-LSTM model are significantly lower than those of the other models in most cases, especially for the 14-day dataset, where the MAPEs of the WND-LSTM are lower than those of the LSTM, W-LSTM, and ND-LSTM by 70.41%, 68.92%, and 46.77%, respectively. In particular, the MAPE value for WND-LSTM is 0.651%, indicating a high predictive power [20].

Also for a more visual illustration, Figure 6 presents the traffic flow prediction results produced by WND-LSTM compared to other LSTM models (given the similarity of

TABLE 2: Comparison of evaluation metrics between WND-LSTM and other advanced models.

Days	MOEs	Models							
		ARIMA	LR	SVR	KNN	SAEs	GRU	LSTM	WND-LSTM
1 day	MAPE	5.297	2.558	3.493	2.458	4.473	4.634	6.122	2.159
	MAE	0.095	0.04	0.062	0.047	0.078	0.076	0.137	0.056
	RMSE	0.123	0.005	0.08	0.066	0.084	0.092	0.184	0.096
	ME	0.302	0.116	0.163	0.245	0.154	0.219	0.369	0.372
3 days	MAPE	6.031	2.819	6.701	4.297	2.308	4.656	2.587	1.795
	MAE	0.138	0.067	0.273	0.16	0.049	0.131	0.145	0.053
	RMSE	0.196	0.096	0.764	0.4	0.069	0.25	0.275	0.102
	ME	0.689	0.438	3.1	1.629	0.269	0.972	1.722	0.410
6 days	MAPE	3.835	1.946	2.466	2.037	2.205	1.988	2.756	0.75
	MAE	0.056	0.030	0.034	0.031	0.032	0.032	0.044	0.012
	RMSE	0.072	0.036	0.041	0.038	0.038	0.042	0.059	0.015
	ME	0.182	0.086	0.095	0.094	0.087	0.114	0.164	0.039
10 days	MAPE	5.842	1.952	2.509	2.061	2.515	2.016	2.988	0.716
	MAE	0.112	0.038	0.042	0.04	0.052	0.039	0.045	0.015
	RMSE	0.139	0.047	0.05	0.05	0.066	0.052	0.054	0.018
	ME	0.42	0.144	0.146	0.167	0.155	0.166	0.141	0.048
14 days	MAPE	5.652	1.903	2.204	2.046	1.97	2.065	2.2	0.51
	MAE	0.084	0.028	0.03	0.03	0.029	0.031	0.03	0.01
	RMSE	0.106	0.036	0.038	0.04	0.037	0.041	0.037	0.014
	ME	0.298	0.1	0.113	0.12	0.103	0.106	0.105	0.044

trends in each set of experimental results, a 10-day dataset was chosen to present the results). As the dataset increases, the accuracy of the WND-LSTM model increases and the timeliness becomes better, as shown in Figure 7.

To further validate the accuracy of the WND-LSTM model, we compared it with advanced differential autoregressive moving average (ARIMA), logistic regression models (LR), support vector regression (SVR), K -nearest neighbour (KNN), stacked autocoding neural networks (SAEs), gated recurrent neural units (GRUs), and long- and short-term memory neural network (LSTM) prediction models, and the experimental results are shown in Table 2.

5. Conclusions

In this paper, we propose a distributed LSTM weighting model, WND-LSTM, which combines time windows and normal distribution to improve the accuracy of short-time traffic flow prediction (TFP). In addition, we implement the proposed WND-LSTM model on a MapReduce parallel processing framework to address the scalability and efficiency of short-time traffic flow prediction and use KF to filter the raw GPS taxi movement trajectory data to remove anomalies for discrete data smoothing. The results of the case study showed that the WND-LSTM model outperformed ARIMA (88.48%), LR (65.79%), SVR (70.46%), KNN (68.21%), SAEs (66.95%), GRU (68.43%), and LSTM (70.41%) in MAPE, respectively, with an average accuracy improvement of 71.25% (MAPE of 0.651%).

Data Availability

The experimental data used to support the findings of this study are available from the corresponding author upon request.

Conflicts of Interest

The authors declare that they have no conflicts of interest regarding the publication of this work.

References

- [1] D. Xia, M. Zhang, X. Yan et al., "A distributed WND-LSTM model on MapReduce for short-term traffic flow prediction," *Neural Computing & Applications*, vol. 33, no. 7, pp. 2393–2410, 2021.
- [2] N. Shamsaimon, N. Matrazali, K. Majid et al., "Traffic flow prediction using long-short term memory technique for connected vehicles in smart cities," in *Proceedings of the International Visual Informatics Conference*, pp. 411–422, Springer, Kajang, Malaysia, November 2021.
- [3] N. A. M. Razali, N. Shamsaimon, K. K. Ishak, S. Ramli, M. F. M. Amran, and S. Sukardi, "Gap, techniques and evaluation: traffic flow prediction using machine learning and deep learning," *Journal of Big Data*, vol. 8, no. 1, p. 152, 2021.
- [4] Y. Wang, R. Jia, F. Dai, and Y. Ye, "Traffic flow prediction method based on seasonal characteristics and SARIMA-NAR model," *Applied Sciences*, vol. 12, no. 4, p. 2190, 2022.
- [5] Y. C. Chen and D. C. Li, "Selection of key features for PM2.5 prediction using a wavelet model and RBF-LSTM," *Applied Intelligence*, vol. 51, no. 4, pp. 2534–2555, 2021.
- [6] X. Su, M. Fan, M. Zhang, Y. Liang, and L. Guo, "An innovative approach for the short-term traffic flow prediction," *Journal of Systems Science and Systems Engineering*, vol. 30, no. 5, pp. 519–532, 2021.
- [7] P. An, Z. Wang, and C. Zhang, "Ensemble unsupervised autoencoders and Gaussian mixture model for cyberattack detection," *Information Processing & Management*, vol. 59, no. 2, Article ID 102844, 2022.
- [8] A. Cao, F. Wang, J. Tao, Z. Liu, and Z. Chen, "Traffic flow prediction model using an integrated framework of improved intelligent optimization algorithms and deep learning

- models,” in *Proceedings of the 2021 Chinese Intelligent Systems Conference*, pp. 613–624, Springer, Singapore, January 2022.
- [9] D. Xia, S. Jiang, N. Yang et al., “Discovering spatiotemporal characteristics of passenger travel with mobile trajectory big data,” *Physica A: Statistical Mechanics and Its Applications*, vol. 578, Article ID 126056, 2021.
- [10] J. F. Torres, F. Martínez-Álvarez, and A. Troncoso, “A deep LSTM network for the Spanish electricity consumption forecasting,” *Neural Computing & Applications*, vol. 34, no. 13, pp. 10533–10545, 2022.
- [11] D. Liu, S. Hui, L. Li, Z. Liu, and Z. Zhang, “A method for short-term traffic flow forecasting based on GCN-LSTM,” in *Proceedings of the 2020 International Conference on Computer Vision, Image And Deep Learning (CVIDL)*, pp. 364–368, IEEE, Chongqing, China, July 2020.
- [12] L. Romo, J. Zhang, K. Eastin, and C. Xue, “Short-term traffic speed prediction via machine learning,” in *Proceedings of the International Conference on Green, Pervasive, and Cloud Computing*, pp. 31–42, Springer, Singapore, 2020 November.
- [13] J. Wang, Y. Cao, Y. Du, and L. Li, “DST: a deep urban traffic flow prediction framework based on spatial-temporal features,” in *Proceedings of the International Conference on Knowledge Science, Engineering And Management*, pp. 417–427, Springer, Cham, 2019, August.
- [14] M. A. Abdelwahab, M. Abdel-Nasser, and R. I. Taniguchi, “Efficient and fast traffic congestion classification based on video dynamics and deep residual network,” in *Proceedings of the International Workshop on Frontiers of Computer Vision*, pp. 3–17, Springer, Singapore, 2020, February.
- [15] Sun, Y. Wang, Z. Qu, N. N. Xiong, BeatClass: a sustainable ecg classification system in IoT-based eHealth,” *IEEE Internet of Things Journal*, vol. 9, no. 10, pp. 7178–7195, Aug. 2022.
- [16] Y. Wang, L. Sun, and S. Subramani, “Classifying arrhythmias based on imbalanced sensor data,” *KSII Transactions on Internet & Information Systems*, vol. 15, no. 7, pp. p2304–2320, Jul. 2021, (Computer Science Q3, 0.858).
- [17] L. Sun, Q. Yu, D. Peng, S. Subramani, and X. Wang, “Fogmed: a fog-based framework for disease prognosis based medical sensor data streams,” *Computers, Materials & Continua*, vol. 66, no. 1, pp. 603–619, 2020.
- [18] Z. Qu, H. Sun, and M. Zheng, “An efficient quantum image steganography protocol based on improved EMD algorithm,” *Quantum Information Processing*, vol. 20, no. 2, p. 53, 2021.
- [19] N. Zafar and I. Ul Haq, “Traffic congestion prediction based on estimated time of arrival,” *PLoS One*, vol. 15, no. 12, Article ID e0238200, 2020.
- [20] W. Elleuch, A. Wali, and A. M. Alimi, “Neural congestion prediction system for trip modelling in heterogeneous spatio-temporal patterns,” *International Journal of Systems Science*, vol. 51, no. 8, pp. 1373–1391, 2020.
- [21] A. R. Abdellah and A. Koucheryavy, “Deep learning with long short-term memory for iot traffic prediction,” in *Lecture Notes in Computer Science*, vol. 12525, pp. 267–280, Springer, Cham, 2020.
- [22] P. Sun, A. Boukerche, and Y. Tao, “SSGRU: a novel hybrid stacked GRU-based traffic volume prediction approach in a road network,” *Computer Communications*, vol. 160, pp. 502–511, 2020.
- [23] L. Han and Y. S. Huang, “Short,” *IET Intelligent Transport Systems*, vol. 14, no. 6, pp. 495–503, 2020.
- [24] Z. Chen, Q. Chen, J. Zhang et al., “Traffic Flow Prediction Based On Cooperative Vehicle Infrastructure For Cloud Control Platform,” in *Proceedings of the 3rd International Forum on Connected Automated Vehicle Highway System through the China Highway & Transportation Society*, December 2020.

Research Article

A Lightweight CNN Model Based on GhostNet

Zhong Wang and Tong Li 

School of Computer Science and Technology, Hefei Normal University, Hefei 230601, China

Correspondence should be addressed to Tong Li; kamilt@foxmail.com

Received 2 June 2022; Accepted 9 July 2022; Published 31 July 2022

Academic Editor: Le Sun

Copyright © 2022 Zhong Wang and Tong Li. This is an open access article distributed under the Creative Commons Attribution License, which permits unrestricted use, distribution, and reproduction in any medium, provided the original work is properly cited.

The existing deep learning models have problems such as large weight parameters and slow inference speed of equipment. In practical applications such as fire detection, they often cannot be deployed on equipment with limited resources due to the huge amount of parameters and low efficiency. In response to this problem, this paper proposes a lightweight smoke detection model based on the convolutional attention mechanism module. The model is based on the YOLOv5 lightweight framework. The backbone network draws on the GhostNet design idea, replaces the CSP structure of the FPN and head layers with the GhostBottleNeck module, adds a convolutional attention mechanism module to the backbone network layer, and uses the CIOU loss function to improve the regression accuracy. Using YOLOv5s as the benchmark model, the parameter amount of the proposed lightweight neural network model is 2.75 M, and the floating-point calculation amount is 2.56 G, which is much lower than the parameter amount and calculation amount of the benchmark model. Tested on the public fire dataset, compared with the traditional deep learning algorithm, the model proposed in the paper has better detection performance and the detection speed is significantly better than the benchmark model. Tested under the unquantized simulator, the speed of the proposed model to detect a single picture is 60 ms, which can meet the requirements of real-time engineering applications.

1. Introduction

In 2021, a total of 748000 fires were reported in China, including 1987 deaths, 2225 injuries, and 6.75 billion yuan in direct property losses. In 2020, a forest fire in Yunnan burned for three days and nights. The area of the fire reached 170 hectares, and 5800 people were involved in suppressing the fire. In addition, a bush fire in Australia burned for more than four months, burning an area of 170000 square kilometers and resulting in the loss of many vegetation and animals. The smoke generated by the fire poured into the stratosphere, and the impact cannot be fully restored for a long time [1]. Fire not only seriously threatens the safety of human life but also has a great effect on the ecological environment. Fire prevention is very important to protect people's lives and property and has important scientific research significance [2, 3].

Traditional fire detection technologies include contact-type fire detectors such as temperature detectors [4] and smoke detectors [5, 6], which are commonly used in most

public places. However, the disadvantages of this kind of detector are limited to indoor detection, aging, alarm time delay, etc. Thus, it is difficult to carry out fire monitoring in outdoor spaces. Compared with traditional contact fire detectors, noncontact video fire detection technology has the characteristics of fast response, wide detection range, and low hardware cost and is suitable for fire monitoring in large indoor and outdoor spaces and forests. Video fire detection technology can be divided into flame detection [7] and smoke detection [8] according to the detection object. Generally, in the early stages of a fire, the smoke appears earlier than the flame and is not easy to cover, and the flame will only be generated in the middle of the fire. When the flame is detected, the fire has occurred, which makes it impossible to prevent and control it for the first moments. Therefore, the current video fire detection technology mainly focuses on detecting smoke.

Smoke detection technologies include traditional machine learning-based methods and deep learning-based methods. The smoke detection technology based on

traditional machine learning includes two parts: feature extraction and classifier design. The core research is smoke feature research. Commonly used smoke features mainly include artificially designed features such as the color [9], texture [10], motion [11], background contrast [12], and combinations of various features [13]. Smoke detection technology based on traditional machine learning has difficulty meeting the application requirements of real-time detection in terms of accuracy and false alarm rate. With the successful application of deep learning technology in the field of computer vision, deep convolutional neural networks are widely used in smoke detection. At present, smoke detection algorithms based on deep learning are mainly divided into two categories. One is a two-stage target detection model based on region extraction, such as R-CNN (regions convolutional neural network) [14–16], Fast R-CNN [17], and Faster R-CNN [18], which divide the target detection into the following two steps: feature extraction and feature classification. The other category is a one-stage target detection model that directly performs location regression, such as the SSD (single-shot multibox detector) [19] and YOLO (you only look once) [20] series, which converts target detection into a regression problem.

Most smoke detection algorithms based on deep learning rely on convolutional networks for feature extraction. To solve the problems of efficiency and storage, researchers adopt network pruning [21], network parameter quantization [22], and knowledge distillation [23] and design lightweight networks to improve the speed of inference. For example, MobileNet v1-v3 [24–26] and EfficientDet [27] were proposed by Google, GhostNet [28] was proposed by Huawei, and ShuffleNet [29, 30] and SqueezeNet [31] were proposed by Megvii. These networks are well constructed. It can reduce the number of model parameters and improve the accuracy of the network detection, which plays an important role in real-time smoke detection.

Although smoke detection technology has been widely used, the smoke detection scene is complex and changeable, and the accuracy and robustness of the existing technology in complex smoke scenes still have difficulty meeting the needs of popularization and application. Therefore, this paper designs a lightweight network based on the YOLOv5 framework, draws on the design ideas of GhostNet, and adds the CBAM attention mechanism [32] to achieve model compression and speed up inference without reducing the accuracy of the model. This model greatly reduces the need for hardware environment and uses MNN as the framework for unquantified testing. The specific work is as follows:

- (1) Improve the focus structure to reduce the parameters and calculation amount of the focus layer.
- (2) The backbone network adopts the GhostNet module, and the CSP of the FPN and the head layers is modified to a Ghost bottleneck.
- (3) Add an attention mechanism CBAM to the backbone network layer.

The rest of the paper is arranged as follows: Section 2 introduces the work related to smoke detection; Section 3

focuses on the description of lightweight smoke detection models and implementation details; Section 4 compares the performance of different smoke detection models on smoke detection datasets; finally, a summary and outlook are given.

2. Related Works

Traditional smoke detection technology tries to obtain the characteristics of smoke to distinguish from other interfering substances and performs smoke detection by manually setting the smoke characteristics, but the detection rate and false alarm rate have difficulty meeting the application requirements. With the application of deep learning techniques in the field of computer vision [33–35], researchers have used deep convolutional neural networks for smoke detection [36–39], which can learn deeper feature models. Luo et al. [40] combined convolutional neural networks with traditional foreground extraction methods for smoke detection, extracted suspected smoke regions based on motion and color information, and used a CNN to extract regional features for classification. Pundir and Raman [41] input texture features into deep belief texture learning to train the smoke recognition model. Zhang et al. [42] solved the problem of insufficient sample data by inserting real smoke images in the forest background and adopted Faster R-CNN to detect wildland forest fire smoke. Filoneko et al. [43, 44] adopted classical convolutional neural networks (including AlexNet, Inception-V3, Inception-V4, ResNet, VGG, and Xception) to conduct experimental verification on four large-scale smoke image databases. Sharma et al. [45] used two pretrained deep convolutional neural networks, VGG and ResNet50, to test unbalanced datasets and found that deeper CNNs performed better on more challenging datasets. Yin et al. [46] proposed a 14-layer deep normalization and convolutional neural network (DNCNN) to achieve automatic feature extraction and classification. To further reduce the problem of model overfitting caused by insufficient training samples, more training samples are generated from the original training set by using various data enhancement techniques. Muhammad et al. [47] proposed an energy-saving edge-assisted smoke detection method based on a deep convolutional neural network for foggy monitoring scenes, and the early smoke detection methods outperformed the state-of-the-art methods. Xu et al. [48] proposed a new video smoke detection method based on a deep saliency network, which uses a circular convolutional structure to construct a pixel-level saliency detection network and uses the fused features for saliency reasoning. Li et al. [49] proposed extracting suspicious smoke regions by smoke region proposal, pruning and reconstructing a convolutional neural network to improve real-time detection, and proposing a regularized loss function called score clustering to improve the accuracy of the model. Liu et al. [50] proposed a two-stage smoke detection method. In the first stage, block DNCNN is used to detect the suspicious smoke area from each frame image and put forward the concept of visual change image. In the second stage, the SVM classifier is used to classify the HOG features of the visual change image of the suspected smoke area.

Although smoke detection technology based on deep learning has achieved good results, with the improvement of the performance of the smoke detection algorithm, the number of convolutional layers also increases, resulting in the problems of large weight parameters and slow equipment reasoning speed. In practical applications, it is often unable to be deployed on equipment with limited resources because of the high parameter quantity and low efficiency. To solve the problem of efficiency and storage, researchers have designed lightweight networks to improve the inference speed. For example, the YOLOv3-Tiny [51] network launched for high parameters and inference speed is a simplified version of the YOLOv3 network. Iandola et al. [52] proposed SqueezeNet. The main idea is to replace the 3×3 convolution with a 1×1 convolution and reduce the amount of computation and parameters by reducing the number of channels of the 3×3 convolution. Howard et al. [53] proposed MobileNet, which mainly uses many neural networks designed with depthwise separable convolutions, which can greatly reduce the number of parameters and computations. MobileNetv2 employs a reverse residual block, while MobileNetv3 achieves better performance with fewer floating-point numbers. Based on MobileNetv3, GhostNet [54] adopts an inexpensive linear operation method to obtain richer output feature maps at a lower cost of model parameters to increase the feature extraction capability to solve the redundancy of feature maps. Zhang et al. [55] proposed ShuffleNet, which uses group convolution and channel shuffling operations to effectively reduce the computational complexity of point convolution and achieve superior performance. ShuffleNetV2 further considers practical speed in compact model design. In the field of smoke detection, Silva et al. [56] proposed a novel lightweight CNN model through RGB images, which can be used from aerial images of UAVs and video surveillance systems and combined with edge computing equipment to process images through a convolutional neural network. Pan et al. [57] used weakly supervised fine segmentation and lightweight Faster R-CNN to propose a collaborative area detection and classification framework for fire smoke, which can simultaneously achieve early warning, area detection, and classification of fire smoke. To reduce the complexity of Faster R-CNN, this method introduces knowledge distillation technology to compare the structure of the model. With the advancement of mobile devices and the diversified development of application scenarios, lightweight networks show higher engineering value. This paper balances between the accuracy and speed of the model, reasonably optimizes the YOLOv5 model, and designs a lightweight improved model based on the GhostNet and CBAM attention mechanisms. Without reducing the accuracy of the model, it realizes model compression and improves the reasoning speed, which greatly reduces the dependence on the hardware environment.

3. Methodology

3.1. YOLOv5. YOLO (you only look once) is widely used as a general object detection model. YOLOv1 uses one stage to

complete the classification and positioning of objects, and then YOLOv2 [58] and YOLOv3 [59] further improve the speed and accuracy to accelerate object detection in the industrial world. YOLOv4 [60] can achieve training on an ordinary GPU. Currently, the YOLO series has developed into YOLOv5. Compared with YOLOv4, YOLOv5 is more flexible. To some extent, the YOLOv5 model is the most state of the art of all the known YOLO series. It provides four versions in the following ascending sizes: YOLOv5s, YOLOv5m, YOLOv5l, and YOLOv5x. The model size and accuracy of the four versions increase in turn and are distinguished by the number of bottlenecks. The channel and layer control factors are used to realize the version change, and the appropriately sized model can be selected according to the application scenario. This paper mainly implements model compression and acceleration, making it easier to apply to the embedded devices with limited resources. Therefore, YOLOv5s is used as the benchmark model with the smallest network depth and feature map width. YOLOv5s is mainly composed of the backbone and head. The backbone includes the focus, C3, and SPP modules, and the head includes the neck and detect modules for extracting fusion features.

3.2. Lightweight YOLOv5. Compared with the traditional YOLOv5s, this paper first gives the implementation method of some modules. The main improvements include the Focus_mod module, the GBN module (Ghost bottleneck), and the attention mechanism CBAM. The specific details are presented in the following subsections.

3.2.1. Focus_mod Module. First, we downsample the original image ($640 \times 640 \times 3$) to reduce the calculation of spatial information, then form a $320 \times 320 \times 16$ feature map through convolution, and reduce the loss of image information caused by the downsampling. Next, we perform 16 convolution kernels with 3×3 convolutions to obtain the feature map of complete information, implement MaxPooling again to reduce the layer size, expand the perceptual field, pool to form a feature map of $320 \times 320 \times 16$, and finally combine the residuals and output a $320 \times 320 \times 32$ feature map. Pooling removes redundant information, compresses features, simplifies the network complexity, reduces computation, reduces memory consumption, and makes the smoke feature layer more obvious. Compared with the original focus module, the parameters of the improved Focus_mod module are reduced by 6 times, and the calculation amount is reduced by 7 times, as shown in Figure 1.

3.2.2. GBN (Ghost Bottleneck) Module. GhostNet proposes an innovative Ghost module that generates more feature maps through cheap operations. This new basic unit of the neural network successfully achieves more feature maps with fewer parameters and computations. The implementation of this module is divided into two parts. First, GhostNet uses a normal convolutional calculation to obtain feature maps with fewer channels, then uses a cheap operation to obtain

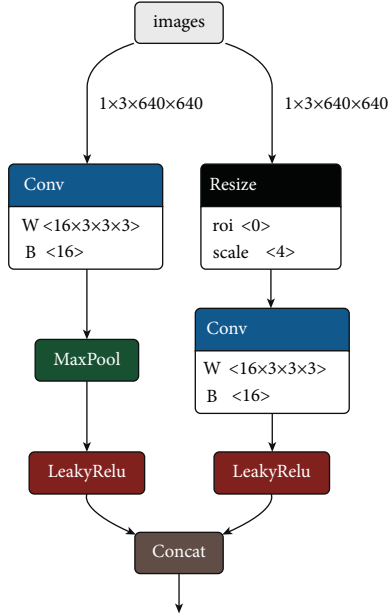


FIGURE 1: Focus_mod module.

more feature maps, and finally concatenates different feature maps together and combines them into a new output, as shown in Figure 2.

In GhostNet, the Ghost bottleneck module is divided into two types according to the stride. The Ghost bottleneck module structure when stride = 1 is modeled on ordinary residuals and is composed of two Ghost modules. The first module acts as an extension layer to increase the number of channels. The second module reduces the number of channels to match the shortcut path and then uses the shortcut to connect the inputs and outputs of these two Ghost modules. The Ghost bottleneck module when stride = 2 has the layout of the standard bottleneck structure and maintains the structural characteristics when stride = 1. By learning from the experience of the linear bottleneck module of MobileNetv2, an intermediate block is added in the middle of the stride = 1 structure. For a lightweight two-dimensional depthwise convolution, the amount of computation is reduced. This method draws on the experience of MobileNetv2. During the design process of the module and when the ReLU activation function is not used after the second Ghost module, the other layers use batch normalization (BN) and the ReLU nonactivation function after each layer. The structure design of the Ghost bottleneck is shown in Figure 3.

3.2.3. Attention Mechanism. The convolutional block attention module (CBAM) is a lightweight convolutional attention module that combines channel and spatial attention mechanism modules [61]. CBAM includes two sub-modules, the channel attention module (CAM) and the spatial attention module (SAM), which perform channel and spatial attention, respectively. This not only saves parameters and computing power but also ensures that it can be integrated into the existing network architecture as a plug-and-play

module. CAM is an adjustment to the structure of the SE module. Based on the SE module, a global maximum pooling operation is added to the CAM. CAM compresses the feature map into a one-dimensional vector in the spatial dimension, uses global average pooling and global maximum pooling to aggregate the feature information of the spatial map, and performs an element-by-element sum operation on the results by sharing the fully connected layer. The structure setting of the double pooling operation can make the extracted high-level features richer and provide more detailed information. SAM performs the concatenating operation on the result of the CAM operation based on the channel and performs single-channel dimensionality reduction through convolution. Similar to CAM, SAM adopts a double pooling operation. CBAM is similar to the SE module. The module structure mostly uses a 1×1 convolution to operate and completes the information extraction of the feature map through the entire channel dimension of the SAM, as shown in Figure 4.

3.3. Lightweight YOLOv5. Figure 5 shows the lightweight YOLOv5 network structure. Based on the YOLOv5s framework, the main improvements involve the two parts of backbone and neck. Combined with the introduction in Section 3.2, the overall structure of the improved lightweight network in this paper can be obtained. The multiscale output of the traditional model is output by the bottleneck module, and the modified multiscale output of the improved model is output by concatenating the two characteristic diagrams.

Table 1 shows the comparison between the parameter quantities of different sub-modules and the calculation quantities of traditional YOLOv5 sub-modules (focus, Conv, and CSP). The number of parameters and calculations of Focus_mod and GBN are significantly reduced. The parameter quantity of the Focus_mod module is 232, and the calculation quantity is 27.85 M. The parameter quantity of the GBN module is 317, and the calculation quantity is 136.4 M.

Table 2 shows the important parameters of the lightweight network model. GBN modules are used in the backbone network and head portion, and the Focus_mod and CBAM attention mechanisms are used in the backbone network portion.

3.4. Loss Function. The loss function of the target detection task consists of classification loss and bounding box regression loss. IoU and its improved algorithm are the most used in the bounding box regression loss. The full name of the IoU algorithm is the intersection over union, which is obtained by calculating the ratio of the intersection and union of the predicted box and ground-truth box, that is, $\text{IoU}(A, B) = (A \cap B) / (A \cup B)$, where A is the prediction box and B is the ground-truth box. IoU can be used as a distance; then, $\text{Loss}_{\text{IoU}} = 1 - \text{IoU}$. The advantage of IoU is that it can reflect the detection effect of the prediction box and ground-truth box. This paper takes CIoU as the loss function of the depth convolutional model, and the specific formula is as follows:

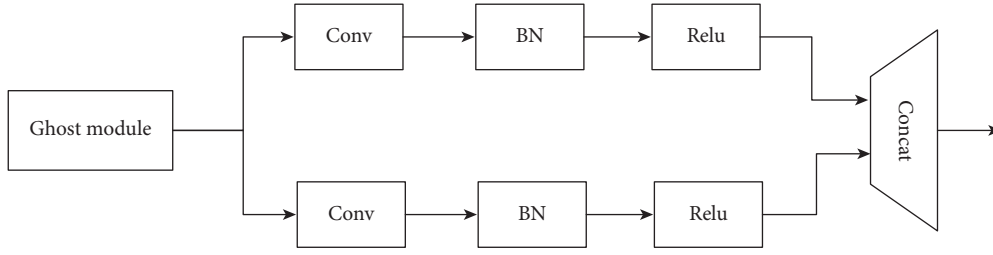


FIGURE 2: Ghost module.

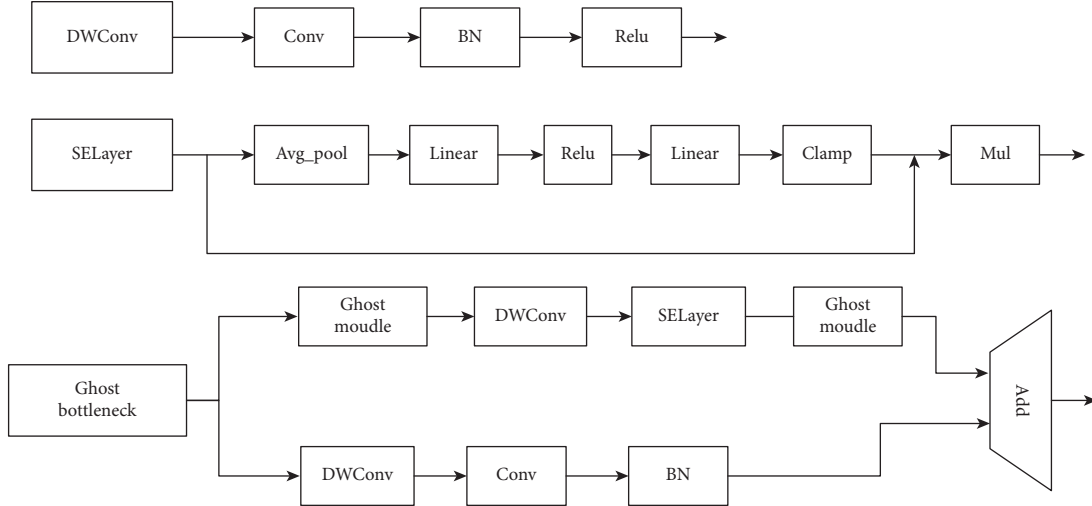


FIGURE 3: Ghost bottleneck module.

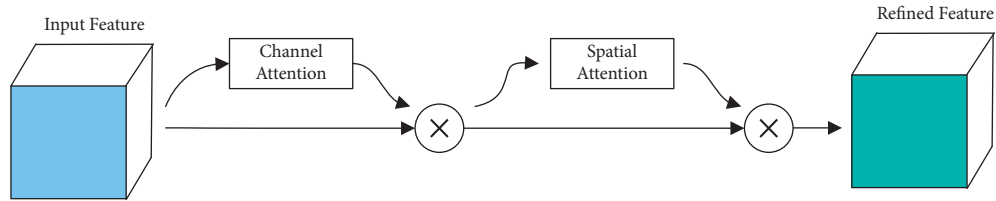


FIGURE 4: CBAM module.

$$\begin{aligned} \text{IoU} &= \text{IoU} - \left(\frac{p^2(b, b^{gt})}{c^2} + \alpha v \right), \\ \text{Loss} &= 1 - \text{IoU} + \frac{p^2(b, b^{gt})}{c^2} + \alpha v, \\ v &= \frac{4}{\pi^2} \left(\arctan \frac{w^{gt}}{\pi^{gt}} - \arctan \frac{w}{h} \right)^2, \\ \alpha &= \frac{v}{(1 - \text{IoU}) + v}, \end{aligned} \quad (1)$$

where b and b^{gt} represent the center points of prediction Box B and ground-truth Box B^{gt} , respectively; c represents the square of the diagonal length of the minimum bounding Box C ; p represents the calculation of the Euclidean distance between the two center points; α is the

weight parameter; and v is used to measure the similarity of the aspect ratio.

4. Experimental Results

4.1. Experimental Data and Environment. There is currently no authoritative dataset similar to ImageNet for smoke detection. The dataset used in this paper comes from the dataset published by the Fire Monitoring Technology Laboratory [62] and some network images, including a total of 4829 real smoke images. The sample images are shown in Figure 6. The smoke dataset covers the smoke pictures collected in different scenarios, including indoor monitoring, outdoor monitoring, field monitoring, field monitoring tower, drone shooting, and network pictures. The smoke and background of some images are confusing to some extent. At the same time, we collected many nonsmoke background images as negative samples and

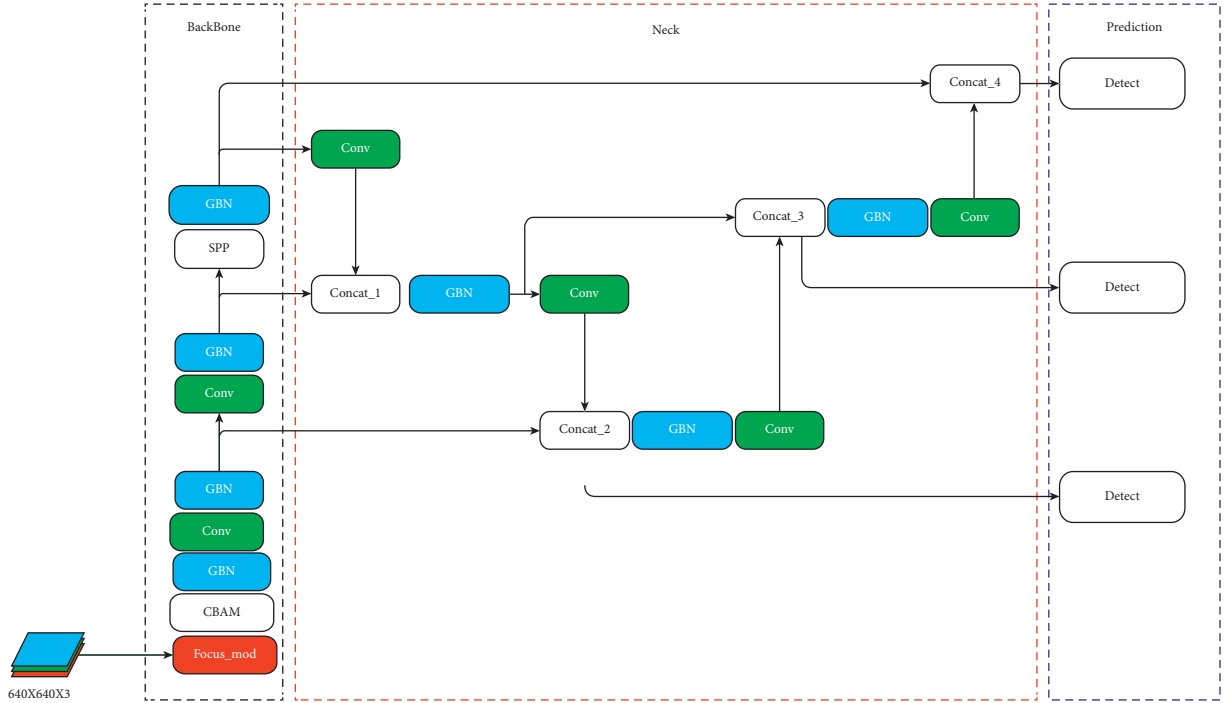


FIGURE 5: Lightweight network model.

TABLE 1: Parameters and calculations of the sub-modules.

Module	Parameters	FLOPs/M
Focus	1760	181.86
Focus_mod	232	27.85
Conv	464	196.61
CBAM	594	230.2
CSP	1120	481.69
GBN	317	136.4

TABLE 2: Overall architecture of lightweight network model.

Input	Operator	Conv	Stride	SE
640 × 640 × 3	Focus_mod	3 × 3	1	—
320 × 320 × 64	CBAM	3 × 3	2	—
160 × 160 × 64	GBN	5 × 5	2	1
160 × 160 × 64	Conv	3 × 3	2	—
80 × 80 × 64	GBN	3 × 3	1	1
40 × 40 × 128	Conv	3 × 3	2	—
40 × 40 × 128	GBN	3 × 3	1	—
20 × 20 × 256	Conv	3 × 3	2	—
20 × 20 × 256	GBN	3 × 3	1	—
20 × 20 × 256	SPP	1 × 1	2	—
20 × 20 × 512	GBN	3 × 3	1	1
20 × 20 × 256	Conv	1 × 1	1	—
40 × 40 × 256	Upsample	—	—	—
40 × 40 × 256	GBN	3 × 3	1	1
40 × 40 × 128	Conv	1 × 1	1	—
80 × 80 × 128	Upsample	—	—	—
80 × 80 × 128	GBN	3 × 3	1	1
40 × 40 × 128	Conv	3 × 3	2	—
40 × 40 × 256	GBN	3 × 3	1	1
20 × 20 × 512	Conv	3 × 3	2	—

divided the smoke dataset into a training set and a test set at a ratio of 7 : 3.

The experimental environment in this paper is the operating system Windows 10, graphics card NVIDIA GeForce RTX3070, memory 16G, processor Intel(R) i7-11700k, software environment CUDA11.4, and PyTorch 1.8.1.

4.2. Evaluation Standard. In this paper, the precision rate, recall rate, average precision (AP), and mean average precision (mAP@0.5) are used as model accuracy evaluation indicators, where AP represents the area under the PR curve, and mAP@0.5 represents the average AP of all categories when IOU is set to 0.5. The specific formula is as follows:

$$\begin{aligned}
 P &= \frac{TP}{TP + FP}, \\
 R &= \frac{TP}{TP + FN}, \\
 AP &= \int_0^1 PdR, \\
 mAP &= \frac{\sum_{i=1}^N AP_i}{N},
 \end{aligned} \tag{2}$$

where TP is the number of correctly classified bounding boxes that are predicted, the bounding box coordinates are correct, FN is the number of all unpredicted bounding boxes, and FP is the number of predicted bounding boxes that are misclassified or whose bounding box coordinates are not up to standard.



FIGURE 6: Sample images from the dataset.

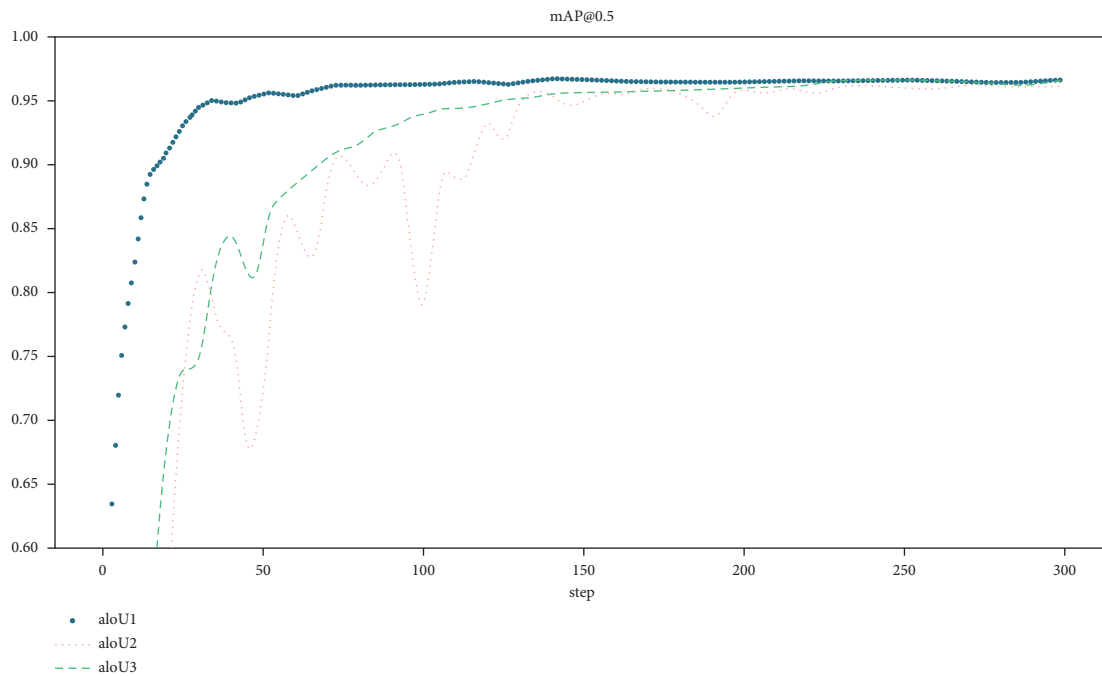


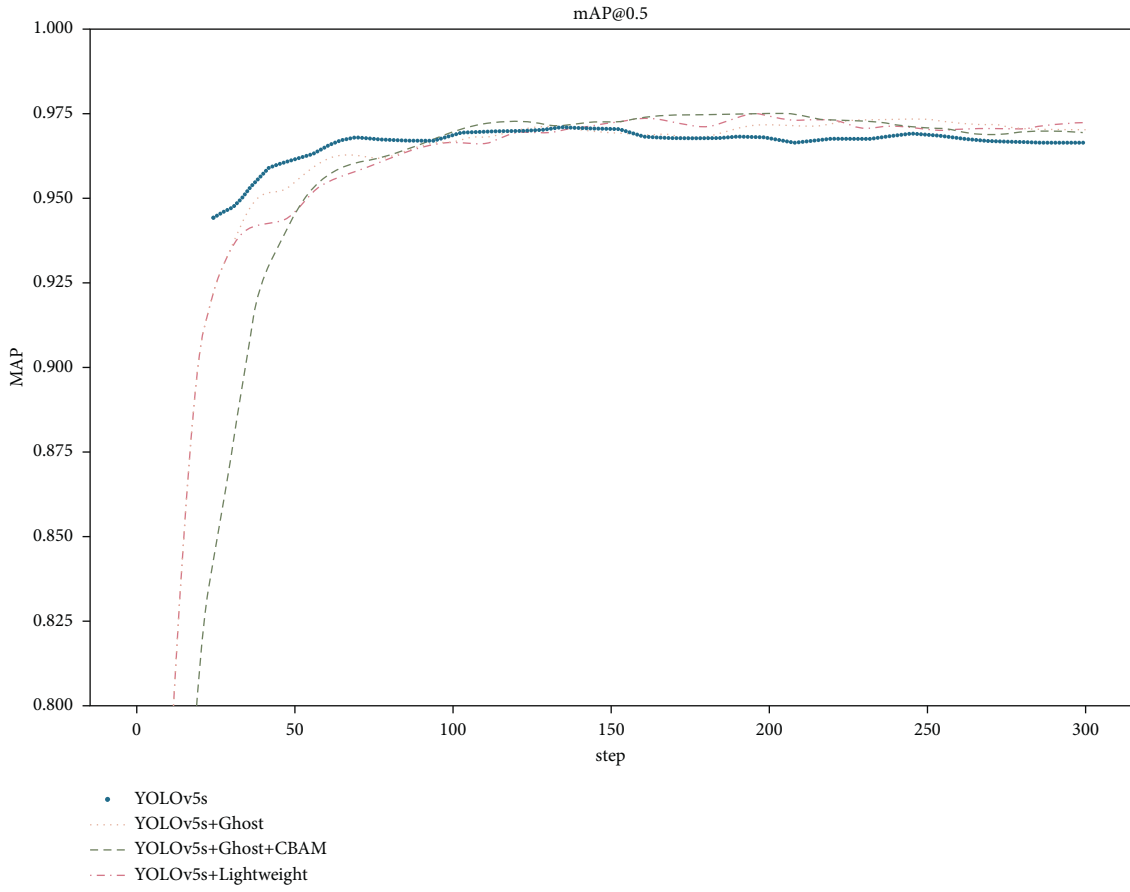
FIGURE 7: Performance curves of different loss functions.

4.3. *Experimental Results.* In the network model training phase, the iteration batch size was set to 32, the decay coefficient was 0.0005, the initial learning rate was 0.001, and the total number of iterations was 300.

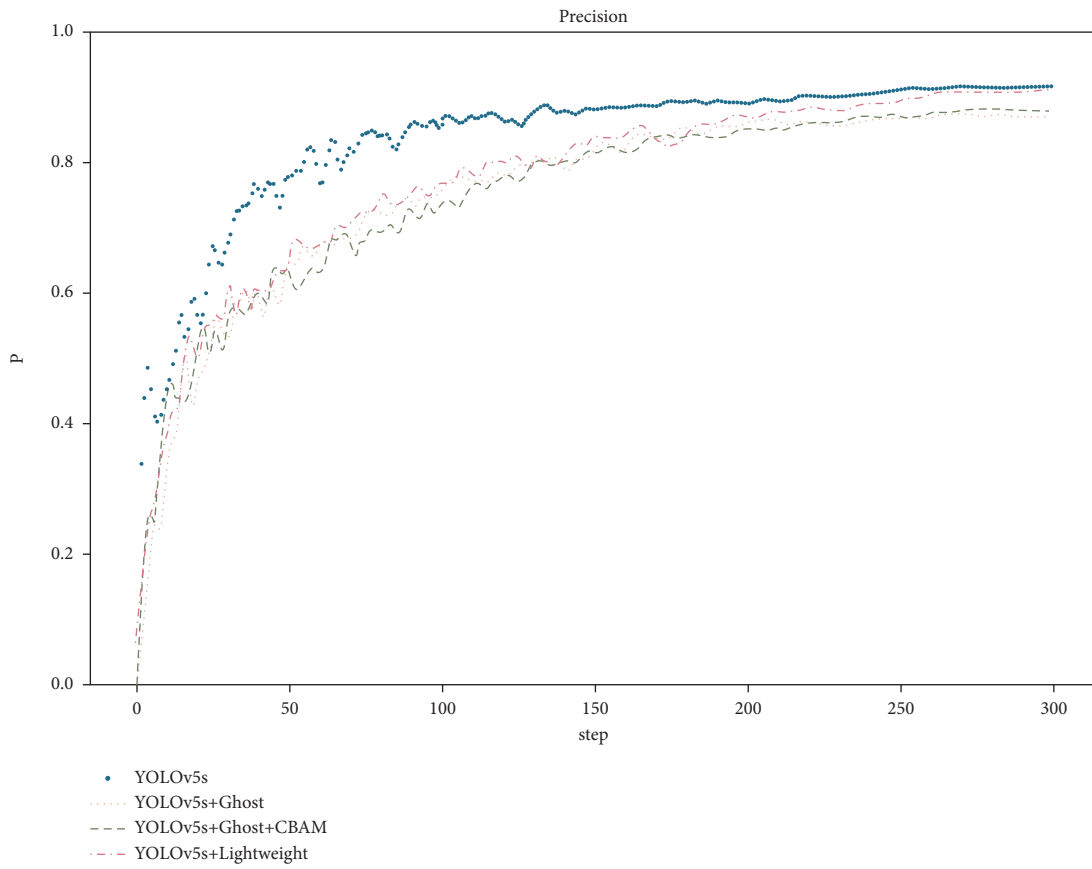
In order to verify the performance of the loss function, the paper uses Alpha-IoU [63] as a comparative experiment and uses CIoU as the benchmark loss function, setting alpha

TABLE 3: The performance of different models.

Model	Parameters	FLOPs (G)	mAP@0.5 (%)
YOLOv5s	7255094	16.86	97.04
YOLOv5s + Ghost	4434246	8.88	97.09
YOLOv5s + Ghost + CBAM	3624520	6.28	97.23
YOLOv5s-Lightweight	2751176	2.56	97.45



(a)



(b)

FIGURE 8: Continued.

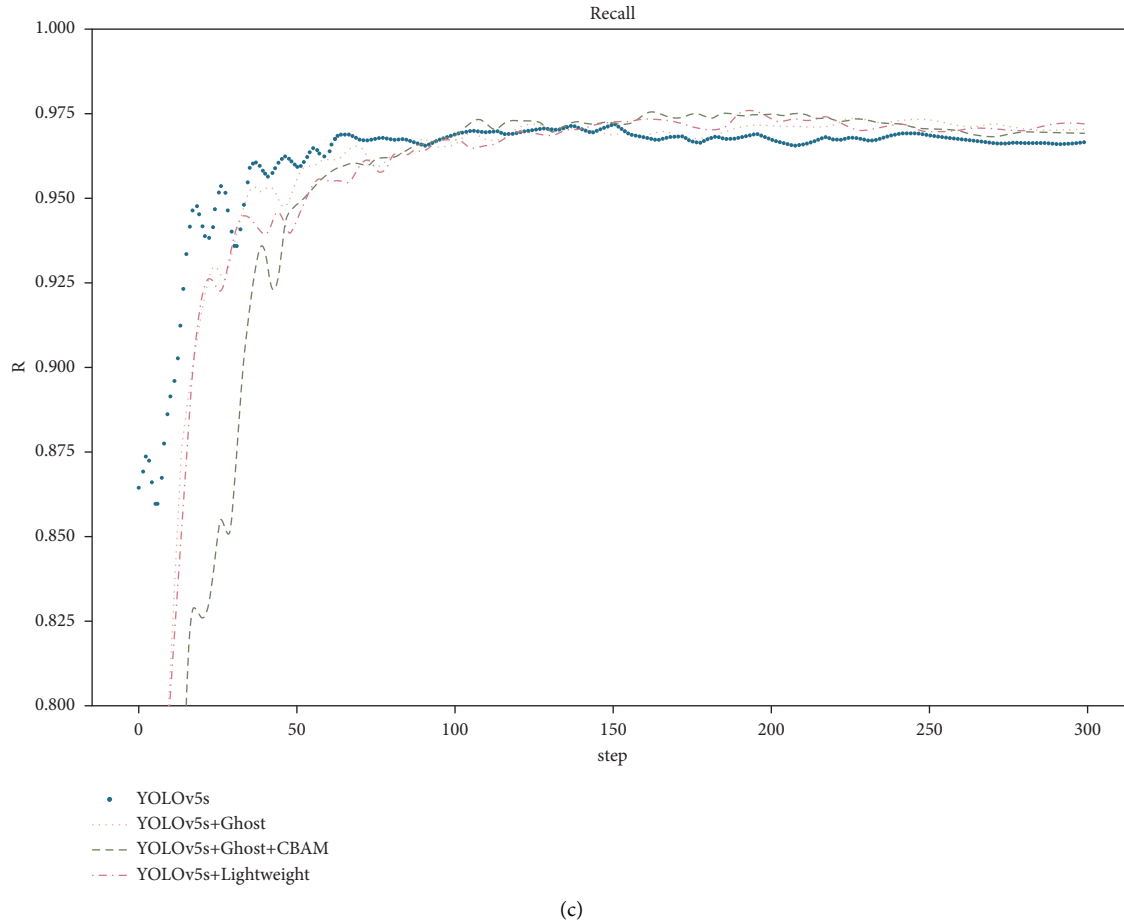


FIGURE 8: Performance detection curves of different models. (a) mAP@0.5. (b) Precision. (c) Recall.

values of 1, 2, and 3, respectively. Among them, $\alpha = 1$ corresponds to the method proposed in the paper. Figure 7 shows the loss function curves corresponding to different α values. It can be seen from the figure that the overall performance of the method proposed in the paper is better. When $\alpha = 2$ or 3, the detection curve has obvious fluctuations in the early stage. This means that α is invalid for smoke detection when the value is high.

To verify the overall performance of the proposed method, the paper gives the following comparison algorithms:

- (1) YOLOv5s: YOLOv5s model without optimization.
- (2) YOLOv5s + Ghost: modify the focus structure to Focus_mod, and all the computing modules of the backbone network use the GhostNet module.
- (3) YOLOv5s + Ghost + CBAM: modify the head layer, modify the CSP module to the Ghost bottleneck, and add the CBAM module.
- (4) YOLOv5s-Lightweight: modify the stride = 2 of the first Ghost bottleneck of the backbone network based on the previous network.

In addition, the traditional multiscale output of YOLOv5s is output after the CSP module directly extracts

features, and the lightweight network model is modified to CONCAT to connect dual feature maps for the output. Table 3 shows the parameters and floating-point calculation of the different algorithms. The parameter of the lightweight network model is only 2.75 M, and the floating-point calculation is 2.56 G, which is approximately 38% of the YOLOv5s parameter (7.25 M) and 15% of floating-point computation (16.86 G). Figure 8 shows the precision, recall, and mAP@0.5 curves of the four models. It can be seen from the figure that the accuracy of the lightweight network model is slightly better than that of the other models, the detection speed is the fastest, and the number of parameters is the lowest.

Figure 9 shows the detection results of the lightweight network model in different scenarios (including indoor and outdoor, wild, etc.). It can be seen from the figure that the lightweight network model can accurately identify smoke targets in different scenarios. In addition, we use the deep network inference engine MNN as the framework to conduct unquantified tests on smoke images on a single-core Intel i7. The traditional YOLOv5s network model needs 140 ms, while the lightweight network model only needs 60 ms, which further improves the inference speed, reaching requirements for engineering applications.



FIGURE 9: Detection results with the lightweight network model.

5. Conclusion

To solve the problem of the smoke detection algorithm with large weight parameters and slow device reasoning speed, this paper proposes a lightweight smoke detection model based on GhostNet and CBAM. The model uses Ghost convolution instead of general convolution to improve the detection speed, uses Ghost bottleneck to replace the CSP structure in the original YOLOv5 to reduce model parameters, and increases the CBAM attention mechanism. Finally, CIOU is used as the loss function to improve the detection accuracy. Compared with the benchmark YOLOv5s model, the parameter amount and calculation amount of the improved model are significantly improved, the mAP is slightly better than that of the benchmark model, and the detection speed meets the requirements of engineering applications. The paper strikes a balance between the model accuracy and speed, optimizes the YOLOv5 model reasonably, realizes model compression, speeds up inference without reducing model accuracy, and greatly reduces the dependence on the hardware environment. At present, we have completed the development of the prototype. In the future, we will complete the quantitative processing and deployment of the model on the mobile terminal and further apply it to the field to realize real-time smoke detection.

Data Availability

The data used to support the findings of this study are included within the article.

Conflicts of Interest

The authors declare that there are no conflicts of interest regarding the publication of this paper.

Acknowledgments

This research was funded by the National Natural Science Foundation of China (no. 61976198), Natural Science Research Key Project for Colleges and University of Anhui

Province (no. KJ2019A0726), High-level Scientific Research Foundation for the Introduction of Talent of Hefei Normal University (no. 2020RCJJ44), 2021 School-level Natural Science Key Project of Hefei Normal University (no. 2020KJZD16), the University-Industry Collaborative Education Program (no. 202102373013), and the Scientific Research Project by Enterprises of Hefei Normal University (HXXM2022007).

References

- [1] E. Hirsch and I. Koren, "Record-breaking aerosol levels explained by smoke injection into the stratosphere," *Science*, vol. 371, no. 6535, pp. 1269–1274, 2021.
- [2] N. Asiri, O. Bchir, M. M. B. Ismail, M. Zakariah, and Y. A. Alotaibi, "Image-based smoke detection using feature mapping and discrimination," *Soft Computing*, vol. 25, no. 5, pp. 3665–3674, 2021.
- [3] S. Chen, Y. Cao, X. Feng, and X. Lu, "Global2Salient: self-adaptive feature aggregation for remote sensing smoke detection," *Neurocomputing*, vol. 466, pp. 202–220, 2021.
- [4] R. Jevtić and M. Blagojević, "Smoke and heat detectors arrangement in hallways," *Safety Engineering*, vol. 7, no. 2, pp. 67–72, 2017.
- [5] H. Y. Jang and C. H. Hwang, "Revision of the input parameters for the prediction models of smoke detectors based on the FDS," *Fire Science and Engineering*, vol. 31, no. 2, pp. 44–51, 2017.
- [6] H. Y. Jang and C. H. Hwang, "Obscuration threshold database construction of smoke detectors for various combustibles," *Sensors*, vol. 20, no. 21, p. 6272, 2020.
- [7] M. Mueller, P. Karasev, I. Kolesov, and A. Tannenbaum, "Optical flow estimation for flame detection in videos," *IEEE Transactions on Image Processing*, vol. 22, no. 7, pp. 2786–2797, 2013.
- [8] R. Xu, H. Lin, K. Lu, L. Cao, and Y. Liu, "A forest fire detection system based on ensemble learning," *Forests*, vol. 12, no. 2, p. 217, 2021.
- [9] G. Miranda, A. Lisboa, D. Vieira, Q. Francisco, and N. Carlos, "Color feature selection for smoke detection in videos," in *Proceedings of the 2014 12th IEEE International Conference on Industrial Informatics (INDIN)*, pp. 31–36, IEEE, Porto Alegre, Brazil, July 2014.

- [10] W. Ye, J. Zhao, S. Wang, Y. Wang, D. Zhang, and Z. Yuan, "Dynamic texture based smoke detection using Surfacelet transform and HMT model," *Fire Safety Journal*, vol. 73, pp. 91–101, 2015.
- [11] Z. Zhou, Y. Shi, Z. Gao, and S. Li, "Wildfire smoke detection based on local extremal region segmentation and surveillance," *Fire Safety Journal*, vol. 85, pp. 50–58, 2016.
- [12] J. Chen, Y. Wang, Y. Tian, and H. Tiejun, "Wavelet based smoke detection method with RGB Contrast-image and shape constrain," in *Proceedings of the 2013 Visual Communications and Image Processing (VCIP)*, pp. 1–6, IEEE, Kuching, Malaysia, November 2013.
- [13] F. Yuan, J. Shi, X. Xia, Y. Fang, Z. Fang, and T. Mei, "High-order local ternary patterns with locality preserving projection for smoke detection and image classification," *Information Sciences*, vol. 372, pp. 225–240, 2016.
- [14] R. Girshick, J. Donahue, T. Darrell, and M. Jitendra, "Rich feature hierarchies for accurate object detection and semantic segmentation," in *Proceedings of the IEEE Conference on Computer Vision and Pattern Recognition*, pp. 580–587, Columbus, OH, USA, June 2014.
- [15] W. Tan, P. Huang, X. Li, G. Ren, Y. Chen, and J. Yang, "Analysis of segmentation of lung parenchyma based on deep learning methods," *Journal of X-Ray Science and Technology*, vol. 29, no. 6, pp. 945–959, 2021.
- [16] W. Tan, L. Zhou, X. Li, X. Yang, Y. Chen, and J. Yang, "Automated vessel segmentation in lung CT and CTA images via deep neural networks," *Journal of X-Ray Science and Technology*, vol. 29, no. 6, pp. 1123–1137, 2021.
- [17] R. Girshick, "Fast R-CNN," in *Proceedings of the IEEE international conference on computer vision*, pp. 1440–1448, Santiago, Chile, December 2015.
- [18] S. Ren, K. He, R. Girshick, and R. C. N. N. Faster, "Towards real-time object detection with region proposal networks," *Advances in Neural Information Processing Systems*, vol. 9199, 2015.
- [19] W. Liu, D. Anguelov, D. Erhan et al., "Ssd: single shot multibox detector," in *Proceedings of the European Conference on Computer Vision*, pp. 21–37, Berlin, Heidelberg, Germany, October 2016.
- [20] J. Redmon, S. Divvala, R. Girshick, and A. Farhadi, "You only look once: unified, real-time object detection," in *Proceedings of the IEEE Conference on Computer Vision and Pattern Recognition*, pp. 779–788, Las Vegas, NV, USA, June 2016.
- [21] P. Molchanov, A. Mallya, and S. Tyree, "Importance estimation for neural network pruning," in *Proceedings of the IEEE/CVF Conference on Computer Vision and Pattern Recognition*, Article ID 11264, March, 2019.
- [22] D. Zhang, J. Yang, D. Ye, and G. Hua, "Lq-nets: learned quantization for highly accurate and compact deep neural networks," in *Proceedings of the European Conference on Computer Vision (ECCV)*, pp. 365–382, Munich, Germany, July 2018.
- [23] G. Hinton, O. Vinyals, and J. Dean, "Distilling the knowledge in a neural network," 2015, <https://arxiv.org/abs/1503.02531>.
- [24] D. Gope, J. Beu, U. Thakker, and M. Mattina, "Ternary mobilenets via per-layer hybrid filter banks," in *Proceedings of the IEEE/CVF Conference on Computer Vision and Pattern Recognition Workshops*, pp. 708–709, Seattle, WA, USA, June 2020.
- [25] M. Sandler, A. Howard, M. Zhu, A. Zhmoginov, and L. C. Chen, "Mobilenetv2: inverted residuals and linear bottlenecks," in *Proceedings of the IEEE Conference on Computer Vision and Pattern Recognition*, pp. 4510–4520, Manhattan, New York, USA, June 2018.
- [26] A. Howard, M. Sandler, G. Chu et al., "Searching for mobilenetv3," in *Proceedings of the IEEE/CVF International Conference on Computer Vision*, pp. 1314–1324, Manhattan, New York, USA, May 2019.
- [27] M. Tan, R. Pang, and Q. V. Le, "Efficientdet: scalable and efficient object detection," in *Proceedings of the IEEE/CVF Conference on Computer Vision and Pattern Recognition*, pp. 10781–10790, Salt Lake City, UT, USA, July 2020.
- [28] K. Han, Y. Wang, Q. Tian, J. Guo, and C. Xu, "Ghostnet: more features from cheap operations," in *Proceedings of the IEEE/CVF Conference on Computer Vision and Pattern Recognition*, pp. 1580–1589, Salt Lake City, UT, USA, March 2020.
- [29] P. Wang, J. Zhang, and H. Zhu, "Fire detection in video surveillance using superpixel-based region proposal and ESE-ShuffleNet," *Multimedia Tools and Applications*, pp. 1–28, 2021.
- [30] N. Ma, X. Zhang, H. T. Zheng, and J. Sun, "Shufflenet v2: practical guidelines for efficient cnn architecture design," in *Proceedings of the European Conference on Computer Vision (ECCV)*, pp. 116–131, Munich, Germany, July 2018.
- [31] L. Su, L. Ma, N. Qin, D. Huang, and A. H. Kemp, "Fault diagnosis of high-speed train bogie by residual-squeeze net," *IEEE Transactions on Industrial Informatics*, vol. 15, no. 7, pp. 3856–3863, 2019.
- [32] S. Woo, J. Park, J. Y. Lee, and I. S. Kweon, "Cbam: convolutional block attention module," in *Proceedings of the European Conference on Computer Vision (ECCV)*, pp. 3–19, Munich, Germany, October 2018.
- [33] Z. Qu, H. Sun, and M. Zheng, "An efficient quantum image steganography protocol based on improved EMD algorithm," *Quantum Information Processing*, vol. 20, no. 2, pp. 1–29, 2021.
- [34] M. Wu, L. Tan, and N. Xiong, "A structure fidelity approach for big data collection in wireless sensor networks," *Sensors*, vol. 15, no. 1, pp. 248–273, 2014.
- [35] Z. Qu, S. Chen, and X. Wang, "A secure controlled quantum image steganography algorithm," *Quantum Information Processing*, vol. 19, no. 10, pp. 1–25, 2020.
- [36] X. Li, Z. Chen, Q. M. J. Wu, and C. Liu, "3D parallel fully convolutional networks for real-time video wildfire smoke detection," *IEEE Transactions on Circuits and Systems for Video Technology*, vol. 30, no. 1, pp. 89–103, 2020.
- [37] M. Yin, C. Lang, Z. Li, S. Feng, and T. Wang, "Recurrent convolutional network for video-based smoke detection," *Multimedia Tools and Applications*, vol. 78, no. 1, pp. 237–256, 2019.
- [38] S. Huang, A. Liu, S. Zhang, N. N. Wang, and N. N. Xiong, "BD-VTE: a novel baseline data based verifiable trust evaluation scheme for smart network systems," *IEEE transactions on network science and engineering*, vol. 8, no. 3, pp. 2087–2105, 2021.
- [39] H. Li, J. Liu, K. Wu, Z. Yang, R. W. Liu, and N. Xiong, "Spatio-temporal vessel trajectory clustering based on data mapping and density," *IEEE Access*, vol. 6, Article ID 58939, 2018.
- [40] Y. Luo, L. Zhao, P. Liu, and D. Huang, "Fire smoke detection algorithm based on motion characteristic and convolutional neural networks," *Multimedia Tools and Applications*, vol. 77, no. 12, Article ID 15075, 2018.
- [41] A. S. Pundir and B. Raman, "Deep belief network for smoke detection," *Fire Technology*, vol. 53, no. 6, pp. 1943–1960, 2017.

- [42] Q. x. Zhang, G. h. Lin, Y. m. Zhang, G. Xu, and J. Wang, "Wildland forest fire smoke detection based on faster R-CNN using synthetic smoke images," *Procedia Engineering*, vol. 211, pp. 441–446, 2018.
- [43] A. Filonenko, L. Kurnianggoro, and K. H. Jo, "Comparative study of modern convolutional neural networks for smoke detection on image data," in *Proceedings of the 2017 10th International Conference on Human System Interactions (HSI)*, pp. 64–68, IEEE, Ulsan, Korea, July 2017.
- [44] A. Filonenko, L. Kurnianggoro, and K. H. Jo, "Smoke Detection on Video Sequences Using Convolutional and Recurrent Neural networks," in *Proceedings of the International Conference on Computational Collective Intelligence*, pp. 558–566, Springer, Berlin, Heidelberg, Germany, September 2017.
- [45] J. Sharma, O. C. Granmo, M. Goodwin, and J. T. Fidge, "Deep convolutional neural networks for fire detection in images," in *Proceedings of the International Conference on Engineering Applications of Neural Networks*, pp. 183–193, Springer, Berlin, Heidelberg, Germany, August 2017.
- [46] Z. Yin, B. Wan, F. Yuan, X. Xia, and J. Shi, "A deep normalization and convolutional neural network for image smoke detection," *IEEE Access*, vol. 5, Article ID 18429, 2017.
- [47] K. Muhammad, S. Khan, V. Palade, I. Mehmood, and V. H. C. de Albuquerque, "Edge intelligence-assisted smoke detection in foggy surveillance environments," *IEEE Transactions on Industrial Informatics*, vol. 16, no. 2, pp. 1067–1075, 2020.
- [48] G. Xu, Y. Zhang, Q. Zhang et al., "Video smoke detection based on deep saliency network," *Fire Safety Journal*, vol. 105, pp. 277–285, 2019.
- [49] C. Li, B. Yang, H. Ding, H. Shi, X. Jiang, and J. Sun, "Real-time video-based smoke detection with high accuracy and efficiency," *Fire Safety Journal*, vol. 117, Article ID 103184, 2020.
- [50] T. Liu, J. Cheng, and Z. Yuan, "Video smoke detection with block DNCNN and visual change image," *KSII Transactions on Internet and Information Systems (TIIS)*, vol. 14, no. 9, pp. 3712–3729, 2020.
- [51] R. Cheng, X. He, Z. Zheng, and Z. Wang, "Multi-scale safety helmet detection based on SAS-YOLOv3-tiny," *Applied Sciences*, vol. 11, no. 8, p. 3652, 2021.
- [52] F. N. Iandola, S. Han, M. W. Moskewicz, K. Ashraf, W. J. Dally, and K. Keutzer, "SqueezeNet: AlexNet-level accuracy with 50x fewer parameters and < 0.5 MB model size," 2016, <https://arxiv.org/abs/1602.07360>.
- [53] A. G. Howard, M. Zhu, and B. Chen, "Mobilenets: efficient convolutional neural networks for mobile vision applications," 2017, <https://arxiv.org/abs/1704.04861?context=cs>.
- [54] M. E. Paoletti, J. M. Haut, N. S. Pereira, J. Plaza, and A. Plaza, "Ghostnet for hyperspectral image classification," *IEEE Transactions on Geoscience and Remote Sensing*, vol. 59, no. 12, Article ID 10378, 2021.
- [55] X. Zhang, X. Zhou, M. Lin, and J. Sun, "Shufflenet: an extremely efficient convolutional neural network for mobile devices," in *Proceedings of the IEEE Conference on Computer Vision and Pattern Recognition*, pp. 6848–6856, Salt Lake City, UT, USA, June 2018.
- [56] J. Silva, C. Huang, F. Nogueira, S. Bhatia, and V. Albuquerque, "EdgeFireSmoke: a novel lightweight CNN model for real-time video fire-smoke detection," *IEEE Transactions on Industrial Informatics*, 2022.
- [57] J. Pan, X. Ou, and L. Xu, "A collaborative region detection and grading framework for forest fire smoke using weakly supervised fine segmentation and lightweight faster-RCNN," *Forests*, vol. 12, no. 6, p. 768, 2021.
- [58] J. Redmon and A. Farhadi, "YOLO9000: better, faster, stronger," in *Proceedings of the IEEE conference on computer vision and pattern recognition*, pp. 7263–7271, Honolulu, HI, USA, July 2017.
- [59] J. Redmon and A. Farhadi, "Yolov3: An Incremental improvement," 2018, <https://arxiv.org/abs/1804.02767>.
- [60] A. Bochkovskiy, C. Y. Wang, and H. Y. M. Liao, "Yolov4: optimal speed and accuracy of object detection," 2020, <https://arxiv.org/abs/2004.10934>.
- [61] Z. Wang, L. Wu, T. Li, and P. Shi, "A smoke detection model based on improved YOLOv5," *Mathematics*, vol. 10, no. 7, p. 1190, 2022.
- [62] U. S. T. C. State Key Laboratory of Fire Science, "Research Webpage about Smoke Detection for Fire Alarm," 2021, <http://smoke.ustc.edu.cn>.
- [63] J. He, S. Erfani, X. Ma, J. Bailey, Y. Chi, and X. S. Hua, "Alpha-IOU: a family of power intersection over union losses for bounding box regression," *Advances in Neural Information Processing Systems*, vol. 34, Article ID 20230, 2021.

Research Article

Optimization and Analysis of Intelligent Accounting Information System Based on Deep Learning Model

Suzhen Feng¹ and Ran Zhong² 

¹*School of Accountancy, Shandong Youth University of Political Science, Jinan 250103, China*

²*School of Economics and Management, Hebei Oriental University, Langfang 065000, China*

Correspondence should be addressed to Ran Zhong; zhongran@hou.edu.cn

Received 15 April 2022; Revised 1 June 2022; Accepted 20 June 2022; Published 31 July 2022

Academic Editor: Le Sun

Copyright © 2022 Suzhen Feng and Ran Zhong. This is an open access article distributed under the Creative Commons Attribution License, which permits unrestricted use, distribution, and reproduction in any medium, provided the original work is properly cited.

Accounting information often accounts for more than 70% of an enterprise's financial report information. Accounting information is an important reference for an enterprise to make major decisions, and it is also the fundamental guarantee for an enterprise to remain invincible under the increasingly fierce business competition. With the vigorous development of enterprise informatization, traditional accounting information processing methods can no longer meet the needs of the information age. Therefore, an excellent enterprise must have a complete set of intelligent accounting information systems. How to extract the information we want from the dazzling accounting information data is a hot topic in the current financial industry. On the basis of analyzing the significance of establishing an information system, this paper creates an intelligent recognition model, which solves the shortcomings of traditional methods such as large calculation errors, time-consuming, and labor-intensive. The research results of the article show that (1) the standardized coefficients of the four influencing factors of CSR, ROE, CEO, and SCALE are relatively large, indicating that these four influencing factors have a significant impact on the development of corporate accounting and you can pay attention to these four aspects. (2) To test the performance of the article model, the experiments are compared with other models. The results show that the model proposed in this paper has the highest running success rate on the two test sets, with a success rate of more than 98%, indicating that the model in this paper has certain advantages in accounting information processing. (3) In the page response time experiment, the financial module has the shortest response time, the number of tests is 60 times, the average response time is 0.5 s, and the success rate can reach 100%. It can reach 0.8 s, and the success rate can be kept above 98%, indicating that the system can work normally. In the system operation stability test, the number of test cases designed for the financial module is 70, the number of executed test cases is 70, and the execution rate can reach 100%. This means that the system can work properly and will not fail during operation.

1. Introduction

In today's highly competitive business competition, enterprises must meet the complex and diverse personalized needs of the market. Enterprises must not only formulate internal management systems to ensure the normal operation of enterprises. Traditional computing methods have been gradually eliminated by society. We are in an era of informationization and intelligence. How to combine big data intelligent technology with accounting management work is a problem we need to consider. Accounting information management of an enterprise is related to the

long-term development of an enterprise, so when formulating an enterprise accounting information system, we must consider many aspects. This paper proposes a rational risk assessment model that will help managers assess risk exposure due to potential threats to internal control in computer-based accounting information systems [1]. In this paper, we propose a new algorithm for risk assessment of accounting information systems using AHP [2]. The purpose of this paper is to explain how case-based reasoners can be used to support inexperienced information systems auditors in evaluating controls and making audit recommendations [3]. Based on the author's work and study experience, this

paper analyzes the accounting data processing problems under the background of the times [4]. This paper analyzes the application of intelligent accounting information systems in industrial and commercial enterprises and puts forward relevant suggestions [5]. This paper studies how to identify accounting events expressed in natural language and constructs an expert system [6]. This paper studies how to identify accounting events expressed in natural language and proposes a word transfer method in accounting text analysis by introducing natural language processing technology [7]. According to the method of the Analytic Hierarchy Process, the article assigns the weights to the scheme layer and constructs a complete system of accounting information disclosure indicators in colleges and universities [8]. The article illustrates that e-accounting is a new information technology term based on the changing role of the accountant, where advances in technology have relegated the mechanical aspects of accounting to computer networks [9]. By studying the relationship between the network environment and the accounting information system and the influence of the network environment on the accounting information system, this paper proposes that the internal control measures should have a diversified development trend and proposes specific measures [10]. The article explains the development status of domestic accounting information systems and risk control methods [11]. The article summarizes the development of accounting information and accounting software in China and points out that the new changes in the future will include the birth of social responsibility accounting, the widening of accounting information, and social supervision [12]. This paper describes in detail the necessity of designing an intelligent accounting information system for enterprise accounting management [13]. This study tested the influence of intrinsic and extrinsic motivation on the behavioral intentions of Libyan SMEs to adopt accounting information systems [14]. The purpose of the article is to explain the impact of accounting environmental variables on the relationship between AIS and Iraqi performing SMEs [15].

2. Detailed Design of Accounting Information System

2.1. Introduction to Accounting Information System. The accounting information system is mainly composed of four major modules. The main module is the core part of the accounting information system. The accounting module is the basis of the information system. Interact in real-time. The budget management module realizes budget preparation through the preparation of budget drafts, enters the budget index allocation module based on the enterprise decision-making system, uses intelligent vouchers to transmit indicators to the accounting system, and uses the network to implement departmental transmission between projects. The database records all the accounting information of the enterprise and can be consulted at any time. All accounting databases are combined to form a data management system, which contains all the accounting information data of the enterprise. The functional modules of the

intelligent accounting information system are shown in Figure 1.

2.2. The Significance of Accounting Information System. At present, big data has transitioned from the conceptual stage to the large-scale application stage. The multifunctional and globalized accounting information system based on big data is a brand-new production tool for enterprises. The application of this transformed processing mode can enable enterprises to have more powerful process optimization. Create a more dynamic organizational structure, lead new changes in the field of financial accounting, realize complex business logic management and intelligent decision-making on uncertain markets and organizational methods, and create a full ecological balance system of internal and external, horizontal and vertical dimensions, to help the leap-forward development of smart business and smart enterprises. The management concept and management work of many enterprises have undergone earth-shaking changes, and an intelligent accounting information management system has also been born in the accounting management work. Accounting management is an important part of the operation process of an enterprise. After years of precipitation, the accounting management field has developed a relatively complete and mature development model. The integration of intelligent computing technology into the work of enterprise accounting management not only greatly reduces the complexity and tediousness in the process of enterprise accounting information processing but also solves the problems of low efficiency and large errors caused by manual calculation and also liberates the labor force. In the increasingly competitive business competition, an excellent enterprise must conform to the development of society and the times, make corresponding changes, adjust the development goals of the enterprise, and formulate relevant development strategies.

3. System Establishment of Deep Learning Model

3.1. Model Establishment. To establish an enterprise indicator model, this paper adopts the following model [16]:

$$ZL_{fy} = \sum F + \sum Y + \partial_0 + \partial_1 * P_{fy} + \partial_2 * M_{fy} + \dots \quad (1)$$

Among them, F represents the industry in which the company is located, Y represents the year, and ZL_{fy} represents the change in the strategic value of the company in F industries and Y years; the changes in various accounting indicators of the company and the comprehensive benefits of the changes in the strategy of the entire company are reflected by this value, and ∂_i ($i = 1, 2, \dots, 7$) represents the index coefficient corresponding to the i -th indicator, P_{fy} represents the investment in sales expenses, M_{fy} represents the investment in management expenses, F_{fy} represents the investment in fixed asset renewal costs, D_{fy} represents capital intensity, I_{fy} represents R&D investment, L_{fy} represents corporate financial leverage, and C_{fy} represents cloud computing ability value.

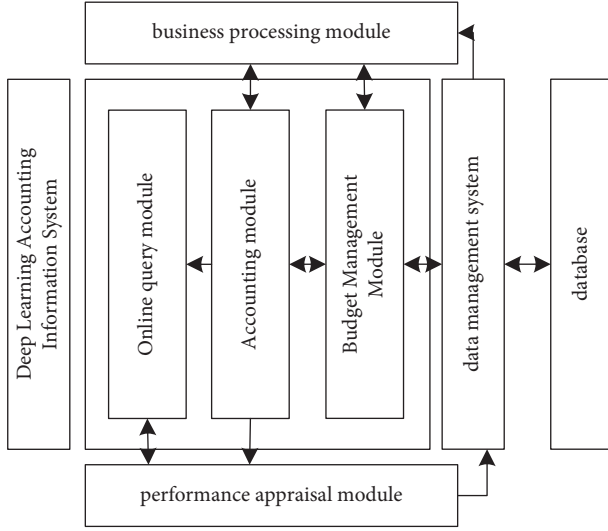


FIGURE 1: System function module.

Sales expense input is as follows [17]:

$$P_{fy} = \frac{SE}{R}. \quad (2)$$

Management fee input is as follows [18]:

$$M_{fy} = \frac{ME}{R}. \quad (3)$$

Fixed assets renewal cost input is as follows:

$$F_{fy} = \frac{NE}{OF}. \quad (4)$$

Capital intensity is as follows [19]:

$$D_{fy} = \frac{NF}{SN}. \quad (5)$$

R&D investment is as follows:

$$I_{fy} = \frac{IF}{R}. \quad (6)$$

Corporate financial leverage is as follows [20]:

$$L_{fy} = \frac{SD + LD + BP}{V}. \quad (7)$$

3.2. Financial Risk Forecast. Financial risk prediction formula is [21]

$$DD = \frac{E(V) - D}{E(V)\sigma_A}. \quad (8)$$

Assuming that the price fluctuations of the real assets of the target company can obey the Wiener process, there are

$$dV_A = \mu V_A dt + \sigma_A V_A dz. \quad (9)$$

The relationship between asset value and equity value can be constructed as follows [22]:

$$V_E = V_A N(d1) - e^{-rt} \times N(d2), \quad (10)$$

$$\sigma_E = \frac{V_A}{V_E} \sigma_A. \quad (11)$$

Expected default rate is as follows:

$$Pt = \text{prob}[V_A^t \leq X_t | V_Z^0 = V_A]. \quad (12)$$

Company asset value is as follows:

$$\ln V t_A = \ln V_A + \left[\mu - \frac{\sigma_A^2}{2} \right] \tau + \sigma_A \sqrt{\tau} \varepsilon. \quad (13)$$

Final default rate is as follows:

$$P_t = N \left[\frac{\ln V_A / X_t + \left(\mu - \frac{\sigma_A^2}{2} \right) \tau}{\sigma_A \sqrt{\tau}} \right]. \quad (14)$$

The evaluation index of enterprise financial risk is as follows [23]:

$$X = (X_1, X_2, \dots, X_p). \quad (15)$$

Linear combination of evaluation metrics is

$$\hat{P} = W_0 + W_1 X_1 + W_2 X_2 + \dots + W_p X_p, \quad (16)$$

in

$$W^* = (W_0, W_1, W_2, \dots, W_p), \quad (17)$$

$$X^* = (X_1, X_2, \dots, X_p). \quad (18)$$

Financial risk prediction model is as follows [24]:

$$P = \frac{\exp(W_0 + W_1 X_1 + \dots + W_p X_p)}{1 + \exp(W_0 + W_1 X_1 + \dots + W_p X_p)}. \quad (19)$$

4. Simulation Experiments

4.1. Model Construction. In order to find out the factors that affect the development of corporate accounting, the experiment selected 11 secondary indicators as impact factors and recorded the data of each impact factor from 2014 to 2018, so as to determine the important indicators that affect the development of corporate accounting. The value of the standardization coefficient is an important reference factor for determining the impact factor and the development degree of enterprise accounting. The larger the coefficient value, the more significant the degree of influence. The specific experimental operation is as shown in Figure 2. The definition of factor variables is described in Table 1.

According to the experimental data in Table 2, in 2014, the standardized values of 11 secondary indicators were all 1. Since 2015, the standardized values of each factor began to change. In 2015, the standardized coefficient of the ownership structure was 3.75, which is 11 items. The highest one of the test indicators indicates that the ownership structure has a greater impact on accounting information. The standardized coefficient of operational management

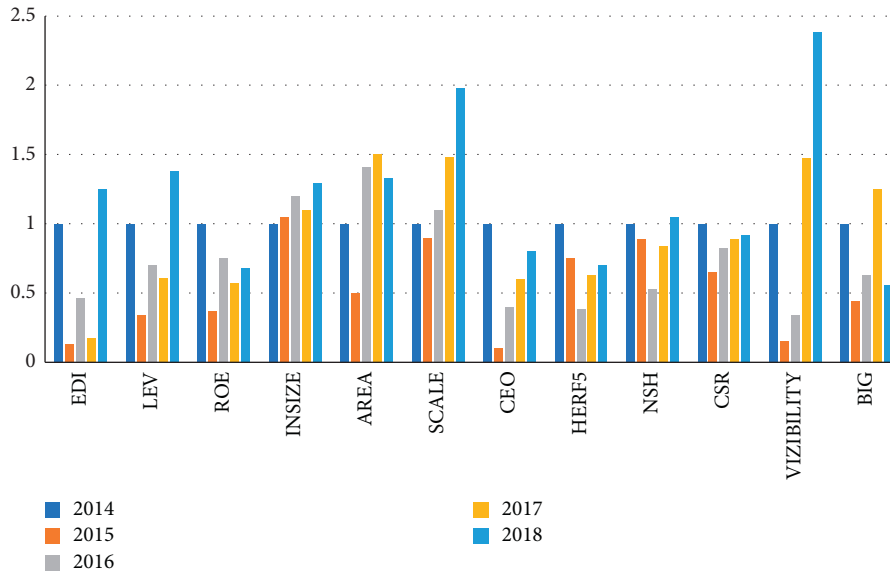


FIGURE 2: Standardized data statistics for each factor.

TABLE 1: Factor variable definition description table.

First-level indicator	Secondary indicators	Representative symbol	Definition explanation
Company financial variables	Financial leverage	LEV	Measure the financial risk of the company by the company's asset-liability ratio Reflect the company's profitability
	Roe	ROE	
Company characteristic variables	Company size	INSIZE	The logarithm of the company's total assets East, middle, and west are represented by 3, 2, and 1, respectively
	Your area	AREA	
Corporate governance variables	Board size	SCALE	Expressed by the number of board members It is represented by the combination of the chairman and the general manager
	Operational management independence	CEO	
	Shareholding structure	HERF5	
	Enterprise nature	NSH	
External environment variables	Government intervention	CSR	1 for publishing social responsibility report, 0 for not publishing Select the financial media attention related to the industry to which the company belongs Indicated by firm ranking, the top ten firms take 1, otherwise take 0
	Media attention	VIZIBILITY	
	Firm influence	BIG	

TABLE 2: Standardized data of each factor.

Index	2014	2015	2016	2017	2018
EDI	1.00	0.13	0.46	0.17	1.25
LEV	1.00	0.34	0.70	0.61	1.38
ROE	1.00	0.37	0.75	0.57	0.68
INSIZE	1.00	1.05	1.20	1.10	1.29
AREA	1.00	0.50	1.41	1.50	1.33
SCALE	1.00	0.90	1.10	1.48	1.98
CEO	1.00	0.10	0.40	0.6	0.80
HERF5	1.00	3.75	3.38	0.63	0.70
NSH	1.00	0.89	0.53	0.84	1.05
CSR	1.00	0.65	0.82	0.89	0.92
VIZIBILITY	1.00	0.15	0.34	1.47	2.38
BIG	1.00	0.44	0.63	1.25	0.56

TABLE 3: Description of accounting information impact factors.

Index	2014	2015	2016	2017	2018
EDI	0.73	0.09	0.33	0.12	0.89
LEV	0.59	0.20	0.41	0.36	0.81
ROE	0.29	0.11	0.22	0.41	0.20
INSIZE	0.89	0.95	1.12	1.30	1.73
AREA	0.20	1.00	0.82	1.25	1.33
SCALE	0.89	0.86	0.92	1.34	1.65
CEO	0.05	0.10	0.02	1.00	0.40
HERF5	0.08	0.30	0.27	0.45	0.56
NSH	0.95	0.85	0.50	0.80	1.00
CSR	0.05	0.25	0.45	0.89	0.50
VIZIBILITY	0.69	0.15	0.24	1.53	2.38
BIG	0.80	0.35	0.50	1.00	0.45

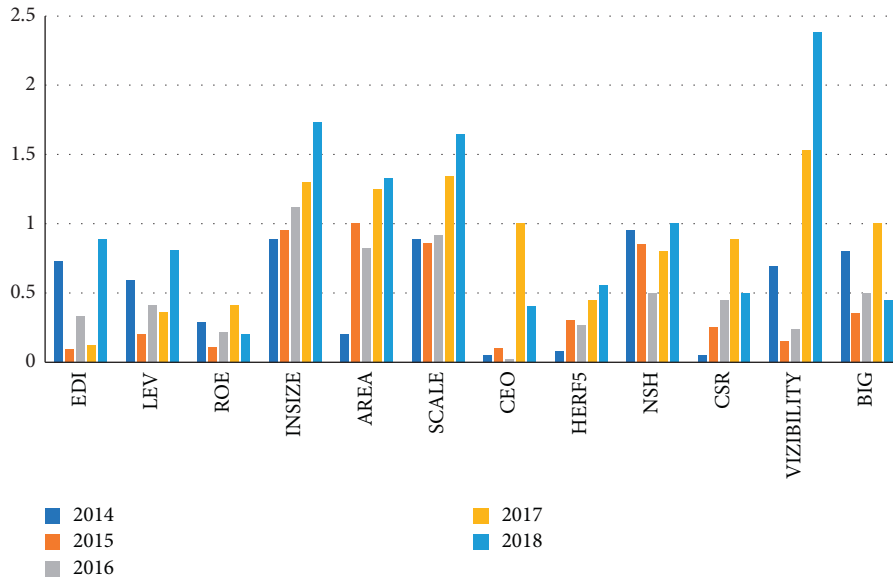


FIGURE 3: Statistics of factors affecting the level of accounting information disclosure.

independence is 0.1, which is the lowest of the test indicators, indicating that operational management independence has the lowest impact. From 2016 to 2018, the standard coefficients of company size and region are all higher than 1.0, indicating that the two independent variables have a relatively large degree of influence. The description of the impact factors of the secondary indicators is shown in Table 3 and Figure 3.

According to the data in Table 3, in 2014, the standardization coefficient of enterprise nature reached 0.95, indicating that the influence factor of enterprise nature was the largest. From 2015 to 2016, the standardized coefficient decreased, and the coefficient reached 1 in 2018. In 2015, except for the AREA coefficient, which reached 1 after that, the other coefficients are all less than 1, indicating that except for the region where the influence factor of the enterprise is relatively large, other influence factors have no significant influence on the development of the enterprise. In 2016, the standard coefficient of company size exceeded 1. From 2017 to 2018, the standardized coefficients of many indicators exceeded 1, indicating that these influencing factors have an increasingly significant impact on enterprise development.

4.2. Model Comparison Study. In order to test the performance of the accounting recognition model established in the article, the experiment will run the model and the other two models on different test sets and record the experimental results. Model evaluation classification is the last step in building a model; it can effectively help us choose an excellent classifier and improve its performance and plays a very important role. Generally speaking, the training set is used to evaluate the parameters of the model, so that the model can reflect the reality and then predict the future or other unknown information, and the test set is used to evaluate the prediction performance of the model. The experimental results under the two different test sets are as

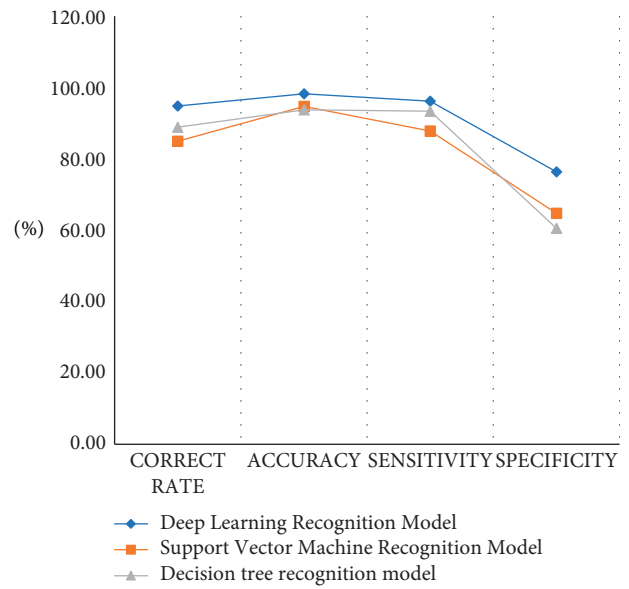


FIGURE 4: Statistics of model evaluation results.

shown in Figure 4. The model evaluation indicators are shown in Table 4.

According to the data in Table 5, we can conclude that after the training set runs, the correct rate of the model proposed in this article can reach 94.8%, and the accuracy rate can reach 98.23%, which is the highest among the test models. The correct rate is 84.95%, and the accuracy rate is 94.71%, which is the lowest among the test models. The correct rate of the decision tree recognition model is 88.87%, and the sensitivity is 93.36%. The detection results are in the model proposed in the article and the support vector machine recognition model in between.

According to the above model test results in Figure 5 and Table 6, the running accuracy of the model in the training set

TABLE 4: Evaluation index table.

	Formula	Definition
Accuracy	$PPV = TP / (TP + FP)$	Indicates the proportion of the model identified correctly among all results identified by the model as correct samples
Sensitivity	$TPR = TP / (TP + FN)$	Indicates that the model recognizes the correct proportion in the true value of the sample
Specificity	$TNR = TN / (TN + FP)$	Indicates that the model recognizes the correct proportions in which the true value is negative

TABLE 5: Training set model evaluation result table.

Recognition model	Correct rate (%)	Accuracy (%)	Sensitivity (%)	Specificity (%)
Deep learning recognition model	94.80	98.23	96.15	76.32
Support vector machine recognition model	84.95	94.71	87.76	64.71
Decision tree recognition model	88.87	93.75	93.36	60.53

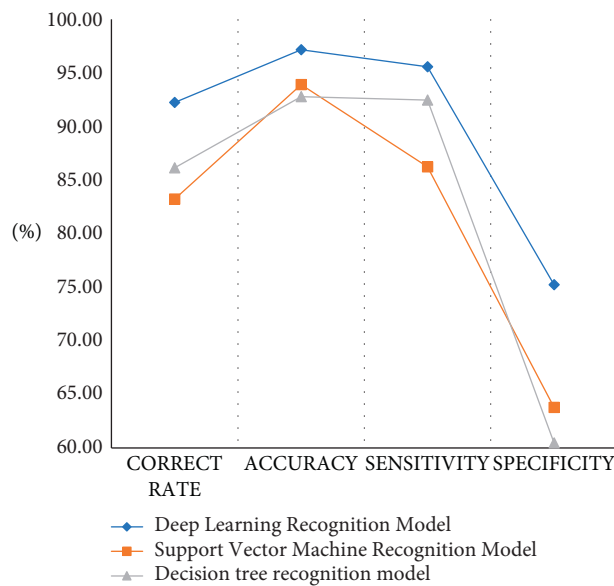


FIGURE 5: Statistics of model evaluation results.

TABLE 6: Evaluation effect of the test set model.

Recognition model	Correct rate (%)	Accuracy (%)	Sensitivity (%)	Specificity (%)
Deep learning recognition model	92.23	97.14	95.56	75.23
Support vector machine recognition model	83.21	93.89	86.22	63.79
Decision tree recognition model	86.14	92.78	92.46	60.48

and the test set is 94.80% and 92.23% respectively, and the running accuracy in the training set and the test set is 81.95% and 92.23% respectively. The accuracy rate is 93.21%. The correct rate of the decision tree recognition model is 88.87% in the training set and 86.14% in the test set. Although the performance of the three detection models is reduced to a certain extent after the test set is run, the detection value of the model in this paper is still the highest among all detection models. The experimental results also show that the detection efficiency of the model proposed in this article is optimal whether it is in the training set or the test set.

4.3. System Test. System testing is to test whether the system can work normally under a certain load [25]. The performance test of the intelligent accounting information system based on the deep learning model studied in this paper is mainly tested from the two indicators of page response time and system operation stability. The method of page response test is to record the system response time under different test times and then observe the response time and operation stability of the system by continuously increasing the number of tests and the ratio of numbers. The components of intelligent accounting information are shown in Table 7

TABLE 7: Components of intelligent accounting information system.

Component	Function
Financial section	Mainly responsible for the company’s daily financial work and financial budget, accounting and financial management, and fundraising, etc., early warning and monitoring of financial risks, and guiding the company’s business activities through financial data analysis
Purchase and sale part	According to the needs of the enterprise, in order to solve the problems of confusing accounts, inaccurate inventory, and untimely information feedback, the purchase, sale, and storage system integrates procurement, sales, inventory management, and receivable and payable management, providing order, procurement, sales, the management of returns, inventory, current invoices, current accounts, salesmen, etc., helps enterprises handle daily invoicing and inventory business, and provides rich real-time query and statistical functions
Management analysis section	Management analysis can make full use of the historical data and other relevant information provided by financial accounting, use certain mathematical methods to process them scientifically, conduct scientific forecasting and analysis for business operations, and help leaders at all levels to make decisions accordingly. Correct decision analysis

TABLE 8: Page response time test results.

Testing frequency	60	70	80	90	100	110	120	130
Financial section	0.5	0.6	0.7	0.8	0.9	1.0	1.1	1.2
Purchase and sale part	0.8	0.9	1.0	1.1	1.2	1.3	1.4	1.5
Management analysis section	1.1	1.2	1.3	1.4	1.5	1.6	1.7	1.8

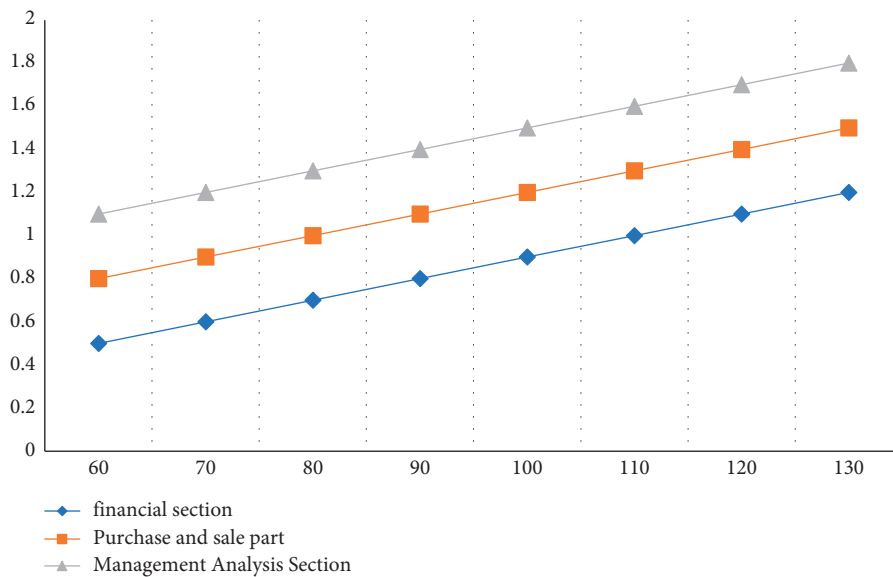


FIGURE 6: Average response time curve.

TABLE 9: System operation stability test.

Design test cases	70.00	80.00	90.00	100.00	110.00	120.00	130.00	140.00
Financial section	70.00	80.00	90.00	100.00	110.00	120.00	130.00	140.00
Purchase and sale part	68.00	77.00	88.00	99.00	109.00	119.00	129.00	139.00
Management analysis section	67.00	76.00	87.00	98.00	108.00	118.00	128.00	138.00

4.3.1. Page Response Time Test. According to the above experimental results in Table 8 and in Figure 6, the average response time will increase with the increase of the number of tests. The average response time of the financial part is the lowest among all the test modules. When the number of tests is 130, the average response time of the financial part is 1.2

seconds; the average response time of the purchase, sale, and storage part is 1.5 seconds, and the average response time of the management analysis part is 1.8 seconds. The management analysis part contains a huge database, so the response time is the longest, and the response time of the purchase, sale, and storage part is between the financial part

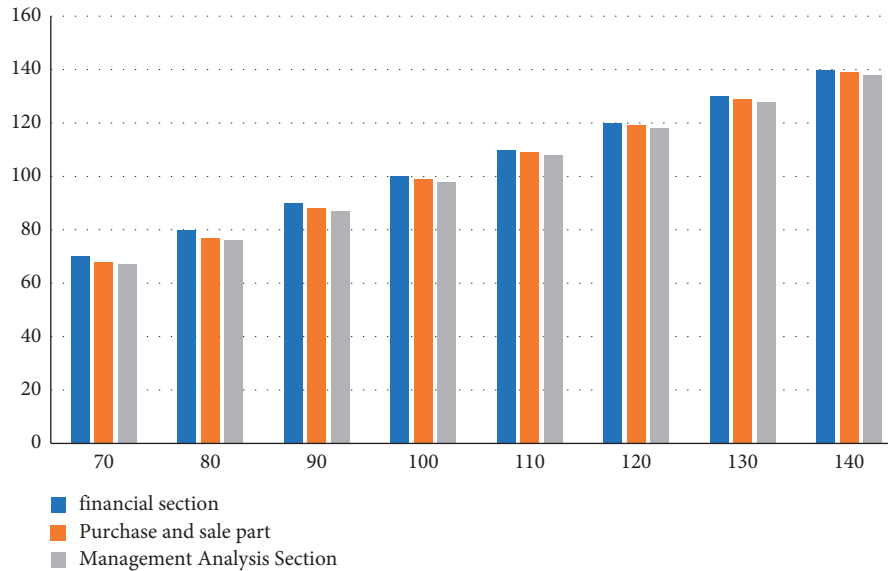


FIGURE 7: Execution test case statistics.

and the management analysis part. Moreover, the execution success rate of the three modules has remained above 98% (Table 9).

4.3.2. System Operation Stability Test. According to the execution rate test of the system in Figure 7, we can know that when the number of design test cases is 140, the number of executed use cases of the financial module is 140, the number of executed use cases of the purchase, sale, and storage module is 139, and the number of executed use cases of the management analysis part is 138. The execution rates of the three modules are kept above 98%, close to 100%, indicating that the system can operate normally.

5. Conclusion

Applying the processing mode transformed by intelligent computing can enable enterprises to have more powerful process optimization, create a more dynamic organizational structure, promote new changes in the field of financial accounting, and realize complex logical management of business and business operations in uncertain markets and organizational methods. Intelligent decision-making, as well as building a comprehensive ecological balance system of internal and external, horizontal, and vertical dimensions, helps smart businesses and smart enterprises to develop forward. The model proposed in this paper solves the problems of long calculation process and high error rate in the human computing process, and the model has a short response time and a high success rate, but the model still has some shortcomings. The model of this paper is to calculate only the accounting information data of a certain enterprise, and the calculation sample capacity is small. In future research work, the calculation capacity should be increased. Accounting management is a very complex task. In the process of accounting work, there will be many accounting calculation methods and related systems that cannot be explained clearly. The relevant departments of the enterprise should pay attention to revising the

relevant policies of accounting management. Effective calculation of accounting information will reduce the occurrence of any illegal operations, thereby promoting the long-term development of enterprises. The construction of the new accounting information system is the result of the development of science and technology of the times. The integration of big data and accounting information processing is a new development trend. Enterprises should seize the opportunity and strive to improve their own development deficiencies. The enterprise accounting information system under big data will develop better and better and can adapt to the pace of scientific and technological development and form an accounting information system with Chinese characteristics in the process of continuous development. Enterprises need to develop and progress. The traditional audit method is inefficient and consumes a lot of manpower and material resources. Before auditing the company's financial statements, auditors can use the identification model in this study to test the possibility of accounting information distortion, clarify the key points and doubts of the audit, form a preliminary evaluation, and then determine the audit scope and audit scope. The review process is a procedure to improve the quality of accounting information audit.

Data Availability

The experimental data used to support the findings of this study are available from the corresponding author upon request.

Conflicts of Interest

The authors declare that they have no conflicts of interest.

Acknowledgments

This research was supported by Research on the construction of a practical teaching system of "big accounting" in the

digital intelligence era (Project No.: 2020yb005), the 13th Five Year Plan Project of Educational Science in Shandong Province. 2. Teaching reform research project of the Shandong Youth University of Political Science “reform and practice of experimental teaching system of auditing from the perspective of cooperation education” (Project No.: jgxm202005).

References

- [1] A. de Korvin and M. F. Shipley, “Assessing risks due to threats to internal control in a computer-based accounting information system: a pragmatic approach based on fuzzy set theory[J],” *Intelligent Systems in Accounting, Finance and Management*, vol. 03, no. 11, pp. 45–49, 2004.
- [2] L. S. Yuan and R. P. Dong, “A Novel risk assessment algorithm for accounting information system using Analytic Hierarchy process[C]. International Conference on intelligent Computation technology & Automation,” *IEEE*, vol. 06, no. 07, pp. 11–17, 2016.
- [3] B. W. Morris, “SCAN: a case-based reasoning model for Generating information system control recommendations,” *Intelligent Systems in Accounting, Finance and Management*, vol. 3, no. 1, pp. 47–63, 1994.
- [4] F. Jiao, “Cloud accounting: the transition of accounting information model in the big data background[C],” in *Proceedings of the 2015 International Conference on Intelligent Transportation, Big Data and Smart City*, pp. 65–74, IEEE, Halong Bay, Vietnam, 2015.
- [5] L. Huimin, “Research on the application of accounting information system intelligence on business enterprises[C],” in *Proceedings of the 2018 5th International Conference on Electrical & Electronics Engineering and Computer Science (ICEECS 2018)*, pp. 89–99, Beijing, China, 2018.
- [6] G. L. Geerts and W. McCarthy, “Expert opinion [accounting],” *IEEE Intelligent Systems*, vol. 14, no. 4, pp. 89–94, 1999.
- [7] L. Wu, X. Cong, and S. O. Accounting, “The intelligent accounting event identification method based on natural language[J],” *Communication of Finance and Accounting*, vol. 3, no. 10, pp. 31–52, 2017.
- [8] L. He and W. Chen, “Index design and model construction of accounting information disclosure of universities based on Analytic Hierarchy process,” *Journal of Advanced Computational Intelligence and Intelligent Informatics*, vol. 22, no. 7, pp. 1093–1098, 2018.
- [9] K. Kitwiboon, “Analysis of an accounting information system [C],” *Digital Information & Communication Technology & Its Applications-international Conference*, vol. 11, no. 4, pp. 114–121, 2000.
- [10] W. Wei and S. Y. Lu, “Study on internal control mode of accounting information system under network environment [C],” in *Proceedings of the 2018 International Conference on Intelligent Transportation, Big Data & Smart City (ICITBS)*, pp. 44–53, IEEE, Xiamen, China, January 2018.
- [11] X. Jiang, “The research on internal control of accounting information system based-on ERP[J],” in *Proceedings of the 2011 International Conference on Business Computing and Global Informatization*, pp. 78–89, IEEE, Shanghai, China, July 2011.
- [12] Z. S. Fang, “Beginning and development of data-processing accounting information system and its effects on future accounting [J],” *Journal of Zhengzhou Institute of Aeronautical Industry Management*, vol. 5, no. 9, pp. 63–74, 2006.
- [13] Y. Raymond and A. Chadi, “Generic Skills to reduce failure rates in an Undergraduate accounting information system Course [J],” *Asian Social Science*, vol. 4, no. 10, pp. 60–72, 2009.
- [14] K. Abduljalil and Y. Zainuddin, “Intrinsic and extrinsic motivation as Attitude factors towards adoption of accounting information system (AIS) in Libyan SMEs [J],” *International Journal of Academic Research in Accounting, Finance and Management Sciences*, vol. 5, no. 1, pp. 36–45, 2015.
- [15] E. Harash, “The role of environmental uncertainty in the Link between accounting information system and performance Small and Medium enterprises in Iraq,” *Global Journal of Management and Business*, vol. 9, no. 11, pp. 33–41, 2015.
- [16] L. Ying, “Basic architecture and function realization of accounting information system based on computer network environment [J],” *Microcomputer Applications*, vol. 34, no. 3, pp. 77–79, 2018.
- [17] R. Dai, “Research on the architecture of intelligent management accounting information system [J],” *China Economic and Trade Tribune*, vol. 3, no. 23, pp. 119–121, 2019.
- [18] L. Suo, “Research on the construction and impact of accounting information system based on blockchain technology [J],” *Value Engineering*, vol. 38, no. 20, pp. 125–127, 2019.
- [19] L. Xin, “Design and analysis of accounting information system architecture based on computer network [J],” *Automation Technology and Application*, vol. 38, no. 10, pp. 135–137, 2019.
- [20] W. Min and G. Li, “Analysis of the current situation and trend of accounting informatization research in my country [J],” *Northern Economic and Trade*, vol. 15, no. 1, pp. 99–101, 2021.
- [21] H. Fang, “Research on the application of A textile trade enterprise management accounting information system under the background of big data [D],” pp. 147–152, Hefei University of Technology, Hefei, 2020.
- [22] C. Xu, “Problems and solutions of accounting information processing of power enterprises under the background of big data [J],” *Fortune Life*, no. 24, pp. 174–175, 2019.
- [23] R. Dai, “Reconstruction of accounting information system in digital Economy - accounting information system in enterprise cloud Platform [J],” *Productivity Research*, vol. 21, no. 5, pp. 156–160, 2019.
- [24] X. Zhao and M. Yang, “Research on the relationship between the quality of environmental accounting information disclosure and corporate governance structure - based on data analysis of resource-based enterprises [J],” *China Certified Public Accountants*, vol. 4, no. 8, pp. 45–49, 2016.
- [25] G. Xu and S. Wan, “Environmental information disclosure, media attention and research on corporate value [J],” *Friends of Accounting*, vol. 10, no. 10, pp. 35–42, 2017.

Research Article

Research on the Evaluation of Moral Education Effectiveness and Student Behavior in Universities under the Environment of Big Data

Rui Zhu 

Publicity Department, Shandong Management University, Jinan, Shandong 250000, China

Correspondence should be addressed to Rui Zhu; 14438120030030@sdmu.edu.cn

Received 1 June 2022; Revised 17 June 2022; Accepted 6 July 2022; Published 30 July 2022

Academic Editor: Le Sun

Copyright © 2022 Rui Zhu. This is an open access article distributed under the Creative Commons Attribution License, which permits unrestricted use, distribution, and reproduction in any medium, provided the original work is properly cited.

Traditional moral evaluation relies on artificial and subjective evaluation by teachers, and there are subjective errors or prejudices. To achieve further objective evaluation, students' classroom performance can be identified, and the effectiveness of moral education can be evaluated based on student behavior. Since student classroom behavior is random and uncertain, in order to accurately evaluate its indicators, a large amount of student classroom behavior data must be used as the basis for analysis, while certain techniques are used to filter out valuable information from it. In this paper, an improved graph convolutional network algorithm is proposed to study students' behaviors in order to further improve the accuracy of moral education evaluation in universities. The technique of video recognition is used to achieve student behavior recognition, thus helping to improve the quality of moral education evaluation in colleges and universities. First, the multi-information flow data related to nodes and skeletons are fused to improve the computing speed by reducing the number of network parameters. Second, the spatiotemporal attention module based on nonlocal operations is constructed to focus on the most action discriminative nodes and improve the recognition accuracy by reducing redundant information. Then, the spatiotemporal feature extraction module is constructed to obtain the spatiotemporal association information of the nodes of interest. Finally, the action recognition is realized by the Softmax layer. The experimental results show that the algorithm of action recognition in this paper is more accurate and can better help moral evaluation.

1. Introduction

Moral evaluation is a guide and an initiative to carry out moral education in schools. Moral evaluation is defined in the Dictionary of Education as "the process of making value judgments on the performance of moral behavior of individuals using the acquired moral standards" [1]. The broad perspective of school moral evaluation content is to examine the ideological, moral, and political qualities of individuals, and the narrow perspective is to examine the moral qualities of individuals. Both focus on the moral cognition and moral behavior of individuals, especially the moral behavior that is more easily observed [2].

To adhere to "people-oriented" means to maintain human dignity, respect human rights, give full play to human potential, meet human needs, and promote the all-round development of people. By insisting on the college students as

the center, we should not only educate them, guide them, inspire them and spur them on but also respect them, understand them, care for them, and help them to develop good ideological and moral qualities and excellent ideological and political qualities, so as to achieve the purpose of moral education and realize the fundamental goal of establishing moral education for people [3].

In the current reform of quality education, colleges and universities pay more and more attention to the moral education quality cultivation of students, and no longer focus not only on the teaching of students' professional courses but also begin to focus on the overall development of students' comprehensive quality. In order to implement the requirements of quality education cultivation and promote the vigorous development of moral quality education, a matching moral quality evaluation system for college students should be formulated. The traditional evaluation

method of students' moral quality has been rather backward, and it is difficult to ensure the fairness and scientificity by simply relying on human for evaluation, which does not meet the needs of quality education, so it needs technology updating. Innovate student moral quality evaluation mode, introduce information technology support, and use big data technology and computer information technology to create a sound moral quality evaluation system for college students. Scientific design and optimization of system structure in order to improve the efficiency of moral quality education in colleges and universities and guarantee the quality of moral quality education for college students.

Literature [4] constructed the spatiotemporal graph with the natural connections of human joints and proposed the spatiotemporal network model with the graph convolution layer as the basic module. Literature [5] integrated a discrete multiscale aggregation scheme and the spatiotemporal graph convolution operator called G3D to form a powerful feature extraction structure. Literature [6] introduces a context-encoded network for enhancing contextual feature relevance and automatically learning the skeleton topology. Literature [7] incorporates third-order features to effectively capture the relationship between joints and body parts. Literature [8] introduced a novel progressive multiscale convolution for capturing long- and short-term correlations in the spatial and temporal domains. Literature [9] used multiscale temporal convolution and exploited the correlation of the original data to better model the channel topology. Literature [10] describes the skeleton features using Lie groups, then describes the relationship of these features in time order by dynamic temporal regularization, and finally uses multiclass support vector machines for the behavior recognition task. Literature [11] designs a multifeature fusion coding method based on VLAD. Literature [12] designs the spatiotemporal weight coding method based on skeleton features. Literature [13] constructs a motion feature generator based on the existing generative adversarial network framework to perform the learning of judgment optical flow features. Literature [14] investigates temporal pooling and long-term information dependence of behavioral features on the basis of CNNs. In the literature [15], the decomposition model of convolutional networks on spatiotemporal sequences is investigated, i.e., the 3D spatiotemporal convolution is decomposed into 2D spatial convolutional kernel and 1D temporal convolutional layer to accomplish the representation and recognition of human behavior. Literature [16] further investigates the combined strategy of 2D spatial convolution and 1D temporal pooling. Literature [17] extends 2D convolutional operations into 3D convolution and implements a dual-stream I3D. In the literature [18], in order to complete the extraction of human behavior on spatiotemporal features, a dual-stream pooling network is designed to further enhance the feature representation. In the literature [19], a synchronous appearance and relationship module SMART are proposed, and the learning of spatiotemporal features of behavior is accomplished by stacking the model. Literature [20] designs a multi-Fiber network, each Fiber uses lightweight convolution, and the speed of behavior recognition is greatly improved.

In the process of moral education evaluation in colleges and universities, schools can conduct in-depth mining based on big data and provide reference for student management and education service supply by analyzing student classroom behavior data to achieve overall improvement of education level. In order to make full use of the action features in the human skeleton sequence and achieve lightweight action recognition model with improved recognition accuracy, this paper proposes a lightweight adaptive graph convolutional network combining multi-information flow data fusion and spatiotemporal attention mechanism. The human skeleton-based action recognition is very little affected by factors such as illumination and background and has great advantages over the RGB data-based methods. The joint skeleton data of human body are a topological graph, and each joint point in the graph has different number of neighboring joints. Traditional convolutional neural networks cannot directly use the same size convolutional kernel for convolutional computation to process such non-Euclidean data. Therefore, in the field of skeleton-based behavior recognition, a graph convolutional network-based approach is more suitable. The experimental results show that the recognition accuracy of the algorithm in this paper is high, and it can do the work of moral evaluation better.

2. Methodology

2.1. Student Behavior Algorithm

2.1.1. Graph Convolutional Network. In the Euclidean space represented by an image, each pixel in the image is treated as a node, then the nodes are arranged regularly and the number of neighboring nodes is fixed, and the points on the edges can be padding operation. However, in a non-Euclidean space like the graph structure, the nodes are disordered and the number of neighbor nodes is not fixed, and feature extraction cannot be achieved by a traditional convolutional neural network with a fixed size convolutional kernel. A convolutional kernel capable of handling variable-length neighbor nodes is needed [21]. For the graph, features need to be extracted by inputting a feature matrix I of dimension $T \times \nu F$ and an adjacency matrix G of $T \times T$, where T is the number of nodes in the graph and F is the number of input features per node. The nodal feature transformation formula for the adjacent hidden layer is shown below.

$$B^{x+1} = f(B^x, G), \quad (1)$$

where x is the number of layers, the first layer ($B^0 = IB^0$). $f(\cdot)$ is the propagation function, and the propagation function varies for different graphical convolutional network models. Each layer B^x corresponds to the $T \times F^x$ -dimensional feature matrix, and the aggregated features are transformed into the features of the next layer by the propagation function $f(\Delta)$, which makes the features more and more abstract.

2.1.2. Lightweight Graph Convolutional Network Framework. In order to make full use of the action features in human skeleton sequences and to achieve a lightweight action recognition model with improved recognition accuracy, this

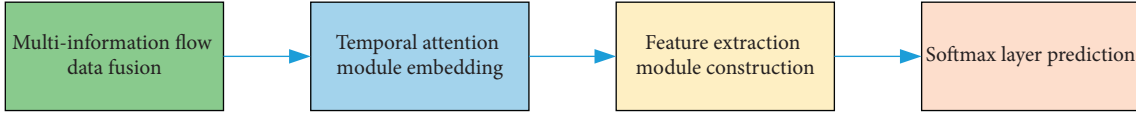


FIGURE 1: Network framework.

paper proposes a lightweight adaptive graph convolutional network combining multiple information streams data fusion and spatiotemporal attention mechanism. Taking the input human skeleton sequence as the research object, we first fuse four kinds of data information: joint point information flow, bone length information flow, joint point offset information flow, and bone length change information flow. Then, an embeddable spatiotemporal attention module based on nonlocal operations is constructed to focus on the most action discriminative joints in the human skeleton sequence after the information flow data fusion. Finally, the recognition results of the action fragments are obtained by Softmax, and the main framework of the network is shown in Figure 1.

2.1.3. Multi-Information Flow Data Fusion. At present, the methods based on graph convolution [22] mostly adopt multiple training under a variety of different data sets and carry out decision-making level fusion according to the training results, resulting in a large amount of network parameters. Therefore, the original joint point coordinate data are preprocessed before training to realize the data-level fusion of joint point information flow, bone length information flow, joint point offset information flow, and bone length change information flow, so as to reduce the network parameters and reduce the calculation requirements. The definition of joint points of human skeleton sequence is shown in formula (2).

$$s = \{Q_{x,n} / x = 1, 2, \dots, T; n = 1, 2, \dots, N\}, \quad (2)$$

where N is the total number of frames in the sequence, T is the total number of nodes 18, and x is the nodes at the moment n . Before fusing the multiple information streams, a diverse preprocessing of the skeleton sequence s is required. The node information stream is obtained from the coordinates of 18 nodes obtained by the human pose estimation algorithm OpenPose, which is a significant cost reduction compared to motion capture devices. Other information streams are defined as follows.

Bone Length Information Flow: the node near the center of gravity of the body is defined as the source node, and the coordinates are used to obtain the bone length information flow by making the difference between the two nodes, as shown in the formula (3).

$$H_{x,y,n} = Q_{y,n} - Q_{x,n} = (i_{y,n} - i_{x,n}, j_{y,n} - j_{x,n}). \quad (3)$$

Joint Difference Information Flow: the coordinates of the joint point x of the n th frame are defined as $(Q_{x,n} = (i_{x,n}, j_{x,n}))$, and the coordinates of the joint point x

of the $(n+1)$ -th frame are expressed as $(Q_{x,n+1} = (i_{x,n+1}, j_{x,n+1}))$. The joint difference information Fflow can be obtained by making a difference between the coordinates of the same joint point in adjacent frames, and the formula is shown in formula (4).

$$YD_{x,n,n+1} = Q_{x,n+1} - Q_{x,n} = (i_{x,n+1} - i_{x,n}, j_{x,n+1} - j_{x,n}). \quad (4)$$

Change of Bone Length Information Flow: in two adjacent frames, the same section of the bone due to the action changes caused by the different lengths, defined by the formula (3) the n th frame of the bone length information flow is $H_{x,y,n}$, then the $(n+1)$ th frame of the bone length information flow is $H_{x,y,n+1}$, by the same bone length of adjacent frames for the difference to obtain the bone length change information flow. The formula is shown in formula (5).

$$CH_{x,n,n+1} = H_{x,y,n+1} - H_{x,y,n}. \quad (5)$$

As shown in Figure 2, the multiple data streams are weighted and fused into a single feature vector according to the definitions of articulation point information stream, bone length information stream, articulation point offset information stream, and bone length change information stream. The skeleton sequence dimension is changed from $(4 \times N \times Y \times C_1)Q$ to $1 \times N \times Y \times 4C_1$ as shown below.

$$\text{Fusion} = \{ \omega_1 Q_{x,n} + \omega_2 H_{x,y,n} + \omega_3 YD_{x,n,n+1} + \omega_4 CH_{x,n,n+1}, x = 1, 2, \dots, T; n = 1, 2, \dots, N \}, \quad (6)$$

where the weight $\omega_1 \sim \omega_4$ is determined by the joint point offset degree ($\sigma_1 (\sigma_1 \in [0^\circ \sim 360^\circ])$) and the bone length change degree ($\sigma_2 (\sigma_2 \in [0 \sim 100\%])$). σ_1 is the angle of the line formed by the coordinate point $Q_{x,n}$ in the previous frame and the coordinate point $Q_{x,n+1}$ in the next frame and the coordinate origin, respectively, and σ_2 is defined as formula (7).

$$\sigma_2 = \frac{|Q_{y,n+1} - Q_{x,n+1}| - |Q_{y,n} - Q_{x,n}|}{|Q_{y,n} - Q_{x,n}|}, \quad (7)$$

where the absolute value operation represents the bone length, when $\sigma_1 \geq 30^\circ$ and $\sigma_2 \leq 50\%$, ω_1 and ω_3 weights are 2, ω_2 and ω_4 weights are 1.

When $\sigma_1 \leq 30^\circ$ and $\sigma_2 \geq 50\%$, the weights of ω_1 and ω_3 are 1, and the weights of ω_2 and ω_4 are 2. When σ_1 and σ_2 are less than the threshold, the weights are 1. When both σ_1 and σ_2 are greater than the threshold, the weights are 2. By calculating the offset degree of joint points and the change

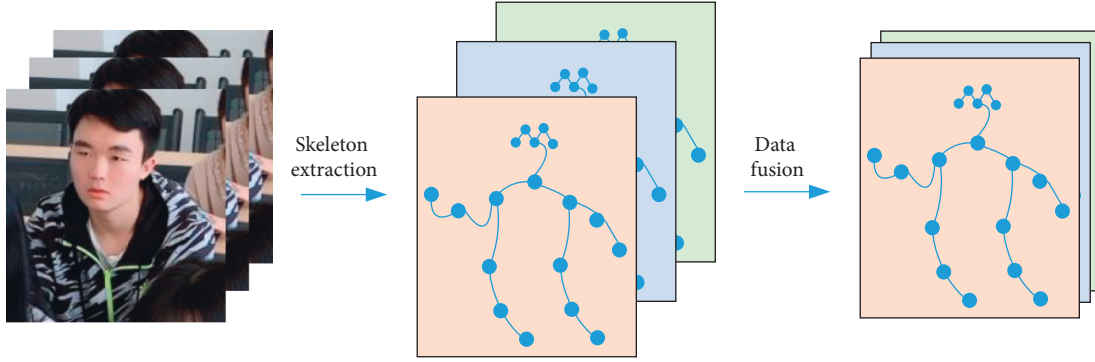


FIGURE 2: Data fusion of information flow.

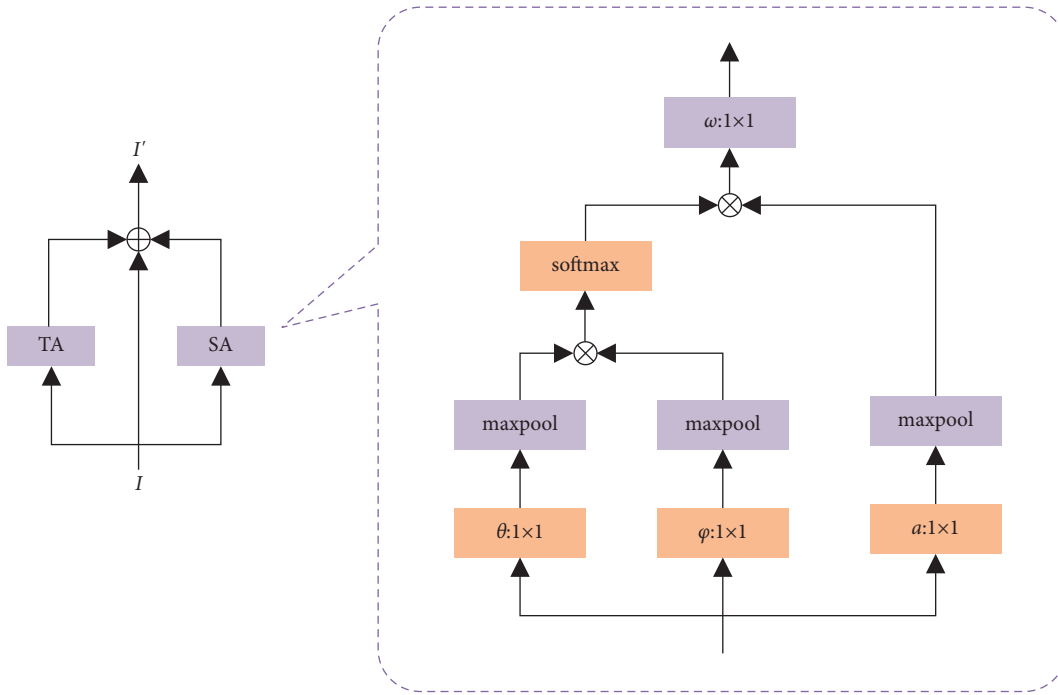


FIGURE 3: Spatio-temporal attention module.

degree of bone length, higher weight is given to the information flow data with large change degree, so as to enhance the representation of action by information flow. Then the fused single feature vector is used to represent the multi information flow data, and the training times are reduced from 4 times to 1 time, which reduces the amount of overall parameters, so as to improve the network operation speed.

2.1.4. Temporal Attention Module Construction. It is also important to ensure the accuracy of action recognition on the basis of the increased speed of network computing. A human skeleton sequence contains all information in the temporal and spatial domains, but only the nodal association information that is discriminative for some of the actions is worthy of attention. The attention mechanism mostly just removes irrelevant terms and focuses on the action region of interest, and the real redundant information comes from other aspects.

The joint point with offset degree $\sigma_1 \geq 30^\circ$ of each joint point is defined as the source joint point, and one source joint point is selected at a time, while the other joint points are the target joint points. The local operation method in the neural network can only calculate the correlation between two individually after traversing the target nodes, so that the source nodes lose the global characterization ability. In order to characterize the correlation of all target nodes to source nodes, as shown in Figure 3. The idea of nonlocal operations is incorporated into the spatiotemporal attention module, and a max pool layer of size 2×2 and step size 2 is added after the feature input to ensure that the number of data and parameters are compressed while preserving the original features as much as possible.

The spatiotemporal attention module (STA) contains a spatial attention module and a temporal attention module. The spatial attention module (SA) captures the intraframe joint correlation, and the temporal attention module (TA) captures the interframe joint correlation, and finally the two

are summed and fused with the input features. The output features of the temporal attention module have the same dimension as the input, and thus can be embedded between the network structures of the graph convolutional network.

The implementation of the module features is divided into 4 steps.

- (1) The dimension of the infeed feature I is $N \times T \times C$, where T, N , and C correspond to the number of frames, joints, and channels, respectively. The input features of the spatial attention module are represented as $k = [k_1^s, k_2^s, \dots, k_T^s] \in R^{N \times T \times C}$.
- (2) Embedding the features into the Gaussian function (θ and φ , convolution kernel dimension 1×1) calculates the correlation of two joints i and j at any position, enumerated by j , and obtains the weighting of the joints i , represented as shown below.

$$j_x^s = \frac{1}{C(k^s)} \sum_{qy} f(k_x^s, k_y^s) a(k_y^s), \quad (8)$$

where k_x^s and k_y^s denote the features of the nodes x and y , respectively. The function a is used to calculate the feature representation of the node y , and ($a(k_y^s) = M_a^s k_y^s$) M_a^s is the weight matrix to be learned. The Gaussian function f is defined as shown below.

$$f(k_x^s, k_y^s) = e^{\theta(k_x^s) \varphi(k_y^s)}. \quad (9)$$

Where ($\theta(k_x^s) = M_\theta^s k_x^s$, $\varphi(k_y^s) = M_\varphi^s k_y^s$), ($C(k^s) = \sum_{qy} f(k_x^s, k_y^s)$) is set as the normalization factor of the correlation representation. In order to reduce the computational cost and maximize the retention of low-order features, a maximum pooling layer of size 2×2 and step size 2 is added after the functions θ , φ , and a .

- (3) The spatial attention information o_x^s ($o_x^s \in R^{N \times T \times C}$) is obtained by making the function weighted.

$$o_x^s = M_o^s j_x^s. \quad (10)$$

- (4) Denote the infant features of the temporal attention module as $k^n = [k_1^n, k_2^n, \dots, k_T^n] \in R^{N \times T \times C}$. The temporal attention information o_x^n ($o_x^n \in R^{N \times T \times C}$) is obtained by repeating (2) and (3), and the temporal attention information o_x ($o_x \in R^{N \times T \times C}$) is obtained by adding and fusing with the spatial attention information and the infant features.

$$o_x = o_x^s + o_x^n + k_x. \quad (11)$$

The discriminative spatiotemporal association information of the nodes is obtained by the attention mechanism based on nonlocal operations, and the interference of irrelevant terms in the action region and the input redundant node information is removed, which reduces unnecessary calculations and thus improves the accuracy.

2.1.5. Spatio-Temporal Feature Extraction Module Construction. In order to extract the features of the skeleton sequence in spatial and temporal dimensions, the dynamic skeleton is first modeled using the spatiotemporal graph convolutional network and a spatial partitioning strategy, and the original expression is shown below.

$$I_{\text{out}} = \sum_x^Z M_x (I_{xt} G_x) \odot W_x, \quad (12)$$

where I_{in} and I_{out} are the graph convolutional input and output features, respectively, Z is the spatial domain convolutional kernel size, M_x is the weight, G_x is the adjacency matrix of node x , \odot represents the dot product, and W_x is the mapping matrix of nodes given connection weights.

Since all mnemonic actions cannot be accurately identified using predefined skeleton structure data, an adaptive adjacency matrix G_x is needed to make the graph convolutional network model adaptive. Therefore, in order to change the topology of the skeleton sequence graph in network learning, the adjacency and mapping matrices that determine the topology in formula (12) are divided into (G_x, B_x) and L_x . The block diagram of the adaptive graph convolution module is shown in Figure 4, and the output features are reconstructed as shown below.

$$I_{\text{out}} = \sum_x^z M_x I_{xt} (G_x + B_x + L_x). \quad (13)$$

In Figure 4, θ and φ are the Gaussian embedding functions in formula (9), and the convolution kernel size is 1×1 . The first part G_x is still the adjacency matrix of the node x . The second part B_x is an additive complement to the original adjacency matrix, which can be updated iteratively through network training. The third part L_x is continuously driven by the data to learn the connection weights, and the node correlation can be calculated by formula (8) and then multiplied with the 1×1 convolution to obtain the similarity matrix L_x .

$$L_x = \text{soft max}(I_{xt}^N M_{\theta x}^N M_{\varphi x} I_{xt}). \quad (14)$$

Through the above calculation, the adaptive graph convolution module is constructed, and then the spatiotemporal information contained in the skeleton sequence is extracted.

The spatiotemporal feature extraction module proposed in this paper is shown in Figure 5. The data are normalized by BN (batch normalization) layer after each convolution operation, and then the model expression capability is improved by ReLU layer. The embeddable spatiotemporal attention module STA has been built in Section 2.1.1, and the features are input to the extraction module to extract the action nodes of interest. Then, the correlation of each joint point of the same frame in the skeleton data is obtained in the spatial dimension by the adaptive GCN, and the relationship of the same joint point of adjacent frames is obtained in the temporal dimension by the temporal convolutional network (TCN). The dropout layer reduces the interaction of hidden layer nodes to avoid overfitting of

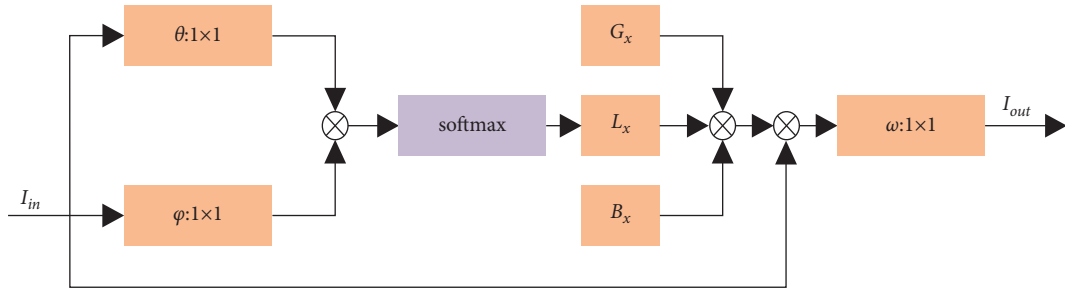


FIGURE 4: Adaptive graph convolutional module.

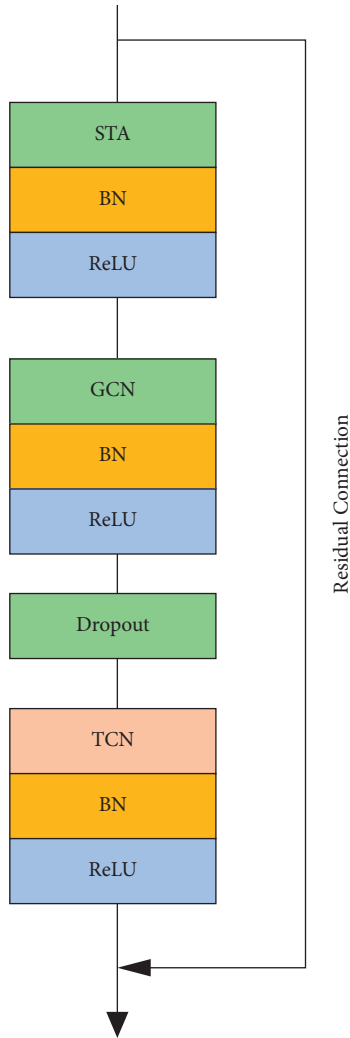


FIGURE 5: Spatiotemporal feature extracting module.

the graphical convolutional network, and the parameter is set to 0.5, while the residual connection is performed to increase the stability of the model.

2.1.6. Overall Network Structure Construction. As shown in Figure 6, the nine spatiotemporal feature extraction modules B1~B9 are stacked. In the direction from feature input I to behavior label output, BN layer is used for normalization after skeleton map input, B1~B3 output feature dimension is

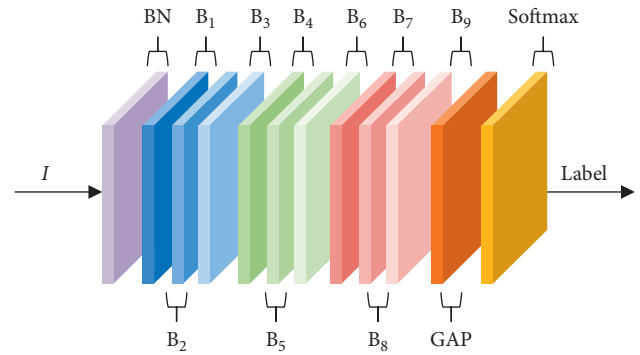


FIGURE 6: Overall network architecture.

Batch $\times 64 \times T \times N$, B4~B6 output feature dimension is Batch $\times 128 \times N/2 \times T$, B7~B9 output feature dimension is Batch $\times 256 \times N/4 \times T$, where the number of channels are 64. The global average pooling (GAP) operation is applied in the spatial and temporal dimensions to unify the feature map sizes of the samples, and finally the data from 0 to 1 are obtained using the Softmax layer for the recognition of human behavior.

2.2. Moral Education Evaluation System in Colleges and Universities

2.2.1. Database Design. In the design of moral education quality evaluation system for college students, the database system is an important material basis for carrying out the work related to comprehensive quality evaluation system for college students, and it plays an important role in the system design and application. Scientific design of database can provide efficient ways and technical support for data storage, avoid data redundancy, and also realize data integrity and unity. The corresponding system can be combined with the basic database structure to build an effective input interface and input format to ensure convenient and effective data input and build a complete basic database for comprehensive student quality evaluation.

2.2.2. System Software and Hardware Design. The hardware design of the moral quality evaluation system for students in colleges and universities should focus on the data collection terminal and data receiving terminal. The specific management software design is the core part of the whole fault

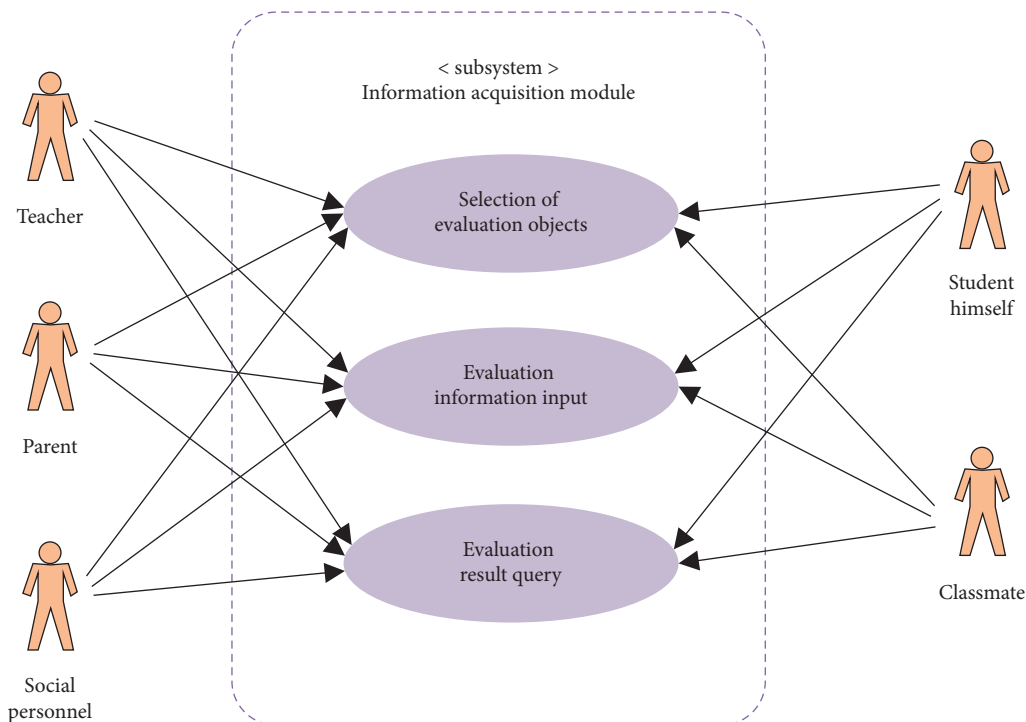


FIGURE 7: UML use case diagram for information acquisition module.

management system, which has a direct impact on the system being able to find the data source quickly and accurately in the data information management. In the software design, the data information management program is designed to achieve effective search of data sources, while the simulation program is used to simulate the parameter signals of large electromechanical integration equipment after docking between the management system and the integration equipment to achieve effective data extraction. In this regard, the management software design takes Windows 2000 as the basic software platform, with the help of VC for interface design, and stores the management mode related to the electronic control system through the database management of access to realize the effective system management program design. The sensor, MCU, AD chip, and other components constitute the data acquisition side. The receiving end is also connected by multiple asynchronous serial ports and also connected with LCD, chip, and other components. And the bus is connected to the wireless transmission module, whose function is equivalent to the terminal receiving device, which can transmit the signal to the control center with the help of antenna, and then transmit the received data information to the host location. In the system hardware design, focus on effective control system architecture and good wiring design. And in the system software design, it contains the data acquisition node, coordinator node, and the main controller design. Through the serial port to receive environmental information from the wireless network, do a good job of parsing and processing, and then save the relevant information and transmit it to the GPRS module to receive relevant control commands or other student quality information data with the help of the

TABLE 1: Compared with different algorithm on NTU RGB + D.

Algorithm	C-sub/%	C-view/%
Literature [23]	62.1	71.4
Literature [24]	70.9	79.5
Literature [25]	77.3	84.8
Literature [26]	81.7	86.2
Literature [27]	86.8	91.9
Proposed	90.5	96.5

TABLE 2: Compared with different algorithm on N-UCLA.

Algorithm	Top-1/%
Literature [23]	73.1
Literature [24]	77.2
Literature [25]	83.6
Literature [26]	89.1
Literature [27]	92.7
Proposed	95.5

serial port. The functional design of this system is shown in Figure 7.

3. Result Analysis and Discussion

3.1. Algorithm Performance Comparison. The model performance of this paper's model is compared with those of literature [23–27] on the NTU RGB + D and N-UCLA data sets, as listed in Tables 1 and 2. Also, Table 3 comparison results are presented visually in the form of bar graphs in Figures 8 and 9. The comparison shows that the proposed algorithm of this paper has the best performance.

TABLE 3: Classroom action recognition accuracy.

Action	Accuracy (%)
Sit down	97.4
Raise hands	98.7
Play phone	95.3
Check time	96.8
Drink water	93.5
Eat food	90.8
Pick up	98.2
Stand up	97.8
Write	82.6

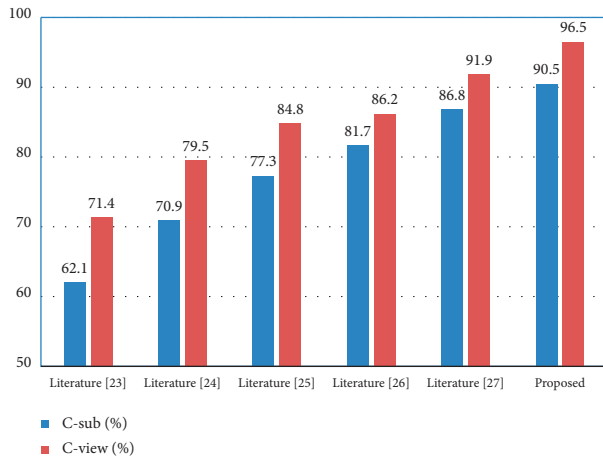


FIGURE 8: Compared with different algorithm on NTU RGB + D.

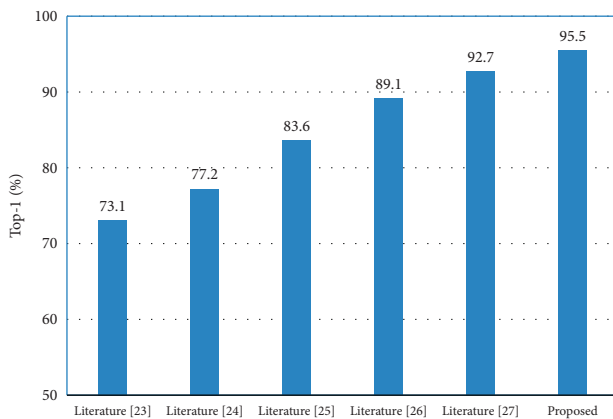


FIGURE 9: Compared with different algorithm on N-UCLA.

3.2. Analysis of Classroom Behavior Recognition Accuracy. Table 3 lists the classification accuracy rates of 10 types of behaviors commonly seen by teachers and students in the classroom when the model of this paper is used. It can be seen that the classification accuracy rates of most behaviors are over 90%, among which picking up actions and raising hands actions are more easily recognized accurately because of the larger magnitude of the whole body, reaching 98.2% and 98.7% recognition accuracy rates, respectively. For the offending actions (such as playing with the phone), a high recognition rate of 95.3% was also achieved. However, for the recognition of static actions such as writing, although it

did not reach the recognition accuracy of other actions, it still had 82.6% recognition accuracy.

4. Conclusion

The behavior recognition technology based on big data can effectively analyze the classroom behaviors of teachers and students, provide support for moral education evaluation in colleges and universities, and improve the efficiency and comprehensiveness of moral education evaluation in colleges and universities. In this paper, we propose a lightweight graph convolutional network combining multi-information flow data fusion and spatiotemporal attention mechanism to address the core problem in the field of moral education effect evaluation and student behavior analysis in colleges and universities, namely, the recognition speed and recognition rate of two types of algorithms for convolutional neural networks and graph convolutional networks are not high. By combining multi-information stream data fusion with adaptive graph convolution and also improving feature utilization by embedding spatiotemporal attention module, the performance of the model in this paper is optimal and also the recognition accuracy is improved substantially when tested and compared on NTU RGB + D and N-UCLA data sets. The design and improvement of this system can help universities to better carry out comprehensive student assessment and improve their human education. The follow-up work can make more improvements in two aspects: improving the accuracy of individual action recognition and continuing to propose a more lightweight model.

Data Availability

The labeled data set used to support the findings of this study is available from the author upon request.

Conflicts of Interest

The author declares that there are no conflicts of interest.

References

- [1] M. Chowdhury, "Emphasizing morals, values, ethics, and character education in science education and science teaching," *MOJES: Malaysian Online Journal of Educational Sciences*, vol. 4, no. 2, pp. 1–16, 2018.
- [2] H. Baharun, "Total moral quality: a new approach for character education in pesantren," *Ulumuna*, vol. 21, no. 1, pp. 57–80, 2017.
- [3] F. Zhang, "Quality-improving strategies of college English teaching based on microlesson and flipped classroom," *English Language Teaching*, vol. 10, no. 5, p. 243, 2017.
- [4] S. Liu, X. Bai, M. Fang, L. Li, and C. C. Hung, "Mixed graph convolution and residual transformation network for skeleton-based action recognition," *Applied Intelligence*, vol. 52, no. 2, pp. 1544–1555, 2022.
- [5] L. Meng and R. Li, "An attention-enhanced multi-scale and dual sign language recognition network based on a graph convolution network," *Sensors*, vol. 21, no. 4, Article ID 1120, 2021.

- [6] R. Guo, X. Shao, C. Zhang, and X. Qian, "Sparse adaptive graph convolutional network for leg agility assessment in Parkinson's disease," *IEEE Transactions on Neural Systems and Rehabilitation Engineering*, vol. 28, no. 12, pp. 2837–2848, 2020.
- [7] T. Hu, "Research on human behavior recognition based on deep learning convolutional neural network," *Public Communication of Science & Technology*, vol. 12, no. 6, pp. 130–131, 2020.
- [8] J. J. Q. Yu, C. Markos, and S. Zhang, "Long-term urban traffic speed prediction with deep learning on graphs," *IEEE Transactions on Intelligent Transportation Systems*, vol. 9, no. 20, pp. 1–12, 2021.
- [9] X. Shao, C. S. Kim, and P. Sontakke, "Accurate deep model for electricity consumption forecasting using multi-channel and multi-scale feature fusion CNN-lstm," *Energies*, vol. 13, no. 8, p. 1881, 2020.
- [10] H. Mohammadzade, S. Hosseini, M. R. Rezaei-Dastjerdehei, and M. Tabejamaat, "Dynamic time warping-based features with class-specific joint importance maps for action recognition using kinect depth sensor," *IEEE Sensors Journal*, vol. 21, no. 7, pp. 9300–9313, 2021.
- [11] K. Xu, H. Huang, Y. Li, and G. Shi, "Multilayer feature fusion network for scene classification in remote sensing," *IEEE Geoscience and Remote Sensing Letters*, vol. 17, no. 11, pp. 1894–1898, 2020.
- [12] Z. Yang, Y. Li, J. Yang, and J. Luo, "Action recognition with spatio-temporal visual attention on skeleton image sequences," *IEEE Transactions on Circuits and Systems for Video Technology*, vol. 29, no. 8, pp. 2405–2415, 2019.
- [13] W. Ullah, A. Ullah, T. Hussain, Z. A. Khan, and S. W. Baik, "An efficient anomaly recognition framework using an attention residual LSTM in surveillance videos," *Sensors*, vol. 21, no. 8, p. 2811, 2021.
- [14] A. U. Rehman, A. K. Malik, B. Raza, and W. Ali, "A hybrid CNN-lstm model for improving accuracy of movie reviews sentiment analysis," *Multimedia Tools and Applications*, vol. 78, no. 18, pp. 26597–26613, 2019.
- [15] M. C. Leong, D. K. Prasad, Y. T. Lee, and F. Lin, "Semi-CNN architecture for effective spatio-temporal learning in action recognition," *Applied Sciences*, vol. 10, no. 2, p. 557, 2020.
- [16] H. Zhang, Y. Li, Y. Zhang, and Q. Shen, "Spectral-spatial classification of hyperspectral imagery using a dual-channel convolutional neural network," *Remote sensing letters*, vol. 8, no. 5, pp. 438–447, 2017.
- [17] K. Zhang, D. Li, J. Huang, and Y. Chen, "Automated video behavior recognition of pigs using two-stream convolutional networks," *Sensors*, vol. 20, no. 4, p. 1085, 2020.
- [18] W. Zhou, Z. Chen, and W. Li, "Dual-stream interactive networks for No-reference stereoscopic image quality assessment," *IEEE Transactions on Image Processing*, vol. 28, no. 8, pp. 3946–3958, 2019.
- [19] S. Martin, S. Vora, K. Yuen, and M. M. Trivedi, "Dynamics of driver's gaze: explorations in behavior modeling and maneuver prediction," *IEEE Transactions on Intelligent Vehicles*, vol. 3, no. 2, pp. 141–150, 2018.
- [20] H. Jiang, Y. Pan, J. Zhang, and H. Yang, "Battlefield target aggregation behavior recognition model based on multi-scale feature fusion," *Symmetry*, vol. 11, no. 6, p. 761, 2019.
- [21] X. Zhang, C. Xu, X. Tian, and D. Tao, "Graph edge convolutional neural networks for skeleton-based action recognition," *IEEE Transactions on Neural Networks and Learning Systems*, vol. 31, no. 8, pp. 3047–3060, 2020.
- [22] S. Zhang, H. Tong, J. Xu, and R. Maciejewski, "Graph convolutional networks: a comprehensive review," *Computational Social Networks*, vol. 6, no. 1, p. 11, 2019.
- [23] J. Liu, A. Shahroudy, D. Xu, A. C. Kot, and G. Wang, "Skeleton-based action recognition using spatio-temporal LSTM network with trust gates," *IEEE Transactions on Pattern Analysis and Machine Intelligence*, vol. 40, no. 12, pp. 3007–3021, 2018.
- [24] W. Ratanavivan and R. J. Ricard, "Effects of a motivational interviewing-based counseling program on classroom behavior of children in a disciplinary alternative education program," *Journal of Counseling and Development*, vol. 96, no. 4, pp. 410–423, 2018.
- [25] V. Peltokorpi, "Host country national employees' prosocial behavior toward expatriates in foreign subsidiaries: a common ingroup identity model perspective," *International Business Review*, vol. 29, no. 2, Article ID 101642, 2020.
- [26] J. Guo, H. Liu, X. Li, D. Xu, and Y. Zhang, "An attention enhanced spatial-temporal graph convolutional LSTM network for action recognition in karate," *Applied Sciences*, vol. 11, no. 18, p. 8641, 2021.
- [27] P. F. Zhang, C. L. Lan, and J. L. Xing, "View adaptive neural networks for high performance skeleton-based human action recognition," *IEEE Transactions on Pattern Analysis and Machine Intelligence*, vol. 41, no. 8, 2018.

Research Article

Analysis of Strategies and Skills of English Translation Based on Coverage Mechanism

Bin Liu ^{1,2} and Jing Wang¹

¹School of Foreign Studies, Suqian University, Jiangsu, Suqian 223800, China

²College of Education, Taylor University, Subang Jaya 47500, Selangor, Malaysia

Correspondence should be addressed to Bin Liu; binliuandy@squ.edu.cn

Received 27 May 2022; Accepted 28 June 2022; Published 21 July 2022

Academic Editor: Le Sun

Copyright © 2022 Bin Liu and Jing Wang. This is an open access article distributed under the Creative Commons Attribution License, which permits unrestricted use, distribution, and reproduction in any medium, provided the original work is properly cited.

In order to alleviate the problem of over translation and missing translation in NMT, based on the consistency and complementarity of information stored in different covering models, a multicoverage fusion model is proposed, which uses coverage vector and coverage score to guide the attention mechanism at the same time. First, the concept level definitions of words are covered. Then, two kinds of translation history information stored in the cover vector and cover score are used to guide the calculation of the attention score at the same time. Finally, the dual attention decoding method based on the fusion coverage mechanism is adopted. The experimental results show that the multicoverage fusion model can improve the translation quality of NMT.

1. Introduction

Due to the diversity and complexity of natural languages, it is still difficult to translate one language properly into another. At present, neural machine translation (NMT) has shown great potential under the condition of large corpus and computational capacity and has developed into a new machine translation method [1, 2]. This method requires only bilingual parallel corpus, which is convenient for training large-scale translation models. It not only has high research value but also has a strong industrialization ability, which has become a hot spot in current machine translation research [3].

Neural machine translation based on encoder and decoder structure is a general model, which is not fully designed for the machine translation task itself, so there are still some problems to be solved. It requires bilingual dictionaries to be fixed in size. Considering the complexity of training, dictionary size, and sentence length are usually limited to a small range [4, 5]. As a result, NMT is faced with more severe problems of unknown words and long sentences. Only bilingual training data are used, and no

additional prior knowledge is required, such as large-scale monolingual corpus, annotated corpus, and bilingual dictionary. In addition, the structural characteristics of machine translation make it difficult to use external resources. Monolingual corpus, annotated corpus, bilingual dictionary, and other resources can significantly improve translation quality in statistical machine translation [6], but prior knowledge has not been fully applied overtranslation and inadequate translation are the problems of NMT. The overlay mechanism is a common method in statistical machine translation to ensure the integrity of the translation. It is difficult to directly model the covering mechanism in NMT [7]. The attention mechanism is a significant improvement on NMT, but its deficiency is that historical attention information is not taken into account in the generation of target language words, and the constraint mechanism is weak. In addition, in some cases, the generation of target language words does not need to pay too much attention to the source language information. For example, in Chinese-English translation, when the function word “The” is generated, more attention should be paid to the target language information. In addition, there are

problems of OverTranslation and UnderTranslation in NMT [8], and the existing attention mechanism also needs to be improved. Although the above-given methods can alleviate the problems of over translation and missing translation in NMT to a certain extent, due to the structural characteristics of a word for word prediction of the NMT model cannot be completely avoided.

Therefore, in this paper, firstly, the problems of existing coverage models and the possibility of fusion between different coverage models and the possibility of fusion between different methods are analyzed. Then, multiple coverage information fusion methods are used to record translation history information complementary to guide the calculation of attention weight, which can reduce the loss of historical information updating and improve the distribution of attention weight, so as to inhibition the phenomenon of over translation and missing translation.

2. Translation Model Based on Fusion of Multiple Coverage Strategies

2.1. Basic Ideas. The covering idea is proposed in the phrase based statistical machine translation model. In each decoding, all untranslated phrases and their translation results are added to the candidate set. Whenever a phrase translation result is added to the output sequence, the corresponding source language phrase should be marked as “translated,” which ensures that each source language phrase is covered by translation, and is not translated repeatedly.

Covering information is also very important for NMT. Due to the lack of a covering mechanism in the NMT model, it is an effective method to improve the over translation and missing translation problem by adding a covering mechanism to the NMT model.

Specifically, assuming that a sentence sequence of the source language $X = \{x_1, x_2, x_3, x_4, x_5\}$ is given, Its initial coverage set $C = \{0, 0, 0, 0, 0\}$. Among them, “0” indicates that the corresponding source language word has not been translated, while “1” indicates that the source language word has been covered by translation. In addition, assuming that the corresponding target phrase source language phrase $\{x_2, x_3, x_4\}$ is $\{y_m, \dots, y_n\}$, then after $\{y_m, \dots, y_n\}$ is added to the translation output sequence, the overlay set will be updated to $C = \{0, 1, 1, 1, 0\}$. If it is specified that a phrase can only be translated once in the process of translation, then follow this step to translate until the translation is completed, and the overlay set should be $C = \{1, 1, 1, 1, 1\}$. At this point, the phrase and the source language are effectively translated only once.

2.2. Coverage Model

2.2.1. Covering Vector. In the statistical machine translation model, all source language phrases can only be translated once, so its coverage mechanism is a hard alignment. However, the attention mechanism of the NMT model is a kind of soft alignment; that is, the words covered by attention are still allowed to participate in the prediction of the next word. Therefore, it is very difficult to model the

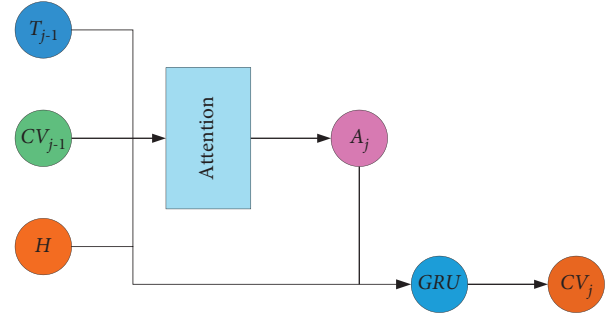


FIGURE 1: Structure of coverage-based attention model.

coverage mechanism directly [9]. In Literature [6], a covering model is proposed, in which a covering vector is set up to explicitly store the historical coverage information of each word in the source language sentence. In order to provide historical information for the translation process, the coverage vector is incorporated into the original attention mechanism model, where more attention is allocated to untranslated words and the weight of translated words is reduced. The structure of the coverage vector guided attention model is shown in Figure 1.

After fusing the covering vector, the calculation method of the attention mechanism is as follows:

$$\begin{aligned} e_{i,j} &= a(t_{j-1}, h_i, CV_{i,j-1}) \\ &= v_a^T \tan h(W_a t_{j-1} + U_a h_i + V_a CV_{i,j-1}). \end{aligned} \quad (1)$$

Among them, $CV_{i,j-1}$ represents the coverage vector corresponding to the source language word x_i before time j , and V_a is the weight matrix.

Since the history information changes after each step of decoding, the coverage vector of each source word needs to be updated. Its method is shown in the following equation:

$$CV_{i,j} = f(CV_{i,j-1}, a_{ij}, h_i, t_{j-1}), \quad (2)$$

where $F(\cdot)$ is a recurrent neural network whose basic neural unit can use only a simple tanh layer or GRU with a more complex structure to capture long-distance dependencies.

2.2.2. Coverage Score. It is used to indicate the degree of source language translation. If the translation results have high coverage of the source language words, the corresponding coverage score is also high; on the other hand, if the translation results have low coverage of the source language, the corresponding coverage score is also low. Suppose a sentence pair (X, Y) is given, the number of Chinese words in X and Y is expressed as $|X|$ and $|Y|$ separately. For any source language word x_i , its coverage is defined as all target words y_j . The sum of the attention scores of the words in the source language is shown in the following equation:

$$\text{coverage}_{x_i} = \sum_{j=1}^{|Y|} a_{ij}. \quad (3)$$

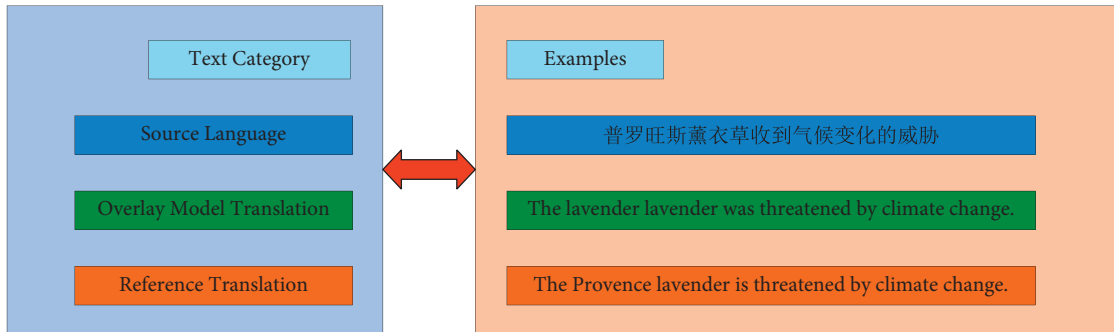


FIGURE 2: An example of NMT model translation based on covering vector.

On this basis, the coverage score of source language sentences is calculated by using the coverage of all source language words. The calculation method is shown in the following equation:

$$cs(X, Y) = \sum_{i=1}^{|X|} \log \varphi(\text{coverage}_{x_i}, \beta). \quad (4)$$

Among them, β is an adjustable parameter, $\varphi(\cdot)$ is truncation function. The coverage score is linearly combined with the original conditional probability function of the model to obtain the final evaluation function. The improved evaluation function is shown in the following equation:

$$\text{score}(X, Y) = a \cdot \log P(Y|X) + b \cdot cs(X, Y). \quad (5)$$

Among them, $\log P(Y|X)$ represents the value of conditional probability predicted by the model, a and b represent an adjustable parameter used to balance the effect of conditional probability and coverage score. The introduction of the coverage score makes the model consider the coverage of source language sentences and reduce the bias of translation results of a short sentence.

2.3. Translation Model Based on Multiple Coverage Strategies

2.3.1. Problem Description. Although the NMT model based on covering vector can alleviate the phenomenon of over translation and missing translation, this problem still exists. As shown in Figure 2, “Lavender” in the original text has been translated twice, while “Provence” has been omitted. When the first lavender is generated, the Coverage vector based NMT model mistakenly allocates more attention to lavender than Provence, which results in repeated translation and missing translation.

From the above-given examples, it can be seen that the NMT model based on covering vector still has further improvement space in attention allocation. As mentioned above, both coverage vector and coverage score can record the coverage information in the translation process in an explicit way. In the decoding stage, the former stores and updates the information abstractly in the form of a vector, calculate and guide the translation of attention through history; the latter is accumulated in the form of constant and used as the coverage of translation results for the selection of

translation results. Compared with the coverage score, the coverage vector cannot directly quantify the coverage of translation results, and there is information loss when using GRU update; while it is difficult to determine the upper and lower limits of the coverage of each source language vocabulary with a fixed value, so it is impossible to compare the coverage between words.

2.3.2. Model Decoding. Coverage vector and coverage score are complementary in the storage of coverage information. In order to combine the advantages of the two methods, this paper proposes a multicoverage fusion model which combines the coverage vector and the coverage score. The coverage score is used to reduce the impact of information loss when the coverage vector is updated, and improve the distribution of attention weight. The concept of word level coverage score is defined first. Then, according to the different fusion methods of coverage vector and coverage score, two kinds of multicoverage fusion models, hierarchical and parallel, are proposed. The overall framework is shown in Figure 3.

The coverage vector and the updated attention vector of each target word in the predicted sentence are obtained through the coverage mechanism layer. The coverage mechanism is shown in Figure 4.

During decoding, the attention weight vector α_t^{src} of text is obtained from the hidden state s_{t-1} at the previous moment, the hidden state sequence H of the source language through the double attention mechanism layer. The key point of the coverage mechanism layer is to maintain a coverage vector C_t in the prediction project. It is the accumulative sum of attention distribution of all previous prediction steps, which records the historical information that the model has paid attention to and avoids focusing on repetitive information, as shown in the following equation:

$$C_t^{\text{src}} = \sum_{\hat{t}=0}^{t-1} \alpha_{\hat{t}}^{\text{src}}. \quad (6)$$

The obtained coverage vector is applied to the attention layer to obtain the updated attention weight, as shown in equations (7) and (8).

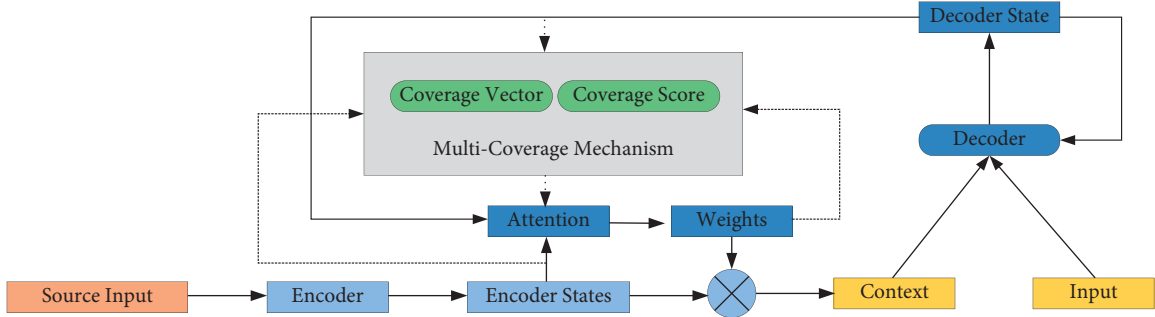


FIGURE 3: NMT model based on multicoverage.

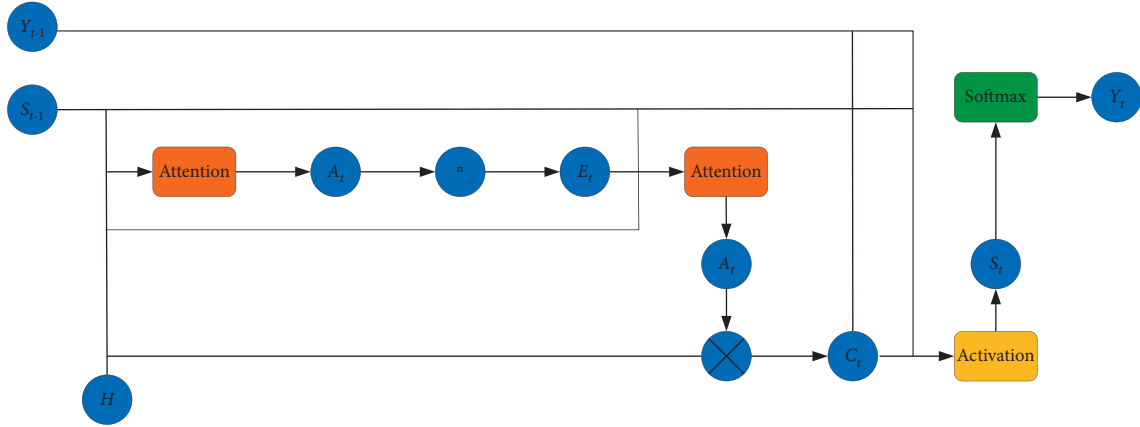


FIGURE 4: Coverage mechanism.

$$e_{t,i}^{\text{src}} = (v_a^{\text{src}})^T \tan h(U_a^{\text{src}} s_t + W_a^{\text{src}} h_i + V_a^{\text{src}} c_{t,i}^{\text{src}}). \quad (7)$$

$$\alpha_{t,i}^{\text{src}} = \frac{\exp(e_{t,i}^{\text{src}})}{\sum_{j=1}^N \exp(e_{t,j}^{\text{src}})}. \quad (8)$$

Among them, $\tan h$ is the nonlinear activation function, $v_a^{\text{src}}, U_a^{\text{src}}, W_a^{\text{src}}$ are the parameters used for learning in the model. The weight $e_{t,i}^{\text{src}}$ can be interpreted as the correlation between the target word generated by the decoder and the source sequence word x_i at t . $\alpha_{t,i}^{\text{src}}$ represents the normalization of the obtained similarity score.

The coverage vector is added as an additional input to affect the prediction of the target language. Then, get the updated context attention vector c_t . The text attention vector c_t at time t is obtained by the weighted sum of the source language implicit state sequence h_i and the weight $\alpha_{t,i}^{\text{src}}$ obtained by the text attention model, as shown in the following equation:

$$c_t = \sum_{i=1}^N \alpha_{t,i}^{\text{src}} h_i. \quad (9)$$

With the updated i_t as the additional input, the candidate implicit state s'_t is used, and the source language attention vector c_t calculates the final implicit state s_t at time t , as shown in equations (10)–(13).

$$z_t = \sigma(W_z^{\text{src}} c_t + U_z s'_t), \quad (10)$$

$$r_t = \sigma(W_r^{\text{src}} c_t + U_r s'_t), \quad (11)$$

$$\underline{s}_t = \tan h(W^{\text{src}} c_t + r_t \odot (U s'_t)), \quad (12)$$

$$s_t = (1 - z_t) \odot \underline{s}_t + z_t \odot s'_t, \quad (13)$$

where z_t is the renewal gate, r_t is the reset gate, \underline{s}_t is the candidate hidden state, s_t is the final hidden state, $W_z^{\text{src}}, U_z, W_r^{\text{src}}, U_r, W^{\text{src}}, U$ is the parameter used for learning in the model.

Finally, output the model, the prediction of the target word y_t at the t moment is related to the implicit state s_t of the target word at the current moment, the target word y_{t-1} generated by the prediction at the previous moment, and the text attention vector c_t , as shown in the following equation:

$$P(y_t | y_{<t}, C, A) = \text{softmax}(f(s_t, y_{t-1}, c_t, i_t)) \propto, \quad (14)$$

$$\exp(L_o \tanh(L_s s_t + L_w E_y[y_{t-1}] + L_o c_t + L_c i_t)),$$

where f and softmax are nonlinear activation functions, and $L_o, L_s, L_w, L_c, L_{ci}$ are parameters used by the model for learning.

3. Experiment and Analysis

3.1. Evaluation Method. BLEU (Bilingual Evaluation Understudy) algorithm evaluates translation performance by calculating the n-element words co-occurring in the translation result and the translation [10]. Firstly, MaxRefCount (n-gram) is calculated as the maximum number of possible occurrences of an n-word in a sentence. Then, it is compared with the number of occurrences of this n-word in the candidate translation, Count(n-gram), and the minimum value between them is taken as the final number of matches of this n-word. As shown in the following equation:

$$\begin{aligned} \text{Count}_{\text{clip}}(n\text{-gram}) \\ = \min\{\text{Count}(n\text{-gram}), \text{MaxRefCount}(n\text{-gram})\}. \end{aligned} \quad (15)$$

And, then the precision P_n of the later co-occurrence n-element words is defined as follows:

$$P_n = \frac{\sum_{c \in \text{candidates}} \sum_{n\text{-gram} \in C} \text{Count}_{\text{clip}}(n\text{-gram})}{\sum_{C \in \text{candidates}} \sum_{n\text{-gram} \in C} \text{Count}(n\text{-gram})}. \quad (16)$$

Since n-gram's matching degree tends to choose shorter sentences, a translation result that only translates part of the original sentence accurately will still have a high matching degree, BLEU introduces Brevity Penalty into the final scoring result to avoid the bias of scoring, as shown in the following equation:

$$\text{BP} = \begin{cases} 1, & \text{if } l_c > l_s, \\ e^{1-l_s}, & \text{if } l_c \leq l_s, \end{cases} \quad (17)$$

where l_c represents the length of the translation result, and l_s represents the length of the reference translation. When there are multiple references, the length closest to the translation result is selected as the length of the reference. It can be found that only when the length of the interpretation result is not exactly the length of the reference text will the punishment factor be presented.

BLEU usually only considers the accuracy of 4-GRAM at most, since the accuracy of n-gram statistics decreases exponentially with the increase of order. In order to balance the effect of statistics of each order, a geometric average is used for weighted summation, and then the length penalty factor is multiplied to obtain the final calculation formula as shown in the following equation:

$$\text{BLEU} = \text{BP} \times \exp\left(\sum_{n=1}^N W_n \log P_n\right), \quad (18)$$

where N is the maximum order of n-element words, W_n is the weight coefficient, $N=4$, $W_n=1/N$.

3.2. Parameter Setting. About 6.5 million sentence pairs were extracted from the bilingual parallel corpus provided by CWMT2018. Using newsdev2017 as a validation set for

parameter tuning and model selection that a total of 2002 sentences are included. Three datasets, newstest2017, cwmt2018, and newstest2018, were selected as test sets to verify the model, each containing 2000, 2481, and 3981 sentences. Before training and testing, the corpus is generalized, the word segmentation of the Chinese and English corpus is carried out by using the open-source tool of NiuTrans, and the subword segmentation is carried out by using byte pair encoding.

The baseline system uses seq2seq, and the settings of the model are displayed in Table 1. The initial learning rate is set to 0.0001. In decoding, the beam search algorithm is adopted, and the length penalty, beam size, and length penalty coefficient are introduced and set to 15 and 1.3, respectively. 350000 steps were trained iteratively on the training set, and the 15 checkpoints with the highest BLEU are saved in the verification set for model testing. The coverage model based on the coverage vector is set up as the control. The coverage vector dimension is set to 10 and the GRU gate function is used to update. In the hierarchical multicoverage model, the balance coefficient is set to 0.5.

3.3. Result Analysis. During training, the 15 models with the highest BLEU were saved on the verification set corpus. In the test, the parameters are averaged first, and the final translation is generated on this basis. The specific experimental results are shown in Figure 5.

According to the experimental results in Figure 5, the average BLEU value of the baseline system on three test sets is 26.78%. On the basis of the baseline system, the coverage model has little improvement, and BLEU is only increased by 0.15%. The results of the two multicoverage fusion models are significantly improved compared with the baseline system and are better than the coverage model. The average BLEU of the HMC model was 27.43%. Compared with the baseline system and coverage model, BLEU increased by 0.65% and 0.5%, respectively; while the average BLEU value of the PMC model is 27.21%, which is 0.43% and 0.28% higher than the baseline system and coverage model, respectively. Compared with the two multicoverage models, the overall promotion effect of the HMC model is more obvious.

The interpretation impact of long sentences is one of the significant records to assess the exhibition of the NMT model. In order to research on the performance of the multicoverage fusion model in different source language sentence length intervals, the source dialects in the test set were assembled by the strategy for Reference [6], and the BLEU of the HMC model was compared with the baseline system and coverage model in the range of translation results on source language length (0, 10], (10, 20], (20, 30], (30, 40], (40, 50] and (50, +∞). The results are shown in Figure 6.

The performance of the HMC model is better than the baseline system and coverage model. Compared with baseline system, BLEU increased by 0.47%, 0.65%, 0.48%, and 0.79%, respectively, and on the basis of coverage model, it increased 0.22%, 0.55%, 0.44%, and 0.63%, respectively. Through the analysis of the corpus, it can be found that this

TABLE 1: Parameters setting.

Parameter	Value
Neural network cell unit	LSTMCell
Encoder layers	2
Decoder layers	4
Dimension vector words	512
Hidden layer state dimension	512
Vocab	32 k
Batch_size	32
Max_length	50

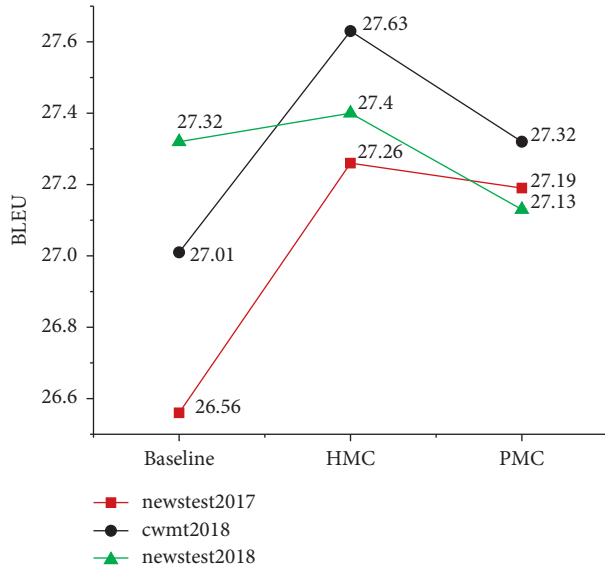


FIGURE 5: BLEU of translation.

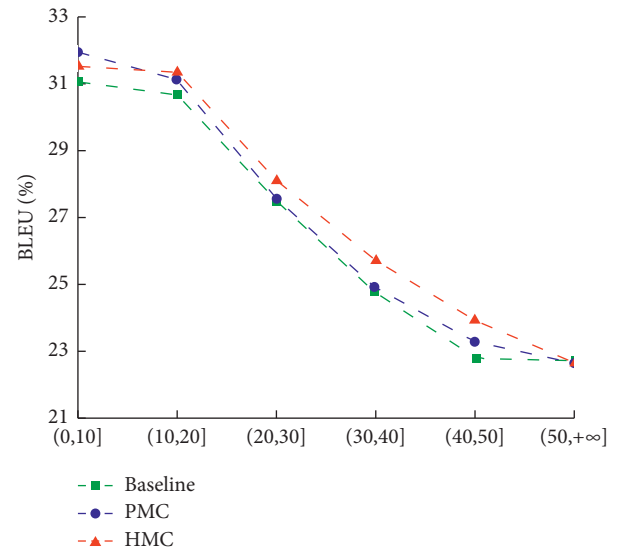


FIGURE 6: BLEU under different source language length.

length interval contains many fragments of long sentences after segmentation. The structure and meaning of these sentences are not complete enough, so the translation performance of the model is affected to a certain extent.

As shown in Figure 7, there are over translation problems in the Baseline system, Coverage model and HMC model, but the number of words in the translation of the coverage model and HMC model is less than that of the baseline system. Among them, the coverage model is 13.5% less than the baseline system, and the HMC model is further reduced by 10.5% on the basis of the coverage model, which shows that the HMC model can further alleviate the over translation problem in NMT on the basis of covering model.

In Figure 2, because the source language word “普罗旺斯 Provence” wrongly establishes a corresponding relationship with “薰衣草Lavender,” which makes the word “薰衣草Lavender” appears in repeated translation. This problem is corrected in the HMC model, as shown in Figure 8. HMC model correctly translates “普罗旺斯薰衣草” into “Provence Lavender.”

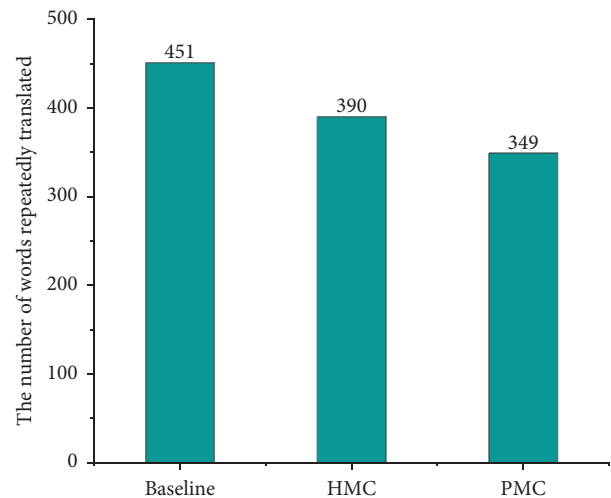


FIGURE 7: Evaluation of repeated translation.

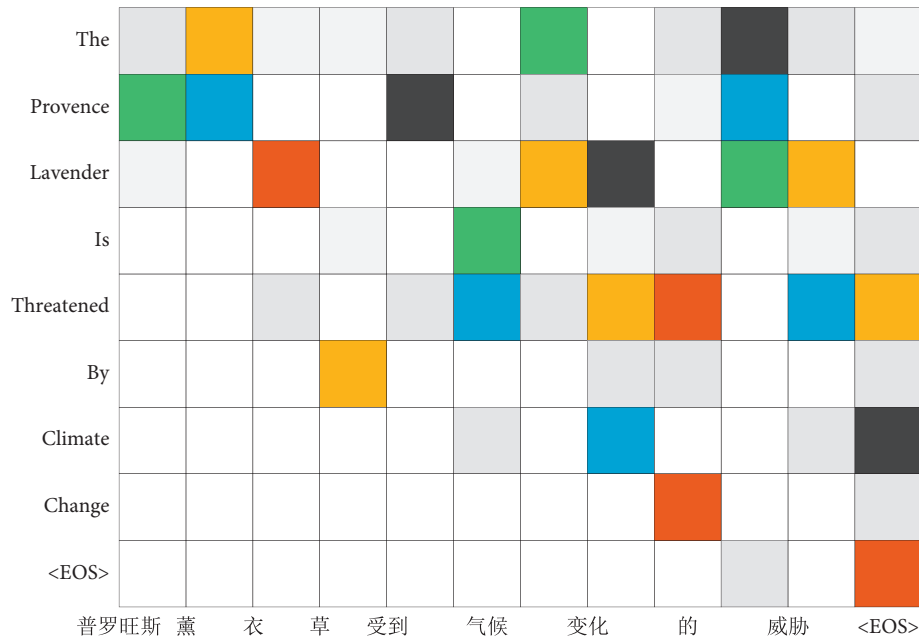


FIGURE 8: Solution of over translation problem.

4. Conclusion

Introducing coverage mechanism into the NMT model can alleviate the over translation and missing translation problems. However, the coverage information stored by the covering vector or coverage score is not perfect. Therefore, this paper discusses the information storage, usage, advantages, and disadvantages of different coverage models, and based on the consistency of translation history information and the complementarity between models, a multicoverage fusion model is proposed. Firstly, the concept of word level covering score is defined; Then, the information stored in the coverage score and coverage vector is used to guide the calculation of attention weight. According to the different fusion methods of coverage vector and coverage score, two methods, hierarchical multicoverage model and parallel multicoverage model, are proposed. The experimental results show that compared with the PMC model, the overall promotion effect of the HMC model is more obvious, and the multicoverage fusion method can further reduce the phenomenon of over translation and omission translation.

Data Availability

The dataset can be accessed from the corresponding author upon request.

Conflicts of Interest

The authors declare that there are no conflicts of interest.

References

- [1] W. Gao, Yaosong Li, D. Li, Z. Chen, and Z. Meng, "Machine translation based on bidirectional codec," *Computer engineering and design*, vol. 42, no. 05, pp. 1479–1484, 2021, in Chinese.
- [2] D. Xu, J. Li, and Z. Gong, "Semantic learning analysis based on NMT encoder," *Chinese Journal of information*, vol. 35, no. 03, pp. 60–68+77, 2021, in Chinese.
- [3] M. Zheng, "Research on Intelligent English translation method based on improved attention mechanism model," *Electronic Technology*, vol. 33, no. 11, pp. 84–87, 2020, in Chinese.
- [4] X. Zhou, Z. Zhang, and J. Wen, "Natural language information hiding based on neural network machine translation," *Computer science*, vol. 48, no. S2, pp. 557–564 + 584, 2021, in Chinese.
- [5] R. Wang, "Analysis of English grammar error correction methods based on NMT," *Automation technology and application*, vol. 40, no. 08, pp. 57–60 + 74, 2021, in Chinese.
- [6] R. Dabre, C. Chu, and A. Kunchukuttan, "A Survey of Multilingual Neural Machine Translation," *ACM Computing Surveys*, vol. 53, no. 5, pp. 1–38, 2020.
- [7] Li Qiang, Y. Han, and X. Tong, "etc. Data generalization and phrase generation in NMT," *Chinese Journal of information technology*, vol. 32, no. 08, pp. 42–52, 2018, in Chinese.
- [8] H. T. Mi, B. Sankaran, Z. G. Wang, and A. Ittycheriah, "Coverage Embedding Models for NMT," in *Proceedings of the 2016 Conference on Empirical Methods in Natural Language Processing*, pp. 955–960, Association for Computational Linguistics, Austin Texas, November 2016.
- [9] Z. Li, S. Zhang, Y. Hong, W. Zhenkai, and J. Yao, "Multimodal NMT with covering mechanism," *Chinese Journal of information technology*, vol. 34, no. 03, pp. 44–55, 2020, in Chinese.
- [10] W. Guo and F. Hu, "Translation evaluation and post editing of NMT," *Journal of Beijing Institute of foreign studies*, vol. 43, no. 05, pp. 66–82, 2021, in Chinese.

[1] W. Gao, yaosong Li, D. Li, Z. Chen, and Z. Meng, "Machine translation based on bidirectional codec," *Computer*

Retraction

Retracted: Construction and Analysis of Performance Evaluation Index System for Chinese Small and Medium-Sized Enterprises Based on Fuzzy Hierarchical Analysis Model

Computational Intelligence and Neuroscience

Received 25 July 2023; Accepted 25 July 2023; Published 26 July 2023

Copyright © 2023 Computational Intelligence and Neuroscience. This is an open access article distributed under the Creative Commons Attribution License, which permits unrestricted use, distribution, and reproduction in any medium, provided the original work is properly cited.

This article has been retracted by Hindawi following an investigation undertaken by the publisher [1]. This investigation has uncovered evidence of one or more of the following indicators of systematic manipulation of the publication process:

- (1) Discrepancies in scope
- (2) Discrepancies in the description of the research reported
- (3) Discrepancies between the availability of data and the research described
- (4) Inappropriate citations
- (5) Incoherent, meaningless and/or irrelevant content included in the article
- (6) Peer-review manipulation

The presence of these indicators undermines our confidence in the integrity of the article's content and we cannot, therefore, vouch for its reliability. Please note that this notice is intended solely to alert readers that the content of this article is unreliable. We have not investigated whether authors were aware of or involved in the systematic manipulation of the publication process.

Wiley and Hindawi regrets that the usual quality checks did not identify these issues before publication and have since put additional measures in place to safeguard research integrity.

We wish to credit our own Research Integrity and Research Publishing teams and anonymous and named external researchers and research integrity experts for contributing to this investigation.

The corresponding author, as the representative of all authors, has been given the opportunity to register their agreement or disagreement to this retraction. We have kept a record of any response received.

References

- [1] M. He and R. P. Estebanez, "Construction and Analysis of Performance Evaluation Index System for Chinese Small and Medium-Sized Enterprises Based on Fuzzy Hierarchical Analysis Model," *Computational Intelligence and Neuroscience*, vol. 2022, Article ID 1230786, 8 pages, 2022.

Research Article

Construction and Analysis of Performance Evaluation Index System for Chinese Small and Medium-Sized Enterprises Based on Fuzzy Hierarchical Analysis Model

Mengning He  and Raquel Pérez Estebanez

Facultad de Ciencias Economicas y Empresariales, Universidad Complutense Madrid, Madrid 28040, Spain

Correspondence should be addressed to Mengning He; mhe01@ucm.es

Received 10 May 2022; Accepted 25 June 2022; Published 21 July 2022

Academic Editor: Le Sun

Copyright © 2022 Mengning He and Raquel Pérez Estebanez. This is an open access article distributed under the Creative Commons Attribution License, which permits unrestricted use, distribution, and reproduction in any medium, provided the original work is properly cited.

It is of great theoretical and practical significance to introduce the supply chain concept into micro and small manufacturing enterprises and to build a cost management evaluation model for micro and small manufacturing enterprises based on the supply chain to improve the cost management of micro and small manufacturing enterprises. To this end, based on combing the relevant literature on supply chain and cost management evaluation at home and abroad, this paper analyzes the characteristics of cost management of micro and small manufacturing enterprises because of the problems of cost management of micro and small manufacturing enterprises, adopts the gray fuzzy hierarchical analysis method to assign and evaluate, which takes into account the nonindependence among the elements of each level and the elements of the same level, and also considers the characteristics of grayness and fuzziness of qualitative indicators so that the evaluation results are more credible. The evaluation of cost management of micro and small manufacturing enterprises based on the supply chain was carried out by using gray fuzzy analysis, and the empirical analysis was based on the research data of company B. The evaluation result was “poor,” which verified the applicability of the cost management performance evaluation model of micro and small manufacturing enterprises and indicated the direction for the improvement of cost management of micro and small manufacturing enterprises. And, the proposed intuitionistic fuzzy hierarchical analysis has greater advantages in evaluation accuracy than the traditional fuzzy hierarchical analysis.

1. Introduction

In the context of economic globalization, the competition among enterprises is becoming increasingly fierce. Large and medium-sized manufacturing enterprises can obtain a place for the development and growth of their companies with the advantages of strong capital, advanced technology level, and good reputation [1]. However, SMEs, especially small and micromanufacturing enterprises, are facing a severe test due to factors such as continuous interest rate increase of RMB, rising labor costs, continuous escalation of raw material prices, and difficulties in financing [2].

Facing various difficulties such as difficult survival, high cost, and low profit, the development of small and micro-manufacturing enterprises is seriously restricted. Although

small and micromanufacturing enterprises attach great importance to cost management, the actual effect is not good [3]. The reason is that the cost management evaluation system adopted by micro and small manufacturing enterprises is to emphasize the evaluation of production cost management, but not the evaluation of other cost management links and to emphasize the evaluation of financial indicators, but not the evaluation of nonfinancial indicators [4]. However, the factors affecting the cost of micro and small manufacturing enterprises are extremely complex, especially the lack of a specific and effective cost management evaluation system, so it is urgent to build a set of indicators and methods suitable for the evaluation of cost management of micro and small manufacturing enterprises [5]. This paper analyzes the current situation of cost management performance evaluation of micro and small

manufacturing enterprises by combining the research literature of domestic and foreign scholars, introduces the idea of supply chain management, and focuses on building a cost management evaluation system for micro and small manufacturing enterprises from the perspective of the supply chain, to provide a reference for cost management evaluation of micro and small manufacturing enterprises.

The business characteristics of small and micro manufacturing enterprises are mainly reflected in two aspects: (1) the small scale of production, and (2) risk resistance is weak [6]. As the employees of small and micro manufacturing enterprises are usually only a few dozen, the staff turnover is frequent, the business type is single, it is difficult to realize the production scale, and the market share is weak, which affects the profit source. Any change of external factors will affect the change of internal business environment, and the ability to resist risks is lower than that of large and medium-sized enterprises. Second is the lack of professional quality of managers. Most of the founders of small and micro-manufacturing enterprise's own knowledge structure is not perfect, and they lack a complete corporate development strategy, so it is difficult to lead the enterprise to break the development bottleneck, out of the predicament [7]. Therefore, it is especially important to focus on cost management and effectively improve the level of cost management to enhance the competitiveness of small and micromanufacturing enterprises. However, the evaluation of the financial indicators of cost management of a single link is not a comprehensive and correct evaluation of the level of cost management of micro and small manufacturing enterprises [8].

The globalization of the economy has transformed the competition among enterprises into the competition among supply chains. Large and medium-sized manufacturing enterprises have realized the importance of supply chain management and successfully applied it in their daily activities, which has become a powerful weapon for enterprises to achieve competitiveness, while micro and small manufacturing enterprises have little awareness of supply chain management. Therefore, this paper selects small and micromanufacturing enterprises as the research object, introduces the concept of supply chain management into small and micro manufacturing enterprises, and constructs a cost management evaluation system based on the supply chain for small and micromanufacturing enterprises to provide some reference for theoretical research on cost management evaluation of small and micromanufacturing enterprises.

2. Related Work

The bottom-up evaluation of the performance of bootstrapped enterprises at home and abroad mostly has different perspectives: the authors of [9] conducted a qualitative study on the indicators of social benefits, economic returns, innovation, and entrepreneurship and business activities of SBIC; the authors of [10] argued that Finland's venture capital bootstrapped enterprises focused too much on profitability indicators in the early stage leading to poor performance; the authors of [11] examined the effect of VCs, enterprise support, and indicators of business operations in the evaluation of UK EIS and VCT. The evaluation

of YOZMA introduces the exit success rate, best exit, number of exits, listing and mergers and acquisitions, the effect of government demonstration and guidance, and total asset size; [12] in the evaluation of Australia IIF, the qualification of venture capital enterprise managers and clear guidance direction in the early stage of the venture are considered to be more important in performance evaluation; [13] using the data envelopment analysis (DEA) method to include enterprise size in the performance evaluation assessment, although there is no direct linear relationship between performance score and size, large-scale enterprises tend to perform better. Since the main problem of venture capital bootstrapped enterprises at the local and municipal levels in China is capital sinking and large disparities exist in different regions, enterprise size is not suitable as a direct evaluation index. The authors of [14] argued that bootstrapped enterprises have greater gains in sales and efficiency than supported enterprises within 3 to 4 years, while there is no significant improvement in employment, so the performance evaluation will mainly examine the sales and efficiency of enterprises. The performance evaluation of foreign bootstrapped enterprises focuses on the design of indicators, and the performance evaluation of YOZMA in Israel and EIF in Europe is the most applicable to China because of the parent company model of equity participation [15].

The performance evaluation of bootstrapped enterprises in China is mostly top-down, so the performance evaluation ideas should be clarified based on policies and regulations: the authors of [16] argue that the leverage effect, industrial support, and sustainability factors need to be considered; the authors of [17] argue that the performance evaluation of public financial expenditure, financial science, and technology investment and commercial investment enterprises is of great reference; the authors of [18] argue that strategic bootstrapped enterprises should be evaluated from three perspectives: financial, management, and sustainability; the authors of [19] argue the performance evaluation of strategic Emerging industry bootstrapping enterprises; the authors of [20] consider bootstrapping enterprises as enterprises and applies TOPSIS model for performance evaluation based on the principle of enterprise-balanced scorecard, but the position is not clear.

To sum up, at present, the performance evaluation of guiding enterprises lacks research from a third-party perspective; there are more studies on policy and economic aspects and not enough studies on managerial indicators; there are more studies on hierarchical constructing indicators and not enough studies on practical details; there are more qualitative discussion and not enough empirical studies. Therefore, this paper wants to enrich the detailed indicators of performance evaluation research from the perspective of third-party rating and carry out empirical tests on the constructed evaluation system.

3. Gray Fuzzy Hierarchical Analysis Method

3.1. Hierarchical Analysis Method

3.1.1. Construction of Hierarchical Analysis Structure. As shown in Figure 1, the hierarchy is divided, such as the target layer, criterion layer, and indicator layer.

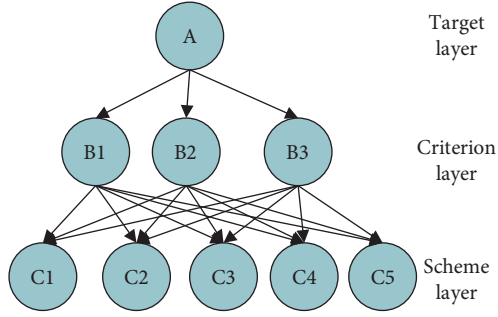


FIGURE 1: Hierarchical chart.

3.1.2. *Construction of the Judgment Matrix.* The constructed matrix judgment should satisfy the following conditions:

$$\begin{aligned} x_{ij} &= 1, x_{ij} = \frac{1}{x_{ji}}, \\ x_{ij} &> 0 \quad (i, j = 1, 2, 3, \dots, n). \end{aligned} \quad (1)$$

3.1.3. *Hierarchical Single Ranking and Consistency Test.* Calculate the consistency index CI : $CI = (\lambda_{\max} - n) / (n - 1)$, where n is the matrix order. Based on of this, make $CR = CI/RI$ and find the value of CR .

If $CR < 0.1$, the consistency of the matrix can be judged as satisfactory. Otherwise, the matrix should be adjusted for the matrix.

3.1.4. *Hierarchical Total Ranking and Its Consistency Test.* The weight vector of layer 2 to layer 1 is expressed as $\omega_i^{(3)} = (\omega_{i1}, \omega_{i2}, \dots, \omega_{im})^T$, $(i = 1, 2, \dots, n)$, $\omega_i^{(3)}$ for the column vectors to form the matrix: $W^{(3)} = [\omega_1^{(3)}, \omega_2^{(3)}, \dots, \omega_n^{(3)}]$, and then the third layer is $\omega_{ij}^{(3)} = W^{(3)}\omega^{(2)}$ for the first layer combination.

If $CR^{(3)} < 0.1$, the consistency of the judgment matrix passes.

Calculate the weights of each index.

3.2. *Gray Fuzzy Evaluation Method.* Since fuzzy comprehensive evaluation can consider fuzzy factors when judging problems, the fuzzy comprehensive evaluation method has wide applicability. The gray comprehensive evaluation is also applied with incomplete or insufficient information is also applied on some specific occasions. As a combination of gray theory and fuzzy theory, gray fuzzy hierarchical analysis can solve not only fuzzy problems but also gray problems, so it is more widely applicable.

\tilde{A} is a fuzzy subset on the space $X = \{x\}$, while $\mu_A(x)$ is a gray number on $[0, 1]$, then the affiliation of x is with respect to \tilde{A} , then its point grayness is $v_A(x)$, which is denoted as $\tilde{A}_{\otimes} = \{(x), \mu_A(x), v_A(x) | x \in X\}$. It is represented as $\tilde{A}_{\otimes} = (\tilde{A}, A_{\otimes})$ by set pairs, in which $\tilde{A} = \{(x), \mu_A(x) | x \in X\}$ is called the fuzzy part of \tilde{A}_{\otimes} and $A_{\otimes} = \{(x), v_A(x) | x \in X\}$ is called the gray part of \tilde{A}_{\otimes} . If $\mu_A = (0, 1)$, then $\tilde{A}_{\otimes} = A_{\otimes}$. If $v_A(x) = 0$, then $\tilde{A}_{\otimes} = \tilde{A}$.

The space $X = \{x\}$ and $Y = \{y\}$ and the gray fuzzy set $X \times Y$ in the direct product space $\tilde{R}_{\otimes} = \{(x, y), \mu_R(x, y), v_R(x, y) | x \in X, y \in Y\}$ are the gray fuzzy relations on $X \times Y$.

With $\tilde{A}_{\otimes} = [(\mu_{ij}^A, v_{ij}^A)]_{m \times 1}$ and $\tilde{B}_{\otimes} = [(\mu_{ij}^B, v_{ij}^B)]_{1 \times n}$ are two gray fuzzy relations, the synthetic relation of $\tilde{A}_{\otimes} \tilde{B}_{\otimes}$ can be expressed as $\tilde{A}_{\otimes} \circ \tilde{B}_{\otimes} = (\tilde{A} \circ \tilde{B}, A_{\otimes} \circ B_{\otimes}) = [(+F_{j=1}^1(\mu_{ik}^A \bullet F\mu_{ik}^B)), (\bullet G_{j=1}^1(v_{ik}^A \bullet G\mu_{ik}^B))]_{m \times n}$.

4. The Gray Fuzzy Evaluation Method

This paper adopts the hierarchical analysis method and gray fuzzy evaluation method to build a scientific, reasonable, and practical evaluation model. The construction idea of the model is as follows: firstly, starting from the internal supply chain process of micro and small manufacturing enterprises, based on analyzing the characteristics and influencing factors of cost management of micro and small manufacturing enterprises and following the principle of constructing evaluation index system, the evaluation system of cost management of micro and small manufacturing enterprises based on the supply chain is established; secondly, the gray fuzzy hierarchical analysis method is used to carry out the research, to analyze the cost management level of enterprises, and its evaluation idea as shown in Figure 2.

4.1. *Determination of the Weights of Each Index.* The cost management evaluation index system of micro and small manufacturing enterprises based on the supply chain studied in this paper is divided into three layers: target layer, criterion layer, and indicator layer. The criterion layer consists of six aspects: procurement cost management evaluation study, production cost management evaluation study, inventory cost management evaluation study, sales cost management evaluation study, distribution cost management evaluation study, and after-sales cost management evaluation study [21, 22].

① Criterion layer judgment matrix construction and consistency test is shown in Table 1.

The data scored by the experts are input into the MATLAB program, and the maximum characteristic roots of the judgment matrix and the corresponding eigenvectors are found as

$$\lambda_{\max} = 6.2484$$

$$W_0 = [0.4954, 0.7801, 0.0721, 0.3154, 0.1460, 0.1418]^T. \quad (2)$$

The feature vector is normalized to obtain the weight vector of each element as

$$W = [0.2539, 0.3999, 0.0370, 0.1617, 0.0748, 0.0727]^T. \quad (3)$$

A consistency test on this judgment matrix yields

$$CI = \frac{\lambda_{\max} - n}{n - 1} = 0.0497. \quad (4)$$

Checking the table, we can see that when $n = 6$, $RI = 1.24$, and the consistency ratio can be calculated as

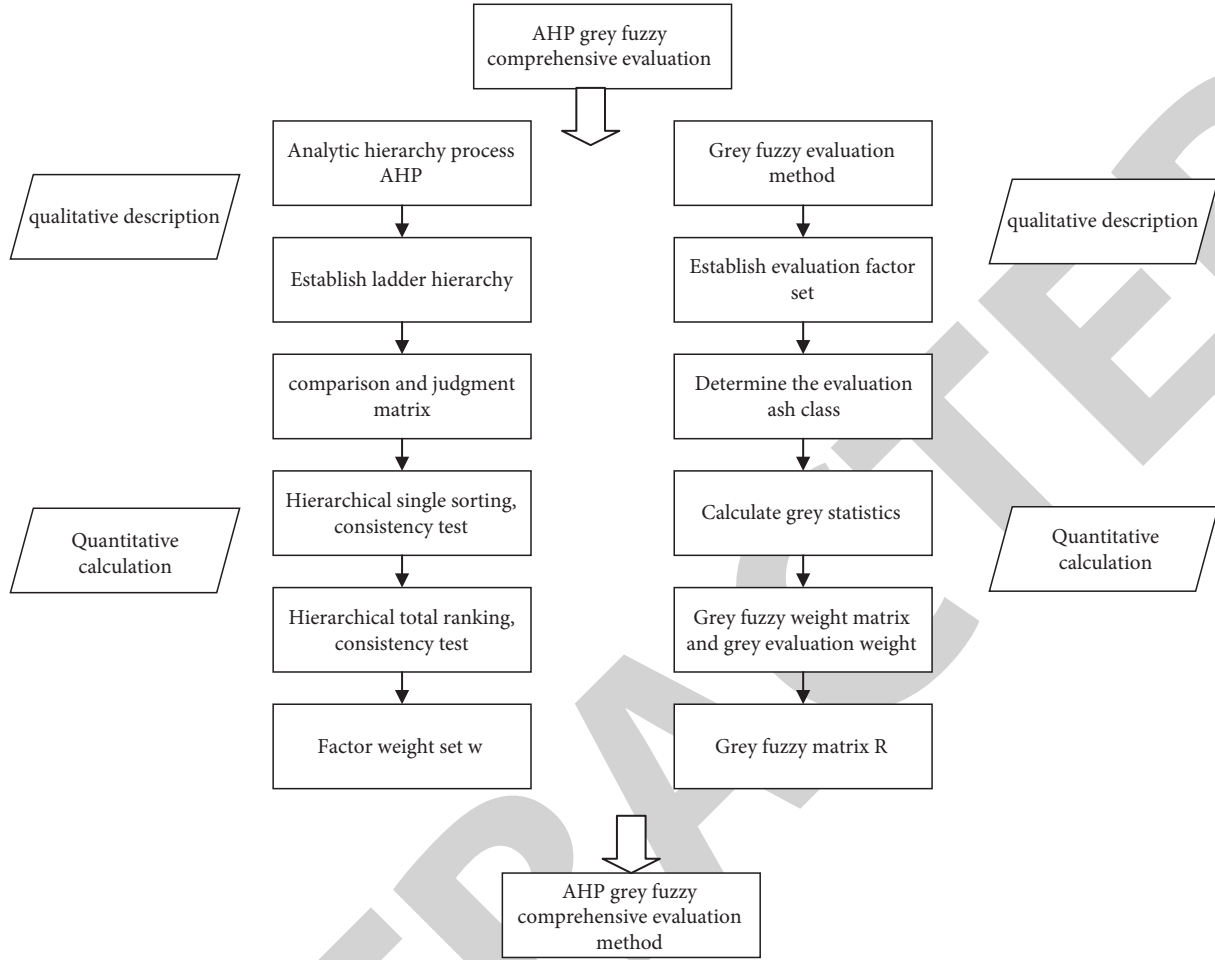


FIGURE 2: Cost management evaluation ideas of small and micromanufacturing enterprises.

TABLE 1: Criterion layer judgment matrix.

Index item	A_1	A_2	A_3	A_4	A_5	A_6
Purchase cost A_1	1	3	5	1/2	2	6
Production cost A_2	1	2	7	4	6	5
Inventory cost link A_3	1/5	1/7	1	1/3	1/2	1
Sales link cost A_4	1/3	1/2	3	2	3	3
Distribution link cost A_5	1/4	1/5	4	1	1/2	1
After sales cost A_6	1/5	1/5	3	1/3	3	2

$$CR = \frac{CI}{RI} = 0.0401. \quad (5)$$

$CR < 0.1$, which passes the consistency test. The judgment matrix construction and consistency test of purchasing link cost (A_1) are shown in Table 2.

The data scored by the experts are input into the MATLAB program, and the maximum characteristic roots of the judgment matrix and the corresponding eigenvectors are found as

$$\lambda_{\max} = 7.4922, \quad (6)$$

$$W_0 = [0.3326, 0.7396, 0.2491, 0.2127, 0.1242, 0.4628, 0.0742]^T.$$

The feature vector is normalized to obtain the weight vector of each element as

$$W = [0.1515, 0.3369, 0.1135, 0.0969, 0.0566, 0.2108, 0.0338]^T. \quad (7)$$

A consistency test on this judgment matrix yields

$$CI = \frac{\lambda_{\max} - n}{n - 1} = 0.0820. \quad (8)$$

Checking the table shows that when $n = 7$ and $RI = 1.32$, the consistency ratio can be calculated as

$$CR = \frac{CI}{RI} = 0.0621. \quad (9)$$

TABLE 2: Cost of procurement (A_1) judgment matrix.

	A_{11}	A_{12}	A_{13}	A_{14}	A_{15}	A_{16}	A_{17}
Purchase batch and purchase batch A_{11}	1	1/2	3	2	3	1/3	4
Supplier stability A_{12}	2	3	2	5	4	4	5
Capital investment ratio of purchasing staff A_{13}	1/3	1/3	2	1/2	3	1/2	6
Online purchase rate A_{14}	1/3	1/4	2	2	3	1/3	3
Standardization of procurement cost management system A_{15}	1/2	1/4	1/2	1/3	1	1/3	3
Intact fulfillment rate of purchase order A_{16}	3	1/3	2	5	4	1	3
Exchange rate and tax rate A_{17}	1/5	1/5	1/6	1/2	1/3	1/4	1

$CR < 0.1$, which passes the consistency test.

4.2. Determination of Evaluation Levels. Based on the views of domestic and foreign scholars, this paper borrows the expert scoring method and scores according to the 10-point system. This paper will be divided into five evaluation levels [23], which are poor, poor, average, good, and good, and the score of each level is $C = \{1, 3, 5, 7, 9\}$, and the whitening weight function of the level “good” is

$$f_j^1(x) = \begin{cases} 0, & x \notin [7, +\infty), \\ \frac{x-7}{9-7}, & x \in [7, 9], \\ 1, & x \in [9, +\infty). \end{cases} \quad (10)$$

The whitening weight function for the grade “better” is

$$f_j^2(x) = \begin{cases} 0, & x \notin [5, 9], \\ \frac{x-5}{7-5}, & x \in [5, 7], \\ \frac{9-x}{9-7}, & x \in [7, 9]. \end{cases} \quad (11)$$

Calculation of gray fuzzy judgment matrix is as follows:

$$B = (b_1, b_2, \dots, b_m) = W \cdot R = (a_1, a_2, \dots, a_n) \begin{bmatrix} r_{11}, r_{12} \dots r_{1n} \\ r_{21}, r_{22} \dots r_{2n} \\ \dots \\ r_{n1}, r_{n2} \dots r_{nm} \end{bmatrix}. \quad (12)$$

Of these, $b_j = \sum_{i=1}^m W_i \cdot r_{ij}$, $j = 1, 2, \dots, m$, normalized to give $\sum_{j=1}^m W_i b_{ij}$.

5. Analysis of the Evaluation Results of Enterprise Cost Management

According to the evaluation results, $3 \leq 3.0695 \leq 5$, which is between “poor” and “average”. It means that the overall cost management level of enterprise B is low.

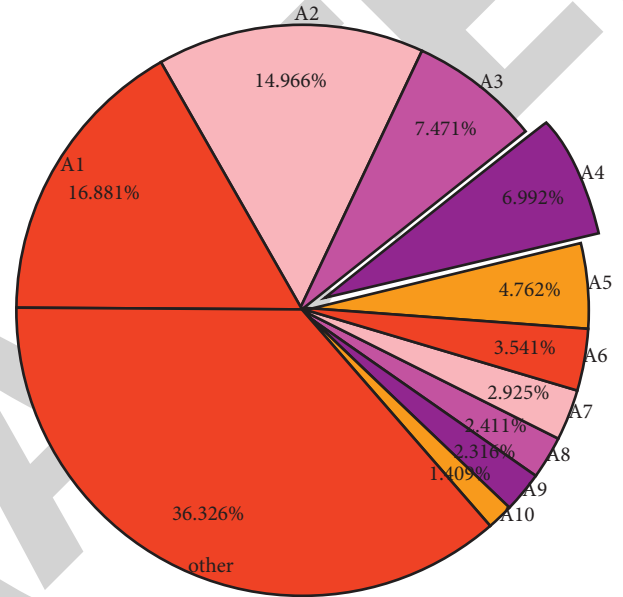


FIGURE 3: Criteria layer index weights.

5.1. Calculation of Indicator Weights. According to the calculated weight results of the criterion level indicators, we make a graph of the criterion level indicators and get the relative importance of each factor in the criterion level according to the size of the weight value [24, 25]. From Figure 3, it can be seen that the weights of the three indicators, namely, cost management evaluation of production process A_2 , cost management evaluation of procurement process A_1 , and cost management evaluation of sales process A_4 , are 39.99%, 25.40%, and 16.17% respectively, accounting for 80% of the total weights, which are the most important indicators in the criterion level indicators.

5.2. Weighting of Indicators in the Indicator Layer to the Target Layer. Based on the results of the calculated weights of the indicators of the indicator layer, the indicators of the indicator layer are plotted, and the relative importance of the factors of the indicator layer can be obtained according to the magnitude of the weight values. From Figure 4, it can be seen that from the greenness of unit production cost A_{26} , product qualification rate A_{27} , online sales rate A_{44} , distribution method and distribution route A_{51} , purchasing batch, and purchasing lot A_{11} , the weights of these six indicators are greater than 3%, which belong to the more important indicators in the indicator of the guideline layer [26].

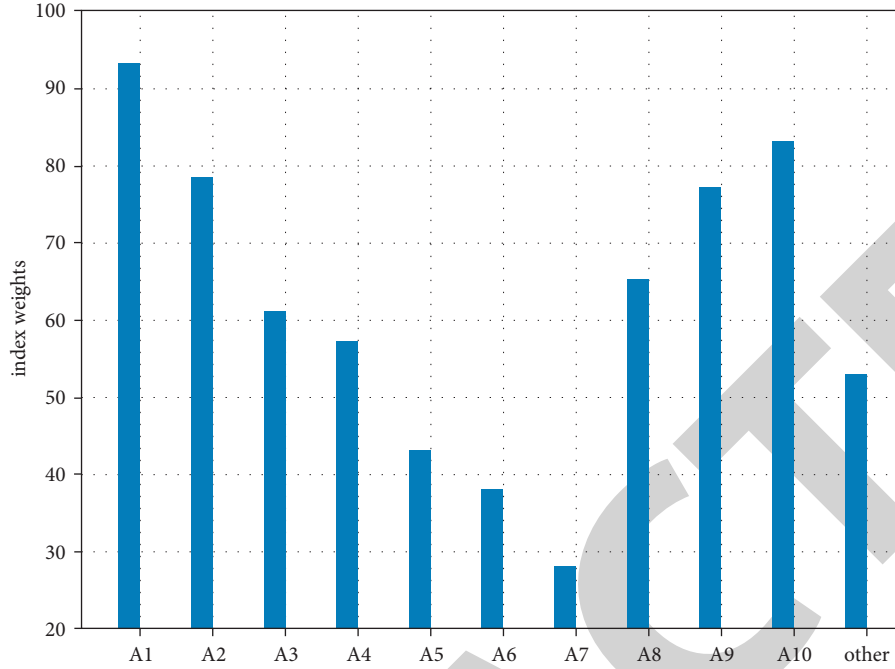


FIGURE 4: Index layer index weights.

TABLE 3: Intuitive preference relationship of the first level indicators.

(0.55, 0.55)	(0.35, 0.55)	(0.65, 0.3)
(0.35, 0.55)	(0.55, 0.55)	(0.65, 0.35)
(0.2, 0.55)	(0.4, 0.5)	(0.55, 0.55)

TABLE 4: Intuitive preference relationships under indicators.

(0.55, 0.55)	(0.35, 0.55)	(0.3, 0.65)
(0.55, 0.35)	(0.55, 0.55)	(0.65, 0.35)
(0.55, 0.35)	(0.25, 0.58)	(0.55, 0.55)

TABLE 5: Intuitive preference relationships under indicators.

(0.55, 0.55)	(0.35, 0.55)
(0.55, 0.35)	(0.55, 0.55)

TABLE 6: Intuitive preference relationships under indicators.

(0.55, 0.55)	(0.35, 0.55)	(0.55, 0.35)
(0.55, 0.35)	(0.55, 0.55)	(0.5, 0.4)
(0.4, 0.55)	(0.4, 0.5)	(0.55, 0.55)

5.3. Enterprise Performance Evaluation by Fuzzy Hierarchical Analysis. Based on the situation of enterprises A and B, the intuitionistic fuzzy preference relationships derived from the scoring of five experts are partially shown in the attached table (Tables 3, 4, 5, and 6).

Calculating the distance of R_1 and \bar{R}_1 , we get $d(R_1, \bar{R}_1) = 0.1568 > 0.1$, which does not pass the consistency test. Therefore, further parameters are set for adjustment, so that $\sigma = 0.6$, and we get

$$\bar{R}_1 = \begin{bmatrix} (0.55, 0.55), (0.35, 0.60), (0.2468, 0.5005) \\ (0.60, 0.35), (0.55, 0.55), (0.60, 0.35) \\ (0.5005, 0.2468), (0.35, 0.60), (0.55, 0.55) \end{bmatrix}, \quad (13)$$

$d(R_1, \bar{R}_1) = 0.0997 > 0.1$. Then, matrix \bar{R}_1 passes the consistency test, and \bar{R}_1 is substituted to calculate the weights. Obtain

$$\omega^1 B_1 = (0.1999, 0.6626), \omega^1 B_2 = (0.3400, 0.5125), \quad (14)$$

$$\omega^1 B_3 = (0.2601, 0.5749).$$

Similarly, we can derive the weights of the other indicators where the weights of C_1 are

$$\omega^1 C_1 = A_1 \otimes B_1 \otimes C_1 = (0.3712, 0.5997) \otimes (0.5476, 0.3421) \otimes (0.1999, 0.6626) = (0.0406, 0.9111). \quad (15)$$

Similarly, we can also get the weights of other indicators. Further substitution yields

$$W_1 = \oplus_{j=1}^{24} (\omega_j \otimes \omega_{1j}) = (0.0406, 0.9111) \otimes (0.0265, 0.9396) \otimes (0.0160, 0.8502) \otimes (0.0211, 0.9402) \otimes (0.0317, 0.9200) \otimes (0.0256, 0.9287) \otimes (0.0257, 0.9232) \otimes (0.0182, 0.9462) \otimes (0.0318, 0.9137) \otimes (0.0103, 0.9445) \otimes (0.0173, 0.9305) \otimes (0.0208, 0.9210) \otimes (0.0132, 0.9394) \otimes (0.1316, 0.7243) \otimes (0.0106, 0.9548) \otimes (0.0186, 0.9307) \otimes (0.0129, 0.9439) \otimes (0.0118, 0.9521) \otimes (0.0177, 0.9342) \otimes (0.0240, 0.9174) \otimes (0.0068, 0.9627) \otimes (0.0053, 0.9696) \otimes (0.0096, 0.9632) \otimes (0.0078, 0.9589) = (0.4343, 0.1677). \quad (16)$$

TABLE 7: Comparison of the results of intuitionistic fuzzy hierarchical analysis and fuzzy hierarchical analysis.

	Intuitive fuzzy hierarchical analysis method	Fuzzy hierarchical analysis method
Fund A	0.3893	0.5189
Fund B	0.4447	0.4064

Similarly, for firm B , we can obtain

$$\begin{aligned}
W_2 = \oplus_{j=1}^{24} (\omega_j \otimes \omega_{2j}) &= (0.0220, 0.8871) \otimes (0.0167, 0.9106) \\
&\otimes (0.0100, 0.9403) \otimes (0.0138, 0.9300) \otimes (0.0138, 0.9300) \\
&\otimes (0.0138, 0.9300) \otimes (0.0141, 0.9241) \otimes (0.0154, 0.9207) \\
&\otimes (0.0116, 0.9375) \otimes (0.0184, 0.9061) \otimes (0.0133, 0.9321) \\
&\otimes (0.0227, 0.9018) \otimes (0.0272, 0.8864) \otimes (0.0173, 0.9100) \\
&\otimes (0.1646, 0.8218) \otimes (0.0109, 0.9379) \otimes (0.0154, 0.9241) \\
&\otimes (0.0188, 0.9060) \otimes (0.0086, 0.9513) \otimes (0.0064, 0.9616) \\
&\otimes (0.0111, 0.9409) \otimes (0.0080, 0.9505) = (0.3990, 0.1370).
\end{aligned} \tag{17}$$

Substituting the above results, we get

$$\begin{aligned}
\rho(W_1) &= 0.5 \times (1 + 1 - 0.4343 - 0.1677) \times (1 - 0.4343) = 0.3954, \\
\rho(W_2) &= 0.5 \times (1 + 1 - 0.3990 - 0.1370) \times (1 - 0.3990) = 0.4399, \\
\rho(W_1) &= 0.3954 < \rho(W_2) = 0.4399.
\end{aligned} \tag{18}$$

Comparing the two venture capital bootstrapped enterprises A and B, enterprise A is more focused on policy effect, with standardized management but lack of professionalism, while enterprise B is more focused on economic benefits. Through the performance evaluation method proposed in the paper, we know that enterprise A scores more than enterprise B. This indicates that, for venture capital bootstrapped enterprises, the policy effect is more important, which is in line with the basic idea of venture capital bootstrapped enterprise establishment, that is, weakening economic benefits and favoring policy effect.

5.4. Comparative Analysis with Fuzzy Hierarchical Analysis. Based on the same information set, we evaluated enterprises A and B with fuzzy hierarchical analysis, and the evaluation results with intuitionistic fuzzy hierarchical analysis are shown in Table 7.

From Table 7, we can see that both intuitionistic fuzzy hierarchical analysis and fuzzy hierarchical analysis conclude that enterprise A is better than enterprise B. However, from the perspective of evaluation methods, intuitionistic fuzzy hierarchical analysis is more in line with the actual situation and can more accurately express the perception of decision participants in the case of incomplete information and evaluate each indicator comprehensively in terms of its strength, weakness, and uncertainty. Secondly, in the process of fuzzy hierarchical analysis evaluation, for the judgment matrix that does not pass the consistency test, we can only carry out a new round of test calculation by rescoring from experts, while the intuitionistic fuzzy hierarchical analysis

method sets parameters for judgment matrix adjustment, a process that does not require the participation of decision-makers and is faster and more effective.

6. Conclusion

In this paper, the performance evaluation index system of an enterprise is constructed from the three dimensions of policy benefit, economic benefit, and management benefit by combining the specific conditions of the enterprise; the enterprise performance evaluation method based on intuitionistic fuzzy hierarchical analysis is proposed for the characteristics of the enterprise evaluation index system in obtaining information and the advantages of intuitionistic fuzzy numbers in processing information; finally, the evaluation process is demonstrated using the actual data of an enterprise, and finally, the evaluation process is demonstrated using the actual data of an enterprise, and the proposed intuitionistic fuzzy hierarchical analysis is compared with the traditional fuzzy research, showing that the index system constructed in this paper is applicable to my enterprise performance evaluation and the proposed intuitionistic fuzzy hierarchical analysis has greater advantages in evaluation accuracy than the traditional fuzzy hierarchical analysis.

Data Availability

The experimental data used to support the findings of this study are available from the author upon request.

Conflicts of Interest

The author declares no conflicts of interest regarding this work.

References

- [1] J. Wang, "Empirical study and evaluation system construction based on hierarchical fuzzy index for low carbon economy," *Journal of Industrial Technological Economics*, vol. 6, no. 20, pp. 8180–8186, 2014.
- [2] S. Zhang and X. Li, "A hybrid performance evaluation model of TPL providers in agricultural products based on fuzzy ANP-TOPSIS," *Custos. Agronegocio. Line*, vol. 11, pp. 144–165, 2015.
- [3] Y. Deng, S. Zou, and D. You, "Financial performance evaluation of nuclear power-related enterprises from the perspective of sustainability," *Environmental Science and Pollution Research*, vol. 27, no. 10, Article ID 11349, 2020.
- [4] H. Gao, H. Chen, J. Feng et al., "Balanced scorecard-based performance evaluation of Chinese county hospitals in underdeveloped areas," *Journal of International Medical Research*, vol. 46, no. 5, pp. 1947–1962, 2018.

Research Article

Research on Perceptual Integrity of Distributed Digital Media Based on AWTC-TT Algorithm Optimization

Xiaobo Zhang ¹ and Rongrong Shen ²

¹School of Art, Shandong Jianzhu University, Jinan 250101, China

²School of Law, Shandong Jianzhu University, Jinan 250101, China

Correspondence should be addressed to Rongrong Shen; 13916@sdjzu.edu.cn

Received 24 April 2022; Revised 6 June 2022; Accepted 10 June 2022; Published 19 July 2022

Academic Editor: Le Sun

Copyright © 2022 Xiaobo Zhang and Rongrong Shen. This is an open access article distributed under the Creative Commons Attribution License, which permits unrestricted use, distribution, and reproduction in any medium, provided the original work is properly cited.

Digital media can spread data and information. Its wide use not only enriches people's work and life but also brings high efficiency and convenience. However, due to different devices, different data quality, network stability, and other reasons, data quality is usually difficult to guarantee, so it is necessary to evaluate its perceptual integrity. In this paper, the group intelligence sensing technology in the sensor field and AWTC-TT optimization algorithm integrating blockchain technology are proposed to collect users' sensing data and build a model to discuss the complete performance. The experimental results show that (1) for the AWTC-TT algorithm, the processing time of 200 data tasks is less than 60 s; moreover, after optimization, the performance is efficient, which can effectively reduce the running time of data processing, and the performance loss is only 4%. (2) The perceptual quality of data was evaluated, the gain value of the first 0.4 is above 0.3, and the interference of abnormal data on integrity was explored. (3) The test results of the four integrality indexes of the model are good and the quality is stable. (4) The income value of CS2 is 5.8, and the income of distribution with the highest quality is the highest. Finally, the model constructed in this paper is mature, the experimental data and results are good, and the data perception integrity is discussed. The use of various fusion technologies can provide a reference for more subsequent research and application and lay a solid foundation.

1. Introduction

With the rapid changes of the times, many new branches have gradually emerged from the technology with the Internet as the core. With the support of 5G network and computer technology, the idea of connecting and communicating between people and things is no longer a dream [1]. At the same time, a large number of digital media terminal devices enter people's daily life, creating massive data that is difficult to estimate by manpower every day. In this case, a new paradigm of group intelligence perception was born. Through mobile devices and media, people can share perceptual data, which greatly expands the service scope of the Internet of Things. Therefore, the backwardness of some traditional technologies has brought an unbearable burden to the network, and people have to face new problems of data integrity. In addition, the group intelligence awareness

service requires high network nodes and speed. Facing challenges, blockchain technology stands out because of its many advantages and outstanding performance in financial transactions. In this paper, the distributed structure of digital media is the main research object, for its perceptual integrity experiments. In this paper, the AWTC algorithm, which is mainly based on blockchain technology, will be optimized, assisted by a consensus algorithm, incentive mechanism, security and trust guarantee, etc. In order to increase the performance of the experiment, the paper also introduces edge computing, the Internet of Things, and blockchain to integrate technologies, so as to reduce some computing pressure and carry out technological reform and integration innovation.

In order to better provide a relevant theoretical basis and experimental data support for our paper, we collected some literature for reference, as follows: Explore the framework

and typical application of blockchain technology in energy Internet [2]. Collect data through sensors, study MCS system, and explore many aspects from sensor communication to system management and data storage [3]. Analyze some open source projects of blockchain technology, and deeply analyze the basic principles of blockchain [4]. This paper studies the task allocation problem perceived by mobile people for multitasking participants [5]. Critically evaluate the superiority of blockchain technology, analyze the current situation and look forward to the future of this technology [6]. Learn from the successful experience of blockchain in the application of digital crypto currency and explore the theory of trusted data management [7]. The consistent hash algorithm is used to solve the problems of storage space, repeated verification, and data hierarchical management [8]. Considering 6G and the Internet of Things, the data sharing and storage mechanism of blockchain based on the Gossip protocol is proposed [9]. Objectively expound on the hot spots and trends in the field of integrating blockchain and the Internet of Things at the technical and application levels [10]. A multi-layer blockchain network model for edge computing and an adaptive workload proof algorithm are proposed [11]. The basic network structure of blockchain is realized through various encryption means and consensus algorithms, and the security architecture of edge computing and the Internet of Things is designed [12]. The incentive mechanism based on blockchain technology adopts the distributed architecture of blockchain security and applies group intelligence perception [13]. The transaction information is recorded by a three-tier cognitive radio system based on a blockchain of reputation value auction, and the perceived revenue distribution mechanism is constructed [14]. Based on discrete logarithm and computational Diffie-Hellman proposed a node exit mechanism suitable for a signcryption scheme [15]. This paper studies the influence of blockchain technology on ordinary netizens' perception of public opinion information quality and willingness to accept behavior [16].

2. Theoretical Basis

2.1. Distributed Digital Media. "Digital media" [17]: it can be interpreted as an information carrier, mainly in the form of binary numbers, which is closely related to computer information technology. However, from a broad perspective, the recording, processing, dissemination, and acquisition functions of digital media have already penetrated into all aspects of the human world. The coverage of intelligent products promotes the advent of the information explosion era, and digital media is widely used by people for its information acquisition and output technology. Its development is no longer only linked with the Internet and IT technology, but with the development of the whole industry and the whole world. Human society can no longer leave digital media technology. Without this technology, the world will lack the energy and driving force to develop the future.

Combine digital technology and media organically. Digital media is usually carried by terminal devices such as

TV, mobile phone, computer, and tablet, and output in the form of audio, image, and video. In the output process, it will generate massive data, transmit data according to different goals and needs, and share it with people or things. Not only can human-computer interaction be carried out but also the entertainment interest can be enhanced. Cutting-edge technologies in almost all fields can be integrated with digital media technology, and the digital products created fully reflect the value of commerce and spread culture and art.

Compared with the centralized client/server structure, each network node in the distributed structure has multiple paths, and its database is composed of several related databases on the network. Each network node is not closely related, and they all have the ability to process independently. Therefore, when a node goes wrong, it will not cause the whole system to crash. Moreover, the distributed structure is easy to upgrade and maintain, costs less money, and has multiple servers for local operations. When digital media is combined with distributed architecture, it can effectively divide the number of tasks, improve the efficiency of the whole system, balance the load problem, and run multiple applications at the same time.

2.2. Blockchain Technology. BC [18]: it is called "blockchain." BC can be interpreted as an open distributed digital ledger, which is mainly based on a peer-to-peer network (i.e., P2P network). This ledger can record the information of all transactions, and even every node of the whole network keeps a copy of the ledger. Therefore, only one node is needed, and we can obtain and query the whole transaction data. However, we can't change all the data copies on the whole network by modifying the copy on a certain node. Initially, blockchain technology mainly served the network "mining," that is, commercial transactions with Bitcoin as the trading currency. With the success of this technology in the financial field, BC has attracted the attention of experts and scholars at home and abroad because of its encryption mechanism, various computing algorithms, consensus mechanism and other technologies. So far, the research on it has become mature. BC technology is not a new single technology, but a new product of the integration of multiple fields and frontier science and technology. It is a continuous and related data system from the perspective of trust, and it is also a decentralized data recording method. Apart from decentralization, most of BC's network data is open and transparent, but users' true identities can be anonymous. Trust is generated between nodes through the hash algorithm. When data is written, in order to ensure the integrity of data, BC can eliminate all modification interventions without authority. Only when you are authorized to control 51% of the nodes can you change the data content or modify the status in BC.

2.2.1. AWTC-TT Algorithm. AWTC [19]: it is called "account-wise transaction chain" in English. It is also better known as "nano block lattice." Running in the way of winding blockchain, it belongs to a DAG type. It is its existence that enables each account to have a separate

blockchain bookkeeping record, which is the core technology of blockchain. Because BC technology is the main medium of economic transactions, it is necessary to ensure fast, safe, effective, and reliable transactions. Although other methods can achieve the above goals, only AWTC can achieve it quickly and stably. Through this algorithm, we can increase the number of network nodes and transactions in the blockchain. While increasing the number steadily, it can also keep the transaction time stable under the maintenance of the algorithm, without being affected by the increasing number of nodes and transactions, thus avoiding other problems. The AWTC algorithm can improve the computational efficiency and provide faster transaction speed for the network and its users. The Locus Chain protocol based on AWTC can upgrade the processing capacity and solve the problem of data scale expansion after introducing dynamic state fragmentation technology. In addition, even in the most stringent network environment, the Locus Chain protocol can support intelligent contracts of blockchain and avoid malicious attacks on the network. After some excellent transformation to improve the performance, we use the AWTC-TT algorithm in this paper.

2.2.2. Consensus Algorithm. The main function of the consensus algorithm is to make all nodes have distributed structure and reach an effective consensus. Its core principles are safety, fault tolerance, and activity. We analyze and compare several commonly used consensus algorithms, and introduce some of their characteristics, as shown in Table 1.

Among them, the calculation operation of POW is as follows:

$$\text{Hash}(\text{PreHash}, M\text{root}, T\text{stamp}, \text{Nonce}) < \text{Target}. \quad (1)$$

Implementation algorithm of POS:

$$\text{Hash}(\text{block_header}) \leq \text{Target} * \text{coinage}. \quad (2)$$

PBFT is a practical Byzantine fault-tolerant algorithm. In this paper, we propose to use LS-PBFT without removing centralization, so as to combine with edge computing to make the model more efficient.

$$p = v \bmod |R|, \quad (3)$$

$$\langle \langle P, v, n, d \rangle, m \rangle, \quad (4)$$

$$P \in \{\text{PRE_PREPARE}, \text{PREPARE}, \text{COMMIT}\},$$

$$m = m * II\{P = \text{PRE PREPARE}\}. \quad (5)$$

Among them, the view number is represented by v , which can express the status of leader nodes; $|R|$ represents the total number of replica nodes and master nodes in the collection. Formulas (3) and (4) are the messaging normal form of nodes. P refers to the message type; v represents the message view; n represents the message sequence number; d represents the message index; m is the concrete expression of the content of the message itself. In the process of message

delivery, m is passed to other nodes only in the first stage, and m is not passed again in other stages.

2.3. Group Intelligence Perception. ‘‘Crowdsensing’’ [24]: it originated from the use of sensing devices in the Internet of Things. At first, the service purpose of group intelligence perception was only for individuals. However, with the increment of information and the popularity of the Internet, because of the high cost of sensors, people prefer to collect sensing data from mobile phones, computers, and other terminal devices and upload them to servers in the cloud. It can be provided to the party in need. Generally speaking, for different tasks, the perceived time can change, and the perceived data quality is also different. Swarm intelligence sensing technology can process data on a large scale and analyze the quality of sensing data with low cost and quick access.

2.3.1. Incentive Mechanism. In this paper, a user-centered strategy is introduced to obtain perceptual information. Participants provide data and optimization goals that RADP needs to consider the following:

$$\text{RADP: } \max \frac{1}{b_i}. \quad (6)$$

MSensing method [25]: considering the selection of participants, the RADP strategy is improved. Its optimization goal is as follows:

$$\text{MSensing: } \max v(w) \sum_{i \in w} b_i. \quad (7)$$

MAA utility function [26] is as follows:

$$S(x) = \sum_{m=1}^M \omega_m S(x_m), \quad (8)$$

$$\sum_{m=1}^M \omega_m = 1.$$

Then, the optimization objectives of MAA are as follows:

$$\text{MAA: } \max S(x_i), \quad i \in \mu. \quad (9)$$

If the policy is platform-centric, the optimization function is as follows:

$$\text{GBMC: } \max \frac{W'_i}{b_i}, \quad (10)$$

$$\text{ISAM: } \max \frac{d_i}{b_i = \min E(y'_i - y_i)^2 / b_i}, \quad (11)$$

where b_i is the user’s bidding price; w is the chosen winner. And $S(x_m)$ refers to the utility function of attributes; Generation w_m refers to attribute weight; M can represent the number of attributes; W'_i of formula (9) is interpreted as the range that the user can perceive; y'_i and y_i can be interpreted as estimated mean and accurate mean, respectively.

TABLE 1: Compare the performance of the consensus algorithm.

Consensus algorithm name	Characteristics of algorithm	Efficiency	Aggressive resistance	Applicable scenarios
Solo [20]	Single-node consensus model; there is no high availability and scalability	High	Low	Alliance chain or private chain
Kafka [21]	High throughput, low latency, no intentional evil node	High	Low	Alliance chain or private chain
PBFT [22]	Consistency, security, and the number of malicious nodes do not exceed 1/3	High	High	Alliance chain [23]
POW	The hash function is the core; decide who gets out of the block by the calculation difficulty value	Low	High	Public chain
POS	Provide incentive mechanism; it is an improvement of POW	Low	High	Public chain

2.3.2. *Trust Management.* Updatable ways to manage reputation values:

$$\begin{aligned} r_i &= \beta r_i(t) + \alpha r_i^-, \\ \alpha + \beta &= 1, \end{aligned} \quad (12)$$

$$r_i(t) = \frac{(p(t) + \varepsilon)}{(p(t) + n(t) + \varepsilon)}$$

Redefine according to credible value:

$$\text{TSCM: } \max_{i \in w} \sum v_i^r - \frac{b_i}{r_i} \quad (13)$$

3. Research on Perceptual Integrity of Group Intelligence Based on AWTC-TT

3.1. *Evaluate Perceived Quality.* Data quality includes accuracy, completeness, consistency, and other attributes. Exploring the integrity of perceived data is an important aspect to ensure the quality of information data. When the data in the database is input, it may lead to input errors or invalid data due to various reasons. Therefore, integrity is put forward to ensure that the data of data digital media conforms to the rules. Generally speaking, data integrity mainly refers to accuracy and reliability, and this experiment will be based on these two points. In addition, the integrity of data can be divided into three categories: domain, entity, and reference.

Before formally exploring completeness, it is necessary to establish standards to evaluate the quality of perceived data. The higher the quality of the data collected, the higher the return given; low returns should be given to low-quality data that fail to meet the standards. Data classification and sorting algorithms are used for evaluation. It is worth noting that every evaluation standard should be based on energy data. Use the following data set:

$$D = \{D_1, D_2, \dots, D_m\}, \quad (14)$$

$$C = \{C_1, C_2, \dots, C_k\}, \quad (15)$$

$$Z = \{(Z_1^{\min}, Z_1^{\max}), (Z_2^{\min}, Z_2^{\max}), \dots, (Z_k^{\min}, Z_k^{\max})\}. \quad (16)$$

Among them, formula (14) describes the data collected about the task. Formula (15) represents the criteria used for data quality assessment. Formula (16) represents each quantifiable effective range, which is related to the evaluation value of the evaluation standard. Get the evaluation value:

$$s_{i,j} = f_j(D_i). \quad (17)$$

The evaluation value matrix is obtained:

$$S = \begin{bmatrix} s_{1,1} & \dots & s_{1,k} \\ \vdots & \ddots & \vdots \\ s_{m,1} & \dots & s_{m,k} \end{bmatrix}. \quad (18)$$

(1) Classify

Before judging whether the evaluation requirements are met, calculate the deviation degree. Negative correlation:

$$e_{i,j} = \begin{cases} \frac{s_{i,j} - z_j^{\min}}{z_j^{\max} - z_j^{\min}}, & z_j^{\min} < s_{i,j} < z_j^{\max} \\ 1 + \omega, & \text{other.} \end{cases} \quad (19)$$

Positive correlation:

$$e_{i,j} = \begin{cases} \frac{z_j^{\max} - s_{i,j}}{z_j^{\max} - z_j^{\min}}, & z_j^{\min} < s_{i,j} < z_j^{\max} \\ 1 + \omega, & \text{other.} \end{cases} \quad (20)$$

Determine whether the maximum value meets the requirements:

$$e_i^{\max} = \max\{e_i\} = \max\{e_{i,1}, e_{i,2}, \dots, e_{i,k}\}. \quad (21)$$

(2) Quality ranking

Single deviation vector:

$$\begin{aligned} e_i &= (\theta_1 e_{i,1}, \theta_2 e_{i,2}, \dots, \theta_k e_{i,k}), \\ \sum_{j=1}^k \theta_j &= 1. \end{aligned} \quad (22)$$

Bias vector of population:

$$r_i = \left(\sum_{j=1}^k (\theta_j e_{i,j})^2 \right)^{1/2}. \quad (23)$$

Sort the data of HD and LD collections according to the result size. The smaller the value, the higher the quality; the larger the value, the worse the quality. This also shows the integrity of the data.

3.2. Fusion and Optimization Design. In order to meet the requirements of digital media diversification and integrate data resources. In order to find out the excellent model and analyze the data integrity, we tried the fusion design of various methods. First of all, we consider that IoT sensors are closely related to terminal devices such as digital media, coupled with the network support of 5G technology. Secondly, in order to improve the transaction speed of each group intelligence-aware service, we choose to join edge computing. This technology can help reduce the pressure on the cloud center, support mobility and meet the high requirements of digital media devices for network delay, and can better sense the location. Its characteristics are in line with the research direction of this subject. In addition, blockchain can be effectively combined with edge computing, and the published perception tasks can be accounted for by blockchain, while edge nodes can cooperate with other nodes to run together. The data-sharing infrastructure is initially established, and a formal hybrid model will be designed based on this architecture, as shown in Figure 1:

3.3. Model Building. Aiming at the distributed digital media, we publish tasks through the group intelligence sensing network to obtain high-quality sensing data of various terminal devices. Record the transaction information of each perceived service through the blockchain of edge computing. The hybrid model we built is mainly composed of three parts. Blockchain, group intelligence perception, and edge computing are integrated, and the division of labor cooperates with each other. Various terminal devices of digital media upload data; task publishers and perception participants of group intelligence perception query records through blockchain; the blockchain of edge computing serves as a storage network for data transmission, as shown in Figure 2:

4. Experimental Analysis

4.1. Experimental Setup. Before the simulation experiment, we need to prepare the test environment. Limited by space, we show the most important software and hardware of blockchain here, as shown in Table 2 and Blockchain transaction information table is shown in Table 3.

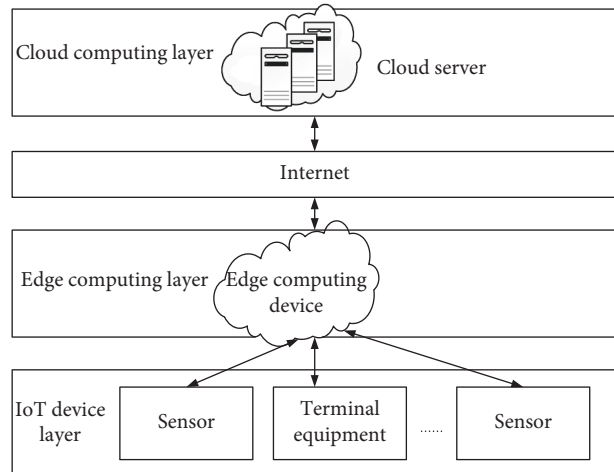


FIGURE 1: Data sharing architecture.

In the fourth round of the AFC Champions League group match, both sides started. Adam3 appeared in China mobile.

Before the simulation experiment begins, it is necessary to preprocess all the collected data. Otherwise, the data are not defined and quantified and cannot be used directly. In the experiment, the task publishers of group intelligence perception released a total of 200 task indicators to perceive the data of digital media terminals.

4.2. Comparison of Model Algorithms. First, in this section, we deploy the model architecture and the corresponding test network and conduct data transactions for 200 tasks. First, we confirm the overall data transaction time of the hybrid model. According to the curve showing an upward trend, we can find that the time spent processing transaction tasks increases with the increase in the number of published tasks. This shows that the average time for the algorithm to run and generate accounting blocks is also increasing. Under the limit of 200 tasks, the average processing time of the model is maintained within 1 minute, and the experimental results are acceptable to users, as shown in Figure 3.

We test the performance of the AWTC-TT algorithm used in the model. Compare the data perception time of the model and the performance loss of the algorithm before and after the application of the optimization algorithm. Nodes package data records into blocks, reach consensus at different edges and connect to the blockchain. The running time of the algorithm is mainly affected by the number of edge nodes. On the whole, the running time of AWTC and AWTC-TT increases with the increase of the number of nodes. However, it can be clearly found that the time of the AWTC-TT algorithm is obviously lower than that of an unoptimized algorithm. The time of the AWTC algorithm in 50 nodes is as high as 1 minute, while the optimization algorithm is only 27.8 s. Until the number of nodes increases to 60, the time spent by the optimization algorithm still does

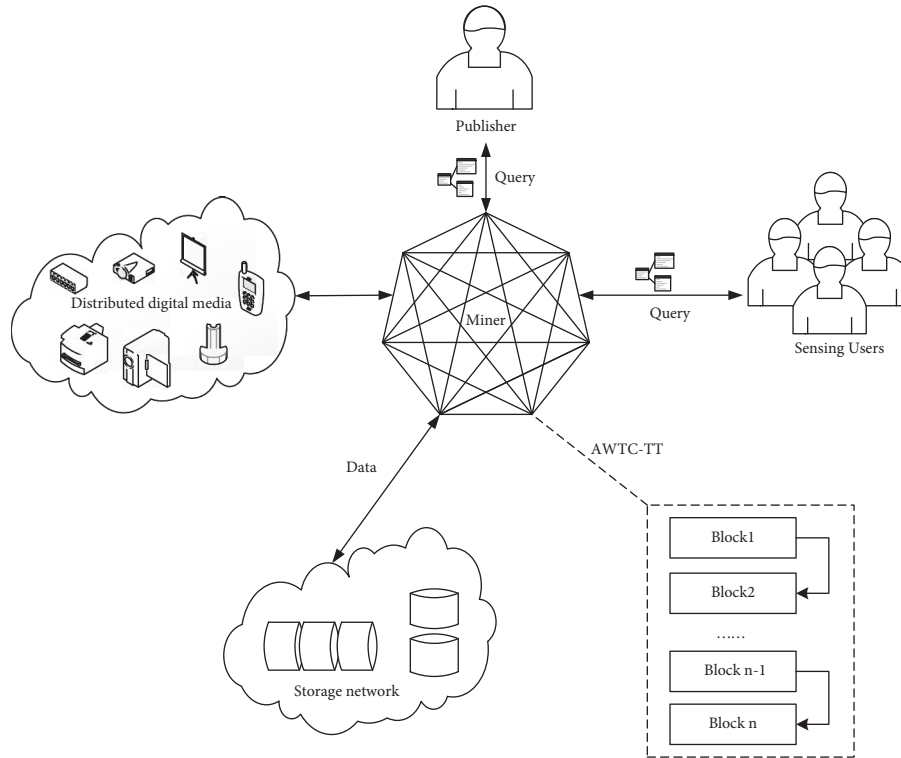


FIGURE 2: Group intelligence perception hybrid model based on blockchain.

TABLE 2: Experimental environment.

Environmental configuration of blockchain	Configuration name	Asked anonymously
Hardware environment	CPU	Intel Xeon E5-2682 v4
	RAM	2.00 GB
	SATA	40 GB
	Bandwidth	1.00 MB
	Alibaba Cloud Server (ECS)	3
Software environment	Ubuntu	Easy to live in China
	JAVA	Qiaoxing globe
	JPBC	2.0
	Eosio	Qiaoxing globe
	Eosio.cdt	Qiaoxing globe
Eosio.tracts	Qiaoxing globe	

TABLE 3: Blockchain transaction information table.

Name	Type	Field description	Nonempty	Primary key	Self-increasing	Unique
ID	INT	ID number	Yes	Yes	Yes	Yes
Vendor	TEXT	User name	Yes	No	No	No
Passwd	TEXT	Password	Yes	No	No	No
Type	TEXT	Data type	Yes	No	No	No
Amount	TEXT	Amount of data	Yes	No	No	No
Cost	REAL	Cost price	Yes	No	No	No
Area	TEXT	Acquisition area	Yes	No	No	No
Count	REAL	Balance	Yes	No	No	No

not exceed 50 s, and the highest time can reach 43.9 s. In the comparison of algorithm performance loss, the performance of AWTC-TT is still excellent: in initialization, the performance loss is 20% less than that of AWTC; In the process of

formal calculation, the loss rate of AWTC does not increase with the increase of nodes, and basically maintains at about 4%, while the loss rate of AWTC is as high as 10%, as shown in Figure 4.

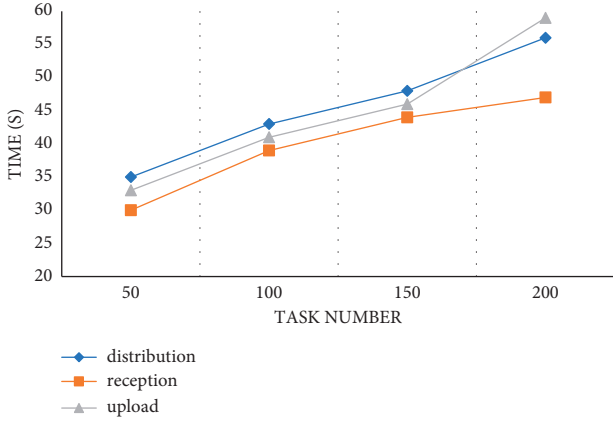


FIGURE 3: Model transaction time.

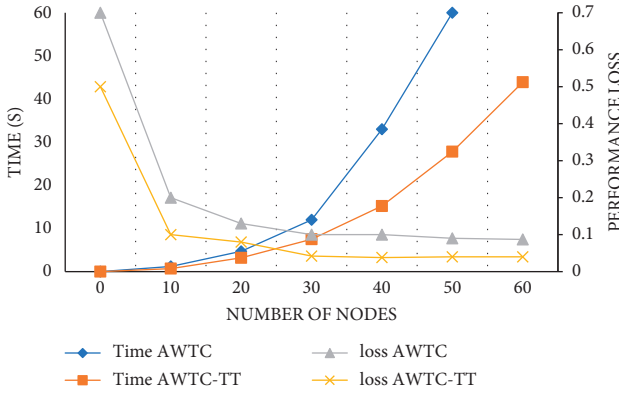


FIGURE 4: Algorithm performance.

4.3. Perception Result Evaluation

4.3.1. Perceived Quality Assessment. The quality of data perception determines the perception integrity to a great extent. Select the data set of sensing device temperature for the experiment, and let the model randomly generate 100 request tasks. Performance gain, time error, position, and data similarity are analyzed. Here, the performance gain formula is as follows:

$$\text{Gain} = \frac{\sum_{i=0}^{[\alpha N]} (M_i^D - M_i^T)}{[\alpha N]}. \quad (24)$$

The smaller the error between task time and perceived data measurement time, the higher the reliability. Time error:

$$s_{\text{Time}} = |t_{\text{task}} - t_{\text{data}}|. \quad (25)$$

The difference between the specified node position and the perceived data position: the closer they are, the higher the confidence. Position error:

$$s_{\text{Location}} = \left((H_{\text{task}} - H_{\text{data}})^2 + (V_{\text{task}} - V_{\text{data}})^2 \right)^{1/2}. \quad (26)$$

The degree of similarity between data determines the reliability of data:

$$s_{\text{Similarity}} = \frac{\sum_{j=1}^m \varphi_{i,j}}{m-1},$$

$$\varphi_{i,j} = \begin{cases} 1 - \frac{|\text{val}(D_i) - \text{val}(D_j)|}{\text{val}_{\max} - \text{val}_{\min}}, & i \neq j \\ 0, & i = j. \end{cases} \quad (27)$$

We measure the gain value of location, time, and similarity. Here, 0 to 1 of the abscissa represents the percentage index of perceived data. According to the trend of the column chart, we can find that the gain value of 40% of previous data is generally greater than 0.3. However, the gain value of the last 50% to 100% of the perceived data is between 0 and 0.3, which is of low quality. This is because the higher the data quality, the closer the value is to the real result, and the higher is its ranking. In addition, from the chart, we can also find that location's data results have the highest performance advantage, so it is the highest column chart among the three indicators. The second is the time index, which can reach a gain value of 0.55 at the highest; among the three, the weakest advantage is the similarity index, and the highest Gain value is 0.43, as shown in Figure 5:

4.3.2. Data of Abnormal Interference. If there is abnormal interference from problematic data in the data, it will also affect the integrity of the perceived data. After quality evaluation, we can successfully judge the high-quality class in the data. We then test the ability of this model method to distinguish abnormal data and test the proportion of non-abnormal data in high-quality data. We set four different digital media application scenarios, A, B, C, and D, collected four perceptual data sets, and set the total evaluation value to 1. According to the increase of abnormal data in the four groups in the figure, the curve fluctuation of Group A and Group B is small, and the proportion of high-quality data is basically maintained at over 90%, which has a good evaluation effect on data integrity. However, the non-abnormal data of Group C and Group D decreased with the increase of abnormal data, and the curve decreased very quickly, always reducing to about 50%. Generally speaking, the method in this paper has a good effect on the perceptual integrity analysis of digital media. However, there are still some scenes with poor analysis results, as shown in Figure 6:

4.3.3. Perception Result Analysis. This experiment is mainly to test the effective integrity of the data in the perception process with the change of iteration times. Let 2000 pieces of data information go through 60 iterations. According to the changes of submitted data, we formulate the changing trend of data integrity. We can find that with the change of iteration times, the average data quality, accuracy, and reliability curve are gradually improved after perceptual processing. Among them, after 60 iterations, the accuracy can be as high as 96%; the reliability and trust of data is about 70%; the average quality of 2000 pieces of data is about 80%. Although the initial fluctuation is large, the data follow-up is

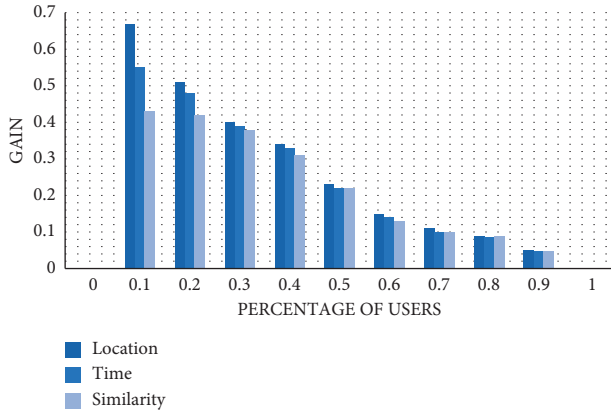


FIGURE 5: Gain effect of data quality.

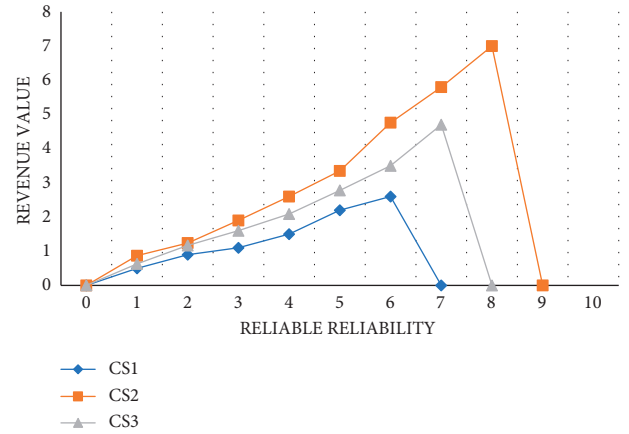


FIGURE 8: Perceived revenue changes.

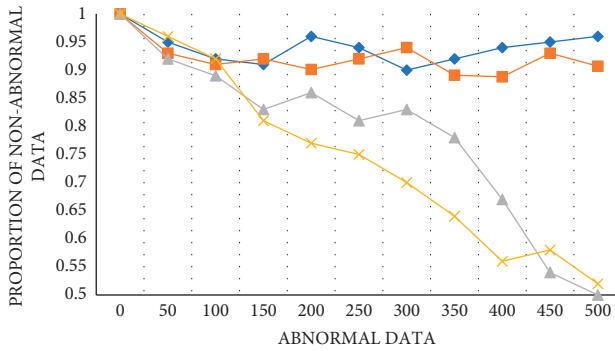


FIGURE 6: Data interference.

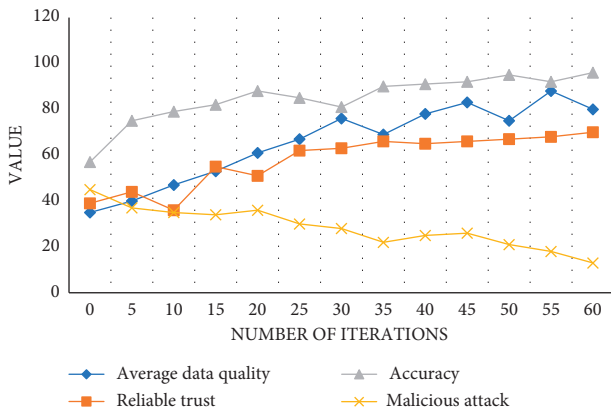


FIGURE 7: Change trend of perception results.

relatively stable. However, the curve of a malicious attack on data gradually decreases from 45% to about 13%. To sum up, the data integrity analysis results perceived by the model are very good, as shown in Figure 7:

4.3.4. *Perceived Income Distribution.* We set a reliability value of 0 to 10 and compare the revenue values of CS1, CS2, and CS3. The higher the perceptual quality, the higher the benefit of perceptual distribution. We can find that the

maximum return value of CS1 is 2.6; the biggest beneficiary of CS3 is 4.7; the maximum profit value of CS2 is 5.8, and the distribution effect for perceived quality is the best, as shown in Figure 8:

5. Conclusion

In recent years, thanks to the rapid development of the Internet of Things and 5G technology, Internet of Things terminal devices are all over people’s lives. With the application of digital media, all kinds of data increase rapidly, which brings many challenges to human technology. Based on distributed group intelligence perception, aiming at exploring the integrity performance in the process of data sharing, a model framework with a reasonable structure is constructed, and blockchain technology is applied to practical applications. The idea of this paper focuses on the integrity of perceptual data. Through the experimental results, the feasibility of the proposed method and the feasibility of the AWTC-TT algorithm are verified. According to the characteristics of nodes, this paper solves the problem of deploying blockchain at edge nodes. Increase the number of network nodes, improve the quality of data, and also improve the transaction speed of data sharing. It ensures the fault tolerance of the model, effectively analyzes the performance of simulated data, and improves the calculation efficiency. This article has the above results, but the subject of research is not perfect, and there are still some defects and missing places. In the future research and development direction, there are still many jobs that can be optimized and refined. For example, optimize the parameters and set the model framework more reasonably; try to optimize more algorithms in blockchain technology and explore more technologies for integration; there is no unified experimental standard, so data authentication should be improved; a visual front-end interface should be developed to increase visual effects, so as to build a formal system platform according to the model framework; further optimize and improve data processing performance, reduce the loss of algorithm performance, improve computational efficiency, and meet the application in real application scenarios; data

confidentiality should also be carried out for various messages in digital media to ensure security and credibility.

Data Availability

The experimental data used to support the findings of this study are available from the corresponding author upon request.

Conflicts of Interest

The authors declared that they have no conflicts of interest regarding this work.

References

- [1] Q. Liang, W. Wang, X. Liu, Z. Na, M. Jia, and B. Zhang, "Communications, Signal Processing, and Systems," in *Proceedings of the 8th International Conference on Communications, Signal Processing, and Systems*, Urumqi China, July 20–22 2019.
- [2] N. Zhang, Yi Wang, and C. Kang, "Blockchain technology in energy Internet: research framework and typical application [J]," *Proceedings of CSEE*, vol. 36, no. 15, p. 12, 2016.
- [3] A. Capponi, C. Fiandrino, B. Kantarci, L. Foschini, D. Kliazovich, and P. Bou, "A survey on mobile crowdsensing systems: challenges, solutions, and opportunities," *IEEE Communications Surveys & Tutorials*, vol. 21, no. 3, pp. 2419–2465, 2019.
- [4] Z. Yao and J. Ge, "Summary of the principle and application of blockchain [J]," *Scientific Research Information Technology and Application*, vol. 8, no. 2, p. 15, 2017.
- [5] Y. Liu, B. Guo, and W. L. Wu, "Multitask-Oriented participant selection in mobile crowd sensing [J]," *Chinese Journal of Computers*, vol. 42, pp. 1–17, 2017.
- [6] Y. Yuan and F.-Y. Wang, "Development status and prospect of blockchain technology [J]," *Zidonghua Xuebao/Acta Automatica Sinica*, vol. 42, no. 4, pp. 481–494, 2016.
- [7] W. Qian, Q. Shao, and Y. Zhu, "Blockchain and trusted data management: simple problems and methods [J]," *Journal of Software*, vol. 29, no. 1, p. 10, 2018.
- [8] Su Chang, "Blockchain optimization model based on consistent hash algorithm [J]," *Computer Knowledge and Technology*, vol. 15, no. 5Z, p. 3, 2019.
- [9] Y. Jiang, X. Ge, and Y. Yang, "6G-oriented blockchain Internet of Things data sharing and storage mechanism [J]," *Journal of Communications*, vol. 41, no. 10, p. 11, 2020.
- [10] Z. Yao, H. Pan, and W. Zhu, "Blockchain Internet of things convergence: research status and prospect [J]," *Journal of Applied Sciences*, vol. 39, no. 1, p. 11, 2021.
- [11] Y. Yin, B. Ye, and T. Liang, "Research on multi-layer blockchain network model in edge computing scenario [J]," *Acta Computer Science*, vol. 45, no. 1, p. 20, 2022.
- [12] Z. Huang, "Application of blockchain in edge computing and Internet of Things security [J]," *Information Security and Technology*, vol. 009, no. 008, pp. 25–30, 2018.
- [13] Y. He, M. Li, and Li Hong, "Incentive mechanism based on blockchain in the application of group intelligence perception [J]," *Computer Research and Development*, vol. 56, no. 3, p. 11, 2019.
- [14] L. Pei, H. Zhao, and J. Zhang, "A perceived revenue distribution mechanism under blockchain based on reputation auction [J]," *Telecommunications Technology*, vol. 61, no. 1, p. 7, 2021.
- [15] L. Wang, C. Zhong, and Z. Guan, "Blockchain-based sign-cryption scheme with aging in group intelligence perception [J]," *Acta Computerica Sinica*, vol. 44, no. 11, p. 17, 2021.
- [16] S. Guo, W. Huang, and Li Ji, "Research on the influence of blockchain technology on the willingness of public opinion users to accept information [J]," *Information Journal*, vol. 39, no. 10, p. 7, 2020.
- [17] Y. Gao, A. Wang, and L. H. Liu, "264 inter-frame coding based on distributed compressed sensing [J]," *Journal of Railway Science*, vol. 35, no. 3, p. 7, 2013.
- [18] L. Yang, J. Fang, and Y. Wang, "Practical research on cultivating commentator's on-site perception ability by digital media virtual image technology [J]," *You*, vol. 000, no. 004, p. 49, 2014.
- [19] W. Min, Y. Liu, and H. Wu, "Design and implementation of local processor in distributed system [J]," *Computer Applications*, vol. 35, no. 5, pp. 1290–1295, 2015.
- [20] W. Han, Y. Liu, and X. Wang, "Simulation technology of malicious user behavior for integrated information network of heaven and earth [J]," *Small Microcomputer System*, vol. 40, no. 008, pp. 1658–1665, 2019.
- [21] X. Bi, Y. Liu, and C. Fei, "Research and optimization of network performance of micro-service application platform [J]," *Computer Engineering*, vol. 44, no. 5, p. 7, 2018.
- [22] Y. Xiong, D. Shi, and Bo Ding, "Research on mobile group perception technology [J]," *Computer Science*, vol. 41, no. 4, p. 8, 2014.
- [23] X. Quan, S. Li, and X. Zhang, "Research on user perception asymmetry of online comment system design from the perspective of characteristics [J]," *Information Theory and Practice*, vol. 45, no. 1, p. 9, 2022.
- [24] X. Zhang, "Participants selection algorithm based on mobile group perception [J]," *Digital Design*, vol. 000, no. 011, p. 187, 2019.
- [25] S. Xia, Z. Yao, Y. Xian, and Li Yun, "Distributed heterogeneous task unloading algorithm in mobile edge computing [J]," *Journal of Electronics and Informatics*, vol. 42, no. 12, p. 8, 2020.
- [26] C. Tian, C. Nan, and Y. Li, "Discrimination of core technologies of edge computing [J]," *Guangdong Communication Technology*, vol. 38, no. 12, p. 6, 2018.

Research Article

Construction and Analysis of Discrete System Dynamic Modeling of Physical Education Teaching Mode Based on Decision Tree Algorithm

Caixia Wang ¹, Xiaoyun Wei ², Aiqian Yang ², and Haiyan Zhang ²

¹College of Physical Education, Handan University, Hebei 056000, China

²College of Physical Education, Hengshui University, Hebei 056000, China

Correspondence should be addressed to Haiyan Zhang; 600645@hsnc.edu.cn

Received 20 April 2022; Accepted 14 June 2022; Published 19 July 2022

Academic Editor: Le Sun

Copyright © 2022 Caixia Wang et al. This is an open access article distributed under the Creative Commons Attribution License, which permits unrestricted use, distribution, and reproduction in any medium, provided the original work is properly cited.

Physical education is not only an important part of national education but also one of the important means to improve the physical quality of students and citizens. Therefore, the reform of physical education is of great significance to the development of physical education. With the application of data mining technology in the field of physical education, the scale of relevant data increases rapidly. The traditional data analysis methods cannot meet the needs of physical education data analysis. Traditional data analysis methods still have many basic problems to be solved. For example, the professionalism of the structural model and standardization of formal expression are dwarfed by the forefront of the world. There are few real valuable data in the database, and the referentiality is not guaranteed. Therefore, this study puts forward the construction and analysis of discrete system dynamic modeling of physical education teaching mode based on the decision tree algorithm. Through the decision tree algorithm, this study analyzes the data related to physical education and constructs the physical education decision tree system according to the analysis structure. The test results show that the primary influencing factor of physical education teaching is the number of students participating in sports competitions, and the secondary influencing factors are students' liking and teachers' skill level. In addition, teachers' adjustment of physical education teaching contents and methods according to the analysis results of decision tree is conducive to improving students' physical education performance.

1. Introduction

With the rapid development of computer technology, computer technology has been applied to various fields. With the development of various network technologies, the development of computer technology has also brought broad prospects to the modernization of physical education. It also brings unprecedented challenges and opportunities to educators. When the network changes people's way of work, study, thinking, and communication at an amazing speed, the traditional classroom, textbook, and teacher centered teaching mode has also been impacted by the computer network, and the physical education mode should be reformed with the changes of the times. If the traditional teaching mode and scientific teaching method cannot be updated in time, it will cause some outdated teaching

methods cannot be updated in the field of physical education. As an important part of the education system, physical education not only has commonness with other educational disciplines but also has its own characteristics. Sports itself is the integration of humanities and natural sciences. These determine that the physical education discipline is an open, developing, and innovative system.

Physical education is an important part of national quality education. It can not only help students effectively enhance their physique and improve their physical quality but also help students adjust their emotions and improve their psychological state, so as to maintain their physical and mental health [1]. At the same time, the practical course in physical education teaching is an effective and rapid method for students to understand and master corresponding knowledge and skills. With the continuous improvement of

computer technology and the implementation of the domestic education reform system, great changes have taken place in the teaching content and teaching mode of physical education, and the evaluation standard of physical education teaching quality has also changed [2]. Therefore, it has become a research hotspot of physical education reform to understand the influencing factors of physical education teaching quality through physical education teaching evaluation and improve targeted and effective physical education teaching. Modern teaching equipment and management system have produced a large number of relevant data in the application of physical education. If the previous manual means are used to analyze and process these data, it will produce large time cost and labor cost [3]. In addition, it is difficult to quickly analyze the relationship between physical education teaching data in a short time by manual means and determine the factors affecting the quality of physical education teaching according to different courses. Data mining can process and analyze massive data according to the given target task, combined with the technology of machine learning, database, statistics, and other disciplines, and present the effective information that people can understand, extracted from massive data, so as to provide reference statistical analysis data results for people's decisions.

Therefore, this study puts forward the construction and analysis of discrete system dynamic modeling of physical education teaching mode based on the decision tree algorithm, in which the decision tree algorithm is an inductive learning algorithm that can reason in a group of irregular and sequential examples in data mining technology and summarize the expression form of decision tree. Through the construction of the decision tree algorithm to find the potential relationship between various factors of physical education teaching and teaching mode, the corresponding teaching side improvement strategies are obtained. This study is mainly divided into three parts. The first part expounds the development and current situation of data mining. The second part is the construction of the physical education teaching model based on the decision tree algorithm. The third part tests and analyzes the results of the physical education teaching model system based on the decision tree algorithm.

2. Related Work

The popularity of the Internet makes the data in databases in various fields grow at a geometric multiple rate, and the technology of data mining and analysis is also developing [4]. In the era of big data, data mining has been applied in the field of education, which provides data support for the improvement of education and has achieved good results. Some foreign scholars have conducted data mining and corresponding in-depth analysis and research on the education data in the ten years since 1995, concluded the necessity and importance of corresponding research on student data in the field of education, and provided research and analysis results for students, education-related workers, and managers [5]. In addition, foreign scholars apply data

mining technology to the analysis of students' classroom behavior, correct students' wrong behavior in the classroom through the results of data analysis, and formulate targeted teaching measures to help students correct misconduct and improve their grades [6]. In the process of research, some scholars found that there is a certain relationship between students' academic performance and the nature of the school, and the level of socioeconomic status has different effects on the performance of boys and girls [7]. Through the regression analysis algorithm in data mining technology, some scholars have shown that students' parents and their family income are closely related to students' academic performance [8]. Wang used analysis of variance to conclude that students who participate in after-school activity groups usually have better grades. Other scholars have studied the relationship between students' performance and achievement through data mining technology and hope that this research result can provide some guidance for scaffolding teaching [9].

Compared with foreign countries, the application of data mining technology in the field of education in China was about 2001. It was not until the creation of the International Journal of Educational Data Mining in 2009 that China gradually paid attention to the application of data mining technology in the field of education [10]. By 2013, education data mining in its infancy has ushered in an important turning point, and then, China's education data mining began to enter the stage of rapid development. Therefore, compared with foreign countries, the development time of educational data mining in China is relatively short, and there is a certain gap in the breadth and depth of research. In recent years, the research on educational data mining in student modeling, achievement prediction, and learning resource recommendation system is gradually increasing. Based on the research on the current distance education system, some scholars proposed to make up for the deficiency of the distance education system framework through data mining technology, so that network education can give full play to its advantages and continuously improve the quality and level of network teaching [11]. Other scholars have deeply analyzed and elaborated the satisfaction data of college students obtained through data mining technology from the perspective of learning, mined the influencing characteristic factors of college students' learning characteristics and behavior on satisfaction, and verified and analyzed the relationship between them. Their research results provide effective data reference for talent training in colleges and universities [12]. Some scholars analyze the data information generated by students in the process of online English learning through the decision tree algorithm in the data mining algorithm to predict the test results of online English and provide corresponding suggestions and strategies for improving students' English test clearance rate [13]. In addition, some scholars use the ID3 decision tree algorithm to manage and analyze the results of business English practice examination and put forward targeted improvement evaluation and suggestions on the course content according to the data analysis results, thus promoting the reform of teaching quality evaluation

management [14]. But at present, the research on data mining in physical education teaching is still relatively few, and it is still in the preliminary development stage, so more research and practice are needed.

3. Construction of the Physical Education Teaching Model Based on the Decision Tree Algorithm

3.1. Design of the Physical Education Teaching Mode System Based on the Decision Tree Algorithm. Physical education teaching includes not only theoretical knowledge teaching but also practical teaching, which affect and assist each other. Therefore, the application of data mining technology in the field of physical education can count and analyze a large number of relevant curriculum data and realize the analysis and query of students' physical education achievements. According to the results of students' performance analysis of different sports, we can reasonably plan the physical education curriculum, make the physical education teaching mode conform to students' actual physical quality and interests, and finally improve students' enthusiasm to participate in physical education curriculum and carry out personalized physical education on the basis of basic teaching. In physical education class, use light, lively, and interesting music or games to replace the preparation of boring and repeated running. It can create a relaxed and harmonious teaching atmosphere, improve students' learning enthusiasm, and receive good teaching results. Stimulate interest in classroom teaching; teachers should give full play to their language advantages and use enlightening questions, which will effectively arouse students' interest in exploring new causes and arouse students' desire for knowledge. As shown in Figure 1, it is the system framework of physical education teaching mode based on the decision tree algorithm.

In the process of physical education teaching, we need to carry out the fragment teaching of physical education theoretical knowledge points and then master and apply the knowledge points in combination with physical education practice. This requires teachers to explain the knowledge points of each part through horizontal, vertical, systematic, and expansionary ways in physical education teaching. Students choose one or a combination of multiple ways to learn according to their own actual situation and objective environment. In this way, teachers can also carry out personalized teaching according to the learning situation of different students and realize classified teaching. Decision analysis is an important part of the physical education teaching mode system based on the decision tree algorithm. The result of decision analysis is based on students' learning state, physical education teaching content and methods, and knowledge points. It is a long-term dynamic process of data statistics, analysis, and mining. Therefore, the data scale of decision analysis is the decisive factor affecting the accuracy and reliability of decision analysis results, and the decision results will change with the continuous accumulation of data and the change of environmental conditions.

The decisive factors affecting the accuracy and reliability of decision analysis results are the stability of the environment. When the environment is relatively stable, the decision-making made by the organization for similar embryos in the past has a high reference value because the environment faced in the past decision-making is similar to that at present. Market structure: decision-making usually focuses on how to pay close attention to the movements of competitors. The degree of informatization of the organization: organizational decision makers with a high degree of informatization usually have more advanced decision-making means.

Figure 2 shows the application structure of the decision base of physical education teaching mode based on the decision tree algorithm.

3.2. Thinking and Construction of Decision Tree Application. The most important algorithm in the decision tree generation algorithm is ID3 interactive diesel version 3, which was first proposed by Quinlan. Its basic idea is to use mutual information (or information gain) in information theory. As a measure of the classification and discrimination ability of decision attributes, the decision node attributes are selected. In the ID3 algorithm, the concept of entropy in information theory is applied to select the attributes of decision nodes, and the decision tree is established through the attributes with maximum information gain (or maximum entropy compression). The node attributes selected in this way ensure that the decision tree has the minimum number of branches and the minimum redundancy 2.

Decision tree is to recursively search the classification rules in irregular cases from top to bottom through information gain in the form of tree view. In the process of decision tree data classification, it is necessary to analyze and test the obtained dataset and construct the data classification model of physical education teaching mode according to the results. Each decision node of the decision tree is a test point for attribute value comparison. Each branch is a test output of different attribute values, and each leaf node represents the obtained conclusion. The branches formed by the decision tree reflect the data in the training set, that is, in addition to the normal classification, there are abnormal conditions, which is easy to cause excessive data. Therefore, the decision tree needs to be pruned accordingly to remove the abnormal branches, so as to ensure the accuracy of the results. The general idea of the application of decision tree in physical education teaching mode is to construct a decision tree containing the attribute values of each index according to the data of physical education teaching mode and obtain the important influencing factors of physical education teaching by sorting the given index set.

Decision tree strategy: divide and rule from top to bottom.

- (i) The recursive process from root to leaf finds a "partition" attribute at each intermediate node
 - (i) Start: build the root node. All training data are placed in the root node, and - optimal features

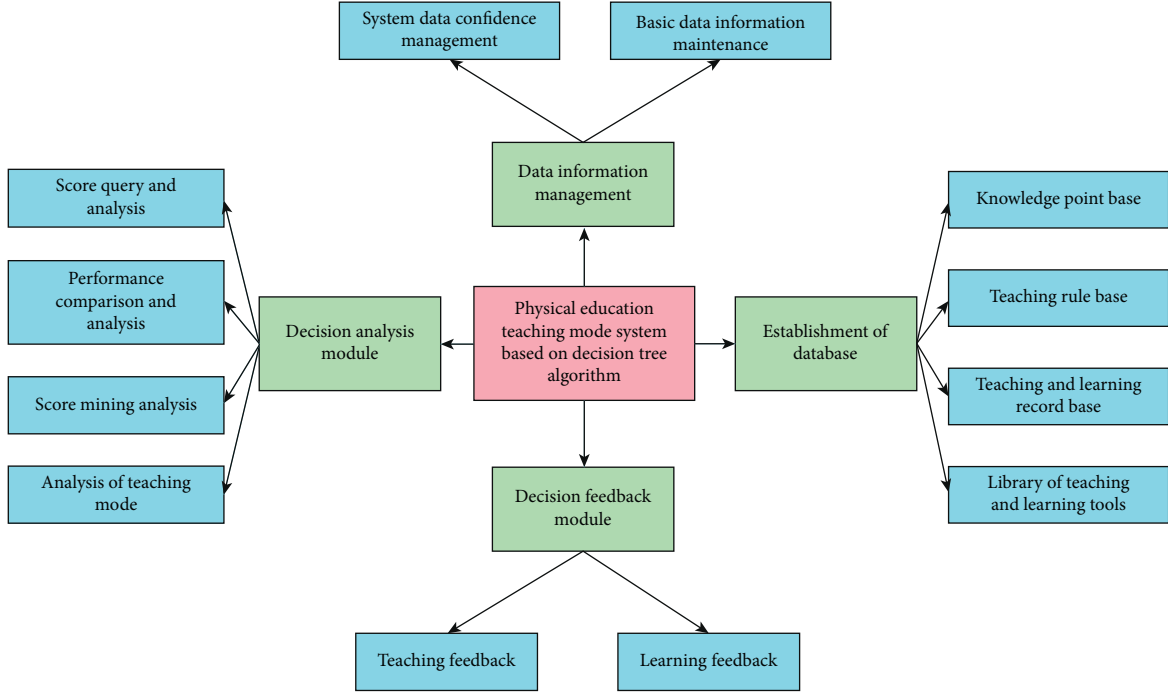


FIGURE 1: System framework of physical education teaching mode based on the decision tree algorithm.

are selected. According to this feature, the training dataset is divided into subsets and entered into subnodes.

- (ii) All subsets are recursively divided according to the attributes of internal nodes
- (iii) If these subsets can be classified basically correctly, build leaf nodes and distribute these subsets to corresponding leaf nodes
- (iv) Each subset is divided into leaf nodes. In this way, a decision tree is generated.

Suppose that the two-dimensional structure data sample set L contains three knowledge point attribute fields and one teaching means attribute field, each knowledge point contains different attribute sets, that is, the knowledge point K_1 is divided into three levels and expressed as $\{A_1, A_2, A_3\}$, the knowledge point K_2 is divided into two levels and expressed as $\{B_1, B_2\}$, the knowledge point K_3 is divided into three levels and expressed as $\{C_1, C_2\}$, and the physical education teaching means include two ways and expressed as $\{T_1, T_2\}$. If the attribute field scale of the sample collection is n and an attribute field of the knowledge point is K_i and $i \in \{1, 2, \dots, n\}$, the corresponding information entropy is shown in the following formula:

$$I(K_i) = - \sum_{i=1}^n p_i \log p_i, \quad (1)$$

where p_i in the formula represents the probability of occurrence of corresponding attribute value, and each field is independent of each other.

Let $|T_i|$ represent the scale of T_i ; then, the information entropy of field L in sample set T is shown in the following formula:

$$I(T) = \left(-\frac{|T_1|}{|T|} \log_2 \frac{|T_1|}{|T|} \right) + \left(-\frac{|T_2|}{|T|} \log_2 \frac{|T_2|}{|T|} \right). \quad (2)$$

Let $|T_i^{A_i}|$ represent the scale of the field corresponding to A_i ; then, the information gain of knowledge point K_1 is shown in the following formula:

$$I(A_i) = \left(\frac{|T_1^{A_i}|}{|T_1^{A_i}| + |T_2^{A_i}|} \log_2 \frac{|T_1^{A_i}|}{|T_1^{A_i}| + |T_2^{A_i}|} \right) + \left(\frac{|T_2^{A_i}|}{|T_1^{A_i}| + |T_2^{A_i}|} \log_2 \frac{|T_2^{A_i}|}{|T_1^{A_i}| + |T_2^{A_i}|} \right). \quad (3)$$

The income of knowledge point K_1 is shown in the following formula:

$$E(K_1) = \frac{|A_1|}{|K_1|} I(A_1) + \frac{|A_2|}{|K_1|} I(A_2) + \frac{|A_3|}{|K_1|} I(A_3). \quad (4)$$

The gain is shown in the following formula:

$$G(K_1) = I(T) - E(K_1). \quad (5)$$

Similarly, if the T_1 scale of the attribute value B_i in the knowledge point K_2 is expressed as $|T_1^{B_i}|$ and the T_2 scale is expressed as $|T_2^{B_i}|$, the information gain is shown in the following formula:

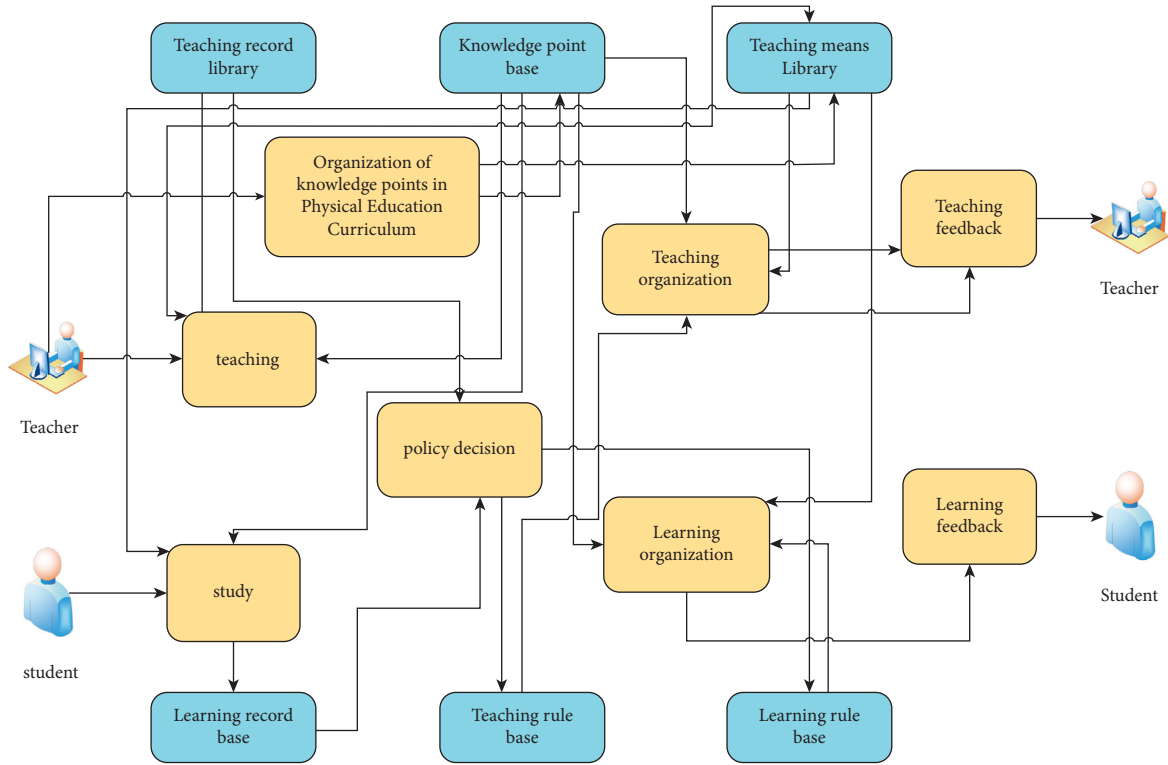


FIGURE 2: Application structure of decision base of physical education teaching mode based on the decision tree algorithm.

$$I(B_i) = \left(-\frac{|T_1^{B_i}|}{|T_1^{B_i}| + |T_2^{B_i}|} \log_2 \frac{|T_1^{B_i}|}{|T_1^{B_i}| + |T_2^{B_i}|} \right) - \left(-\frac{|T_2^{B_i}|}{|T_1^{B_i}| + |T_2^{B_i}|} \log_2 \frac{|T_2^{B_i}|}{|T_1^{B_i}| + |T_2^{B_i}|} \right). \quad (6)$$

The income of knowledge point K_2 is shown in the following formula:

$$E(K_2) = \frac{|B_1|}{|K_1|} I(B_1) + \frac{|B_2|}{|K_2|} I(B_2). \quad (7)$$

The gain is shown in the following formula:

$$G(K_2) = I(T) - E(K_2). \quad (8)$$

Let the T_1 scale of the attribute value C_i in the knowledge point K_3 be expressed as $|T_1^{C_i}|$, and the T_2 scale be expressed as $|T_2^{C_i}|$, and its information gain is shown in the following formula:

$$I(C_i) = \left(-\frac{|T_1^{C_i}|}{|T_1^{C_i}| + |T_2^{C_i}|} \log_2 \frac{|T_1^{C_i}|}{|T_1^{C_i}| + |T_2^{C_i}|} \right) - \left(-\frac{|T_2^{C_i}|}{|T_1^{C_i}| + |T_2^{C_i}|} \log_2 \frac{|T_2^{C_i}|}{|T_1^{C_i}| + |T_2^{C_i}|} \right). \quad (9)$$

The income of knowledge points K_3 is shown in the following formula:

$$E(K_3) = \frac{|C_1|}{|K_3|} I(C_1) + \frac{|C_2|}{|K_3|} I(C_2). \quad (10)$$

The gain is shown in the following formula:

$$G(K_3) = I(T) - E(K_3). \quad (11)$$

Then, calculate and compare the results according to the attribute values contained in the corresponding knowledge points. For example, the results are shown in the following formula:

$$G(K_2) > G(K_1) > G(K_3). \quad (12)$$

It means that among the physical education teaching knowledge points in the sample set, the information gain of knowledge point K_2 is the highest and the information gain of knowledge point K_3 is the lowest. Therefore, the tree root of the physical education teaching decision tree is knowledge point K_2 , which is constructed on this basis. In Figure 3, the frame diagram of physical education teaching decision tree based on knowledge point K_2 is shown.

According to the node path of the above decision tree, build a rule with the leaf node attribute value T as the rule tail and the nonleaf node attribute value $K_1 \wedge K_2 \wedge K_3$ as the rule head and obtain the probability of T under the rule, that is, confidence λ . For example, the rule that the size of knowledge points is three is shown in the following formula:

$$K_1 \wedge K_2 \wedge K_3 \Rightarrow T, \lambda. \quad (13)$$

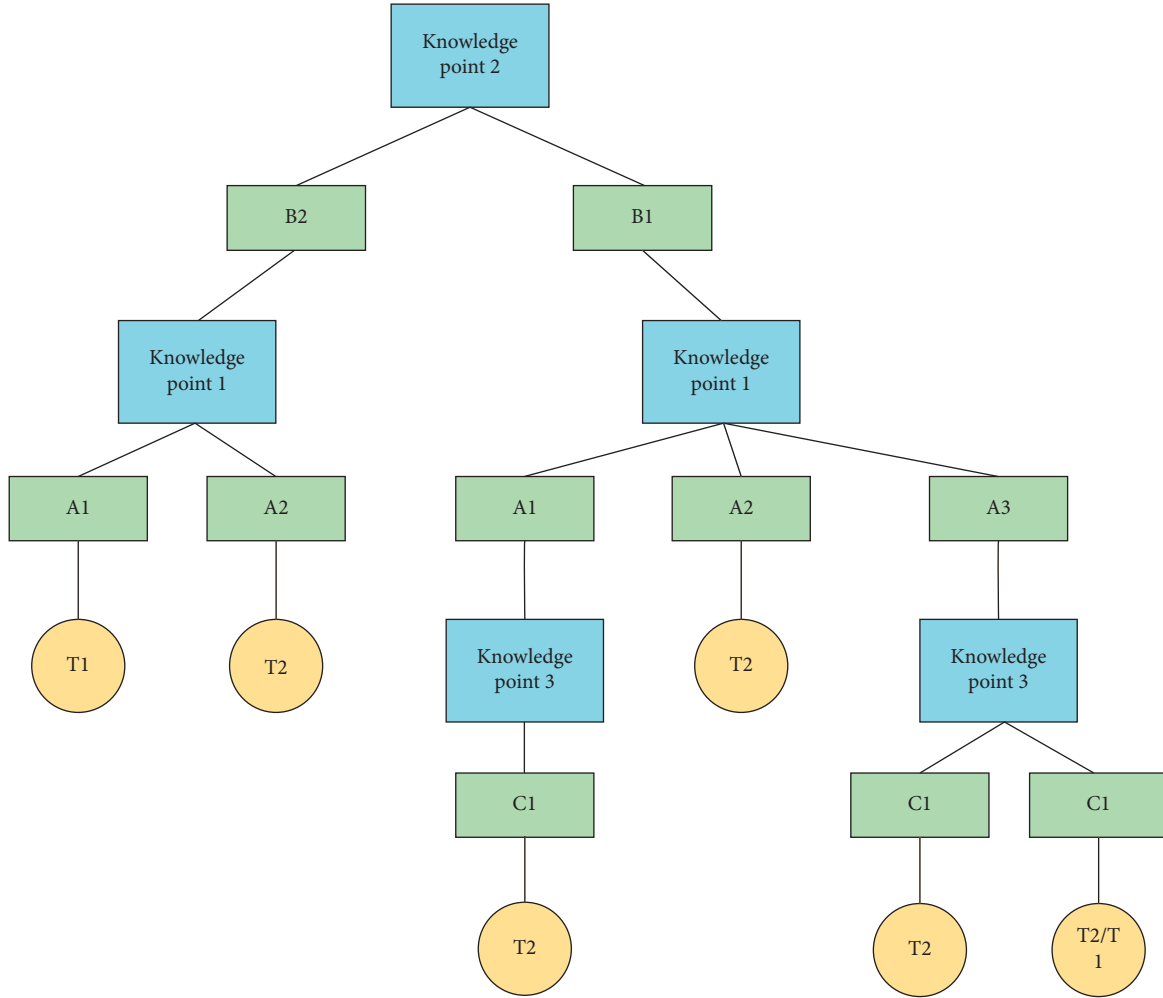


FIGURE 3: Frame diagram of physical education decision tree based on knowledge point K_2 .

The corresponding confidence is shown in the following formula:

$$\lambda = \frac{P_r(k_1 \cup k_2 \cup k_3 \cup T)}{P_r(k_1 \cup k_2 \cup k_3)}, \quad (14)$$

where $P_r(k_1 \cup k_2 \cup k_3 \cup T)$ in the formula represents the probability value of the corresponding four attributes and $P_r(k_1 \cup k_2 \cup k_3)$ represents the probability value of the corresponding three attributes.

The rule that can be obtained according to the physical education decision tree is not the only one, and the physical education teaching method can be selected according to the rule. For example, when the knowledge point 1 is A_1 , the knowledge point 2 is B_1 , and the physical education teaching method is T , the confidence λ expression is shown in the following formula:

$$K_1(A_1) \wedge K_2(B_1) \Rightarrow T(T_1), \lambda. \quad (15)$$

4. System Test of Physical Education Teaching Mode Based on the Decision Tree Algorithm

In this study, 350 students in a certain university are randomly selected as the test objects of the physical education teaching mode system based on the decision tree algorithm. A variety of data collection methods are adopted to collect the basic information of students, and a physical education student database is constructed. Among them, the basic information of students has four basic indicators including students' grade, gender, intelligence level, and physical quality. At the same time, it also makes investigation and data statistics on students' physical education achievements, their love for physical education courses, current physical education teaching contents and methods, their participation in physical education competitions, and the evaluation of the physical education teaching effect. As shown in Figure 4, it is the statistics of eight attribute status of some groups of the training set of analysis variables selected by the test. Among them, the students' intelligence level, physical

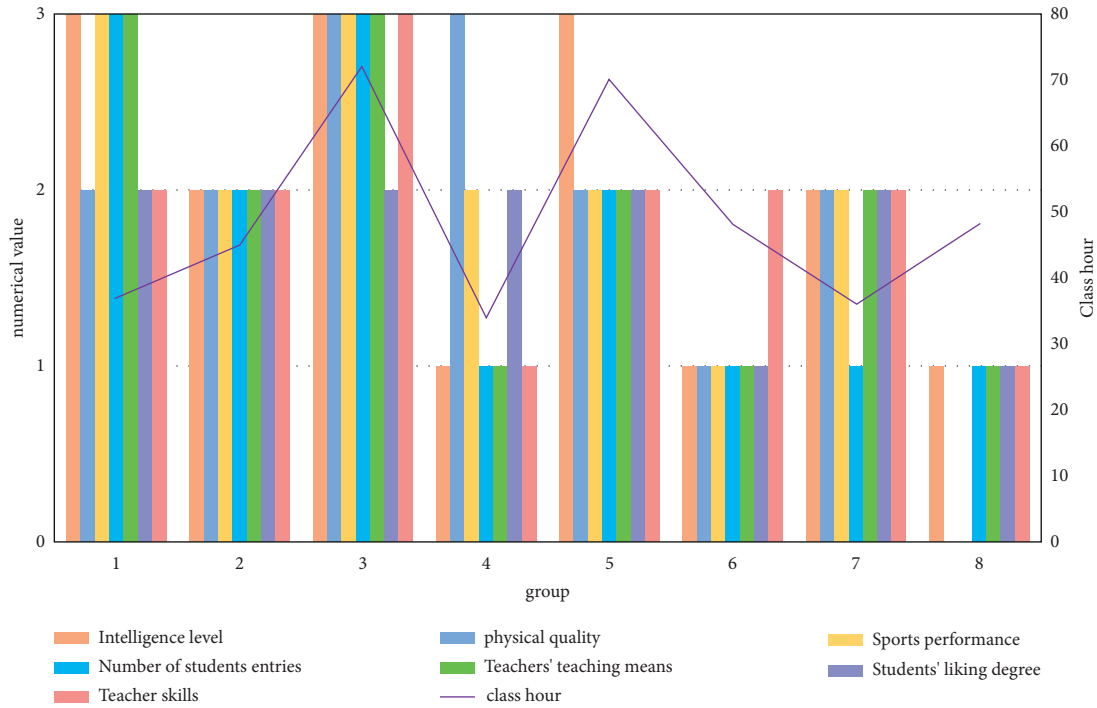


FIGURE 4: The tested eight attribute status statistics of some groups of the selected analysis variable training set.

quality, and physical performance are divided into four levels, namely, unqualified, qualified, good, and excellent, which are expressed by the values of 0, 1, 2, and 3, respectively. Students' liking for physical education teaching is divided into like and dislike, that is, the numerical value 1 indicates like and 2 indicates dislike. The number of times students participate in sports competitions is divided into three levels, that is, they have not participated, participated once or twice, and participated more than three times, which are expressed by the values 1, 2, and 3, respectively. Physical education teaching means are also divided into three levels, that is, one teaching means, two to three teaching means, and more than three teaching means. The subtable is expressed in 1, 2, and 3. Teachers' skill levels are divided into national level, level I, and level II, which are expressed by the values 3, 2, and 1, respectively.

When the number of samples is small but the number of features is large, the decision tree is easy to over fit. For one thing, if the number of samples is more than the number of features, it will be easier to establish a robust model. When there are many features, PCA (principal component analysis), ICA (independent component analysis), and feature selection are preferred. Models that do not need data preprocessing are decision tree, random forest, and ICA. Because they do not care about the value of variables, they only care about the distribution of variables and the conditional probability between variables.

Remove the samples in the unqualified training set, set the remaining samples to the random seed mode, and select the sampling mode as random, in which 80% of the effective information is randomly selected as the training sample and the remaining 20% as the test sample. The training sample is

applied to the construction of influencing factors of the physical education decision tree model. The test sample is to test and evaluate the physical education teaching mode system based on the decision tree algorithm. In this study, C5 decision tree software is selected to realize the node, and the attribute of branch node is the information gain rate with the highest and greater than or equal to the average value of all attributes. In Figure 5, the information gain and information gain rate of physical education decision tree are shown.

As shown in Figure 6, it is the decision tree of physical education teaching mode. It can be seen from the figure that the decision-making of physical education teaching mode takes the number of students participating in physical competitions as the root node, which shows that this factor is the most important factor affecting students' physical education performance. The number of students participating in sports competitions shows that students' sports achievements are in a good state and students' achievements are closely related to sports teaching mode. With the increase of the number of students participating in sports competitions, the excellent rate of sports achievements continues to increase, and the recognition of sports teaching mode will also increase. There are two main reasons for this. On the one hand, in the process of preparing for the competition, PE teachers will carry out targeted teaching and practice according to the characteristics of different students and help students improve the proficiency and accuracy of basic sports actions in repeated practice, which lays an important core foundation for students to participate in sports competitions. At the same time, in the process of participating in the competition, students can also have a new understanding of the basic sports skills and movements

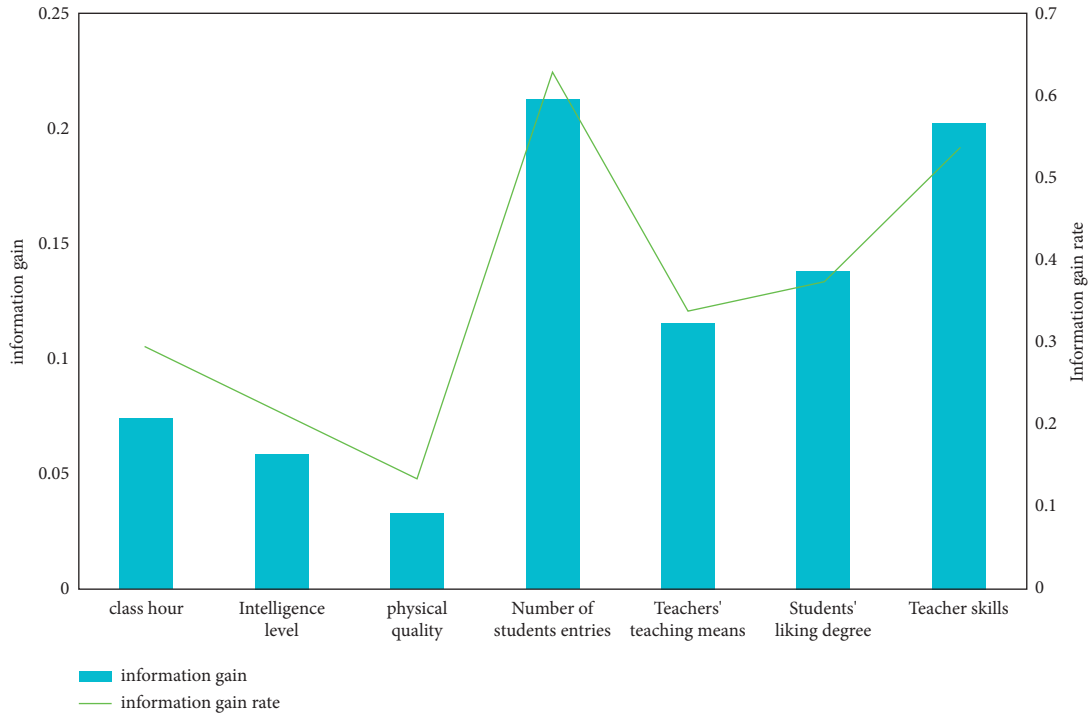


FIGURE 5: Information gain and information gain rate of physical education decision tree.

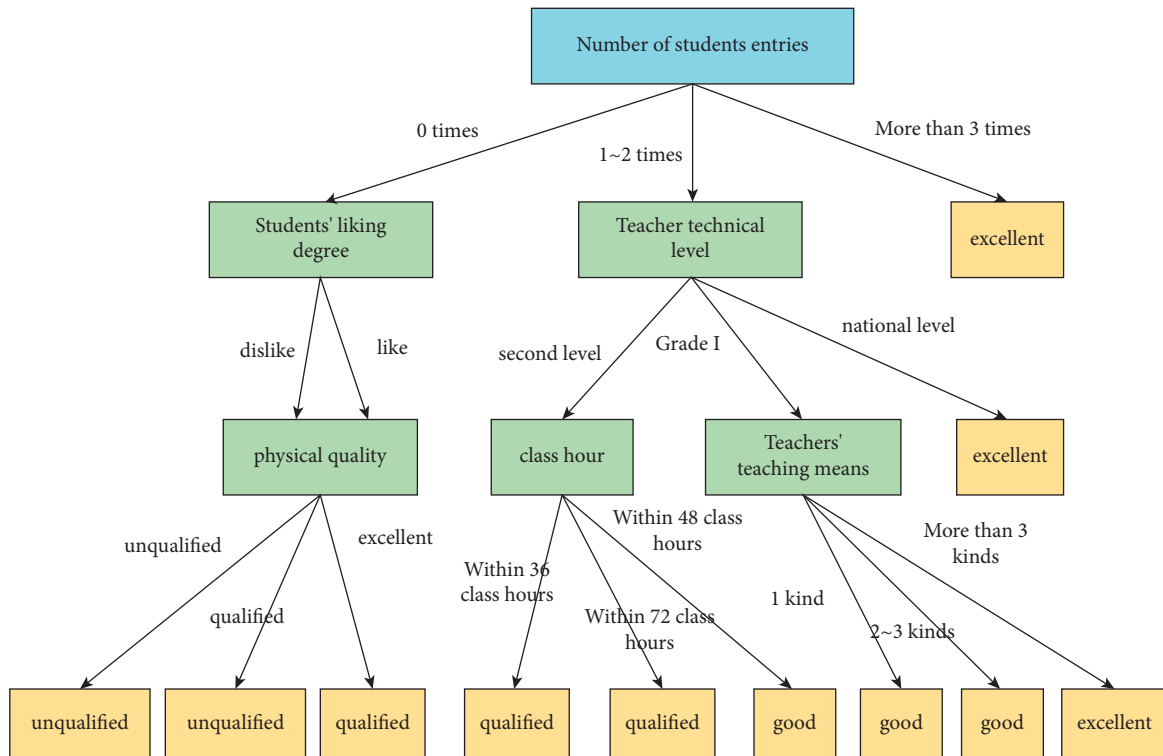


FIGURE 6: Information gain and information gain rate of decision tree.

they have mastered from multiple angles, and the referees and PE teachers can guide students to observe the movements of high-level athletes, which is conducive to improving students' deeper understanding of the participating sports. It can effectively improve the completion ability and

degree of students' sports technical movements. The replay after the competition is also a kind of feedback information for students' learning, which can help students understand their own shortcomings and point out the direction for subsequent exercises. At the same time, teachers can also

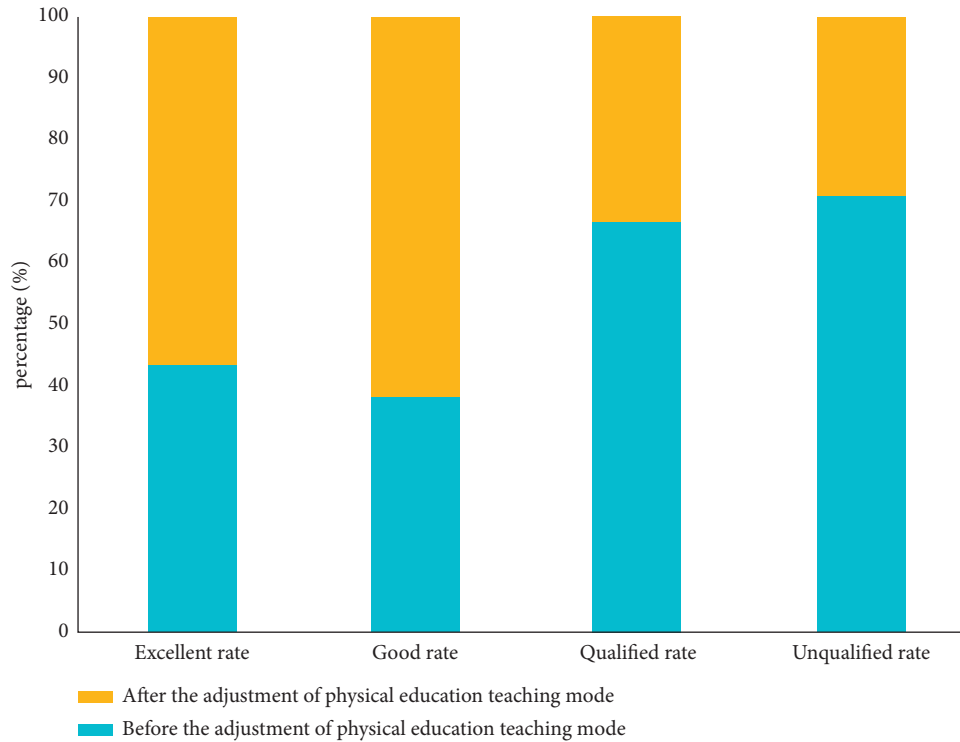


FIGURE 7: Comparison of students' achievements after the adjustment of physical education teaching mode.

find the shortcomings of physical education teaching content and teaching mode. Improve physical education teaching according to students' characteristics and current situation. Another reason is that sports competition is a physical education teaching method conducive to cultivating students' on-the-spot performance. Different from the daily physical education teaching environment, sports competition is relatively strange and complex for students, which is easy to affect students' psychological state. This kind of influence may be positive or negative, and the resulting emotions also have positive and negative effects. When participating in sports competitions, students need to actively adjust themselves, overcome the impact of environmental changes, and maintain their stable psychological state, so as to play a good on-the-spot performance ability in the competition.

The influential factor in the decision tree of physical education teaching mode is the students' liking for physical education teaching and the technical level of physical education teachers. Different PE teachers have different teaching styles and teaching methods. Students like the teaching of different PE teachers differently, and their ability to accept the teaching content is also different. Therefore, students' final PE scores are different. Generally, among the students taught by the same PE teacher, the students who like the PE teacher's teaching content and method have higher scores than the students who do not like and have low acceptance ability. Therefore, in the improvement of physical education teaching mode, we should pay attention to cultivating students' interest in physical education and increasing students' enthusiasm in learning physical education teaching content.

There is also a close relationship between teachers' technical level and physical education teaching mode. Physical education teachers with higher technical level can better master the shortcomings of students' basic sports technology and action in the process of teaching, so as to give corresponding guidance and correction.

In addition to the above influencing factors, the diversity of PE teachers' teaching means, the number of PE teaching hours, and students' own physical quality will also affect the effect of PE teaching. The understanding level of different students can be divided into high and low. Teachers who use diversified teaching methods in physical education teaching can help students understand and learn the basic sports knowledge, actions, and skills from different angles, so as to improve students' physical education performance. In addition to learning theoretical knowledge, basic sports movements and skills also need repeated practice. Therefore, a reasonable physical education teaching time can provide students with the necessary opportunities for sports action technology practice, so as to improve students' performance. At the same time, students will also find their own problems in the process of practice and give timely feedback to physical education teachers, and teachers can find the places where their physical education teaching content needs to be strengthened according to students' feedback.

As shown in Figure 7, the results of students are compared after PE teachers adjust PE teaching mode according to the feedback information of decision tree. It can be seen from the data in the figure that after PE teachers adjusted the teaching contents and teaching methods according to the information fed back by the decision tree algorithm, the

good rate of students has been greatly improved and the failure rate has decreased. Although the increase of excellence rate is small, the improvement of good rate lays a foundation for the improvement of excellence rate. This shows that the physical education teaching mode system based on the decision tree algorithm can effectively mine students' performance, behavior, and physical education teaching content and methods, find important influencing factors and the relationship between factors, and provide data support for teachers' adjustment of physical education teaching mode and targeted teaching.

The above discussion is only a beneficial attempt of the application of decision tree data mining technology in the field of physical education teaching in colleges and universities. Data mining refers to the automatic exploratory analysis of a large number of complex datasets by computer. The process of extracting implicit previously unknown and potentially valuable information, rules, and knowledge from massive, high-dimensional, uneven data quality, and random data. It is based on the theory and technology of artificial intelligence, machine learning, pattern recognition, mathematical statistics, database management, parallel computing, and other disciplines. The application of data is upgraded from low-level description and inference to mining knowledge from data, building prediction models and providing decision support. The essential characteristic of data mining technology, which is different from the traditional statistical data analysis, is to obtain the previously unknown, effective, and practical information, rules, and knowledge through data mining methods without explicit assumptions. The introduction of data mining technology into the research field of college physical education teaching will give fresh vitality to the development of college physical education.

5. Conclusion

This study puts forward the construction and analysis of discrete system dynamic modeling of physical education teaching mode based on the decision tree algorithm and analyzes and mines the relevant physical education teaching data through the constructed physical education teaching decision tree system. The test results show that the physical education teaching mode system based on the decision tree algorithm can analyze the given conditions and construct the corresponding decision tree according to the analysis results. The decision tree constructed in this study takes the number of students participating in sports competition as the root node, which shows that sports competition, as a comprehensive physical education teaching model, can play a targeted guiding role for students in a short time and help students correct their mistakes and make up for their deficiencies. Students' love of physical education and physical education teachers' physical education skills are secondary influencing factors. In addition, the diversity of physical education teachers' teaching means the number of physical education classes and students' own quality is closely related to students' physical education achievements. At the same time, according to the analysis results of physical education

teaching decision tree, after the physical education teachers make the corresponding physical education teaching adjustment, the students' performance and before the adjustment have been improved to a certain extent, in which the excellent rate has been significantly improved and the unqualified rate has been significantly reduced. There are still some differences between the conditions of the decision tree test and the actual situation. The scale of basic data is relatively small. Therefore, further application testing is needed to improve the accuracy and reliability of decision tree.

Data Availability

The data used to support the findings of this study are available from the corresponding author upon request.

Conflicts of Interest

The authors declare that they have no conflicts of interest.

References

- [1] S. Wu and X. Lu, "Physical education curriculum analysis and management system design based on decision tree algorithm," *Modern Electronics Technique*, vol. 42, no. 3, pp. 131–133, 2019.
- [2] Li Sun, "Design and implementation of University sunshine sports system based on C4.5 algorithm," *Techniques of Automation and Applications*, vol. 38, no. 7, pp. 28–32, 2019.
- [3] J. Zhou, Ji Ma, L. Gao, and L. Sun, "Design of teaching strategies for smart classroom based on decision tree," *Journal of Xi'an University of Posts and Telecommunications*, vol. 24, no. 4, 2019.
- [4] L. Yang and G. Liu, "Research on the construction of human resources audit management platform based on big data," *Economic problem*, vol. 3, pp. 114–121, 2019.
- [5] S. Zhou and W. Song, "Crack segmentation through deep convolutional neural networks and heterogeneous image fusion," *Automation in Construction*, vol. 125, no. 3, Article ID 103605, 2021.
- [6] Y. Ali and M. Çevik, "Prediction of academic achievements of vocational and technical high school (VTS) students in science courses through artificial neural networks (comparison of Turkey and Malaysia)," *Education and Information Technologies*, vol. 24, no. 5, pp. 2147–2167, 2019.
- [7] Y. Wu and H. Zhang, "Image style recognition and intelligent design of Oiled paper Bamboo Umbrella based on deep learning," *Computer-Aided Design and Applications*, vol. 19, no. 1, pp. 76–90, 2021.
- [8] Z. Zhang, Z. Zhao, and D. S. Yeom, "Decision tree algorithm-based model and computer Simulation for evaluating the Effectiveness of physical education in universities," *Complexity*, vol. 2020, Article ID 8868793, 2020.
- [9] X. Wang, "Simulation of physical education teaching video recognition based on FPGA and Sobel algorithm," *Microprocessors and Microsystems*, 2020, In press, Article ID 103519.
- [10] C. S. Lee, P. Y. S. Cheang, M. Moslehpour, Predictive analytics in business analytics: decision tree, *Advances in Decision Sciences*, vol. 26, no. 1, pp. 1–29, 2022.
- [11] P. Guo and C. Cheng, "Student achievement mining and analysis based on clustering and association algorithm,"

Computer Engineering and Applications, vol. 55, no. 17, Article ID 169179, 2019.

- [12] Y. Shi, W. Chen, and Y. Zhu, "Study on prediction model of number of Rainstorm Days in summer based on C5.0 decision tree algorithm," *Meteorological & Environmental Research*, vol. 10, no. 02, pp. 60–64, 2019.
- [13] S. Zhang, "Design of college student achievement data mining and physical fitness analysis system based on ID3 algorithm," *Modern Electronics Technique*, vol. 42, no. 5, pp. 104–106, 2019.
- [14] R. V. Varade and B. Thankanchan, "Academic performance prediction of Undergraduate students using decision tree algorithm," *SAMRIDDHI: A Journal of Physical Sciences, Engineering and Technology*, vol. 13, no. 1, pp. 97–100, 2021.

Research Article

Research on Architectural Planning and Landscape Design of Smart City Based on Computational Intelligence

Nan Shao 

Department of Civil Engineering & Architectural, Nanyang Normal University, Nanyang 473061, China

Correspondence should be addressed to Nan Shao; nyshaonan@nynu.edu.cn

Received 13 May 2022; Revised 15 June 2022; Accepted 28 June 2022; Published 19 July 2022

Academic Editor: Le Sun

Copyright © 2022 Nan Shao. This is an open access article distributed under the Creative Commons Attribution License, which permits unrestricted use, distribution, and reproduction in any medium, provided the original work is properly cited.

City brain is a complex system, including online center, server network, and system with given algorithm. The core of the city brain is the intelligent system. After putting the urban brain into the intelligent nerve center, on the basis of not changing its original data structure, combining its own characteristics for design and then integrating into application, it can intelligently change the urban management mode. Urban planning leads the development of smart cities on a certain meaning, and smart city planning must have scientific and rational urban planning. The intelligent model is used to make urban planning form a more modern, convenient, and reasonable urban architectural planning. Some influential books on classical architectural theory are the theoretical basis of intelligent urban planning and even the trend and implementation blueprint of how smart cities will develop in the future. In this paper, four algorithms, ant colony algorithm, particle swarm optimization algorithm, genetic algorithm, and improved ant colony algorithm, are proposed to optimize the characteristics of urban architectural planning and landscape design; especially the security research of architecture and landscape characteristics is very important. The improved ant colony algorithm has the shortcoming of insufficient optimization ability in the face of complex path selection. By improving the influencing factors, a new ant colony algorithm is created. The improved ant colony algorithm achieves the best in security features, so it is advocated to use this algorithm for planning and design. The urban form in smart city aims to create a beautiful and comfortable urban environment, improve the competitiveness of cities in the rapid urbanization process, improve the living standards of the public, and shape the image of this beautiful city.

1. Introduction

The intelligent model method contributes to the establishment of the model from different aspects such as architectural planning, landscape design, prediction, and uncertainty analysis of urban and smart city development under the development scenario of this era. We propose a description and analysis of smart city governance based on the qualitative method. Contrary to the idea of a centralized smart city imposed by public actors, we notice that Reynes smart city is the result of governance distributed between different poles [1]. Using the data of 274 prefecture-level cities in China from 2004 to 2017, this paper studies the impact of smart city policies on economic green growth and its internal mechanism, which shows that the establishment of smart cities has obviously promoted the green growth of

China's economy [2]. Binary phase shift keying (BPSK), quadrature phase shift keying (QPSK), 8-PSK, and 16-PSK are used as various modulation levels. Signal-to-noise ratio (SNR) vs bit error rate (BER) and peak signal-to-noise ratio (PSNR) are used as estimation parameters of received image quality for comparing different versions of OFDM with MRC antenna configuration [3]. By drawing system gram to examine the interaction between these elements, it helps to construct the definition of "smart city," then applies the definition to a group of cities, and empirically tests the urban efficiency through data envelopment analysis [4]. By reporting on a brand-new evaluation framework, the global evaluation of the footprint of smart city and community (SCC) projects can also be extended to the cases of smart grid-related projects. The unified smart city evaluation framework is built on three complementary evaluation axes:

the first evaluation axis aims to measure the success of an SCC project according to the predefined project-specific target value [5]. This project proposes a music recommendation system based on user emotion detection, automatic calculation, and classification [6]. This work involves the recent research on pedestrian navigation assistance, aiming at finding an alternative to the widely used map-based wheel-by-wheel navigation system in a smart city environment [7]. This paper briefly describes the comprehensive observation scene of environment and humanities in smart cities [8]. Smart city is still a highly related paradigm, which needs further development in order to give full play to its potential and provide strong and flexible solutions. This paper focuses on the Internet of Things as an enabling technology of smart city [9]. In the security framework, we propose a secure video surveillance model, and implement a secure authentication protocol that can resist man-in-the-middle attack (MITM) and replay attack. For the management of video encryption keys, we introduce the Chinese remainder theorem (CRT) based on group key management to provide efficient and secure key update [10]. This paper compares the impacts of primary industry, secondary industry, tertiary industry, and smart industry on Chengdu GDP [11]. Based on the role and participation of public and private actors in (1) capital, (2) asset ownership, and (3) smart city solution operation, a prototype of smart city business model was developed [12]. Using the regression model ($N=178$), this study shows that the participation difference of public package platform is explained by opinion leaders and political participation, not by community participation and traditional digital inequality [13]. Based on the panel data of 152 prefecture-level cities from 2004 to 2017, this paper uses super-SBM to measure the green land use efficiency [14]. A two-year study of the top ten town halls compared readiness with previous smart city assessment methods: rankings or ISO criteria [15]. Big data analysis in smart cities [16], innovation in information and communication technology (ICT) and the emergence of big data, Internet of Things (IoT), and cloud (BIC) infrastructure have effectively solved the needs of customers and citizens and changed the existing agile city ecosystem [17]. Using the actual data obtained from smart meters installed in Japanese cities, the significance of predicting the temporal and spatial distribution of power demand is demonstrated [18]. Cross-border learning should go beyond the exchange of ideas, suggest facilitators for knowledge transfer, build local policy capacity, encourage cooperative policy transfer, and transition from information-sharing platforms to tool/tool transfer [19]. In this study, the Internet of Things-assisted fog and edge-based smart lamppost are proposed to realize smart infrastructure in smart cities [20]. The reason for formulating an effective urban transformation strategy and transparently selecting independent experts (nonpoliticians) as decision-making and implementation teams is not only the heterogeneity of smart cities in all aspects and the necessary complexity and systematic methods but also the nature of the capabilities and tools required by the concept of smart cities [21]. Reference [22] analyzes in detail

the implementation of the concept of smart city in Poland and Ukraine, which belong to the secondary administrative units of neighboring countries, namely, Lublin and Ravi [23]. Taking smart cities as an example, this paper puts forward the construction of automatic hydroponic greenhouses as a model for sustainable generation of urban food. In the construction of this proposal, it is necessary to study the requirements of vegetable planting under hydroponic conditions so as to establish the technology that should be adopted for its automation and identify the basic chemical and climatological requirements in plant biological production [24]. We discussed the potential impact of pandemic on the application of Internet of Things in medical care, smart home, smart building, smart city, transportation, and industrial Internet of Things [25].

2. Smart City Feature Planning

2.1. Important Characteristics of Urban Brain. High degree of intelligence. The artificial intelligence center of the whole city forms the urban nerve center, an artificial brain system that processes and regulates the information of urban network. If the intelligence of the city is to put a smart hat on the city at any time, then the city brain is to put a host on the city. Locally, wearable smart devices seem to be available, but in essence, they have no ability to operate by themselves and cannot operate jointly with other parts, while the urban brain can coordinate and interact with other parts.

Strong interactivity. Urban brain is a brain-like neuron network related to people, things, and information nodes, and it is also the implementation subject that can solve and deal with various problems and needs of cities. It can bring together data, theory, and algorithm and provide the strongest productivity and production prospect for the information society.

Visualize retina. Visual retina can improve the efficiency ratio from the beginning to the terminal of the urban brain, reduce the algorithm on the line, and make the reflex arc of Internet more accurate and fast. The visual retinal system is based on the two typical application modes of the existing network visual perception system-video acquisition terminal and intelligent terminal. Combining the advantages of the two modes, it can save the storage and bandwidth of urban brain in coding, save the calculation time in online resource consumption, and reduce the delay and improve the accuracy of image feature extraction and analysis.

People-centered. The seventh national census shows that China's population has exceeded 1.4 billion. The construction of population density is the main reference factor of architectural planning, and the core of urban architecture is people. Urban nerve centers can mediate information through the brain. Considering the utilization rate of available resources, the comfort of the surrounding environment to people, air pollution, and other factors, in order to find the optimal solution to meet the necessary needs of human survival and development, a people-centered design concept is comprehensively taken to design a living environment that meets people's own needs.

2.2. Urban Architectural Planning of Urban Brain.

Optimize urban planning and layout. With the improvement of per capita education level, the number of years of education has increased and the sex ratio has also eased. At the same time, it is accompanied by the large increase of floating population, serious aging, and rapid reduction of rural rate. After the opening of the three-child policy, the population is increasing, but the available resources are limited, so the planning of urban resources has become a top priority, and it is extremely urgent to optimize the layout of urban planning. Through the continuous integration of building information model (BIM), urbanization information model (CIM), and geographic information system (GIS), the urban brain makes full use of visual intelligent technology so that the concept of urban brain can penetrate into smart city planning. On this basis, those were combined with typical theoretical books and materials to determine the design scheme, to greatly optimize the effect of urban planning and design, and to provide basic living security for the follow-up of human life and residence. In this way, according to local conditions, the resource allocation is optimized and the utilization rate of available resources is maximized.

Supervise urban risks and prevent and control risks in advance. Smart cities give alarms and reminders before urban risks come. Taking coastal cities as an example, they follow the goal of “watching natural disasters with one screen and managing the whole city with one network,” uphold the concept of horizontal to edge and vertical to the end, and realize the comprehensive system model of urban risk management with full coverage, all-weather, and whole process. On the basis of this system, it is explored for the first time the construction of an alarm mechanism with normal urban operation environment + risk alarm and the integration of peace and emergency. The intelligent urban management platform can play the role of real-time risk monitoring and unified management of postrisk behavior in the urban planning and operation stage, which can not only effectively prevent and deal with some specific measures of risk coming but also make timely response measures in the face of unexpected situations such as tsunami, earthquake, and other natural disasters.

Sustainable development is an inevitable choice. In urban planning and design, the traditional life concept model has delayed people’s pursuit of high-quality life, and the comfort and happiness of people’s life have been greatly reduced, and some commercial and trade industries have also been affected to some extent. Infiltrating the concept of smart city into urban architectural planning and landscape optimization design can improve the practicality of planning in an all-round way and make more usable space. With the help of intelligent and visual technology, the coordination of available resources can be more rational, and the overall coordination of resource utilization can improve the overall quality of life of people in urban planning and promote the sustainable development of other industries in a wide range, led by the real estate industry.

Information sharing. In recent years, with the development of Internet and Internet of Things, information sharing has gradually penetrated into all aspects of life. However, urban architectural planning and landscape design are closely related to the future trend of the city and the quality of human life, so it is necessary to fully collect and obtain information from all aspects and consider the influence of each factor. To a certain extent, the traditional architectural planning will affect people’s quality of life and cannot keep up with the needs of the development of the times. The urban brain permeates the urban planning, collects information at the same time, and establishes a systematic information online sharing platform, which will help coordinate the communication and mutual assistance performance among personnel in various departments, greatly improve work efficiency, and provide experience and reference blueprint for later urban planning. In this way, information sharing is more thorough, the utilization rate is higher, and the information becomes visual, which can effectively promote the accelerated development of society.

3. Programming Algorithm

3.1. *Principle of Ant Colony Algorithm.* If the number of ants on path X is n_x and the number of ants on path Y is n_y , then the total number of ants n is

$$n = n_x + n_y. \quad (1)$$

The probability of choosing path X and Path Y is

$$P_x(n) = \frac{(n_x + k)^h}{(n_x + k)^h + (n_y + k)^h}, \quad (2)$$

$$P_y(n) = 1 - P_x(n),$$

h and k adjust to simulate the real environment of ant colony routing.

Modeling

$$\begin{cases} x = \text{mod}(i, N) - 0.5, \\ y = N + 0.5 - \text{ceil}\left(\frac{i}{N}\right). \end{cases} \quad (3)$$

3.1.1. *Probability Planning.* Ants have two important factors when searching paths, which are the concentration of information and the heuristic function of distance. At one moment, ants move from one grid to another to form a probability, which is expressed as follows:

$$P_{ij}^k(t) = \begin{cases} \frac{\tau_{ij}^a(t)\eta_{ij}^B(t)}{\sum_{s \in \text{allowed}} \tau_{ij}^a(t)\eta_{ij}^B(t)}, & s \in \text{allowed}, \\ 0, & s \in \text{allowed}. \end{cases} \quad (4)$$

The distance heuristic function is expressed in the above formula as follows:

$$\eta_{ij} = \frac{1}{d_{ij}}, \quad (5)$$

$$d_{ij} = \sqrt{(x_i - x_j)^2 + (y_i - y_j)^2}.$$

When the heuristic factor α of pheromone concentration is larger, the follow-up ants are more inclined to walk through the nodes they have walked through before, which reduces the diversity of paths and makes the ant colony fall into local optimum. When the heuristic factor α of pheromone concentration is small, the feedback mechanism of ant colony will be weakened, which is not conducive to the convergence of the algorithm. When the visibility heuristic factor β is large, the randomness of ant selection will decrease; otherwise, it will increase. Therefore, it is necessary to adjust these two parameters in the simulation experiment

3.1.2. Update of Information Elements. The update formula of information elements is as follows:

$$\tau_{ij}(t+1) = (1 - \rho)\tau_{ij}(t) + \Delta\tau_{ij}, \quad (6)$$

$$\tau_{ij}(t) = \sum_{k=1}^m \Delta\tau_{ij}^k(t).$$

3.2. Model Updates

(1) In the Ant-Cycle model, the formula $\Delta\tau_{ij}(t)$ is as follows:

$$\Delta\tau_{ij}(t) = \begin{cases} \frac{Q}{L_k}, \\ 0, \text{ otherwise.} \end{cases} \quad (7)$$

(2) In the Ant-Quantity model, the formula $\Delta\tau_{ij}(t)$ is as follows:

$$\Delta\tau_{ij}(t) = \begin{cases} \frac{Q}{d_{ij}} \\ 0, \text{ otherwise} \end{cases} \quad (8)$$

(3) In the Ant-Density model, the formula $\Delta\tau_{ij}(t)$ is as follows:

$$\Delta\tau_{ij}(t) = \begin{cases} Q, \\ 0, \text{ otherwise.} \end{cases} \quad (9)$$

3.2.1. Classical Improvement of Algorithm. The difference between the elite ant algorithm and basic ant colony algorithm lies in the different pheromone updating methods, and its pheromone updating formula is as follows:

$$\tau_{ij}(t+1) = \rho\tau_{ij}(t) + \Delta\tau_{ij}(t) + e\Delta\tau_{ij}^{bs}(t) \quad e = (0, 1). \quad (10)$$

The pheromone increment formula of ant sorting algorithm is as follows:

$$\tau_{ij}(t+1) = \rho\tau_{ij}(t) + \Delta\tau_{ij}(t) + e\Delta\tau_{ij}^{bs}(t),$$

$$\tau_{ij}(t+1) = \sum_{k=1}^w \Delta\tau_{ij}, \quad (11)$$

$$\Delta\tau_{ij}(t) = \begin{cases} \frac{(v-k)Q}{L_k}, \\ 0, \text{ otherwise.} \end{cases}$$

The max-min ant algorithm is a classical improved ant colony algorithm, which effectively improves the slow convergence speed and is easy to fall into the local optimum of basic ant colony algorithm. The update formula of information elements is as follows:

$$\tau_{ij}(t+1) = \rho\tau_{ij}(t) + \Delta\tau_{ij}(t) + \Delta\tau_{ij}^{bs}(t). \quad (12)$$

When the basic algorithm is used to plan the path, the ant colony has not left pheromones on the path at the initial stage, and the pheromones on the path are scarce at this time, so the feasible path cannot be searched quickly. The new heuristic function is as follows:

$$\eta_{ij} = \frac{1}{(d_{ij} + d_{jE})^2}. \quad (13)$$

Considering the influence of volatilization factor on algorithm performance, the improved information element updating strategy in this chapter is as follows:

$$\rho(t+1) = \frac{T}{T+t} \times \frac{1}{e^{1-\rho(t)}}, \quad (14)$$

where T is the total number of iterations and t is the current number of iterations.

The volatilization factor in the basic ant colony algorithm has a very important influence on the performance of the algorithm. If the value is set irrationally, the ant may lose the ability of global search, and the convergence speed will also be affected. ρ is always constant in the basic algorithm. If ρ is too small, when ants find a better path instead of the optimal path, pheromone volatilization is slow due to the influence of ρ , which leads to more pheromone accumulation on this path and attracts ants, so it is difficult for ants to find other better paths, which makes the search results fall into local optimal solution. On the contrary, if the ρ setting is too large, the pheromone will volatilize at a faster speed, and the residual amount on the path cannot attract ants to search, so it is difficult for ants to choose the next moving grid depending on the pheromone concentration, which reduces the search ability and leads to slow convergence speed.

3.3. Ant Colony Algorithm

3.3.1. *Modeling.* Specific process of initializing population is as follows:

- (1) Set the parameters needed by the algorithm.
- (2) Judge whether the grid is continuous, and its judgment method is as follows:

$$\Delta = \max\{abs(x_{i+1} - x_i), abs(y_{i+1} - y_i)\}. \quad (15)$$

When $\Delta = 1$, the two grids are continuous; otherwise, the grid is inserted using the average method, which is calculated by

$$\begin{cases} x'_i = \text{int}\left[\frac{1}{2}(x_i + x_{i+1})\right], \\ y'_i = \text{int}\left[\frac{1}{2}(y_i + y_{i+1})\right], \\ P'_i = x'_i + y'_i. \end{cases} \quad (16)$$

3.3.2. *Algorithm Improvement.* Influencing factors are considered in the fitness function, and the new fitness function is as follows:

$$\text{fit} = a \times \text{fit}_1 + b \times \text{fit}_2, \quad (17)$$

where a and b are their weights, and fit_1 is the length factor. fit_1 is the length factor:

$$\text{fit}_1 = \frac{1}{\text{length}}, \quad (18)$$

fit_2 is the smoothness factor:

$$\text{fit}_2 = \sum_{i=1}^{\text{end}} \frac{1}{\theta}, \theta = \sum_{i=1}^{\text{end}-1} \left| \arccos \left| \frac{x_i - x_{i+1}}{y_i - y_{i+1}} \right| - \arccos \left| \frac{x_i - x_{i+1}}{y_i - y_{i+1}} \right| \right|. \quad (19)$$

The max-min ant algorithm is a classical improved ant colony algorithm, which effectively improves the slow convergence speed and is easy to fall into the local optimum of basic ant colony algorithm. The algorithm mainly consists of three parts. First, like the idea of sorting ant algorithm, the shortest path in the current iterative path is strengthened by pheromone, which improves the convergence speed of the algorithm; second, in order to reduce the influence of pheromone concentration on the search results of the algorithm, the range of pheromone quantity on each path is set; and finally, in order to avoid negative feedback leading to pheromone accumulation, set a maximum value for pheromone.

4. Experiment

4.1. *Simulation Experiment.* Set the total number of ant experiments to 50, the maximum iteration times to 100, and

TABLE 1: Results of four simulation experiments.

Parameters	First	Second	Third	Fourth
Optimal path length	31.23	31.28	31.25	31.26
Average number of iterations	31.19	32.03	32.19	30.75
Average operation time	11.06	10.98	11.31	11.24

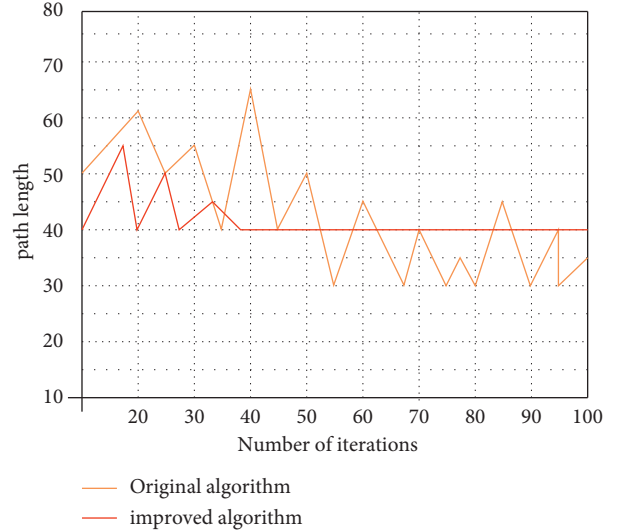


FIGURE 1: Convergence curve of the algorithm before and after improvement.

carry out four simulation experiments with different iteration times. The simulation results are as shown in Table 1.

When the path becomes complex, the path searched by the basic ant colony algorithm becomes more complicated and tortuous, and it still does not converge when the iteration times reach the maximum, and its optimization ability is extremely unsatisfactory. Its shortcomings are very obvious in a large-scale environment. After improving the ant colony algorithm, we compare the convergence ability of the two, as shown in Figure 1:

The comparison of simulation results shows that the improved algorithm has superiority in optimization effect; that is, it reflects the effectiveness of the algorithm in terms of operation time and shortest path. The improved AG algorithm has obvious advantages in convergence speed and optimal path. It can be well applied in architectural planning and landscape design, and the relative path between buildings can be optimally designed. Smart city landscape design has to bring the best experience to tourists and can bring better time advantage to users visually and temporally.

4.2. *Model Comparison.* The urban landscape pattern is the representative of regional characteristics. 500 residents are selected for statistical investigation, and the characteristics of residents' urban architectural planning are counted by the ant colony improvement algorithm. The data are shown in Figure 2.

According to the statistical investigation of residents' desire for urban architectural landscape and the factors of

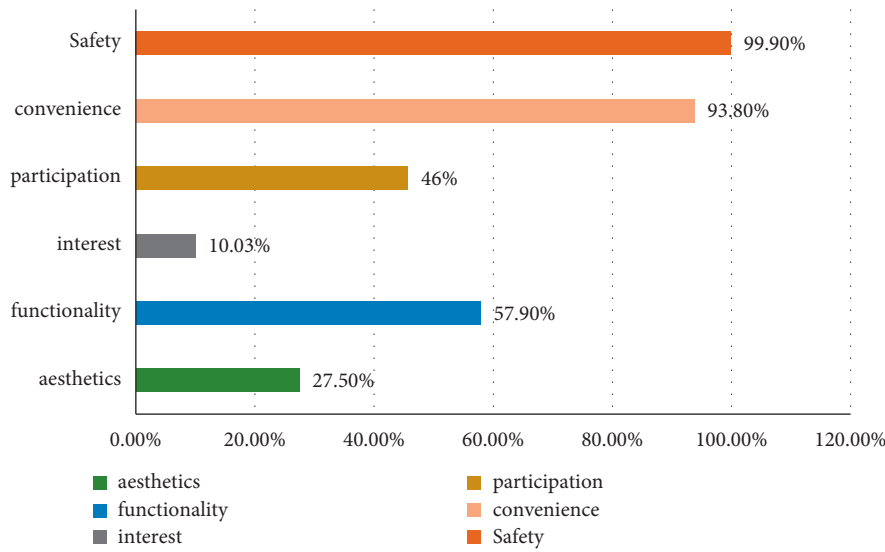


FIGURE 2: Architectural characteristics.

TABLE 2: Optimal design of landscape tree-lined by each algorithm.

Algorithm	Rationality (%)	Safety (%)	Aesthetics (%)	Participation (%)
ACO	56.8	66.6	64.3	45.8
IACO	82.5	98.5	87.5	58.6
PSO	76.8	87.7	54.4	77.9
GA	45.5	76.3	80.1	69.8

TABLE 3: Optimal design of landscape lawn by each algorithm.

Algorithm	Rationality (%)	Safety (%)	Aesthetics (%)	Functionality (%)
ACO	72.3	55.5	64.8	45.7
IACO	86.8	98.8	90.5	58.6
PSO	93.8	87.7	54.4	79.9
GA	56.5	76.3	80.1	68.8

TABLE 4: Optimal design of architectural entertainment square by each algorithm.

Algorithm	Convenience (%)	Security (%)	Aesthetics (%)	Functionality (%)
IACOAPGA	90.8	98.8	90.5	59.6
ACO	68.6	67.4	75.4	43.2
PSO	93.8	84.7	54.4	78.9
GA	59.9	76.3	85.1	66.8

TABLE 5: Optimal design of public toilets in buildings by each algorithm.

Algorithm	Convenience (%)	Security (%)	Aesthetics (%)	Functionality (%)
IACO	90.6	98.8	90.5	88.6
ACO	80.1	78.1	66.6	67.7
PSO	95.8	87.7	59.4	88.9
GA	66.9	76.3	85.1	69.8

use behavior, private space belongs to personal space demand, semiopen and semiprivate space belong to rest facilities demand, open space belongs to vision demand, and large outdoor square belongs to activity place demand.

Using the ant colony improvement algorithm, the relationship between residents' activity mode and behavior mode and urban landscape should be established, as shown in Tables 2, 3, 4 and 5.

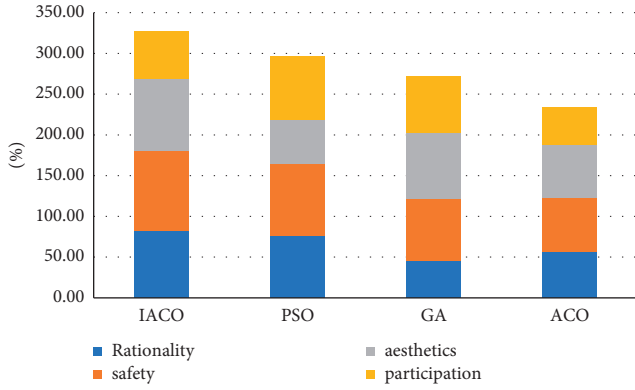


FIGURE 3: Visual diagram of tree-lined characteristics.

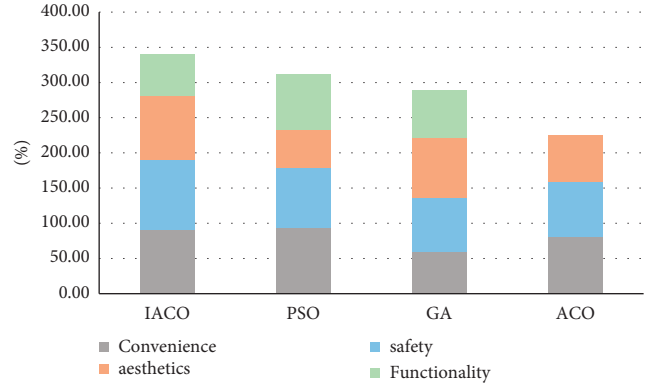


FIGURE 6: Visual diagram of public toilet characteristics.

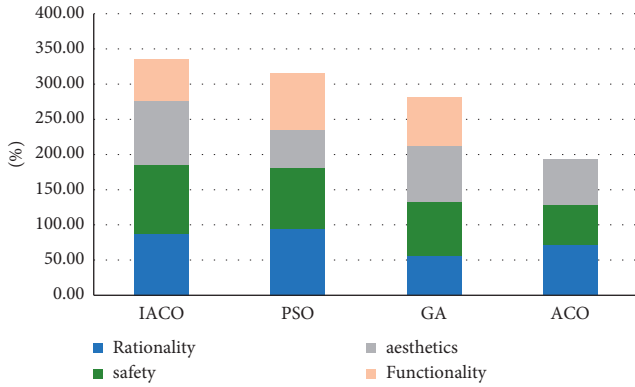


FIGURE 4: Visual map of lawn characteristics.

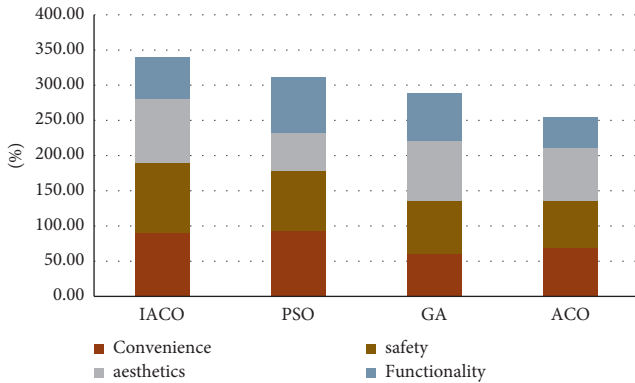


FIGURE 5: Visual diagram of entertainment square characteristics.

Visual statistics of stacked column chart for the data in the above table, as shown in Figure 3:

Visual statistics of stacked column chart for the data in the above table, as shown in Figure 4:

The data in the above table are visually counted by stacking column chart, as shown in Figure 5:

Visual statistics of stacked column chart for the data in the above Table 5, as shown in Figure 6:

TABLE 6: Performance of each algorithm in landscape tree-lined.

Algorithm	Recall (%)	F1 (%)	Roc (%)	Accuracy (%)
IACO	82.5	88.5	87.5	85.6
ACO	66.3	56.5	60.9	67.3
PSO	80.8	87.7	86.4	85.9
GA	76.5	76.8	78.1	82.8

TABLE 7: Performance of each algorithm in landscape lawn.

Algorithm	Recall (%)	F1 (%)	Roc (%)	Accuracy (%)
IACO	80.5	86.5	84.5	85.8
ACO	56.9	65.2	59.4	66.9
PSO	81.8	85.7	82.4	84.9
GA	77.5	74.8	76.3	80.8

TABLE 8: Performance of each algorithm in architectural entertainment square.

Algorithm	Recall (%)	F1 (%)	Roc (%)	Accuracy (%)
IACO	82.5	85.5	88.5	86.6
ACO	56.8	76.3	66.4	63.5
PSO	80.8	84.7	86.9	85.8
GA	78.5	79.8	78.8	80.8

TABLE 9: Performance of each algorithm in building public toilets.

Algorithm	Recall (%)	F1 (%)	Roc (%)	Accuracy (%)
IACO	82.5	88.5	85.9	85.6
ACO	45.8	65.8	58.4	61.2
PSO	83.6	86.7	86.4	83.9
GA	77.5	76.9	79.1	81.5

4.3. Contrast Experiment. We carry out characteristic statistical analysis on urban buildings and landscapes, respectively, and then compare the performance of four intelligent models, and study the performance of four buildings and landscapes, respectively, to find the best

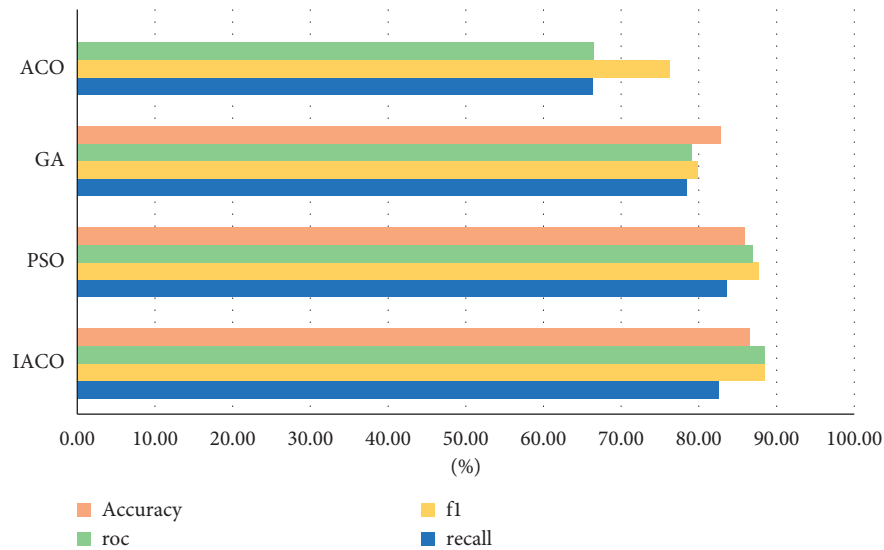


FIGURE 7: Comprehensive comparison of algorithm performance.

intelligent model. The research data are shown in Tables 6, 7, 8, and 9:

Choose the best value of each performance in the above table to compare the comprehensive performance of the four algorithms, as shown in Figure 7:

5. Conclusion

Urban planning leads the intelligent development of cities on a certain meaning, and smart urban planning must have scientific and logical urban planning. For the development of smart cities, smart city planning must have scientific and logical urban planning. The architectural planning and landscape design of smart cities make the urban planning more modern, convenient, and rational. In this paper, intelligent model is used for planning and design, and the research results are as follows:

- (1) In the simulation experiment, the improved ant colony algorithm before and after the optimal path, average moving times, average calculation time, three parameters comparison, and the improved algorithm is indeed more excellent.
- (2) According to the convergence curve of the algorithm, it can be seen that under the complex path, the convergence ability of the ant colony algorithm without improvement is poor, but it increases greatly after improvement.
- (3) Three algorithms are used to study and compare the characteristics of four kinds of architectural landscapes: tree-lined, lawn, entertainment square, and public places.
- (4) In the comparison experiment, the improved ant colony algorithm is slightly superior to the particle swarm optimization algorithm by comparing the optimal values of the performance comparison table of the three kinds of algorithms mentioned in this paper.

Data Availability

The experimental data used to support the findings of this study are available from the corresponding author upon request.

Conflicts of Interest

The authors declare that they have no conflicts of interest regarding this work.

Acknowledgments

This work was sponsored in part by Key scientific research projects of Henan Province colleges and universities (22A790016).

References

- [1] B. M. A. Le, G. Mathilde, and B. Helene, "From open data to smart city governing innovation in the rennes metropolitan area (France)," *International Journal of E-Planning Research*, vol. 10, no. 4, pp. 1–22, 2021.
- [2] Y. Qian, "Does the smart city policy promote the green growth of the urban economy Evidence from China," *Environmental Science and Pollution Research International*, vol. 28, no. 47, Article ID 66709, 2021.
- [3] K. Lavish, "Efficient and robust image communication techniques for 5G applications in smart cities," *Energies*, vol. 14, no. 13, p. 3986, 2021.
- [4] A. Singh and A. R. Singla, "Constructing definition of smart cities from systems thinking view," *Kybernetes*, vol. 50, no. 6, pp. 1919–1950, 2021.
- [5] K. Konstantinos, "Assessing impact, performance and sustainability potential of smart city projects: towards a case agnostic evaluation framework," *Sustainability*, vol. 13, no. 13, p. 7395, 2021.
- [6] R. Rohit, P. Yadav, and R. S. J. Yadav, "Statistical analysis of human emotions to suggest suitable music as per individual's mood: an application of AI and ML for NextGen smart cities,"

- International Journal of Cyber Behavior, Psychology and Learning*, vol. 11, no. 3, pp. 34–67, 2021.
- [7] S. Lisa, G. Ioannis, and R. Martin, “Evaluation of pedestrian navigation in smart cities,” *Environment and Planning B: Urban Analytics and City Science*, vol. 48, no. 6, pp. 1728–1745, 2021.
- [8] Z. Fang, S. L. Shaw, B. Yang, P. Santi, and W. Tu, “Integrated environmental and human observations for smart cities,” *Environment and Planning B: Urban Analytics and City Science*, vol. 48, no. 6, pp. 1375–1379, 2021.
- [9] M. Bauer, L. Sanchez, and J S. Song, “IoT-enabled smart cities: evolution and outlook,” *Basel Sensors*, vol. 21, no. 13, p. 4511, 2021.
- [10] H. Li, C. Yang, L. Deng, and P. Yi, T. Xiezhang, Secure video surveillance framework in smart city,” *Sensors*, vol. 21, no. 13, p. 4419, 2021.
- [11] L. Wang and W. Liu, “Study on the influence of smart city construction on regional economic output value—taking Chengdu for example,” *Sustainable Development*, vol. 11, no. 04, pp. 467–474, 2021.
- [12] C. Edoardo and M. Tania, “Business models for smart city solutions: an overview of main archetypes,” *International Journal of Urban Planning and Smart Cities (IJUPSC)*, vol. 2, no. 2, pp. 94–109, 2021.
- [13] B. Bastiaan and De Marez Lieven, “Co-shaping smart cities: participation inequalities in civic crowdsourcing,” *International Journal of Urban Planning and Smart Cities (IJUPSC)*, vol. 2, no. 2, pp. 34–47, 2021.
- [14] A. Wang, W. Lin, B. Liu, H. Wang, and H. Xu, “Does smart city construction improve the green utilization efficiency of urban land,” *Land*, vol. 10, no. 6, p. 657, 2021.
- [15] A. Orłowski, “Smart cities concept - readiness of city Halls as a measure of reaching a smart city perception,” *Cybernetics & Systems*, vol. 52, no. 5, pp. 313–327, 2021.
- [16] C. Tania, M. Sara, and C. Silvia, “Big data analytics for smart cities,” *Electronics*, vol. 10, no. 12, p. 1439, 2021.
- [17] M. Arunmozhi, “Contactless technologies for smart cities: big data, IoT, and cloud infrastructures,” *SN Computer Science*, vol. 2, no. 4, p. 334, 2021.
- [18] M. Ayumu, “Spatial demand forecasting based on smart meter data for improving local energy self sufficiency in smart cities,” *IET Smart Cities*, vol. 3, no. 2, pp. 107–120, 2021.
- [19] SiY. Tan, A. Taeihagh, and K. Sha, “How transboundary learning occurs: case study of the ASEAN smart cities network (ASCN),” *Sustainability*, vol. 13, no. 11, p. 6502, 2021.
- [20] G. Anita, “Internet of things and long-range-based smart lampposts for illuminating smart cities,” *Sustainability*, vol. 13, no. 11, p. 6398, 2021.
- [21] M. Kelemen, V. Polishchuk, B. Gavurova et al., “Model of evaluation and selection of expert group members for smart cities, green transportation and mobility: from safe times to pandemic times,” *Mathematics*, vol. 9, no. 11, p. 1287, 2021.
- [22] C. Dimmer, “Smart cities in asia: governing development in the Era of hyper- connectivity,” *Pacific Affairs*, vol. 94, no. 2, pp. 401–403, 2021.
- [23] L. Roman, P. Viktoriya, and S. Anna, “The smart city concept in Poland and Ukraine: in search of cooperation opportunities,” *Bulletin of Geography. Socio-Economic Series*, vol. 52, no. 52, pp. 95–109, 2021.
- [24] S. A. Sánchez, A. D. Morales, J. C. Castillas, C. A. Martinez, and A. Z. Meza, “Proposal for an automated greenhouse to optimize the growth of hydroponic vegetables with high nutritional content in the context of smart cities,” *IOP Conference Series: Materials Science and Engineering*, vol. 1154, no. 1, Article ID 012012, 2021.
- [25] U. Muhammad, “Impact of COVID-19 on IoT adoption in healthcare, smart homes, smart buildings, smart cities, transportation and industrial IoT,” *Sensors*, vol. 21, no. 11, p. 3838, 2021.

Research Article

GMAIR: Unsupervised Object Detection Based on Spatial Attention and Gaussian Mixture Model

Weijin Zhu ¹, **Yao Shen** ¹, **Mingqian Liu** ² and **Lizeth Patricia Aguirre Sanchez** ¹

¹Department of Computer Science, Shanghai Jiao Tong University, Shanghai 200240, China

²Winning Health Technology Co., Ltd, Shanghai 200135, China

Correspondence should be addressed to Yao Shen; yshen@cs.sjtu.edu.cn

Received 7 May 2022; Revised 8 June 2022; Accepted 15 June 2022; Published 18 July 2022

Academic Editor: Le Sun

Copyright © 2022 Weijin Zhu et al. This is an open access article distributed under the Creative Commons Attribution License, which permits unrestricted use, distribution, and reproduction in any medium, provided the original work is properly cited.

Recent studies on unsupervised object detection based on spatial attention have achieved promising results. Models, such as AIR and SPAIR, output “what” and “where” latent variables that represent the attributes and locations of objects in a scene, respectively. Most of the previous studies concentrate on the “where” localization performance. However, we claim that acquiring “what” object attributes is also essential for representation learning. This study presents a framework, GMAIR, for unsupervised object detection. It incorporates spatial attention and a Gaussian mixture in a unified deep generative model. GMAIR can locate objects in a scene and simultaneously cluster them without supervision. Furthermore, we analyze the “what” latent variables and clustering process. Finally, we evaluate our model on MultiMNIST and Fruit2D datasets. We show that GMAIR achieves competitive results on localization and clustering compared with state-of-the-art methods.

1. Introduction

The perception of human vision is naturally hierarchical. We can recognize objects in a scene at a glance and classify them according to their appearances, functions, and other attributes. It is expected that an intelligent agent can also decompose scenes to meaningful object abstraction, which is known as an object detection task in machine learning. In the last decade, there have been significant developments in supervised object detection tasks. However, its unsupervised counterpart continues to be challenging.

Recently, there has been some progress in unsupervised object detection. Attend, infer, repeat (AIR, [1]), which is a variational autoencoder (VAE [2])-based method, achieved encouraging results. Spatially invariant AIR (SPAIR [3]) replaced the recurrent network in AIR with a convolutional network that attained better scalability and lower computational cost. SPACE [4], which combines spatial attention and scene-mixture approaches, performed better in background prediction.

Despite the recent progress in unsupervised object detection, the results of previous studies remain unsatisfactory. One of the reasons for this could be that previous studies on unsupervised object detection were mainly concentrated on object localization. They lacked analysis and evaluation of the “what” latent variables, which represent the attributes of objects. These variables are essential for many tasks such as clustering, image generation, and style transfer. Another important concern is that they do not directly reason about the category of objects in the scene, which is beneficial to know in many cases, unlike most of the studies on corresponding supervised tasks.

This study presents a framework for unsupervised object detection that can directly reason about the category and localization of objects in the scenes and provide an intuitive way to analyze the “what” latent variables by simply incorporating a Gaussian mixture prior assumption. In Section 2, we introduce the architecture of our framework, GMAIR. We introduce related works in Section 3. We analyze the “what” latent variables in Section 4.1 and Section

4.4. We describe our model for image generation in Section 4.2. Finally, we present quantitative evaluation results of both clustering and localization in Section 4.3.

Our main contributions are as follows:

- (i) We combine spatial attention and a Gaussian mixture in a unified deep generative model, enabling our model to cluster discovered objects.
- (ii) We analyze the “what” latent variables, which are essential because they represent the attributes of the objects.
- (iii) Our method achieves competitive results on both clustering and localization compared with state-of-the-art methods.

2. Gaussian Mixture Attend, Infer, Repeat

In this section, we introduce our framework, GMAIR, for unsupervised object detection. GMAIR is a spatial attention model with a Gaussian mixture prior assumption for the “what” latent variables, and this enables the model to cluster discovered objects. An overview of GMAIR is presented in Figure 1.

2.1. Structured Object-Semantic Latent Representation. To attain object abstraction latent variables, the image is divided into $H \times W$ regions. Latent variables $\mathbf{z} = (\mathbf{z}_1, \mathbf{z}_2, \dots, \mathbf{z}_{HW})$ are a concatenation of HW latent variables, where \mathbf{z}_i is the latent variable for the i th region representing the semantic feature of the object centered in the i th region. Furthermore, for each region we divide \mathbf{z}_i into five separate latent variables, $\mathbf{z}_i = (\mathbf{z}_i^{\text{pres}}, \mathbf{z}_i^{\text{what}}, \mathbf{z}_i^{\text{cat}}, \mathbf{z}_i^{\text{where}}, \mathbf{z}_i^{\text{depth}})$, where $\mathbf{z}_i^{\text{pres}} \in \{0, 1\}$, $\mathbf{z}_i^{\text{what}} \in \mathbb{R}^A$, $\mathbf{z}_i^{\text{cat}} \in \{0, 1\}^C$, $\mathbf{z}_i^{\text{where}} \in \mathbb{R}^4$, $\mathbf{z}_i^{\text{depth}} \in \mathbb{R}$, A is the dimension of “what” latent variables, and C is the number of clusters. $\mathbf{z}_i^{\text{pres}}$ is a binary variable indicating the existence of the object. $\mathbf{z}_i^{\text{what}}$ is a vector representing the object’s attribute. $\mathbf{z}_i^{\text{where}}$ specifies the relative position between the object and the i th region of an image. $\mathbf{z}_i^{\text{depth}}$ is a real number specifying the relative depth of the object, and $\mathbf{z}_i^{\text{cat}}$ is an one-hot vector for category.

GMAIR imposes a prior on those latent variables as follows:

$$p(\mathbf{z}) = \prod_{i=1}^{HW} p(\mathbf{z}_i^{\text{pres}}) \cdot p(\mathbf{z}_i^{\text{cat}})^{\mathbf{z}_i^{\text{pres}}} \cdot p(\mathbf{z}_i^{\text{what}} | \mathbf{z}_i^{\text{cat}})^{\mathbf{z}_i^{\text{pres}}} \cdot p(\mathbf{z}_i^{\text{where}})^{\mathbf{z}_i^{\text{pres}}} \cdot p(\mathbf{z}_i^{\text{depth}})^{\mathbf{z}_i^{\text{pres}}}. \quad (1)$$

2.1.1. Gaussian Mixture Prior Assumption. Latent variables \mathbf{z}^{cat} are one-hot vectors that act as classification indicators. They obey the categorical distribution, $\text{Cat}(\pi)$, where $\pi \in [0, 1]^C$. For simplicity, we assume that $\pi_k = (1/C)$ for all $1 \leq k \leq C$.

We assume that $\mathbf{z}_i^{\text{what}}$ conditional on $\mathbf{z}_i^{\text{cat}}$ obeys a Gaussian distribution. In that case, $\mathbf{z}_i^{\text{what}}$ obeys a Gaussian mixture model, that is,

$$p(\mathbf{z}_i^{\text{what}}) = \sum_{k=1}^C p(\mathbf{z}_{i,k}^{\text{cat}} = 1) p(\mathbf{z}_i^{\text{what}} | \mathbf{z}_{i,k}^{\text{cat}} = 1) \\ = \sum_{k=1}^C p(\mathbf{z}_{i,k}^{\text{cat}} = 1) f(\mathbf{x}; \mu_k, \sigma_k^2), \quad (2)$$

where $f(x; \mu, \sigma^2) = (1/\sigma\sqrt{2\pi})\exp(-(x - \mu)^2/2\sigma^2)$ is the probability density function of Gaussian distribution, and μ_k, σ_k ($k = 1..C$) are the mean and standard derivation of the k th Gaussian distribution. We let μ_k and σ_k be learnable parameters that are jointly trained with other parameters. During the implementation, $\mu_k = \mu(\mathbf{z}_i^{\text{cat}})$ and $\sigma_k = \sigma(\mathbf{z}_i^{\text{cat}})$ if $\mathbf{z}_{i,k}^{\text{cat}} = 1$, where μ and σ can be modeled as linear layers. They are called “what priors” module in Figure 1.

For other latent variables, \mathbf{z}^{pres} is modeled using a Bernoulli distribution, $\beta(p)$, where p is the present probability. $\mathbf{z}^{\text{where}}$ and $\mathbf{z}^{\text{depth}}$ are modeled using normal distributions, $\mathcal{N}(\mu_{\text{prior}}^{\text{where}}, \sigma_{\text{prior}}^{\text{where}^2})$ and $\mathcal{N}(\mu_{\text{prior}}^{\text{depth}}, \sigma_{\text{prior}}^{\text{depth}^2})$, respectively. All priors of latent variables are listed in Table 1.

2.2. Inference and Generation Model

2.2.1. Inference Model $q_\phi(\mathbf{z}|\mathbf{x})$. In the inference model, latent variables conditional on data \mathbf{x} are modeled as follows:

$$q(\mathbf{z}|\mathbf{x}) = \prod_{i=1}^{HW} q(\mathbf{z}_i^{\text{pres}}|\mathbf{x}) \cdot q(\mathbf{z}_i^{\text{where}}|\mathbf{x})^{\mathbf{z}_i^{\text{pres}}} \cdot q(\mathbf{z}_i^{\text{depth}}|\mathbf{x})^{\mathbf{z}_i^{\text{pres}}} \\ \cdot q(\mathbf{z}_i^{\text{cat}}|\mathbf{x}, \mathbf{z}_i^{\text{where}})^{\mathbf{z}_i^{\text{pres}}} \cdot q(\mathbf{z}_i^{\text{what}}|\mathbf{x}, \mathbf{z}_i^{\text{where}}, \mathbf{z}_i^{\text{cat}})^{\mathbf{z}_i^{\text{pres}}}. \quad (3)$$

During implementation, feature maps with dimension $H \times W \times D$ are extracted from a backbone network using data \mathbf{x} as input, where D is the number of channels of feature maps. Further, the posteriors of \mathbf{z}^{pres} , $\mathbf{z}^{\text{where}}$, and $\mathbf{z}^{\text{depth}}$ are reasoned by pres-head, where-head, and depth-head, respectively. Input images are cropped into $H \times W$ glimpses by a spatial transformer network, and each of these is transferred to the cat-encoder module to generate posteriors of \mathbf{z}^{cat} . Subsequently, we use the concatenation of the i th glimpse and $\mathbf{z}_i^{\text{cat}}$ ($1 \leq i \leq HW$) as the input of the what-encoder to generate posteriors of \mathbf{z}^{what} .

2.2.2. Generation Model $p_\theta(\mathbf{x}|\mathbf{z})$. In the generation model, each $\mathbf{z}_i^{\text{what}}$ ($1 \leq i \leq HW$) is changed back into a glimpse using a glimpse decoder. Then, a renderer combines HW glimpses to generate $\hat{\mathbf{x}}$. We use the same render algorithm as in previous studies [1, 3].

2.3. The Loss Functions

2.3.1. Evidence Lower Bound. In general, we learn parameters of VAE jointly by maximizing the evidence lower bound (ELBO), which can be formulated as follows:

$$\text{ELBO} = \mathbb{E}_{q(\mathbf{z}|\mathbf{x})} \left[\log \left(\frac{p(\mathbf{x}, \mathbf{z})}{q(\mathbf{z}|\mathbf{x})} \right) \right] \\ = \mathbb{E}_{q(\mathbf{z}|\mathbf{x})} [\log(p(\mathbf{x}|\mathbf{z}))] - \mathbb{E}_{q(\mathbf{z}|\mathbf{x})} \left[\log \left(\frac{q(\mathbf{z}|\mathbf{x})}{p(\mathbf{z})} \right) \right], \quad (4)$$

where the first term is called the reconstruction term denoted by $-L_{\text{recon}}$, and the second term, the regularization

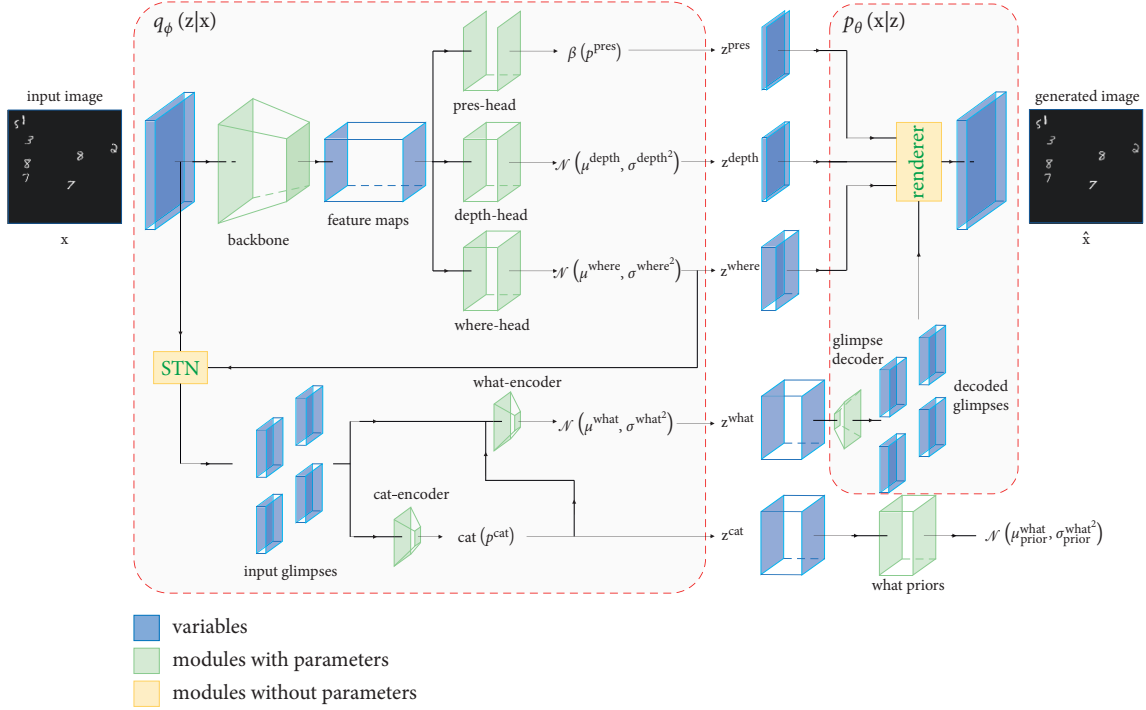


FIGURE 1: Architecture of GMAIR. This is a VAE-based model that consists of a probabilistic encoder, $q_\phi(\mathbf{z}|\mathbf{x})$, and a probabilistic decoder, $p_\theta(\mathbf{x}|\mathbf{z})$. In encoder $q_\phi(\mathbf{z}|\mathbf{x})$, feature maps with dimension $H \times W \times D$ are extracted from data \mathbf{x} going through a backbone network representing feature of $H \times W$ divided regions. They are then fetched into three separated modules: pres-head, depth-head, and where-head, which produce the posterior of \mathbf{z}^{pres} , $\mathbf{z}^{\text{depth}}$, and $\mathbf{z}^{\text{where}}$, respectively. A cat-encoder module generates the posterior of \mathbf{z}^{cat} with $H \times W$ input glimpses transformed by a spatial transformer network (STN) as input, and the posterior of \mathbf{z}^{what} is generated by a what-encoder module with $H \times W$ input glimpses and \mathbf{z}^{cat} as input. In decoder $p_\theta(\mathbf{x}|\mathbf{z})$, each $H \times W$ latent \mathbf{z}^{what} is fetched into a glimpse decoder to generate decoded glimpses rendered by the renderer to recover to the final generated image. Finally, the priors of \mathbf{z}^{pres} , $\mathbf{z}^{\text{depth}}$, $\mathbf{z}^{\text{where}}$, and \mathbf{z}^{cat} are fixed, whereas the prior of \mathbf{z}^{what} is generated by a “what priors” module using \mathbf{z}^{cat} as input.

TABLE 1: Priors of latent variables.

Latent variables	Priors
\mathbf{z}^{pres}	$\beta(p)$
\mathbf{z}^{what}	$\mathcal{N}(\mu(\mathbf{z}^{\text{cat}}), \sigma(\mathbf{z}^{\text{cat}})^2)$
\mathbf{z}^{cat}	Cat(π)
$\mathbf{z}^{\text{where}}$	$\mathcal{N}(\mu_{\text{prior}}^{\text{where}}, \sigma_{\text{prior}}^{\text{where}^2})$
$\mathbf{z}^{\text{depth}}$	$\mathcal{N}(\mu_{\text{prior}}^{\text{depth}}, \sigma_{\text{prior}}^{\text{depth}^2})$

term. The regularization term can be further decomposed into five terms by substituting (1) and (3) into (4), and each of the five terms corresponds to the Kullback–Leibler divergence (or its expectation) between a type of latent variables and its prior:

$$\mathbb{E}_{q(\mathbf{z}|\mathbf{x})} \left[\log \left(\frac{q(\mathbf{z}|\mathbf{x})}{p(\mathbf{z})} \right) \right] = L_{\text{pres}} + L_{\text{where}} + L_{\text{depth}} + L_{\text{cat}} + L_{\text{what}} \quad (5)$$

The terms in (5) are as follows:

$$L_{\text{pres}} = \sum_{i=1}^{HW} KL^{\text{pres}}, \quad (6)$$

$$L_{\text{where}} = \sum_{i=1}^{HW} q(\mathbf{z}_i^{\text{pres}} = 1|\mathbf{x}) KL^{\text{where}}, \quad (7)$$

$$L_{\text{depth}} = \sum_{i=1}^{HW} q(\mathbf{z}_i^{\text{pres}} = 1|\mathbf{x}) KL^{\text{depth}}, \quad (8)$$

$$L_{\text{cat}} = \sum_{i=1}^{HW} q(\mathbf{z}_i^{\text{pres}} = 1|\mathbf{x}) \mathbb{E}_{q(\mathbf{z}_i^{\text{where}}|\mathbf{x})} [KL^{\text{cat}}], \quad (9)$$

$$L_{\text{what}} = \sum_{i=1}^{HW} q(\mathbf{z}_i^{\text{pres}} = 1|\mathbf{x}) \mathbb{E}_{q(\mathbf{z}_i^{\text{where}}, \mathbf{z}_i^{\text{cat}}|\mathbf{x})} [KL^{\text{what}}], \quad (10)$$

where $KL^x = KL(q(\mathbf{z}_i^x|\cdot) \| p(\mathbf{z}_i^x|\cdot))$. A complete derivation is given in Appendix A.

2.3.2. Overlap Loss. During actual implementation, we find that penalizing on overlaps of objects sometimes helps. Therefore, we introduce an auxiliary loss called overlap loss. First, we calculate HW images with size $3 \times H^{\text{img}} \times W^{\text{img}}$, where H^{img} and W^{img} are, respectively, the height and width of the input image, transformed by HW decoded glimpses by a spatial transformer network. The overlap loss is then calculated as the average of the sum subtract by the maximum for each $H^{\text{img}} \times W^{\text{img}}$ pixels.

This loss, inspired by the boundary loss in SPACE [4], is utilized to penalize if the model tries to split a large object into multiple smaller ones. However, we achieve this using a

different calculation method that incurs a lower computational cost.

2.3.3. *Total Loss.* The total loss is as follows:

$$L = \sum_{x \in S} \alpha_x L_x, \quad (11)$$

where $S = \{\text{recon, overlap, pres, where, depth, cat, what}\}$, and α_x is the coefficients of the corresponding loss terms.

3. Related Works

Several studies on unsupervised object detection have been conducted, including spatial attention methods such as AIR [1], SPAIR [3], and SPACE [4], and scene-mixture methods such as MONet [5], IODINE [6], GENESIS [7], and GENESIS-v2 [8]. Most of them including our work are based on the VAE [2] model.

3.1. *AIR.* The AIR framework uses a VAE-based hierarchical probabilistic model marking a milestone in unsupervised scene understanding. In AIR, latent variables are structured into groups of latent variables $\mathbf{z}_{1:N}$, for N discovered objects, each of which consists of “what,” “where,” and “presence” variables. A recurrent neural network is used in the inference model to produce $\mathbf{z}_{1:N}$, and there is a decoder network for decoding the “what” variables of each object in the generation model. A spatial transformer network [9] is used for rendering.

3.2. *SPAIR.* Because AIR attends one object at a time, it does not scale well to scenes that contain many objects. SPAIR attempted to address this issue by replacing the recurrent network with a convolutional network that follows a spatially invariant assumption. Like YOLO ([10]), in SPAIR, the locations of objects are specified relative to local grid cells. SPAIR achieved a better performance and scalability than AIR.

3.3. *MONet.* MONet [5] is a scene-mixture model for unsupervised scene decomposition. Like AIR, MONet also uses a recurrent neural network to infer objects. However, it learns the attention masks to obtain the segmentation results of objects instead of the bounding boxes.

3.4. *IODINE.* IODINE [6] is also a scene-mixture model for unsupervised scene decomposition. Unlike MONet, which infers a mask for one object at a time, in IODINE, all segmentation results are inferred simultaneously. A recurrent neural network is used to refine the segmentation results further.

3.5. *GENESIS.* GENESIS [7] replaced the recurrent neural networks in previous works with the convolutional neural networks. This improvement makes GENESIS more scalable to inputs with a larger number of scene components.

3.6. *GENESIS-v2.* GENESIS-v2 [8] also performs unsupervised object segmentation. It is similar to GENESIS but uses a parameter-free clustering algorithm to avoid iterative refinements.

The scene-mixture models such as MONet, IODINE, GENESIS, and GENESIS-v2 perform segmentation instead of explicitly finding the $\mathbf{z}^{\text{where}}$ location of the objects. The bounding boxes of the discovered objects need to be calculated by the object masks.

3.7. *SPACE.* SPACE [4] employs a combination of both methods. It consists of a spatial attention model for the foreground and a scene-mixture model for the background. By detecting the foreground and background separately, SPACE achieved a better detection result when the background is complicated.

In the area of deep unsupervised clustering, recent methods include AAE [11], GMVAE [12], and IIC [13]. AAE combines the ideas of generative adversarial networks and variational inference. GMVAE uses a Gaussian mixture model as a prior distribution. In IIC, objects are clustered by maximizing mutual information of pairs of images. All of them show promising results on unsupervised clustering.

GM AIR incorporates a Gaussian mixture model for clustering, similar to the GMVAE framework (the authors also refer to a blog post (<http://ruishu.io/2016/12/25/gmvae/>) published by Rui Shu). It is worth noting that our attempt may simply be a choice among many given options. Unless previous research, our main contribution is to show the feasibility of performing clustering and localization simultaneously. Moreover, our method provides a simple and intuitive way to analyze the mechanics of the detection process.

4. Models and Experiments

The experiments were divided into three parts: (a) the analysis of “what” representation and clustering along with the iterations, (b) image generation, and (c) quantitative evaluation of the models.

We evaluate the models on two datasets:

- (i) MultiMNIST: A dataset generated by placing 1–10 small images randomly chosen from MNIST (a standard handwritten digits dataset [14]) to random positions on 128×128 empty images.
- (ii) Fruit2D: A dataset collected from a real-world game. In the scenes, there are 9 types of fruits of various sizes. There is a large difference between both the number and the size of small objects and large objects. The ratio of the size of the largest type of objects to that of the smallest type of objects is ~ 6 , and there are ~ 31 times objects in the smallest size than in the largest size. These settings make it difficult to perform localization and clustering.

In the experiments, we compared GM AIR with two models, SPAIR and SPACE, both of which achieve state of the art in unsupervised object detection in localization

performance. Separated Gaussian mixture models are applied to the “what” latent variables generated by the compared models to obtain the clustering results. We set the number of clusters $C = 10$ and Monte Carlo samples $M = 1$ except as otherwise defined for all experiments. All experiments were conducted on a Ubuntu 16.04.6 server with an Intel(R) Xeon(R) Silver 4110 CPU with 8 cores and 2 TITAN RTX GPUs. We present the details of the models in Appendix B.

It is worth mentioning that the model sometimes successfully locates an object and encloses it with a large box. In that case, IoU between the ground truth and the predicted one will be small and, therefore, will not count to be a correct bounding box when calculating AP. We fix this issue by removing the empty area in generated glimpses to obtain the real size of predicted boxes.

4.1. “What” Representation and Cluster Analysis. We conducted the experiments using the MultiMNIST dataset. We ran GMAIR for 440k iterations and observed the change in the values of the average precision (AP) of bounding boxes, accuracy (ACC), and normalized mutual information (NMI) of clustering until 100k iterations. We also visualized the “what” latent variables in the latent space during the process, as shown in Figure 2. Although all values continued to increase even after 100k iterations, the visualization results were similar to those at the 100k iteration. For integrity, we reserved the results from 100k to 440k iterations in Appendix D. Details of calculating the AP, ACC, and NMI are discussed in Appendix C.

The results showed that at an early stage ($\sim 10k$ iterations) of training, models can already locate objects well with $AP > r_{bin}0.9$ (Figure 2(a)). At the same time, \mathbf{z}^{what} , representations of objects, was still evolving, and the results of clustering (in Figure 2(b)) were not desirable ((ACC, NMI) was (0.24, 0.15)); the digits were a blur in Figure 2(f). After 50k and 100k iterations of training, the clustering effect of \mathbf{z}^{what} was increasingly apparent, and the digits were clearer (Figures 2(g) and 2(h)). The clustering results ((ACC, NMI) was (0.55, 0.43) at 50k and (0.65, 0.55) at 100k iterations) were improved (Figures 2(c) and 2(d)).

The explanation relates to the fact that while the model learns general features of objects and can locate the objects, object classification presents a new challenge for the model. As a result, the model is forced to cluster the feature vector of discovered objects into a small number of categories, which requires the model to learn the similarities between objects and thus requires a large number of training iterations.

It should be noted that even if the clustering effect of \mathbf{z}^{what} is sufficiently enough, the model may fail to locate the centers of clusters (e.g., the large cluster in light red in Figure 2(d)), leading to poor clustering results. In the worst case, the model may learn to converge all μ_k, σ_k ($1 \leq k \leq C$) to the same values, μ^*, σ^* , and the Gaussian mixture model may degenerate to a single Gaussian distribution, $\mathcal{N}(\mu^*, \sigma^{*2})$, resulting in a miserable clustering result. In general, we found that this phenomenon usually occurs at the early stage of training and can be avoided by adjusting

the learning rate of relative modules and the coefficients of the loss functions.

4.2. Image Generation. It is expected that μ_k ($1 \leq k \leq C$) represents the average feature of the k th type of objects, and \mathbf{z}_i^{what} latent variable can be decomposed into the following:

$$\mathbf{z}_i^{what} = \mathbf{z}_i^{avg} + \mathbf{z}_i^{local}. \quad (12)$$

$\mathbf{z}_i^{avg} = \mu_k$ ($1 \leq k \leq C$) if the i th object is in the k th category, and \mathbf{z}_i^{local} represents the local feature of the object. By altering \mathbf{z}_i^{avg} or \mathbf{z}_i^{local} , we should obtain new objects that belong to other categories or the same category with different styles, respectively. In the experiment, we altered \mathbf{z}_i^{avg} and \mathbf{z}_i^{local} and observed the generated images for each object, as shown in Figure 3. In Figure 3(a), objects in each cluster correspond to a type of digit, which is exactly what we expected (except for digit 8 in column 3). In Figure 3(b), categories with a large number of objects are grouped into multiple clusters, while categories with a small number are grouped into one cluster. This is due to the significant difference in number between various types. However, objects in a cluster come from a category in general.

The structure of GMAIR ensures its ability to control object categories, object styles, and the positions of each object of the generated images by altering \mathbf{z}_i^{avg} , \mathbf{z}_i^{local} , and \mathbf{z}^{where} . Examples are shown in Figure 4.

This could provide a new approach for tasks such as style transfer, image generation, and data augmentation. Note that previous methods such as AIR, SPAIR, and its variants can also obtain similar results, but we achieve them in finer granularity.

4.3. Quantitative Evaluations. We quantitatively evaluate the models in terms of the AP of bounding boxes and ACC and NMI of the clusters, and the results are listed in Table 2. In the first part, we show the results of GMVAE for unsupervised clustering on MNIST dataset for comparison. In the second part and the third part, we compare GMAIR to the state-of-the-art models for unsupervised object detection on MultiMNIST and Fruit2D dataset, respectively. The clustering results of SPAIR and SPACE are obtained by the Gaussian mixture models (GMMs). The results show that GMAIR achieves competitive results on both clustering and localization.

4.4. Ablation Study on the Importance of a Gaussian Mixture. The most significant difference between GMAIR and other models is that GMAIR uses a Gaussian mixture model for the “what” latent variables. To investigate whether the Gaussian mixture structure does affect the “what” representation, we also visualized “what” latent variables in latent space generated by SPAIR and SPACE, which have a similar structure of GMAIR and use a Gaussian model instead of a Gaussian mixture model for “what” latent variables. The results are shown in Figure 5. They show that without a Gaussian mixture model, “what” latent variables of different categories tend to follow a single distribution. This is

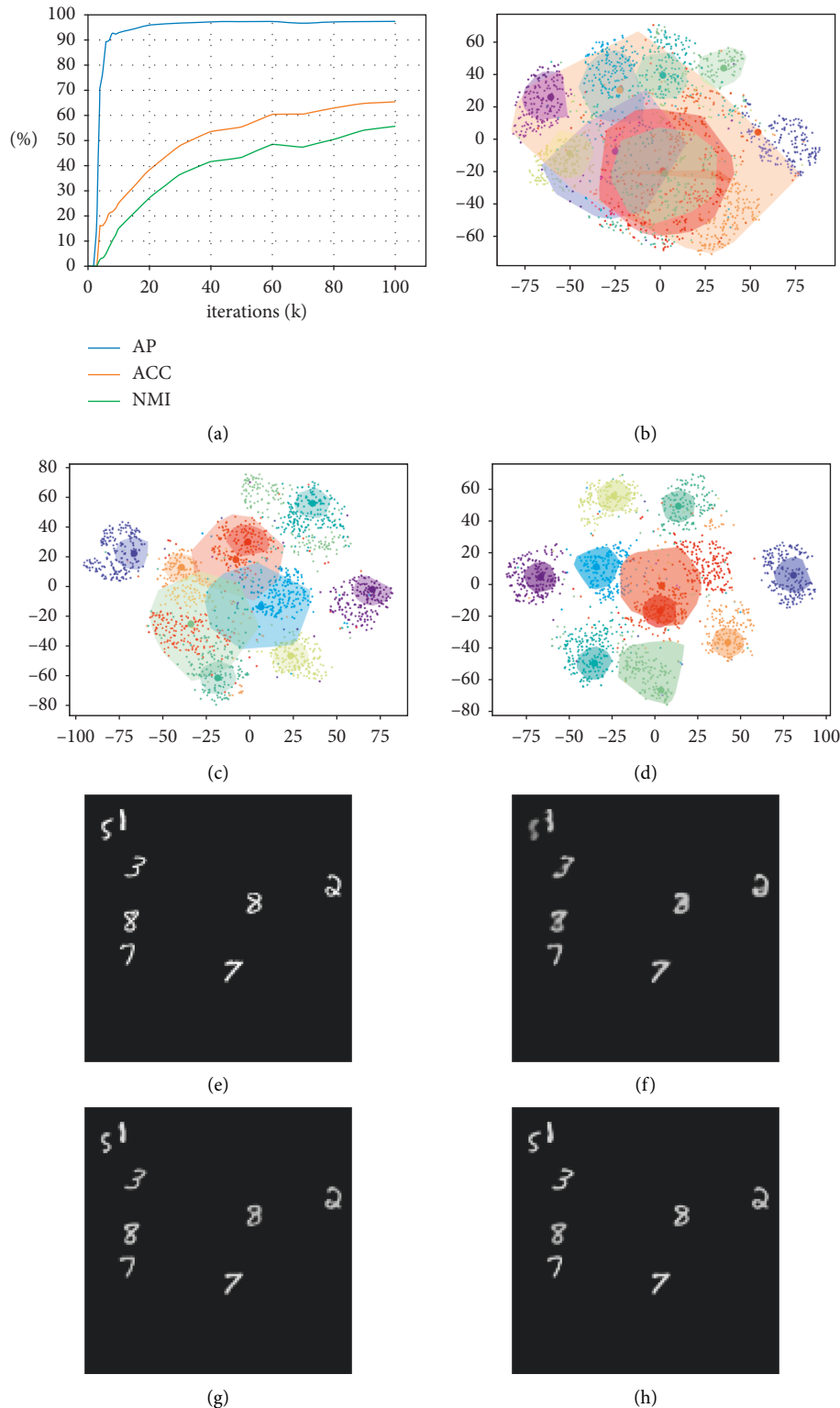


FIGURE 2: "What" representation and cluster analysis. (a) Average precision (AP), accuracy (ACC), and normalized mutual information (NMI) during training. (b-d) Visualized "what" latent space by t-SNE ([15]) at 10k, 50k, and 100k iterations, respectively. Each small dot represents a sample of \mathbf{z}^{what} , and different colors represent the ground truth categories of the corresponding objects. The large dots are μ_k ($1 \leq k \leq C$) described in Section E 2.1, and each of these can be seen as the center of a cluster. The closures represent results of clustering, which are closures of the closest $n\mathbf{z}^{\text{what}}$ points to μ_k that are assigned to the k th cluster (where $1 \leq k \leq C$ and we choose $n = 200$). The color of μ_k ($1 \leq k \leq C$) and closures are decided by a matching algorithm such that a maximum number of \mathbf{z}^{what} are correctly classified to the ground truth label. (e) Sample of original image. (f-h) Samples of generated image at 10k, 50k, and 100k iterations, respectively. (a) AP (IoU = 0.5), ACC, and NMI during training. (b) "What" latent space, at 10k iterations. (c) "What" latent space, at 50k iterations. (d) "What" latent space, at 100k iterations. (e) Original image. (f) Generated image, at 10k iterations. (g) Generated image, at 50k iterations. (h) Generated image, at 100k iterations.

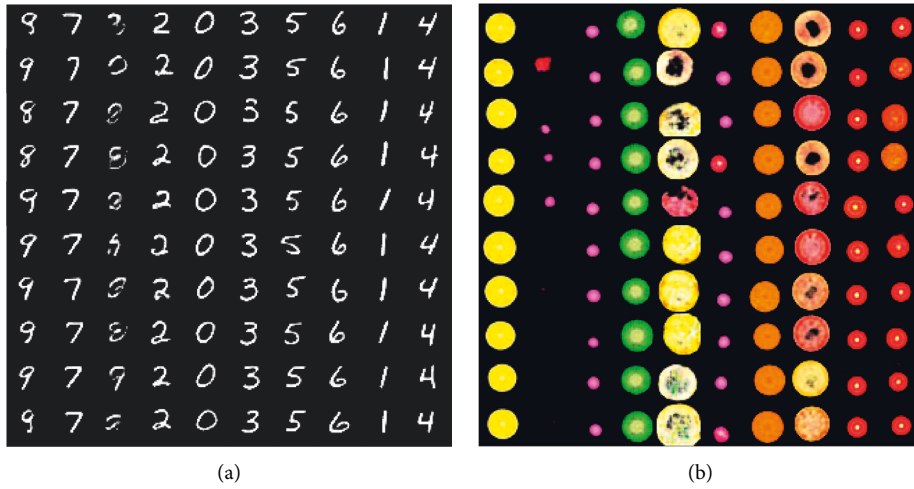


FIGURE 3: Generated objects by varying z^{avg} and z^{local} . The horizontal axis represents varying z^{avg} , and the vertical axis represents varying z^{local} , on both (a) and (b). (a) MultiMNIST. (b) Fruit2D.

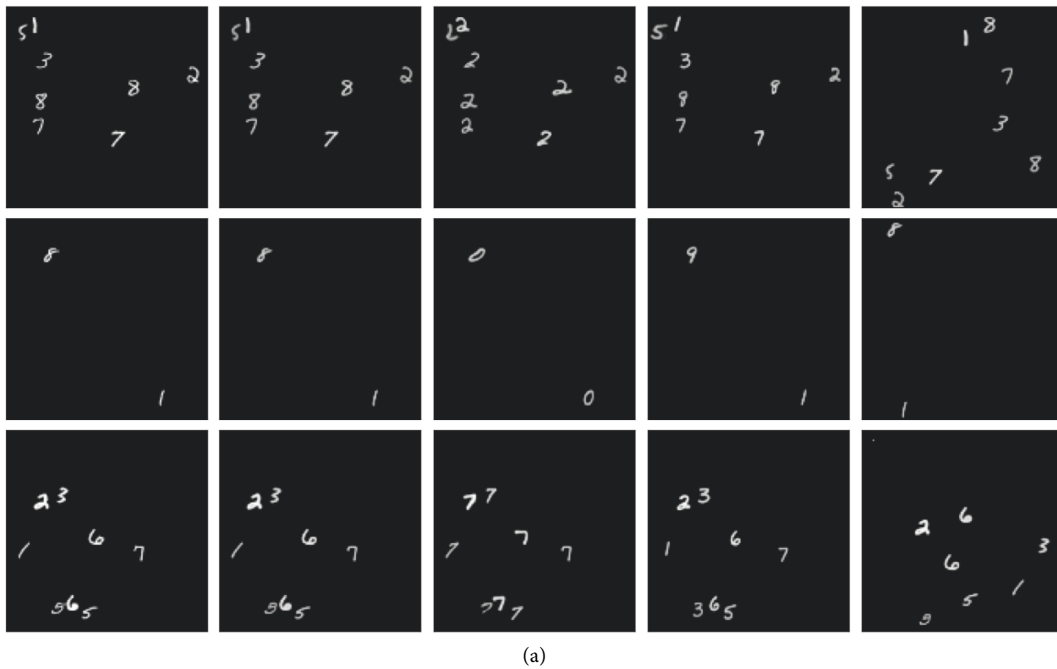


FIGURE 4: Continued.

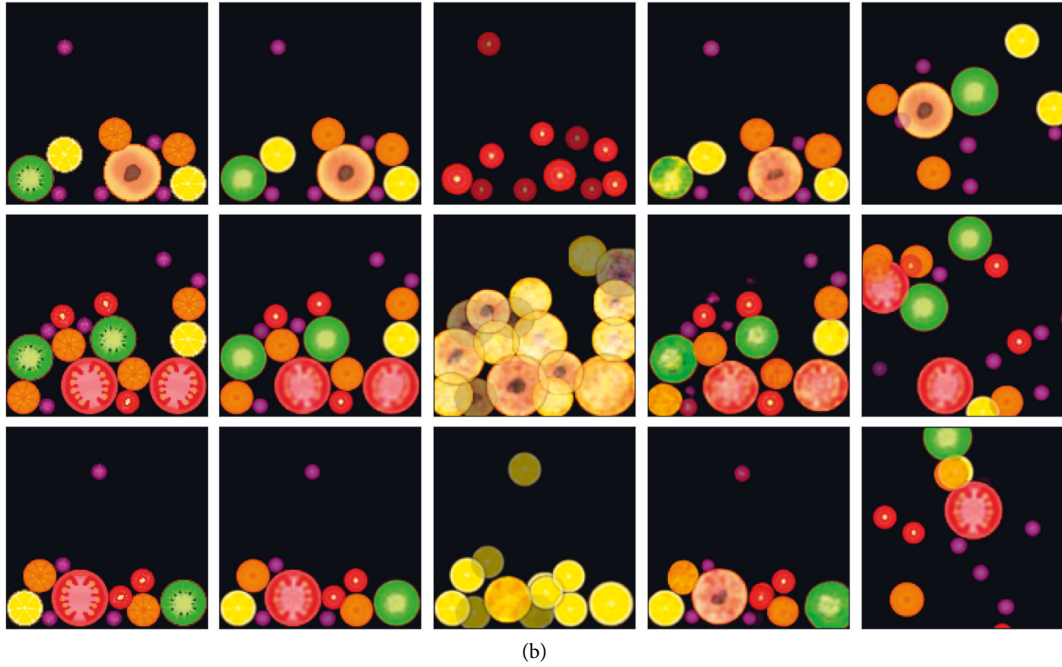


FIGURE 4: Generated images by varying attributes and locations of objects. Columns 1 to 5 are numbered from left to right. Column 1 shows original images. Column 2 shows the generated images without varying \mathbf{z}^{avg} , $\mathbf{z}^{\text{local}}$, and $\mathbf{z}^{\text{where}}$. Column 3 presents images generated by setting all \mathbf{z}^{avg} to the same random μ_k ($1 \leq k \leq C$). Column 4 depicts images generated by varying $\mathbf{z}^{\text{local}}$. Column 5 shows images generated by applying a random shuffle to \mathbf{z}_i . (a) MultiMNIST. (b) Fruit2D.

TABLE 2: Quantitative results on localization (AP) and clustering (accuracy and NMI).

Model	Dataset	AP (% , IoU = 0.5)	ACC (%)	NMI (%)
IIC	MNIST	—	98.4 ± 0.652	—
AAE ($C=16$)	MNIST	—	90.45 ± 2.05	—
AAE ($C=30$)	MNIST	—	95.90 ± 1.13	—
GMVAE ($M=1$)	MNIST	—	77.78 ± 5.75	—
GMVAE ($M=10$)	MNIST	—	82.31 ± 3.75	—
GMAIR	MultiMNIST	97.3 ± 0.10	80.4 ± 0.48	75.5 ± 0.66
SPAIR + GMM	MultiMNIST	90.3	59.4 ± 1.50	56.3 ± 1.41
SPACE + GMM	MultiMNIST	96.7	68.8 ± 3.43	65.8 ± 2.85
GMAIR	Fruit2D	84.9 ± 1.56	90.9 ± 0.32	85.7 ± 1.25
SPAIR + GMM	Fruit2D	83.3	88.1 ± 0.70	78.4 ± 0.51
SPACE + GMM	Fruit2D	93.8	95.0 ± 1.99	87.0 ± 2.20

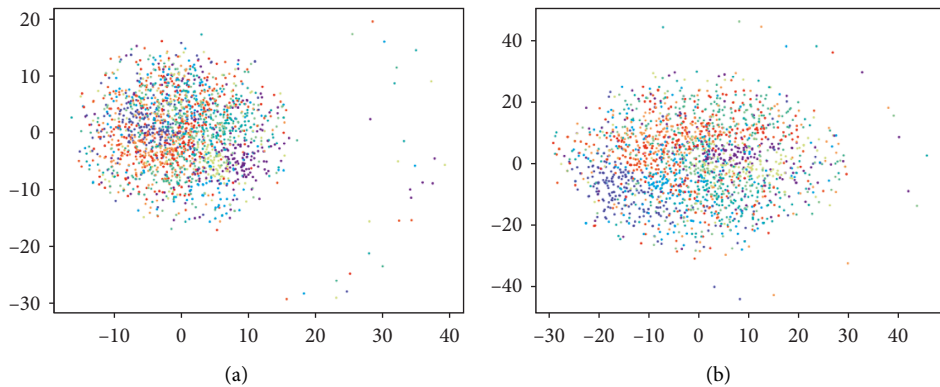


FIGURE 5: “What” representation of (a) SPAIR and (b) SPACE by t-SNE. Each dot represents a sample of \mathbf{z}^{what} , and different colors represent the ground truth categories of the corresponding objects. (a) “What” latent space of SPAIR. (b) “What” latent space of SPACE.

TABLE 3: Architecture of backbone.

Layer	Type	Size	Act./Norm.	Output size
ResNet	ResNet18 (w/o fc)			$512 \times 4 \times 4$
Deconv layer 1	Deconv	128	ReLU/BN	$128 \times 8 \times 8$
Deconv layer 2	Deconv	64	ReLU/BN	$64 \times 16 \times 16$

TABLE 4: Architectures of pres/depth/where-head.

Layer	Type	Size	Act./Norm.	Output size
Input				$64 \times 16 \times 16$
Hidden	Conv	$[3 \times 3, 128] \times 3$	ReLU	$128 \times 16 \times 16$
Output	Conv	$1 \times 1, (1/(1/4))$		$(1/(1/4)) \times 16 \times 16$

TABLE 5: Architectures of what/Cat-encoder.

Layer	Type	Size	Act./Norm.	Output size
Input	Flatten			$(3 \times 32 \times 32 =) 3072$
Layer 1	Linear	3072×128	ReLU	128
Layer 2	Linear	128×256	ReLU	256
Layer 3	Linear	256×512	ReLU	512
Output	Linear	$512 \times (A/C)$		(A/C)

TABLE 6: Architecture of glimpse decoder.

Layer	Type	Size	Act./Norm.	Output size
Input	Linear	$A \times 256$	ReLU	$256 \times 1 \times 1$
Layer 1	Deconv	128	ReLU/GN(8)	$128 \times 2 \times 2$
Layer 2	Deconv	128	ReLU/GN(8)	$128 \times 4 \times 4$
Layer 3	Deconv	64	ReLU/GN(8)	$64 \times 8 \times 8$
Layer 4	Deconv	32	ReLU/GN(8)	$32 \times 16 \times 16$
Conv	Conv	$3 \times 3, 32$	ReLU/GN(8)	$32 \times 16 \times 16$
Layer 5	Deconv	16	ReLU/GN(4)	$16 \times 32 \times 32$
Output	Conv	$3 \times 3, 3$		$3 \times 32 \times 32$

TABLE 7: Base hyperparameters.

Description	Variable	Value
Base box size	(a_h, a_w)	$(72, 72)$
Batch size		16
Dim. of $\mathbf{z}_i^{\text{what}}$	A	256
Dim. of $\mathbf{z}_i^{\text{cat}}$	C	10
Glimpse size	$(H_{\text{obj}}, W_{\text{obj}})$	$(32, 32)$
Learning rate		$[5e - 5, 1e - 4]$
Loss coef. of L_{cat}	α_{cat}	1
Loss coef. of L_{overlap}	α_{overlap}	$2 \rightarrow 0$
Loss coef. of L_{depth}	α_{depth}	1
Loss coef. of L_{pres}	α_{pres}	1
Loss coef. of L_{recon}	α_{recon}	8, 16
Loss coef. of L_{what}	α_{recon}	1
Loss coef. of L_{where}	α_{recon}	1
Prior on \mathbf{z}^{cat}	π	$((1/C), \dots, (1/C))$
Prior on $\mathbf{z}^{\text{depth}}$	$(\mu_{\text{prior}}^{\text{depth}}, \sigma_{\text{prior}}^{\text{depth}})$	$(0, 1)$
Prior on \mathbf{z}^{pres}	p	$1 \rightarrow 6e - 6$
Prior on $\mathbf{z}^{\text{where}}$	$(\mu_{\text{prior}}^{\text{where}}, \sigma_{\text{prior}}^{\text{where}})$	$(0, 1)$
Prior on \mathbf{z}^{what}	$(\mu_{\text{prior}}^{\text{what}}, \sigma_{\text{prior}}^{\text{what}})$	$(0, 1)$

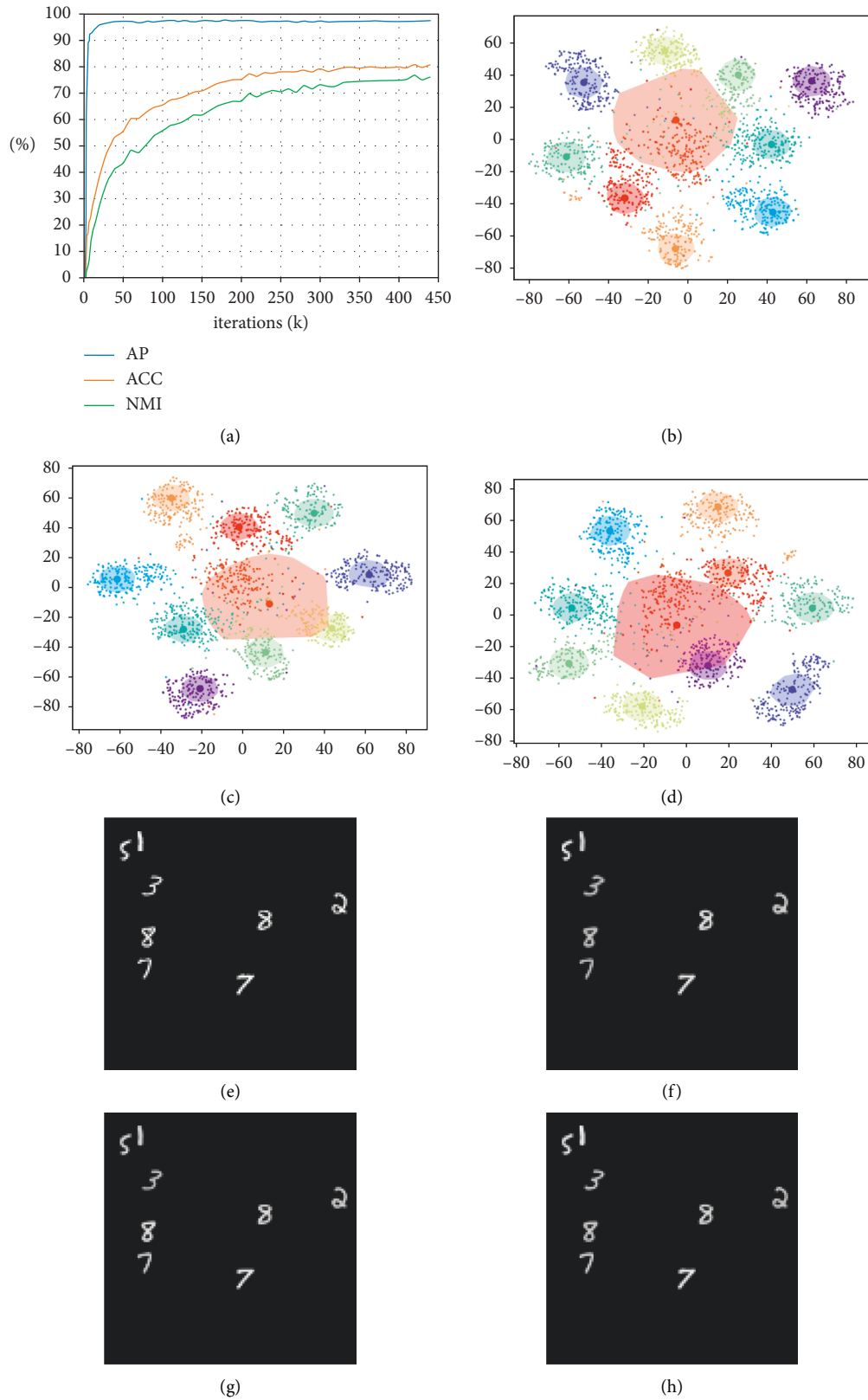


FIGURE 6: “What” representation and cluster analysis after 100k iterations. (a) Average precision (AP), accuracy (ACC), and normalized mutual information (NMI) during training. (b-d) Visualized “what” latent space by t-SNE ([15]) at 220k, 330k, and 440k iterations, respectively. (e) Sample of original image. (f-h) Samples of generated image at 220k, 330k, and 440k iterations, respectively. (a) AP (IoU=0.5), ACC, and NMI during training. (b) “What” latent space, at 220k iterations. (c) “What” latent space, at 330k iterations. (d) “What” latent space, at 440k iterations. (e) Original image. (f) Generated image, at 220k iterations. (g) Generated image, at 330k iterations. (h) Generated image, at 440k iterations.

reasonable since we try to minimize the KL divergence of \mathbf{z}^{what} and a Gaussian model in these models. Therefore, the Gaussian mixture model structure helps to gather “what” latent variables of a category and keep those of different categories away from each other.

5. Limitations and Societal Impact

The biggest limitation of GMAIR is that it can currently only be applied to simple compositing scenarios, such as games. However, the automatic mining of object localization and category from simple scenes is still a step towards artificial general intelligence. Although the current detection performance of GMAIR for complex scenes is poor, it cannot be ruled out that it may be applied to some scenes for unethical automatic detection or that it may learn biased or discriminatory features that may cause negative social impact. All these aspects are to be further investigated.

6. Conclusion

We introduce GMAIR, which combines spatial attention and a Gaussian mixture such that it can locate and cluster unseen objects simultaneously. We analyze the “what” latent variables and clustering process, showing that the model has the ability to detect and cluster similar objects automatically. For the downstream task, we show an

example of image generation that may be applied to data augmentation or synthetic data generation. We also evaluate GMAIR quantitatively compared with SPAIR and SPACE, showing that GMAIR archives the state-of-the-art detection performance.

As the number of data increases and the cost of annotation rises, unsupervised object detection will play an increasingly important role in the future. Future research should be devoted to improving the detection performance for complex scenes. One possible option is to make use of advanced results in supervised learning. Another important topic is to balance multiple loss functions better.

Appendix

A. Derivation of the KL Terms

In this section, we derive the KL terms in Eqn. (6). By assumption of $q(\mathbf{z}|\mathbf{x})$ and $p(\mathbf{z})$ (Eqn. (3) and Eqn. (1)), we have the following:

$$\mathbb{E}_{q(\mathbf{z}|\mathbf{x})} \left[\log \left(\frac{q(\mathbf{z}|\mathbf{x})}{p(\mathbf{z})} \right) \right] = \sum_{i=1}^{HW} \mathbb{E}_{q(\mathbf{z}_i|\mathbf{x})} \log \left(\frac{q(\mathbf{z}_i|\mathbf{x})}{p(\mathbf{z}_i)} \right). \quad (\text{A.1})$$

The term $\mathbb{E}_{q(\mathbf{z}_i|\mathbf{x})} \log(q(\mathbf{z}_i|\mathbf{x})/p(\mathbf{z}_i))$ can further be expanded as follows:

$$\begin{aligned} \mathbb{E}_{q(\mathbf{z}_i|\mathbf{x})} \log \left(\frac{q(\mathbf{z}_i|\mathbf{x})}{p(\mathbf{z}_i)} \right) &= q(\mathbf{z}_i^{\text{pres}} = 0|\mathbf{x}) \log \left(\frac{q(\mathbf{z}_i^{\text{pres}} = 0|\mathbf{x})}{p(\mathbf{z}_i^{\text{pres}} = 0)} \right) + q(\mathbf{z}_i^{\text{pres}} = 1|\mathbf{x}) \\ &\cdot \left(\log \left(\frac{q(\mathbf{z}_i^{\text{pres}} = 1|\mathbf{x})}{p(\mathbf{z}_i^{\text{pres}} = 1)} \right) + \mathbb{E}_{q(\mathbf{z}_i^{\text{where}}, \mathbf{z}_i^{\text{depth}}, \mathbf{z}_i^{\text{cat}}, \mathbf{z}_i^{\text{what}}|\mathbf{x})} \left[\log \left(\frac{q(\mathbf{z}_i^{\text{where}}, \mathbf{z}_i^{\text{depth}}, \mathbf{z}_i^{\text{cat}}, \mathbf{z}_i^{\text{what}}|\mathbf{x})}{p(\mathbf{z}_i^{\text{where}}, \mathbf{z}_i^{\text{depth}}, \mathbf{z}_i^{\text{cat}}, \mathbf{z}_i^{\text{what}})} \right) \right] \right) \\ &= KL(q(\mathbf{z}_i^{\text{pres}}|\mathbf{x})\|p(\mathbf{z}_i^{\text{pres}})) \\ &+ q(\mathbf{z}_i^{\text{pres}} = 1|\mathbf{x}) \mathbb{E}_{q(\mathbf{z}_i^{\text{where}}, \mathbf{z}_i^{\text{depth}}, \mathbf{z}_i^{\text{cat}}, \mathbf{z}_i^{\text{what}}|\mathbf{x})} \left[\log \left(\frac{q(\mathbf{z}_i^{\text{where}}, \mathbf{z}_i^{\text{depth}}, \mathbf{z}_i^{\text{cat}}, \mathbf{z}_i^{\text{what}}|\mathbf{x})}{p(\mathbf{z}_i^{\text{where}}, \mathbf{z}_i^{\text{depth}}, \mathbf{z}_i^{\text{cat}}, \mathbf{z}_i^{\text{what}})} \right) \right]. \end{aligned} \quad (\text{A.2})$$

Eqn. (A.2) is continued to expand:

$$\begin{aligned} &\mathbb{E}_{q(\mathbf{z}_i^{\text{where}}, \mathbf{z}_i^{\text{depth}}, \mathbf{z}_i^{\text{cat}}, \mathbf{z}_i^{\text{what}}|\mathbf{x})} \left[\log \left(\frac{q(\mathbf{z}_i^{\text{where}}, \mathbf{z}_i^{\text{depth}}, \mathbf{z}_i^{\text{cat}}, \mathbf{z}_i^{\text{what}}|\mathbf{x})}{p(\mathbf{z}_i^{\text{where}}, \mathbf{z}_i^{\text{depth}}, \mathbf{z}_i^{\text{cat}}, \mathbf{z}_i^{\text{what}})} \right) \right] \\ &= \mathbb{E}_{q(\mathbf{z}_i^{\text{where}}|\mathbf{x})} \log \left(\frac{q(\mathbf{z}_i^{\text{where}}|\mathbf{x})}{p(\mathbf{z}_i^{\text{where}})} \right) + \mathbb{E}_{q(\mathbf{z}_i^{\text{depth}}|\mathbf{x})} \log \left(\frac{q(\mathbf{z}_i^{\text{depth}}|\mathbf{x})}{p(\mathbf{z}_i^{\text{depth}})} \right) \\ &+ \mathbb{E}_{q(\mathbf{z}_i^{\text{cat}}, \mathbf{z}_i^{\text{where}}|\mathbf{x})} \log \left(\frac{q(\mathbf{z}_i^{\text{cat}}|\mathbf{x}, \mathbf{z}_i^{\text{where}})}{p(\mathbf{z}_i^{\text{cat}})} \right) \\ &+ \mathbb{E}_{q(\mathbf{z}_i^{\text{what}}, \mathbf{z}_i^{\text{where}}, \mathbf{z}_i^{\text{cat}}|\mathbf{x})} \log \left(\frac{q(\mathbf{z}_i^{\text{what}}|\mathbf{x}, \mathbf{z}_i^{\text{where}}, \mathbf{z}_i^{\text{cat}})}{p(\mathbf{z}_i^{\text{what}}|\mathbf{z}_i^{\text{cat}})} \right). \end{aligned} \quad (\text{A.3})$$

By the definition of the Kullback–Leibler divergence, the four terms in the RHS of Eqn. (A.3) are indeed:

$$\begin{aligned} &KL(q(\mathbf{z}_i^{\text{where}}|\mathbf{x})\|p(\mathbf{z}_i^{\text{where}})), \\ &KL(q(\mathbf{z}_i^{\text{depth}}|\mathbf{x})\|p(\mathbf{z}_i^{\text{depth}})), \\ &\mathbb{E}_{q(\mathbf{z}_i^{\text{where}}|\mathbf{x})} [KL(q(\mathbf{z}_i^{\text{cat}}|\mathbf{x}, \mathbf{z}_i^{\text{where}})\|p(\mathbf{z}_i^{\text{cat}}))], \text{ and} \\ &\mathbb{E}_{q(\mathbf{z}_i^{\text{where}}, \mathbf{z}_i^{\text{cat}}|\mathbf{x})} [KL(q(\mathbf{z}_i^{\text{what}}|\mathbf{x}, \mathbf{z}_i^{\text{where}}, \mathbf{z}_i^{\text{cat}})\|p(\mathbf{z}_i^{\text{what}}|\mathbf{z}_i^{\text{cat}}))], \end{aligned} \quad (\text{A.4})$$

respectively. Therefore, we complete the proof of Eqn. (5).

During the implementation, we model discrete variables \mathbf{z}^{pres} and \mathbf{z}^{cat} using the Gumbel-Softmax approximation ([17]). Therefore, all variables are differentiable using the reparameterization trick.

B. Implementation Details

Our code is available at <https://github.com/EmoFuncs/GMAIR-pytorch>.

B.1 Models. Here, we describe the architecture of each module of GMAIR, as shown in Figure 1. The backbone is a ResNet18 ([18]) with two deconvolution layers replacing the fully connected layer, as shown in Table 3. Pres-head, depth-head, and where-head are convolutional networks that are only different from the number of output channels, as shown in Table 4. What-encoder and cat-encoder are multiple layer networks, as shown in Table 5. Finally, the glimpse decoder is a deconvolutional network, as shown in Table 6.

For other models, we make use of code from https://github.com/yonkshi/SPAIR_pytorch for SPAIR and <https://github.com/zhixuan-lin/SPACE> for SPACE. We utilize most of the default configuration for both models and only change A (the dimension of $\mathbf{z}_i^{\text{what}}$) to 256 for comparison, the size of the base bounding box to 72×72 for large objects.

B.2 Training and Hyperparameters. The base set of hyperparameters for GMAIR is given in Table 7. The value p (the prior on \mathbf{z}^{pres}) drops gradually from 1 to the final value $6e - 6$, and the value α_{overlap} drops from 2 to 0 in the early stage of training for stability. The learning rate is in the range of $[5e - 5, 1e - 4]$.

B.3 Testing. During testing phase, to obtain deterministic results, we use the value with the largest probability (density) for latent variables \mathbf{z} , instead of sampling them from the distributions. To be specific, we use π , μ^{depth} , p , μ^{what} , and μ^{where} for \mathbf{z}^{cat} , $\mathbf{z}^{\text{depth}}$, \mathbf{z}^{pres} , \mathbf{z}^{what} , and $\mathbf{z}^{\text{where}}$, respectively.

C. Calculation of AP, ACC, and NMI

The value of AP is calculated at threshold IoU = 0.5 using the calculation method from the VOC ([19]). Before calculating the ACC and NMI of clusters, we filter the incorrect bounding boxes. A predicted box PB is correct if there is a ground truth box GB such that $\text{IoU}(PB, GB) > 0.5$, and the class of a correct predicted box PB is assigned to the class of the ground truth box GB such that $\text{IoU}(PB, GB)$ is maximized. After filtering, all correct predicted boxes are used for the calculation of ACC and NMI. Note that we still have many ways to assign each predicted category to a real category when calculating the value of ACC. In all of the ways, we select the one such that ACC is maximized, following [12]. Formulas are shown in Eqn. (C.1) and Eqn. (C.2) for the calculation of ACC and NMI:

$$\text{ACC} = \frac{\sum_{k=1}^C \max_{1 \leq j \leq C'} \left| \{i | G_i = j, P_i = k\} \right|}{|P|}, \quad (\text{C.1})$$

$$\text{NMI} = \frac{2I(G, P)}{H(G) + H(P)}, \quad (\text{C.2})$$

where G and P are, respectively, the ground truth categories and predicted categories for all correct boxes, C and C' are

the number of clusters and real classes, and $H(\cdot)$ and $I(\cdot, \cdot)$ are the entropy and mutual information function, respectively.

D. Additional Experimental Results

The graphs of “what” representation after 100k iterations are shown in Figure 6.

Data Availability

The data included in this study are available without any restriction.

Disclosure

This article was published on arXiv in preprint form [16].

Conflicts of Interest

The authors declare that there are no conflicts of interest regarding the publication of this study.

Acknowledgments

This work was partially supported by the Research and Development Projects of Applied Technology of Inner Mongolia Autonomous Region, China, under grant no. 201802005, the Key Program of the National Natural Science Foundation of China under grant no. 61932014, and Pudong New Area Science and Technology Development Foundation under grant nos. PKX2019-R02.

References

- [1] S. Eslami, N. Heess, T. Weber et al., “Attend, infer, repeat: fast scene understanding with generative models,” 2016, <https://arxiv.org/abs/1603.08575>.
- [2] D. P. Kingma and M. Welling, “Auto-encoding variational bayes,” 2013, <https://arxiv.org/abs/1312.6114>.
- [3] E. Pineau and J. Pineau, “Spatially invariant unsupervised object detection with convolutional neural networks,” in *Proceedings of the AAAI Conference on Artificial Intelligence*, vol. 33, pp. 3412–3420, Honolulu, HI, USA, January 2019.
- [4] Z. Lin, Y.-F. Wu, S. V. Peri et al., “Space: unsupervised object-oriented scene representation via spatial attention and decomposition,” 2020, <https://arxiv.org/abs/2001.02407>.
- [5] C. P. Burgess, L. Matthey, N. Watters et al., “Monet: unsupervised scene decomposition and representation,” 2019, <https://arxiv.org/abs/1901.11390>.
- [6] K. Greff, R. L. Kaufman, R. Kabra et al., “Multi-object representation learning with iterative variational inference,” in *Proceedings of the International Conference on Machine Learning*, pp. 2424–2433, PMLR, Long Beach, CA, USA, March 2019.
- [7] M. Engelcke, A. R. Kosiorek, O. P. Jones, and I. Posner, “Genesis: generative scene inference and sampling with object-centric latent representations,” 2019, <https://arxiv.org/abs/1907.13052>.
- [8] M. Engelcke, O. Parker Jones, and I. Posner, “Genesis-v2: inferring unordered object representations without iterative refinement,” *Advances in Neural Information Processing Systems*, vol. 34, 2021.

- [9] M. Jaderberg, K. Simonyan, A. Zisserman, and K. Kavukcuoglu, "Spatial transformer networks," 2015, <https://arxiv.org/abs/1506.02025>.
- [10] J. Redmon, S. Divvala, R. Girshick, and A. Farhadi, "You only look once: unified, real-time object detection," in *Proceedings of the IEEE conference on computer vision and pattern recognition*, pp. 779–788, Las Vegas, NV, USA, June 2016.
- [11] A. Makhzani, J. Shlens, N. Jaitly, I. Goodfellow, and B. Frey, "Adversarial autoencoders," 2015, <https://arxiv.org/abs/1511.05644>.
- [12] N. Dilokthanakul, P. A. Mediano, M. Garnelo et al., "Deep unsupervised clustering with Gaussian mixture variational autoencoders," 2016, <https://arxiv.org/abs/1611.02648>.
- [13] X. Ji, J. F. Henriques, and A. Vedaldi, "Invariant information clustering for unsupervised image classification and segmentation," in *Proceedings of the IEEE/CVF International Conference on Computer Vision*, pp. 9865–9874, Seoul, Korea, 2019.
- [14] Y. LeCun, "The mnist database of handwritten digits," 1998, <http://yann.lecun.com/exdb/mnist/>.
- [15] L. Van der Maaten and G. Hinton, "Visualizing data using t-sne," *Journal of Machine Learning Research*, vol. 9, no. 11, 2008.
- [16] W. Zhu, Y. Shen, L. Yu, and L. P. A. Sanchez, "Gmair: unsupervised object detection based on spatial attention and Gaussian mixture," 2021, <https://arxiv.org/abs/2106.01722>.
- [17] E. Jang, S. Gu, and B. Poole, "Categorical reparameterization with gumbel-softmax," 2016, <https://arxiv.org/abs/1611.01144#:~:text=Categorical%20variables%20are%20a%20natural,inability%20to%20backpropagate%20through%20samples>.
- [18] K. He, X. Zhang, S. Ren, and J. Sun, "Identity mappings in deep residual networks," *Computer Vision - ECCV 2016. In European conference on computer vision*, 645 pages, Springer, Manhattan, NY, USA, 2016.
- [19] M. Everingham, L. Van Gool, C. K. I. Williams, J. Winn, and A. Zisserman, "The pascal visual object classes (voc) challenge," *International Journal of Computer Vision*, vol. 88, no. 2, pp. 303–338, 2010.

Research Article

Secure Clustering Strategy Based on Improved Particle Swarm Optimization Algorithm in Internet of Things

Zhanbiao Bao 

Center of Education Technology, Henan University of Economics and Law, Zhengzhou, Henan 450046, China

Correspondence should be addressed to Zhanbiao Bao; bao@huel.edu.cn

Received 10 May 2022; Revised 10 June 2022; Accepted 28 June 2022; Published 16 July 2022

Academic Editor: Le Sun

Copyright © 2022 Zhanbiao Bao. This is an open access article distributed under the Creative Commons Attribution License, which permits unrestricted use, distribution, and reproduction in any medium, provided the original work is properly cited.

This paper proposes a secure clustering strategy based on improved particle swarm optimization (PSO) in the environment of the Internet of Things (IoT). First, in the process of cluster head election, by considering the residual energy and load balance of nodes, a new fitness function is established to evaluate and select better candidate cluster head nodes. Second, the optimized adaptive learning factor is used to adjust the location update speed of candidate cluster head nodes, expand the local search, and accelerate the convergence speed of global search. Finally, in the stage of forwarding node election and data transmission, in order to reduce the energy consumption of forwarding nodes, each cluster head node elects a forwarding node among the ordinary nodes in its cluster, so that the elected forwarding nodes have the optimal energy and location relationship. Experiments show that the proposed method effectively prolongs the network lifetime compared with the comparison methods. The average node degree of the proposed method is less than 2.5.

1. Introduction

With the development of information society, the information industry is more and more vigorous, and the scope of information application is more and more extensive [1]. Especially in the process of the big data era, the acquisition of information has attracted more and more attention, and become one of the important hotspots of scientific research and value-added industry [2–4]. Effective information acquisition is the basis of information transmission, processing, mining, and application. Sensors connect the physical world and the digital world by capturing and revealing the physical phenomena of the world and transforming them [5]. Wireless sensor network (WSN) is a self-organized network composed of a large number of sensor nodes with information collection, processing, and transmission functions. Each sensor node can realize the data collection, processing, and transmission of the sensing area, and the whole network can cooperate to complete the information collection in the target area [6–8]. Through the deployment and use of the network, the ability of human society

to obtain information can be enhanced. It has changed the situation that people only rely on their own feelings and simple tools to perceive information since ancient times and greatly improved the accuracy and sensitivity of human access to data and information [9, 10].

WSN is often used to monitor events of interest in the surrounding environment. A typical WSN monitoring system consists of sensor nodes, base stations, and monitoring centers [11–13]. The remote user or monitoring center can send data acquisition, processing, and transmission commands to the sensor nodes in the network through the base station, and finally, receive the interested data through the base station [14–16].

In the environment of IoT, aiming at the problems of large node energy consumption and short network life cycle caused by the unbalanced location distribution of cluster head nodes screened by clustering routing protocol of wireless sensor networks and unreasonable data transmission path of forwarding nodes, a secure clustering strategy based on improved PSO algorithm in the IoT environment is proposed. The innovations of the proposed method lie in the following:

- (1) In the process of cluster head election, considering the residual energy and load balance of nodes, a new fitness function is established to evaluate and select better candidate cluster head nodes, which effectively shortens the communication distance.
- (2) The optimized adaptive learning factor is used to adjust the position update speed of candidate cluster head nodes, and the concave function nonlinear decreasing strategy is used to improve the inertia weight, which speeds up the convergence speed of global search.
- (3) For each cluster head node, a forwarding node is selected from the ordinary nodes in its cluster, so that the selected forwarding node has the optimal energy and location relationship, and the node communication overhead is reduced.

The remaining chapters of this paper are arranged as follows. Section 2 introduces the related research in this field; Section 3 introduces the system model; Section 4 introduces the proposed clustering routing algorithm based on improved PSO algorithm; Section 5 is the experiment, and Section 6 summarizes this study.

2. Related Works

Compared with plane routing, cluster routing saves the energy consumption of the network to the greatest extent, facilitates data fusion, and is easier to expand [17–19]. As a simple and effective random search algorithm, intelligent algorithm has good application prospects in finding the optimal solution of function and neural network recognition [20]. In the late 19th century, James Kennedy of the United States proposed PSO for the first time. It is famous for its simplicity and effectiveness. Therefore, scholars at home and abroad choose PSO algorithm in cluster head selection. Reference [21] defined a new cost function to minimize the communication distance between cluster members and cluster heads and used the PSO to select cluster heads with higher energy to optimize network clustering. Reference [22] proposed a new clustering mode EECS for wireless sensor networks, which specified the size of clusters in the network. Clusters far from the base station have a larger radius, and clusters close to the base station have a smaller radius, so as to balance the energy consumption of cluster heads. Reference [23] proposed a new hierarchical clustering protocol PSO-HC, which balanced the network energy consumption by reducing the number of cluster heads and transmitted the information collected by cluster heads to the base station by multihop. Based on the clustering of the LEACH protocol, reference [24] used the ant colony algorithm to optimize the distance location between each node and the base station and obtained the best path. Through this path, the cluster head transmitted the information to the next cluster head in sequence until the information was transmitted to the base station.

Reference [25] proposed an improved PSO algorithm to optimize the running time of the network. The algorithm comprehensively considered the factors of energy and distance to realize the selection of target nodes and proposed the introduction of relay nodes to share the transmission

work of cluster head nodes. Reference [26] combined harmony search (HS) algorithm and PSO to select cluster head nodes. The algorithm not only had the efficient search efficiency of harmony search algorithm but also had the dynamic ability of the PSO algorithm, which could better improve the performance of the network. According to the uneven clustering algorithm, reference [27] used ant colony optimization algorithm to calculate the optimal distance between the node and the base station and transmitted the data of each cluster head node to the base station through the selected optimal path. The disadvantage of this algorithm is that the path from each cluster head to the base station needs to be calculated, so it will lead to excessive energy consumption. Reference [28] proposed a clustering strategy based on FBECs (fuzzy based enhanced cluster head selection). In the clustering stage, fuzzy logic algorithm was used to calculate the qualification index of each node according to the residual energy of the node and the distance between the node density and the base station. The node generated the cluster head by comparing the randomly generated random number with the qualification index. Reference [29] proposed a clustering method based on energy center search using PSO (EC-PSO), which used geometric method to select CHs and searched energy centers in CHs selection.

3. System Model

3.1. Network Model. In order to better optimize the algorithm, this model makes the following assumptions.

- (1) The nodes are randomly deployed in the target area. After deployment, the nodes will no longer move, and each node has a unique ID.
- (2) All nodes have the same initial energy, computing power, and communication ability and can automatically adjust the transmission power.
- (3) Each node can communicate with the base station independently, and the location of the base station is known.
- (4) The node can calculate its relative position according to the angle of arrival and signal strength.

3.2. Energy Model. The same energy model as LEACH is used for communication between nodes. According to the distance $d_{ij} = \sqrt{(x_i - x_j)^2 + (y_i - y_j)^2}$ between node i and node j , the channel model is selected. The energy consumed by a node to send k bit data to the node with a distance of d is

$$E_{TX}(k, d) \begin{cases} k(E_{elec} + \alpha_{fs}d^2), d < d_0, \\ k(E_{elec} + \alpha_{mp}d^2), d > d_0, \end{cases} \quad (1)$$

$$d_0 = \sqrt{\frac{\alpha_{fs}}{\alpha_{mp}}}$$

The energy consumed by the node to receive and fuse k bit data is

$$\begin{aligned} E_{RX}(k) &= kE_{elec}, \\ E_{DA}(k) &= kE_{da}, \end{aligned} \quad (2)$$

where E_{elec} is the energy consumed to receive or send 1 bit data and E_{da} is the energy consumed by the node to fuse 1 bit data. The transmission model selected by the node for communication is determined by d_0 . α_{fs} and α_{mp} are the energy required for power amplification of free space channel model and multipath fading model. When the distance between nodes $d < d_0$, choose the free space channel model; otherwise, choose the multipath fading model.

4. Clustering Routing Algorithm Based on Improved PSO Algorithm

4.1. Cluster Head Election

4.1.1. Cluster Head Initialization. Because the calculation of the PSO algorithm is relatively complex, in order to avoid increasing the energy consumption of nodes in election calculation, the clustering and routing calculation based on the PSO algorithm will be completed by the base station with unlimited energy. In the initialization process, all nodes send their residual energy, location, and number information to the base station, and the base station receives and saves the information of each node. After the base station completes the clustering calculation based on the PSO algorithm, the base station broadcasts the calculation results. Each surviving node obtains the specific location information of the elected node and routing node according to the received broadcast information. PSO algorithm selects particles randomly, which is easy to fall into local optimization, resulting in uneven distribution of nodes in the cluster. To solve this problem, the energy of nodes participating in cluster head node election is limited.

Suppose there is N surviving nodes in the WSN, the energy of node i is $E(i)$, and the base station calculates the average residual energy of all nodes in the WSN as $E_a = 1/N \sum_{i=1}^N E(i)$.

In order to ensure that the selected cluster head nodes have sufficient energy to process the data in the cluster, the base station forms a set EA of all nodes with energy greater than or equal to E_a , then randomly selects K nodes from the EA, and stores them in the candidate cluster head node set to form a particle. After initially determining a group of candidate cluster head nodes, other noncluster head nodes join the cluster head nodes closest to them, respectively, to complete the establishment of initial clustering. Then, continue to select K nodes in EA in a random way, conduct a total of M times of screening, and finally generate the M groups of initial cluster head node set; that is, M particles, and form the M groups of clusters.

4.1.2. Fitness Function. The cluster head node is responsible for most activities and needs to consume more energy, which may lead to premature failure due to excessive energy

consumption and reduce the performance of the whole network. Therefore, when selecting the cluster head node, it should consider the following two aspects: select the cluster head node with large residual energy and balance the load of the cluster head node at the same time.

First, consider selecting the cluster head node set with large residual total energy. Suppose that K is the number of cluster head nodes selected by the current particle. CH represents the cluster head set and CH_k represents the cluster head node of k cluster. The ratio f_1 of the current residual energy of all nodes to the residual energy of the cluster head node set is

$$f_1 = \frac{\sum_{i=1}^N E(i)}{\sum_{i=1}^N E(CH_k)}, \quad (3)$$

where $E(i)$ represents the residual energy of the sensor node i in the particle.

After the current particle selects the cluster head node, the set CS_k is used to represent the member node set of the cluster k . C_k is used to count the number of member nodes in the cluster k . If the node j joins the cluster k , it can be expressed as $j \in CS_k$, and the C_k plus 1.

After clustering the current particles, it should further consider the load of the current cluster. The load of the cluster mainly includes the load in the cluster and the load between clusters. For the load balancing in the cluster, it is considered from two aspects: the number of member nodes in the cluster and the distance from the member nodes in the cluster to the cluster head.

Let f_2 represent the average of the deviation between s and the maximum distance between each cluster head node and its nodes in the cluster.

$$f_2 = \sum_{k=1}^K \frac{1}{K} \left| \max \left(\sum_{j=1}^N d(j, CH_k) - s \right) \right|. \quad (4)$$

Let f_3 represent the difference between the number of member nodes in each cluster and the average number of members in the cluster. The smaller the difference, the closer the number of members between clusters, and the more effective it is to balance the energy consumption between cluster heads, so as to prolong the life cycle of the network:

$$f_3 = \sum_{k=1}^K \frac{1}{K} \left| \frac{N}{C_k} - K \right|, \quad (5)$$

where $d(x, y)$ refers to the distance between node x and node y . r is the radius of clusters when the whole network area can be covered. Ideally, the area of each cluster is evenly distributed in the network area, and there is no coverage area between each cluster. The area of each cluster should be $A/(\text{pro} \times N)$, where A is the area of the whole network area, pro is the preset proportion of cluster heads and $\text{pro} \times N$ is the number of cluster heads, so the ideal r value is $\sqrt{A/(\text{pro} \times N)}$.

f_4 represents the average distance between cluster heads. The smaller the average distance between cluster heads, the smaller the load between clusters, which can reduce the communication energy consumption of the network.

$$f_4 = \frac{2(\sum_{k=1}^{K-1} \sum_{j=k+1}^K d(CH_k, CH_j))}{((K-1)/K)}. \quad (6)$$

In the fitness function, the node residual energy and load balance are comprehensively considered, and the multi-objective optimization problem is transformed into a single objective optimization problem by means of weighted sum:

$$F = \alpha f_1 + \beta f_2 + \chi f_3 + \delta f_4, \quad (7)$$

where α , β , χ , and δ are weighting factors.

4.1.3. Update Method of Speed and Position. According to the initial fitness calculation and the initially generated local optimal location and global optimal location, start a round of iterative calculation. First, update the location of the candidate cluster head node set, and then calculate the fitness of the candidate cluster head node after location update. In order to complete the location update of the candidate cluster head node set and obtain the optimization results, let the velocity components of the candidate cluster head nodes in the x and y directions be v_x and v_y , respectively, and the position components be x_x and x_y , respectively.

The calculation of the two velocity components is initially generated randomly, but in each subsequent iteration, it is determined according to the change relationship between the velocity component of the previous round of the candidate cluster head node set and the local optimal position (p_{xi}, p_{yi}) and the global optimal position (p_{xg}, p_{yg}) . The specific calculation is as follows:

$$\begin{cases} v_x(t) = wv_x(t-1) + c_1 l_1 (p_{xi}(t-1) - x_{xi}(t-1)), \\ \quad + c_2 l_2 (p_{xg}(t-1) - x_{xi}(t-1)), \\ v_y(t) = wv_y(t-1) + c_1 l_1 (p_{yi}(t-1) - x_{yi}(t-1)), \\ \quad + c_2 l_2 (p_{yg}(t-1) - x_{yi}(t-1)), \end{cases} \quad (8)$$

where w is the inertia weight, which indicates the influence of the speed of the previous $t-1$ iteration of the candidate cluster head node set on the speed of the candidate cluster head node set in this t iteration. c_1 is a cognitive learning factor and c_2 is a social learning factor, which, respectively, represent the acceleration weight of the candidate cluster head node set close to the local optimal position and the global optimal position. $l_1, l_2 \in (0, 1)$ are the random numbers.

Based on the two velocity components, the calculation method of the position components $x_{xi}(t)$ and $x_{yi}(t)$ of the candidate cluster head node in the direction x and y is as follows:

$$\begin{cases} x_{xi}(t) = x_{xi}(t-1) + v_{xi}(t), \\ x_{yi}(t) = x_{yi}(t-1) + v_{yi}(t). \end{cases} \quad (9)$$

4.1.4. Improved Inertia Weight. Among the parameters that can be adjusted by the PSO algorithm, researchers often improve the important parameter of inertia weight. A larger

inertia weight value is conducive to improve the global search ability of the PSO algorithm, and a smaller weight value will enhance the motion ability of particles.

Under the same convergence accuracy, the concave function decreasing strategy greatly improves the convergence speed of PSO compared with other improved strategies, and can more effectively control the balance between global search and local search.

The rule for improving inertia weight by using concave function nonlinear decreasing strategy is as follows:

$$w = (w_{\max} - w_{\min}) \left[\left(\frac{C_{\text{Cur}}}{C_{\text{Loop}}} \right)^2 + 2 \frac{C_{\text{Cur}}}{C_{\text{Loop}}} \right] + w_{\max}, \quad (10)$$

where $w \in [0.5, 0.9]$ and C_{Cur} represent the number of rounds of the current iteration and C_{Loop} represents the total number of iterations.

4.1.5. Location Mapping Strategy. After each round of iteration, the location of the candidate cluster head node set will be updated, and the updated node location may not find a matching surviving node in the WSN. At this time, location mapping is needed. The basic idea is to adopt the proximity principle to map the updated location to the location of the nearest surviving node. Take x_{xi} and x_{yi} as the updated node coordinates and CM_{nx} and CM_{ny} as the coordinates of the surviving node CM_n in the network. The location mapping process is as follows:

$$\begin{aligned} CM_n &= \left\{ (CM_{nx}, CM_{ny}) \mid \min \sqrt{(CM_{nx} - x_{xi})^2 + (CM_{ny} - x_{yi})^2} \right\}. \end{aligned} \quad (11)$$

The location mapping strategy solves the mismatch between the updated location and the actual surviving node location caused by the discrete distribution of network nodes. When the updated position coordinates of multiple nodes are the same, it is necessary to set a flag while updating the node. When updating and mapping the positions of other nodes, first check whether the flag has been identified as the cluster head node. If so, select the next closest node position in turn for mapping.

After completing the location mapping, take the candidate cluster head node set after the location update as the optimization result, and calculate the fitness value of each candidate cluster head node set. According to the calculation results, the local optimal location of each group of candidate cluster head node set and the global optimal location of M groups of cluster head node sets in this round are updated. If the iteration is not finished, continue to update and map the location of candidate cluster head nodes. Otherwise, the candidate cluster head node set of the global optimal position is calculated as the optimal cluster head node set, and the cluster head election is completed.

After completing the cluster head election, the base station further calculates the distance from the noncluster head node to each cluster head node and adds the noncluster

head node to the nearest cluster head node to complete clustering. Ordinary nodes only send data. After receiving the data from ordinary nodes, the cluster head node performs data fusion and then sends it to the corresponding forwarding node. The forwarding node needs to be further selected from ordinary nodes. It receives the data from the cluster head, selects the optimal path to the base station, and sends the data to the base station.

4.2. Election and Data Transmission of Forwarding Nodes

4.2.1. Election of Forwarding Nodes. After the cluster head node election is completed, the corresponding forwarding node will be selected for the cluster head node. If there are too few forwarding nodes in the network, multiple cluster head nodes send data to the base station through a small number of forwarding nodes, which will increase the energy consumption of forwarding nodes. To solve this problem, the existing WSN routing protocol adopts the way that one cluster head node corresponds to one forwarding node to increase the number of forwarding nodes, but it selects all nodes randomly without considering whether the residual energy and location of the selected nodes are balanced.

In the forwarding node election, the improved PSO algorithm of the above cluster head node election is adopted to elect a forwarding node for each cluster head node among the ordinary nodes in its cluster, so that the elected forwarding node has the optimal energy and location relationship, and avoid speeding up its energy consumption due

to too few forwarding nodes in WSN. In the calculation and evaluation of forwarding nodes, because forwarding nodes can only be elected in one cluster, the calculation methods of energy factor and location balance factor are different from those of cluster head node election. Similarly, N represents the number of surviving nodes in the WSN. After selecting K cluster head nodes, the WSN is divided into K clusters. During initialization, according to the cluster head node screening method, candidate forwarding nodes with high residual energy are screened out in each cluster to form a set of candidate forwarding nodes. Each candidate set contains K nodes. After initialization, the number of ordinary nodes is $N - 2K$. Let $E_{RN}^r(i)$ represent the residual energy of candidate forwarding node RN_i in round r , and $E_{CN}^r(i)$ represent the residual energy of ordinary node CN_j in round r . The calculation formula of energy factor fit_1 is

$$fit_1 = \frac{(N - 2K) \sum_{j=1}^{N-2K} E_{RN}^r(i)}{K \sum_{j=1}^{N-2K} E_{CN}^r(i)}. \quad (12)$$

Let $d(CN_k, CH_j)$ represent the distance between the ordinary node CN_k and the corresponding cluster head node CH_j , $d(RN_i, BS)$ represent the distance between the forwarding node RN_i and the base station BS , $d(RN_i, CH_j)$ represent the distance between the forwarding node RN_i and the corresponding cluster head node CH_j , and $d(RN_i, RN_m)$ represent the distance between the forwarding nodes RN_i and RN_m . The calculation method of the location equalization factor fit_2 of the forwarding node is as follows:

$$fit_2 = \frac{K^2 \sum_{j=1}^{N-2K} d(CN_k, CH_j)}{(N - 2K) \left(\sum_{i=1}^K d(RN_i, BS) + \sum_{i=1}^K d(RN_i, CH_j) + \sum_{i=1}^{K-1} \sum_{m=i+1}^K d(RN_i, RN_m) \right)}, \quad (13)$$

where the ordinary node CN_k is located in the cluster where the cluster head node CN_k is located and the candidate forwarding node RN_i corresponds to the cluster head node CH_j . The closer the candidate forwarding node set is to the base station, the smaller the distance between the cluster head node and the forwarding node in each cluster; the smaller the distance between the forwarding nodes in the candidate forwarding node set, the more balanced the location distribution of the candidate forwarding node set, and the greater the fit_2 value.

Based on the ability factor and location balance factor of candidate forwarding node election, the fitness function F_2 for the evaluation of candidate forwarding node set constructed by weighting method is as follows:

$$F_2 = bfit_2 + (1 - b)fit_2, \quad (14)$$

where $b \in (0, 1]$ is the weight. The higher the residual energy of the candidate forwarding node set and the more balanced the location, the greater the fitness value of the candidate forwarding node set, indicating that the candidate forwarding node set is better. In the iterative election process of candidate forwarding node set, the

speed update and location mapping method similar to cluster head node election is used to select the optimal forwarding node set.

4.2.2. Data Transmission. WSN forward routing mainly selects relay nodes for cluster heads far away from the base station, and relay nodes reduce the load of cluster heads by forwarding data packets from cluster heads. Assuming that the data packet needs to be sent to the base station through n hop; that is, through $n - 1$ relay nodes, the optimal relay node should have the following characteristics:

- (1) The distance between relay nodes should be as balanced as possible.
- (2) The relay node should have high energy to meet the data transmission requirements.
- (3) The total distance should be as close as possible to the direct communication distance between the cluster head and the base station.
- (4) The selection of relay nodes should avoid selecting other cluster heads.

- (5) The load of relay nodes should be as small as possible to avoid over development.

According to the above requirements, the corresponding fitness function is designed, which can be expressed as

$$F_3 = \varepsilon \left(\frac{E_{\min}}{E_{\text{init}}} + \frac{1}{\text{load}_{\max}} \right) + \phi \left(\frac{d_{\min}}{d_{\max}} + \frac{d_{\text{init}}}{d_{\text{total}}} \right), \quad (15)$$

where E_{\min} is the node with the smallest energy among the relay nodes; the load of the node is determined by the number of data packets received by the node. load_{\max} is the node with the largest load in the relay nodes; d_{\min} and d_{\max} are the minimum and maximum distance between adjacent nodes in the forward routing path, respectively; d_{init} and d_{total} are the sum of the distance between the cluster head and the base station and the sum of distance of the whole forward routing path; $\varepsilon = 0.5 + 0.5E_{\text{loss}}/E_{\text{total}}$; $\phi = 1 - \varepsilon$. The total energy consumption of the nodes in the cluster is changed into the energy consumed by the cluster head that needs to plan the route, and the total energy in the cluster is changed into the initial energy of the cluster head. With the operation of the network, the parameter weight ratio is dynamically adjusted.

5. Experiments and Analysis

5.1. Experimental Setup. Simulating the generation of WSN in MATLAB and setting the base station outside the network, in this environment, the secure clustering strategy based on improved PSO algorithm is tested. The experimental computer is configured with 2.3 GHz, Intel Core I7, 8 GB RAM, and 64bit Windows10. The experimental environment and parameter settings related to WSN initialization, cluster head node, forwarding node election, and data processing are shown in Table 1.

5.2. Performance Index Comparison of Topology Generated by Different Schemes. In order to prove the performance of the proposed method under the same experimental conditions, the proposed method is compared with the methods in references [28, 29], and the comparison results are shown in Figure 1. In order to compare the algorithms effectively without losing generality, it is assumed that n sensor nodes are randomly deployed in the target monitoring area of 200×200 .

As can be seen from Figure 1(a), the average link length of the three methods continues to decrease with the growth of n . The proposed method can maintain the global connectivity of the network with a short average link length and has strong advantages in reducing the overall energy consumption of the network.

Figure 1(b) shows the comparison results of the average node degree of the three control schemes. It can be seen from the figure that the average node degree of the other two methods tends to rise with the increase of the network scale, while the topology obtained by the proposed method has a low average node degree, which is basically maintained below 2.5, and the average node degree is relatively stable

TABLE 1: Experimental parameters setting.

Parameter name	Value
Number of nodes	150
Base station location	(50,100)
Network scale	200 m \times 200 m
E_{fs} (pJ.(bit·m ²) ⁻¹)	10
E_{mp} (pJ.(bit·m ⁴) ⁻¹)	0.002
E_{elec} (nJ.bit ⁻¹)	60
$d0$ (m)	70
Maximum number of rounds	2500
The number of iterations of the algorithm	200
Optimal number of clusters	10
Number of particle	20
Data packet length/bit	5000
Control packet length/bit	100
Node initial energy $E0$ (J)	0.7

and will not change greatly with the change of the network scale. It shows that this method has good stability and low interference.

As can be seen from Figure 1(c), when the network size is 70, the average number of joint points of the methods in references [28, 29] is 3.0 and 2.3, respectively, and the number of joint points of the proposed method is 0. The number of joint points of the methods in references [28, 29] decreases with the continuous growth of the network size, but the method in this paper has better stability and can ensure that there are basically no joint points under different network sizes. This is because the proposed method comprehensively considers the residual energy and load balance of nodes, establishes a new fitness function, and can select better candidate cluster head nodes. Therefore, compared with the other two methods, the proposed method can better ensure the connectivity of topology when clusters are connected.

5.3. Location Balance Test of Cluster Head Nodes. The location balance factor reflects the distribution balance of cluster head node set and forwarding node set in WSN. The more balanced the node distribution is, the smaller the total communication distance in WSN communication is, and the lower the node energy consumption will be. Based on the above experimental environment, the total distance from all ordinary nodes to cluster heads and the total distance from all cluster head nodes to base stations in multiple iterations of the methods proposed in this paper, references [28, 29] are tested, respectively. The experimental results are shown in Figures 2 and 3, respectively.

As can be seen from Figures 2 and 3, with the increase of the number of iterations, the total distance from all ordinary nodes to cluster heads and the total distance from all cluster heads to base stations in the three methods become smaller and smaller. In the method of reference [28], the energy and location of nodes are not considered in cluster head election. Initially, the two distances in Figures 2 and 3 are the largest, but the two distances drop rapidly after 2600 rounds. This is because their communication distance is large, energy consumption is large and unbalanced, and node death is fast.

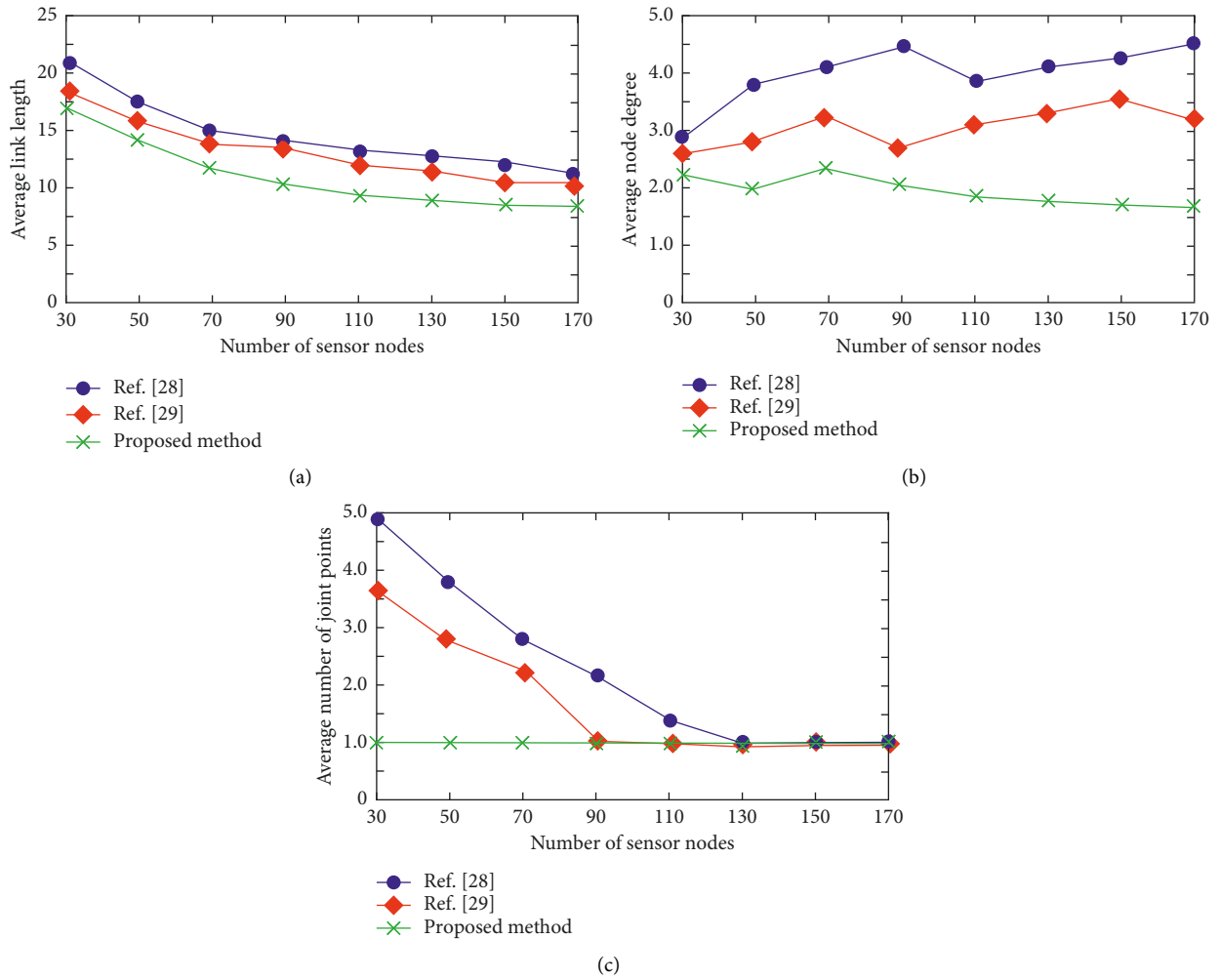


FIGURE 1: Comparison of performance indices of topologies generated by different schemes: (a) comparison of average link length; (b) comparison of average node degree; (c) comparison of average number of joints.

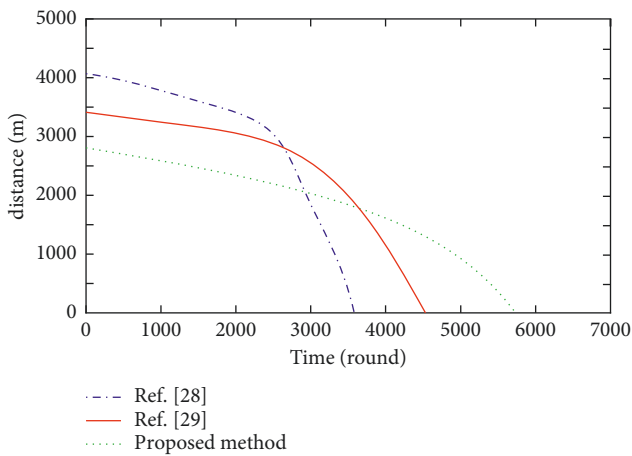


FIGURE 2: Sum of distances from ordinary nodes to cluster heads in different methods.

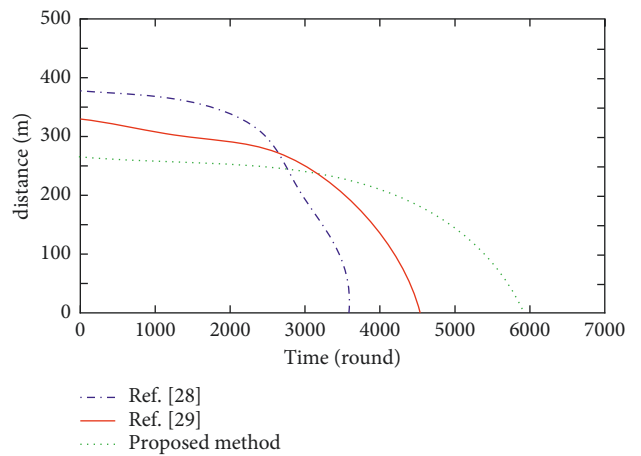


FIGURE 3: Sum of distances between cluster heads and base station in different methods.

With the large reduction of surviving nodes, their communication distance decreases, and the life cycle of WSN is greatly shortened. This is because, the proposed method elects a forwarding node for each cluster head node among the ordinary nodes in its cluster so that the selected forwarding node has the optimal energy and location relationship, which effectively reduces and balances the node energy consumption. The number of dead nodes decreases linearly and slowly, the change is relatively stable and prolongs the life cycle of WSN.

The method in reference [29] considers the location information. At the beginning, the two distances are relatively reduced, the energy consumption is reduced, and the life cycle of WSN is prolonged. The optimization of the inertia weight in the method of reference [29] makes the elected cluster head nodes close to the global optimization. The two distances measured at the beginning are lower than those in the method of reference [28], the node energy consumption is reduced, and the life cycle of WSN is longer than that in the method of reference [28]. The methods in references [28, 29] have fewer surviving nodes due to the proliferation of dead nodes in the later stage of iteration. The measured two distances are smaller than the proposed method, but the life cycle is smaller.

6. Conclusion

A secure clustering strategy based on improved PSO algorithm in the environment of IoT is proposed. Considering the residual energy and load balance of nodes, a new fitness function is established, the better candidate cluster head nodes are evaluated and selected. The location update speed of candidate cluster head nodes is adjusted through the optimized adaptive learning factor, so as to elect a forwarding node for each cluster head node among the ordinary nodes in its cluster for reducing the energy consumption of forwarding nodes. Experiments show that under the same conditions, the average node degree of the proposed method is less than 2.5, which is better than the comparison methods. Compared with the comparison methods, the proposed method can significantly improve the network life cycle of clustering method and optimize node energy consumption.

In WSN clustering routing protocol, the selected cluster head nodes usually accounts for only a small part of the total nodes, so it has sparse characteristics. In future research work, sparse theory can be introduced to solve the problem of cluster head node selection in WSN clustering routing. In addition, in practical applications, the location of sensor nodes is not fixed, so energy optimization can be studied for large-scale dynamic networks.

Data Availability

The data used to support the findings of this study are included within the article.

Conflicts of Interest

The author declares that there are no conflicts of interest regarding the publication of this paper.

Acknowledgments

This work was supported by the Natural Science Foundation of China (No. 61502434).

References

- [1] N. Li, J. Chen, and Y. Yuan, "A Wi-Fi indoor localization strategy using Particle Swarm Optimization based artificial neural networks[J]," *International Journal of Distributed Sensor Networks*, vol. 12, no. 3, pp. 458–467, 2016.
- [2] C. Li and S. Yang, "A Clustering Particle Swarm Optimizer for Dynamic optimization[C]," in *Proceedings of the 2009 IEEE congress on Evolutionary Computation*, pp. 439–446, IEEE, Trondheim, Norway, 2009.
- [3] X. Liang, W. Li, Y. Zhang, and M. Zhou, "An adaptive particle swarm optimization method based on clustering," *Soft Computing*, vol. 19, no. 2, pp. 431–448, 2015.
- [4] G. T. Pulido and C. A. Coello, "Using clustering techniques to improve the performance of a multi-objective particle swarm optimizer," in *Proceedings of the Genetic and Evolutionary Computation - GECCO 2004*, pp. 225–237, Springer, Berlin, Heidelberg, 2004.
- [5] A. A. A. Esmine, R. A. Coelho, and S. Matwin, "A review on particle swarm optimization algorithm and its variants to clustering high-dimensional data," *Artificial Intelligence Review*, vol. 44, no. 1, pp. 23–45, 2015.
- [6] S. Yang and C. Li, "A clustering particle swarm optimizer for locating and tracking multiple optima in dynamic environments," *IEEE Transactions on Evolutionary Computation*, vol. 14, no. 6, pp. 959–974, 2010.
- [7] C. L. Huang, W. C. Huang, H. Y. Chang, Y. C. Yeh, and C. Y. Tsai, "Hybridization strategies for continuous ant colony optimization and particle swarm optimization applied to data clustering," *Applied Soft Computing*, vol. 13, no. 9, pp. 3864–3872, 2013.
- [8] B. Jarboui, M. Cheikh, P. Siarry, and A. Rebai, "Combinatorial particle swarm optimization (CPSO) for partitional clustering problem," *Applied Mathematics and Computation*, vol. 192, no. 2, pp. 337–345, 2007.
- [9] S. Paterlini and T. Krink, "Differential evolution and particle swarm optimisation in partitional clustering," *Computational Statistics & Data Analysis*, vol. 50, no. 5, pp. 1220–1247, 2006.
- [10] M. Omran, A. P. Engelbrecht, and A. Salman, "Particle swarm optimization method for image clustering," *International Journal of Pattern Recognition and Artificial Intelligence*, vol. 19, no. 03, pp. 297–321, 2005.
- [11] S. Rana, S. Jasola, and R. Kumar, "A review on particle swarm optimization algorithms and their applications to data clustering," *Artificial Intelligence Review*, vol. 35, no. 3, pp. 211–222, 2011.
- [12] L. Y. Chuang, C. J. Hsiao, and C. H. Yang, "Chaotic particle swarm optimization for data clustering," *Expert Systems with Applications*, vol. 38, no. 12, pp. 14555–14563, 2011.
- [13] Q. Cai, M. Gong, L. Ma, S. Ruan, F. Yuan, and L. Jiao, "Greedy discrete particle swarm optimization for large-scale social network clustering," *Information Sciences*, vol. 316, no. 8, pp. 503–516, 2015.
- [14] X. Cui, T. E. Potok, and P. Palathingal, "Document Clustering Using Particle Swarm Optimization[C]," in *Proceedings of the 2005 IEEE Swarm Intelligence Symposium*, pp. 185–191, IEEE, Pasadena, CA, USA, 2005.
- [15] M. G. H. Omran, A. Salman, and A. P. Engelbrecht, "Dynamic clustering using particle swarm optimization with application

- in image segmentation,” *Pattern Analysis & Applications*, vol. 8, no. 4, pp. 332–344, 2006.
- [16] Y. Lu, S. Wang, S. Li, and C Zhou, “Particle swarm optimizer for variable weighting in clustering high-dimensional data,” *Machine Learning*, vol. 82, no. 1, pp. 43–70, 2011.
- [17] R. Kuo and L. M. Lin, “Application of a hybrid of genetic algorithm and particle swarm optimization algorithm for order clustering,” *Decision Support Systems*, vol. 49, no. 4, pp. 451–462, 2010.
- [18] G. Kannan and T. Sree Renga Raja, “Energy efficient distributed cluster head scheduling scheme for two tiered wireless sensor network,” *Egyptian Informatics Journal*, vol. 16, no. 2, pp. 167–174, 2015.
- [19] J. Wang, Y. Cao, B. Li, HJ Kim, and S Lee, “Particle swarm optimization based clustering algorithm with mobile sink for WSNs,” *Future Generation Computer Systems*, vol. 76, no. 6, pp. 452–457, 2017.
- [20] R. Liu, Y. Chen, L. Jiao, and Y Li, “A particle swarm optimization based simultaneous learning framework for clustering and classification,” *Pattern Recognition*, vol. 47, no. 6, pp. 2143–2152, 2014.
- [21] P. Kuila and P. K. Jana, “Energy efficient clustering and routing algorithms for wireless sensor networks: particle swarm optimization approach,” *Engineering Applications of Artificial Intelligence*, vol. 33, no. 1, pp. 127–140, 2014.
- [22] M. Ye, C. Li, and G. Chen, “EECS: an energy efficient clustering scheme in wireless sensor networks[C],” in *Proceedings of the PCCC 2005. 24th IEEE International Performance, Computing, and Communications Conference 2005*, pp. 535–540, IEEE, Phoenix, AZ, USA, 2005.
- [23] R. S. Elhabyan and M. C. E Yagoub, “Particle swarm optimization protocol for hierarchical clustering in Wireless Sensor Networks[C],” in *Proceedings of the 10th IEEE international conference on collaborative computing: networking, applications and worksharing*, pp. 417–424, IEEE, Miami, FL, USA, 2014.
- [24] A. Salehpour, B. Mirmobin, and A. Afzali-Kusha, “An Energy Efficient Routing Protocol for Cluster-Based Wireless Sensor Networks Using Ant colony optimization[C],” in *Proceedings of the 2008 International Conference on Innovations in Information Technology*, pp. 455–459, IEEE, Al Ain, United Arab Emirates, 2008.
- [25] Y. Zhou, N. Wang, and W. Xiang, “Clustering hierarchy protocol in wireless sensor networks using an improved PSO algorithm,” *IEEE Access*, vol. 5, no. 3, pp. 2241–2253, 2017.
- [26] T. Shankar, S. Shanmugavel, and A. Rajesh, “Hybrid HSA and PSO algorithm for energy efficient cluster head selection in wireless sensor networks,” *Swarm and Evolutionary Computation*, vol. 30, no. 4, pp. 1–10, 2016.
- [27] J. Du and L. Wang, “Uneven Clustering Routing Algorithm for Wireless Sensor Networks Based on Ant colony optimization[C],” in *Proceedings of the 3rd IEEE International Conference on Computer Research and Development*, pp. 67–71, IEEE, Shanghai, China, 2011.
- [28] P. S. Mehra, M. N. Doja, and B. Alam, “Fuzzy based enhanced cluster head selection (FBECS) for WSN,” *Journal of King Saud University Science*, vol. 32, no. 1, pp. 390–401, 2020.
- [29] J. Wang, Y. Gao, W. Liu, A. Sangaiah, and H. J Kim, “An improved routing schema with special clustering using PSO algorithm for heterogeneous wireless sensor network,” *Sensors*, vol. 19, no. 3, p. 671, 2019.

Research Article

Design and Implementation of Trace Inspection System Based upon Hyperspectral Imaging Technology

Yuchen Wang^{1,2} and Zhongyuan Ji ^{1,3}

¹College of Criminal Justice, Shandong University of Political Science and Law, Jinan 250014, China

²Key Laboratory of Evidence-Identifying in Universities of Shangdong, Shandong University of Political Science and Law, Jinan 250014, China

³College of Electronic and Information Engineering, Nanjing University of Aeronautics and Astronautics, Nanjing 211106, Jiangsu, China

Correspondence should be addressed to Zhongyuan Ji; 000929@sdupsl.edu.cn

Received 23 March 2022; Revised 29 April 2022; Accepted 27 May 2022; Published 15 July 2022

Academic Editor: Le Sun

Copyright © 2022 Yuchen Wang and Zhongyuan Ji. This is an open access article distributed under the Creative Commons Attribution License, which permits unrestricted use, distribution, and reproduction in any medium, provided the original work is properly cited.

Trace inspection is a key technology for collecting crime scenes in the criminal investigation department. A lot of information can be obtained by restoring and analyzing the remaining traces on the scene. However, with the development of digital technology, digital trace inspection has become more and more popular. So, the main research of this article is the design and realization of the trace inspection system based on hyperspectral imaging technology. This article proposes nondestructive testing technology in hyperspectral imaging technology. Combining basic principles of spectroscopy and the image of residual traces such as car tires, shoe soles, and blood stains, it can identify the key traces. Then, based on the image denoising and least squares support vector machine method, this study improves the accuracy and restoration of the image. Therefore, this study designs a test for the trace inspection system for testing hyperspectral imaging technology. The test items include the performance of the trace inspection system, the noise reduction of the trace inspection system, and the ability of the trace inspection system to inspect blood stains. The final collected data are improved to get the trace inspection system based on hyperspectral imaging technology proposed in this study. Compared with the traditional trace inspection system, the experimental results show that the trace inspection system based on hyperspectral imaging technology can improve the accuracy by 5%–28%, compared with the traditional trace inspection system. The image restoration degree of the hyperspectral imaging technology trace inspection system can be improved by 1%–19%, compared with the traditional trace inspection system.

1. Introduction

The universality of traces at the crime scene, material objectivity, close correlation with criminal behavior, and obvious intuition play an important role in criminal activities. Through the analysis and investigation of traces, we can judge the implementation process and specific circumstances of the crime and provide the direction and clues of the investigation. It provides a reliable basis for compound investigations and important physical evidence to prove facts. The last trace may be file storage to provide clues and evidence for investigating the current incident. Traditional trace inspection technology cannot

adapt to the current complex and intelligent crime situation due to its low accuracy and inspection efficiency. Therefore, it is necessary to reform the past trace inspection technology.

With the maturity of hyperspectral imaging technology, it has been applied to many fields such as aerospace tongue coating imaging and pork detection. Its powerful functions are gradually brought into play and have attracted the attention of various countries. The research of tracking detection system based on hyperspectral imaging technology has a wide range of research space and application prospects. So, this study designs a trace inspection system based on hyperspectral imaging technology.

Saliency detection is a hot topic in recent years, and the results of saliency detection are difficult to use in general applications. Wang et al. believed that the main reason is the unclear definition of salient objects. In order to solve this problem, he claimed that the saliency should be defined in the context and took the saliency band selection in the hyperspectral image (HSI) as an example [1]. He studied the application of hyperspectral images in saliency detection, and this article mainly studies the application of hyperspectral images in trace inspection. Deep learning that represents data through hierarchical networks has been proven effective in computer vision. In order to study the role of depth features in hyperspectral image (HSI) classification, Ma et al. focused on how to extract and use depth features in the HSI classification framework [2]. Ma et al. studied the results of hyperspectral images in deep learning. If trace detection can be analyzed, it will be more in line with the purpose of this article. In order to study the application of hyperspectral images in SAJSRC, Fu et al. proposed a new shape-adaptive joint sparse representation classification (SAJSRC) method for hyperspectral image (HSI) classification. The method he proposed adaptively explores spatial information and incorporates it into a joint sparse representation classifier [3]. He is studying the application of hyperspectral images in adaptive joint sparse representation classification, and this article mainly focuses on trace inspection. The objective function of the classical non-negative matrix factorization (NMF) is nonconvex, which affects the obtaining of the optimal solution. Yan et al. proposed an NMF algorithm, which is based on the constraints of minimizing endmember spectral correlation and maximizing endmember spectral difference [4]. The method he proposed is based on the endmember spectrum, and this article studies hyperspectral images. Although there is little correlation, it still has a certain reference value. Shao et al. introduced an effective method for estimating the structure of probability classes. The SSL graph based on sparse representation adopts a method based on edge weighting, adding probability structure information to the sparse representation model. The graph construction method he proposed is superior to several traditional methods [5]. In September 1991, while hiking in the mountains of southern Austria, very close to northern Italy, Erika, and Helmut Simon stumbled upon the upper part of a human corpse protruding from a glacier. Larcher judged by the method of trace inspection that this was a hiker who disappeared in the area a few years ago [6]. He used the method of trace inspection to determine the identity of the corpse, which has a certain reference value for this article, but it is not great. In the oxygen minimum zone (OMZ), the oxygen concentration is at the limit of analytical detection. However, it does not undergo sulfate reduction, which is called hypoxia. Nitrate is usually used as the terminal electron acceptor for heterotrophic respiration. This respiration is highest near the top of the OMZ, where Cutter et al. observed the maximum of nitrite and other redox-active substances [7]. Its research is to detect the lowest area of oxygen, and this article mainly studies trace inspection. Hyperspectral images provide a wealth of spectral information for remotely distinguishing

subtle differences in ground cover plants. The ever-increasing spectral dimensions and information redundancy make the analysis and interpretation of hyperspectral images a challenge. Zhao et al. proposed a new nonlinear feature extraction method for hyperspectral images [8]. The nonlinear feature extraction method of hyperspectral image proposed by Zhao et al. mainly studies feature extraction, while this article mainly studies trace inspection. Most of the documents cited in this article are about hyperspectral images, and trace inspection is rare, so this article needs to study the related knowledge of trace inspection in depth.

The innovation of this study is to combine the nondestructive testing technology with the hyperspectral imaging technology to analyze residual traces such as car tires, shoe soles, and blood stains. Through the method of image denoising and least square support vector machine, this study further refines and restores the trace image. Compared with the traditional trace inspection system based on hyperspectral imaging technology, the trace inspection system has the characteristics of high accuracy and high image recovery ability. This study also designed experiments to verify the performance of the trace inspection system, the noise reduction of the trace inspection system, and the ability of the trace inspection system to inspect blood stains.

2. Combined with the Application Method of Hyperspectral Imaging Technology in Trace Inspection

2.1. Hyperspectral Image Acquisition Method. Hyperspectral imaging technology [9] uses an imaging spectrometer with a spectral range from ultraviolet to near infrared (200–2500 nm). Tens or hundreds of spectral bands are continuously imaged within the spectral coverage of the target object. While acquiring the spatial feature image of the object, it also acquires the spectral information of the measured object [10]. It includes comprehensive technologies including precision optical technology, detector technology, mechanics, computer technology, signal detection technology, and information analysis technology knowledge. Its application area is shown in Figure 1.

Hyperspectral imaging technology can not only obtain the spatial information of the object but also obtain the spectral information of the object. Hyperspectral imaging technology can obtain continuous spectral bands of objects [11], and the number of bands reaches hundreds. Each pixel of the collected hyperspectral image has a complete reflectance spectrum curve. Compared with multispectral imaging technology, hyperspectral imaging technology can obtain more information in a narrower frequency band, and the spectral resolution can be accurate to a few nanometers.

2.1.1. Nondestructive Testing Technology. Nondestructive testing technology [12] is a comprehensive application discipline developed with modern physics, material science, electronic science, and computer science. According to different measurement principles and information processing methods, there are more than 70 types of

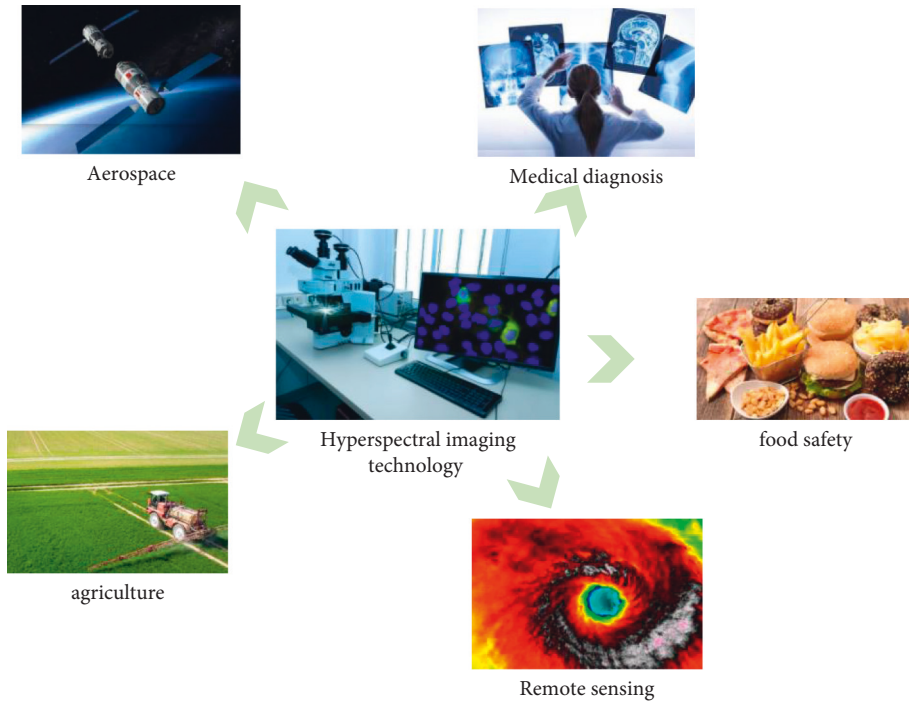


FIGURE 1: Application of hyperspectral imaging technology.

nondestructive testing, covering all branches of modern physics. The basic measurement principle is shown in Figure 2. According to the different responses of the test object to external stimulation, the output information of the test object is collected, the correlation relationship with the input information is established, and then the physical and chemical properties of the test object can be diagnosed.

2.1.2. Basic Principles of Spectroscopy. The matter is always in motion, and the atoms and molecules that makeup matter are also in motion. The rotation of electrons in molecules around atoms is called electronic movement. The vibration of atoms in a molecule is called molecular vibration. The rotation of the molecule itself is called molecular rotation [13]. Different exercise methods have different energies, divided by energy level, that is, electronic energy level, vibration energy level, and rotational energy level. When a substance is stimulated by a specific external energy, the state of molecular motion will change, and the energy level will also change accordingly. This form of change is achieved through the absorption or divergence of energy photons, as shown in Figure 3. Particles absorb energy photons and then transit from the ground state to the excited state, and from the excited state back to the ground state, and they emit energy photons. This form of energy is electromagnetic radiation, commonly known as light. Arranging electromagnetic radiation according to a certain energy level or frequency order is the electromagnetic radiation spectrum or spectrum [14]. As shown in Figure 4, according to the difference between absorption and divergence energy, it is divided into absorption spectrum and divergence spectrum.

Near-infrared spectroscopy [11] (780–2526 nm) is the earliest nonvisible spectrum discovered by mankind, and it

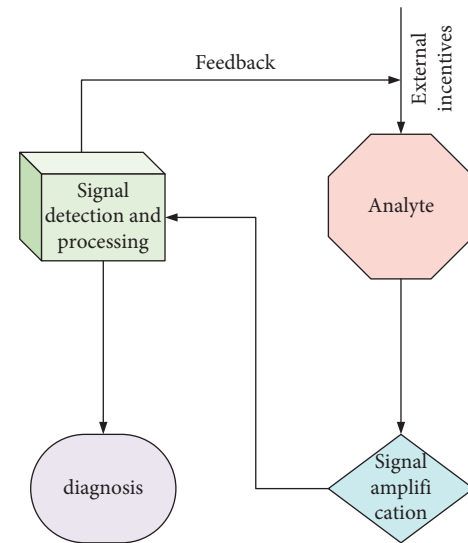


FIGURE 2: Basic measurement principle of nondestructive testing technology.

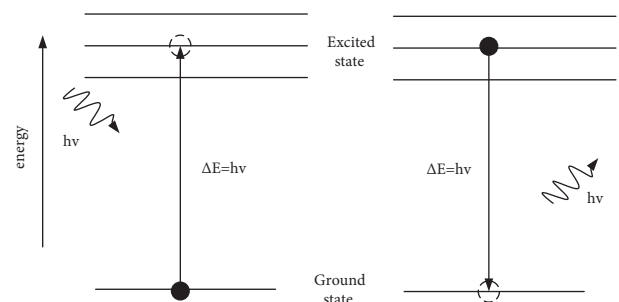


FIGURE 3: Schematic diagram of particle absorption or dissipation of energy.

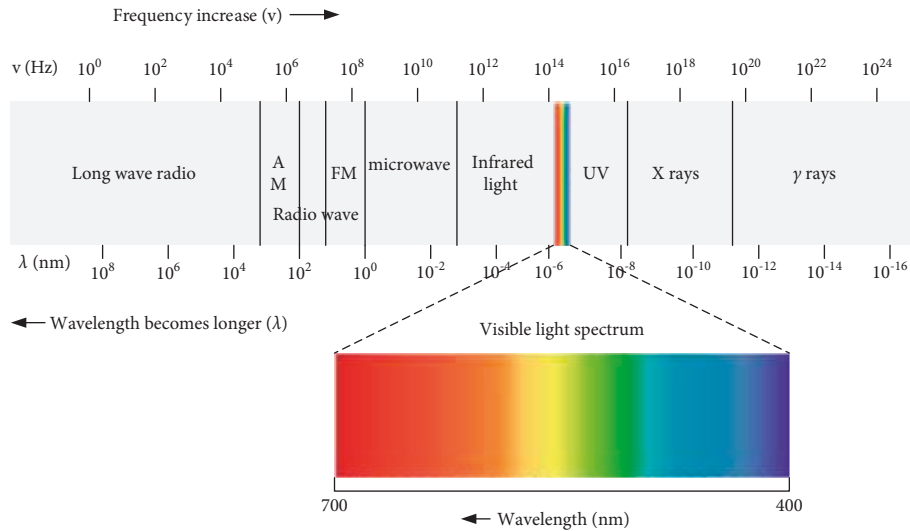


FIGURE 4: Spectral images of different ranges and the molecular motion modes generated by energy.

is also one of the earliest researched spectra. The generation of near-infrared light is mainly caused by the internal vibration of polyatomic molecules. It contains a wealth of chemical bond information, such as hydrogen bond, bond strength, chemical species, and dielectric properties.

2.2. Trace Inspection. Trace inspection [15] is the analysis, identification, and judgment of various characteristics of the formation and change characteristics of criminal traces and the object of trace creation [16]. Therefore, in the process of trace inspection, the collection of traces is very important. The main method is shown in Figure 5.

In the process of trace inspection, any on-site traces need to be used as evidence and should be extracted from the site and preserved in their original form for use by inspectors. The main methods of extracting traces are as follows: transfer method, such as transferring trace materials to a specific carrier by a specific method; molding methods, such as using silicone rubber or plaster liquid to make trace models for three-dimensional traces; photocopying methods, such as the use of electrostatic adsorption to extract traces of dust; the original extraction method, such as direct collection and extraction of small-volume trace objects and trace-bearing objects. The photographic method is a method that can be used for all kinds of trace extraction in the process of trace collection. It can not only achieve lossless acquisition [17] but also perform multiple acquisition processes. Moreover, the photographic method is also a work step that must be carried out before trace extraction, and it is a necessary means to ensure the originality of traces.

The collection of traces includes the collection of pictures and text. It is a highly professional work. Only comprehensive and correct collection can reflect the actual work situation of on-site investigation and trace inspection, and the basic role of traces can be brought into play.

Image [18] has been used in forensics since it was invented in 1839. After entering the digital age, the frequency of use of images has become higher, an alternative to

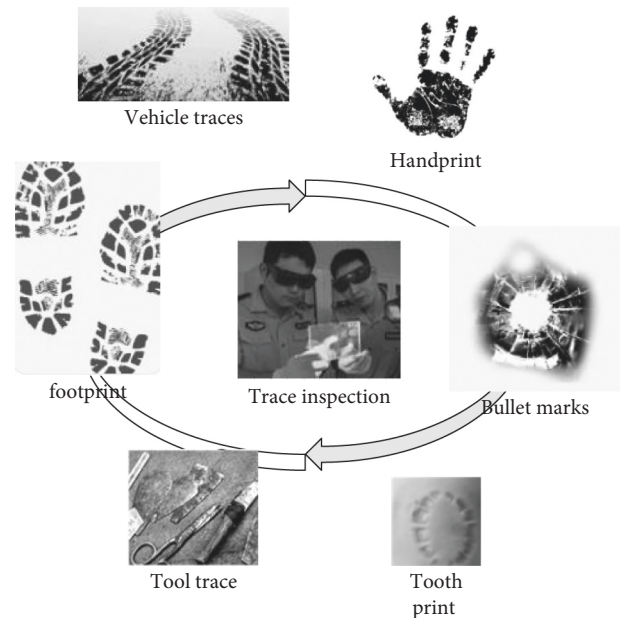


FIGURE 5: Main methods of trace inspection.

analog images—digital images have the advantages of environmental protection, low collection error rate, and convenient use, and it plays an increasingly important role in the process of trace inspection.

In the digitization of trace inspection, the collection of digital images is one of the important methods of trace collection. It mainly refers to the process of receiving light waves reflected or emitted by objects in the scene, recording and storing them, or obtaining image data through other scientific and technological equipment.

There are many ways to collect images. At present, there are four most commonly used collection methods in this article: using a digital camera to take photos directly, using a scanner to scan analog images, capturing video frames, and creating using drawing software. In the trace inspection, the

collection of traces must be a true and objective reflection, so the image collection of traces mainly uses the first three methods.

2.2.1. Tire Tracks on the Road. As the main component of the vehicle, tires play a role in supporting the weight of the vehicle, changing the direction of travel, transmitting braking and driving force, and alleviating road impact. Carbon black, which is a compounding agent for tire rubber materials, adheres to the road surface and leaves marks. In the case of high friction between the mud and the road, the heat release rate is lower than that of the mud of the tire, and the melting point of the tire and the road is relatively low, so the mud rubber becomes soft, black, peeling, and black when attached to the road. The tire traces on the road, such traces can be extracted from the debris of mud rubber [19], and the principle is shown in Figure 6.

In the process of collecting tire traces at the accident site, the tire traces of vehicles related to the accident can be judged according to the new degree of tire traces. The tire marks of a puncture on the road are flat sandwich marks with dust marks and rubber particle marks. Dust traces are usually only displayed on newly repaired roads. In most cases, those are potential traces. In contrast, the rubber particles of cement are easier to observe on the road track (usually displayed when the mud and the road slide against each other). The new tire truck leaves a lot of rubber particles on the road, and the color becomes darker. If the tire of the vehicle involved in the accident slips, then there will be obvious scars on the road surface. Old tire trucks generally have no particles of tire marks. Generally speaking, the new tire tracks are the tire tracks of the vehicles involved in the accident.

2.2.2. On-Site Shoe Sole Trace Pattern Image Extraction Method. There are various methods for extracting pattern images of shoe sole traces on-site [20], but the determination of the extraction method is mainly based on various conditions such as the trace-bearing object of sole traces and the complexity of the site.

The photographic extraction method is the most frequently used method of fixing and extracting on-site traces without damage. Physical evidence photography is mainly used to take photos of shoe sole traces at the scene. This is also an effective way to faithfully record the original state, location, and surrounding relationships of the sole trace pattern image. However, the use of photography to extract images of shoe sole traces will also encounter some problems. If the scale bar and the sole trace surface are not in the same plane, and the height difference is still relatively large, then this will cause the measurement error to become larger due to the perspective deformation of the near and far. The requirements for photographing conditions are relatively strict, so when using photographing methods to extract the image of shoe sole trace patterns, it must be strictly in accordance with the specifications.

The photocopy extraction method is mainly aimed at flat footprints, especially flat dust footprints. The photocopy

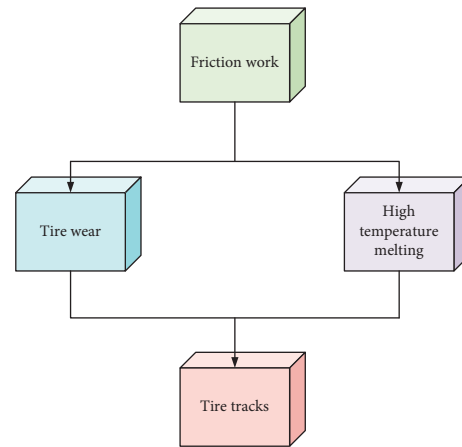


FIGURE 6: The formation mechanism of tire marks.

extraction method transfers the sole traces from the trace-bearing object to other objects with larger color contrast, which is convenient for observation and photo fixation. Copy extraction methods include the electrostatic copy method and paste copy method. Among them, the electrostatic photocopying method is mainly to add or subtract layers of dust sole traces left on the surface of relatively flat and dry objects such as cement floors, terrazzo floors, wooden surfaces, floors, towels, and textiles. The paste copying method is to use relatively a wide palm print tape or sole trace special tape to attach clear dust flat sole traces or sole traces after powder brushing and stained fixed sole traces, etc.

The mold extraction method is mainly aimed at the three-dimensional sole traces. After taking photos of the three-dimensional sole traces, a model of the sole traces must be made. Molding methods include the plaster molding method and cassia gum molding method. Molding methods are also different for different mark-bearing objects. For example, mold making on snow cannot use water at room temperature to prepare plaster liquid. It is necessary to use water temperature close to snow to mold, or use snow trace wax, snow sole trace fixative, etc. to fix the snow sole traces before molding. The cost of cassia glue molding is higher, but in major cases, the cassia glue molding method can be used for local small sole traces. The model made of cassia glue is elastic, not easy to break or break, and the shape is delicate, which can better reflect the characteristics of the traces of the sole.

For the visualization of potential footprints at the crime scene, powder and chemical visualization methods are often used. The chemical display method also includes the red blood salt color method of dust sole traces, the value indicator method of dust sole traces, the "502" glue display method, and the tetramethylaniline solution method of blood footprints.

No matter which extraction method is used, the extraction must be performed in accordance with the specifications; otherwise, the extracted sole trace pattern image will lack information and affect the subsequent processing work.

2.2.3. Footprint Detection Research Technology

(1) *Height Identification.* Most surveys and statistics show that there are many types, many patterns, and high overlapping characteristics of footprints left on crime scenes. To a certain extent, it affects the reflection of traditional footprint features, such as the interaction between legs and bearing objects during walking. At the same time, the extraction method of on-site footprints is also one of the important factors affecting the inspection results [21]. First of all, in order to improve the accuracy of the inspection, before analyzing and inspecting the footprints, it is necessary to determine the symptom extraction method to be used based on various footprints and various on-site environments.

(2) *Age Analysis.* In the past, in some films and TV works, it was often seen that the police judged the age of the characters left by the footprints left at the crime scene. Judging their age through footprints is very helpful in investigating criminal cases.

Age is the length of time from birth to death, usually expressed in “years.” Age is not only a natural sign based on biology but also an important time sign in physiological processes. The characteristics of human footwork are also closely related to age. The characteristics of footwork reflect a person’s physiological state and can correctly reflect person’s various physiological states.

2.3. *Image Denoising.* At present, many methods have been proposed to filter out the noise in the image. The smoothing of images is generally divided into two categories: global processing and local processing. Global processing is to correct the entire image or most of the image. This method is relatively computationally expensive. Local processing is the use of local operators on the image. Calculating the neighborhood of a specific pixel greatly reduces the amount of calculation.

The following sections describe several commonly used image denoising methods:

2.3.1. *Neighborhood Average Method.* The neighborhood average method [22], called the average filtering method, is a simple spatial region processing method. The basic idea is to replace the gray value of each pixel with the average value of the gray values of several pixels. $f(a, b)$ is a noisy specific $K \times K$ image. After the neighborhood averaging process, the image $h(a, b)$ is obtained. $h(a, b)$ is determined by the following formula:

$$h(a, b) = \frac{1}{j} \sum_{(i, j) \in D} f(i, j). \quad (1)$$

2.3.2. *Median Filtering Method.* The median filter method [23] is the most widely used statistical filter in image processing, and it is also the most famous sequential statistical filter. The neighborhood averaging method blurs the edges

of the image while removing noise. In contrast, the middle finger filtering is better than neighborhood averaging.

Median filtering is done on the one-dimensional sequence $f_1, f_2, f_3, \dots, f_k$. The length of the window is taken as j , and the number of j from the sequence $f_{x-v}, \dots, f_{x-1}, f_x, f_{x+1}, \dots, f_{x+v}$ is extracted as the center point of the window, where

$$v = \frac{(j-1)}{2}. \quad (2)$$

The number of j is arranged by size at a time, and the middle value is taken as the output value:

$$b_x = \text{med}\{f_{x-v}, \dots, f_{x-1}, f_x, f_{x+1}, \dots, f_{x+v}\} \quad x \in k. \quad (3)$$

The two-dimensional median filter is represented by the following formula:

$$b_x = \text{med}\{f_{xy}\}. \quad (4)$$

2.3.3. *Low-Pass Filtering Method.* Both the neighborhood averaging method and the median filtering method process the image in the spatial domain. The low-pass filtering method [24] is a method of processing images in the frequency domain.

The mathematical expression of the filter is as follows:

$$H(a, b) = G(a, b)F(a, b). \quad (5)$$

Among them, $F(a, b)$ is the Fourier transform of the original image, $H(a, b)$ is the Fourier transform of the image smoothed by the filter, and $G(a, b)$ is the transfer function of the filter.

The edges, jumps, and grain noise of the image are the high-frequency components of the image. The background area represents the low-frequency components, so the simplest low-frequency filter is to obtain the high-frequency components in the Fourier transform of the image. The corresponding filter is called a two-dimensional ideal low-pass filter (ILPF), and its transfer function is as follows:

$$G(a, b) = \begin{cases} 1, & S(a, b) \leq S_0, \\ 0, & S(a, b) > S_0. \end{cases} \quad (6)$$

Among them, S_0 is the designated non-negative value, and $S(a, b)$ is the distance between point (a, b) and the origin of the frequency rectangle. In addition to ideal low-pass filters, low-pass filters also include Butterworth low-pass filters (BLPFs) and Gaussian low-pass filters (GLPFs). This article uses the Gaussian slow path filter. The transfer function of the Gaussian slow path filter is as follows:

$$G(a, b) = q^{-S^2(a, b)/2S_0^2}. \quad (7)$$

Among them, $S(a, b)$ is the distance from the origin of the Fourier transform.

There are many methods for image sharpening, such as high-pass filtering, gradient sharpening, and Laplacian sharpening. The high-pass filter includes ideal high-pass filter (IHPF), Butterworth high-pass filter (BHPF), and

Gaussian high-pass filter (GHPF). This article only introduces gradient sharpness and Laplacian sharpening.

(1) *Gradient Sharpening*. Gradient processing is often used in industrial inspections, auxiliary manual defects, or more general automatic inspection preprocessing. For image f , the gradient at point (a, b) is as follows:

$$H[f(a, b)] = \left[\left(\frac{\gamma f}{\gamma a} \right)^2 + \left(\frac{\gamma f}{\gamma a} \right)^2 \right]^{1/2}. \quad (8)$$

For discrete images, the above formula can be approximated by the difference method to obtain the following equation:

$$H[f(a, b)] = \{ [f(a, b) - f(a-1, b)]^2 + [f(a, b) - f(a, b-1)]^2 \}^{1/2}. \quad (9)$$

In order to facilitate programming and improve calculations, it can be further simplified as follows:

$$H[f(a, b)] = |f(a, b) - f(a-1, b)| + |f(a, b) - f(a, b-1)|. \quad (10)$$

(2) *Laplacian Sharpening*. Like the gradient, Laplace operation is also a linear combination of partial differential operations, which is a linear operation accompanied by rotation invariance as follows:

$$\nabla^2 f = \frac{\gamma^2 f}{\gamma^2 a} + \frac{\gamma^2 f}{\gamma^2 a}. \quad (11)$$

For discrete digital images, the Laplacian operator can be expressed as follows:

$$\begin{aligned} \nabla^2 f &= \frac{\gamma^2 f}{\gamma^2 a} + \frac{\gamma^2 f}{\gamma^2 a} = f(a+1, b) + f(a-1, b) \\ &+ f(a, b+1) + f(a, b-1) - 4f(a, b). \end{aligned} \quad (12)$$

The following formula is used to deal with the image blur caused by the diffusion effect:

$$h(a, b) = f(a, b) - k\theta \nabla^2 f(a, b). \quad (13)$$

Among them, $k\theta$ represents the coefficient related to the diffusion effect. The value of $k\theta$ must be moderate; otherwise, it will affect the sharpening effect of the image. If $k\theta = 1$ is taken, then the formula is transformed as follows:

$$\begin{aligned} h(a, b) &= 5f(a, b) - f(a+1, b) - f(a-1, b) \\ &- f(a, b+1) - f(a, b-1). \end{aligned} \quad (14)$$

2.4. Least Squares Support Vector Machine. There is a modeling set $\{a_n, b_n\}_{n=1}^K$ composed of K data, where the input data are $a_n \in R^K$ and the output data are $b_n \in R$. Using a nonlinear function $\gamma(\cdot)$, the input data are mapped to a high-dimensional feature space and a relationship model is established:

$$b(a) = w^S \gamma(a) + y. \quad (15)$$

In the formula, $w \in R^K$ is the weight vector and b is the bias value. When using least squares support vector machine to solve, the function fitting problem can be described as the following optimization problem:

$$\min M(w, q) = \frac{1}{2} w^S w + \frac{1}{2} \mu \sum_{n=1}^K q_n^2. \quad (16)$$

The constraints are as follows:

$$b_n = w^S \gamma(a) + y + q_n, n = 1, \dots, K. \quad (17)$$

In the formula, $R^k \rightarrow R^{k_n}$ is the kernel space mapping function, μ is the penalty coefficient, and q_n is the error variable. According to the formula, the model is transformed into the dual space to solve it, and the following Lagrange function is obtained:

$$L(w, y, q, x) = M(w, q) - \sum_{n=1}^K x_n \{ w^S \gamma(a_n) + y + q_n - b_n \}. \quad (18)$$

In the formula, the Lagrange multiplier $x_n \in R$ is called the support value. The partial derivative of each variable is obtained to get the following conditional equation:

$$\begin{aligned} \frac{\phi L}{\phi w} = 0 &\rightarrow w = \sum_{n=1}^K x_n \gamma(a_n), \\ \frac{\phi L}{\phi y} = 0 &\rightarrow \sum_{n=1}^K x_n = 0, \end{aligned} \quad (19)$$

$$\frac{\phi L}{\phi q_n} = 0 \rightarrow x_n = \mu q_n, n = 1, \dots, K,$$

$$\frac{\phi L}{\phi x_n} = 0 \rightarrow w^S \gamma(a_n) + y + q_n - b_n = 0, n = 1, \dots, K.$$

After eliminating the variables w and q , the system of linear equations can be obtained:

$$\begin{bmatrix} 0 & \vec{1}^S \\ \vec{1} & \rho + \mu^{-1} I \end{bmatrix} \begin{bmatrix} y \\ x \end{bmatrix} = \begin{bmatrix} 0 \\ b \end{bmatrix}. \quad (20)$$

$$\text{In the formula, } \begin{cases} b = [b_1, \dots, b_K], \\ \vec{1} = [1, \dots, 1], \\ x = [x_1, \dots, x_K], \\ \rho = \{\rho_{nl} | n, l = 1, \dots, K\}, \end{cases} \text{ and}$$

$$\rho_{nm} = \gamma(a_n)^S \gamma(a_l) = N(x_k, x_l), n, l = 1, \dots, K.$$

$N(x_k, x_l)$ is the kernel function that must satisfy Massa's theorem. The commonly used kernel functions include linear kernel functions, polynomial kernel functions, radial basis kernel functions, and multilayer acceptor kernel functions. The kernel function used in this article is a nonlinear radial basis kernel function:

$$N(x_k, x_l) = \exp \frac{-(a-b)^2}{2e^2}. \quad (21)$$

Thus, the fitting model of the least squares support vector machine can be obtained as follows:

$$b(a) = \sum_{n=1}^K x_n N(a, a_n) + y. \quad (22)$$

3. Test Experiment of Trace Inspection System Based on Hyperspectral Imaging Technology

3.1. Retrieval Performance Experiment of Trace Inspection System. In order to verify the retrieval performance of the imaging spectrum image trace inspection system proposed in this study, the average retrieval accuracy before and after feature randomization encryption is compared in the experiment. It also compares the average precision and retrieval time of the encryption method in this study and the order-preserving encryption method in image retrieval. It is a comparison of the retrieval performance of the imaging spectral image security retrieval system before and after the introduction of relevant feedback.

In order to prove the effectiveness of the feature randomization encryption method, this experiment compares the recall curve and average accuracy of image retrieval before and after encryption. Figure 7 shows the recall-precision ratio curve before and after feature encryption. It can be seen from the figure that the precision and recall rates after feature encryption have not changed much compared with that before feature encryption.

In order to visually see the impact of feature encryption on the retrieval accuracy, Table 1 lists the results of the average retrieval accuracy before and after encryption.

It can be seen from the table that the average precision before encryption using feature randomization is 86.10% and after encryption is 85.25%, and the overall performance of the image retrieval average precision before and after encryption is equivalent. That is, the method in this study has little effect on the accuracy of the retrieval system. The method in this study can effectively protect the image feature information while ensuring the accurate retrieval of imaging spectral images.

In order to further prove the effectiveness of the feature randomization encryption method in this study, this experiment compares the exact recall rate and the average precision rate with order-preserving encryption. Figure 8 shows the recall-precision curve of the two encryption methods. It can be seen from the figure that the retrieval performance of the feature randomization encryption method in this study is better than that of the existing order-preserving encryption methods in the laboratory.

In order to compare the retrieval performance of the two methods intuitively, the average precision of image retrieval of the two methods is given in Table 2.

It can be seen from the table that the average precision of the randomized encryption method in this study is 85.25%, and the average precision of the order-preserving encryption method is 83.26%, which is about 2% higher. It proves the

effectiveness of this method. The table also lists the comparison of encryption time and retrieval time of two different feature encryption methods. The feature encryption time of the method in this study is 5.0×10^{-3} s, the time to retrieve an image after encryption is 1.0 s, the order-preserving encryption method requires 1.10 s for feature encryption, and the time to retrieve an image after encryption is 3.0 s. Whether in terms of feature encryption or retrieval speed, the performance of this method is optimal. The main reason is that the form of the hash code of the depth spectrum-spatial feature in this article speeds up the calculation speed.

3.2. Hyperspectral Image Denoising Experiment. If there is a large amount of hyperspectral image data, then it will affect the subsequent processing. Therefore, the ENVI software is used to cut a part of the calibration image without data and delete redundant data information. Since hyperspectral technology was originally used in the field of remote sensing, it was originally used to process hyperspectral remote sensing images.

The amount of data in hyperspectral images is very large, the number of bands is large, and the data and information between bands are repetitive and redundant. The original CCD detection that records the reflection spectrum of each band is very sensitive, and the existence of dark current has an impact on the experimental data. The steps to reduce hyperspectral image noise are as follows: open the ENVI software, select the hyperspectral image after the black and white frame calibration, click [MNF Rotation] under the [Conversion] function key, select [Forward MNF], and perform the positive change with minimum noise.

The spatial subset adjusts the size of the sensing area of the hyperspectral image, so that the tracking range to be processed is included in the sensing area, and redundant background information is suppressed to a minimum. In the second step, the inverse transformation of the MNF rotation algorithm is performed. The noise-free file processed in the previous step is selected, the image size is set to be the same as the size of the sensing area in the previous step, and the noise-reduced file and the noise-removed hyperspectral image are saved, as shown in Figure 9.

It can be seen from the figure that after the noise reduction of the hyperspectral image, the burrs of the reflection spectrum curve of the traces are reduced and become smoother.

3.3. Hyperspectral Image Fusion of Different Bloodstain Samples. Because the pictures obtained in this experiment are hyperspectral images of all bands, not all of them are suitable for image fusion processing. This article needs to find images that are valuable for the experiment to be fused. As far as blood handwriting pictures are concerned, there are two factors that affect the fusion effect: one is the clarity of the blood handwriting itself and the other is the clarity of the background image of the blood handwriting carrier. Generally speaking, blood writing and carrier background under different wavebands will not reach the clearest degree at the same time, because the degree of absorption and response to

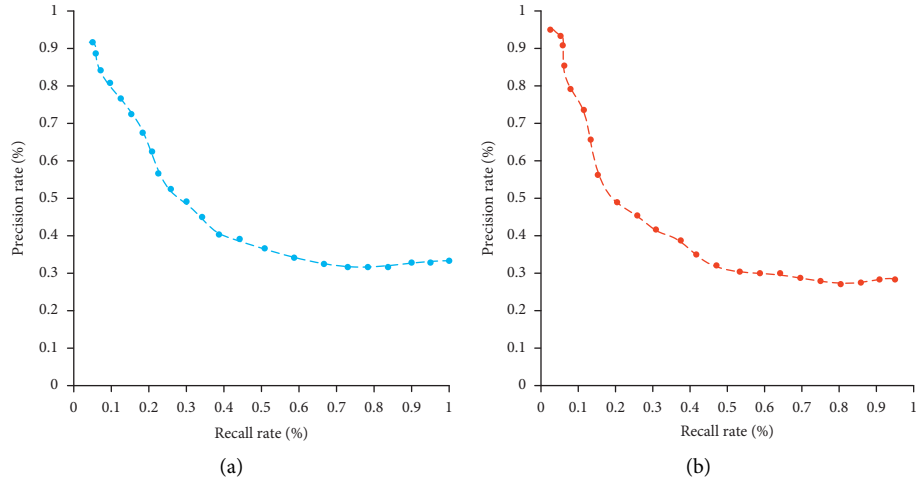


FIGURE 7: Recall rate-precision rate curve before and after feature encryption. (a) Before feature randomization and encryption. (b) After feature randomization and encryption.

TABLE 1: Comparison of average precision before and after feature encryption.

Type	Characteristic encryption time	Retrieve time after encryption	Traditional method
Feature randomization encryption	$5.0 * 10^{-3}$ s	1.10 s	2.13 s
Order-preserving encryption	1.10 s	3.0 s	5.12 s
Average precision rate (%)	86.10	85.25	—

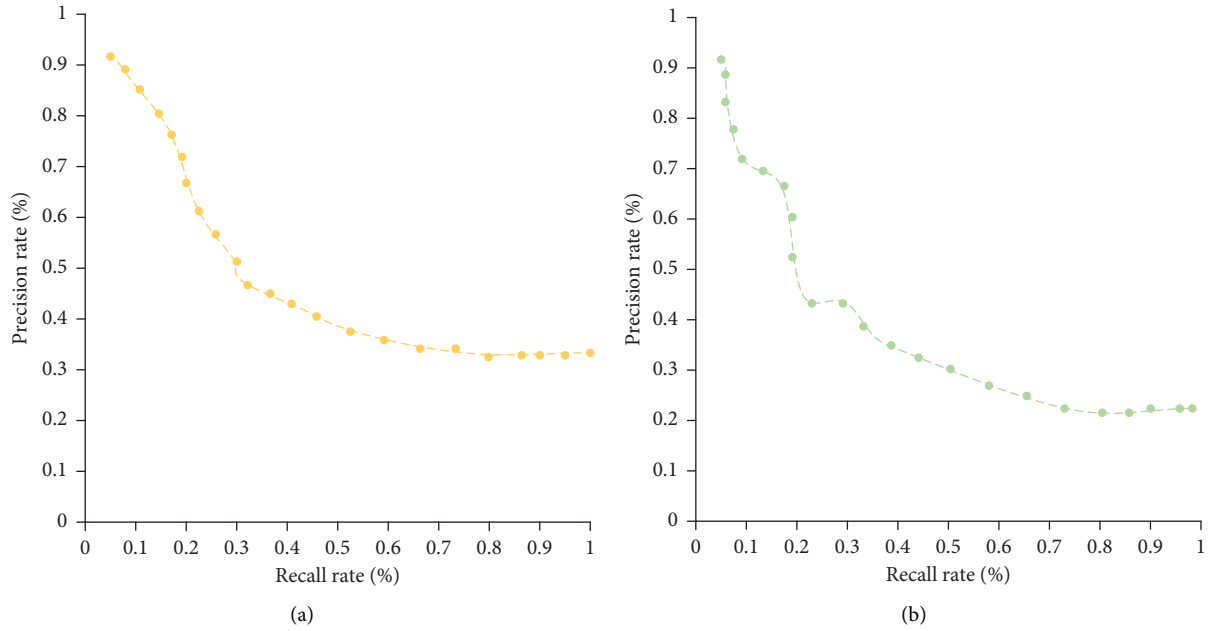


FIGURE 8: Recall rate-precision rate curve of two different feature encryption methods. (a) Characteristic randomization encryption. (b) Order-preserving encryption.

TABLE 2: Comparison of average precision of two different feature encryption methods.

Type	Characteristic encryption time	Retrieve time after encryption	Traditional method
Feature randomization encryption	$5.0 * 10^{-3}$ s	1.10 s	2.13 s
Order-preserving encryption	1.10 s	3.0 s	5.12 s
Average precision rate (%)	85.25	83.26	—

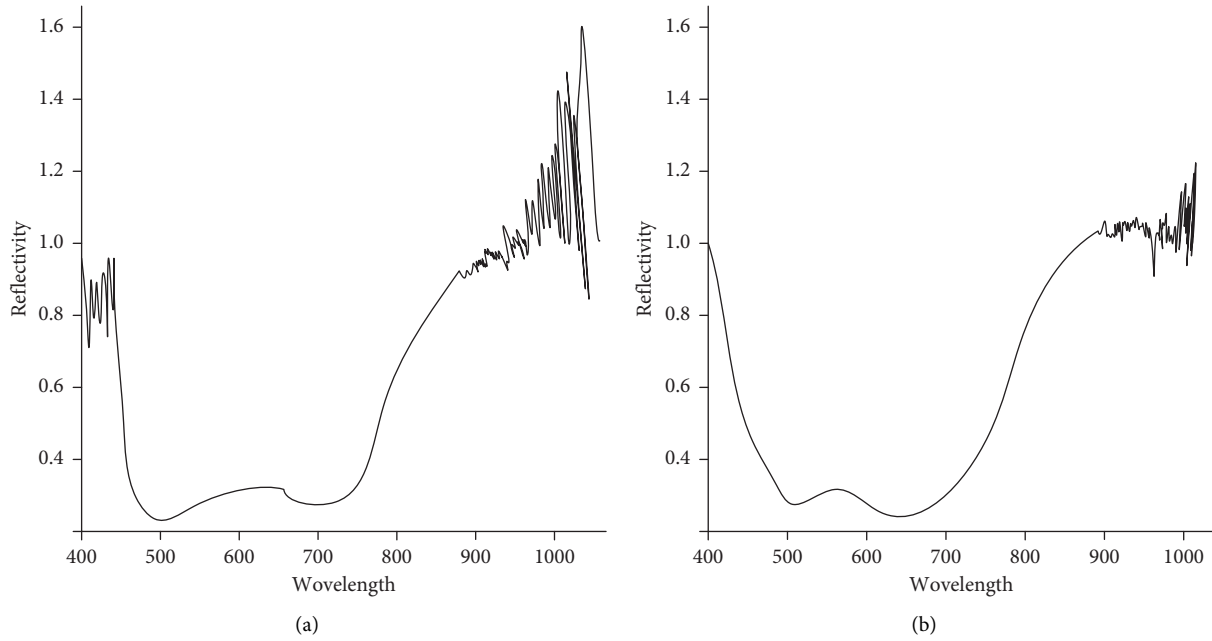


FIGURE 9: The difference of the reflectance spectrum curve of the hyperspectral image before and after noise reduction. (a) Reflectance spectrum curve of original hyperspectral image. (b) Reflectance spectrum curve of hyperspectral image after noise reduction.

TABLE 3: Related evaluation indexes of blood handwriting wavelet fusion image.

Image	Information entropy	Average gradient	Average value	Standard deviation
A	4.26	5.55	26.43	28.94
B	4.82	6.23	30.34	29.65
C	4.51	6.13	25.76	33.21
D	5.35	5.82	27.43	30.84
E	4.36	5.31	29.43	27.65
F	5.21	6.33	32.84	25.64
G	5.56	5.71	23.45	29.34
H	5.04	5.16	28.64	31.54
I	6.21	10.26	55.27	47.68

the same wavelength of light is different between the blood and the carrier. Therefore, this article needs to select two types of pictures for fusion: one is the picture with the clearest blood writing and the clearness of the carrier background. The second is the clearest background image of the carrier, and the clearness of blood handwriting is uncertain. Combining the two pictures together can get a clear picture of the blood handwriting image and the carrier background image. The experimental results are listed in Table 3.

Through the evaluation indicators in the table, it can be found that after the fusion, the average value of the blood handwriting image increases, and the visual effect of naked-eye observation is improved. The standard deviation of blood handwriting images increases, and the amount of information tends to maximize. The average gradient of the blood handwriting image increases, and its sharpness increases. The information entropy increases, and the amount of information increases. It shows that the image obtained by wavelet fusion is clearer and more informative than the blood handwriting image of a single band, which can greatly improve the ability of hyperspectral bloodstain detection.

Regarding the hyperspectral image fusion of blood fingerprint samples, 6 images that meet the requirements were selected for fusion in the experiment. The selected images and the fusion results are listed in Table 4.

Through the evaluation indicators in the table, it can be found that after the fusion, the average value of the blood fingerprint image increases, and the visual effect of naked-eye observation is improved. The standard deviation of blood fingerprint images increases, and the amount of information tends to maximize. The average gradient of the blood fingerprint image increases, and its sharpness increases. The information entropy increases, and the amount of information increases. It shows that the image obtained by wavelet fusion is clearer than a single-band blood fingerprint image and has a larger amount of information, which can greatly improve the ability of hyperspectral bloodstain detection.

For the hyperspectral image fusion of conventional bloodstain samples, three images that meet the requirements are selected for fusion processing in the experiment. The selected images are listed in Table 5.

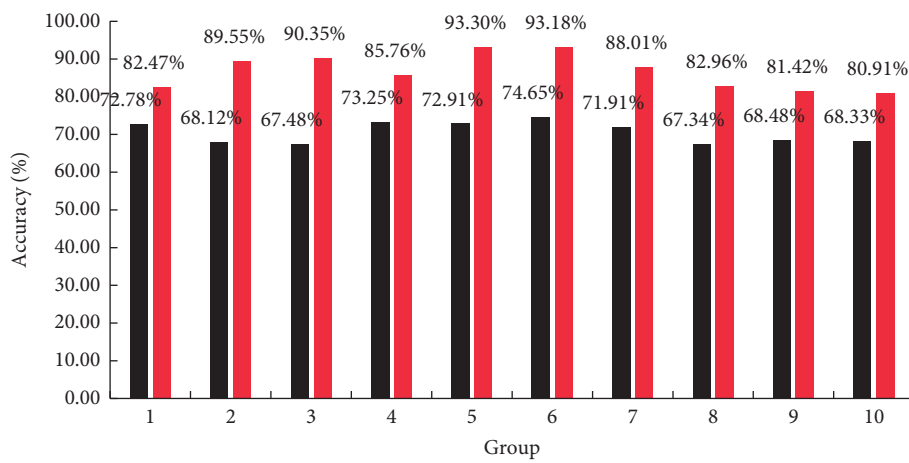
Through the evaluation indicators in the table, it can be found that after fusion, the average value of conventional

TABLE 4: Related evaluation indexes of blood fingerprint wavelet fusion image.

Image	Information entropy	Average gradient	Average value	Standard deviation
A	4.35	5.31	26.41	29.46
B	5.31	6.71	30.54	28.64
C	4.67	6.13	26.64	31.56
D	6.13	6.81	28.64	31.64
E	6.23	6.12	29.64	32.91
F	5.12	8.61	25.31	26.94

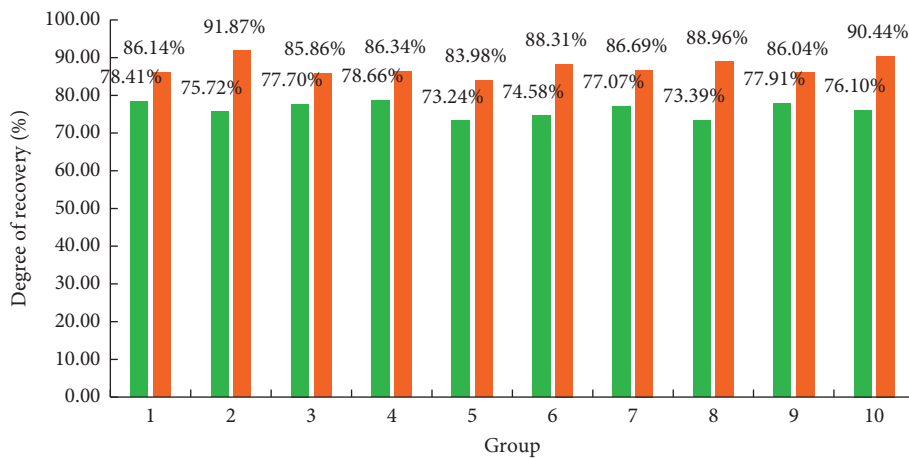
TABLE 5: Related evaluation indexes of conventional bloodstain wavelet fusion image.

Image	Information entropy	Average gradient	Average value	Standard deviation
A	4.58	5.39	30.77	22.51
B	4.21	5.67	31.23	25.39
C	5.33	10.37	43.46	40.23



■ New trace inspection system
 ■ Traditional trace inspection system

(a)



■ New trace inspection system
 ■ Traditional trace inspection system

(b)

FIGURE 10: Comparison result of trace inspection system based on hyperspectral imaging technology and traditional trace inspection system. (a) Accuracy comparison. (b) Comparison of recovery.

bloodstain images increases, and the visual effect of naked-eye observation is improved. The standard deviation of conventional bloodstain images increases, and the amount of information tends to maximize. The average gradient of the conventional bloodstain image increases, and its sharpness increases. The information entropy increases, and the amount of information increases. It shows that the image obtained by wavelet fusion is clearer and more informative than the conventional bloodstain image of a single band, which can greatly improve the ability of hyperspectral bloodstain detection.

4. The Image Trace Inspection Capability of the Trace Inspection System on Account of Hyperspectral Imaging Technology

Based on the hyperspectral imaging technology and the knowledge of trace inspection, this study designs a trace inspection system based on hyperspectral imaging technology. The system can improve the degree of trace recovery and also improve the accuracy of the image. The system can inspect residual traces such as car tires, shoe soles, and blood stains. In this regard, this study designs a set of controlled experiments. They were compared with a trace inspection system based on hyperspectral imaging technology and a traditional trace inspection system. There are 10 sets of pictures in each group, and the detection accuracy and recovery degree are compared respectively. The experimental results are shown in Figure 10.

It can be seen from the figure that the accuracy of the trace inspection system based on hyperspectral imaging technology can reach 80%–95%, while the traditional one is only 67%–75%. Therefore, the trace inspection system of hyperspectral imaging technology designed in this study can improve the accuracy by 5%–28%. The recovery degree of the trace inspection system of hyperspectral imaging technology can reach 80%–92%, while the traditional one is only 73%–79%. It shows that the trace inspection system of hyperspectral imaging technology can be improved by 1%–19%, compared with the traditional one. By analyzing the experimental results, the trace inspection system based on hyperspectral imaging technology has the characteristics of high accuracy and high image recovery ability compared with the traditional trace inspection system. This is very important for criminal investigation trace inspection.

5. Conclusion

This study mainly studies the application of hyperspectral imaging technology in trace inspection. In order to explore how it can be used in trace inspection, this article combines the nondestructive testing technology of hyperspectral imaging technology. By recognizing images of residual traces such as car tires, shoe soles, and blood stains, and then combining image denoising and least squares support vector machine methods, this article denoises and restores the images. This study also designs the retrieval performance experiment of the trace inspection system to verify the performance problems of the hyperspectral imaging

technology. It designed a hyperspectral image noise reduction experiment to verify its degree of noise reduction. It also designed a hyperspectral image fusion experiment of blood stain samples to verify the fusion recovery capability of hyperspectral imaging technology.

Data Availability

The experimental data used to support the findings of this study are available from the corresponding author upon request.

Conflicts of Interest

The authors declare that they have no conflicts of interest.

Acknowledgments

This study was supported by the Youth Innovation Team Development Project of Shandong Universities, China (grant no. 2019KJE018).

References

- [1] Q. Wang, J. Lin, and Y. Yuan, "Salient band selection for hyperspectral image classification via manifold ranking," *IEEE Transactions on Neural Networks and Learning Systems*, vol. 27, no. 6, pp. 1–11, 2017.
- [2] X. Ma, H. Wang, and G. Jie, "Spectral–spatial classification of hyperspectral image based on deep auto-encoder," *Ieee Journal of Selected Topics in Applied Earth Observations and Remote Sensing*, vol. 9, no. 9, pp. 1–13, 2016.
- [3] W. Fu, S. Li, L. Fang, X. Kang, and J. A. Benediktsson, "Hyperspectral image classification via shape-adaptive joint sparse representation," *Ieee Journal of Selected Topics in Applied Earth Observations and Remote Sensing*, vol. 9, no. 2, pp. 556–567, 2016.
- [4] Z. Yan, Z. Zhen, D. Wang, Y. C. Huang, and M. H. Yu, "Hyperspectral image unmixing algorithm based on end-member-constrained nonnegative matrix factorization," *Frontiers of Optoelectronics*, vol. 9, no. 4, pp. 627–632, 2016.
- [5] Y. Shao, N. Sang, C. Gao, and C. X. Li, "Probabilistic class structure regularized sparse representation graph for semi-supervised hyperspectral image classification," *Pattern Recognition*, vol. 63, no. Complete, pp. 102–114, 2016.
- [6] A. Larcher, "How isotopes traced ötzi's origins," *Australasian Science*, vol. 40, no. 4, pp. 16–20, 2019.
- [7] G. A. Cutter, J. G. Moffett, M. C. Nielsdóttir, and V. Sanial, "Multiple oxidation state trace elements in suboxic waters off Peru: in situ redox processes and advective/diffusive horizontal transport," *Marine Chemistry*, vol. 201, no. APR.20, pp. 77–89, 2018.
- [8] B. Zhao, L. Gao, W. Liao, and B. Zhang, "A new kernel method for hyperspectral image feature extraction," *Geo-Spatial Information Science*, vol. 20, no. 4, pp. 309–318, 2017.
- [9] W. Fu, S. Li, L. Fang, X. Kang, and J. A. Benediktsson, "Hyperspectral image classification via shape-adaptive joint sparse representation," *Ieee Journal of Selected Topics in Applied Earth Observations and Remote Sensing*, vol. 9, no. 2, pp. 556–567, 2016.
- [10] H. Hong, F. Luo, Z. Ma, and H. Feng, "Semi-supervised dimensionality reduction of hyperspectral image based on

- sparse multi-manifold learning,” *Journal of Computer and Communications*, vol. 03, no. 11, pp. 33–39, 2017.
- [11] F. Luo, B. Du, L. Zhang, L. Zhang, and D. Tao, “Feature learning using spatial-spectral hypergraph discriminant analysis for hyperspectral image,” *IEEE Transactions on Cybernetics*, vol. 49, no. 7, pp. 2406–2419, 2019.
- [12] P. Ghamisi, N. Yokoya, J. Li, W. Liao, and A. Plaza, “Advances in hyperspectral image and signal processing: a comprehensive overview of the state of the art,” *IEEE Geoscience & Remote Sensing Magazine*, vol. 5, no. 4, pp. 37–78, 2018.
- [13] R. Hang, Q. Liu, H. Song, and Y. Sun, “Matrix-based discriminant subspace ensemble for hyperspectral image spatial-spectral feature fusion,” *IEEE Transactions on Geoscience and Remote Sensing*, vol. 54, no. 2, pp. 783–794, 2016.
- [14] D. Liao, Y. Qian, J. Zhou, and Y. Y. Tang, “A manifold alignment approach for hyperspectral image visualization with natural color,” *IEEE Transactions on Geoscience and Remote Sensing*, vol. 54, no. 6, pp. 3151–3162, 2016.
- [15] T. Reinbacher, J. Brauer, D. Schachinger, A. Steininger, and S. Kowalewski, “Automated test-trace inspection for micro-controller binary code,” *Lecture Notes in Computer Science*, vol. 7186, 2012.
- [16] L. Jie, Q. Yuan, H. Shen, and Z. Liangpei, “Noise removal from hyperspectral image with joint spectral-spatial distributed sparse representation,” *IEEE Transactions on Geoscience and Remote Sensing*, vol. 54, no. 9, pp. 1–15, 2016.
- [17] L. Wei, D. Qian, Z. Fan, and H. Wei, “Hyperspectral image classification by fusing collaborative and sparse representations,” *Ieee Journal of Selected Topics in Applied Earth Observations and Remote Sensing*, vol. 9, no. 9, pp. 4178–4187, 2016.
- [18] H. Su, Y. Cai, and Q. Du, “Firefly-algorithm-inspired framework with band selection and extreme learning machine for hyperspectral image classification,” *Ieee Journal of Selected Topics in Applied Earth Observations and Remote Sensing*, vol. 10, no. 1, pp. 309–320, 2017.
- [19] G. Cheng, F. Zhu, S. Xiang, W. Ying, and P. Chunhong, “Semisupervised hyperspectral image classification via discriminant analysis and robust regression,” *Ieee Journal of Selected Topics in Applied Earth Observations and Remote Sensing*, vol. 9, no. 2, pp. 1–14, 2017.
- [20] X. Ma, H. Wang, and J. Wang, “Semisupervised classification for hyperspectral image based on multi-decision labeling and deep feature learning,” *ISPRS Journal of Photogrammetry and Remote Sensing*, vol. 120, no. oct, pp. 99–107, 2016.
- [21] S. Jia, H. Hu, X. Xie, L. Shen, X. Jia, and Q. Li, “Gabor cube selection based multitask joint sparse representation for hyperspectral image classification,” *IEEE Transactions on Geoscience and Remote Sensing*, vol. 54, no. 6, pp. 3174–3187, 2016.
- [22] Z. Wang, D. Bo, L. Zhang, Z. Liangpei, and J. Xiuping, “A novel semisupervised active-learning algorithm for hyperspectral image classification,” *IEEE Transactions on Geoscience and Remote Sensing*, vol. 55, no. 99, pp. 3071–3083, 2017.
- [23] X. Zhang, Q. Song, R. Liu, W. Wenna, and J. Licheng, “Modified Co-training with spectral and spatial views for semisupervised hyperspectral image classification,” *Ieee Journal of Selected Topics in Applied Earth Observations and Remote Sensing*, vol. 7, no. 6, pp. 2044–2055, 2017.
- [24] Z. Yang, “Hyperspectral image target detection improvement based on total variation,” *IEEE Transactions on Image Processing*, vol. 25, no. 5, pp. 2249–2258, 2016.

Research Article

Short-Term Demand Forecast of E-Commerce Platform Based on ConvLSTM Network

Zan Li ¹ and Nairen Zhang²

¹College of Business, Zhengzhou College of Finance and Economics, Zhengzhou 450000, China

²Department of Decision Consultation, Henan Administration Institute, Zhengzhou 451000, China

Correspondence should be addressed to Zan Li; lizan@zzufe.edu.cn

Received 30 March 2022; Accepted 2 June 2022; Published 14 July 2022

Academic Editor: Le Sun

Copyright © 2022 Zan Li and Nairen Zhang. This is an open access article distributed under the Creative Commons Attribution License, which permits unrestricted use, distribution, and reproduction in any medium, provided the original work is properly cited.

Based on real sales data, this article constructed LGBM and LSTM sales prediction models to compare and verify the performance of the proposed models. In this article, we forecast the product sales of stores in the future $T + 3$ days and use MAPE as the evaluation index. The experiment shows that the product sales prediction model based on the convolutional LSTM (ConvLSTM) network has better prediction accuracy. From a store point of view, ConvLSTM prediction model MAPE was 0.42 lower than the long short-term memory (LSTM) network and 0.68 lower than LGBM. From the perspective of commodity categories, different commodity categories are suitable for different forecasting methods. Some categories are suitable for regression forecasting, while others are suitable for time-series forecasting. Among the categories suitable for time-series forecasting, the ConvLSTM model performs the best.

1. Research Background

In recent years, the Internet has developed rapidly with the passage of time, and enterprises have accumulated massive valuable data, which contains a huge value and is waiting for people to dig. In addition, due to the rise of big data and artificial intelligence, our life has undergone great changes, and many emerging fields of science and technology have emerged. Traditional enterprises also want to take the ride of big data and artificial intelligence to bring scientific analysis and guidance to companies and enterprises.

New retail, supported by artificial intelligence, big data, mobile Internet, and other cutting-edge technologies, emerges in the trend of China's residents' consumption upgrading. With new concepts such as scenarioization, fragmentation, and experientialization, new retail formats are reconstructed, leading to the transformation and upgrading of China's retail market. The traditional retail has come to the stage of contraction, the development of traditional e-commerce has reached a bottleneck today, and the sales industry is in a very challenging period. In the near future, the traditional offline or pure online form may no longer exist, and the full integration of online and offline new retail will be the general trend.

While the new retail industry has been changed, there are also many new challenges. Competitors from a variety of online and offline channels and an increasingly rich variety of goods, especially in the face of changing user needs, force enterprises to constantly make adjustments in the process of pursuing market profits [1]. The development direction of new retail is still to meet the changes of users' needs. As a result, predicting users' needs accurately is very important and presents more challenges in the context of the new retail industry.

2. Related Works of Demand Forecasting

Research on demand forecasting has always been a hot topic for experts at home and abroad. Accurate forecast results are extremely important in different industries, especially for the emerging new retail, which will directly affect the sales of enterprises. Combined with the research of domestic and foreign experts on demand forecasting, the forecasting method is divided into qualitative forecasting and quantitative forecasting.

Qualitative sales forecasting methods mainly include the subjective probability method, expert judgment opinion

method, Delphi method, mutual influence method, scenario prediction method, etc [2–4]. Quantitative sales forecasting methods mainly include the time-series method (e.g., autoregressive series analysis [5], ARIMA model [6]), machine learning method [7] (e.g., artificial neural network [8, 9], extreme learning machine [10], support vector machine (SVR) [11], and ensemble algorithms), and deep learning method.

Because the qualitative prediction method is mainly to predict the future demand through experts combined with their rich business experience, this method is more applicable when there are few influencing factors and the sales information cannot be fully quantified. However, due to its shortcomings such as subjective factors and poor reproducibility, in the face of an increasingly complex business environment, this method is not accurate in demand forecasting. Therefore, this article mainly expounds the research status of demand forecasting at home and abroad from the quantitative forecasting methods, namely the time-series method, machine learning method, and deep learning method.

2.1. Time-Series Prediction. Autoregressive series analysis is one of the most popular methods in time-series application, which only uses single-dimension sales data for forecasting. Back in 1927, some mathematicians proposed the earliest autoregressive model for analyzing sequence data, referred to as the AR model [12]. On the basis of the AR model, scientists combined the autoregressive process AR with the moving average process MA to produce the autoregressive moving average model, referred to as ARMA [13, 14]. AR and ARMA models have good model effects when facing stationary time-series scenes, but they are not suitable for nonstationary sequence scenes which are common. Therefore, people consider introducing difference transformation to stabilize them and generate the differential autoregressive moving average model with difference transformation, ARIMA for short [15].

For example, researchers used the beverage sales data of an enterprise, which only included sales data without other additional features; established stationary series models such as MA and ARMA for analysis and prediction, respectively, and nonstationary ARIMA models for comparative analysis; and obtained very ideal prediction results. In 2018, Facebook opened the time-series prediction algorithm Prophet, which represents the time series as the sum of trend term, period term, holiday term, and error term, which can well fit and predict the time series in the business field.

2.2. Machine Learning Prediction. With the development of machine learning, it is found that the time-series problem can be transformed into a machine learning regression problem, that is the future target data can be regression as “label.” This method can not only use the sales dimension, but also add time, holidays, weather, and other characteristics of different dimensions. Common machine learning algorithms include support vector regression (SVR) algorithm, decision tree regression algorithm, Leo Breiman and

Adele Cutler-proposed bagging ensemble learning on the basis of decision tree, and the random forest algorithm generated by the fusion of multiple decision trees. Boosting ensemble learning is introduced, which iterates multiple base learning devices, and the generated GBDT algorithm, a series of extended tree model algorithm, and an artificial neural network can solve the regression problem [16].

Avanija et al. used XGBoost to predict the house price in 2021 [17], which improved the accuracy of sales forecast and realized effective control of inventory. Experimental results show that XGBoost can fully consider the influence of external factors and historical data on sales volume and effectively predict sales volume. SVR model is used to predict the sales volume [18]. Through comparative experimental analysis with the ARIMA model and linear regression model, it was proved that the SVR model has higher prediction accuracy. Because the SVR algorithm can transform complex nonlinear regression problem into linear regression problem of high-dimensional feature space, it can be widely used in various time-series prediction problems, such as weather prediction, traffic flow prediction, etc.

2.3. Deep Learning Prediction. In recent years, with the growing enterprises accumulating the amount of data, the sales environment is becoming more and more complex and the traditional prediction method of machine learning also exposed the shortcomings, such as training time being too long, it is not easy to convergence. Therefore, people have thought more deeply about the prediction model and started to use deep learning methods to build the prediction model [19]. In terms of prediction, Shih et al. proposed a model to forecast short-term goods demand in an e-commerce context [20]. They found that short-term demand for goods could not be predicted by the periodicity of historical data, so they built a database based on buyers’ reviews to predict short-term demand for goods from this unique perspective. Based on the combination of traditional statistical model and deep learning model, the demand for e-commerce products is predicted, and good prediction results are obtained [21].

3. Sales Forecasting Modeling

The sales volume forecast of commodities can be predicted by the regression method, or the sales data can be fitted by time series. Whether regression prediction or time-series prediction, there is a specific assumption that the features are independent of each other, and the samples are independent of each other. Features are independent of each other and can be solved by constructing associative features. However, the samples are independent of each other, and there are some defects in the scenario where multiple commodities need to be predicted, that is the interaction between different commodities is not considered. There is a certain relationship between commodities, which are mutually exclusive and complementary. Some commodities are of the same type. If you select commodity A, you will not select commodity B with the same attributes. Similarly, some

commodities have complementary relationships and can be sold together, after you select commodity A, you need to match commodity C.

This chapter introduces the sales prediction model based on related commodities. Word2Vec model is used to group the predicted commodities first, and then the ConvLSTM network is used to predict the sales of the commodities after grouping in the future $T + 3$ days, as shown in Figure 1. First, Word2Vec is used for low-dimensional spatial mapping of feature words, which can make words with similar context have similar spatial mapping and extract the semantic characteristics of words. Starting from the receipt data of goods, the vector representation of goods is obtained, so as to extract the association of different goods. Then, ConvLSTM can learn the long-term dependence of data and extract the spatial characteristics of data to predict the sales volume of associated goods.

3.1. Commodity Association Clustering Based on Word2Vec. At present, there are many association analysis algorithms, such as Apriori and FP-growth. The basic idea is to select the commodity combination with high frequency by counting various commodity combinations. However, these algorithms have some disadvantages, they need to traverse all the collections in the data set globally, which consumes a lot of time. At the same time, in the face of a large amount of data, the commodity associations that can be mined are limited.

Word2Vec is a shallow neural network model, which is often used for natural language tasks. It can map feature words into low-dimensional word vectors and map semantically similar feature words into similar projection spaces. First, we need to build a Word2Vec model for commodity ticket data, train the vector representation of commodities, and then conduct association clustering according to the vector representation of commodities.

3.1.1. Commodity Word Vector Model. The vector representation of Word2Vec training commodity needs to be preprocessed for commodity receipt data according to the input requirements of the model, and then appropriate training methods are selected for unsupervised learning. Finally, the vector mapping space of the commodity is obtained. In the model, the vector space of the commodity is the network parameters from the input layer to the hidden layer.

(1) Data Preprocessing. To train the word vector of goods by using the receipt data of goods, the receipt data need to be processed according to the algorithm requirements of the Word2Vec model. The discovery of receipt data shows that (1) there are some dirty data in receipt data, such as shopping bags, price difference compensation, and returns; (2) the same user makes multiple receipts when shopping at one time; (3) the user buys fewer goods; and (4) there are multiple same goods in the same receipt. Figure 2 shows the processing process of receipt data.

First, it is necessary to remove the dirty data in the data and delete nonpredictive goods in the receipt. These dirty

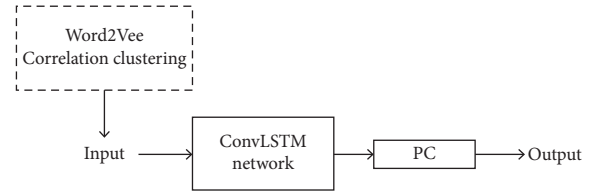


FIGURE 1: The structure of the model.

data are similar to stop words in natural language, which will interfere with model training and destroy the mapping space of vectors. Then, data integration is carried out on the receipt data. There may be multiple receipts for one user and multiple same goods in one receipt. We need to summarize the goods purchased by the same user in the same day and then eliminate the duplicate goods in the receipt data.

Word2Vec model is a three-layer neural network, which predicts its context according to known characteristics or predicts the feature word according to the context of the feature word. The input of the model is the unique heat coding of the known feature word. When used for vector representation of goods, it is necessary to carry out unique thermal coding for the goods contained in the invoice data first and establish a mapping dictionary to transform the goods into the form of unique thermal coding before the commodity input model is known.

(2) Commodity Word Vector Training. Word2Vec has two models. CBOW model is used this time. The input layer is other commodities in the same receipt data of the commodity to be predicted, and the output layer is the one-hot vector of the predicted commodity.

When training the Word2Vec model, you need to set the size of the context window, and the dimension of the word vector. In general, the input is $2n$ commodities up and down the commodity w_t , because the location relationship of commodities is not considered in the receipt data, the user checks out randomly during shopping, and any commodity in the ticket data should be associated with other commodities in the same ticket. Therefore, n should include all commodities as much as possible. Assuming that the total number of commodities in the ticket is m at most, $n = m - 1$ should be set.

As for the dimension of the word vector, the decisive factor is the number of neurons in the hidden layer N , and the input data are spatially mapped through matrix $W_{V \times N}$, where vector $\{h_1, h_2, \dots, h_i, \dots, h_n\}$ is the commodity of commodity w_t and $W_{V \times N}$ is the transfer matrix of the transformation of the word vector.

3.1.2. Commodity Association Clustering. According to the commodity vector trained by Word2Vec, the commodities are correlated and clustered. Similar commodities have similar distances. The clustering algorithm can be used to group commodities and predict the relevance of commodities. The commonly used clustering algorithms include K-means clustering, mean-shift clustering, DBSCAN clustering, expectation-maximization (EM) clustering using

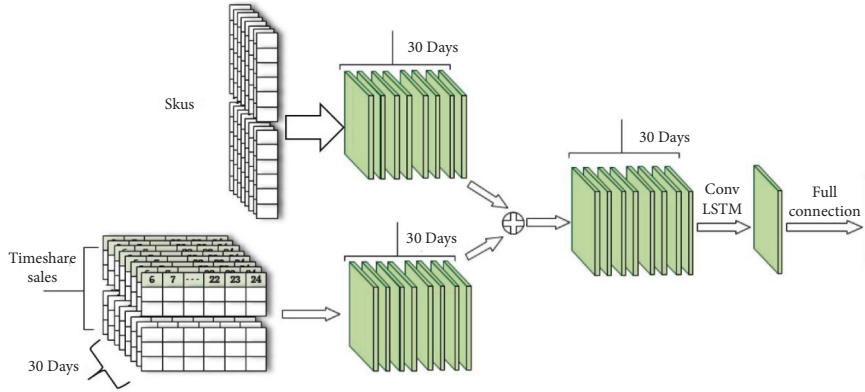


FIGURE 2: Model network structure.

Gaussian mixture Model (GMM) clustering, hierarchical clustering, etc. Each clustering has its advantages and disadvantages, and it is necessary to select the appropriate clustering method according to the manifestation of data samples.

In combination with the vector representation of commodities, this article will select the appropriate clustering method based on K-means clustering and DBSCAN clustering. K-means clustering is a clustering algorithm based on partition. Its main idea is to make the spacing of data samples within clusters as small as possible and the spacing of samples between clusters as large as possible, and it is a local optimal algorithm, and the results of multiple clustering will be different. The time complexity of the K-means algorithm is low, and the algorithm has excellent performance and high efficiency when facing the scene of large data sets. However, the algorithm is sensitive to outliers, and the selection of the total number of cluster classes and the initial cluster center has a great influence on the clustering effect. K-means is suitable for processing data sets with spherical data distribution.

Among the clustering algorithms, DBSCAN clustering is based on density, the general idea is to find a high density of samples first. Then the high density around samples will gradually come together, eventually forming a cluster around each sample point. However, unlike K-means clustering, DBSCAN does not specify the number of clusters to be formed. Under the same settings, the results of multiple DBSCAN clustering are consistent. The advantage of DBSCAN is that it is insensitive to noise and can cluster clusters of different sizes and arbitrary shapes. However, it is sensitive to the radius of the circle and the threshold value of samples in the circle. When the density of data clusters is different, it is difficult to select an appropriate radius, thus affecting the clustering effect. DBSCAN works with clusters of any shape, but requires roughly the same density between clusters.

Through data visualization, it can be found that the total number of commodities to be clustered is not large, which is 500, the distribution of commodity vectors is irregular, there is a small amount of noise, and the density between clusters is roughly the same. Therefore, the DBSCAN algorithm is selected to represent the association clustering of commodity

vectors. Taking the vector representation of 500 commodities trained by Word2Vec as input, using the DBSCAN algorithm, the distance threshold EPS is set as 0.1 and the sample number threshold min_Samples as 10, and the Euclidean distance is used as the distance measurement parameter to cluster the commodities.

4. Forecast Model of Commodity Sales Based on ConvLSTM

In the previous chapter, we constructed a commodity relevance clustering model based on Word2Vec, whose practical significance is to mine the association relationships between different products, the input of ConvLSTM prediction model is constructed, and the prior knowledge of product association is integrated. This section will mainly introduce the commodity sales forecast model based on ConvLSTM, including model input and output, network structure design, activation function selection, model training, etc.

4.1. Input and Output Structure Design of Network. The product sales forecast based on ConvLSTM is actually a supervised learning, which uses the sales data of stores to predict the product sales on the n th day in the future. Input data should not only contain sales data, discount information, and time characteristics of stores, but also conform to the requirements of the ConvLSTM neural network for input data.

In the figure, we splice the data of N days before time T into a two-dimensional tensor, and then sort these two-dimensional tensors according to time, thus forming an example of neural network input. It is worth noting that each two-dimensional tensor is combined according to the sales situation of each commodity and the results of commodity association clustering. Among them, the two-dimensional tensor acts as the time-sharing sales volume of a single commodity in each time period every day, and the column first puts the similar commodities in each cluster together according to the clustering results of commodities, and then according to the distance between clusters, the clusters close to each other are combined to arrange all the commodities to be predicted.

S_T can be considered as the sales data of the day T , then each example is composed of samples $\{S_{T-H}, \dots, S_{T-I}, \dots, S_{T-1}, S_T\}$ and label, where H is the number of ConvLSTM network neurons, that is the sales data of consecutive H days in history input at one time, N is the time span to be predicted, and the output of ConvLSTM network is the sales data S_{T+N} of the $T+N$ day. The input of the whole model requires S_T fusion with other external data of the day T , which will be explained in detail in the model network design in the next section.

4.2. Model Network Design. LSTM network model is very suitable for dealing with problems with time-series characteristics. The network transmits information according to the forward propagation of time step, and the cell state will be updated gradually, and the information is transmitted and forgotten through three gated systems. LSTM sales prediction model can add a feature extraction layer before data input LSTM to improve the prediction effect. For example, the prediction model based on the WaveNet-LSTM network adds a layer of the WaveNet network before the LSTM layer and uses causal convolution to obtain local and global information of the whole time series.

The convolutional neural network has a strong representation learning ability and can recognize features of different locations in space by using convolution operation and pooling operation of data samples. The convolutional neural network takes advantage of the feature that convolution operation can capture local information of data and uses multiple filters (convolution kernel) to extract information at the same time, thus realizing local perception to obtain global information. In this chapter, the advantages of convolution operation for spatial feature extraction will be utilized, and the vector operation of LSTM will be replaced by convolution operation, and combined with external influencing factors of sales volume, a sales prediction model for associated goods will be constructed. The model network diagram is shown in Figure 2.

The model is divided into two parts. In the first part, the store's sales characteristics, discount information, time characteristics, and other features are fused to form the input of the ConvLSTM network. For the input data of the model, first, the attribute features such as daily discount information and time features are fully connected, then the extracted feature reshape is the same size as the sales feature, and finally the concat operation is used to form the input of the ConvLSTM network for the sales features and the reshaped features. The second part consists of a ConvLSTM network prediction module, which consists of a ConvLSTM network layer and a fully connected layer. After the extracted features are inputted into the network, the prediction information is outputted, and the final prediction result is obtained through the full connection layer.

ConvLSTM network can be used to extract time-series characteristics and spatial characteristics of sales volume of various commodities for the following reasons:

First, traditional sales forecasting methods assume that different commodities are independent of each other and

can only forecast independent commodities. The prediction method based on time series can use single-dimension sales data to forecast, but only one kind of commodity can be predicted. To forecast multiple commodities, multiple models need to be constructed. Regression-based prediction method can predict multiple commodities simultaneously by constructing feature engineering, but it cannot obtain time-series characteristics. The idea of the ConvLSTM network is to extract and transfer information of time series from two-dimensional matrix data, so that time-series prediction of multiple commodities can be made simultaneously.

Second, in real life, commodities often interact with each other. When shopping, people will consider the repetition and collocation of commodities. For commodities with repetitive functions, they will choose only one of them, while for commodities with complementary functions, they will buy them with each other. Based on this, the ConvLSTM network can not only capture the time-series characteristics of various commodities, but also extract spatial information of data and capture the interaction between commodities through convolution operation. However, the introduction of convolution operation may bring a series of problems, such as the selection of convolution kernel and poor fitting effect.

The model needs to capture the interaction between goods through the convolution operation, but convolution can only capture part of the local information; it is difficult to obtain global information, that is when there are too many goods, the convolution operation often cannot capture the association between goods with a long distance. If the convolution is extended, more commodity association information can be obtained at the same time, but too many parameters will affect the fitting effect. We integrate the association information of commodities in advance to obtain the prior knowledge of the association relations of commodities and put the commodities with certain association relations together, and then spliced them into the two-dimensional matrix form required by the network, so that even if the size of the convolution kernel cannot contain all commodities and cannot capture the association relation of commodities with relatively distant positions, the influence will not be great. In the process of data preparation, the relationship between goods located far away from each other is poor.

4.3. Selection of Activation Function. The activation function can introduce nonlinearity into the network model and enhance the expression ability of the model. In the gated mechanism of ConvLSTM, information is also forgotten and transmitted through activation functions, commonly used activation functions are as follows:

- (1) *The Sigmoid Function.* The sigmoid function expression is as follows:

$$y = \frac{1}{1 + e^{-x}}. \quad (1)$$

Sigmoid is a commonly used nonlinear activation function. The value range of expression is $[0, 1]$, and

the range of derivative is $[0, 0.25]$. The function is easy to fall into the saturation zone on both sides, and the gradient disappears, and the output is not zero mean, which makes the model convergence slow.

- (2) *Tanh Function*. Tanh function is expressed as follows:

$$y = \frac{e^x - e^{-x}}{e^x + e^{-x}}. \quad (2)$$

The range of the Tanh function is $[-1, 1]$, and the range of its derivative is $[0, 1]$, which solves the problem that the sigmoid output is not zero mean value, but the problem of gradient disappearance still exists.

- (3) *The ReLU Function*. ReLU function is expressed as follows:

$$y = \max(0, x). \quad (3)$$

When the input value of the function is greater than 0, the output of the ReLU function is equal to the input value. When the input value of the function is less than 0, the output is 0. Function can solve the problem of gradient disappearance in the process of model back propagation, but it can only be used in the hidden layer.

According to the network structure of ConvLSTM, the default activation function of input gate and output gate is the Tanh function, and its output range is $[-1, 1]$. However, according to the actual data, it can be found that most of the sales data of commodities are too large, which will change the distribution of data, cause the gradient to disappear, and the dimensions between different commodities are the same. If the data are forcibly normalized, some data will be extremely small, which will affect the effect of the model. In addition, when the sales data of commodities is relatively large, it is not necessary to consider the negative semi-axis when selecting the activation function. Therefore, the ReLU function is chosen.

4.4. Model Training. The training process of a neural network mainly includes two stages: the first stage is the forward propagation stage, and the second stage is the back propagation stage. Specifically, once the data set is ready and the model is built, model training can be carried out. First, it is necessary to set initial values for network parameters and then input model training data. Data samples enter the model network one by one and generate model predicted values through the forward propagation of network. The back propagation process uses an optimizer to update network parameters according to the error between the predicted value and the target value of the model until the termination condition of the model is met.

The effect of model training is affected by many factors, including initialization of parameters, selection of optimizer, selection of learning rate, etc.

4.4.1. Initialization of Parameters. The training effect of the neural network model mainly depends on the updating of parameters by the optimizer. The optimizer back propagates the parameters through the gradient descent method, and the initialization of parameters greatly affects the convergence result of the model. If the initial value of the parameter is set too large, the gradient value of the parameter during back propagation will be too large, the gradient explosion will occur, and the amplitude of network update will be too large, which will make the model difficult to converge. If the initial value of the parameter is set too small, the gradient will be too small and the gradient will disappear, which will slow down the convergence speed of the parameter and make the model converge to the local optimal solution.

The initial value of network parameters should not be too large or too small and should keep the parameter positive or negative half as much as possible, and the expectation is 0. Network parameters can be initialized to small random numbers, such as random sampling with a Gaussian distribution with a standard deviation of 1 and mean of 0, or initialization with Xavier, but requires the activation function to be symmetric with respect to 0.

4.4.2. Selection of Optimizer. In a neural network, parameter optimization mainly relies on the back propagation of the optimizer. The optimizer takes advantage of network errors, calculates gradients, and updates parameters so that the model approaches or achieves the optimal solution, that is, minimizes the objective function. The most basic optimizer is gradient descent, but in the optimization process, each epoch needs to consider all samples, which wastes time and occupies memory. In order to solve the inefficiency of the gradient descent method and accelerate the convergence speed, SGD (stochastic gradient descent) is introduced. Each iteration only uses one sample of all data to update the parameter gradient. Although SGD accelerates the model training speed, it will lead to convergence oscillation and lower accuracy, so it is not a globally optimal optimization algorithm. In order to accelerate the convergence of the model and improve the fitting accuracy, researchers also put forward a momentum optimization algorithm and adaptive learning rate optimization algorithm.

In this application, there is a large amount of actual data. A store has more than 300 examples a year, a total of more than 1000 stores, and the sales data will continue to increase and accumulate, and the data are sparse, so the Adam algorithm is selected. The Adam algorithm can adaptively change the learning rate of each parameter. It is very suitable for processing sparse data. It is not only conducive to the first-order distance estimation mean, but also makes full use of the gradient second-order distance estimation variance.

4.4.3. Selection of Learning Rate. Learning rate is an important super parameter in network training; it plays a decisive factor in whether the objective function can converge to the local optimal value and how long it takes to converge to the optimal value. If the learning rate is small, the convergence speed of the model will become very slow. A

small learning rate can ensure that the model will not miss any local optimal solution, but it will consume more time to make the model converge, especially when the model converges to the plateau area. When the learning rate is large, the model training speed becomes faster, but it may not converge, it is easy to cross the optimal value, and the gradient fluctuates back and forth around the optimal value.

Choosing an appropriate learning rate can ensure that the model can converge to the local optimal solution in a short time. This article will choose the method of learning rate attenuation to continuously adjust the learning rate in the training process. In the training process, a smaller learning rate training model is selected first and the learning rate after each round of iteration is gradually increased. By drawing a two-dimensional chart of learning rate and loss, we can find the optimal learning rate before the loss is no longer reduced.

5. Data Processing

5.1. Data Introduction. The data set of this experiment selects real commodity sales data of Q company, including sales statistics and receipt data of stores, covering four categories of commodities: meat, vegetables, cooked food, and aquatic products. This experiment selects the sales data of 5 stores, covering the period from January 1, 2017 to December 31, 2018, with a total of 11,393,481 pieces of data, including about 500 kinds of goods that appeared in the last 4 months.

5.2. Dividing Data Sets. In the experiment, the sliding window method is used to divide the data set, and the time step is 1 and the sequence length is 30. As shown in Figure 3, the feature in each example is the historical sales data of the store within 30 days, and lable is $T + 3$ to predict the sales volume of goods on the day.

6. Ablation Experiments

6.1. Comparison Method. The previous chapter mainly introduces the sales forecasting model based on the ConvLSTM network. This section will introduce the experimental comparison model, LightGBM prediction model, and LSTM prediction model. The two models will transform the sales forecasting model into a regression problem and a time-series problem, respectively:

- (1) LightGBM prediction model: GBDT is used as the base learner to make regression prediction of sales volume through feature engineering.
- (2) LSTM prediction model: it consists of one dense layer and one LSTM layer and then outputs the prediction results of the model through the full connection layer.

6.2. Parameter Setting. In experiment 1, the LightGBM prediction model, the features used are as follows: historical seven-day sales feature, time-sharing sales feature, pedestrian flow feature, weather feature, monthly feature, weekly

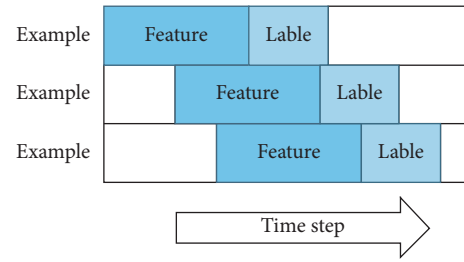


FIGURE 3: Data set partitioning by sliding window method.

TABLE 1: Parameter configuration of LightGBM sales prediction model.

Parameter	Setting
boosting_type	GBDT
objective	Regression
metric	MSE
nthread	5
learning_rate	0.01
num_leaves	25
max_depth	15
max_bin	255
subexample	0.8
colexample_bytree	0.8
feature_fraction	0.9
lambda_ll	0.1
lambda_l2	0.0

feature, weekend feature, price change feature, promotion feature, temperature feature, weekly feature, and quarterly feature. The LightGBM prediction model adopts the grid search method for parameter tuning, and parameter settings are shown in Table 1.

In experiment 2, LSTM prediction model, the input data were first extracted through a Dense Layer to reduce the network parameters of the LSTM layer. Here, the dimension of the full connection layer was set as $1 * 10$, and the specific parameters of the model were set as follows:

- (1) *Optimizer.* Adam optimizer is selected to adaptively adjust the learning rate.
- (2) *Learning Rate.* Set this parameter to 0.001 in the experiment.
- (3) *Activation Function.* The three gating devices for information transmission in LSTM are equipped with activation functions, and the activation function is the ReLU function.
- (4) *Dropout Random Inactivation Rate.* To prevent overfitting, set dropout to 0.1.
- (5) *Error Function.* The error function is set as MSE in the experiment.
- (6) *Batch Size.* Batch size (batch_size) is set to 256 in the experiment.
- (7) *Iteration Times.* The training iteration times epoch is set to 1000 in the experiment.

Experiment 3 was based on the sales prediction model of the ConvLSTM network. In order to compare with

TABLE 2: Comparison of forecast results of different stores.

Shop_Number	MAPE_LGBM	MAPE_LSTM	MAPE_ConvLSTM	MAPE_SVR	MAPE_ARIMA
101015	37.00	36.45	36.25	36.01	35.23
101016	40.31	39.83	38.50	37.1	38.21
101031	35.70	36.34	36.80	35.33	36.41
101044	40.83	41.95	40.00	39.89	38.98
101166	41.06	39.07	39.95	38.34	38.9
Mean value	40.98	38.728	38.03	37.34	37.55

TABLE 3: Comparison of prediction results for different categories.

Category_Number	MAPE_LGBM	MAPE_LSTM	MAPE_ConvLSTM	MAPE_SVR	MAPE_ARIMA
10001	36.65	39.72	42.86	35.45	36.67
10002	40.41	39.56	37.69	38.55	36.43
10003	38.50	41.88	41.32	39.41	37.54
10004	39.60	37.47	35.89	39.31	36.52
10005	40.46	41.04	39.52	38.99	38.12
10006	38.28	32.15	32.50	36.81	33.23
Mean value	38.92	38.64	38.02	38.08	36.41

experiment 2, the training mode of the ConvLSTM prediction model was the same as experiment 2. Adam optimizer was selected, and the learning rate was 0.001, etc. The difference is that ConvLSTM network will conduct convolution operation in the process of state transfer, and convolution-related parameters need to be set:

- (1) *Number of Convolution Kernels.* Here, the convolution kernels extract spatial features of two-dimensional data and set filters to 16.
- (2) *The Size of the Convolution Kernel.* In the experiment, the kernel_size of the convolution kernel is set to $10 * 10$.
- (3) *Convolution Step.* Set strides to (1,1).
- (4) *Zero-Complement Strategy.* In order to retain the convolution result at the boundary, the padding is set to the same in the experiment.

In this experiment, all models will be compared on the basis of the same original data set, and the model will predict the product sales within 3 days ($T + 3$) of the input data, and MAPE will be selected as the evaluation index of the model.

7. Analysis of Experimental Results

In this section, the prediction results of the three models will be compared and analyzed from two perspectives: the prediction results of the three models in different stores and the prediction results of the three models for different categories of goods. The prediction results used for comparison are all the best prediction results after the adjustment of the three models.

7.1. Comparison of Forecast Results of Different Stores. The comparison of the prediction errors of the three models in different stores is shown in Table 2, which shows the optimal performance of the three models in the evaluation index MAPE after the adjustment. On the whole, it can be

seen that the prediction effect of the LSTM model is better than that of LGBM model. The average MAPE of the LGBM model's five stores is 38.98, which is 0.26 percentage points higher than that of the LSTM model. It can be seen that LSTM has advantages in dealing with time series, and the same applies when forecasting sales.

Most importantly, the ConvLSTM model performed best among the three prediction models, with an average MAPE of 38.3, 0.68 percentage points lower than that of the LGBM model and 0.42 percentage points lower than that of the LSTM model, indicating a significant performance improvement.

7.2. Comparison of Forecast Results of Different Categories of Commodities. As can be seen from the clustering results in the previous section, the whole commodity is divided into ten categories, six of which are selected in the experiment to show the prediction performance of the model in different categories, as shown in Table 3, and the comparison of prediction errors of the three models in different categories of commodity.

As shown in Table 3, the error performance of the three models is compared for different categories of goods. It can be found that models have different performance for different categories. For example, the LGBM model has better prediction effect for categories numbered 10001 and 10003, while the LSTM model and ConvLSTM model have better prediction effect for categories numbered 10002, 10004, 10005, and 10006. And the difference between the models is obvious. Categories 10001 and 10003 were suitable for regression prediction, and categories 10002, 10004, 10005, and 10006 were suitable for time-series prediction, and ConvLSTM outperformed LSTM in terms of the categories suitable for time-series prediction.

The above experiments show that the ConvLSTM model has better predictive performance than the LSTM model and LGBM model on the whole, but for individual commodities,

some commodities are more suitable for regression prediction, and the LGBM model performs better. ConvLSTM network can learn the association information between goods through convolution operation and extract the dependence information of time series by LSTM, which realizes the capture of spatial information and time information and greatly improves the prediction ability of the model.

8. Conclusion

This article combines the real sales data set of Q company to make an example application of commodity sales forecasting model based on ConvLSTM. Before modeling, the data set was fully explored, and the whole modeling process of data preprocessing, feature engineering, and experimental result analysis was described in detail, in which the experimental result analysis made a detailed analysis of commodity clustering results, experimental comparison results, and model prediction effect. We found that by using ConvLSTM network, the model can not only extract the characteristics of time series, but also capture the characteristics of data space and predict the future sales of associated goods, and the ConvLSTM network model performs well in most of the time, but sales forecasting is a very complicated task, which is affected by many factors and still faces great challenges.

Data Availability

The experimental data used to support the findings of this study are available from the corresponding author upon request.

Conflicts of Interest

The authors declare that they have no conflicts of interest regarding this work.

Acknowledgments

This work was sponsored in part by the National Social Science Fund of China (20BGL239). Experience, Law and Mechanism Design of Community Construction of Urban and Rural Grass-roots Social Governance.

References

- [1] E. Pantano, "Innovation drivers in retail industry," *International Journal of Information Management*, vol. 34, no. 3, pp. 344–350, 2014.
- [2] E. E. Ameyaw, H. Yi, and S. Ming, "Application of Delphi method in construction engineering and management research: a quantitative perspective," *Journal of Civil Engineering and Management*, vol. 42, no. 8, pp. 1–10, 2016.
- [3] Y. Min, L. Fuyan, S. Mengdi, L. Jinpeng, and C. Chao, "Quantitative analysis and scenario prediction of energy-consumption carbon emissions in urban agglomerations in China: case of Beijing-Tianjin-Hebei region," *IOP Conference Series: Earth and Environmental Science*, vol. 227, no. 6, p. 62042, 2019.
- [4] S. E. Dragomirescu and D. C. Solomon, "A case study concerning sales prediction using sales quantitative prediction methods," *The Annals of "Dunarea de Jos" University of Galati Fascicle III Electrotechnics Electronics Automatic Control and Informatics*, vol. 33, no. 1, 2010.
- [5] X. Fan, Y. Lei, Y. Wang, and Y. Lu, "Long-term intuitionistic fuzzy time series forecasting model based on vector quantisation and curve similarity measure," *IET Signal Processing*, vol. 10, no. 7, pp. 805–814, 2016.
- [6] T. V. Calster, B. Baesens, and W. Lemahieu, "ProfARIMA: a profit-driven order identification algorithm for ARIMA models in sales forecasting," *Applied Soft Computing*, vol. 60, pp. 775–785, 2017.
- [7] M. Bohanec, B. Marko, and M. R. Šikonjac, "Explaining machine learning models in sales predictions," *Expert Systems with Applications*, vol. 71, pp. 416–428, 2017.
- [8] S. Vhatkar and J. Dias, "Oral-care goods sales forecasting using artificial neural network model - ScienceDirect," *Procedia Computer Science*, vol. 79, pp. 238–243, 2016.
- [9] P. Doganis, A. Alexandridis, P. Patrinos, and H. Sarimveis, "Time series sales forecasting for short shelf-life food products based on artificial neural networks and evolutionary computing," *Journal of Food Engineering*, vol. 75, no. 2, pp. 196–204, 2006.
- [10] W. K. Wong and Z. X. Guo, "A hybrid intelligent model for medium-term sales forecasting in fashion retail supply chains using extreme learning machine and harmony search algorithm," *International Journal of Production Economics*, vol. 128, no. 2, pp. 614–624, 2010.
- [11] Q. Wu, H. S. Yan, and B. Wang, "Product sales forecasting model based on robust wavelet v-support vector machine," *Acta Automatica Sinica*, vol. 35, no. 7, pp. 1027–1032, 2009.
- [12] G. U. Yule, "On a method of investigating periodicities in distributed series, with special reference to wolfer's sunspot numbers," *Philosophical Transactions of the Royal Society of London - A*, vol. 226, pp. 267–298, 1927.
- [13] B. Friedlander, "A recursive maximum likelihood algorithm for ARMA spectral estimation," *IEEE Transactions on Information Theory*, vol. 28, no. 4, pp. 639–646, 1982.
- [14] J. A. Cadzow, "High performance spectral estimation--A new ARMA method," *IEEE Transactions on Acoustics, Speech, & Signal Processing*, vol. 28, no. 5, pp. 524–529, 1980.
- [15] H. Liu, H. Q. Tian, and Y. F. Li, "Comparison of two new ARIMA-ANN and ARIMA-Kalman hybrid methods for wind speed prediction," *Applied Energy*, vol. 98, pp. 415–424, 2012.
- [16] S. Deng, C. Wang, M. Wang, and Z. Sun, "A gradient boosting decision tree approach for insider trading identification: an empirical model evaluation of China stock market," *Applied Soft Computing*, vol. 83, Article ID 105652, 2019.
- [17] J. Avanija, G. Sunitha, K. R. Madhavi, P. Kora, and R. Hitesh, "Prediction of house price using XGBoost regression algorithm," *Turkish Journal of Computer and Mathematics Education (TURCOMAT)*, vol. 12, no. 2, pp. 2151–2155, 2021.
- [18] F. C. Yuan, "Parameters optimization using genetic algorithms in support vector regression for sales volume forecasting," *Applied Mathematics*, vol. 03, no. 30, pp. 1480–1486, 2012.

- [19] H. Wei and Q. T. Zeng, "Research on sales Forecast based on XGBoost-LSTM algorithm Model," *Journal of Physics: Conference Series*, vol. 1754, no. 1, Article ID 012191, 2021, (6pp).
- [20] YS. Shih and MH. Lin, "A LSTM approach for sales forecasting of goods with short-term demands in E-commerce," in *Intelligent Information and Database Systems. ACIIDS 2019*, N. Nguyen, F. Gaol, T. P. Hong, and B. Trawiński, Eds., Lecture Notes in Computer Science, vol 11431, pp. 244–256, Springer, Cham, 2019.
- [21] I. Kim, K. Na, S. Yang et al., "T-commerce sale prediction using deep learning and statistical model," *Journal of KIISE*, vol. 44, no. 8, pp. 803–812, 2017.

Research Article

Design of Intelligent Evaluation System for College Students' Mental Health Based on Big Data

Tao Hu,¹ Xiaojun Zhang^{ID},² and Na Li³

¹School of Medical Information Engineering, Gannan Medical University, Ganzhou 341000, China

²First Affiliated Hospital of Gannan Medical University, Ganzhou 341000, China

³Gannan Medical University, Ganzhou 341000, China

Correspondence should be addressed to Xiaojun Zhang; gyfy5236@gmu.edu.cn

Received 6 May 2022; Revised 6 June 2022; Accepted 20 June 2022; Published 13 July 2022

Academic Editor: Le Sun

Copyright © 2022 Tao Hu et al. This is an open access article distributed under the Creative Commons Attribution License, which permits unrestricted use, distribution, and reproduction in any medium, provided the original work is properly cited.

The mental health problems of college students have attracted the attention of all sectors of society. In order to keep college students in a good mental state and effectively analyze their mental health, an intelligent evaluation system of college students' mental health based on big data is designed. Based on big data technology, this article constructs an intelligent evaluation system for college students' mental health, which is divided into six layers, namely, application layer, decision layer, interface layer, analysis layer, data layer, and basic layer. Then, the mental health data of college students were collected based on C/S architecture. On the basis of extracting and integrating data characteristics, six evaluation indexes of personality, will, emotion, depression, fear, and psychosis were screened, and then, the intelligent evaluation was completed according to the weight of indexes. On the basis of the preliminary verification of the performance of the system in this article, according to the comparative experimental results, the mental health data acquisition time of the system is less, the accuracy of data feature extraction and the recall rate of evaluation results are higher.

1. Introduction

Mental health refers to the various aspects of psychology and activity process in a good or normal state. The ideal state of mental health is to maintain intact character, normal intelligence, correct cognition, appropriate emotion, reasonable will, positive attitude, appropriate behavior, and good adaptation [1, 2]. Mental health is influenced by both heredity and environment, especially the upbringing style of the family of origin in childhood. Mental health is prominent in social, production, and life to maintain good communication or cooperation with others, and can well deal with various situations in life. Individuals can adapt to the developing environment and have perfect personality characteristics. Their cognition, emotional response, and volitional behavior are in a positive state and can maintain normal regulation ability. In life practice, people can correctly understand themselves, consciously control themselves, and correctly treat external influences, so as to

maintain psychological balance and coordination, and have the basic characteristics of mental health [3, 4].

Affected by the pressure of life, work, and study, psychological problems often baffle all kinds of people. Taking college students as an example, in the face of high intensity of academic pressure and inevitable employment pressure, psychological level often produces drastic changes, and mental health is greatly affected. With the increasingly fierce competition in modern society, the competition of physical strength and intelligence is far from satisfying the development of society, and the competition of psychological quality is the core competitiveness of this era. If the psychological quality is poor, it will seriously affect the study and life and even more seriously affect the future development and employment [5]. The mental health of college students is related to their own growth and the future development of the country, and more and more tragedies caused by mental health problems occur in the society, which not only affect their own life and future, but also cause serious harm to their

families and others. Therefore, the mental health problems of college students have attracted the attention of all sectors of society. Early detection of whether college students have mental health problems is conducive to timely treatment or auxiliary prevention programs to help students develop healthily, and it is also of great social significance to promote the stable operation of schools [6].

Reference [7] designed a woA-improved random forest-based mental health assessment system for college students. The system divides college students' mental health into nine dimensions: psychosis, paranoia, terror, hostility, depression, anxiety, interpersonal sensitivity, compulsion, and somatization. Then, according to scl-90 total score, Chinese Conventional Model Evaluation Guide, and College Students' Mental Health Evaluation Standard, the mental health data are processed and evaluated discretely. Reference [8] designed an RFC college student mental health evaluation system based on the whale optimization algorithm. The system first collected RFC college students' mental health data, and then according to the current five common mental health problems of college students and the relevant evaluation criteria and data processing, the whale optimization algorithm was used to complete the mental health evaluation, which provided the decision basis for college students whether to carry out psychological counseling and treatment. Reference [9] designed a college student mental health assessment system based on VPMCD. Firstly, from the social environment, campus environment, family environment, and personal environment, the main factors that affect the mental health of contemporary college students are analyzed in detail, and then, the evaluation index system of mental health is established by using analytic hierarchy process, and the numerical calculation method of each level index is given. On this basis, a mental health assessment model based on VPMCD was established.

However, in practical application, it is found that the above traditional intelligent evaluation system of college students' mental health has some problems such as timeliness and accuracy. Therefore, this study designed an intelligent evaluation system for college students' mental health based on big data. The design ideas are as follows:

- (1) Build the overall system structure from the application layer, decision layer, interface layer, analysis layer, data layer, and base layer.
- (2) Build a data collection model of college students' mental health based on the C/S architecture.
- (3) Extracting and integrating the data characteristics of college students' mental health.
- (4) Select 6 evaluation indexes of personality, will, emotion, depression, fear, and psychosis.
- (5) Assign value to index weight, and then, complete intelligent evaluation according to index weight.

2. Design of Intelligent Evaluation System for College Students' Mental Health

Based on big data technology, this study constructs an intelligent evaluation system for college students' mental

health. Big data refers to the huge amount of data involved, which cannot be retrieved, managed, processed, and sorted into more active information to help enterprises make business decisions in a reasonable time through mainstream software tools. "Big data" requires a new processing mode to have stronger decision-making power, insight and discovery power, and process optimization ability to adapt to a massive, high growth rate and diversified information assets. The strategic significance of big data technology lies not in mastering huge data information but in the professional processing of these meaningful data. In other words, if big data is compared to an industry, the key to the profitability of this industry lies in improving the "processing capacity" of data and realizing the "value-added" of data through "processing." Technically, big data cannot be processed by a single computer and must adopt distributed architecture. Its feature is that distributed data mining for massive data must rely on the distributed processing, distributed database, cloud storage, and virtualization technology of cloud computing. The system is divided into six layers, namely, application layer, decision layer, interface layer, analysis layer, data layer, and basic layer. The overall structure of the system is shown in Figure 1.

2.1. Hierarchical System Design. According to the overall structure of the college students' mental health intelligent evaluation system constructed above, the hierarchical design is carried out.

2.1.1. Based Layer. The basic layer of the system is the database software, dynamic environment, network environment, and hardware equipment necessary for the construction of the system and is also responsible for data collection, which is transferred to the data layer for storage.

2.1.2. Data Layer. The system data layer mainly includes mental health assessment database, expert team database, and student information database, which provides data support for the analysis layer.

The data layer also includes two parts: student information management module and online consulting module. Among them, the student information management module includes student registration and login and other related operations. Online psychological counseling services can be provided for students only after they log in successfully. After entering the function interface, students can view and modify personal information and other related operations. When the student information is modified, the system will immediately notify online teachers and students to contact. The online counseling module is mainly responsible for providing psychological counseling services for students. The system of psychological counseling for students is free of charge, and the main purpose of psychological counseling is to help students better understand themselves, at the same time to solve the students' mental health problems. In special cases, psychology teachers can also turn off the SMS notification function.

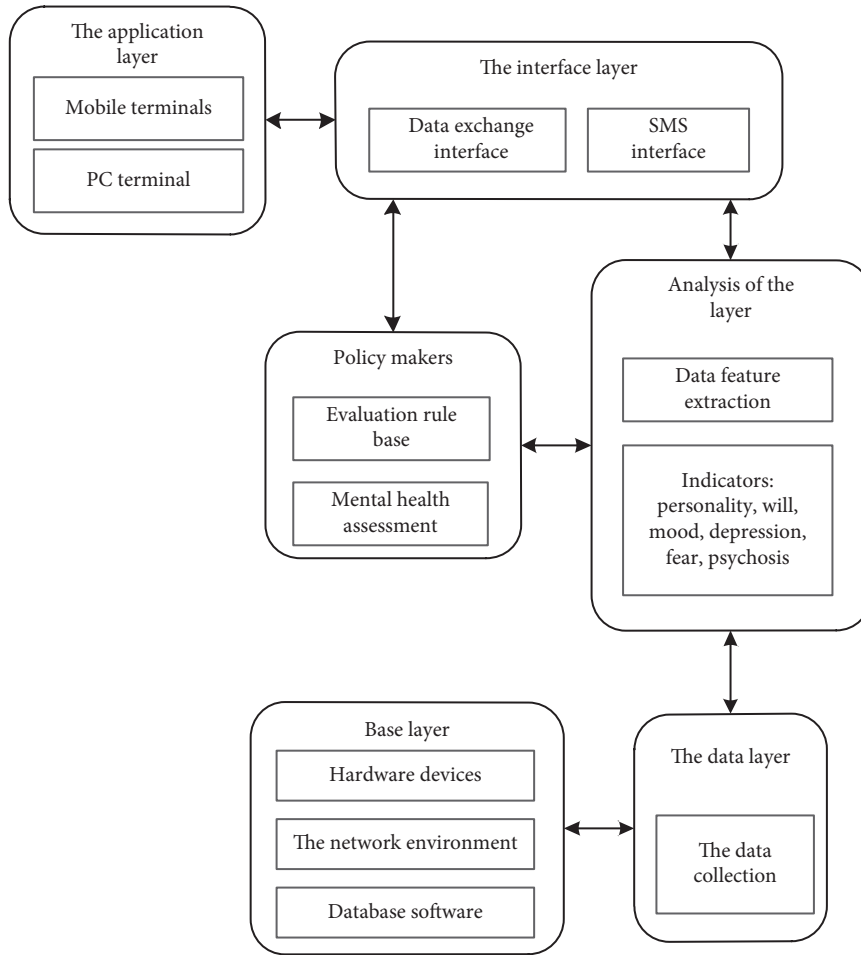


FIGURE 1: Overall structure diagram of intelligent evaluation system for college students' mental health.

2.1.3. *Analysis Layer.* The main work of the system analysis layer consists of two parts. One part is the classification of evaluation reference cases summarized based on existing evaluation results and the classification of mental health evaluation materials [10–12]. The other part of the work is to use big data technology as the basis to extract students' personality, emotions, preferences, and other characteristics.

The analysis layer includes two parts: psychological test module and psychological test topic management module. Among them, the psychological test module is the core module of the system, but also the functional module that students mainly use, which mainly contains the emotion test and social test submodules. According to the data results generated by the module, the mental health problems of college students are divided into three levels: serious, general, and potential psychological problems or no psychological problems, which correspond to the three levels of screening of the mental health intelligent evaluation system. The psychological test topic management module mainly manages the psychological test topic of the student mental health intelligent evaluation system. Among them, it mainly includes the operation of adding and deleting evaluation topics. Among them, the classification of topic types is completed by teachers, and the operation of adding and deleting psychological test topics is completed by administrators.

TABLE 1: Evaluate the field setting of the scale.

The serial number	The field name	The field type
1	Test topics	The integer
2	Content of the test	Character
3	Test time	The date type
4	The user information	The integer

2.1.4. *Policy Makers.* After the analysis, the results were transmitted to the decision-making layer of the system, which evaluated the mental health of college students based on the evaluation rule base and iterative optimization rules.

At the decision-making level, scale test and social software data analysis are combined to conduct research, and the scale test results include test topic, test content, test time, user information, and other contents. Field settings of the evaluation scale are shown in Table 1.

2.1.5. *Interface Layer.* The system interface layer has SMS interface and data exchange interface, which can be connected to the system for data exchange.

2.1.6. *Application Layer.* The application layer of the system feeds back the mental health evaluation results to the

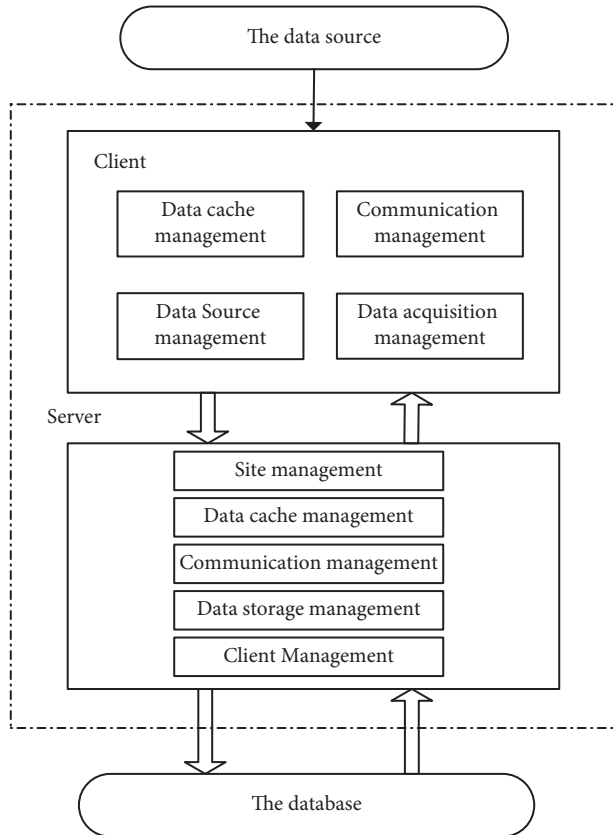


FIGURE 2: Structure diagram of data collection model for college students' mental health.

application layer through the interface layer and provides the evaluation results to college students through the mobile terminal or PC terminal.

2.2. Intelligent Evaluation Process Design

2.2.1. Mental Health Data Collection of College Students.

This study constructs a data collection model for college students' mental health based on the C/S architecture, and its overall structure is shown in Figure 2.

The server side uses the basic attributes of the measurement points to realize the mapping between the data source measurement points and the target measurement points and provides the client with the required information related to the mental health data of college students. In order to facilitate management and search, the attributes of measurement points are generally stored in real-time database, and the client can only save the copy without manual revision [13–15]. If the monitoring point configuration changes, the server will immediately push the modification information to the client and get the updated local copy.

Client management includes configuration management and real-time situation management. Configuration management can achieve rapid client basic information fusion, and real-time situation management can test the current client binding information, obtain the specific value of data link traffic, evaluate the client operating mode and form, and

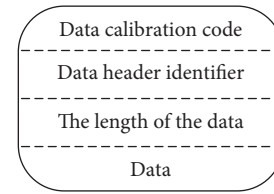


FIGURE 3: Schematic diagram of mental health packet pattern of college students.

monitor the network communication, and complete independent management. In the process of mental health data collection of college students, the server side uses the identification string to sort out the logical relationship between the measurement points and the client side [16–18].

The specific collection process is as follows:

Step 1: Configure preprocessing. Configuration preprocessing is the basis of mental health data collection of college students. Firstly, double calibration of data is carried out to remove the point data that is not available in the mental health data source, so as to prevent the inaccurate data collection caused by the difference between the server side and the data source of the measurement point category [19, 20]. In the preprocessing stage, select some attribute values to complete the mapping table reconstruction, which can enhance the search rate, reduce the packet length, and improve the transmission quality.

Step 2: Data transformation. After reading the current mental health data from the source database, three data transformations are performed according to the point configuration. Numerical quadratic transformation can deal with unit and reference value of metadata. The one-to-many transform can solve the problem of a single source measuring point responding to several target measuring points and maintain the completeness of data collection by using the transform process.

Step 3: Data transfer. The important function of the acquisition model is data transmission [21, 22]. In order to enhance the timeliness of data transmission, data transmission is processed from the following two perspectives in the system interface layer:

- The network link shall use the long connection mode. Due to the long distance between the data source and the target server, long connection is used for data transmission in order to obtain a faster transmission rate. If the amount of transmitted data is not large, periodically transmit heartbeat packets to keep the link stable and reduce network transmission disconnection due to timeout policies of routers and firewalls.
- Use of variable-length packets. According to the data packet header message, realize the data overall verification, subcontracting and analysis. The variable-length packet pattern is shown in Figure 3.
- The introduction of data caching in the transmission sector. Based on the collection characteristics

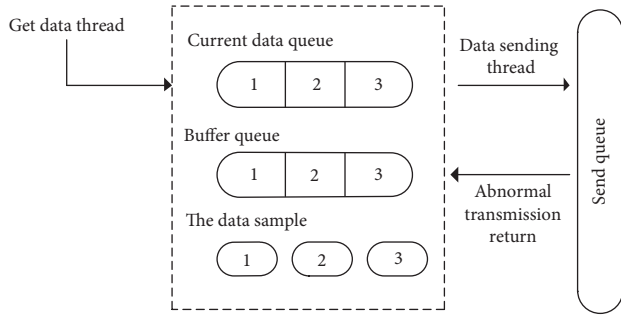


FIGURE 4: Data cache architecture diagram of college students' mental health.

of college students' mental health data, the data cache is substituted in the transmission plate. If the network fails in a short period of time, the data will be cached to the memory, and the system does not contain any running cost [23, 24]. If the collection model fails for a long time, the data will be saved in a local file to maintain the authenticity of the later collection results.

Figure 4 shows the data cache architecture of college students' mental health. In order to maintain the safety of college students' mental health data, thread-safe queues were used to reduce the correlation between functional plates of the model and achieve the goal of high-quality data collection when multifunctional plates of the model interact.

2.2.2. Feature Extraction and Fusion of College Students' Mental Health Data. The characteristics of college students' mental health mainly include behavioral characteristics, attribute characteristics, content characteristics, and social relationship characteristics, among which behavioral characteristics refer to the user's behavior on social network, including likes, comments, and online browsing traces. Attribute characteristics refer to the user's individual information, including name, age, gender, occupation, and hobbies. [25, 26]. Content features include users' chat content and posts on social software. Social relationship features refer to the interaction between users in the whole social network, which is manifested in the number of mutual attention and fans.

Firstly, the validity of the collected data information is inferred. If it is valid, the collected data information is converted into the data form directly processed by the system, which requires the introduction of the concept of time window to extract the mental health features of college students. The scale data and users' social network data are converted in batches, and different samples are divided. One sample corresponds to one window. The data in this time window are used to complete feature extraction, and the feature extraction results are classified and labeled. The time window selected here is 24 hours in order to obtain more comprehensive mental health data information of college students.

In order to further excavate the mental health state of college students and obtain more accurate psychological

characteristics of users, the multifeature fusion analysis is carried out on the mental health data of college students. The mental health data obtained from multiple channels are analyzed as a whole to provide a basis for intelligent evaluation.

Neural network is an effective nonlinear data fusion method, which can transform input space into hidden space and analyze data more conveniently in hidden space. Therefore, neural network has strong data processing ability, and meets the requirements of large-scale data processing and is suitable for multifeature fusion analysis.

Assuming that the transformation function used by the hidden layer in the neural network is Gaussian function, the radial basis function output by the first element is

$$F(i) = \exp\left(-\frac{\sum_{i=1}^n x_i - y_i}{2\partial^2}\right)^2, \quad (1)$$

where x_i represents the input quantity of mental health features of unit i , y_i represents the feature transformation quantity of unit i in the hidden layer, and ∂ represents the control parameter of unit i .

By inputting and extracting the characteristic data of college students' mental health and calculating the radial basis function according to the above formula, the multifeature fusion processing of college students' mental health data features can be realized.

2.2.3. Determine Evaluation Indicators. Scl-9 mental health measurement form is the standard for the evaluation of indicators in this study. The selected evaluation indicators are personality $I1$, willpower $I2$, emotion $I3$, depression $I4$, fear $I5$, and psychosis $I6$, and the target layer is mental health evaluation. The psychological test data of college students in a certain university in recent three years were collected, and 90 samples were randomly selected as mathematical model samples according to the scl-90 scale integral method. The statistical results are shown in Table 2.

2.2.4. Intelligent Evaluation of College Students' Mental Health. In this article, the mental health evaluation module in the decision-making layer of the system uses analytic hierarchy process to evaluate the mental health of college students. First, assign a value to the index weight and then complete the intelligent evaluation according to the index weight. The specific process is as follows:

Step 1: construct the judgment matrix model. Use 1–9 scaling and reciprocal measurement, and compare the importance of one indicator to another indicator pairwise, according to the comparison results to construct judgment matrix J .

Step 2: Use formula (2) to obtain the eigenroot solution of matrix J , and obtain the weight value of importance between the corresponding index of the same level and another index after normalization. Then, perform consistency test on the judgment matrix, and the process is as follows:

TABLE 2: Scl-90 scale score.

Evaluation indicators	The serial number					The mean	The variance
	1	2	3	...	90		
I1	1.44	1.77	1.45	...	1.21	1.55	0.59
I2	1.41	1.70	1.86	...	3.35	1.87	0.70
I3	1.67	1.10	1.40	...	2.90	1.90	0.71
I4	1.65	1.12	1.42	...	2.19	1.86	0.72
I5	1.11	1.85	1.27	...	2.25	1.55	0.55
I6	1.44	1.90	1.63	...	2.45	1.74	0.66

$$\sigma J = \mu_{\max} \sigma^{-1}, \quad (2)$$

σ and μ_{\max} represent eigenvectors and maximum eigenvalues, respectively.

In the implementation of consistency test, the critical index value C_I of each matrix should be calculated first, and the random consistency index R_I should be searched at the same time, and the random consistency C_R can be obtained through calculation:

$$C_R = \frac{C_I}{R_I}, \quad (3)$$

where C_I and R_I represent the consistency index and consistency ratio, respectively. When the value of C_R is less than or equal to 0.1, it is proved that the hierarchical single-sort structure has a relatively suitable consistency. When C_R value is greater than 0.1, the index value of the matrix needs to be obtained again:

$$\left\{ \begin{array}{l} \mu_{\max} = \sum_{j=1}^m \frac{(\sigma J)_j}{(\sigma J_j)} CI = \frac{R_{\max} - m}{m - 1}, \end{array} \right. \quad (4)$$

where m represents the dimension of the matrix.

Step 3: use expert evaluation method to calculate index weight. Experts score the indicators based on rules relating to mental health status. The results can avoid the subjective opinions in the expert reference opinions and have rationality and objectivity.

Assuming that there are k experts, k_I represents the scoring value of experts for each indicator, then the weight calculation formula of mental health evaluation indicators is as follows:

$$\omega_I = \sum_1^k \frac{k_I}{k}. \quad (5)$$

Step 4: construct independent factor evaluation matrix. Let the fuzzy subset of factor U_I be u_I , and obtain the membership degree of each evaluation index of mental health status through expert judgment method. When there are κ experts whose judgment grade of factor U_I is L_j , the evaluation matrix expression formula is as follows:

$$V = \frac{\kappa \times u_I \times L_I}{k}. \quad (6)$$

Step 5: Use the linear weighted sum of objectives to construct intelligent evaluation, and the process is as follows:

$$M = \sum_{I=1}^6 \frac{V \times P_I \times \omega_I}{k}. \quad (7)$$

where P_I represents the scoring value of item I . Input the extracted mental health feature data of college students, and calculate the target linear weighted sum according to the above formula, so as to realize multifeature fusion, further mine the mental health status of college students, obtain more accurate user psychological features, and conduct multifeature fusion analysis on the mental health data of college students. Analyze the mental health data obtained from multiple channels as a whole to provide basis for intelligent evaluation. The calculation process of target linear weighting sum is an effective nonlinear data fusion method, which can transform the input space into hidden layer space, and it is more convenient to analyze data in hidden layer space. Therefore, it has strong data processing ability, meets the needs of large-scale data processing, and is suitable for multifeature fusion analysis, so as to complete the design of College Students' mental health intelligent evaluation system.

3. Experiment and Result Analysis

In order to verify the practical application effect of the above designed intelligent evaluation system for college students' mental health based on big data, the source of mental health data of college students is the knowledge base of machine learning data set, which collects open datasets contributed by data scientists participating in machine learning projects; the following test process is designed.

3.1. Experimental Design. The simulation environment test system was built under MATLAB software. Experimental environmental parameters are shown in Table 3.

The experiment invited 50 students from the third grade of a university as the research object, including 25 boys and 25 girls. During the period of school, the experimental subjects generally have excellent academic performance and good comprehensive development.

First of all, preliminary validation is carried out to verify the quality of the system application indicators and the

TABLE 3: Experimental environmental parameters.

Parameter	The numerical
Runtime environment	Java 1.8
Server memory	16 GB
CPU	Intel Core i-2410 m
Programming language	Java
The hardware carrier	Fourth- and third-generation B raspberry pie

TABLE 4: The score of each index.

Evaluation indicators	Weight of indicators	Index scoring
I_1	0.4841	0.9460
I_2	0.1385	0.8643
I_3	0.0457	0.7120
I_4	0.0174	0.8325
I_5	0.2600	0.7605
I_6	0.1433	0.88326

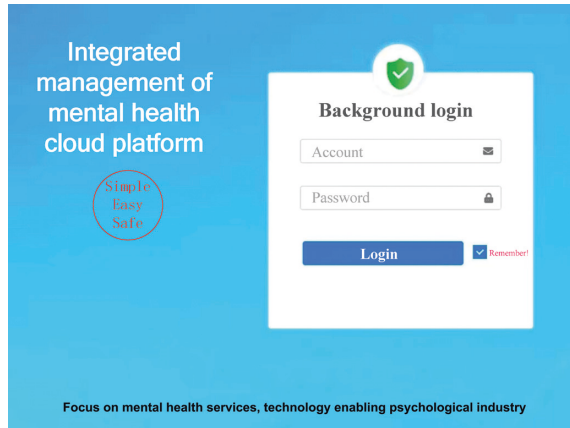


FIGURE 5: System login interface.

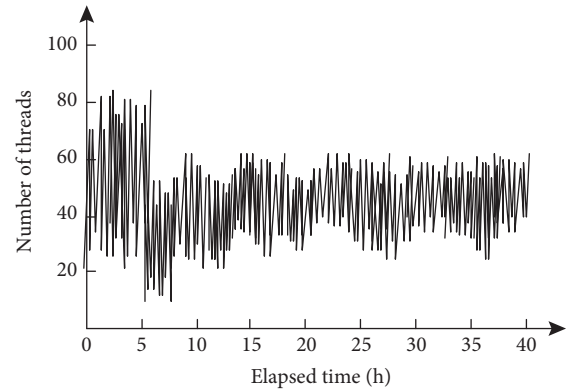


FIGURE 6: System stability test results.

stability of the system. Then, the woA-improved random forest college student mental health evaluation system in reference [7] and RFC college student mental health evaluation system based on the whale optimization algorithm in reference [8] are compared. Comparative verification was carried out from the three perspectives of data acquisition time of college students' mental health, data feature extraction accuracy, and recall rate of the evaluation results.

Finally, the system is applied to test the mental health of 50 students and comprehensively analyze the mental health of college students from the perspectives of social factors, family factors, and personal factors.

3.2. Test Analysis

3.2.1. Preliminary Verification. First, verify the quality of the system application index and the stability of the system. The system login interface is shown in Figure 5.

On the basis of assigning index weights, formula (4) is used to calculate the scores of each index, and the results are shown in Table 4.

As can be seen from Table 4, the calculation results of index scores are between 0 and 1. The score is divided into different grades: 0.9-1 is excellent, 0.8-0.9 is good, 0.7-0.8 is good, 0.6-0.7 is passing, and 0.6 is poor. It can be seen that all the indicators in the index layer have reached the good level, indicating that all the indicators are of the same importance to college students' mental health evaluation.

Then, the number of system running threads was used as an indicator to measure the stability of the system, and the system stability was tested. The results are shown in Figure 6.

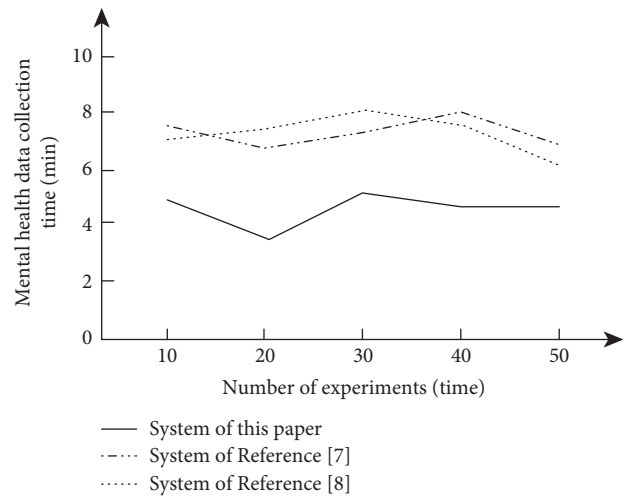


FIGURE 7: Comparison of mental health data collection time of different systems.

Analysis diagram 6 shows that with the increase in the system running time, the system thread count showed a trend of rise at first and then remained stable, and 15 hours before the system running, the system number of threads increases slowly, but the increase is not obvious, and when the system running time exceeds 15 hours, the number of system running threads always stays within the range (20, 60). It can be seen that the number of threads is stable and the running state of the system is always stable.

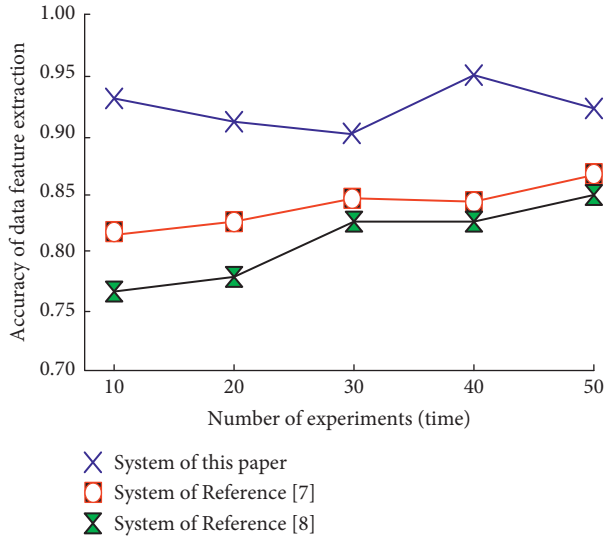


FIGURE 8: Statistical graph of data feature extraction accuracy of different systems.

3.2.2. *Comparison Verification.* Firstly, the mental health data acquisition time of different systems was tested, and the results are shown in Figure 7.

According to the results shown in Figure 7, with the increase in the number of experiments, the mental health data acquisition time of different systems also changes. The acquisition time of system of reference [8] rises first and then decreases, and the global maximum value is 8.1 min. The acquisition time of system of reference [7] fluctuates frequently, and the global maximum value is 7.9 min. In contrast, the collection time of system of this article is less, which is always less than 6 minutes, indicating that the timeliness of system of this article is higher.

Then, the accuracy of data feature extraction is taken as the index to verify the reliability of different systems, and the results are shown in Figure 8.

By analyzing the results shown in Figure 8, it can be seen that when the number of experiments is 50, the data feature extraction accuracy of reference [7] system and reference [8] system reaches their maximum. When the number of experiments is 40, the accuracy of data feature extraction of this system reaches the global maximum, which can reach 0.95. It can be seen that the data feature extraction accuracy of this system is higher, which shows that the reliability of this system is higher.

Finally, the recall rate of evaluation results of different systems was tested, as shown in Figure 9.

By analyzing the results in Figure 9, it can be seen that with the increase in the number of experiments, the recall rate of evaluation results of different systems shows a downward trend. After more than 30 experiments, the recall rate of the evaluation results of the system in this article is gradually stable, while the two comparison systems do not show a stable trend of data, and the recall rate of the evaluation results of the system in this article is always higher than that of the two comparison systems, indicating that the method in this article is more effective.

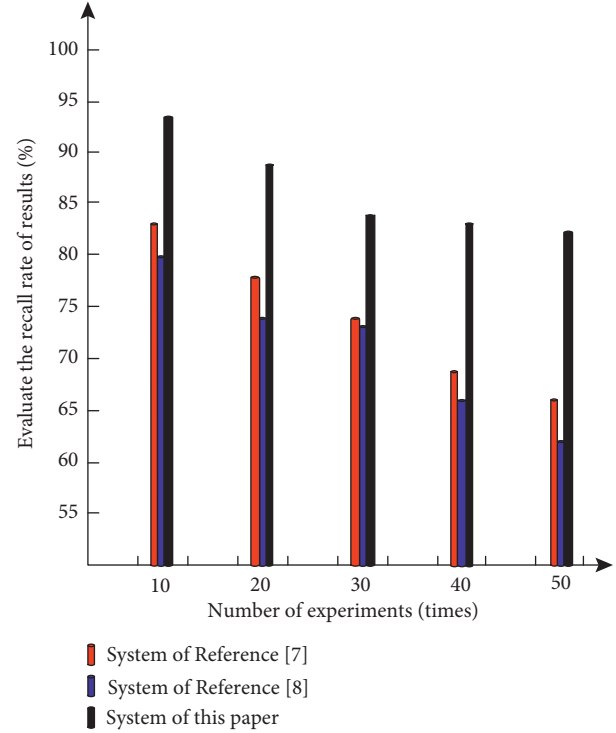


FIGURE 9: Comparison diagram of recall rate of evaluation results of different systems.

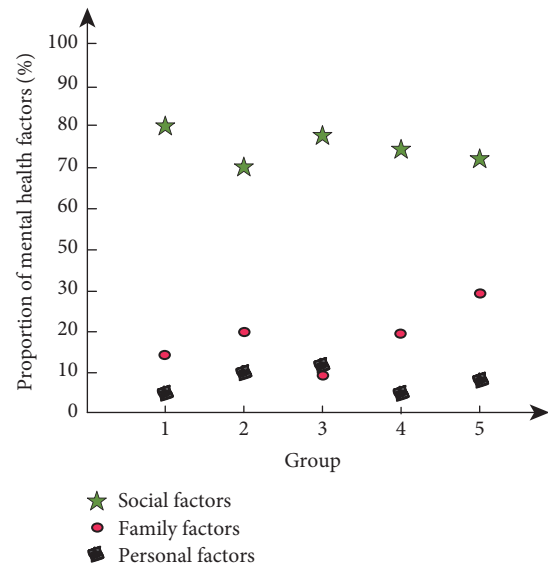


FIGURE 10: Mental health assessment and analysis.

3.2.3. *The Practical Application.* Fifty students were divided into groups on average, and the mental health status of 50 students was tested by using the system of this article. The proportion of factors leading to mental health status of students in each group was tested from the perspectives of social factors, family factors, and personal factors, and the mental health status of college students was comprehensively analyzed, as shown in Figure 10.

As can be seen from Figure 10, among the test results of the mental health status of the 5 groups of students, the

primary factors affecting their mental health status are social factors, followed by family factors and personal factors. Among the students in the third group, the family factors are lower than the personal factors, which is due to the difference of test subjects. In the five groups of assessment, social factors accounted for more than 70%, and family factors accounted for the highest proportion of about 32%; it can be seen that the social environment and small family environment are the main factors affecting students' mental health status, and compared with social and family factors, personal factors accounted for a relatively small.

To sum up, the designed intelligent evaluation system of college students' mental health based on big data has good performance, all indicators in the index layer reach a good level, and all indicators have the same importance to the evaluation of college students' mental health. In this article, the number of threads is stable when the system is running, and the running state of the system always remains stable. The acquisition time is less, which is always kept below 6 min, and the timeliness is higher. The data feature extraction of this system has higher accuracy and reliability. Social environment and family environment are the main factors affecting students' mental health. Compared with social factors and family factors, personal factors account for a relatively small proportion.

4. Conclusion

In order to provide effective data support for college students' mental health project, this study designed an intelligent evaluation system for college students' mental health based on big data.

Based on big data technology, the system of this article builds an intelligent evaluation system for college students' mental health on the basis of designing six layers: application layer, decision layer, interface layer, analysis layer, data layer, and basic layer. Then, based on the C/S framework, the mental health data of college students are collected and the data characteristics are extracted. Secondly, six evaluation indexes—personality, will, emotion, depression, fear, and psychosis—were screened, respectively, and then, the intelligence evaluation was completed according to the index weight.

In the experiment, the quality of the application index of the system is good and the stability of the system is high. After comparison and verification, it is found that the mental health data acquisition time of the system is less, the accuracy of data feature extraction and the recall rate of evaluation results are higher. Finally, a comprehensive analysis of the mental health of college students is made with the practical application of the system of this article.

Data Availability

The raw data supporting the conclusions of this article can be obtained from the corresponding author upon request.

Conflicts of Interest

The authors declared that they have no conflicts of interest regarding this work.

References

- [1] Y. Zou, "Intelligent evaluation of college students' mental health based on grey clustering algorithm," *Computer and Digital Engineering*, vol. 49, no. 12, pp. 2562–2567, 2021.
- [2] S. North, "Addressing students' mental health needs via telehealth," *North Carolina Medical Journal*, vol. 81, no. 2, pp. 112–113, 2020.
- [3] L. Gu and R. Lu, "An exploration of college students' mental health education model based on APP Platform," *Journal of Huainan Vocational & Technical College*, vol. 18, no. 04, pp. 41–42, 2018.
- [4] Li Gao, "Big Data-driven mental health evaluation model of college students," *Information & Technology*, no. 01, pp. 32–36+43, 2022.
- [5] X. Yang, M. Jin, and L. Zheng, "A predictive model of the influence of life stressors on mental health of college students," *China Journal of Health Psychology*, vol. 26, no. 05, pp. 775–778, 2018.
- [6] Q. Y. Fang, *Personality Characteristics, Mental Health, Self-Efficacy and Related Research of Drug Addicts in Compulsory Isolation in Chongqing*, PLA Army Military Medical University, Beijing, 2020.
- [7] Y. W. Huang, *Research on Ecg Identification Method Based on Feature Learning and Multi-Feature Fusion*, Shandong University, Jinan city Shandong Province, 2021.
- [8] F. Li, M. Jin, and Y. Wang, "Research on mental health evaluation of RFC college students based on whale optimization algorithm," *Modern Scientific Instruments*, vol. 38, no. 1, pp. 5–9, 2021.
- [9] C. Ran, "Mental health evaluation model for university students based on VPMCD," *Bulletin of Science and Technology*, vol. 35, no. 07, pp. 218–221+226, 2019.
- [10] F. Yang and B. Zhou, "Research on mental health intelligent evaluation based on decision tree algorithm," *Modern Electronics Technique*, vol. 44, no. 13, pp. 135–139, 2021.
- [11] Z. Wang, Q. Peng, Y. Chen, and Z. Guo, "Analyzing the influencing factors of mental health among college students under the COVID - 19 epidemics based on random forest model," *The Chinese Health Service Management*, vol. 39, no. 03, pp. 215–220, 2022.
- [12] X. Chen, B. Zhang, and Y. Zhao, "College students' mobile phone addiction and personality characteristics, the relationship between mental health," *Journal of Guangxi college of education*, vol. 5, no. 5, pp. 112–117, 2021.
- [13] S. I. Yang, *Research on Physical and Mental Health Assessment Method Based on Multi-Sensory Feature Fusion of Wearable Bracelet*, University of Electronic Science and Technology of China, Chengdu, Sichuan, 2020.
- [14] J. Zhang and L. Liang, "Performance optimization of mental health online assessment system based on time-division design for high concurrent users," *Computer Engineering & Software*, vol. 41, no. 09, pp. 204–206, 2020.
- [15] X. Zhou and M. I. E. Lin, "Design of mental health intelligence evaluation system based on big data technology," *Modern Electronics Technique*, vol. 44, no. 14, pp. 95–99, 2021.
- [16] Q.-ji Zhang and T. Y. Man, "Research on the relationship between personality, mental health and life satisfaction of

- college students with suicidal ideation,” *Science and Education Guide (The first ten-day)*, vol. 19, no. 13, pp. 245-246, 2013.
- [17] L. Xu and H. Shi, “Research on the relationship between employee satisfaction and personality characteristics,” *Chinese journal of health psychology*, vol. 20, no. 07, pp. 997-999, 2012.
- [18] D. Liu and J. Peng, “Design and research of WeChat small program for college students’ mental health test,” *Computer Engineering & Software*, vol. 41, no. 12, pp. 39-41, 2020.
- [19] T. Wang and J. Park, “Design and implementation of intelligent sports training system for college students’ mental health education,” *Frontiers in Psychology*, vol. 12, no. 2, pp. 978-988, 2021.
- [20] S. Williamson, L. Packel, L. Hunter, S. Facente, M. De Zuzuarregui, and Y. Li, “Impacts of COVID-19: a longitudinal study on university students mental health during the COVID-19 pandemic,” *Journal of Depression & Anxiety*, vol. 10, no. 11, pp. 1-5, 2021.
- [21] Q. Marine, P. Aude, E. Pereira, T. Christophe, G. Juan Luis, and M. Ilaria, “An interactive video increasing French students’ mental health literacy: a mixed-methods randomized controlled pilot study,” *Health Promotion International*, vol. 56, no. 12, pp. 325-337, 2021.
- [22] L. I. Li Zhang, “Research on reading therapy of College students’ mental health and ideological and political education under the situation of COVID-19 -- based on the survey of reading promotion activities of some college libraries in China,” *Journal of north China university of technology (social science edition)*, vol. 22, no. 02, pp. 49-55, 2022.
- [23] Y. Li and L. I. Fei, “Based on feature fusion of college students’ mental health intelligent evaluation system design,” *Journal of modern electronic technology*, vol. 44, no. 18, pp. 149-152, 2021.
- [24] Y. Liu, “Research on the innovative path of College students’ mental health Education from the perspective of positive psychology,” *Journal of Urumqi Vocational University*, vol. 31, no. 01, pp. 57-60, 2022.
- [25] P. Wang, K. Wu, and J. Zhou, “Design and implementation of Web-based psychological evaluation system,” *Chinese Medical Equipment Journal*, vol. 42, no. 10, pp. 30-34, 2021.
- [26] L. Ha, L. Yan, Q. Li, and Y. Wang, “Course education under the background of college students’ mental health education curriculum reform empirical study,” *Journal of medical education management*, vol. 8, no. 02, pp. 150-155, 2022.

Research Article

Innovation and Integration Development of the Cultural Industry Based on Mapping Knowledge Domains

Jiangong Lian ¹ and Dan Liang²

¹School of Tourism, Henan University of Animal Husbandry and Economy, Zhengzhou 450006, Henan, China

²School of Geography and Tourism, Zhengzhou Normal University, Henan, Zhengzhou 450044, China

Correspondence should be addressed to Jiangong Lian; 81768@hnuah.edu.cn

Received 24 May 2022; Revised 15 June 2022; Accepted 20 June 2022; Published 9 July 2022

Academic Editor: Le Sun

Copyright © 2022 Jiangong Lian and Dan Liang. This is an open access article distributed under the Creative Commons Attribution License, which permits unrestricted use, distribution, and reproduction in any medium, provided the original work is properly cited.

In view of the less current user data of the cultural industry, its classification and presentation form are complex. This paper constructs the MKD of the cultural industry integration through the RDF graph model and realizes the distributed vector representation of cultural project semantic information by using the fine-tuning translation distance model TransH. The semantic information of cultural industry fusion is mapped to a continuous vector space, and the distributed vector representation of cultural projects is realized. The results show that it is helpful to accurately express the correlation between different regions and cultural types and to explore the data association and implicit relationship of innovation and integration development in the cultural industry.

1. Introduction

Artificial intelligence should support the development and growth of cultural operators, enhance innovation function, accumulate innovation value, promote cultural products and related services to take on a new look, and fully display its cultural connotation, so as to realize the good dissemination of the mainstream value. The massive accumulation of cultural big data and the development of algorithms are the technical basis of the advanced AI cultural industry. It is the increasing amount of data provided by the big data industry that makes deep learning algorithms possible and brings the application and development of computer vision, voice technology, natural language processing, and planning decision systems in the field of the cultural industry.

The integration development of the cultural industry includes the realization of cultural knowledge inheritance and the dissemination of cultural knowledge on this basis. Therefore, how to use digital technology to promote the inheritance and dissemination of the cultural industry has become the key. However, there are still some problems in the digital development of China's cultural industry. First of all, cultural knowledge inheritance aims to realize the

continuity of knowledge, and the emphasis is on the standardization and integrity of knowledge organization. However, the existing organization of cultural knowledge still stays in the single-line organization mode based on a certain feature, and the internal relevance and complexity of the cultural industry have not been effectively described [1, 2]. Therefore, organizing the cultural industry to realize its standardized description and revealing the relevance and complexity of industries have become the primary problems to be solved in the integration and development of the cultural industry; second, the change of technology has changed the communication environment. The birth of media technology has reshaped the existing communication environment, and the traditional mode of communication has gradually declined; the innovation of the cultural industry has to comply with the development of technology and the needs of users, make good use of the relationship between the cultural industry and users, find effective ways of communication, and build a bridge between users [3].

In recent years, mapping knowledge domains (MKDs) have been favored by researchers in various fields for its advantages of extensive data collection, comprehensive knowledge coverage, quantitative analysis macro, and data

graphic visualization. With regard to the development of the cultural industry, the relevant research has a long history, a large number of studies, and a wide range of achievements, which has a strong practical value and theoretical significance to objectively and comprehensively show the historical context of the development of the cultural industry, focus on research hotspots, explore the future development trend, and optimize the protection path.

2. Related Works

2.1. MKD. MKD is a technology that presents the relationship between knowledge in a graphical way, which is widely used in the field of culture, mainly focusing on ontology and semantic relations. The national network cultural heritage advocacy organization of the United States specializes in the digital construction of intangible cultures, such as semantic information architecture, semantic relations, keyword index presentation, and digital reconstruction of cultural content [4]. The European digital museum has earlier adopted the semantic web technology to unify the information resources of different institutions and metadata standards through the semantic association between scattered and heterogeneous digital cultural resources, which has become an important European cultural resource platform [5]. Lamborao et al. [6] proposed to use RDF technology of MKD to code and classify Italian cultural resources, and finally use SPARQL language to query and retrieve the association between various cultural industries.

According to the classification and presentation of different cultural industries, researchers focus on the digitization of cultural industries and semantic relations. Sun [7] used knowledge representation, knowledge engineering, and other technologies to construct a knowledge framework model of folk dance, providing a reference for the digital protection of folk dance. By combing the application status of MKD, it is found that resource integration based on linked data is applied in the fields of network information resources, digital libraries, etc., showing a trend from theoretical research to applied research, and a large number of practical projects appear [8]. At present, the construction and application of cultural industry digitization is rich, mainly in ontology, semantic relationship, data association, resource aggregation, and so on. Besides, it is a hot topic in the research of MKD to establish related data by using semantic relation and making it a part of ontology construction. Few researches based on MKD focus on digital human semantic web and data association construction, while there is a lack of deep understanding and application of knowledge and services in the field of culture. The construction of MKD is an important part of the presentation of digital resources in the cultural industry, which involves not only semantic knowledge analysis, expression framework design, and knowledge representation methods but also complex links such as character relationship presentation and knowledge reasoning.

2.2. Recommendation Algorithm Based on MKD. In recent years, as a knowledge network containing a large number of

entities and the relationships between entities, the MKD can discover rich relationships between objects or users, and enhance the semantic information of data. It has important research significance for some recommendation algorithms that need semantic information of items and users. Literature [9, 10] shows a kind of embedding method, which can map the entities in the MKD and the relationship between them to the low dimensional vector space, and take the learned entities or relationship vectors with semantic information as the knowledge representation of the original objects. Literature [11] regards MKD as a heterogeneous information network to assist in the construction of a recommendation system by constructing a metagraph. The feature of a meta graph is that only one start node and one end node are required, and the middle structure is not constrained. Therefore, more complex semantic information can be integrated into the recommendation problem to fully mine the item information. Path-based approaches can use MKD in a more intuitive way, but they rely heavily on manually designed meta paths or meta graphs, whereas domain knowledge is usually required to define the type and the number of meta paths, which is difficult to tune in practice [12]. According to the literature [13], most of the previous recommendation studies only considered a single relationship type, but in fact, in many cases, the recommendation problem exists in the scenario of heterogeneous information networks.

At present, most of the recommendation algorithms based on the MKD are based on the existing recommendation algorithms. While the integration of the cultural industry is in the development stage, the available user data is less. Therefore, in this paper, the semantic information of cultural industry fusion is mapped to a continuous vector space to realize the distributed vector representation of cultural projects. In addition, the accuracy of the representation vector of the cultural projects is verified by link prediction.

3. Construction of Cultural Industry Integration MKD

This paper starts from the content, type, and presentation of cultural industry information, and follows the logic from knowledge construction, knowledge storage, knowledge management to knowledge application, and constructs a cultural knowledge base characterized by regional distribution, so as to solve the problems of low coupling, weak relevance, low response, and high delay of cultural industry digital resources. The construction framework is shown in Figure 1. In terms of semantic search, RDF is used as the description framework to describe resource entities and attributes, reveal their semantic relations, and form data association of the cultural industry, which is convenient for network retrieval and digital dissemination.

3.1. Knowledge Construction. As shown in Figure 2, there are mainly unstructured, structured, and semi-structured data of cultural industry integration.

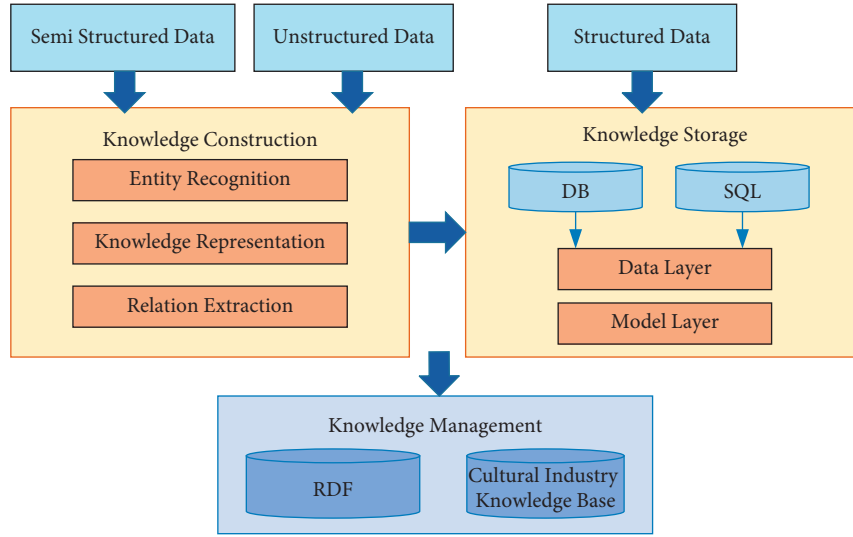


FIGURE 1: Construction of the MKD framework.

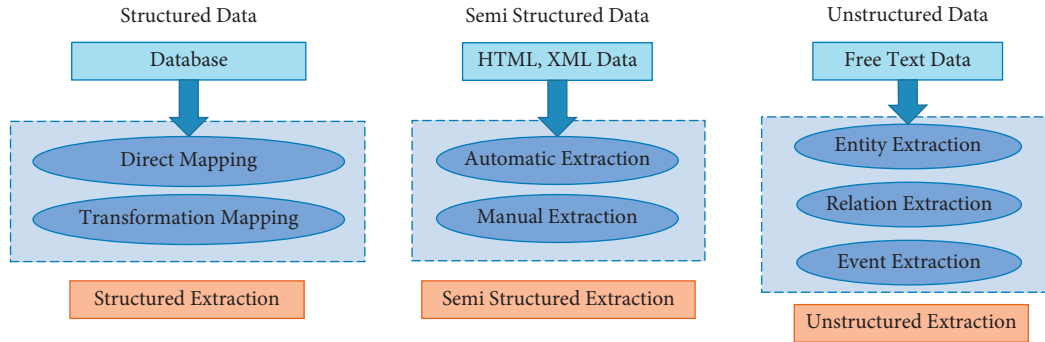


FIGURE 2: Integration data of the cultural industry.

Structured data itself already exists in the database, and its knowledge organization computer can identify and extract it easily. It only needs to directly map or transform the knowledge in relational data to RDF data. The semi-structured data from web pages and tags do not conform to the rules. Unstructured extraction is to extract knowledge from free text, including the following three modules: entity, relationship, and event. The extraction process is mainly based on the existing annotation rules and knowledge base, which is the most difficult among the three data sources; noise and error may exist in data collection, text processing, entity extraction, and relationship extraction, which seriously affect the accuracy of knowledge acquisition. The purpose of entity extraction is to extract entity information from the analysis text of the cultural industry, such as project name, inheritor, region, time, and cultural category. When dealing with unstructured data, API interface technology is used to allow users to extract text information entities and relationships according to rules, so as to ensure the accuracy of the construction of the cultural industry MKD.

In the knowledge base, the relationship name is single, while the corresponding relation language expression in the network resources is diverse. The accuracy of relation extraction will be reduced if the relation is matched directly,

and the introduction of relation keywords can solve this problem well, where the optimization of classifier corpus is different from manual annotation, which often leads to omissions or errors, and it can only be used for simple MKD relationship extraction. Classifier corpus optimization is used to set the tagged corpus as a positive example, and set the unlabeled corpus as a negative example. According to this algorithm, the final text classification is completed. In the classifier model, conditional probability is the key to relation extraction, as shown in the following formula:

$$P(x | y) = \frac{1}{Z(x)} \exp \left[\sum_{i=1}^k \lambda_i f_i(x, y) \right], \quad (1)$$

where x is the context, y is the keyword label, $Z(x)$ is the normalization factor, λ_i is the weight of the equation, and $f_i(x, y)$ is the characteristic equation. In relational extraction, it is 1 when x and y meet the conditions, and 0 otherwise.

Event extraction mainly refers to extracting the event information that users are concerned about from natural text and presenting it in a structured form, which includes meta-event extraction and topic-event extraction. Topic events refer to certain core events and related activities. For

example, for a certain cultural industry project, we can get its cultural industry name, inheritor, region, heritage category, and other information from the cultural industry text library. Event extraction can collect relevant information from unstructured text data to achieve a complete description of entities. Meta event refers to the occurrence or state change of action, involving time, place, and participants.

3.2. Knowledge Storage. In the graph database storage, the cultural industry data is huge, so it is necessary to build a graph database framework which can access the data efficiently to improve the efficiency of MKD storage. There is a big difference between graph database storage and traditional database storage; traditional database storage needs to consider the dynamic read-write operation of data, while the storage of MKD is based on triples, and the information of triples exists in the form of subject, predicate, and object, and its data organization is fragmented and flexible. It is necessary to consider the cost of data storage, such as fast access to data and data storage graph. When the data scale is large, distributed storage can be used to improve the scalability of the storage system. In distributed storage, each RDF data node is distributed and relatively independent. Therefore, there are two ways to store the MKD of the cultural industry: attribute storage and graph data storage. In the distributed environment, based on the data structure of MKD, attribute storage is used to manage the relationship between data and reduce the number of self-joins, which has high efficiency. In the graph data storage, RDF data is stored in a three-column structure table that corresponds to the subject, predicate, and object data of the triple. When a user makes a query request, the system will make multiple self-joins in the triple table to get the user search results. Efficient MKD storage architecture includes a data layer and a model layer, as shown in Figure 3.

In the MKD, different entity types are stored in a block mode, and the undefined objects are treated by the feature clustering method and are classified into similar semantic types. The stored procedure of the graph database follows the principle of unified semantic relationship and centralized storage, that is, the same storage structure is used to process different types of data, and different database query languages are compatible in semantic search.

In the triple, the nodes and edges are labeled to show the semantic association of MKD. The definition of the RDF graph model is as follows: assuming U , B , and L are the uniform resource identifier, empty node, and literal of the finite set, respectively, while each RDF triple $(S, P, O) \in (U \cap B) \times U \times (U \cup B \cup L)$ is a declarative sentence, where S is the subject, P is the predicate, and O is the object, then (S, P, O) represents the attribute of resource S , and P takes the value of O .

In the RDF graph model, the ellipse represents an entity, the rectangle represents an attribute value, and the edge represents a triple predicate. Taking the inheritance of music culture and industrial integration in ethnic areas as an example, the triple (Changyang folk song, cultural category,

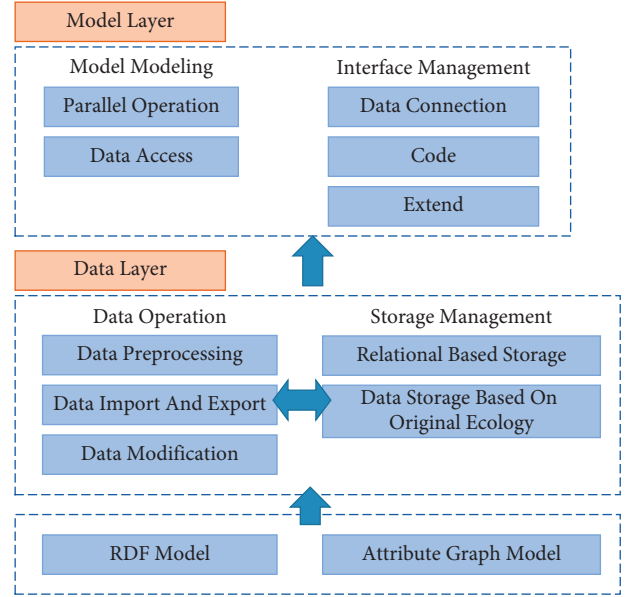


FIGURE 3: Data storage model.

and traditional music) indicates that the heritage category of the Changyang folk song is traditional music. The Changyang folk song belongs to Changyang Tujia Autonomous County. However, information on the specific declaration area cannot be obtained. In fact, the edge attributes represented by the RDF graph model are not clear, so it is necessary to introduce extra points to represent the whole triple, and the original edge attributes are represented as new triples.

As shown in Figure 4, Dec_area is introduced in this paper for Changyang folk song, declaration area, and Changyang Tujia Autonomous County, using three elements of the triple RDF: subject and RDF; predicate and RDF; object. In this way, a new triplet is formed, whose set form is as follows: $G = ((Dec_area, RDF: subject, Changyang folk song), (Dec_area, RDF: predicate, declaration area), (Dec_area, RDF: object, Changyang Tujia Autonomous County))$

The RDF graph model is a special directed tag graph. In this paper, we use these tag graphs to connect all resources to form a large-scale MKD of the cultural industry. In the label graph, the predicate of a triple can also be the subject or object of another triple, which is mapped in the data label graph.

4. Recommendation Algorithm Based on MKD

The basic idea of the recommendation algorithm based on the MKD of cultural industry projects is that on the basis of the MKD of cultural industry projects constructed in the previous chapter, through the use of TransH (translation on hyperplanes), the distributed vector representation containing semantic information of cultural industry projects is learned, and the historical behavior data of users are used to calculate and compare with the cultural industry projects; finally, a top-N recommendation list is generated according

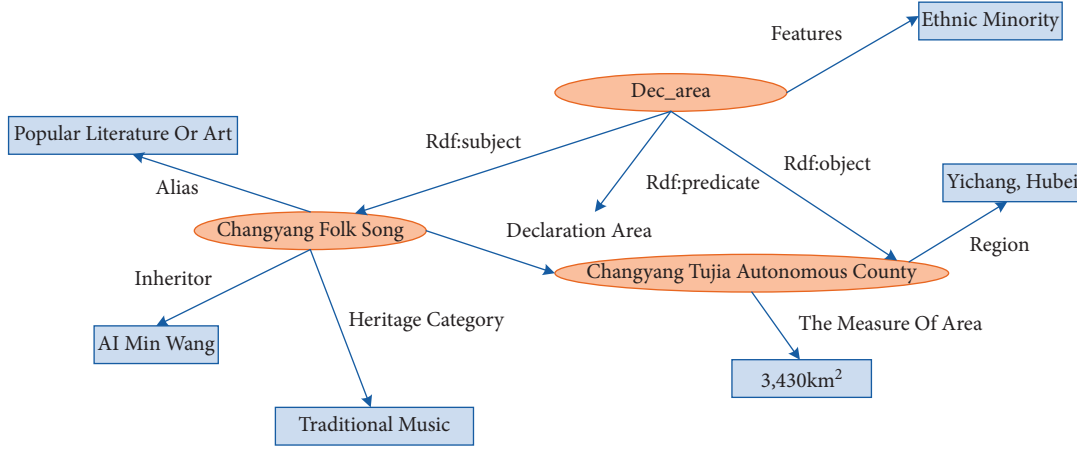


FIGURE 4: RDF edge attribute of Changyang folk song.

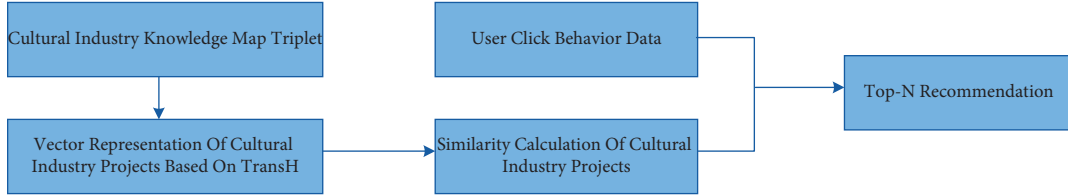


FIGURE 5: Recommendation algorithm flow.

to the calculated similarity. The specific algorithm flow is shown in Figure 5.

4.1. Scoring Function. The main purpose of knowledge representation learning in MKD is to embed the semantic information of the research object into the low-dimensional vector space, and express it as a dense low-dimensional real value vector, so as to pave the way for the subsequent semantic similarity calculation and recommendation operation. The TransH algorithm is adopted after fine-tuning to train, and the project of cultural industry integration is expressed by vectorization.

The head entity h and tail entity t are projected onto the hyperplane determined by the normal vector Wr to obtain vectors h_{\perp} and t_{\perp} . On this hyperplane, there exists a relation to represent the vector dr . After training, equation (2) can be satisfied:

$$h_{\perp} + d_r = t_{\perp}. \quad (2)$$

In TransH, a scoring function is defined to measure the accuracy of the mapping entity vector and relation vector in triple.

$$f_r(h, t) = h_{\perp} + d_r - t_{\perp}^2. \quad (3)$$

Through constraints $\|Wr\| = 1$, there are

$$h_{\perp} = h - w_r^T h w_r, t_{\perp} = t - w_r^T t w_r. \quad (4)$$

The modified scoring function can be obtained as follows:

$$f_r(h, t) = (h - w_r^T h w_r) + d_r - (t - w_r^T t w_r)^2. \quad (5)$$

4.2. Objective Function. For the above scoring function of a single triplet, we define the margin-based ranking loss (formula (6)) as the objective function of model training

$$\mathcal{L} = \sum_{(h,r,t) \in \Delta} \sum_{(h',r',t') \in \Delta'} [f_r(h, t) + \gamma - f_r(h', t')]_+. \quad (6)$$

In the objective function, $[x]_+ \triangleq \max(0, x)$ is a hinge loss function, which can avoid the negative loss value and lead to failure of convergence, Δ is the collection of positive example triples in the MKD of cultural industry projects, Δ' is a set of negative example triples formed by randomly replacing the head entity or tail entity of a positive example triple, and γ is the distance between the positive and negative triples.

When minimizing the loss value, the following constraints (formula (7)–(9)) should be considered:

$$\forall e \in E, \|e\|_2 \leq 1, // \text{scale}, \quad (7)$$

$$\forall r \in R, \left| \frac{w_r^T d_r}{d_{r2}} \right| \leq \epsilon, // \text{orthogonal}, \quad (8)$$

$$\forall r \in R, w_{r2} = 1, // \text{unit normal vector}, \quad (9)$$

where formula (7) ensures that the vectors of all entities are normalized; formula (8) is used to ensure that the normal vector Wr and the relation vector dr are orthogonal and

perpendicular, and dr is on the hyperplane; formula (9) guarantees that the modulus of the normal vector is 1.

The loss function is converted into the following unconstrained loss function by using soft constraint:

$$\mathcal{L} = \sum_{(h,r,t) \in \Delta} \sum_{(h',r',t') \in \Delta'} \sum_{(h,r,t)} [f_r(h,t) + \gamma - f_r(h',t')]_+ + C \left\{ \sum_{e \in E} [\|e\|_2^2 - 1]_+ + \left[\sum_{r \in R} \frac{(w_r^T d_r)^2}{d_r^2} - \epsilon^2 \right]_+ \right\}, \quad (10)$$

where C is a super parameter of weighted soft constraint importance.

5. Experiment and Analysis

5.1. Model Training. Based on the abovementioned objective function, this paper uses the adaptive moment estimation (Adam) optimization algorithm to train the cultural industry triples, update the model parameters, and keep a single learning rate different from the traditional random gradient descent. The Adam algorithm introduces a momentum factor, where independent adaptive learning rates are calculated for different parameters by calculating the first and second moment estimates of the gradient, which accelerates the convergence of the loss function [14]. When the loss function converges or reaches the maximum number of iterations, the training ends and the distributed representation vectors of entities and relationships in the MKD are obtained. The steps of the algorithm are as follows:

Step 1. Initialize and normalize the entity and relation vectors

Step 2. Select batch training data of m in training set S

Step 3. the current loss function gradient $\alpha L/\alpha\theta$ was and multiply it by the learning rate ϵ to obtain the current gradient descent distance to update model parameters, $\theta = \theta - \epsilon \cdot \alpha L/\alpha\theta$

Step 4. Repeat Step 3 until the maximum number of iterations is reached, stop traversing the sample, and output model parameter values, entity, and relationship vectors.

5.1.1. Experimental Data. From the MKD of the cultural industry project, the data set of the relationship between various industries is derived, and the abovementioned model is used for training. There are three tables in the dataset: entity table, relation table, and triple table. Among them, the entity table contains MKD class of the cultural industry, some data attributes, and a generated unique ID. There are 700 entities, including 493 cultural project entities, 106 regional entities, 61 project type entities, and 5 ethnic attribute entities. The relationship between the ID and the unique relationship includes the type of relationship generated by the set. In addition, 4781 groups of triples are in the

triple table, which are divided into a training set, verification set, and test set according to the ratio of 8:1:1.

5.1.2. Evaluation Index. In this paper, the method of link prediction is used to evaluate the effect of model training. A triplet is broken into incomplete triples, and each entity is used to fill in the vacancy, then, a new triplet is reconstructed. The score of the triplet is calculated by using the scoring function. The correct triplet is sorted according to the score that is based on the ranking results, and two evaluation criteria are used to evaluate the effectiveness of model training: MeanRank (average ranking of correct triples) and Hits10 (the probability that the correct triples are in the top 10 bits).

5.1.3. Results and Discussion. In order to make the TransH model perform better, we set different values for the parameters in the model. The initial learning rate of the Adam algorithm is set to 0.001, the batch size of single batch data is selected in {8, 12, 16}, γ is {0.25, 0.5, 1}, and the iteration times of each experiment are 50. Many experiments show that when the batch size is equal to 12, γ of 1 is a better choice. The experimental results of the model in different entity embedding dimensions are shown in Figure 6.

As shown in Figure 6, the evaluation index of MeanRank under different dimensions generally shows a trend of high on both sides and low in the middle. With the increase of dimensions, when the dimension is in 20 dimensions, the best accurate value is obtained, and the average rank of correct triples reaches 22.43.

As shown in Figure 7, the Hit10 under different dimensions tends to be low on the left and high on the right. When the embedded dimension is set to 10, the value of Hit10 is the lowest. With the increase of the dimension, when the dimension is 30, the most accurate index value is obtained. At this time, the Hit10 reaches 67.78%, indicating that the average probability of correct triples ranking in the top 10 is 67.78%.

To sum up, when embedded in the vector space with dimensions between 20 and 30, the evaluation indexes of MeanRank and Hit10 perform best, which realizes the accurate embedding of the entity vector and the relation vector of MKD of cultural industry projects. In this paper, the 30 embedded dimension is selected to train the representation vector containing semantic information of cultural industry projects, which provides the following recommendation algorithm based on the MKD of the cultural industry.

5.2. Effectiveness of the Recommendation Algorithm. Formula (11) is used to calculate the similarity P_{ui} between the cultural industry i and industry j :

$$P_{ui} = \sum_{j \in C(u) \cap S(i,k)} \omega_{ij}^l r_{uj}, \quad (11)$$

where $C(u)$ is the set of items that the user u has fed back, and the feedback here refers to the user's implicit feedback behavior. $S(i, k)$ is the set of k items most similar to item i ,

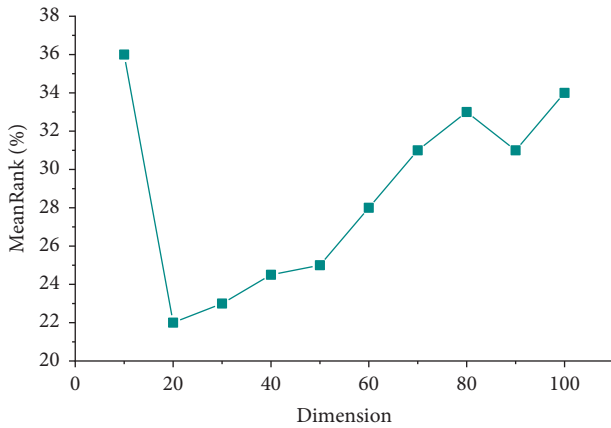


FIGURE 6: MeanRank in different dimensions.

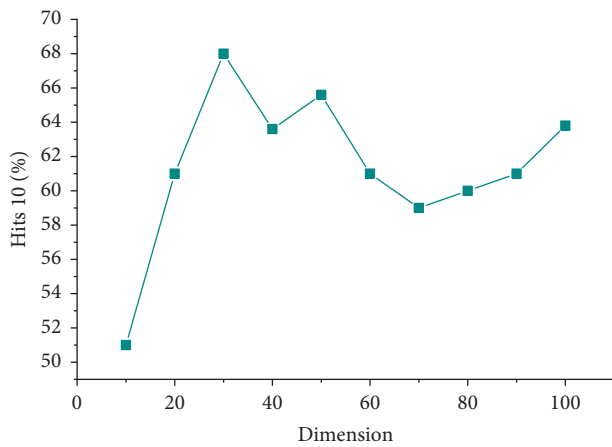


FIGURE 7: Hits10 in different dimensions.

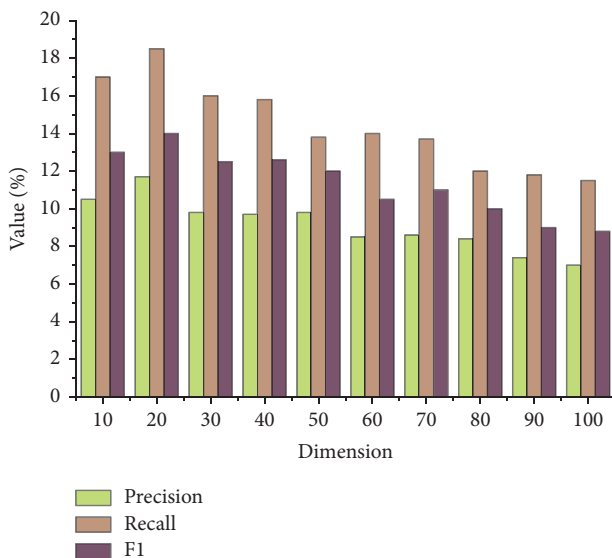


FIGURE 8: Effectiveness of the recommendation algorithm.

that is, the set of items composed by the first k items after they are arranged according to the size of item similarity, and k is called the number of neighbors. r_{uj} is user u 's interest in project j . If user u has clicked project i , r_{uj} can be set to 1; otherwise, it is 0. ω_{ij} is the similarity between items i and j .

The specific calculation process is as follows: Extract all items clicked by user u and find out the similarity degree of the first k items similar to each item clicked by user u . Add all the similarity degrees of item I to obtain the similarity degree of item I . In this way, the items are sorted in the order of similarity, and the first N items are recommended to users, that is, top- N recommendations.

The effect of top- N recommendation is usually measured by precision, recall, and $F1$. The results are shown in Figure 8.

It can be seen from Figure 8 that the accuracy rate of the proposed recommendation algorithm based on the MKD of the cultural industry is between 7% and 11%, the recall rate is between 11% and 18%, and the $F1$ value is between 8% and 14%. By comprehensive comparison, when k value is 20, a higher accuracy rate, recall rate, and $F1$ value can be obtained, and the top- N recommendation effect is the best. To sum up, the feasibility of the top- N algorithm is verified; when the number of neighbors is 20, the recommendation effect is the best.

6. Conclusion

In the era of big data, the development of the MKD provides a new direction for innovation and development of the cultural industry. This paper analyzes the data storage architecture, main models, and management methods. From the perspective of cultural communication pragmatics, this paper applies the MKD of the cultural industry to the recommendation algorithm, and designs a top- N recommendation algorithm; a link prediction experiment is designed to evaluate the training effect of the model. The results show that when it is embedded into the vector space with a dimension between 20 and 30, the evaluation indexes of MeanRank and Hit10 are the best, which realizes the accurate embedding of the entity vector and relation vector of the MKD of the cultural project; in addition, when K is 20, top- N recommendation has the best recommendation effect.

Data Availability

The dataset can be accessed upon request.

Conflicts of Interest

The authors declare that they have no conflicts of interest.

Acknowledgments

This work was supported by Soft science project of science and Technology Department of Henan Province: "Research on the construction and competitiveness improvement of cultural tourism circle in the middle reaches of the Yellow River," the project number is 222400410363.

References

- [1] J. Zhou, *Technological Innovation Promotes the Development of New Formats of Cultural Industry*Hunan University, 2013.
- [2] R. Huang, Xu Qian, and X. Li, “Evolutionary game research on digital transformation of cultural industry,” *Financial Theory and Practice*, vol. 42, no. 02, pp. 125–133, 2021.
- [3] Q. Dong, “The integration mode and regulation path of artificial intelligence and cultural industry,” *Industrial innovation research*, vol. 2021, no. 23, pp. 55–57, 2021.
- [4] J. Cowie and W. Lehnert, “Information extraction,” *Communications of the ACM*, vol. 39, no. 1, pp. 80–91, 1996.
- [5] P. Wang and X. Huang, “Research on semantic fusion of digital cultural resources based on linked open data: a case study of European digital libraries,” *Library and information work*, vol. 60, no. 12, pp. 29–37, 2016.
- [6] L. Lombardo, P. Pizzo, and D. Damiano, “Safeguarding and accessing drama as intangible cultural heritage,” *Journal on Computing and Cultural Heritage*, vol. 9, no. 1, pp. 1–26, 2016.
- [7] C. Sun, *Research on Digital Technology of Folk Dance Intangible Cultural Heritage*Central China Normal University, Wuhan, 2013.
- [8] C. Xia and L. Zhang, “Application of linked data in genealogy Digital Humanities service,” *Library Journal*, vol. 35, no. 10, pp. 26–34, 2016.
- [9] A. Bordes, N. Usunier, and A. Garcia-Duran, “Translating embeddings for modeling multi-relational data,” *Advances in Neural Information Processing Systems*, vol. 26, 2013.
- [10] Z. Wang, J. Zhang, and J. Feng, “Knowledge graph embedding by translating on hyperplanes,” *Proceedings of the AAAI Conference on Artificial Intelligence*, vol. 28, no. 1, 2014.
- [11] H. Zhao, Q. Yao, and J. Li, “Meta-graph based recommendation fusion over heterogeneous information networks,” in *Proceedings of the 23rd ACM SIGKDD international conference on knowledge discovery and data mining*, pp. 635–644, Canada, August 2017.
- [12] X. Yu, X. Ren, Y. Sun, and Q. Gu, “Personalized entity recommendation: a heterogeneous information network approach,” in *Proceedings of the 7th ACM international conference on Web search and data mining*, pp. 283–292, Canada, February 2014.
- [13] X. Cui, “Recommendation system based on heterogeneous information network,” *Computer and Modernization*, vol. 56, no. 12, pp. 13–19, 2020.
- [14] X. Fan and C. Zhang, “Research on recommendation system model based on Adam,” *Journal of Wuxi University of Light Industry*, vol. 39, no. 01, pp. 62–67, 2020.

Research Article

Research on the Application of Artificial Neural Network-Based Virtual Image Technology in College Tennis Teaching

Ruizhe Hu  and Xiaocan Cui 

School of Physical Education (Main Campus), Zhengzhou University, Zhengzhou 450001, Henan, China

Correspondence should be addressed to Xiaocan Cui; cuixiaocan999@zzu.edu.cn

Received 5 April 2022; Revised 29 May 2022; Accepted 8 June 2022; Published 8 July 2022

Academic Editor: Le Sun

Copyright © 2022 Ruizhe Hu and Xiaocan Cui. This is an open access article distributed under the Creative Commons Attribution License, which permits unrestricted use, distribution, and reproduction in any medium, provided the original work is properly cited.

At the same time that my country has shifted from high-speed development to high-quality development, my country has also put forward new requirements for education development. Due to the limited study time during college, each student's study habits and learning process are also different, and the degree of connection between tennis lessons is high, so there will be polarization when learning tennis. With the development of science and technology, more and more technological innovations are integrated into the classroom, and traditional teaching methods can no longer keep up with the pace of the times. Tennis teaching is a subject of equal proportion between theory and practice. The traditional teaching method simplifies the theory, which makes students to have some bad phenomena when they practice. Aiming at this series of problems, this paper uses algorithms such as softmax function and threshold function to construct an application model of virtual image technology based on the artificial neural network in tennis teaching. The research results of the article show that: (1) the average accuracy rate of the method in this paper is 97.22%, and the highest accuracy rate is 99.17%. The average accuracy rate also tends to increase with the increase of sample size; the recall rate is the highest, and the highest recall rate is 99.36%. The average recall rate is 96.77%; the highest correct rate is close to 100% and is significantly higher than the other three methods; the average correct rate reaches 98.8%; the response time is the shortest; the average response time is 33 ms; and the response time increases with the increase of the sample size. (2) After using this model, tennis skills have been improved, with an average of 12 in situ flips, an average of 7 in situ rackets, an average of 5 in situ forehand draws, and an average of 3 in situ backhand draws. (3) The average forehand and backhand scores of the class after the experiment were 90 and 86; the average forehand and backhand stability were 8 and 7; and the average forehand and backhand accuracy were 31 and 29, respectively. The average depth of forehand and backhand is 36 and 32. (4) Most of the students are satisfied with this model, and they all choose to strongly agree and relatively agree, and the percentage of very agree that helps stimulate learning has reached 60.52%, and no students choose to disagree very much.

1. Introduction

At present, although the traditional teaching methods of tennis in colleges and universities are helpful for students to understand and master the basic tennis movements, the traditional methods are relatively simple and cannot provide deeper guidance to students. Therefore, this paper uses the softmax function and threshold function to construct the application model of virtual image technology based on an artificial neural network in tennis teaching. Improve students' learning ability of tennis through virtual imaging technology. This paper has received a lot of support on the

basis of previous results. Artificial neural networks solve many problems that are difficult for modern computers to solve in the field of model recognition [1]. It exhibits good intelligence properties [2]. Artificial neural networks are proposed in the technology of modern neuroscience research results [3]. Neuron processing units can represent different objects [4]. Artificial neural networks enable parallel distributed systems [5]. It adopts a completely different mechanism from traditional artificial intelligence and information processing technology [6]. And it has the characteristics of self-adaptation, self-organization, and real-time learning [7]. Virtual is a description of distance and

impossibility [8]. The most favorable narrative method of digital images is its virtuality [9]. Virtual imaging technology uses information as material and transforms information into perceived reality [10]. Virtual can merge the vast and the subtle into one [11]. Virtual image technology combines art design and computer technology [12]. Virtual imaging technology is a general term for existing virtual reality, augmented reality, and projection technologies [13]. The artificial neural network model mainly considers the topology of network connections [14]. An artificial neural network is a nonlinear, adaptive information processing system composed of a large number of interconnected processing units [15].

2. Basic Knowledge

2.1. Artificial Neural Network

2.1.1. Neural Network Model. Artificial Neural Network (ANN for short) [16] is an information processing system established by humans based on the understanding of the operating rules of the brain neural network. The system can imitate the structure of the brain neural network to achieve certain functions. A neural network is an adaptive nonlinear dynamic system composed of multiple linear and nonlinear neurons connected to each other according to a certain method, in which neurons are the storage and processing units of information, and the learning process of the neural network is based on the input between neurons. The pattern connection weights are continuously adjusted to form a memory for the input pattern. A simple neuron model is shown in Figure 1.

In Figure 1, the input of the neuron is represented by $X = (x_1, x_2, x_3, \dots, x_n)$; the corresponding weight value of each input is represented by $W = (w_1, w_2, w_3, \dots, w_n)$; the bias value of the neuron is represented by b ; the activation function of the neuron is represented by $f(\cdot)$; and the input of the neuron is represented by y .

$$\cdot = \sum_{i=1}^n w_i x_i + b, \quad (1)$$

$$y = f(\cdot). \quad (2)$$

2.1.2. Neuron Activation Function. The activation function is the main processing method of artificial neural network information. The activation functions proposed according to different research problems can be divided into three categories:

(1) Linear activation function: the main function of the linear activation function is to linearly process the input information of the neuron, that is, the output information and the input information satisfy a linear relationship. The most common linear activation function is the pure-line activation function [17]. The function expression is

$$f(x) = kx. \quad (3)$$

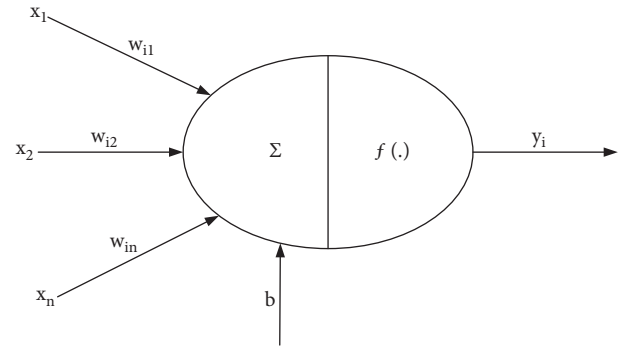


FIGURE 1: Artificial neural network model.

(2) Nonlinear activation function: the main function of the nonlinear activation function is to nonlinearly process the input information of the neuron. The two activation functions of Sigmoid and Tanh are mainly used. The function expressions are as follows:

Sigmoid function:

$$f(x) = \frac{1}{1 + e^{-x}}. \quad (4)$$

Tanh function:

$$f(x) = \frac{1 - e^{-x}}{1 + e^{-x}}. \quad (5)$$

(3) Threshold function: the threshold function adopts a step function, and the output of the neuron is a binary variable [18]. Its function expression is

$$f(x) = \begin{cases} 1, & x \geq 0 \\ 0, & x < 0 \end{cases}. \quad (6)$$

(4) Softmax function: the softmax function is defined as follows:

$$S_i = \frac{e^{y_i}}{\sum_j e^{y_j}}. \quad (7)$$

The softmax function shows the concept of mutual exclusion, that is, the closer the judgment result is to a certain class, the closer the corresponding value of this class is to 1, and the closer to 0 for other classes.

(5) Gaussian error linear unit: the Gaussian error linear unit (GELU) adjusts the output value through a gating mechanism, defined as follows:

$$GELU(x) = xP(X \leq x), \quad (8)$$

where $P(X \leq x)$ is the cumulative distribution function of the Gaussian distribution.

The Gaussian error linear unit is approximated by the Tanh function:

$$GELU(x) \approx 0.5x \left(1 + \tanh \left(\sqrt{\frac{2}{\pi}} (x + 0.044715x^3) \right) \right). \quad (9)$$

Approximate using the logistic function:

$$GELU(x) \approx xL(1.702x). \quad (10)$$

2.1.3. Loss Function. The loss function is usually used to describe the difference between the prediction result of the model on the sample value and the actual value, which represents the accuracy of the model to a certain extent. The loss function includes the mean square error function and the cross-entropy function.

(1) Mean square error function: the mean square error function uses the mean square error in statistics to characterize the deviation of the predicted value from the actual value and is defined as follows:

$$\text{Loss} = \frac{\sum (y - y')^2}{n}, \quad (11)$$

where y is the label value, y' is the predicted value, and n is the number of samples.

(2) Cross-entropy function: the cross-entropy function represents the deviation between two probability steps. Assuming that both p and q represent the law of probability, the cross entropy of p represented by q is

$$H(p, q) = - \sum_x p(x) \log_2 q(x). \quad (12)$$

2.2. Artificial Neural Network Algorithm. The learning process of the artificial neural network is composed of forward propagation and back propagation [19]. The algorithm process is as follows.

Initialize weights and thresholds [20]: after the network BP (n, q, m) is determined, the network algorithm includes the weight from the i unit of the input layer to the j unit of the hidden layer, the weight of W_{ij}^1 ($i = 1, \dots, n; j = 1, \dots, k$) from the j unit of the hidden layer to the k unit of the output layer, and the weight of W_{ij}^0 ($j = 1, \dots, q; k = 1, \dots, m$). The activation threshold of the j unit of the hidden layer is θ_j^H ($j = 1, \dots, q$), and the activation threshold of the j unit of the output layer is θ_k^0 ($k = 1, \dots, m$). The above weights and initial thresholds are randomly generated before the network is trained.

Training sample information [21]: assuming that P is a common training sample, input the r ($r = 1, \dots, p$) training sample information to the first hidden layer of forward propagation and obtain the output information of the hidden layer through the action of the activation function $f(x)$.

$$H_{jr} = f\left(\sum_{i=1}^n w_{ij}^1 x_{ir} \theta_j^1\right), \quad (j = 1, \dots, q; r = 1, \dots, p). \quad (13)$$

The hidden layer output information is transmitted to the output layer, which may be the final output result [22].

$$Y_{kr} = f\left(\sum_{j=1}^q w_{jk}^0 H_{jr} \theta_k^0\right), \quad (k = 1, \dots, m; r = 1, \dots, p). \quad (14)$$

In the process of forward propagation of learning information in the network, the error of another process is backpropagated [23]. If there is an error between the network output and the desired output value, then backpropagate the error, using all adjusted network weights and thresholds.

$$\Delta w(t+1) = \eta \frac{\partial E}{\partial w} \alpha \Delta w(t), \quad (15)$$

where $\Delta w(t)$ is the modified value of the t training weight and threshold [24] and η and α are the scale factor and momentum factor, respectively.

$$E = \frac{1}{2} \sum_{k=1}^m \sum_{r=1}^p (Y_r - t_r)^2. \quad (16)$$

The above two procedures are repeated until the error between the network outputs reaches a certain requirement and desired output.

2.3. The Basic Principle of Artificial Neural Network. The input net_j^m for the j neuron in layer m is

$$\text{net}_j^m = \sum_{i=1}^n w_{ij}^{m-1} o_i^{m-1} + b_j^m. \quad (17)$$

Then, the output o_j^m of the j neuron in the m layer is

$$\begin{aligned} o_j^m &= f_j^m(\text{net}_j^m) \\ &= f_j^m\left(\sum_{i=1}^n w_{ij}^{m-1} o_i^{m-1} + b_j^m\right). \end{aligned} \quad (18)$$

$$\begin{aligned} o^n &= f^n\left(w^{n-1} f^{n-1}\left(\frac{\dots (w^{i+1} f^{i+1}(w^i o^i + b^{i+1})) \dots}{n-2}\right)\right) \\ &\quad + b^{n-1} + b^n, \end{aligned} \quad (19)$$

where w_{ij}^{m-1} is the weight between the i neuron in the $m-1$ layer and the j neuron in the m layer, b_j^m is the bias value of the j neuron in the m layer, and o_i^{m-1} is the second layer. Three neurons were applied to output; f_j^m is the activation function of the j neuron in the m layer.

Thus, the expression of the final output information of the neural network about the input information can be obtained. The expression is represented by a vector as follows:

$$o^n = f^n(w^{n-1} f^{n-1}(w^{n-2} o^{n-2} + b^{n-1}) + b^n). \quad (20)$$

2.4. Learning Rules of Artificial Neural Networks. The error function generated for sample a and the h output neuron is defined as follows:

$$e_h = d_h - o_h. \quad (21)$$

In order to make the partial derivative continuous, a quadratic error function is generally used, and the total error function for sample a is

$$E = \frac{1}{2} \sum_h^L (d_h - o_h)^2. \quad (22)$$

When training, when p training sample is input at a time, the total error function is

$$E_p = \frac{1}{2} \sum_{p=1}^P \sum_{h=1}^L (d_h^p - o_h^p)^2. \quad (23)$$

When using the fastest gradient descent algorithm [25]. The formula is

$$w_{ij}^m(k+1) = w_{ij}^m(k) - lr \frac{\partial \hat{E}_p}{\partial w_{ij}^m}, \quad (24)$$

$$b_j^m(k+1) = b_j^m(k) - lr \frac{\partial \hat{E}_p}{\partial b_j^m}, \quad (25)$$

where $w_{ij}^m(k+1)$ and $w_{ij}^m(k)$ are the weight values between the i neuron in the $m-1$ layer and the j neuron in the m layer in the $k+1$ and k iterations, respectively; $b_j^m(k+1)$ and $b_j^m(k)$ are the $k+1$ and the bias value of the j neuron in the m layer at the k iteration, respectively; lr is the learning rate; and \hat{E}_p is the approximate error at the k iteration.

3. Application of Virtual Image Technology in College Tennis Teaching

3.1. Overview of Virtual Imaging Technology

3.1.1. Concept of Virtual Image Technology. The virtual image is a visual technology and art based on digital technology. Virtual imaging technology is a combination of photography technology, projection technology, display technology, and other technologies, which can help people better understand the known real space and the unknown virtual space. It simulates and reorganizes text, images, and other information through digital technology to form abstract or real spatial scenes with interactivity, virtuality, and immersion.

3.1.2. Classification of Virtual Imaging Technology. Virtual imaging technology can be divided into virtual reality technology, augmented reality technology, holographic projection technology, fog screen stereo imaging technology, wall projection technology, and interactive projection technology as shown in Table 1.

3.1.3. Technical Characteristics of Virtual Images. Virtual imaging technology has the characteristics of integration, fidelity, immersion, imagination, artistry, and interaction as shown in Table 2.

3.2. Basic Principles of Tennis Teaching. Tennis teaching has the principle of health, which means that the physical safety of students should be guaranteed first in the tennis teaching process; in the process of tennis teaching, the teaching content should be gradual and the principle of low level to high level, starting from the actual principle, from simple to complex and gradually improve. According to the students' physical load and practice venues to arrange teaching, students consciously and actively participate in learning activities; students should firmly grasp the knowledge of all aspects of tennis.

3.3. Model Construction. In this paper, a model of college tennis teaching based on virtual image technology based on an artificial neural network is constructed, as shown in Figure 2. The tennis teaching model in colleges and universities is divided into three steps: the first step is audition learning, the second step is practical mastery, and the third step is interactive analysis.

In the first step in tennis teaching, students first need to wear virtual imaging technology equipment to gain a preliminary understanding of tennis teaching through the equipment and then take off the equipment, and the teacher will demonstrate and explain the standard movements; after the teacher's explanation, the students need to wear the equipment again and watch a continuous tennis movement to speed up their understanding of the action.

In the second step, the students take off the instrument again and practice freely. The teacher guides the students' movements during this process; after the teacher finds the students' problems, the students wear the instruments again to compare their movements to find their own problems; Remove the instrument again, repeat the previous practice, and correct the problems found in the process; and the teacher also corrects the problems of the students in the process.

Finally, in the third step, students form groups to practice and supervise each other and wear the instrument again to consolidate the practice.

4. Experimental Analysis

4.1. Model Testing. In this paper, an application model of artificial neural network-based virtual image technology in college tennis teaching is constructed, and algorithms such as softmax function and threshold function are used in the model. First, the model will be tested, and the advantages of the model will be checked by comparing it with BP neural network, deep neural network, and traditional methods, and whether it meets the requirements.

In the model testing stage, in order to test the accuracy, recall, correctness, and response time of the model under different sample sizes, the standard degree of students' actions in the learning process was selected as the research object. The experimental sample sizes were divided into 6 groups, namely 10, 30, 50, 70, 90, and 110.

TABLE 1: Classification of virtual imaging technology.

Classification	Content
Virtual reality (VR)	Virtual reality technology is a general term for a technical system used to establish a virtual environment for the experimenter to observe and interact with. Use 3dmax, Unity3d, and other software to model and create virtual scenes, capture and simulate human movement through hardware facilities such as Kinect and Arduino, and interact with virtual scenes; generate instructions through C language and Java programming; and form feedback.
Augmented reality (AR)	Augmented reality technology will recognize and analyze images observed with the camera; classify and identify matching images, images, and other digital information in a database; and display it on the screen overlaid with the actual scene.
Holographic projection technology	Holographic imaging technology projects the image onto the actual environment or transparent medium without the audience wearing the device, creating the illusion that the image is suspended in the air. Then, interact with the image through the interactive device.
Fog curtain stereo imaging technology	Fog screen stereo imaging technology uses a spray device instead of a traditional projection screen to generate an artificial water mist wall and generates a flickering fog screen projection image through an electric device to form a holographic image.
Wall projection technology	Wall projection technology is mainly used for the outer panels of urban buildings. The urban exterior wall projection is mainly composed of a laser projector, a screen segmentation control matrix technology, and an exterior wall laser projection system composed of an intelligent central control system.
Interactive projection technology	Interactive projection technology is a projection system composed of projection equipment, infrared sensors, motion capture equipment, and computers. The captured data is analyzed using infrared cameras and sensors to track and identify data such as body movements and the voice of the experimenter. Combined with real-time image interaction tracking, it produces real-time interaction effects between participants and projects.

TABLE 2: Technical characteristics of virtual images.

Feature	Content
Integration	Virtual image technology is the product of technology development and traditional images. Virtual image technology is a new image technology supported by projection technology, display technology, sensing technology, and other technologies.
Fidelity	Virtual imaging technology is to reproduce reality through the current simulation or focus on the current image; contrary to the real optical illusion, the user's visual authenticity and the authenticity of the image are unified. There are many real experiences in real vision, intelligence, vision, and relationships.
Immersion	In fact, outside of the ideal visual image, people are really confused about pain. The combined behavior of public experience and sensory psychological factors creates an illusion of interest in the user's real environment. Through sensory technology and real-time, users can connect to virtual environments to create physical and mental experiences.
Imaginative	Virtual images not only can reproduce the real environment but also can imagine an illustrative environment, satisfying the curiosity as well as the visual and psychological needs of the experimenter. The creative process of virtual image technology is special, so it can be integrated into the imagination of the creative stage, increase the scale of the work, and increase the scope of human knowledge and imagination.
Artistry	The production of virtual image content is people's thinking and behavior, and art is also designed and used based on people's main aesthetic preferences, emotions, thinking, and behavior.
Interactivity	Through the recognition of the experienced expressions and sounds, the information of body movement is captured and temporarily returned in real time, and the interaction of images is formed.

The criteria for the model to meet the requirements are as follows: the average accuracy rate of the test samples is more than 97%, the average recall rate is greater than 96%, the average accuracy rate is greater than 98%, and the average response time is less than 34%; then the model meets the requirements.

According to the results in Figure 3 and Table 3, the average accuracy rate of the method in this paper is 97.22%, and the highest accuracy rate is 99.17%. The average accuracy rate also tends to increase with the increase of the sample size, indicating that the method in this paper meets the requirements. And, by comparing the method in this paper with the other three methods, it can be seen that the

method in this paper has obvious advantages and the highest accuracy.

As can be seen from Table 4, the recall rate of the method in this paper is the highest; the highest recall rate is 99.36%; and the average recall rate is 96.77%, which meets the inspection standard. According to Figure 4, it can be clearly seen that the overall recall rate is on the rise, and it is concentrated between 94% and 96%.

The results in Figure 5 and Table 5 show that the highest accuracy rate of the method in this paper is close to 100%, which is significantly higher than that of the other three methods, and the average accuracy rate reaches 98.8%, indicating that the method in this paper meets the

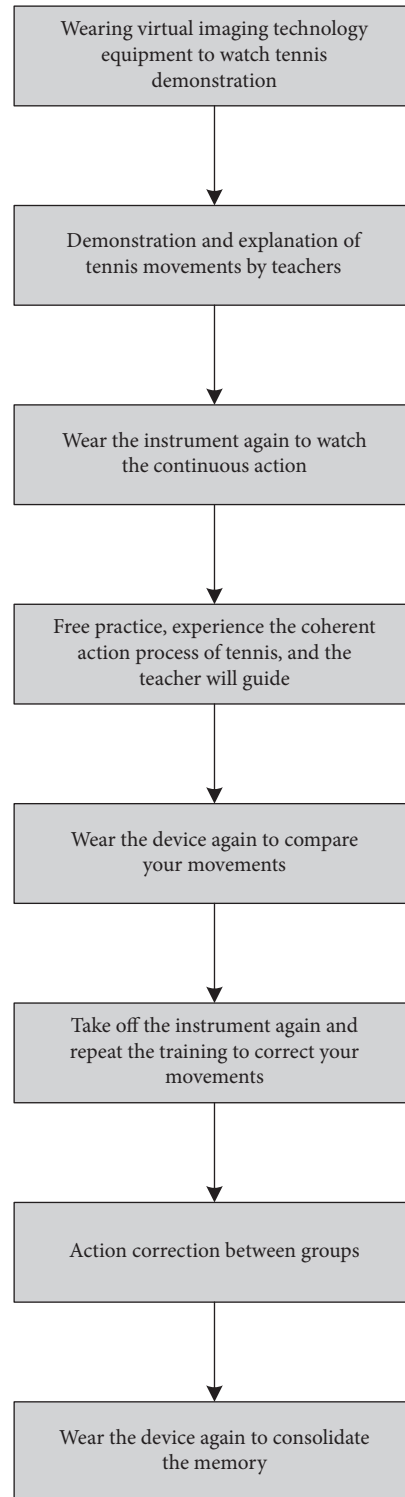


FIGURE 2: Tennis teaching model.

requirements. On the whole, the correct rate of the four methods is above 94%; the average correct rate of the BP neural network is 97.3%; the average correct rate of the deep neural network is 96.6%; and the average correct rate of the traditional method is 96.9%.

The experimental results in Figure 6 and Table 6 show that the method in this paper requires the shortest response

time, with an average response time of 33 ms, and the response time increases with the increase of the sample size. The traditional method had the highest response time, which was twice as high as the other methods with a sample size of 30.

It can be seen from the experimental results that the method in this paper has reached the standard in terms of

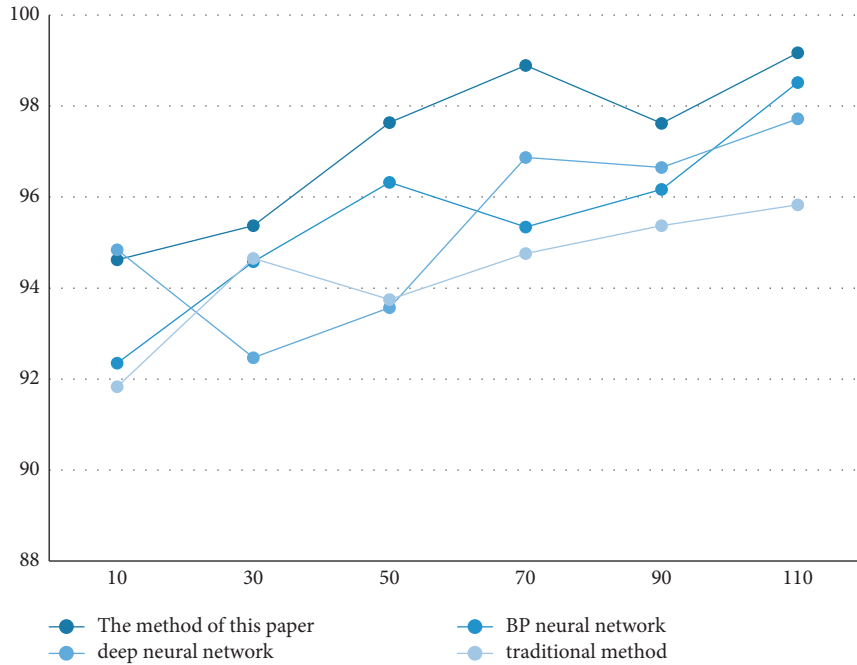


FIGURE 3: Accuracy.

TABLE 3: Accuracy (%).

Model	10	30	50	70	90	110
The method of this paper (%)	94.62	95.37	97.64	98.89	97.62	99.17
BP neural network (%)	92.35	94.58	96.32	95.34	96.17	98.52
Deep neural network (%)	94.84	92.47	93.57	96.87	96.65	97.72
Traditional method (%)	91.83	94.65	93.75	94.76	95.37	95.83

TABLE 4: Recall rate (%).

Model	10	30	50	70	90	110
The method of this paper (%)	94.58	95.37	94.46	97.83	99.02	99.36
BP neural network (%)	91.85	94.57	95.67	95.27	96.53	98.74
Deep neural network (%)	92.57	93.48	96.35	95.53	97.58	96.75
Traditional method (%)	90.75	94.53	94.75	93.58	96.53	96.28

average precision, average recall, average correct rate, and average response time and meets the requirements. Compared with the other three methods, the method has obvious advantages and is feasible.

4.2. Experimental Simulation. After the model meets the test criteria, it will be used in formal teaching. In order to test the students' learning effect under the model, the students' learning results will be compared with those before the experiment.

4.2.1. Comparison of Student Tennis Skills. Students in one class were randomly selected to conduct the experiment, and their average number of in situ hits, average in situ rackets, average in situ forehand draws, and average in situ backhand draws were recorded before and after the experiment. The experimental results are shown in Figure 7.

From the results in Figure 7, it can be seen that the tennis skills of the students before the experiment were relatively weak. After using the model, the tennis skills were improved. The average number of in situ flips was 12 times; the average number of in situ racquets was 7; and the average in situ strokes were 7 times. There is an average of five forehand draws and three backhand draws.

4.2.2. Comparison of Forehand and Backhand Performance. Forehand and backhand assessment, stability, accuracy, and depth of stroke are also important components of tennis assessment in tennis teaching.

Forehand and backhand skill evaluation is to score students' actions during the hitting process; forehand and backhand stability is based on students hitting the ball 10 times with forehand and backhand, respectively, and the number of hits is the final score. Forehand and backhand

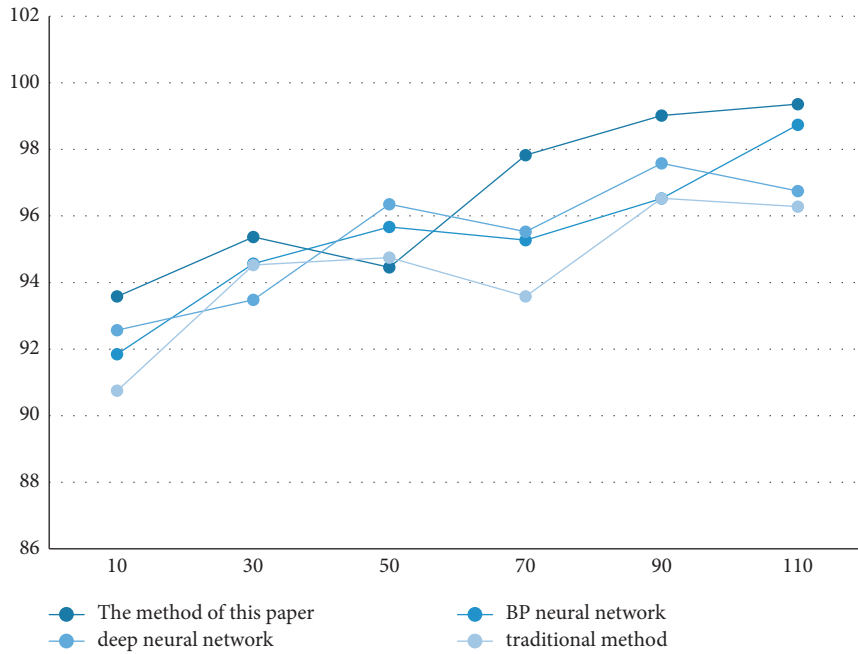


FIGURE 4: Recall rate.

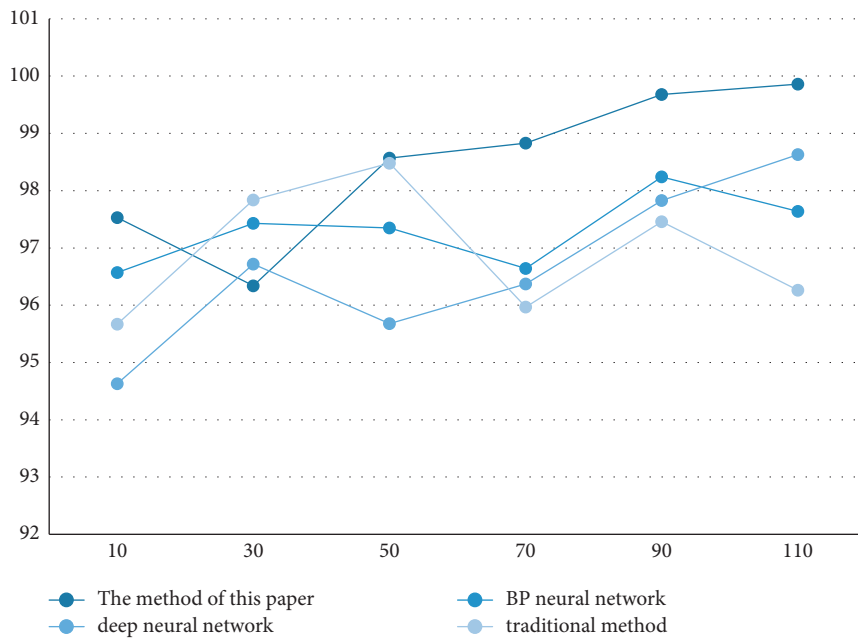


FIGURE 5: Correct rate.

TABLE 5: Correct rate (%).

Model	10	30	50	70	90	110
The method of this paper (%)	97.53	98.34	98.57	98.83	99.68	99.86
BP neural network (%)	96.57	97.43	97.35	96.64	98.24	97.64
Deep neural network (%)	94.63	96.72	95.68	96.37	97.83	98.63
Traditional method (%)	95.67	97.84	98.48	95.97	97.46	96.26

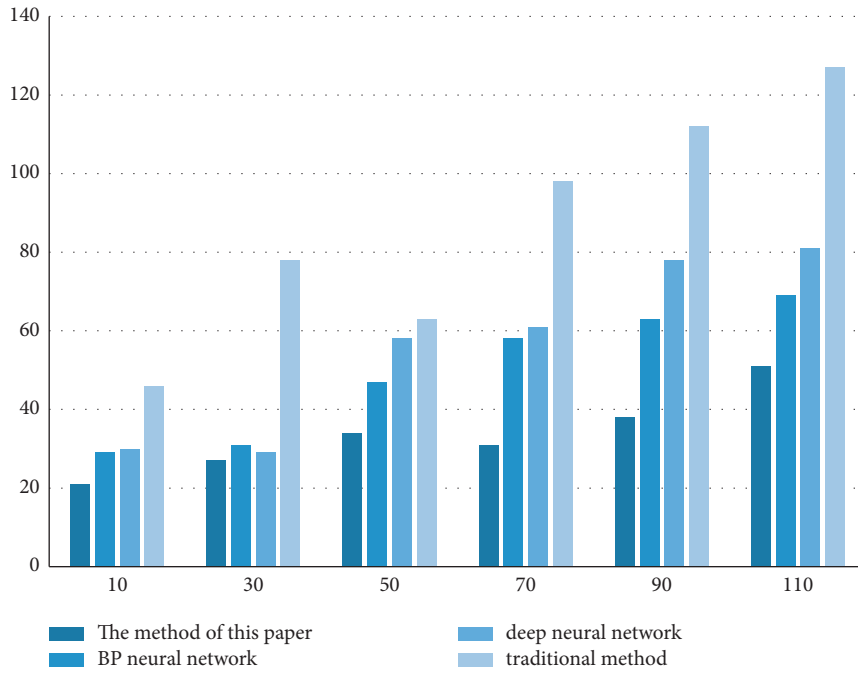


FIGURE 6: Response time.

TABLE 6: Response time (ms).

Model	10	30	50	70	90	110
The method of this paper (ms)	21	27	34	31	38	51
BP neural network (ms)	29	31	47	58	63	69
Deep neural network (ms)	30	29	58	61	78	81
Traditional method (ms)	46	78	63	98	112	127

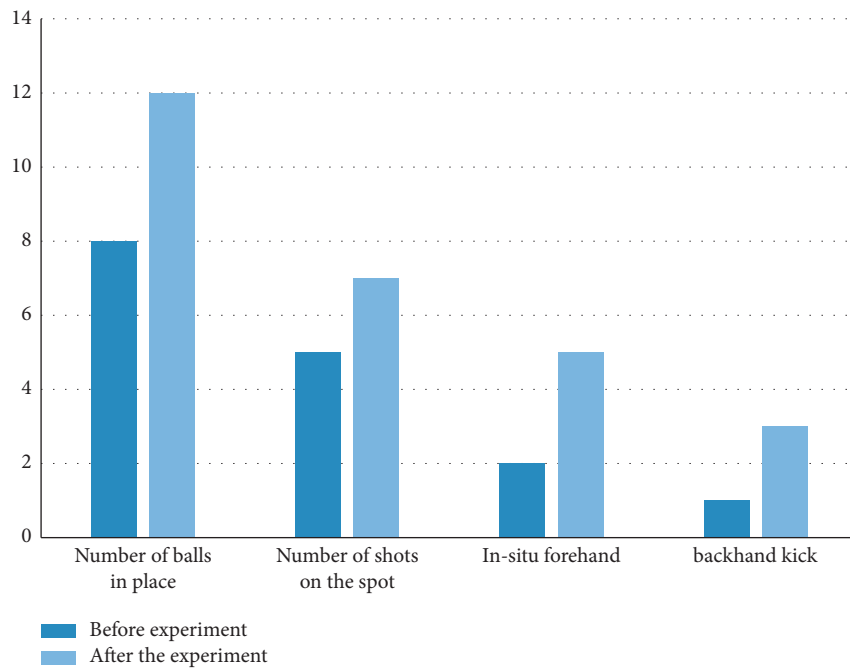


FIGURE 7: Comparison of student tennis skills.

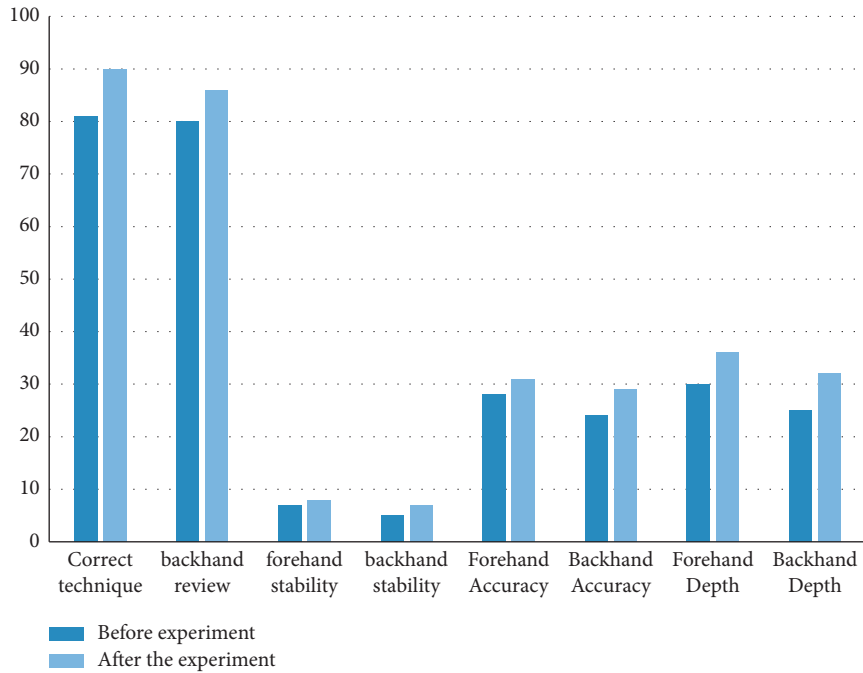


FIGURE 8: Comparison of forehand and backhand scores.

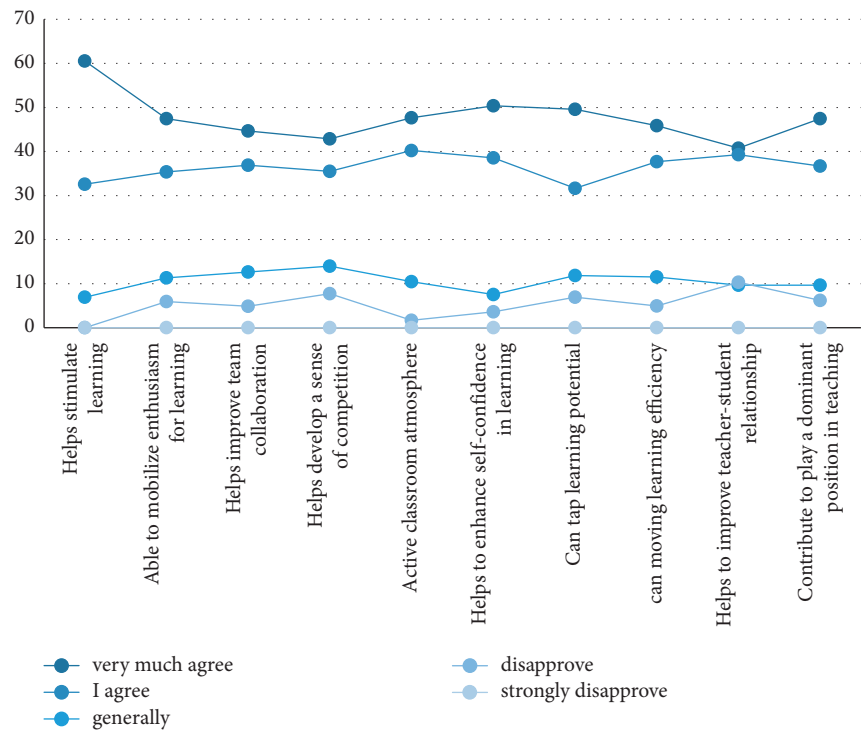


FIGURE 9: Model evaluation.

accuracy: it means that each student hits the ball 10 times alternately within the specified different score areas and hits the ball to get the corresponding score; the depth of forehand and backhand hitting is the depth area corresponding to each student's different scores. Figure 8 shows the average scores of the students in this class before and after using the model in this paper:

The results in Figure 8 show that the average forehand and backhand scores of the class before the experiment were 81 and 80, the average forehand and backhand stability were 7 and 5, and the average forehand and backhand accuracy were 28 and 24, respectively. Forehand and backhand depths are 30 and 25. The average forehand and backhand scores of the class after the experiment were 90 and 86 points,

respectively; the average forehand and backhand stability were 8 and 7 times, respectively; and the average forehand and backhand accuracy were 31 points and 29 points, with an average forehand and backhand depth of 36 and 32 points, respectively. And the scores of the students in this class have improved after using the model, indicating that the model has obvious advantages in improving students' performance.

4.3. Model Evaluation. After the experiment, the classmates' evaluation of the tennis teaching model using virtual image technology was statistically analyzed by means of questionnaires. It is evaluated in 7 aspects: to cultivate a sense of competition, activate the classroom atmosphere, enhance self-confidence in learning, tap learning potential, improve learning efficiency, enhance teacher-student emotion, and play a dominant role in teaching. The evaluation results are shown in Figure 9.

It can be seen from Figure 9 that most of the students are satisfied with this model, and they all choose to strongly agree or agree, indicating that the students have a high degree of recognition of the tennis teaching model using virtual image technology. And the percentage of very agreeable to help stimulate learning reached 60.52%, and no classmates chose to be very disapproved.

5. Conclusion

College physical education is an important part of the teaching process in colleges and universities, and tennis teaching is a subject that combines theory and practice, so the teaching mode of tennis is different from that of other subjects. With the development of the times, the traditional tennis teaching method has a certain lag in the teaching process. Therefore, this paper uses various algorithms such as softmax function and threshold function to construct a virtual image technology based on an artificial neural network in tennis teaching. Improve students' tennis skills through a combination of tennis teaching and virtual technology.

The findings of the article show that

- (1) The average accuracy rate of the method in this paper is 97.22%, and the highest accuracy rate is 99.17%. The average accuracy rate also tends to increase with the increase of the sample size, indicating that the method in this paper meets the requirements.
- (2) The recall rate of the method in this paper is the highest; the highest recall rate is 99.36%; and the average recall rate is 96.77%, which meets the inspection standard.
- (3) The highest accuracy rate of the method in this paper is close to 100%, which is significantly higher than that of the other three methods, and the average accuracy rate reaches 98.8%, indicating that the method in this paper meets the requirements.
- (4) The response time required by the method in this paper is the shortest, with an average response time

of 33 ms, and the response time increases with the increase of the sample size.

- (5) The tennis skills of the students before the experiment were relatively weak. After using the model, the tennis skills were improved. The average number of in situ flips was 12; the average number of in situ rackets was 7; and the average in situ forehand was drawn. The ball is 5 times, and the average backhand kick is 3 times.
- (6) The scores of the students in this class have improved after using the model, indicating that the model has obvious advantages in improving students' performance.
- (7) Most of the students are satisfied with this model, and they all choose to strongly agree or agree, indicating that the students have a high degree of recognition of the tennis teaching model using virtual imaging technology.

According to the experimental results, in the following teaching process, students' interest in learning and autonomous learning ability should be strengthened; teachers' own teaching ability professional level should be improved; an open and free learning division should be created to increase students' interest in the class. Although the artificial neural network-based virtual image technology constructed in this paper has obvious advantages in the application model experimental results of tennis teaching, there are still many shortcomings and certain limitations. The model constructed in this paper is limited to tennis teaching. It is hoped that in the following research, researchers can conduct in-depth research on the scope of application so that the model is not limited to tennis teaching and increases the scope of application of the model.

Data Availability

The experimental data used to support the findings of this study are available from the corresponding author upon request.

Conflicts of Interest

The authors declared that they have no conflicts of interest regarding this work.

References

- [1] W. T. Katz, J. W. Snell, and M. B. Merickel, "[29] Artificial neural networks," *Methods in Enzymology*, vol. 210, no. 210, pp. 610–636, 1992.
- [2] R. S. Govindaraju, "Artificial neural networks in hydrology," *Journal of Hydrologic Engineering*, vol. 5, no. 2, pp. 124–137, 2000.
- [3] B. D. Dalziel, J. M. Morales, and J. M. Fryxell, "Fitting probability distributions to animal movement trajectories: using artificial neural networks to link distance, resources, and memory," *The American Naturalist*, vol. 172, no. 2, pp. 248–258, 2008.

- [4] R. Andrews, J. Diederich, and A. B. Tickle, "Survey and critique of techniques for extracting rules from trained artificial neural networks," *Knowledge-Based Systems*, vol. 8, no. 6, pp. 373–389, 1995.
- [5] D. Silverman and J. A. Dracup, "Artificial neural networks and long-range precipitation prediction in California," *Journal of Applied Meteorology*, vol. 39, no. 1, pp. 57–66, 2000.
- [6] H. White, "Learning in artificial neural networks: a statistical perspective," *Neural Computation*, vol. 1, no. 4, pp. 425–464, 1989.
- [7] Y. Xin, "A review of evolutionary artificial neural networks," *International Journal of Intelligent Systems*, vol. 8, no. 4, pp. 539–567, 2010.
- [8] C. A. Linte, J. White, R. Eagleson, G. M. Guiraudon, and T. M. Peters, "Virtual and augmented medical imaging environments: enabling technology for minimally invasive cardiac interventional guidance," *IEEE Reviews in Biomedical Engineering*, vol. 3, no. 1, pp. 25–47, 2010.
- [9] J. Buckland, "Imaging technology acts as a 'virtual skin biopsy' in SSc," *Nature Reviews Rheumatology*, vol. 9, no. 4, p. 196, 2013.
- [10] H. Kitaoka and S. Tamura, "Virtual imaging of the lung based on computational morphology," *Medical imaging technology*, vol. 18, no. 2, pp. 139–156, 2000.
- [11] Y. Wu and Y. Chen, "Influence of virtual imaging technology based on Html5 technology on digital painting," *Microprocessors and Microsystems*, vol. 82, no. 9, Article ID 103855, 2021.
- [12] F. Leong, A. K. Graham, and J. O. Mcgee, "Virtual histological imaging utilising next generation telepathology technology," *The Journal of Pathology*, vol. 190, p. 50A, 2000.
- [13] X. Han and Q. Yang, "Construction and application of the network-based platform for virtual practice teaching of medical imaging technology specialty in higher vocational education," *China Medical Education Technology*, vol. 151, no. 3, pp. 51–61, 2014.
- [14] B. R. Szkuta, L. A. Sanabria, and T. S. Dillon, "Electricity price short-term forecasting using artificial neural networks," *IEEE Transactions on Power Systems*, vol. 14, no. 3, pp. 851–857, 1999.
- [15] J. Sietsma and R. J. Dow, "Creating artificial neural networks that generalize," *Neural Networks*, vol. 4, no. 1, pp. 67–79, 1991.
- [16] G. Schwarzer, W. Vach, and M. Schumacher, "On the misuses of artificial neural networks for prognostic and diagnostic classification in oncology," *Statistics in Medicine*, vol. 19, no. 4, pp. 541–561, 2000.
- [17] C. M. Zealand, D. H. Burn, and S. P. Simonovic, "Short term streamflow forecasting using artificial neural networks," *Journal of Hydrology*, vol. 214, no. 1-4, pp. 32–48, 1999.
- [18] I.-C. Yeh, "Modeling of strength of high-performance concrete using artificial neural networks," *Cement and Concrete Research*, vol. 28, no. 12, pp. 1797–1808, 1998.
- [19] P. Coulibaly, F. Anctil, and B. Bobée, "Daily reservoir inflow forecasting using artificial neural networks with stopped training approach," *Journal of Hydrology*, vol. 230, no. 3-4, pp. 244–257, 2000.
- [20] D. A. Pomerleau, "Efficient training of artificial neural networks for autonomous navigation," *Neural Computation*, vol. 3, no. 1, pp. 88–97, 1991.
- [21] B. Samanta, K. R. Al-Balushi, and S. A. Al-Araimi, "Bearing fault detection using artificial neural networks and genetic algorithm," *Soft Computing*, vol. 2004, no. 3, pp. 264–271, 2004.
- [22] H. Gómez and T. Kavzoglu, "Assessment of shallow landslide susceptibility using artificial neural networks in Jabonosa River Basin, Venezuela," *Engineering Geology*, vol. 78, no. 1-2, pp. 11–27, 2005.
- [23] M. Conforti, S. Pascale, G. Robustelli, and F. Sdao, "Evaluation of prediction capability of the artificial neural networks for mapping landslide susceptibility in the Turbolo River catchment (northern Calabria, Italy)," *Catena*, vol. 113, pp. 236–250, 2014.
- [24] Q. J. Qi-Jun Zhang, K. C. Gupta, and V. K. Devabhaktuni, "Artificial neural networks for rf and microwave design—from theory to practice," *IEEE Transactions on Microwave Theory and Techniques*, vol. 51, no. 4, pp. 1339–1350, 2003.
- [25] J. Olden, M. Joy, and R. Death, "An accurate comparison of methods for quantifying variable importance in artificial neural networks using simulated data," *Ecological Modelling*, vol. 178, no. 3–4, pp. 389–397, 2004.

Review Article

MRI Radiogenomics in Precision Oncology: New Diagnosis and Treatment Method

Xiao-Xia Yin ¹, Mingyong Gao,² Wei Wang,² and Yanchun Zhang^{1,3}

¹Cyberspace Institute of Advanced Technology, Guangzhou University, Guangzhou 510006, China

²Department of Radiology, The First People's Hospital of Foshan, Foshan 528000, China

³Pengcheng Laboratory, Shenzhen, China

Correspondence should be addressed to Xiao-Xia Yin; xiaoxia.yin@gzhu.edu.cn

Received 2 March 2022; Revised 4 May 2022; Accepted 25 May 2022; Published 7 July 2022

Academic Editor: Le Sun

Copyright © 2022 Xiao-Xia Yin et al. This is an open access article distributed under the Creative Commons Attribution License, which permits unrestricted use, distribution, and reproduction in any medium, provided the original work is properly cited.

Precision medicine for cancer affords a new way for the most accurate and effective treatment to each individual cancer. Given the high time-evolving intertumor and intratumor heterogeneity features of personal medicine, there are still several obstacles hindering its diagnosis and treatment in clinical practice regardless of extensive exploration on it over the past years. This paper is to investigate radiogenomics methods in the literature for precision medicine for cancer focusing on the heterogeneity analysis of tumors. Based on integrative analysis of multimodal (parametric) imaging and molecular data in bulk tumors, a comprehensive analysis and discussion involving the characterization of tumor heterogeneity in imaging and molecular expression are conducted. These investigations are intended to (i) fully excavate the multidimensional spatial, temporal, and semantic related information regarding high-dimensional breast magnetic resonance imaging data, with integration of the highly specific structured data of genomics and combination of the diagnosis and cognitive process of doctors, and (ii) establish a radiogenomics data representation model based on multidimensional consistency analysis with multilevel spatial-temporal correlations.

1. Introduction

Tumor heterogeneity, one of the main characteristics of malignant tumors, poses great challenges to its accurate diagnosis and treatment, which is also manifested by multiple genotypes and multiple gene expression patterns in the same tumor cells [1]. The same tumor presents distinctly different therapeutic effects and prognosis in different individuals, and even tumor cells in the same individual present varied characteristics though with the same genome [2]. As shown in Figure 1, tumor heterogeneity is manifested in both space and time. In terms of space, the combined effects of molecular variation and tumor microenvironment lead to differences in tumor regions [3], which can be classified as follows: (i) intertumor heterogeneity, that is, differences between tumors in different patients; (ii) intratumor heterogeneity, that is, completely different or even opposite patterns of the expression patterns of cells in different tumor regions, which may result in the changes in

structure and differential responses to therapeutic drugs [4]. In terms of time, tumor is a dynamic system, and tumor cells evolve over time with multiple variations and temporal heterogeneity, which requires the reproducible detection in time. However, current genomics technology is static and can only reflect the information of a point (snapshot) on the time axis. Current molecular profiling analysis on locally extracted tumor tissues at a single time point reflects only a small part of the information of the entire tumor in both the spatial and temporal dimensions and fails to fully analyze the characteristics of the tumor. Quantitative description of tumor heterogeneity may lead to one-sided or even erroneous diagnosis, affecting the treatment options, and leading to drug resistance and disease recurrence in patients.

Genome analysis technology attempts to solve the problem of tissue sampling and analysis under tumor heterogeneity, such as the multiregion sampling strategy for spatial heterogeneity, and the micro-cutting of different tumor tissues for the isolation of small tissue fragments.

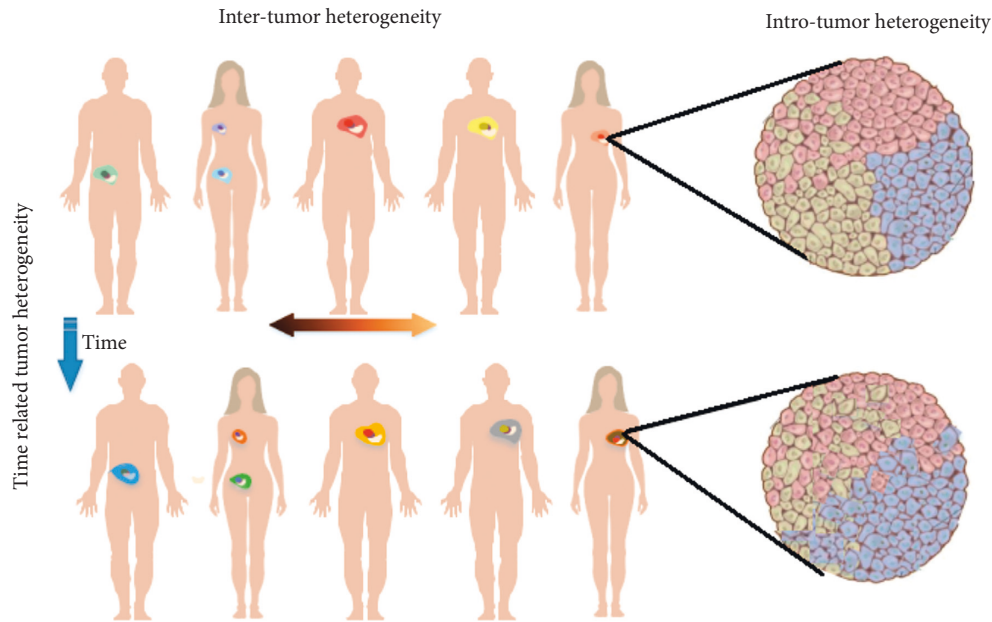


FIGURE 1: Intertumoral, intratumoral, and time related (temporal) heterogeneity of tumors (from Burrell et al., Nature, 2014 [5]).

DNA of these fragments has been analyzed [6]. However, this method requires precise localization of the tumor area during sampling to ensure the sampling genes obtained coming from tumor cells, which greatly limits the success rate of such a method. Longitudinal sampling attempts to solve the problem of temporal heterogeneity. Pathological sections are obtained at different stages of tumor treatment to track the variation of tumor-related genes and accurately analyze tumor heterogeneity [7–9]. However, the longitudinal sampling method requires multiple acquisition of patient tissue samples, and the invasive nature of this method terribly limits its feasibility in clinical practice. In short, the heterogeneity of tumors brings considerable challenges to precise diagnosis and treatment. Merely relying on linear, invasive, and single-time-point genomics technology cannot well meet the needs of precise clinical diagnosis and treatment, making it necessary to explore a three-dimensional, noninvasive, and reproducible method.

Broadly speaking, tumors are made of evolved and heterogeneous populations of cells that are resistant to matched targeting therapy. Thus, it is not enough reliable to evaluate effects of tumor treatment and diagnosis only from the perspective of tumor abnormality [10, 11]. Tumor genome analysis has been the gold-standard technique for molecular mapping [12, 13]. Nevertheless, the study on genomic heterogeneity has revealed that individual tumor may be clonally independent without shared driver gene alterations [14]. There is a proof-of-concept study demonstrating that morphological heterogeneity reflects structural and functional divergence. Moreover, there is a close link between morphological phenotypes and stromal and cancer-cell-related features that allow prediction of the morphological pattern [15]. Furthermore, a better understanding of the molecular background is conducive to preventing adverse drug reactions for defined patient groups [16, 17].

However, drug therapy matched to the molecular target does not necessarily produce positive results [18, 19]. This is affected by multiple factors such as tumor microenvironment and tumor heterogeneity. In summary, the foregoing findings demonstrate that the genetically, morphologically, phenotypically, and topologically distinct primary cancers can not only be present in an individual patient but also are of great significance to personalized medicine approaches, as they can limit therapeutic efficacy, and they are resistant to therapy.

This paper was aimed at reviewing the methods in literature regarding the precise diagnosis and prognosis prediction of neoadjuvant chemotherapy for tumors, using breast MRIs, for example. Taking tumor heterogeneity as the core issue, the deep learning-based radiogenomics analysis of breast tumor heterogeneity was studied, and the relationship between the imaging characteristics of heterogeneous tumors and molecular expression features was correspondingly explored as well. At the same time, geometric algebra was applied to design a framework for analyzing dynamic contrast enhanced MRI radiogenomics, and fully mining the rich spatial images, spatial signals, and semantic features in breast multidimensional magnetic resonance imaging. According to the heterogeneity of different tumors, an individualized model of neoadjuvant chemotherapy efficacy prediction was established by combining MRI information, molecular typing information, and clinical information of patients suffering from breast cancer, which provided scientific guidance for accurate diagnosis, treatment, and prognosis of patients, improved the survival rate of tumor patients, enhanced the life quality of patients after surgery, and achieved effective and rational utilization of medical resources.

The remainder of the paper is structured as follows: Section 2 discusses challenges in the analysis of tumor

heterogeneity using radiogenomic approaches; the main framework for radiogenomics analysis in literature is presented in Section 3, where the mathematical models applied for tumor diagnosis and the evaluation of tumor treatment and prognosis performance via multiomics are presented; Section 4 addresses outlook and future work, where a multilevel deep learning model named BiGRU-RNN is proposed for predicting the efficacy of neoadjuvant chemotherapy using radiogenomics. It is represented by introducing geometric algebra and enables the multidimensional unified analysis of dynamic contrast enhanced MRI radiogenomics; finally, Section 5 summarizes the most significant parts in each section in a simplified manner.

2. Challenges in the Analysis of Tumor Heterogeneity Using Radiogenomic Approaches

In biomedical analysis, tumor heterogeneity characteristics and multiple physiological tumor characteristics are not combined, and multimodal (parametric) imaging technology is not widely used [20]. Various “spectrum” analyses of images from different perspectives describing these physiological characteristics have led to the one-sidedness and singularity of the research. In addition, current radiogenomics analysis on tumor heterogeneity assumes that the voxel of each tumor image presents a single specific tissue characteristic. However, tumors are highly heterogeneous. Current resolution of clinical diagnostic images is rather finite, and the observed signal at a certain position (voxel) of the tumor may be a mixture and superposition of components of different characteristics [21, 22]. From the perspective of signal processing, tumor image heterogeneity is manifested as a multivariate (component) mixed signal processing problem. In this regard, a lot of preliminary researchers work on the DCE-MRI subcomponent decomposition [23, 24], the corresponding molecular information decomposition [25, 26], and an unsupervised convex analysis analyzing the components of different tissue characteristics of heterogeneous tumors [6]. These researches afford a further understanding of the physiology and molecular characteristics of tumors.

At present, this method is only applied for two-dimensional analysis of DCE-MRIs [27–29], and there is no further development of heterogeneous analysis of tumors based on three-dimensional multi-modal MRIs [30–32]. The radiogenomics issues such as the correlation between different subcomponents after decomposition and the application of tumor diagnosis and treatment also need further exploration. Additionally, current heterogeneity analysis and subregion/subcomponent decomposition research mainly focus on the tumor itself, ignoring the fact that tumor does not exist in isolation, which constantly exchanges information with the surrounding substance and microenvironment during the growing process, and is also affected by the surrounding substance. Tumor cells can reshape the microenvironment, and the changed microenvironment can

further affect the behavior and status of tumor cells, leading to tumor progression and metastasis. Therefore, the formation of tumor heterogeneity is the result of the joint action of the tumor body and its surrounding substance. Currently, heterogeneity analysis is mostly limited to the structure and function of the tumor itself, and there is few literatures reporting the heterogeneity of tumor stroma [33, 34].

In recent years, there have been several researches concerning the radiomics research of tumor stroma. For example, King et al. found that the increase in the dynamic enhancement rate of fibroglandular mammary glands was associated with higher mammary cancer morbidity [35], who divided the body into several band-shaped regions according to the distance from the tumor and investigated the relationship between these regions and the disease-free survival of breast cancer [36]. However, the analysis of tumor heterogeneity in these studies was still preliminary, qualitative, or semiquantitative analysis. No systematic work has been performed to quantitatively analyze the relationship between the tumor and the surrounding substance or analyze the heterogeneity of the substance. In addition, the analysis of tumor heterogeneity in radiogenomics research at this stage generally focuses on image feature analysis. The collected gene molecular information is assumed to be homogeneous by default, but in fact, the tissue collected in molecular expression analysis may be a mixture of tissues with different “content” and different characteristics [37]. Besides, current radiogenomics research does not analyze the heterogeneity of the tumor itself, resulting in the inaccuracy of the associated study, and even the appearance of “false relationships.” Previous research was conducted in terms of signal subcomponent decomposition analysis, biological verification research on gene expression values of different tissue characteristics (human brain, liver, and lung), and unsupervised identification of mixed tissue characteristics [31, 32]. The gene expression signal of heterogeneous tumors has not been further analyzed. Therefore, the research of radiogenomics based on the decomposition of gene information is urgently required.

3. Methodology of Radiogenomics in Literature

As a noninvasive modality, the multidimensional radiogenomics analysis based on Magnetic Resonance Imaging (MRI) has become a special field of study on the tumor grading. The field of radiogenomics has been advanced substantially by novel MR imaging sequences that reflect underlying oncogenic processes. MRI-based radiogenomics combines a mass of quantitative data extracted from multidimensional MR images with individual genomic phenotypes and builds a prediction model through deep learning, which aims to make a diagnosis for patients, offer guidance for therapeutic strategies, and make an evaluation on clinical outcomes [38]. Additionally, some issues existing in radiogenomic analysis are specified, and corresponding solutions from prior works are provided [39]. Illustratively, the abundance of immune and stromal cells in the Tumor Microenvironment (TME) indicates the levels of

inflammation, angiogenesis, and desmoplasia. It has been proven that radiomics, an approach of extracting quantitative features from radiological imaging to characterize diseases, can predict molecular classification, cancer recurrence risk, etc. However, the ability of radiomics to predict the abundance of various cells in the TME remains unknown. Arefan et al. [40] carried out studies by applying a radiogenomics approach and building machine learning models to capture one-to-one relationships between radiomic features from Dynamic-Contrast Enhanced Magnetic Resonance Imaging (DCE-MRI) and cell abundance of gene expression data and then predict the infiltration of multiple cells in breast cancer lesions. It is concluded that radiogenomics contributes to computer-aided diagnosis, treatment, and prognostic prediction for patients with tumors in a routine clinical setting.

3.1. Tumor Diagnosis Research Based on Radiogenomics. Radiogenomics, as an important application, reveals and reflects the molecular pathological characteristics of tumor tissues, such as dynamic enhancement characteristics for tumor and mammary-gland tissue [33, 34] and breast asymmetry characteristics [34] in distinguishing benign and malignant tumors using noninvasive and dynamic imaging technology.

Tumor molecular classification is an important index in clinical diagnosis. In several studies, quantitative image features, such as the dynamic enhancement ratio of the lesion to the background area, gray-scale histogram features, and 66texture, are used to predict these molecular indicators [37, 41]. It has been reported that there are 90 extracted image features, including the morphology, dynamic enhancement, and bilateral asymmetry of breast cancer tumors and their background regions, all of which are used to distinguish four molecular subtypes of breast cancer [42]. In recent years, radiomics features, including tumor volume, shape, edge morphology, and dynamic characteristics, have also been used to predict the expression of gene chips for clinical diagnosis, such as MammaPrint, Oncotype DX, and PAM50 gene arrays [43–45]. Additionally, some researchers have studied the MR image characteristics of breast cancer in the TCIA database and the molecular information such as miRNA, gene somatic mutation, protein expression, and copy number variation of these patients in the corresponding TCGA database. It has been found that there are several genetic signaling pathways, gene mutation sites, and image feature modules significantly related to gene expression modules [46]. The above-mentioned study in image group characteristics and gene expression correlation is to explore the imaging biomarkers of tumor molecular characteristics, thus providing services for clinical diagnosis [47].

3.2. Tumor Treatment and Prognosis Research Based on Imaging Group Feature Analysis. Currently, a large amount of research regarding radiogenomics focuses on exploring the relationship between imaging group and molecular features.

Some work bypasses the association between imaging and molecular information and directly uses imaging features to predict treatment results.

It has been investigated that the imaging phenotype of the tumor can be used to provide information on the outcome of tumor treatment, such as chemotherapy efficacy and prognosis. Fan et al. extracted 156 image features of breast tumors and background regions using DCE-MRIs and selected several distinguishing heterogeneous features reflecting gray-scale unevenness, such as kurtosis and skewness, to predict the effectiveness of NAC for breast cancer [48]. Huang et al. extracted the gray-scale texture features of colorectal cancer images to predict lymph node metastasis (disease-free survival) before surgery [49]. Some researchers used cluster analysis to divide the imaged tumor into different regions according to the dynamic enhancement mode, analyzed the differences in the texture characteristics of these regions before and after chemotherapy, and predicted the efficacy of chemotherapy using the detected features [26], proving that the imaging characteristics of different tumor areas could be used to predict the efficacy of NAC. Additionally, key tumor genes were detected and identified by analyzing the differences in the network structure of the tumor genome before and after treatment, combined with the analysis of the tumor volume growth pattern of MRIs in terms of its longitudinal time, to predict the treatment response of tumors [50].

With the use of perfusion magnetic resonance (MR) imaging, Wu et al. characterized intratumoral spatial heterogeneity and studied the tumor homogeneity to predicate the recurrence-free survival (RFS) of the patients with breast cancer [51]. Figure 2 proposed a two-stage intratumor partition framework, including stage I: individual level cluster; and stage II: population level cluster. Primarily, at a personal level, every tumor is exceedingly segmented via superpixels using four kinetic features, that is, percentage and signal enhancement ratios, as well as the wash-in and wash-out slopes, according to DCE-MRIs [52–54]; secondly, at the population level, a consensus cluster can be used to aggregate and uniformly mark all superpixels from the entire population. Additionally, it is possible to establish the congruent relationship between tumor subregions across patients among the given population. Breast cancer is constituted by several subregions with different spatial features, and the intratumoral spatial heterogeneity is characterized and quantified via the defined multi-regional spatial interaction (MSI) matrix. As a distinct independent prognostic factor, imaging heterogeneity is beyond those traditional predictive risk factors; similar radiogenomics is also used for predicting NAC efficacy [50, 55–57], prognosis [26, 48], survival period [58], distant metastasis [59], etc. However, most tumor treatments based on radiogenomics regimen only focus on describing and analyzing the overall gray-scale unevenness (texture, etc.) of imaged tumors [43], and the influence for diagnosis and treatment is rarely analyzed and measured in terms of the subregions (components) of heterogeneous tumors [44].

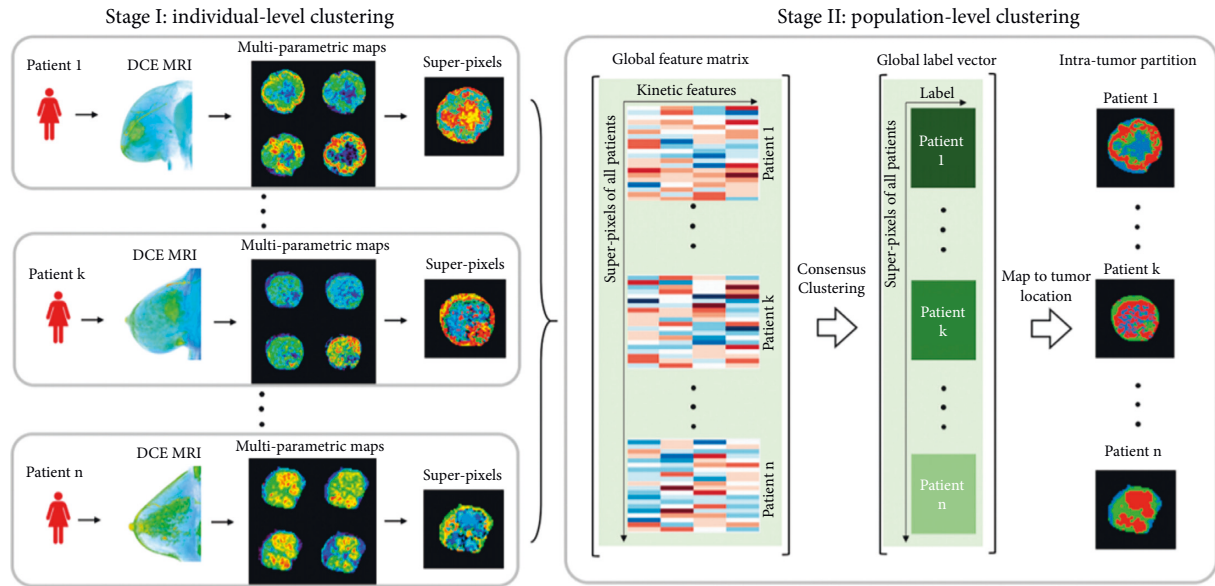


FIGURE 2: Introduction of the Two-Stage Intratumoral Partition Framework, that is, stage I: individual level cluster; and stage II: population level cluster, showing the use of matrix originating from intratumor partition diagrams. Quantitative imaging characteristic were obtained from MSI matrix for the sake of the measurement towards the spatial heterogeneity in tumors [51].

3.3. Tumor Treatment and Prognosis Research Based on Multiomics Approaches. Apart from the mentioned analysis of imaging group features, some researchers have also attempted to establish a multiomics approach for tumor diagnosis and treatment by combining image features and molecular features. For example, it was found that imaging methods exhibited different prediction results for patients with different molecular subtypes of breast cancer. Specifically, HER2-positive breast cancer was found to have a higher accuracy rate for its NAC treatment, while human epidermal growth factor receptor 2 (HER2) and triple-negative breast cancer (TNBC) had a lower accuracy rate [60], since patients with HER2-NBC and TNBC types presented high heterogeneity. During the establishment of tumor diagnosis and treatment models, intrinsic molecular characteristics shall be combined (HER2, etc.) to increase prediction accuracy. Sutton et al. found in the study of predicting breast cancer molecular subtypes based on image features that the accuracy of the model was significantly improved after adding clinical data and pathological data, including age of patients, tumor volume, tumor pathological grade, and accumulation of lymph node [61].

It was revealed that imaged tumor features and patient symptoms could be complementary, and the combination of the two could improve the accuracy of the prediction model. Although researchers have made considerable efforts on tumor diagnosis and treatment based on the analysis of clinical and molecular pathology information and image characteristics, there are few results in the research of precision diagnosis and treatment models combining the two features, and the methods and technologies in this area shall be studied and resolved. Besides, repeatability and reproducibility are the two relatively major problems [62] regarding radiogenomics analysis. The former refers to the consistency of multiple measurements under the same

environment and experimental conditions, while the latter denotes that of grouped image features in different locations, imaging parameters, and experimental subjects. Solutions to these two problems, especially the latter, are the key to the radiogenomics diagnosis and treatment model, which requires the combination of theory and practice. Although some scholars have made exploratory attempts in this regard, such as the use of validation sets to analyze the consistency of radiogenomics [63], there are still few basic methods of radiogenomics, especially tumor heterogeneity analysis, radiogenomics study, and evaluation of the application of scientific methods and models in clinical tumor diagnosis and treatment.

Tumor heterogeneity poses challenges to the precise diagnosis and treatment of breast tumors. Its systematic analysis provides extensive information for the characterization of breast tumors, and effective application of this information is of great significance to improve the accuracy of breast cancer diagnosis and treatment. Fan et al. [48] explored the heterogeneity of tumors by analyzing the subclones with a mass of gene modifications and functional effects, which offered a deeper understanding of the method to identify the bioactivity of certain subclones with a radiogenomic analysis, and predicted the prognosis non-invasively and clinically.

Besides, a modelling framework was proposed by Fan et al. [48], as shown in Figure 3, where multiscale intratumor heterogeneity was modelled, and the radiogenomic analysis was carried out regarding 1310 patients suffering from breast cancer on 5 datasets of 3 data groups. This modelling framework consisted of three phases. Firstly (Phase 1), a nonsupervision deconvolution analysis on gene expression profiles was adopted to achieve genomic subclones, including prognostic genomic signatures; secondly (Phase 2), radiogenomic genomic characterization was established by

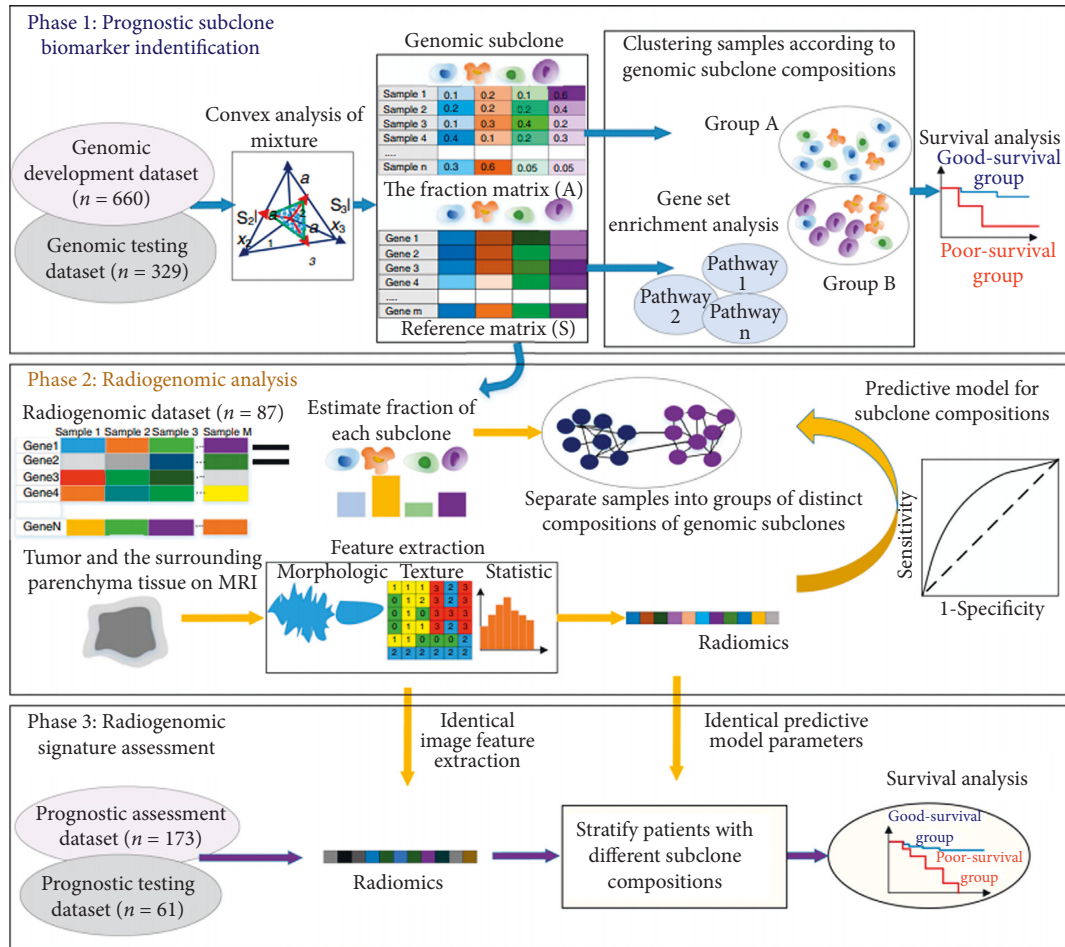


FIGURE 3: Framework of the Three-phase Study. Firstly (Phase 1), the nonsupervision deconvolution analysis on gene expression profiles is conducted to recognize prognostic subclone biomarkers. The gene set enrichment analysis is conducted to infer the biological functions of subclones; secondly (Phase 2), radiomic features onto compositions of prognostic subclones are mapped to establish radiogenomic signatures; thirdly (Phase 3), radiogenomic signatures are evaluated on another two independent datasets containing imaging and survival outcomes data [48].

means of mapping radiomic features onto compositions of prognostic subclones in an independent dataset containing the suited imaging and gene expression data from each tumor; thirdly (Phase 3), the predicated value of the recognized radiogenomic signatures was further investigated using another two independent datasets containing imaging and survival data. The findings provided a noninvasive and reproducible method to be used to identify tumor genomic subclones and their underlying biological clinical functions.

Table 1 is designed to intuitively classify and introduce the mentioned radiogenomics techniques and approaches in literature for diagnosis, treatment, and prognosis research.

4. Outlook and Future Work

Based on the radiogenomics techniques, this section aims to develop novel multidimensional mining algorithms, focusing on the key core issue of tumor heterogeneity. The proposed algorithms will lead to the identification of tumor patterns in complex geometric spaces. Through the analysis of multimodal images and molecular information reflecting

different functional characteristics of tumors, we aim (1) to deeply mine the spatial, temporal, and semantic features of breast multidimensional images across scales; (2) to reveal the relationship between the overall and regional imaging phenotypes of tumors and recognize their joint functional characteristics with gene expression together with molecular typing; (3) to provide new intelligent solutions for breast tumor clinical diagnosis and neoadjuvant chemotherapy efficacy prediction, which can effectively assist doctors to make correct treatment decisions and improve patients' health.

4.1. Temporal-Spatial Consistent Correlation Model Based on MRI Radiogenomics. According to different description methods for tumor heterogeneity, the analysis on tumor radiogenomic correlation is to be carried out at three levels, that is, analysis of the whole tumor region, tumor subregions, and tumor subcomponents; regarding a single time point; and longitudinal time axis. Different levels of tumor heterogeneity can be mapped using geometry algebraic

TABLE 1: is designed to intuitively classify and introduce the mentioned radiogenomics techniques and approaches in literature for diagnosis, treatment, and prognosis research. The bold text is the categories of radiogenomics techniques for tumor heterogeneity.

Genome sampling analysis technology for tumor heterogeneity	Gene expression modules [46].	Tumor treatment and prognosis research
Multi-region sampling strategy [6]	Imaging phenotype of the tumor [48, 49]	Predicting NAC efficacy [50, 55–57]
Micro-cutting of tumor tissues [6]	Imaging characteristics of different tumor areas [26]	Survival period [58], distant metastasis [59]
Longitudinal sampling [7–9]	Key tumor genes [27]	Predicate the recurrence-free survival (RFS) [48]
Radiogenomic approaches for tumor heterogeneity	Molecular information decomposition [25, 26],	Multiomics approaches [61]
DCE-MRI subcomponent decomposition [26, 27]	Unsupervised convex analysis [6]	Intratumor heterogeneity
Unsupervised identification of mixed tissue characteristics [34, 35].	Radiomics research for tumor heterogeneity	Multiscale intratumor heterogeneity [48]
Tumor molecular classification [40–42]	Dynamic enhancement rate of fibroglandular mammary glands [33–35]	Perfusion magnetic resonance (MR) imaging via a two-stage intratumor partition framework [51]

decomposition in relation to the multidimensional image space, image subspaces in different directions corresponding to the same dimensional image vector, and the cross-dimensional image signal vector features in different directions.

It is a crucial basis for accurate analysis of radiogenomics to realize the rapid and automatic parameter extraction of unstructured breast radiomics data and the effective fusion of unstructured feature vectors with diagnostic value found in structured data.

Based on the theory of geometric algebra, tumor images with different structures are transformed from complex geometric objects to straightforward geometries like dots, lines, and polygons that can be directly expressed in Euclidean space, so as to realize the hierarchical decomposition of the complex geometric data of breast tumors. Appropriate image segmentation and deep clustering methods should be adopted to analyze multiple geometric vectors in different dimensions. The final aim is to achieve deep learning and feature extraction of tumor heterogeneity based on multidimensional uniformity analysis in a multivector space and achieve the transition from unstructured imaging to structured genomics data.

As discussed in [64], it is easy to extend a scalar product to Clifford or geometric product to explain errors caused by patient movement, extract nonlinear features from images, or clarify observed scaling changes across the dimensions of a tumor, as illustrated in Figure 4.

4.2. Deep Association Learning between MRI Radiomics and Genomics. There are three parts proposed below for further realization of the deep association learning between MRI radiomics and genomics, as illustrated in Figure 5.

4.2.1. Global Heterogeneity Analysis via the Correlation between Image and Molecular Features. Weak supervision can facilitate the acquisition of the datasets marked manually. Weak supervision learning enables the application of inexpensive weak labels, and such labels can be exploited to build a powerful prediction model. The overall heterogeneity

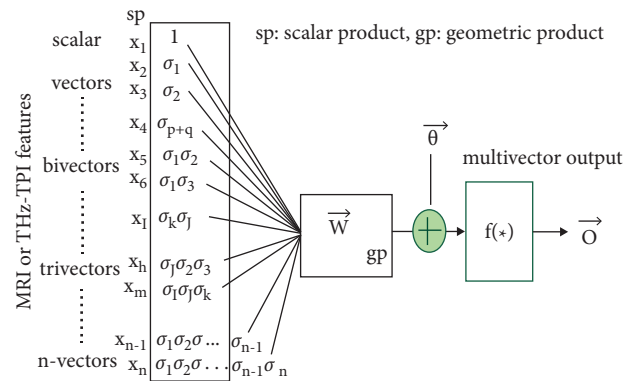


FIGURE 4: Geometric neuron based on McCulloch-Pitts neuron for MRI Imaging Datasets based on General Framework mentioned in References [64, 69] where sp presents a scalar product; $\{\sigma_i\}$, $i = 1, 2, \dots, n$ orthonormal basis vectors; and gp, geometric product.

of tumors can be measured, analyzed, and classified using weakly supervised learning [66–69] of imaged tumors. Weakly supervised spatial clustering can be used to sort the decomposed subregions according to the value of the cluster center position.

Taking DCE-MRI as an example, the clustering results of the initial enhancement speed and the later decline speed of the enhancement curve can be sorted out to obtain several (i) “omics” features, and this process for all tumor images (j) can be sorted out to obtain an $i \times j$ matrix, so that feature calculation and classification research can be performed on the same time signal dimension.

Meanwhile, in view of the characteristics of biomedical functions reflected in tumor images, it is proposed to study the correlation based on multimodal (parametric) image features and molecular analysis features. In order to comprehensively analyze the heterogeneity of different functional characteristics of tumors, image registration [70–73] is performed for calculating different functional images of tumors, including DCE-MRI and DWI, to obtain multiple “dimensions,” which means that each pixel point corresponds to dynamic characteristics, diffusion characteristics,

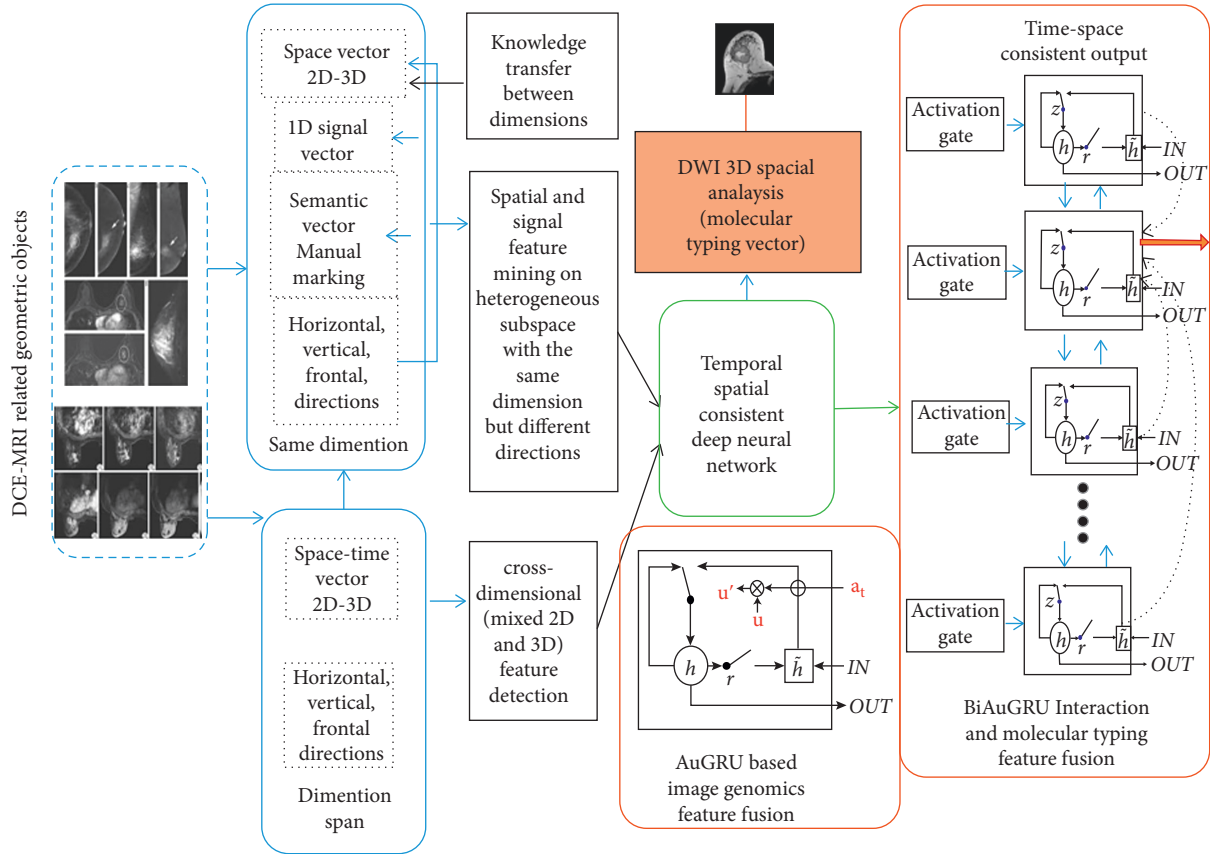


FIGURE 5: Framework regarding the association of MRI group and genome based on the analysis of spatial-temporal consistency.

etc. Such characteristic can be further used to calculate high-dimensional characteristics of imaged tumor heterogeneity and their correlation with molecular fractal characteristics.

4.2.2. Correlation between Heterogeneous Image and Molecular Features via Subdomain Decomposition. To fully analyze the correlation between heterogeneous image features and molecular features, the mixed images and gene molecular expression signals are suggested to be decomposed separately. This practice is to realize high- and multidimensional vector analysis in an integral space, also the multidimensional subspace region analysis, and spatial-temporal consistency analysis of heterogeneous subcomponents. The goal is to establish correlation models at different levels and achieve more accurate relationship to highlight key entities for the image or signal processes and the relationship between multiple entities (spatial-temporal) in multidimensional vector space or subspace.

Simultaneously, the gene expression data can be analyzed using subpathways, submodules, and enrichment methods, thereby dividing them into several representative pathways, marked modules, and gene clusters. The expression signal is expected to break down according to different tissue and cell characteristics using the signal decomposition method, which will in turn constitute a “convex hull,” each containing some “marked” genes [74].

In order to study the correlation between characteristic components in terms of different tissues, the correlation

between the subregions (components) of the tumor heterogeneity should be analyzed and sorted by the spatial-temporal consistency-based algorithm after the decomposition of the image group and gene expression data, as shown in Figure 5. Taking the dynamic enhanced image as an example, it is supposed that there are three subcomponents with different tissue features sorted into three levels according to the enhancement curve of each subcomponent after decomposition, that is, fast blood flow, medium blood flow, and slow flow velocity.

Each sample is decomposed into these three types of subcomponents, and then the radiogenomic association of each subcomponent (fast, medium, and slow) is analyzed separately for all samples. Unlike traditional analysis methods, the attention-based deep learning network aims to study and analyze the correspondence between high-dimensional image vectors and gene expression subcomponents and try to obtain more accurate map of relationships based on the relationship between “pure” subcomponents with the directions of themselves.

4.2.3. Bidirectional Threshold Recurrent Neural Network (BiGRU-RNN) Model. The effective embedding of radiomics and genomics information plays a key role in establishing spatial-temporal consistent model of radiogenomics. The genomics information of breast multi-dimensional dynamic imaging is intricate, including image sequence information, and time series information, both unstructured

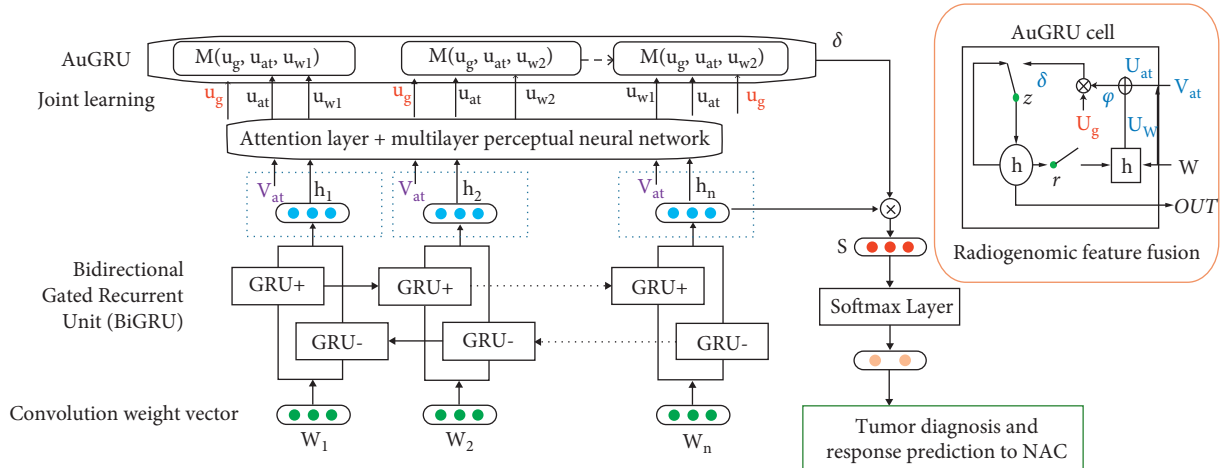


FIGURE 6: BiGRU-RNN network model based on attention. Symbols $\{w_1, \dots, w_n\}$ are input parameters in relation to MRI radiomics, and the output vectors $\{u_w\}$ and $\{u_{at}\}$ regard the hidden layer vector $\{h_1, \dots, h_n\}$ and the radiomics feature vector V_{at} through the multilayer perceptual network. Similarity matrix δ contains the similarities between the genomics vector u_g and output attention weight vector ψ : namely, the ultimate output of radiogenomics eigenvector is achieved in accordance with the concealed layer vector $\{h_1, \dots, h_n\}$ and AuGRU weight vector δ . Radiogenomic feature fusion is conducted as an AuGRU cell.

data of magnetic resonance imaging and structured vector of genomics. The design of gated loop unit with memory mechanism is important not only for timing information, but also for the memory and integration of image and genomics information.

Therefore, the two-way activation embedding method of the gated cyclic unit is designed based on the lightweight BiGRU, and the activation gate is introduced to process the genomics data of breast cancer patients with individual differences. The AuGRU model enables effective fusion of the genome sequence-related output and tumor heterogeneity analysis via radiogenomics, along with molecular typing for classification.

Additionally, it is of importance to design a bidirectional threshold recurrent neural network (BiGRU-RNN) model based on memory and attention mechanism, which highlights tissue-level radiomics feature input and molecular typing feature vector and encodes the contextual interaction mechanism of the genomics feature vector of tumor. Such a model plays a key role in carrying out the effective correlation of the spatiotemporal features of dynamic images and constructing a joint representation model of image data and genomics data. The schematic diagram summarizing the proposed attention-based BiGRU-RNN network model is shown in Figure 6.

5. Discussion

Radiogenomics characteristics reveal multiscale intratumoral heterogeneity concerning biological functions and survival in breast cancer. These studies performed diagnosis and treatment analysis by measuring the characteristics of overall tumor heterogeneity. For example, the research group of Huang et al. used 132 texture features of CT images to forecast the Disease-Free Survival (DFS) of non-small cell lung cancer (NSCLC) [49], and Goh et al. used fractal dimension features to diagnose and analyze colorectal cancer

[75]. However, the heterogeneity features extracted by these methods are basically a measure of the degree of overall tumor heterogeneity (inhomogeneity) based on the gray-scale of tumor images, which fails to reflect the basic facts that heterogeneous tumors are composed of tissues with different characteristics. Biomedical analysis of tumors shows that different spatial regions may exhibit changed physiological characteristics [76], leading to specific regions corresponding to different cancer treatment responses, molecular subtypes [77], etc. In order to analyze the heterogeneity of subfunction regions, Diehn et al. selected two regions with high dynamic enhancement rate and low enhancement rate in DCE-MRIs in gliomas. The hypoxia gene expression values of these two tissue regions also showed corresponding high expression values and low expression values; that is, the tumor heterogeneous expression regions are significantly related to imaging characteristics [78]. The first international study explored the correlation between tumor imaging regional features and molecular features. However, the study only detected the heterogeneity between different tumor regions through imaging methods but failed to achieve precise positioning and quantitatively describe the distribution and characteristics of the heterogeneous regions.

In order to accurately locate and describe the imaging heterogeneity of tumor subregions, researchers around the world have made some preliminary attempts to describe the heterogeneity of different tissue characteristics using different imaging modalities [63, 77, 79]. Tumor heterogeneity analysis must first define “content” from the perspective of the image and assign different “attribute” at each voxel to tissue characteristics in the image. For instance, DCE-MRIs measure the status of tumor blood flow and blood vessels; diffusion-weighted images reflect the diffusion and permeability of tumor water molecules; perfusion images measure tumor vascular proliferation, etc. [80] In this way, different tumor tissue characteristics and pathological

characteristics can be reflected through a variety of imaging techniques from different perspectives. Taking DCE-MRI as an example, it is reported that DCE-MRIs can be divided into several different representative feature regions according to a certain threshold, and texture features are calculated in these regions to measure the heterogeneity degree of these regions [77, 81, 82]. An increasing number of sophisticated methods cluster similar dynamic enhancement patterns [13, 83, 84] and describe the heterogeneity of vascular characteristics in tumor spaces through DCE-MRIs. But technically, the current stage of tumor heterogeneity analysis is still in its infancy.

As mentioned previously, malignant tumor has become one of the most common diseases harmful to human health, whose precise diagnosis and treatment are studied internationally, but remains unsettled. This paper focused on the precise diagnosis and prognosis prediction of neoadjuvant chemotherapy for cancer disease. Centering the tumor heterogeneity, this paper investigated radiogenomic methods for tumor heterogeneity analysis based on machine learning and explored the relationship between the imaging characteristics and molecular expression characteristics of heterogeneous tumors. A multidimensional MRI radiogenomics data analysis framework was designed based on geometric algebraic representation model to comprehensively explore the rich spatial images, spatial signals, and semantic features in multidimensional multimode MRIs. Besides, a spatial-temporal representation model was designed by focusing on both local and the global feature spaces in different hierarchy, and diversified self-attention mechanisms were implemented. Regarding the heterogeneity of different tumors, this paper proposed an individualized radiogenomic model combining the information about tumor imaging, molecular classification, and tumor clinical treatment for predicting the curative effect of neoadjuvant chemotherapy. It provides scientific guidance for accurate diagnosis, treatment, and prognosis of breast tumor patients, for the purpose of improving the cure rate of the patients with tumor, enhancing the well-being of patients after surgery, and using medical resources effectively and reasonably.

6. Conclusions

Tumor heterogeneity is a determinant playing a key role in therapeutic effect and is scarcely known from the perspective of molecular [85]. This paper aims to review the leading research on MRI radiogenomics methods based on the research frontiers in the fields of artificial intelligence and machine learning and focuses on the key core issue of tumor heterogeneity. By analyzing multimodal MR images and molecular information, it is expected to afford methods that can reflect the different functional heterogeneities of tumors. This paper provides a new framework related to temporal-spatial consistent correlation model based on MRI radiogenomics and offers novel intelligent solutions for tumor clinical diagnosis and curative effect prediction in aspects of neoadjuvant chemotherapy, aiming to effectively assist doctors in making correct treatment decisions and improve

patients' survival rate and well-being. Two contributions are represented in this paper: (1) an in-depth exploration is conducted for the cross-scale spatial, temporal, and semantic features of multidimensional MR images to be analyzed to reveal the spatial and temporal heterogeneity of tumors with geometric algebra onto radiogenomic methods and achieve correlation analysis from the local functional area to the global semantic space; (2) a novel bidirectional Gated Recurrent Unit (GRU) recurrent neural network (BiGRU-RNN) model is proposed to establish a multidimensional consistent deep learning of tumor heterogeneity with integrating MR imaging parameters and gene expression and predict the curative effect of tumor neoadjuvant chemotherapy.

Conflicts of Interest

The authors declare that they have no conflicts of interest.

Acknowledgments

This work was funded by Science and Technology Projects in Guangzhou, China (Grant no. 202102010472) and National Natural Science Foundation of China (NSFC) (Grant no. 62176071).

References

- [1] S. W. Piraino, V. Thomas, O. Peter, and S. J. Furney, "Mutations: driver versus passenger," *Paolo Boffetta, Pierre Hainaut, Encyclopedia of Cancer* pp. 551–562, Academic Press, Massachusetts, MA, USA, Third Edition, 2019.
- [2] D. L. Longo, "Tumor heterogeneity and personalized medicine," *New England Journal of Medicine*, vol. 366, no. 10, pp. 956–957, 2012.
- [3] L. A. Garraway, J. Verweij, and K. V. Ballman, "Precision oncology: an overview," *Journal of Clinical Oncology*, vol. 31, no. 15, pp. 1803–1805, 2013.
- [4] J. P. O'Connor, C. J. Rose, J. C. Waterton, R. A. Carano, G. J. Parker, and A. Jackson, "Imaging intratumor heterogeneity: role in therapy response, resistance, and clinical outcome," *Clinical Cancer Research*, vol. 21, no. 2, pp. 249–257, 2015.
- [5] R. A. Burrell, N. McGranahan, J. Bartek, and C. Swanton, "The causes and consequences of genetic heterogeneity in cancer evolution," *Nature*, vol. 501, no. 7467, pp. 338–345, 2013.
- [6] A. Marusyk and K. Polyak, "Tumor heterogeneity: causes and consequences," *Biochimica et Biophysica Acta (BBA) - Reviews on Cancer*, vol. 1805, no. 1, pp. 105–117, 2010.
- [7] Please provide complete details.
- [8] Please provide complete details.
- [9] Please provide complete details.
- [10] P. L. Bedard, A. R. Hansen, M. J. Ratain, and L. L. Siu, "Tumour heterogeneity in the clinic," *Nature*, vol. 501, no. 7467, pp. 355–364, 2013.
- [11] L. Ding, T. J. Ley, D. E. Larson et al., "Clonal evolution in relapsed acute myeloid leukaemia revealed by whole-genome sequencing," *Nature*, vol. 481, no. 7382, pp. 506–510, 2012.
- [12] H. Bai, A. S. Harmanci, E. Z. Erson-Omay et al., "Integrated genomic characterization of IDH1-mutant glioma malignant progression," *Nature Genetics*, vol. 48, no. 1, pp. 59–66, 2016.

- [13] J. Wu, G. Gong, Y. Cui, and R. Li, "Intratumor partitioning and texture analysis of dynamic contrast-enhanced (DCE)-MRI identifies relevant tumor subregions to predict pathological response of breast cancer to neoadjuvant chemotherapy," *Journal of Magnetic Resonance Imaging*, vol. 44, no. 5, pp. 1107–1115, 2016.
- [14] R. Nazarian, H. Shi, Q. Wang et al., "Melanomas acquire resistance to B-RAF(V600E) inhibition by RTK or N-RAS upregulation," *Nature*, vol. 468, no. 7326, pp. 973–977, 2010.
- [15] F. Janku, J. J. Lee, A. M. Tsimberidou et al., "PIK3CA mutations frequently coexist with RAS and BRAF mutations in patients with advanced cancers," *PLoS One*, vol. 6, no. 7, Article ID e22769, 2011.
- [16] H. El-Osta, D. Hong, J. Wheler et al., "Outcomes of research biopsies in phase I clinical trials: the MD Anderson cancer center experience," *The Oncologist*, vol. 16, no. 9, pp. 1292–1298, 2011.
- [17] E. S. Kim, R. S. Herbst, I. I. Wistuba et al., "The BATTLE trial: personalizing therapy for lung cancer," *Cancer Discovery*, vol. 1, no. 1, pp. 44–53, 2011 Jun.
- [18] M. C. Haffner, W. Zwart, M. P. Roudier et al., "Genomic and phenotypic heterogeneity in prostate cancer," *Nature Reviews Urology*, vol. 18, no. 2, pp. 79–92, 2021.
- [19] P. Sántha, D. Lenggenhager, A. Finstadsveen et al., "Morphological heterogeneity in pancreatic cancer reflects structural and functional divergence," *Cancers*, vol. 13, no. 4, p. 895, 2021.
- [20] R. G. Amado, M. Wolf, M. Peeters et al., "Wild-type KRAS is required for panitumumab efficacy in patients with metastatic colorectal cancer," *Journal of Clinical Oncology*, vol. 26, no. 10, pp. 1626–1634, 2008.
- [21] E. Van Cutsem, C. H. Köhne, E. Hitre et al., "Cetuximab and chemotherapy as initial treatment for metastatic colorectal cancer," *New England Journal of Medicine*, vol. 360, no. 14, pp. 1408–1417, 2009.
- [22] R. Dienstmann, D. Serpico, J. Rodon et al., "Molecular profiling of patients with colorectal cancer and matched targeted therapy in phase I clinical trials," *Molecular Cancer Therapeutics*, vol. 11, no. 9, pp. 2062–2071, 2012.
- [23] L. De Mattos-Arruda, M. Oliveira, A. Navarro, M. Vilaro, P. Nuciforo, and A. Vivancos, "Molecular profiling of advanced breast cancer patients and benefit obtained from matched targeted therapy in early phase clinical trials," in *Proceedings of the European Cancer Congress Amsterdam*, Netherlands, 2013.
- [24] A. R. Padhani and K. A. Miles, "Multiparametric imaging of tumor response to therapy," *Radiology*, vol. 256, no. 2, pp. 348–364, 2010.
- [25] M. R. Junttila and F. J. de Sauvage, "Influence of tumour micro-environment heterogeneity on therapeutic response," *Nature*, vol. 501, no. 7467, pp. 346–354, 2013.
- [26] A. Kreso, C. A. O'Brien, P. van Galen et al., "Variable clonal repopulation dynamics influence chemotherapy response in colorectal cancer," *Science*, vol. 339, no. 6119, pp. 543–548, 2013.
- [27] L. Chen, P. L. Choyke, N. Wang et al., "Unsupervised deconvolution of dynamic imaging reveals intratumor vascular heterogeneity and repopulation dynamics," *PLoS One*, vol. 9, no. 11, Article ID e112143, 2014.
- [28] L. Chen, P. L. Choyke, and T. H. Chan, "Tissue-specific compartmental analysis for dynamic contrast-enhanced MR imaging of complex tumors," *IEEE Transactions on Medical Imaging*, vol. 30, no. 12, pp. 2044–2058, 2011.
- [29] N. Wang, T. Gong, R. Clarke et al., "UNDO: a Bioconductor R package for unsupervised deconvolution of mixed gene expressions in tumor samples," *Bioinformatics*, vol. 31, no. 1, pp. 137–139, 2015.
- [30] N. Wang, E. P. Hoffman, L. Chen et al., "Mathematical modelling of transcriptional heterogeneity identifies novel markers and subpopulations in complex tissues," *Scientific Reports*, vol. 6, no. 1, Article ID 18909, 2016.
- [31] L. Sun, J. He, X.-X. Yin et al., "An image segmentation framework for extracting tumors from breast Magnetic Resonance Images," *Journal of Innovative Optical Health Sciences*, vol. 11, no. 4, Article ID 1850014, 2018.
- [32] D. Pandey, X. Yin, H. Wang et al., "Automatic and fast segmentation of breast region-of-interest (ROI) and density in MRIs," *Heliyon*, vol. 4, no. 12, Article ID e01042, 2018.
- [33] X. X. Yin, S. Hadjiloucas, Y. Zhang, M. Y. Su, Y. Miao, and D. Abbott, "Pattern identification of biomedical images with time series: contrasting THz pulse imaging with DCE-MRIs," *Artificial Intelligence in Medicine*, vol. 67, pp. 1–23, 2016.
- [34] X.-X. Yin, S. Hadjiloucas, J. H. Chen, Y. Zhang, J.-L. Wu, and M.-Y. Su, "Tensor based multichannel reconstruction for breast tumours identification from DCE-MRIs," *PLoS One*, vol. 12, no. 3, Article ID e0172111, 2017.
- [35] X.-X. Yin, B. W.-H. Ng, K. Ramamohanarao, A. Baghai-Wadji, and D. Abbott, "Exploiting sparsity and low-rank structure for the recovery of multi-slice breast MRIs with reduced sampling error," *Medical, & Biological Engineering & Computing*, vol. 50, no. 9, pp. 991–1000, 2012.
- [36] X.-X. Yin, B. W.-H. Ng, Q. Yang, A. Pitman, K. Ramamohanarao, and D. Abbott, "Anatomical landmark localization in breast dynamic contrast enhanced MR imaging," *Medical, & Biological Engineering & Computing*, vol. 50, no. 1, pp. 91–101, 2012.
- [37] S. DeCordova, A. Shastri, A. G. Tsolaki et al., "Molecular heterogeneity and immunosuppressive microenvironment in glioblastoma," *Frontiers in Immunology*, no. 1402, p. 11, 2020.
- [38] A. Habib, N. Jovanovich, M. Hoppe et al., "MRI-based radiomics and radiogenomics in the management of low-grade gliomas: evaluating the evidence for a paradigm shift," *Journal of Clinical Medicine*, vol. 10, no. 7, p. 1411, 2021.
- [39] L. Shui, H. Ren, X. Yang et al., "The era of radiogenomics in precision medicine: an emerging approach to support diagnosis, treatment decisions, and prognostication in oncology," *Frontiers in Oncology*, vol. 10, Article ID 570465, 2020.
- [40] D. Arefan, R. M. Hausler, J. H. Sumkin, M. Sun, and S. Wu, "Predicting cell invasion in breast tumor microenvironment from radiological imaging phenotypes," *BMC Cancer*, vol. 21, no. 1, 2021.
- [41] Q. Yang, L. Li, J. Zhang, G. Shao, and B. Zheng, "A computerized global MR image feature analysis scheme to assist diagnosis of breast cancer: a preliminary assessment," *European Journal of Radiology*, vol. 83, no. 7, pp. 1086–1091, 2014.
- [42] Q. Yang, L. Li, J. Zhang, G. Shao, and B. Zheng, "A new quantitative image analysis method for improving breast cancer diagnosis using DCE-MRI examinations," *Medical Physics*, vol. 42, no. 1, pp. 103–109, 2014.
- [43] A. Karahaliou, K. Vassiou, N. S. Arikidis, S. Skiadopoulou, T. Kanavou, and L. Costaridou, "Assessing heterogeneity of lesion enhancement kinetics in dynamic contrast-enhanced MRI for breast cancer diagnosis," *British Journal of Radiology*, vol. 83, no. 988, pp. 296–309, 2010.
- [44] U. Preim, S. Glaßer, B. Preim, F. Fischbach, and J. Ricke, "Computer-aided diagnosis in breast DCE-MRI-

- quantification of the heterogeneity of breast lesions,” *European Journal of Radiology*, vol. 81, no. 7, pp. 1532–1538, 2012.
- [45] H. Li, Y. Zhu, E. S. Burnside et al., “MR Imaging radiomics signatures for predicting the risk of breast cancer recurrence as given by research versions of mammaprint, oncotype DX, and PAM50 gene assays,” *Radiology*, vol. 281, no. 2, pp. 382–391, 2016.
- [46] L. J. Grimm, J. Zhang, and M. A. Mazurowski, “Computational approach to radiogenomics of breast cancer: luminal A and luminal B molecular subtypes are associated with imaging features on routine breast MRI extracted using computer vision algorithms,” *Journal of Magnetic Resonance Imaging*, vol. 42, no. 4, pp. 902–907, 2015.
- [47] M. A. Mazurowski, J. Zhang, L. J. Grimm, S. C. Yoon, and J. I. Silber, “Radiogenomic analysis of breast cancer: luminal B molecular subtype is associated with enhancement dynamics at MR imaging,” *Radiology*, vol. 273, no. 2, pp. 365–372, 2014.
- [48] M. Fan, G. Wu, H. Cheng, J. Zhang, G. Shao, and L. Li, “Radiomic analysis of DCE-MRI for prediction of response to neoadjuvant chemotherapy in breast cancer patients,” *European Journal of Radiology*, vol. 94, 2017.
- [49] Y. Huang, Z. Liu, L. He et al., “Radiomics signature: a potential biomarker for the prediction of disease-free survival in early-stage (I or II) non-small cell lung cancer,” *Radiology*, vol. 281, no. 3, pp. 947–957, 2016.
- [50] A. Ashraf, B. Gaonkar, C. Mies et al., “Breast DCE-MRI kinetic heterogeneity tumor markers: preliminary associations with neoadjuvant chemotherapy response,” *Translational Oncology*, vol. 8, no. 3, pp. 154–162, 2015.
- [51] J. Wu, G. Cao, X. Sun et al., “Intratumoral spatial heterogeneity at perfusion MR imaging predicts recurrence-free survival in locally advanced breast cancer treated with neoadjuvant chemotherapy,” *Radiology*, vol. 288, pp. 26–35, 2018.
- [52] N. Bhooshan, M. L. Giger, S. A. Jansen, H. Li, L. Lan, and G. M. Newstead, “Cancerous breast lesions on dynamic contrast-enhanced MR images: computerized characterization for image-based prognostic markers,” *Radiology*, vol. 254, no. 3, pp. 680–690, 2010.
- [53] N. Hylton, “Dynamic contrast-enhanced magnetic resonance imaging as an imaging biomarker,” *Journal of Clinical Oncology*, vol. 24, no. 20, pp. 3293–3298, 2006.
- [54] T. E. Yankeelov and J. C. Gore, “Dynamic contrast enhanced magnetic resonance imaging in oncology: theory, data acquisition, analysis, and examples,” *Current Medical Imaging Reviews*, vol. 3, no. 2, pp. 91–107, 2007.
- [55] X. Li, H. Kang, L. R. Arlinghaus et al., “Analyzing spatial heterogeneity in DCE- and DW-MRI parametric maps to optimize prediction of pathologic response to neoadjuvant chemotherapy in breast cancer,” *Translational Oncology*, vol. 7, no. 1, pp. 14–22, 2014.
- [56] X. Li, L. R. Arlinghaus, G. D. Ayers et al., “DCE-MRI analysis methods for predicting the response of breast cancer to neoadjuvant chemotherapy: pilot study findings,” *Magnetic Resonance in Medicine*, vol. 71, no. 4, pp. 1592–1602, 2014.
- [57] J. R. Teruel, M. G. Heldahl, P. E. Goa et al., “Dynamic contrast-enhanced MRI texture analysis for pretreatment prediction of clinical and pathological response to neoadjuvant chemotherapy in patients with locally advanced breast cancer,” *NMR in Biomedicine*, vol. 27, no. 8, pp. 887–896, 2014.
- [58] D. A. Gutman, L. A. D. Cooper, S. N. Hwang et al., “MR imaging predictors of molecular profile and survival: multi-institutional study of the TCGA glioblastoma data set,” *Radiology*, vol. 267, no. 2, pp. 560–569, 2013.
- [59] T. P. Coroller, P. Grossmann, Y. Hou et al., “CT-based radiomic signature predicts distant metastasis in lung adenocarcinoma,” *Radiotherapy & Oncology*, vol. 114, no. 3, pp. 345–350, 2015.
- [60] J. H. Chen, S. Bahri, R. S. Mehta et al., “Breast cancer: evaluation of response to neoadjuvant chemotherapy with 3.0-T MR imaging,” *Radiology*, vol. 261, no. 3, pp. 735–743, 2011.
- [61] E. J. Sutton, B. Z. Dashevsky, J. H. Oh et al., “Breast cancer molecular subtype classifier that incorporates MRI features,” *Journal of Magnetic Resonance Imaging*, vol. 44, no. 1, pp. 122–129, 2016.
- [62] J. P. O’Connor, “Cancer heterogeneity and imaging,” *Seminars in Cell & Developmental Biology*, vol. 64, , 2016 In Press.
- [63] J. Wu, Y. Cui, X. Sun et al., “Unsupervised clustering of quantitative image phenotypes reveals breast cancer subtypes with distinct prognoses and molecular pathways,” *Clinical Cancer Research: An Official Journal of the American Association for Cancer Research*, vol. 23, no. 13, pp. 3334–3342. In Press, 2017.
- [64] X.-X. Yin, S. Hadjiloucas, Y. Zhang, and Z. Tian, “MRI radiogenomics for intelligent diagnosis of breast tumors and accurate prediction of neoadjuvant chemotherapy responses—a review,” *Computer Methods and Programs in Biomedicine*, vol. 214, Article ID 106510, 2022.
- [65] X.-X. Yin, L. Yin, and S. Hadjiloucas, “Pattern classification approaches for breastcancer identification via MRI: state-of-the-art and vision for the future,” *Applied Sciences*, vol. 10, no. 20, p. 7201, 2020.
- [66] Z.-Z. Zhou, “A brief introduction to weakly supervised learning,” *National Science Review*, vol. 5, no. 1, pp. 44–53, 2018.
- [67] S. Shikha, H. Bharat, K. Prathamesh, M. Justna, and G. Harsha, “Weakly supervised learning for categorization of medical inquiries for customer service effectiveness,” *Frontiers in Research Metrics and Analytics*, vol. 6, 2021.
- [68] D. W. Sajila and M. Md. Shaad, “Conditional-GAN based data augmentation for deep learning task classifier improvement using fNIRS data,” *Frontiers in Big Data*, vol. 4, 2021.
- [69] L. Torresani, “Weakly supervised learning,” in *Computer Vision*, K. Ikeuchi, Ed., Springer, Boston, MA, USA, 2014.
- [70] F. Oliveira and J. Tavares, “Medical image registration: a review,” *Computer Methods in Biomechanics and Biomedical Engineering*, vol. 17, pp. 73–93, 2014.
- [71] J. B. Antoine Maintz and M. A. Viergever, “A survey of medical image registration,” *Medical Image Analysis*, vol. 2, no. 1, pp. 1–36, 1988.
- [72] F. El-Zahraa Ahmed El-Gamal, M. Elmogy, and A. Atwan, “Current trends in medical image registration and fusion,” *Egyptian Informatics Journal*, vol. 17, no. 1, pp. 99–124, 2016.
- [73] D. L. G. Hill, P. G. Batchelor, M. Holden, and D. J. Hawkes, “Medical image registration,” *Physics in Medicine and Biology*, vol. 46, pp. R1–R45, 2001.
- [74] S. Mohammadi, V. Ravindra, D. F. Gleich, and A. Gramav, “A geometric approach to characterize the functional identity of single cells,” *Nature Communications*, vol. 9, no. 1, p. 1516, 2018.
- [75] V. Goh, B. Sanghera, D. M. Wellsted, J. Sundin, and S. Halligan, “Assessment of the spatial pattern of colorectal tumour perfusion estimated at perfusion CT using two-dimensional fractal analysis,” *European Radiology*, vol. 19, no. 6, pp. 1358–1365, 2009.

- [76] R. J. Gillies, P. E. Kinahan, and H. Hricak, "Radiomics: images are more than pictures, they are data," *Radiology*, vol. 278, no. 2, pp. 563–577, 2016.
- [77] R. A. Gatenby, O. Grove, and R. J. Gillies, "Quantitative imaging in cancer evolution and ecology," *Radiology*, vol. 269, no. 1, pp. 8–14, 2013.
- [78] M. Diehn, C. Nardini, D. S. Wang et al., "Identification of noninvasive imaging surrogates for brain tumor gene-expression modules," *Proceedings of the National Academy of Sciences*, vol. 105, no. 13, pp. 5213–5218, 2008.
- [79] O. Grove, A. E. Berglund, M. B. Schabath et al., "Quantitative computed tomographic descriptors associate tumor shape complexity and intratumor heterogeneity with prognosis in lung adenocarcinoma," *PLoS One*, vol. 10, no. 3, Article ID e0118261, 2015.
- [80] S. H. Kim, H. S. Lee, B. J. Kang et al., "Dynamic contrast-enhanced MRI perfusion parameters as imaging biomarkers of angiogenesis," *PLoS One*, vol. 11, no. 12, Article ID e0168632, 2016.
- [81] A. R. Padhani, "MRI for assessing antivasular cancer treatments," *British Journal of Radiology*, vol. 76, no. suppl_1, pp. S60–S80, 2003.
- [82] B. Chaudhury, M. Zhou, D. B. Goldgof et al., "Heterogeneity in intratumoral regions with rapid gadolinium washout correlates with estrogen receptor status and nodal metastasis," *Journal of Magnetic Resonance Imaging*, vol. 42, no. 5, pp. 1421–1430, 2015.
- [83] X.-X. Yin, L. Yin, and S. Hadjiloucas, "Pattern classification approaches for breastcancer identification via MRI: state-of-the-art and vision for the future," *Applied Sciences*, vol. 10, no. 20, 2020.
- [84] XX. Yin, Y. Zhang, J. Cao, JL. Wu, and S. Hadjiloucas, "Exploring the complementarity of THz pulse imaging and DCE-MRIs: toward a unified multi-channel classification and a deep learning framework," *Computer Methods and Programs in Biomedicine*, vol. 137, pp. 87–114, 2017.
- [85] K. H. Allison and G. W. Sledge, "Heterogeneity and cancer," *Oncology*, vol. 28, no. 9, pp. 772–778, 2014.

Research Article

Analysis of Diversified Radio and Television Data Based on Adaptive Least Squares Support Vector Machine

Jing Liu¹ and Minnan Cang² 

¹College of Liberal Arts, Chifeng University, Neimenggu 024000, China

²Xi'an University of Technology the School of Art and Design, Xi'an 710000, China

Correspondence should be addressed to Minnan Cang; cangminnan@xaut.edu.cn

Received 30 March 2022; Revised 18 May 2022; Accepted 7 June 2022; Published 5 July 2022

Academic Editor: Le Sun

Copyright © 2022 Jing Liu and Minnan Cang. This is an open access article distributed under the Creative Commons Attribution License, which permits unrestricted use, distribution, and reproduction in any medium, provided the original work is properly cited.

Under the current big data background, the training mode of radio and television director technology is obsolete, and the technical means do not meet the needs of modern development. In this article, a self-adaptive multivariate data statistical model of radio and television directors based on the least squares support vector machine is proposed, which combines the students' views with the diversified teaching methods and teaching contents needed by university teachers in the process of vocational education and television education. This article applies the technology integration degree measurement, market integration degree measurement, business integration degree measurement, and integration degree comprehensive analysis to analyze the data of major video websites and major radio and television media. It is found that the market share of major radio and television media is increasing, and the number of broadcasts of major video online stores is also excellent.

1. Introduction

According to China's demand for talents in radio and television industry and the status of education professionals, the director of experimental teaching of radio and television specialty should actively introduce the advanced teaching concept of postmodernism; evaluate and innovate from the aspects of experimental teaching mode, process, method, and behavior; build an experimental teaching system with the characteristics of postmodern teaching theory; and cultivate the innovative spirit and practical ability of radio and television art complex [1]. With the continuous development of new media technology, the market demand for employment is gradually increasing, but the market competition is becoming increasingly fierce. The development of radio and television specialty in China needs more radio and television professionals, and the requirements for talents' skills and quality are also improved. With the rapid development of new media, the demand for applied talents of radio and television director specialty is gradually increasing [2]. A new discrete particle swarm optimization method is

proposed to induce rules from discrete data. The proposed algorithm initializes the population by considering the discrete nature of the data. It assigns different fixed probabilities to the current, local, and global optimal positions. Based on these probabilities, each member of the population iteratively updates its position [3]. The explicit model-based approach to phylogenetic analysis of discrete morphological data opens up several new research approaches, including combined data likelihood analysis (morphological + sequential data), likelihood ratio test, and Bayesian analysis [4]. Linear hybrid models have become the main parameterization tool for analyzing continuous longitudinal data. This article shows how to implement different methods in the SAS software package [5]. Data interpolation is created under two models: multivariate normal model with rounding and discrete model with conditional designation. JM method introduces deviation in reference curve, while FCS does not. This article concludes that FCS is a useful and easy-to-apply flexible alternative to JM [6] when convenient and realistic joint distribution cannot be specified. Cha-meleon algorithm technology focuses on finding clusters in

datasets and detailed information of its main functions, dynamic modeling information of chameleon and comparison between interconnectivity and similarity (limitations of traditional clustering algorithms) [7]. This article evaluates the changing role of dynamic modeling in understanding and discrete dynamic modeling of diversified adaptive data for broadcast and television directors. It discusses new modeling tools for problem scoping and consensus building among a wide range of stakeholders and describes four case studies where dynamic modeling has been used to collect and organize data, synthesize knowledge, and build consensus on the management of complex systems [8]. Two methods to solve the problem of dynamic allocation and route guidance are studied: first, the optimal control method to realize the optimization of a dynamic system or user; second, to establish the feedback concept of dynamic user optimal conditions [9]. Landscape and physical environment shape migration schedules and affect people's ability to interpret patterns observed during stop-overs. Modeling these factors may lead to new insights into migration adaptation in heterogeneous environments [10]. Scale dependence and spatiotemporal dynamics are the two issues that underpin the considerable attention that modelers and statisticians now devote to the quantitative study of ecological edges and boundaries. We introduced the links between methods for demarcating boundaries, monitoring boundary changes, and modeling edge-related dynamics. In this process, we clarify the statistical and mathematical methods of ecological edge and boundary research and discuss the important remaining problems in the field of quantitative edge research [11]. In order to adapt to the gradual diversified development, a diversified training mode for graduate students has been formed. At the same time, in order to meet the needs of people's learning and creation in modern society, graduate education presents an international, diversified, modern, and personalized development trend [12]. Their most influential discrete imaging (DT) uses nanoscale technology to generate a large amount of data. Data footprint production (DFR) is a process that uses almost all of given ETF data at a shorter storage speed. His very advanced lossless compressor or classical probability model is very suitable for final application requirements, such as "arbitrary depth" (ABD) solutions and "dynamic data scale, exploring data-related information" [13]. The moving window detection process of discrete data is studied. The probability of detection waiting time and the limit of expected value are derived. The boundary is evaluated for independent and identically distributed zero-Bernoulli test, binomial and Poisson random variables, and two-state stationary Markov chain. The results are applicable to radar detection theory, time-sharing system, and quality control [14]. For goals and training programs, by constructing a scientific curriculum system, establishing characteristic curriculum relations, expanding diversified teaching forms, strengthening innovative practical teaching concepts, and developing digital laboratories and other measures, we can train talents, explore Sino-foreign cooperative training methods suitable for the development of China's digital media design industry, and improve the quality and level of

digital media design talents training [15]. The development of big data technology has brought new opportunities and challenges to the development of various industries. The radio and television director industry has been widely favored by the broad masses of the people, and its development is directly related to everyone's daily life. People's daily life can no longer be separated from big data technology, whether it is the TV we watch every day or a mobile phone. They all use the technical support of big data, better demonstrate the skills developed in the data age, and show stronger conditions for the progress and formation of the data age. Therefore, in the current development of education, we must master the technical support of big data, expand the content and form of TV director better, help the content of TV education show more power, and lay a solid foundation for improving the quality of TV director content. In order to better cope with the impact and challenges of the big data era and the relevant requirements for talents in the era of big data, colleges and universities need to implement diversified training modes, cultivate high-skilled and high-quality talents, and provide college students with due guarantee in the ability to use big data technology and the ability to use and build big data technology. It can show the creativity of talents in TV choreography and the significance of TV choreography more deeply, and optimize, improve, and systematically train the existing talent training system, so as to provide talent support for the development of radio and TV choreography industry. Based on this, this article introduces the diversified literacy requirements of radio and television directors in the era of big data and summarizes the diversified training strategies of radio and television directors in the era of big data, so as to better promote the development and technical requirements of TV directors in the era of big data and promote the further formation of talents.

2. The Strategy of Cultivating Diversified Applied Talents of Radio and Television Directors

2.1. Cultivating Students' Ability to Analyze and Control Big Data. In the era of big data, the most important thing is information. The available material found in several lines of information is ability. According to big data, it is skill to analyze the development trend of events. Using big data to guide public opinion to develop in the expected direction depends on skills.

If you want to create excellent radio and television programs, you can select useful information on the big data platform and then recombine the useful information. At present, the idea of many reality shows is to find out what the audience likes to watch through big data analysis and then summarize and extract useful information for innovative creation, which is the source of the embryonic form of reality shows.

It is necessary to cultivate students' ability of information prediction and early warning. In the era of big data, a large amount of information is released all the time. As a radio

and television-related worker, he must have the form of predicting the future development through this information. When some events are constantly fermenting, he should be aware of the seriousness of the situation in time, so as to make preventive plans in advance.

Finally, it is the ability to use big data to guide the trend of public opinion. Choreographers need to put forward their views in a timely manner, which should be novel and attract the attention of a broad audience, so as to make public opinion tilt towards the favorable side.

2.2. Curriculum Setting of Diversified Choreography Specialty.

The purpose of the curriculum is to increase the content of education. In addition to the original editorial guidance courses, students must broaden their horizons, edit art and news programs, and add data and information courses. Teachers should not only let students stay in the studio and broadcast live, but also go out, use big data to keep abreast of the latest developments, capture creative inspiration, and apply the latest technology and film and television processing technology to their programs. In order to help students learn how to analyze, acquire, edit, and transmit information to capture creative themes, data information courses can be added to break through the bottleneck of choreography and creation and become diversified talents.

2.3. Focusing on Cultivating Students' All-Media Thinking Mode.

With the popularization of the Internet and the development of information technology, the types and functions of broadcasting are constantly updated, and the program content is gradually diversified. The TV also adds images and text based on video data. In this context, the director talent training strategy should be further refined, focusing on cultivating students' all-media thinking, so that students can choose the most suitable media mode according to the content of radio and television programs and the characteristics of media audiences. At present, different forms of media are developing together. If radio and television students do not have all the media and energy to study professional knowledge, while ignoring literature, society, and nature, they are likely to limit your major and your own development.

2.4. Perfecting the Practical Teaching Function of Choreography Specialty.

First of all, we can join practical activities in the teaching process of choreography. Practice is the basic work of radio and television director, and it is the materials close to life that are more likely to resonate with the audience, so as to ensure attention and click-through rate. Second, schools can work with major media to provide students with more practical opportunities. After graduation, media work is no stranger to students, which effectively shortens the adjustment time. Schools and media organizations will benefit from this process. Students can help the media analyze and organize information. Schools can take the advantage of big data analysis and visual advantages to

gain more practical communication opportunities between schools. The media are more closely linked. In the past teaching activities, students majoring in choreography cannot finish news writing or program creation because they do not have practical materials. With the advent of the era of big data, students have realized their dream of seeing what is going on in the world without leaving home. Students can grasp the current audience's interest trend by analyzing research reports and news information and then summarizing these contents. After analysis and screening, they can provide themselves with complete director materials.

2.5. Cultivating Students' Ability to Interpret Radio and Television Programs.

Schools can improve students' ability to interact with big data. When cultivating choreographers' storytelling ability, they can use big data to analyze social current affairs, explore the information value behind big data, and use topics that can attract social attention to create big data and create inspiration for their own creative inspiration. At present, topics with high attention in society often come from people's daily life. Topic content with life as the theme and high statistical attention is likely to become radio and television content with less investment and high popularity. The cultivation of this ability is especially suitable for the current choreography major, and stories supported by big data analysis will be more convincing.

3. Improvement in Online Adaptive Least Squares Support Vector Machine Algorithm

3.1. Online Adaptive Least Squares Support-Oriented Computer Algorithm. Let the sample set be $T = \{(x_1, y_1), \dots, (x_l, y_l)\}$, where $x_i \in R^n$, $y_i \in R$, $i = 1, 2, \dots, l$ constructs the decision function $f(x) = w^T \Phi(x) + b$ and use the sample data to solve the objective function of minimizing structural risk, which is expressed as

$$\min_{w,b} \frac{1}{2} \|w\|^2 + c \sum_{i=1}^l \zeta_i^2, \quad (1)$$

$$y_i = w \cdot \Phi(x) + b + \xi_i, \quad i = 1, 2, \dots, l, \quad (2)$$

where $\Phi(x_i)$ is x_i nonlinear mapping, w and b are function parameters, c is a parameter, and ξ_i is a prediction error.

The above problem can be transformed into formula (3) by using the related Lagrange function:

$$L(w, b, \xi, a) = \frac{1}{2} \|w\|^2 + c \sum_{i=1}^l \xi_i^2 - \sum_{i=1}^l a_i (w \cdot \Phi(x) + b + \xi_i - y_i), \quad (3)$$

where $a = [a_1, a_2, \dots, a_l]$ is the Lagrange multiplier; $\xi = [\xi_1, \xi_2, \dots, \xi_l]$ is the training set prediction error vector. According to the optimization conditions, formula (4) can be obtained as

$$\frac{\partial L}{\partial w} = 0, \frac{\partial L}{\partial b} = 0, \frac{\partial L}{\partial \xi_i} = 0, \frac{\partial L}{\partial a_i} = 0. \quad (4)$$

Formula (5) can be solved as

$$\begin{cases} w = \sum_{i=1}^l a_i \Phi(x_i), \\ \sum_{i=1}^l a_i = 0, \\ 2c\xi_i = a_i. \end{cases} \quad (5)$$

Formula (6) can be obtained by substituting formula (5) into formula (2).

$$y_i = \sum_{j=1}^l (a_j \cdot \langle \Phi(x_i), \Phi(x_j) \rangle) + b + \frac{1}{2c} a_i. \quad (6)$$

If $K(x_i, x_j) = \langle \Phi(x_i), \Phi(x_j) \rangle$ is defined as a kernel function, formula (6) is transformed into a set of linear equations, which is expressed as

$$\begin{bmatrix} 0 & 1 & 1 & \cdots & 1 \\ 1 & K(x_1, x_1) + \frac{1}{2c} & K(x_1, x_2) & \cdots & K(x_1, x_l) \\ 1 & K(x_2, x_1) & K(x_2, x_2) + \frac{1}{2c} & \cdots & K(x_2, x_l) \\ \vdots & \vdots & \vdots & \ddots & \vdots \\ 1 & K(x_l, x_1) & K(x_l, x_2) & \cdots & K(x_l, x_l) + \frac{1}{2c} \end{bmatrix} \cdot \begin{bmatrix} b \\ a_1 \\ a_2 \\ \vdots \\ a_l \end{bmatrix} = \begin{bmatrix} 0 \\ y_1 \\ y_2 \\ \vdots \\ y_l \end{bmatrix}. \quad (7)$$

To cause

$$H = \begin{bmatrix} K(x_1, x_1) + \frac{1}{2c} & K(x_1, x_2) & \cdots & K(x_1, x_l) \\ K(x_2, x_1) & K(x_2, x_2) + \frac{1}{2c} & \cdots & K(x_2, x_l) \\ \vdots & \vdots & \ddots & \vdots \\ K(x_l, x_1) & K(x_l, x_2) & \cdots & K(x_l, x_l) + \frac{1}{2c} \end{bmatrix},$$

$$y = [y_1, y_2, \dots, y_l]^T,$$

where $e = [1, \dots, 1]_{1 \times l}^T$; $a = [a_1, a_2, \dots, a_l]^T$.

Formula (8) can be derived as

$$\begin{cases} a = H^{-1}y - H^{-1}e \cdot \frac{e^T H^{-1}y}{e^T H^{-1}e}, \\ b = \frac{e^T H^{-1}y}{e^T H^{-1}e}. \end{cases} \quad (8)$$

To solve the decision function, formula (8) is substituted into formula (9), which is expressed as

$$f(x) = \sum_{j=1}^l a_j K(x, x_j) + b. \quad (10)$$

When the prediction of the model has a large deviation, it is updated online.

First, the sample point i closest to the current new sample $\{x_{new}, y_{new}\}$ is found in the original sample space, as in formula (10).

$$i = \arg \left(\min_{k=1, \dots, l} \|x_{new} - x_k\| \right). \quad (11)$$

Second, the row and column corresponding to the i sample in Matrix H are exchanged with the last row and column to obtain H_1 , as shown in formula (11).

$$H_1 = I_{Ri \leftrightarrow Rl} H I_{Li \leftrightarrow Ll}, \quad (12)$$

$$\text{where } H_1 = \begin{bmatrix} K(x_1, x_1) + 1/2c & \cdots & K(x_1, x_i) & \cdots & K(x_1, x_l) \\ \vdots & \ddots & \vdots & \ddots & \vdots \\ K(x_i, x_1) & \cdots & K(x_i, x_i) + 1/2c & \cdots & K(x_i, x_l) \\ \vdots & \ddots & \vdots & \ddots & \vdots \\ K(x_l, x_1) & \cdots & K(x_l, x_i) & \cdots & K(x_l, x_l) + 1/2c \end{bmatrix};$$

$I_{Ri \leftrightarrow Rl}$ and $I_{Li \leftrightarrow Ll}$ represent row i and l interchange and column i and l interchange of identity matrix, respectively.

$$I_{Ri \leftrightarrow Rl} = I_{Li \leftrightarrow Ll} = I_{Ri \leftrightarrow Rl}^{-1} = I_{Li \leftrightarrow Ll}^{-1}.$$

To cause

$$H_1 = \begin{bmatrix} G & g_1 \\ g_1^T & k_1 \end{bmatrix},$$

$$k_i = K(x_i, x_i) + \frac{1}{2c},$$

$$g_i = [K(x_1, x_i), \dots, K(x_{i-1}, x_i), K(x_l, x_i), K(x_{i+1}, x_i), \dots, K(x_{l-1}, x_i)]^T.$$

Because $A^{-1} = \begin{bmatrix} A_{11} & A_{12} \\ A_{21} & A_{22} \end{bmatrix}^{-1} = \begin{bmatrix} A_{11}^{-1} + A_{11}^{-1}A_{12}B^{-1}A_{21}A_{11}^{-1} & -A_{11}^{-1}A_{12}B^{-1} \\ -B^{-1}A_{21}A_{11}^{-1} & B^{-1} \end{bmatrix}$,
of which $B^{-1} = A_{22} - A_{21}A_{11}^{-1}A_{12}$, so

$$H_1^{-1} = \begin{bmatrix} G & g_i \\ g_i^T & k_i \end{bmatrix}^{-1} = \begin{bmatrix} G^{-1} + G^{-1}g_i r_i^{-1} g_i^T G^{-1} & -G^{-1}g_i r_i^{-1} \\ -r_i^{-1} g_i^T G^{-1} & r_i^{-1} \end{bmatrix}$$

$$= \begin{bmatrix} G^{-1} & 0 \\ 0 & 0 \end{bmatrix} + \begin{bmatrix} G^{-1}g_i r_i^{-1} g_i^T G^{-1} & -G^{-1}g_i r_i^{-1} \\ -r_i^{-1} g_i^T G^{-1} & r_i^{-1} \end{bmatrix},$$

(14)

where $r_i = k_i g_i^T G^{-1} g_i$.

At the same time, we might as well make:

$$H_1^{-1} = \begin{bmatrix} G^{-1} & 0 \\ 0 & 0 \end{bmatrix} + \begin{bmatrix} \tilde{h}_{11} & \tilde{h}_{12} \\ \tilde{h}_{21} & \tilde{h}_{22} \end{bmatrix} = \begin{bmatrix} h_{11} & h_{12} \\ h_{21} & h_{22} \end{bmatrix},$$

where $\tilde{h}_{11} = G^{-1}g_i r_i^T G^{-1}$; $\tilde{h}_{12} = -G^{-1}g_i r_i^T$; $\tilde{h}_{21} = -r_i^{-1} g_i^T G^{-1}$; $\tilde{h}_{22} = r_i^{-1}$; $G^{-1} = h_{11} - \tilde{h}_{11} = h_{11} - h_{12} h_{22}^{-1} h_{21}$.

Therefore, G^{-1} can avoid direct inversion of matrix.

The parameters related to the new sample are calculated to replace the original wrong data.

$$g_{\text{new}} = [K(x_1, x_{\text{new}}), \dots, K(x_{l-1}, x_{\text{new}}), K(x_l, x_{\text{new}}), K(x_{i+1}, x_{\text{new}}), \dots, K(x_{l-1}, x_{\text{new}})]^T,$$

$$k_{\text{new}} = K(x_{\text{new}}, x_{\text{new}}) + \frac{1}{2c},$$

$$r_{\text{new}} = k_{\text{new}} - g_{\text{new}}^T G^{-1} g_{\text{new}},$$

$$\text{So: } H_2^{-1} = \begin{bmatrix} G^{-1} + G^{-1}g_{\text{new}} r_{\text{new}}^{-1} G^{-1} & -G^{-1}g_{\text{new}} r_{\text{new}}^{-1} \\ -r_{\text{new}}^{-1} g_{\text{new}}^T G^{-1} & r_{\text{new}}^{-1} \end{bmatrix}.$$

Finally, the updated decision function coefficient can be obtained from the following equation:

$$\begin{cases} \hat{a} = H_2^{-1} \hat{y} - H_2^{-1} e \cdot \frac{e^T H_2^{-1} \hat{y}}{e^T H_2^{-1} e}, \\ \hat{b} = \frac{e^T H_2^{-1} \hat{y}}{e^T H_2^{-1} e}, \end{cases} \quad (17)$$

where $\hat{y} = [y_1, \dots, y_{i-1}, y_l, y_{i+1}, y_{\text{new}}]^T$.

4. Fusion Degree Measurement

4.1. Measurement of Technology Integration Degree

- (1) This article collates the investment scale of the central nervous system and broadband fees from 2012 to 2016 of four major video websites and four major radio and television media (Table 1)

In order to better reflect the classification of advertising revenue, the classification data of major video websites and major radio and television media are sorted out (Table 2)

- (2) Sample unit HI value calculation (Table 3)

- (3) Evaluation of fusion degree

From Table 4, the HI values of CND and broadband fee investment scale of major video websites and major radio and television media from 2012 to 2016 are substituted into different integration degree interval values. It can be seen that the technology integration degree of major video websites and major radio and television media is generally low, among which, in 2012, 2013, 2015, and 2016, it was in a low-to-medium integration state, and in 2014, it was relatively good and in a moderate integration state.

According to the HI value of CND and broadband fee investment scale of major video websites and major radio and television media in each year, the change chart of CND and broadband fee investment HI value from 2012 to 2016 is drawn, as shown in Figure 1.

4.2. Measurement of Market Integration Degree

4.2.1. Collation of Sample Unit Data. According to the statistics of State Administration of Press, Publication, Radio, Film and Television in 2016, this article collates the

TABLE 1: Investment scale of CND and broadband fees of major video websites and major radio and television media.

Unit	CND and broadband fee investment scale (10,000 yuan)				
	2012	2013	2014	2015	2016
Unity group	44,586.84	52,708.30	74,000.15	80,923.80	160,833.00
Tencent video	15,432.12	32,431.00	80,000.00	100,000.00	213,960.00
Sohu video	79,522.62	14,493.00	103,610.00	119,377.67	29,400.00
Iqiyi	1,410.98	29,211.41		78,971.72	129,948.00
CCTV	19,349.55	26,806.33	50,423.16	23,632.02	36,386.21
China Central People's Broadcasting and Television Station	347.00	379.00	422.00	590.00	386.00
China Radio and Television International		25.00	75.00	61.00	64.00
Hunan Radio and Television Station	1,085.61	1,639.34	26,655.48	40,010.74	61,620.00
Total	161,755.72	157,703.38	335,185.79	443,556.95	632,597.21

TABLE 2: Classification of CND and broadband fee investment scale.

Unit	2012	2013	2014	2015	2016
Major video sites	0.76	0.67	0.59	0.73	0.71
Major radio and television media	0.02	0.03	0.05	0.02	0.024
Total	0.78	0.70	0.64	0.75	0.74

TABLE 3: HI value of CND and broadband fee investment scale of major video websites and major radio and television media.

Unit	2012	2013	2014	2015	2016
Major video sites	0.76	0.67	0.59	0.73	0.71
Major radio and television media	0.02	0.03	0.05	0.02	0.024
Total	0.78	0.70	0.64	0.75	0.74

TABLE 4: Analysis of HI value of broadband fee investment scale.

Unit	HI value of CND and broadband fee investment scale				
	In 2012	In 2013	In 2014	In 2015	In 2016
Low fusion (1.0–0.84)					
Medium and low fusion (0.84–0.68)	0.78	0.70		0.75	0.74
Moderate fusion (0.68–0.52)			0.64		
Medium-high fusion (0.52–0.36)					
Highly integrated (0.36–0.2)					

radio and television advertising revenue of four major video websites, including Unity group, Tencent video, Sohu video, and Iqiyi, and four major radio and television media, including CCTV, China National Radio, China Radio International, and Hunan Radio and Television Station, from 2012 to 2016 (Table 5).

In order to better reflect the classification of advertising revenue in major video websites and major radio and television media, the classified data of four major video websites, such as Unity group, Tencent video, Sohu video, and Iqiyi, and four major radio and television media, such as CCTV, China National Radio, China Radio International, and Hunan Radio and Television Station, are sorted out (Table 6).

4.2.2. Sample Unit HI Value Calculation. HI value of advertising revenue is given in Table 7.

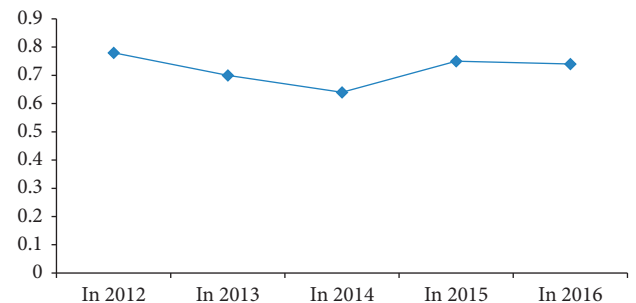


FIGURE 1: HI value change chart.

4.2.3. Evaluation of Fusion Degree. According to the HI value of advertising revenue calculated in Table 7, the HI value of advertising revenue of major video websites and major radio and television media from 2012 to 2016 is

TABLE 5: Advertising revenue of major video websites and major radio and television media.

Unit	Advertising revenue (10,000 yuan)				
	In 2012	In 2013	In 2014	In 2015	In 2016
Unity group	142,632.96	167,272.51	280,791.54	295,631.25	335,540.00
Tencent video	4,945.65	11,696.00	235,666.68	400,000.00	599,700.00
Sohu video	55,660.64	13,074.00	110,980.65	103,391.44	100,232.00
Iqiyi	44,598.74	75,278.09	179,755.38	172,111.28	514,785.00
CCTV	25,868.48	24,916.90	34,615.43	28,705.33	38,277.27
China Central People's Broadcasting and Television Station					1,085.57
China Radio and Television International	113.00	664.00	847.00	434.00	696.84
Hunan Radio and Television Station	4,925.45	3,667.18	7,618.66	53,472.86	84,978.00
Total	278,744.92	296,568.68	850,338.34	1,053,746.16	1,675,294.68

TABLE 6: Classification of advertising revenue.

Unit	Advertising revenue (10,000 yuan)				
	In 2012	In 2013	In 2014	In 2015	In 2016
Major video sites	247,837.99	267,320.60	807,194.25	971,133.97	1,550,257.00
Major radio and television media	30,906.93	29,248.08	43,144.09	82,612.19	125,037.68
Total	278,744.92	296,568.68	850,338.34	1,053,746.16	1,675,294.68

TABLE 7: HI value of advertising revenue.

Unit	HI value of advertising revenue				
	In 2012	In 2013	In 2014	In 2015	In 2016
Major video sites	0.79	0.81	0.90	0.85	0.86
Major radio and television media	0.01	0.01	0.003	0.01	0.006
Total	0.80	0.82	0.903	0.86	0.866

TABLE 8: Analysis of HI value of advertising revenue.

Unit	HI value of advertising revenue				
	In 2012	In 2013	In 2014	In 2015	In 2016
Low fusion (1.0–0.84)			0.90	0.86	0.86
Medium and low fusion (0.84–0.68)	0.80	0.82			
Moderate fusion (0.68–0.52)					
Medium-high fusion (0.52–0.36)					
Highly integrated (0.36–0.2)					

substituted into different integration degree interval values, respectively, and it can be seen that the market integration degree of major video websites and major radio and television media is in a low integration state (Table 8).

According to the HI value of advertising revenue of major video websites and major radio and television media in each year, the change chart of advertising revenue HI value from 2012 to 2016 is drawn, as shown in Figure 2.

4.3. *Measurement of Service Convergence Degree.* Collation of sample unit data. From 2012 to 2016, the PC page playback, PC client playback, mobile page playback, and mobile client playback are given in Tables 9–12, respectively.

According to Tables 9–12, we calculate the average number of times that Heyi group, Tencent video, Sohu video, and Iqiyi play on PC page side, PC client side, mobile page side, and mobile client side, and then draw a histogram as shown in Figure 3.

In order to better observe and judge the abovementioned major video websites and major radio and television media from 2012 to 2016, the overall classification of playing platforms such as PC page side, PC client side, mobile page side, and mobile client side, the overall development trend and development stage of major video websites and major radio and television media in terms of business integration degree are calculated. Figure 3 shows the video development of four different platforms in different years. Mobile clients have developed rapidly, and in 2016, mobile clients are

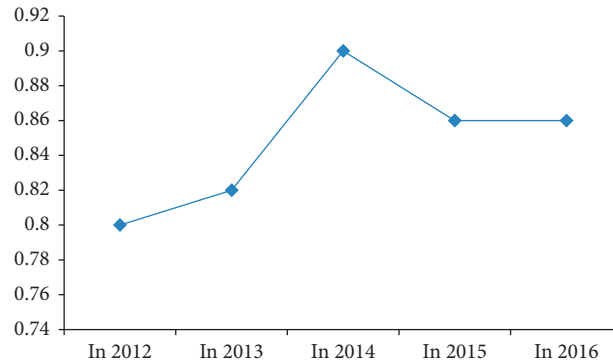


FIGURE 2: Change chart of HI value of advertising revenue.

TABLE 9: PC page playback.

Unit	PC page playback times (100 million times)				
	In 2012	In 2013	In 2014	In 2015	In 2016
Unity group	1,501.91	1,654.31	1,745.10	1,539.62	3,542.31
Tencent video	783.40	704.68	549.44	400.29	356.08
Sohu video	152.26	201.86	214.39	151.46	622.02
Iqiyi	227.67	295.68	384.00	434.72	251.71
CCTV	300.00	390.00	500.00	450.00	1,519.00
China Central People's Broadcasting and Television Station	32.62	48.44	58.14	41.9	547.33
China Radio and Television International	0.52	0.69	1.30	1.00	0.25
Hunan Radio and Television Station	4.82	5.36	5.20	5.31	5.87
Total	0.63	7.60	32.63	54.95	200.05

TABLE 10: PC client playback.

Unit	PC client playback times (100 million times)				
	In 2012	In 2013	In 2014	In 2015	In 2016
Unity group	1,228.51	1,160.80	1,431.91	1,490.53	1,383.21
Tencent video			77.55	119.60	245.54
Sohu video	269.15	226.37	214.65	166.97	199.54
Iqiyi	341.51	443.52	576.00	652.08	13.46
CCTV	610.00	480.00	550.00	540.00	870.00
China Central People's Broadcasting and Television Station	7.85	10.91	13.72	11.89	14.53
China Radio and Television International					
Hunan Radio and Television Station					
Total					40.15

TABLE 11: Mobile page playback.

Unit	Number of plays on the mobile page (100 million times)				
	In 2012	In 2013	In 2014	In 2015	In 2016
Total	175.86	313.56	1,184.98	2,483.81	3,494.55
Unity group		53.82	114.60	226.50	241.56
Tencent video		1.88	472.36	1,650.64	2,657.01
Sohu video	170.76	221.76	288.00	326.04	137.72
Iqiyi	5.10	36.10	300.00	266.00	340.00
CCTV					35.60
China Central People's Broadcasting and Television Station					
China Radio and Television International			0.43	0.51	2.35
Hunan Radio and Television Station			9.60	14.12	80.30

TABLE 12: Mobile client playback.

Unit	Mobile client playback times (100 million times)				
	In 2012	In 2013	In 2014	In 2015	In 2016
Total	637.34	1,635.54	4,004.29	4,865.63	9,753.45
Unity group	88.91	552.22	1,101.25	1,180.93	1,524.45
Tencent video		112.54	710.38	1,289.79	2,614.28
Sohu video	398.43	517.44	672.00	760.75	227.63
Iqiyi	150.00	450.00	1,500.00	1,500.00	4,871.00
CCTV		3.34	11.06	8.95	33.05
China Central People’s Broadcasting and Television Station					1.24
China Radio and Television International					
Hunan Radio and Television Station			9.60	125.21	481.80

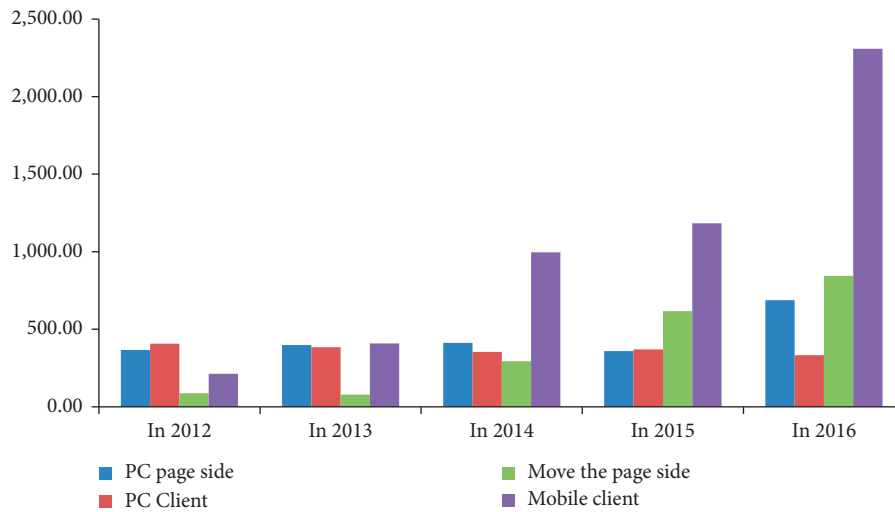


FIGURE 3: Comparison of average playback times from 2012 to 2016.

TABLE 13: Classification of PC page playback.

Unit	PC page playback times (100 million times)				
	In 2012	In 2013	In 2014	In 2015	In 2016
Total	1,501.91	1,654.31	1,745.10	1,539.62	3,542.31
Major video sites	1,463.32	1,592.22	1,647.82	1,436.47	2,788.81
Major radio and television media	38.58	62.09	97.27	103.16	753.50

almost the sum of other platforms. On the whole, the development of PC as a media is slow, and the basic processing stops. According to the relevant data calculated in Tables 9–12 above, this article analyzes and summarizes the classified data of major video websites and major radio and television media (Tables 13–16).

According to Tables 13–16, we calculate the average number of times played by major video websites and major radio and television media on PC page side, PC client side, mobile page side, and mobile client side, and then draw a histogram as shown in Figure 4.

Sample unit HI value calculation: according to the calculation model of Herfindahl index method, the HI values of PC page playback, PC client playback, mobile page playback, and mobile client playback of major video websites

and major radio and television media from 2012 to 2016 are calculated, as given in Tables 17–20.

According to Tables 17–20, we calculate the average HI values of the playing times of major video websites and major radio and television media on PC page side, PC client side, mobile page side, and mobile client side, and then draw a histogram as shown in Figure 5.

Evaluation of fusion degree: according to Tables 17–20, the playback frequency of major video websites and major radio and television media on PC page side, PC client side, mobile page side, and mobile client side was in a low convergence range from 2012 to 2016, and only in 2016, the playback frequency on PC page side showed moderate convergence, among which major video websites were superior to major radio and television media as a whole.

TABLE 14: Classification of PC client playback.

Unit	PC client playback times (100 million times)				
	In 2012	In 2013	In 2014	In 2015	In 2016
Total	1,228.51	1,160.80	1,431.91	1,490.53	1,383.21
Major video sites	1,220.66	1,149.89	1,418.19	1,478.64	1,328.53
Major radio and television media	7.85	10.91	13.72	11.89	54.68

TABLE 15: Classification of mobile page playback.

Unit	Number of plays on the mobile page (100 million times)				
	In 2012	In 2013	In 2014	In 2015	In 2016
Total	175.86	313.56	1,184.98	2,483.81	3,494.55
Major video sites	175.86	313.56	1,174.95	2,469.18	3,376.30
Major radio and television media	-	-	10.03	14.63	118.26

TABLE 16: Mobile client playback classification.

Unit	Mobile client playback times (100 million times)				
	In 2012	In 2013	In 2014	In 2015	In 2016
Total	637.34	1,635.54	4,004.29	4,865.63	9,753.45
Major video sites	637.34	1,632.21	3,983.63	4,731.47	9,237.36
Major radio and television media	-	3.34	20.66	134.16	516.09

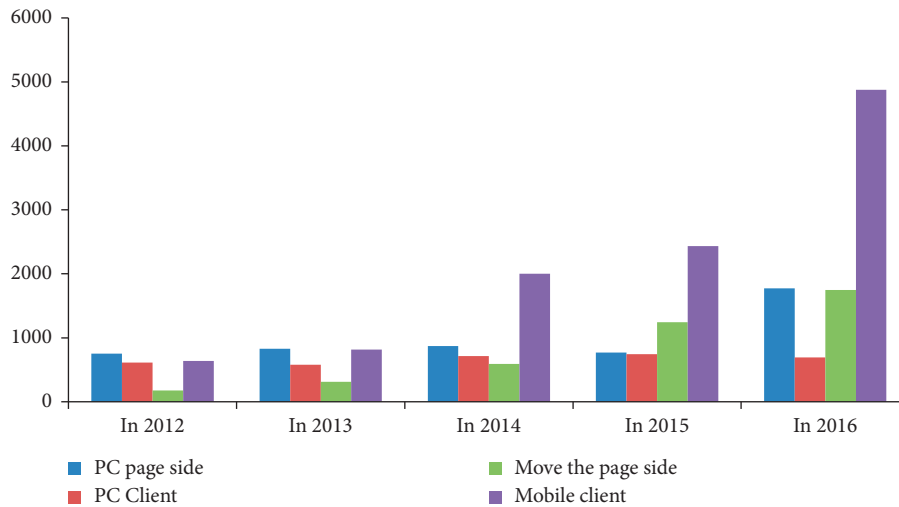


FIGURE 4: Comparison of average playback times from 2012 to 2016.

The smaller the HI value, the higher the degree of industrial integration, and the greater the HI value, the lower the degree of integration. Through comparative analysis in Table 21, the overall integration of radio and television media and new media is low. Among them, the performance of technology integration, market integration, and business integration of radio and television media lags far behind the new media industry. The new media based on the Internet undoubtedly has great communication power, influence, and mobilization power and has been in a comprehensive leading state in technology, market, and business, occupying the strategic highland of various media. Compared with the

telecommunications industry, the radio and television media as a whole are dwarfed.

Generally speaking, the media integration of radio and television industry is divided into three levels. First, the initial integration, that is, the programs are uploaded to the network platform and transformed into terminals suitable for mobile phones, desktops, and tablet computers by means of disassembly, packaging, and reorganization, so as to adapt to network communication. The second is moderate integration, that is, in news collection and editing, news materials are collected through handheld terminals, desktops, and radio and television channels, and news events are

TABLE 17: PC page side playback HI values.

Unit	HI value of PC page playback times				
	In 2012	In 2013	In 2014	In 2015	In 2016
Total	0.95	0.93	0.89	0.87	0.67
Major video sites	0.95	0.93	0.89	0.87	0.62
Major radio and television media	0.001	0.001	0.003	0.004	0.05

TABLE 18: PC client play HI values.

Unit	HI value of PC client playback times				
	In 2012	In 2013	In 2014	In 2015	In 2016
Total	0.99	0.98	0.98	0.98	0.92
Major video sites	0.99	0.98	0.98	0.98	0.92
Major radio and television media	0.00004	0.0001	0.0001	0.0001	0.0016

TABLE 19: Mobile page play HI values.

Unit	HI value of playing times on mobile page side				
	In 2012	In 2013	In 2014	In 2015	In 2016
Total	1.00	1.00	0.98	0.99	0.93
Major video sites	1.00	1.00	0.98	0.99	0.93
Major radio and television media			0.00007	0.00003	0.0011

TABLE 20: Mobile client play HI value.

Unit	HI value of playing times on mobile page side				
	In 2012	In 2013	In 2014	In 2015	In 2016
Total	1.00	1.00	0.99	0.95	0.90
Major video sites	1.00	1.00	0.99	0.95	0.90
Major radio and television media		0.000004	0.000027	0.00076	0.0028

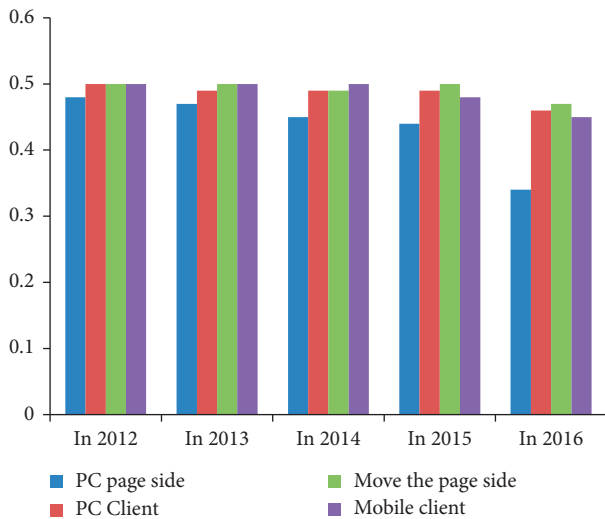


FIGURE 5: Comparison of average HI value of play times from 2012 to 2016.

broadcasted by editors on new media platforms and then made into audio and video programs for broadcasting on radio and television stations. This way can realize the linkage

transmission mechanism of the same news content in different carriers such as radio and television, WeChat Weibo, network, car and outdoor TV, newspapers, and periodicals. Third, deep integration, through cooperation with professional video websites and portal websites, expands the transmission path of radio and television through advantageous network platforms, so as to increase the penetration rate and influence of radio and television programs. At present, although the vast majority of radio and television stations above the prefecture level have set up video and audio websites, and some have set up Weibo accounts, WeChat official account, and developed boutique program applications and clients, they are still in the initial and moderate integration stage as a whole. As the market continues to mature and become more perfect, social capital will become more important and the competition between industries will intensify further, especially with the diversification of TV audience program signal receiving methods. With the increase in traditional media and the emerging audio and media integration services, users' consumption habits change gradually, and cable TV users turn to IPTV, OTT, video websites, and other new media. The market share of cable TV is declining day by day, and the

TABLE 21: Calculation results of convergence degree between radio and television and new media.

Project	In 2012	In 2013	In 2014	In 2015	In 2016
Degree of technology integration	0.78	0.70	0.64	0.75	0.74
Market integration	0.80	0.82	0.90	0.86	0.86
Degree of business integration	0.98	0.98	0.96	0.95	0.86
PC page side	0.95	0.93	0.89	0.87	0.67
PC client	0.99	0.98	0.98	0.98	0.92
Move the page side	1.00	1.00	0.98	0.99	0.93
Mobile client	1.00	1.00	0.99	0.95	0.90

TABLE 22: Proportion of CDN and broadband fee investment in advertising revenue.

Unit	Specific gravity (%)				
	In 2012 (%)	In 2013 (%)	In 2014 (%)	In 2015 (%)	In 2016 (%)
Major video sites	57	48	32	39	34
Major radio and television media	67	99	180	78	246

TABLE 23: Total play times of play platform.

Unit	Total number of plays (100 million times)				
	In 2012	In 2013	In 2014	In 2015	In 2016
Major video sites	3,497.18	4,687.88	8,224.60	10,115.76	16,731.01
Major radio and television media	46.43	76.34	141.67	263.83	1,442.52

competitive pressure of radio and television industry will be increasing.

4.3.1. Degree of Technology Integration. On the one hand, we can see that the degree of technology integration is better than the degree of market integration and business integration as a whole, and the overall performance is getting better from 2012 to 2016, which reflects the efforts made by radio and television media in technology integration to a certain extent. For example, CCTV is committed to China's video cloud service platform; integrates CCTV news, mobile TV platform, and CCTV audio-visual and other new media platforms; promotes the preinstallation of CCTV audio-visual and news clients and China Mobile cooperative models; establishes collaborative linkage between different receiving terminal platforms; and distributes content to desktop computers, tablet computers, mobile phones, televisions, outdoor large screens, and other terminals. China National Radio connects the car network and the mobile Internet market by building a China broadcasting cloud platform. From the analysis of the proportion of major video websites and major radio and television media (CND and broadband fee investment in advertising revenue in Table 22), it can be seen that major radio and television media still attach great importance to the investment in technology, and the related investment in 2014 and 2016 even exceeded the total advertising revenue of that year. From 2012 to 2016, CCTV, China National Radio, China Radio International, and Hunan Radio and Television have invested a total of 2.899 billion yuan in CND and broadband. The four major video websites have invested a total of 14.4 billion yuan in

CND and broadband, with a difference of 4.97 times. Among them, the investment of any of the four major video websites in CND and broadband far exceeds the total investment of the four major radio and television media. The capital strength of new media and the high investment in technology integration can be seen. Generally speaking, some radio and television organizations have not paid enough attention to the subversive impact brought by media convergence, and still muddle along in the hotbed of vested interests of radio and television; and some simply transplant traditional radio and television programs to websites and new media platforms, but do not interpret the programs as the suitable broadcasting form and customer acceptance habit paradigm for the Internet, especially the mobile Internet.

4.3.2. Degree of Market Integration. Advertising revenue is a barometer of the media market. In the new media market, four major video websites have occupied a dominant position, among which the advertising revenue in 2016 was 15.5 billion yuan, accounting for 41% of the national related advertising revenue of 37.5 billion yuan. On the other hand, the related advertising revenue of the four major radio and television media in 2016 was 1.25 billion yuan, accounting for only 3.33% of the national related advertising revenue. It is precisely because of the versatility of assets brought about by technological progress and media convergence that once news and other audio and video programs are produced, due to the noncompetitive sharing and weak increase in reproduction costs, the production cost is saved, and due to the pressure of external competition, the price competition is

obvious. Compared with the business packages of telecommunication departments that provide three-in-one services of TV, telephone, and Internet, the price competitive disadvantage of radio and television media is self-evident and directly affects the share of advertising revenue. Generally speaking, affected by administrative monopoly factors, the market behavior of radio and television industry is extensive, and the efficiency of market resource allocation needs to be further improved. It is necessary to make rational use of radio and television resources, further reduce market access, and effectively form a good competitive situation. With the in-depth integration with new media, the editing process and organizational structure of radio and television media will undergo profound changes; form a production process of collecting multimedia generation and multi-channel and multiplatform information release; realize collaborative communication and integrated production; improve the productivity of various departments; promote the improvement in the economic benefits of the whole media; realize the multiple appreciation of media assets and resources; realize the full utilization and reallocation of common elements and common assets; change the weak cost increase between radio and television media into the weak cost increase within the new media; and realize the improvement in market performance. Of course, radio and television media have also made a lot of efforts in market integration and actively explore new ways of marketing on the basis of continuing to adhere to the principle of “content is king.”

4.3.3. Degree of Business Integration. The performance of the three integration indicators is the worst, and there is a slow upward trend in the later period, indicating that the business integration of the two industries is gradually deepening, but the pace is relatively slow. Of course, the contribution of major video websites in this respect is major. As given in Table 23, the total playing frequency of major video websites on PC page side, PC client side, mobile page side, and mobile client side has increased rapidly, reaching 1,673.101 billion times in 2016, which is 11.6s times of the 144.252 billion times of major radio and television media. Although the total broadcast frequency of major radio and television media is also increasing greatly, it is generally inadequate, especially the broadcast frequency of PC clients, which is basically blank in China National Radio, China Radio International, and Hunan TV Station. Media convergence will give birth to a large number of new products and services, which not only enrich the audience’s choices, but also become the tools and fields for radio and television media to compete with new media. Audience’s choice of radio and television programs is voted by remote control. When the program is broadcast, netizens can express their views to the contestants, and the TV screen can also present the opinions of Weibo netizens in real time, so as to realize the three-screen interaction among TV screen, mobile phone screen, and computer screen, which meets the audience’s opinion expression and interaction needs and successfully attracts young network users to the TV screen. Hunan

Satellite TV pays attention to the integration with its own new media to produce programs and realizes the deep integration of traditional media and new media content production by means of joint research and planning, separate organization and implementation, unified arrangement and production, and external integration and presentation.

The data in above tables are missing, mainly because there is no corresponding data source. Some media have not been applied on the Internet before, and many data cannot be verified or have no relevant data application.

5. Conclusion

Big data endows the radio and television director industry with new characteristics. In order to meet the needs of the times and find the space for students to survive and develop in surgical guidance, colleges and universities need to transform their skills, adopt diversified open teaching methods, optimize the existing professional personnel training mode, rationally organize radio and television teacher courses, and form a double-qualified team. Strong teachers cultivate data, better cultivate more radio and television directors to meet the development needs of the big data era, contribute to the sustainable and long-term development of cultural enterprises, and study and formulate a brand-new talent training strategy. The next step is to analyze the application characteristics of different media in communication effect and commercial value. From different business recommendations, the media application in precision business model has a new application prospect, which is suitable for the method proposed in this article and needs further verification.

Data Availability

The data used to support the findings of this study are available from the corresponding author upon request.

Conflicts of Interest

The authors declare that they have no conflicts of interest.

References

- [1] Z. W. Chen, “On experiment teaching reform of radio and television director specialty,” *Journal of Chengdu University of Technology (Science & Technology Edition)*, vol. 3, pp. 28–31, 2009.
- [2] Q. Qu, C. Jiang, and F. Gao, “Research on the applied talents training of radio and television directing major under the employment orientation,” in *Proceedings of the 2017 4th International Conference on Education, Management, Arts, Economics and Social Science(ICEMAESS 2017)*, pp. 382–386, Seoul, Korea (South), 2017.
- [3] N. K. Khan, A. R. Baig, and M. A. Iqbal, “A new discrete PSO for data classification,” in *Proceedings of the 2010 International Conference on Information Science and Applications*, pp. 1–6, Seoul, Korea (South), April 2010.
- [4] P. O. Lewis, “A likelihood approach to estimating phylogeny from discrete morphological character data,” *Systematic Biology*, vol. 50, no. 6, pp. 913–925, 2001.

- [5] G. Chen, Q. Pei, and M. M. Kamruzzaman, "Remote sensing image quality evaluation based on deep support value learning networks[J]," *Signal Processing: Image Communication*, vol. Volume 83, Article ID 115783, 2020.
- [6] S. van Buuren, "Multiple imputation of discrete and continuous data by fully conditional specification," *Statistical Methods in Medical Research*, vol. 16, no. 3, pp. 219–242, 2007.
- [7] G. Karypis, E.-H. Han, and V. Kumar, "Chameleon: hierarchical clustering using dynamic modeling. (cover story)," *Computer*, vol. 32, pp. 55–63, 1999.
- [8] R. Costanza and M. Ruth, "Using dynamic modeling to scope environmental problems and build consensus," *Environmental Management*, vol. 22, no. 2, pp. 183–195, 1998.
- [9] G. Sun, C.-C. Chen, and S. Bin, "Study of cascading failure in multisubnet composite complex networks," *Symmetry*, vol. 13, no. 3, p. 523, 2021.
- [10] G. B. Chen, Z. Sun, and L. Zhang, "Road identification algorithm for remote sensing images based on wavelet transform and recursive operator," *IEEE Access*, vol. 8, pp. 141824–141837, 2020.
- [11] W. F. Fagan, F. Marie-josée, and S. Candan, "Integrating edge detection and dynamic modeling in quantitative analyses of ecological boundaries," *BioScience*, vol. 8, pp. 730–738.
- [12] C. Wang, H. Li, and J. Wei, "The research of construction of the diversified training mode to graduate students," *IEEE*, vol. 3, pp. 29–34, 2011.
- [13] R. A. Fiorini and G. Laguteta, "Discrete tomography data footprint reduction by information conservation," *Fundamenta Informaticae*, vol. 6, pp. 14–21, 2013.
- [14] L. Sze-wing, M. Stephen, and L. P. Bill, "Using a real-time integrated communication system to monitor the progress and quality of construction works," *Automation in Construction*, vol. 17, no. 6, pp. 749–757, 2008.
- [15] Y. Yuan, "Research on talent training mode for Digital Media Design major with Chinese and foreign cooperation," *Experimental Technology and Management*, vol. 4, pp. 55–59, 2018.

Retraction

Retracted: Railway Traffic Emergency Management Relying on Image Recognition Technology in the Context of Big Data

Computational Intelligence and Neuroscience

Received 3 October 2023; Accepted 3 October 2023; Published 4 October 2023

Copyright © 2023 Computational Intelligence and Neuroscience. This is an open access article distributed under the Creative Commons Attribution License, which permits unrestricted use, distribution, and reproduction in any medium, provided the original work is properly cited.

This article has been retracted by Hindawi following an investigation undertaken by the publisher [1]. This investigation has uncovered evidence of one or more of the following indicators of systematic manipulation of the publication process:

- (1) Discrepancies in scope
- (2) Discrepancies in the description of the research reported
- (3) Discrepancies between the availability of data and the research described
- (4) Inappropriate citations
- (5) Incoherent, meaningless and/or irrelevant content included in the article
- (6) Peer-review manipulation

The presence of these indicators undermines our confidence in the integrity of the article's content and we cannot, therefore, vouch for its reliability. Please note that this notice is intended solely to alert readers that the content of this article is unreliable. We have not investigated whether authors were aware of or involved in the systematic manipulation of the publication process.

Wiley and Hindawi regrets that the usual quality checks did not identify these issues before publication and have since put additional measures in place to safeguard research integrity.

We wish to credit our own Research Integrity and Research Publishing teams and anonymous and named external researchers and research integrity experts for contributing to this investigation.

The corresponding author, as the representative of all authors, has been given the opportunity to register their agreement or disagreement to this retraction. We have kept a record of any response received.

References

- [1] F. Dong and Y. Ma, "Railway Traffic Emergency Management Relying on Image Recognition Technology in the Context of Big Data," *Computational Intelligence and Neuroscience*, vol. 2022, Article ID 1920196, 12 pages, 2022.

Research Article

Railway Traffic Emergency Management Relying on Image Recognition Technology in the Context of Big Data

Fei Dong¹ and Yuanyuan Ma² 

¹School of Railway Transport, Shaanxi Railway Institute, Weinan 714000, Shaanxi, China

²School of Urban Rail Engineering, Shaanxi Railway Institute, Weinan 714000, Shaanxi, China

Correspondence should be addressed to Yuanyuan Ma; 161841288@masu.edu.cn

Received 9 March 2022; Revised 1 April 2022; Accepted 28 April 2022; Published 30 June 2022

Academic Editor: Le Sun

Copyright © 2022 Fei Dong and Yuanyuan Ma. This is an open access article distributed under the Creative Commons Attribution License, which permits unrestricted use, distribution, and reproduction in any medium, provided the original work is properly cited.

With the full popularity of China's railwayization process, it has brought about the problem of the management ability of railway traffic safety. Railway traffic safety emergency management capabilities are low. When an accident occurs, clearer data cannot be obtained in the first time to have a general understanding of the accident. Therefore, the problem of organizing rescue has always plagued relevant railway workers. This study aims to study the improvement of railway traffic emergency management based on image recognition technology in the context of big data. To this end, this study proposes image recognition technology based on deep learning, and through the relay of the railway traffic emergency management system, so that the railway traffic problems can be dealt within time as soon as they occur, and designed an experiment to explore the ability of image recognition. The results of the experiment show that the efficiency of the improved railway traffic emergency management system has increased by 27%, and the recognition capability has increased by 64%. It can very well help current railway workers to carry out emergency management for railway traffic safety.

1. Introduction

Transportation is an important driving force for economic development, and railway transportation is the main driving force for transportation. Railway transportation plays a basic role in stimulating social and economic development and protection. In today's China, with the rapid development of the railway transportation industry, railway emergencies frequently occur, which bring more and more serious harm to society. After in-depth digging, it was discovered that there are obvious loopholes and defects in the domestic railway disaster prevention system and organizational structure, application mechanism, and resource guarantee, which will inevitably bring bad effects. Therefore, perfecting the domestic railway traffic emergency management system from a systematic level has a very important fundamental role in the overall rapid development of the domestic social economy.

With the rapid development of domestic railway traffic, railway traffic accidents are frequently seen in social life, and this has exposed many loopholes in the construction of

railway emergency response systems and accident resolution implementation actions. Therefore, the cause of casualties and losses of personnel and property is not only due to the occurrence of the accident itself. The imperfect emergency response plan, the unfavorable command, the inability to rescue in time, and the lack of relevant medical rescue knowledge are the important reasons for the vicious development of sudden accidents and even the related secondary accidents. Therefore, building a complete accident emergency management system is an important factor in preventing, controlling, and handling accidents. A region or department needs a relatively perfect emergency management system.

With the comprehensive popularization of railway construction in China, the total length of railway lines in China has become the world's number one, and what follows is the emergency safety management of railway traffic. Through the research and application of image recognition technology, the emergency management of railway traffic safety has been greatly improved, and this has made more

and more people begin to invest in related research. Luan X proposed distributed optimization, calculated the real-time traffic management efficiency of large railways, and carried out separate planning for each area [1]. Thielen SV proposed a conflict prevention strategy to quickly and efficiently solve the huge and complex railway network security problems [2]. Yongfu pointed out that we urgently need to innovate and improve the past railway traffic safety management model [3]. In his research, Duan Z conducted a careful investigation of the collision on the Metro Line 10 in Shanghai, China, on September 27, 2011, based on data recorded by anonymous mobile phones. He conducted research on the evacuation process of the accident and analyzed the impact of the accident on urban commuting. After analyzing 7 billion cell phone records for 11 days, the author found that the evacuation followed a two-stage pattern [4]. Liu Z believes that the improvement of the urban traffic emergency management system can start with the optimization of the internet of things and network mining technology to improve its response level [5]. Mauro Z developed a sensor to monitor chicken farms but observed some limitations related to the time required to detect hens. In this research, he proposed a major improvement to the sensor. They are achieved through image pattern recognition technology, which is applied to thermal imaging images obtained from the housing system [6]. Zhang R proposed a segmentation algorithm for large-scale flower species identification. His method is based on identifying potential object areas during detection [7]. Wei L believes that in order to quickly determine the effective bentonite content, the selection of the process is very important. He proposed that based on image recognition technology, he developed a fast automatic analyzer for the effective content of bentonite in waste clay sand [8]. Tai F believes that with the continuous development of science and technology, people can apply more and more technologies to the cultivation of children's abilities. In the process of cultivating children's abilities, the most important thing is the research on executive function, which is also the research topic of this study. In the past, in the research on children's executive ability, training methods such as music, mindfulness, and exercise were used to promote the development of executive function in preschool children. While various approaches have yielded some results, researchers have been exploring more comprehensive approaches to effective training. He aims to study how to use image recognition technology to analyze the intervention analysis of break dance to promote executive function in preschool children. To this end, he proposed image recognition technology based on deep learning neural network, and researched, analyzed, and improved related technologies obtained from deep learning. This makes it more suitable for the research topic of this study and to design related experiments and analyses to explore its relevant performance. His experimental results showed that the improved image recognition technique improved the accuracy by 31.2%. The performance of its algorithm has also improved by 21%, which can be very effective in monitoring the performance of preschool children in break dance [9]. The above documents are quite good for the research on image recognition

technology and railway traffic emergency management, and the instructions for the use of related technologies are quite detailed. However, the depth of research on image recognition technology is still not enough. Basically, it stays at a shallow level. If want to conduct in-depth research on it, it needs to have a certain understanding of image recognition algorithms.

The innovation of this study is based on the theory of system establishment and the technical support of image recognition technology based on deep learning, improving the emergency management system of railway traffic, and improving the image recognition ability and feature extraction efficiency, thereby greatly improving the efficiency of emergency response in the event of a railway accident.

2. Railway Traffic Management Methods

2.1. Railway Traffic Emergency Management System

2.1.1. System Function Goal. The railway hub train monitoring system monitors the railway tracks, platforms, passages, and other scenes in real time, analyses and processes the monitored sequence images, and recognizes the state of the vehicles in the images. In this way, it is judged that there is an accident or danger at the scene and responds to different levels of alarms according to the identification results. According to the degree of danger, it is divided into three levels, namely, the highest level in red, the more dangerous level in orange, and the safe level in blue. The railway staff take corresponding emergency measures according to the corresponding alarm level to achieve the purpose of reducing the accident rate, thereby greatly improving the safety of railway transportation [10].

According to the characteristics of railway transportation and railway trains that need to be guaranteed strong and continuous, the train image monitoring system of railway hubs must have the following characteristics:

- (1) Real time: the system requires the ability to collect real-time train images and perform image recognition in real time, so that the real-time situation can be reflected to the staff in order to take emergency measures in time [11]. Therefore, there is no doubt that the system requires extremely high real-time performance.
- (2) Accuracy: only accurate image recognition can ensure that the alarm will not be responded to by mistake, not only to ensure the safety of the train but also to ensure that the alarm is correspondingly accurate [12]. Therefore, the judgment of the on-site identification of the railway hub must be accurate and there must be no errors.
- (3) Stability: due to the differences in the pros and cons of different monitoring environments, no matter what the environment, the system needs to stably and reliably work for a long time; otherwise, it will bring trouble to the railway passenger transport service [13].



FIGURE 1: Train image monitoring system structure.

2.2. System Design. The train monitoring system is mainly composed of four interconnected parts: display screen, digital hard disk video recorder, high-performance computer, camera, and alarm equipment [14].

2.2.1. Display. Completing one-to-one or one-to-many video surveillance tasks, it can monitor different locations such as railway tracks and platforms in the office to monitor the jurisdiction [15].

2.2.2. Digital Hard Disk Video Recorder. The basic function of a digital hard disk video recorder is to convert analog audio and video signals into MPEG digital signals, store them on the hard disk (HDD), and provide functions corresponding to recording, playing, and managing programs, and voice and alarm interfaces.

2.2.3. Camera. It is mainly responsible for collecting real-time images of trains [16].

2.2.4. Alarm Equipment. The alarm equipment mainly sends out an alarm when the train encounters an accident or is in danger [17]. The structure of the train image monitoring system is shown in Figure 1:

The train monitoring system captures the train image through the CCD camera and then transmits the moving image sequence to the computer for real-time processing. The system designed in this study includes image capture, preprocessing, background extraction, target detection, postprocessing, train number statistics,

etc. [18]. The image recognition process is shown in Figure 2.

Each part has a certain relationship with the previous part, which can be said to have a feedback effect. For example, it can be segmented through preprocessing, and the system is not separated. In order to perform that function, each part effectively plays a role so that it can obtain necessary information from the outside world [19]. This external information refers to the opinions, ideas, and personal laws on handling and solving problems. According to that features of the actual image, an appropriate preprocessing method is adopted. The image is segmented in the recognition part, the feature are extracted, the sizes are classified, and finally the structural information required for analysis is provided. The relationship between image processing and recognition and image understanding is shown in Figure 3.

In this system, the result of the whole system is the description and interpretation of the image [20]. Image feature extraction and image classification belong to image recognition, while structure syntax analysis involves the process from image segmentation to image structure analysis. When a new object (image) is fed into the system, it can be explained to show what it is.

The train image target detection is located in the lower part of the train image recognition system. Whether the target area of the train image can be extracted from the train image correctly and quickly, this will be the key to the subsequent train target recognition processing [21]. Among them, in the train image recognition of railway hubs studied in this study, the interference of light intensity changes is particularly important [22].

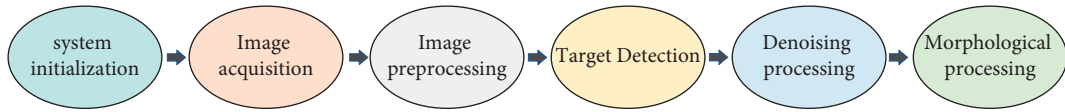


FIGURE 2: Image recognition process.

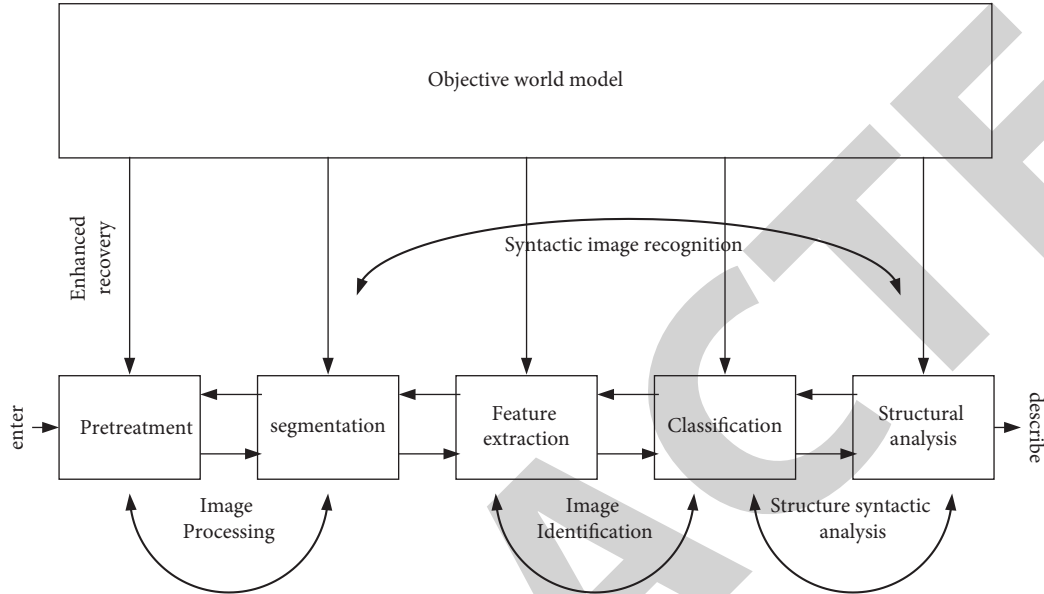


FIGURE 3: The relationship between image processing and recognition and image understanding.

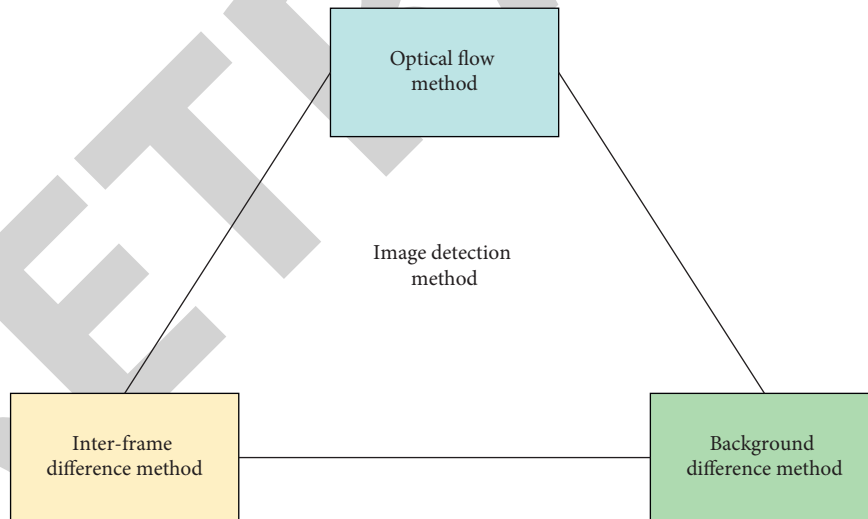


FIGURE 4: Three kinds of train image detection methods.

Generally speaking, there are two classification methods for moving target detection algorithms. One is divided into indoor scene monitoring and outdoor scene monitoring according to the monitored scene; the other classification method is divided into target detection of static background and moving background according to the image sequence formed by the moving target. When the camera and the scene are relatively static in the video

surveillance system, the size and position of the background image will not change at different frame rates [23]. The scene studied in this study belongs to the indoor scene of a railway hub, and the camera and scene are relatively static [24].

In railway train image recognition, real-time segmentation of moving targets from train video image sequences is a basic and important link [25]. At present, there are mainly

three types of train image detection methods, as shown in Figure 4.

2.3. Image Recognition Technology Based on Deep Learning. Deep learning is a subfield of machine learning, which attempts to abstract deep learning of data through a series of multilayer nonlinear transformations. By stimulating the nervous system of the human brain, a hierarchical model structure similar to the human brain is established, and the input data are extracted step by step to form a more abstract high-level representation.

2.3.1. Neuron Model. Simply put, a neuron node is a nonlinear activation function that receives multiple input values and records them as follows:

$$w = (w_1, w_2, \dots, w_n). \quad (1)$$

Then, the input signal W is weighted and summed to obtain Z . Finally, Z passes through a nonlinear activation function to output the activation value a , as shown in formulas (2) and (3).

$$z = \sum_{i=1}^n x_i * w_i + b, \quad (2)$$

$$a = f(z). \quad (3)$$

Among them, X_i represents the weight parameter, and b is the bias term.

2.3.2. Feedforward Neural Network. Given a group of neurons, we can form a hidden layer or input and output layer, and further connect these layers to form a network. Neural networks can have many topological structures, and the simplest and most commonly used is the feedforward neural network. The data propagation formula of the feedforward neural network is as follows:

$$\begin{aligned} z^{(l)} &= W^{(l)} \cdot a^{(l-1)} + b^{(l)}, \\ a^{(l)} &= f_i(z^{(l)}). \end{aligned} \quad (4)$$

We combine the above two formulas to get the following:

$$z^{(l)} = W^{(l)} \cdot f_l(z^{(l-1)}) + b^{(l)}. \quad (5)$$

According to the above formula, the feedforward neural network transfers the input information layer by layer to the next layer, and finally, the output of the network is as follows:

$$\begin{aligned} w &= a^{(0)} \longrightarrow z^{(1)} \longrightarrow a^{(1)} \longrightarrow z^{(2)} \longrightarrow \dots \longrightarrow a^{(l-1)} \\ &\longrightarrow z^{(l)} \longrightarrow a^{(l)} = y. \end{aligned} \quad (6)$$

2.3.3. Backpropagation Algorithm. In order for the neural network to work normally, we need to train the parameters in the neural network. The most common method is the

backpropagation algorithm. In general, as long as there is a large enough dataset and training samples, we can train a well-performing Xianjing network. The objective function is as follows:

$$I(W, b) = \sum_{i=1}^N L(y^{(i)}, f(x^i | W, b)) + \frac{1}{2} \lambda \|W\|_F^2, \quad (7)$$

$$I(W, b) = \sum_{i=1}^N J(X, b; w^{(i)}, y^{(i)}) + \frac{1}{2} \lambda \|W\|_F^2.$$

In order to minimize the weight and bias vector, we modify its parameters, as shown in the following formula:

$$\begin{aligned} w^{(l)} &= w^{(l)} - \alpha \frac{\partial J(Wb)}{\partial W^{(l)}}, \\ w^{(l)} &= w^{(l)} - \alpha \sum_{i=1}^N \left(\frac{\partial J(w, b; x^{(i)}, y^{(i)})}{\partial W^{(l)}} \right) - \lambda W^{(l)}, \\ b^{(l)} &= b^{(l)} - \alpha \frac{\partial J(W, b)}{\partial b}, \\ b^{(l)} &= b^{(l)} - \alpha \sum_{i=1}^N \left(\frac{\partial J(w, b; x^{(i)}, y^{(i)})}{\partial b} \right), \end{aligned} \quad (8)$$

where α is the learning rate of the parameter.

In order to update $W^{(l)}$, we transform the above formula as follows:

$$\frac{\partial J(w, b; x, y)}{\partial W_{ij}^{(l)}} = \text{tr} \left(\left(\frac{\partial J(w, b; x, y)}{\partial z^{(l)}} \right) \right)^T \frac{\partial z^{(l)}}{\partial W_{ij}^{(l)}}. \quad (9)$$

For the l th layer, we define an error term as follows:

$$\delta^{(l)} = \frac{\partial J(w, b; x, y)}{\partial z^{(l)}} \in R^{n'}. \quad (10)$$

Let us analyze the second item on the right first, because

$$z^{(l)} = W^l \cdot a^{(l-1)} + b^l. \quad (11)$$

So we can get the following:

$$\frac{\partial z^{(l)}}{\partial W_{ij}^{(l)}} = \frac{\partial (w^l \cdot a^{(l-1)} + b^l)}{\partial W_{ij}^{(l)}}, \quad (12)$$

$$\frac{\partial J(w, b; x, y)}{\partial W_{ij}^{(l)}} = \delta^{(l)} a_j^{(l-1)}.$$

We further sort out the following:

$$\frac{\partial J(w, b; x, y)}{\partial W^{(l)}} = \delta^{(l)} (a^{(l-1)})^T. \quad (13)$$

The same can be obtained as follows:

$$\frac{\partial J(w, b; x, y)}{\partial b^{(l)}} = \delta^{(l)}. \quad (14)$$

Next, we further solve the error term of the L th layer as follows:

$$\begin{aligned}\delta^{(l)} &= \frac{\partial J(w, b; x, y)}{\partial z^{(l)}}, \\ \delta^{(l)} &= \frac{\partial a^{(l)}}{\partial z^{(l)}} \frac{\partial z^{(l+1)}}{\partial a^{(l)}} \frac{\partial J(W, b; x, y)}{\partial z^{(l+1)}}, \\ \delta^{(l)} &= \text{diag}(f'_l(z^{(l)})) \cdot (W^{(l+1)})^T \cdot \delta^{(l+1)}, \\ \delta^{(l)} &= f'_l(z^{(l)}) \Theta (W^{(l+1)})^T \delta^{(l+1)}.\end{aligned}\quad (15)$$

After calculating the error term of each layer, we can update the parameters according to the gradient of the parameters of each layer, and the training process of the feed-forward neural network is basically completed within three steps. The steps are as follows: (1) calculating the state and activation value of each layer according to the forward propagation formula; (2) calculating the error term of each layer according to the backpropagation formula; and (3) calculating the partial derivative of each layer and update parameter.

2.4. Railway Traffic Safety Emergency Management. Railway accident analysis and application, with the goal of preventing accidents and faults in advance, integrate the unstructured accident fault text data of various business departments, for example, safety supervision report, accident fault tracking report, accident library, and fault library, and gradually realize the functions of full-text search, feature extraction, intelligent classification, correlation analysis, cause recommendation, key accident fault analysis, and key area analysis of unstructured accident fault text.

2.4.1. Overall Structure. The railway big data service platform mainly includes data collection, storage, management, exchange, sharing, analysis, and visualization systems. Railway accident fault text big data analysis is based on a unified railway big data service platform, applying text big data analysis technology to realize massive unstructured railway accident text data analysis. Railway accident fault text big data analysis application standard system is mainly to clarify the scope of railway accident fault text data, data interface, access method, and the use standard of accident fault terminology. It covers the standard specifications of the whole process of railway accident fault text data collection, storage, analysis, and visualization application. The railway accident fault text big data application guarantee system mainly includes railway safety guarantee, railway talent guarantee, railway evaluation, and assessment guarantee. Railway accident fault text big data analysis application logic architecture is mainly composed of a data source layer, data integration layer, data storage layer, data service layer, data analysis layer, data application layer, visualization layer, data standard system, and data guarantee system. Here, we focus on the data storage layer, data application layer, and

visualization layer. Among them, the logic architecture of railway traffic safety management big data analysis application is shown in Figure 5.

- (1) Data source layer. It is mainly unstructured text data related to accidents and failures, and structured data related to equipment structure, basic information of accidents and failures, and safety-related business system monitoring.
- (2) Data integration layer. It is mainly for the data at the data source layer, according to the characteristics of the data type and real-time requirements, and the data are extracted and converted through different collection methods such as ETL tools, JDBC/ODBC, FTP/SFTP, and real-time data collection for storage.
- (3) Data storage layer. It is mainly for the data collected by the data integration layer to store the original accident and fault text data in the distributed file system. At the same time, an index is established on the distributed database Elasticsearch, and the content of the unstructured text is stored on Elasticsearch.
- (4) Data service layer. It is mainly to realize the processing of railway unstructured accident fault text data and related structured data, and to provide processed data for the analysis of accident fault text.
- (5) Data analysis layer. It is the structured data for the structured accident fault text data and the related equipment structure, and the basic information of the accident fault and the monitoring of the safety-related business system after the feature is extracted. The unstructured analysis platform is unstructured data analysis based on Hadoop, Spark, Mahout, Python, TensorFlow, etc. [26].
- (6) Data application layer. Through the mining results of the big data analysis application of the accident fault text, the full-text retrieval of the accident fault document is realized.
- (7) Data visualization. Through GIS, pie charts, data dashboards, chord charts, character clouds, line charts, etc., the result data of the accident fault analysis are dynamically displayed so that the railway-related staff can view and apply them [27].

2.4.2. Functional Architecture. Railway accident fault text big data analysis application functions mainly include the following: accident fault feature extraction, accident full-text retrieval, accident failure area, key accident failure analysis, accident failure reason recommendation, accident failure correlation analysis, system management, and other functions. On the basis of a unified railway big data service platform, each function realizes the digital management of railway unstructured accident fault text and the analysis, diagnosis, rectification, management and control, and prevention of the accident fault through the mutual cooperation between the modules, dig out the evolution law of accidents and failures, analyze the main factors of accidents

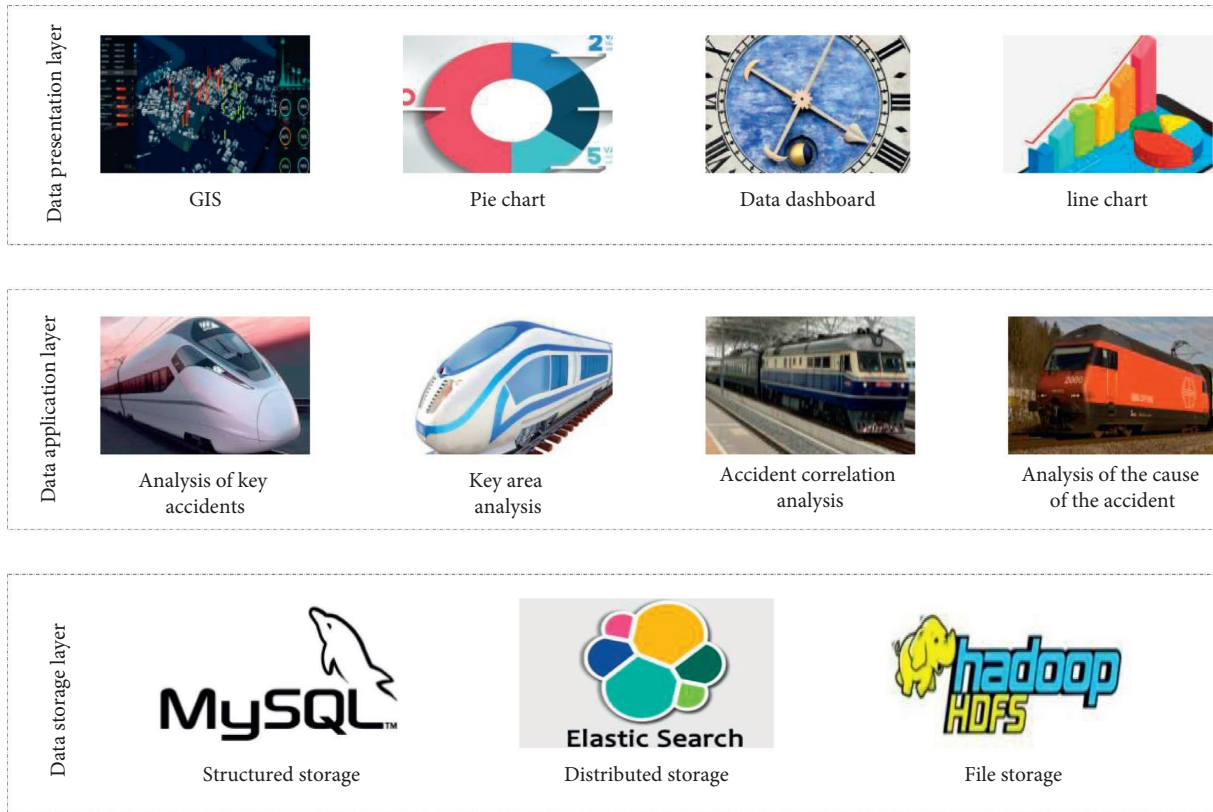


FIGURE 5: Logical architecture of railway traffic safety management big data analysis application.

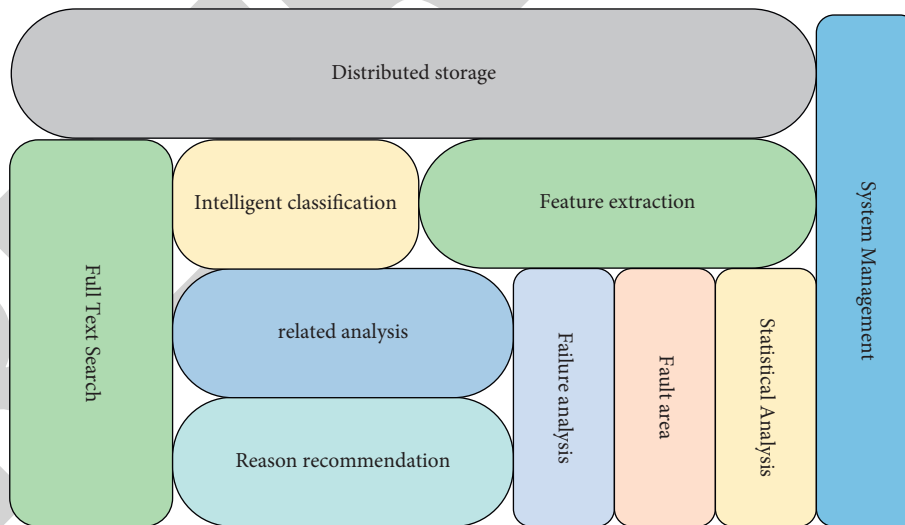


FIGURE 6: The functional architecture of railway traffic emergency management application.

and failures, and prevent the occurrence of similar accidents and failures in the future. The functional architecture diagram of the railway accident fault text big data analysis application is shown in Figure 6.

The distributed storage of railway accident fault text big data is the basis of railway accident fault text big data analysis application. On this basis, a section of accident fault text description can be converted into a certain type of accident

fault, and then based on the accident fault entity and cause entity data extracted from the railway accident fault feature, the relevant analysis and cause intelligent recommendation of the railway accident fault can be realized. The analysis of key accidents and the failure areas of frequent accidents are mainly based on the dynamic display of structured data after the extraction of the characteristics of railway accidents and the use of character clouds. System management is mainly to

TABLE 1: Character recognition results.

Character type	Number of samples	Correct number	Number of errors	Correct rate (%)
Man	1200	1172	28	97.7
Letter	1200	1180	20	98.3
Number	2400	2370	30	98.8

TABLE 2: Train number recognition results.

Train number composition	Letter	Number	Correct rate
Chinese character			
4	1	3	90.34%
5	1	4	90.94%
6	1	5	90.52%

realize the management of functional authority, data authority, user management, etc. of different professional users.

3. Train Number Image Recognition Experiment

3.1. Train Number Character Recognition Test. In the experiment of character recognition, the three types of characters, namely, Chinese characters, English letters, and numbers, are trained with 320 images of each type, and the training model is obtained by using the OC-SVM classifier and the MC-SVM classifier joint classifier. During the test, 1200, 1200, and 2400 images of Chinese characters, English letters, and numbers were taken, respectively, for testing. The results are shown in Table 1.

From the data results shown in Table 1, it is not difficult to see that the recognition rate for the three different characters is still relatively high. According to the recognition results, we can calculate the recognition rate, as shown in Table 2.

From the data results shown in Table 2, it can meet the requirements of the application.

3.2. Comparison of Test Results of Recognition Algorithms in Multiple Environments. The correct rate and error rate are compared with the number character recognition algorithm based on template matching, train number feature, and image recognition. The number of train number image samples participating in the test is 1000, and the results are shown in Table 3.

From the data results shown in Table 3, it can be seen that the correct rate of the algorithm proposed in this study is the highest among several algorithms, which proves that the algorithm has practical application value.

4. Recognition Efficiency and Accuracy

4.1. Experimental Analysis Based on the Integrated Fault Classification Model

4.1.1. BiGRU and BiLSTM Overall Weight Distribution. The training set and the verification set synthesized by ADASYN are extracted and expressed by TF-IDF and input into the BiGRU and BiLSTM network for training. The loss

TABLE 3: Comparison of correct rate.

Number character recognition algorithm	Correct number	Correct rate (%)	Number of errors	Error rate (%)
Template-based	864	86.4	136	13.6
Feature-based	859	85.9	141	14.1
Based on neural network	877	87.7	123	12.3
Image-based recognition	921	92.1	79	7.9

function value of the first-level training process is shown in Figure 7.

In order to view the change in the loss function value in the second-level training process, we compare it with the change in the loss function value in the first-level training process and explore the law of its change. This study designs an experiment to train it, and the results are shown in Figure 8:

From the comparison in Figure 8, it can be seen that the loss function of the second-level classification is smaller than that of the first-level classification.

After $K=5$ times of training, 30% of real samples are used to evaluate the BiGRU and BiLSTM training models. The evaluation results are shown in Table 4:

4.2. Classification of Integrated Models. It can be concluded from the above experiments that the weight of each category of image recognition and BiGRU should be higher than the overall weight of BiLSTM. Different overall weights are given to BiGRU and BiLSTM, the two image recognitions are combined by combining weights, and the output of the two networks will be recalculated to obtain a common classification prediction result. The classification index of the model is shown in Figure 9:

The representative algorithm of integrated image recognition model bagging is the random forest, and the representative algorithm of boosting is gradient boosting tree. It can be seen from Table 5 that the image recognition integrated model designed in this study has a significantly

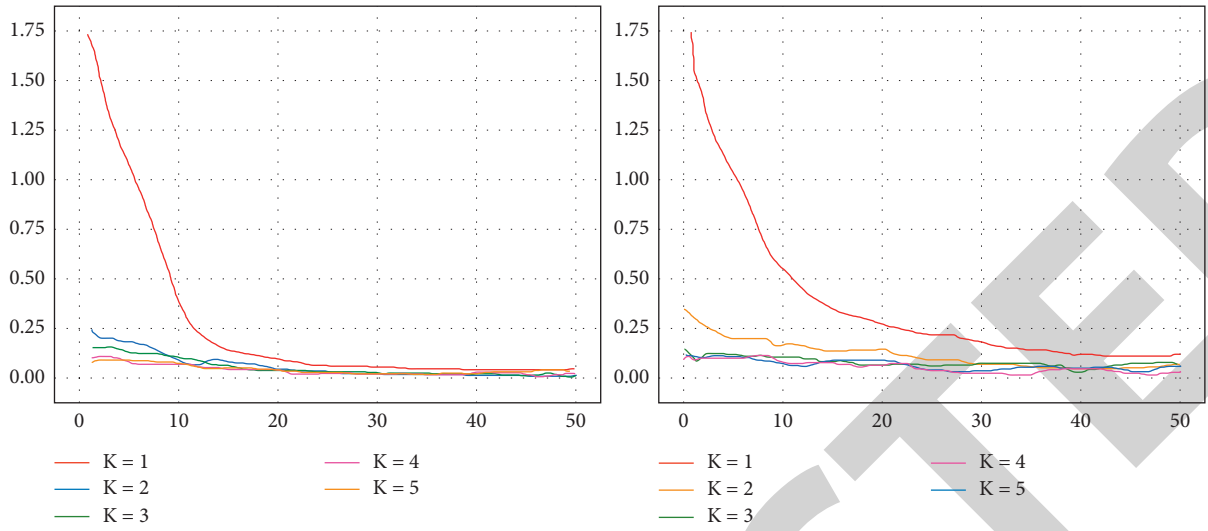


FIGURE 7: First-level classification training under two different weights.

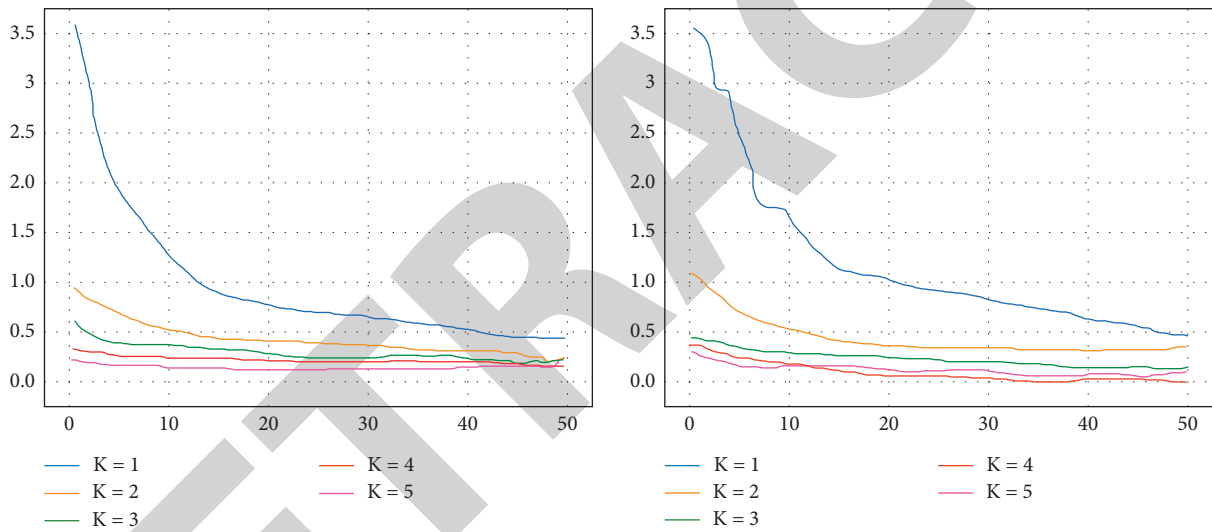


FIGURE 8: Changes in the loss function value of the secondary training process.

TABLE 4: Accuracy training results.

Method	Level	Accuracy	Recall rate	F1 value
ADASYN + BiGRU	First-level fault classification	0.8726	0.8819	0.8773
	Secondary fault classification	0.7826	0.7431	0.7689
ADASYN + BiLSTM	First-level fault classification	0.8622	0.8759	0.8619
	Secondary fault classification	0.7624	0.7538	0.7519
BiGRU	First-level fault classification	0.7336	0.7094	0.7245
	Secondary fault classification	0.7083	0.6722	0.6893
BiLSTM	First-level fault classification	0.6932	0.7122	0.7011
	Secondary fault classification	0.6314	0.6235	0.6287

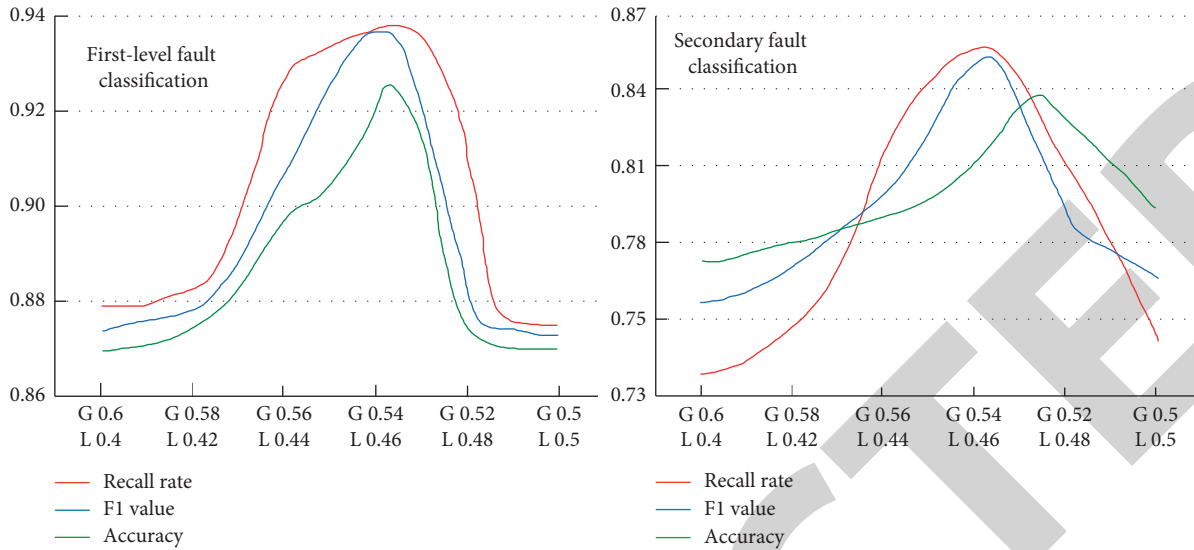


FIGURE 9: Integrated model evaluation index values under different overall weight distribution.

TABLE 5: Experimental results of ensemble model classification.

Method	Level	Accuracy	Recall rate	F1 value
RF	First-level fault classification	0.8549	0.8433	0.8429
	Secondary fault classification	0.7513	0.7648	0.7549
GBDT	First-level fault classification	0.8516	0.8347	0.8499
	Secondary fault classification	0.7613	0.7459	0.7594
Integrated model	First-level fault classification	0.9124	0.9345	0.9248
	Secondary fault classification	0.8549	0.8614	0.8536

higher evaluation index than the mature integrated recognition algorithms RF and GBDT.

4.3. Feature Extraction Analysis in Different Environments.

This section is based on a self-built train number image library. For number recognition, a feature extraction method with rotation invariance and scale invariance is selected, that is, improved SIFT feature extraction. Because the train recognition is affected by the natural environment, rain and snow when capturing the image, the interference items of the image must be removed. At the same time, the image capture is performed on the

wireless client, which requires the image to have a certain degree of adaptability to its own rotation and scaling, and the improved SIFT feature satisfies these performance requirements well.

In order to meet a wider range of actual matching marks, this study divides the images to be matched into two types of simple images and complex images for experimental testing. The test result is shown in Figure 10.

Through the understanding of Figure 10, we can see that in terms of the accuracy of feature extraction, basically all extraction methods can reach more than 85%, but the relative advantage of SIFT is more obvious.

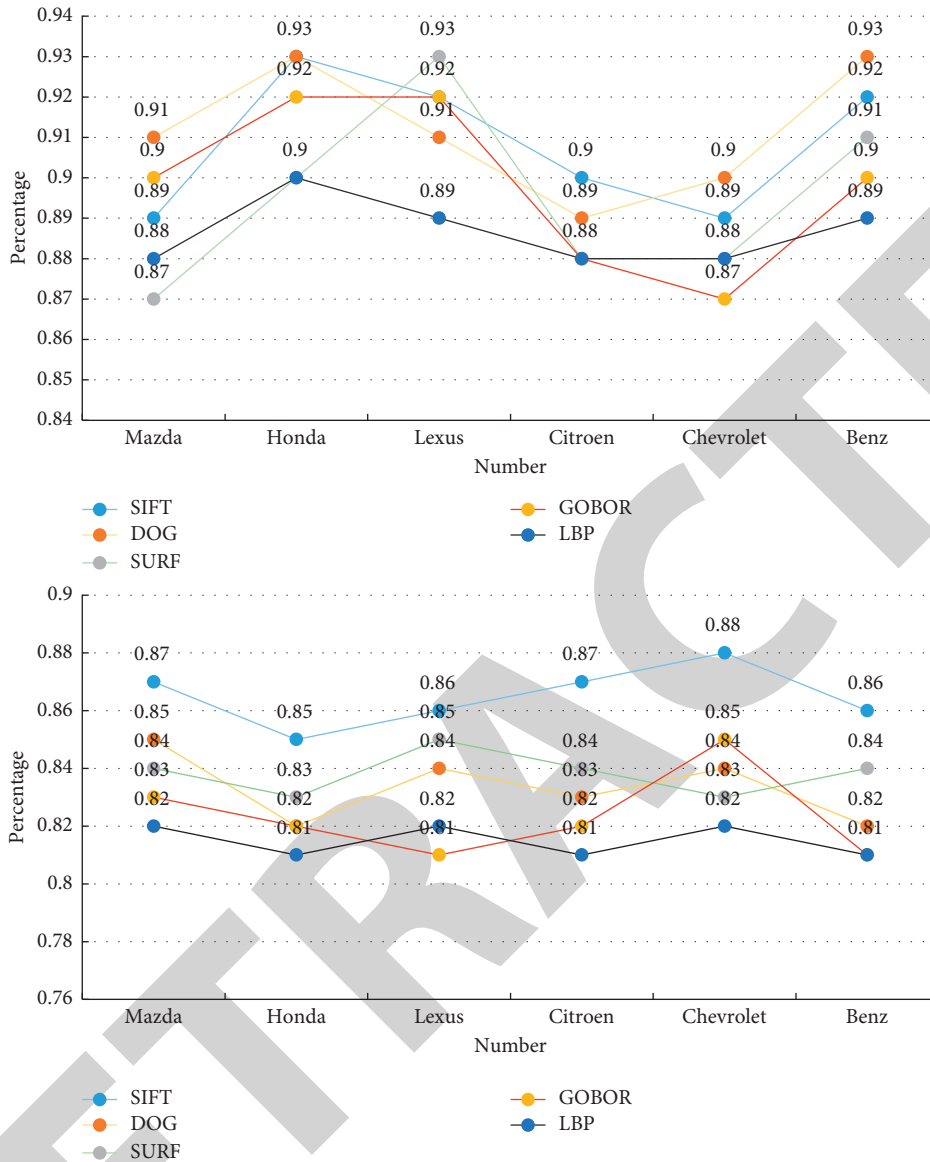


FIGURE 10: Feature vector extraction in different environments.

5. Conclusions

This study is mainly about the research of railway traffic emergency management, through the use of image recognition technology under the background of big data to improve the accident risk monitoring in the actual train operation process. For image recognition technology, this study uses image recognition technology based on deep learning to identify traffic emergency handling problems during train operation. When an accident occurs, the train number can be effectively identified, and the identification ability in the identification process is analyzed and explored experimentally. The results show that the improved image recognition technology based on deep learning has increased the recognition ability of trains by 64%, and the efficiency of emergency handling of railway traffic safety has increased by 27%, which effectively solves the monitoring and

management capabilities for railway traffic safety, and improves the efficiency of emergency accident handling.

Data Availability

The experimental data used to support the findings of this study are available from the corresponding author upon request.

Conflicts of Interest

The authors declare that they have no conflicts of interest regarding this work.

References

[1] X. Luan, B. D. Schutter, T. van den Boom, F. Corman, and G Lodewijks, "Distributed optimization for real-time railway

Research Article

Application of Human Posture Recognition Based on the Convolutional Neural Network in Physical Training Guidance

Qingyu Wang 

College of Sport, Xuchang University, Xuchang 461000, Henan, China

Correspondence should be addressed to Qingyu Wang; 12014246@xcu.edu.cn

Received 19 April 2022; Revised 30 May 2022; Accepted 2 June 2022; Published 28 June 2022

Academic Editor: Le Sun

Copyright © 2022 Qingyu Wang. This is an open access article distributed under the Creative Commons Attribution License, which permits unrestricted use, distribution, and reproduction in any medium, provided the original work is properly cited.

The application of sports game video analysis in athlete training and competition analysis feedback has attracted extensive attention, but the traditional sports human body posture estimation method has a large error between the athlete's human body posture estimation results and the actual results in the complex environment and the athlete's body parts are blocked. Therefore, this study proposes a convolutional neural network for athlete pose estimation in sports game video. Based on the improved model, multiscale model, and large perception model, a superimposed hourglass network is constructed, and the gradient disappearance problem of the convolutional neural network is solved using intermediate supervision. The experimental results show that the athlete pose estimation model based on the convolutional neural network can improve the accuracy of athlete pose estimation and reduce the negative impact of occlusion environment on athlete pose estimation to a certain extent. In addition, compared with other athletes' standing posture estimation methods, the model has competitive advantages and high accuracy under widely used standard conditions.

1. Introduction

With the continuous development of computer vision technology, sports video analysis technology has been widely used in the event analysis of sports competitions. It can provide athletes and coaches with corresponding data as a reference through video analysis and make a relatively systematic evaluation of individual athletes' and groups' performance in sports competitions [1]. In recent years, the number of sports videos has increased geometrically, and at the same time, there is a large amount of interference information in the huge amount of sports videos [2]. The information that athletes and coaches need and pay attention to occupies relatively little in the game video, so how to quickly find the needed information in the massive video information has become a research hotspot in sports video technology.

Sports competition training analysis is mainly divided into technical analysis and tactical analysis, in which technical analysis is the analysis of athletes' personal technical ability, movement standardization, and physical quality in

the competition, and tactical analysis is the guidance of the competition and the application of tactical methods, etc. [3, 4]. Through the analysis of sports competition videos, it can effectively help athletes understand their competitive level and competitive strength of competitors and learn the competitive technology of excellent athletes [5]. With the continuous application of human posture estimation and human motion recognition technology based on the deep neural network, sports training analysis technology based on human posture estimation has also developed rapidly. The athlete's human posture recognition and estimation technology can recognize and estimate the athlete's posture in the high-resolution recorded competition video, decompose the athlete's posture in multiple dimensions, obtain the real action data of the athlete in the competition, and then combine the analysis algorithm with scientific analysis to obtain the final evaluation result of the athlete's performance [6, 7]. In addition, the same movement of athletes in the same sport can be compared horizontally to find out the gap and problems between athletes' movements and standard movements, which will help athletes improve and reduce the

possibility of repeated training [8]. At the same time, it allows athletes to more intuitively understand the training content and give rapid feedback to reduce sports injuries caused by irregular sports [9]. However, the traditional athlete posture recognition and estimation methods cannot fully extract image features. Although the time required is relatively small, when the athlete's posture changes greatly in training, the error between the estimation results and the actual results will become larger [10]. Therefore, estimating the posture recognition of skilled athletes in complex environment has become a challenge for sports video analysis technology.

Combined with the convolution neural network, this study studies the method of athlete posture estimation in sports training. This study creatively constructs a layered hourglass network based on improved module, multiscale module, and large perception field module. The intermediate supervision method is used to avoid the gradient vanishing problem of the convolutional neural network. Compared with the traditional athlete posture estimation method in image feature information extraction, this method has more practical application value. It solves the problem that there is a large error between the estimated results and the actual results when the environment in the sports video is complex or the athletes' body parts are blocked.

To solve the above problems, this study proposes a convolutional neural network research on athletes' human posture estimation technology in sports game training, which is mainly divided into three parts. The first part introduces the development of human posture estimation technology. The second part is the construction of the athlete posture estimation model based on the convolutional neural network and introduces the adopted model. In the third part, the performance experiment and simulation experiment of the athletes' human posture estimation model based on the convolutional neural network are carried out, and the experimental results are analyzed.

2. Related Work

Since the 1980s and 1990s, people have proposed and studied the corresponding human posture estimation methods. However, in the early research stage, computer equipment and deep learning technology are still in the exploration and development stage. Therefore, most of the traditional human posture estimation methods are based on the graphical structure model [11]. Some scholars have improved the graph structure based on statistical combination to obtain the tree structure, which can reduce the computational complexity, but it is difficult to correctly estimate the human posture in the case of complex environment scene or partial occlusion of the human body [12, 13]. To solve these problems, it is suggested to add corresponding constraints to the occluded part of the human body to achieve improvement and combine the confidence propagation algorithm to estimate the corresponding human posture. Therefore, even in the case of human occlusion, human joint points can be predicted relatively accurately [14]. With the in-depth study of human posture

and the development of learning technology, many algorithms have achieved good results in the field of human posture estimation.

The current human pose estimation is mainly divided into overall human pose estimation algorithms and human pose component estimation algorithms [15]. The algorithms for overall human pose estimation usually use a nonlinear mapping between images and nodal positions to achieve human pose estimation [16, 17]. A deep neural network-based human pose estimation algorithm has been proposed to obtain pose estimation values with high accuracy using DNN regression quantities, which has the advantage over other algorithms in that it performs pose inference through a holistic approach [18]. It has also been proposed to incorporate domain prior knowledge in the DCNN framework and combine the variability mixture component for end-to-end human pose estimation [19]. Normalized distances in overall human pose estimation methods like this can have a large impact on the localization of nodes. For the human component estimation algorithm, the human model is built based on the appearance and position of the component or joint, and then, the corresponding optimization is performed to obtain the corresponding energy function [20]. Traditional joint point models are manually performed with image feature design, which makes the real appearance of their representations have a large error, while deep learning can solve this problem. It has been proposed to combine human joints, parts affinity force fields combined with greedy algorithms for learning body parts and individual connections in images through non-parametric representations, and such an approach can achieve real-time performance while maintaining low error regardless of the number of individuals in the image [21, 22]. However, body pose estimation by body parts is prone to loss of body information, while the bottom-up approach increases the chances of joint point misdetection. Therefore, in the field of sports game training and analysis, there are many problems in human posture estimation technology, which need to be further developed and solved.

3. Construction of the Athlete Posture Estimation Model Based on the Convolutional Neural Network

The convolutional neural network has two characteristics: local sensing and parameter sharing. Local sensing, namely, the convolution neural network, proposes that each neuron does not need to perceive all pixels in the image. Only the local pixels of the image are sensed, and then, the local information is combined at a higher level to obtain all the representation information of the image. The nerve units of different layers are connected locally; that is, the nerve units of each layer are only connected with some nerve units of the previous layer. Each nerve unit only responds to the areas within the receptive field and does not care about the areas outside the receptive field. Such local connection mode ensures that the learned spatial local mode of convolution check input has the strongest response. Due to the complex background of the application scene, the flexibility of

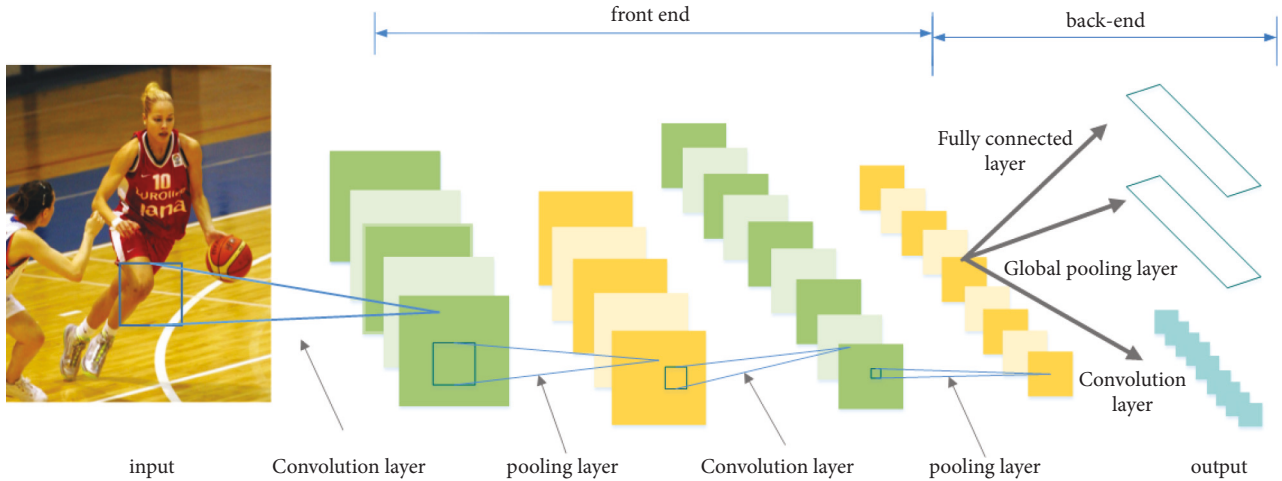


FIGURE 1: Simplified architecture of the convolutional neural network.

athletes' limbs, and the serious occlusion of various parts of the human body, the traditional human posture estimation methods show limited representation performance in practical application and produce unsatisfactory posture estimation results. The athletes' attitude estimation method based on the convolutional neural network has good non-linear transformation ability, and the improvement of the convolutional neural network and other auxiliary methods can further improve the athletes' attitude estimation accuracy in game training.

3.1. Multiresidual Modular Convolutional Neural Network Athlete Pose Evaluation Model. Among the deep learning models of human pose estimation algorithms, convolutional neural networks have the unique advantage of being feed-forward neural networks with deep structure and after continuous development currently contain mainly convolutional layers, pooling layers, fully connected layers, activation functions, normalization layers, inputs, outputs, etc. The pool layer is sandwiched in the middle of the continuous convolution layer to compress the amount of data and parameters and reduce overfitting. If the input is an image, the main function of the pooling layer is to compress the image [23]. A simplified architecture of the convolutional neural network is shown in Figure 1.

In convolutional neural networks, the convolutional layer is a feature extraction layer by having convolutional kernels for abstract feature extraction, to reduce the number of parameters; it mainly takes local sensing and weight sharing methods [24]. The pooling layer, on the other hand, reduces the number of neurons by counting and down-sampling the features [25]. The following equation is the convolution operation.

$$F(i, j) = X(3 \times 3)_{i \times j} \otimes f(3 \times 3), \quad (1)$$

where the $F(\cdot)$ denotes the features after convolution, (i, j) denotes the pixel points of the image, $X(\cdot)$ denotes the matrix of the pixel points and the neighboring pixel points at the corresponding position, and $f(\cdot)$ denotes the filter. If the

size of the input image is denoted as $H \times W$ and the size of the convolution kernel is N , the size of the feature map obtained after the operation with the convolution step is shown in S as follows:

$$H_{\text{feat}} = \frac{H - N}{S} + 1, \quad (2)$$

$$W_{\text{feat}} = \frac{W - N}{S} + 1. \quad (3)$$

If the complementary zero operation is added, the input image size is M , as shown in equation:

$$W_{\text{feat}} = \frac{M + 2K - N}{S} + 1. \quad (4)$$

Although the performance of the convolutional neural network in athlete posture estimation is better than that of traditional methods, there are still some problems, such as gradient problem and small sensing domain of the feed-forward network. Therefore, this study selects a convolutional neural network with stacked hourglass structure and improves it combined with multiple modules [26]. The superimposed hourglass grid is constructed using grid and intermediate supervision method, which not only solves the problem of gradient disappearance, but also has high network performance and athlete attitude estimation accuracy. However, the performance of a single module cannot meet the requirements of athletes' posture estimation technology. Therefore, this study selects large sensory field module, improved module, and multiscale module for network construction.

The accurate performance of the neural network is improved to estimate athletes' posture, so that the neural network can carry out very in-depth training. However, its own unit mapping will also make the response change increase with the increase in depth. Therefore, the laminated hourglass network will have a great response impact when training deeper networks, which increases the difficulty of parameter optimization and estimation error. Based on the traditional laminated hourglass grid, the improved

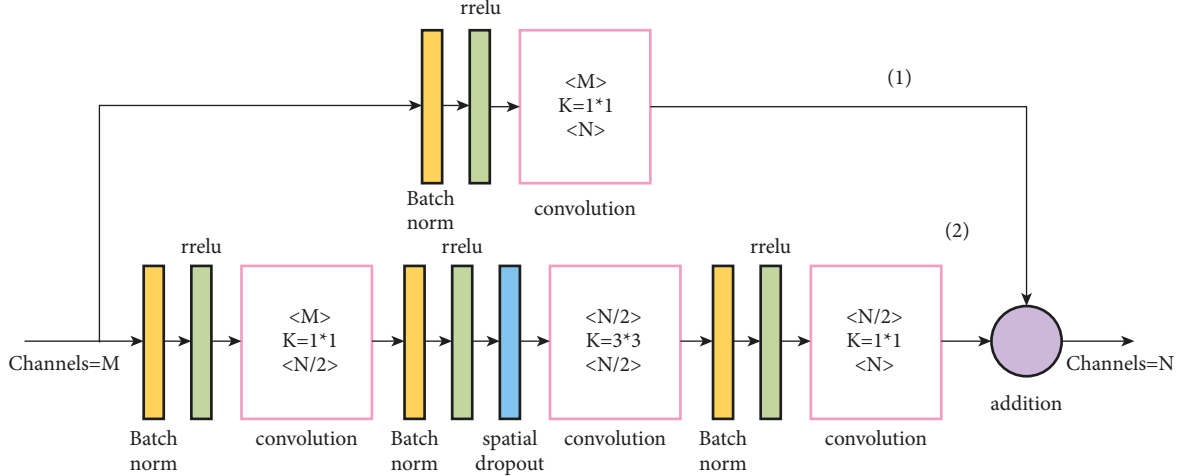


FIGURE 2: Improved hourglass grid stacking diagram.

laminated hourglass grid replaces the unit mapping with normalization layer, ReLU, and convolution and introduces spatial attenuation layer 3×3 before the convolution, as shown in Figure 2.

When estimating athletes' posture in game training, the correlation and connection between the whole body parts and joints are affected by the effective receptive field of neurons to the surrounding area. The size of the mapping range of the pixel points corresponding to each layer of the output feature mapping in the convolution neural network on the original image is the receptive field, which corresponds to the receptive field of the first layer, as shown in the following equation:

$$F_i = F_{i-1} + (k - 1) * \text{stride}(i), \quad (5)$$

where is the F_{i-1} perceptual field size of the previous layer, k denotes the current convolution kernel size, and $\text{stride}(i)$ denotes the step product of the previous $(i - 1)$ layers; i.e., $\text{stride}(i) = \text{stride}(1) * \text{stride}(2) * \dots * \text{stride}(i - 1)$.

The effective receptive field of the improved module is still very small, so a large receptive module is constructed based on the improved module. The schematic diagram of large magnetic field residual module is shown in Figure 3.

When helping the deep residual learning to achieve a breakthrough in the task of image recognition and classification, the module is shown in the following equation:

$$p_{i+1} = h(p_i) + F(p_i, W_i^F). \quad (6)$$

The corresponding input of the first i residual module is denoted as p_i , and the output is denoted as p_{i+1} , F denotes the convolution that forms the stack, and $h(p_i) = p_i$ denotes the unit mapping. The large sensory field residual module is shown in the following equation:

$$p_{i+1} = h(p_i) + F(p_i, W_i^F) + Q(p_i, W_i^Q). \quad (7)$$

The offset problem is one of the common problems faced by equipment manufacturers who use stepping or servo motors in the process of equipment setting, commissioning, and use. The deviation is caused by improper mechanical fittings, mutual interference of equipment in

the workshop, or improper grounding wire treatment in the equipment setting. The problem of large positioning error of joint points is caused by the change in athletes' body shape in the competition video. This requires the integration of multiscale modules on the basis of large receiving field modules. This requires the integration of multiscale modules on the basis of large receiving field modules, as shown in Figure 4.

As can be seen from the figure, the multiscale module in (1), (2), and (3) is the same as the large sensory field module, while branch (4) $Q(p_i, W_i^Q)$ is a new addition with the structure of $\text{pool}2 * 2 + \text{conv}3 * 3 + \text{pool}2 * 2 + \text{conv}3 * 3 + \text{upsample}2 * 2 + \text{upsample}2 * 2$, from which we can see that there are two downsamples in this branch, which means that the feature map size is 25% of the input feature map, and after upsampling to the input feature mapping size, it is fused with the other three branches in series. In the other branches, the feature map size of branch (3) is 50% of the input feature map, and the feature map sizes of branches (1) and (2) remain unchanged. The expressions are shown in the following equation:

$$p_{i+1} = h(p_i) + F(p_i, W_i^F) + Q(p_i, W_i^Q) + G(p_i, W_i^G). \quad (8)$$

Figure 5 shows the overall framework of the convolutional neural network. As shown in the figure, it can be divided into two parts, the first half and the second half. The first half of the framework is composed of convolution, large field of view module, and pool, which is used to learn athletes' pose estimation in the feature map. After convolution kernel operation, the size of the feature map remains in the second half. The second half of the frame is composed of hourglass subgrid structure, with intermediate supervision at the end of each hourglass, and the feature map is processed multiple times between high resolution and first resolution to form a stacked hourglass grid.

3.2. Off-Node Prediction and Athlete Pose Estimation Dataset. The predicted positions of the joint nodes are mainly regressed by the score map, i.e., the score map

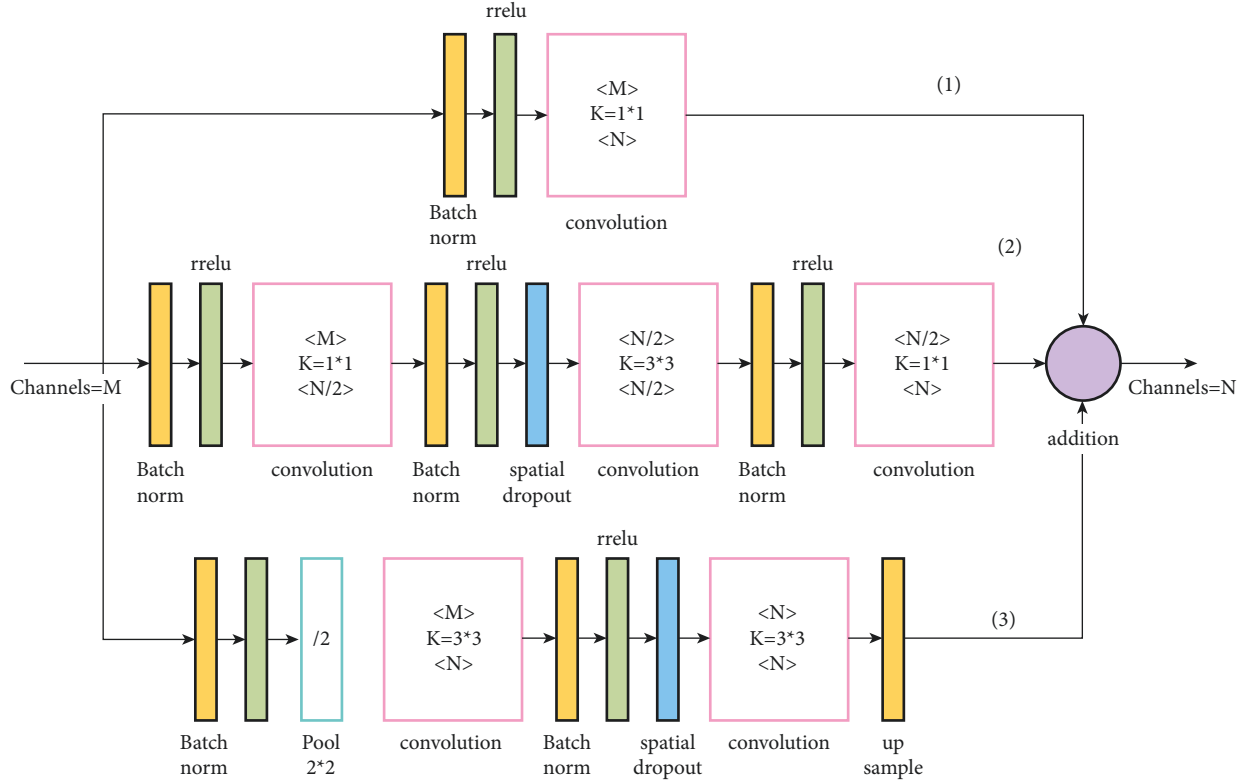


FIGURE 3: Schematic diagram of large receptive field residual module.

corresponding to each hourglass subnetwork and human joint point in the multi-residual convolutional neural network. Let the actual labeled position of the joint point be denoted as $V = \{V_k\}_{k=1}^K$ and position of the first k joint point is denoted as $V_k = (x_k, y_k)$, and then, the fractional map of the actual position is calculated as shown as follows:

$$S_k(t) \sim N(v_k, \Sigma), \quad (9)$$

where the predicted positions of the nodes are denoted as $t \in \mathbb{R}^2$, and Σ denotes the unit matrix. If the number of nodes is K one, the number of predicted score maps obtained for each hourglass subnetwork is K , i.e., $\hat{S} = \{\hat{S}_k\}_{k=1}^K$. The hourglass end loss function is shown in the following equation:

$$L = \sum_{m=1}^M \sum_{k=1}^K \left\| S_k - \hat{S}_k \right\|_2^2, \quad (10)$$

where M denotes the number of samples. The position at the highest score on the score graph of the last hourglass subnetwork after the prediction process is marked as the prediction node position, which is denoted as \hat{v}_k , as shown in the following equation:

$$\hat{v}_k = \arg \max_t \hat{S}_k(t), \quad k = 1, 2, \dots, K. \quad (11)$$

The MPII dataset, LSP dataset, and MS COCO dataset are commonly used for experimental training of athlete's pose estimation in competition video, and the LSP dataset and its extensions are included in this study. In the LSP

dataset, there are many pictures of athletes with rich posture and recognized high difficulty in posture estimation, and the number of joints for human posture estimation is 14 joints, which is challenging for the experiment. The estimated number of joints in human posture is sixteen joints, and the evaluation criterion is the percentage of correct joints, i.e., PCK; after normalizing the data annotation, if the joints are still within the distance of the threshold value, then the joints are correct, as shown in the following equations:

$$D_p = \frac{\sqrt{(x^p - x^g)^2 + (y^p - y^g)^2}}{\text{HoH}}, \quad (12)$$

$$\text{PCKh}@s = \frac{\sum_p \delta(D_p < s)}{\sum_p 1}, \quad (13)$$

where s is the threshold value and $s \in \{0.1, 0.2, 0.3, 0.4, 0.5\}$, p is the number of nodes, and $(x^p - x^g)$ and $(y^p - y^g)$ are the predicted and actual values, respectively. The prediction is wrong when $D_p > s$ and correct when the opposite is true, $\text{PCKh}@s$.

The number of estimated joints of human posture in the MS COCO dataset is 17, which is evaluated in terms of the average accuracy, i.e., mAP, as shown in the following equations:

$$\text{mAP} = \text{mean}\{AP@ (0.5: 0.005: 0.95)\}, \quad (14)$$

$$AP@s = \frac{\sum_p \delta(\text{OKS}_p > s)}{\sum_p 1}. \quad (15)$$

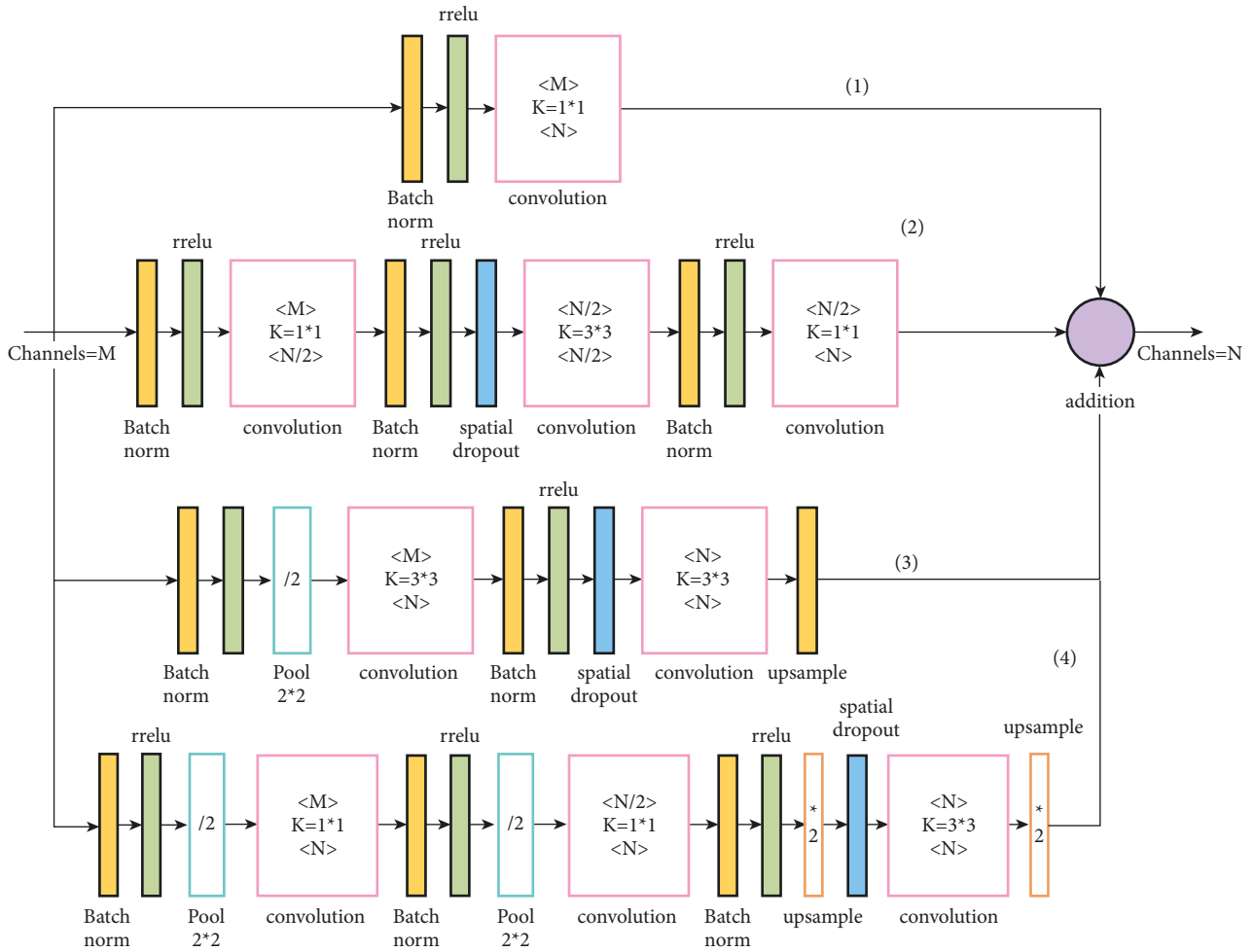


FIGURE 4: Schematic diagram of multiscale residual module.

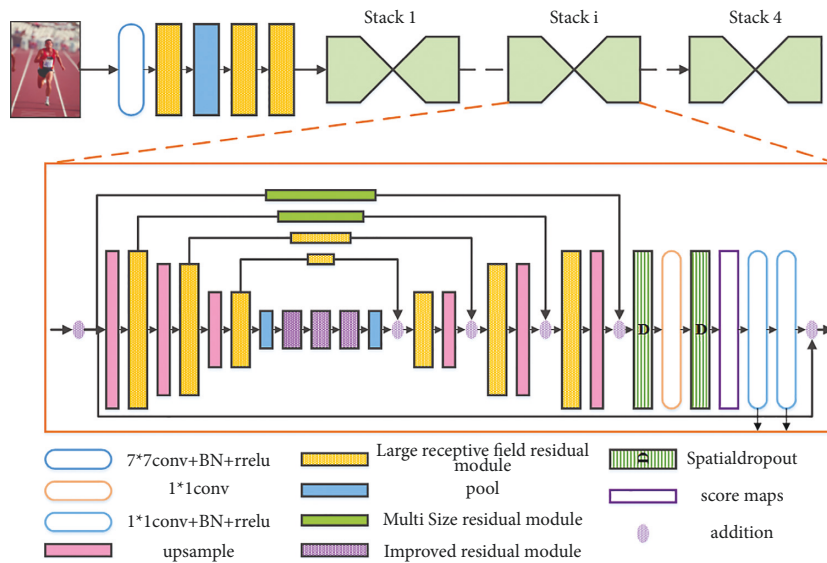


FIGURE 5: Overall framework of the convolutional neural network.



FIGURE 6: Examples of joint points in three datasets.

The threshold value of OKS $s \in [0, 1]$, which is the evaluation criterion for the similarity between the actual and predicted values of the nodes. An example of three dataset nodes is shown in Figure 6.

4. Experimental Results of Athlete Pose Estimation in Sports Game Video Combined with the Convolutional Neural Network

4.1. Experimental Results of Performance of the Athlete Posture Estimation Model Based on the Convolutional Neural Network. The convolutional neural network human posture estimation model is mainly composed of the sand leak subnetwork. Therefore, this study makes an experimental study on the impact of the establishment of sand leak subnetwork on the performance of athletes' human posture estimation. Under the same other experimental conditions, experiments are carried out on different numbers of sand leak subnetworks on the dataset. As shown in Figures 7 and 8, the experimental results of the training model composed of different number of sand leakage subnetworks under the evaluation standard conditions are shown. Figures 9 and 10 show the overall PCK and PCP curves, respectively. The horizontal coordinate represents the threshold of measurement, and the vertical coordinate represents the accuracy of each joint or different part of the athlete in the video.

From the results in the figure, we can know that the performance of the athlete pose estimation model based on the multi-residual module convolutional neural network effectively improves with the increase in the number of

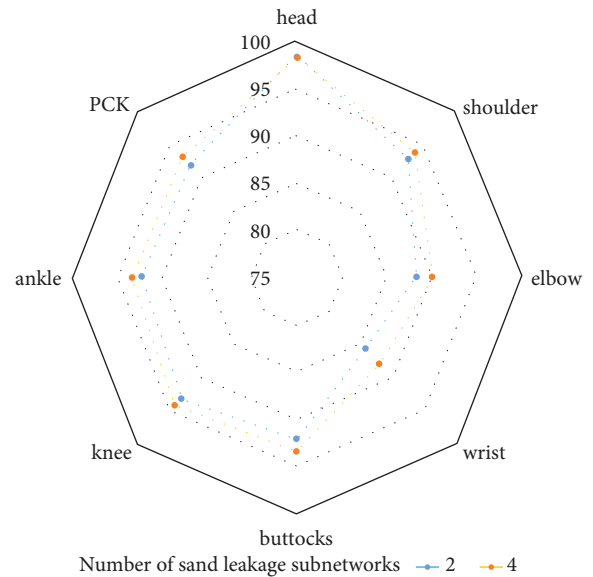


FIGURE 7: PCK results on the LSP dataset.

hourglass subnetworks. This is mainly because the individual hourglass subnetworks can only learn a limited number of image features and their effective perceptual field is relatively small, but the stacked hourglass networks are much more capable of learning feature information and can acquire more feature information. After related experiments, the number of hourglass subnetworks finally selected in this study is 4, which has the best performance in the experiment and has a certain degree of positive impact on the accuracy of the athlete's pose estimation.

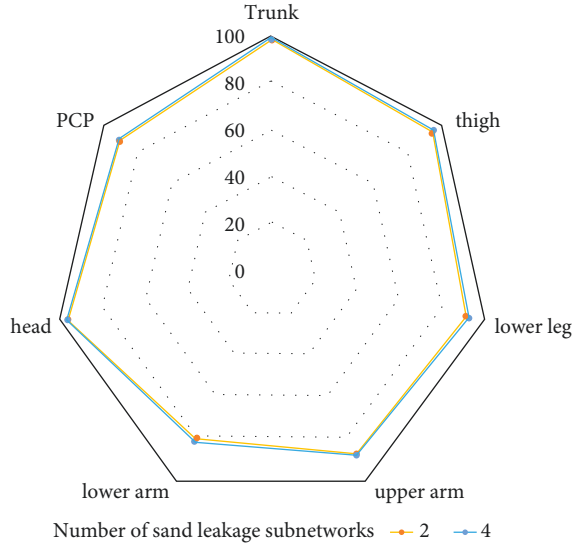


FIGURE 8: PCP results on the LSP dataset.

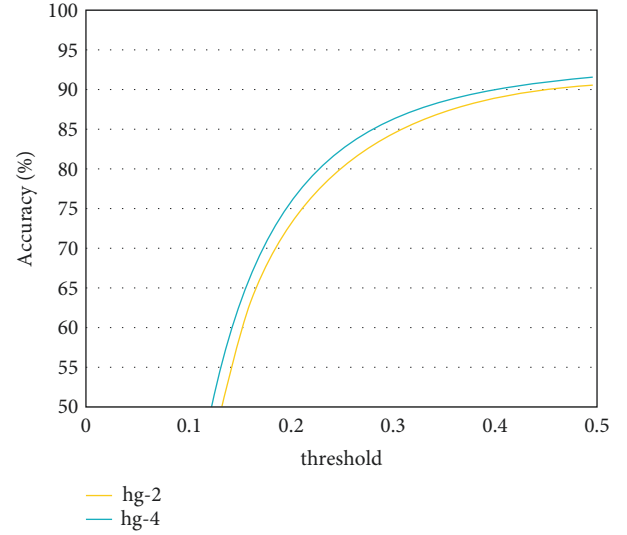


FIGURE 10: Overall PCP curve.

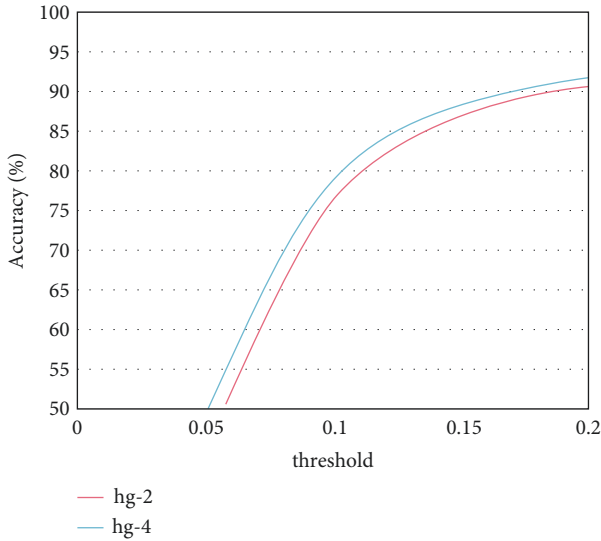


FIGURE 9: Overall PCK curve.

4.2. Experimental Results of the Athlete Posture Evaluation Model Based on the Convolutional Neural Network. To help the athletes' posture estimation model based on the convolutional neural network learn better, this study combines the LSP dataset and MPII dataset for model training. Through the performance test, the experimental comparison results of PCK and PCP are obtained, while the results of other competition video athlete posture estimation methods are from the corresponding references. As shown in Figure 11, the PCK standard comparison results of the athlete posture estimation model based on the multimodule convolutional neural network on the LSP dataset are shown. Figure 12 shows the comparison results of PCP standard of athlete posture estimation model based on the convolutional neural network on the LSP dataset.

It can be seen from the results in the figure that the athlete posture estimation model based on the convolutional

neural network is competitive with other athlete posture estimation methods. Its experimental results on LSP data show that the prediction accuracy of posture estimation is high. In the standard of athletes' posture estimation results, the index to measure and evaluate the estimation accuracy of athletes' body parts is PCP. In sports training, the upper and lower arms of athletes are most affected in the fuzzy environment. However, the data results in the figure show that the accuracy of the upper arm and lower arm of the athlete posture evaluation model based on the multiresidual module convolution neural network is 88.7% and 82.3%, respectively, both of which are relatively accurate. It can be seen that the athlete posture estimation model based on the convolutional neural network can reduce the negative impact of occlusion on athlete posture estimation to a certain extent.

As given in Table 1, after training on the MPII dataset, the results of the athlete posture evaluation model based on the convolutional neural network are compared with other widely used human posture estimation methods.

It can be seen from the table that the simple superimposed hourglass model and the improved superimposed hourglass model used for athlete posture evaluation are slightly higher than the convolution neural network based on multimodule. However, in the network design of laminated hourglass, either the simple laminated hourglass model or the improved laminated hourglass model selects 8 hourglass subnetworks, while the athlete posture evaluation model based on the multimode convolution neural network only uses 4 hourglass subnetworks. This shows that the athlete posture evaluation model based on the convolutional neural network has a certain degree of improvement in the accuracy of human posture estimation. This is mainly because the athlete posture evaluation model based on the multimode convolution neural network fully considers the influence of human body part size and model large perception field when reasoning athletes' human joints. Thus, in the model training, we can fully learn the image feature

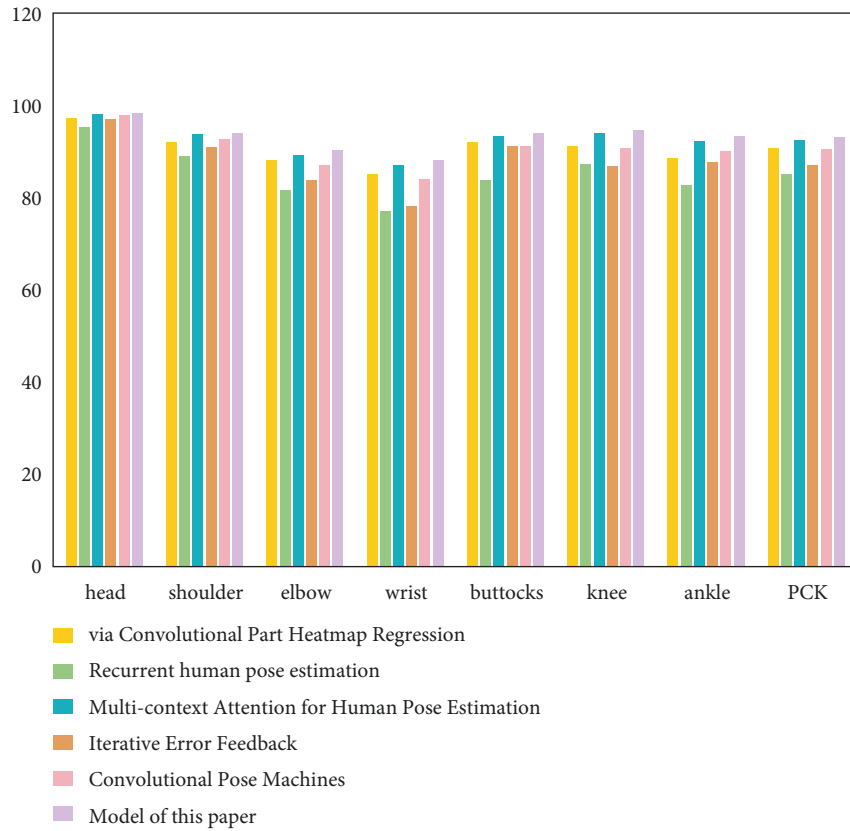


FIGURE 11: PCK standard comparison results of different athlete posture evaluation models on the LSP dataset.

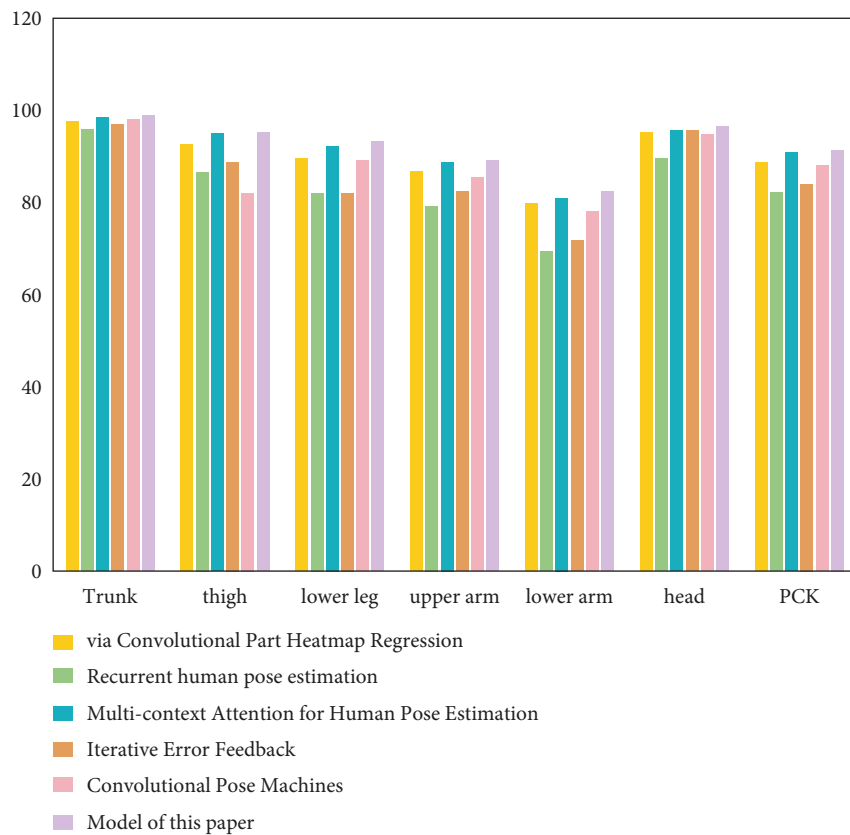


FIGURE 12: PCP standard comparison results of different athlete posture evaluation models on the LSP dataset.

TABLE 1: PCKh comparison results on the MPII dataset.

Method	Head	Shoulder	Elbow	Wrist	Buttock	Knee	Ankle	PCKh
Iterative error feedback	95.5	91.5	81.6	72.3	82.6	73.0	66.3	79.5
Simple stacked hourglass network model	98.1	96.0	91.1	86.9	90.1	87.2	83.4	90.1
Network model based on improved stacked hourglass	98.3	96.2	91.7	88.0	90.5	87.8	84.9	90.7
Joint subset partition and labeling	94.0	90.0	83.3	77.2	82.5	75.6	68.5	81.6
Convolutional pose machines	97.6	94.9	88.5	83.8	88.1	82.5	79.1	87.8
Model of this study	97.7	96.0	90.6	86.0	89.7	86.3	82.6	89.7

information of different sizes, and the extended perception field provides a good basis for learning the correlation of human joints. Therefore, the accuracy of athlete pose estimation in sports game video can be improved.

With the continuous diffusion of sports training data, it becomes more and more difficult for coaches and athletes to find relevant data in a large number of videos. Sports training analysis technology has been widely used in sports and sports competitions. It can not only improve the viewing experience of the audience but also systematically evaluate the performance of individual and team athletes in high-resolution video. We can also analyze athletes' postures in visual training from multiple dimensions to obtain the real movement data of athletes in the competition. These data can help coaches and athletes understand the gap between their own movements and standard movements and can also understand the economic level of other athletes through parallel comparison, to reduce the possibility of repeated training.

5. Conclusion

Combined with the convolution neural network, this study studies the method of athlete posture estimation in sports training. In this study, a layered hourglass network based on improved module, multiscale module, and large perceptual field module is constructed. The intermediate supervision method is used to avoid the gradient vanishing problem of the convolutional neural network. The experimental results show that the athlete posture evaluation model based on the multimode convolution neural network can effectively realize the learning of multiscale image feature information in the training process. To a certain extent, it reduces the negative impact of occlusion environment on athletes' posture estimation and improves the accuracy of athletes' joint position prediction. Compared with other athletes' pose estimation methods, the athletes' pose estimation model based on the dataset convolution neural network has certain advantages and competitiveness and shows high accuracy under the widely used standard conditions. However, this method only estimates the pose of a single athlete in the sports game video and cannot solve the pose estimation problem of multiple athletes. It has shortcomings in practical application and needs further research.

Data Availability

The data used to support the findings of this study are included within the article.

Conflicts of Interest

The authors declare that there are no conflicts of interest.

References

- [1] P. Dognin, I. Melnyk, Y. Mroueh et al., "Image captioning as an assistive technology: lessons learned from VizWiz 2020 challenge," *Journal of Artificial Intelligence Research*, vol. 73, pp. 437–459, 2022.
- [2] S. Yadav and S. Payandeh, "Critical overview of visual tracking with kernel correlation filter," *Technologies*, vol. 9, no. 4, p. 93, 2021.
- [3] F. Zhou and F. De la Torre, "Spatio-temporal matching for human pose estimation in video," *IEEE Transactions on Pattern Analysis and Machine Intelligence*, vol. 38, no. 8, pp. 1492–1504, 2016.
- [4] B. Pu, K. Xiang, J. Ji, and X. Wang, "High-speed tracking with multi-templates correlation filters," *Journal of Electronic Imaging*, vol. 30, no. 6, Article ID 063020, 2021.
- [5] I. Mironică, I. C. Duță, B. Ionescu, and N. Sebe, "A modified vector of locally aggregated descriptors approach for fast video classification," *Multimedia Tools and Applications*, vol. 75, no. 15, pp. 9045–9072, 2016.
- [6] D. Mehta, S. Sridhar, O. Sotnychenko et al., "VNect," *ACM Transactions on Graphics*, vol. 36, no. 4, pp. 1–14, 2017.
- [7] R. Girshick, J. Donahue, T. Darrell, and J. Malik, "Region-based convolutional networks for accurate object detection and segmentation," *IEEE Transactions on Pattern Analysis and Machine Intelligence*, vol. 38, no. 1, pp. 142–158, 2015.
- [8] G. Ning, Z. Zhang, and Z. He, "Knowledge-guided deep fractal neural networks for human pose estimation," *IEEE Transactions on Multimedia*, vol. 20, no. 5, pp. 1246–1259, 2018.
- [9] J. D. Oliveira, J. A. L. de Moraes Junior, and R. H. Bordini, "Ambient intelligence technologies for visually impaired: a mapping study," in *Proceedings of the ITNG 2021 18th International Conference on Information Technology-New Generations*, pp. 163–168, Springer, Berlin, German, February 2021.
- [10] H.-B. Zhang, Q. Lei, B.-N. Zhong, J.-X. Du, and J. Peng, "A survey on human pose estimation," *Intelligent Automation & Soft Computing*, vol. 22, no. 3, pp. 483–489, 2016.
- [11] F. Rezazadegan, S. Shirazi, N. Sunderhauf, and M. Milford, "Enhancing human action recognition with region proposals," *Ultrasound in Obstetrics and Gynecology*, vol. 32, no. 3, p. 335, 2015.
- [12] M. Rohrbach, A. Rohrbach, M. Regneri et al., "Recognizing fine-grained and composite activities using hand-centric features and script data," *International Journal of Computer Vision*, vol. 119, no. 3, pp. 346–373, 2016.

- [13] G. Varol, I. Laptev, and C. Schmid, "Long-term temporal convolutions for action recognition," *IEEE Transactions on Pattern Analysis and Machine Intelligence*, vol. 40, p. 1, 2017.
- [14] A. Richard and J. Gall, "A bag-of-words equivalent recurrent neural network for action recognition," *Computer Vision and Image Understanding*, vol. 156, pp. 79–91, 2017.
- [15] L. Fu, J. Zhang, and K. Huang, "ORGM: occlusion relational graphical model for human pose estimation," *IEEE Transactions on Image Processing*, vol. 26, no. 2, pp. 927–941, 2017.
- [16] B. Ni, V. R. Paramathayalan, T. Li, and P. Moulin, "Multiple granularity modeling: a coarse-to-fine framework for fine-grained action analysis," *International Journal of Computer Vision*, vol. 120, no. 1, pp. 28–43, 2016.
- [17] M. Ma, N. Marturi, Y. Li, R. Stolkin, and A. Leonardis, "A local-global coupled-layer puppet model for robust online human pose tracking," *Computer Vision and Image Understanding*, vol. 153, pp. 163–178, 2016.
- [18] N. Sarafianos, B. Boteanu, B. Ionescu, and I. A. Kakadiaris, "3D Human pose estimation: a review of the literature and analysis of covariates," *Computer Vision and Image Understanding*, vol. 152, pp. 1–20, 2016.
- [19] G. Pavlakos, X. Zhou, K. G. Derpanis, and K. Daniilidis, "Coarse-to-fine volumetric prediction for single-image 3D human pose," *IEEE Conference on Computer Vision and Pattern Recognition*, vol. 139, no. 1, pp. 1263–1272, 2016.
- [20] R. Dunne, T. Morris, and S. Harper, "A survey of ambient intelligence," *ACM Computing Surveys*, vol. 54, no. 4, pp. 1–27, 2022.
- [21] S. E. Wei, V. Ramakrishna, T. Kanade, and Y. Sheikh, "Convolutional pose machines," *IEEE Conference on Computer Vision and Pattern Recognition*, vol. 511, no. 1, pp. 4724–4732, 2016.
- [22] S. Ren, K. He, R. Girshick, and J. Sun, "Faster r-cnn: towards real-time object detection with region proposal networks," in *Proceedings of the IEEE Conference on Transactions on Pattern Analysis & Machine Intelligence*, pp. 91–99, Montreal Canada, December 2015.
- [23] I. U. Yasin and K. Bjorn, "A dual-Source Approach for 3D Pose Estimation from a Single Image," *Computer Vision and Image Understanding*, vol. 2010, no. 1, pp. 4948–4956, 2017.
- [24] J. Deng, S. Shi, P. Li, W. Zhou, Y. Zhang, and H. Li, "Voxel r-cnn: towards high performance voxel-based 3d object detection," *Proceedings of the AAAI Conference on Artificial Intelligence*, vol. 35, no. 2, pp. 1201–1209, 2021.
- [25] M. Gams and M. Gjoreski, "Artificial intelligence and ambient intelligence," *Electronics*, vol. 10, no. 8, p. 941, 2021.
- [26] W. Bao, Y. Yang, and D. Liang, "Multi-residual module stacked hourglass networks for human pose estimation," *Journal of Beijing Institute of Technology (Social Sciences Edition)*, vol. 29, no. 1, pp. 110–119, 2020.

Research Article

Deep Learning-Based Optimization Algorithm for Enterprise Personnel Identity Authentication

Tiejun Chen 

School of Management, Zhejiang University of Technology, 310014 Hangzhou, Zhejiang, China

Correspondence should be addressed to Tiejun Chen; ctj@zjut.edu.cn

Received 19 April 2022; Accepted 15 June 2022; Published 28 June 2022

Academic Editor: Le Sun

Copyright © 2022 Tiejun Chen. This is an open access article distributed under the Creative Commons Attribution License, which permits unrestricted use, distribution, and reproduction in any medium, provided the original work is properly cited.

Enterprise strategic management is not only an important part of enterprise work, but also an important factor to deepen the reform of management system and promote the centralized and unified management of enterprises. Enterprise strategic management is to study the major problems of survival and development of enterprises in the competitive environment from the overall and long-term point of view. It is the most important function of senior leaders of modern enterprises. Starting from the characteristics of the recognition object, this paper analyzes the individual differences of biometrics through intelligent face image recognition technology to identify biometrics, which can be used to identify different individuals. This paper studies the main problems of personnel identity authentication in the current enterprise strategic management system. Based on identity management and supported by face image recognition technology, deep learning, and cloud computing technology, the personnel management model of the management system is constructed, which solves the problems of personnel real identity authentication and personnel safety behavior control. Experiments show that the model can simplify the workflow, improve the operation efficiency, and reduce the management cost. From the perspective of enterprise system development, building a scientific enterprise strategic management system is of great significance to improve the scientific level of enterprise system management.

1. Introduction

Enterprise strategic management is not only an important guarantee for the orderly operation of the government, but also an important content of the government's own construction. The centralized management of enterprise office area is an important part of enterprise affairs and an important factor to deepen the reform of enterprise management system and promote the centralized and unified management of affairs [1]. Integrity function is the most basic function of the system. In general, the system not only has more quantitative provisions than the simple superposition of partial forces, but also has some new properties that do not have qualitative Provisions [2]. Investigating the integrity of things and understanding and handling problems from the perspective of integrity will improve the work efficiency of the organization [3]. Enterprise strategic management is an important part of system management, especially in enterprise reform and development. It plays an

important role in ensuring, coordinating, advising, and encouraging them [4]. The enterprise system urgently needs a technology that can effectively and quickly identify and control enterprise managers. Biometric technology can meet this requirement. Biometric recognition technologies such as fingerprint, iris, and face image recognition have been more and more widely used in the market because of their efficient, stable, fast, and unique characteristics [5]. Face image recognition technology is a biometric recognition technology based on face feature information. Relevant personnel can use mobile phones, tablets, and other devices to collect face image information or video stream and compare it with the template face image information in the database [6].

Enterprise strategic management innovation is the overall innovation of the system and the attribute of metabolism and self-renewal of the enterprise system itself [7]. The goal, core, and value orientation of enterprise management innovation is to realize the overall leap and

overall efficiency of the management system and promote the coordinated development and overall progress of the social system [8]. Because the existing identity information samples in the enterprise strategic management system are extremely limited, there is usually only one employee face sample. This brings challenges to the deep neural network model that needs to rely on a large number of samples for training, resulting in that the recognition results are vulnerable to various external factors, and false recognition occurs from time to time [9]. This poses a potential threat to the safe production of the strategic management system. The conditions for realizing enterprise management innovation are to improve the overall quality of managers, build a scientific and reasonable management system structure, straighten out the boundary between management system and environment, and create a good institutional environment [10]. Promoting the scientific, information, and intensive construction of centralized office areas is of great significance for organ affairs management and building a service-oriented and efficient government [11]. This paper studies the main problems of personnel identity authentication in the current enterprise strategic system and constructs an enterprise system personnel management model based on identity management, face image recognition technology, deep learning, and cloud computing support, so as to solve the problems of personnel real identity authentication and personnel security behavior control.

Face image recognition technology is a research hotspot in the field of recognition in recent years. In terms of the characteristics of the recognition object, it realizes biometric recognition by analyzing the individual differences of the characteristics of the organism itself. Therefore, it can be used to identify different individuals [12]. Face image recognition products have been widely used in people's production and life. For example, the construction of examinee authentication system using face image recognition technology can effectively improve the accuracy and speed of examinee authentication in educational examination [13]. At this stage, the enterprise strategic management system has insufficient binding force on people and lacks the management of personnel identity security, unclear personnel identity information, and nonstandard employment, resulting in management problems in the management process, but it can not accurately locate the person in charge [14].

Based on the theoretical research of face image recognition and combined with work practice, this paper discusses the application of face image recognition technology in centralized office area. There are many changes in the details of face images, and the related motion changes also have different forms. It is the nonlinear characteristics of human face that increase the difficulty of face detection and recognition technology. The personnel management model of enterprise system based on cloud computing intelligent image recognition can simplify the workflow, improve the operation efficiency, and reduce the management cost. From the perspective of the development of enterprise strategic system, the construction of scientific personnel management

system is of great significance to improve the scientific level of enterprise work in the future.

This paper studies the main problems of personnel identity authentication in the current enterprise strategic management system. The contribution of research and innovation includes the construction of the personnel management model of the management system, which solves the problems of personnel real identity authentication and personnel safety behavior control. Simplify workflow, improve operation efficiency, and reduce management cost. From the perspective of enterprise system development, building a scientific enterprise strategic management system is of great significance to improve the scientific level of enterprise system management. Based on innovation, through face image recognition technology, face image recognition technology is organically combined with anti-violation inspection and safety performance evaluation to achieve comprehensive improvement.

2. Related Work

Face recognition is a kind of biometric recognition technology, which integrates multifeilds and multidisciplines. The research direction covers a large number of basic theories, classical algorithms, and mathematical models. It is the in-depth study of these theories that makes the face recognition technology develop continuously [15]. Especially, with the remarkable improvement of computer computing ability, the algorithms and models of face image recognition can break through the bottleneck of hardware, thus entering a period of rapid development. Tong [16] puts forward a face feature point detection method based on region point projection, converts the extracted features into feature vectors, and performs similarity matching with the feature vectors processed in the database, thus completing face image recognition. In order to overcome the potential influence of external environmental factors and self-factors on face image recognition, Chen [17] proposed a geometric feature extraction method based on active appearance model, thus realizing the accurate location and extraction of face feature points. Liu et al. [18] propose to use the edge detection method in image preprocessing combined with projection function to locate the key parts of the face and construct the corresponding feature vectors. Yang [19] introduces the idea of feature vector weighting according to the correlation degree of the importance of different feature vectors to the final recognition result, so that good recognition results can be achieved in different types of data sets.

Because the face image can be regarded as a high-dimensional matrix, the subspace-based method aims to perform a series of complex algebraic transformations on the matrix, so that it can be projected from the high-dimensional space to the low-dimensional space, and keep the contents with different degrees of correlation with the face image according to the actual needs, thus reducing the computational complexity and improving the recognition accuracy. Forlano et al. [20] adopt a method combining bidirectional two-dimensional principal component analysis and neural

network. The former is used to extract features and transform them into feature vectors, while the latter uses the extracted features for training, thus completing face image recognition. In order to fully extract the information contained in the sample, Eriyanti and Noekent [21] put forward a weighted combination of principal component analysis algorithm and linear discriminant analysis algorithm for feature extraction and adopt genetic algorithm to optimize the obtained feature space. Using multitask cascade deep learning network, it can identify the individual's age, gender, and other characteristics and attributes, which has powerful functions. The above recognition algorithms with high recognition rate are based on larger learning and training libraries and more advanced computing processors and supported by a cloud platform with larger capacity. It is a big expense to install these devices or use cloud services in a single mine.

3. Principle of Face Image Recognition Technology

3.1. Face Detection. The strategic management system includes the formulation of strategy, implementation strategy, and evaluation strategy, which form a cycle of three stages. The purpose of promoting the sound development of enterprises' strategic management is to tap and create new development opportunities, obtain sustainable competitive advantage, and realize the long-term development goal of enterprises. The premise of strategic management is that enterprises must adapt to the external economic environment. The foundation of strategic management is based on the internal resource capability of the enterprise. The key to strategic management is to formulate a correct development strategy. The core issue of strategic management is to adapt the enterprise's own resources and capabilities to the external business environment.

Face image recognition technology is to judge the existence of face on the input face image or video stream and identify the face according to the face features compared with the face in the known database. At present, the commonly used face databases in the field of face recognition mainly include FERET face database and so on. Created by FERET project, it contains 14051 gray face images illuminated by multipose light. It is one of the most widely used face databases in the field of face recognition. This paper uses this database [22]. The problems of face image recognition mainly include face detection, recognition, and type judgment. Face detection is a prerequisite for all work. It is necessary to extract faces from various data sources to provide effective data support for subsequent research work [23]. Face detection is generally divided into two categories: (1) based on still images: judge the existence of the face part in the image and circle it; (2) based on video image: the video recorded by the camera can be used for image detection, which can mark the area containing the face. This method has high requirements for the algorithm. It can also be divided into detection methods based on color image (screening by skin color) and detection methods based on

gray image (matching by face feature, appearance, and face template).

3.2. Face Image Recognition Technology and Method

3.2.1. Face Image Recognition Method Based on Geometric Features. Geometric feature method regards the unique contour information, size, and position of a certain part or obvious organ of human face as the feature vector for identifying the features of individual information, and human face can be regarded as a whole, composed of ears, mouth, nose, and chin [24]. Face parts can be identified and determined according to the geometric relationship and position relationship between these parts. Firstly, a face feature extraction model is established to accurately extract and locate the geometric features of the face in the image. Secondly, the extracted geometric features are used to construct face feature vectors. Finally, the constructed feature vector is quickly compared with the feature vector in the database. If the similarity with a feature vector in the database is higher than the threshold, the comparison is successful. Under different facial expressions, facial ornaments, and different illumination, these geometric features may be deformed, so the robustness of the algorithm needs to be enhanced. If only geometric features are used for recognition, its effect is extremely unstable, so it is difficult to popularize its practicability.

3.2.2. Face Image Recognition Method Based on Feature Template. After transforming the high-dimensional image space, a new set of orthogonal bases is obtained, and the important orthogonal bases are retained, from which the low-dimensional linear space can be constructed [25]. If the projections of face in these low-dimensional linear spaces are separable, these projections can be used as feature vectors for recognition, which is the basic idea of feature template method. Firstly, the face in the original database is encoded. Secondly, the coded face images are stored. Finally, the detected images are coded in the same way. When matching is identified, the coded images are compared with the coded images in the library, and the results are obtained. The number of features in a template refers to the number of features in a subwindow. The so-called feature refers to every form formed by the feature template sliding in a subwindow with any size in turn. The form types of all features of the window can be determined by sliding various features in sequence in the window to be checked. After determining the form of features, the number of rectangular features is only related to the size of subwindows.

3.2.3. Face Image Recognition Method Based on Neural Network. The input of neural network can be face image with reduced resolution, autocorrelation function of local area, second moment of local texture, etc. [26]. This kind of method also needs more samples for training. Neural cognitive machine is a special case of neural network, and its weight sharing network structure is its greatest advantage.

This structure is very similar to the biological neural network, so that the network model can be simplified. When the input of the network is a multibit image, this advantage can be more obvious. The method of face detection based on neural network mainly studies the problems of noise and shaking caused by the natural acquisition of face images, and it is sometimes difficult to detect between a face and a nonhuman face by methods based on geometric features or templates. The detection method based on neural network needs to train and learn a large number of face samples and nonhuman face samples and determine the rule information of the two types of samples, which can distinguish between face and nonhuman face. The learning performance depends on the representative ability of the sample library to face and the accuracy of the model.

3.3. Processing Process of Face Image Recognition System. Regional feature analysis algorithm is widely used in face image recognition technology. It integrates computer image processing technology and the principle of Biostatistics, uses computer image processing technology to extract human image feature points from video, and uses the principle of biostatistics to analyze and establish mathematical model, namely, face feature template [27]. The built face feature template is used to analyze the face image of the tested person, and a similar value is given according to the analysis results. Through this value, whether it is the same person can be determined. Face feature extraction is mainly realized by algorithm, including the following steps: (1) face detection and location: detect whether there is a face in the picture. (2) Image preprocessing: process the extracted face to enhance face features. (3) Face feature extraction: extract the key features of face information. (4) Face image recognition: match the input face with the face in the database, find the face image with the smallest distance, and verify the matching degree. The face image recognition and matching process is shown in Figure 1.

The personnel behavior identification process in the enterprise strategic management system is shown in Figure 2.

Generally, the input of the system is a face image or a series of face images with undetermined identities, and several face images with known identities or corresponding codes in the face database, while the output is a series of similarity scores, indicating the identities of faces to be recognized.

4. Face Feature Recognition Based on Convolutional Neural Network

The basic structure of the convolutional neural network is shown in Figure 3. Although it is a lightweight model, it already has the basic framework of depth model, which is mainly composed of convolution layer, pooling layer, full connection layer, and Softmax layer [28].

4.1. Convolution Layer. In the convolution layer, after convolution operation, the image matrix is added with an

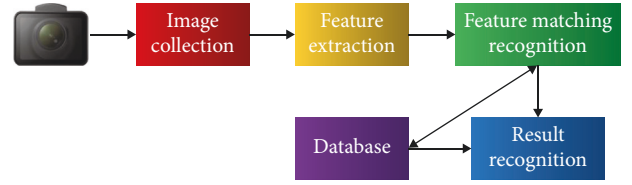


FIGURE 1: Face image recognition matching process.

offset, and a new feature plane can be obtained by activating the activation function. The specific calculation is as follows:

$$u_j^i = \sum_{i \in M_j} x_i^{l-1} * w_{ij}^l + b_j^l, \quad (1)$$

$$x_j^{l-1} = f(u_j^l),$$

x_j^{l-1} represents the pixel value of a point in the feature image of the previous layer; w_{ij}^l represents the $N \times N$ matrix formed by the internal parameters of the convolution kernel; $*$ represents the convolution operation when extracting features; M_j represents the feature of the previous layer involved in the operation A subset of the image; b_j^l represents the bias term, which is used to increase the nonlinearity of the model; l represents the current calculation is in the first layer.

4.2. Pool Layer. The pooling layer is used to select the features extracted by convolution. In the convolution neural network, the dimension of feature space is reduced, but the depth will not be reduced. The convolution kernel of “1 times 1” plays the role of reducing the depth. When the maximum pooling layer is used, the maximum number of input areas is used, and when the average pooling is used, the average value of input areas is used. Pooling layer is usually connected behind convolution layer and used together with convolution layer [29]. The purpose of pooling is to cluster the same features at different positions in the image, thus greatly reducing the calculation parameters in the network and effectively avoiding overfitting. At the same time, the features obtained by pooling are robust to changes such as translation, scaling, and rotation.

4.3. Full Connection Layer. Generally, the full connection layer appears after the convolution layer and the pooling layer and is used to realize the complete connection between the neurons in this layer and the neurons in the previous layer. Its main function is to transform the two-dimensional feature map output by the convolution-pooling layer into a one-dimensional vector and finally enter the Softmax layer.

4.4. Softmax Layer. The appearance of Softmax layer extends the traditional two-classification problem to multi-classification. This layer can map the input value of the fully connected layer into a probability value, and the sum of all probability values is always 1. Suppose that the input feature is recorded as $x^{(i)}$, and the sample label is recorded as $y^{(i)}$, thus forming the training set $s = \{(x^{(1)}, y^{(1)}), \dots, (x^{(m)}, y^{(m)})\}$.

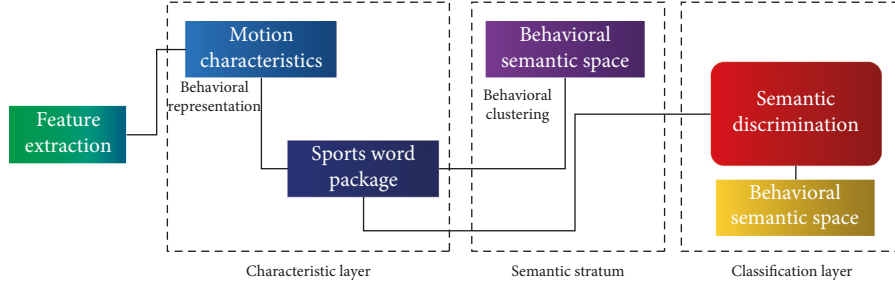


FIGURE 2: Enterprise personnel behavior identification process.

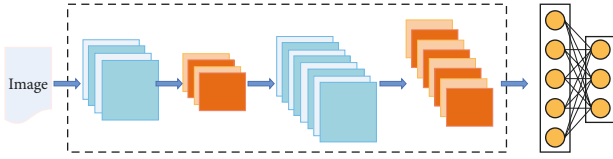


FIGURE 3: Basic structure of convolutional neural network.

When given input x , use the model to estimate each category j and get its probability value $p(y = j|x)$, where the hypothesis function is

$$h_{\theta}(x^{(i)}) = \begin{bmatrix} p(y^{(i)} = 1|x^{(i)}; \theta) \\ p(y^{(i)} = 2|x^{(i)}; \theta) \\ \dots \\ p(y^{(i)} = k|x^{(i)}; \theta) \end{bmatrix} = \frac{1}{\sum_{j=1}^k e^{\theta_j^T x^{(i)}}} \begin{bmatrix} e^{\theta_1^T x^{(i)}} \\ e^{\theta_2^T x^{(i)}} \\ \dots \\ e^{\theta_k^T x^{(i)}} \end{bmatrix}. \quad (2)$$

Among them, $\theta_1, \theta_2, \dots, \theta_k$ is a trainable parameter in the model, and $\sum_{j=1}^k e^{\theta_j^T x^{(i)}}$ is a normalized term. It aims to make the sum of all probabilities equal to 1, thereby obtaining the cost function:

$$J(\theta) = -\frac{1}{m} \left[\sum_{i=1}^m \sum_{j=1}^k 1\{y^{(i)} = j\} \log \frac{e^{\theta_j^T x^{(i)}}}{\sum_{l=1}^k e^{\theta_l^T x^{(i)}}} \right], \quad (3)$$

$1\{\bullet\}$ is the judgment function. When the value in the brackets is true, the function outputs the result 1, and if the value in the brackets is false, the output is 0. Equation (3) is a generalization of logistic regression, so the cost function can be changed to

$$\begin{aligned} J(\theta) &= -\frac{1}{m} \left[\sum_{i=1}^m (1 - y^{(i)}) \log(1 - h_{\theta}(x^{(i)})) + y^{(i)} \log h_{\theta}(x^{(i)}) \right] \\ &= -\frac{1}{m} \left[\sum_{i=1}^m \sum_{j=0}^1 1\{y^{(i)} = j\} \log p(y^{(i)} = j|x^{(i)}, \theta) \right]. \end{aligned} \quad (4)$$

For the partial derivative of the SoftMax cost function $J(\theta)$, the gradient formula is obtained:

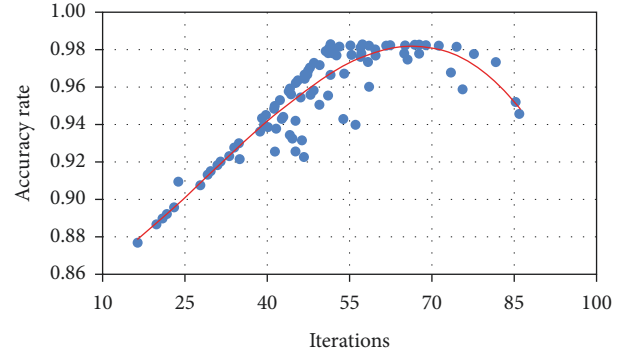


FIGURE 4: Trend chart of the accuracy of the deep convolutional neural network verification set.

$$\nabla_{\theta_j} J(\theta) = -\frac{1}{m} \left[\sum_{i=1}^m x^{(i)} (1\{y^{(i)} = j\} - p(y^{(i)} = j|x^{(i)}, \theta)) \right], \quad (5)$$

$\nabla_{\theta_j} J(\theta)$ is a vector, and its l th element $\partial J(\theta)/\theta_{jl}$ is the partial derivative of $J(\theta)$ with respect to the l th component of θ_j . After obtaining the above formula for solving the partial derivative, use the relevant optimization algorithm to minimize the cost function $J(\theta)$. Then, the parameters need to be updated at each iteration:

$$\theta_j = \theta_j - \alpha \nabla_{\theta_j} J(\theta) \quad (j = 1, 2, \dots, k). \quad (6)$$

Finally, the SoftMax multiclassification model is obtained.

The face image recognition method based on convolutional neural network mainly relies on feature extraction from a large number of face samples. Compared with the traditional artificially designed feature extraction operator, the advantage of convolutional neural network is that it can complete the whole recognition process through its own learning mechanism without excessive human intervention. That is, using its own deep structure, the input face images are convoluted and pooled layer by layer, and after continuous nonlinear mapping transformation, the best feature extractors and classifiers can be obtained from a large number of samples.

5. Result Analysis and Discussion

During the training phase of the model, it will be tested on the verification set regularly. After continuous analysis and comparison, we finally chose 65 training times as the best training times under the condition that the batch size is 30. Figure 4 shows the trend of accuracy on the verification set along with the training process. Therefore, we can know that increasing the training times in a certain range can improve the performance of the model. On the contrary, too many training times will lead to overfitting, and the performance of the model will decrease. It can be seen that the accuracy of the verification set of the network is increasing with the convergence of the model, which verifies the correctness of the convergence of the network and the effectiveness of the network in feature extraction.

In feature extraction, it is necessary to select the most representative or prominent feature according to the application scenario, so as to ensure that the staff to be detected can successfully distinguish from other objects and achieve the best classification and recognition effect. In the detection part of neural network, several initial modules and several convolution layers are adopted, which has good nonlinear fitting characteristics. At the same time, in the part of enhanced recognition, the object features related to behavior are combined to enhance the recognition ability. The influence of feature differences between a block and its surrounding image blocks decreases with the increase of distance. The relationship between visual sensitivity and eccentricity is shown in Figure 5.

The initial model is adjusted horizontally and vertically; that is, the training times, convolution layers, convolution kernel size, optimizer type, and learning rate are changed. Finally, the structure of the neural network model is 8 layers, including 3 convolution layers, 3 pooling layers, 1 fully connected layer, and 1 output layer. Figure 6 is the accuracy curve of the model, and Figure 7 is the loss function curve. With the increase of training times, the accuracy of the network is increasing, and the loss function value is decreasing gradually, and the network basically converges after training 73 times.

During training, the loss function reflected by verification is gradually increasing rather than decreasing, which indicates that network training has entered the trap of local optimization. Figure 8 shows the relationship between iteration times and normal training and overfitting training.

The establishment of enterprise strategic management organization and its relationship depend on the long-term plan. In the process of strategic planning, the mission and vision always guide the direction and requirements of strategic formulation. The core values guide the way of thinking and implementation strategy of strategy. External environment includes macro environment and industrial environment. Corporate culture: the impact of corporate culture on corporate strategy mainly includes the following points: decision-making style, preventing strategic change, overcoming obstacles to strategic change, leading values, and cultural conflict.

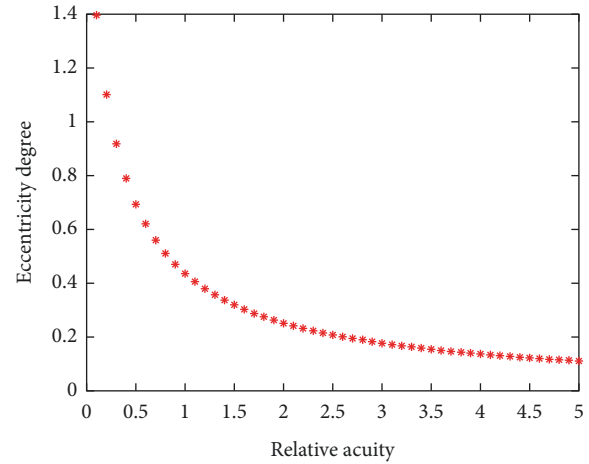


FIGURE 5: The relationship between visual acuity and eccentricity.

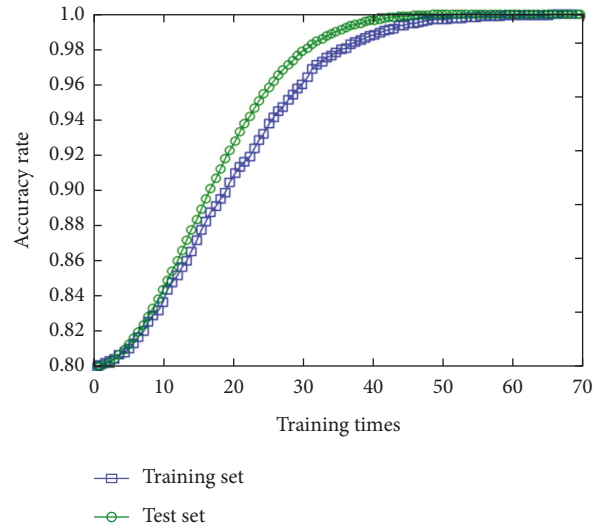


FIGURE 6: Accuracy rate curve.

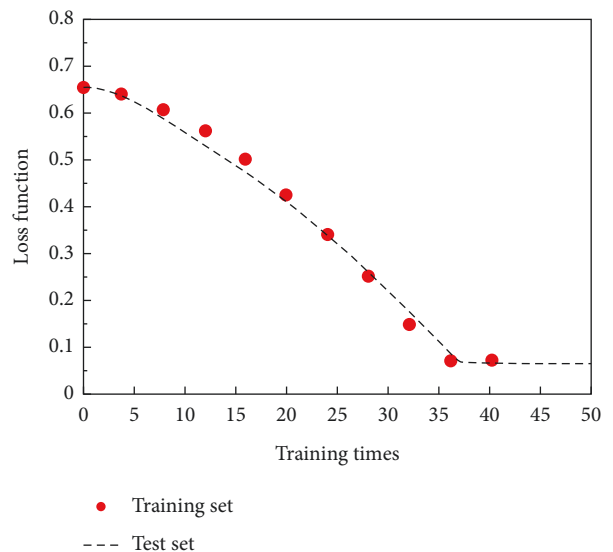


FIGURE 7: Loss function curve.

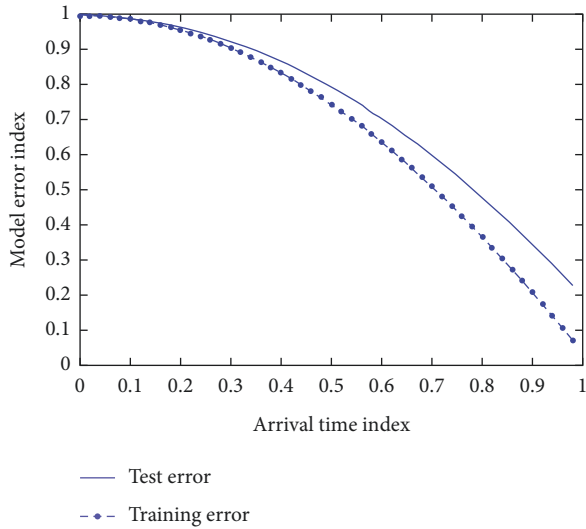


FIGURE 8: The relationship between the number of iterations and normal training and overfitting training.

Enterprise strategic management is an organic whole system composed of multiple institutions, and its structure is the contact between institutions. The establishment of its institutions and the relationship between them must be subject to the overall objectives and efficiency of enterprise management. The general model searches the image to obtain the best matching window with the tracking manager. In the training process, the classification results are obtained through the data processing process of convolution neural network and compared with the corresponding label data to calculate the corresponding relative error. After a certain number of training, the weights on the convolution window in the convolution neural network are continuously modified to reduce the relative error and finally converge.

By manually marking the reference frame as the reference true value of each frame of the actual scene video, the distance accuracy curve and success rate curve of tracking the actual scene video can be drawn, as shown in Table 1 and Figure 9. From the experimental results, it can be seen that video analysis based on convolutional neural network has better tracking effect for practical application scenes.

In the tracking process, the algorithm will give a rectangular tracking box to represent the area identified as the target, and we already know the real area box of the target in advance. By evaluating the overlap between two frames, we can effectively judge the effect of the algorithm. Figure 10 shows the tracking results of different pixels of the video by the deep convolution neural network.

In the calculation of loss function, in addition to the classification information and location information of the original target, the shape information of the target is also considered. Because the marking method of mask is more detailed than that of rectangular box, pixel level recognition can be realized. Experiments show that the model can simplify workflow, improve operation efficiency, and reduce management cost. The goal, core, and value orientation of enterprise strategic innovation are an organic

TABLE 1: Tracking performance of actual scene video.

Frame number	Distance accuracy (%)	Success rate (%)
Frame 5	98.25	95.58
Frame 15	99.72	97.4

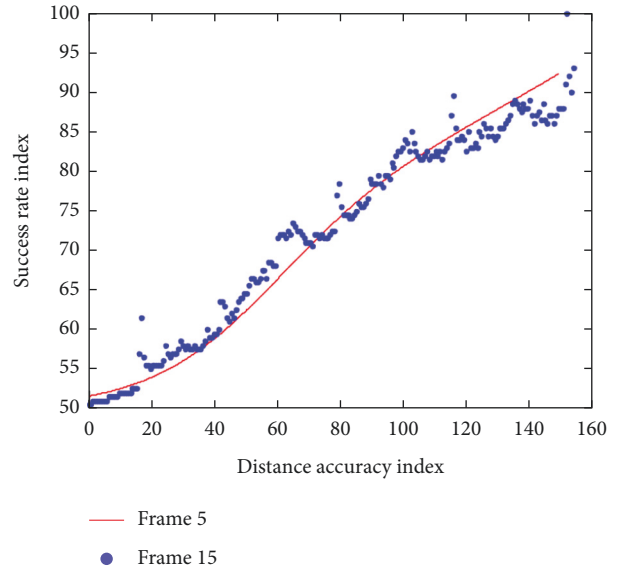


FIGURE 9: Tracking performance of actual scene video.

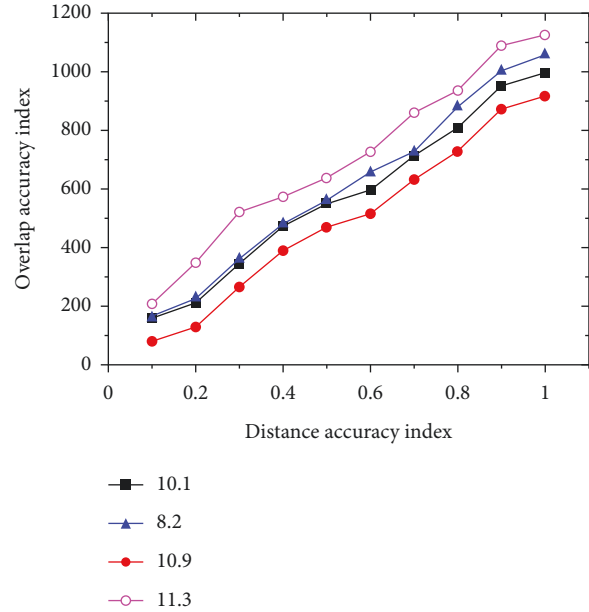


FIGURE 10: Tracking results of deep convolutional neural network.

whole with internal relations. The primary goal of strategic innovation is to realize the overall leap of the enterprise itself, including the perfection and integration of its constituent elements, structure, and function. As an enterprise system, its basic elements are enterprise system and enterprise personnel. The overall efficiency of the strategic system depends on the work efficiency of various

departments and personnel. From the perspective of the development of enterprise strategic system, building a scientific enterprise strategic management system is of great significance to improve the scientific level of enterprise management. Only by establishing a scientific and reasonable overall structure of the system and coordinating the relationship between the whole and the part and between the part and the part can we ensure the consistency of the whole and the part in the operation direction and speed, reduce mutual interference, restrict and offset them, and improve the overall function of the system.

6. Conclusions

Intelligent video surveillance system is the inevitable product of the development of video surveillance technology. At present, face image recognition technology is mainly used in the fields of enterprise and residential security management, e-passport and ID card, public security, judicial and criminal investigation, information security, and so on. The overall innovation of enterprise strategic system is a process of theoretical innovation, practical innovation, and their interaction and organic combination. This process needs not only theoretical innovation to guide the direction, but also practical innovation to open up the road. From the perspective of institutional development, building a scientific enterprise management system is of great significance to improve the scientific level of management in the enterprise system. Any social organization is composed of people. Therefore, the overall progress of the enterprise system depends on the general improvement of personnel quality and creativity. In the final sense, both the goal of innovation and the efficiency of innovation should be subject to the overall interests of the whole society and the needs of long-term sustainable development.

Based on the idea of parallel computing, the improved multiface real-time detection algorithm in this paper transforms the multiface detection problem into a single face detection problem through image segmentation technology, so as to realize the real-time detection of multifaces in video images. The enterprise strategic system management model based on cloud computing intelligent image recognition can simplify the workflow, improve the operation efficiency, and reduce the management cost. Based on innovation, the management system can organically combine face image recognition technology with anti-violation inspection and safety performance evaluation through face image recognition technology to achieve all-round improvement. However, there are still some problems that need to be modified. There are still some problems in the face image recognition algorithm in intelligent video surveillance system, such as the optimization of big data video image and the stability of the algorithm, which need to be further studied.

Data Availability

The data used to support the findings of this study are available from the author upon request.

Conflicts of Interest

The author declares no conflicts of interest.

Acknowledgments

This study was supported by Zhejiang Federation of Social Sciences Project (2021n70).

References

- [1] W. Kang, G. Wang, Z. Pu, and X. Wang, "Research on image recognition technology based on cloud computing platform [J]," *Sensors and Microsystems*, vol. 037, no. 6, pp. 30–32+35, 2018.
- [2] Y. Weng, C. Zhang, and S. Ling, "Massive ship target image recognition based on cloud computing platform[J]," *Ship Science and Technology*, vol. 39, no. 24, pp. 128–130, 2017.
- [3] S. Wang and X. Wang, "Design and research of face recognition and homomorphic encryption scheme based on image subspace and kernel sparse representation [J]," *Computer Science and Application*, vol. 008, no. 5, pp. 582–590, 2018.
- [4] D. Yang, H. Qin, Y. Fan, and M. Caron, "Research on comprehensive personnel safety management and control platform based on face recognition[J]," *Microcomputer Applications*, vol. 326, no. 6, pp. 28–32, 2020.
- [5] H. Song, L. Wan, Yu Lei, and S. Wang, "Design of power grid construction safety management and control system based on face recognition[J]," *Digital Technology and Application*, vol. 37, no. 4, pp. 152–153, 2019.
- [6] X. Yang and Z. Wang, "Cloud desktop identity authentication system based on face recognition[J]," *Manufacturing Automation*, vol. 42, no. 4, pp. 7–10+29, 2020.
- [7] K. Grm, V. Štruc, A. Artiges, M. Caron, and H. K. Ekenel, "Strengths and weaknesses of deep learning models for face recognition against image degradations," *IET Biometrics*, vol. 7, no. 1, pp. 81–89, 2018.
- [8] M. Hayat, S. H. Khan, and M. Bennamoun, "Empowering simple binary classifiers for image set based face recognition [J]," *International Journal of Computer Vision*, vol. 123, no. 3, pp. 1–20, 2017.
- [9] A. K. Bedi and R. K. Sunkaria, "Mean distance local binary pattern: a novel technique for color and texture image retrieval for liver ultrasound images," *Multimedia Tools and Applications*, vol. 80, no. 14, pp. 20773–20802, 2021.
- [10] D. Yu and Z. Wei, "The application of specific foreign personnel's face recognition technology in fine management [J]," *Communication World*, vol. 26, no. 12, pp. 60–61, 2019.
- [11] M. Wan, X. Wang, G. Yang, H. Zheng, and W. Huang, "Feature extraction via sparse fuzzy difference embedding (SFDE) for robust subspace learning," *Neural Processing Letters*, vol. 53, no. 3, pp. 2113–2128, 2021.
- [12] X. Lu, L. Wang, S. Zeng, and C. Zhu, "Multi-pose facial image recognition algorithm based on neural network learning [J]," *Computer Technology and Development*, vol. 029, no. 11, pp. 57–61, 2019.
- [13] Y. Chu, L. Zhao, and T. Ahmad, "Multiple feature subspaces analysis for single sample per person face recognition[J]," *The Visual Computer*, vol. 35, no. 1, pp. 1–18, 2018.
- [14] I. R. Panner Selvam and M. Karuppiah, "Gender recognition based on face image using reinforced local binary patterns," *IET Computer Vision*, vol. 11, no. 6, pp. 415–425, 2017.

- [15] S. Banerjee and S. Das, "LR-GAN for degraded face recognition," *Pattern Recognition Letters*, vol. 116, no. 12, pp. 246–253, 2018.
- [16] D. Tong, "Application of RFID and face recognition technology in open laboratory management [J]," *Digital Design*, vol. 6, no. 3, pp. 28-29, 2017.
- [17] T. Chen, "Research on the application of dynamic face recognition technology in university management[J]," *Electronic Commerce*, vol. 251, no. 11, pp. 95-96, 2020.
- [18] J. Liu, C. Zhu, and C. Zhou, "Application of video face recognition technology in railway personnel management and control[J]," *China Railway*, vol. 682, no. 4, pp. 105–109, 2019.
- [19] H. Yang, "Application of face recognition technology in university campus security management [J]," *Technology and Market*, vol. 026, no. 8, p. 213+215, 2019.
- [20] C. Forliano, P. De Bernardi, and D. Yahiaoui, "Entrepreneurial universities: a bibliometric analysis within the business and management domains," *Technological Forecasting and Social Change*, vol. 165, Article ID 120522, 2021.
- [21] H. F. Eriyanti and V. Noekent, "Effect work-life balance on organizational commitment: role of organizational citizenship behavior?" [J]. *Management Analysis Journal*, vol. 10, no. 4, 2021.
- [22] S. A. Jilani and M. Gilani, "A survey to explore the role of organizational justice on organizational citizenship behavior among Irish healthcare employees," *DBS Business Review*, vol. 4, 2021.
- [23] N. F. Garmann-Johnsen, M. Helmersen, and T. R. Eikebrokk, "Employee-driven digitalization in healthcare: codesigning services that deliver," *Health Policy and Technology*, vol. 9, no. 2, pp. 247–254, 2020.
- [24] K. S. Sambaiah and T. Jayabarathi, "Loss minimization techniques for optimal operation and planning of distribution systems: a review of different methodologies," *International Transactions on Electrical Energy Systems*, vol. 30, no. 2, Article ID e12230, 2020.
- [25] H. Chunliang, X. Liu, Y. Sun, and Bo Fan, "Research and standardization of face recognition security issues[J]," *Information Technology and Standardization*, vol. 430, no. 10, pp. 63–67, 2020.
- [26] G. Peckham, S. Taylor, and S. Jeong, "Cloud computing acceleration for high-performance image recognition[J]," *Electronics World*, vol. 123, pp. 18-19, 2017.
- [27] V. Nagrath, O. Morel, A. S. Malik, M. N. B. M. Saad, and F. Meriaudeau, "Peer to peer trade in HTM5 meta model for agent oriented cloud robotic systems," *Peer-to-Peer Networking and Applications*, vol. 9, no. 2, pp. 328–343, 2016.
- [28] J.-H. Lee, K. Goswami, B.-G. Kim, S. Jeong, and J. S. Choi, "Fast encoding algorithm for high-efficiency video coding (HEVC) system based on spatio-temporal correlation," *Journal of Real-Time Image Processing*, vol. 12, no. 2, pp. 407–418, 2016.
- [29] M. Najmabadi and P. Moallem, "Local symmetric directional pattern: a novel descriptor for extracting compact and distinctive features in face recognition," *Optik*, vol. 251, Article ID 168331, 2022.

Research Article

Research on Image Recognition of Gymnastics Sports Injuries Based on Deep Learning

Peng Jia ¹ and Yixiong Xu²

¹*School of Physical Education, Jiangxi Normal University, Nanchang 330022, China*

²*School of Physical Education, Nanchang Normal University, Nanchang 330032, China*

Correspondence should be addressed to Peng Jia; jiapeng@jxnu.edu.cn

Received 6 May 2022; Revised 6 June 2022; Accepted 11 June 2022; Published 28 June 2022

Academic Editor: Le Sun

Copyright © 2022 Peng Jia and Yixiong Xu. This is an open access article distributed under the Creative Commons Attribution License, which permits unrestricted use, distribution, and reproduction in any medium, provided the original work is properly cited.

Gymnastics is an increasingly popular sport and an important event in the Olympic Games. However, the number of unavoidable injuries in sports is also increasing, and the treatment after the injury is very important. We reduce the harm caused by the injury through the identification and research of pictures. Image preprocessing and other methods can in-depth learn about gymnastics sports injuries. We identify the injured pictures of athletes to know the injury situation. Through the analysis of the force of the athletes during exercise, they can be better integrated into picture recognition for sports injuries. More appropriate prevention and treatment measures are suggested.

1. Introduction

The purpose of this article is to recall NCAA monitoring data on women's gymnastics injuries and to identify areas of potential injury prevention measures. Between 1988 and 1989, 1,550 people participated in the women's varsity gymnastics team. In 2003, the number of varsity teams decreased, affecting many participants. The results showed that the average annual injury rate during the sample period decreased, but not in practice. In 16 years, the injury rate in the competition was higher than the actual rate, and the lower half of the body was injured more frequently. The reason for the injury was explained, and suggestions were made for those with bare feet. Athletes use prophylactic tape to reduce the risk of injury, and preventative measures will add more planning to training to enhance the correct mechanism and make the device more absorbent [1]. Sports trainers collected injury information from many participants and looked at a wide variety of injuries. Compared to other sports, injuries to the back and lumbar regions were more frequent, and bare feet injuries were also common because the thigh and the leg were overused; it can be seen from the above that

women's gymnastics has great room for improvement in many aspects [2]. This article examines the number and types of injuries in non-professional gymnasts. At the same time, it can also know what are most dangerous, and investigate whether various factors such as the proportion of participants' coaches affect the injury rate. Survey data show that professional gymnasts have higher injury rates and non-athletes have lower rates. To sum up, the level of competition has a great relationship with the injury rate [3]. College-level injury testing data are limited. The researchers still have not caught non-time-loss injuries. The purpose was to describe the epidemiology of injuries in women's gymnastics by pooling injury and exposure data from 11 sports. Athletic data, injury rates, injury rates for body parts, diagnoses, and equipment for collegiate athletes participating in women's gymnastics were derived from 28 seasons of data [4]. Long-term exercise for youth training and competitions can lead to back pain that must not be relaxed. Measures should be taken to treat it when one is young, and treat it in the early stage to achieve a higher therapeutic effect. For pain that lasts for a long time, one should pay attention to the need for careful inspection, and bone scans and other techniques should be performed

if necessary. Diagnose the cause [5]. Gymnastics has a lower frequency of injuries in sports. At the same time, based on objective information such as gender and age, the pattern of injury can be predicted. Girls are more likely to be injured. Most of them have wrist pain and low back pain, while some spinal abnormalities were also found. Imaging can also guide the recovery of injured athletes, and parents should know that recreational gymnastics has fewer injuries while more injuries have been found in high-level athletes [6]. According to sports clinic observations, patellar joint pain syndrome is higher, sprains are the biggest problem in emergency surgical treatment, overuse is related to the training intensity, and motor skills can also lead to serious leg injuries [7]. Michelle is the club's project manager. With a large number of gymnasts, Michelle is an integral part of the national team plan, who has been training athletes and has produced many gold medal winners. Michelle has an excellent educational background and wrote the Gymnastics School of Excellence program. Michelle will talk about the prevalence of injuries to better care about the growth of youth sports [8]. Infrared images have many advantages, which can make up for the deficiencies of infrared image face clarity. This technology is an important research direction in the field of face recognition. On the basis of analyzing the characteristics of infrared images, it also analyzes humans. The characteristics of a facial recognition software and a new infrared image recognition method are proposed. Experiments show that this method is feasible [9]. Image recognition methods require a large number of samples to achieve good performance. In some cases, a large number of samples cannot be obtained, which will lead to poor performance. However, commonly used neural network classifiers minimize empirical risk. This paper establishes a method to combine wavelet giant and svm by finding the optimal solution. In the simulation, various tank images are extracted and identified separately. The results show that the algorithms that combine the two are better in small sample cases [10]. The correlation matching algorithm is of great significance, but also faces a key problem. The problem is with sudden changes in the image. This paper examines different application areas and investigates new methods to solve the problem. One is to rotate and rebuild new model diagrams under laboratory conditions. Another approach is to exploit fixed features along with image variance and symbolize them as cells of the correlation matching map [11]. Medical images are the research subject, and the characteristics of images cannot be effectively expressed at present. Therefore, in order to improve the recognition rate, a new algorithm is proposed, which combines two kinds of data. The result is that the fused features can be better expressed for medical images, reducing the workload, and decision-level data fusion can achieve higher recognition rates [12]. In image edge distortion correction, the edge fitting is poor, and hence the correction error is large. In this paper, an image edge true correction algorithm based on the equalization algorithm is proposed, the parameters are adaptively switched by the method, and the image is optimized according to the image

denoising result. According to the extraction results, the optimization function is obtained. This paper considers the noise barrel distortion and pincushion distortion images as the research objects [13]. In order to meet the requirements, a new hot-stamping image recognition algorithm is proposed. The minimum point is the best result through subsequent operations such as digital image conversion and spatial extraction of channels. The results show that identifying the hot-stamping area and improving the matching speed have guiding significance for the quality detection of this technology [14]. At present, image recognition has research value in the field of computer recognition. With the development of national strength, the application of these innovative technologies to pig detection is of great help to the breeding of animal husbandry and the convenience of human beings. This paper makes a great introduction to the individual identification technology of pigs and the current research direction of this innovative technology [15].

2. Image Recognition Research

2.1. Image Recognition of Static Objects. We mainly use the following four methods for image recognition: data feature analysis, image preprocessing, feature extraction, and pattern recognition.

2.1.1. Data Feature Analysis. To achieve static object recognition, the data in a specific object image must first be analyzed to determine what data to retrieve in the object image. According to these characteristics, we analyze the characteristics of the image data, choose the appropriate method during the analysis, and find ways to remove the background and highlight the target. From this, we can see that when performing this step, we need to have a comprehensive understanding of the picture, and different methods need to be used for different picture objects.

2.1.2. Image Preprocessing. Because the image will be damaged and polluted by noise, it will more easily become unsuitable for people's needs or lose the essence of the image during transmission and storage. Therefore, we should preprocess the image to reduce its influence on the image. For simpler image recognition systems, image preprocessing usually includes image enhancement and restoration, but for slightly more complex images, we also perform image segmentation on the image.

This step is mainly to weaken the features that people do not need very much to avoid affecting judgment, and at the same time strengthen the features that people need to pay attention to. Spatial domain methods include processing images directly in the spatial domain, which can be divided into two aspects: point operations and neighborhood operations (local operations). The frequency range method only calculates the image transformation value of the specified image transformation area, calculates the image spectrum of the transformed area, and then inverts the final calculated image in the spatial area. The frequency range

method is generally divided into high magnification filter, low magnification filter, bandpass filter, and notch filter.

Image restoration is to change the image into its original essence, using prior knowledge to change the process of degrading the image. Image restoration technology needs to establish a degradation model and reverse the degradation process to obtain the optimal image before degradation.

Image segmentation first divides the image into several meaningful regions, then determines whether there are objects of interest in these regions, and narrates the content on the image. At present, we divide image recognition and segmentation into two methods. The first is a region-based image segmentation algorithm and the second is a boundary-based segmentation algorithm. Image segmentation also has its own disadvantages, and image segmentation algorithms have certain limitations in their application. For example, the key to the threshold method is the selection and determination of the threshold. Different thresholds have completely different effects. Setting the threshold too low will produce noise, and setting the threshold too high will eliminate noise. With no noise signal, it is difficult to define the starting points and similarity criteria in region growing methods, and the quality of the adjustments greatly affects the efficiency of segmentation. Edge detection difficulty is a way to balance detection accuracy and noise immunity. The watershed method is too sensitive to noise and thin lines and is prone to over-segmentation. In general, some image segmentation algorithms must target specific types of images or specific applications. Thus far, no general and effective image segmentation algorithm suitable for all image segmentation has been found, and there is no generally accepted objective standard to evaluate segmentation performance.

- (1) Information acquisition: It is to convert information such as light or sound into electrical information through sensors. Information can be two-dimensional images such as text, images, etc.; can be one-dimensional waveforms such as sound waves, electrocardiograms, and electroencephalograms; or physical quantities and logical values.
- (2) Preprocessing: It can include A/D, binarization, image smoothing, transformation, enhancement, restoration, filtering, etc., and mainly refers to image processing.
- (3) Feature extraction and selection: In pattern recognition, it is necessary to extract and select features. For example, a 64×64 image can obtain 4096 data, and the original data in the measurement space can be obtained through transformation. Features that reflect the nature of the classification process are feature extraction and selection.
- (4) Classifier design: The main function of classifier design is to determine decision rules through training, such that the error rate is the lowest when classifying according to such decision rules.
- (5) Classification decision: Classify the recognized objects in the feature space.

2.2. Research Status Based on Image Recognition Technology. Image recognition technology uses computer technology to realize the recognition function of human vision, i.e., to detect and recognize objects from images and other information. Most of the applications of recognition technology in modern augmented reality systems are computer vision-oriented image recognition, including sign-based augmented reality and unsigned augmented reality. The basic principle of augmented reality based on symbol recognition is to solve the current pose of the camera by performing image recognition on the symbol points of fixed geometric figures using ARToolKit, ARTagl, etc. However, augmented reality systems based on sign recognition are narrower in scope, as signs must be within the camera's range. Meaningless augmented reality based on natural characteristics is the application of image recognition technology in augmented reality systems. The feature is that there is no need to arrange panels in advance, and the application scenarios are wide. In 1999, Neunn et al in the University of Southern California began to combine in-image target recognition and tracking algorithms to propose an augmented reality system for scene annotation based on industrial 3-D images.

3. Muscle Model

3.1. Muscle Model. One of the most important tasks in sports biodynamic farming is selecting the correct muscle model. The most basic muscle model consists of springs and cushioning materials. The muscle model class proposed by Hill in 1938 reflects a single viscoelastic property of muscle. The ground model consists of linear and viscoelastic elements, and the model has been widely used since then for biomechanical analysis. The hedgehog muscle model consists of three elements: an active contraction element, a parallel elastic element, and a series of elastic elements. Among them, the active contraction element is described by three relational expressions: longitudinal tension ratio, velocity tension ratio, and muscle activation level. Muscle activation levels range from 0 (disabled) to 1 (fully activated). When a muscle becomes fully tonic, both muscle strength and muscle fiber length are within a certain range, indicating a "parabolic" relationship. Maximum contractile force occurs at $-N$. Here death is the optimal length of muscle fibers.

The active force-length curve of a muscle is described by the following parabolic function:

$$\int_L^{\text{act}} = 1 - \left[\frac{(L^M/L_0^M) - 1}{0.5} \right]^2. \quad (1)$$

In this formula, \int_L^{act} is the length tension relationship when main power is supplied; L^M is the muscle length; and L_0^M is the relatively optimal muscle fiber length. The passive dynamic length curve of the muscle is described below.

The relationship between passive force and length:

$$\int_L^{\text{pa}} = \left(\frac{L^M}{L_0^M} \right)^3 \exp \left(8 \frac{L^M}{L_0^M} - 12.9 \right). \quad (2)$$

The relationship between force and velocity can be represented by a hyperbola when the muscle is coaxially isometrically contracted:

$$\int_v = \frac{v_0^M - v^M}{v_0^M + cv^M}. \quad (3)$$

v_0^M and v^M represent the speed of retraction and contraction, and in off-axis isometric contraction; the relationship between force and speed is defined as:

$$\int_v = \frac{2v_0^M - b' + v^M(a'/F_0^M)}{v_0^M - b'}. \quad (4)$$

We assume that the contraction speed of the muscle will be little affected by the viscous effect of the muscle, while the tension speed curve and the tension length N line of the active force of the muscle both need to be scaled by the activation level $a(t)$ before they can be used, and there is feathering angle:

$$a = \arctg\left(\frac{L_0^M \sin \partial_0}{L^{MT} - L_S^T}\right). \quad (5)$$

$L^{MT} = L^T + L^M \cos \partial_0^{MT}$ is the total length of the muscle-tendon component; L_S^T is the relaxed length of the tendon; ∂_0 is the feathering angle at optimal fiber length; thus, the total muscle force F^{muscle} can be expressed as:

$$F^{\text{muscle}} = F_0^M (f_L^{\text{act}} f_v a(t) + f_L^{pa}) \cos(\partial). \quad (6)$$

The expression of muscle activation level $a(t)$ is:

$$a(t) = \frac{(u^2 - ua)}{t_{\text{rise}}} + \frac{(u - a)}{t_{\text{fall}}}. \quad (7)$$

F_0^M represents peak muscle force at optimal muscle length, u indicates muscle excitability, and t_{rise} and t_{fall} represent the ascending and descending processes of muscle activation, respectively.

3.2. Huxley Muscle Model. Although the Hill model is widely used, it cannot directly reflect the biochemical process of muscle energy production. The principle of chemistry was cited in 1957, when Huxley developed the Huxley muscle model, also known as the sliding silk model.

Huxley and later Zahalak used the distributed torque approximation method when using the slip-line model. The distributed torque approximation transforms the Huxley model into a series of ordinary differential equations, allowing the method to be solved numerically.

The Huxley-Huxley muscle model accounts for the speed of myofilament connection and separation, the overlapping function of calcium activation (the relationship between the sarcomere strength and the sarcomere length), and the relationship between calcium concentration and the activation level in fibers when describing muscle contraction. In optimization theory, the frequency of muscle stimulation is a variable that affects the magnitude of the total muscle force. The frequency range for muscle

stimulation is $<1100>124$ Hz. The Huxley muscle model is based on the sliding filament theory and describes the biochemical effects of muscle during the contraction process. The distribution function $n(\theta)$ represents the distributed number of cross-bridge connections, i.e., the logarithm of actin and myosin bonds as a function of cross-bridge length. Since bridging and breaking are assumed to be time-dependent functions $n(\theta, t)$, the muscle force velocity curve becomes an implicit function. The connection rate f and the disconnection rate g of the cross-bridge depend on the normalized cross-bridge length θ .

$$f(\theta) = \begin{cases} 0 - \infty < \theta < 0 \\ 43.3\theta 0 < \theta < 1 \\ 01 < \theta < \infty \end{cases}, \quad (8)$$

$$g(\theta) = \begin{cases} 209 - \infty < \theta < 0 \\ 10\theta 0 < \theta < 1 \\ 10\theta 1 < \theta < \infty \end{cases}.$$

The muscle force-length relationship is included in the overlap factor $\partial(l)$ middle:

$$\partial(l) = \begin{cases} 1 - 6.25(l - 1)^2 l < = 1 \\ 1 - 1.25(l - 1) l > 1 \end{cases}, \quad (9)$$

$l = l_s / l_{s,\text{opt}}$, where $l_{s,\text{opt}}$ corresponds to the sarcomere length when the sarcomere can provide maximum muscle force.

The distribution function $n(\theta, t)$ can be expressed as:

$$\frac{\partial n(\xi, t)}{\partial t} - v(t) \frac{\partial n(\xi, t)}{\partial \xi} = r(t) f(\xi) [\alpha(l) - n(\xi, t)] - g(\xi) n(\xi, t). \quad (10)$$

3.3. Image Recognition Digitization. To process images on a computer, we convert the processed analog images into digital image information. Image digitization refers to the sampling and quantization of images, i.e., converting continuous image signals into discrete digital signals for computer processing.

Sampling is the process of discretizing (coordinates) the real space scene to form a digital representation (i.e., the image is represented by the gray value of some points in space, and these points are called sampling points).

A black and white image can be viewed as a two-dimensional continuous function $f(x, y)$, and its value is expressed as the (x, y) brightness of the location image. A compute digital image is represented by a matrix or two-dimensional matrix $[f]_{m \times n}$. Matrix operation is performed on the digital image to obtain the desired image from a two-dimensional continuous function $f(x, y)$ to digital image matrix $[f]_{m \times n}$. It involves taking the function values of different data as samples, and using the discrete values that can be obtained to represent the two steps to complete the picture.

Sometimes, the original information of the image obtained after scanning cannot be preserved, i.e., the spatial

density of the sample is not suitable or the brightness of the sample is not enough in scale, and the image must be reconstructed from the restoration.

Sampling is the first step in image digitization. In digital images, samples should be taken from two spatial directions. The matrix is obtained by taking M along the x -direction of the image and N points along the y -direction. After a sample has been extracted from an image, the value of the resulting sample must be determined before entering it into a computer. Specifically, span a range of sample values and then use a single value to represent all the values of that layer. According to the integer storage convention in the computer, the value range of the sample value can be divided into $k = 2^i$ level, generally $i = 8, 7, 6$, and the gray pixel value can be divided into 64, 128, 256 levels, generally called 64, 128, 256 grayscale. The higher the number of layers, the closer the actual image retrieved by the quantized value of the sample is to the original image.

Image reconstruction is the inverse process of image sampling done from image $f_s(x, y)$ to consecutive images $f(x, y)$. The commonly used quantization scheme is uniform, namely the length of the sub-cycle. When the sampling theorem is satisfied, we have:

$$F(u, v) = \Delta x \Delta y F_s(u, v) H(u, v), \quad (11)$$

which is:

$$f(x, y) = \Delta x \Delta y h(x, y) * f_s(x, y),$$

$$H(u, v) = \begin{cases} 1 & u \in [-w_u, w_u], \quad v \in [-w_v, w_v] \\ 0, & \text{other.} \end{cases} \quad (12)$$

Thus,

$$h(x, y) = 4w_u w_v \sin c(2\pi w_u x) \sin c(2\pi w_v y). \quad (13)$$

However,

$$f(x, y) = k \sin c(2\pi w_u x) \sin c(2\pi w_v y) * f_s(x, y). \quad (14)$$

Again,

$$f_s(x, y) = \sum_{m=-\infty}^{+\infty} \sum_{n=-\infty}^{+\infty} f(m\Delta x, n\Delta y) \delta(x - m\Delta x, y - n\Delta y). \quad (15)$$

The above derivation shows that the reconstructed image is the result of the weighted summation of many two-dimensional sinc functions located on $x = m\Delta x, y = n\Delta y$.

One-dimensional case:

$$f(x) = k \sum_{m=0}^{M-1} \sin c[2\pi w_u(x - m\Delta x)] f(m\Delta x). \quad (16)$$

The essence of sampling is how many points are used to describe an image, and the quality of the sampling results is measured by the image resolution mentioned above. Quantization refers to the range of values to be used to represent each point after the image is sampled. The result of quantization is the total number of colors that the image can hold, which reflects the quality of the sampling. The amount

of image data obtained after digitization is very huge, and coding technology must be used to compress the amount of information. In a certain sense, coding and compression technology are key to realize image transmission and storage. There are many mature coding algorithms applied to image compression. The most commonly used are image prediction coding, transform coding, fractal coding, and wavelet transform image compression coding.

Quantization is the process of converting the corresponding continuous change interval of brightness on the sampling point into a single specific number. After quantization, the image is represented as an integer matrix. Each pixel has two properties: position and grayscale. Positions are represented by rows and columns. Grayscale is an integer representing the lightness and darkness at that pixel location.

3.4. Image Preprocessing. In the process of image acquisition, due to the influence of signal transmission, camera, brightness, etc., the acquired image will have great noise suppression. In the case of restoring most of the original image, suppress the image noise as much as possible.

Bilateral filtering is a nonlinear filtering method that expresses compromise processing by combining the spatial proximity of images and the similarity of pixel values.

Usually we use: mean filter, median filter, maximum and minimum filter, bilateral filter, and guided filter.

Since the spatial information and grayscale similarity are considered, the purpose of edge preservation and denoising can be achieved. It's native, non-iterative, and simple. The biggest advantage of bilateral filters is that they preserve edges. Since the algorithm in this paper needs to analyze the motion characteristics of gymnastics contours and preserve boundary information, bilateral filters are selected as the image preprocessing method. Bilateral filter is a nonlinear filtering method, which is a compromise processing combining the spatial proximity of the image and the similarity of the pixel value.

The expression for a noisy image is:

$$g(x, y) = f(x, y) + n(x, y), \quad (17)$$

where f refers to the image after noise reduction and n is the noise. The pixel values of the image restored by the bilateral filter are obtained by the method of local weighted average:

$$\hat{f}(x, y) = \frac{\sum_{(i,j) \in S_{x,y}} w(i, j) g(i, j)}{\sum_{(i,j) \in S_{x,y}} w(i, j)}. \quad (18)$$

$S_{x,y}$ is a neighborhood representing the size of the center point A, and $g(i, j)$ represents each pixel in the neighborhood.

$$w_s(i, j) = e^{-|(i-x)^2 + (j-y)^2| / 2\delta_s^2},$$

$$w_r(i, j) = e^{-|g(i, j) - g(x, y)|^2 / 2\delta_r^2}, \quad (19)$$

$$w(i, j) = w_s(i, j) w_r(i, j),$$

w_s represents the spatial proximity factor and w_r represents the luminance approximation factor. The bilateral filter is affected by three parameters: the filter half-width N , and parameters δ_r and δ_s . The larger the N , the stronger the smoothing effect, δ_s and δ_r ; then, control the attenuation degree of the spatial proximity factor and the luminance approximation factor, respectively.

w_s represents the spatial proximity factor and w_r represents the luminance approximation factor. They determine the smoothing effect of image preprocessing. Control the attenuation of the spatial proximity factor as well as the luminance proximity factor.

When we identify objects, the most critical factor is the gradient (a lot of feature extraction, SIFT, HOG, etc. are essentially the statistical information of the gradient); the gradient is the edge and is the most essential part; to calculate the gradient, naturally grayscale images are used. The color itself is very easy to be affected by factors such as light, and there are many changes in the color of similar objects. So the color itself is difficult to provide key information. 2010PAMI has some work of colorSIFT, which is also the gradient of different channels.

4. Analysis of the Experimental Research

4.1. Comparison of the Research Methods. There are various methods for image model recognition. According to the features extracted from image pattern recognition, image recognition methods can be divided into the following categories: feature-based shape recognition technology, color feature-based recognition technology, and texture feature-based recognition technology. Among them, the graph-based learning method finds and describes the shape of the object in the image and completes the classification of different images. The common variables that are used to represent shape include parameters, area, circularity, eccentricity, etc. Color detection technology is mainly based on color images, and the color histogram is relatively simple and insensitive to image size, rotation, and type recognition. To detect texture features, various methods that analyze the statistics of very regularly structured lines in the image or the distribution of color intensity in the image are used as shown in Figures 1–3.

Sports injury pictures need more detailed methods to identify; we usually use texture features to identify sports injuries.

After investigating five sets of data, we can clearly see that the three commonly used image recognition methods have their own advantages and disadvantages. In terms of promotion, the public is accustomed to distinguishing from color first; thus, the color features are the most popular, and texture features are the most rigorous and accurate. The rate is the highest, and the shape features are in between.

According to the difference of pattern features and decision patterns, the types of image recognition patterns can be roughly divided into two categories: statistical methods (decision theory) and syntactic (structural) thinking methods. In addition, with the continuous research of pattern recognition technology in recent years, the fuzzy

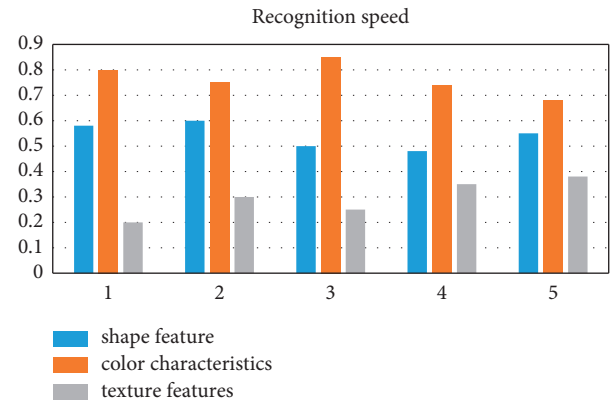


FIGURE 1: Comparison of the recognition speed.

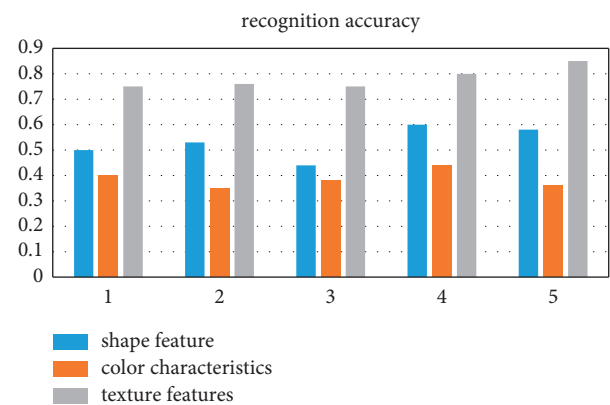


FIGURE 2: Comparison of the recognition accuracy.

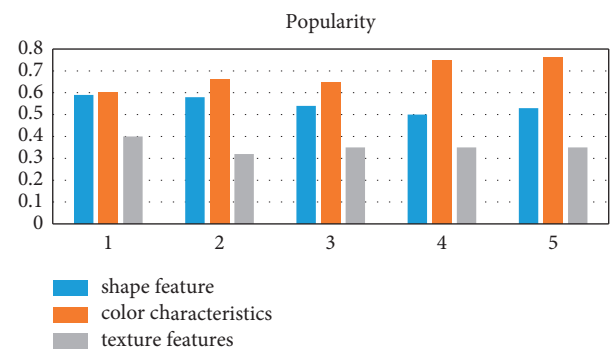


FIGURE 3: Comparison of the recognition promotion degrees.

pattern recognition method and the neural network pattern recognition method have also been widely used.

Various retrieval methods based on shape features can effectively use the target of interest in the image for retrieval, but they also have some common problems, including: ① The current retrieval methods based on shape still lack a relatively complete mathematical model; ② If the target is deformed, the retrieval results are often unreliable; ③ Many shape features only describe the local properties of the target, and a comprehensive description of the target often requires high computing time and storage capacity; ④ Many shape

features reflect that the target shape information is not completely consistent with human intuition, or the similarity in the feature space is different from the similarity perceived by the human visual system. In addition, the 3D object represented from the 2D image is actually just the projection of the object on a certain plane in space. The shape reflected from the 2D image is often not the real shape of the 3D object, due to the change of viewpoint, and various distortions may occur.

It can be clearly seen that the three commonly used image recognition methods have their own advantages and disadvantages. In terms of promotion, the public is accustomed to distinguishing from color first, so color features are the most popular, texture features are the most rigorous, the recognition accuracy is the highest, and shape features are the highest in between.

4.2. Research Objects and Methods

4.2.1. Research Objects. The famous rhythmic gymnasts participating in the “China Art Sports Cup” National Rhythmic Gymnastics Championship are shown in Table 1.

4.2.2. Research Methods. We use sports injury registration in medical research institutes and perform pathological picture recognition on gymnasts. Sports injury identification is related to physical health. We adopt a more rigorous texture identification and mainly investigate the injury situation in the past year.

The above Figure 4 is an example of the injuries caused by gymnastics. We can judge the severity of the injury by performing texture recognition on the pictures and come up with a better treatment plan. After more than 100 case studies, the research results were obtained.

4.3. Research Results

4.3.1. Overall Incidence of Sports Injuries. During the survey, we identified the pathological pictures of the sports injuries of 126 athletes to determine the injuries. The survey results showed that only a small number of athletes were not injured, and the injury rate was as high as 80%. See Table 2 below.

4.3.2. Injury Nature of Sports Injuries. We investigated the injury nature of sports injuries, and the results showed that a total of 172 cases (person) had mild or severe injuries in sports. Our survey results are shown in the following Table 3. (See Table below).

4.3.3. Injury Degree of Sports Injuries. We investigated the injury degree of sports injuries and found that the degrees of sports injuries were different. Mild injuries accounted for 84.30% of the surveyed proportions, moderate injuries accounted for 14.53%, and severe injuries accounted for 1.16%. See Table 4.

4.3.4. Injured Tissue of Sports Injuries. We surveyed 172 injured athletes and found that there were 0 skin injuries, accounting for 0% of the total injuries; 84 injured athletes had muscle injury, accounting for 48.84% of the respondents, 35 injured athletes had joint injury, accounting for 20.35% of the respondents, 52 people had skeletal injury, accounting for 30.23% of the respondents, and 1 person had nerve injury, accounting for 0.58% of the respondents. See Table 5.

4.3.5. Injury Site of Sports Injury. Rhythmic gymnasts were injured in the following order: spine (68), bare feet (45), lower limbs (30), knee joint (20), shoulder (3), wrist (2), elbow (20), head (1), and chest and abdomen (1). See Table 6.

4.3.6. Injury Causes of Sports Injuries. According to consultation documents, expert opinions, and conversations with athletes, techniques, drawbacks, equipment, designated venues, poor physical conditions, insufficient training activities, chronic excessive exercise, inappropriate training methods, etc. are the main causes of injury. A questionnaire based on the same causes was circulated to the athletes. There are 10 types of damage from fatigue, and one or more causes of damage can be selected for each type of damage. The causes of injury were classified as: prolonged excessive exercise (78 cases), improper training methods (38 cases), technique (23 cases), fatigue (14 cases), inertia (10 cases), insufficient preparation (10 cases), and many other specific reasons. See Table 7.

4.3.7. Treatment and Prognosis of Sports Injuries. In this survey, many athletes use traditional Chinese techniques such as acupuncture, massage, cupping, scraping, etc. for treatment, and some also use stretching, fixed reduction, and strength training physiotherapy for rehabilitation. The specific survey results are shown in Table 8. Athletes feel that the treatment effect is not obvious.

4.4. Analysis of the Research Results

4.4.1. Overall Incidence of Sports Injuries. As shown in Figure 5, this study investigated 126 rhythmic gymnasts participating in the “China Rhythmic Sports Cup” National Gymnastics Championships. Among them, 102 athletes had injuries of varying degrees. The high incidence of total injuries is a huge risk for the development of rhythmic gymnastics in our country. It can be seen that in the development process of gymnastics, more attention should be paid to sports injuries and the active measures and the effectiveness of preventive measures to prevent or reduce the occurrence of athletes’ injuries as much as possible.

4.4.2. Injury Nature of Sports Injuries. The ratio of acute to chronic injuries in a survey of 172 injuries is shown. We found that chronic injuries in gymnastics are much higher than in other sports. Chronic injuries are becoming more common as training intensity increases the physical wear

TABLE 1: Basic information of athletes.

$n = 126$	Age (y)	Height (cm)	Weight (kg)	Years of exercise (y)
Woman	15.34 + -2.44	160.39 + -7.18	42.54 + -6.98	6.16 + -2.65



FIGURE 4: Damage site map. (a) Gymnast spinal injury image and (b) Gymnast foot naked sprain image.

TABLE 2: Incidence of sports injuries.

$n = 126$	Number of injuries	No injuries	Total
Woman ($n = 126$)	102	24	125
Percentage%	80.95	19.05	100

TABLE 3: The nature of sports injuries among athletes in rhythmic gymnastics.

Damage nature	Acute injury	Chronic injury	Total
Visits	32	140	172
Percentage%	18.60	81.40	100

TABLE 4: Degree of sports injuries among athletes in rhythmic gymnastics.

Degree of damage	Mild	Moderate	Severe	Total
Visits	145	25	2	172
Percentage%	84.30	14.53	1.16	100

TABLE 5: Organization of sports injuries among athletes in rhythmic gymnastics.

Damaged tissue	Skin	Skeletal muscle	Joint	Skeleton	Nerve	Total
Visits	0	84	35	52	1	172
Percentage%	0	48.84	20.35	30.23	0.58	100

TABLE 6: Sports injuries of athletes in rhythmic gymnastics.

Injury site	Head	Chest and abdomen	Shoulder	Elbow	Wrist	Spine	Lower limbs	Knee joint	Bare feet	Total
Visits	1	1	3	2	2	68	30	20	45	172
Percentage (%)	0.58	0.58	1.74	1.16	1.16	39.53	17.44	11.63	26.16	100

and tear on the body. As with most competitive sports, chronic injuries in rhythmic gymnastics are more common than in other sports. The incidence of chronic injuries has

gradually increased due to the increased technical difficulty and increased exercise duration, load, and intensity in addition to non-systematic rehabilitation after acute injury,

TABLE 7: Causes of sports injuries among athletes in rhythmic gymnastics.

Cause of injury	Technology	Foul	Instrument	Site	Poor health	Insufficient preparation activities	Excessive long-term exercise	Inattention	Improper training methods	Fatigue	Total
Visits	23	1	3	3	9	10	78	10	38	14	317
Percentage %	12.17	0.53	1.59	1.59	4.76	5.29	41.27	5.29	20.11	7.41	100

TABLE 8: Treatment methods for sports injuries.

Treatment method	Visits	Percentage (%)
Acupuncture	86	26.88
Massage	84	26.25
Electric grill	23	7.19
Dressing	18	5.63
Ultrasound	3	0.94
Reset	2	0.63
Closed	10	3.13
Foot bath	5	1.56
Shock wave	9	2.81
Cupping	3	0.94
IF	28	8.75
Scraping	2	0.63
Fixed	1	0.31
Ice	3	0.94
Nutrition	4	1.25
Ultrashort	19	5.94
Limbs	2	0.63
Small needle knife	1	0.31
Magnetic therapy	2	0.63
Pulling	4	1.25
Strength training	8	2.5

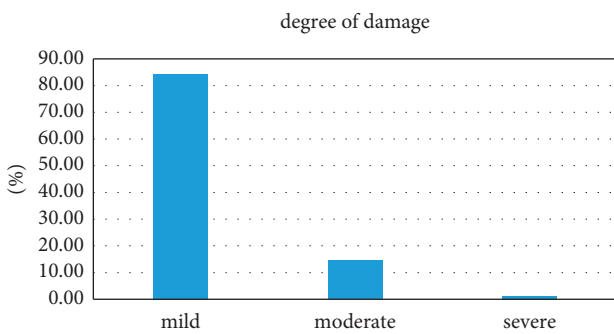


FIGURE 5: Incidence of rhythmic gymnastics injuries.

training with injury, and chronic injury. This suggests that solutions for chronic injury and post-injury training and rehabilitation are still insufficient as shown in Figure 6.

4.4.3. *Injured Tissue of Sports Injuries.* As shown in Figure 7, among the 172 injuries in this investigation, the proportion of injured tissue in each athlete in sports injuries is shown in the figure. Obviously, we can conclude that muscle and spinal cord injuries and keen injuries are due to gymnastics and cause polyrhythmic damage. Skeletal muscle injuries were particularly common, suggesting that problems with

post-exercise muscle strength and rhythm recovery should be of great concern to gymnasts.

4.4.4. *Injury Site of Sports Injury.* Gymnastics sports injuries mainly include three injured parts: the spine, ankles, and lower limbs, as shown in Figure 8, which corresponds to the characteristics of rhythmic gymnastics. Gymnast rhythm is a fighting art that requires various combinations of movements, such as balance, dance, rotation, and similar movements; the spine is the center of the trunk activity, and the muscles are the driving force for spinal movement. Spinal cord injuries include cervical, thoracic, lumbar, the five segments of the coccyx, the muscle and fascia of the vertebral lobe, and the upper vertebral body. The rhythm of gymnasts requires athletes to have good spinal flexibility, strong muscle strength, and three-dimensional dynamics to perfect difficult and complex movements. Rhythmic gymnastics and gymnastics have excellent movements, fast speed, and many darts: if the strength is insufficient, the movements are fierce, and it is easy to cause local cumulative damage. The spinal muscles are rich and different in size and degree; a lack of strength or imbalance results in spinal deformities, such as cervical vertebral arch and thoracic scoliosis. Investigations have shown that the curvature of the spine in athletes is very pronounced and to varying degrees;

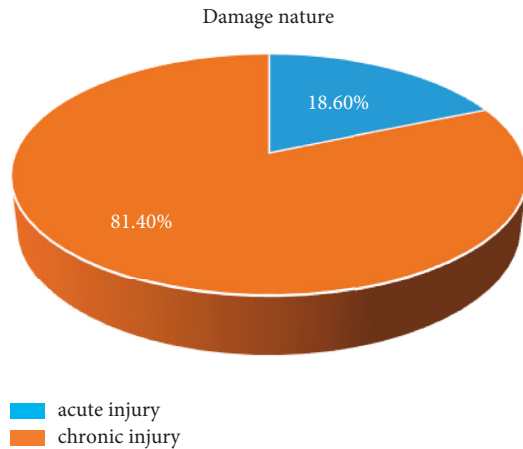


FIGURE 6: Damage nature.

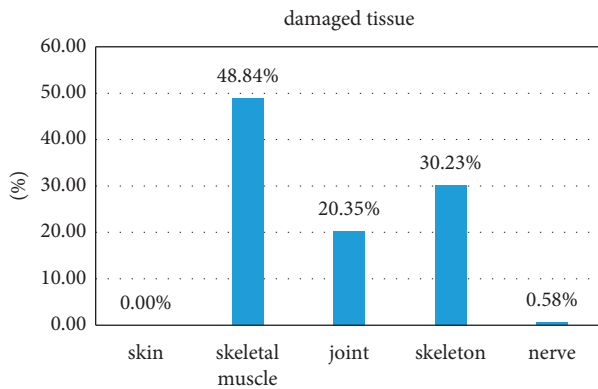


FIGURE 7: Damaged tissue.

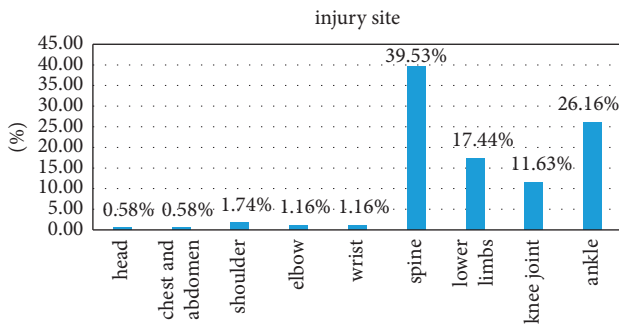


FIGURE 8: Injury site.

the deformation of the spine in turn affects the center of motion of the entire chain, and then a vicious circle begins, affecting most disciplines. In the past, spinal cord injury was much larger than knee joint and other joint injuries, accounting for 39.53% of the total injury, which promoted the solution of the prevention and treatment of spinal cord injury. The spine is the central axis and pillar of the human body and has the function of supporting the load; the spine is an arched structure with good elasticity, which plays the role of transmitting pressure and damping vibration. The lever is attached to this point. The nature of this phenomenon promotes the uneven development of muscle strength on

both sides of the spine, resulting in twisting of the spine, which in turn leads to a series of injuries to the bones, muscles, and fascia. This is a vicious circle that seriously affects the sports discipline and competition. The muscles on both sides of the spine are very rich and are critical to the balanced development of muscle strength in addressing spinal cord injuries. Core strength training reduces spinal cord strain, thereby reducing the damage to various spinal structures. While strengthening both sides, the weak side should be lifted, but the extension of strength should not be neglected. Deep muscles should be strengthened via exercise; the stability of the spine should be strengthened and the physiological structure of the spine should be normalized. In terms of recovery training, therapeutic treatment, spinal manipulation, spinal gun application, and extension, treatment, and rehabilitation methods are coordinated and intersected to achieve the purpose of spinal cord injury rehabilitation. The reason for ankle injuries is that rhythmic gymnastics is a sport based on dance equipment (rings, balls, sticks, belts, and ropes); standing movements are usually done by steps and by weight. In addition, when jumping, balancing, and turning around, the center of gravity of the human body changes, and the gravity falls on the outermost side of the foot, causing uneven force on the swinging part of the foot. The muscles and ligaments on the restless side are prone to cause ankle flexion and foot inversion, joint dislocation, and damage the lateral synovial joint and the anterior fibular ligament. If there is no systematic rehabilitation training, it is easy to hurt the ankle. The correct rhythm of gymnastics is to walk in “beauty” with both feet. Therefore, the form of external opening is necessary, which has a great relationship with the gymnastics rhythm, and the external rotation of the lower limbs must reach the maximum external hip. Herman’s axis is always in a straight line. However, “enlightened measures must be taken to grip the joint so that the inside of the foot touches the ground and ‘falls the foot.’” The high incidence of disc injuries in the foot cannot be underestimated and often affects whether a player is able to train and play. Important: A support band or ring can be applied to the swinging joint prior to exercise to reduce or prevent injury around the joint to be repaired. In addition to structural normalization, tissue rehabilitation must incorporate the complex functional capabilities of this part. The lower extremity is primarily fatigued (periostitis), often doing standing kicks and jumping exercises; fatigue is easily caused by the anterior osseous muscles, and these muscles are not easy to stretch and relax at will. Periostitis is a result of fatigue. The main reason is that there are too many technical jumps but insufficient knee muscle strength, difficult training, unreasonable technical movements, etc. In summary, we can clearly see that young gymnasts have limited physical ability and their physical ability is affected by fiber load. The coach must follow and guide patiently, train step by step, and try to avoid sports injuries.

4.4.5. *Sports Injury Factors.* See Figure 9. Among the injury factors, too long training time, improper training methods, and technical reasons are the main injury factors of sports

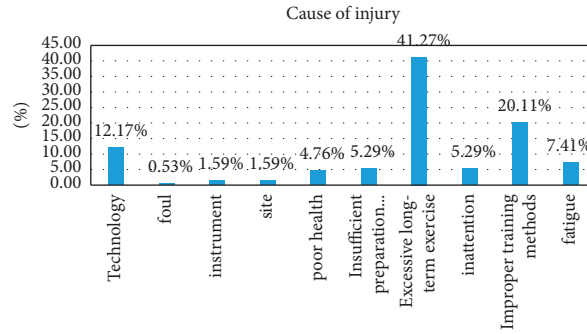


FIGURE 9: Causes of damage.

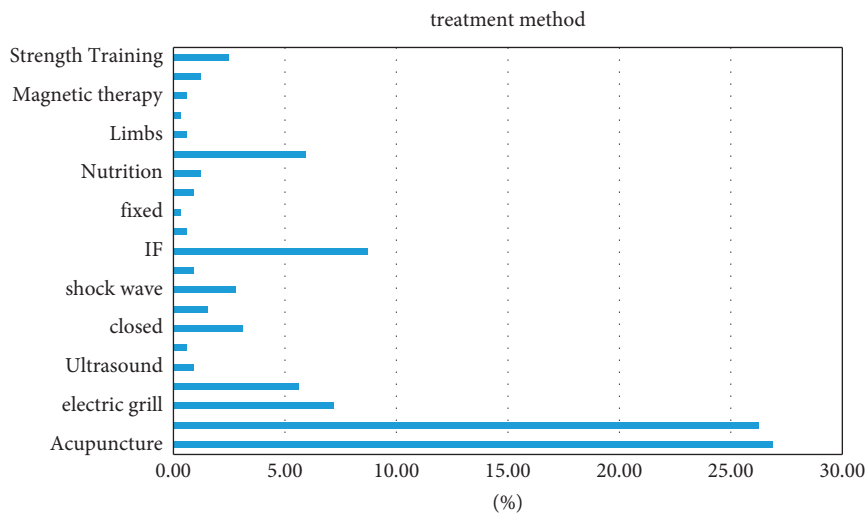


FIGURE 10: Treatment method.

injuries, and preparations for the athlete’s physiological and physical functions, medical monitoring, and follow-up care should be made at all times. The training volume, excessive training, and fatigue can make the athlete’s body more prone to injury. Coaches should have a more comprehensive understanding of each athlete and arrange training reasonably according to each athlete’s situation and should also work harder on the prevention of fatigue.

Fatigue and physical conditions can lead to injuries, suggesting the need to establish precautionary principles. In addition, the lack of preparation and laziness are also completely preventable causes of injury. Coaches should always remind athletes to prepare carefully and fully participate in warm-up exercises, so as to better protect their bodies and devote themselves to training.

4.4.6. Treatment and Prognosis of Sports Injuries. Injury cases in this investigation were treated by the following methods: massage, acupuncture, bandages, sealants, strength training, foot baths, stretching, cupping, ice compresses, scraping, repositioning, limbs, acupuncture, braking, nutritional medicine, and physiotherapy (mainly intermediate frequency current and ultrashort wave). From the above statistics, it can be seen that most injuries are

treated by traditional methods. Acupuncture and massage methods such as active position, tape, ice pack, physiotherapy, rehabilitation training, and other methods still account for a small proportion of the damage. A majority of the athletes who participated in the survey indicated that the treatment methods are effective in relieving pain from acute injuries, but injuries are likely to recur frequently. Complete rehabilitation of the injury site is important in addition to its anatomy to restoring normal tissue and tissue representation. The recovery of this part of complex functional ability requires muscle groups to restore the ability to work in coordination and precision work, and current injury treatments do not include rehabilitation training. It ignores the thorough treatment of the injured party. When this happens, repeat exercise can lead to the accumulation of injuries and gradually step into chronic injuries. Controlling the wearing of joint support belts through the necessary fastening techniques of support belts and the wearing of protective equipment is an important and effective method to protect knee joints and prevent joint injuries. Application of knee pads can protect the knee joint from the impact force after landing. The application of intramuscular action has a good effect on preventing muscle and joint damage. Therefore, it is necessary for us to increase the use of bandages in rhythmic gymnastics to reduce the occurrence

and aggravation of injuries. Strength training includes specific muscle strength training, small muscle group strength training, and core strength training. Core strength training can significantly alter the core stability of rhythmic gymnasts. However, access to scientific training requires good medical supervision. Support belts are used for damaged areas.

Taking preventive measures can help reduce the incidence of injuries, such as exercising before exercising, wearing protective equipment, and performing warm-up activities, which can help reduce the incidence of injuries. After training, athletes can completely relax in various ways, especially active stretching and athlete relaxation, which will not only allow athletes to relax completely, but also improve the flexibility of the athletes' whole bodies and make difficult movement skills go more smoothly; increase the standardization and differentiated treatment of technical gestures during training; effective treatment methods should be adopted in a timely manner after an athlete is injured. Another aspect of scientific training is to monitor the physiological and biochemical functions, and use scientific means to ensure the training level of athletes.

From this article, we can know that gymnastics injuries are mostly chronic injuries, and the treatment of chronic injuries is mostly massage. In sports injuries, we can see from Figure 10 that massage, acupuncture, and other treatments to restore body function are more effective.

5. Conclusion

Through the comparison of various studies and surveys of gymnastics, it can be concluded that the study of injuries in gymnastics is necessary and critical because injuries are inevitable when the general public and professional sportspeople engage in sports. By studying the force analysis of muscle mechanics, we can find the cause of injury during exercise, reduce the probability of injury, and also draw a more effective method of treatment. Our research can better allow the public to participate in gymnastics and reduce the risk of injury. Image recognition research also provides better research conditions for gymnastics sports injury research.

Data Availability

The experimental data used to support the findings of this study are available from the corresponding author upon request.

Conflicts of Interest

The authors declare that they have no conflicts of interest regarding this work.

References

- [1] R. Dick, W. A. Romani, and J. Agel, "Descriptive epidemiology of collegiate women's gymnastics injuries: national collegiate athletic association injury surveillance system, 1988–1989 through 2003–2004," *Journal of Athletic Training*, vol. 42, no. 2, p. 234, 2007.
- [2] J. G. Garrick and R. K. Requa, "Epidemiology of women's gymnastics injuries," *The American Journal of Sports Medicine*, vol. 8, no. 4, pp. 261–264, 1980.
- [3] C. B. Lowry and B. F. Leveau, "A retrospective study of gymnastics injuries to competitors and noncompetitors in private clubs," *The American Journal of Sports Medicine*, vol. 10, no. 4, pp. 237–239, 1982.
- [4] Z. Y. Kerr, R. Hayden, and M. Barr, "Epidemiology of national collegiate athletic association women's gymnastics injuries, 2009–2010 through 2013–2014," *Journal of Athletic Training*, vol. 50, no. 8, pp. 463–479, 2015.
- [5] L. J. Micheli, "Back injuries in gymnastics," *Clinics in Sports Medicine*, vol. 4, no. 1, pp. 85–93, 1985.
- [6] M. S. Keller, "Gymnastics injuries and imaging in children," *Pediatric Radiology*, vol. 39, no. 12, pp. 1299–1306, 2009.
- [7] J. T. Andrich, "Knee injuries in gymnastics," *Clinics in Sports Medicine*, vol. 4, no. 1, pp. 111–121, 1985.
- [8] M. D. Highden, "Gymnastics - sport development and influence on growth related injuries," in *Proceedings of the 30th Annual Conference of Biomechanics in Sports*, Melbourne, Australia, 2012.
- [9] J. Li, W. X. Yu, and G. Y. Kuang, "Research on face recognition approaches of infrared image," *Journal of National University of Defense Technology*, vol. 28, no. 2, pp. 73–76, 2006.
- [10] J. F. Shi and S. Bei, "Research on image recognition based on invariant moment and SVM," in *Proceedings of the 2010 first international conference on pervasive computing, signal processing and applications*, vol. 41, no. 2, pp. 38–40, IEEE, Harbin, China, September 2010.
- [11] M. Tang, "Research of target image recognition based on correlation match," *Proceedings of SPIE - The International Society for Optical Engineering*, vol. 2898, 1996.
- [12] Y. Q. Song, J. M. Chen, and Y. Z. Guo, "Research on multi-feature medical image recognition based on data fusion Research on Medical Image Recognition Based on Multi-feature Fusion," *Application Research of Computers*, vol. 25, no. 6, pp. 1750–1752, 2008.
- [13] Q. Fang, W. Zeng, and R. Liu, "Research on intelligent image recognition technology based on equalization algorithm," *Journal of Physics: Conference Series*, vol. 1748, no. 4, Article ID 042065, 2021.
- [14] D. J. Zhang and W. Y. Tang, "Research of hot stamping image recognition algorithm based on projection feature," *Applied Mechanics and Materials*, vol. 469, pp. 240–245, 2014.
- [15] X. Gu, H. Song, and J. Chen, "A review of research on pig behavior recognition based on image processing," *International Core Journal of Engineering*, vol. 6, no. 1, pp. 249–254, 2020.

Research Article

Financial Data Analysis and Application Based on Big Data Mining Technology

Jinfeng Cheng 

School of Finance and Accounting, Henan Industry and Trade Vocational College, ZhengZhou 451191, China

Correspondence should be addressed to Jinfeng Cheng; chengjinfeng@hngm.edu.cn

Received 19 April 2022; Accepted 27 May 2022; Published 25 June 2022

Academic Editor: Le Sun

Copyright © 2022 Jinfeng Cheng. This is an open access article distributed under the Creative Commons Attribution License, which permits unrestricted use, distribution, and reproduction in any medium, provided the original work is properly cited.

We provide a brief overview of the connotation and characteristics of data mining technology in the era of big data, analyze the feasibility of data mining technology in business management from the economic and technical perspectives, and propose specific application suggestions according to the content and requirements of business management. This paper describes in detail the principles and steps of using the weighted plain Bayesian algorithm and the decision tree algorithm to analyze students' performance; firstly, we need to obtain the plain Bayesian analysis model of college students' learning literacy in physical education and the C4.5 graduation literacy analysis model, and then use certain rules to combine the weighted plain Bayesian algorithm and the decision tree algorithm to obtain the WNB-C4.5 college students' learning literacy analysis model. In addition, in the prediction of financial risks, the classification scheme can be used in the judgment of violation of regulations, but the most used classification scheme is the decision tree. Experiments show that the effectiveness of this scheme in data mining for financial companies is increased by 2% compared to the benchmark method.

1. Introduction

With the rapid development of Internet, cloud computing, and Internet of Things (IoT) technologies in recent years, modern society has gradually stepped into the era of informatization and data-oriented environment [1]. In the development of enterprises, production and operation activities will generate a lot of data and the trend of explosive growth [2]. Comprehensive retrieval, analysis, and application of data can lay a good foundation for the formulation of scientific decision-making, and data information has gradually become an important factor affecting the development capacity of enterprises [3, 4].

With the continuous development of data mining technology, researchers have been expanding data mining technology, which makes its application research fields become more and more extensive [5]. At present, a large number of data mining techniques are successfully applied in many fields such as medical and health care, national

defense science and technology, education and teaching, enterprise applications, and communication industry, which are widely concerned by researchers [6].

For example, in the area of intelligent decision support system, few researchers [7, 8] researched and designed an intelligent decision support system based on data warehouse, OLAP, and data mining methods, and also researched and designed a new intelligent decision architecture framework. In terms of data warehouse applications, Liu et al. [9] researched and implemented a management system applicable to customer data analysis based on data warehousing and data mining techniques, and the combination of the two techniques reflects the advantages of analyzing historical data and is widely used in the mobile communication industry. Few researchers [10, 11] analyzed the intelligent financial decision support system of the ZT Group by combining three key mining techniques, namely association rules, fuzzy methods, and unstructured data mining techniques, and also adopted a function mapping approach to achieve improved

efficiency of operations in response to the shortcomings of the above three techniques. Similar analysis of intelligent decision support system based on data mining technology has many other worthy examples [12].

With the wide application of data mining techniques, most universities also apply the techniques commonly used in data mining to their daily educational teaching activities. Cui and Yan [13] designed and implemented an efficient grade analysis system based on data mining. The system adopts the grade analysis method of data mining, which can quickly and efficiently uncover valuable potential information hidden in a large amount of grade data and help university academic staff to comprehensively analyze students' grades. In [14], data mining technology is applied to the university reader borrowing query and analysis management system, the association rule mining technique is studied in depth, and the classical Apriori algorithm is analyzed, while the Apriori algorithm is improved, thus improving the efficiency of the algorithm to a great extent.

In the metrology business processing, the traditional metrology business often fails to extract valuable data information quickly and effectively when dealing with huge data, which restricts the metrology business management decisions [15]. The use of data mining technology, by building data mining models and data warehouses can effectively handle the huge amount of data generated in metrology business, thus reducing the errors in metrology business to within the standard range and improving the efficiency of metrology business. In [16], the application of data mining technology in WAP business operation is described. By analyzing and comparing the advantages and disadvantages characteristics of various data mining methods, the association algorithm is finally selected to mine the access logs generated by WAP, and some practical optimization solutions are proposed for the performance of data warehouse and data mining.

The deep application of data mining techniques is also widely involved in medical applications. Xu et al. [17] improved the Apriori algorithm by analyzing classical association rule mining algorithms such as AIS algorithm, FP-Growth, and Apriori algorithm, and proposed an array-based mining association rule DRA algorithm, which greatly improves the operation efficiency because the DRA algorithm does not need to generate candidate sets. In [18], a design idea of a data mining system for TCM cases with gastric pain was proposed, and the application of classical association algorithm in TCM cases with gastric pain was effectively verified by mining the medication pattern in 1221 cases for treating a certain disease using the Apriori algorithm.

From the above literature review, it is easy to find that data mining technology is now involved in almost every aspect of people's daily production life, and it is also used in intelligent decision support systems, higher education institutions, metrology business processing, mobile dream network data business, medical business, and other fields with increasing maturity [19, 20]. Based on the respective characteristics of classical Apriori association rule, clustering algorithm, and decision tree algorithm in data mining technology, we decided to use the above three data mining

algorithms to realize the analysis of the enterprise's financial data so as to uncover the potential value information in the enterprise's financial data and provide a reliable decision basis for the enterprise's leadership.

2. System Business Requirements Analysis

2.1. System Process Analysis. The system process analysis mainly describes the execution process of a core business in the main functional modules of the system. Since the financial management system has more functions and the accompanying business process is also relatively large, in view of this, this chapter will focus on analyzing the original financial card management process in the financial management system. The original financial fixed assets card management specification process is shown in Figure 1.

- Step 1: login to the system with the minimum open month.
- Step 2: enter the "Fixed Assets" management operation and enter the original card node; locate an original card at the same time and copy the original card operation.
- Step 3: select the fixed assets category.
- Step 4: enter the items of this fixed assets master card.
- Step 5: save the card.
- Step 6: select the attached card.
- Step 7: make changes to the selected supplementary card, add another supplementary card, and enter the contents again.
- Step 8: save the card.

Through the above eight steps, you can realize the original financial card data entry workflow.

The general ledger of enterprise assets is an accounting of enterprise fixed assets according to certain classification standards in a certain period of all economic operations, the original value of the assets, accumulated depreciation, net value (provision for impairment, net) in a three-column format of debit, credit, and balance of the summary to reflect the changes in their value of the pages of the account. The flow chart of general ledger management is shown in Figure 2.

The general ledger process includes the initial balance entry and after the trial balance, the initial accounts can be created. The general ledger manager can then create some account vouchers and documents based on the initial accounts, and by signing and stamping on the postpayment vouchers, eventually form transfer vouchers for year-end account review and audit role, and finally form bookkeeping methods for year-end transfer.

3. Data Mining Technology in the Era of Big Data

Big data mining technology is an important constituent element of knowledge discovery to analyze data with computer algorithms. In a large number of databases, the

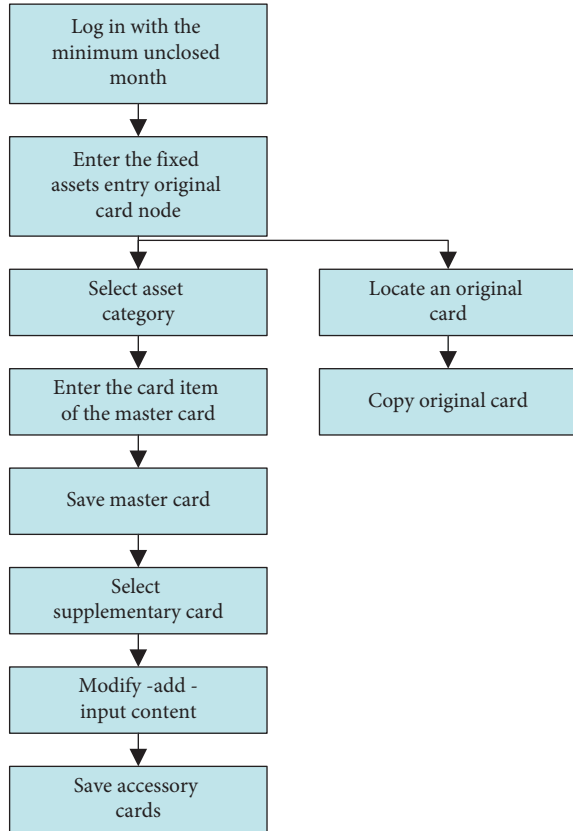


FIGURE 1: Original financial card management process.

required data is obtained, and the data is appropriately transformed, mined, and utilized to obtain valuable information. Generally speaking, the object of big data mining is basically structured, semistructured, or other structured data. The process of data mining is mainly data selection \rightarrow data mining \rightarrow data analysis (see Figure 3).

4. Financial Analysis Method Based on Weighted Multiple Random Decision Trees

The classification problem of financial data is completed by adding a random decision tree scheme to the model, as shown in Figure 4.

The criticality of the attributes in the financial data warehouse varies under different mining objectives, so the criticality of each attribute should be analyzed quantitatively when establishing the decision tree. The current schemes that are often used to confirm the criticality of attributes are the discriminant matrix-based scheme and the information entropy-based scheme. In this study, we use the discriminant matrix scheme to evaluate the importance of attributes. In addition, since financial data are highly specialized, it is not possible to reflect the actual importance of an attribute by relying only on the discriminant matrix, so this project adds artificial weights to modify and intervene in the discriminant matrix to make the calculation of attribute weights more accurate [21, 22].

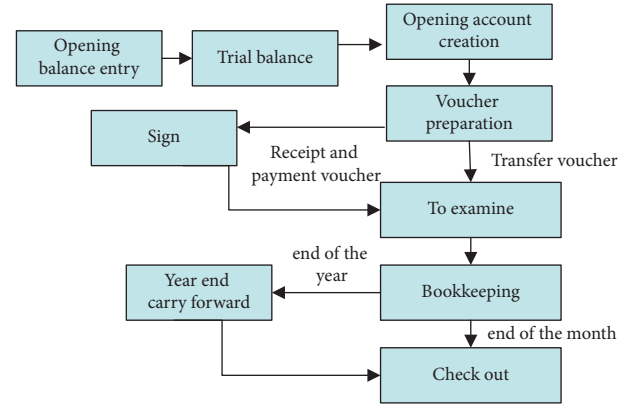


FIGURE 2: General ledger management process.

4.1. *Defining the Resolution Matrix.* A diagonal matrix of $|u| \times |u|$. Each of these terms is defined as

$$C_{ij} = \begin{cases} \{\alpha \in A | \alpha(x_i) \neq \alpha(x_j)\} d(x_i) \neq d(x_j), d(x) \in D \\ \phi \quad d(x_i) = d(x_j), d(x) \in D \end{cases} \quad (1)$$

The number of occurrences and the importance of the attributes in the discrimination matrix are positively correlated; and the shorter the data item with the attribute present, the more critical the attribute.

4.2. *Calculating Attribute Weights for Financial Data.* Initialize all $a_i \in A$ such that $w(a_i) = 0$.

For each term of the diagonal matrix in the resolution matrix C_{jk} calculate

$$w(a_i) = w(a_i) + |C_{jk}|, \quad a_i \in C_{jk}, 0 < k < j = |U|. \quad (2)$$

In the above equation, $|A|$ is the base of all attributes and $|C_{jk}|$ is the base of the discrimination matrix C_{jk} .

After the system presents the weights, it is possible to manually correct the weights in the system, so it is necessary to add the correction coefficients $w^l(a_i)$, $-1 < w^l(a_i) < 1$, if you want to increase the weight of a_i by setting $w^l(a_i)$ to a positive value, and the opposite by setting it to a negative value, then the weight of attribute a_i is $W_{ai} = w(a_i) + w^l(a_i)$.

5. Experimental Validation

This validation data are derived from the financial statistics of more than 1400 company customers who have worked with a commercial bank, and the period of validation data are uniform from 2013 to 2016. The financial information data tables are divided into attributes based on the bank's transaction database, so the financial information data tables provided by the bank can be transformed into 24 attributes that clearly show the financial situation of the company, as presented in Table 1.

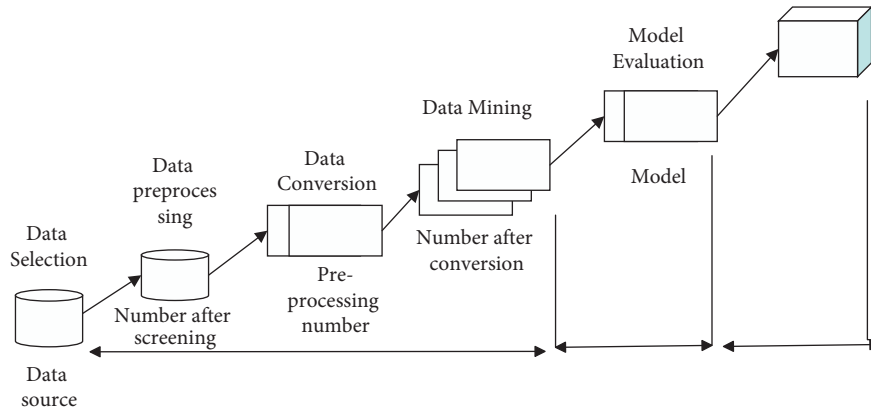


FIGURE 3: Flow of big data mining.

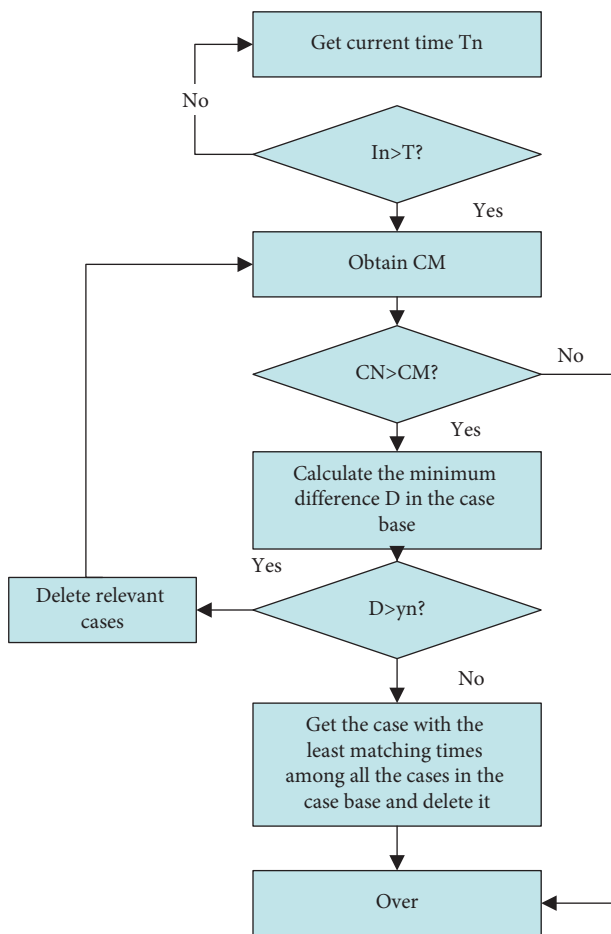


FIGURE 4: Case deletion process.

Due to the actual situation of the company in 2017 and the indicators related to the company, experts in finance classify the company risk into four categories: large, large, small, and small. In this case, companies with high risk are those that will go bankrupt from 2015 to 2017; companies with high risk are those that will default; companies with low risk are those that will not default but their financial situation will deteriorate, and companies with low risk have a

normal financial situation and will not default. The results of the study showed that the best way to apply the decision is to build 10 random decision trees. Therefore, in this study, a total of 10 randomized decision trees were built from the analyzed data because the decision trees were built in a randomized manner, and a total of 5 trials were conducted to verify the stability of the decision trees [23, 24].

The remaining 300 data are test data. The training data were used to build a random decision tree, and the completed decision tree was tested using the test data to finally document the classification accuracy of the decision tree. The experimental results are presented in Table 2 and Figure 5.

The results of the experiment show that this randomized decision tree algorithm classifies companies with large risk, large risk, small risk, and small risk with improved classification accuracy, which has been determined by bank staff to be a practical reference for predicting bank risk. However, because of the small number of large risk data in the training dataset, this branch is not sufficiently trained, making the stochastic decision tree algorithm less accurate than the other branches for large risk classification [25].

Each time, using the same training and validation data, the C4.5 algorithm is applied to classify the risk level, and the final results are presented in Table 3 and Figure 6.

The results of the experiments show that this randomized decision tree algorithm improves the classification accuracy for the risk level of large, risk level of large, risk level of small, and risk level of small by a considerable amount. Similarly, it can be seen that because the number of data with large risk level in the training dataset is relatively small, this class of branches is not trained sufficiently. The accuracy of the C4.5 algorithm is significantly lower for the risky branches compared to the other branches. This is shown in Figure 7.

From Figure 7, we can see that the accuracy of the randomized decision tree algorithm is higher than that of the C4.5 algorithm, which is about 10% higher.

In order to improve the correct rate, 300 data with high risk level are added to the training data set because the training of high risk level is not sufficient. The number of training data with large risk is ensured by replacing the

TABLE 1: Table of experimental attributes.

Attribute code	Attribute	Calculation formula
A1	Return on assets	$(\text{Total profit} + \text{finance costs}) / (\text{Total assets} + \text{total assets of the previous period}) * 2$
A2	Gearing ratio	$\text{Total liabilities} / \text{Total assets}$
A3	Net profit on total assets	$\text{Net Income} / (\text{Total assets} + \text{total assets of the previous period}) * 2$
A4	Return on assets	$\text{Net income} / (\text{Total shareholders' equity} + \text{total shareholders' equity of the previous period}) * 2$
A5	Operating income net profit ratio	$\text{Profit from main business} / \text{income from main business}$
A6	Quick ratio	$(\text{Total current assets} - \text{net inventory}) / \text{total current liabilities}$
A7	Current ratio	$\text{Total current assets} / \text{total current liabilities}$
A8	Fixed assets ratio	$\text{Total fixed assets} / \text{total assets}$
A9	Inventory turnover ratio	$\text{Cost of main business} / (\text{net inventory} + \text{net inventory of previous period}) * 2$
A10	Interest cover multiplier	$(\text{Net profit} + \text{income tax} + \text{finance costs}) / \text{financial costs}$
A11	Total assets turnover ratio	$\text{Income from main business} / (\text{Total assets} + \text{total assets of the previous period}) * 2$
A12	Working capital to total assets ratio	$(\text{Total current assets} - \text{Total current liabilities}) / \text{Total assets}$
A13	Cash from main business ratio	$\text{Cash flow from operating activities} / \text{income from main business}$
A14	Accounts receivable turnover ratio	$\text{Income from main business} / (\text{accounts receivable} + \text{prior period accounts receivable}) * 2$
A15	Fixed assets turnover ratio	$\text{Revenue from main business} / (\text{Total fixed assets} + \text{total fixed assets of the previous period}) * 2$
A16	Accounts receivable turnover ratio	$\text{Income from main business} / (\text{total fixed assets} + \text{total fixed assets of the previous period}) * 2$
A17	Capital adequacy ratio	$\text{Total shareholders' equity} / \text{Total assets}$
A18	Inventory current liability ratio	$\text{Net inventory} / \text{Total liquidity liabilities}$
A19	Cash flow to current liabilities ratio	$\text{Total cash flow from operating activities} / \text{Current liabilities}$
A20	Net income growth rate	$\text{Net profit for the period} / \text{Net profit for the previous period}$
A21	Operating profit growth rate	$\text{Operating profit for the period} / \text{Operating profit for the previous period}$
A22	Main revenue growth rate	$\text{Income from main business for the period} / \text{Income from main business for the previous period}$
A23	Net assets growth rate	$\text{Net assets for the period} / \text{Net assets for the previous period}$
A24	Debt capital ratio	$\text{Total liabilities} / \text{Total shareholders' equity}$

TABLE 2: Comparison of the correct classification rate of multiple stochastic decisions.

Verification times	Small risk %	Less risky %	Risky %	High risk %
1	87.95	78.58	72.71	54.33
2	88.36	79.23	73.98	53.35
3	89.21	80.03	72.55	45.99
4	88.25	79.65	73.39	58.39
5	86.59	78.54	73.38	52.25
Average	88.01	78.61	73.68	52.63

original random sampling with stratified sampling, in which the initial data are stratified by small, small, large, and large risk, and then random sampling is used for each stratum. The classification results using the stratified random sampling method are presented in Table 4 and Figures 8 and 9.

From the above figure, we can see that the correct rate of using the stratified sampling method with high risk is 10% higher than that of the random sampling method with high risk. The underlying reason is that 300 risky data are added to the training data set, which provides more samples for the stratified sampling. Therefore, the number of samples in the training data determines whether the decision tree classification is correct or not, and if the number of samples is

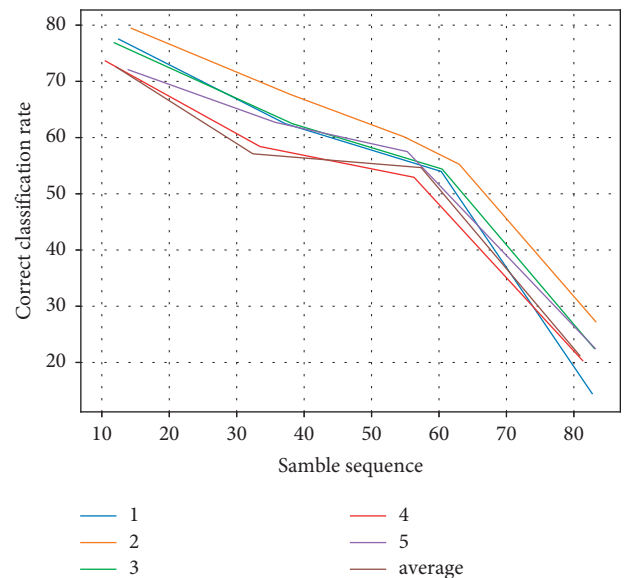


FIGURE 5: Comparison of the correct classification rate of multiple randomized decision trees.

large enough, the decision tree classification will be more correct.

TABLE 3: Comparison of C4.5 classification accuracy.

Verification times	Small risk %	Less risky %	Risky %	High risk %
1	72.58	65.35	6.31	35.59
2	73.36	66.78	62.19	37.12
3	74.55	66.52	66.37	34.39
4	73.98	65.35	62.98	42.86
5	75.91	66.29	63.28	33.98
Average	74.01	66.22	62.58	36.59

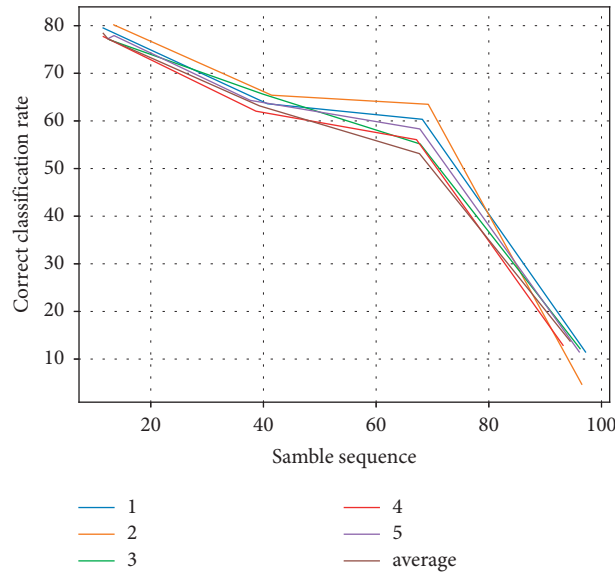


FIGURE 6: Comparison of the correct classification rate of C4.5 algorithm.

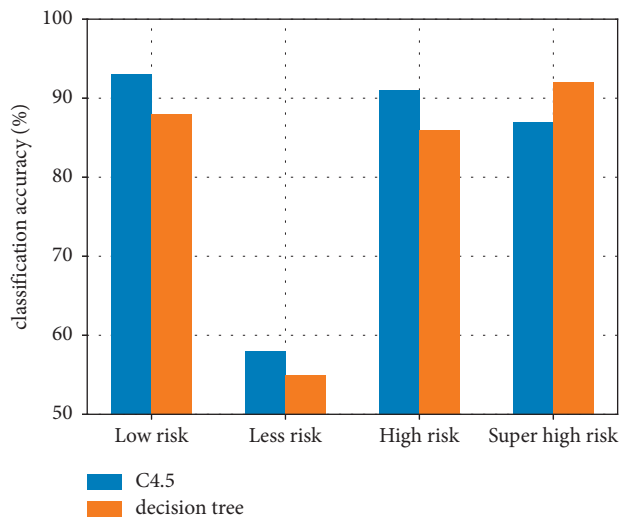


FIGURE 7: Comparison of the classification accuracy of the two algorithms.

TABLE 4: Comparison of the correct rate of stratified sampling for multiple random decision trees.

Verification times	Small risk %	Less risky %	Risky %	High risk %
1	89.33	86.36	77.55	71.03
2	90.32	85.22	76.53	71.98
3	91.39	88.26	78.96	71.65
4	88.36	86.12	79.32	70.11
5	88.96	88.69	79.89	75.97
Average	88.98	84.98	78.03	71.56

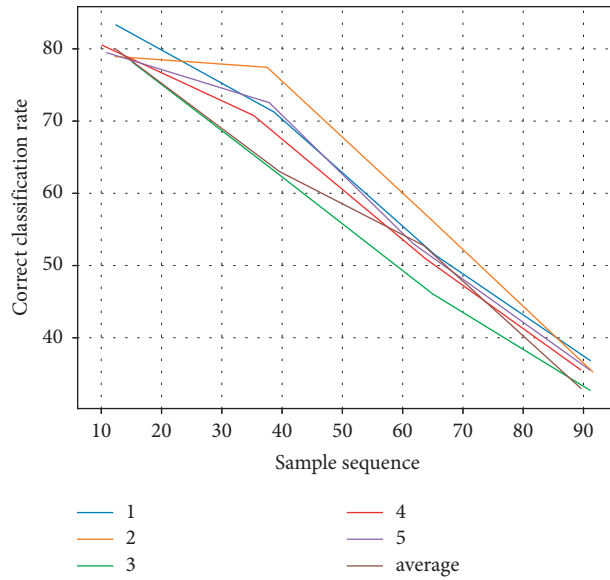


FIGURE 8: Comparison of the correct classification rate for stratified sampling of multiple random decision trees.

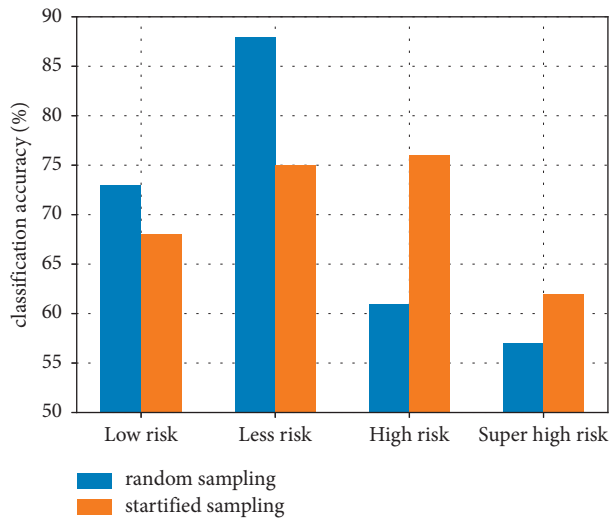


FIGURE 9: Comparison of the correct classification rate of random sampling and stratified sampling.

6. Conclusion

In the era of big data, the content of enterprise financial analysis has increased and the complexity of work is higher. The reasonable application of data mining technology can reduce the work pressure of financial personnel and can improve the quality and efficiency of financial analysis, so it is recommended to promote the use. Good foundation to play the role of data support. During the enterprise cost efficiency accounting, data mining technology can be applied to analyze the association of a certain type of cost and another directly unrelated cost. If it has high correlation characteristics, it needs to be integrated into the process of project budgeting and decision-making to improve the accuracy of cost-benefit accounting.

Data Availability

The experimental data used to support the findings of this study are available from the corresponding author upon request.

Conflicts of Interest

The author declares that they have no conflicts of interest regarding this work.

References

- [1] H. Shang, D. Lu, and Q. Zhou, "Early warning of enterprise finance risk of big data mining in internet of things based on fuzzy association rules," *Neural Computing & Applications*, vol. 33, no. 9, pp. 3901–3909, 2021.
- [2] D. Li, L. Deng, and Z. Cai, "Statistical analysis of tourist flow in tourist spots based on big data platform and DA-HKRVM algorithms," *Personal and Ubiquitous Computing*, vol. 24, no. 1, pp. 87–101, 2020.
- [3] A. Mohamed, M. K. Najafabadi, Y. B. Wah, E. A. K. Zaman, and R. Maskat, "The state of the art and taxonomy of big data analytics: view from new big data framework," *Artificial Intelligence Review*, vol. 53, no. 2, pp. 989–1037, 2020.
- [4] T. Xie, R. Liu, and Z. Wei, "Improvement of the fast clustering algorithm improved by K-means in the big data," *Applied Mathematics and Nonlinear Sciences*, vol. 5, no. 1, pp. 1–10, 2020.
- [5] J. L. Hung, W. He, and J. Shen, "Big data analytics for supply chain relationship in banking," *Industrial Marketing Management*, vol. 86, pp. 144–153, 2020.
- [6] F. Wang, M. Li, Y. Mei, and W. Li, "Time series data mining: a case study with big data analytics approach," *IEEE Access*, vol. 8, pp. 14322–14328, 2020.
- [7] S. Khanra, A. Dhir, and M. Mäntymäki, "Big data analytics and enterprises: a bibliometric synthesis of the literature," *Enterprise Information Systems*, vol. 14, no. 6, pp. 737–768, 2020.
- [8] R. Hou, Y. Kong, B. Cai, and H. Liu, "Unstructured big data analysis algorithm and simulation of Internet of Things based on machine learning," *Neural Computing & Applications*, vol. 32, no. 10, pp. 5399–5407, 2020.
- [9] C. Liu, Y. Feng, D. Lin, L. Wu, and M. Guo, "Iot based laundry services: an application of big data analytics, intelligent logistics management, and machine learning techniques," *International Journal of Production Research*, vol. 58, no. 17, pp. 5113–5131, 2020.
- [10] F. Arena and G. Pau, "An overview of big data analysis," *Bulletin of Electrical Engineering and Informatics*, vol. 9, no. 4, pp. 1646–1653, 2020.
- [11] P. An, Z. Wang, and C. Zhang, "Ensemble unsupervised autoencoders and Gaussian mixture model for cyberattack detection," *Information Processing & Management*, vol. 59, no. 2, 102844 pages, 2022.
- [12] L. Wang and C. A. Alexander, "Big data analytics in medical engineering and healthcare: methods, advances and challenges," *Journal of Medical Engineering & Technology*, vol. 44, no. 6, pp. 267–283, 2020.
- [13] Z. Cui and C. Yan, "Deep integration of health information service system and data mining analysis technology," *Applied Mathematics and Nonlinear Sciences*, vol. 5, no. 2, pp. 443–452, 2020.
- [14] D. Balios, "The impact of Big Data on accounting and auditing," *International Journal of Corporate Finance and Accounting (IJCFA)*, vol. 8, no. 1, pp. 1–14, 2021.
- [15] J. Li, Z. Zhou, J. Wu et al., "Decentralized on-demand energy supply for blockchain in internet of things: a microgrids approach," *IEEE Transactions on Computational Social Systems*, vol. 6, no. 6, pp. 1395–1406, Dec, 2019.
- [16] W. Duan, J. Gu, M. Wen, G. Zhang, Y. Ji, and S. Mumtaz, "Emerging technologies for 5G-IoV networks: applications, trends and opportunities," *IEEE Network*, vol. 34, 2020.
- [17] Z. Xu, C. Cheng, and V. Sugumaran, "Big data analytics of crime prevention and control based on image processing upon cloud computing," *Journal of Surveillance, Security and Safety*, vol. 1, no. 1, pp. 16–33, 2020.
- [18] M. Mohammadpoor and F. Torabi, "Big Data analytics in oil and gas industry: an emerging trend," *Petroleum*, vol. 6, no. 4, pp. 321–328, 2020.
- [19] P. Galetsi, K. Katsaliaki, and S. Kumar, "Big data analytics in health sector: theoretical framework, techniques and prospects," *International Journal of Information Management*, vol. 50, pp. 206–216, 2020.
- [20] O. I. Khalaf and G. M. Abdulsahib, "Design and performance analysis of wireless IPv6 for data exchange," *Journal of Information Science and Engineering*, vol. 37, pp. 1335–1340, 2021.
- [21] U. Srilakshmi, N. Veeraiah, Y. Alotaibi, S. A. Alghamdi, O. I. Khalaf, and B. V. Subbayamma, "An improved hybrid secure multipath routing protocol for MANET," *IEEE Access*, vol. 9, pp. 163043–163053, 2021.
- [22] T. Nguyen, R. G. Gosine, and P. Warrian, "A systematic review of big data analytics for oil and gas industry 4.0," *IEEE Access*, vol. 8, pp. 61183–61201, 2020.
- [23] R. R. Nadikattu, "Research on data science, data analytics and big data," *International Journal of Engineering Science*, vol. 9, no. 5, pp. 99–105, 2020.
- [24] M. Q. Shabbir and S. B. W. Gardezi, "Application of big data analytics and organizational performance: the mediating role of knowledge management practices," *Journal of Big Data*, vol. 7, no. 1, p. 47, 2020.
- [25] S. V. Novikov, "Data science and big data technologies role in the digital economy," *TEM Journal*, vol. 9, no. 2, pp. 756–762, 2020.

Retraction

Retracted: Research on Virtual Interactive Animation Design System Based on Deep Learning

Computational Intelligence and Neuroscience

Received 25 July 2023; Accepted 25 July 2023; Published 26 July 2023

Copyright © 2023 Computational Intelligence and Neuroscience. This is an open access article distributed under the Creative Commons Attribution License, which permits unrestricted use, distribution, and reproduction in any medium, provided the original work is properly cited.

This article has been retracted by Hindawi following an investigation undertaken by the publisher [1]. This investigation has uncovered evidence of one or more of the following indicators of systematic manipulation of the publication process:

- (1) Discrepancies in scope
- (2) Discrepancies in the description of the research reported
- (3) Discrepancies between the availability of data and the research described
- (4) Inappropriate citations
- (5) Incoherent, meaningless and/or irrelevant content included in the article
- (6) Peer-review manipulation

The presence of these indicators undermines our confidence in the integrity of the article's content and we cannot, therefore, vouch for its reliability. Please note that this notice is intended solely to alert readers that the content of this article is unreliable. We have not investigated whether authors were aware of or involved in the systematic manipulation of the publication process.

Wiley and Hindawi regrets that the usual quality checks did not identify these issues before publication and have since put additional measures in place to safeguard research integrity.

We wish to credit our own Research Integrity and Research Publishing teams and anonymous and named external researchers and research integrity experts for contributing to this investigation.

The corresponding author, as the representative of all authors, has been given the opportunity to register their agreement or disagreement to this retraction. We have kept a record of any response received.

References

- [1] B. Liu, "Research on Virtual Interactive Animation Design System Based on Deep Learning," *Computational Intelligence and Neuroscience*, vol. 2022, Article ID 5035369, 10 pages, 2022.

Research Article

Research on Virtual Interactive Animation Design System Based on Deep Learning

Bing Liu 

JMU College of Arts & Design, Xiamen 361000, China

Correspondence should be addressed to Bing Liu; 202161000047@jmu.edu.cn

Received 15 April 2022; Accepted 25 May 2022; Published 25 June 2022

Academic Editor: Le Sun

Copyright © 2022 Bing Liu. This is an open access article distributed under the Creative Commons Attribution License, which permits unrestricted use, distribution, and reproduction in any medium, provided the original work is properly cited.

With the rapid development of computer network technology, the advantages of virtual reality technology in the field of instant messaging are becoming more and more significant. Virtual reality technology plays an important role in communication networks, including enhanced resource utilization, device redundancy, immersion, interactivity, conceptualization, and holography. In this paper, we use the basic theory of Restricted Boltzmann Machine to establish a semisupervised spatio-temporal feature model through the animation capture data style recognition problem. The bottom layer can be pretrained with a large amount of unlabeled data to enhance the model's feature perception capability of animation data, and then train the high-level supervised model with the labeled data to finally obtain the model parameters that can be used for the recognition task. The layer-by-layer training method makes the model have good parallelism, that is, when the layer-by-layer training method makes the model well parallelized, that is, when the bottom features cannot effectively represent the animation features, such as overfitting or underfitting, only the bottom model needs to be retrained, while the top model parameters can be kept unchanged. Simulation experiments show that the design assistance time of this paper's scheme for animation is reduced by 10 minutes compared to baseline.

1. Introduction

Video communication in instant messaging systems usually requires high real time and stability; otherwise, it is prone to data delay, playback lag, and other instability [1]. Due to the influence of unstable network environment, the data is easily disturbed by various factors during transmission, resulting in the data not being broadcasted properly at the receiving end [2]. And the goal of this paper is to design a virtual video chat system combined with virtual reality, which needs to transform from the original transmission video data to the transmission user's face key point data based on the application scenario and handle the transmission abnormality [3]. At the same time, because the content of this paper is not based on video streaming instant messaging, but 3D virtual animation video chat, the user sees the expression animation of the virtual animation model during the chat, so the data format transmitted in the network is the data set of face keypoints and voice data, and this paper has high

requirements for noise reduction and echo cancellation of voice based on the actual application scenario, thus making the voice and animation [4]. Therefore, the synchronization of voice and animation and speech optimization become the urgent problem in the subject.

In recent years, the research on face keypoint localization has become more and more abundant and mature, and the research on deep learning has also made many breakthroughs, bringing better innovative methods and more opportunities for other related research fields [5]. Face keypoint localization is the basis of face recognition and other research, and the application scenarios are very broad. Researchers have proposed many algorithms for face keypoint localization and achieved good results in related fields, but in practical applications, faces are often affected by various internal and external factors such as expression, posture, illumination, and occlusion, making it very difficult to achieve accurate face keypoint localization, which is still a great challenge [6, 7]. This paper will address the design and

optimization of the face keypoint localization model and its application in mobile based on practical application scenarios [8].

Virtual reality technology is an important part of the computer field and has important applications in biochemistry, social entertainment, aerospace, and military industries [9]. However, virtual reality technology is less present in the current popular instant messaging-related research, which indicates that researchers in the field of instant messaging have paid less attention to virtual reality technology and have not well combined the two [10]. In this paper, we combine virtual reality technology and instant messaging, and the client drives the expression animation of 3D virtual model by parsing the key point data of human face to realize the virtual animation real-time communication [11].

In summary, the design of combining virtual reality technology with instant messaging and combining human-computer interaction with video chat will be a very important research direction in the future communication field [12].

2. Related Work

At present, domestic and foreign research in instant communication has made great progress, and communication among people has become more and more convenient and colorful [13]. At the same time, people are more and more willing to try various diversified and personalized instant communication methods, such as using 3D virtual animation models instead of real faces to communicate in real time, and the expression animation of 3D virtual animation models is driven by the real expressions of users in real time [14, 15].

In this paper, we combine deep machine learning-based face keypoint localization technology, virtual reality technology, and instant messaging to design and implement a more personalized instant messaging system [16].

2.1. Face Key Points. Face keypoint localization is the basis of face recognition and expression analysis and has a very broad development and application prospect. Researchers have proposed many face keypoint localization algorithms based on various methods. In [17], a fast face alignment method based on a layer-by-layer model is proposed, which converges after 8~10 iterations and the alignment time of each face image is tested within 40 ms on a Samsung I9300 smartphone. Reference [18] proposed a multitask cascaded convolutional neural network to achieve face detection while achieving face key point localization. Reference [12] et al. used a cascaded convolutional neural network-based method to achieve the localization of five key points of faces with an average localization error of 1.264 pixels, and it only takes 15.9 ms to process a face image. Reference [19] proposed a new cascaded deep design warp network, where the input of the previous cascaded neural network is a certain part of the image, unlike the previous ones, the input of each stage of the DAN (Deep Alignment Network) network is the

whole image, which can extract features from the whole image. The features can be extracted from the whole image to obtain more accurate localization. Reference [20] proposed an edge-aware face alignment algorithm based on the edge as the geometric structure of the face for localization of 98 key points of the face.

From the above studies, it can be seen that there are abundant studies on face keypoint localization techniques and many algorithms are able to achieve better results. In the task of this paper, we are more concerned with the real time of face keypoint localization and the accuracy of face keypoint localization under different postures and expressions.

2.2. Data Transmission and Sound-Image Synchronization. Currently, data transmission is moving in two directions: first, to pursue higher transmission performance at lower transmission rates, that is, to reduce the transmission BER as much as possible; second, to increase the transmission rate as much as possible while the BER meets the requirements. Reference [11] proposes a new method for synchronizing audio and video presynchronization: by designing a presynchronization module based on the RTP/RTCP timestamp in the receive buffer and a new working mechanism, a fast synchronization within the media is achieved, eliminating the intermediate layer bias and adding no additional end-to-end delay before unpacking the RTP packets. Reference [12] proposes a method that uses timestamps to store audio and video data with correlation in acquisition time into a fixed synchronization data structure and always synchronize and control them during acquisition, encoding, transmission, reception, decoding, and playback, which can well meet the demand of audio and video synchronization in application scenarios and has good engineering practice. Reference [15] implemented a virtual reality-based gaze sensitive social communication system for autistic patients, which can measure the gaze-related index of patients during their interaction with virtual companions, and this index can be mapped to their corresponding anxiety level. At the same time, the system can influence the patient's task performance and gaze-related index in response to the virtual companion's emotions.

Technologies such as speech coding and decoding, data transmission, and audio and video synchronization are the basis of research in instant messaging. In the task of this paper, more attention is paid to the effect of special environment on speech, such as external playback under mobile devices and the synchronization of speech with 3D animation models.

3. Animation Design Model Based on Two-Layer RBM

Aiming at the problem that there is often a semantic gap between the underlying features and the high-level semantics of animation capture data, a semantic recognition algorithm for animation capture data that incorporates a restricted Boltzmann machine generative model and a discriminative model is proposed by combining deep

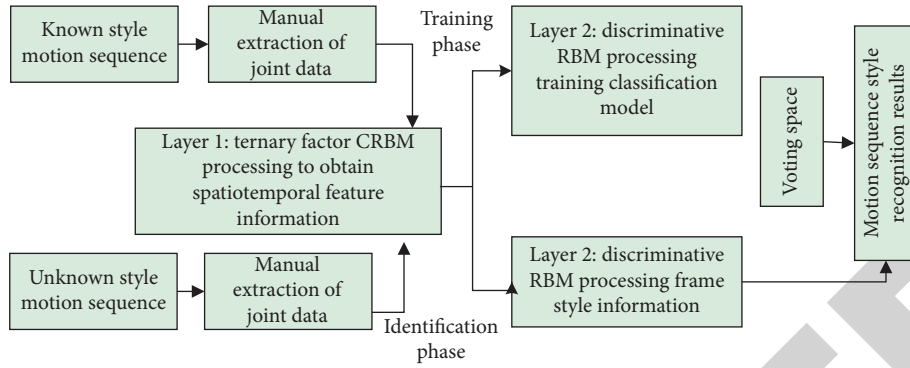


FIGURE 1: Flowchart of animation design based on two-layer RBM model.

learning ideas. The algorithm adopts a two-layer restricted Boltzmann machine to perform discriminative feature extraction (feature extraction layer) and style recognition (semantic discriminative layer) on animation capture data, respectively. Firstly, considering that the autoregressive model has excellent ability to express temporal information, a conditional restricted Boltzmann machine generative model based on single-channel ternary factor interaction is constructed for extracting temporal feature information of animation capture data; then, the extracted features are then coupled with the corresponding style labels as the input of the current frame data layer of the restricted Boltzmann machine discriminative model in the semantic discriminative layer for the training of single-frame style recognition; finally, on the basis of obtaining the parameters of each frame, the voting space is added to the top of the model to achieve the effective recognition of the style semantics of the animation capture sequence. The experimental results show that the algorithm has good robustness and scalability, can meet the needs of diverse animation sequence recognition, and facilitate the effective reuse of data.

3.1. Introduction to Recognition Models and Processes. As one of the representative models of deep learning, the RBM model has the ability to extract static frame features and build a CRBM model by adding autoregressive model constraints to the input layer, which in turn can obtain temporal feature information with contextual semantic scenarios. Reference [19] proposes a nonlinear mapping threshold CRBM binary hidden variable probabilistic model, which uses an unsupervised learning algorithm to extract not only the highly structured feature information that is available when transitions are transferred between video frame images, but also to portray the spatial relationships between each frame's own pixels. In this paper, a voting space layer is added on top of the label layer for animation design, and a segmentation layer with the ability to identify transition frames can also be added. The animation design process using the two-layer RBM model is shown in Figure 1.

3.2. Bottom Feature Extraction Layer. The generative model fully considers the distribution of data and can use joint probability to get the conditional probability from input data

to output data. Therefore, the RBM based on the generative model can reflect the generation process of the target object and the similarity between similar objects through the energy function and the activation state of the hidden layer neurons. The layer 1 generative RBM model developed in this paper takes advantage of the second property.

According to the autoregressive model algorithm, this paper splits the animation into 2 parts and constructs the bottom spatio-temporal feature layer: one part represents the previous n frames of the current animation frame, which is called the history frame; the other part has only one frame, which represents the current animation frame, which is called the current frame. In addition, the interaction factor layer is added to realize the information interaction control between the 2 input layers and the feature layer, aiming to map the latent information and spatio-temporal feature information in the animation data to the feature representation layer through the factor layer so as to obtain more accurate probability distribution of the data in the process of reverse estimation; meanwhile, the factor layer also has the function of reducing the model space complexity from $o(n^3)$ to $o(n^2)$, which is described as follows.

The representation of each neuron in the history frame based on the RBM feature learning is $p = (p_1, p_2, \dots, p_m)$, where $m = (f_r - 1)d$ is the total number of neurons, f_r denotes the length of the historical frame, and d denotes the frame data dimension. The neurons of the current frame are represented as $n = d$, with $v = (v_1, v_2, \dots, v_n)$ representing the total number of neurons of the current frame. The hidden layer neurons are represented as $h = (h_1, h_2, \dots, h_t)$, where t is the total number of hidden layer neurons set. For the convenience of description, p_i is the i th neuron of the history frame, v_j is the j th neuron of the current frame, b_j represents the bias of the j th neuron, h_k represents the k th neuron of the hidden layer, and c_k represents the bias of the k th neuron. c_k is the connection weight from the interaction factor layer to the history frame (directed connection), W_{if}^p is the connection weight from the interaction factor layer to the current frame (directed connection), and W_{if}^v is the connection weight from the interaction factor layer to the hidden layer (undirected connection). W_{kf}^H is the connection weight from the interaction factor layer to the hidden layer (undirected connection), which determines the model parameters and is denoted as $\theta_1 = (W_{if}^p, W_{if}^v, W_{kf}^H, b, c)$. Note

that the history frame and the current frame are both real-parameter visible neurons, while the hidden layer is a binary random hidden unit.

3.3. High-Level Semantic Discriminant Layer. The DRBM model can be considered as a two-layer model, where both the visible layer and the label layer are the input sample data, and the hidden layer can be used to sample the joint probability distribution and conditional probability distribution of the visible and label layer data. Since an animation belongs to only one style, the label layer can be coded as “single heat”; that is, the label layer is set as a binary neuron, and only the neuron corresponding to the label has a value of 1 and is active [21, 22].

The parameters are defined as follows: the label layer neuron is $L(L_1, L_2, \dots, L_o)$, where o represents the number of all styles of training samples, and the bias is $T = (t_1, t_2, \dots, t_o)$; the visible layer is the feature information extracted from the first layer, which is a real unit, denoted as $X = (x_1, x_2, \dots, x_k)$, and the bias is $Q = (q_1, q_2, \dots, q_k)$; the hidden layer is the unit that can represent the correspondence between the label layer and the visible layer, denoted as $Y = (y_1, y_2, \dots, y_n)$, and the bias is $R = (r_1, r_2, \dots, r_n)$. The connection weights of the visible and labeled layers to the hidden layer are W_{yx}, W_{yl} . Since this layer is used for classification rather than prediction of the probability distribution of the animated features, a hybrid discriminant method is used to train the second layer of the RBM, which is a linear combination of the optimal discriminant model

$p(l|x)$ and the generative model $p(l, x)$. The training algorithm is still a comparative scattering algorithm. The log-likelihood function of the function to be optimized takes the form

$$L_{\theta_2} = \sum_{i=1}^s \log P(l_i|x_i) - \alpha \sum_{i=1}^s \log P(l_i, x_i), \quad (1)$$

where s denotes the total number of categories. For the 2nd term, i.e., the generative model part, the parameters are updated according to the steps of the 1st level [23, 24]. For the first discriminant model, the conditional distribution can be calculated as proposed by Larochelle et al.

$$P(l|x) = \frac{e^{(t_l + \sum_j (\log 1 + e^{W_{jl}x_j + W_{jl} + r_j}))}}{\sum_{ls} e^{(t_{ls} + \sum_j \log(1 + e^j))}}. \quad (2)$$

In a sequence of frames, equation (3) represents the magnitude of the probability that each frame belongs to each label, where l is the category label notation to which the training frame belongs, $ls \in (1, 2, \dots, 0)$. Therefore, the conditional probability $p(l|x)$ can be solved by an optimization function using the gradient descent method such that the probability that the animation feature x belongs to the correct label l is maximized. Then, for a single frame of animation $x^{(t)}$ and the corresponding style label $l^{(t)}$, there are

$$\frac{\partial \log P(l^{(t)}|x^{(t)})}{\partial \theta_2} = \sum_j \text{sigmod}(S(x^{(t)})) \frac{\partial S(x^{(t)})}{\partial \theta_2} - \sum_{j,ls} \text{sigmod}(S(x)) P(ls|x^{(t)}) \frac{\partial S(x)}{\partial \theta_2}. \quad (3)$$

Among them, $S(x) = \sum_{i=1}^k W_{ji}x_i + U_{jl} + r_j$, $x^{(t)} \in x$. For label layer, bias update method is

$$\frac{\partial \log P(l^{(t)}|x^{(t)})}{\partial t} = 1_{y=y^{(t)}} - P(l|x^{(t)}), \quad (4)$$

where $1_y = y^{(t)}$ is the label layer neuron activated by the current label after the “single heat” encoding. The model parameters can be updated iteratively at each step by bringing equation (4) into the expression of the hybrid discriminative model in equation (3). The final DRBM model with classification function at layer 2 is trained [25, 26].

4. Experiment and Result Analysis

In order to verify the effectiveness of the two-layer model in animation design, the experiments are conducted on a PC with 3.30 GHz CPU and 8G memory, and the programming test environment is python3.7. In the generated model, the number of neurons in the historical and current frames as input data in the CRBM model is directly determined by the dimensionality of the input data. In the preprocessing, 53

dimensions of data were extracted for each frame, including 48 joint angular degrees of freedom, 3 animation directions, and 2 geodesic velocity data. The first 25 frames are used as the input vector of the history frame, and the 26th frame is used as the input data of the current frame so that the number of neurons of the history frame is 1325 and the number of neurons of the current frame is 53. The number of iterative updates is 250–500, and good feature information can be extracted.

4.1. Two-Layer Model Training. In this paper, we first eliminate the influence of spatial location of animation nodes on recognition and then retain the advantage of autoregressive model to build the first layer of ternary factor CRBM to extract temporal features and finally use the second layer of discriminative Boltzmann machine for classification. The two-layer model is trained to obtain a set of model parameters, including weights and biases, for each layer.

Since the layer 1 RBM uses a generative model, it contains reconstruction errors for the current frame animation data description. Using the reconstruction error, we

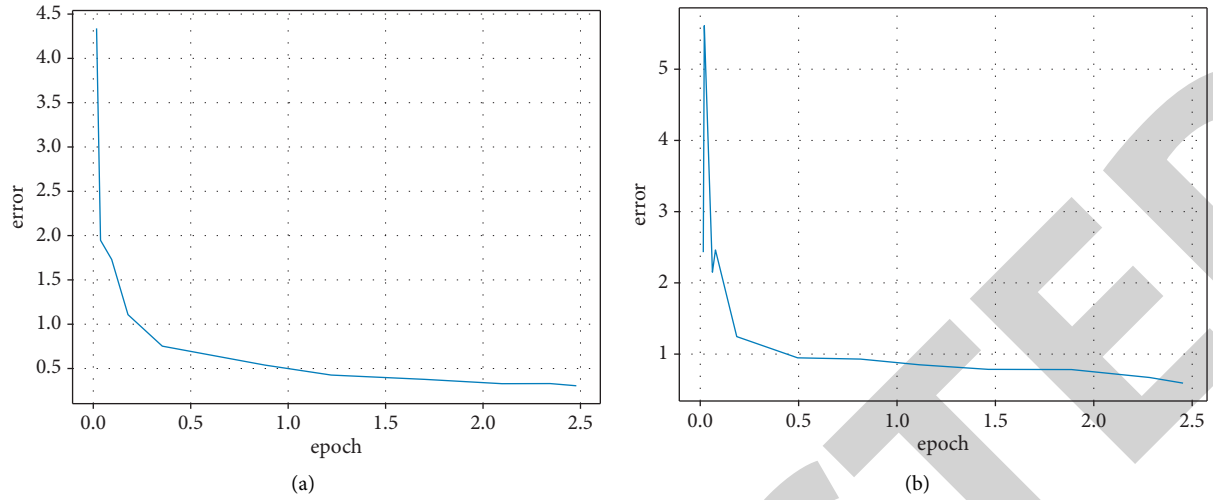


FIGURE 2: Total error of RBM reconstruction in layer 1 versus the number of iterations. (a) Dataset 1. (b) Dataset 2.

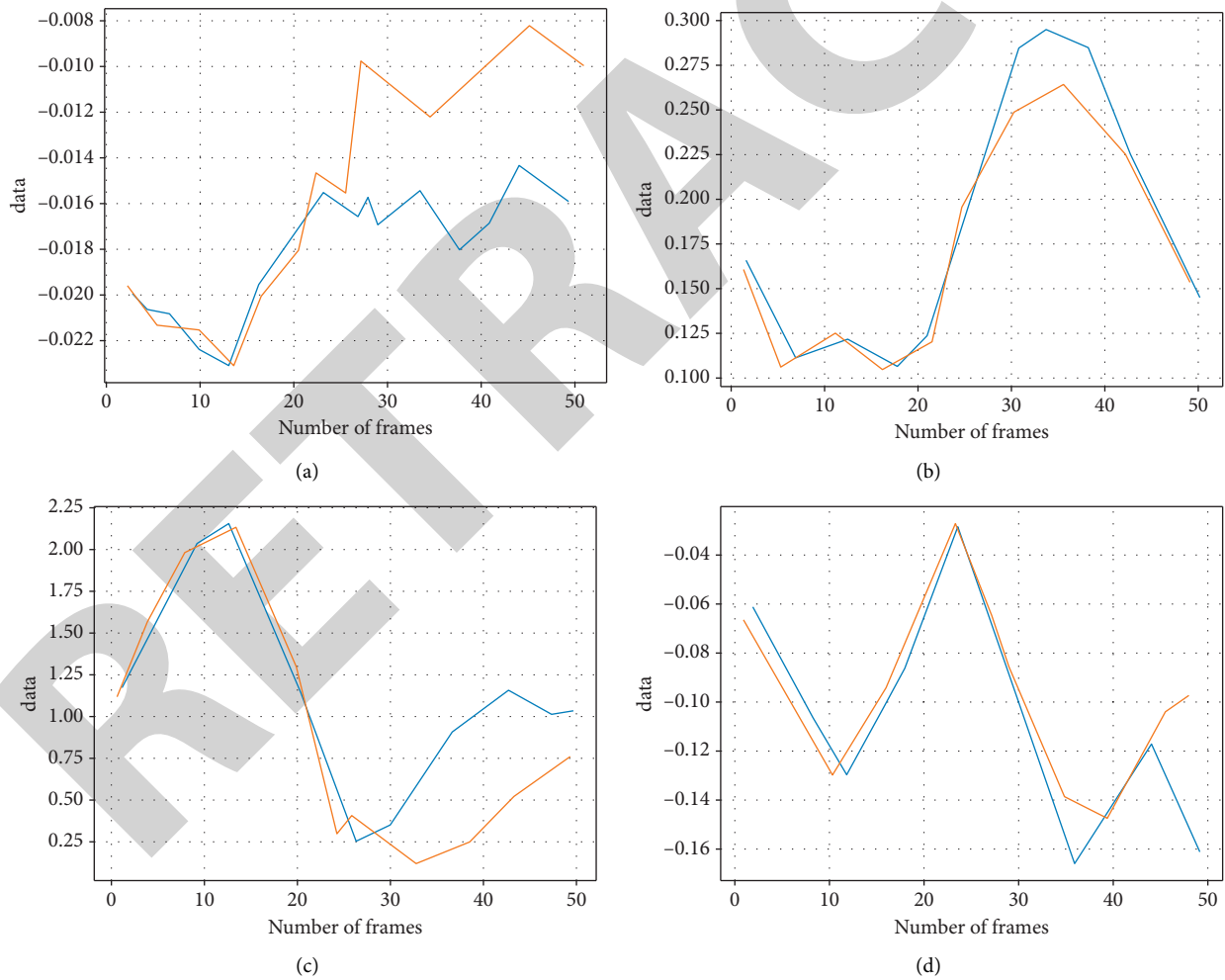


FIGURE 3: Effect of end effector reconstruction. (a) Left foot. (b) Right foot. (c) Left hand. (d) Right hand.

can roughly determine how well the model fits the current 26-frame data distribution. If the error is too large, the parameters are not set properly and the number of neurons

in the feature layer needs to be increased or the number of training sessions needs to be increased. Of course, the reconstruction error should not be too small, as overfitting will

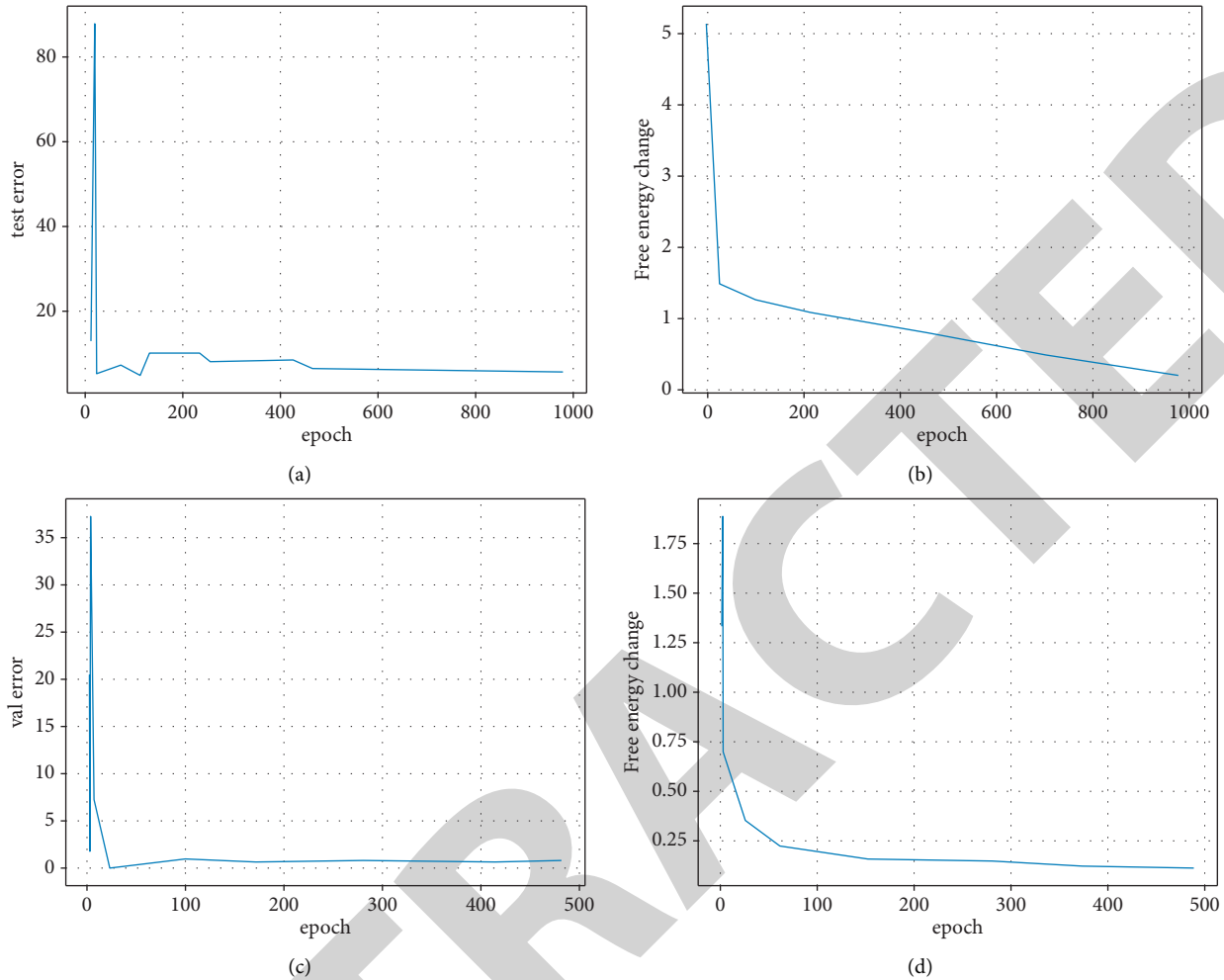


FIGURE 4: Validation set error and energy change for 2 data sets. (a) Validation set error 1. (b) Free energy 1. (c) Validation set error 2. (d) Free energy 2.

occur if it is too small. In the later tuning process, the appropriate number of hidden neurons and other techniques can reduce the occurrence of overfitting. In general, the reconstruction error will be stabilized within a certain range after a certain number of training sessions, which is verified by relevant experiments.

Figure 2 shows the reconstruction errors of layer 1 of the model for the 2 data sets. It can be seen that the reconstruction error obtained from the RBM model based on layer 1 will gradually stabilize after a certain number of iterations. For example, after 200 iterations, the reconstruction error basically tends to a stable level, and the total error of 53 Euler angles per frame does not exceed 0.9. Therefore, it can be judged that the layer 1 model does not change the original characteristics of the animation, and the fitting effect is relatively good.

To verify the reconstruction effect of the model on the animation style, Figure 3 shows the reconstructed effect of the 1st layer generating model part on the 4 end effectors (left and right hands, left and right feet) of the 1st animation style JO (jogging) of data set 1. Analyzing the fluctuation magnitude, we can see that the degree of change of the

reconstructed data is similar to that of the original data animation style, which indicates that the data obtained by reconstructing using the first 25 frames and the model parameters are consistent with the style type of the current animation; that is, the hidden layer can effectively portray the style characteristics of the current animation.

The second semantic discriminative layer uses the RBM discriminative model to construct the mapping relationship between labels and each style animation feature, and the model parameters are updated according to the reconstruction errors of the input data in the label and feature layers. At the same time, a small number of samples are extracted from the training samples as the validation set to verify the accuracy of the model classification in each training cycle. Figure 4 shows the variation of the free energy of the RBM model at layer 2 and the recognition rate of the validation set in Dataset 1 and Dataset 2 as the number of training cycles increases. The free energy is closely related to the probability distribution of the model, and the trend is inversely proportional to the change in the probability distribution, as the energy decreases, the probability distribution becomes closer to the feature distribution, which

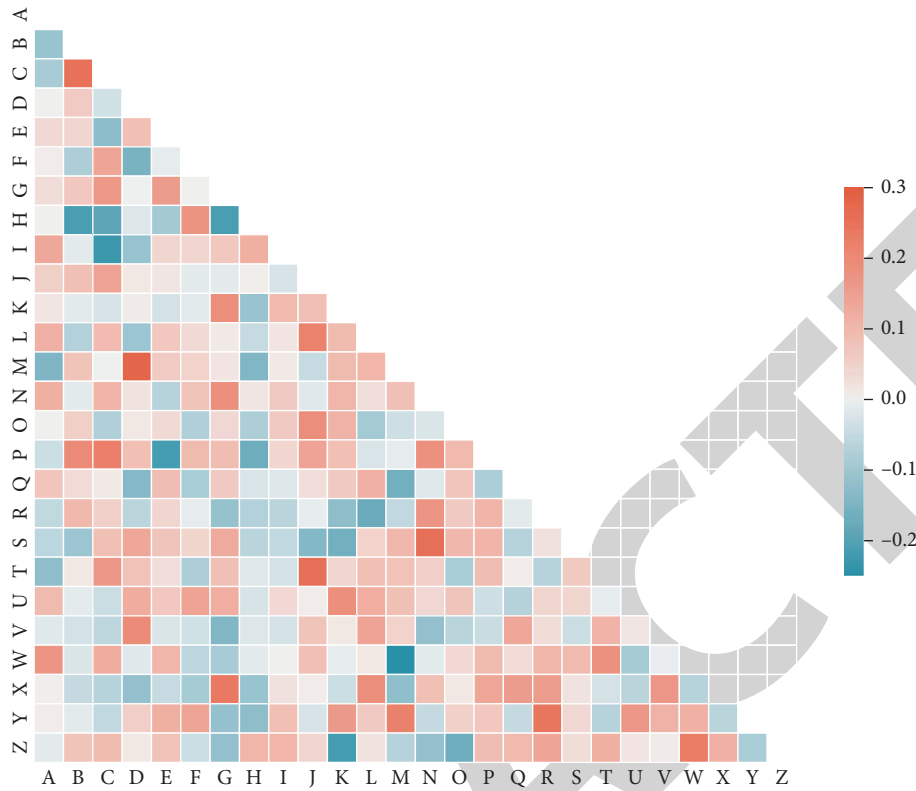


FIGURE 5: Animation style recognition confusion matrix.

also validates the theory that the system is most stable at the lowest energy. The effect of model energy release on the recognition rate can be clearly observed in Figure 4(b): as the system stabilizes, the frame classification error of the validation set is in a decreasing state and gradually tends to be smooth.

4.2. Comparison and Analysis of Experimental Results. In order to further verify the recognition effect of the two-layer RBM model on animation style, the recognition results of this paper’s algorithm are compared with the Adaptive Motion Codebook Classifier (AMCC) algorithm of [12] and the SVM recognition algorithm based on radial basis function, and the spatial locations of 23 nodes are selected as the data preprocessing method. The spatial position information of 23 nodes was selected as the data preprocessing method. From the experimental results of the three recognition algorithms in Figure 5, it can be seen that for simple animations, the two-layer RBM algorithm can also achieve good style determination results, such as JO, KF, and KS simple sequences, and its test discrimination rate reaches 100%. The main reason is that the AMCC and SVM algorithms mainly consider the spatial information of the body joints, which has the greatest influence on the animation style, for classification, and ignore the timing information. The two-layer RBM algorithm proposed in this paper can achieve better semantic discriminative effect, mainly because the first layer extracts discriminative spatio-temporal features for effective pose portrayal; the second layer of DRBM

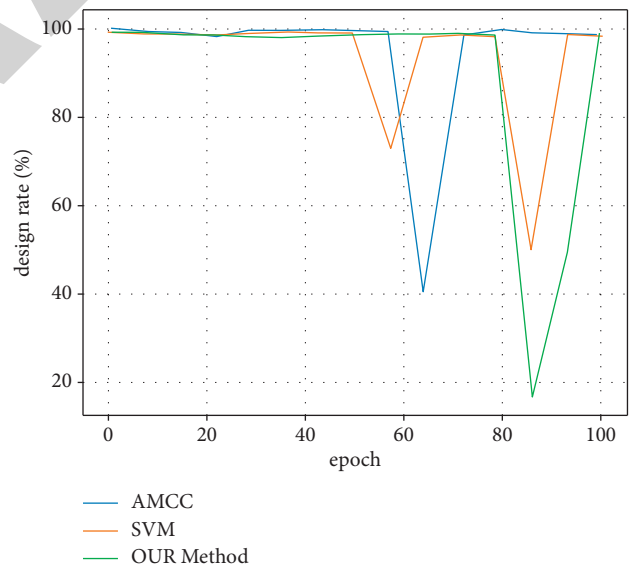


FIGURE 6: Comparison of animation design rates.

model can effectively sample the conditional probability distribution of feature layer and class label data for semantic discriminative effect.

In terms of space storage efficiency, the AMCC algorithm needs to store the entire training set and build codeword templates for different classes of animation sequences, so the space occupation rate is large. In contrast, the depth model built in this paper only needs 2 sets of finite

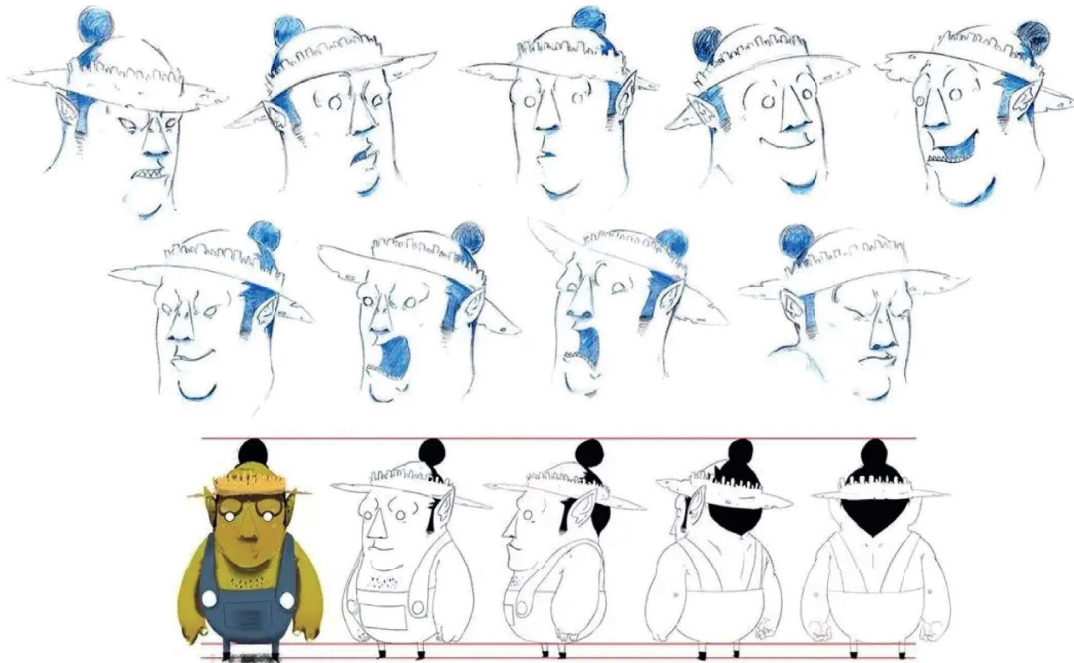


FIGURE 7: Animation design process.



FIGURE 8: Animated character design.

parameters (1 set for each layer) to represent the sequence pose, and only some training samples are needed to learn the model parameters, so the storage space is relatively small. Therefore, the algorithm in this paper is suitable for the learning and modeling work of large data volume animation sequences. In terms of time efficiency, although the deep learning model established in this paper takes some time to learn the underlying features, once trained, the corresponding hidden units can be activated directly according to the model parameters and visible layer data, and the feature distribution of the current animation style can be obtained effectively. Therefore, the algorithm in this paper does not require additional similarity calculation, and in the MATLAB simulation environment, although the training time is long for 13 styles of animation, the recognition time is only

2.6 s. The speed of style recognition is comparable with existing algorithms, as shown in Figure 6.

5. Interactive Animation Design

In interactive animation design, the meaning of fast and slow rhythm is mostly reflected in the process of interactive experience. A fast rhythm can give immediate feedback to younger children. When children select options through the interactive buttons, as shown in Figure 7, the interactive buttons should change color and play corresponding music in an instant; for example, the button turns green with a celebratory tone when correct, and the mobile device vibrates and the button turns red when wrong. The immediate error feedback will provide a kind of error warning to the

younger children so that they can form a psychological gap and pay attention to the subsequent case explanation.

From Figure 8, it can be seen that Dynamic algorithm and this paper's algorithm each have advantages in different styles of animation design. Dyneme vector-based recognition algorithm is weaker in the four animation styles of jump, lie, sit, and stand, because the algorithm does not sufficiently consider the backward and forward timing relationship, such as sitting on the ground and standing up from the ground are inverse animations, but their forward difference vectors are similar to each other. The algorithm in this paper overcomes this drawback by using the past frame cell layer and the current frame cell layer in the visible layer, but the shortcoming is that RBM has transfer invariance, which leads to interference in recognizing animation styles like deposit (picking something up from the ground), jog (running in place), rotate (rotating both arms), and so on, where the animation joint changes are similar but the joint positions are different. Interactive animation design should also anticipate in advance, using the platform's error record to analyze the error-prone content of younger children and insert.

6. Conclusion

In order to meet the demand for spatio-temporal feature representation in human animation design, this paper adopts the two-layer RBM algorithm for animation feature representation and style recognition. The experimental results show that RBM has very good advantages in feature extraction and can extract more discriminative spatio-temporal features of animation sequences after adding autoregressive model constraints; meanwhile, it can achieve very good style recognition effect after introducing Boltzmann machine discriminative model, but the algorithm also has certain shortcomings, mainly because the number of neurons of its deep learning model is difficult to be determined well. Animators can create a moderate risky situation in the interactive animation design. Young children are under the care and attention of parents and lack of emotional catharsis, which leads them to subconsciously like to take risks. Therefore, moderate increase of adventure elements can stimulate their interest and let their playful emotional needs be satisfied put.

Data Availability

The experimental data used to support the findings of this study are available from the corresponding author upon request.

Conflicts of Interest

The authors declare that they have no conflicts of interest regarding the publication of this work.

Acknowledgments

This study was supported by Research on Art Design Education under the Interaction of Art and Technology (no. JAS21104).

References

- [1] J. Zhao, "Research on 3D animation processing technology in modern art design system," in *Journal of Physics: Conference Series*, vol. 1856, no. 1, IOP Publishing, Article ID 01205, 2021.
- [2] J. M. Bern, K.-H. Chang, and S. Coros, "Interactive design of animated plushies," *ACM Transactions on Graphics*, vol. 36, no. 4, pp. 1–11, 2017.
- [3] S. Iizuka, Y. Endo, J. Mitani, Y. Kanamori, and Y. Fukui, "An interactive design system for pop-up cards with a physical simulation," *The Visual Computer*, vol. 27, no. 6–8, pp. 605–612, 2011.
- [4] Z. B. Wang, S. K. Ong, and A. Y. C. Nee, "Augmented reality aided interactive manual assembly design," *International Journal of Advanced Manufacturing Technology*, vol. 69, no. 5–8, pp. 1311–1321, 2013.
- [5] V. Megaro, B. Thomaszewski, M. Nitti, O. Hilliges, M. Gross, and S. Coros, "Interactive design of 3d-printable robotic creatures," *ACM Transactions on Graphics*, vol. 34, no. 6, pp. 1–9, 2015.
- [6] S. Gibet, N. Courty, K. Duarte, and T. L. Naour, "The SignCom system for data-driven animation of interactive virtual signers," *ACM Transactions on Interactive Intelligent Systems*, vol. 1, no. 1, pp. 1–23, 2011.
- [7] Y. Meng, P. Y. Mok, and X. Jin, "Interactive virtual try-on clothing design systems," *Computer-Aided Design*, vol. 42, no. 4, pp. 310–321, 2010.
- [8] S. Coros, B. Thomaszewski, G. Noris et al., "Computational design of mechanical characters," *ACM Transactions on Graphics*, vol. 32, no. 4, pp. 1–12, 2013.
- [9] M. G. Violante and E. Vezzetti, "Virtual interactive e-learning application: an evaluation of the student satisfaction," *Computer Applications in Engineering Education*, vol. 23, no. 1, pp. 72–91, 2015.
- [10] X. I. E. Tao, C. Zhang, and Y. Xu, "Collaborative parameter update based on average variance reduction of historical gradients[J]," *Journal of Electronics and Information Technology*, vol. 43, no. 4, pp. 956–964, 2021.
- [11] Z. Zhengwan, Z. Chunjiang, L. Hongbing, and X. Tao, "Multipath transmission selection algorithm based on immune connectivity model," *Journal of Computer Applications*, vol. 40, no. 12, p. 3571, 2020.
- [12] G. P. Lu, G. H. Xue, and Z. Chen, "Design and implementation of virtual interactive scene based on unity 3D," *Advanced Materials Research*, vol. 317–319, pp. 2162–2167, 2011.
- [13] J. Goedert, Y. Cho, M. Subramaniam, H. Guo, and L. Xiao, "A framework for virtual interactive construction education (VICE)," *Automation in Construction*, vol. 20, no. 1, pp. 76–87, 2011.
- [14] Q. Wu, P. Boulanger, M. Kazakevich, and R. Taylor, "A real-time performance system for virtual theater," in *Proceedings of the 2010 ACM Workshop on Surreal media and Virtual Cloning*, pp. 3–8, 2010 October.
- [15] J. Li, Z. Zhou, J. Wu et al., "Decentralized on-demand energy supply for blockchain in internet of things: a microgrids approach," *IEEE Transactions on Computational Social Systems*, vol. 6, no. 6, pp. 1395–1406, 2019.
- [16] W. Duan, J. Gu, M. Wen, G. Zhang, Y. Ji, and S. Mumtaz, "Emerging Technologies for 5G-IoV Networks: Applications, Trends and Opportunities," *IEEE Network*, vol. 34.
- [17] R. Ali, M. Hameed Siddiqi, and S. Lee, "Rough set-based approaches for discretization: a compact review," *Artificial Intelligence Review*, vol. 44, no. 2, pp. 235–263, 2015.

Retraction

Retracted: Analysis and Prediction of Corporate Finance and Exchange Rate Correlation Based on Machine Learning Algorithms

Computational Intelligence and Neuroscience

Received 3 October 2023; Accepted 3 October 2023; Published 4 October 2023

Copyright © 2023 Computational Intelligence and Neuroscience. This is an open access article distributed under the Creative Commons Attribution License, which permits unrestricted use, distribution, and reproduction in any medium, provided the original work is properly cited.

This article has been retracted by Hindawi following an investigation undertaken by the publisher [1]. This investigation has uncovered evidence of one or more of the following indicators of systematic manipulation of the publication process:

- (1) Discrepancies in scope
- (2) Discrepancies in the description of the research reported
- (3) Discrepancies between the availability of data and the research described
- (4) Inappropriate citations
- (5) Incoherent, meaningless and/or irrelevant content included in the article
- (6) Peer-review manipulation

The presence of these indicators undermines our confidence in the integrity of the article's content and we cannot, therefore, vouch for its reliability. Please note that this notice is intended solely to alert readers that the content of this article is unreliable. We have not investigated whether authors were aware of or involved in the systematic manipulation of the publication process.

Wiley and Hindawi regrets that the usual quality checks did not identify these issues before publication and have since put additional measures in place to safeguard research integrity.

We wish to credit our own Research Integrity and Research Publishing teams and anonymous and named external researchers and research integrity experts for contributing to this investigation.

The corresponding author, as the representative of all authors, has been given the opportunity to register their agreement or disagreement to this retraction. We have kept a record of any response received.

References

- [1] K. Zhang, X. Wang, J. Wang, S. Wang, and F. Hui, "Analysis and Prediction of Corporate Finance and Exchange Rate Correlation Based on Machine Learning Algorithms," *Computational Intelligence and Neuroscience*, vol. 2022, Article ID 2850604, 9 pages, 2022.

Research Article

Analysis and Prediction of Corporate Finance and Exchange Rate Correlation Based on Machine Learning Algorithms

Ke Zhang,¹ Xiaofei Wang ,² Junjie Wang,³ Sinan Wang,⁴ and Feng Hui⁵

¹Guosen Securities Co Ltd, Shenzhen 518000, China

²Shanghai Lilith Technology Corporation, Shanghai 200030, China

³Huafu Securities Co Ltd, Hangzhou 310000, China

⁴Kaiyuan Securities Co Ltd, Xi'an 710000, China

⁵Xigema Certified Public Accountants (Special Ordinary Partnership), Xi'an 710024, China

Correspondence should be addressed to Xiaofei Wang; xiaofeiwang7@njust.edu.cn

Received 1 April 2022; Accepted 4 June 2022; Published 24 June 2022

Academic Editor: Le Sun

Copyright © 2022 Ke Zhang et al. This is an open access article distributed under the Creative Commons Attribution License, which permits unrestricted use, distribution, and reproduction in any medium, provided the original work is properly cited.

Based on the risk management of exposure to foreign exchange assets and liabilities and the application of financial derivatives, this paper provides an in-depth analysis of the financial and exchange rate risks of foreign-funded enterprises. Therefore, a method of evaluating the financial performance of listed financial enterprises based on principal component analysis and neural network model is proposed. First, principal components of alternative financial performance input-output indicators are extracted using principal component analysis. Subsequently, these principal components are used as input-output data for the DEA model to derive the relative validity evaluation results of the financial performance of individual financial enterprises and to provide a reference for decision making to improve the financial performance level of financial enterprises. Combined with the economic business data of the enterprises, an empirical test on exchange rate risk management is conducted and relevant suggestions are made on how foreign enterprises can reduce exchange rate risk losses. It has important theoretical value and practical significance for enterprise finance and exchange rate management.

1. Introduction

For a longer period of time in the future, it will also be difficult for the RMB to become a freely convertible currency on a global scale [1]. Moreover, on a global scale, as the world economy continues to develop, buyers dominate the trade market, which means that “in the settlement of foreign trade exports” [2]. Therefore, against the backdrop of the expected appreciation of the RMB, Chinese enterprises in a passive position are bound to face huge exchange rate risk losses [3]. As the manager of a company, whether the accountant is proficient in financial management will determine the future survival and development of foreign companies [4].

Financial accountants should be actively involved in the signing of foreign trade contracts, and the exchange rate should be taken into account to provide for a mutually acceptable risk ratio as an additional clause in the contract [5]. As foreign trade is a matter of bilateral transactions, both

parties to the transaction wish to reduce the exchange rate risk, and therefore, the choice of currency of denomination is likely to be contradictory [6]. The compromise options available to both parties to foreign trade are the party with the favourable currency of denomination is required to offer other concessions to the party with the unfavourable currency; a mix of soft and hard currencies for denomination, with both parties sharing the risk; and if both parties hold mutual claims and debts, the same currency may be chosen for denomination [7]. Although Chinese foreign companies are in a passive position in the international trade market, if accountants are able to take advantage of favourable contractual terms, they will be able to reduce their exchange rate risk losses to a large extent. As the financial manager of an enterprise, the accountant must not only be proficient in financial accounting but also, and more importantly, be knowledgeable and up-to-date with the relevant knowledge of international trade contract regulations. In the

negotiation of foreign trade contracts, accountants should grasp the elements of the contract terms and conditions and strive to achieve “watertightness” [8].

The use of the buy-sell position balancing method does not aim to completely eliminate foreign exchange risk [9] but to minimise foreign exchange risk losses. Enterprises can achieve a certain degree of balance in their buying and selling positions by adjusting the timing of export receipts and import payments and foreign exchange loan repayments [10]. The buy-sell position balancing method is the most basic method of foreign exchange risk management, and it is also the most effective and lowest cost method; therefore, in foreign exchange risk management, enterprises should first choose this method [11]. Cross-compensation risk refers to the cross-balancing of two different foreign exchange buying and selling positions to hedge foreign exchange risk. For example, if the Hong Kong dollar is linked to the US dollar, the two currencies can be cross-balanced. Cross-balancing risk is a low-cost method of managing foreign exchange risk, whereby companies first balance their buying and selling positions in the same currency and then seek to cross-balance their buying and selling positions [12].

Whether it is a financial enterprise or an enterprise performance evaluation, related research has made some progress, but on how to establish a financial performance indicator system reflecting the financial management level of financial enterprises and how to judge the level of financial performance, these studies are still relatively few. In view of this, this paper integrates the advantages of principal component analysis and data envelopment methods in dealing with the comprehensive evaluation of multiple indicators and proposes a financial performance evaluation method based on PCA-DEA for financial enterprises. Firstly, on the basis of comparing existing studies on financial performance evaluation index systems, principal component analysis is applied to preprocess alternative input-output indicators, i.e., to distil numerous input-output indicators into a few principal components with clear practical significance. Subsequently, these principal components are used as input-output data for the DEA model to derive the relative effectiveness evaluation results of the financial performance of each financial enterprise, which provides a reference for decision making to improve the financial performance level of financial enterprises.

2. Related Work

With the gradual acceleration of China’s economic restructuring, competition in the financial sector is becoming increasingly fierce and the rapid development of financial enterprises depends to a large extent on the level of their financial performance. Therefore, an effective evaluation of the financial performance of financial enterprises can provide a basis for decision making by decision makers and stakeholders and also create new value for the system and promote its healthy development.

Financial enterprises are characterised by high risk and high debt, and if problems arise, they will have a huge impact on the overall operation of the Chinese economy,

therefore, relevant research on financial enterprises has been a hot spot for scholars to focus on. The study in [13] constructed an index system and model for evaluating the symbiotic capacity of financial enterprise clusters, discussed the important factors affecting the symbiotic capacity of financial enterprise clusters; pointing out the direction for the development of financial enterprise clusters in China, the study in [14] constructing a support vector machine-based approach for the measurement of financial instruments and internal accounting control efficiency, which provides a new way for quantitative analysis and evaluation of internal accounting control efficiency of financial enterprises. In order to reduce the technological risk of Chinese financial enterprises, the study in [15] used a fuzzy comprehensive evaluation method to measure the degree of technological innovation risk of Chinese financial enterprises and obtain the risk weights of technological innovation risk provides a decision support for Chinese financial enterprises to carry out technological innovation management [16]. In order to verify whether there is a dynamic relationship between listed financial enterprises and the national macro economy, the study in [17] constructed three dynamic effect models to confirm that the effective introduction of monetary policy can play a significant role in the performance development of listed financial enterprises and provided a basis for the implementation of financial policies in China [18]. The results showed that the two were negatively correlated, and the higher the level of noninternationalisation of financial firms, the greater the negative impact of the degree of internationalisation on performance.

The evaluation of financial performance, which can reflect the operation of enterprises, has been the focus of scholars’ attention, and there are many relevant research results [17] that constructed a set of enterprise value evaluation index system based on the enterprise performance evaluation index system and conducted empirical research using grey clustering hair [18]. Based on the enterprise performance evaluation system promulgated by the Ministry of Finance, the hierarchical analysis method and correlation analysis method were used to evaluate the financial performance of Chinese real estate listed companies. Although these methods can achieve certain results, some evaluation models are not ideal, such as AHP, expert scoring, and other qualitative methods, and are highly subjective and cannot dynamically reflect the change pattern of financial performance data.

3. Corporate Financial Performance Indicator System

3.1. Sample Data. This paper mainly takes the listed financial enterprises in Shanghai and Shenzhen as the research sample, selects a total of 37 listed financial enterprises in the two cities, collects and collates the data of these listed financial enterprises that have passed the annual audit report in the CSMAR database in 2015, and selects the relevant data of the publicly disclosed financial indicators in the financial statements.

3.2. Selection of Indicators. This paper takes financial enterprises as the research subject, and the Ministry of Finance promulgated the measures for evaluating the performance of financial enterprises in 2016, which stipulates that the four dimensions of profitability, operating growth, asset quality, and solvency are required in evaluating the performance of financial enterprises. Therefore, based on these four dimensions and drawing on the financial indicator system constructed in the literature [18], this paper selects 26 common indicators that can measure the financial performance of listed financial enterprises at multiple levels and from multiple perspectives.

Due to the large number of financial indicators and the correlation between them, it is necessary to select the indicators that can best reflect the performance from many indicators. At the present stage, the most commonly used methods for selecting financial performance indicators are the expert consultation method and the hierarchical analysis method, but the evaluation results of these two methods are affected by the structure and number of experts and are highly subjective. Therefore, based on the existing research, this paper uses solvency and asset quality as input indicators and operational growth and profitability as output indicators. In particular, solvency reflects the level of debt burden, the ability to repay various debts and the debt risk faced by financial enterprises; asset quality reflects the efficiency of financial enterprises in utilising their operating assets, asset safety, and management level; operational growth reflects the level of operational growth and capital preservation and appreciation of financial enterprises; profitability reflects the quality of profitability and the level of input and output of financial enterprises within a certain period of time. The specific indicators are shown in Table 1.

The abovementioned indicator system evaluates the financial performance of financial enterprises from several aspects. Although it satisfies the principles of scientificity and diversity in establishing an indicator system, it does not meet the principles of streamlining and feasibility, especially the rules of DEA for input-output indicators.

To solve these problems, the following will use principal component analysis to perform dimensionality reduction in order to reduce the number of dimensions of these financial performance input and output indicators and to find from them the uncorrelated principal components that reflect the main information and subsequently use the values of the principal components as the original input-output variables for DEA model analysis.

3.3. PCA Treatment of Alternative Input Indicators. A factor analysis of the alternative input indicators gives a KMO value of 0.574 (greater than 0.5) and a chi-square statistic significance level of 0.000 after Bartlett's test, which implies that there are common factors among the input indicators and that they are suitable for factor analysis. In terms of the

amount of variance explained, the cumulative variance contribution of the five main components FAC1, FAC2, FAC3, FAC4, and FAC5 selected in the paper was 78.231%. Factor rotation was then performed using the variance maximisation method, and the results are shown in Table 2.

As can be seen from the factor loading matrix, the principal component FAC1 mainly contains information on two indicators, namely, accounts receivable to revenue ratio and accounts receivable to turnover days, reflecting the efficiency of capital recovery of financial enterprises; the principal component FAC2 mainly contains information on four indicators, namely, gearing ratio, net cash flow from operating activities/liabilities, operating debt ratio, and total asset turnover ratio, reflecting the level of indebtedness, riskiness, and ability to repay principal and interest on debt of financial enterprises; the principal component FAC3 mainly contains information on three indicators, namely, long-term capital indebtedness ratio, financial debt ratio, and return on investment, reflecting the long-term capital structure of financial enterprises and their ability to absorb savings; the principal component FAC4 mainly contains information on four indicators, namely, cash assets ratio, fixed assets ratio, consolidated leverage, and return on long-term capital, reflecting the liquidity of financial enterprises, the efficiency of asset utilisation, the impact of changes in sales volume on earnings per share, and the ability of capital profitability; the principal component FAC5 contains information on two indicators, namely, equity multiplier and accounts receivable turnover ratio, reflecting the ability of financial enterprises to achieve financial leverage and liquidity turnover speed.

3.4. PCA Treatment of Alternative Output Indicators. Similarly, a factor analysis of the alternative output indicators gives a KMO value of 0.573 (greater than 0.5) and a chi-square statistic significance level of 0.000 after Bartlett's test, which implies that there are common factors among the output indicators that are suitable for factor analysis. In terms of the amount of variance explained, the cumulative variance contribution of the four principal components FAC1, FAC2, FAC3, and FAC4 selected in the paper was 88.354%. Subsequently, the factor rotation was performed using the variance maximisation method, and the results are shown in Table 3.

As can be seen from the factor loading matrix, the principal component FAC1 contains information on five indicators, namely, the growth rate of total assets, the growth rate of net profit, the growth rate of comprehensive income, the net operating margin, and the growth rate of return on net assets, reflecting the growth scale of financial enterprises' assets, operating results, operating income to generate net profit, and profitability and growth capacity; the principal component FAC2 contains information on three indicators, namely, capital preservation and appreciation rate, return on assets (ROA), and net profit margin on total assets ,

TABLE 1: Financial performance evaluation indicator system for financial enterprises.

Input index	Name	Symbol	Output indicators	Name	Symbol
Solvency	Asset liability ratio	X1	Business growth	Rate of capital accumulation	Y1
	Net cash flow from operating activities/liabilities	X2		Growth rate of total assets	Y2
	Operating debt ratio	X3		Net profit growth rate	Y3
	Financial liability ratio	X4	Profitability	Growth rate of comprehensive income	Y4
	Equity multiplier	X5		Sustainable growth rate	Y5
		X6		Return on assets	Y6
Asset quality	Cash asset ratio	X7	Profit margin on total assets (ROA)	Profit margin on total assets (ROA)	Y7
	Fixed assets ratio	X8		Return on net assets	Y8
	Integrated lever	X9		Operating net interest rate	Y9
	Ratio of accounts receivable to income	X10	Return on net assets growth rate	Total operating cost rate	Y10
	Days sales outstanding	X11		Return on net assets growth rate	Y11
	Total asset turnover	X12			
	Long term return on capital	X13			
	Return on investment	X14			
	Accounts receivable turnover	X15			

TABLE 2: Factor loading matrix for input indicators after orthogonal rotation.

Input indicators	Component				
	FAC1	FAC2	FAC3	FAC4	FAC5
Asset liability ratio	0.224	-0.741	-0.417	-0.174	-0.111
Long term capital liability ratio	0.049	0.075	0.974	-0.017	0.014
Net cash flow from operating activities/liabilities	-0.214	0.551	-0.044	0.357	0.471
Operating debt ratio	0.157	0.921	0.063	-0.17	-0.037
Financial liability ratio	-0.042	0.047	0.978	-0.067	0.054
Equity multiplier	0.197	-0.154	-0.287	0.247	-0.700
Cash asset ratio	-0.557	0.084	-0.063	0.714	0.247
Fixed assets ratio	-0.039	0.165	-0.224	-0.778	0.247
Integrated lever	0.178	-0.367	0.318	-0.687	-0.113
Ratio of accounts receivable to income	0.947	-0.196	-0.182	-0.047	-0.032
Days sales outstanding	0.924	-0.0203	-0.195	-0.062	-0.047
Total asset turnover	-0.387	0.789	-0.082	0.058	0.035
Long term return on capital	-0.437	-0.051	-0.247	0.662	0.017
Return on investment	-0.388	-0.043	-0.097	0.150	-0.208
Accounts receivable turnover	0.245	-0.056	-0.112	0.178	0.768

TABLE 3: Factor loading matrix for output indicators after orthogonal rotation.

Input indicators	Component			
	FAC1	FAC2	FAC3	FAC4
Rate of capital accumulation	0.074	0.861	0.235	-0.167
Growth rate of total assets	0.793	0.247	0.387	-0.094
Net profit growth rate	0.748	0.557	0.192	0.167
Growth rate of comprehensive income	0.857	-0.025	0.338	-0.036
Sustainable growth rate	0.339	0.154	0.871	0.033
Return on assets	0.196	0.952	0.146	-0.070
Total assets net profit margin (ROA)	0.193	0.951	0.157	-0.065
Return on net assets	0.062	0.472	0.834	-0.176
Total operating cost rate	0.038	-0.154	-0.095	0.939
Return on net assets growth rate	0.847	0.080	0.081	0.345

reflecting the operational efficiency and safety of financial enterprises' capital, the efficiency of asset utilisation, and profitability; FAC3 contains the relevant total operating utilization ratio, which reflects the use of human resources in

the financial sector; the principal component FAC4 contains information on the total operating cost ratio, which reflects the overall situation of the financial sector and the position of the financial enterprise in the industry, and provides a

comprehensive understanding of the financial situation of the enterprise.

4. Predictive Modelling Based on Deep Belief Networks

4.1. Deep Belief Network Model. As an efficient deep learning algorithm, deep belief networks have gradually developed into a mainstream technological direction. A random neural network Boltzmann machine model based on statistical principles was generated, containing an implicit layer and a visible layer, as shown in Figure 1.

On these basis, the principle framework of the restricted Boltzmann machine is proposed, as shown in Figure 2.

Where $a = (a_1, a_2, \dots, a_{n_v})^T \in \mathbb{R}^{n_v}$ denotes the bias vector of the visible layer, $b = (b_1, b_2, \dots, b_{n_h})^T \in \mathbb{R}^{n_h}$ denotes the bias vector of the hidden layer and $W = (w_{i,j}) \in \mathbb{R}^{n_h \times n_v}$ denotes the weight matrix between the hidden and visible layers.

The restricted Boltzmann machine introduces a series of related probability distribution functions through the energy function. For a given set of neurons the state vector (v, h) is represented by an energy function, as in

$$E(v, h | \theta) = - \sum_{i=1}^{n_v} a_i v_i - \sum_{j=1}^{n_h} b_j h_j - \sum_{i=1}^{n_v} \sum_{j=1}^{n_h} h_j w_{i,j} v_i, \quad (1)$$

where v denotes the state vector of neurons in the visible layer, h denotes the state vector of neurons in the hidden layer, n_v denotes the total number of all neurons in the visible layer, n_h denotes the total number of all neurons in the hidden layer, and $\theta = \{a_i, b_j, w_{i,j}\}$ denotes the conditioning factor limiting the Boltzmann machine architecture.

With the energy function defined in equation (1), the joint probability distribution of the state (v, h) can be obtained as in

$$P(v, h | \theta) = \frac{1}{Z(\theta)} e^{-E(v,h|\theta)}, \quad (2)$$

where $Z(\theta)$ expressions, as in

$$Z(\theta) = \sum_{v,h} e^{-E(v,h|\theta)}, \quad (3)$$

where $Z(\theta)$ denotes the normalisation parameter. Let $P(v|\theta)$ be the probability distribution of the visible layer vector v . This can be calculated by $p(v, h|\theta)$ the edge distribution for $P(v|\theta)$, as in

$$PP(v|\theta) = \sum_h P(v, h|\theta) = \frac{1}{Z(\theta)} \sum_h e^{-E(v,h|\theta)}. \quad (4)$$

In the same way, we can obtain the probability distribution of the hidden layer vector h $P(h|\theta)$ as in

$$P(h|\theta) = \sum_v P(v, h|\theta) = \frac{1}{Z(\theta)} \sum_v e^{-E(v,h|\theta)}. \quad (5)$$

By analysing equations (4) and (5), it can be seen that in order to obtain $P(v|\theta)$ and $P(h|\theta)$, the key step is to calculate

the normalisation parameter $Z(\theta)$. However, equation (5) shows that its computational complexity is high. However, due to the special principle that restricts the Boltzmann machine model (the visible and hidden layers are conditionally independent), the probability of a neural unit being activated in the hidden layer can be calculated by equation (6) when the states of all neurons in the visible layer are known.

$$P(h_j = 1 | v, \theta) = \sigma \left(b_j + \sum_i v_i w_{i,j} \right), \quad (6)$$

where $\sigma(-)$ denotes the sigmoid activation function.

Because all neural nodes within the same layer are connectionless with each other, the relationship between the values taken by all neural nodes within the same layer and the values taken by a single node is as in

$$P(h|v) = \prod_{j=1}^{n_h} P(h_j | v), \quad (7)$$

$$P(v|h) = \prod_{i=1}^{n_v} P(v_i | h). \quad (8)$$

A randomized gradient algorithm is usually used to find the maximum value of $\sum_{i=1}^i \log P(v^{(i)}|\theta)$ in order to obtain the optimal conditioning factor θ in the network. A deep belief network model is used, as shown in Figure 3.

4.2. Deep Belief Network Training Process. The deep belief network training process is generally divided into 2 steps: a pretraining phase and a fine-tuning phase.

The loss function required for ageing in the fine-tuning phase is given in

$$L(x, y) = \|x - y\|_2^2, \quad (9)$$

where the symbol $\|\cdot\|_2$ denotes the 2-parameter reconstruction error, x denotes the input data, and y denotes the reconstructed data.

5. Corporate Financial Performance Evaluation Model

When the number of evaluation indicators increases to a certain level, it will not only increase the workload of the DEA model in data processing but also make the evaluation results meaningless due to the strong interrelationship between input and output indicators causing the validity of all decision units to be close. Therefore, in order to avoid the above problems, this paper proposes a combined evaluation model based on factor analysis and DEA to evaluate the financial performance of financial enterprises [21, 22].

Using the advantages of the PCA method in extracting the characteristics of indicators, the input and output data required by the DEA model are preprocessed, i.e., multiple indicators are synthesised into a few principal components that can cover their main information, in order to achieve

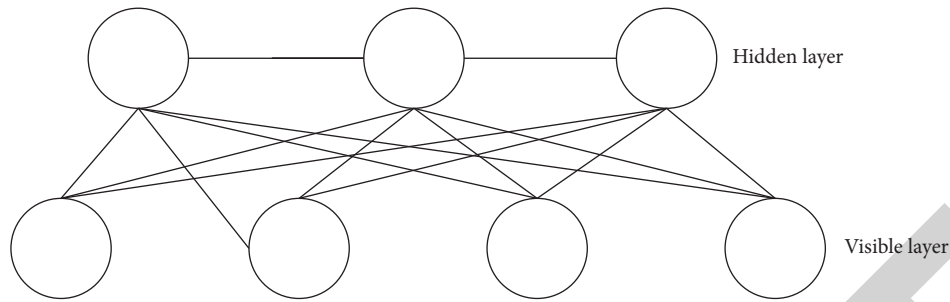


FIGURE 1: Boltzmann machine model.

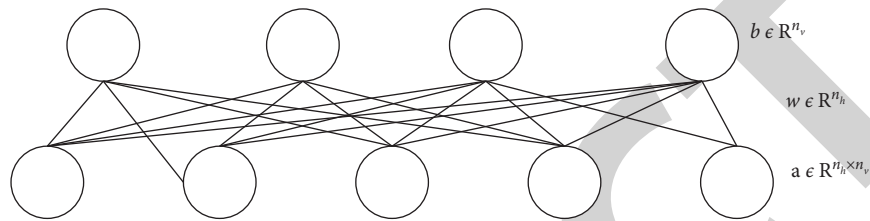


FIGURE 2: Restricted Boltzmann machine model.

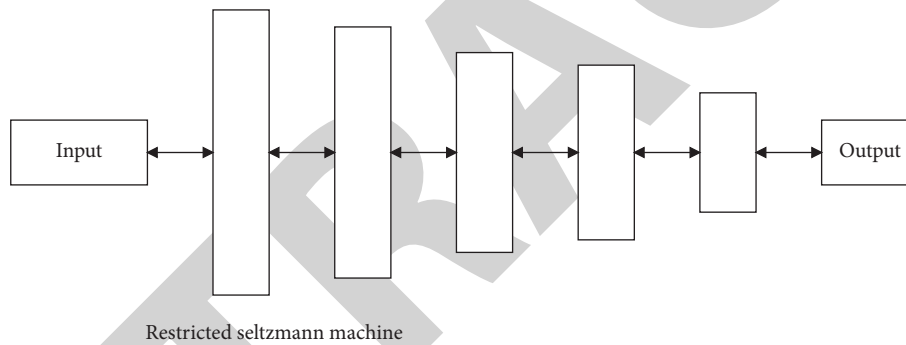


FIGURE 3: Depth generation model.

the purpose of dimensionality reduction of the indicators [23].

The processed input and output indicators are fed into the DEA model in order to calculate the relative efficiency of the financial performance of financial enterprises. This not only retains the complete information of each indicator but also reduces the degree of correlation between indicators, while satisfying the requirements of the DEA model, so that the model can adequately evaluate the relative effectiveness of the decision-making unit and ensure the accuracy and scientificity of the results. The process is shown in Figure 4.

6. Evaluating Model Validity Tests

As some of the principal components obtained above have negative values, they do not meet the DEA model's requirement of positive values for the input and output variables. Therefore, the principal components obtained in the above section were normalised to obtain new input and output data, which were fed into the DEA model to obtain the results, as shown in Table 4.

Technical efficiency can measure an enterprise's ability to allocate resources and its ability to use resources efficiently in

many ways and evaluate whether its industrial structure is in line with the overall requirements to enable the enterprise to maximise its economic efficiency. On the whole, these 37 listed financial enterprises operate well in terms of input-output efficiency in terms of financial performance, with an average value of 0.883 for technical efficiency, indicating that these listed financial enterprises have good capabilities in terms of capital allocation and efficiency of use.

As can be seen from Table 4, there are 24 financial enterprises with all three efficiency values of 1, accounting for 64.9% of the total sample, which are on the DEA efficiency frontier, indicating that these 24 financial enterprises are relatively efficient, achieving "maximum output with existing inputs" and "minimum input on top of existing output." The remaining 13 financial enterprises have achieved the best efficiency in terms of capital allocation and utilisation, with no waste of input resources and no shortfall in output. The technical efficiency of the remaining 13 financial firms ranged from 0.2 to 0.9, accounting for 35.1% of the total sample, indicating that the DEA of these financial firms was ineffective, with the dual problems of inefficient capital allocation and low capital efficiency. There are two main reasons for this: firstly, technical efficiency is 1 and

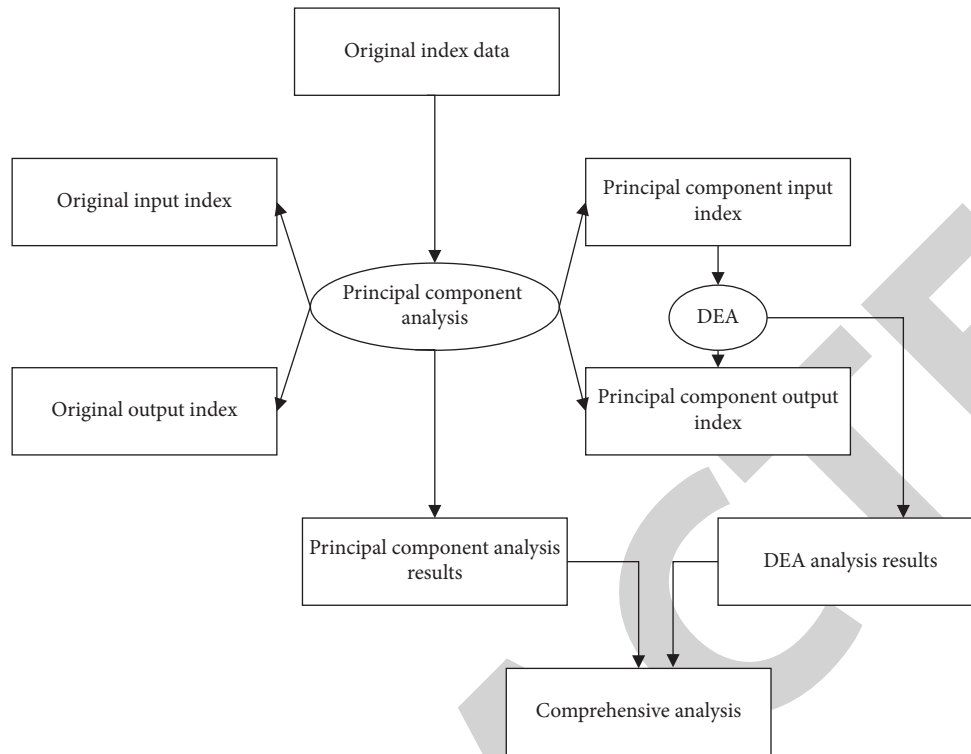


FIGURE 4: Financial performance evaluation process of the financial companies based on PCA and DEA.

scale efficiency is ineffective. For example, DUM19 technical efficiency is 0.452, technical efficiency is 1, and scale efficiency is 0.452. If we want to make this firm DEA effective, we need to increase the scale of investment and adjust to scale, and we can achieve relative optimality after increasing scale efficiency. Second, neither pure technical efficiency nor scale efficiency is 1, but both are at the stage of increasing returns to scale, indicating that it is advantageous for these financial firms to expand their scale at this stage. For example, the technical efficiency of DUM2 is 0.433, the technical efficiency is 0.448, and the scale efficiency is 0.967, which are in the stage of increasing returns to scale. If you want to make this enterprise reach DEA effective, you can adjust the scale of investment to improve the technical efficiency, but you cannot ignore the improvement in technology, and you need to make comparative improvements in both financial efficiency and input scale of the enterprise in order to reach relative optimization [24].

In terms of the value of pure technical efficiency, its overall sample mean reached 0.954 and the pure technical efficiency of the sample was 30, accounting for 81% of the total sample. For the remaining seven financial enterprises with ineffective DEA, they need to upgrade their technology and increase the scale of inputs in order to achieve relative optimality. For example, DUM2 with a pure technical efficiency of 0.448 and a scale efficiency of 0.967 has a low financial efficiency mainly due to a low level of financial management and technical inputs. Therefore, for these financial companies with relatively low values of pure technical efficiency, the management should further improve the scientific nature of their operational and investment

decisions and focus on managing the returns and risks of their investment projects [25, 26].

There are three types of returns to scale: constant returns to scale, diminishing returns to scale, and increasing returns to scale. Production with constant returns to scale is generally the most efficient. Increasing returns to scale indicate that each additional unit of resource input produces greater than one unit of output, while the opposite is true for decreasing returns to scale. In terms of scale efficiency coming to a value, the sample mean is 0.918, which indicates that only 0.82% of resources are underutilised at scale.

In terms of returns to scale, all financial firms are at the stage of constant or increasing returns to scale, indicating the huge potential and prospects for the development of the financial sector, when financial firms continue to increase their capital investment, which can lead to increasing output, thus contributing to the rapid development of the financial system as a whole. Twenty-four financial firms have an efficiency of scale value of 1. They are in a state of constant returns to scale, and their use of resources and scale of inputs are optimal and do not need to be improved. The remaining 13 financial firms, all of which have an efficiency of scale value less than 1, are in a state of increasing returns to scale despite their inefficient scale. For these financial firms, their pure technical efficiency and scale efficiency are inefficient, and in order to reach optimality, improvements must be made in both the input and output efficiency of financial resources.

For the purpose of analysis, assume that a foreign-owned company, Company A, has the following economic operations:

TABLE 4: Results of the 2015 financial performance evaluation of the listed financial companies.

DMU	Technical efficiency	Pure technical efficiency	Scale efficiency	Returns to scale
1	1	1	1	Unchanged
2	0.434	0.449	0.968	Increasing
3	1	1	1	Unchanged
4	1	1	1	Unchanged
5	0.643	0.747	0.847	Increasing
6	0.936	1	0.924	Increasing
7	1	1	1	Unchanged
8	1	1	1	Unchanged
9	1	1	1	Unchanged
10	1	1	1	Unchanged
11	0.727	1	0.728	Increasing
12	1	1	1	Unchanged
13	1	1	1	Unchanged
14	0.877	0.987	0.887	Increasing
15	0.651	0.874	0.744	Increasing
16	1	1	1	Unchanged
17	1	1	1	Unchanged
18	1	1	1	Unchanged
19	0.452	0.879	0.749	Increasing
20	0.231	0.438	0.527	Increasing
21	0.958	1	0.987	Increasing
22	1	1	1	Unchanged
23	1	1	1	Unchanged
24	1	1	1	Unchanged
25	0.857	1	0.858	Increasing
26	1	1	1	Unchanged
27	1	1	1	Unchanged

1. On 4 January 2010, Company A enters into a trade contract with a foreign importer, Company B, which provides that over the next 12 months, with the 15th of each month being the shipment date, Company A will export to Company B goods valued at CNY72 million in 12 batches, with each batch being settled 60 days after the shipment date in the amount of CNY6 million.
2. On 5 January 2010, Company A launched a new domestic production line with a total project investment of CNY60 million, with an expected useful life of five years and a 30% increase in productivity, payable in 12 monthly instalments of CNY5 million from March 2010.
3. On 15 April 2010, Company A borrowed funds of CNY80 million from the Industrial and Commercial Bank of China to resolve its liquidity difficulties. Company A's foreign exchange exposure risk data (as shown in Table 5).

In the example above, the accountant did not apply any exchange rate risk management measures, and against the backdrop of a significant appreciation of the RMB, Company A, a foreign-owned company, suffered significant exchange rate risk losses. However, if the accountant had been able to use flexible foreign exchange exposure management, Company A's situation would have been different, as the price index CPI in China has been increasing since the

TABLE 5: Exposure data for Company A's foreign exchange exposure positions.

Date	Foreign exchange assets	Foreign exchange liabilities	Exchange rate	Open mouth
2010.01.15	USD6000000	2	6.8271	USD6000000
2010.02.15	USD6000000	1	6.8271	USD6000000
2010.03.15	USD6000000	2	6.8271	USD6000000
2010.04.15	USD6000000	2	6.8271	USD6000000
2010.05.15	USD6000000	5	6.8702	USD6000000
2010.06.15	USD6000000	4	6.8243	USD6000000
2010.07.15	USD6000000	4	6.7744	USD6000000
2010.08.15	USD6000000	6	6.8741	USD6000000
2010.09.15	USD6000000	6	6.5742	USD6000000
2010.10.15	USD6000000	5	6.4571	USD6000000
2010.11.15	USD6000000	6	6.5787	USD6000000
2010.12.15	USD6000000	8	6.5654	USD6000000

second half of 2010 and the central bank has adopted a tightening monetary policy, which means that the cost of financing for companies will increase. In contrast, due to the low economic boom in the United States, the Federal Reserve has adopted a quantitative easing monetary policy with lower lending rates in US dollars.

Therefore, Company A should choose a loan in US dollars to introduce advanced production lines from abroad and increase the rate of return of its project investment.

7. Conclusions

The rapid development of an enterprise depends largely on the level of its financial performance. An effective evaluation of its financial performance can create new value for the financial system continuously and promote the healthy development of the financial industry. This paper uses principal component analysis methods and data envelopment methods to conduct a comprehensive evaluation of the financial performance of the listed financial enterprises. While ensuring that the information on the indicators is retained intact, it can also provide a scientific and effective evaluation of the financial performance of financial enterprises and provide financial enterprises with the opportunity to make appropriate adjustments to their own resources or scale in order to achieve the optimal allocation of resources, thereby achieving an improvement in the overall financial performance level of financial enterprises.

Data Availability

The experimental data used to support the findings of this study are available from the corresponding author upon request.

Conflicts of Interest

The authors declare that they have no conflicts of interest regarding this work.

Research Article

Design and Optimisation of an Enterprise Digital Management System Based on IoT Monitoring

Shengwen Wang 

School of Business Administration, Shandong University of Finance and Economics, Jinan 250014, China

Correspondence should be addressed to Shengwen Wang; sw8258@mail.sdufe.edu.cn

Received 22 March 2022; Accepted 26 April 2022; Published 24 June 2022

Academic Editor: Le Sun

Copyright © 2022 Shengwen Wang. This is an open access article distributed under the Creative Commons Attribution License, which permits unrestricted use, distribution, and reproduction in any medium, provided the original work is properly cited.

Modern enterprise management is developing rapidly, and one of the most important components of enterprise management is enterprise digital management. In this paper, the research background of enterprise digital management system is firstly elaborated, current situation of enterprise digital management work in enterprises is elaborated, then the current situation of the system research and development at home and abroad is also analysed and outlined in detail, and finally, according to the actual enterprise digital management situation of enterprises, combined with the system method of software development and corresponding technology, the new system design requirements of enterprises based on Internet of Things are proposed. Simulations show that the overall design and module design of the system in this paper are well managed, a system interface diagram can be given, and the database table structure and entity class diagram are applied to elaborate the database design.

1. Introduction

Digital management is an important aspect of the management of modern enterprises, and the survival and development of enterprises is closely related to strengthening the protection of their digital resources [1]. Enterprises have been using traditional management methods for a long time, manually locating and retrieving digital files, and designing and printing hard copies of digital catalogues [2]. However, this traditional management approach requires human participation, leading to a variety of problems such as inefficiency and difficulty storing and securing documents [3]. In the course of an enterprise's daily operations, large numbers of digital documents are generated at all levels, and these documents all need to be archived [4]. The archiving of corporate documents is generally not undertaken in a timely manner. To meet the management requirements of modern enterprises, a digital enterprise management system should consist of six parts: scanning and entry, digital management, enquiry and statistics, loan management, approval management, and system management [5]. The rapid

development of Internet-based information technology systems has resulted in enterprises attaching increasing importance to digital information management [6]. The use of Internet technology is an important aspect of a digital information system, while the application of digital information resources provides support for the management and transformation of enterprises [7]. Therefore, it is necessary for each enterprise to build a digital management system that meets its specific requirements and enables it to keep up with the trend of increasing informatisation [8]. This study is based on the integration of the main activities of an enterprise with advanced management information system technology, and aims to improve the efficiency of enterprise management by designing a digital enterprise management system [9]. Based on the needs of enterprises, the digital enterprise management system is designed to facilitate information exchange and communication that overcomes problems such as poor information communication caused by inconvenient locations, incompetence, and operational distance, which can hinder the development of the enterprise [10, 11].

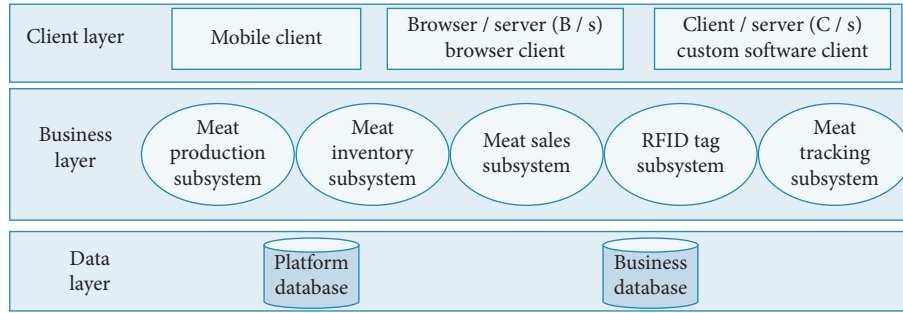


FIGURE 1: RFID-based enterprise digital management platform architecture.

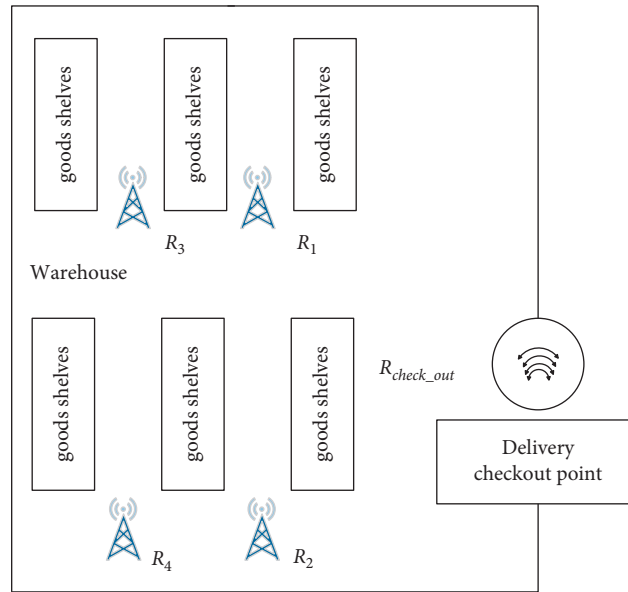


FIGURE 2: Layout of RFID readers in the sales centre warehouse.

2. RFID-Based Enterprise Digital Management Platform Architecture

The architecture of the RFID-based enterprise digital management platform is shown in Figure 1 and is divided into a data layer, a business layer, and a customer layer. The data layer includes the platform database and the business database. The platform database provides the operational data of the basic platform, and the business database provides the business data [11]. The business layer provides the main functions of the system, which mainly consists of five subsystems: RFID tag subsystem, enterprise production subsystem, enterprise inventory subsystem, enterprise sales subsystem, and enterprise tracking and tracing subsystem. The client layer provides the interface for users to use the system in different ways, mainly divided into mobile phone clients, browser clients under the browser/server (B/S) structure, and custom software clients under the client/server (C/S) structure. Users are divided into 3 main categories: consumers, administrators, and supervisors.

The EPC system is mainly responsible for the collection and filtering of RFID data from each subsystem node, which

is transmitted via the network to the respective remote PML database for processing such as storage and query.

The lifecycle of an enterprise, from slaughter to the consumer, can be divided into several stages: slaughter, processing, inventory, transport, sales, and consumption. To achieve enterprise tracking and tracing, it is necessary to identify, record, manage, and track the information in these stages to form a complete enterprise lifecycle information chain [12]. Among them, the enterprise information tracking and tracing in the slaughtering and processing stage has already been discussed in this paper. This paper focuses on the tracking and tracing of information in the sales phase of the enterprise.

2.1. Analysis of Corporate Sales Tracking Systems. In a radio frequency identification (RFID)-based information system environment, the volume of information is so large that efficient RFID event detection and processing is difficult to achieve using existing database and data management technologies [14]. This system uses the stand-alone synchronisation equipment (SASE) event language of complex

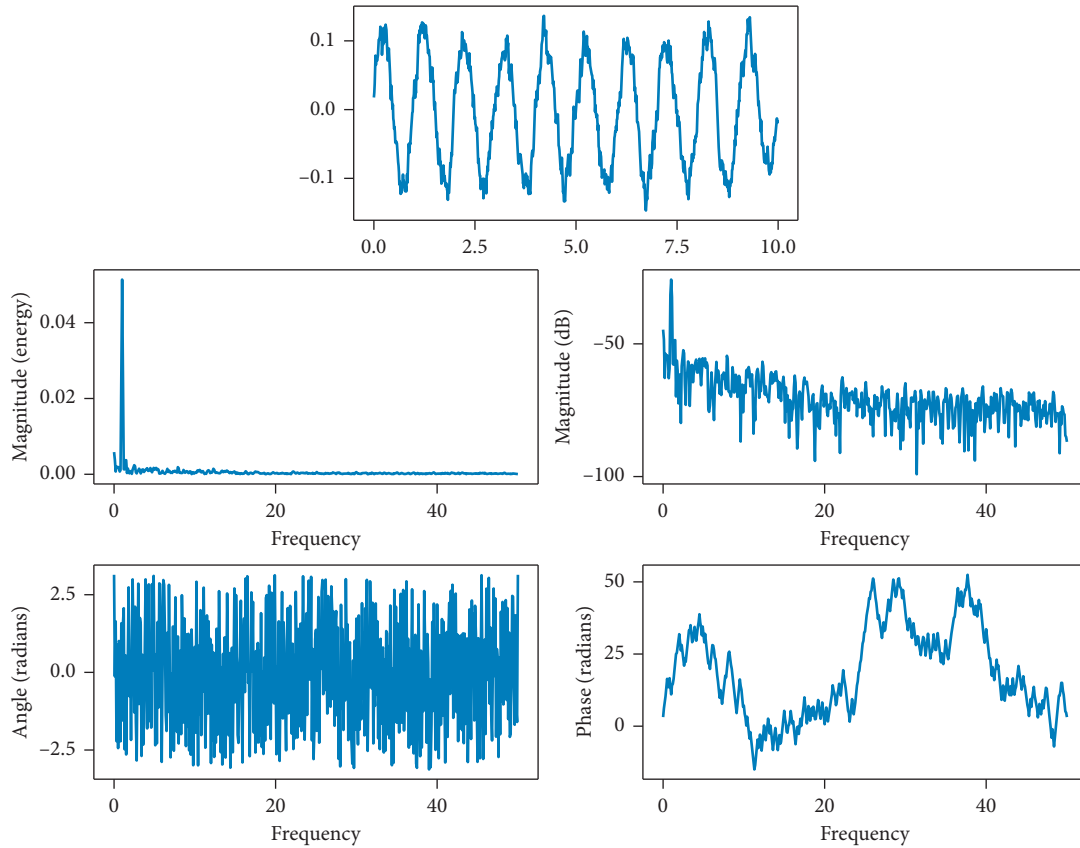


FIGURE 3: Frequency of use of different data information.

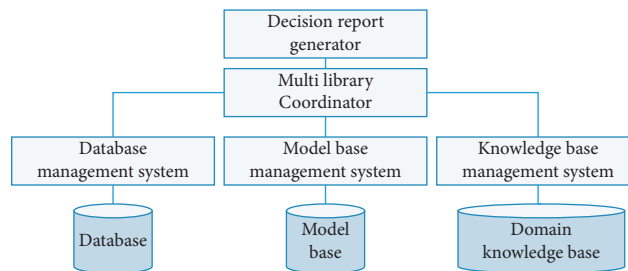


FIGURE 4: Overall structure of the decision support system.

event processing (CEP) technology to process the basic events formed by the filtered data [15]. CEP is an emerging technology for building and managing information systems [16]. CEP defines the basic information to be processed as events, which can be customised by the user, for example, as an event related to an operation in an enterprise application or as an event related to a data transfer on the network, depending on the user’s role and observation point [17]. There are various relationships between simple events, and multiple simple events can be combined to form a complex event. Further, multiple complex events can be combined to form a “more complex” event. The process of using CEP to analyse data is as follows. First, the layout of the RFID reader is designed based on the requirements of each node in the enterprise’s operations. Second, basic events are defined

based on the layout of the RFID reader. Finally, complex events are processed using the SASE event language [18, 19].

2.2. Operating mechanism of corporate sales tracking systems.

The following is an example of RFID data analysis of an enterprise’s inventory node to illustrate the process of RFID data analysis using CEP. 1) The enterprise’s regional sales centre is the main link in the circulation of the enterprise’s products and requires information about the enterprise’s sales, stock, and expired products. Based on an analysis of the functions required by the enterprise’s regional sales centre, it is clear that the information to be collected includes stock stored in the enterprise’s warehouse, sales through the regional sales centre, and expired stock in the enterprise’s

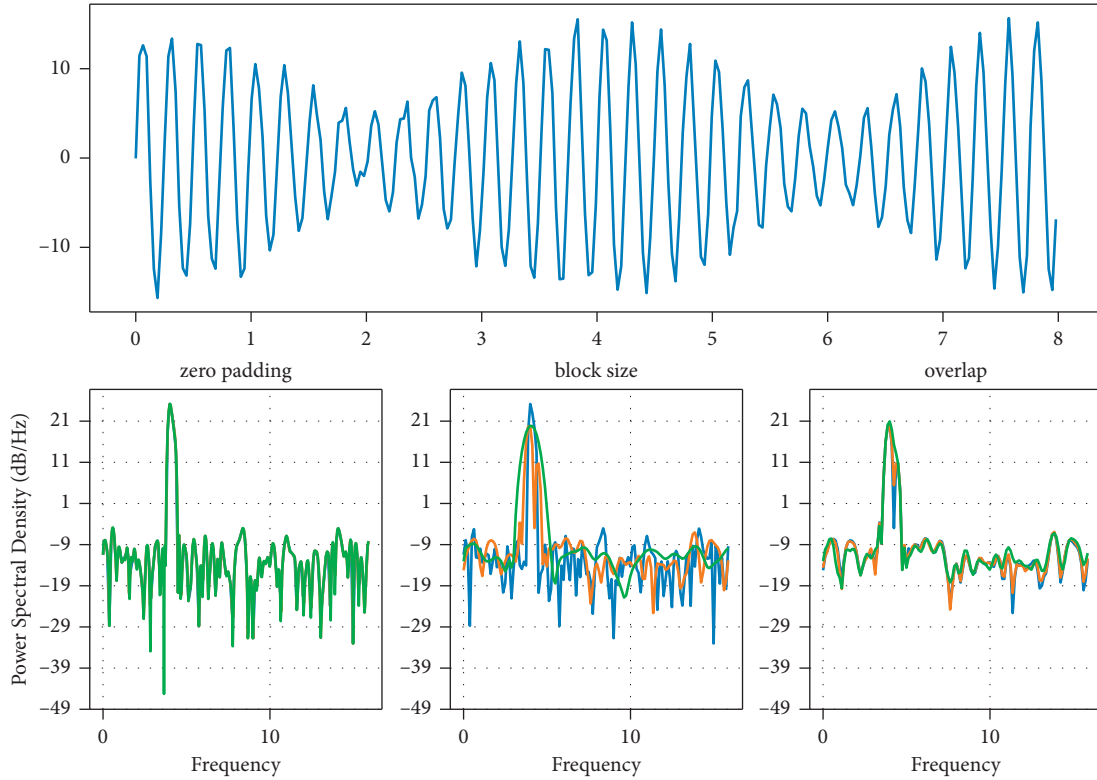


FIGURE 5: Effect of using company documents.

warehouse. Therefore, it is necessary to position RFID readers inside the warehouse, at the warehouse exit, and at the warehouse settlement point, as shown in Figure 2. 2). The three basic events in the warehouse inventory node are WAREHOUSE-READING, CHECK_OUT-READING, and EXIT-READING, where WAREHOUSE-READING represents the data from the RFID readers (R1, R2, R3, R4 in Figure 2) in the warehouse, CHECK_OUT-READING represents the data from the tags read by the checkout reader (Rcheck_out in Figure 2 when the enterprise ships stock, and EXIT-READING represents the data read by the warehouse exit reader (Rcheck_out in Figure 2 when the stock leaves the warehouse [20, 21] 3) Regarding the processing of complex events in the warehouse inventory node, the following is an example of how the SASE event language is processed. The complex event of enterprise sales is represented in the sales centre node model as follows. The stock arrives at the shipping checkout point and then arrives at the warehouse door, which is represented in the basic event set as a sequence of two basic events, CHECK_OUT-READING and EXIT-READING, and is completed within a defined time frame. When this complex event occurs, its EPC code and exit time are provided and this information is stored in the product exit table of the event database. In conjunction with the example shown in Figure 4, the complex event processing in relation to the sale of this stock involves checking that a label with the EPC code 86.0257A08.100167.20100608432 appears in sequence in the two basic events CHECK_OUT-READING and EXIT-READING with a time

interval of less than 1 h. If this is the case, the enterprise is considered to have completed the sale of the stock.

3. Establishment of Decision Support Systems

When the information accumulated by the system reaches a certain scale, advanced data mining technology can be used to intelligently identify information with potential utility from the data warehouse and provide decision support information to the leaders of relevant departments for the purpose of effective accident prevention. The system is designed with decision support interfaces included in both the data layer and the key service layer of the software. The decision support system is an independent subsystem, the overall structure of which is shown in Figure 3. The main functions of the decision support system are as follows. (1) Safety problem causation analysis for decision-making. The safety problem causation analysis decision support system assists managers in the analysis of the causes of safety problems and the assignment of responsibility for those problems. It analyses the internal and external environment in which safety problems arise, uses multidimensional analysis techniques to study the intrinsic connection of safety data, compares problems with similar problems that have occurred in the past, and completes a report on the causes of problems through human-computer interaction. (2) Accident prediction and decision-making. Predictive analysis is carried out using theories and methods such as fuzzy diagrams, grey systems, nonlinear

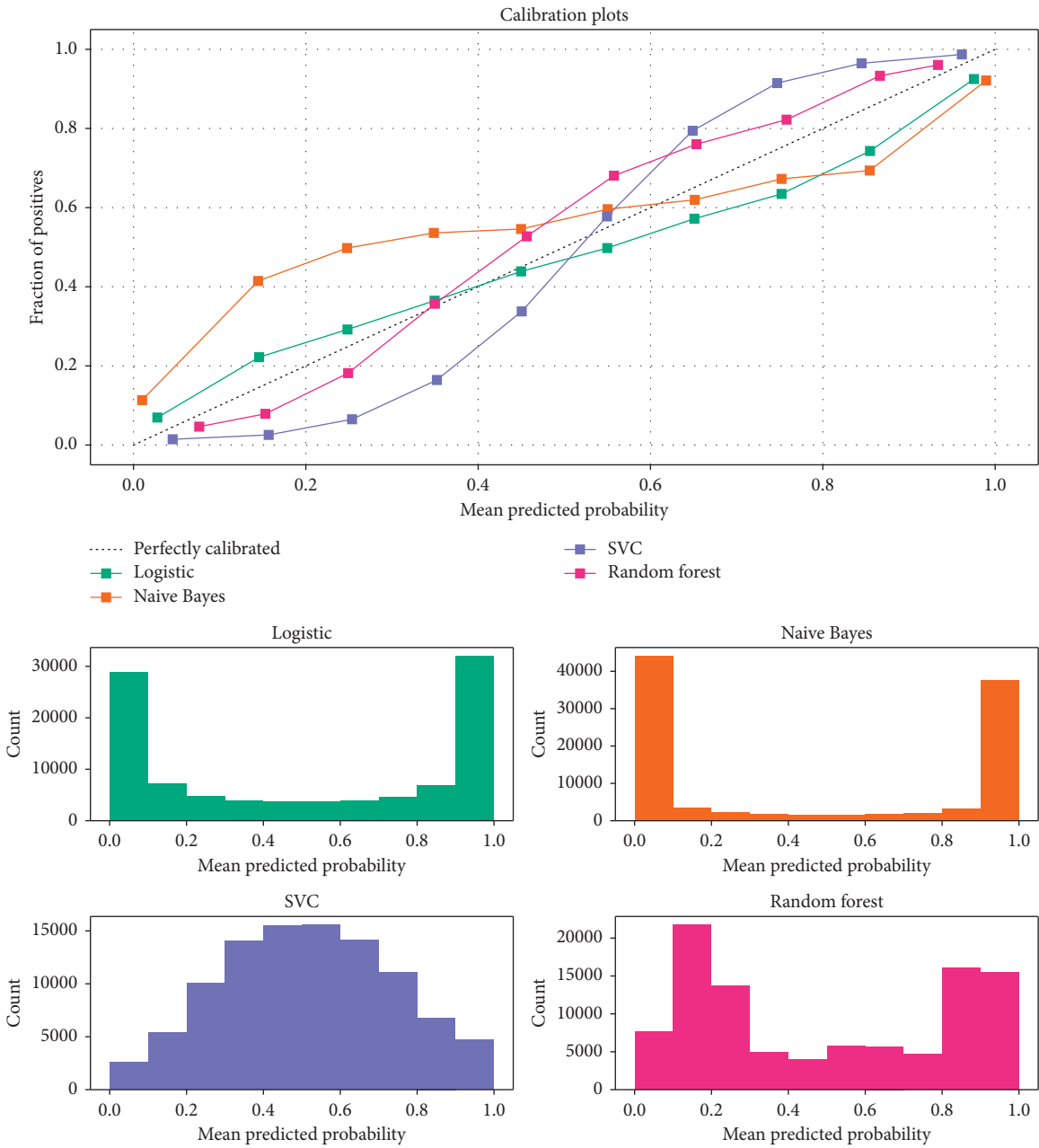


FIGURE 6: Effectiveness of digital management of companies with different solutions.

regression, stochastic processes, and safety system engineering. Correlations between factors affecting safe production and safety problems during production are obtained [19]. The applicability of various prediction methods is examined so that the results produced by the model provide a scientific basis for the prevention and management of safety problems. (3) Research on safety countermeasures. Safety information contains a wide variety of problem types. When the number and severity of problems are within specified limits, general management measures can be applied. However, when they reach or exceed those limits, safety improvements are required. This requires the identification of problem-prone units, lines, or

sections, as well as potentially problematic units, lines, or sections, and then the application of appropriate countermeasures. This mainly includes the identification of accidents, daily safety management countermeasures and safety engineering improvement countermeasures. (4) Safety warning mechanism. This involves the establishment of an assessment mechanism based on conditions such as problem level and unit type, which is then combined with historical data to enable a scientific assessment of the production safety status of each unit. A safety early warning mechanism is also established and regular safety early warning notices are issued in a targeted manner with the aim of preventing seasonal accidents.

4. Simulation Implementation

In summary, the RFID/GIS-based enterprise sales tracking and tracing system, which is a sub-system of the enterprise digital management platform architecture, needs to be integrated with other subsystems to enable the sharing of information. The frequency of data usage by the enterprise's employees is shown in Figure 4. Using the EPC codes of the products the enterprise buys, inputting these into the system through the reader on the traceability terminal and clicking on the product traceability function, it is possible to obtain the product circulation path from the manufacturer to the retailer. The relevant information regarding each product circulation node can be obtained from the GIS system. The digital enterprise management platform features hierarchical architecture containing a customer layer, a business layer, and a data layer. It is feasible to develop an enterprise sales tracking and tracing system using a unified enterprise digital management platform with hierarchical architecture. The enterprise sales link, which includes storage, transportation, sales, and other processes, does not require sales to be divided or combined with other activities, and is particularly suitable for the use of RFID tags. The system design proposed in this study was verified using enterprise documents, as shown in Figure 5. In the life-cycle management of the enterprise, based on the sales process key node RFID data collection and processing, the electronic product code system is used to develop an Internet of Things environment for enterprise information tracking and tracing. However, the system needs to ensure the validity of the data flow, and each key node in the business process must be connected to the entity tag language server of the producer to obtain the necessary information. If the data from one link cannot be updated, the integrity of the tracking and tracing information cannot be guaranteed. The effectiveness of various digital enterprise management solutions is shown in Figure 6. The good results obtained using the model proposed in this study can be attributed to the use of HF/UHF RFID technology, process optimisation and database backend control to ensure that the information is correctly collected and filtered. How to ensure stable operation of the equipment and fast, accurate data collection and processing is a challenging problem that requires further research.

5. Conclusions

In this study, we developed an enterprise information tracking and tracing platform based on GIS using three-tiered architecture. This platform is required to support multiuser and multiterminal devices, and thus requires the installation of the necessary GIS software in different terminals. The model proposed in this study uses process optimisation, database backend data control, and other measures to ensure that the data is safe and secure. However, the best way to ensure the security of information is to focus on the security of the RFID tags used in the front-end solution, which requires further research.

Data Availability

The experimental data used to support the findings of this study are available from the corresponding author upon request.

Conflicts of Interest

The author declares no conflicts of interest.

References

- [1] B. Ç. Uslu, E. Okay, and E. Dursun, "Analysis of factors affecting IoT-based smart hospital design," *Journal of Cloud Computing*, vol. 9, no. 1, pp. 67–23, 2020.
- [2] D. Minoli, K. Sohraby, and B. Occhiogrosso, "IoT considerations, requirements, and architectures for smart buildings—energy optimization and next-generation building management systems," *IEEE Internet of Things Journal*, vol. 4, no. 1, pp. 269–283, 2017.
- [3] Y. Liu, K. Tong, F. Mao, and J. Yang, "Research on digital production technology for traditional manufacturing enterprises based on industrial Internet of Things in 5G era," *International Journal of Advanced Manufacturing Technology*, vol. 107, no. 3–4, pp. 1101–1114, 2020.
- [4] Y. C. Lin and W. F. Cheung, "Developing WSN/BIM-based environmental monitoring management system for parking garages in smart cities," *Journal of Management in Engineering*, vol. 36, no. 3, Article ID 04020012, 2020.
- [5] H. H. Qasim, A. E. Hamza, H. H. Ibrahim, H. A. Saeed, and M. I. Hamzah, "Design and implementation home security system and monitoring by using wireless sensor networks WSN/internet of things IOT," *International Journal of Electrical and Computer Engineering*, vol. 10, no. 3, p. 2617, 2020.
- [6] C. Tuffnell, P. Kral, P. Durana, and T. Krulicky, "Industry 4.0-based manufacturing systems: smart production, sustainable supply chain networks, and real-time process monitoring," *Journal of Self-Governance and Management Economics*, vol. 7, no. 2, pp. 7–12, 2019.
- [7] T. Haaker, P. T. M. Ly, N. Nguyen-Thanh, and H. T. H. Nguyen, "Business model innovation through the application of the Internet-of-Things: a comparative analysis," *Journal of Business Research*, vol. 126, pp. 126–136, 2021.
- [8] A. Moeuf, R. Pellerin, S. Lamouri, S. Tamayo-Giraldo, and R. Barbaray, "The industrial management of SMEs in the era of Industry 4.0," *International Journal of Production Research*, vol. 56, no. 3, pp. 1118–1136, 2018.
- [9] G. Bressanelli, F. Adrodegari, M. Perona, and N. Sacconi, "Exploring how usage-focused business models enable circular economy through digital technologies," *Sustainability*, vol. 10, no. 3, p. 639, 2018.
- [10] K. Leng, L. Jin, W. Shi, and I. Van Nieuwenhuysse, "Research on agricultural products supply chain inspection system based on internet of things," *Cluster Computing*, vol. 22, no. S4, pp. 8919–8927, 2019.
- [11] M. A. Sadeeq and S. Zeebaree, "Energy management for internet of things via distributed systems," *Journal of Applied Science and Technology Trends*, vol. 2, no. 2, pp. 59–71, 2021.
- [12] W. Chen, "Intelligent manufacturing production line data monitoring system for industrial internet of things," *Computer Communications*, vol. 151, pp. 31–41, 2020.
- [13] J. Muñuzuri, L. Onieva, P. Cortés, and J. Guadix, "Using IoT data and applications to improve port-based intermodal supply chains," *Computers & Industrial Engineering*, vol. 139, Article ID 105668, 2020.

- [14] Q. Gao, S. Guo, X. Liu, G. Manogaran, N. Chilamkurti, and S. Kadry, "Simulation analysis of supply chain risk management system based on IoT information platform," *Enterprise Information Systems*, vol. 14, no. 9-10, pp. 1354–1378, 2020.
- [15] G. Tucker, "Sustainable product lifecycle management, industrial big data, and internet of things sensing networks in cyber-physical system-based smart factories," *Journal of Self-Governance and Management Economics*, vol. 9, no. 1, pp. 9–19, 2021.
- [16] D. Xisong, X. Gang, L. Yuantao, G. Xiujiang, and L. Yisheng, "Intelligent ports based on internet of things," in *Proceedings of the 2013 IEEE International Conference on Service Operations and Logistics, and Informatics*, pp. 292–296, IEEE, Dongguan, China, July 2013.
- [17] J. H. Ang, C. Goh, A. A. F. Saldivar, and Y. Li, "Energy-efficient through-life smart design, manufacturing and operation of ships in an industry 4.0 environment," *Energies*, vol. 10, no. 5, p. 610, 2017.
- [18] Z. Qu, H. Sun, and M. Zheng, "An efficient quantum image steganography protocol based on improved EMD algorithm," *Quantum Information Processing*, vol. 20, no. 2, pp. 53–29, 2021.
- [19] Z. Qu, S. Chen, and X. Wang, "A secure controlled quantum image steganography algorithm," *Quantum Information Processing*, vol. 19, no. 10, pp. 380–425, 2020.
- [20] X. Ning, P. Duan, W. Li, and S. Zhang, "Real-time 3D face alignment using an encoder-decoder network with an efficient deconvolution layer," *IEEE Signal Processing Letters*, vol. 27, pp. 1944–1948, 2020, <https://doi.org/10.1109/LSP.2020.3032277>.
- [21] L. Qin, S. Feng, and H. Zhu, "Research on the technological architectural design of geological hazard monitoring and rescue-after-disaster system based on cloud computing and Internet of things," *International Journal of System Assurance Engineering and Management*, vol. 9, no. 3, pp. 684–695, 2018.

Research Article

High-Performance Computing Analysis and Location Selection of Logistics Distribution Center Space Based on Whale Optimization Algorithm

Lijuan Yang ¹ and Xiedong Song²

¹School of Management, Anhui Business and Technology College, Hefei 231131, China

²School of Intelligent Engineering, Yantai Institute of Science and Technology, Yantai 265600, China

Correspondence should be addressed to Lijuan Yang; yanglj@ahbvc.edu.cn

Received 22 April 2022; Revised 23 May 2022; Accepted 2 June 2022; Published 22 June 2022

Academic Editor: Le Sun

Copyright © 2022 Lijuan Yang and Xiedong Song. This is an open access article distributed under the Creative Commons Attribution License, which permits unrestricted use, distribution, and reproduction in any medium, provided the original work is properly cited.

As a meta-heuristic algorithm based on swarm intelligence, the WOA algorithm has few control parameters and searches for the optimal solution by encircling the prey, searching for the prey, and attacking the bubble net. During the whole process, only two internal parameters A and C are utilized for the control of the exploration and development process. BWOA is simple to implement. In the process of algorithm execution, the initial population, global exploration, and local development stages have shortcomings. Therefore, it is necessary to optimize the WOA algorithm. Based on WOA, this study conducts a high-performance computing analysis and location selection of logistics distribution center space. It is concluded that: (1) by using the combination of direct logistics distribution and hierarchical logistics distribution, the WOA algorithm optimizes the cross selection strategy, the population fitness S-LO is improved, the quality of LA is guaranteed, and the chaotic S-LO mapping eliminates inferior individuals in the population. Direct distribution is carried out for bulky goods and important distribution customers, and hierarchical logistics distribution is used for customers in intensive logistics distribution destinations. (2) WOA uses the second reverse learning, chaotic mapping, and logistic chaotic mapping to improve the location update mode. The direct distribution method is mostly used for the logistics business with short journeys, fixed distribution points, and more goods delivered at one time, and logistics enterprises do not need to store and distribute goods. The uniform ergodicity of the Tent chaotic map and logistic chaotic map is improved. Ka adaptive inertia weights are a good complement to optimize the limitations of the Ao whale algorithm. (3) The inertia weight of the levy flight behavior can play a powerful role in balancing the global exploration ability and optimization performance of the intelligent algorithm. The long-term short-distance search of HED and the long-distance jump of KVAR are combined. Variant individuals undergo vector synthesis. It reduces the construction and operation costs of logistics sites and is suitable for logistics distribution under specific conditions.

1. Introduction

Whale Optimization Algorithm (WOA), as a new type of modern intelligent optimization algorithm, has been applied in research fields such as reactive power scheduling optimization, short-term load forecasting, logistics distribution calculation analysis, and location selection and has shown good results. Head whales surround the fish in a circular contraction [1–3]. At the same time, it will swim upward in a spiral upward manner to prey, and by following a “9” or “O”-

shaped path, it is constantly approaching its prey while generating unique bubbles. The position of each humpback whale in the whale algorithm represents a feasible solution. The advantages of this algorithm are that there are few adjustment parameters, simple operation, and strong local optimal ability. For each basic function, define the population size and variable range, run the improved whale optimization algorithm 30 times from randomly generated different populations, and calculate the average and standard deviation as the basis for judging the optimization effect of

the algorithm. In the whale algorithm, each whale can be regarded as a particle, and the position of each particle represents a decision variable. The shrinkage and encirclement mechanism will make the remaining whale individuals move closer to the current optimal whale, and the change in the absolute value of the coefficient will affect the judgment of the remaining whales based on the current position of the corresponding position of the optimal position at the next moment. The spiral update mechanism is based on the distance between the whale's real-time position and the current optimal position, simulating the whale's predation through a spiral trajectory to explore the trajectory range. This makes the population develop towards a single, prone to premature convergence. The optimal individual is mutated [4]. Individuals with high fitness before and after mutation can be used to expand the search range and improve population diversity [5–7]. The core idea of the WOA algorithm is to abstract the hunting mode of humpback whales into a mathematical model, which subtly solves the problem of finding the optimal value in most scenarios, but when faced with some more complex problems or high search space dimensions, in the WOA algorithm, there is insufficient global exploration ability and unsatisfactory convergence accuracy. It is easy to fall into problems such as local optimum [8–10]. In the process of algorithm execution, the initial population, global exploration, and local development stages have shortcomings. For the meta-heuristic algorithm based on group iteration, the quality of the initial population will directly affect the optimization ability and stability of the algorithm and the high-quality initial population with better diversity can lay the foundation for the global search of the group iterative algorithm. Since there is no prior knowledge of the global optimal value of the problem to be solved, the WOA algorithm uses random initialization to generate the initial whale population. The initialized population generated by the random method cannot guarantee the diversity of the population, and it is difficult to effectively extract the useful information of the solution space. To a certain extent, it will affect the convergence speed and optimization ability of the algorithm. The location update of whale individuals in the global exploration phase mainly depends on two parts: the randomly selected search individual location and the product of the coefficient vectors A and D . In the iterative process, A decreases from 2 to 0 and the proportion of A greater than 1 is very small, which leads to a very low probability of global exploration of the whale population, which further weakens the global exploration ability, and it is difficult to get rid of the constraints of local optimality, which leads to the algorithm Precocious and convergent.

As a key node in the express distribution process, logistics distribution sites have received more and more attention. Successful distribution site selection can speed up the circulation efficiency of products and reduce logistics costs, bringing convenience and economic benefits to suppliers and demanders. The development of social productive forces is promoted. Logistics and distribution need to deliver goods from suppliers to customers. For customers, logistics and transportation efficiency is an important determinants of customer experience. In the process of

logistics and transportation, storage, transportation, distribution, and processing are all indispensable. In the process of applying the whale algorithm to solve the optimization problem, since the convergence ability of the algorithm is closely related to the size and randomness of the population, the reasonable setting of the population is very important to the subsequent operation of the algorithm. The differential evolution algorithm performs mutation operations according to the differential strategy. The most prominent feature of the algorithm is its mutation operator. The method of selecting the parent in the mutation operator has an important impact on the search speed of the optimal solution of the differential evolution algorithm. Reasonable allocation of resources is suitable for demand distribution. It also needs to adapt to the overall function and spatial distribution pattern of the city [11–13]. Huge investment, recovery, and relocation are all difficult. The infrastructure of the logistics distribution center is coordinated and balanced with the overall logistics system in terms of spatial distribution, productivity, and technical capabilities. To control the impact of site selection on urban traffic is tried [14, 15]. The whale optimization algorithm has the characteristics of simple structure and easy implementation, but there is a problem of local optimality. It can be improved by simulating the mutation and selection operation of the differential evolution algorithm, so that the improved algorithm not only has the ability to quickly converge but also can optimize globally.

2. Logistics Model

2.1. Enterprise Logistics Distribution Network Model. The multilevel network distribution method is generally used in the logistics network distribution of e-commerce, and the logistics distribution is carried out by establishing a hierarchical logistics site. The current fitness value is calculated and the optimal individual is selected. Using the combination of direct logistics distribution and hierarchical logistics distribution, direct distribution is carried out for bulky goods and important distribution customers and hierarchical logistics distribution is used for customers in intensive logistics distribution destinations. According to the fitness value, the optimal individual of the newly generated population is selected, through the improvement of the whale position update method in the algorithm. The direct distribution method is mostly used in the logistics business where the journey is short, the distribution point is fixed, and there are many goods delivered at one time. The logistics enterprise does not need to store and distribute the goods. After the logistics enterprise obtains the goods from the supplier, it will be delivered directly to the customer, and in this way, the construction and operation costs of logistics sites are reduced, and it is suitable for logistics distribution under specific conditions. However, with the increase of modern logistics business demand, the distribution demand has become scattered and fragmented and most logistics enterprises no longer regard the direct logistics distribution method as the only distribution method of the enterprise but use it in combination with other distribution methods, as shown in Figure 1.

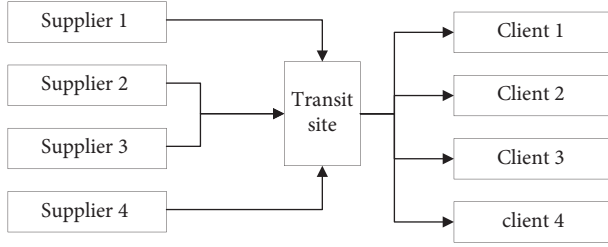


FIGURE 1: Enterprise logistics network.

2.2. Hierarchical Distribution Network. Hierarchical logistics distribution is divided into two logistics methods: for small and medium-sized cities, a two-layer logistics distribution network is established that includes a combination of a general distribution site and several regional distribution sites. When it is delivered to the customer by the regional distribution site and when returning the goods, the goods first enter the regional logistics site, and then the regional logistics site is merged into the general distribution site. For large cities, because there are too many logistics orders, a total distribution site is not enough to complete the distribution and collection of a large number of orders, so an intermediate distribution site will be built between the first and second level distribution sites to assist in the management of logistics, forming a three-level city logistics and distribution network. The transit station means that it is used in the distribution network of large cities, and the distribution network of small and medium-sized cities does not use intermediate distribution stations, as shown in Figure 2.

3. Whale Optimization Algorithm

3.1. BWOA [16–20]. Reactive power scheduling optimization,

$$\min p = \min \sum_{i \in X} L_i * M_i. \quad (1)$$

Short-term load forecasting,

$$x = \frac{\sum_{i \in X} L_i * M_i}{\sum_{i \in X} M_i}. \quad (2)$$

Logistics and distribution calculation analysis selection,

$$\min F = \sum_{i=1}^a \sum_{j=1}^b x_{ij} c_{ij}, \quad (3)$$

$$\min F = \sum_{i=1}^n \sum_{j=1}^m x_{ij} c_{ij} + \sum_{j=1}^m f_j.$$

Surround prey,

$$\min F = \sum_{i=1}^n \sum_{j=1}^m x_{ij} c_{ij} + \sum_{j=1}^m \sum_{k=1}^l h_{jk} x_{jk} + \sum_{j=1}^m v_j (w_j)^\sigma. \quad (4)$$

Bubble attack,

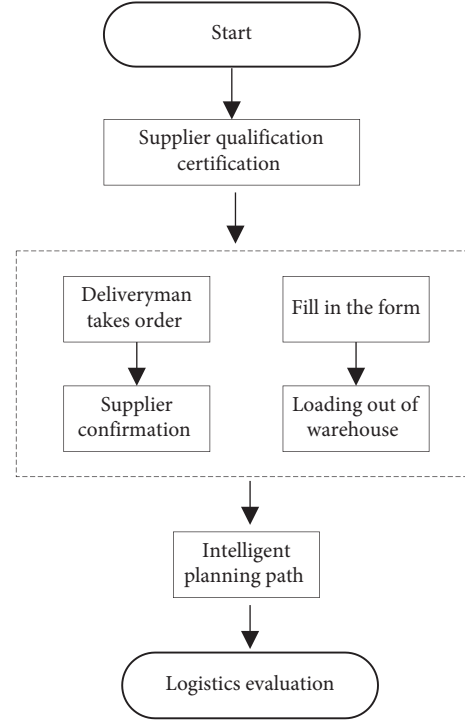


FIGURE 2: Logistics optimization distribution network.

$$F = \sum_{i=1}^k \sum_{x=1}^n a_{xi} d(x, i) + \sum_{i=1}^k \sum_{j=1}^m b_{xi} d(i, j). \quad (5)$$

Explore foraging,

$$W = \sum_{i=1}^k \left[\sum_{x=1}^n \max \left(g_{xi}, \frac{v_{xi}}{60} \right) C d(x, i) \right]. \quad (6)$$

Differential evolution algorithm,

$$\begin{aligned} \sum_1^n i &\geq 1, \\ \sum_1^n \partial_i &\leq 1. \end{aligned} \quad (7)$$

3.2. Rosenbrock [21–23].

$$\sum_{\theta=1}^n m_\theta \leq M. \quad (8)$$

Single population development,

$$\begin{aligned} \left[\sum_{j=1}^n g_{ij}, \sum_{x=1}^n g_{ij} \right] &\geq 0, \\ d(x, i, j) &\geq 0. \end{aligned} \quad (9)$$

Precocious astringent,

$$\left[\sum_{j \in D_i} j, \sum_{x \in D_i} x \right] \geq 1. \quad (10)$$

High-dimensional space search,

$$F = \sum_{i=1}^k \sum_{x=1}^n a_{xi}d(x, i) + \sum_{i=1}^k \sum_{j=1}^m b_{xi}d(i, j) + \sum_{i=1}^k \sum_{j=1}^m t_i g_j, \quad (11)$$

$$A = \{a_1, a_1, \dots, a_i\},$$

$$K_1 = \{K1_1, K2_1, \dots, K j_1\},$$

$$SSE_1 = \sum_{m=1}^j \sum_{a_{m1} \in Km_1} \|a_{m1} - Km_1\|^2.$$

3.2.1. Quartic [24–26].

$$K_2 = \{K1_2, K2_2, \dots, K j_2\}, \quad (12)$$

$$K j_2 = \text{mean}(a_{m1}).$$

Global exploration capability,

$$SSE_2 = \sum_{m=1}^j \sum_{a_{m2} \in Km_2} \|a_{m2} - Km_2\|^2, \quad (13)$$

$$\Delta SSE_2 = |SSE_1 - SSE_2|.$$

Local optimum,

$$\Delta SSE_2 \leq \delta. \quad (14)$$

Species diversity,

$$x(t+1) = x_{\text{best}}(t) + D * e^{bl}. \quad (15)$$

Differential evolution algorithm,

$$x(t+1) = x_{\text{rand}}(t) - A * C * x_{\text{rand}}(t) - x(t). \quad (16)$$

The overall coordination and balance of the logistics system are as follows:

$$p = \frac{|E_x - x|}{E_x}, \quad (17)$$

$$x_i^0 = (a_i - b_i)z_i + b_i.$$

4. Simulation Experiment

4.1. Individual Elimination Strategy. When the WOA searches immediately, it moves closer to a random position. Although this method can ensure the diversity of the population to a certain extent, it is easy to produce inferior solutions that deviate from the optimal direction, which affects the convergence speed. In the cross selection strategy of the genetic algorithm, after each iteration, the population is sorted according to fitness and equally divided into two parts, one part is relatively high-quality individuals and the other part is relatively inferior individuals, and the two parts are subjected to pairwise arithmetic crossover to generate a new one. The population of, where S-LO = 111, S-LA = 107, C-LO = 54, C-LO = 62, WT = 44, and VO = 10. A crossover between high-quality individuals and low-quality individuals can ensure the diversity of the population. The original

TABLE 1: Parameters of individual elimination strategy.

S-LO	S-LA	C-LO	C-LO	WT	Vo
99	116	78	77	28	3
119	102	62	56	27	9
90	111	74	71	20	9
96	111	68	60	28	9
110	94	86	75	46	3
94	107	72	65	22	9
99	96	67	54	42	8
114	102	73	90	31	10
92	109	63	81	40	8
105	117	90	65	48	9
111	107	54	62	44	10

population is merged, and the new population, sorted by fitness, eliminates inferior individuals in the merged population and lets the retained high-quality individuals enter the next iteration, and S-LO = 110, S-LA = 94, C-LO = 86, C-LO = 75, WT = 46, and Vo = 3. S-LA guarantees the high quality of the population. Chaos S-LO mapping can be used to generate chaotic sequences, and C-LO has a better effect than pseudorandom numbers in generating WT chaotic sequences in population initialization as shown in Table 1 and Figure 3.

4.2. Partial Development Stage. The chaotic sequence is added on the basis of secondary reverse learning. The more commonly used discrete chaotic maps are Tent chaotic map and logistic chaotic map, and Ka = 4.08, Ao = 4.47, Io = 4.22, IT = 4.04, To = 4.52, No = 4.47, and $\beta = 4.98$. It is proved that the Tent chaotic map has better uniform traversal properties than the logistic chaotic map. If the current optimum is close to the local optimum, then a small step search pattern around the local optimum will trap the algorithm in a local extremum, and Io = 4.44, IT = 4.78, To = 4.39, No = 4.97, and $\beta = 4$. It is difficult to get rid of the shackles of local extrema. The introduction of Ka adaptive inertial weights is a good complement to optimize the limitations of the Ao whale algorithm. In the local development stage, Ka = 4.68 and Ao = 4.97; an effective mutation strategy makes it difficult for the whale population to get rid of the shackles of local optimum. See Table 2 and Figure 4.

4.3. Levy Flight Strategy. Levy flight is a kind of random walk (Randomly walk) motion of living organisms; bats, fruit flies, cuckoos, people, lights, etc., all have this levy flight behavior. The inertia weight plays an excellent role in balancing the global exploration ability and optimization performance of the intelligent algorithm, and HED = 3.82, ND = 3.58, HDE = 3.45, DIR = 3.66, DIT = 5.51, LAD = 4.7, W = 2.63, and KVAR = 2.16 is used in a variety of algorithms. The walking performance of this mechanism is a combination of the long-term short-distance search of HED and the occasional long-distance jump of KVAR, which is characterized by directional variability. The mutation strategy in the differential evolution algorithm is to randomly select two different individuals in the population, and HDE scales the

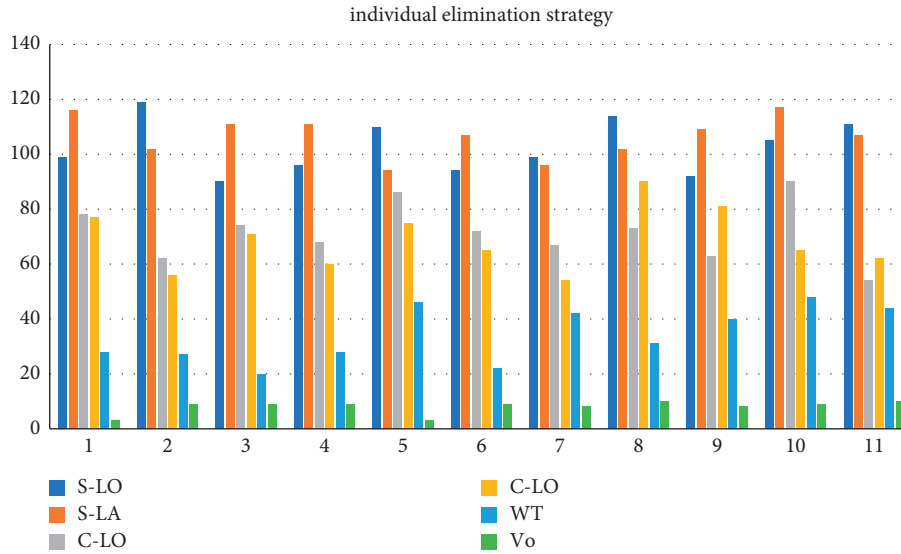


FIGURE 3: Individual elimination strategy parameters.

TABLE 2: Local development parameter settings.

Parameter	Ka	Ao	Io	IT	To	N-o	β
Ka	4.08	4.68	4.46	4.89	4.63	4.08	4.83
Ao	4.13	4.97	4.87	4.01	4.53	4.47	4.77
Io	4.40	4.44	4.39	4.88	4.62	4.22	4.35
IT	4.27	4.78	4.69	4.13	4.77	4.04	4.33
To	4.21	4.39	4.46	4.58	4.43	4.52	4.53
N-o	4.00	4.97	4.94	4.21	4.12	4.47	4.93
B	4.08	4.00	4.01	4.53	4.13	4.98	4.90

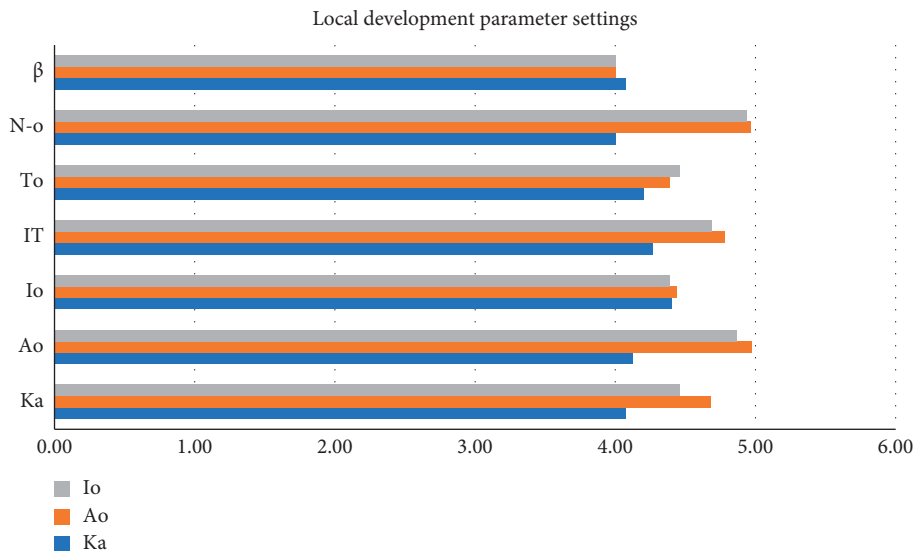


FIGURE 4: Local development parameter settings.

vector difference and then performs vector synthesis with the individual to be mutated. See Table 3 and Figures 5 and 6.

4.4. Improvement Strategies. The whale optimization algorithm simulates the unique bubble network attack

mechanism of humpback whales. By calculating the fitness value of all search agents, the current optimal solution is selected, and then the circular contraction mechanism and the spiral up mechanism are selected. By calculating the fitness value of each whale, the optimal whale position bestX and its corresponding global optimal fitness value best f are

TABLE 3: Flight node parameters.

HED	ND	HDE	DIR	DIT	LAD	W	KVAR
3.41	3.30	3.85	3.16	3.74	3.90	1.59	2.65
3.65	3.73	3.55	3.49	3.19	1.09	1.67	1.25
3.14	3.16	3.84	3.76	1.39	3.73	4.80	2.00
3.82	3.58	3.45	3.66	5.51	4.70	2.63	2.16
3.34	3.46	3.64	3.43	5.47	1.24	5.06	1.77
3.50	3.87	3.31	3.93	2.97	4.42	4.86	3.78
3.34	3.98	3.44	3.41	3.08	2.46	1.64	5.21
3.53	3.85	3.00	3.86	1.17	3.70	4.59	1.02

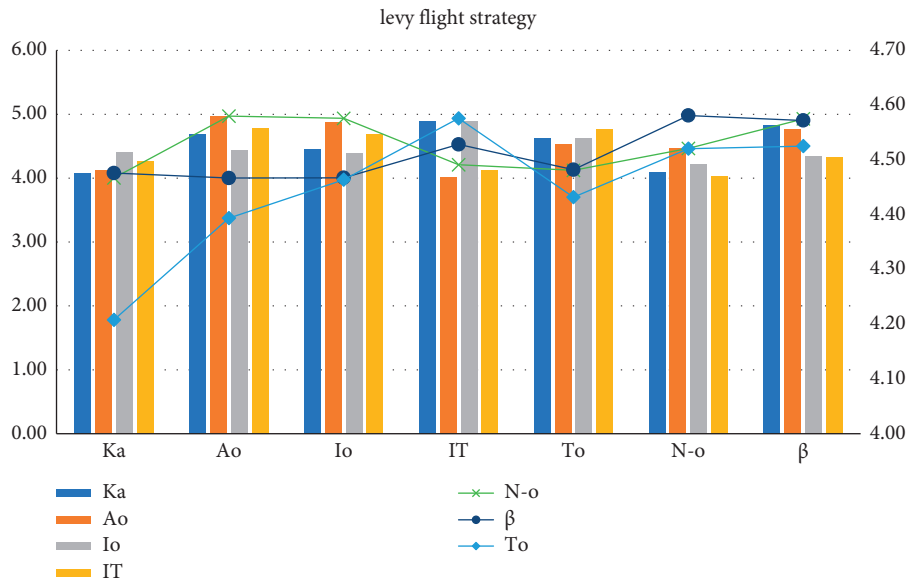


FIGURE 5: Levy flight strategy.

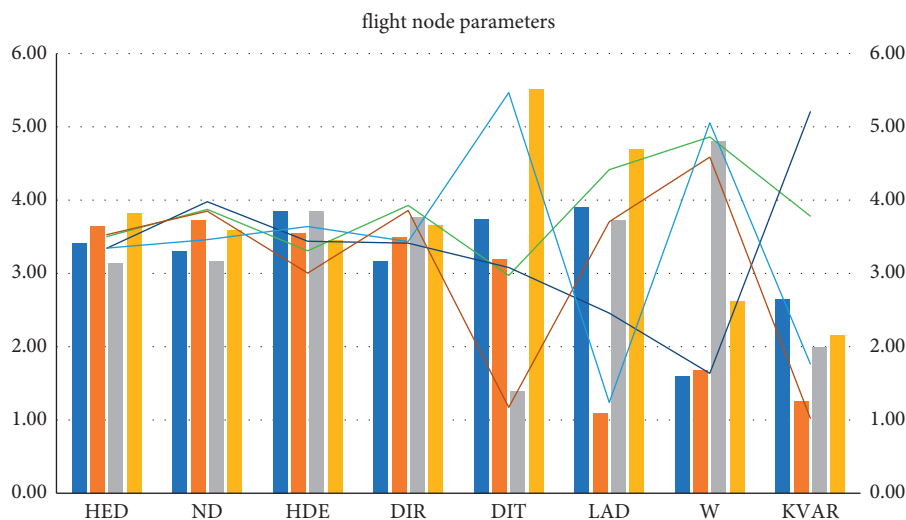


FIGURE 6: Flight node parameters.

found. When the population is initialized, the method of stochastic differential mutation is used in the particle swarm algorithm and the gray wolf algorithm, respectively. test function = 0.4, algorithm = 0.43, optimal = 0.49, average = 0.26, worst = 0.3, encircled prey in whale algorithm

ND = 3.46, bubble attack HED = 3.34, exploration and foraging stage HDE = 3.64, compare current whale individuals, the fitness value LAD = 1.24, and the individual fitness value of the leading whale is DIT = 5.47. DIR = 3.43, W = 5.06, and KVAR = 1.77 to update the leading value and leading

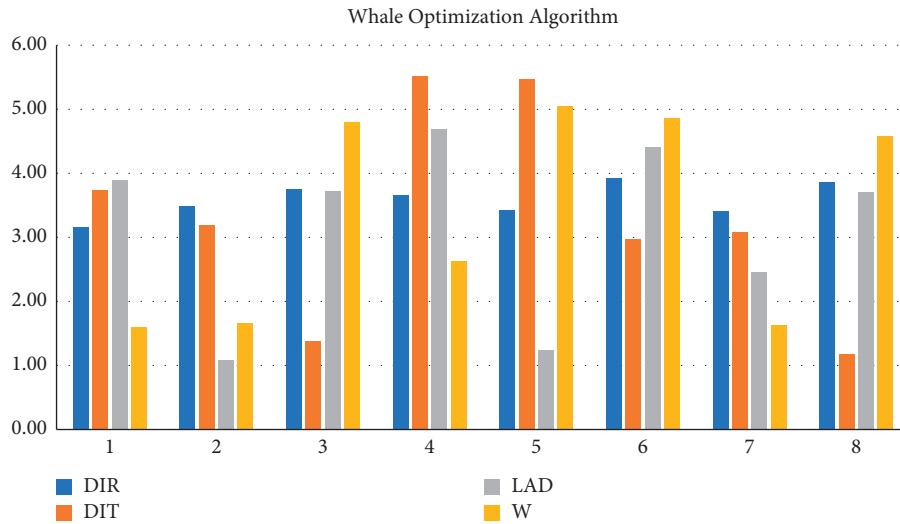


FIGURE 7: Whale optimization algorithm.

TABLE 4: Comparison of algorithms.

Test function	Algorithm	Optimal	Average	Worst	
Sphere	0.60	0.03	0.63	0.84	0.49
BWOA	0.40	0.43	0.49	0.26	0.30
Rosenbrock	0.10	0.35	0.18	0.53	0.04
Quartic	0.35	0.35	0.60	0.37	0.03
Ackley	0.29	0.73	0.82	0.11	0.50
Schwefel's	0.89	0.77	0.14	0.81	0.47

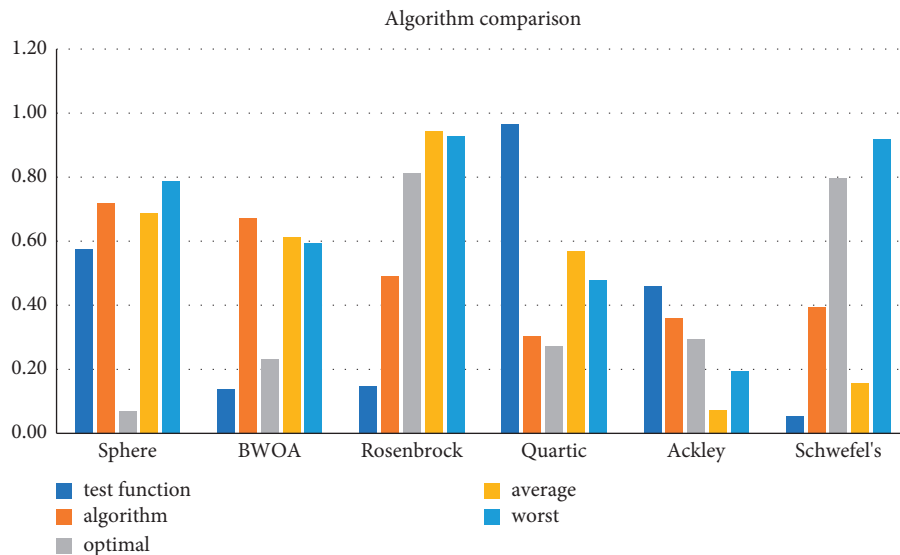


FIGURE 8: Algorithm comparison.

position and record the current global optimum value and optimum position at the same time. The selection of the circular contraction mechanism and the spiral up mechanism is performed (Figure 7).

As a meta-heuristic algorithm based on swarm intelligence, the WOA algorithm is the same as other meta-heuristic algorithms and has the advantages of fewer control parameters, simple implementation, and high flexibility. (1) Sphere

has few control parameters: test function = 0.6, algorithm = 0.03, optimal = 0.63, average = 0.84, and worst = 0.49. The WOA algorithm mainly simulates the predation behavior of humpback whales and searches for the optimal solution by encircling the prey, searching for the prey, and attacking the bubble net. During the whole process, only two internal parameters A and C are utilized for the control of the exploration and development process. (2) BWOA is simple to

implement, test function = 0.35, worst = 0.03, WOA algorithm obtains the optimal solution through algorithm = 0.35, optimal = 0.6 spiral equation, and iterative average = 0.37 position. (3) The flexibility of Rosenbrock is high optimal = 0.82. The implementation process of the WOA algorithm is simple, test function = 0.29, algorithm = 0.73, few parameters, and simple expressions. Practical problems in various fields can be solved by transforming or integrating other algorithms. Average = 0.11, worst = 0.5, which has the characteristics of high flexibility. See Table 4 and Figure 8.

5. Conclusion

As a meta-heuristic algorithm based on swarm intelligence, the WOA algorithm has few control parameters and searches for the optimal solution by encircling the prey, searching for the prey, and attacking the bubble net. BWOA is simple to implement. In the process of algorithm execution, the initial population, global exploration, and local development stages have shortcomings. Therefore, it is necessary to optimize the WOA algorithm.

Based on WOA, this study conducts a high-performance computing analysis and location selection of logistics distribution center space. It is obtained: 1. Using the combination of direct logistics distribution and hierarchical logistics distribution, the two parts perform pairwise arithmetic crossover to generate a new population, where S-LO = 111, S-LA = 107, C-LO = 54, C-LO = 62, WT = 44, and Vo = 10. A crossover between high-quality individuals and low-quality individuals can ensure the diversity of the population. The original population and the new population are merged, sorted by fitness, eliminate inferior individuals in the merged population and let the retained high-quality individuals enter the next iteration, and S-LO = 110, S-LA = 94, C-LO = 86, C-LO = 75, WT = 46, and Vo = 3. S-LA guarantees the high quality of the population. 2. The logistic chaos map $K_a = 4.08$, $A_o = 4.47$, and $I_o = 4.22$. Tent chaotic map has better uniform traversal properties $IT = 4.04$, $T_o = 4.52$, $N-o = 4.47$, and $\beta = 4.98$ than the logistic chaotic map. If the current optimum is close to the local optimum, the small-step search pattern around the local optimum will cause the algorithm to fall into the local extremum, and $I_o = 4.44$, $IT = 4.78$, $T_o = 4.39$, $N_o = 4.97$, and $\beta = 4$, get rid of local extrema bound. 3. The concept of random difference variation is used in the particle swarm algorithm and gray wolf algorithm, respectively. test function = 0.4, algorithm = 0.43, optimal = 0.49, average = 0.26, worst = 0.3, encircled prey in whale algorithm ND = 3.46, bubble attack HED = 3.34, exploration and foraging stage HDE = 3.64, comparing current whale individuals the fitness value LAD = 1.24, and the individual fitness value of the leading whale is DIT = 5.47. DIR = 3.43, $W = 5.06$, and $KVAR = 1.77$ to update the leading value and leading position and record the current global optimum value and optimum position at the same time. 4. Sphere has few control parameters: test function = 0.6, algorithm = 0.03, optimal = 0.63, average = 0.84, and worst = 0.49. The WOA algorithm mainly simulates the predation behavior of humpback whales and searches for the optimal solution by

encircling the prey, searching for the prey, and attacking the bubble net. During the whole process, only two internal parameters A and C are utilized for the control of the exploration and development process. BWOA is simple to implement, test function = 0.35, worst = 0.03, WOA algorithm obtains the optimal solution through algorithm = 0.35, optimal = 0.6 spiral equation, and iterative average = 0.37 position. Rosenbrock flexibility is high optimal = 0.82. The implementation process of the WOA algorithm is simple, test function = 0.29, algorithm = 0.73, few parameters, and simple expressions. Practical problems in various fields can be solved by transforming or integrating other algorithms. Average = 0.11 and worst = 0.5, which has the characteristics of high flexibility. [27].

Data Availability

The experimental data used to support the findings of this study are available from the corresponding author upon request.

Conflicts of Interest

The authors declare that they have no conflicts of interest.

Acknowledgments

This work was sponsored in part by the Quality engineering project of colleges and universities in Anhui Province (Grant no. 2020zyq09).

References

- [1] M. A. Little, "Smartphones for remote symptom monitoring of Parkinson's disease [J]," *Journal of Parkinson's Disease*, vol. 11, pp. 1-5, 2021.
- [2] Y. Gu and M. Liu, "Fair and privacy-aware EV discharging strategy using decentralized whale optimization algorithm for minimizing cost of EVs and the EV aggregator[J]," *IEEE Systems Journal*, vol. 15, no. 99, pp. 1-12, 2021.
- [3] K. E. H. Jenkins, B. K. Sovacool, N. Mouter, N. Hacking, M. K. Burns, and D McCauley, "The methodologies, geographies, and technologies of energy justice: a systematic and comprehensive review," *Environmental Research Letters*, vol. 16, no. 4, Article ID 043009, 2021.
- [4] K. Vanchinathan, K. R. Valluvan, C. Gnanavel, C. Gokul, and J. R. Albert, "An improved incipient whale optimization algorithm based robust fault detection and diagnosis for sensorless brushless DC motor drive under external disturbances," *International Transactions on Electrical Energy Systems*, vol. 31, no. 12, 2021.
- [5] Y. Wang, S. Wang, and D. Li, "An improved multi-objective whale optimization algorithm for the hybrid flow shop scheduling problem considering device dynamic reconfiguration processes [J]," *Expert Systems with Applications*, vol. 174, no. 8, Article ID 114793, 2021.
- [6] J. Zhao, H. Nguyen, and T. Nguyen-Thoi, "Improved Levenberg-Marquardt backpropagation neural network by particle swarm and whale optimization algorithms to predict the deflection of RC beams [J]," *Engineering with Computers*, pp. 1-23, 2021.

- [7] M. Yin, X. Qian, M. Huang, and Q Zhang, "Winner determination for logistics service procurement auctions under disruption risks and quantity discounts," *Engineering Applications of Artificial Intelligence*, vol. 105, no. 1, Article ID 104424, 2021.
- [8] P. Sarir, J. Chen, P. G. Asteris, D. J. Armaghani, and M. M Tahir, "Developing GEP tree-based, neuro-swarm, and whale optimization models for evaluation of bearing capacity of concrete-filled steel tube columns," *Engineering with Computers*, vol. 37, no. 1, 19 pages, 2021.
- [9] J. Feng, "Forecasting of carbon emission in China based on gradient boosting decision tree optimized by modified whale optimization algorithm [J]," *Sustainability*, vol. 13, 2021.
- [10] P. Singh, A. Numa, B. Pethani, A. Bye, M. Cardamone, and D. Flanagan, "assessing the logistics, feasibility and challenges OF establishing continuous eeg service IN a children'S ICU," *Pediatric Critical Care Medicine*, vol. 22, no. Supplement 1 3S, p. 40, 2021.
- [11] A. Uluta and A. Topal, "A new hybrid model based on rough step-wise weight assessment ratio analysis for third-party logistics selection [J]," *Soft Computing*, vol. 26, no. 4, pp. 2021–2032, 2021.
- [12] S. Pathan, P. C. Siddalingaswamy, and T. Ali, "Automated Detection of Covid-19 from Chest X-ray scans using an optimized CNN architecture," *Applied Soft Computing*, vol. 104, no. 10223, Article ID 107238, 2021.
- [13] A. Goodson, S. Parmar, S. Ganesh et al., "Printed titanium implants in UK craniomaxillofacial surgery. Part II: perceived performance (outcomes, logistics, and costs)," *British Journal of Oral and Maxillofacial Surgery*, vol. 59, no. 3, pp. 320–328, 2021.
- [14] A. K. Tripathi, K. Sharma, M. Bala, A. Kumar, V. G. Menon, and A. K. Bashir, "A parallel military-dog-based algorithm for clustering big data in cognitive industrial internet of things [J]," *IEEE Transactions on Industrial Informatics*, vol. 17, no. 3, pp. 2134–2142, 2021.
- [15] N. M. Ashraf, R. R. Mostafa, R. H. Sakr, and M. Z Rashad, "Optimizing hyperparameters of deep reinforcement learning for autonomous driving based on whale optimization algorithm," *PLoS One*, vol. 16, no. 6, Article ID e0252754, 2021.
- [16] W. S. Hassanein, M. M. Ahmed, M. I. Mosaad, and A Abu-Siada, "Estimation of transmission line parameters using voltage-current measurements and whale optimization algorithm," *Energies*, vol. 14, no. 11, p. 3239, 2021.
- [17] M. Tahmasebi, J. Pasupuleti, F. Mohamadian et al., "Optimal operation of stand-alone microgrid considering emission issues and demand response program using whale optimization algorithm," *Sustainability*, vol. 13, no. 14, p. 7710, 2021.
- [18] V. K. Jadoun, G. R. Prashanth, S. S. Joshi et al., "Optimal scheduling of non-convex cogeneration units using exponentially varying whale optimization algorithm," *Energies*, vol. 14, no. 4, p. 1008, 2021.
- [19] M. Huang, Q. Zhai, Y. Chen, S. Feng, and F Shu, "Multi-Objective whale optimization algorithm for computation offloading optimization in mobile edge computing," *Sensors*, vol. 21, no. 8, p. 2628, 2021.
- [20] J. Li, L. Guo, Y. Li, C. Liu, L. Wang, and H Hu, "Enhancing whale optimization algorithm with chaotic theory for permutation flow shop scheduling problem," *International Journal of Computational Intelligence Systems*, vol. 14, no. 1, p. 651, 2021.
- [21] Y. Li, Z. Wang, Y. Tang, and Z. Shang, "Enhanced precision inspection of free-form surface with an improved whale optimization algorithm," *Optics Express*, vol. 29, no. 17, p. 26909, 2021.
- [22] J. Lian, "An optimization model of cross-docking scheduling of cold chain logistics based on fuzzy time window [J]," *Journal of Intelligent and Fuzzy Systems*, vol. 41, no. 2, pp. 1–15, 2021.
- [23] H. Jin, Q. He, M. He, S. Lu, F. Hu, and D Hao, "Optimization for medical logistics robot based on model of traveling salesman problems and vehicle routing problems," *International Journal of Advanced Robotic Systems*, vol. 18, no. 3, 2021.
- [24] H. Zhang and Y. Jin, "Credit system of smart logistics public information platform based on improved neural network," *Neural Computing & Applications*, vol. 33, no. 9, pp. 3987–4000, 2021.
- [25] T. G. Crainic, F. Djeumou Fomeni, and W. Rei, "Multi-period bin packing model and effective constructive heuristics for corridor-based logistics capacity planning," *Computers & Operations Research*, vol. 132, no. 3, Article ID 105308, 2021.
- [26] S. Iranmanesh, F. S. Abkenar, R. Raad, and A Jamalipour, "Improving throughput of 5G cellular networks via 3D placement optimization of logistics drones," *IEEE Transactions on Vehicular Technology*, vol. 70, no. 2, pp. 1448–1460, 2021.
- [27] H. Brdulak and A. Brdulak, "Challenges and threats faced in 2020 by international logistics companies operating on the polish market," *Sustainability*, vol. 13, no. 1, p. 359, 2021.

Retraction

Retracted: Design of a Multimedia-Assisted Distance English Teaching System for College Students

Computational Intelligence and Neuroscience

Received 25 July 2023; Accepted 25 July 2023; Published 26 July 2023

Copyright © 2023 Computational Intelligence and Neuroscience. This is an open access article distributed under the Creative Commons Attribution License, which permits unrestricted use, distribution, and reproduction in any medium, provided the original work is properly cited.

This article has been retracted by Hindawi following an investigation undertaken by the publisher [1]. This investigation has uncovered evidence of one or more of the following indicators of systematic manipulation of the publication process:

- (1) Discrepancies in scope
- (2) Discrepancies in the description of the research reported
- (3) Discrepancies between the availability of data and the research described
- (4) Inappropriate citations
- (5) Incoherent, meaningless and/or irrelevant content included in the article
- (6) Peer-review manipulation

The presence of these indicators undermines our confidence in the integrity of the article's content and we cannot, therefore, vouch for its reliability. Please note that this notice is intended solely to alert readers that the content of this article is unreliable. We have not investigated whether authors were aware of or involved in the systematic manipulation of the publication process.

Wiley and Hindawi regrets that the usual quality checks did not identify these issues before publication and have since put additional measures in place to safeguard research integrity.

We wish to credit our own Research Integrity and Research Publishing teams and anonymous and named external researchers and research integrity experts for contributing to this investigation.

The corresponding author, as the representative of all authors, has been given the opportunity to register their agreement or disagreement to this retraction. We have kept a record of any response received.

References

- [1] H. Feng, "Design of a Multimedia-Assisted Distance English Teaching System for College Students," *Computational Intelligence and Neuroscience*, vol. 2022, Article ID 2184600, 8 pages, 2022.

Research Article

Design of a Multimedia-Assisted Distance English Teaching System for College Students

Haili Feng 

School of Foreign Languages, Qiongtai Normal University, Haikou 571127, China

Correspondence should be addressed to Haili Feng; 030068@hainnu.edu.cn

Received 1 April 2022; Revised 12 May 2022; Accepted 21 May 2022; Published 16 June 2022

Academic Editor: Le Sun

Copyright © 2022 Haili Feng. This is an open access article distributed under the Creative Commons Attribution License, which permits unrestricted use, distribution, and reproduction in any medium, provided the original work is properly cited.

To address the problems of poor compatibility, weak load capacity, and time consumption of existing multimedia-assisted teaching systems, we propose and design a physics multimedia-assisted English teaching system based on a concept network. The architecture of the physics multimedia-assisted teaching system is constructed with the logical layer as the core, and the theoretical knowledge module, experiment module, and student practice module are designed, respectively. Based on the concept network, a large number of rules in the physics teaching system are attached to the concepts to form the concept network knowledge system and complete the design of the theoretical knowledge system. This paper explores the multimedia teaching of college English and points out the advantages and characteristics of this teaching mode and the problems to be paid attention to in the process of application. The design of the physics multimedia-assisted teaching system is completed by realizing students' practice and giving feedback on the practice results. The experimental results show that the system has good compatibility, strong load capacity, low time consumption, and practical application value.

1. Introduction

University education, an important part of the national higher education system, has been developing rapidly in China in recent years. In order to promote the vigorous development of university education and meet the needs of social and economic development, the Ministry of Education has been actively promoting the reform of university education, and the reform of university English courses also needs to meet the needs of the times [1, 2]. The rapid development of information technology and the increasing maturity of computer network technology have made education more and more modernized, and the application of multimedia technology is one of the important symbols of education modernization [3, 4]. Multimedia teaching is the latest stage of development of modern English teaching, which provides a colorful expression for English teaching with the characteristics of large amount of information, fast transmission, graphic and text, human-computer dialogue, clear interface, effective combination of audio-visual, convenient information retrieval and high efficiency, and so on

[5]. It injects new colors and vitality into the classroom and is becoming more and more important in English teaching [6].

Multimedia-assisted English teaching is conducive to giving full play to students' initiative and enthusiasm. Multimedia technology can make teaching forms more lively, further improve the quality of teaching, and change the passive acceptance of information to active acceptance of information, thus stimulating students' initiative and creativity [7]. Multimedia teaching integrates sound, image, video, and text, which can produce a lively effect and help improve students' interest in learning and memory ability [8]. It is better than the traditional teaching mode-textbook, chalk, or blackboard to stimulate students' learning enthusiasm [9]. Computer multimedia will be vivid images, vivid colors, and rich language and cultural scenes real in front of the students, and multimedia courseware with its images, graphics, text, sound, animation, and so on, a variety of functions on the students' multiple senses, can stimulate students' interest in learning, attract students' attention, more mobilize students' enthusiasm for learning, stimulate

students' desire to learn, and give full play to students [10]. It is not only stimulating students' interest in learning and attracting their attention but also stimulating their enthusiasm for learning, stimulating their desire to learn, and giving full play to their initiative and enthusiasm [11].

It is also conducive to improving teaching efficiency and expanding classroom capacity [12]. Multimedia-assisted English teaching can expand the amount of classroom information, make full use of classroom teaching time, greatly enrich and improve the content of foreign language teaching, and fundamentally improve teaching efficiency [13, 14]. Teachers and students can use the information resources stored on CDs, VCDs, floppy disks, CD-ROMs, and hard disks in the multimedia classroom and can also use multimedia courseware for teaching, which can create a vivid, imaginative, authentic, and interesting English language environment for students, which is conducive to their understanding and mastery of teaching contents [15]. In traditional English classroom teaching, teachers spend most of the time on writing and explaining in each lesson, which is less dense and less informative, but teachers can increase the information of each lesson by arranging the board with the courseware, which can save time and make students get more knowledge in the same time and improve the learning efficiency [16, 17].

The use of multimedia technology in teaching puts forward higher requirements for teachers, who should not only know educational technology and teaching theory and have a high level of English but also have a certain ability to use computers [18]. Through multimedia courseware, teachers can design a new teaching process, display subtle teaching ideas and new creativity, expand the capacity of classroom teaching, and attract students' pursuit of knowledge, which is both promotion and challenge for teachers and a process of improving themselves. Multimedia teaching can also effectively use network resources [19]. There is a large amount of information related to English teaching content on the Internet, so teachers can use the Internet to download the content they need and expand the language materials so that students can use and obtain the latest information. This not only enriches the teaching content dynamically but also keeps the teachers' teaching ideas and content up to date with the development of the times [20].

2. System Design Principles and Functional Design

2.1. System Design Follows the Principles. The proposed English teaching system follows the following principles to carry out design: (1) Having complete functions: nowadays, most R&D enterprises are developing toward the level of intensification and scale, and according to the infrastructure and technology already available, all levels are closely united using information flow to achieve the purpose of unified management and data acquisition. (2) Modularity: the English teaching system is designed according to the principle of "modularity," and the configuration is carried out according to the actual requirements of users, with

relatively simple and flexible structured functional modules installed, and all basic and business modules can be combined at will to meet the existing or future system personalized application requirements. (3) Friendly operation interface: the design of a friendly and easy-to-operate interface helps users carry out the functions of each link, thus enhancing the efficiency of the system. The designed information input interface should follow the requirements of simplifying the actual work of users as much as possible and effectively reducing the error rate of data input. Therefore, in the process of designing this English teaching system, the user's memory burden should be reduced as much as possible, and automatic data input should be increased to avoid the situation of user data input errors. (4) High efficiency: the designed system should have high security and operation efficiency so as to provide users with high-quality services and obtain a quick response and relatively stable system. In addition, each program and interface of the system must be designed with a uniform standard to ensure that the system shows good portability and also facilitates timely expansion and application.

2.2. Overall System Architecture. Although the rapid development of computer and network technology has solved many problems, it is still a difficult problem to design and develop an English teaching system with complex information, such as how to secure the front-end of the system. The system architecture is the basis for the proper operation of a system, and its layout directly affects the stability of the system's operation. In the J2EE system, the server-side Web application is divided into several layers. Each of these layers is configured with significantly different functions and promises to be linked to different communication interfaces. The specific architecture of the system is shown in Figure 1.

In Figure 1, the JSP page is seen as the view layer, the main function of which is to smoothly implement the interaction between the system and the user and to display the final interaction combination directly using the JSP page. The view does not unfold the actual business but can accept data update operations so that the system interface can be updated at any time. Action control layer aims to receive response requests from the client user at any time and timely invoke the model in the business layer to smoothly realize the delivery of user requests. If the user submits a request using the page, mainly by sending an HTML form, the controller must respond to the request and finally deliver the result to the user using the view method. In one layer, the controller is implemented mainly through Action, ActionServlet, where Action can be called the corresponding adapter and separates the request from the business logic, thus combining the user's needs and calling the corresponding business logic components in time. The service business layer is located between the persistence layer and the Action layer, which is designed to implement the application logic and check the business, such as login password authentication. The main function of the DAO layer is to smoothly connect with the database, and the main function of the DAO layer is to smoothly connect to the

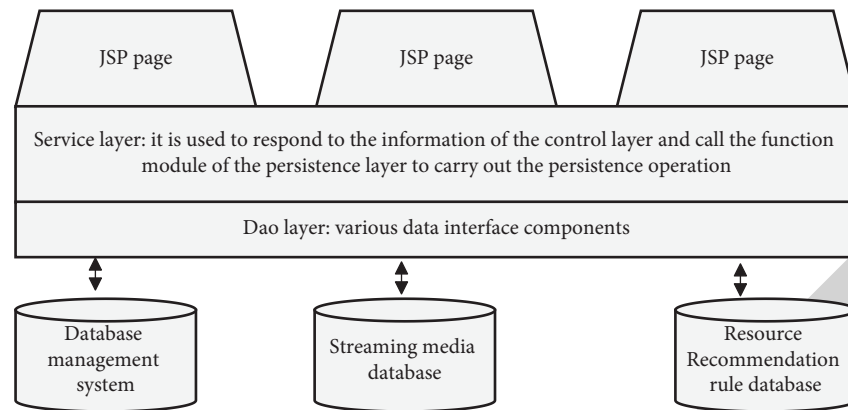


FIGURE 1: Functional design of English teaching system.

database and perform various operations on the database, such as adding, modifying, deleting, and other business functions, but in J2EE development, SQL statements are generally used to smoothly implement the query operations, so that different interfaces can be called to achieve the corresponding functions.

2.3. Design of Each Function of the System. In order to improve the efficiency and level of students' learning English and to solve the time of learning English to a certain extent, the English teaching system designed in this study is based on advanced computer network technology, which is realized through the combination of J2EE, MVC architecture, and other technologies with related business, so that students can learn related services through this system and ensure that students can learn English audio materials, video materials, and so on at the first time. The system is designed to ensure that students have the first access to English audio and video materials. Based on this, combined with the actual needs of English teaching, the system functions are divided into the following functional modules in the paper, as shown in Figure 2.

In Figure 2, the authority management mainly consists of user login, user logout, user management, and other functions. To ensure more convenient system operation, the designed system login interface retains some similarities for different roles, and only some visual differences exist. After users enter their account numbers and passwords, the system automatically determines the user's identity type and quickly opens the operation privileges for that type of user. At the same time, the rights management is used to guide users to register on the website and for registered users to log in; the managerial rights include functions such as classification of user rights and user passwords. The teaching resource check includes two functions of joint and category search, with the help of which the required resource information can be searched according to the actual needs of users and the results can be directly linked to English teaching information. English audio/video on demand aims to realize the playback of English teaching videos or audios, and users can realize the download of English teaching resources with the help of this module. The resource management is mainly in the

audio/video data uploading, deleting, and other operations to meet the needs of learners. The navigation management module is to meet the actual classification needs of the system. With the help of this function module, users can locate the required search resources in a very short time and start the operation of function switching and information finding according to the default order of the classification navigation configuration.

3. System Development Environment and Its Implementation

3.1. System Development Environment. In this study, RealNetworkHelixServer was selected as the streaming media server, which can support different formats, and the server supports some of the current mainstream playback software to better meet the needs of users. The operating system of the system is Win7, the development platform is My Eclipse 3.5, the server used is 70mcat6.5, the development technology is Struts2, Spring3, and Hibernate3, the configuration of MySQL5.0 database has the advantages of simple and easy to learn, the style of programming language is uniform, and the functions can be completed simply by using a few words. The SQL language is unified, simple, and easy to learn, all functions can be realized by combining a few English words, and this standardization makes it show its unique advantages in data storage and update.

3.2. Implementation of System Functions

3.2.1. User Login Implementation. When designing the system login interface, the designers and developers generally use two security technologies to ensure the stability of the system and its safe operation. When users enter their own accounts and passwords, the user accounts and permissions are judged by the system code, and only when the visitors enter the correct accounts and passwords can they successfully enter the system to complete various operations. If the system suggests that the user has entered an incorrect account number or password, the system will restrict the visitor's access to the system and warn the illegal visitor in an appropriate way.

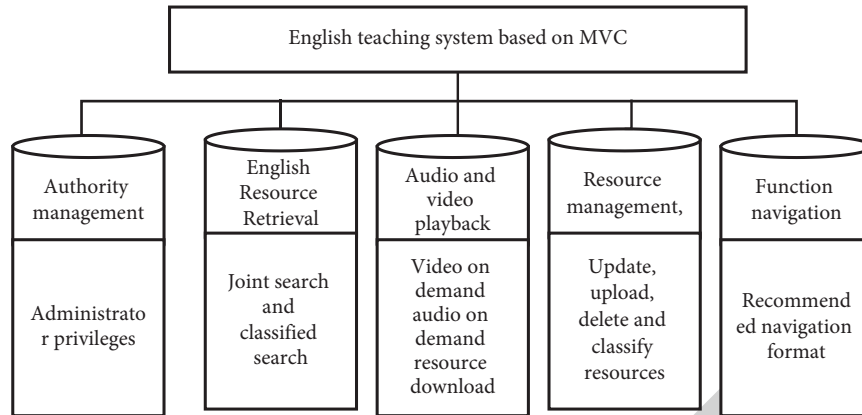


FIGURE 2: Overall architecture of English teaching system.

3.2.2. Implementation of Third-Party Insertion Operation. In this paper, we would like to play the English audio/video material smoothly by inserting the corresponding player in the interface. Therefore, in the development process, we chose the ActiveX control technology, which is based on the principle of inserting an ActiveX control into the HTML file by using the object tag and accessing this space smoothly by using JavaScript.

3.3. Analysis of Application Examples. With the rapid development of computer technology, nowadays, most of the new resources for teaching English in schools are saved in the form of audio and video, which requires higher requirements in terms of real-time transmission and certain quality assurance; RTP/RTCP can provide real-time transmission control services for streaming media and has QoS to ensure that the purpose of teaching resources transmission can be achieved through this protocol. RTP/RTCP real-time video transmission can be based on compression coding to collect English teaching video to perform compression coding operations; the most basic process includes video capture, encoding, decoding, and other operations, as shown in Figure 3.

On the server side, the collected audio and video information is used to generate the corresponding data source through compression coding. If a user requests access to the data information, the server receives the request information, generates a transmission channel at both the client and server endpoints, and then encapsulates the data source information in RTP packets to meet the actual needs of the client. At the same time, the RTCP feedback information is used to monitor the packet loss rate and the quality of service [21, 22].

4. Teaching System Architecture

Multimedia technology is based on animation, image, and other technologies as the core, and the content involves many fields such as communication, communication, and education. The multimedia-assisted teaching system is a new teaching method designed based on multimedia technology,

which includes computer host, input/output devices, storage devices, and logic layer. The system architecture is shown in Figure 4.

In this paper, the logic layer is the core of the system design. Only by ensuring the smooth operation of the theoretical knowledge module, experiment module, and student practice module in the logic layer can the purpose of teaching system design be effectively realized. In this paper, the system design takes the teaching of the inaccuracy relationship in quantum mechanics as an example, and the specific module design is as follows.

4.1. Theoretical Knowledge Module Based on Conceptual Network. Conceptual network is an exploration of artificial intelligence research, using concepts as the basic nodes for describing objective things and the knowledge representation framework system of the association between things. Conceptual networks can integrate cognition, understanding, reasoning, and behavior into a whole and are used to guide the judgment and processing of intelligent systems for expected behaviors. A conceptual network consists of three elements: attributes, behaviors, and relationships [23, 24]. Attributes are inherent properties of things, behaviors are used to distinguish conceptual networks from other networks, and relationships are simple or complex associations formed between concepts. Conceptual network can produce a rule reasoning process, which is used to reflect the behavior of different concepts, so that a large number of rules in the physics teaching system can be attached to the knowledge system construction framework formed by the conceptual network, different things in different fields can form different knowledge systems based on their own characteristics and at the same time based on the framework, and this knowledge system construction method is more in line with the human thinking mode. The conceptual network is applied to the theoretical knowledge module to form the theoretical knowledge system, as shown in Figure 5.

4.2. Experimental Module. The teaching of the inaccuracy relationship of quantum mechanics includes the experiments of electron single slit diffraction, diffraction

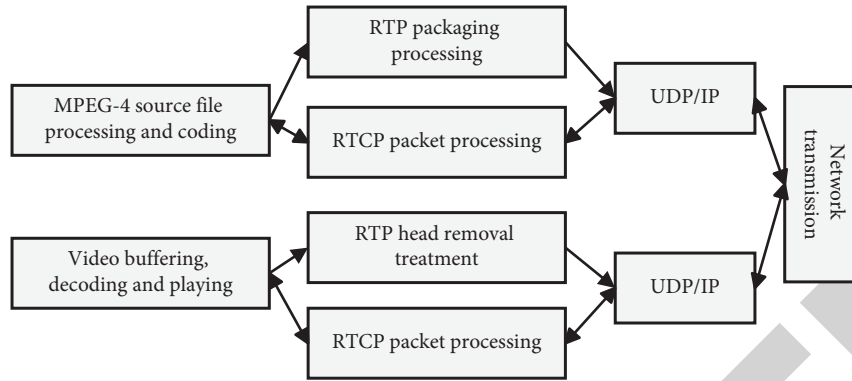


FIGURE 3: Real-time video transmission operation.

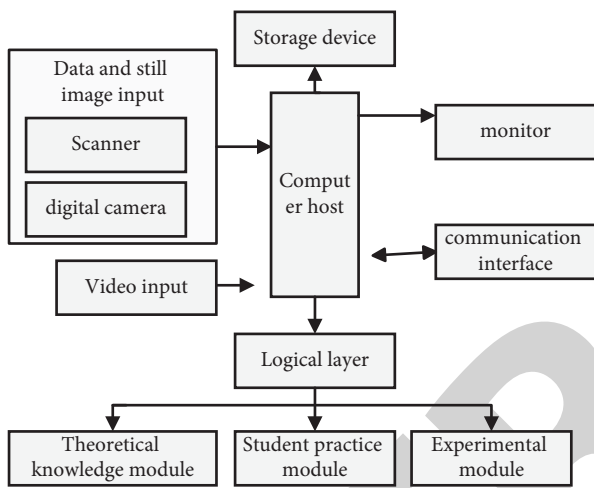


FIGURE 4: Architecture of physics multimedia-assisted teaching system.

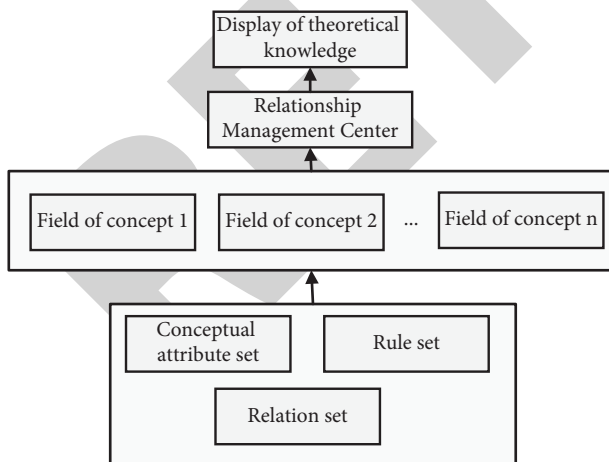


FIGURE 5: Conceptual network theory knowledge system.

influencing factors, and the study of the number of incident particles. The experiments for variables such as single slit width are done by scrolling bars, and through the experimental settings, it is possible to apply the theoretical knowledge to reality and clearly show the particle diffraction

streaks and the curve distribution using images and animations. The image design includes wave function and probability distribution diagram. The animation is an image that is dynamically displayed on the computer with regularity, and the animation is designed with a strong sense of realism, which can increase the interest in teaching. The images and animations formed in the experimental module design are realized through computer programming [25].

4.3. *Student Practice Module.* The design of the multimedia-assisted teaching system needs to incorporate the student-oriented education idea advocated in the current education field, which is a sign of educational progress and the basis for promoting the development of multimedia-assisted teaching. Based on the theoretical knowledge and experimental module mentioned above, student knowledge is modeled to ensure that student knowledge is consistent with theoretical knowledge and experimental knowledge, and student knowledge is compared with the theoretical knowledge system to form a comparison model, as shown in Figure 6.

In Figure 6, a value of 1 is assigned to each attribute node of the knowledge domain, and a range of values [0, 1] is also set in the student knowledge model. 0 means that the student has no knowledge at all, and 1 means that the student has completely mastered the knowledge of the node. In the initial stage of model construction, the values in the student model are set to 0. The student practice module is designed with several multiple-choice questions to complete the student practice based on the above mechanism and obtain the student behavior. Comprehensive analysis of the above modules can complete the design of multimedia-assisted teaching system of physics based on the concept network, as shown in Figure 7.

5. Experimental Results and Analysis

In order to test the performance of this system and conduct experimental analysis, the hardware configuration required for the operation of this system is 64 GB of internal memory, 256-color graphics card, 125 MB hard disk, and a monitor resolution of 1,024 × 768 pixels. The software configuration required for system operation is Windows XP operating system, data access component is MDAC2.8, and .Net

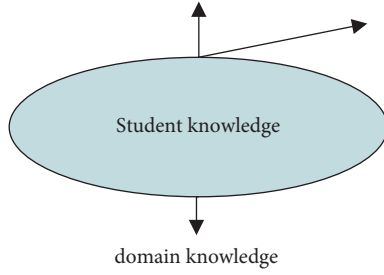


FIGURE 6: Comparison of student knowledge and theoretical knowledge system.

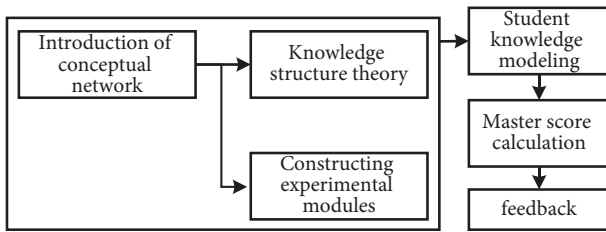


FIGURE 7: Block diagram of multimedia-assisted teaching of physics.

Framework version 2.0 is used for the running environment. The system design is based on the Struts framework, which uses Servlet and JSP technology and has the function of unifying data resources, which can greatly save development time.

In the experimental analysis, 1 million data in the SQL Server database are selected as the data source, of which 500,000 data are used for system training and 500,000 data are used for system testing. The following experimental indexes are selected for experimental validation analysis: system load test and system time consumption.

5.1. Experiment 1. For a complete system, the load capacity size is a direct factor to determine the system performance, this experiment uses Web Application Stress for system load test, and the test parameters settings are shown in Table 1.

The test results were compared with literature [5, 7], and the results are shown in Figure 8.

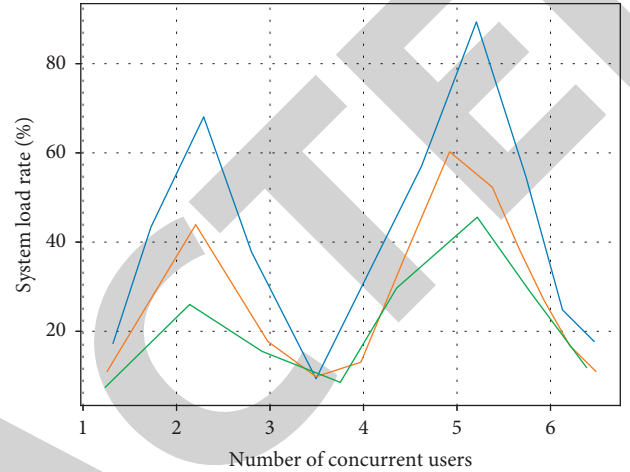
Analysis of Figure 8 shows that no matter how the number of concurrent users changes, the system load rate of this paper is always lower than that of literature [5] and literature [6], and the low load rate means that the system can keep running efficiently for a longer time, which indicates that the system of this paper has better load capacity and is better than other literature methods.

5.2. Experiment 2. The running time of the system in this paper is compared with the systems in literature [5] and literature [7], and the results are shown in Figure 9.

From Figure 9, it can be seen that, with the increase in the amount of test data, the running time of the system in this paper shows a small increase, with the maximum time consumed being 15 s. The curves of literature [5] and literature [6] have a larger change and are more time-

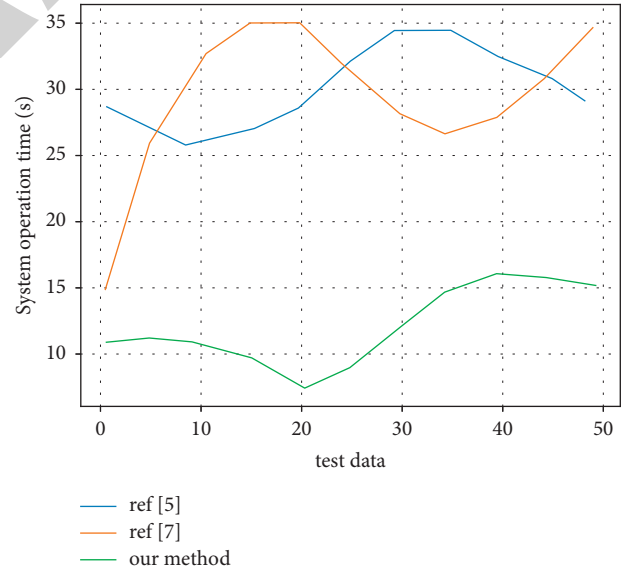
TABLE 1: System load test parameters.

Test parameters	Numerical value
Test tools	Web application stress
Number of concurrent users	7
Running time (S)	5
Line type	Ethernet



— ref [5]
— ref [7]
— our method

FIGURE 8: Comparison of system load test results.



— ref [5]
— ref [7]
— our method

FIGURE 9: Comparison of system running time.

consuming, with a maximum value of 35 s, which is larger than the system in this paper. The low running time consumption and the significant advantage of the system in this paper are due to the fact that this paper uses conceptual networks to construct theoretical knowledge models and forms a knowledge representation framework, and the construction of this framework structure greatly reduces the complexity of model construction and saves time.

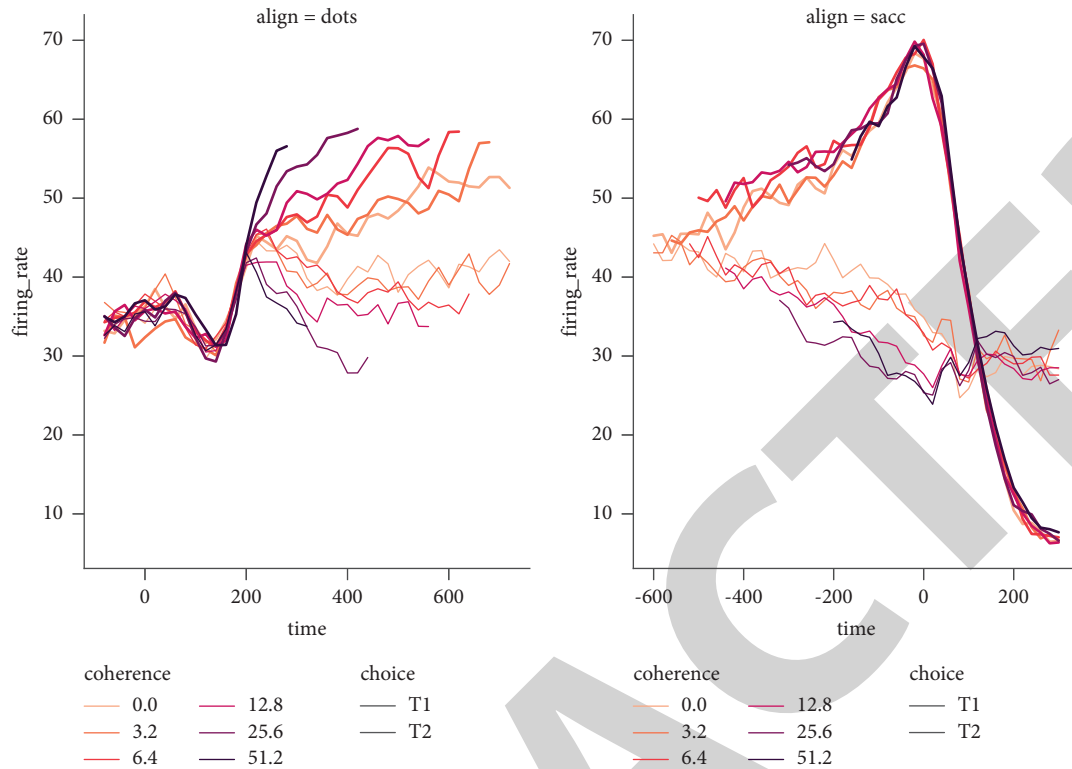


FIGURE 10: Effect of teaching English with different media.

The use of computer-assisted multimedia teaching systems has provided us with great convenience in this area. Its role is to apply modern technology to stimulate and motivate students to think, to inspire their thinking, and to cultivate their ability to find, think, and solve problems. Due to the inertia of thinking, when we use multimedia-assisted teaching, most of the courseware is still stuck in only using the computer to show the phenomenon and impart knowledge, and many of them simply copy and electronize the textbook knowledge. As shown in Figure 10, teachers do not leave enough time for thinking, do not teach in a heuristic way, and show students all through multimedia, which will kill students' ability of independent learning and thinking over time. Therefore, when we design the courseware, we should start by improving students' ability and creating problem situations as much as possible to stimulate students' thinking so as to accelerate students' development. In multimedia-assisted English teaching, if we can pay attention to these problems, use the multimedia teaching system reasonably, create the situation of learning English, and let the advanced modern tools for teaching services so that students can perceive the English language materials through audio-visual.

6. Conclusion

Multimedia-assisted teaching system is a new mode of modern teaching, which can help teachers teach and assist students in completing independent learning. This paper designs a multimedia teaching system based on the concept network. The system design is completed by describing the

theoretical knowledge module, experiment module, and student practice module based on the concept network. And the good performance of the system is verified through experiments, which has a certain reference value. However, there are still some shortcomings in the system design, and the interactive performance between students and teachers is not analyzed. In the subsequent research, we will focus on the analysis of the interactivity and further improve the system performance.

Data Availability

The experimental data used to support the findings of this study are available from the corresponding author upon request.

Conflicts of Interest

The author declare no conflicts of interest regarding this work.

Acknowledgments

The author is grateful to document [26], from which ideas and benchmark schemes were obtained.

References

- [1] N. Yue, "Computer multimedia assisted English vocabulary teaching courseware," *International Journal of Emerging Technologies in Learning (IJET)*, vol. 12, no. 12, p. 67, 2017.

Research Article

Design of Optimum Portfolio Scheme Based on Improved NSGA-II Algorithm

Yiqian Zhou,¹ Weinan Chen,¹ and Deqin Lin ²

¹Faculty of Business, City University of Macau, Macau 999078, China

²Faculty of Finance, City University of Macau, Macau 999078, China

Correspondence should be addressed to Deqin Lin; dqin@cityu.mo

Received 12 April 2022; Accepted 24 May 2022; Published 13 June 2022

Academic Editor: Le Sun

Copyright © 2022 Yiqian Zhou et al. This is an open access article distributed under the Creative Commons Attribution License, which permits unrestricted use, distribution, and reproduction in any medium, provided the original work is properly cited.

In the financial industry, it is of great significance to study the multiobjective portfolio optimization for obtaining a reasonable investment strategy. This paper designs the financial portfolio scheme based on the multiobjective optimization algorithm that is based on the framework of the NSGA-II algorithm. In order to introduce convergence information, aiming at the actual problem of the portfolio, the mixed individual coding mechanism with asset information expands the application of the multiobjective evolutionary algorithm in portfolio optimization. The portfolio scheme obtained is effective, which is helpful to improve the decision-making efficiency of financial investors and enriches the application of modern financial theory.

1. Introduction

With the rapid development of the financial market, investment and financial management are no longer limited to a single way of saving with more investments in securities. How to use more scientific and rational investment strategies to realize capital appreciation has become a problem that investors must consider and pay attention to. Generally speaking, the purpose of investment and financial management is to maximize the income, but benefits and risks often exist at the same time. A portfolio can spread risks, and the key lies in how to allocate assets and how to deal with the relationship between risks and benefits.

At present, the financial industry, as one of the important components of China's economy, has been widely concerned by people in various fields. In reality, the investment fields and fund types are complicated, so the essence of designing a relatively optimal portfolio is a high-dimensional multiobjective optimization problem [1–4]. Meanwhile, the heuristic algorithm can get a satisfactory solution in polynomial time, such as evolutionary algorithm, simulated annealing algorithm, artificial neural network, and quantum algorithm [5–7]. Because of the inherent multiobjective nature of portfolio problem, many scholars

usually use a multiobjective evolutionary algorithm to solve it, such as weighting method, constraint method, objective programming method, and minimax method. A multiobjective optimization algorithm does not need to obtain the derivative information of the problem nor does it need to aggregate optimization objectives with different properties. It can deal with enormous scope search space autonomously, where the problem can be solved by parallel search of cyclic iteration, and the average fitness of the species is improved generation by generation to approach the global optimal solution [8, 9]. Therefore, the customized improvement of the problem model can not only expand its related research but also help to advance the decision-making efficiency of investors.

2. Theoretical Basis of Portfolio

With the rapid development of science and technology and the continuous improvement of the financial system, China's financial market is actively integrated with foreign countries where financial products are becoming more diversified, and bonds, stocks, futures, foreign exchange, and various Internet financial derivatives are gradually moving towards the investment scope of ordinary people [10]. Investment is the

act of converting funds into assets or capital in a certain period of time, so as to obtain economic returns or value-added benefits. No matter what kind of investment is made, the purpose is to obtain higher returns. However, benefits and risks often coexist. Investors want to get as many benefits as possible and at the same time bear as little risk as possible. Therefore, how to maintain and increase the value of assets through investment and financial management is a great challenge.

2.1. Single Investment. The quantitative relationship is applied to the research of portfolio theory, the benefits and risks are quantified, and the two goals of maximizing benefits and minimizing risks are put forward to solve the problems of selection of financial products and allocation of capital proportion for investors [11, 12].

In actual investment activities, the average historical real rate of return is usually used to replace the expected rate of return to measure the pros and cons of the portfolio. Assuming that there are M securities in the securities pool, the actual rate of return of securities is calculated as shown in the following formula:

$$r_i = \frac{S_i(t) - S_i(0)}{S_i(0)}, \quad (1)$$

where r_i is the actual rate of return of a security, $S_i(t)$ is the closing price of the securities at the end of the holding period, and $S_i(0)$ is the closing price of the securities at the initial stage of the cycle.

The company's operation and performance usually have certain stability; therefore, the average historical actual rate of return can be used as the estimate of the expected rate of return of the securities. Assuming that vector $R_i = (r_i^1, r_i^2, \dots, r_i^T)^T$ represents the vector composed of multiperiod historical return rate of the i th asset, so the expected return rate is shown in the following formula:

$$\bar{R}_i = E(R_i) = \sum_{t=1}^T r_i^t p_i^t, \quad (2)$$

where \bar{R}_i is the expected return on a security, T is the number of periods with the historical real return, r_i^t is the real return on the security in term t , and p_i^t is the probability that the real return is r_i^t .

In investment activities, it is uncertain to use the historical rate of return to estimate the expected rate of return because the real return may be higher than expected or lower than expected, which is the risk faced by many investors. Therefore, the risk needs to be quantified by the variance of the expected rate of return. For a single security, the risk can be calculated by the following formula:

$$\sigma^2 = D(R_i) = \sum_t (r_i^t - \bar{R}_i)^2 p_i^t. \quad (3)$$

The above formula uses the volatility of security returns; that is, the variance σ^2 of the expected return rate of a security is adopted to quantify the risk. The larger the variance

is, the greater the deviation between the actual return rate and the expected return rate is, which indicates that the returns of security are highly uncertain, and the investment risk is strong.

2.2. Portfolio Investment. Assuming a portfolio chooses N sorts of resources from the protections pool and joins them as indicated by a specific venture proportion, then in a certain investment cycle, the pay of the portfolio is measured by the weighted normal amount of the return paces of every resource, which can be calculated by the following formula:

$$r_p = \sum_{i=1}^N x_i \bar{R}_i, \quad (4)$$

where r_p represents the expected return rate of the portfolio and x_i represents the proportion of the i th asset in the portfolio, which meets the budget constraint $\sum_{i=1}^N x_i = 1$, $x_i > 0$, \bar{R}_i .

In the actual market, all kinds of securities are not completely independent, and there are always some connections. This correlation between securities is usually expressed by covariance, which is the expectation to measure the overall error between two variables [13]. In the actual portfolio, investors usually want to choose some unrelated assets as far as possible to spread the risk as much as possible, so set $R = (R_1, R_2, \dots, R_N)^T$ as the actual rate of return of each security in the portfolio, and the covariance between i and j securities is calculated by the following formula:

$$\begin{aligned} \sigma_{ij} &= \text{cov}(R_i, R_j) \\ &= \frac{1}{T} \sum_t (r_i^t - \bar{R}_i)(r_j^t - \bar{R}_j). \end{aligned} \quad (5)$$

Using variance σ_p^2 as a measure of portfolio risk, we should consider not only the characteristics of individual securities but also the relationship between them. The portfolio risk is expressed by the following formula:

$$\begin{aligned} \sigma_p^2 &= D(R) \\ &= \sum_i \sum_j x_i x_j \sigma_{ij}. \end{aligned} \quad (6)$$

3. Multiobjective Optimization Algorithm

3.1. Algorithm Design. NSGA-II algorithm is a far-reaching multiobjective optimization algorithm at present. Since it was put forward, because of its simplicity and high efficiency, this algorithm has become one of the basic algorithms in problems of multiobjective optimization [14]. As shown in Figure 1, the main advantages of this algorithm compared with traditional NSGA are as follows.

- (1) The fast nondominated sorting algorithm reduces the computational complexity from the original mN^3 to mN^2 , where n is the species size and m is the quantity of goal capacities.

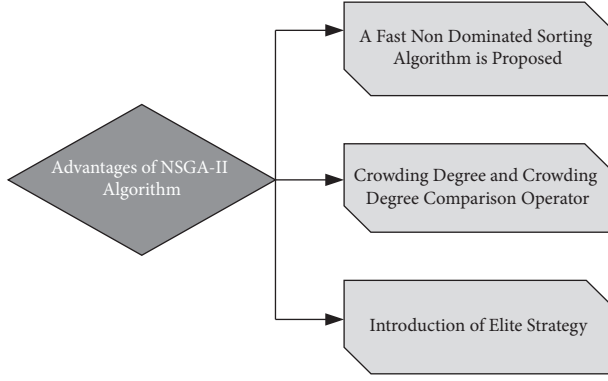


FIGURE 1: Advantages of NSGA-II algorithm.

- (2) The addition of the crowding degree and crowding degree comparison operator not only solves the shortcoming of artificial designation of shared parameters in the algorithm but also enables the species to be homogeneously extended to the whole Pareto domain through crowding degree, thus ensuring the diversity of the species.
- (3) Introduction of elite strategy and expansion of sampling space combine the parent and the offspring together to produce the next generation of the species by competition is beneficial to preserve the excellent individuals of the previous generation of the species. At the same time, the stratified storage of individuals in the species reduces the loss of the best individuals, improves the overall level of the species, and greatly optimizes the accuracy of the algorithm.

The NSGA-II algorithm adopted in this paper can improve the diversity of the species and make the level of the species improve rapidly. The flow chart of the algorithm is shown in Figure 2.

- (1) Initialize the species and set its size as n , after the nondominated sorting of the species with the size of n , execute the traditional genetic algorithm, and obtain the first-generation progeny species through crossover, mutation, and selection
- (2) Combine the parent and offspring species into a species, calculate the crowding degree of individuals in the nondominant layer simultaneously through rapid nondominant sorting, and select suitable individuals to form a new parent species by using crowding degree and nondominant relationship
- (3) Generate a new progeny species through the basic operations of crossover, mutation, and selection in a traditional genetic algorithm, and repeat the above steps until the maximum number of iterations is met

3.2. Optimized Algorithm. t-SNE algorithm is introduced to reduce the problem of target redundancy in high-dimensional multitargets, which greatly decreases the running time and the load of devices and improves the accuracy of the algorithm. The flow chart is shown in Figure 3.

Firstly, the original target set I_0 was selected to initialize the species, and then, the NSGA-II algorithm was performed to optimize the species to form a new parent species P_0 . Then, t-SNE algorithm is optimized for P_0 to obtain the nonredundant target set I_1 . Finally, the above steps are repeated until the maximum number of iterations is satisfied, and the species $P_2, P_3, \dots, P_{t-2}, P_{t-1}$, and target set I_3, \dots, I_t , when $I_{t-1} = I_t$, the Pareto optimal solution P_{t-1} of the target set can be obtained.

3.3. Implementation Process of Algorithm. Assuming that the number of targets is N , the target set is I_t , and gen is the number of iterations.

- (1) Set $t = 0$, the initial target set is $I_0 = \{1, 2, \dots, N\}$, and then, the species of the target set is initialized. P , where selection, suitable individuals are selected to form a new parent species P_0 by fast nondominated sorting and calculating crowding degree. The binary crossover can be simulated as follows:

$$\begin{aligned} x_{1j}(t) &= 0.5 * [(1 + \gamma_j)x_{1j}(t) + (1 - \gamma_j)x_{2j}(t)], \\ x_{2j}(t) &= 0.5 * [(1 + \gamma_j)x_{1j}(t) + (1 - \gamma_j)x_{2j}(t)]. \end{aligned} \quad (7)$$

Among them,

$$\gamma_j = \begin{cases} (2u_j)^{1/(n+1)}, & u_j < 0.5, \\ \left(\frac{1}{2(1-u_j)}\right)^{1/(\eta+1)}, & \text{else.} \end{cases} \quad (8)$$

- (2) Calculate the pairs of Euclidean distances between samples of P_0 species, and calculate the joint probability p_{ij} between pairs of data points in high-dimensional space.

$$p_{ij} = \frac{p_{j|i} + p_{i|j}}{2n}, \quad (9)$$

where δ_i represents the variance of the Gaussian function centered on the data point, x_i represents the initial population characteristic matrix, and p_{ji} represents the conditional probability of similarity between the data point x_i and data point x_j of the species characteristic matrix.

$$p_{j|i} = \frac{\exp(-x_i - x_j^2/2\delta_i^2)}{\sum_{k \neq i} \exp(-x_i - x_k^2/2\delta_i^2)}. \quad (10)$$

- (3) Calculate joint probability q_{ij} between low dimensional spatial data point pairs in P_0 Eigenmatrix.

$$q_{ij} = \frac{(1 + y_i - y_j^2)^{-1}}{\sum_{k \neq l} (1 + y_l - y_k^2)^{-1}}, \quad (11)$$

where y_i, y_j, y_l , and y_k represent the data point of the species characteristic matrix.

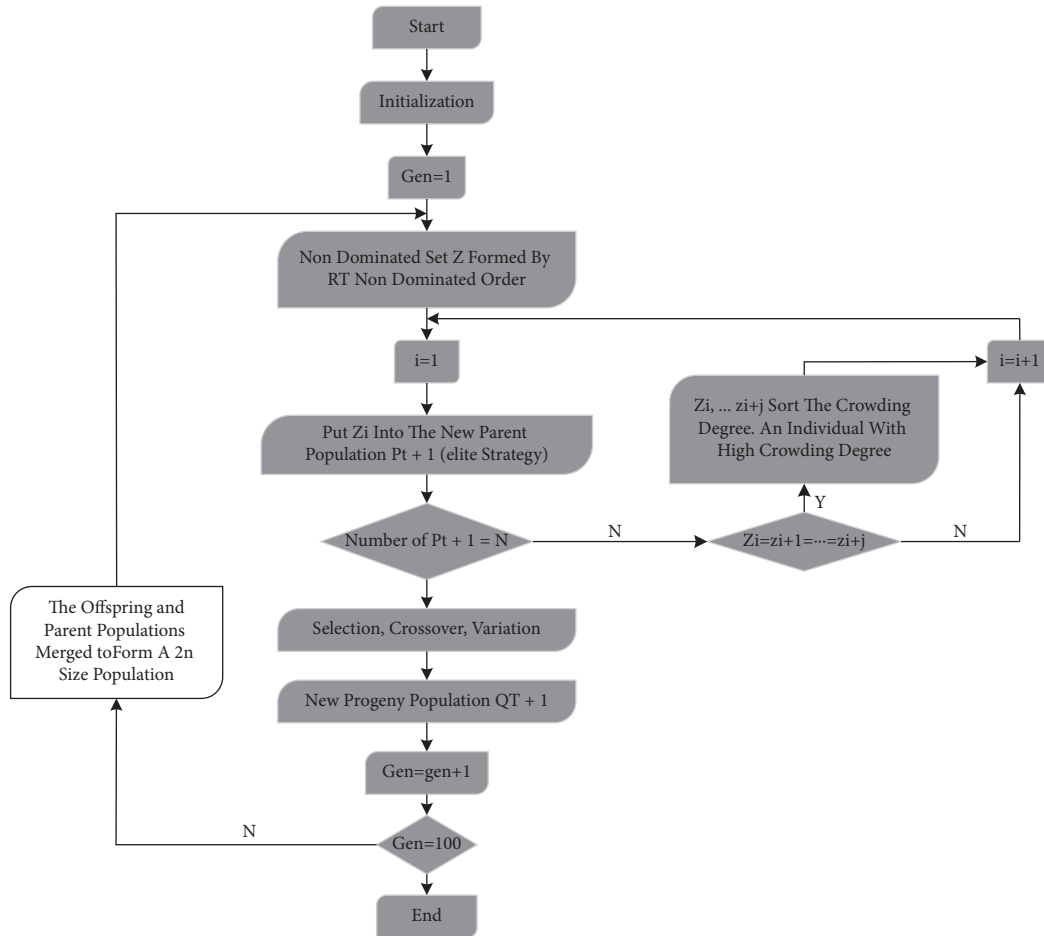


FIGURE 2: Flow chart of NSGA-II algorithm. The fundamental advances are as per the following [15, 16].

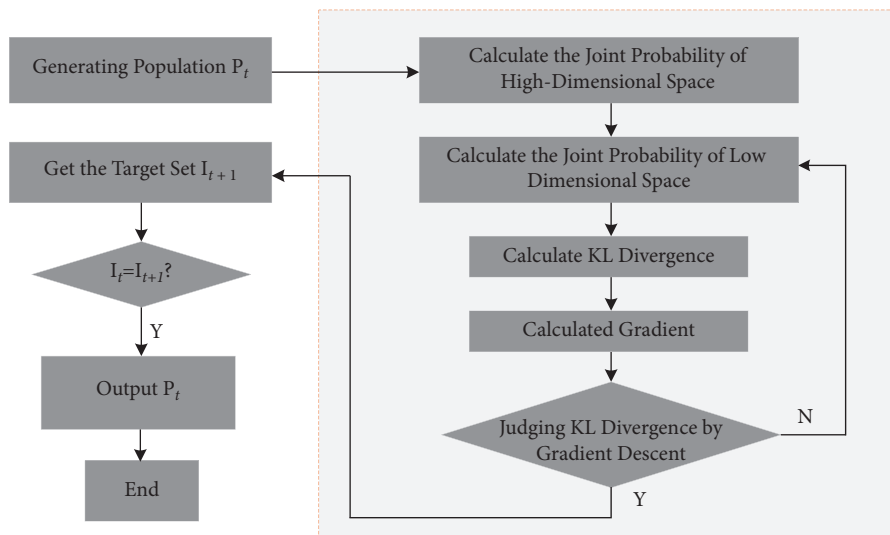


FIGURE 3: Algorithm optimization based on *t*-SNE.

- (4) Calculate the KL divergence between p_{ij} and q_{ij} , and work out the objective function C :

$$C = \text{KL}(PQ) = \sum_i \sum_j p_{ij} \log \frac{p_{ij}}{q_{ij}}. \quad (12)$$

- (5) Solve the gradient of P and Q :

$$\frac{\delta C}{\delta y_i} = 4 \sum_j (p_{ij} - q_{ij})(y_i - y_j)(1 + y_i - y_j^2)^{-1}. \quad (13)$$

- (6) Get the target set I_1 , and repeat (1) ~ (5) until the set maximum iteration algebra is met, and the species is obtained. $P_2, P_3, \dots, P_{t-2}, P_{t-1}$ and target set I_3, \dots, I_t , when $I_{t-1} = I_t$, and find the Pareto optimal solution of the target set P_{t-1} .

Calculate the target set I_1 , and repeat step (1) ~ (5) until the maximum iteration algebra is satisfied, and the species $P_2, P_3, \dots, P_{t-2}, P_{t-1}$ and target set I_3, \dots, I_t , when $I_{t-1} = I_t$, the Pareto optimal solution P_{t-1} of the target set can be obtained.

4. Multiobjective Portfolio Model

4.1. Problem Description. The financial market has many nonrandom factors, such as fuzziness and uncertainty. Therefore, this paper tries to express the fuzzy uncertainty of the financial market with fuzzy theory. Investors usually refer to financial intermediaries. The main reason why diversified investment reduces the risk is that the correlation of different types of companies is poor or even negative. After the formation of the portfolio, the correlation of the portfolio is dissolved, so that the variance of the portfolio decreases; that is, the risk decreases. In investment theory, diversified investment is common that it can effectively reduce risks [17, 18]. Based on the fuzzy theory, a profit-risk optimization model is established with constraints, where the profit and risk are regarded as two optimization objectives in the model.

Assuming that R represents all real numbers, A is the convex fuzzy number defined on R with continuous membership function $\mu_A(x)$, and F is the whole fuzzy set defined on the real number field R .

Definition 1. Assume $A \in F$, $[A]_\gamma = [a(\gamma), \bar{a}(\gamma)]$ ($\gamma \in [0, 1]$), and A represents the γ -horizontal cut set, then the probability mean of fuzzy number A is defined as

$$E(A) = \int_0^1 \gamma [\underline{a}(\gamma) + \bar{a}(\gamma)] d\gamma, \quad (14)$$

$$\text{Var}(A) = \int_0^1 \gamma [(E(A) - \underline{a}(\gamma))^2 + (E(A) - \bar{a}(\gamma))^2] d\gamma.$$

Lower half probability variance of A is

$$\text{Var}^-(A) = 2 \int_0^1 \gamma (E(A) - \underline{a}(\gamma))^2 d\gamma. \quad (15)$$

Upper half probability variance of A is

$$\text{Var}^+(A) = 2 \int_0^1 \gamma (E(A) - \bar{a}(\gamma))^2 d\gamma. \quad (16)$$

If $A = (a, b, \alpha, \beta)$ is a trapezoidal fuzzy number, its membership function $\mu_A(x)$ is shown in Figure 4.

$$\mu_A(x) = \begin{cases} \frac{x - (a - \alpha)}{\alpha}, & a - \alpha \leq x \leq a, \\ 1, & a \leq x \leq b, \\ \frac{b + \beta - x}{\beta}, & b \leq x \leq b + \beta, \\ 0, & \text{else.} \end{cases} \quad (17)$$

So, the γ -horizontal cut set of trapezoidal fuzzy number A is $[A]^\gamma = [a - (1 - \gamma)\alpha, b + (1 - \gamma)\beta]$, $\forall \gamma \in [0, 1]$.

In this paper, we consider the following constraints [19]:

- (1) Constraint on the number of portfolio assets: in the process of real investment decision-making, there are certain requirements for the number of assets held. Assume that the maximum number of assets held is M , then the constraint is $\sum_{i=1}^n \text{sign}(x_i) = M$.
- (2) Investment ratio constraint: the sum of investment ratios for each asset should be 1. Namely, $\sum_{i=1}^n x_i = 1$.

4.2. Model Building. As skewness is introduced as a new goal, cardinality constraints and upper and lower bound constraints are added, historical data are replaced by

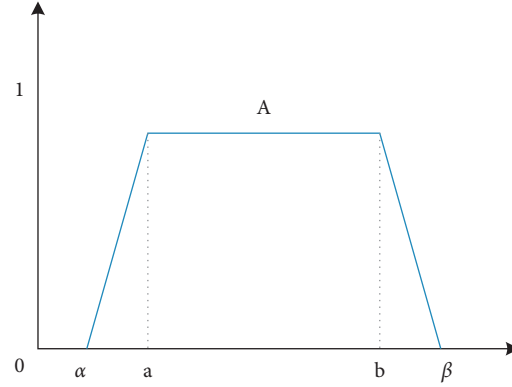


FIGURE 4: Membership function of fuzzy number A.

predicted returns, and the specific portfolio model is shown in function (18).

$$\begin{aligned}
 \max R(\mathbf{x}) &= \mathbf{X}^T \bar{\mathbf{R}} = \sum_i^n x_i \bar{R}_i, \\
 \min V(\mathbf{x}) &= \mathbf{X}^T \mathbf{V} \mathbf{X} \\
 &= \sum_{i=1}^n \sum_{j=1}^n x_i x_j \sigma_{ij}, \\
 \max S(\mathbf{x}) &= E(\mathbf{X}^T (\mathbf{R} - \bar{\mathbf{R}}))^2 \\
 &= \sum_{i=1}^n x_i^3 s_i^3 + 3 \left(\sum_{i=1}^n x_i^2 x_j s_{ijj} + \sum_{j=1}^n x_i x_j^2 s_{ijj} \right) (i \neq j), \\
 \text{s.t. } \sum_{i=1}^n x_i &= 1, \\
 \sum_{i=1}^n K_{\min} &\leq \theta_i \leq K_{\max}, \quad l_i \theta_i \leq x_i \leq u_i \theta_i, \quad i = 1, 2, 3, \dots, n, \quad \theta_i \in \{0, 1\}, \quad i = 1, 2, \dots, n.
 \end{aligned} \tag{18}$$

Among them,

n is the number of available assets

X is the weight vector formed by the proportion of investment into various assets when each goal achieves the optimal tradeoff

x_i is the proportion invested in the i th asset; \bar{R}_i is the expected return on the i th asset

σ_{ij} is the return covariance between asset i and asset j

s_i^3, s_{ii} , and s_{ijj} are skewness and oblique skewness

$R(x)$ is the expected return on the portfolio x

$V(x)$ is the return variance of the portfolio x

$S(x)$ is the skew of the portfolio x

θ_i specifies whether an asset θ_i exists in the portfolio

K_{\min} and K_{\max} are the minimum and maximum number of assets allowed in a portfolio

l_i and u_i are the lowest and highest proportion of the investment in asset i to the total investment, respectively

The advancement objective of the model is to limit the gamble of the portfolio and expand the normal return of the portfolio and the skewness of the portfolio. Therefore, constraints conclude budget constraints, upper and lower limit constraints, and cardinality constraints. Cardinality constraint ensures that the number of assets in the portfolio is within a certain range where substantial diversified income can be achieved by owning 6 to 15 stocks [20].

4.3. Model Solution

4.3.1. *Test Index.* Generation distance (GD) and spatial distribution (SS) are selected to test the convergence and accuracy of the algorithm in this paper.

GD refers to the average minimum distance from each point in the solution set P to the reference set P' , indicating the degree of deviation from the truly optimal boundary. The larger the GD value, the farther away from the true optimal boundary, and the worse the convergence. The specific calculation formula is as follows:

$$GD(P, P') = \frac{\sqrt{\sum_{i=1}^n d_i^2}}{n}, \quad (19)$$

where n is the number of points on the Pareto frontier and d_i is the minimum Euclidean distance between an individual and the real Pareto frontier.

SD indicates the extent of the obtained solution set. The smaller the value of SD, the more homogeneous the solution set. The specific calculation formula is as follows:

$$\Delta = \frac{d_f + d_l + \sum_{i=1}^{N-1} |d_i - \bar{d}|}{d_f + d_l + (N-1)\bar{d}}. \quad (20)$$

4.3.2. Test Environment. The hardware environment used in this experiment is Intel Xeon (R) CPU ES-2620V4 @ 2.10 GHz, NVIDIA Quadro M4000 GPU, and the running memory is 32G. In addition, the experiment is realized by Matlab simulation. In order to test the performance of the algorithm under different numbers of the target, they are set as 3, 5, and 10, respectively, in the test function. DTLZ (I, M) represents the spatial distribution of targets in the I dimension, where I is the target dimension and M is the number of target objects. The specific parameters are shown in Table 1.

4.3.3. Test Results. Function (18) was tested with the NSGA-II algorithm and its improved algorithm, respectively, running independently for 10 times, and the test indexes were GD and SD. The experimental results are shown in Table 2.

Table 2 shows that the indicators of GD and SD obtained by the improved algorithm are $2.6509E-05, 0.33982$, respectively; the GD and SD of the NSGA-II algorithm are $5.7065E-02$ and 0.35211 , respectively, which shows that the optimization algorithm has the smallest deviation from the real optimal boundary, the best convergence, and the smallest breadth of the solution set. Therefore, the optimized multiobjective algorithm has better convergence, and the distribution of the solution set is more homogeneous.

5. Evaluation of Portfolio Design

5.1. Scheme Analysis. By taking the fund as an example, if the original capital Y yuan is used for financial investment, then the investment in $A, B, C, D,$ and E funds can be expressed as

$$\begin{aligned} Y &= A + B + C + D + E, \\ W &= aW_A + bW_B + cW_C + dW_D + eW_E, \end{aligned} \quad (21)$$

where Y is the original fund, a, b, c, d, e and W_A, W_B, W_C, W_D, W_E are the weight and income of funds

TABLE 1: Test parameters.

Name	Expression	Value
Species size	Species size	500
Evolutionary algebra	Generation	10000
Variation probability	Pm	0.1
Cross probability	Pc	0.9
Data dimension	V	12
Analog binary crossover parameter	L	50
Polynomial variation parameter	U	5

TABLE 2: Model test results.

Test categories		NSGA-II	Improved NSGA-II
Generation distance	Standard	$5.7065E-02$	$2.6509E-05$
	Error	$2.1500E-03$	$4.9200E-05$
Spatial distribution	Standard	0.35211	0.33982
	Error	0.00977	0.0103

invested in A, B, C, D, E , respectively, and W is the total income.

5.2. Evaluation Indicators. The raw data of this experiment come from the daily trading data of Chinese funds from December 2014 to December 2021, which contains transaction data of various fund prices, each of which consists of time, opening price, maximum price, minimum price, closing price, increase rate, and turnover rate. The daily price data of 10 kinds of funds are selected as experimental data, and only 733 fund price data are selected.

In this paper, the mainstream measurable performance indicators of investment in the current market are adopted, namely, the annual rate of profit, sharp ratio, and forecast rate of profit [21, 22].

(1) Annualized rate of profit

The annualized rate of profit is a measure of the profitability of investors during the investment period of one year

$$\text{Annualized rate of return} = \frac{\text{Income/capital}}{\text{Investment days}/365} \times 100\%. \quad (22)$$

(2) Sharp ratio

Sharp ratio is a standardized index to evaluate the fund performance

$$\text{Sharpe Ratio} = \frac{E(R_p) - R_f}{\sigma_p}, \quad (23)$$

where $E(R_p)$ represents the expected return rate of risk asset portfolio; R_f is the risk-free rate of return, which can be replaced by the interest rate of 10-year Treasury bonds, that is, 2.85%; $E(R_p) - R_f$ is the risk premium. When the Sharp ratio < 0 , the return on investment is not as good as the return on Treasury bonds.

TABLE 3: Weight of portfolio.

Serial number	NSGA-II algorithm	Optimization algorithm
1	0.265	0
2	0.102	0.196
3	0.249	0.185
4	0	0
5	0.127	0.287
6	0.164	0.234
7	0	0
8	0.045	0.060
9	0	0
10	0.048	0.038

TABLE 4: Performance evaluation.

	NSGA-II algorithm	Optimization algorithm
Annualized rate of profits/%	37.60	41.25
Forecast rate of profits/%	63.24	70.08
Sharp ratio/%	74.26	93.65

(3) Predicted rate of profit

The estimated pace of profit from the venture, otherwise called the speculation benefit rate, alludes to the proportion of the absolute yearly net gain of the speculation plan to the all speculation of the plan in a year subsequent to arriving at the planned limit of creation

$$\text{Predicted rate of profit} = \frac{\text{Annual pre-tax profit}}{\text{Total investment of project}} \times 100\% \quad (24)$$

5.3. *Analysis of Results.* The multiobjective portfolio model algorithm mentioned above is iterated for 50 times to get the weight of each industry coefficient in the scheme of the portfolio. The results are shown in Table 3.

According to a certain capital, the annual return, investment profit, and Sharp ratio within 2 years are calculated, respectively, according to the portfolio scheme obtained by NSGA-II and its optimization algorithm, as shown in Table 4.

From the data in the table, it can be seen that the annualized profits of the portfolio scheme within two years obtained by NSGA-II and its optimization algorithm are 37.60% and 41.25%, respectively. The predicted profits on investment are 63.24% and 70.08%, respectively; the Sharp ratio of the two portfolio schemes is greater than 0, which indicates that the income of investment exceeds that of the Treasury bonds. Therefore, the portfolio scheme obtained by the multiobjective optimization algorithm is the best.

6. Conclusion

Based on the portfolio theory, this paper introduces the t-SNE optimized NSGA-II algorithm to establish a

multiobjective portfolio model for the multiobjective optimization of portfolio investment in the financial industry, where the expected return, risk, skewness, and other indexes of securities are quantified, and the solving algorithm of the model is evaluated by the generation distance and spatial distribution. The evaluation results show that the annualized profits of the portfolio scheme obtained by the optimized algorithm are 41.25%, the predicted profits on investment are 70.08% within two years, and its evaluation of performance is higher than that of the NSGA-II algorithm.

Data Availability

The dataset can be accessed upon request.

Conflicts of Interest

The authors declare that they have no conflicts of interest.

Acknowledgments

This work was supported by the Research on Production Factors of Financial Industry Development in Macao (project number: MF1827).

References

- [1] B. Javad and S. Fatemi Ghomi, "Multi-objective multi-factory scheduling," *RAIRO-Operations Research*, vol. 55, no. 2, pp. S1447–S1467, 2021.
- [2] H. Li and x. Li, "Research on entropy optimization model in securities portfolio," *Journal of Dalian University of Technology*, no. 1, pp. 157–160, 2005, in Chinese.
- [3] W. Han, Q. Deng, G. Gong, L. Zhang, and Q. Luo, "Multi-objective evolutionary algorithms with heuristic decoding for hybrid flow shop scheduling problem with worker constraint," *Expert Systems with Applications*, vol. 168, no. 12, Article ID 114282, 2021.
- [4] B. Zhang, T. Jiang, X. Zhou, and J. Duan, "A new method of portfolio optimization: mean-Co Va R model," *Statistics and Decision*, vol. 35, no. 11, pp. 67–70, 2019, in Chinese.
- [5] M. Guo, N. Masó, Y. Liu, and A. R. West, "Electrical properties and oxygen stoichiometry of Ba_{1-x}Sr_xTiO_{3-δ} ceramics," *Inorganic Chemistry*, vol. 57, no. 1, pp. 64–71, 2018, in Chinese.
- [6] A. Hitaj and G. Zambruno, "Portfolio optimization using modified herfindahl constraint," *International Series in Operations Research & Management Science*, Springer, Berlin, Germany, pp. 211–239, 2018.
- [7] X. Cui, *Multi-objective Evolutionary Algorithm and its Application*, National Defense Industry Press, Beijing, China, 2006, in Chinese.
- [8] X. Yu, "Introduction to evolutionary algorithms," in *Proceedings of the International Conference on Computers & Industrial Engineering*, July 2010.
- [9] M. Zhu and B. Su, "Communication network path optimization based on fuzzy ant colony convergence control," *Computer Simulation*, vol. 33, no. 5, pp. 272–276, 2018, in Chinese.
- [10] X. Lei and Y. Zhou, "Portfolio selection of Chinese households: good health and risk," *Financial Research*, no. 1, pp. 31–45, 2010, in Chinese.

- [11] L. Yang and L. Yu, "Optimal portfolio analysis based on Markovitz theory," *Accounting Monthly*, no. 22, 2013, in Chinese.
- [12] V. Demiguel, L. Garlappi, and R. Uppal, "Optimal versus naive diversification: how inefficient is the 1/N portfolio strategy?" *Review of Financial Studies*, vol. 22, no. 5, pp. 1915–1953, 2009.
- [13] H. Xiao, "Literature review on optimal capital allocation model," *Finance*, no. 24, pp. 374–376, 2016, in Chinese.
- [14] P. Mauren, R. C. Leborgne, A. R. Herrera-Orozco, and A. Suman, "NSGAI optimization for single phase passive filter allocation in distribution systems," *Electric Power Systems Research*, vol. 176, no. 1, Article ID 105923, 2019.
- [15] Y. Yuan, H. Xu, and B. Wang, "An improved NSGA-II procedure for evolutionary many objective optimization," in *Proceedings of the 2014 Annual Conference on Genetic and Evolutionary Computation*, pp. 661–668, Vancouver, Canada, July 2014.
- [16] K. Deb, R. E. Steuer, R. Tewari, and R. Tewari, *Bi-Objective Portfolio Optimization Using A Customized Hybrid Nsga-ii Procedure*, Springer, Berlin, Germany, 2011.
- [17] Y. Liu and C. Gao, "Mean value of risk portfolio -WcVar fuzzy portfolio optimization model," *China Management Science*, vol. 14, no. 6, 2006, in Chinese.
- [18] C. Carlsson and R. Fullér, "On possibilistic mean value and variance of fuzzy numbers," *Fuzzy Sets and Systems*, vol. 122, no. 2, pp. 315–326, 2001.
- [19] F. Qiu, X. Hu, and L. Wang, "Research on multi-objective particle swarm optimization algorithm based on grouping decomposition," *Miniature microcomputer system*, vol. 38, no. 8, pp. 1824–1828, 2017, in Chinese.
- [20] G. Y. N. Tang, "How efficient is naive portfolio diversification? an educational note," *Omega*, vol. 32, no. 2, pp. 155–160, 2004.
- [21] F. Gu, H.-L. Liu, and K. C. Tan, "A hybrid evolutionary multiobjective optimization algorithm with adaptive multi-fitness assignment," *Soft Computing*, vol. 19, no. 11, pp. 3249–3259, 2015.
- [22] J. Tang, *Performance Evaluation and Analysis of China's Private Equity Investment Fund*, Shanghai International Studies University, Shanghai, China, 2020, in Chinese.

Research Article

Design of Cloud Storage-Oriented Sports Physical Fitness Monitoring System

Zhou Zheng¹ and Yang Liu ²

¹Hulunbuir University, Institute of Physical Education, Inner Mongolia, Hulunbuir 021008, China

²Physical Education Institute of Shanxi Normal University, Shanxi 710119, China

Correspondence should be addressed to Yang Liu; liuyang0330@snnu.edu.cn

Received 1 April 2022; Revised 25 April 2022; Accepted 10 May 2022; Published 10 June 2022

Academic Editor: Le Sun

Copyright © 2022 Zhou Zheng and Yang Liu. This is an open access article distributed under the Creative Commons Attribution License, which permits unrestricted use, distribution, and reproduction in any medium, provided the original work is properly cited.

In order to improve the accuracy and response speed of sports fitness monitoring results and make the monitoring results more comprehensive, a new cloud storage-oriented sports fitness monitoring system is designed. Based on cloud storage technology, the overall framework of the sports fitness monitoring system is established; the function of the hardware module of the monitoring system is analyzed, and distributed database is established. The ray-casting image feature scanning method was used to collect the physical condition monitoring image and generate a high-quality human body target frame to realize the physical condition monitoring. Based on the monitoring data, the fitness method recommendation method is designed according to the user's physical condition. The experimental results show that the monitoring results of the proposed system have higher accuracy, faster system response speed, and higher comprehensiveness of the monitoring results, which verifies the application value of the proposed system.

1. Introduction

With the application of computer-related technology in the field of sports [1], sports-related units at all levels have established their own sports information management or sports physical fitness monitoring management systems to systematically manage relevant data [2, 3]. However, at present, the physique data databases established by various units are isolated from each other. Moreover, due to the mobility of the population, it brings great inconvenience to large-scale and effective physique monitoring, longitudinal tracking research, and personal understanding of their own physique [4, 5]. At the same time, how to use the data of national physique monitoring to scientifically guide the national fitness and apply the national physique monitoring results to practice is also the focus and development direction of physique monitoring research [6]. In order to more conveniently manage and utilize the research results in the field of sports science such as national physique monitoring, promote the transformation of the research

results of physique monitoring into practical application results, and facilitate individuals to get the feedback and scientific guidance of physique test results in time, it is urgent to establish a sports physical fitness monitoring system [7, 8].

Reference [9] designs an autonomous fitness monitoring system based on a monocular camera, which relies on the monocular camera of a mobile phone and 3D human key point detection technology to monitor whether the fitness actions of users are standard in real time and give corresponding prompts through voice. The monitoring effect of the system is verified by comparing with the related work in recent years. The results show that the system can accurately evaluate fitness movements in real-time monitoring, but there is a problem of long system response time. Reference [10] designed a video monitoring system for children's sports training based on feature moving frame differential scanning and adaptive compensation. The Internet of Things networking technology was used to collect video monitoring images of children's sports training, and

the three-dimensional data field of three-dimensional reconstruction of video monitoring images of children's sports training was constructed. According to the distribution characteristics of the data field, the physical condition of sports training can be monitored to analyze the video monitoring images of children's sports training and extract the physical condition characteristics. The experimental results show that the real-time performance of the system is poor, and the accuracy of the monitoring results is low. Reference [11] based on Taubin smoothing filter designed a children's sports training image 3D reconstruction of video monitoring systems and children's sports training video monitoring of the surface of the image of 3D reconstruction, according to the result of the reconstruction of physical conditions of sports training in real-time monitoring, but this method is not suitable for monitoring image interference intensity bigger. The response speed cannot meet the real-time requirements, and the monitoring results are not comprehensive enough.

To solve the above problems, this paper designs a sports physical fitness monitoring system for cloud storage. The main research contents are as follows:

- (1) Under the support of cloud storage technology, establish the sports physical fitness monitoring system, establish the system application support platform by using a series of network interconnection and information security technologies, and ensure the safe and reliable transmission of sports physical fitness monitoring information by using firewall technology and data encryption technology.
- (2) The hardware module of the monitoring system is divided into five functional modules: knowledge base management module, perception module, physical fitness data sampling module, physical fitness project information management module, and parameter setting module, and the function of each module is analyzed.
- (3) The ray casting image feature scanning method is used to collect the monitoring image of physical condition in sports training. The image convolution, clipping, translation, scaling, and rotation are given through the spatial transformation network, so that the moving target has spatial invariance, and the image data can be automatically transformed in space to generate a high-quality human target frame to realize the monitoring of the physical condition.
- (4) After realizing the sports physical fitness monitoring, take the monitoring data as the basis, design the fitness mode recommendation method according to the user's physical fitness state, and improve the practical application value of the system.
- (5) Finally, simulation experiments are carried out to show the advantages of the proposed system in improving the sports physical fitness monitoring ability.

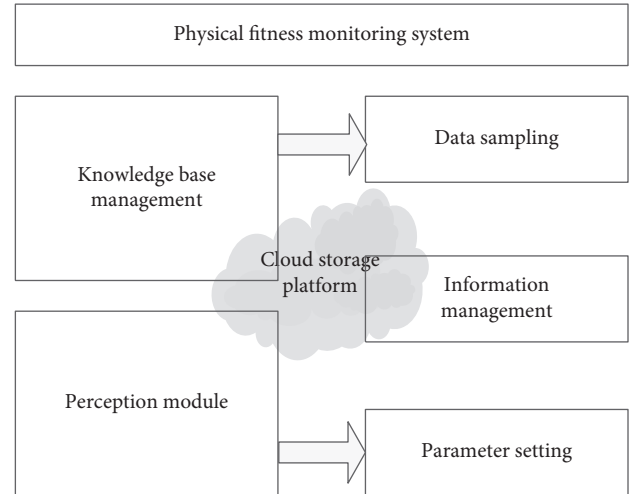


FIGURE 1: Schematic diagram of the overall architecture of the sports fitness monitoring system.

2. Design of Sports Physical Fitness Monitoring System

2.1. Overall Structure and Supporting Platform Design of Sports Fitness Monitoring System

2.1.1. Overall Structure of Sports Physical Fitness Monitoring System. Cloud storage technology [12, 13] is a networked storage concept rising in recent years. It is an emerging technology derived and developed on the basis of cloud computing [14, 15]. Cloud storage is a mode of online storage, that is, data are stored on multiple virtual servers usually hosted by a third party, rather than exclusive servers. Hosting companies operate large data centers. People who need a data storage and hosting can meet the needs of data storage by purchasing or renting storage space from them. According to the needs of customers, data center operators prepare storage virtualized resources at the back end and provide them in the form of a storage resource pool, so that customers can use this storage resource pool to store files or objects by themselves. In fact, these resources may be distributed on many server hosts, which is also the theoretical basis of cloud storage analysis. Combined with developed Internet technology, advanced cluster application, and mature distributed file system, this technology enables the massive types of storage devices in the network to work together to form an overall storage and computing structure model and jointly provide data storage and computing services and interface access functions. This paper transmits the collected data to the cloud platform through the wireless network to realize the cloud storage function [16], which can realize the storage and calculation of massive sports fitness monitoring data. In addition, compared with embedding the algorithm into the sensor terminal module program, the data processing algorithm stored on the remote cloud platform can be continuously optimized and updated in real time to ensure the accuracy and expansibility of the data [17, 18].

According to the characteristics of sports fitness monitoring, relying on cloud storage as the bottom end, through B/S and C/S multilayer architecture, realize the overall architecture design of the sports fitness monitoring system. The overall architecture of the system is shown in Figure 1.

According to Figure 1, based on the architecture of “optical fiber sensing terminal + data processing relay + cloud platform + heterogeneous application terminal” [19, 20], combined with cloud storage technology, the sports fitness monitoring system designs a system framework including sensing layer, cloud platform, management layer, data processing layer, and application layer.

2.1.2. System Application Support Platform. The network application support platform uses the TCP/IP protocol as the network communication protocol and is composed of network servers, communication equipment, security equipment, etc., and applies the latest, the most advanced network core technology also includes existing network application support systems and supports the operation of the upper-layer application software. Establish a safe, stable, reliable, and open network application platform, which is the cornerstone of establishing a comprehensive management environment for sports physical fitness monitoring information.

The network application support platform, based on open protocols and technical standards, is not limited to any hardware platform or network platform, spanning Unix, Windows NT, and other network operating systems and realizing multiplatform, multiprotocol, and multioperating system communication. This feature makes the comprehensive environment for sports physical fitness monitoring information management independent of the network environment, and the network application support platform is completely transparent to the application system to ensure a seamless connection between different systems.

The network application support platform adopts a series of network interconnection and information security technologies, uses firewall technology and data encryption technology to ensure the safe and reliable transmission of sports physical fitness monitoring information, and more importantly, makes full use of and shares various network resources such as existing public information networks by using virtual private network (VPN) technology. Users in different regions of the system can communicate with users in other regions of the system only by connecting with local public information network nodes, which saves investment. Virtual private network (VPN) has higher and stricter requirements for the security of network system and information. It comprehensively adopts appropriate technologies to establish separation around the internal network and external network, protect the internal network, and safely and stably protect the information platform through special firewall software, data encryption software, high-performance hardware, and comprehensive management measures.

2.2. Functional Module Design of Sports Physical Fitness Monitoring System. The sports physical fitness monitoring system can be divided into five functional modules:

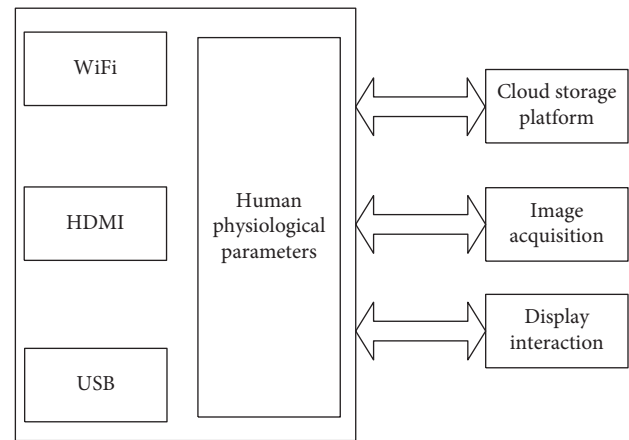


FIGURE 2: The working principle of the perception module.

knowledge base management module, perception module, sports fitness data sampling module, fitness project information management module, and parameter setting module. These functional modules are analyzed in detail below.

2.2.1. Knowledge Base Management Module. The knowledge and experience model of physical fitness analysis and evaluation experts is stored in the knowledge base, which is expressed by production rules. Production rule representation of. By analyzing the data of the inquirer, the system selects the corresponding knowledge base model and method and then generates the physical exercise methods and methods suitable for the inquirer according to the knowledge base [21, 22]. The knowledge base management system is responsible for the acquisition, retrieval, storage, and other functions of knowledge. The knowledge base also stores the technical action essentials, precautions, pictures, animations, videos of exercise methods, and diet adjustment recovered after exercise. The knowledge base is not only the organizer of sports prescription generation but also provides users with the basic knowledge and skills of physical exercise. Through learning and understanding, users can improve their interest in physical exercise, improve the quality of physical exercise, and finally achieve the effect of fitness.

2.2.2. Perception Module. The core chip used in the main control board of the perception module is RK3188 with a quad-core ARM Cortex-A9 architecture of Rockchip, with the main frequency of 1.8 GHz and is equipped with the Android 4.4 operating system. Different peripherals and interface circuits are built around the system functions, as shown in Figure 2.

According to Figure 2, the main control module exchanges data with the acquisition terminal through different transmission methods such as serial port, Bluetooth, and USB and realizes the reception and transmission of human physiological parameters such as bed rest state, heart rate, pulse and respiratory rate, and measurement instructions. GPIO can realize functions such as sound acquisition output and liquid crystal display interaction. It is equipped with

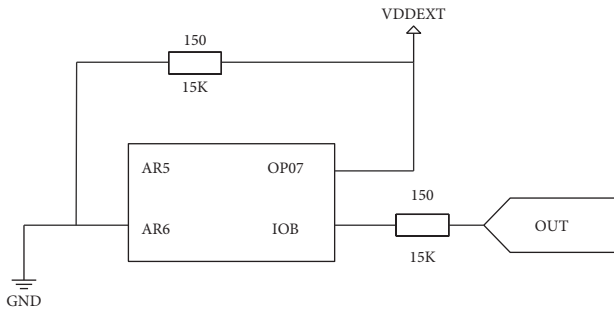


FIGURE 3: Circuit diagram of physical fitness data sampling module.

peripherals such as a liquid crystal display, touch screen, microphone, and speaker and uploads the monitoring data to the cloud storage platform in real time.

2.2.3. Physical Fitness Data Sampling Module. The physical fitness data sampling module realizes the acquisition of video image information of the physical fitness real-time monitoring system [23], and the DM9000 network module of DAVI-COM is used to design the radio frequency interface of the physical fitness real-time monitoring system in sports training. The real-time monitoring system for physical fitness in the design of sports training is divided into four layers, which are the process management layer, AD image processing layer, parameter calculation layer, and interface information interaction layer. The circuit diagram of the physical fitness data sampling module obtained is shown in Figure 3.

2.2.4. Physical Fitness Project Information Management Module. The entry of physical fitness measurement items is the preparation before sports physical fitness monitoring. The name, number, category, measurement unit, measurement instrument, measurement site, and other information of all items are recorded through the physical fitness item information management module. The system manager can view, modify, delete, and add new items at any time.

2.2.5. Parameter Setting Module. The user's personal information settings are shown in Figure 4.

According to Figure 4, the setting of the user's personal information needs to determine the user's name, photo, and source, as well as the user's age and sports level. The determination of the physical fitness index monitoring index is mainly combined with the competitive ability characteristics of users to reflect the advantages and disadvantages of users' physical reserves.

2.3. Database Design. The database is the carrier for storing all information. The database of this system is divided into three modules: basic information database, measurement data storage database, and measurement standard comparison database.

- (1) *Basic Information Database:* store the basic file data of users and the basic information of testers
- (2) *Measurement Data Repository:* record all measurement information, including the results and scores of measurement items
- (3) *Measurement Standard Comparison Library:* records the normal standards of various indicators formulated by the World Health Organization, which are used to compare with the performance of the measured person, so as to obtain the performance grade and physical fitness grade of the measured person

Since more databases will cause a certain burden on the operation of the system, the reconstruction method is adopted to create a distributed database [24, 25]. The reconstruction method is to re-establish a distributed database from the overall design, including the database on each site, according to the implementation environment and user requirements of the system [26], according to the design idea and method of distributed database, and from a unified point of view, as shown in Figure 5.

The advantage of the reconfiguration method is that it can consider various problems in the distributed database according to the unified idea and effectively solve the data consistency, integrity, and reliability of the distributed database.

This completes the design of the sports fitness physique monitoring system. The system is used to monitor people's body temperature, heart rate, and other physiological parameters during sports. At the same time, the data are uploaded to the cloud service center for data monitoring and analysis to prevent people from fainting, sudden death, and other accidents during sports. The application of the system not only provides an effective means for objectively evaluating the intensity of human sports but also promotes the scientific management of people's sports, which is of great significance to promoting sports.

3. Real-Time Monitoring Method of Physical Fitness Based on Video Image

3.1. Image Acquisition of Physical Condition Monitoring. In order to realize the real-time monitoring of physical fitness, it is necessary to reconstruct the three-dimensional contour and collect the sample pixels of the sports physical fitness monitoring image in sports training [27]. The ray-casting image feature scanning method is used to collect the physical condition monitoring image in sports training. The common spatial scanning methods of physical condition monitoring image in sports training are Cell Projection and Splatting. The ZigBee video monitoring network is designed in the environment of the Internet of things [28, 29]. The physical condition video image acquisition model in sports training is shown in Figure 6.

According to the image acquisition results in Figure 6, the sparse linear equations of fitness monitoring image template matching in sports training are obtained as follows:

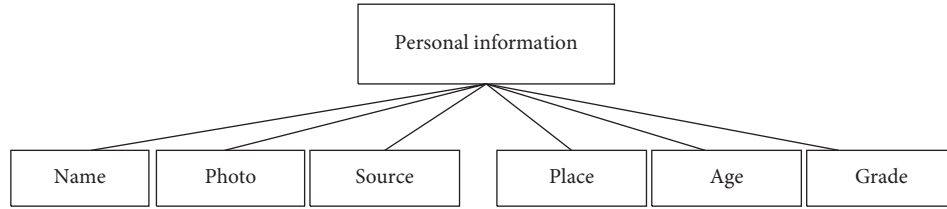


FIGURE 4: User personal information settings.

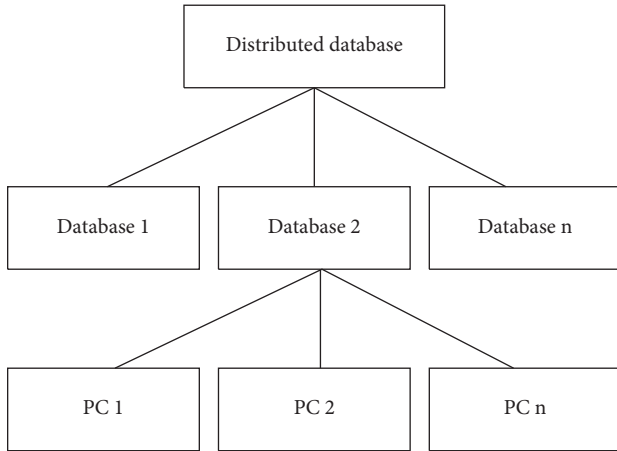


FIGURE 5: Distributed database.

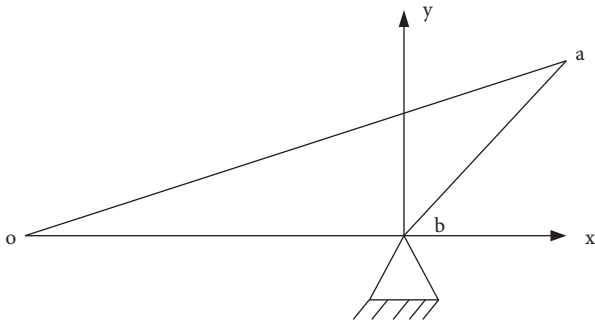


FIGURE 6: Image acquisition model of physical condition monitoring.

$$F(a, b) = h(a, b) * s(a, b) + l(a, b). \quad (1)$$

Here, $h(a, b)$ represents the disparity function of physical condition monitoring in sports training; the symbol $*$ represents the convolution. According to the pixel-level disparity function of sports physical fitness monitoring in sports training, information center pixel calibration and feature information adaptive weighting are performed to solve the parallax template function of physical fitness monitoring in sports training. The subpixel level matching is performed on the feature segmentation regions of the physical fitness monitoring images in sports training [30, 31], and the pixel disparity of the physical fitness monitoring image distribution in sports training is obtained as follows:

$$F(a, b) = \frac{s(a, b) + l(a, b)}{w(a, b)}. \quad (2)$$

Here, $w(a, b)$ represents the weight coefficient of physical condition monitoring in sports training [32]. The estimated value of edge pixels for physical condition monitoring is

$$\hat{s}(a, b) = R_k S(a, b) + \frac{1}{C_i} \phi^2. \quad (3)$$

Here, $S(a, b)$ represents the pixel value of the strong texture set of the physical fitness monitoring image in sports training about the scanning point (a, b) ; R_k represents the weak texture set of the sports physical fitness monitoring part; ϕ^2 represents the local variance; C_i represents the classification pixel set of the physical fitness monitoring image feature information in sports training. $s_1(x)$ and $s_2(x)$ are used to denote the gray value of the reconstructed image of the physical condition monitoring image in the exercise training of young children.

The spectral feature quantity of video surveillance is initialized, a real-time monitoring model is constructed, and combined with the 3D data distribution of the 3D reconstruction of the exercise training video image, the image reconstruction processing of the physical condition monitoring in the exercise training is carried out, thereby realizing the video image acquisition of the physical condition in the exercise training.

3.2. Physical Condition Monitoring. Because the human body's physical fitness target frame provided by the traditional method is not accurate enough, it is not suitable for the key point calibration of the physical condition monitoring image. The research shows that the slight movement of the human body target frame will seriously affect the key point calibration result. Therefore, this paper proposes to give the image convolutional cropping, translation, scaling, and rotation characteristics through the spatial transformation network, so that the moving target has spatial invariance, and the image data can be automatically spatially transformed to generate a high-quality human target frame.

Mathematically, the spatial transformation network can be regarded as a two-dimensional affine transformation [33, 34], which can be expressed as follows:

$$\begin{pmatrix} a_i^2 \\ b_j^2 \end{pmatrix} = [\alpha_1, \alpha_2, \alpha_3] \times \begin{pmatrix} a_i^f \\ b_j^f \end{pmatrix}. \quad (4)$$

Here, α_1 , α_2 , and α_3 represent two-dimensional vectors; (a_i^2, b_j^2) represents the coordinates before the transformation; (a_i^f, b_j^f) represents the coordinates after the transformation.

After the spatial transformation network, a human body physical fitness motion pose estimation network is formed, which is used to perform preliminary pose estimation of the human body target frame. At this time, the generated pose needs to be mapped to the original human body target frame image. Naturally, an inverse spatial transformation network is required to remap the estimated human pose back to the original image coordinates.

The spatial inverse transformation network performs inverse transformation by calculating the threshold value ϑ and generates a grid based on the threshold value ϑ . The calculation method can be expressed as follows:

$$\begin{pmatrix} a_i^f \\ b_j^f \end{pmatrix} = [\vartheta_1, \vartheta_2, \vartheta_3] \times \begin{pmatrix} a_i^2 \\ b_j^2 \end{pmatrix}. \quad (5)$$

Here, (a_i^f, b_j^f) and (a_i^2, b_j^2) are the coordinates before and after the spatial inverse transformation network transformation, respectively. Since the spatial inverse transformation network is the inverse process of the spatial transformation network, it can be derived as follows:

$$\begin{aligned} [\vartheta_1, \vartheta_2] &= [\alpha_1, \alpha_2]^{-1}, \\ \vartheta_3 &= -1 \times [\vartheta_1, \vartheta_2] \alpha_3. \end{aligned} \quad (6)$$

Then, a loss function $\partial(x)$ is set, which can be deduced as follows for α_1 and α_2 when back propagating in the spatial inverse transformation network:

$$\partial(x) = \frac{1}{\mu\alpha_1} + \frac{G_1((1/\alpha_2) + Y_1)}{G_2 + (1/\alpha_1) + Y_2}. \quad (7)$$

Here, μ represents the attitude error of the back-propagation center position of the space transformation network; G_1 and G_2 both represent the similarity between poses; Y_1 and Y_2 both represent the reference pose.

For α_3 , the equation can be derived as follows:

$$\partial(x) = \frac{\partial(x)}{\alpha_3} \times \frac{\lambda\alpha_3}{\lambda\vartheta_3}. \quad (8)$$

During network training, the spatial inverse transformation network and the single-person pose estimation network are fine-tuned together.

According to the above-given derivation results, the corner detection method is used to calibrate the characteristic key points of the video surveillance part of the motion training. The expression of the corner calibration is

$$\begin{cases} D_1 = \max(\tilde{z}_i - z_i), \\ D_2 = \min(\tilde{z}_i - z_i). \end{cases} \quad (9)$$

Here, D_1 and D_2 represent the image pixel difference feature quantity in the secondary matching template. The Harris corner detection method is used to locate the key feature points of the physical condition monitoring image in

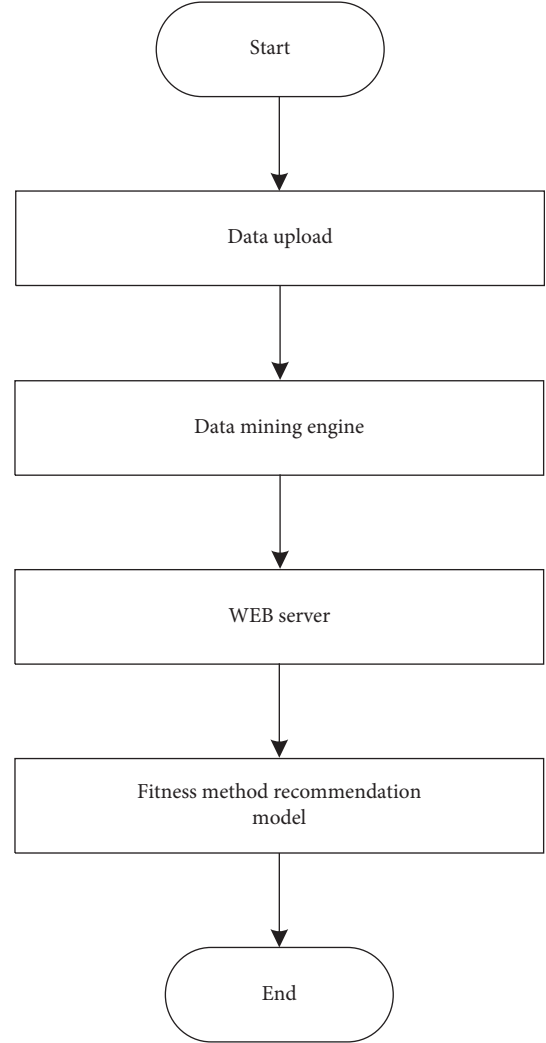


FIGURE 7: Fitness method recommendation process.

exercise training, and the positioning output vector is obtained as follows:

$$W_{ij} = \eta(a_i)\eta(b_j). \quad (10)$$

According to the dynamic distribution of the corners of the sports physical fitness monitoring images during exercise training, the sports physical fitness monitoring is realized.

3.3. Recommended Fitness Methods. After the sports physical fitness monitoring is realized, the monitoring data is used as the basis, and the fitness method recommendation method is designed according to the physical fitness state of the user [35, 36], so as to improve the practical application value of the system. The following are the recommended steps for specific fitness methods:

- (1) Use the browser as the interaction layer, provide a data input interface and data upload function, and transmit the physical fitness test data of individual users to the WEB server;

TABLE 1: Experimental parameter setting.

Number	Equipment or indicators	Model parameter
1	Monitoring system transformer	1500 kV
2	Monitoring system substation host	IdeaCentre K350
3	Rated voltage of monitoring system	380 V
4	Rated current of monitoring system	≤ 51 A
5	Monitoring system resistance	$6.8 \times 10^7 \Omega$
6	Total power consumption information storage of monitoring system	128 Gb

- (2) The server analyzes the physical fitness test data and transmits the physical fitness test indicators after the analysis to the data mining engine. During this stage, for the acquired physical fitness test indicators, in the background database, the data mining engine matches them with the fitness categories in the fitness mode recommendation model and generates the mining results of fitness mode recommendation;
- (3) Send the mining results to the WEB server;
- (4) Individual users will be able to view the mining fitness results through their browsers.

The design of embedding the fitness mode recommendation model into the service application platform focuses on the operation phase of importing the model into the data mining engine and background database.

Import the fitness recommendation model into the database: the model and rule set are processed in a certain format and imported into the database, or the model and the database are connected using a port. The physical fitness test sample data is mined through the data mining engine, and after completion, the mining results are matched with the background fitness method recommendation table to form a recommendation list, which is presented to individual users through the browser. In this way, different users and at different times, individual users see different content on their browsers. Therefore, the fitness mode recommendation based on the individual user's physical fitness test information is realized. Figure 7 is a flowchart of fitness mode recommendations.

4. Experimental Analysis

In order to verify the effectiveness of the cloud storage-oriented sports physical fitness monitoring system, an experimental study is carried out. Configure the relevant experimental parameters according to Table 1 to complete the construction of the basic experimental environment.

The storage space occupied by the compressed electric information can reflect the redundancy degree of information parameters. Generally, the smaller the storage space occupied by the compressed sports fitness monitoring system information, the lighter the redundancy degree of information parameters. At this time, the network host is more capable of eliminating redundant data.

4.1. Test Index Object Setting. Set the experimental test index object: take the autonomous fitness monitoring system based on a monocular camera (system 1) and the video

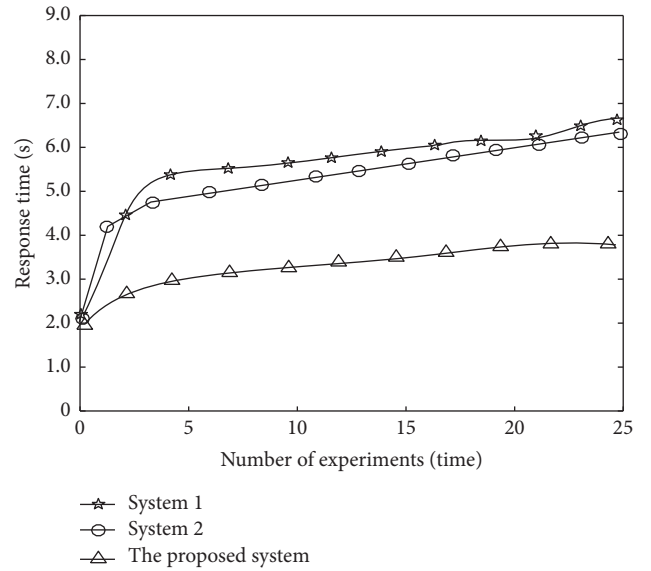


FIGURE 8: Response speed comparison results.

monitoring system for children's sports training based on feature moving frame difference scanning and adaptive compensation (system 2) as the comparison system to compare with the proposed system. In the system application performance test, the focus of the test is to verify whether the accuracy and response speed of the system monitoring results meet the actual use requirements of users and the comprehensiveness of the monitoring results.

4.2. Analysis of Test Results

4.2.1. System Response Speed. In order to verify the application effect of the monitoring system, the system response speed is used as an evaluation index. The faster the system response speed, the better the system application effect is, which indicates that the system can effectively meet the requirements of real-time monitoring of physical fitness status. Using system 1, system 2, and the proposed system to compare, the response speed comparison results of different systems are shown in Figure 8.

According to Figure 8, the response time of different systems increases with the increase of the number of experiments. When the number of experiments is 5, the response time of system 1 is 5.4 s, that of system 2 is 4.8 s, and that of the proposed system is only 2.9 s; When the number of experiments is 15, the response time of system 1 is 5.8 s, that of system 2 is 5.6 s, and that of the proposed system is

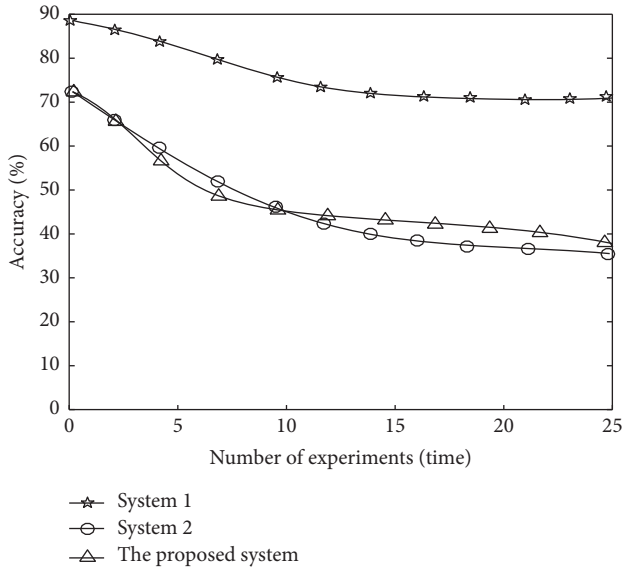


FIGURE 9: Comparison of accuracy of monitoring results.

only 3.3 s. Therefore, the monitoring time of the proposed system is less, indicating that the monitoring response of the proposed system is more timely.

4.2.2. Accuracy of Monitoring Results. In order to verify the monitoring effect of the proposed system, the accuracy of the monitoring results is taken as the evaluation index. The higher the accuracy of the monitoring results, it shows that the system can effectively meet the actual needs of sports physical fitness monitoring, obtain accurate monitoring results, and provide reliable data for the recommendation of fitness methods. Compare system 1, system 2, and the proposed system and get the monitoring results of different systems. The accuracy comparison results are shown in Figure 9.

According to the analysis of Figure 9, with the increase of the number of experiments, the accuracy of monitoring results of different systems decreases. When the number of experiments is 5, the accuracy of monitoring results of system 1 is 60% and that of system 2 is 57%. The accuracy of the monitoring results of the proposed system is 84%; when the number of experiments is 15, the accuracy of monitoring results of system 1 is 41%, that of system 2 is 44%, and that of the proposed system is 74%. It can be seen that the accuracy of the monitoring results of the proposed method is high, and more accurate monitoring results can be obtained.

4.2.3. Comprehensiveness of Monitoring Results. In order to further verify the monitoring effect of the proposed system, the comprehensiveness of the monitoring results is taken as the evaluation index. The index is expressed by numerical value, and the interval is $[0, 1]$. The larger the value is, the more comprehensive the monitoring results are. The monitoring results of different systems are shown in Table 2.

According to the data in Table 2, the highest comprehensive coefficient of the monitoring results of the proposed

TABLE 2: Comprehensive comparison of monitoring results.

Number of experiments/ time	The proposed system	System 1	System 2
2	9.6	7.5	8.0
4	9.4	7.3	7.9
6	9.2	7.2	7.8
8	8.9	7.6	7.5
10	9.0	7.9	7.4
12	9.0	7.1	7.5
14	8.7	7.0	7.3
16	8.7	6.8	7.1
18	9.1	7.0	7.0
20	9.3	7.0	6.9

system is 9.6, and the highest comprehensive coefficient of the monitoring results of system 1 and system 2 are 7.5 and 8.0, respectively. Through comparison, it can be seen that the comprehensiveness coefficient of the proposed system is higher, indicating that its monitoring results are more comprehensive.

To sum up, with the increase of the number of experiments, the monitoring time of the sports fitness monitoring system designed for cloud storage is less, and the monitoring response is more timely; the accuracy of monitoring results is high, and more accurate monitoring results can be obtained. The highest comprehensive coefficient of the monitoring results of the proposed system is 9.6, and the comprehensive coefficient is higher, indicating that the monitoring results are more comprehensive.

5. Conclusion

In order to improve the accuracy of sports fitness monitoring results, the response speed of the system, and the comprehensiveness of monitoring results, a sports fitness monitoring system for cloud storage is designed. Based on cloud storage technology, establish the overall architecture of sports fitness monitoring system, ensure the safe and reliable transmission of fitness monitoring information under the system application support platform, and improve the accuracy of testing results; analyze the function of the hardware module of the monitoring system and establish a distributed database to improve the comprehensiveness of the detection results; ray casting image feature scanning method is used to collect the monitoring image of physical condition, and a high-quality human body target frame is generated through the steps of image convolution, cutting, translation, scaling, and rotation to realize the monitoring of the physical condition. The following conclusions are obtained through the research:

- (1) The physical fitness monitoring system designed for cloud storage can improve the real-time response speed of monitoring
- (2) Based on the monitoring data, the fitness mode recommendation method is designed according to the user's physical condition, so as to improve the application value of the system

- (3) The monitoring results of the designed system are more accurate, the system response speed is faster, the monitoring results are more comprehensive, and the highest value reaches 9.6, indicating that the application value of the proposed system is higher

Data Availability

The raw data supporting the conclusions of this article will be made available by the authors, without undue reservation.

Conflicts of Interest

The authors declare that they have no conflicts of interest regarding this work.

Acknowledgments

This work was supported by Research on teaching reform of higher Education in Jilin University of Architecture and Technology, Topic: Application and Practice of Flipped Classroom in PHYSICAL Education (Grant No. JY2021C006).

References

- [1] A. Nicolò, C. Massaroni, E. Schena, and M. Sacchetti, "The importance of respiratory rate monitoring: from healthcare to sport and exercise," *Sensors*, vol. 20, no. 21, pp. 1–45, 2020.
- [2] I. c. Jeong, D. Bychkov, and P. C. Searson, "Wearable devices for precision medicine and Health state monitoring," *IEEE Transactions on Biomedical Engineering*, vol. 66, no. 5, pp. 1242–1258, 2019.
- [3] F. Bardid, T. Utesch, D. F. Stodden, and M. Lenoir, "Developmental perspectives on motor competence and physical fitness in youth," *Scandinavian Journal of Medicine & Science in Sports*, vol. 31, no. 1, pp. 5–7, 2021.
- [4] R. D. Langer, R. de Fatima Guimarães, E. M. Gonçalves, G. Guerra-Junior, and A. M. de Moraes, "Phase Angle is determined by body composition and cardiorespiratory fitness in adolescents," *International Journal of Sports Medicine*, vol. 41, no. 9, pp. 610–615, 2020.
- [5] H. Root, A. N. Marshall, A. Thatcher, A. R. S. Valier, and B. R. Curtis, "Sport specialization and fitness and functional task performance among youth competitive gymnasts," *Journal of Athletic Training*, vol. 54, no. 10, pp. 1095–1104, 2019.
- [6] T. Zhou, X. Li, and H. Zhao, "Med-PPPHIS: blockchain-based personal healthcare information system for national physique monitoring and scientific exercise guiding," *Journal of Medical Systems*, vol. 43, no. 9, pp. 1–23, 2019.
- [7] X. L. Xu, Y. M. Liu, N. X. Wu, Z. Q. Yue, and Z. L. Lu, "Design of a fitness trainer system based on Kinect 3D somatosensory camera," *Modern Electronics Technique*, vol. 42, no. 8, pp. 11–15, 2019.
- [8] J. Y. Zhao and D. F. Zhang, "Simulation of human motion information capture in time-space domain based on virtual reality," *Computer Simulation*, vol. 38, no. 8, pp. 391–395, 2021.
- [9] P. Yu, L. Liu, Y. Cai, Y. He, and S. H. Zhang, "Home fitness monitoring system based on monocular camera," *Journal of Zhejiang University (Science Edition)*, vol. 48, no. 5, pp. 521–530, 2021.
- [10] F. L. Bian, "Study on the positioning and the collaborative relationship of subjects of the physical fitness and Health monitoring of teenagers," *Journal of Guangzhou Sport University*, vol. 40, no. 2, pp. 24–27, 2020.
- [11] Z. Tian, "Research on damage risk monitoring system relying on human-body motion state recognition," *Modern Electronics Technique*, vol. 40, no. 12, pp. 93–96, 2017.
- [12] A. Karthika and N. Muthukumaran, "An ADS-PAYG approach using trust factor Against economic denial of sustainability attacks in cloud storage," *Wireless Personal Communications*, vol. 122, no. 1, pp. 69–85, 2021.
- [13] W. B. Kim, D. Seo, D. Kim, and I. Y. Lee, "Group delegated ID-based proxy reencryption for the enterprise IoT-cloud storage environment," *Wireless Communications and Mobile Computing*, vol. 2021, no. 4, Article ID 7641389, 12 pages, 2021.
- [14] K. Alsubhi, Z. Imtiaz, A. Raana, M. U. Ashraf, and B. Hayat, "MEACC: an energy-efficient framework for smart devices using cloud computing systems," *Frontiers of Information Technology & Electronic Engineering*, vol. 21, no. 6, pp. 917–930, 2020.
- [15] K. Sreenu and S. Malempati, "MFGMTS: epsilon constraint-based modified fractional grey wolf optimizer for multi-objective task scheduling in cloud computing," *IETE Journal of Research*, vol. 65, no. 2, pp. 201–215, 2019.
- [16] W. A. Shalaby, W. Saad, M. Shokair, F. E. A. El-Samie, and M. I. Dessouky, "COVID-19 classification based on deep convolution neural network over a wireless network," *Wireless Personal Communications*, vol. 120, no. 2, pp. 1543–1563, 2021.
- [17] V. S. Lakshmi and P. P. Deepthi, "A secure regenerating code-based cloud storage with efficient integrity verification," *International Journal of Communication Systems*, vol. 32, no. 9, pp. 1–22, 2019.
- [18] A. Tahir, C. Fei, H. U. Khan, M. Zhong, and M. Shafiq, "A systematic review on cloud storage mechanisms concerning e-healthcare systems," *Sensors*, vol. 2020, no. 5392, pp. 1–32, 2020.
- [19] L. S. Subhash and R. Udayakumar, "Sunflower whale optimization algorithm for resource allocation strategy in cloud computing platform," *Wireless Personal Communications*, vol. 116, no. 4, pp. 3061–3080, 2021.
- [20] A. Pellegrini, N. Stephens, M. Bruce et al., "The arm neoverse N1 platform: building blocks for the next-gen cloud-to-edge infrastructure SoC," *IEEE Micro*, vol. 40, no. 2, pp. 53–62, 2020.
- [21] N. P. V. KoopmansF, M. Andres-Alonso, A. Byrnes, and M. Verhage, "SynGO: an evidence-based, expert-curated knowledge base for the synapse," *Neuron*, vol. 103, no. 2, pp. 217–234, 2019.
- [22] D. R. Doan, "Contributions to the electrical safety knowledge base [electrical safety]," *IEEE Industry Applications Magazine*, vol. 27, no. 2, pp. 7–106, 2021.
- [23] S. Zebhi, S. Almodarresi, and V. Abootalebi, "Converting video classification problem to image classification with global descriptors and pre-trained network," *IET Computer Vision*, vol. 14, no. 8, pp. 614–624, 2020.
- [24] N. R. Chauhan and S. P. Tripathi, "Optimal admission control policy based on memetic algorithm in distributed real time database system," *Wireless Personal Communications*, vol. 117, no. 2, pp. 1123–1141, 2021.
- [25] F. Castro-Medina, L. Rodriguez-Mazahua, A. Lopez-Chau, M. A. Abud-Figueroa, and G. Alor-Hernandez, "FRAGMENT: a web application for database fragmentation,

- allocation and replication over a cloud environment,” *IEEE Latin America Transactions*, vol. 18, no. 6, pp. 1126–1134, 2020.
- [26] R. S. Nasagh, M. Shahidi, and M. Ashtiani, “A fuzzy genetic automatic refactoring approach to improve software maintainability and flexibility,” *Soft Computing*, vol. 25, no. 11, pp. 1–31, 2021.
- [27] W. Takano, “Annotation generation from IMU-based human whole-body motions in daily life behavior,” *IEEE Transactions on Human-Machine Systems*, vol. 50, no. 1, pp. 13–21, 2020.
- [28] H. Khelifi, S. Luo, B. Nour, H. M. SellamiA, S. H. Ahmed, and M. Guizani, “Bringing deep learning at the edge of information-centric Internet of things,” *IEEE Communications Letters*, vol. 23, no. 1, pp. 52–55, 2019.
- [29] S. H. Ahmed, V. H. Cd Albuquerque, and W. Wei, “Guest editorial: special section on advanced deep learning algorithms for industrial Internet of things,” *IEEE Transactions on Industrial Informatics*, vol. 17, no. 4, pp. 2764–2766, 2021.
- [30] L. L. Cui and Z. Li, “Three-dimensional image reconstruction method for human maxillofacial defect images based on block sample feature matching,” *International Journal of Engineering Systems Modelling and Simulation*, vol. 11, no. 3, p. 112, 2019.
- [31] B. Sadeghi, K. Jamshidi, A. Vafaei, and S. A. Monadjemi, “A local image descriptor based on radial and angular gradient intensity histogram for blurred image matching,” *The Visual Computer*, vol. 35, no. 10, pp. 1373–1391, 2019.
- [32] K. K. Yoo, S. L. Jin, and H. W. Yong, “Low-noise high-efficiency double-phase hologram by multiplying a weight factor,” *Optics Letters*, vol. 44, no. 15, pp. 3649–3652, 2019.
- [33] B. Zhao, T. W. Sung, and X. Zhang, “A quasi-affine transformation artificial bee colony algorithm for global optimization,” *Journal of Intelligent and Fuzzy Systems*, vol. 40, no. 4, pp. 1–18, 2021.
- [34] W. Keizer, “Affine transformation for synthesis of low side-lobe patterns in planar array antennas with a triangular element grid using the IFT method,” *IET Microwaves, Antennas & Propagation*, vol. 14, no. 8, pp. 830–834, 2020.
- [35] Y. Yin and W. Zheng, “An efficient recommendation algorithm based on heterogeneous information network,” *Complexity*, vol. 2021, no. 17, Article ID 6689323, 18 pages, 2021.
- [36] S. J. Music, “Recommendation algorithm based on multidimensional time-series model analysis,” *Complexity*, vol. 2021, no. 1, Article ID 5579086, 11 pages, 2021.

Research Article

The Empirical Analysis of Bitcoin Price Prediction Based on Deep Learning Integration Method

Shengao Zhang,¹ Mengze Li,² and Chunxiao Yan ³

¹School of Public Administration, China University of Geosciences, Wuhan 430074, China

²School of Public Finance and Taxation, Capital University of Economics and Business, Beijing 100070, China

³School of Economics and Management, China University of Geosciences, Wuhan 430074, China

Correspondence should be addressed to Chunxiao Yan; yanchunxiao@cug.edu.cn

Received 24 April 2022; Accepted 14 May 2022; Published 10 June 2022

Academic Editor: Le Sun

Copyright © 2022 Shengao Zhang et al. This is an open access article distributed under the Creative Commons Attribution License, which permits unrestricted use, distribution, and reproduction in any medium, provided the original work is properly cited.

As a new type of electronic currency, bitcoin is more and more recognized and sought after by people, but its price fluctuation is more intense, the market has certain risks, and the price is difficult to be accurately predicted. The main purpose of this study is to use a deep learning integration method (SDAE-B) to predict the price of bitcoin. This method combines two technologies: one is an advanced deep neural network model, which is called stacking denoising autoencoders (SDAE). The SDAE method is used to simulate the nonlinear complex relationship between the bitcoin price and its influencing factors. The other is a powerful integration method called bootstrap aggregation (Bagging), which generates multiple datasets for training a set of basic models (SDAES). In the empirical study, this study compares the price sequence of bitcoin and selects the block size, hash rate, mining difficulty, number of transactions, market capitalization, Baidu and Google search volume, gold price, dollar index, and relevant major events as exogenous variables uses SDAE-B method to compare the price of bitcoin for prediction and uses the traditional machine learning method LSSVM and BP to compare the price of bitcoin for prediction. The prediction results are as follows: the MAPE of the SDAE-B prediction price is 0.016, the RMSE is 131.643, and the DA is 0.817. Compared with the other two methods, it has higher accuracy and lower error, and can well track the randomness and nonlinear characteristics of bitcoin price.

1. Introduction

Bitcoin is a decentralized, anonymous, exclusive ownership, and inflation-free currency [1]. Fry and Cheah [2] found that in view of the innovative characteristics of decentralization and traceability of bitcoin, bitcoin has attracted extensive attention from the media and investors. After the rise and fall of cryptocurrency prices in recent years, bitcoin is increasingly seen as an investment asset. Investors see bitcoin as a speculative investment, similar to the Internet stocks of the last century [3]. Bitcoin as a cryptocurrency, itself appears for a short time compared with the sovereign currency [4]. Unlike the sovereign currency, bitcoin is a decentralized digital currency without any government credit support, so the price of bitcoin is highly volatile. It produces much more volatility than sovereign currencies. Its price rose from zero value when

it was established in 2009, to about \$13 per bitcoin in January 2013, and then soared to about \$20000 per bitcoin in December 2017. Since bitcoin started trading, its highly unstable nature has been plaguing investors, and it may be a bubble, threatening the stability of the financial system. Therefore, it is necessary to make a good prediction of the price of the special currency. The possibility of predicting the price trend of bitcoin is a practical problem. It not only affects a country's economic policy at the macro level but also strongly affects investors' decision to buy and sell investment instruments at the micro-level. Matkovskyy and Jalan [5] found that the accurate prediction of bitcoin price can not only provide decision support for investors but also provide reference for the government to formulate regulatory policies.

Equally noteworthy are the factors that influence bitcoin prices. In addition to the internal factors such as block size,

hash rate, mining difficulty, trading volume, and market value of bitcoin, this study thinks that the factors should be more comprehensive: firstly, this study thinks that the Google and Baidu search index is an important factor affecting bitcoin because it is an important indicator to measure investors' attention and media hype and reflects the sentiment of the highly speculative cryptocurrency market [6]. Secondly, this study argues that the irrational factors such as major events and investor sentiment caused by economic policies will also affect the price of bitcoin [7]. Papadopoulos [8] shows that there is good interaction between bitcoin price and gold price. Dyhrberg [9] proved the similarity among bitcoin, gold, and the US dollar through the GARCH model. Therefore, this study takes the gold price and the dollar index as the influencing factors of bitcoin price. By selecting the above external factors, the problem of simplifying bitcoin price prediction is avoided.

The contribution of this study is as follows: compared with traditional financial asset price prediction, bitcoin price prediction is still in the early stage. Because bitcoin lacks seasonality, A. Greaves and Au [10] found that the machine learning model is applicable and useful. Similarly, Shah and Zhang [11] used Bayesian regression to predict the price change of bitcoin. At present, various popular machine learning algorithms such as SVM [12], RNN, LSTM, ARIMA [13], GA, and NARX [14] have also been applied to predict the price of bitcoin. Although the traditional machine learning model has obvious advantages in bitcoin price prediction, the imbalance and poor integrity of relevant data will lead to the problems of low accuracy, poor robustness, and easy to fall into the local optimum of deep network training. With the maturity of machine learning technology, deep learning has gradually become the mainstream of machine learning technology, and related algorithms and applications have also begun to flourish. And it shows strong ability in classification, feature extraction, and other non-linear modeling tasks. A deep denoising self-coding network is a widely used network model in deep learning. With fewer data samples and suitable classification and recognition algorithms, it can obtain higher classification ability and has strong feature extraction ability and robustness. The unsupervised pretraining of self-coding networks can effectively extract the internal features of bitcoin data and reduce the loss of typical features to the greatest extent [13, 15]. Therefore, this study proposes a deep learning ensemble

method (SDAE-B) to predict the price of bitcoin, which combines two technologies: one is the stacking denoising autoencoders (SDAE-B), which is used to simulate the nonlinear complex relationship between bitcoin price and its influencing factors. The other is a powerful integration method called bootstrapping, which generates multiple datasets for training a set of basic models (SDAES). Through the use of the SDAE-B method to compare the price of the special currency and get a good result.

The framework of this study is as follows: Section 2 introduces the methods proposed; Section 3 carries out empirical research and discusses the results; Section 4 gives the conclusion and describes the main contributions of the study.

2. Materials and Methods

2.1. Deep Learning Integration Method (SDAE-B). Stacking denoising autoencoders (SDAE) [16] is a popular DNN model. The results show that it has higher prediction accuracy in a series of classification problems than competitive machine learning models such as stacked autoencoders (SAE) and deep belief networks (DBN). SDAE is constructed by stacking several denoising autoencoders (DAEs), which is a special neural network structure. To illustrate SDAE, the autoencoder (AE) and the DAE are introduced.

2.1.1. Autoencoder (AE). Autoencoder(AE) is a single hidden layer neural network with equal input and output sizes. Firstly, an input vector $x \in [0, 1]^d$ is mapped to a hidden representation $y \in [0, 1]^d$ by a deterministic function:

$$y = f_{\theta}(x) = \phi_f(Wx + b). \quad (1)$$

$F(x)$ parametrization is $\theta = \{W, b\}$, W is a weight matrix of $d' \times d$, b is a bias vector, and $\phi_f(\cdot)$ is a nonlinear activation function. Then, y in the input space maps the return $z \in [0, 1]^d$ as the following equation:

$$z = g_{\theta'}(y) = \phi_g(W'y + b'). \quad (2)$$

With $\theta' = \{W', b'\}$. Therefore, each training $x^{(i)}$ is mapped to the corresponding $y^{(i)}$ and reconstruction $z^{(i)}$. The model parameters are optimized to minimize the average reconstruction error.

$$\theta^*, \theta'^* = \arg_{\theta, \theta'} \min \frac{1}{n} \sum_{i=1}^n L(x^{(i)}, z^{(i)}) = \arg_{\theta, \theta'} \min \frac{1}{n} \sum_{i=1}^n L(x^{(i)}, g_{\theta'}(f_{\theta}(x^{(i)}))), \quad (3)$$

where L is the loss function, which can be the traditional square error:

$$L(x, z) = \|x - z\|^2, \quad (4)$$

or reconstruction fork:

$$L_H(x, z) = H(B_x \bullet B_z) = - \sum_{k=1}^d [x_k \log z_k + (1 - x_k) \log (1 - z_k)]. \quad (5)$$

Vincent et al. [17] believed that the autoencoder (AE) is a self-monitoring algorithm, not an unsupervised algorithm.

It does not need to mark the training samples, and its label is generated from the input data. Therefore, it is easy to train a specific encoder for the input of the specified class without any new work. The autoencoder (AE) is data-related and can only compare data similar to training data. For example, the automatic encoder trained with face has poor performance in compressing other pictures, such as trees, because the features it learns are related to the face.

2.1.2. Denoising Autoencoder (DAE). Based on the autoencoder (AE), the denoising autoencoders (DAE) adds noise to the input data of the input layer to prevent the overfitting problem, which improves the robustness of the learned encoder. The core idea of DAE is to reconstruct a purified input from a corrupted version. First, the corrupted original input data x is randomly mapped $\tilde{x} \sim q_D(\tilde{x}|x)$ to \tilde{x} . Then input the noisy model \tilde{x} and get y by $y = f_\theta(\tilde{x}) = \phi(W\tilde{x} + b)$ mapping. Finally, the pair is mapped $z = g_{\theta'}(y)$ back to z . For the training set, the best parameters θ and θ' are obtained by minimizing the average reconstruction error between z and undamaged input x . The process is shown in Figure 1.

2.1.3. Stacking Denoising Autoencoders (SDAE). The idea of stacking denoising autoencoders (SDAE) is to stack multiple DAEs together to form a deep architecture. Only when the training is complete, the input will be added with noise. It follows layer-by-layer greedy training [18]: each layer of the self-coding layer carries out unsupervised training independently to minimize the error between the input (the input is the hidden layer output of the previous layer) and the reconstruction result. After the former k layer is trained, the $K+1$ layer can be trained, because the output of the k layer has been calculated by forwarding propagation, and then the output of the k layer is used as the input of $K+1$ to train $K+1$ layer.

Specifically, the first DAE uses the training set as the input for independent training and learns through $f_\theta^{(1)}$ mapping function. Then the second DAE uses the hidden representation y of the first DAE as input to train and learn by $f_\theta^{(2)}$ mapping function. All DAEs can train independently according to the same procedure. An independently supervised learning algorithm (such as FNN) is added to the structure, which uses the hidden representation of the last DAE as input. Finally, establish SDAE. Once the SDAE training is completed, its high-level characteristics can be used as the input of the traditional monitoring algorithm. Besides, the parameters of each layer of SDAE can be adjusted synchronously by gradient descent and other training algorithms. The process is shown in Figure 2.

2.1.4. Bagging. Bagging [19] is the abbreviation of bootstrap aggregating. It is a powerful integrated learning algorithm, which can be used for tasks such as two classifications, multiclassification, and regression. Its principle is to give a data set containing m samples, first, take a sample randomly and put it into the sampling set, and then put the sample back, so that the sample will still have the chance to be selected in the next sampling. So, after M times of sampling, we can get a

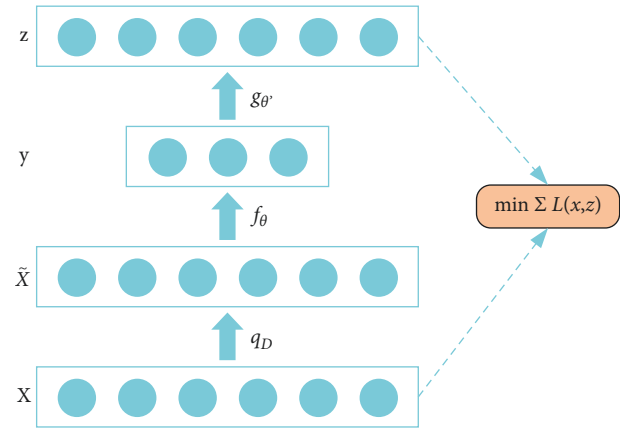


FIGURE 1: The architecture of DAE.

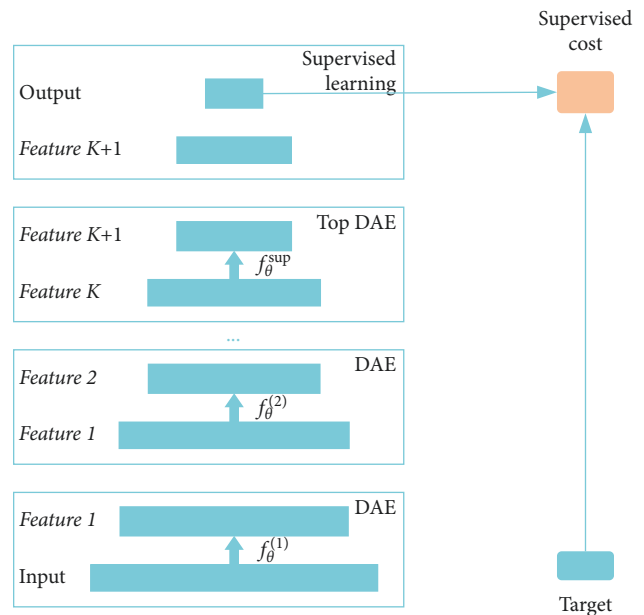


FIGURE 2: The architecture of SDAE.

data set with the same data amount of m from the original data set. Simply speaking, there are put back samples in the statistics and each sample. The probability of samples being taken is the same, which is one of the total samples.

Only when the basic learning algorithm is unstable, bagging can generate different basic models, which can be regarded as a method to improve the prediction accuracy by using this instability. The neural network model is unstable due to the random initialization process of weights, while the bagging neural network has strong robustness. It has been successfully applied in the field of finance and economy [20–22]. For these reasons, bagging can be used to construct an integration based on SDAES.

2.1.5. Multivariate Forecasting. Different from the time series model, the multivariate model not only considers the autoregressive effect of target series but also considers the influence of exogenous variables on the target series. The

multivariate model as a simple but very important method in the process of statistical analysis, it has been widely used in prediction in different fields. For example, Rombouts et al. [23] applied it in the field of option pricing. In recent years, scholars have applied multivariate model and deep learning technology to the field of prediction [24]. The results show that the multivariate model outperforms the univariate model for forecasting. It can be formalized as a function to simulate the relationship between dependent variables and independent variables:

$$y(t+h) = f(s(y), s(x_1), \dots, s(x_C)), \quad (6)$$

where $y(t+h)$ is the value of the dependent variable in $(t+h)$ and $s(x) = x(t), x(t-1), \dots, x(t-l_x+1)$ is a set of past values of exogenous variable x with a total of l_x . Therefore, the input quantity is $m = \sum l_y + l_{x_1} + l_{x_2} + \dots + l_{x_C}$.

2.1.6. The Overall Process of SDAE-B Approach. The main idea of the hybrid model is as follows. The deep learning model SDAE is used to extract useful information from the selected data and generate prediction. The powerful integration method bagging is used to combine the strength of multiple SDAEs to improve the prediction accuracy, so as to generate an integrated model with better performance.

SDAE-B forecasts bitcoin prices based on the following five steps. Figure 3 shows the flow chart of the whole process:

- (1) Data preprocessing: transform the original data into training samples and test samples.
- (2) Generate multiple training sets: generate K sample sets of training samples through the bootstrapping algorithm.
- (3) Training: each group of training samples trained K SDAE models, respectively.
- (4) Prediction: use SDAE models of K training to generate K predictions.
- (5) Result summary: take the average of K predicted values as the final result.

3. Results and Discussion

In this section, we compare the prediction ability of LSSVM and BP with that of SDAE-B. Firstly, the data description is given. Secondly, the model evaluation criteria are given. Then LSSVM, BP, and SDAE-B are used to compare the price of the special currency for prediction. Finally, the comparison results are given and analyzed.

3.1. Datasets. In this study, the data of bitcoin block size, hash rate, mining difficulty, number of transactions, and market capitalization are from Data.Bitcoinity.Org, Blockchain.com, and CoinMarketCAP. Baidu and Google search volume, respectively, come from Baidu Index and Google Trends. Relevant major events come from the review of the 11th anniversary of bitcoin by the blockchain media "Daily Star." Gold prices come from GOLDHUB. Dollar index from Investing.com. The data is from November 29, 2014, to March

30, 2020. This study selects nine indicators of bitcoin, including block size, hash rate, mining difficulty, trading volume, market value, Baidu, and Google search volume, gold price, dollar index, relevant major events (Table 1) as independent variables, and bitcoin price (trend as shown in Figure 4) as dependent variables to build the model, as shown in Table 2.

The reasons for choosing these variables are as follows. First, they are closely related to bitcoin prices. Secondly, the relationship between bitcoin price series and these factors is noisy, fluctuating, and nonlinear, but any of them may provide useful information about bitcoin price trends at a certain point in time. Therefore, we can extract more information through as many variables as possible. Finally, as a deep neural network model, SDAE has a very powerful function in high-dimensional data modeling. Using these variables, we can make full use of the advantages of SDAE to create an ideal environment for the modeling of the bitcoin price series.

Different from previous studies, except for the internal factors such as block size, hash rate, mining difficulty, trading volume, and market value of bitcoin, this study increases Baidu and Google search volume, gold price, dollar index, and relevant major events.

These variables are selected to model the price series of bitcoin for the following reasons: first, they are closely related to bitcoin prices and represent different drivers of bitcoin prices. Secondly, the relationship between bitcoin price series and these factors is noisy, unstable, and nonlinear, but any of them may provide useful information about the movement of bitcoin price at a certain time. Therefore, we can extract more information by including as many variables as possible. Finally, a large number of variables can be used to provide relatively complete bitcoin price change information.

To model, this study divides the data into two parts: the training sample contains the first 80% of the observation values of all series, and the rest is the test sample. For model training, bitcoin price and exogenous variables are pre-processed by the normalization method.

3.2. Model Evaluation Index. To evaluate the prediction performance of the model from different perspectives (i.e., direction prediction and level prediction), three frequently used indicators in recent years include direction accuracy (DA), mean absolute error (MAPE), and mean square root error (RMSE):

$$DA = \frac{1}{N} \sum_{t=1}^N a(t) \times 100\%,$$

$$MAPE = \frac{1}{N} \sum_{t=1}^N \left| \frac{y(t) - \hat{y}(t)}{y(t)} \right|, \quad (7)$$

$$RMSE = \sqrt{\frac{1}{N} \sum_{t=1}^N (y(t) - \hat{y}(t))^2},$$

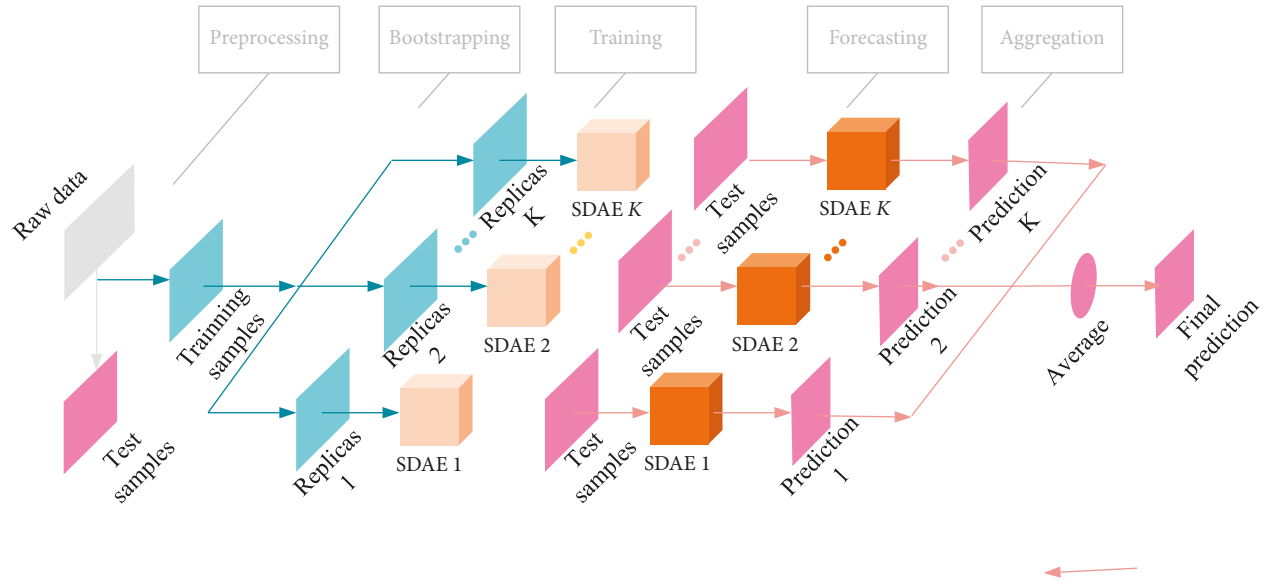


FIGURE 3: The prediction process of SDAE-B model.

TABLE 1: Features.

Future	Definition
Block size	The average block size in MB
Hash rate	The estimated number of tera hashes per second (trillions of hashes per second), the bitcoin network is performing
Mining difficulty	A relative measure of how difficult it is to find a new block. The difficulty is adjusted periodically as a function of how much hashing power has been deployed by the network of miners
Number of transactions	The number of transactions per day
Market capitalization	The total US dollar market value of bitcoin
Baidu and google search volume	The weighted volume for media coverage of the keyword “bitcoin”
Relevant major events	Major events in bitcoin from November 29, 2014, to March 31, 2020 (positive impact expressed as “1” and negative impact expressed as “-1”)
Gold price	XAU gold spot price in US dollars
Dollar index	An indicator that comprehensively reflects the exchange rate of the US dollar in the international foreign exchange market

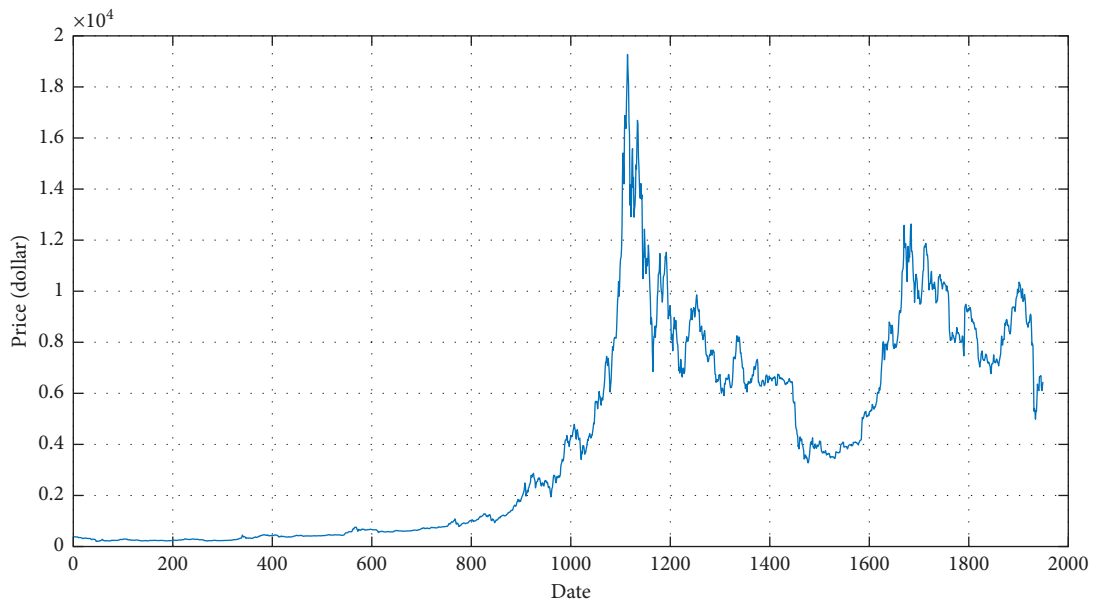


FIGURE 4: Bitcoin price trend in recent five years.

TABLE 2: Summary statistics of features used for bitcoin price prediction.

Future	Count	Mean	Sd	Minimum	Maximum
Block size	1950	734528.0	189090.04	187483.7	998175.2
Hash rate	1950	3.24E + 18	3.86E + 18	9.98E + 15	1.81E + 19
Mining difficulty	1950	3.54E + 12	4.53E + 12	39457671307	1.66E + 13
Number of transactions	1950	238145.4	81220.36	59344	490644
Market capitalization	1950	70265662078	69380000349	2.53E + 10	3.23E + 11
Baidu and Google search volume	1950	594.84	296.41	232	2499
Major events	1950	0.09	0.84	-1	1
Gold price	1950	444.3	40.86	364.63	585.01
Dollar index	1950	96.08	2.88	87.98	103.61

TABLE 3: Forecast results.

Model	DA	MAPE	RMSE
LSSVM	0.658	0.106	272.152
BP	0.740	0.040	540.084
SDAE-B	0.817	0.016	131.643

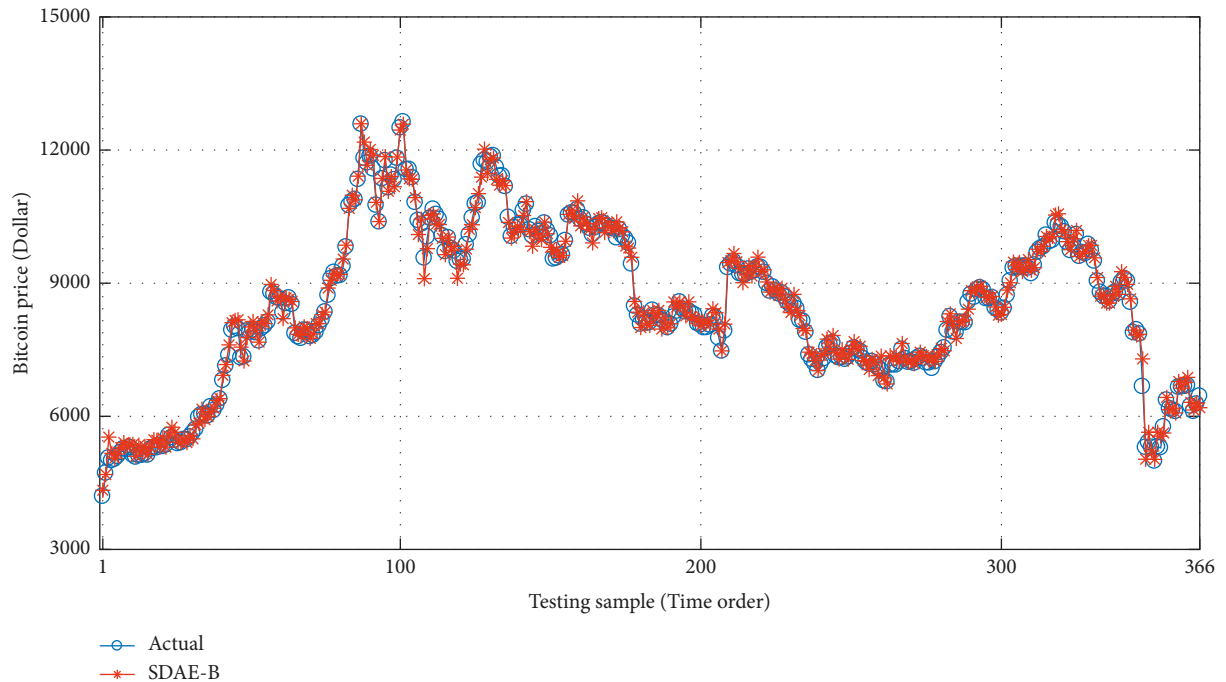


FIGURE 5: Comparison of the true price of Bitcoin and predicted price based on SDAE-B model.

where $y(t)$ and $\hat{y}(t)$ represent true value and prediction respectively when $(y(t+1) - y(t))(\hat{y}(t+1) - y(t)) \geq 0$, $a(t) = 1$; otherwise, $a(t) = 0$. N is the size of the forecast data.

3.3. Parameter Settings. SDAE model is a three-layer hidden neural layer network model. It stacks two DAEs and a supervised FNN on top of the architecture. According to the size of the feature space, set the number of nodes in the first to third hidden layers to 200, 100, and 10. Based on the trial and error method, the number of epochs for DAEs unsupervised pretraining, FNN supervised pretraining, and

global fine tuning are all set to 500. The noise type in DAEs is additive Gaussian noise. According to Vincent et al. [17], the noise ratio is 0.2. The numbers of K is set to 100. The choice of K number is actually a trade-off between computational complexity and accuracy. However, with the increase of K , the prediction error of SDAE-B quickly converges to a certain level, so it is not necessary to select a large number. The lagged order of all variables and bitcoin price in the multivariate prediction model is set to 1, i.e., to learn a function satisfying. Through this method, a short term nonlinear dependency can be learned between input/output data. The number of hidden layers of BP is 1, the network structure is [40, 20, 1] the activation function is sigmoid

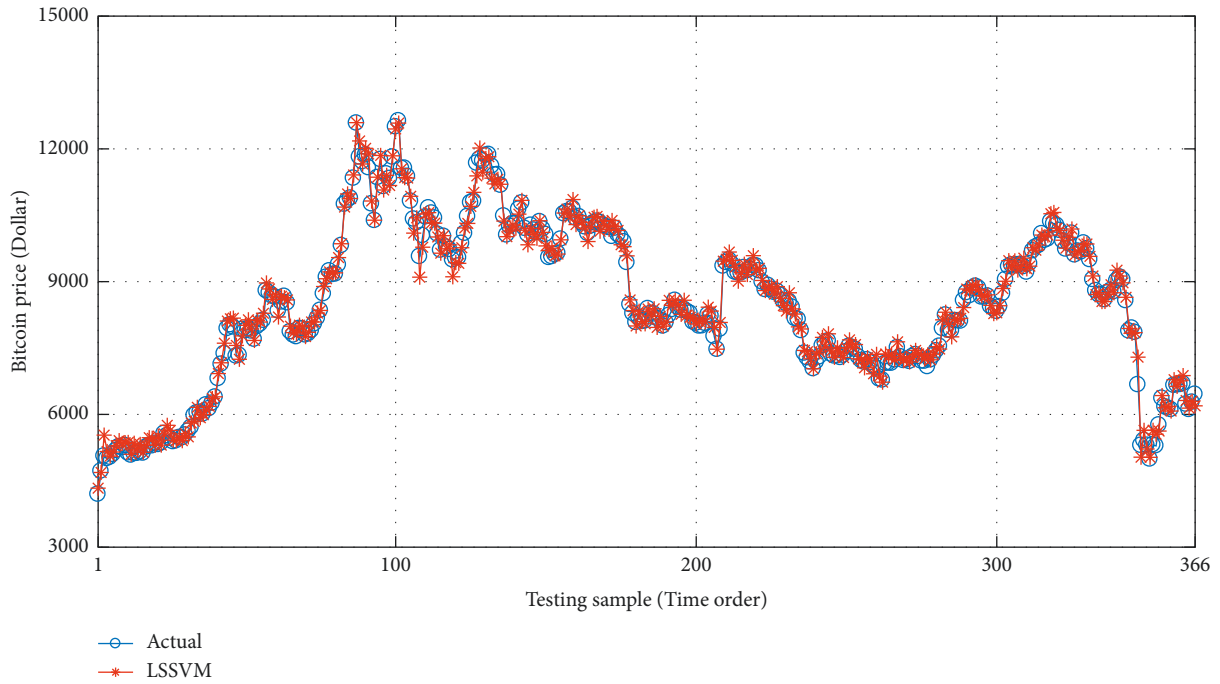


FIGURE 6: Comparison of the true price of Bitcoin and predicted price based on LSSVM model.

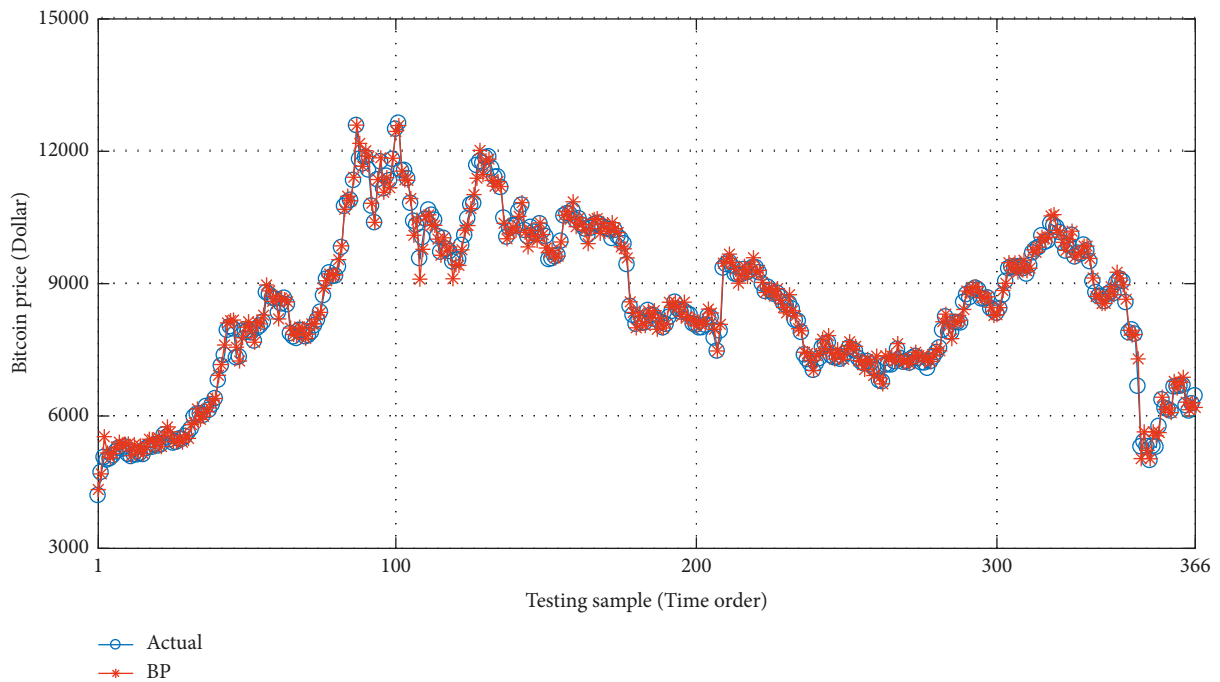


FIGURE 7: Comparison of the true price of Bitcoin and predicted price based on BP model.

function, and the learning rate is 0.1. The Gaussian kernel function is selected as the kernel function of the LSSVM method. Matlab R2016a is used to perform all the computations in this study.

3.4. *Bitcoin Price Forecast.* With the help of MATLAB software, LSSVM, BP, and SDAE-B are used to compare the

price of special currency for forecasting. The results are shown in (Table 3). Also, the research results are shown in Figures 5–7.

The results show that SDAE-B has higher direction accuracy (DA), lower mean absolute error (MAPE), and lower mean square root error (RMSE), and has better prediction performance than LSSVM and BP. The possible reasons are as follows:

- (1) When dealing with data with various features, many traditional machine learning algorithms have a weakness. They cannot extract and organize different information from the data. Since it may be a difficult task to build a model of the relationship between bitcoin price and many variables, traditional models may not be able to learn useful representations, resulting in poor out of sample predictions. Instead, SDAE-B has a deep architecture. It can learn useful information from features by extracting multiple levels of representation, to obtain better prediction ability when the sample data are insufficient.
- (2) The performance of the integrated model is more stable than the traditional single machine learning model, because the traditional single machine learning model excessively relies on the sample data, underestimates the variance, and causes overfitting. The integrated model can reduce overfitting or generalization errors.

4. Conclusions

At present, bitcoin is a good stored value and safe haven, which is the most important use of bitcoin by all those who recognize it. In the long run, with the continuous development of blockchain technology and the recognition of bitcoin by more and more countries, bitcoin is likely to become a national strategic reserve resource like gold. Although the price of bitcoin is of great significance to market practitioners, the theoretical research in this field is very limited. In this study, a deep learning integration method named the SDAE-B is utilized to predict the price of bitcoin. Aiming at the complex relationship between bitcoin price and various factors, this study proposes LSSVM, BP, and SDAE-B to predict bitcoin price. In the data selection, through the analysis of internal and external factors, the limitations of the previous bitcoin price prediction methods, which only consider the historical data of bitcoin price are overcome. In empirical research, the first step is to obtain data, and then do data processing and model training. Through the training results, we can get a bitcoin price prediction based on deep learning and get good results. The SDAE-B model is better than the LSSVM model and BP model, which have higher accuracy and lower error. It shows that this method can be used as a promising tool for bitcoin price prediction.

Nevertheless, this study think there is still room for improvement. As we all know, unconventional factors such as political risk and investor psychology also have a great influence on the price fluctuation of special currency, but how to quantify the influence of these factors is quite challenging. This study believes that better predictions can be generated by quantifying these factors and using the information they provide. Finally, the prediction results of the SDAE-B model proposed in this paper have a certain lag, and the correction of postphenomenon is also the focus of future research.

Data Availability

In this study, the data of bitcoin block size, hash rate, mining difficulty, number of transactions and market capitalization are from Data.Bitcoinity.Org, Blockchain.com, and Coin-MarketCAP. Baidu and Google search volume, respectively, come from Baidu Index and Google Trends. Relevant major events come from the review of the 11th anniversary of bitcoin by the blockchain media "Daily Star.". Gold prices come from GOLDHUB. Dollar index from Investing.com.

Conflicts of Interest

The authors declare that they have no conflicts of interest regarding the publication of this study.

References

- [1] S. Nakamoto, "Bitcoin," *A peer-to-peer electronic cash system*, Decentralized Business Review, vol. 21260, 2008.
- [2] J. Fry and E.-T. Cheah, "Negative bubbles and shocks in cryptocurrency markets," *International Review of Financial Analysis*, vol. 47, pp. 343–352, 2016.
- [3] D. Yermack, "Is Bitcoin a real currency? An economic appraisal," *National Bureau of Economic Research*, vol. 36, no. 2, pp. 843–850, 2015.
- [4] X. Sun, M. Liu, and Z. Sima, "A novel cryptocurrency price trend forecasting model based on LightGBM," *Finance Research Letters*, vol. 32, Article ID 101084, 2020.
- [5] R. Matkovskyy and A. Jalan, "From financial markets to Bitcoin markets: a fresh look at the contagion effect," *Finance Research Letters*, vol. 31, pp. 93–97, 2019.
- [6] L. Kristoufek, "BitCoin meets Google trends and wikipedia: quantifying the relationship between phenomena of the Internet era," *Scientific Reports*, vol. 3, no. 1, p. 3415, 2013.
- [7] P. Wang, X. Li, D. Shen, and W. Zhang, "How does economic policy uncertainty affect the bitcoin market?" *Research in International Business and Finance*, vol. 53, Article ID 101234, 2020.
- [8] S. Vassiliadis, P. Papadopoulos, M. Rangoussi et al., "Bitcoin value analysis based on cross-correlations," *Journal of Internet Banking and Commerce*, vol. 22, no. S7, p. 1, 2017.
- [9] A. H. Dyhrberg, "Bitcoin, gold and the dollar - a GARCH volatility analysis," *Finance Research Letters*, vol. 16, pp. 85–92, 2016.
- [10] A. Greaves and B. Au, "Using the bitcoin transaction graph to predict the price of bitcoin," *No Data*, vol. 8, pp. 416–443, 2015.
- [11] D. Shah and K. Zhang, "Bayesian regression and bitcoin," in *Proceedings of the 2014 52nd Annual Allerton Conference on Communication, Control, and Computing (Allerton)*, pp. 409–414, IEEE, Monticello, IL, USA, October 2014.
- [12] I. Georgoula, D. Pournarakis, C. Bilanakis et al., "Using time-series and sentiment analysis to detect the determinants of bitcoin prices," *Social Science Electronic Publishing*, vol. 24, no. 2, pp. 966–969, 2015.
- [13] S. Shi and G. Xu, "Novel performance prediction model of a biofilm system treating domestic wastewater based on stacked denoising auto-encoders deep learning network," *Chemical Engineering Journal*, vol. 347, pp. 280–290, 2018.
- [14] J. Han, S. Kim, M. Jang et al., "Using genetic algorithm and NARX neural network to forecast daily bitcoin price," *Computational Economics*, vol. 16, pp. 1–17, 2019.

- [15] Y. Zhao, J. Li, and L. Yu, "A deep learning ensemble approach for crude oil price forecasting," *Energy Economics*, vol. 66, no. aug, pp. 9–16, 2017.
- [16] P. Vincent, H. Larochelle, Y. Bengio et al., "Extracting and composing robust features with denoising autoencoders," in *Proceedings of the 25th international conference on Machine learning*, pp. 1096–1103, Helsinki, Finland, June 2008.
- [17] P. Vincent, H. Larochelle, I. Lajoie et al., "Stacked denoising autoencoders: learning useful representations in a deep network with a local denoising criterion," *Journal of Machine Learning Research*, vol. 11, no. 12, pp. 3371–3408, 2010.
- [18] G. E. Hinton and R. R. Salakhutdinov, "Reducing the dimensionality of data with neural networks," *Science*, vol. 313, no. 5786, pp. 504–507, 2006.
- [19] L. Breiman, "Bagging predictors," *Machine Learning*, vol. 24, no. 2, pp. 123–140, 1996.
- [20] M.-J. Kim and D.-K. Kang, "Ensemble with neural networks for bankruptcy prediction," *Expert Systems with Applications*, vol. 37, no. 4, pp. 3373–3379, 2010.
- [21] N. Kourentzes, D. K. Barrow, and S. F. Crone, "Neural network ensemble operators for time series forecasting," *Expert Systems with Applications*, vol. 41, no. 9, pp. 4235–4244, 2014.
- [22] L. Yu, S. Wang, and K. Lai, "Credit risk assessment with a multistage neural network ensemble learning approach," *Expert Systems with Applications*, vol. 34, no. 2, pp. 1434–1444, 2008.
- [23] J. Rombouts, L. Stentoft, and F. Violante, "The value of multivariate model sophistication: an application to pricing Dow Jones Industrial Average options," *International Journal of Forecasting*, vol. 30, no. 1, pp. 78–98, 2014.
- [24] Y. N. Malek, M. Najib, M. Bakhouya, and M. Essaïdi, "Multivariate deep learning approach for electric vehicle speed forecasting," *Big Data Mining and Analytics*, vol. 4, no. 1, pp. 56–64, 2021.

Research Article

Research on Discrete Dynamic Modeling of Learner Behavior Analysis in English Teaching

Junru Fu  and Lingmei Cao 

Department of Foreign Languages, Shanghai University of Finance and Economics Zhejiang College, Jinhua, Zhejiang 321000, China

Correspondence should be addressed to Lingmei Cao; z2011229@shufe-zj.edu.cn

Received 30 March 2022; Accepted 17 May 2022; Published 9 June 2022

Academic Editor: Le Sun

Copyright © 2022 Junru Fu and Lingmei Cao. This is an open access article distributed under the Creative Commons Attribution License, which permits unrestricted use, distribution, and reproduction in any medium, provided the original work is properly cited.

The current English teaching mode focuses on the traditional offline teaching and online teaching. In order to solve the problems that some students are inefficient and cannot teach students according to their aptitude in the teaching process, this paper uses the big data analysis strategy based on a neural network algorithm. This paper studies the discrete dynamic modeling method of learner behavior analysis in English teaching. Firstly, it summarizes the current situation of English teaching and the research status of the hybrid application of discrete dynamic modeling technology. Secondly, combined with English teaching content and teaching objectives, through the analysis of various data of students' learning behavior, this paper evaluates students' English teaching quality from five aspects that affect the students' English teaching quality and puts forward a personalized English teaching quality evaluation model based on discrete dynamic modeling technology and learners' behavior analysis. Finally, through the practical teaching application in a university, the feasibility of the discrete dynamic English teaching model is verified. The results show that compared with the current innovative English teaching methods based on a dynamic iterative decision algorithm, the personalized discrete dynamic English teaching model based on learner behavior analysis significantly improves the quality of English teaching and students' academic performance.

1. Introduction

The mainstream English teaching still focuses on the traditional offline face-to-face teaching, supplemented by online network teaching, so the teaching mode is relatively single [1]. Since the teaching model innovation policies are promoted in different regions at this stage, the vigorous development of a variety of data analysis technologies has also triggered the innovative application of English Classroom Teaching [2]. Manufacturing computer-integrated manufacturing system CIMS, system scheduling, communication network system, database management system, military C3I system, and other systems are typical discrete event systems [3]. Therefore, customization and real-time have become important features of the College English classroom teaching system in China [4]. There are two kinds

of modeling methods for this kind: informal modeling and formal modeling. Informal modeling technology refers to modeling the system with the help of computer technology through graphical representation that people can easily accept and understand, and then converting it into computer language, and analyzing the system through programs [5]. Based on English teaching and the actual situation of learner behavior analysis, this paper studies the modeling and flexible recruitment strategy of the high-tech knowledge-based discrete dynamic system. English teaching behavior is deeply influenced by teaching values, which are usually formed under the guidance of learning theory [6]. In this context, this paper studies the discrete dynamic modeling technology based on a neural network algorithm and the innovative English teaching method of learner behavior analysis.

Compared with the current innovative English teaching methods with dynamic iterative decision-making algorithms as the mainstream, the innovation of this paper is to improve the efficiency of English teaching by combining discrete dynamic modeling technology and neural network algorithm. On this basis, it can make full use of each student's learning behavior, learning data, and test scores in the English classroom through real-time dynamic tracking. It can realize customized analysis, quantitatively describe the similarity and coincidence degree of each learning behavior and teaching strategy with behavior analysis factors, complete the influence ranking of English classroom teaching indicators with quantitative indicators, and effectively conduct multivariate analysis.

Aiming at the problems of low teaching efficiency and poor intelligence in English teaching, this paper studies the construction of a discrete dynamic modeling method for learner behavior analysis in English teaching. Chapter 1 briefly summarizes the background, innovation, and chapter arrangement of this study. Chapter 2 introduces the current research status of English teaching models and influencing factors at home and abroad. Chapter 3 analyzes the teaching classroom model. Based on Gaussian random function and Laplace feature recognition, a classroom teaching model is constructed. At the same time, the three-dimensional target matching analysis is carried out according to the students' classroom performance, and the quantitative characteristics are constructed. Chapter 4 sets up a correlation experiment to verify the relevant indicators of the English classroom teaching model constructed in this paper, analyzes the experimental results, and draws a conclusion.

2. Related Work

China has developed slowly in the mode of innovation and quality evaluation of English teaching, while some foreign developed countries have good basic and phased innovative achievements in the field of English Teaching [7]. It is very necessary and important to evaluate teachers' teaching behavior through the study of English learning theory and find deep theoretical roots for teaching practice, so as to carry out English teaching activities more scientifically in the future [8]. In addition, it is more suitable to analyze the learners' motivation and behavior of their learners [9, 10].

Based on this model, the strategy of a discrete dynamic system for learners' behavior analysis in English teaching is put forward, and the sufficient conditions for the asymptotic stability of the closed-loop system for learners' behavior analysis are analyzed. The designed strategy can ensure that each state of the actual discrete dynamic system tracks the desired state, and the simulation results verify the effectiveness of the discrete dynamic modeling strategy proposed in this paper [11]. The establishment of a reasonable discrete dynamic model and computer simulation has always been an indispensable research method, which has played a great role in reducing losses, saving funds, shortening the cycle, reducing costs, and improving product quality and service quality [12, 13]. With the help of the description and solution methods of learners' behavior analysis problems

provided by English teaching theory, the research on discrete dynamic modeling, analysis, control, and optimization of this kind of system has reached a quite mature and perfect state, at least in relatively simple branches such as linear time-invariant systems, and its effectiveness has been shown in practical applications [14]. According to the idea of neuron node association in neural network algorithm, researcher Zou et al. proposed a distributed parsing model for English teaching based on mixed contexts. The experimental results show that it has a strong speech discrimination ability [15]. Pejpichestakul et al. proposed that the Petri net modeling of discrete dynamic systems should be guided by scientific modeling methods and supported by powerful computer software. Deloitte & ToucheBakkenist of the Netherlands and Eindhoven University of Technology jointly developed ExSpect. The concept of domain model base and the design characteristics of supporting system analysis methods of this language make it a powerful modeling and simulation tool for complex discrete event dynamic systems [16]. Cao et al. proposal is more significant for basic systems such as large-scale computer and communication networks and airport traffic management systems. Therefore, the research on the modeling of discrete event dynamic systems is an urgent need for the current social production to achieve high efficiency and low fault operation [17]. Cao et al. proposed that when designing a feedback controller for modeling discrete dynamic systems, the time-varying perturbation of controller parameters may lead to the performance degradation of closed-loop systems, and even the stability will be destroyed. Therefore, the concept of elastic control was put forward. Elastic control in discrete modeling means that the control behavior can adapt to the changes in the internal conditions and external environment of the organization, and has a certain flexibility and anti-interference [18]. Deng et al. proposed that Petri net can describe the structure of a discrete dynamic modeling system well, and express the relationships of parallelism, synchronization, conflict, and sequence in the system, and the discrete dynamic combination model represented by graphics has the advantages of intuition, easy understanding, and easy use, and has its unique advantages in describing and analyzing concurrency phenomena [19]. Do et al. proposed that the use of the Petri net discrete dynamic model largely depends on the support of sufficient computer tools. To create, store, change, and analyze such discrete dynamic models with computers, it is necessary to choose a computer-friendly representation, which is called language [20]. Zheng et al. proposed to analyze the demand of enterprises for human resources through discrete dynamic modeling and gave a human resource planning scheme conducive to the development of enterprises. Note that most of these methods are based on discrete dynamic, static, and deterministic perspectives [21]. Santini et al. proposed to study and establish the m-sequence discrete dynamic test signal model according to the random characteristics of typical dynamic load, construct the electric energy measurement algorithm of the dynamic test signal, analyze and give the dynamic signal electric energy measurement error caused by the quantization error of IEC61850 protocol, and

provide the basis for testing and evaluating the dynamic error characteristics of all digital electric energy meter [22].

Dynamic iterative decision-making algorithms are mainly differentiated teaching methods, and rarely make effective analyses by combining learners' behavior habits [23]. It does not have a wide application, and rarely has a good construction of differentiated analysis model and discrete dynamic evaluation model [24]. Therefore, it is of great significance to study English teaching based on learner behavior analysis.

3. Methodology

3.1. Research Status of Discrete Dynamic Modeling of English Learners' Behavior Analysis. In this paper, the discrete dynamic modeling is studied under the analysis of English teaching learners' behavior. Teachers' intuitive judgments in the classroom of English teaching learners' behavior analysis are sometimes wrong [25]. Because those students who have introverted and retreating problem behaviors in English classes are often obedient, their behaviors are easily overlooked, and teachers' explanations and solutions to the discovered problem behaviors are not necessarily correct. The discrete dynamic modeling of the whole system under the analysis of English learners' behavior is a kind of discrete dynamic system, which is characterized by the continuous change of the system state caused by the interaction of discrete according to certain operating rules. In this sense, DEDS has the following two basic characteristics [26]: first, DEDS is driven by discrete events, which is the performance of its system attributes; secondly, the running rules of DEDS are all artificial rules, which are the performance of its artificial attributes. Besides, in the process of discrete dynamic modeling of behavior research in English teaching, it is sometimes difficult to find out the real cause of problematic behavior by the commonly used methods such as questionnaire survey and interview, because students' answers are often unwilling or unable to reveal their true inner situation because of face, anxiety, or other psychological factors. For these common problem behaviors of discrete dynamic modeling, teachers should take various countermeasures according to their judgments, and test whether these countermeasures are effective in classroom practice, so as to further improve their strategies and methods.

3.2. Modeling of Learner Behavior Analysis in English Teaching. The teaching behavior in line with the theory of "the essence of learning is trial and error" involved in sanddike's connection theory in the learning view of behavior school runs throughout the whole English teaching activities, especially in the oral training of students. English teachers often have to face the mistakes of students in language learning. This makes students inevitably make mistakes in practice. The usual practice is that no matter what mistakes students make in their expression, they will not interrupt directly, but write down the questions first. When summing up, all students are required to analyze

mistakes together and constantly encourage students to speak out first, which is the first step to success. For those students who are unwilling and unable to participate in classroom activities, teachers should create more opportunities for them to express themselves, but this opportunity is selective, that is, the tasks they are competent for. Modeling is actually an iterative process, which cannot be achieved overnight. The following figure describes the important process of modeling. There are several steps in the figure, which reflect that modeling is a spiral process, and its importance is obvious. Therefore, special attention should be paid to the implementation of these steps. That is, the layer-by-layer decomposition of the system and the use of reusable components. The data analysis process is shown in Figure 1.

Firstly, through image sensing equipment, the current English learning behavior of different types of professional students can be recorded online. It is used in computer language processing and converts it to multi-channel binary numbers. Then the teaching system is used to store students' learning data information in a multidimensional way. Vectorization analysis and feature extraction can be carried out for the first time. In this process, simulation analysis can be carried out on the data collected by different types of learners' behaviors. The results are shown in Figure 2.

As can be seen from Figure 2, with the increase in the number of iterative operations in the process of converting learning behavior information into data vector information dimension, the change law of the analysis error degree of learning behavior data information is also obvious. Different learning behavior analysis methods usually separate the learning process into independent behavior operation units. It is not conducive to grasping the process and analysis of online learning activities from the overall analysis. The time series and relationship between different learning behaviors aim to reveal the learning behavior characteristics of individuals and learning groups. Identify the behavioral differences of different learning groups, diagnose key learning events in learning activities, and predict learners' learning performance. Taking English teaching learners' behavior as the research object, the purpose of this group's English learning is more important to meet the needs of work and life, and their instrumental motivation is strong. However, the self-influence factors of English learners who are under the pressure of family and friends are relatively weak. Different from basic education English learners who are forced to study English full-time under the pressure of entering a higher school, the nature of this group's part-time study of English determines that the variables of second language learning experience related to the learning environment are less influential, but the variables of English learning attitude are relatively more important. According to its characteristics, it is divided into different English teaching center models. The simulation analysis results of customized teaching optimization are shown in Figure 3.

As can be seen from Figure 3, under the discrete dynamic modeling technology based on a neural network algorithm, with the increase in English teaching courses, the optimal customized teaching scheme has been optimized and

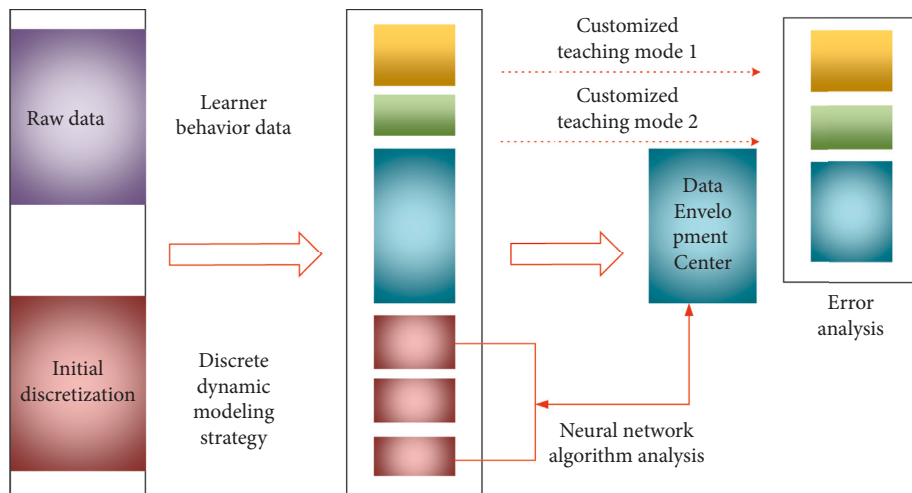


FIGURE 1: Discrete dynamic modeling method in the data analysis process of customized English teaching model.

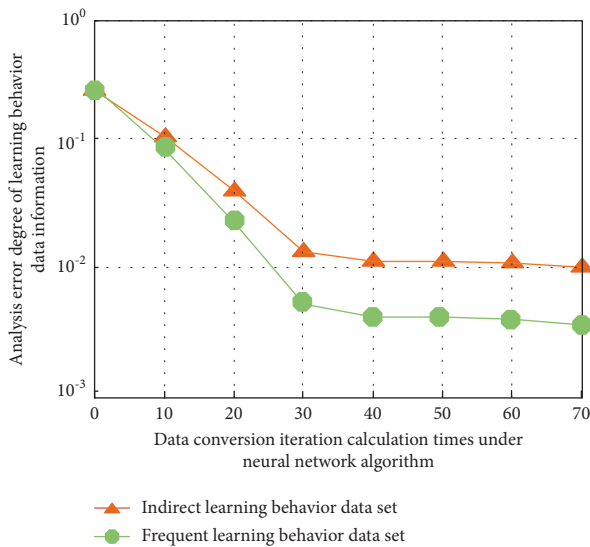


FIGURE 2: Simulation analysis results of different types of learning behavior data.

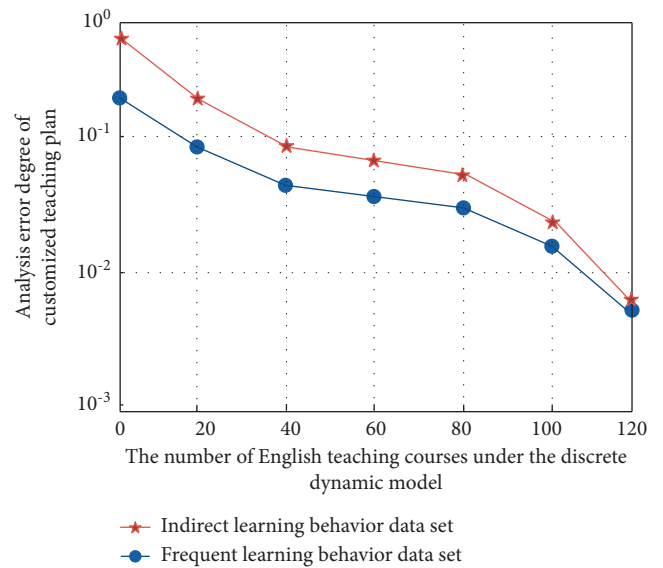


FIGURE 3: Analysis error degree of customized teaching plan based on neural network algorithm discretization dynamic modeling technology.

improved to varying degrees, and shows a trend of gradual decline and then gradually stable. The improvement of students' learning enthusiasm will bring learning interest and satisfaction of success, and this cognitive internal motivation is the most important and stable motivation in classroom learning. Years of education and teaching practice have proved that students' learning enthusiasm has an obvious impact on the teaching effect. Cultivating students' learning enthusiasm is the premise and guarantee to improve teaching efficiency. The most fundamental driving force of learning comes from the enthusiasm for active learning. Therefore, due to the particularity of English learning, teachers' words and behaviors in English classes must be encouraged, and students' language output should not be criticized and attacked easily. They should adopt a tolerant attitude towards mistakes, and those students who have problematic behaviors should not be criticized and punished blindly. They must be more concerned about them

and find out the causes of their problematic behaviors! Then give them continuous help and guidance. In this process, the statistical results of 8 learning behavior types (A-H) under 12 simulation analyses are shown in Figure 4.

It can be seen from the changes of statistical data in Figure 4 that with more classification of learner behavior data information (A-H), the higher the proportion of special data information in the learner's behavior data information (A-H), the greater its role, and the internal differentiation is more obvious. Although the law trend is similar, there are also obvious differences, because of the process of calculation and recognition with high similarities. The process of completing the four stages of data association in turn is defined as "frame," that is, from the beginning of measurement sampling to the end of the physical operation and the beginning of new measurement sampling. At this stage,

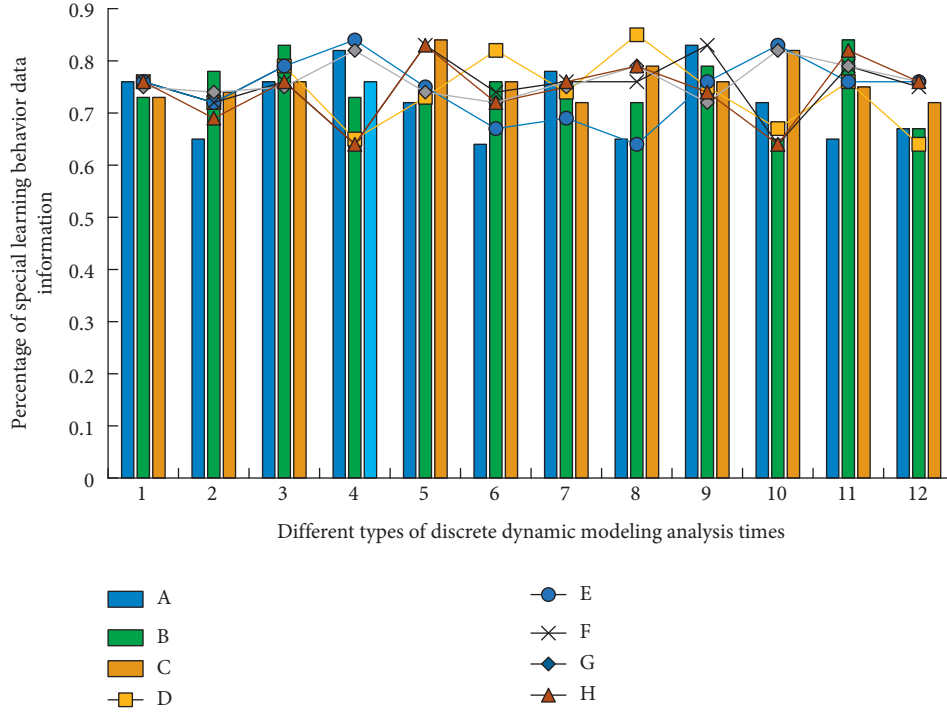


FIGURE 4: The regular relationship between different types of learner behavior data sets and special data information under the discrete dynamic model.

let $x_i = (x_{i1}, x_{i2}, \dots, x_{ip})$ and $x_j = (x_{j1}, x_{j2}, \dots, x_{jp})$ be the observed values of English learning behavior of different students, then the similarity measure function $R(x)$ and correlation function $Q(x)$ between them can be characterized as

$$R(x) = \frac{\left[\sum_{k=1}^p (x_{ik} - \bar{x}_i)^2 \right] + \left[\sum_{k=1}^p (x_{jk} - \bar{x}_j)^2 \right]}{2}, \quad (1)$$

$$Q(x) = \sum_{k=1}^p (x_{ik} - \bar{x}_i)(x_{jk} - \bar{x}_j).$$

The corresponding dispersion function and $W(x)$ correlation function $T(x)$ are

$$W(x) = \frac{\sum_{k=1}^n x_{ki}^2 + \sum_{k=1}^n x_{kj}^2}{2}, \quad (2)$$

$$T(x) = \sum_{k=1}^n \frac{x_{ki} + x_{kj}}{2}.$$

The corresponding Fourier definite function $P(x)$ and European iterative function $Y(x)$ are

$$Y(x) = \sqrt{\frac{1 + (\sum_{k=1}^n x_{ki}^2 + \sum_{k=1}^n x_{kj}^2)}{n}}, \quad (3)$$

$$P(x) = \frac{1 + (\sum_{k=1}^n x_{ki} + x_{kj}/2)}{n}.$$

The corresponding square sum difference s^2 is

$$s_\delta^1 = \frac{1}{n} \sum_{k=1}^n \left[\sum_{k=1}^n x_{ki}^2 + \sum_{k=1}^n x_{kj}^2 \right]^2, \quad (4)$$

$$s_\delta^2 = \frac{1}{n} \sum_{k=1}^n \left[\sum_{k=1}^n \frac{x_{ki} + x_{kj}}{2} \right]^2.$$

3.3. Optimization Process of Discrete Dynamic Model Based on Neural Network Algorithm in English Teaching. In order to support the application of modeling in different fields, the concept of learner behavior analysis in English teaching is proposed. To a certain extent, this language library is similar to the professional language. The domain model library contains reusable components such as predefined system definition, mathematical function definition, and typical type definition. The use of these reusable components produces a high-level specification description of a discrete dynamic modeling system, that is, the specification and complexity of learner behavior analysis in English teaching description are reduced. Reusability is also a way to improve the efficiency of the modeling process. It can describe a discrete dynamic modeling system in less time. A discrete dynamic modeling system, which is different from a continuous dynamic system, has a large number of practical problems in the real world. The solution to such events is far from the maturity of the theory of a continuous dynamic system, which requires the further development of relevant theories. Another way is to modify the existing components in the discrete dynamic modeling system. In order to modify the existing components, users need to know the internal

behavior of the components. The process of a discrete dynamic modeling system is complex and cumbersome, and sometimes it has to go through many steps of derivation. For the data of 8 learning behavior types (A-H), after 12 groups of simulation analysis are carried out on the discrete dynamic model, the data analysis and processing process are shown in Figure 5.

As can be seen from Figure 5, with the increase in data analysis and processing groups, it can be found that within a certain range (1-12), the longer the unified standard processing time is, and it is relatively stable.

$$\begin{aligned}
 M(x) &= \frac{9x^7 + 9x^5 + 5x^3 + 3x^2 + 2}{7x^7 + 3x^5 + 5x^3 + 1}, \\
 L(x) &= \frac{\sum_{k=1}^n (x_{ik}\bar{x}_i/i + x_{jk}\bar{x}_j/j)}{\bar{x}_i + \bar{x}_j}, \\
 Z(x) &= \sqrt{\frac{\sum_{k=1}^n (x_{ik} - \bar{x}_i)(x_{jk} - \bar{x}_j)}{i + j}}, \\
 B(x) &= \frac{\sqrt{\sum_{k=1}^n (x_{ik}\bar{x}_i + x_{jk}\bar{x}_j)}}{i + j}.
 \end{aligned} \tag{5}$$

The information threshold R corresponding to the three functions is

$$\begin{aligned}
 R_L &= \frac{\sum_{k=1}^n (x_{ik}\bar{x}_i/i + x_{jk}\bar{x}_j/j)}{\sqrt{i^2 + j^2}}, \\
 R_Z &= \frac{\sum_{k=1}^n ((x_{ik} - \bar{x}_i)(x_{jk} - \bar{x}_j))}{\sqrt{i^2 + j^2}}, \\
 R_B &= \frac{\sqrt{i^2 + j^2}}{\sum_{k=1}^n (x_{ik}\bar{x}_i + x_{jk}\bar{x}_j/i + j)}.
 \end{aligned} \tag{6}$$

Based on the informal description of learner behavior analysis in English teaching, we distinguish the discrete dynamic modeling system entities involved, such as suppliers, customers, and transporters of the logistics system. We decompose the logistics system into subsystems until each subsystem is a basic material system, a basic information system, a control system, or a component. It has been widely used in many fields because of its strong ability for function distribution and function description. It is a powerful tool for modeling and performance analysis of asynchronous, discrete, and concurrent event dynamic systems. The simulation analysis is carried out, and the data processing process is shown in Figure 6.

4. Result Analysis and Discussion

4.1. Experimental Process of Discrete Dynamic Model for Learner Behavior Analysis in English Teaching. In order to verify the practicability of the English teaching model

constructed in this study, this study carries out practical teaching experiments combined with the actual English curriculum content, teaching process, and students' learning behavior data characteristics in Colleges and universities, and makes quantitative analysis according to students' classroom performance behavior. These external and controllable factors are attributed to the very few external and controllable factors. It shows that students' attribution tendency to their success in learning English has high stability. In foreign language learning, they generally work hard and can control their learning behavior. They believe that they can accept academic challenges. Even if they have unsuccessful experiences, they will not attribute their failure to their ability. This positive attribution will encourage students to actively summarize the experience, stimulate motivation, maintain motivation level, and help them succeed in subsequent learning activities. The simulation analysis results before the experiment are shown in Figure 7, and the results in the experiment are shown in Figure 8.

It can be seen from Figures 7 and 8 that in the discrete dynamic model based on the neural network algorithm, different types of learner behavior data have different characteristics. When determining the experimental data, with the improvement of the completion degree of data analysis times, the corresponding operation and analysis speed shows a changing trend of first decreasing and then increasing, whether in the process of simulation or experiment.

The data analysis times and completion degree of discrete dynamic model based on neural network algorithm increase, and the data operation rate of discrete dynamic model decreases and then increases. These are external controllable factors, which are caused by a very small number of external controllable factors.

Great changes have taken place in its internal relevance, and its changing laws are also different. The difference between the experimental process and the simulation process lies in the difference in minimum value. This is because different simulation data sets have different comprehensive solutions and correlation analyses.

4.2. Experimental Results and Analysis. This experimental study adopts different questionnaire contents. The questionnaire includes the following aspects: English learning habits, oral practice time, English reading habits, classroom student participation, types of homework completion, and English listening status. In the overall process of the experiment, 88.3% of the people have obvious effects, of which 62% are girls and 26% are boys. The error analysis results of the experimental results are shown in Figure 9 (1-10 represents ten groups of students who use discrete dynamic modeling to analyze English teaching, including 1357 groups for freshmen and sophomores, and 2468 groups for juniors and seniors).

It can be seen from Figure 9 that in the discrete dynamic model based on a neural network algorithm, after analyzing the learning behavior of freshmen, sophomores, seniors, and postgraduates (master and doctoral) of the University, the overall teaching quality is relatively good in the process of

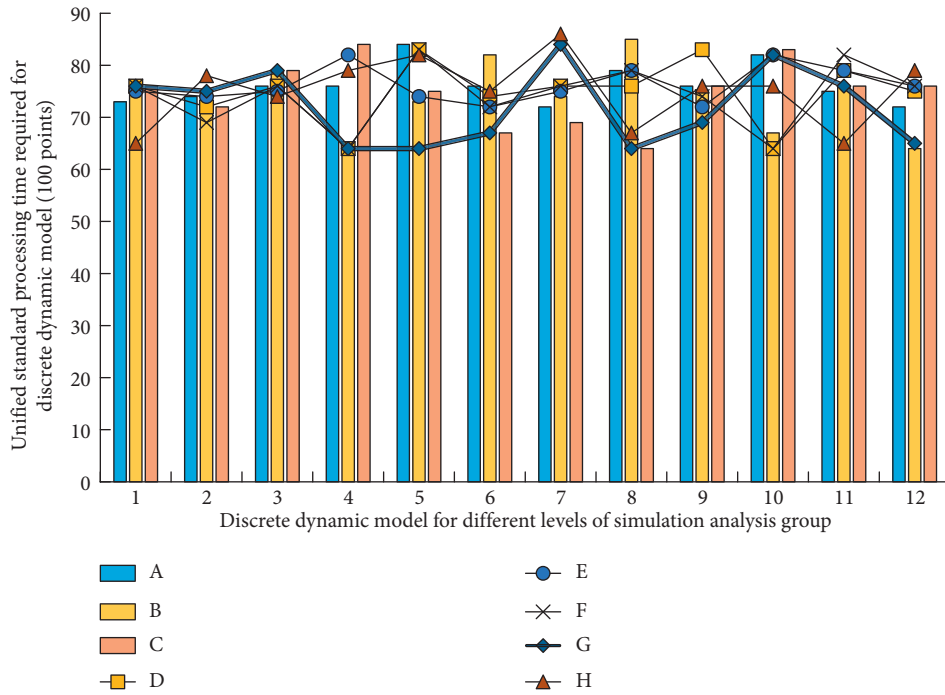


FIGURE 5: Processing time required for discrete dynamic models under different data analysis and processing groups.

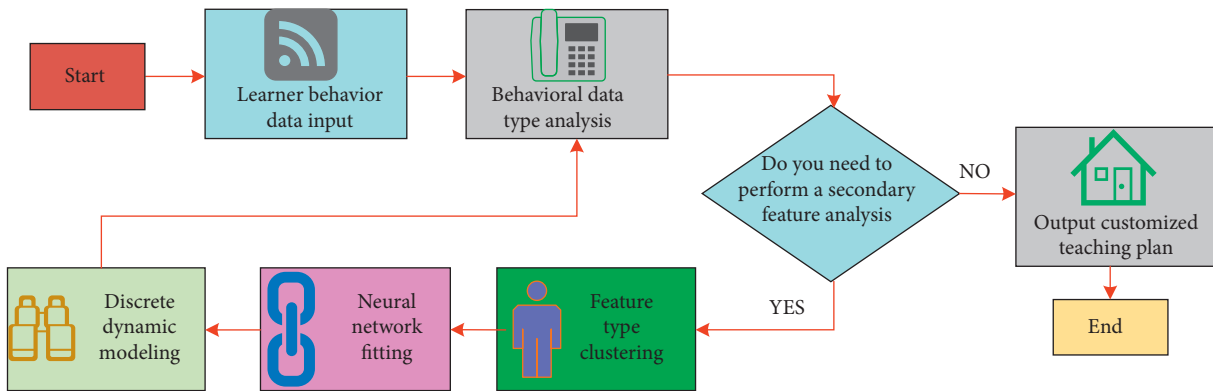


FIGURE 6: The process of analyzing and processing learner behavior data based on the discrete dynamic model of neural network algorithm.

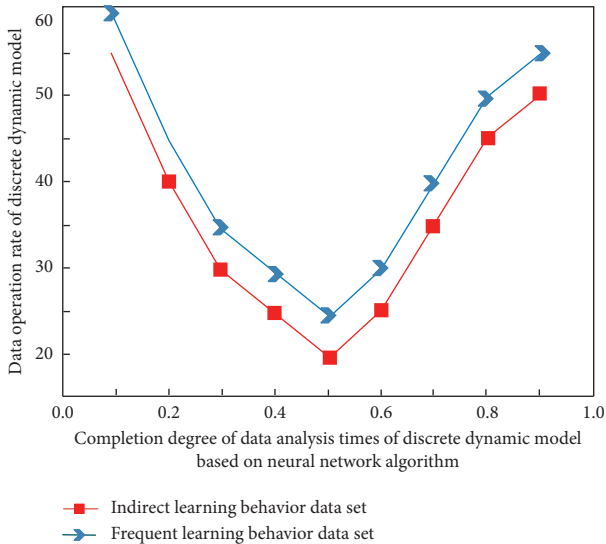


FIGURE 7: Experimental simulation analysis results.

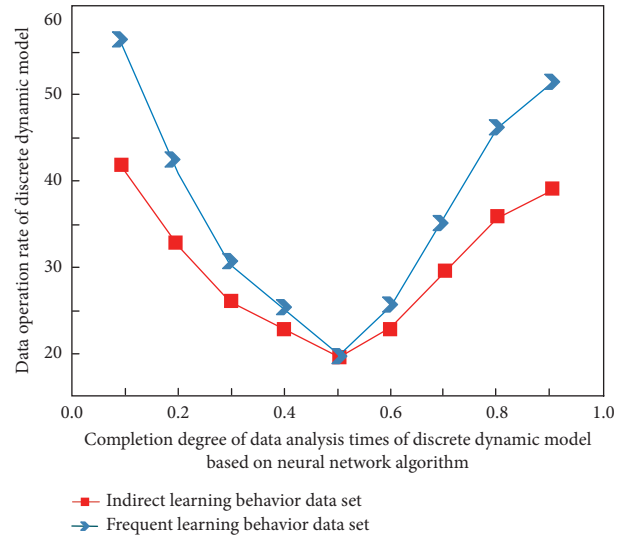


FIGURE 8: Preliminary experimental analysis results.

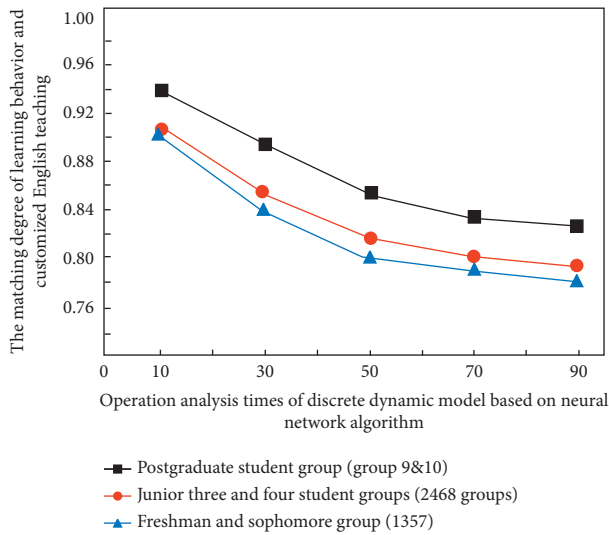


FIGURE 9: The matching degree of the corresponding learning behavior of the discrete dynamic model with the customized English teaching under different operation analysis times.

customized English classroom teaching. Among the research variables, the average change rate of English learning attitude is the highest. Internalized instrumental motivation and ideal second language self-motivation do not produce strong learning motivation among adult English learners in open education, which shows that “the existence mode and degree of ideal second language self in various educational and learning situations are inconsistent, and there are great differences in the impact on learning behavior and learning feeling.”

5. Conclusion

This paper analyzes learners’ behavior in English teaching. In the discrete dynamic model of students’ English classroom teaching, students’ behavior is constantly changing, and the causes of problem behavior are also different. Based on the analysis of English learners’ behavior, a discrete dynamic model suitable for a general hybrid simulation system is established. Firstly, this paper analyzes and expounds on the current research status of English teaching. The application of dynamic modeling technology is analyzed. Secondly, combined with the English teaching content and teaching objectives, through various data analyses of students’ learning behavior, this paper evaluates students’ English teaching quality from five aspects that affect students’ English teaching quality and puts forward a customized English teaching quality evaluation model based on discrete dynamic modeling technology and learners’ behavior analysis. Finally, through the practical teaching application in a university, the feasibility of the discrete dynamic English teaching model is verified. The results show that compared with the current innovative English teaching methods dominated by dynamic iterative decision-making algorithms, the customized discrete dynamic English teaching model based on learner behavior analysis has significantly improved the quality of English teaching and the

improvement of students’ performance. In English teaching, they should also learn and understand the theories and research results of educational psychology, which can help teachers understand “problem-finding and problem-solving behaviors” from different aspects, fundamentally improve students’ interest and enthusiasm, and truly improve the efficiency and quality of behavior analysis of English teaching learners. However, this paper does not consider the personalized teaching model according to the actual situation of different students. Therefore, the model in this paper may deviate from the actual simulation. This requires further discussion in the future.

Data Availability

The data used to support the findings of this study are included in the article.

Conflicts of Interest

The authors declare that they have no conflicts of interest.

References

- [1] L. Wang, Z. Zhen, T. Wo, B. Jiang, and H. Sun, “A scalable operating system experiment platform supporting learning behavior analysis,” *IEEE Transactions on Education*, vol. 63, no. 3, pp. 232–239, 2020.
- [2] A. G. Martín, A. Fernández-Isabel, I. M. D. Diego, and M. Beltran, “A survey for user behavior analysis based on machine learning techniques: current models and applications,” *Applied Intelligence*, vol. 51, no. 3, 2021.
- [3] A. A. Ofshteyn, K. Bingmer, E. Tseng et al., “Effect of “residents as teachers” workshop on learner perception of trainee teaching skill,” *Journal of Surgical Research*, vol. 264, pp. 418–424, 2021.
- [4] A. Mihalik, F. S. Ferreira, M. Moutoussis et al., “Multiple holdouts with stability: improving the generalizability of machine learning analyses of brain-behavior relationships,” *Biological Psychiatry*, vol. 87, no. 4, 2019.
- [5] P. Wang and S. Qiao, “Emerging applications of blockchain technology on a virtual platform for English teaching and learning,” *Wireless Communications and Mobile Computing*, vol. 2020, no. 2, 10 pages, Article ID 6623466, 2020.
- [6] Y. Zeng, “Application of flipped classroom model driven by big data and neural network in oral English teaching,” *Wireless Communications and Mobile Computing*, vol. 2021, no. 1, 7 pages, Article ID 5828129, 2021.
- [7] M. Ramanauskas, D. Šešok, J. Žilinskas, V. Starikovicius, A. Kaceniauskas, and R. Belevicius, “Global optimization of grillage-type foundations using a distributed genetic algorithm,” *Journal of Global Optimization*, vol. 77, no. 1, pp. 157–173, 2020.
- [8] H. Wu, “Multimedia interaction-based computer-aided translation technology in applied English teaching,” *Mobile Information Systems*, vol. 2021, no. 5, 10 pages, Article ID 5578476, 2021.
- [9] X. Liang, H. Lv, J. Liu, and L. Lin, “Reform of English interactive teaching mode based on cloud computing artificial intelligence—a practice analysis,” *Complexity*, vol. 40, no. 5, 13 pages, Article ID 189397, 2020.
- [10] L. Yang and S. Zhang, “English teaching model and cultivation of students’ speculative ability based on internet of

- things and typical case analysis,” *Journal of Surgical Research*, vol. 37, no. 5, pp. 1–9, 2019.
- [11] D. Lunz, G. Batt, and J. Ruess, “To quarantine, or not to quarantine: a theoretical framework for disease control via contact tracing,” *Epidemics*, vol. 34, Article ID 100428, 2021.
- [12] Q. Richard, S. Alizon, M. Choisy, M. T. Sofonea, and R. Djidjou-Demasse, “Age-structured non-pharmaceutical interventions for optimal control of COVID-19 epidemic,” *PLoS Computational Biology*, vol. 17, no. 3, Article ID e1008776, 2021.
- [13] A. Caldwell, S. Brander, J. Wiedenmann, G. Clucas, and E. Craig, “Incidence of microplastic fiber ingestion by common terns (*Sterna hirundo*) and roseate terns (*S. Dougallii*) breeding in the northwestern atlantic,” *Marine Pollution Bulletin*, vol. 177, Article ID 113560, 2022.
- [14] A. S. M. Miraz, W. J. Meng, B. R. Ramachandran, and C. D. Wick, “Computational observation of the strengthening of Cu/TiN metal/ceramic interfaces by sub-nanometer interlayers and dopants,” *Applied Surface Science*, vol. 554, Article ID 149562, 2021.
- [15] D. Zou, S. Li, X. Kong, H. Ouyang, and Z. Li, “Solving the combined heat and power economic dispatch problems by an improved genetic algorithm and a new constraint handling strategy,” *Applied Energy*, vol. 237, pp. 646–670, 2019.
- [16] W. Pejpichestakul, A. Frassoldati, A. Parente, and T. Faravelli, “Kinetic modeling of soot formation in premixed burner-stabilized stagnation ethylene flames at heavily sooting condition,” *Fuel*, vol. 234, pp. 199–206, 2018.
- [17] H. Cao, “Analysis of English teaching based on convolutional neural network and improved random forest algorithm,” *Journal of Intelligent and Fuzzy Systems*, vol. 39, no. 2, pp. 1–11, 2020.
- [18] S. Cao, R. Chen, H. Liu, and R. Shi, “An empirical study on multimodal discourse analysis of college English teaching in the context of new media,” *Journal of Intelligent and Fuzzy Systems*, no. 2, pp. 1–5, 2021.
- [19] B. Deng, “Word order detection in English classroom teaching based on improved genetic algorithm of block coding,” *Bulletin of the American Meteorological Society*, vol. 40, no. 6, pp. 1–12, 2020.
- [20] M. N. Do, J. Y. Lee, and J. R. Kim, “Development of level-differentiated flipped learning model for teaching and learning English language in Korean primary school,” *Asia Life Sciences*, no. 4, pp. 2371–2380, 2018.
- [21] J. Fathi, V. Greenier, and A. Derakhshan, “Self-efficacy, reflection, and burnout among Iranian EFL teachers: the mediating role of emotion regulation,” *Iranian Journal of Language Teaching Research*, no. 9(2), pp. 13–37, 2021.
- [22] J. Santini, T. Bloor, and G. Sensevy, “Modeling conceptualization and investigating teaching effectiveness: a comparative case study of earthquakes studied in classroom practice and in science,” *Science & Education*, vol. 27, no. 9-10, pp. 921–961, 2018.
- [23] Y. Cong, H. Kang, G. Yan, and T. Guo, “Modeling, dynamics, and parametric studies of a multi-cable-stayed beam model,” *Acta Mechanica*, vol. 231, no. 4, pp. 1–24, 2020.
- [24] B. O. Taddé, H. Jacqminadda, J. Dartigues, and C. Daniel, “Dynamic modeling of multivariate dimensions and their temporal relationships using latent processes: application to Alzheimer’s disease,” *Biometrics*, vol. 76, 2020.
- [25] Y. C. Chung and Y. R. Wu, “Dynamic modeling of a gear transmission system containing damping particles using coupled multi-body dynamics and discrete element method,” *Nonlinear Dynamics*, vol. 98, no. 1, pp. 129–149, 2019.
- [26] R. S. J. Pa and K. H. Cho, “Discrete event dynamic modeling and analysis of the democratic progress in a society controlled by networked agents,” *IEEE Transactions on Automatic Control*, vol. 67, no. 99, p. 1, 2021.

Retraction

Retracted: Fuzzy Logic-Based Machine Learning Algorithm for Cultural and Creative Product Design

Computational Intelligence and Neuroscience

Received 13 September 2023; Accepted 13 September 2023; Published 14 September 2023

Copyright © 2023 Computational Intelligence and Neuroscience. This is an open access article distributed under the Creative Commons Attribution License, which permits unrestricted use, distribution, and reproduction in any medium, provided the original work is properly cited.

This article has been retracted by Hindawi following an investigation undertaken by the publisher [1]. This investigation has uncovered evidence of one or more of the following indicators of systematic manipulation of the publication process:

- (1) Discrepancies in scope
- (2) Discrepancies in the description of the research reported
- (3) Discrepancies between the availability of data and the research described
- (4) Inappropriate citations
- (5) Incoherent, meaningless and/or irrelevant content included in the article
- (6) Peer-review manipulation

The presence of these indicators undermines our confidence in the integrity of the article's content and we cannot, therefore, vouch for its reliability. Please note that this notice is intended solely to alert readers that the content of this article is unreliable. We have not investigated whether authors were aware of or involved in the systematic manipulation of the publication process.

Wiley and Hindawi regrets that the usual quality checks did not identify these issues before publication and have since put additional measures in place to safeguard research integrity.

We wish to credit our own Research Integrity and Research Publishing teams and anonymous and named external researchers and research integrity experts for contributing to this investigation.

The corresponding author, as the representative of all authors, has been given the opportunity to register their agreement or disagreement to this retraction. We have kept a record of any response received.

References

- [1] T. Lan, "Fuzzy Logic-Based Machine Learning Algorithm for Cultural and Creative Product Design," *Computational Intelligence and Neuroscience*, vol. 2022, Article ID 7747192, 7 pages, 2022.

Research Article

Fuzzy Logic-Based Machine Learning Algorithm for Cultural and Creative Product Design

Taihua Lan 

College of Fine Arts, Fujian Normal University, Fuzhou, Fujian 350117, China

Correspondence should be addressed to Taihua Lan; lantaihua@fjnu.edu.cn

Received 24 April 2022; Revised 15 May 2022; Accepted 25 May 2022; Published 9 June 2022

Academic Editor: Le Sun

Copyright © 2022 Taihua Lan. This is an open access article distributed under the Creative Commons Attribution License, which permits unrestricted use, distribution, and reproduction in any medium, provided the original work is properly cited.

In order to effectively assist industrial designers in the color scheme design of cultural and creative products and output color schemes that meet users' image preferences, an interactive color scheme design method for cultural and creative products based on triangular fuzzy number is proposed. Through the group consistency decision based on triangular fuzzy number, an interactive genetic evolution of the color scheme population of cultural and creative products is performed to generate color schemes that satisfy the group consistency imagery preference and satisfaction, and the final selection scheme is calculated by color beauty. This paper verifies that the method can effectively integrate the imagery preferences of group users and help industrial designers to better design color schemes for cultural and creative products through the results of multiuser decision consistency.

1. Introduction

Cultural and creative products based on art paintings in the market are mainly divided into two categories based on a certain theme and cultural and creative products based on different artworks of a certain form [1]. For example, cultural creative products based on paintings of Van Gogh, Monet and Klimt, whose forms include functional artifacts such as mugs, mouse pads, scarves and coasters, belong to a series of cultural creative products based on a certain theme [2]. Cultural creative products based on a certain form with fixed forms, such as umbrellas and socks, with different famous paintings printed onto them [3]. To sum up, the current combination of paintings and cultural creative product carriers is rather rigid, without finding the proper entry point, not to mention the factor of personalization, which makes it difficult to win users [4].

The characteristics of cultural and creative products include shape, size, texture, material, color, graphics, and details, but aspects such as novelty style and personalized embodiment of products are not the characteristics of products, but the psychological reactions of people to products [5–7]. At the same time, design triggers emotional reactions in people, and Peter Dismert proposed five types of

emotions: instrumental, aesthetic, social, surprise, and interest [8]. Cultural experiences in products are entertaining, educational, aesthetic, and creative. Entertainment refers to the relaxation of the consumer during the experience, which is an enjoyable experience; education refers to the knowledge gained during the experience, such as understanding the shape and meaning of pottery, and the production process of pottery; aesthetics refers to the pleasure of the consumer immersed in the environment of something; creativity refers to the ability to create a product that is unique and based on a personal experience [9–13]. In this paper, an interactive color scheme design method for cultural creative products based on triangular fuzzy number is proposed. The process and basic principles of interactive genetic color scheme design are investigated, and the interactive genetic evolution of the color scheme population of cultural and creative products is carried out to generate color schemes that satisfy the consistent imagery preference and satisfaction of the group, and the final selection of the scheme is calculated by color beauty, which verifies that the method can effectively integrate the imagery preference of the group users and help industrial designers through the results of consistent multiuser decision making better design color schemes for cultural and creative products [14–16].

In this paper, based on triangular fuzzy number, an interactive genetic evolution of the color scheme population of cultural and creative products is performed to generate color schemes that satisfy the group consistency imagery preference and satisfaction, and the final selection scheme is calculated by color beauty.

2. Related Work

CNNs have been proposed to provide a new approach to image processing and have achieved remarkable success in the field of image recognition [17]. These were created on the basis of generative adversarial networks whose training data included more than 15,000 portraits from the 14th to the 20th century, and the system automatically generated several new works until it successfully fooled specialized tests to determine whether the work was created by a human or a machine. More recently, learned existing styles and aesthetics and were able to generate their own innovative images, and experiments found that 75% of people could not distinguish whether a painting was generated by AICAN or created by the artist [18].

A key issue in image generation is how to ensure that the generated images look realistic. To this end proposed a method for learning the shape of natural image streams directly from data using generative adversarial networks, a model that automatically adjusts the output so that all edits remain as realistic as possible and all operations are represented by constrained optimization. Deep convolutional GAN were developed in to produce some highly realistic images, but currently only for specific classes, such as faces, record covers, and room interiors. Zhang et al. [19] proposed generative adversarial networks to generate images based on text descriptions only, i.e., the model first acquires text descriptions about image synthesis, second learns and captures features in the text that describe important visual information, and then uses these features to synthesize realistic images that can fool people. Nilashi et al. [20] developed a set of image-to-image conversion algorithms and later proposed the CycleGAN framework to migrate the visual style of a set of images to other images. In addition, learning-based interactive coloring methods have been proposed [21].

Although these schemes have improved the color performance, the effect is still not good. Therefore, this scheme is more important for the performance of cultural and creative design.

3. Fuzzy Quantification of Color Imagery Preference

The color imagery of cultural and creative products reflects the users' psychological perceptions of the products, which are often expressed with the help of language and have ambiguity and uncertainty. The triangular fuzzy number helps to solve the problem that quantitative numbers cannot fully express the evaluation opinion, so this paper introduces the triangular fuzzy number to quantify the users' color imagery preference [22–24].

Let the set of comments $I = \{i_0, i_1, \dots, i_n\}$ represent an ordered set of linguistic evaluation values, where $i_m (1 \leq m \leq n)$ is a linguistic evaluation result in this linguistic set, then the triangular fuzzy number of this result can be expressed as

$$\bar{A} = (a^L, a^M, a^U) = \left(\frac{m-1}{n}, \frac{m}{n}, \frac{m+1}{n} \right). \quad (1)$$

In particular, when $m=0$, $\bar{A} = (0, 0, (m+1)/n)$.

The Likert five-level scale is used to determine the evaluation level of color imagery of cultural and creative products ($n=4$), and the corresponding triangular fuzzy numbers and scales are shown in Table 1.

4. Consensus Model of Group Imagery Preference

In order to make the color scheme design of tourism cultural and creative products better reflect the image preference of users, multiple user groups are used to participate in the interactive color scheme design process. The consistency of user groups' perception of the design scheme reflects the reliability of the color scheme design results. Through interactive genetic evolution of the color scheme group of cultural and creative products, generate a color scheme that meets the image preference and satisfaction of group consistency. Therefore, we constructed a consensus model to judge the consistency of group perception [25–27].

Let the set of users be $E = \{e_1, e_2, \dots, e_t\} (t \geq 2)$. According to (1) and Table 1, the triangular fuzzy number of users $e_i (1 \leq i \leq t)$ evaluating the color scheme of cultural and creative products is $a_i = (a_i^L, a_i^M, a_i^U)$, and the group evaluation matrix is

$$A = \begin{pmatrix} \bar{a}_1 \\ \vdots \\ \bar{a}_i \\ \vdots \\ \bar{a}_t \end{pmatrix} = \begin{pmatrix} a_1^L & a_1^M & a_1^U \\ \vdots & \vdots & \vdots \\ a_i^L & a_i^M & a_i^U \\ \vdots & \vdots & \vdots \\ a_t^L & a_t^M & a_t^U \end{pmatrix}. \quad (2)$$

The Euclidean distance is used to measure the difference of user groups' preference for color imagery of cultural and creative products, and the distance between the 2 sets of triangular fuzzy numbers $a_i = (a_i^L, a_i^M, a_i^U)$ and $a_j = (a_j^L, a_j^M, a_j^U)$ is calculated as

$$\frac{\|\bar{a}_i - \bar{a}_j\|}{\sqrt{(a_i^L - a_j^L)^2 + (a_i^M - a_j^M)^2 + (a_i^U - a_j^U)^2}}. \quad (3)$$

Then, the distance between the group evaluation matrices is

$$S = \sum_{i=1}^t \sum_{j=1}^t \|\bar{a}_i - \bar{a}_j\|. \quad (4)$$

Using the arithmetic mean ϕ aggregates all distances as

TABLE 1: Evaluation language sets.

Language evaluation variables	Triangular fuzzy number	Evaluation scale
I do not like it very much	(0, 0, 0.25)	0
Dislike	(0, 0.25, 0.5)	0.25
Commonly	(0.25, 0.5, 0.75)	0.5
Like	(0.5, 0.75, 1)	0.75
Like it very much	(0.75, 1, 1)	1

$$B = \varphi(S). \quad (5)$$

For a certain scheme of color scheme design of cultural and creative products, the consensus degree of imagery preference of user groups is

$$C_r = 1 - B. \quad (6)$$

5. Group Consensus-Driven Interactive Color Scheme Design

5.1. Interactive Color Matching Design Process. Interactive genetic algorithm is an evolutionary algorithm to simulate the superiority and inferiority of biological populations, evolving color schemes through selection, crossover and variation, generating color schemes that satisfy the consistent imagery preference and satisfaction of the population, and finally obtaining a satisfactory color scheme through color beauty calculation. Compared with traditional genetic algorithm, interactive genetic algorithm adds interactive evaluation with users and embeds implicit factors such as users' preferences and perceptions into the algorithm, which can obtain a satisfactory solution more in line with users' perceptions [27]. In this paper, we consider the problem of consistency of user evaluation in the population interactive genetic algorithm, and the process of interactive genetic color matching is driven by both the consensus degree of group opinion and satisfaction based on the quantification of user imagery preference, and its color matching design process is shown in Figure 1.

5.2. Color Matching Interactive Genetic Manipulation

5.2.1. Population Setting. The number of populations is set by the designer according to the actual demand. The individual coding method adopted in the color scheme is

$$D = \{(d_1, r_1, g_1, b_1), \dots, (d_x, r_y, g_y, b_y)\}, (x \geq y), \quad (7)$$

where x is the number of color partitions; d_i is the i -th color scheme of the product, $i = 1, 2, \dots, x$; y is the number of colors included in the product color scheme; r_j, g_j, b_j is the R, G, B color value of a color scheme, respectively, taking values between 0 and 255 [28, 29].

5.2.2. Generate the Initial Population. After obtaining the population individual code by (7), the initialized population is obtained by randomly generating the individual color by adopting the interactive genetic algorithm.

6. Color Beauty Calculation

In order to better reflect the quality of the output solution of interactive color scheme of cultural and creative products, color beauty is introduced to analyze the success degree of color scheme design. The color aesthetics includes the sense of order and the complexity of the color scheme, which is calculated as follows:

$$M = \frac{O}{C}, \quad (8)$$

where M is the degree of beauty, O is the order factor, and C is the complexity factor.

The order factor O is calculated as follows:

$$\begin{cases} O = \sum O_g \\ O = \sum O_h + \sum O_v + \sum O_c \end{cases}, \quad (9)$$

where O_g is the order factor when only uncolored grays are combined; $O_h, O_v,$ and O_c are the order factors determined by the color phase difference, lightness difference, and purity difference, respectively, when there are colors involved in the color scheme.

The complexity of color matching is obtained by calculating the total number of colors and the number of pairs with hue difference, lightness difference, and purity difference among all possible combinations of color pairs, thus obtaining the complexity factor C , as shown in (10).

$$C = C_m + C_h + C_v + C_c. \quad (10)$$

In which, C_m is the total number of colors in the color scheme; C_h is the number of color pairs with hue difference among all possible color pairs; C_v is the number of color pairs with lightness difference among all possible color pairs; C_c is the number of color pairs with purity difference among all possible color pairs. According to (9) to (10), the color order and color complexity are calculated, and the color beauty M is further calculated. When $M > 0.5$, the product color scheme is considered beautiful and conforms to the law of aesthetics, otherwise it is considered unattractive.

6.1. Example Application Results Analysis. The cloisonné tire making is used as an innovative design example for algorithm simulation and genetic algorithm is used as a comparison. The example process finds the specific substructure of cartoon expression modeling to satisfy the target maximum group, and the execution parameters of the algorithm in this paper are shown in Table 2. The execution process of

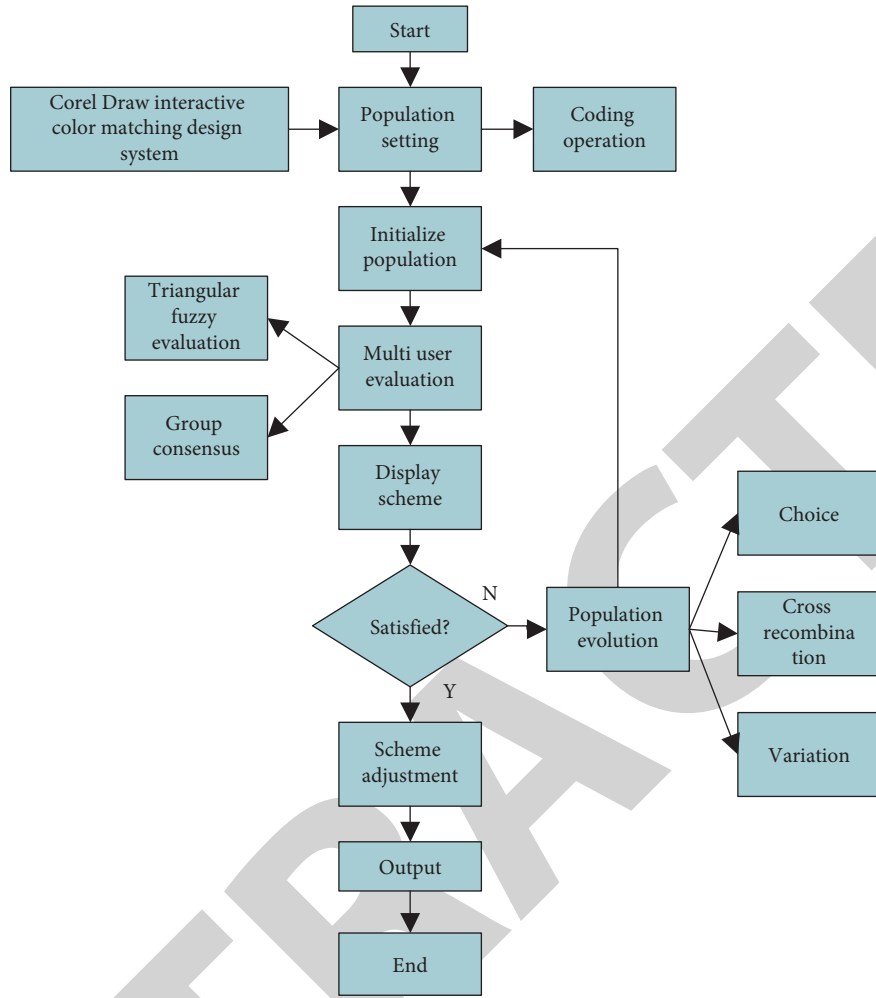


FIGURE 1: Color scheme operation flow.

TABLE 2: Implementation parameters of this paper.

Parameter	Numerical value
Initial temperature	1000
Termination temperature	0.1
Temperature variation coefficient	0.89
Function fitness	0

this paper is shown in Table 3, and the algorithm mining is executed 410 times.

6.2. Emoji Modeling Results. After reaching the target adaptation value of 0, the results of the optimized combination of cartoon expression modeling were obtained, of which the combination modeling results are shown in Figure 2. After the designer and user satisfaction survey, all the 9 cartoon expressions got 85 points (out of 100) or more, which verified the feasibility and effectiveness of the proposed method.

6.3. Cloisonné Making Session. The traditional cloisonné pattern making (tire making) is to cut out different shapes of purple copper sheets according to the drawings, and

TABLE 3: Implementation process of this paper.

Number of executions	Temperature	Fitness value
1	991	10
2	980.9	10
3	971.2	8
4	967.3	8
280	50.6	5
410	37.9	0

hammer them into various shapes of copper tires, then join the parts together and put on the solder, and after high temperature welding, they become the copper tire shape of the vessel [30].

In the process of cloisonné making, the traditional process is optimized through digital technology. Firstly, the traditional cloisonné vessels are measured and collected by laser scanning or photography to generate 3D model data of cloisonné tires, and the 3D scanning modeling is shown in Figure 3. Secondly, using deep learning and innovation engine to create 3D objects, AI achieves modeling of high-level data abstraction through image recognition technology, and deep neural network will analyze and learn from the



FIGURE 2: Cartoon expression modeling optimization results.



FIGURE 3: 3D scanning modeling.

stored traditional ware data to select 3D works that meet the requirements according to the cloisonné tire pattern specification and send them to online 3D printing platform for 3D printing. AI is useful in the model design, material selection, and product production of cloisonné 3D printing, realizing the intelligence of the whole process from design to copper tire forming. The intelligent creation of cloisonné body integrates AI with the “object,” which makes traditional craftsmen more accurate, time-saving, and labor-saving in the production of copper tires, and provides more possibilities for digital innovation design of cloisonné [31]. Taking cloisonné color scheme design as an example, it is verified that the proposed method can effectively integrate the imagery preferences of group users and assist industrial designers to better design the color scheme of cultural and creative products through the results of multiuser decision consistency.

When solving iteratively with Fluent, the flow field needs to be initialized. Still, an initial velocity is added to the liquid

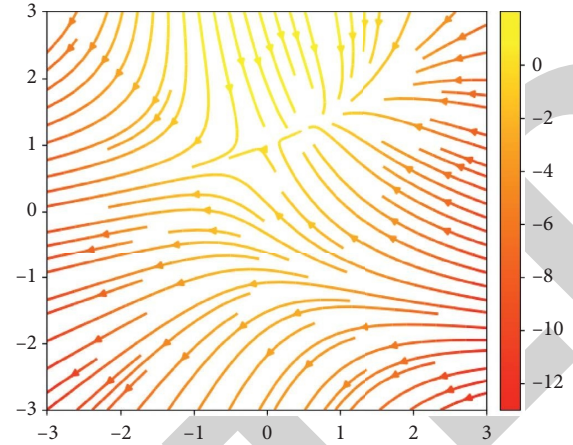


FIGURE 4: Micro bubble generator printhead model speed vector distribution.

drip inlet plane and then the solution is solved iteratively (10 iterations). After solving, the simulation results are observed and analyzed. Figures 4 and 5 show the velocity field distribution vectors obtained after the simulation.

According to the velocity field distribution obtained from the simulation, Figure 4, the velocity field distribution of the main channel shows a decreasing trend, the further away from the drip channel, the smaller the velocity vector, but the velocity field distribution exists in all areas of the main channel, and the velocity vector is distributed in the order of $10\text{--}2\text{--}10^2$ cm/s. Figure 4 shows a partial enlargement of the printhead structure, which shows that the velocity field distribution also exists in the microchamber and capillary channels, with velocity vectors in the order of $10\text{--}2$ to 100 cm/s. This indicates that the velocity field distribution exists in all parts of the printhead in the presence of velocity pressure at the drip inlet [32].

7. Comparative Analysis of Mining Capacity

In addition, in order to evaluate the mining performance of the algorithm quantitatively, the similarity value index is used to compare the maximum cluster structure mining results of the genetic algorithm and the algorithm in this paper, and the similarity value index S is calculated as follows:

$$S = \frac{N_C}{N_s}, \quad (11)$$

where N_C denotes the number of triangular slices of the largest group structure and N_s denotes the number of triangular slices of the template structure. The average excavation index and time comparison of the 9 cartoon expression modeling results are shown in Table 4.

As can be seen from Table 4, compared with the genetic algorithm, the algorithm in this paper consumes less time and has less similarity between structures due to the controllable execution parameters and clear objectives, thus effectively improving the design efficiency while ensuring product diversity and quality.

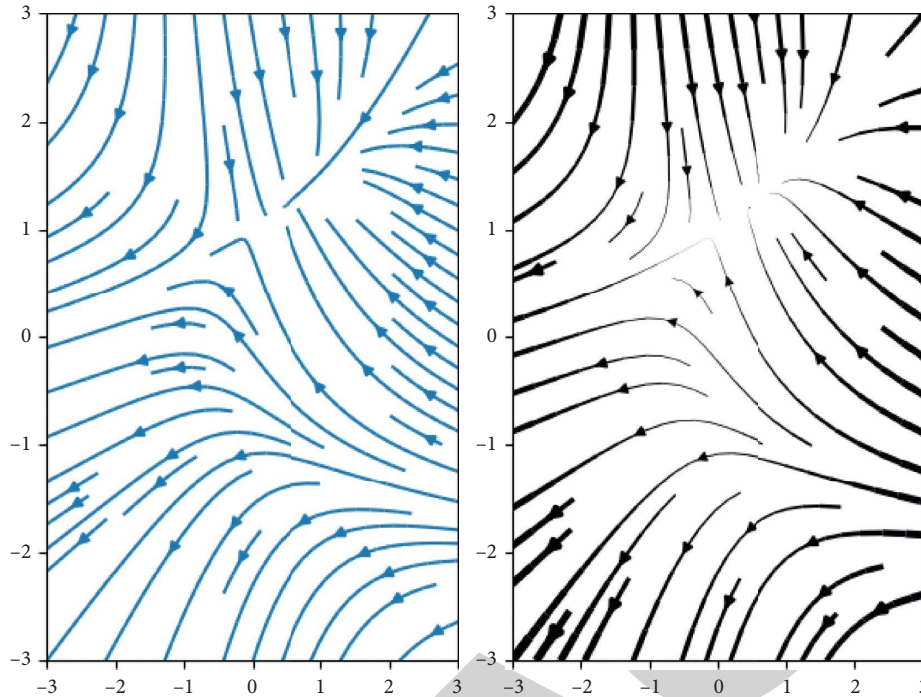


FIGURE 5: Micro bubble generator printhead model velocity vector distribution (partial enlargement).

TABLE 4: Comparison of mining metrics and time.

Algorithm	Similarity (S)	Time (S)
Genetic algorithm	0.79	0.36
Simulated annealing algorithm	0.59	0.21

8. Conclusions

In this paper, an interactive color matching design method for cultural creative products with triangular fuzzy numbers is proposed. The user group's imagery preference is quantitatively described by using triangular fuzzy number, and the interactive genetic evolution of the color matching population of cultural creative products is operated by the group consistency decision based on the triangular fuzzy number. The proposed method is verified to be effective in integrating the imagery preferences of the group users by taking cloisonné color scheme design as an example.

Data Availability

The experimental data used to support the findings of this study are available from the corresponding author upon request.

Conflicts of Interest

The author declares that there are no conflicts of interest to report regarding the present study.

References

- [1] G. Soltani-Fesaghandis and A. Pooya, "Design of an artificial intelligence system for predicting success of new product development and selecting proper market-product strategy in the food industry," *The International Food and Agribusiness Management Review*, vol. 21, no. 7, pp. 847–864, 2018.
- [2] A. A. A. Rostamy, M. Shaverdi, B. Amiri, and F. B. Takanlou, "Using fuzzy analytical hierarchy process to evaluate main dimensions of business process reengineering," *Journal of Applied Operational Research*, vol. 4, no. 2, pp. 69–77, 2012.
- [3] G. Huang, L. Xiao, and G. Zhang, "Decision-making model of machine tool remanufacturing alternatives based on dual interval rough number clouds," *Engineering Applications of Artificial Intelligence*, vol. 104, Article ID 104392, 2021.
- [4] J. Fu and Y. Fu, "An adaptive multi-agent system for cost collaborative management in supply chains," *Engineering Applications of Artificial Intelligence*, vol. 44, pp. 91–100, 2015.
- [5] C.-H. Chen and Z. Lin, "The application of fuzzy theory in the evaluation of visual images of smartphone rear cameras," *Applied Sciences*, vol. 11, no. 8, p. 3555, 2021.
- [6] Y.-J. Chen, "Structured methodology for supplier selection and evaluation in a supply chain," *Information Sciences*, vol. 181, no. 9, pp. 1651–1670, 2011.
- [7] S. Vinodh, S. R. Devadasan, K. E. K. Vimal, and D. Kumar, "Design of agile supply chain assessment model and its case study in an Indian automotive components manufacturing organization," *Journal of Manufacturing Systems*, vol. 32, no. 4, pp. 620–631, 2013.
- [8] F. R. Lima, L. Osiro, and L. C. R. Carpinetti, "A fuzzy inference and categorization approach for supplier selection using compensatory and non-compensatory decision rules," *Applied Soft Computing*, vol. 13, no. 10, pp. 4133–4147, 2013.
- [9] A. N. Fb Saghezchi, M. Albano, A. Radwan, and J. Rodriguez, "A novel relay selection game in cooperative wireless networks based on," in *Proceedings of the 2011 IEEE 73rd vehicular technology conference (VTC Spring)*, pp. 1–6, Budapest, Hungary, 15–18 May 2011.
- [10] A. I. Ban, O. I. Ban, V. Bogdan, D. C. Sabau Popa, and D. Tuse, "Performance evaluation model of Romanian manufacturing

Research Article

Research and Application of Clustering Algorithm for Text Big Data

Zi Li Chen 

Institute of General Aviation Industry, Fujian Chuanzheng Communications College, Fuzhou 350007, China

Correspondence should be addressed to Zi Li Chen; 1999005@fjpc.edu.cn

Received 12 April 2022; Revised 5 May 2022; Accepted 17 May 2022; Published 8 June 2022

Academic Editor: Le Sun

Copyright © 2022 Zi Li Chen. This is an open access article distributed under the Creative Commons Attribution License, which permits unrestricted use, distribution, and reproduction in any medium, provided the original work is properly cited.

In the era of big data, text as an information reserve database is very important, in all walks of life. From humanities research to government decision-making, from precision medicine to quantitative finance, from customer management to marketing, massive text, as one of the most important information carriers, plays an important role everywhere. The text data generated in these practical problems of humanities research, financial industry, marketing, and other fields often has obvious domain characteristics, often containing the professional vocabulary and unique language patterns in these fields and often accompanied by a variety of “noise.” Dealing with such texts is a great challenge for the current technical conditions, especially for Chinese texts. A clustering algorithm provides a better solution for text big data information processing. Clustering algorithm is the main body of cluster analysis, K-means algorithm with its implementation principle is simple, low time complexity is widely used in the field of cluster analysis, but its K value needs to be preset, initial clustering center random selection into local optimal solution, other clustering algorithm, such as mean drift clustering, K-means clustering in mining text big data. In view of the problems of the above algorithm, this paper first extracts and analyzes the text big data and then does experiments with the clustering algorithm. Experimental conclusion: by analyzing large-scale text data limited to large-scale and simple data set, the traditional K-means algorithm has low efficiency and reduced accuracy, and the K-means algorithm is susceptible to the influence of initial center and abnormal data. According to the above problems, the K-means cluster analysis algorithm for data sets with large data volumes is analyzed and improved to improve its execution efficiency and accuracy on data sets with large data volume set. Mean shift clustering can be regarded as making many random centers move towards the direction of maximum density gradually, that is, moving their mean centroid continuously according to the probability density of data and finally obtaining multiple maximum density centers. It can also be said that mean shift clustering is a kernel density estimation algorithm.

1. Introduction

Text detection is the fundamental step in many computer vision applications. This paper introduces a novel text detection technique, and we verify the utility of the method in the YouTube video text dataset and find that the method runs more than 2 times [1] of the classical method. This paper expounds the existing research work on the decomposition and inference of clustering algorithms based on text big data and points out the shortcomings of the existing research work [2]. Big data text analysis is the promoter of knowledge management. This paper believes that, through the big data text analysis, it not only can improve the quality of life of ordinary people but also can make various

enterprises for benign competition, so as to improve the quality of enterprises. This paper provides many different opinions, involving many aspects, from the daily life of ordinary people to different business functions of enterprises, from stock market to finance. Text big data analysis has become a shortcut and a leader of knowledge management [3]. Big data is used in various industries, which contains various value information, and text big data, as an important part of big data, carries countless human knowledge. This paper reviews the feature representation of text big data and finally discusses the future trend of large-text data content understanding [4]. Nowadays, the application of big data is not open in various fields, and the meaningful analysis and extraction of big data are needed in

many fields. In this paper, we study the cluster analysis process based on text big data and propose the whole process [5] from collecting big data to applying various clustering algorithms for cluster analysis. This paper uses K-means text clustering algorithm to analyze the big data talent recruitment information. The results show that big data jobs are concentrated in frontier cities. Most enterprises require undergraduate or graduate students, and a few enterprises see whether the applicant has many years of relevant work experience. There are wage differences between different types of jobs, and the higher the position, the higher the requirements for education and experience will be [6]. Discovering knowledge from text data in a high-speed and accurate manner is a major challenge in large-text data mining. This paper presents a new large-text data mining method, the random walk algorithm, which accurately extracts two basic and complementary words from numerous text data. We show that the proposed random walk algorithm is based on the aggregate relation and the combined relation [7] in recent decades, with the development of the Internet, it is almost normal for people to use mobile phones and computers, while the phenomenon of reading books decreases day and night. This also makes the storage and search of articles in the digital library reach an unprecedented height, but it is limited to indexing the text description of each pseudocode and cannot provide simple algorithm-specific information. Therefore, this paper proposes a set of algorithms to extract and search related information from text big data, and its efficiency is as high as 78% through practical verification [8] accurate. The K-means algorithm is an incremental clustering method. In this paper, we propose improvements of the algorithm to reduce the computational amount without significantly affecting the quality of the solution. It is also tested and showed that the improved K-means algorithm has better results than [9]. This paper presents a new algorithmic model, called the fuzzy c-mean clustering model (or FCM). FCM solves the problem [10] that objects in the dataset cannot partition significantly separated clusters. We discuss three main issues of traditional partitioning clustering, namely, sensitivity to initialization, difficulty determining the number of clusters, and sensitivity [11] to noise and outliers. In this paper, we propose an adaptive spatial fuzzy C mean clustering algorithm for the segmentation of 3D MR images in text big data. We verify the effectiveness of [12] through extensive segmentation experiments on simulation and real MR images and comparison with existing algorithms. Clustering algorithm plays an important role in analyzing the structure and function of biological network. In this paper, a fast local network clustering algorithm SPICI is proposed. It has the most advanced performance and can cluster all the test networks in a very short time. Experiments show that its success rate is the highest among other algorithms. Reference [13] in terms of the quality of the clusters it finds. In the data analysis methods, we often use the cluster analysis. In this paper, we propose K-means clustering algorithms and investigate the problem where the K-means clustering algorithm is limited to small-scale datasets. Finally, this paper presents a method to make the

algorithm more efficient and thus obtain better clustering [14] with reduced complexity. In text big data processing, K-means is our common partitioning clustering algorithm. However, the proposed algorithm is still unsatisfied in some professional fields, and many initialization methods have been proposed to solve this problem. In this paper, we demonstrate that popular initialization methods generally perform poorly, and that there are actually some powerful alternatives to these methods [15].

2. Text Big Data and Cluster Analysis

2.1. Text Big Data. Text big data refers to the document data, which is manifested in the form of documents and contains a large amount of information, fast speed, more types, and low data value. In big data, text big data is an important part of big data. Due to the rapid development of information technology, the growth rate of data sources increases through the media of mobile phones and computers. Text big data has three characteristics: diversity, large quantity, and fast speed. For the data collection technology, there are still huge challenges to ensure its accuracy and effectiveness.

2.2. Mining and Application of Big Data. Data mining refers to a process of searching for the information hidden in the data through algorithms, which is the process of analyzing the hidden and potentially valuable information contained in a large amount of data in a database. Data mining does not need manual operation, can automatically analyze the data of enterprises, can summarize the data, and then make reasoning, to help decision makers to adjust market strategies, reduce risks, and make correct decisions. The practical data analysis of big data can help people make judgments so as to take appropriate actions. Because of the popularity of the network and the convenience of big data application, the application of big data is more and more extensive such as answering customer questions, meeting customer service needs, helping to optimize business processes, improving health care and research and development, and so on. With the continuous innovation of big data in various industries, big data will gradually create more value for human beings. Text clustering is to cluster some documents with similar contents from many documents. Simply speaking, it is to find any two most relevant text information in the text information space and degenerate them into one text information, so as to reduce the amount of information.

2.3. Text Big Data Processing Method. Nowadays, our common text big data processing method is cluster analysis, which is a quantitative method. When processing text big data, clustering score is generally analyzed from two perspectives. First, from the perspective of data analysis, it is a multivariate statistical analysis method for quantitative analysis of multiple samples. Second, from the perspective of data mining, it can be divided into division clustering, hierarchical clustering, density-based clustering, and network-based clustering. Partition clustering is based on distance clustering, which effectively uses mean or center point and

small data. Hierarchical clustering is a very intuitive algorithm, as its name implies, it is to cluster layer by layer. Density-based clustering is to divide data into each category according to the connection of density around it. Grid-based clustering adopts multiresolution grid data structure, which can process data quickly.

2.4. Type of Clustering Algorithm

2.4.1. Cluster Analysis. Clustering is a technology of classifying data by computer, is also a classification of multivariate statistical analysis method, divides a data set according to a specific standard into different classes or clusters, and makes the similarity of the data object as big as possible, not the difference in the same cluster is as big as possible. Text clustering refers to the clustering of documents. Similarly, data with similar characteristics are gathered together as much as possible, and dissimilar data are separated as far as possible. Not only text can be clustered, but anything where features can be extracted. For example, e-commerce websites cluster goods according to features such as price and color, app stores according to the App's user age and downloads, and movie websites according to the theme and year of films. Machine learning including clustering can be performed simply by converting real-life objects into a vector in the mathematical world through feature extraction.

2.4.2. Clustering Algorithm. When dealing with text big data, we all have an algorithm bias, and we use different algorithms to deal with different problems. The following clustering algorithms are commonly used when we cluster data.

3. Cluster Algorithm Analysis

3.1. Definition of the Class

Definition 1. Set the positive number given by the threshold T , if the distance d of any two elements in the set G_{ij} . Everything meets

$$d_{ij} \leq T, \quad (i, j \in G). \quad (1)$$

It is called that G constitutes a class for the threshold T .

Definition 2. Let the threshold T be the given positive number, if each $i \in G$ in the set G satisfies

$$\frac{1}{n-1} \sum_{j \in G} d_{ij} \leq T \lim_{x \rightarrow \infty}, \quad (2)$$

where n is the number of elements in the set G and then G is said to form a class for the threshold T .

Definition 3. Let T and H ($H > T$) be two given positive numbers, if the average pairwise element distance in the set G meets

$$\frac{1}{n(n-1)} \sum_{i \in G} \sum_{j \in G} d_{ij} \leq T, \quad d_{ij} \leq H (i, j \in G), \quad (3)$$

where n is the number of elements in the set G and G is called a class of H for the threshold T .

Formula (2) shows that the average of the sum of distances between any two elements in the set G is less than a given threshold T . Similarly, formula (3) indicates that the average is less than T and less than H .

3.2. Characteristics of the Class. Let the sample contained by class G be $X_{(1)}, X_{(2)}, \dots, X_{(N)}$, where t is the sample of population G and its characteristics can be characterized from different angles. The barycenter of G , sample deviation matrix A_G , and sample covariance matrix S_G and D_G represent the diameter of class G as follows:

$$\bar{X}_G = \frac{1}{n} \sum_{t=1}^n X_{(t)}, \quad (4)$$

$$A_G = \sum_{t=1}^n (X_{(t)} - \bar{X}_G), \quad S_G = \frac{1}{n-1} A_G, \quad (5)$$

$$D_G = \sum_{t=1}^n (X_{(t)} - \bar{X}_G), \quad (X_{(t)} - \bar{X}_G) = \text{tr}(A_G), \quad (6)$$

$$D_G = \max_{i,j \in G} d_{i,j}. \quad (7)$$

3.3. Distance. If n samples are considered as n points in m -dimensional space, then the similarity between two samples is d_{ij} measure. For sample X_i , the distance of X_j , the general requirement is $d_{ij} \geq 0$, for any i, j , when $d_{ij} = 0 \Leftrightarrow X_{(i)} = X_{(j)}$; $d_{ij} = d_{ji}$, for any i, j ; $d_{ij} \leq d_{ik} + d_{kj}$, for any i, j, k (triangle inequality).

The common distances are as follows.

The Minkowski distance is represented as

$$d_{ij}(q) = \left[\sum_{t=1}^m |x_{it} - x_{jt}|^q \right]^{1/q}, \quad (i, j = 1, 2, \dots, n). \quad (8)$$

The first order Ming distance at V is expressed as

$$d_{ij}(1) = \sum_{t=1}^m |x_{it} - x_{jt}|, \quad (i, j = 1, 2, \dots, n). \quad (9)$$

The absolute distance, when X , is expressed as

$$d_{ij}(2) = \left[\sum_{t=1}^m |x_{it} - x_{jt}|^2 \right]^{1/2}, \quad (i, j = 1, 2, \dots, n). \quad (10)$$

Euclidean distance, when to Z , is represented as

$$d_{ij}(\infty) = \max_{1 \leq t \leq m} |x_{it} - x_{jt}| \quad (i, j = 1, 2, \dots, n). \quad (11)$$

That is, the Chebyshev distance.

The Mahalanobis distance is located.

In 1930s, Mahala Mahalanobis, a famous Indian mathematician, put forward Mahalanobis distance, which is

of great significance in data clustering. Σ is the covariance array of the indicator, $\Sigma = (\omega_{ij})_{p \times p}$, as shown in (12) and (13) among

$$\omega_{ij} = \frac{1}{n-1} \sum_{\alpha=1}^n (x_{\alpha i} - \bar{x}_i)(x_{\alpha j} - \bar{x}_j), \quad i, j = 1, 2, \dots, p, \quad (12)$$

$$\bar{x}_i = \frac{1}{n} \sum_{\alpha=1}^n x_{\alpha i}, \quad \bar{x}_j = \frac{1}{n} \sum_{\alpha=1}^n x_{\alpha j}. \quad (13)$$

When Σ^{-1} is present, it is Ma distance, which can be expressed as

$$d_{ij}^2(M) = (X_i - X_j)' \Sigma^{-1} (X_i - X_j). \quad (14)$$

The Mahalanobis distance from sample X factory to population G port is defined as

$$d^2(X, G) = (X - \mu)' \Sigma^{-1} (X - \mu). \quad (15)$$

Here, μ is the mean vector of the population.

The Lance and Williams Distance, also known as the Canberra Distance, is considered a weighted version of the Manhattan distance.

The Rand distance is a kind of distance given by Lance and Williams. The formula is calculated as follows:

$$d_{ij}(L) = \frac{1}{m} \sum_{t=1}^m \frac{|x_{it} - x_{jt}|}{x_{it} + x_{jt}}, \quad (16)$$

$$d_{ij}(L) = \frac{1}{m} \sum_{t=1}^m \frac{|x_{it} - x_{jt}|}{x_{it} + x_{jt}}, \quad i, j = 1, 2, \dots, n. \quad (17)$$

Jeffery and Matasta put forward the distance formula, but there is no related reference. The formula is calculated as

$$d_{ij}(J) = \left[\sum_{k=2}^p (\sqrt{x_{ik} - x_{jk}})^2 \right]^{1/2}. \quad (18)$$

Incline intersection space distance is defined as follows.

Since there are often different correlations between the variables, the distance of the orthogonal space calculates the sample space as variable.

You can use the oblique intersection space distance. The calculation formula is

$$d_{ij} = \left[\frac{1}{p^2} \sum_{n=1}^p \sum_{k=1}^p (x_{in} - x_{jn})(x_{ik} - x_{jk}) r_{hk} \right]^{1/2}. \quad (19)$$

3.4. Similarity Coefficient. To study the relationship between the samples, the similarity coefficient method was used here. First, the samples are classified, and then the relationship between the samples is studied by the similarity coefficient. C_{ij} represents the similarity coefficient between samples X_i and X_j , with $C_{ij} = \pm 1 \Leftrightarrow X_i = aX_j$; $|C_{ij}| \leq 1$, valid for any

i, j ; $C_{ij} = C_{ji}$ is true for any i, j . The closer the absolute value of C_{ij} is to 1 here, the more similar them X_i and X_j are. Conversely, the two are estranged. The common similarity coefficients are angular cosine:

$$c_{ij}(1) = \cos \alpha_{ij} \frac{\sum_{k=1}^n x_{ki} x_{kj}}{\left[(\sum_{k=1}^n x_{ki}^2) (\sum_{k=1}^n x_{kj}^2) \right]^{1/2}}. \quad (20)$$

When X_i and X_j are parallel, the angles $\alpha_{ij} = 0^\circ$ and $C_{ij}(1) = 1$ indicate that the two vectors are completely similar; when X_i and X_j are orthogonal, the angles $\alpha_{ij} = 90^\circ$ and $C_{ij}(1) = 0$ indicate that the two vectors are not correlated.

The correlation coefficient is expressed as

$$c_{ij}(2) = \cos \alpha_{ij} \frac{\sum_{k=1}^n (x_{ki} - \bar{x}_i)(x_{kj} - \bar{x}_j)}{\left\{ \left[\sum_{k=1}^n (x_{ki} - \bar{x}_i)^2 \right] \left[\sum_{k=1}^n (x_{kj} - \bar{x}_j)^2 \right] \right\}^{1/2}}. \quad (21)$$

I indicates the linear correlation of the two vectors.

3.5. K-Means Clustering Algorithm. The original mean clustering algorithm is different from the improved mean clustering algorithm. The specific steps of the original clustering algorithm are as follows: input data set $X = \{x_1, x_2, \dots, x_n\}$, cluster number K ; output K cluster C_j , $j = 1, 2, \dots, k$, make $I = 1$, and randomly select K data points as the initial cluster center $m_j(I)$, $j = 1, 2, \dots, k$. Of K clusters; calculate the distance between each data point and the center of the K cluster $d(x_i, m_j(I))$, $i = 1, 2, \dots, n$, $j = 1, 2, \dots, k$, if it meets

$$d(x_i, m_j(I)) = \min \{ d(x_i, m_j(I)), \quad j = 1, 2, \dots, k \}. \quad (22)$$

Then, calculating S new clustering centers satisfies

$$m_i(I+1) = \frac{1}{N_j} \sum_{i=1, x_i \in C_j}^{N_j} x_i, \quad j = 1, 2, \dots, k. \quad (23)$$

If $m_j(I+1) \neq m_j(I)$, $j = 1, 2, \dots, k$, then $I = I + 1$, return to step 2. Otherwise, the algorithm ends.

K-means clustering algorithm can also add clustering criterion function to terminate the iterative process; generally, the criterion function of sum of squares of clustering errors is adopted, that is, the sum of squares of clustering errors J is calculated in the fourth step of the above algorithm flow, and then judgment is added. If the value of J does not change obviously twice, it means that the value of J has converged, and the algorithm is ended. Otherwise, it is transferred to the second step to continue execution. Specifically, K clustering centers (m_1, m_2, \dots, m_k) are randomly designated as follows. Assign x_i , for any x_i , the nearest to it is divided into the same class. Recalculate the center of each cluster with formula H

$$m_i \frac{1}{N_i} \sum_{j=1}^{N_i} x_{ij}, \quad i = 1, 2, \dots, n. \quad (24)$$

The deviation is then calculated using formula F

$$J = \sum_{i=1}^k \sum_{j=1}^{n_i} \|x_{ij} - m_i\|^2. \quad (25)$$

If J converges, the return (m_1, m_2, \dots, m_k) algorithm ends; otherwise, proceed to the second step.

The idea of the original clustering algorithm is reflected in the above algorithm process, from which we can see that the selection of the initial cluster center point of each cluster is crucial to the final result of the clustering. In the above algorithm, the focus is on the iterative algorithm. In each iteration of the formula, the data points are divided into the cluster with the nearest cluster center and then recalculate the cluster center and then repeatedly iterate until each data point is no longer redivided. Simply put, K-means is a method of dividing data into K parts without any supervision signal.

4. Study on Text Clustering Algorithm

4.1. Improved Global K-Means Clustering Algorithm Analysis. In order to verify the real effect of clustering algorithm, the six data sets Iris, Wine, Soybean-small, Segmentation, Pima Indians Diabetes, and Pen digits are used for global clustering, fast global clustering, and improved clustering. By comparison of clustering time (T) sum of clustering error (E), we prove that the improved algorithm in this paper without seriously affecting the sum of squared of clustering errors. It greatly reduces the clustering time. Comparison of experimental results for the six sets of machine learning database data from UCI is shown in Table 1. Iris and Pen digits specifically refer to the data set of text big data in this paper.

From the above experimental results, compared with the other two algorithms, the improved algorithm obviously reduces the clustering time, without affecting the clustering error, right Soybean-small databases and databases greatly shorten the clustering time without seriously affecting the clustering errors. among Pen digits. It is particularly prominent in the big data sets. Thus, the present algorithm has a superior clustering performance.

In this paper, the improved global K-means clustering algorithm is tested by randomly generated artificial data sets with noise data to prove the anti-interference performance of the improved global K-means clustering algorithm against noise data. The randomly generated data are divided into three categories, each of which contains 120 two-dimensional samples, which conform to normal distribution. In class i , the mean value of abscissa x is μ_x^i , the mean value of ordinate is μ_y^i , and the standard deviation of class i is σ^i . Among them, a certain number of noise points are added to the second class, and the standard deviation of the noise points is expressed as σ^l . The effects of parameter category clustering for the three classes of randomly generated samples are shown in Table 2 and Figure 1. Figure 1 shows the clustering effect diagram of randomly generated three types of data, and its ordinate represents the time required for clustering the three types of data. The larger the value, the longer the time required.

These three sets of random data were tested using the above three algorithms, and the comparison of cluster time (T) and sum of cluster error (E) are shown in Table 3.

As can be seen from Table 3, these three algorithms have the same clustering effect on these three randomly generated data sets with noise points, but the improved algorithm in this paper has obvious advantages in clustering time, far superior to the other two kinds of algorithms. The steering results are shown in Figure 2. It can be seen from the table that the sum of squares of clustering errors of the three algorithms is the same, but the clustering time is gradually shortened, and the time required by this algorithm is the shortest, which also shows that this algorithm has obvious advantages in clustering time.

Visible from Figure 2, the global K-means algorithm, fast global K-means algorithm, and the improved global K-means algorithm in the three sets of randomly generated data sets with noise points has the same clustering effect, but this algorithm has obvious advantages in clustering time, far better than the global K-means algorithm and fast global K-means algorithm.

4.2. K-Means Original Algorithm and Improved Algorithm Analysis. In order to verify the effectiveness of the improved clustering algorithm, the Iris data set of the database was used for experimental test comparison. The comparative performance indexes are the accuracy and convergence rate (specifically the number of cycles of each test). First, the original and the improved algorithm were tested 10 random tests on the dataset, and the test metrics and accuracy comparisons are shown in Table 4 and Figure 3.

The original and the modified algorithms were sub-randomly tested on the dataset, and the results on the loop number index are shown in Figure 4.

Figures 3 and 4 present the results of the experiment: the clustering accuracy of the original algorithm fluctuates between 79% and 89% and 89%, and the number of cycles fluctuates between the second times, while the accuracy of the improved algorithm is always 92%, and the number of cycles is always 3 times. The horizontal and vertical coordinates in Figure 4 represent the number of tests and the number of bad cycles, respectively. The number of bad cycles refers to the number of times it is necessary to classify these data in the process of substituting data into the algorithm for clustering. When the original algorithm is used for clustering in the figure, the number of times to follow the bad is uncertain, which shows that the algorithm is imperfect and the accuracy is unstable. The improved algorithm can be seen in the graph is very stable, which will greatly shorten the clustering time.

To verify the effectiveness of the improved algorithm in practical applications, the original K-means algorithm and the improved algorithm were tested 5 times, respectively, with the dataset, and the metrics randomly run 5 times are shown in Table 5.

The five tests are shown in Figure 5 in terms of the overall accuracy of the algorithm and in Figure 6 in terms of cycle times.

TABLE 1: Comparison of the experimental results for several different clustering methods.

	The global K-means		Fast global K-means		The algorithm in this paper	
	E	T (s)	E	T (s)	E	T (s)
Iris	78.9408	0.438	78.9451	0.078	78.9451	0.031
Wine	2.3707×10^6	0.765	2.707×10^6	0.094	2.3707×10^6	0.015
Soybean-small	96.3984	0.156	96.4702	0.047	96.4702	0
Segmentation	0.9398×10^6	3.765	1.0076×10^6	0.188	1.0198×10^6	0.125
Pima Indians diabetes	5.1363×10^6	3.625	5.1665×10^6	0.109	5.1363×10^6	0.047
Pen digits	9.9830×10^6	186.391	1.0480×10^7	6.844	1.0553×10^7	0.953

TABLE 2: Randomly generated various parameters with the noise data.

	First kind	Second kind	The third class
Mean μ	$\mu_x^1 = 0$	$\mu_y^1 = 0$ $\mu_x^2 = 6, \mu_y^2 = 2$	$\mu_x^3 = 6, \mu_y^3 = -1$
Standard deviation σ	$\sigma^i = 1.5$	$\sigma^2 = 0.5, \sigma^l = 2$	$\sigma^3 = 0.5$

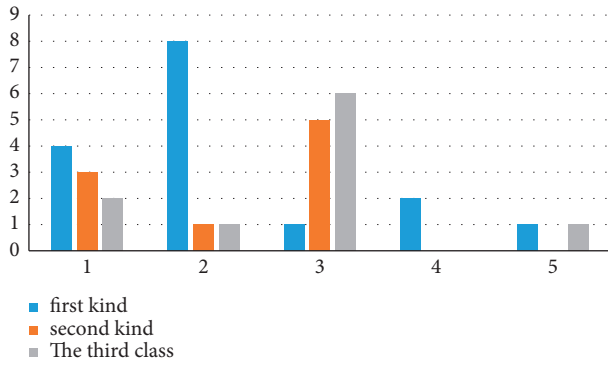


FIGURE 1: Cluster results diagram of the three categories.

TABLE 3: Comparison of the cluster results for the randomly generated data.

	A	B	C
$E (\times 10^3)$	0.6363	0.6363	0.6363
T (s)	1.11	0.062	0.031

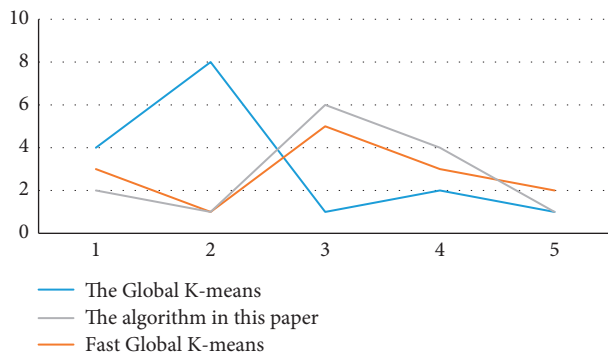


FIGURE 2: Comparison of the cluster results for the randomly generated data.

TABLE 4: The original algorithm and the improved algorithm are 10 random indicators.

Test serial number	The original algorithm		Improve the algorithm	
	Precision	Follow the bad times	Precision	Follow the bad times
1	84	10	93	3
2	83	5	92	3
3	89	7	90	3
4	82	4	92	3
5	85	13	92	3
6	84	3	92	3
7	83	10	89	3
8	79	4	85	3
9	89	5	92	3
10	89	9	92	3

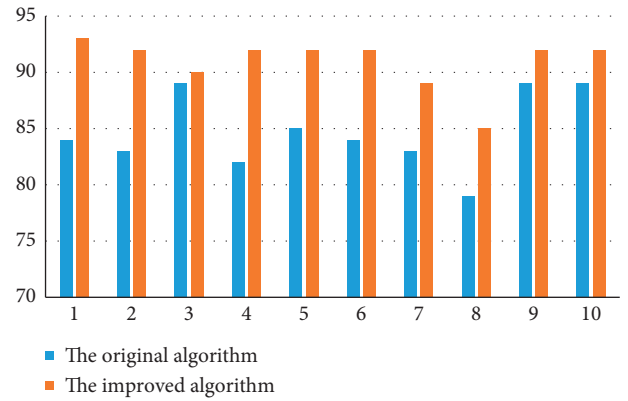


FIGURE 3: Comparison plot of the accuracy of the original and improved algorithms for 10 random tests.

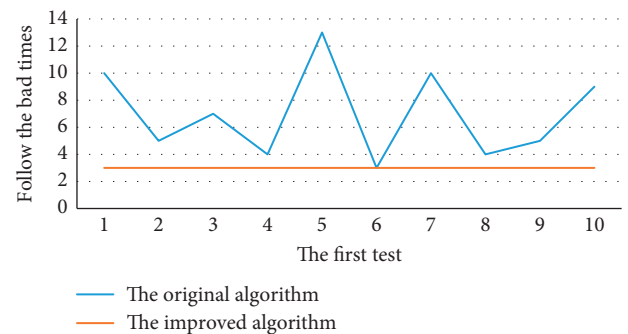


FIGURE 4: Comparison of the number of cycles of the original and improved algorithms.

TABLE 5: Five random runs of the original algorithm and the improved algorithm.

Test serial number	The original algorithm		Improve the algorithm	
	Precision	Follow the bad times	Precision	Follow the bad times
1	59	18	75	9
2	61	24	75	9
3	68	35	75	9
4	73	27	75	9
5	69	11	75	9

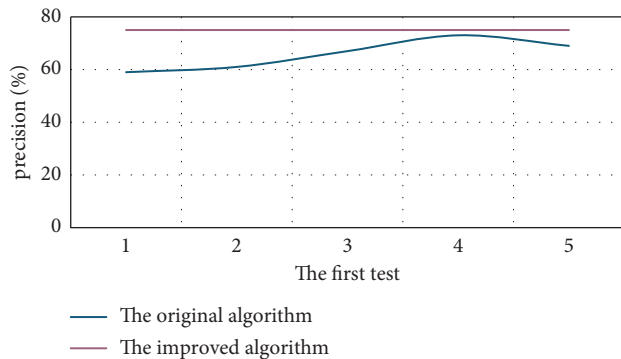


FIGURE 5: Accuracy comparison of the original and improved algorithm randomly run 5 times.

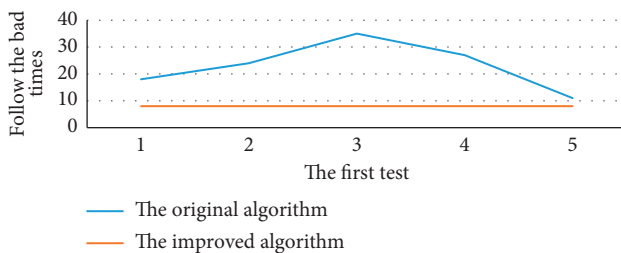


FIGURE 6: Comparison of cycle number for five random runs of the original and improved algorithms.

Figures 5 and 6 show the results of the experiment. The accuracy of the original algorithm fluctuates between times, and the cycle times fluctuate between the next times. Under the condition that the precision of the improved algorithm is unchanged, the number of cycles is unchanged, and the average time consumption is unchanged. Considering the experimental results, it is not difficult to see that the improved algorithm is better than the original algorithm in practice. At present, the automatic classification of text is widely used, such as Baidu news column display. For cluster analysis, category information is unknown and can automatically generate category information is not only critical for cluster mining count but also significant for subsequent data mining work.

5. Conclusion

Now, the data is explosive growth, and the data processing is particularly urgent. This paper studies big data processing, explains the concept and application of text big data, and introduces the processing method of text big data. This paper

studies the clustering algorithm for text-oriented big data and analyzes the sample point similarity measure method and clustering algorithm. In this paper, the K-means algorithm is the main object to solve the adaptive clustering algorithm to optimize the initial clustering center of the clustering algorithm, in order to solve the problems such as failure to handle large-scale data sets, low clustering accuracy, and unstable clustering results. And, the original K-means algorithm of the original algorithm and improved algorithm, global K-means, and fast K-means algorithm, through a large number of real data comparison experiment, demonstrates the proposed new algorithm can solve the problems in the actual problem. Experimental results show that the algorithm is higher, and clustering results are more stable. In the era of big data, text data is exploding every day, and how to deal with text big data quickly and efficiently has become a difficult problem. The scientific significance of this paper lies in the research of clustering algorithm, bringing forth new ideas and putting forward new text data processing algorithm. It makes clustering algorithm more convenient and efficient to deal with practical problems.

Data Availability

The experimental data used to support the findings of this study are available from the corresponding author upon request.

Conflicts of Interest

The author declares no conflicts of interest regarding this work.

References

- [1] A. B. Ayed, M. B. Halima, and A. M. Alimi, "MapReduce based text detection in big data natural scene videos," *Procedia Computer Science*, vol. 53, no. 1, pp. 216–223, 2015.
- [2] J. Zhang, C. Yao, Y. Sun, and Z. Fang, "Building text-based temporally linked event network for scientific big data analytics," *Personal and Ubiquitous Computing*, vol. 20, no. 5, pp. 743–755, 2016.
- [3] Z. Khan and T. Vorley, "Big data text analytics: an enabler of knowledge management," *Journal of Knowledge Management*, vol. 15, no. 3, pp. 456–598, 1997.
- [4] S. Yuan, X. Yang, and E. Shijia, "Text big data content understanding and development trend based on feature learning," *Big Data Research*, vol. 10, no. 6, pp. 156–314, 2015.
- [5] S. Jun, "A big data preprocessing using statistical text mining," *Journal of Wuhan Institute of Physical Education*, vol. 4, no. 7, pp. 236–356, 2015.

- [6] D. Dai, Y. Ma, and M. Zhao, "Analysis of big data job requirements based on K-means text clustering in China," *PLOS ONE*, vol. 16, no. 2, pp. 678–765, 2021.
- [7] J. Shan and C. X. Zhai, "Random walks on adjacency graphs for mining lexical relations from big text data," *IEEE*, vol. 34, no. 6, pp. 387–492, 2015.
- [8] I. Safder, J. Sarfraz, and S. U. Hassan, "Detecting target text related to algorithmic efficiency in scholarly big data using recurrent convolutional neural network model," *Springer*, vol. 53, no. 9, pp. 413–537, 2017.
- [9] A. Likas, N. Vlassis, J. Verbeek, and J. J. Verbeek, "The global k-means clustering algorithm," *Pattern Recognition*, vol. 36, no. 2, pp. 451–461, 2003.
- [10] N. R. Pal, K. Pal, J. M. Keller, and J. C. Bezdek, "A possibilistic fuzzy c-means clustering algorithm," *IEEE Transactions on Fuzzy Systems*, vol. 13, no. 4, pp. 517–530, 2005.
- [11] H. Frigui and R. Krishnapuram, "A robust competitive clustering algorithm with applications in computer vision," *IEEE Transactions on Pattern Analysis and Machine Intelligence*, vol. 21, no. 5, pp. 450–465, 1999.
- [12] A. W.-C. Liew and Y. Hong Yan, "An adaptive spatial fuzzy clustering algorithm for 3-D MR image segmentation," *IEEE Transactions on Medical Imaging*, vol. 22, no. 9, pp. 1063–1075, 2003.
- [13] M. Singh, "SPICi: a fast clustering algorithm for large biological networks," *Bioinformatics*, vol. 26, no. 8, pp. 1105–1111, 2010.
- [14] K. Nazeer and M. P. Sebastian, "Improving the accuracy and efficiency of the k-means clustering algorithm," *Lecture Notes in Engineering & Computer Science*, vol. 21, no. 1, pp. 654–726, 2009.
- [15] M. E. Celebi, K. Ha, and P. A. Vela, "A comparative study of efficient initialization methods for the k-means clustering algorithm," *Expert Systems with Applications*, vol. 9, no. 11, pp. 64–92, 2013.

Research Article

High Performance Computing Simulation of Intelligent Logistics Management Based on Shortest Path Algorithm

Zongchao Wei 

Developing and Planning Department, Yellow River Conservancy Technical Institute, Kaifeng 475004, China

Correspondence should be addressed to Zongchao Wei; weizongchao@yrciti.edu.cn

Received 11 April 2022; Revised 5 May 2022; Accepted 17 May 2022; Published 8 June 2022

Academic Editor: Le Sun

Copyright © 2022 Zongchao Wei. This is an open access article distributed under the Creative Commons Attribution License, which permits unrestricted use, distribution, and reproduction in any medium, provided the original work is properly cited.

At present, e-commerce drives the logistics industry to develop greatly, but at the same time, there is a huge demand in this field, such as lower cost and higher efficiency. Facing the needs of logistics management development, it needs the blessing of intelligent technology, which involves countless fields at present. Intelligent logistics management has become a hot spot at present. What needs to be solved in this respect is how to shorten the transportation distance and save costs. To solve this problem, this paper proposes to introduce the shortest path algorithm. This paper compares the Dijkstra algorithm with the A* algorithm under the background of logistics management and finds that the latter is more suitable for this field with huge amount of information. In order to improve the performance of the A* algorithm, this paper introduces ant colony algorithm, which can better avoid obstacles. Combining these two algorithms, a *-ant colony algorithm is obtained. The algorithm absorbs the advantages of the two algorithms, while maintaining high efficiency and good stability. These characteristics are very satisfying in the field of logistics management. Through the performance test and simulation experiment, it is concluded that the algorithm has excellent optimization ability and can reduce the cost for this field.

1. Introduction

The awakening of e-commerce also awakens the development of logistics industry. At the same time, China pays great importance to logistics management. It is also the idea that the country wants to innovate and change to collide with the field of intelligent technology and logistics management. With the addition of intelligent technology, it can solve the shortest path problem well, thus reducing the cost. The shortest path algorithm is a good medicine to solve this problem. Under the test of the traditional shortest path algorithm, it is found that it can no longer meet the current problem, so it is necessary to innovate and change the algorithm. And, this is undoubtedly the mutual achievement of the two. The level of logistics management can be improved only when the two develop mutually.

In literature [1], the shortest path problem has penetrated into a wide range of fields. The Dijkstra algorithm is not perfect. First, its exit mechanism is not applicable to undirected graphs; second, the problem of adjacent nodes is

a great hidden danger; third, the problems of multivertex are not fully considered. In literature [2], the k -shortest path algorithm also has some defects in some aspects, and the alternative path obtained by the algorithm cannot be proved to be substantially different from the original path. In reality, network extension technology is usually used to solve the problems caused by turning restriction, but this method also has defects. Therefore, researchers introduce links to improve and solve this problem. The advantage of this model is to eliminate overlapping paths and find alternative paths, which can finally reduce similarity and only rely on its own nodes and links to complete the operation. In literature [3], distributed algorithm gives the shortest path problem a shot in the arm, the most important component of which is BHC. The related problems can be solved by calculating the time complexity. For example, each node can use multiple processors and how much time complexity can be calculated through these processors, so that this kind of problem can be well solved. In literature [4], the network shortest path problem is relatively simple to solve. The fact is that a single

objective function is incapable of describing problems appropriately in real life. While pursuing fast time, it may bring high cost. This is like a seesaw, but it still needs a way to balance the seesaw. The force that can balance the seesaw is Pareto. In literature [5], in the field of genes, this algorithm has also made some achievements. Dijkstra algorithm is like a good medicine to diagnose and treat gene-related problems. And, all genes in this path are candidate genes. Only a few genes were selected in the end. In literature [6], all objects have their own sizes and shapes, and researchers suggest that this algorithm has achieved little in motion planning. The idea of shape decomposition is put forward to solve this problem. Decomposition and iteration are a pair of enemies, and it is their choice to have more you and less me. Then, the geometric algorithm is the judge to judge whether there will be a war between them. If there is no hidden danger, the shortest path can be calculated by grass fire algorithm. In literature [7], researchers combine the graph algorithm with active contour restoration. Finding the global minimum is the trick of graph algorithm. Generally speaking, ordinary active contours cannot be run with three or more pixels in mind. Therefore, the researchers put forward a correct definition of deformable template and use the Dijkstra algorithm to track the contour. In literature [8], in order to study the relationship between user interface and satisfaction, the Dijkstra algorithm is used for experiments. Apple and Android are the two kings of mobile models. Students were recruited to conduct experiments on this. After testing, it was found that IOS was more useful than Android for Dijkstra algorithm. In literature [9], China has summarized all aspects of logistics. After analyzing the logistics demand, the researcher proposed to introduce relevant technical software support. For the problems related to the path, the relevant personnel and institutions decided to adopt logical data structure. In literature [10], the article agrees that intelligent technology is unshakable. Therefore, we can only find another way to change from a strategic perspective. At the same time, it shows that the addition of intelligent technology has brought many qualitative changes to this field. Compared with traditional methods, intelligent logistics application has been recognized as the best management method at present. In literature [11], the Internet of Things and cloud computing have propped up a sky, sheltering intelligent logistics from the wind and rain. In literature [12], in order to keep up with the development trend of intelligent logistics demand, it is necessary to shorten the cycle and cost while designing the system. In the whole process, there must be methods to implement both people and things. A series of technologies such as GPS have also been applied. Therefore, intelligent logistics will provide a good ascending ladder for e-commerce. In literature [13], in medical use, logistics management is also very important. Hospitals will encounter a series of problems when quoting a set of logistics management mode, which researchers need to analyze and popularize in hospitals after using the logistics management mode. At the same time, this model also needs to be improved. In this way, hospital consumables can be reduced, and costs can be reduced. In literature [14], it is recognized by most enterprises that production and

transportation become one. Cost and time are important factors in the whole process. If you want to taste the sweetness, you have to give up. This price is the control of information. For logistics management, the ultimate destination must be gradually networked and then set different frameworks according to different needs. In literature [15], Internet of Things has been the backbone of logistics development, which is the development trend of the times. Researchers need to analyze and predict the architecture, which will be a historic change.

2. Shortest Path Algorithm

As its name implies, the shortest path algorithm is a corresponding algorithm proposed to solve the shortest path problem, and the shortest path is the path with the minimum sum of the weights of edges in the process of starting from one vertex to another in a graph.

2.1. Dijkstra Algorithm. Dijkstra algorithm is a classical algorithm for solving the shortest path, and the core of its algorithm is the order of the length of the path. The main purpose of this algorithm is to choose the best route in the logistics transportation nodes.

The Dijkstra algorithm flow is shown in Figure 1:

The final shortest path length $D[j]$ is expressed as follows:

$$D[j] = \min\{D[i] | v_i \in V\}. \quad (1)$$

$D[i]$: shortest path length from shipment starting point to each receiving point. v : logistics starting point. v_i : end point.

After the shortest path is obtained, the shortest path length among the remaining paths is as follows:

$$D[j] = \min\{D[i] | v_i \in V - S\}, \quad (2)$$

$$S = S \cup \{v_j\}. \quad (3)$$

S : the shortest path set obtained. v_j : the shortest path end point of the remaining path starting from v .

At the same time, modify the shortest path that the remaining paths can reach v_k , and the formula is as follows:

$$D[k] = D[j] + arcs[j][k] \text{ if } D[j] + arcs[j][k] < D[k]. \quad (4)$$

2.2. A Algorithm.* The right-hand man of A* algorithm is not only the evaluation function but also the search direction. In the logistics system, in the process of finding the shortest path, there are 8 nodes around the starting point, and these nodes are adjacent to the starting point. With the help of his right-hand man, the node with the lowest value will soon be found out and given the search for the next extended node. Repeat the above operations, and the lowest cost path comes into being.

The A* algorithm flow is shown in Figure 2:

The formula of heuristic function is as follows:

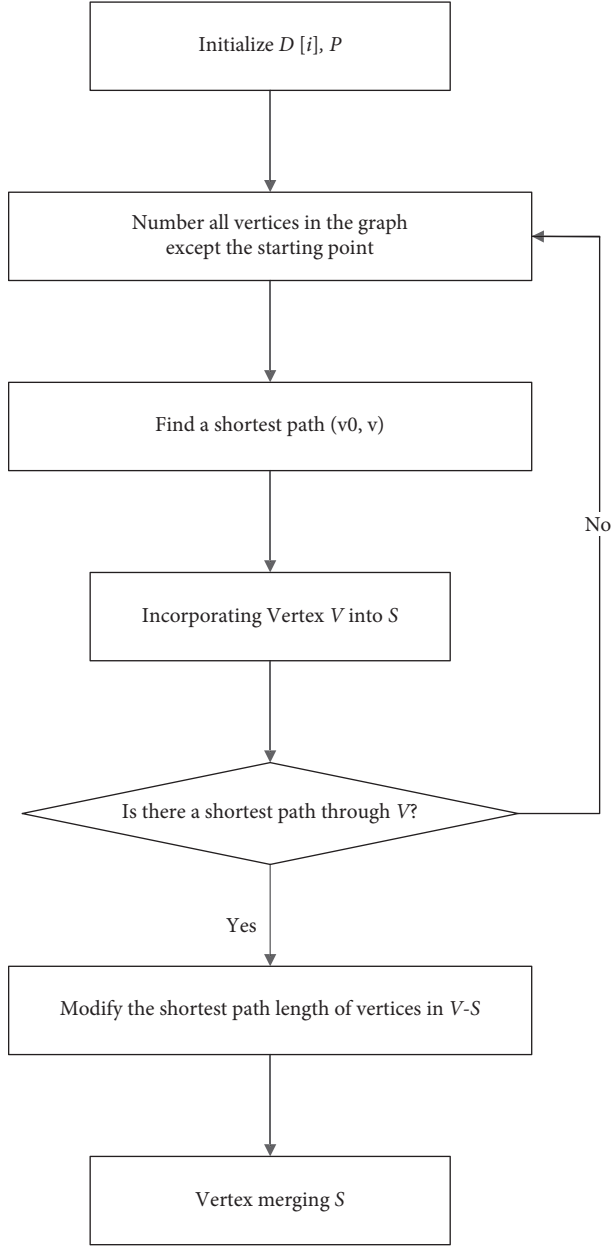


FIGURE 1: Flow chart of Dijkstra algorithm.

$$f(n) = g(n) + h(n), \quad (5)$$

$$g(n) = L_i + \sqrt{(x_n - x_i)^2 + (y_n - y_i)^2}, \quad (6)$$

$$h(n) = L_i + \sqrt{(x_n - x_T)^2 + (y_n - y_T)^2}. \quad (7)$$

$f(n)$: cost function of node n . $g(n)$: actual cost from starting point to node n . $h(n)$: estimated cost of node n to the end point. x_n, y_n : horizontal and ordinate values of node n . x_i, y_i : horizontal and ordinate values of current node i . x_T, y_T : horizontal and ordinate values of the end point. L_i : actual cost from the starting point to the current node i .

3. Optimization Algorithm

In logistics management, the above two algorithms can speed up this field. But even in terms of legal skills, there is still a gap between the two. When the digraph using Dijkstra algorithm has n vertices, the complexity of the algorithm is $O(n^2)$. Obviously, this algorithm is very efficient in solving single source path in directed graphs with all positive weighted edges, but it cannot combine more useful information to search, which is undoubtedly a fatal blow in logistics management with huge amount of information.

A* algorithm has the characteristics of Dijkstra algorithm mentioned above, and A* algorithm can maintain stability; at the same time, it has high-speed operation and accurate results. It can be seen from this that A* algorithm is more efficient in logistics management. But the A* algorithm still needs to be improved.

3.1. Improved A* Algorithm

3.1.1. Improved Node. There are n nodes in a single road section, and the search efficiency for n nodes one by one is too low, so this paper proposes to extract only the beginning and end nodes in a single road section, which greatly improves the search efficiency. Specific improvements are shown in Figure 3:

3.1.2. Improved Database. Logistics transportation usually takes each transfer point as a unit, and the amount of data in the network database of each transfer point is huge. General logistics management is to use direct reading means for data, but this is inefficient. Therefore, this paper puts forward the combination of database and memory and stores it in batches according to time. In this way, data can be obtained from the cache, thus greatly improving the efficiency of data query and search.

3.1.3. Improved Heuristic Function. In this paper, the evaluation standard of the evaluation function is travel time, while the heuristic function can be determined by the ratio of the distance between two nodes to the logistics speed. The formula of travel time estimation $h(n)$ is as follows:

$$h(n) = \frac{d(n, e)}{\bar{v}}, \quad (8)$$

$$d(n, e) = R \times \arccos \left[\cos \left(\frac{\pi x_n}{180} - \frac{\pi x_e}{180} \right) \cos \frac{\pi y_n}{180} \cos \frac{\pi y_e}{180} + \sin \frac{\pi y_n}{180} \sin \frac{\pi y_e}{180} \right], \quad (9)$$

$$\bar{v} = \frac{1}{m} \sum_{i=1}^m v_i. \quad (10)$$

$d(n, e)$: actual distance between node n and target node e . \bar{v} : average vehicle speed. R : radius of the Earth, with the value of. $6.37 \times 10^6 m$. v_i : speed on road section i . m : the

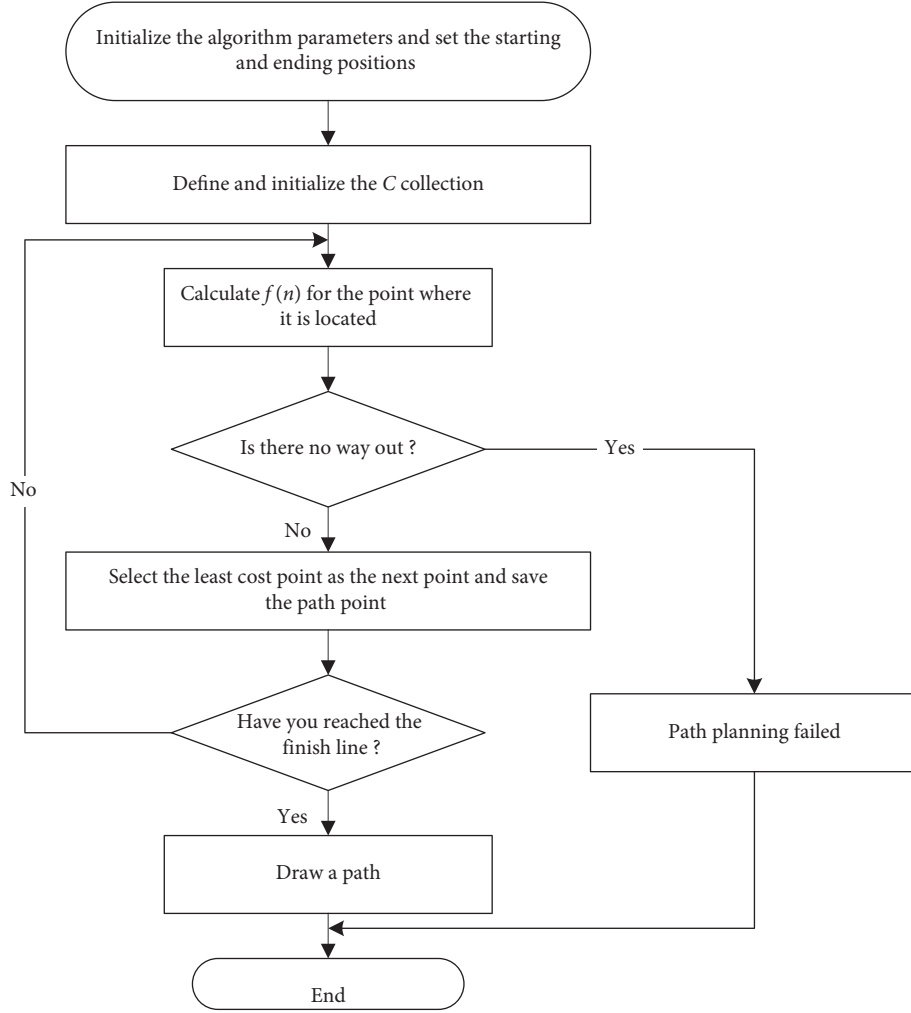


FIGURE 2: A* algorithm flow chart.

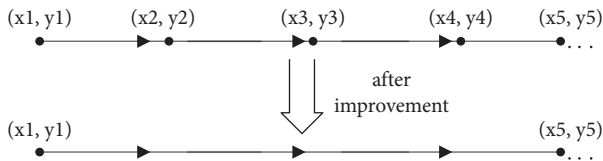


FIGURE 3: Node improvement diagram.

range involved in the formula is the total number of road sections in the logistics area.

3.2. Ant Colony Algorithm. The core content of the algorithm, Ant k , judges the choice path by pheromones and leaves pheromones for stacking. Finally, we can get the shortest path. The flow chart of ant colony algorithm is shown in Figure 4:

At first, when $\tau_{ij}(0) = \tau^0$, this means that ants do not understand the environment, and they need to determine the path by the transition probability $P_{ij}^k(t)$ from node i to j . The transition probability $P_{ij}^k(t)$ is expressed as follows:

$$P_{ij}^k(t) = \begin{cases} \frac{[\tau_{ij}(t)]^\alpha \cdot [\eta_{ij}(t)]^\beta}{\sum [\tau_{ij}(t)]^\alpha \cdot [\eta_{ij}(t)]^\beta}, & j \in a_k, \\ 0, & j \notin a_k, \end{cases} \quad (11)$$

$$\eta_{ij} = \frac{1}{d_{ij}}. \quad (12)$$

$\tau_{ij}(t)$: the pheromone left by ant k on path i, j at time t . $\eta_{ij}(t)$: distance heuristic factor. d_{ij} : distance between nodes i and j . α : relatively important factors about ant information trajectory. β : relative importance factor of heuristic function. a_k : a set of nodes to which goods k in the logistics are allowed to arrive next.

After ants move for a long time, pheromones remaining in the path will volatilize like alcohol. Therefore, the pheromone on the path should be updated after each cycle of ants. The pheromone update formula is as follows:

$$\tau_{ij}(t+1) = \rho\tau_{ij}(t) + \Delta\tau_{ij}(t, t+1), \quad (13)$$

$$\Delta\tau_{ij}(t, t+1) = \sum_{k=1}^m \Delta\tau_{ij}^k(t, t+1). \quad (14)$$

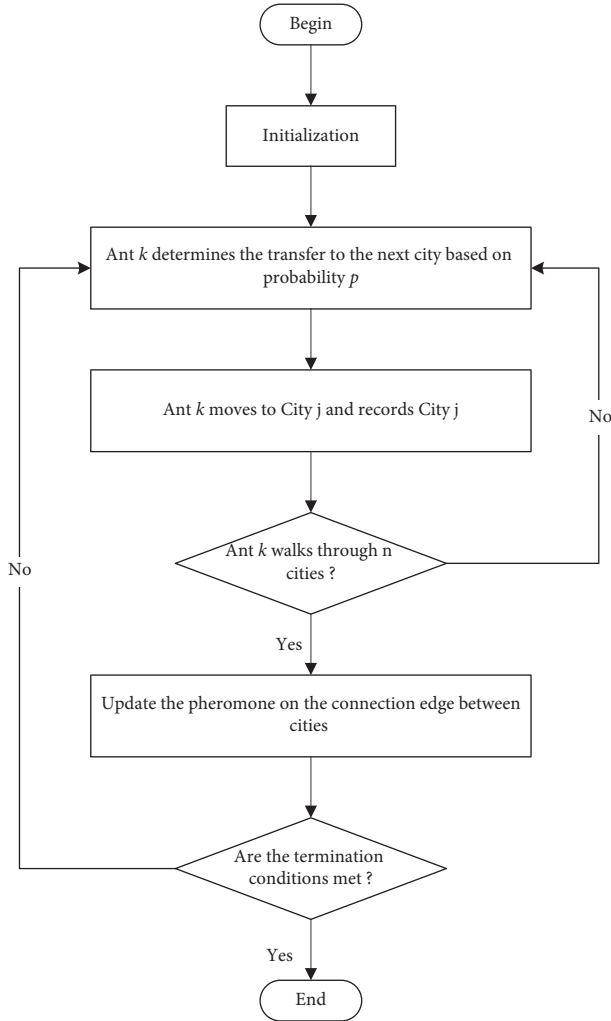


FIGURE 4: Flow chart of the ant colony algorithm.

ρ : pheromone volatilization coefficient. $\Delta\tau_{ij}^k$: pheromones left by ant k on paths i and j . $\Delta\tau_{ij}$: pheromone increment left by ants on paths i and j .

The three formulas for $\Delta\tau_{ij}$ are as follows:

$$\Delta\tau_{ij}^k(t, t+1) = \frac{C}{L_k}, \quad (15)$$

$$\Delta\tau_{ij}^k(t, t+1) = \frac{C}{d_{ij}}, \quad (16)$$

$$\Delta\tau_{ij}^k(t, t+1) = C. \quad (17)$$

L_k : path length of ant k once cycle. C : constant.

3.3. *A*-Ant Colony Algorithm*. A*-ant colony algorithm for logistics path planning is divided into global and local. The initial global planning is to use A* algorithm to calculate, with the passage of time to search for complex environment, the planning problems encountered by ant colony algorithm, which can effectively avoid obstacles and avoid local deadlock. The algorithm flow is shown in Figure 5:

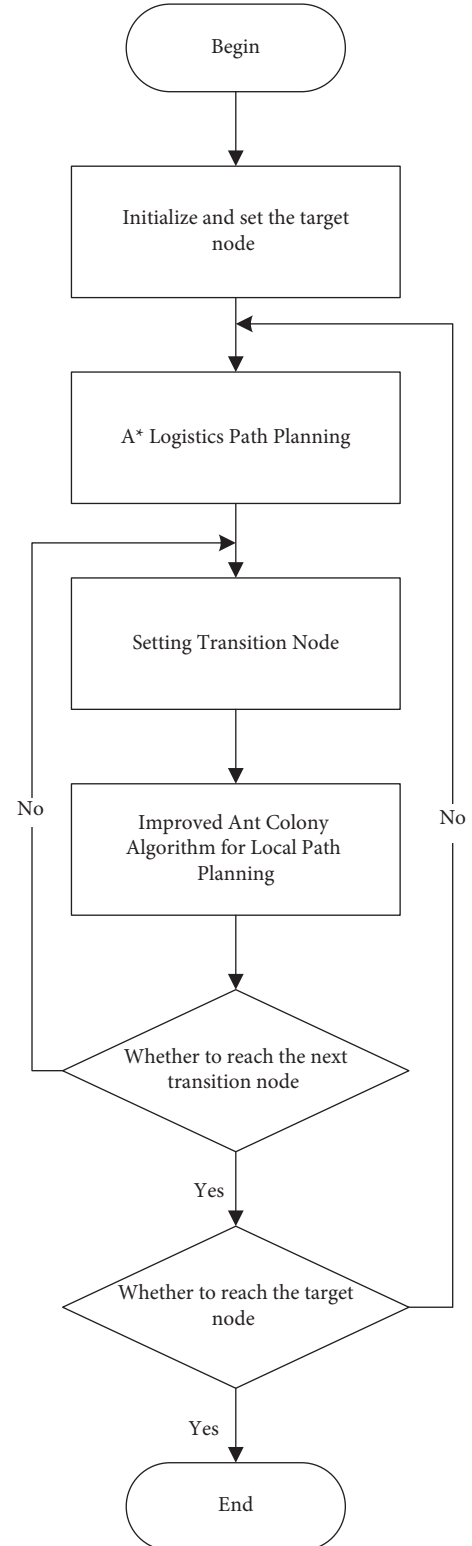


FIGURE 5: A*-ant colony algorithm diagram.

3.3.1. *Node Selection and Information Update*. However, ant colony algorithm also has some defects, such as the global search ability is not strong, convergence speed is not high, and a series of problems. This will make the whole algorithm appear a series of cases such as local optimum. Therefore, it is necessary to further improve the ant colony algorithm

before it can be merged with A* algorithm to obtain A*-ant colony hybrid algorithm.

Assuming that there are m goods to be transported by logistics in this area, the formula for m is as follows:

$$m = \sum_{i=1}^n b_i(t), \quad (18)$$

n : total number of target nodes in this area. $b_i(t)$: quantity of logistics goods at node i at time t .

The formula for the probability of goods k transported by logistics moving from node i to node j is as follows:

$$j = \begin{cases} \max\{\tau_{is}^\alpha(t)\eta_{is}^\beta(t)\}, & S \in a_k, r > \rho_0, \\ \text{choose } j \text{ according to } p_{ij}^k(t), & \text{otherwise,} \end{cases} \quad (19)$$

$$P_{ij}^k(t) = \begin{cases} \frac{\tau_{ij}^\alpha(t)\eta_{ij}^\beta(t)}{\sum_{S \in a_k} \tau_{ij}^\alpha(t)\eta_{ij}^\beta(t)}, & j \in a_k, \\ 0, & \text{others,} \end{cases} \quad (20)$$

$\max\{\tau_{is}^\alpha(t)\eta_{is}^\beta(t)\}$: the node of the path with the largest amount of information in the path set related to the node i .

When the whole iteration is completed, the best path, that is, the shortest path, will be selected, and the pheromones of each node on this path will be updated. The updated formula is as follows:

$$\tau_{ij}(t+1) = (1-\rho)\tau_{ij}(t) + \rho\Delta\tau_{ij}(t, t+1), \quad (21)$$

$$\Delta\tau_{ij}(t, t+1) = \frac{1}{L_i}. \quad (22)$$

L_i : the optimal path length of the whole search in this iteration.

4. Simulation Experiment

4.1. Algorithm Testing

4.1.1. Parameters and Environment Settings. In this test, the grid method is adopted, and 10×10 grids are divided, in which the white grid represents the logistics transportation area and the black grid represents the obstacles. Set the ant size to 50 and the maximum iteration number to 100.

$\alpha = 1$, $\beta = 5$, $\rho = 0.7$, $\tau_0 = 4$, and $Q = 2000$ for Dijkstra algorithm, A* algorithm, and A*-ant colony algorithm for path planning and experiment. The experimental results of Dijkstra algorithm are shown in Figure 6:

The experimental results of A* algorithm are shown in Figure 7:

The experimental results of A*-ant colony algorithm are shown in Figure 8:

The length and running time data of the path are shown in Table 1:

As can be seen from the above chart, for these three algorithms, in terms of time, A* algorithm has the shortest running time and the fastest search speed. But from the shortest path point of view, the shortest path found by the algorithm

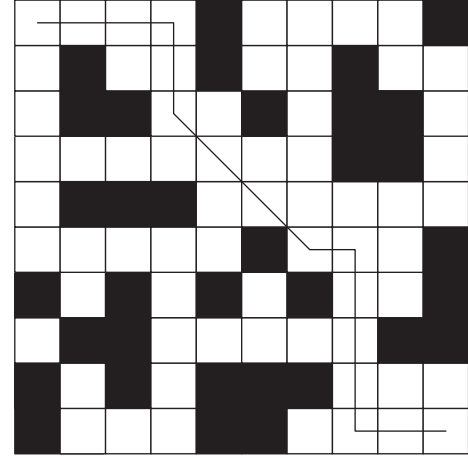


FIGURE 6: Dijkstra algorithm simulation path diagram.

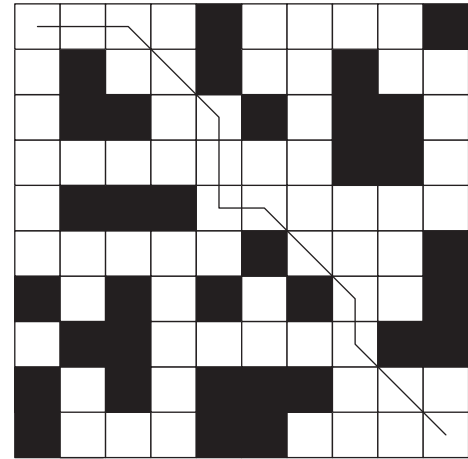


FIGURE 7: A* algorithm simulation path diagram.

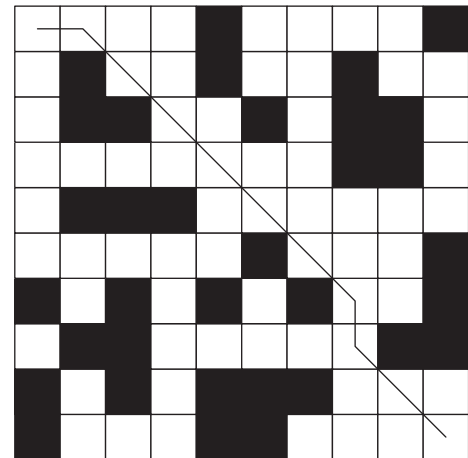


FIGURE 8: A*-ant colony algorithm simulation path diagram.

TABLE 1: Path length and running time data table.

Algorithm	Path length	Running time
Dijkstra	16.24	7.89
A*	13.99	1.32
A*-ant colony algorithm	13.31	3.79

TABLE 2: Shortest path length data table.

Serial number	Dijkstra	A*	A*-ant colony algorithm	Actual value
1	24.5	21.3	15.3	14.1
2	30.7	25.9	20.2	21.1
3	16.9	13.2	11.4	10.2
4	22.5	20.4	13.9	13.9
5	27.9	22.4	17.8	16.9
6	10.5	8.9	5.1	6.4
7	21.1	15.6	10.2	11.3
8	11.6	8.2	4.3	4.6
9	15.4	9.3	4.8	5.1
10	20.4	13.9	10.3	10.5

TABLE 3: Data table for finding the shortest path time.

Serial number	Dijkstra	A*	A*-ant colony algorithm	Actual value
1	32	10	20	11
2	33	15	16	13
3	42	20	30	23
4	41	5	30	12
5	39	20	21	22
6	31	15	13	13
7	32	23	16	17
8	36	19	17	16
9	35	21	18	19
10	46	25	19	19

proposed in this paper is better. From the combination of these two aspects, it can be concluded that the advantages of the A*-ant colony algorithm are not particularly prominent in the simulation environment, but the overall performance is still due to the other two. For the logistics management environment, the A*-ant colony algorithm can better play its advantages. For such a large environment as logistics management, there are much more nodes to search than tests. With iterative updating, the A*-ant colony algorithm can give full play to its advantages, while the first two algorithms are not suitable for such a large amount of data operations.

4.2. Simulation Experiment

4.2.1. Establishment of an Objective Function. This experiment will compare the three algorithms from the path length, cost, and speed.

The formula of the minimum cost is as follows:

$$F_i = \sum_{j \in J} C_{ij} X_{ij} + f_{ki} \quad i \in I, \quad (23)$$

$$\min F' = \sum_{k=1}^q \sum_{j=1}^n C_{kj} X_{kj}, \quad (24)$$

$$\sum_{j=1}^n X_{kj} \leq d_k, \quad (25)$$

$$\sum_{k=1}^q X_{kj} \geq b_j. \quad (26)$$

F_i : cost of transportation from node i . C_{ij} : management fee of goods transported from node i required by user j . X_{ij} : the quantity of goods transported from the node i required by the user j . C_{kj} : management fee of goods at outlet k required by user j . X_{kj} : the quantity of goods from the outlet k required by the user j . f_{ki} : the cost of setting the dot k in the experimental delimited area. d_k, b_j : maximum setting size of outlets and demand of users j .

4.2.2. Simulation Results and Experimental Analysis. Set a certain area as logistics transportation area and transform it into a 50*50 grid range. Suppose it needs to be delivered to 10 users for 10 times, and there are 8 outlets in total. Three algorithms are used to predict the shortest path length, find the shortest path time and transportation cost of these 10 times, and compare with the actual values.

The shortest path length data obtained through experiments are shown in Table 2:

The experimental data of finding the shortest path time are shown in Table 3.

The transportation cost data obtained through experiments are shown in Table 4.

The algorithm for the shortest path pair is shown in Figure 9.

The algorithm pair finds the shortest path time pair as shown in Figure 10.

The algorithm for transportation cost pairs is shown in Figure 11.

It can be seen from the above icon that, in terms of finding the shortest path and transportation cost, it is obvious that the algorithm proposed in this paper can better

TABLE 4: Data sheet of transportation cost.

Serial number	Dijkstra	A*	A*-ant colony algorithm	Actual value
1	2.5	2.1	1.5	1.3
2	3.1	2.6	2.1	2.2
3	1.5	1.9	1.8	2.0
4	2.3	2.5	1.7	1.9
5	2.8	2.9	2.5	2.2
6	1.2	1.1	0.5	0.9
7	2.0	1.7	1.5	1.6
8	1.4	1.2	0.8	0.7
9	1.9	2.2	1.2	1.3
10	2.2	2.4	1.9	1.5

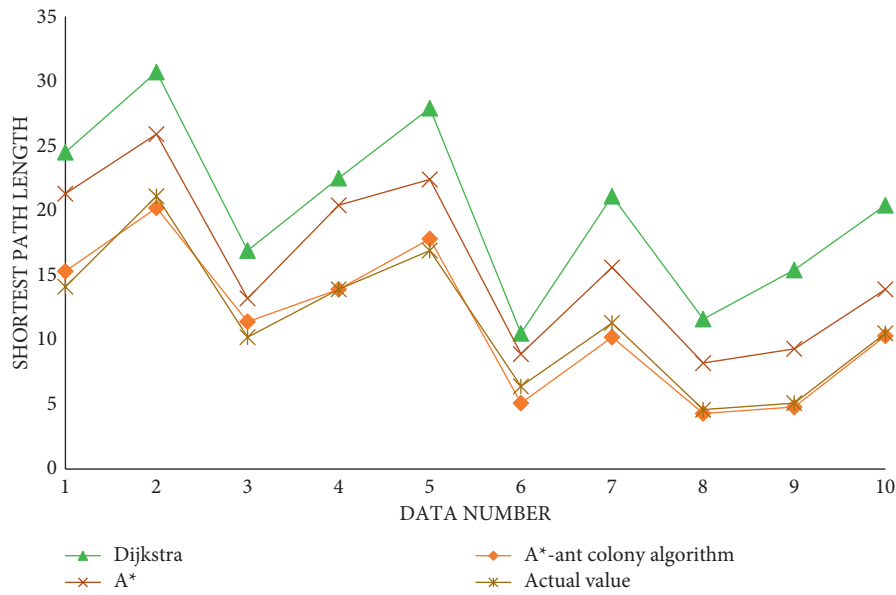


FIGURE 9: Comparison diagram of the algorithm against shortest path.

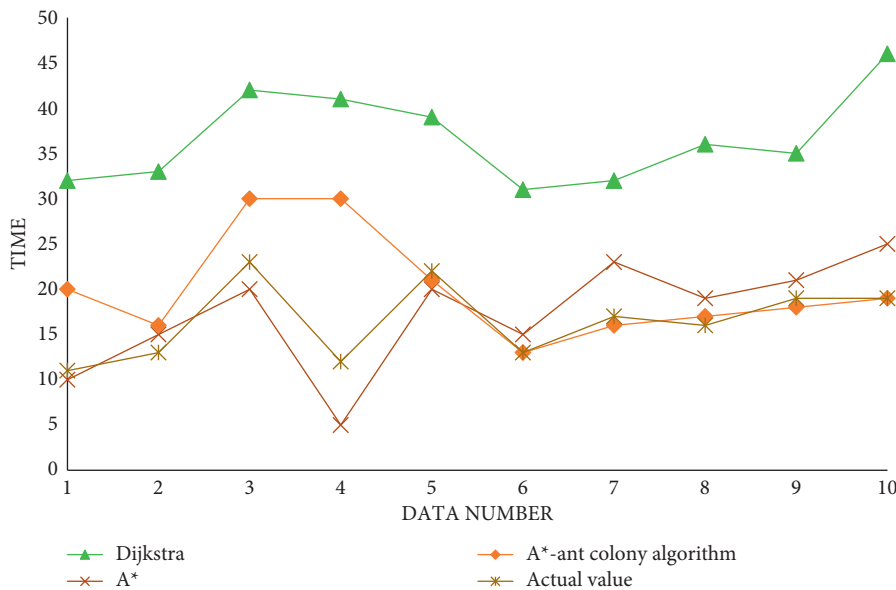


FIGURE 10: Comparison diagram of the algorithm to find the shortest path time.

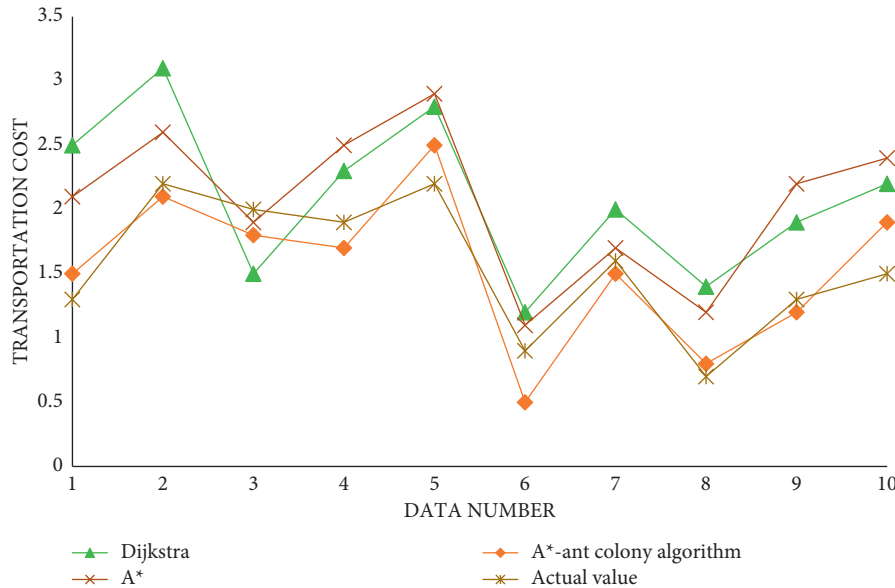


FIGURE 11: Comparison of algorithm and transportation cost.

calculate and find the shortest path, which shows that the algorithm has been improved and greatly improved the optimization ability. In terms of running time, we can see that, in the early stage of running, the speed of the A* algorithm is still relatively fast, but with the increase of iteration times, the increasing number of nodes, and the continuous accumulation of information, the speed of A* algorithm cannot be well maintained, while the algorithm proposed in this paper is more consistent with the data in the later stage.

5. Conclusion

For the Dijkstra algorithm, facing a large amount of information, it does not have the ability to use it reasonably, which makes it and A* algorithm have a gap in logistics and transportation. This is also one of the reasons for choosing the A* algorithm in this paper. A* algorithm is really excellent in terms of running speed, but in terms of logistics and transportation, the algorithm proposed in this paper can provide stable development for later operation. At the same time, it can be found from the experiment that the performance of the algorithm is stable, and the high stability and accuracy can be combined with logistics and transportation. The logistics management in the future tends to be more intelligent, and the intelligent technology is constantly developing, which is a further excavation assistant for intelligent logistics management.

Data Availability

The experimental data used to support the findings of this study are available from the corresponding author upon request.

Conflicts of Interest

The author declares no conflicts of interest regarding this work.

References

- [1] S. X. Wang, "The improved dijkstra's shortest path algorithm and its application[J]," *Procedia Engineering*, vol. 29, no. 1, pp. 1186–1190, 2012.
- [2] Y. Lim and H. Kim, "A shortest path algorithm for real road network based on path overlap[J]," *Journal of the Eastern Asia Society for Transportation Studies*, vol. 6, pp. 1426–1438, 2005.
- [3] J. K. Antonio, G. M. Huang, and W Tsai, "A fast distributed shortest path algorithm for a class of hierarchically clustered data networks," *IEEE Transactions on Computers*, vol. 41, no. 6, pp. 710–724, 1992.
- [4] J. Climaco and E. Martins, "A bicriterion shortest path algorithm[J]," *European Journal of Operational Research*, vol. 11, no. 4, pp. 399–404, 1982.
- [5] Z. Jian, M. Jiang, and F. Yuan, "Identification of age-related macular degeneration related genes by applying shortest path algorithm in protein-protein interaction network[J]," *BioMed Research International*, vol. 2013, no. 4–6, p. 523415, 2013.
- [6] P. L. Lin and S. Chang, "A shortest path algorithm for a nonrotating object among obstacles of arbitrary shapes," *IEEE Transactions on Systems, Man, and Cybernetics*, vol. 23, no. 3, pp. 825–833, 1993.
- [7] M. P. Dubuisson-Jolly and A. Gupta, "Tracking deformable templates using a shortest path algorithm," *Computer Vision and Image Understanding*, vol. 81, no. 1, pp. 26–45, 2001.
- [8] M. Seraj and C. Y. Wong, "Impacts of different mobile user interfaces on students' satisfaction for learning d shortest path algorithm," *International Journal of Interactive Mobile Technologies (ijIM)*, vol. 8, no. 4, pp. 24–30, 2014.
- [9] M. L. Yi, B. Lan, and M. F. Xiao, "Design of GPS-based intelligent logistics management system[J]," *Ence Technology & Engineering*, vol. 6-7, no. 6, pp. 485–490, 2008.
- [10] Ł Marzantowicz, "Changes in contemporary logistics management in the light of intelligent logistics," *Kwartalnik Nauk o Przedsiębiorstwie*, vol. 50, no. 1, pp. 62–71, 2019.
- [11] T. Zhang, Y. Hua, H. Luo et al., *Journal of traditional Chinese medicine = Chung i tsa chih ying wen pan*, vol. 37, no. 3, pp. 341–354, 2017.

- [12] Y. B. Jiao, "Based on the electronic commerce environment of intelligent logistics system construction," *Advanced Materials Research*, vol. 850-851, pp. 1057-1060, 2013.
- [13] C. Yang, X. Hu, W. Gu, and T. Liu, "Research on the c intelligent logistics," *Zhongguo yi liao qi xie za zhi = Chinese journal of medical instrumentation*, vol. 43, no. 6, pp. 462-465, 2019.
- [14] L. X. Zhou and K. Liu, "Intelligent logistics transportation system[J]," *Journal of Tongji University*, vol. 58, no. 58, pp. 55-70, 2002.
- [15] Y. Guo and J. Qu, "Study on intelligent logistics management information system based on IOT and cloud computation in big data era," *The Open Cybernetics & Systemics Journal*, vol. 9, no. 1, pp. 934-941, 2015.

Research Article

Prediction and Planning of Sports Competition Based on Deep Neural Network

Jin Xu 

School of Sports Hunan City University, Yiyang 413000, China

Correspondence should be addressed to Jin Xu; xujin@hncu.edu.cn

Received 31 March 2022; Revised 24 April 2022; Accepted 17 May 2022; Published 8 June 2022

Academic Editor: Le Sun

Copyright © 2022 Jin Xu. This is an open access article distributed under the Creative Commons Attribution License, which permits unrestricted use, distribution, and reproduction in any medium, provided the original work is properly cited.

Physical education curriculum has been paid more and more attention by teachers and parents, and having a healthy body is the foundation. School sports competition is also more and more concerned by major researchers, and scholars have produced in-depth research and analysis of sports competition results prediction because prediction results can better let teachers carry out appropriate sports training for students, so as to achieve the best learning effect. The construction of the prediction model and whether the performance and universality of the model after construction are suitable for predicting sports competitions have also become a major research point. Deep neural network is a complex network method to analyze the structure of the human brain, which plays a core role in the field of sports planning and performance prediction and can know the future performance of athletes or students in advance in sports competitions. This paper establishes the autoregressive summation model prediction model, the complex neural network prediction model, and the improved complex neural network prediction model. It is concluded that only the improved BP neural network model has a remarkable effect on performance prediction, and the prediction value obtained by this prediction model can reduce the systematic error of prediction, so that it can better infer the performance prediction of sports competitions in China and plan which sports events are suitable for which prediction model.

1. Introduction

We live in the education by leaps and bounds in the environment, and our physical education curriculum content and structure of the construction is becoming more and more complete and having rapid development. Based on humidity, dew point, wind speed, and other meteorological parameters, a depth neural network (DNN) model is proposed to predict the minimum and maximum temperature. A particle swarm optimization algorithm is applied to select the correlation and important features of the data set to improve the prediction accuracy of the model. In the face of the multiobjective sinusoidal algorithm (MOSCA), the objective function is optimized [1]. The indexes of the optimized objective function are data rate, signal-to-interference-noise ratio (SINR), power consumption, and energy efficiency, and then the optimized objective function is allocated to a neural network for resource allocation [2]. It expounds a new deep neural network convolution layer-

variable convolution (vConv) layer, which learns the kernel length of data adaptively by its own cycle to realize the motif recognition of data sets with high throughput [3]. It proves the effectiveness of pretraining neural networks on different data sets and shows that in many practical cases, the convolution layer can be replaced by a smaller fully connected layer, and the accuracy degradation is relatively small [4]. In this paper, a machine learning (DL) method is proposed to accurately obtain the performance of components and obtain the key features of typical components, and the data set is prepared and trained based on the extracted indicators [5]. It introduces the method for fault damage. Because of its powerful feature extraction ability, this method can extract more advanced and abstract fault features from massive data. Experiments show that deep neural network has better feature learning and classification performance in the field of fault diagnosis [6]. This paper introduces the background of semantic segmentation, then divides the semantic segmentation methods based on deep learning into five

categories, and presents the advantages and disadvantages of each category [7]. The surrogate model is established by using polynomial chaotic expansion and a deep neural network, and the Sobol exponent needed to identify the influence of soil parameters on dam behavior is calculated [8]. In this paper, a new pruning-based DNNs model is proposed without affecting the expression ability of DNNs. By mining more compact structures and learning the effective weights, the computational overhead of DNNs is reduced [9]. We replace these empirical parameters with dynamic values of machine learning, which perfectly improves the accuracy of the extended model and uses complex neural networks to generate dynamic values to reproduce orbital energy and density based on density functional theory [10]. In this paper, the prediction ability of deep neural network relative to other machine learning technologies is established, and the future range of deep learning in multiparameter time series prediction is shown [11]. Our results are helpful to improve the estimation performance of structural variables of Arctic forests by using the concepts of image sampling and input features proposed in this paper [12]. This method also has the advantage of transfer learning; that is, DNN trained on one battery data set can use less training data to improve the curve estimation of other batteries running in different scenarios [13]. It will make a simple scientific overview of machine learning [14]. Learning-based computer generated holography (CGH) provides a fast way to generate holograms for holographic displays [15]. In REPAID, the multifocus image is first reconstructed from a single all-optical image and then up-sampled by a specially designed depth neural network suitable for real scenes, and finally, a full-focus image with the high spatial and temporal resolution is generated [16]. It introduces a regularized chain of deep and complex brain structure networks to handle classification tasks from multiple annotators [17]. A complex brain structure network for linear B cell epitope prediction is introduced [18]. The most relevant deep learning-based methods and the most advanced graphic page object detection in document images are discussed [19]. Materials informatics is an emerging field, which allows us to predict the properties of materials and has been applied to various research and development fields, such as materials science [20]. A new two-layer depth neural network structure is proposed, which can reconstruct the self-organized humanlike deformation shape from the depth framework by combining the inherent parameters of the camera [21]. Deep neural network for privacy protection becomes essential because of the need to maintain personal privacy and confidentiality of sensitive data and has attracted the attention of many researchers. With the wide application of neural network as a service in the unsecured cloud environment, the importance of privacy protection network is increasing day by day [22]. CNN is a new image recognition technology. Compared with the standard manual feature extraction method, it does not need explicit feature engineering and extraction and produces efficient results [23]. Its performance is satisfactory in both novelty detection and fault diagnosis, which is superior to other advanced methods. This study proposes a new fault diagnosis method,

which can not only diagnose defects of known types but also detect defects of unknown types [24]. We propose a new algorithm called depth feature selection, which is used to estimate sparse parameters and other parameters at the same time [25].

2. Concept and Characteristics of Complex Network Method of Brain Structure

2.1. The Concept of Artificial Neural Networks. Human brain is the most complex, perfect, and effective information processing system known by human beings in exploring unknown fields. It is the advanced product of biological evolution and the cornerstone of advanced spiritual movements such as language, thinking, and emotion of the human brain. At present, human beings have little knowledge of this field. For a long time, scholars have been studying neural networks through the analysis of a series of disciplines such as neurology, psychology, cognition, mathematics, electronics, and computational science and want to dissect the structure of the human brain and its massive information processing modes. Using the complex network structure characteristics of the brain, an intelligent system similar to the human brain, which can perform some functions, is designed to deal with massive information and solve the complex problem of blending different data. It is the core goal of the development of science and technology to replace part of the labor of the human brain with a machine structure composed of electronic parts. Computer is an information processing system which uses some electronic components to carry out some memory, calculation, and information processing functions of the human brain. The speed of every electronic component in modern computers is as high as nanoseconds, while the reflection time of every nerve cell in the human brain is only millisecond units. Therefore, the complex neural network method of the brain is only a neural network which can complete some ideal function after artificial construction and processing on the basis of cognitive understanding of the brain neural network. It is a mathematical network method close to the idealized human brain nerve structure, and it is also a data processing structure based on imitating the complex nervous system structure and function of the brain. In fact, it is a complex network structure constructed by a large number of simple components interconnected with each other, which has complex nonlinearity and can carry out complex logic operations and realize some curvilinear relationships.

2.2. Features of Artificial Neural Networks. Although an artificial neural network is an idealized network structure based on brain structure, the complex network structure of the brain is different from the current computer and artificial intelligence structure. It has many similarities with human intelligence: the performance of a single neural unit is relatively weak, but a large number of neurons converge into a network structure, which will have interoperability and

parallel processing functions and is very powerful. It has the following characteristics:

- (1) *Inherent Parallel Structure and Parallel Processing.* The similarity between an artificial neural network and the human brain in structure is parallel and interoperable, and the processing sequence is also parallel and simultaneous. Neurons in each layer process data at the same time. That is to say, the function of neural network processing data can be distributed and can be carried out simultaneously on multiple processing units.
- (2) *The Storage of Knowledge.* In the complex neural network model of brain structure, knowledge is not only stored in a fixed storage unit but all the memorized information is stored in the weights of interconnection between neurons. The content of stored information can not be seen from the weights of a single neuron, because the knowledge is stored in a distributed way.
- (3) *Strong Fault Tolerance.* The automatic death of brain cells every day will not affect our memory ability and thinking ability. Similarly, artificial neural networks have strong error tolerance; that is, local or partial neuron damage will not affect the subsequent and even global activity changes.
- (4) *Self-Adaptability.* Artificial neural network can acquire various abilities through learning. Input the input and ideal output modes into complex networks; the network adjusts the connection weights between neurons in each layer of the system according to the basic information extracted from the samples given by the original learning algorithm and stores these basic information in a specific system in the form of connection methods between neurons until the network reaches a stable state.

3. Sports Competition Prediction Algorithm

3.1. Traditional Statistical Methods

3.1.1. Determining the Time Series Prediction Model

- (1) *No Change Method.* The premise of this method is that the sports competition results in $T + 1$ period are the same as those in T period. Because this model is too idealistic, it may produce a higher prediction value for Chinese sports competition results with an obvious improvement trend.
- (2) *Proportional Change Method.* It is considered that the results of sports competitions change by a certain percentage with time. The expression is as follows:

$$C_{t+1}^A = C_t \left(1 + \frac{C_t - C_{t-1}}{C_{t-1}} \right). \quad (1)$$

- (3) *Moving Average Model Method.* That is, the average of observed values in the past several periods is used as the predicted value of the prediction period. The expression is as follows:

$$C_{t+1}^A = \frac{C_t + C_{t-1} + \cdots + C_{t-n+1}}{N} \quad (t \geq N). \quad (2)$$

- (4) *Weighted Moving Average Model.* Different weights are given according to the time when each data are away from the prediction period. It is generally believed that the closer the time is away from the prediction period, the greater the weight should be given because the recent prediction value has stronger prediction ability and accuracy. The expression is as follows:

$$C_{t+1}^A = \frac{a_0 C_t + a_1 C_{t-1} + \cdots + a_{N-1} C_{t-n+1}}{N} \quad (t \geq N). \quad (3)$$

- (5) *Exponential smoothing model*

It is a special weighted average method, which uses the weighted average of the previous observation value and the predicted value as the predicted value of the next period. The calculation formula is

$$C_{t+1}^A = a C_t + (1 - a) C_t^A. \quad (4)$$

3.1.2. Stochastic Time Series Model. This is the most commonly used method in the time sequential model method to find out the trend of sports competition results with a certain factor by regression method. The independent variable in the model can be any one of the influencing factors of sports competition results. People usually use time as the independent variable.

3.2. Evaluation Criteria of Sports Competition. The parameters of absolute average error, correlation coefficient, and reliability of output data are used to evaluate the model. Because they are neither affected by the size of the sample nor by the restriction of sample units on other different models, the comparability is strong. They can be obtained by the following formula.

Absolute mean difference:

$$\text{MAPE} = \frac{\sum_{i=1}^n |x_i - y_i| / y_i}{n} \times 100\%. \quad (5)$$

Correlation coefficient:

$$R = \frac{\sum_{i=1}^m (x_i \times y_i)}{\sqrt{\sum_{i=1}^m (x_i)^2 \times \sum_{i=1}^m (y_i)^2}}. \quad (6)$$

Data reliability:

$$Z = \frac{\sum_{i=1}^n j}{n} \times 100\%, \quad (7)$$

where $|x_i - y_i| / y_i \leq 0.15$, $j = 1$, otherwise $j = 0$.

3.3. *Artificial Neural Network Algorithm.* The expression of the input sum of neurons is as follows:

$$\text{net} = \sum_{i=1}^n P_i W_i. \quad (8)$$

Neuron output:

$$o = f(\text{net} - \theta). \quad (9)$$

Artificial neural network learning is carried out under the condition that the input mode and ideal output mode are known. Its comprehensive error often adopts the sum of squares of errors.

$$E_k = \frac{1}{2} \sum_j^Q (O_j^k - o_{kj})^2. \quad (10)$$

3.3.1. BP Neural Network

- (1) Calculate the output values of hidden layer and output layer nodes:

Hidden node output:

$$y_i = f\left(\sum_j w_{x_j} x_j - \theta_i\right). \quad (11)$$

Output node:

$$o_i = f\left(\sum_j T_{ij} y_j - \theta_i\right). \quad (12)$$

- (2) Calculate the error of output layer and hidden layer:

All sample errors:

$$E = \sum_{k=1}^P e_k \leq \varepsilon. \quad (13)$$

One sample error:

$$e_k = \sum_{i=1}^n |t_i^{(k)} - o_i^{(k)}|. \quad (14)$$

Output layer node error:

$$\delta_i = (t_i - o_i) \cdot o_i \cdot (1 - o_i). \quad (15)$$

Hidden layer node error:

$$\delta_i = y_i(1 - y_i) \sum_j \delta_j T_{ij}. \quad (16)$$

- (3) Correct the node weights and closed values of output layer and hidden layer:

Output layer node weight correction:

$$T_{ij}(k+1) = T_{ij}(k) + \eta \delta_i y_j. \quad (17)$$

Output layer node threshold correction:

$$\theta_i(k+1) = \theta_i(k) + \eta \delta_i. \quad (18)$$

Modification of node weight value in hidden layer:

$$W_{ij}(k+1) = W_{ij}(k) + \eta \delta_i x_j. \quad (19)$$

Hidden layer node threshold correction:

$$\theta_i(k+1) = \theta_i(k) + \eta \delta_j. \quad (20)$$

3.3.2. BP Algorithm Improvement

(1) *Additional Momentum Value Method.* The method is based on the back propagation method, adding a dynamic change quantity proportional to the last weight and threshold value to each change of weight and threshold value and generating new changes of weight and threshold value according to the back propagation method. The adjustment formula of weight and threshold value with additional momentum factor is as follows:

$$\Delta X(k+1) = mc \times \Delta X(k) + lr \times \frac{\partial E}{\partial X} \quad (0 < lr \leq 1). \quad (21)$$

(2) *Adaptive Learning Rate Method.* Adjusting the learning rate based on self-adaptation rules is beneficial to shorten the time. The learning rate is too small and the convergence rate is too slow; if the range of learning rate selection is too large, it may change too much, resulting in data dispersion. Therefore, a unique improved algorithm suitable for adaptive adjustment appears, and its weight and gap value update expression is

$$\Delta X = lr \times \frac{\partial E}{\partial X}, \quad (22)$$

$$\Delta X(k+1) = mc \times \Delta X(k) + lr \times mc \times \frac{\partial E}{\partial X}.$$

Adjustment formula of adaptive learning rate lr is as follows:

$$lr(k+1) = \begin{cases} 1.06lr(k)mse(k+1) < mse(k), \\ 0.6lr(k)mse(k+1) > 1.05mse(k), \\ lr(k). \end{cases} \quad (23)$$

(3) *Levenberg-Marquardt Optimization Method.* The weight and threshold update formula is

$$X_{k+1} = X_k - (J^T J + \mu I)^{-1} J^T e. \quad (24)$$

4. Experiment

4.1. *Simulation Experiment.* In order to effectively predict sports performance, 500 data samples of sports performance in a university were collected, of which 400 were used as training samples and 100 as test samples. 400 training samples are trained by a support vector machine algorithm,

TABLE 1: Comparison of forecast data of online computing platform.

Sports events	Prediction result (%)	Prediction error (%)	Actual result (%)
Running	98.7	0.21	98.5
High jump	96.5	0.38	97.2
Long jump	97.3	0.22	96.8
Shot put	98.5	0.13	97.4
Relay race	96.6	0.26	97.3

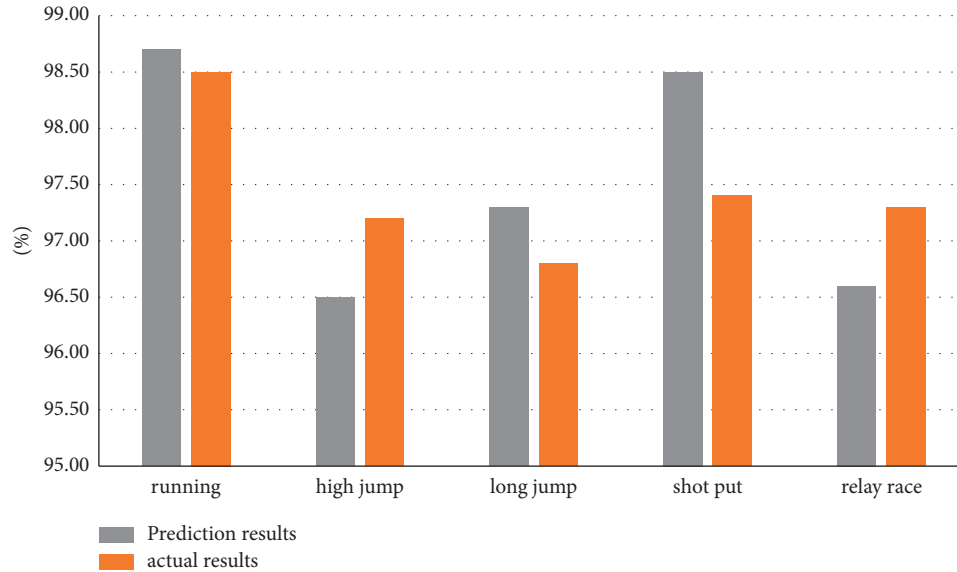


FIGURE 1: Comparison between predicted results and actual values.

and the sports scores of 100 test samples are predicted by an online computing platform. The prediction results and prediction error curves obtained by the online computing platform are shown in Table 1 and Figure 1.

Through the above-given experimental results, we can see that using this model to test the sports performance prediction results are very ideal, the experimental results show that using this model can effectively predict sports performance.

The predicted results and actual results of the above-mentioned sports events are counted into a bar chart as shown in Figure 1.

Five groups of sports data are selected from the training sample data set to test and verify whether the improved BP neural network has good training. The error curve after inspection is shown in Figure 2.

4.2. Model Comparison. The error of predicting sports results by three models is compared, and the comparative data are shown in Table 2.

According to the experimental data in Table 2, we can get that the improved neural network model with complex brain structure has higher accuracy in predicting sports events. Is the prediction result of this model equally accurate for different types of sports events? We further compare and analyze the four kinds of sports: running, ball games, long jump, and improvement. For example, the experimental data are as follows.

Select the results of four kinds of sports events in a high school sports meeting to test the universality of the model.

The model performance indicators for running sports competitions are shown in Table 3.

The model index comparison data of the above-given experimental results are counted into a bar chart as shown in Figure 3.

Model performance indicators for ball games are compared and are shown in Table 4.

The model index comparison data of the above experimental results are counted into a bar chart as shown in Figure 4.

The model performance indicators for long jump sports are shown in Table 5.

The model index comparison data of the above experimental results are counted into a bar chart as shown in Figure 5.

Model performance indicators for high jump sports are shown in Table 6.

The model index comparison data of the above experimental results are counted into a bar chart as shown in Figure 6.

4.3. Contrast Experiment. Through the previous results, it is proved that applying the single prediction of various sports events, the prediction results superior to each single item can be combined, which can further effectively improve the prediction accuracy. Therefore, this study continues to use the improved neural network model construction method of complex brain structure to

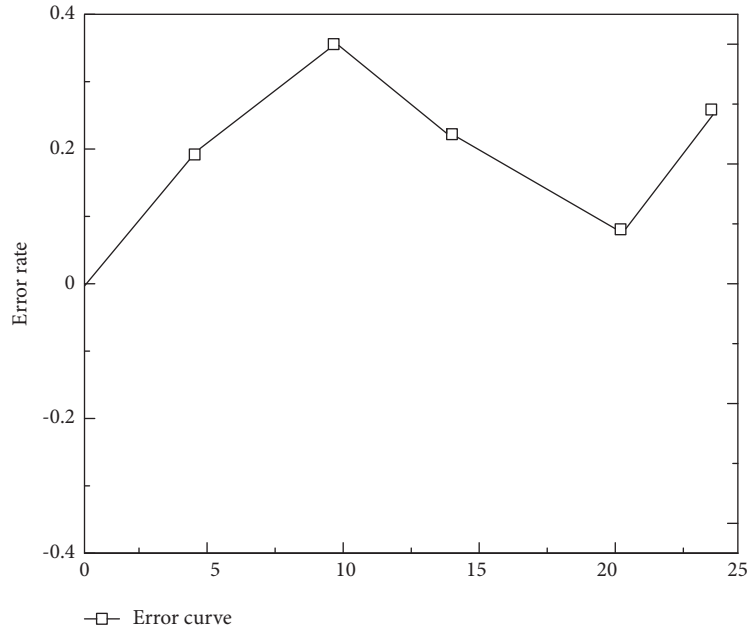


FIGURE 2: Error curve of sports events.

TABLE 2: Error comparison of each prediction model.

Model name	RMSE	MAPE
Autoregressive summation	0.321	0.531
BP neural network	0.217	0.328
Improved BP network	0.142	0.249

TABLE 3: Comparison of performance indexes of model indexes in running sports.

Sports events	Accuracy (%)	Recall (%)	ROC (%)	F1 (%)
Sprints	98.3	87.8	88.4	88.8
Long-distance races	97.6	86.5	89.6	91.2
Team races	95.8	85.9	87.4	87.6

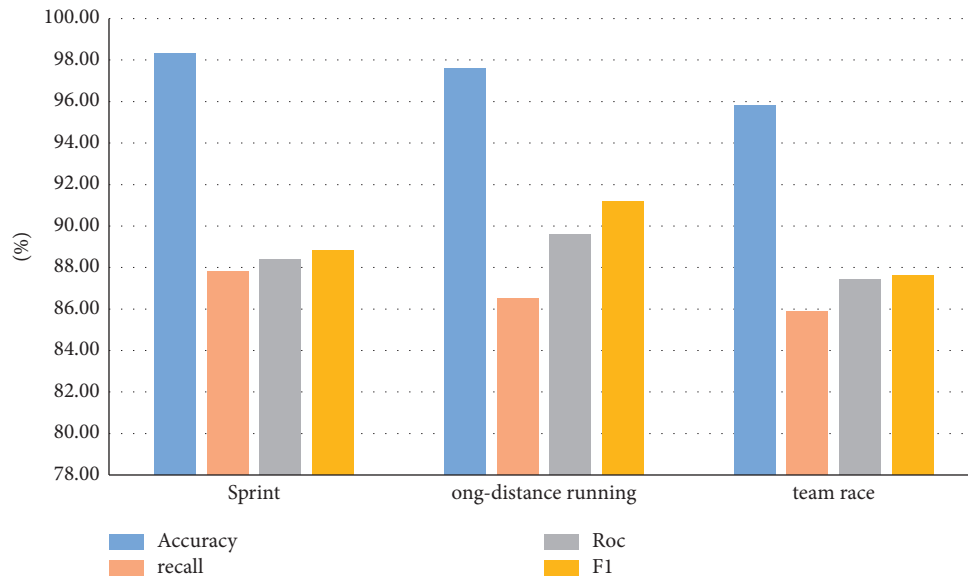


FIGURE 3: Comparison chart of running experimental data.

TABLE 4: Comparison of performance indexes of model indexes in ball games.

Sports events	Accuracy (%)	Recall (%)	Roc (%)	F1 (%)
Basketball	96.3	85.4	87.4	85.8
Football	96.5	87.6	86.6	89.4
Volleyball	97.4	86.9	84.4	84.6

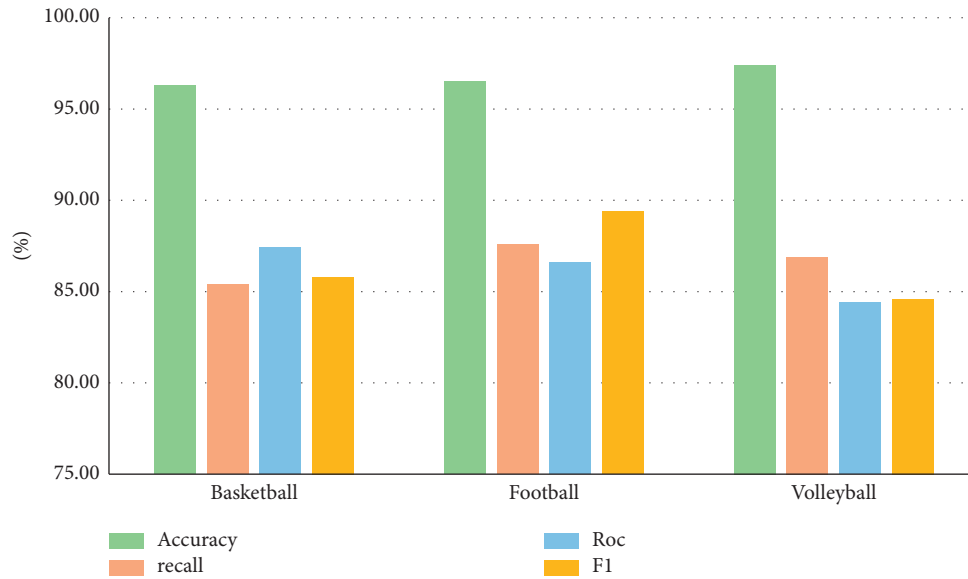


FIGURE 4: Comparison chart of ball experiment data.

TABLE 5: Comparison of performance indexes of model indexes in long jump sports events.

Sports events	Accuracy (%)	Recall (%)	Roc (%)	F1 (%)
Fast walk long jump	95.3	85.4	80.4	82.3
Standing long jump	98.5	90.6	92.6	92.3
Triple jump	97.6	86.7	82.4	85.8

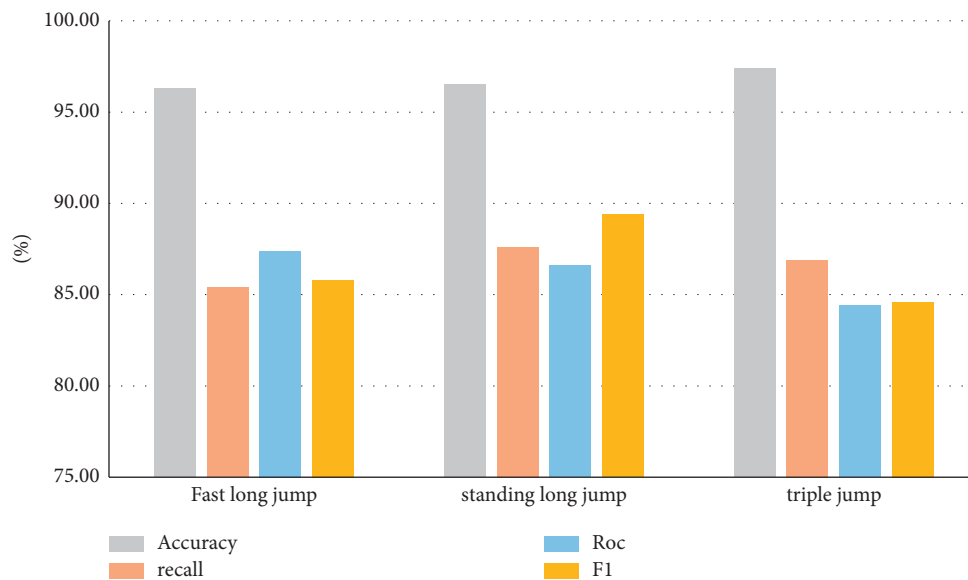


FIGURE 5: Comparison of experimental data of long jump.

TABLE 6: Comparison of performance indexes of model indexes in high jump sports events.

Sports events	Accuracy (%)	Recall (%)	Roc (%)	F1 (%)
Leap-forward	97.8	95.4	90.9	92.3
Scissors high jump	92.3	84.6	82.6	86.5
Boiling high jump	91.0	82.1	78.3	81.8

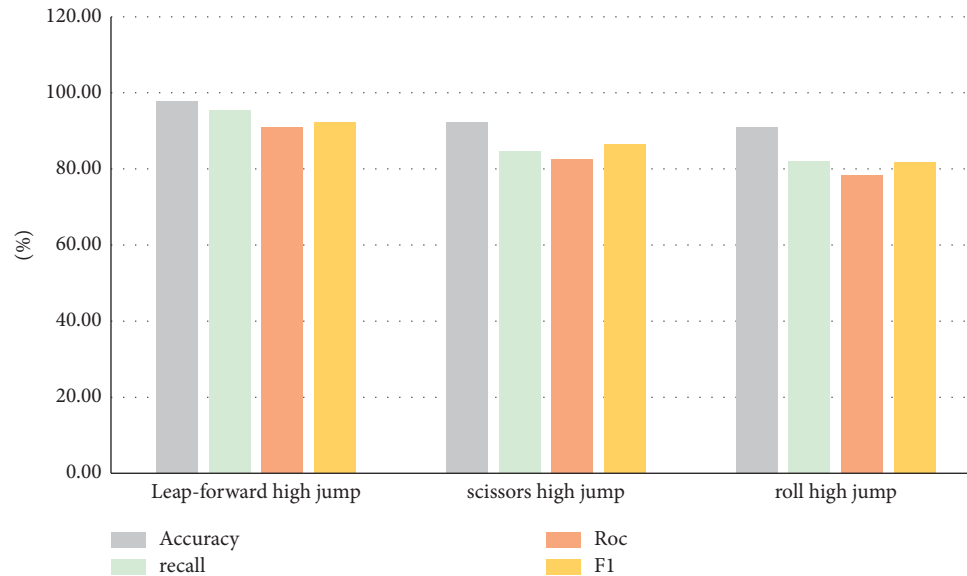


FIGURE 6: Comparison of experimental data of high jump.

TABLE 7: Comparison of prediction accuracy of each model.

Year	Absolute value of prediction error of autoregressive sum model	Absolute value of prediction error of BP neural network model	Absolute value of prediction error of improved BP model
2018	0.8321	1.2093	0.6512
2019	0.9682	0.9827	0.4381
2020	0.7765	0.8821	0.3165
2021	0.5932	0.5411	0.2109
Errors	3.17	3.6152	1.6167

establish a prediction model for all the data from 2018 to 2021 and predict the comprehensive evaluation index values in these years. The prediction results are shown in Table 7.

5. Conclusion

Through the preliminary establishment of the autoregressive summation model prediction model of sports competition development in China, the neural network prediction model of complex brain structure, and the improved network prediction model, it is concluded that the improved complex brain structure model prediction model has a remarkable effect, and its research results are as follows:

- (1) In both the neural network model and traditional regression model, a neural network with a complex brain structure is more inclined to predict the results of sports competitions
- (2) In the model comparison experiment, we predict the individual items of various sports events, and the

prediction effect of the improved prediction model is inconsistent

- (3) Among the four kinds of sports in the article, the prediction effect of running is the most obvious, while the prediction effect of the other three kinds is poor
- (4) The prediction error of the improved neural network model is reduced by about twice as much as that of the original model

Data Availability

The experimental data used to support the findings of this study are available from the corresponding author upon request.

Conflicts of Interest

The author declares that there are no conflicts of interest regarding this work.

Acknowledgments

This work was supported by the Social Science Foundation of Hunan Province: Research on the Development of Urban and Rural Coordinated Public Sports Service under the Background of Rural Revitalization (Grant No. 20TBA042).

References

- [1] K. U. Jaseena and C. Kovoor Binsu, "An improved multi-variate weather prediction model using deep neural networks and particle swarm optimisation," *Journal of Information and Knowledge Management*, vol. 20, no. 3, 2021.
- [2] K. E. Purushothaman and V. Nagarajan, "Evolutionary multi-objective optimization algorithm for resource allocation using deep neural network in 5G multi-user massive MIMO," *International Journal of Electronics*, vol. 108, no. 7, pp. 1214–1233, 2021.
- [3] J. Y. Li, S. Jin, X. M. Tu, Y. Ding, and G. Gao, "Identifying complex motifs in massive omics data with a variable-convolutional layer in deep neural network," *Briefings in Bioinformatics*, vol. 22, no. 6, 2021.
- [4] J. Gusak, T. Daulbaev, E. Ponomarev, A. Cichocki, and I. Oseledets, "Reduced-order modeling of deep neural networks," *Computational Mathematics and Mathematical Physics*, vol. 61, no. 5, pp. 774–785, 2021.
- [5] P. Wang, "Fast and accurate performance prediction and optimization of thermoelectric generators with deep neural networks," *Advanced Materials Technologies*, vol. 6, no. 7, 2021.
- [6] S. Tong, "Application of deep neural network in fault diagnosis," *International Core Journal of Engineering*, vol. 7, no. 7, pp. 76–82, 2021.
- [7] W. Zhou and K. Chen, "A brief survey on semantic segmentation based on deep neural network," *International Core Journal of Engineering*, vol. 7, no. 7, pp. 356–363, 2021.
- [8] G. Shahzadi and A. Soulaïmani, "Deep neural network and polynomial chaos expansion-based surrogate models for sensitivity and uncertainty propagation: an application to a rockfill dam," *Water*, vol. 13, no. 13, p. 1830, 2021.
- [9] Q. Chen, "An efficient pruning scheme of deep neural networks for internet of things applications," *EURASIP Journal on Applied Signal Processing*, vol. 2021, no. 1, 2021.
- [10] T. Zubatiuk, B. Nebgen, N. Lubbers et al., "Machine learned Hückel theory: interfacing physics and deep neural networks," *The Journal of Chemical Physics*, vol. 154, no. 24, Article ID 244108, 2021.
- [11] P. R. Srivastava, E. Prajwal, and J. Z. Zuopeng, "Deep neural network and time series approach for finance systems," *Journal of Organizational and End User Computing*, vol. 33, no. 5, pp. 204–226, 2021.
- [12] A. Heikki, "Deep neural networks with transfer learning for forest variable estimation using sentinel-2 imagery in boreal forest," *Remote Sensing*, vol. 13, no. 12, p. 2392, 2021.
- [13] J. Tian, R. Xiong, W. Shen, J. Lu, and X. G. Yang, "Deep neural network battery charging curve prediction using 30 points collected in 10 min," *Joule*, vol. 5, no. 6, pp. 1521–1534, 2021.
- [14] R. I. Mukhamediev, A. Symagulov, Y. Kuchin, K. Yakunin, and M. Yelis, "From classical machine learning to deep neural networks: a simplified scientometric review," *Applied Sciences*, vol. 11, no. 12, p. 5541, 2021.
- [15] J. Wu, K. Liu, X. Sui, and L. Cao, "High-speed computer-generated holography using an autoencoder-based deep neural network," *Optics Letters*, vol. 46, no. 12, pp. 2908–2911, 2021.
- [16] M. Yu, Y. Gu, Z. Jiang et al., "REPAID: resolution-enhanced plenoptic all-in-focus imaging using deep neural networks," *Optics Letters*, vol. 46, no. 12, pp. 2896–2899, 2021.
- [17] G. G. Julián, "Regularized chained deep neural network classifier for multiple annotators," *Applied Sciences*, vol. 11, no. 12, p. 5409, 2021.
- [18] M. Collatz, F. Mock, E. Barth, M. Holzer, K. Sachse, and M. Marz, "EpiDope: a deep neural network for linear B-cell epitope prediction," *Bioinformatics*, vol. 37, no. 12, p. 1784, 2021.
- [19] J. Bhatt, K. A. Hashmi, M. Z. Afzal, and D. Stricker, "A survey of graphical page object detection with deep neural networks," *Applied Sciences*, vol. 11, no. 12, p. 5344, 2021.
- [20] K. Atsushi, K. Toshifumi, and J. Kikuchi, "Solubility prediction from molecular properties and analytical data using an in-phase deep neural network (Ip-DNN)," *ACS Omega*, vol. 6, no. 22, Article ID 14278, 2021.
- [21] K. Audrius, "HUMANNET—a two-tiered deep neural network architecture for self-occluding humanoid pose reconstruction," *Sensors*, vol. 21, no. 12, p. 3945, 2021.
- [22] E. S. Raghida, E. Sedgh Gooya, A. Alfalou, and M. Khalil, "Privacy-preserving deep neural network methods: computational and perceptual methods—an overview," *Electronics*, vol. 10, no. 11, p. 1367, 2021.
- [23] F. Mushtaq, M. M. Misgar, M. Kumar, and S. S. Khurana, "UrduDeepNet: offline handwritten Urdu character recognition using deep neural network," *Neural Computing & Applications*, vol. 33, no. 22, pp. 15229–15252, 2021.
- [24] Z. Yang, D. Gjorgjevikj, J. Long, Y. Zi, S. Zhang, and C. Li, "Sparse autoencoder-based multi-head deep neural networks for machinery fault diagnostics with detection of novelties," *Chinese Journal of Mechanical Engineering*, vol. 34, no. 1, p. 54, 2021.
- [25] C. Yao, "Nonlinear variable selection via deep neural networks," *Journal of Computational & Graphical Statistics*, vol. 30, no. 2, pp. 484–492, 2021.

Retraction

Retracted: Feasibility Analysis and Discrete Dynamic Modeling of Physical Education Teaching Strategy Based on Intelligent Computing

Computational Intelligence and Neuroscience

Received 25 July 2023; Accepted 25 July 2023; Published 26 July 2023

Copyright © 2023 Computational Intelligence and Neuroscience. This is an open access article distributed under the Creative Commons Attribution License, which permits unrestricted use, distribution, and reproduction in any medium, provided the original work is properly cited.

This article has been retracted by Hindawi following an investigation undertaken by the publisher [1]. This investigation has uncovered evidence of one or more of the following indicators of systematic manipulation of the publication process:

- (1) Discrepancies in scope
- (2) Discrepancies in the description of the research reported
- (3) Discrepancies between the availability of data and the research described
- (4) Inappropriate citations
- (5) Incoherent, meaningless and/or irrelevant content included in the article
- (6) Peer-review manipulation

The presence of these indicators undermines our confidence in the integrity of the article's content and we cannot, therefore, vouch for its reliability. Please note that this notice is intended solely to alert readers that the content of this article is unreliable. We have not investigated whether authors were aware of or involved in the systematic manipulation of the publication process.

Wiley and Hindawi regrets that the usual quality checks did not identify these issues before publication and have since put additional measures in place to safeguard research integrity.

We wish to credit our own Research Integrity and Research Publishing teams and anonymous and named external researchers and research integrity experts for contributing to this investigation.

The corresponding author, as the representative of all authors, has been given the opportunity to register their agreement or disagreement to this retraction. We have kept a record of any response received.

References

- [1] G. Wang, "Feasibility Analysis and Discrete Dynamic Modeling of Physical Education Teaching Strategy Based on Intelligent Computing," *Computational Intelligence and Neuroscience*, vol. 2022, Article ID 4093924, 8 pages, 2022.

Research Article

Feasibility Analysis and Discrete Dynamic Modeling of Physical Education Teaching Strategy Based on Intelligent Computing

Ge Wang 

School of Physical Education and Sport Science, Fujian Normal University, 350117 Fuzhou, Fujian, China

Correspondence should be addressed to Ge Wang; wangge@fjnu.edu.cn

Received 19 April 2022; Accepted 17 May 2022; Published 7 June 2022

Academic Editor: Le Sun

Copyright © 2022 Ge Wang. This is an open access article distributed under the Creative Commons Attribution License, which permits unrestricted use, distribution, and reproduction in any medium, provided the original work is properly cited.

With the advent of the information age, computer technology is also widely used in various fields. In the field of education, physical education teaching strategy has always been the focus of many educators. In order to optimize physical education teaching strategies and improve teaching quality, this paper proposes a new intelligent computing technology. This technology has excellent innovation in the engineering design field of physical education teaching strategy reform and innovation and combines Intelligent Computing with physical education teaching strategy to explore the feasibility and effectiveness of physical education teaching strategy reform and innovation. On the basis of intelligent computing algorithm, this paper analyzes the visualization strategy scheme brought by intelligent computing classroom to physical education teaching. This paper analyzes the feasibility of students' feedback after the reform of the physical education teaching strategy. Finally, the big data discrete dynamic modeling technology is used to dynamically model and analyze the students' learning behavior and effect after the reform and innovation of physical education teaching strategy. Combined with the analysis data and students' behavior feedback, this paper analyzes the feasibility of the physical education teaching strategy after the reform and innovation. The results show that the visualization scheme of physical education teaching strategy based on intelligent computing can help students understand theoretical knowledge and realize the transformation from static classroom to dynamic classroom. It enhances students' practical activities and perceptual knowledge and is of great help to students' physical education learning effect. In the discrete dynamic modeling analysis, the feasibility of physical education teaching strategy reform is very important.

1. Introduction

With the influence of examination-oriented education in China, the decline in students' physical quality in China is very serious (Wan et al. 2021) [1]. There are many diseases such as myopia, obesity, and weakness. Good physical education teaching can help students improve this situation. Therefore, the task of physical education teaching strategy reform in China is imminent (Jennina et al. 2021) [2]. Comprehensively improving students' physical quality and physical education achievements has become one of the teaching objectives of each university. More and more colleges and universities begin to pay attention to the reform of students' physical education teaching strategies. However, there are still many deficiencies in the actual process of teaching strategy reform and innovation. As a result,

students cannot give full play to their strengths and form good learning habits in sports activities (Hao et al. 2021) [3]. Among them, the factors affecting the reform of physical education teaching strategies include the low attention of schools. In carrying out sports activities, many colleges and universities do not pay enough attention to the impact of teaching itself (Yuchen et al. 2021) [4]. Physical education teaching is not only to improve students' physical performance but also to improve students' physical quality and comprehensive quality. Students need to improve their physical environment through physical education and physical exercise. Moreover, in school social communication, a good physical education teaching environment can help students change the introversion trend and expand communicative activities (Li et al. 2021) [5].

Most teachers only regard physical education courses as free activity time in physical education teaching, without clear teaching objectives (Liu et al. 2021) [6]. In the actual teaching process, I did not understand how to highlight the characteristics of sports and training direction. Teachers lack the combination of the theoretical basis and teaching activities, resulting in students' interest in sports cannot be effectively improved (Yang et al. 2021) [7]. The teaching mode of many colleges and universities is relatively backward, and the traditional physical education teaching method still exists in many schools. Teachers' teaching to students is mainly theoretical learning, supplemented by physical training [8]. This traditional teaching mode has a great impact on students' physical education development. In the learning process, it does not reflect that students are the main body of learning and lack of subjective initiative. With the combination of education and information technology, more and more physical education teaching strategies began to appear and achieved good results and teaching results (Lin et al. 2021) [9]. As a modern auxiliary teaching tool, intelligent computing can bring new opportunities for the physical education teaching environment. This method was originally used in the field of engineering and can simulate biological mechanism and evolution process with the help of a computer. It provides technical support for information acquisition and information processing. It has achieved good results in the fields of virtual modeling, image recognition, image processing, information processing, prediction analysis, and so on. Facing the single form of traditional physical education teaching strategy, this paper combines intelligent computing with physical education teaching to explore the reform, innovation, and feasibility analysis of teaching strategy.

Optimizing physical education teaching strategies and improving teaching quality are the main contents of the reform and innovation of physical education teaching strategies, including implementing the guiding principle of health first in teaching guiding ideology. In the relationship between teaching and learning, it emphasizes the equality between teachers and students, cooperation, and interaction, and students are the main body of teaching. In the concept structure of teaching, it emphasizes that teaching activities are the organic unity of three psychological activities: cognition, emotion, and behavior. Teaching design should create conditions for students' independent choice and active exploration in the teaching process, advocate teaching democracy, make students' learning an active and personalized process under the guidance of teachers, and emphasize the formation of students' self-study ability.

This paper is mainly divided into three parts. The first part is a basic understanding of the reform and innovation of physical education teaching strategies and puts forward the teaching strategies and teaching modes of intelligent computing. The research status of discrete dynamic modeling technology used in feasibility analysis is analyzed. The second part first studies the mode of Intelligent Computing physical education teaching strategy and analyzes the application of intelligent computing algorithm in the feasibility study. This paper studies the changes in students' behavior

after the reform of the Intelligent Computing physical education teaching strategy. Finally, the discrete dynamic modeling technology is used to analyze the feasibility of physical education teaching strategy reform and innovation. The third part analyzes the teaching environment after the reform of the physical education teaching strategy and the results of the feasibility study of the Intelligent Computing teaching mode.

2. Related Work

The reform of the physical education teaching strategy is a complex process and structure. Not only do schools need to pay more attention to physical education but also students need to form a good physical education classroom atmosphere (Liao et al. 2021) [10]. In the physical education teaching environment, teachers should give full play to their professional skills, analyze students' physical and mental characteristics, and formulate targeted teaching strategies (Bian et al. 2021) [11]. In the reform of physical education teaching strategy, we first need to solve the importance of this industry, make use of its own advantages to spread and influence in various aspects, improve people's understanding of sports, and use their spare time to help students take physical exercise. In the reform of teaching strategies, it needs to be formulated according to the physical and mental characteristics of students, and the time of sports activities cannot be reduced in order to meet the needs of examination-oriented education (Zhang et al. 2021) [12]. We use the characteristics of intelligent computing to improve physical education teaching strategies in order to explore the feasibility of this method. This paper uses big data discrete dynamic modeling technology to analyze the feasibility. Discrete dynamic modeling technology can quickly deal with the problem of excessive data in big data environment, which provides effective help for system operation and efficiency improvement. In the feasibility analysis, combined with the changes in students' own behavior, we study the dynamic changes before and after the improvement of the Intelligent Computing physical education teaching strategy. Finally, it provides accurate data sources for exploring the feasibility of teaching strategy reform and innovation. Next, we will briefly describe the application status of big data discrete dynamic modeling technology in various countries.

Japan does not pay much attention to the ecological environment. Therefore, with the progress and development of the times, they mainly study the protection and utilization of sustainable energy and renewable energy (Lin et al. 2021) [13]. Wind power generation has always been a large model in renewable energy. With the continuous bad changes in the ecological environment, they pay more attention to the research on the operation process of wind power generation. Wind turbines are prone to damage during operation. In order to effectively monitor the aging degree of components, they apply discrete dynamic modeling technology here to timely grasp the operation state of the motor and ensure stable operation.

Enterprise development in Korea has always been the main source of the national economy. With the

popularization of the Internet, the information system has also changed (Guan et al. 2021) [14]. Enterprises have been slow to use and accept big data. In order to improve this situation, they use big data technology to optimize and dynamically model enterprise management. Mainly combined with various factors affecting the enterprise environment, this paper constructs a dynamic model of data analysis and processing and finally realizes the purpose of optimizing the enterprise development process.

The United States is relatively advanced in the development of the military field. Their military strength is very strong, but computer technology is also a field that cannot be underestimated [15]. They have provided many effective achievements and research in the development of information technology. Military equipment operation system usually has minor faults, which is not conducive to their national security and guarantee. Therefore, they use big data technology to dynamically model and analyze the data source of equipment operation and build a prediction model to give early warning of possible fault factors in the system. Thus, the purpose of reducing maintenance cost and overhaul cost is realized. Based on the development status of discrete dynamic modeling technology in various countries, this paper studies the feasibility analysis of Intelligent Computing physical education teaching strategy reform.

3. Methodology

3.1. Feasibility Study on the Reform and Innovation of Physical Education Teaching Strategy Based on Intelligent Computing.

At this stage, most teaching methods in physical education teaching strategies have undergone basic reform and innovation. Traditional teaching mode and innovative teaching mode are parallel to each other. Most colleges and universities adopt traditional teaching, optional physical education, and free activity teaching. Through literature survey, we know that ordinary teaching methods have been relatively rare. The current physical education teaching mode has been basically improved in combination with modern educational technology. Traditional teaching strategies only appear in track and field, shot put, gymnastics, and other events. The physical education curriculum in most colleges and universities is also relatively single, and practical knowledge and teaching mode are relatively rare. This situation leads to the fact that the physical education curriculum in colleges and universities does not have its own characteristics and cannot attract students to study and stimulate interest. In the teaching strategy of intelligent computing, we use the efficient computer language program MATLAB as the core technology of visual teaching. It can process a large amount of data and information and realize analysis and sorting. It provides technical support in visual physical education teaching strategy. Visual teaching in physical education teaching strategy refers to the concretization of abstract actions by using simulation technology. In sports training, the most common observation methods are video observation and three-dimensional dynamic photography, which are established on the basis of science. Human motion simulation technology mainly

includes the establishment of the human model, the collection of more real physical reaction signals of the human body under specific conditions, the process of computer simulating human real motion, and so on. This technology is a major breakthrough of information technology in the process of sports. It can promote the development of sports and the development of three-dimensional dynamic simulation technology in sports, analyze and extract the theoretical knowledge from the essence, and show it intuitively. In traditional teaching, in addition to using body language to convey information, students can also perceive actions in virtual simulation. We apply MATLAB visualization technology to the teaching strategy of sports intelligent computing, which can enhance students' sensory understanding. In the process of studying the reform of Intelligent Computing physical education teaching strategy, it is necessary to complete three parts: theory teaching, actionability, and curriculum practice. We need to maximize the improvement of the physical education curriculum in a limited time. Compared with ordinary courses, this model has a shorter teaching time. In the reform and innovation of physical education teaching strategies, we need to pay more attention to students' thinking divergence ability and practical ability. Different from the traditional classroom, the optimized classroom can enrich students' ability to acquire knowledge. In Intelligent Computing physical education teaching, theory and practice need to be highly integrated. The traditional physical education teaching strategy only pays attention to the academic achievement and actual effect but does not pay attention to the teaching process. With the continuous development of educational ideas, in the process of education, we no longer only pay attention to the teaching of relevant knowledge and skills. At the same time, we also need to pay more attention to the awakening of students' self-spirit and constantly stimulate students' thinking of self-thinking and self-creation. When this phenomenon is fed back to the computer industry and artificial intelligence teaching, it is necessary to cultivate computing thinking in the process of basic computer knowledge teaching and skill training. Of course, due to the influence of traditional educational thought, the cultivation of computing thinking is relatively weak. However, intelligent computing course needs to cultivate students to combine theory with practice and be able to deal with technical problems by themselves. This cross-teaching strategy mode is shown in Figure 1.

As can be seen from Figure 1, this physical education teaching strategy includes theoretical teaching and innovation as well as practical exercises. It fully reflects the innovation and reform effect of teaching strategies and has a positive impact on students' physical education teaching activities. In order to explore the feasibility of physical education teaching strategy reform and innovation, we need huge data as the basis of analysis results. In dealing with massive data, intelligent computing algorithm can improve the running speed of the system on the premise of ensuring real time. Firstly, the feasibility analysis model is established, and the test values of data accuracy are as follows:

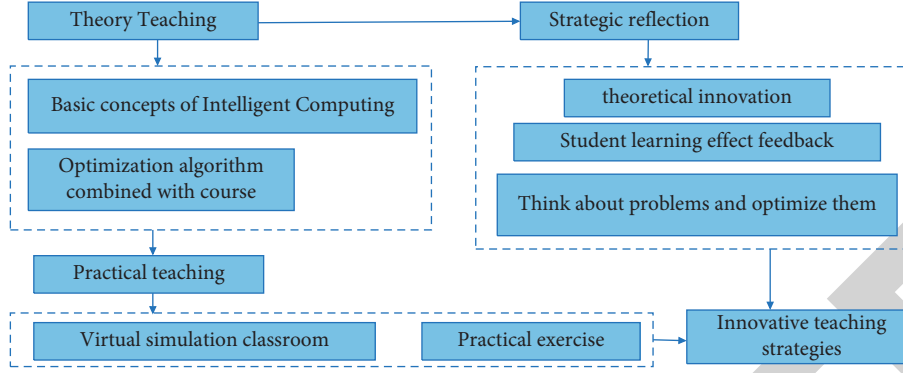


FIGURE 1: Cross-teaching strategy model.

$$M_{t+1} = M_t + w(m_t - M_t), \quad (1)$$

where M_t is the prediction data at each time and w is the weight coefficient. Set that the changes between adjacent data are equal, and the calculation formula is

$$\varepsilon = M_t - M_{k-1}. \quad (2)$$

In order to solve the error coefficient in data calculation, we will test the multiple prediction results in the way of average:

$$M = \frac{\sum_{k=1}^n M_k}{n}. \quad (3)$$

Judge the difference between the two coefficients to illustrate the changing trend of error rate when the current data increase with the number. In order to deal with high-dimensional data sets and prevent the fitting phenomenon, we need to classify and balance the data samples, increase the fault tolerance of the algorithm, and set the calculation formula of the sample characteristic index as follows:

$$G_m = \sum_{k=1}^{|k|} \sum_{k \neq k'} pmkpmk' = 1 - \sum_{k=1}^{|k|} p^2 mk. \quad (4)$$

In the formula, k represents the sample category and pmk represents the proportion of nodes and coefficients. Secondly, the importance of the eigenvector in the calculation node is expressed as follows:

$$VIM_{jm}^{(Gini)} = G_m - G_i - G_r. \quad (5)$$

In the formula, G_i and G_r , respectively, represent the relationship index in the node. If the eigenvalue is in the set state, the weight is

$$VIM_{jm}^{(Gini)} = \sum_{m \in M} VIM_{im}^{(Gini)}. \quad (6)$$

Assuming that there are multiple parent nodes in the algorithm, the formula is defined as follows when calculating the feasibility of characteristic data

$$VIM_i^{(Gini)} = \sum_{j=1}^n VIM_{ji}^{(Gini)}. \quad (7)$$

Finally, the calculated feasibility score is summarized by normalization as follows:

$$VIM_i = \frac{VIM_i}{\sum_{j=1}^m VIM_j}. \quad (8)$$

To sum up, the calculation can obtain the feasibility data of the reform model of physical education teaching strategy and provide accurate data support for the reform process of physical education teaching strategy. We summarize the flow of the intelligent computing model as shown in Figure 2.

As can be seen from Figure 2, first initialize the calculation parameters of the algorithm and arrange the factors affecting the data results. Finally, according to the adaptability of each data, the data are divided and processed uniformly. According to the feasibility results of physical education teaching strategy reform and innovation, the optimized physical education teaching model is more suitable for students' physical activities. The visual teaching of intelligent computing can also optimize the teaching according to the concept of combining theory with practice. With its own advantages of image, vividness, and intuition, visual teaching arranges a large amount of theoretical information into a collection. It is convenient for teachers to summarize teaching priorities and help students show their thinking through practical activities in combination with theoretical knowledge.

3.2. Feasibility Study on the Reform and Innovation of Physical Education Teaching Strategy Based on Discrete Dynamic Modeling Analysis. With the advent of the information age, information-based teaching mode and intelligent teaching mode have been gradually applied in the field of education. With the increasing demand for learning, it is necessary to study the theoretical knowledge that cannot be expressed by action in physical education teaching. We began to explore the practical application of information-based teaching methods in physical education. Intelligent computing visual physical education teaching strategy can make physical education technology and action clearly displayed in front of students. In traditional physical education teaching strategies, teachers can only teach movements through multiple demonstrations. This model is no longer applicable to today's environment. Therefore, a

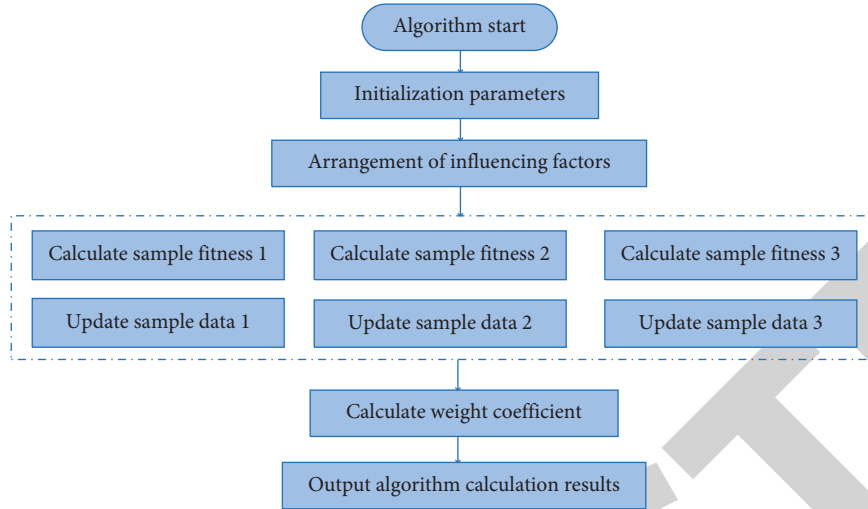


FIGURE 2: Process of intelligent computing model.

series of reforms and innovations have been carried out for physical education teaching strategies. In order to better explore the feasibility of reform and innovation, this paper uses big data discrete dynamic modeling technology to analyze the behavior of physical education learners. Because the work task and processing speed of the database in the big data environment are the main factors affecting the result judgment, the traditional data processing technology cannot face this dynamic and complex environment, so it is necessary to use discrete dynamic modeling to process the data set. In the selection of hardware system, make full use of the modern platform and combine the prediction model with historical experience to make the data processing model more intelligent. Be able to adapt to the changes in dynamic data and work content. Firstly, we reduce the error rate of data results based on Bayesian theory. The behavior of physical education learners is regarded as a feature vector. The eigenvalues are expressed by conditional coefficients. Define the main behavior of data in different categories and different sample characteristics, then

$$P(C_i|X) = \frac{P(X|C_i)P(C_i)}{P(X)}. \quad (9)$$

The assumed independence of the above formula is

$$P(X|C_i) = \prod_{j=1}^M P(X_j|C_i). \quad (10)$$

According to the above formula, we can divide the data processing into three parts. The first part is data mining and sorting, the second part is data visualization calculation, and the third part is to ensure the accuracy and independence of calculation. In learner behavior analysis, the correct rate and error rate of each behavior are different. A sports project needs a variety of learning behaviors to carry out a feasibility analysis. We mark the nodes in the behavior. When the value of the teaching strategy is a fixed value, we can obtain the learners'

learning state. If learners can master this sports skill in this teaching strategy, it can be expressed as

$$P(C_n = \text{false}|K_n = \text{true}),$$

$$P = \frac{\exp(-\sum_{j=1}^n \delta_j s_j^n + \gamma)}{1 + \exp(-\sum_{j=1}^n \delta_j s_j^n + \gamma)}. \quad (11)$$

In the formula, P represents learning efficiency and K_n represents accuracy.

If we cannot master this sports skill in learning, the coefficient of teaching strategy can be expressed by visual data. The calculation equation obtained by logarithmic regression expansion is

$$P(G_n) = P(C_n = \text{true}|K_n = \text{false}),$$

$$P(G_n) = \frac{1}{1 + \exp(-\sum_{j=1}^n \alpha_j s_j^n + \beta)}. \quad (12)$$

In the formula, α_j and s_j^n can represent the factors affecting the correctness and error of feasibility judgment, and β is the calculated deviation. Finally, the learning probability and mastery degree are expressed by the following probability formula:

$$P(K_{n+1} = \text{true}|K_n = \text{false}) = \frac{1}{1 + \exp(-\sum_{j=1}^n \alpha_j s_n^{(j)} + \beta)}. \quad (13)$$

According to the above formula, we can get the feasibility analysis results of discrete dynamic modeling technology on the reform and innovation of physical education teaching strategies. The teaching effect is known through the judgment of learners' behavior correctness and the mastery of sports skills. We will analyze the students' learning effect before and after the reform of the physical education teaching strategy as shown in Figure 3.

It can be seen from Figure 3 that after the reform and innovation of physical education teaching strategies, most

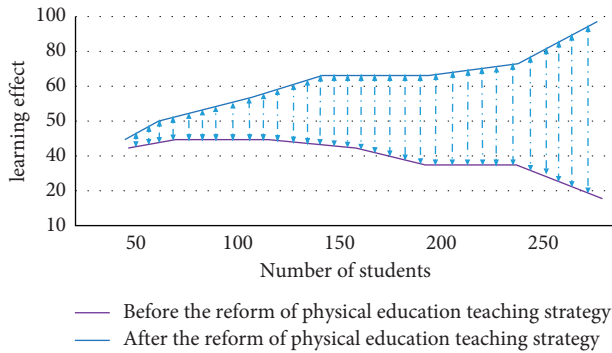


FIGURE 3: Analysis of students' learning effect before and after the reform of physical education teaching strategy.

students can improve their mastery of physical education skills. It has been well applied in sports.

4. Result Analysis and Discussion

4.1. Analysis of Feasibility Study Results of Physical Education Teaching Strategy Reform and Innovation Based on Intelligent Computing. The core content of optimization in the reform and innovation of physical education teaching strategy lies in the teaching mode. In traditional physical education, teachers are the main body and students are the object of imitation. Under this mode, students' own enthusiasm and initiative have been restrained, and their understanding of sports is not deep enough. Teachers' professional level and teaching content can affect students' learning interest to a certain extent. In order to improve this situation, this paper combines the visual teaching design in Intelligent Computing with physical education and puts forward a dynamic and innovative teaching strategy. In order to study the feasibility of physical education teaching strategy reform, we need formal modeling and intelligent calculation of learner evaluation. In the evaluation of physical education teaching, we should emphasize the task of physical education teaching and skill development. In testing, actions are often separated. What students learn are specific skills, which are often practiced under the condition of decomposition. Then, use standardized tests to test their ability to do these decomposition skills. Traditional evaluation methods cannot meet the current needs. We need to dynamically observe students' state and learning performance in sports activities. This demand brings some difficulties to the feasibility evaluation and analysis. We use the intelligent calculation algorithm to analyze the error of the student evaluation coefficient and test whether the evaluation results meet the accuracy requirements, which can be helpful for feasibility judgment. Next, we compare the accuracy changes of data before and after intelligent computing as shown in Figure 4.

It can be seen from Figure 4 that the information data processed by intelligent computing can ensure a certain accuracy in a massive range. According to the evaluation results, we want to intervene students' physical education teaching strategies and determine whether the current interaction state of students meets the expected effect.

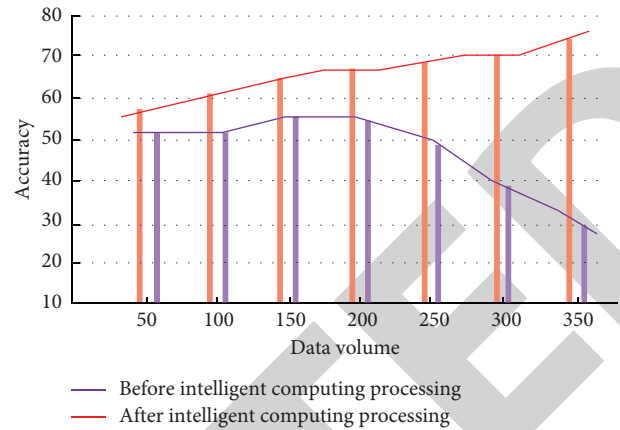


FIGURE 4: Changes in data accuracy before and after Intelligent Computing.

According to the students' feedback, we know that the reform and innovation of physical education teaching strategies can have a positive impact on teaching activities. It has certain feasibility in the actual teaching effect.

4.2. Analysis of Feasibility Study Results of Physical Education Teaching Strategy Reform and Innovation Based on Discrete Dynamic Modeling Analysis. In the reform and innovation of physical education teaching strategies, we find that in order to mobilize students' interest in physical activities, this teaching model must be integrated with information skills, that is, integrated with auditory, tactile, and visual information to improve students' desire for exploration. The use of video or pictures in multimedia technology to explain sports movements separately is of great help to students' understanding and mastering skills. We found that after the reform and innovation of the physical education teaching strategy, it is very helpful for students to master knowledge points. Teachers only need to point out the wrong actions in training in time to help students exercise correctly. The traditional teaching strategy is only simple teaching according to the classroom form. Using the teaching strategy of information combination can make the physical education classroom more vivid in an intuitive and visual way. In the feasibility analysis of physical education teaching strategy reform and innovation, we use discrete dynamic modeling to predict and judge the results. Discrete dynamic modeling technology can quickly process a large amount of data information and ensure the accuracy of data. In terms of data feedback efficiency, discrete modeling technology also has good performance. We compare the feedback of the traditional prediction model with the discrete dynamic model as shown in Figure 5.

It can be seen from Figure 5 that the system model constructed by discrete dynamic modeling technology can stabilize the feedback efficiency when the data are increasing. Compared with the traditional prediction model, it has high applicability. In the reform and innovation of physical education teaching strategies, it can bring accurate judgment and rapid feedback to the calculation results. After feasibility

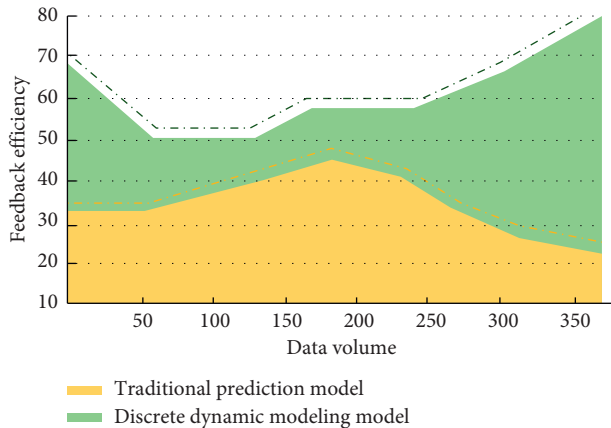


FIGURE 5: Comparison between feedback of traditional prediction model and discrete dynamic model.

analysis, we put forward some suggestions on the reform of the physical education teaching strategy. First, improve the teaching mode and set up physical education courses according to different types. For example, football, basketball, and yoga give full play to these professional advantages to the students. Let students drive students' learning and form a community model. Secondly, improving teaching facilities and sports environment can increase the atmosphere for students' sports activities. At the same time, it can ensure that students will not be injured due to sports conditions. Adding sports facilities can make students pay more attention to exercise. The last is to improve the level of teachers. A good physical education teaching strategy needs a qualified teacher to improve. PE teachers with professional and technical level can make students better understand sports activities and ensure the accuracy of posture in sports movement training.

5. Conclusion

With the improvement of the overall quality of the whole people, sports have become a necessary content in daily life. All colleges and universities have reformed and innovated the physical education teaching mode and strategy. Due to the defects of traditional physical education equipment and the influence of external factors, students' interest in physical activities is not high. Most students have poor physical quality in the examination-oriented education environment. More and more parents and teachers begin to pay attention to students' health. Therefore, it is imperative to reform and innovate physical education teaching strategies. The actual changes after the reform and innovation of physical education teaching strategies need further analysis and research. This paper analyzes the feasibility of physical education teaching strategy reform and innovation by using intelligent computing algorithm and big data discrete dynamic modeling technology. Firstly, according to the defects of physical education teaching strategies, this paper puts forward the ways and methods of reform and innovation. This paper briefly analyzes the application status of big data discrete dynamic modeling technology in various countries.

Combining the traditional classroom with the teaching method of intelligent computing, the teaching effect is analyzed by using the intelligent computing model. Finally, we compare the behavior characteristics of students before and after the reform and innovation of physical education teaching strategies, conduct discrete dynamic modeling analysis, and integrate the data results of dynamic analysis with students' learning attitude and effect to achieve the purpose of feasibility analysis. The results show that the reform and innovation of physical education teaching strategies can help students improve physical exercise activities and lay a foundation for the growth of students' interest in sports and help teachers improve the bad situation of students' sports activities and realize the concept of teaching integration and students' physical and mental growth.

Data Availability

The data used to support the findings of this study are included in the article.

Conflicts of Interest

The author declares that there are no conflicts of interest.

References

- [1] C. Wan, "Difficulties and Reform Strategies of track and field teaching in secondary vocational colleges," *Research on innovation of ice and snow sports*, vol. 18, pp. 54-55, 2021.
- [2] Jennina, "A preliminary study on the reform of Open Physical Education in Colleges and universities," *Research on the innovation of ice and snow sports*, vol. 17, pp. 123-124, 2021.
- [3] H. Yanlong, "Multidimensional analysis of the implementation strategy of quality education in Physical Education," *Journal of Jilin Institute of agricultural science and technology*, vol. 30, no. 4, pp. 110-113, 2021.
- [4] Y. Jia, "Constructing a new physical education teaching model and promoting the reform of School Physical Education," *Contemporary physical education science and technology*, vol. 11, no. 23, pp. 69-71, 2021.
- [5] G. Li, "Research on high school physical education teaching strategy from the perspective of Lifelong Physical Education," *New wisdom*, vol. 21, pp. 7-8, 2021.
- [6] xingai Liu and X. Zhang, "Analysis on the reform strategy of college physical education based on the concept of lifelong physical education," *Wudang*, vol. 7, pp. 93-94, 2021.
- [7] D. Yang, "Analysis of middle school physical education teaching strategies from the perspective of core literacy," *Invention and innovation Vocational Education*, vol. 5, pp. 28-30, 2021.
- [8] D. Bao, "Analysis of higher vocational physical education teaching strategies based on Sports literacy and professional ability," *Research on ice and snow sports innovation*, vol. 10, pp. 39-40, 2021.
- [9] L. Han, "Analysis of higher vocational physical education teaching strategies based on Sports literacy and professional ability," *Journal Of Liaoning Economic Management Cadre College*, vol. 1, pp. 146-148, 2021.
- [10] Z. Jian and Y. Jian, "A HDFS dynamic load balancing strategy using improved niche PSO algorithm in cloud storage,"

Research Article

Research on Cross-Contrast Neural Network Based Intelligent Painting: Taking Oil Painting Language Classification as an Example

Xi Zeng 

Oil Painting Department, School of Drawing and Art, Guangzhou Academy of Fine Art, Guangzhou 123456, Guangdong, China

Correspondence should be addressed to Xi Zeng; zmqp_1234@gzarts.edu.cn

Received 15 April 2022; Accepted 17 May 2022; Published 6 June 2022

Academic Editor: Le Sun

Copyright © 2022 Xi Zeng. This is an open access article distributed under the Creative Commons Attribution License, which permits unrestricted use, distribution, and reproduction in any medium, provided the original work is properly cited.

With the continuous fermentation of the thought of intelligence, artificial intelligence has extended its tentacles into the field of artistic creation and has begun to try intelligent creation. Painting creation based on artificial intelligence is called “intelligent painting.” For oil paintings, the computational language is a relatively complicated description. How to correctly identify the computational language of oil paintings is essential for establishing a large oil painting database. This paper constructs a meaningful learning similarity measure and multiclassification model based on the CCNN model to realize the classification of oil painting language. A cropped CNN model is used to extract language features, and on this basis, oil painting works are cross-compared and multiclassified. This method realizes the classification of oil painting language and the corresponding painter and achieves superior accuracy. This paper constructs a data classification method based on small samples, measures similarity through cross-comparison, and provides a measuring approach for classifying the language of oil paintings. The CCNN model proposed combines the best classification results of oil painting language, which improves the accuracy of oil painting language classification. Moreover, it further enriches the methods of oil painting language classification and image recognition under computational intelligence.

1. Introduction

As a unique symbol of artistic expression, oil painting language conveys the artist’s understanding of the objective world and life and his feelings about life. It is a silent language, a bridge between the work and the audience’s appreciation, and the basic expression of oil painting [1]. Language category is an important aspect of the meaning of an oil painting. For example, a portrait of Pierre-Auguste Renoir (1841–1919) painted in heavy ink and color, or a beautiful landscape painting by Claude Monet, shows the meaning of the work and the painter’s thoughts. Famous artists often have their own unique language of their work, and understanding the language of art is crucial to artistic cognition. In order to better understand work of art, researchers put considerable effort into categorizing the language of work of art.

In computer vision research field, significant progress has been made in the classification of scenes in images and videos due to the improvement of machine learning algorithms and the improvement of image processing technology. Researchers have begun to try to automatically classify the language of work. Research on the use of machine learning methods to classify the language of work involves calligraphy, music, painting, etc. Among them, oil painting image classification can be regarded as two-dimensional signal classification.

Artistic language recognition in oil painting has their own characteristics in image features such as color, texture, and stroke thickness due to different painters [2]. They are hard to detect using traditional algorithms and objective characteristics. This research seeks to establish a CCNN-based oil painting language similarity measurement and classification method. The research done for this study in the

language classification of oil paintings will be a new attempt and possibility for image classification technology.

2. Literature Review

Different painting styles, tools, and materials are all important factors that affect painting recognition. The styles of painters in different eras are extremely different, which is closely related to the artistic movements carried out in different periods [3]. For example, Gauguin, the representative of Post-Impressionism, pays more attention to color harmony rather than contrast when painting. Van Gogh, who is also a postimpressionist, emphasizes the use of colors to highlight themes, and his paintings are always a carnival of colors and brushstrokes.

Painting language classification is a field that people take an interest in. It can apply to painted identification, style classification, and painting database search. The task of painter classification includes classifying a painting by its respective painter. The style classification is a matter of classifying artists based on art schools such as Cubism, Baroque, and Impressionism. Both tasks are expected to be extremely challenging, because even the same painter's work has extremely different styles. Image processing techniques are a quantitative analysis tool that can perform scientific statistics and evaluation of works of art [4, 5]. Stork's comments on this topic use low-level functions that encode colors, shadows, textures, and edges [6]. Lombardi proposed that the style of painting is regarded as a personal label for the artist. Different controlled and uncontrolled teaching methods were utilized to study artists' classification tasks [7]. Lee and Cha proposed using color-based statistical calculations to extract global features and to classify painting styles by segmenting painting objects to extract local features based on composition [8]. On the basis of extracting features, using SOM to classify and visualize painting work provides a new way for artistic quantification.

Research on oil painting language classification has not made much progress in recent years. The main reason is that there is no unambiguous definition of artistic style. Numerous studies have transformed the recognition of oil painting language into the analysis of oil painting's color, texture, composition, and other characteristics and analyzed these specific characteristics in the classification model [9]. However, the results achieved are not good. The definition of language is subjective, and there is no definite quantitative indicator for the language distinction of oil paintings, so it is difficult to say in which aspects the differences between the two works are manifested [10].

In traditional oil painting language classification research, researchers extract oil painting features and then classify the features by modeling. Lombardi developed a system to study the problem of artistic analysis. Quantitative method was used to analyze the characteristics of oil paintings using the work of Van Gogh and painters of the same period as research samples, which are Van Gogh's unique brushstroke language. This paved the way for science [7]. Saleh et al. proposed a measurement method for figuring out the impact of different paintings to evaluate by learning

how to optimize the primary functions of HOG [11]. Condorovici et al. studied the classification of Iranian paintings according to texture features. The characteristics of LBP, LPQ, and LCP oil paintings were extracted and input into KNN, SVM, and other models for classification. Recognition accuracy of painting language using SVM classifier is 96.24%, 96.42%, and 96.5% [12]. In the study of deep learning painting language classification, Bar et al. classified images according to the features obtained by the pretrained convolutional neural network for image classification tasks. A machine was designed to make aesthetically relevant semantic decisions. According to the existing consensus in the field of art history interpretation, predict painting language, genre and artist, and provide the best similarity measure [13]. In addition, 81449 images of 1119 artists were employed in the experiment, and the recognition accuracy reached 43%. In 2016, Tan et al. used neural network method to realize the automatic classification of oil painting language for the first time. They achieved an accuracy of 54.5% in the classification of more than 25 painting languages in Wiki-painting [14]. Lecoutre et al. suggested using deep residual nerve to solve the problem of discovering painting language, and the accuracy rate on the Wiki-paintings data set (for 25 different languages) reached 62% [15].

3. Methods

3.1. Convolutional Neural Networks (CNN). In recent years, in the field of large-scale image classification, CNN has significant advantages, so it has attracted people's attention in the computer vision field. CNN is composed of a collection of multilayer neurons, which process the input image hierarchically [16]. Each layer can be seen as a collection of image filters, where each filter extracts specific characteristics from the input image.

CNN's research history goes back nearly 50 years, from the concept of prescription drugs in biological research in the 1960s to the first model based on prescription drug yards in the 1980s [9]. In 1998, Lecun of New York University proposed that the LeNet-5 model PW has made breakthrough progress in handwriting recognition, which has promoted the process of CNN research [17]. In recent years, CNN research in the field of pattern recognition has come to peak [18]. The above model resulted in the machine recognition error rate of ImageNet gallery approaching 3%, which is equivalent to the error rate of human eye recognition [17, 19, 20]. Although these models' structure is getting more and more complex, the bases of these models are almost the same.

CNN model is composed of three layers, that is, convolutional layer, a pooling layer, and a fully connected layer [21]. The convolutional layer is composed of a series of filter banks, which is of some size. And the depth of the filter is equal to the depth of the input data. The initial parameters can be set randomly, and parameters are updated in the training process.

Most of the current CNN structures will have a pooling layer embedded in it. Generally, a pooling layer is inserted into the fixed structure after the convolutional layer [19]. The

pooling layer has a role of reducing the spatial size of the input data, so that it can reduce the possibility. The number of learning parameters greatly reduces the resource consumption of the computer and can also effectively control the overfitting of the training network [22].

Like a normal neural network, the neurons in the CNN are fully connected to input data of the former layer. The fully connected layer mainly maps the previously learned distribution features to the sample in the space; it plays a role of classification [23]. However, due to the parameter redundancy of the fully connected layer, some models (ResNet, GoogLeNet) have adopted other methods to replace the fully connected layer to avoid parameter redundancy and have achieved good results.

3.2. Information-Based Similarity (IBS). The IBS method combines classification methods based on information and word statistics and is a novel method for effectively classifying symbol sequences based on word frequency and rank statistics [24]. In the research of natural language, it is found that each writer tends to use certain high-frequency words in the word citations in his writing, and the high-frequency words preferred by different writers differ from each other [25]. In 2003, Yang et al. applied this concept to the study of heart rate signals and, for the first time, proposed a method for similarity measurement of two complex sequences [26], which is the prototype of the IBS method. At present, IBS has been successfully applied in various fields, including Interbeat (RR) interval analysis, SARS coronavirus classification, and literary work research [24, 27].

The IBS method is to quantify the degree of difference between two symbol sequences. This degree of difference can be measured by the comparability of repeated patterns, and then the “distance” between the two symbol sequences is defined by the degree of difference. The steps for measuring the degree of difference between two symbol sequences are as follows:

- (1) A sliding window of length m is applied to one of the symbol sequences Ψ_1 , and the sliding window divides the symbol sequence into a “word” of length m ;
- (2) Calculate the number of occurrences of each “word” and sort these words according to the number of occurrences. The more frequent the occurrence, the higher the ranking;
- (3) Step (1) and step (2) are applied to another symbol sequence Ψ_2 to obtain the sequence of the symbol sequence “words.” It can be seen that different symbol sequences correspond to different “words” sequence;
- (4) According to the distribution of the “words” of the two symbol sequences Ψ_1, Ψ_2 , the weight distance formula (1) is used to calculate the difference degree D_m of the two symbol sequences.

$$D_m(\Psi_1, \Psi_2) = \frac{1}{L} \sum_{k=1}^L |R_1(s_k) - R_2(s_k)| F(s_k). \quad (1)$$

In formula (1), s_k is a “word” of length m ; $R_i(s_k)$ is the rank of a specific word s_k in the symbol sequence Ψ_i ; L represents the type of a word of length m , which is 2^m for a two-dimensional symbol sequence; $F(s_k)$ represents the weighting factor of the word s_k .

When Yang et al. first proposed the similarity measurement theory [26], the weighting factor used is as shown in formula (2), and the weighting factor $F_0(s_k)$ represents the proportion of the occurrence probability of the word s_k in the two symbol sequences Ψ_1, Ψ_2 .

$$F_0(s_k) = \frac{p_1(s_k)p_2(s_k)}{z_0 \sum_{k=1}^L p_1(s_k)p_2(s_k)}. \quad (2)$$

In formula (2), $p_i(s_k)$ refers the probability of the occurrence of a specific word s_k in the symbol sequence Ψ_i . Z_0 is a normalization factor, which is used to ensure that the difference degree D_m takes a value in the interval [0,1]. The definition of Z_0 is as follows:

$$Z_0 = 2^m - 1. \quad (3)$$

In order to apply this difference index to the classification of more symbol sequences, Goldberger and Peng [24] proposed to use the Shannon entropy formula to redefine the weighting factor $F(s_k)$, as in formula (4), to obtain the difference, a new definition of the degree index.

$$F(s_k) = \frac{[-p_1(s_k)\log p_1(s_k) - p_2(s_k)\log p_2(s_k)]}{Z}. \quad (4)$$

The normalization factor Z is defined as

$$Z = \sum_{k=1}^L [-p_1(s_k)\log p_1(s_k) - p_2(s_k)\log p_2(s_k)]. \quad (5)$$

The steps for calculating the degree of difference between two sequences using the IBS method are as above. According to the definition of the degree of difference D_m , the more similar the two symbol sequences are in the order of words, the more similar the two sequences are. We can also visually reflect the “distance” between two symbol sequences by drawing a scatter diagram. If the words in the two sequences are more similar, the scatters are more concentrated near the diagonal. In some cases, the average deviation of the distance between these scattered points and the diagonal can be used to represent the “distance” between two sequences. The farther this “distance” is, the lower the similarity between the two sequences is.

Combining the distance measurement method of the IBS model and CNN, this research designs a CCNN model to measure and classify oil painting language.

3.3. Principles and Steps of CCNN. CCNN is built on CNN signal extraction and IBS distance measurement. The goal of CCNN is to determine the similarity of different images, so as to perform multi-image classification. The input data of CCNN are specific [28]. The algorithm uses deep-rolling neural network to extract features of images and generate a set of cross-probability maps through cross-comparison of

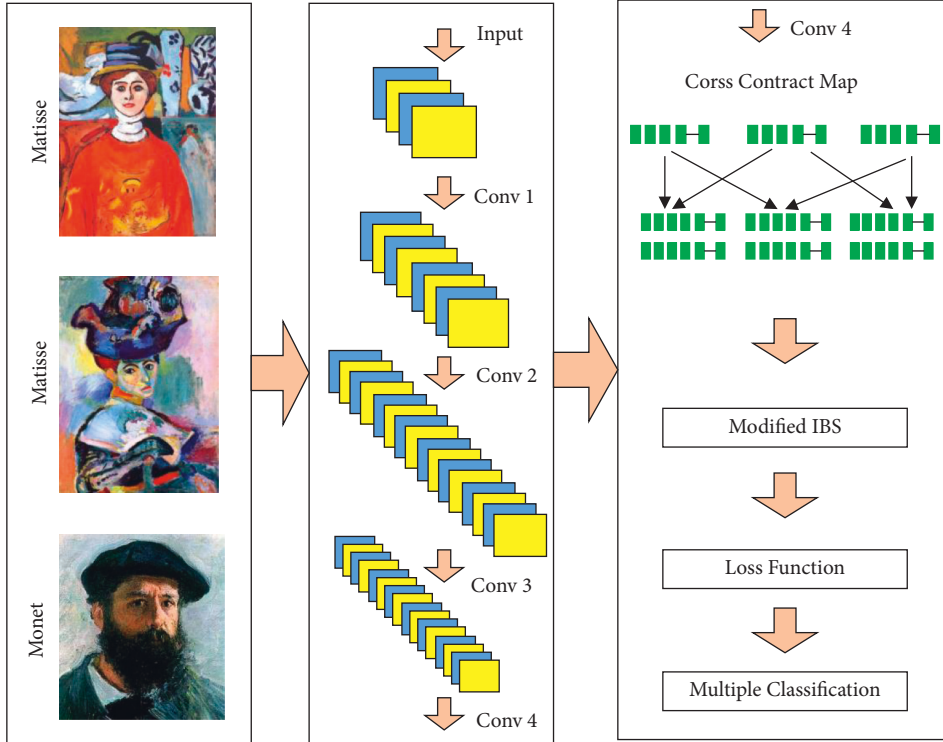


FIGURE 1: Schematic diagram of CCNN structure.

images. In addition, CCNN defines a ModLBS distance to represent the cross similarity between probability map vectors based on IBS. When the distance of ModLBS is 1, it indicates that the reorganized image languages are different. A value of 0 means that the languages are similar and come from the same painter.

CCNN extracts features by comparing the implicit information generated by the input image and obtains a set of cross-probability maps. The purpose of distance measurement is to determine the similarity between images. The two are related to each other, and together, they form a complete network [29]. As shown in Figure 1, the network uses cnN-tuned image extraction mode and ModLBS to measure the similarities between the two images.

3.3.1. Feature Extraction. First, introduce the part of the convolutional neural network used for feature extraction. The input image will be preprocessed before convolution and then pass through different layers of convolutional neural networks. The role of the convolutional layer is to do inner product operations, using multiple the convolution kernel operates on the pixels of a block. The convolution kernel is 3×3 , the step size is 1, and the padding is 1. The convolution output is activated by ReLU and then pooled. The kernel size of the pooling layer is 2×2 , so after the pooling layer, the input feature map will be cropped to $1/4$ of the original, and the output of the pooling layer is the compressed feature map (feature map). Table 1 shows the convolutional layer parameter changes in the convolution process, the ReLU layer is omitted in the table. It should be pointed out that, during the training and testing process, the

TABLE 1: VGGNet network structure of each level.

Input	Layer name	Array size
C-3-64	C 1-1	$224 \times 224 \times 3$
C-64-64	C 1-2	$224 \times 224 \times 64$
Maxpool	Pool1	$112 \times 112 \times 64$
C-64-128	C 2-1	$112 \times 112 \times 128$
C-128-128	C 2-2	$112 \times 112 \times 128$
Maxpool	Pool2	$56 \times 56 \times 128$
C-128-256	C 3-1	$56 \times 56 \times 256$
C-256-256	C 3-2	$56 \times 56 \times 256$
C-256-256	C 3-3	$56 \times 56 \times 256$
C-256-256	C 3-4	$56 \times 56 \times 256$
Maxpool	Pool3	$28 \times 28 \times 256$
C-256-512	Conv 4-1	$28 \times 28 \times 512$

input is a single image rather than a pair. Therefore, this paper can load the trained weight to initialize the CCNN, and no need to perform parameters. Here, this paper uses parameters trained on the ImageNet dataset of VGG19 to initialize the model.

3.3.2. Cross-Comparison of Feature Images. After the convolutional neural network extracts the features, this paper will then perform cross-comparison and similarity measurement of the extracted features. First, it assumes that different convolution kernels correspond to different image features, and then the above output based on CNN feature extraction is a set of features.

The number of image features corresponds to that of convolution kernels. This paper first defines a threshold to

vectorize the output feature images. The $f(v)$ function is used to convert the output of the convolutional neural network into a probability distribution map, so that this paper can calculate the frequency of the feature represented by each convolution kernel. Here, Y is the i -th image of convolution filter in the j -th pixel value. N refers the number of image inputs. D represents the number of convolution kernels; K represents the output value of the last convolution layer.

$$\vec{p}_n = [p_1, p_2, \dots, p_i, \dots, p_D] \Big|_n, n \in [1, N],$$

$$p_i = f(v_i) = \frac{\sum_j \text{softsign}(\max(v_{ij}, 0))}{\sum_i \sum_j \text{softsign}(\max(v_{ij}, 0))}, \quad \begin{array}{l} i \in [1, D], \\ j \in [1, K]. \end{array} \quad (6)$$

This paper constructs feature vectors in the output feature images and then combines them into multiple sets of sample pairs, so that the output of the corresponding convolutional neural network can be converted into many feature vectors with dimensions of $(2, D)$. Figure 2 fully shows the cross-comparison structure. Among them, X_i is the i -th frame of a group of images; p_i is the probability. Combining the probability mapping pair, the pair label is set to 0 if both are in the same category; if they do not belong to the same category, the pair label is set to 1.

Therefore, N ($N \geq 2$) images can generate $C_N^2 = N \times (N - 1)/2$ sample pairs.

After constructing the corresponding feature vector, the language classification problem is transformed into how to measure and classify this group of feature vectors. In this way, an image classification problem is converted to a similarity measurement problem based on feature vectors. The CCNN model proposed in this paper focuses on the similarity of oil painting language, rather than the difference in exact image pixels. Therefore, when doing similarity measurement, in this model, value-sensitive Euclidean distance/Manhattan distance is not included. An improved IBS method is proposed to calculate the distance obtained by weighting information entropy. CCNN uses traditional IBS. Redefine it as NorlBS, and set a RevlBS value randomly.

3.3.3. Similarity Measurement. Based on the idea of IBS, this paper first defines a NorlBS distance. 5 cores are the sum of the entropy of the probability distribution of the two images. NorlBS tends to 0 if they are similar; when they are completely different, it is not positive for the upper limit. Analogous to the principle of IBS, if the two images correspond to the same filter, and the output feature maps are ranked similarly. The scattered points are located close to both sides of the diagonal. The greater the distance, the smaller the similarity. The improved IBS method is based on the following assumption: if a feature is randomly shuffled, and the corresponding ranking changes significantly, then the fluctuation of the feature mapping may not be random and may contain relevant structural information. So, it is necessary to set a cross probability. Assuming that, after random destruction, distribution is still discrete, then the

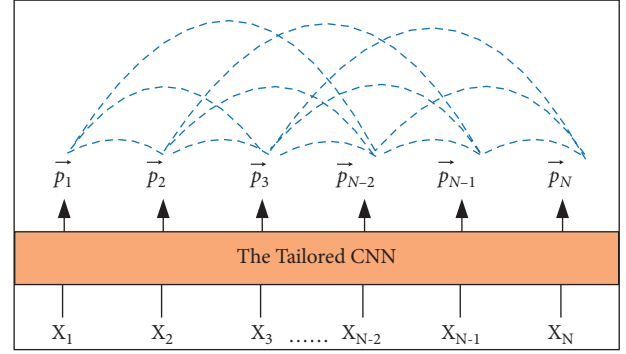


FIGURE 2: Schematic diagram of cross-contrast probability generation.

distance between the points after scrambling is defined as RevlBS.

$$\text{NorlBS} = \frac{\sum_i |R_{xi} - R_{yi}| SE_i}{D \sum_i SE_i},$$

$$SE_i = E_x(p_i) + E_y(p_i), \quad (7)$$

$$E(p) = -p \log p,$$

$$\text{RevlBS} = \text{NorlBS}(\text{random}(\vec{p}_x)).$$

For the two to work in different languages, that is, when the similarity category label is 1, the distribution before and after scrambling does not change much, so the corresponding ReslBS and NorlBS have not changed much. This paper can think that the difference between the two has a tendency to 0. And for two paintings of the same painter, the RevlBS value after scrambling is greater than NorlBS, and the difference between the two is greater than 0. Therefore, this paper defines a distance ModlBS as follows (8), where P is a coefficient, which is in 2~4. ModlBS is in 0~1. For ModlBS, when it tends to 0, the languages of the two works are similar. The value tending to 1 means that the languages of the two paintings are extremely different.

$$\text{ModlBS} = e^{-(\text{RevlBS} - \text{NorlBS}/\text{NorlBS})^P}. \quad (8)$$

Finally, this paper defines a loss function and establishes the optimization goal of the model in this paper to complete the construction of the model. The loss function is as follows, where y is the category similarity label, and $y=0$, indicating that the two oil paintings are the same painter, and vice versa, and $y=1$ means different.

$$L = \sum -[y \log(\text{ModlBS}) - (1 - y) \log(1 - \text{ModlBS})]. \quad (9)$$

3.4. Data Set. To train the model, the Wiki-paintings dataset is used. It is a large-scale image dataset collected by Karayev et al. of WikiArt [30]. The Wiki mapping dataset contains more than 85,000 images, which are divided into 25 languages/genres, such as Abstract Art, Abstract Expressionism, Baroque, Color Field Painting, Cubism, Early

TABLE 2: The number of different genres, painters and works.

Art genres	Painters	Train	Test	Total
Early renaissance	Sandro Botticelli	140	35	175
High renaissance	Leonardo da Vinci	69	17	86
Rococo	Jean-Baptiste Greuze	79	20	99
Baroque	Johannes Vermeer	43	9	52
	Rembrandt Harmenszoon	121	27	150
Neoclassicism	Auguste Dominique Ingres	94	23	117
	William-Adolphe Bouguereau	158	40	198
Impressionism	Pierre-Auguste Renoir	239	66	305
	Claude Monet	55	15	70
Post-impressionism	Vincent Willem van Gogh	160	47	207
	Paul Gauguin	65	18	83
Expressionism	Egon Schiele	149	60	209
	Amedeo Modigliani	78	20	98
Realism	John Singer Sargent	126	31	157
	Edgar Degas	47	12	59
Surrealism	Jean-Francois Millet	56	14	70
Symbolism	Pablo Picasso	115	28	143
Fauvism	Odilon Redon	78	20	98
Else	Henri Matisse	162	40	202
Else	Nicolai Fechin	138	18	156
Total	20	2172	560	2732

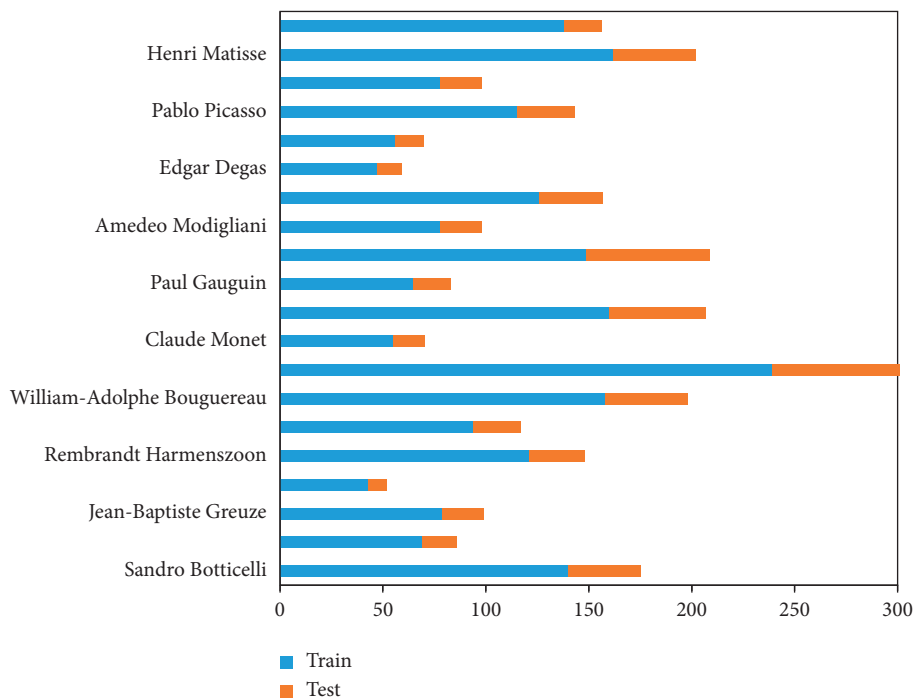


FIGURE 3: Distribution of oil painting data sets.

Renaissance, and Expressionism. The styles of oil painting pictures from the Wiki-paintings dataset include Academicism, Baroque, Expressionism, High Renaissance, Low Renaissance, Impressionism, neoclassicism, Primitivism, Realism, and Rococo.

Some paintings can have similar content, but different languages. This paper selects 20 artists in different languages to form the “Selected-Wiki-Painting” data set of this paper.

The distribution of genres, artists, and the number of works is shown in Table 2.

Each artist contains more than 50 pictures. The specified train/test ratio is about 4:1. As can be seen from Figure 3, Renoir has the largest number of paintings in the data set, and the number of images drawn by Vermeer is drawn by these 20 artists. At least, in order to ensure that the model is based on the classification of the oil painting language, the

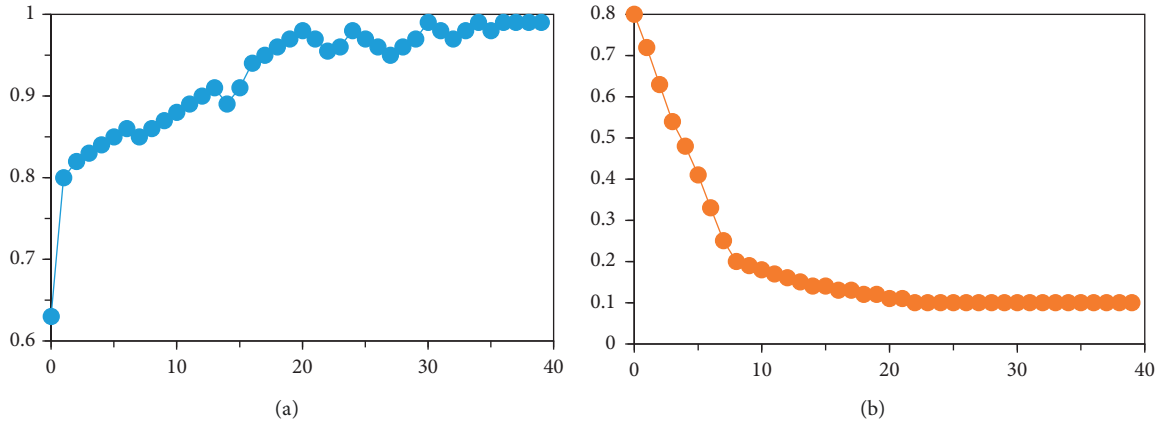


FIGURE 4: Accuracy and loss changes during the training. (a) The classification accuracy change. (b) The loss change.

selected images are all portraits, which guarantees the general similarity of the content.

4. Result and Discussion

4.1. Data Preprocessing. Data preprocessing has a greater impact on the quality of the model, and different data sets and different preprocessing methods should be used. Common image preprocessing methods in deep learning include the following three:

Zero mean: subtract the average value of each dimension of the original data of each dimension, and replace the original data with the result.

$$x_{\text{new}} = x - \mu. \quad (10)$$

Min-max standardization: it is a linear transformation of the original data in $[0,1]$ by mapping, and its mathematical expression is as follows:

$$x_{\text{new}} = \frac{x - x_{\min}}{x_{\max} - x_{\min}}. \quad (11)$$

Z-Score standardization: the data after Z-Score standardization conforms to the standard normal distribution.

$$x_{\text{new}} = \frac{\bar{x} - \mu}{\delta}. \quad (12)$$

In the CCNN-based oil painting language and artist classification process, data preprocessing mainly includes the following steps:

- (i) Crop the original image to a uniform size (224, 224, 3);
- (ii) Perform min-max standardization on the cropped image, and normalize the pixel value of the image to $[0,255]$;
- (iii) Zero-average processing is performed, and each pixel of the three channels of each image is subtracted from its corresponding RGB three-channel pixel average.

Zero-average processing can remove the average brightness value of the image and pay more attention to the

image language or content, and at the same time, data distribution with 0 center is also constructed, so that the gradient descent algorithm can effectively converge.

4.2. Model Training. This section conducts experiments on the data set selected, that is, Wiki-painting. VGG19 model pretrained on ImageNet is used to initialize the parameters. In addition, some related strategies are used, such as early stopping, learning rate, and index decay.

Implementation of the CCNN model is based on the TensorFlow framework. Model training includes image preprocessing, model initialization and training, parameter tuning, and other steps. Model training has two parts: forward propagation and backpropagation. In the back-propagation process, CCNN uses `tf.train.AdamOptimizer` provided by TensorFlow to update its parameters. Taking this into account, CCNN iterates the model parameters. The network gradually approaches the optimal solution and finally achieves the optimal goal. Here, the Adam method is a method founded on gradient descent. The `tf.train.AdamOptimizer` provided by TensorFlow can improve traditional gradient descent by using momentum, promote dynamic adjustment of hyperparameters, and accelerate model convergence. In addition, the CCNN model uses L2 regularization to prevent overfitting, and through loss, the sum of the squares of the parameter w is added to suppress the value of w and make the loss curve smoother, thereby reducing overfitting. The specific implementation of L2 in TensorFlow is `tf.add_n(tf.get_collection('losses'), weight)`. Extract all loss and use `total_loss` to train. In Figure 4, the accuracy and loss of the training set data are changing during the model training process ($lr=4.261487e-05$, $batch_size=21$).

Figure 5 shows the probability graph of similarity between two paintings by Matisse and a painting by Matisse and a painting by Monet. It is found that, in the initial stage, the probability distribution of the two paintings of different authors in the picture tends to be scattered. As the number of training increases, the degree of scatter increases. On the contrary, for the two paintings of the same artist, as the

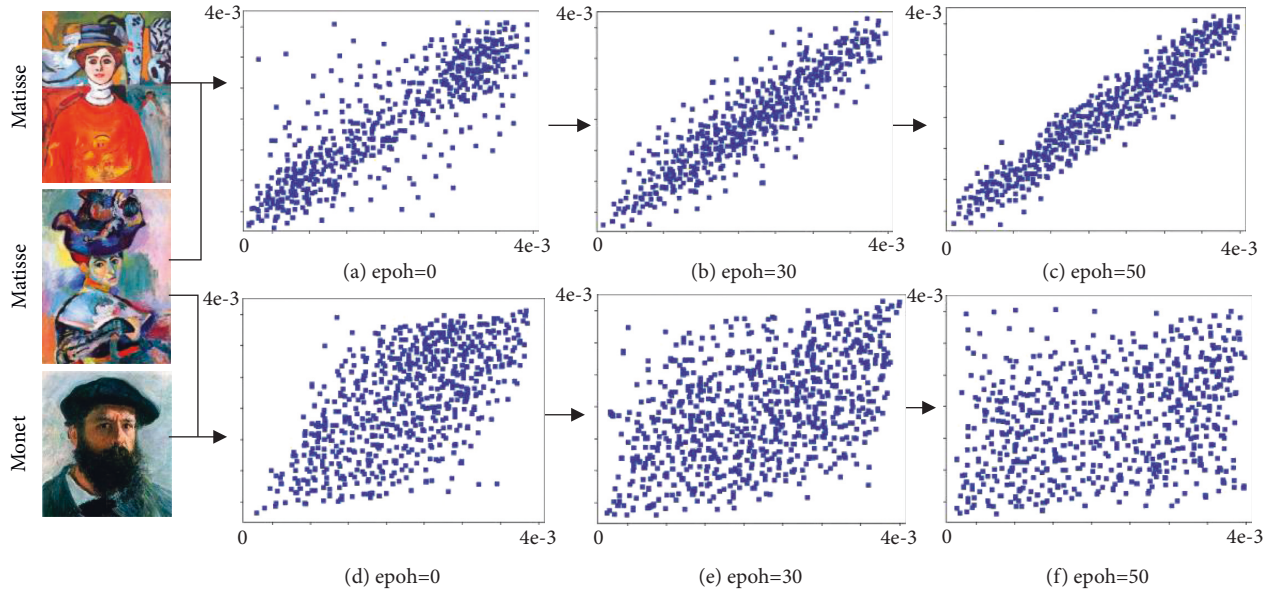


FIGURE 5: The probability distributions of different images.

training goes, it will be better distributed on both sides of the central axis. Observe the loss curve. As the training increases, the average loss is steadily decreasing, which indicates that the model training is converging in the expected direction.

4.3. Model Test. As can be seen from Figure 6, the test process of CCNN oil painting language classification is as follows. One test image and n training set images are combined into a set of inputs, and input into the trained model. 1 test image and 1 one training set image can get 1 ModIBS value, and n training set images can get n ModIBS values.

Three accuracy indicators are included in the model. Similarity accuracy (SA) is defined as the predictive accuracy of all pairs used to determine whether two images are similar, that is, two classifications. LVA is to select the category containing more label0 as the final classification result and calculate the accuracy rate. DVA is to select the category with the smallest average IBS modification value as the final classification. LVA and DVA aim to evaluate the classification accuracy of multiple classifications.

4.4. Classification Result. In the classification task, the goal is to find the similarity between two input images and realize its multiclassification. The model is applied to the identification and language classification of 20 painters. Results are presented in Table 3. Among them, in the classification of artists, the accuracy rate of similarity measurement is 97.95%. The DVA and LVA were 85.75% and 80.26%, respectively. The results of classification and recognition show that the model can effectively classify the two images. In other words, CCNN can estimate the structure from the contrasted images, copying the process of the human brain

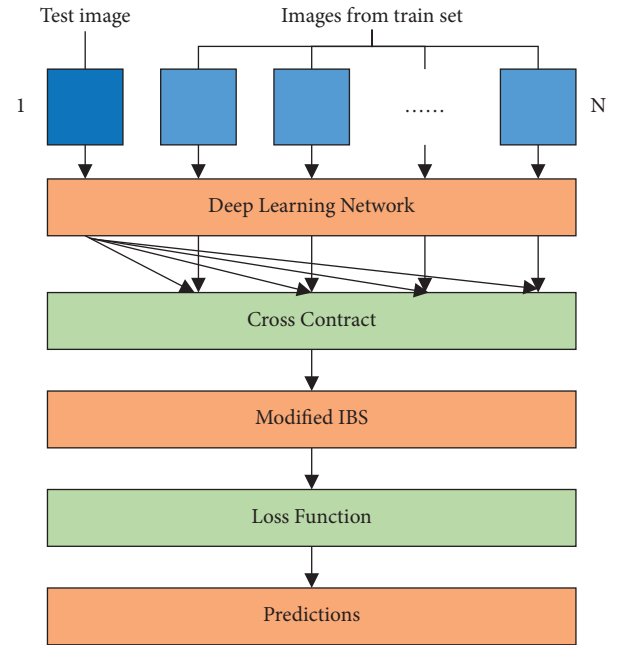


FIGURE 6: CCNN test method.

TABLE 3: Oil painting language classification results based on CCNN.

Classes	Artists/Style	SA (%)	DVA (%)	LVA (%)
13	Styles	86.96	52.77	47.76
20	Selected-wiki paintings	97.95	85.75	80.26

in measuring these images. In the classification of art genres, the accuracy rate of its 13 genres multiclassification is the highest 52.77%.

5. Conclusion

How to correctly identify the artistic language of oil paintings is essential for establishing a large oil painting database. The classification of artistic language cannot rely on any concrete characteristics, especially for those artistic works that are not representative. In response to the above problems, this paper proposes the CCNN model. The model performs well in the multiclassification task of oil painting language. This paper proposes a CCNN multiclassification method, which can measure the similarity and multiclassification of the language of oil painting work and the corresponding artists. Oil painting data set was constructed using the WikiArt library. The data set includes more than 2,000 works by 13 language styles and 20 artists. CCNN achieved an accuracy of 85.75% on the task of artistic classification. The CCNN model proposed dividing the 13 languages of the oil painting data set finds the best combination of the classification results and improves the accuracy of oil painting language classification. Although the CCNN model can be well applied to multiclassification tasks of small samples with obvious language features, its depth should be further expanded, such as extending ResNet for feature extraction.

Data Availability

The dataset can be accessed upon request.

Conflicts of Interest

The authors declare that they have no conflicts of interest.

Acknowledgments

This work was supported by the (1) University-Level Scientific Research Project of Guangzhou Academy of Fine Arts: "Comparative Study of Water-Based Painting Materials and Oil-Based Painting Materials", project number 21XSC46, and (2) the School Level Project of Guangzhou Academy of Fine Arts: "Comparative Study of Oil-Based Materials and Water-Based Materials and Their Practice and Application in Oil Painting Teaching", project number 604091809914.

References

- [1] S. P. Rosenbaum, S. P. Rosenbaum, and S. P. Rosenbaum, *The Art of Clive Bell's Art*, Springer Netherlands, Dordrecht, Netherlands, 2007.
- [2] B. Guo and P. Hao, "Analysis of artistic styles in oil painting using deep-learning features," in *Proceedings of the 2020 IEEE International Conference on Multimedia and Expo Workshops, ICMEW 2020*, Institute of Electrical and Electronics Engineers Inc, London, UK, July 2020.
- [3] V. Vieira, R. Fabbri, D. Sbrissa, L. Da Fontoura Costa, and G. Travieso, "A quantitative approach to painting styles," *Physica A: Statistical Mechanics and its Applications*, vol. 417, pp. 110–129, 2015.
- [4] S. Soleymani, A. Dabouei, S. M. Iranmanesh, H. Kazemi, J. Dawson, and N. M. Nasrabadi, "Prosodic-enhanced siamese convolutional neural networks for cross-device text-independent speaker verification," in *Proceedings of the 9th IEEE International Conference on Biometrics: Theory, Applications, and Systems (BTAS 2018)*, pp. 1–7, 2018, <https://arxiv.org/abs/1808.01026>.
- [5] B. Ranjgar, M. Khoshlahjeh Azar, A. Sadeghi-Niaraki, and S.-M. Choi, "A novel method for emotion extraction from paintings based on lüscher's psychological color test: case study Iranian-islamic paintings," *IEEE Access*, vol. 7, no. 1, pp. 120857–120871, 2019.
- [6] G. S. Kamaledin, "Competitive cross-entropy loss: a study on training single-layer neural networks for solving nonlinearly separable classification problems[J]," *Neural Processing Letters*, vol. 50, pp. 1–8, 2018.
- [7] T. Lombardi, *The Classification of Style in fine-art Painting (Dissertation)*, Pace University, New York, USA, 2005.
- [8] S.-G. Lee and E.-Y. Cha, "Style classification and visualization of art painting's genre using self-organizing maps," *Human-centric Computing and Information Sciences*, vol. 6, no. 1, p. 7, 2016.
- [9] I. Kandel and M. Castelli, "The effect of batch size on the generalizability of the convolutional neural networks on a histopathology dataset," *ICT Express*, vol. 6, no. 4, pp. 312–315, 2020.
- [10] G. U. Hayn-Leichsenring, T. Lehmann, and C. Redies, "Subjective ratings of beauty and aesthetics: correlations with statistical image properties in western oil paintings," *I-Perception*, vol. 8, no. 3, pp. 204166951771547–21, 2017.
- [11] B. Saleh, K. Abe, and A. Elgammal, "Knowledge discovery of artistic influences: a metric learning approach," in *Proceedings of the 5th International Conference on Computational Creativity, ICC3 2014*, Jozef Stefan Institute, Slovenia, June 2014.
- [12] R. G. Condorovici, C. Florea, and C. Vertan, "Automatically classifying paintings with perceptual inspired descriptors," *Journal of Visual Communication and Image Representation*, vol. 26, pp. 222–230, 2015.
- [13] Y. Bar, N. Levy, and L. Wolf, "Classification of artistic styles using binarized features derived from a deep neural network," in *Proceedings of the European Conference on Computer Vision*, Zurich, Switzerland, September 2014.
- [14] W. R. Tan, C. S. Chan, H. E. Aguirre, and K. Tanaka, "Ceci n'est pas une pipe: a deep convolutional network for fine-art paintings classification," in *Proceedings of the IEEE International Conference on Image Processing*, pp. 3703–3707, IEEE, Phoenix, AZ, USA, September 2016.
- [15] A. Lecoutre, B. Negrevergne, and F. Yger, "Recognizing art style automatically in painting with deep learning," *Journal of Machine Learning Research*, vol. 77, pp. 327–342, 2017.
- [16] A. Khan, A. Sohail, U. Zahoor, and A. S. Qureshi, "A survey of the recent architectures of deep convolutional neural networks," *Artificial Intelligence Review*, vol. 53, no. 8, pp. 5455–5516, 2020.
- [17] M. V. Valueva, N. N. Nagornov, P. A. Lyakhov, G. V. Valuev, and N. I. Chervyakov, "Application of the residue number system to reduce hardware costs of the convolutional neural network implementation," *Mathematics and Computers in Simulation*, vol. 177, pp. 232–243, 2020.
- [18] A. Krizhevsky, I. Sutskever, and G. E. Hinton, "ImageNet classification with deep convolutional neural networks," *Communications of the ACM*, vol. 60, no. 6, pp. 84–90, 2017.
- [19] T. Urakawa, Y. Tanaka, S. Goto, H. Matsuzawa, K. Watanabe, and N. Endo, "Detecting intertrochanteric hip fractures with orthopedist-level accuracy using a deep convolutional neural network," *Skeletal Radiology*, vol. 48, no. 2, pp. 239–244, 2019.

- [20] T. Song, W. Zheng, P. Song, and Z. Cui, "EEG emotion recognition using dynamical graph convolutional neural networks," *IEEE Transactions on Affective Computing*, vol. 11, no. 3, pp. 532–541, 2020.
- [21] C. Cheng and K. K. Parhi, "Fast 2D convolution algorithms for convolutional neural networks," *IEEE Transactions on Circuits and Systems I: Regular Papers*, vol. 67, no. 5, pp. 1678–1691, 2020.
- [22] S. Masood, A. Rai, A. Aggarwal, M. N. Doja, and M. Ahmad, "Detecting distraction of drivers using convolutional neural network," *Pattern Recognition Letters*, vol. 139, pp. 79–85, 2020.
- [23] P. Oza and V. M. Patel, "One-class convolutional neural network," *IEEE Signal Processing Letters*, vol. 26, no. 2, pp. 277–281, 2019.
- [24] A. L. Goldberger and C.-K. Peng, "Genomic classification using an information-based similarity index: application to the SARS coronavirus," *Journal of Computational Biology*, vol. 12, no. 8, pp. 1103–1116, 2005.
- [25] F. Mosteller and D. L. Wallace, *Applied Bayesian and Classical Inference: The Case of the Federalist Papers*, Springer Science&Business Media, Berlin, Germany, 2012.
- [26] A. C.-C. Yang, S.-S. Hseu, H.-W. Yien, and A. L. C.-K. Goldberger, "Linguistic analysis of the human heartbeat using frequency and rank order statistics," *Physical Review Letters*, vol. 90, no. 10, Article ID 108103, 2003.
- [27] M. D. Costa, R. B. Davis, and A. L. Goldberger, "Heart rate fragmentation: a symbolic dynamical approach," *Frontiers in Physiology*, vol. 8, no. 827, pp. 1–15, 2017.
- [28] Q. Wang, Z. Wang, Y. Sun et al., "SCCNN: a diagnosis method for hepatocellular carcinoma and intrahepatic cholangiocarcinoma based on siamese cross contrast neural network," *IEEE Access*, vol. 8, pp. 85271–85283, 2020.
- [29] Y. Huang, Y. Chen, H. Zhu et al., "A liver fibrosis staging method using cross-contrast network," *Expert Systems with Applications*, vol. 130, pp. 124–131, 2019.
- [30] S. Karayev, M. Trentacoste, H. Han et al., "Recognizing image style," in *Proceedings of the BMVC 2014 - Proceedings of the British Machine Vision Conference 2014*, November 2013, <https://arxiv.org/abs/1311.3715>.

Research Article

Prediction of Labor Unemployment Based on Time Series Model and Neural Network Model

Xitao Liu and Lihui Li 

School of Public Finance and Administration, Harbin University of Commerce, Harbin 150001, Heilongjiang, China

Correspondence should be addressed to Lihui Li; 102148@hrbcu.edu.cn

Received 2 April 2022; Accepted 14 May 2022; Published 3 June 2022

Academic Editor: Le Sun

Copyright © 2022 Xitao Liu and Lihui Li. This is an open access article distributed under the Creative Commons Attribution License, which permits unrestricted use, distribution, and reproduction in any medium, provided the original work is properly cited.

With the advent of big data, statistical accounting based on artificial intelligence can realistically reflect the dynamics of labor force and market segmentation. Therefore, based on the combination of machine learning algorithm and traditional statistical data under big data, a prediction model of unemployment in labor force based on the combination of time series model and neural network model is built. According to the theoretical parameters, the algorithm of the two-weight neural network is proposed, and the unemployment rate in labor force is predicted according to the weight combination of the two. The outcomes show that the fitting effect based on the combined model is superior to that of the single model and the traditional BP neural network model; at the same time, the prediction results with total unemployment and unemployment rate as evaluation indexes are excellent. The model can offer new ideas for assisting to solve the unemployment of the labor force in China.

1. Introduction

Unemployment is not only a comprehensive economic problem but also a complex social problem [1] which has turned into the focal point of consideration for all nations. Whether unemployment can be properly solved is related to the development of the country. In recent years, China's economy is facing a complicated international economic environment, such as RMB appreciation [2], prices rising of raw materials [3], and pressure increase of inflation input [4], which has led to the decline of export and economic growth, thus bringing about unemployment that deserves our attention. In addition, the government also attaches great importance to the development of a country, which depends not only on the country's economy, science, technology, military affairs, and the gap between the rich and the poor but also on the treatment results of unemployment. If countries with serious unemployment do not have effective policies and measures to ensure the survival of the unemployed labor force, it can easily lead to social instability, which will affect the development of a country in all aspects. Therefore, if the government can predict the number

and proportion of unemployed labor force in advance, they can formulate policies and measures to ensure the prosperity and development of the country according to these predicted data [5].

At present, with the advent of big data, some researchers try to use circumstantial big data to build indicators for measuring the dynamics of China's labor market [6–8]. For example, by using recruitment data on Internet [9], social media data [10], data of digital search [11], etc., to build economic indicators based on nonstatistical accounting methods, which can reflect the dynamics of the whole labor force and market segments in real time. However, these indicators lack a clear definition in the accounting sense, and their scientific and reliability are questioned. For the method of prediction, because the urban unemployment and unemployment rate in China are all differential stationary time series data, the neural network algorithm has been proved to have an excellent approximation ability to nonlinear relationship in theory [12, 13], so it is of practical significance to study a prediction model of unemployment in the labor force, so as to solve the actual unemployment.

Before 2018, the most important unemployment index released by the Chinese government was the registered

urban unemployment rate, which was quite different from the international definition of the unemployment rate, and the value remained stable at around 4% for a long time, so it was difficult to reflect the real unemployment level in China [14]. Since 2018, the Chinese National Bureau of Statistics has released the national urban survey of the unemployment rate on a monthly basis, which is a significant progress in the release of unemployment statistics. To make up for the long-term lack of China's four macro-economic indicators, the data have been generally recognized by all sectors of society. However, due to the limited sample size of the labor force survey, the unemployment rate in the urban survey is not representative of administrative regions at all levels below the provincial level [13]. In 2021, the Chinese National Labor Force Survey will conduct a new round of sampling according to the seventh national census and appropriately expand the sample size to meet the main index data, such as the urban unemployment rate, which is well representative of the country and provinces (autonomous regions and municipalities).

Therefore, in this paper, the above-mentioned combination model is established, and the unemployment situation of the urban labor force with the number of unemployed and unemployment rate as evaluation indexes to explore new ideas that are helpful to manage the urban unemployment in China.

2. Related Theories

2.1. Neural Network Model

2.1.1. BP Neural Network. First proposed by the Parallel Distributed Processing scientific research group represented by Rumelhart and McClelland in the United States, BP neural network is a multilayer perceptron feedforward network [15]. It has strong nonlinear adaptability, excellent nonlinear approximation, and good fault tolerance. Therefore, it can process large-scale data in parallel with outstanding self-organizing, self-learning, and self-adapting abilities, which are widely adopted in the fields of prediction, classification, and clustering. This back propagation algorithm makes multilayer perceptron has the ability to approximate any complex nonlinear function [16]. It is a feedforward neural network using the BP learning algorithm, and Figure 1 shows its topology.

It can be seen that the direction of data flow is that first the data of the input layer flow to the first hidden layer after weighting, then the data flow to the second hidden layer after further weighting, and so on until the output data of the last hidden layer flow to the output layer. The change function between the info and the result of neurons in each layer is known as the activation work. The universal approximation theorem has been proved [17, 18]. A three-layer BP neural organization with a secret layer can surmise any ceaseless capacity in a limited locale with erratic accuracy as long as there are an adequate number of stowed away hubs. The function corresponding to the i th neuron in a certain layer is shown in the following formula:

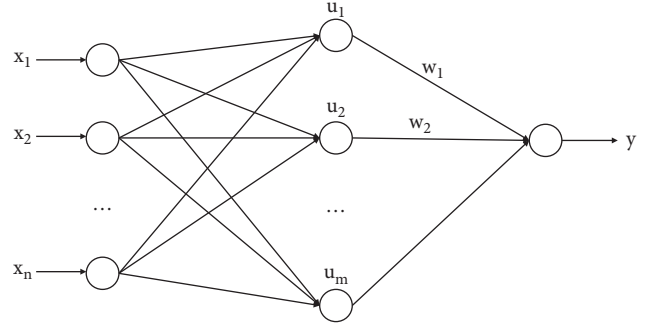


FIGURE 1: Topology of the BP neural network.

$$\begin{aligned} y_j &= f(W_j * X - \theta_j) \\ &= f\left(\sum_{i=1}^n \omega_{ij}x_i - \theta_j\right). \end{aligned} \quad (1)$$

In which, W_j is the weight in the BP neural network, X is the input vector, θ_j is the threshold, and F is the activation function.

2.1.2. RBF Neural Network. The radial basis function neural network (RBF) also belongs to feedforward neural network. It is widely used in function approximation and classification its straightforward design, simple preparation, quick learning combination, and the capacity to estimate any nonlinear combination [19]. Although RBF has only one hidden layer, it has the same excellent nonlinear approximation ability as BP neural network, and Figure 2 shows its topology.

The basis function of hidden nodes in RBF adopts the distance function, and the activation function adopts the Gaussian function. Since RBF has spiral evenness about a middle mark of N -layered space, and the farther the contribution of neurons is from the middle point, the less activated the neurons are. This characteristic is often called "local property" [20].

2.1.3. Two-Weight Neural Network. For the two-weight neural network, by changing parameters of neuron function, it can also be constructed not only as a higher-order neural network [21]. In addition, the neural of the double-weight neural network includes not only the weights of the BP neural network but also the core values (i.e., central data). The neuron function of the neural network is shown in the following formula:

$$y_j = f\left(\sum_{i=1}^n \left(\frac{\omega_{ij}(x_i - c_j)}{|\omega_{ij}(x_i - c_j)|}\right)^s \left|\omega_{ij}(x_i - c_j)\right|^p - \theta\right). \quad (2)$$

Among them, y_i is the output value of the j th neuron in a layer in the two-weight neural network model, f is the activation function, ω_{ij} is the weight of neuron, c is called the kernel value of neuron, x_i is the input value of neuron, θ is the threshold value of neuron, and s and p are two parameters.

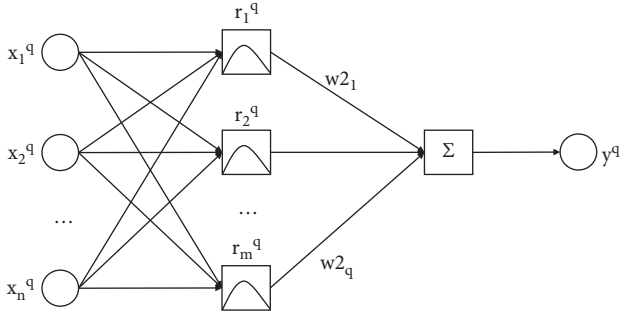


FIGURE 2: Topology of RBF neural network.

In formula (2), when $C_j=0$, $S=1$, and $p=1$, it becomes the neuron function of the BP neural network; When $s=0$ and $p=2$, the function becomes the neuron function of RBF neural network. For the hidden layer, the neuron function of this layer only contains the direction weight but not the core weight. For the hidden layer of the RBF neural network, the neuron function of this layer only contains core weights but does not contain the direction weight; while for the hidden layer of the two-weight neural network, the neural function of this layer contains both the direction weight and the core weight. Therefore, when the parameters of the activation function take specific values, it has more excellent approximation ability for nonlinear continuous functions [22].

In view of this, the algorithm of the two-weight neural network is taken. To apply all training samples to the improved BP algorithm of weight adjustment (batch processing) in the neural network. The minimum mean square error criterion is selected to evaluate the learning rule and its objective function is defined as the following equation:

$$E^{(p)} = \frac{1}{2} \sum_{l=0}^{m-1} (d_l^{(p)} - y_l^{(p)})^2. \quad (3)$$

The total error of all input samples is

$$\begin{aligned} E_T &= \sum_{p=1}^P E^{(p)} \\ &= \frac{1}{2} \sum_{p=1}^P \sum_{l=0}^{m-1} (d_l^{(p)} - y_l^{(p)})^2, \end{aligned} \quad (4)$$

where P is the number of learning sample vectors, $d_l^{(p)}$ ($p=1, \dots, P$) is the expected output, and $y_l^{(p)}$ ($p=1, \dots, P$) is the actual output.

Generally, the gradient descent method is used to modify the weights. In this paper, the formulas for adjusting the weights and the core values are as follows:

$$\begin{aligned} \omega(t+1) &= \omega(t) - (1-\alpha)\eta \frac{\partial E_T}{\partial \omega(t)} + \alpha \Delta \omega(t), \\ c(t+1) &= c(t) - (1-\alpha)\eta \frac{\partial E_T}{\partial c(t)} + \alpha \Delta c(t). \end{aligned} \quad (5)$$

Among them, η represents the learning rate whose value is generally small, $\Delta \omega(t) = \omega(t) - \omega(t-1)$, $\Delta c(t) = c(t) - c(t-1)$, α is the momentum factor, and the value of α is

$$\alpha = \begin{cases} 0, & \text{SS}(t) > 1.04\text{RSS}(t-1), \\ 0.95, & \text{RSS}(t) < \text{RSS}(t-1), \\ \alpha, & \text{others,} \end{cases} \quad (6)$$

where $\text{RSS}()$ is the residual sum of squares of the output.

The learning of network is divided into two processes [23, 24]: one is to calculate the output of each layer by forward propagation from front to back and the other process is to correct the weight or core value of each layer by backward propagation from back to front. The Algorithm 1 steps are as follows:

2.2. Time Series Model. The time series of a random event usually refers to sequence $\{X_t\}$, formed by arranging the numerical values of an index observed at equal intervals in a certain period of time in sequence, which essentially reflects the trend that an index changes with time. The main purpose of time series analysis is to observe and study the existing data, mine the development law of these data with time, and thus analyze and estimate its future situation in the time series model [25]. The analyzed data are differential stationary time series in nonstationary time series. The so-called time series is a series of ordered data recorded according to the time sequence. In daily life, the data of time series can be seen everywhere, and most of these data are nonstationary time series, among which the ARIMA model, as a kind of nonstationary time series analysis, is widely used.

ARIMA (p, d, q) model has the following formula:

$$\begin{cases} (1 - \Phi_1 B - \dots - \Phi_p B^p) \nabla^d x_t = (1 + \theta_1 B + \dots + \theta_q B^q) \varepsilon_t, \\ E(\varepsilon_t) = 0, \text{var}(\varepsilon_t) = \sigma_\varepsilon^2, \\ \text{cov}(\varepsilon_t, \varepsilon_s) = 0 (s \neq t), \\ \text{cov}(X_s, \varepsilon_t) = 0 (\forall s < t). \end{cases} \quad (7)$$

The modeling steps can be summarized as [26, 27] follows:

- (1) Test the stationarity of the original sequence data. There are two most commonly used methods, one is the graph test, and other is the unit root test. If the sequence is stationary, the graph of data changing with time should show that most of the data fluctuate at a constant and its fluctuation range is similar, autocorrelation coefficient will quickly decay to zero. When the sequence is nonstationary, the corresponding characteristic equation contains characteristic roots. Therefore, the unit root test can also be used to verify whether the sequence is stationary. The commonly used ones are DF, ADF test, etc. If the sequence is not stationary, the difference operation will be carried out.
- (2) Test the white noise of the series. It is not meaningful for all stationary series models, but only for those series models that can influence each other.

- (3) Determine the model's order. The model to be established and its order can be determined according to the correlation coefficient diagram of stationary time series, and the order can also be determined according to the identification function.
- (4) Parameter estimation: The AIC criterion can be used to complete the process of order determination and parameter estimation simultaneously.
- (5) Model test. There are usually two types of tests: the significance test of model, whose purpose is to test whether the established model effectively and adequately extracts the information contained in the data. If the established model is effective, the residual has the characteristics of white noise data, and there is no available information; Otherwise, it means that the information in the data has not been extracted completely, and the significance test of the parameters remaining in the residual error is to confirm whether each parameter obtained is obviously different from zero to establish a simpler and more accurate model.

3. The Combined Model of Unemployment Prediction in Labor

Based on the above sample data, we first forecast the number of registered unemployed people and the registered unemployment rate in China by using the two-weight neural network and then forecast the data by using the time series method. Finally, the predicted results of the two methods are combined according to the corresponding weights as the predicted values of the combined model.

3.1. Two-Weight Neural Network Model. In this paper, the parameters in the neurons of the double-weight neural network are $s = 0$, $p = 1$, $\theta = 0$, and the BP algorithm is used. When taking two-weight neural network to analyze, it is important to standardize the information first. The normalization formula for the series of the number of unemployed and unemployment rate is:

$$x(i) = 2 \frac{x_0(i) - x_{0\min}}{x_{0\max} - x_{0\min}} - 1. \quad (8)$$

Among which, $X(i)$ is the i th value in the normalized sequence, $x_0(i)$ is the original data, $x_{0\min}$ is the minimum value, and $x_{0\max}$ is the maximum value.

A training sample is constructed with the normalized data of unemployed and unemployment rate, and the method of sample construction is shown in the following formula:

$$\begin{aligned} X_i &= (x(i), x(i+1), x(i+2)), \\ Y_i &= x(i+3). \end{aligned} \quad (9)$$

In which, X_i and Y_i are the samples i th group, and $x(i)$ is the i th value of the normalized data. The sample data of nearly 30 years are selected in this model, and Table 1 shows some normalized samples as follows:

Through the prediction method of two-weights neural network, the last expectation results are displayed in Table 2.

3.2. Time Series Model. Aiming at analyzing the data that changes with time, the time series analysis uses the time series model to analyze the unemployment and the registered unemployment rate in cities and towns. Because the data series of labor unemployment is nonstationary, it is necessary to make a first-order difference to the original series, and the series after the difference has a very strong short-term correlation. Therefore, the ARIMA model is selected for fitting.

The statistical samples are tested for significance level of $\alpha = 0.05$. The white noise test of the first-order differential sequence of unemployed shows that the P value of the statistics constructed after the sixth-order delay is 0.0122, which is less than 0.05, while for the unemployment rate, the P value is 0.0017 that less than 0.05. It can be considered that the differential sequence is a nonwhite noise sequence; that is, the related information of the differential sequence cannot be ignored and has yet to be extracted. The ARIMA model can be used to fit the differential stationary and nonwhite noise sequence.

After the difference sequence, the autocorrelation coefficient is trailing, so as the partial autocorrelation coefficient. After testing, when the ARIMA model with $p = 1$ and $q = 0$ is adapted to fit the data, the best results are obtained, and the upsides of AIC and SBC compared to the model are additionally the smallest. The results are shown in Table 3.

Under the significance test level of 0.05, the residual sequence test results are shown in Table 4.

The P values of the statistics constructed are far greater than 0.05, so it can be considered that the residual sequence no longer has the significance of extracting information. The results of the coefficient test and residual test show that the ARIMA (1, 1, 0) model implemented in this paper has a decent displaying impact on the sequence of unemployment.

According to the established model, the unemployment of the labor force is predicted, and the prediction results are shown in Table 5.

3.3. The Combined Model. In the previous part, the two-weight neural network model and the ARIMA model were used to analyze the number of unemployed and the unemployment rate in China. The two analysis methods are suitable for fitting the series of unemployed laborers and unemployment rate in China. The fitting values of the two models about the sample data are shown in Table 6:

Figures 3 and 4 describe the fitting situation between the number of unemployed and the unemployment rate under a single model. From the figure, it can be inferred that the fitting value of neural network model and time series model is higher than the actual value, but the curves of the three models are similar, showing that the fitting of single model is better. But for the unemployment rate, there is a certain deviation between the fitting curve and the actual curve.

- (1) Initialize the neural network weights;
- (2) Input P training samples in turn, and assuming that the currently inputted learning sample is the p -th training sample;
- (3) Calculate the output sequentially;
- (4) Solve the back propagation error;
- (5) Record the number that has been examined. If $p < P$, turn to (2), if $p = P$, continue to (6);
- (6) Revise the correction formula of the weight value of each layer or the right;
- (7) Recalculate the output of the hidden layer according to the new weight or core value, and if the maximum learning times are reached for each p and P , end the network learning.

ALGORITHM 1: Process of learning of network.

TABLE 1: Normalized data of sample.

	Unemployment	Unemployment rate
1992	-0.65643843	-0.722222222
1993	-0.505828755	-0.444444444
1994	-0.354343843	-0.388888889
1995	-0.239179954	-0.277777778
...
2018	0.801688329	0.277777778
2019	0.839206753	0.277777778
2020	0.825807316	0.277777778
2021	0.919603377	0.277777778

TABLE 2: Prediction results of unemployment based on two-weight neural network.

	Unemployment (ten thousand people)	Unemployment rate (%)
2022	1076.6072	5.8051
2023	1104.8578	5.7644
2024	1074.7537	5.7468
2025	1114.4804	5.7465
2026	1114.0756	5.8420
2027	1081.8054	5.8074
2028	1082.2029	5.7975
2029	1073.9059	5.7892
2030	1093.9167	5.8136

TABLE 3: Fitting results of time series model.

	Unemployment	Unemployment rate
Parameter	AR(1)	AR(1)
Coefficient	0.59849	0.59901
Standard error	0.10207	0.10189
Statistic	4.53	4.54
P value	<0.0001	<0.0001
AIC	399.7305	8.926
SBC	481.4685	9.564

TABLE 4: Residual sequence test.

Latency	Q_{LB} statistic		P value	
	Unemployment	Unemployment rate	Unemployment	Unemployment rate
6	1.4	1.93	0.9260	0.8582
12	7.9	6.15	0.8652	0.7982
18	10.2	8.65	0.7289	0.8321
24	19.2	15.06	0.8729	0.7765

TABLE 5: Forecast results of unemployment based on time series model.

	Unemployment (ten thousand people)	Unemployment rate (%)
2022	1023.087	5.5954
2023	965.6409	5.3656
2024	982.5995	5.6965
2025	970.6785	5.5118
2026	1004.326	5.3388
2027	956.5798	5.6677
2028	1035.294	5.7514
2029	1030.214	5.3738
2030	1023.087	5.5954

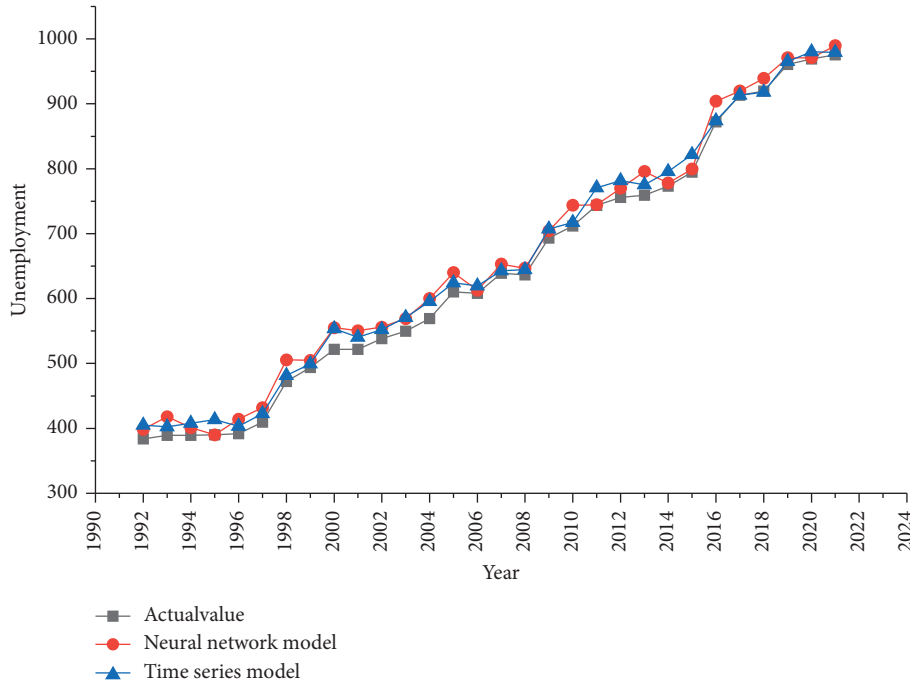


FIGURE 3: Fitting chart of unemployment under single model.

According to the fitting results of the unemployment model, the sum of residual squares between the fitting value and the true value is solved, which is shown in Table 7:

Assuming that y_0 represents the true value, y_1 represents the fitting value of the neural network model, y_2 represents the fitting value of the time series model, W represents the residual value corresponding to the combination model, ω ($0 \leq \omega \leq 1$) represents the weight of the neural network model in the combined model, and $1-\omega$ represents the weight of the time series model in the combined model. The combined model is calculated by the following formula:

$$\begin{cases} W_{\min} = \sum_{k=1}^{i=1} (\omega y_1 + (1-\omega)y_2 - y_0)^2, \\ 0 \leq \omega \leq 1, \end{cases} \quad (10)$$

where k is the number of true values for calculating the residual sum of squares.

After calculation, when ω is 0.4267, the minimum residual error is 21353. Similarly, when ω is 0.598, the minimum residual error of the combined model is 0.6574, which

is smaller than the residual sum of squares fitted by neural network and time series model. According to this weight, the predicted value of the combined model for unemployment is shown in Table 8:

3.4. Other Comparison. Because the fitting effect of the combined model is better than that of the single model, which constitutes the combined model, it is still necessary to compare whether the fitting effect is better for other models. The BP neural network model, the most commonly used network model, is selected as the prediction model. For the number of unemployed, the minimum residual error of BP neural network model fitting is 25,673, and for the unemployment rate of labor force, the minimum residual error is 2.9760. Both of them are higher than the minimum residual error obtained by the combined model in fitting, which shows that in the model built in this paper, there are better fitting results and it seems to be more accurate to predict the unemployment in labor force.

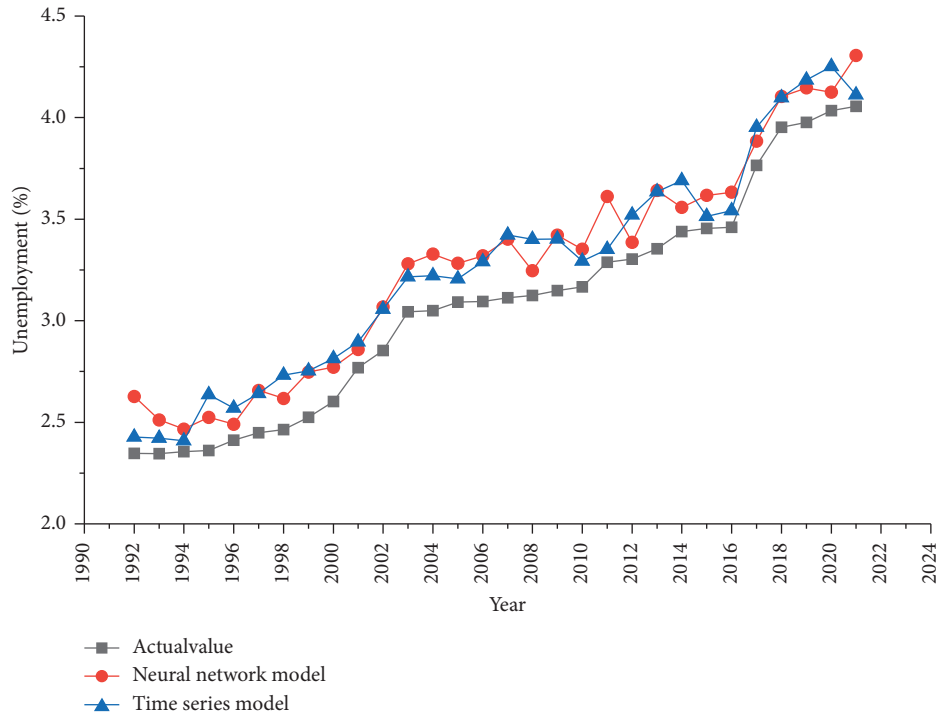


FIGURE 4: Fitting chart of unemployment rate under single model.

TABLE 6: Fitting results of unemployment in labor force under different models.

	Unemployment			Unemployment rate		
	Actual value	Neural network model	Time series model	Actual value	Neural network model	Time series model
1992	363.9	426.06	353.64	2.3	2.59	2.18
1993	420.1	433.63	390.90	2.6	2.51	2.30
1994	476.4	470.81	473.73	2.8	2.55	2.77
1995	519.6	521.65	530.09	2.9	2.68	2.91
...
2018	926	953.03	934.00	4.1	4.13	4.3
2019	952	958.69	951.38	4.1	4.13	4.3
2020	966	985.38	987.56	4.1	4.13	4.2
2021	982	998.52	994.37	4.1	4.13	4.2

TABLE 7: Residual sum of squares of fitting results.

	Neural network model	Time series model
Unemployment	24127	26370
Unemployment rate	0.9736	1.2987

TABLE 8: Prediction of unemployment based on combination model.

	Unemployment (ten thousand people)	Unemployment rate (%)
2022	1039.7289	5.5954
2023	999.6992	5.4756
2024	1010.085	5.7538
2025	1011.403	5.6462
2026	1037.8668	5.8499
2027	1023.6391	5.6047
2028	1038.852	5.3406
2029	987.4474	5.3701
2030	1012.404	5.7903

4. Conclusion

An accurate prediction of unemployment in labor force is helpful to tackle the issue of metropolitan unemployment. In this paper, the data of unemployment obtained by the Chinese National Bureau of Statistics are taken as a statistical sample. A labor unemployment prediction model in light of the combination of the neural network model and time series model is built, while the situation about labor unemployment in China from 2022 to 2030, is forecasted. The results show that the fitting impact of the combined model is superior to that of the single model, which constitutes the combined model. The minimum residuals of the combined model for fitting and the unemployment rate are 21353 and 0.6574, respectively, which are lower than their single models. At the same time, the fitting condition of the combined model is better than that of the commonly used BP neural network model, which has an excellent impact. When the latter is fitted to the unemployed and unemployment rate, the obtained minimum residuals are 25673 and 2.9760, respectively, which are higher than the combined model. The prediction results of the combined model show that from 2022 to 2030, the number of unemployed labor force in China will fluctuate between 999.6992 and 1038.8520, and the unemployment rate will vary between 5.3406 and 5.8499.

Data Availability

The dataset can be accessed upon request.

Conflicts of Interest

The authors declare that they have no conflicts of interest.

References

- [1] Y. Tan and L. Fan, "An analysis of the occupational structure of unemployed people in China in the 1920s and 1930s," *Journal of Northeast Normal University*, vol. 1, no. 255, 2012, in Chinese.
- [2] L. Hong, J. Li, M. Rong, and Y. Song, "Empirical study on unemployment early warning modeling based on regression analysis," *China Soft Science*, vol. 34, no. 5, 2012, in Chinese.
- [3] S. Liu, Y. Dang, and Z. Fang, *Grey Theory and its Application*, Science Press, Beijing, China, 2010.
- [4] G. Zhang and Y. Wu, "Evaluation of enterprise emergency management capability based on grey cluster analysis," *Economic Mathematics*, vol. 28, no. 3, pp. 96–99, 2008, in Chinese.
- [5] A. Jin, "Evaluation of employment promotion effect of unemployment insurance system — taking inner Mongolia autonomous region as an example," *Financial Theory Research*, vol. 26, no. 1, pp. 91–95, 2013, in Chinese.
- [6] T. Jiang, K. Tang, and T. Liu, "Research on the price stickiness of Chinese commodities based on online big data," *Economic Research*, vol. 43, no. 6, pp. 56–72, 2020, Chinese.
- [7] Z. Ren, X. Chai, and Z. Zhou, "China's employment situation report [R/OL]," 2019, <https://MP.weixin.qq.com/s/siqui3infmu0b0s%20%20fzpm-na> in Chinese.
- [8] K. Xu, F. Chen, and X. Liu, "The authenticity of China's economic growth: a test based on global night light data," *Economic Research*, vol. 50, no. 9, pp. 17–29, 2015, Chinese.
- [9] X. Zeng, "Investigating unemployment statistics is a scientific measure to promote higher quality and full employment [EB/OL]," 2018, <http://www.stats.gov.cn/tjsj/sjjd/201804/t20180417%20%201594329.html> in Chinese.
- [10] Y. Zhao, "Thinking about the statistical design of big data," *Statistical Research*, vol. 32, no. 6, pp. 3–10, 2015, in Chinese.
- [11] J. Bailliu, X. Han, M. Kruger, Y.-H. Liu, and S. Thanabalasingam, "Can media and text analytics provide insights into labour market conditions in China?" *International Journal of Forecasting*, vol. 35, no. 3, pp. 1118–1130, 2019.
- [12] L. Breiman, "Random forests," *Machine Learning*, vol. 45, no. 1, pp. 5–32, 2001.
- [13] T. Cajner, L. D. Crane, R. Decker, A. H. Puertolas, C. Kurz, and T. Radler, "Using payroll processor microdata to measure aggregate labor market activity," *FEDS Working paper*, vol. 25, 2018.
- [14] R. Zhang, H. Zeng, and Y. Ye, "Analysis and forecast of registered urban unemployment rate in China based on ARIMA BP model," *Journal of Metals*, vol. 23, pp. 78–80, 2010.
- [15] A. Enriquede, "Constrained forecasting in autoregressive time series models: a bayesian analysis," *International Journal of Forecasting*, vol. 9, no. 1, pp. 95–1083, 1993.
- [16] B. E. Hansen, "Inference in TAR models," *Studies in Non-linear Dynamics & Econometrics*, vol. 28, no. 2, pp. 1–14, 1997.
- [17] D. Van Dijk, P. H. Franses, and R. Paap, "A nonlinear long memory model, with an application to US unemployment," *Journal of Econometrics*, vol. 110, no. 2, pp. 135–165, 2002.
- [18] L. Zhang, *Research on Water Quality Prediction Model Based on RBF Neural Network*, Hebei University of Engineering, Handan, China, 2019, in Chinese.
- [19] H. X. Huan, D. T. Hien, and H. H. Tue, "Efficient algorithm for training interpolation RBF networks with equally spaced nodes," *IEEE Transactions on Neural Networks*, vol. 22, no. 6, pp. 982–988, 2011.
- [20] X. Fan, Li Guang, and X. Zhou, "GA-RBF neural network trajectory tracking control of multi-link manipulator," *Mechanical Science and Technology*, vol. 37, no. 5, pp. 669–674, 2018, in Chinese.
- [21] W. M. Cao and S. J. Wang, "Study of adaptive equalizers based on two weighted neural networks," *International Conference on Computer and Information Technology*, vol. 2, pp. 612–615, 2004.
- [22] H. Zou, W. Chu, and J. Xu, "Application of dual-weight neural network in image segmentation," *Computer Engineering and Application*, vol. 48, no. 13, pp. 163–195, 2012, in Chinese.
- [23] Ji Jin, H. Lu, and S. Wang, "Research on the application of dual weight network in power management," *Microcomputer Information*, vol. 25, no. 1, pp. 197–199, 2009, in Chinese.
- [24] H. Yuan and D. Blind, "Forensics of median filtering in digital images," *IEEE Transactions on Information Forensics and Security*, vol. 6, no. 4, pp. 1335–1345, 2011.
- [25] Z. Hong, H. Hui, and X. Fang, "Application of ARIMA model in prediction of incidence trend of hand, foot and mouth disease in Beijing, Tianjin and Hebei region," *Mathematical Statistics and Management*, vol. 37, no. 2, pp. 191–197, 2018, in Chinese.
- [26] Z. Shen, Y. Wang, and S. Ma, "Application of ARIMA model in predicting the monthly reported incidence of hepatitis B in China," *Chinese Journal of Disease Control*, vol. 22, no. 3, pp. 298–301, 2018, in Chinese.
- [27] Y. Zhang, G. Tang, and W. Wang, "ARIMA model and its application in tuberculosis prediction," *Modern Preventive Medicine*, vol. 35, no. 9, pp. 1608–1610, 2008, in Chinese.

Retraction

Retracted: A Deep Learning-Based Piano Music Notation Recognition Method

Computational Intelligence and Neuroscience

Received 25 July 2023; Accepted 25 July 2023; Published 26 July 2023

Copyright © 2023 Computational Intelligence and Neuroscience. This is an open access article distributed under the Creative Commons Attribution License, which permits unrestricted use, distribution, and reproduction in any medium, provided the original work is properly cited.

This article has been retracted by Hindawi following an investigation undertaken by the publisher [1]. This investigation has uncovered evidence of one or more of the following indicators of systematic manipulation of the publication process:

- (1) Discrepancies in scope
- (2) Discrepancies in the description of the research reported
- (3) Discrepancies between the availability of data and the research described
- (4) Inappropriate citations
- (5) Incoherent, meaningless and/or irrelevant content included in the article
- (6) Peer-review manipulation

The presence of these indicators undermines our confidence in the integrity of the article's content and we cannot, therefore, vouch for its reliability. Please note that this notice is intended solely to alert readers that the content of this article is unreliable. We have not investigated whether authors were aware of or involved in the systematic manipulation of the publication process.

Wiley and Hindawi regrets that the usual quality checks did not identify these issues before publication and have since put additional measures in place to safeguard research integrity.

We wish to credit our own Research Integrity and Research Publishing teams and anonymous and named external researchers and research integrity experts for contributing to this investigation.

The corresponding author, as the representative of all authors, has been given the opportunity to register their agreement or disagreement to this retraction. We have kept a record of any response received.

References

- [1] C. Li, "A Deep Learning-Based Piano Music Notation Recognition Method," *Computational Intelligence and Neuroscience*, vol. 2022, Article ID 2278683, 9 pages, 2022.

Research Article

A Deep Learning-Based Piano Music Notation Recognition Method

Chan Li 

School of Preschool Education, Guangdong Nanhua Vocational College of Industry and Commerce, Guangzhou 510510, China

Correspondence should be addressed to Chan Li; lichen@nhic.edu.cn

Received 20 April 2022; Accepted 20 May 2022; Published 2 June 2022

Academic Editor: Le Sun

Copyright © 2022 Chan Li. This is an open access article distributed under the Creative Commons Attribution License, which permits unrestricted use, distribution, and reproduction in any medium, provided the original work is properly cited.

In the era of rapid development of computer technology, piano music notation and electronic synthesis system can be established using computer technology, and the basic laws of music score can be analyzed from the perspective of image processing, which is of a great significance in promoting piano improvement and research and development, etc. In this paper, the Beaulieu analysis method is used to analyze the piano music notation and electronic synthesis system module. For piano sheet music, sheet music recognition is the main problem in the whole system. Through the digital recognition method, the piano sheet music feature matrix is extracted to get the piano sheet music multiplication frequency points and the envelope function needs to be extracted for better electronic synthesis of piano sheet music. The envelope function can represent the relationship between piano sound intensity and time change and finally achieve the recognition of the piano score. We extract the music information from the digital score, thus converting the music information into MIDI files, reconstructing the score, and providing an audio carrier for the score transmission. The experimental results show that the system has a correct rate of 94.4% in extracting music information from piano scores, which can meet the needs of practical applications and provide a new way for music digital libraries, music education, and music theory analysis.

1. Introduction

In the era of rapid development of computer technology, music and electronic synthesis are widely concerned by musicians, and the use of computer technology allows for the creation of piano music notation and electronic synthesis systems, which are important to promote the improvement and development of the piano, among other things [1]. With the advancement of electronic synthesis technology, computers are producing electronic synthesis scores, especially for the piano, which are very beautiful, and with electronic synthesis, more new scores will appear that perfectly demonstrate the uniqueness of the piano and its application to computer music composition. Computer technology for piano notation and electronic synthesis plays an important role in electronic music; however, computer technology is an important method to achieve piano music notation and electronic synthesis [2, 3].

Piano is a keyboard instrument used in various countries. The sound range of the piano is very wide, and the recognition

of piano music symbols is very important [4–6]. The design of the piano music score and the electronic synthesis system based on the improved linear modulation method is proposed. This method separates harmonic signals according to the edge tone of piano music, transmits the music score, analyzes the continuity of the piano music score signal, and completes the design of the piano music score and the electronic synthesis system, but the performance of this method is poor [7, 8]. The method proposes the design of the piano score setting and the electronic synthesis system based on the audio tampering method, extracts and measures the piano score, enhances the characteristic parameters of the piano score, classifies it, judges whether the score has been tampered, compares the authenticity of the score, and finds that the accuracy of this method for the piano score is low [9–12].

The rapid development and popularity of digital technology and network technology have provided material conditions for the conversion of paper sheet music into music sound dissemination; however, the key problem to be solved is

how to digitize the sheet music, convert the paper sheet music into digital sheet music, and automatically generate the corresponding digital audio to realize the dissemination of music on the Internet. Currently, there are two main methods to realize digital scores: one is to manually input the scores into computers by music professionals through music software (e.g., Cakewalk, etc.), which relies on professionals and has low work efficiency; the other is to use OMR (optical music recognition) technology for an automatic input [13, 14]. OMR integrates image processing, pattern recognition, artificial intelligence, MIDI, and other related technologies and can convert scores within seconds, which greatly improves the work efficiency and is widely used in digital media music libraries, large digital music libraries, reading and playing of robotic scores, computer music teaching, music teaching, and digitization of traditional Chinese scores [15–18].

2. Knowledge in the Field of Music Notation

Notation is a method of recording musical scores. In the course of music development, various notation methods have been created due to the different contents and needs of the music, such as the guqin score for the guqin, the gong score for the gongs and drums, and the five-line score, the short score, and the kongjue score used in our folklore [19]. Notation is very important for creation and performance. Notation must be able to record all aspects of musical activities, including the height, strength, length, musical notation, and expression marks. Notes are symbols that record the progression of notes of different durations [20]. A rest is a symbol that records the interruption of a note of different lengths. In western notation, the common notes and rests are shown in Figure 1.

3. Extraction of Musical Information from Digital Sheet Music Based on Mathematical Morphology

The workflow of digitizing paper sheet music and extracting music information based on the OMR system is shown in Figure 2.

The following is an example of a polyphonic piano score using mathematical morphology to process the digital image of the piano score and extract the musical information from the score. It is unrealistic to extract all the musical information of the score, and the purpose is only to get the sound corresponding to the score, so it is not necessary to identify the large number of performance cues in the score (the sound is originally the result of the performance). However, the basic note pitch, time value, and polyphony must be identified. By combining their information, the sound file (MIDI file) corresponding to this score is created, and the score can be reconstructed using the MI-DI file, as shown in Figure 3.

In the image preprocessing stage, because the background of the pentatonic image is single and the color used for recording music information is single, the binarization image processing technique can be used to transform the

paper pentatonic into a binary image, and at the same time, the pepper-like restless sound is removed by using the mathematical morphology of first erosion and then expansion operation [21, 22].

Let the image to be processed be A , its height be H , and its width be W .

In the music information recognition stage, the Y -projection technique (horizontal statistics) is used to obtain the information of the music score lines. The number of black pixels in each line is counted as a statistical unit, and the array $s[n]$, $1 \leq n \leq W$ is obtained. If the value of each element in $s[n]$ is considered as a grayscale value, the grayscale histogram, called the numerical histogram, can be counted. Obviously, there are two peaks in the numerical histogram, from which we can get the threshold value that divides the two peaks, denoted as f , find the elements in the array $s[n]$ that are greater than f , denoted as a total of m , get the sequence of subscripts of these elements, denoted as R_i , and satisfy $1 < R_i < W, 1 \leq i \leq m, S[R_i] > f$.

Let the width of the spectral line be k ; obviously, there is $k \geq 1$, and there is the property.

If $k = 1$, then $R_{i+1} - R_i \leq 1, 1 \leq i < m$; if $k > 1$, then, there exists i , which satisfies $R_{i+1} - R_i = 1, 1 \leq i < m, t, D$.

Note that there are t different i satisfying conditions $k > 1$ and $R_{i+1} - R_i = 1$.

The distance between spectral lines is defined as d :

$$d = \frac{\sum_{i=1}^{m-1} (R_{i+1} - R_i) - t}{m - t} \quad (1)$$

In this paper, a fragment of Beethoven's "Turkish March" (digital image A) was selected for processing, and the results are shown in Figure 3, where the digital image of the score is shown on the left, the corresponding part on the right is the result of Y -projection, and the numerical histogram is shown on the upper right.

The score and key number can be identified by using the hit and miss operation based on the position of the score line and the distance d from the score line.

The note can be identified using the erosion operation. Let $B1$ be a structural element consisting of black pixels of $(d - k) * (d - k)$, and using the erosion operation, the note head can be identified and the position information of the note head can be obtained. Figure 4 shows the result of the erosion of Tchaikovsky's "Four Little Swans," where the pitch of the note is determined based on the position of the score and the note head. Also, by setting $B2$ as a structural element consisting of $1 * [4 * d + 3 * k]$ black pixels, the stem and bar line of the notes can be obtained by the corrosion operation. Figure 5 shows the corrosion result of Beethoven's "For Alice" [23, 24].

The two operations $A \odot B1, A \odot B2$ can be performed in parallel, and the relationship between the note head position and the note stem position is used to design the structural elements E and F . Using these two structural elements, the temporal information of the notes can be obtained by hitting the hit-miss transformation of the score image.

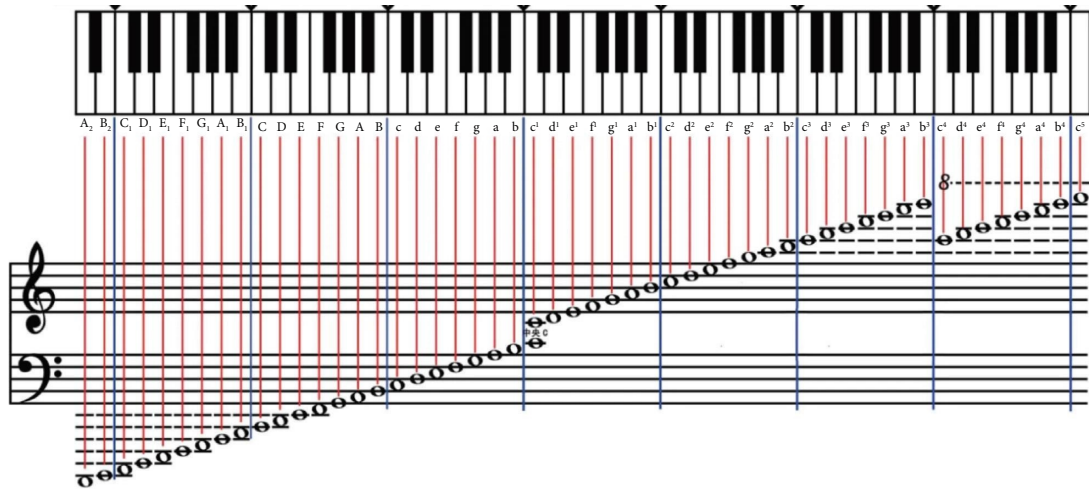


FIGURE 1: Common notes and rests.

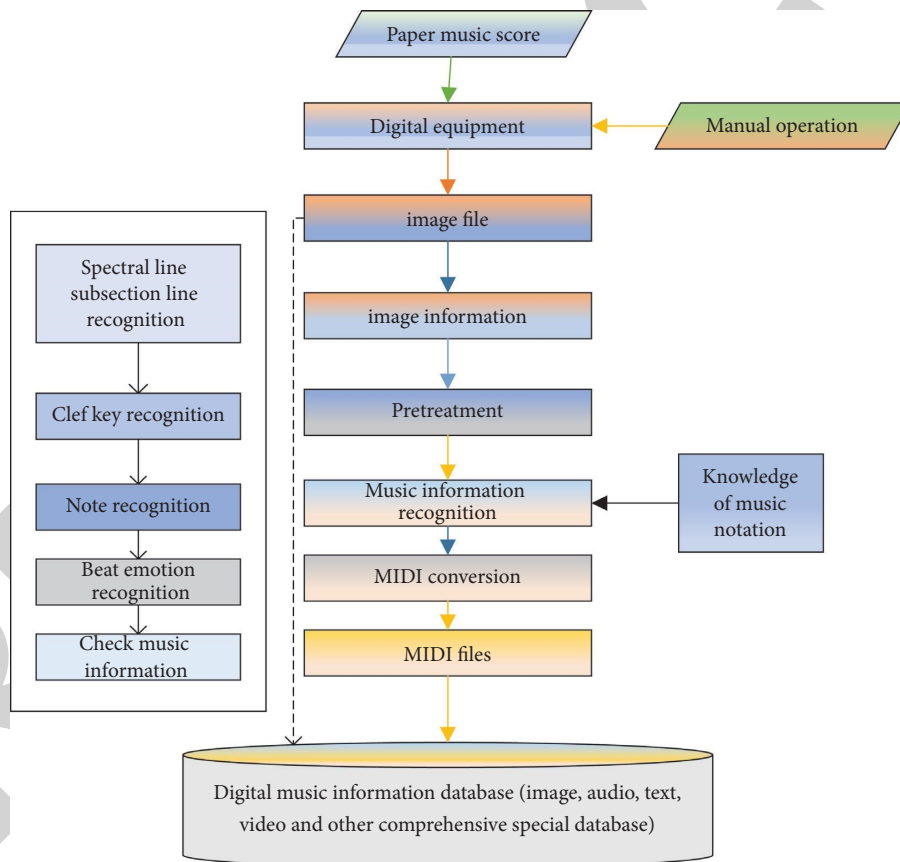


FIGURE 2: Music information extraction process based on the OMR system.

After getting the complete note information, all the notes are divided into bars by bars using bar lines, and each note belongs to one bar only, and the time values in all bars are calculated to determine whether they are equal or not.

Finally, the extracted music information is combined and converted into MIDI files according to the data structure of the MIDI 1.0 protocol.

4. DC-CNN-Based Music Notation Recognition Model

The reduction model proposed in this paper adopts a multilayer convolutional stacking and gate activation function model without a pooling layer similar to PixelCNN. The model is based on an extended causal convolutional

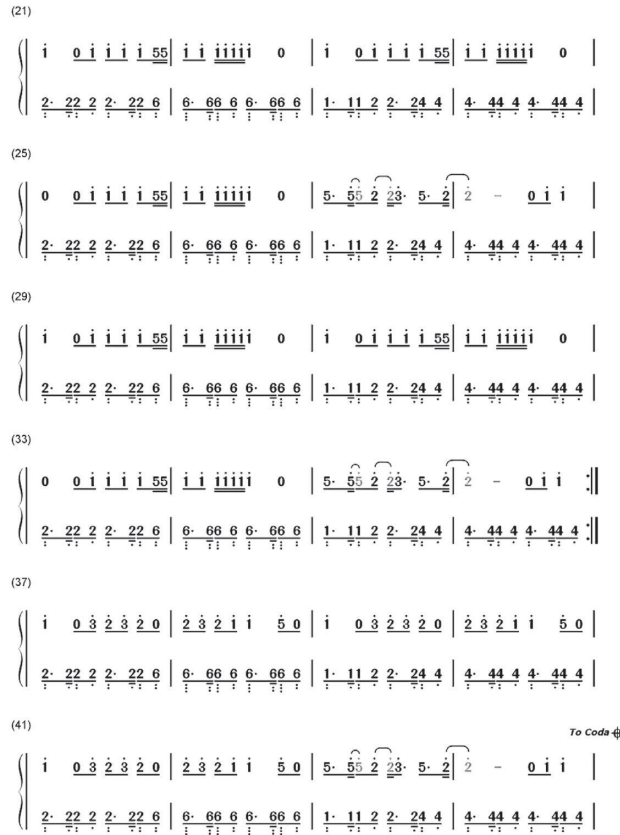


FIGURE 3: Example of Y-projection results and their numerical histograms.

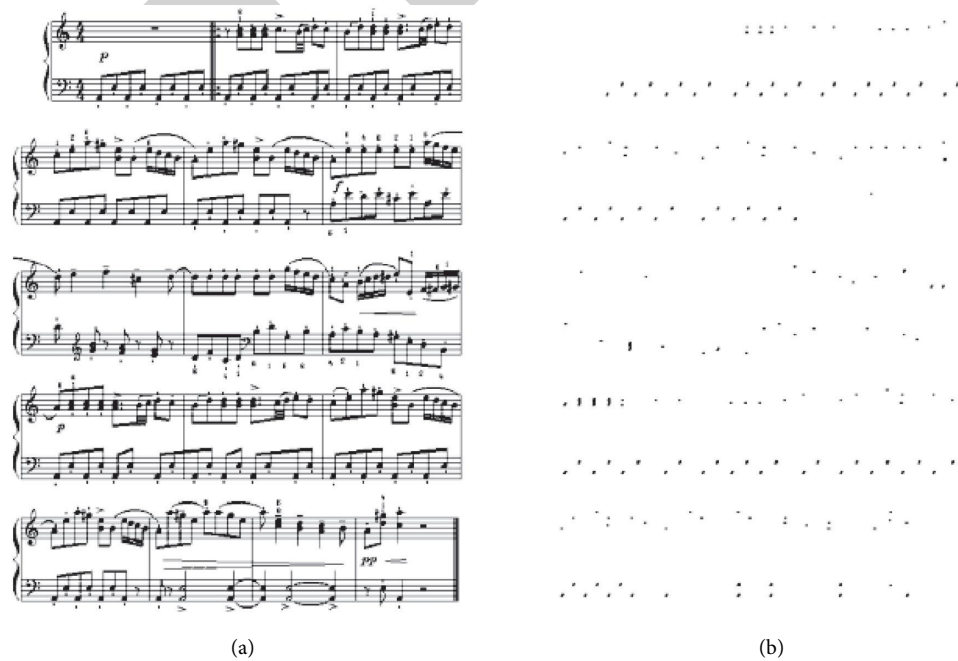


FIGURE 4: The score (a) and the result of the corrosion operation of $A@B1$ (b).

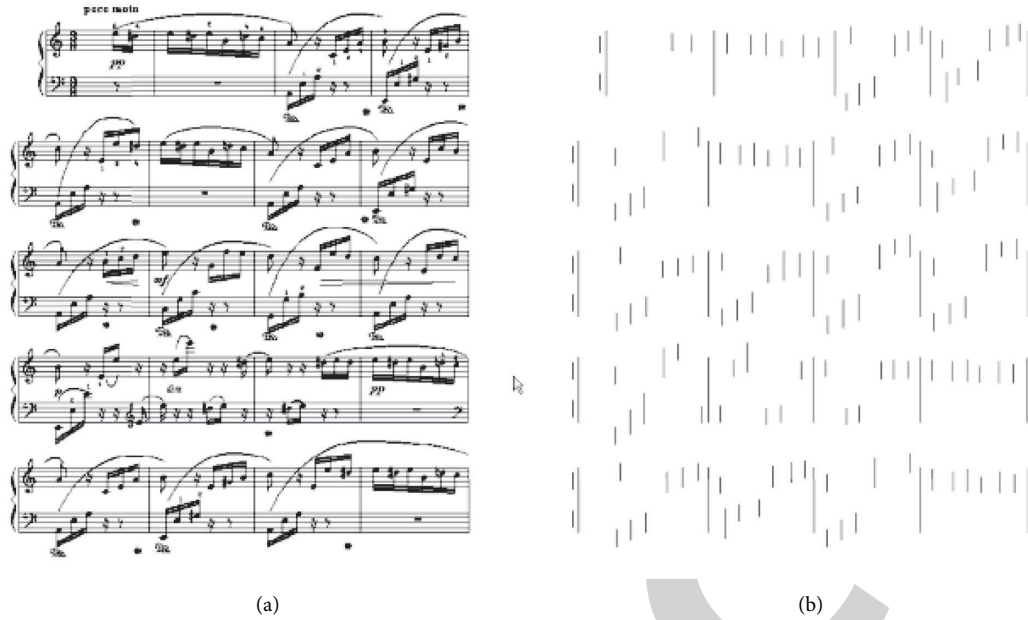


FIGURE 5: The score (a) and the result of the corrosion operation of $A \otimes B2$ (b).

neural network (DC-CNN), and the reduction features are introduced by controlling the gate activation unit of each neuron in the neural network to achieve the reduction of electronic artifacts. The DC-CNN adopted in the model exists in causal convolution and expanded convolution, and the DC-CNN has achieved good results in the speech synthesis model WaveNet [25, 26].

4.1. Expanded Causal Convolutional Neural Network (DC-CNN). Generally, each neuron of a convolutional neural network (CNN) consists of a feature extraction layer responsible for extracting the local features of the previous neuron and a feature mapping layer consisting of multiple feature-mapping planes together required during the computation of that neuron.

As shown in Figure 6, the expanded convolution is combined with causal convolution to form an expanded causal convolutional neural network (DC-CNN). This network can control the speech data to be transmitted backward in an orderly manner in time order but also can expand the perceptual field without increasing the number of layers of the neural network and the size of the convolutional kernel, which makes it have excellent performance in processing speech signal data.

4.2. Structure of the DC-CNN-Based Music Notation Recognition Model. The speech signal x_T is predicted to be reduced by the input speech signal before time T with the reduction factor h . The multidimensional joint variable distribution of speech signal sequences $X = (x_1, x_2, \dots, x_T)$ over a period of time can be expressed as

$$P(X) = \prod_{t=1}^T P(x_t | x_1, x_2, \dots, x_{t-1}, h). \quad (2)$$

As shown in Figure 7, in order to make the music notation recognition sequence generated with the aforementioned conditional probability, the neural network body of the DC-CNN-based music notation recognition model is modeled with a multilayer stack of expanded causal convolutional blocks and a nonlinear mapping is achieved by introducing a gate activation function.

5. Experimental Analysis

A server with a Xeon(R) E5-2620 processor and an NVIDIA Quadro M4000 high-performance computing unit was used to train a reduced model with a 20-layer convolutional neural network. The 20-layer convolutional neural network is divided into 2 convolutional blocks, and the expansion coefficients in each block are (20, 21, 22, . . . , 29) in order. The size of the perceptual field in the reduced model is 128 ms, the number of connected channels in the leap layer is 256, and the initial learning rate is set to 10⁻³. 869 audio segments are selected for the training set, and the test set consists of 2 piano pieces and 503 English speech segments, all of which are sampled at 16 kHz and quantized at 16 bits [27–30].

The average training time per iteration was 5.0316 s for the piano piece and 3.7273 s for the English speech, and the average training time per 1 s speech was about 36.15 s.

5.1. Acoustic Features for Music Notation Recognition. The broadband speech spectrograms of the reduced piano piece and English speech are extracted, and the speech spectral envelope structure is observed, and the vocal pattern features are analyzed. As shown in Figure 8, the restored piano piece is weak in noise, with good audio continuity and a high restoration rate in the low-frequency part.

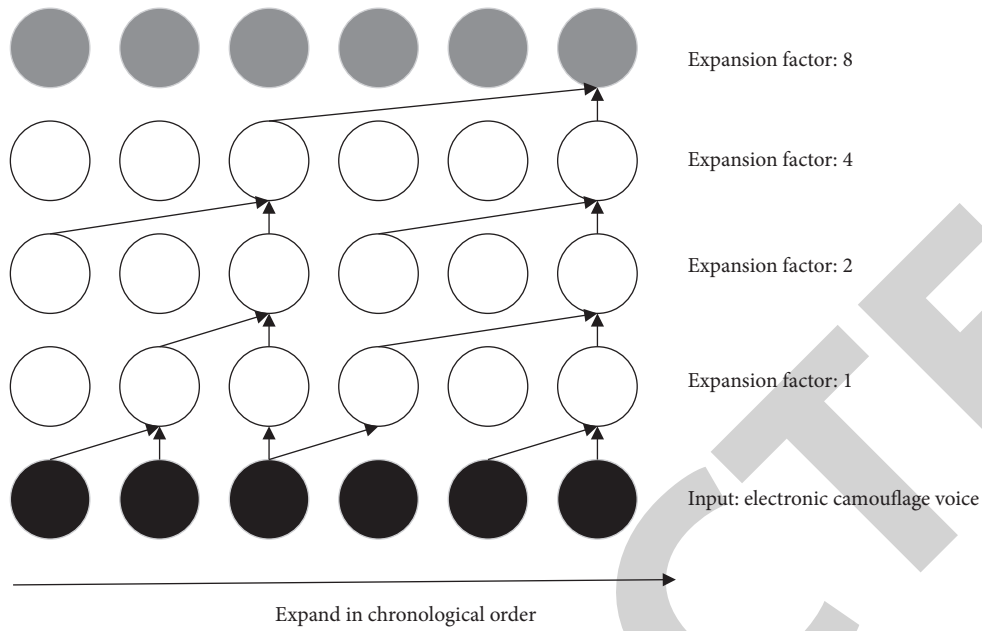


FIGURE 6: Schematic diagram of the expanded causal convolutional neural network.

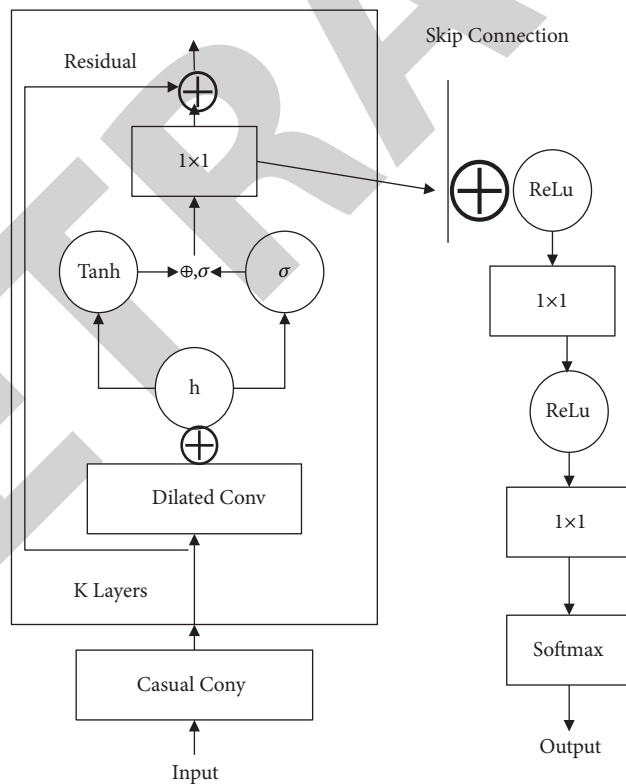


FIGURE 7: Structure of the DC-CNN-based music notation recognition model.

By comparing the broadband spectrograms of piano pieces with those of English speech, we can see that the broadband spectrograms of the model-reduced speech are clear, with obvious waveforms and high reduction rates.

5.2. *LPC Data Analysis for Music Notation Recognition.* Linear predictive coding (LPC) was first applied to speech analysis and synthesis by Itakura et al. in 1967 and has been widely used in speech signal processing technology since then.

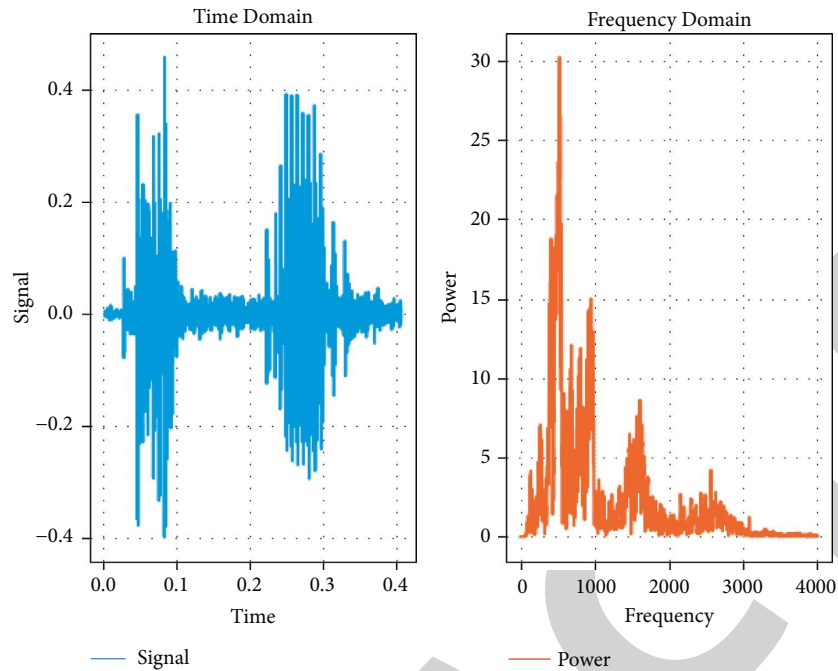


FIGURE 8: Broadband speech spectrogram of music notation recognition and original speech (partial).

As shown in Figures 9 and 10, LPC data were analyzed separately for the reduced piano music and English speech and the resonance peaks of the music notation recognition and the original speech were consistent with each other; the positions of the resonance peaks generally matched, with only deviations in the intensity of the sound. In Figures 9 and 10, the black solid line and gray solid line indicate the LPC data of music notation recognition and original speech, respectively.

The deviation between the arithmetic mean of music notation recognition and the arithmetic mean of the original speech was calculated for these main parameters. From Table 1, it can be seen that the center frequencies of the musical notation recognition of piano pieces and English speech are very close to their corresponding original speech, and the absolute average deviations of the two are 3.79% and 0.97%, respectively; the intensity of the sound is the second, and the absolute deviations of each artifact are within 13%. Only the bandwidth has a certain degree of deviation.

The analysis results prove that the proposed reduction model can achieve high-quality resonance peak waveform recovery; the overall reduction fit rates of the resonance peak parameters of piano music and English speech reach 79.03% and 79.06%, respectively, which are 44.03% and 44.06% higher than the 35% similarity ratio between the electronic artifact speech and the original speech, respectively.

5.3. Human Audiometric Identification of Sameness for Music Notation Recognition. In addition to the electroacoustic instrumentation, 15 volunteers were invited to conduct human ear audiometry to identify the identity of the electronic artifacts and music notation recognition of piano pieces and English speech, respectively, with their corresponding original

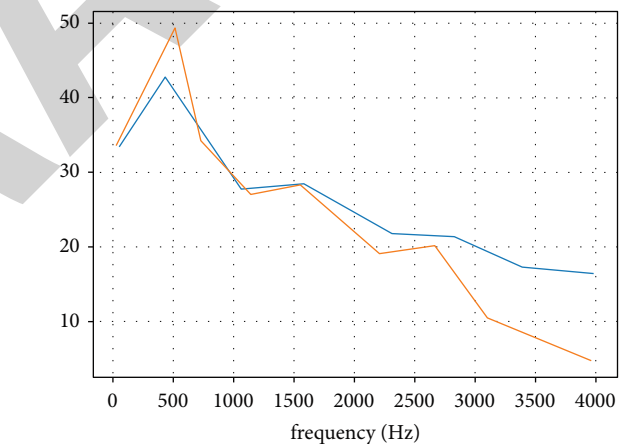


FIGURE 9: Graph of LPC data analysis of music notation recognition of piano pieces with original speech (partial).

speech. In the statistical results listed in Table 2, the percentage of identity between the musical notation recognition and the corresponding original speech for piano and English speech increased significantly compared with the percentage of identity between the electronic artifacts and their corresponding original speech, with a maximum increase of 46.67% and a minimum increase of 26.66%, indicating that the reduction model can effectively reduce the electronic artifacts in the speech and make the musical notation recognition closer to the original speech in terms of human ear primary observation.

Due to the influence of noise, the human auditory recognition results of music notation recognition differed

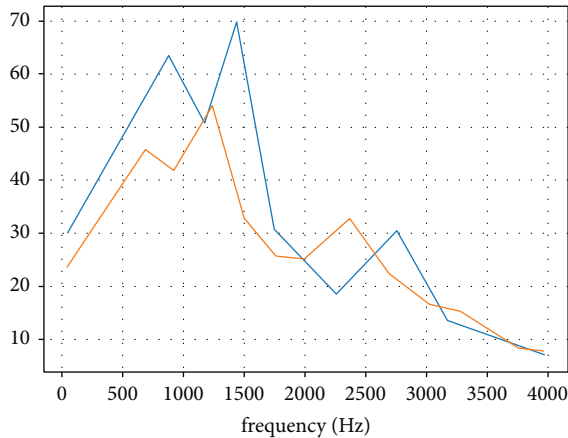


FIGURE 10: Graph of music notation recognition of English speech with LPC data analysis of original speech (partial).

TABLE 1: Deviation of main parameters of music notation recognition and the original speech (unit: %).

Audio	Parameters	Pitch	Rate	Tempo
Piano music	Center frequency	6.29	4.50	0.59
	Bandwidth	26.01	66.69	63.95
	Intensity	-9.99	0.65	-10.12
Overall absolute deviation = 20.97 overall reduction fitting rate = 79.03				
English pronunciation	Center frequency	0.50	-2.11	-0.36
	Bandwidth	49.33	72.01	29.55
	Intensity	-11.22	-10.98	12.88
Overall absolute deviation = 20.97 overall reduction fitting rate = 79.03				

Note: overall restoration fit rate = 100% - overall absolute deviation.

TABLE 2: Speech homogeneity human ear audiometric recognition(unit: %).

Audio	Identity identification	Pitch	Rate	Tempo
Piano music	Electronic camouflage voice	33.22	20.00	45.69
	Restore voice	74.44	60.00	80.11
	Improve proportion	41.01	39.09	33.29
English pronunciation	Electronic camouflage voice	26.68	20.00	26.79
	Restore voice	54.44	67.01	74.44
	Improve proportion	26.77	46.47	47.67

from the vocal pattern characteristics and LPC data analysis, so the percentage of volunteers judged the same source as the original speech during human auditory recognition for the noisy music notation recognition was low. In addition, the quality of the music notation recognition was affected by the μ -law compression and amplification conversion of the original speech and the auditory effect was not good, which made some of the audio less effective in the human auditory recognition experiment.

6. Conclusion

With the advancement of electronic synthesis technology, computer technology for piano notation and electronic synthesis plays an important role in electronic music but also in various musical themes. In this paper, we analyze and study the piano score and electronic synthesis system module using the Beaulieu analysis method. We extract music information from digital scores, thus converting music information to MIDI files, reconstructing the score, and providing an audio carrier for score transmission. The experimental results show that the system has a correct rate of 94.4% in extracting music information from piano sheet music, which can meet the needs of practical applications and provide a new way for music digital library, music education, and music theory analysis.

Data Availability

The experimental data used to support the findings of this study are available from the corresponding author upon request.

Conflicts of Interest

The author declares that there are no conflicts of interest regarding this work.

Acknowledgments

This work was sponsored in part by (1) 2020 Characteristic Innovation Projects of Guangdong Universities, "Research on the Construction of Intelligent Curriculum System for Higher Vocational Preschool Education Majors in Guangdong-Hong Kong-Macao Greater Bay Area" (no. 2020WTSCX217); (2) 2020 Guangzhou Philosophy and Social Sciences Development "Thirteenth Five-Year Plan" Project, "Research and Practice on the Coeducation and Coconstruction Model of Preschool Education," (no. 2020GZGJ249); and (3) 2019 Guangdong Higher Vocational Teachers' Education Steering Committee Education and Teaching Reform Project of "home garden school" integrated early childhood development platform (no. 2019G14).

References

- [1] Y. Zhibin and C. Hong, "Research on household appliances recognition method based on data screening of deep learning," *IFAC-PapersOnLine*, vol. 52, no. 24, pp. 140-144, 2019.
- [2] S. Sigtia, E. Benetos, and S. Dixon, "An end-to-end neural network for polyphonic piano music transcription," *IEEE/ACM Transactions on Audio, Speech, and Language Processing*, vol. 24, no. 5, pp. 927-939, 2016.
- [3] C. T. Cheng-Te Lee, Y. H. Yi-Hsuan Yang, and H. H. Chen, "Multipitch estimation of piano music by exemplar-based sparse representation," *IEEE Transactions on Multimedia*, vol. 14, no. 3, pp. 608-618, 2012.
- [4] C. Wang, "Professional piano education in Chinese piano music culture," *International Education Studies*, vol. 3, no. 1, pp. 92-95, 2010.

Research Article

Analysis of Sentiment and Personalised Recommendation in Musical Performance

Dan Wang 

Huaihua University, School of Music and Dance, Huaihua, Hunan Province 418000, China

Correspondence should be addressed to Dan Wang; wangdanluck@hhtc.edu.cn

Received 22 March 2022; Accepted 14 May 2022; Published 2 June 2022

Academic Editor: Le Sun

Copyright © 2022 Dan Wang. This is an open access article distributed under the Creative Commons Attribution License, which permits unrestricted use, distribution, and reproduction in any medium, provided the original work is properly cited.

Music performance research is a comprehensive study of aspects such as emotional analysis and personalisation in music performance, which help to add richness and creativity to the art of music performance. The labels in this paper in collaborative annotation contain rich personalised descriptive information as well as item content information and can therefore be used to help provide better recommendations. The algorithm is based on bipartite graph node structure similarity and restarted random wandering. It analyses the connection between users, items, and tags in the music social network, firstly constructs the adjacency relationship between music and tags, obtains the music recommendation list and indirectly associated music collection, then fuses the results according to the proposed algorithm, and reorders them to obtain the final recommendation list, thus realising the personalised music recommendation algorithm. The experiments show that the proposed method can meet the personalised demand of users for music on this dataset.

1. Introduction

As an important vehicle to showcase the charm of music, music performance art can play a role in enriching the form of musical expression and enhancing the connotation of music performance art [1]. It is also an important vehicle for the expression of music and the enhancement of its connotation. The addition of modern music aesthetics to music performance art can, on the one hand, inject strong expressive power into the art and, on the other hand, bring audiences the ultimate visual and audio enjoyment [2]. The study of modern music aesthetics can contribute to the progress and innovation of music performance art and can also attract more people to the art of music performance, thus contributing to the overall development of the music industry. The study of contemporary music aesthetics is therefore important and needs to be implemented as soon as possible [3].

Music aesthetics has a long history and culture. As early as the ancient Greeks, Pythagoras and Plato noted the therapeutic effect of musical aesthetics on the human mood and how the good or bad character of music could make the

listener's soul beautiful or ugly [4]. However, they were constrained by their time to explain the reason for this, thus giving a strong mystical dimension to musical aesthetics [5]. As the times have developed, modern musical aesthetics is no longer unknown and has extended into two directions of study, psychological and social [6]. The psychological dimension of modern music aesthetics follows the same direction as that of the ancient Greeks, in that it relates to the psychological knowledge of people's reactions to listening to music in order to find the differences between the general mental activity and the psychological activity of music aesthetics [7]. The social dimension of modern music aesthetics is to relate music to social issues, for example, by analysing the social issues of the time in which the music was composed through the context in which it was written [8].

The art of music performance is a secondary activity of music creation. For the performer, it is a way of presenting the full range of musical achievements in the form of vocal, instrumental, and dramatic music, thus expressing the ideological content of the music [9]. For the listener, the art of music performance is not only an essential way of appreciating and understanding the content and form of music

but also a way of identifying and recognising the different interpretations of music by different music performers through the comparison of different performances. At the same time, different performance styles, genres, and techniques will enhance the audience's understanding of the music, thus giving them a sense of thought and emotional resonance [10].

With the development of information technology and the Internet, people are gradually moving from an era of information scarcity to an era of information overload. In this era, both information consumers and information producers have encountered great challenges: for information consumers, it is very difficult to find the information they are interested in from a large amount of information; according to the different technologies used, music recommendation systems can be broadly divided into three categories: content-based recommendation algorithms, collaborative filtering recommendation algorithms, and hybrid recommendation algorithms [11]. Content-based recommendation algorithms select appropriate items for recommendation based on the item's attribute associations, the location of the item, the item's metainformation (keywords describing the item, in the case of music, album, genre, artist name, lyrics, audio, etc. [12]), and the user's history [13]. However, the keywords used by the user do not correspond well to the item description tags, and converting audio information to digital information leads to increased computation and response time. This content-based approach also ignores the similarity of interests between different users and is therefore not well suited to community-based networks [14].

However, model-based algorithms are usually very time-consuming to build and update, and they do not cover all users as well as memory-based algorithms [15]. Collaborative filtering recommendation algorithms and content-based recommendation algorithms each have their own focus and shortcomings [16]. The main idea of the hybrid recommendation algorithm is to combine the above two recommendation methods in order to make full use of the information of users and resources. One of the most influential systems is the Fab [17] from Stanford University. There are also many research results in China in this area [18].

In order to achieve the recommendation of music that users may be interested in, this paper makes use of the information provided in social networks as much as possible and explores the intrinsic connection between users, tags, and items [19]. First, the two bipartite graphs of the user song and tag song are used to build the adjacency matrices of items and tags, respectively; then, the user vector is used to perform a restart-type random walk on the two adjacency matrices to obtain the list of related songs and related tags of the user; finally, the first N tags of the related tag list are selected. Finally, the top N tags of the relevant tag list are selected and the indirectly associated music set is mined from the tag-song relationship. The indirectly associated music set is used to adjust the ranking of the user's relevant song list and recommend the items with high scores to the user. Experimentation on the corpus collected by Last.fm shows that the proposed method performs better than the collaborative filtering algorithm [20].

2. Theory Related to Recommendation Algorithms

In traditional collaborative recommendation systems, users are required to give explicit ratings to indicate their liking of the item, and these ratings are generally limited and discrete. The memory-based algorithm can be divided into user-based and item-based collaborative filtering recommendation algorithms.

The user-based collaborative filtering algorithm is based on the assumption that if users rate some items similarly, they will also rate other items similarly. The algorithm approximates the target user's ratings of an item based on the ratings of the target user's nearest neighbours (the most similar users). Define the target user a and its unrated item i . Then, predict a 's rating of I as follows:

$$p_{a,i} = \bar{r}_a + \frac{\sum_{u=1}^K (r_{u,i} - \bar{r}_u) \omega_{a,u}}{\sum_{u=1}^N \omega_{a,u}}, \quad (1)$$

where $r_{u,i}$ denotes the rating of item i by the user u , \bar{r}_u and r_u denote the average rating of the user a and the user u , respectively, and $\omega_{a,u}$ denotes the similarity between the user u and the user a .

In contrast, the item-based collaborative filtering algorithm considers that there is similarity in users' ratings of different items, and when it is necessary to estimate users' ratings of an item, it can be estimated using users' ratings of several similar items of that item, as shown in the following equation:

$$p_{a,i} = \bar{r}_i + \frac{\sum_{k=1}^M (r_{a,k} - \bar{r}_k) \omega_{i,k}}{\sum_{k=1}^M \omega_{i,k}}, \quad (2)$$

where \bar{r}_k denotes the average score of the item I and $\omega_{i,k}$ denotes the similarity between the item i and the item k . In practical commercial applications, the user-based collaborative filtering algorithm is more efficient than the item-based one. In the corpus used in this paper, the number of songs is much larger than the number of users, and for efficiency, the user-based collaborative filtering algorithm is used as the comparison experiment in this paper.

Regardless of the method, the similarity between items and items or between users and users is calculated when predicting the score. There are many ways to calculate the similarity, but the most popular Pearson correlation coefficient is used in this paper, as shown in the following equation:

$$\omega_{a,u} = \frac{\sum_{i=1}^M (r_{a,i} - \bar{r}_a)(r_{u,i} - \bar{r}_u)}{\sqrt{\sum_{i \in I_a \cap I_u} (r_{a,i} - \bar{r}_a)^2} \sqrt{\sum_{i \in I_a \cap I_u} (r_{u,i} - \bar{r}_u)^2}}, \quad (3)$$

Obviously, in this algorithm, the more items the users rate together, the higher the similarity. However, assuming that both users only rate the same item, the similarity between the two users calculated by this method is very large, which is not reasonable. In order to reduce this situation, it is set that if the number of items jointly rated by two users, n , is less than the threshold $T\bar{r}$, then the similarity is multiplied by

a factor. In addition, this paper uses the k -nearest neighbour method to select similar users of the target user.

The dataset used in this paper is based on the number of times a user listens to a song to indicate how much the user likes a particular song, rather than an explicit rating of the item by the user based on their own liking. In order to fuse the label information, the similarity between users $\omega(UTr)_{a,u}$, u , and $\alpha\omega(UTr)_{a,u}$ is first calculated from the number of times a user listens to a song and the user's label, respectively, and the sum of the two is used as $\omega_{a,u}$, as shown in the following equation:

$$\omega_{a,u} = \alpha\omega(UTr)_{a,u} + \beta\omega(UTg)_{a,u}, \quad (4)$$

where $\alpha + \beta = 1$.

3. Music Recommendation Algorithm

We present the personalised music recommendation algorithm based on latent semantic mining in the user-tag item starting with the two-part diagram, followed by the latent semantic mining algorithm on the three-part diagram.

3.1. Correlation Matrix for Two-Part Diagrams. The relationship between a user and a song can be represented as a bipartite graph $G1 = \langle U, E1 \rangle$, where the set of vertices U represents the set of users in the recommender system, and if user u_i has listened to music Tr_j , then an edge Tr_j is created between u_i and the number of times the user has listened to the music. Similarly, the relationship between a user and a label can be represented as a bipartite graph $G2 = \langle U, E2 \rangle$, where an edge is created between the user and the label if there is a connection between the two. Then, the above two bipartite graphs are projected onto the dimensions of music and tag, respectively, and the weights of the edges between the node i and the node j after the projection represent the similarity between music (tag) i and music (tag) j . In this paper, the cosine method is chosen to calculate the node similarity, as shown in the following equation:

$$\omega_{i,j} = \frac{|\Gamma_i \cap \Gamma_j|}{\sqrt{|\Gamma_i| |\Gamma_j|}}, \quad (5)$$

where Γ_i is the set of neighbouring nodes of the node i before projection.

3.2. Recommendation Algorithms Based on Bipartite Graphs. The two-part graph-based recommendation algorithm estimates the relationship between users and items by ranking them. The algorithm represents a user node as a vector, and each dimension of the vector represents an item in the association graph, whose value in this paper records the number of times the user has listened to the music node or has used the tag, i.e., the user's interest in the song or tag. The algorithm uses the random walk with the restart model (RWR) to predict the interest of the user node u_i in node Tr_j or Tg_j . The random walk starts from the user node and traverses the whole graph. For any node, the traverser walks

with probability $1 - a$ to the node's neighbouring nodes and returns to the node with probability a to start the walk again. Each walk yields a probability distribution that describes the probability that each vertex in the graph will be visited. This probability distribution is used as input for the next walk, and the process is iterated over and over. The probability distribution of this point converges when the previous and next probability distributions are the same or essentially similar. After convergence, a stable probability distribution is obtained, which represents the closeness of the user node to the project.

For the bipartite graph composed of user music, definition \mathbf{U}_i^{tr} is a user query vector built from the record of songs listened to by user u_i in the training set, with playcount denoting the number of times the user listened to the j th song, and vector q_i is a normalized vector of \mathbf{U}_i^{tr} . Each dimensional element of \mathbf{U}_i^{tr} is defined as shown in the following equation:

$$\mathbf{U}_i^{tr} = \begin{cases} \text{playcount,} \\ 0. \end{cases} \quad (6)$$

The purpose of the algorithm is to obtain the music items that are most closely related to the user. If the association graph consists of N music nodes, the steady-state probability vector $\mathbf{S}_i^{tr} = [S_i^{tr}(1), S_i^{tr}(2), \dots, S_i^{tr}(N)]$ corresponding to u_i is the desired one. After experimental verification, \mathbf{S}_i^{tr} has reached convergence when the number of iterations $t = 10$.

3.3. Semantic Mining. Each user has their own interests, which are presented in the form of tags on their personal description page. When a user listens to music, social media allows the user to tag the item, and these tags reveal the user's perception of the item they are currently listening to. Over time, users' tags become richer and more sophisticated; in addition, a single item can be tagged by multiple users. For these reasons, there is a phenomenon in social media where different users have different perceptions of the same music item and where multiple tags for a music item may imply the same meaning. Therefore, we propose the following idea: a bipartite graph can be used to mine tags with the same meaning; the more tags an item and a user have in common (including similar meanings), the more the user is associated with the item. The workflow of a personalised recommendation system based on potential semantic mining in user-tag music is shown in Figure 1.

The same algorithm is applied to the user-tag bipartite graph to obtain a list of tags associated with the current user. $\mathbf{S}_i^{tg} = [S_i^{tg}(1), S_i^{tg}(2), \dots, S_i^{tg}(M)]$. The difference is that the list of tags obtained by this method does not exclude the tags used by the user itself, as these tags clearly indicate the interests of the user. Then, the N tags with the highest relevance to the user are selected and the music collection corresponding to these tags is extracted, which is defined as the "indirectly related music collection." Finally, the list of song recommendations is modified and reordered according to the song collection, and the final recommendation results are obtained. The weighting equation (7) is used to readjust the song weights:

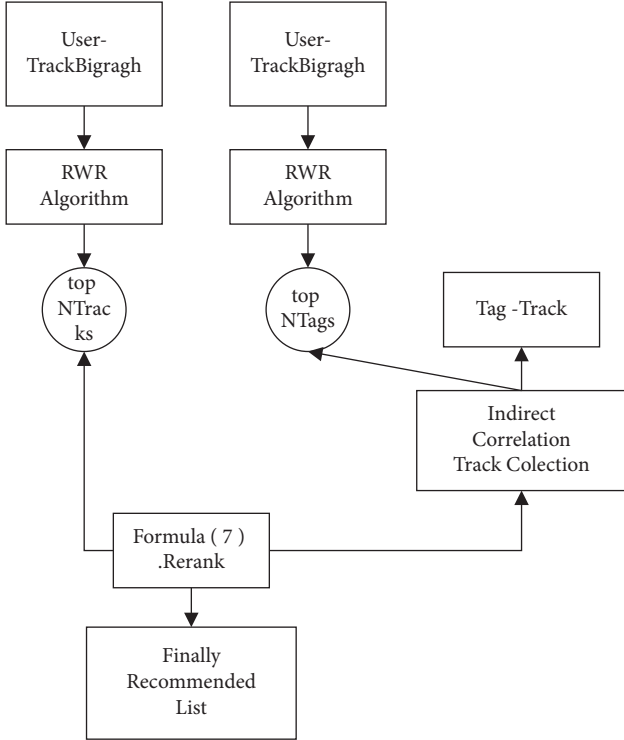


FIGURE 1: Flowchart of the user-tag-music-based recommendation algorithm.

$$\omega'_{i,j} = \omega_{i,j} \times \left(1 + \frac{m}{p}\right), \quad (7)$$

where m denotes the number of occurrences of an identical song corresponding to different tags and p denotes the ranking position of the song in the intersection set (an intersection set is an ordered set of intersections between a collection of indirectly associated music and the original recommendation list by weight). It reflects two ideas: (1) the music corresponding to the tag that is more associated with the user is also more associated with the user; (2) multiple tags associated with the user correspond to the same music, which is more associated with the user. After adjusting the weights, the music is reordered in descending order of weights and top N is rerecommended to users. After counting the data in the dataset, the average number of tags per user is 10. Therefore, the number of relevant tags for a user should be more than the number of tags owned by the user itself, so as to obtain extended tags and more information. However, the more relevant the tags are, the more computationally intensive the algorithm will be and the efficiency of the algorithm will be reduced. Based on the above two points, 30 tags with high relevance to the user will be selected for the calculation in this paper [21, 22].

4. Analysis of Experimental Results

4.1. Last.fm Dataset. Last.fm is a musical social network that allows users to create their own personal pages, make friends, add tags, and record the names and times they listen

to songs. In 2008, the Computer Science and Technology Laboratory at the University of Glasgow collected and extracted a corpus from the music community site Last.fm and made it publicly available for scholarly research. The corpus contains 3,148 users, 30,520 songs, 12,565 tags, and 5,616 friendships among 3,148 users. This paper is a study of this corpus [23, 24].

For each user, all songs in the corpus are divided into three parts: the training set, which is 80% of the songs that the user has listened to; the test set, which is 20% of the songs that the user has listened to; and the set of songs that the user has not listened to.

4.2. Experimental Results and Analysis. In this paper, we compare the user-based collaborative filtering recommendation algorithm with the bipartite graph-based collaborative recommendation algorithm, where each set of experiments is designed to compare the recommendation algorithm with the simple model after adding the label information adjustment. The experiments using the user-music relationship and the experiments adjusted by adding user label information are denoted by UT_r and UT_rTg , respectively. The experiments use $P@N$ as the evaluation index, and for each method, $P@5$, $P@10$, $P@20$, $P@100$, and $P@200$ are calculated for the comparison experiments. Table 1 shows a comparison of the effectiveness of different recommendation algorithms using Last.fm as the dataset [25, 26].

As shown in the last row of Table 1, the two-part graph-based collaborative recommendation algorithm is significantly more effective than the user-based collaborative filtering algorithm in the same dataset, and the RWR algorithm with user labels is optimal. This is because the user-based recommendation algorithm only considers the relevance of the users and ignores the relevance between items.

As shown in Figure 2, after the user-based collaborative filtering algorithm is adjusted with the tag information, the overall recommendation effect does not improve, but the recommendation accuracy rate decreases. The reason for this is that although there are 12565 tags in the dataset, the average number of tags per user is 10 according to the experimental statistics. This means that there are very few edges in the user-tag bipartite graph, making the correlation between users obtained from this bipartite graph very small. When a simple weighted sum is applied to the user association matrix obtained from the user-music bipartite graph, the degree of association between users who are already closely related is reduced to some extent, resulting in a decrease in recommendation accuracy. This is a good algorithm if the density of user labels grows with time. In short, social tagging is still a hot topic and a focus of research.

For the improved bipartite graph-based collaborative recommendation algorithm, the accuracy of the recommendations was improved by adding label information and reordering the recommendations, but the effect was not very obvious. The user's browsing habits are mainly

TABLE 1: Comparison of the experimental results of the RWR and CF algorithms.

Method	Specific methods	MAP	P@5	P@10	P@20	P@100	P@200
CF	UT_r	0.031	0.142	0.124	0.091	0.047	0.035
	UT_rTg	0.021	0.1101	0.0801	0.0701	0.0385	0.0247
RWR	UT_r	0.1024	0.2415	0.3102	0.4412	0.3254	0.2091
	UT_rTg	0.1021	0.2102	0.3251	0.4127	0.3524	0.2021

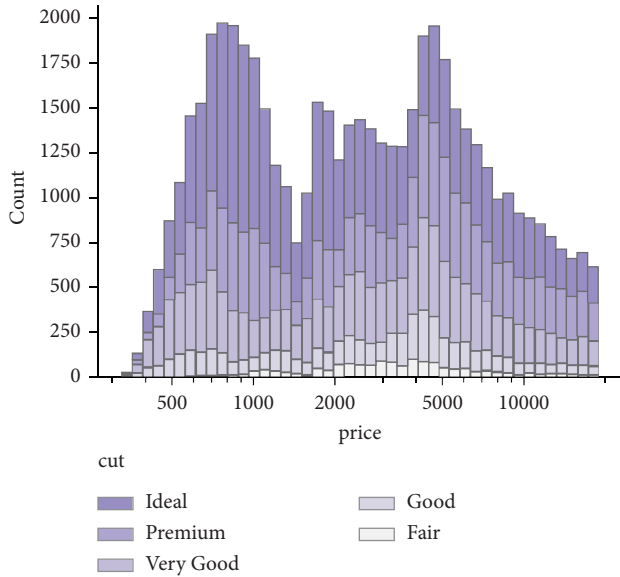


FIGURE 2: Effect of different music recommendations.

focused on the first 20 items in the return list, and the items after that are rarely noticed by the user, so the main goal of this algorithm is to improve the accuracy of the first 20 items in the recommendation list. As can be seen from Figure 3, the algorithm in this paper mainly improves P@10. This is due to the nature of the dataset used. Last.fm has a large number of users and songs, but users rarely tag themselves and their songs, so there are even fewer suitable tags that can accurately locate users and songs. The density of user tags and music tags in the dataset is 4.6×10^{-4} and 3.2×10^{-4} , respectively, making the social tagging information sparse and inevitably mixed with some noisy tags. This makes the application of socially annotated information more difficult. Despite this, the proposed algorithm improves the recommendation results, and as time goes by and the user information and social labeling information become richer, personalised recommendations using community network graphs will be more in line with the interests of users.

As shown in Figure 4, in terms of computational efficiency, given the association matrix TR, the recommendation algorithm based on social annotation and bipartite graphs can obtain a recommendation in $O(n^2)$ time with a small number of iterations. However, one of the problems with this algorithm is that if one node in the association matrix TR is updated, the whole association matrix needs to be updated, which will consume $O(n^2)$ time.

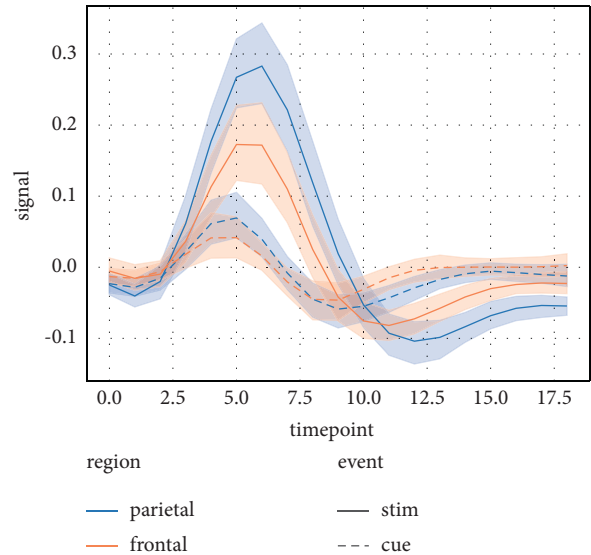


FIGURE 3: Distribution of different levels of music appreciation.

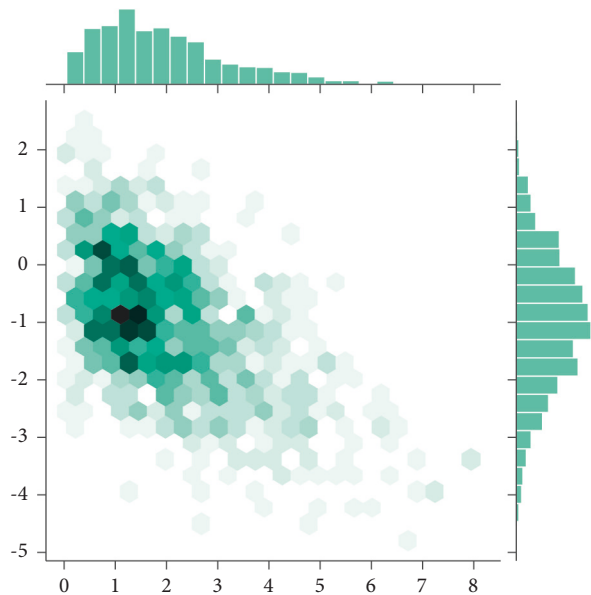


FIGURE 4: Correlation matrix of different music recommendations.

5. Conclusions

The aesthetics of modern music is mainly presented through the art of music performance, which, on the one hand, allows the listener to gain knowledge of the music by learning about

its creator and the context in which it was created. On the other hand, music as an emotional carrier carries the full emotion of the music creator, and by listening to music, listeners can have a spiritual resonance with the music creator across generations. In this paper, the bipartite graph-based collaborative recommendation algorithm is further improved by mining the underlying semantics to make more accurate music recommendations. The results of the comparison with the user-based collaborative filtering algorithm and the bipartite graph-based collaborative recommendation algorithm on the same dataset show that this method is a good strategy for personalised recommendation, especially with the development of Web 2.0 and the increase of tags, this method will show a greater advantage.

Data Availability

The experimental data used to support the findings of this study are available from the corresponding author upon request.

Conflicts of Interest

The authors declare that they have no conflicts of interest regarding the publication of this work.

References

- [1] B. Pang and L. Lee, "Opinion mining and sentiment analysis," *Foundations and Trends in Information Retrieval*, vol. 2, no. 1–2, pp. 1–135, 2008.
- [2] A. Abbasi, H. Chen, and A. Salem, "Sentiment analysis in multiple languages," *ACM Transactions on Information Systems*, vol. 26, no. 3, pp. 1–34, 2008.
- [3] C. Whitelaw, N. Garg, and S. Argamon, "Using appraisal groups for sentiment analysis," in *Proceedings of the 14th ACM International Conference on Information and Knowledge Management CIKM*, pp. 625–631, Gold Coast, Queensland, October 2005.
- [4] M. Taboada, J. Brooke, M. Tofiloski, K. Voll, and M. Stede, "Lexicon-based methods for sentiment analysis," *Computational Linguistics*, vol. 37, no. 2, pp. 267–307, 2011.
- [5] E. Cambria, B. Schuller, Y. Xia, and C. Havasi, "New avenues in opinion mining and sentiment analysis," *IEEE Intelligent Systems*, vol. 28, no. 2, pp. 15–21, 2013.
- [6] M. Ghiassi, J. Skinner, and D. Zimbra, "Twitter brand sentiment analysis: a hybrid system using n-gram analysis and dynamic artificial neural network," *Expert Systems with Applications*, vol. 40, no. 16, pp. 6266–6282, 2013.
- [7] L. Hong and B. D. Davison, "Empirical study of topic modeling in twitter," in *Proceedings of the 1st Workshop on Social Media Analytics*, pp. 80–88, Association for Computing Machinery, New York, NY, USA, July 2010.
- [8] Y. Jo and A. H. Oh, "Aspect and sentiment unification model for online review analysis," in *Proceedings of the 4th ACM International Conference on Web Search and Data Mining*, pp. 815–824, Association for Computing Machinery, New York, NY, USA, February 2011.
- [9] Z. Zhengwan, Z. Chunjong, L. I. Hongbing, and X. Tao, "Multipath transmission selection algorithm based on immune connectivity model," *Journal of Computer Applications*, vol. 40, no. 12, Article ID 3571, 2020.
- [10] Z. W. Zhang, D. Wu, and C. J. Zhang, "Study of cellular traffic prediction based on multi-channel sparse LSTM," *Computer Science*, vol. 48, no. 6, pp. 296–300, 2021.
- [11] X. Ning, P. Duan, W. Li, and S. Zhang, "Real-time 3D face alignment using an encoder-decoder network with an efficient deconvolution layer," *IEEE Signal Processing Letters*, vol. 27, pp. 1944–1948, 2020.
- [12] X. Ning, W. Li, B. Tang, and H. He, "BULDP: biomimetic uncorrelated locality discriminant projection for feature extraction in face recognition," *IEEE Transactions on Image Processing*, vol. 27, no. 5, pp. 2575–2586, 2018.
- [13] L. Sun, Y. Wang, Z. Qu, and N. Xiong, "Beat Class: a sustainable ecg classification system in IoT-based eHealth," *IEEE Internet of Things Journal*, vol. 9, no. 10, pp. 7178–7195, 2022.
- [14] Y. Wang, L. Sun, and S. Subramani, "CAB: classifying arrhythmias based on imbalanced sensor data," *KSII Transactions on Internet & Information Systems*, vol. 15, 2021.
- [15] J. McAuley and J. Leskovec, "Hidden factors and hidden topics: understanding rating dimensions with review text," in *Proceedings of the 7th ACM Conference on Recommender Systems*, pp. 165–172, Association for Computing Machinery, New York, NY, USA, October 2013.
- [16] N. Cook, "Music as performance," in *The Cultural Study of Music*, pp. 206–216, Routledge, Oxfordshire, UK, 2012.
- [17] P. N. Juslin and P. Laukka, "Expression, perception, and induction of musical emotions: a review and a questionnaire study of everyday listening," *Journal of New Music Research*, vol. 33, no. 3, pp. 217–238, 2004.
- [18] B. Sarwar, G. Karypis, J. Konstan, and J. Riedl, "Analysis of recommendation algorithms for e-commerce," in *Proceedings of the 2nd ACM Conference on Electronic Commerce*, pp. 158–167, DBLP, Minneapolis, MA, USA, October 2000.
- [19] S. M. Mudambi and D. Schuff, "Research note: what makes a helpful online review? a study of customer reviews on Amazon.com," *MIS Quarterly*, vol. 34, no. 1, pp. 185–200, 2010.
- [20] Y. Chen and J. Xie, "Online consumer review: word of mouth as a new element of marketing communication mix," *Management Science*, vol. 54, no. 3, pp. 477–491, 2008.
- [21] Y. Zhang and X. Chen, "Explainable recommendation: a survey and new perspectives," *Foundations and Trends in Information Retrieval*, vol. 14, no. 1, pp. 1–101, 2020.
- [22] P. K. Chintagunta, S. Gopinath, and S. Venkataraman, "The effects of online user reviews on movie box office performance: accounting for sequential rollout and aggregation across local markets," *Marketing Science*, vol. 29, no. 5, pp. 944–957, 2010.
- [23] H. Baek, J. Ahn, and Y. Choi, "Helpfulness of online consumer reviews: readers' objectives and review cues," *International Journal of Electronic Commerce*, vol. 17, no. 2, pp. 99–126, 2012.
- [24] N. Archak, A. Ghose, and P. G. Ipeirotis, "Deriving the pricing power of product features by mining consumer reviews," *Management Science*, vol. 57, no. 8, pp. 1485–1509, 2011.
- [25] K. R. Scherer, "Which emotions can be induced by music? what are the underlying mechanisms? and how can we measure them?" *Journal of New Music Research*, vol. 33, no. 3, pp. 239–251, 2004.
- [26] B. N. Macnamara, D. Z. Hambrick, and F. L. Oswald, "Deliberate practice and performance in music, games, sports, education, and professions: a meta-analysis," *Psychological Science*, vol. 25, no. 8, pp. 1608–1618, 2014.

Research Article

Evaluation of Financial Subsidy for Agriculture Based on Combined Algorithm

Kexin Chen^{1,2} and Zhenyu Wang^{1,3} 

¹College of Economics and Management, Shenyang Agricultural University, Shenyang 110866, Liaoning, China

²Business School, Shenyang University, Shenyang 110044, Liaoning, China

³School of Economics, Liaoning University, Shenyang 110036, Liaoning, China

Correspondence should be addressed to Zhenyu Wang; ckx@syu.edu.cn

Received 2 April 2022; Accepted 11 May 2022; Published 1 June 2022

Academic Editor: Le Sun

Copyright © 2022 Kexin Chen and Zhenyu Wang. This is an open access article distributed under the Creative Commons Attribution License, which permits unrestricted use, distribution, and reproduction in any medium, provided the original work is properly cited.

The stable development of agriculture is related to the national economy, and the fragility and foundation of agricultural production determine the inherent requirements of the government for financial support of agriculture. Based on China's policy of agricultural subsidy, in this study, the basic characteristics and classification methods of agricultural subsidies are analyzed, and an evaluation model of agricultural subsidies is established based on a combined algorithm, where the attributes of agricultural subsidies are screened by analytic hierarchy process, and the evaluation process of agricultural subsidies is constructed by data envelopment approach. Moreover, the development level of regional financial subsidies for agriculture is measured by relative efficiency value, and the implementation direction of financial subsidies is evaluated, to enhance the administrative benefits of government finance and deepen the supply-side reform of agricultural financial subsidies, which promote the sustainable development of agricultural insurance and agricultural production.

1. Introduction

Agriculture is the foundation of human existence, which provides necessary conditions for all production activities, and is the foundation of social stability and economic development. However, agricultural production is restricted by the natural environment with inherent weakness, low efficiency, and high risk. At the same time, with the marketization of China's socialist economy, the problem of "agriculture, rural areas, and rural residents" has become increasingly prominent [1–3]. Therefore, in recent years, the Central Committee of the Communist Party of China has issued a series of policies to strengthen agriculture and benefit farmers, where the financial support and protection for agriculture, rural areas, and rural residents have been continuously enhanced. A subsidy is the way that the government provides transferred payment to the production, circulation, and trade of agricultural products through administrative means [4, 5]. It helps to support and protect

the agricultural field, which plays a very important role in promoting agricultural development, healthy operation of national economy, and protecting farmers' interests, and occupies an important position in the economic policies in the world.

However, there are many outstanding problems of supply-side structural contradictions in China's agricultural development at present. Although the total amount of grain is increasing continuously, due to the change in social demand, the imbalance of supply, and demand structure of agricultural products, the costs of agricultural production has been rapidly increased, and the comparative benefits and internal motivation of agricultural development are obviously weakened [6–8]. For a long time, China's cultivated land resources have been relatively short. Under the condition of overexploitation of cultivated land and serious pollution, the pressure on agricultural resources and environment has become greater. In addition, some policies of agricultural subsidy are biased in pertinence due to

imperfect guiding mechanism, which leads to the continuous weakening of agricultural subsidies.

The performance evaluation of agricultural subsidies refers to the use of a method or model to measure the efficiency of agricultural financial subsidies and to measure the achievement of government performance in the process of agricultural financial subsidies or the governance efficiency of government in the process of agricultural development participation [9, 10]. Through the results of performance evaluation, the shortcomings can be found in the process of government administration, which provides guidance for the improvement and stable implementation of the follow-up agricultural financial subsidies.

2. Basis of Agricultural Subsidies

Agricultural subsidies are part of financial subsidies, by implementing specific financial support for some specific projects, and according to certain subsidy basis and standards, the supply and demand structure of agricultural products and agricultural means of production is changed, thus generating the income effect and substitution effect, which is a kind of transfer expenditure of the government with guiding function.

2.1. Basic Characteristics of Agricultural Subsidies. From the connotation of the abovementioned agricultural subsidy policy, it can be known that the characteristics of agricultural subsidy policy mainly include the following points [11–14]:

- (1) The main body of agricultural subsidy policy is the government. No matter what kind of agricultural subsidies are adopted, the subsidy funds will ultimately come from fiscal revenue.
- (2) Agricultural subsidy belongs to the government's transfer expenditure; that is, it is a unilateral and unpaid transfer of funds given by the government to agricultural producers, consumers, or operators. Agricultural producers, consumers, or operators who get agricultural subsidies will inevitably get certain benefits that are not equivalent. A subsidy is a kind of pure benefit increase or cost decrease, so agricultural subsidy must be a behavior of transfer payment.
- (3) The policy objectives of agricultural subsidies are often diversified and phased. There are three main objectives of agricultural subsidy policy: ensuring food security; raising farmers' income level; and realizing the sustainable development of agriculture and rural economy, which will be adjusted correspondingly with the changes in economic development level, industrial structure, and other related economic variables.
- (4) Agricultural subsidies are diversified and flexible. The diversified characteristics of agricultural subsidy policy inevitably require that agricultural subsidy methods have both diversity and flexibility.

2.2. Classification of Agricultural Subsidies. As shown in Figure 1, according to different classification standards, agricultural subsidy policies can be classified in many different ways. In the light of different links of agricultural production, subsidy policies can be divided into productive subsidies, circulation subsidies, and income subsidies, while according to different payment methods, agricultural subsidy policies can be divided into direct subsidy and indirect subsidies [15–17]. Meanwhile, according to different subsidy objects, it can be divided into producer subsidy, consumer subsidy, and operator subsidy.

According to the functional mechanism of agricultural subsidies, this study divides them into four types: income-based agricultural subsidies, cost-based agricultural subsidies, technology-based agricultural subsidies, and price-based agricultural subsidies, as shown in Figure 2.

2.2.1. Income-Based Agricultural Subsidies. It refers to the agricultural subsidy policy that directly subsidizes farmers to increase their income, thus affecting the total expenditure of farmers' agricultural budget. Hook grain direct subsidies and Hook comprehensive agricultural resources subsidies belong to income-based agricultural subsidies, while unhook grain direct subsidy generally takes the taxable farmland or taxable regular production as the basis of grain direct subsidy, where whether farmers actually plant or not, there is subsidy when there is contracted land, which is a kind of inclusive subsidy and belongs to income-based agricultural subsidy policy. The way and mechanism of unhook agricultural comprehensive subsidies are similar to those of unhook grain direct subsidies, so unhook agricultural comprehensive subsidies also belong to income agricultural subsidies.

2.2.2. Cost-Based Agricultural Subsidies. By reducing the cost of grain production, it can mobilize farmers' enthusiasm for growing grain, which promotes the increase in grain production and increases farmers' income level. Unhook direct grain subsidies and unhook comprehensive agricultural subsidies are cost-based agricultural subsidies. Hook grain direct subsidy means that the grain direct subsidy is linked to the current agricultural production and planting situation; that is, linked grain direct subsidy is subsidized according to the actual grain planting area of farmers, and the amount of direct grain subsidy is linked to the planting area. Hook grain direct subsidy can reduce the cost of grain production, mobilize farmers' enthusiasm for growing grain, and thus promote the increase in grain production and farmers' income, so it is a cost-based agricultural subsidy policy. The same argument, hook comprehensive agricultural subsidies also belong to the cost-based agricultural subsidy.

2.2.3. Technology-Based Agricultural Subsidies. It refers to the policy that advances the agricultural production mode through new products and technologies, thus improving the production efficiency of agricultural products. Improved varieties' subsidy, farm machinery purchase subsidies, etc.,

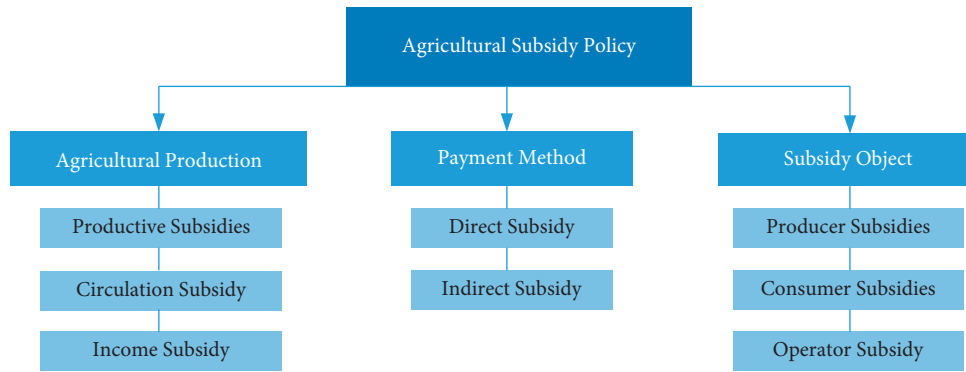


FIGURE 1: Classification of agricultural subsidies.

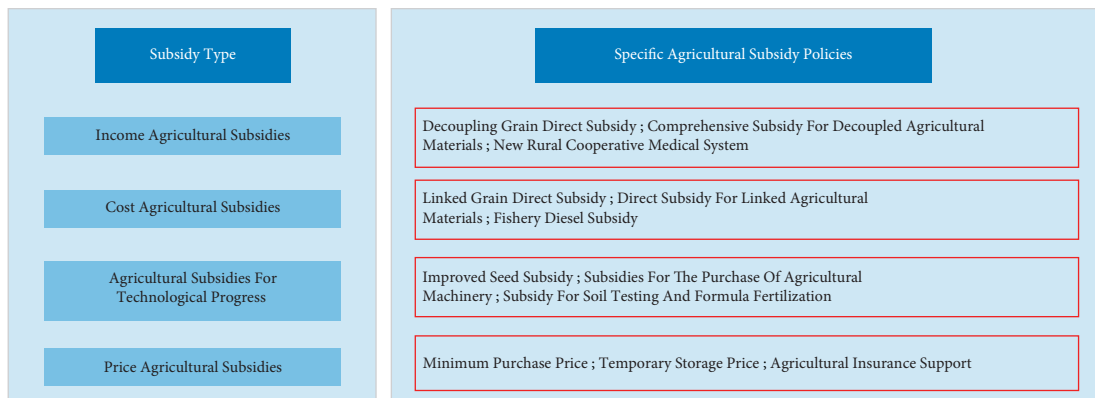


FIGURE 2: Classification of agricultural subsidies based on mechanism of action.

are technology-based agricultural subsidies. Improved varieties’ subsidy is a subsidy given by the government to farmers who use high-quality seed, which guides farmers to adopt new varieties and technologies and improves the output and quality of agricultural products, while farm machinery purchase subsidy is a subsidy given by the government to farmers who purchase farm machinery within the scope specified in the catalogue, which encourages and supports farmers to use advanced and applicable farm machinery, improves the mechanization process, and thus increases the output of agricultural products. Therefore, it belongs to the technology-based agricultural subsidies.

2.2.4. *Price-Based Agricultural Subsidies.* It refers to the policy that promotes the development of grain production, protects farmers’ enthusiasm for growing grain, and guarantees farmers’ income from growing grain by stabilizing or influencing the prices of agricultural products, where the minimum purchase price, temporary purchasing and storage price, etc., are price-based agricultural subsidies.

3. Evaluation Model of Agricultural Subsidy Based on Combined Algorithm

3.1. *Screen of Agricultural Subsidy Attribute Based on AHP.* Analytic hierarchy process (AHP) is a process of modeling and quantifying the decision-making thinking process of

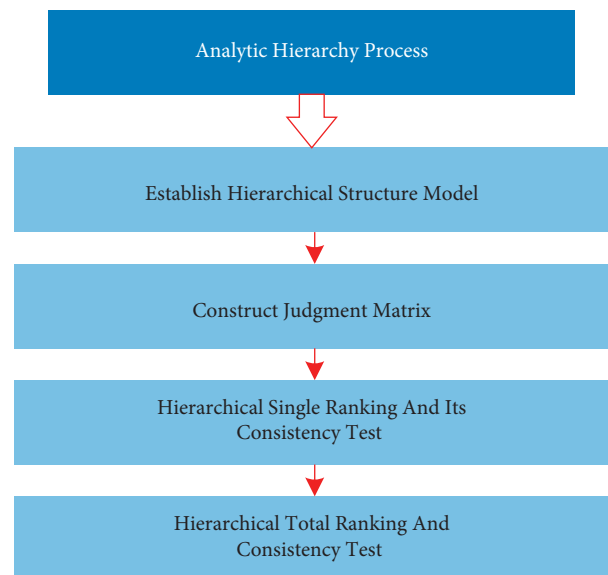


FIGURE 3: Steps of AHP based on classification of agricultural subsidies.

decision-makers on complex systems, which is a hierarchical weight decision analysis method combining qualitative and quantitative analysis, where the decision-maker points out the standard weight of each decision scheme and calculates the ranking of the alternatives using the weight of each decision

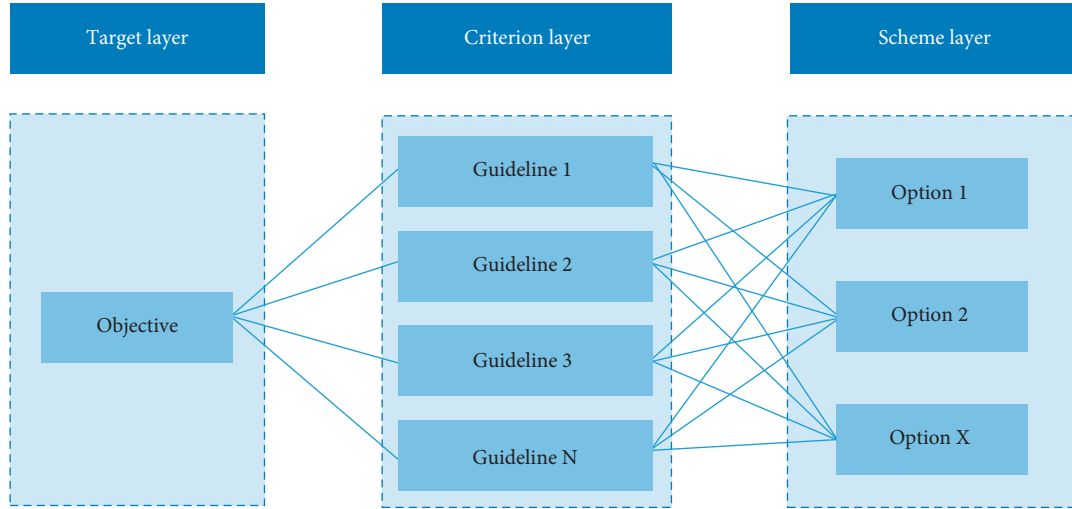


FIGURE 4: AHP hierarchy.

scheme [18]. According to the classification of subsidy mentioned above, the analytic hierarchy process adopted in this study is divided into the steps as shown in Figure 3.

3.1.1. Establish a Hierarchical Structure Model. The targets, factors, and objects are divided into target level, criterion level, and scheme level according to their relationships, and the hierarchical structure is shown in Figure 4.

The decision-makers point out the weight of each scheme and then adopt the weight to calculate the ranking of the advantages and disadvantages of each alternative scheme. When there are many factors at a certain level, the layer can be further divided into sublayer orders of the next order [19].

3.1.2. Construct a Judgment Matrix. The judgment matrix compares each other between pairwise, which is to reduce as little as possible the difficulty of comparing various factors due to different nature, thus improving the accuracy of the decision-making model. Assume that the elements of the judgment matrix are a_{ij} , which is generally given by the Saaty 1–9 scale method, where i and j are horizontal and vertical coordinates, respectively. When using the numerical ratio with practical significance, the construction of the judgment matrix can express the importance degree between pairwise.

3.1.3. Hierarchical Single Sorting and Its Consistency Test. The judgment matrix established in the second step is solved. The formula for characteristic root is as follows: $\bar{A}W = \lambda_{\max}W$. The eigenvector of W is obtained, the hierarchical single sort is solved, and the consistency of hierarchical single sort is checked. Here, you can define the consistency index formula (CI). The formula is as follows, where n is the order of the judgment matrix.

When solving the characteristic root of judgment matrix \bar{A} , which has been established in the second step, the eigenvector W can be obtained in the formula $\bar{A}W = \lambda_{\max}W$. Then, the consistency test of a single order of levels is

implemented; here, the consistency index formula CI is defined as follows, where n is the order of the judgment matrix:

$$CI = \frac{\lambda_{\max} - n}{n - 1}. \quad (1)$$

The consistency ratio (CR) is defined, and its calculation formula is as follows:

$$CR = \frac{CI}{RI} \quad (2)$$

When the consistency ratio $CR < 0.1$, it is considered that the degree of inconsistency of hierarchical single sorting is within the allowable range, and the result has satisfactory consistency; otherwise, the scoring matrix should be reconstructed [20].

3.1.4. Hierarchical Total Sorting and Consistency Test. In this study, it is assumed that the upper level A contains m factors, which are A_1, A_2, \dots, A_m , respectively, and then, the total sorting weights of these elements are a_1, a_2, \dots, a_m , respectively. In addition, it is assumed that the next level B of the elements in the upper level contains n factors, which are B_1, B_2, \dots, B_n , and then the single sorting weights of these elements for factor A_j , including $b_{1j}, b_{2j}, \dots, b_{nj}$ (if B_k and A_j are not related, $b_{kj} = 0$).

If in hierarchy B the consistency index of the hierarchical single ordering of element A_j of some factors is CI_j , then the average random consistency index corresponding to these elements is RI_j , and the calculation formula of the random consistency ratio of the total ordering of element B is shown as follows:

$$CR = \frac{\sum_{j=1}^m a_j CI_j}{\sum_{j=1}^m a_j RI_j}. \quad (3)$$

3.2. Process of Agricultural Subsidy Evaluation Based on Data Envelopment Analysis. As shown in Figure 5, the experimental process of data envelopment method can be divided into four modules [21, 22].

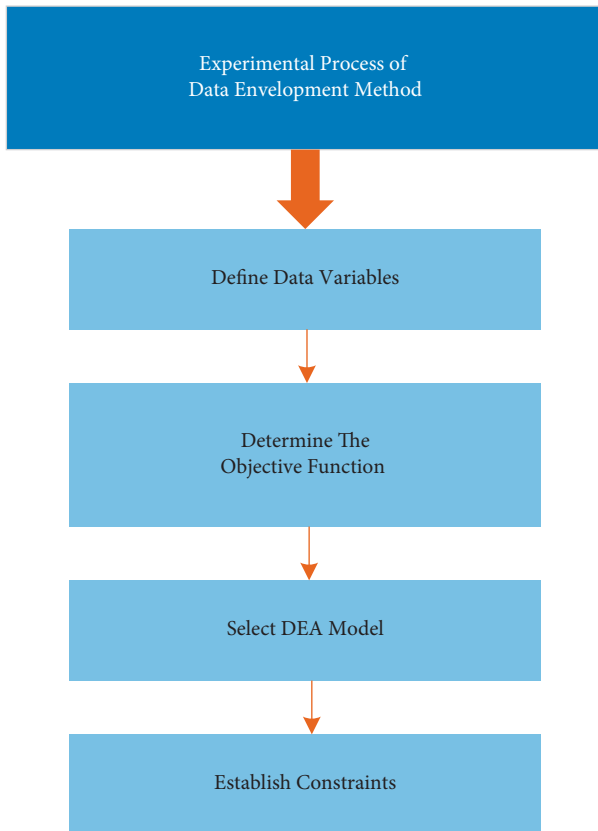


FIGURE 5: Experimental flow of data envelopment method.

3.2.1. Define Data Variables. It consists of two parts: “determine the evaluation target” and “select the decision-making unit.” The evaluation target of this study is to realize performance evaluation of the government’s agricultural financial subsidy policy, whose experimental process mainly refers to DEA, where the input and output of different subsidy categories are selected as decision-making units, including income subsidies, cost subsidies, technology subsidies, and price subsidies.

3.2.2. Determine the Objective Function. It is mainly to establish input and output target system, which is mainly based on a decision-making unit of the module, where the input target and output target systems are based on the selection of AHP indicators, and the indicators in data envelopment method are established as shown in Figure 6.

The determined index system takes the per capita net income of rural residents, the proportion of agricultural employees, the average household population, the per capita common cultivated land area, the amount of chemical fertilizer used per acre, and the effective irrigated cultivated land area as the input indexes of decision-making unit in DEA and takes the agricultural development status, cultivated land endowment, rural labor force, and production factors as the output indexes of DEA decision-making unit.

3.2.3. Choose DEA Model. CCR model is selected as the performance evaluation model of agricultural insurance financial subsidy. CCR model assumes that the production

technology of the decision-making unit is constant to scale return and determines whether the decision-making unit is DEA effective by constructing production front.

3.2.4. Establish Constraints. This module is the regulating variable in the whole performance evaluation process of agricultural financial subsidies, which controls whether the evaluation results are recognized by evaluators or relevant agricultural participants. Model participants can set constraint thresholds according to the existing experience of agricultural subsidies policies. If the evaluation results are accepted, the effectiveness of the DEA evaluation model is recognized and the model evaluation can be implemented. Otherwise, Step 3 is returned, the evaluation model is replaced or the AHP algorithm is adjusted to alter the evaluation index system, and then Step 4 is restarted.

3.3. Evaluation Model of Agricultural Financial Subsidies Based on Combination Algorithm. As shown in Figure 7, the evaluation model of agricultural financial subsidies proposed in this study is mainly divided into two modules: AHP module and DEA module, in which the main function of AHP module is to determine the evaluation index of DEA module; and DEA module establishes the evaluation target system according to the results of AHP, thus determining each decision-making unit and then evaluating agricultural financial subsidies.

The third-order hierarchical model of evaluation index is constructed as shown in Figure 8, in which the first-level index is the evaluation index system of agricultural financial subsidy policy that is also the target level of this evaluation index, the second-level index system includes scale index, efficiency index, influence index, and sustainability index, and the third-level index is the basic index related to the evaluation of agricultural financial subsidy.

The hierarchical total sorting of all judgment matrices is carried out by the index weight values under the single sorting of each level through the consistency test, and the results of the hierarchy total sorting are checked for consistency, as shown in Table 1.

4. Results and Discussion

The decision-making units in this study included income subsidies, cost subsidies, technology subsidies, and price subsidies. According to the results in Table 1, in the ranking of three-level indicators, four indicators with a comprehensive score greater than 0.1 are selected: the amount of financial subsidies, regional per capita income, economic development density, and economic development depth, and the amount of financial subsidies is taken as the input index of DEA decision-making unit, while regional per capita income, economic development density, and economic development depth are taken as the output indicators of DEA decision-making unit. Therefore, the settings of each unit are shown in Table 2.

Relative efficiency is the performance of agricultural insurance financial subsidies related to input index and

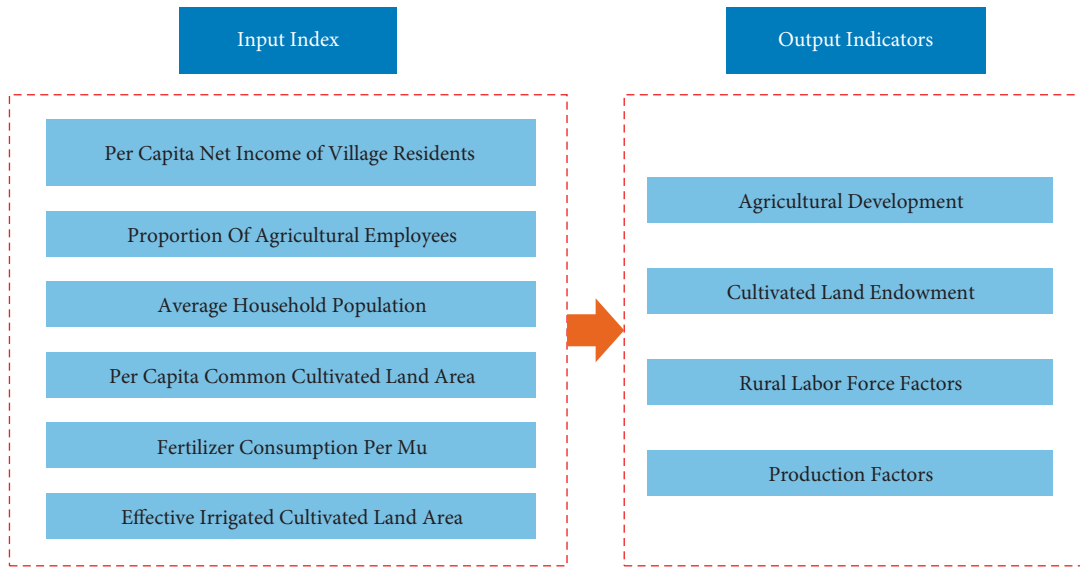


FIGURE 6: Classification of input and output indicators.

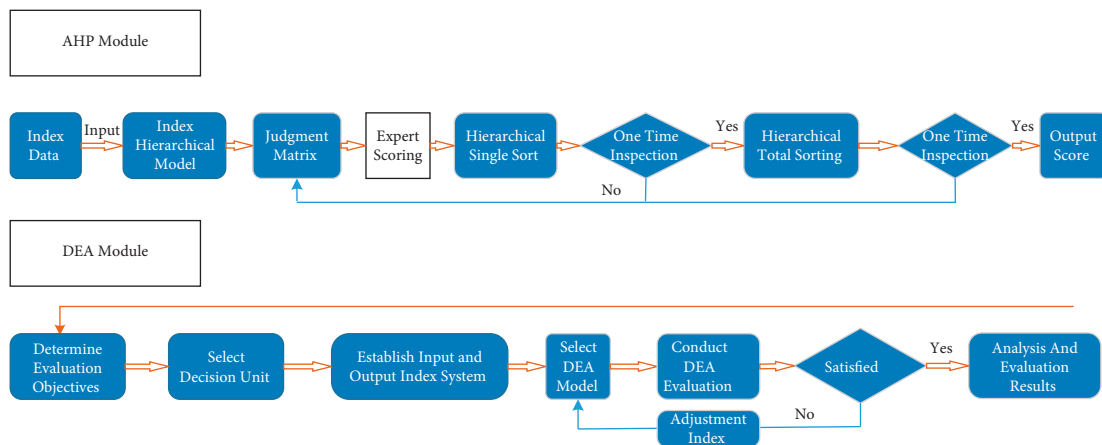


FIGURE 7: Implementation of agricultural financial subsidy model.

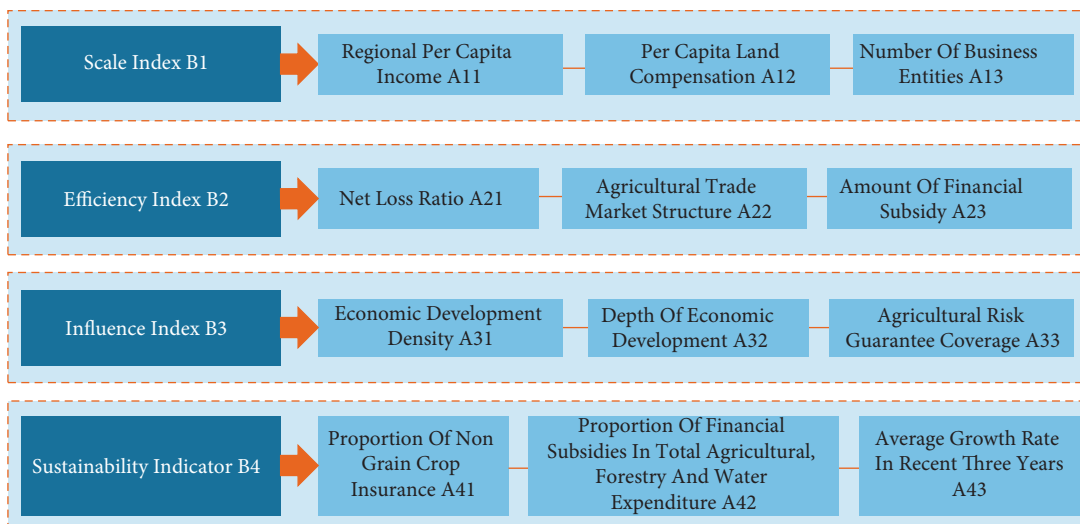


FIGURE 8: Evaluation index of agricultural financial subsidy model.

TABLE 1: Hierarchy total sorting.

<i>W</i>	<i>B1</i>	<i>B2</i>	<i>B3</i>	<i>B4</i>	Weight ranking
A11	0.195	0	0	0	A23
A12	0.074	0	0	0	C11
A13	0.043	0	0	0	C32
A21	0	0.051	0	0	C31
A22	0	0.030	0	0	C12
A23	0	0.214	0	0	C21
A31	0	0	0.146	0	C13
A32	0	0	0.155	0	C22
A33	0	0	0.028	0	C33
A41	0	0	0	0.026	C41
A42	0	0	0	0.021	C42
A43	0	0	0	0.017	C43

TABLE 2: Setting of decision-making unit.

	Invest		Output	
	Amount of financial subsidy	Regional per capita income	Economic development density	Economic development depth
Income-based subsidy	12602.32	282.54	68.44	0.55
Cost-based subsidy	7242.83	127.92	63.22	0.30
Technology-based progress subsidy	9343.28	35.55	25.33	0.19
Price-based subsidy	2794.05	25.97	72.82	0.24

TABLE 3: Calculation results of relative efficiency.

	Input weight vector		Output weight vector		Relative efficiency
	Amount of financial subsidy	Regional per capita income	Economic development density	Economic development depth	
Income-based subsidy	60.89	0.0034	0	0	0.9832
Cost-based subsidy	135.45	0.0075	0	0	0.9583
Technology-based progress subsidy	79.42	0.2190	0	0	0.9023
Price-based subsidy	46.05	0	0.0218	0	0.9345

output index, which can be used as a significant evaluation index to measure the effect of agricultural insurance fiscal subsidies in a certain region. According to the relevant data on agricultural fiscal subsidies provided by the Department of Finance (2015–2021), the input weight vector and output weight vector are calculated and the relative efficiency is calculated according to the evaluation input index and decision unit setting. The results are shown in Table 3.

The above results show that the relative efficiency of agricultural financial subsidies in this region is relatively high, and its comprehensive efficiency exceeds 0.9. Among them, the comprehensive efficiency of income subsidies is the best, which is 0.9832, while that of technological progress subsidies is lower, which is 0.9023. From the relative efficiency index of financial subsidies, the progress of related technologies has effectively promoted the improvement of agricultural productivity. In addition, according to the result of input-output efficiency value, the region still needs to strengthen the innovation of agricultural financial subsidy system, adjust the allocation structure of financial subsidy funds, and improve the allocation management of financial subsidy funds to make

up for the lack of scale efficiency. Moreover, with the implementation of the financial subsidy policy, the stable development of subsidies has better compensated for the economic losses in the process of agricultural production and ensured the healthy production of agriculture.

It can be seen that China is in the new normal period of economy, the market puts forward higher requirements for the quality and safety of agricultural products, and the contradiction between market constraints and resources and environment faced by the development of agricultural industry is prominent, so it is urgent to promote the structural reform of agricultural supply side. Meanwhile, we should strengthen the implementation of technical subsidy policies and advance the rapid development of key agricultural technologies.

5. Conclusion

The evaluation of agricultural subsidies can improve China's agricultural management and promote the agricultural production with sustainable, healthy, and stable

development. Therefore, this study establishes an evaluation model of agricultural subsidies based on a combined algorithm and measures the development level of regional agricultural financial subsidies with relative efficiency value. The evaluation result shows that in the hierarchical total sorting, the comprehensive score of financial subsidy amount, regional per capita income, economic development density, and economic development depth is greater than 0.1, which can be used as the decision-making unit of this model. The relative efficiency of agricultural financial subsidies in this region is relatively high, and its comprehensive efficiency exceeds 0.9. Among them, the comprehensive efficiency of income subsidies is the best, which is 0.9832, while the efficiency of technology-based subsidies is lower, which is 0.9023. The government should adjust the allocation structure of financial subsidy funds and strengthen the implementation of technical subsidy policies, to ensure the healthy production of agriculture.

Data Availability

The dataset can be accessed upon request.

Conflicts of Interest

The authors declare that they have no conflicts of interest.

Acknowledgments

This work was supported by 2019 Social Science Planning Fund Project of Liaoning Province: “Research on the Current Situation and Countermeasures of Liaoning Enclave Economic Development,” and the project number is L19BJL008.

References

- [1] Y. Wang, S. Zhou, and T. Gao, “Analysis and empirical test of the influence effect of China’s agricultural subsidy policy,” *Journal of Social Sciences of Jilin University*, vol. 2017, no. 57, 2017, in Chinese.
- [2] Y. Wang, Y. Cai, and L. Zhu, “Analysis of regional effects and influencing factors of agricultural subsidy policy — taking typical main functional areas such as jingmen huanggang in wuhan, hubei Province as an example,” *Journal of Huazhong Agricultural University (Social Science Edition)*, vol. 2017, no. 1, 2017, in Chinese.
- [3] Ji poop, “Developing agricultural insurance to provide support for farmers’ income to grow steadily,” *Journal of Dongbei University of Finance and Economics*, vol. 2006, no. 02, pp. 75–77, 2006, in Chinese.
- [4] Y. Wang and J. Ge, “Economic analysis of low efficiency of China’s grain subsidy policy,” *Guizhou Social Sciences*, vol. 2009, no. 23, 2009, in Chinese.
- [5] T. Zhang, Y. Guo, and J. Yang, “Retrospect and prospect of China’s agricultural support and protection policy reform for 40 years (part two),” *Rural Work Newsletter*, vol. 2018, no. 21, pp. 24–30, 2018, in Chinese.
- [6] W. Maoqing, *Research on the Implementation Effect of Comprehensive Subsidy Policy for Agricultural Materials in Fujian Province*, Doctoral Dissertation of Fujian Agriculture and Forestry University, Fuzhou, China, 2013, in Chinese.
- [7] S. K. Sharma, “Counter-cyclical payments under doha negotiations: an analysis of agricultural subsidy programme of the US,” *Agricultural Economics Research Review*, vol. 27, no. 2, p. 209, 2014.
- [8] F. Haifa, “Thoughts and measures of agricultural subsidy system reform,” *Agricultural Economic Issues*, vol. 2015, no. 3, 2015, in Chinese.
- [9] N. McCloud and S. Kumbhakar, “Do subsidies drive productivity? A cross-country analysis of Nordic Dairy Farms,” *Bayesian Econometrics*, vol. 23, no. 1, pp. 245–274, 2008.
- [10] J. Yang, Z. Huang, X. Zhang, and T. Reardon, “The rapid rise of cross-regional agricultural mechanization services in China,” *American Journal of Agricultural Economics*, vol. 95, no. 5, pp. 1245–1251, 2013.
- [11] B. Zhou, *Research Progress and Direction of Agricultural Support Policy*, no. 3, 2016, in Chinese.
- [12] W. Wang, *Thoughts on China’s Agricultural Subsidy Policy under the New Situation*, no. 7, China, 2011, in Chinese.
- [13] W. Chang, “Research on regional differential financial subsidies of agricultural insurance in China,” *Agricultural Economics*, vol. 2018, no. 11, pp. 88–89, 2018, in Chinese.
- [14] J. Wang, M. Zhou, and X. Wang, “Discussion on the nature and system construction of rural revitalization planning [J/OL],” *Progress of geographical science*, vol. 2019, pp. 1–9, 2019, in Chinese.
- [15] A. Ma and A. Zhang, “Effect evaluation and optimization of agricultural subsidy policy,” *Journal of Huazhong Agricultural University: Social Science Edition*, vol. 2012, no. 3, pp. 33–37, 2012, in Chinese.
- [16] L. Yang, X. Yuan, and L. Deng, “Efficiency evaluation of local agricultural subsidies in China based on DEA model,” *Local Finance Research*, vol. 2013, no. 4, pp. 25–27, 2013, in Chinese.
- [17] D. Huang, X. Li, and S. Cai, “Research on the impact of agricultural subsidy policy on food security based on Chinese agricultural CGE model,” *[J]. chinese agricultural science bulletin*, vol. 2010, no. 24, pp. 429–435, 2010, in Chinese.
- [18] H. William and X. Ma, “The state-of-the-art integrations and applications of the analytic hierarchy process[J],” *European Journal of Operational Research*, vol. 267, no. 2, pp. 399–414, 2018.
- [19] Z. Jin, D. Li, Y. Jin, and X. Ni, “The performance evaluation index and its weight calculation of local scientific research institutions — a comparative study based on expert analysis and analytic hierarchy process,” *Research on Science and Technology Management*, vol. 29, no. 12, pp. 103–106, 2009, in Chinese.
- [20] W. Pan, Q. Fu, and L. Yang, “Research on the indicators system optimization of China national professional standardization technical committees evaluation based on AHP method,” in *Proceedings of the The 11th International Conference on E-business, Management and Economics*, pp. 232–238, ACM, Beijing China, 15 July 2020.
- [21] Y. Zhang and R. Zhang, “Analysis of financial subsidy efficiency of Jilin agricultural insurance based on DEA model [J],” *Agricultural Outlook*, vol. 17, no. 01, pp. 15–21, 2021, in Chinese.
- [22] Z. Qian, Y. Zhang, and D. Gao, “Evaluation of financial subsidy efficiency of policy-based agricultural insurance based on three-stage DEA model,” *Business Research*, vol. 2014, no. 10, pp. 58–64, 2014, in Chinese.

Retraction

Retracted: A Study on the Impact of Digital Finance on Regional Productivity Growth Based on Artificial Neural Networks

Computational Intelligence and Neuroscience

Received 3 October 2023; Accepted 3 October 2023; Published 4 October 2023

Copyright © 2023 Computational Intelligence and Neuroscience. This is an open access article distributed under the Creative Commons Attribution License, which permits unrestricted use, distribution, and reproduction in any medium, provided the original work is properly cited.

This article has been retracted by Hindawi following an investigation undertaken by the publisher [1]. This investigation has uncovered evidence of one or more of the following indicators of systematic manipulation of the publication process:

- (1) Discrepancies in scope
- (2) Discrepancies in the description of the research reported
- (3) Discrepancies between the availability of data and the research described
- (4) Inappropriate citations
- (5) Incoherent, meaningless and/or irrelevant content included in the article
- (6) Peer-review manipulation

The presence of these indicators undermines our confidence in the integrity of the article's content and we cannot, therefore, vouch for its reliability. Please note that this notice is intended solely to alert readers that the content of this article is unreliable. We have not investigated whether authors were aware of or involved in the systematic manipulation of the publication process.

Wiley and Hindawi regrets that the usual quality checks did not identify these issues before publication and have since put additional measures in place to safeguard research integrity.

We wish to credit our own Research Integrity and Research Publishing teams and anonymous and named external researchers and research integrity experts for contributing to this investigation.

The corresponding author, as the representative of all authors, has been given the opportunity to register their agreement or disagreement to this retraction. We have kept a record of any response received.

References

- [1] J. Li, F. Sun, and M. Li, "A Study on the Impact of Digital Finance on Regional Productivity Growth Based on Artificial Neural Networks," *Computational Intelligence and Neuroscience*, vol. 2022, Article ID 7665954, 7 pages, 2022.

Research Article

A Study on the Impact of Digital Finance on Regional Productivity Growth Based on Artificial Neural Networks

Jia Li,¹ Fangcheng Sun,¹ and Meng Li ²

¹Research Center for Economy of Upper Reaches of the Yangtze River, Chongqing Technology and Business University, Chongqing 400060, China

²School of Tourism and Event Management of Chongqing University of Arts and Sciences, Chongqing 402160, China

Correspondence should be addressed to Meng Li; 20140012@cqwu.edu.cn

Received 15 April 2022; Accepted 14 May 2022; Published 31 May 2022

Academic Editor: Le Sun

Copyright © 2022 Jia Li et al. This is an open access article distributed under the Creative Commons Attribution License, which permits unrestricted use, distribution, and reproduction in any medium, provided the original work is properly cited.

The relationship between financial development and economic growth has become a hot topic in recent years and for China, which is undergoing financial liberalisation and policy reform, the efficiency of the use of digital finance and the deepening of the balance between quality and quantity in financial development are particularly important for economic growth. This paper investigates the utility of digital finance and financial development on total factor productivity in China using interprovincial panel data decomposing financial development into financial scale and financial efficiency; an interprovincial panel data model is used to explore the utility of digital finance on total factor productivity. This involves the collection and preprocessing of financial data, including feature engineering, and the development of an optimised predictive model. We preprocess the original dataset to remove anomalous information and improve data quality. This work uses feature engineering to select relevant features for fitting and training the model. In this process, the random forest algorithm is used to effectively avoid overfitting problems and to facilitate the dimensionality reduction of the relevant features. In determining the model to be used, the random forest regression model was chosen for training. The empirical results show that digital finance has contributed to productivity growth but is not efficiently utilised; China should give high priority to improving financial efficiency while promoting financial expansion; rapid expansion of finance without a focus on financial efficiency will not be conducive to productivity growth.

1. Introduction

The role of financial development in promoting economic growth has been unanimously recognised by scholars at home and abroad [1–3] and it was found that the scale and function of finance can effectively stimulate long-term economic growth as well as total factor productivity growth through their studies. The main emphasis is on a kind of guiding effect of financial development on supply, that is, with the growth rate of economic development as well as the complexity of economic structure, social demand for financial aspects will further stimulate the development of the economy, and financial development and economic growth are causally related to each other [4–6].

A vector error correction model is used to separately verify the existence of a significant positive relationship between financial development and total factor productivity.

There is a large body of research literature, both domestic and international, on the utility of digital finance for economic growth [7]. An endogenous growth model based on digital finance argues that digital finance, as the main carrier of knowledge products, is an alternative to knowledge and innovation. The existence of digital finance overcomes the constraint of diminishing marginal returns to factors and makes long-term economic growth possible [8, 9]. The study points out that the long-term growth rate of the economy is directly proportional to the long-term growth rate of basic knowledge, that the ultimate variable determining the long-term growth rate of basic scientific knowledge is the stock of digital finance in the economy, and that digital finance is the real source of economic growth. Paper [10] concluded that higher education in the eastern, central, and western regions all contributes significantly to the GDP growth rate, but the contribution is distributed in a gradient from higher to lower.

The measurement of total factor productivity growth can be broadly grouped into two categories: the growth accounting approach and the econometric approach [11]. The econometric approach uses various econometric models to estimate total factor productivity, taking into account the effects of various factors in a more comprehensive manner, but the estimation process is more complex [12]. One type of econometric method is the potential output method, also known as the frontier production function method, which has been widely used in current research. These methods use changes in inputs and outputs and the displacement of the frontier production function to measure total factor productivity growth, the key to which lies in the estimation of the frontier production function and the measurement of the distance from observations to the production frontier [13]. Depending on the method of estimating the frontier production function and the distance function, the frontier production function method can be divided into two categories: First, the stochastic frontier analysis (SFA) method, of which the more popular methods are Hildreth and Houck's random coefficient panel models [14] (this is more problematic for empirical studies with small sample sizes); secondly, nonparametric data envelopment analysis (DEA).

2. Data Acquisition and Processing

There is a lot of noise and missing values in all types of real data, which are detrimental from the point of view of training algorithmic models. It is important to carry out the necessary preprocessing before using the data information to improve its quality and make the training of the model smoother, which is important for data mining purposes [15].

2.1. Feature Engineering. For machine learning, feature engineering is required to improve the performance of a model. The original dataset is the input and the relevant dataset used in the future model training process is the output, which can be used to select more desirable training features and thus achieve good results in simple structural models. The current work will address the general process of feature construction and processing, feature selection, and analysis.

Steps are as follows:

- (1) First find the minimum (min) and maximum (max) of the original sample data X .
- (2) Calculate the coefficients k by expressing them as follows:

$$k = \frac{100}{(\max - \min)}. \quad (1)$$

- (3) The data normalized to the interval [0, 100] is obtained y^* as follows:

$$y^* = k(X - \min). \quad (2)$$

In this paper, the data on the number of public cars per 10,000 people ($\times 18$), urban disposable income per capita

($\times 19$), and rural disposable income per capita ($\times 20$) are normalized so that these data become continuous variables in the range of [0, 100].

2.2. Feature Selection. Once the analysis, construction, and processing of the relevant features have been completed, feature selection is performed. Those features that have a high correlation with the target variables are selected and those that are not are eliminated [16]. The selected feature subsets are identified as the input to the model training process, resulting in a significant increase in model accuracy and performance and a corresponding decrease in training time costs.

Fitting a series of features together gives a better fit than fitting individual features, resulting in a significant increase in the predictive power of the model. However, this does not mean that more features will give better results. Random forest is an integrated learning algorithm consisting of multiple decision trees, which is easy to implement, is computationally compact, and has high performance in classification and regression and is one of the representative techniques in current integrated learning technology [17]. If the relevant features are selected by the random forest algorithm, the problem of overfitting caused by a large number of features can be effectively solved on the one hand, and the relatively minor features can be filtered out to make the prediction results more accurate on the other hand.

The key function of the random forest algorithm is to accurately calculate the importance of each feature variable. The basic principle of importance measurement is to calculate the specific contribution of each feature in each tree, to obtain its mean value, and to compare the contribution of different features [18]. The error rate of out-of-bag data is often used as an important metric for evaluation. The importance of each feature is used as an aid in the feature selection process, so that the robustness of the model is increased and the dimensionality of the features is reduced. The actual out-of-bag error rate (i.e., OOB) of each feature allows us to calculate the specific importance of the feature. The specific algorithm is described in equation:

$$FIM_j = \frac{\sum (\text{errOOB2} - \text{errOOB1})}{N}. \quad (3)$$

Here, err OOB2 is the out-of-bag correlation error size when noise is added to feature j in a random way; errOOB1 is the out-of-bag correlation error size under normal conditions; N is the total number of trees in the random forest; j is feature j ; and FIM is the actual rating of the importance of the feature. If noise is added to feature j , it significantly reduces the out-of-bag accuracy level, which means that the final outcome of the prediction is significantly influenced by feature j , and the importance of the feature is high.

3. Estimation of Total Factor Productivity Growth

3.1. Estimation Methodology. This paper draws on the nonparametric DEA-Malmquist index method of [19] to

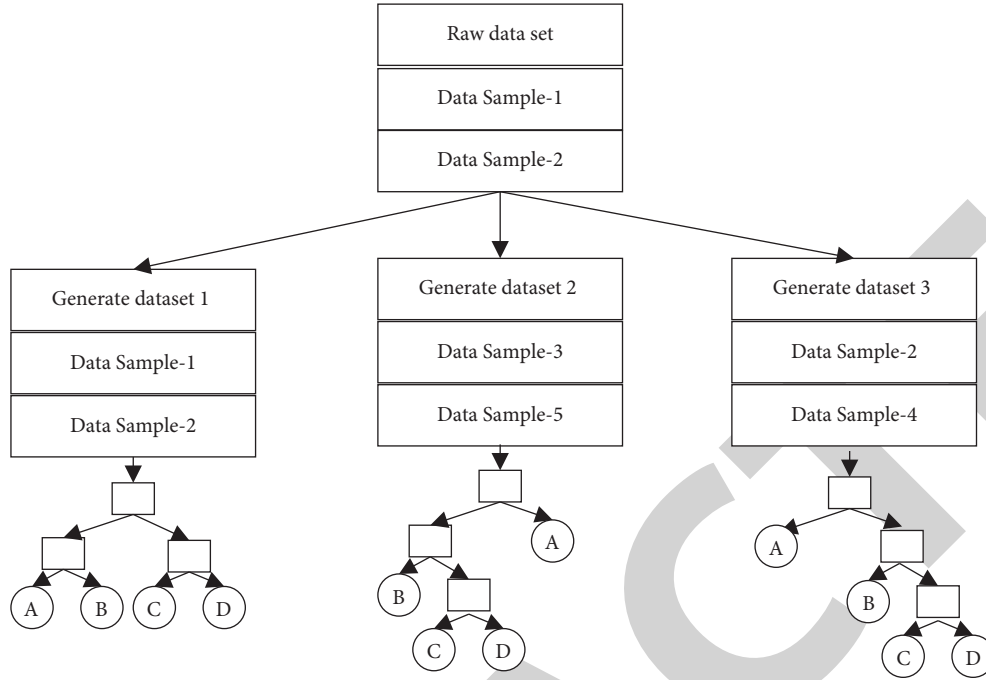


FIGURE 1: Random forest regression model construction process.

estimate total factor productivity growth in China's provinces. Assume that there are H agents, where the input of the h th agent in period t is $x'_h = (K_{ht}, L_{ht})'$, K_{ht} is the capital stock input, and L_{ht} is the labour input. Then the Malmquist index of total factor productivity growth in period $t+1$ for the h th subject is

$$M_h^{t+1}(x'_h, y'_h, x'^{t+1}_h, y'^{t+1}_h) = \left[\frac{D'_h(x'^{t+1}_h, y'^{t+1}_h)}{D'_h(x'_h, y'_h)} \frac{D_h^{t+1}(x'^{t+1}_h, y'^{t+1}_h)}{D_h^{t+1}(x'_h, y'_h)} \right]^{1/2},$$

$$h = 1, \dots, H.$$
(4)

When the total factor productivity growth index is greater than one, it means that total factor productivity growth is positive, while the opposite means that total factor productivity growth is negative.

The Malmquist index has two advantages over traditional growth accounting methods: it eliminates the need for factor price information and economic equilibrium assumptions; and it provides more comprehensive information on total factor productivity growth by decomposing it into two components: efficiency change and rate of technological progress. This method is only applicable to panel data.

4. Construction of a Random Forest Regression Model

The following procedure is involved in the construction of this type of model.

- (1) Samples are randomly drawn from the initial data set in a put-back and unweighted manner, so that each decision tree will be generated from its training set.

- (2) Decision tree can be constructed from each training set; no pruning is required at this point.
- (3) A series of decision trees together form a random forest. The prediction mean of each decision tree forms the final prediction result.

Figure 1 details the modelling process.

4.1. Data Sampling. For each decision tree, it corresponds to a particular training set, so the original dataset is used as the basis for forming the relevant subset of data (so that both have an equal number of decision trees) and thus the random forest is constructed. The corresponding dataset is obtained through a random sampling technique. This technique covers two different types of sampling methods: reverse and one-way.

A specific set of samples is taken from a dataset and not put back when the samples are collected; this is called nonreturn sampling. These include the random number method and the lottery method. The former is the sampling of a data set by means of a random number formation or table. In the case of nonreturn sampling, the initial dataset will continue to get smaller during the sampling process, so that there will be no duplication of samples in the subdataset. In the latter case, the entire data is numbered, the data set is homogenised, and the relevant subsets are extracted by a random method (with a capacity of n). Although the latter method is relatively straightforward, the difficulty of homogenisation increases when there is a large dataset, making the resulting sample unrepresentative.

4.2. Constructing Decision Trees. When constructing a decision tree, it is crucial to choose the random feature

variables appropriately. The basic attributes associated with node splitting are called random feature variables. They are selected in order to reduce the correlation between decision trees and to improve the performance of the random forest algorithm. The random feature variables can be generated by combining input variables or by random selection. The selection process involves a number of indicators, including the Gini index, information gain ratio, and information gain. The CART algorithm is based on the Gini impurity index, which is used as the basis for determining the classification scale for effective selection.

The above process results in a number of decision trees that together form a random forest. The final result of the model is the mean of the predicted values of all the decision trees.

5. Empirical Analysis

5.1. Model Setting. Based on the claim that the level of digital finance can facilitate access to technology, the following equation for total factor productivity growth is proposed:

$$\Delta a_{it} = c + gh_{it} + m \left[\frac{h_{it}(y_{\max t} - y_{it})}{y_{it}} \right] + \theta i, \quad (5)$$

where $y_{\max t}$ represents output per capita in the technologically advanced region and y_{it} is output per capita in period t in region i . h_{it} represents digital finance in period t in region i , a_{it} represents total factor productivity, and i represents individual provincial fixed effects, which are included to control for possible variability between provinces [19, 20]. In this model, total factor productivity growth depends not only on the level of digital finance in the current period, but also on the interaction term between digital finance and the difference in technology levels in technology-led regions. Based on this model, the following model is developed to analyse the utility of digital finance and financial development on total factor productivity growth:

$$a_{it} = c + gh_{it} + m \left[\frac{h_{it}(y_{\max t} - y_{it})}{y_{it}} \right] + \alpha \text{fin}_{it} + \beta_j \text{ctrl}_{jit} + \theta i + \varepsilon_{it}. \quad (6)$$

Among them, fin_{it} is the level of financial development. According to the research of [21–23], the effect of financial scale and financial efficiency on the economy is different. The effect of financial scale and financial efficiency on the economy through the growth of total factor productivity should also be different. Therefore, this paper divides the level of financial development into financial scale and financial efficiency, to explore its role in the growth of total factor productivity. c is the control variable, which is the government intervention, the degree of economic activity, and the degree of opening to the outside world. ε_{ij} is the random disturbance term. Empirical analysis is carried out according to model (4).

Endogenous growth theory holds that digital finance is an important reason to explain total factor productivity. It has a significant impact on total factor productivity through influencing technological innovation ability, technology spillover absorption ability, and other channels.

It can be seen from Table 1 that the statistics of Kao test are statistically significant at the 1% level; that is, the original assumption that there is no cointegration relationship cannot be accepted at the 1% level. Therefore, it is considered that there is cointegration relationship between the two variable systems and regression analysis can be carried out [24, 25].

5.2. Empirical Results. In this paper, fixed and random effects panel data models are used. Table 2 presents the model estimation results, where columns (1) and (2) present the utility analysis of digital finance and financial size on total factor productivity growth, and columns (3) and (4) present the utility analysis of digital finance and financial efficiency on total factor productivity growth. Hausman test p values are 0.9641 and 0.8420, respectively, which are both greater than 0.10; therefore, at the 10% level the original hypothesis that individual effects are correlated with explanatory variables cannot be rejected at the 10% level, so it is decided that a random effects model should be chosen instead of a fixed effects model [26, 27].

From there, the analysis is based on the model estimation results in columns (2) and (4).

The analysis focuses on the core variables to be explored in this paper, digital finance lnhit , the interaction term between digital finance and technology level differences lnhmaxit , and the impact of financial development indicators lnfscit and lnfeft on total factor productivity growth.

Column (2) presents the estimated results of the regression of digital finance and financial scale on total factor productivity growth. From the estimated results, the estimated coefficient of digital finance on total factor productivity growth is 0.0427, which is statistically significant at the 5% level; i.e., when the level of digital finance increases by 1, it will contribute to an increase in total factor productivity growth by 0.0427. Therefore, strengthening education efforts and increasing the level of digital finance are conducive to promoting an increase in total factor productivity growth, which in turn will contribute to economic growth. The interaction term between digital finance and technology level difference is negative (−0.0000984) and statistically significant at the 5% level; i.e., technology level difference shows a negative effect in the effect of digital finance on total factor productivity growth; the greater the technology level difference, the more negative the effect of the utility of digital finance on total factor productivity growth, but this negative effect is relatively small; it can be seen that the use of digital finance in China is relatively inefficient and the ability to learn new technologies is weak. The estimated coefficient of the effect of financial size on TFP growth is −0.177, which is statistically significant at the 1% level, suggesting that every 1 increase in financial size will contribute to a 0.177 decrease in TFP, possibly because state-owned enterprises receive most of the incremental financial resources due to implicit government guarantees, but do not use them effectively or even have idle funds, while the private economy, which operates more efficiently, faces a chronic shortage of capital, and the

TABLE 1: Panel cointegration tests for variables.

	Variable system	Kao test
dfsc	Dtftp dh dhmax dexp dinv dxm dfdi	-5.0319
dfef	Dtftp dh dhmax dexp dinv dxm dfdi	-4.7336

TABLE 2: Panel data model estimation results.

	1	2	3	4
dtfp	dtfp	dtfp	dtfp	dtfp
dh	0.0417	0.0451	0.0524	0.0587
	1.92	2.16	2.47	2.87
dhmax	-0.000906	-0.000947	-0.000847	-0.000874
	-2.02	-2.33	-0.84	-2.13
dfsc	-0.174		-0.1771	
	-4.43		-5.29	
dfef		0.273		0.288
	3.93		4.65	
dexp	0.215	0.223	0.218	0.221
		1.07	1.06	1.09
dinv	-4.83	-0.436	-0.528	-0.458
	-3.5	-3.56	-3.72	-3.67
dxm	-0.0145	0.00047	0.07475	0.0754
	-0.17	-0.13	0.91	0.95
dfdi	-0.0063	-0.00478	-0.00627	-0.00517
	-0.90	-0.74	-0.90	-0.76
_cons	0.00607	0.00419	0.00653	-0.00208
	0.76	0.56	0.07	-0.25
N	318	218	320	320
Adj. R ²		0.165		0.152
rmse	0.104	0.0098	0.105	0.009
Sman test (p value)	1.93	0.09647	3.43	0.8432

expansion of credit is also inflationary, leading to a recession [28, 29].

Column (4) presents the estimated results of the regression between digital finance and financial efficiency on total factor productivity growth. The estimated coefficient is 0.0564, which is statistically significant at the 1% level. The elasticity of financial efficiency to total factor productivity growth is 0.289, which is statistically significant at the 1% level, indicating that an increase in financial efficiency can contribute to an increase in total factor productivity growth, and an increase of 1 in financial efficiency will increase total factor productivity growth by 0.289. In addition, the contribution of financial efficiency in China (0.289) is greater than the inhibiting effect of financial size (0.177), so China should continue to carry out institutional reforms to promote financial efficiency in order to promote economic growth.

For the control variables, the results in columns (2) and (4) are generally consistent. The estimated coefficient of government expenditure on total factor productivity growth is positive, which shows that increased government expenditure is conducive to economic growth and that appropriate government intervention is conducive to healthy economic development. The estimated coefficient for investment is negative and statistically significant at the 1% level, indicating that continued higher investment is not

conducive to increased efficiency in the Chinese economy, thus showing a declining trend in the marginal return to capital. The two variables of foreign development—total exports and imports and FDI—both have negative regression results in column (2), while the estimated coefficients of total exports and imports are positive and FDI remains negative in column (4), and neither is statistically significant, which is somewhat inconsistent with the fact that, according to [14], exports and imports may inhibit firms through the following channels. Firstly, domestic exporters face a latecomer disadvantage in R&D innovation in international markets, with internationally available technologies creating strong patent barriers and barriers to domestic firms’ innovation, which cannot be applied unless domestic firms have a practical innovation. Secondly, international dominant enterprises suppress and control the R&D behaviour of China’s export enterprises, resulting in serious “capture effect” and “lock-in effect,” which will eventually lead to a “ceiling effect” on the technological progress of export enterprises.” Therefore, the impact of international trade on total factor productivity depends on the outcome of the game between positive and negative forces, and only when the technology spillover effect is greater than the “barrier effect” can it significantly contribute to total factor productivity growth. For FDI, some scholars point out that, in places where resources are more scarce, FDI firms as dominant firms may seize the production and market resources of domestic firms, thus causing the decline of domestic firms. Therefore, FDI may have a dampening effect on total factor productivity.

5.3. Comparison of Model Results. The current work has used RF, SVR, and MLR methods in comparative studies. In this work, the bias of the random sampling process is effectively reduced by means of a tenfold cross-validation method, which requires the calculation of the mean value to obtain the relevant indicators for the prediction assessment. In general, the metrics used are RMSE, MSE, and MAPE. The results are given in Table 3.

In the regression models presented in the previous section, the parameters are the default parameters in the computational library and are compared with each other for the same conditions. A detailed analysis of the prediction results shows that these algorithms have generally consistent prediction results, in the following order: MLRRFSVR. The middle of the range of errors was obtained by the random forest method with an error of 22.58%, and the larger error value was obtained by the multiple linear regression method (about 38.98%). Compared to linear regression, prediction by nonlinear regression has relatively better results. It can be found that if a multiple regression correlation model is used, it will have a high training efficiency and convenience, but relatively poor nonlinear learning ability. The random forest approach (based on regression trees) has better prediction results, and the support vector machine regression approach would have better prediction results. In the current work, with a relatively small dataset and a small number of features, the advantages of the random forest approach are difficult to realize, and the factors that affect carbon

TABLE 3: Information on the evaluation indicators of the three models.

Regression model index	RMSE	MSE	MAPE
MLR	0.4714	0.2547	0.3874
SVR	0.7985	0.5674	0.1747
RF	1.534	2.4711	0.2257

TABLE 4: Table of results of the random forest correction model.

Model index	RMSE	MSE	MAPE
RF_opt	1.574	2.547	0.2241
RF_def	1.4527	2.1047	0.1574

productivity in practice are complex, including consumption structure, energy efficiency levels, and differences between cities (regions). By increasing the number of features, the advantages of random forests are highlighted and the accuracy of the prediction results is increased.

The current work uses the best values of the parameters as its input and then compares them with the default parameters, as shown in the data in Table 4.

Here, RF_opt and RF_def are the random forest regression model with optimal and default parameters, respectively. A detailed comparison of the above evaluation metrics shows that, for the case of optimal parameters, the errors of MAPE and RMSE are reduced by about 17.23% and 7.72%, respectively, which means that the prediction results are better than those with default values. The current work is based on the commonly used parameters of interest, and the best values are obtained by a grid search algorithm and optimised, which greatly increases the accuracy.

6. Conclusions

The study points out that the long-term growth rate of the economy is directly proportional to the long-term growth rate of basic knowledge, that the ultimate variable determining the long-term growth rate of basic scientific knowledge is the stock of digital finance in the economy, and that digital finance is the real source of economic growth. The role of financial development in promoting economic growth has been unanimously recognised by scholars at home and abroad. This paper examines the utility of digital finance and financial development on total factor productivity in China using interprovincial panel data. The results show that digital finance has contributed to the improvement of total factor productivity, but there is still a problem of inefficient use of digital finance in China; to this end, this paper proposes a random forest regression model with a related optimisation process. First, a training set is generated using random sampling, and a number of decision trees are constructed using a series of operations to obtain a random forest. The final result of the model is the mean of the predicted values of all the decision trees. The model is then used as the basis for regression. In the current work, the main parameters of the regression function are adjusted in order to optimise the prediction model and improve its accuracy. China should give high priority to improving financial efficiency while promoting financial expansion,

which is detrimental to the growth of total factor productivity, the source of economic growth.

Data Availability

The experimental data used to support the findings of this study are available from the corresponding author upon request.

Conflicts of Interest

The authors declare that they have no conflicts of interest regarding this work.

References

- [1] P. Hajek and R. Henriques, "Modelling innovation performance of European regions using multi-output neural networks," *PLoS One*, vol. 12, no. 10, Article ID e0185755, 2017.
- [2] R. M. Basse, H. Omrani, O. Charif, P. Gerber, and K. Bódis, "Land use changes modelling using advanced methods: cellular automata and artificial neural networks. The spatial and explicit representation of land cover dynamics at the cross-border region scale," *Applied Geography*, vol. 53, pp. 160–171, 2014.
- [3] T. Behrens, H. Förster, T. Scholten, U. Steinrücken, E. D. Spies, and M. Goldschmitt, "Digital soil mapping using artificial neural networks," *Journal of Plant Nutrition and Soil Science*, vol. 168, no. 1, pp. 21–33, 2005.
- [4] J. Bruneckiene, R. Jucevicius, I. Zykienė, J. Rapsikevicius, and M. Lukauskas, "Assessment of investment attractiveness in European countries by artificial neural networks: what competences are needed to make a decision on collective well-being?" *Sustainability*, vol. 11, no. 24, p. 6892, 2019.
- [5] K. Y. Tam and M. Y. Kiang, "Managerial applications of neural networks: the case of bank failure predictions," *Management Science*, vol. 38, no. 7, pp. 926–947, 1992.
- [6] H. Gómez and T. Kavzoglu, "Assessment of shallow landslide susceptibility using artificial neural networks in Jabonosa River Basin, Venezuela," *Engineering Geology*, vol. 78, no. 1–2, pp. 11–27, 2005.
- [7] N. I. Lomakin, O. A. Golodova, and O. M. Burdyugova, "Application of neural networks to studying the impact of the Russian central bank's monetary policy," in *Proceedings of the International Scientific Conference "Far East Con" (ISCFEC 2018)*, pp. 1245–1248, Atlantis Press, Amsterdam, Netherlands, January 2019.
- [8] B. A. Story and G. T. Fry, "A structural impairment detection system using competitive arrays of artificial neural networks," *Computer-Aided Civil and Infrastructure Engineering*, vol. 29, no. 3, pp. 180–190, 2014.
- [9] L. Cavaleri, P. G. Asteris, P. P. Psyllaki, M. G. Douvika, A. D. Skentou, and N. M. Vaxevanidis, "Prediction of surface treatment effects on the tribological performance of tool steels using artificial neural networks," *Applied Sciences*, vol. 9, no. 14, p. 2788, 2019.
- [10] Y. Huang, L. J. Kangas, and B. A. Rasco, "Applications of artificial neural networks (ANNs) in food science," *Critical Reviews in Food Science and Nutrition*, vol. 47, no. 2, pp. 113–126, 2007.
- [11] E. Yesilnacar and T. Topal, "Landslide susceptibility mapping: a comparison of logistic regression and neural networks

Research Article

Intelligent Control Method for Loss Distribution Balance of High-Power Photovoltaic Grid-Connected Inverters

Yi Xu ^{1,2}, ErYong Zou,¹ and FengPing Tang¹

¹Jiaxing Nanyang Polytechnic Institute, Jiaxing, Zhejiang 314000, China

²Key Laboratory of Control of Power Transmission and Conversion (SJTU), Ministry of Education, Shanghai 200240, China

Correspondence should be addressed to Yi Xu; xuyi@jxny.edu.cn

Received 24 March 2022; Revised 15 April 2022; Accepted 25 April 2022; Published 31 May 2022

Academic Editor: Le Sun

Copyright © 2022 Yi Xu et al. This is an open access article distributed under the Creative Commons Attribution License, which permits unrestricted use, distribution, and reproduction in any medium, provided the original work is properly cited.

Aiming at the problem that the loss distribution balance control effect of high-power photovoltaic grid-connected inverter is poor due to the complex loss factors, this paper proposes a loss distribution analysis and balance intelligent control method for high-power photovoltaic grid-connected inverter. The topology structure of high-power photovoltaic grid-connected inverter is constructed and the overall control scheme is designed. The loss of inductance, resonant frequency, harmonic attenuation, and damping resistance in the circuit of PV grid-connected inverter is analyzed, respectively. On this basis, a two-stage loss control model of high-power PV grid-connected inverter is constructed, and the generalized linear decision rule is adopted to schedule PV power supply and fluctuating load. A two-stage loss control model for high-power photovoltaic grid-connected inverter was established and the optimal loss control value was obtained. Experimental results show that the proposed method can accurately suppress voltage and current losses of grid-connected photovoltaic inverters and has strong resonance resistance and robustness.

1. Introduction

In recent years, photovoltaic power generation has accounted for an increasing proportion of the installed capacity in the power system. As a kind of distributed generation, photovoltaic power generation has also been widely studied. According to different needs and applications, photovoltaic grid-connected power generation systems have different structures and power levels, from a single photovoltaic module to a million-level photovoltaic module [1]. With the continuous improvement of requirements for grid-connected voltage level, efficiency, and grid-connected current quality of photovoltaic grid connected inverter, multilevel photovoltaic grid-connected inverter is bred [2–4]. The multilevel conversion technology can avoid the direct series connection of power switching devices. It has the advantages of high output voltage, low harmonic content, small switching stress, low voltage change rate, and low switching frequency. It can be applied to the fields of medium voltage high-power AC speed regulation, high-voltage DC transmission, static var generator, and new energy

power generation [5–7]. When the large-scale photovoltaic power generation system is connected to the grid, the impact on the power quality of the power grid and the operation conditions such as the separation speed of the power grid in case of failure of the photovoltaic power generation system itself has become an important focus [8]. The research on the intelligent control method of loss distribution balance of high-power photovoltaic grid-connected inverter has become the main research content in the current field.

At present, relevant scholars have made research on the loss distribution of high-power photovoltaic grid-connected inverters and proposed an intelligent control method for the balance of loss distribution of photovoltaic grid-connected inverters. Reference [9] presents a control method for a two-stage single-phase grid-connected cascaded H-bridge photovoltaic inverter based on a hybrid control strategy of optimal third harmonic injection and limited power maximum power point tracking. The optimal third harmonic injection can improve the modulation range; limited-power maximum-power point tracking algorithm can limit the power of the photovoltaic module of the unit where the

maximum modulation ratio is located under the condition of exceeding the third harmonic compensation range, so that it can continue to meet the grid-connected operating conditions. Reference [10] proposes a direct power control method based on nonlinear disturbance observer. In the photovoltaic grid-connected power generation system, when the output power of photovoltaic panels suddenly changes, the DC side bus voltage fluctuates greatly. If the control is improper, it will directly affect the normal operation of the system. This method does not need to add additional sensors. The disturbance observer is used to observe the output power of the photovoltaic panel in real time, and it is added to the inner power loop as a feedforward value, so that the given power inner loop contains the input power information. For the power inner loop, the control input is redefined, and the synchronous rotation coordinate transformation is omitted. The design process of the observer and the power inner loop is introduced in detail, and the parameter tuning method of the inner and outer loops is given.

The above methods all provide a certain theoretical support for the control of high-power photovoltaic grid-connected inverters, but the above methods do not fully consider the loss distribution of high-power photovoltaic grid-connected inverters, and the control effect on the loss of photovoltaic grid-connected inverters is relatively low. Difference. For this reason, this paper proposes an intelligent control method for the loss distribution balance of high-power photovoltaic grid-connected inverters, fully analyzes the inductance, resonant frequency, harmonic attenuation, and damping resistance losses in the photovoltaic grid-connected inverter circuit, and a two-stage loss control model is proposed, and the intelligent control of loss distribution balance of photovoltaic grid connected inverter is realized.

2. Topology Structure and Overall Control Scheme of High-Power Photovoltaic Grid-Connected Inverter

2.1. Topology. The function of the high-power photovoltaic grid-connected inverter is to convert the DC power output by the high-power photovoltaic panels into the AC power of the same frequency and phase of the large grid voltage. In order to study the intelligent control method of the loss distribution balance of the high-power photovoltaic grid-connected inverter, this paper chooses a typical two-stage high-power photovoltaic grid-connected inverter topology; its topology is shown in Figure 1.

As shown in Figure 1, U_d represents the output voltage of the high-power photovoltaic array; C_d represents the filter capacitor on the input side; (S_{a+}, S_{a-}) , (S_{b+}, S_{b-}) , and (S_{c+}, S_{c-}) represent the switch tubes that constitute the key components of the inverter; R_l represents the missed filter R_d represents the grid resistance of the large grid; C_l represents the inverter capacitance; N represents the neutral point of the large grid, which is used as the potential reference point [11, 12]. The core of the topology structure of the high-power photovoltaic grid-connected inverter is the realization of the

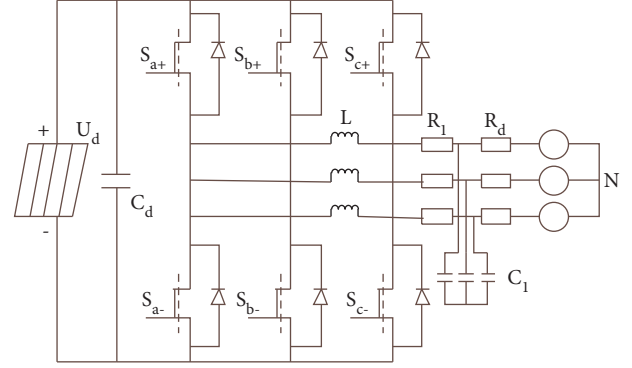


FIGURE 1: Topological structure of high-power photovoltaic grid-connected inverter.

control theory, so the requirements for the topology structure of the high-power photovoltaic grid-connected inverter are relatively high. The voltage space vector control which is easy to digitize is adopted, which has the effect of improving the utilization rate of DC voltage and has the characteristics of many voltage steps of output voltage, so it has small voltage harmonic component, meeting the needs of topology design of high-power photovoltaic grid-connected inverter.

In order to construct the mathematical model of the high-power photovoltaic grid-connected inverter, its switching function is defined [13], as shown in the following formula:

$$\begin{cases} d_1 = \begin{cases} 1 & S_{a+} & \text{turn on} \\ -1 & S_{a-} & \text{shut down} \end{cases} \\ d_2 = \begin{cases} 1 & S_{b+} & \text{turn on} \\ -1 & S_{b-} & \text{shut down} \end{cases} \\ d_3 = \begin{cases} 1 & S_{c+} & \text{turn on} \\ -1 & S_{c-} & \text{shut down} \end{cases} \end{cases} \quad (1)$$

In formula (1), S_{a+} , S_{b+} , and S_{c+} represent the inverter coefficient in the open state, and S_{a-} , S_{b-} , and S_{c-} represent the inverter coefficient in the closed state. The inverter output voltage is the voltage between the inverter output phase and the neutral point plus the neutral point voltage [14]. According to the balance theory and the characteristics of capacitance and inductance on voltage and current, the mathematical model of high-power photovoltaic grid-connected inverter is derived as

$$\dot{x} = Ax + Bi. \quad (2)$$

In formula (2), \dot{x} represents the phase voltage of the inverter output filter; x represents the large grid voltage; A and B represent the coefficient matrix; i represents the inverter output filter current.

2.2. Overall Control Scheme of Photovoltaic Inverter. The adoption of the photovoltaic inverter carrier phase-shift control strategy can avoid the state where the voltage of

the photovoltaic inverter integrated circuit is zero, so that the modulation index $n > 0.462$ in the phase-shift control system can be optimized in the photovoltaic inverter optimization control system to stabilize the control modulation area below 0.462 [15]. Under such conditions, the DC voltage u_b of the photovoltaic inverter integrated circuit drops to 1. If the photovoltaic inverter carrier phase-shift control scheme needs to be adopted in the area of $n < 0.462$, the current in each circuit will have a certain peak value, which reduces the utilization rate of photovoltaic inverters [16, 17]. When n is the domestic standard value of 0.5, the carrier amplitude of the three output terminals of the PV inverter carrier phase-shift control is 2 V, the period is T_2 , the carrier signal reaches the peak value, the sine wave first falls and then rises, and the number of carrier switches increases to 2. Second, the zero state is in a small variation range and lasts for a short time. So the photovoltaic inverter always works under the current light and temperature. In the process of optimizing the modulation strategy of the modulation control system, the level of the differential mode filter supplements the energy in the back-shifted state and is equivalently exchanged with the zero-state voltage of the circuit, thereby effectively improving the mutation of the phase-shifted carrier and maintaining the switching. The number of times does not change. The low-level state appearing in the pulse transformation is regarded as the zero state of the integrated circuit, which is equivalent to the carrier pulse transformation in the equivalent state [18–20]. The carrier pulse translation process is shown in Figure 2.

According to Figure 2, it can be seen that if the pulse signal sine wave is distorted at the intersection of the rectangular wave, the duration of the zero state of the circuit will be prolonged. When the potential of the intersection of the triangular wave is reduced to the lowest point, the duration of the zero state of the integrated circuit is significantly shortened, and the high level jumps. The trigger pulse signal is variable, so when setting the zero state of the photovoltaic inverter integrated circuit, the change of the pulse width causes the output voltage to be uneven to a certain extent, so that the differential mode properties of the pulse are frequently switched, and it needs to be compensated in the shortest time because the voltage bump changes the pulse energy, the pulse modulation strategy of the photovoltaic inverter changes the position of jump and shift, and the number of pulse switches of the photovoltaic inverter is retained [21].

3. Loss Distribution of High-Power Photovoltaic Grid-Connected Inverters

3.1. Basic Current Formula. Since the loss of the switching device has a direct relationship with the current flowing through it, the relationship between the voltage and current of the intermediate bus in the circuit is deduced [22], and the influence of the photovoltaic grid-connected inverter on the current is deduced according to the inverter harmonic circuit model.

$$G_n = \frac{I_{A-n}(s)}{U_{A-n}(s)}. \quad (3)$$

In the above formula, G_n represents the influence of the photovoltaic grid-connected inverter on the current; $I_{A-n}(s)$ represents the phase current harmonic under the n harmonic; $U_{A-n}(s)$ represents the phase voltage harmonic of the grid under the n harmonic.

To sum up, as the harmonics of photovoltaic grid-connected inverters increase, the current harmonics increase rapidly. It can be seen that the quality of photovoltaic grid-connected inverter is extremely sensitive to inverter harmonics, which will cause the power supply quality to fail to meet user needs [23].

3.2. Loss Analysis of Photovoltaic Grid-Connected Inverters

3.2.1. Inductance. According to the L-type filter standard, the total inductance is analyzed for the suppression of harmonics in the low input voltage inverter. According to the grid-connected standard, the harmonic amplitude of each order current in the inverter is set to $i_g(n)$, and the filter is calculated by the following formula. The inductance value of the device Z is

$$Z = \max \left[\frac{u(n)}{n \times \theta_{s0} \times i_g(n)} \right]. \quad (4)$$

In the above formula, $n = 2, 3, 4$ and θ_{s0} represents the fundamental angular frequency; $u(n)$ represents the harmonic amplitude of each order phase voltage output in the inverter.

When calculating the current harmonic amplitude $i_g(n)$ of each order, the parasitic resistance existing in the inductor is not considered:

$$i_g(n) = \frac{u(n)}{\theta_{s0} \times [(Z_1 + Z_2) - Z_1 Z_2]}. \quad (5)$$

In the above formula, Z_1 and Z_2 represent the grid-side inductance and the inverter-side inductance, respectively.

On the basis of the above formula, the inductive loss value Z_{eq} of the n -th current harmonic output in the LCL filter is obtained:

$$Z_{eq} = (Z_1 + Z_2) \times \left(1 - \frac{n\theta_{s0}}{\theta_{res}} \right). \quad (6)$$

In the above formula, θ_{res} represents the resonant angular frequency.

3.2.2. Resonant Frequency. When resonance occurs, the LCL filter with zero impedance resonance point will affect the stability of the power grid control system, resulting in a decrease in power quality and distortion of the output current [24].

Regardless of the parasitic resistance existing in the inductance, the parallel branch of inductance Z_1 on the series inductance side, the inverter inductance Z_2 , and capacitor C , for the midpoint of the bridge arm, the voltage

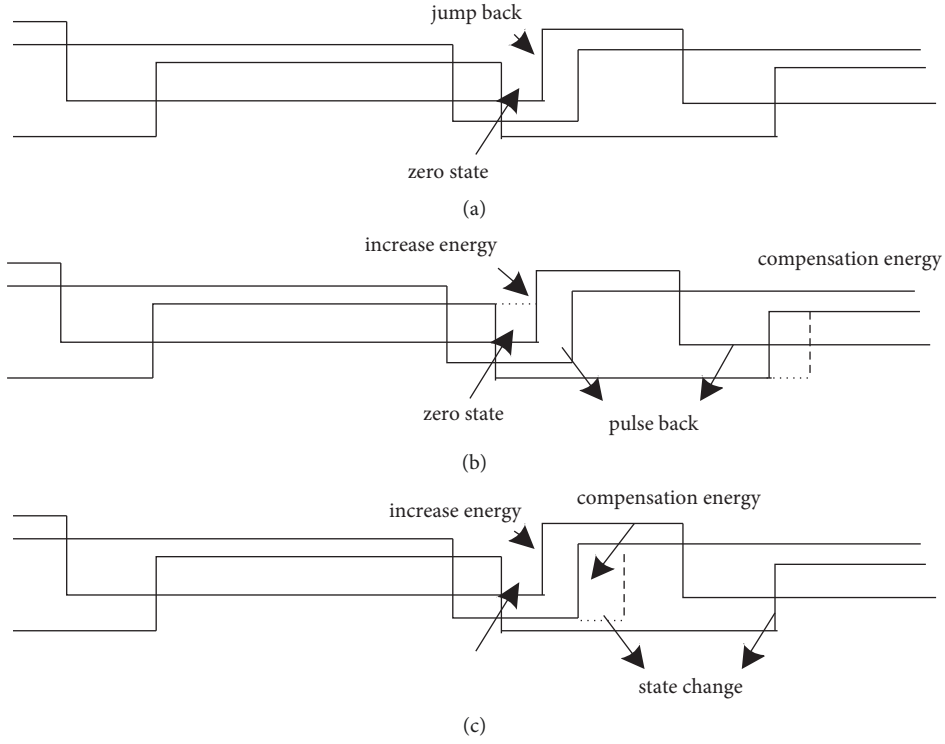


FIGURE 2: The translation process of the carrier pulse of photovoltaic inverter (Jump backward), (Pulse backward), and (State change).

transfer impedance X_1 generated by the output current of the inverter can be calculated by the following formula:

$$X_1 = j\theta(Z_1 + Z_2 - C\theta^2). \quad (7)$$

Set the inverter inductance Z_2 to zero, and calculate the resonant frequency g and the resonant corner frequency θ by

$$\begin{cases} g = \frac{1}{2\pi} C \sqrt{\frac{Z_1 + Z_2}{Z_1 Z_2}}, \\ \theta = C \sqrt{\frac{Z_1 + Z_2}{Z_1 Z_2}}, \end{cases} \quad (8)$$

3.2.3. Harmonic Attenuation. According to the relationship between the output current and the input current of the LCL filter, the current harmonic attenuation of the filter is designed, and the relationship between the output current i_0 and the input current i_i is described by the following transfer function $H_i(s)$ combined with the topology of the filter:

$$H_i(s) = \frac{i_0(s)}{i_i(s)}. \quad (9)$$

Express the above transfer function $H_i(s)$ in current form:

$$i(n) = i_0(n) \left| 1 - \left(\frac{n\theta_0}{\theta} \frac{Z_1 + Z_2}{Z_1} \right) \right|. \quad (10)$$

Solve the above equation to obtain the corner frequency g' of the LCL filter:

$$g' = \frac{1}{2\pi} \sqrt{\frac{2}{Z_2 C}}. \quad (11)$$

If the corner frequency g' is lower than the harmonic current frequency existing in the output current of the low input voltage inverter, after processing by the LCL filter, attenuation will occur. Therefore, the current harmonics whose frequency is higher than the turning frequency have higher suppression ability. However, when the LCL filter is used to process the current harmonics whose frequency is lower than the corner frequency g' , it is easy to reduce the waveform quality and cause the waveform to be distorted. Therefore, when designing the harmonic attenuation of the LCL filter, it is necessary to reduce the corner frequency g' .

3.2.4. Damping Resistor. In order to avoid resonance in the low input voltage converter, it is necessary to introduce a damping resistor to improve the stability. At the same time, it is necessary to consider the influence of the damping resistor and the stability requirements. Adding a damping resistor to the inverter will increase its power loss. By reducing the resistance value of the damping resistor to reduce the power loss of the low input voltage inverter, the resonance suppression effect is not ideal at this time; increasing the resistance value of the damping resistor in the inverter

can improve the stability of the inverter, but, at the same time, it will increase the power loss, which will affect the bypass effect of high-order current harmonics. When suppressing high-frequency harmonics, the ability of the LCL filter is reduced [25].

4. Loss Control of High-Power Photovoltaic Grid-Connected Inverters

4.1. Construction of a Two-Stage Loss Control Model for High-Power Photovoltaic Grid-Connected Inverter Losses. The front-stage DC-DC conversion of the photovoltaic power generation inverter is to track the control of the maximum power. The power output of the photovoltaic cell has a maximum value and a minimum value. By tracking the power change, the required maximum power is output. Under different temperature and illumination conditions, the power of photovoltaic power generation will be affected differently, so the tracking of the maximum power is necessary for the research and control of the utilization rate of the photovoltaic power generation system and the equipment.

The poststage AC converter stabilizes the DC bus voltage between the front and rear stages to achieve the balance between the output power of photovoltaic power generation, the input power of the grid, and the power of the energy storage device; to control the output current of the system; and to control the waveform. The quality is optimized so that the output current can track the voltage of the grid.

In order to make the system reach the maximum power point voltage as soon as possible and avoid the power loss caused by the system searching for the area far from the maximum power point during the startup process, the compound MPPT method of constant voltage tracking method and disturbance observation method is adopted.

In addition, referring to the idea of intermittent scanning method, the photovoltaic array periodically changes the array voltage and works at this point. Since the actual situation is that the operating point of the array does not change much in a short period of time during the operation of the day, the system uses the method of starting MPPT every 500ms. This method does not require the grid-connected inverter to be in the search state all the time, does not generate oscillation, and avoids the power loss caused by other schemes due to the need for real-time search, and it has proved to have almost no impact on accuracy.

The system has the problem of cooperation between MEPT and MPPT. In the stable stage, MEPT is embedded in MPPT due to the large difference in the disturbance time between the two. Different from the ordinary disturbance observation method, in order to make the system perform MEPT as soon as possible in the startup phase to achieve the maximum efficiency, this paper adds a step change counter in the system startup phase; that is, after each disturbance, it is judged whether the disturbance step size has changed. When a change occurs, the counter is incremented by 1. If the step size changes for the first time, it means that the photovoltaic array operating point has

crossed the vertex of the photovoltaic curve; when the second step size changes, it means that the operating point has completed crossing the vertex of the photovoltaic curve twice, and the next beat works. The point will move towards the apex, at which time the array must work near the apex of the photovoltaic curve and oscillate near the apex. The value of the counter is equal to 2, wait for one beat, and trigger the start of MEPT. After the system startup process is over, the design method is the same as the ordinary disturbance observation method.

4.1.1. Calculation of Two-Stage Loss Control Objective Function. Aiming at minimizing the losses of photovoltaic grid-connected inverters, the two-stage loss control objective function is calculated. It is determined that, during the operation of the distribution network, its reactive power is compensated locally, and the structure does not change. Only the optimal scheduling of active power is taken into account, and the photovoltaic power supply and fluctuating load are regarded as the uncertain random variables of loss control. An uncertainty set contains all uncertain random variables in the fluctuation range [26]. In the first stage of optimal scheduling, the predicted values of uncertain random variables, that is, the active power of photovoltaic power sources and loads, are selected as the decision variables of this stage. There is a certain error between the predicted value and the actual value, and the actual value is unknown [27]. The first-stage loss control objective function is

$$C_1 = \sum_{t=1}^N (U_t + A_t + B_t + R_t)t. \quad (12)$$

In the above formula, C_1 is the schedulable operation cost of the first stage, N is the loss control scheduling cycle, U_t is the photovoltaic energy scheduling cost at t time, A_t is the fluctuating load scheduling cost at time t , B_t is the energy storage scheduling cost, and R_t is the distribution network loss cost [28]. In the second stage of optimal dispatching, the load loss and light rejection are taken as decision variables. At this time, the actual value of the uncertain random variable is known, and its loss control objective function is

$$C_2 = \sum_{t=1}^N (H_t + K_t). \quad (13)$$

In the above formula, C_2 is the schedulable operation cost of the second stage, H_t is the reduced penalty cost of light abandonment, and K_t is the reduced penalty cost of load loss. Taking formulas (12) and (13) as the objective functions of loss control, the random variables in the uncertain set can also minimize the total expected cost of the distribution network in the worst case. So far, the calculation of the two-stage loss control objective function has been completed.

4.1.2. Calculation of Two-Stage Loss Control Constraints. When the random variable in the uncertain set takes any value, calculate the various constraints contained in it, obtain the extreme bad scene of the uncertain random

variable, and optimize the objective function. The expression of the first-stage loss control equation constraint is

$$\begin{cases} P = P_1 + P_2 + P_3 - P_4 - P_5, \\ \frac{P^2 + Q^2}{V^2} = I^2. \end{cases} \quad (14)$$

In the above formula, P is the power flow distribution, P_1 is the predicted photovoltaic power output value, P_2 is the maximum fluctuation difference of the active power output value, P_3 and P_4 are the charging and discharging capacities of the distribution network, P_5 is the load active power, and V is the active power of the branch; Q and I are circuit resistance and current, respectively [29–31]. By formula (15), the branch power flow constraint is carried out on the objective function of the first stage. According to the electricity conservation of the distribution network and the limit of charging and discharging power, the loss control is constrained by inequality, and the expression formula is

$$\begin{cases} P_{\min} \leq P_1 \leq P_{\max}, \\ S_{\min} \leq S_1 - S_2 \leq S_{\max}. \end{cases} \quad (15)$$

In the above formula, P_{\min} and P_{\max} are the lower limit and upper limit of the active power of the photovoltaic power supply, S_{\min} and S_{\max} are the lower limit of the discharging power and the upper limit of the charging power, and S_1 and S_2 are the charging power and the discharging power, respectively [32]. The first stage of loss control is used as the reference value to determine the fluctuation range of photovoltaic power output and load. The second stage adopts distributed loss control theory to further reduce the fluctuation of photovoltaic output and load. It provides reactive auxiliary services [33]. Since this process will produce abandoned light, the PV inverter reactive power auxiliary constraint is carried out for the second stage, and the expression is

$$F = \frac{\lambda}{G}. \quad (16)$$

In the above formula, F is the apparent power of the photovoltaic inverter, λ is the binary variable during reactive auxiliary service, and G is the maximum power of the access node. According to the recourse cost, the second-stage loss control is constrained by inequality, and the expression is

$$\begin{cases} 0 \leq \frac{D}{a} \leq D_{\max}, \\ 0 \leq \frac{V}{b} \leq V_{\max}. \end{cases} \quad (17)$$

In the above formula, V is the loss of load, V_{\max} is the maximum loss of the loss of load, D is the amount of abandoned light, D_{\max} is the maximum loss of the amount of abandoned light, and a and b are the penalty coefficients of the loss of load and the amount of abandoned light, respectively [34]. Traverse all the nodes connected to the photovoltaic inverter, set the voltage of node j to U_j , set the

maximum voltage and the minimum voltage of the node to U_{\max} and U_{\min} , respectively, and impose voltage constraints on the uncertain set. The formula is

$$U_{\min} \leq \sum_{j=1}^{\delta} U_j \leq U_{\max}. \quad (18)$$

In the above formula, δ is the number of nodes connected to the PV inverter. Through the objective function and constraints, the loss control scheduling results under the worst distribution of uncertain random variables are expressed. At this point, the calculation of the constraints is completed and the model construction is realized.

4.2. Solving the Two-Stage Loss Control Model of High-Power Photovoltaic Grid-Connected Inverter Losses.

Using generalized linear decision rules, the two-stage loss control model of high-power photovoltaic grid-connected inverter losses is solved, and photovoltaic power sources and fluctuating loads are dispatched. The principles followed in the process of establishing the model are as follows. The first is the simplification principle: the actual model is a multivariable and multilevel complex model, and the establishment of the model requires the necessary simplification of the prototype. Therefore, the model establishment process should be the “simplest” model. The second is the derivation principle: a series of definite conclusions can be deduced through the study of the model. If the model cannot be mathematically deduced and the result of the application prototype cannot be determined, the model will be meaningless. The third is the similarity principle: the model is a form of numerical expression, which needs to have “similarity” with the actual prototype. The key to modeling is to reasonably use the mathematical formula and analytical graphics “similar” to the prototype. The established environment should use new independent variables or existing variables as environment settings. An auxiliary variable is introduced to simulate the change of an uncertain random variable through an affine function to obtain the probability distribution information of the random variable [35]. The calculation formula of auxiliary variable e is

$$e = \frac{f(v)}{E}. \quad (19)$$

In the above formula, v is the random variable in the uncertain set, $f(v)$ is the affine function of the random variable, and E is the random value function of the random variable. The loss control model is solved recursively. Through mixed-integer linear programming, e is transformed into the first-stage auxiliary variable o_1 and the second-stage auxiliary variable o_2 . The transformation formula is

$$\begin{cases} o_1 = \frac{(y_1 - y_2)cP}{h_{\max} - h_{\min}}, \\ o_2 = q(e - o_1). \end{cases} \quad (20)$$

In the above formula, y_1 and y_2 are the adjustment power of the photovoltaic inverter reactive power and active power,

c is the correction coefficient, p is the power of the abandoned light, q is the compensation capacity of the inverter access node, and h is the compensation capacitor. Through auxiliary variables, a fuzzy upper bound is applied to the objective function of the two stages, and the global optimal value in the worst scenario is obtained, the value of the uncertain random variable is continuously updated iteratively, and the set of decision variables which satisfies the expected cost minimization is selected to obtain optimal decisions for two-stage loss control scheduling [36]. So far, the solution of the two-stage loss control model of the high-power photovoltaic grid-connected inverter loss has been completed, and the design of the two-stage loss control scheduling method for the loss of the high-power photovoltaic grid-connected inverter has been realized.

5. Experimental Analysis

5.1. Experimental Environment. In order to verify the overall effectiveness of the intelligent control method of loss distribution balance of high-power photovoltaic grid-connected inverters, it is necessary to carry out relevant tests. An active distribution network is selected as the optimization object of the four methods. The distribution network is a combined electricity-heating type, the installed photovoltaic capacity is 1 MW, the rated capacity of the cogeneration unit is 2500 kW, the rated capacity of the electric energy storage is 2300 kWh, and the photovoltaic capacity is 2300 kWh. The output is fluctuating, and the peak load is taken as the power per unit value. The distributed power and daily load curves are shown in Figure 3.

According to Figure 3, the standard value of distribution network load is 2.95 MW and the PV unit value is 3.02 MW. When the design method is connected to the photovoltaic inverter, the DC voltage source and the controlled current source are, respectively, used to replace the front stage and the rear stage. The key parameters of the power circuit of the photovoltaic inverter are shown in Table 1.

Based on the key parameters of photovoltaic inverter in Table 1, the simulation results of intelligent control of loss distribution balance of high-power photovoltaic grid-connected inverter under the condition of severe uneven sunlight are studied by simulation experiment. The simulation time is 3 s, and the photovoltaic units keep the light intensity at 800 W/m². The corresponding high-power photovoltaic grid-connected inverter output voltage, output current, and loss control effects are given. The antiresonance capability of the high-power photovoltaic grid-connected inverter is analyzed.

5.2. Analysis of Experimental Results. According to the simulation parameter settings, test the waveforms of the output voltage and output current of the high-power photovoltaic grid-connected inverter before and after the application of the method in this paper, and test the regulation effect of the method in this paper in turn. The results are shown in Figures 4 and 5.

It can be seen from Figures 4 and 5 that, after the method in this paper regulates the joint operation of high-power

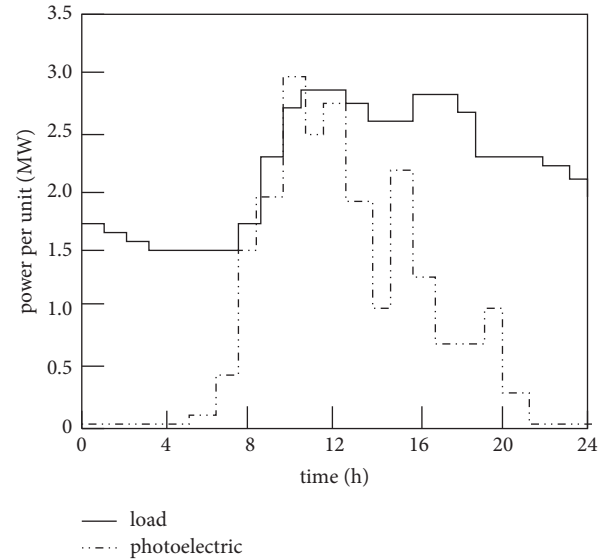


FIGURE 3: Daily operation curves of photovoltaic grid and load.

TABLE 1: Key parameters of PV inverter.

Parameter	Numerical value
Number of PVs installed in the node	8
Inverter rated capacity	4000 kW/h
Maximum charge and discharge power	450 kW
Inverter total capacity	4500 kW/h
Distribution grid voltage	220 V
Output filter inductor	7mH/0 Ω
Reactive power compensation range	-100~300 kvar
DC bus capacitance	2500 uF
DC bus voltage	450 V
Distribution network frequency	60 Hz
Inverter remaining capacity threshold	6.0kVA
Operating frequency	40 kHz
DC boost inductor	5 mH

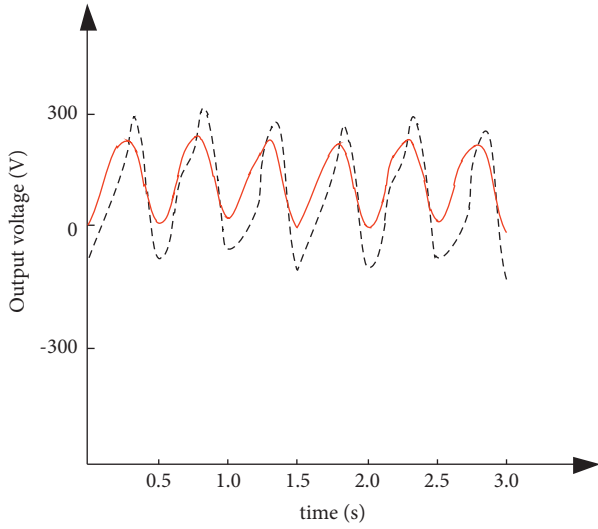
photovoltaic grid-connected inverters in the power grid, the output voltage waveform can be optimized and the current fluctuation can be suppressed, which verifies the effectiveness of the method in this paper for loss control.

The proposed method, the method of [9], and the method of [10] are used to track the grid-connected current of the high-power photovoltaic grid-connected inverter, and the tracking results are shown in Figure 6.

Analysis of Figure 6 shows that, under the same environment, there are errors in the method of [9] and the method of [10] when tracking the incoming current, and the tracking results of the proposed method are basically consistent with the actual current waveform, indicating that the proposed method has better performance and tracking effect.

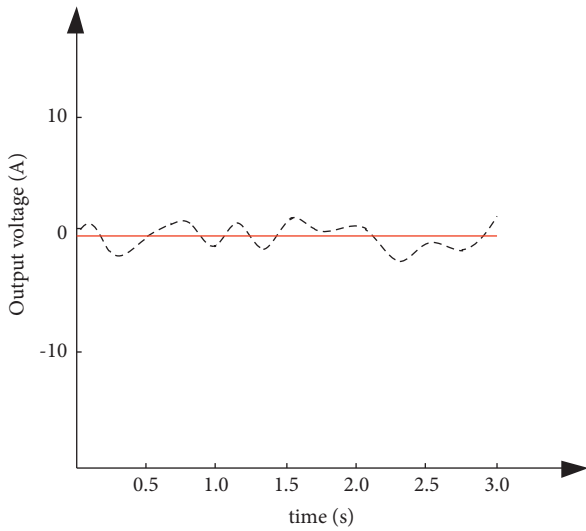
Change the inductance value of the grid-side point, and continue to use the proposed method, the method of [9], and the method of [10] to track the incoming current in the above test environment, and the tracking results are shown in Figure 7.

Analysis of Figure 7 shows that when the grid-side inductance of the proposed method changes, the tracking



— after application
 --- before application

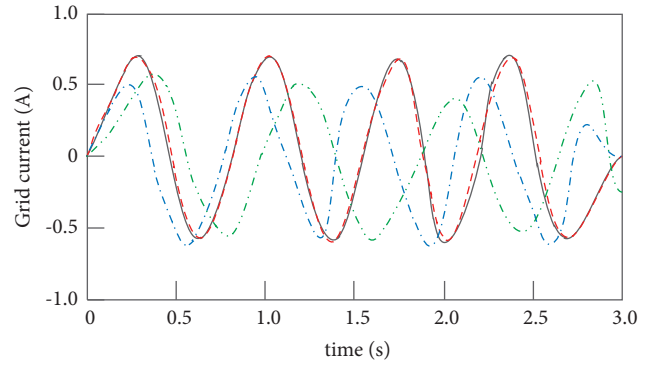
FIGURE 4: Waveform diagrams before and after the output voltage is applied.



— after application
 --- before application

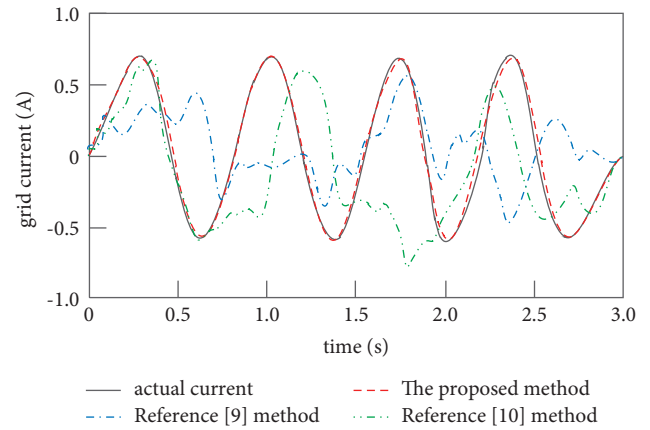
FIGURE 5: Waveform diagrams before and after the output current is applied.

results are still basically consistent with the actual grid-connected current, indicating that the proposed method has high robustness. Changing the grid-side inductance can be regarded as an external disturbance, so the loss affecting the high-power photovoltaic grid-connected inverter was analyzed before the proposed method to control the grid-connected current. On this basis, a two-stage loss control method was designed to control the grid-connected current. Therefore, for the external disturbance in the control process, the proposed method shows good robustness.



— actual current - - - The proposed method
 ··· Reference [9] method - · - Reference [10] method

FIGURE 6: Grid current tracking results.



— actual current - - - The proposed method
 ··· Reference [9] method - · - Reference [10] method

FIGURE 7: Grid current tracking results with changing grid-side point inductance.

A trace disturbance signal of 1000 rad/s is introduced into the control process of the double closed-loop grid-connected current of the inverter, and the antiresonance capabilities of the proposed method, the method in [9], and the method in [10] are compared, as shown in Figure 8.

It can be seen from Figure 8 that, after the introduction of microdisturbance signal, the network access current control curve obtained by the proposed method is relatively smooth, and there is no resonance peak, indicating that the proposed method has strong antiresonance capability. However, after the introduction of microdisturbance signal, there are multiple resonance peaks in the network current control curve and the surface smoothness is low, which shows that the resonance peaks of microdisturbance signal noise cannot be eliminated when the methods in [9] and [10] are used to control the loss of high-power photovoltaic grid-connected inverter. Compared with the proposed method, the network current control effects of the methods in [9] and [10] are poor, with weak antiresonance capability.

To sum up, the output voltage waveform can be optimized and the current fluctuation can be suppressed at 0A after the joint operation regulation of high-power

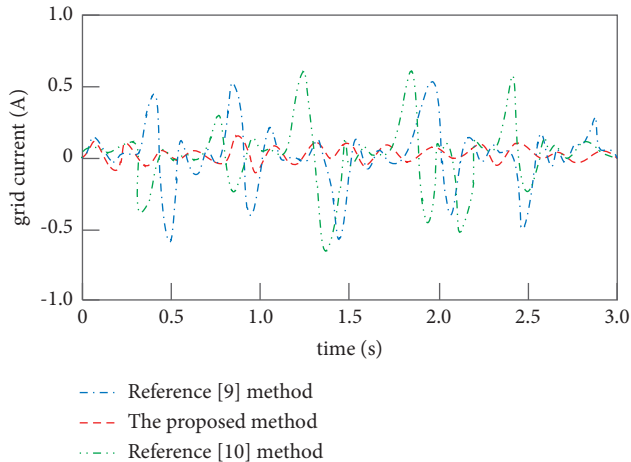


FIGURE 8: Antiresonance capabilities of different methods.

photovoltaic grid-connected inverters in the power grid. Under the same environment, the tracking results of the proposed method are basically consistent with the actual current waveform. When the network side inductance changes, the tracking result is still basically consistent with the actual network current. After introducing micro-disturbance signal, the control curve of network access current obtained by the proposed method at 0A is relatively smooth, there is no resonance peak, and the proposed method has strong antiresonance capability.

6. Conclusion

The control of photovoltaic grid connection is a necessary condition for photovoltaic system power generation and a key technology related to the utilization of new energy. It is very important for the intelligence, efficiency, and popularization of microgrid in the future. This paper proposes an intelligent control method for the loss distribution balance of high-power photovoltaic grid-connected inverter. Based on the analysis of the loss distribution of high-power photovoltaic grid-connected inverter, a two-stage loss control objective function is proposed. In the first stage, the scheduling costs such as photovoltaic energy and fluctuating load are selected, and, in the second stage, the penalty costs of light abandonment and load loss are selected, which are limited by branch power flow and charging and discharging power of distribution network. A two-stage loss control model of distribution network is built and the optimal solution of the model is searched. Finally, through experiments, the correctness and feasibility of the loss analysis and loss control strategy of photovoltaic grid-connected inverter are verified, which reflects the effectiveness of this method for loss control, good tracking effect, strong robustness, and strong antiresonance capability.

Data Availability

The raw data supporting the conclusions of this article will be made available by the authors, without undue reservation.

Conflicts of Interest

The authors declare that they have no conflicts of interest regarding this work.

Acknowledgments

This work was supported by the Key Laboratory of Control of Power Transmission and Conversion (SJTU), Ministry of Education (2020AC02).

References

- [1] H. Bouaouaou, D. Lalili, and N. Boudjerda, "Model predictive control and ann-based mppt for a multi-level grid-connected photovoltaic inverter," *Electrical Engineering*, vol. 30, no. 8, pp. 1–18, 2021.
- [2] L. Kong, W. Wang, and H. Wang, "Parameter optimization design method of LCL filter for photovoltaic grid-connected inverter," *Computer Simulation*, vol. 38, no. 8, pp. 6–16, 2021.
- [3] B. Karanayil, S. Ceballos, and J. Pou, "Maximum power point controller for large-scale photovoltaic power plants using central inverters under partial shading conditions," *IEEE Transactions on Power Electronics*, vol. 34, no. 4, pp. 3098–3109, 2019.
- [4] A. Elmelegi, M. Aly, E. M. Ahmed, and A. G. Alharbi, "A simplified phase-shift pwm-based feedforward distributed mppt method for grid-connected cascaded pv inverters," *Solar Energy*, vol. 187, no. 7, pp. 1–12, 2019.
- [5] K. Takagi, H. Fujita, and F. Hideaki, "A three-phase grid-connected inverter equipped with a shunt instantaneous reactive power compensator," *IEEE Transactions on Industry Applications*, vol. 55, no. 4, pp. 3955–3966, 2019.
- [6] E. Akpinar, A. Balikci, E. Durbaba, and B. T. Azizoglu, "Single-phase transformerless photovoltaic inverter with suppressing resonance in improved h6," *IEEE Transactions on Power Electronics*, vol. 34, no. 9, pp. 8304–8316, 2019.
- [7] P. K. Boggarapu, C. Manickam, B. Lehman, S. I. Ganesan, and N. Chilakapati, "Identification of pre-existing/undetected line-to-line faults in pv array based on preturn on/off condition of the pv inverter," *IEEE Transactions on Power Electronics*, vol. 35, no. 11, pp. 11865–11878, 2020.
- [8] S. Golzari, F. Rashidi, and H. F. Farahani, "A lyapunov function based model predictive control for three phase grid connected photovoltaic converters," *Solar Energy*, vol. 181, no. 3, pp. 222–233, 2019.
- [9] H. Yang, M. Wang, Y. Sun, J. Pan, and W. Yang, "Power balance control strategy for two-stage cascaded H-bridge photovoltaic grid-connected inverter," *Proceedings of the CSU-EPSA*, vol. 33, no. 4, pp. 76–83, 2021.
- [10] X. Liu, C. Gao, and Z. Wang, "DC-bus voltage control for PV grid-connected inverter based on nonlinear disturbance observer," *Power System Technology*, vol. 44, no. 3, pp. 897–906, 2020.
- [11] A. Elkholy, "Harmonics assessment and mathematical modeling of power quality parameters for low voltage grid connected photovoltaic systems," *Solar Energy*, vol. 183, no. 5, pp. 315–326, 2019.
- [12] M. Gharibi and A. Askarzadeh, "Size and power exchange optimization of a grid-connected diesel generator-photovoltaic-fuel cell hybrid energy system considering reliability, cost and renewability," *International Journal of Hydrogen Energy*, vol. 44, no. 47, pp. 25428–25441, 2019.

- [13] M. Khodabandeh, E. Afshari, and M. Amirabadi, "A single-stage soft-switching high-frequency ac-link pv inverter: design, analysis, and evaluation of si-based and sic-based prototypes," *IEEE Transactions on Power Electronics*, vol. 34, no. 3, pp. 2312–2326, 2019.
- [14] A. L. Bukar, C. W. Tan, and K. Y. Lau, "Optimal sizing of an autonomous photovoltaic/wind/battery/diesel generator microgrid using grasshopper optimization algorithm," *Solar Energy*, vol. 188, no. 8, pp. 685–696, 2019.
- [15] X. Ruan, W. Li, D. Pan, C. Bao, X. Wang, and D. Yang, "Control techniques for LCL-type grid-connected inverters," *Springer Singapore*, vol. 8, no. 8, pp. 978–991, 2017.
- [16] V. Behraves, R. Keypour, and A. Akbari Foroud, "Control strategy for improving voltage quality in residential power distribution network consisting of roof-top photovoltaic-wind hybrid systems, battery storage and electric vehicles," *Solar Energy*, vol. 182, no. 4, pp. 80–95, 2019.
- [17] A. Karafil, H. Ozbay, and S. Oncu, "Design and analysis of single-phase grid-tied inverter with pdm mppt-controlled converter," *IEEE Transactions on Power Electronics*, vol. 35, no. 5, pp. 4756–4766, 2020.
- [18] X. Zhang, F. Fang, and J. Liu, "Weather-classification-mars-based photovoltaic power forecasting for energy imbalance market," *IEEE Transactions on Industrial Electronics*, vol. 66, no. 11, pp. 8692–8702, 2019.
- [19] T. Yang, K. T. Mok, S. S. Ho, S. C. Tan, C. K. Lee, and R. S. Y. Hui, "Use of integrated photovoltaic-electric spring system as a power balancer in power distribution networks," *IEEE Transactions on Power Electronics*, vol. 34, no. 6, pp. 5312–5324, 2019.
- [20] R. Dogga and M. K. Pathak, "Recent trends in solar pv inverter topologies," *Solar Energy*, vol. 183, no. 5, pp. 57–73, 2019.
- [21] J. C. d. S. de Morais, J. L. d. S. de Morais, and R. Gules, "Photovoltaic ac module based on a cuk converter with a switched-inductor structure," *IEEE Transactions on Industrial Electronics*, vol. 66, no. 5, pp. 3881–3890, 2019.
- [22] I. Al Siyabi, K. Shanks, T. Mallick, and S. Sundaram, "Indoor and outdoor characterization of concentrating photovoltaic attached to multi-layered microchannel heat sink," *Solar Energy*, vol. 202, no. 5, pp. 55–72, 2020.
- [23] G. A. Farias-Basulto, P. Reyes-Figueroa, C. Ulbrich, B. Szyszka, R. Schlatmann, and R. Klenk, "Validation of a multiple linear regression model for cigsse photovoltaic module performance and pmpp prediction," *Solar Energy*, vol. 208, no. 9, pp. 859–865, 2020.
- [24] V. M. Emelyanov, P. V. Pokrovskiy, N. A. Kalyuzhnyy, M. V. Nakhimovich, and M. Z. Shvarts, "Capacitive characteristics of high-speed photovoltaic converters at combined lighting," *Semiconductors*, vol. 53, no. 14, pp. 1959–1963, 2019.
- [25] S. Tippabhotla, Song, Tay, and A. Budiman, "Effect of encapsulants on the thermomechanical residual stress in the back-contact silicon solar cells of photovoltaic modules - a constrained local curvature model," *Solar Energy*, vol. 182, no. 4, pp. 134–147, 2019.
- [26] S. Kan, X. Ruan, H. Dang, L. Zhang, and X. Huang, "Second harmonic current reduction in front-end DC–DC converter for two-stage single-phase photovoltaic grid-connected inverter," *IEEE Transactions on Power Electronics*, vol. 34, no. 7, pp. 6399–6410, 2019.
- [27] W. A. Xuan, L. A. Qi, A. Wc, B. Ww, A. Yp, and Y. A. Jin, "Parallel interaction influence of single-stage photovoltaic grid-connected/hydrogen production multi-inverter system based on modal analysis sciencedirect," *International Journal of Hydrogen Energy*, vol. 44, no. 11, pp. 5143–5152, 2019.
- [28] F. Yang, H. Ge, J. Yang, and H. Wu, "Dual-input grid-connected photovoltaic inverter with two integrated DC-DC converters and reduced conversion stages," *IEEE Transactions on Energy Conversion*, vol. 34, no. 1, pp. 292–301, 2019.
- [29] J. P. O Avilés, E. Silva, and F. L. Tofoli, "connected photovoltaic system," *IET Circuits, Devices and Systems*, vol. 14, no. 8, pp. 1117–1128, 2020.
- [30] R. Zaim, J. Jamaludin, and N. A. Rahim, "Photovoltaic flyback microinverter with tertiary winding current sensing," *IEEE Transactions on Power Electronics*, vol. 34, no. 8, pp. 7588–7602, 2019.
- [31] T. W. Tsai, C. J. Yang, C. Li, M. Chen, and R. Chang, "Dc-bus dual-level control strategy for pv power system with dual-mode operation," *IEEE Transactions on Energy Conversion*, vol. 34, no. 1, pp. 267–276, 2019.
- [32] V. Ravindran, T. Busatto, S. K. Ronnberg, J. Meyer, and Bollen, "Time-varying interharmonics in different types of grid-tied pv inverter systems," *IEEE Transactions on Power Delivery*, vol. 35, no. 2, pp. 483–496, 2020.
- [33] K. Zaouche, S. M. Benmerabet, A. Talha, and E. M. Berkouk, "Finite-set model predictive control of an asymmetric cascaded h-bridge photovoltaic inverter," *Applied Surface Science*, vol. 474, no. 4, pp. 102–110, 2019.
- [34] A. A. Hussein, X. Chen, M. Alharbi, A. A. Pise, and I. Batarseh, "Design of a grid-tie photovoltaic system with a controlled total harmonic distortion and tri maximum power point tracking," *IEEE Transactions on Power Electronics*, vol. 35, no. 5, pp. 4780–4790, 2020.
- [35] S. Yazdani, M. Ferdowsi, and P. Shamsi, "Internal model based smooth transition of a three-phase inverter between islanded and grid-connected modes," *IEEE Transactions on Energy Conversion*, vol. 35, no. 1, pp. 405–415, 2020.
- [36] S. Dadfar, K. Wakil, M. Khaksar, A. Rezvani, M. R. Miveh, and M. Gandomkar, "Enhanced control strategies for a hybrid battery/photovoltaic system using fgs-pid in grid-connected mode," *International Journal of Hydrogen Energy*, vol. 44, no. 29, pp. 14642–14660, 2019.

Research Article

Correlation-Based Anomaly Detection Method for Multi-sensor System

Han Li ^{1,2}, Xinyu Wang ^{1,2}, Zhongguo Yang ^{1,2}, Sikandar Ali ³, Ning Tong ⁴,
and Samad Baseer ⁵

¹School of Information Science and Technology, North China University of Technology, Beijing 100144, China

²Beijing Key Laboratory on Integration and Analysis of Large-Scale Stream Data, North China University of Technology, Beijing 100144, China

³Department of Information Technology, The University of Haripur, Haripur 22620, Pakistan

⁴School of Software, Dalian Jiaotong University, Dalian 116028, China

⁵Department of Computer Systems Engineering, University of Engineering and Technology Peshawar, Peshawar 25000, Pakistan

Correspondence should be addressed to Han Li; lihan@ncut.edu.cn

Received 2 April 2022; Revised 2 May 2022; Accepted 10 May 2022; Published 31 May 2022

Academic Editor: Le Sun

Copyright © 2022 Han Li et al. This is an open access article distributed under the Creative Commons Attribution License, which permits unrestricted use, distribution, and reproduction in any medium, provided the original work is properly cited.

In industry, sensor-based monitoring of equipment or environment has become a necessity. Instead of using a single sensor, multi-sensor system is used to fully detect abnormalities in complex scenarios. Recently, physical models, signal processing technology, and various machine learning models have improved the performance. However, these methods either do not consider the potential correlation between features or do not take advantage of the sequential changes of correlation while constructing an anomaly detection model. This paper firstly analyzes the correlation characteristic of a multi-sensor system, which shows a lot of clues to the anomaly/fault propagation. Then, a multi-sensor anomaly detection method, which finds and uses the correlation between features contained in the multidimensional time-series data, is proposed. The method converts the multidimensional time-series data into temporal correlation graphs according to time window. By transforming time-series data into graph structure, the task of anomaly detection is considered as a graph classification problem. Moreover, based on the stability and dynamics of the correlation between features, a structure-sensitive graph neural network is used to establish the anomaly detection model, which is used to discover anomalies from multi-sensor system. Experiments on three real-world industrial multi-sensor systems with anomalies indicate that the method obtained better performance than baseline methods, with the mean value of F1 score reaching more than 0.90 and the mean value of AUC score reaching more than 0.95. That is, the method can effectively detect anomalies of multidimensional time series.

1. Introduction

Internet of Things (IoT) is an extended network based on the Internet, which supports more intelligent physical object management. In recent years, a rapid growth of the IoT has been witnessed, and the number of connected IoT devices is estimated to exceed 500 million by 2030 [1, 2]; therefore, IoT-based services will appear on a large scale in different application domains [2]. In the era of “Industry 4.0,” digital twin, which is a “fusion of the real and the virtual entities,” has begun to use data such as sensors, physical models, and

operational histories to represent the entire life cycle processes of physical entities [3]. In the actual production process, the digital twin entity is commonly established by monitoring one or more important, interdependent physical entities through sensors [4]. In general, the function of the sensor is relatively single, so a single sensor cannot fully reflect the physical world [5]. A multi-sensor system is a system that contains multiple sensors. A digital entity constructed by a multi-sensor system can reflect the entity and its behavior more comprehensively and can provide richer data for different kinds of analysis [6].

Hawkins [7] defined anomalies as data that are distinctive in a dataset, which is suspected not to be derived from random deviations but generated by a totally different mechanism. Anomaly detection refers to identifying anomalous data using various data processing models and techniques and is a prerequisite part for fault diagnosis [4]. Anomalies in the equipment or the environment, which reflect production problems, usually cause failures and economic losses and can even lead to catastrophic consequences [8]. Taking the electric power system as an example, we find that abnormal real-time monitoring of electric power and electrical equipment not only can obtain the running state of the equipment, but also will diagnose the fault in time. Therefore, finding anomalies can help to better ensure the safe and stable operation of a power and electrical equipment. On the contrary, failure to discover the anomalies implied in the sensing data will be unfavorable to the timely detection of problems of physical entities and may cause unnecessary losses. Thus, multi-sensor systems which can achieve data monitoring of complex equipment or an environment throughout its whole life cycle have become the main approach in the field of anomaly detection.

The collected data of a multi-sensor system is represented by multivariate time-series data, and different dimensions of the multivariate time-series data originate from different features of sensors. In complex industrial systems, anomalies are not always isolated. Due to the fuzzy physical interaction, small anomalies might spread between different sensors and gradually deteriorate into serious anomalies in some devices [9]. Taking the thermal power plant as an example, there are two devices: coal feeder and coal pulverizer. A coal feeder is responsible for conveying the coal to the coal pulverizer for crushing. In normal conditions, when the amount of coal conveyed by the coal feeder increases, the working load of the coal pulverizer also needs to increase accordingly in time, which indicates that the coal quantity of the coal feeder and the current of the coal pulverizer maintain a stable correlation. On the contrary, if the coal pulverizer is not adjusted within the allowable time range, it will cause coal blockage and insufficient output and even cause equipment damage and production interruption. That is, the complex correlation between sensors is closely related to anomalies.

In recent years, deep learning-based techniques have been used for the anomaly detection of multi-sensor systems. However, the potential relationships between sensors, which are helpful for finding anomalies, are not explicitly learned. That is, when the stable correlation is destroyed, it may indicate the occurrence of anomalies. Therefore, it is necessary to obtain the correlations between sensors in a multi-sensor system, and the main challenge of using these correlations in anomaly detection is that the functions of sensors vary greatly and the relationship between sensors changes dynamically, which requires dynamic discovery, representation, and detection of correlations. Hence, this paper proposes a correlation-based anomaly detection method of a sequential multi-sensor system, which learns a set of temporal correlation graphs from sensors and detects the deviations of these correlations. The proposed method involves two main stages. (1) Correlation-based graph model is constructed: Firstly, the

time-series data generated by the multi-sensor system is divided according to the time window. Nodes and edges are, respectively, used to represent the features and the correlations between pairs of features. Then, temporal correlation graphs are constructed to represent the fluctuation of correlations between features in a sequential multi-sensor system. (2) Graph-based anomaly detection learns the anomaly detection model with a structured-sensitive graph neural network and then identifies the deviations from the learned correlations in the temporal correlation graphs.

To summarize, the main contributions of this work are as follows:

- (i) This paper is a novel attempt to propose and construct the concept of temporal correlation graph by obtaining the correlation between the features in a multi-sensor system.
- (ii) A structured-sensitive graph neural network is used to learn the information in the temporal correlation graph, including attributes such as points, edges, and structure of the graph, and classify the graph based on the collected information for anomaly detection.
- (iii) The accuracy and stability of the proposed method are compared with baselines by conducting numerous experiments on several datasets, and hence accuracy and stability have proven better than those of the baselines.

The rest of this paper is organized as follows. Section 2 briefly introduces the related work of anomaly detection. Section 3 analyzes the correlation characteristics of the sensor data acquired by a multi-sensor system, defines the research problem, and describes the correlation-based anomaly detection method for multi-sensor system. The performance evaluation is given in Section 4, and Section 5 is the conclusion.

2. Related Work

An overview of the current state of anomaly detection is first presented. Then, the data-driven anomaly detection methods are reviewed. Since the proposed method is a deep learning method, the related work of machine learning methods and deep learning methods is also summarized.

2.1. Anomaly Detection. The most important aspect of quality monitoring in the industry is anomaly detection. With the application of multi-sensor systems in the industry, anomaly detection is starting to target more than just outliers. The data acquired by multi-sensor systems is reflected as high-dimensional time-series data with characteristics such as continuity and correlation. Therefore, the anomalies of physical entities characterized by multi-sensor systems are no longer reflected as a single outlier or small number of outliers, but through multiple anomalies of data with certain continuity. Currently, methods for anomaly detection can be broadly classified into two types, i.e., non-data-driven methods and data-driven methods [10].

2.2. Non-data-Driven Methods. The non-data-driven anomaly detection methods include physical model-based methods and signal processing-based methods. The former focus on obtaining the data signals on the system to be tested and analyzing the data processing results with the initially established model in order to obtain the abnormal diagnostic situation. The latter aims at investigating the techniques and methods of highlighting abnormal feature information.

However, the above methods require a priori knowledge and relevant equipment or environment knowledge.

2.3. Data-Driven Methods. The data-driven anomaly detection method can be used without having a priori knowledge such as the physical model of the system. That is, the monitored system data is analyzed to extract information about features and can be combined with historical data to diagnose anomalies in the system. This approach does not require extensive domain knowledge, relevant expert reasoning mechanisms, or establishment of accurate complex system models. This has become an important tool in the field of anomaly detection in the context of IoT and Industry 4.0. Traditional data-driven anomaly detection methods refer to anomaly detection for outliers and can be classified into four types, namely, statistical-based methods [11, 12], distance-based methods [13, 14], density-based methods [15, 16], and clustering-based methods [17, 18]. Statistical-based methods are model-based methods where a model is first created for the data and evaluated based on how well the object fits the model. For example, Laurikkala et al. [10] used box-line plots to identify outliers in the dataset while Kasliwal et al. [16] used a hybrid model of G-LDA which combines Latent Dirichlet Allocation (LDA) and genetic evolution techniques to detect anomalies in the network traffic. Distance-based methods consider a point anomalous if it is far from most of the points, because for the distance measurement, there are various ways. For example, Zhang et al. [17] used Mahalanobis distance for anomaly detection of hyperspectral images while Laxhammar and Göran [19] used Hausdorff distance for phase dissimilarity measure for multidimensional trajectories of arbitrary length. Density-based methods consider outliers as objects that are in low-density regions. Density is commonly defined by proximity. Huang et al. [20] solved the problem of adaptive anomaly detection based on the Local Outlier Factor (LOF) algorithm while Celik et al. [21] discovered the anomalies present in temperature data based on the Density-Based Spatial Clustering of Applications with Noise (DBSCAN) algorithm. Clustering-based methods treat those data that do not belong to any class as anomalies by clustering them into classes. Münz et al. [22] proposed an anomaly detection approach based on the K-means algorithm for detecting anomalies in network monitoring data while Chitrakar and Chuanhe [23] proposed a hybrid method to solve the anomaly detection problem by combining Naïve Bayes classification and k-Medoids clustering method.

Since this paper aims to perform anomaly detection on a multi-sensor system based on extracting and analyzing

potential correlations between features, the above methods do not match the goal of this paper.

2.4. Machine Learning Methods. As a typical representative of data-driven methods, machine learning can comprehensively analyze and mine potential anomalies in the high-dimensional time-series data generated by multi-sensor systems. Rauber et al. [24] designed a raw feature vector based on a set of statistical and signal characteristics and then used Support Vector Machine (SVM) to identify bearing faults. Chine et al. [25] calculated several feature parameters and used Artificial Neural Networks (ANN) for fault diagnosis of photovoltaic (PV) systems.

Although machine learning models, such as SVM [26], ANN [27], clustering algorithms [28], genetic algorithms [29], and fuzzy inference [30], can partially meet the needs of anomaly diagnosis and identification, changes in mechanical equipment load during operation can also affect the generalization ability of the models.

2.5. Deep Learning Methods. Deep learning is a branch of machine learning, and it can automatically discover features to meet the requirements of adaptive feature extraction for mechanical anomaly diagnosis. It effectively overcomes the shortcomings of traditional manual extraction of features, such as poor generalization ability and poor robustness, and reduces the uncertainty of traditional anomaly detection methods in the process of manual design and extraction. In recent years, different deep learning models, such as Deep Belief Networks (DBN), Stacked Autoencoder (SAE), Recursive Neural Network (RNN), and Conventional Neural Network (CNN), have received increasingly wide attention in intelligent anomaly detection [31]. Zhao et al. [32] proposed an approach for multi-sensor fault detection based on DBN, using deep learning models for the classification and prediction of sensor faults. Li et al. [33] used DBN for fault classification of bearings to reduce the manual operations in the detection process and to achieve intelligence in fault detection. Lei et al. [34] proposed a deep learning-based health monitoring method for mechanical equipment using frequency-domain signals as training data for Deep Neural Networks (DNN), completing adaptive feature extraction and intelligent health condition identification without the need for fault feature extraction through signal processing. Wan et al. [35] proposed a function-aware anomaly detection approach, in which both single function and short sequence patterns are considered as the function control characteristics, and a Wavelet Neural Network- (WNN-) based behavior model is established to detect function control misbehaviors caused by cyber intrusions in industrial automation. Kumar and Hati [36] proposed a CNN-based fault detection method for squirrel cage induction motor, in which small convolutional kernel and adaptive gradient optimizer were used to verify the performance of CNN model. Wilson et al. [37] proposed a deep learning-based fault diagnosis method for ship turbines using a deep bidirectional Long Short-Term Memory (LSTM) model for fast detection of turbines. Khorram et al. [38] investigated a

Convolutional Recurrent Neural Network- (CRNN-) based fault diagnosis method, where the authors fused CNN and LSTM to form a Deep Neural Network for end-to-end fault diagnosis. Deng and Hooi [39] proposed an anomaly detection method based on GDN (Graph Deviation Network) in multivariate time series, in which the relationship between sensors is firstly found by GNN (graph neural network). The expected behavior of time series is then predicated, and the anomaly is finally identified by judging whether the predicted data violates the correlation. It considers the correlation as the scoring and judgment basis of whether the prediction data is abnormal.

In a nutshell, all the methods do not consider the potential correlation between features in a multi-sensor system, except for the method proposed in [39], which only uses the correlation as a threshold to judge whether the prediction data is abnormal and does not fully consider the dynamic and continuous characteristics of correlation to directly construct an anomaly detection model. In a multi-sensor system, sensors cooperate with each other to reflect the state of an entity, and the features used to describe the same entity are usually relevant. In general, the correlation is related to the physical characteristics of the entity, so the correlation is relatively stable, and if the correlation is broken, there may be an anomaly. Therefore, it is necessary to introduce correlation into anomaly detection for the purpose of finding potential anomalies caused by feature dependencies. Moreover, due to the time stability of the correlation, using the correlation between features which are obtained by time window for anomaly detection can effectively avoid the wrong detection results caused by discrete noisy data.

3. The Proposed Method

3.1. Correlation Characteristic of Multi-sensor System. Sensor data is generally considered to be the data collected by sensors for continuous sensing of the physical world. A multi-sensor system consists of several or even plenty of sensors. These sensors are used jointly to reflect the physical world. Except for continuity [40] and high dimensionality [41], the sensor data acquired by a multi-sensor system has several correlation characteristics, discussed as follows.

3.1.1. Spatiotemporal Correlation. Sensor data is always applied to collect information about the physical world. Therefore, the sensor data can be correlated with the physical world it senses, especially in terms of time and space. In other words, there is a similarity between sensor data collected by similar sensors located in analogous time and space ranges. For example, multiple air quality monitors set up in the same environmental monitoring station at the same moment detect the same environmental indicators. Therefore, if sensor data is anomalous, the sensor data with which it has spatial-temporal correlation is more likely to be anomalous as compared to other sensor data [40].

3.1.2. Data Similarity. If the sensor's monitoring objects are similar in behavior, the sensor data which is used to portray

their behaviors should also have similarities. Take the power system as an example; the electricity meter data of household users with similar electricity consumption patterns are also approximately similar. It can be assumed that there are similarities between the data collected by similar sensors under similar behavioral, temporal, or spatial conditions. If sensor data is anomalous, the sensor data with which it has data similarity is more likely to be anomalous. That is, sensor data that disrupt data similarity may be anomalous. In a real-life production environment, monitoring data are relatively stable in most cases [42]. When a special event happens, the surrounding sensors usually monitor the situation and obtain data at the same time [43].

3.1.3. Data Correlation. There may be correlations between the collected data of different sensors monitoring the same physical entity, including positive correlation and negative correlation. For example, the current and voltage collected by smart meters are correlated with power while the line loss is positively correlated with the current in the transmission system. When this correlation fluctuates, it may mark an anomaly of the physical entity; therefore, the correlation between different sensor data can also be used as a basis for determining anomalies. In fact, sensors always work together. Even if single sensor data is normal, it might be anomalous when it is calculated jointly with other sensor data [44].

3.2. Problem Statement. In a multi-sensor system, the training data usually consists of multiple sensors' data, that is, multivariate time-series data with M features from N sensors. The multivariate time-series data is expressed as the following formula:

$$S_{t,w} = (s^1, s^2, \dots, s^m)^T \in R^{m \times w}. \quad (1)$$

In (1), t denotes the current timestamp, w denotes the size of the time window, and m denotes the feature dimension of the temporal data. Moreover, s^i ($i = 1, 2, \dots, m$) denotes the column vector composed of the values of feature i in the dataset over the time window from timestamp t to timestamp $t + w - 1$, and $S_{t,w}$ denotes a fragment of the time series. Using $s^k = (s^k_t, s^k_{t+1}, \dots, s^k_{t+w-1})^T \in R^w$ denotes the value vector of the k th feature within a time window.

The goal of this paper is to identify anomalies in physical entities characterized by multivariate time-series data generated by the same sensors but over a different time slice. The output of the proposed method is a group of labels used to show the result of anomaly detection for each time window; i.e., $\text{label}_t \in \{-1, 1\}$, in which $\text{label}_t = 1$ indicates that the time window t is normal, and $\text{label}_t = -1$ is the opposite.

3.3. Method Overview. The goal of the proposed correlation-based anomaly detection method is to capture the temporal correlations between sensors and then identify whether the normal temporal correlation patterns between sensors are violated. As shown in Figure 1, the proposed method mainly

involves two parts, namely correlation-based graph model construction and graph-based anomaly detection.

3.3.1. Correlation-Based Graph Model Construction. It represents the unique characteristics of the multiple sensors for each time window with multivariate time-series data, and these multidimension time series are converted into a set of graph structures.

3.3.2. Graph-Based Anomaly Detection. It trains an anomaly detection model with a structured-sensitive GNN and then identifies deviations from the learned temporal correlations.

3.4. Correlation-Based Graph Model Construction. Data captured by a multi-sensor system are represented as multivariate temporal data; i.e., there are temporal correlations between different sensors. To represent and analyze the correlations, these multidimensional time-series data can be transformed into a set of temporal correlation graphs $G = (V, E)$ according to the time window. A temporal correlation graph is an undirected graph, where the nodes represent features in the multi-sensor systems while the edges represent the correlation between these features.

3.4.1. Construction of Nodes. Each feature of the multi-sensor system is considered as a node in the temporal correlation graph, and the node information consists of $s^i = (s^i_p, s^i_{t+1}, \dots, s^i_{t+w-1})^T$, where $i = 1, 2, \dots, m$, where m is the total number of nodes.

3.4.2. Construction of Edges. The edges in a temporal correlation graph are defined as the temporal correlations between nodes. Take the example of constructing an edge between node V_i and node V_j ; the edge is depicted as a row vector $e = (corr_1, corr_2, \dots, corr_k)$ consisting of k kinds of correlation coefficients between node V_i and V_j on the time series $S_{t,w}$. To comprehensively measure the correlation between nodes, this study fuses multiple correlation coefficients to constitute the edge information, including Manhattan distance, Euclidean distance, Chebyshev distance, Pearson correlation coefficient, and Spearman correlation coefficient.

By calculating the inter-feature correlation coefficients of each pair of features, the corresponding inter-feature correlation coefficient matrix for a time window can be obtained, as shown in Figure 2(a). If the inter-feature correlation coefficient matrices of continuous-time windows are combined, a group of multidimensional temporal correlation matrices are built, as shown in Figure 2(b).

3.4.3. Construction of Temporal Correlation Graphs. To identify the fluctuation of correlations between features, the proposed method converts each matrix array into a temporal correlation graph. Subsequently, the correlation strength between pairs of features is calculated according to the correlation coefficient. Then, the value of correlation

coefficient is further analyzed; if it is within the threshold of the correlation coefficient in the normal mode, the edge is reserved; otherwise, the edge is removed from the graph. That is, a temporal correlation graph can be an incomplete graph, and the structures of different temporal correlation graphs may not be the same, as shown in Figure 3.

When the multidimensional time series are converted into a set of temporal correlation graphs, these graphs are used as an input for the graph-based deep learning algorithm. Besides, the proposed method is still a supervised one; the correlations among features always have high stability. Since anomalies in a multi-sensor system are usually reflected as non-single outliers and the significant fluctuations in the correlations between features in different time windows may exist, a label is assigned to each temporal correlation graph, which is used to mark whether the time series is abnormal or not. If anomalies exist, the graph label is set to positive; otherwise, it is set to negative.

3.5. Graph-Based Anomaly Detection. The method uses temporal correlation graphs to represent features and the correlations between them. Changes in the graph structure, point, and edge attributes can reflect changes in the degree of dependency between features. Therefore, an anomaly detection of multi-sensor systems can be converted into a binary classification problem based on the GNN model.

3.5.1. Construction of Graph-Based Anomaly Detection Model. Figure 4 shows the network architecture of the anomaly detection model.

The correlation between features is also a kind of time-series data, whose fluctuation is universal. In this paper, the edges of temporal correlation graph are conducted based on the strength of correlation between features. If the correlation is very low or even does not exist, there is no edge between features. That is, the temporal correlation graphs are heterogeneous. Therefore, a structure-sensitive graph convolution neural network, GIN (Graph Isomorphism Network), is applied to the temporal correlation graphs by encoding feature and the correlation between features according to the requirements of GIN. Then, Global Add pooling (GAP) which refers to the default pooling function `global_add_pool` in `torch_geometric` maps the features of different samples to the same size and the pooled features are output to the Softmax classifier for classification after being mapped to the sample label space by the fully connected (FC) layer. In addition, for this model, cross-entropy loss is selected as the training loss function, and Adam is used to optimize the neural network.

3.5.2. Anomaly Detection. Figure 5 shows the workflow of graph-based anomaly detection. The multidimensional time series is firstly transformed into a set of inter-feature correlation matrices, and then the corresponding temporal correlation graphs are established. The graph-based anomaly detection model treats these graphs as input and produces output based on the binary classification.

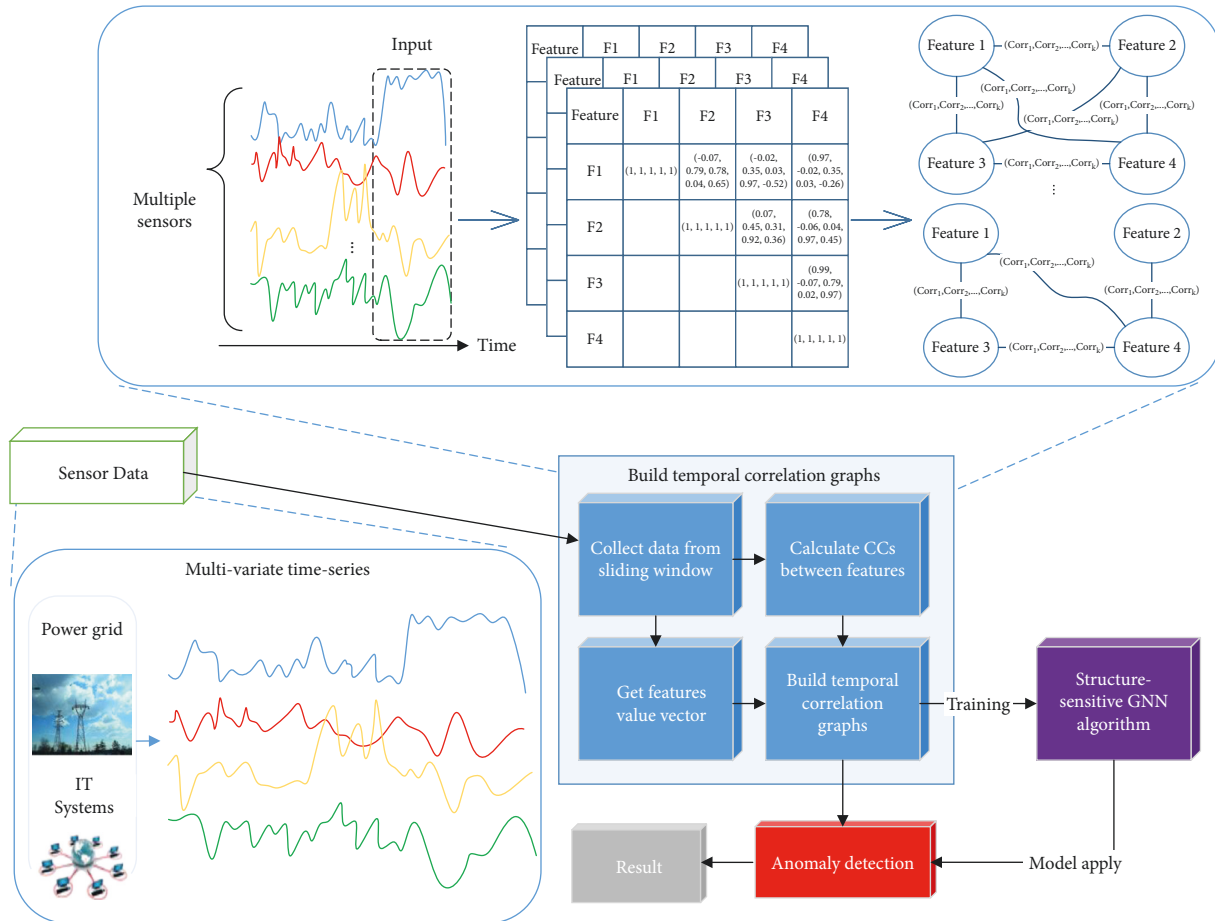


FIGURE 1: Overview of the proposed method.

Feature	F1	F2	F3	F4
F1	(1, 1, 1, 1)	(-0.07, 0.79, 0.78, 0.04, 0.65)	(-0.02, 0.35, 0.03, 0.97, -0.52)	(0.97, -0.02, 0.35, 0.03, -0.26)
F2		(1, 1, 1, 1)	(0.07, 0.45, 0.31, 0.92, 0.36)	(0.78, -0.06, 0.04, 0.97, 0.45)
F3			(1, 1, 1, 1)	(0.99, -0.07, 0.79, 0.02, 0.97)
F4				(1, 1, 1, 1)

(a)

Feature	F1	F2	F3	F4
Feature	F1	F2	F3	F4
F1	(1, 1, 1, 1)	(-0.07, 0.79, 0.78, 0.04, 0.65)	(-0.02, 0.35, 0.03, 0.97, -0.52)	(0.97, -0.02, 0.35, 0.03, -0.26)
F2		(1, 1, 1, 1)	(0.07, 0.45, 0.31, 0.92, 0.36)	(0.78, -0.06, 0.04, 0.97, 0.45)
F3			(1, 1, 1, 1)	(0.99, -0.07, 0.79, 0.02, 0.97)
F4				(1, 1, 1, 1)

(b)

FIGURE 2: Temporal correlation matrices: (a) inter-feature correlation coefficient matrix; (b) multidimensional temporal correlation matrices.

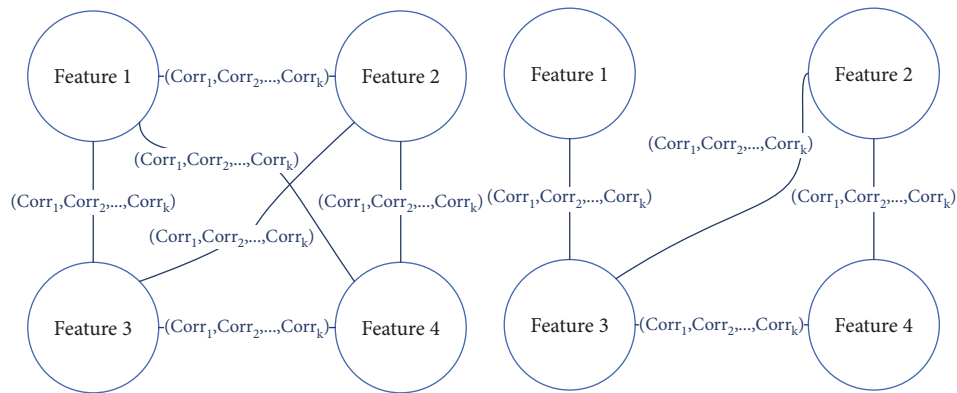


FIGURE 3: Examples of temporal correlation graphs.

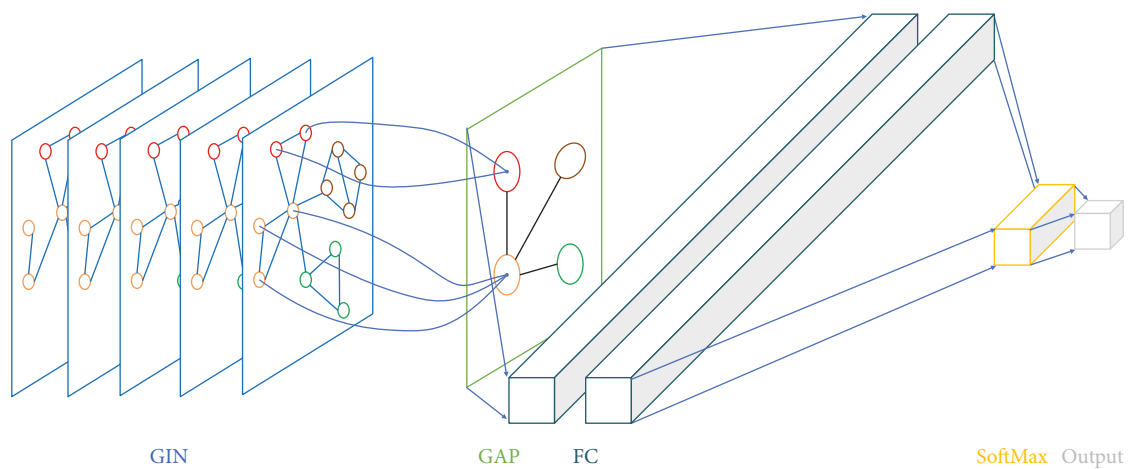


FIGURE 4: Network architecture.

4. Evaluation

4.1. Experimental Setting. Dataset: In order to evaluate the validity of the proposed method, this paper conducted extensive experiments on three industrial datasets. These datasets are described in detail as follows:

Dataset 1: Air Quality1 is from the air quality online detection and analysis platform (<https://www.aqistudy.cn/historydata/>). The platform contains air quality and meteorological data collected hourly in more than 300 cities from December 2013 to December 2021. Dataset 1 selected the historical data from January 2014 to December 2018 in Air Quality1, including AQI, $PM_{2.5}$, PM_{10} , CO, NO_2 , SO_2 , and O_3 . Among them, AQI is used to measure air quality based on the standard of “Technical Regulation on Ambient Air Quality Index (on trial)” [45]. The data description of other features in Dataset 1 is shown in Table 1, in which the unit of each feature is $\mu g/m^3$.

Dataset 2: Air Quality2 is from Kaggle (<https://www.kaggle.com/amritpal333/tps-july-2021-original-dataset-clean>). The installation is in a heavily polluted area of an Italian city, and the data are collected through an embedded air quality chemical multi-sensor unit containing five metal oxide sensors’ data and other relevant data. The five metal oxide sensors’ data refer to carbon monoxide, total nitrogen

oxides, non-methane hydrocarbons, NO_2 , and benzene. Air Quality2 is accumulated according to the “Ambient Air Quality Standards” [46]. The dataset contains six kinds of air quality data from March 2004 to February 2005, with data collected hourly. After data cleaning, a total of 827 time points were included. To ensure the scale, Dataset 2 was constructed by replicating Air Quality2, and the expanded dataset contains data of 414327 time points. The data description of Dataset 2 is shown in Table 2, in which the units are, respectively, mg/m^3 , $\mu g/m^3$, $\mu g/m^3$, $^{\circ}C$, %, and g/m^3 .

Dataset 3: The gas chromatography data was obtained from the industrial dataset of power enterprises, consisting of the dissolved gas content of insulating oil of oil-filled power equipment. It is the basis for power generation and supply enterprises to judge whether there are latent overheating, discharge, and other faults of oil-filled power equipment in operation. Moreover, it is also the necessary data for oil-filled electrical equipment manufacturers to carry out factory inspection of their equipment. Dataset 3 is time-series data consisting of transformer oil chromatography data, containing six data items, namely, H_2 , CH_4 , C_2H_4 , CO, C_2H_6 , and total hydrocarbons, containing 20128 time points. Based on the “Guide to the Analysis and the Diagnosis of Gases Dissolved in Transformer Oil” [47] issued by the National Energy Administration, if the gas

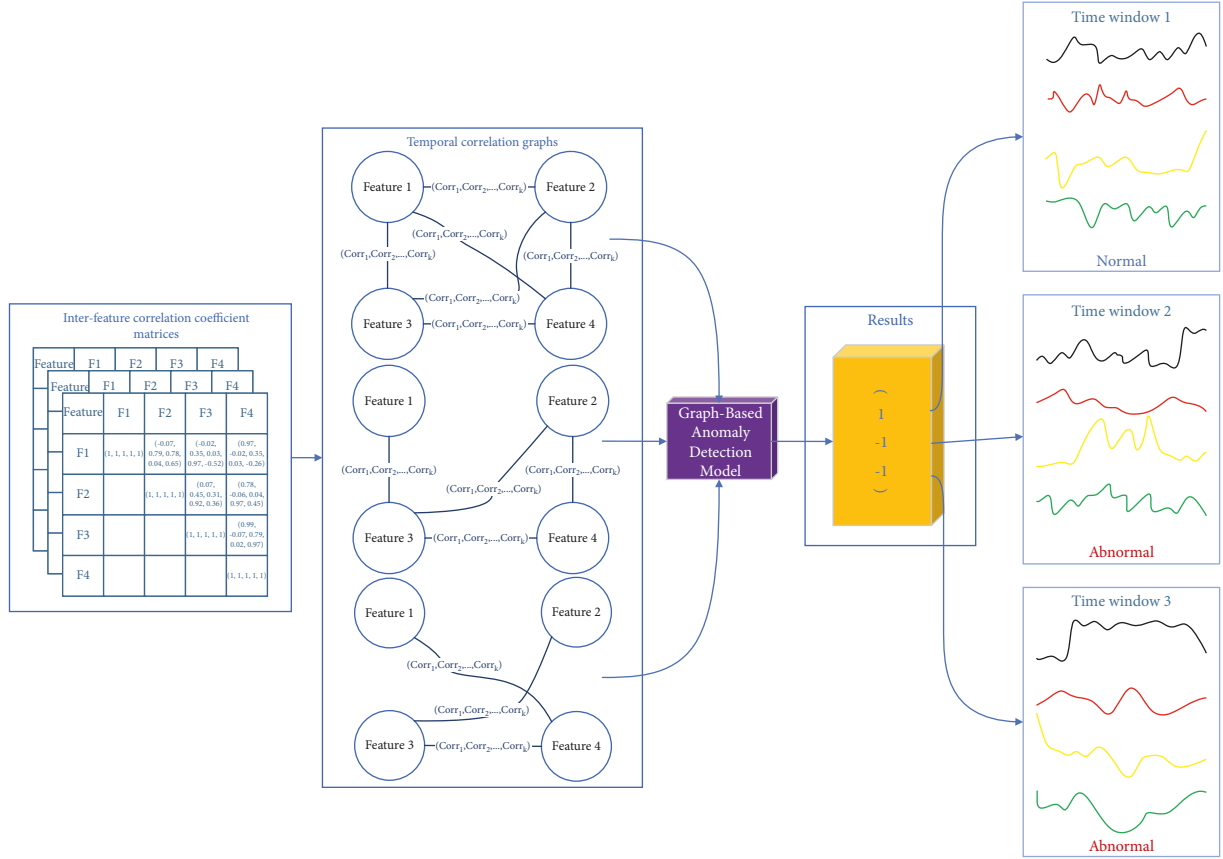


FIGURE 5: The workflow of the graph-based anomaly detection.

TABLE 1: Data description of Dataset 1.

Feature	Range	Threshold
PM _{2.5}	0~885.0	75
PM ₁₀	0~1700.0	150
SO ₂	0~429.0	150
CO	0~10.4	4
NO ₂	0~183.0	80
O ₃	0~311.0	160

TABLE 2: Data description of Dataset 2.

Feature	Range	Threshold
CO	0.3~8.1	4
NO _x	12.0~478.0	100
NO ₂	19.0~196.0	80
Temperature	6.30~30.00	-
Relative humidity (%)	14.90~83.20	-
Absolute humidity	0.4023~1.4852	-

content data exceeds the threshold value, there may be an anomaly, and if multiple gas contents are consistently abnormal, the transformer can be judged to be faulty. The data description of Dataset 3 is shown in Table 3, in which the unit of each feature is $\mu\text{L}/\text{L}$.

In the field of anomaly detection, if the percentage of negative samples is low, it will affect the quality of the fault model and influence the detection effect. In addition, to fully

TABLE 3: Data description of Dataset 3.

Feature	Range	Threshold
H ₂	1.357~171.160	150
CH ₄	0.042~30.183	-
C ₂ H ₄	0~15.082	-
C ₂ H ₂	0~15.000	5
CO	12.996~1202.545	-
Total hydrocarbon	2.242~161.771	150

evaluate the validity of the proposed method, it is essential to conduct experiments on datasets with different anomaly distributions. Therefore, a data enhancement algorithm whose framework is described in Algorithm 1 is used to inject anomalies into the original data. The method of data augmentation is as follows: For each passing step, an attribute is selected, and the original time-series array is modified by the data augmentation sequence array within the data augmentation window.

The distribution of anomalies for the datasets is listed in Table 4.

Baselines: The following algorithms are selected for comparison for the sake of verifying the effectiveness of the proposed method. The detailed description of these comparison algorithms is as follows.

Decision Tree: The purpose of decision trees is to build a model which can forecast the value of a specified variable according to a set of decision rules extrapolated from the

Algorithm 1 : Data augmentation in the dataset.

Input: The moving steps of data augmentation window len_a ; the size of data augmentation window w_a ; the number of attributes of time-series data m ; the data augmentation sequence array S ; the original time-series data array D ;

Output: The time-series data array D_a after data augmentation;

```

(1): function DATAAUGMENTATION ( $D, S, m, w_a, len_a$ )
(2):  $r_m \leftarrow 0$ 
(3):  $i \leftarrow 0$ 
(4):  $length \leftarrow \text{sizeof}(D)$ 
(5): while  $i < length$  do
(6):  $i \leftarrow i + len_a$ 
(7): For  $j = 0 \rightarrow w_a$  do
(8):  $D[i + j][r_m] \leftarrow D[i + j][r_m] + S[r_m]$ 
(9): end for
(10): if  $r_m + 1 < m$  then
(11):  $r_m \leftarrow r_m + 1$ 
(12): else
(13):  $r_m \leftarrow 0$ 
(14): end if
(15): end while
(16):  $D_a \leftarrow D$ 
(17): return  $D_a$ 
(18): end function

```

ALGORITHM 1: Framework of data augmentation in the dataset.

data characteristics. It can be used as a nonparametric supervised algorithm for classification.

Logistic Regression: Logistic regression is used to evaluate the possibility of a particular event by settling binary classification problems through the machine learning method.

Naïve Bayes: As a supervised algorithm, Naïve Bayes is a simple and effective classification algorithm based on Bayes' theorem.

Quadratic Discriminant Analysis: Quadratic Discriminant Analysis (QDA) is a classifier that makes classifications according to the difference in covariance, which is particularly useful for many features.

Support Vector Machine: Support Vector Machine (SVM) is a binary classification algorithm that maps the feature vector of each entity to a point in the space and classifies these space points by finding an optimal separating hyperplane.

Convolutional Neural Networks: As a deep learning model, Convolutional Neural Network (CNN) is a feed forward neural network based on convolution calculation, which can classify the input information according to the hierarchical structure.

Evaluation Metrics: Although anomalies are common, the proportion of anomalies in a dataset is not high, so most of the data used for anomaly detection are unbalanced data. In the classification problem of balanced data, accuracy is a common evaluation metric. In the classification of unbalanced data, F1 score and AUC (Area Under Curve) score are common evaluation metrics. Thus, F1 score and AUC score are used to measure the performance of the proposed method.

F1 Score: Precision focuses on evaluating the proportion of real positive data in all data predicted as positive, while

TABLE 4: Detailed information of datasets in the experiments.

Dataset	Positive samples	Negative samples	Negative ratio (%)
Dataset 1	4142	6807	37.82
Dataset 2	1562	256	85.90
Dataset 3	898	3126	22.30

TABLE 5: Settings of hyperparameters.

Hyperparameter	Dataset 1	Dataset 2	Dataset 3
window_size	5	5	5
threshold_1	0.25	0.25	0.05
threshold_2	2	2	3
learning_rate	0.01	0.01	0.01
batch_size	10	10	10

recall focuses on assessing how much of all the positive data has been successfully predicted as positive. F1 score is a harmonic mean of precision and recall. In general, the value of F1 score will be high only when both precision and recall are good.

AUC Score: Facing the unbalanced data, ROC (Receiver Operating Characteristic) curve ignores the imbalance of samples and only considers the classification ability of the model. That is, when the proportion of positive and negative samples changes, the discrimination ability of the model remains unchanged, and the shape of ROC curve will not change. However, ROC is not intuitive enough, so AUC which refers to the area under the ROC curve becomes a way to reflect the classification ability expressed by the ROC curve. Since AUC score is robust to the data with heterogeneous distribution of positive and negative samples, this

TABLE 6: Anomaly detection accuracy in terms of F1 score, on three datasets.

Method	Dataset 1		Dataset 2		Dataset 3	
	Mean	Standard deviation	Mean	Standard deviation	Mean	Standard deviation
Logistic regression	0.87	0.007	0.82	0.035	0.94	0.006
Decision tree	0.91	0.006	0.83	0.086	0.97	0.011
Naïve Bayes	0.89	0.008	0.70	0.042	0.86	0.017
QDA	0.88	0.027	0.86	0.066	0.87	0.021
SVM	0.52	0.008	0.40	0.047	0.82	0.032
CNN	0.90	0.005	0.86	0.027	0.95	0.005
Proposed method	0.92	0.006	0.90	0.031	0.95	0.004

Bold font is to highlight the results of the proposed method.

paper uses AUC score as a metric for performance evaluation, and the larger the AUC, the better the effect.

Environments: A XenServer virtual machine is used to conduct these experiments, and its configuration is as follows: CentOS7.3, one Intel Core i5-1135G7 processor, 16.00 GB RAM, 500 GB hard disk. The proposed method and the baselines are all implemented in Python and PyTorch 1.6.0.

Hyperparameter Settings: The model in this paper involves five hyperparameters, which are *window_size*, *learning_rate*, *batch_size*, correlation coefficient-related parameter *threshold_1*, and feature value anomaly-related parameter *threshold_2*. *window_size* is the size of the sliding window, which can collect data on the time series according to the specified length; *learning_rate* and *batch_size* are the parameters used to train the deep learning model; *threshold_1* is the upper limit of the inter-feature correlation coefficient fluctuation; *threshold_2* is the upper limit of feature value anomalies within the sliding window. Table 5 gives the setting of these hyperparameters in the experiments.

In addition, the model setting for the structure-sensitive GNN is as follows: the model was trained for 300 epochs with a learning rate of 0.01 and a batch size of 10.

4.2. Experiments

4.2.1. Experiment on Accuracy. The mean and standard deviation are two relevant statistical indicators whose combined use can describe the overall characteristics of the data more comprehensively. The former indicator shows the concentration tendency of the data, while the latter indicator shows the off-center tendency of the data. In other words, the smaller the standard deviation, the better the representativeness of the mean. Table 6 shows the accuracy of anomaly detection by listing the mean and standard deviation of F1 scores of the proposed method and the baselines in three datasets.

As shown in Table 6, the standard deviation values of the F1 score in the three datasets are, respectively, 0.006, 0.031, and 0.004. The two standard deviation values of CNN are 0.001 lower than or equal to those of the proposed method, while the other 16 values are not as good as those of the proposed method. This result shows that the F1 score of the proposed method is more concentrated and the proposed method is more stable. The mean values of the F1 score in the

three datasets are, respectively, 0.92, 0.90, and 0.95. Among all the mean values of F1 score, only the value of the decision tree on Dataset 3 is 0.02 higher than that of the proposed method. This proves that the proposed method outperforms all the other baselines. In addition, all the three mean values of the F1 score of the proposed method are more than 0.90, while the baselines failed to do so. Overall, the F1 score of the proposed method is low for off-center tendency and high for concentration tendency. F1 score is a comprehensive evaluation of the precision and recall of a method. The results indicate that the method proposed in this paper achieves well balanced precision and recall, which shows that both precision and recall are good.

4.2.2. Experiment on Classification Ability. In Table 7, the classification ability of different anomaly detection methods in terms of the mean value and standard deviation of AUC score on the three datasets is given.

As shown in Table 7, the standard deviation values of the AUC score in the three datasets are, respectively, 0.005, 0.009, and 0.005. Only three standard deviation values are, respectively, 0.001, 0.001, and 0.002 lower than those of the proposed method, while the other 15 values are not as good as those of the proposed method. This result indicates that the mean value of the AUC score of the proposed method is quite concentrated. The mean values of the AUC score in the three datasets are, respectively, 0.96, 0.98, and 0.95. Except that the value of the decision tree on Dataset 3 is 0.01 higher than that of the proposed method, the proposed method outperforms all the baselines. The mean values of the AUC score of the proposed method on the three datasets all exceed 0.95, while the other methods do not reach this value. AUC score reflects the classification ability of the models. Therefore, the results illustrate that the method proposed in this paper is superior to the baselines in the classification ability on all the three datasets no matter whether the datasets are balanced or not.

In view of the above experiments, it is found that the method based on the neural network has better performance. Meanwhile, the decision tree method also has good results on Dataset 3. The reason is that Dataset 3 is the actual measurement data of the substation equipment of the National Grid, and the original dataset does not contain anomalies, while the injected anomalies are more obviously different from the normal data. Since the decision tree uses a tree structure, it is easier to decide if the two categories are

TABLE 7: Classification ability of anomaly detection in terms of AUC score, on three datasets.

Method	Dataset 1		Dataset 2		Dataset 3	
	Mean	Standard deviation	Mean	Standard deviation	Mean	Standard deviation
Logistic regression	0.90	0.006	0.98	0.008	0.95	0.008
Decision tree	0.90	0.006	0.89	0.051	0.96	0.012
Naïve Bayes	0.93	0.007	0.96	0.010	0.84	0.025
QDA	0.92	0.009	0.91	0.030	0.92	0.020
SVM	0.75	0.012	0.81	0.022	0.68	0.042
CNN	0.96	0.004	0.96	0.007	0.93	0.006
Proposed method	0.96	0.005	0.98	0.009	0.95	0.005

Bold font is to highlight the results of the proposed method.

completely different when binary classification is performed, so its classification results become better. However, the F1 score and AUC score of the decision tree in Dataset 1 and Dataset 2 are not as good as the proposed method. That is, the stability of the decision tree is lower than that of the proposed method. In brief, the experimental results of the proposed method on all three datasets illustrated that the method introduced in this paper is a better classifier than the baseline methods by combining the two metrics, especially for the anomaly detection problem in which unbalanced data may exist.

5. Conclusion

For the anomaly detection problem of multi-sensor systems, this paper proposes an anomaly detection method which innovatively makes use of the correlation between features and transforms the anomaly detection of multivariate time-series data into graph classification problem. Since the correlation of features fluctuates with time, the concept of temporal correlation graph is firstly proposed, and the method in which both the feature and the correlation between features are, respectively, encoded into nodes and edges is given to construct the temporal correlation graph. Subsequently, the graph classification model is established for the constructed graph structure data which may have structural differences by the structured-sensitive GNN. Finally, the anomalies of the multi-sensor system are identified by determining whether the graph data are anomalous. The results of the experiments show that the mean values of F1 score and AUC score of the proposed method exceed 0.90 and 0.95, respectively, which are better than those of other baseline methods. That is, the proposed method achieves well balanced precision and recall and is a better classifier which provides better discrimination. Therefore, the proposed method can effectively identify the physical entity anomalies reflected by multidimensional time series in multi-sensor systems. Future research will focus on conducting more abundant experiments to analyze the influence of graph-related attributes and labels on the classification effect and to study more domain-targeted anomaly detection methods for multi-sensor systems.

Data Availability

Dataset 1 and Dataset 2 used to support the findings of this study are included within the article. Dataset 3 used to

support the findings of this study was supplied by China State Grid under license and so cannot be made freely available. Requests for access to these data should be made to the corresponding author for an application of joint research.

Conflicts of Interest

The authors declare that there are no conflicts of interest regarding the publication of this paper.

Acknowledgments

This work was supported by the National Natural Science Foundation of China (No. 61902051).

References

- [1] H. Jayakumar, K. Lee, and W. S. Lee, "Powering the internet of things," in *Proceedings of the 2014 international symposium on Low power electronics and design*, vol. 2014, pp. 375–380, La Jolla, CA, USA, August. 11-13. 2014.
- [2] T. R. Gadekallu, Q. V. Pham, D. C. Nguyen et al., "Blockchain for edge of things: applications, opportunities, and challenges," *IEEE Internet of Things Journal*, vol. 9, no. 2, pp. 964–988, 2021.
- [3] Y. Yu, S. Fan, and G. Peng, "Study on application of digital twin model in product configuration management," *Aeronautical Manufacturing Technology*, vol. 526, no. 07, pp. 41–45, 2017.
- [4] J. Jiao, M. Zhao, J. Lin, and K. Liang, "Hierarchical discriminating sparse coding for weak fault feature extraction of rolling bearings," *Reliability Engineering & System Safety*, vol. 184, pp. 41–54, 2019.
- [5] Y. Lei and Z. He, "Advances in applications of hybrid intelligent fault diagnosis and prognosis technique," *Journal of Vibration and Shock*, vol. 30, no. 9, pp. 129–135, 2011.
- [6] H. Shao, J. Cheng, and H. Jiang, "Enhanced deep gated recurrent unit and complex wavelet packet energy moment entropy for early fault prognosis of bearing," *Knowledge-Based Systems*, vol. 188, pp. 1–14, 2020.
- [7] D. M. Hawkins, *Identification of Outliers*, Springer, 1st edition, 1980.
- [8] J. Freeman, "Outliers in statistical data (3rd edition)," *Journal of the Operational Research Society*, vol. 46, no. 8, pp. 1034–1035, 2017.
- [9] P.-C. Chang and J.-L. Wu, "A critical feature extraction by kernel PCA in stock trading model," *Soft Computing*, vol. 19, no. 5, pp. 1393–1408, 2015.

- [10] J. Laurikkala, M. Juhola, E. Kentala et al., "Informal identification of outliers in medical data," in *Proceedings of the 5th International Workshop on Intelligent Data Analysis in Medicine and Pharmacology*, vol. 1, pp. 20–24, Berlin, Germany, August. 20-25. 2000.
- [11] S. Ramaswamy, R. Rastogi, and K. Shim, "Efficient algorithms for mining outliers from large data sets," *ACM SIGMOD Record*, vol. 29, no. 2, pp. 427–438, 2000.
- [12] R. Frank, W. Jin, and M. Ester, "Efficiently mining regional outliers in spatial data," in *Proceedings of the 10th International Conference on Advances in Spatial & Temporal Databases*, vol. 2007, pp. 112–129, Boston, MA, USA, July 2007.
- [13] A. Hinneburg, "An efficient approach to clustering in large multimedia databases with noise," in *Proceedings of the 4th International Conferences on Knowledge Discovery and Data Mining*, vol. 1998, pp. 58–65, New York, NY, USA, August 1998.
- [14] F. Wang, X. Gao, X. Jia et al., "An anomaly detection ensemble algorithm for power dispatching data based on log-interval isolation," *Power System Technology*, vol. 45, no. 12, pp. 4818–4827, 2021.
- [15] L. Portnoy, E. Eskin, and S. Stolfo, "Intrusion detection with unlabeled data using clustering," in *Proceedings of the ACM CSS Workshop on Data Mining Applied to Security*, vol. 2001, pp. 1–14, Philadelphia, USA, Nov 2001.
- [16] B. Kasliwal, S. Bhatia, and S. Saini, "A hybrid anomaly detection model using G-LDA," in *Proceedings of the 2014 IEEE International Advance Computing Conference (IACC)*, vol. 2014, pp. 288–293, Gurgaon, India, Feb. 21-22. 2014.
- [17] Y. Zhang, B. Du, and L. Zhang, "A low-rank and sparse matrix decomposition-based mahalanobis distance method for hyperspectral anomaly detection," *IEEE Transactions on Geoscience and Remote Sensing*, vol. 54, no. 3, pp. 1–14, 2015.
- [18] G. Pu, L. Wang, J. Shen, and F. Dong, "A hybrid unsupervised clustering-based anomaly detection method," *Tsinghua Science and Technology*, vol. 26, no. 2, pp. 146–153, 2021.
- [19] R. Laxhammar and F. Görän, "Sequential conformal anomaly detection in trajectories based on hausdorff distance," in *Proceedings of the 14th International Conference on Information Fusion*, vol. 2011, pp. 1–8, Chicago, IL, USA, July. 5-8. 2011.
- [20] T. Huang, Y. Zhu, and Q. Zhang, "An LOF-based adaptive anomaly detection scheme for cloud computing," in *Proceedings of the 2013 IEEE 37th Annual Computer Software and Applications Conference Workshops*, vol. 2013, pp. 206–211, Kyoto, Japan, Jul. 22-26. 2013.
- [21] M. Celik, F. Dadasercelik, and A. S. Dokuz, "Anomaly detection in temperature data using DBSCAN algorithm," in *Proceedings of the International Symposium on Innovations in Intelligent Systems & Applications*, vol. 2011, pp. 91–95, Istanbul, Turkey, June. 15-18. 2011.
- [22] M. Gerhard, S. Li, and G. Carle, *Traffic Anomaly Detection Using K-Means Clustering*, GI/ITG Workshop MMBnet, Hamburg, Germany, 2007pp. 1–8, Sep. 13-14.
- [23] R. Chitrakar and H. Chuanhe, "Anomaly detection using Support Vector Machine classification with k-Medoids clustering," in *Proceedings of the Third Asian Himalayas International Conference on Internet*, vol. 2012, pp. 1–6, Kathmandu, Nepal, November. 23-25. 2012.
- [24] T. W. Rauber, F. De Assis Boldt, and F. M. Varejao, "Heterogeneous feature models and feature selection applied to bearing fault diagnosis," *IEEE Transactions on Industrial Electronics*, vol. 62, no. 1, pp. 637–646, 2014.
- [25] W. Chine, A. Mellit, V. Lughi, A. Malek, G. Sulligoi, and A. Massi Pavan, "A novel fault diagnosis technique for photovoltaic systems based on artificial neural networks," *Renewable Energy*, vol. 90, pp. 501–512, 2016.
- [26] R. S. Gunerkar, A. K. Jalan, and S. U. Belgamwar, "Fault diagnosis of rolling element bearing based on artificial neural network," *Journal of Mechanical Science and Technology*, vol. 33, no. 2, pp. 505–511, 2019.
- [27] N. Pandeeswari and G. Kumar, "Anomaly detection system in cloud environment using fuzzy clustering based ANN," *Mobile Networks and Applications*, vol. 21, no. 3, pp. 494–505, 2016.
- [28] P. Li, O. Niggemann, and B. Hammer, "A geometric approach to clustering based anomaly detection for industrial applications," in *Proceedings of the 44th Annual Conference of the IEEE Industrial Electronics Society*, vol. 2018, pp. 5345–5352, Washington D.C, USA, October. 21-23. 2018.
- [29] P. Krishnamurthy, F. Khorrami, S. Schmidt, and K. Wright, "Machine learning for netflow anomaly detection with human-readable annotations," *IEEE Transactions on Network and Service Management*, vol. 18, no. 2, pp. 1885–1898, 2021.
- [30] D. Wijayasekara, O. Linda, M. Manic, and C. Rieger, "FN-DFE: fuzzy-neural data fusion engine for enhanced resilient state-awareness of hybrid energy systems," *IEEE Transactions on Cybernetics*, vol. 44, no. 11, pp. 2065–2075, 2014.
- [31] T. Praveen Kumar, M. Saimurugan, R. B. Hari Haran, S. Siddharth, and K. I. Ramachandran, "A multi-sensor information fusion for fault diagnosis of a gearbox utilizing discrete wavelet features," *Measurement Science and Technology*, vol. 30, no. 8, Article ID 085101, 2019.
- [32] G. Zhao, G. Zhang, and Q. Ge, "Research advances in fault diagnosis and prognostic based on deep learning," in *Proceedings of the Prognostics & System Health Management Conference*, vol. 2016, pp. 1–6, Chengdu, China, October. 19-21. 2016.
- [33] W. Li, W. Shan, and X. Zeng, "Bearing fault identification based on deep belief network," *Journal of Vibration Engineering*, vol. 29, no. 02, pp. 340–347, 2016.
- [34] Y. Lei, F. Jia, X. Zhou et al., "A deep learning-based method for machinery health monitoring with big data," *Journal of Mechanical Engineering*, vol. 51, no. 21, pp. 49–56, 2015.
- [35] M. Wan, Y. Song, Y. Jing, and J. Wang, "Function-aware anomaly detection based on wavelet neural network for industrial control c," *Security and Communication Networks*, vol. 2018, Article ID 5103270, 11 pages, 2018.
- [36] P. Kumar and A. Shankar Hati, "Convolutional neural network with batch normalisation for fault detection in squirrel cage induction motor," *IET Electric Power Applications*, vol. 15, no. 1, pp. 39–50, 2021.
- [37] D. Wilson, S. Passmore, Y. Tang et al., "Bidirectional long short-term memory networks for rapid fault detection in marine hydrokinetic turbines," in *Proceedings of the 17th IEEE International Conference on Machine Learning and Applications (ICMLA)*, vol. 2018, pp. 495–500, Orlando, Florida, December. 17-18. 2018.
- [38] A. Khorram, M. Khalooei, and M. Rezaghi, "End-to-end CNN + LSTM deep learning approach for bearing fault diagnosis," *Applied Intelligence*, vol. 51, no. 2, pp. 736–751, 2021.
- [39] A. Deng and B. Hooi, "Graph neural network-based anomaly detection in multivariate time series," in *Proceedings of the 35th AAAI Conference on Artificial Intelligence*, vol. 35, no. 5, pp. 4027–4035, Vancouver, BC, Canada, February. 2-9. 2021.
- [40] C. Zhou, S. Huang, N. Xiong et al., "Design and analysis of multimodel-based anomaly intrusion detection systems in

- industrial process automation,” *IEEE Transactions on Systems, Man, and Cybernetics: Systems*, vol. 45, no. 10, pp. 1345–1360, 2015.
- [41] R. Wan, N. Xiong, and Q. Hu, “Similarity-aware data aggregation using fuzzy c-means approach for wireless sensor networks,” *EURASIP Journal on Wireless Communications and Networking*, vol. 2019, no. 1, pp. 1–11, 2019.
- [42] W. Budgaga, M. Malensek, and S. Lee Pallickara, “A framework for scalable real-time anomaly detection over voluminous, geospatial data streams: scalable anomaly detection over voluminous geospatial data streams,” *Concurrency and Computation: Practice and Experience*, vol. 29, no. 12, pp. 1–24, 2017.
- [43] P. Tamilselvan and P. Wang, “Failure diagnosis using deep belief learning based health state classification,” *Reliability Engineering & System Safety*, vol. 115, pp. 124–135, 2013.
- [44] J. Wang, J. Lü, and B. Zhang, “Correlation-based distributed anomaly detection algorithm,” *Journal of Computer Research and Development*, vol. 47, pp. 241–245, 2010.
- [45] Ministry of Ecology and Environment of the People’s Republic of China, *HJ 633-2012 Technical Regulation on Ambient Air Quality Index (On Trial)*, China Environmental Science Press, Beijing, China, 2012.
- [46] Ministry of Ecology and Environment of the People’s Republic of China, *GB 3095-2012 Ambient Air Quality Standards*, China Environmental Science Press, Beijing, China, 2012.
- [47] National Energy Administration, *DL/T 722-2014 Guide to the Analysis and the Diagnosis of Gases Dissolved in Transformer Oil*, China Electric Power Press, Beijing, China, 2014.

Research Article

Short Sequence Chinese-English Machine Translation Based on Generative Adversarial Networks of Emotion

Hua Wang 

School of Journalism, Nanjing University of Finance & Economics, Jiangsu, Nanjing 210000, China

Correspondence should be addressed to Hua Wang; helen_wang@nufe.edu.cn

Received 26 March 2022; Revised 25 April 2022; Accepted 11 May 2022; Published 31 May 2022

Academic Editor: Mohamed Abdelaziz

Copyright © 2022 Hua Wang. This is an open access article distributed under the Creative Commons Attribution License, which permits unrestricted use, distribution, and reproduction in any medium, provided the original work is properly cited.

With the steady growth of the global economy, the communication between countries in the world has become increasingly close. Due to its translation efficiency and other problems, the traditional manual translation has gradually failed to meet the current people's translation requirements. With the rapid development of machine-learning and deep-learning related technologies, artificial intelligence-related technologies have affected various industries, including the field of machine translation. Compared with traditional methods, neural network-based machine translation has high efficiency, so this field has attracted many scholars' intensive research. How to improve the accuracy of neural machine translation through deep learning technology is the core problem that researchers study. In this paper, the neural machine translation model based on generative adversarial network is studied to make the translation result of neural network more accurate and three-dimensional. The model uses adversarial thinking to consider the sequence of emotion direction so that the translation results are more humanized. We set up several experiments to verify the efficiency of the model, and the experimental results prove that the proposed model is suitable for Chinese-English machine translation.

1. Introduction

Since the twenty-first century, the economic level of all countries in the world has been greatly improved. In the context of economic globalization, cross-language communication between people of all countries has become more and more frequent. Different nations have their own customs and cultures, and there are great differences in language expression. How to communicate effectively across languages is a problem that must be faced and solved. Due to its translation efficiency and other problems, the traditional manual translation has gradually failed to meet the current people's translation requirements. Therefore, many people turn their attention to Machine Translation, which is an important branch of natural language processing. Machine translation is to generate the target language with the semantics of the source language unchanged through relevant computer and algorithm and other techniques. That is, to achieve equal conversion from one natural language to another [1, 2].

In the initial stage of machine translation research, the implementation of translation is mainly through the use of rule-based methods. Linguists manually compile translation rules between source language and target language, that is, rules that enable conversion between two natural languages, and then input these formulated translation rules into the system [3]. Although the method that generate conversion rules between source and destination languages has made great progress, this method almost completely depends on the quality of language rules established by linguists, and it has certain limitations in practical application. Moreover, due to the problems such as its too extensive coverage and the direct relationship between language and national culture, it is difficult to list the translation rules between source language and target language. Therefore, the failure to obtain a complete set of language rules [4, 5] is the main problem faced by rule-based machine translation. IBM put forward the Statistical Machine Translation model in 1993. Statistical Machine Translation mainly adopts the way of word alignment between source language and target language.

Statistical Machine Translation mainly obtains the conversion rules between two natural languages by learning the corpus, without the need to make conversion rules manually. However, there are still many problems in Statistical Machine Translation [6]. It relies too much on the learning of the model in the corpus and has high requirements on the accuracy of the processing steps such as word alignment, word segmentation, and translation rule extraction [7].

In recent years, with the continuous maturity of artificial intelligence technology and the rapid development of machine learning and deep learning-related technologies, deep learning has gradually been combined with different fields. How to improve the accuracy of neural machine translation through related deep learning technology is also a problem that researchers have been studying [8, 9]. Deep learning techniques are used to deal with natural language problems so that some problems faced in natural language processing have been well solved and good results have been achieved. The application of deep learning technology provides many ideas and methods for improving the accuracy and efficiency of machine translation. At present, deep learning technology is mainly used in two models in the machine translation [10]. The first is the Statistical Machine Translation model framework, which adopts neural network to improve and optimize the language model, sequencing model, and other key modules in the model framework. The second method is to construct the encoder and decoder through neural network, and use the end-to-end neural network machine translation model to realize the translation and conversion from source language to target language [11, 12]. With the deepening of research, more and more neural network machine translation algorithms are proposed.

2. Related Work

2.1. Rule-Based Machine Translation. With the birth of computers in the middle of the last century, machine translation began its exploration [13]. In 1954, IBM used the computer to translate several simple Russian sentences into English for the first time. Its translation system consists of six translation rules and 250 words [14, 15]. This experiment shows that the process of machine translation can be realized by using the method based on dictionaries and translation rules. Although it was only a preliminary success, it aroused the enthusiasm of machine translation research in the Soviet Union and other European research institutions. It greatly promoted the research progress of early machine translation. However, machine translation was completely rejected in 1966 by a report titled LANGUAGE AND MACHINES, and machine translation research suffered a setback at that point [16, 17]. With the increasingly close exchanges between countries, the communication barriers between different languages become more and more serious, and people's demand for machine translation is more and more intense. At the same time, the development of corpus linguistics and computer science has provided new possibilities for machine translation. Since then, Machine Translation has entered a period of rapid development. After decades of evolution, it has formed three stages from Rule-based Machine

Translation to Statistical Machine Translation and then to Neural Machine Translation [18–20].

The earliest machine translation method is rule-based machine translation, which realizes the conversion between source language and target language by making relevant translation rules. The process of rule-based machine translation mainly includes three steps: source language parsing, language conversion, and target language generation [21]. The first step is to parse the input source language to obtain the structural representation of the source language. The second step is language conversion. Transform the structural representation of the source language into the structural representation of the target language through the formulated translation rules. In the third step, the representation of the target language is generated into the target language by processing the corresponding rules. Early rule-based machine translation methods require manual transformation rules. Although they have high-translation accuracy for a small number of sentences, their coverage is limited, the system robustness is poor, and is very sensitive to noise in rules. The rule-based machine translation method can perform machine translation to a certain extent, but its application is very limited. This translation method almost completely depends on the language rules established by linguists, which has certain limitations in practical application. Moreover, due to the extensive and profound language, it is difficult to list all the rules contained in various kinds of language. Therefore, the inability to obtain a complete set of language rules is the main problem facing rule-based machine translation research.

2.2. Machine Translation Based on Statistics. In order to solve the problems of rule-based machine translation, statistical machine translation has become the representative method of machine translation research. A landmark event was the launch of Google's free online automatic translation system, also known as Google Translate [22], which really brought the "high-flying" technology of machine translation into people's lives. Statistical machine translation is a data-driven approach that designs probabilistic models on large-scale parallel corpora to achieve automatic translation from source language to target language. Early statistical machine translation was word-based, learning model parameters from words in the corpus. Later, phrases were used as the basis to learn model parameters, and now syntax is used as the basis to build syntactically based statistical machine translation model to further improve translation accuracy. Statistical machine translation model is one of the most widely used machine translation models. This is because statistical machine translation models have excellent translation results in machine translation in unbounded domains.

Statistical machine translation model is to obtain the parameters required by the relevant translation model through the statistical analysis and learning of a large number of parallel corpus, and then to construct the statistical translation model, and then to use the model for translation. Koehn et al. took words as the basic unit of

statistical machine translation model, extracted corresponding words of original language and target language from corpus, and proposed phrase-based statistical machine translation model [23]. Och and Ney proposed statistical machine translation based on the maximum entropy model and constructed the machine translation model through the log-linear model [24]. Later, the processing unit of the translation model is extended to include words, and a phrase-based statistical machine translation model is proposed [25]. All of the above statistical machine translation methods are syntactically based and take syntactic structure as the basic translation unit to construct translation models. Although the basic organizational structure of a sentence can be displayed through the syntax tree, the specific semantic information of the sentence cannot be expressed, which makes it difficult for the final translation to correctly represent the original sentence semantics. People gradually turn their attention to the semantic understanding of source language and target language in machine translation. In order to increase the differentiation of translation rules, Aziz et al. integrated the semantic information generated by the source language as a feature into the existing translation model, and marked the nonterminal symbols in the syntactic translation model to a certain extent through the semantic role information [26]. Wu and Fung preprocessed the translation process to realize the utilization of semantic information, reordered the candidate translation list, and marked semantic information with semantic roles [27]. Zhai et al. [28] through the predicate meta-structure made the statistical machine translation model maintain the semantic information of the original text to the maximum extent, made the semantics of source language and target language more similar, and established a semantic translation model based on the transformation of predicate meta-structure.

The charm of language lies in the fact that different words have different meanings in different situations. However, in the process of translation, these traditional machine translation models ignore the influence of contextual information on sentence semantics, ignore the context in which the sentence exists, and only focus on the translation of the sentence, which results in the lack of structural rationality and semantic coherence. Therefore, many researchers conduct machine translation research based on the whole article as a translation unit. Xiong et al. [29] proposed a statistical machine translation model based on topic transformation in order to improve the quality of discourse-level statistical machine translation. Gong et al. maintained semantic consistency of the same words and phrases in the whole document through semantic caching technology based on cohesive properties [30]. Tu et al. made a preliminary exploration of the discourse translation framework model based on discourse and proposed a statistical machine translation model that takes the rhetorical structure of discourse as the basic translation unit [31]. Statistical machine translation also has some problems. The independent parameter model structure makes the parameters of the translation model independent, which leads to the situation that the translation model cannot consider the relevance between words, leading to the existence of

sparse problem. The process of parameter optimization and training of translation model is independent and not unified. Since learning is carried out in a corpus, statistical machine translation is dependent on the corpus, and the quality of the corpus will directly affect the final translation result. Without in-depth analysis of the source language, if the model does not deal with syntactic and semantic components, it ignores the connection between words and context, which results in the inability to deal with long-distance dependence, resulting in semantic incoherence and unreasonable semantics [32].

2.3. Neural Network Machine Translation. With the development of deep learning theory, researchers have found that deep learning-related technologies can better solve these problems in statistical machine translation. Neural machine translation technology originated from the neural network probabilistic language model proposed by Bengio et al. in 2003 [33]. It represents discrete characters into continuous dense distributed vectors through neural networks, which effectively alleviates the problem of data sparsity. In 2013, Kalchbrenner and Blunsom et al. [34] from Oxford University constructed an encoder-decoder structure by using CNN and RNN. As an encoder, convolutional neural network (CNN) can obtain historical information and process variable length strings. As a decoder, recurrent neural network (RNN) can directly model translation probability. In earlier studies, deep neural network was only used as an auxiliary method for language modeling, while their study was completely composed of deep neural network, which marked the independent application of deep learning methods in machine translation. Subsequently, Sutskever et al. in Google team proposed RNN-RNN model on the basis of the former, which became the general Sequence-to-Sequence model later. The model uses recurrent neural network as the backbone network of an encoder and a decoder. Cho et al. [35] proposed that Gated Recurrent Unit (GRU) could replace LSTM to handle machine translation tasks. GRU is actually an optimization of LSTM, which simplifies the internal structure, reduces training parameters, and improves training efficiency. Sequence-to-sequence structure, understood abstractly, generates a semantic space. Source language and target language are mapped to this semantic space through neural network training. The more semantically similar words are, the closer they are in the semantic space. In 2014, Bahdanau of Youngor University in Germany proposed attention mechanism, which effectively solved this problem and brought machine translation to a new height [36]. They gave the “S-S” model ability to distinguish, so that it pays attention to the more relevant input information. The attention mechanism is essentially a small neural network trained at the same time as the S-S network. Luong et al. from Stanford proposed many variations of attention mechanism, which further enhanced the representational ability of attention mechanism. After the attention mechanism is introduced, the long-distance dependency problem can be better dealt with. The influence of the previous word on the current word can be obtained

through the attention weight, and the representation vector of the current word can be better generated.

With the proposal of attention mechanism [37] and the rapid development in the field of image, attention mechanism is gradually combined with natural language processing. Especially in machine translation, attention mechanism is introduced between the current state of the target language sequence and the hidden layer state of the source language sequence. The matching degree of these two states is measured by attention weight, so as to obtain a better representation vector of the target language. The problems of long-distance dependence and incomplete representation of vector information are effectively solved [38]. Mi et al. used punishment to improve the translation effect. If the completed part of the translation received too much attention, it would be punished and reward the unfinished part of the translation [39]. In order to obtain better translation results, Tang et al. selected the required rules through the attention mechanism in the translation process, but it also caused high-time complexity [40]. Researchers have never stopped improving the neural machine translation model and have made some achievements in improving the memory capacity of the model and expanding the depth of the translation model [41].

Although neural machine translation has surpassed statistical machine translation in many publicly evaluated translation tasks, its actual translation quality is far from the level of human expert translation, and the model of neural machine translation still needs to be optimized. Compared with phrase-based or rule-based statistical machine translation, neural machine translation lacks the basis of theoretical explanation, because deep learning itself is a “black box” approach. Besides, the complex network structure and the large number of parameters mean the need for large-scale and high-quality parallel corpus pairs. However, high-quality parallel corpus pairs are often missing among many less-popular languages. From the cyclic neural network based on attention mechanism to the convolutional neural network based on attention mechanism to the current mainstream Transformer model based on self-attention mechanism, Transformer’s parallel input combined with the self-attention mechanism makes the actual distance between the input words as 1. It effectively alleviates the long-distance dependence problem. At the same time, the computing speed is greatly improved. However, this also leads to inferior representational ability of local information as RNN and CNN, and damages relative location information. In addition to the Transformer model, there is still a lot of room for improvement in the neural machine translation model.

3. Network Framework

Bi-LSTM and Transformer are widely used in various fields of artificial intelligence. How to further improve the translation effect of Bi-LSTM and Transformer neural machine translation models which introduce attention mechanism that is the focus of this paper and also the innovation of this paper. In this paper, the generative adversarial network is added to the neural machine translation model. The

generator adopts Bi-LSTM and Transformer neural machine translation models, respectively. The discriminator uses convolutional neural network to discriminate the translation results and generates feedback to act on the generator. Through the idea of generating antagonism, the effect of generator is improved, that is, the final translation effect of the machine translation model is improved. Language is an important means of expressing emotions. Confrontational training methods can judge positive or negative emotions, and such translation results have emotional effect also.

Based on the end-to-end neural machine translation model, the neural machine translation model adopts the encoder-decoder framework structure. Encoder-decoder model framework is used to encode and decode variable sequences of input and output. In the frame of the model of the encoder and decoder, the decoder corresponds to the output sequence, and the encoder corresponds to the input sequence. The decoding stage decodes the whole target language sequence by maximizing the probability of prediction sequence, and the coding stage encodes the whole source language sequence into a vector. The encoder-decoder framework mainly realizes the probability prediction of target language through the encoding and decoding process of encoder and decoder. Assuming that the source language sequence is $X \in [x_1, x_2, \dots, x_n]$ and the target language sequence is $Y \in [y_1, y_2, \dots, y_m]$, the probability calculation of generating the target language is shown in formula (1). The generation probability of each target language vocabulary is calculated by softmax function as shown in formula (2).

$$P = (y_1, y_2, \dots, y_m | x_1, x_2, \dots, x_n) \quad (1)$$

$$= \prod_{t=1}^{t=m} P(y_t | c, y_1, \dots, y_{t-1}),$$

$$p(y_t | x, y < t; \theta) = \frac{\exp(\phi(y_t, x, y < t, \theta))}{\sum_{y \in Y} \exp(\phi(y, x, y < t, \theta))} \quad (2)$$

$$= \frac{\exp(\phi(v_{y_t}, c_s, c_t, \theta))}{\sum_{y \in Y} \exp(\phi(v_y, tc_s, n, qc_t, h, \theta))},$$

where C is the vector used to represent the source language sequence, contains the relevant information of the source language sequence, and is the vector with fixed dimensions generated by the encoder stage. The ϕ function defines the possibility of generating the current target language term y_n from the source language as well as the generated target translation. The purpose of introducing the softmax function is to generate the probability distribution of the target word and to ensure that the function value satisfies the probability distribution. c_s represents the source language context vector representation, c_t represents the target language context vector representation, Y represents the target language, and v_y represents the word vector representation of the target language. The known source language sentences and generated target language sentences are used to predict the current probability of the target word. Since the source language sentences and generated target language sentences are very sparse, neural machine translation uses continuous

representation to model the conditional probability of the current word in the target language.

3.1. RNN Neural Translation Model. Owing to the network structure of Recurrent Neural Networks, which perfectly fits the sequence problem, it can process the input sequence of any length in theory. In the process of processing the sequence problem, Recurrent Neural Networks can store the time sequence information and store the historical information of the time sequence through the implicit state. Therefore, the structure of cyclic neural network is generally adopted to deal with sequence problems. The output of the recurrent neural network is a hidden layer state, which is used when the current layer processes the next layer, and each layer outputs to the next layer. This structure enables the recurrent neural network to process the input sequence data well, and to process the data samples with contextual dependencies. The hidden layer state at each moment is a functional representation of all the hidden layer states at the previous moment. According to the time sequence, the schematic diagram of the cyclic neural network is shown in Figure 1.

As shown in Figure 1, the input in the network at time t consists of the hidden layer state h_{t-1} at the previous moment and the input x_t at the current moment. The hidden layer state h_t at the current moment can be calculated by h_{t-1} and x_t . The hidden layer state h_t is computed repeatedly until all inputs are complete. In general, the zero vector is used to represent the initial state of the hidden layer. If the neural network contains only one hidden layer, the activation function of the hidden layer will generally adopt sigmoid function, which is represented by σ . For a batch data with n samples, assuming that the length of the hidden layer is h and the dimension of the feature vector of the sample data is X , the output representation of the hidden layer is shown in formula (3):

$$H = \sigma(XW_{xh}^T + b_h), X \in (R^{n \times x}), \quad (3)$$

where b_h, w represents the bias vector parameters and weights of the hidden layer, respectively. In the neural network, the output of the hidden layer is taken as the input of the output layer. Assuming that the dimension of the output vector corresponding to each sample is y , the final output representation is shown in formulae (4) and (5):

$$\hat{y} = \text{softmax}(HW_{hy} + b_y), \quad (4)$$

$$\text{softmax}(x_m) = \frac{e^{x_m}}{\sum_k e^{x_k}}. \quad (5)$$

3.2. Transformer Neural Network Translation Model. Attention mechanism is used for machine translation tasks. Encoder or decoder layers are directly used for attention, which reduces the transmission path of information. In addition, this attention approach can directly mine the semantic combination relationship between words inside sentences, and treat it as a semantic whole, making better use

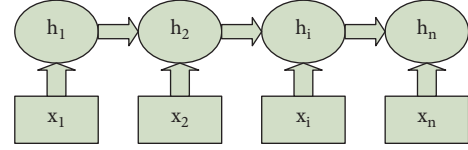


FIGURE 1: Expansion diagram of RNN internal structure.

of word combination and even phrase information in translation, and better encoding semantic matching target language words. The final experimental results show that with the reduction of computation and the improvement of parallel efficiency, the translation result is also improved. Transformer is the encoder and decoder, respectively. The encoder maps the natural language sequence into a hidden layer, that is, the mathematical expression containing the natural language sequence. The decoder is responsible for remapping the hidden layer to a natural language sequence. First of all, text is typed in Transformer for embedding. That is word embedding processing. Text information is transformed into high-dimensional real vector. In order to identify the sequential relationship between statements, position embedding is introduced, and linear transformation of sine and cosine functions is used to provide position information for the model.

In the encoder of Transformer, $N=6$, that is, there are six layers, and each layer includes two sublayers, as shown in Figure 2. The first sublayer refers to the multihead self-attention mechanism, which is mainly used to calculate the self-attention value. The second sublayer is a simple fully connected network. Residual networks are added to each sublayer, and the output of each sublayer is shown in the equation (6):

$$\text{LayerNorm}(x + \text{Sublayer}(x)), \quad (6)$$

where $\text{Sublayer}(x)$ represents the mapping of input x by the sublayer. To ensure dimension consistency, all sublayers and word embedding layers have the same output dimension. Transformer decoder is also composed of $N=6$ layers, each layer includes three sublayers. The first sublayer is masked multihead self-attention, which is also used to calculate self-attention. However, because it is a generation process, there is no result at time i greater than i , and only at time less than i , so mask processing is required. The second layer is the encoder input, related to attention calculation. The third sublayer is also a fully connected network, the same as encoder's sublayer fully connected network. The encoders and decoders of the Transformer model do not contain cyclic neural networks or convolutional neural networks, so it is impossible to capture sequence information. For example, if K, V are scrambled in line, the result will be the same after attention. However, the sequence information is very important, representing the global structure of the sequence, so the relative or absolute position information of each word of the sequence must be used.

3.3. Generative Adversarial Network. The core idea of generative adversarial network is derived from the Nash

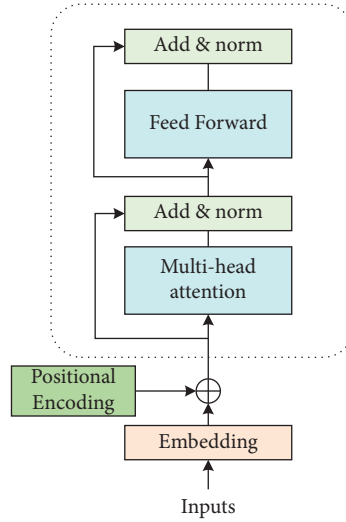


FIGURE 2: Transformer encoder structure diagram.

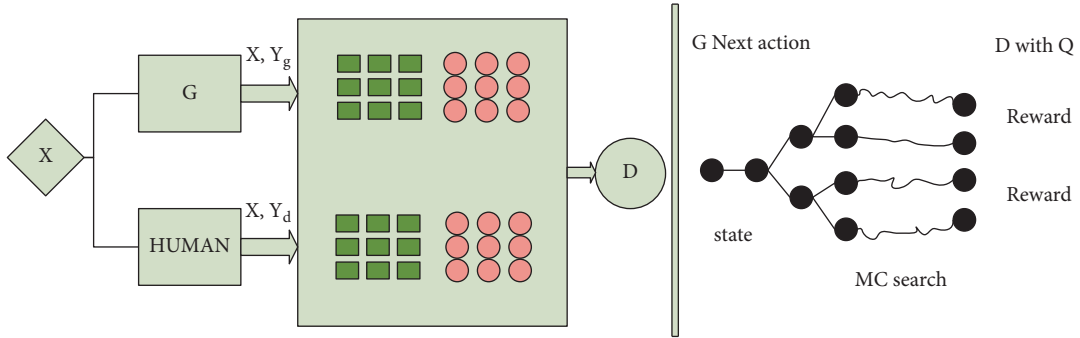


FIGURE 3: Generate an adversarial network diagram.

equilibrium of game theory, which is a two-player game in which the sum of the interests of both sides is a constant. The generation problem is regarded as the competition and game between generator and discriminator networks: the generator generates synthetic data from a given noise (generally evenly distributed or normally distributed), and the discriminator distinguishes the generator's output from the real data [42]. The former tries to produce more realistic data, while the latter, in turn, tries to better distinguish real data from generated data. Thus, the two networks make progress in the confrontation and continue to fight after progress. Then the data obtained from the generative network is more and more perfect, approaching the real data, so that the desired data can be generated. The antagonistic network judges that the text belongs to positive or negative emotion, and the final output results include that the emotional state that is more consistent with the language characteristics. The overall architecture of the model is shown in Figure 3.

The left half of Figure 3 is made up of generator G and discriminator D . Among them, G is our neural machine translation model, which generates target sentences. D discriminates between the sentences generated by G and the artificial translation sentences, and generates feedback results. The right part carries out strategy gradient training for G , and the final feedback is provided by D and Q , where Q is

BLEU value. The model of generator G is similar to the model of neural machine translation. Generator G defines the method of generating the target sentence y , given the source statement x . The generator uses exactly the same architecture as the neural machine translation model. It is noteworthy that we do not assume a specific model structure for generator G . In order to verify the effectiveness of the proposed method, the generator adopts Bi-LSTM and Transformer. Since the length of the target sentence generated by the generator is not fixed, the discriminator model CNN fills the generated sentence to a certain extent and converts the target sentence into a sequence with fixed length T , which is the maximum length of the output target sentence of the generator. Given the source sentence sequence $[x_1, x_2, \dots, x_T]$ and the target sentence sequence $[y_1, y_2, \dots, y_T]$, the source matrices for the source sequence and the target sequence are, respectively, established as shown in the following expressions:

$$\begin{aligned} X_{1:T} &= x_1; x_2; \dots; x_T, (x_t \in R^k), \\ Y_{1:T} &= y_1; y_2; \dots; y_T, (y_t \in R^k). \end{aligned} \quad (7)$$

When l words undergo convolution operation, a series of feature graphs are generated, as shown in the formula (8):

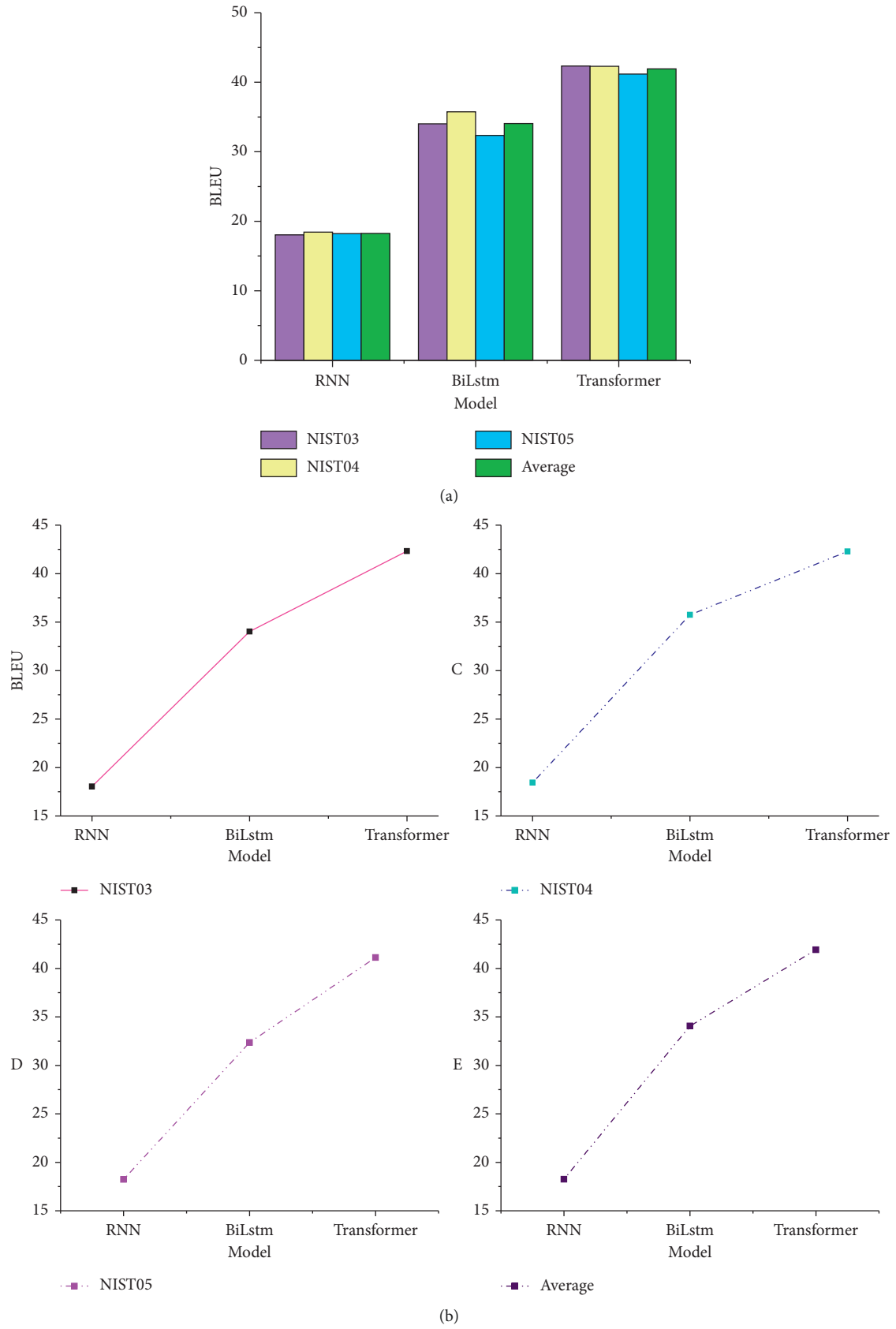


FIGURE 4: BLEU value diagram of baseline experiment. (a) Baseline model BLEU histogram. (b) Baseline experimental grouping diagram.

$$c_{ji} = \sigma \left(BN(w_j \otimes x_{i:i+1} + b) \right), \quad (8)$$

where \otimes represents the sum of principal element multiplications, b is the offset term, and σ is the activation function. Apply the BLEU value to the generator as a specific target. For the target sequence y_g generated by the generator and the real target sequence y_d , by calculating the n-element syntax accuracy of the generated target sequence y_g , the calculated result $Q(y_g, y_d)$ is used as the feedback of the final generation. In order to facilitate the fusion of D and Q , the value range of $Q(y_g, y_d)$ is 0–1, the same as the output of the discriminator. The objective of generator G is defined as maximizing the expected feedback from the beginning state of the generated sequence, and the objective function is shown in the formula.

$$J(\theta) = \sum_{Y_{1:T}} G_\theta(Y_{1:T}|X) \cdot R_{D,Q}^{G_\theta}(Y_{1:T-1}, X, Y_T, Y^*), \quad (9)$$

where θ is the parameter in generator G , $Y_{1:T} = Y_1, Y_2, \dots, Y_T$ is the target sequence generated by generator, x is the source sentence sequence, Y^* is the real existing target sentence sequence. The action value function from the source sentence sequence X given by $R_{D,Q}^{G_\theta}$ to the target sequence indicates that the generated feedback is accumulated from the state. The action value function is calculated by combining the actual probability estimation output of discriminator D with the output of BLEU objective function Q as feedback.

4. Experimental Analyses

The experimental models were done on the Tensor Flow framework and then run on the GPU. When the model ran ten evaluation tests on the test set and the model performance did not improve, we stopped training the model. BLEU value is used as the evaluation index of translation results. In order to ensure the fairness of the experiment, 1 million sentence pairs are randomly selected from the LDC corpus as training data, and the source and target statements are encoded by byte pair encoding, respectively. About 36,000 words are generated in the source language and 32,000 words in the target language. Select NIST04 as the test set and NIST02 as the verification set. The hidden neural units of both the encoder and decoder are set to 512, and the dimension size of word embedding is also set to 512 dimensions.

For the Transformer translation model, the basic structure of the model is used without any changes. We set the dimension size for word embedding to 512 dimensions, Dropout to 0.1, and multiple to 8. Both encoders and decoders have a six-layer network structure. For Bi-LSTM translation model, the number of hidden units of encoder and decoder is set to 512, and the dimension size of word embedding is also set to 512 dimensions. Dropout is not used to train the Bi-LSTM translation model.

4.1. Baseline Experimental. It can be clearly seen from Figure 4(a) that the BLEU score of RNN model is low,

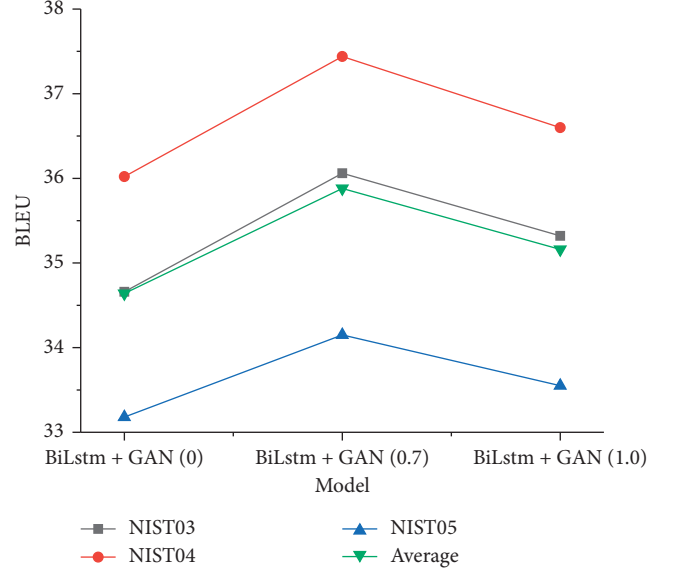


FIGURE 5: Experimental results of Bi-LSTM + GAN.

indicating that the translation effect generated by the original RNN is not very good. This is because in the original RNN translation model structure, the Encoder needs to compress the whole source language sentence into a fixed dimension vector, and then the Encoder-Decoder decodes the whole target language sentence from it. This requires that the fixed dimensional vector contain all the information of the source language sentence, which is obviously difficult to achieve, so it becomes the performance bottleneck of the original RNN as a machine translation model. Although Bi-LSTM and Transformer models are better than traditional RNN models, the effect is still not ideal.

Bi-LSTM model, due to the internal bidirectional time extraction of features, has a stronger timeliness of features, so it reaches the highest 35.74 in NIST04, and the average BLEU value is 34.06. Transformer, due to its own attention mechanism, well explores the potential connection between different time points, and the features obtained have stronger internal connection, and the overall effect is significantly improved. In order to clearly show the changes of the three groups of experiments, we used another way to express the experimental results, as shown in Figure 4(b).

4.2. Generative Adversarial Network Model Experiment. According to the basic experiment, we select Bi-LSTM and Transformer, two models with better performance, to join the generative adversarial network. Experimental results were grouped according to the size of training parameters λ of generating adversarial network (0, 0.7, 0.8, 1.0). As can be seen from the experimental results in Figure 5, when the parameter λ of generating adversarial network is 0.7, the Bi-LSTM model achieves the best effect and the highest average value is 35.88. According to the changes of four curves, the experimental model in this paper conforms to objective laws.

Transformer is the most outstanding model in all fields of artificial intelligence at present, and has been greatly

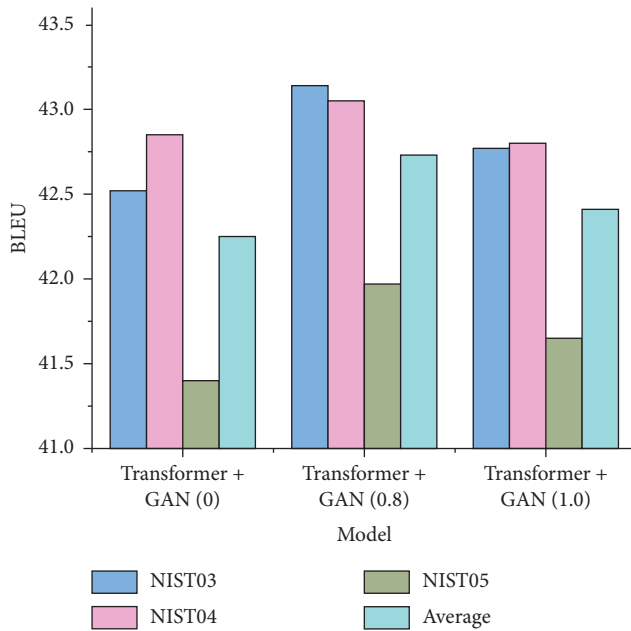


FIGURE 6: Experimental results of transformer + GAN.

improved after the introduction of GAN. As can be seen from Figure 6, the lowest BLEU introduced by Transformer model into generative adversarial network is 41.4, higher than the average of other models. When the parameter λ value of generated admission-network is 0.8, the model achieves the best result of 43.14 and the average value of 42.73. From the overall experimental results, BLEU values of Bi-LSTM and Transformer models have basically the same change rule with parameter λ , both of which are nonlinear changes. It is important for our subsequent improvement. As an expression mode closely related to culture, language deserves more features and models.

5. Conclusion

With the development of economic globalization, communication between countries, industries, and people of all countries are becoming more frequent and closer. Language is the tool of communication between people. How to quickly and accurately realize the free conversion between different languages is vital. Machine translation is an important research direction in natural language processing, and the development of deep learning related technologies has improved the methods and performance of machine translation. Machine translation as an efficient tool for language conversion, is of great practical significance in translating different languages into equivalent languages while preserving original semantics. Aiming at common neural machine translation models, this paper combines generative adversarial network with machine translation and improves the translation effect of translation models through adversarial training of generative adversarial network. In this paper, classic neural network model and attention-based Transformer model are studied. Then, Bi-LSTM model and Transformer model are added with generative adversarial

network, respectively. Through the addition of generative adversarial network, the newly constructed model is analyzed and studied. Through the adversarial idea of generative adversarial network, certain feedback is obtained from discriminator D and acted on generator G to improve the translation effect of the translation model, get two emotional attributes of opposite polarity, and the effectiveness of the improved analysis method is verified through the final experiment. There are many hidden forms of emotion in language, and it is difficult to find the deep meaning of language by ordinary models, which is also the biggest advantage of the model in this paper.

Data Availability

The raw data supporting the conclusions of this article will be made available by the authors, without undue reservation.

Conflicts of Interest

The authors declare that the research was conducted in the absence of any commercial or financial relationships that could be construed as potential conflicts of interest.

References

- [1] S. Ahmadi and M. Masoud, *Towards Machine Translation for the Kurdish Language*, 2020, <https://arxiv.org/abs/2010.06041>.
- [2] M. V. S. Rishita, M. A. Raju, and T. A. Harris, "Machine translation using natural language processing," *MATEC Web of Conferences*, vol. 277, Article ID 02004, 2019.
- [3] H. Zhao and An Yan, "Automatic pragmatic reordering in machine translation," *Journal of Xi'an International Studies University*, vol. 25, no. 4, p. 5, 2017.
- [4] O. Bojar, C. Buck, and C. Callisonburch, "Findings of the 2013 Workshop on Statistical Machine Translation," in *Proceedings of the Eighth Workshop on Statistical Machine Translation, Sofia, Bulgaria*, 2013.
- [5] W. J. Hutchins, *Machine translation: past, present, future*, Ellis Horwood, Chichester, UK, 1986.
- [6] H. Guo and G. Hu, "A Statistical and rule-based approach to target language generation," in *Proceedings of the International Conference on Machine Translation*, Tiburon, CA, USA, 2002.
- [7] X. Tong, T. Li, and R. Chen, "A new approach to statistical machine translation," *The Chinese Journal of International Politics*, no. 1, p. 7, 2010, <https://arxiv.org/abs/1709.02779>.
- [8] V. Dunjko and H. J. Briegel, "Machine learning & artificial intelligence in the quantum domain: a review of recent progress," *Reports on Progress in Physics*, 2018.
- [9] A. O. Basile and M. D. Ritchie, "Informatics and machine learning to define the phenotype," *Expert Review of Molecular Diagnostics*, vol. 18, no. 3, pp. 219–226, 2018.
- [10] R. M. Zbib, *Using Linguistic Knowledge in Statistical Machine Translation*, Massachusetts Institute of Technology, Cambridge, MA, USA, 2010.
- [11] R. Sennrich, H. Schwenk, and W. Aransa, "A multi-domain translation model framework for statistical machine translation," in *Proceedings of the 51st Annual Meeting of the Association for Computational Linguistics*, vol. 1, pp. 832–840, Sofia, Bulgaria, 2013.

- [12] S. Chen, Y. Gao, and B. Zhou, *Systems and Methods for Fast and Memory Efficient Machine Translation Using Statistical Integrated Phase lattice*, US, 2010.
- [13] I. D. Melamed, *Automatic Evaluation and Uniform Filter Cascades for Inducing N-Best Translation Lexicons*, 1995, <https://arxiv.org/pdf/cmp-lg/9505044.pdf>.
- [14] D. N. Posner, "Translating into polyphony: creating a dramaturgical translation for three sisters at steppenwolf," *Theatre Topics*, vol. 23, 2013.
- [15] R. Dholakia, "Real-world use of pivot languages to translate low-resource languages," *Atmosfera*, vol. 4, no. 4, pp. 205–233, 2014.
- [16] National Research Council, "Automatic Language Processing Advisory Committee. Language and machines; computers in translation and linguistics; a report," *Methods in Molecular Biology*, vol. 260, pp. 73–82, 1966.
- [17] S. Nirenburg, H. Somers, and Y. Wilks, *The Proper Place of Men and Machines in Language Translation*, MIT Press, Cambridge, MA, USA, 2003.
- [18] M. F. Alawneh and T. Sembok, "Rule-based and example-based machine translation from English to Arabic," in *Proceedings of the 2011 Sixth International Conference on Bio-Inspired Computing: Theories and Applications*, pp. 343–347, IEEE, Penang, Malaysia, 2011.
- [19] T. H. King and M. Santaholma, *Using Artificially Generated Data to Evaluate Statistical Machine Translation*, in *Proceedings of the 2009 Workshop on Grammar Engineering Across Frameworks (GEAF 2009)*, 2009.
- [20] K. Lingam, E. R. Lakshmi, and L. R. Theja, "Rule-based Machine Translation from English to Telugu with Emphasis on Prepositions," in *Proceedings of the 2014 First International Conference on Networks & Soft Computing (ICNSC2014)*, IEEE, Guntur, India, 2014.
- [21] N. Yusliani, Yunita, and W. Octaviani, *Indonesian-English Machine Translation Using Rule-Based Method*, 2015.
- [22] G. Hadis and H. Mahmood, "A comparative study of Google translate translations: an error analysis of English-to-Persian and Persian-to-English translations," *English Language Teaching*, vol. 9, no. 3, p. 13, 2016.
- [23] P. Koehn, *Statistical Phrase-Based Translation*, Association for Computational Linguistics, in *Proceedings of the Conference of the North American Chapter of the Association for Computational Linguistics on Human Language Technology*, 2003.
- [24] F. J. Och and H. Ney, "Discriminative training and maximum entropy models for statistical machine translation," in *Proceedings of the 40th Annual Meeting on Association for Computational Linguistics*, pp. 295–302, ACL, Philadelphia, PA, USA, 2002.
- [25] F. J. Och and H. Ney, "The Alignment Template Approach to Statistical Machine Translation," *Computational linguistics*, vol. 30, no. 4, pp. 417–449, 2004.
- [26] W. Aziz, M. Rios, and L. Specia, *Shallow Semantic Trees for SMT*, Association for Computational Linguistics, in *Proceedings of the Workshop on Statistical Machine Translation*, New York City, NY, USA, 2011.
- [27] D. Wu and P. Fung, "Semantic roles for SMT: A hybrid two-pass model," in *Proceedings of the Conference of the North American Chapter of the Association for Computational Linguistics*, Association for Computational Linguistics, 2009.
- [28] F. Zhai, J. Zhang, Y. Zhou, and C. Zong, "Machine translation by modeling predicate-argument structure transformation," in *Proceedings of the COLING*, pp. 3019–3036, 2012.
- [29] D. Xiong, M. Zhang, and X. Wang, "Topic-based coherence modeling for statistical machine translation," *IEEE/ACM Transactions on Audio, Speech, and Language Processing*, vol. 23, no. 3, pp. 483–493, 2015.
- [30] M. Gardner, J. Grus, M. Neumann et al., "Allennlp: a deep semantic natural language processing platform," 2018, <https://arxiv.org/abs/1803.07640>.
- [31] M. Tu, Y. Zhou, and C. Zong, "A novel translation framework based on rhetorical structure theory," in *Proceedings of the 51st Annual Meeting of the Association for Computational Linguistics*, pp. 370–374, Sofia, Bulgaria, 2013.
- [32] M. Li and C. Zong, "A Survey of Machine Translation System Fusion Technologies," *Journal of Chinese Information Processing*, vol. 24, no. 4, pp. 74–85, 2010.
- [33] Y. Bengio, R. Ducharme, and P. Vincent, "A neural probabilistic language model," *Advances in Neural Information Processing Systems*, vol. 13, 2000.
- [34] N. Kalchbrenner and P. Blunsom, "Recurrent continuous translation models," in *Proceedings of the 2013 Conference on Empirical Methods in Natural Language Processing*, pp. 1700–1709, Washington, WA, USA, 2013.
- [35] K. Cho, B. van Merriënboer, and Ç. Gülçehre, *Learning Phrase Representations Using Rnn Encoder-Decoder for Statistical Machine Translation*, pp. 1724–1734, EMNLP, 2014, <https://arxiv.org/abs/1406.1078>.
- [36] D. Bahdanau, K. H. Cho, and Y. Bengio, "Neural machine translation by jointly learning to align and translate," in *Proceedings of the 3rd international conference on learning representations, ICLR 2015*, pp. 39–599, San Diego, CA, USA, 2015.
- [37] H.-R. Guo, X.-J. Wang, Y.-X. Zhong, and P. Lu, "Traffic signs recognition based on visual attention mechanism," *The Journal of China Universities of Posts and Telecommunications*, vol. 18, no. 18, pp. 12–16, 2011.
- [38] J. Gehring, M. Auli, and D. Grangier, "Convolutional Sequence to Sequence Learning," in *Proceedings of the International Conference on Machine Learning (PMLR, 2017)*, Paris, France, 2017.
- [39] H. Mi, B. Sankaran, and Z. Wang, *Coverage Embedding Models for Neural Machine Translation*, 2016, <https://arxiv.org/abs/1605.03148>.
- [40] Y. Tang, F. Meng, and Z. Lu, *Neural Machine Translation with External Phrase Memory*, 2016, <https://arxiv.org/abs/1606.01792>.
- [41] M. Pinnis, R. Krišlauks, D. Dekšne, and T. Miks, "Neural machine translation for morphologically rich languages with improved sub-word units and synthetic data," in *Proceedings of the International Conference on Text, Speech, and Dialogue*, pp. 237–245, Springer, Cham, 2017.
- [42] W. Ma, B. Yan, and L. Sun, "Generative adversarial network-based short sequence machine translation from chinese to english," *Scientific Programming*, vol. 2022, Article ID 7700467, 10 pages, 2022.

Research Article

An Efficient Resource Management Optimization Scheme for Internet of Vehicles in Edge Computing Environment

Anqing Zhu  and Youyun Wen 

Management School, South China Business College Guangdong University of Foreign Studies, Guangzhou, Guangdong 510000, China

Correspondence should be addressed to Anqing Zhu; zhuq18@126.com

Received 2 April 2022; Revised 26 April 2022; Accepted 11 May 2022; Published 28 May 2022

Academic Editor: Le Sun

Copyright © 2022 Anqing Zhu and Youyun Wen. This is an open access article distributed under the Creative Commons Attribution License, which permits unrestricted use, distribution, and reproduction in any medium, provided the original work is properly cited.

The contradiction between limited network resources and a large number of user demands in vehicle environment will cause a lot of system delay and energy consumption. To solve the problem, this paper proposes an efficient resource management optimization scheme for Internet of Vehicles in edge computing environment. Firstly, we give a detailed formulation description of communication and computing cost incurred in the resource optimization process. Then, the optimization objective of this paper is clarified by considering the constraints of computing resources, and system delay and energy consumption are considered comprehensively. Secondly, considering dynamic, random, and time-varying characteristics of vehicle network, the optimal resource management scheme of Internet of Vehicles is given by using distributed reinforcement learning algorithm to optimize total system overhead to the greatest extent. Finally, experiments show that when bandwidth = 40 MHz, the total system cost of the proposed algorithm is only 3.502, while that of comparison algorithms is 4.732 and 4.251, respectively. It is proved that the proposed method can effectively reduce the total system overhead.

1. Introduction

In recent years, the automotive industry has developed rapidly, and intelligence and networking have become an important trend in the future development of automotive industry [1]. On the one hand, these technologies enable communication and information exchange between Vehicle to Vehicle (V2V) and Vehicle to Infrastructure (V2I), helping to build safe, collaborative, and intelligent transportation systems. On the other hand, this in turn generates a large amount of data, and at the same time, the demand for computing, communication, and content increases significantly [2–4]. With the development of Internet of Vehicles (IoV) and intelligent connected vehicles, in-vehicle infotainment applications such as road safety, intelligent navigation, autonomous driving, and in-vehicle entertainment continue to emerge. This promotes the development of intelligent transportation and brings a great improvement to driving experience [5–7]. Due to the particularity of the

physical location of vehicles and cloud servers, the backhaul link capacity is limited. Such a high content demand of the Internet of Things will bring a huge burden to the core network [9]. At the same time, they also pose a major challenge to support massive content delivery and meet the low-latency requirements of IoT [10–12].

The introduction of mobile edge computing (MEC) technology makes up for the network instability and delay limitations of cloud computing in IoT scenario and is more suitable for low-latency, high-reliability task computing on IoT requirements [13–18]. The cloud server located in core network is far away from vehicles, and vehicles need to rely on a large base station for multi-hop transmission to offload tasks to the cloud server for processing. However, it is prone to network fluctuations and transmission interruptions and is unreliable for in-vehicle applications, especially safe driving applications [19, 20]. Therefore, using distributed MEC services to replace traditional cloud computing services can effectively solve the resource management optimization problem in IoT [21].

The main factors that affect the decision of computing offloading are the execution delay and energy consumption of task. Thus, optimization goals usually include solutions such as reducing delay, reducing energy consumption, and weighting between delay and energy. Reinforcement learning can capture the hidden dynamics of environment well, so it is often used to optimize resource allocation algorithms. Liu et al. [22] proposed a resource allocation strategy based on deep reinforcement learning (DRL). Zhan et al. [23] designed a strategy optimization method based on DRL by using game theory. Huang et al. [24] studied the wireless charging MEC network and proposed an online decision-making method based on DRL. Hui et al. [25] proposed a content dissemination framework based on edge computing. Combining the selfishness and transmission ability of vehicles, the authors designed a two-level relay selection algorithm to reasonably select relay vehicles to meet different transmission needs. Su et al. [26] used the vehicles parked around the street and the vehicles driving along the road to communicate the vehicle social community through V2V and used the content cached in the parked vehicles to reduce the delay of content download. Zhao et al. [27] proposed a caching strategy in V2V scenario with information as the center and designed a dynamic probabilistic caching scheme. Zhang et al. [28] proposed a MEC scenario computing resource allocation scheme based on DRL network, which avoids falling into the disaster of dimensionality. Zhang et al. [29] proposed a joint optimization scheme of IoT content caching and resource allocation based on MEC in high-speed free-flow scenario, which reduced data acquisition latency. Li [29] proposed a resource allocation strategy for computing unloading in vehicle Internet based on DRL. However, in the case of limited network resources and a large number of user demands, the above research has the problems of excessive resource delay consumption and large energy consumption. Therefore, the optimization of IoT resource management in the MEC system scenario is a challenging problem.

Based on the above analysis, in view of delay and energy consumption caused by the contradiction between limited network resources and a large number of user needs in vehicle environment, this paper proposes an efficient resource management optimization scheme for IoT in edge computing environment. This method takes minimizing the weighted sum of system delay and energy consumption as the optimization goal and constructs a communication model and task offloading optimization model in IoT edge computing scenario. Moreover, a solution algorithm based on distributed reinforcement learning is used to optimize the total system overhead.

2. System Model and Problem Modeling

2.1. System Model. The system model is shown in Figure 1. J road side units (RSUs) are evenly distributed on the road, and all have MEC services configured, denoting MEC server as me_{c_j} , $j \in \{1, 2, \dots, J\}$. Each of C randomly distributed vehicles performs multiple computing tasks. Suppose the sum of computing tasks of all vehicles is N , and the computing

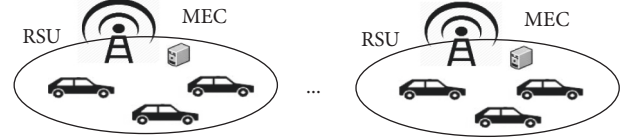


FIGURE 1: IoT system model.

tasks are denoted by L . b represents the size of input data, w represents the task computation amount, and t^{\max} represents the task deadline. If the task processing exceeds the time limit, it means that the task processing fails, and R_L represents MEC cell carried by vehicle-mounted terminal to which the task belongs. ω represents the importance of computing task to distinguish the task is a secure computing task and a common computing task. Therefore, the computational task can be denoted as $L = \{b, w, \omega, t^{\max}, R_L\}$. Let i represent the number of onboard terminals offloading the computing task to MEC server, and $x = 0$ indicates that the task is executed locally. The offloading strategies of N computing tasks constitute the offloading strategy vector set $X = \{x_1, x_2, \dots, x_N\}$.

2.2. Communication Model. When task i chooses to perform computing offloading, a corresponding offloading decision needs to be made to decide which MEC server to offload to and which channel to select to upload data. When the offloading decision vector \mathbf{d} of all users is given, data transmission rate $R_n^m(\mathbf{d})$ on the n channel between user u_i of offloading decision $d_n^0 > 0$ and the j RSU can be obtained. The maximum information transfer rate V is

$$V = W \log_2(1 + \text{SNR}), \quad (1)$$

where W is the channel bandwidth and SNR is the ratio of average power of signal transmitted in the channel to noise power in the channel, that is, the signal-to-noise ratio. Its calculation is

$$\text{SNR} = \frac{p_i g_i^h}{\gamma^2 + \sum_{i \in V} p_i g_i^h}, \quad (2)$$

where p_i represents the transmission power of users, that is, the transmit power of user equipment; g_i^h represents the channel gain of communication channel selected by users; and γ^2 represents the white Gaussian noise power.

The data transfer rate $V_{i,j}^h(d)$ is

$$V_{i,j}^h(d) = B \log_2 \left(1 + \frac{p_i g_i^h}{\gamma^2 + \sum_{i \in V} p_i g_i^h} \right). \quad (3)$$

2.3. Computing Offloading Model

2.3.1. Local Computing. Assuming that task i is only calculated locally, only the calculation delay is considered. e^{loc} represents the computing capability of vehicle terminals. The processing delay of local tasks and the energy required for local computing are expressed as

$$t_i = t_{\text{loc}} = \frac{w_i}{e_{\text{loc}}^{\text{mec}}} \quad (4)$$

$$E_i = t_i P_{\text{loc}}.$$

When MEC server resources are insufficient, the system unloads the task to other servers.

2.3.2. Local Server Computing. When the vehicle communicates directly with the local server, the vehicle will unload the computing task to the server in the cell. After the server completes the execution, the result will be returned to the vehicle immediately. The total task delay includes upload delay, server calculation delay, and return delay. Let $t_{i,j}^{\text{mec}}$ denote the task execution delay, $e_{i,j}^{\text{mec}}$ denote the computing resources, and $v_{i,j}$ denote the wireless transmission rate:

$$t_{i,j}^{\text{mec}} = \frac{w_i}{e_{i,j}^{\text{mec}}} \quad (5)$$

$$t_{i,j}^{\text{trans}} = \frac{b_i}{v_{i,j}}$$

Since the return rate is much higher than the upload rate, the return delay of the calculation result can be ignored. The total time delay of unloading calculation is

$$t_{i,j} = t_{i,j}^{\text{trans}} + t_{i,j}^{\text{mec}}. \quad (6)$$

The energy consumption for unloading calculation is

$$E_{i,j} = P_{\text{loc}}(t_{i,j}^{\text{trans}} + t_{i,j}^{\text{mec}}), \quad (7)$$

where P_{loc} represents the energy consumption per unit cycle of local CPU.

2.3.3. Other Server Computing. When the MEC server in the cell where the vehicle is located is overloaded, the computing task is unloaded to other cell servers. Communication between MEC servers is generally performed through wired communication links such as optical fibers. Assuming that the average task transmission delay on the wired link is t_w and c represents the number of wired link hops between computing tasks offloaded to other servers, the task processing delay at this time is expressed as

$$t_{i,j}^o = 2ct_w + t_{i,j}^{\text{trans}} + \frac{w_i}{e_{i,j}^{\text{mec}}}. \quad (8)$$

Then, the energy consumption of other servers' offloading computing is

$$E_{i,j}^o = P_{\text{loc}} \left(2ct_w + t_{i,j}^{\text{trans}} + \frac{w_i}{e_{i,j}^{\text{mec}}} \right). \quad (9)$$

2.4. Problem Modeling. τ is the calculated weight, and the weighted sum of the total delay is

$$t_{\text{all}} = \sum_{i=1}^N \left(\tau t_i + (1 - \tau) \sum_{j=1}^J t_{ij} \right). \quad (10)$$

The total energy consumption is

$$c_{\text{all}} = \sum_{i=1}^N \left(\tau C_i + (1 - \tau) \sum_{j=1}^J t_{ij} \right). \quad (11)$$

Considering delay and energy consumption, the total cost of local calculation is

$$C_{\text{all}} = \gamma t_{\text{all}} + (1 - \gamma) c_{\text{all}}, \quad (12)$$

where γ is the weight.

The optimization problem can be formulated as

$$\min(C_{\text{all}}). \quad (13)$$

In order to ensure that the task is completed on time, the calculation task is required to complete the task before the vehicle leaves the MEC unit, and the following conditions shall be met:

$$t_i^{\text{stay}} = \frac{S_i}{v_i}, \quad (14)$$

$$t + \frac{w_i}{e_{i,j}^{\text{mec}}} \leq \min[t_i^{\text{max}}, t_i^{\text{stay}}].$$

Computing tasks unloaded to other servers should meet the following conditions:

$$2ct_w + t_{i,j}^{\text{trans}} + \frac{w_i}{e_{i,j}^{\text{mec}}} \leq \min[t_i^{\text{max}}, t_i^{\text{stay}}]. \quad (15)$$

The computing resources required to complete computing tasks are

$$e_{i,j}^{\text{mec}} \geq \max \left\{ \frac{w_i}{\min[t_i^{\text{max}}, t_i^{\text{stay}}] - t_{i,j}^{\text{trans}}}, \frac{w_i}{\min[t_i^{\text{max}}, t_i^{\text{stay}}] - 2ct_w - t_{i,j}^{\text{trans}}} \right\}. \quad (16)$$

The total computing resources required for computing tasks are

$$e_j = \sum_{i=1}^N \sum_{x_i=j} e_{i,j}^{\text{mec}}. \quad (17)$$

The constraints are as follows:

$$\text{C1: } x_i \in \{0, 1, 2, \dots, j\}, \forall i \in N,$$

$$\text{C2: } y_i \in \{0, 1\}, \forall i \in N, \quad (18)$$

$$\text{C3: } e_j < E_j, j \in \{1, 2, \dots, J\}.$$

C1 indicates that a computing task can only be offloaded to one edge server and cannot be offloaded to two or more at the same time. C2 means that the computing task adopts binary offloading, which can choose not to offload or offload entire task at the same time, that is, the task is indivisible. C3 indicates that computing resources required by computing tasks offloaded to edge server cannot exceed the total resources of edge servers.

3. Solutions Based on Reinforcement Learning

3.1. Problem Solving Based on Distributed Reinforcement Learning. In view of dynamic, random, and time-varying nature of in-vehicle networks, artificial intelligence algorithms are more suitable for resource management and task scheduling than traditional mathematical methods. In comparison, Q-learning needs to maintain Q-table and is not suitable for networks with many states. Deep deterministic policy gradient algorithms need to use an experience replay mechanism to eliminate the correlation between training data. For experience playback mechanism, the agent consumes more resources for each interaction with the environment. The off-policy learning method adopted can only be updated based on the data generated by the old policy. Therefore, consider using the actor-critic algorithm to reduce the overhead required for algorithm execution, while providing optimal offloading decisions and resource management based on real-time network environment. Modeling the environment of system with an actor-critic algorithm requires determining its state space, action space, and reward function.

The state space, S , consists of computing resources and cache resources of in-vehicle network, $S = \{F_1, F_2, \dots, F_M, S_1, S_2, \dots, S_M\}$, where F_i and S_i represent the computing capacity and storage capacity of road side unit i , respectively.

The action space consists of offloading decisions of vehicles, caches of road side units, and computing resource management, $A = (x_i, w_i, f_i)$, where $x_i = \{x_{i0}, x_{i1}, \dots, x_{iM}\}$, $w_i = \{w_{i1}, w_{i2}, \dots, w_{iM}\}$, and $f_i = \{f_{i1}, f_{i2}, \dots, f_{iM}\}$ represent the set of vehicle i offloading decision, road side unit storage, and computing resource management, respectively.

Reward Function. The goal of reinforcement learning training is to maximize long-term cumulative reward. According to the objective function of this paper, the reward function is designed as

$$r_{i,t} = 1 - \frac{C_{i,j}}{\max\{C_{i,j}\}}. \quad (19)$$

The public neural network in actor-critic algorithm consists of multiple threads, and each thread has the same 2 modules as public neural network: the policy (actor) network and the critic (critic) network. The actor network is used to optimize the policy $\pi(a_t|s_t; \delta)$ with parameters δ ; the critic network tries to estimate the value function $V(s_t; \delta)$ with parameters δ_v . At time t , the actor network performs action a_t based on current state s_t , gets a reward r_t , and enters the next state s_{t+1} .

Use the advantage function $A(a_t, s_t)$ to represent the difference between the action value function $Q(a_t, s_t)$ and state value function $V(s_t)$:

$$A(a_t, s_t) = Q(a_t, s_t) - V(s_t). \quad (20)$$

To speed up convergence, approximate $Q(a_t, s_t)$ with k step sampling:

$$Q((a_t, s_t)) \approx \sum_{i=0}^{k-1} \gamma^i r_{t+i} + \gamma^k V(s_{t+k}; \delta_v), \quad (21)$$

where γ is the discount coefficient, r_{t+i} represents the instant reward, and $V(s_t)$ is obtained through critic network.

Taking the parameter δ as a variable, differentiate the policy loss function to obtain

$$\nabla_{\delta} f_{\pi}(\delta) = \nabla_{\delta} \log \pi(a_t|s_t; \delta) A(a_t, s_t) + \beta \nabla_{\delta} H(\pi(s_t; \delta)), \quad (22)$$

where H is the entropy of policy and β is the coefficient.

For the value loss function, there are

$$f_v(\delta_v) = (R_t - V(s_t; \delta))^2. \quad (23)$$

Based on RMSProp algorithm, the gradient estimate can be expressed as

$$g = ag + (1 - a)\Delta\delta^2, \quad (24)$$

where a represents momentum and $\Delta\delta$ represents the cumulative gradient of loss function.

The update parameters of RMSProp algorithm are

$$\delta \leftarrow \delta - \eta \frac{\Delta\delta}{\sqrt{g + \varepsilon}}. \quad (25)$$

3.2. Algorithm Flow. The proposed offloading strategy flow based on distributed reinforcement learning is shown in Algorithm 1.

4. Example Verification and Result Discussion

4.1. Simulation Settings. This section uses Python to simulate and verify resource management optimization scheme for IoT and evaluate the pros and cons of different algorithms by comparing the impact of each algorithm on the total system overhead with the number of vehicles, the number of tasks, and the bandwidth. The simulation parameters are set as shown in Table 1. Due to the existence of small-scale fast fading and the mobility of mobile devices in established model, the results of each run are random. Therefore, the mathematical method of statistical averaging is used to obtain average value as the final result. The computer configuration information used for the simulation is Windows Server 2019, Intel(R) Xeon(R) 2.6 GHz processor, and 16 GB RAM.

4.2. Convergence Performance Analysis. Figure 2 describes the convergence of algorithm in this paper under different learning rate scenarios. It can be found from the figure that when the learning rates of actor and critical networks are $L_a = 1 \times 10^{-3}$ and $L_b = 1 \times 10^{-2}$, respectively, although the learning speed of algorithm is very fast, it will degrade the final convergence performance of system. When the learning rate is too small ($L_a = 1 \times 10^{-3}$, $L_b = 1 \times 10^{-2}$), the learning speed will drop sharply. Therefore, the learning rate is set to $L_a = 1 \times 10^{-4}$, $L_b = 1 \times 10^{-3}$ in the follow-up experiment.

4.3. Comparison of Accumulated Average Rewards under Different Schemes. Compare the average reward value of the

Input: actor network, actor target network, critical network and critical target network, learning rate α , discount rate γ , attenuation factor λ .
Output: computing task offloading policy π' .
 Initialize the critical network parameter δ^c and actor network parameter δ^a .
 Initialize the status of experience playback pool and task vehicle s_0
For $t \leq T$ **do**
 Observe the environment status s_t and select actions a_t based on the current policy
 Execute the action a_t , get the reward r_t , and transfer to the state s_{t+1}
 Save array (s_t, a_t, r_t, s_{t+1}) to experience playback pool
 If the memory bank is full, but the stop condition is not met, a small batch of arrays (s, a, r, s') is randomly sampled from the experience playback pool.
 Update critical network parameters, actor network parameters, and target network parameters
End
End

ALGORITHM 1: Resource management algorithm based on distributed reinforcement learning.

TABLE 1: System parameters.

Parameter	Value
Number of concurrent tasks of a single vehicle	2~7
Number of vehicles	5~15
Calculation capability of onboard terminal	5 MHz
Vehicle transmission power	1.5 W
Vehicle speed	30~80 KM/h
Gaussian white noise power	-80 dB
MEC computing power	$[2 \times 10^8, 9 \times 10^8]$ Hz
System bandwidth	10~50 MHz

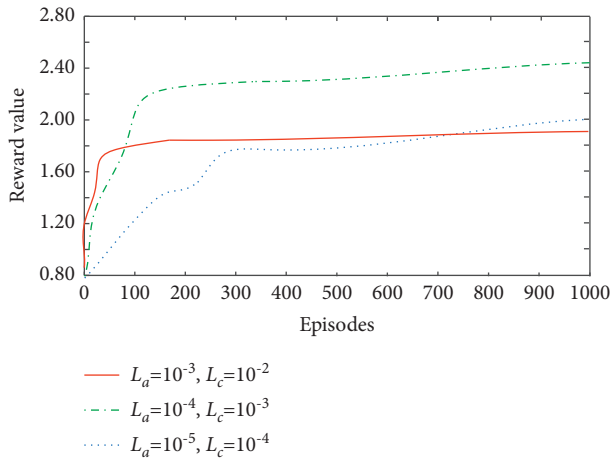


FIGURE 2: Performance comparison under different learning rates.

proposed scheme with the following schemes: (1) all-local strategy; (2) random strategy; (3) all-MEC policy. During DDPG training, there will be violent shocks. Thus, this section observes the convergence of neural network by calculating the cumulative average value of system reward. Figure 3 shows the comparison of cumulative average rewards for different caching schemes. With the increase of training times, it can be seen that all-MEC and random schemes can gradually converge to a stable cumulative

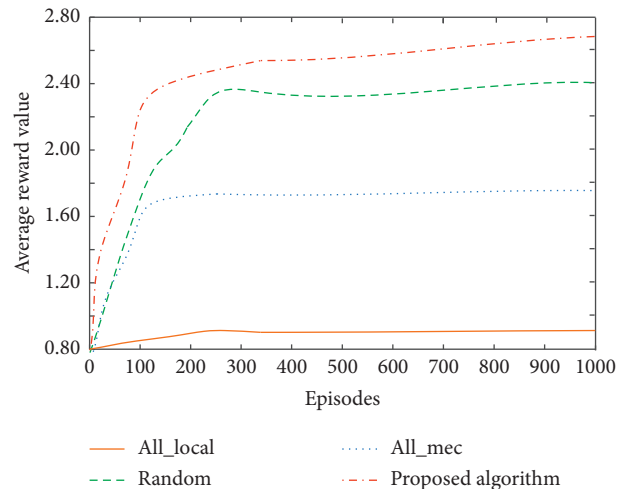


FIGURE 3: Comparison of average rewards under different schemes.

average. All-local strategy behavior is not encouraged, so the reward value is the lowest. Because the proposed algorithm needs to consider the road conditions of adjacent areas, increases the dimension of system state, and improves the complexity, it has poor performance at the beginning of training and obtains the highest average reward value after convergence. Therefore, the proposed resource optimization management scheme for IoT can make full use of communication resources and effectively improve the effectiveness of the system.

4.4. Performance Comparison under Different Algorithms.

In order to prove the advantages of the proposed algorithm, the algorithms in [28–29] are compared with the proposed algorithm under the same experimental conditions. Figure 4 shows the impact of the number of vehicles on the delay. It can be found that the delay of system task processing increases with the increase of the number of vehicles. This is mainly due to the increase of processing tasks and the limitation of computing resources. Among all algorithms, The reference [29] algorithm has the largest delay.

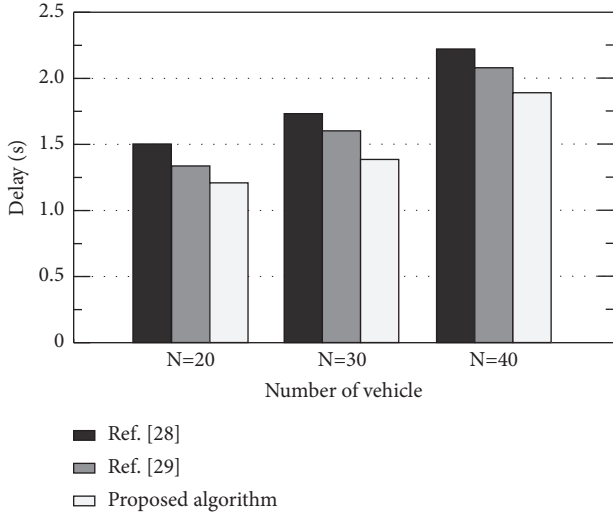


FIGURE 4: Influence of vehicle number on delay of different algorithms.

Compared with the reference [29] algorithm and the proposed algorithm, the vehicle will undertake more tasks. Due to the limitation of the vehicle's own computing resources, processing tasks alone will cause greater delay. Due to the limitation of vehicle computing resources, processing tasks alone will cause large time delay. The proposed algorithm considers the cooperation of terminal, edge, and cloud, improves the utilization efficiency of resources, and minimizes the system delay.

The change of total system overhead with bandwidth under different algorithms is shown in Figure 5. Figure 5 shows that with the increase of bandwidth, the total system overhead of three algorithms shows a downward trend, but the total system overhead of the proposed algorithm is always lower than that of other two algorithms. When bandwidth = 40 MHz, the total system overhead of the algorithm in [28] is 4.732, and the total system overhead of the algorithm in [28] algorithm is 4.251, while the total system overhead of the proposed algorithm is only 3.502. Further analysis shows that when the cloud computing ability of comparison algorithm is relatively weak, most of computing tasks will be completed at the edge node, which cannot make good use of the cloud edge system. Therefore, it produces high total system overhead. Compared with the other two algorithms, the proposed algorithm can achieve the lowest total system overhead because the proposed algorithm considers the dynamic, random, and time-varying characteristics of vehicle network to optimize system performance to the greatest extent.

The change of total system overhead with the number of tasks is shown in Figure 6. With the increase of the number of tasks, the total cost of the three algorithms shows an upward trend. However, the total system overhead of this algorithm is less than that of the algorithms in [28, 29]. This is because the algorithm can collect the state and action information of the whole system and make better decisions according to the global information, so the total cost of the system is low. The comparison algorithm does not fully analyze the state and action information of the system, and

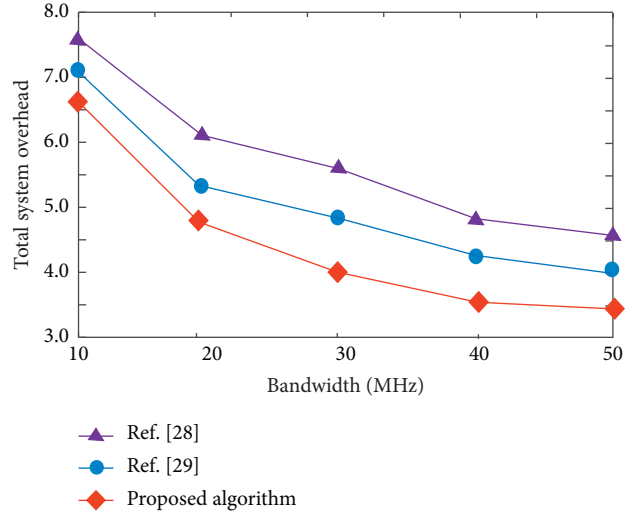


FIGURE 5: Variation of total system overhead with bandwidth under different algorithms.

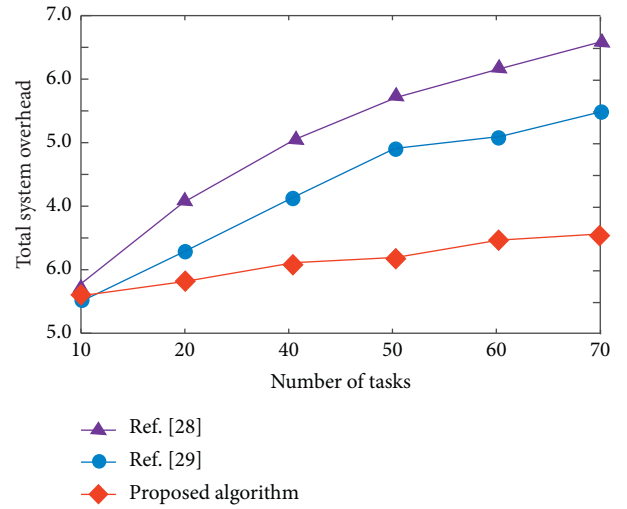


FIGURE 6: Changes of total system overhead with the number of tasks under different algorithms.

the multi-vehicle game increases the energy consumption, resulting in the increase of the total cost of the system.

5. Conclusion

Aiming at the problem of delay and energy consumption caused by the contradiction between limited network resources and a large number of user needs in vehicle environment, this paper proposes an efficient resource management optimization scheme for IoT in edge computing environment. The proposed algorithm builds a communication model and task offloading optimization model in IoT edge computing scenario and solves them based on distributed reinforcement learning to maximize the system performance.

In the future, we will study the content acquisition decision combined with micro-traffic data and the

prediction of vehicle mobility to further improve algorithm performance. Besides, a dynamic situation will be considered, that is, devices may leave the current edge server during computing offloading. In this case, it is necessary to set up a more effective mobile model for devices. In addition, the current blockchain technology provides a powerful solution for the unloading of secure computing tasks in the IoV. In view of the contradiction between the high real time of IoV applications and the low real time of blockchain, we can take advantage of the differences of participants in IoV in terms of security level, computing power, and communication ability to design a hierarchical blockchain structure matching the cloud IoV structure to solve it. It is of great significance to use the blockchain technology to build a secure Internet of Vehicles computing task unloading platform.

Data Availability

The data used to support the findings of this study are included within the article.

Conflicts of Interest

The authors declare that there are no conflicts of interest regarding the publication of this paper.

References

- [1] D. Zhang, L. Cao, H. Zhu, T. Zhang, J. Du, and K. Jiang, "Task offloading method of edge computing in internet of vehicles based on deep reinforcement learning," *Cluster Computing*, vol. 25, no. 2, pp. 1175–1187, 2022.
- [2] M. S. Aslanpour, A. N. Toosi, and C. Cicconetti, "Serverless edge computing: vision and challenges," in *Proceedings of the 2021 Australasian Computer Science Week Multiconference*, pp. 1–10, Dunedin, New Zealand, February, 2021.
- [3] K. Cao, Y. Liu, G. Meng, and Q. Sun, "An overview on edge computing research," *IEEE Access*, vol. 8, no. 2, Article ID 85714, 2020.
- [4] W. Shi and S. Dustdar, "The promise of edge computing," *Computer*, vol. 49, no. 5, pp. 78–81, 2016.
- [5] N. Hassan, K.-L. A. Yau, and C. Wu, "Edge computing in 5G: a review," *IEEE Access*, vol. 7, no. 6, Article ID 127276, 2019.
- [6] D. Zhang, N. Vance, and D. Wang, "When social sensing meets edge computing: vision and challenges," in *Proceedings of the 2019 28th International Conference on Computer Communication and Networks (ICCCN)*, pp. 1–9, IEEE, Valencia, Spain, July, 2019.
- [7] Y. Mao, C. You, J. Zhang, K. Huang, and K. B. Letaief, "A survey on mobile edge computing: the communication perspective," *IEEE communications surveys & tutorials*, vol. 19, no. 4, pp. 2322–2358, 2017.
- [8] Z. Fan, W. Yang, and K. Tian, "An edge computing service model based on information-centric networking," in *Proceedings of the 2019 IEEE 25th International Conference on Parallel and Distributed Systems (ICPADS)*, pp. 498–505, IEEE, Tianjin, China, December, 2019.
- [9] S. Chen, Q. Li, M. Zhou, and A. Abusorrah, "Recent advances in collaborative scheduling of computing tasks in an edge computing paradigm," *Sensors*, vol. 21, no. 3, pp. 779–787, 2021.
- [10] W. Wu, Q. Zhang, and H. J. Wang, "Edge computing security protection from the perspective of classified protection of cybersecurity," in *Proceedings of the 2019 6th International Conference on Information Science and Control Engineering (ICISCE)*, pp. 278–281, IEEE, Shanghai, China, December, 2019.
- [11] S. M. Khan, M. Chowdhury, E. A. Morris, and L. Deka, "Synergizing roadway infrastructure investment with digital infrastructure for infrastructure-based connected vehicle applications: review of current status and future directions," *Journal of Infrastructure Systems*, vol. 25, no. 4, Article ID 03119001, 2019.
- [12] F. Loussaief, H. Marouane, H. Koubaa, and F. Zarai, "Radio resource management for vehicular communication via cellular device to device links: review and challenges," *Telecommunication Systems*, vol. 73, no. 4, pp. 607–635, 2020.
- [13] A. W. Wang, Y. J. Wang, A. M. Zahm, A. R. Morgan, K. J. Wangenstein, and K. H. Kaestner, "The dynamic chromatin architecture of the regenerating liver," *Cellular and molecular gastroenterology and hepatology*, vol. 9, no. 1, pp. 121–143, 2020.
- [14] R. Shrestha, S. Y. Nam, R. Bajracharya, and S. Kim, "Evolution of V2X communication and integration of blockchain for security enhancements," *Electronics*, vol. 9, no. 9, pp. 1338–1345, 2020.
- [15] X. Li, L. Zhou, Y. Sun, S. Zhou, and M. Lu, "Resource allocation schemes based on improved beetle antennae search algorithm for collaborative communication of the unmanned aerial vehicle network," in *Proceedings of the International Conference on Wireless and Satellite Systems*, pp. 275–282, Springer, Harbin, China, January, 2019.
- [16] T. Xue, W. Wu, Q. Wang, and X. Wu, "Radio resource allocation for V2X communications based on hybrid multiple access technology," in *Proceedings of the International Conference on Wireless and Satellite Systems*, pp. 23–35, Springer, Harbin, China, January, 2019.
- [17] C. He, Q. Chen, C. Pan, X. Li, and F.-C. Zheng, "Resource allocation schemes based on coalition games for vehicular communications," *IEEE Communications Letters*, vol. 23, no. 12, pp. 2340–2343, 2019.
- [18] J. Kim, J. Lee, S. Moon, and I. Hwang, "A position-based resource allocation scheme for V2V communication," *Wireless Personal Communications*, vol. 98, no. 1, pp. 1569–1586, 2018.
- [19] F. Wang, J. Liu, L. Zhao, and K. Zheng, "Decentralised resource allocation of position-based and full-duplex-based all-to-all broadcasting," *IET Communications*, vol. 13, no. 15, pp. 2254–2260, 2019.
- [20] M. Chen, T. Wang, K. Ota, M. Dong, M. Zhao, and A. Liu, "Intelligent resource allocation management for vehicles network: an A3C learning approach," *Computer Communications*, vol. 151, no. 1, pp. 485–494, 2020.
- [21] Y. Liu, H. Yu, S. Xie, and Y. Zhang, "Deep reinforcement learning for offloading and resource allocation in vehicle edge computing and networks," *IEEE Transactions on Vehicular Technology*, vol. 68, no. 11, Article ID 11158, 2019.
- [22] Y. Zhan, S. Guo, P. Li, and J. Zhang, "A deep reinforcement learning based offloading game in edge computing," *IEEE Transactions on Computers*, vol. 69, no. 6, pp. 883–893, 2020.
- [23] L. Huang, S. Bi, and Y.-J. A. Zhang, "Deep reinforcement learning for online computation offloading in wireless powered mobile-edge computing networks," *IEEE Transactions on Mobile Computing*, vol. 19, no. 11, pp. 2581–2593, 2020.

- [24] Y. Hui, Z. Su, T. H. Luan, and J. Cai, "Content in motion: an edge computing based relay scheme for content dissemination in urban vehicular networks," *IEEE Transactions on Intelligent Transportation Systems*, vol. 20, no. 8, pp. 3115–3128, 2019.
- [25] Z. Su, Y. Hui, and S. Guo, "D2D-based content delivery with parked vehicles in vehicular social networks," *IEEE Wireless Communications*, vol. 23, no. 4, pp. 90–95, 2016.
- [26] W. Zhao, Y. Qin, D. Gao, C. H. Foh, and H.-C. Chao, "An efficient cache strategy in information centric networking vehicle-to-vehicle scenario," *IEEE Access*, vol. 5, no. 9, pp. 12657–12667, 2017.
- [27] Y. Zhang, T. M. Mirpuri, and C. L. Ho, "Primary epithelioid sarcoma manifesting as a fungating scalp mass - imaging features and treatment options. A case report and literature review," *Journal of Radiology Case Reports*, vol. 15, no. 11, pp. 1–9, 2021.
- [28] C. Zhang, H. Du, and Q. Gao, "DMORA: decentralized multi-SP online resource allocation scheme for mobile edge computing," *IEEE Transactions on Cloud Computing*, vol. 9, no. 1, p. 1, 2020.
- [29] X. Li, "A computing offloading resource allocation scheme using deep reinforcement learning in mobile edge computing systems," *Journal of Grid Computing*, vol. 19, no. 3, pp. 2001–2009, 2021.

Research Article

Intrusion Detection Model for Industrial Internet of Things Based on Improved Autoencoder

Wumei Zhang  and Yongzhen Zhang 

Zhejiang Tongji Vocational College of Science and Technology, HangZhou, Zhejiang 311231, China

Correspondence should be addressed to Yongzhen Zhang; zhangyongzhen@zjtongji.edu.cn

Received 15 March 2022; Revised 14 April 2022; Accepted 29 April 2022; Published 27 May 2022

Academic Editor: Le Sun

Copyright © 2022 Wumei Zhang and Yongzhen Zhang. This is an open access article distributed under the Creative Commons Attribution License, which permits unrestricted use, distribution, and reproduction in any medium, provided the original work is properly cited.

With the gradual advancement of informatization and industrialization, the safety and controllability of industrial Internet of things (IIoT) have attracted more and more attention. Aiming to improve the security of industrial IIoT, a detection method using stacked sparse autoencoder network model is proposed. In this method, the basic units of the network model have been simplified and sparse, and some of basic features are combined with obtaining a higher-level abstract expression, so as to solve the problem of unbalanced network traffic data. The cascaded network structure is adopted to stack its sparse autoencoder network model, so as to improve the data ability of the detection model. In addition, the incorporation of Softmax classifier realizes the dynamic adjustment and optimization of the whole network parameters, which further ensures the efficiency of the detection method. The simulation experiment is based on NSL-KDD dataset. The experiment has proved that the proposed method has excellent network attack identification and detection performance. Its accuracy index is about 95.42%, and the detection time is about 3.42 s.

1. Introduction

The essence of Internet of things (IoT) is the integrated development of industrial automation and interconnection of all things technology [1–3]. The Industrial Internet of things (IIoT) has realized the unprecedented combination of subsystems such as production, monitoring, and management. Different systems can process all kinds of industrial data more efficiently under the unified management of the control center [4, 5]. Its high complexity and openness increase the network security risk faced by the industrial IIoT.

Typical network attacks in industrial control systems are common [6]. In July 2010, the first virus “Stuxnet” targeting the Supervisory Control and Data Acquisition (SCADA) system attacked Iran’s nuclear facilities. In 2012, the “Flame” virus paralyzed Iran’s oil industry network. Since then, the incidents of hacker attacks on industrial control systems have been reported all over the world, and the frequency and impact have shown a rapid upward trend year by year. Industrial control security has become a complex of “network security, equipment security, control security,

application security, and data security” [7]. Therefore, it is particularly urgent to propose an accurate and efficient network intrusion detection method.

Intrusion detection system is widely used in traditional industrial control system and modern industrial IIoT, and it has attracted more and more attention [8, 9]. In [10], the authors detect attacks on the industrial IIoT based on BiLSTM-RNN and use the UNSWNYB15 dataset to train a multilayer neural network. In [11], the authors designed a network intrusion detection system for the SCADA system based on CNN to protect the IIoT from conventional network risk such as DDoS and specific network attacks against SCADA. In [12], the authors studied the power theft attack in the smart grid and proposed a detection method using the multilayer network. However, it should be pointed out that when facing the current high real-time, high-capacity and complex multidimensional data in industrial IIoT, the above methods often need a complex training process, and the accuracy needs to be improved [13].

Deep network can not only obtain the maximum reward from the high-dimensional and massive network data

environment but also have the exploration function and automatically mine more valuable information in the network environment [14–16]. Therefore, many scholars have carried out research studies and analyses using deep learning network. In [17], the authors used a context adaptive intrusion detection system, which realizes the accurate detection of network attacks through the mutual assistance of multiple agents. The IIoT detection model in [18] combines feedforward neural network and long-term and short-term memory network. In [19], the authors used an IIoT detection model based on intelligent algorithm and multilayer network, which can achieve better detection efficiency. In [20], the authors proposed a new multiagent confrontation reinforcement learning model for IIoT detection system to realize steady-state support for the network environment. However, it should be noted that the industrial IoT data has unbalanced characteristics. The current deep learning intrusion detection method cannot achieve accurate data feature extraction in the network data with too many feature dimensions, and it is difficult to support efficient and accurate intrusion attack-type mapping. At the same time, due to the deeper network structure, the deep network model also has the problem of time-consuming in intrusion detection.

Aiming at the above problems, based on the improved autoencoder (AE), a detection method for IIoT is proposed. The main innovations are as follows:

- (1) In this study, the network structure unit of the multilayer network is sparse. By adding sparsity constraints to the hidden layer, some neurons are suppressed, and the problem of industrial network intrusion detection with unbalanced network traffic data is solved, so as to learn more accurate and efficient feature expression.
- (2) The cascade form is used to combine the sparse autoencoder (SAE) network and construct the stacked sparse autoencoder (SSAE) network model, which can realize the continuous deep feature extraction of industrial IoT network data, so as to support the high accuracy of intrusion detection network.

2. Standard Autoencoder Model Learning Algorithm

Industrial control system network dataset presents the characteristics of more normal data, less abnormal data, and uneven data distribution [21]. Algorithms including traditional artificial neural network cannot effectively classify and identify unbalanced data.

AE network is an unsupervised feature detection model, which can learn a feature representation of input data. This model belongs to artificial neural network and is optimized by backpropagation algorithm.

The essence of the algorithm of self-encoder network is an unsupervised training and learning method. In order to make the target value input directly, it introduces the data

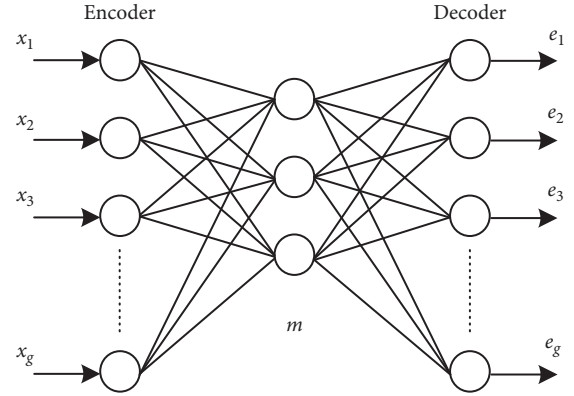


FIGURE 1: Autoencoding network structure.

processing model of backpropagation to maintain the consistency of data.

In addition to being used as the construction module of deep neural network, the AE network can also be used to extract discriminant features with lower dimension than input, so as to solve the dimension disaster.

The standard AE is a multilayer feedforward network, which expects the input and output to be consistent. It can be used to learn identity mapping and extract unsupervised features. Figure 1 is a network structure of a single-layer autoencoder, in which only one hidden layer is used to encode the input and reconstruct the input at the output through decoding. The part from the input layer to the middle layer is called encoder, and the part from the middle layer to the output layer is called decoder. Autoencoder is an unsupervised feature detection model, which can learn another feature representation of input data. Autoencoder learns to generate a hidden layer representation from the input and reconstructs the output as close to the input as possible from the hidden layer representation.

As can be seen from Figure 1, the AE network model is composed of the input layer, the hidden layer, and the output layer. Specifically, the purpose of the self-encoder is to make the output value of the model equal to or as close to the input value of the model as possible with the help of an identity function. $x_i = e_i$.

Encoding refers to the process of mapping input $x \in R$ to implicit representation $h(x) \in R$. The calculation form is

$$h(x) = \alpha_h(Wx + b), \quad (1)$$

where $W \in R$ is the encoding weight matrix, $b \in R$ is the encoding offset vector, $\alpha_h(x)$ is the vector value function, and in the case of nonlinearity, $\alpha_h(x)$ is taken as Sigmoid function.

Decoding refers to mapping the implicit representation $\alpha_h(x)$ to the output layer e , so as to reconstruct the input x . The calculation form is

$$e = \alpha_e(Wh(x) + b'), \quad (2)$$

where $W' \in R$ presents the decoding matrix, $b' \in R$ presents the decoding vector, and $\alpha_e(x)$ is similar to $\alpha_h(x)$.

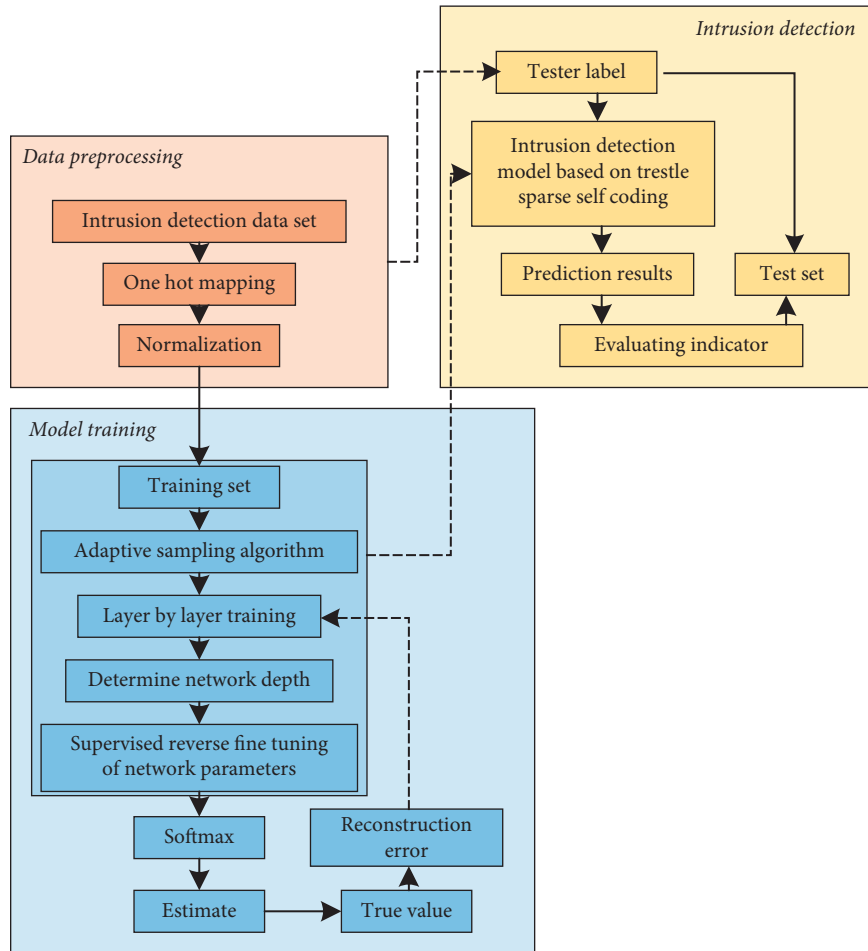


FIGURE 2: Intrusion detection model for IIoT.

3. Intrusion Detection Model of IIoT

Excessive feature dimension is the reason for the low efficiency of industrial control safety anomaly detection [22, 23]. Dimension reduction can be achieved by reducing high-dimensional and nonlinear attribute features. Through the sparse expression of features, a small number of basic features are combined to obtain a higher-level abstract expression.

Therefore, based on the standard AE network, this study adds sparsity constraints to the output of the hidden layer so that most neurons are suppressed and constructs a attacked sparse autoencoder (SSAE) network model.

The SSAE network is used to establish the intrusion detection model of the IIoT. On the premise of maintaining the accuracy of detection, the calculation speed and calculation memory are improved, so as to learn better feature expression.

3.1. Overall Architecture. The proposed overall architecture is shown in Figure 2.

From Figure 2, the identification of industrial IoT intrusion by this model mainly includes the following three steps:

(1) Data preprocessing: build an industrial IoT environment and capture real-time network data, including source address, target address, connection attributes, and other relevant information [24, 25]. The data are preprocessed and transformed into a format that can be processed by the stacked noise reduction convolutional autoencoder. In this study, data preprocessing is divided into three parts:

- ① Attribute mapping: convert character data into numerical data
- ② Data normalization: normalize the data to within 0 to 1 to solve the problem of dimensional inconsistency, which affects the accuracy
- ③ Regional adaptive oversampling algorithm: generate new samples at the algorithm level for minority samples, handle the imbalance of data distribution properly, and then carry out the next operation to optimize minority data

3.2. Stacked Sparse Autoencoder Network. SAE network suppresses most neurons by adding sparsity constraints to the output of the hidden layer, which can learn better feature expression, so as to solve the problem of industrial network

intrusion detection with unbalanced network traffic data. The specific way is to add a sparse penalty term, that is, the function of the average output activation value of neurons.

The goal of SAE is to make the output fit the input features, which is similar to AE, but SAE imposes sparsity restrictions on the middle layer in order to avoid simple mapping output to input.

The simple understanding of sparsity restriction is that when the output of neuron in each layer is 0, it indicates that the state of neuron is inhibited; when the output of neuron is 1, it indicates that the state of neuron is active, and the sparsity restriction makes the state of neuron inhibited most of the time.

The mean activation degree of hidden layer neuron i is defined as follows:

$$\hat{\tau}_i = \frac{1}{n} \sum_{p=1}^n [c_i^{(2)}(v^{(i)})], \quad (3)$$

where n indicates the total number of data sample sets and $c_i^{(2)}$ is the activation parameter of the middle layer neuron i when v is used as input. To get the sparse representation of the middle layer neuron, it should make the activation mean $\hat{\tau}_i$ of the middle layer neuron i as 0 as possible. If making $\hat{\tau}_i = \tau$ as a sparsity parameter, τ should be a decimal close to zero. By introducing a penalty factor into the solution of the objective, those scenarios that $\hat{\tau}_i$ and τ are significantly different are punished, so as to realize such sparsity limitation and continuously optimize the value of the objective function. There are many ways to construct penalty factors. Here, the Kullback–Leible (KL) is used to regularize the network so that the average activation degree $\hat{\tau}_i$ is equal to τ as much as possible:

$$KL(\tau \parallel \hat{\tau}_i) = \tau \log \frac{\tau}{\hat{\tau}_i} + (1 - \tau) \log \frac{1 - \tau}{1 - \hat{\tau}_i}. \quad (4)$$

The penalty factor formula is as follows:

$$\sum_{i=1}^{z^2} \tau \log \frac{\tau}{\hat{\tau}_i} + (1 - \tau) \log \frac{1 - \tau}{1 - \hat{\tau}_i}, \quad (5)$$

where z^2 is the sum of neuron. The above penalty factor can also be expressed as $\sum_{i=1}^{z^2} KL(\tau \parallel \hat{\tau}_i)$.

It can be seen that the loss function of the detection network is

$$\theta_{sparse}(W, b) = \theta_E(W, b) + \mu \sum_{i=1}^{z^2} KL(\tau \parallel \hat{\tau}_i). \quad (6)$$

Usually, in order to avoid the overfitting problem, the L_2 weight penalty is introduced to the objective function; then,

$$\theta_{SAE}(W, b) = \theta_{sparse}(W, b) + \frac{\gamma}{2} \sum_{i=1}^{s_q} \sum_{p=1}^{s_q+1} \sum_{q=1}^{s_q-1} (u_{pi}^{(q)})^2, \quad (7)$$

where γ represents the regularization parameter, q represents the current layer, and s_q and $s_q + 1$ are the sum of neurons.

The formula of descent optimization is as follows:

$$W_{pi}^{(q)} = u_{pi}^{(q)} - \psi \frac{\partial}{\partial u_p^{(q)}} \theta_{SAE}(W, b), \quad (8)$$

$$b_{pi}^{(q)} = b_{pi}^{(q)} - \psi \frac{\partial}{\partial b_p^{(q)}} \theta_{SAE}(W, b), \quad (9)$$

where ψ is the learning rate. The optimal W and b can be obtained by back propagation using the SGD optimization method.

The training process of SSAE network is shown in Figure 3.

The first SAE contains layers x , m_1 , and \hat{x} , uses formula (6) to learn the representation of features in an unsupervised manner, and then obtains U_1 and c_1 through formulae (7) and (8) training. The second SAE contains layers m_1 , m_2 , and \hat{m}_1 . The training method of the second SAE is similar to that of the first SAE, and U_2 and c_2 are obtained through training. By repeating the above training steps, all the parameters in the stacked sparse autoencoder network can be obtained.

The way of weight assignment of neural network through pretraining is better than that of random weight assignment of neural network, and it is conducive to convergence. In the training process, the number of neurons decreases gradually, and finally, the deep sparse feature is obtained.

3.3. Detection Model Training. Softmax classifier is added in the last layer of SSAE network, and the trained parameters are used as the initial optimization parameters of the model, and then, the parameters of the whole network are fine tuned. This layer-by-layer greedy process is proved to produce a better local extremum than random initialization weights and achieves better generalization performance in some tasks.

The proposed detection model used the SSAE network model is as follows (Algorithm 1).

4. Experiment and Result Discussion

4.1. Simulation Environment. Tensorflow and OpcnAlGym are the mainstream machine learning training platforms and environments. We choose them as the software environment for simulation experiments. Meanwhile, the experimental hardware environment is CPU model: AMD Ryzen 7, CPU: NVIDIA GeForce RTX2080Ti, and RAM: 32 GB.

4.2. Data Preprocessing. At present, the public datasets of industrial IoT intrusion mainly include KDDCup99, NSL-KDD, GasPipeline Datasets, WaterDatasets, and UNSW-NB15. These datasets have the problems of redundancy and repetition of data and attributes. This study selects NSL-KDD dataset as the experimental benchmark data.

NSL-KDD dataset solves the problem of redundant data in KDDCup99 dataset. Its original training set

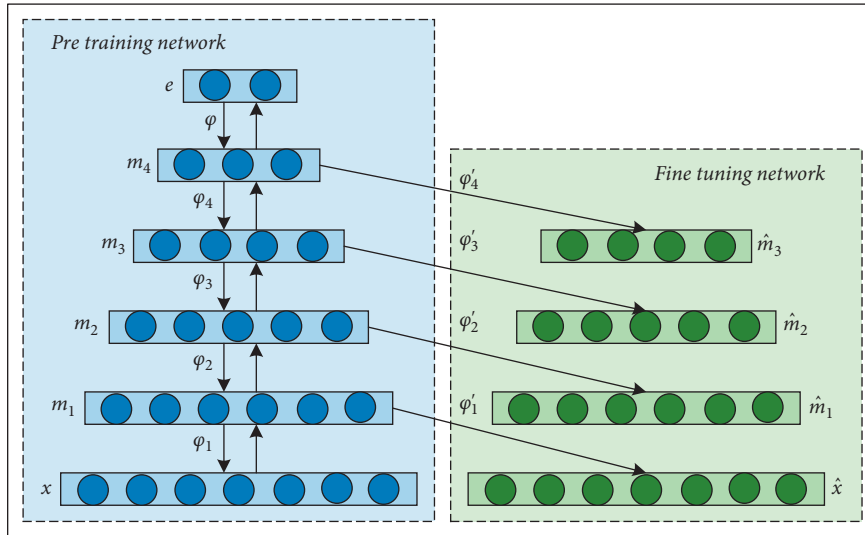


FIGURE 3: Stacked sparse autoencoder network training process.

Input: 256 dimensional data x after high-dimensional mapping and normalization, data \hat{x} with a certain noise proportion κ .

Output: optimal network parameter values $\varphi_1, \varphi_2, \varphi_3, \varphi_4$, and φ_5 .

Step 1: the feature extraction model based on SSAE network takes the training data x as the input. Through the SGD descent method, the input data are analyzed and processed to obtain the network parameters of the hidden layer. Finally, the output m_1 of the first hidden layer is calculated by using the original data x and parameters φ_1 .

Step 2: then, combined with m_1 and φ_1 , the output parameter φ_2 and output m_2 of the hidden layer can be obtained through the calculation and analysis of the second layer.

Step 3: repeat step 1 and step 2, and get the weight parameters $\varphi_1, \varphi_2, \varphi_3$, and φ_4 by layer-by-layer training. With the help of the calculation and analysis of the classifier, the parameter m_5 is obtained.

Step 4: through the above calculation, we can obtain the network parameter $\varphi_1 - \varphi_5$ of the detection model. By introducing random noise, we input it as training data, calculate the loss function between the predicted value and the target, and use various optimization methods to calculate the parameters near the minimum value.

ALGORITHM 1: Training algorithm of intrusion detection model based on SSAE network model.

KDDTrain contains 125973 data and the original test set KDDTest contains 22544 data. In this study, KDDTrain+20% of 25192 data are selected as experimental data.

4.2.1. Character-Type Mapping Numeric Type. “O, tcp, ftp_data, SF, 491, 0, 0, 0, 0, 0, 0, 0, 0, 0, 0, 0, 0, 0, 0, 0, 2, 0, 0, 0, 0, 1, 0, 0, 150, 25, 0.17, 0.03, 0.17, 0, 0, 0, O.OS, O, Normal” is a piece of data in the dataset. According to the analysis, the values in dimension 2, 3, and 4 of the data are character types and need to be converted into numerical types. For example, there are 3 types in dimension 2 (TCP, UDP, ICMP), 70 types in dimension 3 (“auth,” “bgp,” “courier,” etc.), and 11 types in dimension 4 (“OTH,” “REJ,” “RSTO,” etc.), which are processed according to the one-hot coding in Figure 4 and finally convert the 32 dimension into 256 dimension attributes.

4.2.2. Numerical Normalization. Because data order of magnitude and corresponding value range of different feature attributes are obviously different, in order to

facilitate the analysis of experimental results, the Min-Max standardization method is used to uniformly map the numerical data to the $[0, 1]$ interval so that the data is in the same order of magnitude:

$$x_{\text{normal}} = \frac{x - x_{\min}}{x_{\max} - x_{\min}}, \quad (10)$$

where x is the original eigenvalue of data, x_{\min} and x_{\max} represents the minimum and maximum values in the data respectively, and x_{normal} represents the new feature value after normalization of each data.

4.2.3. Low-Frequency Sample Processing. Although current industrial IoT attacks show a rapid growth trend, the individual attack categories still belong to the low-frequency category compared with the normal data flow, which makes it difficult to capture their feature records. Moreover, most AI models have obvious classification bias because they aim at the overall classification accuracy of the largest sample. Therefore, this study improves the sampling algorithm and introduces the Regional Adaptive Synthetic Oversampling algorithm (RASmote) to

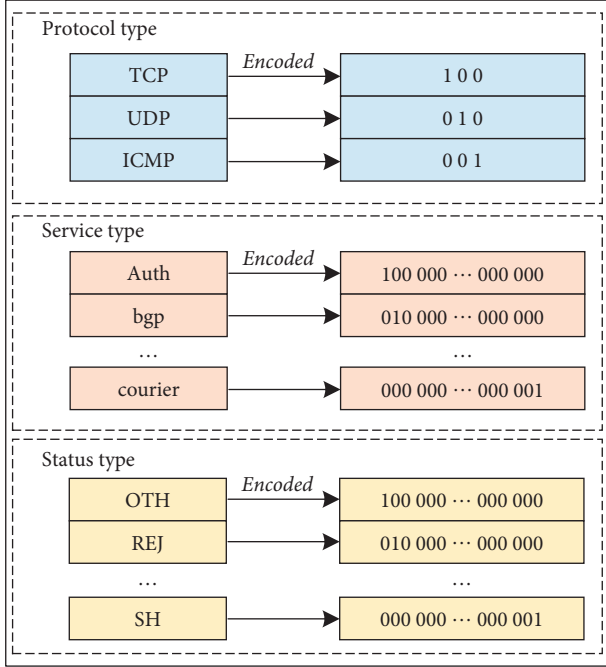


FIGURE 4: One-hot coding digitization.

incrementally process low-frequency samples. The algorithm formula is as follows:

$$\begin{aligned} \eta &= |X_n - X_l| \\ &= \sqrt{\sum_{k=1}^n (X_{nk} - X_{lk})^2}. \end{aligned} \quad (11)$$

Euclidean distance is used to calculate the distance of low-frequency samples in the nearest neighbor radius. n is the nearest neighbor radius, X_n is the nearest neighbor sample set, X_l is the low-frequency sample, and X' is the new sample set:

$$\begin{cases} X' = 0, & 0 \leq \eta \leq \frac{n}{2}, \\ X' = X + \mu(0, 1) \left(\left(\frac{1}{n - \eta} \sum_{i=1}^n X_i \right) - X \right), & \frac{n}{2} < \eta < n, \\ X' = X, & \eta = n, \end{cases} \quad (12)$$

where $(1/n - \eta \sum_{i=1}^n X_i)$ is a low-frequency sample.

4.3. Evaluation Index. The performance of the SSAE intrusion detection model can be evaluated from two aspects: model comparison and classification detection. The model comparison is mainly compared with traditional intrusion detection technology. The main indexes of system detection include accuracy Acc, precision Pre, recall Re, and F1-score F_1 . It should be noted that, for these four indexes, the higher the value, the better the detection performance:

TABLE 1: Distribution of dataset.

Data type	Training set	Test set
Normal	9415	4034
Dos	6500	2734
Probe	1603	786
R2L	145	64
U2R	8	3

TABLE 2: Identification result of different types of network attacks.

Data type	Accuracy (%)
Dos	97.34
Probe	96.81
R2L	91.32
U2R	88.23

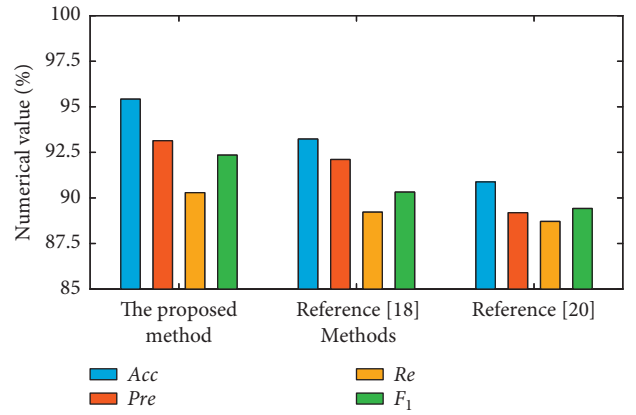


FIGURE 5: Intrusion detection analysis under different methods.

$$\begin{aligned} \text{Acc} &= \frac{|T_P| + |T_N|}{|T_P| + |F_P| + |T_N| + |F_N|}, \\ \text{Pre} &= \frac{|T_P|}{|T_P| + |F_P|}, \\ \text{Re} &= \frac{|T_P|}{|T_P| + |F_N|}, \\ F_1 &= 2 \times \frac{\text{Pre} \times \text{Re}}{\text{Pre} + \text{Re}}, \end{aligned} \quad (13)$$

where T_N is true negative rate, F_P is false positive rate, F_N is false negative rate, and T_P is true positive rate.

4.4. Experimental Analysis. KDDTrain+20% data are used as the experimental data, 70% as the training set, and 30% as the test set. The data distribution is shown in Table 1.

Firstly, based on the experimental dataset, the detection, analysis, and research of industrial IoT under different network attacks are carried out for the proposed model. The

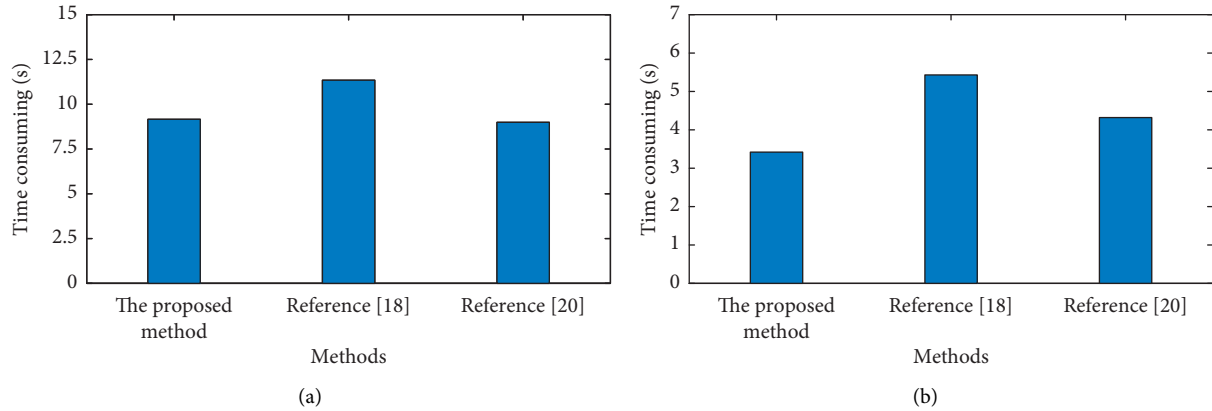


FIGURE 6: Comparison of intrusion detection time under different methods. (a) Training set time consuming. (b) Test set time consuming.

identification results of attacks are displayed in the under table.

From Table 2, we can see that the proposed model can better complete the task of network defense, and the detection accuracy of Dos and Probe attacks is more than 95%. For R2L and U2R attacks, because of the small volume of training data, the identification accuracy is lower than that of the first two attacks, but it is still more than 85%.

In order to further verify the performance of the proposed model, the authors [18, 20] are used as comparison methods to detect KDDTrain+20% datasets, respectively. Figure 5 shows the attack identification results under different intrusion detection methods.

From Figure 5, we can see that the proposed method is better than other comparison methods in terms of network performance. The evaluation indexes of the proposed method are as follows: the accuracy Acc is 95.42%, the precision Pre is 93.14%, the recall Re is 90.29%, and the F1-value F_1 is 92.35%. The accuracy of intrusion detection in [18, 20] is less than 95%, which is less than the detection performance of the proposed method.

The reason is that the proposed model simplifies the network and enhances the autonomous ability and can realize better feature extraction and expression of the network. Meanwhile, with the introduction of Softmax classifier, the detection network parameters can be dynamically adjusted to support accurate network attack identification and analysis. In [18, 20], LSTM network as the benchmark model is taken for modeling and analysis, without considering the imbalance of data, which is not enough to achieve more accurate and efficient intrusion identification analysis.

At the same time, the attack detection efficiency is also compared and evaluated. Figure 6 shows the analysis of detection time under different methods.

As shown in Figure 6, due to the simplification of the network unit, the unit structure of the proposed method needs more autonomous learning time to realize the accurate extraction of data features. Therefore, the training time is 9.16s, which is 0.17s more than that in [20]. Moreover, the time-consuming of the proposed method for

network intrusion detection is only 3.42 s and that of [18] is 5.43 s and that of reference [20] is 4.32 s.

To sum up, while ensuring the accuracy of detection, the proposed method can improve the efficiency of intrusion identification and analysis and reflect its overall efficient performance.

5. Conclusion

This study proposes an intrusion detection method based on stacked sparse autoencoder network. This method constructs an intrusion network model based on autoencoder network, which can effectively improve the feature extraction of industrial Internet data. The autoencoder network is simplified and cascaded, and a small number of basic network units are used to obtain more efficient feature expression. In addition, the introduction of Softmax classifier ensures that the parameters of the detection network can be fine-tuned and optimized, which can further improve the processing and computing efficiency of the network while improving the accuracy of industrial IoT attack recognition. The experimental analysis based on NSL-KDD dataset shows that the proposed method can realize accurate and fast intrusion attack identification and can meet the safe and controllable operation requirements of industrial IoT.

Although this method improves the solution of IIoT intrusion detection, the essence of the proposed model is a centralized processing and computing model. Aiming to support the detection research in the actual complex network environment, the next step will be to study the intrusion detection method of distributed architecture mode.

Data Availability

The data used to support the findings of this study are included within the article.

Conflicts of Interest

The authors declare that there are no conflicts of interest regarding the publication of this paper.

Acknowledgments

This work was supported by Zhejiang Water Conservancy Science and Technology Project (no. RC1974).

References

- [1] X. Gming, S. Xiaorui, Z. Zhihua, and X. Bertino, "Advances in Artificial Intelligence and Security," in *Proceedings of the 27th International Conference, ICAIS 2021*, Dublin, Ireland, July 2021.
- [2] A. A. Suzen, "Developing a multi-level intrusion detection system using hybrid-DBN," *Journal of Ambient Intelligence and Humanized Computing*, vol. 12, no. 2, pp. 1913–1923, 2021.
- [3] Z. Wang, Y. Lai, Z. Liu, and J. Liu, "Explaining the attributes of a deep learning based intrusion detection system for industrial control networks," *Sensors*, vol. 20, no. 14, pp. 3817–3824, 2020.
- [4] A. Ayodeji, Y.-k. Liu, N. Chao, and L. Q. Yang, "A new perspective towards the development of robust data-driven intrusion detection for industrial control systems," *Nuclear Engineering and Technology*, vol. 52, no. 12, pp. 2687–2698, 2020.
- [5] D. Li, L. Deng, M. Lee, and H. Wang, "IoT data feature extraction and intrusion detection system for smart cities based on deep migration learning," *International Journal of Information Management*, vol. 49, no. 1, pp. 533–545, 2019.
- [6] A. Khraisat, I. Gondal, P. Vamplew, J. Kamruzzaman, and A. Alazab, "A novel ensemble of hybrid intrusion detection system for detecting Internet of things attacks," *Electronics*, vol. 8, no. 11, pp. 1210–1218, 2019.
- [7] L. Lv, W. Wang, Z. Zhang, and X. Liu, "A novel intrusion detection system based on an optimal hybrid kernel extreme learning machine," *Knowledge-Based Systems*, vol. 195, no. 1, pp. 105648–105717, 2020.
- [8] I. A. Khan, D. C. Pi, and Z. U. Khan, "HML-DS: a hybrid-multilevel anomaly prediction approach for intrusion detection in SCADA systems," *IEEE Access*, vol. 7, no. 1, pp. 89507–89521, 2019.
- [9] B. Li, Y. Wu, J. Song, R. Lu, T. Li, and L. Zhao, "DeepFed: federated deep learning for intrusion detection in industrial cyber-physical systems," *IEEE Transactions on Industrial Informatics*, vol. 17, no. 8, pp. 5615–5624, 2021.
- [10] B. Roy and H. Cheung, "A deep learning approach for intrusion detection in internet of things using bi-directional long short-term memory recurrent neural network," in *Proceedings of the 28th International Telecommunication Networks and Applications Conference (ITNAC)*, pp. 1–6, Sydney, NSW, Australia, November 2018.
- [11] H. Yang, L. Cheng, and M. C. Chuah, "Deep-Learning-Based Network Intrusion Detection for SCADA Systems," in *Proceedings of the 2019 IEEE Conference on Communications and Network Security (CNS)*, pp. 3–5, IEEE, Washington, DC, USA, June 2019.
- [12] M. Ismail, M. F. Shaaban, M. Naidu, and E. Serpedin, "Deep learning detection of electricity theft cyber-attacks in renewable distributed generation," *IEEE Transactions on Smart Grid*, vol. 11, no. 4, pp. 3428–3437, 2020.
- [13] W. Ding, J. Nayak, B. Naik, D. Pelusi, and M. Mishra, "Fuzzy and real-coded chemical reaction optimization for intrusion detection in industrial big data environment," *IEEE Transactions on Industrial Informatics*, vol. 17, no. 6, pp. 4298–4307, 2021.
- [14] I. A. Khan, D. Pi, P. Yue et al., "Efficient behaviour specification and bidirectional gated recurrent units-based intrusion detection method for industrial control systems," *Electronics Letters*, vol. 56, no. 1, pp. 27–30, 2020.
- [15] W. Liang, K.-C. Li, J. Long, X. Kui, and A. Y. Zomaya, "An industrial network intrusion detection algorithm based on multifeature data clustering optimization model," *IEEE Transactions on Industrial Informatics*, vol. 16, no. 3, pp. 2063–2071, 2020.
- [16] W. Wang, F. Harrou, B. Bouyeddou, S.-M. Senouci, and Y. Sun, "A stacked deep learning approach to cyber-attacks detection in industrial systems: application to power system and gas pipeline systems," *Cluster Computing*, vol. 25, no. 1, pp. 561–578, 2022.
- [17] K. Sethi, E. Sai Rupesh, R. Kumar, P. Bera, and Y. Venu Madhav, "A context-aware robust intrusion detection system: a reinforcement learning-based approach," *International Journal of Information Security*, vol. 19, no. 6, pp. 657–678, 2020.
- [18] I. Almomani, "A multi-layer classification approach for intrusion detection in IoT networks based on deep learning," *Sensors*, vol. 21, no. 9, pp. 1–21, 2021.
- [19] Y. Zhang, P. Li, and X. Wang, "Intrusion detection for IoT based on improved genetic algorithm and deep belief network," *IEEE Access*, vol. 7, no. 1, pp. 31711–31722, 2019.
- [20] A. Chu, Y. Lai, and J. Liu, "Industrial control intrusion detection approach based on multiclassification GoogleNet-LSTM model," *Security and Communication Networks*, vol. 2019, no. 1, pp. 1–11, Article ID 6757685, 2019.
- [21] J. Y. Song, R. Paul, J. H. Yun, H. C. Kim, and Y. J. Choi, "CNN-based anomaly detection for packet payloads of industrial control system," *International Journal of Sensor Networks*, vol. 36, no. 1, pp. 36–49, 2021.
- [22] M. T. R. Laskar, J. X. Huang, V. Smetana et al., "Extending isolation forest for anomaly detection in big data via K-means," *ACM Transactions on Cyber-Physical Systems*, vol. 5, no. 4, pp. 1–26, 2021.
- [23] S. Mubarak, M. Hadi Habaeabi, M. Rafiqul Islam, F. Diyana Abdul Rahman, and M. Tahir, "Anomaly detection in ICS Datasets with machine learning algorithms," *Computer Systems Science and Engineering*, vol. 37, no. 1, pp. 33–46, 2021.
- [24] T. Vaiyapuri, Z. Sbai, and H. Alaskar, "Deep learning approaches for intrusion detection in IIoT networks – opportunities and future directions," *International Journal of Advanced Computer Science and Applications*, vol. 12, no. 4, pp. 86–92, 2021.
- [25] X. Zhou, Y. Hu, W. Liang, J. Ma, and Q. Jin, "Variational LSTM enhanced anomaly detection for industrial big data," *IEEE Transactions on Industrial Informatics*, vol. 17, no. 5, pp. 3469–3477, 2021.

Research Article

Research on Brand Image Evaluation Method Based on Consumer Sentiment Analysis

ZhengMin Li 

School of Journalism & Communication, Wuhan University, Wuhan 430072, Hubei, China

Correspondence should be addressed to ZhengMin Li; 2015101030022@whu.edu.cn

Received 14 April 2022; Revised 28 April 2022; Accepted 10 May 2022; Published 27 May 2022

Academic Editor: Le Sun

Copyright © 2022 ZhengMin Li. This is an open access article distributed under the Creative Commons Attribution License, which permits unrestricted use, distribution, and reproduction in any medium, provided the original work is properly cited.

Brand image assessment is a key step to reasonably quantify the value of a brand and has far-reaching significance for improving the competitiveness of an enterprise. With the rapid development of Internet technology, traditional questionnaires can no longer meet the current needs of brand image assessment. In this environment, the huge amount of fragmented consumer topic data provides a rich data resource and new research ideas for brand image assessment. Therefore, a brand image assessment method based on consumer sentiment analysis is proposed. First, a topic-based brand image cognitive label extraction method is proposed by setting language rules, aggregation rules, and ranking rules according to the characteristics of online topic data. Then, the fusion of cognitive labels and deep features is performed by fusing the deep features extracted from word vectors. Finally, a supervised learning support vector machine is selected as the sentiment classification model. The experimental results show that based on the obtained important cognitive labels, enterprises are able to better understand the unique attributes that consumers have for the brand; the feature fusion approach is better evaluated and can accurately reflect consumers' views on brand image and quantified as brand score.

1. Introduction

With the rapid development of the global market, various brands are becoming more and more colorful, but the trend of product homogeneity is intensifying, leading to increasingly fierce competition among enterprises. For an enterprise to gain lasting vitality, it must have a clear and superior brand image. Brand image assessment is a key step in understanding brand image and is the first step in improving brand quality and developing brand communication strategies. Enterprises need a way to objectively assess their brand image. This will enable companies to better grasp consumers' psychological perceptions and thus develop precise marketing strategies that vary from person to person and can provide support and more insight into future decisions. Internet technology has broken the traditional ecology of information dissemination and changed the previous way of information delivery. The traditional brand evaluation method based on a questionnaire survey can no longer meet the current demand for brand image evaluation.

In the new information communication ecology, user-generated content brings unprecedented opportunities and challenges for brand image mining [1–3]. Based on user-generated data, social networks can improve the feasibility, operability, and flexibility of brand image assessment. Analyzing the sentiment tendency of texts through natural language processing techniques for user-topic texts is a new trend in brand image assessment and has a very practical application value [4–8]. The task process of sentiment analysis includes sentiment feature extraction and sentiment classification. The first task of sentiment feature extraction is to find the words (features) that represent the user's point of view and then classify the features for sentiment tendency [9–11]. From a psychological perspective, the brand image refers to the sum of consumers' psychological feelings about the brand's products and services. Brand image is divided into two main dimensions, one that is the user's perception of the functional attributes of the brand and one that reflects the emotional value of the brand.

Consumer perception of a brand is the overall impression of the consumer of the brand [12]. The most basic

element of brand image assessment is brand perception. The explosive growth of topic texts provides a massive source of data for brand perception analysis. Therefore, this paper focuses on brand research through topic text sentiment analysis techniques, so as to extract the attributes of brands that consumers pay attention to. It also quantifies consumers' attitudes toward brands into brand scores, so that companies can understand consumers' views more intuitively and objectively, understand the strengths and weaknesses of brand images, and provide them with decision support for resource allocation and product strategy adjustment.

The rest of the paper is organized as follows: In Section 2, the related research is studied in detail, while Section 3 provides the detailed methodology of brand image cognitive label extraction. Section 4 provides the detailed brand image evaluation method based on a weighted fusion model. Section 5 provides the results and discussion. Finally, the paper is concluded in Section 6.

2. Related Research

Brand image theory was first proposed in the United States in the 1960s. After that, brand image theory has been developed continuously, and brand image is gradually interpreted as a collection of consumers' perception of various elements and concepts of a brand. Brand image in general can be divided into two categories, one from the image visual perspective and one from the psychological perspective.

The visual image of a brand refers to the visual design and communication elements that are visible to the user. As the differences between products become less and less, brands are anthropomorphized. Rehman et al. [13] mapped consumers' personality traits vaguely to the brand image. Consumers and brands are closely linked, and consumption can interact and communicate through brands. Portal et al. [14] described brands anthropomorphically and considered brands as having their own independent personalities. The relationship between the consumer and the product is also an interpersonal relationship. These early definitions of anthropomorphism were vague until the concept of the brand image became clearer by using the Big Five personality theory to construct a brand personality theory.

From a psychological perspective, the brand image refers to the sum of consumers' psychological feelings about a brand. Psychological image is divided into two main dimensions, one that is the user's perception of the functional attributes of the brand and one that reflects the emotional value of the brand. The perception of functional attributes refers to the ability of the brand to satisfy functional needs [15]. For example, a car can fulfill the function of a substitute, and coffee can refresh the mind. Currently, defining brand image at the psychological level has been dominant in the field of related research. Sentiment analysis from a psychological perspective consists of two components: feature selection of texts and feature-based sentiment classification models. Early sentiment analysis was mainly based on a rule-based feature approach to classification. Recently, many researchers have started to study machine

learning classification for sentiment analysis methods. Suhasini et al. [16] used a fusion of machine learning and rules for sentiment classification of microblog data with good results and solved the problem of sentiment classification of fuzzy words by combining rules and statistics. Kang et al. [17] compared plain Bayes, support vector machine (SVM), and Rocchio (ROC) classification models, where the second classifier effect is the best performance among the three. The above findings suggest that machine learning-based classification methods are more scalable, while rule-based classification methods need to be constrained by the corpus.

In this paper, we analyze massive topic sentiment data for brand evaluation and set language rules, aggregation rules, and ranking rules to extract consumers' cognitive label (CL) of the brand. This cognitive label is used to achieve a shallow portrait of the brand. Meanwhile, the feature selection method incorporating deep features improves the evaluation effect of the classification model. Finally, a supervised learning support vector machine is selected as the sentiment classification model.

The main innovation points and contributions of this paper are as follows.

- (1) A topic sentiment-based brand image cognitive analysis method is proposed to extract the features of topic text and improve the effect of the sentiment recognition algorithm. By regularizing the topic data (constraint rules), consumers' cognitive labels of brands are extracted.
- (2) In order to make up for the defect that shallow features cannot obtain complete semantic information, this paper introduces the method of fusing deep features, fusing shallow learning features with deep learning features to solve the problem of recognizing a large number of nonentity words in the text, enriching the set of features used by the classification algorithm, and improving the correct rate of text classification.

3. Brand Image Cognitive Label Extraction Based on Topic Sentiment

The effect of sentiment classification is crucial with feature selection, and this paper proposes a rule-based cognitive feature extraction method and aggregates cognitive labels with the help of a synonym dictionary and Jaccard similarity. Finally, the TF-MF model is applied to calculate the importance of cognitive labels.

3.1. Language Rules for Cognitive Label Extraction. Definition of cognitive label: users' knowledge and understanding of brand connotation. For example, the Redmi Note, which positions itself in the low and midrange market, users' cognitive labels of its brand are "within one thousand dollars," "teenager," "big screen," "good pixel," "lagging," etc. In this paper, w is used to denote the cognitive labels.

Let the corpus set $T = \{t_1, t_2, \dots, t_n\}$, where t_i denotes a corpus instance. Different users use different lengths of utterances to express their feelings or experiences about a brand. In general, a single phrase may contain several aspects of a user’s perception of a brand. However, one aspect of the user’s perception of a brand is usually not in several phrases, but in a single phrase. For example, “It’s really good! The system is smooth, the screen is good, the performance is good, but unfortunately there is no transparent case. [Big Love] It’s really good!” In this corpus, the idea of “no transparent case” can only be expressed in one phrase. However, the phrase “smooth system, good screen, and good performance” contains the perceptions of “smooth system,” “good screen,” and “good performance.” The corpus is partitioned using the dot mark set $D = \{, ; : ? !\}$ to obtain a set $S = \{s_1, s_2, \dots, s_m\}$ of phrases, where $m > n$. We choose phrase s_i as the basic unit to extract the candidate cognitive labels.

After splitting the input text into a series of phrase collections S , the traditional feature extraction view is to deal with adjectives. However, in addition to adjectives, nouns, adverbs, and verbs are often used to express opinions and perceptions. For example, “big” as an adjective is often used to modify nouns. If “big brand” is the user’s perception of the brand, then this noun phrase can be regarded as the user’s perception label. Similarly, verbal and adverbial phrases such as “stuck” and “trustworthy” are also user awareness, reflecting the user’s perception of a particular aspect of the brand. After splitting and deactivating s_i , the speech chain rule set $R = \{r_1, r_2, r_3, r_4, r_5, r_6\}$ is used to extract candidate cognitive labels w , as shown in Table 1.

The distance between the first word and the last word in the label is L . There are too many interferences in the labels extracted by the lexical chain rule, so we need to use the distance principle to filter the interferences. In the corpus “The phone is very comfortable to operate,” after pre-processing, the corpus becomes “phone/n, operate/vn, very/d, comfortable/a.” We may extract the label “phone comfortable.” At this point, “phone” is in position 1, and “comfortable” is in position 4. Using the principle of closest modification, we design a word spacing constraint. The label extraction is constrained by using the label distance L to improve the readability of the cognitive labels. After the above steps, a series of candidate cognitive tag sets $W = \{w_1, w_2, \dots, w_p\}$ are obtained from the corpus T . The processing schematic is shown in Figure 1.

3.2. Aggregation Strategies for Cognitive Label Extraction.

The initial extracted cognitive labels appear to be messy and voluminous because users freely choose their own terms when expressing their opinions and views. Therefore, we need to further aggregate the initial cognitive labels extracted in the previous section. Although users are free to use words when expressing their perceptions, in most cases, users’ perceptions of a certain side are often near or opposite words. Therefore, we use Jaccard similarity [18–20] to cluster the extracted tags based on a lexicon of near-sense words. For the candidate tags w_i and w_j of the same length, the similarity between them is

TABLE 1: Speech chain rules in label extraction.

Rules	Speech chain	Example
r_1	n + d + a (noun + adverb + adjective)	Cost very effective
r_2	n + h + a (noun + prefix + adjective)	Logistics super-fast
r_3	a + n (adjective + noun)	Smooth system
r_4	d + v (adverb + verb)	Very much like
r_5	d + n (adverb + noun)	Very youth
r_6	d + a (adverb + adjective)	Really good

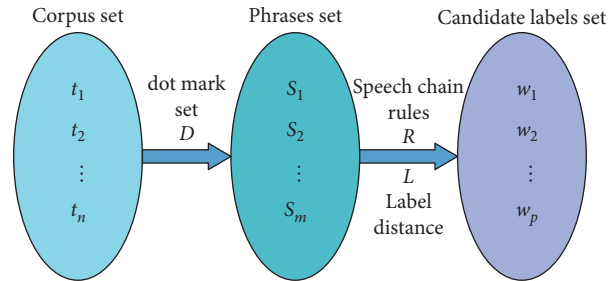


FIGURE 1: Sketch map of candidate labels extracting based on language rules.

$$\text{SIM}(w_i, w_j) = \frac{|w_i \cap w_j|}{|w_i \cup w_j|}. \quad (1)$$

When a pair of elements in a phrase appears in pairs in the list of near-synonyms, we consider them to be the same word. For example, $A = \text{“Beautiful appearance,“}$ $B = \text{“Pretty appearance,“}$ $C = \text{“Fast logistics.“}$ Obviously, A and B have a high similarity. The words “Beautiful” and “Pretty” are a set of near-synonyms, so $\text{SIM}(A, B) = 1$ and $\text{SIM}(A, C) = 1/5 = 0.2$.

Based on the Jaccard similarity and synonym dictionary, we can get the similarity between any two words, which in turn clusters the initial cognitive labels. The word w with the highest frequency in this cluster is selected as the representative of this cluster. At this point, the new set of cognitive labels $W^* = \{x_1^*, x_2^*, \dots, x_k^*\}$, $k \leq p$ is obtained, as shown in Figure 2. For example, after the aggregation of “good endurance, great endurance, OK endurance,” the cognitive label “good endurance” is extracted.

3.3. Importance Ranking of Cognitive Labels. In order to understand the importance of the acquired cognitive labels in the minds of consumers, the importance of the cognitive labels needs to be ranked. The entire corpus set is T , and the set of tags appearing in this corpus is w^* . The elements in the initial tag set W are replaced by representative elements in the same tag cluster. f_{w^*} denotes the number of occurrences of the word w^* in the corpus set T , and B denotes the number of corpus containing the word w^* in the corpus set. Considering that w^* is already a label with actual meaning, the importance of the label w^* can be calculated according to the TF-MF model.

$$\text{TFMF}(w^*) = \frac{f_{w^*}}{\sum_{W^*} f_{w^*}} \times \log\left(\frac{B}{|T|} + 1\right). \quad (2)$$

An example of the TF-MF model is given as follows. Suppose the corpus set T has five different corpora

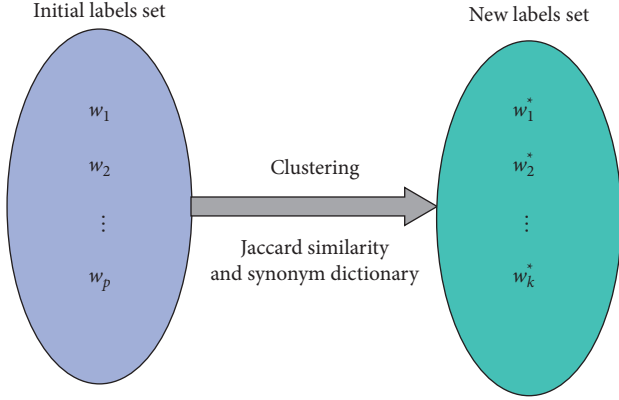


FIGURE 2: Candidate labels aggregation diagram.

t_1, t_2, t_3, t_4, t_5 . Two cognitive labels w_1^* and w_2^* appear in the corpus, and the specific distribution is shown in Figure 3.

The importance of the two was calculated by the TF-MF model.

$$\begin{aligned} \text{TFMF}(w_1^*) &= \frac{5}{10} \times \log\left(\frac{3}{5} + 1\right) = 0.102, \\ \text{TFMF}(w_2^*) &= \frac{5}{10} \times \log\left(\frac{5}{5} + 1\right) = 0.151. \end{aligned} \quad (3)$$

Although the two labels w_1^* and w_2^* appear equally in the corpus in total, the label w_2^* is more important than w_1^* . This coincides with the fact that in practice the more people pay attention to it the more it deserves attention.

4. Brand Image Assessment Method Based on Weighted Fusion Model

The previous section proposed to extract features by cognitive labels, but cognitive labels only address the importance of brand attribute features and cannot explain the meaning of a large number of noncognitive labels. To complement this deficiency, this paper then introduces fusion features to supplement the feature vectors based on the results of deep learning word vector models.

4.1. Features Based on Word Vector Model. Since the implicit meaning of some words can be obtained using deep model parameter passing, this paper uses the CBOW (continuous bag of words) model [21] to train the word vector model. The CBOW model uses the context before and after the target word to predict the probability of occurrence of the target word. We used a three-layer word vector model for training to obtain the word vector representation.

Firstly, a lexicon matching and hidden Markov model-based lexicographer are used to split the text. Then, the lexicon numbers are extracted from the split text, and the numbers are used to convert the training text utterances into id representations. Finally, the word2vec tool [22] is called, and the word vector model is trained according to the belonging parameter settings. The dimensionality of the word vector is set to 200, and the sliding window size in the

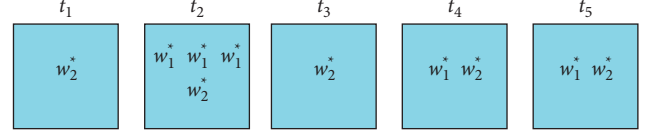


FIGURE 3: Example of TFMF model.

training model is 5. The output results in a vector set of floating-point numbers and the vector values are normalized.

4.2. Emotion Classification Model with Feature Fusion. We fuse shallow cognitive label extraction and deep feature filtering to improve the accuracy of feature selection and optimize the classification results. Then, the training text is trained for classification using an SVM classifier, which we call CL-C-SVM.

The processing of text content in sentiment analysis can be reduced to the processing of a vector of a certain length. For the extracted cognitive labels, they can be represented in the form of one-hot. Each cognitive label represents a dimension, and a sentence may be represented by thousands of dimensions. The position of words that have appeared in the sentence is filled with 1, and the position corresponding to words that have not appeared is filled with 0. This allows the text data to be represented by a high dimensional 0-1 vectorization. The extracted cognitive labels and the word vectors from the training output are fused to generate new feature files, and the flow of feature fusion is shown in Figure 4.

4.3. Definition of Brand Image. For a brand, which contains a lot of products, products at the same time contain a lot of models, different models of goods in the e-commerce site, and a large number of sellers, thus generating a large number of topic comments data. The good or bad topic comments can represent the brand's reputation to a certain extent. According to the principle of statistics, in the context of big data statistics, good or bad user word-of-mouth can be used as a standard for a high or low brand image, so the brand assessment given in this paper is defined as

$$\text{score} = \sum_{i=0}^m w_{ij} - \sum_{i=0}^n w_{ij}, \quad (4)$$

where m denotes the number of positive comments and n denotes the number of negative comments. w_{ij} denotes the ranking of each cognitive label j in the sentence i .

5. Experiment and Result Analysis

5.1. Data Selection and Preprocessing. Two competing cell phone brands, <Huawei mate50> and <Samsung Galaxy S22>, were selected for the experiment. Records about these two brands were searched on three online platforms, namely B2C e-commerce cell phone category comment information, Sina Weibo and Zhongguancun Online, and 10,000 records

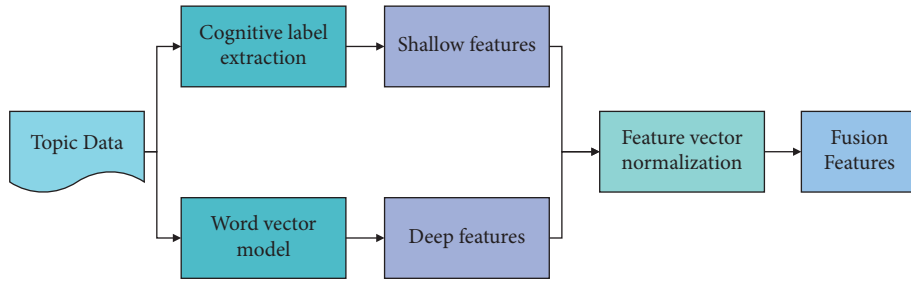
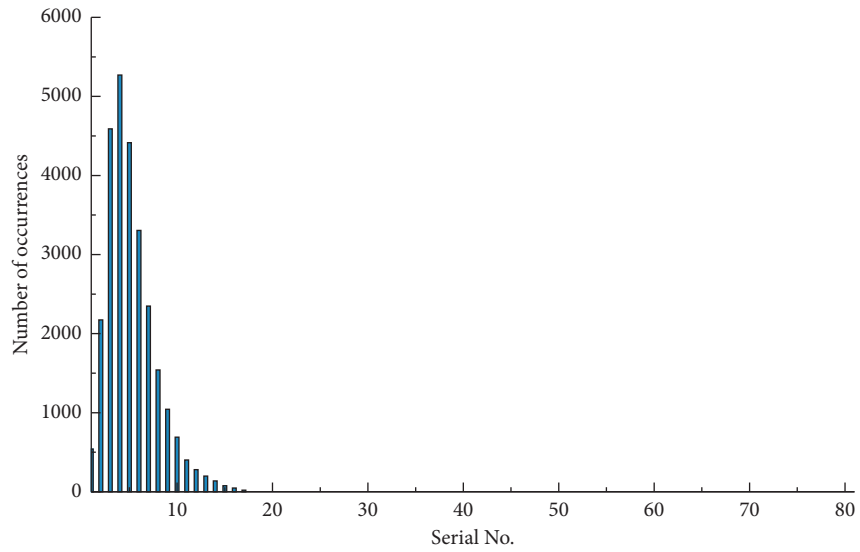
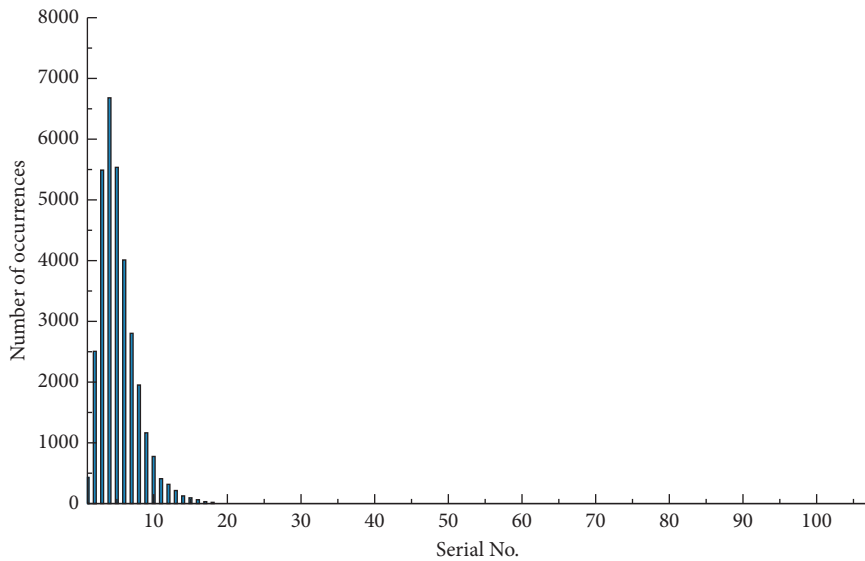


FIGURE 4: The process of feature fusion.



(a)



(b)

FIGURE 5: Short sentences' length distribution. (a) Huawei Mate 50. (b) Samsung Galaxy S22.

each were randomly selected as the experimental data set. Each corpus was segmented with the dot as the separator to obtain the basic unit phrases for label extraction. The NLPiR system was used for word segmentation and lexical

annotation, and the deactivated words in the records were removed using a deactivated word list. The Huawei mate50 dataset has 27575 phrases, with a maximum of 163 words and a minimum of 1 word in the phrase, and an average

length of 5 words. The Samsung Galaxy S22 dataset has 34563 phrases, with a maximum of 195 words and a minimum of 1 word, and each phrase has an average of 5 words. The overall distribution is shown in Figure 5.

5.2. Cognitive Labeling Analysis. Using the speech chain rule, the initial set of cognitive labels is obtained, and the results are shown in Table 2.

The above table shows that the initial cognitive labels extracted at this point are cluttered and disorganized. Next, critical information needs to be obtained through linguistic aggregation and importance ranking methods. Based on Jaccard similarity and synonym dictionary to calculate the similarity between tags, the initial cognitive tags are aggregated, the tags are ranked using TF-MF rules, and the top 5 tags are taken, as shown in Table 3.

From Table 3, it can be seen that the method in this paper can effectively extract the cognitive labels of consumers, so as to obtain the key elements of users' perception of brand image. Through the method in this paper, it can help companies recognize their image in consumers' mind and discover the most and least satisfied areas of users, thus providing strong support for subsequent brand image evaluation.

5.3. Classification Performance. The dataset was annotated manually and labeled with the review data sentiment classification as positive or negative reviews. The labeled data were divided into a training set and a test set in the ratio of 9:1. The classical IG (information gain)-SVM model was selected as the comparison algorithm to compare with the proposed CL-SVM and CL-C-SVM classification algorithms to verify their effectiveness. The metrics for evaluating the algorithms were chosen as accuracy rates commonly used in the field of natural language. The accuracy comparison of the different classification models is shown in Figure 6.

From the accuracy comparison shown in Figure 6, it is clear that the CL-C-SVM algorithm proposed in this paper has the best sentiment classification effect. By analyzing the data, the reason can be obtained that the choice of IG, CL, or feature fusion by the feature extraction algorithm leads to a large difference in the actual results. The fused features are more comprehensive and compensate the problem that shallow features cannot explain the meaning of a large number of non-CL words. Combining the shallow filtered CL with deeper features that contain more hidden meanings can improve the accuracy of feature selection.

5.4. Brand Image Evaluation Experiment. For the two cell phone brands, the results of brand image assessment using the CL-C-SVM model are shown in Table 4.

In order to conduct a manual and subjective assessment of brand image ratings, this paper adopted a user questionnaire + ranking approach. For the above two cell phone brands, 1000 online questionnaires were randomly distributed at the entrance of a large supermarket. The target audience was consumers who had used these two cell phone brands, and they were asked to rate these two cell phone brands. A score of

TABLE 2: The distribution of candidate cognitive label in the speech chain.

Candidate label type	n+d+a	n+h+a	n+a	d+a	d+v	d+n	Total
Huawei Mate 50	2954	27	1171	587	3124	2358	10221
Samsung Galaxy S22	4067	55	1466	794	3458	2783	12623

TABLE 3: Cognitive label extraction results.

Cognitive label of Huawei Mate 50	Cognitive label of Samsung Galaxy S22
Fast speed	Great service
Very satisfied	Nice phone
Cost very effective	Nice screen
Battery not durable	Beautiful appearance
Nice screen	Battery not durable

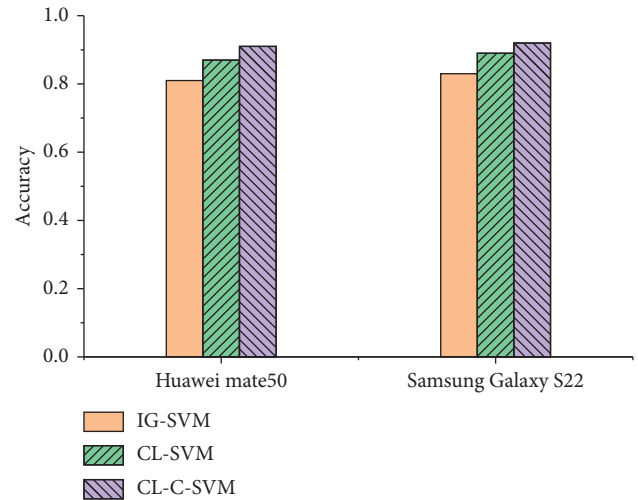


FIGURE 6: Accuracy of different classification models.

TABLE 4: Score of brand image evaluation.

Candidate label type	Good review	Poor reviews	Medium rating	Normalized mean score
Huawei Mate 50	14112	8427	5036	938.3
Samsung Galaxy S22	16036	11402	7125	833.4

1 was set as a passing score, and the higher the score, the better the brand's psychological impression on users. The scores and the number of people were multiplied to obtain the average score and normalized to within 1000, and the final results were obtained as shown in Table 5. The comparison of brand scores for different methods is shown in Figure 7.

The scores of different brands are shown in Figure 7, and it is found that the brand scores calculated by the CL-C-SVM model have the best fit with the scores of the user questionnaire. The brand scores derived from the CL-SVM

TABLE 5: Scoring results of the questionnaire.

Candidate label type	1 score	2 score	3 score	4 score	5 score	Normalized mean score
Huawei Mate 50	65	82	256	366	241	916.5
Samsung Galaxy S22	73	147	386	231	163	816

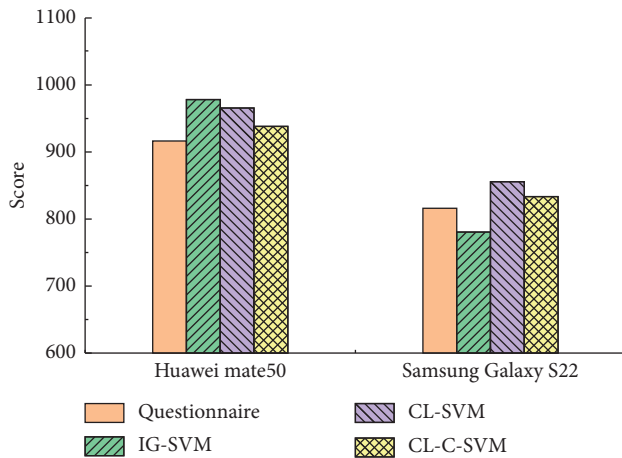


FIGURE 7: Comparison of brand scores.

model are slightly less effective but better than those calculated by the IG-SVM model. The practical value of the CL-C-SVM model was verified by comparing the results with those of the manual questionnaire.

6. Conclusions

In this paper, a brand image cognitive analysis method based on topic sentiment is proposed to extract features of topic text and improve the effect of the sentiment recognition algorithm. At the same time, the feature selection method incorporating deep features makes up for the defect that shallow features cannot obtain complete semantic information and enriches the set of features used by the classification algorithm. The experimental results show that the proposed cognitive label extraction method can effectively obtain the key elements of users' brand image and discover the most and least satisfied areas of users. In addition, the CL-C-SVM model can accurately quantify consumers' brand scores on brand image, and the results are almost consistent with the manual questionnaire approach. However, the extraction of cognitive labels does not take into account the influence of unexpected events, resulting in the assessment of the model failing to reflect the real-time changes in corporate image, which is important in practical applications. Therefore, further work on this issue will be conducted in subsequent studies.

Data Availability

The raw data supporting the conclusions of this article will be made available by the authors, without undue reservation.

Conflicts of Interest

The authors declare that the research was conducted in the absence of any commercial or financial relationships that could be construed as potential conflicts of interest.

References

- [1] É. Ferreiro-Rosende, L. Fuentes-Moraleda, and R. Ferreiro-Rosende, "Artists brands and museums: understanding brand identity," *Museum Management and Curatorship*, vol. 14, no. 17, pp. 1–18, 2021.
- [2] D. Singh, N. Bajpai, and K. Kulshreshtha, "The effect of brand anthropomorphism on customers' behaviour towards the indian hypermarket brands," *Journal of Creative Communications*, vol. 16, no. 3, pp. 266–284, 2021.
- [3] W. Feng, I. Y. Yu, M. X. Yang, and M. Yi, "How being envied shapes tourists' relationships with luxury brands: a dual-mediation model," *Tourism Management*, vol. 86, no. 1, pp. 104344–105113, 2021.
- [4] K. O. Keller, I. Geyskens, and M. G. Dekimpe, "Opening the umbrella: the effects of rebranding multiple category-specific private-label brands to one umbrella brand," *Journal of Marketing Research*, vol. 57, no. 4, pp. 677–694, 2020.
- [5] J. Guo, L. Bai, Z. Yu, Z. Zhao, and B. Wan, "An ai-application-oriented in-class teaching evaluation model by using statistical modeling and ensemble learning," *Sensors*, vol. 21, no. 1, pp. 241–252, 2021.
- [6] X. Zhang, X. Yang, and J. Yang, "Teaching evaluation algorithm based on grey relational analysis," *Complexity*, vol. 2021, no. 1, Article ID 5596518, 9 pages, 2021.
- [7] J. Hu, "Teaching evaluation system by use of machine learning and artificial intelligence methods," *International Journal of Emerging Technologies in Learning (iJET)*, vol. 16, no. 5, pp. 87–96, 2021.
- [8] T. Uzunkaya, "Relationship between the customer expectations from websites performance and e-wom: a study on sport shoes brands," *Pressacademia*, vol. 7, no. 2, pp. 80–94, 2020.
- [9] H. Yuzhong, "Students' emotional analysis on ideological and political teaching classes based on artificial intelligence and data mining," *Journal of Intelligent and Fuzzy Systems*, vol. 40, no. 2, pp. 3801–3809, 2021.
- [10] A. Khan, J. P. Li, A. U. Haq, I. Memon, S. H. Patel, and S. Din, "Emotional-physic analysis using multi-feature hybrid classification," *Journal of Intelligent and Fuzzy Systems*, vol. 40, no. 1, pp. 1681–1694, 2021.
- [11] J. Chen, B. Hu, P. Moore, X. Zhang, and X. Ma, "Electroencephalogram-based emotion assessment system using ontology and data mining techniques," *Applied Soft Computing*, vol. 30, no. 3, pp. 663–674, 2015.
- [12] M. Thenmozhi, R. Indira, and R. Dharani, "Using lexicon and random forest classifier for twitter sentiment analysis," *International journal of computer sciences and engineering*, vol. 7, no. 6, pp. 591–594, 2019.
- [13] A. Rehman, J. Jaafar, M. Omar, S. Basri, I. Abdul, and Q. Uddin, "Suitable personality traits for learning programming subjects: a rough-fuzzy model," *International Journal of Advanced Computer Science and Applications*, vol. 8, no. 8, pp. 153–162, 2017.
- [14] S. Portal, R. Abratt, and M. Bendixen, "Building a human brand: brand anthropomorphism unravelled," *Business Horizons*, vol. 61, no. 3, pp. 367–374, 2018.
- [15] Z. Liu, "Research for public opinion of charitable organizations based on microblogging sentiment analysis," *Journal of*

- Information and Computational Science*, vol. 12, no. 3, pp. 1011–1019, 2015.
- [16] M. Suhasini and S. Badugu, “Two step approach for emotion detection on twitter data,” *International Journal of Computer Application*, vol. 179, no. 53, pp. 12–19, 2018.
 - [17] Q. Kang, L. Shi, M. Zhou, X. Wang, and Q. Wu, “A distance-based weighted undersampling scheme for support vector machines and its application to imbalanced classification,” *IEEE Transactions on Neural Networks and Learning Systems*, vol. 29, no. 9, pp. 4152–4165, 2018.
 - [18] S. Kakad and S. Dhage, “Cross domain-based ontology construction via jaccard semantic similarity with hybrid optimization model,” *Expert Systems with Applications*, vol. 178, no. 3, pp. 115046–115123, 2021.
 - [19] R. B. Lanjewar, S. Mathurkar, and N. Patel, “Implementation and comparison of speech emotion recognition system using Gaussian mixture model (gmm) and k- nearest neighbor (k-nn) techniques,” *Procedia Computer Science*, vol. 49, pp. 50–57, 2015.
 - [20] Q. Hou, C. Li, M. Kang, and X. Zhao, “Intelligent model for speech recognition based on svm: a case study on English language,” *Journal of Intelligent and Fuzzy Systems*, vol. 40, no. 2, pp. 2721–2731, 2021.
 - [21] B. Liu, “Text sentiment analysis based on cbow model and deep learning in big data environment,” *Journal of Ambient Intelligence and Humanized Computing*, vol. 11, no. 2, pp. 451–458, 2020.
 - [22] Z. Xiong, Q. Shen, Y. Xiong, W. Yijie, and W. Li, “New generation model of word vector representation based on cbow or skip-gram,” *Computers, Materials & Continua*, vol. 60, no. 1, pp. 259–273, 2019.

Research Article

Research on Audio Recognition Based on the Deep Neural Network in Music Teaching

Yun Cui ¹ and Fu Wang ^{1,2}

¹School of Music and Performing Arts, Mianyang Teachers' College, Mianyang 621000, China

²College of Management Science, Chengdu University of Technology, Chengdu 610059, China

Correspondence should be addressed to Fu Wang; fwang@mtc.edu.cn

Received 30 March 2022; Revised 25 April 2022; Accepted 6 May 2022; Published 27 May 2022

Academic Editor: Le Sun

Copyright © 2022 Yun Cui and Fu Wang. This is an open access article distributed under the Creative Commons Attribution License, which permits unrestricted use, distribution, and reproduction in any medium, provided the original work is properly cited.

Solfeggio is an important basic course for music majors, and audio recognition training is one of the important links. With the improvement of computer performance, audio recognition has been widely used in smart wearable devices. In recent years, the development of deep learning has accelerated the research process of audio recognition. However, there is a lot of sound interference in music teaching environment, which leads to the performance of the audio classifier that cannot meet the actual demand. In order to solve this problem, an improved audio recognition system based on YOLO-v4 is proposed, which mainly improves the network structure. First, Mel frequency cepstrum number is used to process the original audio and extract the corresponding features. Then, try to apply the YOLO-v4 model in the field of deep learning to the field of audio recognition and improve it by combining with the spatial pyramid pool module to strengthen the generalization ability of data in different audio formats. Second, the stacking method in ensemble learning is used to fuse the independent submodels of two different channels. Experimental results show that compared with other deep learning technologies, the improved YOLO-v4 model can improve the performance of audio recognition, and it has better performance in processing data of different audio formats, which shows better generalization ability.

1. Introduction

Music is an abstract art form with sound as its means of expression. In the process of music teaching, solfeggio can strengthen students' musical memory ability, enable students to accurately identify music works, and thus obtain better "musical perception." As an important link in solfeggio, audio recognition training is very difficult for junior students. This is because students need to master all kinds of clefs, distinguish the length and duration represented by different notes, and the pitch difference between different notes.

Audio signal analysis based on embedded intelligent devices has attracted more and more researchers' attention [1–7]. Intelligent wearable devices with audio recognition function can help students solve the above problems and realize music teaching assistance. The task of audio

recognition needs to preprocess the collected audio signals first, extract useful features for distinguishing music scores from them, and finally classify them according to these features. Classification is a very important method of data mining [8–10]. Classification refers to generating a classification function according to certain rules on the basis of training set data. This function can map the data of the test set to one of the given categories, thus realizing the category prediction of unknown data. At present, common classifiers include decision tree, logistic regression, support vector machine (SVM), Naive Bayes, k -nearest neighbor algorithm (KNN), BP neural network, and deep learning [11–13].

The previous machine learning methods often need to manually extract the features that can represent the original data as the input of the classifier. However, deep learning can automatically extract the high-dimensional features of samples (without manual feature extraction), as long as the

input data cover the information of the original data as much as possible, which is suitable for large-scale data. The deep learning method can realize specific audio recognition tasks with the help of a large amount of audio data collected by intelligent devices. The convolutional neural network (CNN), as a kind of deep learning architecture, is widely used in image classification, speech recognition, natural language processing, and other fields because of its superior performance in local feature learning [14]. Different from other neural network models (such as Boltzmann machine and recurrent neural network), the CNN characterized in that core operation is convolution operation. The YOLO network draws lessons from the CNN classification network structure and shows good advantages in the field of image recognition, which has attracted the attention of many researchers.

Therefore, this study tries to apply the YOLO-v4 model to the field of audio recognition and improves its network structure. In addition, the stacking method in ensemble learning is used to fuse two independent submodels of different channels, and the classification performance of the fused system is further improved compared with the single submodel.

2. Related Works

Nowadays, with the emergence of a large number of smart devices, the excellent computer performance and the development of deep learning technology have jointly promoted the research process in the audio field. Combined with the main research contents of this study, the current research status will be introduced from two aspects: convolutional neural network and audio recognition.

The convolutional neural network structure originated from a study by Yann LeCun in 1998 is called the Le Net-5 artificial neural network. The convolutional neural network, like other neural networks, can be trained by the back propagation algorithm [15]. In 2012, Alex Krizhevsky and others adopted CNN technology for the first time in complex computer vision tasks. By using 3 fully connected layers, 5 convolution layers, and Softmax classifier, a convolutional neural network with 8 layers is constructed, which is named AlexNet. AlexNet uses ReLU activation function, and at the same time, it also uses regularization (dropout) to prevent overfitting. In 2014, the Google' computer vision team puts forward the GoogLeNet network [16], with a network depth of 22 layers, which contains a new structure, incident. It integrates the features of different depths and the same scale, and the detection accuracy is improved. On the basis of the GoogLeNet network, YOLO and SSD algorithms appeared. Both methods are based on a single end-to-end network, which can complete the input from the original image to the output of the object position and category.

In the aspect of audio recognition, Yang and Zhao [17] proposed an acoustic scene classification method based on the support vector machine (SVM), which enhanced the sound texture to improve the classification accuracy. Greco et al. [18] proposed a voice recognition system based on the heuristic deep learning method. Demir et al. [19] proposed a

new pyramid cascade CNN method for environmental sound classification. Zhu et al. [20] proposed an improved YOLO-v4 algorithm for sound imaging instruments, which effectively improved the accuracy of acoustic phase cloud image detection. The above methods all show excellent performance in dealing with audio recognition tasks in a single acoustic scene, but there are many sound disturbances in the music teaching environment, and it is necessary to deal with a variety of different audio format data.

Therefore, this study proposes an audio recognition system based on the improved YOLO-v4 network model. The main innovations and contributions include the following: (1) try to apply YOLO-v4 network architecture, which is excellent in the field of deep learning, to the field of audio recognition, and improve it by combining the spatial pyramid pool module. The improved YOLO-v4 network architecture effectively utilizes the spatial information in audio files, thus strengthening the generalization ability of data in different audio formats. (2) The stacking method in ensemble learning is used to fuse two independent submodels of different channels, and the classification performance of the fused system is improved.

3. Extraction and Processing of Audio Features

Extracting the best parameter representation of audio signal is one of the important tasks to produce better recognition performance. The feature extraction in this stage is very important for the classifier classification in the next stage because it will directly affect the classification efficiency.

In the classification task, especially the audio classification task, the Mel frequency cepstrum coefficient (MFCC) which describes the spectral shape has a long history. Although the MFCC extraction process will cause lossy compression of data, its classification and recognition effect are quite available even when the data rate is very low. In addition, compared with other classification features, MFCC is widely used because it is more in line with the auditory frequency response curve of human ears.

The reason why human beings can judge different environments in complex sound environment lies in the credit of the cochlea. The cochlea can be seen as a filter bank to help people filter 20-20 kHz audio. The problem is that the sensitivity of the cochlea to frequencies in the auditory range is not linear, but there is a mapping relationship. MFCC can simulate the frequency response of the human ear. MFCC feature extraction consists of seven steps, and the whole process is shown in Figure 1.

Common audio signals have the phenomenon that the low-frequency energy is large, but the high-frequency energy is small. If it is transmitted directly, it will lead to high signal-to-noise ratio at low frequency and insufficient signal-to-noise ratio at high frequency. In order to make up for this loss of audio signal during transmission, preemphasis is introduced to compensate the input signal, so that the high-frequency characteristics of audio signal can be highlighted. Preemphasis is usually achieved by means of a high-pass filter [21–23].

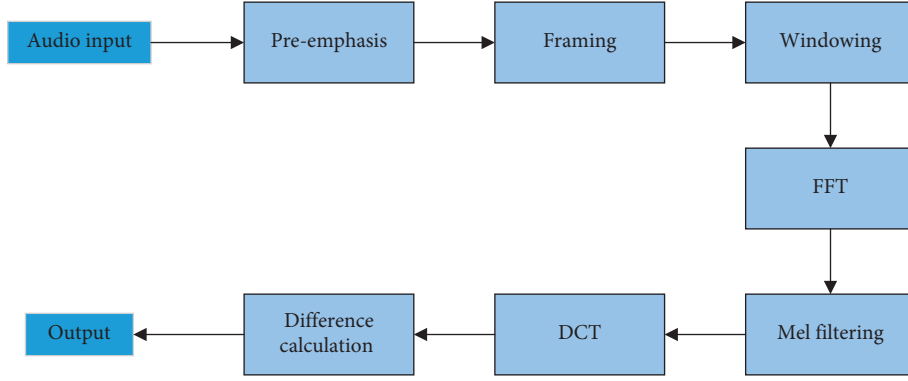


FIGURE 1: MFCC feature extraction steps.

Let the voice sample value at the n^{th} time be $X[n]$, and the result after preemphasis is

$$Y[n] = X[n] - aX[n-1], \quad (1)$$

where a is the preemphasis coefficient, usually within 0.9-1.0.

Framing divides audio samples obtained from analog-to-digital conversion (ADC) into small frames with a length in the range of 20-40 milliseconds. After preemphasis and framing are completed, it is necessary to add a Hamming window to each frame. Windowing is to control the amount of data processing, and only the data in the window are processed at a time. The frequency range in the fast Fourier transform spectrum is very wide, which leads to the speech signal not following the linear scale [24-26]. Therefore, it is necessary to pass the Mel scale filter bank as shown in Figure 2.

Figure 2 shows a set of triangular filters, which are used to calculate the weighted sum of the spectral components of the filters, so that the processed output approximates Mel scale. The amplitude-frequency response of each filter is triangular. The Mel spectrum of a given frequency f is calculated as follows:

$$F(\text{Mel}) = 2595 \cdot \log_{10} \left(1 + \frac{f}{700} \right). \quad (2)$$

Discrete cosine transform (DCT) transforms the Mel spectrum into time domain. The result of the transforms is called Mel frequency cepstrum coefficient. The coefficient set is called acoustic vector. Therefore, each input is converted into an audio vector sequence.

In order to improve the signal recognition performance, the differential spectrum based on the static characteristics of audio signals is used to describe the dynamic characteristics of audio signals. 13 first-order difference features and 39 second-order difference features are introduced. The frame energy of signal x in the window from time t_1 to t_2 is as follows:

$$\text{Energy} = \sum_{t=t_1}^{t_2} X^2(t). \quad (3)$$

13 first-order differential features represent the changes between frames of cepstrum in MFCC features, while 39 second-order differential features represent the changes between frames in first-order differential features. The first-order difference is calculated as follows:

$$d(n) = \frac{c(n+1) - c(n-1)}{2}, \quad (4)$$

where $c(n+1)$ represents the cepstrum coefficient at time $n+1$.

4. SPP-YOLO-v4 Network Structure

4.1. Spatial Pyramid Pool (SPP) Module. SPP can avoid information distortion caused by scaling, stretching, clipping, and other operations and provide output that is not affected by the input size, which cannot be achieved by sliding window pooling technology [27]. Second, SPP can pool with multiple scales, while sliding window pooling only uses one window scale. The basic structure of the SPP module is shown in Figure 3. It can be seen that because the input size is flexible, SPP can combine the features of data in different audio formats. The dimension of the transformed feature vector is the same as that of the fully connected layer, while alleviating the generalization problem.

4.2. SPP-YOLO-v4. YOLO-v4 is a high-precision real-time single-stage detection algorithm integrating YOLO-v1, YOLO-v2, and YOLO-v3. YOLO-v4 constructs the CSP cross-stage partial network (CSPNet) in the residual module, in which the feature layer is the input and the feature information of the higher layer is the output. This shows that the learning objectives of YOLO-v4 in the ResNet module are different between output and input. Therefore, residual learning is realized, and the model parameters are reduced, so the feature learning ability is enhanced. Considering the application environment of music teaching, some changes are made on the basis of the original network, and the final network structure is shown in Figure 4.

First, the feature layer is convolved three times, and then, the input feature layer is maximally pooled by using the maximum pooled cores of different sizes. After convolution and upsampling, different feature layers are connected in

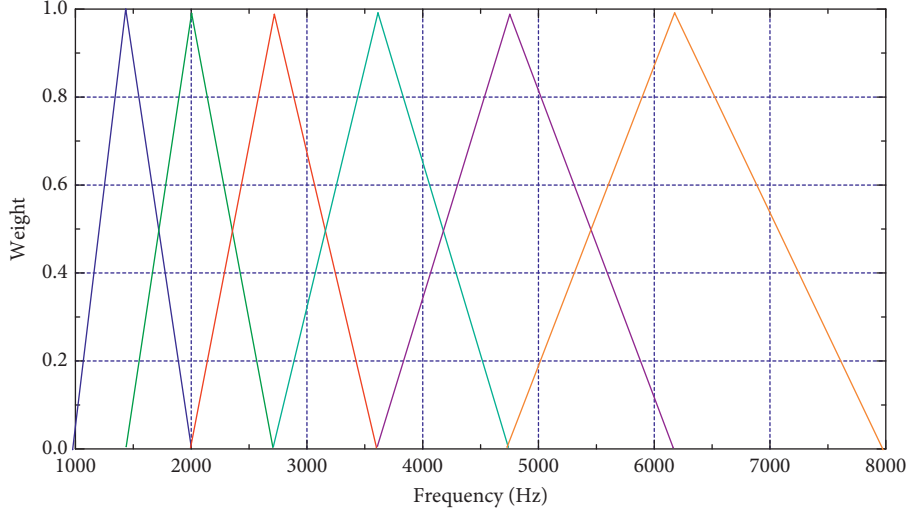


FIGURE 2: Mel scale filter bank.

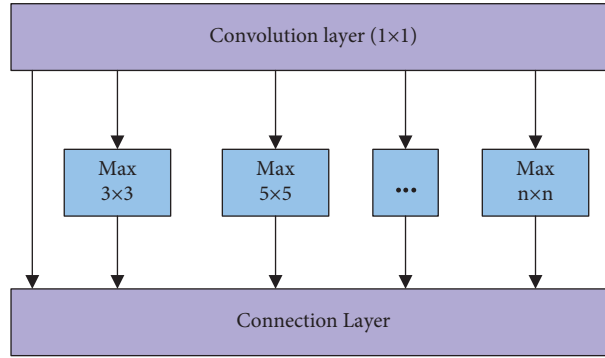


FIGURE 3: Basic module structure of SPP.

series to realize feature fusion. Then, perform down-sampling, compress height and width, and finally stack with the previous feature layer to realize more feature fusion (5 times). The classification module uses the features extracted from the network to make classification judgment. Take the 13×13 grid as an example, which is equal to dividing the input Mel spectrogram into 13×13 squares; then, each square will be preset with three prior frames. The classification results of the network will adjust the positions of these three prior boxes and finally filter by the nonmaximum suppression (NMS) algorithm [28], so as to get the final classification results.

5. Audio Recognition System Based on SPP-YOLO-v4

5.1. System Architecture. As shown in Figure 5, after audio input, the proposed audio recognition system first divides the audio sequence data into two parts. The first part comes from stereo channel, while the second part is compressed into mono. The audio signals of the two channels are extracted by MFCC spectrogram and input into the SPP-YOLO-v4 model as features. Then, two groups of SPP-YOLO-v4 models are integrated, and the stacking method is adopted in the

integration. After the integrated learning of the two models, the audio classification results are finally output. The details of the SPP-YOLO-v4 model are shown in Figure 4.

5.2. Stacking Integrated Learning. As shown in Figure 5, the system uses ensemble learning technology to get the final classification result. The basic idea of ensemble learning is to form a strong classifier through the combination of several weak classifiers. Even if some weak classifiers make wrong predictions, they can be corrected by other weak classifiers with correct predictions, thus achieving the effect of improving the system performance.

Assuming that x is an input, m_i ($i = 1, 2, \dots, k$) is a group of classifiers and the output of the classifiers is the probability distribution $m_i(x, c_j)$ of each class c_j ($i = 1, 2, \dots, k$), the final output $y(x)$ of the integrated classifier can be expressed as

$$y(x) = \operatorname{argmax}_{c_j} \sum_{i=1}^k w_i m_i(x, c_j), \quad (5)$$

where w_i is the weight of classifier m_i . Ensemble is a method to calculate the best weight of each classifier according to the

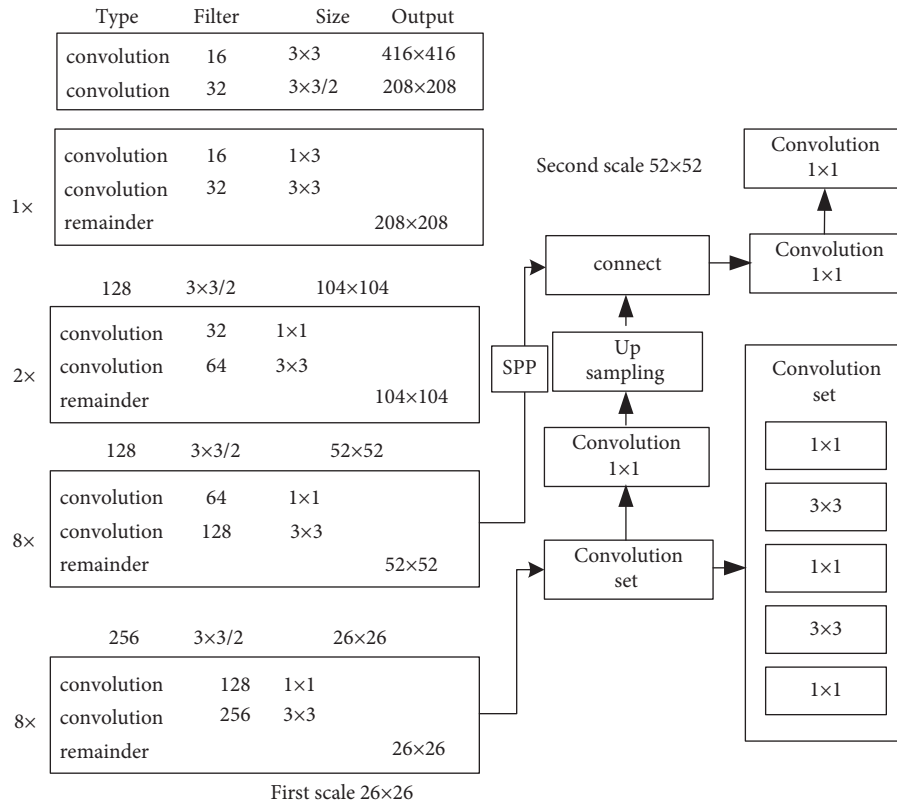


FIGURE 4: SPP-YOLO-v4 network structure.

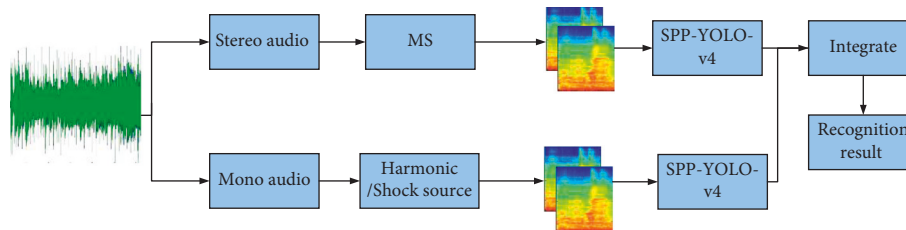


FIGURE 5: Overall architecture of the audio recognition system.

classification target. At present, popular ensemble learning algorithms include stacking, bagging, boosting, ensemble selection, and so on. The ensemble learning algorithm selected in this study is the stacking method.

Stacking is a process of second-order learning with the output of the first-order learning process as input, also known as “meta-learning.” The stacking method has become a popular ensemble learning method, not only because its implementation is quite simple but also because it can significantly improve the generalization ability of the system, which is very consistent with the purpose of this study. The basic principle of the stacking method is shown in Figure 6.

6. Experiment and Result Analysis

6.1. Experimental Environment and Dataset. The hardware platform of this study is Intel Core i3-M350 CPU@ Dual-core 2.20 GHz, 8 GB of DDR2 memory, Nvidia RTX2080Ti GPU, and 11 GB of video memory. The PyCharm integrated

development tool is developed in Python 3.5.0 language. The YOLO annotation framework written in Python is used to convert the numerical format, so that it can be read by YOLO. The comparison methods are the Gaussian mixture model (GMM), CNN, and R-CNN.

The experimental dataset is recorded audio files in the real teaching environment. The dataset consists of audio types of four different labels (D1, D2, D3, and D4). All audio files are cut into 30-second clips. There are 12 audio file formats including MPEG, MP3, and WMA. Each recording is performed at a different location, and the average recording duration is 3–5 minutes. The recording equipment includes two-channel Soundman OKM II Classic/studio A3 in-ear microphone and Roland Edirol R09 waveform recorder with 44.1 kHz sampling rate and 24 bit resolution.

The used dataset contains 1404 audio files, and the number of audio files of each type is 351. About 70% of the data is used for training the audio recognition model, and the remaining 30% is used for testing. The system settings are given in Table 1.

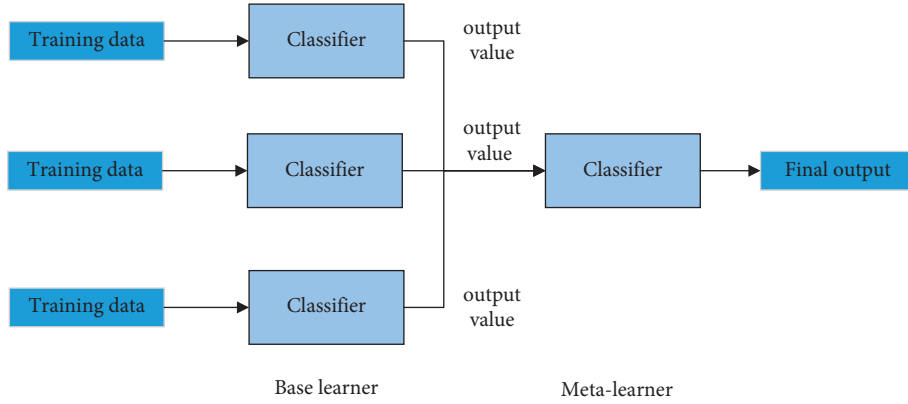


FIGURE 6: Basic principle of the stacking method.

TABLE 1: The system settings.

Settings	Parameter
Audio channel	Single channel
Audio type	MFCC
Audio window length	40 ms
Audio frame shift	20 ms
Feature vector	Static MFCC + first-order + second-order
Feature vector length	60

6.2. *Evaluation Criteria.* The mean accuracy (mAP) is calculated as follows:

$$\text{mAP} = \int_0^1 p(\tau) d\tau, \quad (6)$$

where $p(\tau)$ is the accuracy of audio classification.

Precision and recall are defined as follows:

$$\text{Pr} = \frac{\text{TP}}{\text{TP} + \text{FP}}, \quad (7)$$

$$\text{Recall} = \frac{\text{TP}}{\text{TP} + \text{FN}},$$

where TP is the positive alarm rate, FP is the false alarm rate, and FN is the missed alarm rate.

F1 score is the harmonic value of precision and recall rate. The higher the value, the better the performance. It is defined as follows:

$$\text{F1} = 2 \frac{\text{Recall} \times \text{Pr}}{\text{Recall} + \text{Pr}}. \quad (8)$$

6.3. *Verification of SPP-YOLO-v4 Performance.* In order to verify the promotion effect of the proposed improved YOLO-v4 (SPP-YOLO-v4) on generalization ability, it is compared with the traditional YOLO-v4 model. In the experiment, 3 of 12 audio file formats were selected: MPEG, MP3, and WMA. The generalization ability of SPP-YOLO-v4 is given in Table 2.

From Table 2, it can be found that the overall accuracy of SPP-YOLO-v4 is higher than that of traditional YOLO-v4, which verifies its generalization ability for data in different

TABLE 2: Generalization ability analysis of SPP-YOLO-v4.

Model	Audio file format	Accuracy				
		1	2	3	4	Average
YOLO-v4	MPEG	0.931	0.914	0.901	0.933	0.919
	MP3	0.889	0.961	0.894	0.880	0.906
	WMA	0.921	0.910	0.900	0.913	0.911
SPP-YOLO-v4	MPEG	0.951	0.969	0.961	0.959	0.956
	MP3	0.889	0.982	0.911	0.889	0.918
	WMA	0.937	0.989	0.919	0.938	0.945

audio formats. This is because compared with the original method, SPP of SPP-YOLO-v4 contains more layers, but it also increases the processing time.

6.4. *Comparison of Test Results.* Table 3 provides the results of training loss, mAP, and so on for all categories after 8000 rounds of training. It can be seen that the training model of the proposed method can effectively identify audio types. It has certain advantages in accuracy, recall rate, and F1 score, and its loss value is also the lowest of all methods, only 0.0122. Therefore, the stability and accuracy of the proposed method are better. This is mainly due to the high resolution and receptive field (RF) of SPP-YOLO-v4, and the addition of SPP module in the connection layer retains the advantages brought by SPP. In terms of training time, SPP-YOLO-v4 is only slightly more than GMM. The CNN needs to train a lot of convolution operations, so its training time is longer.

Finally, the experiment uses data of 12 different audio formats to test and compare the four methods. Table 4 provides the values of test accuracy and test time. It can be seen that the average accuracy of the method proposed in this study is 99.0%, and the average detection time is 0.449ss. Therefore, the proposed method achieves better performance among the four methods compared. It can be concluded that the upsampling and maximum pooling of SPP-YOLO-v4 brought significant benefits. Maximum pooling selects the maximum value from adjacent areas to slightly delete some maximum frequency noise in the audio sequence. Therefore, convolution subsampling can be better operated in the subsequent sampling layer. Through these advantages, SPP can improve the performance of the backbone network.

TABLE 3: Performance comparison of different methods for different types.

Model	Loss value	Training time	Type	mAP (%)	TP	FP	Precision	Recall	F1
CNN	0.0143	2 h 40 min	D1	97.5	77	0	0.98	0.97	0.98
			D2	98.81	83	0			
			D3	99.92	62	1			
			D4	98.74	76	2			
GMM	0.0151	2 h	D1	97.53	78	0	0.98	0.96	0.97
			D2	100	83	0			
			D3	99.85	61	3			
			D4	98.01	75	3			
R-CNN	0.0131	2 h 20 min	D1	97.50	77	0	0.98	0.97	0.97
			D2	98.81	83	0			
			D3	99.92	59	0			
			D4	97.75	72	5			
SPP-YOLO-v4	0.0122	2 h 10 min	D1	97.51	78	0	0.99	0.99	0.99
			D2	98.82	83	0			
			D3	99.90	62	1			
			D4	98.94	79	3			

TABLE 4: Accuracy and detection time of different methods.

Format	CNN		GMM		R-CNN		SPP-YOLO-v4	
	Accuracy	Time (s)	Accuracy	Time (s)	Accuracy	Time (s)	Accuracy	Time (s)
CD	0.960	0.459	0.987	0.448	0.973	0.456	0.994	0.454
WAVE	0.791	0.453	0.963	0.442	0.826	0.459	0.993	0.452
AIFF	0.991	0.459	0.991	0.435	0.994	0.448	1.000	0.451
MPEG	0.970	0.473	0.990	0.448	0.994	0.457	0.997	0.443
MP3	0.951	0.445	0.990	0.447	0.931	0.452	0.982	0.457
MPEG-4	0.900	0.462	0.922	0.448	0.963	0.443	0.981	0.439
MIDI	0.907	0.460	0.870	0.449	0.901	0.451	0.982	0.448
WMA	0.787	0.453	0.880	0.462	0.841	0.460	0.996	0.449
RealAudio	0.869	0.457	0.982	0.464	0.947	0.447	0.993	0.433
VQF	0.863	0.447	0.961	0.442	0.866	0.459	0.992	0.450
AMR	0.957	0.453	0.960	0.443	0.990	0.459	0.991	0.451
AAC	0.881	0.452	0.632	0.471	0.961	0.466	0.989	0.459
Average	0.902	0.456	0.927	0.450	0.933	0.491	0.990	0.449

7. Conclusions

This study presents an audio recognition system suitable for music teaching environment. Use SPP to improve YOLO-v4 network architecture, that is to say, use SPP to select local areas on different scales of the same convolution layer to learn the characteristics of the multiscale system. In addition, the stacking method in ensemble learning is used to fuse independent submodels of two different channels. The experimental results show that the proposed method can improve the recognition accuracy of audio types and has better performance for different audio file formats. Due to the limitation of audio recording conditions, there are few audio types in the experimental dataset and the classification performance of audio files recorded by different devices has yet to be verified. More tests will be conducted on these two issues in the future.

Data Availability

The data used to support the findings of this study are available from the corresponding author upon request.

Conflicts of Interest

The authors declare that they have no conflicts of interest.

References

- [1] S. Wu, D. Zhang, Z. Zhang, N. Yang, M. Li, and M. Zhou, "Dependency-to-Dependency neural machine translation," *IEEE/ACM Transactions on Audio, Speech, and Language Processing*, vol. 26, no. 11, pp. 2132–2141, 2018.
- [2] J. Zou, W. Li, C. Chen, and Q. Du, "Scene classification using local and global features with collaborative representation fusion," *Information Sciences*, vol. 348, no. 2, pp. 209–226, 2016.
- [3] H. Phan, L. Hertel, M. Maass, P. Koch, R. Mazur, and A. Mertins, "Improved audio scene classification based on label-tree embeddings and convolutional neural networks," *IEEE/ACM Transactions on Audio, Speech, and Language Processing*, vol. 25, no. 6, pp. 1278–1290, 2017.
- [4] S. Bayatli, "Unsupervised weighting of transfer rules in rule-based machine translation using maximum-entropy approach," *Journal of Information Science and Engineering*, vol. 36, no. 2, pp. 309–322, 2020.

- [5] A. Rakotomamonjy, "Supervised representation learning for audio scene classification," *IEEE/ACM Transactions on Audio, Speech, and Language Processing*, vol. 25, no. 6, pp. 1253–1265, 2017.
- [6] W. Yang and S. Krishnan, "Combining temporal features by local binary pattern for acoustic scene classification," *IEEE/ACM Transactions on Audio, Speech, and Language Processing*, vol. 25, no. 6, pp. 1315–1321, 2017.
- [7] A. S. Dhanjal and W. Singh, "An automatic machine translation system for multi-lingual speech to Indian sign language," *Multimedia Tools and Applications*, vol. 81, no. 3, pp. 4283–4321, 2021.
- [8] M. A. . Alamir, "A novel acoustic scene classification model using the late fusion of convolutional neural networks and different ensemble classifiers," *Applied Acoustics*, vol. 172, no. 3, pp. 112–122, 2020.
- [9] J. G. Makin, D. A. Moses, and E. F. Chang, "Machine translation of cortical activity to text with an encoder–decoder framework," *Nature Neuroscience*, vol. 23, no. 4, pp. 575–582, 2020.
- [10] S. Waldekar and G. Saha, "Two-level fusion-based acoustic scene classification," *Applied Acoustics*, vol. 170, no. 5, Article ID 107502, 2020.
- [11] J. Sangeetha, R. Hariprasad, and S. Subhiksha, "Analysis of machine learning algorithms for audio event classification using Mel-frequency cepstral coefficients," *Applied Speech Processing*, vol. 27, no. 3, pp. 175–189, 2021.
- [12] M. Blochberger and F. Zotter, "Particle-filter tracking of sounds for frequency-independent 3D audio rendering from distributed B-format recordings," *Acta Acustica*, vol. 5, no. 5, pp. 20–118, 2021.
- [13] P. Yu, S. Zhang, X. Feng, Z. Liu, and Y. Shen, "Selecting program material by audio features for low-frequency perceptual evaluation of loudspeakers," *Applied Sciences*, vol. 11, no. 5, pp. 2302–2311, 2021.
- [14] Y. Xi, Q. Li, M. Zhang, L. Liu, and J. Wu, "Characterizing the time-varying brain networks of audiovisual integration across frequency bands," *Cognitive Computation*, vol. 12, no. 6, pp. 1154–1169, 2020.
- [15] C. P. Dadula and E. P. Dadios, "Fuzzy logic system for abnormal audio event detection using Mel frequency cepstral coefficients," *Journal of Advanced Computational Intelligence and Intelligent Informatics*, vol. 21, no. 2, pp. 205–210, 2017.
- [16] K. W. Church, "Emerging trends: APIs for speech and machine translation and more," *Natural Language Engineering*, vol. 24, no. 6, pp. 951–960, 2018.
- [17] L. Yang and H. Zhao, "Sound classification based on multi-head attention and support vector machine," *Mathematical Problems in Engineering*, vol. 2021, no. 5, 11 pages, Article ID 9937383, 2021.
- [18] A. Greco, N. Petkov, A. Saggese, and M. Vento, "AReN: a deep learning approach for sound event recognition using a brain inspired representation," *IEEE Transactions on Information Forensics and Security*, vol. 15, no. 1, pp. 3610–3624, 2020.
- [19] F. Demir, M. Turkoglu, M. Aslan, and A. Sengur, "A new pyramidal concatenated CNN approach for environmental sound classification," *Applied Acoustics*, vol. 170, no. 6, pp. 107520–108116, 2020.
- [20] Q. Zhu, H. Zheng, Y. Wang, Y. Cao, and S. Guo, "Study on the evaluation method of sound phase cloud maps based on an improved YOLOv4 algorithm," *Sensors*, vol. 20, no. 15, pp. 4314–4322, 2020.
- [21] A. Venturini, L. Zao, and R. Coelho, "On speech features fusion, α -integration Gaussian modeling and multi-style training for noise robust speaker classification," *IEEE/ACM Transactions on Audio, Speech, and Language Processing*, vol. 22, no. 12, pp. 1951–1964, 2014.
- [22] J. Zhang and C. Zong, "Deep neural networks in machine translation: an overview," *IEEE Intelligent Systems*, vol. 30, no. 5, pp. 16–25, 2015.
- [23] P. L. Son, "On the design of sparse arrays with frequency-invariant beam pattern," *IEEE/ACM Transactions on Audio, Speech, and Language Processing*, vol. 29, no. 5, pp. 226–238, 2021.
- [24] S. Ketu and P. K. Mishra, "India perspective: CNN-LSTM hybrid deep learning model-based COVID-19 prediction and current status of medical resource availability," *Soft Computing*, vol. 26, no. 2, pp. 645–664, 2022.
- [25] M. Jia, Y. Wu, C. Bao, and C. Ritz, "Multi-source DOA estimation in reverberant environments by jointing detection and modeling of time-frequency points," *IEEE/ACM Transactions on Audio, Speech, and Language Processing*, vol. 29, no. 2, pp. 379–392, 2021.
- [26] M. S. Akhtar, P. Sawant, S. Sen, A. Ekbal, and P. Bhattacharyya, "Improving word embedding coverage in less-resourced languages through multi-linguality and cross-linguality: a case study with aspect-based sentiment analysis," *ACM Transactions on Asian and Low-Resource Language Information Processing*, vol. 18, no. 2, pp. 1–22, 2019.
- [27] G. Pepe, L. Gabrielli, S. Squartini, and L. Cattani, "Designing audio equalization filters by deep neural networks," *Applied Sciences*, vol. 10, no. 7, pp. 2483–2491, 2020.
- [28] X. Sun, T. Liu, X. Yu, and B. Pang, "Unmanned surface vessel visual object detection under all-weather conditions with optimized feature fusion network in YOLOv4," *Journal of Intelligent and Robotic Systems*, vol. 103, no. 3, pp. 55–72, 2021.

Research Article

Efficient Linkable Ring Signature Scheme over NTRU Lattice with Unconditional Anonymity

Qing Ye , Mengyao Wang , Hui Meng , Feifei Xia , and Xixi Yan 

School of Software, Henan Polytechnic University, Jiaozuo 454000, China

Correspondence should be addressed to Hui Meng; menghui@hpu.edu.cn

Received 18 March 2022; Revised 2 April 2022; Accepted 7 April 2022; Published 13 May 2022

Academic Editor: Le Sun

Copyright © 2022 Qing Ye et al. This is an open access article distributed under the Creative Commons Attribution License, which permits unrestricted use, distribution, and reproduction in any medium, provided the original work is properly cited.

In cloud and edge computing, senders of data often want to be anonymous, while recipients of data always expect that the data come from a reliable sender and they are not redundant. Linkable ring signature (LRS) can not only protect the anonymity of the signer, but also detect whether two different signatures are signed by the same signer. Today, most lattice-based LRS schemes only satisfy computational anonymity. To the best of our knowledge, only the lattice-based LRS scheme proposed by Torres et al. can achieve unconditional anonymity. But the efficiency of signature generation and verification of the scheme is very low, and the signature length is also relatively long. With the preimage sampling, trapdoor generation, and rejection sampling algorithms, this study proposed an efficient LRS scheme with unconditional anonymity based on the e-NTRU problem under the random oracle model. We implemented our scheme and Torres et al.'s scheme, as well as other four efficient lattice-based LRS schemes. It is shown that under the same security level, compared with Torres et al.'s scheme, the signature generation time, signature verification time, and signature size of our scheme are reduced by about 94.52%, 97.18%, and 58.03%, respectively.

1. Introduction

In most scenarios involving data transmission, including blockchain, cloud computing, edge computing, etc., the sender of data usually wants to be anonymous, while the receiver of data always expects the data to be reliable. Ring signature (RS) proposed by Rivest et al. [1] is a good technology that can meet the above requirements. RS has two essential security properties: (1) unforgeability, which requires the verifier is able to verify whether the signature was signed by a reliable signer; and (2) anonymity, which requires the verifier could not identify the real signer from a group of users. Similar to group signature [2, 3], RS is group-oriented. However, different from group signature, in RS, the group is formed spontaneously, that is, there is no special manager, and the setup and revocation procedures are not required. Any user can select a group of ring members and sign any message with his own private key and the public keys of other members without their consent. And the verifier only can verify whether the signature comes from a member in the ring without knowing which member the signer is.

Due to the anonymity of RS, it is widely used in anonymous tip off, e-cash [4], and other fields. It is worth noting that while protecting the anonymity of signers, RS also brings a new problem, that is, the same signer can sign multiple times without being detected.

In 2004, Liu et al. [5] introduced an extended property called linkability to RS, and the corresponding primitive is now known as linkable ring signatures (LRS). LRS not only satisfies the properties of ordinary RS (such as correctness, unforgeability, and anonymity) but also can be used to judge whether two different signatures are signed by the same signer (linkability). LRS is useful in situations where anonymity and nonrepeatability are required. For example, in the system of blockchain [6], if some user signs the same amount of money twice, LRS will help the verifier detect it and the verifier will deny the second signature, thus avoiding the so-called “double spending” problem. In smart grid systems [7], the electricity consumption data of users are automatically collected by the smart meter, and specific electricity consumption information is fed back to the service provider. Thus, malicious attackers can infer the life and rest rules of the user from the large amount of electricity

consumption data recorded by the smart meter. LRS can not only conceal the specific information of the meter user but also eliminate the redundant data of the same meter and provide the system with abnormal user monitoring and tracking functions.

In 2013, Liu et al. [8] constructed an unconditional anonymous linkable ring signature (UALRS) scheme, which addressed the open problem that RS could not have linkability and strong anonymity simultaneously and made it more secure. RS schemes have two types of anonymity: computational anonymity and unconditional anonymity. Computational anonymity refers to the protection of anonymity under certain number theory problems. The anonymity of RS is destroyed if this potential problem can be solved by an adversary. By contrast, unconditional anonymity means that the probability that any adversary with unlimited computing power and time knows the actual signer of a given RS is no better than random guessing. In other words, assuming that there are l users in RS, the probability of any adversary with unlimited computing power and time correctly indicating the public key of the actual signer is no more than $1/l$.

It is not difficult to design a RS scheme with unconditional anonymity. In fact, most traditional RS schemes can satisfy unconditional anonymity [1, 9–16]. However, it is not an easy work to construct a UALRS scheme. The difficulty lies in the following two aspects. First, in a computational anonymous linkable ring signature (CALRS) scheme, the linking tag can always be designed as a pseudorandom function about the private key of the signer based on some mathematical problem. But unconditional anonymity means that the adversary has unlimited computing power, that is it can calculate out the solution of any NP-hard problem, such as NTRU-SIS, large integer factorization, discrete logarithm, and the preimage of a given hash value. Therefore, only designing the linking tag using mathematical problems is not enough, and it should consider more skills. Second, in order to achieve unconditional anonymity, the generation and verification of a linking tag are often more complex, which may increase the length of public and private keys and signatures, as well as reduce the computational efficiency of the scheme. In fact, from 2004 to 2013, only the LRS scheme proposed by Liu et al. [8] can achieve unconditional anonymity.

The above schemes are all constructed based on classical number theory problems, that is, discrete logarithm and the decomposition of large integer problems. With the development of quantum computers, cryptosystems under classical number theory problems are faced with severe challenges. Shor [17] constructed a quantum algorithm in 1994 to solve the problem of large integer factorization in polynomial time under quantum computing conditions, and this algorithm made most existing public key cryptosystems no longer secure under quantum attacks.

In this case, post-quantum cryptography began to be studied by scholars in the field of cryptography. In the alternatives, lattice-based cryptography appeals to scholars because of its high efficiency, simplicity, high parallelizability, and strong provable security guarantees. In 2016,

Libert et al. [18] constructed a lattice-based RS scheme based on zero-knowledge proofs and accumulators. Thereafter, other lattice-based RS schemes have been proposed [19–21]. In 2017, Yang et al. [22] proposed a lattice-based LRS scheme based on weak pseudorandom functions, accumulators, and zero-knowledge proofs. In 2018, Baum et al. [23] proposed the lattice-based one-time LRS scheme based on the module-SIS problem (a variant of SIS problem) and module-LWE problem (a variant of LWE problem). In the same year, Alberto Torres et al. [24] proposed a lattice-based one-time LRS scheme based on the ring-SIS problem. Subsequently, Zhang et al. [25] proposed a LRS scheme over ideal lattice based on the homomorphic commitment scheme and Σ protocol. In 2019, Liu et al. [26] proposed a lattice-based LRS scheme supporting stealth addresses under the module-SIS and module-LWE problems. In 2020, Beullens et al. [27] constructed a LRS scheme whose signature size scales logarithmically with the ring size from isogeny and lattice assumptions.

However, in the above lattice-based LRS schemes, only Alberto Torres et al.'s scheme [24] satisfies unconditional anonymity. By analyzing Torres et al.'s scheme, it is found that in order to achieve unconditional anonymity, the linking tag of Torres et al.'s scheme is generated using an m -dimensional polynomial vector over a polynomial ring. Since the linking tag is so large, Torres et al.'s scheme generates signatures m times longer than a normal CALRS scheme over a polynomial ring, and its efficiency in generating and verifying signatures is also significantly reduced.

Hoffstein et al. [28] proposed the NTRU lattice-based cryptosystem in 1996. Considering that it only involves multiplication on polynomial rings and small integer modulo operations, the NTRU-based cryptosystem usually requires smaller public and private keys and is more efficient compared with that on the general lattice. Therefore, it has received extensive attention from scholars. In 2016, Zhang et al. [29] proposed an efficient RS scheme on NTRU lattice whose security can be reduced to the e-NTRU problem (a variant of the SIS problem on NTRU lattice) in the random oracle model. In 2019, Lu et al. [30] constructed Raptor, a practical NTRU lattice-based LRS scheme based on a variant of chameleon hash functions. In 2021, Tang et al. [31] constructed an identity-based LRS scheme over NTRU lattice by employing the technologies of trapdoor generation and rejection sampling. The security of this scheme relies on the small integer solution (SIS) problem on NTRU lattice.

1.1. Our Contribution. To reduce the signature size, as well as promote the efficiency of signature generation and verification of lattice-based UALRS scheme [24], in this study, a LRS scheme is reconstructed on NTRU lattice, and its architecture is shown in Figure 1. The main contributions of this article are as follows:

- (1) In the key generation stage, the public and private keys of the LRS scheme are generated by the trapdoor and the preimage sampling algorithms on NTRU lattice. Then, the linking tag is produced by the public and private keys of the signer, and a LRS

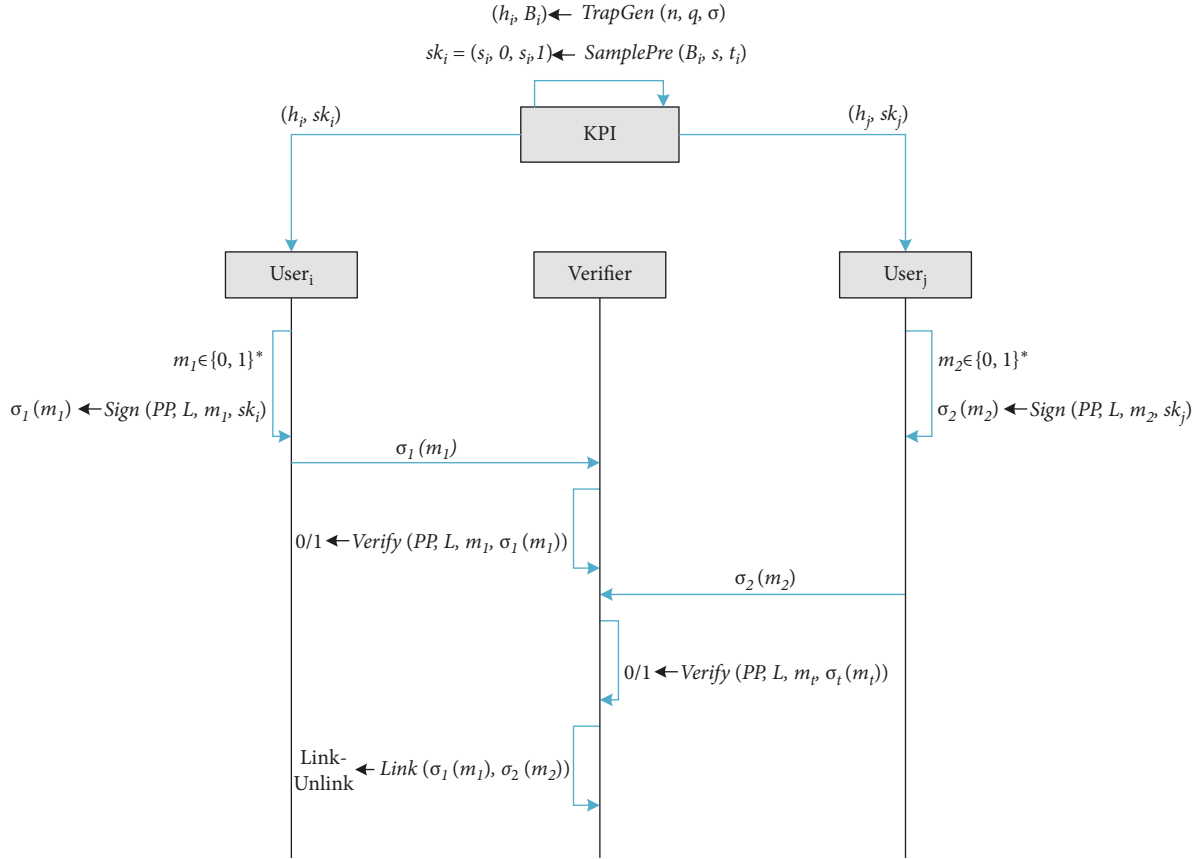


FIGURE 1: Linkable ring signature on NTRU lattice.

is generated based on the signature algorithm of Zhang et al. [29] combined with the rejection sampling algorithm.

- (2) In terms of security analysis, strict security proof is conducted based on the security model of UALRS proposed by Liu et al. [8]. The result of the proof shows that the unforgeability and linkability of the proposed scheme can be reduced to the difficulty of e-NTRU problem under the random oracle model, and, meanwhile, the proposed scheme satisfies unconditional anonymity.
- (3) In terms of performance analysis, the proposed scheme is compared with the latest and efficient lattice-based LRS schemes in [23, 24, 26, 27, 30], and a detailed analysis is given. The possible parameter settings of the proposed scheme are also analyzed and provided under the premise of ensuring the security of the proposed scheme.
- (4) We implement our scheme and Torres et al.'s scheme [24], as well as other four efficient lattice-based LRS schemes [23, 26, 27, 30], and it is shown that under the same security level, the signature generation and verification time of the proposed scheme are respectively reduced by 56.61% and 65.18%. Especially compared with Torres et al.'s scheme, the signature generation and verification time of the proposed scheme are respectively reduced by 94.52% and

97.18%, and the signature size of the proposed scheme is reduced by 58.03% on average.

1.2. Paper Organization. In Section 2, we introduce some definitions, lemmas, difficult problems, and related algorithms which we will use to construct the scheme. We introduce the definition of LRS and the relevant security model in Section 3. Section 4 contains the construction and correctness statement of the LRS scheme and the proof of correctness. Section 5 contains the security statements of the proposed scheme and the proofs of unforgeability, unconditional anonymity, and linkability. In Section 6, we discuss the parameter settings and post-quantum security of the proposed scheme. Finally, in Section 7 and Section 8, we respectively give the performance analysis and experimental results of the proposed scheme and the lattice-based LRS schemes of [23, 24, 26, 27, 30] and also make a comparison between them.

2. Preliminaries

2.1. Symbol Definition. Descriptions of the used notations are listed in Table 1.

2.2. Related Definitions of NTRU Lattice

Definition 1 (lattice). Lattice Λ generated by m linearly independent vectors $\mathbf{b}_1, \mathbf{b}_2, \dots, \mathbf{b}_m \in \mathbb{R}^n$ is the set of linear

TABLE 1: Symbol description.

Notations	Explanation
\mathbb{R}	Set of real numbers
\mathbb{Z}	Set of integers
\mathbb{Z}_q	Set of integers modulo q
\mathbb{Z}^m	Set of m -dimensional column vectors over \mathbb{Z}
$\mathbb{Z}_q^{n \times m}$	Set of matrices of n rows and m columns over \mathbb{Z}_q
R	Polynomial ring $\mathbb{Z}[x]/(x^n + 1)$
R_q	Polynomial ring $\mathbb{Z}_q[x]/(x^n + 1)$
\mathbf{A}	Matrix
\mathbf{x}	Vector
$\mathbf{x} \leftarrow D$	Randomly choosing vector \mathbf{x} from probability distribution D
$\ \mathbf{x}\ $	Euclidean norm of vector \mathbf{x}
$f \cdot g$	Multiplication of polynomials
$negl(n)$	Negligible function about n
$g(n) = \omega(f(n))$	$g(n) > f(n)$

combinations of all integer coefficients of the m linearly independent vectors, namely

$$\Lambda = L(\mathbf{b}_1, \mathbf{b}_2, \dots, \mathbf{b}_m) = \left\{ \sum_{i=1}^m a_i \mathbf{b}_i \mid a_i \in \mathbb{Z} \right\}, \quad (1)$$

where m and n are the rank and dimension of lattice Λ , respectively, and $\mathbf{b}_1, \mathbf{b}_2, \dots, \mathbf{b}_m$ is called a basis of lattice Λ .

Definition 2 (convolutional polynomial ring). Let $R = \mathbb{Z}[x]/(x^n + 1)$ be an ordinary polynomial ring. If the addition operation remains unchanged and the multiplication operation is replaced by a convolution operation on R , then R is called a convolution polynomial ring. Similarly, given a prime number q , the modulus convolution polynomial ring is $R_q = R/qR$.

Let $f = \sum_{i=0}^{n-1} f_i x^i, g = \sum_{i=0}^{n-1} g_i x^i \in R_q$, then the two operations on R_q are defined as follows:

(i) Addition operation $+$:

$$f + g = \sum_{i=0}^{n-1} (f_i + g_i) x^i \bmod q \in R_q. \quad (2)$$

(ii) Convolution operation $*$:

$$f * g = f \cdot g \bmod (x^n + 1) \bmod q \in R_q. \quad (3)$$

Definition 3 (anticirculant matrix). Let the coefficient vector of polynomial f be $(f_0, f_1, \dots, f_{n-1})$. Then, the coefficient vector of polynomial $x \cdot f$ is $(-f_{n-1}, f_0, \dots, f_{n-2})$ and the coefficient vector of polynomial $x^{n-1} \cdot f$ is $(-f_1, -f_2, \dots, f_0)$. The anti-circulant matrix defined by polynomial f is as follows:

$$\mathbf{A}_n(f) = \begin{bmatrix} f_0 & f_1 & \cdots & f_{n-1} \\ -f_{n-1} & f_0 & \cdots & f_{n-2} \\ \vdots & \vdots & \cdots & \vdots \\ -f_1 & -f_2 & \cdots & f_0 \end{bmatrix} = \begin{bmatrix} f \\ x \cdot f \\ \vdots \\ x^{n-1} \cdot f \end{bmatrix}. \quad (4)$$

Definition 4. (NTRU lattice). Let a positive integer $q \geq 2$, n is a power of two and $f, g \in R_q, f^{-1} \in R_q$ be the inverse of $f, h = g * f^{-1} \bmod q$. The NTRU lattice corresponding to q and h is as follows:

$$\Lambda_{q,h} = \{(u, v) \in \mathbb{R}^2 \mid u + v * h = 0 \bmod q\}. \quad (5)$$

Apparently, lattice $\Lambda_{q,h}$ is a $2n$ -dimensional full-rank lattice, and $\mathbf{A}_{q,h} = \begin{pmatrix} -\mathbf{A}_n(h) & \mathbf{I}_n \\ q\mathbf{I}_n & \mathbf{O}_n \end{pmatrix} \in \mathbb{Z}_q^{2n \times 2n}$ is a set of basis matrices. $\mathbf{A}_{q,h}$ can be uniquely determined by the polynomial $h \in R_q$, whereas the others can be compressed during storage. Thus, the storage space required is relatively small. However, in NTRU lattice-based cryptographic schemes, $\mathbf{A}_{q,h}$ cannot be used as a trapdoor basis because it has poor orthogonality.

Definition 5. (discrete gaussian distribution) [32]. For any $\sigma > 0$ and m -dimensional integer lattice Λ , the discrete Gaussian distribution on integer lattice Λ with vector $\mathbf{c} \in \mathbb{R}^m$ as the center and σ as the parameter is defined as follows:

$$\forall \mathbf{x} \in \Lambda, D_{\Lambda, \mathbf{c}, \sigma}^m(\mathbf{x}) = \frac{\rho_{\mathbf{c}, \sigma}^m(\mathbf{x})}{\rho_{\mathbf{c}, \sigma}^m(\Lambda)}, \quad (6)$$

where $\rho_{\mathbf{c}, \sigma}^m(\mathbf{x}) = \exp(-\pi \|\mathbf{x} - \mathbf{c}\|^2 / \sigma^2)$. When $\mathbf{c} = 0$, let ρ_{σ}^m and $D_{\Lambda, \sigma}^m$ be abbreviated as ρ_{σ}^m and $D_{\Lambda, \sigma}^m$, respectively. And throughout the article, $D_{\mathbf{c}, \sigma}^m$ denotes the discrete Gaussian distribution over \mathbb{Z}^m .

2.3. Hardness Assumption

Definition 6 (NTRU small-integer solution, NTRU-SIS) [33]. For a polynomial $h = g * f^{-1} \bmod q \in R_q$ and a real number $\beta > 0$, to find two nonzero polynomials $(u, v) \in R_q^2$ such that $u + v * h = 0 \bmod q$ and $\|u\|, \|v\| \leq \beta$.

Definition 7 (extended NTRU, e-NTRU) [29]. Given N polynomials $h_i = g_i * f_i^{-1} \bmod q \in R_q, i \in \{1, \dots, N\}$, where $N \ll q$, to find a tuple of short polynomials $(u_i, v_i) \in R_q^2, u_i, v_i \neq 0 \bmod q, i \in \{1, \dots, N\}$ such that

$$\sum_{i=1}^N (u_i + v_i * h_i) = 0 \bmod q, \|u_i\|, \|v_i\| \leq \beta, i \in \{1, \dots, N\}. \quad (7)$$

Theorem 1 (see [29]). *Let integer $k > 0, n = 2^k, q = 1 \bmod 2n$ and integer $N \ll q$, then the e-NTRU problem is polynomially equivalent to the NTRU-SIS problem.*

2.4. Related Algorithm

Lemma 1 (see [34]). *Let an integer $n = 2^k$ for $k > 0$, a prime number $q = 1 \bmod 2n$, and a parameter $\sigma = 1.17\sqrt{q/2n}$. Then, a probabilistic polynomial time (PPT) algorithm TrapGen(n, q, σ) can output a sample matrix $\mathbf{B}_{f,g} \in \mathbb{Z}_q^{2n \times 2n}$ from (a distribution close to) $D_{h, \sigma}^{2n \times 2n}$ and a polynomial $h = g * f^{-1} \bmod q \in R_q$ on the NTRU lattice $\Lambda_{h,q}$.*

Lemma 2 (see [34]). *Given a matrix $\mathbf{B}_{f,g}$ and a parameter $s = 0.585/\pi\sqrt{q} \ln(2 + 2/\eta)$ for $\eta = 2^{-\lambda}/2n$, where λ is the security parameter. For any polynomial $t \in R_q$, a PPT algorithm $\text{SamplePre}(\mathbf{B}_{f,g}, s, t)$ may output $\mathbf{z} = (z_1, z_2) \leftarrow D_{h^{\dagger+c,s}}$, such that $z_1 + z_2 * h = t$, $\|\mathbf{z}\| \leq s\sqrt{2n}$.*

Definition 8 (rejection sampling algorithm) [35]. In 2012, Lyubashevsky proposed rejection sampling technique for the first time and gave the first signature scheme without trapdoor on lattice with this technique. It can be applied to the signature system and can make the distributions of the signature and private key independent of each other. Thus, it can effectively prevent the leakage of the private key.

Lemma 3. *Let $V = \{\mathbf{v} \in \mathbb{Z}^m : \|\mathbf{v}\| < t\}$, $\sigma = \omega(t\sqrt{\log m})$, and $h: V \rightarrow \mathbb{R}$ is a probability distribution. Then, for constant $M = O(1)$, the statistical distance of output distributions of Algorithms 1 and 2 is less than $2^{-\omega(\log m)}/M$.*

Algorithm 1. $v \leftarrow h$, $\mathbf{z} \leftarrow D_{\mathbf{v},\sigma}^m$, output (\mathbf{z}, v) with probability $\min(D_{\sigma}^m(\mathbf{z})/MD_{\mathbf{v},\sigma}^m(\mathbf{z}), 1)$.

Algorithm 2. $v \leftarrow h$, $\mathbf{z} \leftarrow D_{\sigma}^m$, output (\mathbf{z}, v) with probability $1/M$.

Furthermore, the output probability of Algorithm 1 is at least $1 - 2^{-\omega(\log m)}/M$.

3. Security Model

In this section, we present our security model and define related security concepts.

3.1. LRS Definition. A LRS scheme consists of the following five PPT algorithms:

- (1) **Setup**(1^λ): On input a security parameter λ , it outputs system public parameters PP .

- (2) **KeyGen**(PP): On input the public parameters PP , it outputs a public/private key pair (pk_i, sk_i) . We denote by SK and PK the domains of possible private and public keys, respectively.
- (3) **Sign**(PP, L, m, sk_k): On input the public parameters PP , a public key list L , a message $m \in \{0, 1\}^*$, and private key sk_k , it outputs a signature $\sigma(m)$, which contains a linking tag I .
- (4) **Verify**($PP, L, m, \sigma(m)$): On input the system public parameters PP , a public key list L , a message $m \in \{0, 1\}^*$, and a signature $\sigma(m)$, if $\sigma(m)$ is valid, it outputs “1”; otherwise, it outputs “0.”
- (5) **Link**($\sigma(m_1), \sigma(m_2)$): On input two signatures $\sigma_1(m_1), \sigma_2(m_2)$, where $\sigma_1(m_1)$ and $\sigma_2(m_2)$ are the signatures of different messages m_1 and m_2 under the same ring, which contain linking tags I_1 and I_2 , respectively. It checks whether $I_1 = I_2$ and outputs “Link” if $I_1 = I_2$; otherwise, it outputs “Unlink.” “Link” means that the two signatures are generated by the same signer, and “Unlink” means that the two signatures are generated by different signers.

Definition 9 (correctness). Correctness for LRS contains verification correctness and linking correctness simultaneously.

- (i) **Verification Correctness:** For a valid signature $\sigma(m)$, the probability of the algorithm $\text{Verify}(PP, L, m, \sigma(m))$ outputting “0” is negligible.
- (ii) **Linking Correctness:** For two valid signatures $\sigma_1(m_1), \sigma_2(m_2)$ generated by using the same private key, the probability of the algorithm $\text{Link}(\sigma(m_1), \sigma(m_2))$ outputting “Unlink” is negligible. The formal definition of the correctness of the LRS scheme is shown in the following expressions:

$$\Pr \left[\begin{array}{l} \text{“0”} \leftarrow \text{Verify}(PP, L, m, \sigma(m)) \\ (pk, sk) \leftarrow \text{KeyGen}(PP) \\ \sigma(m) \leftarrow \text{Sign}(PP, L, m, sk) \end{array} \right] \leq \text{negl}(\lambda). \quad (8)$$

$$\Pr \left[\begin{array}{l} \text{“Unlink”} \leftarrow \text{Link}(\sigma(m_1), \sigma(m_2)) \\ (pk, sk) \leftarrow \text{KeyGen}(PP) \\ \sigma(m_1) \leftarrow \text{Sign}(PP, L_1, m_1, sk) \\ \sigma(m_2) \leftarrow \text{Sign}(PP, L_2, m_2, sk) \end{array} \right] \leq \text{negl}(\lambda). \quad (9)$$

3.2. Security Model. Generally, a LRS scheme should satisfy three security properties, namely unforgeability, anonymity, and linkability. According to the security model of UALRS proposed by Liu et al. [8] in 2013, this study uses a series of games between an adversary A and a challenger S to describe the security model of LRS. Supposing there are l

members in the ring, these three properties are described as follows:

Before defining unforgeability, anonymity, and linkability, we consider the following oracles, which together simulate the adversary’s ability to break the security of the scheme.

JO (Joining Oracle): A inputs member index k , and S outputs the corresponding public key $pk_k \in PK$ to A

CO (Corruption Oracle): A inputs a public key $pk_k \in PK$, which is a query output of *JO*, and S returns the corresponding private key $sk_k \in SK$

SO (Signing Oracle): A inputs a public key list $L = \{pk_i\}_{1 \leq i \leq l} \in PK$, and a message $m \in \{0, 1\}^*$, and S returns a valid signature $\sigma(m)$

In addition, in the random oracle model, a random oracle model *HO* is provided for users to query.

3.2.1. Unforgeability. It means that users outside the ring cannot successfully forge a legal signature under the ring. That is, if there is no private key of a member in the ring, even if the adversary obtains multiple valid message signature pairs, the probability of the adversary forging a valid signature successfully is negligible. Unforgeability for the LRS scheme is defined by the following game between an adversary A and a challenger S , in which A is given access to oracles *JO*, *CO*, *SO*, and *HO*:

- (i) The system public parameters PP are generated by challenger S and given to A
- (ii) A can access the oracles adaptively
- (iii) A gives S a list $L = \{pk_i\}_{1 \leq i \leq l}$ of public keys, a message $m \in \{0, 1\}^*$, and a signature $\sigma(m)$

A wins the game if

- (i) $\text{Verify}(PP, L, m, \sigma(m)) = "1"$
- (ii) All public keys in L are obtained by querying *JO*
- (iii) Any public key in L has not been input to *CO*
- (iv) $\sigma(m)$ is not obtained by querying *SO*

We express it as

$$\text{Adv}_A^{\text{Unf}} = \Pr[A \text{ wins the game}]. \quad (10)$$

Definition 10 (unforgeability). If the advantage $\text{Adv}_A^{\text{Unf}}$ of any PPT adversary A to win the unforgeability game is negligible, then the LRS scheme is unforgeable.

3.2.2. Unconditional Anonymity. It means that given a ring signature, no one can guess the real signer. In other words, given the public keys of all the members of the ring, it is impossible for anyone to tell the public key of the actual signer with a probability larger than $1/l$, where l denotes the cardinality of the ring, even the adversary has unlimited computing time and resources. The unconditional anonymity of LRS is described by the following game between an adversary A and a challenger S , where A is granted access to oracle *JO*:

- (i) The system public parameters PP are generated by challenger S and given to A ;
- (ii) A can access the oracle *JO* adaptively;

(iii) A gives S a public key list $L = \{pk_i\}_{1 \leq i \leq l}$, which are query outputs of *JO*, and a message $m^* \in \{0, 1\}^*$. S randomly samples $b \in \{1, \dots, l\}$, uses the signature key sk_b corresponding to pk_b to run algorithm $\text{Sign}(PP, L, m, sk_b)$, and generates and gives A the signature $\sigma(m^*)$; and

(iv) A returns the guess value $b' \in \{1, \dots, l\}$.

We express it as

$$\text{Adv}_A^{\text{Anon}} = |\Pr[b' = b] - 1/l|. \quad (11)$$

Definition 11 (unconditional anonymity). If the advantage $\text{Adv}_A^{\text{Anon}}$ of any unbounded adversary A to win the anonymity game is negligible, then the LRS scheme is called to be unconditional anonymous.

It is worth noting that though only *JO* is given to A , since A has unbounded computation power, it can calculate out the solution of any NP-hard problem, such as NTRU-SIS, large integer factorization, discrete logarithm, as well as the preimage of a given hash value. Therefore, unconditional anonymity in fact requires that in this case, A is still unable to reveal the public key of the actual signer of a RS with a probability higher than $1/l$.

3.2.3. Linkability. It means that two signatures generated by the same ring member can be linked. That is, an adversary who has less than two members' private keys in the ring cannot generate two valid signatures determined by the linking algorithm as "Unlink." The linkability of a LRS scheme is described by the following game between an adversary A and a challenger S , where A is granted access to oracles *JO*, *CO*, *SO*, and *HO*:

- (i) The system public parameters PP are generated by challenger S and given to A
- (ii) A can access the oracles adaptively
- (iii) A gives S two sets $L_1 = \{pk_i\}_{1 \leq i \leq l_1}$ and $L_2 = \{pk_i\}_{1 \leq i \leq l_2}$, messages $m_1, m_2 \in \{0, 1\}^*$, and signatures $\sigma(m_1)$ and $\sigma(m_2)$, where $\sigma(m_1)$ and $\sigma(m_2)$ contain the corresponding linking tags I_1, I_2 , respectively

A wins the game if

- (i) All public keys in $L_1 \cup L_2$ are query outputs of *JO*
- (ii) For $i = 1, 2$, $\text{Verify}(PP, L_i, m_i, \sigma(m_i)) = "1"$ such that $\sigma(m_i)$ is not an output of *SO*
- (iii) *CO* has been queried less than two times
- (iv) $\text{Link}(\sigma(m_1), \sigma(m_2)) = \text{"Unlink"}$

We express it as

$$\text{Adv}_A^{\text{Link}} = \Pr[A \text{ wins the game}]. \quad (12)$$

Definition 12 (linkability). If the advantage $\text{Adv}_A^{\text{Link}}$ of any PPT adversary A to win the linkability game is negligible, then the LRS scheme is linkable.

4. Scheme Construction

- (1) Setup($1^\lambda, 1^n$): On input the security parameter λ and integer $n = 2^k$, where $k > 0$, a ring of $l = \omega(\log n)$, a prime $q = 1 \bmod 2n$, two parameters $\sigma = 1.17\sqrt{q}/2n$ and $s = 0.585/\pi\sqrt{q \ln(2 + 2/\eta)}$, where $\eta = 2^{-\lambda}/2n$, choose a collision-resistant hash function $H: \{0, 1\}^* \rightarrow \{0, 1\}^n$, and output $PP = (q, \sigma, s, H)$.
- (2) KeyGen(PP): On input the system public parameters PP , the following steps should be performed:
 - (i) Run the trapdoor generation algorithm $\text{TrapGen}(n, q, \sigma)$ to generate $\{h_i \in R_q, \mathbf{B}_i \in \mathbb{Z}_{2n \times 2n}^q\}$;
 - (ii) Randomly choose $t_i \in R_q$, and let $sk_i = (s_{i,0}, s_{i,1}) = \text{SamplePre}(\mathbf{B}_i, s, t_i)$ such that $s_{i,0} + s_{i,1} * h_i = t_i$, $\|(s_{i,0}, s_{i,1})\| \leq s\sqrt{2n}$; and
 - (iii) Output a public key list $L = \{h_i\}_{1 \leq i \leq l}$ and the private key for the member i : $sk_i = (s_{i,0}, s_{i,1})$.
- (3) Sign(PP, L, m, sk_k): On input the system public parameters PP , the public key list $L = \{h_i\}_{1 \leq i \leq l}$, a message $m \in \{0, 1\}^*$, and a private key $sk_k = (s_{k,0}, s_{k,1})$, the member k performs the following steps:
 - (i) Compute linking tag
$$I = s_{k,0} + s_{k,1} * h_k. \quad (13)$$
 - (ii) For $1 \leq i \leq l$, sample random vectors $\mathbf{r}_{i,0}, \mathbf{r}_{i,1} \leftarrow D_s^n$.
 - (iii) Let
$$\mathbf{v} = H\left(\sum_{1 \leq i \leq l} (\mathbf{r}_{i,0} + \mathbf{r}_{i,1} * h_i), L, m, I\right). \quad (14)$$
 - (iv) If $i \neq k$, compute
$$\mathbf{z}_i = (\mathbf{z}_{i,0}, \mathbf{z}_{i,1}) = (\mathbf{r}_{i,0}, \mathbf{r}_{i,1}). \quad (15)$$

if $i = k$, compute

$$\mathbf{z}_k = (\mathbf{z}_{k,0}, \mathbf{z}_{k,1}) = (s_{k,0} * \mathbf{v} + \mathbf{r}_{k,0}, s_{k,1} * \mathbf{v} + \mathbf{r}_{k,1}). \quad (16)$$
 - (v) Continue with probability $\min(D_s^n(z_k) / MD_{s^*v,s}^n(z_k), 1)$, where $M = O(1)$; otherwise restart.
 - (vi) Output signature $\sigma(m) = (m, (\mathbf{z}_i)_{1 \leq i \leq l}, \mathbf{v}, I)$.
- (4) Verify($PP, L, m, \sigma(m)$): On input the system parameters PP , the public key list $L = \{h_i\}_{1 \leq i \leq l}$, a message $m \in \{0, 1\}^*$, and a signature $\sigma(m) = (m, (\mathbf{z}_i)_{1 \leq i \leq l}, \mathbf{v}, I)$, output “1” if and only if the following conditions are true; otherwise, output “0”:
 - (i) $\mathbf{v} = H\left(\sum_{1 \leq i \leq l} (\mathbf{z}_{i,0} + \mathbf{z}_{i,1} * h_i) - I\mathbf{v}, L, m, I\right). \quad (17)$
 - (ii) For $1 \leq i \leq l$, $0 \leq \|\mathbf{z}_{i,0}, \mathbf{z}_{i,1}\| \leq s\sqrt{2n}. \quad (18)$
- (5) Link($\sigma(m_1), \sigma(m_2)$): On input two signatures $\sigma(m_1)$ and $\sigma(m_2)$, which contains linking tags I_1 and I_2 ,

respectively, the following steps should be performed:

Verify whether $I_1 \stackrel{?}{=} I_2$. If $I_1 = I_2$, then return “Link”; otherwise, return “Unlink.”

Theorem 2 (correctness). *The proposed LRS scheme satisfies correctness.*

Proof. Assuming $\sigma(m) = (m, (\mathbf{z}_i)_{1 \leq i \leq l}, \mathbf{v}, I)$ is a signature generated by a member of the ring according to the algorithms under public key set $L = \{h_i\}_{1 \leq i \leq l}$, then the following equation holds:

$$\begin{aligned} & \sum_{1 \leq i \leq l} (\mathbf{z}_{i,0} + \mathbf{z}_{i,1} * h_i) - I\mathbf{v} \\ &= \mathbf{z}_{k,0} + \mathbf{z}_{k,1} * h_k - I\mathbf{v} + \sum_{1 \leq i \leq l, i \neq k} (\mathbf{z}_{i,0} + \mathbf{z}_{i,1} * h_i) \\ &= (s_{k,0} + s_{k,1} * h_k)\mathbf{v} + \mathbf{r}_{k,0} + \mathbf{r}_{k,1} * h_k - I\mathbf{v} \\ & \quad + \sum_{1 \leq i \leq l, i \neq k} (\mathbf{r}_{i,0} + \mathbf{r}_{i,1} * h_i). \end{aligned} \quad (19)$$

Given that $s_{k,0} + s_{k,1} * h_k = I$, we have

$$\sum_{1 \leq i \leq l} (\mathbf{z}_{i,0} + \mathbf{z}_{i,1} * h_i) - I\mathbf{v} = \sum_{1 \leq i \leq l} (\mathbf{r}_{i,0} + \mathbf{r}_{i,1} * h_i). \quad (20)$$

Hence,

$$\mathbf{v} = H\left(\sum_{1 \leq i \leq l} (\mathbf{z}_{i,0} + \mathbf{z}_{i,1} * h_i) - I\mathbf{v}, L, m, I\right). \quad (21)$$

By using the rejection sampling algorithm described in Definition 8, the distribution of $(\mathbf{z}_{i,0}, \mathbf{z}_{i,1})$ is close to $D_s^n(\mathbf{z}_i)$ for $1 \leq i \leq l$. Thus, by Lemma 3, we have $\mathbf{z}_i = (\mathbf{z}_{i,0}, \mathbf{z}_{i,1})$ satisfies $\|\mathbf{z}_i\| \leq s\sqrt{2n}$ with a probability at least $1 - 2^{-\omega(\log n)}$. Therefore, the proposed scheme satisfies verification correctness.

Assume member k calculates the linking tags of messages m_1 and m_2 as I_1 and I_2 , respectively. In the proposed scheme, $I_1 = s_{k,0} + s_{k,1} * h_k$ and $I_2 = s_{k,0} + s_{k,1} * h_k$ are generated by the signer’s public and private keys, and thus this scheme satisfies linking correctness. This completes the proof. \square

5. Security Analysis

Theorem 3 (unforgeability). *Under the random oracle model, when the e-NTRU problem is intractable, the proposed LRS scheme is unforgeable.*

Proof. Setup Phase: To solve the e-NTRU problem, S gets an instance $(h_i)_{1 \leq i \leq l}$

Query Phase: Adversary A is allowed to access oracles JO , CO , SO , and HO , and S responds as follows:

- (i) H : A inputs $((\mathbf{r}_{i,0}, \mathbf{r}_{i,1})_{1 \leq i \leq l}, L, m, I, k)$, S first checks whether there is the relevant record in the list $list_H$. If so, then the same query result is returned to A . Otherwise, S randomly picks and gives A an integer

\mathbf{v} , and adds the tuple $((\mathbf{r}_{i,0}, \mathbf{r}_{i,1})_{1 \leq i \leq l}, L, m, I, \mathbf{v}, k)$ to the list $list_H$.

- (ii) *JO*: Suppose A can only access the oracle JOI' times at most, where $l' \geq l$. S selects a subset X_l with l random indexes. S assigns $(h_i)_{1 \leq i \leq l}$ to these l indexes as their public keys, respectively. Moreover, for these l indexes, S does not know the corresponding private keys. We use $l+1, \dots, l'$ to denote other indexes. With regard to other $l' - l$ indexes, S obtains the public and private keys according to the algorithm $KeyGen(PP)$. A inputs index j to query, and S outputs the corresponding public key.
- (iii) *CO*: A inputs a public key $pk_i = h_i$, S checks whether i belongs to X_l . If so, then S stops; otherwise, S outputs the corresponding private key.
- (iv) *SO*: A inputs a ring public key set $L = \{h_i\}_{1 \leq i \leq l}$ a public key h_k , where $k \in \{1, \dots, l\}$, and a message $m \in \{0, 1\}^*$. S performs as follows:

- (1) If h_k does not correspond to any element in the subset X_l , then S knows its private key and generates the signature according to the signature algorithm $Sign(PP, L, m, sk_k)$. Otherwise, we assume that h_k is obtained by JO .
- (2) S checks the list $list_H$ to find the record $((\mathbf{r}_{i,0}, \mathbf{r}_{i,1})_{1 \leq i \leq l}, L, m, I, \mathbf{v}, k)$ corresponding to the index k . Then, S randomly chooses $\mathbf{z}_{i,0}, \mathbf{z}_{i,1} \leftarrow D_s^n$ and sets the output of $H(\sum_{1 \leq i \leq l} (\mathbf{z}_{i,0} + \mathbf{z}_{i,1} * h_i) - I\mathbf{v}, L, m, I)$ to \mathbf{v} .
- (3) S returns a signature $\sigma(m) = (m, (\mathbf{z}_i)_{1 \leq i \leq l}, \mathbf{v}, I)$ with probability $\min(D_s^n(z_k)/MD_{s_k * v, s}^n(z_k), 1)$, where $M = O(1)$.

Forgery Phase: After the simulation, A gives signature $\sigma(m^*) = (m^*, (\mathbf{z}_{i,0}^*, \mathbf{z}_{i,1}^*)_{1 \leq i \leq l}, \mathbf{v}^*, I^*)$ about $\{PP, m^*, L\}^*$ to S satisfying the following conditions:

- (i) $Verify(PP, L^*, m^*, \sigma(m^*)) = "1"$
- (ii) All of the public keys $pk_i = h_i$ in L^* are query outputs of JO
- (iii) A did not query *CO* about the public keys in L^*
- (iv) $\sigma(m^*)$ is not a query output of *SO*

Analysis. Assuming the signature $\sigma(m^*)$ is a valid signature, the following shows how S can solve the e-NTRU problem using the forged results of A . We will consider the following two situations:

- (i) If \mathbf{v}^* appears in the *SO*, and assume that $\sigma(m) = (m, (\mathbf{z}_{i,0}, \mathbf{z}_{i,1})_{1 \leq i \leq l}, \mathbf{v}, I)$ is a query output of *SO*. Given that the signature is valid, it satisfies

$$\mathbf{v}^* = H\left(\sum_{1 \leq i \leq l} (\mathbf{z}_{i,0} + \mathbf{z}_{i,1} * h_i) - I\mathbf{v}^*, L, m, I\right). \quad (22)$$

Given that A successfully forged the signature, there is

$$\mathbf{v}^* = H\left(\sum_{1 \leq i \leq l} (\mathbf{z}_{i,0}^* + \mathbf{z}_{i,1}^* * h_i) - I^* \mathbf{v}^*, L^*, m^*, I^*\right). \quad (23)$$

When the function H collides, S aborts (Abort I). Otherwise, from (22) and (23), there is

$$\begin{aligned} L^* &= L, m^* = m, I^* = I, \\ \sum_{1 \leq i \leq l} (\mathbf{z}_{i,0} + \mathbf{z}_{i,1} * h_i) - I\mathbf{v}^* &= \sum_{1 \leq i \leq l} (\mathbf{z}_{i,0}^* + \mathbf{z}_{i,1}^* * h_i) - I^* \mathbf{v}^*. \end{aligned} \quad (24)$$

$$\sum_{1 \leq i \leq l} (\mathbf{z}_{i,0} - \mathbf{z}_{i,0}^*) + (\mathbf{z}_{i,1} - \mathbf{z}_{i,1}^*) * h_i = 0 \text{ mod } q. \quad (25)$$

Therefore, $[(\mathbf{z}_{i,0}^* - \mathbf{z}_{i,0}), (\mathbf{z}_{i,1}^* - \mathbf{z}_{i,1})]_{1 \leq i \leq l}$ is a solution to the e-NTRU problem.

- (ii) If \mathbf{v}^* appears in the H query and is stored as $((r_{i,0}, r_{i,1})_{1 \leq i \leq l}, L, m, I, \mathbf{v}^*, k)$ in $list_H$, then,

$$\mathbf{v}^* = H\left(\sum_{1 \leq i \leq l} (\mathbf{r}_{i,0} + \mathbf{r}_{i,1} * h_i), L, m, I\right). \quad (26)$$

When the function H collides, S aborts (Abort II). Otherwise, from (23) and (26), there is

$$\begin{aligned} L^* &= L, m^* = m, I^* = I, \\ \sum_{1 \leq i \leq l} (\mathbf{z}_{i,0}^* + \mathbf{z}_{i,1}^* * h_i) - I^* \mathbf{v}^* &= \sum_{1 \leq i \leq l} (\mathbf{r}_{i,0} + \mathbf{r}_{i,1} * h_i). \end{aligned} \quad (27)$$

S performs the following: when $i \neq k^*$, let $\mathbf{z}_{i,0} = \mathbf{r}_{i,0}$ and $\mathbf{z}_{i,1} = \mathbf{r}_{i,1}$; when $i = k^*$, let $\mathbf{z}_{k^*,0} = \mathbf{r}_{k^*,0} + \mathbf{v}^* I$ and $\mathbf{z}_{k^*,1} = \mathbf{r}_{k^*,1}$. Then, we have

$$\begin{aligned} \mathbf{v}^* &= H\left(\sum_{1 \leq i \leq l} (\mathbf{r}_{i,0} + \mathbf{r}_{i,1} * h_i), L, m, I\right) \\ &= H\left(\sum_{1 \leq i \leq l, i \neq k^*} (\mathbf{r}_{i,0} + \mathbf{r}_{i,1} * h_i) + \mathbf{z}_{k^*,0} \right. \\ &\quad \left. - \mathbf{v}^* I + \mathbf{z}_{k^*,1} * h_{k^*}, L, m, I\right) \\ &= H\left(\sum_{1 \leq i \leq l} (\mathbf{r}_{i,0} + \mathbf{r}_{i,1} * h_i) - \mathbf{v}^* I, L, m, I\right). \end{aligned} \quad (28)$$

Given (23), (27), and (28), we have

$$\sum_{1 \leq i \leq l} (\mathbf{z}_{i,0} - \mathbf{z}_{i,0}^*) + (\mathbf{z}_{i,1} - \mathbf{z}_{i,1}^*) * h_i = 0 \text{ mod } q. \quad (29)$$

Thus, the solution to the e-NTRU problem is $[(\mathbf{z}_{i,0}^* - \mathbf{z}_{i,0}), (\mathbf{z}_{i,1}^* - \mathbf{z}_{i,1})]_{1 \leq i \leq l}$.

Probability Analysis. The challenger S fails when Aborts I and II occur. The probability of H colliding is $1/2^n$. Assume A can successfully forge the signature with probability ξ ,

then the probability of S solving the e-NTRU problem is $\xi - 1/2^n \times 2 = \xi - 1/2^{n-1}$. This completes the proof. \square

Theorem 4 (unconditional anonymity). *The proposed scheme satisfies unconditional anonymity.*

Proof. The anonymity proof of the signature is completed by the following game between adversary A and challenger S . If the signature distributions of l different members in the ring are computationally indistinguishable to adversary A , then this scheme satisfies anonymity.

Query Phase: A is allowed to access JO , and S responds as follows:

JO: A inputs an index j to query. S runs the algorithm $\text{KeyGen}(PP)$ to generate the public key $pk_j = h_j$ and returns it to A .

Challenge Phase: A inputs a public key list $L = \{h_i\}_{1 \leq i \leq l}$ and a message $m^* \in \{0, 1\}^*$. S randomly chooses $b \in \{1, \dots, l\}$, then runs $\text{Sign}(PP, L, m^*, sk_b)$ to generate the signature $\sigma(m^*) = \text{Sign}(PP, L, m^*, sk_b)$ and gives it to A , where sk_b is the private key corresponding to index b .

Guess Phase: A gives a value $b' \in \{1, \dots, l\}$ as a guess for b .

Analysis. Suppose A is an adversary with unlimited computing power. Next, we will show the advantage $\text{Adv}_A^{\text{Anon}}$ of A in winning the anonymous game is negligible. We need to prove that the distributions of signatures generated with the private keys of different users are computationally indistinguishable.

First, even A is an adversary with unlimited computing power, from the JO query, or from the challenger signature (which contains a linkability tag), A still cannot deduce the private key, as well as the corresponding index. That is because the randomness of the algorithms TrapGen and SamplePre makes each public key h_b correspond to multiple pairs $(s_{b,0}, s_{b,1})$, and which one is the actual private key of member b cannot be determined. Moreover, given a linking tag $I = s_{b,0} + s_{b,1} * h_b$, to know which member generated the linking tag I , it is no better than random guessing for the adversary. In addition, it should be noticed that the signature $\sigma(m^*)$ is generated by using not only a private key $(s_{b,0}, s_{b,1})$ but also a set of random numbers. Lemma 3 guarantees that the distributions of $(z_{b,0}, z_{b,1})$ and $(z_{i,0}, z_{i,1})_{i \neq b}$ are indistinguishable, and the distribution of $(z_{b,0}, z_{b,1})$ is independent of $(s_{b,0}, s_{b,1})$. That is, in the view of the adversary, the signature $\sigma(m^*)$ is independent of the index b of the actual signer. Hence, we can conclude that even an unbounded adversary cannot guess the index b with a probability greater than $1/l$.

We can infer that when A is a normal adversary, that is, A has limited computing power and time, obviously it cannot destroy the anonymity of the scheme. This completes the proof. \square

Theorem 5 (linkability). *Under the random oracle model, if the proposed scheme is unforgeable, then for any PPT adversary A , the proposed scheme is linkable.*

Proof. We will show that if the proposed scheme satisfies unforgeability, then it will satisfy linkability. The linkability proof of the scheme is completed by the following game interaction between an adversary A and a challenger S .

- (i) S generates the system public parameters PP and public and private keys $(pk_i, sk_i)_{1 \leq i \leq l}$, and then sends PP to A
- (ii) A can access JO , CO , SO , and HO , and the process of accessing JO , CO , SO , and HO in the linkability game is the same as that in the unforgeability game
- (iii) Suppose A outputs two signatures $\sigma_1(m_1) = (m_1, (z_{i,0}, z_{i,1})_{1 \leq i \leq l}, v_1, I_1)$ and $\sigma_2(m_2) = (m_2, (z_{i,0}, z_{i,1})_{1 \leq i \leq l}, v_2, I_2)$ under public key set L , which satisfy the following conditions:
 - (1) All public keys in L are outputs of JO
 - (2) For $i = 1, 2$, $\text{Verify}(PP, L, m_i, \sigma_i(m_i)) = "1"$ such that $\sigma_i(m_i)$ is not an output of SO
 - (3) A accesses CO once at most

Analysis. Assume A can generate two signatures $\sigma_1(m_1)$ and $\sigma_2(m_2)$ with a nonnegligible probability η while holding only one private key sk_k , and $"1" \leftarrow \text{Verify}(PP, L, m_i, \sigma_i(m_i))$ for $i = 1, 2$. Given that the proposed LRS scheme is unforgeable, these two signatures can be validated by the Verify algorithm if and only if A honestly generates signatures $\sigma_1(m_1)$ and $\sigma_2(m_2)$ using his private key sk_k . In other words, we have $I_1 = s_{k,0} + s_{k,1} * h_k$ and $I_2 = s_{k,0} + s_{k,1} * h_k$. And since there is also only one public key corresponding to this private key, that is, $h_k = h'_k$, we have $I_1 = I_2$. This indicates that the algorithm $\text{Link}(\sigma_1(m_1), \sigma_2(m_2))$ returns "Link" when given two signatures $\sigma_1(m_1)$ and $\sigma_2(m_2)$. Hence, the advantage $\text{Adv}_A^{\text{link}}$ of A is negligible. This completes the proof. \square

6. Discussion

6.1. Parameter Selection. The security of the proposed scheme is based on the e-NTRU problem, which is reduced to the NTRU-SIS problem. The NTRU-SIS problem is to find two polynomials $(u, v) \in \mathbb{R}_q^2$ that satisfies $u + v * h = 0 \text{ mod } q$ and $\|u\|, \|v\| \leq \beta$ in the NTRU lattice, which is in turn reduced to γ -Ideal-SVP problem. Similar to [34, 36], we use the "root Hermite factor γ " which measures the hardness of γ -Ideal-SVP problems to select the parameters.

If we look for a polynomial v in an n -dimensional lattice, which is greater than the n -th root of the determinant, then the associated γ is

$$\frac{\|v\|}{\det(\Lambda)^{1/n}} = \gamma^n. \quad (30)$$

According to [37], if we look for a small-size polynomial v in the NTRU lattice, the associated γ is

$$\frac{\sqrt{n/(2\pi e)} \cdot \det(\Lambda)^{1/n}}{\|v\|} = 0.4\gamma^n. \quad (31)$$

From the results in [36, 38], if the value of γ is approximately 1.007, to find the polynomial is at least 80 bits

TABLE 2: Parameter settings.

Parameter	Recommended choice	
λ	80	192
γ	1.0069	1.0040
n	256	512

TABLE 3: Comparison of time costs and difficult assumption.

Scheme	Signature cost	Verification cost	Unconditional anonymity	Difficult assumption
[23]	$nT_{SD} + kn(2l-1)T_{Mul} + nT_{RS}$	$2knT_{Mul}$	No	MSIS, MLWE
[24]	$knT_{SD} + k^2n(2l+1)T_{Mul} + knT_{RS}$	$2k^2nT_{Mul}$	Yes	R-SIS
[26]	$knT_{SD} + kn(2l+1)T_{Mul} + knT_{RS}$	$2knT_{Mul}$	No	MSIS, MLWE
[27]	$vnT_{SD} + 5knT_{Mul} \log l$	$2knT_{Mul} \log l$	No	MSIS, MLWE
[30]	$2n(l+1)T_{SD} + 2n(l+1)T_{Mul}$	$2nT_{Mul}$	No	R-SIS, R-ISIS
Ours	$2nT_{SD} + nT_{Mul} + 2nT_{RS}$	nT_{Mul}	Yes	e-NTRU

hard. If the value of γ is less than 1.004, to find the polynomial is at least 192 bits hard.

The methods to attack the proposed scheme are mainly to attack the ring member's public key and the signature.

The public key of the member i is a polynomial $h_i = g_i * f_i^{-1} \text{mod } q \in R_q$. The attack on h_i is to find two nonzero small-size polynomial $(u_i, v_i) \in R_q^2$ that satisfies $u_i + v_i * h_i = 0 \text{mod } q$. By Lemma 1 we know, $\|(u_i, v_i)\| \leq \sigma\sqrt{2n}$. So using (32) to calculate the value of γ , we have $\gamma = (\sqrt{n}/1.368)^{1/2n}$. When $n = 256$, $\gamma \approx 1.0048$, it is at least 80 bits hard to attack the ring member's public key, and when $n = 512$, $\gamma \approx 1.0027$, it is at least 192 bits hard to attack the ring member's public key.

The attack on the signature of the member i is to find a vector $(\mathbf{z}_{i,0}, \mathbf{z}_{i,1})$ passing the verification algorithm without member i 's private key. It can be seen from Lemma 3, $\|(\mathbf{z}_{i,0}, \mathbf{z}_{i,1})\| \leq s\sqrt{2n}$. Since $s = 0.585/\pi\sqrt{q} \ln(2+2/\eta)$, where $\eta = 2^{-\lambda}/2n$, there is $s = 1.4708\sqrt{q}$ for $n = 256$ and $s = 2.2089\sqrt{q}$ for $n = 512$. So, computing the value of γ by (28), we have

$$\frac{\sigma\sqrt{2n}}{\sqrt{q}} = \gamma^{2n} \implies \begin{cases} \gamma = (2.080\sqrt{n})^{1/2n}, & n = 256 \\ \gamma = (3.124\sqrt{n})^{1/2n} & n = 512 \end{cases}. \quad (32)$$

When $n = 256$, $\gamma \approx 1.0069$, to attack the ring member's signature is at least 80 bits hard, and when $n = 512$, $\gamma \approx 1.0041$, to attack the ring member's signature is at least 192 bits hard. The recommended choice of the parameters is shown in Table 2.

6.2. Post-Quantum Security. The proposed scheme is based on the hard assumption over lattice which is generally recognized to provide anti-quantum security. The security proof of the proposed scheme is unlikely to be extended to the Quantum Random Oracle Model [39] (QROM): in the security proof (Theorems 3 and 5), we use the adaptive programming of random oracle (RO) H , and this proof technique is inherent in the structure to some extent.

We note that other schemes built on QROM, such as [40, 41], also use the form of RO programming (even if not

TABLE 4: Comparison of communication costs.

Scheme	Public key size (bits)	Private key size (bits)	Signature size (bits)
[23]	$kn \log q$	$n \log q$	$O(n \cdot l)$
[24]	$n \log q$	$kn \log q$	$O(kn \cdot l)$
[26]	$3kn \log q$	$kn \log q$	$O(kn \cdot l)$
[27]	$kvn \log q$	$vn \log q$	$O(n \cdot \log l)$
[30]	$n \log q$	$9n \log q$	$O(n \cdot l)$
Ours	$n \log q$	$2n \log q$	$O(n \cdot l)$

TABLE 5: Parameter settings for our scheme.

Parameter	n	k	v	q	Security level
Recommended choice	256	5	4	2^{32}	80 bits

adaptive). In addition, although Fiat–Shamir seems unlikely to be proved in QROM, to the best of our knowledge, there are no attacks on the protocols using these proof technologies, which stems from the use of RO.

7. Performance Analysis

In this section, the proposed LRS scheme is compared with the schemes [23, 24, 26, 27, 30] in terms of efficiency. We mainly compare these schemes in terms of elapsed time and storage space.

Comparison terms in Table 3 include signature generation cost, signature verification cost, unconditional anonymity, and difficult assumption. Comparison terms in Table 4 include public and private key, as well as signature size of each user. In Tables 3 and 4, n is the degree of polynomials, $q = 1 \text{mod } 2n$ is a large prime number, l represents the cardinality of the ring, and k and v are integers. The time cost for the discrete Gaussian sampling algorithm and the rejection sampling algorithm running once are represented by T_{SD} and T_{RS} , respectively. In general, $T_{SD} > T_{RS}$. The time cost for polynomial-polynomial multiplication is represented by T_{Mul} , and $T_{Mul} > T_{SD}$. The time overhead of hash, matrix-matrix addition, and polynomial-

TABLE 6: Comparison of time costs (ms) at security level $\lambda = 80$.

Scheme	Signature time					Verification time										
	$l=1$	$l=8$	$l=64$	$l=128$	$l=256$	$l=512$	$l=1024$	$l=2048$	$l=1$	$l=8$	$l=64$	$l=128$	$l=256$	$l=512$	$l=1024$	$l=2048$
[23]	3.42	33.44	218.09	421.31	817.84	1532.27	2953.14	5666.39	5.73	35.46	200.10	379.92	750.35	1410.44	2699.05	5189.23
[24]	32.87	154.36	1019.57	1906.38	3693.68	7084.92	14018.56	27925.31	24.32	133.12	950.27	1769.47	3440.64	6619.14	13120.31	23855.36
[26]	9.25	48.87	282.71	525.43	1002.42	1890.29	3659.71	7106.84	5.63	36.86	201.19	389.94	753.65	1428.68	2752.51	5295.31
[27]	34.97	101.14	202.98	239.61	281.36	330.24	381.64	447.12	14.02	41.56	83.32	100.15	121.06	150.38	176.86	237.63
[30]	3.78	14.88	82.87	151.91	265.57	514.81	986.62	1898.85	1.23	7.78	49.81	94.37	162.53	316.15	622.34	1172.31
Ours	1.71	10.36	59.56	109.04	199.47	364.63	688.64	1367.06	0.73	4.63	29.13	49.81	94.37	162.53	316.15	622.34

TABLE 7: Comparison of storage overhead (KB) at security level $\lambda = 80$.

Scheme	[23]	[24]	[26]	[27]	[30]	Ours
Size of public key	5.45	1.09	16.35	31.80	1.09	1.09
Size of private key	1.09	5.45	5.45	6.36	9.81	2.18
Signature size for $l = 1$	6.54	6.54	7.63	33.39	4.36	3.27
Signature size for $l = 8$	14.17	44.69	45.78	36.57	27.25	18.53
Signature size for $l = 64$	75.21	349.89	350.98	41.34	210.37	140.61
Signature size for $l = 128$	144.97	698.69	699.78	42.93	419.65	280.13
Signature size for $l = 256$	284.49	1396.29	1397.38	44.52	838.21	559.17
Signature size for $l = 512$	563.53	2791.49	2792.58	46.11	1675.33	1117.25

polynomial addition is ignored because these operations take less time. We mainly focus on time-consuming operations, such as matrix-matrix multiplication and polynomial-polynomial multiplication.

In terms of signature generation cost, the proposed scheme mainly uses the Gaussian sampling algorithm $2l$ times, the polynomial-polynomial multiplication l times, and the rejection sampling algorithm once, respectively. Hence, the signature generation cost is $2nlT_{SD} + nlT_{Mul} + 2nT_{RS}$. In terms of signature verification cost, since the proposed scheme primarily runs polynomial-polynomial multiplication l times, the signature generation cost is about nlT_{Mul} . From Table 3, due to $T_{Mul} > T_{SD} > T_{RS}$, compared with the four schemes of [23, 24, 26, 30], the proposed scheme has higher signature generation and verification efficiency. The signature generation and verification time of the proposed scheme is linearly related to the number of ring members l , while that of the scheme of [27] has a logarithmic relationship with l . Therefore, when l is large, the signature generation and verification efficiency of the scheme of [27] is better than that of the proposed scheme. But when l is small, the proposed scheme is more efficient by the settings of relevant parameters. In addition, only Alberto Torres et al.'s scheme [24] and our scheme can achieve unconditional anonymity, while other four schemes only have computational anonymity. And the efficiency of signature generation and verification of our scheme is obviously higher than that of Torres et al.'s scheme.

In the proposed scheme, the public key of the member in the ring is a small polynomial $h_i \in R_q$ generated by the trapdoor generation algorithm TrapGen, and the private key corresponds to two small polynomials in R_q . Therefore, the public and private key lengths of the proposed scheme are $n \log q$ and $2n \log q$, respectively. As shown in Table 4, the public and private key lengths of [23, 24, 26, 27, 30] are $(kn \log q, n \log q)$, $(n \log q, kn \log q)$, $(3kn \log q, kn \log q)$, $(kvn \log q, vn \log q)$, and $(n \log q, 9n \log q)$, respectively. Hence, in terms of public key size, the public key size of the proposed scheme is similar to that of [24, 30] and smaller than that of [23, 26, 27]. With respect to private key size, the private key size of the proposed scheme is larger than that of [23] and they are both smaller than that of [24, 26, 27, 30]. For signature size, the signature size of the scheme [27] has a logarithmic relationship with l , while that of the other five schemes including the proposed scheme has a linear relationship with l . But the growth rate of signature size of

[23, 30] and the proposed scheme is obviously slower than that of [24, 26].

8. Implementation and Evaluation

We implemented and evaluated the proposed LRS scheme on a typical laptop configured with a Windows 8.1 system, an Intel(R) Core(TM) i5-4210U CPU@1.70 GHz processor, and a 4.00 GB running memory. We selected parameters to make the proposed scheme secure, and detailed parameter settings are given in Table 5. We ran the signature generation and verification algorithms for 1000 times. And at security level $\lambda = 80$, the average running time of these algorithms of the five schemes under different numbers of ring members is shown in Table 6. It can be seen from Table 6 that the signature generation and verification of [24] take the longest time among the six schemes, while the signature generation and verification time of the proposed scheme is shorter than that of [23, 24, 26, 30]. Compared with [27], when $l \leq 256$, the proposed scheme has higher signature efficiency, but when $l \geq 512$, the signature efficiency of the proposed scheme needs to be improved. On average, compared with the other five schemes, the signature generation and verification time of the proposed scheme is reduced by about 56.61% and 65.18%, respectively. Especially compared with [24], which also has unconditional anonymity as ours, the signature generation and verification time of the proposed scheme is reduced by about 94.52% and 97.18%, respectively.

At security level $\lambda = 80$, the comparison between the proposed scheme and the other five schemes on public/private key size and signature size under different numbers of ring members is shown in Table 7. As for the public key size, the public key size of the proposed scheme is equal to that of [24, 30] and smaller than that of [23, 26, 27]. With respect to private key size, the private key size of the proposed scheme is larger than that of [23] but is significantly smaller than that of [24, 26, 27, 30]. In the case of signature size, the signature size of the proposed scheme is larger than that of [23] but is significantly smaller than that of [24, 26, 30]. When $l \geq 64$, the signature size of the scheme in [27] is shorter than that of the proposed scheme. However, the scheme of [27] only has computational anonymity, while the proposed scheme has unconditional anonymity. Especially compared with [24], the signature size of the proposed scheme is reduced by 58.03% on average.

In addition, in the above experiment, we only completed the proof-of-concept work and did not consider potential

optimization algorithms, such as the polynomial-polynomial multiplication based on FFT.

9. Conclusions

Based on the e-NTRU problem, this study constructed a LRS scheme on NTRU lattice by combining preimage and rejection sampling techniques. Under the random oracle model, the security of our LRS scheme was analyzed in detail. The analysis results show that our scheme satisfies the requirements of correctness, unforgeability, and linkability based on the intractability of the e-NTRU problem in the random oracle model. In particular, our scheme can achieve unconditional anonymity. The efficiency of the proposed scheme was analyzed in detail, and the optional parameter settings of the proposed scheme that meet the security requirements are given. Finally, the proposed scheme and other five latest lattice-based LRS schemes are implemented, which shows that under the same security level, the proposed scheme has higher signature generation and verification efficiency as well as shorter signature size compared with other five LRS schemes.

Data Availability

The data that support our findings are available at <https://github.com/wang-0218/ring-signature>.

Conflicts of Interest

The authors declare that they have no conflicts of interest.

Acknowledgments

This work was supported by the National Natural Science Foundation of China (Grant no. 61802117), Support Plan of Scientific and Technological Innovation Team in Universities of Henan Province (Grant no. 20IRTSTHN013), the Youth Backbone Teacher Support Program of Henan Polytechnic University (Grant no. 2018XQG-10), and Key Scientific Research Project of Henan Higher Education Institutions (Grant no. 20A413005).

References

- [1] R. L. Rivest, A. Shamir, and Y. Tauman, "How to leak a secret, Advances in Cryptology - ASIACRYPT 2001," in *Proceedings of the 7th International Conference on the Theory and Application of Cryptology and Information Security: Advances in Cryptology*, pp. 552–565, Berlin, Heidelberg, November 2001.
- [2] D. Chaum and E. van Heyst, "Group Signatures," *Workshop on the Theory and Application of Cryptographic Techniques*, Springer, Berlin, Heidelberg, pp. 257–265, 1991.
- [3] D. Boneh, X. Boyen, and H. Shacham, "Short group signatures, Advances in Cryptology - CRYPTO 2004," in *Proceedings of the Annual International Cryptology Conference*, pp. 41–55, Santa Barbara, CA, USA, August 2004.
- [4] P. P. Tsang and V. K. Wei, "Short Linkable Ring Signatures for E-Voting, E-Cash and Attestation," in *Proceedings of the International Conference on Information Security Practice and Experience*, pp. 48–60, Singapore, April 2005.
- [5] J. K. Liu, V. K. Wei, and D. S. Wong, "Linkable spontaneous anonymous group signature for ad hoc groups, Information Security and Privacy," in *Proceedings of the Australasian Conference on Information Security and Privacy*, pp. 325–335, Sydney, Australia, July 2004.
- [6] X. Li, Y. Mei, J. Gong, F. Xiang, and Z. Sun, "A blockchain privacy protection scheme based on ring signature," *IEEE Access*, vol. 8, pp. 76765–76772, 2020.
- [7] F. Tang, J. Pang, K. Cheng, and Q. Gong, "Multiauthority traceable ring signature scheme for smart grid based on blockchain," *Wireless Communications and Mobile Computing*, vol. 2021, Article ID 5566430, 2021.
- [8] J. K. Liu, M. H. Au, W. Susilo, and J. Zhou, "Linkable ring signature with unconditional anonymity," *IEEE Transactions on Knowledge and Data Engineering*, vol. 26, no. 1, pp. 157–165, 2013.
- [9] M.-J. Qin, Y.-L. Zhao, and Z.-J. Ma, "Practical constant-size ring signature," *Journal of Computer Science and Technology*, vol. 33, no. 3, pp. 533–541, 2018.
- [10] X. Zhang and C. Ye, "A Novel Privacy protection of Permissioned Blockchains with Conditionally Anonymous Ring Signature," *Cluster Computing*, vol. 25, pp. 1–15, 2022.
- [11] H. Yu and W. Wang, "Certificateless Network Coding Ring Signature Scheme," *Security and Communication Networks*, vol. 2021, Article ID 8029644, 2021.
- [12] F. Tang, J. Pang, K. Cheng, and Q. Gong, "Multiauthority Traceable Ring Signature Scheme for Smart Grid Based on Blockchain," *Wireless Communications and Mobile Computing*, vol. 2021, Article ID 5566430, 2021.
- [13] K. Gu, X. Dong, X. Dong, and L. Wang, "Efficient traceable ring signature scheme without pairings," *Advances in Mathematics of Communications*, vol. 14, no. 2, pp. 207–232, 2020.
- [14] T. X. Khuc, T. N. Nguyen, H. Q. Le et al., "Efficient unique ring signature for blockchain privacy protection," in *Proceedings of the Australasian Conference on Information Security and Privacy*, pp. 391–407, Australia, Nov 2021.
- [15] S. Bouakkaz and F. Semchedine, "A certificateless ring signature scheme with batch verification for applications in VANET," *Journal of Information Security and Applications*, vol. 55, Article ID 102669, 2020.
- [16] H. Lin and M. Wang, "Repudiable Ring Signature: Stronger Security and Logarithmic-Size," *Computer Standards & Interfaces*, vol. 80, 2022.
- [17] P. W. Shor, "Polynomial Time Algorithms for Discrete Logarithms and Factoring on a Quantum Computer," in *Proceedings of the International Algorithmic Number Theory Symposium*, London, May 1994.
- [18] B. Libert, S. Ling, K. Nguyen, and H. Wang, "Zero-knowledge arguments for lattice-based accumulators: logarithmic-size ring signatures and group signatures without trapdoors, Advances in Cryptology - EUROCRYPT 2016," in *Proceedings of the Annual International Conference on the Theory and Applications of Cryptographic Techniques*, pp. 1–31, Zagreb, Oct 2016.
- [19] M. F. Esgin, R. Steinfeld, J. K. Liu, and D. Liu, "Lattice-based Zero-Knowledge Proofs: New Techniques for Shorter and Faster Constructions and Applications," in *Proceedings of the Annual International Cryptology Conference*, pp. 115–146, CA, USA, Aug 2019.
- [20] V. Lyubashevsky, N. K. Nguyen, and G. Seiler, "SMILE: set membership from ideal lattices with applications to ring signatures and confidential transactions, Advances in

- Cryptology - CRYPTO 2021,” in *Proceedings of the Annual International Cryptology Conference*, pp. 611–640, Aug 2021.
- [21] C. Cao, L. You, and G. Hu, “Fuzzy Identity-Based Ring Signature from Lattices,” *Security and Communication Networks*, vol. 2021, 2021.
- [22] R. Yang, M. H. Au, J. Lai, Q. Xu, and Z. Yu, “Lattice-based techniques for accountable anonymity: composition of abstract stern’s protocols and weak PRF with efficient protocols from LWR,” *IACR Cryptol. ePrint Arch.*, p. 781, 2017.
- [23] C. Baum, H. Lin, and S. Oechsner, “Towards Practical Lattice-Based One-Time Linkable Ring Signatures,” in *Proceedings of the International Conference on Information and Communications Security*, pp. 303–322, Lille, France, October 2018.
- [24] W. A. Alberto Torres, R. Steinfeld, A. Sakzad et al., “Post-quantum one-time linkable ring signature and application to ring confidential transactions in blockchain (lattice RingCT v1.0), Information Security and Privacy,” in *Proceedings of the Australasian Conference on Information Security and Privacy*, pp. 558–576, Perth, WA, Australia, NOV 2018.
- [25] H. Zhang, F. Zhang, H. Tian, and M. H. Au, “Anonymous post-quantum Cryptocash,” in *Proceedings of the International Conference on Financial Cryptography and Data Security*, pp. 461–479, Nieuwpoort Curaçao, February 2018.
- [26] Z. Liu, K. Nguyen, G. Yang, H. Wang, and D. S. Wong, “A Lattice-Based Linkable Ring Signature Supporting Stealth Addresses,” in *Proceedings of the European Symposium on Research in Computer Security*, pp. 726–746, Luxemburg, September 2019.
- [27] W. Beullens, S. Katsumata, and F. Pintore, “Calamari and Falafel: Logarithmic (Linkable) Ring Signatures from Isogenies and Lattices,” in *Proceedings of the International Conference on the Theory and Application of Cryptology and Information Security*, pp. 464–492, Daejeon, South Korea, December 2020.
- [28] J. Hoffstein, J. Pipher, and J. H. Silverman, “NTRU: a ring-based public key cryptosystem,” in *Proceedings of the Algorithm Number Theory (ANTS III)*, pp. 267–288, Oregon, USA, June 1998.
- [29] Y. Zhang, Y. Hu, J. Xie, and M. Jiang, “Efficient ring signature schemes over NTRU Lattices,” *Security and Communication Networks*, vol. 9, no. 18, pp. 5252–5261, 2016.
- [30] X. Lu, M. H. Au, and Z. Zhang, “Raptor: a practical lattice-based (linkable) ring signature, Applied Cryptography and Network Security,” in *Proceedings of the International Conference on Applied Cryptography and Network Security*, pp. 110–130, Bogota, Colombia, June 2019.
- [31] Y. Tang, F. Xia, Q. Ye, M. Wang, R. Mu, and X. Zhang, “Identity-based Linkable Ring Signature on NTRU Lattice,” *Security and Communication Networks*, vol. 2021, 2021.
- [32] D. Micciancio and O. Regev, “Worst-case to average-case reductions based on Gaussian measures,” *SIAM Journal on Computing*, vol. 37, no. 1, pp. 267–302, 2007.
- [33] D. Stehlé and R. Steinfeld, “Making NTRU as Secure as Worst-Case Problems over Ideal Lattices,” in *Proceedings of the Annual International Conference on the Theory and Applications of Cryptographic Techniques*, pp. 27–47, Tallinn, Estonia, May 2011.
- [34] L. Ducas, V. Lyubashevsky, and T. Prest, “Efficient identity-based encryption over NTRU lattices,” *Lecture Notes in Computer Science*, vol. 8874, pp. 22–41, 2014.
- [35] V. Lyubashevsky, “Lattice Signatures without Trapdoors,” in *Proceedings of the Annual International Conference on the Theory and Applications of Cryptographic Techniques*, pp. 738–755, Cambridge, UK, April 2012.
- [36] N. Gama and P. Q. Nguyen, “Predicting lattice reduction,” in *Proceedings of the Annual International Conference on the Theory and Applications of Cryptographic Techniques*, pp. 31–51, Istanbul, Turkey, April 2008.
- [37] L. Ducas, A. Durmus, T. Lepoint, and V. Lyubashevsky, “Lattice Signatures and Bimodal Gaussians,” in *Proceedings of the Annual Cryptology Conference*, pp. 40–56, Santa Barbara, CA, USA, August 2013.
- [38] Y. Chen and P. Q. Nguyen, “Bkz 2.0: better lattice security estimates,” Advances in Cryptology-ASIACRYPT 2011-, in *Proceedings of the 17th International Conference on the Theory and Application of Cryptology and Information Security*, pp. 1–20, Seoul, South Korea, December 2011.
- [39] D. Boneh, Ö. Dagdelen, M. Fischlin, A. Lehmann, C. Schaffner, and M. Zhandry, “Random Oracles in a Quantum World,” in *Proceedings of the International Conference on the Theory and Application of Cryptology and Information Security*, pp. 41–69, Seoul, South Korea, 2011.
- [40] R. Del Pino, V. Lyubashevsky, N. Gregory, and G. Seiler, “Practical quantum-safe voting from lattices,” in *Proceedings of the 2017 ACM SIGSAC Conference on Computer and Communications Security*, pp. 1565–1581, New YorkNY-United State, Oct 2017.
- [41] D. Leo, T. Lepoint, V. Lyubashevsky, P. Schwabe, G. Seiler, and D. Stehlé, “Crystals–dilithium: Digital Signatures from Module Lattices,” 2017, <http://eprint.iacr.org/2017/633>.

Retraction

Retracted: Analysis of Psychological Changes and Intervention Mechanism of Elderly Groups Based on Deep Learning Analysis Technology

Computational Intelligence and Neuroscience

Received 3 October 2023; Accepted 3 October 2023; Published 4 October 2023

Copyright © 2023 Computational Intelligence and Neuroscience. This is an open access article distributed under the Creative Commons Attribution License, which permits unrestricted use, distribution, and reproduction in any medium, provided the original work is properly cited.

This article has been retracted by Hindawi following an investigation undertaken by the publisher [1]. This investigation has uncovered evidence of one or more of the following indicators of systematic manipulation of the publication process:

- (1) Discrepancies in scope
- (2) Discrepancies in the description of the research reported
- (3) Discrepancies between the availability of data and the research described
- (4) Inappropriate citations
- (5) Incoherent, meaningless and/or irrelevant content included in the article
- (6) Peer-review manipulation

The presence of these indicators undermines our confidence in the integrity of the article's content and we cannot, therefore, vouch for its reliability. Please note that this notice is intended solely to alert readers that the content of this article is unreliable. We have not investigated whether authors were aware of or involved in the systematic manipulation of the publication process.

In addition, our investigation has also shown that one or more of the following human-subject reporting requirements has not been met in this article: ethical approval by an Institutional Review Board (IRB) committee or equivalent, patient/participant consent to participate, and/or agreement to publish patient/participant details (where relevant).

Wiley and Hindawi regrets that the usual quality checks did not identify these issues before publication and have since put additional measures in place to safeguard research integrity.

We wish to credit our own Research Integrity and Research Publishing teams and anonymous and named external researchers and research integrity experts for contributing to this investigation.

The corresponding author, as the representative of all authors, has been given the opportunity to register their agreement or disagreement to this retraction. We have kept a record of any response received.

References

- [1] Y. Gao and Q. Fan, "Analysis of Psychological Changes and Intervention Mechanism of Elderly Groups Based on Deep Learning Analysis Technology," *Computational Intelligence and Neuroscience*, vol. 2022, Article ID 1686219, 8 pages, 2022.

Research Article

Analysis of Psychological Changes and Intervention Mechanism of Elderly Groups Based on Deep Learning Analysis Technology

Yue Gao¹ and Qi Fan ²

¹Department of Psychology, School of Medicine & Holistic Integrative Medicine, Nanjing University of Chinese Medicine, Nanjing 210023, China

²Institute of Mental Health, Nanjing Xiaozhuang University, Nanjing 210017, China

Correspondence should be addressed to Qi Fan; fanqi@njxzc.edu.cn

Received 9 March 2022; Accepted 19 April 2022; Published 30 April 2022

Academic Editor: Le Sun

Copyright © 2022 Yue Gao and Qi Fan. This is an open access article distributed under the Creative Commons Attribution License, which permits unrestricted use, distribution, and reproduction in any medium, provided the original work is properly cited.

The elderly group is a unique social phenomenon in China. This study analyzes the typology of psychological changes in the elderly group based on the analysis of deep learning techniques and also combines crisis intervention theory to study the intervention strategies of social workers in different stages of emotional changes in the elderly group. A questionnaire survey of the elderly was conducted using the survey method, in which 10,948 valid questionnaires were screened from the Psychological Condition Self-check Scale and 11,040 valid questionnaires were screened from the Mental Health Survey Questionnaire for the Elderly. The degree of negative emotions of the elderly group in public emergencies was not related to age, but significantly correlated with age (p value < 0.05), and there was a tendency that the higher the age, the deeper the degree; in addition, elderly people of different professions also showed significant differences ($p < 0.05$); elderly people of different regions also showed significant differences ($p < 0.05$). In crisis intervention, social workers mainly provide services such as initial diagnosis, primary intervention, secondary intervention, and assessment for the caseworkers. The practical study found that social workers need to use strategies such as short-term focal solutions, avoiding guiding clients with their own values; crisis intervention programmes should be flexible, proactively helping clients to rebuild their support network, developing clients' self-solving skills, and implementing inter-professional teamwork and whole-person rehabilitation services.

1. Introduction

As the first generation of only-child parents move into old age, more and more problems are emerging for the elderly parents of only children. According to some scholars, nearly 100 million only child have been born in China over the past 30 years [1]. Most of the young couples who responded strictly to the national family planning policy and had only one child are now in their middle and old age. If they lose their only child, they become China's new generation, the "lost generation" [2]. Although there are no official statistics on the number of older people, demographic survey data and reports show that the number of older people is increasing and cannot be ignored. As they are past their child-bearing years, many of them are

facing great trauma, with problems such as the breakdown of their family of origin and the inadequacy of the social security system causing them to suffer both physical and psychological blows, and they may face problems such as "no one to rely on, no one to turn to, no one to defend their rights, no one to interact with, no one to seek medical treatment for their illness, no one to support them in their old age, and no one to send them to their death" [3].

At present, both the government and civil society are still not paying enough attention to this group. Social workers can, to a certain extent, help this group to effectively integrate multiple resources, repair the broken social network, and rebuild social support, thus restoring and enhancing their ability to adapt to their environment [4].

There are three main perspectives in the study of older people in China. One is the study of the number and growth trend, which is a macrolevel study by scholars, but lacks consideration of the microlevel of the single-parent group [5]. The second is the perspective of family-planning policy risks, where scholars have mainly explored the interrelationship between family planning policies, but lacked research on practical services for different family risks [6]. Thirdly, from the perspective of research on protection mechanisms, academics have studied the issue of social assistance for older people at the external levels of material and spirituality, but not enough research has been conducted on crisis interventions for older people to cope with risks and their ability to live independently [7]. Crisis intervention aims to help older people deal with emotional crises that they cannot cope with, provide them with social resources to avoid further harm, and help them return to the good state they were in before the crisis, in the process promoting their growth and improving their ability to cope [8]. Overseas research on the problems associated with only children focuses on the education and psychological aspects of growing up as an only child and comparisons with non-only children, but little research has been conducted on the issue of “lost children.” In addition, children need to become self-reliant as adults and are thus removed from the parental relationship [9]. In response to the lack of research on practical interventions for older people, this study attempts to answer the following questions: what are the aspects of the emotional crisis of older people, what are the practical theoretical foundations of crisis intervention, how to apply crisis intervention theory in the process of serving older people, what are the strategies and techniques of crisis intervention, how to reflect on the practice of crisis intervention, and so on [10].

The elderly population is a special group that is easily affected during major public emergencies. The primary reason for this is that the elderly population is in a stage of rapid physical and mental development and change, with a high degree of instability; secondly, as the lifestyle of the elderly is inclined towards cerebral activities, their inner world has a relatively complex. Thirdly, as the lifestyle of older people is inclined towards mental activities, their inner world has a relatively complex nature [11]. As a result, the overall psychological needs of older people are high and may lead to psychological crises in times of social change, family conflicts, and setbacks in personal development [12]. As a result, the psychological crisis of the elderly population is the most important issue in the event of a major public emergency. The increasingly fierce competition in contemporary society and the gradually accelerating pace of life are bound to have an impact on the academic life of older people [13]. From a historical perspective, the great abundance of material conditions means that people will gradually face less stress in life and have less capacity to cope with unexpected events. There are numerous contemporary cases of psychological crises among the elderly due to various problems, and universities are paying more and more attention to mental health education for the elderly [14]. Therefore, it is of great importance to establish a perfect

psychological crisis intervention mechanism for the elderly, to cultivate a positive psychological concept among them, to provide them with correct mental health education, and to guide them to face possible psychological crises by using strong will qualities, appropriate achievement motivation, and correct attribution methods, both for maintaining the life safety of the elderly and for building a harmonious society [15].

2. Practical Theory of Emotional Crisis Intervention for the Elderly

2.1. Theoretical Foundations. Lindemann, one of the founders of crisis theory, began with his study of the grief reactions of refugees and families of those who died in the Boston fire of 1943 and divided crisis intervention into four stages [16]: disruption of equilibrium, short course therapy or grief intervention for the client, overcoming the crisis or coming out of discomfort, and regaining equilibrium (see Figure 1).

This theory suggests that the longer an older person is in a state of severe depression, especially in bereavement, the higher the risk of falling into excessive grief, leading to a loss of balance and a state of crisis. The social worker should help the client to get out of the emotional crisis as soon as possible by giving them adequate support and linking them to resources to restore their pre-crisis state of equilibrium [17].

The Kubler–Ross model, which describes the emotional reactions that people experience when facing their impending death, has since been widely applied to the study of grief following the loss of a loved one. Figure 2 shows the extended crisis theory model.

First is the period of denial. When people hear news of a terminal illness or death of themselves or a family member, they will first feel shocked and numb and psychologically deny the truth of the information they receive about the death. Second is the period of anger. After the shock and numbness have passed, the case worker becomes very angry, lashing out at those around him or her and blaming himself or herself or others for the death. Third is the bargaining period. During this period, the caseworker enters a period of self-deception, hoping for another chance to make up for what was not accomplished in the past. The caseworker will bargain with God for a series of things in exchange for or to prolong life. Fourth is the depression phase. During this phase, the caseworker has two depressive tendencies, reactive depression, which is an ineradicable emotional reaction, and preparatory depression, which is an internal emotional preparation to give up on everything. Fifth is the period of acceptance. After going through the whole grief journey, the caseworker begins to accept the status quo and shows a state of calmness, but this phase is the most melancholic period.

As with bereavement in general, older people who have lost someone go through this series of emotional changes, but not everyone will go through every stage, some will skip certain stages and some will stay at a certain stage. Older people who have lost someone may take longer to move

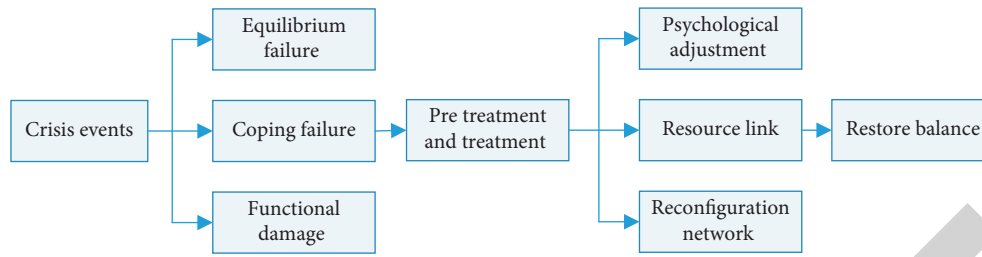


FIGURE 1: Lindemann crisis theory model.

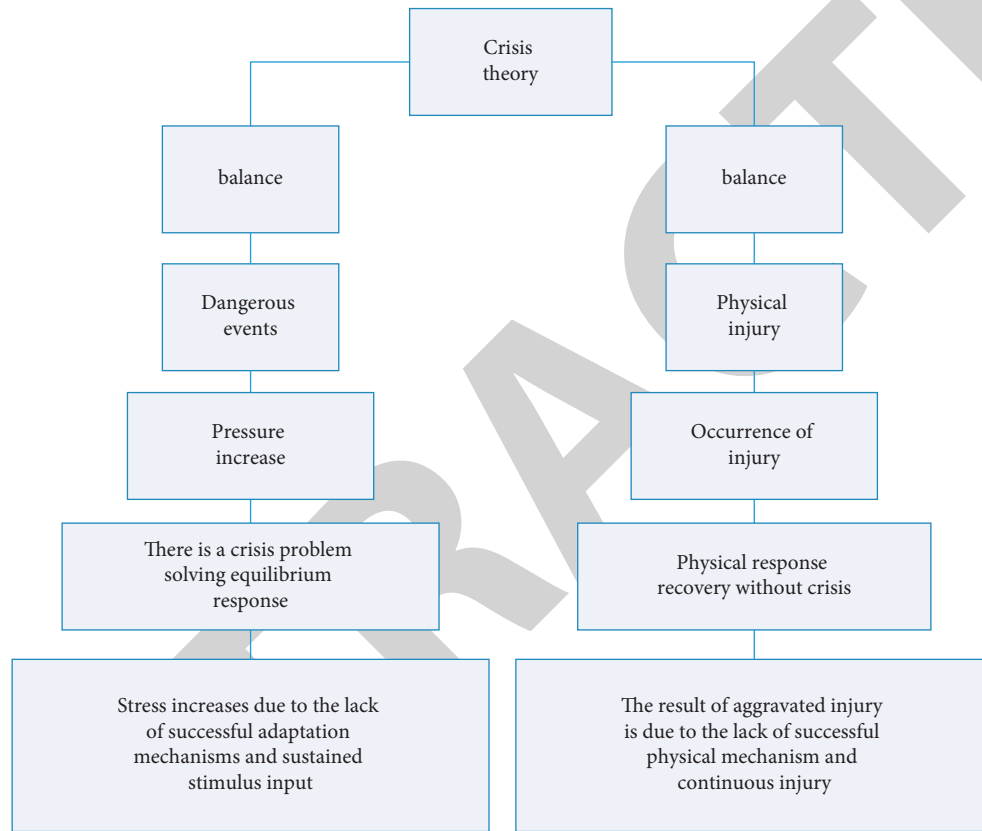


FIGURE 2: Extended crisis theory model.

through each stage of emotional change than at other ages or other bereavement events.

Without grief counselling from professionals, it can be difficult for the bereaved elderly to get out of their situation on their own. Moreover, feelings of self-blame and irrational emotions will be more pronounced in the elderly who have lost a parent, and the worse their physical and mental state, the greater the likelihood of depression.

2.2. Support Network Rupture and Reconstruction: A Case Intervention in an Emotional Crisis. Crisis assessment requires the identification of the client’s crisis situation, the planning of crisis intervention services, and a specific diagnosis of post-traumatic stress disorder [18]. The assessment is generally done in a funnel style, moving from an assessment of the client’s wider social environment to a

focused assessment of the core issues, which is a subjective and uncertain process (see Figure 3).

This case is an emotional crisis and a developmental crisis. Through crisis management strategies, the social worker helped the client to cope with the internal or external stress caused by the loss of her son (see Figure 4). In the intervention, the principles of immediate response, time limitation, focus on the crisis structure, problem solving, self-determination of the client, and social network connection were followed.

3. Modelling Mental Health Status Calculations

3.1. Data Collection. This study used a self-developed online experiment platform to collect data from Sina Weibo users (Figure 5). During April 2012, a total of 563 Sina Weibo users volunteered to participate in the experiment. In order to

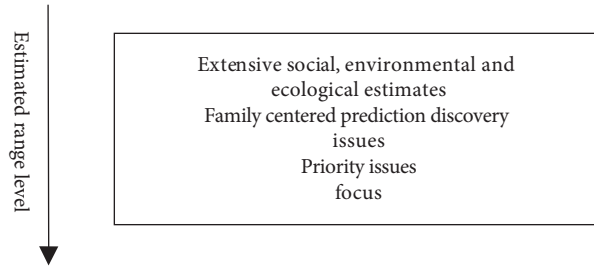


FIGURE 3: Hierarchy of prognosis in a funnel.

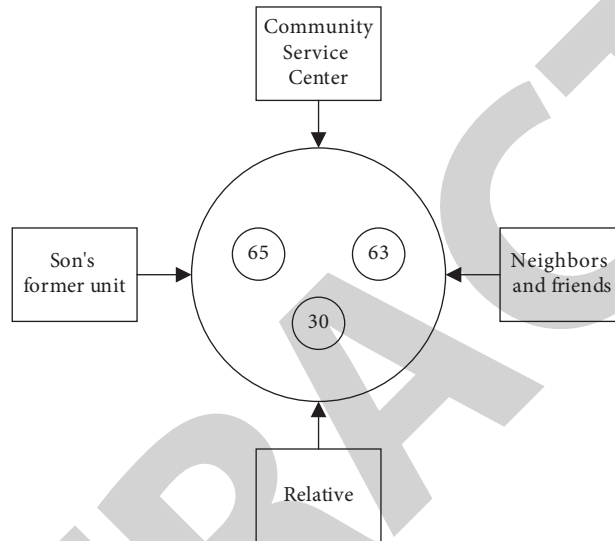


FIGURE 4: Ecological map of the case owner's family.

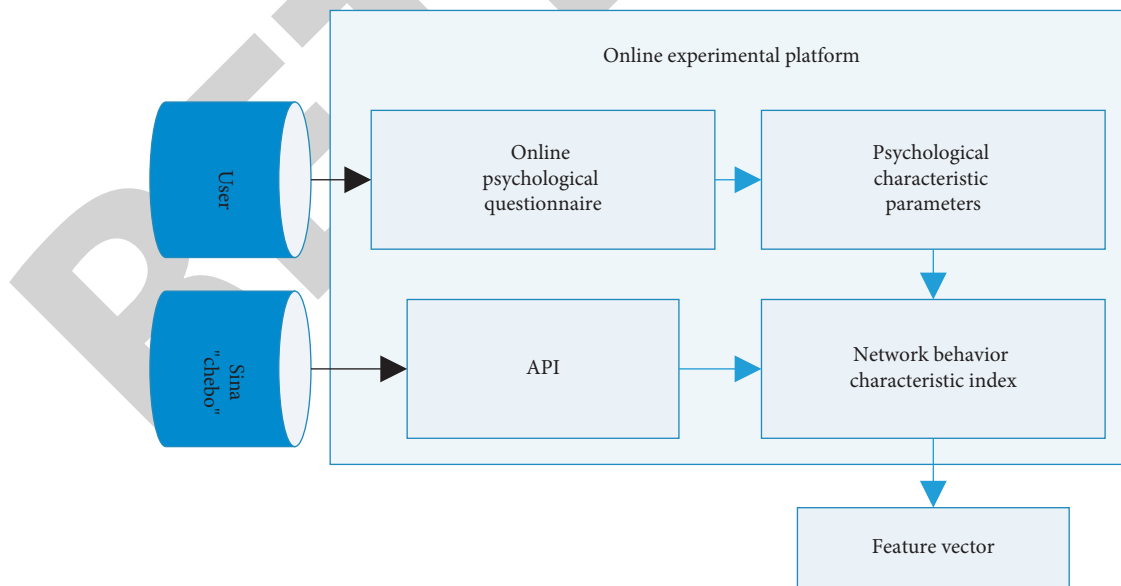


FIGURE 5: Subject data collection process.

ensure a sufficient amount of online data for the subjects, active users were selected from the recruited users with requirement that they had posted at least 500 tweets before

the experiment and that the latest tweet was posted within 3 months before the experiment, thus effectively eliminating inactive users from the data. In order to ensure the quality of

the psychological characteristics of the subjects, the subjects were required to fill in the online psychological questionnaire according to the standard. In this study, subjects who failed to answer the questionnaire were excluded [19]. After the screening process, 444 subjects (171 males and 273 females, average age 23.8 years old) remained, and their education level was mainly undergraduate (43%) and college (24%). The monthly per capita disposable income of the subjects was concentrated in the range of 1000–2000 RMB (25%) and 2000–5000 RMB (22%). Data from eligible subjects were used for subsequent model training.

3.2. Data Measurement

3.2.1. Mental Health Status. In this study, the Symptom Checklist 90 (SCL-90) [20] was used to measure the depression and anxiety levels of the subjects. The SCL-90 is a widely used international instrument for measuring mental health status, with good reliability and validity [21]. The questionnaire consists of a series of mental health symptoms, and subjects are asked to rate the severity of each mental health symptom on a 5-point Likert-type scale (0 being never and 4 being severe). The number of questions measuring depression and anxiety was 13 and 10, respectively, with higher scores indicating more severe mental health problems.

3.2.2. Online Behavioural Characteristics. In this study, based on the common types of online behavioral characteristics, we designed four categories of online behavioral characteristics based on the functions and data format of Sina Weibo, and the characteristics of the modeling target (mental health status). Based on the features of Sina Weibo, we designed 45 online behavioral characteristics in 4 categories [22]. Among them, (1) user information features describes the basic personal information of the subjects (e.g., gender and place of origin), (2) self-presentation features describe how the subjects create a virtual personal image on the online platform and present it to other users (e.g., whether to use the system's default virtual avatar), (3) privacy settings' features describe the subjects' preferences for personal privacy protection (e.g., whether to allow strangers on their personal pages), (4) privacy settings' features describe the subjects' preferences for privacy protection (e.g., whether to allow strangers on their personal pages), and (5) social network characteristics describe subjects' interpersonal interactions on online platforms (e.g., number of "followers" and number of "mutual followers"). For the Boolean features, they were binary coded, while for the floating-point features, the original values were retained.

3.3. Data Modeling. Mental health includes a range of different mental health dimensions (e.g. depression and anxiety), which are related to each other to a certain extent. The effectiveness of data modeling can be improved if common information between different mental health dimensions is

taken into account when building a computational model for a specific mental health dimension.

The basic idea of the multitask regression approach is that there are assumed to be T tasks and N instances, each with a training dataset $\{(x_{tn}, y_{tn})\} (t = 1, 2, \dots, T; n = 1, 2, \dots, N)$. Each instance can be represented as $x \in \mathbb{R}^d$ and $y \in \mathbb{R}^T$ (with feature number d) and matched with a multidimensional output vector (e.g., depression and anxiety dimensions), with the aim of finding a $T \times d$ matrix of coefficients, e.g.,

$$\mathbf{W} = \arg \min \{L(x, y, \mathbf{W}; 1:T) + \lambda \Omega(\mathbf{W})\}. \quad (1)$$

In this study, $L(x, y, \mathbf{W}; 1:T)$ is denoted as the empirical loss function, $\Omega(\mathbf{W})$ is denoted as the regularizer, and λ is denoted as the tradeoff constant [23]. In this study, $L(x, y, \mathbf{W}; 1:T)$ is set as the least square error, and $\Omega(\mathbf{W})$ is set as the Frobenius norm. That is,

$$\begin{aligned} L(x, y, \mathbf{W}; 1:T) &= \mathbf{Y} - \hat{\mathbf{Y}} = \sum_{t=1}^T \sum_{n=1}^N (y_{tn} - \hat{y}_{tn})^2 \\ &= \sum_{t=1}^T \sum_{n=1}^N \left(y_{tn} - \sum_h w_{th} x_{nh} \right)^2, \end{aligned} \quad (2)$$

$$\Omega(\mathbf{W}) = \|\mathbf{W}\|^2 = \text{tr}(\mathbf{W}^T \cdot \mathbf{W}). \quad (3)$$

Substituting (2) and (3) into equation (1), i.e.,

$$\mathbf{W} = \left(\lambda \mathbf{I} + \sum_n \mathbf{x}_n \mathbf{x}_n^T \right)^{-1} \left(\sum_n \mathbf{x}_n \mathbf{y}_n^T \right). \quad (4)$$

For the selection of λ , a bias-variance decomposition method was used to minimize the expected loss of [(error)+variance]. In view of this, the multitask regression method [24, 25] was used to develop models for depressive and anxiety states based on network data analysis. This study also used linear regression and feedforward neural network to develop the same mental health state model, which was used as a baseline model to evaluate the effectiveness of the multitask regression method.

4. Study Results

After tuning the model parameters, the learning rate of the feedforward neural network method was set to 0.9 and the parameter λ of the multitask regression method was set to 1.70 ($\ln(\lambda) = 0.53$). The correlation coefficients between the results of the mental health state model and the psychological questionnaire are shown in Table 1, and the network behavioral characteristics that were significantly correlated with depression and anxiety are shown in Table 2. For the same modeling target (depression or anxiety), the results of the mental health state model based on different modeling methods were different [26]. It is noteworthy that the correlation coefficient between the results of the mental health state model and the results of the psychological questionnaire was the highest among the three different

TABLE 1: Calculated results of the mental health state model and the results of the psychological questionnaire: correlation coefficients between the results of the mental health model and the results of the psychological questionnaire.

	Linear regression	Feedforward neural network	Multitask regression
Depressed	0.12	0.26	0.41
Anxious	0.14	0.21	0.34

TABLE 2: Correlation coefficient values for selected online behavioural characteristics and mental health dimensions.

Features	Depressed	Anxious
Gender	-0.137	-0.148
Original “microblog” ratio	-0.085	-0.094
Screen name length	0.166	0.073

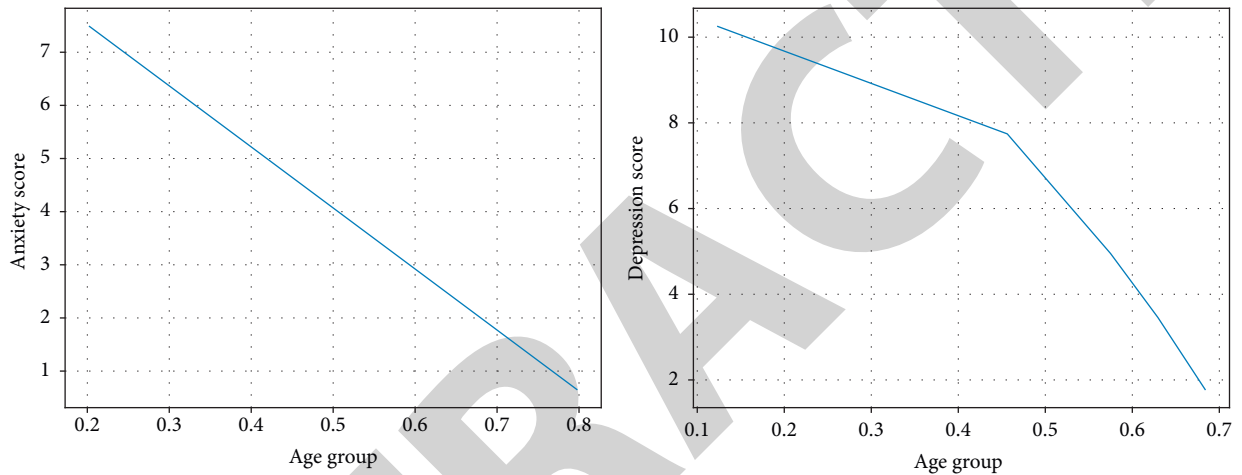


FIGURE 6: Comparison of psychological profiles between ages.

modeling approaches for both the depression and anxiety dimensions.

Analysis of the data showed no significant gender differences in anxiety and depression during major public events, anxiety $t = -0.865$, $p = 0.387$; depression $t = -0.011$, and $p = 0.991$; but regionally, significant differences were shown, anxiety $F(31, 10\ 916) = 1.713$, $p = 0.008$, and depression $F(31, 10\ 916) = 3.687$, $p = 0.000$; unexpectedly, the region with the highest levels of both anxiety and depression among older people was Guangxi (M (anxiety) = 9.38, $SD = 3.264$, and M (depression) = 12.05, $SD = 4.011$). The data showed that the levels of anxiety and depression among older people in this major public event differed between groups of older people, with anxiety $F(9, 10\ 938) = 3.757$, $p = 0.000$, and depression $F(9, 10\ 938) = 3.840$, $p = 0.000$, and the differences were highly significant. It is noteworthy that there were no significant differences in anxiety and depression between ages, but there were significant differences between ages, with anxiety $F(2, 10\ 945) = 5.495$, $p = 0.004$, and depression $F(2, 10\ 945) = 5.117$, $p = 0.006$, and it is easy to see from the images that, as age increases, the levels of anxiety and depression caused by major public events increased significantly and linearly with age, see Figure 6.

TABLE 3: Test of variance for each dimension of the Older People’s Mental Health Survey questionnaire.

Dimension	F	Sig
Growth experience	0.66	0.517
Personality traits	4.646	0.01
Life events	69.206	0
Social support	8.688	0

However, significant age differences were found in only some of the older adult groups. Again, not all regions showed significant age differences, with the most significant differences being in Inner Mongolia, where $F(2, 1,147) = 5.221$, $p = 0.006$, and in depression, $F(2, 1,147) = 4.997$, $p = 0.007$. Anxiety was $F(2, 231) = 3.966$, $p = 0.020$, and depression was $F(2, 231) = 6.034$, $p = 0.003$.

The analysis of the results of the mental health questionnaire for older people showed results that were largely consistent with the results of the Psychological Status Self-Assessment Scale [27]. There were no significant differences in total questionnaire scores by age, but there were significant differences by age, $F(2, 11,037) = 4.916$, $p = 0.007$. Tests of variance for each dimension of the Psychological Screening Questionnaire for Older People showed that the

most significant differences between ages were for life events, followed by social support and personality traits, see Table 3.

5. Conclusions

By collating and analysing the results of psychological assessments conducted on older people through big data, we can accurately identify groups with potential psychological crises and develop psychological support programmes to promote psychological resources to groups in greater need, which is of great guidance in helping counsellors to complete psychological crisis screening, effectively improve the timeliness of psychological counselling work, and improve the directionality of psychological support and psychological construction. Combined with the results of big data analysis, the construction of a complete psychological crisis intervention system will help to give full play to the important role of cadres and counsellors of the elderly, form a four-level crisis prevention and intervention system of schools, psychological centres, counsellors of elderly groups, and class-level psychological members, monitor the psychological dynamics of the elderly in real time, carry out psychological health education, improve the response rate when facing psychological crises, and effectively help the elderly cope with potential psychological crises arising from major emergencies.

Data Availability

The experimental data used to support the findings of this study are available from the corresponding author upon request.

Conflicts of Interest

The authors declare that they have no conflicts of interest regarding this work.

Acknowledgments

This work was sponsored in part by Philosophy and Social Science Research in Colleges and Universities in Jiangsu Province (2017SJB0304).

References

- [1] M. G. Cole and N. Dendukuri, "Risk factors for depression among elderly community subjects: a systematic review and meta-analysis," *American Journal of Psychiatry*, vol. 160, no. 6, pp. 1147–1156, 2003.
- [2] D. Shen, G. Wu, and H.-I. Suk, "Deep learning in medical image analysis," *Annual Review of Biomedical Engineering*, vol. 19, no. 1, pp. 221–248, 2017.
- [3] M. Porumb, S. Stranges, A. Pescapè, and L. Pecchia, "Precision medicine and artificial intelligence: a pilot study on deep learning for hypoglycemic events detection based on ECG," *Scientific Reports*, vol. 10, no. 1, pp. 170–216, 2020.
- [4] N. T. Duc, S. Ryu, M. N. I. Qureshi, M. Choi, K. H. Lee, and B. Lee, "3D-Deep learning based automatic diagnosis of alzheimer's disease with joint MMSE prediction using resting-state fMRI," *Neuroinformatics*, vol. 18, no. 1, pp. 71–86, 2020.
- [5] N. T. Lautenschlager, K. L. Cox, L. Flicker et al., "Effect of physical activity on cognitive function in older adults at risk for alzheimer disease," *JAMA*, vol. 300, no. 9, pp. 1027–1037, 2008.
- [6] Y. Engeström and A. Sannino, "Studies of expansive learning: foundations, findings and future challenges," *Educational Research Review*, vol. 5, no. 1, pp. 1–24, 2010.
- [7] M. Mahmud, M. S. Kaiser, T. M. McGinnity, and A. Hussain, "Deep learning in mining biological data," *Cognitive computation*, vol. 13, no. 1, pp. 1–33, 2021.
- [8] Q. Jones, G. Ravid, and S. Rafaei, "Information overload and the message dynamics of online interaction spaces: a theoretical model and empirical exploration," *Information Systems Research*, vol. 15, no. 2, pp. 194–210, 2004.
- [9] Y. Liu, L. Zhang, Y. Yang et al., "A novel cloud-based framework for the elderly healthcare services using digital twin," *IEEE Access*, vol. 7, pp. 49088–49101, 2019.
- [10] R. Kachouie, S. Sedighadeli, R. Khosla, and M.-T. Chu, "Socially assistive robots in elderly care: a mixed-method systematic literature review," *International Journal of Human-Computer Interaction*, vol. 30, no. 5, pp. 369–393, 2014.
- [11] X. Ning, K. Gong, W. Li, and L. Zhang, "JWSAA: Joint weak saliency and attention aware for person re-identification," *Neurocomputing*, vol. 453, pp. 801–811, 2021.
- [12] X. Ning, P. Duan, W. Li, and S. Zhang, "Real-time 3D face alignment using an encoder-decoder network with an efficient deconvolution layer," *IEEE Signal Processing Letters*, vol. 27, pp. 1944–1948, 2020.
- [13] J. X. Li, Y. Hong, and K. M. Chan, "Tai chi: physiological characteristics and beneficial effects on health," *British Journal of Sports Medicine*, vol. 35, no. 3, pp. 148–156, 2001.
- [14] A. Chiesa and A. Serretti, "Mindfulness-based stress reduction for stress management in healthy people: a review and meta-analysis," *Journal of Alternative & Complementary Medicine*, vol. 15, no. 5, pp. 593–600, 2009.
- [15] P. D. Bamidis, A. B. Vivas, C. Styliadis et al., "A review of physical and cognitive interventions in aging," *Neuroscience & Biobehavioral Reviews*, vol. 44, pp. 206–220, 2014.
- [16] Y. Wang, L. Sun, and S. Subramani, "CAB: classifying arrhythmias based on imbalanced sensor data," *KSII Transactions on Internet & Information Systems*, Jul. vol. 15, no. 7, pp. p2304–2320, 2021, (Computer Science Q3, 0.858).
- [17] L. Sun, Q. Yu, D. Peng, S. Subramani, and X. Wang, "Fogmed: a fog-based framework for disease prognosis based medical sensor data streams," *Computers, Materials & Continua*, vol. 66, no. 1, pp. 603–619, 2021.
- [18] Z. Qu, H. Sun, and M. Zheng, "An efficient quantum image steganography protocol based on improved EMD algorithm," *Quantum Information Processing*, vol. 20, no. 53, pp. 1–29, 2021.
- [19] M. Koufaris, "Applying the technology acceptance model and flow theory to online consumer behavior," *Information Systems Research*, vol. 13, no. 2, pp. 205–223, 2002.
- [20] R. T. Proyer, W. Ruch, and C. Buschor, "Testing strengths-based interventions: a preliminary study on the effectiveness of a program targeting curiosity, gratitude, hope, humor, and zest for enhancing life satisfaction," *Journal of Happiness Studies*, vol. 14, no. 1, pp. 275–292, 2013.
- [21] T. Xie, C. Zhang, and Y. Xu, "Collaborative parameter update based on average variance reduction of historical gradients," *Journal of Electronics and Information Technology*, vol. 43, no. 4, pp. 956–964, 2021.
- [22] Z. Zhang, C. Zhang, H. Li, and T. Xie, "Multipath transmission selection algorithm based on immune connectivity

Research Article

Redactable Blockchain Trust Scheme Based on Reputation Consensus for MEC

YongLi Tang ¹, Shuai Wu ¹ and XiaoJun Wang ²

¹School of Computer Science and Technology, Henan Polytechnic University, Jiaozuo 454003, China

²School of Electronic Engineering, Dublin City University, Dublin 9, Ireland

Correspondence should be addressed to XiaoJun Wang; xiaojun.wang@dcu.ie

Received 9 March 2022; Revised 3 April 2022; Accepted 11 April 2022; Published 28 April 2022

Academic Editor: Le Sun

Copyright © 2022 YongLi Tang et al. This is an open access article distributed under the Creative Commons Attribution License, which permits unrestricted use, distribution, and reproduction in any medium, provided the original work is properly cited.

Blockchain technology can build trust, reduce costs, and accelerate transactions in the mobile edge computing (MEC) and manage computing resources using the smart contract. However, the immutability of blockchain also poses challenges for the MEC, such as the smart contract with bugs cannot be modified or deleted. We propose a redactable blockchain trust scheme based on reputation consensus and a one-way trapdoor function in response to the problem that data on the blockchain, which is an error or invalid needs to be modified or deleted. The scheme calculates each user's reputation based on their currency age and behavior. The SM2 asymmetric cryptography algorithm is used as the one-way trapdoor function to construct a new Merkle tree structure, which guarantees the legitimacy of the modification or deletion after verification and vote. The simulation experiments show that the modification or deletion does not change the existing blockchain structure and the links of blocks. Furthermore, the consensus verification accurately passes after the modification or deletion operations, which indicates the proposed scheme is feasible.

1. Introduction

The mobile edge computing (MEC) reduces latency and network load by consolidating computing resources that are close to mobile users in edge networks. However, there are problems in system security and resource management. The security and privacy of MEC have been a concern in recent years, and blockchain can provide the best solution. Blockchain technology is one of the revolutionary emerging technologies in recent years. The immutability of blockchain technology facilitates it to establish a consensus in a trustless environment [1]. Furthermore, blockchain has the advantages of decentralization, distrust, anonymity, and data incorruptibility, and makes the transmission of secret information in the MEC more secure [2]. Therefore, it has broad development prospects. The smart contract can realize the decentralized resource management and ensure the security of system data. Using the decentralized characteristics of blockchain to perform task allocation and scheduling in mobile edge computing can effectively eliminate the attack behavior to the central server and ensure the correctness of data transmission.

Blockchain brings benefits to the MEC but also challenges. The immutability ensures the information security of the computing devices on the chain. It also means the wrong or invalid information cannot be modified or deleted and will be permanently stored in the blockchain. The smart contract can facilitate the intelligent management of MEC devices. Still, bugs in the smart contract will lead to irreparable damage, as in the well-known DAO attack. However, illegal information has been maliciously uploaded to the blockchain time and again since the creation of blockchain, providing opportunities for criminals to disrupt the order of the blockchain network for benefit. The current research and application of blockchain emphasize the security of storage and transmission of data on the blockchain, while ignoring the security of data contained on the blockchain from the perspective of information regulation [3]. Data on the blockchain can only be appended, not deleted or modified [4]; the storage burden of the entire blockchain increases due to the increasing amount of data on the blockchain, which cannot be deleted or altered, which is not conducive to maintaining. The General Data Protection Regulation

(GDPR) mandated by the European Union in 2018 sets new standards for collecting, storing, protecting, and using users' data. Companies need to ask for each user's permission before collecting their personal data. The user has the right to be forgotten, and the data controllers must ensure that personal data are accurate and kept up to date. It means that users can withdraw their permission at any time and ask companies to modify or delete their personal data. Therefore, the blockchain system applied in this context must provide users with a convenient way to modify or delete. The decentralization of blockchain does not mean that the system data cannot be modified, but the data on the blockchain can be modified with the approval of the majority of the system users, and the modification operation is performed by the system users, which does not violate the concept of decentralization. Therefore, the study of redactable blockchain technology under specific conditions is of great research significance.

After Satoshi Nakamoto proposed "Bitcoin: A Peer-to-Peer Electronic Cash System" in 2008 [5], blockchain came into the public eye. As the core technology of blockchain, the consensus mechanism determines blockchain's security, scalability, decentralization, and other essential characteristics [6]. It solves the Byzantine problem so that communication between untrustworthy nodes is possible and makes the distributed data of blockchain consistent. A suitable consensus mechanism improves the performance and efficiency of a blockchain system, provides a robust security guarantee, and supports complex application scenarios [7]. The initial Bitcoin blockchain used the Proof-of-Work (PoW) mechanism, which relies highly on the HashRate of nodes, to ensure the consistency of the distributed data. However, PoW proved to be a severe waste of resources and an inefficient transaction. The Proof-of-Stake (PoS) consensus created by Peercoin solves the problem of waste of resources of PoW. However, it cannot resist the permanent divergence. It may lead to polarization, widening the gap between rich and poor nodes, and a low level of decentralization is detrimental to currency circulation [8]. Liu proposed a new consensus mechanism based on reputation in 2019 (Proof of Reputation, PoR) [9]. It distributes a reputation value to each node and determines who has the right to create a new block according to the reputation value. The PoR consensus mechanism does not waste the HashRate or power resources; it has a low computational cost and is more efficient compared with the PoW consensus mechanism. The PoR also does not lead to polarization compared with the PoS consensus mechanism. The reputation value is logarithmically proportional to the amount of currency. The reputation value increases with the increasing amount of currency, but the growth rate decreases. It allows moderately wealthy nodes to create a new block for rewards.

Krawczyk H proposed the chameleon hash function in 2000 [10], which has a trapdoor that can construct a hash collision. The Accenture company applied for a patent of redactable blockchain that having a trapdoor can modify the block data without changing the block's hash value. Still, the scheme is not secure because the trapdoor is controlled by only one party, and the scheme is highly centralized. Li

proposed a study of redactable blockchain technology based on chameleon hash functions and verifiable secret sharing in 2018 [11]. Li's scheme solves the problem of high centralization, with N nodes cooperating to perform modification operations. Still, most of the blockchains are mainly based on traditional collision-resistant hash functions, so the application value of Li's scheme is low. Ren proposed a redactable blockchain scheme based on Proof-of-Space consensus and collision-resistant hash functions in 2020 [12], using one-way trapdoor functions to modify the data on the blockchain. The blockchain structure of Proof of Space is different from Proof of Work and Proof of Stake, due to the features of Proof-of-Space consensus, and this scheme [13] is only limited to Proof-of-Space consensus, which has substantial limitations; the modification involves the inverse operation of Q users. The more users there are in the blockchain network, the larger the Q is, and the lower the efficiency is. Therefore, the Proof of Reputation has many advantages compared with Proof of Space. First, the Proof of Reputation selects a Leader to create a new block according to user's reputation value, and it does not waste the HashRate resources compared with Proof of Space; second, the efficiency of Proof of Space will decrease with the increasing number of Q users in the network, there are Q inverse operations, and the efficiency of Proof of Reputation will not decrease because there is only one inverse operation.

This paper uses a collision-resistant hash function to implement a redactable blockchain scheme based on the Proof of Reputation consensus mechanism (PoR). We propose a new Merkle tree structure using a one-way trapdoor function. As a result, legitimate modification of invalid or error information could be performed after verification without changing the existing blockchain structure; all users can verify the validity of modified data [14].

2. Basic Knowledge

2.1. One-Way Trapdoor Function. A one-way trapdoor function contains two features: a one-way function and a trapdoor. The one-way function is irreversible. For a one-way function $y=f(x)$, it is easy to calculate y given x but is computationally infeasible to compute x given y . There exists a z such that we can easily calculate $x=f^{-1}(y)$ if we have z and y . The function $y=f(x)$ is called one-way trapdoor function, and z is called the trapdoor. The character of the one-way function determines its computational complexity, and the character of the trapdoor determines that z will be the key to cracking the one-way function.

2.2. PoR Consensus-Based Blockchain. A new consensus mechanism based on Proof of Reputation (PoR) was proposed in [9]. The PoR consensus mechanism has certain merits in energy-saving and computation efficiency compared with PoW. Furthermore, PoR can avoid the waste of resources caused by PoW and create a secure network atmosphere.

As shown in Figure 1 [9], the block structure of the PoR consensus mechanism has three parts: block header,

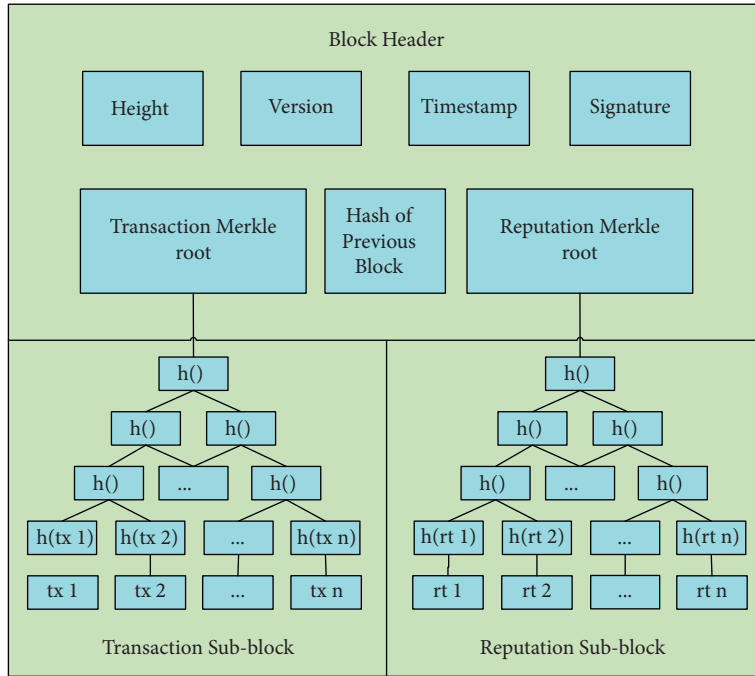


FIGURE 1: Block structure [9].

transaction sub-block, and reputation sub-block. Detailed contents of the three parts are as follows:

- (1) Block header: contains block height, version, timestamp, signature of the block header, hash of the previous block (only hash the block header), transaction Merkle root, and reputation Merkle root.
- (2) Transaction sub-block: contains transactions stored as a Merkle tree. The root of Merkle tree in the transaction sub-block links to the transaction Merkle root in the block header.
- (3) Reputation sub-block: contains the vote information. As shown in Figure 2, the vote information includes explicitly: the voter’s public key, reputation value, opinion of agreement or disagreement, signature, and the block hash. The vote information, stored as a Merkle tree, is used to verify the legitimacy of the created block. The Merkle root links to the reputation Merkle root in the block header.

In the PoR consensus mechanism, the highest reputation node can create a new block. The factors that affect a node’s reputation are as follows: currency age R_s ; transaction activities with other nodes R_a ; and contribution to consensus R_c . The currency age is the product of currency amount and time; transactions with other honest nodes and participation in consensus validation voting will increase a node’s reputation value, and the reputation values of each participating node will change when each block is published, whether the block is approved or rejected by the network. The following equations computing the constituting components, R_s , R_a , and R_c , of the reputation values are formulated in [9].

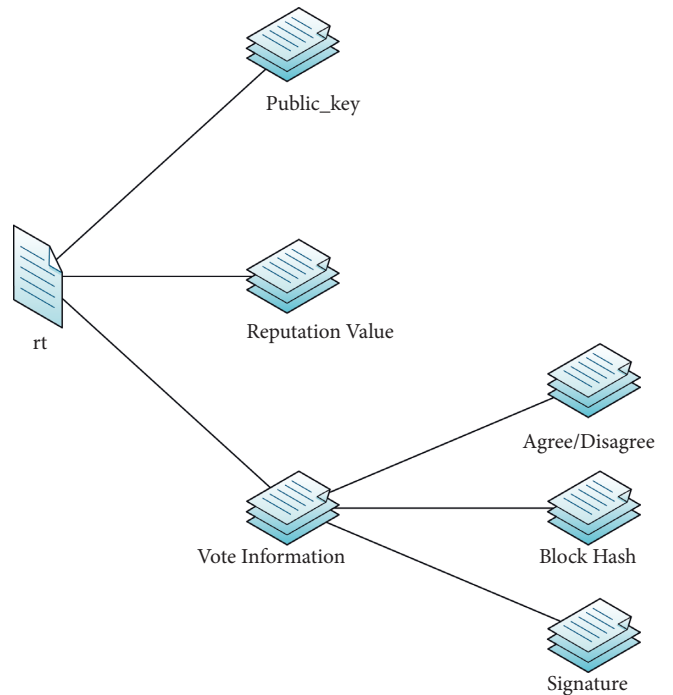


FIGURE 2: Details of a vote information.

$$R_s(S_i, t) = \alpha \log(S_i t), \quad (1)$$

$$R_a(A_k, V_k) = \sum_{k=1}^j A_k \log(V_k) S(k), \quad (2)$$

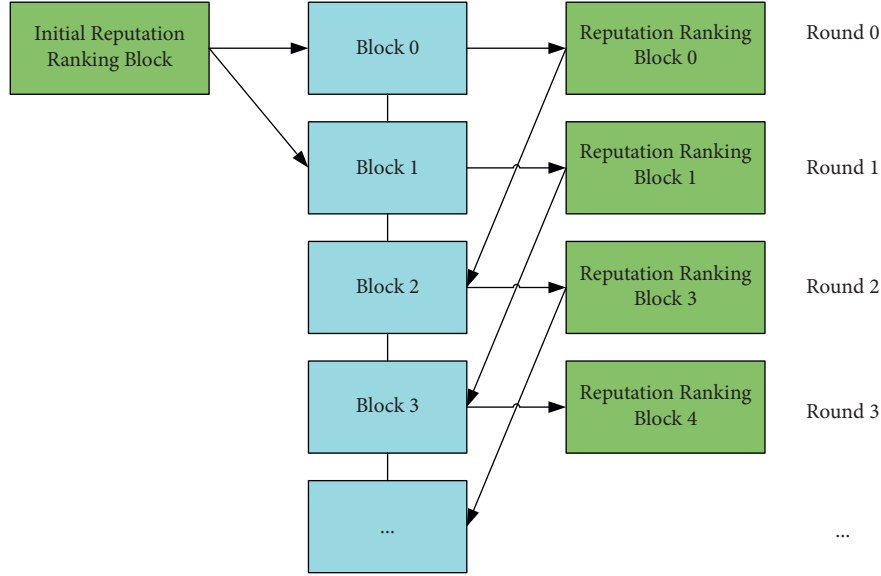


FIGURE 3: Process of creating new blocks [9].

$$R_c(N_i) = \gamma_1 N_{ic} T_{\text{total}} - \gamma_2 N_{ie} T_{\text{total}} \quad (3)$$

In (1), the S_i denotes the currency amount of the i^{th} node; the t represents the time length that node i has owned this currency, $S_i t$ is the currency age, and α is a conversion factor. The PoR consensus mechanism uses the logarithmic formula to calculate reputation value. The reputation value growth rate decreases as the wealth increases; this reduces the gap between the rich and the poor so that people of moderate wealth also have the opportunity to create new blocks for reward of increasing its reputation value.

The j in (2) is the number of transactions related to node i . With the appropriate settings of the weighting factor A_k and the scaling factor $S(k)$, nodes would prefer to trade with other high reputation nodes to achieve or maintain their high reputation status.

The R_c in (3) incentivize nodes to frequently make positive contributions to consensus voting to increase their reputation values.

The reputation value R_i for each node in the network can be calculated using the following (4) from [9], where β_1 , β_2 , and β_3 are weighting parameters. Readers are referred to [9] for a more detailed description of each of the parameters in following equations:

$$R_i = \beta_1 R_s(S_i, t) + \beta_2 R_a(A, V) + \beta_3 R_c(N_i). \quad (4)$$

There is also a positive causal connection between the system currency and the reputation values; the high reputation nodes are likely responsible for the system's security because system security is inseparable from their wealth.

The process of creating a new block is as follows.

- (1) Select a Leader to create a new block. As shown in Figure 3, an initial reputation ranking block is generated during the system initialization. The highest reputation node of the initial reputation ranking block is selected as the Leader to create

blocks 0 and 1. Then, reputation ranking blocks 0 and 1 are built according to the blocks 0 and 1 created by the Leader. The highest reputation node of block 0 creates block 2, the highest reputation node of block 1 creates block 3, and so on. After creating a new block, the Leader needs to sign and broadcast it to the network and wait for the other nodes in the network to vote on it.

- (2) Votes on the new block. The validation group consists of high reputation nodes, and the sum of their reputation values is over 80% of the system's total reputation values. The nodes in the validation group are usually in the top 20% of the highest reputation nodes. All nodes in the network can verify whether the transactions and signature are legitimate and then vote on it. The Leader needs to collect the voting information and store it in the reputation sub-block as a Merkle tree. The block will be uploaded to the blockchain when (i) more than 2/3 of the validation group nodes vote in favor; (ii) the sum of the YES voters' reputation values exceeds 1/2 of the system total reputation value. The block is rejected in the opposite scenario.
- (3) The other nodes in the blockchain network verify the new block. Other nodes verify the newly released block and update their local blockchain data for consistency.

3. Redactable Blockchain

We propose a redactable blockchain based on the blockchain structure of PoR, using a new Merkle tree and a one-way trapdoor function. The specific transaction in the *Request* can only be legitimately modified when the nodes who agree to perform the requested modification have more than 1/2 of the whole reputation value in the network, so the

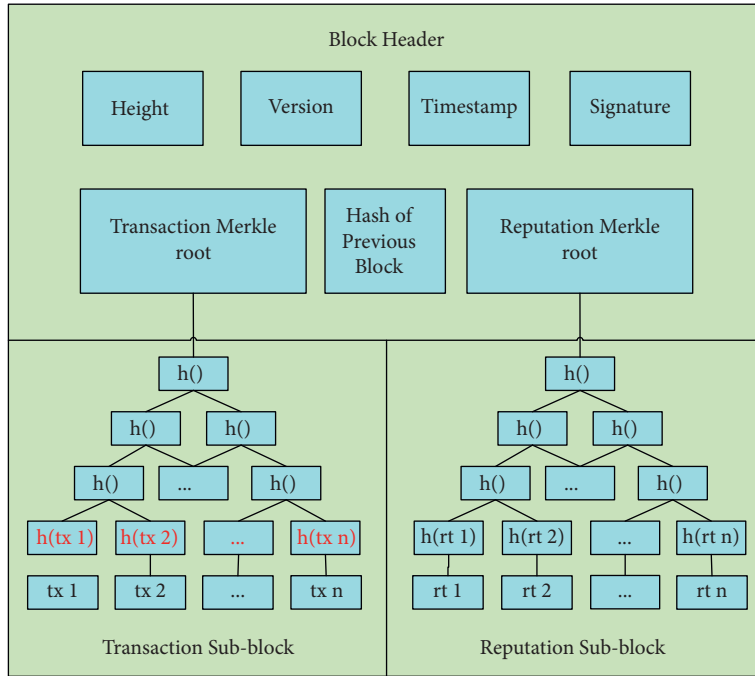


FIGURE 4: Structure of redactable block.

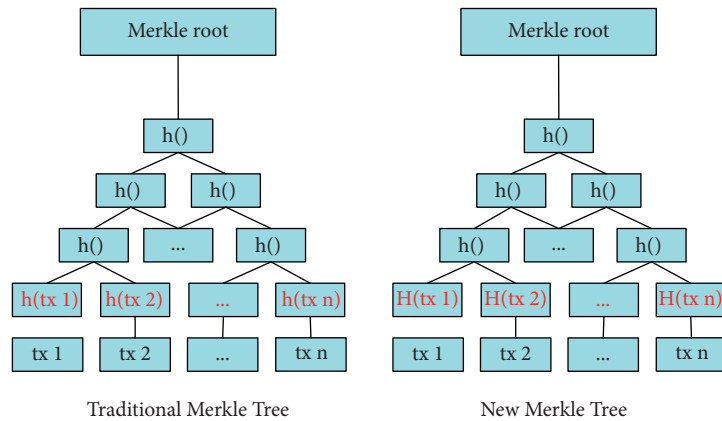


FIGURE 5: Traditional Merkle tree and new Merkle tree.

amendment represents the system’s will. Furthermore, the blocks’ link and other data remain unchanged after the amendment. Thus, the proposed redactable blockchain prevents illegal or malicious modifications. We first introduce the redactable blockchain structure and then analyze the modification principle and security.

3.1. Structure of Redactable Blockchain. As shown in Figures 4 and 5, the structure of the redactable block uses a new Merkle tree that incorporates the XOR operation $H(tx)$ on the one-way trapdoor function and the hash function. This operation ensures that the transaction Merkle root, the signature, and the hash value of the block header will remain unchanged after the modification, keeping the links of blocks intact.

The difference between the traditional Merkle tree and the new Merkle tree is in the hashing of the leaf nodes.

In the traditional Merkle tree, the value of each leaf node is the $SHA256$ hash $h(tx)$ of a transaction tx . The parent node’s value is the hash of two hash values, $h(tx1)$ and $h(tx2)$, of the two children nodes, and this hashing process is repeated until the transaction Merkle root is generated. Therefore, we can detect any tamper of transactions according to the Merkle root to ensure the transaction data’s integrity [15]. If a transaction is tampered with, its hash value and the transaction Merkle root will also change; therefore, the transactions on the blockchain cannot be modified without being detected at the Merkle root.

In the new Merkle tree structure, the value of the leaf node is $H(tx)$, which is the XOR of the hash value $h(tx)$ of the

transaction tx and the one-way trapdoor function $g(x)$ (the calculation process of the other nodes remains unchanged):

$$H(tx) = h(tx) \oplus g(x). \quad (5)$$

x is the Leader's exclusive random number, automatically generated when the public and private keys are created and recorded as a common parameter. $g(x)$ is the result of encrypting the random number x with the public key. When the transaction tx is modified to tx_{new} , the block Leader can use its private key to compute a new number $x' = g^{-1}$, ($h(tx) \oplus g(x) \oplus h(tx_{new})$), to satisfy the formula:

$$h(tx) \oplus g(x) = h(tx_{new}) \oplus g(x'). \quad (6)$$

Although the transaction is modified, with the calculated number x , the transaction Merkle root, the signature, and the other data in the block header remain unchanged; the block header's hash is also intact, therefore maintaining the links of blocks. Thus, the new Merkle tree can still achieve the functions of the traditional Merkle tree as follows:

- (1) Providing a Merkle proof. *Light nodes* can verify whether a transaction exists by Merkle proof with the help of *full nodes*, even if only the block header is stored (a *full node* has all transactions in the network, while a *light node* only has transactions related to itself).
- (2) Verifying whether a transaction has been modified. Suppose an attacker wants to change a transaction maliciously. Because only the Leader owns the trapdoor, an attacker cannot calculate the number x' to ensure the transaction Merkle root is unchanged. So, we can judge whether a transaction is modified according to the different transaction Merkle root.

3.2. The Principle of Redactable Blockchain. In a redactable blockchain, the data on the blockchain can be legitimately modified in the interest of the system if nodes with more than 1/2 of the system total reputation value agree the modification. Furthermore, the modification does not break the links between the blocks. The following section describes how to implement modification operation and ensure it is legal.

3.2.1. Implementing Data Modification

(1) *Legitimacy Verification of a Modification Request.* When a node has a valid reason to modify a transaction, the node can send a modification *Request* to the network. All nodes in the network could vote on whether the *Request* is legitimate. The *Request* is approved if the sum of the yes voters' reputation values is greater than 1/2 of the system's total reputation value; otherwise, the *Request* is rejected if the voting result is in the opposite. The modification *Request* information includes the height of the block to be modified, the serial number of transactions, the reason of redaction, and the set after redaction.

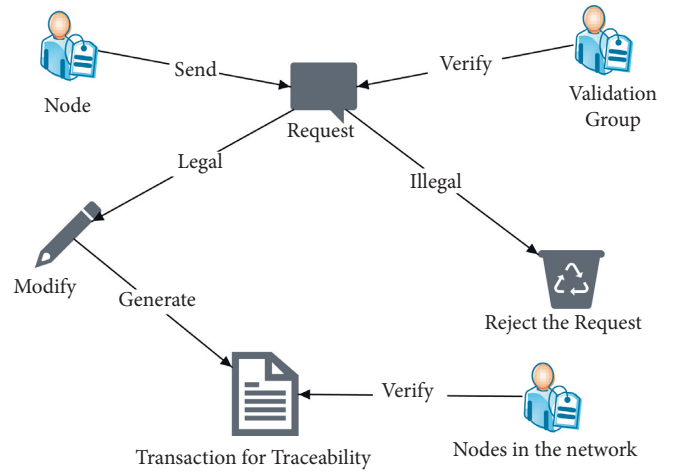


FIGURE 6: Process of data modification.

$$\text{Request} = \{\text{Height, ID, Action, data}_{\text{new}}\}. \quad (7)$$

The requirement of high reputation yes voters' sum of reputation values is more than 1/2 of the system's total reputation values ensures the "legality" of the modification *Request*, and prevent malicious nodes in the network from destroying the modification operation. Higher reputation nodes are more likely honest nodes, so these nodes are entrusted with more decision-making power.

(2) *Process of Implementing Data Modification.* The Leader needs to calculate a new number $x' = g^{-1} (h(tx) \oplus g(x) \oplus h(tx_{new}))$, to guarantee that the Merkle root and the data in the block header remain unchanged after the transaction modification. Hence, the links of the blocks are not affected, and there is no need to adjust the data of the subsequent blocks. Furthermore, all nodes in the network can verify the legitimacy of the data at any time.

(3) *Update of System Status.* The Leader generates a new transaction message called $txorg$ for traceability after the modification operation is executed. The content of $txorg$ is as follows:

$$txorg = \{\text{id, Height, ID, Action, data}_{\text{new}}, x, x', \text{Pubkey}_{\text{leader}}, \text{time, rt_set}\}. \quad (8)$$

The contents of the $txorg$, in sequential order, are as follows:

- (i) The serial number of the $txorg$, id
- (ii) The height of the block, $Height$
- (iii) The serial number of transactions, ID
- (iv) The reason of redaction, $Action$
- (v) The set after redaction, $data_{\text{new}}$
- (vi) The Leader's random number, x
- (vii) The calculated new number, x'
- (viii) The Leader's public key, $\text{Pubkey}_{\text{leader}}$
- (ix) The time of modification, $time$

(x) The voting record to the Request, rt_set

All network nodes can verify the modification's legitimacy according to *txorg* and update their local blockchain data for the consistency of the chain.

Figure 6 illustrates the data modification process.

First, the node sends a transaction modification *Request*.

Second, all nodes send in the network vote on the legitimacy of the *Request*. The *Request* is considered legitimate if the favorable votes come from nodes whose sum of reputation values is more than 1/2 of the system's total reputation values. Then, the Leader executes the legitimate modification *Request* by calculating a new number x' so that the links of blocks are not affected after the modification. Otherwise, reject the modification *Request* and vastly reduce the reputation value of the node sent the *Request*.

Third, the Leader issues a transaction for traceability, and the nodes of the whole network verify whether the executed modification is legitimate and update their local blockchain data.

3.2.2. Ensuring the Legality of Modification. The redactable blockchain does not compromise blockchain security while addressing the limitations of immutability. Because only legal changes voted and verified through by the network's nodes can be performed, the "redactable" blockchain can still ensure the data's security, guaranteed by the characteristics of the one-way trapdoor function and our scheme.

We can only adjust the number x' to match the modification of transactions, which guarantees that data and the links of the blocks remain unchanged after the modification. The property of the one-way trapdoor function determines that only the node knowing the trapdoor can find the only number x' that can match the transaction change to execute the modification. In this paper, the trapdoor is the Leader's private key, so only the Leader can calculate the new number, and only the Leader can execute the modification authorized by the network.

Specifically, we choose the SM2 asymmetric cryptography algorithm as the one-way trapdoor function. In essence, the Leader encrypts its selected random number x with its *public key*. According to the one-way trapdoor function properties, all nodes can use the Leader's *public key* to calculate $g(x)$ given x . However, only the Leader can do the reverse calculation, that is, calculate x given $g(x)$, with the corresponding *private key*. Therefore, the Leader's private key is the trapdoor generated by one-way trapdoor function. Furthermore, the blockchain modification request needs to be approved by the nodes in the network before execution and verified by all other nodes after implementation. Therefore, the modification operation represents the will of the system and is legitimate.

3.2.3. Security Analysis of Data Modification. To illustrate the security of the redactable blockchain scheme, we simulate the attacks of a malicious adversary on modifying block transactions. The adversary can take the following methods:

- (1) Modify the target block data, modify the data of all blocks on the chain from the targeted block up to the latest block, and keep the links of blocks unchanged
- (2) Calculate a new number for the modification so that the new Merkel tree root is unchanged after modifying the targeted block data

Attack scenario 1 is not feasible because only the block Leader can modify the block. Furthermore, the Leader of each block on the path from the targeted block up to the latest block may be different. The Leaders of each block on the block path are all high reputation nodes. A high reputation node is likely trustworthy because its wealth is closely related to the system's security. According to the principle of maximum wealth, high reputation nodes will not damage the system, negatively affecting their wealth. So, the adversary cannot perform all modification operations from the targeted block up to the latest block. Therefore, the adversary's attack is not feasible.

The attack scenario 2 is also infeasible because only the Leader knows the trapdoor of the new Merkel tree, so only the Leader can calculate the unique number to keep the Merkel root unchanged after the transaction modification. And the Leader with a high reputation is more likely to be honest because blockchain security is closely related to its wealth. However, suppose the Leader does not faithfully execute the modification request in the network. In that case, the unauthorized modification cannot pass the verification of the other nodes, and the modification operation cannot complete. The Leader's reputation value is also significantly reduced as a consequence. In this way, the attacker cannot obtain benefits but loses his wealth, violating the principle of attack. Therefore, the scheme is safe. In conclusion, the redactable blockchain scheme is safe and effective.

4. Experimental Simulation

Smart contracts can be used for computing devices management in MEC. However, if a smart contract with bugs is released in MEC, and the bugs can cause devices to fail to alert potential warning conditions, it can cause irreparable damage. In this scenario, the proposed redactable blockchain scheme can modify the uploaded buggy smart contract to prevent damage that the buggy smart contract can cause. For easier understanding, the information in the buggy smart contract can be treated as transaction data in the system blockchain to implement the modification. Furthermore, the proposed redactable blockchain also facilitates companies' compliance to GDPR, the EU law on data protection and privacy. For example, in a blockchain-based electronic health record system, the medical institute should ensure that customer's personal data are accurate and up to date, and be able to modify customers' personal data or completely erase a customer's health record at the customers' request. In these scenarios, the customers' health records can be treated as transaction data modified or deleted.

TABLE 1: Node information.

Id	Public key	Wealth	Random number
1	87979b12e898279dfae24641faf44b10b9c623484224e5b0b8929731e31276af41d3d810d04038fece131e38c28106429bbfe325d6bc0f9a46f34a8b2b0f4a82e9f783b762a864afb2b2483a8d92f4a0f979fd49b89506092b6b7c7fb1bba914fd193514171f9eeb480424275fde4bb8d1e895f4afb315f012137135d33ed0de31612374ea9e9a8f7e7d2d6650f32bdcc780f2749f4edb25f9e09d7726f8bf2a623e2fbf708dfacee87c68abd5072c830cc350832f8cace015f57b8897f887e88f5ce03fa86f77b19f42d59c59e1a69f4ab714ba9006f50255165a530be1d54a9899009bcb895636c90079f92938b902ffb4f570a80859e585f2668fdc108783f6eb2bbd6265db7f6ef738ccb294d5078c64071804e6b81863f049bf5b630caefa0918f850449eb37bd16796b4e3295f969f0e1306952374dcfa9011bd50f3d36906b0d14e4280b2a74ec925a574f1d632378b8a2efd25ac30f17c02c6d2b793a888cd3c8253fa216bba67e8324c8e3de5da8d9e3abc3bfd9b4bde6ea0748ab479c2bd550973e773f336ca94612bfa404723ddc0000f6d76eae32d2f82787484dec28e603f3b6a9f8ec01509c0a742a4de7ffe467c4c62e091dd124a4f157d36518d966e5015274c7a78c19620b71e0771838c0e779eb5ca2bd070bd81951a8030f0a455e2c7b752ac35c885f3f41d3f36c1d8c1ba8b4860dc312bca65961388661dd35fdf73b8da16f9c49d6420ce780c95fa0a6fb7ef73ac3d87debb15ca44be28820e3b113641c8351c759a6bd73f5d598b724e5367611f23dfc11d098dd03004e355417668d8ea016085e8dd64a2f788ea95052b1a2058ca8ea81cf3366f883b4279762414b5e68c7f9fd35c27cbbc1174df00fb222ec0b83f557c0	10000	635635635
2		6000	359147852
3		3000	972951361
4		8000	168752164
5		500	160789451
6		800	938852164
7		2000	543163456
8		100	700785426
9		0	844111594
10		50	162111021

TABLE 2: Ranking of initial reputation.

Id	Wealth	Reputation value
1	10000	8.30482023
4	8000	8.14385619
2	6000	7.93633744
3	3000	7.43633744
7	2000	7.14385619
6	800	6.48289214
5	500	6.14385619
8	100	4.98289214
10	50	4.48289214
9	0	0

We simulated the data modification on a blockchain under the PoR consensus mechanism. The experiment uses Python as the language, PyCharm, as the compiler and imports the encrypted package of gmssl.sm2 for the encryption, decryption, and signature operations.

4.1. Competition of Bookkeeping Rights. Table 1 shows the information of the nodes in the initial system. There are no transactions and validation votes in the initial system, so the reputation values are only related to the nodes' wealth.

The system converts the amount of currency into a reputation value using the conversion formula in equation (1), that is, $R_s(S_i, t) = \alpha \log(S_i t)$, and generates an initial ranking of reputation value, as shown in Table 2. We set the conversion factor α as 1/2. The initial reputation value is only related to currency amount because no transactions have been generated yet.

Figure 7 shows the nodes' reputation values.

The consensus mechanism selects the highest reputation node as the Leader to create a new block. Then, other nodes

in the network vote on the legitimacy of the new block, and all nodes can verify the legitimacy of the new block.

4.2. Generation of New Blocks. The system sets each block to pack four transactions. The initial reputation ranking determines that node 1 is the Leader to create blocks 0 and 1. The Leader collects four transactions in the transaction pool, packs them into a block, and releases it to the network with a signature. All nodes in the network vote on the legitimacy of the transaction and verify the signature. If passing the validation, the block is uploaded as block 0, and a new reputation ranking table 0 is generated. The highest reputation node in reputation ranking table 0 generates block 2. Similarly, the highest reputation node in reputation ranking Table 1 generates block 3, and so on. Figure 8 shows the detailed structure of blocks 0 and 1.

Let's use block 1 as an example to introduce the computation of the transaction Merkle root.

- (1) Block 1 contains four transactions, and node 1 is the Leader of block 1. The one-way trapdoor function $g(x)$ can be calculated using SM2 encryption on the Leader's exclusive random number x using the public key of the Leader (node 1). The $g(x)$ is at least 776 bits in length. We calculate the $SHA256(tx)$ of each transaction first and then pass the value of $SHA256(tx)*3$ to the first 768 bits of $h(tx)$, and padding the remaining bits of $h(tx)$ with zero to make $h(tx)$ and $g(x)$ equal in length. Then, calculate the hash value $H(tx)$ of each leaf node.
- (2) After calculating the $H(tx_i)$ of each Merkle tree leaf node i , we compute the hash value of the parent node of two leaf nodes by performing $SHA256()$ hashing of the concatenation of their hash values. These steps

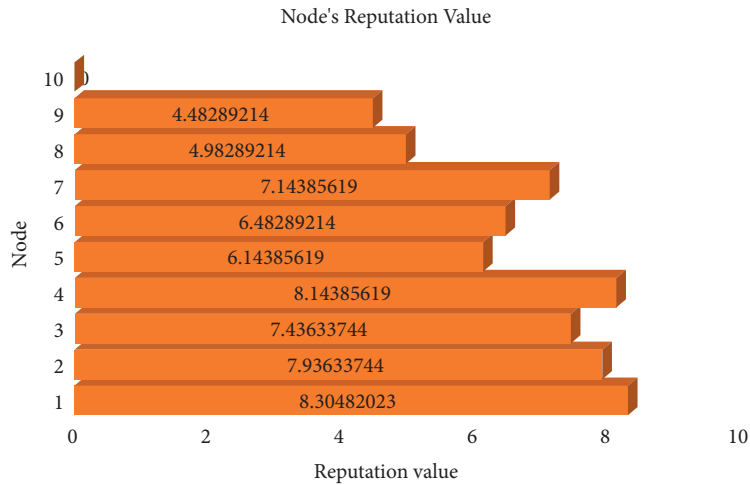


FIGURE 7: Nodes' reputation values.

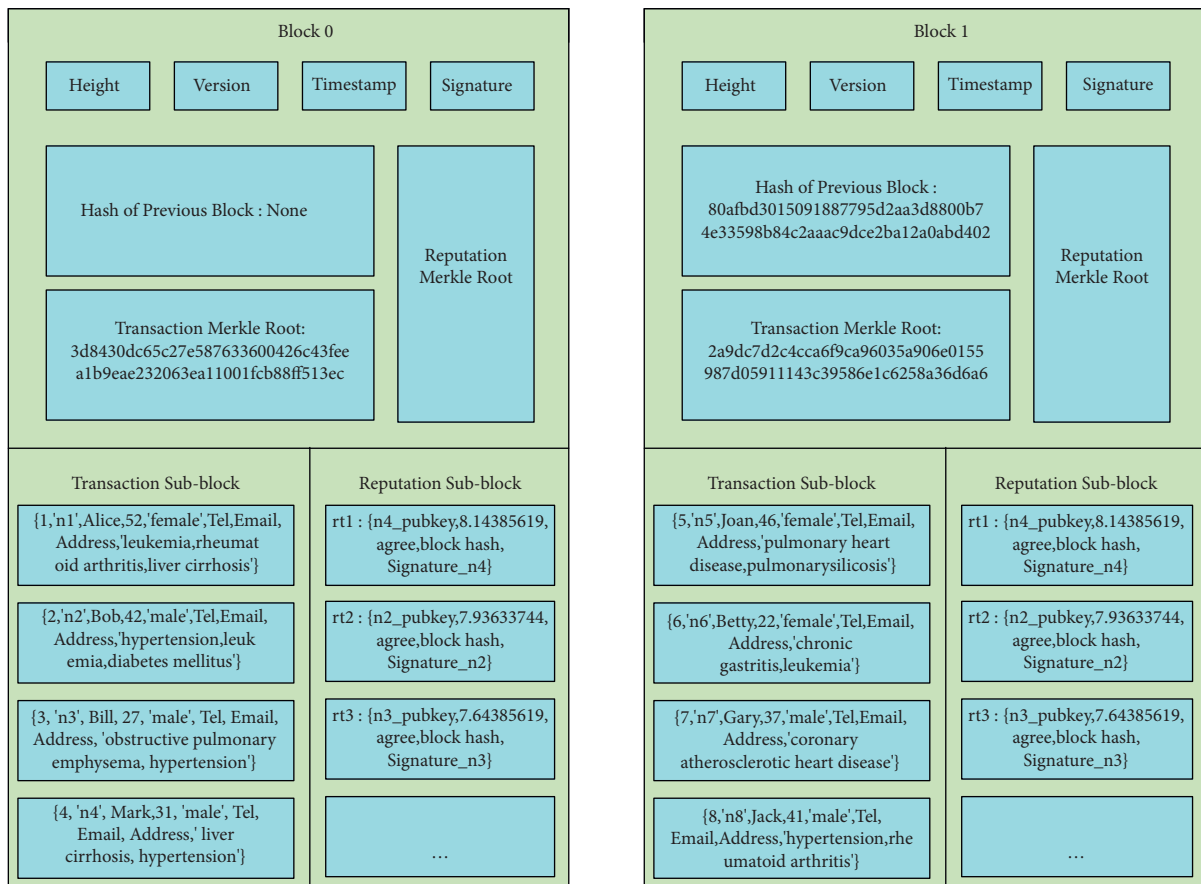


FIGURE 8: Blocks 0 and 1.

are repeated until the transaction Merkle root is generated.

$$\text{Merkle root} = \text{SHA256}(\text{SHA256}(H(tx1)\|H(tx2))\|\text{SHA256}(H(tx3)\|H(tx4))). \tag{9}$$

TABLE 3: Hash of transactions.

Transaction	SHA256()
<i>tx1</i>	70d78a190451aaeadfbccc0ddf1043c7a6851595dcc01cb13a1953df57e9cbee
<i>tx2</i>	ca5c4a603d75c6a9d32c7ee36f4ffe0674d473f26760d4c09d658cb175569580
<i>tx3</i>	6de64c719e4d7604af8c3120ecd559217a68246389b4ba4422fbc6c381d924
<i>tx4</i>	8586e0ec5a2f382394cc04d57f1b032cb22b94927f468d2c21b142f227b27f35

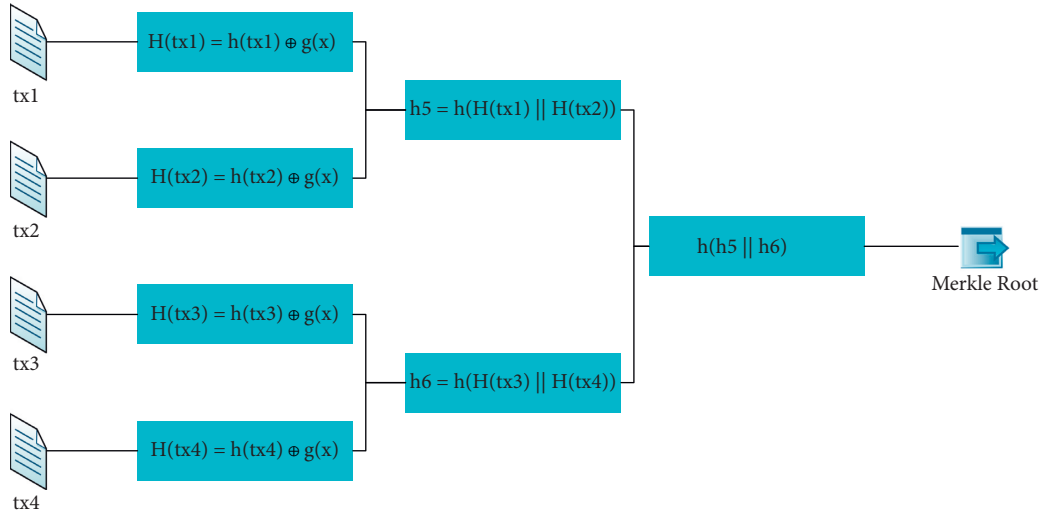


FIGURE 9: Computation of the Merkle root.

The value of $g(x)$ is as follows:

$$g(x) = \text{efcd19ddc10422480f18792b6d77be29f288f644cb4b1625c9754f7aa00c8f93304df99bcf6188b139e429d07d78d} \\ \text{8177a90babaec7e7b7b42b6cb0ed6e9712e9c986111fda10b602d99f4a0d64f2e9a566324432d} \\ \text{8990810412e3d215f0083a5df14ec.} \tag{10}$$

Table 3 shows the hash of transactions.

We can calculate the Merkle root according to Figure 9:

$$\text{Merkle root: } \text{3d8430dc65c27e587633600426c43feea1b9eae232063ea11001fcb88ff513ec.} \tag{11}$$

The private key of block Leader (node 1) is as follows:

$$\text{private_key: } \text{2b40bbd922b8cb4f99a67875b35440562133d7cf6ac9710a60d0baaeafdca6b54.} \tag{12}$$

The signature of the block Leader (node 1) to the block header is as follows:

$$\text{Sign: } \text{94532e3d3d8afa58838c4f5c2137fa3c3dc7e4eaf290b1d2595e2ad633e7d13e} \\ \text{7aeae4656ff1d317952245b795cff894316e9bad0714be778569be9225e525e9.} \tag{13}$$

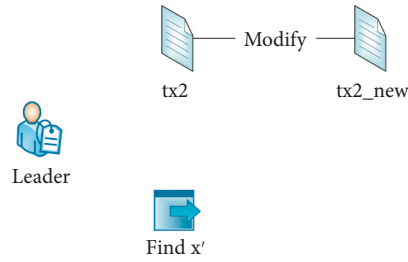


FIGURE 10: Operation of the Leader.

```

h(tx):
ca5c4a603d75c6a9d32c7ee36f4ffe0674d473f26760d4c09d658cb175569580ca5c4a603
d75c6a9d32c7ee36f4ffe0674d473f26760d4c09d658cb175569580ca5c4a603d75c6a9d
32c7ee36f4ffe0674d473f26760d4c09d658cb1755695800000000

g(x):
efcd19ddc10422480f18792b6d77be29f288f644cb4b1625c9754f7aa0c8f93304df99bc
f6188b139e429d07d78d8177a90babaec7e7b7b42b6bcb0ed6e9712e9c986111fda10b6
02d99f4a0d64f2e9a566324432d8990810412e3d215f0083a5df14ec

h(tx) XOR g(x):
259153bdfc71e4e1dc3407c80238402f865c85b6ac2bc2e55410c3cbd55a1a13fa11b3fb
f2144e18eac85733123726110e44c9488b1eafbbdfd33001983802922395cc7122afd61f
d1f5e1a9622b0cefd1b241b655b84dc88d24a28c54099503a5df14ec

h(txnew):
5f03ca15f22bf2fae168783fdb976a740e00744eb9b7b7240b6586b8b12695f03ca15f
22bf2fae168783fdb976a740e00744eb9b7b7240b6586b8b12695f03ca15f22bf2faeb
ea168783fdb976a740e00744eb9b7b7240b6586b8b1269000000000

g(x'):
7a9299a80e5a161b37de114f81c5f959211c65b1e8c0599e26507593bed1087aa51279ee
003fbce2012241b491ca9f67a904294cfff534c0ad938659f3b310fb7c960664d08424e53a
1ff72ee1d6b59976f2a1b11153d6b3ff6414d43f82876aa5df14ec

h(txnew) XOR g(x'):
259153bdfc71e4e1dc3407c80238402f865c85b6ac2bc2e55410c3cbd55a1a13fa11b3fbf
2144e18eac85733123726110e44c9488b1eafbbdfd33001983802922395cc7122afd61fd
1f5e1a9622b0cefd1b241b655b84dc88d24a28c54099503a5df14ec

Merkle root:
3d8430dc65c27e587633600426c43feea1b9eae232063ea11001fcb88ff513ec
    
```

FIGURE 11: Program result.

The block Leader (node 1) publishes the packaged block and signature to the network. Then, all nodes in the network vote on the legitimacy of the transactions and verify the signature in the block. Next, the block Leader (node 1) collects the vote information and stores it in the reputation sub-block. After the nodes finish the validation and vote in agreement for the block, block 1 is officially uploaded. After block 1 Leader (node 1) uploads block 1, the rest nodes in the network verify the legitimacy of block 1 and update their local blockchain data to achieve the consistency of the distributed data if passing the verification.

4.3. Modification of Block Data. Suppose a blockchain-based health record system needs to update a customer’s personal data in compliance with GDPR at the customer’s request. Under the EU General Data Protection Regulation (GDPR), Bob as a customer is entitled to demand his personal data be accurate, be up to date, or be deleted. For example, Bob can request that his contact information be updated after he has changed a phone number or moved to a new address. For example, Bob informs his hospital that he has moved home. His hospital is obliged to update Bob’s personal information, and the hospital can send an “Address change” Request to the medical blockchain system with Bob’s ID.

```

txorg = {
  id : 1,
  Height : 0,
  Patient_ID:2:
  Action : customer change address,
  datanew:{Address : 78 some street,zhengzhou},
  x : 635635635,
  x' : 1183451931,
  Public_key of Leader :
    87979b12e898279dfae24641faf44b10b9c623484224e5b0b8929731e3127
87979b12e898279dfae24641faf44b10b9c623484224e5b0b8929731e31276af
  41d3d810d04038fece131e38c28106429bbfe325d6bc0f9a46f34a8b2b0f4
41d3d810d04038fece131e38c28106429bbfe325d6bc0f9a46f34a8b2b0f4a82,
  time : 2021-06-21,
  rt_set : {
    Public_key of voter1 :
      e9f783b762a864afb2b2483a8d92f4a0f979fd49b89506092b6b7cdc
e9f783b762a864afb2b2483a8d92f4a0f979fd49b89506092b6b7cdc7fb1bba9
  14fd193514171f9eeb480424275fde4bb8d1e895f4afb315f0121371
14fd193514171f9eeb480424275fde4bb8d1e895f4afb315f012137135d33ed0,
      Reputation Value : 7.93633744,
      Opinion : Agree,
      Block Hash :
e438533e762e25be6141aed6efbc55e37c4fa428ed4e2b0a897c6cad15b4567,
      Signature:
94532e3d3d8afa58838c4f5c2137fa3c3dc7e4eaf290b1d2595e2ad633e7d13e
bc3f08a3ed14c4e1761de5426d56346e4d58059837bf75685828301cf7038173,
    }, {
      Public_key of voter2 :
        e88f5ce03fa86f77b19f42d59c59e1a69f4ab714ba9006f50255165a530be
e88f5ce03fa86f77b19f42d59c59e1a69f4ab714ba9006f50255165a530be1d54
        a9899009bcb895636c90079f92938b902ffb4f570a80859e585f2668fdc10
a9899009bcb895636c90079f92938b902ffb4f570a80859e585f2668fdc1087,
        Reputation Value : 8.14385619,
        Opinion : Agree,
        Block Hash :
e438533e762e25be6141aed6efbc55e37c4fa428ed4e2b0a897c6cad15b4567,
        Signature:
94532e3d3d8afa58838c4f5c2137fa3c3dc7e4eaf290b1d2595e2ad633e7d13e
9d4a74d72bccfc3a10c3c6686907cd3b2d1b49b46597f22c85c444b385708d01,
    }, {
      Public_key of voter3 :
        de31612374ea9e9a8f7e7d2d6650f32bdcc780f2749f4edb25f9e09d7726f8bf2
de31612374ea9e9a8f7e7d2d6650f32bdcc780f2749f4edb25f9e09d7726f8bf2
        a623e2fbf708dface87c68abdd5072c830cc350832f8cace015f57b8897f8
a623e2fbf708dface87c68abdd5072c830cc350832f8cace015f57b8897f887,
        Reputation Value : 7. 43633744,
        Opinion : Agree,
        Block Hash :
e438533e762e25be6141aed6efbc55e37c4fa428ed4e2b0a897c6cad15b4567,
        Signature:
94532e3d3d8afa58838c4f5c2137fa3c3dc7e4eaf290b1d2595e2ad633e7d13e
25fb066cc7c7f862f826525f7f9325132fb915580929f60a94e788f9dba73156,
    },
    ...
  }
}

```

FIGURE 12: Details of transaction record *txorg*.

$$\text{Request} = \{ 'Height : 0', 'ID : 2', 'Action: customer changed address, Address : 78 some street, zheng zhou' \}. \quad (14)$$

All nodes (participating hospitals) in the blockchain-based health record system validate whether the modification request is legitimate. If they approve the modification request, the Leader of block 1 performs the modification as shown in Figure 10 to update this customer's personal record. Block 1 Leader (node 1) can calculate a new number x'

$$\text{SHA256}(tx_{2_{\text{new}}}) = 5f03ca15f22bf2faebea168783fdb976a740e00744eb9b7b7240b6586b8b1269. \quad (15)$$

The value of $g(x')$ is as follows:

$$g(x') = 7a9299a80e5a161b37de114f81c5f959211c65b1e8c0599e26507593bed1087aa51279ee003fbce2012241b491ca9f67a904294fcff534c0ad938659f3b310fb7c960664d08424e53a1ff72ee1d6b59976f2a1b11153d6b3ff6414d43f82876aa5df14ec. \quad (16)$$

Decryption to calculate the new number is as follows:

$$x' = 1183451931(468a0b1b). \quad (17)$$

Figure 11 shows the result of the program. We can calculate the result of XOR operation. Therefore, the transaction Merkle root is the same after updating this customer's health record.

The signature and the hash of the block header will not change if the transaction Merkle root does not change after the modification, so the links of blocks are not affected. After completing the modification, block 1 Leader (node 1) generates a new transaction record called tx_{org} and publishes it to the network, as shown in Figure 12, for legitimacy verification by the rest nodes in the network.

The other nodes in the network verify whether the modification is legal according to tx_{org} , and update their local blockchain data if the amendment is legitimate, which completes the modification operation.

After the modification, both the transaction Merkle root and the block header's hash are unchanged; the links of blocks are not affected, so the modification operation is feasible.

5. Conclusion

A redactable blockchain scheme based on the PoR consensus mechanism is put forward in this paper to address the problem of amending or removing erroneous or sensitive data on blockchains of MEC applications. The proposed Merkle tree structure uses the one-way trapdoor function characteristics, which ensures the Merkle root does not change after modifying a transaction, so the links of blocks are not affected. Although only the block Leader node with the trapdoor can legally perform the modification operation, the modification operation also needs to be validated and

to execute the amendment without affecting the transaction Merkle root and the links of blocks.

The new number $x' = g^{-1}(h(tx) \oplus g(x) \oplus h(tx_{\text{new}}))$ is calculated, which satisfies (6).

The hash of $tx_{2_{\text{new}}}$ is as follows:

agreed upon by the nodes of the whole network to ensure the integrity and security of the blockchain.

Data Availability

Our experimental results are available from the corresponding author upon request.

Conflicts of Interest

The authors declare that they have no conflicts of interest.

Acknowledgments

This work was supported by the Henan University Science and Technology Innovation Team Support Plan (20IRTSTHN013), Shaanxi Key Laboratory of Information Communication Network and Security, Xi'an University of Posts & Telecommunications, Xi'an, Shaanxi 710121, China (ICNS202006), the Fundamental Research Funds for the Universities of Henan Province (NSFRF210312), and the Youth Talent Support Program of Henan Association for Science and Technology (2021HYTP008).

References

- [1] S. Guo, Y. Dai, S. Guo, and X. F. Qiu, "Blockchain meets edge computing: stackelberg game and double auction based task offloading for mobile blockchain," *IEEE Transactions on Vehicular Technology*, vol. 69, no. 5, pp. 5549–5561, 2020.
- [2] Z. Qu, H. Sun, and M. Zheng, "An efficient quantum image steganography protocol based on improved EMD algorithm," *Quantum Information Processing*, vol. 20, no. 2, pp. 53–29, 2021.
- [3] M. Zhaofeng, W. Xiaochang, D. K. Jain, and H. G. W. Khan, "A blockchain-based trusted data management scheme in edge computing," *IEEE Transactions on Industrial Informatics*, vol. 16, no. 3, pp. 2013–2021, 2020.

- [4] Y. Yuan and F.-Y. Wang, "Blockchain and cryptocurrencies: model, techniques, and applications," *IEEE Transactions on Systems, Man, and Cybernetics: Systems*, vol. 48, no. 9, pp. 1421–1428, 2018.
- [5] E. Zaghloul, T. Li, M. W. Mutka, and J. Ren, "Bitcoin and blockchain: security and privacy," *IEEE Internet of Things Journal*, vol. 7, no. 10, pp. 10288–10313, 2020.
- [6] N. Z. Tomić, "A Review of consensus protocols in permissioned blockchains," *Journal of Computer Science Research*, vol. 3, no. 2, pp. 32–39, 2021.
- [7] Y. Xiao, N. Zhang, W. Lou, and Y. T. Hou, "A survey of distributed consensus protocols for blockchain networks," *IEEE Communications Surveys & Tutorials*, vol. 22, no. 2, pp. 1432–1465, 2020.
- [8] Z. Qu, Y. Huang, and M. Zheng, "A novel coherence-based quantum steganalysis protocol," *Quantum Information Processing*, vol. 19, no. 10, pp. 362–419, 2020.
- [9] Q. W. Zhuang, Y. Liu, L. S. Chen, and Z. Ai, "Proof of Reputation: A Reputation-Based Consensus Protocol for Blockchain Based Systems," in *Proceedings of the the 2019 International Electronics Communication Conference*, pp. 131–138, Okinawa, Japan, November 2019.
- [10] K. Huang, X. Zhang, Y. Mu et al., "Building redactable consortium blockchain for industrial internet-of-things," *IEEE Transactions on Industrial Informatics*, vol. 15, no. 6, pp. 3670–3679, 2019.
- [11] c. Li, H. Rao, A. Xu, and X. H. Guo, "Strategic research on China energy technology revolution system," *Chinese Journal of Engineering Science*, vol. 20, no. 3, pp. 1–8, 2018, In Chinese.
- [12] Y. L. Ren, D. T. Xu, X. P. Zhang, X. Eng, and G. D. Wu, "Scheme of revisable blockchain," *Journal of Software*, vol. 12, pp. 3909–3922, 2020, In Chinese.
- [13] E. Politou, F. Casino, E. Alepis, and C. Patsakis, "Blockchain mutability: challenges and proposed solutions," *IEEE Transactions on Emerging Topics in Computing*, vol. 9, no. 4, pp. 1972–1986, 2021.
- [14] Z. Qu, S. Chen, and X. Wang, "A secure controlled quantum image steganography algorithm," *Quantum Information Processing*, vol. 19, no. 10, pp. 380–425, 2020.
- [15] D. Lee and N. Park, "Blockchain based privacy preserving multimedia intelligent video surveillance using secure Merkle tree," *Multimedia Tools and Applications*, vol. 80, no. 26-27, pp. 34517–34534, 2021.

Research Article

Research on Video Captioning Based on Multifeature Fusion

Hong Zhao, Lan Guo , ZhiWen Chen, and HouZe Zheng

School of Computer and Communication, Lanzhou University of Technology, Lanzhou, Gansu, China

Correspondence should be addressed to Lan Guo; guolan@lut.edu.cn

Received 22 March 2022; Revised 9 April 2022; Accepted 15 April 2022; Published 28 April 2022

Academic Editor: Le Sun

Copyright © 2022 Hong Zhao et al. This is an open access article distributed under the Creative Commons Attribution License, which permits unrestricted use, distribution, and reproduction in any medium, provided the original work is properly cited.

Aiming at the problems that the existing video captioning models pay attention to incomplete information and the generation of expression text is not accurate enough, a video captioning model that integrates image, audio, and motion optical flow is proposed. A variety of large-scale dataset pretraining models are used to extract video frame features, motion information, audio features, and video sequence features. An embedded layer structure based on self-attention mechanism is designed to embed single-mode features and learn single-mode feature parameters. Then, two schemes of joint representation and cooperative representation are used to fuse the multimodal features of the feature vectors output by the embedded layer, so that the model can pay attention to different targets in the video and their interactive relationships, which effectively improves the performance of the video captioning model. The experiment is carried out on large datasets MSR-VTT and LSMDC. Under the metrics BLEU4, METEOR, ROUGEL, and CIDer, the MSR-VTT benchmark dataset obtained scores of 0.443, 0.327, 0.619, and 0.521, respectively. The result shows that the proposed method can effectively improve the performance of the video captioning model, and the evaluation indexes are improved compared with comparison models.

1. Introduction

With the rapid development of the mobile Internet and the rapid popularization of intelligent devices, from “Internet + Plus” to “AI + Plus,” the process of human informatization has entered a new stage. As a new type of user-generated content, short video has widely appeared on various social platforms. While people interact through video, some unhealthy videos such as terrorist violence and pornography take advantage of it, which seriously endanger the physical and mental health of young people. Therefore, the audit of short video content is of great significance. Most of the existing video auditing methods use manual means, but manual auditing has poor real-time performance and low efficiency. Using the deep learning for video content auditing can not only improve the accuracy of the audit but also support the video screen, text, and speech for multi-dimensional audit. Therefore, how to obtain the main information from short videos and convert it into natural language, analyze, and understand it has become a hot research topic in the field of text expression of video content. Video captioning is a cross-modal, cross-disciplinary

research, and has been a challenging research topic in the computer and multimedia fields [1, 2]. The video captioning aims at expressing the objects, attributes, and mutual relationships presented in the video in natural language. The research has broad application prospects, including helping visually impaired people to understand visual content such as movies and short videos, and helping existing video social platforms to identify the objectionable content.

The early work of video captioning is based on the fixed template structure [3–5], which mainly includes two phases, content recognition, and sentence generation from template. The content recognition stage is to visually recognize and classify the main objects in the video. The stage of generating sentences according to the template is to match the entities identified by the content with the categories required by the template, such as subject, predicate, object, and location. However, the method relies too much on the preset template, resulting in poor flexibility in generating descriptions and the simplex sentences. Inspired by the machine translation direction encoder-decoder framework, the current mainstream methods of video captioning use convolutional neural networks (CNNs) [6–8] in advance, which are widely

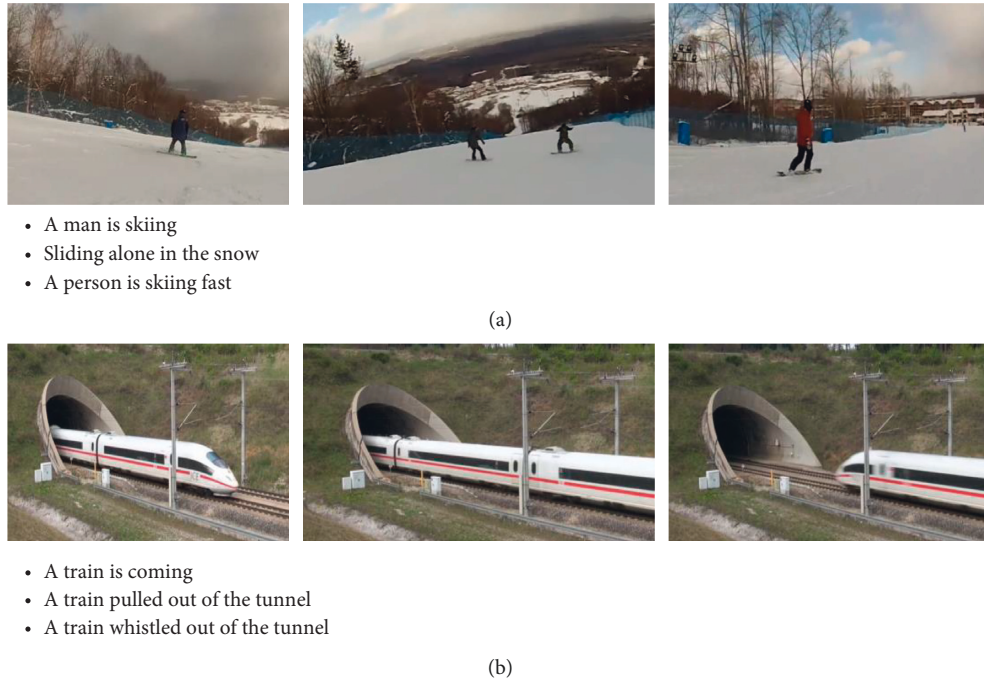


FIGURE 1: The video contains not only physical objects, but also features such as sound. When we pay more attention to these supplementary features, the generated text will be more complete. (a) Video example of fast skiing. (b) Video example of a train honking out of a tunnel.

used in the field of object recognition and detection, to obtain visual information and generate vision representation vector, and then use recurrent neural networks (RNNs) [9–11] that have made great progress in natural language processing as the encoder to receive the visual representation vector for encoding, generate the intermediate hidden vector, and send it to the decoder composed of RNN so as to generate serialized natural language expression. For example, literature [12] uses CNN to extract the image features of each frame in the video, sends it to the RNN encoder for encoding in time sequence, generates the intermediate hidden vector, and sends it to the decoder to generate the description text of the video. Literature [13] improves the performance of the video description text network by adding explicit high-level semantic attributes of images and videos, but these attributes are extracted from a single modality, which is not enough to fully understand the video. The actual video is constructed from a number of different modal contents, which contains not only a single image information, but the information such as the motion of the object in the video, the audio in the background, and the timing of the context, and the information of different modalities. There is a high degree of correlation and complementarity between them, and these modalities cooperate with each other to provide complete information. As depicted in Figure 1(a), the example video can be described as “a person is skiing fast,” in which “fast” is highly related to sports information; in Figure 1(b), the example video can be described as “there is a train whistling out of the tunnel,” in which “whistling” is closely correlated to the audio information.

Video is a recording carrier based on static pictures, but it is a higher expression than static pictures. With the movement of the object and the camera, the composition

structure and plot focus of the video screen will change accordingly, and the perspective relationship of the objects in the video will also change. This change is called the motion feature of the video; the optical flow graph of video has apparent feature invariance and contains coherent motion trajectory information. The accuracy of optical flow at the boundary and small displacement has a strong correlation to the capture of video motion information. The audio signal carried by the video is also of great significance to the video. Video dubbing can explain the main points and themes of the video in the form of sound. For example, applause and whistle can only be captured from audio information. Aiming at the problem of low accuracy of video captioning based on a single visual feature, and the high correlation and complementarity between different modal information, this article uses the fusion of multiple complementary modal information to train the video captioning model. Firstly, each frame of video in the dataset is converted into a single JPEG image, and the audio information of each extracted video is stored as an audio file in wav format. Then, the representation information of static image, audio, motion, optical flow, and other modes is extracted from the extracted modal data to cross-modal information fusion, and to generate a richer and more accurate video captioning. The main work of the research is as follows:

- (1) According to different video modal information, various models pretrained by large-scale datasets are used to extract static, dynamic, and audio information in video, which improves the accuracy of the text expression of the video content.
- (2) An embedded layer based on self-attention mechanism is designed to embed the single-mode

eigenvector and learn the network parameters needed in sentence generation. The complementary information between different modes can be fitted better when encoding.

- (3) Two schemes of joint representation and collaborative representation are used for cross-modal feature fusion, and it is verified that the collaborative representation strategy has better experimental results in this model when fusing multiple complementary video modal information.

2. Related Work

The video captioning aims at analyzing, understanding, and expressing the content displayed in the video through the use of natural language. At present, the mainstream methods of video captioning are based on the “coding decoding” architecture, which can be divided into three types: methods based on visual feature mean/maximum, video sequence memory modeling, and three-dimensional convolution features.

The method based on the mean/maximum value of visual features extracts the visual features by employing the mean value or the maximum value, and then encodes the features and decodes them to generate the natural language text. Venugopalan et al. [14] adopted an LSTM-MY model that uses mean pooling to extract visual features, and its performance is improved compared with the template-based method. Dong et al. [15] proposed the ruc-uva model to solve the problem of insufficient relevance of generated text and video content. This model extracts video keywords by combining the video tagging method and then combines the keywords and video frame features as the input of the decoder, which effectively improves the accuracy of the generated text. However, these methods are difficult to capture the time-series characteristics in video clips, which could cause the loss of dynamic features easily.

The method based on video sequence memory modeling effectively solves the problem that time-series features in video clips are difficult to capture. Literature [16] adopted a temporal attention (TA) model for video data preprocessing, which combines attention mechanism in the time dimension, generates text from the resulting feature input decoder, and selects the frame with the greatest correlation with the content to be generated in a time step to make the generated sentences more adaptable. Literature [17] applies the sequence-to-sequence model to the video to text task to solve the problem of variable length of video to text, and realizes the end-to-end video description of video frame sequence input and text sequence output. Although this type of model can realize the time-series feature extraction and end-to-end training of the language module, the CNN feature could easily lead to the destruction and loss of the spatial information in the video frame after the sequence transformation.

The method based on 3D convolution features can mine the static and temporal dynamic features of video at the same time by encoding the spatiotemporal features of video. In literature [18], the proposed model uses the 3D convolutional network to extract the three-dimensional features of

different video segments, calculates the average value of multiple three-dimensional feature vectors, and then combines them with the average value of the CNN feature extracted from the video frame as the feature representation of the video. The features extracted by the 3D convolution network contain some dynamic information of video, which improves the performance of the model to a certain extent. Literature [19] proposed the M^3 – inv3 model that jointly models visual information and language information by extracting the 2D and 3D features of the video frame, which better solved the problem of the long-term dependence of multimodal information and semantic dislocation in LSTM. Literature [20] proposes a hierarchical LSTM with the adaptive attention method for image and video captions, which uses spatial or temporal attention to select regions to predict related words. Literature [21] presents a grammar prediction action module that combines the region target features with the spatial location information of the corresponding region to form a new region target feature to guide the description generation. To further selectively integrate semantic features into the description generation model, Ryu et al. (2021) [22] used semantic alignments to establish the correlation between a word phrase and a video frame and used semantic focusing mechanism to group semantically related frames. The visual and semantic features are then passed to the codec to generate the description.

The proposed model does not fully utilize the extracted single-mode representation information and take into account the audio information carried by the video to the model. Therefore, considering the complementarity between single-mode feature parameter learning and video multimodal representation information, the semantic attributes expressed by each mode are obtained by extracting the representation information of multiple modes of video, so as to improve the performance of the video captioning model.

3. Video Captioning Model

3.1. Model Structure. The structure of the cross-modal video captioning model based on multilayer attention is shown in Figure 2. It mainly includes four parts: video preprocessing, single-modal feature extraction, coding (single-modal information embedding, multimodal information fusion), and decoding. Among them, the video preprocessing module mainly extracts the video frame and the video audio information. The single-mode feature extraction module uses the improved ResNet network [23], FFmpeg, two-stream inflated 3D convolution network [24] (I3D) to extract 2D frame features, audio MFCC features, and optical and 3D motion features of the video after increasing channel attention. The designed embedded layer is composed of a self-attention mechanism [25] and a two-layer LSTM network [26], and the encoder takes the feature vectors of the frame, motion, and audio modes as input, feeds different modal features into the embedded layer for single-mode modeling, and finally codes them into three hidden vectors $\{h_v, h_{I3D}, h_{audio}\}$ and maps the information of multiple modes together to a single multimodal vector space V_{multi} through collaborative representation. The decoder receives

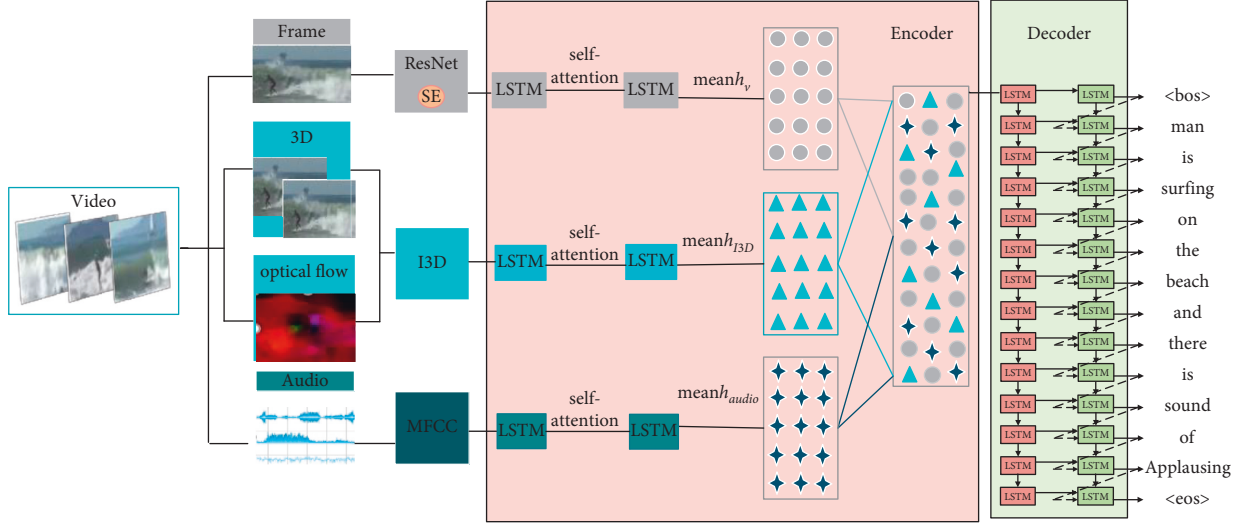


FIGURE 2: The architecture of the MM-V2T (multimodal video content text generation model). Specifically, the MM-V2T is composed of three parts as follows: video preprocessing, single-modal feature extraction, coding (single-modal information embedding, multimodal information fusion), and decoding.

V_{multi} for decoding, predicts the hidden state of the current time, outputs the probability distribution vector of each time step in turn, and uses the greedy search algorithm to take the word with the highest probability at each time step at the decoding time as the predicted output result. The word probability model of time T is shown in

$$P_t(Y)_t = \arg \max(\text{softmax}(h_t, Y_{t-1}, V_{multi})), \quad (1)$$

where h_t is the current hidden state, Y_{t-1} is the result of the last time step, V_{multi} is a unified multimodal vector space, softmax is a normalized exponential function, mapping the result to (0,1) as a probability value, and $P_t(Y)_t$ represents the probability distribution of each word in the current time step. When all probability distributions are calculated, the greedy search algorithm is used to extract the word with the highest probability in each time step at the decoding time as the prediction output until the output is $\langle eos \rangle$ and the decoding is completed.

3.2. Feature Extraction. Video data differ from picture data in that video is multiframe snapshot, which makes video more suitable for describing continuous actions or pictures. Meanwhile, the video is attached with corresponding real-time sound information, so that the video can record an event more stereoscopically and vividly. Compared to a single image, the video contains not only spatial features but also temporal features, as well as audio and motion features. Because the continuous frame structure in the video conveys a wealth of information, it is difficult to determine in the context of the more significant content to accurately describe. For this reason, we use multimodal features of video to express video content text.

For the static feature extraction of video frames, a channel attention framework unit squeeze and excitation (SE) proposed in literature [27] is added to the residual

network ResNet152 network [28] to extract frame-level 2D features.

For the extraction of dual-stream 3D features of video, the two-stream inflated 3D convolution network (I3D) proposed by the DeepMind team is adopted [29]. This network structure adds the idea of dual stream into 3D convolution, which can make the network better extract the spatiotemporal information of video and capture fine-grained temporal features.

For the extraction of audio information in the video, FFmpeg is used to extract the Mel frequency cepstral coefficient (MFCC) of the voice signal.

3.2.1. Channel Attention. The attention mechanism in deep learning draws lessons from the human visual system. For example, the human visual system tends to focus on the key information that assist judgment in the image and ignore the irrelevant information [30]. Therefore, the attention mechanism is essentially similar to the human selectivity mechanism. Attention in deep learning refers to the weight of learning parameters. The core task is to select the information more related to the current model goal from the extracted information. The extraction of video frame-level features actually extracts different information from each frame picture in different channels, so adding channel attention can give greater weight to important features. In the SE module [27], the interdependence between channels is explicitly modeled and the channel-type feature response is adaptively recalibrated. Through this mechanism, the model can learn to use global information to selectively emphasize important features and suppress redundant features. SE module realization and its structure are shown in Figure 3.

In the SE module, there are three key operations: squeeze, excitation, and reweight. In Figure 3, (a) network input matrix X is given, and its characteristic channel is C' .

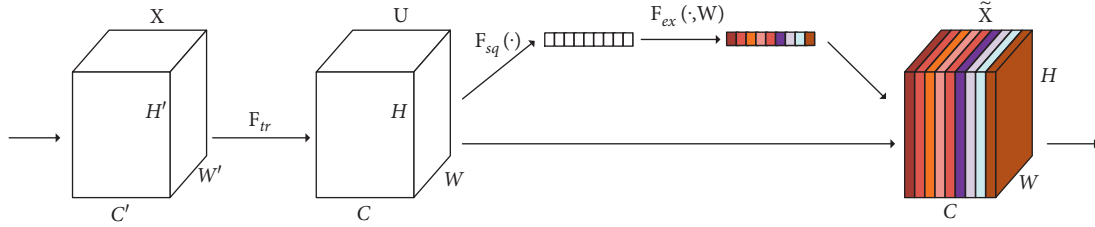


FIGURE 3: SE network structure.

After a series of convolution and other operations, a characteristic diagram with the number of characteristic channels of C is obtained. Then, the three operations of the SE module are used to recalibrate the previously obtained feature map U .

The first is the squeeze operation. This operation compresses the feature map U along the spatial dimension. The two-dimensional information of each characteristic channel is compressed into a real number Z_C , which has a global receptive field to a certain extent. Z_C represents the global information of the response on the characteristic channel. Formally, the statistic Z_C is generated by reducing the space dimension ($H * W$) of the characteristic graph U , so the c th element of z is calculated in the following:

$$Z_C = F_{sq}(U_c) = \frac{1}{H \times W} \sum_{i=1}^H \sum_{j=1}^W u_c(i, j). \quad (2)$$

In order to take advantage of the information gathered in the squeeze operation, the second important operation exception is carried out. The exception is similar to the design of the gate in the cyclic neural network structure. This operation aims at capturing the channel dependence completely. The excitation operation is implemented with two fully connected (FC) structures to reduce the model complexity and to improve the model generalization ability. The first FC layer reduces the C channel into c/r channels, and the dimension reduction factor r is a super parameter. The second FC layer is used to restore the original dimensions of the feature map. Finally, a weight coefficient S is obtained, which is calculated as in the following equation:

$$S = F_{ex}(z, w) = \sigma(g(z, w)) = \sigma(w_2 \delta(w_1 z)), \quad (3)$$

where σ represents the sigmoid function and δ represents the ReLU function, $w_1 \in R^{c/r \times c}$, $w_2 \in R^{c \times c/r}$

Finally, the reweight operation is performed. The weight output from the previous operation is weighted to the previously obtained feature map U channel by channel, and the recalibration of the original feature on the channel dimension of the feature map is completed to obtain the final attention feature \tilde{X}_C . The calculation of \tilde{X}_C is shown in the following equation:

$$\tilde{X}_C = F_{scale}(u_c, s_c) = s_c \cdot u_c, \quad (4)$$

where F_{scale} refers to the channel multiplication between the attention weight s_c and the feature map u_c .

The SE module finally performs an attention or gating operation in the channel dimension. This attention mechanism allows the mode to pay more attention to the channel features with the largest amount of information and suppress the unimportant channel features.

3.2.2. Feature Extraction of Video Frame. For the video frame feature extraction part, the SE (squeeze and excitation) module is added to the improved ResNet152 network structure and used as the video frame feature to extract the network. As shown in Figure 4, the SE module is embedded in the ResNet152 network to readjust the important features extracted by the network, so that the global information can be used to measure the importance of each feature and obtain the correlation between two channels, so as to assist in the recalibration of features. In order to simplify the complexity of model parameters, a $1 * 1$ full connection layer is adopted at both ends of the ReLU activation function of the SE module [31]. The advantages of this approach are as follows: (1) making the network more nonlinear and better fitting the complex correlations between channels; and (2) promoting useful features and suppressing features that are of little use to the current task.

Each video in the dataset is preprocessed into fixed frames, and 80 of them are taken as sample frames at equal intervals. Then, these sample frames are sent to the SE-ResNet model pretrained on the large-scale image dataset ImageNet to extract the feature information of the frames and obtain a high-dimensional feature vector of $80 * 2048$.

3.2.3. Feature Extraction of Two-Stream I3D. Two-stream inflating 3D convolution network [29] I3D is one of the latest 3D convolutional networks proposed by the deep mind team. Since two-stream can capture action information simply and effectively, this network structure adds the idea of dual stream to construct an I3D network in 3D convolution. One 3D structure is used to receive RGB information, and the other is used to receive optimized smooth optical flow information. These two 3D convolution structures are derived by improving the 2D convolution structure Inception v1, as shown in Figure 5(a). The convolution kernel parameters in the 2D structure are repeated in the time dimension to form the parameters of the 3D convolution kernel, and then, the parameters are divided by N to ensure that the network output is the same as the 2D convolution.

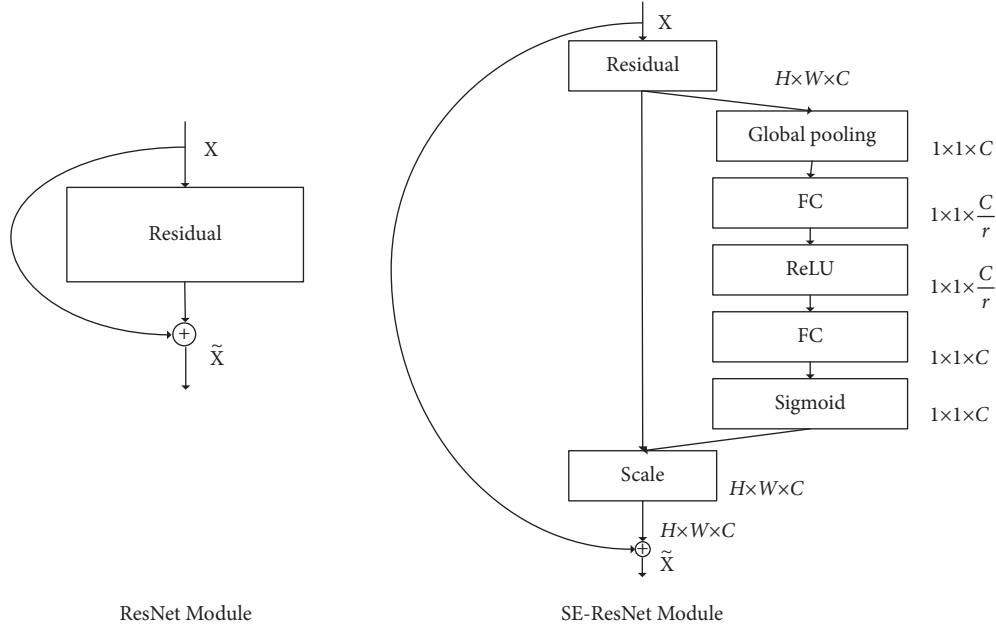


FIGURE 4: ResNet original structure and ResNet structure embedded with SE module.

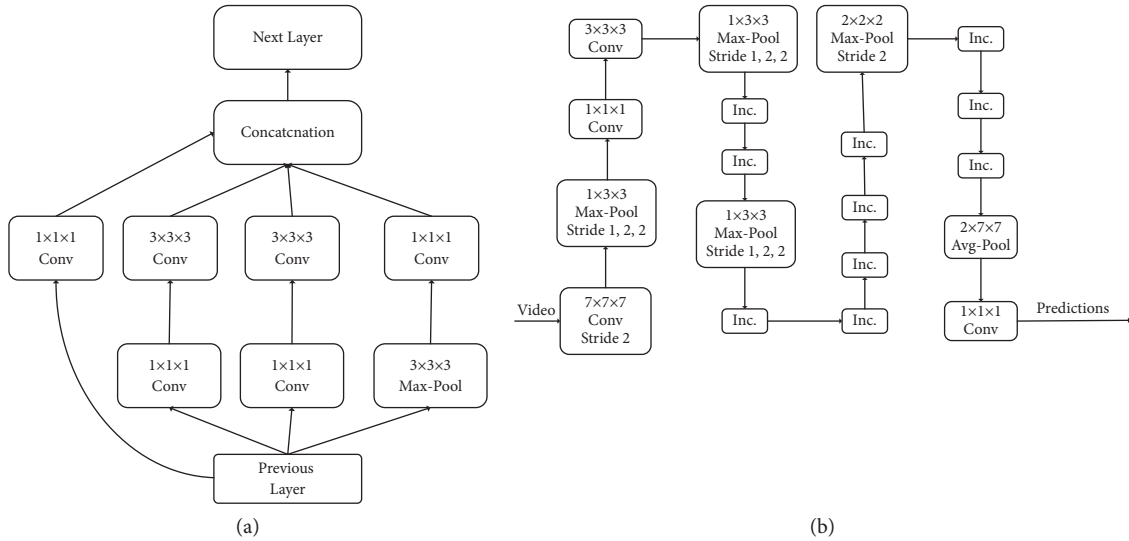


FIGURE 5: Three-dimensional convolution and two-stream expansion 3D convolution network structure. (a) 3D Inception V1. (b) I3D.

Therefore, the convolution kernel and pooling increase the time dimension, and other nonlinear layer structures remain unchanged. The network connection details are shown in Figure 5(b). Although 3D convolution can learn the time features of a video directly, it only performs pure forward propagation, and the optical flow algorithm provides some iterative ideas in it, the recognition accuracy of the network can be improved by adding optical flow.

Each video in the dataset is preprocessed into a $224 * 224$ fixed frame and sent it to the I3D model pretrained on the large-scale image dataset ImageNet and the video dataset kinetics to extract the dynamic features of the video to obtain a feature vector.

3.2.4. Feature Extraction of Audio MFCC. At present, the commonly used speech feature extraction methods include linear prediction cepstral coefficient extraction method [32], linear predictive cepstral coefficient (LPCC), and Mel frequency cepstral coefficient extraction method [33], and Mel frequency cepstral coefficient (MFCC). MFCC was proposed by Stevens, Volkman, and Newman in 1937. MFCC is mainly based on human nonlinear auditory mechanism to simulate the function of the human ear for speech frequency analysis, so as to better extract speech signal features. Mel is the measurement unit of perceived tone or tone frequency, and 1 Mel is 1/1000 of the tone perception degree of 1000 Hz. The specific definition is shown in the following equation:

$$f_{mel} = 2595 \log_{10} \left(1 + \frac{f_{Hz}}{700} \right), \quad (5)$$

$$f_{mel} = 1125 \ln \left(1 + \frac{f_{Hz}}{700} \right),$$

where f_{Hz} is the actual linear frequency and f_{mel} is the Mel frequency standard.

The cepstrum parameter feature of the Mel filter plays an important role in speech feature extraction. Its calculation is simple, and its discrimination ability is prominent. The feature parameter extraction principle of MFCC is shown in Figure 6.

First, the audio signal extracted from the dataset is preprocessed, such as pre-emphasis, framing, and windowing, and then, the corresponding discrete Fourier

transform is performed on the single frame signal after framing to obtain the frequency-domain data, as shown in the following equation:

$$X_i(k) = \sum_{n=1}^N x_i(n) \text{ExponentialE} \left[\frac{-j^2 \pi n k}{N} \right]; \quad 1 \leq k, n \leq N, \quad (6)$$

where $x(k)$ represents the time domain signal; $x_i(k)$ is the data of the i -th frame; and K represents the k th spectral line in the frequency domain.

Secondly, the frequency-domain data obtained above are filtered by W Mel frequency filters, and the spectrum, Mel filter banks, and frequency envelope are extracted. The frequency-domain response of the filter $H_w(k)$ is in the following equation:

$$H_w(k) = \begin{cases} 0, & k < f(w-1) \\ \frac{2(k-f(w-1))}{(f(w+1)-f(w-1))(f(w)-f(w-1))}, & f(w-1) \leq k < f(w) \\ \frac{2(f(w+1)-k)}{(f(w+1)-f(w-1))(f(w)-f(w-1))}, & f(w) \leq k \leq f(w+1) \\ 0, & k > f(w+1) \end{cases}, \quad (7)$$

where $\sum H_w(k) = 1$; $f(w)$ is the center frequency of the filter.

Then, the logarithm of the processed energy spectrum is taken so that the amplitude multiplication in the Fourier transform is converted into addition to obtain the logarithmic energy, which is calculated in the following equation:

$$S_i(w) = \ln \left(\sum_{k=0}^{N-1} |X_i(k)|^2 H_w(k) \right); \quad 0 \leq w < W, \quad (8)$$

where i is the i -th frame and k is the k -th spectral line in the frequency domain.

Finally, it is substituted into the discrete cosine transform (DCT) to obtain the MFCC coefficient, which is calculated in the following equation:

$$MFCC(i, n) = \sum_{w=0}^{W-1} S(w) \cos \left(\frac{\pi n (w + 0.5)}{W} \right), \quad (9)$$

$$0 \leq w < W, n = 1, 2, \dots, L.$$

where W is the w -th Mel filter, i is the i -th frame, and n is the spectral line obtained after DCT.

The audio extracted from each video in the dataset is divided into 1120 frames, and the MFCC signal of 20 dimensions is extracted from each frame and stored as an $1120 * 20$ high-dimensional audio feature matrix.

3.3. Feature Fusion. The information fusion of different modes is a key point in multimodal research, which integrates the information extracted from different modes into a stable multimodal representation. There are two multimodal feature fusion strategies [34]: joint representations and coordinated representations.

Joint representation is shown in Figure 7; this method maps the information of multiple modes together into a unified multimodal vector space. After multiple modal features x_1, \dots, x_m are obtained, the characteristic $X = f(x_1, \dots, x_m)$ is obtained by splicing and fusing. When the splicing vector dimension is high, principal component analysis (PCA) dimensionality reduction operation is carried out to form a multidimensional feature vector space $F = PCA(X)$.

Collaborative representation is shown in Figure 8. Instead of seeking fusion, this method models the correlation among various modal data but maps the information of

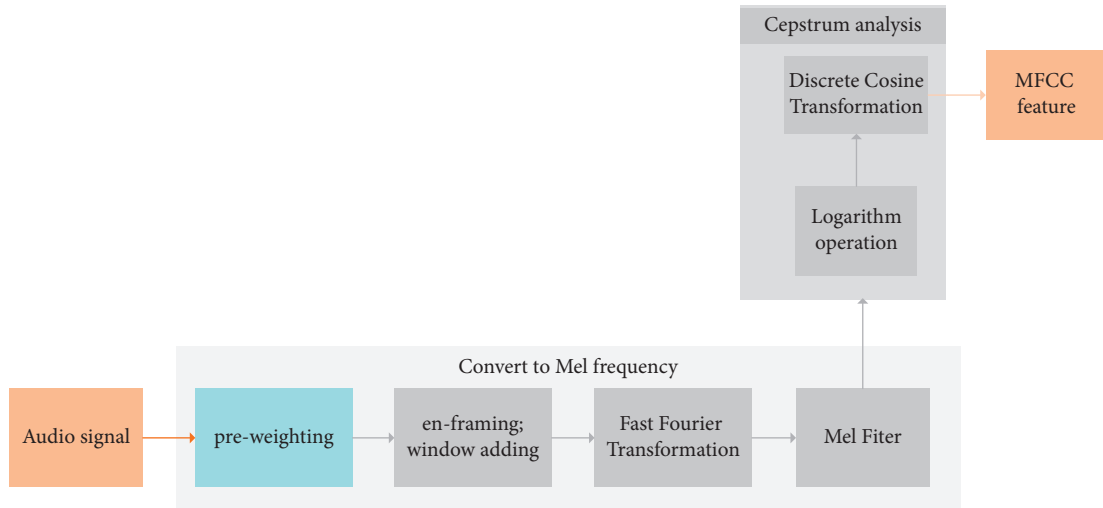


FIGURE 6: MFCC feature parameter extraction.

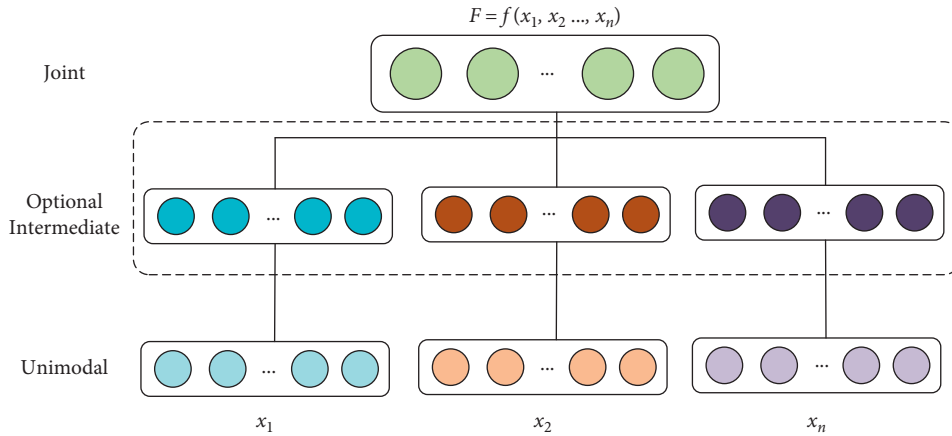


FIGURE 7: Joint representation.

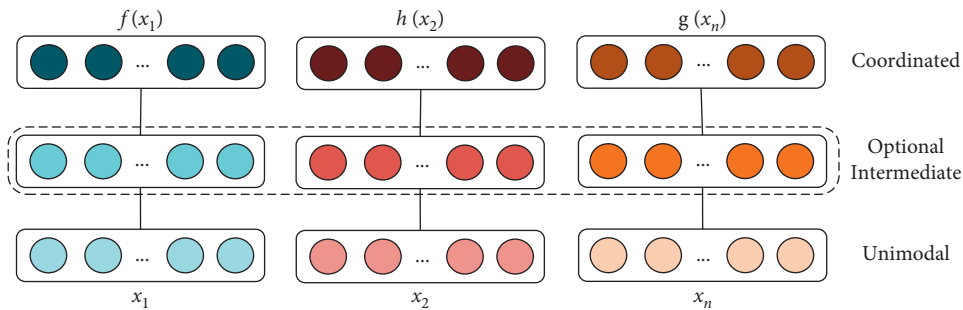


FIGURE 8: Collaboration representation.

multiple modalities to a collaborative space, which is expressed as $f(x_1) \sim f(x_n)$, where \sim represents a collaborative relationship. The goal of network optimization is to optimize the cooperative relationship.

As shown in Figure 2, the various modal features extracted from the pretraining model are input into the embedded layer based on the self-attention mechanism for

single-mode parameter learning. Then, the extracted multimodal feature vectors are fused by the above two fusion methods. As shown in Table 1, in the ablation experiment results, it is found that for the field of video captioning, the performance of cooperative representation and fusion of multimodal features is better than joint representation. The joint representation structure retains

TABLE 1: Comparison of the experimental results of the model obtained by different experimental parameters and different modal information fusion training under the MSR-VTT dataset.

Number layer	Feature	Score							
		BLEU4		METEOR		ROUGEL		CIDEr	
		Coordinated	Joint	Coordinated	Joint	Coordinated	Joint	Coordinated	Joint
1	$V_f + V_{I3D}$	0.306	0.299	0.255	0.251	0.517	0.518	0.391	0.400
	$V_f + V_{au\ di\ o}$	0.359	0.352	0.214	0.200	0.603	0.598	0.397	0.395
	$V_f + V_{au\ di\ o} + V_{I3D}$	0.401	0.410	0.290	0.287	0.619	0.586	0.422	0.410
2	$V_f + V_{I3D}$	0.334	0.325	0.235	0.220	0.520	0.499	0.394	0.396
	$V_f + V_{au\ di\ o}$	0.386	0.381	0.243	0.244	0.609	0.587	0.424	0.422
	$V_f + V_{au\ di\ o} + V_{I3D}$	0.443	0.430	0.327	0.319	0.612	0.600	0.521	0.517
3	$V_f + V_{I3D}$	0.325	0.319	0.227	0.231	0.542	0.539	0.389	0.391
	$V_f + V_{au\ di\ o}$	0.379	0.377	0.246	0.237	0.597	0.585	0.463	0.459
	$V_f + V_{au\ di\ o} + V_{I3D}$	0.393	0.390	0.292	0.293	0.599	0.571	0.497	0.469

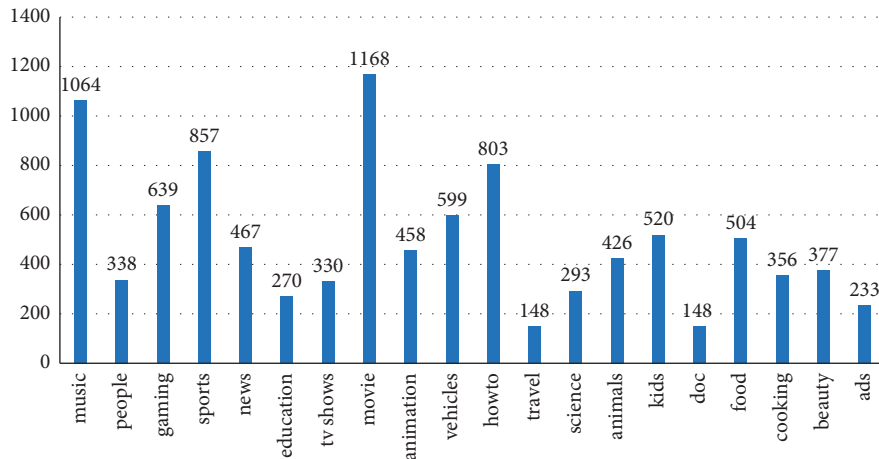


FIGURE 9: MSR-VTT dataset content distribution.

the independent representation space of multiple modes, which is more suitable for applications with only one mode as input, such as cross-modal retrieval and translation. However, the cooperative representation structure pays more attention to capture the complementarity of multimodes and obtains multimode representation X by fusing multiple input modes X , which is more suitable for multimode as input.

4. Experimental Design and Result Analysis

4.1. Experimental Hardware Platform. In this experiment, the server CPU is 48-core Intel(R) Xeon(R) Gold 5118, the running memory is 128G, the GPU card is NVIDIA Tesla V100, the video memory is 32G, and the operating system is Ubuntu18.04. NVIDIA CUDA 11.3, cuDNN V8.2.1 deep learning acceleration library, and PyTorch deep learning framework supporting GPU acceleration are installed.

4.2. Datasets

4.2.1. MSR-VTT. MSR-VTT [35] is a large public dataset released by Microsoft in 2016 for research into video-

generated text. We used the updated MSR-VTT from the 2017 competition, which contains 10,000 training video clips and 3,000 test video clips for a total of 41.2 hours. On average, each clip contains 20 natural language tags, 200000 statements in total. The dataset contains the most comprehensive and representative video content that consists of 257 popular categories from 20 representative categories (including cooking and movies) of the real video search engine, which is conducive to enhance and verify the generalization ability of the video semantic description algorithm. The content distribution of the dataset is shown in Figure 9. The x -axis is the video category, a total of 20 categories, and the y -axis is the total number of videos under each category.

4.2.2. Large-Scale Movie Deion and Understanding Challenge Dataset. The large-scale movie description challenge LSMDC dataset is based on the joint presentation of MPII Movie Description Dataset (MPII-MD) [36] and Montreal Video Annotation Dataset (M-VAD) [37]. The dataset contains more than 128K sentence fragment pairs and 158-h video. The training, validation, public, and blind test sets contain 101079, 7408, 10053, and 9578 video clips,

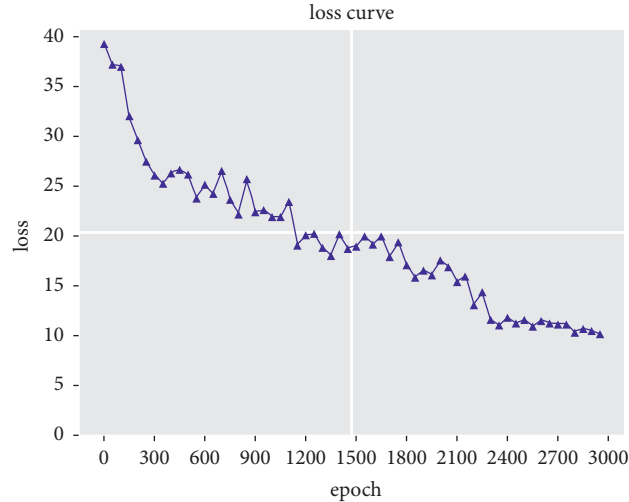


FIGURE 10: Decline curve of the training loss value.

respectively. Since the vocabulary used to describe action movies may be quite different from those used in comedy movies, this division balances the types of movies in each group, making the data more evenly distributed.

4.3. Evaluation Metrics. For model performance evaluation, four algorithms widely used in the field of video caption, namely, consensus-based image description evaluation (CIDEr) [38], Metric for Evaluation of Translation with Explicit Ordering (METEOR) [39], Recall-Oriented Understudy for Gisting Evaluation Longest Common Subsequence (ROUGEL) [40], and Bilingual Evaluation Understudy (BLEU) [41], are used as evaluation indicators to calculate evaluation scores for the model in this article and the comparison model, thereby objectively evaluating the effect of the model's sentence description generation.

4.4. Experimental Parameters and Result Analysis

4.4.1. Experimental Parameter Settings. Scaling the extracted original frame size to $256 * 256$ pixels before the model reads each frame. When extracting features, perform 15° random rotation on each frame of the image, which is needed firstly, and then perform random clipping to obtain an image with the size of $224 * 224$ pixels. Summarize and count the text vocabulary after the word segmentation, and then form a vocabulary list that consists of the words that are larger than the low-frequency threshold, and remove the vocabulary below the low-frequency threshold. Finally, select the vocabulary threshold as 5 and get 16860 words.

In the training phase of the model, Adam's algorithm [42] is used to optimize the parameters of the model. The parameters of the optimizer are $\alpha = 0.9$, $\beta = 0.999$, $\epsilon = 10^{-8}$. The initial learning rate of the model is 0.001, and the learning rate decay rate is 0.8. The model is trained with a learning rate decay of 0.8 for 50 consecutive rounds without loss, and the negative log-likelihood loss function is used to measure the distance between the labeled statements of the

dataset and the generated statements of the model, and the batch size is set to 128. The single-mode embedding layer adopts a two-layer LSTM network, and the numbers of LSTM layers of the fusion feature encoder and decoder are set to 1, 2, and 3.

4.4.2. Analysis of Experimental Results. During the training of the model, the average loss value is kept every 50 rounds. The curve of the loss value is shown in Figure 10. The initial loss decreases obviously. After 2300 rounds of training, the overall loss value tends to be stable.

To verify the validity of the model and the impact of specific parameters on the model, two-mode $V_f + V_{I3D}$, $V_f + V_{audio}$ and three-mode $V_f + V_{I3D} + V_{audio}$ video captioning models were trained for static frame feature V_f , motion feature V_{I3D} , and MFCC feature V_{audio} of the video. On the basis of each mode combination, the number of layers of LSTM network is set as 1 layer, 2 layers, and 3 layers for the single-mode embedded module and encoder module, and the model training experiments are carried out, respectively. The model comparison experiment is carried out under the MSR-VTT dataset, and the experimental results are shown in Table 1. Through nine sets of experiments, it can be seen that the monomodal embedding-multimodal fusion video captioning model constructed in this study can optimize the model by learning the parameters of monomodal information and fusing the representation information of multiple complementary modalities. The performance of the model also proves that there is a high degree of correlation and complementarity among different modal information. According to the data in the table, when the number of LSTM layers is fixed, the fusion of three complementary modal information including 2D frame features, I3D features containing 3D and optical flow information, and MFCC features of audio have the highest evaluation score for the model. When the mode is fixed, selecting 2 layers of LSTM layers in the embedded layer and encoder module is the best for the experiment. In the case of fixed modes and the number of layers of the LSTM network,

TABLE 2: Comparing the experimental results with the top five model structures in the second MSR-VTT challenge.

Rank	Organization	BLEU4	METEOR	ROUGEL	CIDEr
1	RUC&CMU	0.390	0.255	0.542	0.315
2	TJU	0.359	0.226	0.515	0.249
3	NII	0.359	0.234	0.514	0.231
4	Tongji University	0.351	0.226	0.509	0.236
5	IIT Delhi	0.304	0.213	0.494	0.206
	Ours	0.443	0.327	0.619	0.521

TABLE 3: Comparing the experimental results with the representative research work in the field of video captioning.

Models	BLEU4	METEOR	ROUGEL	CIDEr
MPool [14]	0.304	0.237	0.520	0.350
Ruc-uva [13]	0.387	0.269	—	0.459
S2VT [17]	0.314	0.257	0.559	0.352
TA [16]	0.285	0.250	0.533	0.371
SAAT [21]	0.399	0.277	0.612	0.510
M ³ -Inv3 [19]	0.381	0.266	—	—
SGN [22]	0.408	0.283	0.608	0.495
PickNet [12]	0.389	0.272	0.595	0.421
Ours	0.443	0.327	0.619	0.521

the model trained by cooperative representation has a higher test score than that obtained by joint representation, which proves that the effect of modal information fusion by cooperative representation in the video captioning is better. The experimental results show that the joint representation structure retains independent representation space of multiple modes and is more suitable for applications with only one mode as input, such as cross-modal retrieval and translation. The cooperative representation structure pays more attention to capture the multimode complementarity, fusing multiple input modes x_1, \dots, x_m to obtain the multimode representation $X = f(x_1, \dots, x_m)$, which is more suitable for multimode as input.

First, three modal features are fed into the embedded layer structure to learn the parameters that related to the single mode. Then, the multimodal information is fused through the joint representation and fed into the encoder-decoder. The ablation results show that the performance of the model is improved by fused audio information compared with single-mode and dual-mode cases. Compared with the single-mode fusion score evaluation indexes BLEU4, METEOR, ROUGEL, and CIDEr increased by 0.137, 0.072, 0.102, and 0.130, respectively. Compared with dual-mode fused score evaluation index, BLEU4, METEOR, ROUGEL, and CIDEr are improved by 0.084, 0.113, 0.016, and 0.124, respectively.

This study is compared with the top five model structures in the second MSR-VTT challenge, and the results are shown in Table 2.

This article also compares the results with the representative research work in the field of video captioning, as shown in Table 3.

As can be seen from Tables 2 and 3, in the evaluation indexes such as BLEU4, METEOR, ROUGEL, and CIDEr,

TABLE 4: In this article, the model is compared with the experimental results of the large-scale film description challenge in the LSDC dataset.

User or model	Meteor
frcnnBigger	0.033
rakshithShetty	0.046
EITanque	0.056
Yj	0.070
S2VT	0.070
Ours	0.072

the model improved 0.139, 0.114, 0.125, 0.315, respectively, compared with the top five models in the MSR-VTT challenge. Compared to the authoritative models in this field, the proposed model improves 0.158, 0.090, 0.099, and 0.171, which verifies the performance improvement of the video captioning model and the superiority of the proposed model.

This article also conducts experiments based on the latest large-scale movie description challenge (LSMDC) dataset. Table 4 shows the comparison of the METEOR results of the model on the LSMDC public dataset.

The model extracts multiple modal information of the video and uses it to train the model so that the model can obtain more complementary and diversified characterization information, making the model more robust and adaptable to multiple types of video clips. The text description is more specific and accurate, which further proves that the different modal information of the video has a high degree of correlation and complementarity.

In the split test set from the MSR-VTT dataset, different categories of video were selected. Figure 11 shows the effect of the text generation of the video content under four different categories, and each dataset selected the first five true

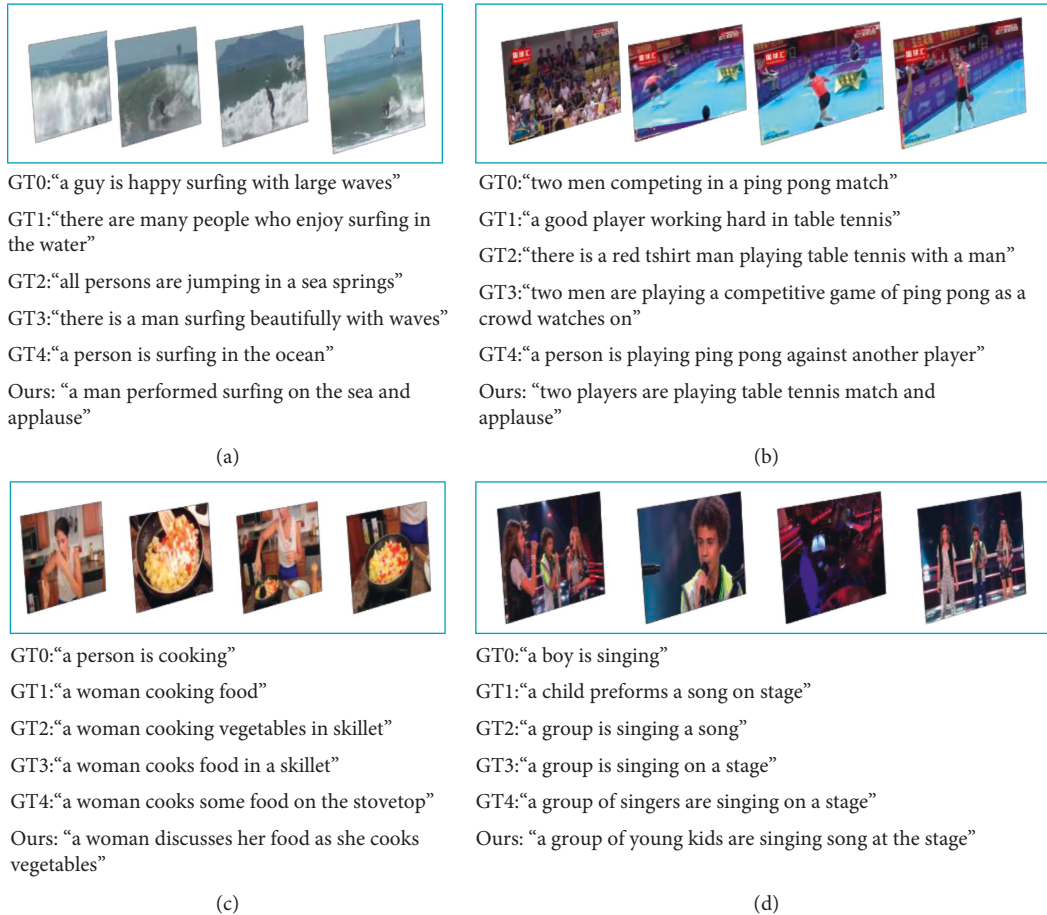


FIGURE 11: Dataset test visualization case.

markup statements (ground truth, GT), from which the visual model is generated to improve the accuracy and richness of video content text generation, and it shows that the performance of the model is improved by the fusion of multiple complementary modes.

5. Conclusion

In this article, a single-mode embedding multimode fusion video captioning model is proposed. Through a variety of efficient pretraining models, various modal representations contained in the video are effectively extracted, and static frame information, dynamic 3D, optical flow information, and audio information are complementary. The embedded layer based on self-attention is designed to learn the characteristic parameters of a single mode, which can enhance the complementarity of each mode better. Provide comprehensive and plentiful representation information for video generation text. And make the model generate more rich and accurate natural language. The above methods are verified by a series of ablation experiments and comparative experiments on MSR-VTT and LSMDC datasets. The experimental results show that the performance of the proposed model is significantly better than other models, and the generated text is more accurate.

In the later research work, we will make further improvements on the method of cross-modal information fusion and the complementarity of modal information. Combined with the attention mechanism to do further improvement work, make the alignment of various modal information with the text more accurate, and make the model obtain more accurate and rich representation information, so as to generate high-quality text and ensure the lightweight of the model.

Data Availability

The experimental data used to support the findings of this study are available from the corresponding author upon request.

Conflicts of Interest

The authors declare that they have no conflicts of interest to report regarding this study.

Acknowledgments

This research work was supported by the National Natural Science Foundation of China (Grant nos. 62166025 and 51668043), the Science and Technology Project of Gansu

Province (No. 21YF5GA073), and the Gansu Educational Science and Technology Innovation (Project nos. 2021CXZX-511 and 2021CXZX-512).

References

- [1] J. Ji, C. Xu, X. Zhang, B. Wang, and X. Song, "Spatio-temporal memory attention for image captioning," *IEEE Transactions on Image Processing*, vol. 29, pp. 7615–7628, 2020.
- [2] J. Yang, C. Wang, B. Jiang, H. Song, and Q. Meng, "Visual perception enabled industry intelligence: state of the art, challenges and prospects," *IEEE Transactions on Industrial Informatics*, vol. 17, no. 3, pp. 2204–2219, 2020.
- [3] S. Guadarrama, N. Krishnamoorthy, G. Malkarnenkar et al., "Youtube2text: recognizing and describing arbitrary activities using semantic hierarchies and zero-shot recognition," in *Proceedings of the IEEE international conference on computer vision*, pp. 2712–2719, Sydney, NSW, Australia, 2013.
- [4] J. Perez-Martin, B. Bustos, and J. Pérez, "Improving video captioning with temporal composition of a visual-syntactic embedding," in *Proceedings of the IEEE/CVF Winter Conference on Applications of Computer Vision*, pp. 3039–3049, Waikoloa, HI, USA, 2021.
- [5] M. Zhu, "Video captioning in compressed video," in *Proceedings of the 2021 6th International Conference on Image, Vision and Computing (ICIVC)*, pp. 336–341, IEEE, Qingdao, China, 2021.
- [6] C. Szegedy, W. Liu, Y. Jia et al., "Going deeper with convolutions," in *Proceedings of the IEEE conference on computer vision and pattern recognition*, pp. 1–9, Boston, MA, 2015.
- [7] Y. Li, R.-G. Zhou, R. Xu, J. Luo, and W. Hu, "A quantum deep convolutional neural network for image recognition," *Quantum Science and Technology*, vol. 5, no. 4, Article ID 044003, 2020.
- [8] J. Park, S. Woo, J.-Y. Lee, and I. S. Kweon, "A simple and light-weight Attention module for convolutional neural networks," *International Journal of Computer Vision*, vol. 128, no. 4, pp. 783–798, 2020.
- [9] H. Yousuf, M. Lahzi, S. A. Salloum, and K. Shaalan, "A systematic review on sequence-to-sequence learning with neural network and its models," *International Journal of Electrical and Computer Engineering*, vol. 11, no. 3, p. 2315, 2021.
- [10] D. W. Otter, J. R. Medina, and J. K. Kalita, "A survey of the usages of deep learning for natural language processing," *IEEE Transactions on Neural Networks and Learning Systems*, vol. 32, no. 2, pp. 604–624, 2020.
- [11] J. Xiao and Z. Zhou, "Research progress of RNN language model," in *Proceedings of the 2020 IEEE International Conference on Artificial Intelligence and Computer Applications (ICAICA)*, pp. 1285–1288, IEEE, Dalian, China, 2020.
- [12] Y. Chen, S. Wang, W. Zhang, and Q. Huang, "Less is more: Picking informative frames for video captioning," in *Proceedings of the European conference on computer vision (ECCV)*, pp. 358–373, Springer, Munich, Germany, 2018.
- [13] Q. Wu, C. Shen, L. Liu, A. Dick, and A. Van Den Hengel, "What value do explicit high level concepts have in vision to language problems?" in *Proceedings of the IEEE conference on computer vision and pattern recognition*, pp. 203–212, Las Vegas, NV, USA, June 2016.
- [14] S. Venugopalan, H. Xu, J. Donahue, M. Rohrbach, R. Mooney, and K. Saenko, "Translating videos to natural language using deep recurrent neural networks," 2014, <https://arxiv.org/abs/1412.4729>.
- [15] J. Dong, X. Li, W. Lan, Y. Huo, and C. G. M. Snoek, "Early embedding and late reranking for video captioning," in *Proceedings of the 24th ACM international conference on Multimedia*, pp. 1082–1086, Amsterdam, The Netherlands, October 2016.
- [16] L. Yao, A. Torabi, K. Cho et al., "Describing videos by exploiting temporal structure," in *Proceedings of the IEEE international conference on computer vision*, pp. 4507–4515, Santiago, Chile, December 2015.
- [17] S. Venugopalan, M. Rohrbach, J. Donahue, R. Mooney, T. Darrell, and K. Saenko, "Sequence to sequence-video to text," in *Proceedings of the IEEE international conference on computer vision*, pp. 4534–4542, Santiago, Chile, December 2015.
- [18] Y. Pan, T. Mei, T. Yao, H. Li, and Y. Rui, "Jointly modeling embedding and translation to bridge video and language," in *Proceedings of the IEEE conference on computer vision and pattern recognition*, pp. 4594–4602, Las Vegas, NV, USA, June 2016.
- [19] J. Wang, W. Wang, Y. Huang, L. Wang, and T. Tan, "M3: multimodal memory modelling for video captioning," in *Proceedings of the IEEE conference on computer vision and pattern recognition*, pp. 7512–7520, Salt Lake City, UT, USA, June 2018.
- [20] L. Gao, X. Li, J. Song, and H. T. Shen, "Hierarchical LSTMs with adaptive attention for visual captioning," *IEEE Transactions on Pattern Analysis and Machine Intelligence*, vol. 42, no. 5, pp. 1112–1131, 2020.
- [21] Q. Zheng, C. Wang, and D. Tao, "Syntax-aware action targeting for video captioning," in *Proceedings of the IEEE/CVF Conference on Computer Vision and Pattern Recognition*, pp. 13096–13105, Seattle, WA, USA, June 2020.
- [22] H. Ryu, S. Kang, H. Kang, and C. D. Yoo, "Semantic grouping network for video captioning," in *Proceedings of the AAAI Conference on Artificial Intelligence*, vol. 35, no. 3, pp. 2514–2522, Vancouver, Canada, 2021.
- [23] N. Wang, H. Liu, and C. Xu, "Deep learning for the detection of COVID-19 using transfer learning and model integration," in *Proceedings of the 2020 IEEE 10th International Conference on Electronics Information and Emergency Communication (ICEIEC)*, pp. 281–284, Beijing, China, July 2020.
- [24] Q. Wu, A. Zhu, R. Cui et al., "Pose-Guided Inflated 3D ConvNet for action recognition in videos," *Signal Processing: Image Communication*, vol. 91, Article ID 116098, 2021.
- [25] L. Guo, J. Liu, X. Zhu, P. Yao, S. Lu, and H. Lu, "Normalized and geometry-aware self-attention network for image captioning," in *Proceedings of the IEEE/CVF Conference on Computer Vision and Pattern Recognition*, pp. 10327–10336, Seattle, WA, USA, June 2020.
- [26] S. Hochreiter and J. Schmidhuber, "Long short-term memory," *Neural Computation*, vol. 9, no. 8, pp. 1735–1780, 1997.
- [27] J. Hu, L. Shen, and G. Sun, "Squeeze-and-excitation networks," in *Proceedings of the IEEE conference on computer vision and pattern recognition*, pp. 7132–7141, Salt Lake City, UT, USA, June 2018.
- [28] K. He, X. Zhang, S. Ren, and J. Sun, "Deep residual learning for image recognition," in *Proceedings of the IEEE conference on computer vision and pattern recognition*, pp. 770–778, Las Vegas, NV, USA, June 2016.
- [29] J. Carreira and A. Zisserman, "Quo vadis, action recognition? a new model and the kinetics dataset," in *Proceedings of the IEEE Conference on Computer Vision and Pattern Recognition*, pp. 6299–6308, Honolulu, HI, USA, July 2017.

- [30] W. Zhang, S. Tang, J. Su, J. Xiao, and Y. Zhuang, "Tell and guess: cooperative learning for natural image caption generation with hierarchical refined attention," *Multimedia Tools and Applications*, vol. 80, no. 11, pp. 16267–16282, 2021.
- [31] Q. Liu and C. Wang, "Within-component and between-component multi-kernel discriminating correlation analysis for colour face recognition," *IET Computer Vision*, vol. 11, no. 8, pp. 663–674, 2017.
- [32] M. A. A. Albadr, S. Tiun, M. Ayob, and M. Mohammed, "Mel-frequency cepstral coefficient features based on standard deviation and principal component analysis for language identification systems," *Cognitive Computation*, vol. 13, no. 5, pp. 1136–1153, 2021.
- [33] N. Yang, N. Dey, R. S. Sherratt, and F. Shi, "Recognize basic emotional states in speech by machine learning techniques using mel-frequency cepstral coefficient features," *Journal of Intelligent and Fuzzy Systems*, vol. 39, no. 2, pp. 1925–1936, 2020.
- [34] L.-P. Morency and T. Baltrušaitis, "Multimodal machine learning: integrating language, vision and speech," in *Proceedings of the 55th Annual Meeting of the Association for Computational Linguistics: Tutorial Abstracts*, pp. 3–5, Canada: Vancouver, 2017.
- [35] J. Xu, T. Mei, T. Yao, and Y. Rui, "Msr-vtt: a large video description dataset for bridging video and language," in *Proceedings of the IEEE conference on computer vision and pattern recognition*, pp. 5288–5296, Las Vegas, NV, USA, June 2016.
- [36] A. Rohrbach, M. Rohrbach, N. Tandon, and B. Schiele, "A dataset for movie description," in *Proceedings of the IEEE conference on computer vision and pattern recognition*, pp. 3202–3212, Boston, MA, USA, June 2015.
- [37] Y. F. Huang, L. P. Shih, C. H. Tsai, and G. T. Shen, "Describing video scenarios using deep learning techniques," *International Journal of Intelligent Systems*, vol. 36, no. 6, pp. 2465–2490, 2021.
- [38] R. Vedantam, C. Lawrence Zitnick, and D. Parikh, "Cider: Consensus-based image description evaluation," in *Proceedings of the IEEE conference on computer vision and pattern recognition*, pp. 4566–4575, Boston, MA, USA, June 2015.
- [39] M. Denkowski and A. Lavie, "Meteor universal: language specific translation evaluation for any target language," in *Proceedings of the ninth workshop on statistical machine translation*, pp. 376–380, Baltimore, Maryland, USA, June 2014.
- [40] C.-Y. Lin, "Rouge: a package for automatic evaluation of summaries," in *Text Summarization Branches Out*, pp. 74–81, Association for Computational Linguistics, Barcelona, Spain, 2004.
- [41] K. Papineni, S. Roukos, T. Ward, and W.-J. Zhu, "Bleu: a method for automatic evaluation of machine translation," in *Proceedings of the 40th annual meeting of the Association for Computational Linguistics*, pp. 311–318, Philadelphia, Pennsylvania, USA, July 2002.
- [42] D. P. Kingma and J. Ba, "Adam: a method for stochastic optimization," 2014, <https://arxiv.org/abs/1412.6980>.

Research Article

Intelligent Tourism Information Service Model considering Tourist Experience in the Environment of Internet of Things

Han Liu ^{1,2}

¹*School of Education and Management, Bozhou Vocational and Technical College, Bozhou 236800, Anhui, China*

²*Gujing School of Management, Bozhou 236800, Anhui, China*

Correspondence should be addressed to Han Liu; 0430070130@bzy.edu.cn

Received 2 March 2022; Revised 22 March 2022; Accepted 31 March 2022; Published 28 April 2022

Academic Editor: Le Sun

Copyright © 2022 Han Liu. This is an open access article distributed under the Creative Commons Attribution License, which permits unrestricted use, distribution, and reproduction in any medium, provided the original work is properly cited.

Due to the narrow range of route search and the single choice of the optimal route during the peak period of tourists' tourism, resulting in a long walking time and relatively high route cost, an intelligent tourism information service model considering tourists' experience is proposed in the environment of Internet of things. Firstly, the overall architecture of the Internet of things environment is designed to obtain the characteristic data of the carrying capacity of scenic spots, including tourism resources, psychology, ecology, and economic carrying capacity, based on which the tourist perception experience model is constructed; different service functions such as in-depth mining of Web content, personalized information push, and data information conversion under the environment of Internet of things and the construction of intelligent tourism information service model are realized. The experimental results show that the passenger flow prediction error of the designed model is small and has a good prediction effect of tourist attraction selection demand.

1. Introduction

Driven by the rapid development of information technology and Internet technology, tourism has ushered in a golden period of rapid growth. With the gradual development of the national economy and the increase in leisure time and disposable income, tourism has become an important way of entertainment for residents [1]. Because ecotourism has the characteristics of objectivity, dynamics, and management, it is difficult to measure its environmental carrying capacity. There are still great disputes on the selection of indicators and influencing factors [2]. In the open Internet of things environment, the total amount of data information shows a geometric growth, which causes great resistance to the rapid retrieval service of data information [3]. In the Internet of things environment, it is impossible to quickly confirm the current location and return to the specified node. Secondly, due to the limited receiving and holding capacity of information users, it is difficult to correctly understand and apply information [4,5]. Although the emergence of various

search engines has satisfied the basic needs of information users to a certain extent, the quality of information retrieved is poor due to the huge amount of Internet information and the existence of information overload [6, 7]. Considering the tourist experience, the intelligent tourism information service model is established, which not only has the function of fast retrieval and collection but also integrates the Internet of things retrieval functions such as personalized database, favorites, and hyperlinks, which significantly improves the information retrieval efficiency.

Reference [8] presents an assessment of the comparative advantage shown by Ukraine's export of tourism services to the EU. For those countries where tourism is an important source of national income and a job-creating activity, the question of tourism and the revitalization of the tourism sector become urgent following the devastating consequences of the pandemic. Tourism stimulates the development of small- and medium-sized enterprises, has great potential for a creative economy, enables rapid recovery of costs, has a significant environmental impact, and enables a

high degree of social inclusion, including the use of women and youth labour. Reference [9] proposed the impact of applied quality standards on improving environmental tourism services in nature reserves in southern Jordan. The study population included tourists from all nature reserves in southern Jordan. Descriptive analysis was used to conduct a field survey of 600 visitors to a nature reserve in southern Jordan, selected by a simple random method, through questionnaires. Using statistical analysis of social science statistical procedure according to the results, in the south of Jordan nature reserves, tourist service quality standards to improve the environment have a significant statistical effect, and the study suggested southern Jordan nature reserve management department to make a plan, through continuous application of quality standards, to ensure to improve its ecological tourism services.

Although the above research has made some progress, there is less consideration of tourists' experience. Therefore, an intelligent tourism information service model considering tourists' experience in the Internet of things environment is proposed to adapt. The overall architecture of the Internet of things environment was designed to obtain the characteristic data of tourist attractions' carrying capacity, and based on this, the tourist perception experience model was constructed. Different service functions such as in-depth mining of Web content, personalized information push, and data information conversion can be realized in the Internet of things environment, to adapt and meet the personalized information retrieval and use needs of tourists in the Internet of things environment.

2. Intelligent Tourism Information Service Model considering Tourist Experience in the Environment of Internet of Things

2.1. Overall Architecture of Internet of Things Environment. The overall architecture of the Internet of things environment can be divided into four main levels of "cloud management edge end."

2.1.1. Cloud Level. The "cloud" layer can realize the functions of intelligent tourism information service terminal connection, system deployment, data decoupling, and so on, which meets the conditions of high-speed response to the demand for tourism information service and intensive system operation and maintenance [10].

2.1.2. Pipe Level. This layer uses the system of the integration of remote communication network and local communication network to meet the needs of intelligent tourism information service through channel IP, network protocol, and resource self-description.

2.1.3. Edge Level. The architecture of "unified hardware system + edge operation + business software" is used to integrate the functions of network, computing, and storage, combined with edge computing to improve the real-time processing performance and reduce the computing pressure; the terminal

is defined according to the software to realize the flexible deployment of intelligent tourism information service [11].

2.1.4. End Level. This level can collect information such as the operation of intelligent tourism information service, equipment, and environmental status and can execute decision-making commands to realize timely communication with tourists. The overall architecture of the Internet of things environment is shown in Figure 1.

2.2. Obtain the Characteristic Data of Carrying Capacity of Scenic Spots. From the perspective of tourists' experience and keeping the tourism demand and tourism supply of the scenic spot in a relatively ideal state, the transportation carrying tools of tourists and the facilities or space occupied by them in a specific time are determined through the combination of quantitative and qualitative methods, to obtain the characteristic data of the carrying capacity of the scenic spot, including the carrying capacity data of tourism resources, tourism psychological carrying capacity data, tourism ecological carrying capacity data, and tourism economic carrying capacity data [12,13]. The specific contents of data acquisition are shown in Table 1.

For the data of tourism resource carrying capacity, the calculation formula is as follows:

$$R_j = \frac{T_a}{T_1} \times \frac{S_a}{S_1} \quad (1)$$

In formula (1), R_j represents the actual limit daily capacity of resources, T_a represents the opening time of tourist destination every day, T_1 represents the actual visiting time of each tourist, S_a represents the resource area, and S_1 represents the minimum space standard of each tourist.

For the data of tourism psychological carrying capacity, the calculation formula is as follows:

$$C_{zl} = \frac{T_a}{T_1} \times k \times S_a \quad (2)$$

In formula (2), C_{zl} represents daily psychological capacity and k represents reasonable capacity per unit area of space.

For the data of tourism ecological carrying capacity, the calculation formula is as follows:

$$S_{tc} = \frac{\sum_{i=1}^n S_i T_i + \sum_{i=1}^n Q_i}{\sum_{i=1}^n P_i} \quad (3)$$

In formula (3), S_{tc} represents the daily ecological capacity, n represents the specific number of pollutants, and S_i represents the specific number of i pollutants absorbed and purified by the ecological environment, T_i represents the specific purification time of each pollutant, Q_i represents the amount of Q_i pollutants treated manually every day, and P_i represents the actual amount of pollutants (type i) produced by each tourist every day.

For the data of tourism economic carrying capacity, the calculation formula is as follows:

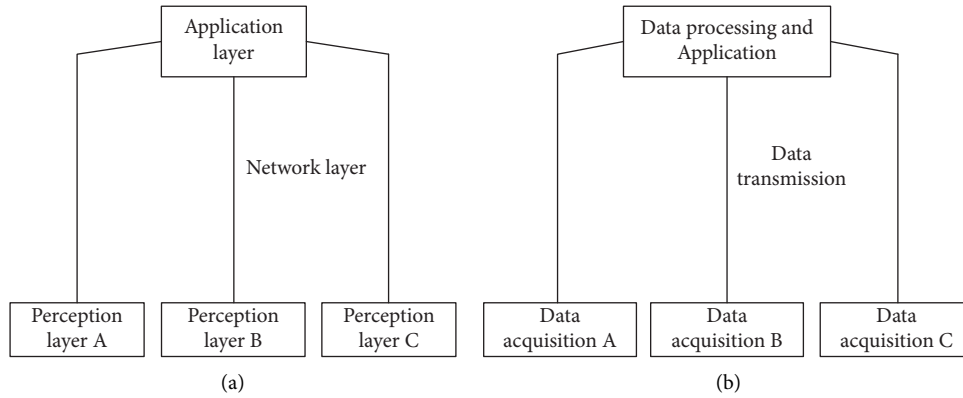


FIGURE 1: Overall architecture of Internet of things environment.

TABLE 1: Specific contents of data acquisition.

Serial number	Data type	Specific content of data
1	Tourism resources carrying capacity	Actual limit daily capacity of resources
2	Tourism psychological carrying capacity	When tourists can get greater satisfaction, the maximum tourism activity capacity that the region can carry
3	Tourism ecological carrying capacity	The ability to treat tourism pollutants through artificial methods and ecological environment absorption and purification methods
4	Tourism economic carrying capacity	It refers to the reception capacity of basic tourism facilities, related facilities, and industrial supporting facilities, represented by the actual supply capacity of entertainment and accommodation facilities

$$\begin{cases} T_e = \frac{\sum_{i=1}^m D_l}{\sum_{i=1}^m E_l} \\ T_h = \sum_{i=1}^{n_l} B_j \end{cases} \quad (4)$$

In formula (4), T_e represents the daily carrying capacity of food supply tourism, m represents the specific types of food consumed by tourists, D_l represents the supply of l kinds of food per day, E_l represents the l food demand per person per day, T_h represents the daily carrying capacity of accommodation bed tourism, B_j represents the specific number of accommodation beds in class j tourism areas, and n_l represents the actual types of accommodation facilities.

2.3. Tourist Perception Experience Model. Tourism activities involve many factors, not only taking tourists as the main participation but also taking the image of the scenic spot as the main behavior. Scenic spots attract tourists with specific resources and carry out relevant activities. Whether tourism resources have a certain tourism attraction depends not only on the tourism resources of the scenic spot but also on the comprehensive object environment of the scenic spot [14, 15]. The tourism environment is an important carrier of tourism activities. The tourism environment is one of the important factors for tourists to consider whether the scenic spot is worth traveling. For example, the quality of the natural environment often affects the experience of tourists

in this process. If the scenic spot has good tourism resources, but it rains or earthquakes frequently all year round, then tourists will not come to visit. It can be seen that tourism environmental factors are very important.

Tourists bring economic benefits, promote employment, promote the protection of ecological environment and traditional culture, and inevitably bring many negative effects caused by their own lifestyle and behavioral habits to the scenic spot. Therefore, it is of great practical significance to study tourism information services from the perspective of tourists [16].

ACSI represents the core concept and architecture of tourism motivation, purchase policy, tourism, and tourism process when tourists play. As a dynamic and continuous experience process, the end of tourism can establish a tourist perception experience model through the dynamic process of tourists' comprehensive experience [17, 18]. The specific content is shown in Figure 2.

As can be seen from Figure 2, the tourist perception experience model is built on the basis of tourist resettlement experience. Tourist perception experience is a kind of social perception that tourists perceive the impact of tourism, including the perception of economy, social culture, environment, self, interpersonal relationship, and social role. Tourism experience is generated in every link of tourism product consumption, from landscape appreciation to the acquisition of various services, and the quality of service in each link will affect the quality of tourist experience [19,20]. The accuracy, safety, comfort, and reliability of information transmission determine the service quality of each element.

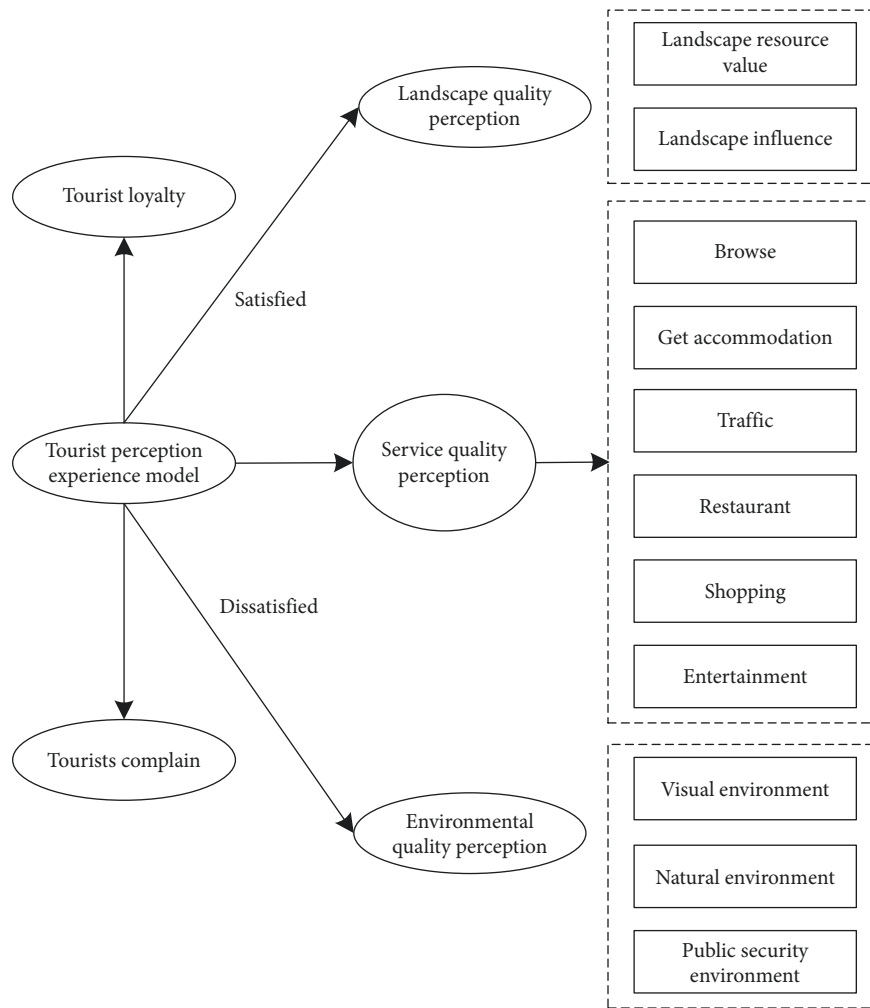


FIGURE 2: Tourist perception experience model.

Therefore, tourists can obtain more accurate comprehensive perception experience through the perception of tourism landscape quality, service quality, and environmental quality.

3. Realize the Design of Intelligent Tourism Information Service Model considering Tourist Experience

3.1. Design of Information Service Function Module. Consider intelligent tourism information service model of tourist experience, which is divided into four modules, respectively, as tourism information module, the network data retrieval module, push module, and database module, to realize the Internet environment, the depth of the Web content mining, data conversion and other personalized information push service function, the structure of the model, and the main function module design, as shown in Figure 3.

- (1) *Visitor Module.* The intelligent tourism information service model based on multimode takes tourists as the service center. The functions of the tourist module include basic information management and customized management of tourists' information needs. All personal information and account

information of tourists are stored in the module. After authorization, you can enter the account and password to log in to the system. After entering the system, tourists can add, edit, and modify tourist information by themselves after being authorized by the system administrator; through this module, tourists can put forward specific tourism information retrieval needs, customize the database list, and select the retrieval and classification query methods of tourism information. The module has the function of automatic storage and retrieval, and the historical retrieval content can be queried through keywords.

- (2) *Network Data Retrieval Module.* This module is the core module of the tourism information service model, through which tourists can retrieve and customize the content of interested weblogs [21]. To adapt to the compound multi-data transmission mode, a data retrieval network is designed. The network has good compatibility and supports different modes such as static data transmission and dynamic data transmission. The bus matrix can process 64 bit data input and output in parallel, with four I/O interfaces. The network data retrieval module can deeply mine and

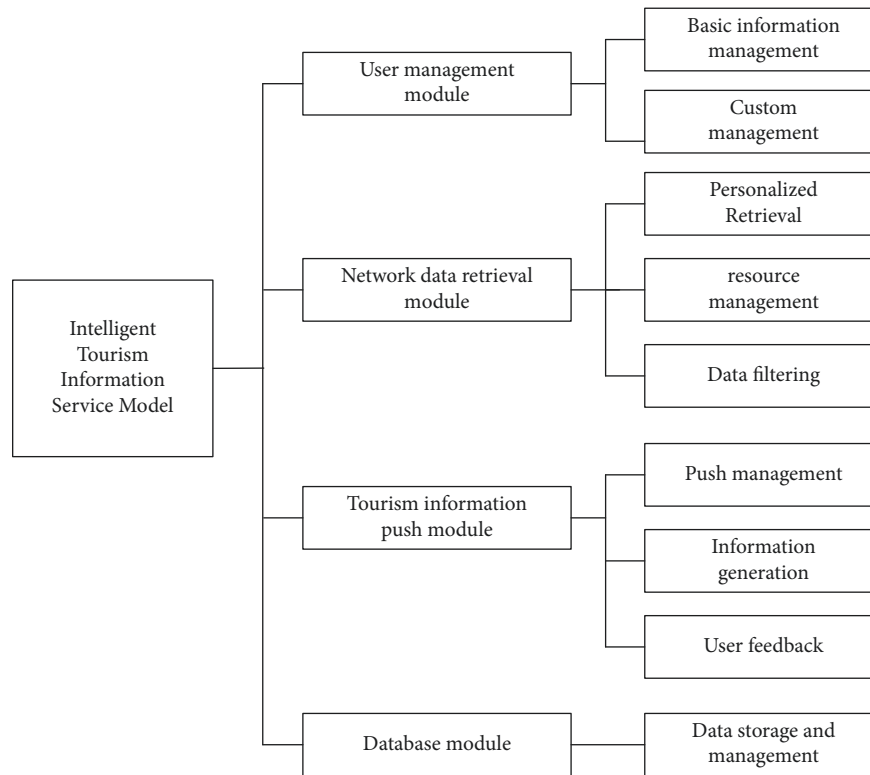


FIGURE 3: Structure diagram of main functional modules of intelligent tourism information service model.

analyze the contents of the network log and actively switch the mode of tourism information retrieval according to the use habits and preferences of tourists, to obtain the retrieval habits of tourists and store keywords and characteristic words in the database, to facilitate the subsequent data call of tourists.

- (3) *Tourism Information Push Module*. The tourism information push module includes the specific functions of pushing tourism information management, tourism information generation, and tourists' use feedback. The total amount of tourism information in the network is huge, and the total amount of data information collected according to tourists' habits and preferences is huge. Push management is to preprocess and classify this redundant and wrong tourism information first, retain useful tourism information, and eliminate interference information [22,23]; through the classified retrieval of customized tourism information for tourists, the most economical tourism information transmission mode is selected in the Internet of things environment, the tourism information categories required by tourists are generated, and directional and regular push is realized [24]. The tourism information push module has a two-way information interaction function; that is, on the one hand, it transmits basic tourism information to tourists, and on the other hand, it also receives tourists' feedback, to optimize each module of the system and continuously improve the database [25].

- (4) *Database Module*. According to the above three modules, the list category of the database is divided into tourist basic tourism information data, tourist search tourism information table, and personalized data table, as shown in Tables 2–4, respectively.

Other forms in the database are extended and expanded on the basis of the basic form and connected with the basic form through the primary key field, which is convenient for tourists' retrieval and query.

3.2. Realize Intelligent Tourism Information Service Model. The Internet of things is taken as the goal of tourists' experience perception, an intelligent tourism information service model is established through intelligent perception, a large number of tourism-related real-time information are mined through the Internet of things, such as scenic spot tickets, accommodation places, weather, and meteorology, this information is gathered and analyzed, and the tourism information available for service is summarized [26,27].

To establish an intelligent tourism information service model, we need to take the big data of the Internet of things as the goal and use multi-agent technology to divide the establishment of the model into multiple modules, namely data acquisition, data perception, data decomposition, data storage, data integration, central control, and data display modules. Among them, data acquisition is responsible for the input of the model, collecting the tourism big data of the Internet of things through the compiled crawler program,

TABLE 2: Basic tourism information data of tourists.

Field	Meaning	Type	Length	Can it be blank	Primary key
UID	Number	Int	16	No	Yes
Name	Full name	Var	10	No	No
Sex	Gender	Var	4	No	No
Bd	Birth	Date	10	No	No
Add	Date	Var	50	Yes	No
Edu	Address	Var	40	Yes	No

TABLE 3: Tourist information retrieval.

Field	Meaning	Type	Length	Can it be blank	Primary key
UID	Number	Int	16	No	Yes
Id	Data	Int	20	No	Yes
Cta	Number	Int	20	No	No
Ctn	Classification	Var	10	No	No
Cat	Number	Var	8	Yes	No

TABLE 4: Personalized datasheet.

Field	Meaning	Type	Length	Can it be blank	Primary key
UID	Number	Int	16	No	Yes
Id	Data	Int	20	No	Yes
Kw	Number	Int	20	Yes	No
Ty	Key tourism information number	Var	20	Yes	No
Ind	Data	Flo	10	Yes	No

making preliminary selection and filtering, and submitting the data to the data decomposition module after completing the preliminary processing; the data decomposition module decomposes the collected data into multiple parts through extraction, filtering, decomposition, and other operations and submits them to the perception module [28]; after sensing the tourism information, the perception module in the platform selects the tourism data with service value in a unified format through weighted calculation and normalization processing and then integrates this data information with service value into independent data through the data integration module, which is stored in the data storage module, managed storage, and provided to the data display module, and the data are displayed in front of tourists.

The central control module is responsible for connecting each module in the perception model, controlling the information exchange of each module, and the processed request link queue established by the manager in the process of obtaining the tourism data of the Internet of things, so that the whole platform can effectively process the tourism big data and communicate information [29].

In the above, the data collection is mainly realized through the Web page analysis algorithm, which is not simply judged according to whether all the text of the Web page is related to the given subject. This judgment method lacks certain reliability. In the process of establishing the intelligent tourism information service model [30], the data

collection is mainly based on the theme relevance of the parent Web page of the Internet of things. The correlation between the current Web page and the theme and the location of the Web page link is comprehensively determined. The final result may be a continuous value between 0 and 1. The closer the value is, the higher the correlation between the collected data and tourism service information, which proves that the collected data are the target data of the platform [31,32].

Assuming that the 0/1 mode is used to represent whether tourists have been to the scenic spot, the check-in times of tourists correspond to the degree of interest of tourists in the scenic spot. Therefore, the similarity between tourist interest points is solved using the check-in times of tourists in the scenic spot, and the expression is as follows:

$$X_{qd} = \frac{\left(\sum y_{i,j} \times y_{k,j}\right)}{\sum y_{i,j}}. \quad (5)$$

In formula (5), $y_{i,j}$ represents the check-in frequency of a tourist $y_{i,j}$ in scenic spot j and $y_{k,j}$ represents the check-in frequency of another tourist in scenic spot j .

The first N' tourists with the greatest similarity are selected according to the similarity between tourists. These tourists are used to form a set U_I , and the possibility that tourists will go to the scenic spot without checking in is solved according to the collaborative filtering model based on tourists. Then, the formula is as follows:

$$Y_{qd} = \frac{\left(\sum X_{qd} \times y_{k,j}\right)}{\sum X_{q,d}}. \quad (6)$$

Assuming that a tourist has been to m cities, the expression of the number of interest points that can be mined is obtained according to the sign-in times and stay time of his activity track:

$$Z_{qd} = \left(\frac{\sum l_c}{m}\right) \times X_{qd} \times Y_{qd}. \quad (7)$$

In formula (7), l_c represents the vector set represented by the points of interest. To ensure that the mining of interest points is comprehensive enough, it is necessary to use the characteristics of tourist similarity, social relations, and geographical location information to realize the mining [33,34]. Because the probability values of interest points are different, the standardized weighting method should be used for processing during integration, and the processing results should be substituted into the model of mining interest points. The construction of intelligent tourism information service model can be realized [35,36], and its expression is as follows:

$$S_{ab} = P_{ab} \times Z_{qd} \times \lambda. \quad (8)$$

In formula (8), P_{ab} represents the collection of users check-in interest points, and λ represents the training parameters. Intelligent tourism is a highly complex and dynamic field. Intelligent tourism information service providers often need to rely on models to predict the marketing objectives of

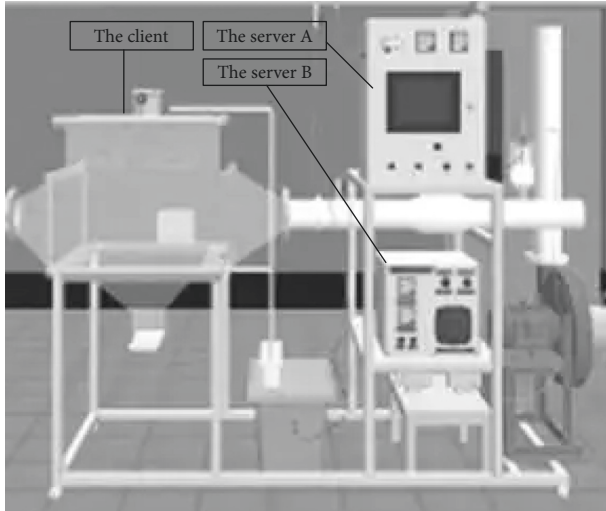


FIGURE 4: Environment diagram of simulation experimental platform.

the tourism market and explore the potential market. Users also need tourism information to assist decision-making. These need to be realized through the organization and integration of intelligent tourism information service models. There is an urgent need for an Internet of things processing technology to organize them in depth. In the Internet of things environment, various network information technologies are used as a structured data application specification, to realize the construction of intelligent tourism information service model considering tourist experience in the Internet of things environment.

4. Experimental Analysis

In the experimental platform of this study, the CPU is Intel (R) Q4800, the frequency is 2.66 GHz, the computer memory is 512 GB, the simulation programming environment is MATLAB 2016 under windows 10 system, the classifier uses LIBSVM and grid search method for parameter optimization, and the kernel function used is Gaussian kernel. The experimental equipment includes two servers and one client, which stores the communication transmission information in the cloud. The experimental environment is shown in Figure 4.

According to Figure 4, to ensure the time synchronization between sampling and updating, the time can be calibrated by smoothing and extrapolation. To ensure the reliability of the experiment, the experiment is carried out according to the method in Figure 5.

In the simulation platform, the initial parameters of the sensor are set: the position coordinate is $(X, Y) = (120km, 120km)$, the observation radius r_1 is 100 km, the ranging error σ_{l_1} is 150m, and the angle measurement error σ_{θ_1} is 1° . In the simulation experiment, five data sets of wine, forest, glass, iris, and segmentation used for identification in the UCI standard database are used. The basic information of the data set is shown in Table 5.

Under the five authoritative data sets in Table 5 above, the model in this study, the model in reference [8], and the

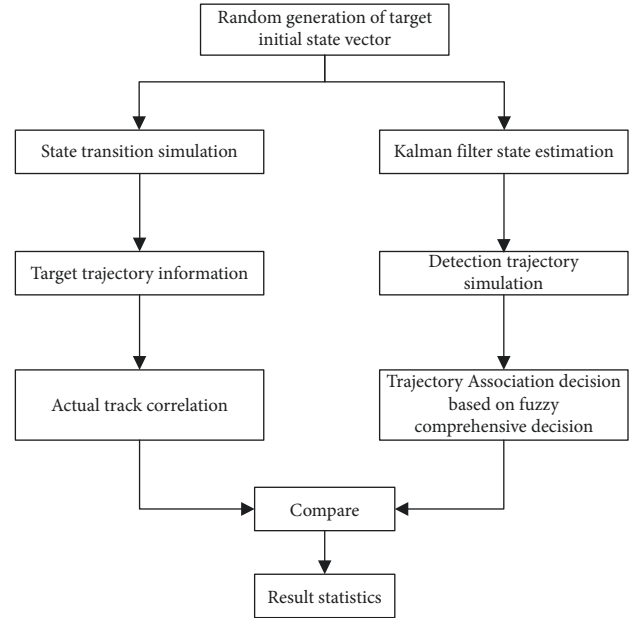


FIGURE 5: Simulation principle of intelligent tourism information service model.

TABLE 5: Basic information of data set.

Data set	Sample input dimension	Number of training samples	Number of test samples	Number of identifications
Wine	24	133	133	4
Forest	47	247	317	7
Glass	18	159	114	2
Iris	11	121	84	3
Segmentation	37	331	3310	5

TABLE 6: Experimental environmental parameters.

Experimental configuration	Experimental parameters
CPU	Dual-core 2 GHz
Effective memory, memory	3.4 GB, 4 GB
The server	ASUA RS100-X5

model in reference [9] are used for experimental verification, respectively. The experimental environmental parameters are shown in Table 6.

The dynamic virtual variable of the intelligent tourism information service model is set to 0, and the three models are used to predict the passenger flow of a scenic spot on a working day and compared with the actual value. The overall scatter diagram of the predicted passenger flow and the real passenger flow is shown in Figure 6.

According to the analysis of Figure 6, the scattered points of the passenger flow prediction results of the model in this study are roughly distributed at the 45° boundary, while the scattered points of the passenger flow prediction results of the model in reference [8] and the model in reference [9] are relatively scattered. This shows that the passenger flow prediction error of this model is small and has good effect.

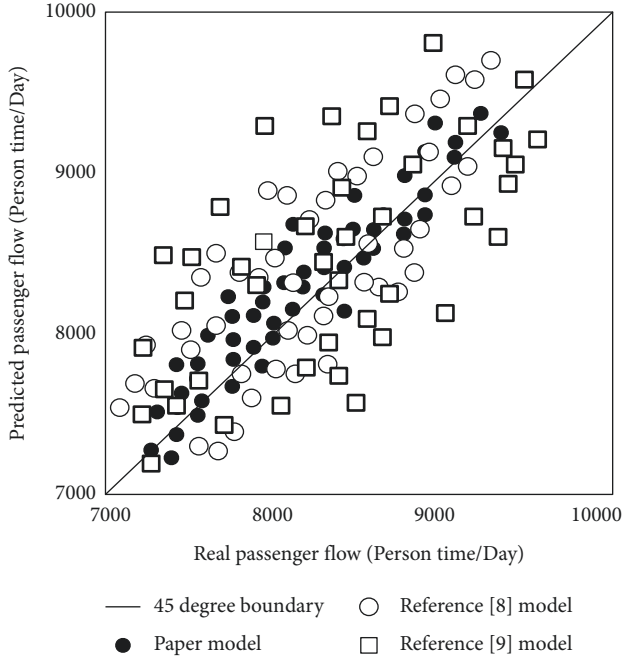


FIGURE 6: Scatter diagram of model prediction period.

TABLE 7: Forecast results of tourists' demand for scenic spot selection.

Scenic spot category	Actual person times	Predicted person times	Absolute quantity difference	Relative difference (%)
Resort	10222	11433	1221	5.6
Ecological farm	25340	24200	1140	2.3
Water hole	34586	35442	-856	-1.2
Drift	38351	37607	744	0.9
Picking point	21004	19412	1592	3.9

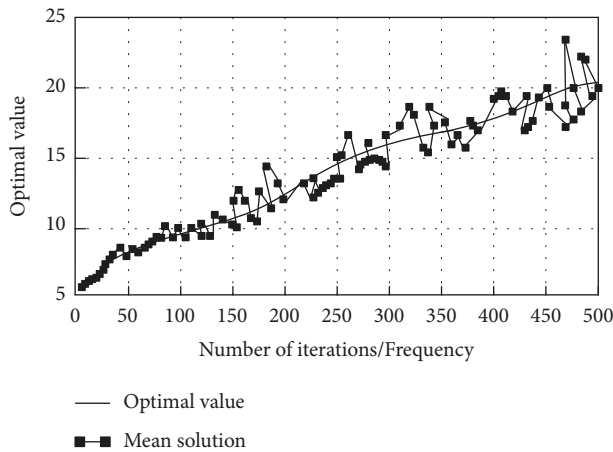


FIGURE 7: Optimal travel route search results.

To test the intelligent tourism information service performance of the model in this study, 2021 is taken as an example to predict the demand for tourists for scenic spot selection. The prediction results are shown in Table 7.

As shown in Table 2, the relative error between the number of tourists choosing scenic spots and the actual number of tourists in 2021 predicted by the model in this study is less than 6%. The experimental results show that the model in this study has a good prediction effect on the demand for selecting scenic spots. The method in this study is used to search the optimal tourism route, and the results are shown in Figure 7.

According to Figure 7, with the increase in iteration algebra, the optimal solution of the search results of the optimal tourism route shows an upward trend, the average value fluctuates up and down in the optimal solution, and the fluctuation range of iteration oscillation is small. When the number of iterations reaches 470 generations, the peak value of iteration fluctuation appears, indicating that the optimal path has been found and has good convergence.

To sum up, the prediction error of the model in this study is small and has a good prediction effect. The intelligent tourism information service model considering tourist experience in the Internet of things environment can effectively find the optimal path.

5. Conclusions and Prospects

5.1. Conclusions.

- (1) Under the environment of Internet of things, the prediction error of passenger flow of intelligent tourism information service model considering tourist experience is small
- (2) The intelligent tourism information service model has a good effect on the demand prediction of tourist attraction selection
- (3) When the number of iterations reaches 470 generations, the peak value of iteration fluctuation appears, indicating that the intelligent tourism information service model considering tourist experience in the designed Internet of things environment has found the optimal path

5.2. Prospects

- (1) As the infrastructure construction of intelligent tourism information service is still relatively backward, which is the biggest obstacle to the intelligent development of tourism industry, in the future, we can design intelligent tourism information service system under the background of intelligent tourism and use all kinds of network information technology under the environment of Internet of things to provide intelligent tourism services for tourists. Therefore, whether the establishment of the model can be truly implemented remains to be verified by the development of the times.
- (2) The next step is to establish an intelligent tourism information service model based on the tourism consumption model, user needs, and functional needs, through the current situation and investigation and analysis, and establish an intelligent tourism

information service model considering the experience of tourists using the service design methods such as tourist experience map, tourist role model, and interview. At the same time, it also needs to be verified by testing.

- (3) To facilitate the travel needs of tourists, the operation mode of intelligent tourism information service model is set as tourism app, the main functional modules of tourism app are determined according to the priority of tourist behavior path and service contact point, the corresponding service blueprint and app information architecture diagram are drawn, and the interactive interface prototype of tourism app is designed in combination with the design principles of interactive interface, and the visual design is improved.

Data Availability

The raw data supporting the conclusions of this article will be made available by the authors, without undue reservation.

Conflicts of Interest

The authors declare that they have no conflicts of interest regarding this work.

Acknowledgments

This work was supported by the Project of Anhui Vocational Education Innovation and Development Pilot Zone “Bozhou Internet + Traditional Chinese Medicine Tourism Town Cultivation and Construction” (WB-ZJYQ-034), the Scientific Research Planning Project of Anhui Institute Vocational and Adult Education “Exploration and Practice of Talents Co-Cultivation Mode between Enterprises and Colleges in Higher Vocational Colleges” (Azcj111), and the Key Project of Humanities and Social Sciences of Bozhou Vocational and Technical College “Bozhou Cultural Tourism Industry Think Tank” (ypzk003).

References

- [1] J. Zelenka, T. Azubuike, and M. Pásková, “Trust model for online reviews of tourism services and evaluation of destinations,” *Administrative Sciences*, vol. 11, no. 2, pp. 34–40, 2021.
- [2] M. A. Asnawi, “Synergy of tourism services based on local wisdom in south sulawesi,” *OSF Preprints*, vol. 7, no. 4, pp. 1–10, 2021.
- [3] S. Jardim and C. Mora, “Customer reviews sentiment-based analysis and clustering for market-oriented tourism services and products development or positioning,” *Procedia Computer Science*, vol. 196, no. 2022, pp. 199–206, 2022.
- [4] M. Nekomahmud and A. Hassan, “Tourism products and services in bangladesh: in search of policy and development frameworks,” *Tourism Products and Services in Bangladesh*, vol. 1, no. 8, pp. 3–24, 2021.
- [5] B. Zheng, Z. Mei, L. Hou, and S. Qiu, “Application of internet of things and edge computing technology in sports tourism services,” *Security and Communication Networks*, vol. 2021, no. 3, pp. 1–10, 2021.
- [6] J. P. Faggidae and P. Seran, “Willingness to Pay for Premium Tourism Services,” *Advances in Social Science, Education and Humanities Research*, vol. 544, no. 1, pp. 221–224, 2021.
- [7] F. Hemmati, F. Dabbaghi, and G. Mahmoudi, “Investigating prevalence job stress and illness among hospital staff providing health tourism services (hsphts) in iran,” *BMC Health Services Research*, vol. 20, no. 1, pp. 906–6, 2020.
- [8] N. Pochernina, “Assessment of the revealed comparative advantages of ukraine’s tourism services export to the eu,” *Black Sea Economic Studies*, vol. 1, no. 62, pp. 1–10, 2021.
- [9] L. Turkey Al-Khawaldeh and G. Ali Al-Badayneh, “The impact of applying quality standards on improving environmental tourism services for natural reserves in southern jordan,” *International Journal of Business and Management*, vol. 16, no. 7, pp. 119–126, 2021.
- [10] N. T. Hoa, “Vietnam tourism services development during and after covid 19 pandemic: situation and solutions,” *Revista Gestão Inovação e Tecnologias*, vol. 11, no. 3, pp. 23–34, 2021.
- [11] S. F. Schubert, “Covid-19,” *Revista Brasileira de Pesquisa em Turismo*, vol. 15, no. 1, pp. 2297–2305, 2021.
- [12] A. Oi, A. Mg, and B. Ms, B. Jr and B. Bs, City tourism services with mobile geolocation sharing - sciencedirect,” *Procedia Computer Science*, vol. 191, no. 2021, pp. 49–56, 2021.
- [13] M. Roy and A. H. M. Salimullah, “Application of technology for tourism products and services in bangladesh,” *Technology Application in the Tourism and Hospitality Industry of Bangladesh*, vol. 12, no. 10, pp. 37–62, 2021.
- [14] O. Hulych, “Trends, features and reserves of the development of the tourism services sector in ukrainian regions,” *Regional Economy*, vol. 3, no. 3(97), pp. 109–119, 2020.
- [15] S. M. Sergeev, A. A. Kurochkina, O. V. Lukina, and V. E. Zasenka, “Interactive algorithm for estimating consumer demand for tourism services for sustainable operation of the transport industry,” *IOP Conference Series: Materials Science and Engineering*, vol. 918, no. 1, Article ID 012219, 2020.
- [16] M. A. Khalaf, W. Elias, and G. Wafek, “Assessing tourism services quality and its effect on egyptians tourists satisfaction in hurghada,” *International Journal of Heritage, Tourism and Hospitality*, vol. 14, no. 2, pp. 73–87, 2020.
- [17] N. M. Al-Hazmia, “A study on the dimensions of the quality of tourism services in the kingdom of saudi arabia,” *Management Science Letters*, vol. 10, no. 1, pp. 1115–1120, 2020.
- [18] S. Turabekov, L. Toshnazarova, and N. Mukumova, “Foreign experience in providing employment in the field of tourism services in uzbekistan,” *Journal of Central Asia Economy*, vol. 4, no. 4, pp. 361–366, 2020.
- [19] M. Stelmach, “Purchase of trips for employees. tourism services provided by the employer,” *Doradztwo Podatkowe - Biuletyn Instytutu Studiów Podatkowych*, vol. 3, no. 283, pp. 15–18, 2020.
- [20] N. Dekhtyar, “Availability of free time as a factor of forming the demand for tourism services,” *Economic Scope*, vol. 1, no. 1, pp. 1–10, 2020.
- [21] M. Ka-Kan-Dee and S. Nonthapot, “Communication factors affecting the tourism services in the upper northeast of thailand,” *Management Science Letters*, vol. 10, no. 7, pp. 1437–1444, 2020.
- [22] R. A. Zahid, A. I. Suroso, A. I. Suroso, and S. Hannan, “Development of bussines model in sentulfresh agrotourism services,” *Jurnal Aplikasi Manajemen*, vol. 18, no. 1, pp. 46–56, 2020.

- [23] N. M. Al-Hazmi, "The impact of market targeting strategies on tourism services," *Management Science Letters*, vol. 10, no. 12, pp. 2799–2804, 2020.
- [24] N. M. Al-Hazmi and Y. A. G. Hassan, "Barriers on marketing tourism services and their impacts on customer awareness," *Management Science Letters*, vol. 10, no. 1, pp. 2603–2608, 2020.
- [25] V. F. Mayer, G. E. d. O. Santos, and O. R. B. Marques, "Option framing for upselling tourism services: does cognitive availability prevent irrational choices?" *Tourism Economics*, vol. 28, no. 2, pp. 476–494, 2020.
- [26] S. Polkovnychenko and A. Krasny, "Ukraine's attractiveness at the european tourism services market," *Efektivna Ekonomika*, vol. 1, no. 1, pp. 14–21, 2020.
- [27] J. Dědková and O. Ungerma, "Analysis of tourism services in the czech-polish part of the euroregion neisse," *Trendy v podnikání*, vol. 10, no. 1, pp. 21–30, 2020.
- [28] Z. Al-Quraishi, "The effect of tourism communication on the marketing of tourism services: a field study in the marshes of southern iraq," *International Journal of Psychosocial Rehabilitation*, vol. 24, no. 8, pp. 2020–2030, 2020.
- [29] Q. Wei, "Simulation of Integrated Integration Method of Smart Tourism Time and Space Database Resources," *Computer Simulation*, vol. 37, no. 5, pp. 399–402, 2020.
- [30] J. L. Cordova, "Digital platforms and the demand for international tourism services," *Policy Research Working Paper Series*, vol. 5, no. 14, pp. 9147–9156, 2020.
- [31] M. Roy and R. Saha, "Market design for tourism products and services in bangladesh: an ecotourism perspective on sylhet," *Tourism Products and Services in Bangladesh*, vol. 1, no. 5, pp. 365–396, 2021.
- [32] Y.-C. Lee and P.-T. Liao, "The effect of tourism on tele-connected ecosystem services and urban sustainability: an emergy approach," *Ecological Modelling*, vol. 439, no. 1, Article ID 109343, 2021.
- [33] M. Alauddin, S. M. M. A. Dipu, and M. R. Uddin, "Tourism products and services in bangladesh: challenges and suggestions," *Tourism Products and Services in Bangladesh*, vol. 3, no. 3, pp. 445–459, 2021.
- [34] M. Mohiuddin, M. Mesbah Uddin, S. Nowreen, and A. Nahian, "Tackling climate change effects and sustainable tourism products and services development through innovation in bangladesh," *Technology Application in the Tourism and Hospitality Industry of Bangladesh*, vol. 6, no. 6, pp. 301–315, 2021.
- [35] M. Alauddin, J. J. Li, and M. A. I. Chowdhury, "General medical tourism products and services in bangladesh," *Tourism Products and Services in Bangladesh*, vol. 1, no. 14, pp. 27–44, 2021.
- [36] M. Moura, B. Sousa, M. A. Malheiro, and C. M. Veloso, "The quality of services in tourism: a study applied to transport companies," *Quality - Access to Success*, vol. 22, no. 183, pp. 124–129, 2021.

Research Article

Design of Multimedia English Online Teaching Platform under Wireless Network Communication Technology

He Dan 

Department of College English, Liaoning University of International Business and Economics, Shenyang, China

Correspondence should be addressed to He Dan; hedan@luibe.edu.cn

Received 2 March 2022; Revised 26 March 2022; Accepted 7 April 2022; Published 23 April 2022

Academic Editor: Le Sun

Copyright © 2022 He Dan. This is an open access article distributed under the Creative Commons Attribution License, which permits unrestricted use, distribution, and reproduction in any medium, provided the original work is properly cited.

The traditional online teaching platform has poor compatibility due to the high data delay in practical applications. Therefore, a Multimedia English online teaching platform under wireless network communication technology is designed. Aiming at the actual functional requirements of online teaching, the overall architecture of the Multimedia English online teaching platform is designed. In this architecture, the hardware of the data collector, memory, and main controller is deployed to build the platform. Based on the wireless network communication technology, the software modules are divided into two parts. It is made of a number of functional modules. The design of the platform functional modules is mainly based on the main functions of the administrator submodule, the teacher submodule, and the student submodule. At the same time, the weight of the indicators is determined by combining the analytic hierarchy process and the evaluation domain for the quality evaluation of Multimedia English online teaching is established. The level model completes the platform design. The experimental results show that the test results of the designed platform meet the expected goals and can effectively improve the quality and efficiency of Multimedia English online teaching. The teaching quality is always higher than 95%, and the average teaching efficiency is 96.27%.

1. Introduction

In order to improve the stability of the Multimedia English online teaching platform and meet the needs of Multimedia English online teaching in larger colleges, it is really necessary to improve the management mode of resources in the platform [1]. At the same time, how to carry out Multimedia English online teaching in a more vivid form is also the key to improving teaching quality [2, 3]. Wireless network communication technology refers to the long-distance transmission of signals between multiple nodes without transmission through conductors or cables. Wireless network communication can be carried out by using various fixed, mobile, and portable applications, such as two-way radio, mobile phones, personal digital assistants, wireless networks, and radio, which can make students pay more attention to learning situations and minimize the interference of the surrounding environment [4]. The Multimedia English online teaching platform breaks the restrictions of time and space, but it is more dependent on the network

environment [5]. Therefore, improving the operation ability of the platform is also the focus of future research [6].

Relevant scholars have carried out research on this; the study in [7] provides a platform for online teaching to adapt to large concurrent visits. The Multimedia online teaching platform is one of the important contents of the Internet plus education platform. Constructing an online teaching platform suitable for large concurrent access is an urgent requirement for the transmission of university information. Compared with the construction of the Multimedia English online teaching platform in colleges and universities under the new situation, there are some new problems. Large concurrent access puts forward new requirements for platform performance, network bandwidth, and teachers' and students' literacy. Based on the new objectives and main problems of educational informatization 2.0, this paper puts forward countermeasures and suggestions from the aspects of new objectives of platform construction, network bandwidth, quality of teachers and students, new platform selection concept, new platform deployment mode, new

network unblocked mode, new teaching evaluation method, new quality improvement requirements, etc. The study in [8] puts forward the practice and research of hybrid teaching of sports anatomy courses based on the Multimedia English online teaching platform and demonstrates the superiority and feasibility of the hybrid teaching mode through experimental comparison, mathematical statistics, and literature review. The results show that the students in the experimental group with a mixed teaching mode had better knowledge and understanding of the relevant contents of the experiment than the students in the control group with traditional teaching methods. The mixed teaching mode is especially suitable for the characteristics of students majoring in physical education, and it is worth popularizing and applying in the teaching of sports anatomy.

Although the above research has made some progress, the application under wireless network communication technology is not enough. Therefore, the design of a Multimedia English online teaching platform under wireless network communication technology is proposed. Wireless network communication technology is a communication method for information exchange by using the characteristics that electromagnetic wave signals can propagate in free space. It can be point-to-point communication, point-to-multipoint communication, broadcasting, cellular network, other wireless networks, and WiFi technology. Its application in the Multimedia English online teaching platform had a good effect. Setting the actual functional requirements of online teaching as the goal, the author designs the overall architecture of the Multimedia English online teaching platform, deploys hardware and software modules in this architecture, determines the index weight combined with the analytic hierarchy process, establishes the evaluation-domain level model of Multimedia English online teaching quality evaluation, and completes the design of the Multimedia English Online teaching platform. The results show that the designed platform can meet the expected objectives and improve the quality and efficiency of Multimedia English online teaching.

2. Multimedia English Online Teaching Platform Based on Wireless Network Communication Technology

2.1. Architecture Design of the Multimedia English Online Teaching Platform. The Multimedia English online teaching platform is based on the open-source platform for architecture and secondary development. In order to standardize the development process and improve the development efficiency, the overall architecture of the Multimedia English online teaching platform is designed with wireless network communication technology to achieve the design goal of the platform [9, 10]. The upper layer does not need to completely rely on the specific implementation details of the lower layer. Changing the structure of the upper layer will not affect the lower layer, making the code more concise, so as to meet the coupling requirements of various modules of the Multimedia English online teaching platform [11].

When the server receives the user's request to access the page, it first loads the global configuration file, initializes the loading core framework, such as data operation, routing, and security, schedules the controller according to the configured route, requests the business logic layer and data layer to load data, and renders the data to the page, thus completing the whole process of request operation and rendering and outputting the data to the page [12, 13]. The overall architecture of the Multimedia English online teaching platform is shown in Figure 1.

As shown in Figure 1, the Multimedia English online teaching platform adopts a hierarchical tree structure design, which can be divided into five modules: user layer, application layer, middle layer, data layer, and basic environment layer for the user [14]. According to the actual functions of these five modules, a Multimedia English online teaching platform is designed.

2.2. Platform Hardware Design. Platform hardware refers to the physical equipment that constitutes the computer and is the realistic carrier for the operation of various logic programs. In the Multimedia English online teaching platform [15, 16] designed with wireless network communication technology, the key hardware used includes a data collector, memory, and master controller, which will be analyzed in detail as follows.

2.2.1. Data Collector. The data collector is a programmable logic chip equipped with a crawler program, which can be used to complete the search and collection of user history learning data, including web browsing information, user retrieval keywords, resource download records, exchange and interaction information, and other data that can understand user preferences [17]. The programmable logic chip in this platform is EPM240T100I5N TQFP-100 CPLD. The basic parameters of the chip are shown in Table 1.

According to the basic parameters of the chip in Table 1, it can be seen that the programmable logic chip in the Multimedia English online teaching platform plays an important role and, at the same time, it needs to meet the requirements of low noise and high precision during use.

2.2.2. Storage. Massive English teaching resources and a large amount of user historical behavior data are not enough to be stored only by the storage space carried by the platform itself. Therefore, after the data collector completes a collection task, it is necessary to transfer the collected data to the external memory [18, 19]. The memory in this platform is a disk array with 12 disks, which is equipped with a 4-bit Annapurna Labs Alpine AL-324 ARM@Cortex@-A57 Quad-Core 1.7 GHz processor and 46BDDR4 memory (up to 16 GB) support SATA6Gb/s hard-disk transmission interface to provide faster read and write speed. In addition, two GbE SFP+ and two 2.5Gbe network ports are built in the disk array. Using the disk array can realize the reasonable deployment of the network environment, so as to realize the

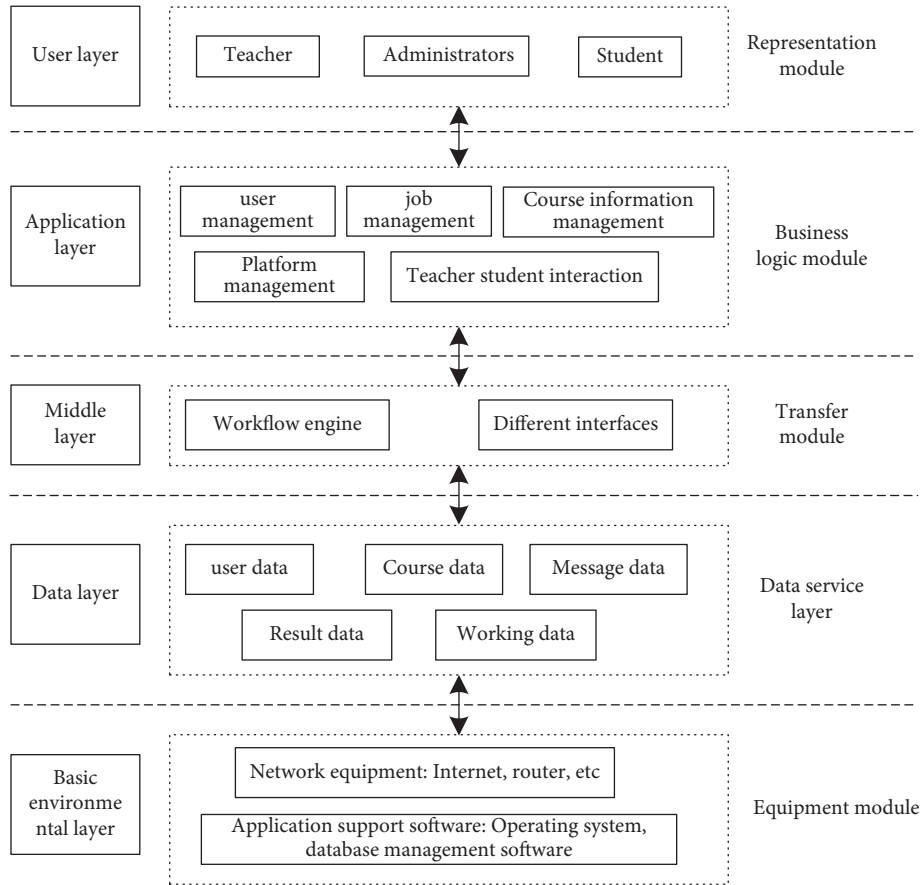


FIGURE 1: Overall structure of the Multimedia English online teaching platform.

TABLE 1: Basic parameters of the chip.

Attribute	Parameter
Name	Embedded CPLD
Model	EPM240T100I5N
Encapsulation	100-TQFP
Editable type	Editable in the platform
Delay time	≤ 4.7 ns
Supply voltage-internal	2.5 V, 3.3 V
Number of logical elements/blocks	240
Number of macrocells	192
I/O count	80
Working temperature	$-40^{\circ}\text{C}\sim 100^{\circ}\text{C}$

tasks of copying, saving, repairing, and restoring massive data.

2.2.3. Master Controller. The main controller is the core hardware of the Multimedia English online teaching platform, which is mainly used for the overall operation control of the platform and the execution of various business logic operations [20]. The main controller of this platform is dtb-1022 J1900-embedded industrial computer, and its basic parameters are shown in Table 2.

According to the basic parameters of the embedded industrial computer in Table 2, it can be seen that the power supply, CPU, I/O interface, and other components are

centrally installed in a chassis, which has the characteristics of compact structure, small size, and low price and generally adopts an integral structure.

2.3. Platform Software Design. In order to further improve the overall function of the Multimedia English online teaching platform [12, 21], the software part of the platform can be divided into three modules: administrator management submodule, teacher management submodule, and student management submodule. The specific module function flow chart is shown in Figure 2.

The specific contents of the platform software design are given as follows.

2.3.1. Administrator Submodule. This module is the manager of the Multimedia English online teaching platform. Its main responsibility is platform maintenance and website management [22, 23], to ensure the stable operation of the platform and the effective development of teachers' teaching interaction. This module is the core part of the whole Multimedia English online teaching platform. The specific functions are described as follows:

- (1) *Role Division.* When logging into the Multimedia English online teaching platform with the browser for the first time, it is necessary to provide the e-mail and other contact information of new users and

TABLE 2: Basic parameters of the embedded host controller.

Name	Parameters
CPU	On-board Intel J1900 processor
Memory	One 204 pin DDR3L1600 MHZ SO-DIMM memory socket, maximum 8 G
Display	1 HDM interface, 1 VGA interface
Hard disk	1 SATA interface, 1 msata interface
Network	2 gigabit network ports
Extension	1 half height Mini pcie plug-in
COM	8 COM interfaces
USB	5 USB2 0 interface, 1 usb3 0 interface
GPIO	4-bit DI, 4-bit DO
Audio frequency	Line-in interface, line-out interface
Power support	DC 12V power input
Working temperature	-10°C to 70°C

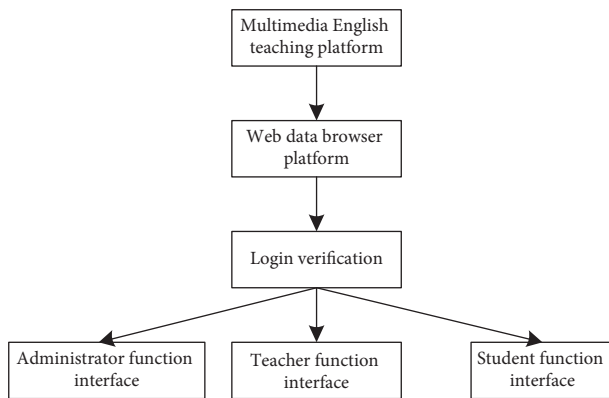


FIGURE 2: Specific design flow chart of the Multimedia English online teaching module.

realize role matching and authority division for new users according to the information provided by users [24, 25]. For example, if the new user is a teacher, the permissions that the new user can use include applying for adding or deleting courses and uploading teaching resources to the network platform; if the new user is a student, the permissions of the user include online course selection, online testing, and viewing results. At the same time, the administrator has the functions of increasing or decreasing users and managing user-level permissions.

- (2) *Course Management.* By this function, the administrator can add or delete the function categories in the platform through the actual situation of English teaching. At the same time, the administrator also has the right to move, modify, or import new courses for each function, as well as the right to restore and backup courses [26, 27].
- (3) *Web Page Setup.* The website administrator can choose to install different skin plug-ins to make the platform layout and appearance design more beautiful.
- (4) *Other Settings and Information Query.* The website administrator can view the online time, offline time, course selection, and listening and other activities of

users on this platform; notices and announcements can be issued on the platform, and multiple information can be accurately managed by using this module. The operation flow chart of the specific administrator submodule is shown in Figure 3.

2.3.2. Teacher Management Submodule. One of the main users of the Multimedia English online teaching platform is teachers. The main responsibility of the design is to provide teachers with various permissions and functions through the platform, which can better complete teaching activities. Using the characteristics of the network platform, we can vividly design the English teaching process and carry out effective interactive activities, so as to achieve the purpose of teaching in a fun manner [28, 29]. The specific functions are described as follows:

- (1) *Applying for Courses.* After receiving the notice of teaching, teachers can apply for adding new courses through the platform and simply design the new courses. At the same time, they can realize the functions of adding, deleting, modifying, moving, and so on. After the administrator imports the students into the platform in batches, group teaching can be realized according to the situation of the students.
- (2) *Teaching Design and Organizing Activities.* According to the course content and the characteristics of each course, teachers can upload teaching plans, teaching materials, teaching dynamic videos, teaching courseware, and other resources to the Multimedia English online teaching platform to facilitate the teaching process [30]. Based on the above teaching resources, they can achieve the predesigned teaching purpose, so as to improve the teaching quality and promote students to effectively acquire knowledge.
- (3) *Online Test Management.* In this function module, teachers can use the topic selection function of the question bank in the module to select the test questions in the question bank by random selection or manual selection to form the test paper. At the same time, teachers can also set the test time, the option of whether to answer again, and the number of answers and have the authority to delete, add, and change the order of the test questions. After the end of the semester teaching course, you can also use the network platform to prepare the final examination paper, in which the objective test questions can be judged by yourself through the platform.
- (4) *Personal Data Management.* Teachers can view and change personal information and also have the functions of setting up personal microblogs and transmitting personal messages. The specific operation flow of the teacher management submodule is shown in Figure 4.

2.3.3. Student Management Submodule. In the Multimedia English online teaching platform, another main user is students. In order to facilitate students to browse the network

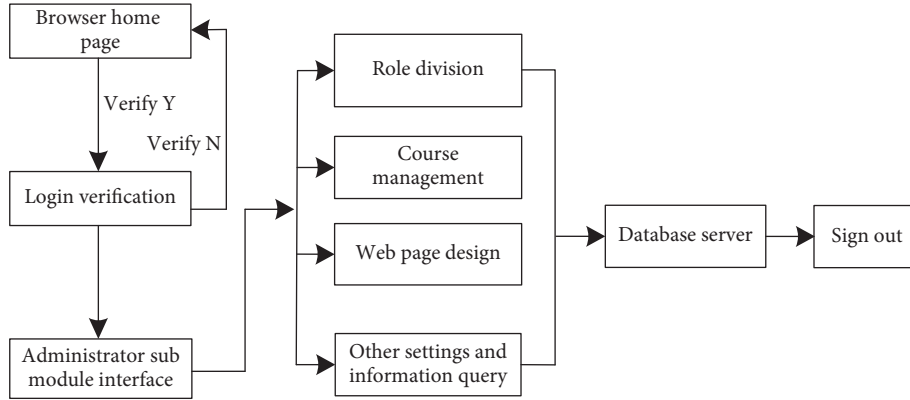


FIGURE 3: Operation flow chart of the administrator submodule.

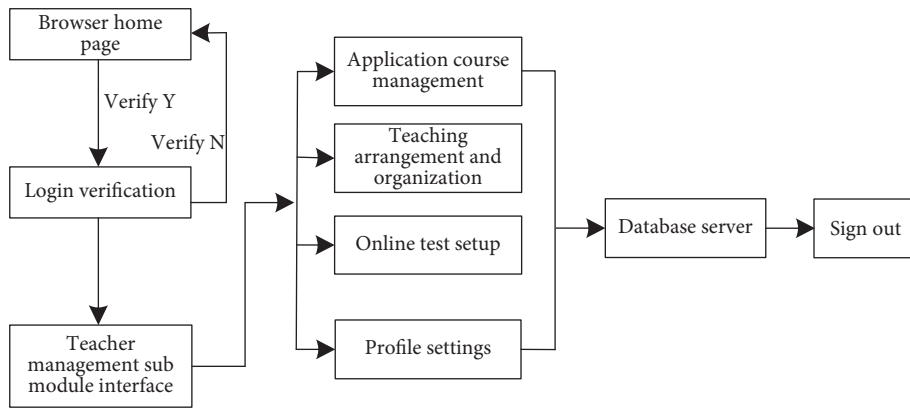


FIGURE 4: Operation flow chart of the teacher management submodule.

platform, functions such as selecting course learning, course's interactive activities, online test answers, and setting up personal data are added to the student management submodule [31, 32]. The specific functions are described as follows:

- (1) *Course Learning*. After successfully registering new users through the browser, students can view the teaching introduction and courses, as well as all learning courses in the semester.
- (2) *Teaching Interaction*. In the Multimedia English online teaching platform, according to the scene of teachers' curriculum, students can discuss relevant problems with teachers and other students to realize a series of interactive activities, so as to improve students' learning ability [33].
- (3) *Online Answers*. In order to understand students' mastery of knowledge, students can conduct online self-evaluation according to the unit test provided by teachers after the unit course. After completing the test, they can also enter the Multimedia English teaching platform to realize the score query function, which can consolidate and review knowledge [34, 35].
- (4) *Personal Data Management*. Students can change their basic personal information in the Multimedia English online teaching platform and establish a

personal learning space according to their interests and hobbies. The specific operation flow of the student management submodule is shown in Figure 5.

To sum up, the overall framework of the Multimedia English online teaching platform is preliminarily designed using wireless network communication technology. On the basis of this framework, each functional module is analyzed and designed in detail. A planning decision-making goal is set as M_b , and the expression is as follows:

$$M_b = Y_x \times Q_s. \quad (1)$$

Here, Y_x represents the influencing factors and Q_s represents the importance data of Y_x corresponding to the planning objectives. Due to the difference in influence degree of influencing factors on the target M_b , it is necessary to compare the influence degree, and all the comparison results can be expressed by D matrix:

$$D = \begin{bmatrix} d_{11}, d_{12}, \dots, d_{1m} \\ d_{21}, d_{22}, \dots, d_{2m} \\ \vdots \\ d_{m1}, d_{m2}, \dots, d_{mm} \end{bmatrix}. \quad (2)$$

Here, d_{mm} represents the influence degree coefficient in row m and column m . Assuming that the matrix D satisfies

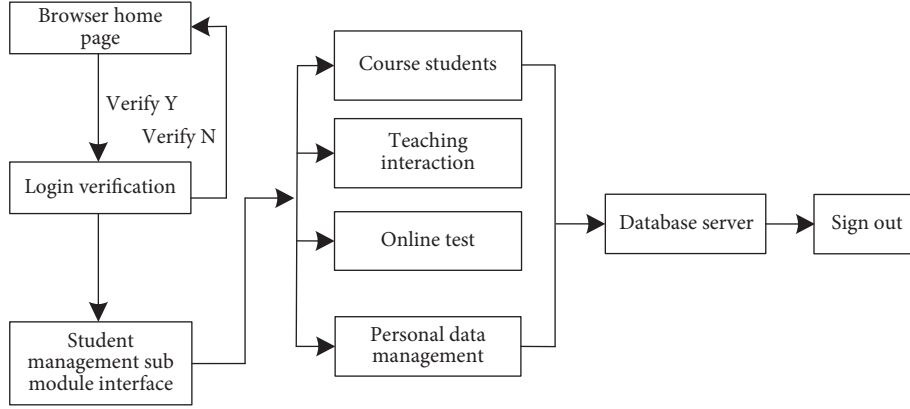


FIGURE 5: Operation flow chart of the student management submodule.

the consistency condition, the corresponding solution to the eigenvalue problem is as follows:

$$D' = d_{mm} \times R_u. \quad (3)$$

Here, R_u represents the fuzzy comprehensive evaluation coefficient. The fuzzy comprehensive evaluation method is a mathematical evaluation method. It mainly deals with the fuzzy things in the real world quantitatively through the basic theories and methods of fuzzy mathematics and makes an objective, accurate, and practical Multimedia English online teaching evaluation, so as to effectively solve the problems in the actual teaching process. The basic principle of a fuzzy comprehensive evaluation is as follows: give priority to collecting materials for accurate evaluation of Multimedia English online teaching and determine the main factors and grades of evaluation; then, the weight distribution of the online teaching evaluation index is determined by the above analytic hierarchy process, and the fuzzy mathematical model is established. Assuming that the analytic hierarchy process is used to determine the weight, the evaluation-domain level model is set as follows:

$$A = (a_1, a_2, \dots, a_n). \quad (4)$$

Here, a_1 , a_2 , and a_n all represent the evaluation grade coefficient. The teaching quality evaluation results of different teachers are obtained through the evaluation-domain level model, and the corresponding improvement measures are given in time combined with the evaluation results to ensure the effective improvement of the quality of the Multimedia English online teaching platform, so as to complete the design of the Multimedia English online teaching platform under the wireless network communication technology.

3. Experimental Analysis

In order to verify the feasibility of the designed Multimedia English online teaching platform under wireless network communication technology, the following experiments are designed. Taking the course teaching of a college English major as an example, the teaching content is set as the experimental object. On this basis, combined with the virtual

TABLE 3: Platform test environment.

Name	Parameter
Platform	Windows 10
CPU	Intel Zhiqiang E5-2600
Development tool	Sublime
Deep learning tools	Theano

simulation platform, the host used for the test is Microsoft Windows Professional Tomcat7.0 host, using Myeclipse software as the simulation environment, the database type is SQL SERVER2012 Database 5.3, and the expansion device is Web Server, equipped with FTPServer, Mail Server, and Database Server subplatforms. The platform is controlled using Adobe Dreamweaver CS, PhotoImpact12, and Acrobat9, the network program language is JSP, and the TCP/IP communication protocol is executed. Other test environments are shown in Table 3.

According to the platform test environment in Table 3, the experiment uses English books in a university library as English teaching resources to test the application performance of the platform. The test process is shown in Figure 6.

Based on the test process of the Multimedia English online teaching platform in Figure 6, the simulation test parameters are set, as shown in Table 4.

In order to verify the practicability of the designed platform, the function and performance of the platform are simulated and tested, respectively. Functional testing is to use test cases to verify the function of the platform. The platform teaching function and platform management function are tested, and the results are shown in Tables 5 and 6.

Through the function tests in Tables 5 and 6, it can be seen that during the operation of the platform data function, the client has relatively completed verification measures. Without going through the server, the client can complete reliable information category calibration, prevent the input of dirty data, ensure the quality of teaching resources of the platform, and quickly save the complete information to the database. All test results are passed, and the test results meet the expected objectives.

In order to further verify the effect of the Multimedia English online teaching platform under wireless network

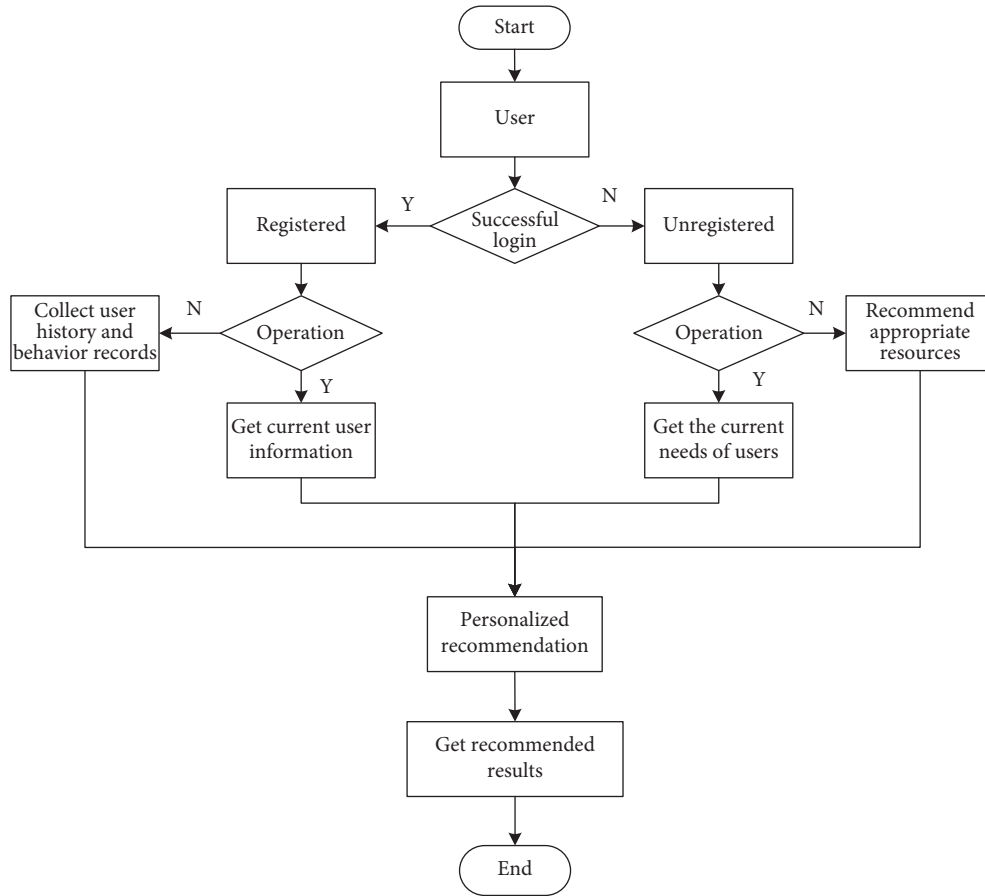


FIGURE 6: Test flow chart of the Multimedia English online teaching platform.

TABLE 4: Experimental parameters of the platform simulation test.

Name	Parameter
Average crawl processing time of web crawler nodes	≤ 2 h
Enter data batch size	128 Mb
Training rounds	5 rounds
Number of different convolution kernels	70
Convolution kernel type	3 kinds
Hidden layer size	18×2
	Layer 1 input $128 \times L \times (18 \times 5)$
	Layer 1 output 200
Full connection layer	Layer 2 input 200
	Layer 2 output $128 \times L \times (18 \times 5)$
	Layer 3 input 200
	Layer 3 output 200

Note. L stands for the characteristic scale.

communication technology and compare the teaching quality of three different platforms for testing, 150 students with equivalent academic achievements are selected as the test objects, of which every 50 students are a group, and three different platforms are used to teach the same content, of which the full score of the test score is 100, where $100 \sim 85$ points mean excellent; $84 \sim 60$ points mean qualified; and if the score is below 60, it means unqualified. The comparison

TABLE 5: Platform teaching function test.

Number	Test items	Test method	Result
1	Admin/12345	Is the format correct	Adopt
2	Course view	Whether the course is displayed or not	Adopt
3	Search courses	Can I search	Adopt
4	Job submission	Can I submit normally	Adopt
5	Video playback	Can it play normally	Adopt

results of teaching quality of each teaching platform are given in Figure 7.

By analyzing the experimental data in Figure 7, we can see that the teaching quality of the designed platform is always higher than 95%, while the teaching quality of the platform in reference [7] and the platform in reference [8] is lower than 90%. Our platform uses analytic hierarchy process to evaluate the quality of Multimedia English online teaching, so as to obtain the evaluation results of Multimedia English online teaching in time. Through the evaluation results, the corresponding improvement measures are given in time to ensure the effective improvement of the teaching quality of the designed platform. The student test scores of the designed platform are significantly higher than those of the other two platforms, which shows that the designed platform can obtain more satisfactory teaching results. The

TABLE 6: Platform management function test.

Number	Test items	Test method	Result
1	Courseware management	Can you find the required courseware correctly	Adopt
2	User management	Can you effectively query the number of users	Adopt
3	Job management	Can I use keywords to browse jobs	Adopt
4	Online interaction	Can you use this function to complete online topic answers	Adopt

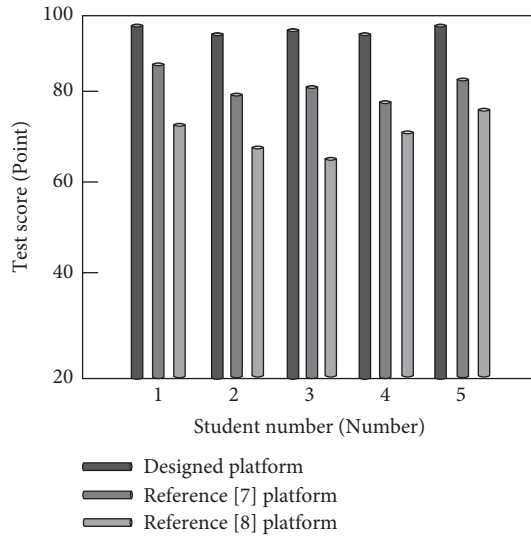


FIGURE 7: Comparison results of teaching quality on different platforms.

TABLE 7: Comparison results of teaching efficiency of different Multimedia English online teaching platforms.

Number of experiments/frequency	Teaching efficiency of the Multimedia English online teaching platform/%		
	Designed platform	Reference [7] platform	Reference [8] platform
2	99.69	98.63	93.52
4	99.37	96.09	92.03
6	98.44	95.25	90.09
8	97.85	94.59	89.21
10	96.33	93.85	87.63
12	96.12	92.43	85.14
14	95.99	91.52	84.22
16	95.47	89.20	82.30
18	94.58	88.30	80.25
20	94.44	86.72	79.12
22	93.29	83.45	77.41
24	93.65	81.43	77.22
Average value	96.27	90.96	84.85

following experimental tests compare the teaching efficiency of three different platforms. The specific experimental comparison results are shown in Table 7.

By analyzing the experimental data in Table 7, we can see that the teaching efficiency of each platform is constantly changing with the increase in the number of experiments. The average teaching efficiency of the designed platform is 96.27%, the average teaching efficiency of the platform in reference [7] and the platform in reference [8] are 90.96%

and 84.85%, respectively, and the decline trend of literature platform teaching efficiency is very obvious, mainly because the two teaching platforms failed to evaluate the teaching quality in the process of practical application, resulting in the cumbersome whole teaching process; it also proves that it is feasible and effective to add analytic hierarchy process to the designed platform for teaching quality evaluation.

To sum up, the designed Multimedia English online teaching platform under wireless network communication technology has a good effect in practical application and can produce positive results. As a practical technical scheme, it is not something in the abstract thinking stage but something that can be implemented in the industry and has the characteristics of enforceability, reproducibility, and usefulness. Compared with other literature platforms, the teaching quality and teaching effect of the designed platform are better and the performance is improved to a greater extent.

4. Conclusions and Prospects

4.1. Conclusions

- (1) During the operation of the data function of the Multimedia English online teaching platform under the designed wireless network communication technology, the client has relatively complete verification measures, which can complete reliable information category calibration and ensure the quality of platform teaching resources. A passing status is presented, and the test results meet the expected goals.
- (2) The designed platform uses the analytic hierarchy process to evaluate the quality of Multimedia English online teaching and obtains the evaluation results of Multimedia English online teaching in time to ensure that the teaching quality of the designed platform is effectively improved, and more satisfactory teaching results can be obtained.
- (3) The teaching efficiency of the designed platform is good, and it is effective to add the analytic hierarchy process to the platform to evaluate the teaching quality.

4.2. *Prospects.* Due to the limitation of time and other factors, there are still some deficiencies in the designed platform. The follow-up research will focus on the following aspects:

- (1) We will expand the scope of research, make teachers give more targeted teaching, and ensure the effective improvement of teaching quality and efficiency

- (2) In the follow-up, we will comprehensively analyze the learning situation of different students, so that the platform can comprehensively summarize and analyze them and give the corresponding teaching plan in time

Data Availability

The raw data supporting the conclusions of this article will be made available by the author, without undue reservation.

Conflicts of Interest

The author declares that there are no conflicts of interest regarding this work.

References

- [1] R. J. Musa, O. M. Ejovi, and F. O. Oghenerhovweya, "Re-thinking the design of English language teaching online using the flipped classroom approach," *Social Science Electronic Publishing*, vol. 4, no. 3, pp. 9–18, 2021.
- [2] A. Cheung, "Synchronous online teaching, a blessing or a curse? insights from efl primary students' interaction during online English lessons," *System*, vol. 100, no. 8, pp. 102–126, 2021.
- [3] N. T. H. Thu, "Communication skills and reflection practice in smart English teaching and learning environment: a case study," *International Journal of Emerging Technologies in Learning (IJET)*, vol. 15, no. 17, pp. 221–237, 2020.
- [4] K. Wilson, "Balancing the disruptions to the teaching and learning equilibrium-responsive pedagogic approaches to teaching online during the covid-19 pandemic in general chemistry classes at an arabian gulf university," *Journal of Chemical Education*, vol. 97, no. 9, pp. 2895–2898, 2020.
- [5] A. Mehrpouyan and E. Zakeri, "Approaches using social media platforms for teaching English literature online," *European Journal of Language and Literature Studies Articles*, vol. 7, no. 7, pp. 1–10, 2021.
- [6] W. Ho and K. Tai, "Doing expertise multilingually and multimodally in online English teaching videos," *System*, vol. 94, no. 3, pp. 102–124, 2020.
- [7] X. H. Xiao, G. L. Zhang, and H. P. Pu, "New thoughts on the construction of college online teaching platform adapting to a large concurrent access," *Creative Education*, vol. 12, no. 5, pp. 1047–1056, 2021.
- [8] L. Mirong, "The practice and research of blended teaching of sports anatomy course based on network teaching platform," *Journal of Advances in Education Research*, vol. 5, no. 4, pp. 1–10, 2020.
- [9] P. Alicia, "Teaching email writing through online teaching platform," *International Journal of Clinical Medicine*, vol. 1, no. 1, pp. 14–29, 2020.
- [10] B. Vadivel, M. Mathuranjali, and N. R. Khalil, "Online teaching: insufficient application of technology," *Materials Today Proceedings*, vol. 23, no. 1, pp. 10–18, 2021.
- [11] R. Munirah and R. Refnaldi, "An evaluation of assessment designed by English language education student teachers during teaching practice," *Journal of English Language Teaching*, vol. 9, no. 1, pp. 1–10, 2020.
- [12] T. Al-Habsi, S. Al-Busaidi, and A. Al-Issa, "Integrating technology in English language teaching through a community of practice in the Sultanate of Oman: implications for policy implementation," *Educational Research for Policy and Practice*, vol. 21, no. 1, pp. 1–10, 2021.
- [13] M. S. Yadav and M. K. Yadav, "Role of the transformational generative grammar and other language learning theories in English language teaching," *SSRN Electronic Journal*, vol. 2, no. 1, pp. 142–153, 2020.
- [14] H. Ssf and F. Ans, "Online teaching during covid-19: how to maintain students motivated in an efl class," *Social Science Electronic Publishing*, vol. 6, no. 2, pp. 157–171, 2020.
- [15] N. R. Moteanu, "Teaching and learning techniques for the online environment. how to maintain students' attention and achieve learning outcomes in a virtual environment using new technology," *International Journal of Innovative Research and Scientific Studies*, vol. 4, no. 4, pp. 278–290, 2021.
- [16] J. E. Pineda, L. H. T. Cano, and M. A. Peralta, "An inquiry-based framework for teaching English in synchronous environments," *International Journal of Computer-Assisted Language Learning and Teaching*, vol. 11, no. 1, pp. 38–58, 2021.
- [17] M. J. Ennis, Ed., *Online Submission*, vol. 230, no. 1, pp. 1–10, 2020.
- [18] R. J. Pearson, "Clickers versus pickers: comparing two audience response systems in a smartphone-free teaching environment," *Journal of Chemical Education*, vol. 97, no. 8, pp. 2342–2346, 2020.
- [19] H. A. Öztürk, "My quest for negotiating meaning. Reflections on my dilemmas about practices of English language teaching in public school context in Turkey," *Technium Social Sciences Journal*, vol. 7, no. 1, pp. 36–48, 2020.
- [20] N. Oeamoum and C. Sriwichai, "Problems and needs in English language teaching from the viewpoints of pre-service English teachers in Thailand," *Asian Journal of Education and Training*, vol. 6, no. 4, pp. 592–601, 2020.
- [21] M. Bhat, H. P. Palanyswamy, and U. Varsha, "Development and Validation of an automated Dichotic double word test in Indian English using MATLAB," *International Journal of Pediatric Otorhinolaryngology*, vol. 144, no. 5, pp. 110–119, 2021.
- [22] M. Lin, C. H. Shi, and H. J. University, "An exploration of objective question assessment of English teaching platform under the background of big data," *Journal of Hubei Open Vocational College*, vol. 32, no. 13, pp. 187–188, 2019.
- [23] Z. H. Yuan, "Research and practice of mixed teaching mode of online course—taking the advanced mathematics based on "learning pass + ding talk" as an example," *Creative Education Studies*, vol. 9, no. 1, pp. 221–226, 2021.
- [24] I. You, G. Pau, W. Wei, and C. Fung, "IEEE access special section editorial: green communications on wireless networks," *IEEE Access*, vol. 8, no. 10, pp. 187140–187145, 2020.
- [25] H. Chen, "The influence of online English writing platform on writing metacognitive strategies and writing performance—a study based on English majors in vocational colleges," *Journal of Shaanxi Xueqian Normal University*, vol. 35, no. 3, pp. 97–100, 2019.
- [26] W. Chen and F. Wang, "Practical application of wireless communication network multimedia courseware in college basketball teaching," *EURASIP Journal on Wireless Communications and Networking*, vol. 2021, no. 1, pp. 73–10, 2021.
- [27] S. Sartini, "Kahoot in maritime English teaching: its impact on nautical science cadet's oral reproduction and vocabulary," *English Language Teaching Educational Journal*, vol. 3, no. 1, pp. 41–51, 2020.
- [28] F. Desmeules-Trudel and M. F. Joannis, "Discrimination of four Canadian-French vowels by native Canadian-English

- listeners,” *Journal of the Acoustical Society of America*, vol. 147, no. 5, pp. 391–395, 2020.
- [29] X. X. Yan, X. W. An, W. B. Dai, and N. L. Sun, “Image segmentation teaching system based on virtual scene fusion,” *Computer Simulation*, vol. 38, no. 4, pp. 331–337, 2021.
- [30] P. A. Boda and B. Brown, “Priming urban learners’ attitudes toward the relevancy of science: a mixed-methods study testing the importance of context,” *Journal of Research in Science Teaching*, vol. 57, no. 1, pp. 567–596, 2020.
- [31] A. E. Yastibas, “An anthropocentric approach to evaluate English language teaching course books,” *Shanlax International Journal of Education*, vol. 8, no. 3, pp. 24–29, 2020.
- [32] T. Gan, “Language regulation in English as a lingua franca: focus on academic spoken discourse,” *ELT Journal*, vol. 73, no. 1, pp. 101–104, 2019.
- [33] A. Tarafdar, M. Debnath, S. Khatua, and R. K. Das, “Energy and quality of service-aware virtual machine consolidation in a cloud data center,” *The Journal of Supercomputing*, vol. 76, no. 1, pp. 9095–9126, 2020.
- [34] L. Gashi, “Intercultural awareness through English language teaching: the case of kosovo,” *Interchange*, vol. 52, no. 2, pp. 357–375, 2021.
- [35] T. G. Durand, L. Visagie, and M. J. Booysen, “Evaluation of next-generation low-power communication technology to replace GSM in IoT-applications[J],” *IET Communications*, vol. 7, no. 7, pp. 1–10, 2019.